HYDROCARBON EVOLUTION OF THE BREDASDORP BASIN, OFFSHORE SOUTH AFRICA: FROM SOURCE TO RESERVOIR

CHRISTOPHER PAUL NORMAN DAVIES

DECEMBER 1997

Dissertation presented for the Degree of Doctor of Philosophy at the University of Stellenbosch.

Promoter: Professor A. Rozendaal

Co-Promoter: Professor B.V. Burger

I the undersigned hereby declare that the work contained in this dissertation is my own original work and has not previously in its entirety or in part been submitted at any university for a degree.

Signature: C P N Davies Date: 27 November 1997

ABSTRACT

This first comprehensive study of the petroleum geochemistry of the Bredasdorp Basin, and the adjacent Southern Outeniqua Basin, documents the characteristic large number of hydrocarbon shows and the four regionally distinctive marine source rocks. Detailed correlation of reservoired hydrocarbons with source rock bitumens shows that two source rocks have expelled oil in commercial quantities and two others have expelled commercial quantities of wet gas/condensate.

In contrast with earlier studies which indicated that thermal 'gradualism' prevailed, this study indicates that the post-rift thermal history of the basin is very complex. Post-rift cool-down is punctuated by periods of rapidly increasing heat flow resulting in much of the maturation being localised in time. These periods of increased heating coincide with regional plate tectonism. The associated thermal uplift and downwarp effects govern the periods of trap formation and control the hydrocarbon migration direction.

Migration distances of these hydrocarbons are described and show *inter alia* that oil migrates no more than ~7-10 km but gas migrates regionally. Two regional episodes of meteoric water flushing reduce sandstone cementation in palaeo-highs forming potential reservoirs at specific times. The unusually low salinity of remnants of this water in some sandstones help characterise these two main migration conduits.

A highly detailed hydrocarbon correlation scheme derived from gas, light oil and biomarker data has been established which differentiates products of the four active source rocks and helps characterise the oil-oil, oil-source and source-source pairs. It is evident from these correlations that two periods of migration and reservoiring occurred at 50-60 Ma and 0-10 Ma. As a result, source-reservoir plays which characterise certain areas of the basin as predominantly oil or gas prone can be described. These correlations also highlight areas where mixtures of hydrocarbons are common and where some of the early reservoired oil has been displaced to new locations, constituting potential new exploration plays.

Source rocks for some of the analysed hydrocarbons have yet to be found and may not even have been drilled to date. One such source rock appears to be located in the Southern Outeniqua Basin, making that area a potential target for further exploration.

This study resolved the common heritage of the source rocks and reservoir sandstones which form part of the Outeniqua(!) petroleum system. The hydrocarbon volumes available to this system show that by world standards it is indeed significant.

ABSTRAK

Die groot aantal koolwaterstof voorkomste asook vier streekskenmerkende mariene brongesteentes word in hierdie eerste omvattende studie van die petroleumgeochemie van die Bredasdorp-kom en die aangrensende Suidelike Outeniqua-kom saamgevat. Gedetaileerde korrelasies van die opgegaarde koolwaterstowwe met brongesteente bitumen, dui daarop dat twee van die vier geidentifiseerde brongesteentes olie in kommersiële hoeveelhede uitgeset het. Die ander twee het kommersiële hoeveelhede nat gas-kondensaat uitgeset.

In teenstelling met vroeër studies wat daarop gedui het dat termale 'gradualisme' voorgekom het, dui hierdie studie daarop dat die na-rif termale geskiedenis van die kom baie meer kompleks is. Verskeie periodes van versnelde toename in hittevloei het voorgekom in die na-rifse verkoeling. Dit het daartoe gelei dat veroudering plaaslik binne 'n beperkte tydsverloop plaasvind. Hierdie periodes van hittetoename stem ooreen met die regionale plaattektoniek. Die geassosieerde termiese opheffing en afwaartse vervormingseffek, beheer die totstandkoming van opvanggebiede en die migrasierigting van die koolwaterstowwe.

Migrasie-afstande van die koolwaterstowwe word bespreek en wys inter alia daarop dat olie nie verder as ~7-10 km beweeg nie, maar gasmigrasie vind regionaal plaas. Twee kort episodes van meteoriese wateruitsetting, het sandsteensementasie in palaeo-hoogsliggende gebiede verminder wat potensiële reservoirs gevorm het op spesifieke tye. Die ongewone lae soutvlakte van oorblyfsels van dié water in sekere sandstene help om die twee vernaamste migrasieroetes te kenmerk.

'n Hoogs omvattende koolwaterstof-korrelasieskema wat van gas, ligte olie en biomerkerdata verkry is, is opgestel. Die skema het onderskei tussen produkte van die vier aktiewe brongesteentes en help om die olie-olie, olie-bron en bron-bron pare te karakteriseer. Dit is duidelik van die korrelasies dat twee periodes van migrasie en opgaring plaasgevind het ongeveer teen ~50-60 Ma en 0-10 Ma. Gevolglik kan bron-reservoir omskrywings wat sekere dele van die kom karakteriseer as grotendeels olie- of gas-ontvanklik beskryf word. Hierdie korrelasies beklemtoon ook areas waar mengsels van koolwaterstowwe algemeen voorkom en waar sekere van die vroeër opgegaarde olie verplaas is na nuwe lokaliteite, wat nuwe eksplorasieteikens daarstel.

Brongesteentes vir sekere van die ge-analiseerde koolwaterstowwe, moet nog gevind word en is tot op hede nog nie raakgeboor nie. Een so 'n brongesteente kom voor in die Suidelike Outeniqua-kom, wat daardie area 'n potensiële teiken vir verdere eksplorasie maak.

Die studie het die gesamentlike oorsprong van die brongesteente en reservoirsandsteen, wat deel is van die Outeniqua(!) Petroleumsisteem, geidentifseer. Die koolwaterstofvolumes wat beskikbaar is vir die sisteem wys dat, gemeet teen wêreld standaarde, dit wel beduidend is.

Ex Africa semper aliquod novi

Pliny the Elder (AD23-79). "Historia Naturalis", **VIII**, 17.

CONTENTS LIST

VOLUME 1: CHAPTERS 1-6

LIST OF FIGURES AND TABLES

CHAPTER 1

CHAPTER 2

CHAPTER 3

Figure 3.12: Part of NW-SE seismic line through the eastern part of the basin crossing that in Figure 3.13 at the location shown. Vertical noise (esp. at shotpoints 1350-1850) i.e. in the vicinity of well 8 are probably igneous intrusions but appear very different from the 'knolls' in Figure 3.13 suggesting a different mode of origin. The line is located on the regional map, Figure 3.30.

Figure 3.13: Part of N-S seismic line through the south flank of the basin showing possible reef knolls. A more regional location map of the line is shown in Figure 3.30.

Figure 3.14: Map of the Bredasdorp Basin showing the distribution of oil, wet gas and dry gas shows in syn-rift sandstones.

Figure 3.15: Map of the Bredasdorp Basin showing the distribution of oil, wet gas and dry gas shows in early drift sandstones.

Figure 3.16: Map of the Bredasdorp Basin showing the distribution of oil, wet gas and dry gas shows in late Barremian deep-water turbidite sandstones.

Figure 3.17: Map of the Bredasdorp Basin showing the distribution of oil, wet gas and dry gas shows in Aptian shelf-edge channel sandstones immediately below the Aptian regional source rock/seal.

Figure 3.18: Map of the Bredasdorp Basin showing the distribution of oil, wet gas and dry gas shows in Albian outer shelf channel and lobe sandstone complexes (elongate distribution) and overbank sandstones (localised individual reservoirs).

Figure 3.19: Palaeo-topographic map of the Bredasdorp Basin and its environs at lowest Plio-Pleistocene sea-level lowstand. This glacially-related lowstand reached approximately 150 metres below present sea-level (Dingle et al., 1983) and resulted in exposure of faulted northern and southern flank highs and possibly the highs which range largely N-S across the eastern part of the basin. Rainfall is likely to enter the marginal highs (especially where faulted) and migrate down to the porous/permeable sandstones - particularly those in the 14A sequence - diluting or even replacing the formation water with low salinity water (<10 000 ppm, Davies, 1995c).

Figure 3.20: Northwest-southeast section through the Bredasdorp Basin and into the onshore hinterland at lowest Plio-Pleistocene sea-level lowstand. The low salinities in 14A sandstones in wells 27, 37 and 156 either entered the system through the fractures associated with Early Tertiary intrusives (viz. in Well 3) or through the faulted highs (out of plane of section). It is possible that fresh water entered the system through the outcropping Enon conglomerate (cf. Table 2.03) but since these rocks have essentially no porosity where encountered offshore, the conduit to post-basement sandstones is unknown.

Figure 3.21: Palaeotopographic map of Bredasdorp Basin as in Figure 3.19 but showing the low salinity formation waters in pre1At1 sediments largely in the north flank. As in the south of the basin, fresh water may have entered the system through one of two conduits; vertically downwards through the faulted highs or via the pre1At1 sandstones to the west. In well 2 the salinity in these sandstones is so low (<2000 ppm, Davies, 1995c) that it may indicate the fluid migration conduit. Alternatively long distance migration through fractured basement from onshore is not impossible but less likely as conduits are not evident.

Figure 3.22: North-south section from onshore through the Bredasdorp basin, paralleling that of Hälbich (1983), showing another possible ingress route - through the faults which extend (at least) to Late Cretaceous in wells 71 and 41. This route is much less likely than the western ingress route because shallow formation water salinities are close to normal marine, suggesting minimal alteration.

Figure 3.23: Plot of RFT and DST pressures vs depth for reservoirs in the Bredasdorp Basin. Most of these are hydrostatically pressured but the deepest reservoirs (below 3000 metres) are often overpressured. A few of these reach pressures thousands of psi above hydrostatic and in three wells the pressure gradient (to sea floor) reaches 0.73 psi/ft.

Figure 3.24: Map of the western half of the Outeniqua Basin showing the wells and major faults, the nearshore and deep water limits of the initially deposited pre-slump Tertiary sediments, the post Early Miocene slump and its estimated thickness, the slump scars and the location of the two burial history diagrams in the Southern Outeniqua Basin used to characterise the slump.

Figure 3.25: Map of the western half of the Outeniqua Basin showing the 1972 and 1974 reconnaissance seismic lines used in the study of the Southern Outeniqua Basin.

Figure 3.26: Part of one of the reconnaissance seismic lines (L72-021) showing the most recent interpretation of the slump and the pre-slump deposits. Several sea-floor 'steps' near the Infanta high are considered to be slump scars.

Figure 3.27: Depth-converted schematic diagram of composite seismic section through central Bredasdorp Basin into western Southern Outeniqua Basin along a traverse shown in Figure 3.30. Onlap of the 6At1-13At1 sediment package across the eastern high (between wells 8 and 12/13) is shown as well as the near constant Early Tertiary sediment thicknesses out to the slump 'glide

CHAPTER 4

Figure 4.34: Map of the Bredasdorp Basin showing the distribution of the surface offsets of the exponential trend line constructed through the vitrinite reflectance data for each of the 72 wells in which continuous data are available.

Figure 4.35: Plot of the vitrinite reflectance data for four wells in which the sea floor regression intercept ranges between the expected value (0.15%) and an unusually high value (0.49%).

Figure 4.36: Cross-plots of sample depth range and top sampled interval showing a lack of relationship with vitrinite reflectance extrapolated surface intercepts.

Figure 4.37: Plot of Tmax versus depth for DSDP 361 data (data courtesy IFP). In spite of the wide data scatter, there is a definite trend of increasing Tmax with depth which, if extrapolated, would result in a Tmax of 430°C being reached at ~1500m. This low maturity agrees with the low maturity interpreted from lipid and GC data presented by Foresman (1978).

Figure 4.38a and b: Plots of averaged free hydrocarbon (S1) and remaining potential (S2) values for all measured oil prone 13A source rock intervals in the Bredasdorp Basin (from Davies, 1990). These data show that peak S1 values vary considerably but tend to cluster around 1.0-1.5 kg/tonne rock whilst S2 values are proportionally less variable. Palaeotemperatures are measures of maturity derived from a summation of all maturity parameters as shown in Table 4.05.

Figure 4.39: Partial gas chromatogram of saturates fractions of two 13A oil prone source rock samples from well 14, one from the edge of the source and one from the centre (the latter being sample no. 62 in the biomarker dataset). The light ends are clearly more reduced in both normal alkane carbon number and in quantity (Table 4.09). Other source data (e.g. pyrolysis data also confirm that a higher proportion of the more mobile hydrocarbons have escaped, probably by expulsion. (The loss of all alkanes <C14 and proportionally up to ~nC18 is a result of the bitumen extraction process used).

Figure 4.40: Map of the eastern Bredasdorp basin showing the 14A sandstone-rich trends and the gas:oil ratios of produced samples therefrom (GOR in scft/bbl). Well 94 is included even though the flow was from a 13B sandstone because the shows in the 14A sandstone indicate the two sandstones are connected nearby.

Figure 4.41: Schematic chronographic cartoon showing the proposed development, modification and dissipation of gas wetness profiles across a standard shale sandstone sequence as a function of reservoir fill.

Figure 4.42: Ditch gas wetness diffusion and gamma ray profiles for Well 156. The small peak at 2455-60m is due to a thin gas-charged sandstone rather than a break-in-slope.

Figure 4.43: Ditch gas wetness diffusion and gamma ray profiles for Well 166. The change in slope at 2475-80m is interpreted to result from a change in the reservoir fill - possibly related to influx of late gas (which was tested by the RFT).

Figure 4.44: Ditch gas wetness diffusion and gamma ray profiles for Well 165. A continuous oil fill curve is interpreted below~2200m down to ~2355m (although the top section may represent a background gas profile) and a possible diffusion gap below.

Figure 4.45: Ditch gas wetness diffusion and gamma ray profiles for Well 132. There is evidently a normal oil fill curve extending down to ~2660m, a possible diffusion gap down to ~2680m and a steep wet gas fill curve down to the top of the reservoir.

Figure 4.46: Map showing the two main depositional trends of the 14A sandstone fairways with the region of low formation water salinity shown and the probable hydrocarbon migration direction outlined. The two trends end at the possible diagenetic seal trend, believed formed by the deposition of diagenetic carbonates in the thin crevasse splay sands adjacent to the 14A channels due to pressure reduction, salinity change or reduced flow rate precipitation (Brown, 1991, Davies, 1995c and Noble and Davies, 1996).

Figure 4.47a: Map showing the location of the three north flank hydrocarbon and salinity sections.

Figure 4.47b: Section showing the distribution of low salinity formation water (values in NaCl $_{equiv.}$) in syn-rift sandstones on the north-west flank of the basin.

Figure 4.47c: Section showing the distribution of low salinity formation water (values in NaCl $_{equiv.}$) in the syn-rift sandstones on the north-central flank of the basin.

Figure 4.47d: Section showing the distribution of low salinity formation water (values in NaCl $_{equiv.}$) in the syn-rift sandstones on the north-east flank of the basin.

Table 4.01: Table of available kinetic data evaluated from low maturity Outeniqua Basin samples from several different sequences (using the same equipment etc.) and used in the modelling carried out in the Bredasdorp Basin. Non-Bredasdorp data used only for models in the Southern Outeniqua Basin.

CHAPTER 6

CHAPTER 7

schematically demonstrate the amount of tilting which might have occurred. Fluid and heat flows up and across faults are assumed from the known heat regime in the basin.

Table 7.01: Casing shoe depths and static borehole temperatures for wells on which the five Bredasdorp basin models are based.

Table 7.02: All vitrinite reflectance values measured from late Cretaceous and Tertiary SWC samples.

CHAPTER 8

Figure 8.01: Relative yields of hydrocarbon and non-hydrocarbon gases (after Hunt, 1979, p163)

Figure 8.02a: Cross-plot of C1 vs CO_2 from recombined formation fluid samples (PVT) showing distinction of the samples into five main Families and their maturation trends.

Figure 8.02b: Cross-plot of C1 vs CO_2 from separator gas samples showing distinction of the samples into four of the five Families.

Figure 8.03: Map of 13A source rocks (after Figure 4.15) and with the distribution of Family 1 gases (large circles) and gases containing mixtures of Family gas with other gases (small circles).

Figure 8.04: Map of 9A-12A source rocks (after Figure 4.13) and with the distribution of Family 2 gases (large triangles) and mixtures of family 2 gases with other gases (small triangles).

Figure 8.05: Map of 5A-8A source rocks (after Figures 4.09 and 4.11) with the distribution of Family 3 gases (large squares) and mixtures of Family 3 gas with other gases (small squares).

Figure 8.06: Two-way time thickness map of drift and syn-rift sediment (after Figure 4.03) showing the locations of the Family 4 and 5 gases (star and diamond respectively).

Figure 8.07a: Cross-plot of C1 x CO_2 (from recombined formation fluid samples) vs static borehole temperature showing that gases generated from Bredasdorp Basin drift sediments (Families 1, 2 and 3) are present in different proportions than in gases from non-Bredasdorp/non-drift sediments (Families 4 and 5).

Figure 8.07b: Cross-plot of C1 x CO_2 vs vitrinite reflectance (of adjacent shales) for all recombined formation fluid gases showing the different regression lines of the three Families of gases which were not separated in Figure 8.07a.

Figure 8.08a: Partial ternary plot of C1, C2 and C3-6 (as proportions of C1-6) for recombined formation fluid samples. The overall trend towards the C1 apex denoting increasing maturity is modified by slightly offset groups of samples from different Families.

Figure 8.08b: Partial ternary plot of C1, C2 and C3+ for non-recombined separator gas samples. The overall trend towards the C1 apex matches that in Figure 8.08a but the distinction of the different Families is less clear.

Figure 8.08c: Cross-plot of C1 vs C2/C3 for recombined formation fluid samples. The separation of the different Families is clear as is the marginal locations of data from certain wells (48, 59 and 126) which are later shown to be mixtures of two families.

Figure 8.08d: Cross-plot of C1 vs C2/C3 for non-recombined separator gas samples. Data from different Families plots largely separate although a few samples (e.g. well 59) do appear out of place.

Figure 8.09a: Cross-plot of CO_2 vs N_2 proportions for recombined formation fluid samples. Some Families are clearly separated but there are outlier data (e.g. wells 126 and 59) which denote mixtures. In particular, the consistent Family 3 trend shows the continuously changing ratio between the gases is largely as a function of temperature.

Figure 8.09b: Cross-plot of CO_2 vs N_2 proportions for non-recombined separator gas samples. The fewer data result in more scatter but some families are clearly distinguished (e.g. Families 1 and 2).

Figure 8.10: Plot of CO_2 partial pressure showing the trend of the undistinguished Families 1-3 (possibly later drift sourced) gases separate from the trend for Families 4 and 5 gases which are possibly non-Bredasdorp Basin drift-sourced.

Figure 8.11: Plot of the iso/normal butane ratio for recombined formation fluid samples. Families 1, 2 and 5 are inseparable but plot almost completely separate from the family 3 gases. The only two data which overlap are those from wells 59 and 102 DST4, both of which are later shown to represent mixtures. The representative sample of Family 4 plots completely separate from the other gases further supporting the interpretation that it was sourced outside the basin.

Table 8.01: Differences between sampling and analytical methods used for PVT and SABS analyses.

CHAPTER 9

Figure 9.01: Examples of whole oil gas chromatograms showing (a) an oil fill, (b) mixed fill of oil and later gas, (c) residual oil with gas and (d) post-production evaporated sample.

Figure 9.02: Examples of (a) C4-9 and (b) C9-20 annotated gas chromatograms (Well 109, DST1, Column 3).

Figure 9.03: Plot of Heptane and Iso-Heptane values showing the aromatic and aliphatic source trends of Thompson (1983). Trends of Bredasdorp Basin data subparallel those of Thompson. The four labelled outlying samples have unusually high ratios methyl hexanes: dimethyl cyclopentanes indicative of high maturity (Mango, 1994) and recent charge.

Figure 9.04: Plot of iso-heptane ratios used (Mango, 1987) in interpreting thermo-catalytic activity from the invariance of the C7 hydrocarbon proportionation

Figure 9.05: Ternary plot of the first stage thermo-catalytic break-down of parent nC7 (after Mango, 1994).

Figure 9.06: Ternary plot of the second stage thermo-catalytic break-down of parent nC7 (after Mango, 1994).

Figure 9.07: Plot of C7 ratios with the evaporative fractionation trend of Thompson (1988) superimposed. Most of these samples locate below the trend, in the area Thompson indicated to contain biodegraded oils. In this case though, this probably a result of the different peak size measuring method. Two samples (both condensates from well 65) locate so far along the trend that they are thought to represent in-reservoir evaporation.

Figure 9.08: Crossplot of C6 ratios used by Osadetz et al. (1992) to test for water-washing.

Figure 9.09: Plot of ratio between high and low solubility C7 hydrocarbons vs formation water salinity. Of the four hydrocarbon families with more than one data point, only that of Family 1 displays the expected trend of decreasing MCH/Toluene with increasing formation water salinity and even there the samples with low ratios are mostly the mixed samples.

Figure 9.10a: Ternary plots of major C7 hydrocarbon proportions for each column type showing separation into the main hydrocarbon Families. Selected DST and RFT samples are located where outside their group.

Figure 9.10b: Partial ternary plot of the major C7 hydrocarbons summarised from Figure 9.10a showing separation into the main hydrocarbon families. Mango (1988) shows the proportions of these components to be largely a function of source type and thermo-catalysis.

Figure 9.11: Cartoon of definitions of fluid communication used with interpreted C9-20 GC data (from Davies, 1995d).

Figure 9.12: Chromatographic plots (a) nC9-16, (b) nC17-25 (c) nC26-36 of oils from separate flow zones but the same structure illustrating peak-pair differences (Hwang et al., 1994).

Figure 9.13: Plots of a low carbon number ratio [Toluene/(nC7+nC8)] vs (a) separator temperature and (b) separator pressure showing no temperature or pressure correlation. Family 5 data plot offscale because of their high proportions of Toluene.

Figure 9.14: Plots of a high carbon number ratio [6/15] vs (a) separator temperature and (b) separator pressure showing no temperature or pressure correlation.

Figure 9.15: Crossplot of ratios 6/15 and 2/2a showing partial separation between the different hydrocarbon families

Figure 9.16: Schematic diagram comparing hypothetical mixing proportions of Family 1 and 2 liquid phases with carbon-number range and selected peak-pair ratios.

Figure 9.17: Crossplot of ratios 1 vs 2 showing the partial separation between data points of Families 1 and 2.

Figure 9.18: Plot of ratio 3 vs static borehole temperature showing the temperature dependant separation of Families 1, 2 and 3 and the Family 1+2 mixed hydrocarbons.

Figure 9.19: Plot of ratio 17 (between C15 and C16 isoprenoids) vs static borehole temperature showing the largely complete temperature dependant separation of Family 3 from the other Families.

Figure 9.20: Plot of ratio 8 vs static borehole temperature showing the temperature-dependant distinction of Family 1 from Families 2, 4 and 5.

Figure 9.21: Crossplot of the first and second canonical variables showing the separation of the 'pure' Families and the intermediate locations of the hydrocarbon mixtures.

Figure 9.22: Crossplot of RFT pressures for the sands in the eastern part of the north flank showing the isolation of the DST1 sandstone in well 18 from the other wells as suggested by the discriminant function analysis.

Figure 9.23a: Location map of the section line across the southern master fault (after Figure 3.04).

Figure 9.23b: Part of seismic line across the southern master fault through which hydrocarbons could migrate from pre13A sediments into pre1A sandstones on the uptilted fault blocks and thence to the north flank.

Figure 11.01b: Gas chromatogram of part of the urea non-adduct fraction of sample 51 showing the steranes and pentacyclic terpanes in more detail. Compare this chromatogram to the GC-MS fragmentograms of the m/z 191 and m/z 217 ions for this sample in Appendix E, Figure E.50.

Figure 11.02: Gas chromatogram of the aromatic fraction of sample 51 showing the location of the trimethyl naphthalenes (TMN), dibenzo thiophenes (DBT), mono-aromatic and tri- aromatic steroids (MAS and TAS), phenanthrenes (P) and chrysenes (C) in detail. Labelling as detailed in Appendix G.

Figure 11.03: Partial fragmentogram of the total ion current (TIC) of an Aptian (13A) oil prone source rock (sample 59) with the regular C18-21 isoprenoids indicated. Labelling as detailed in Appendix G.

Figure 11.04: Partial fragmentogram of the m/z 177 ion of sample 59, characteristic of demethylated hopanes showing the steranes and pentacyclic terpanes. Labelling as detailed in Appendix G.

Figure 11.05: Partial fragmentogram of the low temperature part of the m/z 191 ion of sample 59, characteristic of the tricyclic terpanes (labelled T) and the C24 tetracyclic terpane (24/4). The doublets evident for the C26 and C27 homologues record the development of isomerisation at C-22. Labelling as detailed in Appendix G.

Figure 11.06: Partial fragmentogram of the high temperature part of the m/z 191 ion of sample 59, characteristic of the high molecular weight tricyclic terpanes, pentacyclic terpanes and gammacerane (Gam). Labelling as detailed in Appendix G.

Figure 11.07: Partial fragmentogram of the m/z 217 ion of sample 59 showing the C27-30 steranes and C27-29 diasteranes. Labelling as detailed in Appendix G.

Figure 11.08: Partial fragmentogram of the m/z 218 ion characteristic of the C27-29 $\beta\beta$ steranes of sample 59. Labelling as detailed in Appendix G.

Figure 11.09: Partial fragmentogram of the m/z 231 ion characteristic of the C28-30 4-methyl steranes of sample 59. Labelling as detailed in Appendix G.

Figure 11.10: Partial fragmentogram of the m/z 259 ion of sample 59 characteristic of the $\beta\alpha$ diasteranes and showing the C27-29 homologues. Labelling as detailed in Appendix G.

Figure 11.11: Partial fragmentogram of the total ion current from GC-MS analysis of the aromatic fraction of sample 59 with the phenanthrenes and chrysenes located. Labelling as detailed in Appendix G.

Figure 11.12: Partial fragmentogram of the m/z 170 ion of sample 59 characteristic of the trimethyl naphthalenes. Labelling as detailed in Appendix G.

Figure 11.13: Partial fragmentogram of the m/z 198 ion of sample 59 characteristic of the methyl dibenzothiophenes. Labelling as detailed in Appendix G.

Figure 11.14: Partial fragmentogram of the m/z 212 ion of sample 59 characteristic of the dimethyl dibenzothiophenes. Labelling as detailed in Appendix G.

Figure 11.15: Partial fragmentogram of the m/z 226 ion of sample 59 characteristic of the trimethyl dibenzothiophenes. Labelling as detailed in Appendix G.

Figure 11.16: Partial fragmentogram of the m/z 231 ion of sample 59 characteristic of the C20-28 triaromatic steroids. Labelling as detailed in Appendix G.

Figure 11.17: Partial fragmentogram of the m/z 253 ion of sample 59 characteristic of the monoaromatic steroids (MAS). This fragmentogram shows the MAS which eluted with the saturated hydrocarbon fraction. Labelling as detailed in Appendix G.

Figure 11.18: Partial fragmentogram of the m/z 253 ion characteristic of the C27-29 monoaromatic steroids (MAS). This fragmentogram shows the MAS eluting with the aromatic fraction. Labelling as detailed in Appendix G. Compare this plot with that in Figure 11.17.

Figure 11.19: Partial fragmentograms of the m/z 178, 192 and 206 ions of sample 58 characteristic of phenanthrene, methyl phenanthrenes and dimethyl phenanthrenes. Labelling detailed in Appendix G.

CHAPTER 12

Figure 12.01: Map showing the wells in the Bredasdorp Basin in which GC-MS (biomarker) analyses were carried out (✖) (this map copied from Figure 2.10).

Figure 12.02: Depth map showing the distribution of source rocks in the 15A sequence and the wells from which samples were taken from the source rock for GC-MS (biomarker) analyses (□). Sample codes indicated. Map after Fig. 4.17.

Figure 12.03: Depth map to 14At1 showing the wells from which samples of reservoired fluids were taken for GC-MS (biomarker) analyses (O). Sample codes indicated.

Figure 12.04: Depth map to 13At1 showing the distribution of source rocks and the wells from which samples of source rocks (□) and reservoired hydrocarbons (O) were taken for GC-MS (biomarker) analyses. Sample codes indicated. Map after Fig. 4.15.

Figure 12.05: Depth map to 9At1 showing the distribution of source rocks and the wells from which samples of source rocks (□) and reservoired hydrocarbons (O) were taken for GC-MS (biomarker) analyses. Sample codes indicated. Map after Fig. 4.13.

Figure 12.06: Depth map to 6At1 showing the distribution of source rocks and the wells from which samples of source rocks (□) and reservoired hydrocarbons (O) were taken for GC-MS (biomarker) analyses. Sample codes indicated. Map after Fig. 4.11.

Figure 12.07: Depth map to 5At1 showing the distribution of source rocks and the wells from which samples of source rocks (□) and reservoired hydrocarbons (O) were taken for GC-MS (biomarker) analyses. Sample codes indicated. Map after Fig. 4.09.

Figure 12.08: Depth map to 1At1 showing the distribution of source rocks and the wells from which samples of source rocks (□) and reservoired hydrocarbons (O) were taken for GC-MS (biomarker) analyses. Sample codes indicated. Map after Fig. 4.07. All hydrocarbon samples shown are from below horizon 1At1.

Figure 12.09: Partial mass fragmentograms of examples of characteristic ions from each of the main source rocks. Relevant peaks are highlighted and connected to indicate the differences between each unit of source rock.

Figure 12.10: Partial mass fragmentograms of examples of characteristic ions from each of the two inactive source rocks. Relevant peaks are highlighted and connected to indicate the differences between each unit of source rock.

Figure 12.11: Partial mass fragmentograms of examples of characteristic ions from representative samples of each hydrocarbon family. Relevant peaks are highlighted and connected as in Figures 12.09 and 12.10 to indicate the differences which distinguish each hydrocarbon family.

Figure 12.12: Partial m/z 191 mass fragmentograms of (a) a high maturity source rock sample (no. 63) and (b) a low maturity source rock sample (no. 49) showing the development of the C29-33 homologous series of diahopanes in the high maturity and the C29-30 moretane series in the low maturity samples.

Figure 12.13: Plots of ratio between two triaromatic steroid peaks i.e. c/d (C28 20S/C27 20R) vs vitrinite reflectance data calculated for (a) each source rock and (b) each hydrocarbon sample. Each data point is coded to indicate (a) the source rock intervals sampled and (b) the hydrocarbon families. Regression lines for source rock intervals are drawn through the majority of the data which display a maturity-dependency. These figures are discussed in section 12.1.2.7.

Figure 12.14: Plots of the C29 $\alpha\alpha$ 20S/(20S+20R) sterane isomer ratios vs vitrinite reflectance data for all (a) source rock and (b) hydrocarbon samples. Data zone after Waples and Machihara (1991, p. 25).

Figure 12.15: Plots of the C29 $\beta\beta/(\alpha\alpha+\beta\beta)$ 20S+R epimer ratio vs vitrinite reflectance data for (a) all source rocks and (b) all hydrocarbon samples. Trend zone after Cornford et al. (1983), Goodarzi et al. (1989) and Burwood et al. (1990). Samples from northern source rocks plot within the low side of the trend.

Figure 12.16: Ternary plots of the total 20S+R C27-29 14α,17α steranes for (a) source rock and (b) hydrocarbon samples. Maturation envelope after Mackenzie et al. (1984), Brassell et al. (1986) and Peters et al. (1989).

Figure 12.17: Ternary plots of the total 20S+R C27-29 13β,17α diasteranes for (a) each source rock and (b) each hydrocarbon sample. Although the points appear to form an unstructured group, there is a general structure. All Family 1B (and upper 9A-12A source rocks) locate furthest from the C27 apex, all Family 2 samples (and lower 9A-12A and possibly basal 13A source rocks) locate furthest from the C29 apex and all Family 1 samples locate centrally.

Figure 12.18: Cross-plots of rearranged/regular hopanes vs steranes for (a) source rock and (b) hydrocarbon samples. The envelope was constructed to encompass all matching data from Farrimond and Telnaes (1996). Sample 67 does not fit, perhaps because it contains impregnating condensate.

Figure 12.19: Plot of total sterane/hopane ratios vs equivalent vitrinite reflectance data for samples from Van Graas (1990) showing the distinction between two different source rocks.

Figure 12.20: Plots of total sterane/hopane ratios vs vitrinite reflectance data for all Bredasdorp Basin samples of (a) source rock and (b) hydrocarbons to scales matching those used in Figure 12.19.

Figure 12.21: Plots of C24 tetracyclic/average C25+26 tricyclic terpane ratios vs vitrinite reflectance data for (a) all source rock and (b) all hydrocarbon samples. The possible maturity trend(s) differ from that expected from increased C24 tetracyclic terpane contents predicted by Aquino Neto et al. (1983). Supporting this unusual trend(s), all Family 1B hydrocarbons and upper 9A-12A (possibly basal 13A) source rocks locate with high values whilst all Family 2 hydrocarbons, and lower 9A-12A source rock samples, locate with very low ratios.

Figure 12.22: Cross-plots of C24 tetracyclic/average C25+26 tricyclic terpane ratios vs C23/C21 tricyclic terpane ratios for (a) all source rock samples and (b) all hydrocarbon samples. The predicted maturity-dependency for the C23/21 ratio is not evident in either data set.

Figure 12.23: Plots of total tricyclic terpanes/total terpanes vs vitrinite reflectance data for (a) all source rock and (b) all hydrocarbon samples. Most sub-parallel trends of source rock data are not matched by the hydrocarbon data.

Figure 12.24: Plots of C30 diahopane/hopane vs vitrinite reflectance data for (a) all source rock and (b) all hydrocarbon samples. Maturation-dependent trends are weakly developed for upper 9A-12A source rock and Family 1B hydrocarbon samples and for 5A-8A source rocks and Family 3 hydrocarbons.

Figure 12.25: Plots of C32 homohopane 22S/R epimerisation ratio vs vitrinite reflectance data for (a) all source rock and (b) all hydrocarbon samples. Two trends are shown, for the 13A and 15A source rocks.

Figure 12.26: Cross-plots of C29 norhopane/C28 bisnorhopane vs C29 norhopane/C30 diahopane for (a) all source rock and (b) all hydrocarbon samples. The group of source rocks with unusually high bisnorhopane proportions are all from relatively low maturity shales deposited in highly anoxic environments.

Figure 12.27: Plots of C27 18α(H) norneohopane/17α(H) norhopane vs vitrinite reflectance data for (a) all source rock and (b) all hydrocarbon samples. Several sub-parallel trends are evident in the source rock data. In the hydrocarbon data, the Family 2 (and Family 2 mixture) data locate close to their possible source, the lower 9A-12A interval.

Figure 12.28: Plots of the C29 norhopane/(nor- and norneo-) hopane ratio vs vitrinite reflectance data for (a) all source rock and (b) all hydrocarbon samples. Two maturity-dependent trends are seen in the source rock samples (except sample 66) but are not evident in the hydrocarbon samples.

Figure 12.29: Ternary plots of C27-31+ hopanes. All Family 2 and 1B hydrocarbons and source rocks (9A-12A) locate in distinct regions but not matching the depositional environments of Fan Pu et al. (1991).

Figure 12.30: Cross-plots of trimethyl naphthalene ratios for (a) all source rock and (b) all hydrocarbon samples. All Family 1B and 2 hydrocarbons and source rock samples (9A-12A) locate in two distinct trends with most Family 3 hydrocarbon/5A-8A source rock samples located between.

Figure 12.31: Plots of MPI1 (methyl phenanthrene index) for (a) all source rock and (b) all hydrocarbon samples. Data envelope trends of Radke (1987) and Boreham et al. (1988) are shown.

Figure 12.32: Plots of DPR (dimethyl phenanthrene ratio) after Radke (1987) for (a) all source rock and (b) all hydrocarbon samples.

Figure 12.33: Plots of total C26-28 triaromatic /(triaromatic and C27-29 monoaromatic) steroids for (a) all source rock and (b) all hydrocarbon samples. Trend up to R_o~0.9% after Mackenzie (1987) and after R_o~0.9% after Davies (1997, in press). Out of place data due to, in source rock figure (i) peak overlap by contaminating normal alkane (sample 68) and (ii) different source rock type in the lacustrine sample (45) and in the hydrocarbon figure (iii) hydrocarbon migration.

Figure 12.34: Plots of the C27 rearranged/total monoaromatic steroids vs vitrinite reflectance data for (a) all source rock and (b) all hydrocarbon samples. The apparent reversal in the source rock data is not matched by the hydrocarbon data but that may be because there are too few hydrocarbon data above the inflection point (R_o 0.8-0.9%).

Figure 12.35: Cross-plots of triaromatic steroid ratios (peaks c/d and d/e) for (a) all source rock and (b) all hydrocarbon samples. Equivalent reflectances given for the two trends are based on the available measured data. The slopes of the sub-parallel trends of the Family 1, 1B and 3 data in the hydrocarbon plot match the source rock trends, but are slightly offset.

Figure 12.36: Cross-plots of methyl dibenzothiophene ratios (4MDBT/1MDBT vs 4MDBT/2+3MDBT) for (a) all source rock and (b) all hydrocarbon samples. All the source rock and hydrocarbon data locate in the same zone but within that there are subtly different trends for each source rock interval - however only the Family 1B hydrocarbons show any matching trend.

Figure 12.37: Plots of dimethyl dibenzothiophene ratios (C/E) and (D/F) vs vitrinite reflectance data for source rock sample only. Both datasets show differences between the trends of Family 1, 3 and 7 samples. The different molecule shapes, which are thought to affect the relative rates of expulsion, are shown.

Figure 12.38: Cross-plots of dimethyl dibenzothiophene ratios (C/E vs D/F) for (a) all source rock and (b) all hydrocarbon samples. Well defined trends are apparent in both the plots - although the hydrocarbon trend is offset somewhat. Equivalent vitrinite reflectances have been annotated on the Family 1+1B+2 trends and the Family 3 trend and achieve precisions of R_o~0.1%.

CHAPTER 13

Figure 13.12: Plots of measured and calculated vitrinite reflectance data at the central basin location (see section 7.2.1) comparing the maturity level of the 13A source rock at present and at end of the hotspot transit.

Figure 13.13: Chronographic chart showing the major heating events, the backstripped maturity levels and the biomarker-calculated maturities of oil samples in the southern 14A oil-rich trend (after Davies, 1997a).

Figure 13.14: Schematic paragenesis of hydrocarbon fills and spills since the start of the hotspot transit to the present, explaining the possible reservoir fills and the biomarker maturity differences between the residual and flowed oils.

Figure 13.15: Schematic section across the 14A trend sandstones showing the faulting and the hydrocarbon migration routes.

Figure 13.16: Schematic section through the basin margin showing the fault juxtaposition of younger source rock and older reservoir rock which allows stratigraphic down-stepping of migrating oil.

Figure 13.17: Schematic 3-D sections through the north flank of the basin showing the fault juxtaposition of source and reservoir, the migration trends of the different hydrocarbon Families and the probable generally updip migration route by which Family 1 oil reached the northern traps.

Figure 13.18: Schematic section through sandstone reservoir subjacent to the 13A source rock showing the likely oil and gas migration routes which created the hydrocarbon fills seen today.

Figure 13.19: Schematic section through the southern 14A trend showing the probable migration routes for the gas and oil known to be in place and the emplaced hydrocarbon (after Davies, 1995c).

Figure 13.20: Schematic section through the Family 1B reservoirs and their probable source rocks showing the likely migration routes by which the gas and oil migrated into the present structures.

Figure 13.21: Schematic section through the north flank of the basin showing the juxtaposition of the 5A gas prone source rock and the regional pre1At1 regressive coastal sandstone complex through which Family 3 gas probably migrated to the north flank.

Figure 13.22: Schematic section through the pre13A central basin area where the 13A source acts as a seal as it is mostly gas prone and immature. Sandstones beneath this barrier are gas charged from below, from the lower 9A-12A gas prone source rocks developed immediately below and possibly also from remigrated gas from breached pre1At1 reservoirs up to 2 km below. Graben-bounding tensional faults, rejuvenated during compressional events exist in the area and may be gas conduits.

Figure 13.23: Schematic section through the syn-rift fill of a pre-rift graben showing the probable development of lacustrine source rocks (after those found in the A-J1 well on the west coast, Muntingh, 1993) and possible migration routes into adjacent structures.

Figure 13.24: Petroleum System Chart showing the development chronology of the various parts of the system (after Davies, 1997i).

Table 13.01: Quantities of oil and gas which could be expelled from each source rock interval in the Bredasdorp Basin, to the present day. These numbers are calculated from measured source rock richness, mapped extent, measured and extrapolated maturity levels and from empirical examples of proportions of expellable hydrocarbons.

ABBREVIATIONS USED IN TEXT

ααα	5α(H), 14α(H), 17α(H) sterane
αβ	13α(H), 17β(H) diasterane
αββ	5α(H), 14β(H), 17β(H) sterane
βα	13β(H), 17α(H) diasterane
‰	parts per thousand
24DMP	2,4-dimethyl pentane
28,30 bis	norhopane with no methyl group at C-28 and C-30
AFFZ	Agulhas-Falklands Fracture Zone
AFR	Agulhas Fracture Ridge
API	American Petroleum Institute
AROM	hydrocarbons containing at least 1 aromatic ring
ASPH	asphaltenes
Bbls	barrels (US)
Bcf	billion standard cubic feet
mbKb	metres below Kelly bushing
C3....	hydrocarbon with 3 carbon atoms
CO_2	carbon dioxide
CPI	carbon preference index (odd/even numbered alkanes)
CSIR	Council for Scientific and Industrial Research
DG	dry gas prone source rocks
DPR	dimethyl phenanthrene ratio
DSDP	Deep Sea Drilling Project well
DST	drill stem test
EOM	extracted organic matter
EWT	extended well test
GC	gas chromatography or gas chromatogram
GC-MS	GC-mass spectrometry
GHG	GH Geochemical services
GLR	gas-liquid ratio (inc. condensates)
GOR	gas-oil ratio
HI	hydrogen index
HTAC	high temperature Agulhas Current
HV	heptane value
IHV	isoheptane value
IP15...	regular acyclic head-to-tail isoprenoid with 15 carbon atoms
KFA	KernForschungZentrum, Jülich
LSM	lower shallow marine sandstones
Ma	million years before present
MH	methyl hexane
MCH	methyl cyclohexane
MCI	methyl chrysene index
MCR	methyl chrysene ratio
MPI1	methyl phenanthrene index 1
MPR	methyl phenanthrene ratio
MW_{equiv}	mud weight equivalent (lb/gal)
NBS22	National Bureau of Standards ^{13}carbon isotope standard no. 22
nC15....	normal (straight-chain) alkane with 15 carbon atoms
N_2	nitrogen gas
NSO	nitrogen, sulphur and oxygen containing polycyclic compounds ≡ resins
OAE	oceanic anoxic event
OIL	oil prone source rocks
OM	organic material
PAH	polycyclic-aromatic hydrocarbons
PDB	Pee Dee Belemnite ^{13}carbon isotope standard
Ph	phytane
PI	Rock-Eval production index =S1/(S1+S2)
Pr	pristane
PVT	samples at reservoir formation pressure, temperature and volume
RFT	Repeat Formation Tester
R_o	mean random vitrinite reflectance measured in oil
ROP	rate-of-penetration
20S/R	optical isomers at C-20
S1	peak 1 from Rock-Eval data (free hydrocarbons)
S2	peak 2 from Rock-Eval data (total pyrolysable hydrocarbons)
S3	peak 3 from Rock-Eval data (total pyrolysable oxycarbons)
SABS	South African Bureau of Standards
SAT	fully saturated hydrocarbons
SBHT	static borehole temperature (corrected for mud cooling effect)
Scft	standard cubic feet (gas measurement)
SCOT	support-coated open tubular
SP	Spontaneous Potential log
S-R	Simon-Robertson, N. Wales
SWC	sidewall core
t1	type 1 unconformity (where sea level falls to below shelf edge)
TAI	thermal alteration index (maturity parameter based on colour of organic material in transmitted light)
TD	total drilled depth
Tmax	temperature at maximum rate of hydrocarbon generation (from Rock-Eval pyrolysis data)
TOC	total organic carbon
Tol	toluene
Tm	C27 trisnorhopane
Ts	C27 trisnorneohopane
UCM	unresolved complex mixture
US	University of Stellenbosch
USM	upper shallow marine sandstones
WCOT	wall-coated open tubular
WG	wet gas prone source rocks
WOB	weight on bit (drilling parameter)

CHAPTER 1. INTRODUCTION

1.1. BACKGROUND

The Bredasdorp Basin and its environs, is located on the South African continental shelf between Cape Agulhas and Mossel Bay (Figs. 1.01; 1.02). The basin, one of four delineated by the results from seismic surveys and the ~200 wells drilled during the course of exploration for hydrocarbons, extends for approximately 150 km E-W and 100 km N-S, having a total area of ~15 000km^2.

Prior to the start of hydrocarbon exploration in the South African offshore in the late 1960's, there had been no geological studies of the continental shelf of South Africa. The presently understood geologic history of the area in general and of the Bredasdorp Basin in particular therefore stems from this hydrocarbon exploration effort, which is still continuing. Indeed, it is only during the past 10 years, after many regional and local studies, that the geologic history has become well enough understood for exploration success rates to improve dramatically. However, few of these studies have been published apart from some general reviews (e.g. Burden, 1992) and presentations at Geocongress, Cape Town (1990). In step with this advancement has come an explosive growth in the understanding of the petroleum geochemistry of the basin. Many regional and well-specific studies of this nature have also been undertaken in offshore areas, almost entirely by SOEKOR. Very little of this information has been published.

Within the Bredasdorp Basin many hydrocarbon reservoirs have been found in Cretaceous sandstones. It is thought that the gas and oil they contain have been generated in one or more of the carbon-rich source rocks found within the limits of the basin or in the western part of the Southern Outeniqua Basin.

These hydrocarbons comprise liquid oils and traces of high molecular weight hydrocarbons, considered to be residues after earlier oil charges, and wet gas with condensate. Concentrations of these hydrocarbons are commercially significant and are actively explored. Two reservoirs are currently producing gas-condensate and oil. The commercial viability of these occurrences is primarily related to the high monetary value of the liquid fraction compared to that of gas. Therefore it is of paramount importance to the exploration efforts to concentrate their search in those parts of the basin where such hydrocarbons are preferentially reservoired. This is achieved if (a) the route(s) these hydrocarbons took when migrating from their source rock to the present reservoir rock are known, (b) where the timing of the migration episodes is understood and (c) the volume available for migration through each route can be

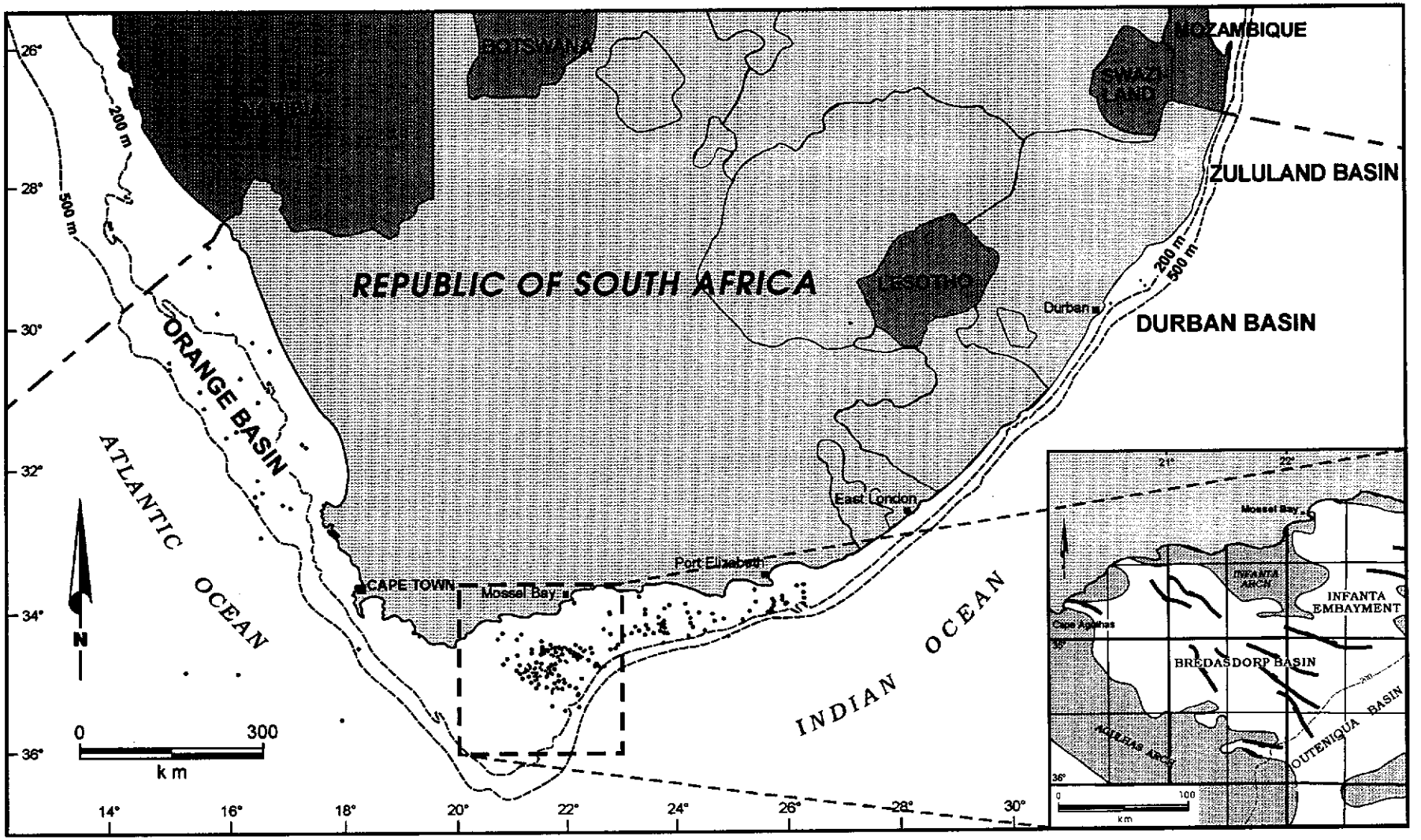

Figure 1.01: Location map of the offshore Bredasdorp Basin and its relation to the other major basins on the west and east coasts of South Africa.

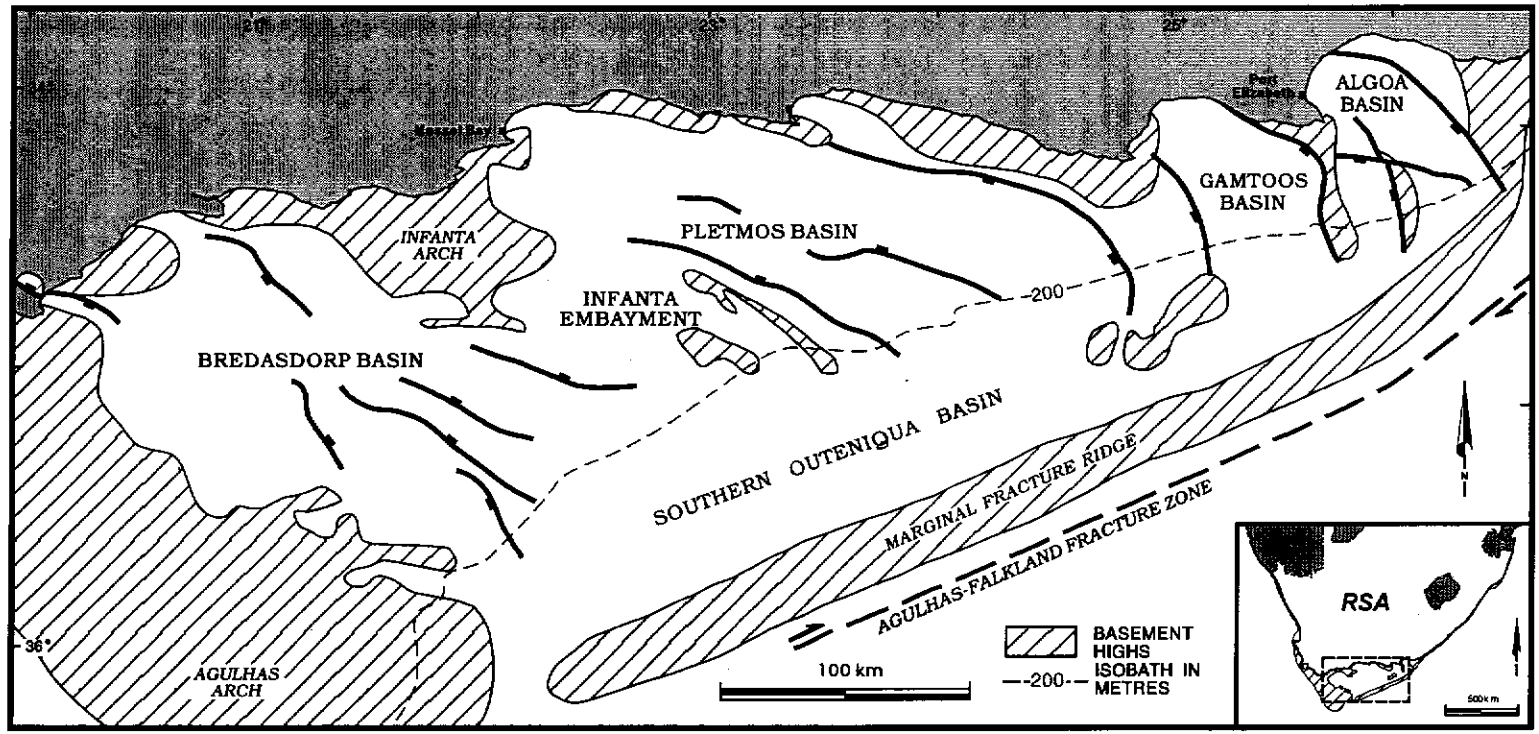

Figure 1.02: Location map of the south coast of South Africa showing the five separate basins that comprise the Outeniqua Basin.

reliably estimated. These can only be evaluated once (a) the source rock for the hydrocarbon is identified, (b) the fetch area is delineated, (c) the maturation history is known and (d) the relative quantities expellable from each source are calculated. Each of these is very difficult to determine and represents major challenges to the explorationist.

Prior to the present study, the distribution, thickness and richness of source rocks in the Bredasdorp Basin wells were established from inter-well comparisons using pyrolysis analyses (>24000) and optical studies (>3500) carried out on core and sidewall core samples from 150 wells and 75 wells respectively. From these data it was determined that there were several different source rocks and that some were within the oil window, whereas some had passed through the oil window. No intersections of immature wet gas or oil-prone source rocks have been found.

The search for inherited characteristics of source rocks has been actively pursued by petroleum geochemists elsewhere for some time (e.g. Philippi, 1956 and Bray and Evans, 1965). These earliest efforts concentrated on the composition of the oil amenable to gas chromatographic analysis. Those early methods were quickly adopted by other companies and refined so that correlations between source rocks and oils were frequently attempted using ever more detailed comparisons of the chemical and physical properties of hydrocarbons, with similar properties of bitumens in the supposed source rocks (e.g. Dow, 1974 and Williams, 1974). Those comparisons were based on the premise that hydrocarbons derived from each source rock should be distinguishable because they inherit characteristics of the original biological source material. Since it is known that some hydrocarbons are left behind in the source rock as bitumens after migration (Tissot and Welte, 1984), it is likely that chemical 'fossils' in the bitumens should match those found in reservoired hydrocarbons (Eglinton and Calvin, 1967).

These early correlation studies largely addressed characteristic aspects of low maturity whole oil and bulk source rock extracts using medium resolution gas chromatography. As the techniques became more widely used, the complexity of the hydrocarbons became apparent. The high molecular weight fractions of the oils were evidently comprised of mixtures of hundreds of components which could only be separated by high resolution gas chromatography and later by mass spectrometry analysis. However, these methods proved less successful when dealing with higher maturity condensates and their sources, because the proportions of bulk and chromatographically resolvable groups of hydrocarbons decreased with increasing maturity. As a result, various fractionation and concentration steps were employed. The added advantage of using high resolution analyses of specific fractions was that

they were able to establish identities of characteristic groups of compounds which could differentiate oils and source rocks without recourse to the short to medium-chain alkanes previously employed. This was a step forward as those alkanes were often subject to severe in-reservoir alteration by biodegradation (Rogers et al., 1974).

During the 1970's and 1980's, source rock-oil correlation methods available in South Africa were largely limited to those developed prior to the imposition of trade sanctions and technical embargo's in the early 1970's. These methods mostly comprised the high resolution gas chromatography techniques. Low resolution mass spectrometry analyses were possible but without calibration samples, the biological fossils or marker compounds could not be readily identified and compared with published literature. In addition, until the mid-1980's almost all the discovered hydrocarbons which were reservoired in quantity, and on which exploration focus was placed, were high maturity condensates. The known lack of success in determining oil:source correlations from such high maturity hydrocarbons, left little incentive for further study especially in view of the inaccessibility of the more modern analytical methods.

The discovery in 1986 of reservoired oil in the previously unexplored centre of the Bredasdorp Basin led to a concerted effort to discover further reserves of oil, which in turn led to a need to understand the sourcing and migration timing of oil in the basin. This could only be done using the techniques of biological marker (or 'biomarker') analysis and provided a new impetus for the use of these analyses. A few such analyses were carried out at the University of Stellenbosch but equipment problems, and the inability to correlate the peaks found with those of published biomarkers because of the lack of suitable standards, led to a cessation of the attempt. However, after the easing of sanctions in the early 1990's it became possible to have samples from South Africa analysed for their biomarker contents and to use those results as standards to calibrate the local equipment.

The arrival of the first available biomarker results in 1992 sparked a fresh start to oil:source correlation studies. The ability to carry out these analyses in-house led to a rapid growth in their utilisation and helped in the understanding of the hydrocarbon history of the basin. In addition, most of the work has been targeted at local studies which have immediate commercial benefits and not at the long-term aims of regional appraisal. This study, however, aims at redressing the imbalance and shows that studies outside the main hydrocarbon trend can also yield information which is of direct importance to more local oil and gas exploration projects.

A second major advance came with the adoption of a commercial burial history programme (Basinmod) in the late 1980's for use in basin modelling studies aimed at

understanding the generation history of the basin. This capability was further enhanced by the acquisition of the OPTKIN programme for the Rock-Eval pyrolysis instrument which allowed for the determination of kinetic generation parameters from source rock samples. These two techniques together allowed a more rigorous assessment of the generation and expulsion of hydrocarbons from source rocks, which in turn led to the appreciation that the previously accepted gradualistic thermal history model of the basin, i.e. continuous cool-down after Late Jurassic rifting, did not take account of all the facts. Hence a new thermal model of the basin had to be formulated.

1.2. AIMS

From the above discussion, it is clear that five specific aspects of petroleum geochemistry need to be addressed in the basin to further the aims of exploration namely:

(i) To analyse representative samples of oils, oil traces, condensates and potential source rocks for their characteristic chemical features in order to correlate the hydrocarbons with their source rocks
(ii) To determine the source interval (and fetch area) for hydrocarbons found in the basin
(iii) To use the available mapping and modelling techniques to indicate probable fetch areas, to determine the timing of migration and to suggest possible migration routes
(iv) To determine whether any of these hydrocarbons were generated in source rocks which are presently undrilled in the basin but whose presence and character can be inferred from the data
(v) To delineate fluid migration trends in time and space.

1.3. METHODS

Several methods are used to achieve these aims:
Regional fluid distribution studies were initiated. These studies mostly addressed hydrocarbons but also included studies of the formation waters distributed through sandstones. The latter was done by determining formation water salinities from SP, resistivity and porosity log data as well as from the available measured data, and mapping the results through regional sandstone trends. Apart from the demonstrated source rock potential of the Bredasdorp Basin, it was considered that the western part of the undrilled Southern Outeniqua Basin may have been a source for hydrocarbons. Major sequence boundaries and characteristic seismic amplitude signatures of source rocks were mapped throughout on a reconnaissance basis using the available seismic data. Depth conversion using calibrations from nearby wells was used to evaluate the

distribution and depths to potential source rocks and to estimate the volumes of fluids which might be expelled from modelled estimates of the maturity.

A regional assessment of seal effectiveness in the Bredasdorp Basin was carried out which utilised the proportions of hydrocarbon gases absorbed in seal lithologies. This study used gas data recorded during drilling operations at the more than 160 wellsites in the basin. Parallel to this, several in-house studies were aimed at correlating sandstones and also at establishing preferential trends of sandstone deposition and preservation through the basin (Gilbert, 1990; Brink et al., 1991; Smit, 1992; Burden and Gasson, 1992; Benson et al., 1993; Wickens, 1993).

Chemical and optical maturity data were calculated to determine the local maturation profiles in each well and establish the regional patterns of heat flows in the area. As part of this study, a regional assessment of the thickness, distribution and richness of all source rocks encountered in the basin was carried out. Both these studies drew heavily on the large database of pyrolysis and optical analyses available from borehole samples in the basin. These results are presented in the form of a series of source rock and maturity maps.

Burial history modelling was carried out at selected wellsites in the Bredasdorp Basin and at centres of potential fluid fetch areas. These models draw extensively on the geologic, palaeontologic and seismic horizon evaluations carried out by geoscientists in SOEKOR over the years and reported in SOEKOR databases. The results from these models, together with measured kinetic data, allow for the calculation of quantities of hydrocarbons available for expulsion.

Detailed chemical analyses of reservoired hydrocarbons and representative samples of source rocks - in particular high resolution gas chromatography (GC), GC-mass spectrometry (GC-MS) and stable ^{13}carbon isotopic analyses have been carried out. These results are interpreted in a similar way to that done in published reports in order to demonstrate the validity of conclusions reached, but in some cases the published form of the data was unable to discriminate between hydrocarbon types and new formats were utilised. Many of these results are examined statistically to help confirm the conclusions reached and demonstrate their support by the data.

All chemical biomarker data and all of the burial history modelling parameters determined for this study are reported in the Appendices. Maturation levels of hydrocarbons are assessed by comparison with published biomarker-maturity parameters.

Pyrolysis analyses for source rock and maturation studies were carried out from 1978 in the SOEKOR laboratory and some medium resolution GC studies were done by the SABS, Pretoria. More recently, GC analyses were carried out by SOEKOR and most GC-MS analyses at the University of Stellenbosch

Throughout the last 10 years, the exploration focus has been almost wholly on oil, and analyses carried out by the laboratory were prioritised to suit those exploration needs. They were aimed specifically at establishing characteristics of oil-prone source rocks and oil-rich hydrocarbons. Consequently, few of the gas condensates or possible gas-prone source rocks were effectively analysed by these wet chemical and chromatographic methods. Detailed whole oil, biomarker isotopic analyses have now been carried out on some of these samples and characteristics of the hydrocarbon families are now well established.

CHAPTER 2. REGIONAL GEOLOGICAL SETTING

2.1 PRE-RIFT GEOLOGY

Cape Supergroup sandstones and shales were deposited on the southern perimeter of the Kaapvaal Craton during the late Palaeozoic and were overlain, at least in the present day onshore regions, by sedimentary rocks of the Karoo Supergroup (Table 2.01). These rocks were deposited in a retro-arc foreland basin (McLachlan and McMillan, 1979; Johnson, 1990). Deposits of the Cape Supergroup are recognised in offshore wells, specifically Bokkeveld Series shales and slates and Table Mountain Series metasandstones. There is no evidence that Witteberg Series rocks were present across the area. Their absence, and that of Karoo rocks, may reflect non-deposition (Biddle et al., 1986) or erosion (Rowsell and De Swardt, 1976; Cole, 1992).

There is evidence that these rocks did indeed extend further south than the southern African continental shelf. Deposits of Devonian age, possibly equivalent to Bokkeveld Group rocks, comprise basement in the Falkland Islands (Lawrence and Johnson, 1995). Banks et al. (1993) show that sediments equivalent to Lower Ecca Beds of the Karoo Supergroup are present in the Falklands showing that at least some earliest Karoo rocks were present south of the Cape Fold Belt mountains. Indeed, Lawrence and Johnson (1995) show that some of these possess source potential.

Rowsell and De Swardt (1976) show that burial of pre-Karoo rocks to a depth of several thousand metres is necessary to account for the high maturity of the Bokkeveld Series rocks both onshore and offshore. Indeed, Bokkeveld Series slates, intersected in two offshore wells, have vitrinite reflectances commensurate of burial to 4000-6000 metres at moderate heat flow rates, whilst reflectances in the overlying Mesozoic deposits in those wells have maturity levels typical of <2000 metres of burial at similar heating rates. The maturation levels of the Bokkeveld rocks have been confirmed by fission track analyses in the southern Cape (Brown et al., 1990; Duane and Brown, 1992).

It may be that these Bokkeveld rocks represent the basal formations and that burial caused by the originally great thickness of Bokkeveld rocks (interpreted to have exceeded 4 kilometres, Theron, 1970) plus a small thickness of early Karoo rocks could have caused the evidence of deep burial. It is therefore considered that Karoo rocks, of at least early Karoo age, were originally present in southernmost South Africa and possibly even reached as far as southern South America. During the Cape Orogeny (215-278 Ma; Hälbich et al., 1983) which was largely coeval with Karoo sedimentation, Cape Supergroup (and possibly early Karoo Supergroup rocks) were folded and faulted to form the present-day WNW-ESE structural grain which now underlies all the offshore

MEGASEQUENCES	FORMATION NAME	ENVIRONMENT	LITHOLOGY	PERIOD	AGE
KAROO SUPERGROUP	STORMBERG SERIES	continental-to-shallow marine	Largely extrusives with some sandstones	Late Triassic and Early Jurassic	~180-230 Ma
	BEAUFORT SERIES	Fluvial - transitional marine	Siltstones and occ. shales	Late Permian and Triassic	~230-255 Ma
	ECCA SERIES	Two upward-coarsening deep-marine megacycles	Claystones with occ. coals	Permian	255-270 Ma
	DWYKA TILLITE	Glacio-marine	Tillites and claystones	Carboniferous	278-~290 Ma
CAPE SUPERGROUP	WITTEBERG SERIES	Shallow marine and transitional	Shoreface sandstones and siltstones	Late Devonian - Early Carboniferous	~320-390 Ma
	BOKKEVELD SERIES	Deep marine	Turbidity claystones and sandstones	Devonian and Late Silurian	~390-410 Ma
	TABLE MOUNTAIN SERIES	Continental and nearshore	Sandstones and occ. claystones	Ordovician	410-500 Ma
BASEMENT	CAPE GRANITE AND METASEDIMENT	Continental	Sandtones and arkoses	Cambrian and Pre-Cambrian	>500 Ma

Table 2.01: Generalised chronostratigraphic, environmental and lithologic descriptions of Basement, Cape and Karoo Supergroup rocks in the Western Cape (after Wickens, 1987, pers. comm.)

basins of Southern Africa (Hälbich et al., op cit.). The orogeny is considered to have commenced when the Gondwana landmass started to override the Pacific plate producing oblique subduction (Dingle et al., 1983). A recent plate reconstruction of western Gondwana (Fig. 2.01) records this disposition just after this event (Lawver et al., 1992). Subsequent to this early deformation, Gondwana started to fragment resulting in the development of the subsequent syn-rift and post-rift basins (Fig. 2.02). Dingle et al. (1983) and Biddle et al. (1986) show that the Magellanes basin of S. Argentina, based on its present day position west of the Falklands Islands, was located south of the Agulhas Bank prior to continental separation. The Falklands Islands and Falklands Plateau Basin were probably south-east of Port Elizabeth.

The present day southern African offshore is considered to comprise the Outeniqua Basin (Du Toit, 1976; Dingle et al., 1983), which is subdivided into five basins, separated by ridges of Palaeozoic metasediments (Dingle et al., 1983). The four inboard basins (Bredasdorp, Pletmos, Gamtoos and offshore Algoa) arbitrarily extend to the 200 metre isobath. The outboard deep water basin is the Southern Outeniqua Basin (Fig. 1.02).

2.2 SYN-RIFT GEOLOGY

2.2.1. Regional igneous events

It has been suggested that regional igneous events herald the break-up of continents as a result of the increasingly focussed heat flow along mantle trends (Condie, 1989). There is support for this suggestion from the igneous events around Southern Africa/South America.

An extensive igneous episode affected the eastern part of South Africa and adjacent plates and resulted in the extrusion of basaltic material forming the Drakensberg basalts and Lebombo igneous centres in Southern Africa and basaltic intrusions in the Trans Antarctic mountains (Dingle et al., 1983; Dalziel, et al., 1987) (Fig. 2.02). The age of this episode is reportedly between 162 Ma and 200 Ma (Dingle et al., 1983; Duane and Brown, 1991) although there is evidence that intermittent volcanism probably extended as late as 130 Ma. Indeed, Brown et al. (1990) record a period of uplift and unroofing at 135 Ma from fission track data. On the western side of Africa, a somewhat later igneous episode formed the Etendeka Formation volcanics of central Namibia and the Paraña volcanic province of South America (Fig. 2.03) dated around 134 ±5 Ma (Milner, 1992). Igneous and extrusive basaltic material has also been found in Cretaceous sediments in several wells drilled in the Orange Basin (Gerrard and Smith, 1983; Erlank et al., 1990).

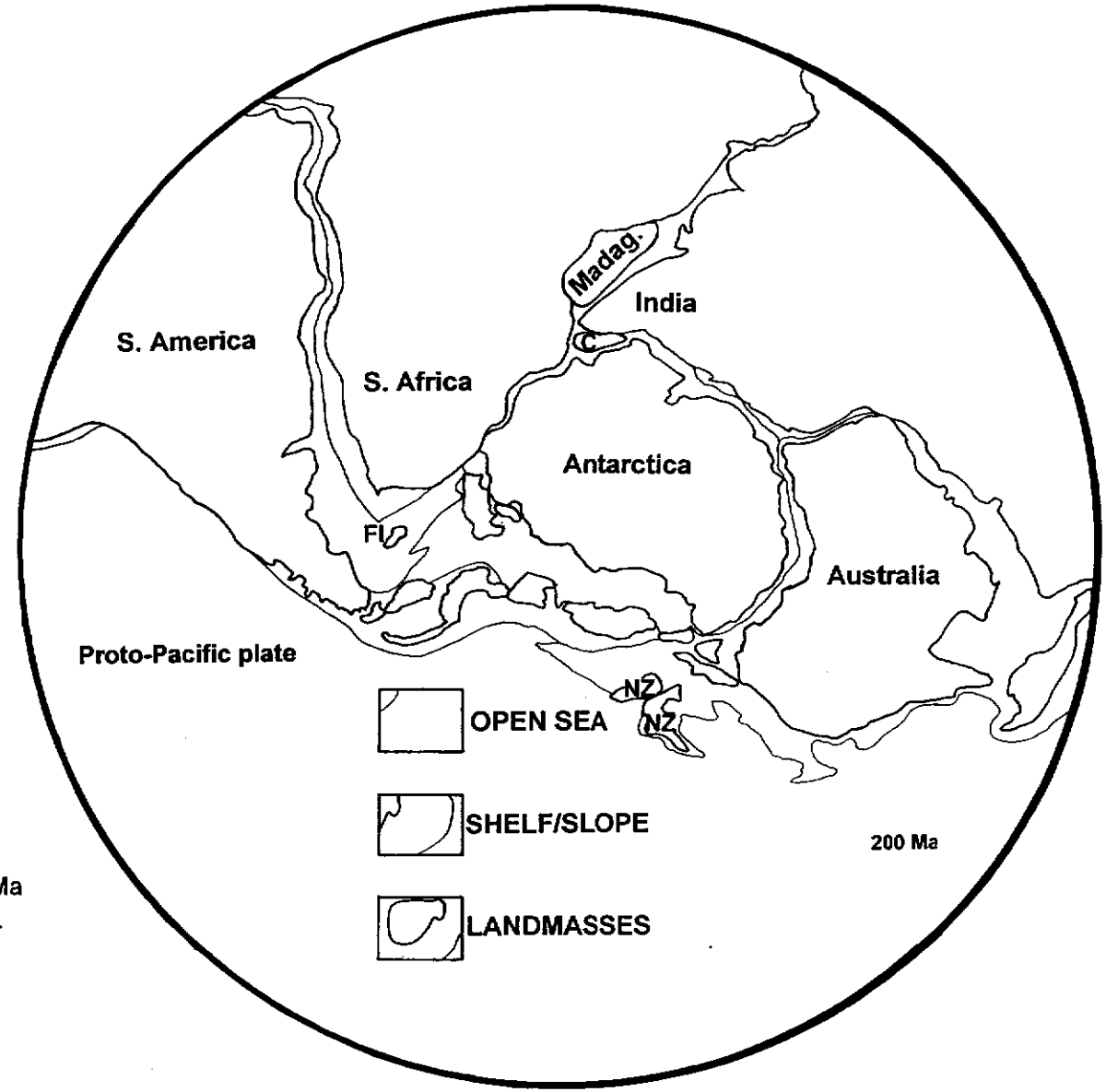

Figure 2.01: View of Gondwana plate reconstruction at 200 Ma prior to the commencement of proto-Pacific subduction (after Lawver et al., 1992).

FI = Falkland Islands, C = Sri Lanka/Ceylon, NZ = New Zealand.

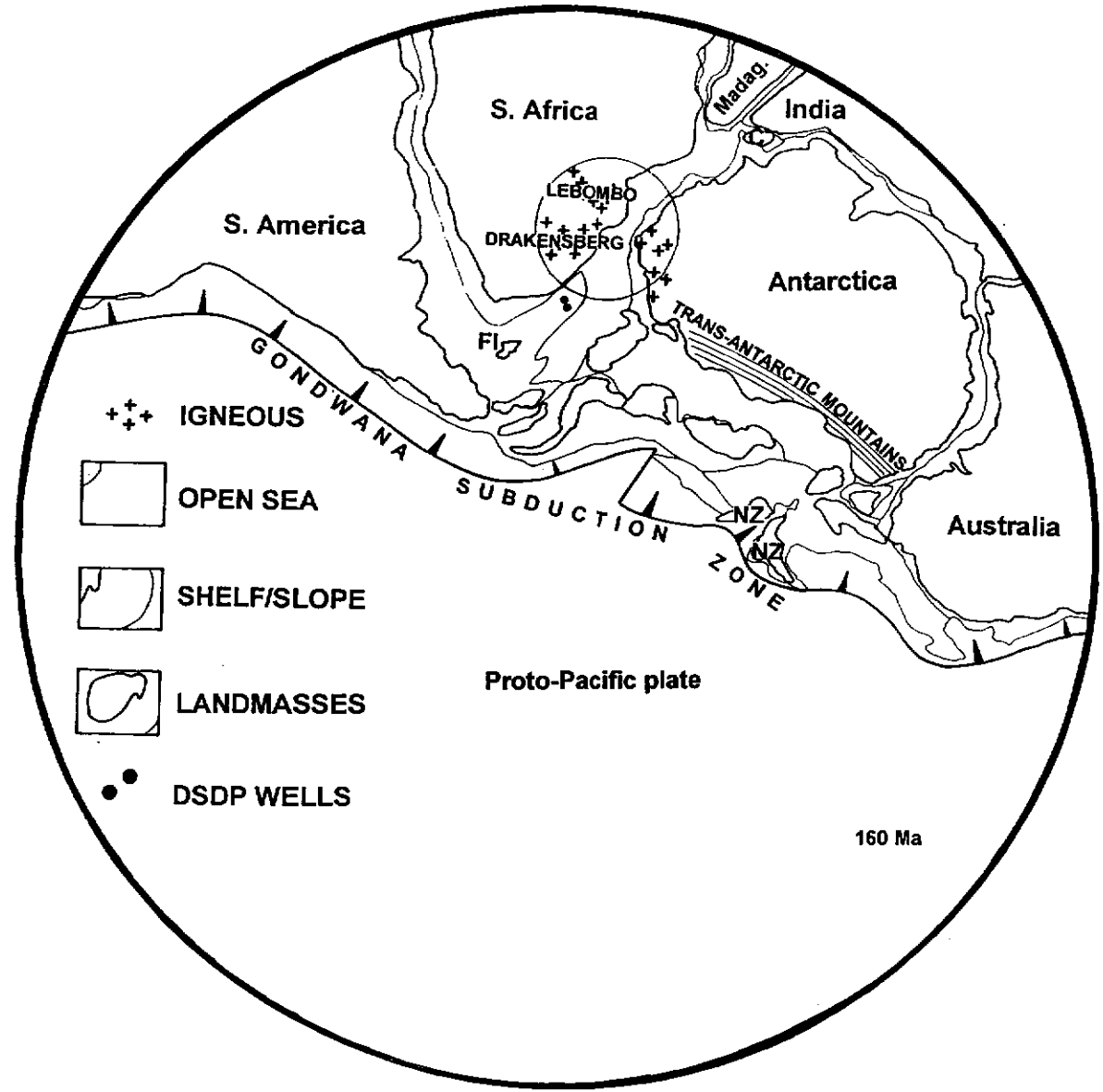

Figure 2.02: View of Gondwana plate reconstruction at 160 Ma (after Lawver et al., 1992). Proto-Pacific plate subduction started at 180-190 Ma. Location of relevant DSDP wells are shown in the vicinity of Southern Africa. Igneous activity believed related to the early Bouvet hotspot is shown where it affects southwestern Africa and southeastern South America. Coeval intrusive activity is found associated with the Trans-Antarctic Mountains and may be related to back-arc igneous activity.

FI = Falkland Islands, C = Sri Lanka/Ceylon, NZ = New Zealand.

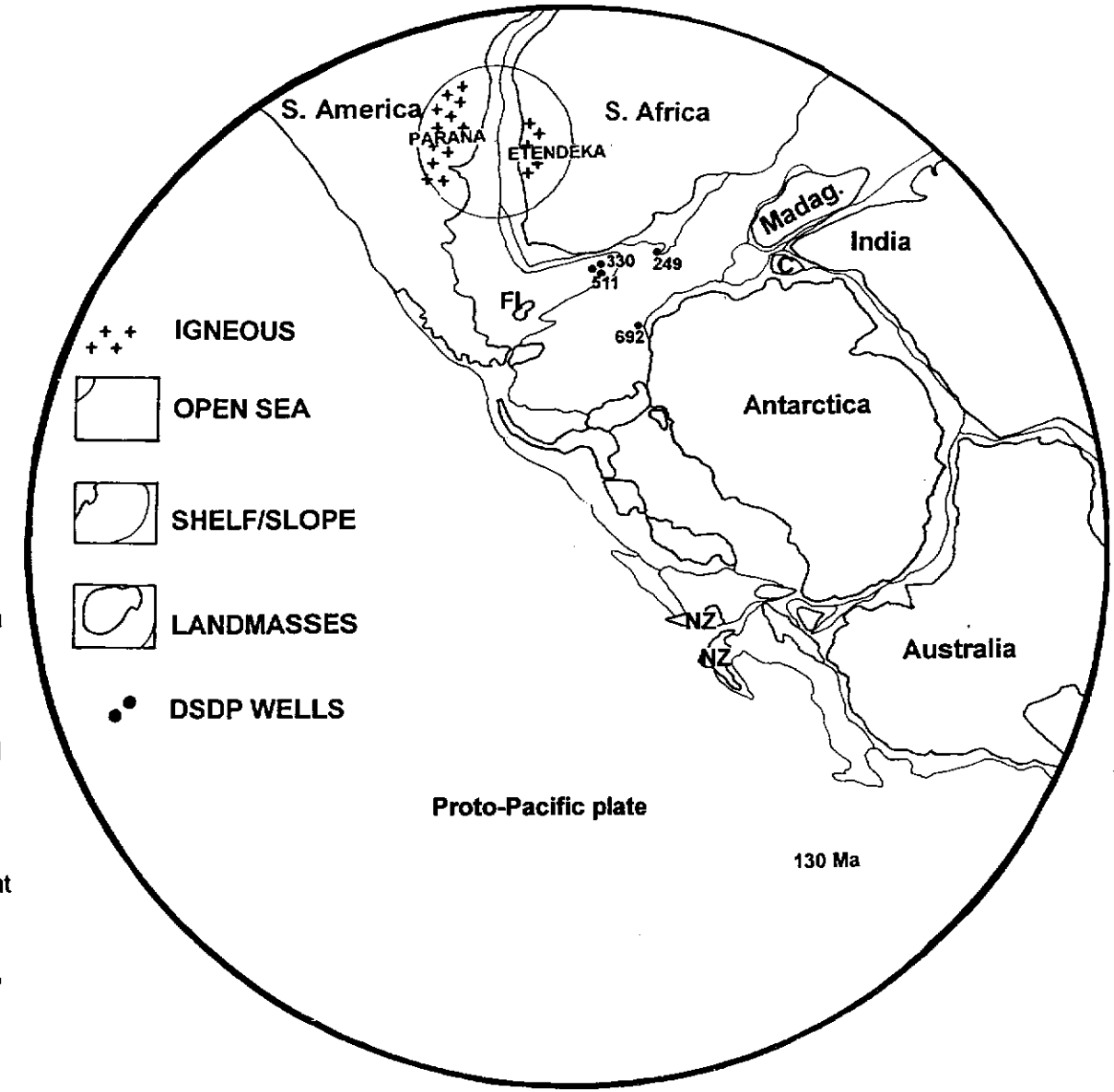

Figure 2.03: View of Gondwana plate reconstruction at 130 Ma close to the time of earliest sag basin formation. Well DSDP 692 in the western Antarctic Basin records the presence of coeval Jurassic sediments to those recorded in DSDP 327 and 511 in the Falklands Plateau Basin. Regional igneous activity (Paraña and Etendeka areas of South America and southern Africa respectively) related to early Walvis hotspot development are shown. Early opening of the rift between East and West Gondwana, connecting the region to Tethyan marine influence, is evident between Africa and Madagascar.
FI = Falkland Islands, C = Sri Lanka/Ceylon, NZ = New Zealand.

The date of the earliest break-up of Gondwana, based on the volcanic evidence from eastern South Africa is therefore taken to be approximately 160 ±30 Ma, whilst in the western part of South Africa it is approximately 150 ± 15 Ma. Rifting appears to have started earlier in the east than in the west. This conclusion agrees well with the proposed time of the first rifting events in the southern part of Africa based on the presence of mid-late Jurassic (possibly Oxfordian) rocks in DSDP 327 and 511 in the South Atlantic (Gilbert, 1977). It is considered that the Agulhas-Falklands Fracture Zone is characterised by ultramafic rocks which upwelled into the fracture zone (Talwani and Eldholm, 1973) and which cause the strong magnetic signature evident in the regional aeromagnetic survey (GETECH, 1992).

2.2.2. Plate separation

Separation between East and West Gondwana started along the progressively foundering rift zone between the Australasian plate (comprising India, Madagascar, Seychelles, Antarctica and Australia) and the African plate comprising South America, Africa and the Falklands (Khanna and Pillay, 1986; Lawver et al, 1992). During this phase, continental (fluvial and lacustrine) sediments were deposited on the early syn-rift surface. During later stages of the sag, a seaway developed along the eastern margin of Africa (Figs. 2.02 and 2.03) gradually transgressing further south and bringing marine conditions to the southern coastal areas.

An example of this transgression is developed in DSDP 327 where below the Late Jurassic marine shales, 12 metres of Mid-Jurassic silts and limestones overlie 10 cm of kaolinitic soil resting unconformably on oceanic basalts. This sequence of rocks is not developed in the Bredasdorp Basin but may be found further offshore, possibly in the Southern Outeniqua Basin (Martin et al., 1981). Further east of that location, the earliest oceanic crust, found in DSDP 249 (SE of Mozambique) is of Kimmeridge age (McMillan et al., 1992) This provides an earliest date for the separation and confirms that the Mid-Jurassic continental sediments in DSDP 327 pre-date the first opening of the rift.

There has been considerable speculation on whether the separation between South Africa and the Falklands Islands was either rotational or straight pull-apart. In support of the former view, Banks et al. (1993) show that early Karoo-age sediments in West Island (Falkland Islands) are intruded by dolerites of similar type and age to those intruding the Karoo rocks in the African Craton. In order to match these to those on the African plate requires the islands to be relocated between Port Elizabeth and the Transkei where the present day limit of Karoo intrusives intersects the coast (Dingle et al., 1983), but rotated through 180°. This interpretation is also favoured by Mitchell, et al. (1986); Cole (1992); Marshall (1994).

In support of the latter view, Lawver et al. (1992) show that a restricted marine basin developed between the Falklands Plateau and western Antarctica (Fig. 2.02). Uneroded remnants of these rocks were encountered in DSDP 692 off the Antarctic Peninsula. These appear to be coeval with the organic-rich rocks in DSDP's 327 and 511 indicating that the two areas must have been adjacent during the depositional phase. The separation of the Falkland Islands from Antarctica was therefore a straight-forward pull-apart. Recent seismic data acquired offshore from the Falkland Islands, show pre-rift structures which match those on the African plate (Lawrence and Johnson, 1995; Platt and Philip, 1995). These structures match those on the African landmass when replaced without rotation. As a result of the pull-apart separation, marine sag basins developed along the coastal margins of all the affected plates (Fig. 2.04) and source rocks similar in age and type to those in the South African basins developed there (Table 2.02).

2.2.3. Sedimentary deposits

The earliest of the post-basement and pre-rift sediments were deposited in continental fluviatile, lacustrine and estuarine environments and comprise mainly red and green sandstones and shales. Rigassi and Dixon (1970) subdivided these rocks into three main units which they interpreted as Lower Cretaceous based on field evidence only:

1. Sundays River Beds (marine to estuarine grey shales and clastics)
2. Marls and Wood Beds (estuarine to lacustrine clastics and shales)
3. Enon Conglomerates (fluviatile coarse red beds).

Du Toit (1976) also stated that both the Kirkwood Bridge Formation (previously called Marls and Wood Beds) and the Enon Formation were of Early Cretaceous age (Table 2.03) and both were overlain by the Sundays River Formation. The latter was subdivided into two units separated by a major unconformity, seismic horizon C.

From microfaunal data, McLachlan and McMillan (1979) showed the Kirkwood Bridge and Enon Formations to be Late Jurassic in age and that Du Toit's seismic horizon B was in fact the Jurassic-Cretaceous boundary (dated to 131 Ma by Haq et al., 1987). Later work (McMillan et al., in press) has shown that Du Toit's seismic horizon C (now named 1At1, Burden, 1992) is of Valanginian age.

During the earliest stages of the rifting, when the crust had just started to sag and prior to the development of the marine environment, lacustrine sediments might be expected to have developed due to ponding of rivers in the lowest areas. Where such sediments were deposited in large lakes, source rocks could have formed. Such sediments have not only been encountered in a number of wells in the Algoa Basin (McLachlan and

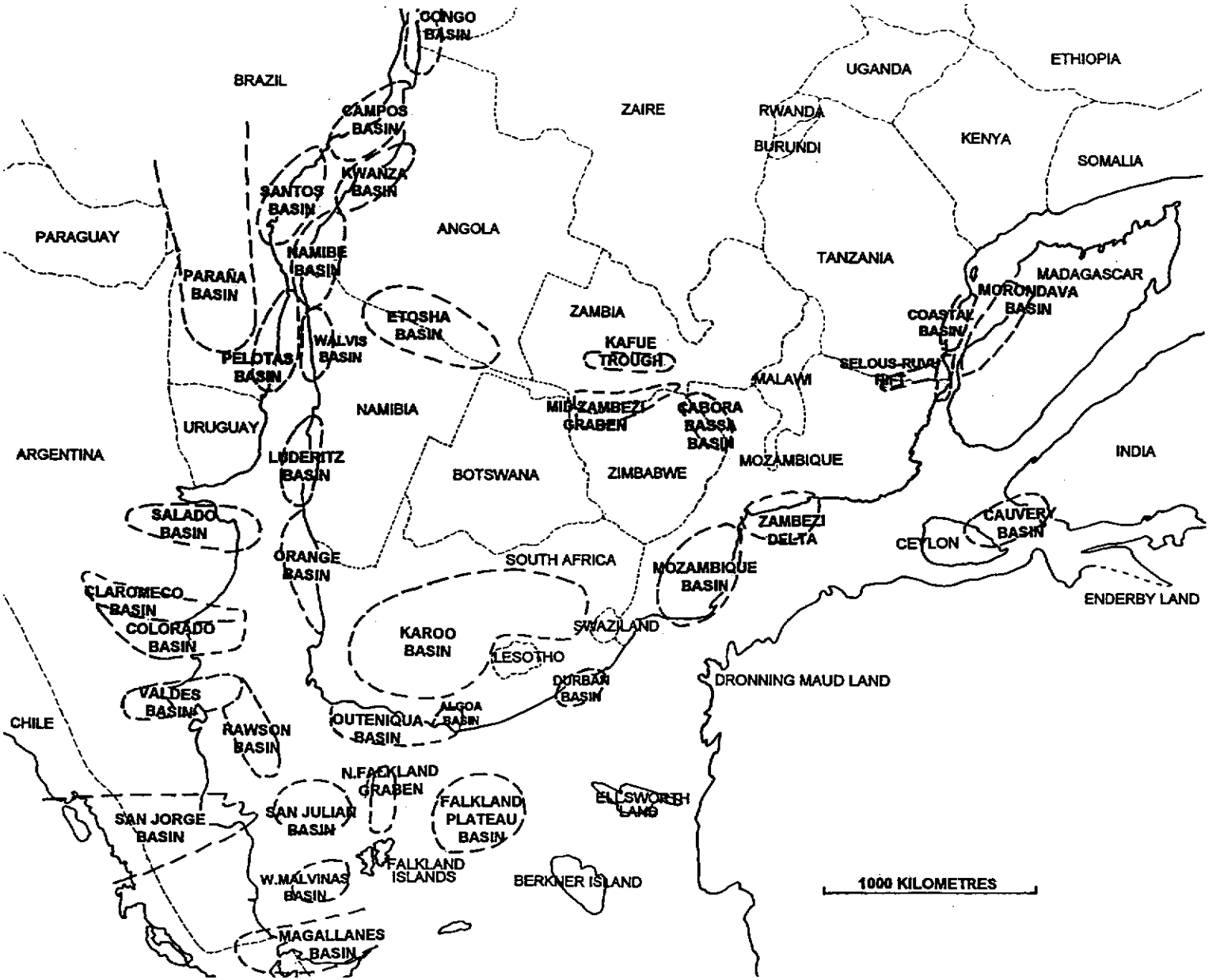

Figure 2.04: Regional map of plate reconstruction at ~121 Ma (after De Wit et al., 1988) showing the location of Mesozoic basins along the proto-coastlines. Source rocks in the basins close to Southern Africa are listed in Table 2.02.

SOUTH-WESTERN GONDWANA: PHANEROZOIC (including pre-Rift) SOURCE ROCKS

COUNTRY	AREA	PERIOD/STAGE	LOCAL NAME	ENVIRONMENT	QUALITY	REFERENCE	REMARKS
TERTIARY							
ANGOLA	Kwanza Basin	Palaeogene		deltaic	GAS	Mello et al. (1988)	
MID-CRETACEOUS							
BRAZIL	Campos Basin	Turonian	Campos	anoxic marine	OIL	Mello et al. (1988)	carbonate-rich shale
SOUTH AFRICA	Outeniqua Basin	Turonian	15A	anoxic marine	WG/OIL	Burden (1992) Davies (1996c)	
ANGOLA	Namibe Basin	Turonian	? Unit 4	marine	WG/OIL	Schlumberger 1991a Light and Shimutwikeni (1991)	postulated source rock based on intersection in DSDP 364.
MOZAMBIQUE	Mozambique Basin	Neocomian	Lower Grudja Lower Domo	marine/deltaic	GAS	Coster et al. (1989) Flores (1986)	
ANGOLA	Congo Basin	Cenomanian-Turonian	Iabe	marine	GAS/OIL	Light and Shimutwikeni (1991) Burwood et al. (1992)	
ANGOLA	Kwanza Basin	Cenomanian-Turonian	Itombe	marine	GAS/OIL	Burwood et al. (1992) Schlumberger (1991a)	Known onshore but postulated offshore source rocks
SOUTH ATLANTIC	Atlantic	Turonian		marine	GAS/OIL	Herbin et al. (1986)	Known quality but unknown generation and expulsion
EARLY CRETACEOUS							
SOUTH AFRICA	Bredasdorp, Pletmos and Gamtoos Basins	Early Aptian	13A	dysoxic marine	OIL	Davies (1990 and 1996c) Burden (1992) Malan (1993)	sometimes called Upper Sundays River Formation
NAMIBIA	Orange Basin	Early Aptian	P-P1	dysoxic marine	WG/OIL	Davies and Van der Spuy (1990)	sometimes referred to as 13A sequence
SOUTH ATLANTIC	Atlantic	Early Aptian	Unit 6	dysoxic marine	WG-OIL	Herbin et al. (1986) Deroo et al. (1983)	intersected in DSDP 361
CHILE	Magellanes Basin	Early Aptian	Margas Verdes	dysoxic marine	WG-OIL	Pittion and Goudain (1991)	
BRAZIL	Santos Basin	Aptian - Cenomanian		dysoxic marine	WG-OIL	Abreu and Savini (1994)	
ARGENTINA	Colorado Basin	Barremian-Albian	El Fortin	lacustrine/deltaic	GAS	Keeley and Light, (1993) Riccardi (1989)	
ANGOLA	Kwanza	Barremian	Upper Cuzo	lacustrine	GAS/OIL	Schlumberger (1991a)	
ANGOLA	Congo	Barremian-Aptian	Bucomazi	lacustrine/saline	OIL	Burwood et al. (1992)	
SOUTH AFRICA	Bredasdorp and Pletmos Basins	Hauterivian-Barremian	1A-9A	dysoxic marine	WG-OIL	Burden (1992) Davies (1996c)	also known as earliest Upper Sundays River Formation
FALKLANDS	San Julian	Hauterivian-Barremian		marine	GAS/OIL	Richards and Fannin (1994)	undrilled basin - source rocks postulated from seismic/geological reasoning
NAMIBIA	Orange Basin	Hauterivian	6A	marine	GAS	Davies and Van der Spuy (1990)	
SOUTH AFRICA	Orange Basin	Hauterivian	6A	lacustrine	OIL	Muntingh (1993)	known from a limited graben but suspected widespread development

Table 2.02: Source rocks, their depositional environment and kerogen type in Phanerozoic basins of the Southern African region, their depositional environment and kerogen type (from published data).

ARGENTINA	Neuquen Basin	Hauterivian-Valanginian	Vaca Muerta	lacustrine	OIL/GAS	Riccardi (1989)	
CHILE	Magallanes Basin	Hauterivian	Inoceramus Inferior	dysoxic marine	GAS/OIL	Pittion and Goudain (1991)	
CEYLON/INDIA	Cauvery Basin	Hauterivian-Barremian		marine	GAS/OIL	Barnard and Thompson (1992) Berry and Rawat (1990)	Equivalent to the Dalmiapurum shlaes of Cauvery Basin
BRAZIL	Campos Basin	Hauterivian - Barremian	Lagoa Feia	lacustrine/ saline	OIL	Mohriak et al. (1989) Mello et al. (1988 and 1991)	
CHILE	Magallanes Basin	Berriasian	Springhill Continental	lacustrine	GAS/OIL	Pittion and Goudain (1991)	
LATE JURASSIC							
CHILE	Magellanes Basin	Portlandian-Hauterivian	Estratos con Favrella	marine deltaic	OIL/GAS	Natland et al. (1974) Davies, 1994b	
FALKLAND ISLANDS	Falkland Plateau	Portlandian and Kimmeridgian		marine	WG-OIL	Herbin et al.(1986)	identified as late Jurassic
SOUTH AFRICA	Algoa/Gamtoos Basins	Portlandian	Colchester	lacustrine	WG-OIL	Davies et al. (1991) (for Haasvlakte Graben) Malan (1993) McLachlan and McMillan (1979)	
SOUTH AFRICA	Haasvlakte Graben Bredasdorp Basin	Kimmeridgian		lacustrine	OIL	Davies et al. (1991)	
ARGENTINA	San Jorge Basin	Kimmeridgian - Berriasian (and Valanginian?)	D-129, Cerro Guadal and Aguaba Bandero	lacustrine	OIL	Biddle et al. (1986) Fitzgerald et al. (1990) Riccardi (1989) Maslanyj et al. (1992)	Riccardi identifies the D-129 source rock as Aptian age. Earliest source = lacustrine in A-J1 graben.
ARGENTINA	Waldes Basin	Kimmeridgian-Berriasian	Cerro Guadal and Aguaba Bandero	lacustrine	OIL	Herbin et al. (1986)	
CHILE	Magallanes Basin	Callovian	Tobifera	lacustrine	WG-OIL	Maslanyj et al. (1992) Davies (1993d; 1994b) Natland et al. (1974)	
TANZANIA	Coastal Basin	Bathonian - Callovian		deltaic shales	GAS (?OIL)	Kajato (1982)	
TANZANIA	Selous-Ruvu Basin	Bajocian	Makarawe shale	deltaic coaly shale	GAS/OIL	TPDC (1992)	
TANZANIA	Eastern Marginal Basins	Late Jurassic		marine	oil	Barnard and Thompson (1992)	
MADAGASCAR	Morondava Basin	Bajocian		marine shales	GAS/OIL	Coster et al. (1989)	thought to be the equivalent of the Makarawe shales of Tanzania
TANZANIA	Ruvuma	Early Jurassic	Nondwa	deltaic	GAS/OIL	SADCC (1992)	
TRIASSIC							
MADAGASCAR	Morondava Basin	late Triassic	Mid-Sakamena	lacustrine	GAS	Ravelosan et al. (1991)	

Table 2.02: Regional source rocks (continued)

ARGENTINA - CHILE	Cuyo Basin	late Triassic		lacustrine	GAS	Valicenti, 1995, pers comm.	
PERMIAN							
ARGENTINA	Colorado Basin	late Permian	Pillahuinco	lacustrine	OIL/GAS	Keeley and Light (1993)	
TANZANIA	Coastal Basin	Permian		coaly shales	GAS	Kajato (1982)	
ZAMBIA	Kafue Trough Mid-Zambezi Graben	late Permian	Gwembe coal measures	coals	GAS/(OIL)	Reimann (1985)	
ZIMBABWE	Mid-Zambezi Graben	late Permian	Mkanga shales Lower Madumabisa shales	coaly shale (locally alga!)	(GAS)/OIL	Hiller and Shoko (1996)	
FALKLANDS	Falklands Plateau	? late Permian	? Port Sussex	lacustrine or marinite	OIL	Lawrence and Johnson (1995)	Whitehill-type shale postulated in this basin
FALKLANDS	North Falklands Graben	? late Permian	? Port Sussex	lacustrine or marinite	OIL	Lawrence and Johnson (1995)	Whitehill-type shale postulated in this basin
SOUTH AFRICA	Karoo Basin	late Permian	Whitehill shale	lacustrine or marinite	OIL	Christie (1990) Cole and McLachlan (1990) Marshall (1994).	Christie (1990) identifies this source rock as a 'marinite' meaning a large lake ie one with tides, waves and possibly salinity more similar to marine conditions.
SOUTH AFRICA	Karoo Basin	mid Permian	Molteno Coals	cannel coal	GAS	Christie (1990) Maslanyj et al. (1992)	
SOUTH AFRICA	Karoo Basin	mid Permian	Vryheid	lacustrine/deltaic	GAS	Christie (1990)	these sediments are thought by some to be equivalents of the upper Whitehill Formation (Cole and McLachlan, 1990) or an earlier turbidite equivalent (Wickens, et al., 1995)
URUGUAY	Paraña Basin	mid-late Permian	Irati shale	lacustrine	OIL	Marshall (1994)	
BRAZIL	Rio Grande do Sul Basin	mid-late Permian	Irati shale	lacustrine	OIL	Maslanyj et al. (1992). Correa Da Silva and Cornford (1985)	
CARBONIFEROUS							
NAMIBIA ANGOLA	Etosha Basin	Westphalian	Owambo shale	marine	OIL/?GAS	Momper (1982)	oil traces in adjacent sands considered to have been locally generated.
DEVONIAN							
SOUTH AFRICA	Kaapvaal Craton	Devonian	Bokkeveld shale	marine	?OIL	Rowsell and De Swardt (1979)	all intersections now over-matured

Table 2.02: Regional source rocks (continued)

McMillan, 1979) but also in the Bredasdorp Basin and in the onshore Haasvlakte Graben (Fig. 2.05). In addition, since the Southern Outeniqua Basin too contains great thicknesses of syn-rift sediments (Wenham et al., 1991), it is possible that a similar lithology could be present there.

The best known example of such lacustrine source rock is the Colchester Member of the Infanta Formation (Table 2.03). This is locally well developed in the onshore Algoa Basin in the form of pyritic black shales interspersed with fluviatile and deltaic sands and silts (McLachlan and McMillan, 1979). Ostracode datings show it to be Kimmeridgian-Portlandian in age (Valicenti and Stephens, 1984).

As the separation of Gondwana continued, the marine transgression continued southwards along the eastern seaboard of Africa and into the more westerly basins, progressively overstepping the earlier continental sediments and heralded the drift onset unconformity. Late Jurassic marine source rocks deposited in a deep marine environment, have been found only in the Algoa and Gamtoos offshore basins and match those in DSDP 511 and 330 on the Falkland Plateau (Barker et al., 1977a; Herbin et al. 1986; Davies et al., 1991).

2.3 POST-RIFT GEOLOGY

More recent studies have addressed the post-rift geology because of the importance of that time interval to commercial exploration. As a result of these studies, the classification table of Du Toit (1976) (Table 2.03) has been found to be inadequate and a more correct chronostratigraphic table was constructed (Fig. 2.06). This table is used exclusively hereafter.

The drift onset unconformity has been determined from ostracode, foram and palynologic data to be at ~126 Ma in the Bredasdorp Basin (Valicenti and Broad, 1994). The oldest rocks overlying horizon 1At1 are deep marine shales of the Upper Sundays River Formation. These shales have occasional interbeds of basin floor turbiditic and fan sandstones, deposited following the major sea level rise during the Valanginian which was due in part to post-rift thermal subsidence. They overlap a basin-wide veneer of transgressive coastal sandstones (part of the 'V' formation, VH Valicenti, 1995, pers. comm.) considered equivalent to the lower part of sequence LZB 2.1 of Haq et al. (1987). The base of the shales is marked by a characteristic angular unconformity mapped as seismic horizon 1At1. Seismically this is characterised by a surface of downlap onto an impedance contrast. The regional extent of this seismic evidence suggests the shales have a basin-wide distribution. The location of this shale immediately above extensive shallow marine sandstones, where there is no evidence

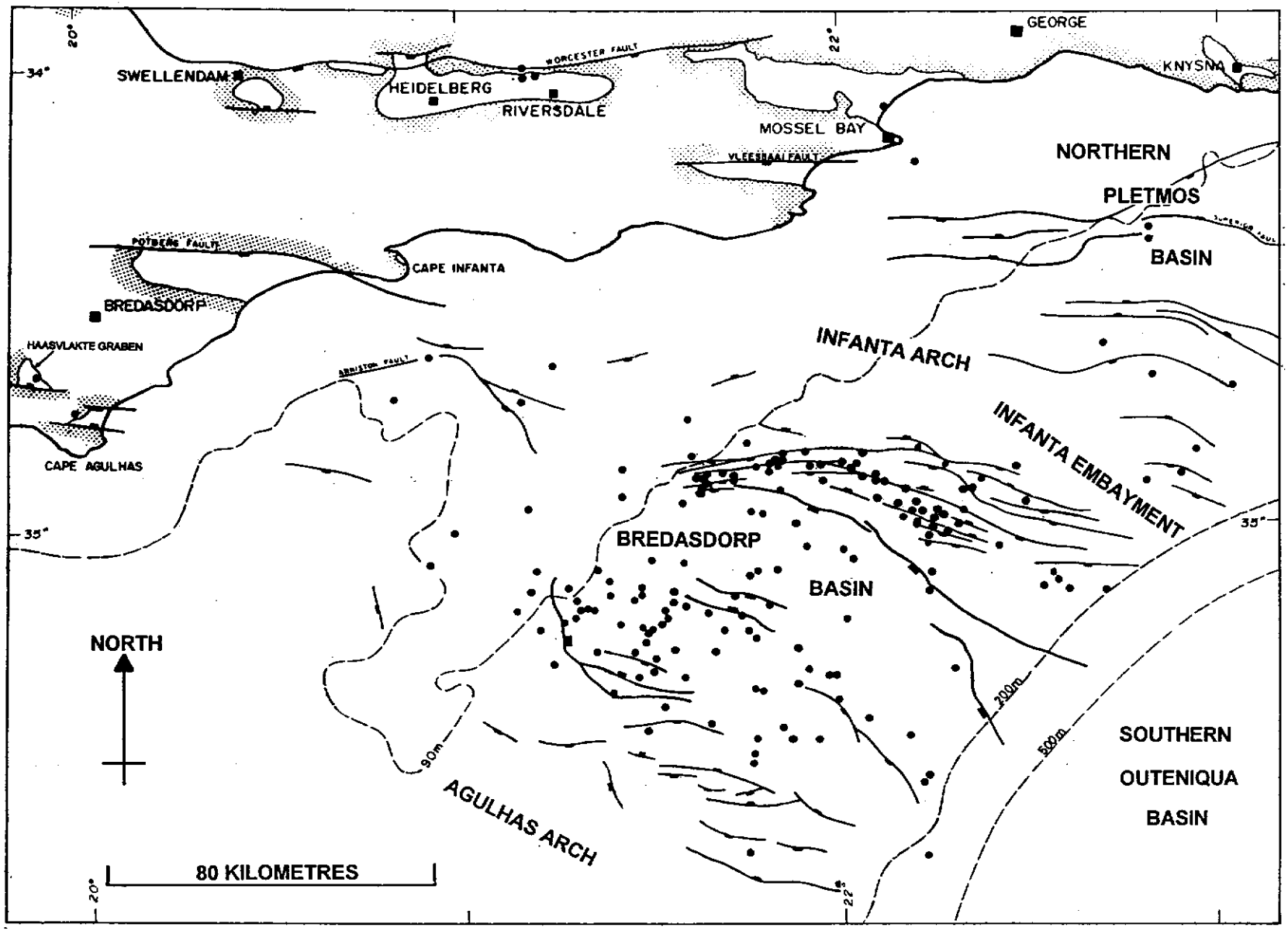

Figure 2.05: Map of wells drilled to date in the western part of the Outeniqua Basin. This locates the Bredasdorp Basin, Southern Outeniqua Basin, western Pletmos and Infanta Embayment, the onshore Haasvlakte Graben and major onshore and offshore faults.

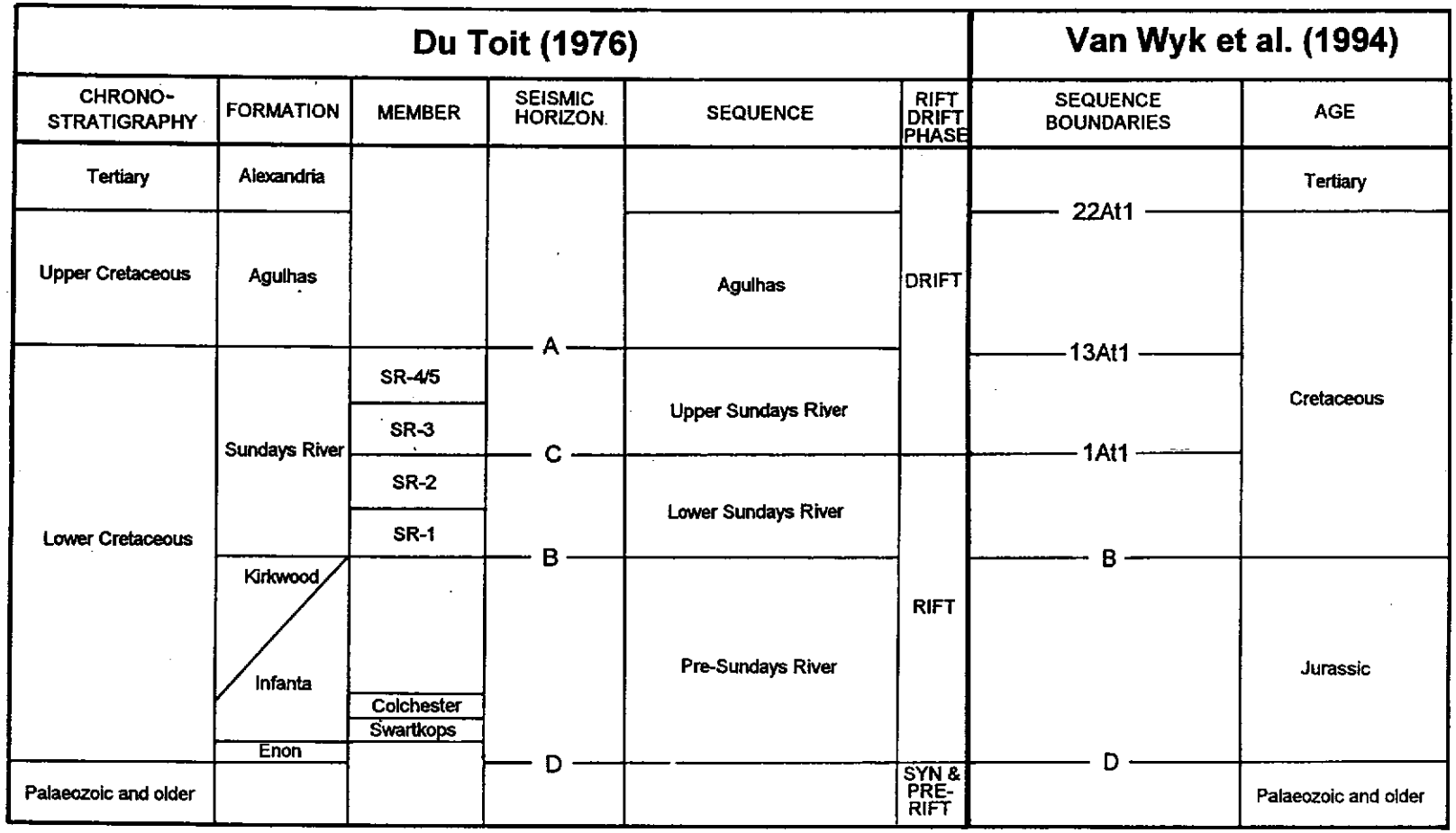

Table 2.03: Classification of Mesozoic and Tertiary sediments (and their bounding horizons) after Du Toit (1976) compared to the recent biostratigraphically and seismically characterised sequence stratigraphic boundaries. Modern sequence stratigraphic and tectonic subdivisions are now used in preference to this less practical classification.

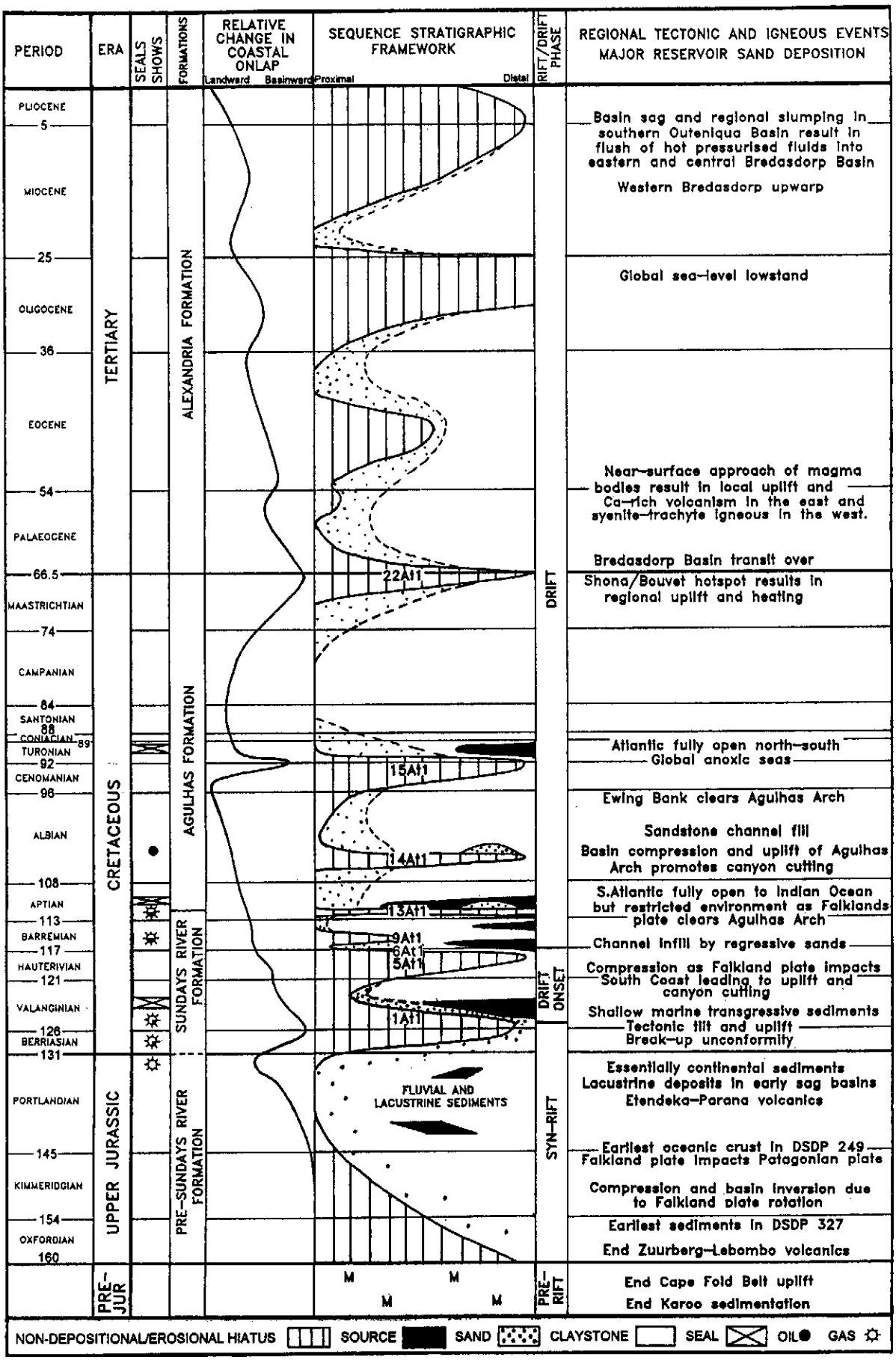

Figure 2.06: Chronostratigraphic column of the Mesozoic and Tertiary strata in the Bredasdorp Basin (after Dingle et al., 1983; Burden, 1992 and McMillan et al., in press). The sequence of events and the stratigraphy are generally applicable for the greater southern African region and the Mesozoic part of the succession in the DSDP wells in the Falklands Plateau Basin.

either lithologically or seismically of intervening transgressive sediments, shows that the basin subsided rapidly (McMillan et al., 1997).

During the Hauterivian, a second major tectonic episode resulted in rejuvenation of many of the earlier horst and graben features (Jungslager, 1996). This episode probably resulted from transpression during early movement along the Agulhas-Falklands Fracture Zone (AFFZ). Coevally, a tectonically-enhanced sea level fall resulted in a major regression in the Bredasdorp Basin, mapped as seismic horizon 5At1 (Fig. 2.06). Deep marine rocks of the ensuing 5A sequence have not been intersected to data owing to their great depth of burial. They are only likely to be found in the centre of the basin and are largely infill. No evidence of progradation or aggradation is recorded from seismic or drilling data to date (Jungslager, 1996). However, remnant shelf rocks have been intersected in boreholes around the basin edge.

Further regional sag occurred after Hauterivian times and the transgression brought the coastline close its present day location. Marine sedimentation dominated up to the present, but owing to the closeness of the Falkland Islands Plateau which was a positive feature, circulation was restricted during Early to Mid-Cretaceous. During this period, the seafloor (and probably much of the water column) was intermittently depleted of oxygen, perhaps because of short periods of restriction, resulting in the development of dysoxic conditions which promoted the better preservation of organic material. These organic-rich intervals have source potential for gas and oil.

Oceanic circulation improved after the rift had opened further and open marine conditions extended around the southern tip of Africa joining the incipient North Atlantic rift during the Mid-Cretaceous (Zimmerman et al., 1987). Evidence for this is that Early Aptian marine conditions extend up the west coast of Africa, at least as far as the Kudu wells (Wickens and McLachlan, 1990; Benson 1990), the DSDP 361 well (Herbin et al., 1986) and probably as far as the Walvis Ridge (Schlumberger, 1991a).

The presence in Angola of thick Aptian salt deposits, formed by the occasional overtopping of the Walvis Ridge during highstands, demonstrate that the transgression was regionally extensive. Four of these spill-over events are demonstrated to have occurred in the Angola Basin (Schlumberger, 1991a). Several sea level adjustments during the Cretaceous resulted in widespread erosive events mapped regionally (partly because of their downlapping relationship with underlying reflectors) as type 1 unconformities (Vail et al., 1977). These occurred notably during the Aptian (13At1), Albian (14At1), Turonian (15At1) and at the Cretaceous-Tertiary boundary (22At1) (Fig. 2.06). Post-Hauterivian, active progradation can be seen on seismic records to

continue up to the Cretaceous-Tertiary boundary. Above this, the sedimentation appears largely aggradational although seismic data near the sea-floor are badly affected by noise multiples. The biostratigraphic definition of several of these hiatuses has been discussed by McMillan (1990). He addressed the susceptibility of the benthic and pelagic fauna to changes in water depth and commented on the environmental implications of the faunal changes across the boundary, pointing out that most of these unconformities are of relatively short duration.

Deep marine sediments deposited immediately after many of the hiatuses during periods of transgression and early highstand sedimentation, are associated with sediments with elevated contents of organic carbon. Many of these intervals have source potential. The most widespread of these is found in Upper Barremian to Lower Aptian transgressive-to-highstand sediments in the 13A sequence. These marine source rocks are also inferred to be developed on the opposite side of the AFFZ as hydrocarbon source rocks of matching age and quality have also been found in DSDP 511 on the Falklands Plateau (Gilbert, 1977) and in the Magallanes Basin (Pittion and Goudain, 1991).

Cretaceous rocks can separated into four units based on the oxygen level in the water: (i) 1A-4A rocks tend to be dominated by relatively low levels of oxygen (ii) 5A-12A rocks tend to be generally oxidising although in some areas oxygen levels are lower (iii) 13A rocks which were deposited under low oxygen (dysoxic-anoxic) conditions and (iv) post-13A rocks which, with one exception in the Turonian, were deposited in oxygen-rich water.

The exception is found in the Turonian 15A sequence which is dominated by a sediment-starved environment in which organic-rich claystones are found (McMillan, 1990). The claystones are considered to be equivalent to the Turonian source rocks accumulated in the Tethyan region and thought to represent a Regional Oceanic Anoxic Event, possibly related to the final opening of the Atlantic (Schlanger et al., 1987) (Fig. 2.07). Arthur et al (1987) show that this was a short-lived period of intense organic carbon burial coinciding with a maximum sea-level highstand when strong upwellings enhanced the surface productivity. This highstand is believed to be due to higher global temperatures which reduced ice caps to a minimum and which led to greater precipitation and higher surface runoff. This would in turn lead to larger quantities of fresh water entering the marine environment resulting in density stratification in deep basins and an increase in deep marine salinity and anoxicity. These conditions have been noted in Angola and Nigeria as probably being responsible for the presence of source rocks and oils with dominant biomarkers which are characteristic of hypersaline conditions (Burwood et al., 1990; Ekweozor and Telnaes,

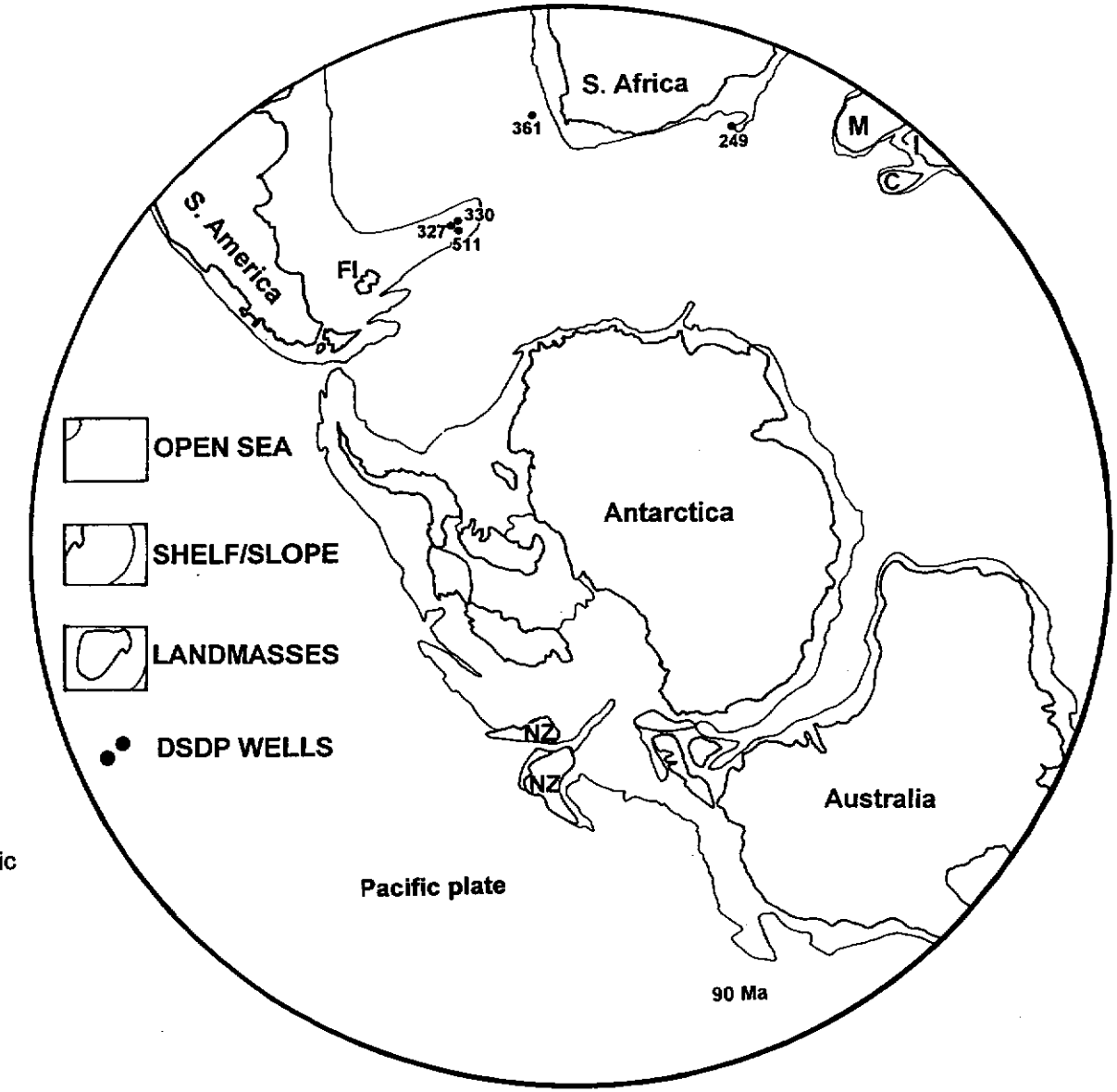

Figure 2.07: View of Gondwana plate reconstruction at 90 Ma showing the disposition of the continents at the time the Atlantic Ocean was fully open for the first time. At this time there was also a connection between the proto-Pacific ocean and the Indian/ South Atlantic Oceans between southern South America and the West Antarctic Peninsula (after Lawver et al., 1992).

1990). More locally, there is microfaunal evidence of uplift of the western South African offshore and downwarp of the eastern area (McMillan, 1990; McMillan et al., 1997)

Above these Turonian source rocks, a thick package of Mid-Late Cretaceous claystones and siltstones prograded across the basin from the west. These argillites are devoid of source potential, mainly because the dominantly oxygenated environment precluded preservation of aliphatic organic matter (Cornford et al., 1983). The persistent influx of cold, oxygen-rich Antarctic bottom water is given as the main reason for the largely oxygenated sedimentary environment (Zimmerman et al., 1987).

2.4 TERTIARY

The Tertiary sediments were deposited in a strongly oxidising environment in higher water temperatures and have low organic carbon contents. The sediments are calcite-rich, largely biogenic and occasionally form caliche layers. These are thought to be associated with winnowing current action resulting from the occasional warm water eddies which separate from the Agulhas Current and sweep the shelf.

The core of the Agulhas Current is at a temperature of 25-29°C, i.e. 10-15°C warmer than the water on the Atlantic side of South Africa, and >20°C warmer than the bottom water in the Outeniqua Basin (Derbyshire, 1964). The current is considered to have been active at least since the Early to Mid-Tertiary (Winter and Martin, 1990; McMillan, 1986; McMillan, 1989) and to have influenced the nearshore land temperatures (Frakes and Kemp, 1972). The core of the current generally flows near the surface along the shelf break (Fig. 2.08) although it occasionally deflects southwards or northwards impinging on the bottom water of the shelf. Examples of this happening recently have been demonstrated from anchored current meter data (Gründlingh, 1984). During periods of northern hemisphere glaciation, though, it has been shown that the current swings southwards (Winter and Martin, 1990) so that the present day shelf and continental rise were no longer swept by the current.

The Tertiary sedimentary history of the continental shelf of the south coast has been studied using shallow seismic profiles in conjunction with bottom dredged and gravity cored samples (Dingle, 1971) and occasional samples from offshore wells (McMillan, 1989). These data allowed for the subdivision of the Tertiary into three packages separated by major unconformities during the Late Palaeocene, Eocene-Early Oligocene and Late Miocene-Pliocene. Tertiary sediments commonly have a large biogenic component and include phosphatic muds, chalks and chalky marls.

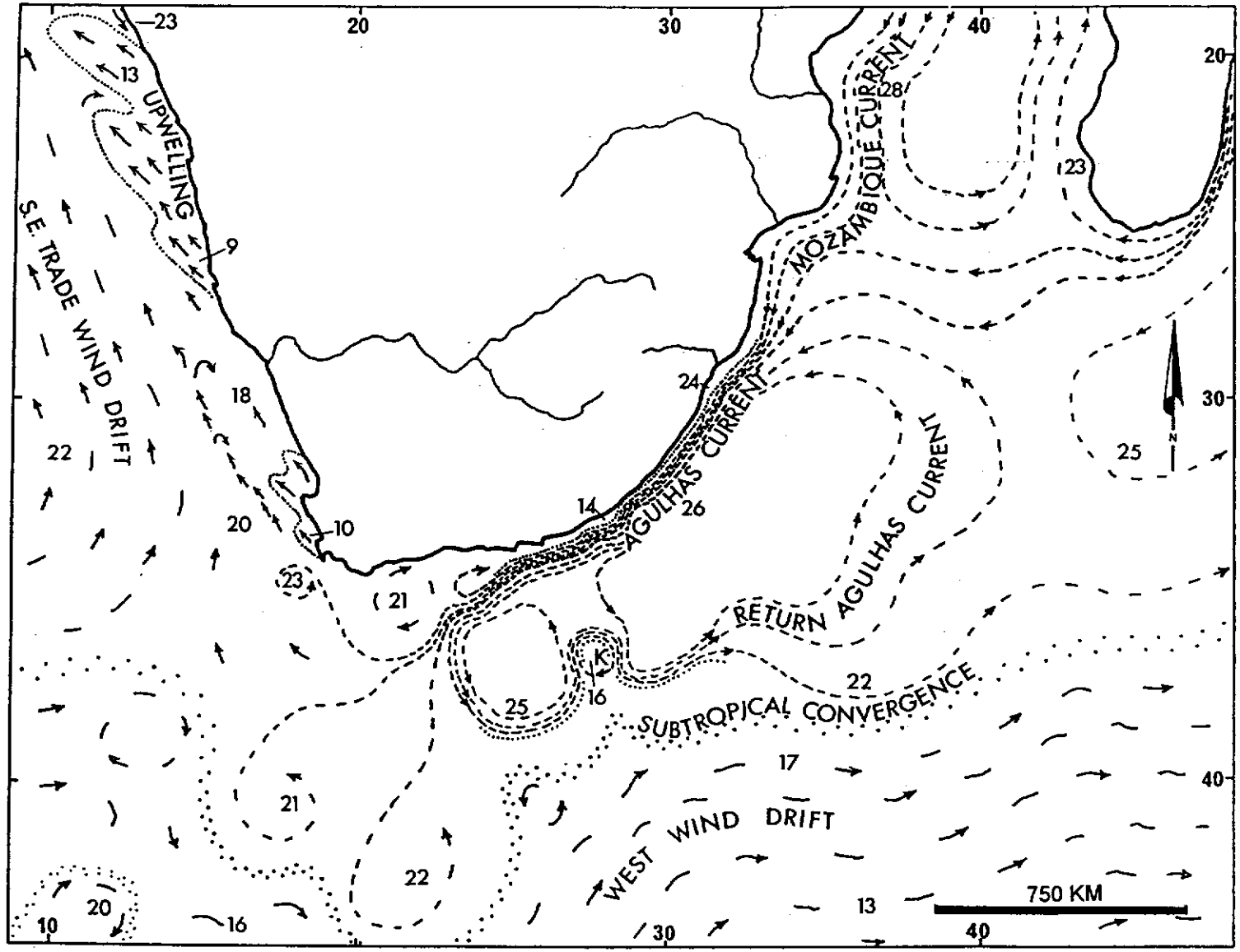

Figure 2.08: Oceanography of the southern African region showing the direction and temperature in degrees celsius of the major marine surface water bodies - in particular the Agulhas Current which flows alongside the southern and eastern coastlines of South Africa - based on data acquired during the 1960's (NASOU, 1973).

McMillan (1989) confirmed the latter two of these unconformities and pointed out that no boreholes on the South African offshore had ever intersected deposits of Late Oligocene. This supports the conclusions of Vail et al. (1977) who showed that the Mid- to Late Oligocene was a period of major world-wide sea-level fall during which sedimentation probably continued, but only in the deepest parts of the basin. Unfortunately, the Late Tertiary is consistently thin in all the basins, and seismic sea-bottom noise multiples mask evidence of possible erosion at this horizon. Microfaunal studies (McMillan, 1996, pers comm.) have shown evidence of reworked Mid-Oligocene fauna indicating that there had been at least some erosion.

No sediments of Late Oligocene age were reported from the DSDP 361 well, although they were expected because the well is in a more distal location than any oil exploration well drilled in the South African offshore to date. The incompleteness of the core record in the well (less than 10% of the upper 1000 metres was sampled) may be responsible for this absence. Lower Oligocene sediments have also been eroded from the Bredasdorp Basin, most severely in the proximal portions. Locally this planation extends down to the latest Eocene (McMillan, 1993; pers comm.).

McMillan (1989) demonstrates that Upper Miocene, lime-rich sediments have also been eroded leaving only the Lower Miocene. This surface forms a calcrete on which Late Pliocene, Early Pleistocene and Holocene fauna are preserved.

2.5. IGNEOUS BODIES, MANTLE SWELLS AND HOTSPOTS

2.5.1. Post-rift igneous bodies

Alkaline, locally undersaturated, igneous bodies have been found in two regions of the Bredasdorp Basin and in one region of the Orange Basin (Broad and Turner, 1982; Gerrard and Smith, 1983 and unpubl. SOEKOR data). In the Bredasdorp Basin, these areally extensive intrusives are readily detected from seismic data and a map of their distribution has been compiled (Fig. 2.09). Similar igneous bodies are also found in a number of onshore locations (Duncan et al., 1978; Duncan, 1981). A number of samples of these igneous bodies, both onshore and offshore, have been subjected to isotopic age dating (K-Ar and Rb-Sr) as indicated in Table 2.04.

Nepheline-syenite and aegirine-trachyte dykes and sills intruded the western Bredasdorp Basin in the area around well 3 during the Early Tertiary (Fig. 2.09, drawn after Broad and Turner, 1982 and unpublished SOEKOR data; Fig. 2.10). Isotopic dating of sea floor and borehole samples of these intrusives provides dates ranging from 52-59 Ma (Dingle and Gentle, 1972; Rowsell et al., 1979). Coevally, calc-alkaline lamprophyric and possibly carbonatitic dykes and sills intruded the eastern end of the

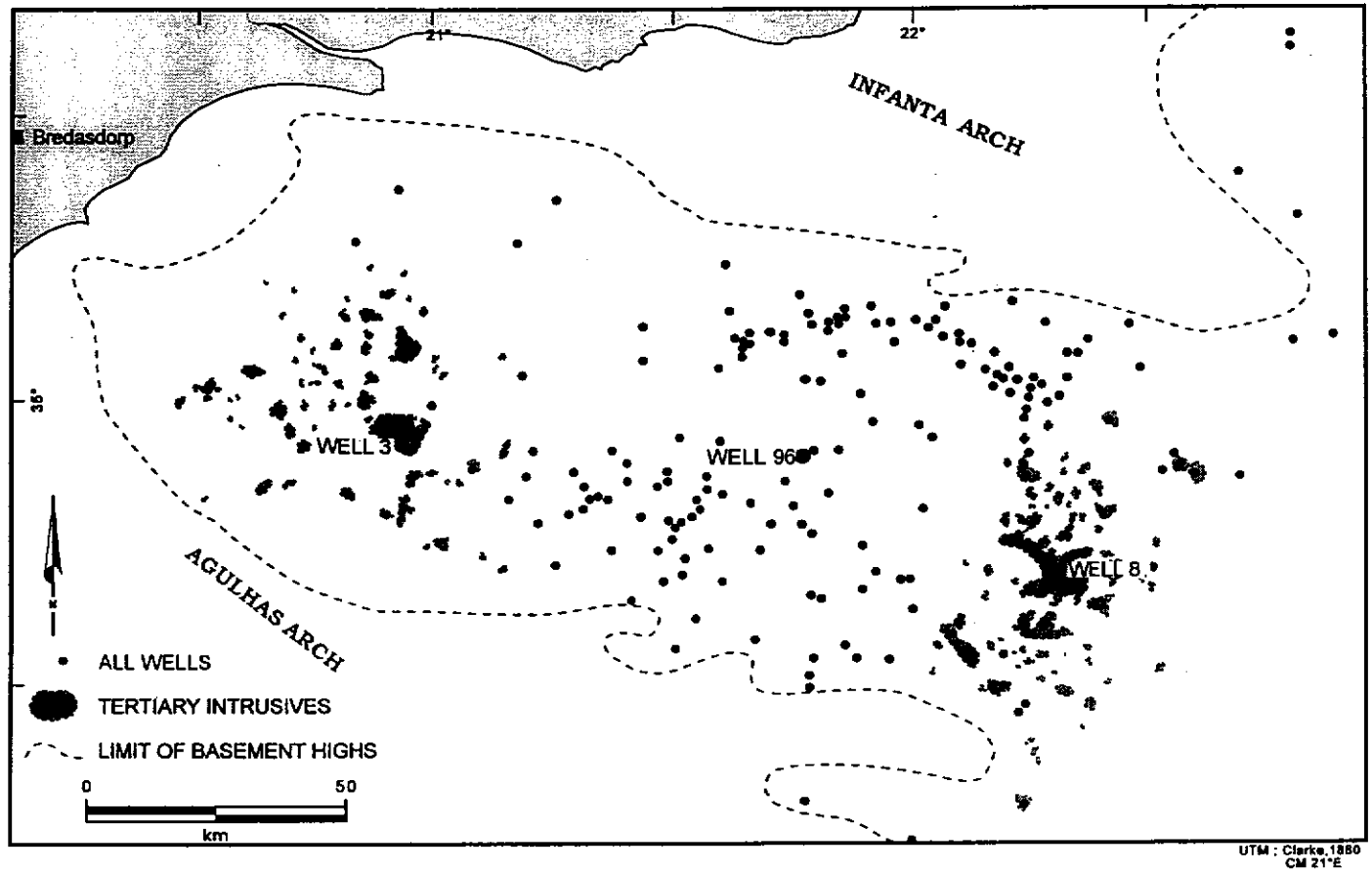

Figure 2.09: Map showing the distribution of igneous rocks in the Bredasdorp Basin after Broad and Turner (1982) modified using unpublished SOEKOR seismic and borehole data. Recent detailed seismic interpretations in the eastern Bredasdorp Basin (e.g. Mlaba, 1996) show the distribution of the igneous bodies follow the NNE-SSW trend of the Bouvet/Shona hotspot track of Duncan (1981) and Hartnady and Le Roex (1985). The less complete definition of the distribution of intrusives in the western basin is probably a function of the limited exploration in the area.

AGE	LOCATION	LITHOLOGY	ANALYSIS METHOD	REFERENCE
38.5 Ma	30°43'S,17°59'E, near Garies.	melilite basalt plug	?	Kroner, 1973.
35.7 Ma and 37 Ma	'Klinghardt Mountains, nr Luderitz, SWA' (27°20.1'S 15°42.7'E)	phonolite plugs and melilite basalt	?	"
74.9 ±1.3 Ma	Sutherland	melilite basalt	K-Ar	Duncan et al., 1978.
74.7 ±3.0 Ma	Saltpetrekop	biotite from alkaline trachytic basalt	K-Ar	"
63.7 ±1.3 Ma	Robertson	melilite basalt	K-Ar	"
62.6 ±1.0 Ma	Spiegal River	melilite basalt	K-Ar	"
58 ±2.4 Ma	Alphard Bank, sea floor	sanidine from aegirine trachytic basalt	K-Ar	Dingle and Gentle, 1972.
59.0 ±3.5 Ma	D-A1 (2446-2500m)	amphibole from undersaturated nepheline syenite'	K-Ar	FM Consultants, 1973.
52.3 ±2.9 Ma	Sea floor, D-A1	sanidine from aegirine-trachytic basalt	K-Ar	FM Consultants, 1972.
55 ±2 Ma	F-F2 and F-O1	biotites from Ca-lamprophyres	Rb-Sr	Eglington et al., 1990.
32.8±2.6 Ma (alteration date)	KUDU 9A-1 (4452.7m)	altered amygdaloidal olivine-basalt	K-Ar	FM Consultants, 1974.
41.9 ±2.0 Ma (alteration date)	KUDU 9A-1 (core 1, as above)	altered basalt	K-Ar	Kreuger Enterprises Inc.
37.6 ±1.1 Ma	Ba-A2 (213m)	peralkaline nosean phonolite basalt	K-Ar	FM Consultants, 1976.

Dingle, RV and Gentle, RI (1972). Early Tertiary volcanic rocks on the Agulhas Bank, South African continental shelf. Geol. Mag., **109**, 127-136.
Duncan, RA, Hargraves, RB and Brey, GP (1978). Age, palaeomagnetism and chemistry of melilite basalts in the Southern Cape, South Africa. Geol. Mag., **115/5**, 317-327.
Eglington, BM, Auret, JM and Retief, EA (1990). Results of a Rb-Sr isotopic study of biotites from boreholes F-F2 and F-O1. EMATEK, CSIR, unpubl. rept., EMA-C 90119, 5pp.
Kroner, A (1973). Comment on "Is the African plate stationary". Nature, **243**, 29-30.
Kreuger Enterprises Inc, Geochron Laboratories Ltd., Potassium-Argon Age determination, 1pp.
FM Consultants (1972). Geochronological report on an aegirine-trachyte sample. Unpubl. rept. to SOEKOR No. FMK/1105, 5pp.
FM Consultants (1973). Geochronological report on syenite cuttings D-A1. Unpubl. rept. to SOEKOR No. FMK/1138, 4pp.
FM Consultants (1974). Geochronological report on sample no. FM7396, KUDU 9A-1. Unpubl. rept. to SOEKOR No. FMK/1178 , 3pp
FM Consultants (1976). Geochronological report: age determinations on Ba-A2 samples. Unpubl. rept. to SOEKOR No. FMK/1271, 3pp.

Table 2.04: Ages, types and locations of dated igneous rocks in Southern Africa which pertain to the hotspot tracks of Duncan (1981), Hartnady and Le Roex (1985) and Martin (1990, pers. comm.).

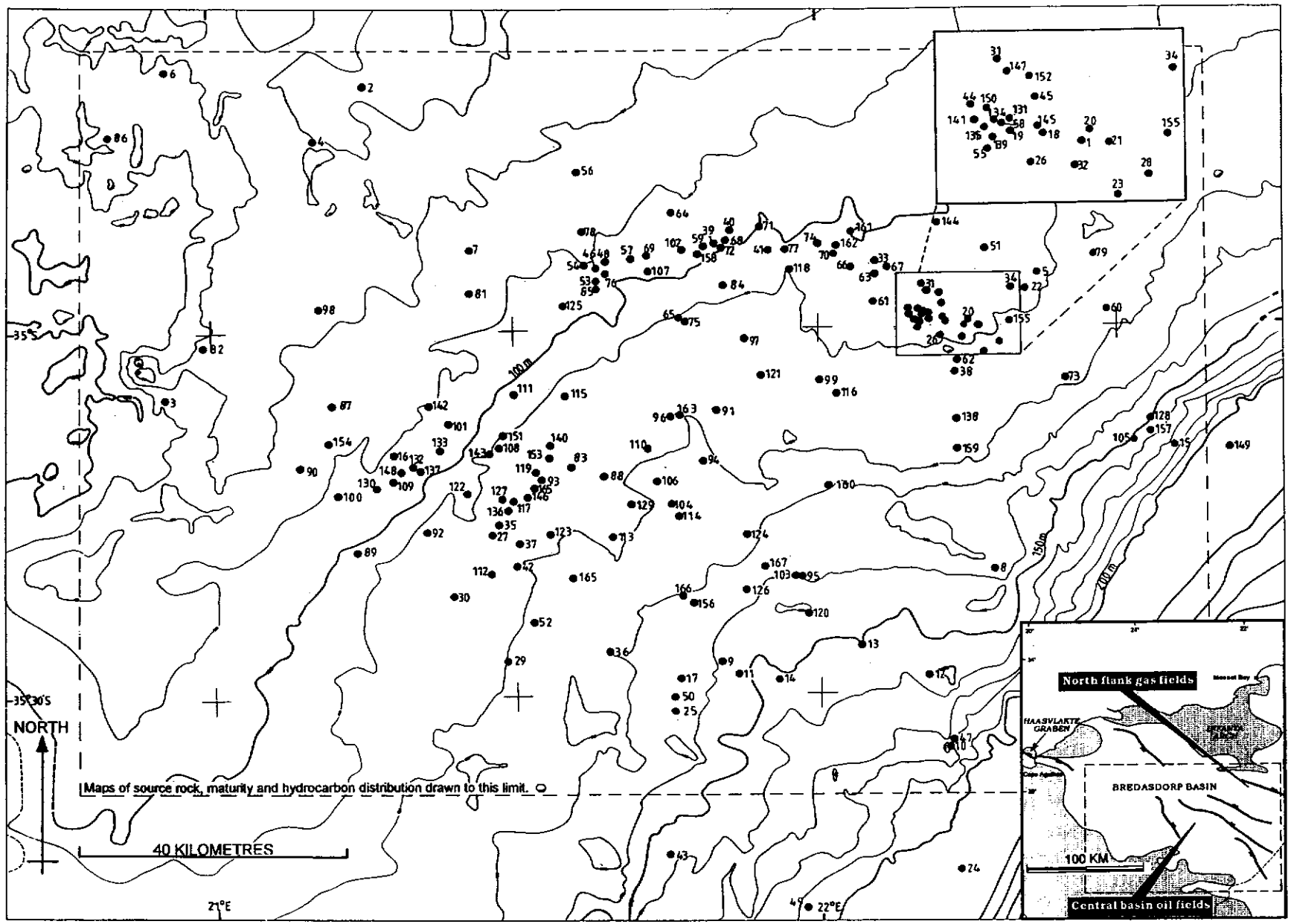

Figure 2.10: Distribution of wells in the Bredasdorp Basin drawn on regional bathymetric contours constructed from seismic records, after Birch et al., 1986 and unpublished data from the SA Navy (Teuteberg, 1995). Wells are numbered in chronological sequence. The boundaries of the source rock, maturity and hydrocarbon distribution maps in subsequent chapters are also shown.

basin (Rowsell et al., 1979) especially in the vicinity of well 8. Isotopic dating of these revealed ages ranging from 53-57 Ma (Eglington et al., 1990). Although from the descriptions they appear to differ chemically and petrologically, Rowsell et al. (1979) and Eglington et al. (1990) considered these intrusives to represent early and late fractions of the same magma which may be related (Hatch et al., 1961, p. 373-379). Alternatively, the differences may result from biased sampling because the more basic intrusions are often severely altered, apparently by hydrothermal fluids. Examples of this were noted in well 8, (Marot, 1990, pers comm.). Some of the lamprophyre samples effervesce strongly in dilute acid and may represent either carbonate intrusives, hydrothermally altered sediments or lamprophyre (Rowsell et al., 1979). Trace element analysis of some sidewall core samples from these rocks record locally high contents of Rb, Y and Zr suggesting a non-sedimentary origin (McCarthy, 1978) but do not to help confirm whether they are original carbonatites or altered lamprophyres.

Onshore, alkaline melilite-rich basalts plugs are reported from several locations in the south-western Cape and some of these have been dated as Latest Cretaceous and Early Tertiary (Table 2.04 and references therein). The melilite basalts at Saltpeter Kop, in the southern Cape, which Duncan (1981) considers to be part of this igneous trend, are indeed chemically similar to the intrusions in the western Bredasdorp Basin (McIver and Ferguson, 1978; Duncan et al., 1978).

2.5.2. Mantle swells and Cretaceous-Tertiary hotspot

It has been suggested that these intrusions are associated with proposed mantle swells and the ensuing hotspot activity (Duncan, 1981; Hartnady and Le Roex, 1985).

Mantle swells are considered to originate at the lower mantle boundary where periodic outbursts of excess heat initiate rising plumes from the mantle (White and McKenzie, 1989; Condie, 1989). These rising plumes of mantle material usually develop large heads up to 1000 km in diameter (Underhill and Partington, 1993) and can result in the transfer of large quantities of heat to the lithosphere where they form 'hotspots'. Where these hotspots result in decompressive melting of localised buoyant upwellings (DePaolo et al., 1996) they often take the form of regional lava extrusion (e.g. Drakensburg lavas). With time the head dissipates leaving a persistent plume, which may be only a few hundred kilometres across but which continues to give rise to repeated outbursts of igneous activity in a series of loosely associated intrusive events. Since hotspots tend to be fixed relative to crustal motion, they leave distinct linear tracks of volcanic emanations which are especially noticeable in oceanic crust as bathymetric highs (Wright, 1973; Duncan, 1981; Morgan, 1983). Some hotspots leave a very narrow surface track because they have essentially no plume head. The hotspot

considered to have formed the Hawaiian chain is of this type (Wright, 1973). It is also possible that the Bouvet/Shona hotspot is of this type.

The African plate is unusual in being characterised by a large number of hotspots. Each has a surface expression of a volcanic centre (Fig. 2.11). The separation of the African and South American continents after initiation of the Agulhas-Falklands Fracture Zone (AFFZ) transform motion resulted in the northward rotational movement of the African plate (Duncan, 1981; Lawver et al., 1992) about a pole located off north-west Africa - hence these hotspot tracks are arcuate. Duncan (1981) suggested that one of these hotspots migrated past the Bredasdorp Basin during the Late Cretaceous-Early Tertiary. There are also abrupt changes in the direction of the bathymetric tracks which may be a result of the impingement of the hotspot plume alternately on opposite sides of transform faults (Hartnady and Le Roex, 1985). In addition to this explanation, a change in the pole of rotation also resulted in the tracks showing a matching change in direction at about 40 Ma (Fig. 2.11, Duncan, 1981).

The increments of motion of this hotspot indicate that the Bredasdorp Basin would have overlain the hotspot at ~70 Ma, i.e. there is a discrepancy between the date of transit of the hotspot and the dates of the intrusions. DePaolo et al. (1996) show that hotspot volcanoes tend to have an active lifetime of only about 1 Ma. It is considered likely that magma generated in the upper mantle could have taken 10-20 Ma to travel to the lithosphere (Condie, 1989; Underhill and Partington, 1993), hence ages of the near-surface bodies would be expected to have a range of 50 Ma.

Many of the dated intrusives lie on a track from the Bouvet/Shona hotspot, which continues into the Bredasdorp Basin. This may extend to the kimberlite intrusions of the Northern Cape (Duncan, 1981; Hartnady and Le Roex, 1985, Fig. 2.11). The 'footprint' of this track is relatively narrow, apparently about 200 km wide, typical of an ascending plume without plumehead (Wright, 1973). The present day position of the hotspot is shown by Duncan (1981) to be near Bouvet Island, although Hartnady and Le Roex (1985) suggest it may be closer to the probable 'Shona' hotspot several hundred kilometres north-west of Bouvet Island.

Fission track analyses of two Late Cretaceous samples from well 96, located at least 50 km distant from the nearest intrusive either intersected or visualised seismically, are available for temperature study (Fig. 2.09). These data record a heating event to 100°C or more during the period 60 ±5 Ma (Eurotrack, 1996). This high Palaeocene temperature may be due to a more regional heat input such as might arise during the hotspot transit. This needs to be tested by study of fission track data from other wells in the basin.

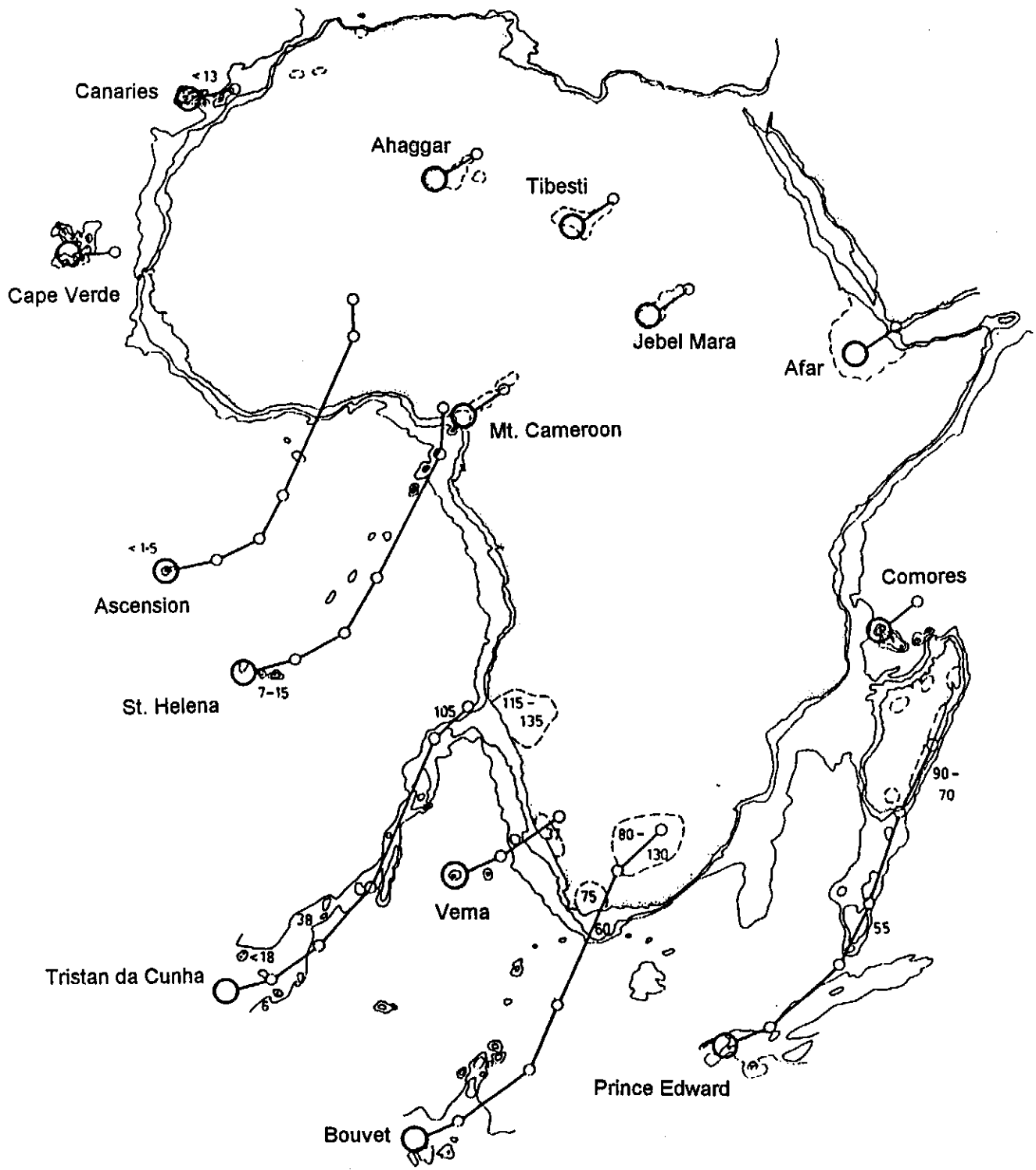

Figure 2.11: Map of African plate showing hotspot motion since 100 Ma BP (after Duncan, 1981). Presently active hotspots are large open circles (~110 km in diameter). Bathymetric contours are 4000 m and 2000 m, continental volcanic provinces are bounded by dashed lines, and where known, the ages of these provinces (from radiometric data and stratigraphic inference) are shown. A best-fitting series of rotation poles constructed from the geometry of the hotspot paths produces the solid line segments, connected by 'bubbles' at 20 Ma increments.

Further evidence of the passage of a hotspot may be gained from regional uplifts which cannot be explained in terms of either eustatic changes (Vail et al., 1977) or regional tectonism. For example, the presence of unabraded Late Maastrichtian benthic fauna in Mid-Palaeocene deposits in wells on the south flank of the Bredasdorp Basin show that the nearby Agulhas Arch must have experienced uplift of several hundred metres during Late Maastrichtian (McMillan, 1986 and 1994, pers. comm.). Although Late Jurassic and Early Cretaceous tectonism in the Southern Offshore was caused by wrenching and block faulting resulting from transform motion along the AFFZ (Van der Merwe and Fouché, 1992), this cannot be invoked for the Late Cretaceous tectonism. This is because the spreading centre transit was complete by Mid-Cretaceous and the fracture zone inactive after Late Cretaceous (Hartnady and Le Roex, 1985). Hence there is no cause for a regional event, other than the hotspot transit, which could have caused such a large uplift.

Vitrinite reflectance gradients using data interpreted and compiled from all wells throughout the south and west coast offshore areas (Davies, 1996a) are plotted on Fig. 2.12. The distribution of high gradients (>0.35% R_o/km) are indeed found only in the regions where hotspot tracks are accentuated by igneous rocks.

The separation of the onshore and offshore igneous events into two apparently parallel tracks (Figs. 2.12), between 90 and 130 km apart, may be due to there being either two separate magma reservoirs (accounting for the chemical differences between the igneous material sampled from the Bredasdorp basin) or one magma reservoir with two outlets. Examples of the latter case are found in Pacific hotspot tracks in the Tuamotu Archipelago (Condie, 1989) and the Hawaiian-Emperor chain (Condie, 1989; Ernst et al., 1995; DePaolo et al., 1996). The lack of evidence of igneous material between the main onshore intrusive centres and those in the Bredasdorp Basin may result from magma being formed at irregular intervals from the hotspot plume. Such an explanation is given for the discontinuous nature of the Hawaiian-Emperor chain (Vogt, 1972; Condie, 1989). In addition, outpourings will tend to be localised where major fault lineaments intersect the hotspot track (Condie, 1989). The Bredasdorp Basin and the onshore Outeniqua Fault trend are such regions where intrusives are concentrated (Figs. 2.11-2.13).

2.5.3. Other Tertiary hotspots

Duncan (1981) also shows a hotspot located at the Vema sea-mount (Fig. 2.11). A bathymetric track approaches the coastline near Lüderitz and Duncan (op cit.) attributes the melilite basalt and phonolitic intrusions in the Klinghardt Mountains to the east, dated at 35.7-37.0 Ma, as being due to the passage of the hotspot. The Kudu gasfield

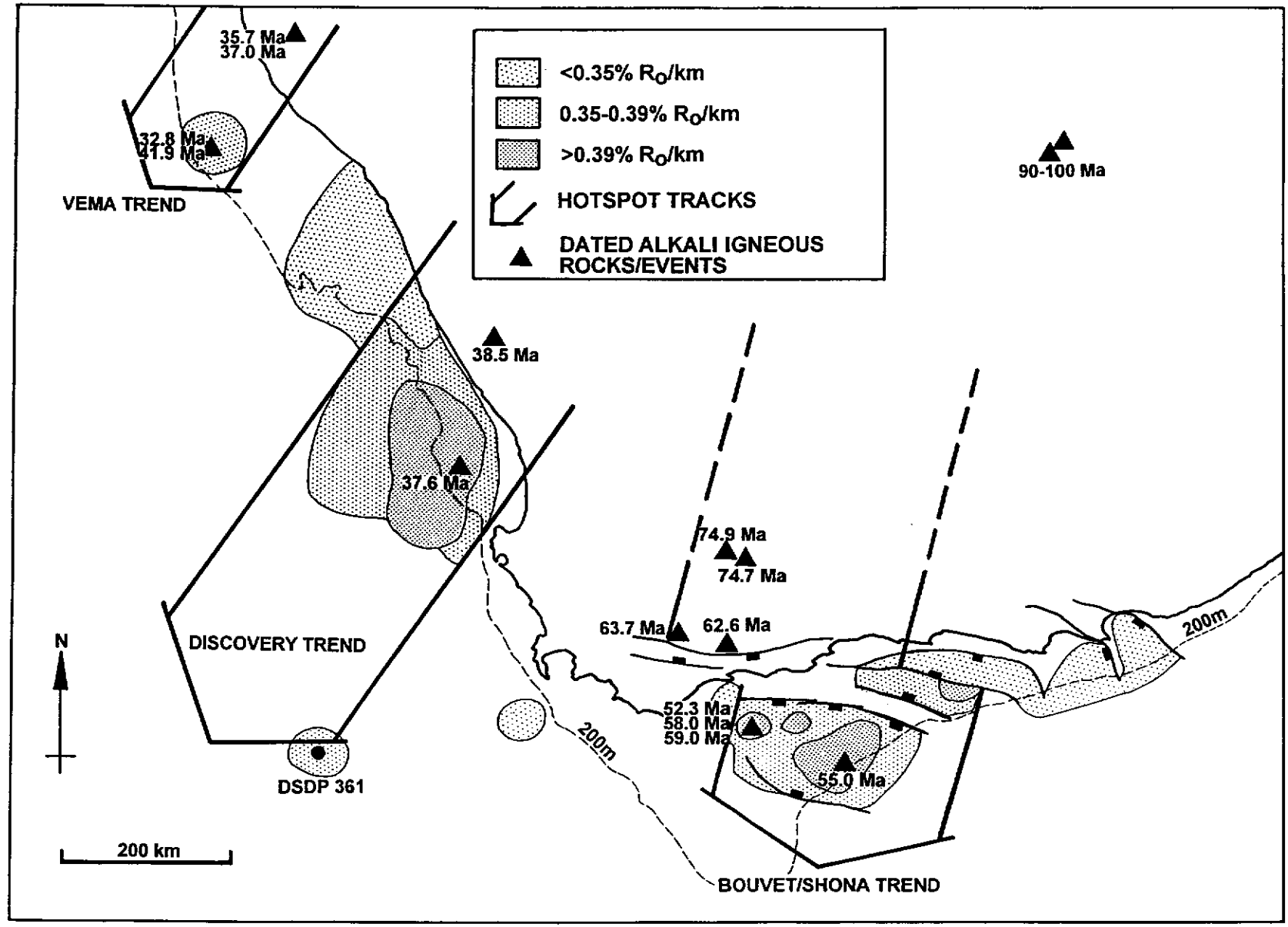

Figure 2.12: Map of southern Africa showing the distribution of dated alkali igneous events, hotspot tracks (after Duncan, 1981, Hartnady and Le Roex, 1985 and Martin, 1990, pers. comm.) regional vitrinite reflectance gradients measured in wells (or calculated from Tmax after Espitalié et al., 1985) and major south coast faults.

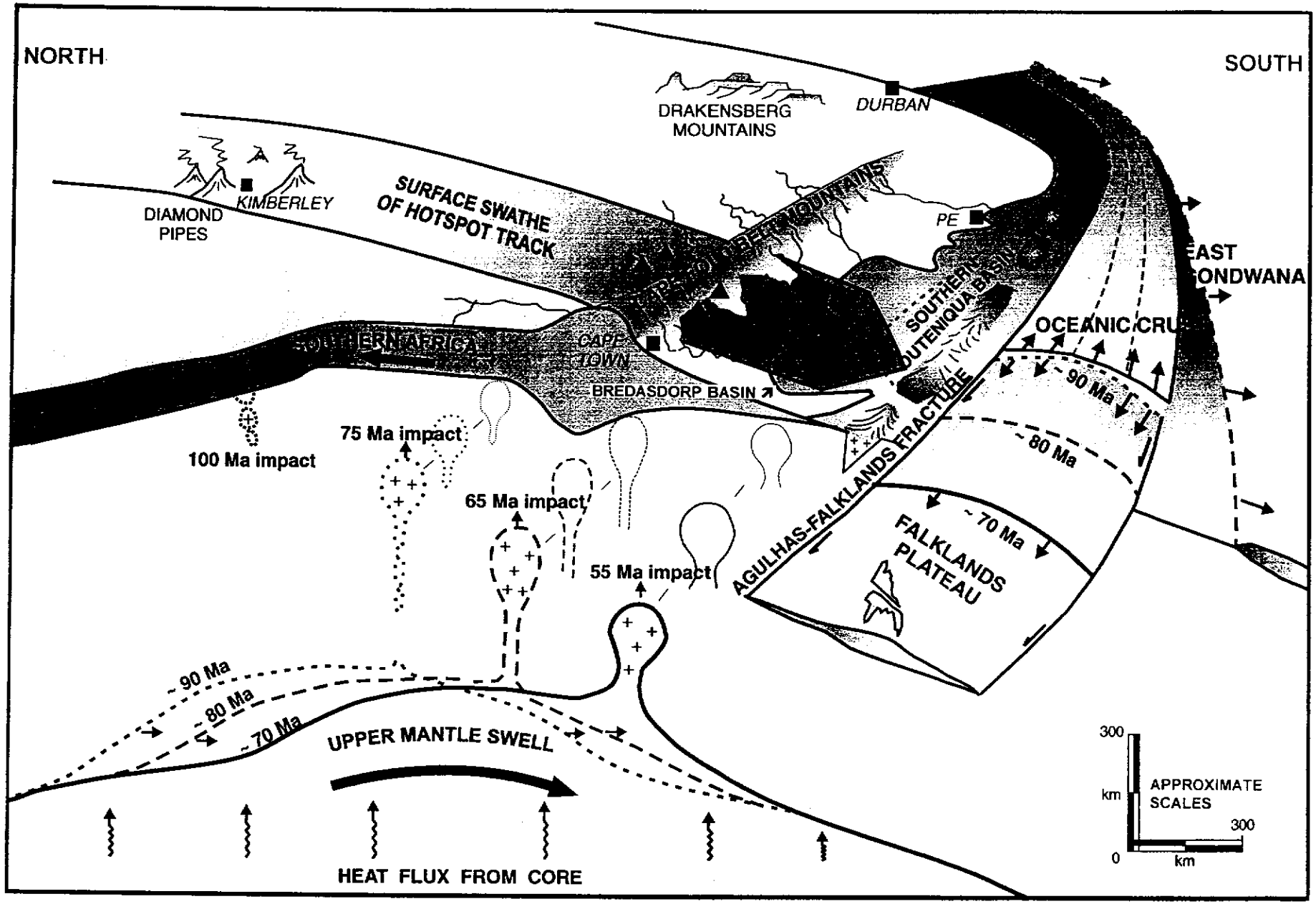

Figure 2.13: Schematic 3-dimensional cross-section showing interpreted plate and mantle swell motion and the extrapolated hotspot track during the period ~90-55 Ma relative to Southern African geologic features (Davies, 1997d).

(Davies and Van der Spuy, 1990 and 1992/93) is located on the track (Fig. 2.12). There are no known Tertiary intrusives in those wells but igneous bodies in one well, considered to be Early Cretaceous lavas, were dated at 32.8 ±2.6 Ma and 41.9 ±2.0 Ma (Kreuger, 1974; FM Consultants, 1974). These dates are thought to represent a period of late hydrothermal activity (DM Rowsell, unpubl. SOEKOR data, 1974) which supports the Mid-Tertiary track age. An alternate interpretation of these data suggests that this represents early sea-water ingress and alteration (Erlank et al., 1990). Yet if this were the case, the alteration must have happened at around the time of the final rifting in the area which is dated at 117,5 Ma (Valicenti and Broad, 1994) hence the date would be wrong.

In addition, (Martin, 1990, pers. comm.) speculated on the possibility of another bathymetric track through the southern part of the Orange Basin (Figs. 2.12) which may indicate another hotspot. If so, the dates of 37.6 ±1.1Ma for an alkaline phonolitic lava in the Ba-A2 well (FM Consultants, 1976) and 38.5 Ma from a melilite basalt plug near Garies (Kroner, 1973) confer a Mid-Tertiary age on this possible hotspot transit.

Approximately 10 Ma ago, a new swell, the 'African Superswell', formed in the mantle beneath Southern Africa (Nyblade and Robinson, 1994; Hartnady and Partridge, 1995). Heating effects of this swell seem to be slight because offshore wells in the eastern basins do not have higher geothermal gradients than in the Bredasdorp or Pletmos Basins (Davies, 1996e). Tectonic effects are, however, significant as the swell resulted in differential uplift of the eastern part of Africa of 700-800 metres (Hartnady and Partridge, 1995). The tilting is believed to have caused instability of slope sediments on the Agulhas Plateau resulting in the Agulhas Slump, and possibly the Chamais Slump on the west coast (Dingle, 1977). This tilting also caused the Agulhas-Falklands fracture ridge to founder (Fig. 2.14; Davies, 1996e). As a result, some 20 000km^3 of sediments slumped from the present-day shelf edge into the basin (Dingle, 1977). Most of these sediments remained within the Southern Outeniqua Basin but a proportion crossed the Agulhas Fracture Ridge and were deposited in the Transkei Basin (Dingle et al., 1987). The relevance of this slumping to hydrocarbon generation and migration in South Coast basins is discussed in Chapter 7.

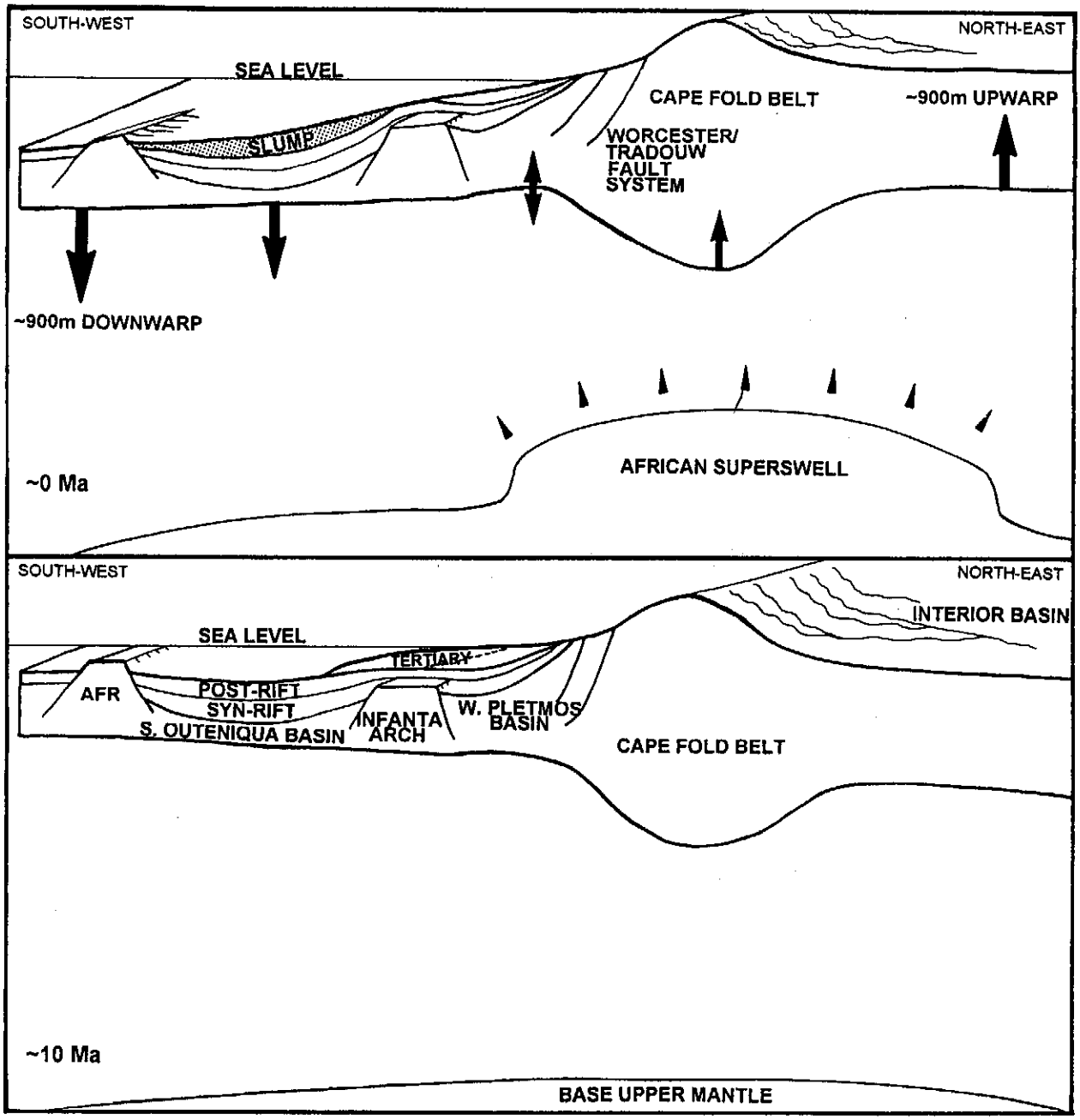

Figure 2.14: Schematic 3-dimensional cross-section showing the results of plate tilting (or buckling) during the initial period of development of the "African Superswell" (Hartnady and Partridge, 1995). The pre-slump Tertiary sediment wedge is shown at 10 Ma together with an approximation of the slump glide plane. The slump fill and localised downwarping of the Mesozoic sediments are shown at 0 Ma as well as the supposed wave-cut eroded surface of the Agulhas Fracture Ridge (after Ben-Avraham et al., 1993).

CHAPTER 3. GEOLOGY OF THE BREDASDORP BASIN

3.1. STRUCTURAL CONFIGURATION AND DEVELOPMENT

The Bredasdorp Basin is the westernmost of five south-easterly trending rift basins on the southern border of the African continent (Fig. 3.01). These basins comprise the greater Outeniqua Basin. This basin is arbitrarily divided in two at the 200 metre isobath - the inboard component is subdivided into four basins (Bredasdorp, Pletmos, Gamtoos and Algoa) whilst the outboard component is the Southern Outeniqua Basin (Fig. 1.02). The Bredasdorp Basin is underlain by metasedimentary rocks of the Palaeozoic Table Mountain and Bokkeveld Groups which also form the dividing highs (e.g. the Agulhas and Infanta Arches, Figs. 3.01; 3.02). The geometry of the basin follows the grain of the underlying Cape Fold Belt (Fouché et al., 1992) raising the possibility that structural control is related to reactivation of earlier lines of weakness. To the east, the basin is separated from the western part of the Southern Outeniqua Basin by a north-south lineation of early structural horsts (Roux, 1996).

Much of the tectonism affecting the basin after formation is attributable to differential plate motion during the separation of Africa and South America, the transit of the Bouvet/Shona hotspot and the initiation of the African Superswell.

3.1.1. Periods of tectonic adjustment

A phase of compression in the Mid-Jurassic, probably coincident with early separation of the Falklands Plate, affected all offshore basins (Van der Merwe and Fouché, 1992). It resulted in uplift and erosion of Palaeozoic metasediments, and extant Lower Mesozoic Karoo sedimentary rocks, Rowsell and De Swardt (1976). Later downwarp, associated with the initial southward propagation of the rift between East and West Gondwana along the East African seaboard, was initiated as early as Oxfordian based on palaeontological results (Barker et al., 1977a and 1977b).

The second phase of compression, during the Hauterivian, possibly related to impact of the Falklands Plate on the south coast of Africa, coincided with a major uplift and erosive event resulting in an angular unconformity at horizon 5At1 (Fig. 3.03).

The third phase of compression occurred shortly after deposition of the Albian 14A sequence (Van der Merwe and Fouché, 1992) and formed the central basin structural highs. This phase of compression is probably related to the passage of the eastern end of the Falklands Plate past the Agulhas Arch. Subsequently the basin subsided again, probably when the Falkland Islands finally cleared the southern tip of the Agulhas Arch (Honiball, 1995), and no further compressional events occurred.

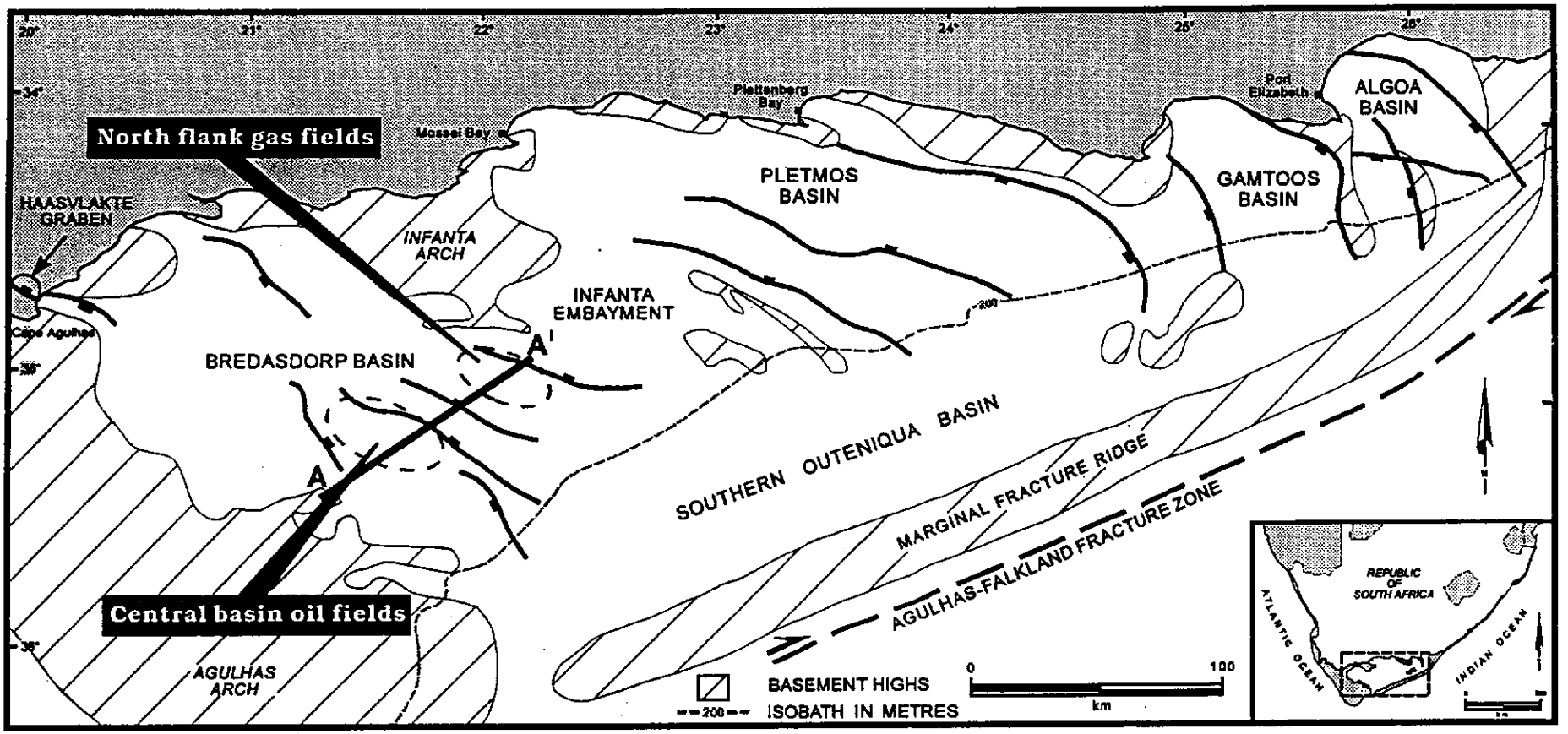

Figure 3.01: Cartoon map showing the disposition of the five South African offshore basins which comprise the greater Outeniqua Basin and their bounding faults and highs, the Marginal Fracture Ridge (MFR) and Agulhas-Falklands Fracture Zone (AFFZ) after Broad and Mills, (1993). The main hydrocarbon-bearing regions of the Bredasdorp Basin are indicated.

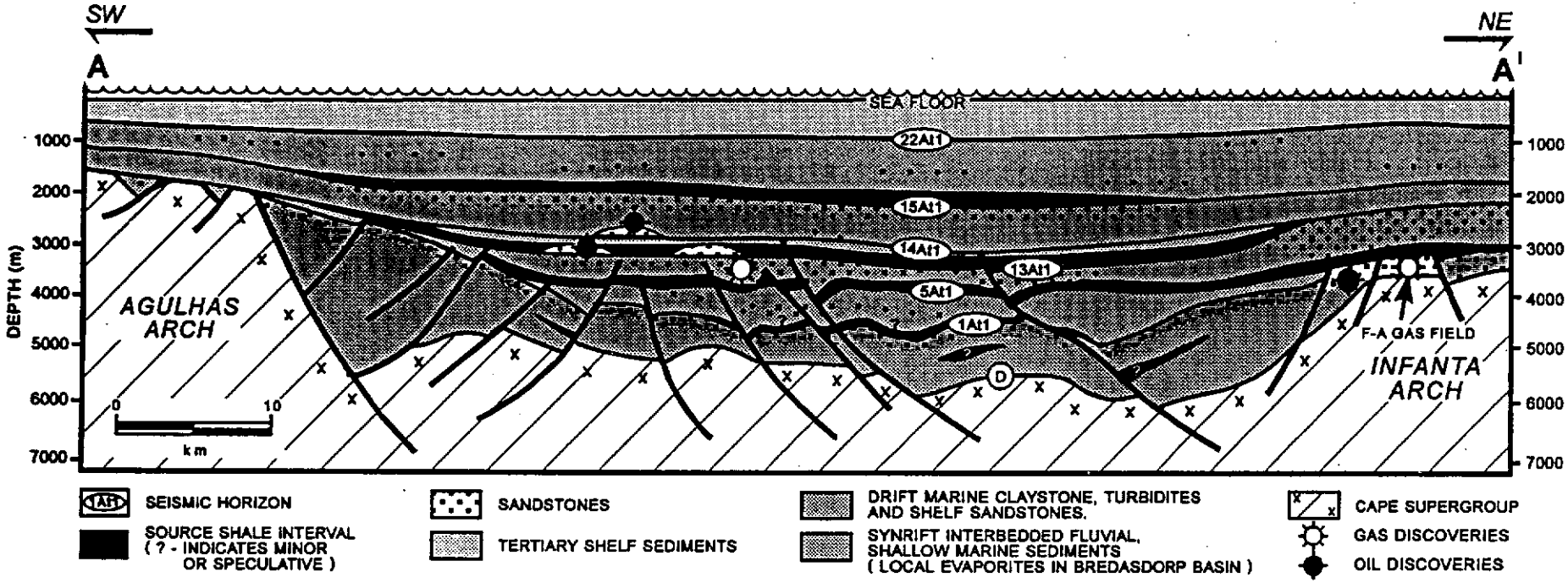

Figure 3.02: North-south cartoon section through the Bredasdorp Basin showing major faults, hydrocarbon and source rock distribution and major sequence boundaries. The location of the section line is shown in Figure 3.01.

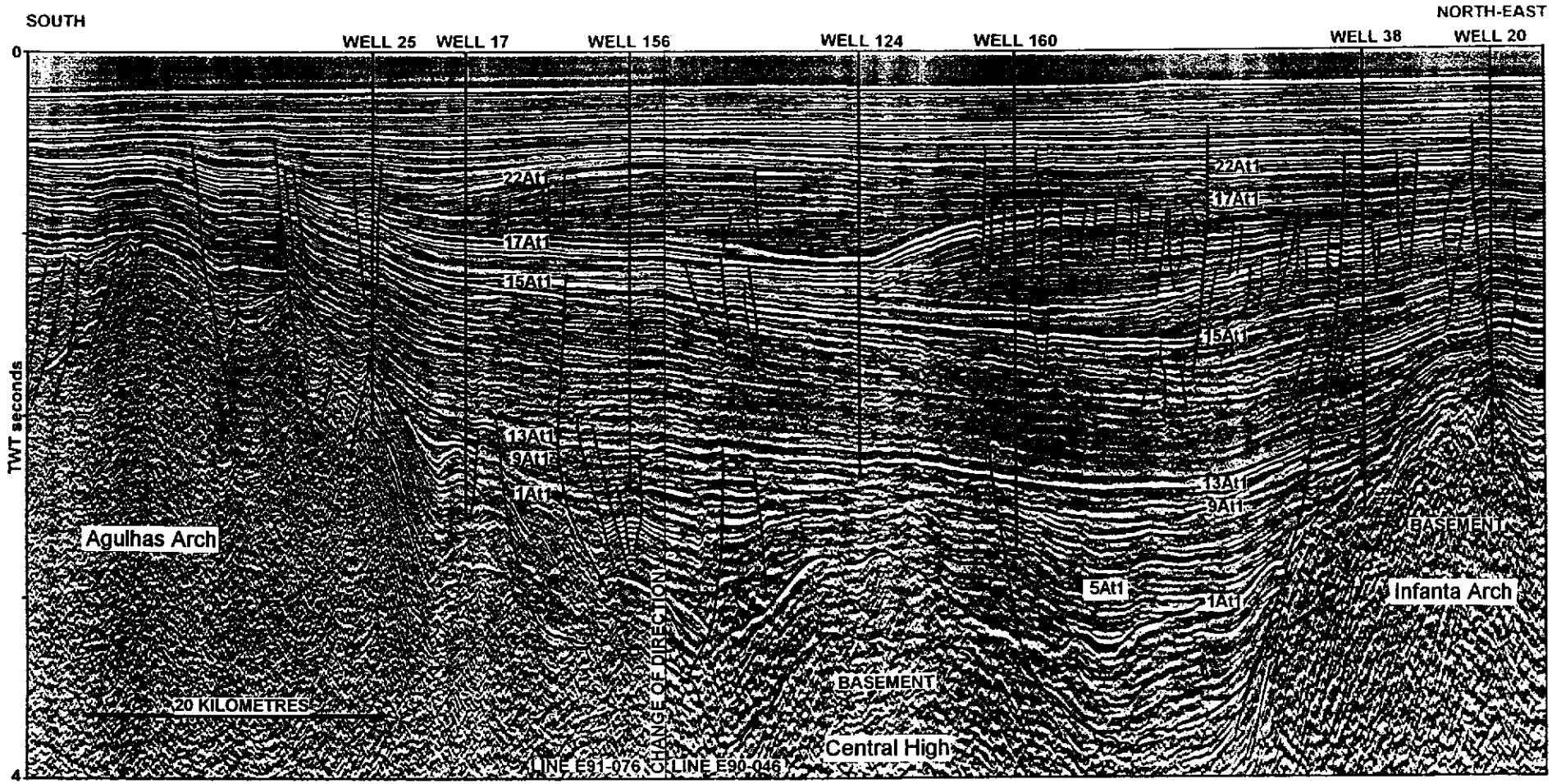

Figure 3.03: North-south seismic section across the Bredasdorp Basin showing the Agulhas Arch, the southern part of the Infanta Arch, the central basement high, the angular contacts at the 1At1 and 5At1 unconformity surfaces and the blanketing effect of the post-Barremian sediment cover.

The last major uplift of the Agulhas Arch started in Late Maastrichtian (McMillan, 1986) reaching a maximum of ~300 metres during the period 66-64 Ma, although the arch only became exposed during the Early Palaeocene (McMillan, 1986). This uplift, and associated erosion, were probably due to heat flux during passage of the Bouvet/Shona hotspot. A more detailed appraisal of the tectonic development of the basin is provided in McMillan et al. (1997).

A major uplift of the western end of the basin, evident from seismic data, reaches a maximum in the D-block wells where Cenomanian deposits are at the sea floor (Figure 8 of Brink et al., 1991) indicating probable erosion of >1000 metres. This uplift is thought to have been the result of mid-Oligocene tilting (McMillan, 1996, pers. comm.) but did not affect the central and eastern areas. Alternatively, the tilting may reflect initiation of the African Superswell (Hartnady and Partridge, 1995).

3.1.2 Faulting

Early rift-faulting during the period of formation of the Bredasdorp Basin resulted in a WNW-ESE parallel-sided graben with a number of marginal half-graben. This fault trend is most evident in the north and south flanks (Fig. 3.04). At the same time, in the eastern part of the basin, on both north and south flanks, as well as in the eastern central basin, a series of structural highs developed (Friedinger, 1988; Roux, 1995; Pferdekämper, 1996, pers. comm.). These highs include all the eastern highs (wells 10, 12, 13, 24 and 47) and the high immediately to the south-west (wells 9, 11. 14 and 17) (Fig. 2.10). The regional WNW-ESE fault trend is modified in the Bredasdorp Basin (and indeed in other south coast basins) by trending NW-SE at the western and eastern ends (Fig. 3.04). All these similar fault trends are considered to be due to drag along the Agulhas-Falklands Fracture Zone (Du Toit, 1976; Fouché et al., 1992) or to inherited Cape Fold Belt faults (Cartwright, 1989) or possibly to 'tension gash' style faulting (Cartwright, 1989; Malan et al., 1990).

Some of these faults are thought to have rejuvenated at 5At1 times (Late Hauterivian, ~118 Ma) as many extend to this surface. Details of these movements are given in Jungslager (1996). Some of the faults have been rejuvenated much later and extend to 9At1 (Hodges, 1996), probably representing a combination of compactional drape over the central high and Albian compression, and locally even into the Tertiary (Strauss and Noble, 1996) (Fig. 3.05). These faults have been suggested to be conduits for gas migration into those wells from deeper in the succession (Davies, 1996c). Indeed, in the western part of the basin, in the area of well 16 and particularly near well 3, sea-floor steps and ridges are evident on seismic lines which may be surface manifestations

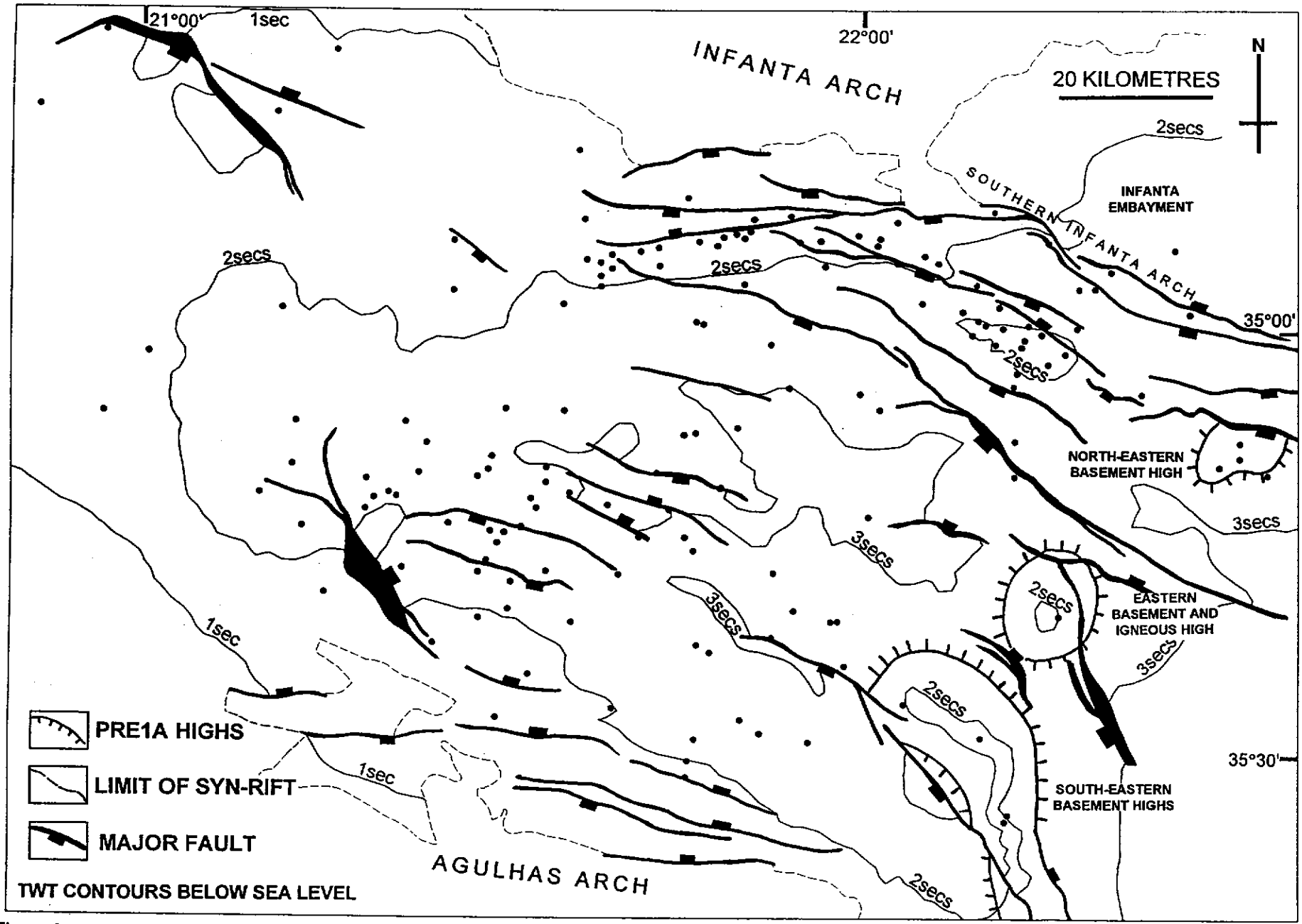

Figure 3.04: Map of two-way time (TWT) to horizon 1At1 in the Bredasdorp Basin showing the disposition of major faults, the region of thickest syn-rift graben fill and the location of the eastern basin highs.

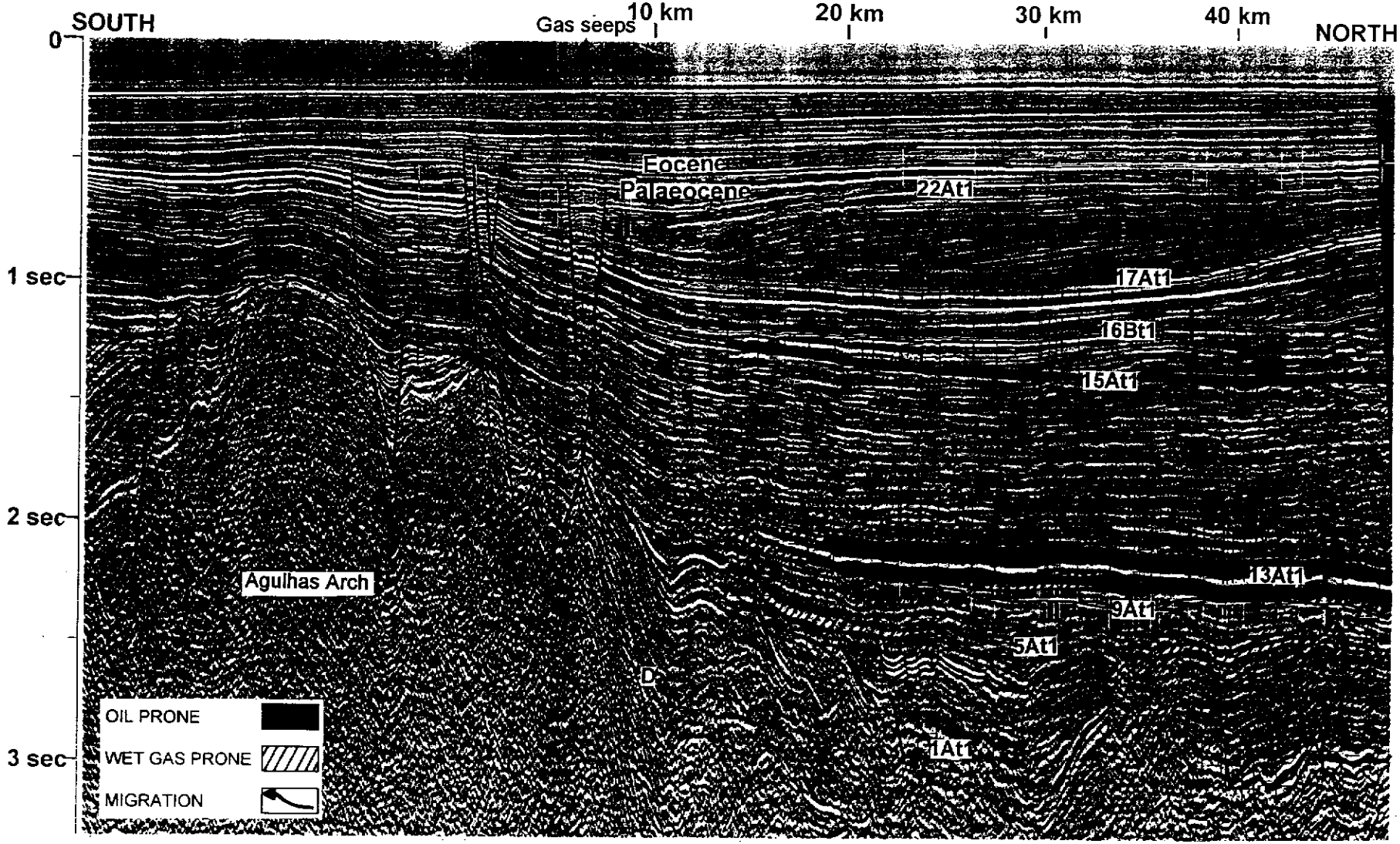

Figure 3.05: Seismic section across part of the southern flank of the Bredasdorp Basin showing rejuvenated mid-Cretaceous faults extending into Palaeogene sediments. Sea floor gas seeps, recorded during the 'Sniffer' survey (Davies, 1988b) provide evidence that gassy hydrocarbons, possibly generated in local source rocks, migrate updip to the faults and thence to surface.

of very shallow faults. However, few faults smaller than ~10 metres are seismically mapped because they cannot be effectively imaged. Hence most of the faults which intersect the sea floor cannot be mapped at depth.

On the north flank, a few faults extend shallower than 6At1 (Latest Hauterivian) but none appear to reach the Tertiary. The most readily mappable of these faults is in the area of well 78 due north of the E-M structure. The presence of apparently bacterially degraded oil in syn-rift sandstones downdip of the fault intersection may be evidence that the fault allowed the ingress of fresh, oxygenated water. There is, however, no evidence of a step in the sea floor although the movement may have been too small (<2 metres).

In general, although the basin has been extensively faulted during at least three episodes in the Late Jurassic, Early Hauterivian and Barremian, (syn-rift, 5At1 and post 9At1 times) and there are also faults which appear to be related to an inherited Cape Fold Belt trend, there are essentially only four main fault regions. These four regions all have similar trends i.e. W-E to NW-SE:

1. south flank essentially between wells 16 and 9, downthrowing north and north-east
2. north flank essentially between wells 46 and 1, downthrowing to the south
3. central basin near wells 96 and 163, forming a deep-seated horst block
4. north of the central basin between wells 46 and 8, downthrowing to the south (this fault acts as the main pressure boundary between high pressure 9A sandstones to the south and low pressure 1A-10A sandstones to the north).

The hydrocarbon migration effects of these four fault trends are discussed later.

3.2. SEDIMENTATION

The pattern of sediment distribution in the Bredasdorp Basin has been broadly controlled by global sea level changes (Haq et al., 1987) superimposed on regional tectonism. Since some of these sediments are potential source rocks for hydrocarbons and others are possible reservoir rocks, the tectonic control on the sediment distribution is of importance. The developing Mid-Late Jurassic rift created accommodation space for fluvial sedimentation. Intersections of up to 900 metres of largely fluvial sandstones and claystones have been made in wells around the margins of the Bredasdorp Basin. There is only one intersection of these sediments in the basin centre as only that well (no. 160) was targeted at the break-up unconformity (horizon 1At1) - elsewhere it is far below the temperature limit for oil preservation (Figs. 3.06 and 3.07). Basement rocks too, have only been intersected by a few wells around the edges of the basin and in each case, seismic data suggest great thicknesses of pre-rift sedimentary rocks were eroded during this period (Du Toit, 1976).

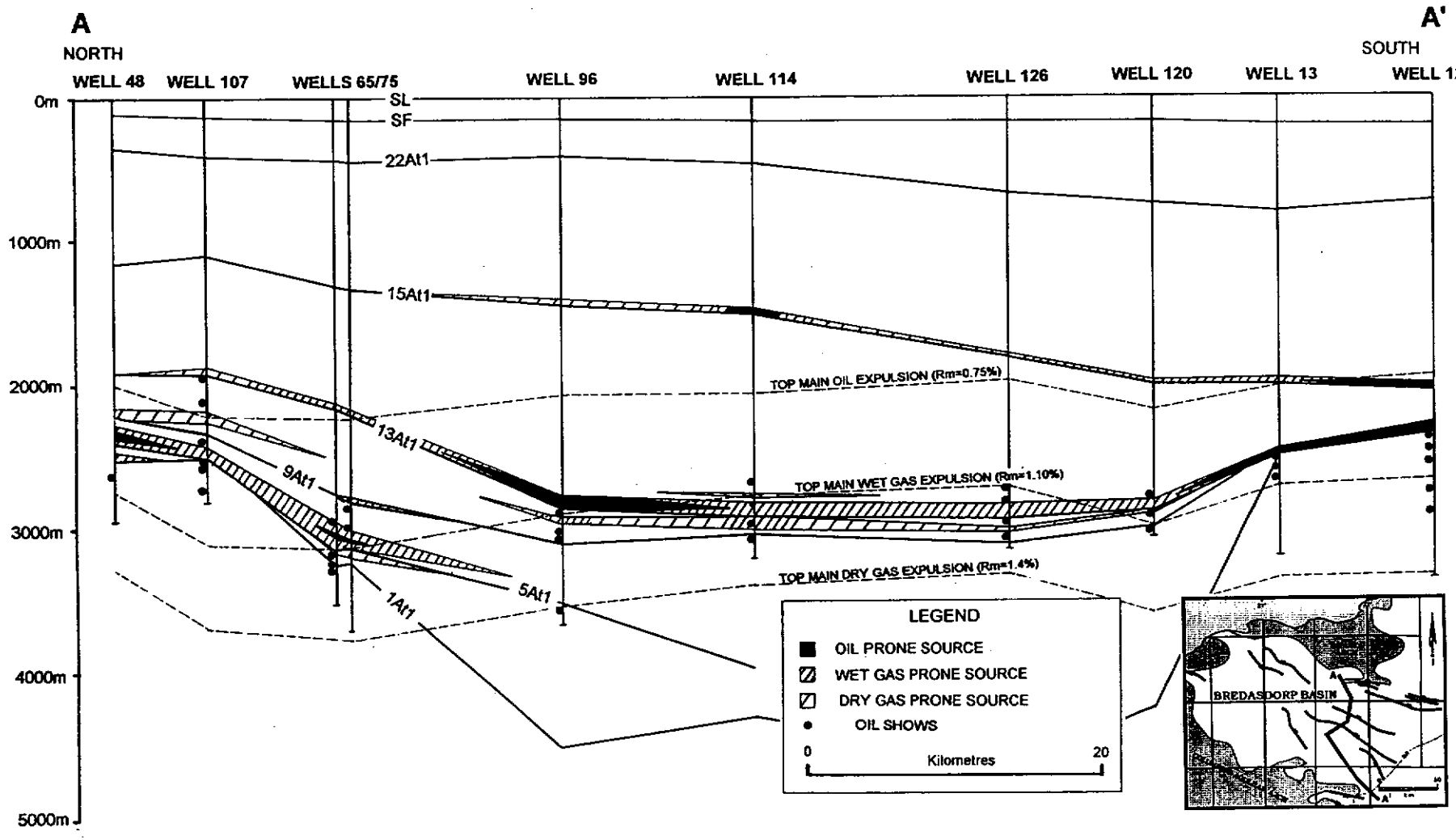

Figure 3.06: Scaled N-S section-line across the Bredasdorp Basin through wells used in this study showing the distribution of source rocks, oil shows and maturity windows and the disposition of the major sequence boundaries.

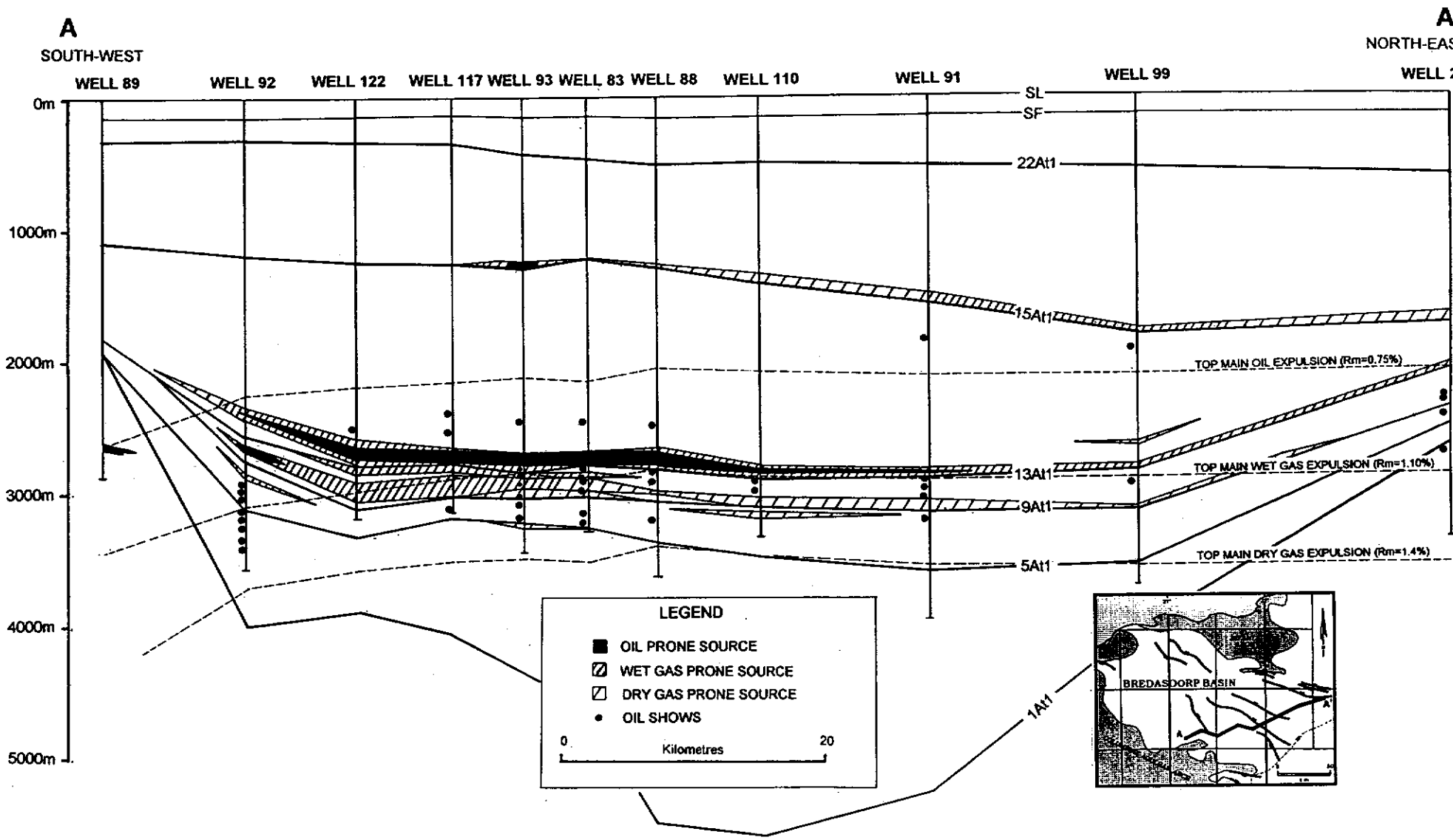

Figure 3.07: Scaled southwest-northeast section-line across the Bredasdorp Basin through wells used in this study showing the distribution of source rocks, oil shows and maturity windows and the disposition of the major sequence boundaries.

3.2.1. Syn-rift period, Jurassic-to-Earliest Cretaceous

Early sedimentological studies subdivided post-Palaeozoic metasediments into four main intervals of non-marine deposits separated by major erosive unconformities (Du Toit, 1976) (Table 2.03). The non-marine Kirkwood, Infanta and Enon Formations (collectively known as the Pre-Sundays River sequence) were stratigraphically defined in the onshore Algoa Basin and interpreted as Lower Cretaceous (Du Toit, 1976) or Upp0er Jurassic-Uppermost Cretaceous (McLachlan and McMillan, 1979). These intervals were deposited during the pre-rift period. The Lower Sundays River Formation extended from the pre-rift sedimentary rocks up to the onset of drift, horizon C≡1At1 (Du Toit, 1976 and Burden, 1992). This formation comprises transitional-to-shallow marine sedimentary rocks. The distribution of the pre-Sundays River rocks has been tentatively extended into the offshore basins and time-equivalent intervals have been intersected in the Bredasdorp Basin. These formations separate the Devonian and older basement rocks from the Cretaceous marine sedimentary rocks.

Continuation of the rift caused increased sag which resulted in the lowering of base level in the Bredasdorp Basin causing fluvial systems to locally pond, resulting in the formation of lakes. Shaly and silty intervals containing freshwater fauna (e.g. carophytes) were found in a few wells and are considered to indicate a nearby lacustrine environment (Valicenti, 1995, pers. comm.). Thin (<30m) Early Tithonian (?Kimmeridgian) lacustrine shales with local oil source potential, are found in one well in a marginal half-graben in the Bredasdorp Basin and another well (DWK-1) in the coeval onshore Haasvlakte Graben (Davies et al., 1991). The source potential is variable but locally very high, as seen in the type intersection for Late Jurassic lacustrine source rocks, the Colchester shales of the onshore Algoa Basin (McLachlan and McMillan, 1979). However, well 89 did not continue deep enough to establish the overall thickness of these sedimentary rocks. In addition, their presence elsewhere in the area has not been confirmed largely because most wells did not penetrate deep enough.

It is likely that lacustrine shale development in the Bredasdorp Basin is not as sparing as these few intersections show and could be similar to the distribution of coeval sedimentary rocks in the Springhill Formation, Magellanes Basin, South America (Biddle et al., 1986; Maslanyi et al., 1992) i.e. in the basal parts of most marginal half-graben.

3.2.2. Evaporites

Well 16 drilled into a small sub-basin in the western part of the basin and intersected a 409 metre thick interval of red siltstones and claystones thinly interbedded with halite-

rich sediments. A total of 53 individual salt layers up to several metres thick in places were found, totaling ~209 metres, although more may be present as seismic data show that the interval continues below TD (Fig. 3.08). Salt swells are evident on seismic lines throughout this region. Evaporites are unexpected because Southern Africa was located further south (~55°S) during the Earliest Cretaceous (Dingle et al., 1983; Lawver et al., 1992) and from the present day climatic regime (cool and moist) formation of evaporites is unlikely. However, warm water ostracode species found in sediments of similar age in the onshore Algoa Basin, indicate that the water temperature was higher than today implying significantly warmer weather (Valicenti and Stephens, 1984). These warmer conditions may have been a consequence of the higher proportions of CO_2 interpreted to characterise the Mesozoic atmosphere and which resulted in the development of 'greenhouse' conditions (Barron and Moore, 1993; Larsen, 1991).

It is thought that this evaporite-bearing sub-basin was located close to the palaeo-coast-line and filled with sea-water each time the barrier between it and the sea was breached - most likely during periodic highstands. Log data (Fig. 3.09) show the thickness of the salt layers to vary between 1-8 metres with a mean of 3.5 metres (Fig. 3.10). Evaporation of a 220 metre column of present-day sea-water is required to deposit this average thickness of salt, although the actual thicknesses of salt layers most probably reflect frequent fill and evaporation episodes – enhanced by intermittent tectonism. After each major tectonic deepening event, the basin gradually filled with both salt and sediments reducing the accommodation space. Hence salt layer thicknesses progressively decrease (Fig. 3.10). These sediments are time-equivalents of 3rd order transgressive and highstand portions of the earliest Valanginian LZB 2.1 sequence (Haq et al., 1987 and Valicenti, 1995, pers comm.) and represent some 60% of the sequence duration, i.e. ~1.9-2.1 Ma. Hence each average salt layer could equate to a period of ~40000 yrs. This time interval could differ if the salt layers resulted from partial or multiple fill and evaporation episodes as shown for Messinian salt layers in the Mediterranean (Butler et al., 1995). This figure is close enough to the accepted average period of global orbital obliquity (Hays et al., 1976; Heckel, 1986; Smith, 1990) of 41000 yrs to tempt comparison. Elsewhere in the basin, high gamma claystones are thought to characterise equivalents of these highstands, e.g. in wells 65/75 (Valicenti, 1995, pers comm.).

3.2.3. Syn-rift period, Early Cretaceous

Regional relative sea level rise in the Early Valanginian brought an extensive marine incursion into the Outeniqua Basin and with it a diachronous coastal environment which transgressed the region. Littoral, shallow marine and marine glauconitic sandstones up to 100-200 metres thick, the latter originally interpreted to be lag sands, were deposited

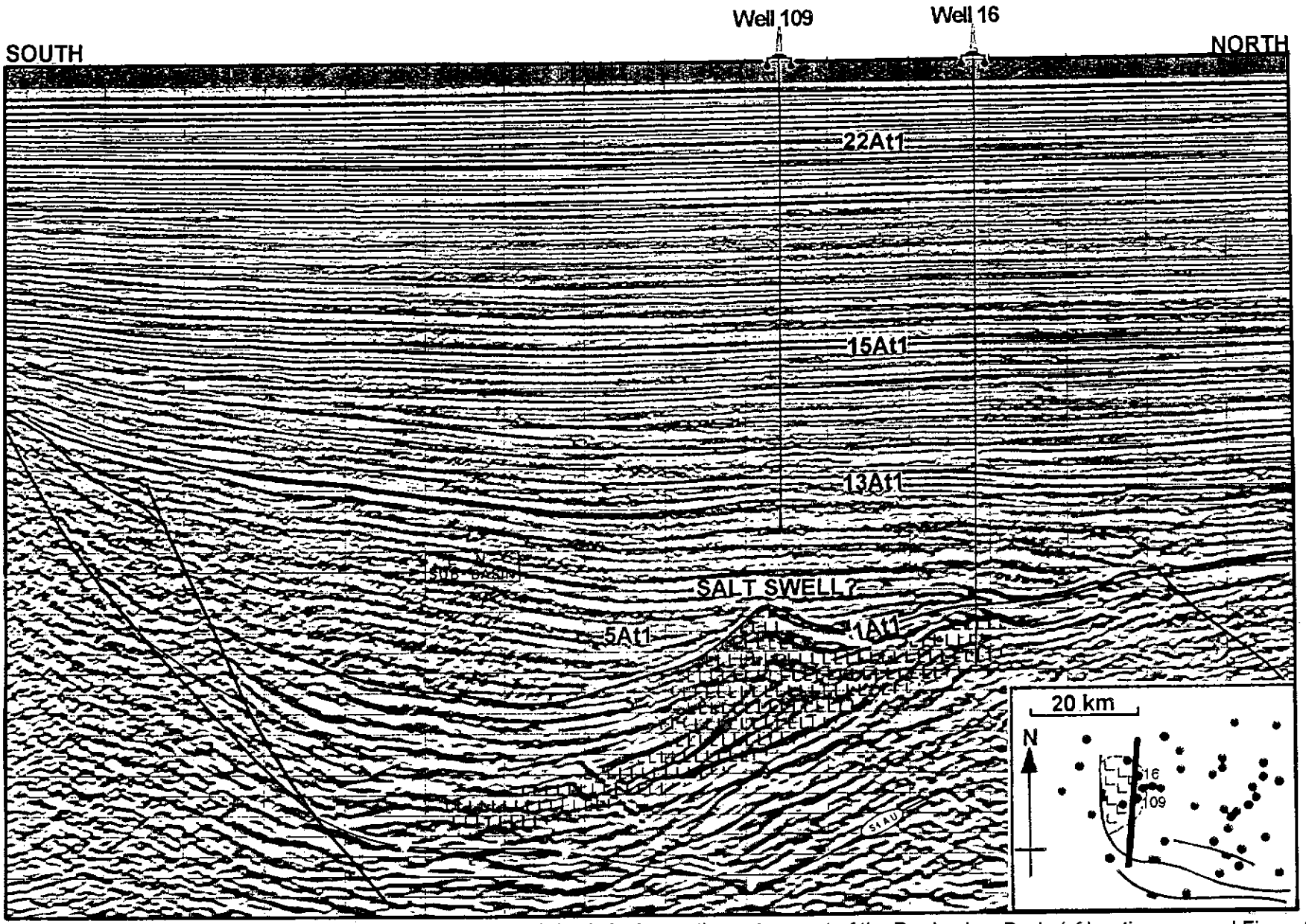

Figure 3.08: North-south seismic line through the evaporite-rich sub-basin in the south-western part of the Bredasdorp Basin (cf location map and Figure 2.05). Well 16 intersected a halite-bearing interval >400 metres thick. The nearby (possible) salt swell (below well 109) is considered to have formed just prior to the localised sand deposition at the 13At1 surface in which oil is reservoired because there is no thinnning evident above the 13At1 surface but there is below.

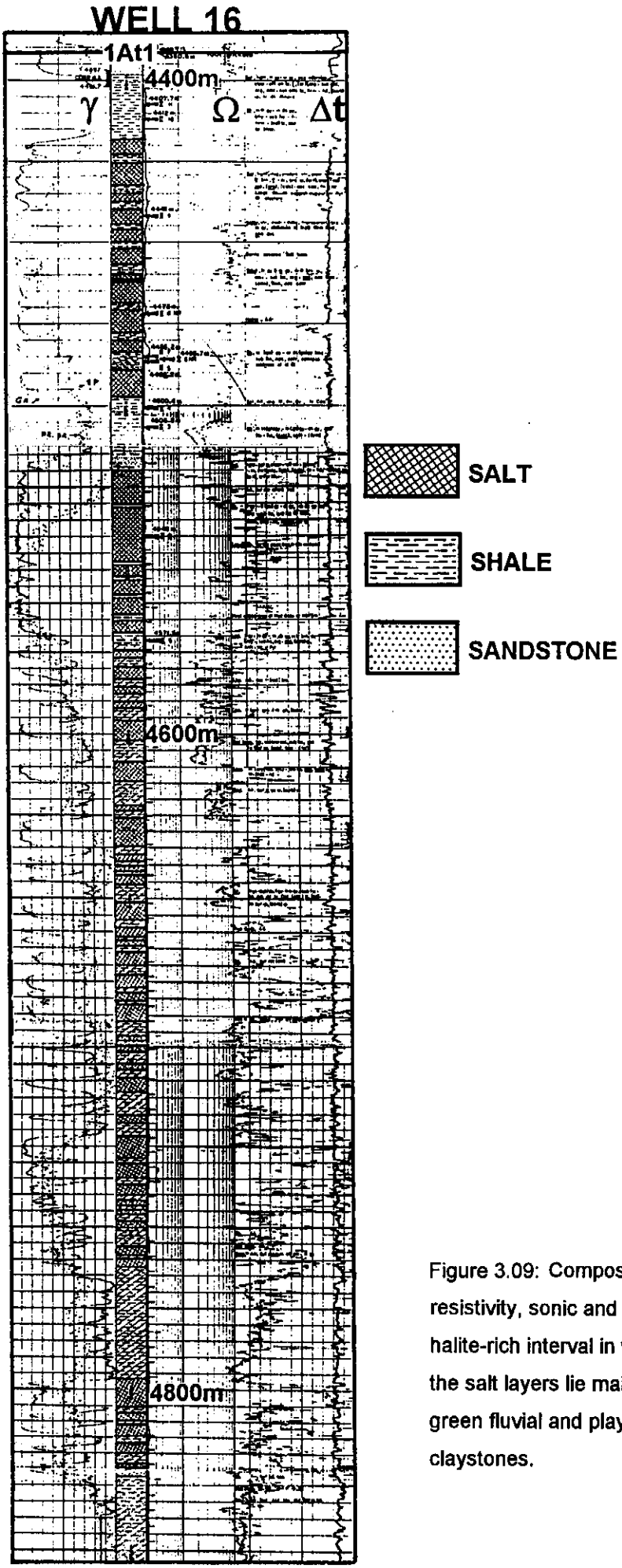

Figure 3.09: Composite log (gamma, resistivity, sonic and lithology) of the halite-rich interval in well 16. Between the salt layers lie mainly red and green fluvial and playa lake silts and claystones.

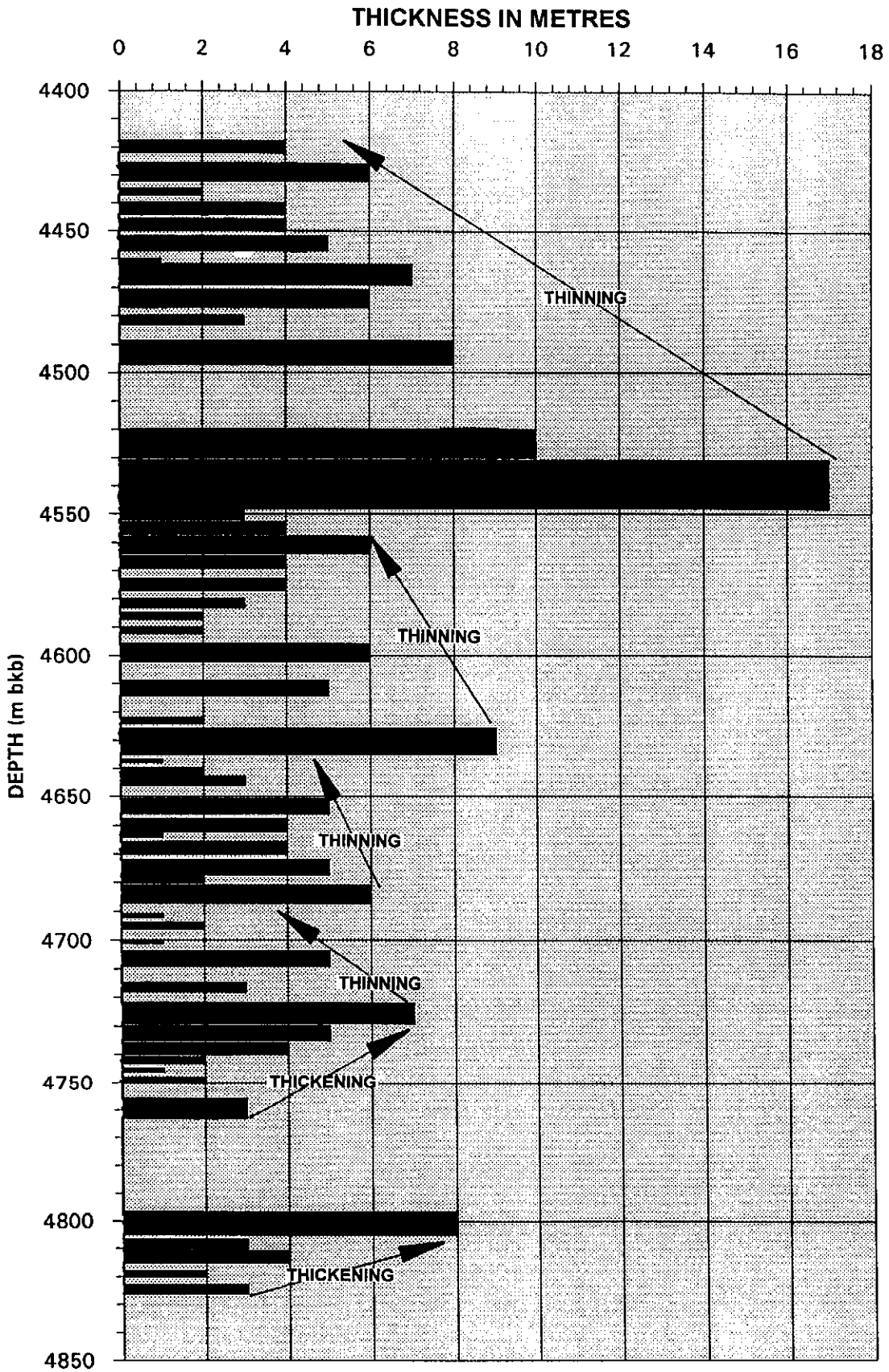

Figure 3.10: Bar chart diagram of the interval of sediments in Figure 3.09 showing the distribution and thickness of individual log-defined halite-rich intervals. There are major upward-thinning intervals with bases at 4540m, 4630m, 4685m and 4730m and thickening-upwards intervals with bases at 4760m and 4830m.

(Du Toit, 1976). Recent studies show that they represent the earliest phase of marine incursion during the final stages of rifting and sag (Valicenti and Broad, 1994 and McMillan et al, in press). Indeed, the most recent biostratigraphic interpretations place the 1A type 1 unconformity (1At1) at the base of these transgressive coastal sandstones rather than the top (Valicenti, 1995). However, the top of these sandstones is still called 1At1 for purely descriptive reasons. As the transgression continued into the western Bredasdorp Basin, the coastal sands were in turn overlain by basin-wide deep marine infill sediments of the Upper Sundays River Formation which encroached from the east. The contact is diachronous (Valicenti and Broad, 1994).

3.2.4. Post-rift period, Mid-Cretaceous

Subsequent sea level rise resulted in the establishment of open marine conditions in the basin which prevailed to the Albian. Sediments deposited during this episode were shelf and slope shales and silts but several persistent channelised sandstones have been identified. These sandstones are important petroleum migration conduits. The upper boundary of the Upper Sundays River Formation, seismic horizon A≡E≡13At1 (Du Toit, 1976; McLachlan and McMillan, 1979; Burden, 1992) also marks the base of the Agulhas Formation (cf. Table 2.03 and Fig. 2.06).

Dominantly argillaceous marine sedimentation continued in the Lower Agulhas Formation deposits until global lowering of sea level in Early Albian (14At1) resulted in a major erosive period when the shelf edge was dissected by submarine canyons. These canyons subsequently filled with further channelised sandstones which are important oil reservoirs. Sediments in the 1At1-to-13At1 interval belong to the Upper Sundays River Formation

3.2.5. Cretaceous sequence stratigraphy

Recent seismic studies of marine Cretaceous sediments (Van Wyk, 1990; Brown et al., 1995) saw the application of sequence stratigraphic concepts to the Bredasdorp Basin. A sequence is defined as 'a relatively conformable succession of genetically related strata bounded by unconformities and their correlative conformities' (Vail et al., 1977). Benefits of this interpretation method are the ability to predict lithology, particularly that of reservoir quality sandstone, and the basin-wide correlation of sedimentary units. After the sequences in the Cretaceous had been fully delineated, the success rate of the technique for lithological prediction was evaluated by Brown and Doherty (1992). They showed that the ability to predict the continuation of individual units across the basin was high by comparison with the results obtained from previous facies correlation methods. Results from drilling confirmed the predicted depositional system in 75% of all cases although only approximately 50% of predicted lithologies were found.

The application of the method resulted in the basin-wide correlation of 22 Cretaceous third-order sequences, each bounded by type 1 unconformity surfaces (Van Wyk, 1990). Such surfaces (labelled 't1') are considered to reflect sea level fall below the shelf break (Vail, 1987) and so indicate episodes of shelf edge erosion (Fig. 3.11). Individual sequences have been established from seismic and borehole data. Precise ages of sequences and their boundaries, based on biostratigraphic information (using palynological, ostracode and foraminiferal datings), match the major sequence boundaries of Haq et al. (1987). Their basin-wide definition has allowed the construction of detailed distribution and isopach maps for the 14A sequence (Benson et al., 1993 and Wickens, 1993), the 13A sequence (Brink et al., 1991), the 9A-12A sequences (Smit, 1992) and 1A-8A sequences (Burden and Gasson, 1992). The studies also confirmed that the stratigraphic subdivision of the Sundays River Formation of Du Toit (1976) (Table 2.03) was essentially valid but too imprecise for current detailed exploration work. Therefore horizon correlations used in this report all reflect the sequence stratigraphic concept.

Each sequence commenced with deposition of isolated or amalgamated lowstand fan deposits on the unconformity surface (Van Wyk, 1990). These deposits are inferred to be connected by channels to submarine canyons incised into the previous shelf. Seismic evidence of shelf-edge canyons and the channels themselves is largely lacking - perhaps because of their small size and lack of lithologic contrast - although recent developments in seismic continuity mapping show some features which could be channels (Barton and Grobbler, 1997). Many of the clastic sediments derived from onshore are polycyclic and where reworked, especially into lowstand deposits. They generally comprise fine sandstones and silts. Occasionally, however, coarse material was transported into the basin. Examples of these deposits are found in the basin floor sandstones of the 14A sequence which form the reservoir facies for some of the oil reservoirs sampled for this study (Wickens, 1993). In general, sandstones nearest the shelf are poorly sorted and characteristic of mass-flow deposits (Gilbert, 1990) but more distally they are well-sorted and channels and lobes dominate (Beamish, 1990).

One important consequence of the continued and extensive transgression is that the central part of the basin became progressively sediment starved - typified by thinly bedded pelagic, organic-rich shales draped over the basin floor fans (Fig. 3.11). At the time of greatest landward transgression (13A mfs), these shales are characterised by maximum sediment starvation i.e. greatest concentration of fauna (especially radiolaria), maximum preservation of organic matter and lowest oxygen contents (McMillan et al., 1997). Development of oil-prone source rocks in the 13A sequence is considered to be an example of this process (Demaison et al., 1988). Shelf progradation or aggradation, following the period of highstand sedimentation,

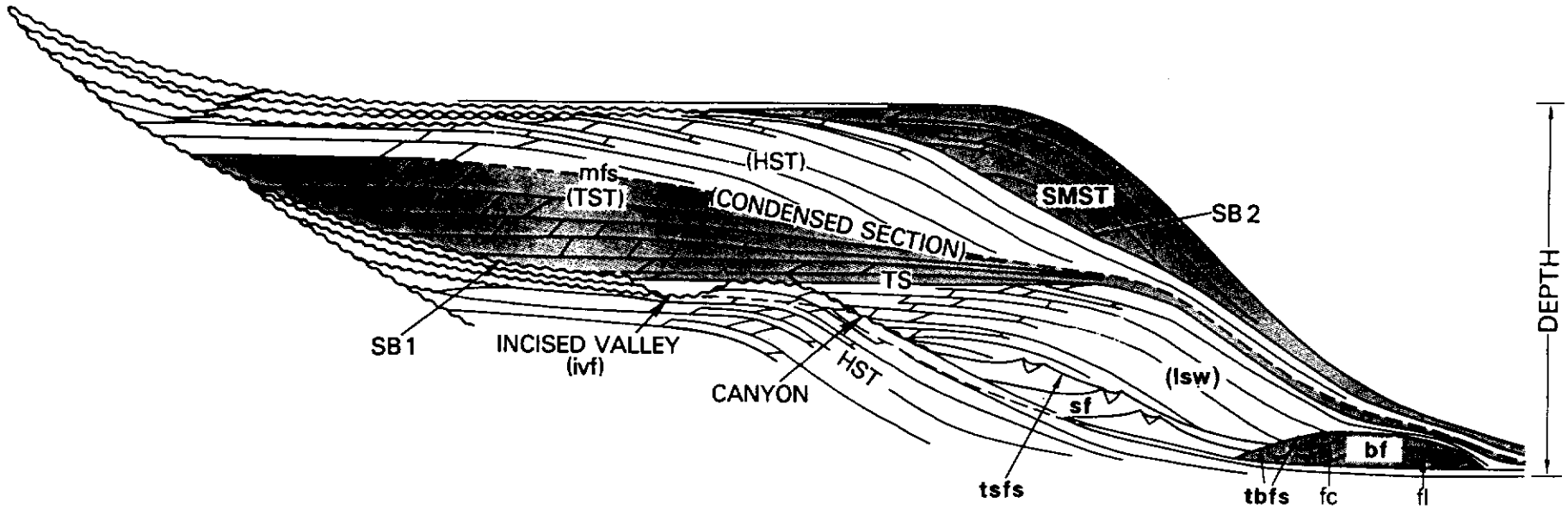

LEGEND

SURFACES

(SB) SEQUENCE BOUNDARIES
- (SB 1) = TYPE 1
- (SB 2) = TYPE 2

(DLS) DOWNLAP SURFACES
- (mfs) = maximum flooding surface
- (tbfs) = top basin floor fan surface
- (tsfs) = top slope fan surface

(TS) TRANSGRESSIVE SURFACE
- (First flooding surface above maximum progradation)

SYSTEMS TRACTS

HST = HIGHSTAND SYSTEMS TRACT

TST = TRANSGRESSIVE SYSTEMS TRACT
- ivf = incised valley fill

LST = LOWSTAND SYSTEMS TRACT
- ivf = incised valley fill
- lsw = lowstand wedge-prograding complex
- sf = lowstand slope fan
- bf = lowstand basin floor fan
  - fc = fan channels
  - fl = fan lobes

SMST = SHELF MARGIN SYSTEMS TRACT

Figure 3.11: Diagrammatic section showing the cyclicity of sequence stratigraphy tracts in depth and their terminology (after Vail, 1987).

accompanied a return to oxygenated conditions, and resulted in dilution of faunal concentrations and decreased preservation of organic matter in shales. Associated deltaic systems, rich in clastic debris, advanced into the basin and deposited extensive, mainly fine-grained, sandstones across the shelf edge. Eventually these systems advanced across the pre-existing shelf edge and onto the slope following discreet channels as in the present day Mississippi delta. Depending on distance from the sediment source, these resulting deposits can be fine-grained (as in the 9A-10A sandstones) or relatively coarse (as in the 14A channel sandstones).

3.2.6. Post-rift period, Late Mid-to-Late Cretaceous

Environments of deposition prevailing through the later part of the Cretaceous were dominated by gradual cooling from 'greenhouse' conditions (Veevers, 1990; Barron and Moore, 1993; Larsen 1991) and a long period when temperate conditions dominated. Deposits during this period are dominated by relatively high energy sedimentary rocks (sandstones and siltstones) and only occasional shales indicative of erosion of pre-existing sediments. The greater rate of sediment input (from burial history diagrams in Chapter 7) reflect the wetter climate and elevated hinterland topography. The remainder of the Cretaceous comprises the clastic-rich later parts of the Agulhas Formation and is separated from the overlying carbonate-rich Tertiary Alexandria Formation by the basal Palaeocene unconformity horizon L≡22At1 (Du Toit, 1976; Burden, 1992).

Completion of separation between Africa and South America in the Early Turonian allowed the establishment of open marine circulation between northern and southern hemispheres throughout the Atlantic. This resulted in changed global oceanic circulation (Arthur et al., 1987; Schlanger et al., 1987; Zimmerman et al., 1987) which is inferred to have initiated the formation of locally anoxic bottom waters and caused the deposition of thin, but persistent, organic-rich shales in the 15A sequence. These constitute a regional source rock overlying the 15At1 unconformity. Matching sediments are found in wells in the offshore Gamtoos and Pletmos Basins and in many wells on the west coast of South Africa, although without the rich source potential of the Bredasdorp Basin. Climatic changes culminated in cooler conditions in the Campanian and Maastrichtian (Huber and Watkins, 1992). These sedimentary rocks contain significant amounts of calcite, mostly in the form of abundant inoceramus spines, reflecting the change to cooler water.

3.2.7. Post-rift period, Tertiary

Palaeocene and Eocene sedimentary rocks comprise about two-thirds of the preserved Tertiary thickness and well data indicate a nearly complete succession. These rocks are typically carbonate-dominated (marls, limestones and chalks) but can be locally

silty. The high carbonate content was largely due to regionally increased water temperatures, perhaps as a result of the initiation of the Agulhas Current (McMillan, 1986; O'Connell et al., 1996). Indeed, local coral reefs may have developed, particularly where the warm Agulhas Current impinged on the shelf. Oligocene and Miocene rocks, where studied, are thinly laminated, frequently interrupted by hiatuses and comprise less than one-third of the Tertiary thickness. They tend to be even more calcite-rich than the Lower Tertiary rocks and limestones and calcretes abound. Pliocene deposits are rarely recorded because of lack of sampling, but are essentially a continuation of the largely biogenic sedimentation of the Late Tertiary.

Tertiary sedimentary rocks rarely exceed 300m in total thickness except in the easternmost part of the basin where thicknesses of 500m are attained (Petrie, 1996). The apparent thickness of Tertiary rocks in the adjacent western part of the Southern Outeniqua Basin is much greater and locally reaches 1000 metres (Wenham et al., 1991). No biostratigraphic studies have been carried out in the basin centre but seismic data show that the Tertiary rocks are not significantly thicker there. Unfilled and uncompacted foram tests, including many in which the aragonite has yet to convert to calcite, are common in Oligocene and later deposits (McMillan, 1989 and 1996, pers. comm.) and attest to maximum burial depths of little more than a few hundred metres.

During the Tertiary, the basin experienced three periods of widespread sea-level lowstands during the Earliest Palaeocene, Mid-Eocene and Late Oligocene. There is biostratigraphic evidence of only small amounts of erosion during each event (Burden, 1992; McMillan, 1994, pers. comm.) totalling <~200 metres.

From seismic evidence, Tertiary sedimentary rocks basinward of the most distal Bredasdorp Basin wells (e.g. well 149 in 251m water) are probably similar, i.e. muds, marls, limestones and occasional chalks (Dingle et al., 1983). SOEKOR evidence from the distal wells (McMillan and Valicenti, 1986; McMillan, 1995, pers. comm.) suggests a shelfal environment for those rocks in ~100 metres water. The rapid bathymetric increase just seaward of these wells places these rocks in water up to 700-1000 metres deep implying considerable subsidence since deposition (Fig. 3.01).

3.3. IGNEOUS

The Bredasdorp Basin is characterised by two areas, some ~80 km apart, where essentially coeval Tertiary igneous intrusive bodies (plugs, dykes and sills) are found (Fig. 2.09). They are considered to have formed during the Late Cretaceous-to-Early Tertiary hotspot transit. Where individual intrusions are intersected by boreholes they are seen to be small, metres to tens of metres, (Broad and Turner, 1982). Where

inferred from seismic data they appear larger but this is probably an effect of the aureole or alteration halo (Fig. 3.12). The intrusives in the eastern region are a mixture of lamprophyres and carbonatites (Rowsell et al., 1979). Such material is known to contribute very little heat to the host rocks (Tarling, 1973). This reduced thermal effect, combined with their individually limited areal extent, means they make little contribution to the thermal maturity in the area. However they are a manifestation of a more regional heating event, the mantle swell and hotspot transit, which affected the whole basin. Confirmation of this more regional heating comes from palaeotemperature data from the centre of the basin (well 96, Fig. 2.09). This well is located at least 40 kms from either seismically or sampled intrusions so is unaffected by the intrusions (Funnell and Allis, 1996). Spontaneous uranium fission tracks in apatite grains from samples of Upper Cretaceous sandstones, at present-day depths ranging 440 –550 metres bKb, were largely annealed during a heating event at 60 ±5 Ma (Eurotrack, 1996). This degree of annealing indicates that formation temperatures briefly reached 100-120°C shortly after deposition. The coincidence of this heating event with the postulated hotspot transit is further support for the latter.

Vertical bodies associated with these two intrusive events are seen in many seismic lines. Mlaba (1996) shows magnetic susceptibilites as high as 10-15 nTesla's above background recorded above some of these vertical bodies which penetrate basal Palaeocene strata (Fig. 3.12) suggestive of an igneous origin. On at least one seismic line through the south-western part of the basin (F80-048) there are build-ups on the Late Maastrichtian surface which appear to represent reef knolls (Fig. 3.13). They do not match the presumed igneous bodies (cf. Figs. 3.12-3.13) but match published examples of isolated reefs (Hovland et al., 1994; O'Brien and Woods, 1995).

Another possibility is that the 'knolls' are unusually prominent igneous intrusions especially since they are only found near the eastern intrusive centre. However, since they are developed on the Late Maastrichtian surface, based on extrapolation along seismic lines from wells 9-13, and onlapped and capped by Lower Palaeocene sedimentary rocks (considered to be ~64 Ma, McMillan, 1994, pers. comm.) they must have formed pre-Palaeocene. This is 9 Ma earlier than the Rb-Sr dated intrusives in the area (Eglington et al., 1990) and 6-12 Ma earlier than intrusives in the western igneous region (Table 2.04 and references therein). If these are intrusions, and due to the Late Cretaceous-Early Tertiary hotspot, then the time span of igneous activity is unusually long compared to similar hotspot activity elsewhere (Condie, 1989, p159; Funnell and Allis, 1996).

There are no magnetic data across the knolls (and they have not been physically sampled) but even if later study shows a small increased magnetic susceptibility in the

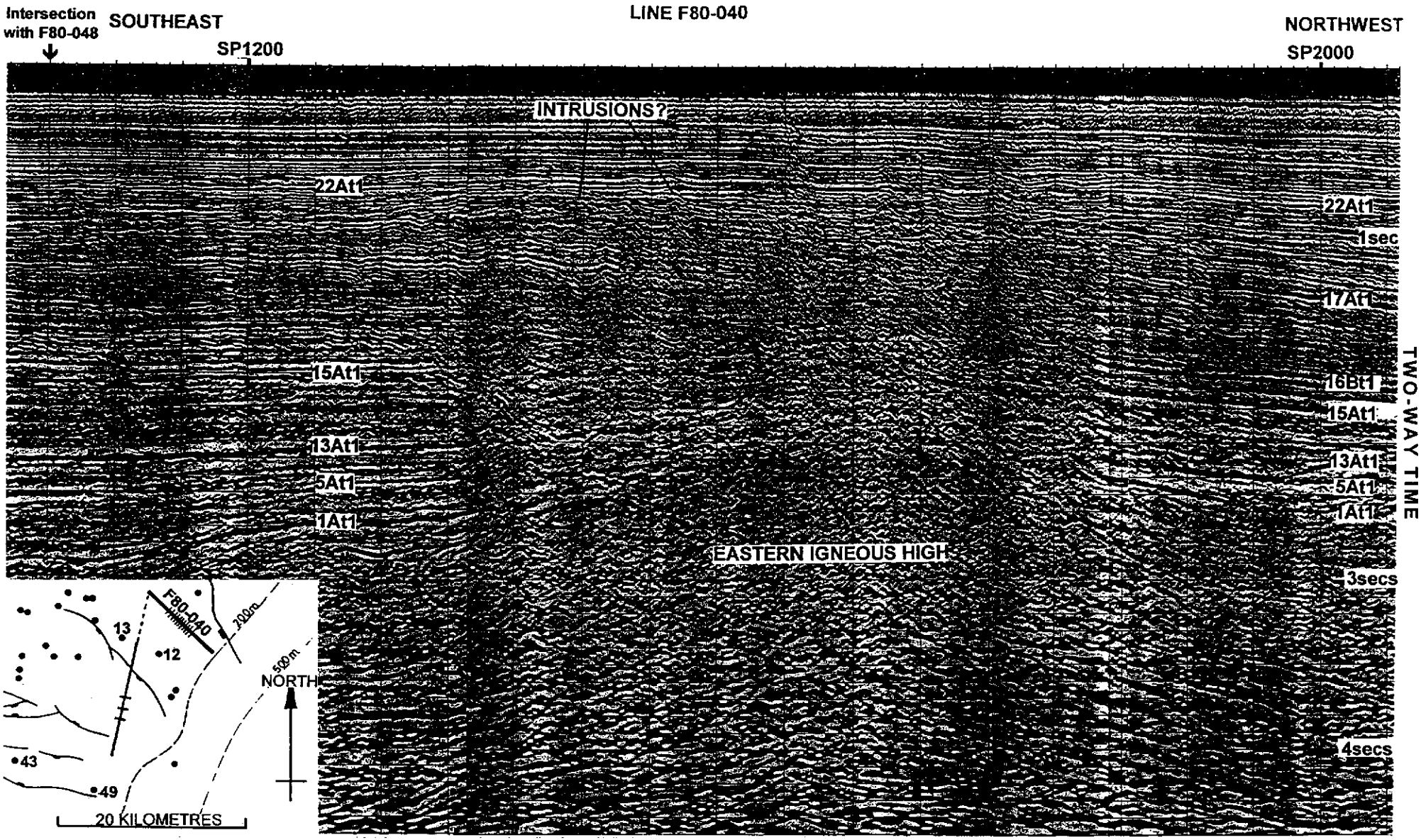

Figure 3.12: Part of NW-SE seismic line through the eastern part of the basin crossing that in Figure 3.13 at the location shown. Vertical noise (esp. at shotpoints 1350-1850) ie. in the vicinity of well 8 are probably igneous intrusions but appear very different from the 'knolls' in Figure 3.13 suggesting a different mode of origin. The line is located on the regional map, Figure 3.30.

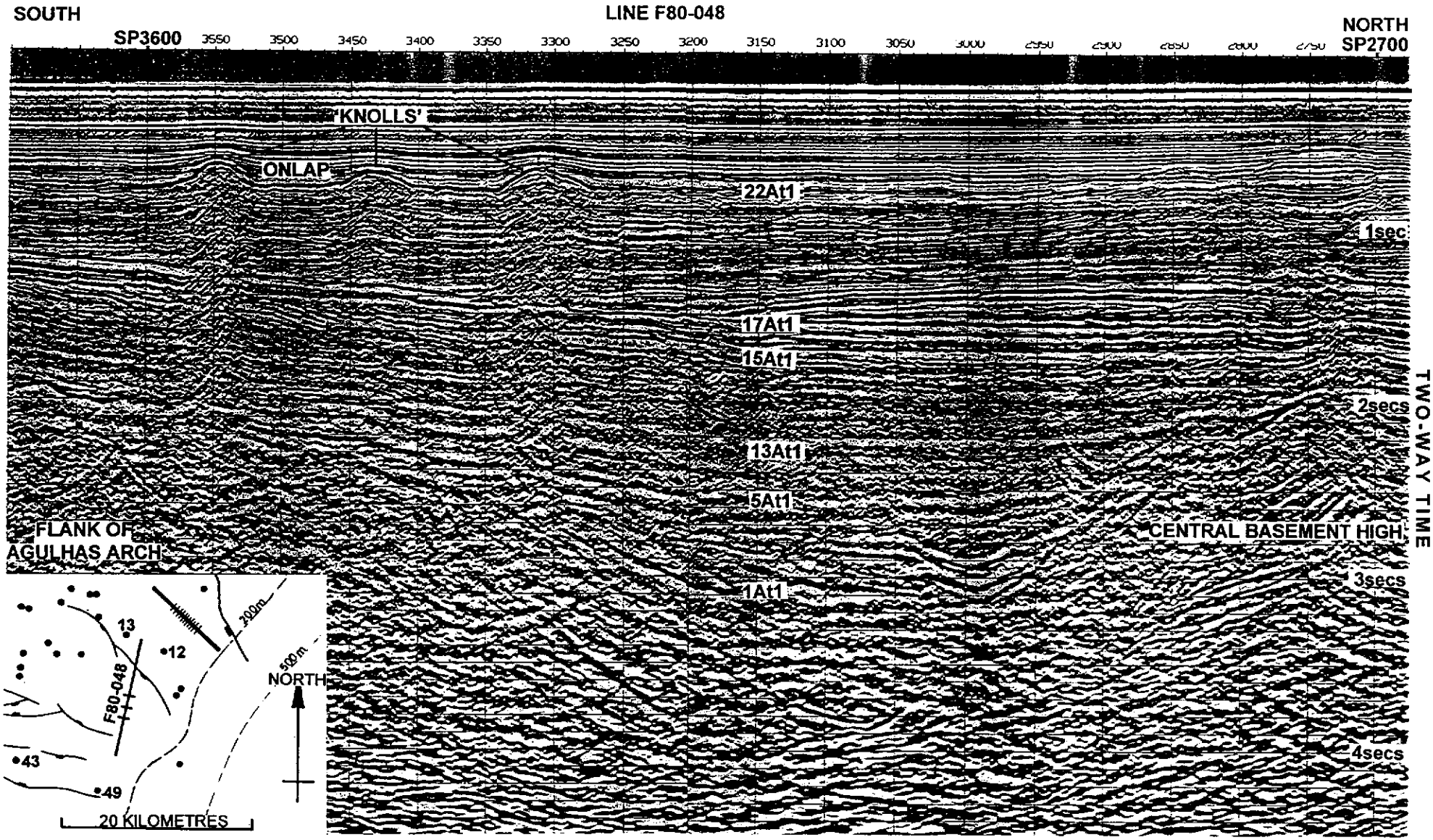

Figure 3.13: Part of N-S seismic line through the south flank of the basin showing possible reef knolls. A more regional location map of the line is shown in Figure 3.30.

case of the three 'reef knolls', a bacterial origin is still possible. This is because one mode of formation, over gas seeps where bacterially-induced reducing conditions occur, results in concentrations of pyrrhotite and magnetite causing elevated magnetic susceptibility (Barton et al., 1988; Gay, 1992). The importance of this mode of origin is that it implies a deeper gas source than previously known (see Chapter 7).

3.4. FORMATION FLUIDS

3.4.1. Hydrocarbons

Reservoirs containing gas with condensate or oil have been found below horizon 13At1 throughout the basin. Those gases reservoired below 9At1 tend to be condensate-rich whilst those below 1At1 generally have very little condensate. Oil reservoirs have been found mostly in Albian (14A) sandstones in the basin centre and occasionally in north flank area wells below horizon 1At1 (wells 48, 59, 70, 102 and 162). The distribution of these oil and gas reservoirs is shown in Figs. 2.06, 3.01-3.02 and in detail in Figs. 3.14-3.18. Details of hydrocarbons in many of these reservoir trends and in individual reservoirs are addressed later.

The results of drilling offshore have shown that Palaeozoic metasediments contain neither significant hydrocarbon source potential nor potential reservoir rocks (except where locally fractured) and they are currently considered to be the economic limit for hydrocarbon exploration. It is possible that locally the Bokkeveld Group slates could source non-hydrocarbon gases (e.g. CO_2, H_2S) as well as some methane (Chapter 4).

3.4.2. Water

Where the Agulhas (and possibly Infanta) Arch were subaerially exposed, they could have been sources of water influx to the basin, especially where highly faulted. Recent mapping has shown faults which extend to the basal Palaeocene on the Agulhas Arch (Strauss and Noble, 1996). Rain falling on such exposed highs percolated through these faults, entering juxtaposed sandstone bodies where through-flow of fluids was possible (Figs. 3.19-3.22). Also, porosity resurrection prevails in syn-rift reservoir sandstones in the north flank of the basin, caused by dissolution of intergranular poikilotopic calcite cement (Hill, 1995a and b) probably by meteoric fluids. Even today, formation water salinities in these reservoirs are low (locally <20000 ppm NaCl, Davies, 1995a). This dissolution must have occurred late, after the period of Cretaceous rapid burial, otherwise the secondary pores would have been compacted. This could be at, or shortly after, the Cretaceous-Tertiary boundary because sedimentation rates decreased greatly during Late Cretaceous (McMillan et al., 1997) leading to a reduced likelihood of further compaction.

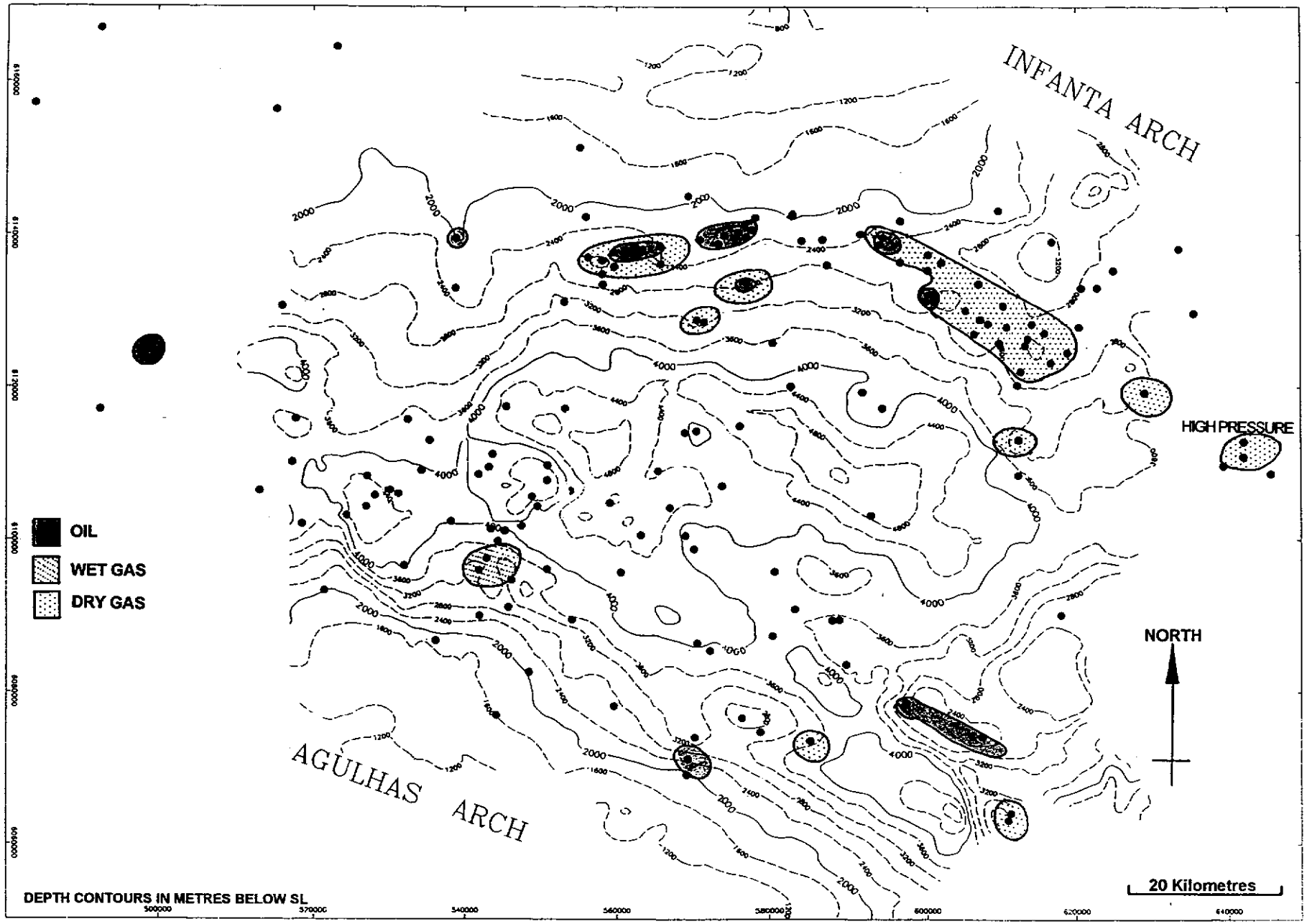

Figure 3.14: Map of the Bredasdorp Basin showing the distribution of oil, wet gas and dry gas shows in syn-rift sandstones.

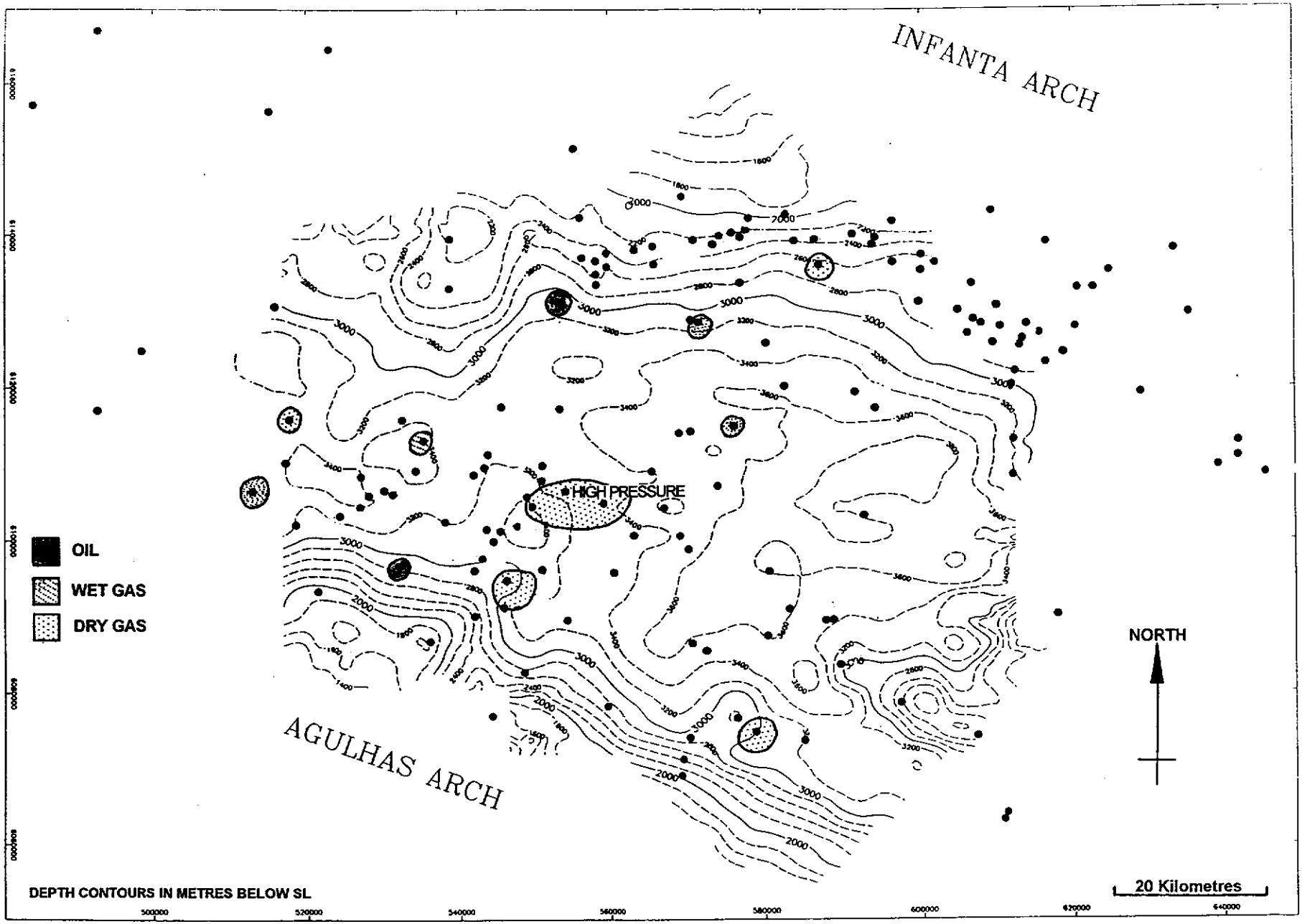

Figure 3.15: Map of the Bredasdorp Basin showing the distribution of oil, wet gas and dry gas shows in early drift sandstones.

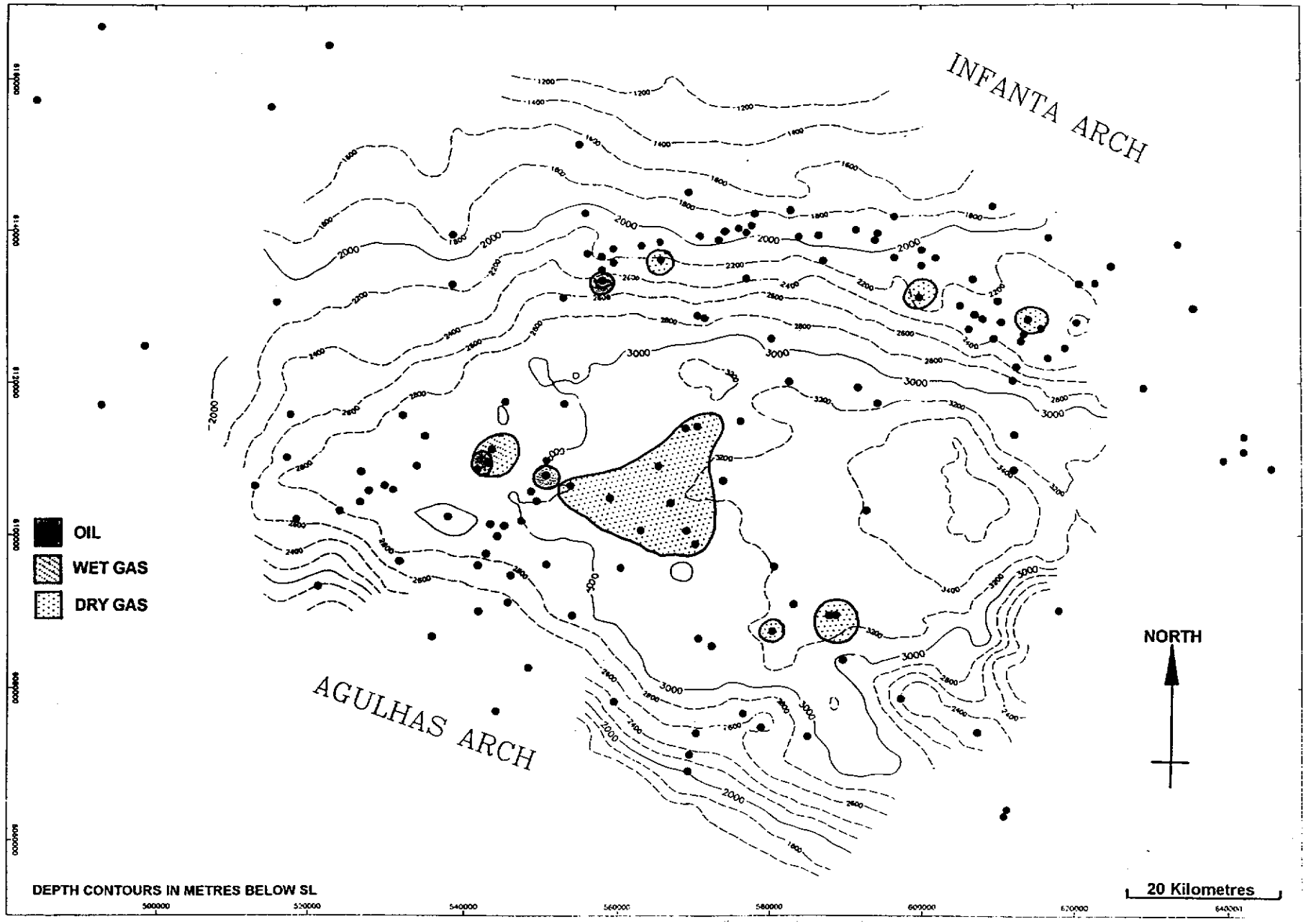

Figure 3.16: Map of the Bredasdorp Basin showing the distribution of oil, wet gas and dry gas shows in late Barremian deep-water turbidite sandstones.

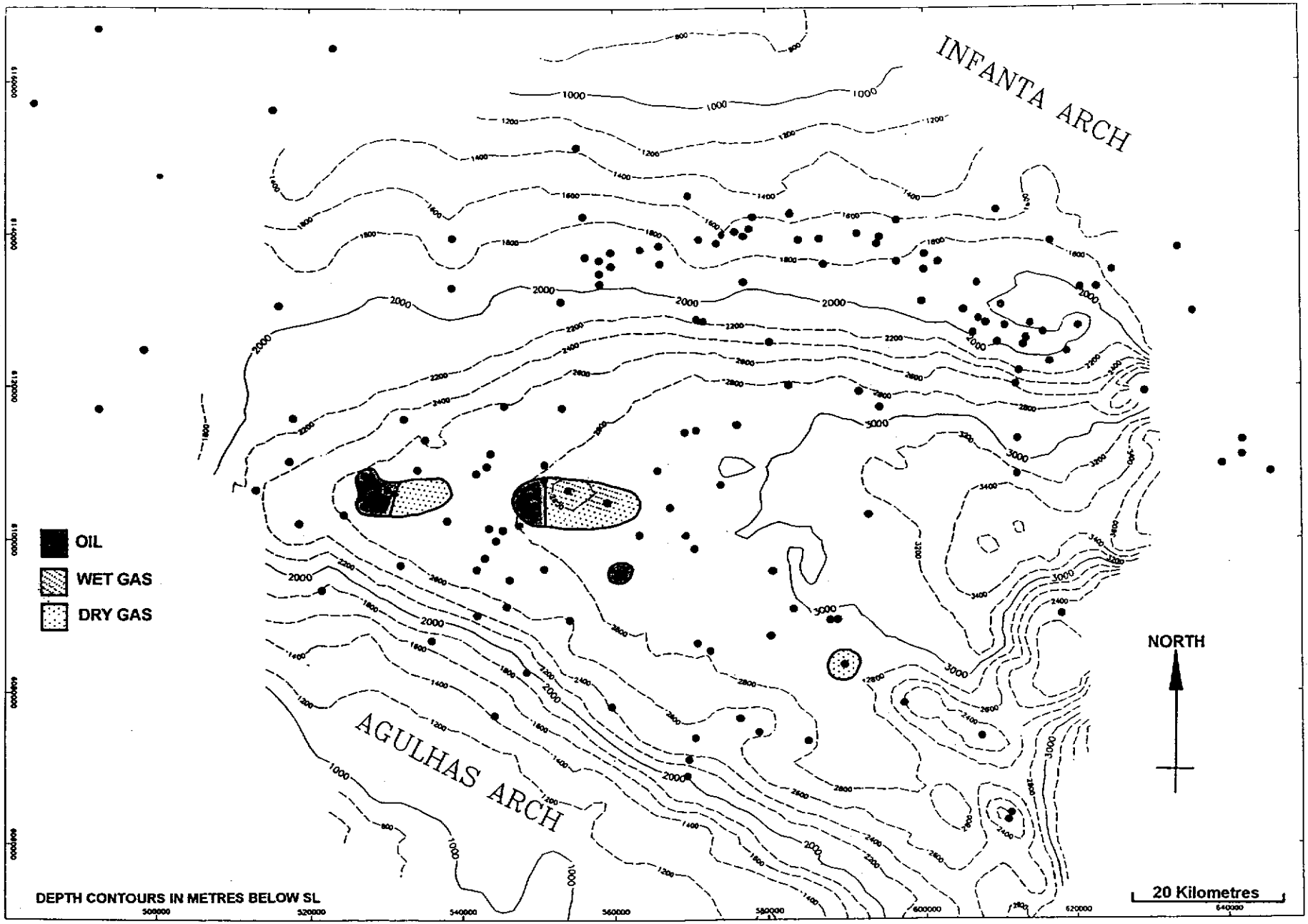

Figure 3.17: Map of the Bredasdorp Basin showing the distribution of oil, wet gas and dry gas shows in Aptian shelf-edge channel sandstones immediately below the Aptian regional source rock/seal.

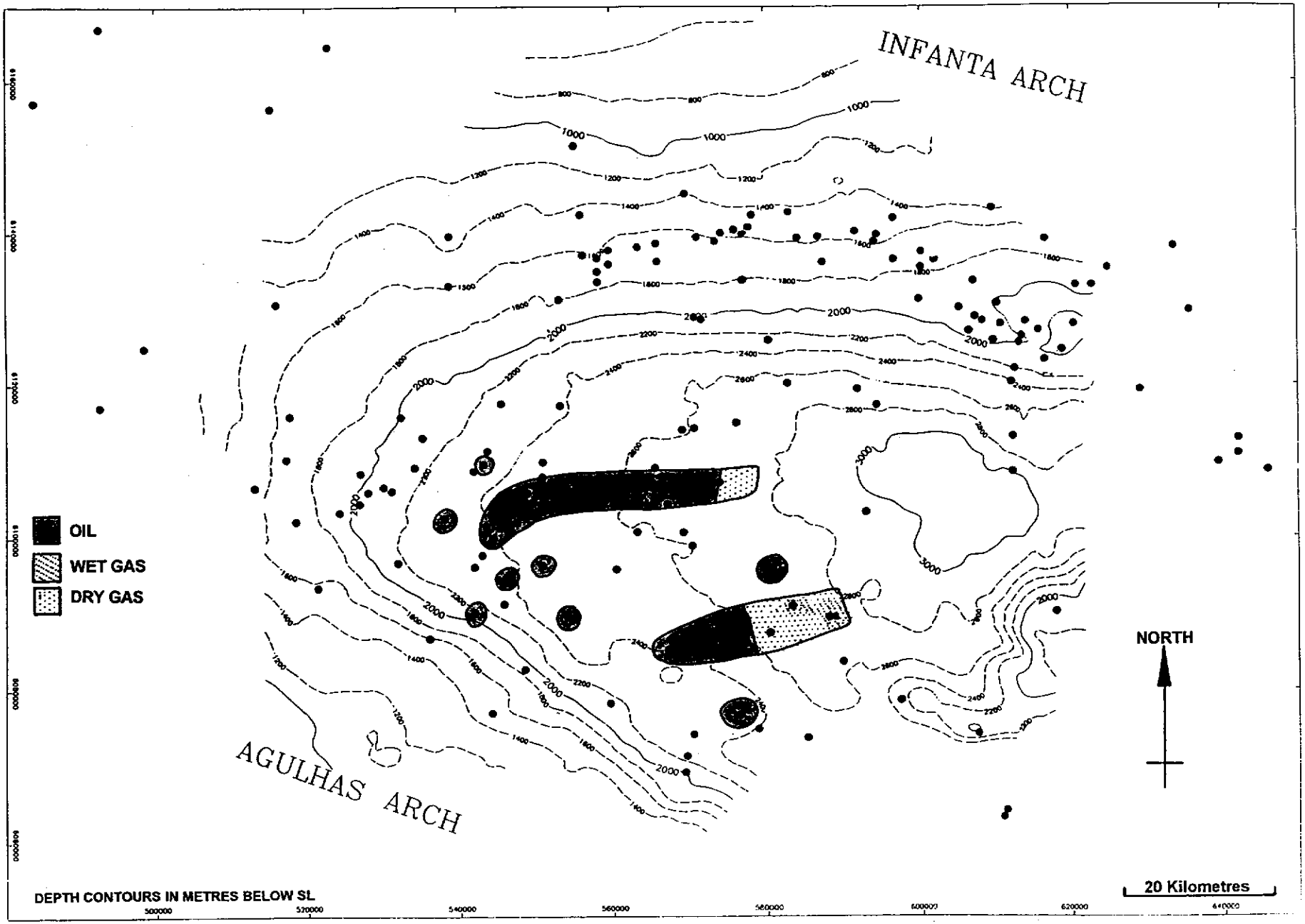

Figure 3.18: Map of the Bredasdorp Basin showing the distribution of oil, wet gas and dry gas shows in Albian outer shelf channel and lobe sandstone complexes (elongate distribution) and overbank sandstones (localised individual reservoirs).

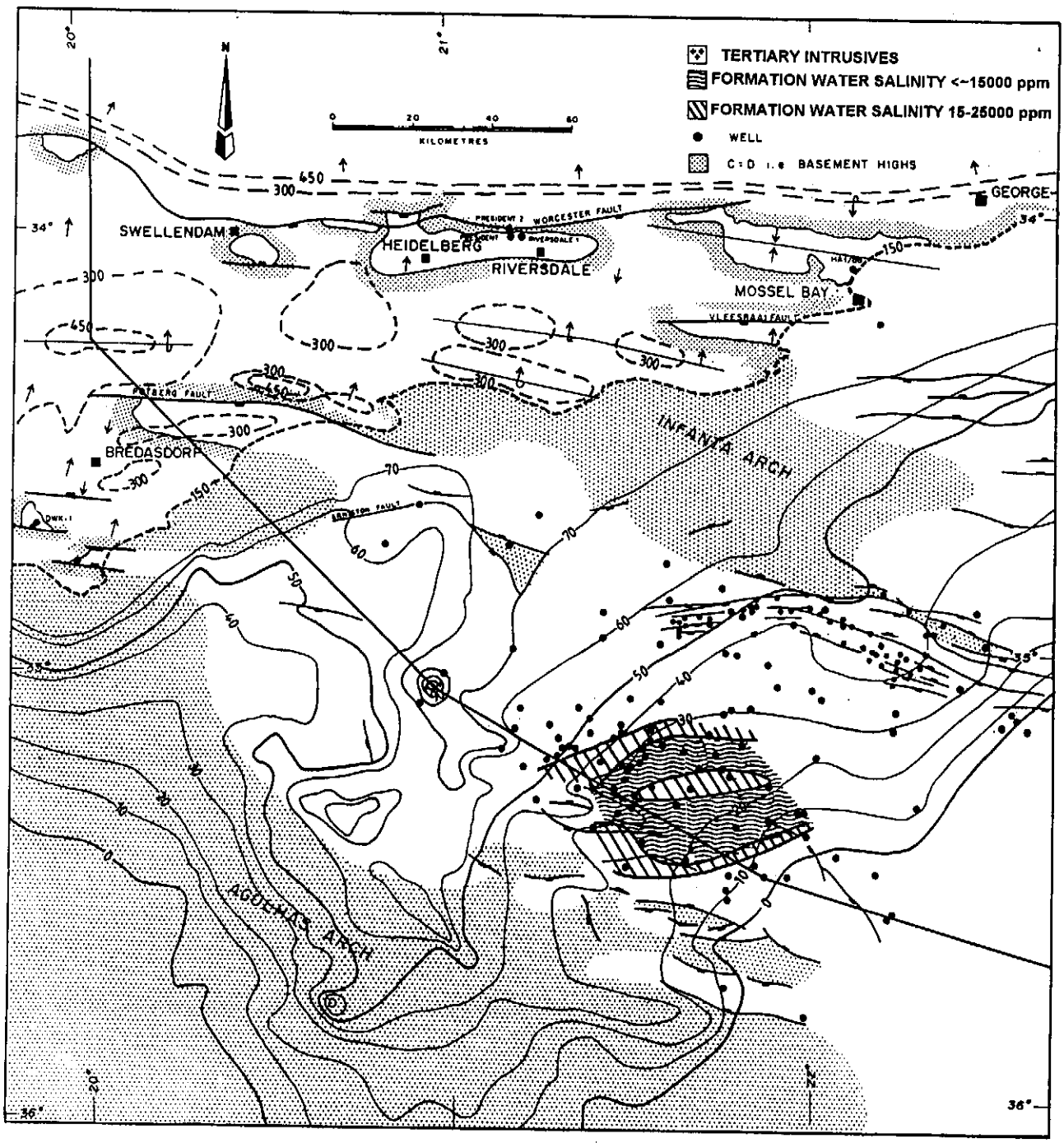

Figure 3.19: Palaeo-topographic map of the Bredasdorp Basin and its environs at lowest Plio-Pleistocene sea-level lowstand. This glacially-related lowstand reached approximately 150 metres below present sea-level (Dingle et al., 1983) and resulted in exposure of faulted northern and southern flank highs and possibly the highs which range largely N-S across the eastern part of the basin. Rainfall is likely to enter the marginal highs (especially where faulted) and migrate down to the porous/permeable sandstones - particularly those in the 14A sequence - diluting or even replacing the formation water with low salinity water (<10 000 ppm, Davies, 1995c).

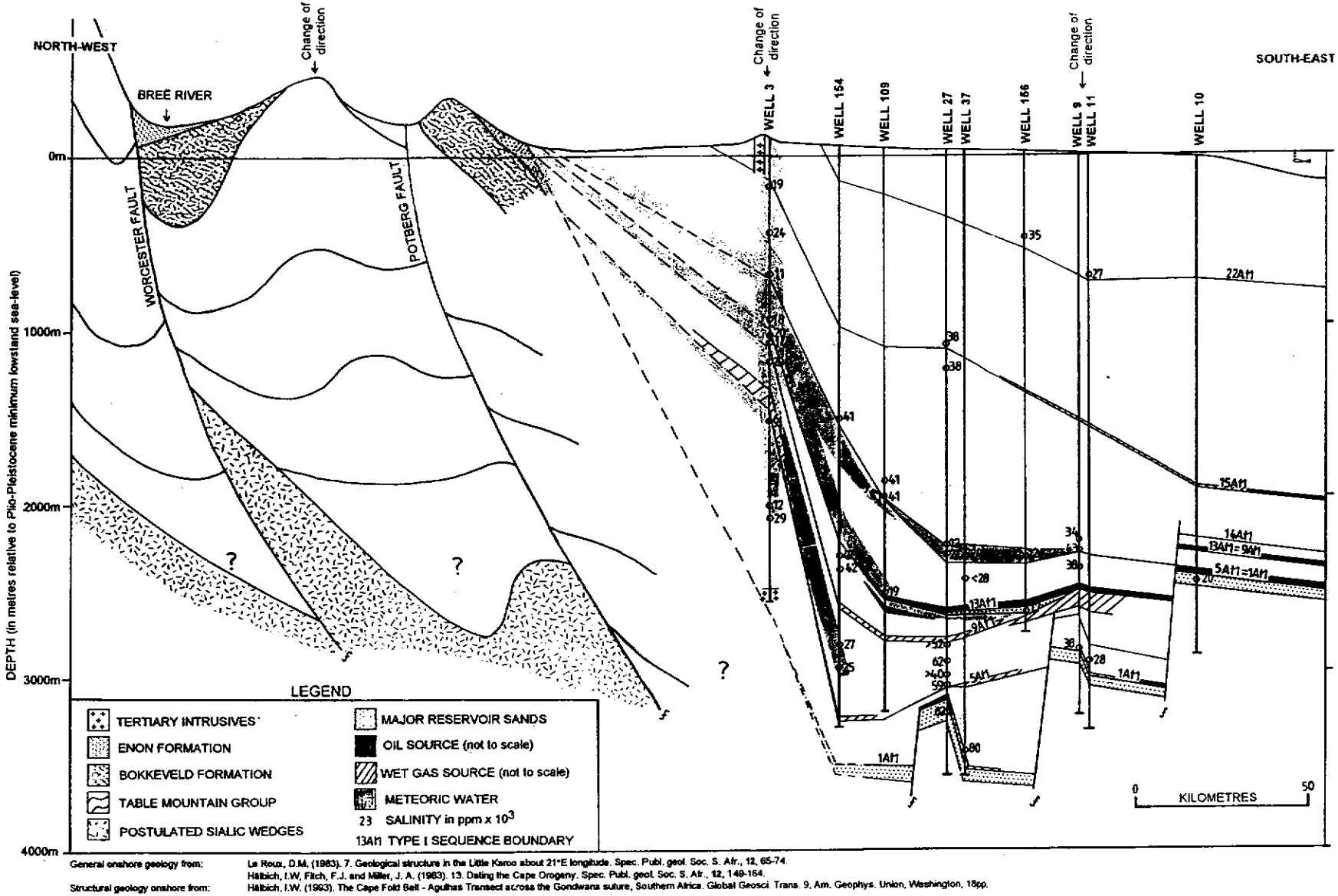

Figure 3.20: Northwest-southeast section through the Bredasdorp Basin and into the onshore hinterland at lowest Plio-Pleistocene sea-level lowstand. The low salinities in 14A sandstones in wells 27, 37 and 156 either entered the system through the fractures associated with Early Tertiary intrusives (viz in Well 3) or through the faulted highs (out of plane of section). It is possible that fresh water entered the system through the outcropping Enon conglomerate (cf Table 2.03) but since these rocks have essentially no porosity where encountered offshore, the conduit to post-basement sandstones is unknown.

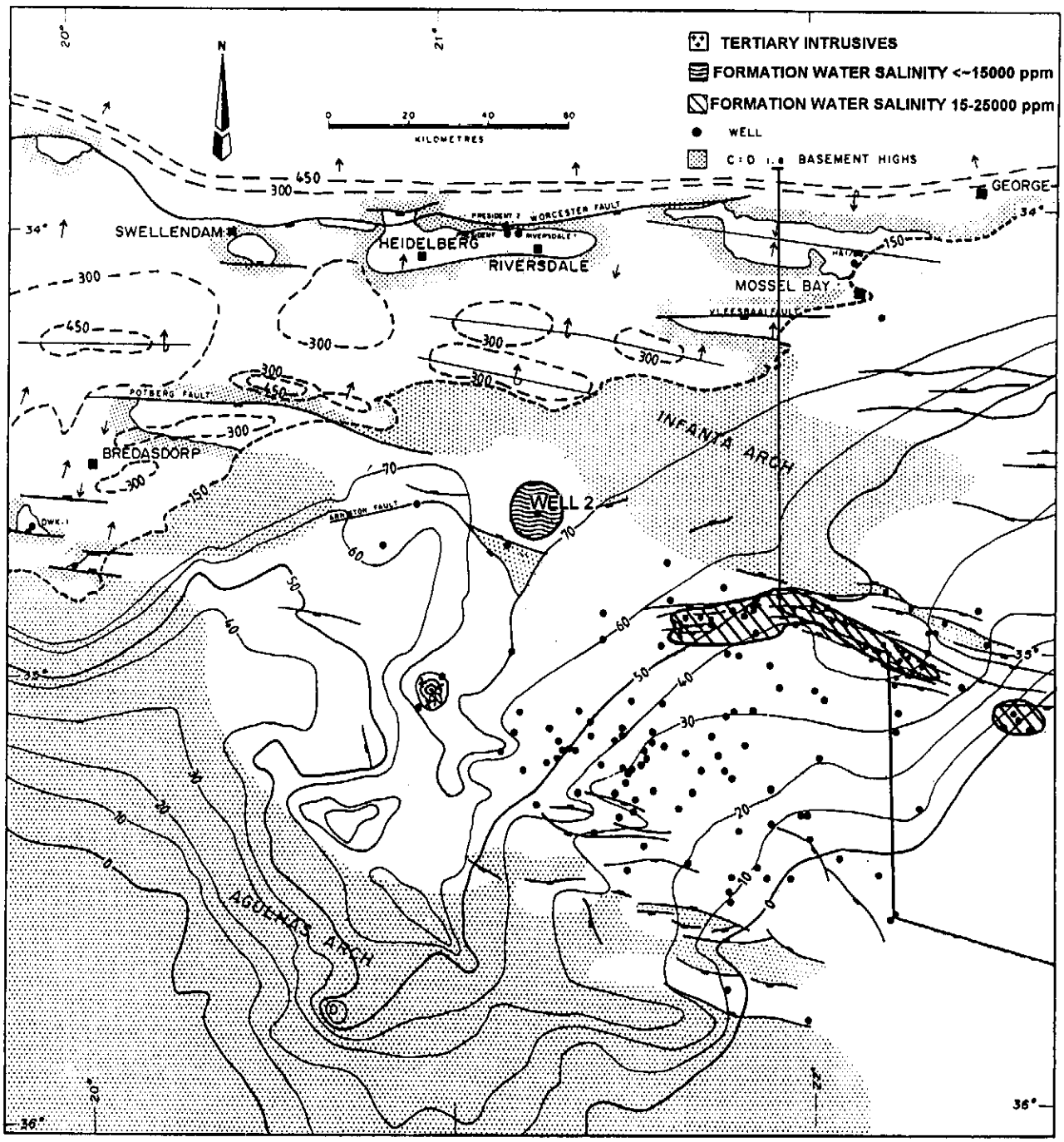

Figure 3.21: Palaeotopographic map of Bredasdorp Basin as in Figure 3.19 but showing the low salinity formation waters in pre1At1 sediments largely in the north flank. As in the south of the basin, fresh water may have entered the system through one of two conduits; vertically downwards through the faulted highs or via the pre1At1 sandstones to the west. In well 2 the salinity in these sandstones is so low (<2000 ppm, Davies, 1995c) that it may indicate the fluid migration conduit. Alternatively long distance migration through fractured basement from onshore is not impossible but less likely as conduits are not evident.

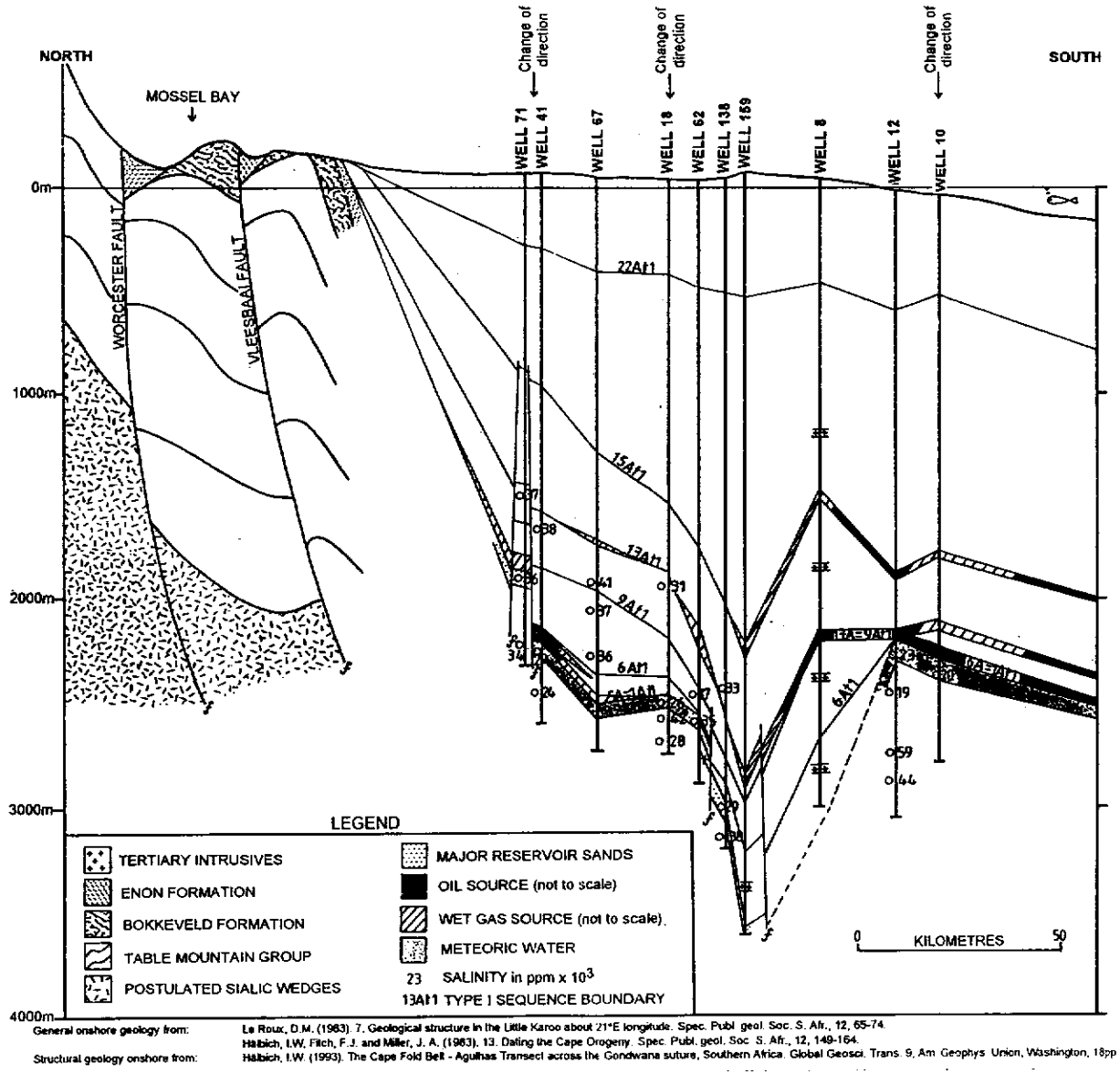

Figure 3.22: North-south section from onshore through the Bredasdorp basin, paralleling that of Hälbich (1983), showing another possible ingress route - through the faults which extend (at least) to Late Cretaceous in wells 71 and 41. This route is much less likely than the western ingress route because shallow formation water salinities are close to normal marine suggesting minimal alteration.

In addition, recent studies have shown evidence of a possible bolide impact at the Cretaceous/Tertiary boundary (Alvarez et al., 1980; Hildebrand et al., 1991). One global consequence was markedly elevated rain-water acidity during the succeeding 0.01-0.1 Ma (Retallack, 1996). This rain-water would have been able to percolate from the exposed basin margins into the sandstones resulting in dissolution of calcite-rich pore-filling material. In support of this scenario, an apparently partly biodegraded oil, with depleted normal alkanes, was found in well 78 close to a major fault which extends close to the Early Tertiary palaeo-surface. Burial and thermal history modelling of the well data show the sandstone is presently at ~80°C (at which temperature any bacteria are essentially inactive), but during the Early Tertiary, formation temperatures were closer to 60°C, when bacteria were active (Connan, 1984). In other areas, compaction resulted in expulsion of saline water from deeper sediments, and this connate water flowed updip, locally mingling with the incoming meteoric water and possibly resulting in the brackish water found in many sandstones in marginal highs (Davies, 1995a).

Erosion during the Early Eocene mainly occurred on the north flank and reached a maximum at the eastern end of the basin - but was still <50-100 metres. It was probably caused by thermal uplift due to the near-surface intrusion of the alkaline igneous bodies. Erosion during the latter part of the Mid-Oligocene is considered to be a result of the global sea-level lowstand (Haq et al., 1987; McMillan, 1989) rather than local tectonic uplift. Erosion of Early to Mid-Oligocene (and presumably Late Eocene) sedimentary rocks may have reached 100 metres during this lowstand (McMillan, 1995, pers. comm.). The event has only been recognised very locally from biostratigraphic data, mainly because few samples of the interval were collected from the wells.

Flushing by meteoric water of north flank pre1A and central basin 13B-14A (Albian) channel sandstones may also have happened during Plio-Pleistocene sea-level falls caused by northern hemisphere glaciation. The resulting eustatic sea level falls could have reached 200 metres and probably averaged 150 metres for each glacial advance (Dingle et al., 1983; Malan, 1990; Ben-Avraham, 1994, pers comm.). At that time, various topographic subsea highs around the margins of the basin - and to some extent the centre of the basin - would have been exposed to rainfall. In addition, annual rainfall rates are shown to have been at least twice as high as presently for periods of several tens of thousands of years within the Plio-Pleistocene (Butzer et al., 1973). Fresh-water flushing might have occurred during this period but until samples of formation water have been dated (possibly using ^{14}C isotope techniques) this will remain uncertain.

3.4.3. Formation pressures

Regional pressure studies, based almost wholly on data from Cretaceous reservoirs, show three pressure regimes to exist in the basin (Winter, 1981; Brink and Winters, 1989; McAloon et al., 1990; Larsen, 1995). These are:
(i) a normally pressured zone, largely down to ~3000m. In parts of this zone, fluids readily interchange with surface water causing low salinity trends and locally gas seeps (Davies, 1988b),
(ii) a second zone, largely associated with thick source rocks (mainly 13A Aptian), in which the equivalent mud weight (MW_{equiv}) reaches values up to 1.15 ppg,
(iii) a third zone in which very high overpressures are developed (up to >3000 psi above hydrostatic or $MW_{equiv.}$ >1.60). These pressures are estimated in many sandstones from the drilling and log parameters but are locally recorded from RFT and DST pressures (Verfaille, 1993) (Fig. 3.23 and Tables 3.01 and 3.02).

Very high formation pressures are also found in Valanginian sandstones in well 128 some 80 kilometres east (Table 3.02 and Fig. 3.14). In the highest pressured reservoirs, Hauterivian (5A) sandstones in wells 83 and 88 (Fig. 2.10), pressures approach ~0.73 psi/ft, similar to that found in North Sea reservoirs (Miles, 1990) and possibly represent the local fracture gradient (Tables 3.01 and 3.02). Indeed, their matching pressure and close proximity suggest they are part of the same pressure cell although it is possible that the matching overpressures reflect matching seal efficiencies rather than connectivity. It is possible that thermally-induced hydrocarbon cracking during hotspot events or pulses of migration may have caused pressures to locally exceed this amount only to be almost instantly reduced by seal rupturing.

In a few reservoirs, the regional pressure distribution shown above differs. For example, in well 123, overpressure is recorded in Lower Albian (13B) sandstones just above ~2600 metres bKb. Associated oil-bearing fractures in apparently diagenetically calcitised sandstones attest to possible intermittent pressure build-up/release episodes (Brown, 1991; Davies, 1995c). In well 142, Barremian (9A-12A) sandstones are also overpressured and fractured (although not to the same extent as above) and contain gas shows and fluorescence traces (possibly residual condensate) below ~2700 metres bKb.

3.5. LATE TERTIARY SLUMP

3.5.1. Evidence

Large volumes of Tertiary (and locally Upper Cretaceous) sediments were removed from the present day shelf edge by Late Tertiary slumping (or creep) along a composite glide plane resulting in the present day rugose sea floor topography (Dingle, 1977). Indeed De Swardt and McLachlan (1982) comment that up to 1000 metres of sediment

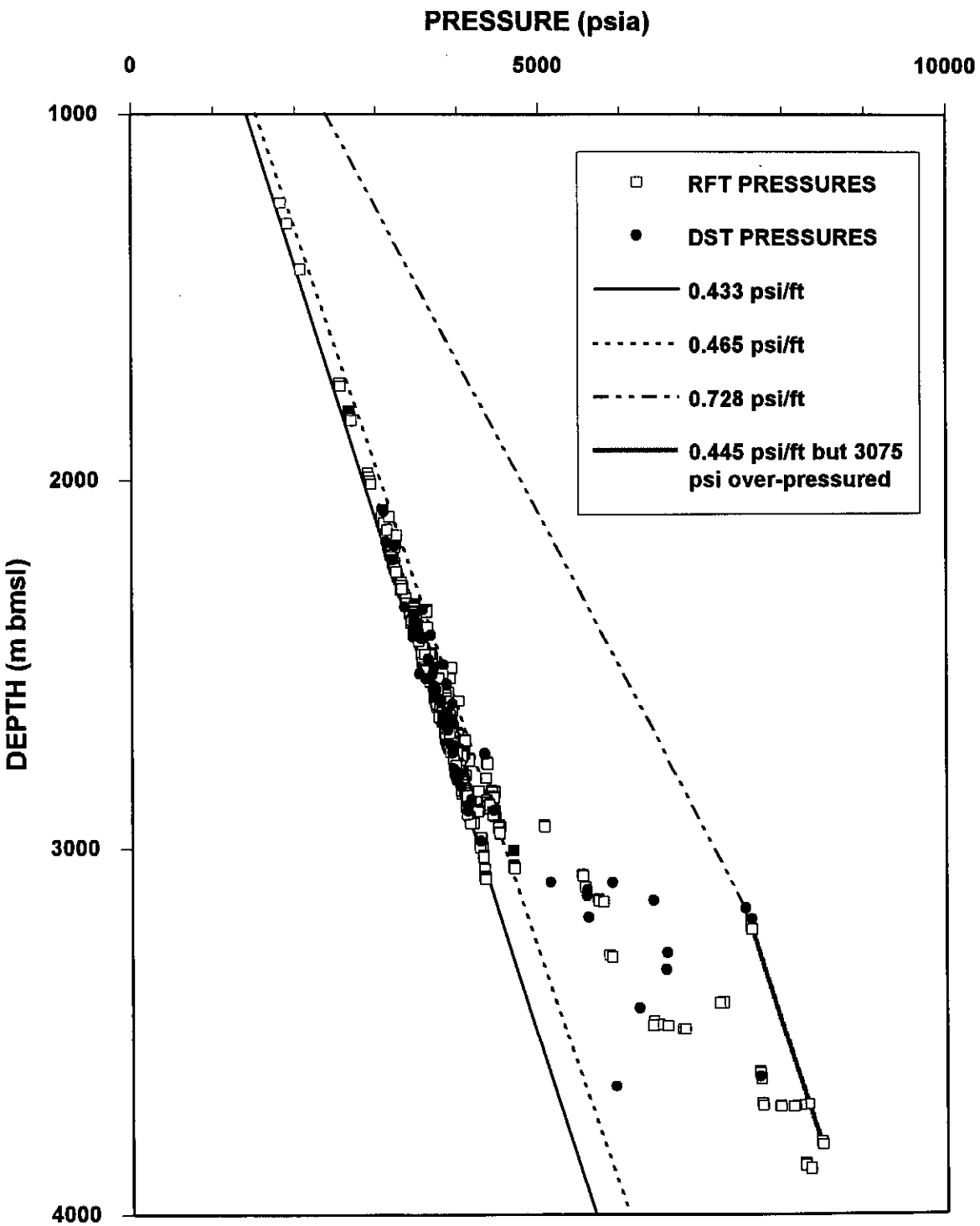

Figure 3.23: Plot of RFT and DST pressures vs depth for reservoirs in the Bredasdorp Basin. Most of these are hydrostatically pressured but the deepest reservoirs (below 3000 metres) are often overpressureed. A few of these reach pressures thousands of psi above hydrostatic and in three wells the pressure gradient (to sea floor) reaches 0.73 psi/ft.

BREDASDORP BASIN INTERVAL RFT DATA				
WELL	DEPTH (mbmsl)	PSIA (strain)	HORIZON	GRADIENT TO SURFACE
153	2453-2459	3570.4-3584.0	14A	0.444
88	2473-2499	3608.2-3637.2	14A	0.445
88	2805.9	3998.2	11A	0.434
88	2858.9	4095.7	10A	0.437
88	2887.5	4124.7	10A	0.435
88	2928.0	4190.7	9A	0.436
88	2932.0	4196.7	9A	0.436
88	3193-3218	7603.8-7620.7	5A	0.725
102	2217-2308	3203.3-3328.8	PRE1A	0.440
90	2444.0	3552.2	9A	0.443
95	2653.52704.5	3877.3-3923.7	14A	0.445
95	2987.6	4292.7	12A	0.438
95	2993.6	4301.9	10A	0.438
95	3056.1	4325.7	9A	0.431
103	2675.0-2690.0	3881.7-3903.7	14A	0.442
103	2802.0	4098.7	13A	0.446
103	2989.0-3082.0	4268.7-4340.7	9A	0.430
94	1425.0	2077.7	15A	0.444
94	2713.0-2728.0	3938.7-3956.7	14A	0.442
94	2768.5-2771.0	4358.1-4366.7	13B	0.480
114	2886.0-2899.0	4108.7-4225.9	12A	0.438
114	2900.0	4248.7	9A	0.447
114	3004.5	4681.7	9A	0.475
114	3045.0-3053.0	4683.5-4698.0	9A	0.469
123	2366.5-2487.5	3464.3-3634.2	14A	0.446
93	2429.0-2458.0	3549.7-3583.7	14A	0.445
93	2780.0-2814.0	3960.9-4002.1	13A	0.434
93	2847.0-2850.0	4048.7-4052.7	12A	0.433
119	2423.8-2452.5	3532.5-3565.8	14A	0.444
119	2783.4-2808.0	3959.2-3992.7	13A	0.433
108	2771.0-2820.5	4018.7-4081.7	10A	0.442
108	2845.3-2846.6	4248.7-4252.7	9A	0.446
143	2742.5-2759.5	3982.0-3994.2	11A	0.443
143	2793.1-2793.5	4055.4-4054.7	10A	0.443
143	2841.0-2843.0	4102.7-4105.4	10A	0.440
151	2386.5-2387.6	3494.6-3495.8	13B	0.446
151	2691.1-2698.1	3994.9-4004.2	12A	0.452
151	2811.0-2811.5	4339.7-4346.7	10A	0.471
151	2844.8-2861.6	4416.7-4442.2	9A	0.473
151	2895.2-2913.5	4435.0-4451.0	9A	0.467
129	2511.5	3730.3	14A	0.453
129	2825.0-2844.0	4038.7-4045.9	12A	0.435
129	2876.0-2933.0	4106.2-4158.6	10A	0.434
109	2597.5-2625.0	3777.7-3811.1	13A	0.443
124	2711.0-2713.0	4091.2-4091.0	14A	0.460
107	2355.0-2360.0	3621.7-3625.7	8A	0.469
107	2501.0-2614.0	3697.9-3793.7	PRE1A	0.449
110	2614.5-2619.5	3804.1-3805.7	14A	0.443
110	2972.5	4288.1	11A	0.440
110	2995.0-3023.0	4271.7-4317.9	10A	0.435

Table 3.01: RFT pressures and pressure gradients in sandstones in wells in the Bredasdorp Basin.

WELL	DEPTH (mbmsl)	PSIA (strain)	HORIZON	GRADIENT TO SURFACE
113	2886.5-2907.0	4094.7-4119.7	13A	0.432
126	2600.0-2685.0	3799.2-3904.6	14A	0.445
146	2357.1-2375.1	3456.7-3473.5	14A	0.447
146	2492.0-2511.1	3643.5-3666.2	13B	0.446
117	2364.5-2391.4	3455.1-3486.2	14A	0.445
117	2514.0-2521.0	3670.2-3680.7	13B	0.445
136	2391.0-2393.0	3488.1-3491.9	14A	0.445
136	2417.0-2419.0	3524.7-3527.3	13B	0.444
136	2472.0-2477.0	3611.2-3617.8	13B	0.445
136	2518.2-2523.1	3674.6-3681.2	13B	0.445
122	1245.0-1299.9	1834.6-1914.0	14C	0.449
122	2388.0-2466.9	3495.2-3604.9	13B	0.446
122	2491.4	3663.6	13A	0.448
122	2737.0	3969.9	13A	0.442
140	2452.0-2453.9	3571.1-3573.6	14A	0.444
140	2760.0	4146.3	12A	0.458
140	2761.0-2763.0	4144.0-4144.9	10A	0.458
140	2869.0-2908.5	4355.7-4429.6	10A	0.463
140	2909.2-2910.0	4433.0-4433.2	9A	0.465
140	29437.0-2959.0	4506.1-4513.4	9A	0.468
156	2488.6-2520.0	3637.6-3672.7	14A	0.445
156	2548.6-2550.6	3740.8-3742.3	14A	0.447
156	2556.6-2557.6	3766.7-3768.5	14A	0.449
156	2573.1-2575.0	3745.7-3748.7	14A	0.444
166	2481.5-2572.6	3634.7-3745.8	14A	0.446
133	2685.0-2695.0	3892.8-3906.5	13A	0.442
132	2635.0-2707.0	3861.8-3965.5	13A	0.446
132	2770.0	4022.4	10A	0.443
137	2655.0-2727.0	3852.2-3945.9	13A	0.442
148	2588.5-2592.5	3767.7-3771.7	13A	0.444
148	2652.6-2666.5	3867.5-3876.1	13A	0.443
142	2659.0-2662.0	3850.8-3853.1	11A	0.441
142	2937.6-2941.5	5058.9-5061.8	8A	0.525
165	2347.0-2381.0	3436.2-3479.9	13A	0.446
163	3069.1-3102.2	5529.1-5563.2	8A	0.549
163	3136.1-3139.6	5723.0-5730.5	8A	0.556
163	3143.1	5792.0	8A	0.562
167	2655.1-2694.5	3878.1-3935.4	14A	0.445
167	2749.5-2750.6	4020.3-4023.3	13B	0.446
84	2731.0-2739.4	3967.7-3973.9	PRE1A	0.443
84	2742.9-2752.9	4061.1-4049.2	PRE1A	0.451
84	2761.4-2858.5	3986.7-4101.7	PRE1A	0.439
37	3465.0-3475.0	6406.7-6476.7	1A-5A	0.568
37	3476.0	6576.7	1A-5A	0.577
37	3485.0-3486.0	6772.7-6795.7	1A-5A	0.593
69	2351.5-2361.5	3471.7-3474.7	1A-5A	0.449
69	2373.0-2383.0	3477.7-3481.7	PRE1A	0.446
69	2399.0-2506.1	3486.7-3623.2	PRE1A	0.442
46	2203.1	3213.2	6A-10A	0.445
46	2473.6-2483.7	3683.7-3687.7	PRE1A	0.454
46	2491.6-2501.5	3688.7-3692.7	PRE1A	0.450
46	2518.6-2555.6	3696.7-3705.7	PRE1A	0.445
46	2584.1-2660.6	3713.7-3806.7	PRE1A	0.437

Table 3.01 (cont.)

WELL	DEPTH (mbmsl)	PSIA (strain)	HORIZON	GRADIENT TO SURFACE
48	2574.2-2576.2	3712.7-3715.7	PRE1A	0.440
48	2582.0-2602.2	3711.7-3737.7	PRE1A	0.438
48	2611.9-2620.1	3737.7-3747.7	PRE1A	0.436
53	2539.5-2542.5	3903.7-3905.2	1A-6A	0.469
54	2533.1-2536.0	3698.2-3699.2	PRE1A	0.445
54	2546.0-2565.9	3696.2-3705.2	PRE1A	0.441
54	2573.9-2637.1	3706.7-3775.2	PRE1A	0.438
54	2689.9-2724.0	3855.2-3902.2	PRE1A	0.437
54	2743.9	3994.7	PRE1A	0.444
57	2485.5	3568.7	1A-6A	0.438
57	2485.5-2552.5	3573.7-3666.7	PRE1A	0.438
76	2533.7-2553.0	3717.7-3718.1	PRE1A	0.446
76	2555.9-2630.0	3716.7-3816.7	PRE1A	0.442
76	2636.0-2679.0	3936.7-3948.7	PRE1A	0.455
50	2513.9	3923.7	1A-5A	0.476
50	2594.0-2594.4	3796.7-3800.7	PRE1A	0.446
50	2595.0-2596.4	3833.7-3889.7	PRE1A	0.453
50	2604.0	4009.7	PRE1A	0.469
50	2607.2	3883.7	PRE1A	0.454
50	2613.9-2630.2	3783.7-3810.7	PRE1A	0.441
39	1735.9-1742.9	2549.7-2561.7	1A-6A	0.448
39	2181.5-2193.0	3199.7-3200.7	PRE1A	0.447
39	2196.9-2291.0	3202.7-3324.7	PRE1A	0.444
39	2477.1	3662.7	PRE1A	0.451
39	2498.5-2549.9	3633.7-3663.2	PRE1A	0.443
59	2150.0-2151.2	3119.7-3121.7	PRE1A	0.443
59	2173.4-2252.4	3140.7-3248.7	PRE1A	0.440
59	2300.5	3300.7	PRE1A	0.437
59	2343.1	3422.7	PRE1A	0.445
59	2389.9-2390.4	3431.7-3431.7	PRE1A	0.438
59	2419.0	3522.2	PRE1A	0.444
59	2421.5	3521.7	PRE1A	0.443
59	2474.2	3557.7	PRE1A	0.438
59	2509.0	3587.7	PRE1A	0.436
68	2281.9-2405.1	3314.5-3484.7	PRE1A	0.442
72	2290.5-2425.5	3307.7-3492.7	PRE1A	0.440
72	2498.5-2519.9	3572.7-3613.7	PRE1A	0.436
72	2647.4	3777.7	PRE1A	0.435
72	2673.4-2765.3	3844.7-3953.7	PRE1A	0.438
75	3285.2-3290.0	5864.7-5897.7	PRE1A	0.545
18	2573.2-2583.5	3857.7-3858.7	PRE1A	0.457
18	2587.4-2602.2	3855.7-3856.7	PRE1A	0.453
18	2614.5-2623.0	3858.7-3865.7	PRE1A	0.450
18	2666.1-2671.4	3873.7-3887.7	PRE1A	0.443
21	2525.5-2527.3	3811.7-3812.7	PRE1A	0.460
19	2654.6	3914.7	PRE1A	0.449
19	2666.0-2669.0	3900.7-3901.7	PRE1A	0.446
20	2672.2	3872.7	PRE1A	0.442
20	2737.1	3945.7	PRE1A	0.439
44	2151.4	3189.1	11A	0.452
44	2401.4	3631.7	6A-8A	0.461
44	2687.5-2691.5	3840.7-3841.7	PRE1A	0.436
44	2706.4-2729.0	3844.7-3883.7	PRE1A	0.433

Table 3.01 (cont.)

WELL	DEPTH (mbmsl)	PSIA (strain)	HORIZON	GRADIENT TO SURFACE
45	2157.0-2184.1	3187.7-3231.7	9A-12A	0.450
45	2740.0-2777.0	3927.7-3975.7	PRE1A	0.437
45	2858.5	4118.7	PRE1A	0.439
55	2636.0-2643.0	3867.2-3868.2	PRE1A	0.447
58	2081.7-2086.6	3081.7-3086.7	9A-12A	0.451
58	2586.2-2609.7	3852.2-3957.2	PRE1A	0.453
58	2615.7-2637.8	3859.2-3865.2	PRE1A	0.449
58	2658.7-2679.8	3867.2-3874.2	PRE1A	0.443
58	2727.7-2740.7	3889.2-3911.2	PRE1A	0.435
131	2616.2-2626.2	3865.21-3866.7	PRE1A	0.450
131	2632.5-2634.3	3867.7-3868.3	PRE1A	0.448
131	2647.4-2653.6	3875.1-3877.4	PRE1A	0.445
134	2580.5	3884.5	PRE1A	0.459
134	2585.5-2587.6	3855.4-3856.6	PRE1A	0.455
134	2595.2-2620.3	3858.9-3865.7	PRE1A	0.452
134	2649.2-2654.2	3873.2-3874.6	PRE1A	0.446
60	2088.0-2138.0	3070.7-3136.7	9A-12A	0.447
60	2152.4	3256.7	9A-12A	0.461
60	2703.7-2718.7	3942.2-3949.2	PRE1A	0.444
70	2387.0	3489.7	PRE1A	0.446
70	2389.0-2475.0	3490.7-3596.7	PRE1A	0.443
70	2541.5	3765.7	PRE1A	0.452
74	2339.5-2356.0	3476.7-3480.7	5A-6A	0.452
74	2371.0-2382.0	3482.7-3485.7	PRE1A	0.447
74	2389.0-2399.0	3486.9-3488.9	PRE1A	0.444
74	2403.0-2450.0	3491.7-3571.9	PRE1A	0.442
74	2571.5	3758.1	PRE1A	0.445
162	1812.0-1839.0	2660.5-2695.4	9A	0.447
162	2347.5-2349.5	3464.5-3464.9	PRE1A	0.450
162	2357.5-2367.5	3467.3-3489.4	PRE1A	0.448
162	2370.5	3470.1	PRE1A	0.446
161	2366.0-2439.5	3417.0-3522.9	PRE1A	0.440
63	2636.0-2649.1	3816.7-3826.7	PRE1A	0.441
63	2651.0-2662.0	3816.7-3840.7	PRE1A	0.439
66	1982.5-2011.0	2900.7-2941.7	9A	0.446
66	2102.0	3159.7	9A	0.458
66	2709.5-2712.4	3904.7-3922.7	PRE1A	0.439
67	2691.2	3901.7	PRE1A	0.442
72	3413.7-3415.7	7225.7-7272.7	PRE1A	0.649
105	3692.0-3700.0	7747.7-7751.4	PRE1A	0.640
128	3605.0-3625.0	7712.3-7732.2	PRE1A	0.652
157	3696.0	8302.9	PRE1A	0.685
157	3700.1	8205.0	PRE1A	0.676
157	3702.0-3702.5	8129.7-8144.7	PRE1A	0.670
157	3799.0-3808.0	8466.9-8485.1	PRE1A	0.679
157	3860.0-3875.0	8271.2-8336.7	PRE1A	0.654
149	3700.5-3703.0	7966.2-7967.8	PRE1A	0.656

Table 3.01 (cont.)

FORMATION PRESSURES AND TEMPERATURES IN DST INTERVALS (psia, degC, bKb) (55 wells)								
WELL	DEPTH	DST	Hor.	psia	Water	Airgap	Gradient	Temperature
83	2460	3	14A	3580	121	26	0.448	98.9
83	2894	2	10A	4169	121	26	0.443	113
83	3186	1	5A	7546	121	26	0.728	128.5
88	2555	5	14A	3535	123	26	0.426	112
88	2839	4	10A	3990	123	26	0.432	117
88	2910	3	9A	4127	123	26	0.436	119.4
88	2925	2	9A	4133	123	26	0.435	120
88	3215	1	5A	7620	123	26	0.728	131.7
102	2240	4	PRE1A	3207	99	22	0.441	106.7
102	2594	2	PRE1A	3743.1	99	22	0.444	106
95	2703	2	14A		142	26	0.000	120
103	2708	2	14A	3886	142	25	0.441	93.3
94	2769	1	13B	4334	124	22	0.481	126
96	3113	1	9A	5139	120	23	0.507	126.1
114	3030	1	9A	4682	129	26	0.475	135
93	2458	2	14A	3549	120	26	0.445	102.8
93	2815	1	10A	3966	120	26	0.433	112.8
119	2807	1	10A	3961	120	22	0.434	114.4
108	2805	2	10A		115	22	0.000	112.2
108	2820	1A	10A	4047	115	22	0.441	116.7
151	2915	2	10A		114	22	0.000	118
151	2919	1B	10A	4437	114	22	0.467	118.3
129	2855	2	10A	4038	122	22	0.434	118.3
129	2935	1	10A		122	22	0.000	123.9
109	2625	1	13A	3792	101	26	0.445	109.4
107	2379.8	3	10A	3579.3	98	26	0.463	97.8
107	2517.4	2	PRE1A	3646.9	98	26	0.446	106.7
107	2567.8	1	PRE1A	3610.3	98	26	0.433	106.7
110	3010	2	10A		122	23	0.000	121.1
110	3003	1B	10A	4280	122	23	0.438	121.1
126	2633	1	14A	3803	139	25	0.444	116.7
120	2931	1	12A		145	25	0.000	121.1
117	2397	1	14A	3465	118	22	0.445	106.7
146	2388	1	14A	3460	118	22	0.446	101.7
156	2510	1	14A	3643	135	22	0.446	111
166	2517	1	14A		133	22	0.000	113.8
132	2658	2	13A	3873	102	22	0.448	104.4
132	2665	1	13A	3857	102	22	0.445	110
148	2684	1	13A		101	22	0.000	110.6
11	2949	2	5A		147	30	0.000	127.2
14	3675	1	PRE1A	5939.7	156	30	0.497	
17	3259	3	PRE1A		139	30	0.000	
17	3335	2	PRE1A		139	30	0.000	
17	3365	1	PRE1A		139	30	0.000	

Table 3.02: DST pressures and temperatures recorded in sandstone reservoirs in wells in the Bredasdorp Basin (some of the temperatures shown rely on static borehole temperatures data).

84	2753	1	PRE1A	3951	110	26	0.442	108.9
25	2205	1	PRE1A		139	26	0.000	
27	3136	2	PRE1A	5595	120	26	0.548	
27	3152	1	PRE1A	5585	120	26	0.545	136.1
35	3309	3	PRE1A	6580	118	30	0.612	134.4
35	3354	2	PRE1A	6565	118	30	0.602	134.4
37	3458	1	5A	6230	120	30	0.554	136.7
69	2435	2	PRE1A	3463	97	28	0.439	107.2
46	2540	2	PRE1A	3715	93	28	0.451	109.4
48	2620	2	PRE1A	3714.7	94	30	0.437	109.4
48	2625	1	PRE1A	3755	94	30	0.441	104.4
54	2588	1	PRE1A	3715	94	26	0.442	112.8
76	2556	1	PRE1A	3695	97	26	0.445	107.8
39	2209	2	PRE1A	3229	101	28	0.451	100.6
39	2451	1	PRE1A	3675	101	28	0.462	110.6
59	2195	1	PRE1A	3120	100	25	0.438	99.2
65	3167	2	PRE1A	6409	114	28.4	0.622	126.1
65	3212	1	PRE1A	5605	114	28.4	0.537	127.8
18	2602	4	PRE1A		109	30	0.000	124.4
18	2641	3	PRE1A	3939	109	30	0.460	121.1
18	2696	1	PRE1A	3955	109	30	0.452	120
21	2532	2	PRE1A	3827	112	28	0.466	112.8
21	2585	1	PRE1A	3867	112	28	0.461	117.2
19	2680	2	PRE1A	3900	108	31	0.449	118.3
20	2503	4	PRE1A		110	30	0.000	101.1
20	2569	3	PRE1A		110	30	0.000	100.6
20	2692	2	PRE1A		110	30	0.000	99.4
44	2750	1	PRE1A	3911	106	28	0.438	128.7
55	2659	2	PRE1A	3865	108	26	0.447	118.3
61	2113	3	10A	3095	107	25	0.452	99.3
61	2768	2	PRE1A	3940	107	25	0.438	121.7
62	2549	1	?5A		116	28	0.000	110.6
70	2411	2	PRE1A	3475	106	26	0.444	107.2
70	2440	1	PRE1A	3498	106	26	0.442	108.3
162	2369.1	2	PRE1A	3355	106.5	22.5	0.436	
162	2450	1	PRE1A	3451	106.5	22.5	0.433	
31	2691	1	PRE1A	3898	105	30	0.446	117.8
63	2690	1	PRE1A	3820	103	26	0.437	107.2
128	3644	2	PRE1A	7721	152	25	0.650	154.3
138	3113	1a	PRE1A	5900	118	22	0.582	
Depths are top depth of interval with measured pressure.								

Table 3.02 (cont.)

was removed at this time (although they considered that erosion was the cause). Several prominent, regionally sub-parallel slump scars are interpreted on the available seismic records from the area (Fig. 3.24). These sediments were redeposited further downdip in a partially consolidated state (Dingle, 1977; Dingle et al., 1983, p. 307). The exact timing of the slump event is not known but is discussed in section 3.9.5. Dingle (1977) comments on a core sample from the slump which contains Upper Miocene sedimentary rocks suggesting a Pliocene age for the slump although this may only reflect the age of the last slump. Certainly the disposition of the apparent slump scars lends support to the suggestion of multiple slumps over a period of time (Fig. 3.24).

3.5.2. Age

Biostratigraphically dated horizons in nearby SOEKOR wells can be extrapolated into the Southern Outeniqua Basin using seismic data and it is evident that the slumps do affect the latest correlatable sediments, which are Early Miocene in age. Available seismic data (Fig. 3.25) were recently re-interpreted to take into account recent stratigraphic data from distal wells drilled around the northern and western rim of the Southern Outeniqua Basin. Palaeocene rocks are shown to be consistently thick as far offshore as the main slump scar whilst the Eocene rocks appear to gradually thin (Figs. 3.26-3.28). This supports the contention of Partridge and Maud (1987) that the Early Palaeogene sedimentation rate was high but gradually decreased into the Neogene. All Tertiary and Latest Cretaceous sediment packages terminate at the glide plane which suggest that the strata were originally continuous into the basin. If so, this indicates that large volumes of these sediments (up to ~20000 km^3, Dingle, 1977) must have existed further offshore prior to the slump (Fig. 3.27).

The timing of the slump event has been modelled using Basinmod 1D (Platte River Associates, 1995), details of the modelling are provided in Chapter 7. The timing of slumping has been assumed as between 10-9 Ma, midway between the latest microfaunal age dating in the nearest well (McMillan and Valicenti, 1986), the suggestion of an Early Pliocene date by Dingle (1977). The model shows the subsequent build-up and dissipation of excess pressure to occur during the succeeding 9 Ma. The slumping may, however, have occurred later than this and it is possible that the event was Pliocene in age rather than Late Miocene. It is unlikely that the slumping took as long as 1 Ma - rather each of the several slump episodes would have been considerably more rapid. In geological terms, slumping is essentially instantaneous although some develop over periods of weeks or years (probably more likely creep) whilst other slumps occur within a day. In the marine environment, slumps could be much more rapid (Holmes, 1965, p.482-486; Piper et al., 1985). However, where slumps are caused by slope-steepening as a result of a regional tilting event, it is likely that each slump was separated from the next by a lengthy hiatus during which the

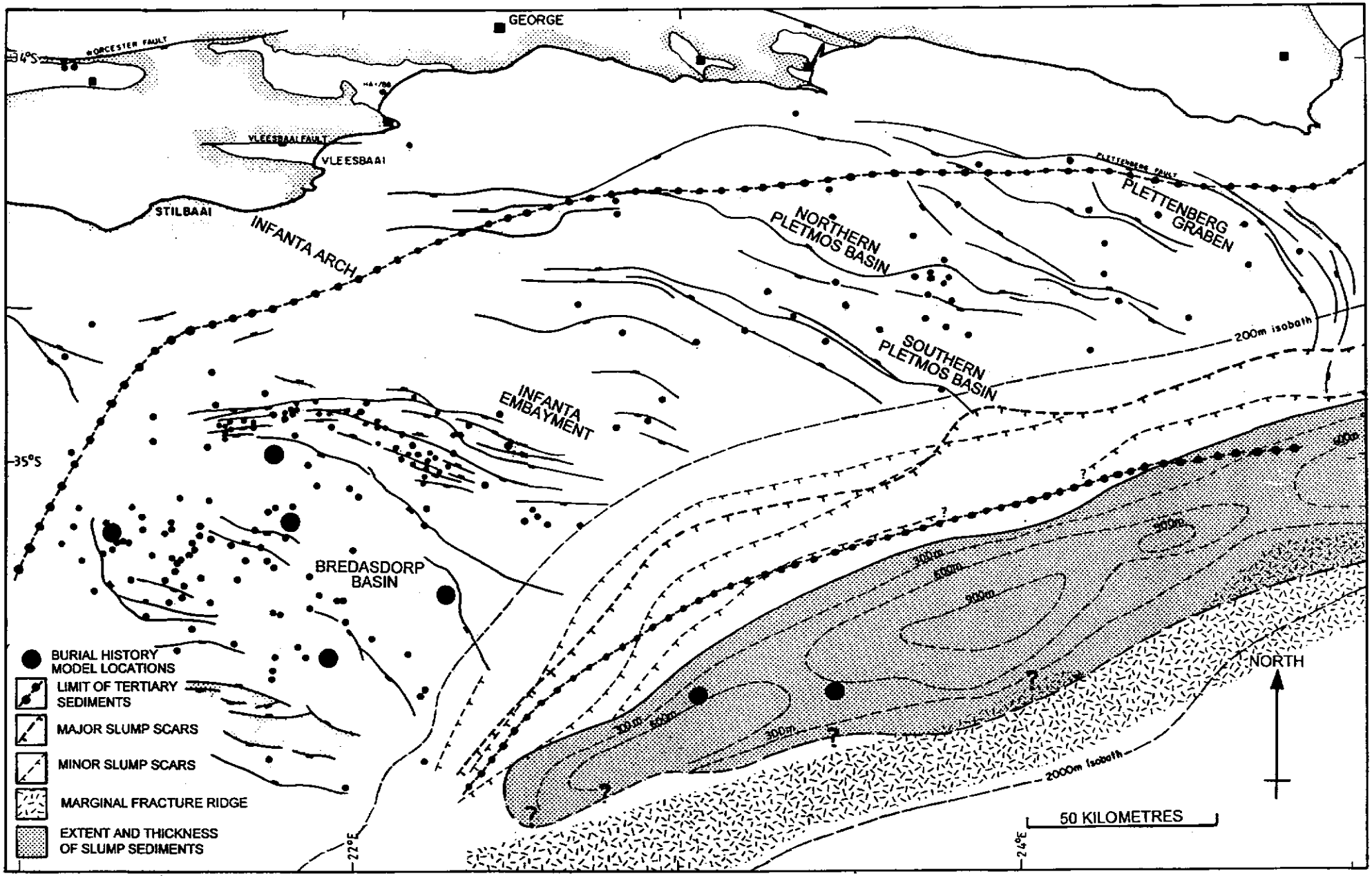

Figure 3.24: Map of the western half of the Outeniqua Basin showing the wells and major faults, the nearshore and deep water limits of the initially deposited pre-slump Tertiary sediments, the post-Early Miocene slump and its estimated thickness, the slump scars and the location of the two burial history diagrams in the Southern Outeniqua Basin used to characterise the slump.

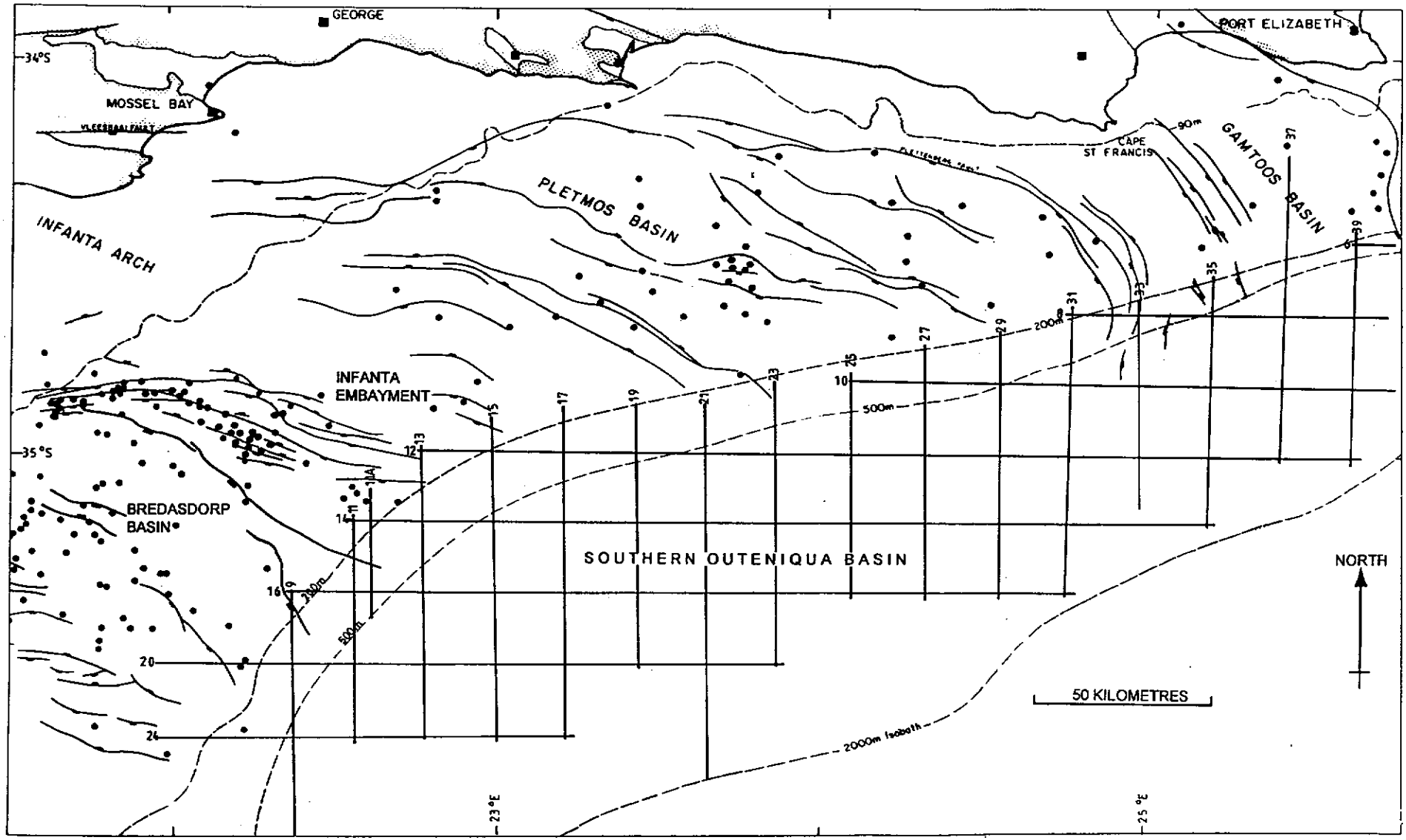

Figure 3.25: Map of the western half of the Outeniqua Basin showing the 1972 and 1974 reconnaissance seismic lines used in the study of the Southern Outeniqua Basin.

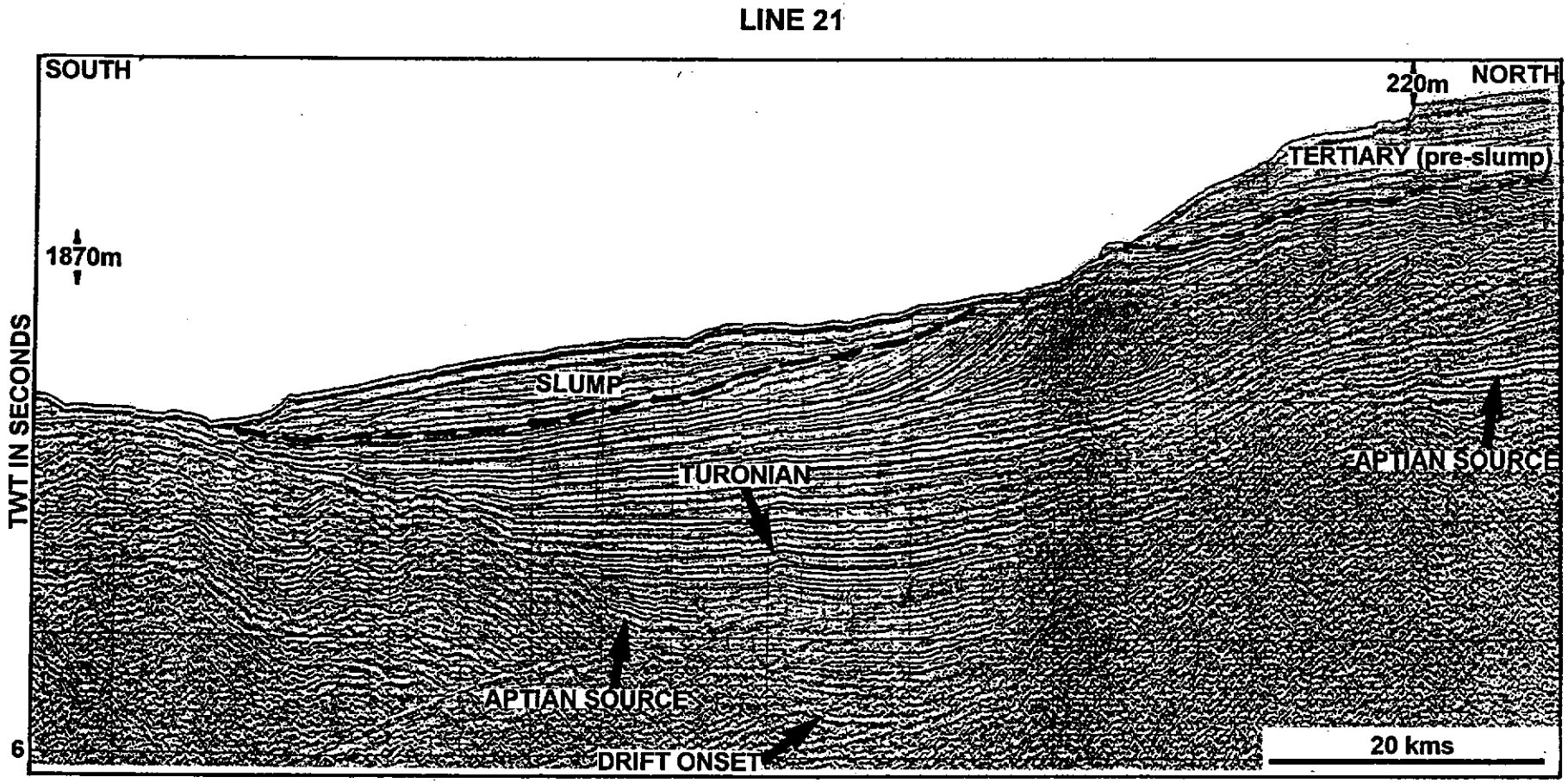

Figure 3.26: Part of one of the reconnaissance seismic lines (L72-021) showing the most recent interpretation of the slump and the pre-slump deposits. Several sea-floor 'steps' near the Infanta high are considered to be slump scars.

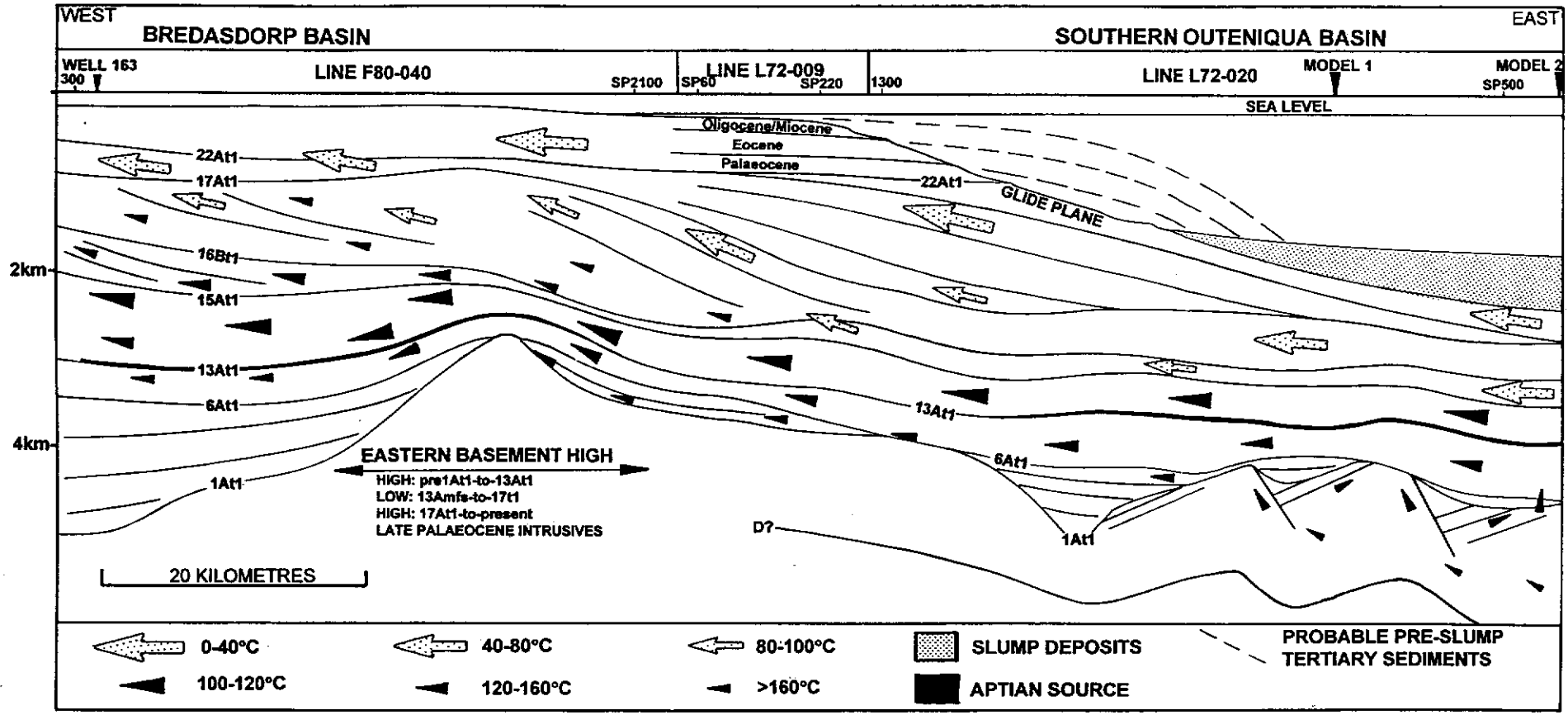

Figure 3.27: Depth-converted schematic diagram of composite seismic section through central Bredasdorp Basin into western Southern Outeniqua Basin along a traverse shown in Figure 3.30. Onlap of the 6At1-13At1 sediment package across the eastern high (between wells 8 and 12/13) is shown as well as the near-constant Early Tertiary sediment thicknesses out to the slump 'glide plane'. The position of basement is based on seismic character and is highly tentative. The central section of this traverse across the high is a portion of seismic line F80-040 across the high as shown in Figure 3.12. Intrusives evident on that line are omitted from this figure for clarity.

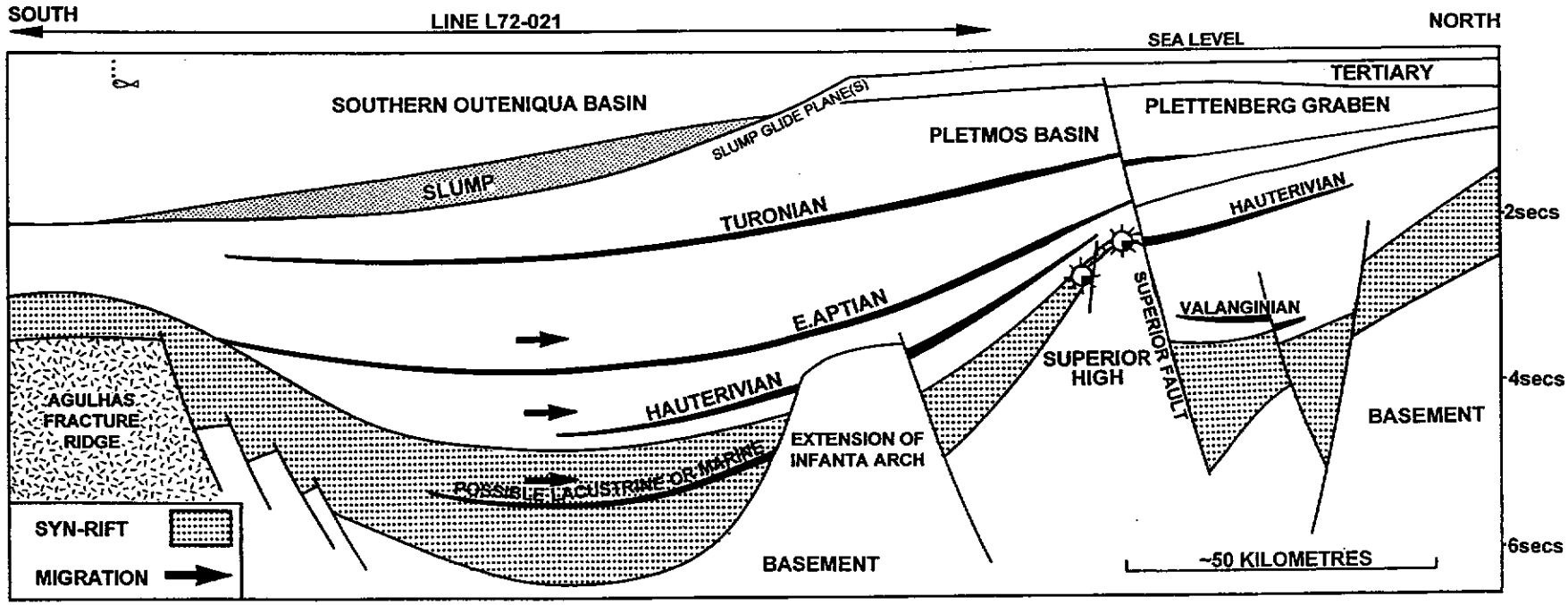

Figure 3.28: Diagrammatic section along seismic line L72-021 and further landward across the southern Pletmos Basin towards the Plettenberg Graben (after B. Munro-Perry, 1982, pers. comm.). The general seaward dip means that most fluids expelled from the Southern Outeniqua Basin migrate landward - in this case toward the Pletmos Basin.

expelled water migrated updip dissipating the excess pressure. Thus the period of slumping and hot-water flow could have spanned several million years.

3.5.3. Volumetrics

These large volumes of sediment removed from the shelf and redeposited in the basin must have profoundly affected the compaction and fluid flow from the pre-existing sediments. Not only would the flow direction of water from the sediment pile due to normal compaction have been directed toward the Bredasdorp Basin by the relative uplift of the continental plate and downwarp of the oceanic plate, but water expressed from the sediment pile as a result of the slumping would also migrate into the Bredasdorp Basin (Figure 3.29). Dingle (1977) comments on a maximum estimated thickness of the slump debris of 324 metres from the interpretation of a few seismic lines, whilst De Swardt and McLachlan (1982) comment on thicknesses up to 700 metres. This study shows up to 750 milliseconds (TWT) of sediments on some lines and up to 720 milli-seconds (two-way time) thickness of slump sediments in the central part of the Southern Outeniqua Basin (Roux, 1997, pers. comm.). Since these sediments could have been redeposited in a partly consolidated state (Dingle, 1977) and almost certainly were if they were affected by creep (Paull et al.,1996), they would be equivalent to at least 800 metres (possibly in excess of 900 metres) based on equivalent non-slumped sediments in surrounding wells (Fig. 3.24).

The area of the Southern Outeniqua Basin covered by the slump, from where expressed water could migrate into the Bredasdorp Basin, is shown in Fig. 3.29. The area is essentially that south of the southern Infanta Arch and its south-eastward projection.

3.5.4. Cause of slumping

The reasons for the slope instability, and by extension the age of slumping, are not known for certain because of the lack of suitable rock samples, although several possibilities exist:

(i) seismic shocks from fault movements (Dingle, 1977) although few faults extend shallower than the base of the Oligocene (Strauss et al., 1996),

(ii) increased sediment load from rapid deposition (Dingle, 1977) although Partridge and Maud (1987) show this to be unlikely,

(iii) slope undercutting by shelf edge erosion (see below)

(iv) dip steepening as the Southern Outeniqua Basin (and probably the Agulhas Fracture Ridge) foundered (Dingle et al., 1983) (see below),

(v) release of gas from hydrates during pressure reduction by low sea level acting as a plane of decollement (Paull et al., 1996).

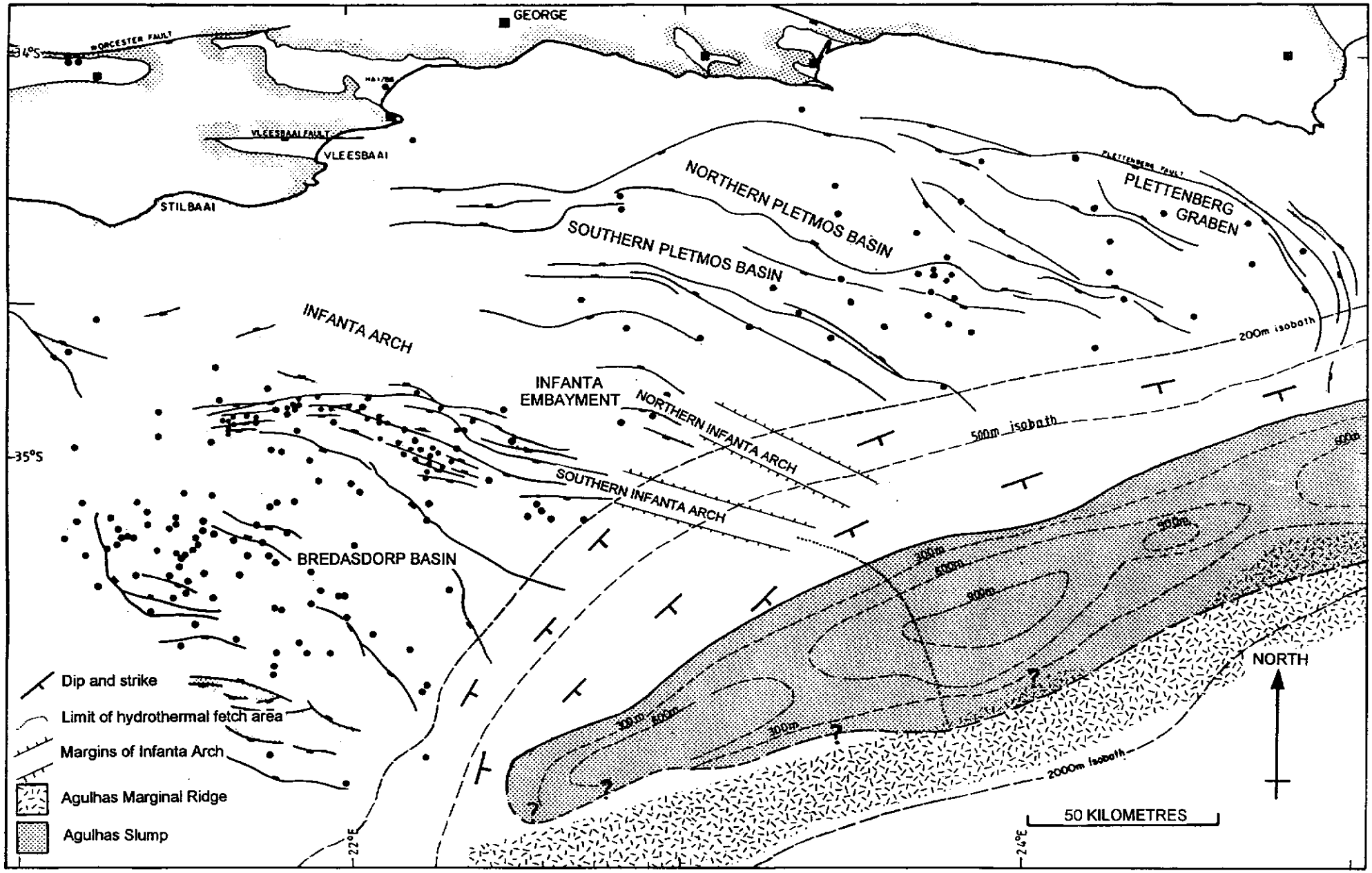

Figure 3.29: Map of the western half of the Outeniqua Basin showing wells, major faults, the distribution of slump sediments and the dip directions of the underlying sediments evaluated from reconnaissance seismic data.

Slope undercutting by shelf edge erosion

Sea-level oscillation was more intermittent during the Plio-Pleistocene than at present, but shelf edge erosion could not have happened then because the Agulhas Current was much further south - as far as latitude 38°S - and only weakly developed (Winter and Martin, 1990). In addition, there is little likelihood of the wave-base erosion of sediments downdip because the maximum Late Tertiary sea-level lowstand was only ~150m (Partridge and Maud, 1987) yet the slumped area is now in >700 metres of water. Erosion due to the Agulhas Current has been postulated (Winter and Martin, 1990). If erosion were the cause of the sediment planation, the current velocity would have to be higher than the minimum needed to remove claystone (i.e. ~0.2-0.4 m/s) in order to overcome the cohesion of the sediments and to remove partially compacted Upper Cretaceous sediments (Potter et al., 1980, pp. 10-12).

However, the Agulhas Current velocity decreases markedly with depth (Derbyshire, 1964). For example, the high velocity part of the Agulhas Current, where velocities attain 2 metres/second, is the warmest part where temperatures generally exceed 20°C. This is called the high temperature Agulhas Current (HTAC) and it flows near surface. By contrast, the cool Agulhas Current barely reaches temperatures of 17-20°C and generally flows at much less than half the speed of the HTAC. In fact, at depths below ~140 metres, the temperature rapidly decreases to <<15°C (SOEKOR unpublished Sniffer survey data, Davies, 1988a, Table 3.03 and Figs. 3.30-3.31) and the velocity drops substantially. Below 170 metres the mean velocity falls to <~0.2 metres/second (Derbyshire, 1964; Lutjeharms et al., 1981; Van Heerden, 1984) and it is this water which locally impinges on the sea floor. Indeed, silt and clay deposition dominates where the velocity drops below ~0.2 metres/second (Birch et al., 1986).

Dip steepening

A strong possibility for the cause of slumping is dip oversteepening. The driving force behind this could be tilting of the continental plate and localised downwarping of the oceanic plate as a result of the physical and thermal doming during development of a new mantle plume below south-eastern Africa, the 'African Superswell' (Hartnady and Partridge, 1995). The earliest evidence of formation of this swell is given as Late Miocene (Hartnady and Partridge, op cit.), i.e. coincident with the estimated age of slumping. Uplift during this event is thought to be ~900 metres on the east coast but only ~100 metres on the south-western coast. Accompanying the tilting, there would likely have been considerable seismic activity which could have added to the sediment instability as seen in other examples (Piper et al., 1985).

AGULHAS CURRENT DATA

PROFILE 1
S end of line 64
580000, 5960000, 21degE

DEPTH (m)	TEMP (degC)
4	23.1
15	23
39	20.5
66	18.1
91	17.1
115	15.6
136	14.55
164	14.35
190	14.05
214	13.85
239	12.45
263	11.8
289	11.25

PROFILE 2
S end of line 25
578000, 6029000, 21degE

DEPTH (m)	TEMP (degC)
10.5	20.8
20	20.75
25	18.1
29	17
37	16.4
46	15.95
52	15.7
63	15.6
73	15.2
83	15
92	14.55
101	14.2
104	13.9
115	13.4
123	13.55
127	13.5

PROFILE 3
S end of line 29
643000, 6099000, 21degE

DEPTH (m)	TEMP (degC)
9	20.9
16	16.3
27	15.2
49	13
64	11.9
84	10.8
101	10.1
125	9.6
156	9.1
168	9.1
184	8.8

PROFILE 4
S end of line 23E
631000, 6141000, 21degE

DEPTH (m)	TEMP (degC)
5	21.2
12	21.1
15	20.4
23	16.3
30	13.8
45	12.2
56	12
71	11.8
84	11.8
96	11.6
108	11.5

PROFILE 5
S end of line 42
237000, 6144000, 27degE

DEPTH (m)	TEMP (degC)
30	15.6
49	12.2
71	11.4
89	10.6
108	10.3
131	9.35
149	9.3
171	9.15
190	9.2

PROFILE 6
S end of line 57
395000, 6199000, 27degE

DEPTH (m)	TEMP (degC)
8	19.25
9	19.4
13	19.5
15	18.8
25.5	16
26	15.4
34	14.1
39	14.1
40	14
48	13.2
55	13.2
57	12.9
64	11.6
71	11
85	10.8
92	10.5
100	10.2

Table 3.03: Depth vs temperature data from six locations in the Outeniqua Basin used to construct the water column temperature profiles shown in Figure 3.21.

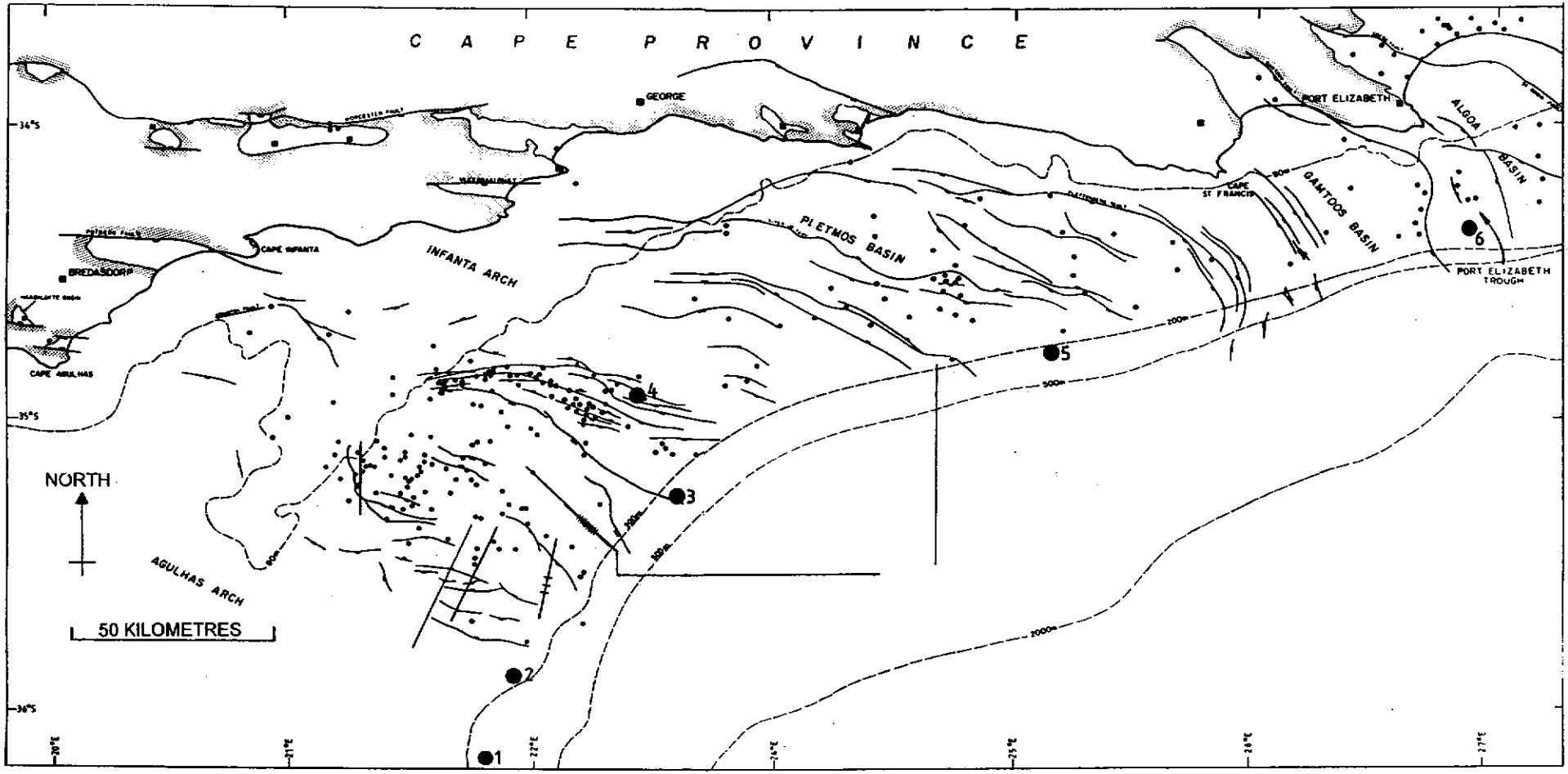

Figure 3.30: Map of Outeniqua basin showing the position of the six sea-water temperature profiles near the shelf edge recorded during the 'Sniffer' survey (Davies, 1988a). The tracks of seismic lines (from Figures 3.03, 3.04, 3.08, 3.12, 3.13, 3.26 and 3.27) and the plan location of the 'knolls' and intrusions, are shown.

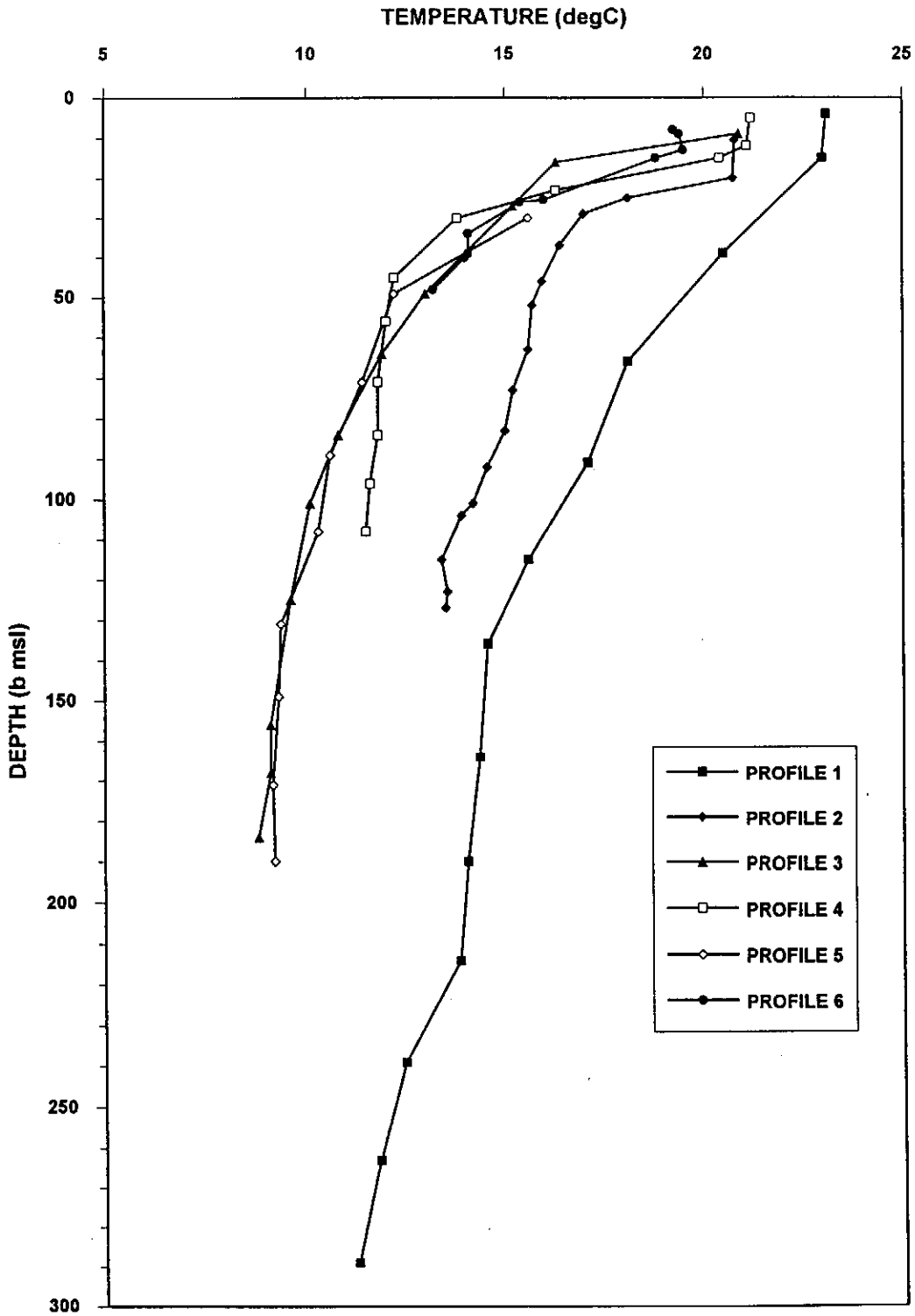

Figure 3.31: Composite plot of the 6 sea-water temperature vs depth profiles located on Figure 3.30. The two higher temperature profiles are from the south-western part of the Southern Outeniqua Basin where the edge of the Agulhas Current (see Figure 2.08b) impinges on the shelf - and shows the high temperature Agulhas Current (HTAC) barely extends deeper than 80 metres. Along the south-facing shelf break, south of the Pletmos Basin, the profiles show that the HTAC (considered the fastest part of the current and therefore the most likely to erode shelf sediments) extends no deeper than 30 metres. Data for these profiles are given in Table 3.03.

3.5.5. Fluid flow

The sudden addition of several hundred metres of partly compacted overburden would rapidly increase pore pressures in those sediments and since the pressure could not dissipate rapidly because of the overburden, it would bleed off slowly (Deming, 1994). Basinmod 1D modelling of the pressure build-up in these sediments (Fig. 3.32) has been carried out. This type of modelling is, however, less than perfect as it takes no cognisance of lateral fluid movements. In addition, the model is poorly unconstrained because of the lack of well data in the area. Nevertheless, it indicates pore pressure increases of several hundred psi and a 'bleed-off' period of some Ma, both dependent on assumptions of the lithologic type based on data from the surrounding wells (Fig. 3.32). Immediately after each slump, pressure would build up in the sediments deeper than ~2000 metres (bmsl), i.e. below the Turonian source rock claystones (but not above as those sediments are too porous and permeable to sustain overpressures). This claystone layer forms a regionally extensive seal to fluid flow and would channel fluids laterally updip rather than vertically. Modelled excess pressure does not build up in sediments in the top 2000 metres, probably because their high permeability allow near-instantaneous expulsion of water (Chapter 7). Below that depth the model shows a rapid rise in the excess pressure and a slow fall-off over the succeeding few million years.

The top 1500-2000 metres of original (pre-Miocene) sediments presently retain high permeability and porosity. Partial compaction of these sediments by deposition of 800 metres (or more) of sediment, would result in the expulsion of large volumes of water which should be able to flow essentially unimpeded updip and out of the basin through the shallow overburden. The remainder of the Cretaceous and Jurassic rocks in the basin, locally in excess of 8 kilometres thick (Ben Avraham et al., 1993), were already partially compacted and slump-related compaction effects would be less but nevertheless likely. The volumes of water expelled during this slump event could be very large. Estimates can be made from modelled porosity changes. Based on compilations of porosity versus depth data (North, 1985), and the calculated depths to the seismic horizons (Van Wyk et al., 1992; Wenham et al., 1991), models of the porosity changes (Fig. 3.33) match those shown by North (1985). From this, estimates of the amounts of water possibly expelled during the event are shown in Table 3.04. Evaluation of log porosities in sandstones in wells at the margins of the Southern Outeniqua Basin support these estimates.

The hydrothermal charge due to this slumping significantly altered the thermal regime of the Bredasdorp Basin, influencing hydrocarbon generation, and is discussed, together with the methodology of the temperature calculations, in great detail in Chapter 7.

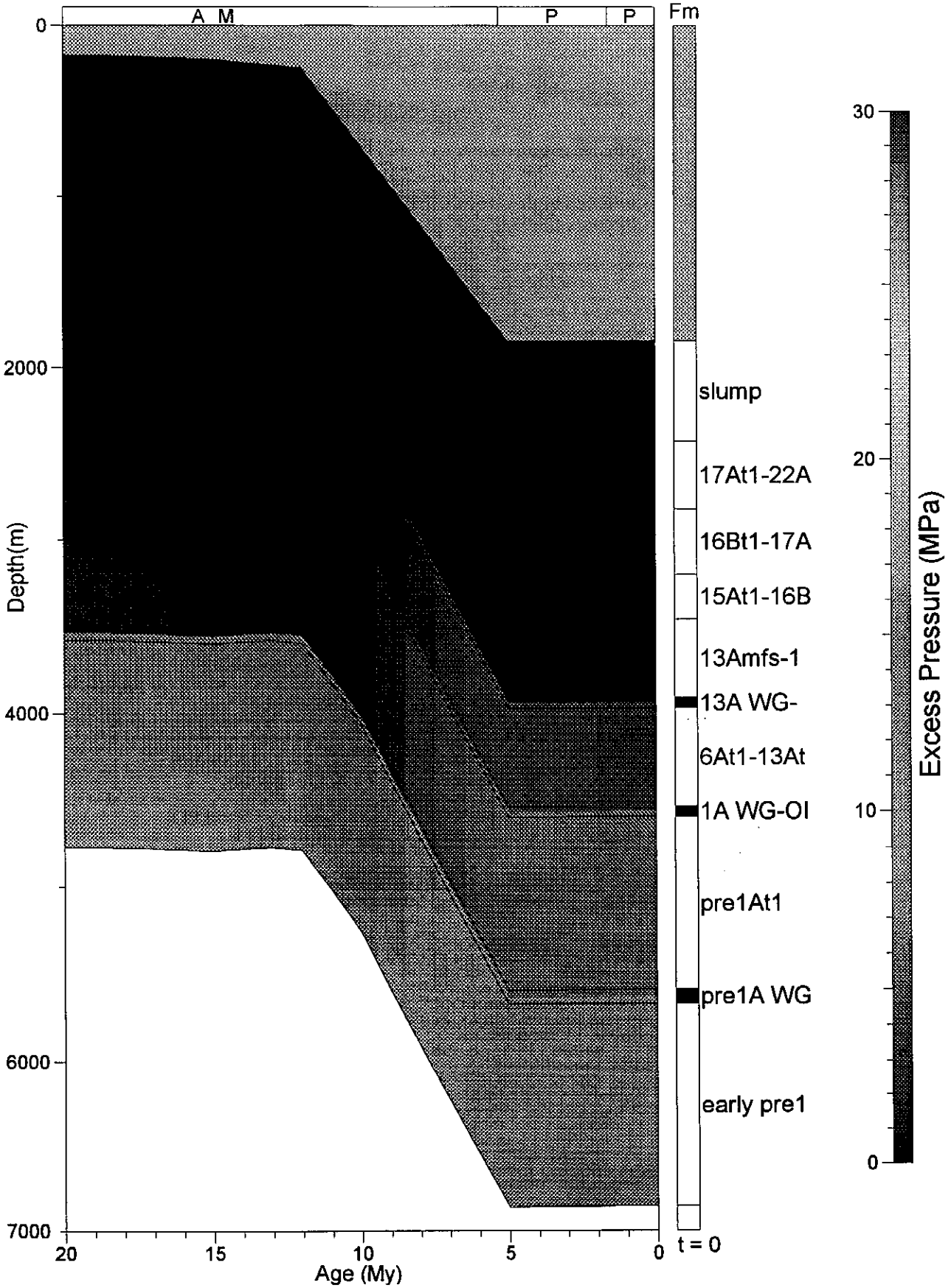

Figure 3.32: Basinmod plot of excess pressure (ie above hydrostatic) during the period of slumping (assumed to be 10-9 Ma) and thereafter. The model shows there is essentially no post-slump pressure increase in the uppermost 2000 metres of sediments in spite of large porosity reductions and concomitant release of water, probably because the high permeability and porosity of these sediments allow geologically instantaneous migration of fluids. Below 2000 metres, and especially below 3000 metres, fluid expulsion rates are limited due to modelled compaction-induced poroperm reductions and excess pressure of nearly 2000 psi is modelled to develop. Depending on the lithology, the model shows that this pressure decreases to hydrostatic over a few Ma.

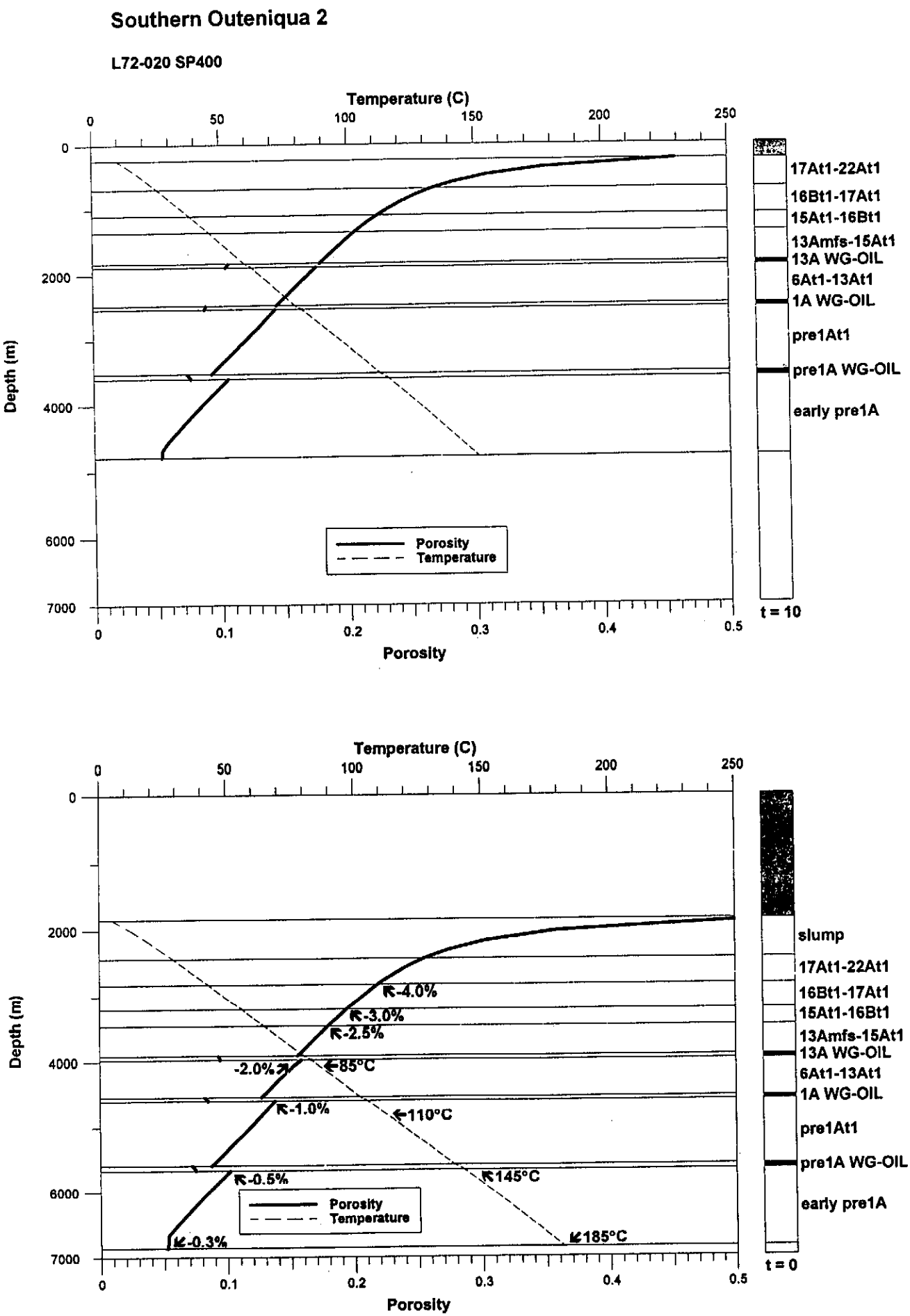

Figure 3.33: Porosity/temperature vs depth plots from Basinmod modelling at the eastern model location in Figure 3.28 for the period before and after the slump deposition. Modelled porosity losses and maximum temperature at selected horizons are used to calculate the volumes and temperature of expelled fluids.

ESTIMATED VOLUMES (km3) OF WATER EXPELLED BY THE AGULHAS SLUMP										
SLUMP	AVERAGE	POROSITY	AREA	0-800m	800-1600m	1600-2000m	2000-2400m	2400-3200m	3200-4000m	>4000m
THICKNESS	THICKNESS	LOSS	km X km	0-40degC	40-80degC	80-100degC	100-120degC	120-160degC	160-200degC	>200degC
	(metres)	proportion of		av. 8%	av. 5%	av. 3.5%	av. 2.5%	av. 1.5%	av. 0.75%	av. 0.3%
		600m loss		0.1	0.1	0.0	0.0	0.0	0.0	0.0
0-300m	200	0.33	1050	5.5	3.5	2.4	1.7	1.0	0.5	0.2
300-600m	500	0.83	1890	62.7	39.2	27.5	19.6	11.8	5.9	2.4
600-900m	750	1.23	1210	89.3	55.8	39.1	27.9	16.7	8.4	3.3
>900m	950	1.58	50	6.0	3.8	2.6	1.9	1.1	0.6	0.2
				163.6	102.2	71.6	51.1	30.7	15.3	6.1
		TOTAL	4200	TOTAL COLD-WATER LOSS			TOTAL HOT-WATER LOSS			
		AREA	km2	in km3 at <100degC =		337.4	in km3 at >100degC =		103.3	

POROSITY LOSS FOR 600m SLUMP		
Depth range	Porosity loss	Av. loss
0-800m	6-10%	8%
800-1600m	4-6%	5%
1600-2000m	3-4%	3.50%
2000-2400m	2-3%	2.50%
2400-3200m	1-2%	1.50%
3200-4000m	0.5-1%	0.75%
>4000m	0.2-0.5%	0.35%

Table 3.04: Thickness of Agulhas Slump sediments and areal extent of thickness increments. Volumes of water expelled and the modelled temperatures (derived from assumptions in Chapter 7-"Modelling") are also listed.

CHAPTER 4. PETROLEUM GEOCHEMISTRY OF BREDASDORP BASIN AND ADJACENT SOUTHERN OUTENIQUA BASIN

The Bredasdorp Basin and adjacent Southern Outeniqua Basin contain all the factors usually considered necessary for hydrocarbon prospectivity namely:

(i) source rocks that have demonstrably expelled hydrocarbons (this study)
(ii) conduits for hydrocarbon migration and reservoiring (i.e. continuous sandstones and fault-connected sandstones) exist at several levels in the basin
(iii) sandstones retain enough original porosity (or have diagenetically-enhanced porosity) to reservoir large volumes of hydrocarbons
(iv) many of these sandstones are over- and underlain by claystones which are locally over-pressured capillary seals preventing escape of hydrocarbons
(v) several families of hydrocarbons have been reservoired and can be correlated to nearby source rocks (this study).

Relevant aspects of each of these factors will be addressed in this section whilst the samples and analyses are discussed in subsequent chapters.

4.1 SOURCE ROCKS

Source rocks have been defined as "a volume of rock that has generated, or is generating, and expelling hydrocarbons in sufficient quantities to form commercial oil and gas accumulations" (Brooks et al., 1987). A potential source rock is one which "could generate hydrocarbons given the right conditions" (Brooks et al., 1987). Other authors omit the commercial reference but comment on maturation, e.g. "rocks containing sufficient organic matter of a suitable chemical composition to generate and expel hydrocarbons at appropriate maturity levels" (Miles, 1989). In order to be a viable source rock, the quantities of hydrocarbons which can be (or have been) generated must exceed the amount necessary to fill a portion of the pore spaces in the source rock and satisfy the adsorbency of the maceral grains before expulsion can commence. Indeed many source rock definitions include comment on both the quantity of sedimentary organic matter and the amount of hydrocarbons generated.

Source rocks can form in both non-marine (fluvial and lacustrine) and marine detrital environments and can be clastic-dominated or carbonate-rich and biogenic-dominated.

4.1.1. Source potential of clastic lithologies

Clastic source rocks are fine-grained, clay-rich sediments containing larger than average quantities of organic matter. Clay-rich rocks are generally only considered to

be potential source rocks if the total organic carbon (TOC) content exceeds 1% by weight (Tissot and Welte, 1984). Since the average organic carbon content of several of these fine-grained sediments is <1% by weight, they are considered potential source rocks (Ronov, 1958; Dow, 1977). This cut-off is an empirical one, based on data from various studies which show that sedimentary rocks with TOC contents less than this, even though they may generate hydrocarbons, do not expel them in any significant quantity. This is largely because smaller amounts of organic matter are generally widely dispersed through the rock and not concentrated in one region. In practice, effective source rocks often contain >2% TOC and may even exceed 10%, e.g. Bakken Shale (Williston Basin, Canada) and Kimmeridge Shale (North Sea). It is also shown (Ronov, 1958; Dow, 1977; Demaison and Moore, 1980) that many non-source argillaceous sediments contain <<1.0% TOC and that the difference between TOC contents in prolific source rocks and non-source rocks can be greater than an order of magnitude.

Large amounts of organic matter, suitable to form source rocks, can be concentrated in clastic sedimentary rocks as a result of three processes:
(i) enhanced preservation
(ii) high organic productivity
(iii) sediment starvation
Considerable study has taken place during the past two decades in attempting to understand the relative importance of each TOC enhancement process.

4.1.1.1. Enhanced preservation of organic matter.
Enhanced preservation is due mainly to the development of anoxia. In low oxygen environments, there are few organisms at the sea-floor or in the topmost sediments which can scavenge organic material (Demaison et al., 1988) - hence, the organic matter content of sediments preserved under such conditions is higher than in oxidising environments.

Anoxia can develop regionally for a number of reasons but dominates in one of two main depositional settings:
(i) restricted circulation due to the presence of a barrier (such as a landmass) to open ocean circulation (Fig. 4.01)
(ii) water stratification due either to the development of a halocline or separate water masses having different temperatures (Fig. 4.02).

4.1.1.2. Enhanced productivity of organic matter
Pederson and Calvert (1990) showed that biogenic decomposition of organic matter occurred at the same rate whether the seafloor conditions were oxic or anoxic. Hence

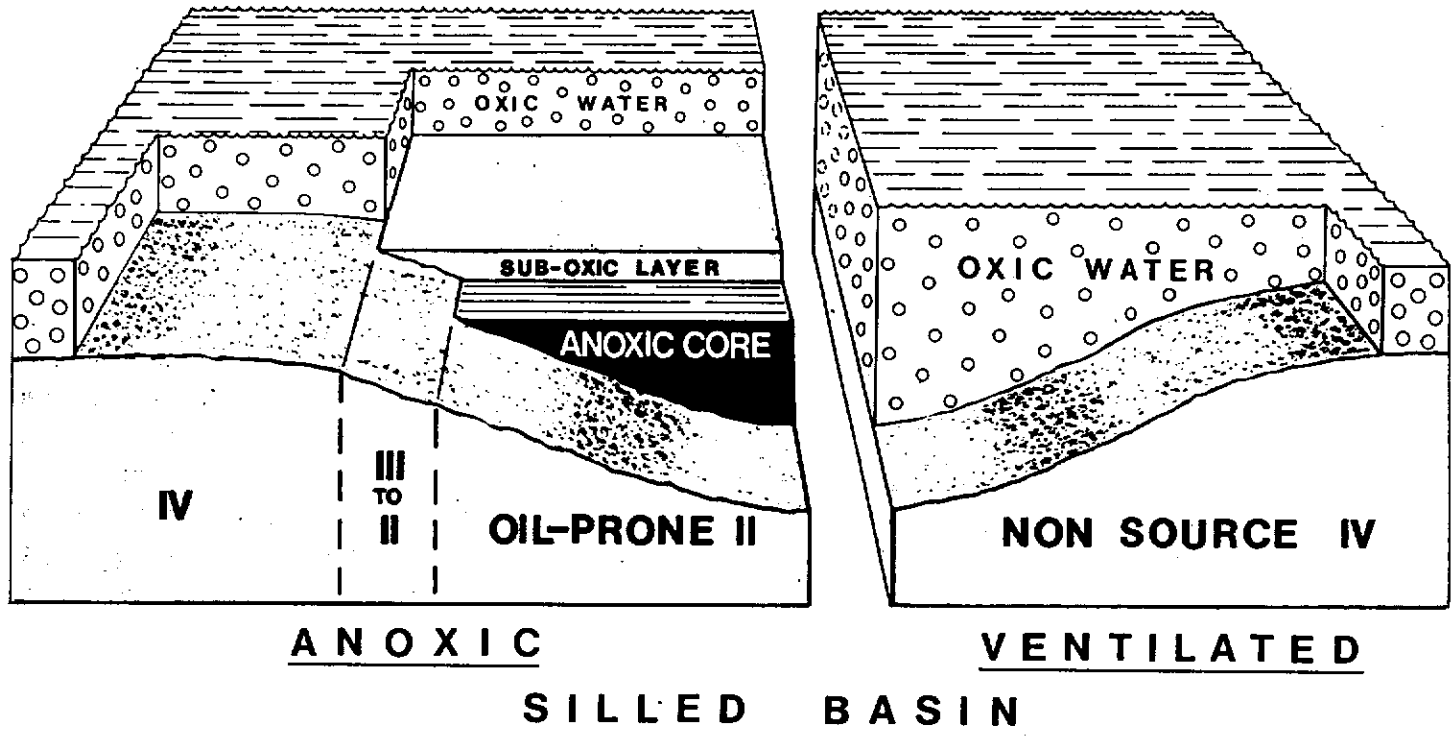

Figure 4.01: Schematic sections through anoxic and ventilated silled basins (from Demaison et al., 1988). The anoxic basin has a core in which oxygen levels are low. In such situations, organic matter generation is high in the surface waters and its preservation through the passage from sea level to sea floor is enhanced because of the limited scavenging of organisms. Hence high proportions of organic matter, in particular high hydrogen material, is preserved.

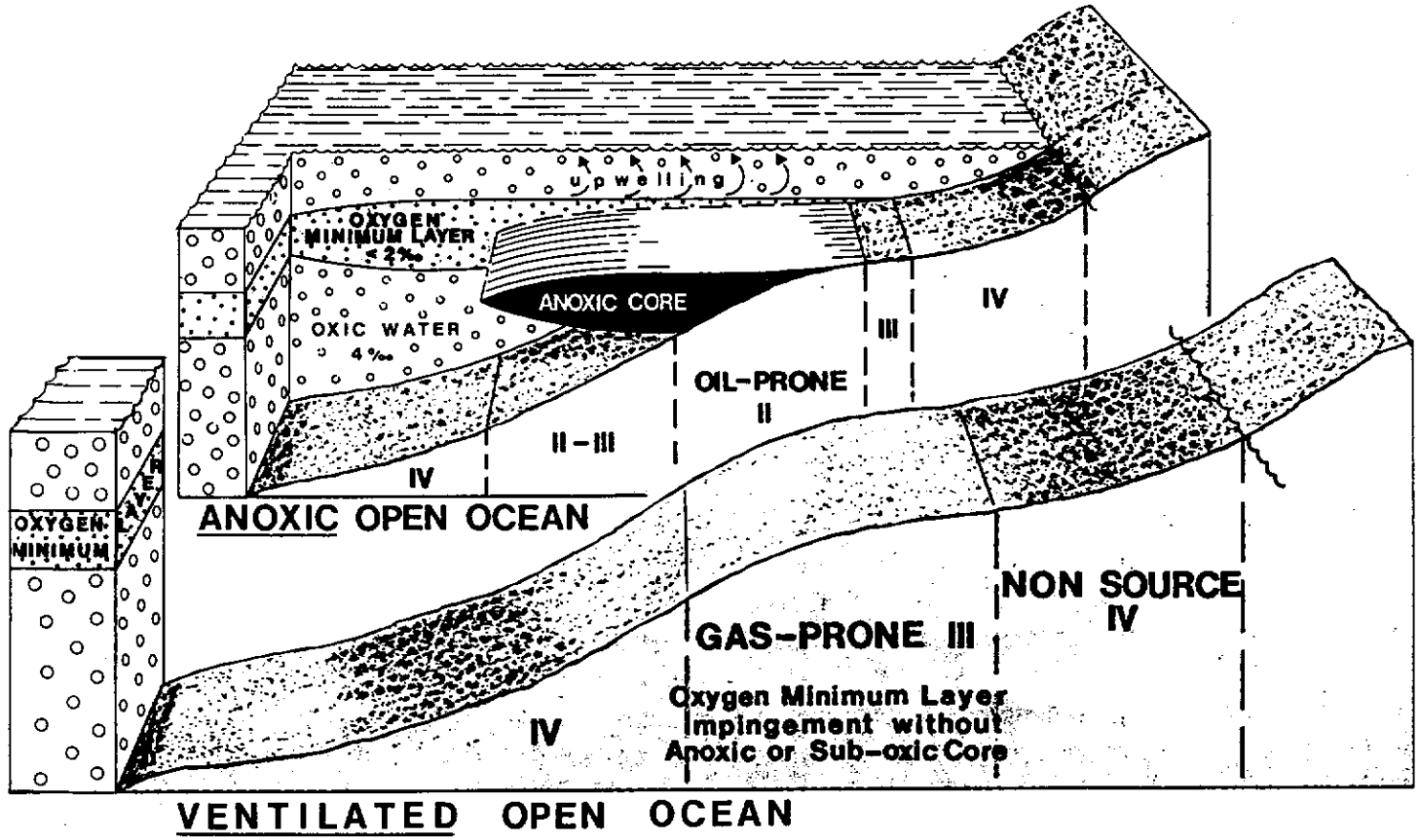

Figure 4.02: Schematic section through a basin in which open oceanic circulation prevails but where high organic productivity occurs and bacterial decay is enhanced which results in development of an oxygen minimum layer (after Demaison et al., 1988). Where this layer impinges on the basin floor and margins, or even where it closely approaches these regions, scavenging destruction of the most lipid material is largely prevented - large amounts of high hydrogen organic matter becomes deposited and incorporated in the sediments. In this situation, a mixed oil and gas prone zone is commonly found seaward of the main oil prone (oxygen minimum) zone.

they favour a model which relies on an increased organic productivity to result in the formation of source rocks. In this model, the oxygen minimum is located in the mid-water column (rather than at the sea floor) and organic-rich sediments are deposited directly beneath it. One such location where this commonly occurs is in mid-latitudes (i.e. 30-40°S and N) where a large temperature difference exists between deep, cold, oxygen-rich bottom water and warm, oxygen-poor surface water. This results in a relatively stable water column with essentially no mixing (Demaison et al., 1988). At the contact between these two layers, a prolific food-chain develops and oxidation of the resulting large amounts of organic material uses up the free oxygen in the water - resulting in a low oxygen layer (Fig. 4.02).

This is occasionally enhanced where trade winds blow continuously on the south-western sides of southern hemisphere continents. Warmer surface waters are forced westwards, cold water wells up from below and the waters mix, so that in the nutrient-rich water, an explosive organic growth results. Decay processes, operating with consumption of the organisms by bacteria and plankton, uses up oxygen in the water column and 'blooms' of phytoplankton occur. This effect is likely to result in high concentrations of organic matter entering the sediment cycle - partly because the scavenging organisms are overwhelmed by the large amounts of organic matter and cannot reduce it.

Demaison and Moore (1980), however, suggest that periodic wholesale mixing of water columns, thought to be responsible for much of the source rock deposition, is likely to occur where there is a stable warm upper-water surface column. Under those conditions, the high rate of input of organic matter to the bottom water is exacerbated during overturning events when high-oxygen, nutrient-rich, cold bottom-water upwells and biotic blooms occur. Assuming present climatic conditions prevailed, the early Cretaceous palaeo-location of South Africa at ~55°S (McMillan, 1986) places the continent in a cool surface water environment where continuous mixing is likely, which would result in the development of a large scavenging community in the water column and at the sea floor so that periodic development of anoxia would not occur. Pederson and Calvert (1990) consider that these conditions may not have been operative in South African waters during the Late Jurassic and Early Cretaceous because open marine conditions had not developed. However, once the continents had separated enough to allow establishment of open marine conditions, during the Mid-Late Cretaceous (and even into the Tertiary (Frakes and Kemp. 1972), such stability would occur. Under the 'greenhouse conditions prevailing in Mid-Late Cretaceous, stable warm water columns extended further south (Barron, 1983: Pederson and Calvert, 1990) and water-column mixing was less regular, resulting in periodic development of biotic blooms which, where preserved, resulted in source rock formation. Cornford et

al. (1986) suggest that the Kimmeridge Shale may be an example of this type of source rock and it is thought that the Hauterivian-Aptian sources in the Bredasdorp Basin also represent such an example.

4.1.1.3. Sediment starvation

Loutit et al., (1989) show that organic carbon enrichment and source rock development usually occur during periods of highstands associated with sediment starvation episodes. Burden (1992) therefore suggested that the 13A source rock interval was deposited during a period of sediment starvation. However, the average sedimentation rate of this source sequence (SOEKOR unpublished biostratigraphic data) is ~47 metres/Ma (using the time scale of Haq et al., 1987) which does not indicate any significant sediment starvation.

By way of contrast, in the northern part of the North Sea, the richest source shales are approximately 200 metres thick (Bailey et al., 1990). They were deposited during the Brent and Early Heather periods, which Thomas et al. (1985) show to extend from Bajocian through Callovian (i.e. ~18 Ma). This indicates a sedimentation rate of about 11 metres/Ma, typical of that in periods of sediment starvation (Loutit et al., op cit.).

In the Bredasdorp Basin, the Turonian source rock interval was deposited at an even lower sedimentation rate (~7 metres/Ma) suggesting sediment starvation as the prime cause. However, the existence of intervals of sediment starvation (typified by 'condensed sequences') without source rock development (Benson et al., 1993) demonstrates that starvation does not always ensure source rock development.

4.1.1.4. Other factors

Whichever model of source rock development is more likely - if indeed it is possible to select one or the other - the conditions responsible for their formation were enhanced by the following additional factors:

(i) the period of major development of Mid-Cretaceous source rocks has been correlated with sea level fluctuations, palaeo-surface temperature maxima and the 'Long Cretaceous Normal' magnetic non-reversal period. All of these can be related to periods of increased mantle activity and initiation of plume generation (Veevers, 1990; Larsen, 1991) and related increases in carbon recycling from the mantle. These result in a propensity of Mid-Upper Mesozoic sedimentary rocks to be organic-rich.

(ii) Pederson and Calvert (1990) and Larsen (1991) also demonstrate that with the high CO_2 contents thought to have dominated during the Mesozoic (Barron and Moore, 1993) a global 'greenhouse' could have prevailed. This would have resulted in higher

water temperatures. Warmer water tends to have reduced oxygen levels resulting in sediments being deposited in a dominantly low oxygen environment with fewer bottom-living organic matter scavengers.

(iii) Pederson and Calvert (1990) also suggest that globally, wind speeds would have been higher because of enhanced Hadley cells. This could result in increased influx of moist air from high latitudes to the tropics and hence globally, rainfall would have been higher. This generally moister climate would be enhanced in southern Africa by the presence of the Cape Fold Belt mountains which acted as an obstacle to the northward movement of these air masses. These conditions would result in greater plant growth and increased runoff resulting in larger inputs of terrigenous organic material to the marine environment, which would become more organic-rich. In offshore basins, all sediments contain some terrigenous material. Sediments deposited during the syn-rift period are generally coarse and oxidised so that remnant organic matter tends to be only the most refractory material. Indeed, many of the sediment intersections contain wood in the form of tree trunks or fragments of wood (Du Toit, 1954, p. 374-387; Rigassi and Dixon, 1970; McLachlan and McMillan, 1979). Where recognised in the onshore Algoa and offshore Bredasdorp Basins, lacustrine rocks contain remnants of lake flora such as reeds and limnological fauna. Sedimentary rocks preserved from post-rift periods, especially Mid-Cretaceous, locally contain woody material (Du Toit, 1954, p. 393-395) and thick coals are developed (wells 3 and Ga-D1, Davies, 1979). A significant proportion of organic material in the marine sediments is also shown optically or chemically to be terrigenous. Much of this material probably comes from a coastal vegetated belt, similar to the present, as Du Toit (1954, p. 408) shows that most of the interior of the continent was relatively dry throughout the Late Mesozoic.

4.1.2. Source potential of carbonate lithologies

Carbonate sediments deposited in shallow, warm-water, low-oxygen environments are common world-wide and often prolific source rocks. Their kerogen is often comprised of finely disseminated amorphous material with a high oil potential. The Bredasdorp Basin has been a deep, cool-water mud-rich basin (McMillan et al., 1997) and contains little carbonate sediment except in the Tertiary. In those carbonates, source potential is uniformly low.

4.1.3. Types of organic matter and their products

There are four main types of detrital organic matter found in source rocks:
(i) refractory (e.g. inertinite or vitrinite) with low hydrogen
(ii) structured (lipid-rich, e.g. algal, exinite) fluorescent, high hydrogen
(iii) amorphous/sapropelic (e.g. lipid-rich), fluorescent, high hydrogen
(iv) amorphous (low hydrogen, non-fluorescent), low hydrogen.

The relative proportions of these four types of organic matter determine the source potential.

(i) Refractory organic matter is comprised largely of condensed, polycyclic aromatic rings with few alkyl groups and little hydrogen so they cannot be readily converted to hydrocarbons. They also require a high activation energy to crack their condensed structures and tend to mature later than aliphatic material. Such material is generally terrigenous, being mainly comprised of cellulose-rich woody material rich in oxygen. Most woody material is deposited in nearshore estuarine and deltaic-continental environments where plant input is high and sediment reworking common - both contributing to continual attack by scavengers. Woody material has a high preservation potential because it has few chemically reactive moieties - hence the lipid fraction is generally removed from the material leaving the highly condensed core of the lignin. If this kerogen has any source potential, it is largely for gas although some forms of terrigenous material can generate waxy oil (Fleet and Scott, 1994).

(ii) Structured high-hydrogen material generally comprises exinite (e.g. spores, pollen) and has the potential to generate wet gas and oil. Algal material, which is also structured but often only in the form of flowed structures, has a very high oil potential.

(iii) Amorphous organic material is usually assumed to be high-hydrogen forms such as bacterially altered marine organic matter. This is formed under low oxygen conditions where anaerobic bacteria reduce sulphates and oxygenated organic matter for oxygen and deposit the sulphur as H_2S, pyrite or other metal sulphides. Thus these amorphous sapropelic claystones are often black - partly from the finely disseminated organic matter and partly from the presence of sulphides. In the oil window, this material fluoresces - which distinguishes it from low-hydrogen material.

(iv) Low-hydrogen amorphous material is commonly found only where humic acids are incorporated into the sediment in large volumes. Even where matured into the oil window, this material does not fluoresce, by contrast with high-hydrogen material. Fluorescence is therefore only used to differentiate the two types in the oil window. In the absence of first cycle vitrinite, this maturity level can only be determined from chemical parameters, such as Tmax, production index and extracted hydrocarbon GC's and other optical parameters such as TAI, spore fluorescence (Chapter 6).

4.1.3.1. Distribution of organic-rich sediments in Bredasdorp Basin

In the oxygen minimum model, the basin would be expected to have a band of source rock around the edge of the basin coinciding partly with the intersection of the oxygen

minimum layer and its shadow with the sea floor. Hence, where source rocks are present mainly in the basin centre this provides support for the restricted anoxic basin model, whilst where source rocks are absent from the centre but present around the edges, it lends support to the oxygen minimum model. Where source rocks are only locally developed (and not restricted for tectonic reasons) it could indicate the local sediment starvation model. Each of these three types of source rocks are found developed in the marine drift sediments in the Bredasdorp Basin - and discussed in detail in Section 4.2.

Isolated half-graben infilled with clastic non-marine sediments characterised the pre-rift sedimentation. In some of them, lacustrine argillites are found, and in two wells, DWK-1 onshore (Davies et al., 1991; Fig. 3.30) and well 89 offshore (Figs. 2.05 and 4.03), these locally possess oil source potential.

Marine source rocks are associated with rapid sea-level rise and continental shelf flooding during which explosive colonisation of hitherto exposed (nutrient-rich) shelf occurred. Yet the rate of subsidence needed to generate each sequence boundary is far greater and far more rapid than could be accounted for by regional thermal decay and probably indicates a tectonic influence. In general, each post-rift transgression extended further landward culminating in the Turonian when sea-level advance reached a maximum. Under these conditions, increasing distance from the sediment input results in sediment starvation which in turn leads to increased proportions of organic matter incorporated into the sediment.

The general trend of rising sea-level through the Early and Mid Cretaceous may be related to post-rift thermal decay which gradually lowered base level (Haq et al., 1987). Hence most source rocks are formed partly as a result of sediment starvation. After deposition, diagenetic alteration of the organic material in the first few hundred metres of burial reduces most of the oxygenated functional groups and converts most hydrolyzable material to polycondensed macro-molecules, while micro-organisms recycle amino acids and sugars. Below these depths, the resulting organic material has a much higher preservation potential than detrital organic matter and is referred to as kerogen (Tissot and Welte, 1984).

The type of hydrocarbons generated and expelled classify the source rocks as "oil-prone", "wet gas-prone" and "dry gas-prone". In general, all source rocks generate both oil and gas but in different proportions, e.g. oil represents 60-70% of the hydrocarbons generated by oil-prone (i.e. sapropelic) source rocks but only ~5% of the product of dry gas-prone (i.e. refractory) source rocks.

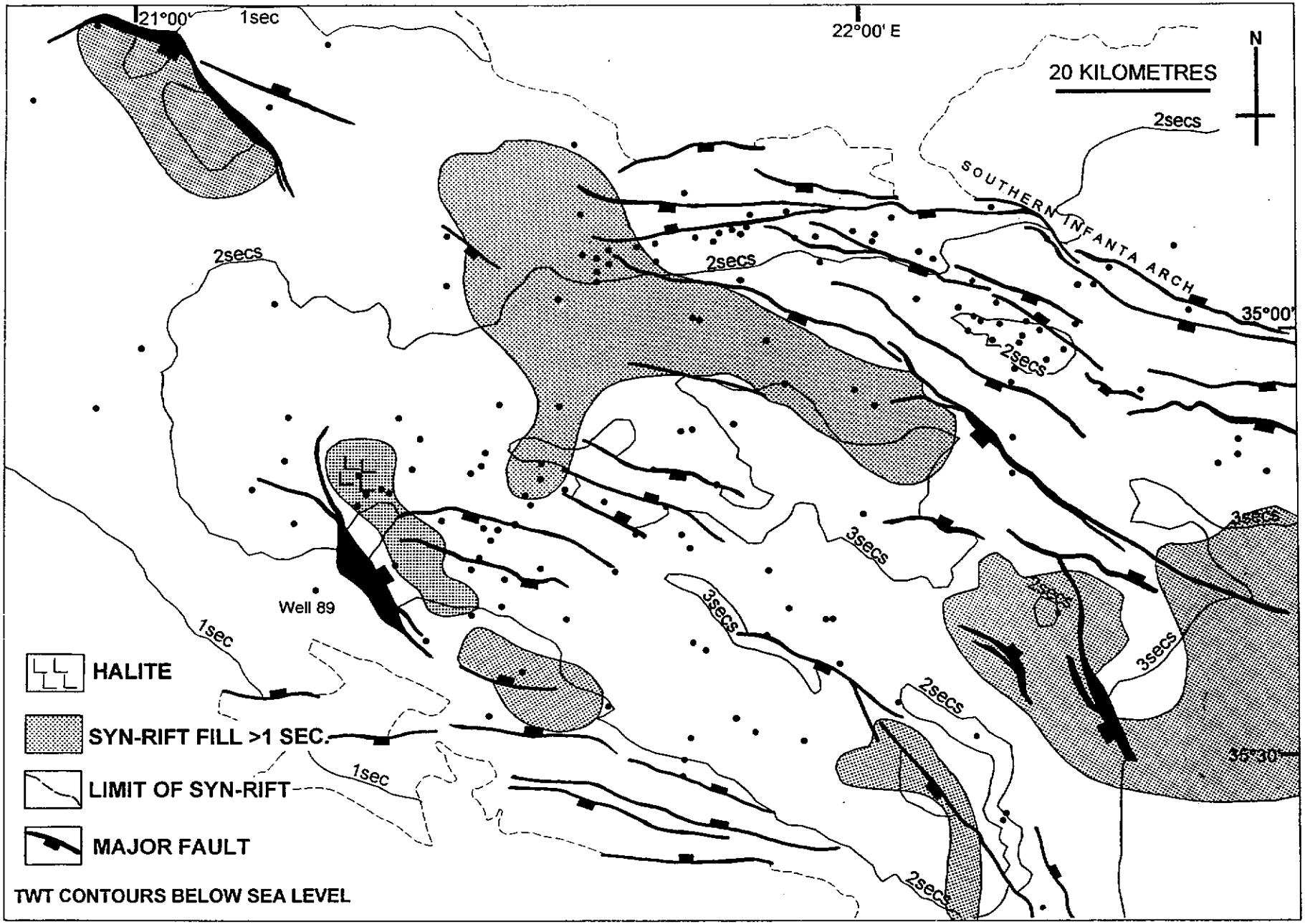

Figure 4.03: Two-way time contour map to horizon 1At1 in the Bredasdorp Basin showing the graben in which syn-rift sediments exceed 1500 ms in TWT thickness (from Burden, 1993).

4.1.3.2. Distribution of organic-rich sediments in Southern Outeniqua Basin

As the western part of this basin lies immediately down-dip of the Bredasdorp Basin, mature organic-rich rocks could act as sources for hydrocarbons in the Bredasdorp Basin. Predictions of source rock development can be made based on the known distribution of source rocks in the surrounding basins, their regional synchroneity and their matching seismic signatures, namely a high impedance contrast with the super- and subjacent rocks. In addition, DSDP wells on the Maurice Ewing Bank, east of the Falkland Islands, which was conjugate with the Outeniqua Basin, also contain matching Aptian and Upper Jurassic source rocks. There is no reason to suppose they were not deposited in the Southern Outeniqua Basin when the landmasses were in contact. However, as no wells have yet been drilled in this basin, discussion of source rocks there is speculative.

4.1.4. Measurements of source rock quality and quantity

Source rocks are usually characterised in terms of the quantity and hydrogen richness (often referred to as quality) of the organic matter, their log character and their seismic expression. These analytical methods are briefly described here and discussed in detail in Chapter 6.

4.1.4.1. Chemical and optical analyses

The minimum amount generally regarded as necessary to constitute a source rock is TOC 1% (mass). For convenience, this is usually measured by combustion (e.g. using a LECO instrument) although a wet chemical process (Loring and Rantala, 1992) was used for some of the earliest analyses. An estimation of the quantity of kerogen can be made from the amount of material recovered during the kerogen separation process, but this depends largely on which processed fraction is used. Of equal importance to the study of quantity and quality are (i) the type of organic material, as this must be able to generate hydrocarbons within the oil or gas windows and (ii) its thermal maturation, which determines the depth at which hydrocarbons are generated.

Fine-grained sediments generally contain larger proportions of hydrogen-rich organic matter (e.g. sapropels) and constitute source rocks for oil, in contrast with coarse-grained rocks (e.g. silts) in which the organic carbon is generally refractory, hydrogen-poor, (e.g. vitrinite) and largely gas-prone (Tissot and Welte, 1984).

The character of the organic matter is often best determined from optical studies in which the kerogen is separated from the mineral matrix (by acid dissolution of the minerals) and studied under transmitted light. Structurally distinct hydrogen-rich material (e.g. spores, algal masses) or amorphous matter, usually fluoresces except where over-mature. As the material is matured, hydrogen-rich chemical compounds

are generated and the organic matter becomes less hydrogen-rich - hence any evaluation of the potential of source rocks should be carried out in conjunction with maturity analyses.

The hydrogen proportion can also be estimated from chemical analyses using the Rock-Eval method (section 6.2.1.) This is a method which requires minimal sample work-up and is carried out routinely on all samples. Chemically, hydrogen-rich macerals have high S2 (remaining hydrocarbon potential) and low S3 oxycarbon (≡ carbon dioxide and monoxide) potential at low maturity, whereas structured low-hydrogen high-oxygen macerals (e.g. vitrinite, inertinite) have low S2 and high S3 values. The ratio S2/TOC is the hydrogen index (HI), and is a measure of the amount of hydrocarbons which can be generated from each unit mass of kerogen. Similarly, the ratio of the S3 peak to TOC is called the oxygen index (OI) a measure of the oxygen content of the kerogen. Rich source rocks, including some coaly kerogens (Espitalié et al., 1985; Fleet and Scott, 1994) have original HI values in excess of 400. This figure reduces with increasing maturation as hydrocarbons are generated and expelled but some are retained as increased S1.

A further analytical approach used with immature samples is that of kerogen kinetic analysis. The results of these analyses provide not only a detailed understanding of the chemical kinetic break-down rate of the organic material but also the maturation levels at which that occurs. A detailed description of the hydrocarbon characteristics of source rocks is summarised in Tissot and Welte (1984) and Brooks et al. (1987).

During maturation, the kerogen breaks down at characteristic rates initiated above specific energy thresholds. These break-down characteristics have been measured on a number of samples using a Rock-Eval 2 instrument. The results of these analyses are used in the hydrocarbon generation modelling carried out for this study (Table 4.01).

4.1.4.2. Log character

Source rocks are often recognisable by their geophysical log characteristics. For example higher-than-background log responses, i.e. gamma log (+10 API), slow sonic travel time (commonly accentuated by compaction disequilibrium and overpressure) (+15 μsec/ft), high resistivity (+2-5 Ω/m) and lower density are common in source rocks (Cornford, 1986; Davies, 1990; Van der Spuy, 1991; Creaney and Passey, 1993). The common paucity of accurately located samples in wells (e.g. sidewall cores and cores) frequently leads to a reliance on log character to extrapolate between samples.

4.1.4.3. Seismic character

KINETIC DATABASE																										
BASIC DATA						PYROLYSIS DATA					KINETIC DATA															
			SOURCE								Frequency	Activation energies														
WELL	DEPTH	Sequ.	TYPE	PalT	Ro%	HI	S1	S3	TOC	Tmax	A (Ma-1)	<46	46	48	50	52	54	56	58	60	62	64	66	68	TOTAL
95	1994m	15A	OIL	80	0.81	384	0.57	0.51	2.47	434	1.0760E+27	13	2	0	0	283	77	7	2						384
95	2007m	15A	OIL	80	0.85	397	0.61	0.42	3.21	429	1.0555E+27	6	2	0	0	303	68	13	4	1					397
114	1530.5m	15A	OIL	60	0.61	443	0.15	1.02	4.23	424	3.8159E+27	5	1	0	4	173	191	54	12	3					443
116	1875m	15A	WG	75	0.68	383	0.24	0.64	3.04	421	7.0988E+27	5	4	0	0	6	224	123	18	2	1				383
116	1933m	15A	WG	76	0.70	510	0.55	0.89	4.28	424	1.9861E+27	5	1	1	0	22	293	152	28	7	1				510
12	2052m	15A	OIL	81	0.70	452	1.02	0.52	2.50	430	1.4365E+27	31	13	3	1	304	97	3							452
Pletmos	1777.5m	15A	WG	72	0.67	500	0.21	0.90	3.47	426	2.3180E+28	2	3	4	1	0	100	263	98	23	5	1			500
92	2410m	13A	OIL	91	~0.80	370	0.48	0.89	2.49	431	1.1044E+27			1	2	278	73	8	5	3					370
25	2010m	13A	OIL	79	~0.75	405	0.54	0.82	2.91	425	1.4980E+27	12	3	1	4	274	98	10	2	1					405
50	2410m	13A	WG	96	0.94	504	0.76	0.88	3.02	430	2.0724E+28	6	5	2	3	4	18	319	125	19	3				504
36	2400m	13A	?OIL	88	~0.80	263	0.54	1.06	4.00	428	1.4650E+27	6	1	0	1	191	56	5	2	1					263
36	2410m	13A	WG	88	~0.80	335	0.53	1.10	2.60	427	5.9040E+27	4	3	2	0	2	239	73	7	3	2				335
12	2315m	13A	WG	97	~0.90	306	0.94	0.78	2.00	438	9.9938E+27	7	7	5	8	1	1	206	52	11	6	2			306
Pletmos	2504m	13A	WG	105	0.91	380	0.94	0.13	3.10	431	1.1511E+28	6	4	4	3	0	2	272	70	14	5				380
78	2171m	6A	OIL	84	~0.70	383	0.34	0.42	2.41	434	5.2890E+27	3	5	3	0	0	273	81	11	4	2	1			383
36	2560m	6A	OIL	94	~0.90	284	0.76	0.96	2.42	432	4.3830E+27	7	5	6	1	1	207	50	2	2	2	1			284
Algoa	2105.9m	pre1A	OIL	67	0.87	299	0.17	0.71	3.70	430	1.9730E+27	4	2		8	166	94	16	6	2	1				299
msgen2: kinetic.xls																										

Table 4.01: Table of available kinetic data evaluated from low maturity Outeniqua Basin samples from several different sequences (using the same equipment etc.) and used in the modelling carried out in the Bredasdorp Basin. Non-Bredasdorp data used only for models in the Southern Outeniqua Basin.

Marine source rocks are usually found in sediments deposited in specific deep marine environments (e.g. overlying transgressive system tracts and in basal highstand tracts) and these often have a characteristic and recognisable seismic signature (Loutit et al, 1989). As a result of their slower travel time and lower densities (because of the organic matter contents and the commonly high proportions of undercompacted clays) they often show strong impedance contrasts with normally compacted and organic-poor beds above and below. This results in the characteristic "tramline" response i.e. high contrast parallel reflectors enclosing a low contrast interval (Brink et al., 1991). Indeed source rock distributions in the distal Bredasdorp and the Southern Outeniqua Basins are largely extrapolated from adjacent wells using this aspect (Figs. 3.19, 4.04 and 4.05). However, the distinction of source rocks near the edge of the basin is made more difficult because sequences thin below seismic resolution, by onlap, offlap and erosion (Beamish, 1990).

4.1.4.4. Measurement of source potential

Estimates of the proportions of different macerals, essentially that proposed by Correia and Peniguel (1975) are used to evaluate the quality of the organic matter. The fourfold subdivision used, with certain diagnostic chemical parameters, is given in Table 4.02.

4.2. BREDASDORP BASIN SOURCE ROCKS

Source rocks have been intersected in wells in the Bredasdorp Basin in each of the major sequences as shown in Table 4.03.

4.2.1. Syn-rift source rocks (Late Jurassic)

Syn-rift source rocks have been intersected in only one offshore well (no. 89) in the Bredasdorp Basin and in one onshore well (DWK/1) in the Haasvlakte graben an onshore extension from the western end of the Bredasdorp Basin (Figs. 2.05 and 4.03). In both wells, thin intervals of interbedded lacustrine source rocks and coaly silts were intersected - in each case totalling <20 metres. TOC contents vary from 1-3% and in many samples, a large proportion of the organic matter is amorphous although bottryococcus masses do occur (Davies et al., 1991).

In well 89, the WG-OIL prone lacustrine shales have a total thickness of 13 metres spread over a 70 metre section, i.e. ~20% of the whole interval has source potential (Table 4.04 for definitions). Potential ranges up to ~20 kg/tonne rock (HI=764) but averages 7 kg/tonne (HI=523) (Fig. 4.06). The few data points plot in the Type 1 region of the HI vs Tmax plot. (This plot style, commonly called the Espitalié plot, was pioneered by Espitalié et al., 1977). The maturation level is recorded at R_O~0.8%

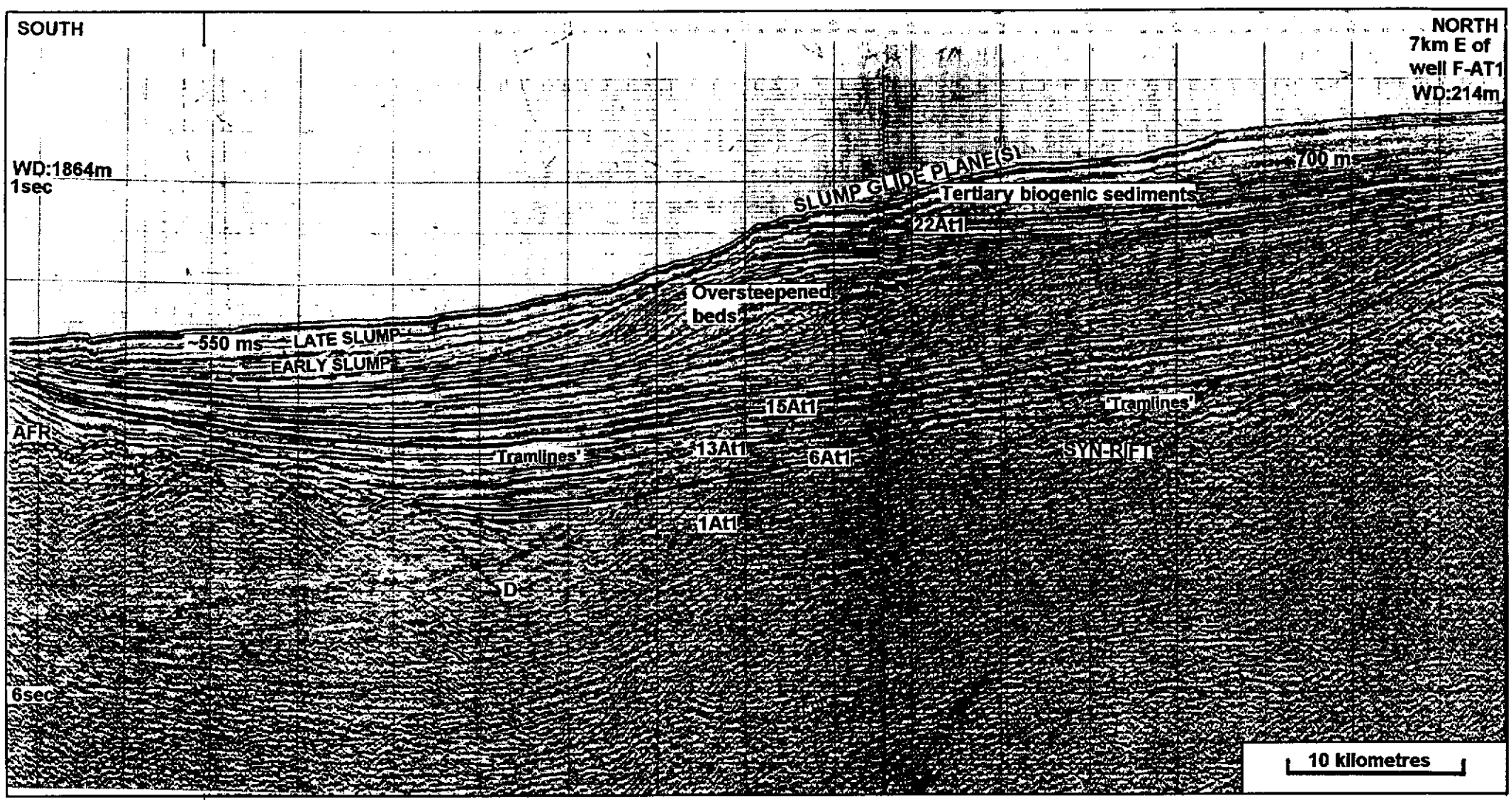

Figure 4.04: North-south seismic line across the western Southern Outeniqua Basin showing the characteristic "tramline" signature of the early Aptian source rocks (for location, see Figure 3.16). The source potential is assumed to be at its highest and the rocks have the lowest density and the slowest sonic travel-time, where this signature is most strongly developed.

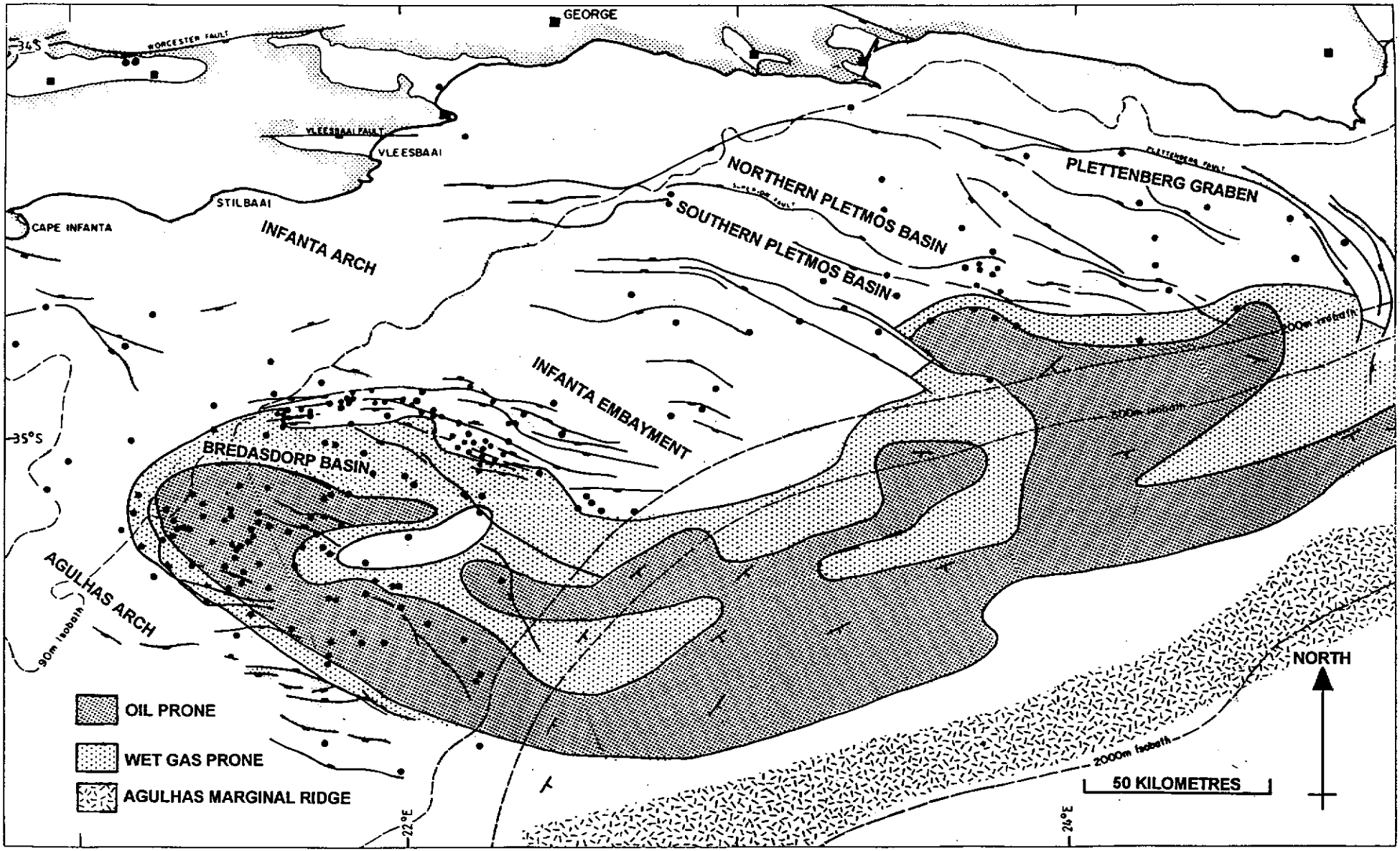

Figure 4.05: Map of the greater Outeniqua Basin showing the distribution of wet gas and oil prone source rocks in the early Aptian 13A sequence. The distribution recorded in the Southern Outeniqua Basin is derived from mapping of the characteristic high impedance contrast of these source rocks with the over- and underlying clastic sediments.

Kerogen type	Optical description	Hydrocarbon/ oxycarbon ratio S2/S3	Hydrogen index S2 mg/gm TOC	Oxygen index S3 mg/gm TOC
MOC	amorphous/sa propelic	>10	>400	<30
MOV	structured terrigenous	~5	250-450	20-50
	algal	>20	>600	10-30
MOT	tracheid	1-3	150-300	40-100
MOL	lignitic	≤1	<150	>80

Table 4.02: Chemical source potential of the four main types of organic matter distinguished by optical means (after Correia and Peniguel, 1975).

AGE	SOEKOR SEQUENCE NAME	OVERALL HYDROCARBON POTENTIAL	OVERALL MATURITY (R_o%)
Turonian	15A	Oil	0.5-0.7%
Early Aptian	13A	Oil	0.7-1.2%
Barremian	9A-12A	Wet gas-oil	0.8-1.3%
Early Barremian	6A-8A	Wet gas-oil	0.8-1.3%
Late Hauterivian	5A	Gas	0.9-1.5%
Late Valanginian-Early Hauterivian	1A-4A	Gas	1.0-1.5%
Late Jurassic-Early Valanginian	Syn-rift	Dry gas or Oil	1.0-1.5%
Devonian	Bokkeveld	Dry gas and non-hydrocarbons	>3%

Table 4.03: Overall maturity and gas/oil potential of source rocks in the Bredasdorp Basin.

TOTAL GENERATION POTENTIAL

RICHNESS	TOC%	HYDROCARBON POTENTIAL (S2 kg/tonne rock)
Excellent	10-20%	>50
Very good	5-10%	10-50
Good	2-5%	5-10
Fair	1-2%	2-5
Poor	<1%	<2

HYDROCARBON POTENTIAL AND ORGANIC MATTER TYPES

TYPE (organic matter types	HYDROGEN INDEX (estimated original) (100*S2/TOC)	S2/S3	OPTICAL	HALF-HEIGHT (Width in T°C of S2 peak at half maximum height)
OIL (I/II)	>>400	>5 (>10 where TOC >5%)	>60% amorphous, exinitic or liptinite	<45°C
WG-OIL (II)	300->400			
WG (II/III)	250-350	2.5-5 (>5 where resinous or woody OM)	40-60% amorphous, liptinite and exinite	50-60°C
DG-WG (III/II)	200-300			
DG (III)	100-200	1-2.5 (>5 where resinous or woody OM)	>60% structured exinite, vitrinite and inertinite	>70°C

Table 4.04: Values of each parameter used to describe source rocks of various types and potential (from Davies et al., 1994).

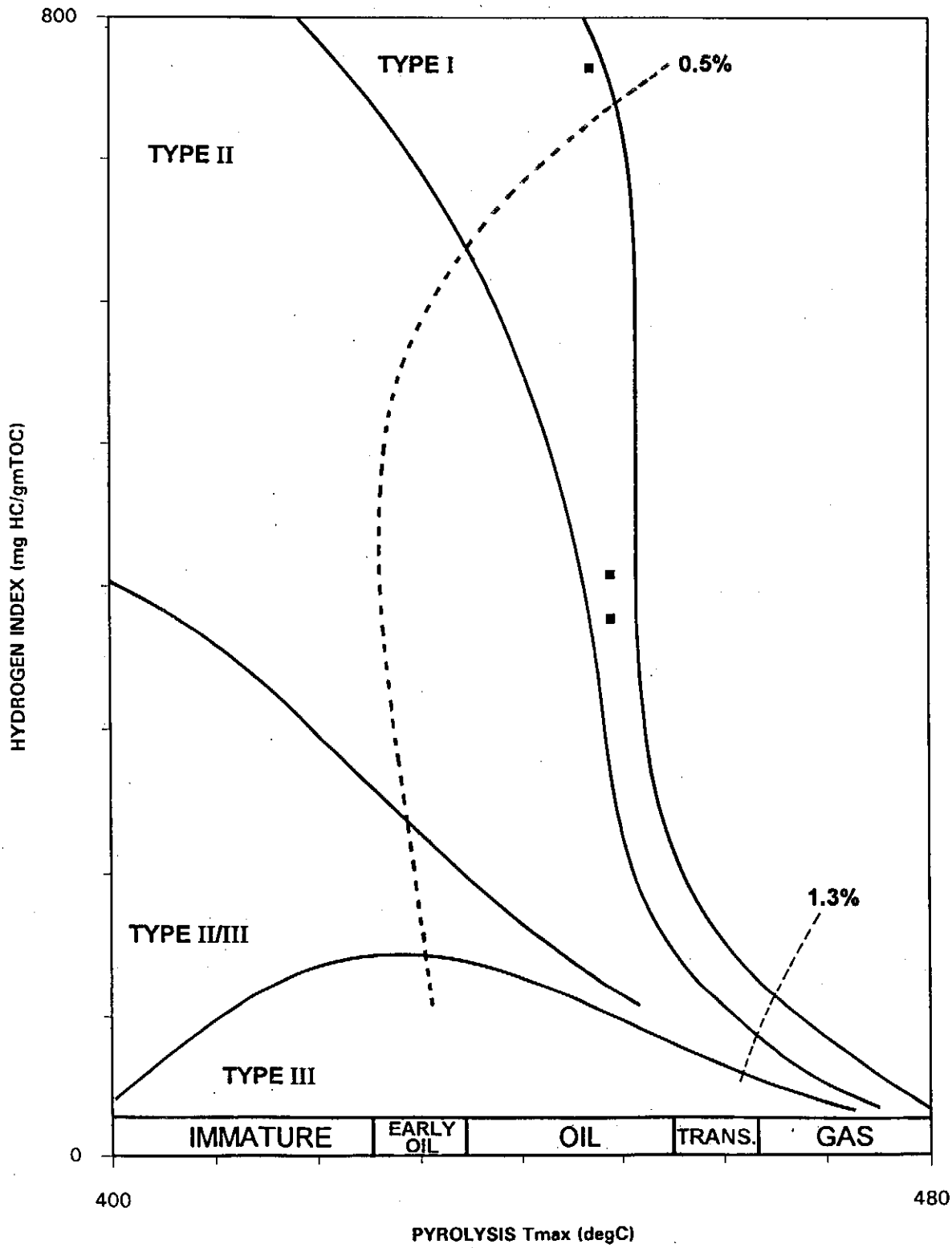

Figure 4.06: Plot of the hydrogen index (HI) versus the Rock-Eval Tmax (temperature at peak rate of pyrolysis) for the late Jurassic lacustrine source rock samples from Well 89 (in the western Bredasdorp Basin).

(Tmax=447-449°C). Similar source rock richness variations are found in other examples of Mesozoic lacustrine source rocks, e.g. in borehole DWK-1 and in wells in other onshore and offshore basins (Davies et al., 1991, Davies et al., 1994a and 1994b, McLachlan and McMillan, 1979).

In the two Bredasdorp Basin examples, source potential varies widely from thin laminae of oil-rich Type 1, oil-prone source rocks to thicker beds of coarser, coaly shales and silts. Within the shales, variations are indicative of widely changing rates of production or preservation of organic material. Similar variability was also found in Hauterivian lacustrine shales encountered in borehole A-J1 on the west coast of South Africa (Muntingh, 1993; Davies et al., 1994a) and in Kimmeridgian age (Colchester Unit) continental sediments in several onshore wells in the Algoa basin (McLachlan and McMillan, 1979).

Lacustrine syn-rift sediments appear to have a very restricted distribution as only two of the 168 wells in the Bredasdorp Basin intersected such source rocks. Lacustrine source rocks, where intersected, were deposited prior to the main marine incursion and will be found at or near the base of the graben. Few wells have intersected more than the top few hundred metres of graben fill which can be in excess of 2 kilometres thick (Burden, 1993; Jungslager, 1996) hence the paucity of source rock intersections may be due to limited drilling coverage.

It is considered that hydrocarbons in sandstones far below 1At1, for which there is no demonstrable migration route from a post-1At1 source, indicate the presence of syn-rift source rocks. For example, in the south-east part of the basin (near wells 12 and 13 and wells 9, 11, 14 and 17) residual hydrocarbons are present throughout a thick interval (>400 metres) of syn-rift sands. Pores in many of the sandstones are filled with hard, chloroform-insoluble bitumenous material and traces of chloroform-soluble oil (McLachlan et al., 1979). In many cases, solid bitumen is seen as thin strings on compacted grains and between quartz overgrowths. These shows could represent migration from a pre1At1 source.

Elsewhere, Hill (1996) shows that quartz overgrowths tend to occur after early diagenesis. Some of the sandstone samples are characterised by the presence of so much solid bitumen that the sand grains apparently float in bitumen suggesting emplacement before early compaction or after removal of a pore-filling material. It is possible that the oil entered the reservoir pore spaces after a period of flushing which removed early calcite cement (McLachlan et al., 1979) the oil being coked during the igneous phase associated with the hotspot transit. It is less likely that oil entered after this main heating event as there was not enough residual heat to coke the oil. Yet

post-1At1 source rocks in the vicinity (Valanginian-Aptian) are not so deeply buried that they would have been mature enough to generate such large quantities of oil pre-transit. Hence the widespread presence of pyrobitumen suggests a common pre-1At1 oil source.

The wedge-shaped fetch area common to these structures measures 10x15 kilometres and is bounded by highs to the north, east and south. Burden (1993) shows the area does indeed contain a deep pre1-At1 graben. Aeromagnetic data in this area show strikingly low magnetic susceptibility (GETECH, 1992) possibly indicating the presence of evaporites similar to those in the west of the basin where oil-prone lacustrine source rocks are found nearby. Such conditions prevailed in the Angola Basin, offshore Angola (Schlumberger, 1991a). Coincidentally, formation water salinities calculated from SP logs in pre-1At1 (?Late Jurassic) sandstones in the closest well, no. 14, are close to 100 000 ppm NaCl equivalent (Davies, 1995a) supporting the likelihood of salt deposits.

Chemical and optical data from these samples show the TOC content ranging 1.1-2.7% and extrapolation of Rock-Eval data shows the original HI was >600 (Fig. 4.06). The original potential was >10 kg oil/tonne rock although the individual samples are widely variable. One sample of lacustrine shale (sample 35 from well 89) is used in detailed analysis for this study.

4.2.2. Source rock in sequences 1A-4A (Valanginian)

Wet gas to oil-prone source rock is known to be present in the 1A-4A sequences although it is likely that only one interval in these four sequences has source potential. The range of intervals included reflects the difficulty of seismic correlation of these four sequences. Examples of 1A-4A source rock are seen in 6 wells on the south flank (Davies, 1996a), especially around well no. 42 (Fig. 4.07), mostly because these sequences onlap basin margins and highs away from structural crests. Locally these sequences have been eroded, mostly during the Late Hauterivian tectonic readjustment (Jungslager, 1996). Therefore the paucity of source rock data throughout these source rocks is a function of both the few wells and the limited areal extent of the source.

Burden (1993) and Jungslager (1996) indicate that after the Early Valanginian rift phase, the basin was dissected into several deep topographic lows into which early marine transgressions occurred over the 1At1 surface. The localised nature of the lows would have meant that there would be limited sediment provenance for some of the lows and sedimentation could have been largely pelagic. It is possible that the highly dissected and restricted nature of the 1A-4A graben results in locally very distinct source rocks, some graben may even have interbedded evaporites. This geological

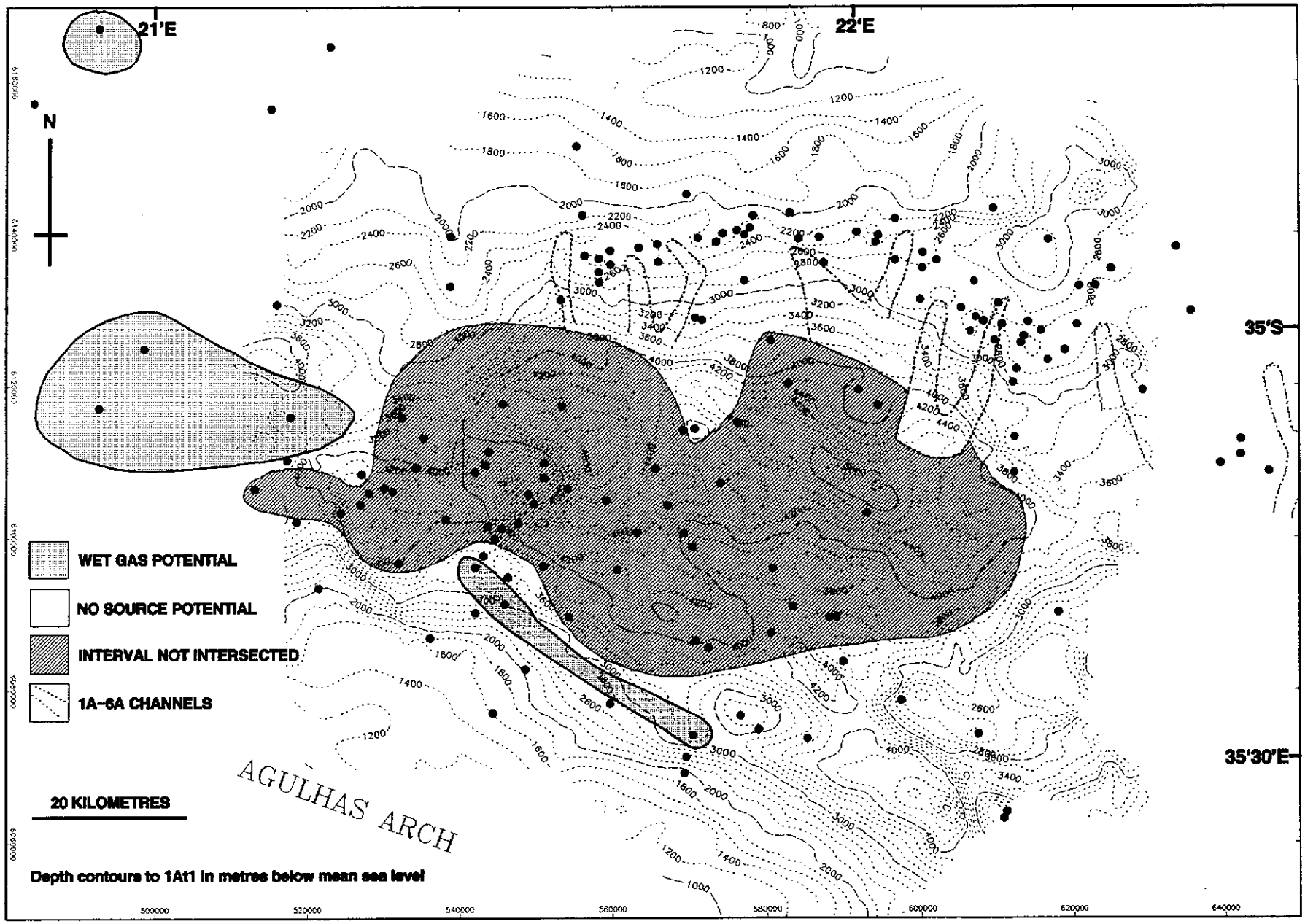

Figure 4.07: Map of the distribution of source rock quality in the 1A-4A sequences in the Bredasdorp Basin.

setting is very favourable for deposition and preservation of oil-prone source rocks (Cornford, 1986).

Optical and chemical analyses of samples from these intervals indicate a largely terrigenous input mixed with some fluorescent amorphous organic matter. The TOC content is moderate, ranging from 1.0-1.5%, and extrapolation of the HI data (after Davies, 1990) suggests the original potential to have been some 5-8 kg/tonne rock and an HI of~400-500 (Fig. 4.08). One sample of this source rock (no. 63 from well 42) is used in detailed analyses for this study.

4.2.3. Source rocks in sequence 5A (Latest Hauterivian)

The basal 5A sequence contains a thin, locally oil-prone, source rock interval averaging 28m in thickness. The distribution map shows the minimum extent because only a few wells intersect the interval over much of the basin (Fig. 4.09). Seismic data, though, confirm the extrapolation from the known intervals across the basin. The sediments were deposited in a restricted pelagic - hemi-pelagic environment (Jungslager, 1996). These conditions are favourable for source rock development because organic matter preservation is more likely under dysoxic conditions especially where restricted sedimentation occurs (Demaison and Moore, 1980).

There is a possibility that the slow sedimentation allowed for localised oxidation of sediments before they were buried and hence oxidation of the kerogen. This may explain why these shales are only moderately rich, having up to 1.8% TOC and HI averaging 200 (Fig. 4.10). Locally, however, the kerogen is quite hydrogen-rich and in wells on the north flank of the basin, some samples retain HI >250 even where maturity is above R_o=0.9%. The very localised potential of the 5A shales suggests local carbon maxima - typical of the high productivity model.

If the source rock had been deposited under the same conditions basin-wide, then the potential should be similar. The available data from wells scattered across the basin all locate in the same area of the HI vs Tmax plot (Fig. 4.10) and trend parallel to the boundary between Type 2 and Type 1 organic matter, barely intersecting the Type 3 limit. Optical data confirm the largely WG to locally WG-OIL potential.

Samples have been selected for detailed analyses from wells in the north flank only (no's. 41, 65 and 67) because they are representative of the largest area of source development. There are intervals of marginally oil-prone source rocks in the 5A sequence on the south flank, but as they are very thin, they may have limited areal extent. In addition, the source character in these wells is impersistent, very localised and generally at low maturity.

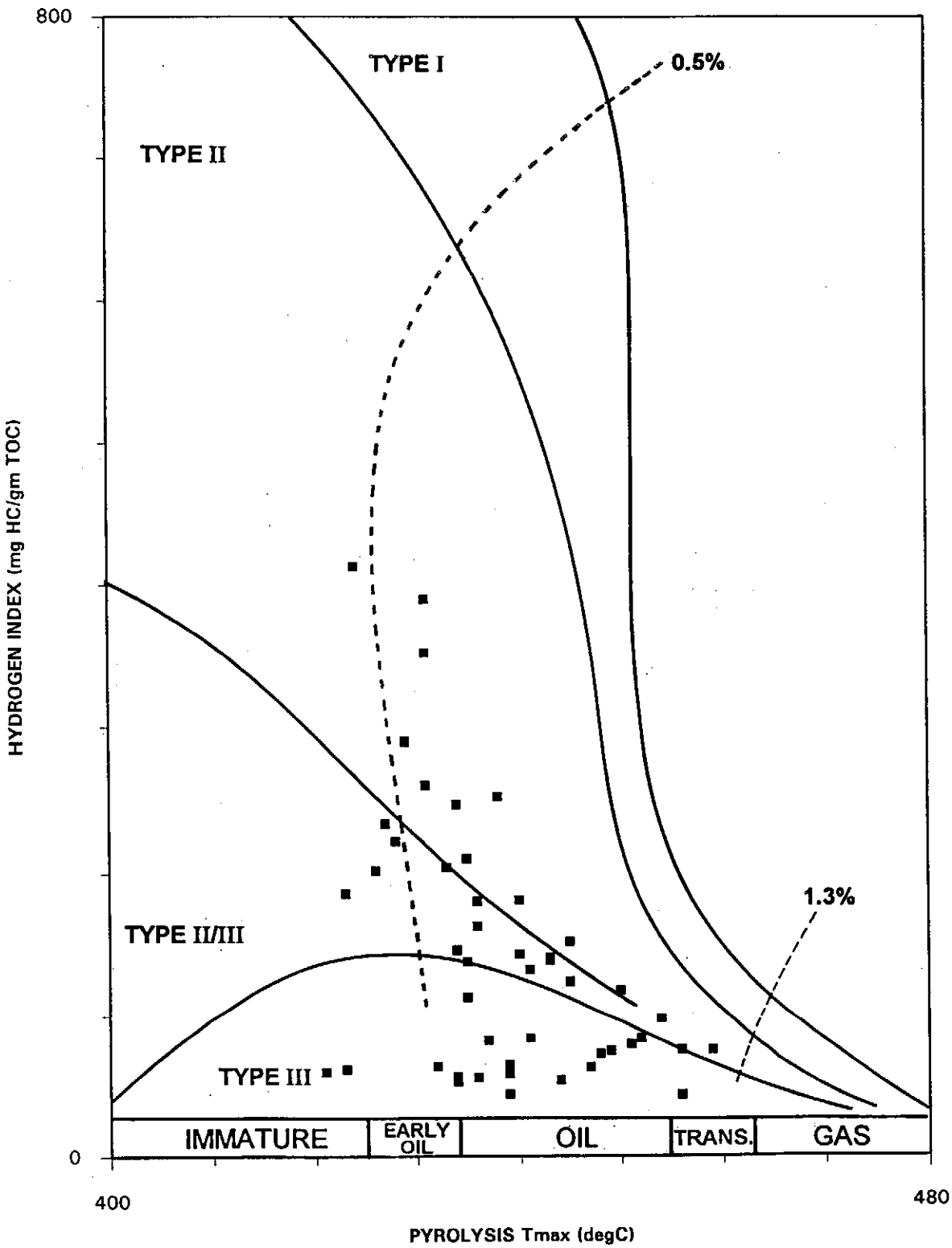

Figure 4.08: Plot of hydrogen index (HI) vs Tmax for all sequence 1A-4A source rock samples that have potential for wet gas or oil generation.

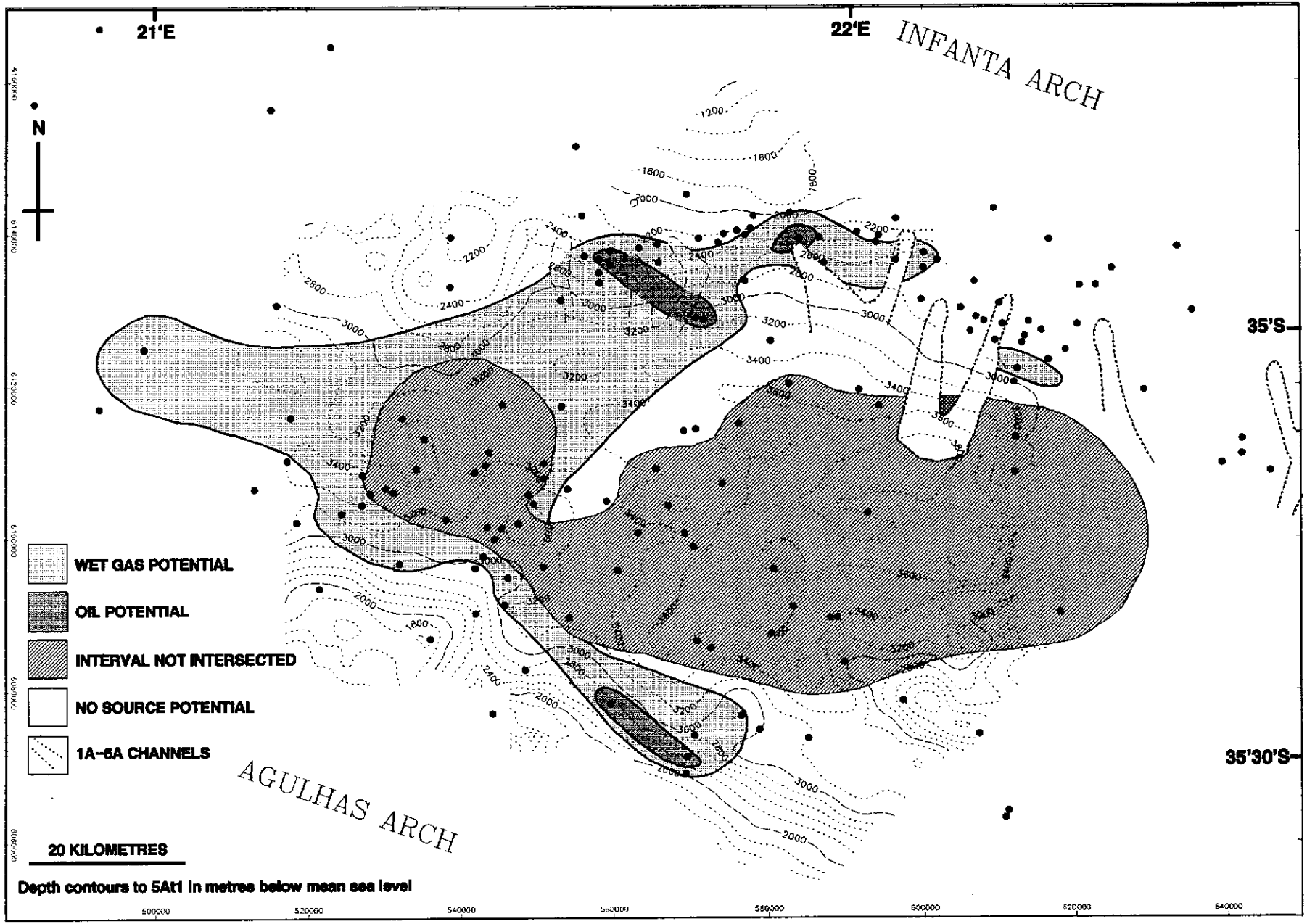

Figure 4.09: Map of the distribution of source rock quality in the 5A sequence in the Bredasdorp Basin.

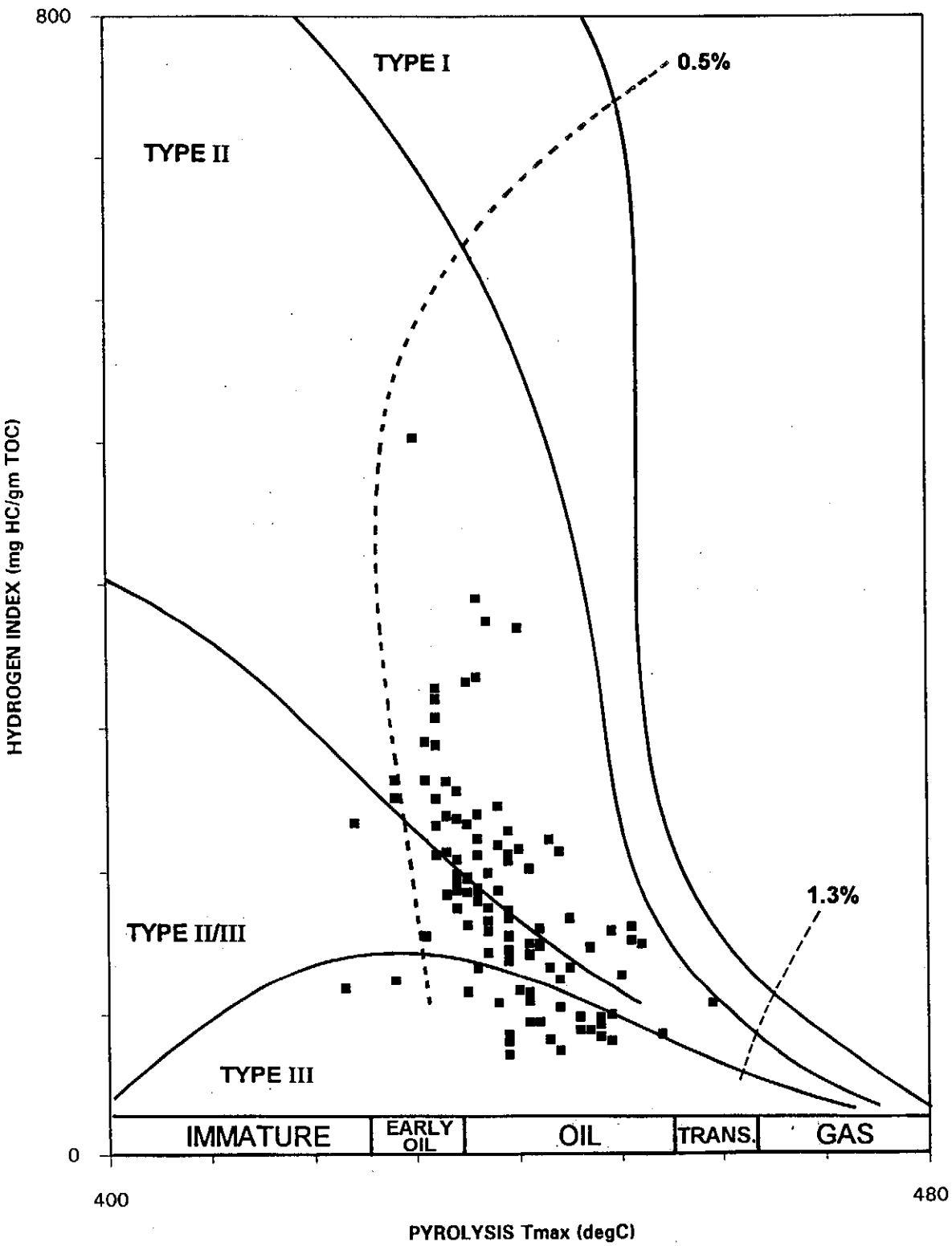

Figure 4.10: Plot of hydrogen index (HI) vs Tmax for all sequence 5A source rock samples that have potential for wet gas or oil generation.

4.2.4. Source rocks in sequences 6A-8A (Early Barremian)

Source potential in this interval is largely developed immediately above 6At1 (Fig. 4.11). In some cases, source rocks have been assigned to the 7A or 8A sequences but there is some doubt regarding the correctness of those assignments. Indeed, these horizons are no longer routinely picked because at the basin edge they become indistinguishable from other horizons. Biostratigraphic data is not able to differentiate these individual sequences. Horizon 6At1 is relatively easy to pick on seismic records as it is often an angular break and marks the base of basin-wide progradation. The present distribution of source rocks in the interval, i.e. largely away from the south flank, may be a function of tectonism in post-6A times when the south flank was uplifted relative to the north flank and eroded. It may also be that, as with the 5A sequence, source rocks are better developed in the depositional lows which are undrilled.

The distribution of these source rocks cluster in two distinct zones, one in the south-east and the other in the north-western part of the basin (Fig. 4.11). These two marginal zones show that the location of better quality source rocks is not a function of water depth, which was greatest near the basin centre, or of sediment starvation. The 6A-8A source rocks may be an example of the high productivity model in which the prevalence in the western end of the basin indicates an input point for organic carbon. There is, however, no evidence for sediment input from that direction (Burden and Gasson, 1992).

These source rocks have thicknesses of a few tens of metres with variable but generally modest TOC contents (1.8-2.5%). Overall the source potential is shown in the HI vs Tmax plot (Fig. 4.12) as wet gas – oil-prone. All the data locate within the Type 2 limits but are widely scattered. This wide variation is mirrored by the chemical data which locally show the potential to range from oil-prone to dry gas-prone within just a few metres (e.g. well no. 93, core 1, 2850.85-2852.30m, where maturity is high (R_o=1.03%), HI varies between 275 and 119). Notwithstanding the location of many points to the left of the Espitalié et al. (1985) 0.5% line, the samples are not of such low maturity. Other chemical and optical maturity data place all of these samples in the main oil window at R_{equiv} = >0.7%.

As with the 5A sequence source rocks, the reduced Tmax is probably due to a large proportion of bitumen (Peters, 1986). Some of this bitumen is detrital as many of the lowest maturity samples have significant free hydrocarbon contents (S1 >0.2 and generally >0.6 kg/tonne rock). Three representative samples from this interval are used in the detailed study.

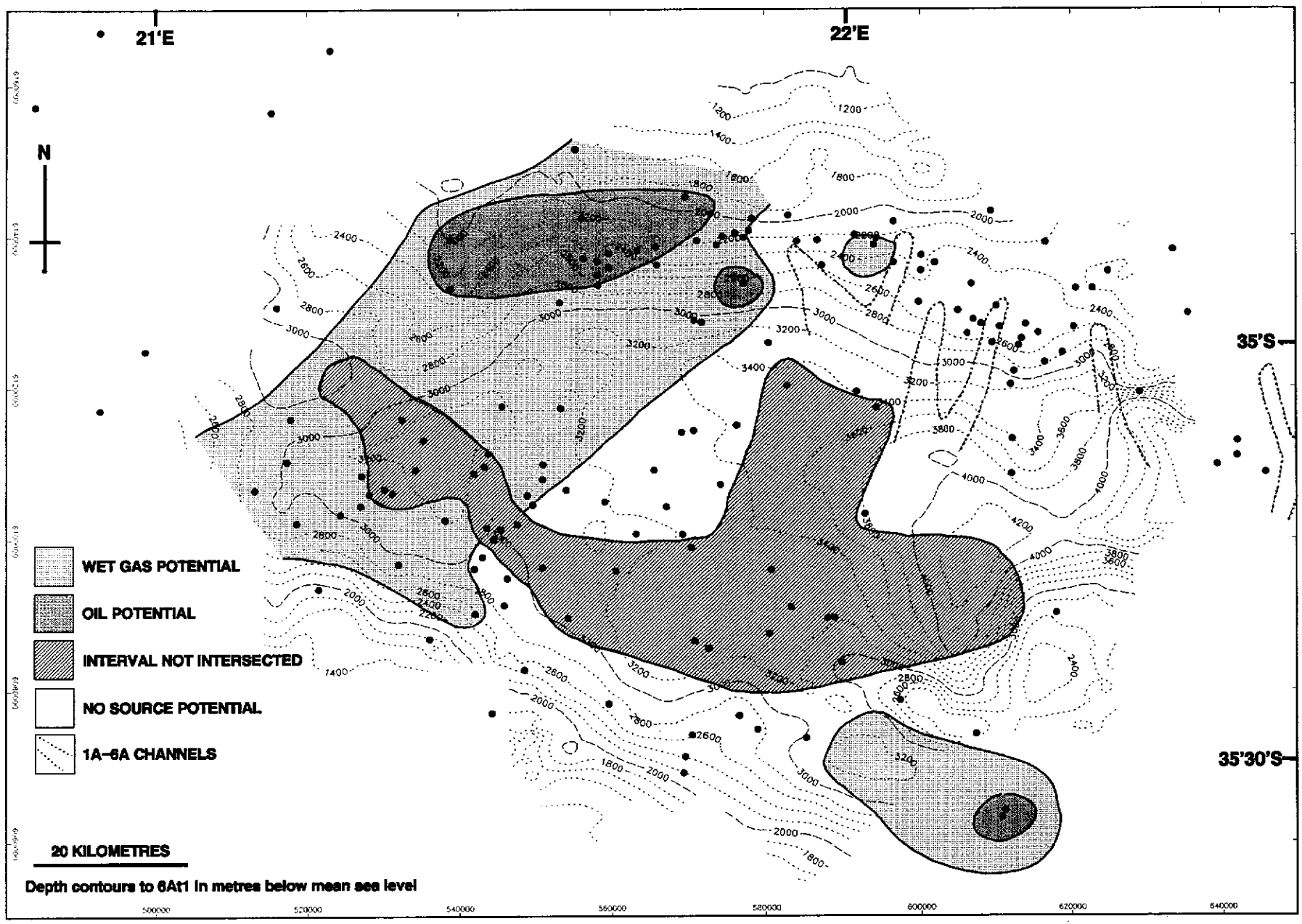

Figure 4.11: Map of the distribution of source rock quality in the 6A sequence in the Bredasdorp Basin.

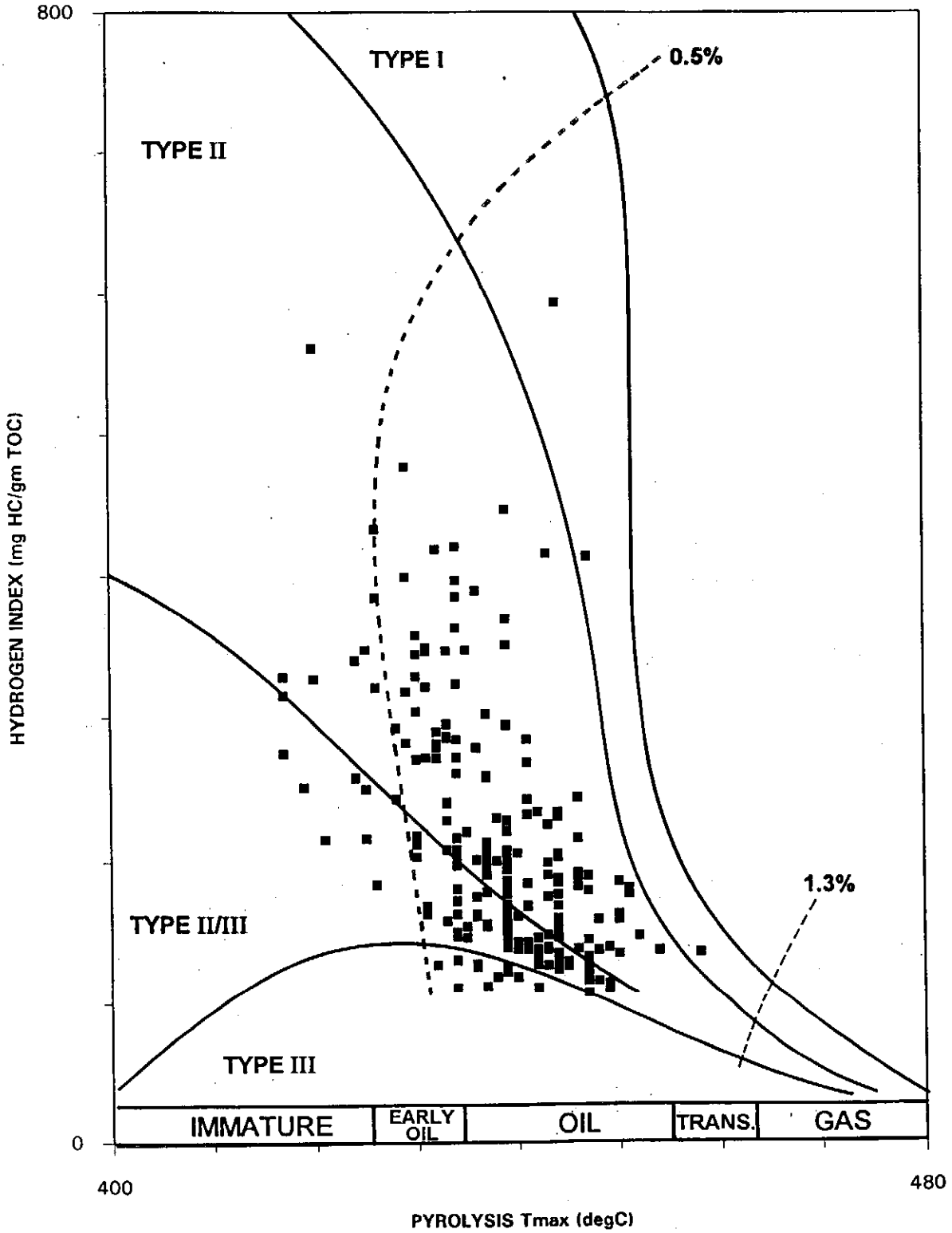

Figure 4.12: Plot of hydrogen index (HI) vs Tmax for all sequence 6A source rock samples that have potential for wet gas or oil generation.

4.2.5. Source rocks in sequences 9A-12A (Late Barremian)

In most cases, the source rocks are located at the base of the 9A sequence. This makes the interval relatively easy to pick on seismic lines as it marks the start of widespread aggradation. In the central part of the basin, early lowstand channelisation of pre-existing sediments and later infill of the channel with relatively coarse clastic late lowstand sediment fill (Hodges, 1996), result in the source rocks being found stratigraphically higher in the succession. Source rocks are found largely in the basal section of the 9A-12A sequences, but only along the south flank and in the western central parts of the basin (Fig. 4.13). The maturation data show that these source rocks are buried through the base of the oil window and into the top of the gas window (R_O~1.1%) in different locations. The HI vs Tmax plot (Fig. 4.14) shows a wide maturity variation but the source quality data all locate within the Type 2 region. Unusually, the best quality source potential is found associated with the southern flank highs (near wells 9, 35 and 42) and not with the onlap position on the Agulhas Arch.

One possible explanation is that these highs are inverted lows although the distribution of onlaps of the preceding sequences do not support this interpretation (Burden, 1992). Alternatively the distribution may indicate the development of a shallow oxygen minimum which impinged on the highs, yet where the oxygen minimum layer deepens, sediment starvation resulted in widespread oxidation. Source rocks are unlikely to have been present in this interval closer to the arch (and consequently eroded during later lowstands) because there is no evidence of an angular break between these rocks and the later 13A sediments. These source rocks have TOC's ranging from 1.8-2.5% with quite high original HI values (Table 4.03). Areally, the distribution of oil-prone source rocks is very limited (~300 km^2) but some of the intersections of wet gas-prone shales may, based on the log character, actually be interlaminated oil- and wet gas-prone shales. However, overlaying the source map with the maturity map shows that only the central area of wet gas-prone source rocks is buried deeper than R_o=1.1% - and therefore the source rocks are largely immature for gas. Yet the oil-prone source rocks are all buried into the oil window and are mature - hence there is oil potential in 9A-12A source rocks although it is restricted to the areas shown. Five representative samples of these wet gas- and oil-prone source rocks are selected from the interval for detailed study.

4.2.6. Source rocks in sequence 13A (Early Aptian)

Source rocks in the 13A sequence are developed across most of the basin (Davies, 1988b and Brink et al., 1991). The considerable thickness and extent of this source (Fig. 4.15) and its significantly higher richness than any of the other source rocks make it highly prospective. The Early Aptian source is considered to have been formed in an anoxic basin in which organic matter deposited in the core of the basin was dominated

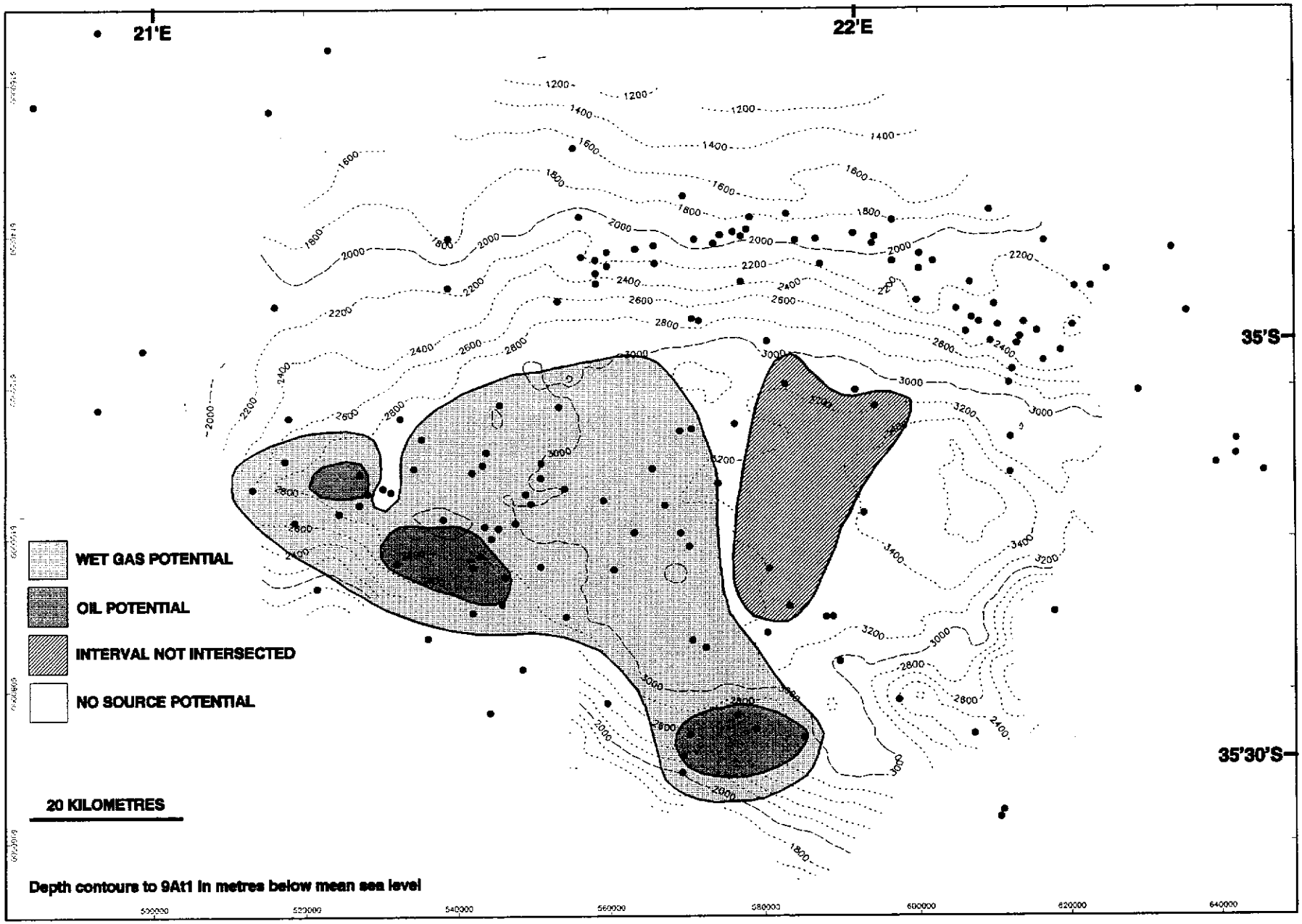

Figure 4.13: Map of the distribution of source rock quality in the 9A-12A sequences in the Bredasdorp Basin.

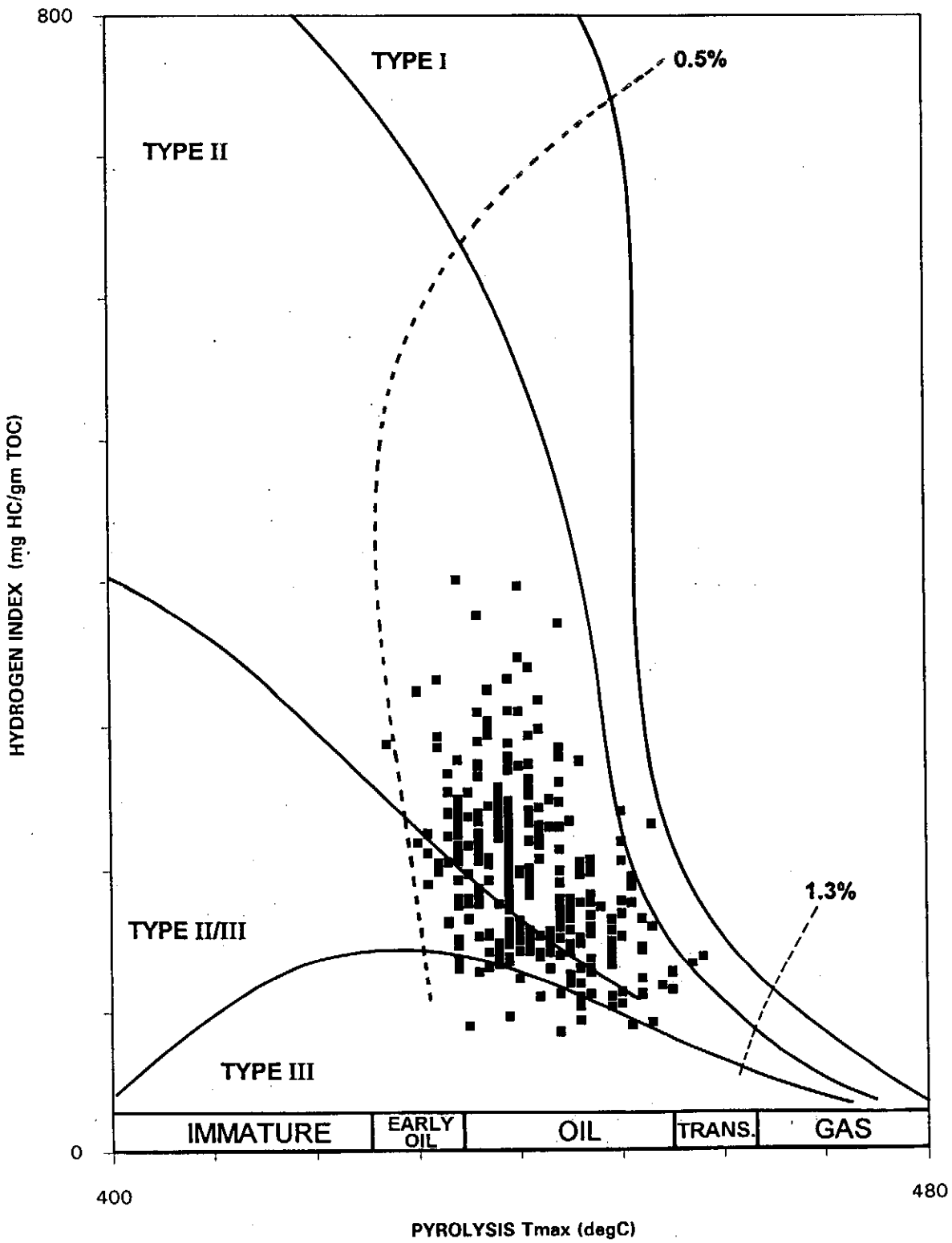

Figure 4.14: Plot of hydrogen index (HI) vs Tmax for all sequence 9A-12A source rock samples that have potential for wet gas or oil generation.

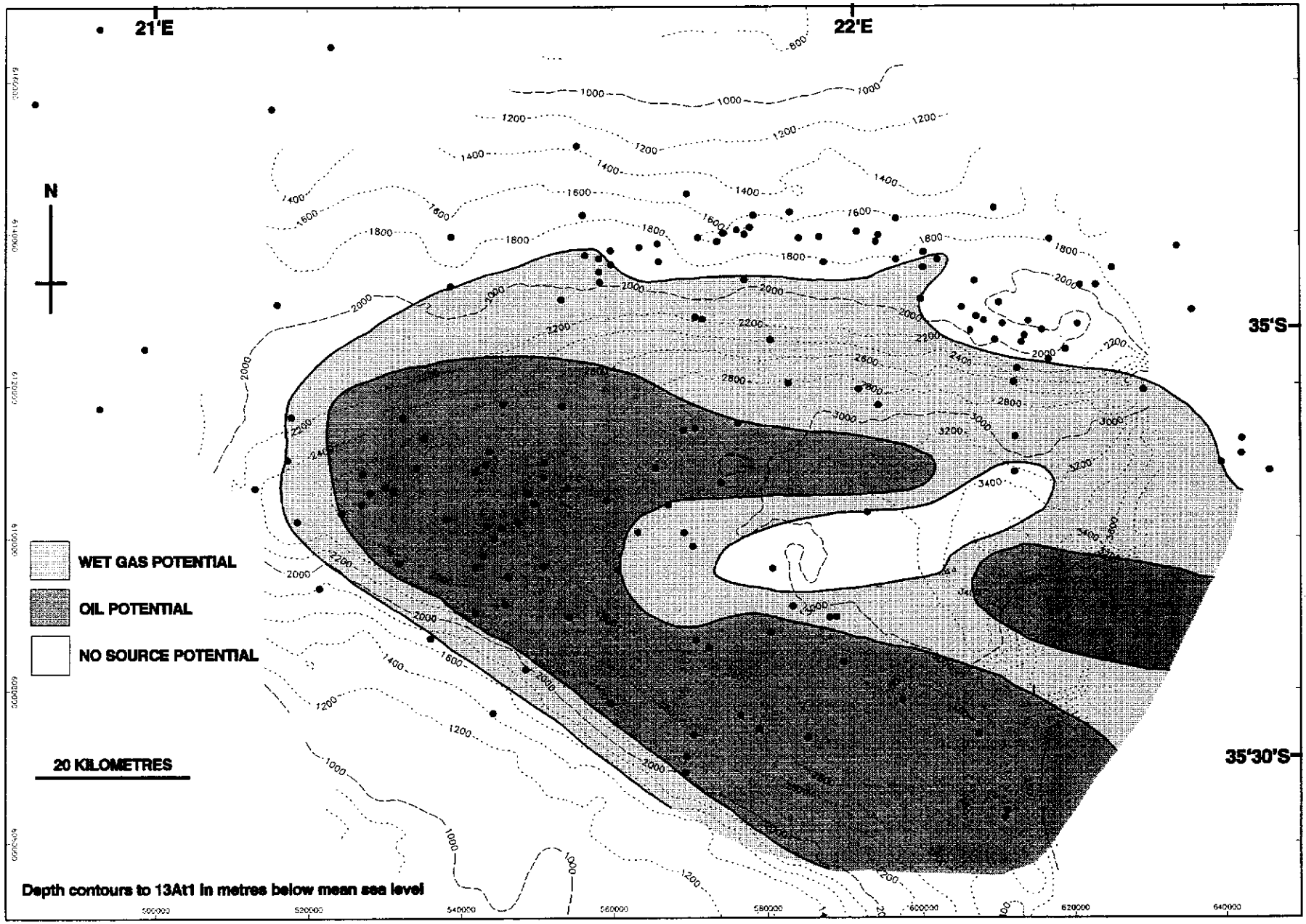

Figure 4.15: Map of the distribution of source rock quality in the 13A sequence in the Bredasdorp Basin.

by oil-prone material and was rimmed by gas-prone source rocks. There is a small area near the basin centre where no source rocks have been found (between wells 124 and 160). This does not negate the anoxic basin model as it is thought that this was a high during deposition of Lower Aptian rocks, possibly a relict of an earlier inversion (perhaps during Hauterivian), when the sea floor may have been above the oxygen minimum. Support for this comes from the thinly bedded nature of the sands in over- and underlying sequences, evidence of a topographic high lasting a considerable time. Indeed, this region is still a relative high in post-13A, based on the bifurcation of the 14A sandstone-rich trend around it (Hill, 1991). In well 123 at the western end of this high there are thin intervals of source rock indicating that potential existed at least intermittently for source rock deposition This suggests the 13A source rock was deposited in the "silled basin" model - probably silled by the early eastern highs (Fig. 3.04). The 13A sequence is seen to blanket all the highs in the eastern part of the basin and it is therefore likely that the source rock was deposited by hemi-pelagic sedimentation (Benson, J.M., 1993, pers. comm.).

In the northern flank of the basin, in spite of the considerable areal extent of wet gas-prone source rocks, the maturation level is generally too low to result in significant gas generation, except in the eastern region were sediments have been matured into the gas window by the intrusions.

The bulk of the oil-prone material is found to the south of the present day basin axis. As with other source rock intervals, the HI vs Tmax plot (Fig 4.16) shows all samples located in the Type 2 region, but towards the upper side in contrast with all other intervals. This indicates a greater oil potential in this interval than in any other. Average TOC's are significantly higher than in other intervals, ranging up to 4.0% with HI's ranging up to >500. Generation potentials exceed 12 kg/tonne at the present day. Extrapolation along the trend shown in Davies (1990) suggests that original potentials could have been in excess of 14 kg/tonne rock.

4.2.7. Source rocks in sequence 15A (Early Turonian)

Source rocks in this interval are located at the eastern end of the basin (Fig. 4.17). The richness distribution away from the edges of the basin bears little relation to the shape of the palaeobasin and suggests it was not deposited under either the oxygen minimum model or the restricted basin model. Based on the known rate of deposition, it is probably an example of the sediment starvation model. The interval is thin (generally 10m maximum) and at such low maturation level that only the most deeply buried rocks are in the oil expulsion window - and even then only just.

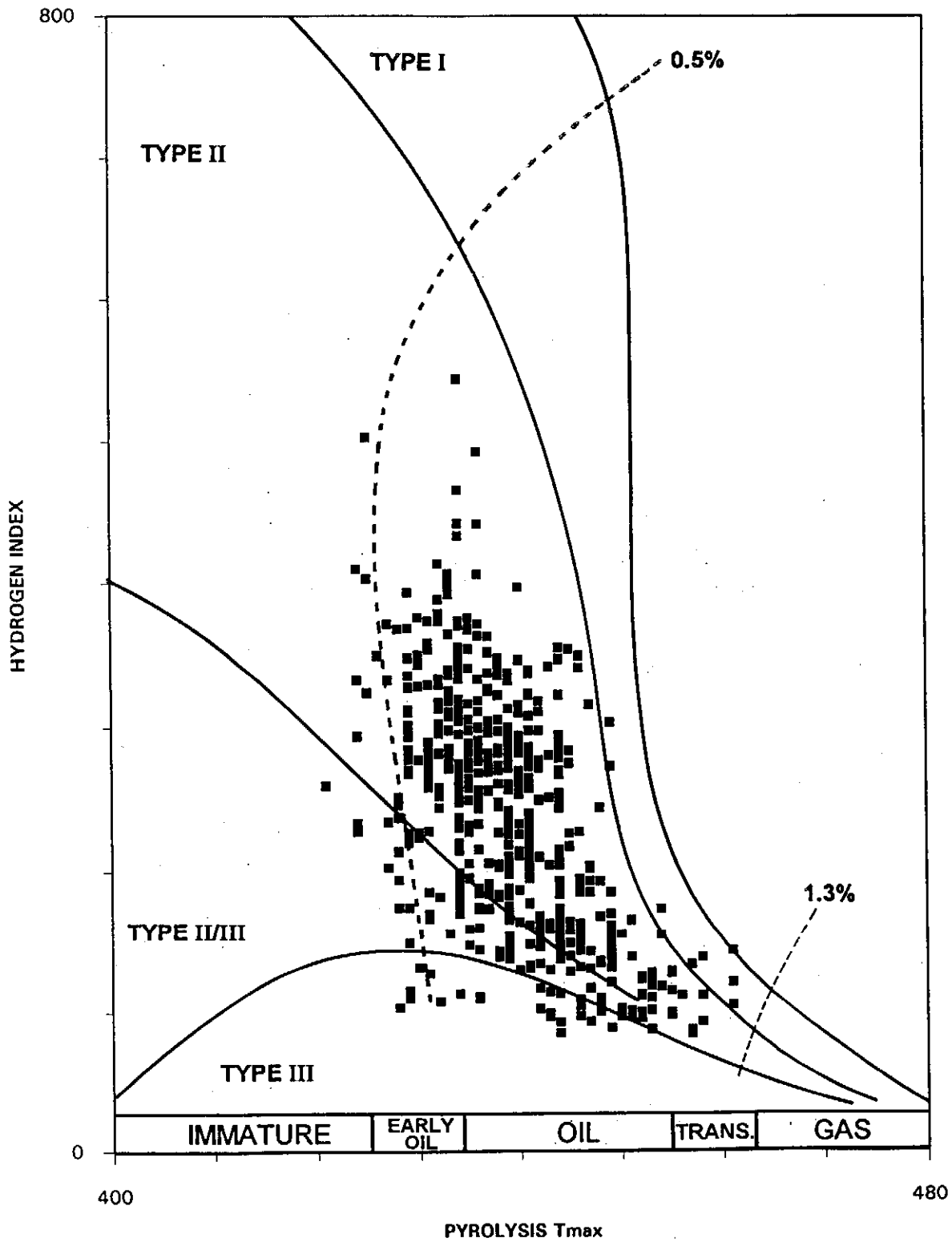

Figure 4.16: Plot of hydrogen index (HI) vs Tmax for all sequence 13A source rock samples that have potential for wet gas or oil generation.

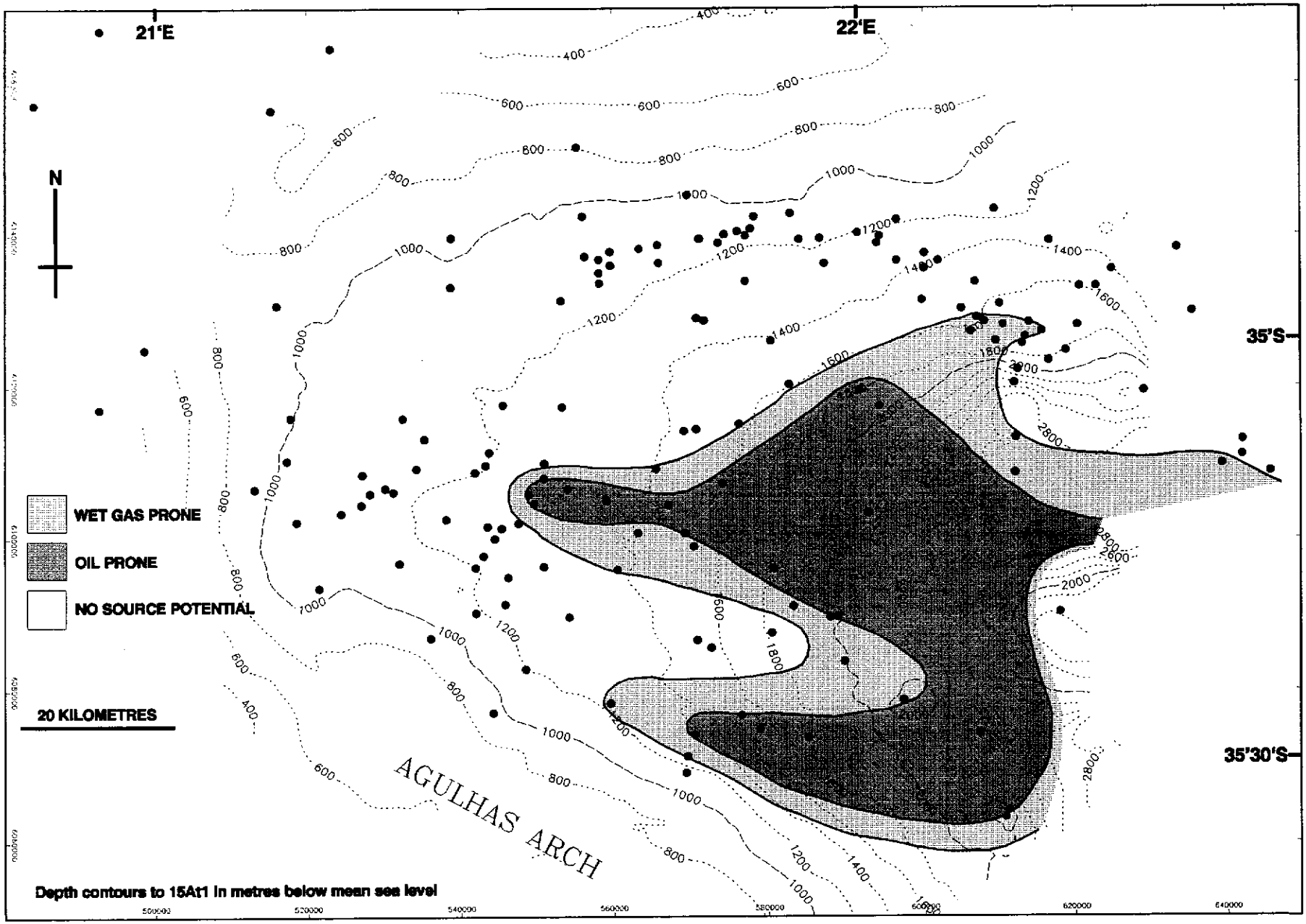

Figure 4.17: Map of the distribution of source rock quality in the 15A sequence in the Bredasdorp Basin.

This interval is not considered to have a significant potential because it is thin and barely mature enough to generate large quantities of oil. There are, however, three wells which have traces of oil post-15At1 (wells 21, 32 and 47). Analyses of these oils record low maturity - probably generated by a source similar to the 15A source although a biomarker match has not been attempted (Fig. 4.18).

There are very few samples of this source. This is partly because it is thin and masked by cuttings caving downhole. In addition there are no cores and only a few sidewall cores (a total of 12 are available). Hence the sample data may not adequately represent the true potential. The zone of increased gamma and slower travel time, recorded by the gamma and sonic logs respectively, is ~10 metres thick. The truly oil-prone samples all come from the centre of this interval where these logs record their highest values. Hence the oil potential may be only a few metres in extent.

4.3. SOUTHERN OUTENIQUA SOURCE ROCKS

Source rock distribution in the Southern Outeniqua Basin is estimated by extrapolation from known source rocks in surrounding wells because no wells have been drilled in the basin. Source rocks are most likely to be found in the Turonian OAE sediments, Upper Barremian-Lower Aptian transgressive and basal highstand tracts and Hauterivian pelagic infill sequences because of their regional nature. Upper Jurassic syn-rift lacustrine (or later restricted marine) rocks are also expected as this area has been a regional low since the time of early rifting. Organic richness and quality of these intervals could be as high as in the Bredasdorp Basin, although the examples of restricted-basin source rocks may need to invoke restriction due to an elevated AFFR. The characteristically strong impedance contrast, occasionally a 'tramline' signature, of the Upper Barremian-Lower Aptian source rock is seen on many lines across the basin suggesting it has a widespread distribution (Figs. 4.04-4.05). Source potential in syn-rift sediments, similar either to lacustrine shales in well 89 or marine shales in DSDP 330 and 511 and in the Algoa and Gamtoos basins (Malan, 1993) are more likely to be present than 1A-6A infill sediments. The Turonian source rock, which is widely developed in regions bordering the southern Atlantic (Table 2.02), may be present but is unlikely to be significantly thicker than in the Bredasdorp Basin because of the great distance from sediment supply.

4.4. MATURATION

In general, regional heat flow from the mantle provides most of the heat necessary for maturation of organic material. Additionally, considerable amounts of heat are released from igneous events. These are generally limited in time and space particularly where

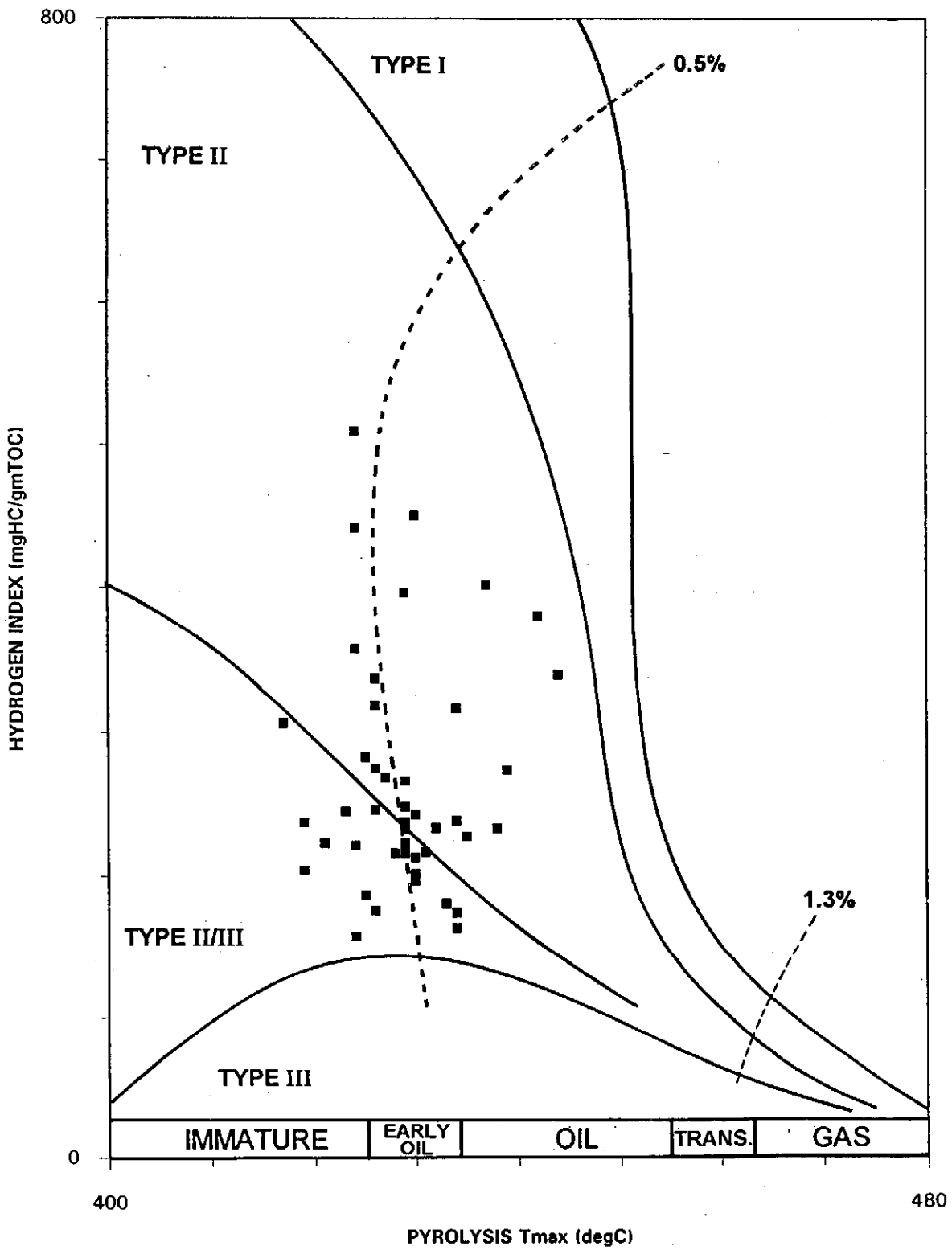

Figure 4.18: Plot of hydrogen index (HI) vs Tmax for all sequence 15A source rock samples that have potential for wet gas or oil generation.

alkali igneous rocks such as carbonatites occur, as these are relatively low temperature intrusions (Tarling, 1973). Heat input during fluid flow events are generally of limited importance (Hermanrud, 1986) but can be regionally effective where proportionally large amounts of fluids are involved, whether for short periods only (Barker, 1983) or for long duration (Jessop and Majorowicz, 1994).

Present-day heat flow calculated for the Bredasdorp Basin (using Basinmod) from calibrated bottomhole temperatures and default thermal conductivities derived from known lithologies, averages 53±5 mW/m^2. This falls within the range for oceanic basins which are not associated with active rifting (Tissot and Welte, 1984, p. 598) or for cratonic basins (Jessop and Majorowicz, 1994). During early rifting, heat flow from the mantle is likely to have been higher (Condie, 1989, p. 91) partly because of the thinned crust. Heat flow in the Bredasdorp Basin has therefore been modelled at 80-100 mW/m^2 at 130 Ma (the variation depending on distance from the AFFZ). Heat flow was probably effectively higher during the Turonian when the active spreading centre traversed the AFFZ (Dingle et al., 1983) and possibly until the ridge 'jump' occurred in the Late Cretaceous (Hartnady and Le Roex, 1985). Higher regional heat flow during the transit of the Shona/Bouvet hotspot (and more locally from the related igneous events) would result in increased maturation. Lastly, during and after the Agulhas slump, the subsequent dewatering of the hot overpressured water from the Southern Outeniqua Basin could have ensured a further local heat input (discussed later).

These heat inputs resulted in three phases of heating which matured source rocks throughout the Bredasdorp Basin (Fig. 4.19). Evidence of these are found in the common coexistence of gas and oil shows in reservoir sediments below ~2000 metres and in source rocks which retain traces of early-formed oil.

4.4.1. Optical parameters

Vitrinite reflectance measurements comprise a widely used high precision technique to ascertain the level of organic diagenesis (Bustin et al., 1990) and the parameter is the base against which other maturity data are compared (Dow, 1977; Table 4.05).

With increasing maturation (heating through time), vitrinite becomes chemically altered, trending towards higher proportions of condensed aromatic ring components. Because of this, the material becomes harder and will take a higher polish. The proportional reflectance of a known beam of light from the surface of the material is therefore a measure of its surface hardness and has been compared with coal rank parameters to evaluate the maturity level (Hood et al., 1975) i.e. the rate of alteration of the maceral is largely dependent on the time and temperature achieved since maturation started. However, it is also partly dependent on the rate of heating the organic matter has

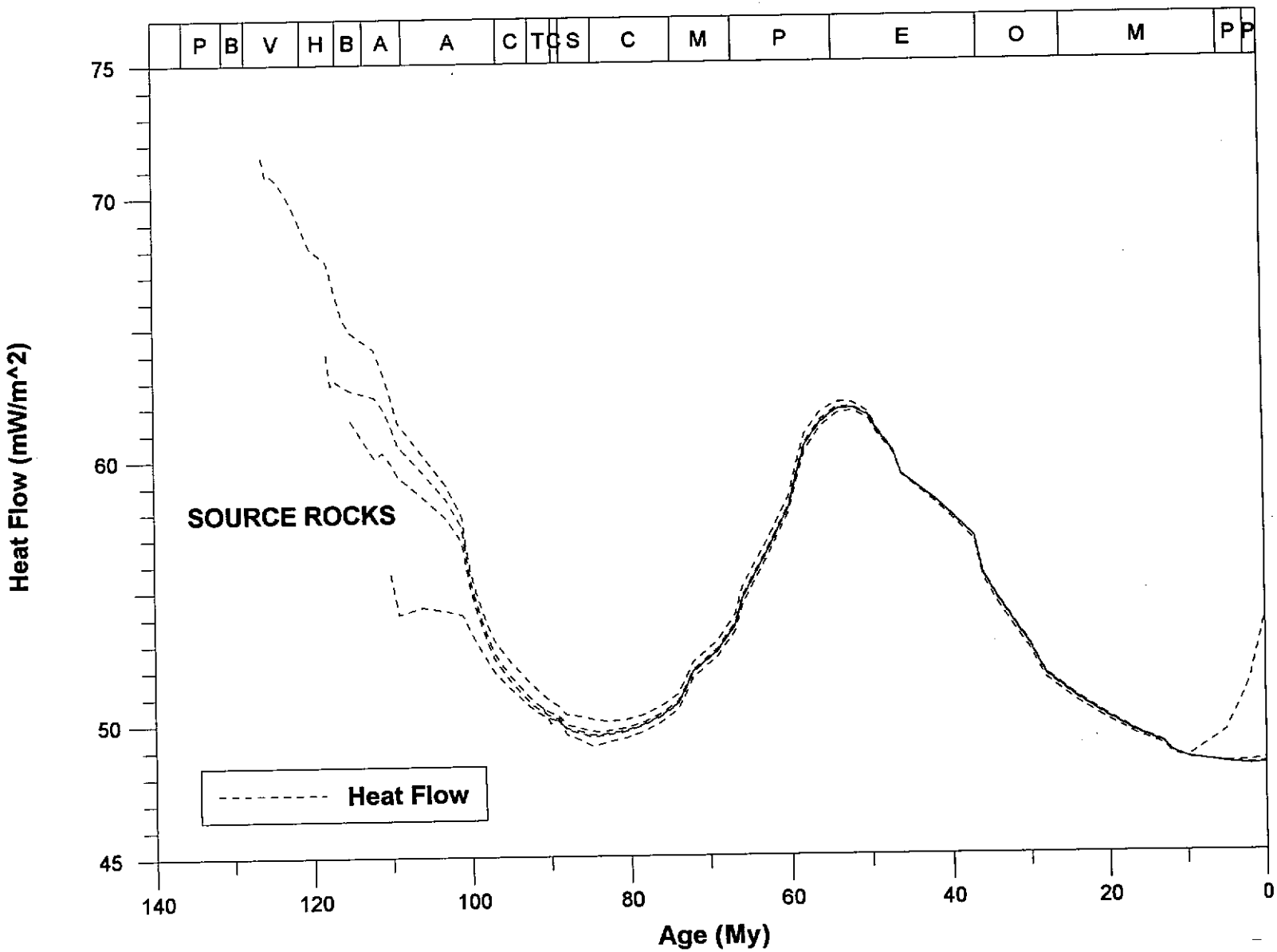

Figure 4.19: Plot of modelled heat flow since syn-rift sediment deposition started (~140 Ma). The three periods of high heat flow correspond to the thermal cool-down phase after Gondwana rifting, the late Cretaceous-early Tertiary hotspot transit and the heating effects associated with the Great Africa Swell. The heat brought into the basin by the hot fluid flush is largely a shallow effect and only the Turonian source in the basin is affected.

MATURATION WINDOWS

WINDOWS	VITRINITE REFLECTANCE (R_0)	PALAEOTEMPERATURE
Oil (main generation)	0.5-1.3%	60-135°C
Wet gas (main generation)	1.3-1.5%	135-160°C
Dry gas (main generation)	1.5-~2.0%	160-200°C

EXPULSION WINDOWS

EXPULSION WINDOWS	VITRINITE REFLECTANCE (R_0)	PALAEOTEMPERATURE
Main oil (expulsion)	0.75-1.10%	85-115°C
Main wet gas (expulsion)	1.10-1.40%	115-140°C

BULK MATURATION PARAMETERS

OPTICAL				CHEMICAL	
Vro	SCI	Spore flu	Spore colour	Tmax	PI
<0.5%	<<5	yellow	lemon	<430°C	<0.1
0.5%	<5		yellow	430°C	0.1-0.2
0.6%	6	yellow-orange	yellow-orange		
0.7%	7			440°C	~0.2
0.9%	8	orange	orange	450°C	0.2-0.4
1.1%		orange-red		460°C	0.2-0.4
1.2%	9	nil	red at edges	465°C	<0.2
>1.4%	10	nil	brown at edges	475°C	
2.2%		nil	black	520°C	<0.1

MATURATION WINDOWS	PRESENT TEMPERATURE	VITRINITE REFLECTANCE
Top oil window	60°C	0.5%
Early stage oil formation	60-80°C	0.7%
Main stage oil generation	80-135°C	0.7-1.3%
Peak oil generation	100°C	1.0%
Oil-gas transition	135-160°C	1.3-1.55%
Dry gas stage	160-200°C	1.55->1.8%
Thermal basement	200°C	>1.8->2.0%

Table 4.05: Table of maturation parameter correlations (from Davies et al., 1994).

undergone, the amount of absorbed oil and the amount of amorphous material (Hutton and Cook, 1980; Barker, 1983; Price and Barker, 1984; Yukler and Thomsen, 1989).

In company with the chemical re-ordering of the vitrinite macerals, there is a progressive colour change of the organic material in transmitted light from yellow to black. This change affects amorphous and structured organic material (Peters et al., 1977; Staplin, 1982a; Gutjahr, 1966). Other optical parameters which are comparable to vitrinite reflectance and organic matter coloration are conodont colour changes and bitumen reflectance (North, 1985, p.61; Riediger, 1993) although these have not been used here.

4.4.2. Chemical parameters

The most commonly used chemical maturation parameters are those derived from artificial maturation analyses such as Rock-Eval. In those analyses, rock samples are artificially matured and the temperature at which the peak output of hydrocarbons is measured is a comparable measure of maturity to the vitrinite reflectance (Espitalié et al., 1985). In addition, the ratio of generated hydrocarbons to remaining potential (PI) is also used as a maturation parameter (Peters, 1986). Both these parameters are often used to evaluate maturity levels where optical data are absent or sparsely available (Espitalié et al., 1985). Progressive changes in the proportions of bitumen which are solvent-extractable from the rock, of the ratios of the individual fractions (Phillippi, 1965) as well as more specific parameters such as the carbon preference index (Bray and Evans, 1961) and aromatic compound ratios (Radke, 1988) are also commonly used to estimate maturity. Ditch and cuttings gas data (analyses of gas adsorbed and absorbed in rock) are well suited to the evaluation of maturity levels (Le Tran, 1975). They are recorded regularly throughout the drilling of the well, in contrast to most geochemical parameters which are only measured on selected samples, and are often analysed automatically or semi-automatically eliminating much potential operator bias. These data can be directly compared to the more commonly used optical and chemical parameters (such as vitrinite reflectance and Tmax) as shown for wells 83, 91, 93 and 99 in Figs. 4.20-4.23.

4.4.3. Maturation distribution

In order to use maturation data in the construction of maps or sections, it is most useful to have maturity data in a linear scale but Tmax and vitrinite data vary exponentially with maturation. Hence it is usual to convert maturation thresholds to a linear scale. Various authors have calibrated different maturation parameters to each other and have derived 'palaeotemperatures' to provide different linear scales (Le Tran, 1975; Heroux et al., 1979; Dow and O'Connor, 1982; Espitalié and Joubert, 1987). This type of calibration study has also been carried out in the Bredasdorp Basin (Benson et al.,

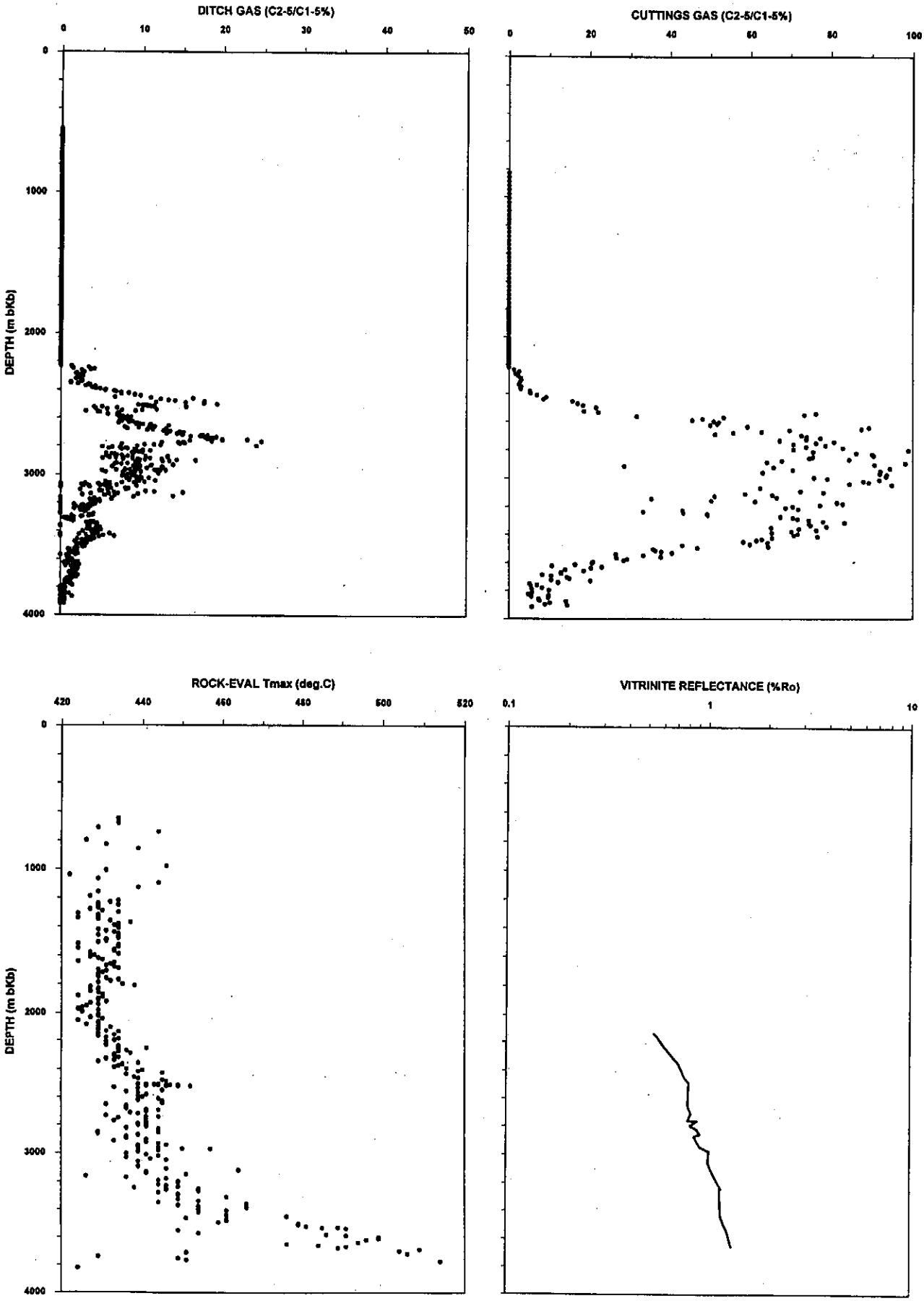

Figure 4.20: Plot of ditch and cuttings gas methane wetness, Rock-Eval Tmax and vitrinite reflectance data for Well 83.

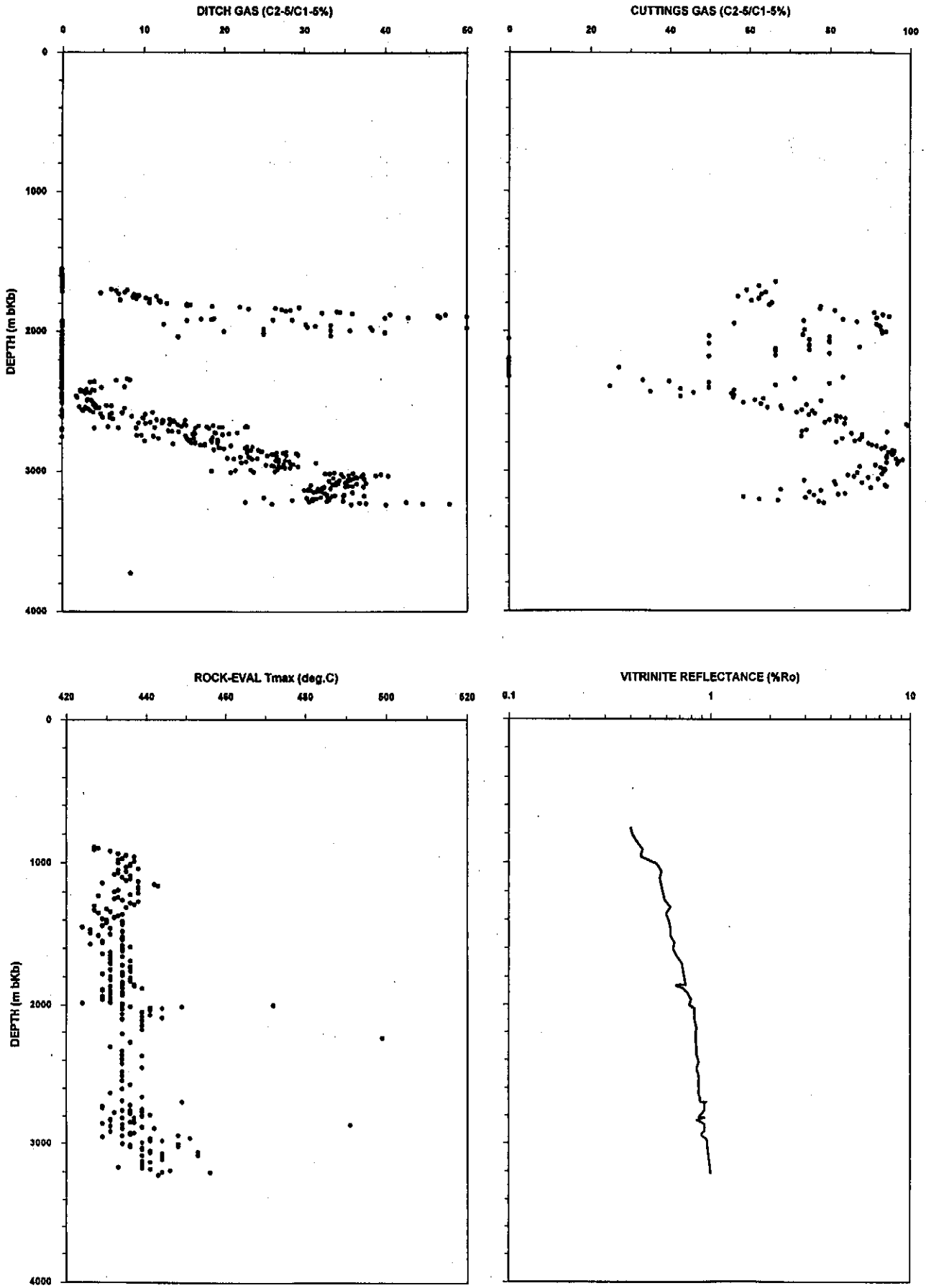

Figure 4.21: Plot of ditch and cuttings gas methane wetness, Rock-Eval Tmax and vitrinite reflectance data for Well 98.

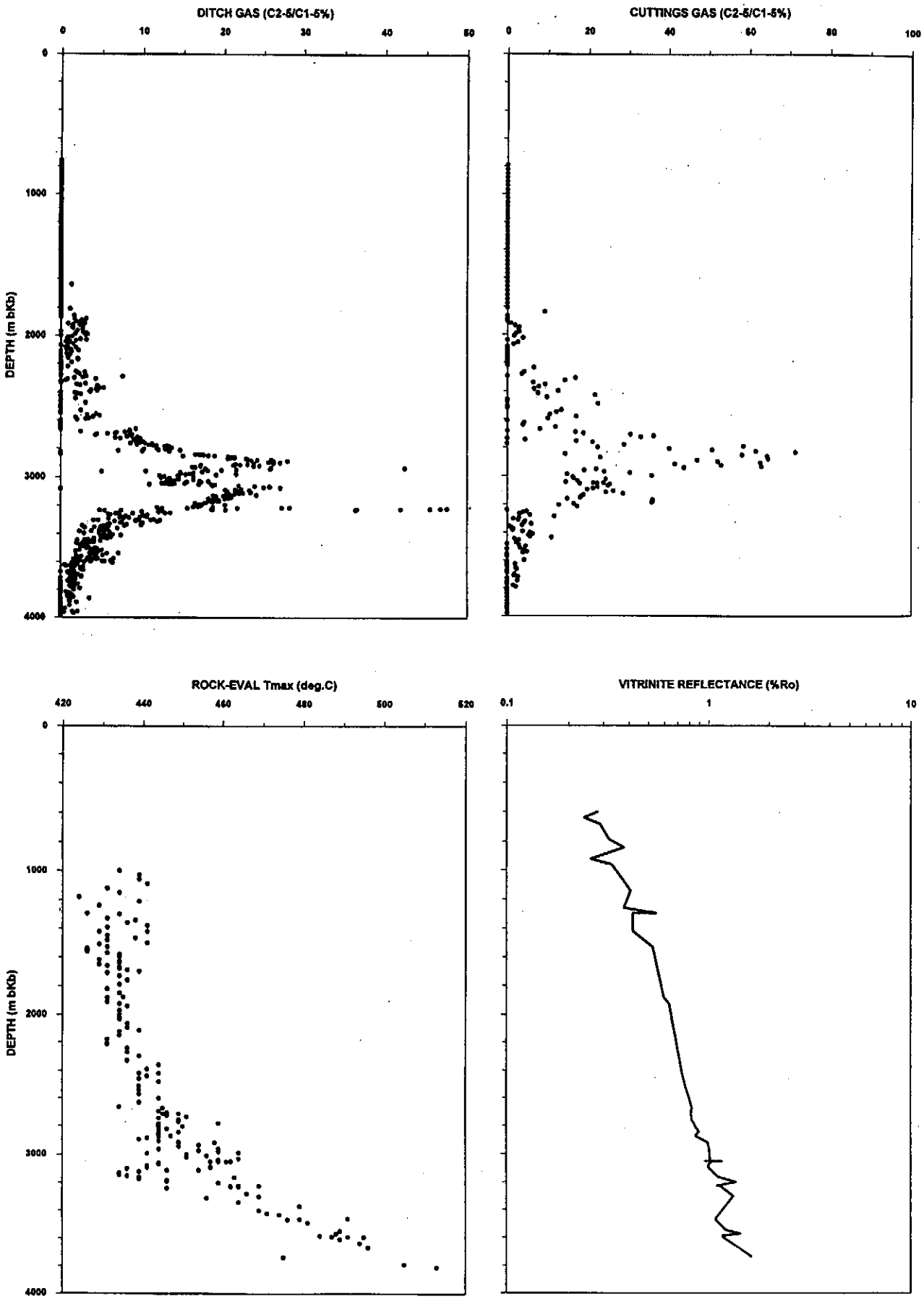

Figure 4.22: Plot of ditch and cuttings gas methane wetness, Rock-Eval Tmax and vitrinite reflectance data for Well 91.

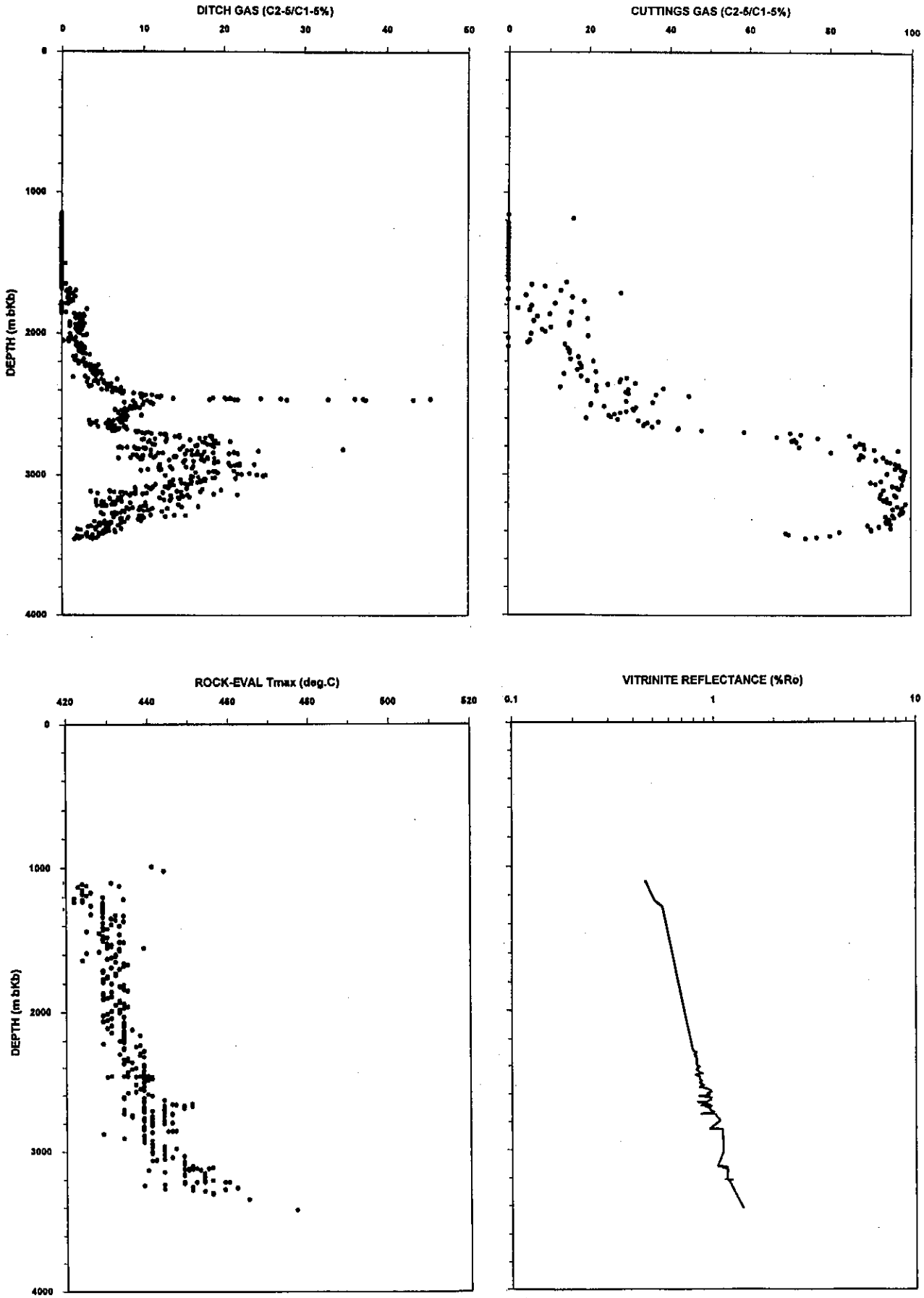

Figure 4.23: Plot of ditch and cuttings gas methane wetness, Rock-Eval Tmax and vitrinite reflectance data for Well 93.

1990). The results generally confirm (Table 4.02) that many of the parameters are essentially interchangeable in their ability to measure maturity.

The only compilation of South African offshore maturity data to date, which includes a summation of regional temperature gradients, is that of Leith and Rowsell (1978). They reported an average geothermal gradient of 3.5°C/100m but this was based mainly on data from the first wells in the Pletmos Basin and included data from only two wells in the Bredasdorp Basin. The result of this study, which drew extensively on the models of Karweil (1956), Correia and Peniguel (1975) and Cornelius (1975) in matching optical and chemical evidence to palaeotemperatures, introduced the concept of 'effective generation time' to offshore data. They (as Rowsell and De Swardt, 1976 had done for the onshore data), showed that palaeotemperatures estimated from the known burial time and the vitrinite reflectance data, recorded a close similarity with present-day temperatures (Table 4.05). Effective generation time refers to burial of the source rock close to the maximum temperature for a significant period of time - in the case of these offshore source rocks, for ~75 Ma (North, 1985). To achieve such a close similarity required that present day temperatures were essentially the maximum achieved (Cornelius, 1975). Such data were modelled using the TTI method (Waples, 1980), and many early Bredasdorp Basin reports quote 'palaeotemperatures' according to this format. However, in this thesis, vitrinite reflectance results have been used as the standard parameter for characterisation of thermal maturity. Isoreflectance contour maps have been constructed (Davies, 1996a) for all major horizons which underlie the main source intervals namely 15At1, 13At1, 9At1, 6At1, 5At1 and 1At1. They are shown in Figs. 4.24-4.29.

4.4.4. Maturation Thresholds

Estimation of depths to maturation thresholds is essentially empirical – i.e. some of the methods used are less accurate than others and all are affected by aspects other than maturity. Hence a variety of parameters should be used to determine maturity thresholds rather than just one. Some of the more important of these effects are discussed below.

4.4.4.1. Organic matter type

Different types of organic matter have different reaction rates and thresholds. Hence, each parameter is most effective in specific maturity ranges. Maturation parameters derived from light hydrocarbons (Thompson, 1979) are effective through the oil window. The carbon preference index, however, (Erdman, 1975) attains its equilibrium value (1.0) by the mid-oil window. Some parameters also react at different rates to increasing maturity so that they cannot always be correlated with each other. For example the rate of change of vitrinite reflectance parallels the increase in Tmax only until the

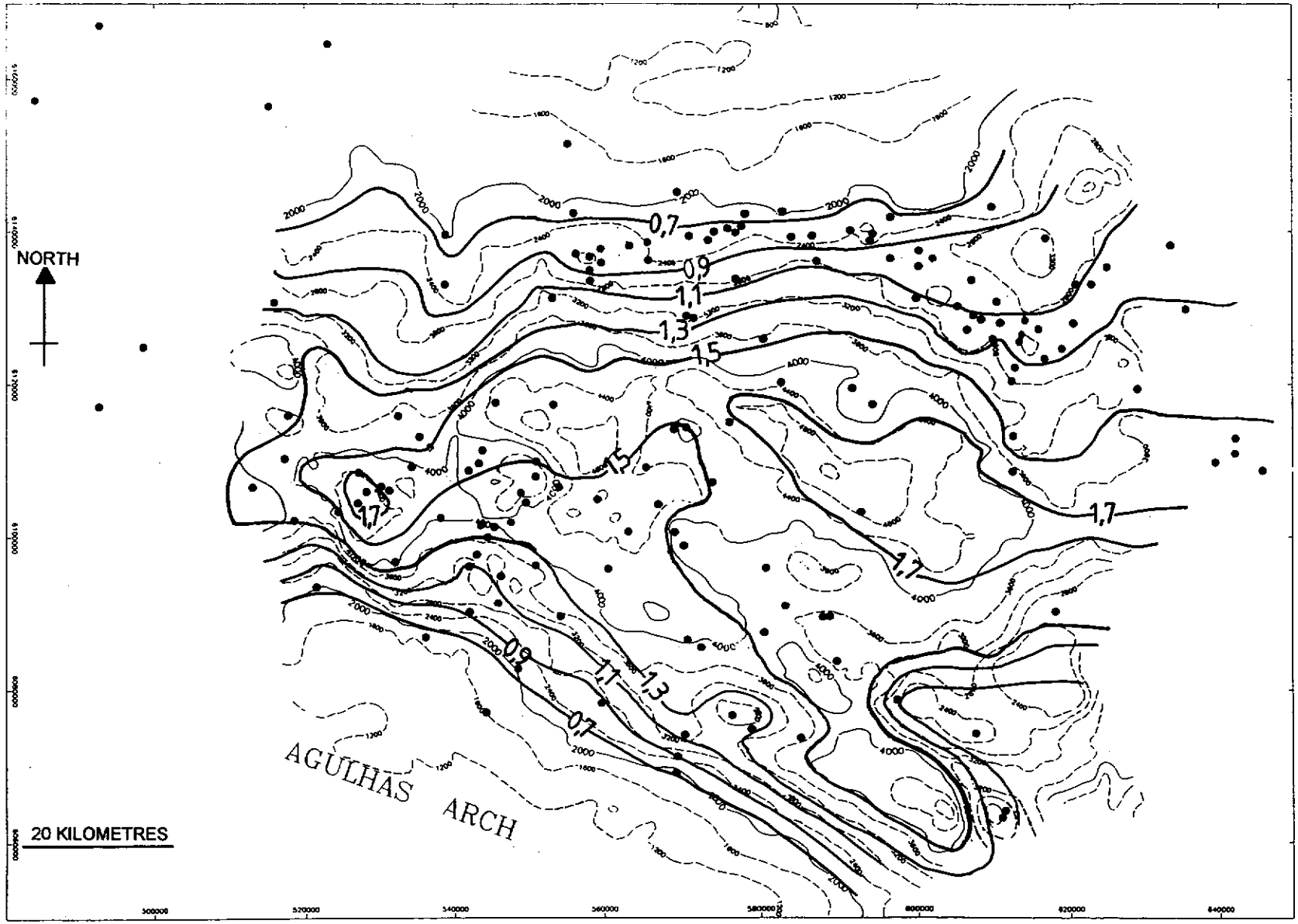

Figure 4.24: Depth map to horizon 1At1 with vitrinite iso-reflectance contours superimposed.

Figure 4.25: Depth map to horizon 5At1 with vitrinite iso-reflectance contours superimposed.

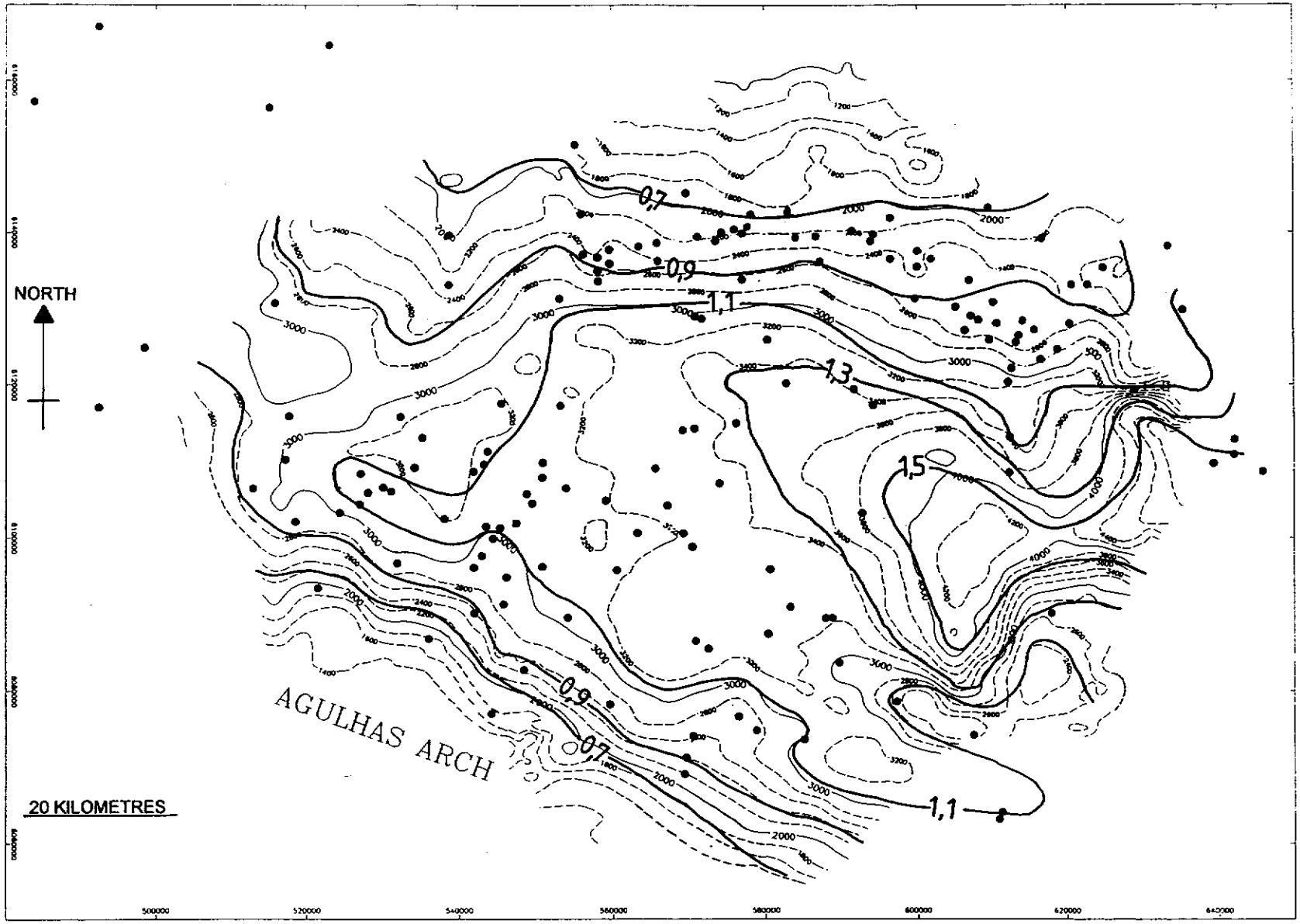

Figure 4.26: Depth map to horizon 6At1 with vitrinite iso-reflectance contours superimposed.

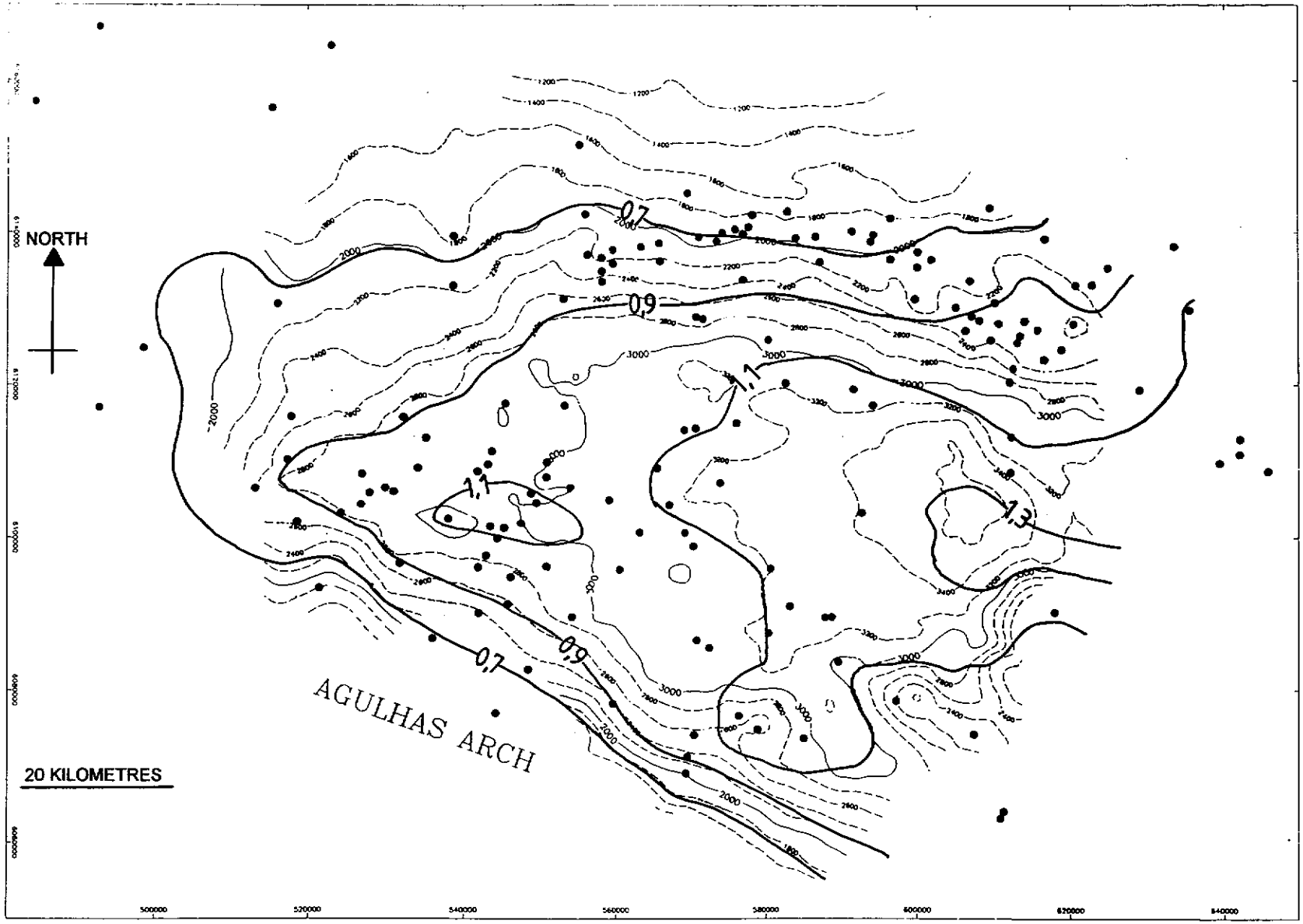

Figure 4.27: Depth map to horizon 9At1 with vitrinite iso-reflectance contours superimposed.

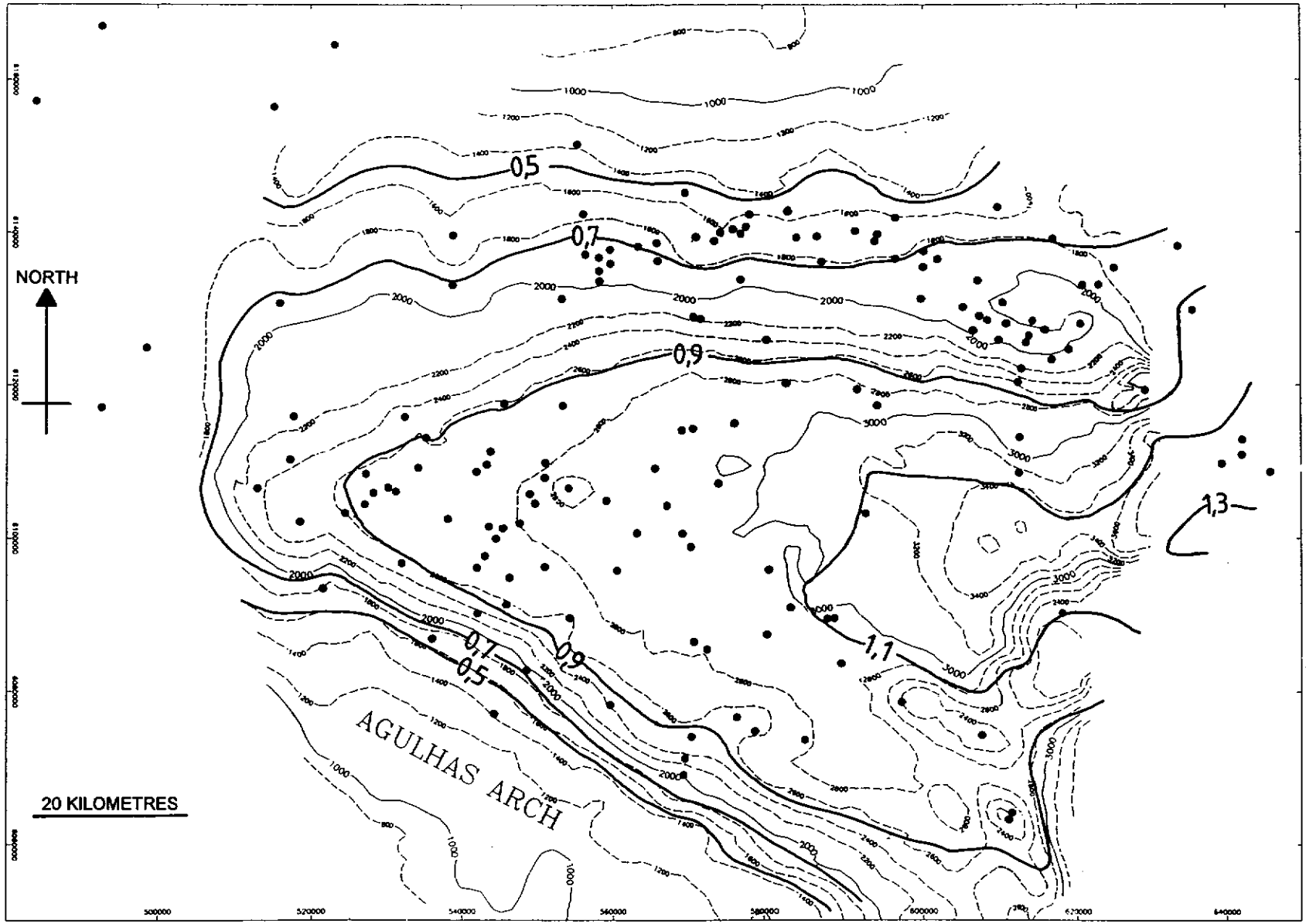

Figure 4.28: Depth map to horizon 13At1 with vitrinite iso-reflectance contours superimposed.

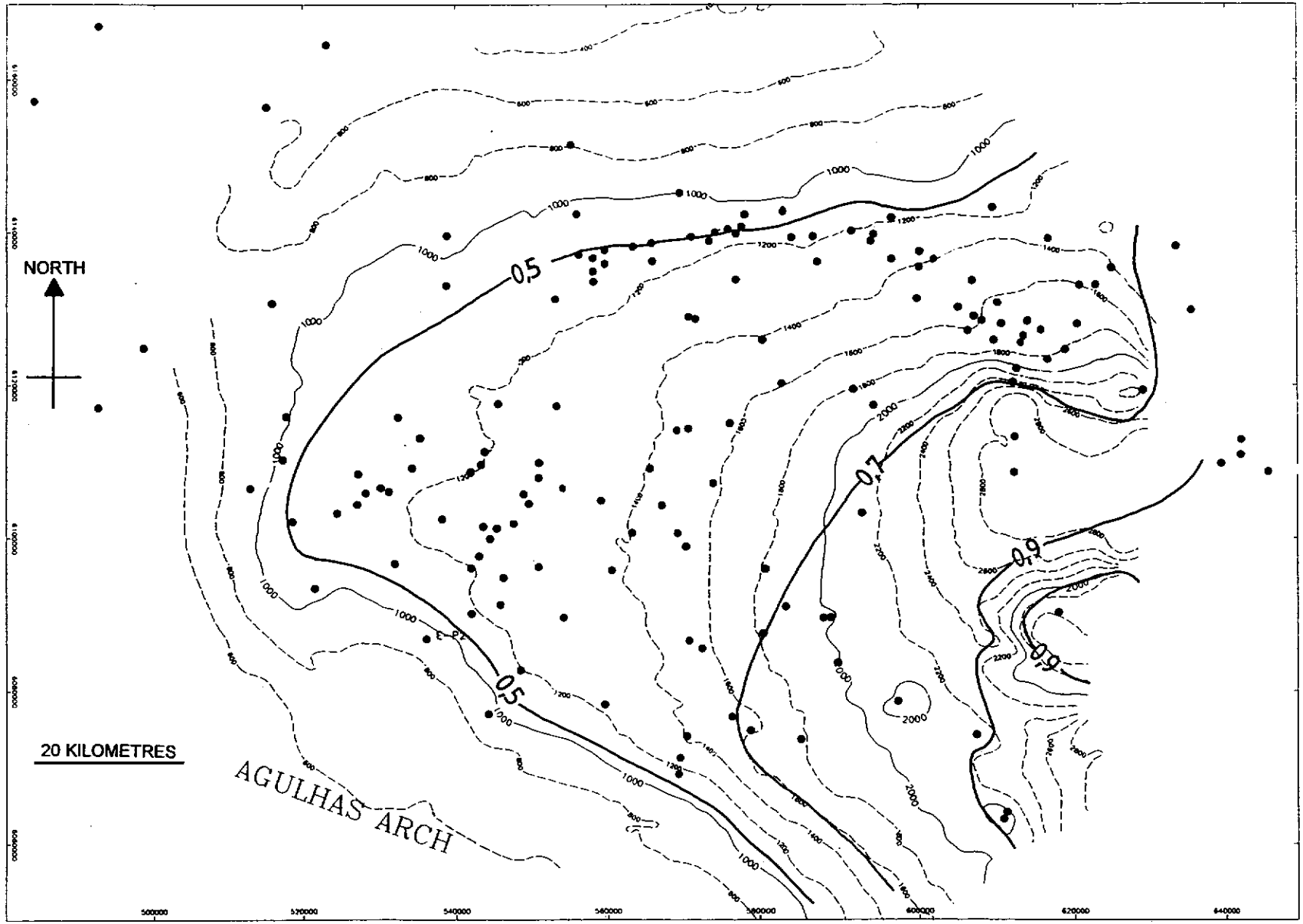

Figure 4.29: Depth map to horizon 15At1 with vitrinite iso-reflectance contours superimposed.

middle of the oil window after which the Tmax increases more rapidly (Espitalié et al., 1977; Senftle and Landis, 1991).

4.4.4.2. Lithology effects

The presence of varying amounts of free oil or unusual mineral matter in the shale can also affect maturation parameters by altering their rate of response to temperature or time. Tmax values too, can be similarly reduced in oil-rich rocks due to the influence of absorbed oils (Peters, 1986). However, the peak due to the oil is usually at such a low temperature and is present in such large quantities relative to the organic matter content, that it can be readily identified as an impregnation.

4.4.4.3. Catalytic effects.

Catalysis also plays a role in accelerating or retarding generation relative to temperature. Studies have been carried out to address this effect using individual minerals and hydrocarbons (Shimoyama and Johns, 1972; Radke, 1987) or on whole rock samples (Evans and Felbeck, 1983). However, such catalysis is considered likely to be significant only where there is 'intense contact' between the minerals and the organic matter. Prior to generation, most of the organic matter is essentially solid. Hence the contact areas between the two are very limited, which limits the catalytic effects. Once some of the organic matter has been converted into bitumen, there is a greater and more intimate contact between the mineral matter and the bitumen. Therefore the effect of catalysis can be much greater. Smectitic clays have been shown to be active catalysts (Peters and Moldowan, 1993) partly because they have readily transferable cations. These clays are commonly found in fine-grained argillaceous source rocks but less commonly in reservoir rocks - in addition, many of the transition metals found largely in deep water claystones may act as catalysts (Mango, 1992). Hence, catalysis is generally only effective in mature source rocks and the effects may be difficult to separate from those prevailing due to normal maturation processes.

Generally, the optical and chemical parameters used in this study are those which are readily determined, e.g. Tmax, R_o, production index, spore fluorescence. The palaeotemperature thresholds of the oil and gas windows derived from these parameters, and from the modelling using the reaction rate data, do not always compare to those reported in other basins. This is mainly due to differences in the heat flow, lithology and compaction between the basins. However, Waples (1984) pointed out that an empirical study should be made of each basin to determine these differences. This has been done only for the Upper Barremian to Lower Aptian source rocks (13A and 9A) in the Bredasdorp Basin (Davies, 1988b and 1990). This is because these are the only intervals intersected basin-wide and which are present in

both the oil and wet gas windows. This variety of samples has provided a wide range of remnant potentials which can be used to estimate the original potential and from these data, it is possible to estimate the quantity of hydrocarbons generated.

4.4.5 Vitrinite reflectance data

It was noted early on that vitrinite reflectance values recorded from source rock samples were consistently higher at hydrocarbon generation thresholds than expected relative to other maturity parameters (Figs. 4.20-4.23; Heroux et al., 1979). Indeed, Banks et al. (1993) commented on the large number of shale samples with high vitrinite reflectances which had 'low mature'-looking normal alkane profiles. Vitrinite reflectance models constructed using the thermal history estimated from the regional geology and extrapolated using available biostratigraphic, lithologic and heat flows, did not match measured vitrinite reflectances. Even using kinetic data from several source rocks failed to eliminate the significant disagreement between modelled and actual values.

It was thought that this was an effect of the rapid burial of the source rocks into the oil window and very slow burial through the window (North, 1985) which resulted in an unusually low heating rate during the past 50-100 Ma. An effect similar to this was reported by Teichmüller and Teichmüller (1981), Quigley et al. (1988), Field (1985) and Williamson (1992). Burial history and thermal modelling shows that the heating rate of post-rift source rocks has been below 0.3-0.6°C/Ma for most of the past 100 Ma resulting in higher reflectance values e.g. 0.95-1.10% at peak oil, than in more rapidly heated rocks e.g. 0.7-0.9% (Dahl and Spears, 1985; Yukler and Thomsen, 1989; Peters and Moldowan, 1993). The higher reflectances at the various oil thresholds were therefore considered to be solely a function of the unusually low heating rates. However, the differences were still not fully explained by this.

In the Bredasdorp Basin, there are 72 wells with vitrinite reflectance data extending for at least 1000 metres above TD. In these wells, reflectance profiles generally describe a convex trace in Mid-Upper Cretaceous rocks. Modelled reflectances, however, describe a straight line. In a few wells, there are enough data from high in the succession, to show that the reflectances become less anomalously high as the sea floor is approached, contrary to the expected trend if erosion were the cause (Dow, 1977). The profiles therefore show a 'normal' data trend near TD and a bulge which is offset from the trend towards the usual seafloor intercept value of ~0.2% (Dow, 1977; Fig. 4.30).

Four possible causes of this offset were identified and studied:
(i) a Late Tertiary erosion event
(ii) unusual source rock kinetics or vitrinite reflectances

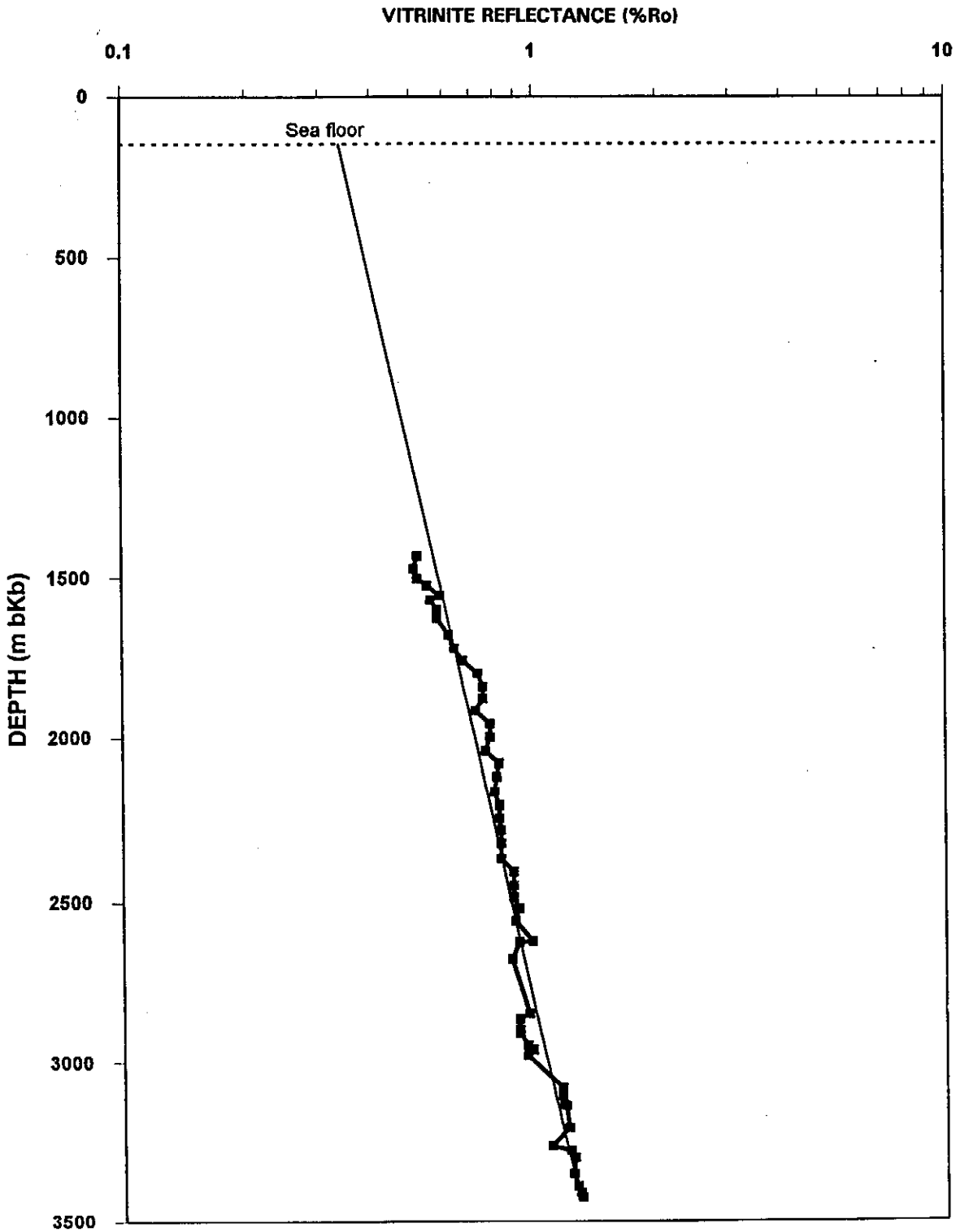

Figure 4.30: Plot of vitrinite reflectance versus depth for a central Bredasdorp well (Well 106) showing the very narrow range of data either side of an exponential trend fitted to the vitrinite reflectance data.

(iii) erroneous vitrinite reflectance data
(iv) a late pulse of heat shallow in the section

(i) Late Tertiary erosion event
The regression line through reflectance data from many wells intercepts the sea-floor at >>0.3% whilst in other wells the sea floor intercept is nearer 0.2%. Such large variations cannot be explained by late stage erosion of >1500 metres (Dow, 1977) (Table 4.06), because the vitrinite reflectance data are not consistently high throughout the profile. Biostratigraphic and seismic data throughout the basin showed no indications of major Tertiary erosive events in either the flank wells or the central region. Upper Oligocene through Miocene rock samples from piston cores off Mossel Bay and from wellsite sampling recorded no unexplained timegaps (McMillan, 1996, pers. comm. and SOEKOR unpubl. biostratigraphic data). Hence a major, Late Tertiary phase of erosion cannot be invoked to explain the anomalous vitrinite reflectance data.

(ii) Unusual source rock kinetics or vitrinite reflectances.
The reflectance of vitrinite is known to be affected by the admixture of large amounts of amorphous organic material (Price and Barker, 1984), algal debris (Hutton and Cook, 1980) or traces of sorbed oil (Peters, 1986). However, in each case these do not increase reflectance - rather, the opposite happens. Moreover, most kerogen samples in the wells concerned are neither dominated by algal or amorphous debris nor by oil traces. The similarity of published source rock kinetic data (Burnham et al., 1987) with those measured on Bredasdorp Basin samples (Table 4.01) showed the kerogen types were not unusual.

(iii) Erroneous vitrinite reflectance data
The large maturation dataset in the Bredasdorp Basin (3760 vitrinite data points from 99 wells, >50% from core samples) were measured relative to internationally accepted standards. A set of reflectance measurements made with SOEKOR equipment were compared to measurements by other exploration and contracting companies on the same or matching samples (Fig. 4.31 and Table 4.07). The SOEKOR reflectance data (ranging from R_o 0.49-1.64%) matched those reported by other companies to a standard deviation of 17%. Published comparisons of reflectance data from coal samples ranging from R_o~0.4-0.6% were 11% (Lin, 1994) but for Mesozoic shales ranging from R_o~0.5-3.0%, deviations ranged 5-66% (Claypool and Magoon, 1985). The SOEKOR data are therefore considered to reliably represent the maturation of the samples. These reflectance data are backed up by pyrolysis maturation parameters (Tmax and PI) calculated from 22423 Rock-Eval and Leco data from 143 wells in the basin as well as wellsite cuttings and ditch gas data from all but four wells in the basin (e.g. Figs. 4.20-4.23). In addition, the R_o : Tmax comparison of all matching core and

TABLE OF VITRINITE REGRESSION INTERCEPTS (72 WELLS)						
WELL	SAMPLES	INTERCEPT	ABOVE 15At1	TOP SAMPLE	BOTTOM SAMPLE	DEPTH RANGE
3	13	0.46	0	915	2342.5	1427.5
6	22	0.28	0	460	2108	1648
83	28	0.22	0	2134.5	3657	1522.5
85	42	0.43	0	1410	2500	1090
88	81	0.40	0	2010	3823	1813
118	32	0.36	0	1424	2746.2	1322.2
102	32	0.27	7	797	2228.5	1431.5
90	78	0.42	0	1592	3530	1938
89	6	0.23	0	1630	2665	1035
95+103	44	0.41	10	1879.5	3482	1602.5
91	51	0.23	13	600	3810	3210
94	43	0.34	7	794	3567.4	2773.4
104	52	0.35	1	1452.5	3269.1	1816.6
114	20	0.35	1	1530.5	3055	1524.5
98	72	0.41	3	760	3211	2451
123	48	0.44	0	2245	2960	715
93	109	0.32	4	1101	3415	2314
119	145	0.28	1	1213.5	2976	1762.5
97	30	0.22	0	2600	3348.9	748.9
99	66	0.23	2	1625.1	3683.6	2058.5
111	21	0.35	0	1496.5	2954.08	1457.58
106	53	0.34	1	1434.5	3424	1989.5
108	47	0.35	1	1176.5	3118.9	1942.4
129	44	0.48	0	1615	3295	1680
109	53	0.35	0	1625	3227	1602
130	20	0.36	0	1794.9	2855.2	1060.3
124	32	0.39	4	1654.7	3038	1383.3
107	14	0.33	0	1603	2485	882
121	47	0.34	1	1601	3190	1589
110	33	0.39	0	2390	3321	931
112	30	0.46	0	1534	2500	966
113	53	0.41	0	2312.4	3059.5	747.1
126	34	0.35	0	2205	3092.5	887.5
120	29	0.37	0	2451.7	2929.7	478
116	46	0.25	16	1324	3070	1746
115	49	0.49	0	2450.1	3348.5	898.4
125	54	0.33	0	1893.5	3066	1172.5
117	101	0.34	0	1552	3105.6	1553.6
122	103	0.31	0	1394	3183	1789
156	31	0.48	0	2203.2	3065.2	862
133	42	0.46	0	2111.1	2955.5	844.4
132	54	0.38	0	1476	2924	1448
137	40	0.53	0	2249	2796.5	547.5
142	34	0.39	0	1537.5	3047.5	1510
160	57	0.33	12	1514.5	3627.6	2113.1
163	19	0.30	0	2145	3975	1830
9	38	0.46	5	515	2780	2265
11	30	0.41	5	806	3015	2209
14	45	0.41	4	720	3749	3029
27+35+37	6	0.35	0	3163	3505	342
87	48	0.44	0	1765	2245	480
46	22	0.47	0	1250	2455	1205
16	76	0.41	9	625	4506.5	3881.5

Table 4.06: Sea floor intercepts of exponentially regressed vitrinite reflectance data (using the Excel GROWTH function).

50	19	0.42	3	1010	2410	1400
41	83	0.38	0	2000	2592	592
52	14	0.49	2	510	2902	2392
65+75	36	0.45	0	1310	3326.5	2016.5
101	39	0.29	11	950	3271	2321
18	40	0.37	16	640.8	2580	1939.2
55	10	0.35	0	1975	2652	677
70	68	0.25	0	2210	2646	436
63	6	0.31	0	2055	2455	400
66	46	0.28	0	2250	2888	638
60	21	0.58	0	960	2662	1702
159	22	0.15	2	2320	3723	1403
8	17	0.40	0	2117	2894	777
73	24	0.25	0	2100	3481	1381
47	24	0.48	20	791.5	2311	1519.5
105	46	0.28	24	1532	3660	2128
128	30	0.29	6	1524	3738.1	2214.1
13	6	0.14	4	1283	2134	851
138	48	0.29	0	2201	3110	909
TOTALS	2983	av.=0.36	195			

Table 4.06 (cont.)

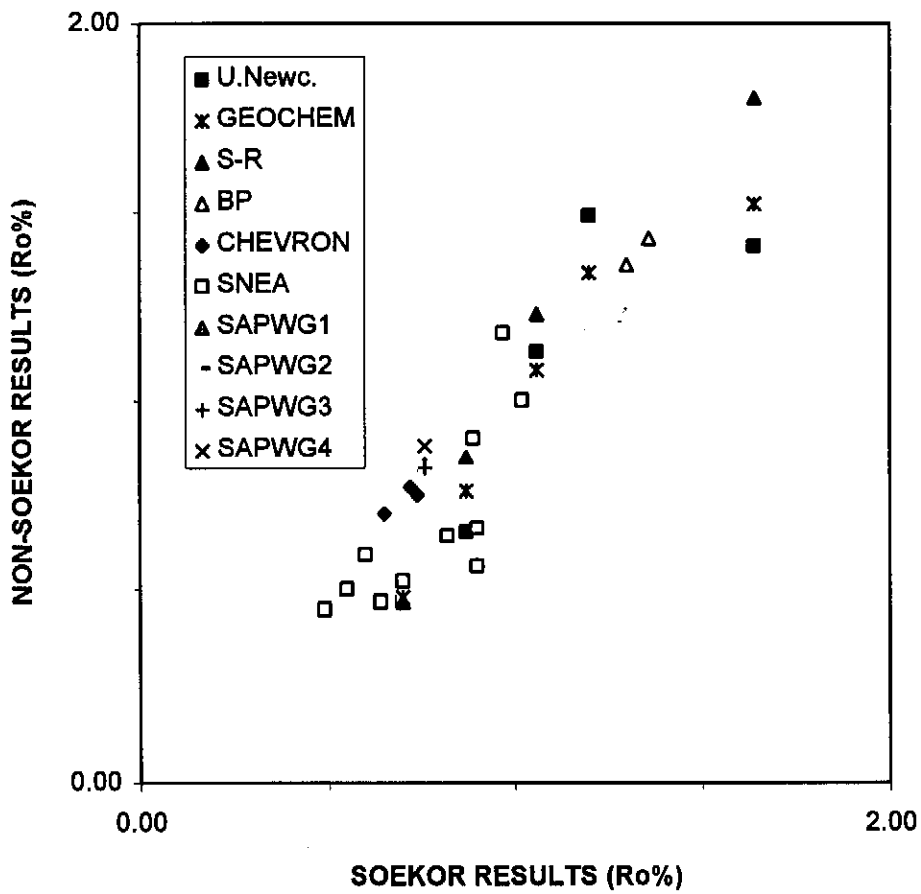

Figure 4.31: Comparison of SOEKOR-generated vitrinite reflectance data with results from the same or matching samples carried out by other laboratories as listed in Table 4.06.

VITRINITE REFLECTANCE VALIDATION DATA												
WELL	Depth	SOEKOR	U.Newc.	GEOCHEM	S-R	BP	CHEVRON	SNEA	SAPWG1	SAPWG2	SAPWG3	SAPWG4
128	3738.8	1.64	1.41	1.52	1.80							
West coast 'O'	4166.7	1.20	1.49	1.34								
16	3380.5	1.06	1.13	1.08	1.23							
90	2478.5	0.70	0.47	0.48	0.47							
90	3159.2	0.87	0.65	0.76	0.85							
West coast 'K'	3830.0	1.30				1.36						
West coast 'K'	3930.0	1.36				1.43						
West coast 'J'	2950.0	0.65					0.70					
West coast 'J'	3049.0	0.74					0.75					
West coast 'J'	3262.0	0.72					0.77					
coal	stub	0.76							0.83			
coal	stub	0.76								0.82		
coal	stub	0.76									0.82	
coal	stub	0.76										0.88
Pletmos 'G'	1380.0	0.55						0.50				
Pletmos 'G'	1600.0	0.49						0.45				
Pletmos 'G'	1703.0	0.60						0.59				
Pletmos 'G'	1793.0	0.64						0.47				
Pletmos 'G'	1903.0	0.82						0.64				
Pletmos 'G'	2063.0	0.70						0.52				
Pletmos 'G'	2255.0	0.90						0.66				
Pletmos 'G'	2324.0	0.89						0.90				
Pletmos 'G'	2465.0	0.97						1.18				
Pletmos 'G'	2543.0	0.90						0.56				
Pletmos 'G'	2765.0	1.02						1.00				
from Van der Spuy, D. (1995). The vitrinite reflectance validation exercise: results and discussion. Soekor unpubl. cons. rept., HALGEO R003/95, 10pp.												
SAPWG = South African Petrographers Working Group.												

Table 4.07: Correlation of vitrinite reflectance data determined by SOEKOR versus equivalent data from analyses by other laboratories on the same or matching samples.

sidewall core samples (Fig. 4.32) correlates closely with published data (Espitalié et al., 1985)

(iv) Late heating event

A shallow heat input, late in the maturation history, could also explain the 'bulge' (C. Cornford, 1994, pers comm.), but this unusual explanation can only be used where a reasonable geological model is employed. Several published studies have addressed this effect showing that regional hot fluid flow can influence maturation levels.

The result of a heat and fluid flow study carried out over the Troll field in the North Sea (Hermanrud, 1986) showed that hot water expelled from sediments in the near vicinity of the wells by burial compaction could have caused only minor maturation deviation. In an example from the Halten Terrace, North Sea, a recent heat increase had to be applied to match the measured maturity data to known lithological, burial and thermal history. Jensen and Doré (1993) showed that overpressured rocks affect modelled thermal conductivities which in turn influence the modelled fluid flow, and concluded that the apparent heat 'spike' was a result of the inability of the programme algorithms to fully model the events.

In contrast, Grigo et al. (1993), from 3-D modelling of fluid flow across the Haltenbanken area, considered there was justification for the modelling of a late fluid flow-related heat pulse. Jessop and Majorowicz (1994), in their review of the maturation effects of fluid flow, showed that laterally flowing fluids in the Williston (and other) basins supplied up to a third of the total heat input and caused much of the maturation.

In the case of the Bredasdorp Basin, the shallowness of the heat flow anomalies (~1000-3000 metres) indicates that the heat pulse needs to be applied mainly to Upper Cretaceous rocks. Tertiary rocks too may be affected by this event, but there are too few data to confirm that. By contrast, the deep, least permeable rocks require the least modification to the maturation profile to balance the heat flows. This favours a late, shallow heat input instead of a deep basement source.

One possible initiator of the heating anomaly is the Agulhas Slump (Dingle, 1977; Section 3.5). Tilting and compaction associated with this event are thought to have influenced pore fluid migration patterns throughout the southern offshore basins. In particular, they resulted in the expulsion of water from ~4200 km^2 of the Southern Outeniqua Basin towards the Bredasdorp Basin. Burial history modelling was carried out at two locations in the Southern Outeniqua Basin (Fig. 3.24). Depth-time correlations were made using data from wells around the edge of the basin whilst the

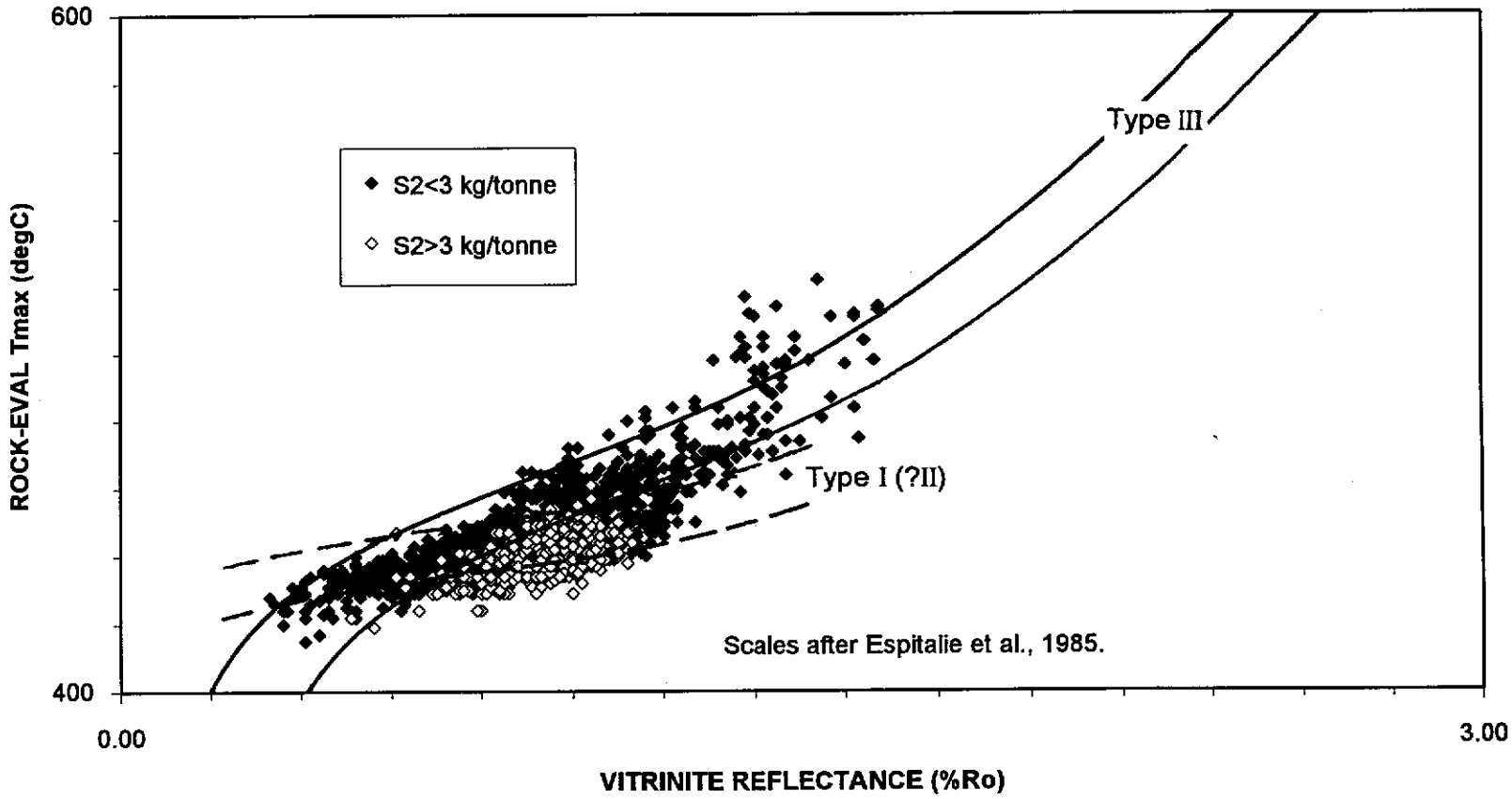

Figure 4.32: Cross-plot of all vitrinite reflectance and Rock-Eval Tmax data from the same core and sidewall core samples where the original source potential exceeds (or is extrapolated to exceed) 3kg/tonne rock. The trend lines are after Espitalié et al. (1985). The close agreement of these data with published results supports the assumption that the reflectance data are correctly measured and representative of the maturity level experienced by the rock.

horizon correlation was extended along seismic lines which intersected wells around the basin. Modelled porosities have been shown to reduce by 4.0-0.3% after the 'slump' in sediments at depths ranging from 1500-4000 metres bmsl (Table 3.04). Temperatures modelled in these sediments ranged up to 240°C (i.e. beyond the gas window) in the deepest portion where porosity reductions of ~0.3-0.5% were modelled.

Modelling of total porosity loss from sediments in the Southern Outeniqua Basin directly downdip of the Bredasdorp Basin indicated that >100 km^3 of hot water (>100°C) was expelled during the Agulhas Slump (Table 4.08). Pressure modelling at those locations show that excess pressure bled off rapidly from the upper 2000 metres but more slowly from the sediments below. The rapid bleed-off could have caused localised mud volcano formation. One possible example was recorded near well no. 8 (Burden 1991; Fig. 4.33). In view of the ease of erosion at this location by occasionally severe wave action, the occasional impingement of the Agulhas Current on the shelf and soft-sediment slumping, such a cone could be preserved only if recently formed. Similar examples are found in other overpressured areas (Limonov et al., 1997).

Also, the sections with anomalously high reflectance rarely coincide with over-pressured sediments (cf. Brink and Winters, 1989; McAloon et al., 1990; Verfaille, 1993; Larsen, 1995). Indeed little overpressure was found above 3000 metres bsf (Larsen, 1995). It is likely that there was no lasting effect of overpressuring - except possibly in the central basin where the pre-9At1 rocks are still largely overpressured (Larsen, 1995; Davies, 1996c). Nevertheless, 1-D modelling may not be adequate to fully explain the compaction and regional fluid flow effects or correctly model the decreasing temperature gradients below the heat pulse. These should be tested using 3-D modelling when available.

4.4.6. Evidence for flow of hot fluids

A map of the distribution of the maximum reflectance offset value in the basin shows a central area with low values and a marginal area with high values (Fig. 4.34). There is no evidence that the intercept value is related to the number of samples, the depth range or the shallowest depths of the sampled interval (Fig. 4.35). If the offset values are a function of the vertical diffusion of the hot water, then where the greatest depth range of sediments has been affected should be where there has been the most extensive heating from the hot water charge, i.e. in those wells with the highest overall maturity gradients. Plots of reflectance data which demonstrate this effect are shown in Fig. 4.36.

In addition, maturity gradients have been estimated through the oil window (60-130°C) derived from summation of optical and chemical maturity parameters (North, 1985;

ESTIMATED VOLUMES (km3) OF WATER EXPELLED BY THE AGULHAS SLUMP										
SLUMP	AVERAGE	POROSITY	AREA	0-800m	800-1600m	1600-2000m	2000-2400m	2400-3200m	3200-4000m	>4000m
THICKNESS	THICKNESS	LOSS	km X km	0-40degC	40-80degC	80-100degC	100-120degC	120-160degC	160-200degC	>200degC
	(metres)	proportion of		av. 8%	av. 5%	av. 3.5%	av. 2.5%	av. 1.5%	av. 0.75%	av. 0.3%
		600m loss		0.1	0.1	0.0	0.0	0.0	0.0	0.0
0-300m	200	0.33	1050	5.5	3.5	2.4	1.7	1.0	0.5	0.2
300-600m	500	0.83	1890	62.7	39.2	27.5	19.6	11.8	5.9	2.4
600-900m	750	1.23	1210	89.3	55.8	39.1	27.9	16.7	8.4	3.3
>900m	950	1.58	50	6.0	3.8	2.6	1.9	1.1	0.6	0.2
				163.6	102.2	71.6	51.1	30.7	15.3	6.1
		TOTAL	4200	TOTAL COLD-WATER LOSS			TOTAL HOT-WATER LOSS			
		AREA	km2	in km3 at <100degC =		337.4	in km3 at >100degC =		103.3	

POROSITY LOSS FOR 600m SLUMP		
Depth range	Porosity loss	Av. loss
0-800m	6-10%	8%
800-1600m	4-6%	5%
1600-2000m	3-4%	3.50%
2000-2400m	2-3%	2.50%
2400-3200m	1-2%	1.50%
3200-4000m	0.5-1%	0.75%
>4000m	0.2-0.5%	0.35%

Table 4.08: Table of the sediment thicknesses, porosity losses, temperatures and volumes affected by the slump and the volumes and temperatures of water expelled therefrom.

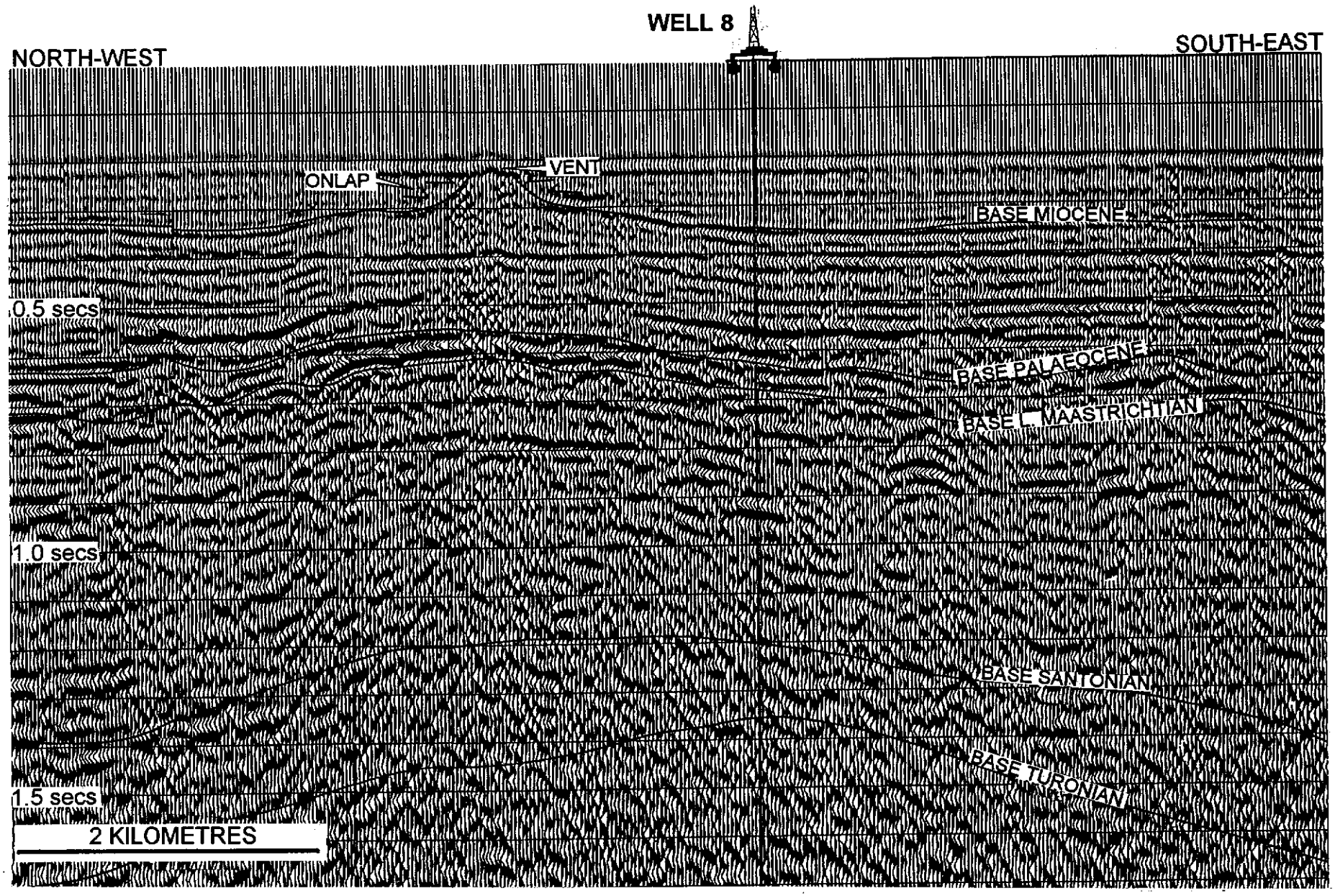

Figure 4.33: East-west seismic line through a Miocene sea-floor cone (near well 8) which may be the result of a mud volcano.

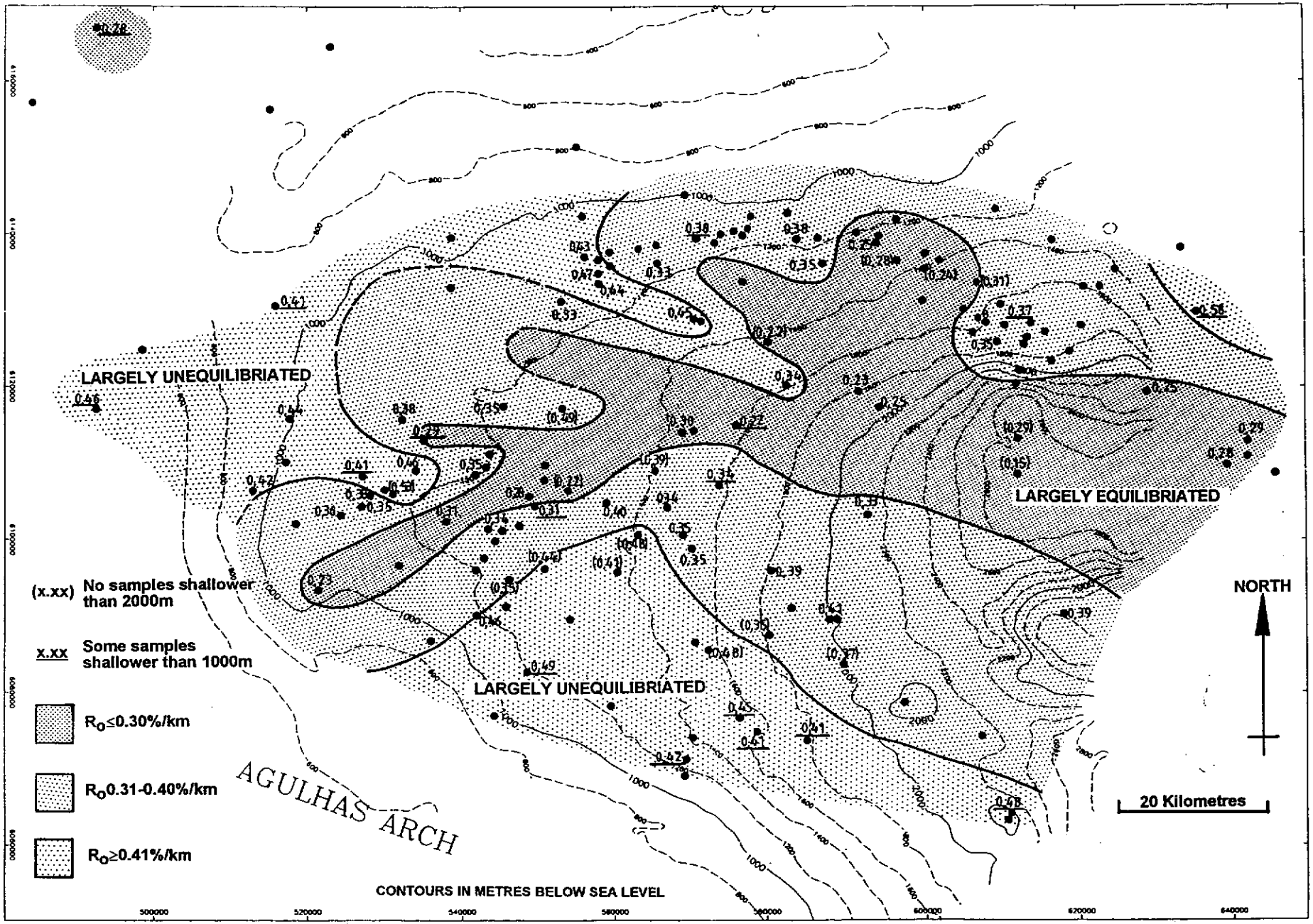

Figure 4.34: Map of the Bredasdorp Basin showing the distribution of the surface offsets of the exponential trend line constructed through the vitrinite reflectance data for each of the 72 wells in which continuous data are available.

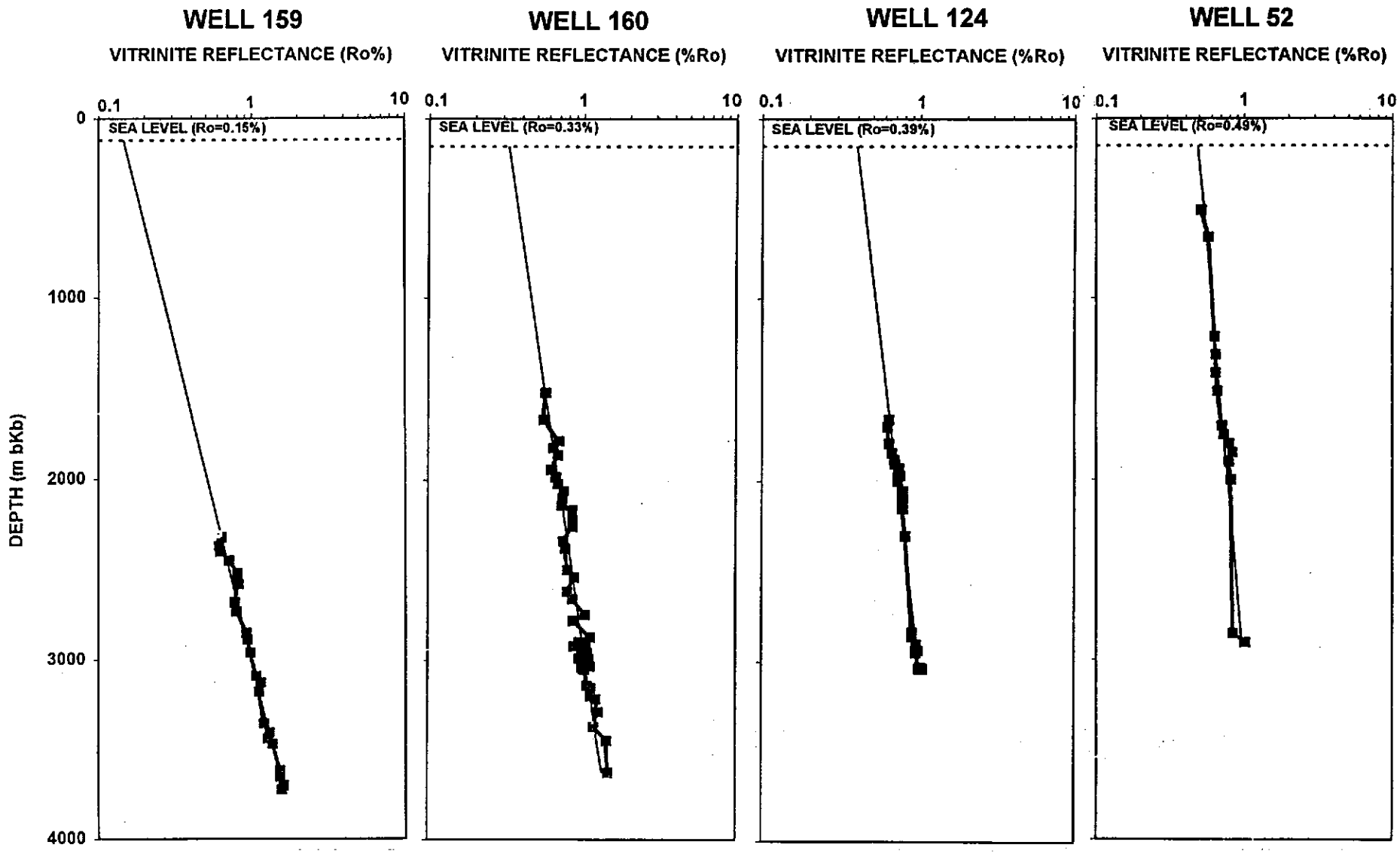

Figure 4.35: Plot of the vitrinite reflectance data for four wells in which the sea floor regression intercept ranges between the expected value (0.15%) and an unusually high value (0.49%).

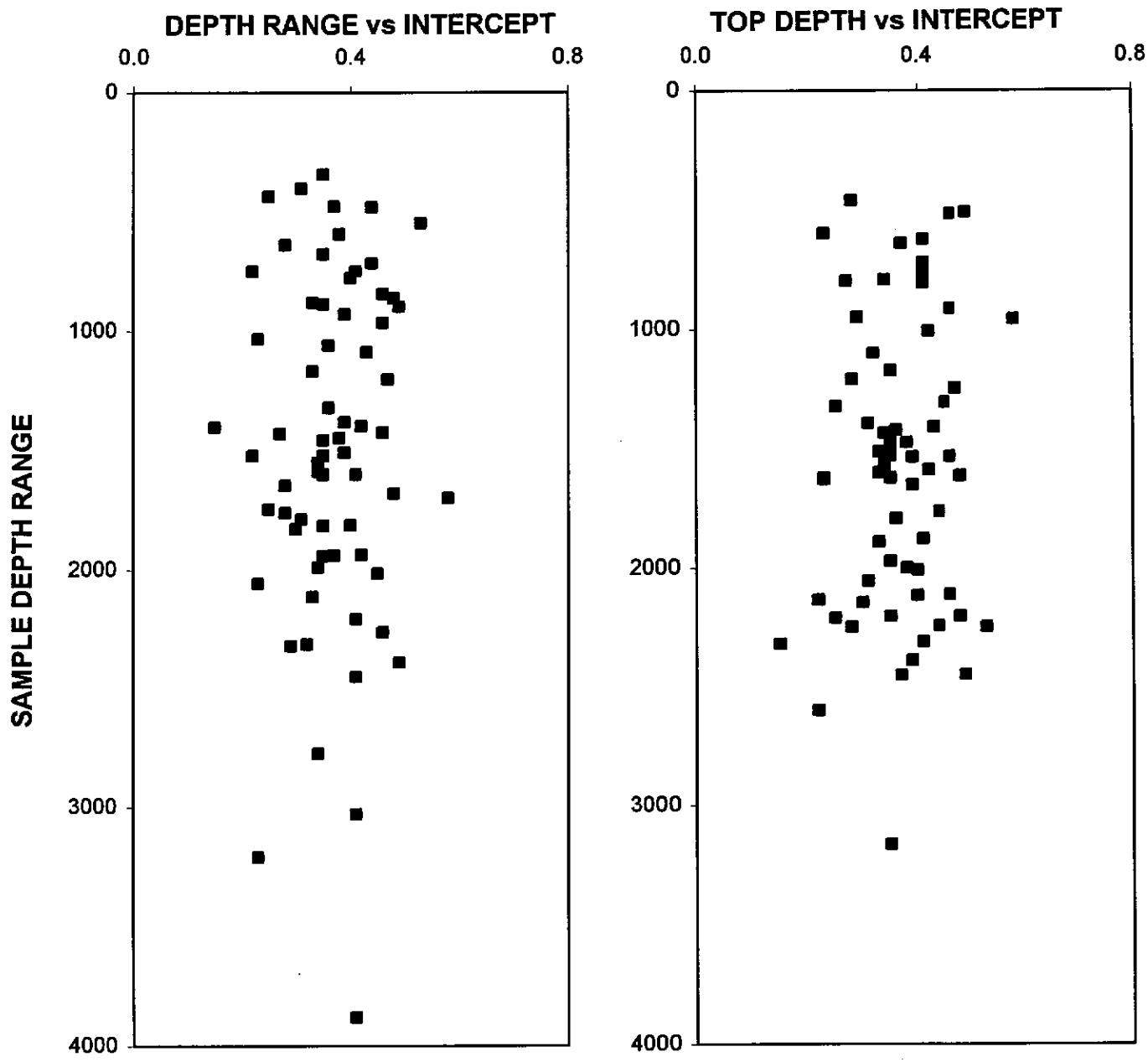

Figure 4.36: Cross-plots of sample depth range and top sampled interval showing a lack of relationship with vitrinite reflectance extrapolated surface intercepts.

Davies, 1996a) as this particular maturity range lies below the interval of reflectance offset in virtually all Bredasdorp basin wells. The maturity gradients calculated in the Bredasdorp Basin are still higher than in the eastern basins where the hotspot effects were not felt. Indeed, other hotspot tracks are also evident from these data although less strongly developed than the Bredasdorp Basin trend. These other high gradient areas (e.g. central West Coast, Southern Namibia) match the locations of interpreted 'hotspot tracks' (Duncan, 1981; Hartnady and Le Roex, 1985; AK Martin, 1993, pers comm.).

4.4.7. Southern Outeniqua Basin Maturation

The thermal history of the Southern Outeniqua Basin is extrapolated from surrounding wells where temperature gradients increase towards the Southern Outeniqua Basin (Wenham, 1991; Van Wyk and Guest, 1992). A thinner crust near the AFFZ may be largely responsible for this.

In the nearest location where a well was located on basaltic oceanic crust and drilled through most of the post-rift sediments (DSDP 361), Tmax data show the oil window (Tmax=430°C) would be reached at ~1500 metres bsf (Fig. 4.37). This results in a geothermal gradient of ~3.6°C/100m, assuming the top of the oil window for Aptian rocks, buried for >70 Ma near their present maximum temperature, is ~60°C, (Leith and Rowsell, 1978; North, 1985), i.e. close to the Bredasdorp Basin average. The location of DSDP 361 is hundreds of kilometres from the track of an active spreading centre, whereas the Southern Outeniqua Basin, at its furthest, is less than 100 kilometres from the AFFZ (Fig. 2.12). In the latter location, the AFR is a deep-seated, thermally conductive ridge composed of granitic or metamorphosed basement (Scrutton and Du Plessis, 1972; Ben-Avraham et al., 1993) which could 'mine' heat from depth. There is also a major crustal fault system (the AFFZ) against which are juxtaposed highly-thermally conductive basic igneous rocks (Talwani and Eldholm, 1973). Hence effective basal heat flow in the Southern Outeniqua Basin could be up to 30% higher than in the vicinity of DSDP 361 or in the eastern Bredasdorp Basin.

Basal heat flow in eastern wells in the Bredasdorp Basin, located far away from the area of intrusions, are modelled from static borehole temperatures and known lithologies (Chapter 7) to average 53 mW/m^2. Average heat flows in the western Southern Outeniqua Basin probably range 20-30% higher than this. Indeed, during hotspot transits (~70-40 Ma and 10-0 Ma) and passage of the active spreading centre (~90 Ma), these values were probably even higher. Therefore, the western model (junction of lines L72-15 and L72-20) and the central model (Fig. 3.24) (at the junction

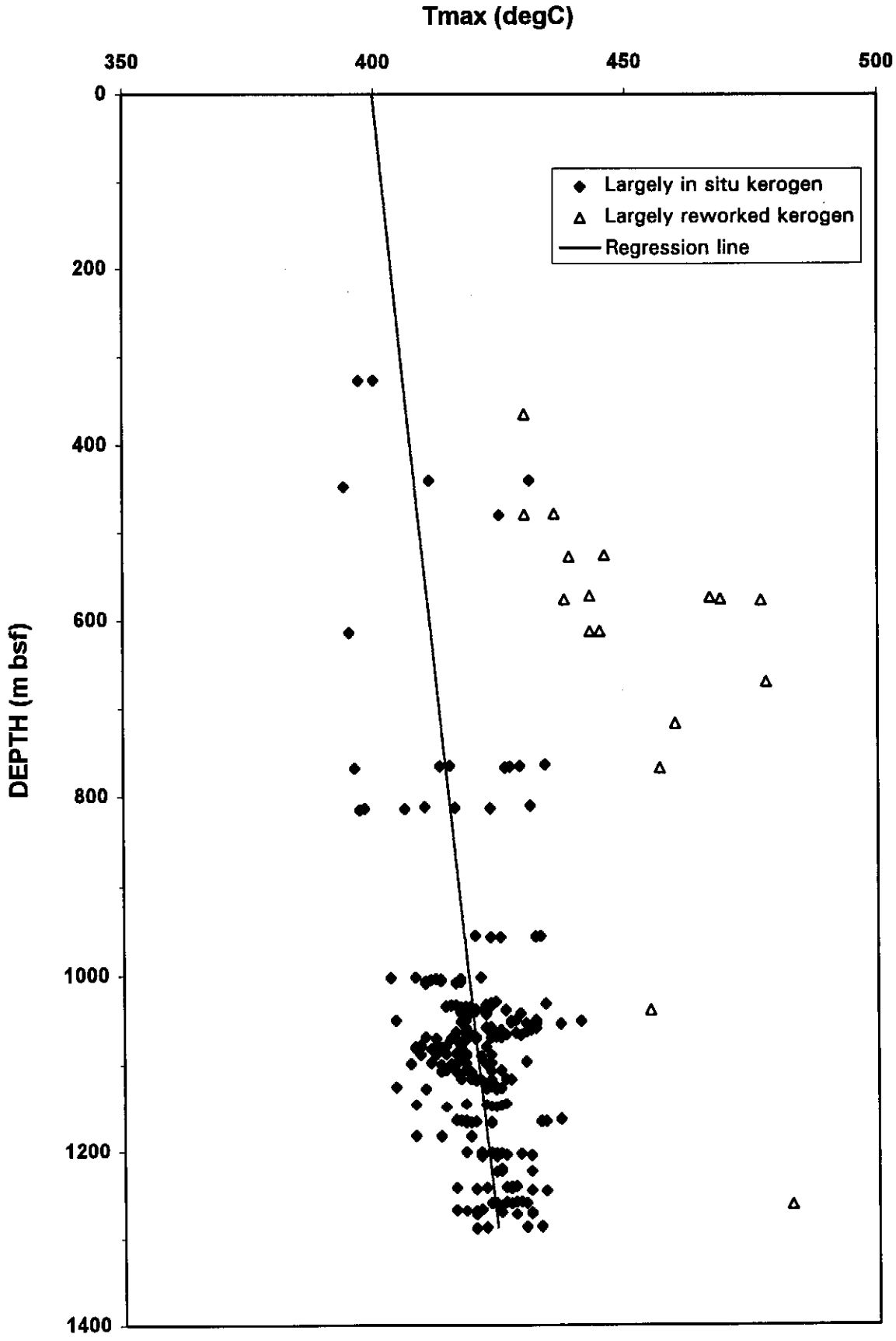

Figure 4.37: Plot of Tmax versus depth for DSDP 361 data (data courtesy IFP). In spite of the wide data scatter, there is a definite trend of increasing Tmax with depth which, if extrapolated, would result in a Tmax of 430°C being reached at ~1500m. This low maturity agrees with the low maturity interpreted from lipid and GC data presented by Foresman (1978).

of lines L72-20 and L72-21) were constructed using averages of 65mW/m^2 and 70 mW/m^2 respectively.

4.4.8. Basement maturity

Basement sediments are largely composed of metasandstones of the Table Mountain Series, and locally, Bokkeveld Series shales and slates. The latter contain coaly organic material (Rowsell and De Swardt, 1976) at high maturity, based on the available analytical coverage (R_o=3.6-4.3%) close to the base of the dry gas window (Dow, 1977; Price, 1982). Bokkeveld Series rocks at similar maturity levels are believed to source the dry gas in Ecca Series rocks in the onshore CR1/68 well (Rowsell and De Swardt, 1976). Source rocks at this maturity level are well within the window in which nitrogen and carbon dioxide release from coaly organic material prevails (Smith and Ehrenberg, 1989 and Littke, et al., 1995). Many of the deeper gases encountered, contain increased amounts of CO_2 and N_2 (see Chapter 8) and it is possible that the source for at least some of these gases in deep offshore reservoirs lies in basement rocks.

4.5. EXPULSION

4.5.1. Migration processes

Various processes have been advocated to account for primary and secondary migration (Tissot and Welte, 1984, p.293-295), e.g. separate phase droplets or bubbles, colloidal and micellar solution, molecular solution in water or CO_2, diffusion, and continuous hydrocarbon phase migration. However, theoretical and empirical data have shown that most of these are likely to be quantitatively ineffectual (Pepper, 1991), because of pressure variances (Magara, 1977), pore size exclusion (Tissot and Welte, 1984, p. 306-307), chemical composition effects (McAuliffe, 1966; Price, 1976), high gas maturities (Leythauser and Poelchau, 1991; Smith and Ehrenberg, 1989; Littke et al., 1995) and liquid diffusion rates (Krooss et al., 1988).

The timing of expulsion is also dependent on the thickness of the source rocks and the efficiency of the adjacent migration conduits. Leythauser et al. (1983) demonstrate that migration of low-medium molecular weight normal alkanes and isoprenoids from thin shales is more rapid than from thicker, more continuous shales.

4.5.2. Dominant migration process

Continuous hydrocarbon-phase migration is presently considered to be the dominant migration process (Tissot and Welte, 1984; Pepper, 1991) although it probably occurs only where source rocks have potential for 5 kg hydrocarbons/tonne rock or better, because there is a minimum saturation needed to connect individual pore fillings. Also

migration usually takes place only where generation has been rapid and compaction is not too severe - otherwise the pore throats become too narrow by compaction for build-up of a continuous oil phase. Pepper (1991) envisages that in a rich source, oil droplets displaced from mineral surfaces by ionically-bound water, are located in pore centres. If enough oil is generated prior to pore throat closure, the oil phase links up between pores, and continuous stringers form. Once the stringers reach the edge of the shale, they continue to flow, driven by pressure, partly from the ionic attraction of other water layers reducing the available space and partly from compaction, until the stringer exhausts the oil supply. Hence expulsion efficiencies can be very high. However, in a less rich source the time taken to build the stringer may be so long that expulsion delays until oil cracking occurs, leading to gas-condensate expulsion. Later sequential exsolution of the gas as pressure declines with depth, can result in reservoirs with gas:oil ratios which match expected values very closely (Heums et al., 1986).

Since hydrocarbon generation is continuous (while maturation increases) until all potential is exhausted, so residual oil stains are transient as generation in the source rock continues and pore spaces become reconnected, resulting in pulsed expulsion. Migration of freshly generated droplets and stringers utilise the same pore throat fill/lining and conduit - until either all the oil is generated or the oil generation rate is too low to keep the pore throat open. They can be opened again but only where oil-to-gas cracking builds enough pressure to micro-fracture the rock (Barker, 1990).

4.5.3. Initiation of migration

Ejedawe (1986) suggested that generation occurs without expulsion until oil saturates a certain proportion of the pore space. Once this threshold has been reached expulsion starts and continues until the pore space saturation falls below the threshold level. In the Tertiary Agbaba source rock in the Niger delta, the threshold was found to be equivalent to approximately 25% of the pore space. The threshold is largely dependent on the ratio between pore volumes, pore throat sizes and the molecular weight of the oil. For example, high molecular weight oils tend to be less mobile, hence a higher proportion of the pore space needs to be occupied before expulsion starts.

The pore saturation threshold can also vary due to porosity reduction by compaction (which changes the relative proportions between the pore throats and pore volumes) and to the adsorptive properties of the lithologic grains in relation to the polarity of the oil (Ekweozor and Strausz, 1983). Pepper (1991) confirmed much of Ejedawe's conclusions by showing the proportion of pore space filled with oil had to be high enough to form a continuous network to initiate expulsion. Depending on the amount of 'bound water', the adsorbed volume could vary significantly. Since the lithology

determined the proportions of active clay adsorption sites, so the lithology determines the expulsion initiation. He demonstrated that the quantity absorbed in the pore spaces, in joints and fractures, was large but still only a small proportion of the total generated. This is supported by data from the Bredasdorp Basin - where the amount of oil lost to absorption (~1.0-1.5 kg/tonne rock) is approximately 15-20% of the total oil which can be generated (5-7 kg/tonne rock) (Davies, 1988b, 1990 and 1996d).

Talukdar et al. (1986) showed that expulsion takes place through micro-fractures. However, it is also possible to use such data to show that expulsion through fractures is probably limited, because they become bitumen-plugged quite rapidly, as seen in rocks in the south-eastern Bredasdorp Basin highs (McLachlan et al., 1979).

4.5.4. Pressure-driven migration

Volume expansion of organic matter by 10-15% accompanies the process of oil generation resulting in increased internal pressure. In addition, compaction and thermal expansion of water can help to increase pressure to the point where oil is forcibly expelled. But much more volume increase occurs when oil is cracked to gas - hence gas expulsion is favoured (Barker, 1990). Conversely, asphaltenes can be precipitated in overpressured zones because compressible light hydrocarbons have a reduced solvating power (Hunt, 1996).

4.5.5. Quantitative expulsion

Quantitative studies of generation and expulsion from Kimmeridge claystone source rock (North Sea) were made by Cooles et al. (1986). They determined an empirical relationship from pyrolysis and extract data between the quantity of the free hydrocarbons and the remaining potential to arrive at estimates of the timing and quantity of expulsion.

Empirical calculations of the oil and wet gas expulsion windows of 13A source rocks in the Bredasdorp Basin, (Davies, 1988b and 1990) are used widely to determine expulsion timing (e.g. Strauss et al., 1996). The calculations used these assumptions:

(i) the source rocks, based on micropalaeontological and palynological evidence, were composed of similar types of organic material

(ii) the original potential was a function of the total organic carbon content

(iii) the reduction in the original potential during burial through the oil and wet gas windows was due to the generation of hydrocarbons

(iv) the amount of hydrocarbons lost during sample collection and processing was estimated following the method in Davies (1988b), namely 25% of the original oil is lost during processing and all the original gas (probably under-estimated at 0.02% m/m rock) lost during sample collection at the wellsite

(v) free hydrocarbons included those in pore spaces and adsorbed on mineral grains
(vi) the amount expelled ('missing' from the calculation) was equal to the original potential less the remaining potential, the free hydrocarbons and the amount lost in collection/processing.

The calculations showed a high proportion (up to 80%) of the generated hydrocarbons was expelled as wet gas and oil. S1 and S2 values plotted against maturity (Fig. 4.38a and 4.38b) show a general decrease of several kg/tonne rock with most of the expulsion at palaeotemperatures of 85-115°C (≡R_o~0.75-1.10%) (Davies, 1988b). From Fig. 4.38b the original source potential was estimated by extrapolation to the top of the oil window. The results showed free hydrocarbon contents to be highly variable (~0.5-1.8 kg/tonne rock, Fig. 4.38a). Oil extract data too varies but at higher values (900-3500 ppm, Table F.01) which may include material which is not freely available in pore spaces or is adsorbed on rock surfaces. The range of Rock Eval data corresponds to pore saturations of ~20% based on modelling carried out using the BASINMOD programme. A similar process of estimation of original potential and expulsion potential, was carried out for all source rock intervals, using the Aptian source as a model (reported in Davies, 1996b).

The variation between the low and high free hydrocarbon contents may indicate source intervals which have expelled oil or not, respectively. It is possible that continuous generation increases the oil content of the rock up to the expulsion threshold. Expulsion then takes place but in pulses of ~1.0-1.5 kg/tonne rock. Hence average oil saturation in source rocks before expulsion is related to the source richness, the rate of generation, the distance from the conduit and the permeability of the source rock.

4.5.6. Evidence of expulsion

Direct evidence of expulsion is derived from saturates GC data. Many samples of shales with relatively minor amounts of extracted organic matter (EOM) are found to have significantly reduced proportions of nC15-nC20 alkanes and to peak at higher carbon numbers (sometimes as high as nC22). By contrast, those with large amounts of EOM were generally found to contain apparently complete normal alkane profiles peaking at nC16-18 (components with smaller molecular size than this being largely lost in processing). This matches results reported by Leythauser et al. (1988) and Leythauser and Poelchau (1991), which are interpreted to show preferential expulsion of the low molecular weight components. An example of this effect is shown in Fig. 4.39 and Table 4.09.

Some biomarkers are thought to be expelled early while others of similar size and mass are expelled late (Seifert and Moldowan, 1978). Although this may be due to the early

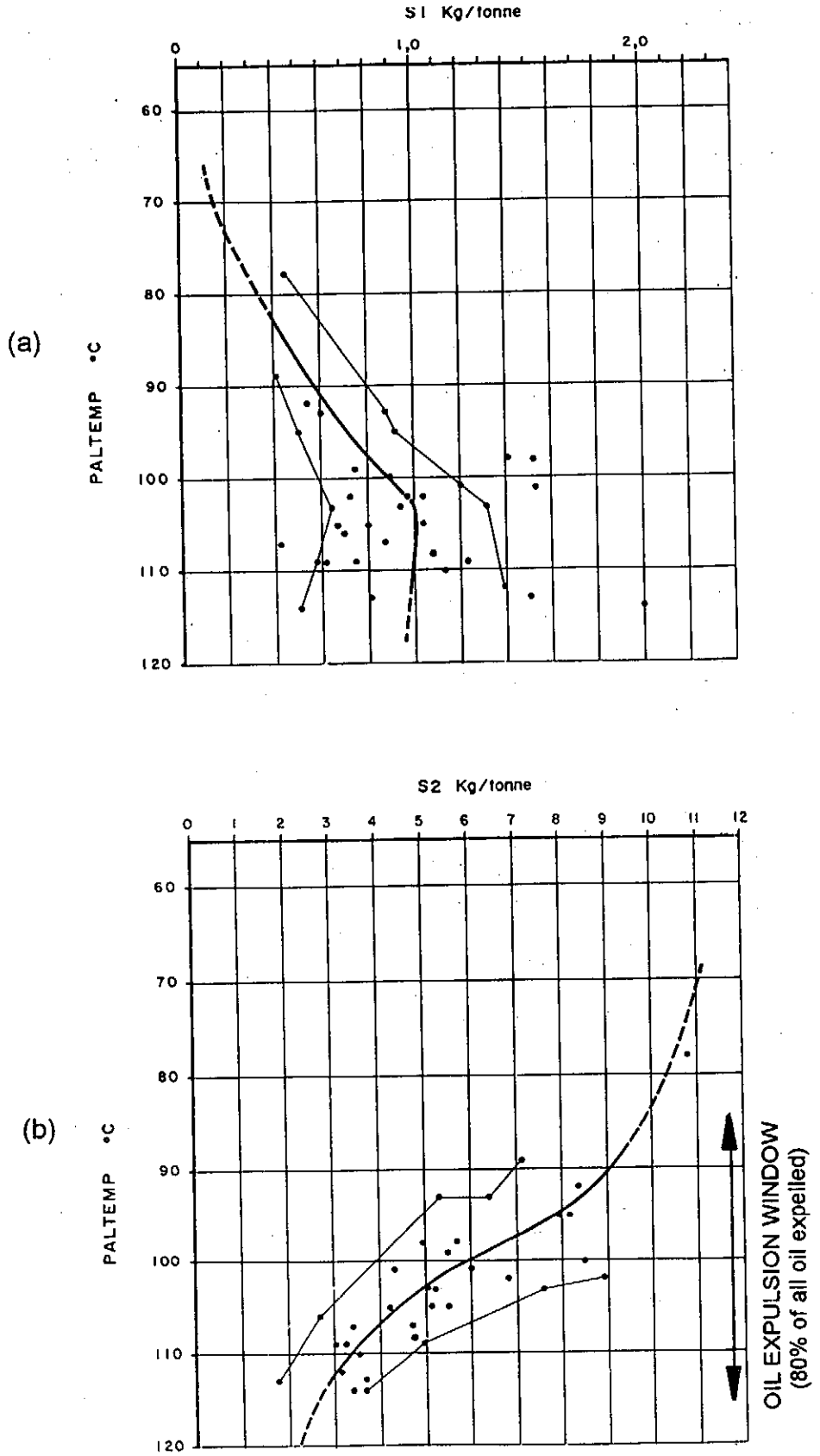

Figure 4.38a and b: Plots of averaged free hydrocarbon (S1) and remaining potential (S2) values for all measured oil prone 13A source rock intervals in the Bredasdorp Basin (from Davies, 1990). These data show that peak S1 values vary considerably but tend to cluster around 1.0-1.5 kg/tonne rock whilst S2 values are proportionally less variable. Palaeotemperatures are measures of maturity derived from a summation of all maturity parameters as shown in Table 4.05.

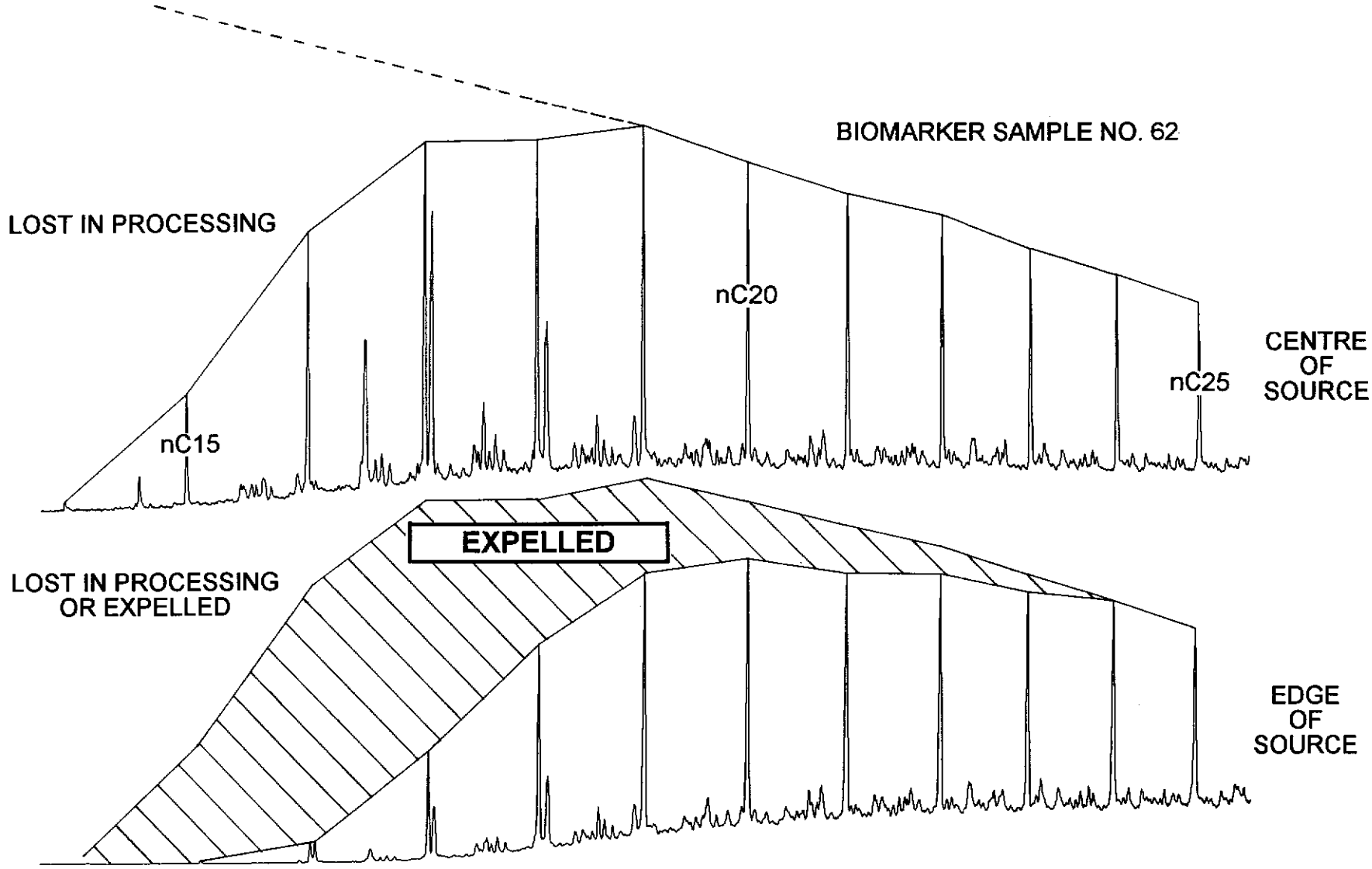

Figure 4.39: Partial gas chromatogram of saturates fractions of two 13A oil prone source rock samples from well 14, one from the edge of the source and one from the centre (the latter being sample no. 62 in the biomarker dataset). The light ends are clearly more reduced in both normal alkane carbon number and in quantity (Table 4.09). Other source data (eg pyrolysis data also confirm that a higher proportion of the more mobile hydrocarbons have escaped, probably by expulsion. (The loss of all alkanes <C14 and proportionally up to ~nC18 is a result of the bitumen extraction process used).

LOCATION	WELL	DEPTH	TYPE	EOM	SAT	AROM	NSO	ASPH
CENTRE	14	2721m	RC	2830 ppm	53%	23%	22%	3%
EDGE	14	2766m	RC	694 ppm	32%	22%	29%	18%

WELL	DEPTH	TYPE	S1	S2	TOC	Tmax	Ro
14	2721m	RC	1.20‰	2.90‰	2.28%	440°	~1.04%
14	2766m	RC	0.97‰	3.04‰	2.66%	443°	~1.04%

Table 4.09: Quantities of bitumen and its fractions, as well as pyrolysis analytical data, from samples of oil prone early Aptian 13A source rocks selected from central and edge locations to test for oil expulsion.

or late achievement of the expulsion threshold due to richer or poorer source rock quality respectively, in some cases it has been considered to be a manifestation of geochromatography (Zhusheng et al., 1988).

4.6. SECONDARY MIGRATION CONDUITS

Secondary migration is defined as movement of hydrocarbons through porous and permeable conduits after expulsion from the source rocks. Migration conduits are pathways for fluid movement and can be vertical or horizontal, or more likely a combination of both. They are treated separately here for convenience, but in reality grade into one another. Migration routes can be highly complex, and are usually in crestal locations. They are often areally restricted although their size does not detract from the ease with which hydrocarbons can pass through extremely small conduits (Downey, 1984). Since structures are generally drilled off-crest to prove-up minimum volumes of hydrocarbons, migration conduits are unlikely to be intersected during exploration drilling.

Migration takes place initially in the highest permeability sediments in a structure in a direction governed by several factors, *inter alia* sedimentary dip, buoyancy, compaction pressure versus pore entry pressure and tortuosity of conduit. The most important driving force in secondary migration is considered to be buoyancy.

Migration along a carrier bed takes place by the progressive buoyant fill of the most accessible pores either by oil droplets or by gas bubbles. These gradually coalesce to form a stringer which eventually may be long enough to overcome the pore entry pressures ahead of it. The stringer then starts to migrate and continues to do so while there is a supply of hydrocarbons and until it can no longer overcome the pore entry pressures. Such stringers may migrate quite slowly on their own but they soon catch up with further stringers which are about to migrate and add their buoyancy together. In this way migration may be slow to initiate but can be quite rapid once started. In addition, pore entry pressures decrease with shallowing depth (because compaction and mineral growth have not degraded the pore throats) hence migration tends to speed up further as the hydrocarbon train migrates.

During migration, the composition of the oil may be changed by the effects of geochromatography. This effect has also been investigated by Philp and Engel (1987) who concluded that low molecular weight alkanes migrate most rapidly of all hydrocarbons. Certain biomarkers too are reported to migrate at different speeds - for example 14ß,17ß steranes are reported to migrate faster than 14α,17α steranes and tricyclic terpanes faster than pentacyclic terpanes (Seifert and Moldowan, 1978).

However these effects could equally well be ascribed to different thermal histories (Mackenzie, 1984).

In one example, compositional differences resulting from migration of an oil through an alumina/silica chromatographic column were large (Zhusheng et al., 1988). However, the artificial nature of their method over-accentuated the differences between the oils as their investigation of a natural series showed. Durand (1988) commented that there was no convincing evidence for measurable geochromatographic effects and that another explanation for minor changes in oil compositions must be sought.

4.6.1. Lateral migration

Subsurface pathways along which lateral migration mostly occurs are coarse-grained sediments such as sandstones or siltstones found on unconformity surfaces, where braided and lag sandstones are deposited during coastline retreat, in channels and fans deposited during lowstand periods, and on reworked surfaces, formed during transgressive sea level rise. Examples of all of these are found in the Bredasdorp Basin:

(i) coastline retreat sandstones in the 9A-12A sequences: sandstones interbedded with gas-prone claystone source rock, considered to represent braided shelf deposition, are found to host gas (Barton, 1996).

(ii) lowstand sandstones: deep marine channel/splay sandstones are found in the 14A sequence in the area of wells 156 and 166 where they locally host oil (Van Wyk, 1995 and Davies, 1997a).

(iii) reworked surfaces: extensive sandstones are commonly found at the base of the drift sediments, where the latest syn-rift transgressions resulted in reworking of syn-rift fluvial rocks and deposition of glauconite-rich coastal sands. These rocks have been intersected in most wells around the basin and in many locations host gas (Hill, 1995a and b).

4.6.2. Vertical migration

Pathways for vertical migration can be created through joints, faults, and alongside igneous bodies (due partly to shrinkage cooling). Vertical migration can also be as a result of leakage through syn-sedimentary faulting in thinned sediments at onlap positions around the basin. Evidence for vertical migration through faulted areas is found along the south flank of the basin where Sniffer anomalies overlie a heavily faulted region (Davies, 1996b). It is also seen in localised bitumen emplacement in fractures (McLachlan et al., 1979). Indeed igneous conduits are thought to have acted as the probable migration pathway for the shows of mature oil in well 47 (Davies, 1997b).

4.6.3. Combination migration

Horizontal and vertical migration both take place through fault juxtaposition of porous and permeable rocks. Where this happens, the only major impediment to flow is the nature of the fault-plane fill. If ductile shales are present between the sandstones, they can smear along the fault plane (Downey, 1984; Nybakken, 1991; Weber, 1994). The resulting shale smears are suggested to dominate in relatively shallow rocks (<600 metres, Nybakken, 1991) because of the lower overburden pressure and the greater ductility of the shales.

In the Bredasdorp Basin, many of the faults which influence the stratigraphically deep rocks (pre-6A) during either of the two phases of rifting (Jungslager, 1996) or during later compressional events which affect rocks into the 9A sequence in the central basin (Hodges, 1996), also extend quite shallow. In the pre-13A sequences, claystones dominate over sandstones but are thinly interbedded. Such a situation is highly favourable for the development of shale smears in fault zones forming excellent lateral seals. This concept may help to explain the common presence of overpressured, gas-saturated sandstones in the highly faulted central part of the basin (Barton, 1996 and Fouché, 1996a).

Although it is not possible to show that any specific oil or gas show represents a migration conduit, the likelihood is that some of the mostly strongly fluorescing shows in non-source rocks may represent a migration route. An example of this is the oil shows in the 14A sands in well 94 which match those in 14A sands further updip, yet contain no gas and little of the light ends. That migration has taken place in the basin is unquestionable, but the most favoured direction can be assessed from the known reservoir fills. An example of this is the 14A channel-and-splay sandstones (in the central and southern basin trends) where gas:oil ratios steadily decrease in a westerly (updip) direction, due to decreased gas proportions (Davies, 1995c; Fig. 4.40).

4.7. TERTIARY MIGRATION

Further migration of hydrocarbons either within or out of a reservoir can take place. For example, hydrocarbons can migrate out of the reservoir due to displacement or because the seal has been breached. Alternatively hydrocarbons can migrate within the reservoir either due to tectonic tilting and subsequent remigration to the crest of the structure or to hydraulic flow.

One example of displacement out of a reservoir is known at a gas-bearing structure in the Pletmos Basin. During the 'Sniffer' survey, gas seepage with a methane concentration of ~1ppm approximately 10 metres was detected above the sea-floor

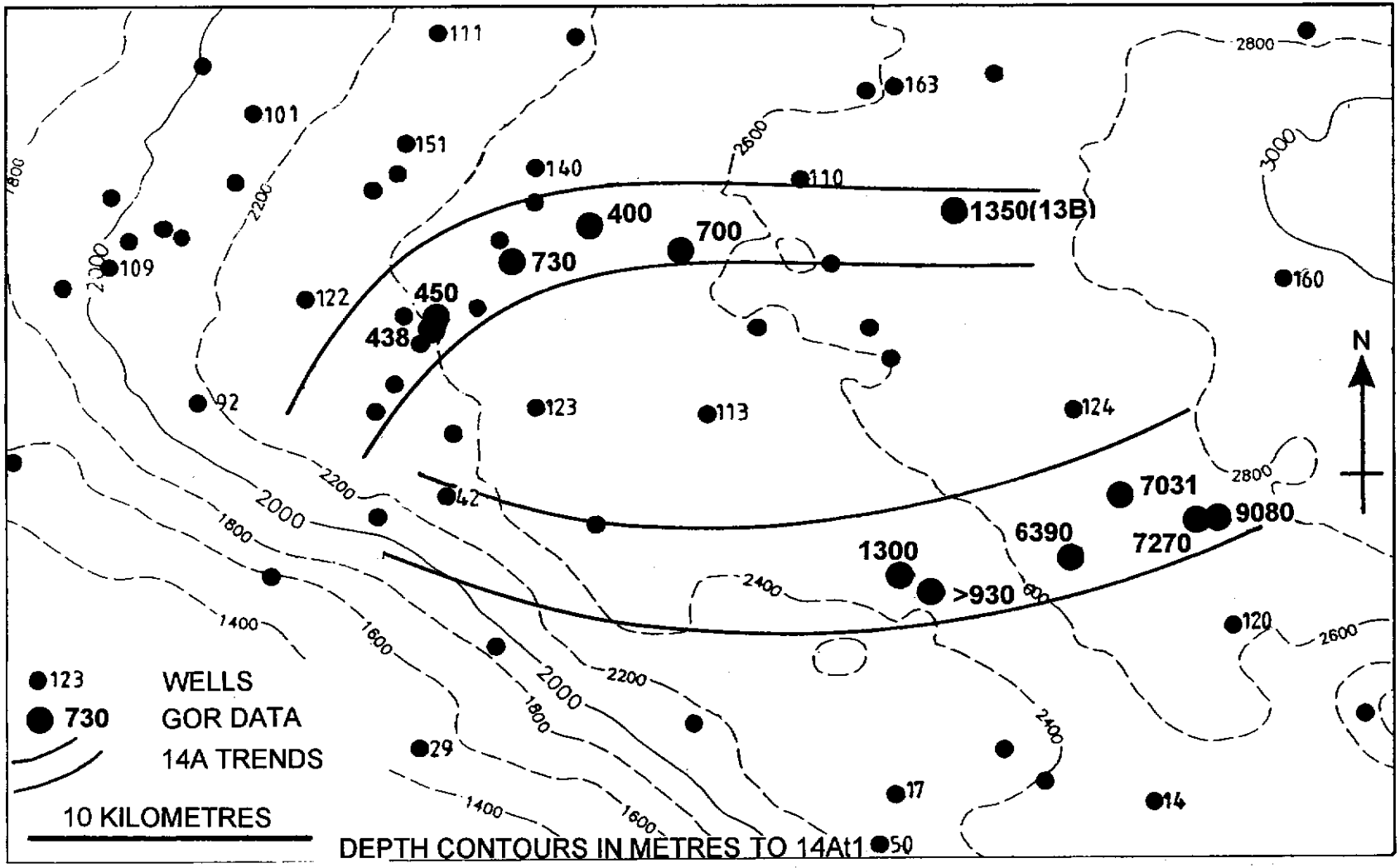

Figure 4.40: Map of the eastern Bredasdorp basin showing the 14A sandstone-rich trends and the gas:oil ratios of produced samples therefrom (GOR in scft/bbl). Well 94 is included even though the flow was from a 13B sandstone because the shows in the 14A sandstone indicate the two sandstones are connected nearby.

over a 1 km wide area. The location of this seep was directly above the spill point of the Ga-A structure (Davies, 1988a; Fig. 2.05). Bearing in mind the volumes of gas that such a small seep represents, the structure would need to be constantly replenished otherwise it would empty in a matter of a few million years. A weekly gas seepage equivalent to a concentration of 1ppm v/v in the bottom 10 metres of water and an areal extent of 1 km^3 is equivalent to 18 Bcf/Ma. Since the structure still contains gas, it is likely that the seep indicates continued migration to the present day. Similarly, the seeps associated with wells 10, 12 and 47 in the south-eastern area also support the indication of a recent loss of reservoir fill (Davies, 1997b).

Compositional changes can occur in the reservoir during such leakage due to pressure and temperature fractionation effects. Such changes, in which the most volatile hydrocarbons are lost from the reservoir almost instantaneously when the seal is breached, may explain the effects of geochromatography. Heums et al. (1986) showed that the different compositions of hydrocarbons in parts of the Troll field could be explained by intermittent loss of the gas cap. They proposed that light hydrocarbons partition and equilibriate into the gas cap and that when the seal is breached and the gas cap lost, the more volatile hydrocarbons are lost in higher proportions than the less volatile compounds. Hence, intermittent seal leakage can result in the reservoir becoming depleted of certain hydrocarbons.

Thompson (1987) invoked a similar process, called 'evaporative fractionation', to explain different types of condensates found in Gulf Coast reservoirs. He showed that oils which had lost their equilibriated gas cap were characterised by significantly reduced proportions of normal alkanes and moderately reduced cyclo-alkanes, but increased proportions of aromatic hydrocarbons. He showed that the result of such a process would be a condensate which was significantly more paraffinic than the original reservoir fill, whilst the residual oil would become more aromatic.

Larter and Mills (1991) also investigated the fractionation of the gas and oil constituents of a petroleum system and found similar changes to those encountered by Thompson (1987) in the <nC12 fraction, but only minor differences in the biomarker contents. They concluded that biomarker studies could still be useful for differentiating between fractionated oils, providing light-hydrocarbon data were available to confirm that such fractionation had occurred.

4.8. SEALS

Seals are rocks which are able to stop or retard fluid migration. They are fine-grained rocks in which either the porosity and permeability is essentially zero (e.g. igneous

rocks or fault mylonite) or sedimentary rocks in which the pore entry pressures are so high that they essentially act as impermeable membranes. The effectiveness of a seal is determined by how large a hydrocarbon column it can hold.

Grunau (1987) showed that, theoretically, only a few centimetres of shale could act as a seal to large column heights of oil. In practice, though, there is little likelihood that such thin shales would be continuous across a structure. He showed from empirical studies that a typical minimum thickness for a cap-rock of a commercial-size deposit must be of the order of tens of metres. He also pointed out that a cap-rock which is effective at present may leak over time as a result of tectonism (e.g. faulting), loss of hydrocarbons due to gaseous diffusion or to diagenesis (modification of its sealing capabilities). Seals are rarely perfect, they generally leak over time and with compaction tend to become more brittle allowing fracturing to destroy their integrity. However, evaporitic seals are likely to seal hydrocarbons most effectively. Yet it is not so much the thickness of the seal or its lithology which is important (at least for top seals) but its continuity and ductility (Downey, 1984).

4.8.1. Effect of seals

Identification of migration seals is at least as important to the understanding of the type and quantity of hydrocarbons trapped as the lithology of the reservoir or the source type and richness. This is partly because regional sealing layers help to channel hydrocarbons from the fetch area to the trap and partly because they can 'filter out' lighter or more polar gases. Indeed, the seal efficiency is largely dependent on the type of hydrocarbon being retained, e.g. fine siltstones can seal oil but not gas. Yet highly efficient seals can be detrimental to the quality of hydrocarbons trapped in a number of different ways as well as being beneficial, as they can:

(i) retain large amounts of gas in the structure which, on going into solution, precipitate asphaltenes in pore spaces, reducing porosity and permeability,
(ii) allow gaseous displacement of large amounts of oil from structures (Gussow, 1954),
(iii) reduce the economic value of the structure if a gas cap forms.

Indeed, Sales (1994) show that there are four types of hydrocarbon traps, namely:

(a) those which retain all the gas supplied so that the pre-existing fill is displaced
(b) those which leak all the gas supplied but retain the oil;
(c) those which hold some oil and some gas;
(d) those which do not hold either enough oil or gas to attain the spill-point.

4.8.2. Formation of seals

Most argillaceous rocks can be effective seals and their effectiveness develops through time because of the effects of diagenesis and compaction. Seals can occur regionally

either in lithologies which over- or underlie the reservoir rock (cap-rocks or seat-seals) or in lithologies which constitute edge-seals (pinchouts or fault seals). They are often transient and can form and dissipate rapidly due to local deposition of minerals from migrating fluids at pore-throats or pH/Eh boundaries. However, transient seals are generally short-lived as they can be removed by solution or are susceptible to damage during compaction and faulting or buoyancy pressure. Their ductility increases with reducing grain-size and increasing organic matter content.

4.8.3. Pressure retention

A lithotype is considered as a seal when the rate of diffusion and leakage of hydrocarbons through it is less than the rate of influx. Under these conditions, a column of trapped hydrocarbons can build up below or downdip of the seal. Seals can be breached in many ways. Rapid loss of hydrocarbons takes place when the buoyancy pressure of the trapped column exceeds the entry pressure to the pore throats and gas is forced through the seal. In addition, seals can be fractured where the pressure below exceeds the compressive strength of the rock. This is usually considered to occur where the pressure gradient exceeds 1.0 psi/ft (Magara, 1978, p.112) although in some cases, it can be considerably lower (e.g. ~0.73 psi/ft, Miles, 1990). In the Bredasdorp Basin, some reservoirs are effectively sealed with pressure gradients exceeding 0.7 psi/ft (Fig. 3.14-3.15) and since all argillaceous seals leak, these formation pressures may have been higher in the past. Apart from the possible catastrophic loss of seal integrity, in many cases continuous loss of hydrocarbons from the reservoir takes place as a result of molecular diffusion through the pore throats by partitioning on the mineral surfaces.

Downey (1984) showed the number and disposition of shales on each side of the fault to be of importance in determining whether it formed a lateral seal to migration or not.

4.8.4. Hydrocarbon diffusion

Leith et al. (1993) determined that diffusion processes played only a small role in the escape of higher hydrocarbons from a reservoir through the cap-rock. Their calculations showed that the diffusion coefficients of >nC10 hydrocarbons through typical shales were so low that the molecules were essentially unable to migrate. In the Bredasdorp Basin, there are many wells where gas leakage through the cap-rock occurs (Davies, 1993b).

Krooss (1987) and Krooss et al. (1988) investigated the rate of diffusion of light hydrocarbons through shale. They found that shale top-seals allow passage of some light C1-6 hydrocarbons only by diffusion and that the proportions of each component escaping at any time are functions of:

(i) the permeability of the shale to gas
(ii) the composition of the reservoired HC
(iii) the pressure differential between reservoir and seal
(iv) the time since diffusion began.

Where the seal lithology and reservoired hydrocarbons are unvarying and the seal has no source potential, the proportions of gases in the seal will be constant. Since the amount and proportions of hydrocarbons diffusing through the seal are also a function of the buoyancy, there will be a gradual upward movement of each iso-concentration line, i.e. the same proportions of HC will be found shallower and shallower with increments of time (Fig. 4.41a-c). Therefore, the height to which gas has diffused above the reservoir is a function of (a) the diffusivity of the seal and (b) the time since filling started. Therefore the time of reservoir filling can be estimated.

Should the reservoir lose its charge, gas diffusion into the seal will stop, but the gas already in the seal will both slowly diffuse upwards and downwards and partially migrate upwards in response to fluid movements due to compaction. A break-in-slope of the profile could develop between the base of the migrated diffusion profile and the top of the reservoir, within which the gas will become proportionally less with time, approaching background values (Fig. 4.41d). As the diffusion profile migrates upwards in response to solution in migrating fluids, buoyancy etc., it will gradually dissipate becoming less evident.

It can take 10^6-10^7 years for a gas diffusion profile to reach equilibrium (Krooss, 1987) so it can take an equally long time for the profile to reach a new equilibrium position after the sudden loss of reservoired HC. Effects of the loss will therefore be noticeable for a long time. By extension, should the gas proportions in the reservoir change, the proportions of individual gases diffusing upwards will also change. Hence, the profile built up from the first fill will be superseded by a second profile building up immediately below. Since each gas component diffuses at the much same rate, the two patterns should remain largely distinct, only merging gradually with time (Fig. 4.41e).

In addition, since gas proportions characterise the hydrocarbon type (Schoell, 1983a; 1983b), the gas composition in the seal above a hydrocarbon-bearing sand will broadly characterise the fill. By extension, where gas is present in a seal above a non-reservoiring sandstone it can indicate a pre-existing hydrocarbon fill. Therefore, study of gases in seal lithologies above reservoir sandstones can yield data which allow the sequential fill-and-spill histories to be determined.

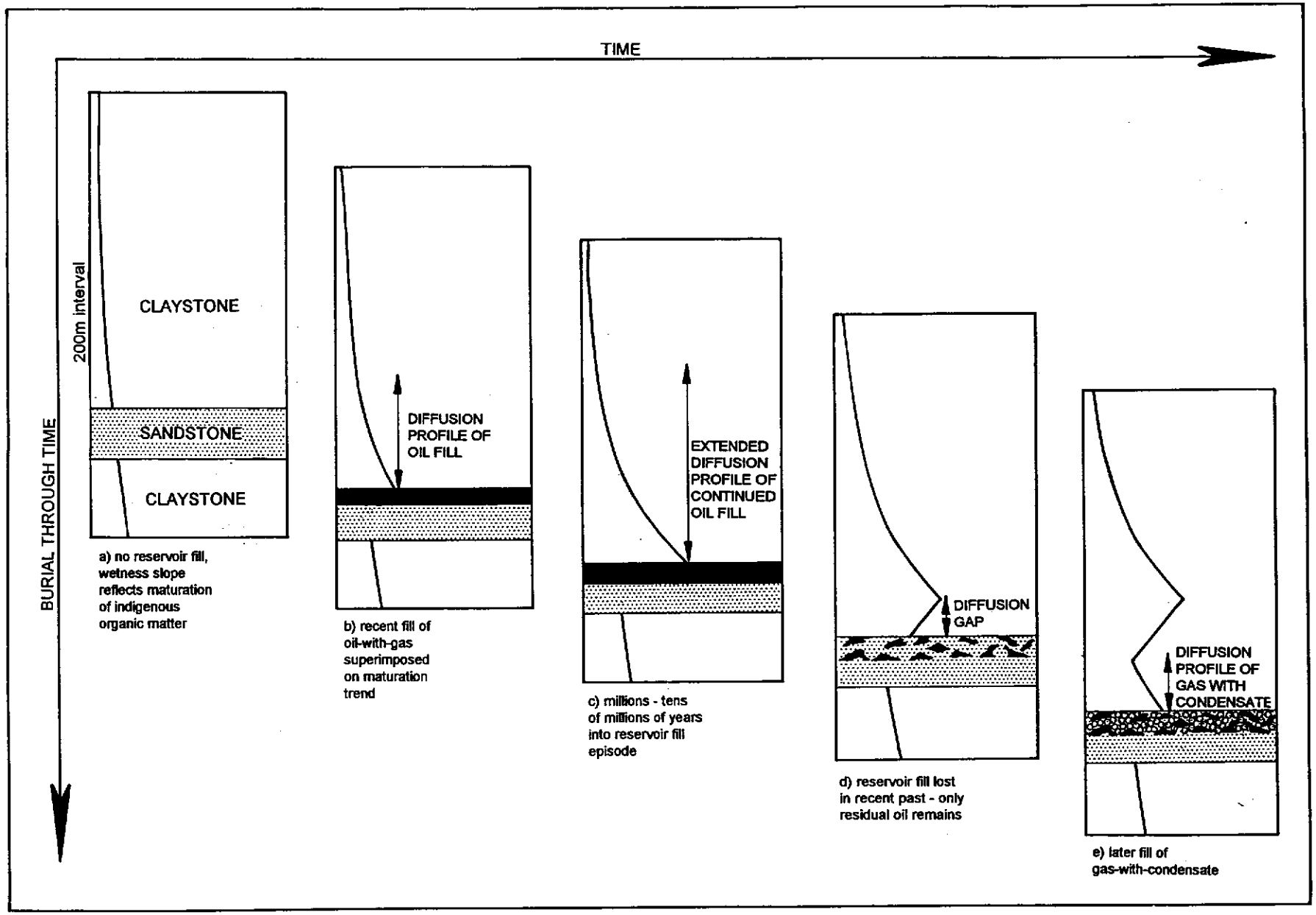

Figure 4.41: Schematic chronographic cartoon showing the proposed development, modification and dissipation of gas wetness profiles across a standard shale sandstone sequence as a function of reservoir fill.

4.8.5. Hydrocarbon data

Proportions of gases in the seal are evaluated from ditch gas data. Cuttings gas data are not used in this study because operator bias can be introduced in the sample selection, washing and in the gas extraction. Both biases add to the uncertainty that the gas is truly representative of the interval drilled. Ditch gas data are not perfectly suited to this task as there are several possible complicating factors (discussed below) but these complications can be overcome by careful adoption of well selection criteria and the data can be largely representative. Three factors are listed below and discussed in further detail:

(i) incomplete sampling of gas in ditch samples
(ii) generation of gases in the seal lithology
(iii) adsorption of gas by the seal lithology.

(i) Incomplete sampling of gas is likely where the position of the ditch gas trap is altered.

(ii) Gas generation in the seal in large amounts can overprint the diffusion profile and may be a significant effect where the source rock is rich and mature. However, the locations of rich source rocks and maturation thresholds are known in each well from pyrolysis and optical data. Therefore, where source rocks are mature or close to the reservoir-seal boundary, diffusion profiles in these wells are not studied further.

(iii) Hydrocarbons can be readily adsorbed on kerogen (Peters, 1986). For example, if the kerogen type and quantity is consistent throughout the sealing interval, a consistent proportion of each gas will be adsorbed, maturation differences between the top and bottom of the usual seal interval (<100m) being relatively minor (Fig. 4.41). Therefore, any well in which the effective kerogen type and content in the sealing shale can vary with depth is also not included in the study. Since log characteristics too can be used to assess organic matter content (Cornford, 1986), where gamma, sonic and resistivity logs show large variations with depth, diffusion profiles have been excluded.

Comparison of the gas proportions recorded in ditch gas measurements with gas proportions in sampled formation fluids shows no unusual depletion of components indicative of poor sample quality. Therefore, included in this study are those reservoir-seal combinations which meet the following criteria:

(i) all in the same basin
(ii) reservoirs have large amounts of gas
(iii) reservoirs have been flow tested and some fully analysed
(iv) consistent topseal shales which are tens of meters thick
(v) consistently low source potential in seals
(vi) ditch gas data available throughout the reservoir-seal interval.

4.8.6. Discussion

An example of a reservoir-seal combination, where chemical evidence suggests that only one type of hydrocarbon diffusion has occurred, is found in well 156 (Fig. 4.42). The ditch gas data plots show a smooth and consistently varying methane profile (ethane and propane profiles not shown for clarity) above the reservoir-seal boundary extending upward for at least 100 metres. These data confirm the chemical evidence from hydrocarbon analyses that only one fill has occurred and that there has been no significant input of later high maturity gas. The height the profile extends above the base seal is a measure of the length of time the hydrocarbons have been in the reservoir, in this case possibly since an early generation episode. Modelling has shown the first arrival of oil in this reservoir was some 60 Ma ago (Davies, 1993b).

The adjacent well (no. 166) is known to contain a small gas cap as well as oil. The diffusion profile above the reservoir is largely similar to that at well 156, with the exception of a thin (~20m) zone of different wetness gas immediately above the reservoir (Fig. 4.43), unrelated to any significant change in chemical, optical log, lithological or drilling parameter change (e.g. ROP, WOB, bit change). Gas and light oil data (Chapters 8 and 9) confirm this later gas condensate input (Davies, 1997b).

An example of an apparent loss of reservoir fill is seen in well 165 (Fig. 4.44) where the smoothly increasing wetness of the profile with depth suggests a long-term hydrocarbon fill. However, the few values immediately above the reservoir do not fall on this trend suggesting a recent loss of fill. The 14A sandstone, on the main 14A trend, has a trace of oil as do the thin sandstones above 2280m. An example of a reservoir-seal combination which provides evidence of a large gas input to a pre-existing oil reservoir, is found well 103. The ditch gas data (Fig. 4.45) record two zones with very different gas profiles. The lower zone is wetter, suggesting an influx of wet gas some time after the reservoir first filled with oil. This is supported by the gas-condensate and biomarker data from samples of DST 2 (sample no. 28 in this report) which show mixed HC compositions.

Indeed, investigations of the 26 reservoir-seal combinations which fit all the above criteria show that those which are known to consist of mixtures of hydrocarbons mostly record evidence of mixed diffusion profiles (Table 4.10). In addition, there are a number of wells in which the profiles do not match the present reservoir fill. These may indicate where the fill has recently changed. For example, wells in which diffusion profiles are developed but where there is no underlying reservoir of hydrocarbons probably indicate loss of hydrocarbons from pre-existing reservoirs either very recently or, where the profile is separated from the reservoir-seal boundary, in the distant past. Those wells may provide evidence of onward migration and could lead to exploration

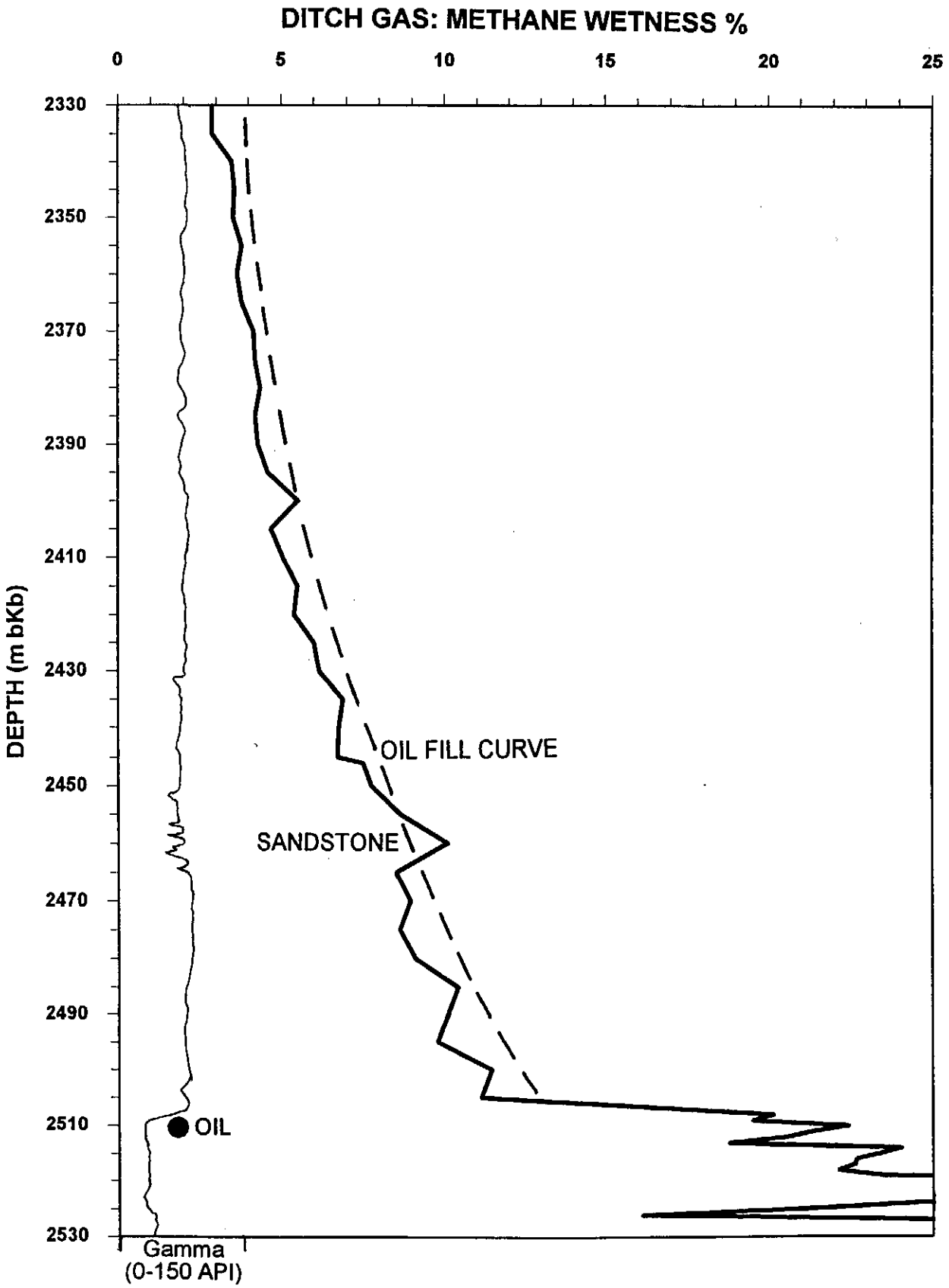

Figure 4.42: Ditch gas wetness diffusion and gamma ray profiles for Well 156. The small peak at 2455-60m is due to a thin gas-charged sandstone rather than a break-in-slope.

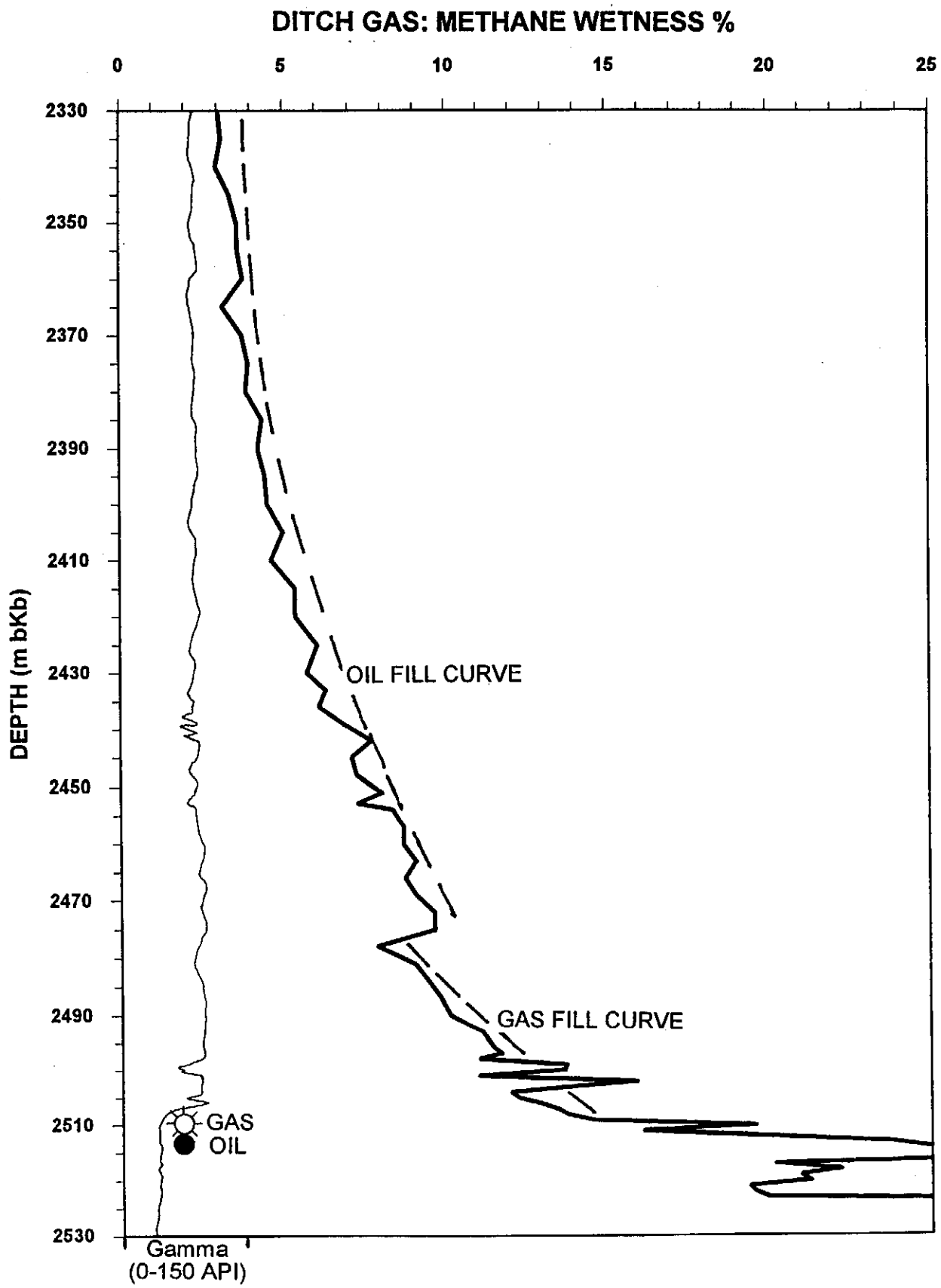

Figure 4.43: Ditch gas wetness diffusion and gamma ray profiles for Well 166. The change in slope at 2475-80m is interpreted to result from a change in the reservoir fill - possibly related to influx of late gas (which was tested by the RFT).

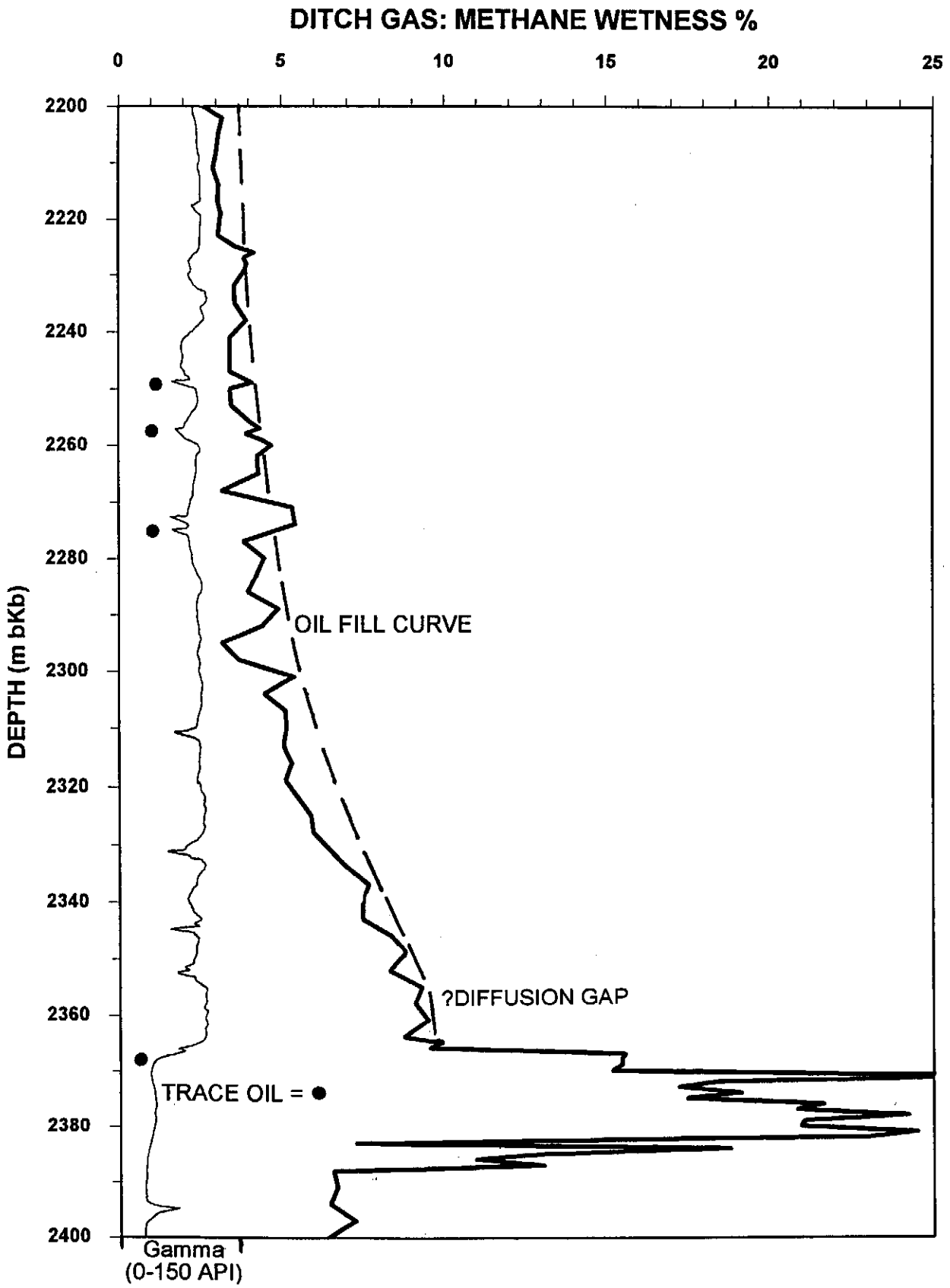

Figure 4.44: Ditch gas wetness diffusion and gamma ray profiles for Well 165. A continuous oil fill curve is interpreted below~2200m down to ~2355m (although the top section may represent a background gas profile) and a possible diffusion gap below.

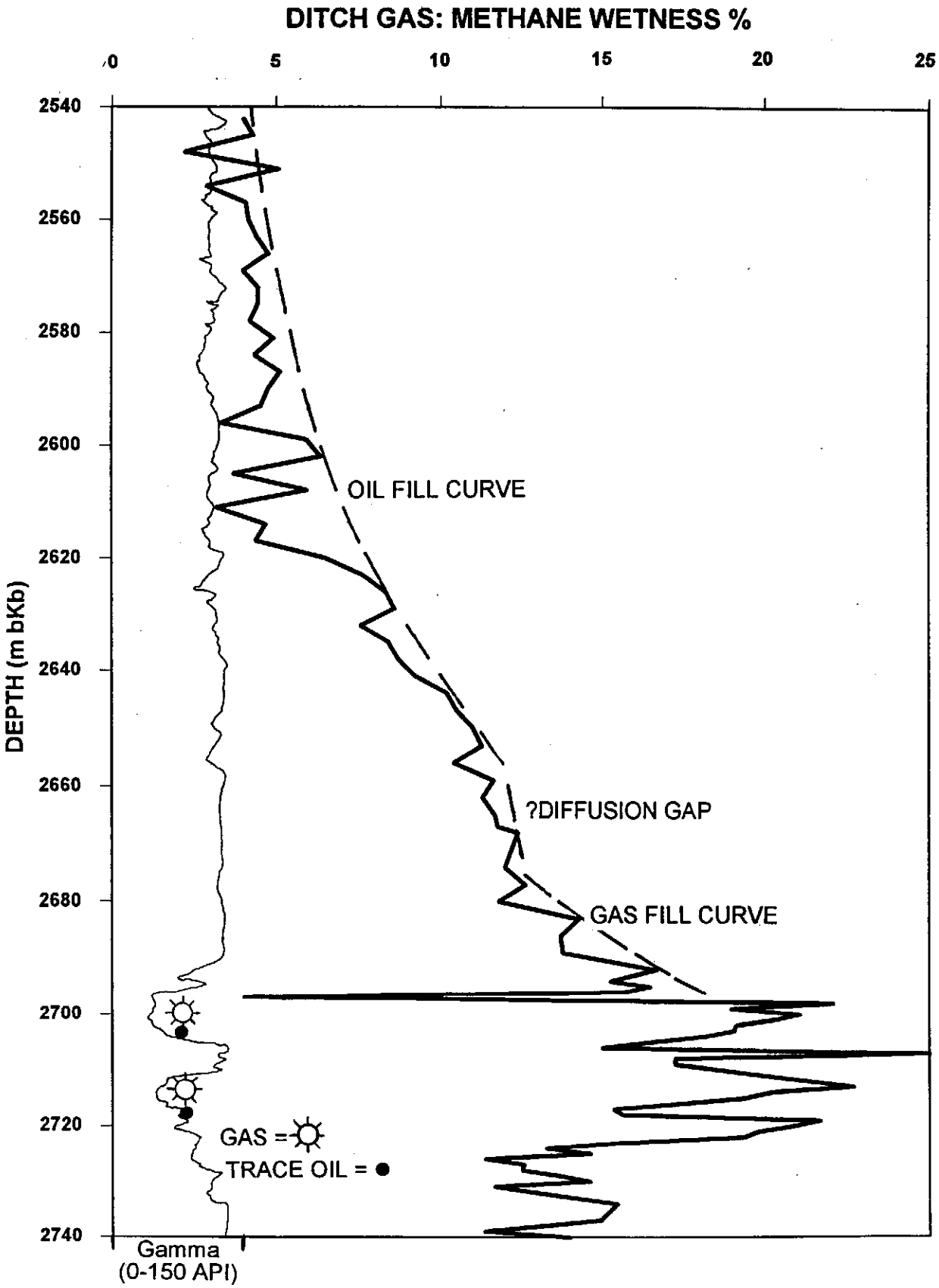

Figure 4.45: Ditch gas wetness diffusion and gamma ray profiles for Well 132. There is evidently a normal oil fill curve extending down to ~2660m, a possible diffusion gap down to ~2680m and a steep wet gas fill curve down to the top of the reservoir.

SEALS: DIFFUSION HEIGHTS												
WELL	RESERVOIRED HYDROCARBON FAMILIES	TOP RESERVOIR ZONE	NUMBER OF DIFFUSION PROFILES	HEIGHT OF PROXIMAL DIFFUSION	HEIGHT OF DISTANT DIFFUSION	HEIGHT OF FURTHEST DIFFUSION	SUPPORT FROM GC	No. OF RESERVOIR FILLS	DO SOURCE DATA SUPPORT PROFILE CONCLUSIONS?	UPWARD SHAPE OF GAS CURVES	REMARKS	SEQUENCE
83	FAMILY 1	2460m	Single	110m			Y	1	Y	drying	DST3	14A
83	none	2500-2700m	Single	gap	50m		nd	?1	Y	drying	40m diffusion gap above 13B sand.	13B
85	none	1723m	Single	80m			nd	?1	y	drying	RESERVOIR LOST	14A
85	live oil	2496m	Single	gap	120m		nd	1	Y	drying	10m diffusion gap. Minor reservoir	9A
88	FAMILY 1	2496m	Single	>160m			Y	1	Y	drying	DST5	14A
88	none	2670m	Double	gap	25m	?30m	nd	2	?	drying	5m diffusion gap above 13B sand.	13B
92	none	2171m	Single	gap	35m		nd	?1	?Y	drying	15m diffusion gap. Doubtful profile.	14A/13B
92	none	2777m	Single	gap	30m		nd	?1	?	wetting	5m diffusion gap above 9A sand.	9A
92	none	2939m	Double	gap	25m	30m	nd	?2	Y	mixed	25m diffusion gap above first seal (6A).	6A
102	FAMILY 1+2	2236m	Double	10m	?		Y	2	Y	drying	Source rock interferes. DST4	pre1A
103	FAMILY 1	2692m	Double	10m	80m	?20m	?Y	?2	Y	drying	Early trends separated by 50m gap. DST2	14A
94	trace oil	2708m	Single	gap	35m		nd	1	Y	drying	60m diffusion gap above 14A sand.	14A
94	FAMILY 1	2790m	Single	gap	20m		nd	1	Y	drying	20m diffusion gap. DST1	13B
96	trace oil	2877m	Single	gap	35m		nd	1	?	wetting	10m diffusion gap, source interference	13A
96	FAMILY 2	3100m	Single	90m	nil		Y	1	Y	wetting	Gas sand above diffusion. DST1	9A
104	trace oil	2215m	Single	20m			nd	?1	Y	drying		14B
114	none	2525m	Single	?gap	40m		nd	none	Y	drying	?5-10m diffusion gap. No gas in place.	14A
98	none	2675m	Double?	30m	50m		nd	?2	Y	drying	?Two fills or two leaks?	7A
123	FAMILY 1	2583-2678m	Inconclusive	80m	?20m		?	1	?	mixed	Sands interfere with diffusion	14A/13B
119	FAMILY 1	2446m	Single	~100m	nil		Y	1	Y	drying		14A
108	FAMILY 2	2791m	Single	>120m	nil		Y	1	Y	wetting	DST2	11A
129	none	2533m	Single	?gap	90m		nd	1	nd	drying	?5m diffusion gap.	14A
109	FAMILY 1B	2621m	Inconclusive	60m	75m		Y	2	?	wetting	Source rock interferes.	13A
107	FAMILY 3	2378m	Single	40m			Y	1	Y	drying	DST3	10A
107	FAMILY 2+3	2522m	several	45m	40m	40m	?	Y	2	wetting	DST2	pre1A
110	FAMILY 2	several	Inconclusive	25m	20m	10m	N	1	?	drying	Sands interfere with diffusion. DST1A	9A
112	?FAMILY 1B	2083m	Single	gap	35m		nd	1	Y	drying	~10m diffusion gap above 14Aff.	14B
113	?FAMILY 1B	2144m	Single	gap	50m		Y	1	Y	drying	~20m diffusion gap above 14At1.	14A
126	FAMILY 1+2	2624m	?Double	30m	>100m		Y	2	Y	drying		14A
125	trace	3135m	Single	gap			nd	?	N	none	SR interference with profile.	5A
125	none	3266m	none				nd	none	Y		?SR interference with profile.	pre1A
125	trace	3350m	none									pre1A

Table 4.10: Table of intervals in Bredasdorp basin wells in which diffusion profiles can be characterised. The intervals have been grouped according to the number of families of hydrocarbons found in mixtures in the reservoirs.

117	FAMILY 1	2383m	Single	113m	nil		Y	1	Y	drying	DST1	14A
154	trace	2883m	Single	gap	30/100m		nd	?1	Y	drying	SR/csg interference but 50m diffusion gap.	6A
154	trace	3088m	Single	gap	>40m		nd	1	Y	drying	15m diffusion gap. Sands interfere with profile.	6A
122	none	2399m	none	?20m			nd	?	Y	mixed	No show.	14A
122	FAMILY 1B	2511m	Single	20m			Y	1	?	drying	Live oil show in 13B sequence.	13B
156	FAMILY 1	2508m	Single	>150m	?nil		Y	?2	Y	drying	DST1	14A
166	FAMILY 1	2504m	Double	25m	>120m		Y	2	nd	drying	DST1	14A
132	FAMILY 1B+2	2654m	Double	40m	70m		Y	2	Y	wetting	DST1 and DST2	13A
132	none	2675m	Double	20m	?60m		?	2	Y	wetting	Two lost reservoirs? Source above.	13A
165	none	2366m	Single	gap	50m		nd	?1	nd	drying	?11m diffusion gap above barren sand.	14A
9	FAMILY 1	2247m/2283m	none				nd	none	Y	none	Tar and oil show.	14A
11	none	?2316m	Single	gap	50-70m		nd	none	nd	drying	?15m gap. Leak through silt @ 'H'.	14A
11	FAMILY 2	2950m	Double	60m	40m		N	1	Y	wetting	DST2 (5A)	5A
14	none	?2453m	none				nd	none	Y	none	Essentially no sand.	14A
17	none	none	none				nd	none	Y	none	Essentially no sand.	14A
27	none	2313m	Single	gap	>120m		nd	1	Y	drying	20m diffusion gap.	14A
35	none	2330m	?none					none				14A
37	none	2366m	?Single	gap	40m		nd	?1	nd	drying	20m diffusion gap. Silty diffusion zone. No flu.	14A
37	none	2479m	none				nd	none	nd	none	Lithologic interference. Probably never sealed.	13B
42	none	2285m	Single	gap	50m		nd	1	N	drying	10m diffusion gap. Depth shift. TOC increase.	14A
76	FAMILY 2+3	2541m	Double	60m	>40m		?N	2	No data	wet/dry	Some source rock interference. DST1	pre1A
50	none	?2252m	none				nd	none	Y	none	Interference from TOC, S2.	13B
36	none	2099m	Single	gap?	50m		nd		Y	Q only	Methane only - increasing upwards.	14A
59	FAMILY 1+3	2174m	Double	60m	50m		Y	2	Y	wetting	Barren sand above DST1.	pre1A
52	trace	1863m	Single	gap	35m		?nd	?1	Y	drying	15m diffusion gap.	14A
65	FAMILY 2	3167m	Single	160m	nil		Y	1	Y	wetting	Source rocks interfere. DST1	pre1A
18	FAMILY 3	2600m	Single	65m	nil		Y	1	Y	drying	Lithologic interference above DST3+DST4.	pre1A
19	FAMILY 3	2677m	Double	17m	127m		N	1	Y	wetting	DST2	pre1A
61	FAMILY 2	2717m	Single	~100m	nil		Y	1	Y	wetting	DST2	pre1A
62	FAMILY 2	2522m	Single	60m	nil		Y	1	Y	drying	60m diffusion gap above waxy DST1	5A
162	FAMILY 1+3	2369m	Double	25m	?100m		Y	2	No data	dry/wet	DST1+DST2	pre1A
63	FAMILY 2+3	2657m	Double	70m	55m		?N	?2	?	dry/wet	DST1	pre1A
128	FAMILY 4	3614m	Double	43m	35m		?N	1	Y	wetting	Two migration episodes? DST1	pre1A
138	FAMILY ?4	3111m	Single	>150m	nil		nd	?	Y	wetting	No condensate. DST1	pre1A

Table 4.10 (cont.)

targets being delineated further updip. Alternatively, if gas has entered the reservoir very recently, as may be the case in wells 156 and 166, there may be little or no evidence of diffusion into the overlying seal.

4.9. FLUIDS

Fluids found in the basin comprise three types, namely water, gas and oil.

4.9.1. Water

There are several different types of water in the subsurface. They can be separated on the basis of their chemistry, and in some cases the source of the water can be distinguished. Meteoric water is fresh and tends to bring excess iron into the subsurface. Fresh water is also often $CaSO_4$-rich - although reduction processes operating within the first few hundred metres of burial tend to largely eliminate this. Fresh water in the subsurface is generally considered to have been sourced by rainfall on elevated areas which then act as recharge areas.

Another source of fresh water is early expulsion from compacting claystones. Magara (1978, p.222-229) showed that claystones act as ionic traps for large cations and anions (such as Na^+ and Cl^-) and generally retain them. Water expelled from claystones during the first few hundred meters of burial tends to be fresher than the original pore water. Volumetrically these amounts can be large but they often go unnoticed during drilling because the changes happen in shallow rocks where the seabed riser has not been installed and there are no samples.

As depth increases, pore water salinity tends to increase and the later compaction water is usually more saline. This is because of the ionic bonding process in which clays develop surface ionic activity and are able to hold several layers of fresh water to their surface. This late connate water, although volumetrically limited, can be significantly more saline. However, the highest salinity fluids in a basin are often found where connate water has been in contact with (or within a few hundred metres) of evaporites where formation water salinity can exceed 100000 ppm NaCl (Bjørlykke and Gran, 1994). In the Bredasdorp Basin, the only interval where evaporites are known is in syn-rift rocks in well 16 (Fig. 4.03). These halite-rich rocks reach to within 50 metres of the pre1At1 sandstones. Water salinities, calculated from SP log deflections and confirmed from resistivity logs (Davies, 1995a), are in excess of 220000 ppm NaCl equivalent.

Where hydraulic communication occurs, formation water salinities are similar. Formation waters with matching salinities are seen in the basin-wide 14A hydrocarbon

migration trend (Fig. 4.46) and in the north flank pre-1At1 sandstones (Fig. 4.47a, b, c and d). Correlation of migration trends of fluids, including hydrocarbons, can often be investigated by mapping formation water salinity trends (Davies, 1995a and Grobbler, 1995). The method can be misleading, though, as sandstones with matching salinities are not necessarily from the same trend, so that a combination of correlative trends needs to be considered before a regional fluid flow trend can be assumed.

Formation water salinities can also be an indicator of previous tectonic effects. For example, the low salinity water in wells in the extensive (~40 km long) 14A trend must have come either from a meteoric source or a fresh connate input. It is unlikely to be the latter as (i) such water from the basin centre would only be available at that depth and in those quantities from syn-rift rocks and (ii) the 13A shale acts as a regional seal to migration of fluids (Davies, 1996c). Hence the more likely source is meteoric.

Maps of the present basin configuration suggest that meteoric input could have happened during the Plio-Pleistocene glaciation when sea levels were 100-200 metres below present (Dingle et al., 1983; Malan, 1990; Figs. 3.09 and 3.11). Sections through the basin show how fresh water might have been distributed through the rocks (Figs. 3.10 and 3.12). This flushing is unlikely to have occurred significantly earlier because those longer periods of major sea-level fall (e.g. Oligocene, Palaeocene) would have resulted in more severe effects in which:
(i) biodegradation would have been widespread in the affected hydrocarbon-bearing sandstone trends (discussed later)
(ii) water-washing of hydrocarbons would have been more prevalent in affected sandstones (discussed later) and
(iii) the continuing outflow of saline water from the basin centre (and from the western part of the Southern Outeniqua Basin) from compaction would have resulted in more complete replacement of the fresh water with saline water.

If this scenario is correct, the direction of formation water freshening in each sandstone indicates that the recharge areas must lie towards the western parts of the south and north flanks. Interestingly, one well (no. 2, Fig. 2.05) drilled in the westernmost part of the north flank has essentially fresh water at ~2400 metres bmsl (Davies, 1996c), suggestive of recent flushing. In support of this, a well to the east (no. 78), located near a fault which extends near-surface, contains apparently biodegraded oil.

4.9.2. Gas

Gases are found throughout the Bredasdorp Basin. They are largely comprised of hydrocarbons (~>95%) and show distinct proportions of 'wet' components in specific areas:

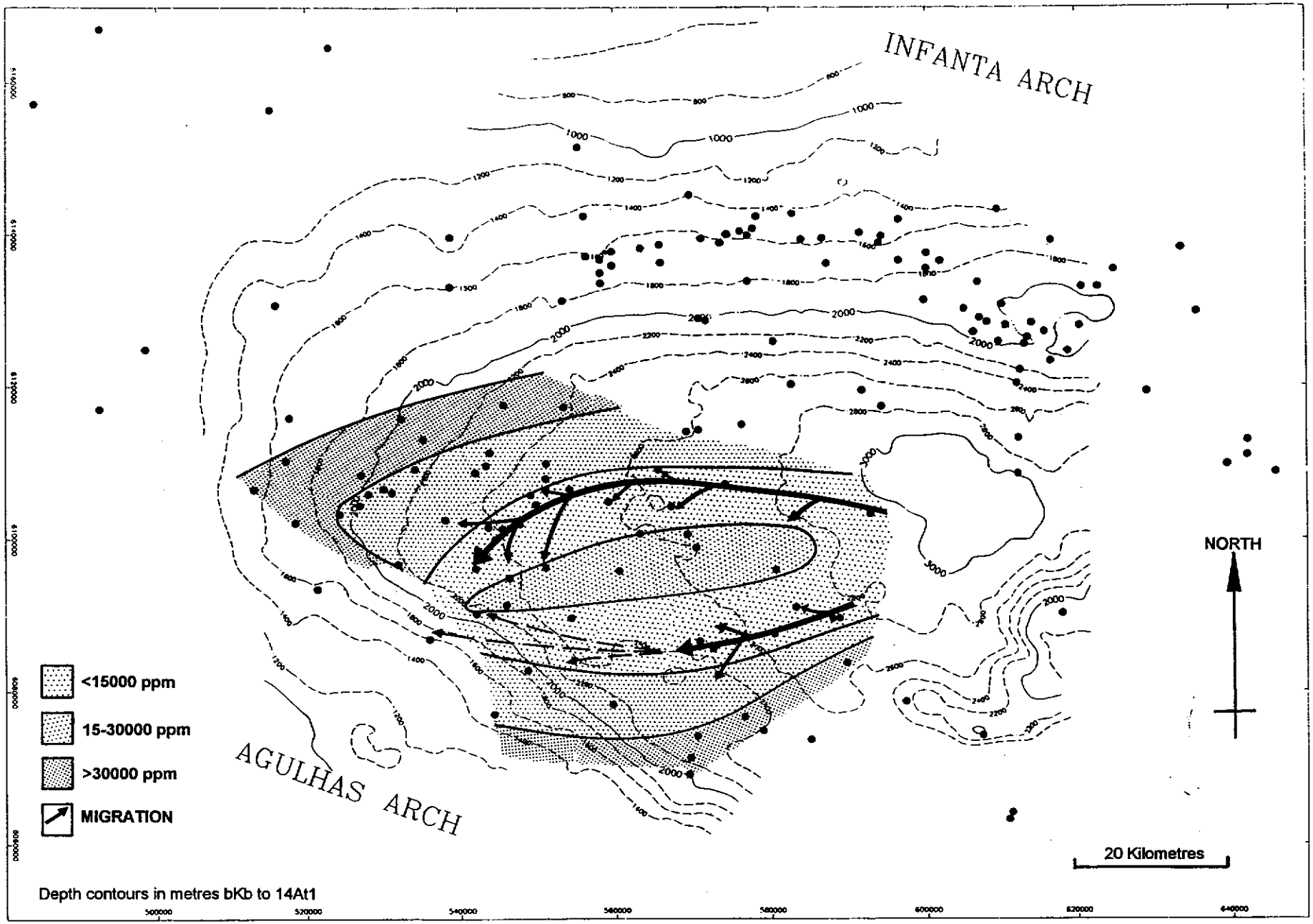

Figure 4.46: Map showing the two main depositional trends of the 14A sandstone fairways with the region of low formation water salinity shown and the probable hydrocarbon migration direction outlined. The two trends end at the possible diagenetic seal trend, believed formed by the deposition of diagenetic carbonates in the thin crevasse splay sands adjacent to the 14A channels due to pressure reduction, salinity change or reduced flow rate precipitation (Brown, 1991, Davies, 1995c and Noble and Davies, 1996).

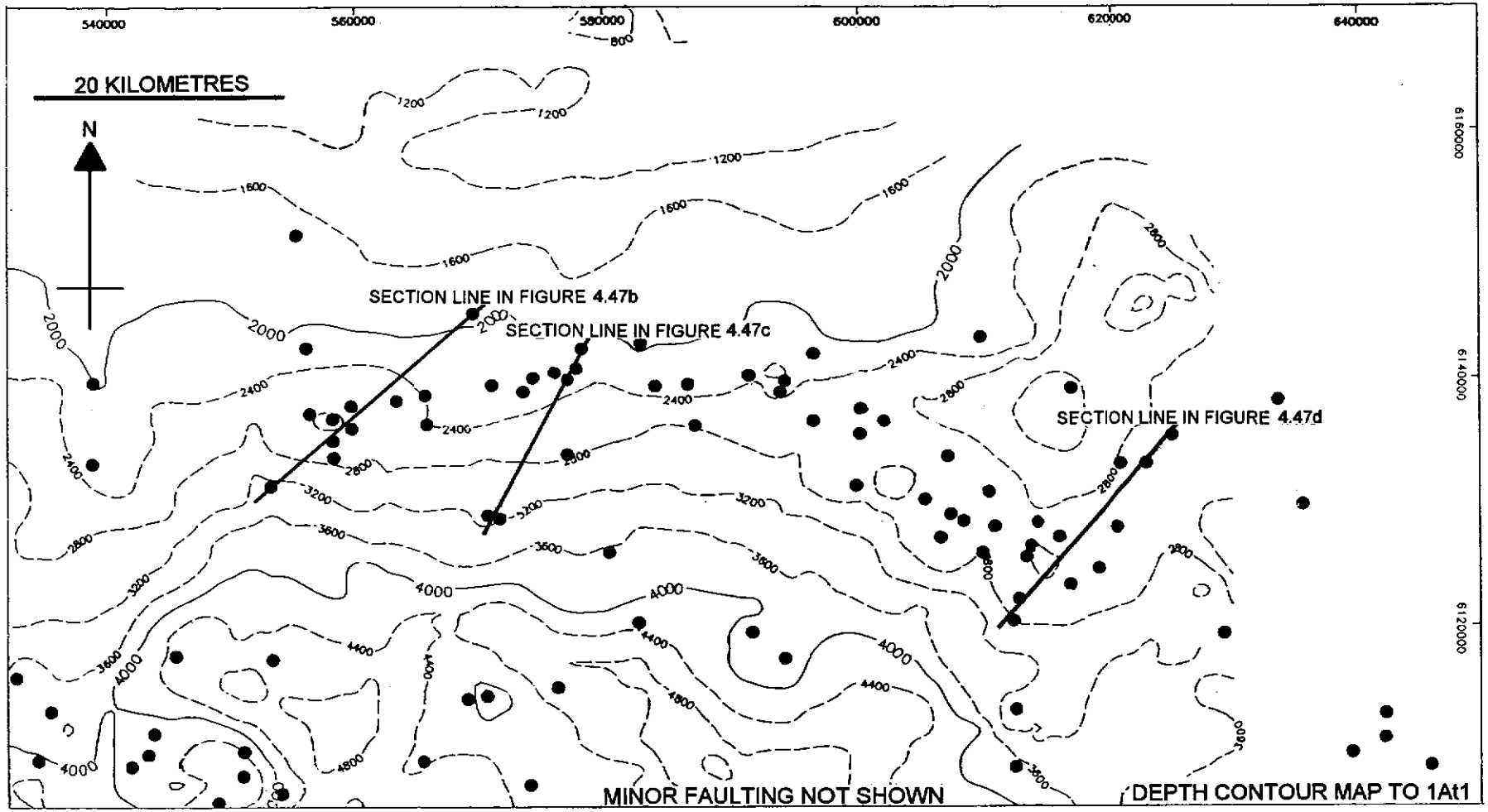

Figure 4.47a: Map showing the location of the three north flank hydrocarbon and salinity sections.

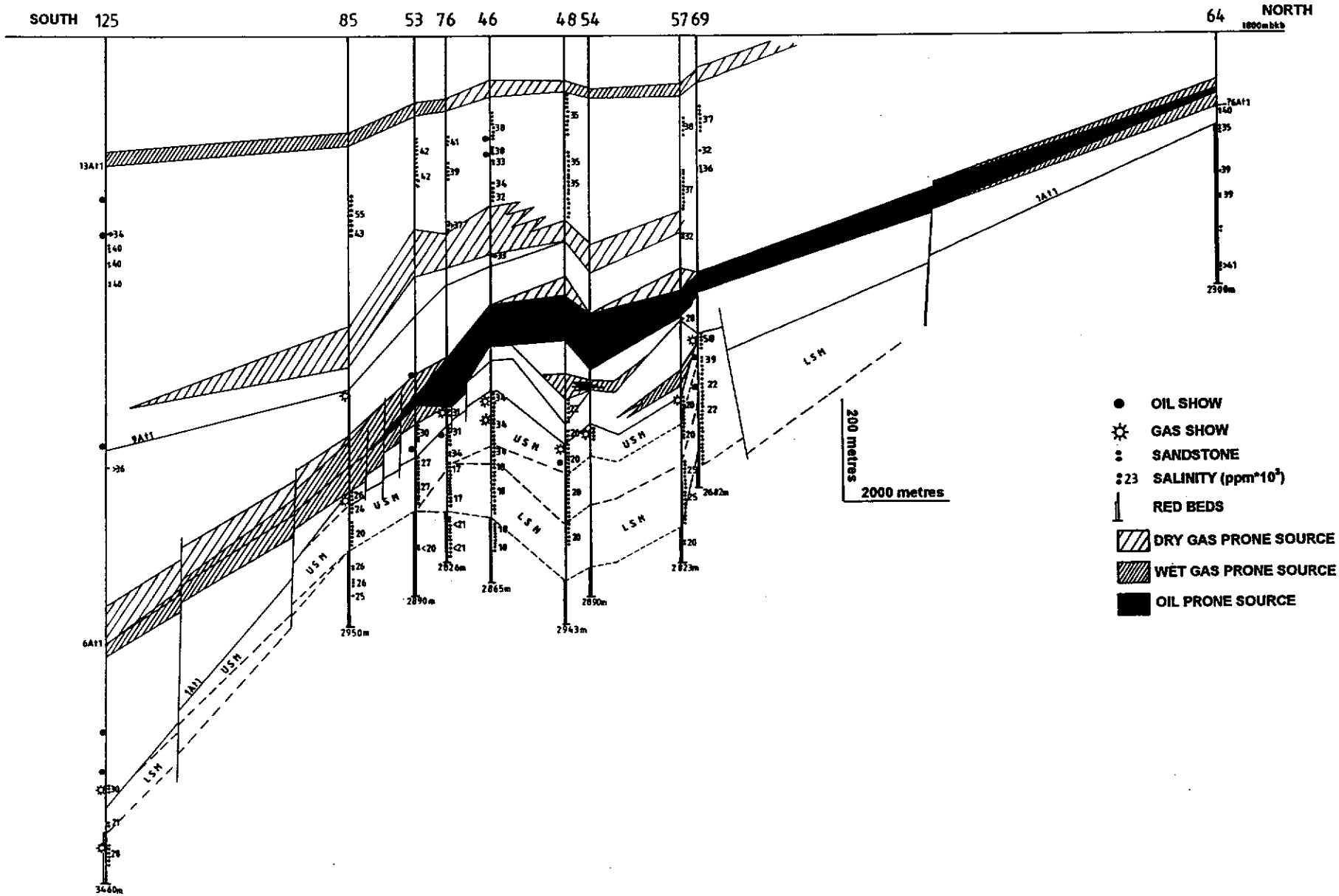

Figure 4.47b: Section showing the distribution of low salinity formation water (values in $NaCl_{equiv.}$) in syn-rift sandstones on the north-west flank of the basin.

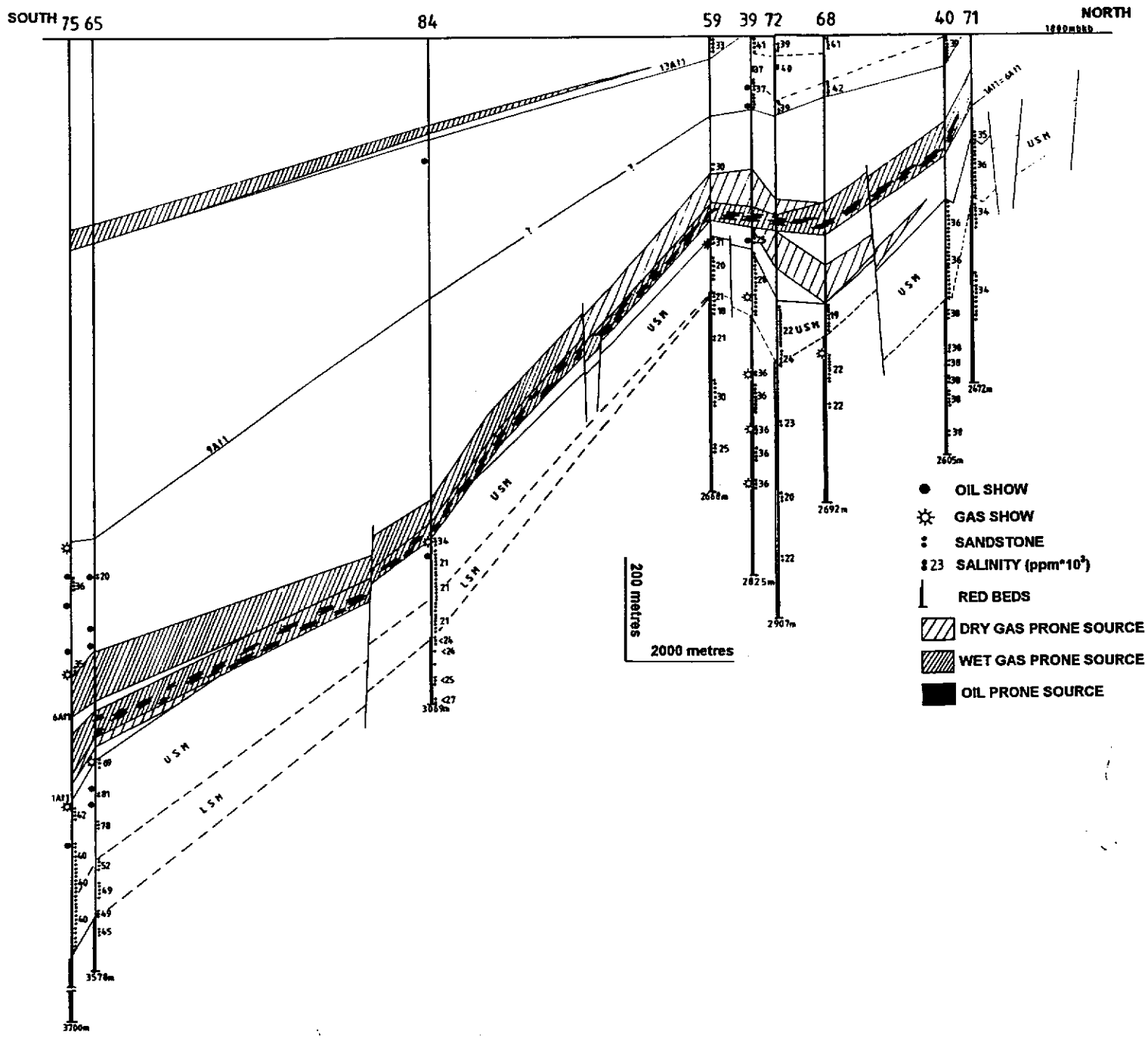

Figure 4.47c: Section showing the distribution of low salinity formation water (values in $NaCl_{equiv.}$) in the syn-rift sandstones on the north-central flank of the basin.

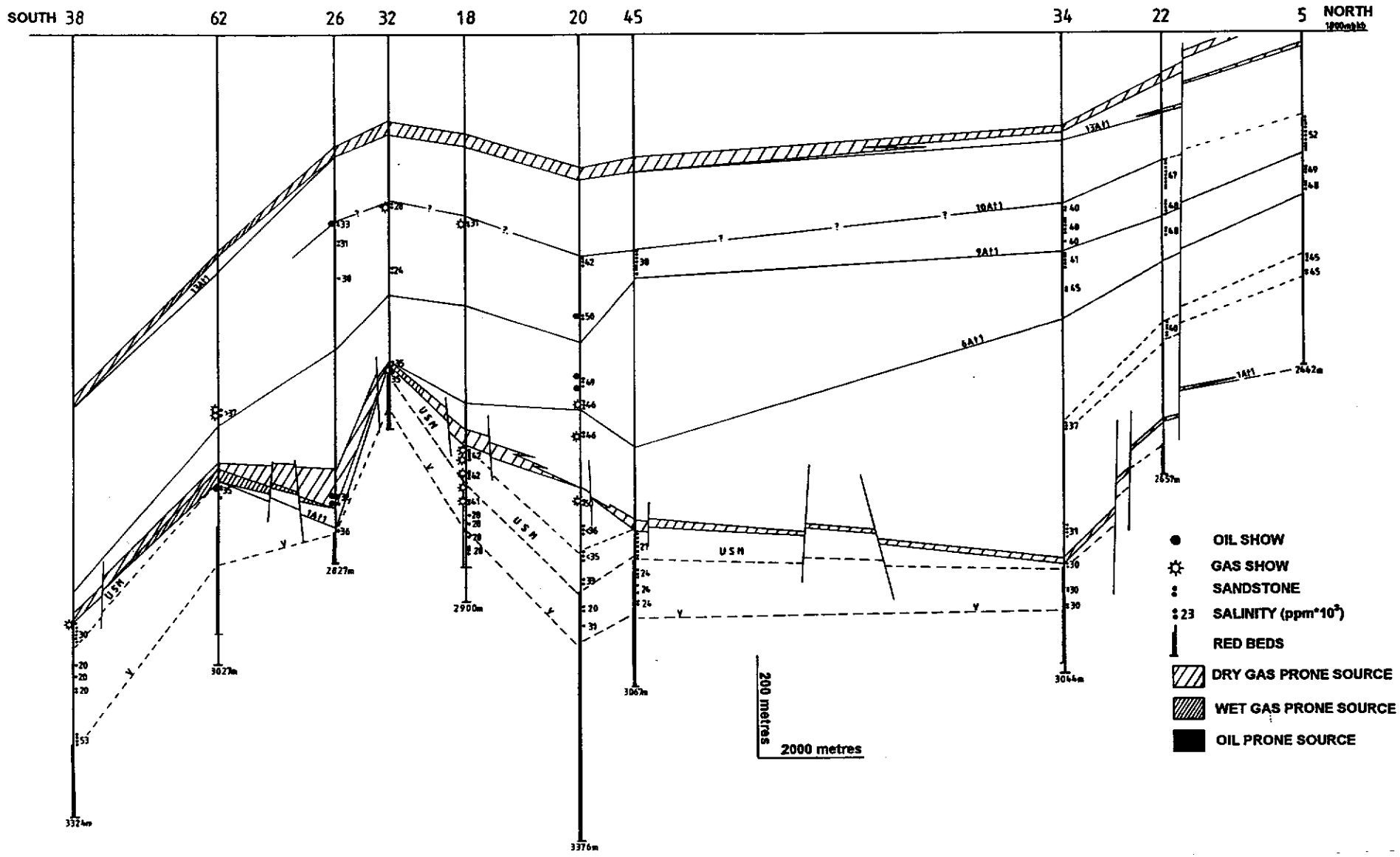

Figure 4.47d: Section showing the distribution of low salinity formation water (values in $NaCl_{equiv.}$) in the syn-rift sandstones on the north-east flank of the basin.

(i) ubiquitous minor gas traces in both sandstones and shales
(ii) largely dry gas in syn-rift targets
(iii) mildly wet gas in early post-rift sandstones
(iv) strongly wet gas associated with oil in Mid-Cretaceous sandstones

Ditch and cuttings gas analyses investigate the traces which are present in all wells below the top of hydrocarbon generation and represent the ubiquitous presence of light hydrocarbons. Gas and liquid reservoirs, on the other hand, are usually found in isolated locations and represent significant concentrations. Gas is more commonly reservoired in stratigraphically and structurally deep locations largely because of the higher maturity with depth and the more gas-prone nature of the kerogen in the earlier sedimentary rocks. Significant gas reservoirs are found in pre-1A, 9A-10A and immediately pre-13A rocks.

Most of the reservoired gases have been analysed for their non-hydrocarbon contents and small proportions of carbon dioxide and nitrogen are commonly detected (~1-4%). Other non-hydrocarbon gases such as hydrogen and helium are also found, but in smaller quantities (~0.01-0.1%). Gases in the basin also contain hydrocarbons which are in the gas phase in the reservoir, but are in the liquid phase at ambient conditions. These hydrocarbons contain trace amounts of high molecular weight components, including biological markers. Condensates are generally considered to be generated at relatively high maturity and their presence usually signifies the level below which oil is unlikely to be found. This is certainly the case in the Bredasdorp Basin.

4.9.3. Oil

Oil is commonly found in Cretaceous and Upper Jurassic rocks in the form of traces, distinct droplets or large reservoired volumes. Oil traces could be sourced in three distinct ways (i) as remnants of migrated oil (ii) locally generated from nearby kerogen (possibly even in the conduit) and (iii) as residue of lost reservoirs. Since traces are largely soluble in condensates, these traces may be removed from their original reservoir to be later redeposited in other sandstones by evaporative fractionation. However, the amount of oil soluble in condensates is generally quite small and unless the condensate migrates through an oil-rich location, the amount available for redeposition is small. In this case, they are not strictly 'oil' shows, but are usually characterised as that because fluorescence was noted at the wellsite. Hence, only the strongest of oil shows should be sampled for analysis. All oil shows are listed in Noble (1996) and plotted schematically in Figs. 3.27-3.31.

An alternative source of oil traces is in mature source rocks which have yet to expel oil. In such circumstances, a light oil migrating past the base of the source might be able to

dissolve material from the source. In this case the biomarker analysis would respond to the dissolved oil and not the light oil, giving a false impression of the maturity and the source. Although this situation does occur (Hughes and Dzou, 1995 and Davies, 1996d), it usually requires special circumstances to prevail and in general is considered an unlikely source of large amounts of high molecular weight hydrocarbons. In the example given by Hughes and Dzou (1995), thick sequences of low maturity coals were juxtaposed with the light oil-filled reservoir and the source. The coals had TOC contents near 52% and were richly endowed with biomarkers.

The different sources of the chemicals in the oil shows are often difficult to separate. However, where there are mixtures of hydrocarbons in produced fluids, whole oil analysis usually provides enough data to identify the mixture, as has been shown from oil/source rock correlation studies in the Pletmos Basin (Davies, 1996d and 1997c).

CHAPTER 5. SAMPLES

Sample types studied from wells in the Bredasdorp Basin are the following:

- drilling mud (M)
- drilling cuttings (RC)
- sidewall cores (SWC)
- cores (C)
- DST fluid samples
- RFT fluid samples

Each type of sample is collected in a different manner (see below) and hence can represent different parts of the formation drilled. For example, liquid samples will test the pore filling fluids whilst rock samples test the rock; sidewall core samples very precisely test a small interval whilst the matching cuttings sample tests an interval of some 10 metres. Since each type of sample reflects the sampled interval in a different way, the pros and cons of each type as well as their usage is addressed.

5.1. DRILLING MUD SAMPLES

Drilling mud is used to remove drilled rock from the borehole, especially from the area of the drill bit, and to cool and lubricate the bit. In Bredasdorp Basin wells, drilling mud commonly comprises a mixture of various additives (often cellulose and bentonite) in suspension in sea-water. It also often contains some of the drilled formation, although generally only the finest grain-size fraction, as well as some of the formation fluids. In many of the earliest wells (up to ~ well no. 50) a lignosulphonate mud was used below the 13 $^{3}/_{8}$''' casing. This resulted in the addition of quantities of lignite to the mud. Since a mud system is intimately mixed with drilled formation material, it can contaminate the rock samples and this is a particular problem with muds made of cellulose polymers or lignite as these have high organic contents. For this reason, samples of the mud are usually analysed every hundred metres or so by routine chemical methods, to establish background values of various parameters and help determine the level of contamination of formation samples.

The mud also contains gas entrained during drilling, commonly called 'ditch gas', which is considered representative of the gas in pore spaces in the formation. This gas can be used to characterise the hydrocarbons likely to be found in the rock and is a useful first indication of nearby reservoirs.

Samples of mud used for analysis are dried at ~35°C and ground finely (<125μ). Two wells (no's. 54 and 55) were drilled using an oil-based mud system for at least some of the section. Source rock and mud samples from these wells were not analysed

geochemically because of the likelihood of hydrocarbon contamination even where the samples were cleaned of as much mud as possible.

5.2. CUTTINGS SAMPLES

Rock chips, fractured from the formation by the action of the drilling bit, are removed from the well in suspension in the mud at intervals of 3-9 metres. Collection procedures at the wellsite shale shakers mean that these samples represent the whole of the interval of formation drilled and therefore comprise a mixture of the different rocks. In addition, they can also be affected by other contaminants in one of several ways:

(i) chips from previously drilled formations can remain incorporated in the mud, often because of inadequate cleaning procedures

(ii) chips from other formations can be knocked from the wellbore during drilling

(iii) contaminants can be introduced directly from the mud, e.g. mud chemicals

(iv) contaminants can be brought into the hole on drilling equipment such as thread grease, pipe dope or casing thread bitumen

(v) contaminants can be added during other operations, e.g. paint from new drill bits, rubber seals from casing, diesel added to free stuck pipe.

Because of all these possible sources of contaminants, cuttings samples are thoroughly cleaned on collection by washing them in water, sieving to remove the largest chips (>2 mm, which are generally representative of caving) and hand-picking pieces of solid contaminant (Davies and Ellis, 1981). During this process, the finest clay fraction, generally assumed to be representative of mud, is removed. However, *in situ* chips of soft shale can disaggregate if the washing process is too severe. Since these shales often contain high proportions of organic matter, the cuttings samples commonly under-estimate the source potential of the sampled interval.

Cuttings samples are routinely used to describe the drilled formation to provide a complete, but general, geological description of the lithology intersected. Cuttings samples used for routine analyses in this study were cleaned and processed at the wellsite as part of the reference set of washed cuttings, hence the geological description can be applied directly to the reference cuttings used in this study. In addition, a fraction of this material is always tested at the wellsite for hydrocarbon fluorescence and cut. From these descriptions samples of oil traces are selected.

On receipt in the laboratory, the samples are dried at ~35°C, cleaned of remaining pieces of rubber, paint etc., a brief description is made of the lithology and of any contaminants removed. Where larger samples are necessary and are selected from unwashed samples which have been stored for a long time, the water in which they are

washed in the laboratory is made up to a similar salinity to that used during drilling. This is to stop the expandable clays from undergoing cation exchange which causes them to swell and disaggregate.

5.3. CORE SAMPLES

When drilling reservoir quality sandstones, they are often cored. These cores are largely uncontaminated and can provide large samples of specific lithologies. However, pore fluids are sometimes lost or interchanged with mud chemicals during drilling. In addition, most of the light fractions of hydrocarbons are lost during the core slabbing process but remnants of the oils are usually found in large enough quantity to justify their analysis. Core samples are generally analysed after removal of the outer edge/end of each core piece so that mud contamination and evaporative losses are minimised.

5.4. SIDEWALL CORE SAMPLES

Sidewall core samples are collected from the borehole during logging runs. The sample intervals are generally selected after inspection of the logs so that specific rock types are collected. The samples are up to 50 mm in length, and have a maximum weight of ~50 grams. Because they are sampled through the mud system they can be subject to severe contamination due to mud injection into and onto the sample.

It is possible to remove much of the mud, leaving some 20-30 g of *in situ* rock - enough for most routine optical and chemical analyses. These samples are generally too small for bitumen extraction analyses (except where high proportions are present) especially if petrographic studies are needed. In addition these samples are generally too small to allow for repeat analyses. Hence it is advantageous to have two samples shot at the same location. This second shot can usually be made to an accuracy of about 50 centimetres. Nevertheless, the facility to be able to return to a formation which was not adequately sampled during drilling and to obtain a largely uncontaminated sample, is of great value and far outweighs the problems associated with the small size of the samples.

5.5. DRILL STEM TEST SAMPLES

Intervals which are considered likely to contain enough hydrocarbon (and where sandstones have adequate porosity and permeability) to permit hydrocarbon flow are usually subjected to drill stem testing (DST). Samples can be collected during these tests either at the point of flow into the wellbore or from fluids which flowed to the

surface and separated into gas and liquid fractions. In cases where the formation pressure is not high enough to allow for flow of fluids all the way to the surface, they can be reverse circulated from the well bore and sampled at the well head - although in this case, the lightest gas fractions are usually lost.

Two sets of samples are usually collected in containers filled downhole at flowing pressure and one set in containers filled from the separator at near atmospheric pressure. These comprise the samples for fluid recombination analyses at reservoir conditions (PVT analyses). The PVT sample set is analysed at a laboratory outside South Africa where rigorously controlled recombination of the gas and oil samples is carried out. By contrast, the geochemical set is analysed locally at ambient conditions. As a result, there is an inherent difference between the two samples sets, related largely to the volatility of their different components. These tests usually result in the collection of essentially uncontaminated gas and liquid samples of the reservoir fluids and as such are preferred to sampling oil traces from sandstone samples. Drill stem testing is usually expensive in terms of rig time and only carried out in selected reservoirs, hence only a small proportion of the known hydrocarbons found in the basin are properly sampled. Also produced at the surface are water samples. These are usually a mixture of formation water and mud filtrate, and are normally not used to characterise the formation water. Where a large volume of water has been produced, these can be composed wholly of formation water, providing there has been no drop-out of condensation water.

5.6. RFT SAMPLES

A cheaper alternative to acquiring hydrocarbon or water samples from a specific formation is that of the repeat formation tester (RFT). As the name implies, it is used to carry out repeat tests of formations, up to 30 in one run. The downhole tool has the facility not only to measure formation pressure and estimate permeability from the rate of build-up of pressure at each sample point, but can also collect fluid samples. The technique does not allow for flow-through of liquids to obtain a clean uncontaminated sample and fluid samples collected this way are usually contaminated by varying amounts of mud filtrate. In addition, any liquid hydrocarbons collected may be merely residual oil that was not flushed from the sandstone by filtrate invasion. However, in cases where an expensive DST cannot be justified, RFT samples can be invaluable and can be used for the same range of hydrocarbon analyses.

CHAPTER 6. ANALYSES

Analysis of sampled lithologies and fluids is subdivided into 3 different categories namely onsite, routine offsite and non-routine offsite.

6.1. ONSITE ANALYSES

6.1.1. Drilling parameters

Various parameters are recorded during drilling, such as gas contents, mud weight and rate-of-penetration, and used in estimation *inter alia* of lithology and formation overpressure (Baird, 1986). The estimated pore pressure, usually quoted in mud weight equivalents, is usually calibrated by log pressure measurements (RFT) after drilling but where not, can still be used to compare pressure regimes. Only the most pertinent of the many parameters are employed in this study.

6.1.2. Ditch gas analyses

These data record the amount and proportions of free gas which can be separated from the mud returning from the drilling bit by agitation and evacuation. The gas is analysed every 1-3 metres drilled for C1-C5. The results are used to evaluate the gas present in the porosity of the drilled rock and in studying the type of hydrocarbon in place and its retention in the reservoir (Deroo et al., 1977).

6.1.3. Cuttings gas analyses

These analyses determine the amount and proportions of C1-C5 gases which can be desorbed from rock cuttings. It is usually assumed that unless the lithology is unusually impermeable, gas in pore spaces is released during drilling. A small portion of the rock chips is collected every 3-9 metres, washed free of mud in fresh water and split into three portions. One portion is introduced into a blender and macerated, releasing any gas remaining in closed pores and on sorption sites on mineral and maceral grains. This gas is usually more representative of gas generated in situ, as opposed to ditch gas data being more representative of gas reservoired in situ. These gas data can be interpreted to provide a first approximation of the source potential and maturity (Le Tran, 1975). Of the remaining two portions of washed cuttings, one is dried at low temperature in an oven and used for lithologic description. The second, larger portion, is retained wet in a sealed container for later geochemical analyses.

6.1.4. Hydrocarbon shows

Shows are signs of reservoired hydrocarbons. These can take the form of gas increases whilst drilling, such as large increases in background ditch gas or from oil sheen on the mud pits or oil fluorescence in samples from the well. Only compounds

containing aromatic rings fluoresce. These tests really 'see' only a small fraction of the oil, but since aromatics are almost always found in oils, they are an easily detectable pointer to oil. Some minerals also fluoresce (e.g. calcite, fluorite), so samples with fluorescence are checked for hydrocarbons by 'cutting' with an organic solvent (usually trichlorethane). Where there is a cut (i.e. some of the fluorescing material dissolves in the solvent) this is an indication of reservoired oil. Samples can be crushed before testing to expose as much surface area as possible to the solvent, which highlights weak hydrocarbon shows but can be confused with traces of unexpelled oil found in source rocks. This latter result is also useful as it provides a check on interpretations of source quality and maturity derived from ditch and cuttings gas data.

The presence of fluorescence in specific lithologies in cuttings samples is often used to determine which samples should be subjected to further oil extraction analyses. Tests for fluorescence can also be carried out after the well has been completed to check that no fluorescence was missed. However, because the lightest and most strongly fluorescing hydrocarbons evaporate very quickly, the fluorescence dulls quite soon after drilling. Nevertheless, some fluorescence is almost always present for months or years after collection. Very few of these data are specifically presented in this report as a full description of their accuracy, use and interpretation is beyond the scope of this study. The data are widely used to plan sample selection, to support pressure measurements from RFT and DST data, to investigate source potential and maturity and to characterise seals. These data are all available in well completion reports and a comprehensive listing of shows in wells in this basin has been compiled (Noble, 1996).

6.1.5. Downhole logs

Downhole logs are usually recorded for prospective intervals, but generally only where drilling deeper than 1500 metres below surface, i.e. in regions where hydrocarbons are generated or reservoired. These logs are the same as those used elsewhere in the world and comprise gamma ray, sonic travel time, resistivity (deep and shallow) and spontaneous potential. If reservoir rocks are present, density and porosity logs are run as well as specialist logs such as RFT and SWC. Interpretation of the results of all these logs are used to determine *inter alia* the extent of reservoired hydrocarbons, fluid contacts, lithologic type, source rock quality and formation pressure. A full description of all these logs is beyond the scope of this report but can be found in Schlumberger (1989; 1991b). Several logs are particularly useful in assessing the petroleum potential of the well (Cornford, 1986; Schmoker and Hester, 1990; Creaney and Passey, 1993) and a brief description is given below. A number of logs are run in the open-hole section of the well (usually) to determine various parameters relating to the lithology and pore-filling fluids. These logs are run sequentially and sometimes repeated in

different logging runs. Extensive use of these logs world-wide has shown that they provide accurate and repeatable records of the down-hole parameters.

The spontaneous potential (SP) log is used to determine the electrical resistivity of fluids in both water- and hydrocarbon-bearing sands. The calculated resistivity in largely hydrocarbon-free sands is a measure of the formation water salinity. Such calculated salinities are available for all sands thicker than 3 metres in Bredasdorp Basin wells (Davies, 1995a). Since fluids migrating through common conduits have essentially the same salinities, mapping the salinity data at all levels throughout the basin has allowed distinction of preferential fluid migration routes (Davies, 1995a; Grobbler, 1995).

The gamma log is probably the most widely used log for litholog correlation as it readily distinguishes low gamma sandstones from high gamma claystones. Uranium salts are insoluble in anoxic environments hence they are common where better quality source rocks are found. Hence an anomalously high gamma log response often indicates better quality source rock. Kimmeridge Clay Formation shales in the North Sea area, in which the gamma response exceeds 250 API in the richest oil-prone source rock, provide a good example of this effect (Bailey et al., 1990). In addition, gamma response is often high where high proportions of smectite is found because of their content of potassium, which decays giving off beta particles. Smectite is commonly found closely associated with pelagic sedimentation and is therefore a facies indicator.

Resistivity logs are particularly useful for evaluation of mature source rocks which tend to have higher proportions of oil in pore spaces. This effect is especially marked in rich source rocks, partly because of the presence of detrital resins and lipid-rich organic matter and partly because of the retention of oil generated from the in-situ kerogen. Since oil has a much higher electrical resistivity than salt water, such rocks have higher electrical resistivity (Price et al., 1986). Logs obtained from the 13A oil-prone source rock intersected in the well 83 (Davies, 1988b) provide clear evidence of this effect. There, shales at the edge of the source rock from which oil has been expelled, can be differentiated from the centre of shales from which little oil has been expelled by the variations in free hydrocarbon contents.

Gas can also be an electrical resistor but, because of its high compressibility, occupies a smaller pore space volume per unit mass than oil. Hence, increased resistivity would be more evident in source rocks buried into the oil window than those which are immature or in the gas window.

The sonic (or time travel) log is often used as an indicator for better than average source rocks (Cornford, 1986) and for compaction studies (Magara, 1986). Shales with high contents of hydrogen-rich lipid organic material tend to be associated with the finest-grained clays deposited in the same hydraulic regime (Morris and Calvert, 1975). These are usually smectites which have very slow sonic travel times. Their importance stems not only from the fact that they are usually deposited with the lowest density, lipid-rich organic material but also because they are able to absorb lipid material (Bishop and Philp, 1994). Smectitic clays are expandable and retain water during compaction longer than illitic or kaolinitic clays (Burst, 1969) and they compact more slowly becoming overpressured and hence have slower sonic velocities. Excess pressure is accentuated by generation of low density hydrocarbons during maturation. The sonic log readily records changes in shale compaction, which allows for the interpretation of formation pressures higher than normal (Magara, 1977). Knowledge of the level of overpressure is very important when assessing the likelihood of hydrocarbon expulsion from source rocks and comparing fluid flow regimes.

The neutron density log responds to the total flux of neutrons in the rock. Source shales tend to have an apparently low neutron density because hydrocarbons have higher hydrogen contents than water. This apparent low density is less marked in gaseous source rocks because gas has a much higher proportion of hydrogen than oil.

Formation temperature measurements are routinely made at maximum logging depths. Original formation temperatures are evaluated from these data relying on the assumption that the rock is cooled by drilling mud circulation and after cessation of circulation, warms up following an exponential function. The warm-up period can last many weeks long and in order to more quickly provide an estimate of the true formation temperature, they are corrected using the Horner function:

$T°C \alpha$ [(time since last circulation+time of last circulation)/time since last circulation]=1.

The resulting temperatures are called 'static borehole temperatures' (SBHT) and are a close approximation of formation temperatures (Dowdle and Cobb, 1975). Some geochemists consider that the SBHT is still not accurate enough and that a correction factor based on DST data should be applied (D.W. Waples, 1996, pers. comm.).

The Repeat Formation Tester (RFT) is designed to gather pressure data (validated by rate build-up data) but does have the facility to divert some fluid during pressure testing into two small chambers (1.75 US gal and 3.5 US gal.). These chambers can be sealed at reservoir pressure and sampled at surface (Verfaille, 1993). However, the chambers are small relative to the volume of filtrate which could have entered the sand,

hence sampled fluids may be contaminated with mud filtrate. Nevertheless, if gas and oil or condensate are present, their proportions can be used to calculate a gas:oil ratio (GOR) for correlation between connected and unconnected flow units (Davies, 1995b).

The Drill Stem Test (DST) is designed to test the flow characteristics of the formation and to capture some of the flowing fluids - either within the tool or flowed to the well bore and thence to surface. Temperatures and pressures are also recorded during the DST, both down-hole and at surface. DST temperatures theoretically provide a better approximation of the formation temperature because, providing the test is not very short, the fluids are flowed from the formation which is far away from that cooled directly by the mud. Hence flowing temperatures should be closer to the true formation temperatures. To address this concern, a comparison of DST and static borehole temperatures has been carried out for wells in the Bredasdorp Basin (cf. Fig. 2.10 and Table 6.01). A regression line drawn through the data shows DST temperatures to be approximately 3% higher than comparable SBHT values (Figs. 6.01 and 6.02).

Although the DST temperature error bar is generally small, the values can occasionally be either too high (because of friction at high flow rates) or too low (due to gas expansion cooling). In addition, DST data are available for a total of 85 intervals in only 52/164 wells. As a result, the data base is not representative, indeed one quarter of these DST's are from the greater F-A structure which covers <0.01% of the basin area). Therefore in view of the small and non-random sample set, and because the difference between the two temperature measurements is small, SBHT data are not adjusted.

During the DST, there may be several periods when hydrocarbons flow and several shut-in pressures recorded. These can be extrapolated to confirm the formation pressure determined from the RFT logging run or estimated from drilling parameters. The ratio of the hydrocarbon gas:oil (GOR), reported in standard cubic feet of gas per barrel of oil, is used in determining the fluid type (Prior, 1984) and in estimating the source type. Data acquired from DST's in Bredasdorp Basin wells are shown in Table 6.02 and their regional distribution reported in Davies (1995b). GOR data are often used to characterise the hydrocarbons as either gas or oil (Prior, 1984; Table 4.03).

6.2. ROUTINE OFFSITE ANALYSES

These analyses are carried out on most samples by shore-based laboratories. The analyses can be further subdivided into four groups as shown below:

(i) pyrolysis and calcimetry analyses
(ii) optical analyses
(iii) fluid samples (hydrocarbon and water).

DST vs SBHT TEMPS				
WELL	DEPTH	DST	SBHT	DSTT
83	2470m	DST3	101	98.9
83	2889m	DST2	112	113.0
83	3254m	DST1c	128	128.5
88	2507m	DST5	100	112.0
88	2839m	DST4	117	117.0
88	2916m	DST3	120	119.4
88	2929m	DST2	121	120.0
88	3243m	DST1	131	131.7
102	2241m	DST4	95	106.7
102	2632m	DST2	110	106.0
95	2703m	DST2	120	120.0
103	2718m	DST2	117	93.3
94	2799m	DST1	113	126.0
96	3131m	DST1	126	126.1
114	3085m	DST2	132	135.0
93	2463m	DST2	107	102.8
93	2808m	DST1A	111	111.1
93	2817m	DST1	112	112.8
119	2816m	DST1	112	114.4
108	2820m	DST2	117	112.2
108	2829m	DST1	117	116.7
151	2915m	DST1c	118	118.3
151	2919m	DST1b	118	118.3
129	2865m	DST2	116	118.3
129	2946m	DST1	120	123.9
109	2630m	DST1	100	109.4
107	2388m	DST3	98	97.8
107	2565m	DST2	104	106.7
107	2590m	DST1	105	106.7
110	3051m	DST1B	120	121.1
110	3051m	DST1A	120	121.1
113	2914m	DST1	125	114.4
126	2643m	DST1	112	116.7
120	2931m	DST1	117	121.1
117	2399m	DST1	95	106.7
146	2564m	DST1	96	101.7
156	2522m	DST1	100	111.0
166	2520m	DST1	99	113.8
132	2662m	DST2	103	104.4
132	2706m	DST1	104	110.0
148	2684m	DST1	104	110.6
167	2679m	DST1	108	115.0
11	2950m	DST2	125	127.2
84	2771m	DST1	109	108.9
27	3161m	DST1	136	136.1
35	3309-3416m	DST3	130	134.4
35	3354-3416m	DST2B	132	134.4
35	3397-3416m	DST1	134	135.6
37	3495m	DST1	137	136.7
69	2436m	DST1	92	107.2
46	2560m	DST2	98	109.4

Table 6.01: Temperatures recorded during each DST and the matching temperature calculated from the corrected static borehole temperature.

46	2620m	DST1	101	109.4
48	2620m	DST2	109	109.4
48	2634m	DST1	110	104.4
54	2617m	DST1	104	112.8
76	2610m	DST1	109	107.8
39	2229m	DST2	89	100.6
39	2567m	DST1	99	110.6
59	2212m	DST1	93	99.2
65	3189m	DST2	129	126.1
65	3267m	DST1	131	127.8
18	2635m	DST4	105	124.4
18	2673m	DST3	107	121.1
18	2703m	DST1	109	120.0
21	2559m	DST2	107	112.8
21	2585m	DST1	108	117.2
19	2709m	DST2	109	118.3
20	2515m	DST4	100	101.1
20	2579m	DST3	105	100.6
20	2699m	DST2	110	99.4
44	2750m	DST1	112	128.7
55	2680m	DST2	111	118.3
61	2128m	DST3	90	99.3
61	2770m	DST2	114	121.7
62	2549m	DST1	109	110.6
70	2428m	DST2	103	107.2
70	2452m	DST1	104	108.3
162	2349m	DST2	92	107.0
162	2450m	DST1	95	110.0
31	2753m	DST1	105	117.8
63	2691m	DST1	109	107.2
128	3661m	DST1	149	154.3
12	2371m	DST4	97	102.8
12	2426m	DST3	99	110.0
12	2460m	DST2	100	106.1
12	2489m	DST1	101	100.0

Table 6.01 (continued)

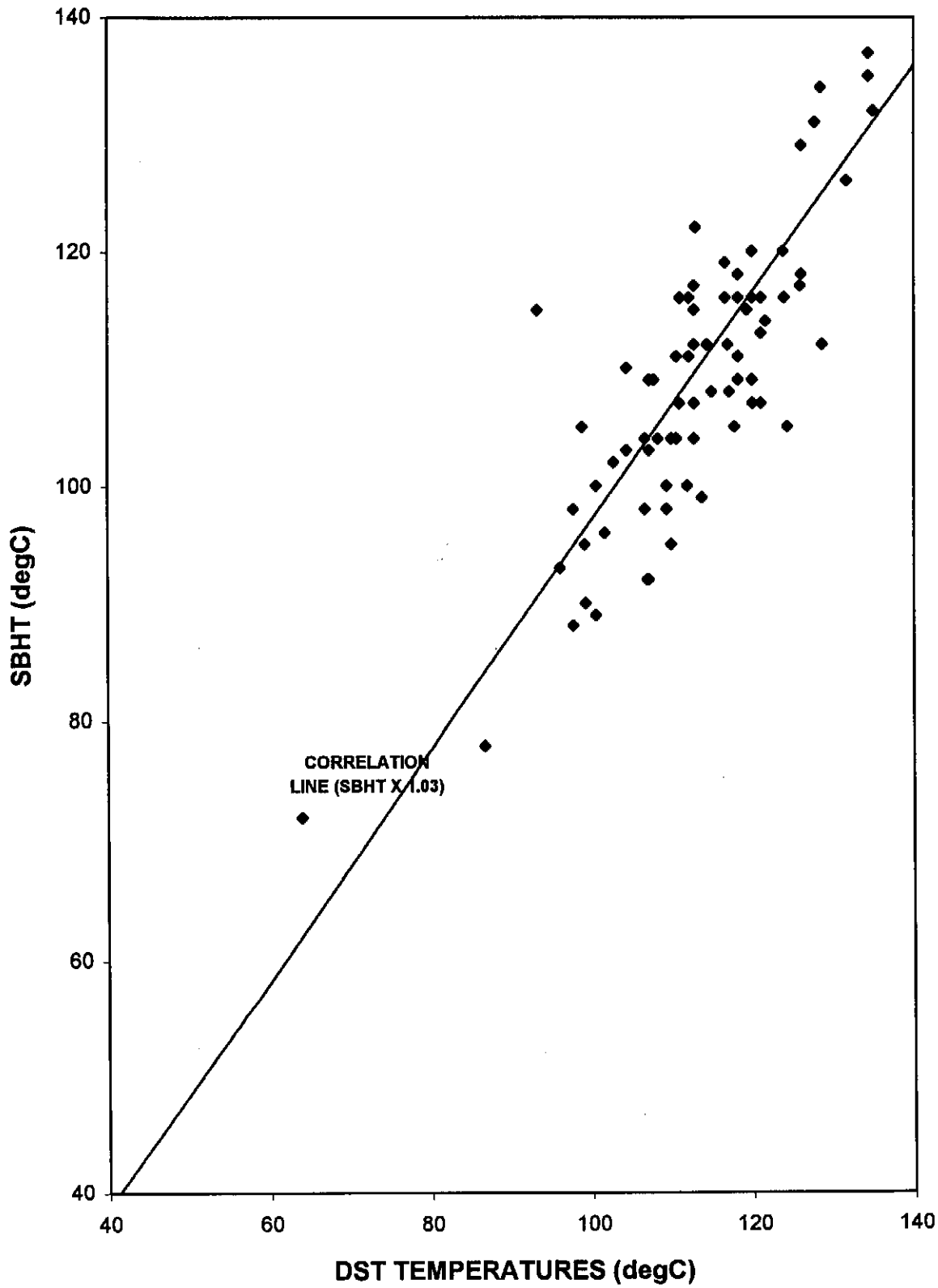

Figure 6.01: Crossplot of temperatures from DST locations with extrapolated corrected borehole temperatures (SBHT).

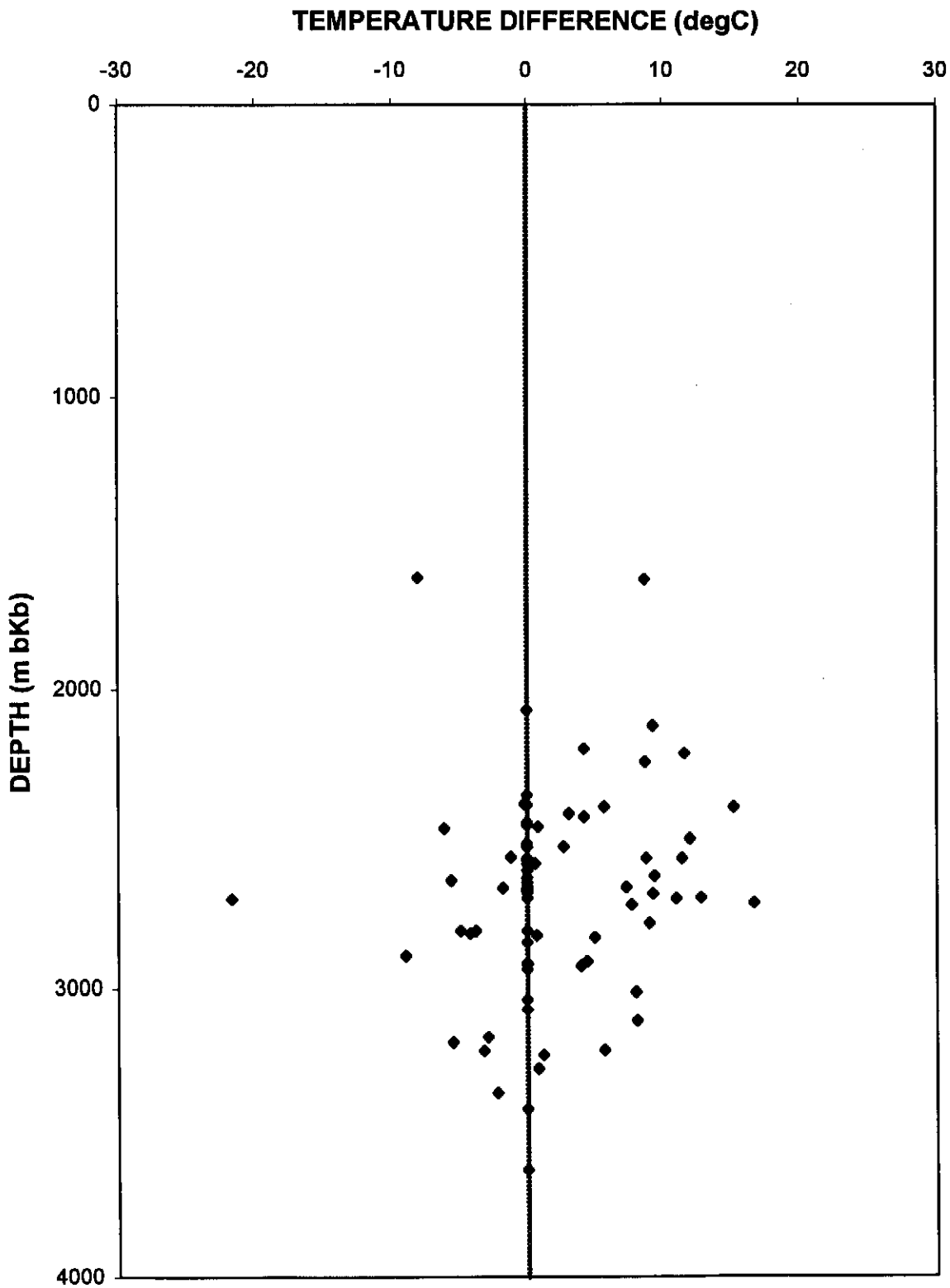

Figure 6.02: Differences between DST temperatures and extrapolated corrected borehole temperatures (SBHT).

BREDASDORP BASIN WELLS: GAS:OIL RATIO AND RELATED DATA											
WELL	DST	DEPTH	GOR	PVT GOR	DSTT	SBHT	SBHTGrad	SEQU.	API	Salinity	Pressure
83	3	2460	400	454	98.9	105	4.10	14A	43.0	13000	3580
83	2	2889	5750	5464	113.0	122	4.10	9A	41.1	24500	4169
83	1	3186	40000		128.5	134	4.10	9A	51.1	57000	7546
88	5	2495	700	503	112.0	100	3.81	14A	45.4	12000	3608
88	4	2827	7600	8750	117.0	112	3.81	9A	41.1	25000	3998
88	3	2909	29900	26873	119.4	115	3.81	9A	54.7	23000	4124
88	2	2924	25700	24393	120.0	116	3.81	9A	54.7	23000	4133
88	1	3213	29200	24667	131.7	126	3.81	9A	52.3	53000	7620
102	4	2241	580	576	106.7	98	4.19	pre1A	45.4	17000	3203
95	2	2693	9080		120.0	120	4.34	14A	57.2	14000	3884
103	2	2698	7270		93.3	115	4.14	14A	57.2	17000	3850
94	1	2779	1350		126.0	117	4.05	13B	46.3	20000	4353
96	1	3113	132000	130300	126.1	118	3.97	9A	44.7	68000	5139
114	1	3070	35000	33694	135.0	132	4.17	9A	49.9	8000	4683
93	2	2454	730	630	102.8	102	4.01	14A	43.2	12000	3549
93	1A	2804	6260		111.1	116	4.01	13A	57.2	17000	3960
93	1	2813	3100		112.8	117	4.01	13A	43.4	17000	3964
119	1	2804	1203		114.4	112	3.80	13A	39.4	13000	3958
108	2	2805	6720		112.2	116	3.97	9A	54.7	13000	4024
108	1	2820	7300	6211	116.7	116	3.97	9A	52.3	13000	4031
151	1c	2915	13733		118.3	118	3.88	9A	53.5	18000	4437
151	1b	2919	15588		118.3	118	3.88	9A	50.6	18000	4437
129	2	2845	14760	17726	118.3	116	3.90	12A	43.0	5800	4038
129	1	2935	31520		123.9	120	3.90	12A	46.5	8000	4145
109	1	2620	660		109.4	100	3.63	13A	38.0	19000	3781
124	3	2378	20600		97.8	98	3.21	8A	60.8	27000	3621
107	2	2522	47023	45482	106.7	104	3.21	pre1A	59.7	25000	3778
110	2	3010	14300		124.0	116	3.68	9A	51.6	21000	4275
110	1	3037	11840	8429	121.1	116	3.68	9A	50.4	16000	4315
126	1	2625	6390	6134	116.7	119	4.44	14A	56.2	10000	3799
120	1	2917	74067		121.1	113	3.75	12A	54.2	20000	4154
117	1	2383	450	411	106.7	104	4.20	14A	42.8	15000	3465
146	1	2390	438	376	101.7	96	3.82	14A	43.2	22000	3460
156	1	2522	930	1581	111.0	107	4.14	14A	44.3	8000	3643
166	1	2510	1299		113.8	99	3.78	14A	48.1	8000	3646
132	2	2655	7145	6497	104.4	103	3.64	13A	55.9	22000	3861
132	1	2694	980		110.0	104	3.64	13A	41.9	21000	3880
148	1	2674	5917		110.6	111	3.96	13A	57.2	20000	3870
167	1	2676	7031		115.0	108	3.89	14A	62.3	10000	3867
35	3	3416	3000	2851	134.4	135	3.96	pre1A	49.9	59000	6565
35	2B	3416	3200		134.4	137	3.42	pre1A	50.1	59000	6550
69	1	2389	31300		107.2	92	3.61	pre1A	56.4	58000	3469
46	2	2560	62200	53448	109.4	98	3.64	pre1A	49.9	34000	3694
48	1	2634	0.01	580	104.4	110	4.01	pre1A	31.1	22000	3755
54	1	2560	86200	89235	112.8	104	3.86	pre1A	50.4	0	3714
76	1	2556	68600	46139	107.8	109	4.03	pre1A	53.0	31000	3702
39	2	2212	65289	78486	100.6	89	3.81	pre1A	53.7	28000	3260
39	1	2567	55417	61820	110.6	104	3.81	pre1A	57.2	36000	3660

Table 6.02: Maximum gas:oil ratios (scft/bbl) recorded at the wellsite during flow periods when samples were collected for PVT analyses, actual gas:oil ratios recorded at the time of DST sampling, API gravity of the flowed liquids, salinity (from SP log data) and formation temperatures at the test interval.

BREDASDORP BASIN WELLS: GAS:OIL RATIO AND RELATED DATA											
WELL	DST	DEPTH	GOR	PVT GOR	DSTT	SBHT	SBHTGrad	SEQU.	API	Salinity	Pressure
59	1	2195	400	368	99.2	95	4.10	pre1A	35.4	31000	3169
65	2	3168	142000		126.1	129	3.93	pre1A	43.2	69000	6400
65	1	3215	294000		127.8	131	3.71	pre1A	45.4	81000	5606
1	3	2070	133000		97.8	88.1	4.04	9A	71.8	23000	3090
18	4	2601	45200	40220	124.4	105	4.29	pre1A	55.9	42000	3900
18	3	2641	36700	42789	121.1	107	4.09	pre1A	55.2	42000	3939
18	2	2664	76000		120.1	107	4.09	pre1A	53.7	42000	3900
18	1	2696	53800	46584	120.0	109	3.86	pre1A	57.2	41000	3940
21	2	2559	58000		112.8	107	4.08	pre1A	82.9	26000	3827
21	1	2579	42000		117.2	108	3.95	pre1A	50.6	26000	3668
19	2	2680	34400	31665	118.3	109	3.79	pre1A	54.9	26000	3885
20	3	2578	63200		100.6	100	3.81	5A-1A	49.4	46000	0
44	1	2711	26190	19368	128.7	112	3.96	pre1A	52.5	50000	3848
55	2	2658	51000	38766	118.3	111	4.01	pre1A	49.2	0	3877
61	3	2123	17100	12443	99.3	90	4.01	9A	65.0	32000	3084
61	2	2717	57600	44919	121.7	114	4.01	pre1A	51.6	28000	3960
70	2	2422	30800	28897	107.2	103	4.07	pre1A	57.4	34000	3460
70	1	2440	0.01		108.3	104	4.07	pre1A	34.5	34000	3498
162	2	2349	32321		107.0	92	3.63	pre1A	57.2	30000	3355
162	1	2450	0.01	0.433	110.0	95	3.63	pre1A		37000	3451
31	1	2692	23000	21227	117.8	105	3.73	pre1A	54.7	36000	3898
63	1	2659	48900	36478	107.2	109	3.89	pre1A	53.7	56000	3805
128	1	3627	376270		154.3	149	4.00	pre1A	46.3	18000	7712
Flow rate data taken from wellsite records. Depth is of top sand in m bKb.											
Salinity data from report by Davies, 1995. (NB: no data for wells drilled with oil-based muds).											
Calculated salinity at well 94 was <<29000 and has been assumed to be closer to 20000.											
Calculated salinity at well 167 was <<20000 and is assumed to be probably ~10000 ppm.											
Pressure = psia from RFT or DST. Horizons from SOEKOR ORACLE database.											
SBHT Gradient from wellsite calculations, DST Temp and pressure from petroleum engineering data.											
Total number of DST's = 71, total number of wells = 167.											

Table 6.02 (continued)

Flow charts for the pyrolysis/calcimetry and optical analyses and processing are given in Figs. 6.03 and 6.04.

6.2.1. Pyrolysis and calcimetry analyses

Pyrolysis and calcimetry analyses comprise total organic carbon pyrolysis (TOC), calcimetry (CALC) and Rock Eval pyrolysis (RE). These are usually carried out on most wellsite processed cuttings samples, sidewall core and selected core samples (Venter at al., 1994a and b). Each analysis method is briefly described below:

(i) Total Organic Carbon

A small amount of each sample (250-500 mg) is decarbonated by three reactions with 5ml each of warm (40°C) 1N hydrochloric acid in an inert filtering crucible. The crucibles are rinsed five times with de-ionised water to remove chloride salts and dried at 35°C. The dried crucibles with the decarbonated samples are pyrolysed in an oxygen-rich atmosphere at ~1200°C for 1 minute in a LECO WR12 carbon analyser. This converts all the remaining carbon to carbon dioxide. Assuming that all the carbonates are removed by this process (Davies, 1991; Van der Spuy, 1994a) the resulting quantity of CO_2 is proportional to the original TOC. The result is automatically reported as mass percent carbon (Jarvie, 1991).

(ii) Calcimetry

A small amount of the sample (125-250 mg) is treated with warm (40°C), dilute 1N hydrochloric acid in a sealed chamber to which a pressure transducer has been attached (Venter, 1992). Carbon dioxide generated during the 8 minute reaction period creates a pressure build-up proportional to the amount of carbonate in the sample. Calcite reacts faster than dolomite and the pressure build-up from calcite is therefore faster. Hence the graphical response for calcite produces a steeper slope on the real-time graphical output than does dolomite (Davies, 1991; Venter et al., 1994a). This method of analysis approximates the proportions of calcite and dolomite and cannot distinguish between other members of the carbonate series. However, it does provide repeatable data which have been used in several cases for lithological correlation, (Davies, 1993a and 1993c; Littke et al., 1991).

(iii) Rock-Eval Pyrolysis

Small amounts (50-80mg) of each sample are progressively heated under an inert (helium) atmosphere (250-550°C at 25°C/min.). The products of this pyrolysis are split into two streams. One stream is passed to a flame ionisation detector to quantitatively record the hydrocarbons output and the other to a thermal conductivity detector to record the oxycarbons. During the analysis, any hydrocarbons already present in the sample are volatilized at moderate temperatures (<300°C) and recorded as S1. Further

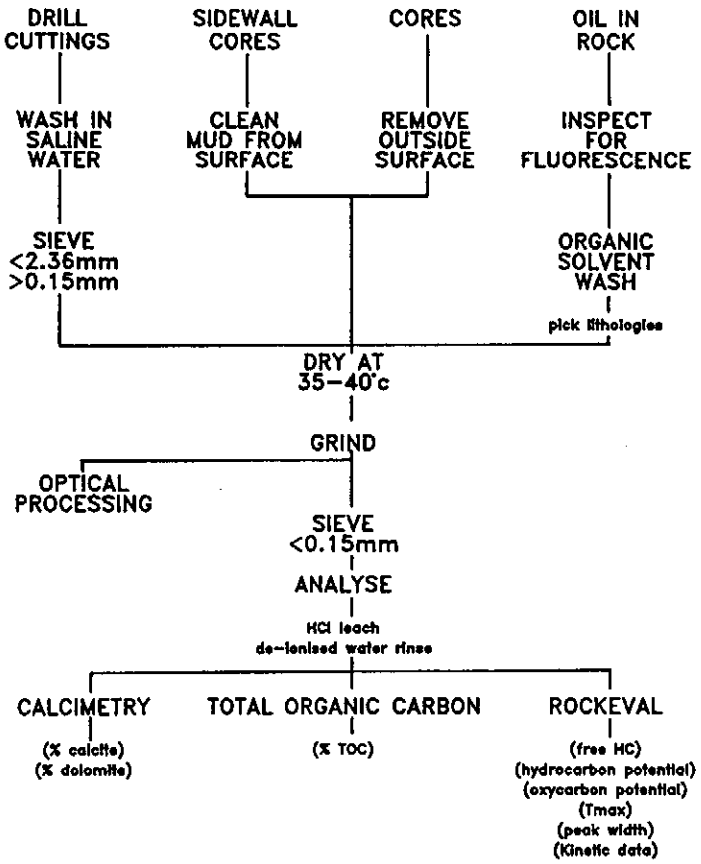

Figure 6.03: Flow chart of the processing steps necessary for the preparation of samples for routine pyrolysis and wet chemical analyses.

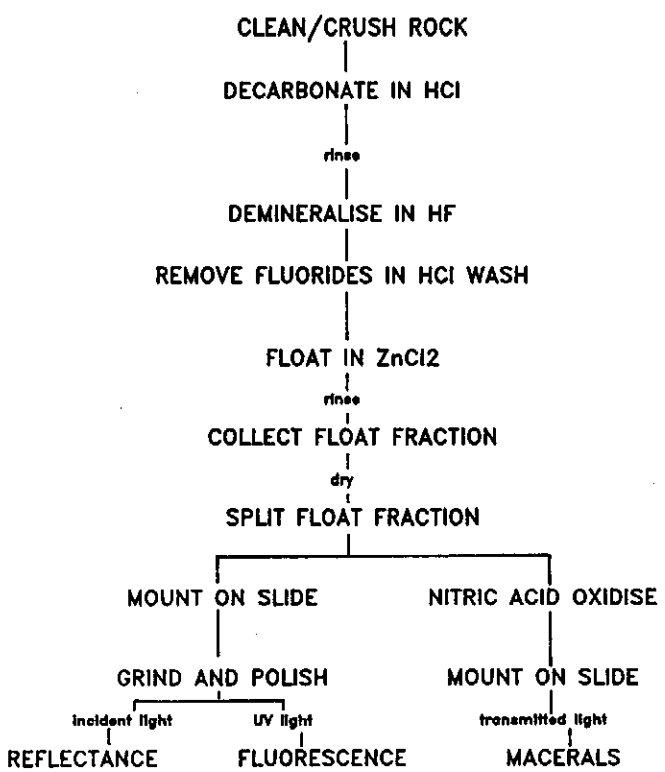

Figure 6.04: Flow chart of the processing techniques used for the separation of kerogen from rock samples and the analytical steps for transmitted, reflected and incident light analysis.

heating pyrolyzes the kerogen so that it generates hydrocarbons (S2) and oxygen containing volatiles (S3) such as carbon dioxide and water. The oxycarbons are only collected during pyrolysis at temperatures less than 390°C to ensure that no CO_2 from carbonate dissociation is included. Espitalié et al. (1985) show that dissociation of carbonates starts at temperatures higher than 400°C.

The temperature corresponding to the maximum of the hydrocarbon generation (Tmax) is accurate to ~2°C. The size of the S2 peak records the remaining potential of the organic material to generate hydrocarbons, whereas the S3 peak measures the remaining potential to generate oxycarbons (Tissot and Welte, 1984, p. 509-513). The production index (or transformation ratio) maturation parameter (S1/(S1+S2)) is commonly calculated from the data. The parameter is preferred by some authors because it is the only easily obtained parameter which is derived directly from the generation of hydrocarbons (Miles, 1989), all other bulk parameters being related to hydrocarbon generation by inference only.

Other ratios derived from Rock-Eval and TOC data are the hydrogen and oxygen indices, HI and OI respectively (HI=100*S2/TOC, OI=100*S3/TOC). They are synonymous with the $^{H}/_{C}$ and $^{O}/_{C}$ ratios used by Van Krevelen (1984) to characterise source potential (Fig. 6.05a). These indices are essentially interchangeable with the atomic ratios (Fig. 6.05b). Clementz et al. (1979) showed that the ratio S2/S3 could also describe the type of hydrocarbons which could be generated by the organic material in the source rock (Fig. 6.06)

6.2.2. Optical studies

These are usually carried out on lightly crushed rock chips selected from sidewall cores or cores after extensive processing to concentrate the kerogen. However, pieces of TOC-rich shale or lignites extracted from cuttings or core samples, can be mounted on slides and polished without further processing (Van der Spuy, 1994b).

(i) Vitrinite Reflectance

Vitrinite reflectance studies are made on all concentrates collected after hydrochloric and hydrofluoric acid digestion and dense liquid separation using zinc chloride (Fig. 6.04). This organic material is called kerogen. It is split into two fractions for vitrinite and palynological studies, the former being oxidised to remove fluorides before being mixed with resin, made into a plug and polished (McLachlan and Fülop, 1975).

The small size of the disaggregated fragments of kerogen requires magnification of several hundred times. The reflectance of grains of vitrinite are measured relative to a standard beam of white light, the reflectivity of which has been shown to be related to

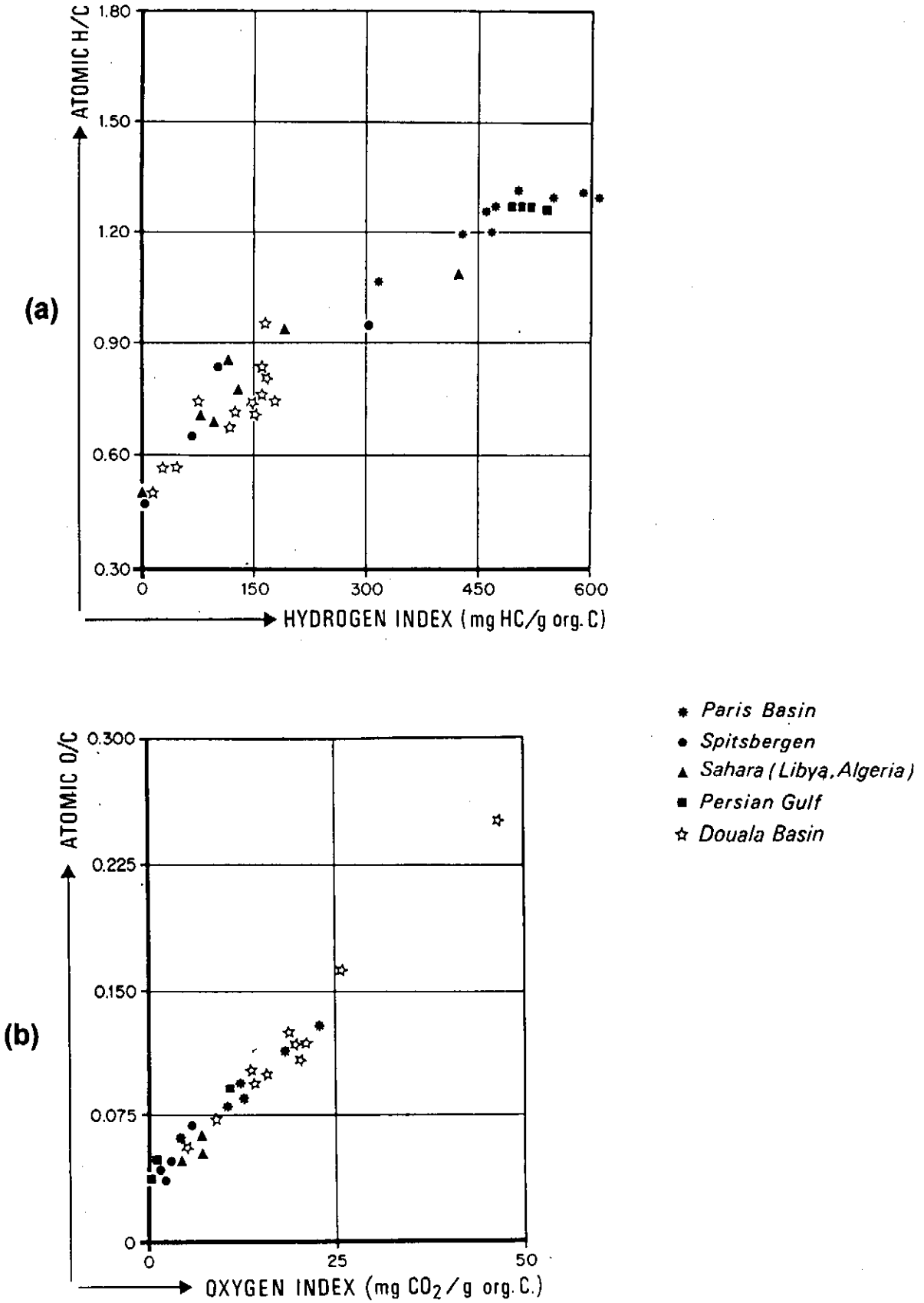

Figure 6.05: (a) Crossplot of the Hydrogen Index (from Rock-Eval analyses) vs atomic H/C ratios and (b) Oxygen Index vs atomic O/C ratios for samples from different basins (from Espitalié et al., 1977).

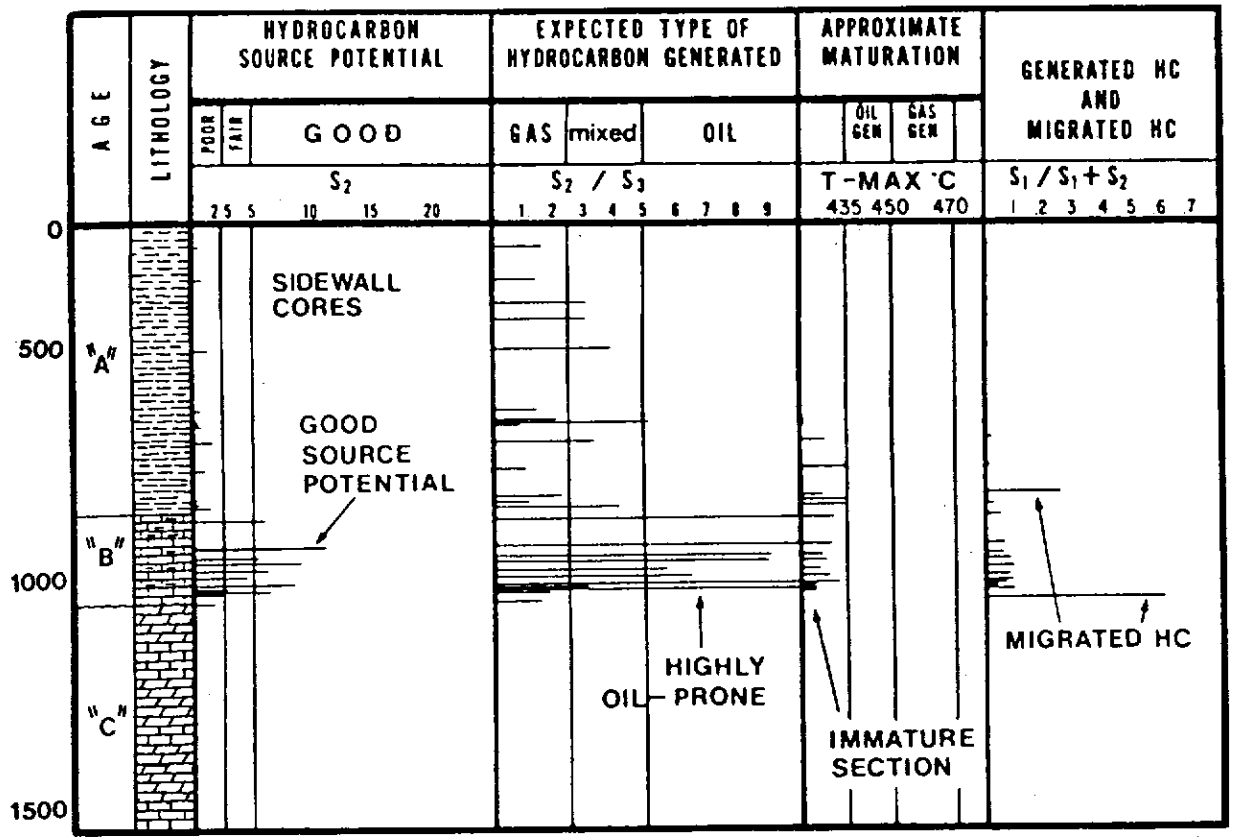

Figure 6.06: Geochemical log (from Clementz et al., 1979) showing *inter alia* the estimation of generated hydrocarbon type from the S2/S3 ratio.

the maximum maturity level achieved (Bostick, 1975; Pocock, 1982). An attempt is made to record 50 reflectance measurements from each sample for statistically correct evaluation (Robert, 1988, p102). However, due to the dispersed nature and very small grain size of the organic material after processing, it is not always possible to achieve this maximum. The final quoted value is the mean of measurements of first order vitrinite, all readings from caved or reworked vitrinite having been excluded (Senftle and Landis, 1991; Van der Spuy, 1994c). This value is plotted either on a logarithmic scale against depth or on a normal scale against other major maturation parameters. Values range from R_O~0.25% at surface (Katz et al., 1988) to R_O>1.5% at depth. Few wells are drilled to intersect rocks more mature than this, except where igneous bodies approach the well or where basement intersection is confirmed. Where basement rocks are intersected, e.g. Devonian Bokkeveld slates, reflectances can be considerably higher (R_O>4%). Oil window maturation ranges from R_O 0.5-1.3% although the main expulsion window is characterised by values of R_O 0.75-1.15% (Table 4.05).

(ii) Thermal Alteration Index (TAI)

The second fraction of the kerogen is mixed with resin and mounted in a random orientation strew slide and ground thin to permit study of the kerogen in transmitted light. This method is used to determine the type of organic matter present in the sample as well as colour changes of some organic material with maturity. For example, *classopolis* spores change colour with increasing maturity from pale yellow to black through the oil and gas windows (Staplin, 1982b; Benson et al., 1990).

(iii) Maceral Proportion Count

Maceral studies are usually carried out on the same strew slides used for TAI (Benson, 1990). The types of organic material commonly found in source rocks (e.g. inertinite, vitrinite, exinite, sporinite and amorphous material) are detailed in Tissot and Welte (1984) and Falcon and Snyman (1986). The amorphous proportion is often distinguished as either fluorescing or non-fluorescing as these have been shown (where R_O<~1.2%) to represent high and low hydrogen kerogen respectively. Since the hydrogen content of kerogen is an indicator of oil or gas potential, the distinction is important. In these samples, the amorphous material is considered to be of the high-hydrogen type from its fluorescence response. In summarising the results of several authors, Tissot and Welte (1984) showed that, in general, in clastic sediments where >60% of the kerogen is amorphous (high-hydrogen) the expelled product is largely oil. Where the amorphous percentage ranges from 30-60%, the product is wet gas with light oil and where there is <30% amorphous material, the product is essentially dry gas. These distinctions are also affected by the proportions of other macerals and the lithology and these are taken into account when determining the source potential.

(iv) Sporinite Fluorescence

Characteristic spores, in the southern hemisphere usually *Classopolis sp*, fluoresce at different wavelengths when buried through the oil window (Table 4.03) and the sequence of colour change can be equated with other maturity parameters (Robert, 1988, p.86). In addition, all fluorescence is lost by a maturity level of R_O~1.2%. All fluorescence was observed in short wavelength ultra-violet (UV) light (490 nm wavelength). Not all kerogen is able to fluoresce naturally (some fluorescence is due to later oil impregnation) so that precautions need to be taken when considering which data are used to validate the description of the source rock kerogen.

6.2.3. Fluid sample analysis

Fluid sample analyses entailed two analysis routes, one for water samples and one for hydrocarbon samples.

(i) Water tests

Where DST's or RFT's produce water which may represent formation water, samples are usually analysed by a dedicated laboratory. Analyses are carried out to determine the resistivity, specific gravity, pH, total dissolved solids, and concentrations of major cations and anions. From these data, it is possible to characterise the water and indicate its source. The data are also useful in confirmation of log calculated formation water salinity and flow unit connectivity. Available data are shown in Table 6.03.

Where the water is not produced to surface during the test, samples are derived from reverse circulation after the test. The doubt about which sample corresponds to true formation water is often resolved by analysing a sequence of samples from throughout the reverse circulation. Such sampling analyses have been carried out and data from two such test series are reported here (Figs. 6.07 and 6.08). Results of ionic concentration analyses are usually reported in mg/litre. These have to be converted to milli/equivalents in order to take into account the mass and valence of each ion and the cation/anion combination ratios. The cations for which analyses are usually carried out are Na, Ca, K, Mg, Fe, Ba and Sr and the anions are Cl, SO_4, CO_3/HCO_3 and F.

Of the 107 drill stem tests carried out in the Bredasdorp Basin, 33 produced large enough volumes of water to be analysed. In addition, two extended well tests (EWT) and 9 RFT samples were analysed. Data gained from these analyses are presented in Table 6.03 and discussed where relevant throughout the following chapters.

FORMATION WATER ANALYSES

(Analyses carried out by A L Abbott Ltd., Anglovaal, McLachlan and Lazar, J Muller and Serck Baker laboratories)

WELL	DST	DEPTH RANGE	SP LOG	MEASURED		COMMENT		MATCH	IONIC	ANALYST	DATE
		(mbKb)		NaCl (meq.)	TDS	Notes	Samples		BALANCE		
88	3	2912-2916m	<29000	1829	3127	water of condensation	3	N	Y	J. Muller	25-07-1990
103	2	2695-2718m	17000	5793	13134.24		2	?	Y	J. Muller	25-07-1990
103	1	3075-3109m	16000	7245	10021.19		4	?	Y	J. Muller	25-07-1990
114	1	3068-3085m	8000	10998	14298.53		5	Y	Y	J. Muller	25-07-1990
93	EWT	2454-2462m	10000	13099	18360		5	Y	Y	J. Muller	25-07-1990
93	EWT	2454-2463m	10000	10720	14174		10	Y?	N	A.L. Abbott	30-03-1992
119	1	2804-2816m	13000	4778	8241.97	water cushion?	9	N	Y	J. Muller	09-01-1991
107	1	2586-2590m	20000	17294	23158.2		9	Y	Y	J. Muller	25-07-1990
110	1B	3037-3051m	16000	6800	8242.23	water cushion?	1	?	N	A.L. Abbott	30-03-1992
113	1	2906-2914m	5000	4596	12092.6		7	Y	Y	J. Muller	25-07-1990
117	RFT1	2411.8	15000	17159	37391.7		1	Y	N	A.L. Abbott	30-03-1992
164	DST1	2414-45m	11500	12298	13369	chambers above sands	2	Y	Y	Serck Baker	1995
164	DST1	2440	11500	17921	21030	?filtrate	2	N	Y	J. Muller	17-05-1995
166	RFT3	2508m	<14000	30367	36756	filtrate	4	N	~	A.L.Abbott	21-11-1995
166	RFT2	2518m	9500	27968	35512	filtrate	1+1	N	~	A.L.Abbott	21-11-1995
166	RFT1	2558.6m	10000	30782	37580	filtrate	2	N	~	A.L.Abbott	21-11-1995
84	1	2753-2771m	17000	16523	29073.13		1	Y	N	A.L. Abbott	30-03-1992
25	1	2205-2217m	33000	24557	289200	suspect SP log	2	?	Y	McLachlan and Lazar	26-02-1982
27	2B	2314-2335m	12000	70416	77385	contaminated by filtrate	4	N	Y	McLachlan and Lazar	23-03-1982
27	1	3152-3164m	62000	28471	40780		1	N	Y	McLachlan and Lazar	08-02-1982
46	2	2540-2560m	34000	2669	6310		2	N	Y	McLachlan and Lazar	23-03-1984
46	1	2635-2655m	18000	17687	18400		66	Y	Y	McLachlan and Lazar	23-03-1984
46	RFT1	2672.4	18000	28480	32900		1	N	Y	McLachlan and Lazar	23-03-1984
48	1	2635-2657m	22000	22243	22700		2	Y	Y	McLachlan and Lazar	02-05-1984
48	RFT2	2658.9	22000	29507	31700		1	N	Y	McLachlan and Lazar	02-05-1984
48	RFT1	2668.9	20000	28925	32400		1	N	Y	McLachlan and Lazar	02-05-1984
54	1	2560-2618m	1	491	956	oil-based mud	2	obm	Y	McLachlan and Lazar	02-10-1984
39	2	2209-2229m	25000	1648	2390	water of condensation?	1	N	Y	McLachlan and Lazar	25-08-1983
39	RFT	2255.4	28000	25947	30390		1	Y	Y	McLachlan and Lazar	25-08-1983

Table 6.03: Results of analyses of all water samples collected during DST's, RFT's and EWT's in the Bredasdorp Basin. Comments on the samples and the results and whether these measured salinities match those calculated from the SP log are included. There are no consistent differences between the results from different analysts except for the small ionic imbalance in examples from the same analyst.

WELL	DST	DEPTH RANGE	SP LOG	MEASURED		COMMENT		MATCH	IONIC	ANALYST	DATE
39	RFT	2338.4	28000	25222	30450		1	Y	Y	McLachlan and Lazar	25-08-1983
39	1	2451-2567m	36000	685	1180	water of condensation?	1	N	Y	McLachlan and Lazar	25-08-1983
18	4	2602-2635m	42000	2747	5477	water of condensation?	1	N	Y	Anglo-Vaal	24-02-1981
23	2	2365-2380m	23000	28741	38300		9	Y	Y	McLachlan and Lazar	15-12-1981
19	1	2770-2775m	26000	23408	30328		2	Y	Y	Anglo-Vaal	30-07-1981
20	3	2570-2579m	46000	17413	21850		1	N	Y	McLachlan and Lazar	08-01-1982
20	2	2692-2699m	<<40000	5239	7710		1	?	Y	McLachlan and Lazar	08-01-1982
20	1	2735-2740m	48000	63064	77900		2	?	Y	McLachlan and Lazar	08-01-1982
55	2	2659-2680m	1	428	550	oil-based mud	1	obm	Y	McLachlan and Lazar	25-02-1985
61	3	2123-2130m	32000	9561	11412	water cushion?	1	N	Y	McLachlan and Lazar	12-09-1985
61	2	2717-2770m	28000	4121	5028	water cushion?	2	N	Y	McLachlan and Lazar	12-09-1985
70	1	2440-2446m	34000	23737	27107		25	?	Y	McLachlan and Lazar	16-04-1986
31	1	2691-2753m	36000	15835	18576.5		1	N	Y	McLachlan and Lazar	25-08-1983
63	1	2660-2691m	56000	10218	12688.3		1	N	Y	McLachlan and Lazar	18-11-1985
10	1	2195-2654m	20000	17144	33013.1		1	Y	N?	Anglo-Vaal	29-03-1979

meq/l = (mg/l x valence)/atomic mass

Element	Valence	Atomic mass
Na	1	22.99
K	1	39.102
Ba	2	137.34
Sr	2	87.62
Ca	2	40.08
Mg	2	24.31
Fe	2	55.85
Cl	1	35.453
HCO3	1	61.017
CO3	2	60.009
SO4	2	96.062

42 zones tested: Y=15, N=19, ?=7 and OBM=6.

WELL 117 RFT chamber 1: Rmf=0.194 ohmm@73.4degF = 33000ppm.

WELL 117 RFT chamber 2: Rmf=0.211 ohmm@68.0degF = 32000ppm.

Table 6.03 (continued)

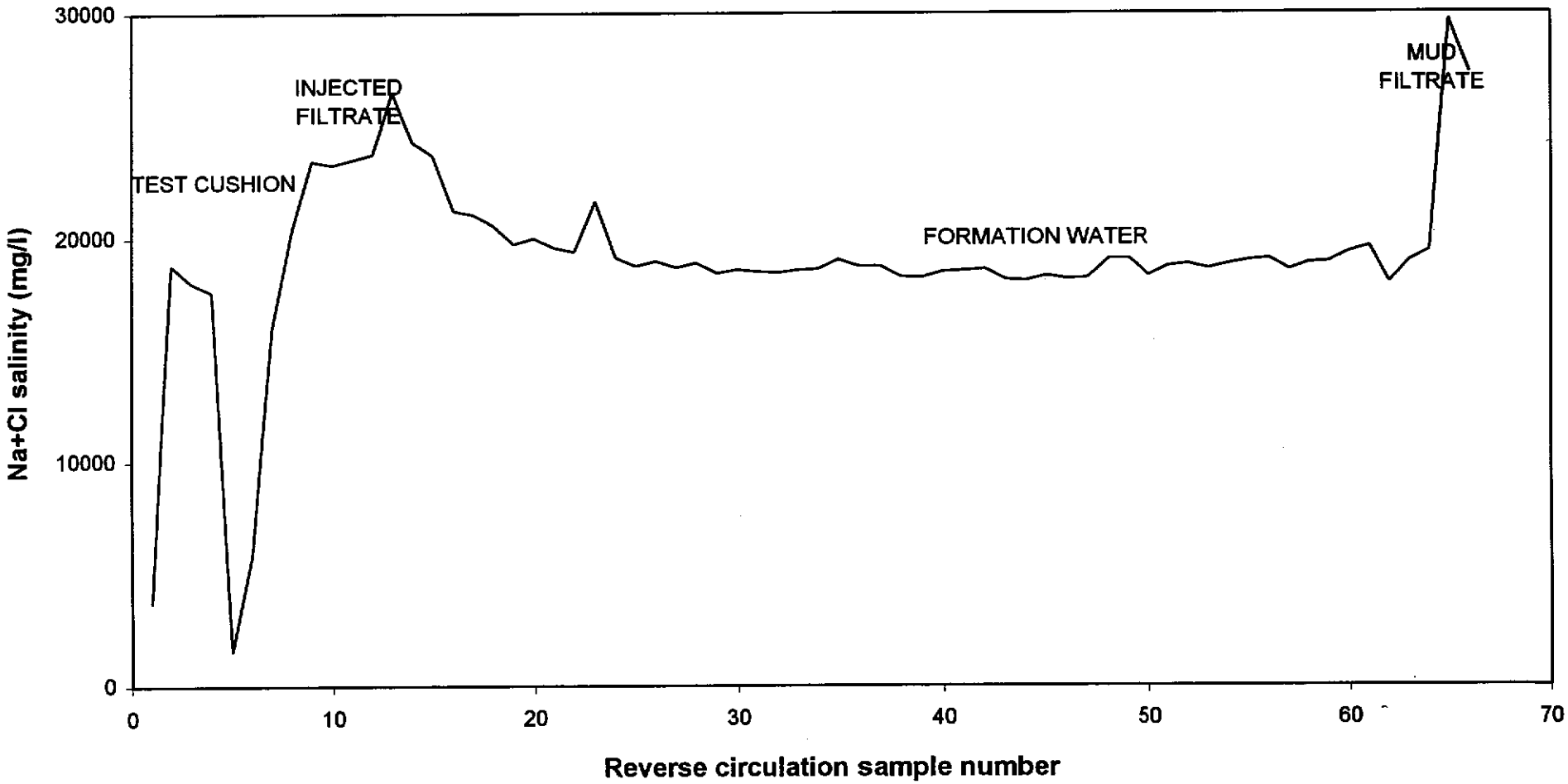

Figure 6.07: Plot of Na and Cl salinity for reverse circulation samples collected after DST1 in well 46 showing the four different salinity fluids represented in the test sample. Salinities gradually decrease after initial flow of filtrate to the probable formation fluid.

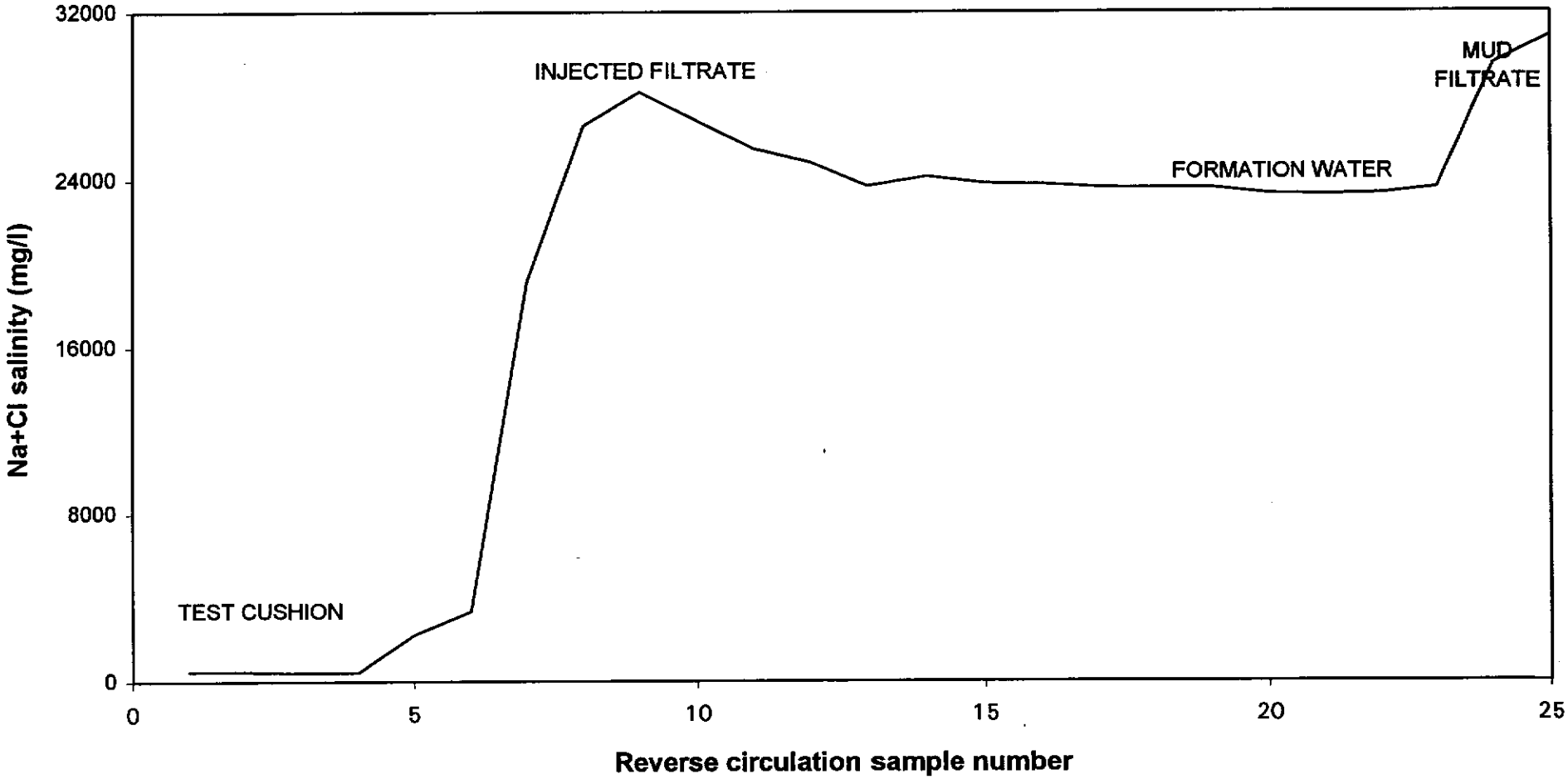

Figure 6.08: Plot of Na and Cl salinity for reverse circulation samples collected after DST1 in well 70 showing the four different salinity fluids represented in the test sample. Salinities decrease systematically after initial flow of filtrate to the probable formation water salinity before increasing again as mud is circulated out.

(ii) PVT analyses

From the 107 drill stem tests carried out in the Bredasdorp Basin, some 85 produced fluids in quantity. Of these, a total of 59 were subjected to hydrocarbon recombination analyses at reservoir conditions (PVT) although some were only partly analysed. In other cases, analyses were not begun because the flow rates were deemed uneconomic. The result is that a total of 55 sets of DST samples were subjected to PVT analyses (Tables 6.04 and 6.05a).

Gas and liquid samples are recombined in the same proportions in which they were produced at the separator and at the known reservoir pressure and temperature. Analysis of these recombined samples provides a view of the reservoir fill at the time of the DST. Several aliquots of the recombined fluid are sampled at reduced pressures and temperatures and analysed for their bulk hydrocarbon composition and properties to simulate the effects on the hydrocarbon composition of decreasing reservoir pressure and temperature during production. Table 6.04 provides a listing showing the number of samples for which PVT recombination analyses were carried out and Table 6.05 gives the relevant gas and light oil data for each coded well.

In addition, gas analyses were also carried out on non-recombined separator samples at the SABS (Pretoria). These samples (Table 6.05b) are usually of lower quality than those used for PVT analysis because they were unsuitable for PVT analysis. For example they were not so rigorously collected and stored, none of them are downhole samples and cylinders were sampled at ambient conditions. Nevertheless they constitute a large dataset and are used in the regional interpretations as they generally represent gaps in the sample database.

6.3. NON-ROUTINE OFFSITE ANALYSES

Analyses in this group comprise the following:

1. kerogen kinetic analyses
2. elemental analyses
3. stable isotope analyses
4. wet chemical processing analyses

6.3.1. Kerogen kinetic analyses

Analyses of source rock kerogen kinetics are carried out with a Rock-Eval II using a minimum of 3 different heating rates ranging over at least one order of magnitude. The rate and amount of heat input to produce the pyrolysis curves for each of the analyses are used to assign a single curve-fitting algorithm to all three curves. The algorithm describes the break-down of the kerogen in terms of activation energies and frequency

SAMPLE LISTING																		
	RE/LECO/CALC		MACERAL		VITRINITE		PVT		GAS (SABS)		FINGERPRINT GC		SALINITY		FISSION TRACK		STABLE ISOTOPE	
SAMPLES					REFLECTANCE													
	samples	wells	samples	wells	samples	wells	samples	wells	samples	wells	samples	wells	samples	wells	samples	wells	samples	wells
MUD	551	41	-	-	-	-	-	-	-	-	-	-	-	-	-	-	-	-
CUTTINGS	18652	139	630	23	948	31	-		-	-	-	-	-	-	7	1	-	-
SWC	2883	99	1666	55	2037	67	-	-	-	-	-	-	-	-	-	-	-	-
CORE	1307	73	160	22	463	37	-	-	-	-	-	-	-	-	1	1	-	-
TOTAL	**22842**	**147**	**2456**	**72**	**3533**	**90**	-	-	-	-	-	-	-	-	-	-	-	-
SURFACE GAS	-	-	-	-	-	-	-	-	39	24	-	-	-	-	-	-	-	-
SURFACE OIL	-	-	-	-	-	-	-	-	-	-	79	47	-	-	-	-	-	-
SURFACE WATER	-	-	-	-	-	-	-	-	-	-	-	-	42	27	-	-	-	-
DOWNHOLE FLUIDS	-	-	-	-	-	-	55	42	-	-	-	-	-	-	-	-	-	-
SP LOG	-	-	-	-	-	-	-	-	-	-	-	-	900	154	-	-	-	-
BITUMEN EXTRACT	-	-	-	-	-	-	-	-	-	-	-	-	-	-	-	-	20	14
PVT: 1 repeat analysis. Fingerprint GC: 7 repeat analyses on different columns.																		
SABS gas: no repeat analyses but 26 samples match PVT analyses. Water analyses: 1 repeat interval.																		
Carbon isotope: 2 repeat analyses, 1 shale sample only. Fission track: 8 samples but only 2 found adequate amounts of apatite.																		

Table 6.04: List of the number of each type of analyses (other than GC and GC-MS of bitumen and oil fractions) carried out in the Bredasdorp Basin.

DST DATA									
SAMPLE			DEPTH (mbKb)		WELLHEAD		TEMPS		Remarks
WELL	DST	Sequ.	TOP	BASE	psi	GLR	DST	SBHT	(cylinder, ratios)
83	3	14A	2461	2470	1118	454	98.9	101.0	1116-583
83	2	10A	2864	2889	755	5464	113.0	112.0	22400/125
88	5	14A	2495	2507	1262	503	112.0	100.0	20524-21
88	4	12A	2827	2839	2418	8750	117.0	117.0	A-8504
88	3	10A	2909	2916	1835	26873	119.4	120.0	22226/78
88	2	10A	2924	2929	1965	24393	120.0	121.0	20524-51
88	1	5A	3213	3243	1596	24667	131.7	131.0	20524/57
102	4	pre1A	2237	2241	996	576	106.7	95.0	8008/100
96	1	8A	3117	3131	633	130300	126.1	126.0	9214/385
114	1	9A	3068	3085	2346	33694	135.0	132.0	8008N329
93	2	14A	2454	2463	730	630	102.8	107.0	16251-28
93	1	13A	2805	2817	2000	6256	112.8	112.0	9214/319 (GLR)
119	1	13A	2804	2816	1375	1203	114.4	112.0	8008N10 (GLR)
108	1	10A	2820	2829	1625	6211	116.7	117.0	8488N429
151	1	10A	2915	2927	537	12500	118.3	113.0	8554-184 (GLR)
129	2	12A	2845	2865	2204	17726	118.3	116.0	1116-449
109	1	13A	2620	2630	1060	660	109.4	100.0	1116/314 (WHFP,GLR)
107	2	pre1A	2522	2565	2758	45482	106.7	104.0	1116/449
110	1	10A	3037	3050	1335	8429	121.1	120.0	2226/78
126	1	14A	2624	2643	2043	6134	116.7	112.0	1116-256
117	1	14A	2382	2399	1098	411	106.7	95.0	73FA230-27 (GLR)
146	1	14A	2371	2400	1005	376	101.7	96.0	108
156	1	14A	2512	2522	793	1581	111.0	100.0	8008/253 (WHFP,GLR)
132	2	13A	2654	2662	2500	6497	104.4	103.0	9214-323
132	1	13A	2696	2706	3828	980	110.0	104.0	8008N13 (GLR)
148	1	13A	2674	2684	2431	6309	110.6	104.0	((SLS03) (WHFP,GLR)
35	3	pre1A	3309	3416	2128	2851	134.4	130.0	16251/28 (Schlumberger)
35	3	pre1A	3354	3416	2128	2851	134.4	130.0	22226/78 (Expro)Gas at 2455psi
35	2B	pre1A	3397	3416	2555	4300	134.4	132.0	STX-7-11 (WHFP,GLR)(Expro)as at 2226psi
69	1	pre1A	2388	2436	1767	31348	107.2	92.0	(WHFP,GLR)
46	2	pre1A	2540	2560	2520	53448	109.4	98.0	

Table 6.05a: List of available PVT samples from DST's, analysed from the Bredasdorp Basin.

SAMPLE			DEPTH (mbKb)		WELLHEAD		TEMPS		Remarks
WELL	DST	Sequ.	TOP	BASE	psi	GLR	DST	SBHT	(cylinder, ratios)
48	1	pre1A	2625	2634	12	580	104.4	110.0	
54	1	pre1A	2558	2617	2195	89235	112.8	104.0	20524/6
76	1	pre1A	2556	2610	2330	46129	107.8	109.0	8008N328
39	2	pre1A	2209	2229	1341	78486	100.6	89.0	2811/12
39	1	pre1A	2451	2567	2679	61820	110.6	99.0	2641/13
59	1	pre1A	2195	2212	489	368	99.2	93.0	
18	4	pre1A	2602	2635	1185	40220	124.4	105.0	20524/63
18	3	pre1A	2641	2673	1355	42789	121.1	107.0	A 4403
18	1	pre1A	2696	2703	830	46584	120.0	109.0	2641/13
21	2	pre1A	2552	2559	2880	47684	112.8	107.0	M 810878.(GLR) Bottom-hole spls.
19	2	pre1A	2680	2709	724	31665	118.3	109.0	20524/61
44	1	pre1A	2715	2750	3000	19368	128.7	112.0	16251/30
55	2	pre1A	2659	2680	2730	38766	118.3	111.0	20524/61
61	3	9A	2113	2128	1685	12443	99.3	90.0	20524/1
61	2	pre1A	2718	2770	2054	44919	121.7	114.0	2811/30
70	2	pre1A	2411	2428	1654	28897	107.2	103.0	9214/208
31	1	pre1A	2691	2753	2704	21227	117.8	105.0	2401/11
63	1	pre1A	2659	2691	2470	36478	107.2	109.0	2641/13
131	1	pre1A	2669	2752	2634	17207	120.0	107.0	814272
135	1	pre1A	2629	2734	2612	19821	126.3	107.0	814282
141	1	pre1A	2624	2734	1475	24477	125.1	107.0	814273
145	1	pre1A	2626	2678		21998	126.3	107.0	814283
147	1	pre1A	2728	2765		14624	121.7	107.0	814287
128	1	pre1A	3627	3661	3935	376271	154.3	149.0	2657-9 (GLR)

Table 6.05a (continued)

SABS GAS RESULTS							
ENVIRONMENTAL DATA							
WELL	DST	HOR.	DEPTH	DEPTH	PSIA	SBHT	REMARKS
			top mbkb	bot.mbkb		degC	
83	3	14A	2461	2470	3580	105.0	Final flow
83	2	10A	2864	2894	4169	112.0	Final flow
83	1	5A	3160	3254	7546	132.0	Choke 0.75"
88	5	14A	2495	2507	3535	100.0	Final flow
88	4	12A	2827	2839	3990	112.0	Flow 3
88	3	10A	2909	2916	4127	115.0	Final flow
88	2	10A	2924	2929	4133	116.0	Final flow
88	1	5A	3213	3243	7620	126.0	Flow 3
93	2	14A	2454	2463	3549	102.0	Flow 6
93	1A	13A	2805	2808	3966	117.0	Flow 4
93	1	13A	2805	2817	3966	117.0	Final flow
11	2	5A	2949	2952	0	130.6	Wellhead sample.
17	2C	pre1A	3337	3352	0	123.4	Flow 3. Air contamination?
17	1B	pre1A	3365	3398	0	124.4	PCT
84	1	pre1A	2753	2771	3951	110.8	Final flow
35	3	pre1A	3309	3417	6580	135.0	Servipetrol cylinder.
35	2B	pre1A	3354	3417	6565	137.0	Servipetrol cylinder.
37	1C	pre1A	3458	3495	6230	135.7	Final flow. Air contamination
69	1	pre1A	2388	2435	3463	92.0	Flow 2
46	2	pre1A	2540	2560	0	98.0	Flow 2
54	1	pre1A	2558	2617	3715	104.0	Flow 2
39	1	pre1A	2451	2576	3675	105.0	Flow 4. Air contamination
59	1	pre1A	2195	2212	3120	95.0	Final flow
65	2	pre1A	3167	3189	6409	131.0	Final flow
65	1	pre1A	3213	3267	5605	132.8	Final flow
18	4	pre1A	2602	2635	0	105.0	Flow 6
18	3	pre1A	2641	2673	3939	107.0	Flow 5
18	1	pre1A	2696	2702	3955	109.0	Flow 4
23	2	pre1A	2365	2380	0	104.6	APR
21	2	pre1A	2552	2559	3827	107.0	Flow 4
19	2	pre1A	2680	2709	3900	109.0	APR-M lower.
20	3	1A-6A	2569	2578	0	96.7	Flow 2
20	2	pre1A	2692	2699	0	101.1	Flow 2
44	1B	pre1A	2715	2750	3911	112.0	Flow 2
55	2	pre1A	2659	2682	3865	109.0	Final flow
61	3	9A	2113	2130	3095	90.0	Choke 0.625"
61	2	pre1A	2718	2770	3940	114.0	Choke 0.50"
70	2	pre1A	2411	2428	3475	103.0	Flow 2
63	1	pre1A	2659	2691	3820	109.0	Final flow
Partial pressure of CO_2(bars) = 1470 * mol% CO_2/reservoir pressure.							
NB: F-A2 DST4 and DST 3 DATA are suspect and not used in correlating between PVT and SABS data .							
Molecular mass of gas = sum of each component's volume percent*its molecular weight/100.							
Mole percent of a gas is its molecular mass (vol*mol.wt.)/molecular mass.							

Table 6.05b: Samples used for gas analyses at the SABS (Pretoria).

factors. These descriptions of kerogen break-down are considered to be valid over geologic time and hence describe kerogen maturation (Ungerer et al., 1986). The samples used should ideally be of low maturity rather than immature because the break-down starts with kerogen, i.e. post-diagenetic reduction and reorganisation of organic material.

6.3.2. Elemental analyses

Confirmation of hydrogen richness can be gained from elemental analysis of kerogen. Analyses were carried out using a Fisons EA 1108 CHNS-O analyzer at Fisons Instruments, Milan. Samples of kerogen are loaded into tin capsules in a sealed catalytic combustion chamber. Oxygen is flowed through the chamber and catalytic oxidation at up to 1800°C converts the kerogen into N_2, CO_2, H_2O and SO_2. The quantities of these gases are determined using a thermal conductivity detector. Jacobson (1991) showed that source potential evaluated from such data reasonably reflect kerogen properties determined from other optical and chemical analyses.

Financial constraints meant that only two samples could be analysed using this technique. One sample was of an oil-prone Aptian source rock and the other sample was of a Hauterivian dry gas-prone source rock - both in the oil window. The results of these analyses (Table 6.06) are compared to published results showing variations in CHNS ratios from known source rocks at different maturity levels (Tissot and Welte, 1984, p.511). The oil-prone source rock sample has a high H/C ratio whilst the poorer quality gas-prone source has a low H/C ratio, both matching their source quality and richness determined from the more usual pyrolysis and optical analyses.

6.3.3. Stable carbon isotope analyses

Two analysts were used to generate $\delta^{13}C$ data from saturated and aromatic fractions, namely CSIR, Pretoria and GH Geochemical Services, Bebington, UK (GHG). Analyses reported in IGI (1994) were also carried out by GH Geochemical Services but on samples of topped oil (100°C). In the case of one set of data from GHG, the only saturated fraction available was the residue after urea adduction and contained no normal alkanes. However, results of branched-cyclic fraction analyses are likely to be nearly synonymous with the more usual total saturated hydrocarbon fraction. Recent studies using isotope ratio mass spectrometry have shown only minor differences between these two fractions (Bjorøy et al., 1991).

The processing used by GH Geochemical was as follows:

(i) excess copper oxide is placed in a pyrex tube

(ii) the sample is dissolved in excess dichloromethane, injected into the tube and allowed to evaporate at ambient conditions

COMPARISON OF CHEMICAL AND OPTICAL DATA WITH ELEMENT PROPORTIONS														
SAMPLE DATA			ATOMIC %				SOURCE TYPE						MATURITY	
WELL	DEPTH/SAMPLE	FORMATION	C	H	N	S	H/C	HI	OI	TOC	S1	DOMINANT MACERAL	Tmax	Ro
109	2453m SWC 1-37	13A	5.484	6.349	0.130	0.260	1.158	433	28	2.32%	0.64	Sporinite and flu. amorphous	430	0.80%
118	2402.7m SWC 1-28	6A	6.706	4.853	0.100	0.120	0.724	121	45	1.04%	0.22	Vitrinite	447	0.79%

Table 6.06: Table of the elemental analytical data from the two samples analysed to date. Included are optical and chemical source rock quality, richness and maturity data.

(iii) excess silver wire is added to remove chlorides and the tube is evacuated
(vi) pyrolysis is carried out at >1000°C in the reaction oven of a VG ISOTECH isotope ratio mass spectrometer
(v) after completion, the tube is removed from the reaction oven, cooled and opened and the volume of generated gas equilibriated with reference gas.

The isotope ratio of a reference gas, calibrated to NBS 22 standard, was used to calibrate the unknown gases and several aliquots of the pyrolysed gas are analysed and averaged.

6.3.4. Wet chemical processing analyses

These analyses comprise methods used to prepare samples for gas chromatographic (GC) and mass spectrometric (GC-MS) analyses (Venter et al., 1994c). They result in a detailed record of the bulk composition of reservoired and unexpelled oils which is used in oil:source rock correlation and in maturation and environmental characterisation of the source rock. A flow chart of the processing steps is given in Fig. 6.09. The analyses are oil extraction, topping, desulphurization, deasphaltening, column fractionation and normal alkane removal.

Samples from which oil is to be extracted are washed with a hydrocarbon solvent to remove surface contaminants introduced during drilling and handling. The samples are finely ground and soxhlet extracted for 16 hrs using either boiling chloroform or dichloromethane. Studies by Price et al. (1986) have shown that exhaustive extraction is only achieved after some 24 hours but that chemically the difference between the extracts of 8 hours and those resulting from longer periods of extraction, is minimal. Theoretically the two solvents could extract different hydrocarbons although the results of a test using the two solvents (section 6.3.4.2.) showed no evidence of this. Tests were carried out to determine whether differences exist between proportions of hydrocarbons extracted using two common solvents - chloroform and dichloromethane. An oil-bearing core sample was ground using a ball mill to <125 μm and riffle split. Each half was treated as a separate sample for the extraction processes, which used dichloromethane for one half of the sample and chloroform for the other half. The total amounts of extracted hydrocarbons differed by ~6% (1428 and 1342 ppm respectively) but some of this difference can be ascribed to the small sample size used (~25 gm) and the balance accuracy (~0.5 mg). Gas chromatographic analyses of the saturated and aromatic hydrocarbon fractions were carried out on fractions extracted using the two solvents (Figs. 6.10 and 6.11) but no difference was found. Thus the different solvents had extracted the same proportions of hydrocarbons.

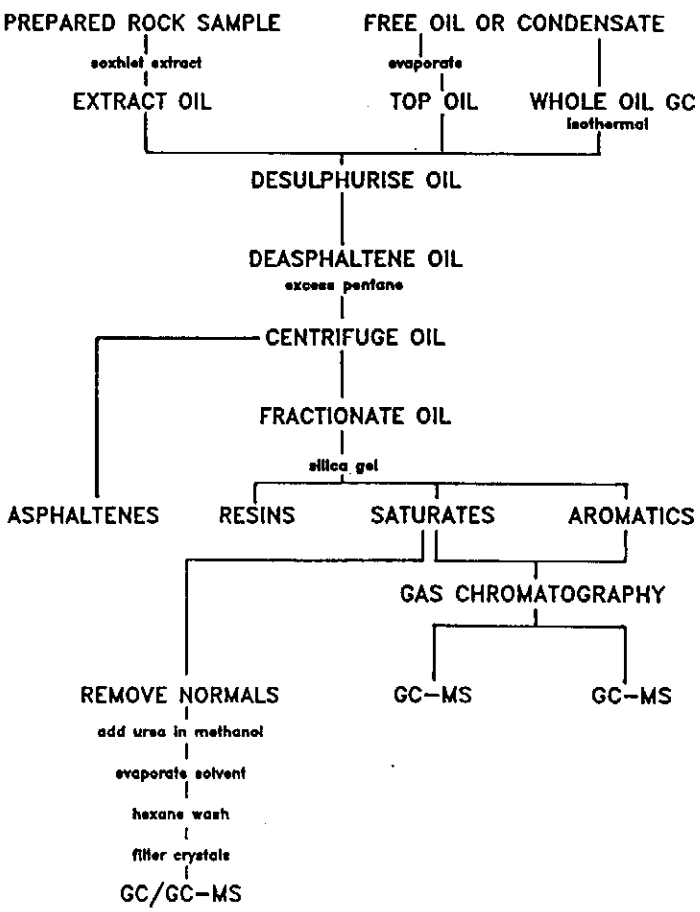

Figure 6.09: Flow chart of the steps taken to process shale extract bitumen and oil samples for analysis.

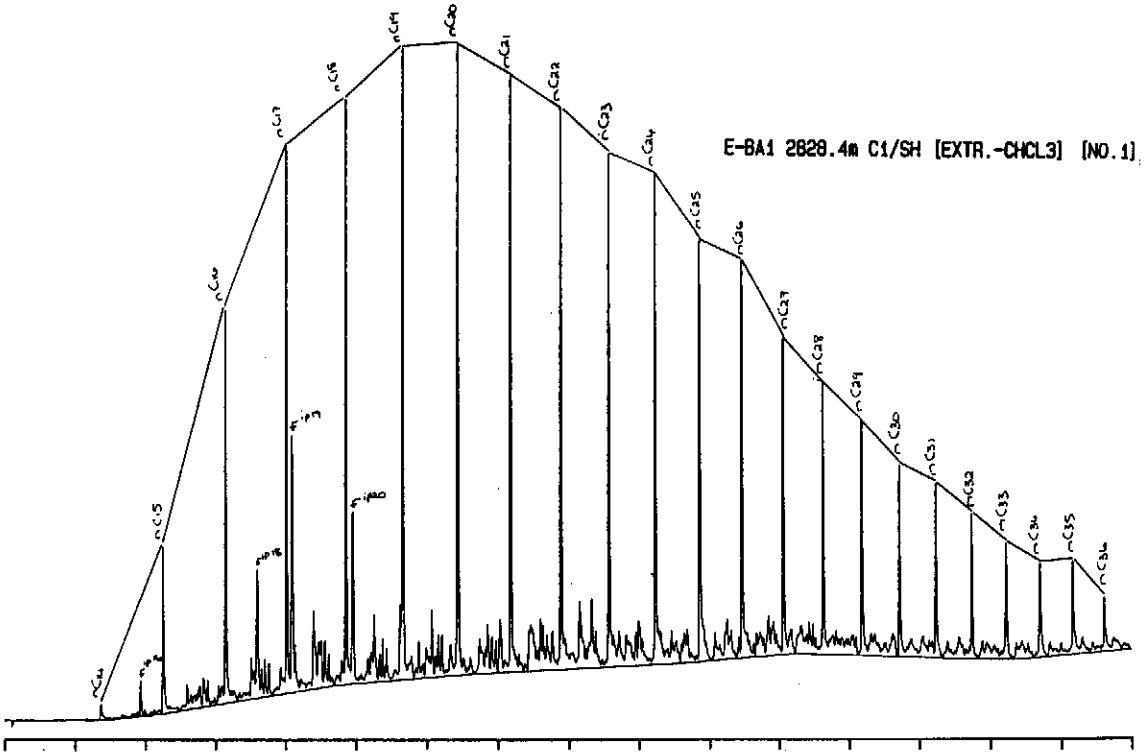

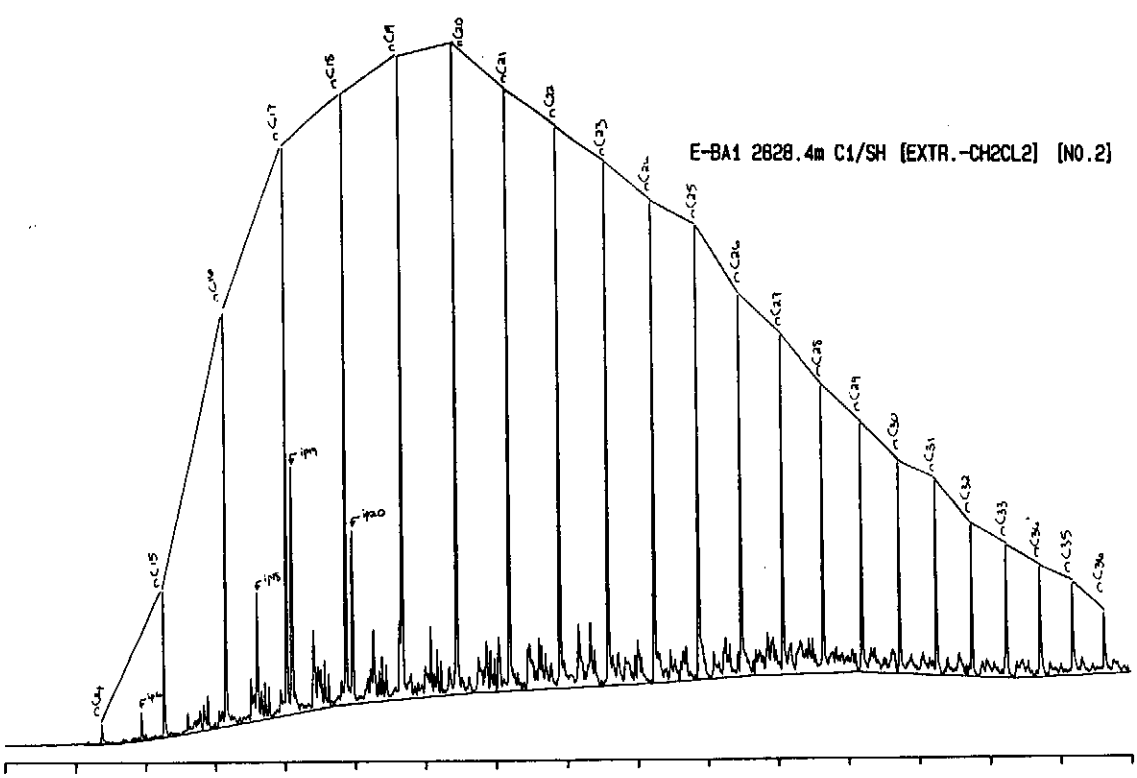

Figure 6.10: Gas chromatograms of the saturated fraction of a source rock sample processed with (a) chloroform ($CHCl_3$) and (b) dichloromethane (CH_2Cl_2).

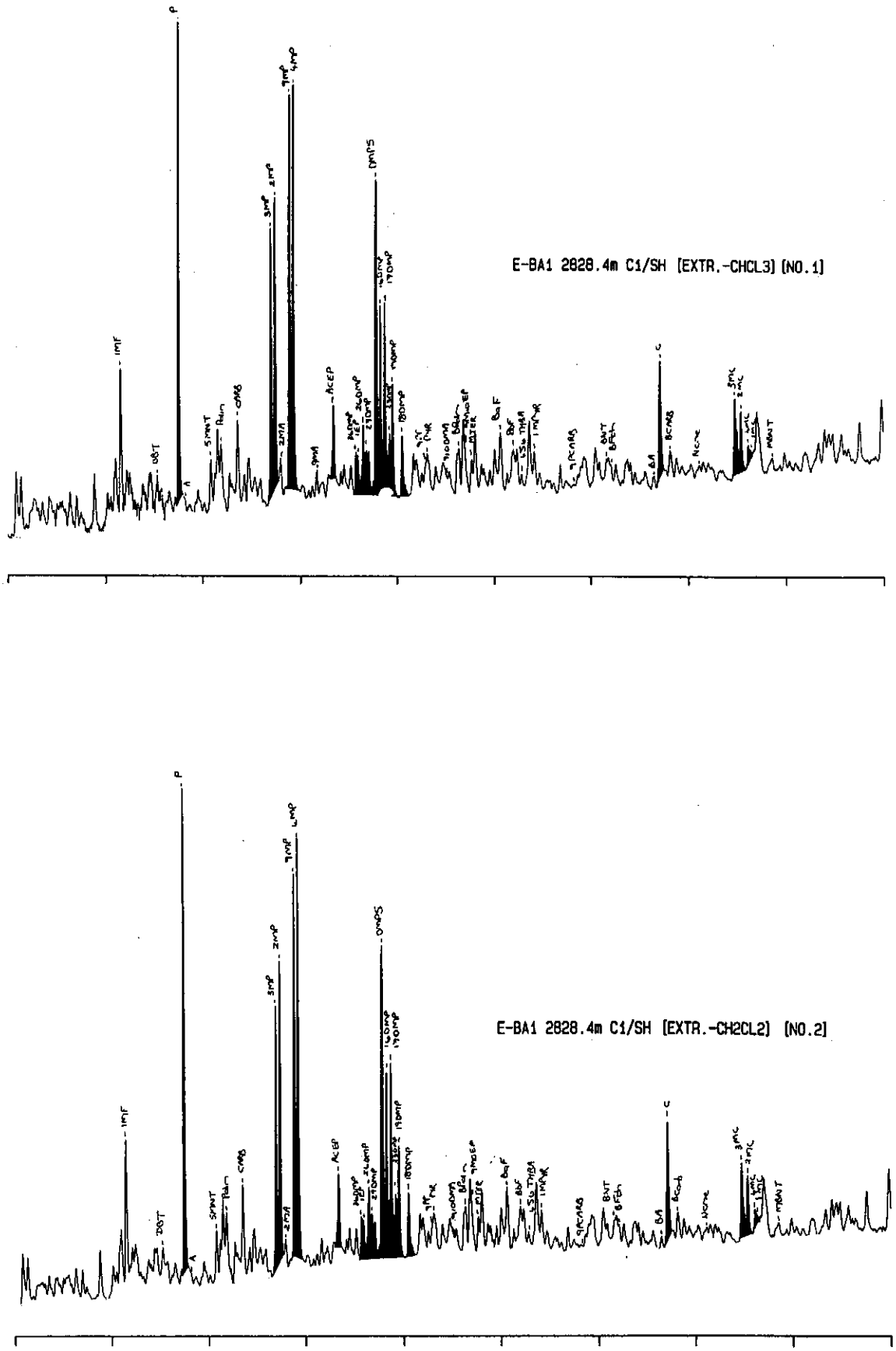

Figure 6.11: Gas chromatograms of the aromatic fraction of a source rock sample processed with (a) chloroform ($CHCl_3$) and (b) dichloromethane (CH_2Cl_2).

Hydrocarbon samples produced during DST's and sampled from the test separator, contain light hydrocarbons (C2-4) which can provide valuable information on reservoir conditions. A portion of the sample is analysed as received to ensure that these light compounds are not lost during processing. A second portion of the sample is 'topped' (evaporated) at 35°C to remove light components (to mimic the effect of the oil extraction process) and processed as below. The extract from the soxhlet (or oil topping process) is treated with activated copper to remove free sulphur to ensure that sulphur does not enter the separation column where it can deactivate the alumina. The copper is activated by removing oxides in concentrated (5N) hydrochloric acid.

Deasphaltening is carried out after the desulphurization step. Each sample is treated with excess (50 volumes) normal pentane to precipitate the asphaltenes. These are separated from the oil by repeated centrifuging until the sample dissolved in pentane remains clear. The sample is evaporated to dryness at near ambient conditions (<35° C) with forced inert gas ventilation to preserve as much of the medium molecular weight material as possible. Each deasphaltened sample is separated into its constituent hydrocarbon class fractions by low pressure liquid-solid chromatography. The samples are loaded onto columns charged with silica gel and alumina and sequentially eluted using n-pentane, benzene and benzene-methanol under a slight positive pressure of inert gas. This yields three fractions:
(i) total saturated hydrocarbons (i.e. essentially no aromatic rings)
(ii) total aromatic hydrocarbons (at least one aromatic ring)
(iii) resins (containing at least one heteroatom such as N, O, or S).

The complete separation between multi-ring condensed saturated and aromatic hydrocarbons can be difficult to accomplish, because of overlap of compounds bearing a single aromatic ring with high molecular weight non-aromatic compounds. Some monoaromatic steroids are generally found in the saturated hydrocarbon fraction.

The non-hydrocarbon fraction ('resins') comprises those compounds containing condensed polycyclic structures with heteroatoms (oxygen, nitrogen or sulphur). They are in many ways similar to the asphaltenes, some authors considering that the two major differences are the latter's higher aromatic proportion and higher mass (1200 Daltons vs >50 000 Daltons, Tissot and Welte, 1984, p.405-406). Partly as a result of their polarity, these high molecular weight compounds retain oil (or oil precursors) which are released as oil-like mixtures during pyrolysis and form part of the Rock-Eval S2 peak. This facility has proved useful in source-rock:oil correlation (Cassani and Eglinton, 1986).

Normal alkanes are often removed from saturated fractions to concentrate the branched and cyclic fraction which contains the biomarkers and to remove components which overlap with certain of the biomarkers. It is usually not carried out on samples which are very small because of the potential for loss of part of the sample, and also because the chance of contamination increases as the processing length and complexity increase. There are two widely used methods to accomplish this, namely molecular sieving (absorption of normal alkanes into a man-made zeolite by size exclusion effects) and urea adduction (adduction of normal alkanes into the interstices of crystallising urea). Literature results record no consistent differences between the resultant fractions. Nevertheless, the choice was the subject of a detailed study which confirmed that both processes were equally capable of removing the normal paraffins. However, the urea adduction process was far quicker and had fewer process steps in which contamination could occur (Van der Weide, 1969) and the method was eventually adopted. In detail, the method followed that of Hall et al. (1985) and most samples were processed that way (Table 6.07). Two oils (no's 1 and 2) and one shale (no. 34) were processed using the molecular sieve method for comparison.

One sample, no. 4 (DST5 in Well 88) was analysed by GC-MS prior to removal of the normal alkanes. The sample was subsequently adducted and re-analysed using the same equipment and column (new sample number 5). Comparison of the results of the analyses shows essentially no difference except where compounds coeluted.

The molecular sieving process involves refluxing a solution of the saturated hydrocarbon fraction in iso-octane (2,2,4,trimethyl pentane) in benzene with 20x its volume of activated powdered molecular sieve (5A) for 100 hours. The molecular sieve is activated by drying in a vacuum at 240°C for 24 hours and stored over phosphorus pentoxide. Tests showed that the molecular sieving methods used by KFA and by SOEKOR produced results essentially indistinguishable from each other and from the results obtained by urea adduction.

The urea adduction process involves the retention of normal alkanes in the interstices of crystallised urea. The saturates sample (4-10 mg) is dissolved in n-hexane (2 ml) and 1ml of acetone is added. A saturated solution of urea in 1ml of methanol is added dropwise while stirring at ambient temperature and pressure and the urea is allowed to crystallise. The process is repeated twice, each time with the solvents removed under inert gas evaporation. The crystallised urea together with the adducted normal alkanes are washed in n-hexane (3x5ml) and filtered through pre-extracted cotton wool covered with activated alumina. The branched and cyclic alkanes are retained in the liquid fraction. Eleven samples were processed by Simon-Robertson (N. Wales) using a

HYDROCARBON SAMPLES							
SAMPLE	WELL	TYPE	DEPTH	SEQUENCE	ANALYST	REMARKS	CODE
1	83	DST3	2470m	14A	KFA	few fragmentograms brown oil	●
2	83	DST2	2889m	10A	KFA	few fragmentograms light condensate	◬
3	83	"	"	"	US (CE)	brown oil/condensate	◬
4	88	DST5	2507m	14A	US (CE)	sample not adducted	●
5	88	"	"	"	"	urea adducted sample	●
6	88	DST4	2827m	10A	US (CE)	brown oil/condensate	◬
7	92	Core1	2949.0m	5A	US (CE)	live oil trace	⊞
8	118	Core1	2563.1m	8A	US (F)	residual oil trace	▩
9	102	DST4	2241m	pre1At1	US (CE)	brown oil/condensate	●
10	102	DST2	2556m	pre1At1	US (CE)	condensate	◬
11	91	Core1	3220.05m	6A	US (F)	residual oil trace	◬
12	104	Core2	3017.46m	10A	US (F)	live oil trace	▲
13	93	Core4	3212.4m	5A	S-R	residual oil trace	■
14	109	DST1	2630m	13A	S-R	brown oil	○
15	107	DST2	2565m	pre1At1	US (F)	light condensate	◬
16	110	DST1	3051m	9A	US (F)	condensate	▲
17	126	DST1	2643m	14A	US (F)	light condensate	◬
18	122	SWC	2517m	13B	S-R	live oil trace	○
19	132	DST2	2662m	13A	S-R	brown condensate	○
20	132	Core1	2702.43m	13A	S-R	oil trace below OWC	○
21	48	DST2	2620m	pre1At1	US (F)	brown condensate	▩
22	16	RC	2614m	13A	US (F)	live oil trace	▩
23	59	DST1	2212m	pre1At1	US (CE)	brown oil	▩
24	75	Core1	2830.5m	8A	US (F)	residual oil trace	▲
25	101	Core1	2987.5m	7A	S-R	residual oil trace	■
26	20	DST2	2699m	pre1At1	US (CE)	light condensate	■
27	13	Core1	2518.86m	pre1At1	US (F)	live oil show	●
28	103	DST2	2718m	14A	GHG	light condensate/?oil	◬
29	94	DST1	2799m	13B	GHG	brown oil	●
30	156	DST1	2522m	14A	US (CE)	brown oil	●
31	156	Core1	2525m	14A	US (CE)	residual oil trace	●
32	166	RFT	2508m	14A	US (CE)	light condensate	◬
33	166	Core1	2510.43m	14A	US (CE)	asphalt layer ('mini-tarmat')	○
34	166	DST	2520m	14A	US (CE)	brown oil	●
35	166	Core1	2522.5m	14A	US (CE)	residual oil trace	●
36	165	RC	2256m	14A	US (CE)	residual heavy oil	●
37	167	DST1	2679m	14A	US (CE)	light condensate	▲
38	167	Core1	2681.65m	14A	US (CE)	residual oil	◬

Biomarker analysts:

KFA=Institute of Petroleum and Organic Geochemistry (ICH-5) at the Research Centre (KFA), Julich, Germany.
S-R=Simon-Robertson Laboratories, Simon Petroleum Technology, Llandudno, N.Wales, UK.
US=University of Stellenbosch, Laboratory for Ecological Chemistry. Sats:(F)=Fisons 8000 GC-MS, (CE)=Carlo-Erba MD1000 GC-MS.
GHG=GH Geochemical services, Bebington, Wirral, Cheshire, UK.

Table 6.07a: List of the oil, condensate, residual oil and trace oil samples from the Bredasdorp Basin for which biomarker data are presented in this report.

SOURCE ROCK SAMPLES							
SAMPLE	WELL	TYPE	DEPTH	SEQUENCE	ANALYST	REMARKS	CODE
41	83	RC	2702m	13A	US (CE)	WG-OIL prone	●
42	83	RC	2741m	13A	US (CE)	OIL prone	●
43	83	RC	2792m	13A	US (CE)	WG-OIL prone	●
44	92	RC	2610m	?13A	US (CE)	WG-OIL prone	△
45	89	RC	2660m	pre1At1	US (CE)	WG prone	✚
46	93	RC	2720m	13A	S-R	OIL prone	●
47	93	RC	2761m	13A	US (CE)	OIL prone	●
48	93	"	"	"	"	SE52 column	●
49	99	RC	1820m	15A	US (CE)	WG prone	⊙
50	109	RC	2461m	13A	US (CE)	OIL prone	●
51	109	Core3	2654.15m	13A	S-R	OIL prone	△
52	130	RC	2331m	13A	US (CE)	OIL prone	●
53	110	RC	2830m	13A	US (F)	WG prone	●
54	110	RC	2902m	13A	US (F)	WG prone	●
55	112	RC	2392m	6A	US (F)	WG prone	■
56	117	SWC	2918.5m	9-12A	S-R	WG prone	▲
57	117	"	"	"	US (CE)	WG prone	▲
58	117	"	"	"	US (F)	WG prone	▲
59	122	RC	2682m	13A	S-R	OIL prone	●
60	122	RC	2832m	9-12A	S-R	WG prone	△
61	11	RC	2682m	9-12A	US (F)	WG-OIL prone	▲
62	14	RC	2721m	13A	US (F)	WG-OIL prone	●
63	42	RC	3021m	1A-4A	US (F)	WG-OIL prone	⊕
64	48	RC	2490m	6A	US (F)	WG prone	■
65	41	RC	2320m	5A	US (F)	OIL prone	■
66	65	RC	3160m	5A	US (F)	WG prone	■
67	75	Core1	2829.0m	8A	US (F)	WG-OIL prone	■
68	67	RC	2651m	5A	US (F)	WG prone	■
69	12	RC	2057m	15A	US (F)	OIL prone	⊙
70	156	RC	2835m	13A	US (CE)	OIL prone	●

Table 6.07b: List of the shale source rock samples from the Bredasdorp Basin for which biomarker data are presented in this report.

proprietary 'hot' urea adduction process (Table 6.07). Tests of matching samples show no discernable differences between the results of the two urea processes.

6.3.5. Gas chromatography analyses

High resolution gas chromatography (GC) analyses were carried out on each sample using two different separation columns. Analyses of saturates and whole oils were done on Macherey-Nagel FS-OV101DF-0.25 columns whilst aromatic fractions were separated on SE52 columns (Macherey-Nagel, FS SE52-DF-0.25). These analyses were carried out using a Varian 3300 GC employing split injection for the whole oils, split/splitless for the aromatics and programmed cold on-column injection for the saturated fraction. The latter technique was used to ensure that no discrimination effects (i.e. undue accentuation of either heavy or light components) occurred. Different columns were used for the whole oil analyses, the three Macherey-Nagel columns and one Quadrex column, coded 1, 2, 3 and Q. Operating conditions for all three types of GC analyses are given in Table 6.08a. All data generated from these analyses were handled by the DAPA processing system on the dedicated computer. Results of whole oil GC analyses are in Appendix C, fractional GC analyses in Appendix D. Peak heights measurements are in Appendix F.

6.3.6. GC-Mass Spectrometry (GC-MS)

Gas chromatography-mass spectrometry (GC-MS) analyses were carried out using five different equipment systems in four different laboratories (Table 6.08b). This lack of consistency of laboratories and equipment was due to the great difficulty initially experienced in obtaining a regular supplier of data. Repeat analyses on locally processed and analysed material have demonstrated that the different equipment and techniques gave essentially the same results (Tables 6.09 and 6.10). Most analyses were carried out using a low resolution single quadrupole MS in multiple ion detection mode. Metastable ion monitoring of the 414/400/386/372/358 - 217 daughter ions were carried out for the two DST samples (no's. 1 and 2) analysed at KFA (Rullkötter et al., 1991). Single ion monitoring was also used for high resolution analyses by GH Geochemical for two light oil samples (samples 28 and 29; IGI, 1994). These results allowed for confirmation of saturates peak assignments used in this study. Results of GC-MS analyses are given in Appendix E, peak heights listed in Appendix F, evidence to support peak assignments in Appendix G and peak codes explained in Appendix F. The individual systems and conditions used for the analyses are given in Table 6.08b.

Columns used for GC and GC-MS analyses were essentially of two types: methyl silicone (OV101, DB-1, CPSil5CB, PS349.5) and methyl, phenyl silicone (DB-5, SE52). The methyl silicone columns are non-polar whilst the methyl phenyl silicone columns are slightly polar. Both column types separated the hydrocarbons relative (essentially)

METHOD		WHOLE OIL	SATURATES	AROMATICS
Equipment	GC	Varian 3300	Varian 3300	Varian 3300
	Column	MN OV101	MN OV101	MN SE52
		Q OV101 (for some)		
Carrier gas	Type	Helium	Helium	Helium
	Splitter flow	60ml/min (col. 1)	No split	10ml/min
		100ml/min (col. 2, 3, Q)		
	Column flow	1ml/min (split)	1ml/min	1ml/min
Programme	Initial	40°C	50°C	80°C
	First ramp	None	15°C/min.	None
	First final	None	80°C	None
	First hold	6 min.	none	2 min.
	Main ramp	5°C	2.5°C	2.5°C
	Final temp.	280°C	300°C	280°C
	Final hold	46 min.	40 min.	8 min.
Temperatures	Injector start	270°C	75°C	270°C
	Injector ramp	None	150°C/min.	none
	Injector final	270°C	300°C	270°C
	Detector	320°C	320°C	320°C
Injection	Volume	0.1µl	1µl	1µl
	Solvent	None	n-hexane	Benzene
	Dilution	None	50-100µl	50-100µl

MN = Macherey-Nagel. Q = Quadrex.

Table 6.08a: Gas chromatography equipment and operating conditions.

SYSTEM		1	2 (saturates)	2 (aromatics)	3 and 4 (saturates)	3 and 4 (aromatics)	5
Analyst		KFA	S-R		US	US	GHG
No. of samples		2	11		44		2
GC		CE 4160	HP5890A		3=CE5270 4=Fisons 8350		HP5890A
GC column	Type	Bonded	Bonded		Glass	Glass	Bonded
	Size	50m x 0.25mm	30m x 0.32mm		40m x 0.28mm	40m x 0.28mm	25m x 0.28mm
	Phase	CPSil5CB (≡ OV1)	DB-1	DB-5		PS349.5 (≡ SE30)	DB-5
	Film	0.4µ	0.25µ	0.25µ	0.4µ	0.4µ	0.25µ
Injection	Volume		1µl		0.2µl	0.2µl	1µl
	Solvent		n-hexane	Benzene	n-hexane	Benzene	Benzene
	dilution		100µl	100µl	50-100µl	50-100µl	100µl
GC programme	Injector	-	-	-	250°C	250°C	-
	Detector	-	-	-	300°C	300°C	-
	Oven start	110°C	20°C	50°C	40°C	30°C	60°C
	First hold	-	1 min.	1 min.	3 min.	-	-
	First ramp	-	30°C/min.		40°C/min.	40°C/min.	-
	First final	-	130°C		100°C	60°C	-
	Ramp	3°C/min.	5°C/min.	7.5°C/min.	2°C/min.	2°C/min.	5°C/min.
	Final	320°C	300°C		300°C	300°C	310°C
	Hold	20 min.	20 min.		35 min.	20 min.	12 min.
Carrier gas	Type	Helium	Helium		Helium	Helium	Helium
	Rate	3.5ml/min.	30cm/sec.		27cm/sec.	27cm/sec.	35cm/sec.
	Split rate	~4:1	Splitless		Splitless	Splitless	Splitless
MS	Type	VG7070E	Finnegan 4500		3=CE MD1000 4=Fisons MD800		VG TS250
	Source energy	70eV	70eV		70eV	70eV	70eV
	Source temperature	220°C	260°C		200°C	200°C	220°C
	Cycle time	1300msec.	1000msec.	4000msec.	1100msec.	1100msec.	1000msec.

Analyst abbreviations as on Table 5.01.

Table 6.08b: Gas chromatography-mass spectrometry equipment and operating conditions.

SATURATED HYDROCARBON FRACTION									
DIFFERENCES BETWEEN DATA FROM DIFFERENT SYSTEMS (error from mean)									
PARAMETER		SYS1:SYS3	SYS3:SYS5				SYS4:SYS2	SYS3:SYS4	
		WELL 83 DST2	WELL 70 DST1	WELL 123 2622m	Pletmos	WELL 62 DST1	WELL 117 2918.5m	WELL 117 2918.5m	WELL 92 2949m
STERANES	C27 βα S+R	11.6%	1.1%	1.8%	4.4%	5.0%	12.5%	0%	3.2%
m/z 217	C28 βα S+R	0%	5.1%	3.9%	2.4%	6.1%	0%	4.3%	4.3%
	C29 βα S+R	16.8%	3.4%	1.3%	4.1%	1.6%	11.8%	4.6%	0%
	C27 αα S+R	1.8%	8.4%	0%	5.9%	3.3%	2.6%	5.1%	8.7%
	C28 αα S+R	6.5%	16.6%	6.9%	11.7%	0%	7.5%	2.8%	8.0%
	C29 αα S+R	2.0%	3.7%	5.7%	0%	7.7%	2.0%	10.0%	6.7%
	C29 αα S/(S+R)	4.3%	1.9%	6.8%	0.9%	4.4%	7.4%	2.4%	0%
	C29 ββ/(αα+ββ)	2.4%	5.4%	0.9%	4.7%	0.8%	4.4%	0.8%	2.5%
	(20+21)/(C27 βαS)		15.3%	4.5%		3.2%	???		
m/z 218	C27 ββ S+R	8.3%	3.6%	0	1.2%	6.3%	2.9%	3.1%	4.6%
	C28 ββ S+R	8.9%	2.9%	1.4%	11.3%	7.6%	3.8%	0%	0%
	C29 ββ S+R	9.1%	0%	1.5%	3.6%	0%	1.6%	3.2%	6.0%
TRI- AND TETRA-	C23T/C21T	nil	nil	nil	nil	nil	2.9%	1.9%	5.1%
CYCLIC-TERPANES	C24/4Tetra/C24T	nil	nil	nil	nil	nil	9.4%	9.4%	10.7%
m/z 191	C25T/C26T	nil	nil	nil	nil	nil	4.5%	14.1%	11.2%
PENTA-CYCLIC	Ts/Tm	19.1%	13.3%	2.1%	3.0%	nil	8.3%	6.0%	11.4%
TERPANES m/z 191	C29 nH/C29 Ts	11.4%	3.5%	19.1%		nil	5.9%	2.9%	15.9%
	C29 nH/C30 Dia	9.1%	8.7%	5.7%	17.6%	nil	13.6%	0%	0.8%
	C29 nH/C30 H	15.9%	1.6%	2.0%	5.5%	nil	11.3%	5.7%	6.6%
	C31 hH S/R	23.4%	15.3%	3.1%	2.2%	nil	0.4%	5.8%	13.1%
	C32 hH S/R	0.9%	5.8%	0.7%	5.3%	nil	2.1%	0.7%	19.7%
	C33 hH S/R	0.4%		2.1%	2.6%	nil	2.6%	4.8%	
m/z 177	C27 βα S/C29 H			0.9%	nil	nil	11.6%	12.5%	nil

SYS1 = System 1 (KFA), SYS2 = System 2 (Simon-Robertson), SYS3 and SYS4 = Systems 3 and 4 (University of Stellenbosch Carlo-Erba and Fisons respectively), SYS5 = System 5 (GHG).

Table 6.09: Comparison of proportional differences between ratios of saturated hydrocarbon biomarkers from repeat analyses carried out using different GC-MS systems.

AROMATIC HYDROCARBON FRACTION									
DIFFERENCES BETWEEN DATA FROM DIFFERENT SYSTEMS (error from mean)									
PARAMETER		SYS3:SYS5				SYS2:SYS3	SYS3:SYS3		
		WELL 70 DST1	WELL 46 DST2	Pletmos	WELL 62 DST1	WELL 117 2918.5m	WELL 117 2918.5m	WELL 88 DST4	WELL 92 2610m
m/z 170 TRIMETHYL-NAPHTHALENES	1,3,6/1,3,7					4.7%	0.8%	3.2%	2.5%
	(1,3,5+1,4,6)/2,3,6					8.6%	2.9%	3.8%	1.9%
METHYL DIBENZO THIOPHENES m/z 198	4M/(2M+3M)	19.8%	nil	3.1%	8.4%	8.0%	2.2%	6.5%	9.1%
	4M/1M	22.9%	nil		7.9%	5.8%	10.5%	1.8%	4.5%
DIMETHYL DIBENZO THIOPHENES m/z 212	D/B					7.8%	1.6%	6.8%	3.5%
	C/E					2.3%	1.5%	3.3%	4.6%
TRIMETHYL DIBENZO THIOPHENES m/z 226	c/b					6.6%	11.1%	9.3%	15.8%
	e/f					3.3%	0.4%	9.6%	0.7%
TRIAROMATIC STEROIDS m/z 231	f/g					7.7%	2.5%	3.2%	7.4%
	b/a					17.0%	0.2%	3.8%	9.9%
MONOAROMATIC STEROIDS m/z 253	9/6					17.8%	5.6%	4.8%	15.4%
	2/3					32.3%	4.5%	4.6%	5.0%
PHENANTHRENES m/z 178+192	MPR	5.1%	5.6%	11.6%	8.6%	5.6%	0.7%	5.0%	1.8%
	MPI1	0.6%	8.8%	14.5%	15.6%	8.1%	2.1%	4.5%	3.0%

SYS2 = System 2 (Simon-Robertson), SYS3 = System 3 (University of Stellenbosch, Carlo-Erba), SYS5 = System 5 (GH Geochemical).

Table 6.10: Comparison of proportional differences between ratios of aromatic hydrocarbon biomarkers from repeat analyses carried out using different GC-MS systems.

to their boiling points. One sample (no. 37) was also analysed by GC-MS using both types of column (Appendix D, Figs. D.35 and D.36) and the results show that the analyses are essentially identical. Chromatogram and fragmentogram peak distributions compared very closely with published distributions. More rigorous compound identification methods were also used in order to confirm the comparisons. The three methods used include matching of mass spectra, co-injection of standard samples and relative retention indices.

(i) Mass spectra of selected peaks are compared with published examples in order to demonstrate that the name of the compound responsible for each interpreted peak selected from the GC-MS plots was correctly assigned. To avoid duplication, it was decided not to compare spectra from all compounds but to use at least one from each homologous series. In some series, the spectra of only a few compounds have been published. Thus the range of compounds selected for spectral comparison have been based on the availability of published spectra rather than because they were the best available spectra. The results of these comparisons are given in Appendix G.

(ii) Co-injection of standards was carried out where standards were available. Standards of normal and branched alkanes including isoprenoids and C5-15 aromatics and cycloalkanes were used. No standards were available for biomarker compounds.

(iii) Relative retention indices were used to compare the majority of the peaks between samples. These were selected by reference to published examples of characteristic patterns and from identifications made at each of the overseas laboratories. Some of the samples analysed in other laboratories (e.g. Simon-Robertson, N.Wales, GHG, Liverpool and KFA, Jülich) where standardisation had been carried out, were used as general standards and frequently analysed. This had a twofold purpose in ensuring that the equipment was optimised and the peak identification was rigorously controlled.

Because of the number of different systems used for the analyses, various tests were carried out to determine if they imposed any variation in the peak sizes or retention.

(i) Tests of matching analyses were carried out to compare the five different GC-MS systems. In the case of systems 3 and 4, the columns matched very well because they were manufactured from 80 metre columns which were broken in half to provide two matching 40 metre columns. In the case of other systems, this was not possible and repeat analyses were carried out to demonstrate that use of the different equipment did not significantly affect the results.

An SWC sample from well 117 (2918.5m) was analysed for its saturates content using systems 2, 3 and 4 (samples 46-48). The saturated fraction of a DST sample from well 83 (DST2, 2889m) was analysed using systems 1 and 3 (samples 2-3). Samples 21, 34, and 43 (well 92, 2949m, well 110, 2830m and well 48, 2620m) were re-analysed using systems 3 and 4. The results demonstrated no major difference between the peak heights obtained from each analysis, although slight variances between the fragmentograms dependent on different injector configurations were apparent. Hence, there were no obvious systematic differences in the ratios between nearby peaks. The two samples analysed by system 5 were not reanalysed because the remaining sample was too small. However, another sample studied using this system (well 123, 2622m) was analysed on systems 3 and 5. The results of these repeat analyses also showed no significant difference between the two datasets and the peak ratios matched within an error range of ~5% (Tables 6.07 and 6.08).

(ii) Analytical repeatability was thought to pose a problem especially with the samples of light condensates, which contained only small amounts of biomarkers. Consideration was therefore given to the possibility that the peaks could be reliably reproduced during multiple analyses. Several samples were repeatedly analysed to test for this effect. The sample from well 102, DST2 (2241m) was analysed three times using the same system. The sample from well 20, DST2 (2699m) was analysed twice using the same system and again using different programmes. The SWC sample from well 117 (at 2918.5m) was used as the laboratory standard and was analysed many times during a 20 month time period. In each case all peaks matched, even those which were no more than twice the noise level and barely visible above the baseline, were reproduced.

(iii) Peak size measurements were made using the same analog equipment throughout these tests. Repeats of randomly selected samples were made to confirm the consistency of the measurements. Semi-quantitative evaluation of the content of each component was made by measuring the peak heights from the valley-to-valley (V-V) baseline. This was done for the following reasons:

The KFA results (Rullkötter et al., 1991) did not provide the areal measurement of the peaks so that the only measure of the peak sizes was the peak height. Since the KFA results were the first available and were used as initial laboratory standards, it was decided to measure peak heights for all future analyses.

The Simon-Robertson (S-R) results provided tables of peak heights and areas. Peak areas were determined from triangulation using a manually controlled baseline with perpendiculars drawn from the peaks and shoulders to baseline. In some cases the

perpendiculars did not always separate individual peaks in the same proportions, hence their method to determine peak areas was potentially suspect.

The version of the Lab-Base data programme used for systems 3 and 4 did not have the facility to integrate every peak using a baseline derived from the complete fragmentogram. Hence, a crowded area of the fragmentogram might, especially if the peaks were small and partly overlapping, have a different baseline depending on where the integration started. In each case, therefore, baselines were manually constructed (from valley to valley) producing a baseline which largely approximated a blank analysis. Peak heights were measured perpendicularly above this baseline. This procedure, although time-consuming, resulted in two definite advantages as it allowed for internal consistency between data which had been supplied with either areal or areal-plus-height measurements and also ensured that peaks were not assigned different sizes because of variations in the method of integration.

(iv) Differences could also be expected in the measured peak sizes due to other factors such as low signal-noise ratios and data system or column overload (Peters and Moldowan, 1993, p.98). However, repeat analyses at different sensitivities showed variations <1% which barely affected the calculated ratios.

(v) Quantification against standards is the optimal method of data presentation but such standards were not available. Where quantification has been carried out for published studies, a common method relies on extrapolation from single standards assuming that response factors for each compound in the interval of interest are 1.00 (Hughes and Dzou, 1995). The implication of this is that assumes that the ratio between areas under peaks of two different compounds in a similar area of a chromatogram (and similarly in a fragmentogram where the fragmentation patterns are similar) is the same as the ratio of the mass concentration of the two compounds. One result of this is that a range of components can be quantified using the same standard, as done with the C27-29 steranes and C21-23 tricyclic terpanes using a 5β cholane standard (Dzou et al., 1995).

(vi) Peak broadening with increasing column temperature in the chromatogram or fragmentogram does not appear to significantly affect peak height comparisons where the compounds locate close together. Hence the heights of the two peaks are also in proportion to the ratio of the mass concentration of the components.

HYDROCARBON EVOLUTION OF THE BREDASDORP BASIN, OFFSHORE SOUTH AFRICA: FROM SOURCE TO RESERVOIR

VOLUME 2: CHAPTERS 7-15

CHAPTER 7. MODELLING

There are many reservoired oils, oil traces, 'condensates' and wet gases in the Bredasdorp Basin between horizons 15At1 and pre-1At1. None, however, is present in such intimate spatial association with a source rock that its origin is unambiguous.

The data and discussion presented in Chapter 4 show that there are a number of source rocks in the basin which are able to generate and expel high molecular weight hydrocarbons during burial through the oil and wet gas windows. Since all the source rocks have the potential to generate some oil and all (with the exception of the 15A source) were at some time during their history buried through the oil expulsion window, any one of them could be responsible for the oil shows. Because wells target reservoirs rather than source rock kitchens, very few source rock intersections are from the main part of the relevant kitchen. Hence evaluation of the amounts of oil generated and available for migration is only estimate.

It is important to know which source was responsible for which hydrocarbon, as this allows for confirmation of the individual generation kitchen and evaluation of the downdip fetch areas. Oil:source correlation studies can then establish which source was effective. It is also important to know how much hydrocarbon was expelled, to determine whether there were enough to fill the available reservoirs. That can be determined from knowledge of the areal extent and richness of the mature source rock. It is equally important to know when the hydrocarbons migrated relative to the time of formation of the reservoir and trap. This constrains the effective migration direction, especially where the basin has tilted through time, and can only be determined from reconstruction to the time of migration. The time when each source was generating, the type and quantity of product and the time when migration occurred are therefore of great importance in the assessment of the prospectivity of the basin. In order to assess these factors, it is necessary to know the burial and thermal history of the basin. Modelling is therefore used to reconstruct the burial, thermal and hydrocarbon generation history at selected locations throughout the basin. This provides an estimate of the time when hydrocarbon generation and expulsion from the different source rocks occurred and when they reached their maxima (Durand, 1983; Durand et al., 1987).

Potential reservoir-rock facies have been found mainly in Lower to Mid-Cretaceous rocks ranging from late syn-rift (pre-1At1) to mid-drift (pre-15At1). Structural and stratigraphic traps could have formed in these sandstones at different times during the basin history because of the varied rates of sedimentation and tectonism. Models of

generation, expulsion and migration in different parts of the basin can indicate areas where hydrocarbon generation and migration was timeous for reservoiring.

7.1. MODELLING TECHNIQUES.

An early modelling method, using a mathematical simulation of hydrocarbon generation introduced by Tissot (1969), was described in detail in Tissot and Espitalié (1975). The model comprised a two-step kinetic process for kerogen degradation, in which first heteroatomic bonds, then carbon-carbon bonds, were broken sequentially as depth and temperature increased. The model included a series of parallel reactions which describe first the generation of CO_2 and H_2O plus residues and then later oil generation. With increased maturation, the oil fractions were modelled to crack forming lighter oil plus residue and more gas. It was also assumed that once generated, the gases and residues would be essentially excluded from further reactions. These reactions are considered to be first-order, i.e. in which the rate of reaction is proportional to the concentration of the reactants. Recent oil cracking studies show that some reactions are second order, i.e. they do not proceed at a rate determined by the concentration of the reactants, but as a result of *inter alia* thermocatalysis (Mango, 1992). The energies involved in each step of these parallel reactions are summed to provide the energy profile of the sample. With mono-maceralic samples, the profiles readily describe a gaussian curve but are skewed where several types of kerogen are present.

Mathematical modelling has become commonplace in recent years (Tissot and Welte, 1984, p.583-590) and a number of computer programmes have been designed for these calculations. The 'n-component model' in the 1-D version of Basinmod version 5.00 (Platte River Associates, 1995) uses a refinement of the Tissot and Espitalié method in which oil cracking proceeds by multiple reactions, resulting in simultaneous conversion of kerogen to liquid, gaseous hydrocarbons and residues. Each of these products continue to crack until essentially only methane and char remain. The kinetic data used in the modelling of these wells describe the reaction rates for each component. They were derived from analyses of source rock samples carried out at SOEKOR and listed in Tables 4.01 and in Appendix A, Tables A1 and A2.

For each well, several different types of modelling are carried out, each of which calculate different aspects of the geological history:
(i) tectonic (based on subsidence curves, geology and plate tectonic history)
(ii) burial (based on sediment thicknesses and biostratigraphic formation ages)
(iii) compaction (derived from empirical lithology-based porosity relationships)
(iv) permeability (used to evaluate the effects of diagenesis on fluid flow rates)
(v) thermal/maturity (derived by matching calculated and estimated heat flow)

(vi) generation (derived from measured kinetic reaction rate data)
(vii) expulsion (based on proportions of generated oil less minimum pore saturation)
(viii) cracking reactions (using chemical degradation rates).

To evaluate these various models, certain assumptions are made:
(i) cracking reactions occur in the heavier components first and progress to lighter fractions as maturity increases (i.e. from oil through condensates and wet gas to methane) in a regular sequence
(ii) oil expulsion starts when the threshold of porosity saturation exceeds a certain threshold and ends when the saturation falls below that threshold
(iii) there is no expulsion fractionation and hydrocarbons are expelled in the same proportions as they are generated
(iv) expelled hydrocarbons are not accessible to further cracking reactions
(v) petroleum density is a function of kerogen type and maturation.

7.1.1. Tectonic History.
Major uplift and rifting events (Figs. 2.06 and 7.01) affect the elevation and structural configuration of the basin and these are included in the models. This helps to constrain some of the periods of excess heat flow and to detail sea level changes and the effect these have on the sediment type. In addition, the periods of local tectonism following regional uplift, are also modelled where they too affect the Bredasdorp Basin.

7.1.2. Burial History.
Age dating of the sediments, hiatuses and estimates of eroded sediments are derived from biostratigraphic studies carried out on Bredasdorp Basin wells during the course of exploration. Ages of sediments are based on faunal correlation with series identified by Haq and Van Eysinga (1987). Environments of deposition of each package of sediment are derived from microplankton distribution (McMillan et al., 1997) locally confirmed by available palynofacies studies (J.M. Benson, 1992, pers. comm.). These studies assign possible water depth ranges to sediment packages which largely match those inferred from seismic data (e.g. top-to-base of clinoforms) although they are locally adjusted to match global sea level subsidence curves (Haq et al., 1987). Data used in this modelling are listed in Appendix A, Tables A3 and A4.

7.1.3. Compaction and Porosity.
Rates of compaction can be modelled empirically and used to derive an algorithm which predicts porosity changes with depth. Many such algorithms are available, each able to predict porosity in different lithologies to varying degrees of accuracy depending on the empirical relationship used. In the absence of routine measurements of sandstone grain density and grain size, default Basinmod values are used (Appendix A,

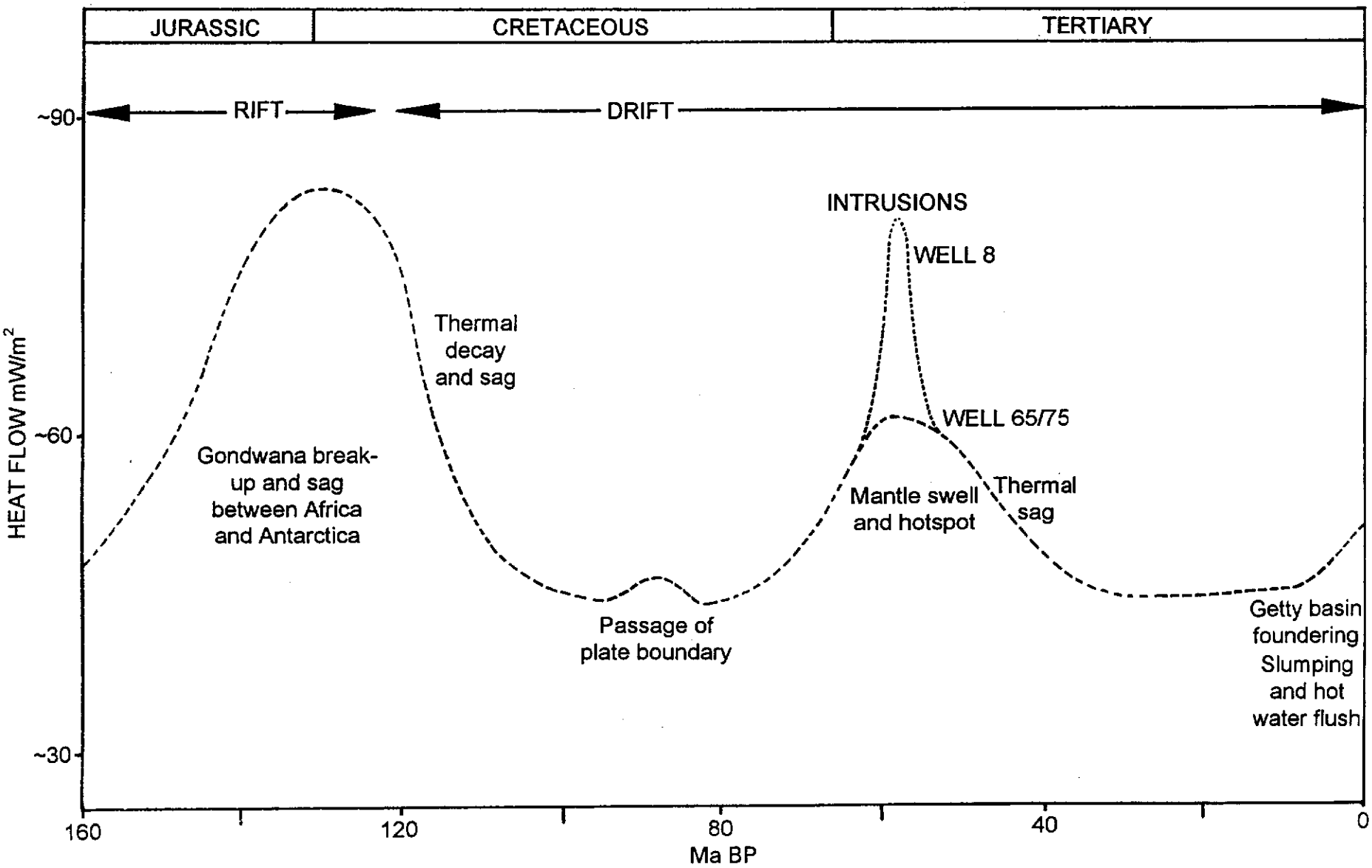

Figure 7.01: Model of heat flow after start of syn-rift sediment deposition (~140 Ma) showing three periods of high heat flow at - (i) cool-down phase after Gondwana rifting (ii) late Cretaceous-early Tertiary hotspot transit and (iii) heating effects associated with African Superswell.

Table A5). The few available values from petrographic and core analysis studies do not differ markedly from these defaults.

Source rocks in the models were decompacted using the Baldwin and Butler (1985) algorithm of shale porosity reduction. This algorithm, derived from measured compaction data for mildly overpressured shales, was used in preference to others available in Basinmod because all mature source rocks in the basin exhibit slight overpressure (Brink and Winters, 1989). For all other sequences, coupled fluid flow modelling was used. In this method, parameter calculations take into account not only other parameters of that layer but also values calculated for previously deposited layers. The advantage of this method is that results of pressure calculations are reflected in porosity, thermal conductivity and temperature changes. During this modelling, depth and time maturity integration were routinely maximised at 400 metres and 5 Ma respectively (with local variations to handle the rapid events). Models predict the onset of significant overpressure to start near 3000 metres as is the case in many wells in the Bredasdorp Basin, independent of their chronostratigraphic level (Brink and Winters, 1989; Larsen, 1995). The depth to top overpressure worldwide is also ~3000 metres (Hunt, 1990) and because this is depth-related rather than temperature-related, the cause is considered to be compaction. Indeed, the 'frame pressure' calculation in fluid flow modelling which results in this pressure evaluation, is solely a function of void ratio (porosity changes) and its density derivative, both of which are dependent on compaction processes (Lerche, 1990, p274).

7.1.4. Permeability.

The effective permeability of a formation is related not only to the formation lithology and pore space configuration but also includes effects due to viscosity of the flowing fluid and its temperature and rate of flow. The effective permeability of any formation is governed to a large degree by the presence of a variety of clay minerals in different crystal forms in the pores and pore throats. For example, detrital illite can be granular and behaves like other grains but diagenetic illite, in its fibrous form, can significantly affect the effective permeability - particularly in the case of high molecular weight fluids. Permeability parameters used in the modelling are listed in Appendix A, Table A6.

Since the form and proportions of the component minerals can be locally variable, and therefore difficult to predict, several algorithms are available in Basinmod to estimate permeability - each of which is derived from empirical studies of various types of lithologies. The permeability power function is used here as it better describes essentially normally-pressured claystones and sandstones than do other algorithms. This method combines lithologic parameters together to calculate permeability. The default function (5.5, after Lerche, 1990, p275) was used for this modelling. However,

for source rocks, permeability calculations used the modified Kozeny-Carman method as it handles low permeability rocks better.

No detailed grain/matrix compaction data are available, hence a regional study of permeability parameters is not possible and the Basinmod default values are used. Since the computation of palaeo-compaction is only an estimate, only a nominal pore saturation value is used, in this case 10%. The amounts of oil and gas estimated to be expelled from each source rock take into account the measured unexpelled proportions of free hydrocarbons in known examples of each source rock, after the empirical method used by Davies (1988b and 1990). These are essentially absorption of ~1.0-1.5 kg oil/tonne rock and gas absorption of 0.1-0.2 kg/tonne rock above 115°C.

7.1.5. Maturity.

Maturation parameters described in chapter 6 are used to determine the maximum maturation level presently attained. Changes in these parameters through time are a function of all the temperature changes affecting that formation. Although the parameters do not measure individual temperature changes at each time step, they can be used to inverse model the palaeo heating rates and hence to evaluate palaeotemperatures. This is most conveniently done using the heat flow method which assumes that surface heat flow is a measure of the amount of energy passing through the sediment column. This heat flow is largely a function of (i) mantle heat flux and (ii) thermal conductivity of the sediments below. Localised igneous, radiogenic or other heat sources can perturb regional heat flow and allowance is made where relevant (Green et al., 1993; Jessop and Majorowicz, 1994).

7.1.5.1. Heat flow evaluation

Heat flow at the present day at each wellsite is calculated from the current thermal regime, i.e. the temperature difference between the measured sea floor and bottom-hole temperatures and the thermal conductivity of each layer (Table 7.01 and Fig. 7.02). In the absence of measured sediment thermal conductivities, Basinmod default values are used to represent the known lithologies. Estimates of palaeo-heat flow use present day values as a starting point (Appendix A, Table A7) and model the tectonic, thermal and lithologic history and palaeo-thermal conductivities to derive estimates of the heat flow through time. These are tested (using the Basinmod EasyRo% module) by iterative adjustments to match the measured vitrinite reflectance.

Estimates of heat flows at the start of the cool-down period (~130 Ma), are based on the Red Sea model (Barnard et al., 1992), i.e. ~100 mW/m^2 with a cool-down period of ~30 Ma. Heat flows likely during the hotspot transit period were modelled at up to 40% above background, reaching a peak in the middle of the 30 Ma time span (75-45 Ma)

WELL	20" casing	13 3/8" casing	9 5/8" casing	SBHT (°C)	7" liner	TD	SBHT (°C)
14	481m	1746m	3706m	161.7		3996m	nil
65	321m	900m	2140m	nil	3331m	3578m	135
75	332m	1600m	3135m	nil	3458m	3700m	150.6
16	409m	1507m	3385m	125	nil	4866m	179
91	328m	1600m	3063m	nil	nil	3989m	165
94	337m	1306m	2894m	nil	nil	3634m	151
8	457m	1233m	2805m	104	nil	3147m	129

NB: only two log temperature measurements at TD in well 65, hence value from well 75 preferred.

Table 7.01: Casing shoe depths and static borehole temperatures for wells on which the five Bredasdorp basin models are based.

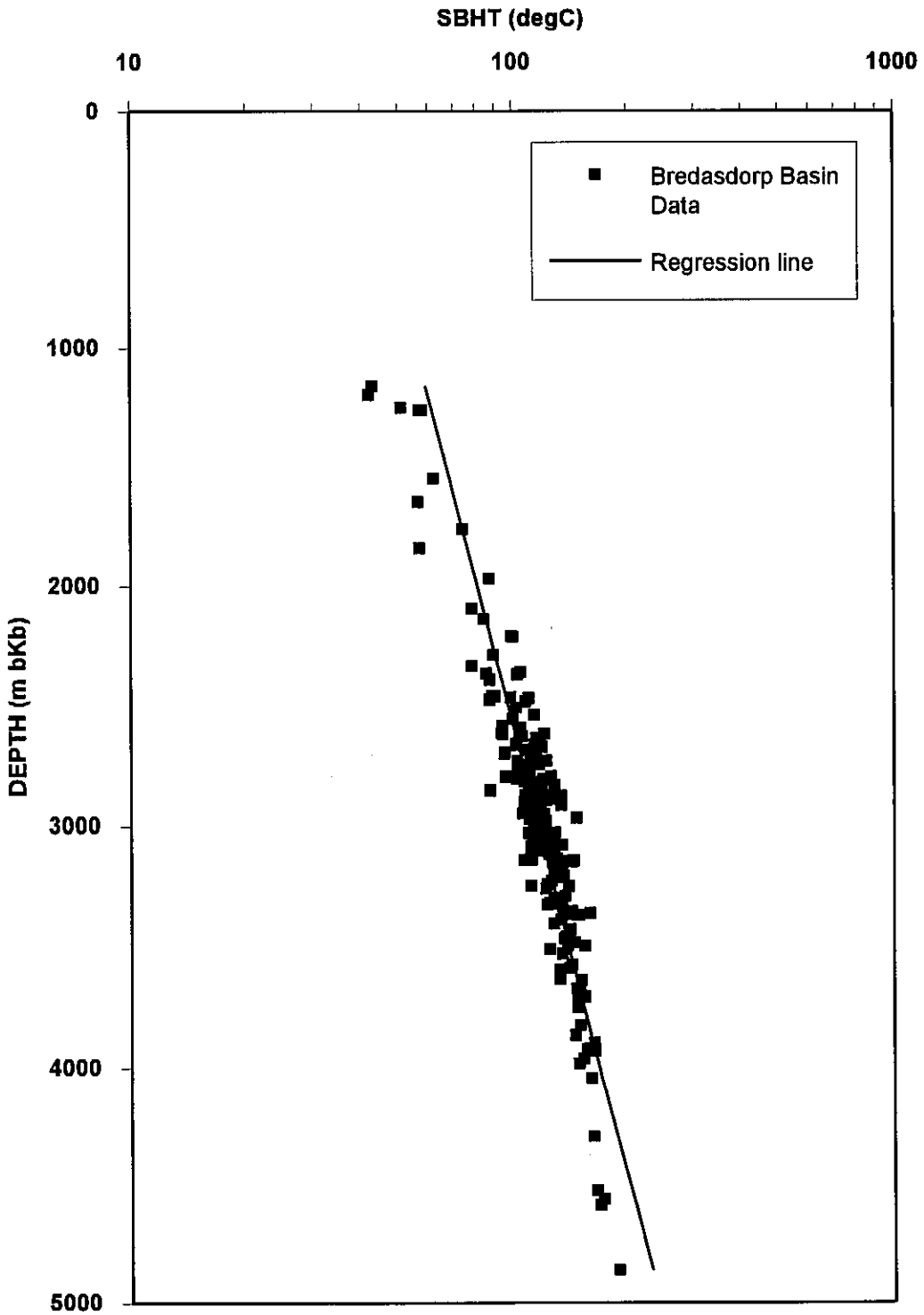

Figure 7.02: Static borehole temperatures at each casing point from Bredasdorp Basin wells. The data describe an approximately straight line indicating that all locations where temperatures were measured in the basin are affected by the same heat regime.

estimated for the duration of the proposed mantle swell. Hence the peak was reached at ~60 Ma to match the period of maximum heating from the more localised hotspot. In addition, in the two regions where intrusions are known, the heat flows were increased to reach 50% above background where intrusions are present either in the well or in the near vicinity (cf. wells 65/75 and 8) as idealised in Fig. 7.01. The Arrhenius-based EasyRo% programme using vitrinite reaction rates (Burnham and Braun, 1985), permits simulation of vitrinite reflectance changes through time by forward modelling based on first order chemical reactions (Morrow and Issler, 1993). Maturation proceeds by a series of parallel reactions each resulting in a series of products of different molecular size. Collectively these reactions are responsible for the broad activation energy range used for many type 2 and 3 kerogens. In the kerogen generation calculation programme (OPTKIN) activation energies ranging ~46-60 mcal/mole approximate the kerogen reaction (Appendix A, Tables A1; A2). Kinetic data are available for samples from wells shown in Figs. 7.03; 7.04.

7.1.5.2. Heat flow modelling

This modelling provides estimates of the heat flows and surface temperatures necessary to achieve the present day maturity level (Appendix A, Table A7). However, the calculation does not always give perfect matches of modelled and measured reflectances, perhaps because of imperfect data (e.g. thermal conductivities). Over recent years, Basinmod studies have been carried out for many wells in the Bredasdorp Basin. In each case it is only possible to match modelled and measured reflectances by assuming a small heat input, focussed shallow in the section during late Tertiary (Fig. 7.05a; Appendix A, Table A7) averaging 30$\mu W/m^3$ for the period 10-0 Ma.

A second possible thermal model (Fig. 7.05b) by which measured and modelled Cretaceous reflectances could approximately match assumes an unrecognised Mid- to Late Tertiary burial of 1500 metres followed by uplift and erosion of at least 1500 metres. This is unlikely (McMillan, 1986; McMillan, 1996, pers. comm.), because of:

(i) the common presence of uncrushed and unfilled Miocene and Oligocene fauna,

(ii) the widespread presence of aragonite in Late Tertiary rocks indicative of burial shallower than ~300m (≡23°C) at which temperature aragonite converts to calcite in <3 months (Bathurst, 1976, p. 240),

(iii) the absence of a large enough time gap for deposition and removal of 1500m of sediment (assuming similar sedimentation rates to those prevailing through the remainder of the Tertiary),

(iv) no seismic evidence (e.g. truncation, offlap),

(v) the lack of log evidence for unexpectedly compacted sediments below the supposed erosion surface.

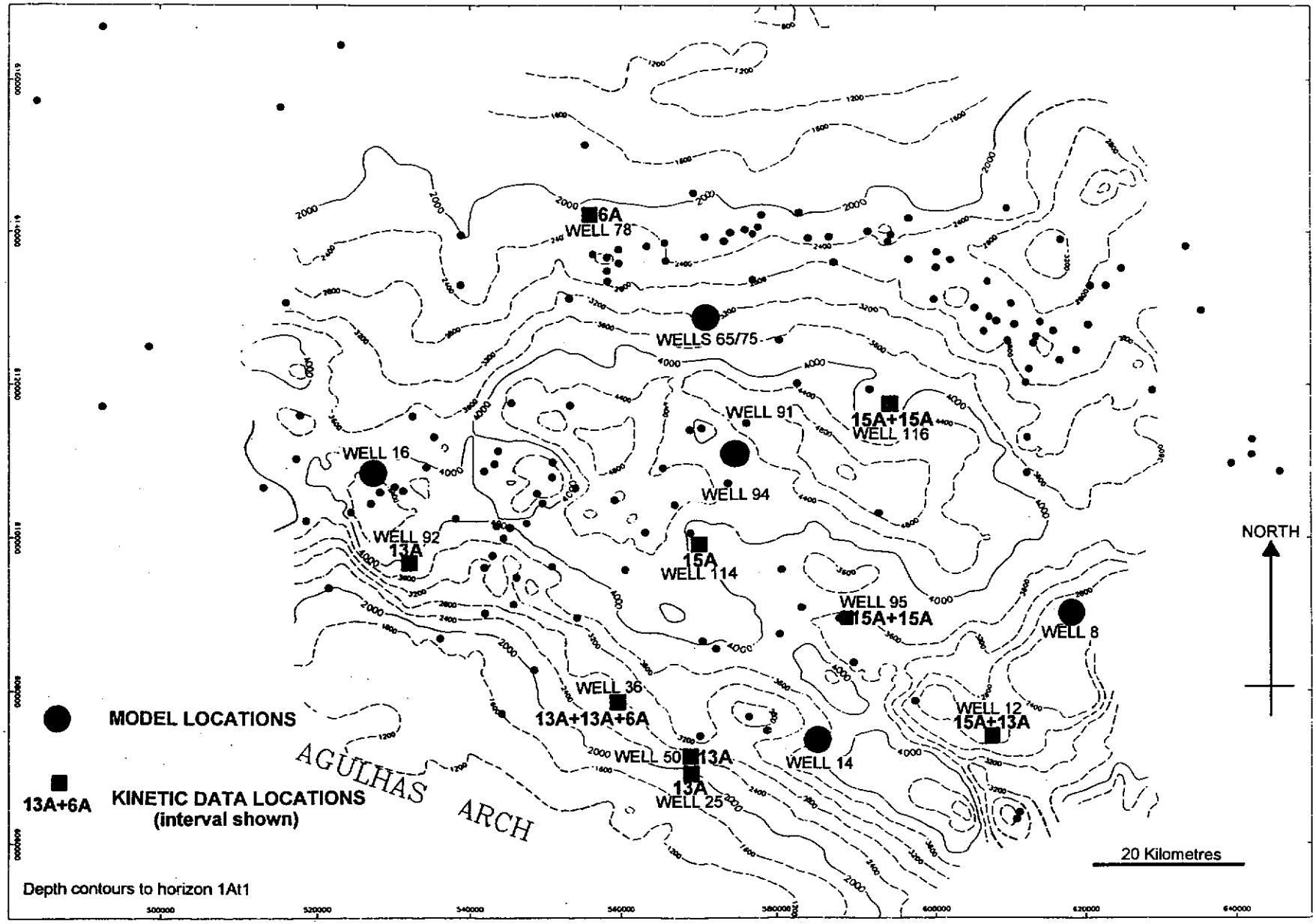

Figure 7.03: Location map of Bredasdorp Basin wells from which samples were taken for kinetic analyses and locations of burial history models.

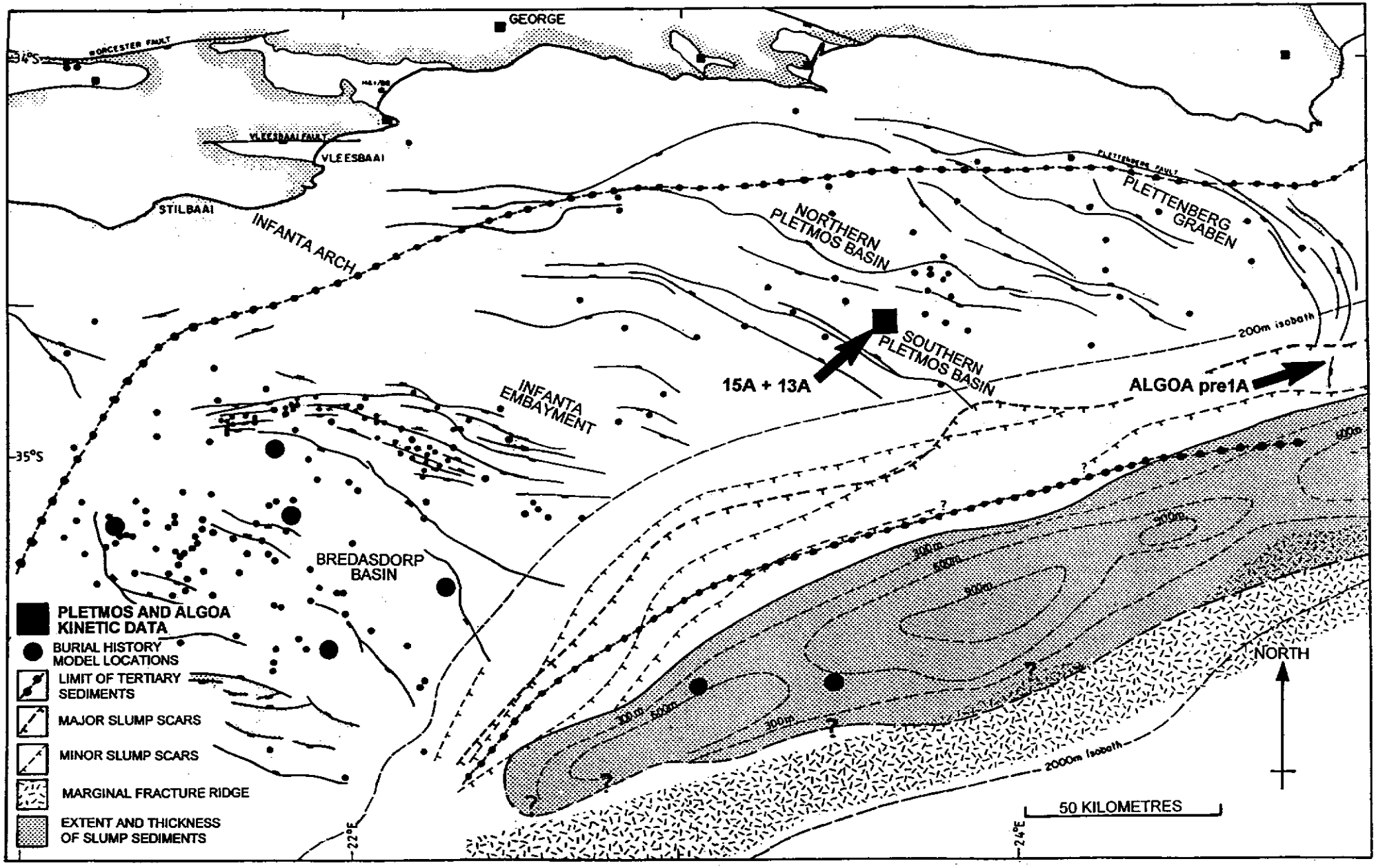

Figure 7.04: Location map of non-Bredasdorp Basin wells from which samples were taken for kinetic analyses and locations of all burial history models.

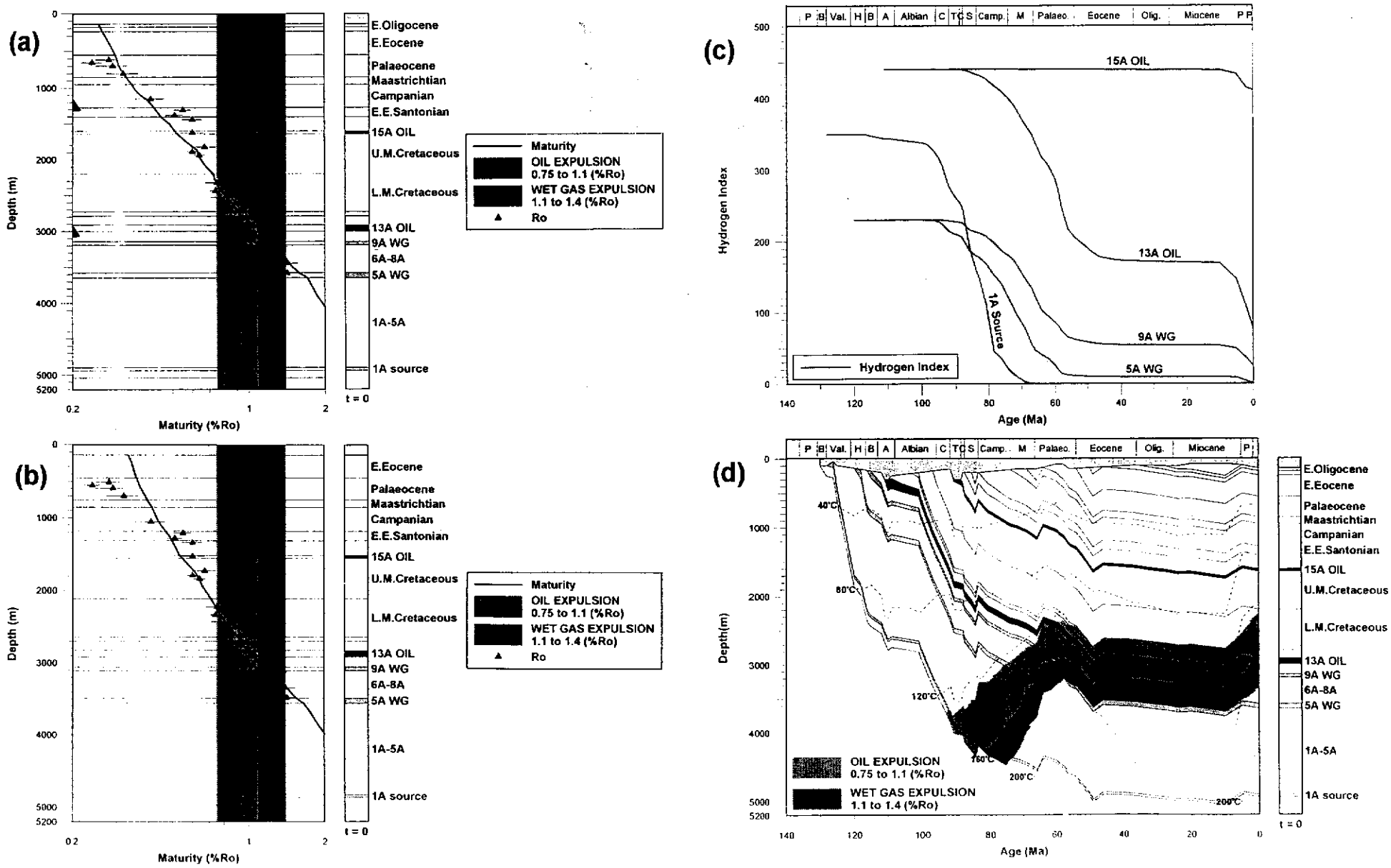

Figure 7.05: Basinmod plots for the central basin location showing (a) modelled vs measured vitrinite reflectance for the model excluding the 1500m of Tertiary erosion, (b) as before but for the model including 1500m of Tertiary erosion (c) calculated hydrogen indices vs time and (d) the burial history diagram.

This lack of major deposition and erosion is largely confirmed from sonic and density logs which do not show unusually high compaction states. In addition, modelled reflectances using the erosion model still do not fully match available reflectance data from Tertiary and Uppermost Cretaceous sidewall core samples from wells in the vicinity of the basin centre (Table 7.02).

Vitrinite reflectance data were inverse-modelled for three of the wells (K.L. Gallagher, 1996, pers. comm.). The results of this modelling showed that a close match with the reflectance values could be obtained by addition of heat late in the Tertiary, but because the stratigraphic data were not then available, the model method could not be pursued.

7.1.5.3. Heat input from fluid flow

One possible model for this focussed heat input has been discussed in Chapter 4 - namely the migration of large volumes of hot water expelled following slumping off the continental shelf in the Southern Outeniqua Basin. Whether this is the only reason or not, the coincidence of the event and the 'missing' heat is remarkable.

A similar need for a late heat input was discussed by Jensen and Doré (1993). They concluded that the 'missing' heat was a function either of the inability of their modelling programme to properly handle recent geological processes (glaciation, overpressuring, rapid subsidence, fluid flow) or of these processes themselves. However, the case they considered was different from the Bredasdorp Basin examples because:

(i) their reflectance curve was concave upwards whereas it is convex upwards in this basin, indicating a shallow heating phase

(ii) recent Bredasdorp Basin sedimentation rates were much slower

(iii) the rocks where the heat event is needed for the model are normally-pressured whereas they are strongly over-pressured in Jensen and Doré's example

(iii) there has been no recent glaciation to perturb the near-surface heat flow

(iv) present day temperatures record a straight-line increase with depth in the Bredasdorp Basin (Fig. 7.02) but not in the example of Jensen and Doré (op cit.).

Similar hot water focussing was used by Zielinski and Bruchhausen (1983) to explain local near-surface heat flow anomalies (~20 mW/m^2 above background) recorded in Tierra del Fuego. They showed that considerable lateral migration of hot water from the compacting basin centre at relatively slow rates (~5 cm/yr.) could account for the thermal anomaly. Gibbons and Herridge (1984) and Gibbons and Fry (1986) invoked similar hydrothermal flows to explain unusual maturity effects in Mesozoic and Cenozoic rocks.

VITRINITE DATA FROM LATE CRETACEOUS AND TERTIARY SAMPLES.					
SAMPLE DATA			16Bl1-17At1	17At1-22At1	22At1-SF
			K-X	X-L	L-SF
			L. Sant.-E. Camp	L. Camp.-Maas.	Palaeo.-Holoc.
WELL	DEPTH	TYPE	89-80 Ma	80-66 Ma	66-0 Ma
102	752.5	SWC		0.43	
102	797	SWC	0.34		
102	842	SWC	0.45		
102	900	SWC	0.32		
102	952	SWC	0.4		
91	600	SWC		0.28	
91	639	SWC		0.24	
91	682	SWC		0.29	
91	786	SWC	0.32		
91	842	SWC	0.38		
91	920	SWC	0.26		
91	960	SWC	0.33		
94	794	SWC		0.44	
94	1123	SWC	0.66		
94	1149	SWC	0.44		
160	1514.5	SWC	0.57		
160	1620	SWC	0.43		
160	1660	SWC	0.55		
9	515	SWC		0.52	
9	585	SWC		0.57	
9	620	SWC		0.52	
11	806	SWC		0.45	
11	1190	SWC	0.56		
11	1240	SWC	0.57		
11	1345	SWC	0.62		
14	720	RC			0.54
14	1370	RC		0.55	
14	1440	RC	0.56		
16	625	SWC	0.49		
50	1010	RC	0.58		
52	510	RC		0.51	
52	660	RC	0.57		
18	640.8	SWC	0.51		
18	830	SWC	0.47		
18	878	SWC	0.58		
18	931	SWC	0.56		
18	993	SWC	0.56		
18	1042.6	SWC	0.6		
18	1067.5	SWC	0.55		

			K-X	X-L	L-SF
			L. Sant.-E. Camp	L. Camp.-Maas.	Palaeo.-Holoc.
WELL	DEPTH	TYPE	89-80 Ma	80-66 Ma	66-0 Ma
47	791.5	SWC		0.57	
47	850	RC		0.55	
47	870	RC		0.61	
47	890	RC		0.6	
47	924	SWC		0.74	
47	930	RC		0.7	
47	963.5	SWC		0.66	
47	1000	SWC		0.62	
47	1023	SWC		0.64	
47	1080	RC		0.7	
47	1082	SWC		0.62	
47	1110	RC		0.78	
47	1124	SWC		0.63	
47	1150	RC		0.7	
47	1200	RC		0.75	
47	1260	RC		0.74	
47	1450	RC	0.83		
47	1560	RC	0.8		
105	1532	RC	0.52		
105	1612	RC	0.53		
105	1635.5	SWC	0.58		
105	1944	SWC	0.64		
105	1969.5	SWC	0.63		
128	1524	RC	0.6		
13	1283	SWC		0.36	
13	1378.7	SWC		0.4	
13	1486.5	SWC	0.4		
WELLS	SAMPLES		K-X	X-22At1	22At1-SF
15	66		36	29	1

Table 7.02: All vitrinite reflectance values measured from late Cretaceous and Tertiary SWC samples.

Hot water generated by this process, together with any hot fluids circulating at the plate boundary and released during subsidence of the AFR ('heat-mining') would be able to migrate into the Bredasdorp Basin mainly below the regionally-developed 15A source rock. A second regional seal, that of the 13A source shale, onlaps the eastern basin highs, essentially closing off these highs to water ingress. Hence much of the water which entered the Bredasdorp Basin would probably have migrated between these shales, focussed in the area between the eastern and north-eastern highs (Fig. 4.34). The volume of fluids migrating below the 13A seal is probably only a small proportion of the total expelled as calculations show only ~20% being derived from rocks deeper than ~3200m (Table 4.09). The interval between these two regional seals is dominantly argillaceous, although there are several thin, probably discontinuous silty intervals, and through-flow of fluids would be slow and tortuous.

Input of large volumes of fluid to this region after each of the several slumps would result in local fluid build-up and development of overpressure. Faulting coeval with overpressured fluid build-up in the northern half of the basin (Cartwright, 1994) is evident on the cross-basin seismic line shown in Fig. 3.03. The faults are well-developed above and below horizon 15At1, suggestive of periodic pressure break-through into post-15At1 rocks. Hydrocarbon generation is unlikely to cause this overpressure as there are no mature source rocks nearby and maturity levels are not high enough to cause oil-to-gas cracking (Barker, 1990).

This periodic flow of heated water could have been the mechanism for the increased reflectance values. Indeed, this part of the basin is the area in which the low vitrinite reflectance offsets, and the high maturities suggest that it was most affected by the hydrothermal input (Fig. 4.34). Rocks in this area are now no longer overpressured (Brink and Winters, 1989; Larsen, 1995) indicating that if a hydrothermal charge was the source, it was not recent.

Fluid flow rates are likely to range between 5-100 cm/yr. (Zielinski and Bruchhausen, 1983; Jessop and Majorowicz, 1994; Ungerer et al., 1990), suggesting that the last hydrothermal event could have been as recent as 2 Ma ago. It is not known how long a period the slumping occupied of the past ~10 Ma. Slumping probably started after ~10 Ma and extended at least until the Plio-Pleistocene glaciation when water levels were lower. If the period lasted for most of the 10Ma, then additional heating of only 30-50 mW/m^3, focussed in Upper Cretaceous sediments, is needed to match modelled and measured reflectances. If the period of heating lasted a shorter time, then additional heating would be proportionally greater.

7.1.6. Modelled hydrocarbon generation.

In this study, the LLNL model of hydrocarbon generation is applied. This calculates generation rates of four major hydrocarbon groups (C1, C2-4, C5-14, C15+) plus residue for each oil-generative source rock, using the kinetic data in Table 4.01.

Activation energies and frequency factors of cracking reaction kerogen rate constants effective during hydrocarbon formation, can be used to predict the rates of generation of hydrocarbons from different types of kerogen (Ungerer et al., 1986). Such data are acquired from multiple Rock-Eval pyrolyses using the OPTKIN programme. The hydrocarbon generation rates calculated by this method are used to determine pseudo-activation energies for the sample. In each example from the Bredasdorp Basin, the distribution is skewed showing the mixture of organic material. The available data include samples from outside the Bredasdorp Basin which are used only in confirming that the average values used in the Bredasdorp Basin are valid for the western Southern Outeniqua Basin models.

In general, immature samples should be used to evaluate kinetic models, although it is preferable to use samples in which most of the early diagenetic reactions are complete and the reactive kerogen is largely de-oxygenated. However, few such samples are available in this basin. Indeed there are no samples of immature oil-prone source rocks in the Bredasdorp Basin. The least mature are from the basal 15A sequence in well 99 where R_O=0.58% (sample 39). All other samples used to determine kinetic reaction rate parameters are known to have higher reflectances than this (Table 4.01). Therefore the low activation energy organic material had already been generated and kinetic data acquired from these samples indicate an initial activation energy which may be too high, and a total generation potential which is too low.

7.1.7. Kinetic data

Reaction kinetics data have been generated from 14 samples representing the 3 major source rocks in the Bredasdorp Basin (Table 4.01). All available kinetic data generated from borehole samples from the Bredasdorp Basin are given in Table 4.01. Averages of the 15A, 13A (both oil-prone and wet gas to oil-prone) and 6A data are used in modelling basinwide, even though all of the 13A and 15A samples are from the southern flank (Fig. 7.03). This sample concentration results from the concentration of SWC samples in those wells, because few of the central wells penetrate deeper than 13At1, and because few north flank wells encountered rich source rocks in post-6A rocks.

There are several source intervals (pre-1A, 5A and 9A-12A) for which kinetic data are not available. In these cases, values from the most similar 15A, 13A and 6A source

rocks are used. In addition, default network structures, kerogen constants and product properties have been modified taking into account the proportions and properties of known hydrocarbon types, resulting in four regionally distributed source rocks (BREDOIL, BREDWGOIL, BREDWG, BREDDG). A favourable comparison between volumes of hydrocarbons likely to be generated from source rocks in certain parts of the basin (Davies and Van der Spuy, 1997) and the actual volumes of reservoired hydrocarbons suggests the generation assumptions are valid.

Kinetic data employed are derived from open-cell Rock-Eval pyrolysis. In that process, products are free to evaporate as soon as they are formed, taking no further part in reactions (although products are sometimes retained on cell walls, rock fragments and remaining kerogen). This is in contrast with hydrous pyrolysis methods where water is included as a reactant (as in natural sediment) and the cell is sealed so that none of the products escape. The result of this is that the products of hydrous pyrolysis react through several steps and produce more 'natural-looking' compounds with few iso-alkane doublets (Lewan, 1985). Because of this, the range of components produced in anhydrous pyrolysis is only an approximation of the range generated in the subsurface and leads to an apparently faster reaction rate compared to hydrous pyrolysis. Burnham et al. (1987) suggest that at geologically important maturation rates, this may constitute only a minor difference.

Analyses of each sample were carried out at programmed heating rates of 5°C/min., 15°C/min., 25°C/min. and 50°C/min. These rates were determined from temperatures recorded by the oven thermo-couple and calibrated against known heating rates for IFP standard samples. The rates of build up and decline of the S2 peak were modelled in the OPTKIN programme to determine the activation energy distribution between 35 and 85 kcal/mole and calculate the reaction rate frequencey factor.

7.1.8. Expulsion.

The total amount of hydrocarbons available for expulsion from each source rock is commonly calculated by subtracting the amount needed to fill a proportion of the pore space, from the amount of hydrocarbons generated. Estimates of the proportion of pore space which must be filled before expulsion can take place range from 10-25% (Ejedawe, 1986; Ekweozor and Strausz, 1983). The proportions of each class of hydrocarbon expelled (methane, wet gas, condensate or oil) are based on analytical data (Tissot et al., 1982; Ozkaya and Akbar, 1991). The Basinmod programme does not allow for differentiating between oil and gas retention. Since this is a geologically unreasonable situation, minimal pore saturations have been used in the modelling, and empirically derived proportions of unexpelled oil quantities are subtracted from the modelled amounts (Davies, 1988b; 1990) to approximate the start of expulsion.

7.1.9. Cracking

Hydrocarbon cracking in response to increasing maturity has been investigated by Espitalié et al. (1988) and Ungerer et al. (1986; 1988). They simulated cracking reactions of different types of kerogen to establish a general cracking-rate algorithm. They modelled oil cracking to gas following certain basic reactions and determined the activation energies of those reactions. These are used in Basinmod. The default values calculate the rates of generation of gas and condensate from cracked oil, but cracking is now thought to dominate at only high maturities (Mango, 1991).

7.1.10. Regional events

One further regional event likely to have introduced heat to the basin heat flow and which affected maturation is the transit of the plate trailing edge spreading centre during the Turonian. However, it is likely to have a minimal effect in the basin except in the south-eastern region and in the southern part of the Southern Outeniqua Basin.

7.2. BREDASDORP BASIN MODELS

To evaluate the hydrocarbon generation history of the Bredasdorp Basin, five burial history models have been constructed at widely distributed locations across the basin. They are located in the east central part (well 8), in the west (well 16), on the north flank (wells 65 and 75), on the south-eastern flank (well 14) and in the basin centre between wells 91 and 94 (Fig. 7.03). Each model location was selected to highlight characteristic features of the burial history of that part of the basin and to show differences in hydrocarbon maturation rates across the basin.

All models take into account the effects of rifting and associated thermal subsidence. They all address regional maturation from heat flows associated with the movement of the African continent over the Shona/Bouvet hotspot and all take account of uplift and downwarp events (Fig. 2.11). Water depth variations derived from sequence stratigraphic studies in the basin are also included. (Brown et al., 1995). In addition, all take into account heating associated with the hydrothermal charge from slump-induced compaction of western Southern Outeniqua Basin sediments considered to have resulted from the Miocene initiation of a new mantle swell, the 'African Superswell'.

In general, the most important results of the modelling are used in well by well correlation of the timing of hydrocarbon generation and in the quantification of hydrocarbon expulsion. In this study, one of the most important aspects is the appreciation that earlier models showing post-rift cool-down alone are inadequate and that even when the transit of the known Late Mesozoic mantle swell and associated

hotspot are included, the models still do not fit all the data. Modelling of a late near-surface heat input from an unknown source was suggested by C. Cornford (1994, pers. comm.) in order to balance modelled and actual vitrinite reflectance values. The match between this requirement of a late heat input and the initiation of the African Superswell (Hartnady and Partridge, 1995) and timing of the 'Agulhas Slump' is close (Dingle, 1977).

7.2.1. Basin Centre Model

The model uses lithology and temperature data from wells 91 and 94. Neither of these wells extended far below horizon 5At1, so depths of deeper horizons are modelled from seismic data using regional time:depth curves. Lithologic data is extrapolated from nearby wells. The model is characterised by a moderate present day heat flow (57 mW/m^2) calculated from static borehole temperatures in wells 91 and 94. Similar heat flows are found in other wells in the area and temperatures match closely (Tables 3.02, 3.03 and Appendix, Table A3). It is possible that regional heat flows were locally accentuated by flow of hot fluids up the *en echelon* WNW-ESE faults, which cut the late syn-rift sediments in the region and which extend close to horizon 13At1 in the central basin (Fig. 4.03). There are no intrusions in this or the surrounding boreholes and there is no evidence of intrusions on seismic lines from the area. Regional palaeoheat flow is likely to have been high during the Early Tertiary (~60 Ma) resulting in partial annealing of apatite grains in Uppermost Cretaceous sediments at 440 m (Eurotrack, 1996).

This report shows that a Late Campanian sandstone sample, composited across the interval 440-550m, contains apatite grains in which spontaneous fission tracks were encountered. The track density confirmed the biostratigraphically determined age. All these tracks were largely annealed indicating partial erasure by temperatures between 100-115°C reached at 60 ±5 Ma. They also show that cooling was rapid after the event and remained below 60°C to the present day. The present day temperature, extrapolated between a static (corrected) borehole temperature of 96°C at 2690m and a sea floor temperature of 10°C at 143m, show the sample is at ~ 20°C. Backstripping the Tertiary sediments from the area results in this sediment being within 100m of sea floor. The lack of intrusions in the area indicate another major source of heat is necessary to result in these high temperatures so shallow in the succession.

Heat flows modelled during the hotspot transit result in a match of measured and modelled reflectances (Fig. 7.05a; Duncan, 1981). The model results in a high generation rate in the Early Tertiary for 5A-13A source rocks (Figs. 7.05c; 7.05d). However, it barely affects generation from the 1A source as this traversed both gas and oil windows before the hotspot heating became effective (Figs. 7.05c, 7.05d). Therefore gas and oil could have been generated in quantity from these deeper source

rocks long in advance of any basin tilting resulting from the hotspot transit (see section 7.4).

The 5A wet gas-prone source rock, which is not present at the wellsite, but is probably developed just east of the model location (Fig. 4.09), completed its traverse of the wet gas window and entered the dry gas window at the same time (Fig. 7.06c). Some of this wet gas might have been expelled from the source and was retained in reservoirs during later tectonism. The high pressure gas-condensates found below horizon 9At1 in the basin centre may have come form this source.

7.2.2. East Central Model.

Well 8 is located on the eastern igneous high (Fig. 3.04). This area has been significantly affected by localised heating from Upper Cretaceous-Lower Tertiary intrusives as well as from the mantle swell and hotspot transit. Based on pyrolysis data, present day hydrocarbon potential of 13A source rocks in the well is low (HI~150) but it was originally higher because it is presently highly mature (R_O~1.0-1.1%). Indeed, maceral data record that fluorescing amorphous kerogen dominates (Rowsell et al., 1979), hence the original potential was wet gas-to-oil and the HI could have been >400. The S1 is unusually low (~0.5‰) for such a good quality mature source rock, although this could reflect steam distillation of generated oil and any detrital bitumens out of the sandstones by later hydrothermal fluids.

The coincidence between reflectances modelled from estimated palaeo-heat flows and measured reflectances is evident in Fig. 7.07a suggesting that modelled heat flows provide a reasonable representation of geologic events. The high rate of maturation increase of the 1A sequence is inferred from its rapid rate of hydrogen index reduction (Figs. 7.07b and 7.08b) coincident with the period of maximum heat input. Yet the burial history and maturation modelling of this well show that younger source rocks did not enter the oil window prior to the intrusive event (Fig. 7.07c). Generation of oil and wet gas from possible 1A source rocks in expellable volumes just prior to the main intrusive event (Fig. 7.08b), is an effect both of rapid burial during the Maastrichtian (Fig. 7.05) and incipient heat from the mantle swell.

The HI of the 13A source rock matches the measured values quite well (~150), confirming the correctness of the modelling parameters used (Fig. 7.07b). The burial history model shows this source rock to have entered only the top third of the oil window during the igneous phase and to have become more fully mature quite recently (Fig. 7.08a). Kinetic modelling of hydrocarbon generation shows a short expulsion pulse from the 13A source rock associated with the hotspot transit and intrusive event (Fig. 7.08a). Slow thermal subsidence through the Eocene after the hotspot transit may

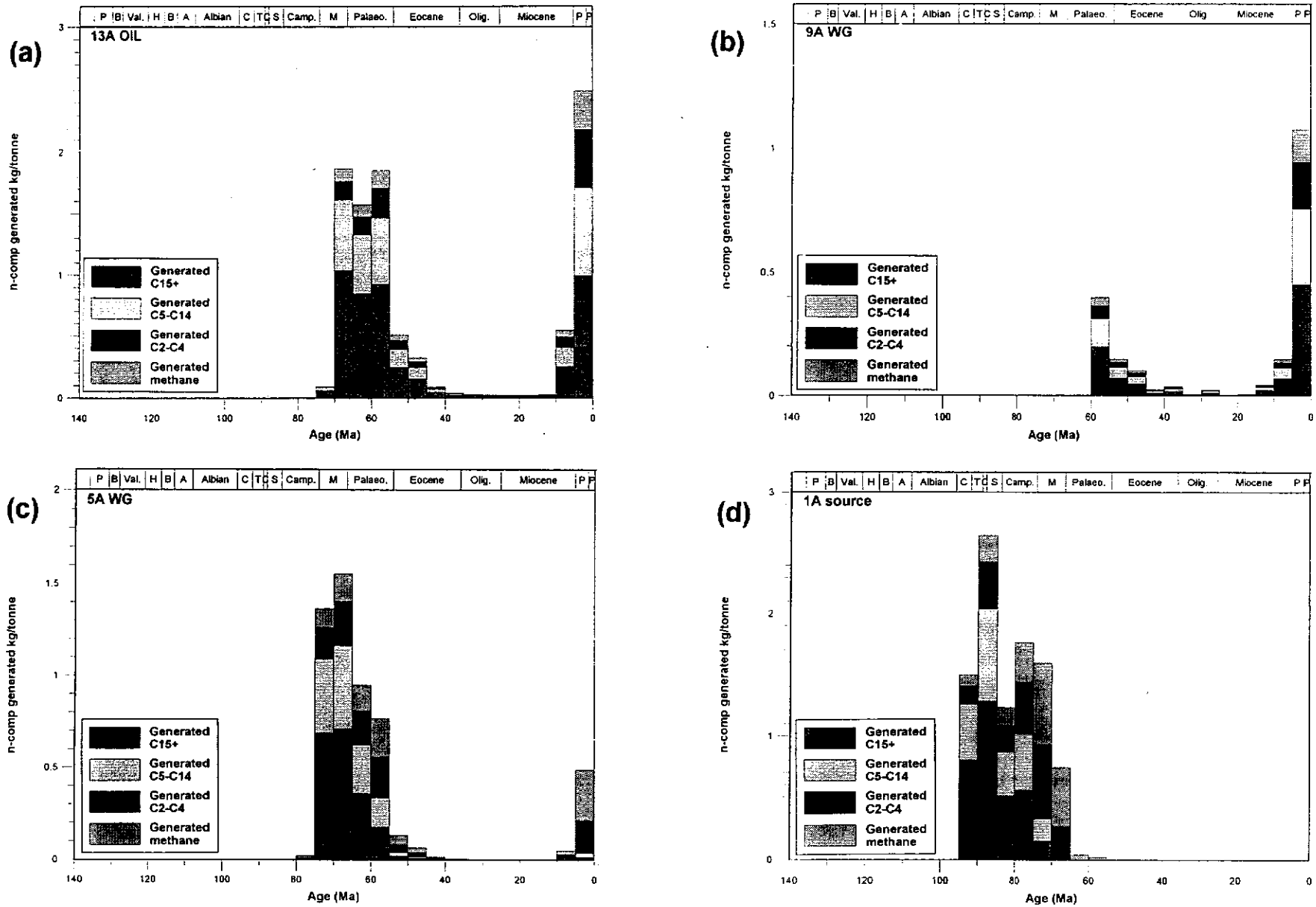

Figure 7.06: Basinmod plots for central basin location showing mass of hydrocarbons generated from (a) 13A, (b) 9A-12A, (c) 5A and (d) 1A source rocks.

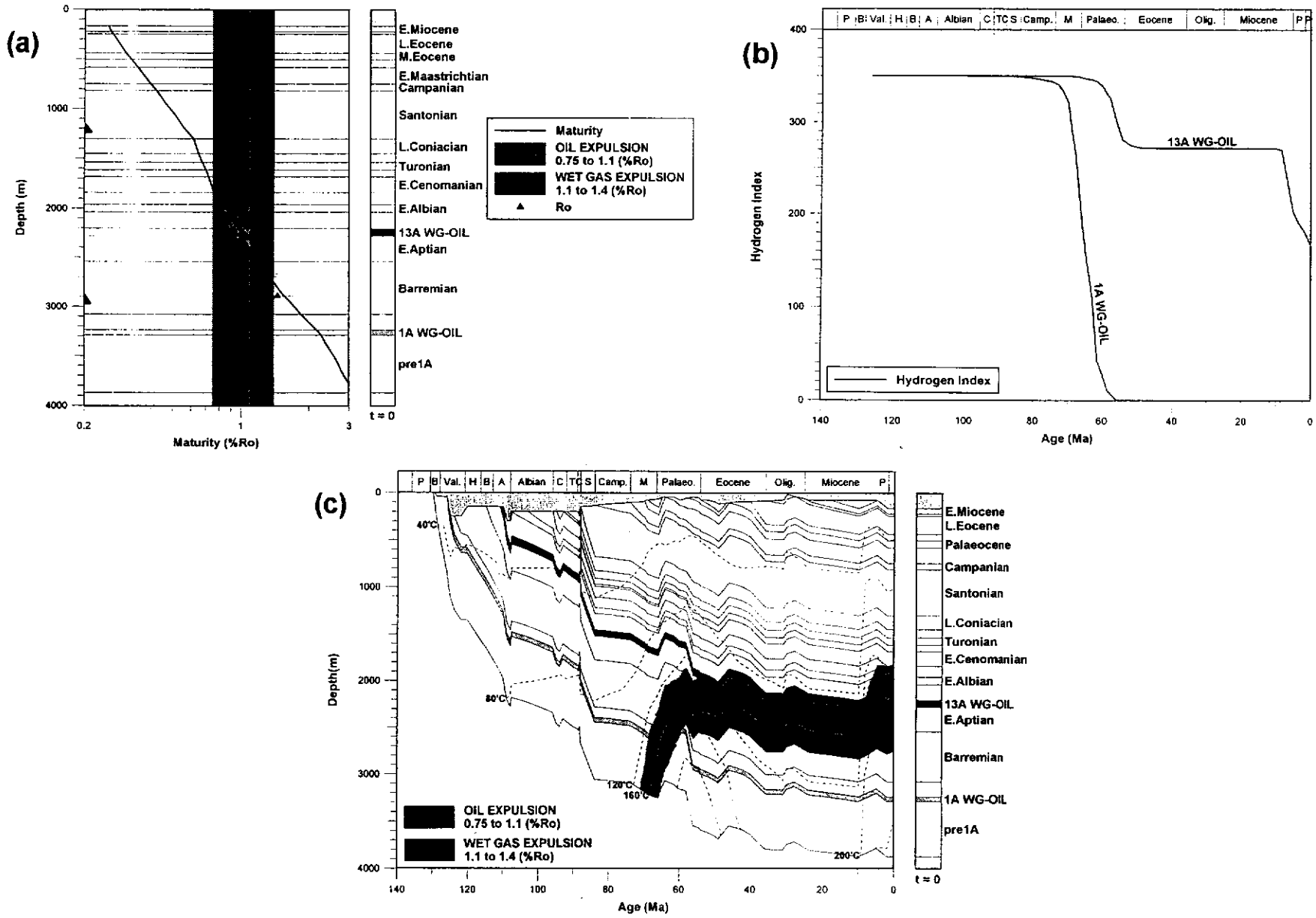

Figure 7.07: Basinmod plots for eastern basin location showing (a) modelled vs measured vitrinite reflectance, (b) calculated hydrogen indices vs time and (c) burial history diagram.

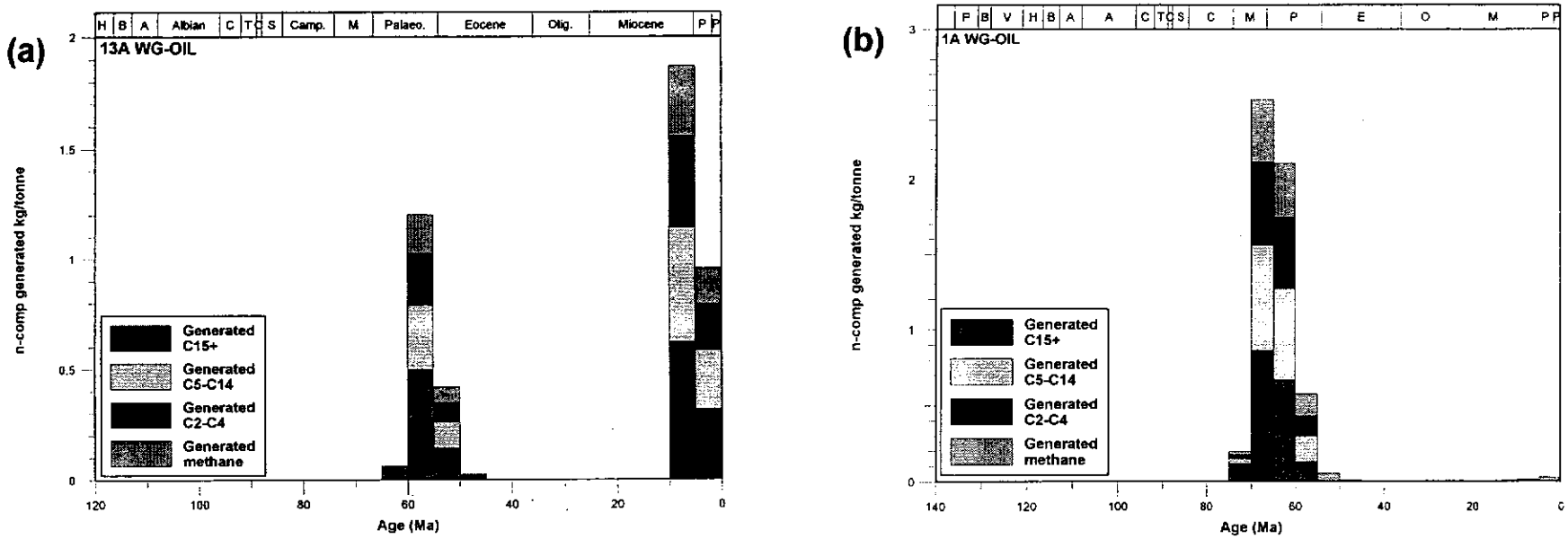

Figure 7.08: Basinmod plots for eastern basin location showing mass of hydrocarbons generated from (a) 13A and (b) 1A source rocks.

be the cause of the increased water depth prevailing during later Tertiary sedimentation, which could also have been the cause of the reduced calcite dominance (McMillan, 1986).

Apart from the erosion due to the great topographic elevation of the still partly emergent Agulhas Arch, which supplied clastic sediments in abundance to the south-eastern basin (McMillan, 1986), most of the Eocene rocks in the whole of the Bredasdorp Basin area are sand-rich. This may also be partly an effect of current winnowing by the early Agulhas Current (McMillan, 1986; Winter and Martin, 1990).

During the Mid-Oligocene, the effects of the excess heating diminished and thermal subsidence prevailed as a result of the African continent drifting further away from the hotspot. This culminated in subsidence of the Agulhas Arch (McMillan, 1986). The rate of maturation continued to decrease until the Early Miocene when heat input resulting from the incipient mantle swell and the resulting shallow hydrothermal event increased maturation enough to mature the Aptian source further into the oil window. Indeed, the generation modelling shows that half the oil generation from the 13A source rock took place during the past 10 Ma (Fig. 7.08a).

7.2.3. Western model

Well 16 was drilled to intersect a deep pre-1At1 half-graben (Figs. 3.08 and 3.04) close to the Alphard Banks region of Tertiary intrusives (Fig. 2.09, Dingle and Gentle, 1972). In nearby wells which intersected intrusives, downhole maturation parameters show only local effects of igneous heating, but regional heating during the hotspot transit was more pervasive. The heat flows required to match measured and modelled reflectance values appear higher in this well than in the basin centre well. However, some of this high maturity effect may be spurious as there is reworked vitrinite in this well (Van der Spuy, 1996).

There are no known syn-rift source rocks in well 16. However, several hundred metres of halite-bearing siltstones are present in the well in syn-rift sediments. These deposits represent a sabkha environment of limited areal extent (P.B. Burden, 1995, pers comm.) or a marginal half-graben (Banks et al., 1993; Jungslager, 1996) of possibly greater extent. In similar situations elsewhere, such environments can host significant oil source potential (Barnard et al., 1992). In addition, there were no reservoired quantities of hydrocarbons in intercalated sandstones either within or below the evaporitic section. This may indicate either that source rocks do not exist below or that if they do, the halite-bearing rocks continue below TD, sealing off any deeper hydrocarbons.

Halites also impact on the maturity modelling because of their high thermal conductivity. In well 16, the halite-rich interval below 4400m is marked by a near-vertical vitrinite reflectance trend (Fig. 7.09a) capped by thick (up to ~1000m) shales which produce a much flatter trend.

The modelled maturation history shows the two main heating events to have influenced the region (i.e. Late Jurassic-Early Cretaceous cool-down and a Late Cretaceous-Early Tertiary hotspot transit) and a small effect due to the Late Tertiary hydrothermal charge. However, there was also a rapid maturation increase of the 1A source rock during the Albian-Santonian (Fig. 7.09b). This is possibly a function of thermal subsidence or base level change (due to continued graben growth) and halokinesis initiated by rapid sediment deposition during the Albian (Burden, 1993; Jungslager, 1996).

The HI plot shows close agreement between measured and modelled reflectances which result in modelled generation of hydrocarbons from 1A source rocks as early as Mid-Cretaceous (Fig. 7.09b). However, modelled generation started as late as the Miocene from the youngest source rocks,(Fig. 7.10d). The live oil show in deep marine sandstones within the 13A source interval may reflect recent generation.

First hydrocarbon generation from 9A-12A source rocks started in the Late Maastrichtian (Fig. 7.10b), although the main oil generation window is reached only during the Early Eocene. In addition to this late start, absorption and micro-reservoiring of 1.0-1.5 kg oil/tonne rock (Davies, 1988b and 1990) largely deplete the shales of 'free' oil so that they become gas expellers only.

7.2.4. North Flank Model

The two wells (65 and 75) on this structure are only a kilometre apart and for modelling purposes are treated as one well. They are characterised by the presence of earliest drift (1A-6A) source rocks in contrast with the later drift (9A-13A) source rocks dominating in the southern and western regions. Other thin and discontinuous source rocks, such as those in the 8A interval in well 75 (sample 24 in this study) do not appear separately on the source rock distribution maps (Figs. 4.07-4.17) but are included in the summed thickness of the major interval (i.e. 6A-8A).

The wells are at least 50 km from the nearest expression of igneous activity but the model still needed a small, Early Tertiary heating input during the hotspot transit to match modelled and measured reflectances. Indeed, overall palaeotemperature gradients of many north flank wells are higher than those in the basin centre. This may reflect rapid heat flow up flank faults and through the sediment cover in contrast to wells in the basin centre, which is blanketed by thick shales (Fig. 3.03). Indeed the maturity

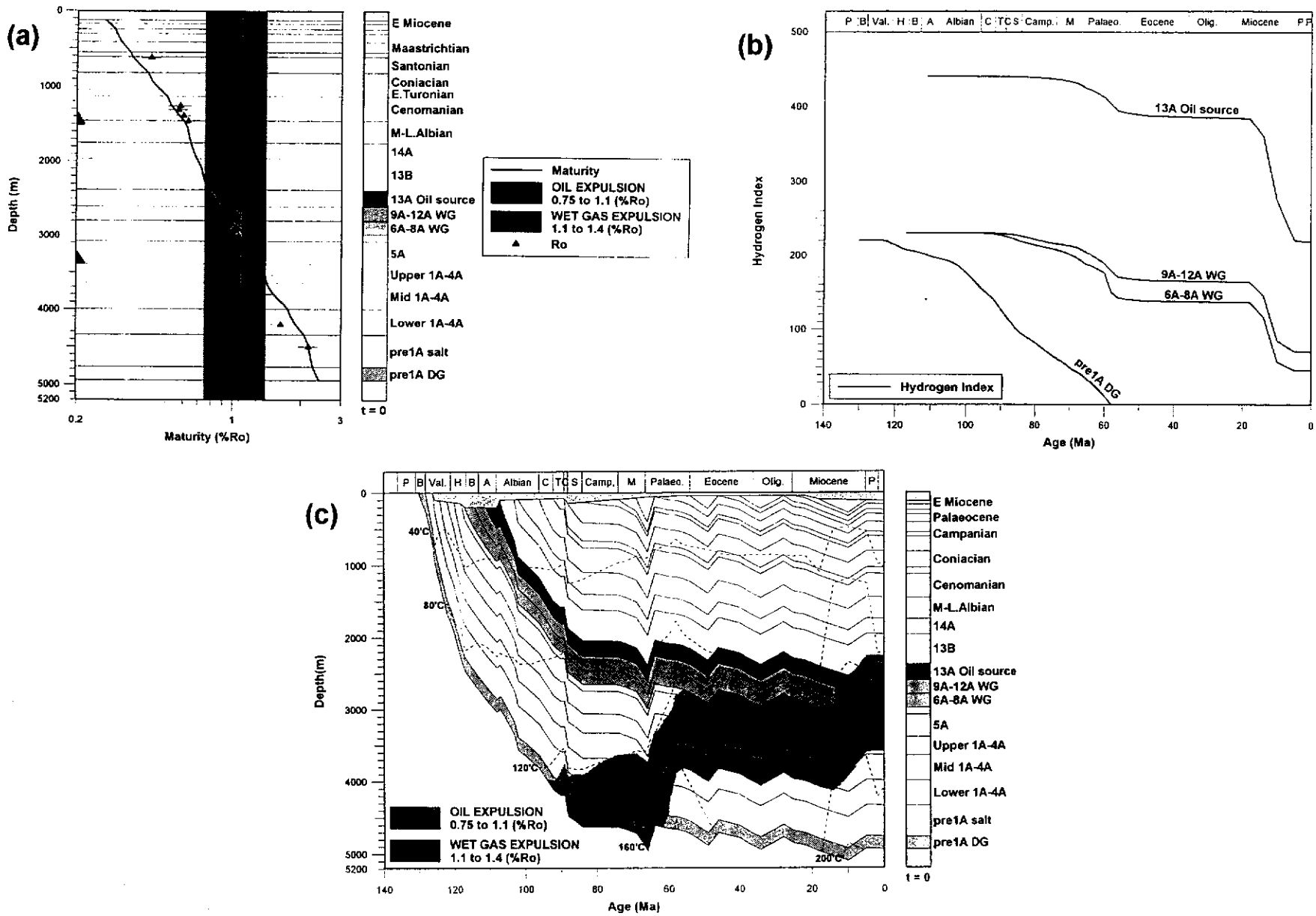

Figure 7.09: Basinmod plots for western basin location showing (a) modelled vs measured vitrinite reflectance, (b) calculated hydrogen indices vs time and (c) burial history diagram.

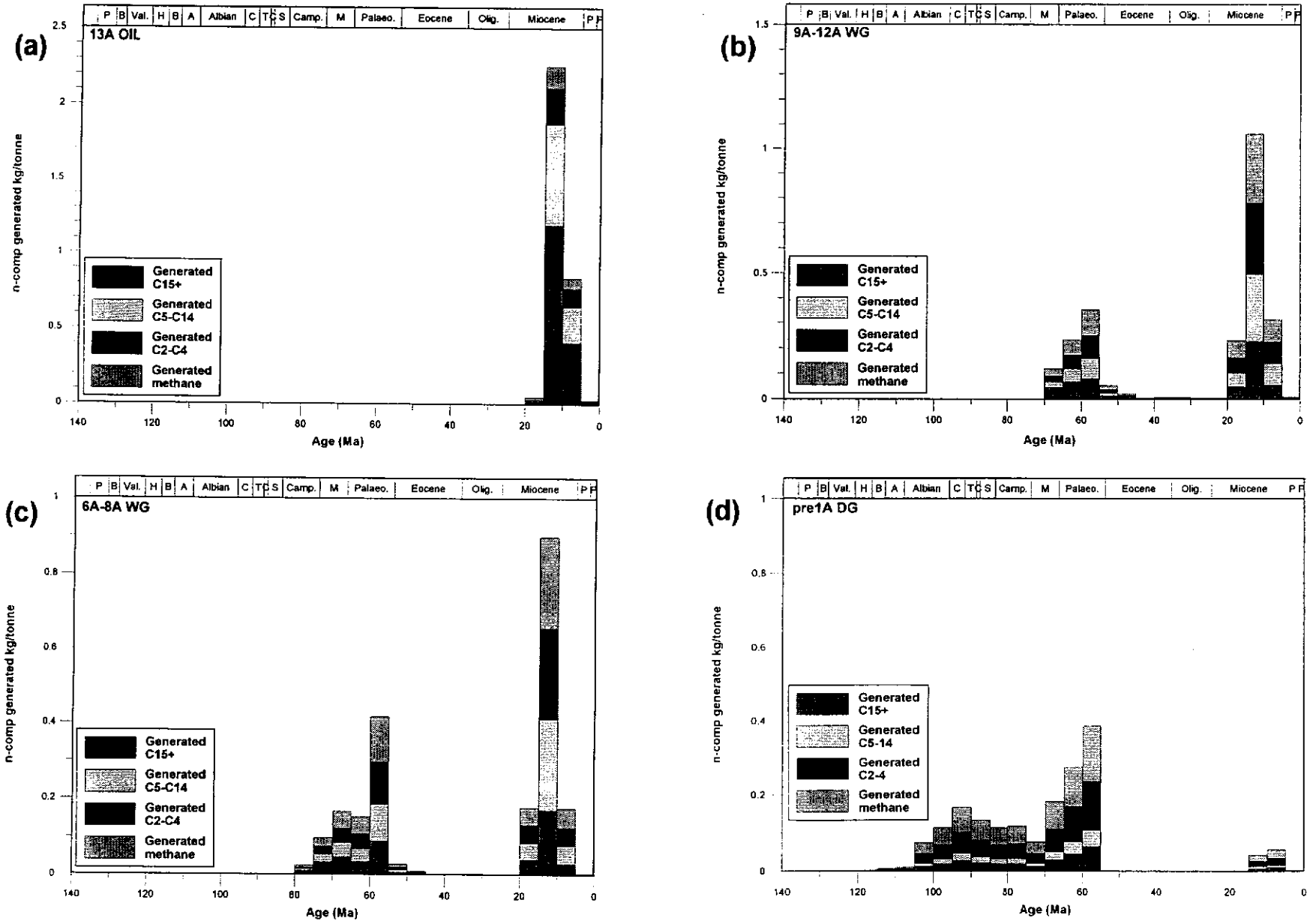

Figure 7.10: Basinmod plots for western basin location showing mass of hydrocarbons generated from (a) 13A, (b) 9A-12A, (c) 6A-8A and (d) pre1A source rocks.

plot (Fig. 7.11a) shows a slight mismatch between modelled and measured reflectances both above and below the 9A rocks (barely within the error range), which may be caused by this heat flow. However, the wells are located in an area from where much of the early rocks were eroded and transported into the basin (Burden and Gasson, 1992). Incorporation of oxidised kerogen from these reworked shelf rocks during the erosion of the pre-9A unconformities may be responsible for the slight residual mismatch.

Modelling of HI changes shows a significant period of wet gas and oil generation from 5A-6A source rocks in the Late Cretaceous, largely resulting from rapid post-Turonian burial - although it is unlikely that any Turonian-sourced oil was expelled (Fig. 7.11b). This rapid burial is evident on the burial history diagram (Fig. 7.11c) and on plots of generated hydrocarbons (Figs. 7.12c and 7.12d). However, rapid burial does not appear to have significantly influenced generation from 13A source rocks (Fig. 7.12b) because they are much shallower.

Through the Late Cretaceous and Tertiary the overall burial rate was minimal and little further generation or expulsion occurred. However, a small maturation increase during the past 10 Ma from the hydrothermal charge added to the quantities of hydrocarbons generated. In any event, the 13A shales are unlikely to expel any oil or even large amounts of gas owing to their poor quality. Hence reservoired hydrocarbons found in wells 65 and 75 which prove to be locally sourced, most likely result from the Mid- to Late Cretaceous fill rather than the hotspot transit or Late Tertiary heating.

7.2.5. South Flank Model

South flank wells, of which well 14 is a typical example, were mostly drilled early in the exploration of the basin and were only recently analysed using modern methods. In many cases, the cuttings samples dried out prior to preparation for analysis and as a result disaggregated on washing. For this reason, these samples were less rigorously washed than usual and consequently a higher proportion of mud was retained. Since most of these early wells were drilled with a lignosulphonate mud system, the cuttings do occasionally contain lignite additive which increases TOC in pyrolysis analyses. Fortunately the lignite has low reflectance (R_o~0.3%), which influences reflectance only in those samples with low *in situ* reflectance. Where *in situ* reflectance is high, contamination is readily distinguished. Downhole caving too was more of a problem in the early wells but where core or SWC samples were interspersed with cuttings the results still largely match (Appendix A, Table A7).

Reflectance values recorded in well 14 (Fig. 7.13a) display three major changes in slope at ~1600m, ~2850m and ~3520m. Two of these (~1600m and ~3250m) coincide

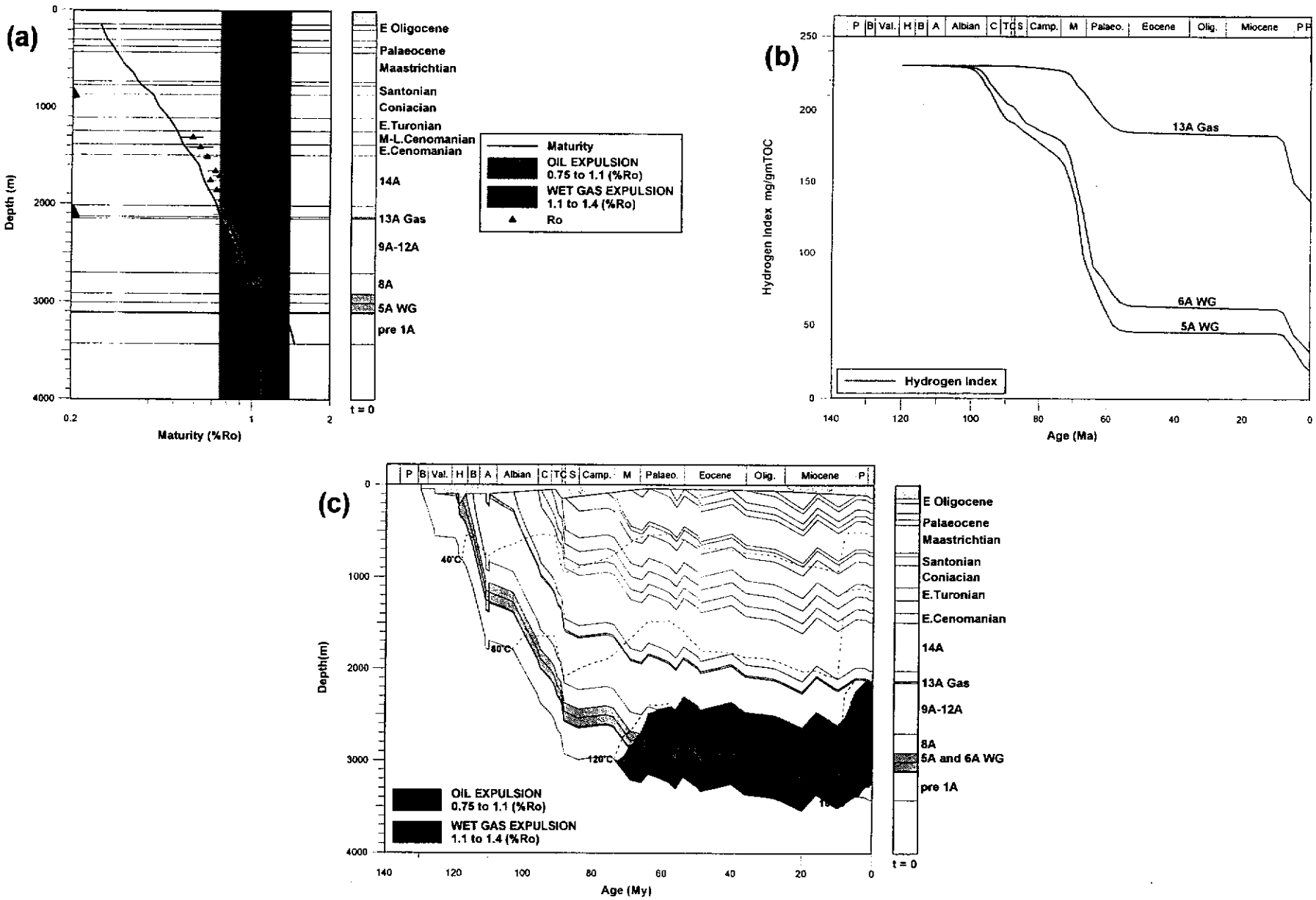

Figure 7.11: Basinmod plots for northern basin location showing (a) modelled vs measured vitrinite reflectance, (b) calculated hydrogen indices vs time and (c) burial history diagram.

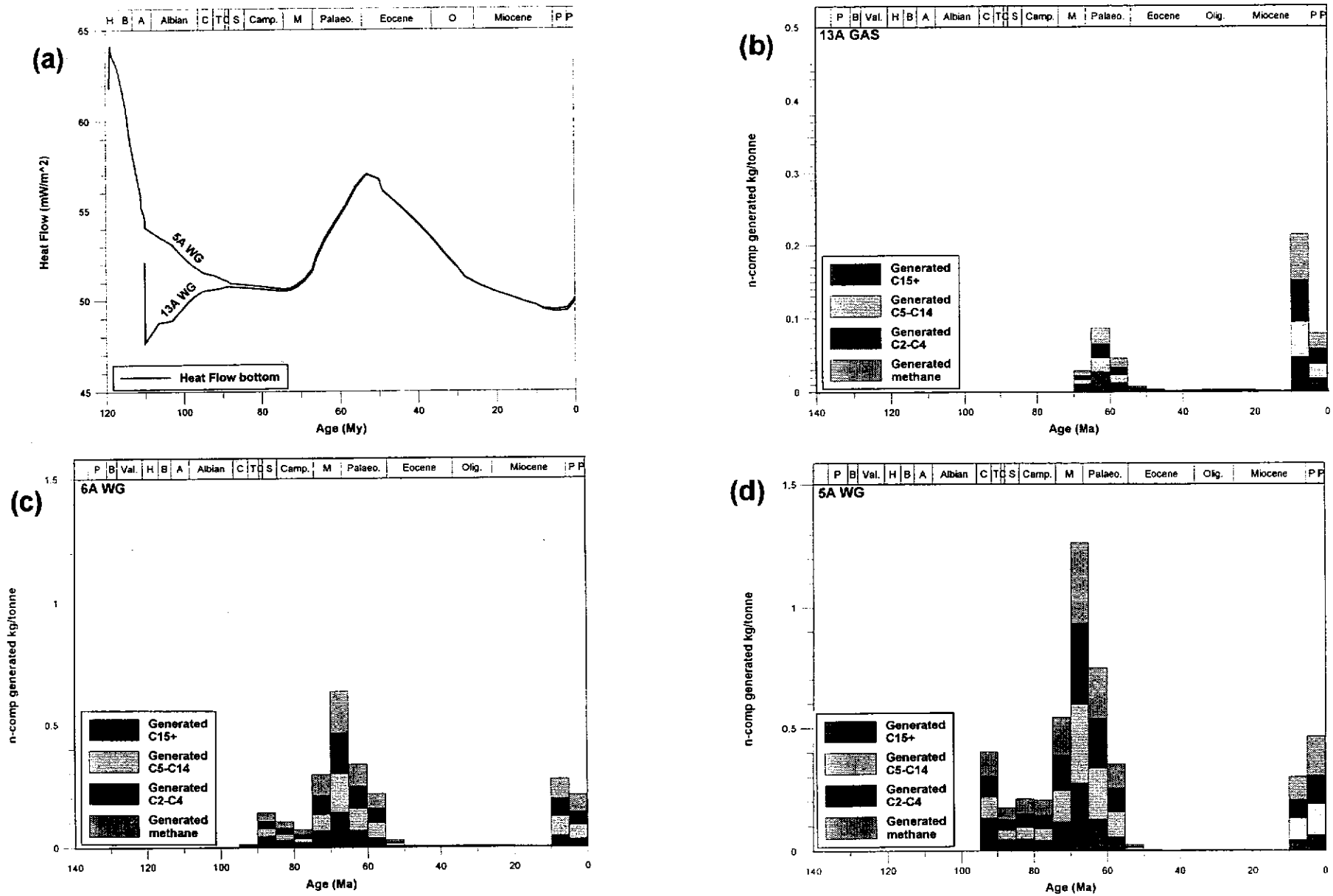

Figure 7.12: Basinmod plots for northern basin location showing matching heat flows for uppermost and lowermost source rocks (a) and mass of hydrocarbons generated from (b) 13A, (d) 6A and (d) 1A source rocks.

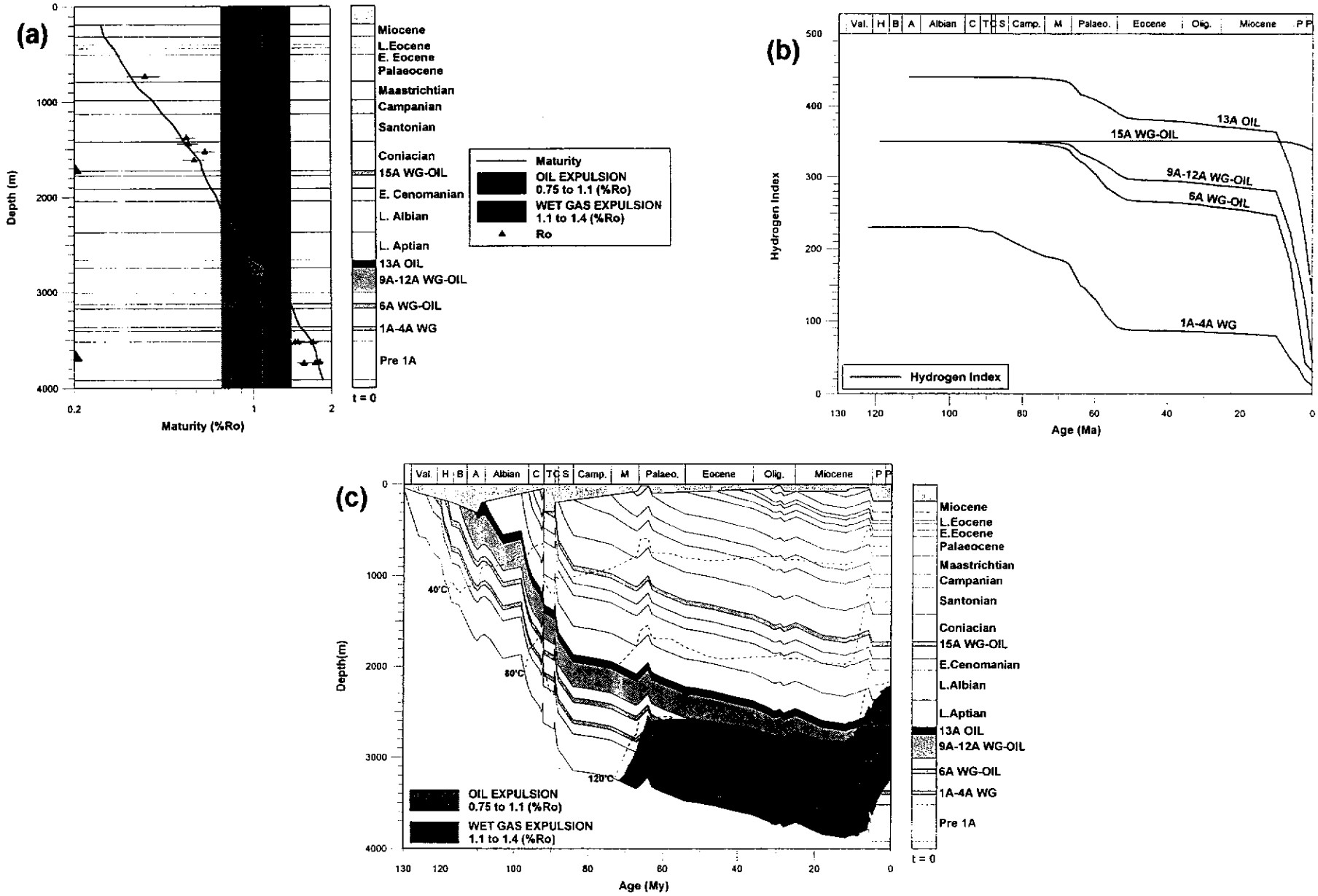

Figure 7.13: Basinmod plots for south flank basin location showing (a) modelled vs measured vitrinite reflectance and (b) calculated hydrogen indices vs time and (c) burial history diagram.

with SWC or core samples (Table A7) and may reflect a return to *in situ* values from contaminants or cavings above. The third coincides with the base of the 13A source rock, below which the reflectance values are significantly lower than would be expected. This shale is considered to act as a fluid seal elsewhere because of its mild overpressure (Brink and Winters, 1989), and probably acts as a seal to heat-carrying fluids here, which should result in higher rather than lower reflectances below. In this case, low reflectance values below ~3000m (and low Tmax values too) probably reflect downhole caving of 13A source rock.

Modelling results indicate that the upper two source intervals (13A and 9A-12A) mature mainly through the Miocene-Recent heating episode (Figs. 7.14a and b) whilst only the older source rocks traverse a significant proportion of the oil window during the Late Cretaceous-Early Tertiary hotspot transit (Fig. 7.14c and d). Only small amounts of liquid hydrocarbons are modelled to be generated in the older (1A-4A, 6A) source rocks (Figs. 7.13c and d) and they are probably not in large enough quantity to exceed the 'absorbency' of the shale. Hydrocarbon expulsion from the younger source rocks is largely restricted to the Late Tertiary. Hence the hydrocarbon shows which are found near 1At1 in this well, and in other nearby wells, are not locally sourced.

7.3. MODELLING IN THE SOUTHERN OUTENIQUA BASIN

Burial history models have been constructed at 2 locations in the western Southern Outeniqua Basin, in order to address hydrocarbon generation within potential fetch areas for the Bredasdorp Basin (Fig. 7.04). Because of the lack of well intersections, the models are based on thermal and burial histories extrapolated from the Bredasdorp and Pletmos Basins. The western model investigates the effects of the edge of the Agulhas Slump where it is ~300 metres thick, whereas the central model (no. 2) deals with the centre of the slump where thicknesses exceed 600m. In each case, the presence and thicknesses of source rocks are derived from the seismic character of the interval. Pressure modelling at the central location (model no. 2) demonstrates the transient nature of the pressure effects of the slump.

7.3.1. Western model

The model was constructed for the location at the junction of lines 15 and 20 (Figs. 3.04 and 4.05). Lithologies of the major sequences are modelled as similar to those in the Bredasdorp Basin, but somewhat more argillaceous as a result of the greater distance from sediment input. Maturation parameters are also assumed to be similar to those in the central Bredasdorp Basin but without igneous activity. Modifications however include increased heat flow during the Turonian transit of the Agulhas-Falklands

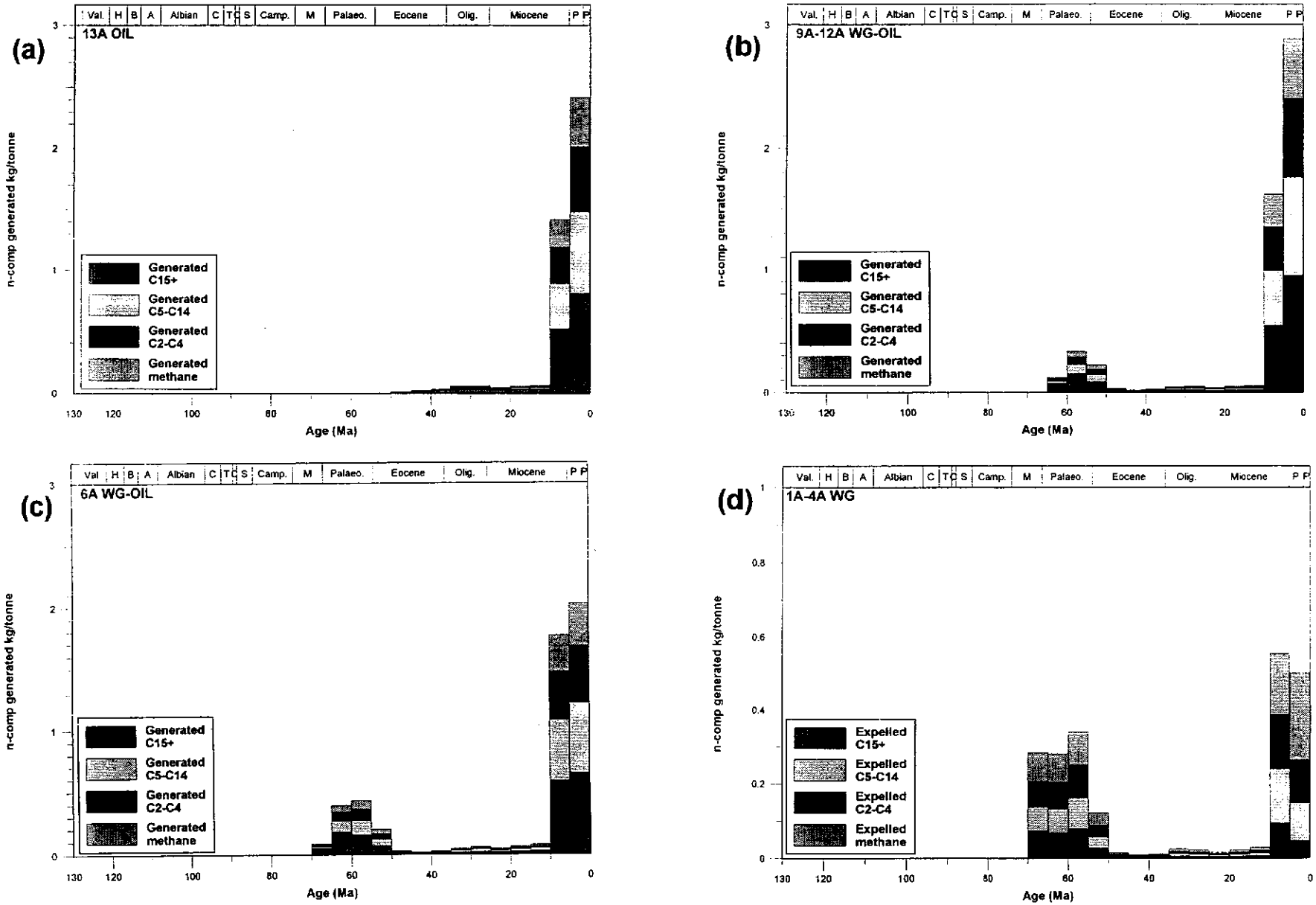

Figure 7.14: Basinmod plots for south flank basin location showing mass of hydrocarbons generated from (a) 13A, (b) 9A-12A, (c) 6A and (d) 1A-4A source rocks.

spreading centre (section 4.4) and reduced thermal effects of the Agulhas Slump because of the reduced downdip fetch area.

Adoption of this thermal history results in modelling 13A wet gas to oil-prone source rocks as generating hydrocarbons (Fig. 7.16a), but not entering the oil expulsion window at all (Figs. 7.15a and b). However, possible syn-rift source rocks, which may be lacustrine (as in well 89), apparently traverse the oil window during the Palaeocene and nearly exit the wet gas expulsion window (Fig. 7.15b). Earlier Late Jurassic marine pre-1A source rocks, such as those found in the Gamtoos and Algoa Basins (Malan, 1993) and in DSDP 330 on the Falklands Plateau (Gilbert, 1977), are unlikely to be present because of the relatively late sag of this area, although they are modelled to develop in the eastern half of the Southern Outeniqua Basin.

Heat input during the hotspot transit was small because the area was near the edge of the affected zone. Therefore, much of the effective heat input results from the period of the Agulhas Slump. There was likely only a small hydrothermal input from water displaced from further east in the Southern Outeniqua Basin. However, the area was closer to the thermally conductive AFR, which 'mines' heat from the oceanic plate, and closer to the African Superswell mantle heat source.

As a result, 1A and pre-1A source rocks are modelled to generate >>1.5 kg oil/tonne rock. In the case of a pre-1A lacustrine source rock, this could total 5 kg oil/tonne rock (Fig. 7.16c). Any of this material not trapped locally in pre-1A fault-blocks (Fig. 3.28) could migrate updip to the flanks of the eastern highs and beyond - perhaps some bitumen traces in pre-1A sandstones in those highs are a result of this migration.

7.3.2. Central model

This model was constructed for a location some 50 km east of the western model at the junction of seismic lines 19 and 20 (Figs. 3.24, 3.25, 3.28 and 7.04). The model uses lithologic, thermal and burial histories similar to the more westerly model, but with two differences (i) a larger heat increase at the time of the passage of the Agulhas-Falklands spreading centre and (ii) a smaller heat increase at the time of the Bouvet/Shona hotspot transit. Notwithstanding these heating differences, the 13A source rock still does not enter the oil expulsion window although, as in model 1, some oil is generated (Figs. 7.17; 7.18a).

The 1A source only enters the top of the oil window very late (10-0 Ma) and generates enough to satisfy the micro-reservoir capacity of the source rock - hence some could be available for expulsion. The pre-1At1 interval is modelled to contain the only source rock to enter the wet gas window (Fig. 7.18c). The modelling shows ~3 kg oil/tonne

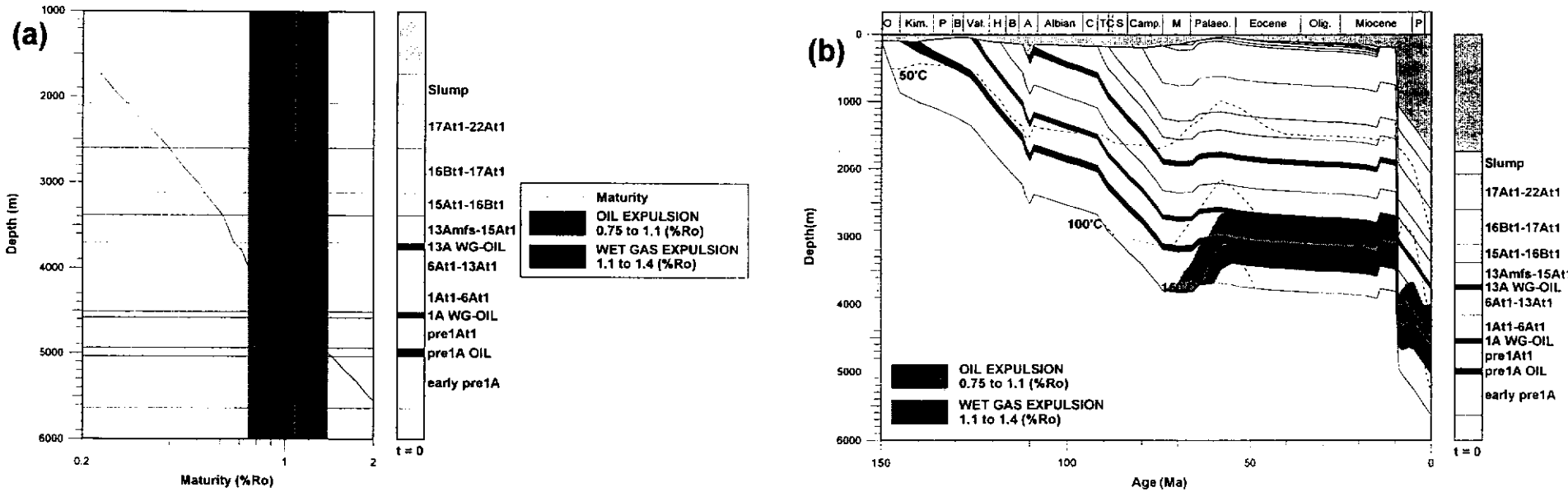

Figure 7.15: Basinmod plots for western Southern Outeniqua location showing (a) modelled vitrinite reflectance and (b) burial history diagram.

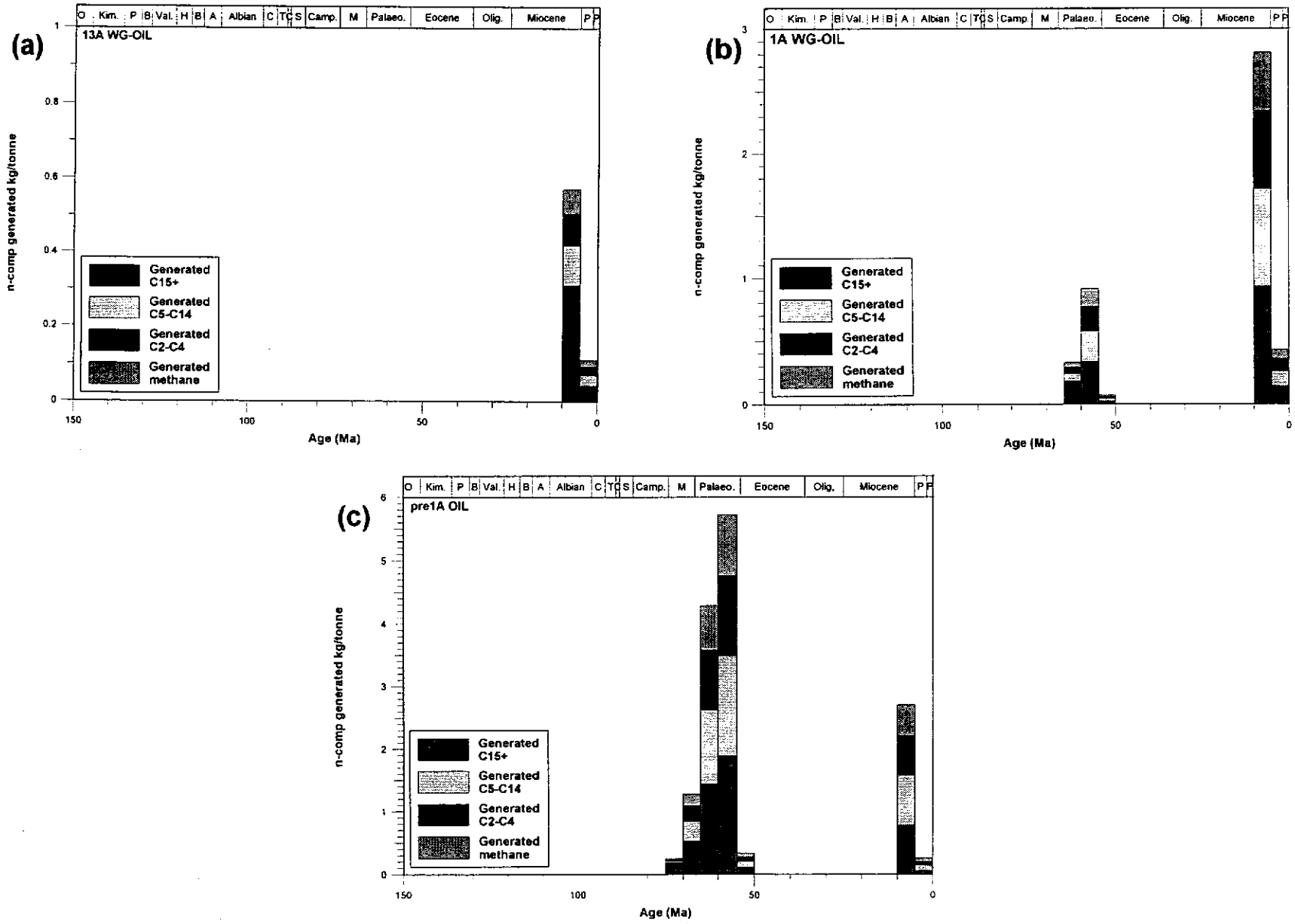

Figure 7.16: Basinmod plots for western Southern Outeniqua location showing mass of hydrocarbons generated from (a) 13A, (b) 1A and (c) pre1A source rocks.

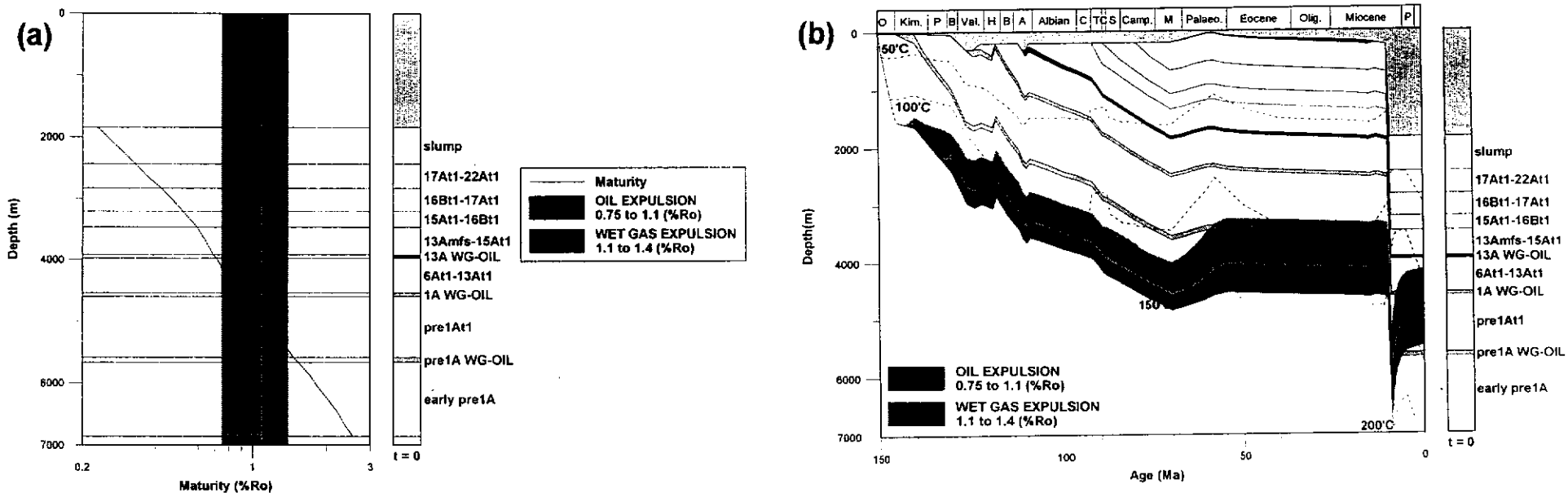

Figure 7.17: Basinmod plots for central Southern Outeniqua location showing (a) modelled vitrinite reflectance and (b) burial history diagram.

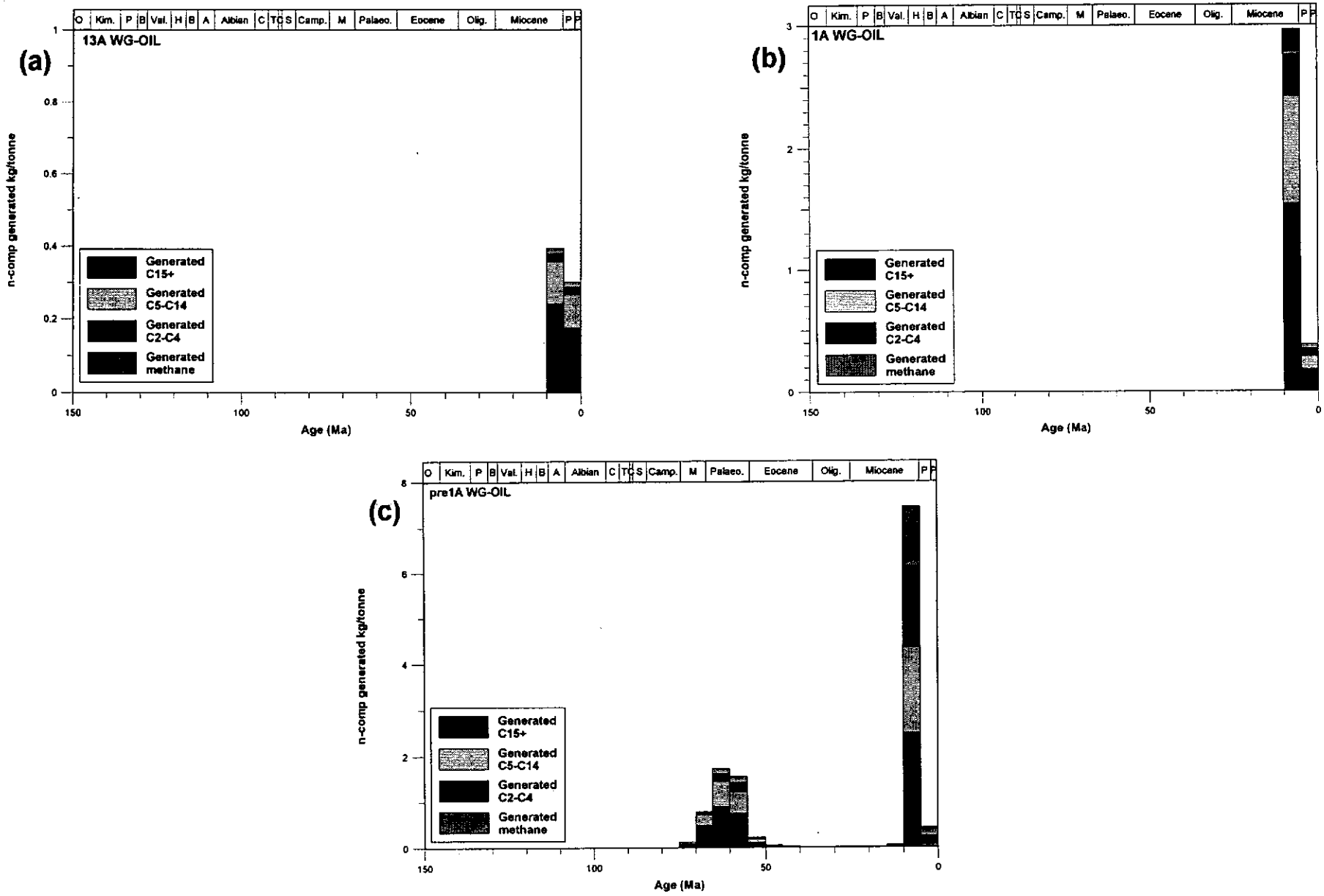

Figure 7.18: Basinmod plots for central Southern Outeniqua location showing mass of hydrocarbons generated from (a) 13A, (b) 1A and (c) pre1A source rocks.

rock to be generated during the hotspot transit (of which 1-2 kg oil/tonne rock might be expelled) and a further 3-3.5 kg oil/tonne rock more recently.

7.4. DISCUSSION

The modelling assumes that high heat flows prevail during rifting and continue into the early drift phase, but thereafter rapidly decrease to a low level. This cooling effect resulted in thermal subsidence which provided the space necessary for the rapid Albian - Santonian sedimentation. Each burial history diagram shows this as the period of most rapid burial and even though the heat flow was decreasing, the added burial resulted in an increased maturation level during this period. The deeper source intervals in the north flank and basin centre, and in the Southern Outeniqua Basin traverse much of the oil window during this period.

Burial through the Coniacian to present was generally at a much slower rate. Three of the Bredasdorp Basin burial history diagrams record only 400-500 metres of burial during this ~84Ma period (a fourth shows ~750m of burial but mostly during the Maastrichtian). Of the Bredasdorp Basin model locations, only the south flank model records any amounts of significant Tertiary burial - and even there a maximum of ~500 metres is recorded.

Present day heat flows, modelled in the five Bredasdorp Basin wells from known temperatures, are similar (50-57 mW/m^2), and largely match those modelled to prevail in oceanic basins (Condie, 1989, p.94-96) during the cool periods in the Late Cretaceous and through much of the Tertiary. At this level of heat, there would be little further maturation after the post-rift heat-flow decline so that those source rocks which did not attain the oil window during the rapid Mid-Cretaceous burial, would have approached it only extremely slowly (if at all) by the end of the Tertiary. The same situation applies to the Southern Outeniqua Basin models - although the regional heat flow is modelled to be higher there (i) because of the proximity of the oceanic crust and (ii) because of the thinned continental margin.

However, subsequent to the cool-down post-rifting, two major heating events are shown to have affected the Bredasdorp and western Southern Outeniqua Basins. These are (i) the heat input during the Late Palaeocene transit of the continent across the Bouvet/Shona hotspot (Duncan, 1981; Hartnady and Le Roex, 1985) and (ii) heat resulting from the African Superswell and associated Agulhas Slump (Dingle, 1977; Hartnady and Partridge, 1995).

Half of the maturation of the 9A-13A oil-prone source rocks in the Bredasdorp Basin is modelled to have occurred during the first event and half during the second event. Condensate-prone source intervals in the Bredasdorp Basin, mainly in the 1A-5A sequences, mostly traverse the oil window before the heat effects of the hotspot transit become apparent. Because those intervals had little oil potential, they did not generate enough hydrocarbon for expulsion. In the northern, eastern and central Bredasdorp models, these wet gas-prone source rocks also traversed the gas generation window during the Palaeocene. Thus, other than for unknown, but possible deep basin oil-prone and wet gas-prone source rocks, most gas generation and expulsion took place during or after the Bouvet/Shona hotspot transit.

A regional tectonic event is thought to have affected the distribution of hydrocarbons in the basin - specifically the movement of the Bredasdorp Basin resulting from the progressive north-to-south thermal uplift and decay during passage of the Bouvet/Shona hotspot. This could result in a southward tilt during the early part of the transit when the hotspot was located to the north and a northward tilt during the later part as the hotspot moved south. If tilting by even 1-2° did occur, it could alter the flow regime in the basin as well as previous tectonic trapping mechanisms. Five chronographic N-S sections across the basin address possible tilting through this period (Fig. 7.19). These sections take into account the probable 300-500 metres of uplift through this period and show that early-formed reservoirs could have been breached and most of the hydrocarbons lost. It is possible that this mechanism explains the ubiquitous residual bitumen traces in syn-rift sandstones in the south-east flank where oil would be expected (McLachlan et al., 1979). It may also help to explain the presence of residual traces of low maturity oil, especially in wells 156 and 166 (Davies, 1997a), particularly if these traces are remnants of early expulsion from the 1A or pre-1A source rocks in the Southern Outeniqua Basin.

Tilting associated with the initiation of the 'African Superswell' in the Early Miocene (i.e. a slight upwarp to the NE) might also have affected trapping and sealing of hydrocarbons. However, since the tilting affects were minor, except probably near the plate edge (Hartnady and Partridge, 1995; Ben-Avraham et al., 1997) and in the western part of the Bredasdorp Basin (Brink et al., 1991; section 3.1.1.), the likelihood of large volumes of reservoired hydrocarbons escaping past the spill points of structures is low.

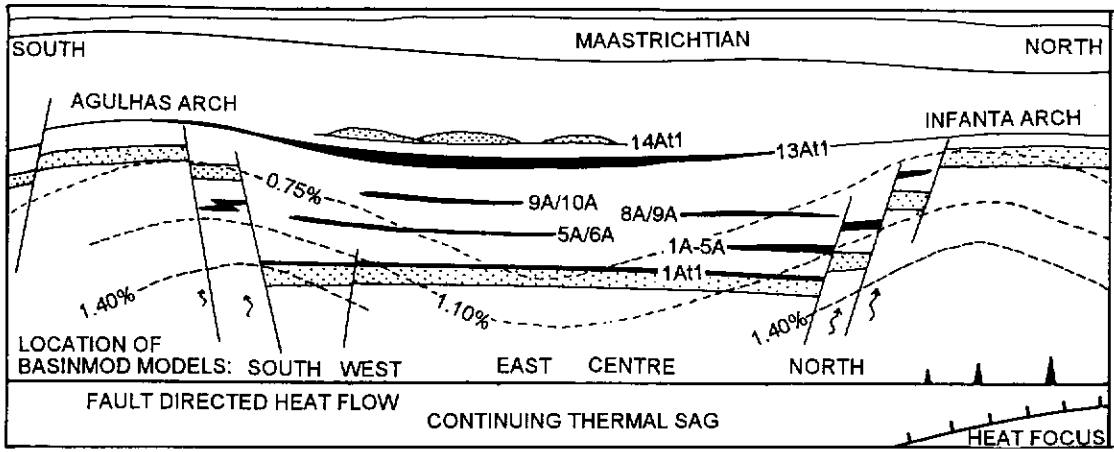

1. BASIN VIEW AT ~70 Ma (MAASTRICHTIAN)

1. Low overall heat flow and continued thermal subsidence.
2. Elevated heat flow at faulted margins.
3. Only the deepest source rocks are mature.
4. Slow burial and heating rate - ~0.4°C/Ma.
5. Barely mature lacustrine source rock in south flank.
6. Maastrichtian sediments thickest near north flank.
7. Earliest effects of approaching hotspot.
8. HIghest formation water salinities deep in basin centre.

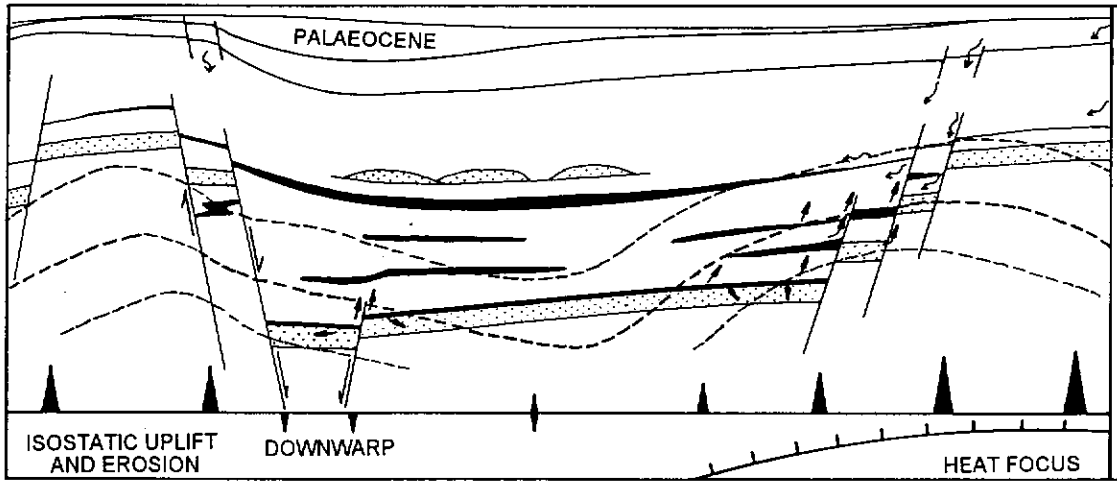

2. BASIN VIEW AT 62 Ma (EARLY PALAEOCENE)

1. Regional heat increase but locally centred in north flank.
2. Gas generation from 1A, 5A and 9A sources near north flank.
3. Some oil generation from 5A source.
4. Basin tilts southwards and south flank pop-up due to isostacy.
5. Maastrichtian eroded from south flank.
6. Thickest Palaeocene near south flank.
7. Meteoric water ingress mainly near north flank.
8. Water flush distance limited by adverse dip and salinity contrast.

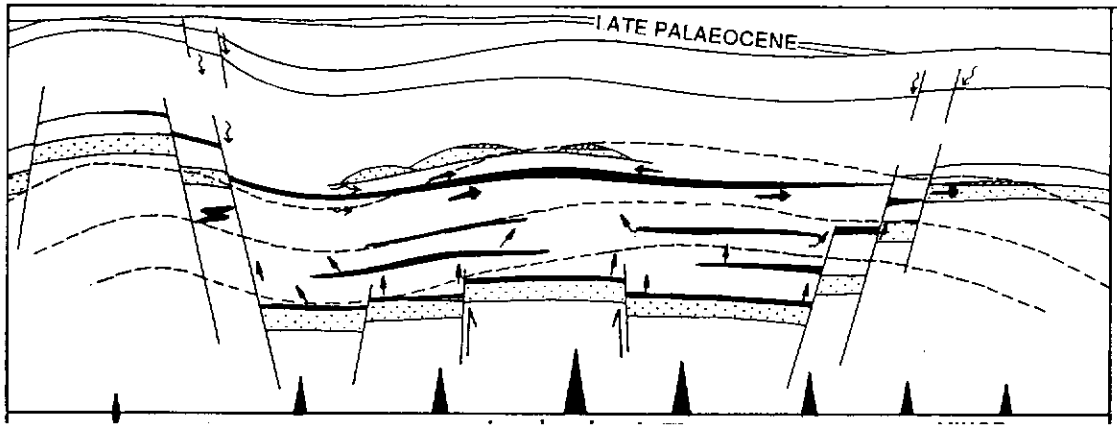

3. BASIN VIEW AT 58 Ma (LATE PALAEOCENE)

1. Heat focus located centrally - main vulcanism phase.
2. Central basin thermal uplift, flanks relatively downwarped.
3. Water ingress at south flank as well as north.
4. Water flow towards basin centre due to basin inversion.
5. Oil generation and expulsion from 13A source in basin centre.
6. Migration up to 14A assisted up faults by water flow.
7. Oil flows northwards: partly updip, partly hydrodynamic drive.
8. Hydrodynamically tilted oil and gas contacts in 14A sands.

CHAPTER 8 GASEOUS COMPONENTS

In this study, 'gas' refers to hydrocarbon and non-hydrocarbon compounds which are gaseous at ambient conditions. In the more usual reservoir engineering characterisation, 'gas' includes large volumes of light oils present in the gas phase at reservoir conditions. In addition, almost all source rocks expel a mixture of gas and heavier components, i.e. gas-prone source rocks also expel oils. Hence, surface conditions rather than source rock, migration route or reservoir conditions are used to characterise gas compositions. The aim of the study is to determine the source of this low molecular weight material separate from the heavier material in order to highlight any source-related similarities or differences. For example, low maturity biomarkers can be dissolved by the condensates associated with wet gases. Separating the two allows the distinction to be fully interpreted.

8.1. SAMPLES

Gases at ambient conditions are mostly normal C1-5 alkanes and some iso-alkanes, plus nitrogen and carbon dioxide. Other hydrocarbon and non-hydrocarbon gases are also present (such as H_2, He, cyclo-C_5H_{10}) but in small proportions only. Two gas datasets are available: the one from bottom-hole or recombined separator samples was used for PVT analyses and the other from non-recombined surface samples collected at the separator was analysed at the South African Bureau of Standards (SABS). Bottom-hole samples need no recombination as they sample the whole flowing fluid. Recombination of flowed gas and liquid samples is done in the proportions recorded at the separator during the flow period. Both these sample types are described in more detail in Chapter 6 and the results of analyses are given in Appendix B, Tables B1 and B2. All but two of the PVT samples were analysed in the Schlumberger Flopetrol laboratories in France: the remaining two were analysed at Expro laboratories in Scotland. Since PVT and SABS sample types are not the same (Table 8.01), they are addressed separately allowing only inter-group direct comparison. Several samples are from the same test interval and although the gas proportions are different because of differences in handling, the ratios between gases (except for those compared with methane) are similar to the PVT ratios. Hence comparisons between the two data sets are possible. For example, in both data sets the CO_2 proportions in Family 2 samples are generally twice as high as in the other families and both are close to 4%. Nitrogen contents in Family 3 samples are generally the highest of all the families, maximising at ~5% in each data set.

Where large volumes of gas are intersected in a reservoir interval, the producibility of the gas is tested, usually by drill stem test (DST). Oil reservoirs too contain some gas

Samples used for PVT analyses	Samples used for SABS analyses
hydrogen and helium not measured.	hydrogen and helium both measured.
samples collected at working pressure	samples collected at near ambient pressure
samples stored in guaranteed pressure-tight containers	samples not stored in guaranteed pressure-tight containers.
gas and liquid samples recombined before analysis	gas and liquid samples are not recombined.
analyses done by flow loop sampling	analyses done by syringe extraction
results repeatable to ±~0.1%	results repeatable to (min) ±2%

Table 8.01: Differences between sampling and analytical methods used for PVT and SABS samples.

which is also sampled by DST's. Hence bottom-hole samples, collected during the DST, are preferred, but where these are not available, surface samples are recombined to recreate the reservoir fluid.

Circumstances under which surface samples are used to evaluate reservoir production are as follows:
- where the flow rate was indicative of a sub-commercial reservoir
- where there is a need for early results (PVT analyses can take several months)
- where one of the samples is found to have lost pressure
- where there is uncertainty regarding the correct recombination ratio.

Analyses of PVT samples are carried out by flow-loop sampling, where a sample of the cylinder fluid is displaced by mercury into a small calibrated flow loop and thence to the GC column. Gas and liquid separator samples are however analysed at ambient pressures by water-displacement sampling. In this technique, the gas is displaced from the sampling cylinder by water and thence into a small container, from which a sample is withdrawn using a syringe and injected into the GC. Under these conditions, there can be loss of some of the light ends through solubility and from the open syringe. In addition, some of the liquid fraction originally held in the gas phase can condense on the surface of the gas bomb during water displacement sampling, because displacement is done at ambient conditions whereas sampling was at separator conditions (~300 psi and ~60°C) and is lost from the analyses.

A further complication is that during surface separation into gas and liquid fractions, some volatile hydrocarbons remain within the liquid phase (and vice versa). Hence hydrocarbons in the C4-6 range, many of which are liquid at ambient conditions, can be present in both gas and liquid fractions. Separator gas analyses therefore at best reliably evaluate gas compositions up to ~nC3. Fortunately as most gases are dominated by C1-3 components and contain only small proportions of non-hydrocarbons, the interpretation plots can be considered largely representative. Almost all C7+ hydrocarbons are separated into the liquid phase at the wellsite so that data from analyses of these hydrocarbons can be readily used to identify hydrocarbon characteristics.

Gas compositional data are amongst the first hydrocarbon data to be generated as the analyses are carried out during (ditch gas data) and also shortly after (cuttings gas data) the drilling of any well. The gases collected are rarely fully representative of gas in the formation and give only a first approximation of the contents of the reservoir drilled. In that format, the data are commonly used in first interpretations of the organic maturity and source quality (Le Tran, 1975).

8.2. MATURITY INTERPRETATION

The parameter most commonly addressed by interpretation of gas data is an estimate of the maturity level of the reservoir fluids. This is often thought to be related to rock temperature, probably because thermal cracking reactions also take place in the reservoir and during migration as well as in the source rock. However, where hydrocarbon maturity is higher than the equivalent formation temperature, long distance migration is a probable explanation. Since this would indicate the availability of larger volumes of hydrocarbons than are likely from local sourcing, maturity estimation is very important. To obtain consistent interpretations, the gas maturity is usually compared to other maturity parameters - in this case vitrinite reflectance (Heroux et al., 1979).

8.2.1. Hydrocarbons

Gas maturity estimates are usually derived from the proportion of methane relative to that of ethane and the heavier hydrocarbon gases - higher maturity being signified by lower proportions of heavier gases. During early maturation, initially high proportions of biogenic gas, essentially methane (Hunt, 1979a, p.425) are gradually superseded by increased amounts of wet gas - hence the dryness index ($^{C1}/_{(C1\text{-}5)}\%$) decreases. Once the peak of oil generation has been passed, there are fewer lipid fractions left to crack in the source rock and the average gas molecule chain length decreases, leading to a late stage rise in methane proportion. These changes are most commonly recorded by the dryness index but can also be evaluated from the proportions of other gases. A common plot type is the ternary plot comparing methane to ethane to propane. Through increasing maturity, the proportions of C1, C2 and C3+ are expected to describe a smooth continuum from the wettest (in low maturity oil reservoirs) to the driest (in the high maturity methane-rich reservoirs). Fig. 8.01 shows how these ratios change with increasing maturity.

8.2.2. Non-hydrocarbons

Proportions of non-hydrocarbon gases, the most commonly encountered in the basin being carbon dioxide (CO_2) and nitrogen (N_2), also have interpretative uses and display both source and maturity dependency. Hunt (1979a, p. 163) shows the proportions of both these gases to increase, then decrease, with depth and maturity - but along different trends for different source rock types (Fig. 8.01).

8.2.2.1. Nitrogen

Littke et al. (1995) show non-coaly kerogen to contain only small amounts of nitrogen. They interpret this to be partly because atmospheric gases are largely excluded from marine source rocks and partly because nitrogen-fixing bacteria are far less common in

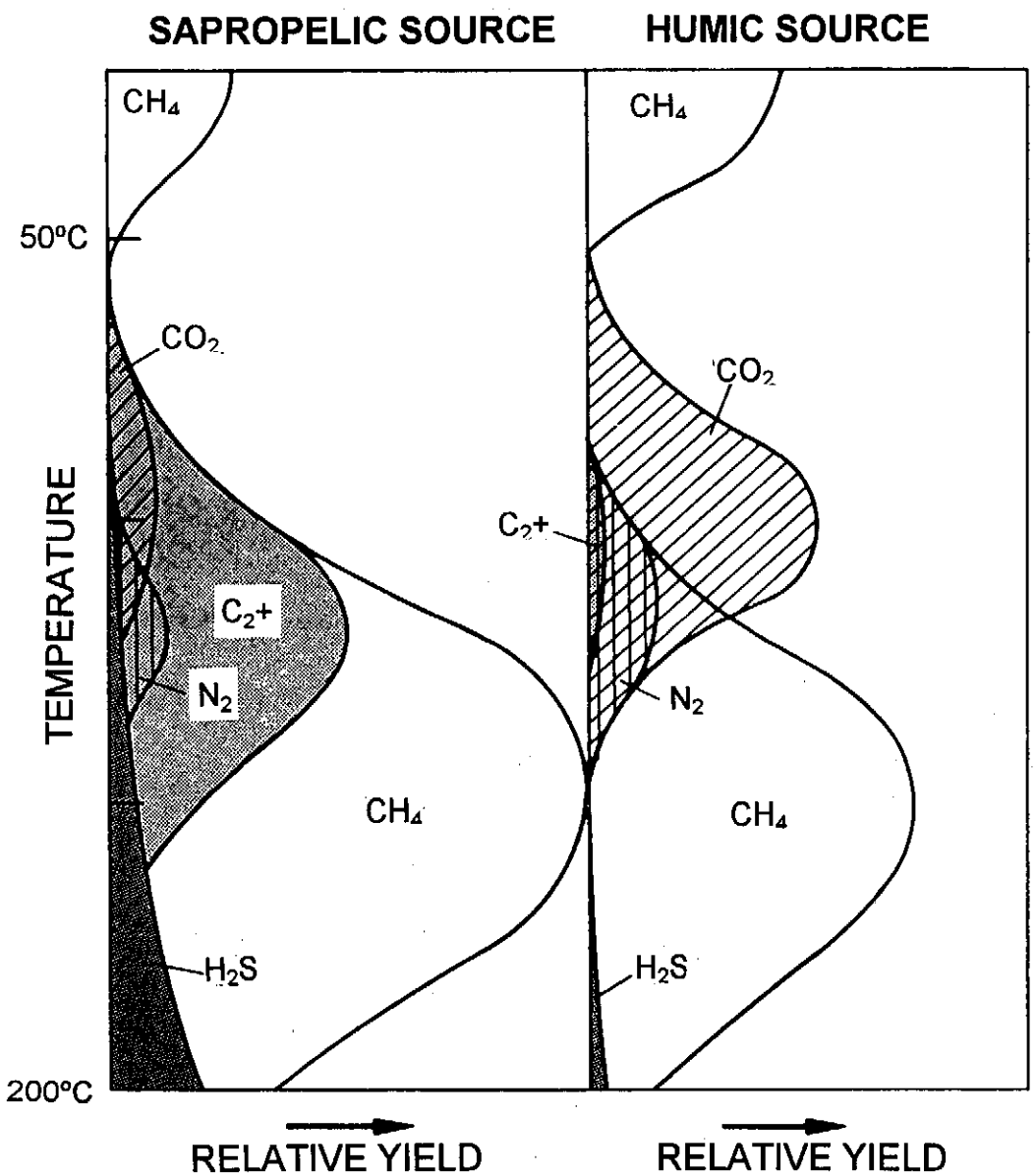

Figure 8.01: Relative yields of hydrocarbon and non-hydrocarbon gases (after Hunt, 1979, p163)

the marine environment. They also show that the highest proportions of nitrogen (>10%) are found in TOC-rich coaly sediments at high maturation levels at vitrinite reflectances >3%R_o. These results are in contrast to those of Hunt (1979a, p.163-166) who shows nitrogen to be largely present near 120°C (≡R_o 1,1%). However, the nitrogen gas proportion evaluated for humic sources (Hunt, op cit.) appears to continue slightly deeper than the equivalent value for sapropelic sources. Hence it may be that Littke et al. (1995) used an even more coal-rich kerogen in their study.

In the Bredasdorp Basin none of the gases contain much N_2 (the highest proportion being ~5%) and these low proportions suggest the gases are not of very high maturity. The only rocks known in the basin which might be at the right maturity level and have high organic matter contents (TOC locally exceeds 2%), namely the Devonian Bokkeveld Series shales, contain very little hydrocarbon or non-hydrocarbon gas. Whilst this paucity may be because they did not source large amounts of this gas it is more likely that most of the gas generated has escaped since the main generation period in the pre-Jurassic (Rowsell, 1974; Davies et al., 1995).

8.2.2.2. Carbon Dioxide

Smith and Ehrenberg (1989) show that the highest CO_2 content is usually found in carbonate-rich rocks. They demonstrate that the conversion of carbonates to CO_2 is a response to changing inorganic equilibria between carbonate, clay and feldspar minerals and that the proportion of CO_2 is generally a function of partial pressures. Their cross-plot describes a log curve (at least on a small scale).

In the Bredasdorp Basin, carbonate and CO_2 contents are limited, partly owing to the absence of both warm water and evaporitic environments. The one group of gases which has a higher CO_2 contents may be at least partially sourced by syn-rift lacustrine rocks which have been shown to be locally evaporitic. The generally low CO_2 contents may also be a function of the relatively low temperature because Smith and Ehrenberg (1989) show that CO_2 proportions generally only increase above 150°C. Hunt (1979a, p.166-167) however shows that large proportions of CO_2 are also found at temperatures no higher than ~100°C (≡mid-oil window).

The relatively modest proportions of CO_2 in Bredasdorp Basin gases, even from the high maturity central basin (e.g. wells 96 and 110, Table 8.01), confirm a lack of input of CO_2-rich gas during the igneous phase of carbonatite intrusions in the eastern region (around well 8, Rowsell et al., 1979), which must have been associated with copious CO_2 input. This supports the indication from apatite fission track data that the substantial annealing which took place in very shallow samples (well 96) was caused by

a regional heat increase rather than local heating by CO_2-rich hydrothermal fluids (Eurotrack, 1996).

8.2.2.3. Hydrogen sulphide

Hydrogen sulphide gases are generated by bacterial degradation of organic material in anoxic conditions, either of lipid material during diagenesis producing 'marsh gas' or of liquid hydrocarbons in low temperature reservoirs (Jobson et al., 1979; Connan, 1984). H_2S can also be generated from anhydrite at high temperature, however, no concentrations of anhydrite have been found. Low concentrations of H_2S (0-100 ppm) are conspicuously odiferous. Since H_2S is poisonous in larger concentrations, a monitor is permanently connected to the returning mud system as a safety measure. No concentrations of H_2S have been detected. Since H_2S readily combines with iron, samples collected in steel cylinders will retain little free gas after a short time, hence analyses for H_2S are rarely carried out. In the few tested samples from gases flowed during production, concentrations <3 ppm have very rarely been noted.

8.3. SOURCE INTERPRETATION

In addition to the already discussed dominance of N_2-rich gas in terrigenous source rocks and of CO_2 in gases from evaporitic environments, studies have shown that hydrocarbon gas composition can also indicate source environment (Deroo et al., 1977; Powell, 1978; Tissot and Welte, 1984, p.219-221). The kerogen in oil-prone source rocks is largely composed of lipid-rich kerogen, such as that found in marine or bacterially altered terrigenous organic material. The latter has a preponderance of long alkyl side-chains, which crack during maturity to yield high proportions of long-chain alkanes. Gas-prone source rocks are comprised largely of terrigenous, refractory organic matter dominated by condensed aromatic structures with few short, side-chains (Hunt, 1979a, p.174). This yields mostly aromatic and short chain paraffin molecules. Therefore gases from oil-prone source rocks are generally wetter than gases from gas-prone source rocks and are usually present in the reservoired hydrocarbons in larger quantities (Hunt, 1979a, p.163-164).

Distinction of the 5 hydrocarbon families is based on the interpretation of gas, condensate, oil fractional, isotopic and biomarker data and correlation with the different source rocks is also based on oil fraction, isotopic and biomarker data. For convenience, each data type is discussed separately but there are some familial correlations which are less evident from single data types. In those cases, the relevant data type is indicated.

8.4. DATA INTERPRETATION AND DISCUSSION

The source and maturity responses of gas compositions are inter-related, hence they are not discussed individually herein. Results of gas analyses from PVT and SABS analyses are shown in matching plots and the samples located on the relevant source rock distribution maps. The pair of parameters which appears to hold the facility to best differentiate reservoired hydrocarbons are carbon dioxide and methane. A cross-plot of their proportions in PVT data (Fig. 8.02a) allows for the delineation of 5 separate hydrocarbon families (with only two intermediate points). Data from three of the families show clear parallel, but offset, reservoir maturity relationships. The SABS data, by contrast, shows little such distinction (Fig. 8.02b), perhaps because CO_2 is the component most readily lost from imperfectly sealed gas bombs or contaminated during water displacement sampling (Table 8.01).

Family 1 gases are commonly found associated with oil-rich hydrocarbons, reservoired in sandstones above the 13A source rock (Figs. 8.02a; 8.03) and with the immediately pre-13A oily condensates, which are probably mixtures of oil and wet gases (Chapters 9-12). They are distinctly separate from the gas-rich hydrocarbons and show an obvious maturity trend of increasing CO_2 and C1 with higher vitrinite reflectances.

Family 2 gases, characteristically those associated with the over-pressured central basin near-9At1 reservoirs, e.g. wells 96 and 114, are clearly distinguished (Figs. 8.02a; 8.04). They too display a maturation trend which parallels that of Family 1. Mixtures of Family 1 oil and Family 2 gas samples from wells 48 and 126 plot clearly between the two trends (Fig. 8.02a). The produced hydrocarbons comprise relatively dry gas with oil residues (Winters et al., 1984; Labuschagne, 1993). Within Family 2, a few samples locate slightly separate from the others (Fig. 8.02b). These are the samples from the north flank of the basin in wells 65 and 84 and because of their separate location they are called Family 2A. They are characterised by *inter alia* the highest CO_2, C1, and N_2 of Family 2 hydrocarbons.

Family 3 gases represent mostly hydrocarbons found in the north flank of the basin and they too can be subdivided into two regions, viz. eastern (near wells 18-23) and western (near wells 48 and 59; Figs. 8.02a; 8.05). Family 3 gases do not display such dramatic maturity trends as Families 1 and 2, but do show a slight reservoir maturity trend in the same direction as those of the other families.

Family 4 gas is clearly separate from Family 3 as it has significantly higher CO_2 and C1 proportions (Fig. 8.02a). The reservoir is at much higher maturity than the Family 3 reservoirs (R_o 1.6% vs 0.9-1.1%) and is located outside the basin (Figs. 3.04; 8.06). On

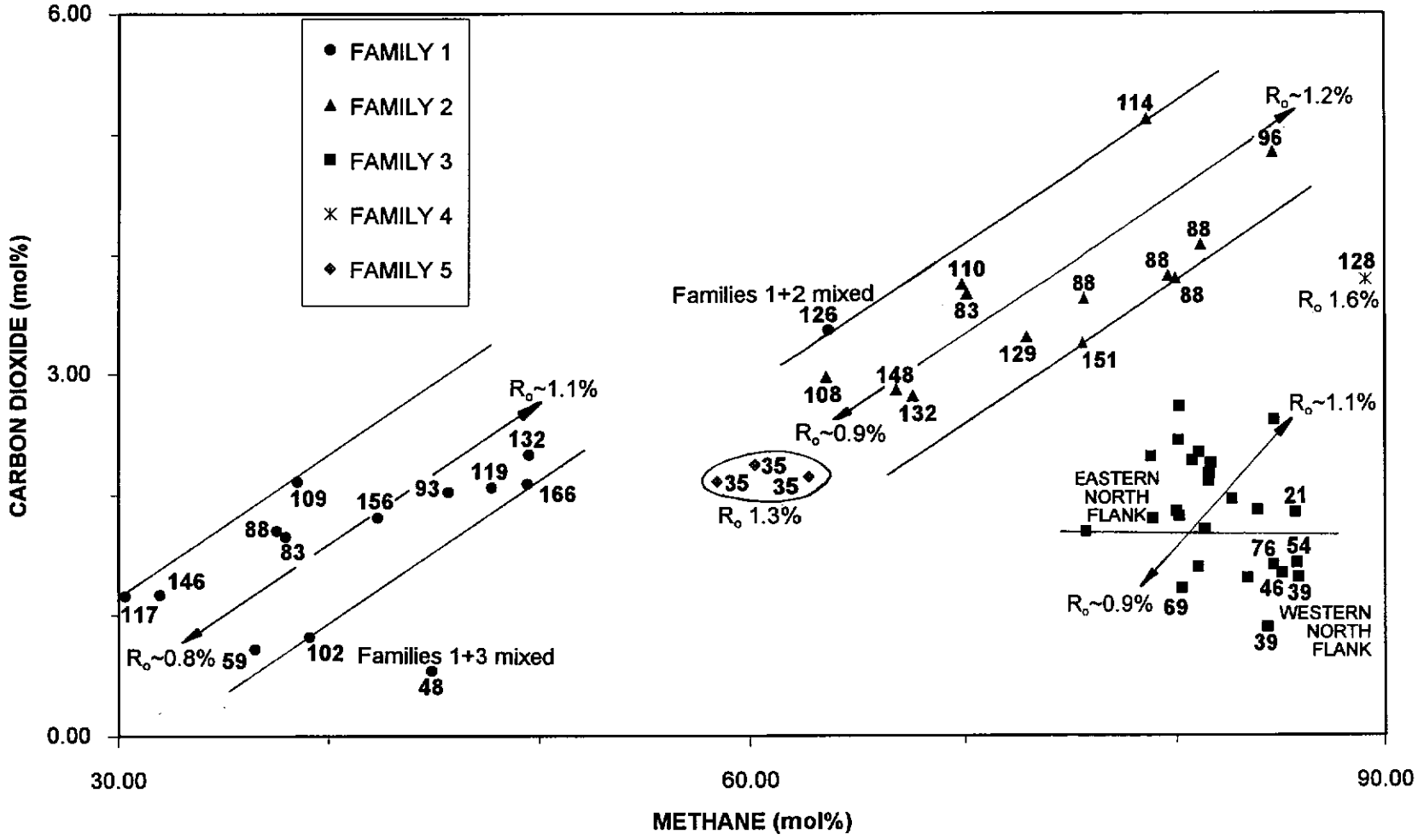

Figure 8.02a: Cross-plot of C1 vs CO_2 from recombined formation fluid samples (PVT) showing distinction of the samples into five main Families and their maturation trends.

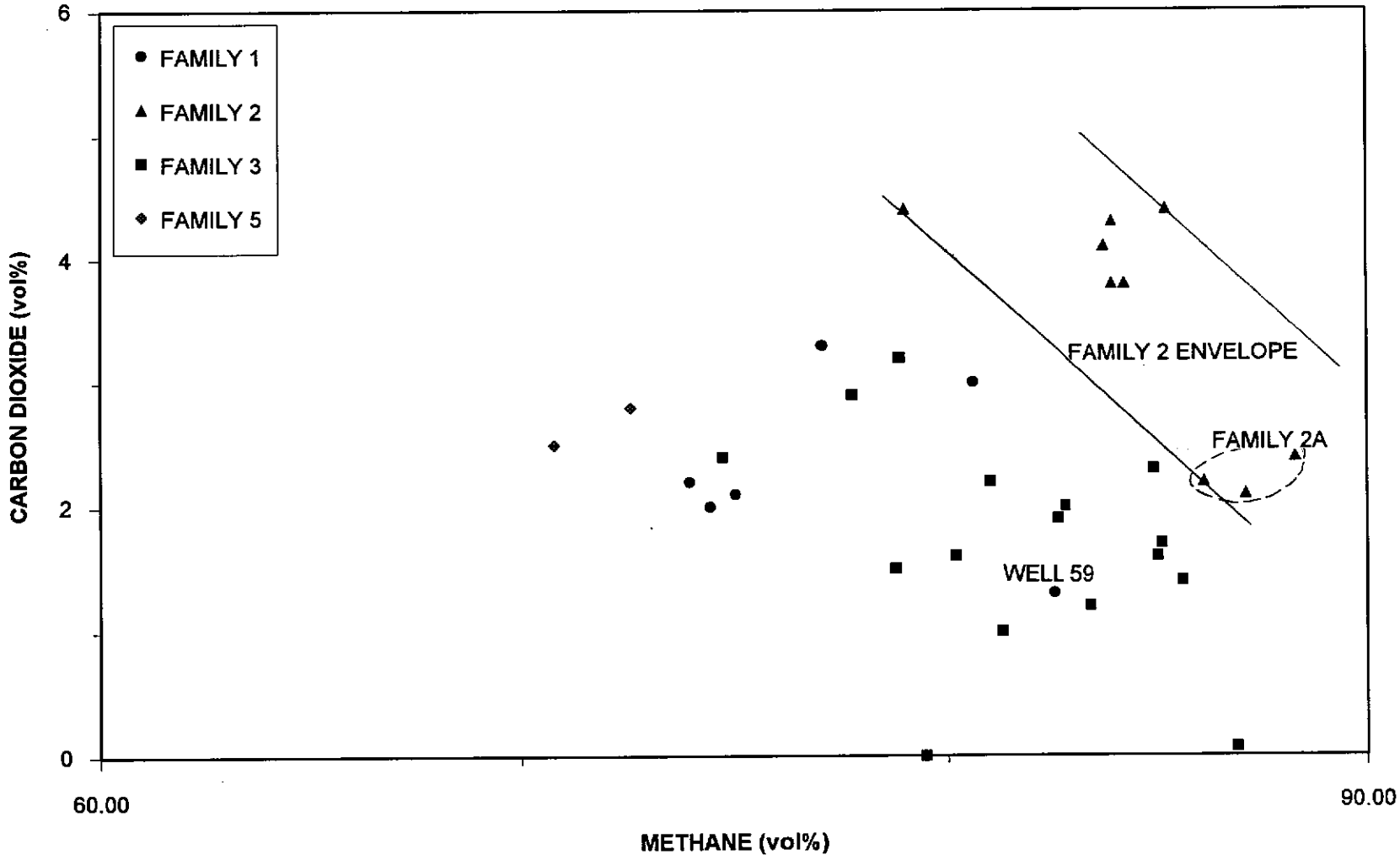

Figure 8.02b: Cross-plot of C1 vs CO_2 from separator gas samples showing distinction of the samples into four of the five Families.

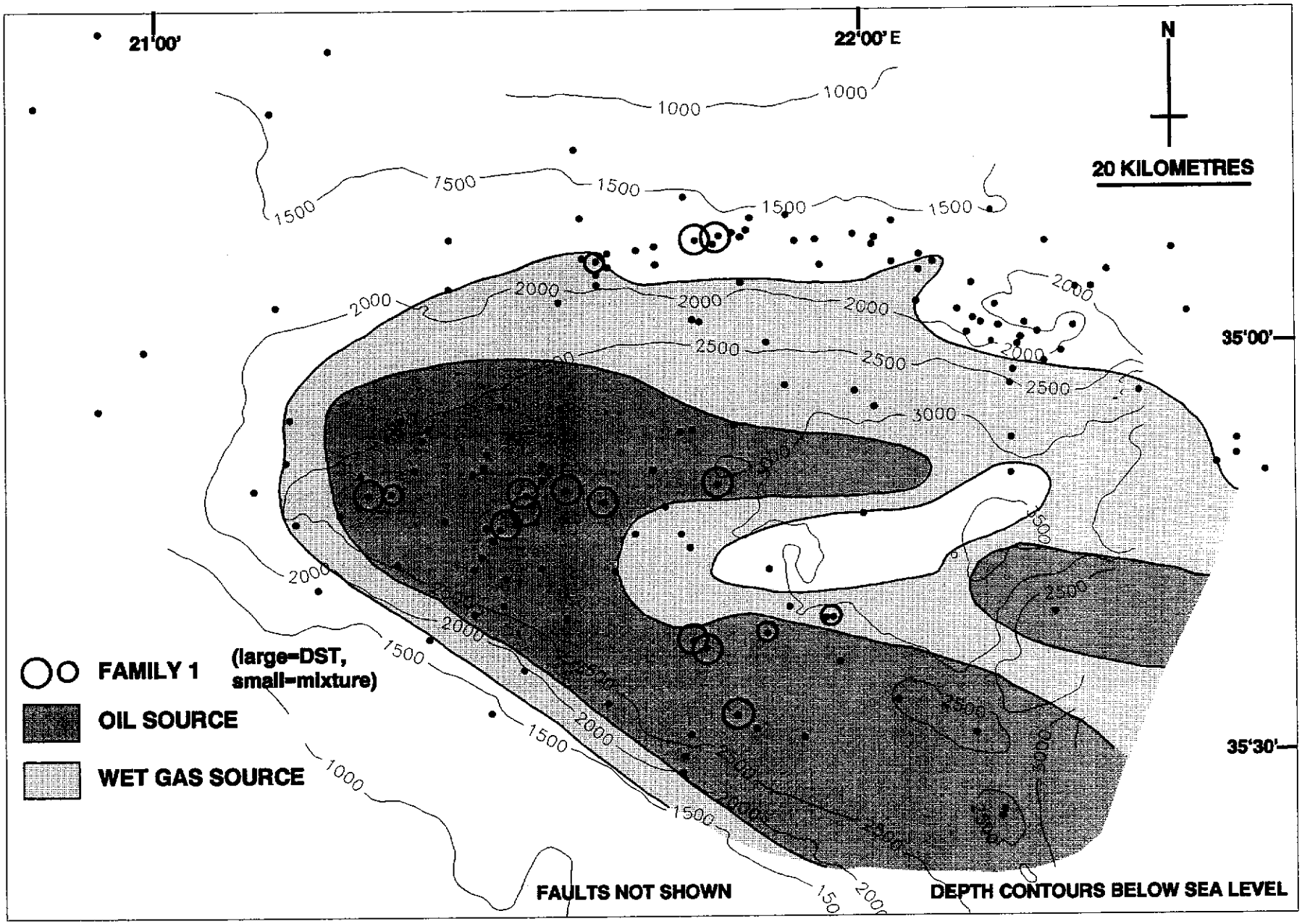

Figure 8.03: Map of 13A source rocks (after Figure 4.15) and with the distribution of Family 1 gases (large circles) and gases containing mixtures of Family gas with other gases (small circles).

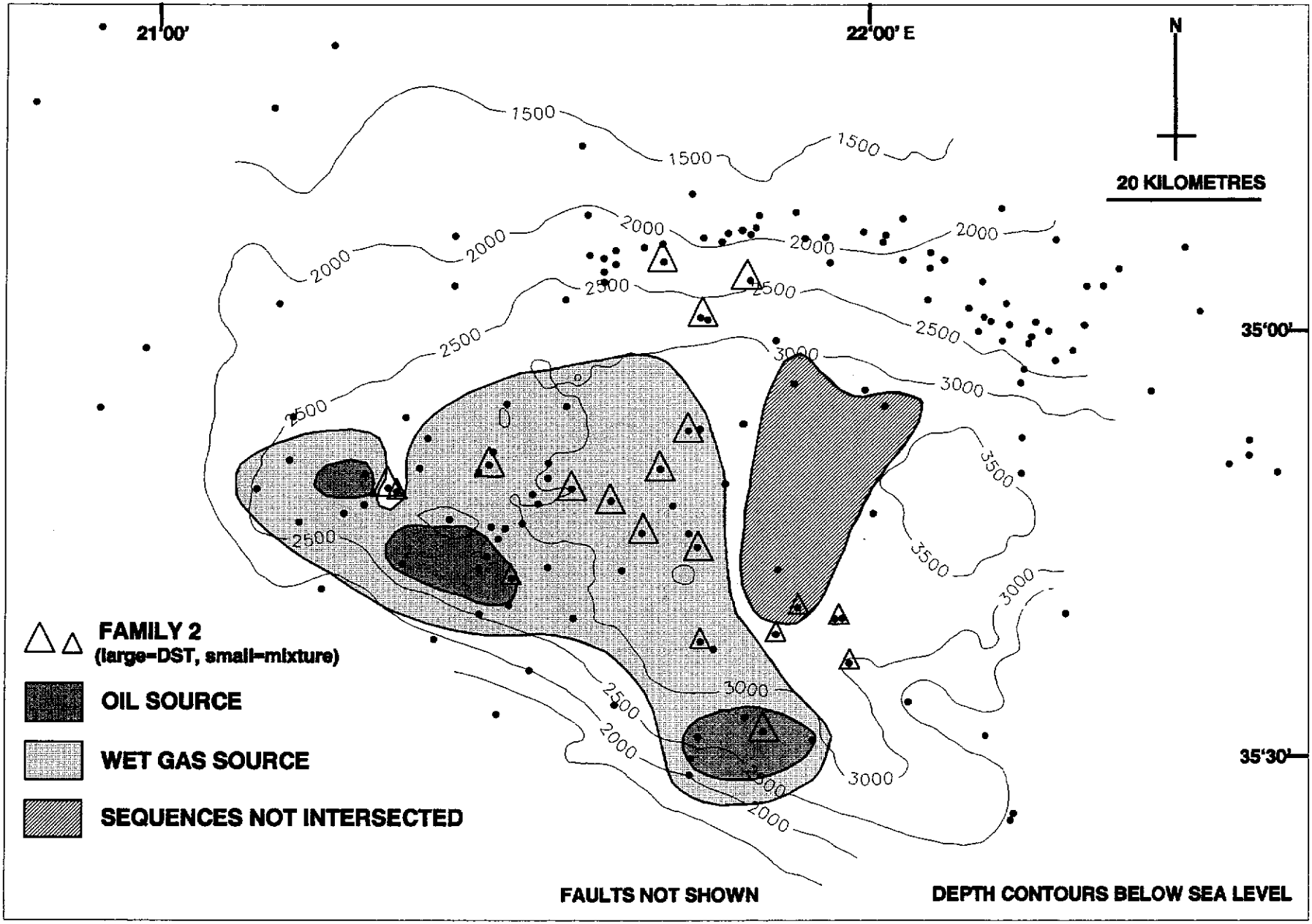

Figure 8.04: Map of 9A-12A source rocks (after Figure 4.13) and with the distribution of Family 2 gases (large triangles) and mixtures of family 2 gases with other gases (small triangles).

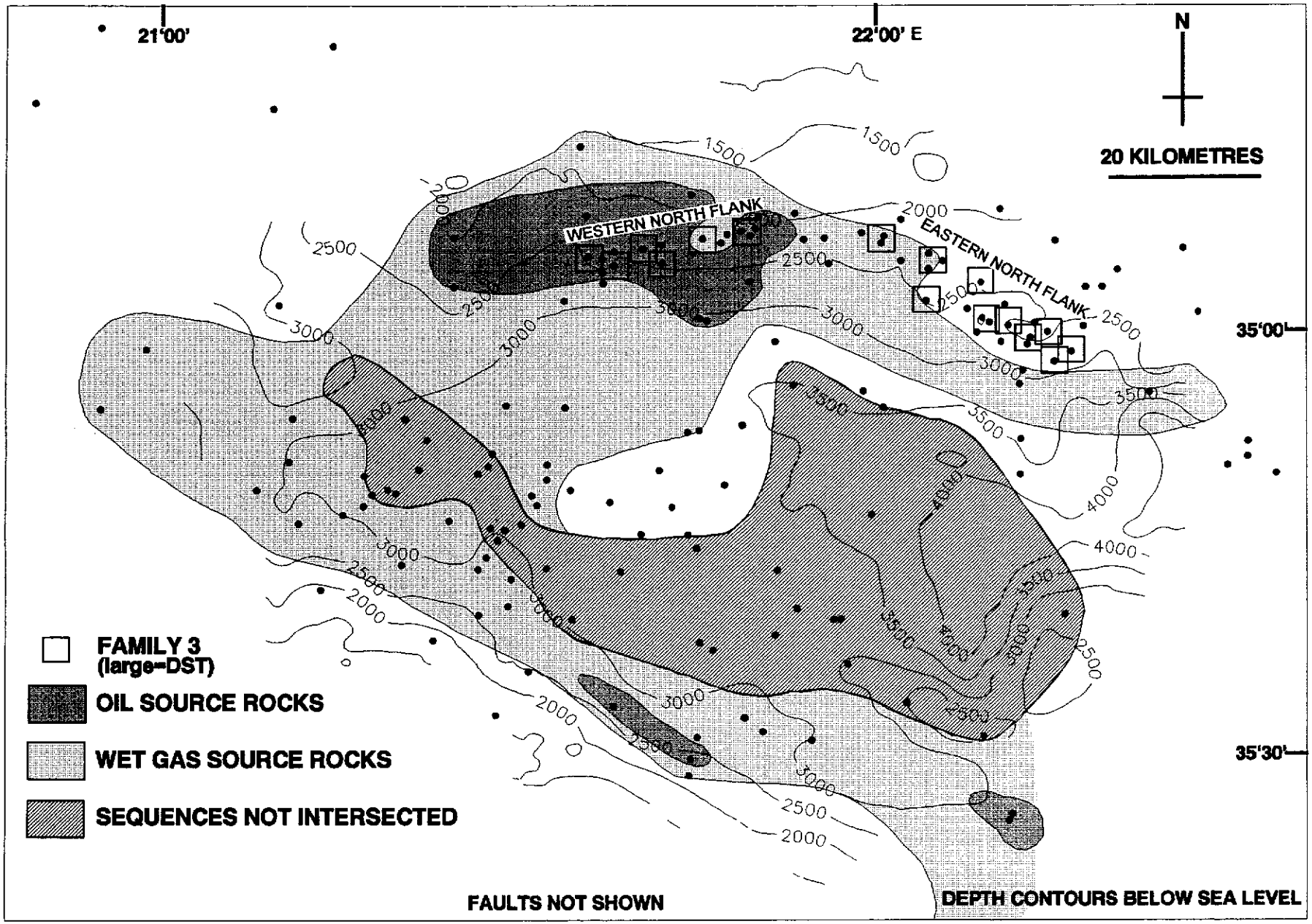

Figure 8.05: Map of 5A-8A source rocks (after Figures 4.09 and 4.11) with the distribution of Family 3 gases (large squares) and mixtures of Family 3 gas with other gases (small squares).

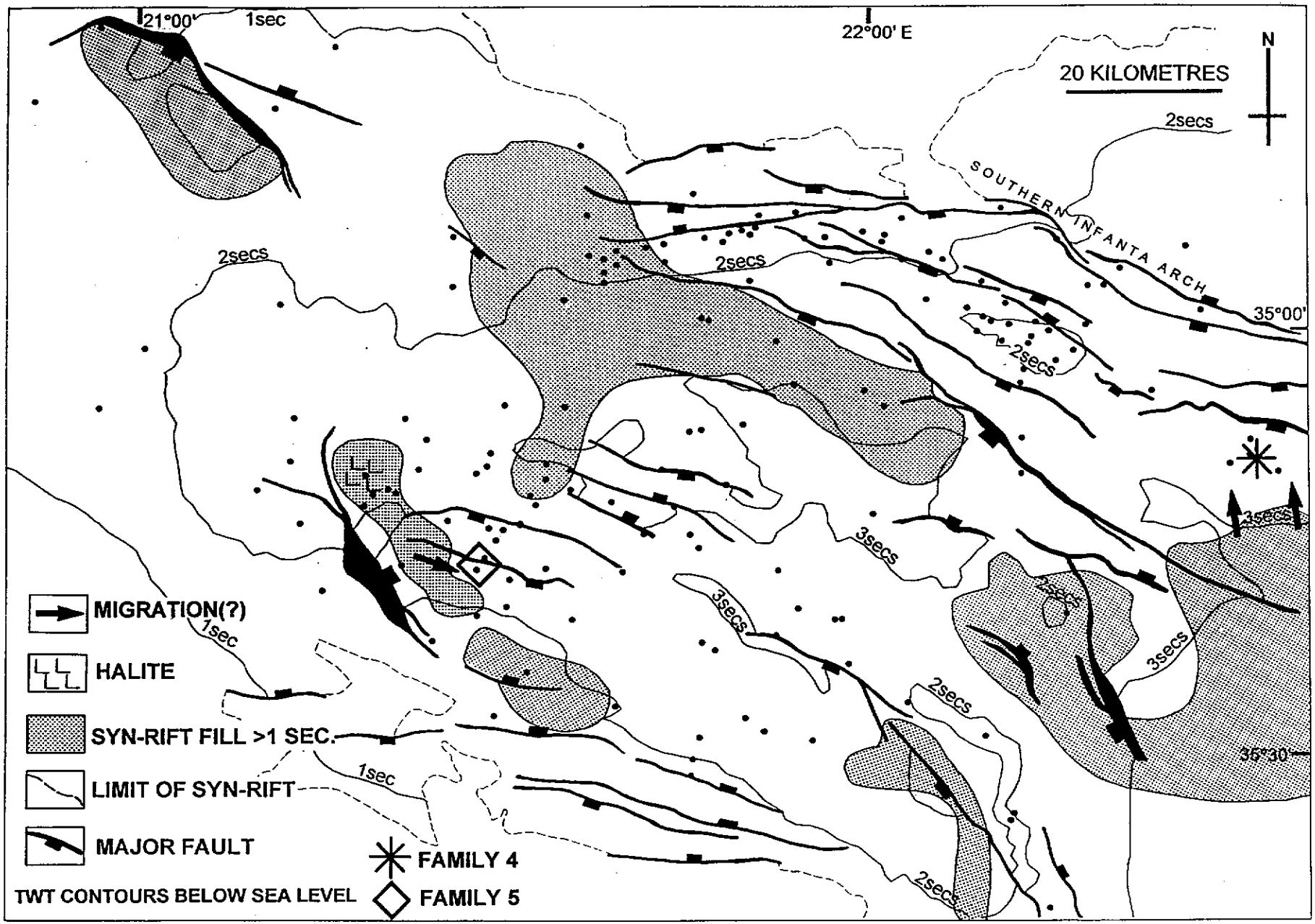

Figure 8.06: Two-way time thickness map of drift and syn-rift sediment (after Figure 4.03) showing the locations of the Family 4 and 5 gases (star and diamond respectively).

Fig. 8.02a, this gas locates a similar direction away from Family 3 as would be expected by a small maturity difference, even though the maturity difference is close to R_o~0.6%. Hence, these data suggest that the Family 4 condensate could be from a similar, but not matching, source. Indeed, Banks et al. (1993) suggested from geological considerations that these gases could be from the same source. The great dissimilarity between the Family 4 sample and the trend of the Family 3 samples is accentuated by the C1*CO_2 trend (Figs. 8.07a, 8.07b). The C1:C2/C3 plot (Fig. 8.08c) and the CO_2:N_2 plot (Fig. 8.09a) indicate the two to be dissimilar. In addition, GC and isotopic data (Chapters 9-10) confirm this difference.

The region of the Family 5 gases is located near the low reservoir maturity end of the Family 2 field (Fig. 8.02a). They are from a geographically restricted location distant from other Family 2 gases (Fig. 8.06) and up to 800 metres deeper than the nearest Family 2 reservoir to the north-west. They may even have been generated in adjacent syn-rift sediments. These Family 5 hydrocarbons are clearly not wholly distinguished from the Family 2 hydrocarbons in Fig. 8.02a but they plot in very different locations in Figs. 8.07a; 8.07b; 8.09a. They are more clearly separated from any of the other families by fingerprint data in Chapter 9.

Ternary plots of the proportions of methane, ethane and propane+ are shown in Figs. 8.08a and 8.08b. In both (particularly in the PVT data) there is a typical maturity trend from wet gas associated with oil, to largely dry gas with high GOR condensates. Cross-plots of these data (Figs. 8.08c; 8.08d) also clearly show the separation of the different hydrocarbon types, and since the ratio C2/C3 has been shown to indicate the type of source material, so the distinction between the values of Families 1, 2 and 3 may indicate different source intervals. The western Family 3 gases are slightly drier and have higher gas:oil ratios (Davies, 1996c) and have higher proportions of N_2 than those in the east (Fig. 8.09a; 8.09b). This could suggest dilution of Family 3 low N_2 gas by a high N_2 gas. There are several deep pre-1At1 graben near the western north flank reservoirs which could source this high N_2 gas (Figs. 3.04, 8.05a; 8.05b; 8.06).

Samples from well 48 and 59 both seem to represent mixtures of families. Gas produced from the latter well is shown to be unusually dry for an oil-associated gas (Stear et al., 1985) and more likely represents a later gas injection. Biomarker data show the oil fractions of these two belong to Family 1 (Chapters 11-12) but they include relatively dry gases, possibly from Family 3. The gas sample from well 48 locates outside the Family 1 margin in Fig. 8.02a. The sample from well 59 locates close to the edge of that region in Fig. 8.02a but in the Family 3 region in Fig. 8.02b and on the extension of the Family 3 trend in Fig. 8.08a.

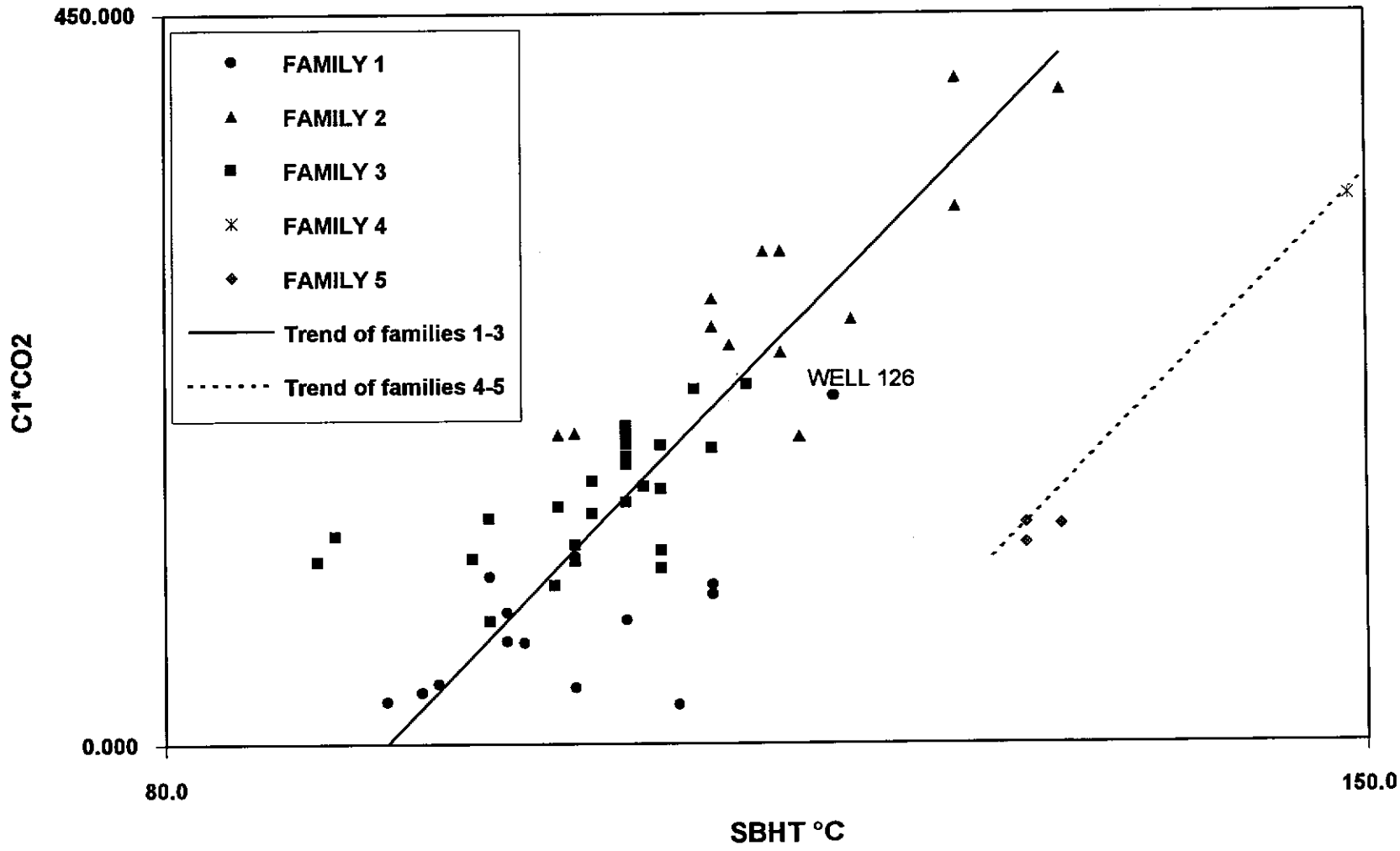

Figure 8.07a: Cross-plot of C1 x CO_2 (from recombined formation fluid samples) vs static borehole temperature showing that gases generated from Bredasdorp Basin drift sediments (Families 1, 2 and 3) are present in different proportions than in gases from non-Bredasdorp/non-drift sediments (Families 4 and 5).

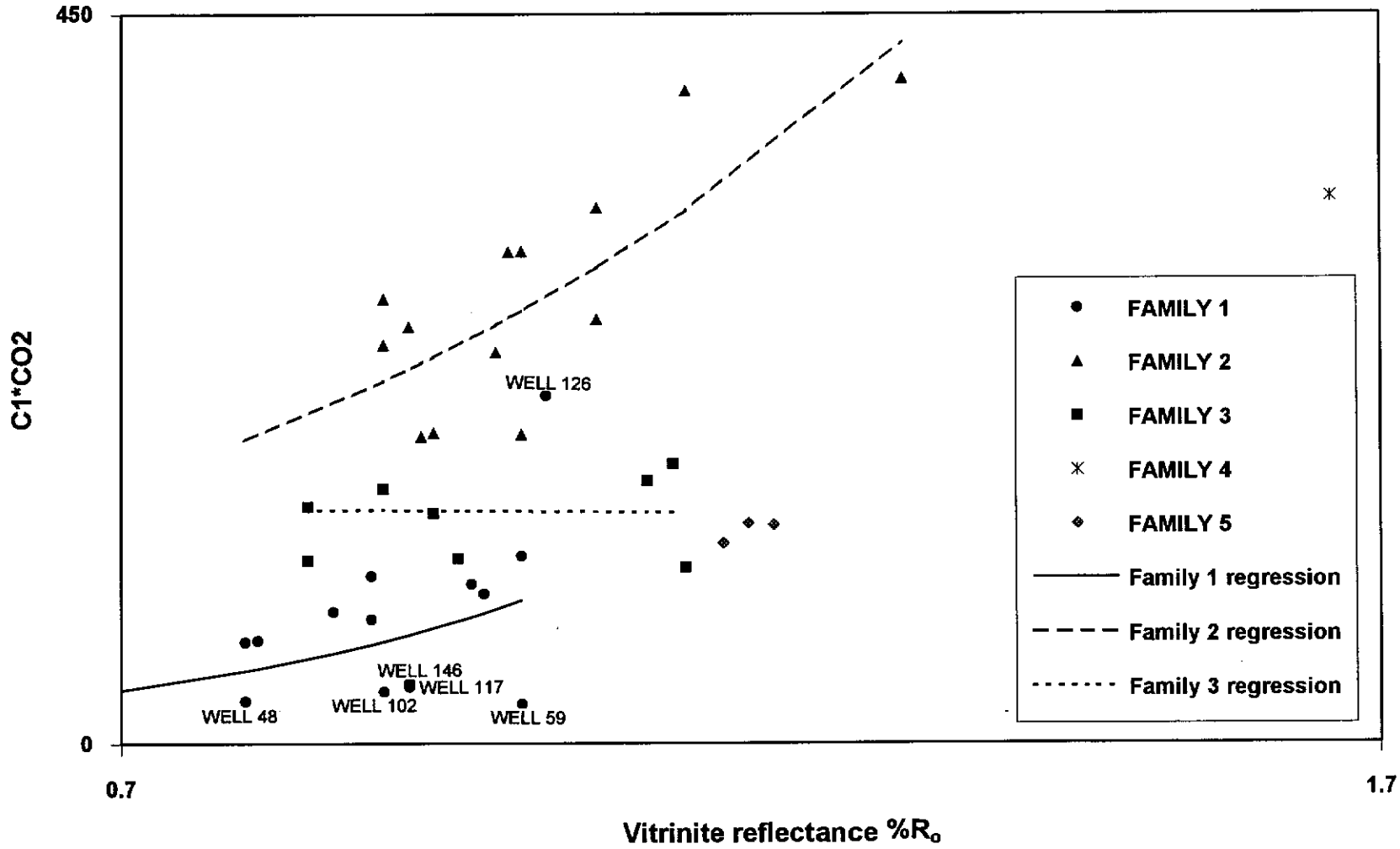

Figure 8.07b: Cross-plot of C1 x CO_2 vs vitrinite reflectance (of adjacent shales) for all recombined formation fluid gases showing the different regression lines of the three Families of gases which were not separated in Figure 8.07a.

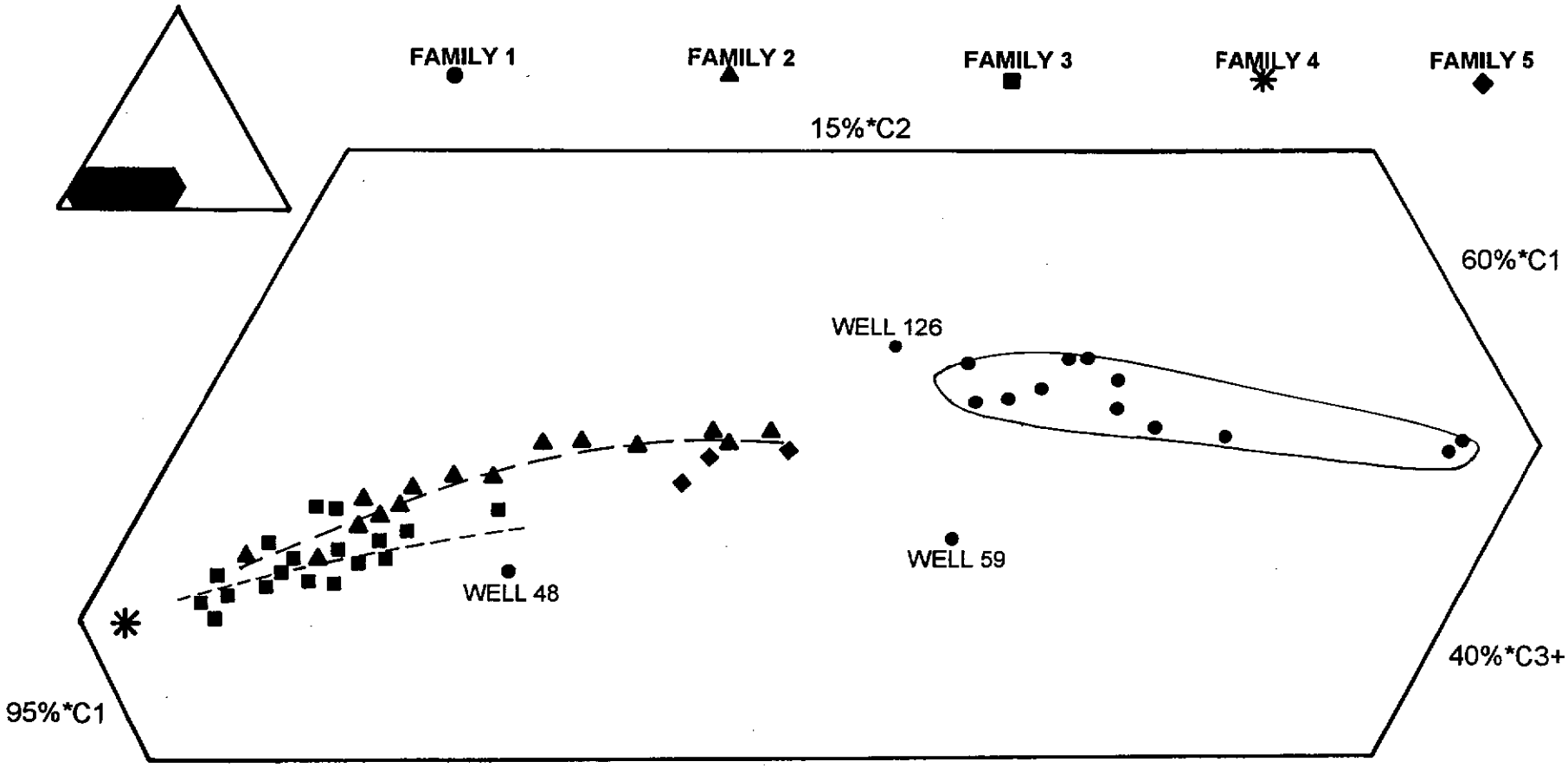

Figure 8.08a: Partial ternary plot of C1, C2 and C3-6 (as proportions of C1-6) for recombined formation fluid samples. The overall trend towards the C1 apex denoting increasing maturity is modified by slightly offset groups of samples from different Families.

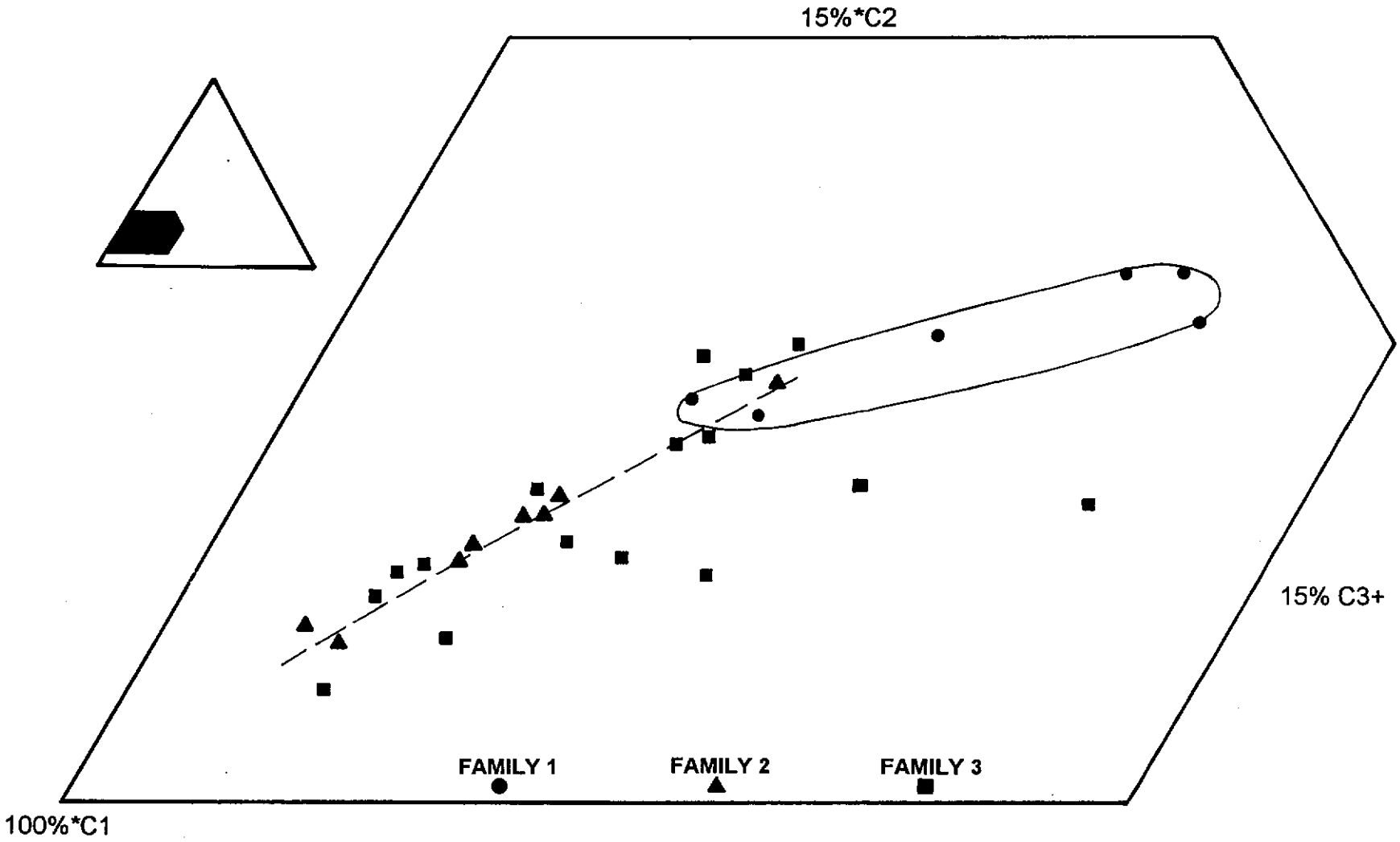

Figure 8.08b: Partial ternary plot of C1, C2 and C3+ for non-recombined separator gas samples. The overall trend towards the C1 apex matches that in Figure 8.08a but the distinction of the different Families is less clear.

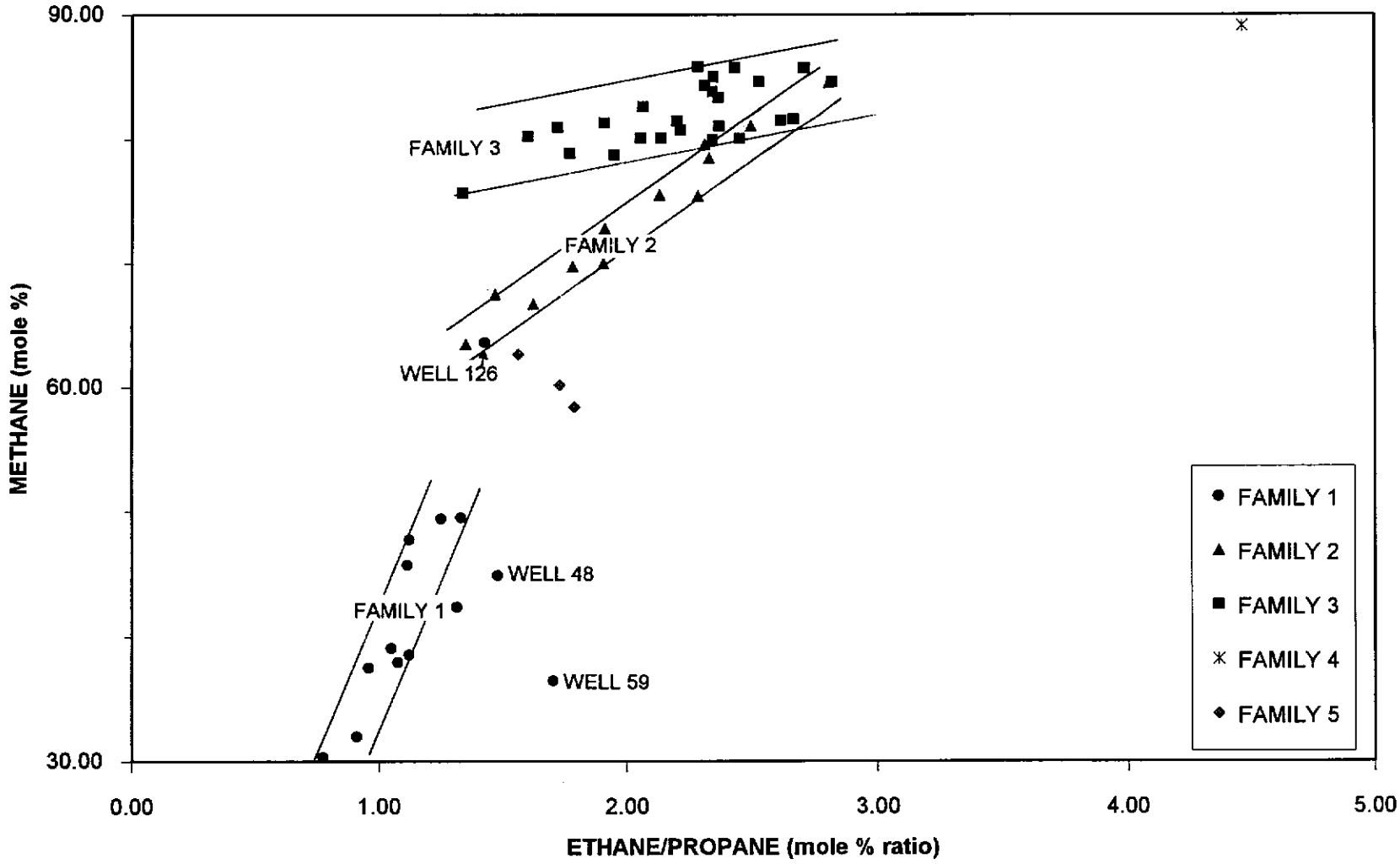

Figure 8.08c: Cross-plot of C1 vs C2/C3 for recombined formation fluid samples. The separation of the different Families is clear as is the marginal locations of data from certain wells (48, 59 and 126) which are later shown to be mixtures of two families.

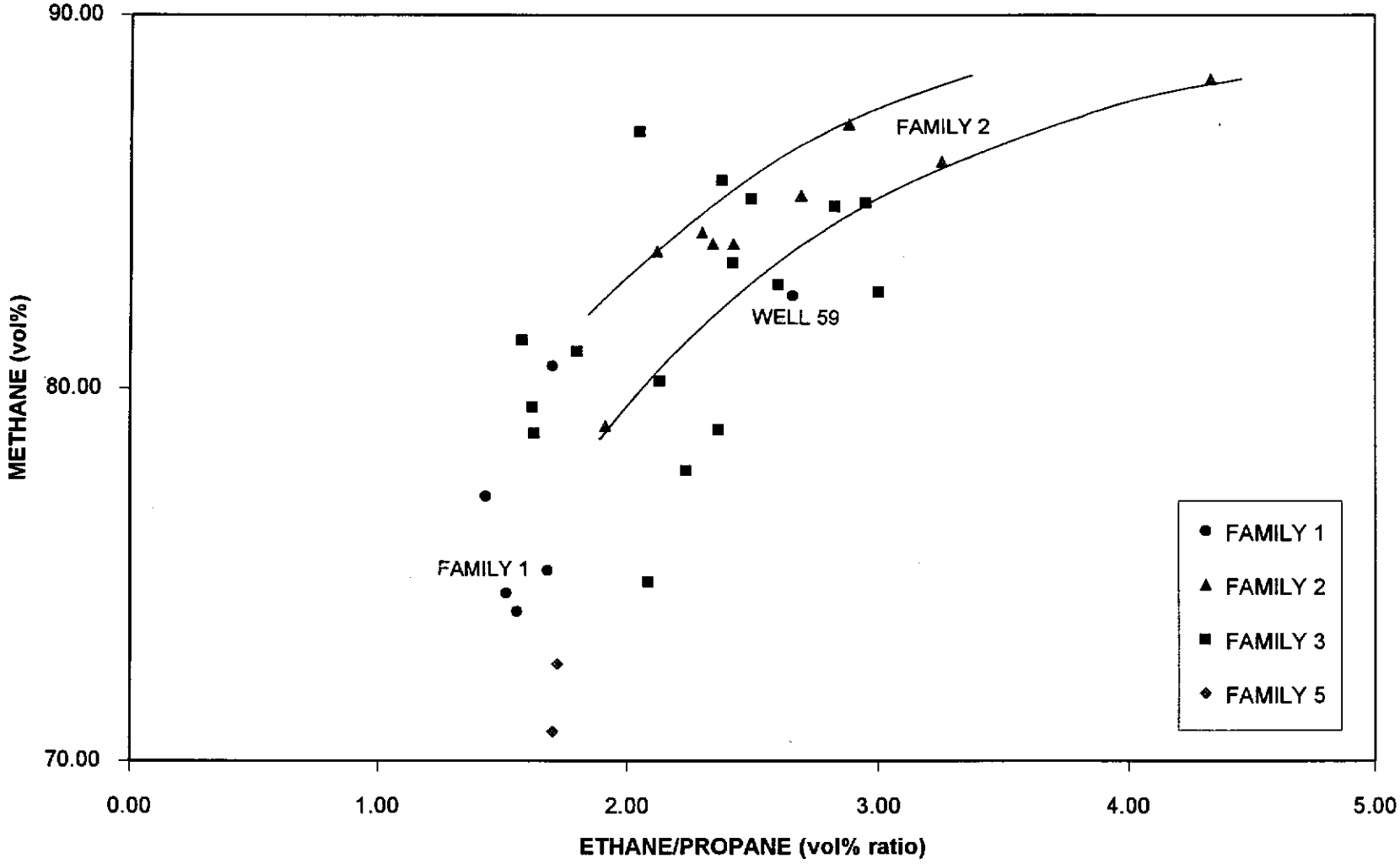

Figure 8.08d: Cross-plot of C1 vs C2/C3 for non-recombined separator gas samples. Data from different Families plots largely separate although a few samples (eg well 59) do appear out of place.

In fact, non-hydrocarbon data may be equally characteristic of source rocks as the hydrocarbon data. For instance, the cross-plot of the two main non-hydrocarbons (i.e. CO_2 and N_2) show a diffuse inverse relationship (Figs. 8.09a and 8.09b). Indeed, the highest maturity gases (Families 2 and 4) tend to have low N_2 proportions - quite dissimilar to the trend predicted by Littke et al. (1995). It is possible that the different N_2 trend is a function of source type rather than maturity. If so, this suggests that Family 3 and 4 gases are substantially different from all others because of their overall relatively higher N_2 proportions (Fig. 8.05a). More specifically, Family 1 gases have low CO_2 and N_2 contents (except for well 126 which is shown later to be a mixture of Family 1 oil and Family 2 gas), Family 2 gases have high CO_2 but low N_2 contents whereas Family 3 gases have low CO_2 but high N_2 contents.

Fig. 8.09a also shows Family 4 gas to lie off the Family 3 trend confirming that it is not directly related to these gases. This distinction, supported by other data (Chapters 9-12) is important as it shows that the fetch area and possibly also the source for Family 4 gas was not the same as for Family 3 gas. The location of the Family 4 gas outside the main Bredasdorp Basin suggests a Southern Outeniqua Basin source.

Smith and Ehrenberg (1989) show a log normal correlation between CO_2 partial pressures and formation temperatures for two contrasting basins. They interpret this to indicate that a thermodynamic equilibrium exists between the two parameters. They show that an equilibrium constant (which matches acidity to temperature changes) accommodates decreased equilibrium between feldspar and clays as maturity increases. However, this assumes that formation temperature is a measure of gas source maturity and that excess CO_2 is taken up by mineralisation. By contrast, the Bredasdorp Basin data (Fig. 8.10) show two separate log-normal distributions; one for gases reservoired in Hauterivian rocks and one for gases reservoired in Aptian-Barremian rocks. It also shows that Families 4 and 5 plot far away from these trends. This difference may indicate either different mineral-types in these sediments or different effective thermal histories for the two hydrocarbon groups, the latter being more likely based on the known unusual thermal histories (Davies, 1997c; 1997d).

Variations in formation temperatures do affect the ratio between normal butane and iso-butane (Alexander et al., 1983a), but these authors reported no strong source rock effect on the ratio. It is not clear from the text whether the wells sampled different source sequences or whether the wells were far enough apart to sample different facies of the same source. However, they commented on minor differences in the proportions of long-chain alkyl groups in different source intervals and noted that this was largely a function of free radical reactions rather than carbonium ion reactions. Alexander et al. (1983a) and Heroux et al. (1979) comment on the initial decrease in iso-butane

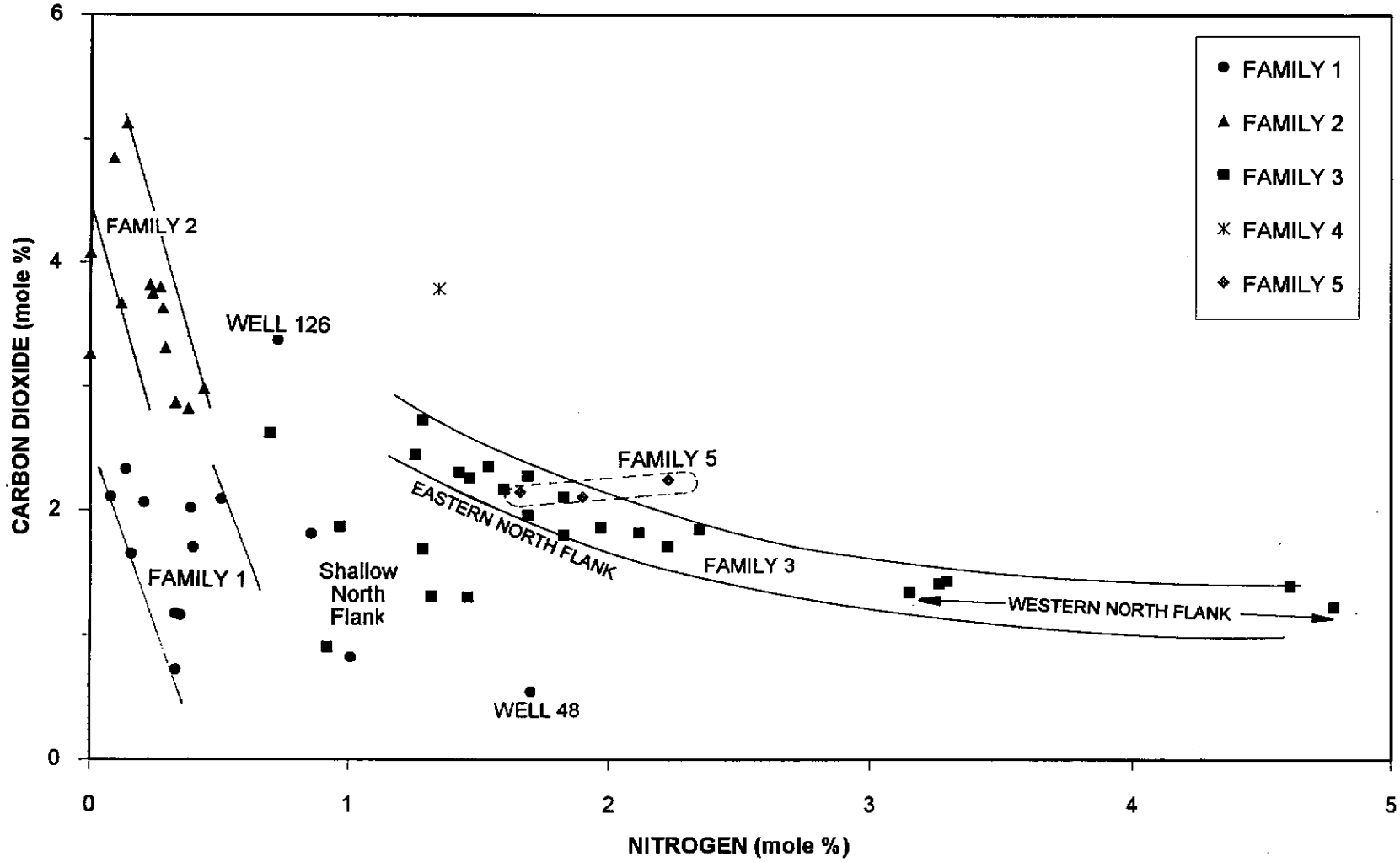

Figure 8.09a: Cross-plot of CO_2 vs N_2 proportions for recombined formation fluid samples. Some Families are cleraly separated but there are outlier data (eg. wells 126 and 59) which denote mixtures. In particular, the consistent Family 3 trend shows the continuously changing ratio between the gases is largely as a function of temperature. There is also a region in which some shallow north flank samples are located (eg wells 39, 61 and 63).

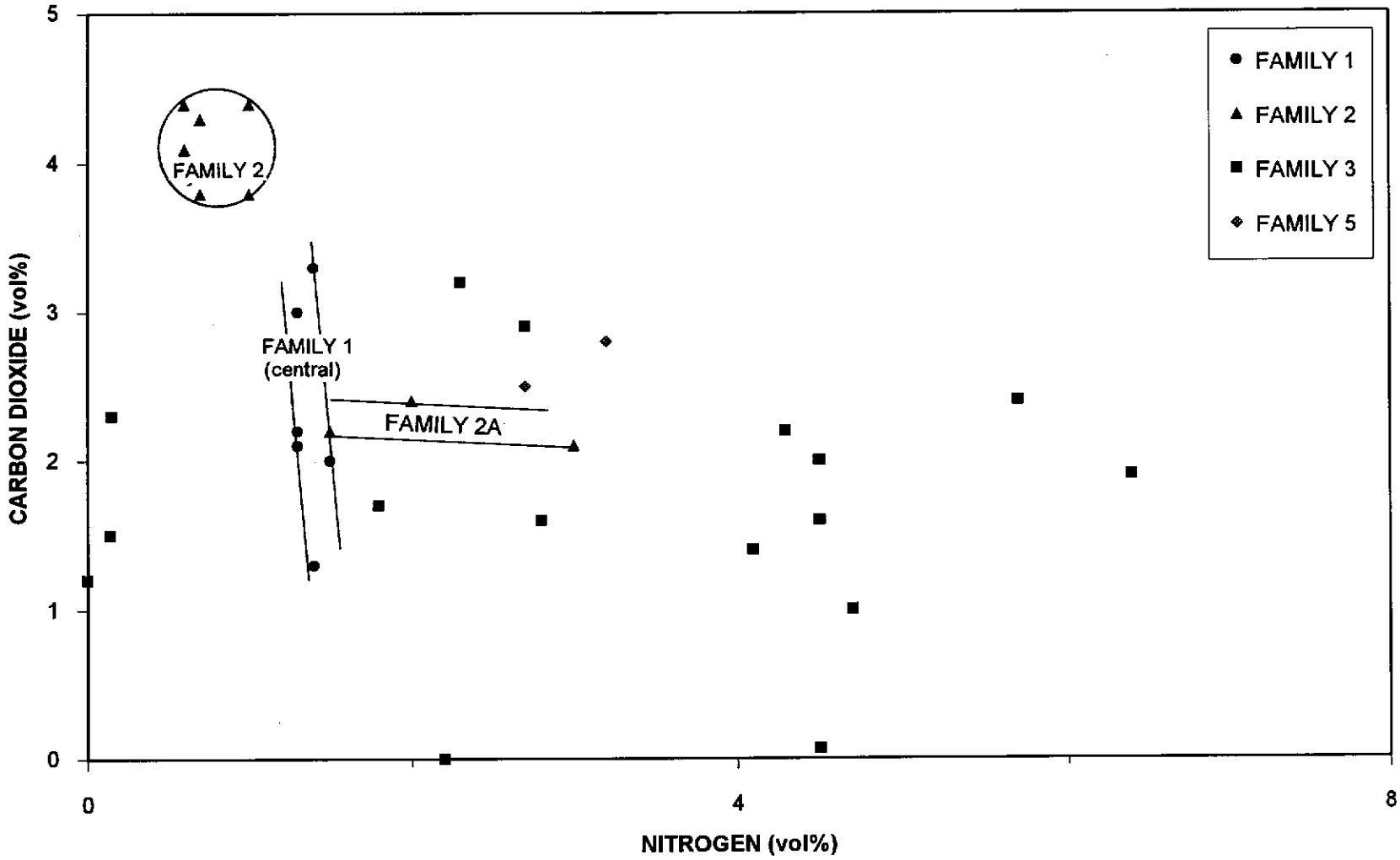

Figure 8.09b: Cross-plot of CO_2 vs N_2 proportions for non-recoombined separator gas samples. The fewer data result in more scatter but some families are clearly distinguished (eg. Families 1 and 2).

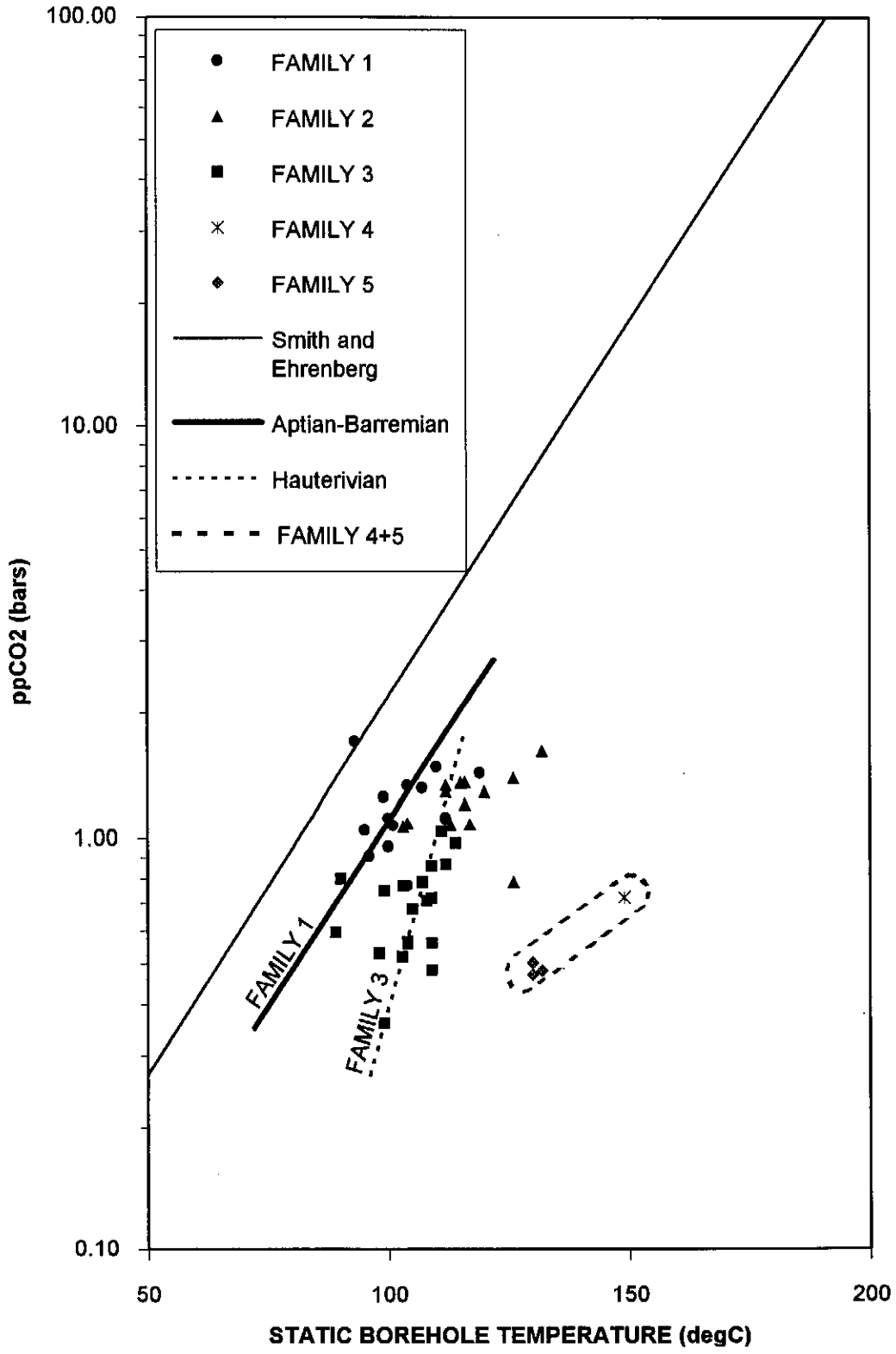

Figure 8.10: Plot of CO_2 partial pressure showing the trend of the indistinguished Families 1-3 (possibly later drift sourced) gases separate from the trend for Families 4 and 5 gases which are possibly non-Bredasdorp Basin drift-sourced.

contents which later reverses until iso- and normal butane are nearly equal. Alexander et al. (op cit.) suggest that this is a result of the initial preference for free radical reactions being succeeded by later carbonium ion reactions.

In the Bredasdorp Basin data, the decrease in the iso/normal ratio which Alexander et al. (1983a) and Heroux et al. (1979) reported to extend from ~40-100°C is barely evident amongst the PVT data because there are few data from reservoirs at temperatures less than 90°C. The increase they reported at temperatures higher than ~100°C is matched by the Bredasdorp data (Fig. 8.11). In addition, there is an evident separation between the Family 3 region and the trend of Families 1, 2 and 5. The Family 4 sample locates far outside the other Bredasdorp data trends or the trend of Alexander et al. (1983a) further suggesting that it is derived from a different source area. Alexander et al. (1983a) do indeed show that source rock differences would be expected to result in differences in the ratio - presumably within the stage when carbonium ion formation is prevalent (i.e. above the 100-110°C ratio minimum).

8.5. CONCLUSION

High quality samples are preferred for provision of meaningful analytical results. In this study, the samples used for PVT analyses are considered to be better quality than the water-displacement sampled cylinders, because the recombination method results in rigorous quality control and because the water-displacement method can lead to solution and discrimination effects. The latter analyses are useful for general guidance and were not analysed by PVT methods. Where pressures are not retained in the sample cylinders during storage, gas losses are largely the light components, e.g. C1, CO_2, N_2 - hence these gases cannot be fully interpreted in the SABS samples. However, the heavier components remain largely unaffected by leakage so that relationships are still valid.

The data record the effects of maturity and source rock type. The clear separation between compositional trends of different gases permits distinction of five separate families of hydrocarbons. These families are characterised by dominances and paucities of certain compounds and are overprinted by reservoir maturity trends. It is suggested that between the data trends of the different families, "out-of-place" data may result from mixing of two or more hydrocarbon streams in the reservoir. Indeed gases from wells 48, 59 and 126 all represent mixtures of different hydrocarbon families (Chapters 9-12). Data trends of Families 1, 2 and 3 are sub-parallel in many of the figures and can be extrapolated to higher maturities. Family 4 and Family 5 data do not lie on those extrapolated trends suggesting that they are both representative of different hydrocarbon sources than that of the other gases. In general it is found that Family 1

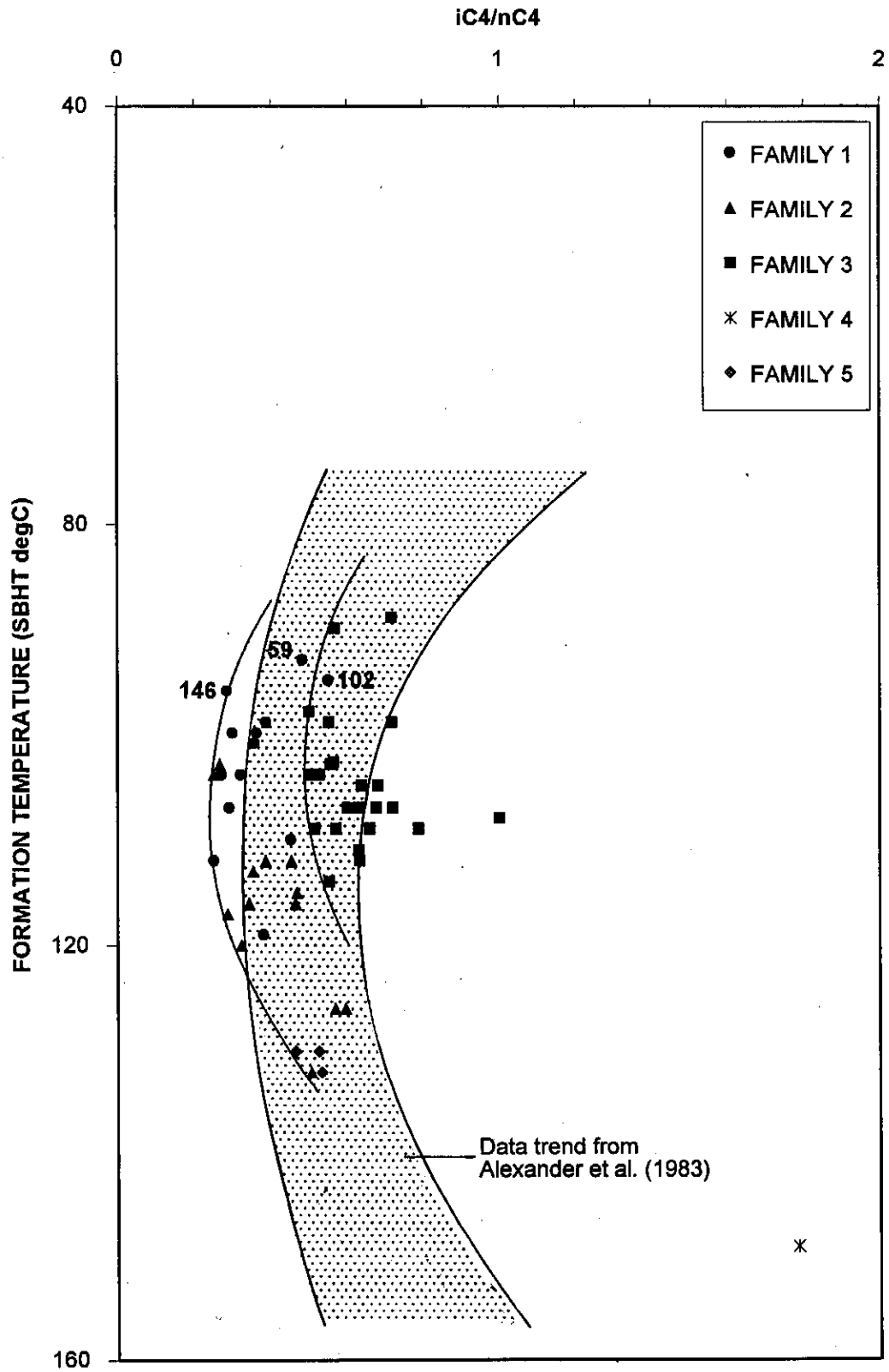

Figure 8.11: Plot of the iso/normal butane ratio for recombined formation fluid samples. Families 1, 2 and 5 are inseparable but plot almost completely separate from the family 3 gases. The only two data which overlap are those from wells 59 and 102 DST4 both of which are later shown to represent mixtures. The representative sample from Family 4 plots completely separate from the other gases further supporting the interpretation that it was sourced outside the basin.

hydrocarbons are almost all oils and are closely associated with the oil-prone 13A source rock, Family 2 hydrocarbons are associated with 9A-12A source rocks and Family 3 hydrocarbons are associated with 5A-6A source rocks. Families 4 and 5 are possibly associated with Southern Outeniqua Basin and syn-rift sources respectively. These correlations indicate that gas data do provide guidance on source characteristics. Other data (Chapters 9-12) confirm these correlations with specific source intervals

Although based on only one sample, the distinction of Family 4 is important because it probably represents a previously unknown source rock in the Southern Outeniqua Basin. Modelling in Chapter 7 demonstrates that hydrocarbons could be expelled from this basin if the expected source rocks are present. Family 4 gas may confirm that at least one of those source rocks is present.

CHAPTER 9: WHOLE OIL GAS CHROMATOGRAPHY DATA

Samples of hydrocarbon liquids produced from reservoirs are routinely analysed unprocessed by high resolution whole oil gas chromatography (GC) (Table 9.01). Such samples always contain some gaseous components in solution and range through to asphaltenes. Analyses are carried out on whole oil samples, in spite of the potential for column contamination by dissolved asphaltene molecules, for three reasons:
(i) to gain a general overview of the complete oil envelope
(ii) to investigate the components up to C9 which are susceptible to in-reservoir alteration
(iii) to correlate the hydrocarbons using the light oil 'fingerprint' components, in the range nC9-16, which are usually lost or in reduced proportions in extracted oils.

The analysis results in delineation of many hundreds of chromatographic peaks - each representing one or more compounds, between nC4 and >nC37. Data are plotted to three scales namely 0-80 minutes (i.e. full scan), 0-10 mins. (i.e. nC4-nC9) and 6-36 minutes (i.e. C9-C20) (Fig. 9.01). The nC4-9 fraction is commonly referred to as the condensate fraction since it is the largest fraction in gas-condensates and the C9-20 fraction as the 'fingerprint' fraction, recently brought into use as a low cost fingerprint of oil. In petroleum engineering terms, condensate refers to the liquid which forms when the pressure and temperature of a reservoired gas are reduced below the dew point. This liquid is often referred to as light oil as it remains in the gas phase in the reservoir, because of physical as opposed to chemical conditions.

Analytical conditions are given in Table 6.08a. Analyses were carried out using matching conditions (Table 6.08a), which resulted in chromatograms of matching length (to within ~3 seconds at 10 minutes, or ~10 seconds at 35 minutes) hence peak widths and heights are comparable. However, analyses carried out with different columns are slightly different (Appendix C, Figs. C33-34, C.37-38 and C.60-61). Some peaks in column 1 analyses are slightly displaced relevant to the other chromatograms, although overall fingerprints matched closely. Two of these peaks are known from injection of authentic standards to be aromatic and the other displaced peaks may be also. This is unlikely to be related to the different split ratio (60:1 vs 100:1, Table 6.08a), because the analyses were carried out with the split open. It may be an effect of a non-standard OV101 loading. In any event, these 'out-of-place' components were not used in the fingerprint correlation. Comparison of peak height ratios show that columns 1 and 3 give similar results whereas results of analyses on column 2 differ slightly (< ~10%); column Q differs by a further by ~10% from column 2. Repeat analyses of sample batches a few months apart using the same column show that sample handling repeatability is better than 3% and that column degradation (resulting from ~100

WELL	TOP DEPTH	TYPE	COL.	FAM.	DSTTemp	API	Wellsite GOR	Hydrocarbon types	REMARKS
Family 1: Aptian oils									
83	2470	DST3	1	1	98.9	43.0	400	O	nC9 low
88	2507	DST5	1	1	112.0	45.4	700	O	nC9 low
102	2241	DST4	2	1	106.7	45.4	5880	[G]+O	
95	2703	DST2	2	1	120.0	57.2	9080	G+[[O]]	
103	2718	DST2	1	1	93.3	57.2	7270	G+[O]	
94	2799	DST1	2	1	126.0	46.3	1350	O	low gas = evaporated
93	2463	DST2	1	1	102.8	43.2	730	G+[O]	
93	2808	DST1A	3	1	111.1	57.2	6260	G+[O]	
93	2817	DST1	1	1	112.8	43.4	3100	G+O	
119	2816	DST1	2	1	114.4	39.4	1203	G+O	
109	2630	DST1	2	1	109.4	38.0	660	[G]+O	
126	2643	DST1	1	1	116.7	56.2	6390	G+O	
146	2398	DST1	3	1	101.7	43.2	438	O	
117	2399	DST1	3	1	106.7	42.8	450	O	
156	2522	DST1	Q	1	111.0	44.3	930	O	
166	2520	DST1	Q	1	113.8	48.1	1299	O	
48	2634	DST1	2	(1)	105.0	0.0	0	G+O	reverse circulation
59	2212	DST1	2	1	99.2	35.4	400	[G]+O	
Family 2: Barremian wet gas									
83	2889	DST2	1	2	113.0	41.1	5750	G+O	
83	3254	DST1	1	2	128.5	51.1	40000	G+O	
88	2839	DST4	1	2	117.0	41.1	7600	G+O	
88	2916	DST3	1	2	119.4	54.7	29900	G+[O]	
88	2929	DST2	2	2	120.0	54.7	25700	?	little gas = evaporated
88	3243	DST1	1	2	131.7	52.3	29200	G+[[O]]	
102	2625	DST2	2	2	106.0	57.2	9080	G	
96	3131	DST1	3	2	126.1	44.7	132000	G	
114	3085	DST1	1	2	135.0	49.9	35000	G+O	
108	2820	DST2	2	2	112.2	54.7	6720	G	
108	2829	DST1	2	2	116.7	52.3	7300	G	
129	2855	DST2	1	2	118.3	43.0	14760	G+O	
129	2945	DST1	1	2	123.9	46.5	31520	G+[O]	
107	2388	DST3	2	2	97.8	60.8	20600	G	
110	3051	DST1B	3	2	121.1	50.4	11840	G	similar to DST1A
120	2931	DST1	1	2	121.1	54.2	74057	G+O	
166	2508	RFT	Q	2	?112.5	0.0	~6000	G	RFT sample
132	2662	DST2	2	2	104.4	55.9	71451	G	
132	2706	DST1	2	2	110.0	41.9	980	G+[O]	
148	2684	DST1	3	2	110.6	57.2	5917	G	
167	2676	DST1	Q	2	115.0	62.3	7031	G	
11	2950	DST2	2	2	127.2	0.0	0	G	reverse circulation
84	2771	DST1	2	2	108.9	42.4	0	G+O	reverse circulation
37	3495	DST1	2	2	136.7	43.1	0	G	reverse circulation
65	3189	DST2	2	2	126.1	43.2	142000	G	
65	3267	DST1	2	2	127.8	45.4	294000	?	little gas

Table 9.01: List of all samples, the analysis columns, the hydrocarbon Families, the reservoir temperature (DST Temp.), the API gravity and gas:oil ratios (scft/bbl) and the type of hydrocarbon (including mixtures).

WELL	TOP DEPTH	TYPE	COL.	FAM.	DSTTemp	API	Wellsite GOR	Hydrocarbon types	REMARKS
Family 3: Hauterivian wet-dry gas									
107	2565	DST2	2	3	106.7	59.7	47023	G	
107	2590	DST1	2	3	106.7	0.0	0		reverse circulation
69	2435	DST1	2	3	107.2	56.4	31300	G	
46	2560	DST2	2	3	109.4	49.9	62200	G	
48	2620	DST2	3	(1)	104.4	31.1	0	[G]+O	reverse circulation
54	2588	DST1	2	3	112.8	50.4	86200	G+[[O]]	
76	2610	DST1	3	3	107.8	53.0	68600	G	
39	2229	DST2	2	3	100.6	53.7	65289	G	
39	2556	DST1	1	3	110.6	57.2	55417	G+??	
18	2635	DST4	2	3	124.4	55.9	45200	G+[[O]]	
18	2673	DST3	2	3	121.1	55.2	36700	?	little gas = evaporated
18	2703	DST1	2	3	120.0	57.2	53800	G	
21	2552	DST2	3	3	113.0	54.0	58000	G	
21	2577	DST1	3	3	117.2	50.6	42480	G	
19	2700	DST2	2	3	118.3	54.9	34400	G	
20	2515	DST4	1	3	101.1	50.4	0	G	reverse circulation
20	2579	DST3	1	3	100.6	49.4	63200	?	little gas
20	2699	DST2	1	3	99.4	44.4	281000	G	low pressure, little gas
44	2750	DST1	2	3	128.7	52.5	26190	G	
55	2681	DST2	2	3	118.3	49.2	51000	G	
61	2128	DST3	2	3	99.3	65.0	17100	G	
61	2770	DST2	2	3	121.7	51.6	57600	G	
62	2549	DST1	2	3	110.6	35.9	0	G+O	low pressure = evaporated
70	2428	DST2	2	3	107.2	57.4	30800	G	
70	2452	DST1	2	3	108.3	34.5	0	G+O	reverse circulation
31	2753	DST1	1	3	117.8	54.7	23000	G+[[O]]	
63	2690	DST1	1	3	107.2	53.7	48900	G+O	
Family 4: ?Southern Outeniqua dry gas									
128	3640	DST1	1	4	154.3	46.3	376270	G	little gas
Family 5: ?Valanginian wet gas									
27	3164	DST1	2	5	136.1	37.8	0	?G	rev. circ., little gas, evaporated
35	3309	DST3	1	5	134.4	49.9	3000	?G	little gas = evaporated
35	3354	DST2B	2	5	134.4	50.1	3200	?G	little gas = evaporated
35	3397	DST1	2	5	135.6	52.2	0	?G+[?O]	rev. circ., little gas, evaporated
G = gas, ?G = possible gas peak but uncertain, O = oil hump, [O] = possible oil hump.									

Table 9.01 (cont.)

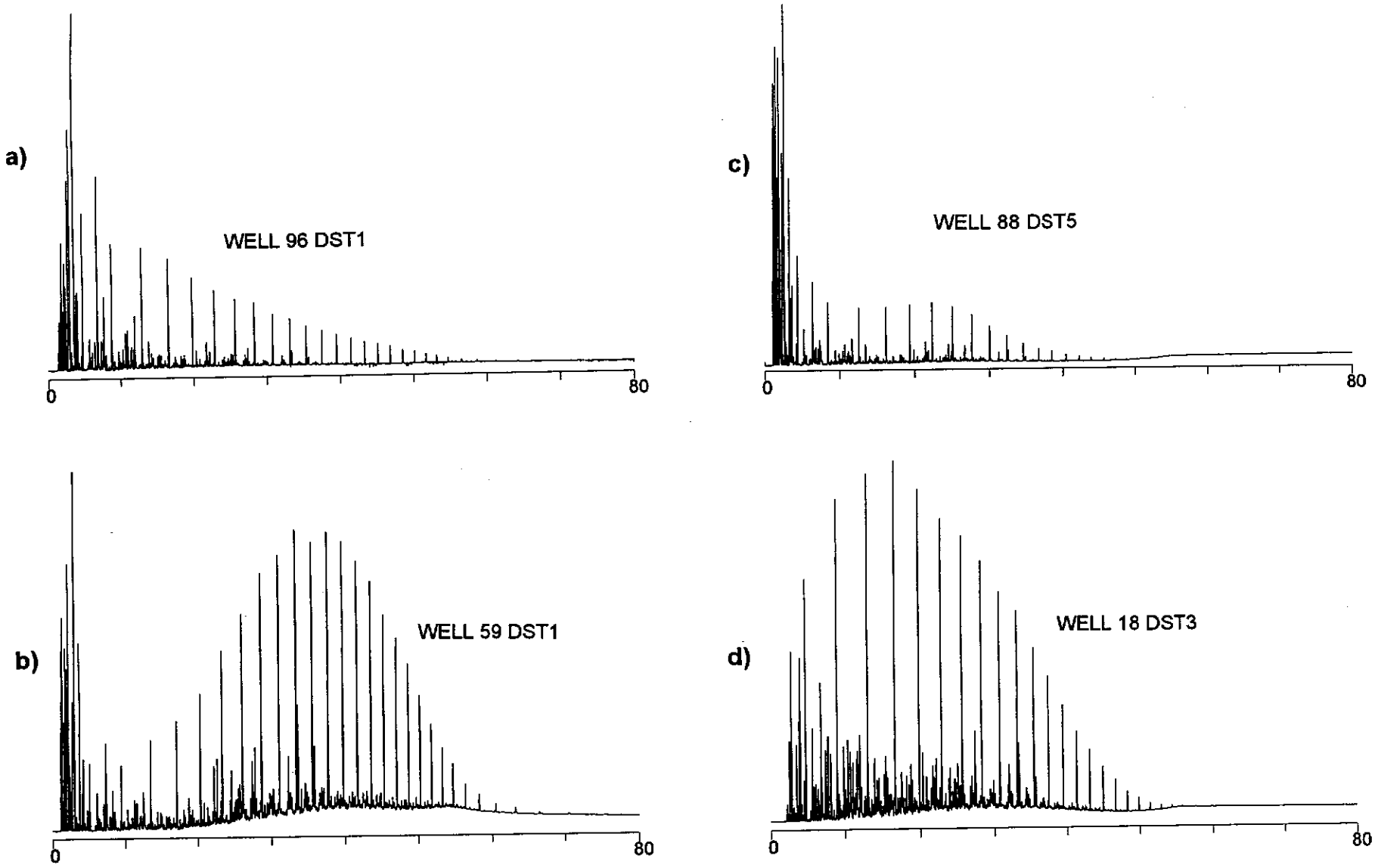

Figure 9.01: Examples of whole oil gas chromatograms showing (a) an oil fill, (b) mixed fill of oil and later gas, (c) residual oil with gas and (d) post-production evaporated sample.

analyses) gives progressive peak height differences of <2% from the mean (Davies, 1996e). Apart from these analyses, repeat analyses have also been carried out on a number of samples in the Bredasdorp Basin, reported here in Table 9.02.

Most of the components in the nC4-9 fraction are assigned unambiguously to specific compounds. Many of these were confirmed by co-injection with authentic standards. This was done during analytical work at SABS (Pretoria) on a standard sample (SABS, 1983), at Soekor (1989-1992) and by Hunt (1979b), identifying a total of 48 compounds. Within this fraction, there are usually traces of nC3 but they are not included in any calculations. The locations of these compounds in a whole oil GC are shown in Fig. 9.02 and listed in Appendix H. Only a small proportion of the peaks in the fingerprint fraction have been unambiguously assigned to particular compounds and few of those are used in this study. Because of the lack of suitable standards for many peaks, compounds are located by relative retention times. Moreover, because most of the peaks are not assigned to specific compounds, none are referred to by name. Elsewhere, peaks have been attributed to specific compounds, most of which are saturated hydrocarbons (Hwang et al., 1994; C.C. Magnier, 1995, pers. comm.).

Individual peak heights are used for correlation in the nC4-9 fraction. However, to avoid changes due to slight differences in the GC oven temperature (accurate to <1°C) and carrier gas flow rates, fingerprint correlation ratios are constructed of adjacent or near-adjacent peaks instead of using individual peak heights. Gas chromatograms generated during these analyses are given in Appendix C, Figs. C.1-C.85 and tabulated peak heights are given in Appendix F, Table F.3.

Samples are assigned to hydrocarbon families based on their liquid fraction. This allows for correlation with reservoired hydrocarbons which were solvent-extracted from the formation and hence have no gas fraction, and with source rocks which are not sampled for their gas and lightest oil fractions. Gas and whole oil analyses, therefore, do not allow for confident assignment of all samples, as some are assigned based on other distinguishing features such as biomarkers and isotopic data, discussed in Chapters 10-12.

9.1. INTERPRETATION OF WHOLE OIL ENVELOPE

The main interpretation made from the whole oil GC data is whether the liquid represents a mixture of oil and gas, perhaps indicating different migration episodes or different sources, or a single hydrocarbon type migrated during a single episode. These differences are often evident from the shape of the whole oil envelope (Fig. 9.01 and Appendix C, Figs. C.01-C.85). Where a sample represents a single fill of high

MSCHEV PEAKS						PEAK-PAIR RATIOS									
					Analysis	1	2	2a	3	4	5	6	7	8	9
WELL	DEPTH	TEST	Col.	BH	Date	Branched and cyclo-alkanes									
Family 1															
83	2470	DST3	1	105	20-08-91	2.51	0.85	3.04	0.33	0.94	0.59	1.59	0.83	2	1.22
88	2507	DST5	1	100	21-08-91	2.25	0.90	2.58	0.39	1.17	0.54	1.37	0.81	2	1.13
102	2241	DST4	2	98	1-04-92	1.62	1.26	1.01	0.48	0.80	0.70	1.80	0.47	1	1.44
103	2718	DST2	1	115	26-08-91	1.85	1.00	2.73	0.60	0.73	0.59	1.68	0.98	3	1.36
94	2799	DST1	2	117	2-04-92	1.29	0.93	1.53	0.65	0.74	0.95	1.35	0.66	4	1.38
93	2463	DST2	1	102	27-08-91	3.23	0.88	4.27	0.65	1.05	0.90	1.83	0.83	2	1.16
93	2808	DST1A	3	116	16-02-93	4.29	1.22	1.17	1.01	0.87	1.24	0.79	0.79	5	1.44
93	2817	DST1	1	117	26-08-91	2.82	0.79	1.28	0.84	0.87	0.54	0.44	0.60	3	0.57
119	2816	DST1	2	112	2-04-92	2.31	1.27	0.86	1.34	0.85	1.46	0.48	0.60	6	1.72
109	2630	DST1	2	100	23-12-92	2.91	1.20	0.79	2.68	0.13	1.06	0.47	0.82	4	1.11
109	2630	DST1	3	100	18-02-93	4.09	1.45	0.74	1.32	0.89	1.39	0.45	0.65	6	1.29
126	2643	DST1	1	119	27-08-91	2.12	1.06	2.90	0.58	0.85	0.80	1.68	0.80	3	1.32
126	2643	DST1	Q	119	07-11-95	2.47	0.96	1.55	0.93	0.49	0.87	1.07	1.14	4	1.56
146	2398	DST1	3	96	18-05-93	2.03	0.84	2.03	0.56	1.00	0.71	1.65	0.84	3	1.53
117	2399	DST1	1	104	28-08-91	2.92	0.85	2.79	0.37	0.96	0.61	1.63	0.90	2	1.19
117	2399	DST1A	3	104	22-02-93	3.16	0.86	2.04	0.48	0.99	0.93	1.88	0.80	6	1.72
156	2522	DST1	Q	100	07-11-95	3.53	1.01	1.58	0.79	0.64	0.69	1.00	1.02	5	1.87
166	2520	DST1	Q	99	09-11-95	2.93	1.08	1.41	0.85	0.61	0.71	1.04	0.94	5	1.95
48	2634	DST1	1	110	4-09-91	2.30	1.51	0.96	0.55	0.82	0.54	0.77	0.51	2	0.88
59	2212	DST1	1	95	29-08-91*	1.41	1.54	0.69	1.39	0.48	0.37	0.45	0.65	2	0.56
59	2212	DST1	2	95	3-04-92	1.21	1.62	0.43	2.10	0.50	0.86	0.40	0.30	3	0.94
Family 2															
83	2889	DST2	1	122	21-08-91	1.92	1.69	0.96	1.09	0.66	0.47	0.46	0.57	2	0.56
83	3254	DST1	1	134	21-08-91	0.52	0.95	0.59	1.65	0.49	0.31	0.50	0.58	3	0.30
88	2839	DST4	1	112	22-08-91	1.72	1.47	0.71	1.33	0.59	0.37	0.38	0.59	3	0.55
88	2916	DST3	1	115	22-08-91	1.35	1.30	0.85	1.32	0.46	0.43	0.64	0.68	3	0.73
88	2929	DST2	2	116	1-04-92	1.11	1.09	0.70	2.06	0.41	0.55	0.58	0.55	5	0.86
88	3243	DST1	1	126	22-08-91	0.60	1.06	0.72	1.64	0.53	0.29	0.57	0.55	3	0.40
102	2625	DST2	2	110	2-04-92*	1.26	1.11	0.86	2.23	0.46	0.22	0.57	0.48	3	1.03
95	2703	DST2	2	120	2-04-92	1.30	0.91	1.29	0.77	0.59	0.89	1.41	0.70	3	1.34
96	3131	DST1	3	118	16-02-93	1.13	0.93	0.55	1.95	0.27	0.46	0.67	0.60	4	0.74
96	3131	DST1	2	118	30-11-92	0.54	1.04	0.51	2.85	0.25	0.45	0.55	0.66	3	0.93
61	2770	DST2	2	114	6-05-92	1.79	0.90	0.67	3.95	0.46	1.13	0.22	0.53	5	0.81
114	3085	DST1	1	132	2-08-91	0.91	1.27	0.42	1.84	0.34	0.35	0.50	0.63	3	0.64
108	2820	DST2	2	116	28-04-92	3.59	1.03	1.32	2.18	0.95	0.69	0.58	0.70	4	1.44
108	2829	DST1	2	116	28-04-92	3.47	1.04	1.29	2.11	0.94	0.68	0.59	0.69	5	1.37
129	2855	DST2	1	116	27-08-91	2.39	1.71	0.83	1.28	0.70	0.54	0.58	0.64	2	0.71
129	2945	DST1	1	120	19-08-91	1.28	1.28	0.57	1.79	0.38	0.35	0.55	0.64	4	0.61
107	2388	DST3	2	82	28-04-92	3.28	0.92	1.36	2.16	0.74	0.66	0.63	0.65	3	1.42
110	3051	DST1A	2	116	29-04-92	2.68	1.01	1.13	2.53	0.66	0.71	0.57	0.71	4	1.16
110	3051	DST1B	3	116	19-02-93	2.17	1.30	0.88	1.37	0.60	0.52	0.77	0.75	4	0.87
110	3051	DST1B	2	116	29-04-92	2.50	0.97	1.18	2.48	0.66	0.65	0.56	0.70	4	1.18
120	2931	DST1	1	117	28-08-91	0.91	0.99	0.69	1.53	0.32	0.37	1.16	0.88	2	1.09
120	2931	DST1	Q	117	08-11-95	0.83	0.99	0.60	2.02	0.22	0.38	1.28	0.93	3	0.86
166	2508	RFT	Q	98	09-11-95	2.84	1.00	1.70	0.83	0.56	0.88	1.37	1.06	4	1.82
132	2662	DST2	2	103	30-03-92	3.14	1.46	0.85	1.82	0.82	1.02	0.58	0.62	5	1.27
132	2706	DST1	2	104	30-03-92	2.97	1.47	0.83	1.73	0.84	1.20	0.45	0.52	6	1.17
148	2684	DST1	3	111	19-05-93	2.08	1.34	0.96	1.82	0.78	0.61	0.84	0.76	6	1.18
167	2679	DST1	Q	108	07-12-95	2.18	1.01	1.51	0.75	0.45	0.79	1.36	1.12	4	1.72
11	2950	DST2	2	125	29-04-92*	3.09	0.82	0.52	8.52	0.24	0.70	0.11	0.41	10	2.60
84	2771	DST1	2	109	29-04-92	4.38	0.85	0.62	4.83	0.65	1.74	0.28	0.69	5	0.95
37	3495	DST1	2	137	30-04-92	1.96	1.35	0.86	2.53	1.00	0.59	0.53	0.43	1	1.64
65	3189	DST2	2	129	4-05-92	1.98	0.70	0.46	6.99	0.36	1.28	0.32	0.81	6	0.44
65	3267	DST1	2	131	4-05-92	1.59	0.69	0.68	2.15	0.35	0.95	0.49	0.98	4	0.65

Table 9.02: Peak height ratios and separator conditions for all samples

					Analysis	1	2	2a	3	4	5	6	7	8	9
WELL	DEPTH	TEST	Col.	BH	Date	Branched and cyclo-alkanes									
Family 3															
107	2565	DST2	2	105	28-04-92	2.56	1.02	1.33	1.06	0.79	0.82	1.33	0.58	1	1.48
107	2590	DST1	2	106	07-05-92	2.91	1.03	1.08	1.28	0.96	0.58	0.87	0.47	3	1.40
69	2435	DST1	2	92	30-04-92	1.95	0.98	1.77	0.63	0.81	0.52	1.62	0.60	1	1.68
46	2560	DST2	2	98	31-03-92	1.95	1.31	0.86	1.00	0.66	1.05	1.79	0.55	1	1.52
48	2620	DST2	3	110	19-02-93	3.18	1.66	0.64	0.88	0.76	1.43	0.90	0.49	2	1.18
54	2588	DST1	2	104	5-05-92	2.69	0.92	1.04	1.67	0.70	1.24	1.15	0.57	2	1.37
76	2610	DST1	3	109	19-02-93	2.74	1.36	0.88	0.79	0.66	1.14	1.78	0.65	2	1.55
39	2229	DST2	2	89	3-04-92	1.88	1.41	0.58	2.12	0.29	0.68	0.69	0.46	2	1.06
39	2229	DST2	1	89	29-08-91*	0.88	1.49	0.66	2.02	0.16	0.73	1.51	0.72	0	0.56
39	2556	DST1	1	104	29-08-91	0.60	1.21	1.17	1.28	0.26	0.51	1.43	0.67	1	0.90
18	2635	DST4	2	105	18-05-92	1.85	0.89	0.93	2.50	0.43	0.64	0.95	0.59	2	0.94
18	2673	DST3	2	107	18-05-92	1.22	0.91	1.18	1.41	0.41	0.33	1.31	0.55	2	0.92
18	2703	DST1	2	109	4-05-92	1.06	1.00	2.27	0.71	0.42	0.30	1.62	0.61	1	1.09
21	2559	DST2	3	109	16-02-93	1.37	0.97	0.82	1.04	0.33	0.45	1.72	0.63	3	1.17
21	2585	DST1	2	108	5-05-92	1.15	0.72	1.19	1.40	0.35	0.60	1.33	0.65	2	0.97
19	2700	DST2	2	109	30-03-92	1.31	1.19	0.79	1.36	0.38	0.69	0.93	0.46	3	0.89
20	2515	DST4	1	100	4-09-91	1.53	1.74	1.04	0.73	0.54	0.30	1.57	0.48	2	0.78
20	2579	DST3	1	102	29-08-91	1.36	1.71	0.70	1.57	0.48	0.50	1.71	0.69	2	0.77
20	2699	DST2	1	110	20-08-91*	0.44	1.00	1.48	0.54	0.36	0.24	2.25	0.80	2	0.68
44	2750	DST1	2	112	5-05-92	1.85	0.92	0.95	2.35	0.45	1.12	0.74	0.52	3	0.95
55	2681	DST2	2	111	5-05-92	1.79	0.90	0.87	2.75	0.48	0.91	0.63	0.98	3	0.86
61	2128	DST3	2	90	6-05-92	1.52	1.14	1.25	1.50	0.54	0.44	1.24	0.52	1	1.20
62	2549	DST1	2	109	6-05-92	1.84	1.17	0.74	3.32	0.75	1.16	0.31	0.53	4	1.00
70	2428	DST2	2	103	7-05-92	1.89	1.00	0.88	2.72	0.50	0.45	0.76	0.49	2	0.91
70	2452	DST1	2	104	6-05-92	2.24	1.07	0.76	3.08	0.57	0.48	0.42	0.44	3	0.83
31	2753	DST1	1	105	30-08-91	1.31	1.46	0.84	1.36	0.37	0.82	1.77	0.74	1	0.56
63	2690	DST1	1	109	30-08-91	1.27	1.78	0.56	1.60	0.41	0.36	1.45	0.55	2	0.33
Family 4															
128	3640	DST1	1	149	20-08-91	0.44	0.75	0.63	0.91	0.35	0.13	2.28	0.59	1	0.84
Family 5															
27	3164	DST1	2	136	29-04-92	1.49	1.28	1.91	0.90	0.96	0.67	1.13	0.50	1	1.45
35	3309	DST3	1	135	28-08-91	1.57	1.24	2.78	0.42	0.99	0.61	1.35	0.59	1	1.05
35	3354	DST2B	2	137	7-05-92	1.87	1.22	1.39	1.41	1.06	0.67	1.03	0.58	1	1.65
35	3397	DST1	2	138	18-05-92	1.59	1.12	1.80	1.01	1.03	0.70	1.16	0.60	1	1.69

REPEAT SAMPLES

WELL	DST	SAMPLE DEPTH	FAMILY	COLUMN
39	2	2229m	3	M-N 1
39	2	2229m	3	M-N 2
59	1	2212m	2	M-N 1
59	1	2212m	2	M-N 2
96	1	3131m	2	M-N 2
96	1	3131m	2	M-N 3
108	2	2820m	2	M-N 2
108	1	2829m	2	M-N 2
109	1	2630m	1	M-N 3
109	1	2630m	1	M-N 3
110	1A	3051m	2	M-N 3
110	1B	3051m	2	M-N 2
110	1B	3051m	2	M-N 3
117	1	2399m	1	M-N 1
117	1A	2399m	1	M-N 3
120	1	2931m	2	M-N 1
120	1	2931m	2	QUADREX
126	1	2643m	1	M-N 1
126	1	2643m	1	QUADREX

M-N = Macherey-Nagel.

Table 9.02 (cont.)

PEAK-PAIR RATIOS														
10	11	12	13	14	15	16	17	18	19	20	6(15)	2(2a)	Separator	
Branched and cyclo-alkanes					Isoprenoids								psi	T'F
0.64	0.42	1.47	1.16	2.23	1.25	0.74	0.85	1.12	0.86	1.99	1.27	0.28	140	70
0.63	0.47	1.40	1.13	1.92	1.21	0.77	0.86	1.15	0.85	2.02	1.13	0.35	255	64
1.18	0.33	0.94	1.38	1.45	0.74	1.31	0.59	1.85	0.56	2.49	2.42	1.25	135	60
0.74	0.37	1.56	1.00	1.84	1.31	0.89	0.88	1.20	0.89	2.31	1.28	0.37	219	99
1.06	0.57	1.08	1.35	1.54	0.87	1.62	0.72	1.71	0.64	1.99	1.55	0.61	160	75
0.85	0.59	1.64	0.94	2.06	1.36	0.88	0.98	1.38	0.89	1.89	1.35	0.21	237	110
1.12	0.63	1.41	1.74	1.65	0.88	1.35	0.81	1.79	0.60	1.95	0.90	1.05	169	66
0.82	0.88	1.53	0.68	2.15	1.11	0.46	0.94	0.76	0.67	1.51	0.39	0.62	263	103
0.51	0.90	1.21	1.39	1.73	0.45	2.12	0.71	1.28	0.52	1.71	1.06	1.48	89	84
0.86	0.91	1.23	1.79	1.48	0.67	0.76	1.33	1.34	0.61	1.68	0.70	1.51	83	59
1.59	0.73	1.55	1.85	1.72	0.60	1.63	0.71	1.41	0.52	1.84	0.75	1.97	83	59
0.82	0.39	1.39	1.03	1.68	1.24	0.90	0.87	0.61	0.55	1.20	1.36	0.36	164	80
0.79	0.31	1.87	1.35	1.54	1.29	1.18	0.86	1.42	0.85	2.25	0.83	0.62	164	80
0.77	0.45	1.14	1.15	1.13	1.16	1.07	0.79	1.38	0.65	1.77	1.42	0.41	385	97
0.61	0.45	1.53	1.09	1.86	1.27	0.80	0.90	1.16	0.81	1.99	1.28	0.30	135	59
0.99	0.43	1.41	1.46	1.63	1.18	1.11	0.78	1.44	0.62	1.96	1.59	0.42	135	59
0.66	0.40	1.81	1.33	1.62	1.21	1.11	0.80	1.17	0.82	1.91	0.83	0.64	388	106
0.75	0.37	1.73	1.24	1.65	1.17	1.10	0.81	1.24	0.77	2.05	0.89	0.77	278	120
0.58	0.48	1.20	1.16	1.57	1.18	0.60	0.59	0.86	0.72	1.67	0.65	1.57	0	0
0.30	0.44	1.42	0.97	1.43	0.86	0.78	0.48	0.87	0.72	1.79	0.52	2.23	140	89
2.73	0.63	0.87	1.28	1.34	0.36	1.91	0.48	1.23	0.54	1.67	1.11	3.75	140	89
0.74	0.69	1.42	0.81	2.12	1.15	0.48	0.99	1.15	0.72	1.80	0.40	1.75	165	102
0.58	0.64	0.93	0.95	1.24	1.09	0.63	0.97	1.85	0.89	2.34	0.46	1.61	200	48
0.67	0.71	1.34	0.72	1.81	1.10	0.49	1.11	1.17	0.72	1.78	0.34	2.08	390	151
0.70	0.61	1.30	1.02	1.95	1.17	0.64	1.08	1.82	0.81	2.27	0.54	1.54	220	90
2.03	0.71	0.94	1.32	1.41	0.58	2.23	0.69	2.07	0.60	2.05	0.99	1.56	391	111
0.60	0.74	1.00	0.91	1.38	1.16	0.64	0.91	1.29	0.82	2.28	0.49	1.47	420	93
1.12	0.55	0.93	1.19	1.93	0.25	2.31	0.77	2.48	0.75	1.84	2.27	1.28	67	68
1.09	0.34	1.10	1.33	1.46	0.92	1.56	0.73	1.88	0.63	2.21	1.52	0.70	0	0
2.40	0.39	1.17	1.88	1.54	1.08	1.22	0.70	1.80	0.66	1.84	0.62	1.71	105	72
1.59	0.60	0.87	1.48	1.04	1.04	0.59	0.90	1.09	0.71	1.46	0.53	2.02	105	72
2.04	1.20	0.88	1.03	1.53	0.43	2.07	0.61	2.05	0.75	2.24	0.52	1.35	197	50
0.57	0.49	1.06	0.89	1.83	1.30	0.54	1.00	1.05	0.77	1.61	0.39	3.05	253	78
0.77	0.91	1.04	0.96	1.71	0.98	1.24	0.78	1.65	0.62	2.14	0.59	0.78	312	82
0.75	0.94	1.05	0.92	1.83	1.00	1.20	0.78	1.67	0.63	1.96	0.59	0.80	309	80
1.25	0.63	1.52	0.81	2.23	1.14	0.57	0.99	1.16	0.73	1.87	0.51	2.05	135	83
0.62	0.58	1.23	1.04	1.71	1.19	0.61	1.01	1.24	0.71	1.82	0.46	2.24	495	101
0.91	0.65	0.92	0.97	1.54	1.09	1.28	0.90	2.04	0.67	2.13	0.58	0.67	477	118
0.85	0.66	0.96	1.03	1.53	1.09	1.07	0.81	1.59	0.59	1.70	0.52	0.90	158	69
0.83	0.55	1.29	1.73	1.61	1.04	1.20	0.87	1.73	0.57	1.91	0.74	1.47	160	95
0.83	0.63	0.95	1.00	1.59	1.11	1.07	0.79	1.73	0.58	1.88	0.51	0.82	160	95
0.71	0.32	1.28	0.97	1.96	1.28	0.74	0.88	1.14	0.79	1.60	0.90	1.45	298	77
0.67	0.24	1.58	1.13	1.61	1.28	1.10	0.78	1.53	0.87	1.93	1.00	1.65	298	77
0.73	0.32	1.83	1.18	1.48	1.33	1.28	0.91	1.61	0.84	2.28	1.03	0.59	0	0
1.20	0.91	1.22	1.19	1.73	0.54	2.27	0.77	1.79	0.60	1.87	1.08	1.71	464	80
1.42	1.02	1.22	1.36	2.01	0.43	2.47	0.69	1.42	0.62	1.67	1.05	1.78	419	99
0.81	0.57	1.12	1.37	1.50	0.80	1.46	0.84	1.84	0.60	2.01	1.04	1.40	256	62
0.72	0.30	1.74	1.40	1.44	1.35	1.31	0.94	1.72	0.90	2.49	1.00	0.67	387	64
2.84	1.77	0.40	0.94	1.67	0.27	7.76	0.61	2.23	1.01	1.54	0.40	1.56	0	0
2.10	1.12	0.62	0.97	1.71	0.46	2.66	0.58	1.44	0.69	1.83	0.61	1.39	65	59
0.89	0.50	0.72	1.15	1.79	1.08	1.12	0.65	1.94	0.60	2.48	0.49	1.58	11	61
1.57	1.09	0.47	1.03	1.39	0.79	1.77	0.56	1.55	0.96	1.54	0.40	1.52	200	64
1.93	6.32	0.50	1.11	1.28	0.96	1.41	0.61	1.51	0.95	1.38	0.52	1.02	255	115

Table 9.02 (cont.)

10	11	12	13	14	15	16	17	18	19	20	6(15)	2(2a)	Separator	
Branched and cyclo-alkanes					Isoprenoids								psi	T°F
1.05	0.46	0.75	1.09	1.21	1.17	1.16	0.79	2.40	0.70	2.77	1.14	0.77	124	51
1.07	0.57	0.79	1.11	1.50	0.93	0.85	0.49	1.17	0.55	1.89	0.96	0.93	0	0
0.96	0.42	0.76	1.29	1.45	1.12	1.28	0.76	2.93	0.67	3.01	1.45	0.56	465	59
1.39	0.45	0.91	1.22	1.40	0.82	1.49	0.64	1.93	0.60	2.21	2.18	1.52	325	97
1.94	0.54	1.22	1.38	1.34	0.83	1.07	0.55	1.30	0.55	1.80	1.08	2.59	0	0
1.33	0.65	0.64	1.12	1.41	1.21	1.06	0.67	1.85	0.66	2.10	0.96	0.88	320	97
1.53	0.40	1.14	1.18	1.27	1.19	1.19	0.63	1.98	0.62	2.36	1.49	1.54	360	77
2.51	0.65	0.87	1.33	1.26	0.57	2.77	0.62	2.26	0.77	2.06	1.20	2.43	420	72
0.55	0.18	0.76	0.83	1.29	1.24	1.10	0.65	1.56	0.81	1.84	1.22	2.27	420	72
0.60	0.17	1.04	0.91	1.27	1.13	1.06	0.60	1.49	0.84	2.07	1.27	1.03	570	72
1.46	0.57	0.68	1.09	1.32	1.17	1.21	0.62	1.67	0.68	1.01	0.81	0.96	345	91
1.28	0.50	0.71	1.15	1.41	1.13	1.14	0.60	1.75	0.67	2.07	1.16	0.77	220	72
0.80	0.42	0.63	1.04	1.22	1.06	0.97	0.61	1.69	0.75	1.68	1.52	0.44	155	56
1.68	0.37	0.92	1.31	1.13	1.39	1.42	0.68	2.49	0.86	2.31	1.24	1.19	300	50
1.35	0.43	0.61	1.18	1.29	1.44	1.26	0.66	2.35	0.91	2.00	0.92	0.61	0	0
2.13	0.60	0.86	1.27	1.33	0.66	2.04	0.62	1.98	0.67	2.08	1.41	1.50	195	56
0.61	0.56	1.10	1.07	1.54	1.37	0.86	0.71	1.35	0.79	1.93	1.15	1.67	0	0
0.51	0.17	0.94	0.98	1.41	1.10	1.08	0.65	1.64	0.85	2.43	1.55	2.44	130	100
0.53	0.58	1.11	1.00	1.54	1.94	1.04	0.87	1.50	0.87	1.40	1.16	0.68	0	0
1.70	1.15	0.42	1.10	1.49	1.15	1.26	0.64	1.90	0.73	2.02	0.65	0.97	295	66
1.74	0.77	0.62	1.11	1.49	1.09	1.35	0.61	1.88	0.71	1.99	0.58	1.03	225	84
0.74	0.40	0.94	1.20	1.50	1.07	1.35	0.73	2.62	0.71	2.59	1.15	0.91	310	70
1.14	0.89	0.73	1.10	1.58	0.67	1.60	0.61	1.42	0.62	1.75	0.47	1.58	0	0
1.60	0.70	0.67	1.11	1.40	1.20	1.10	0.62	1.92	0.66	2.07	0.63	1.13	285	72
1.78	0.83	0.65	1.17	1.51	0.61	1.31	0.48	1.18	0.60	1.60	0.69	1.40	0	0
0.51	0.13	0.98	0.90	1.49	1.20	1.15	0.65	1.26	0.81	1.92	1.48	1.74	355	82
0.57	0.53	0.61	0.67	1.49	1.26	0.49	0.98	1.05	0.69	1.70	1.15	3.18	330	68
0.46	0.13	0.78	1.14	1.00	1.68	0.80	0.74	1.86	1.71	2.30	1.36	1.18	365	101
0.85	0.44	0.79	1.02	1.68	0.95	1.12	0.60	1.77	0.57	2.26	1.19	0.67	0	0
0.79	0.11	1.23	0.87	1.68	1.08	0.65	0.73	1.06	0.73	2.08	1.25	0.44	210	93
0.76	0.37	0.77	1.15	1.64	1.16	1.14	0.69	1.82	0.61	1.70	0.89	0.88	155	95
0.73	0.30	0.73	1.15	1.65	1.07	1.10	0.63	1.69	0.62	2.13	1.09	0.62	0	0

Table 9.02 (cont.)

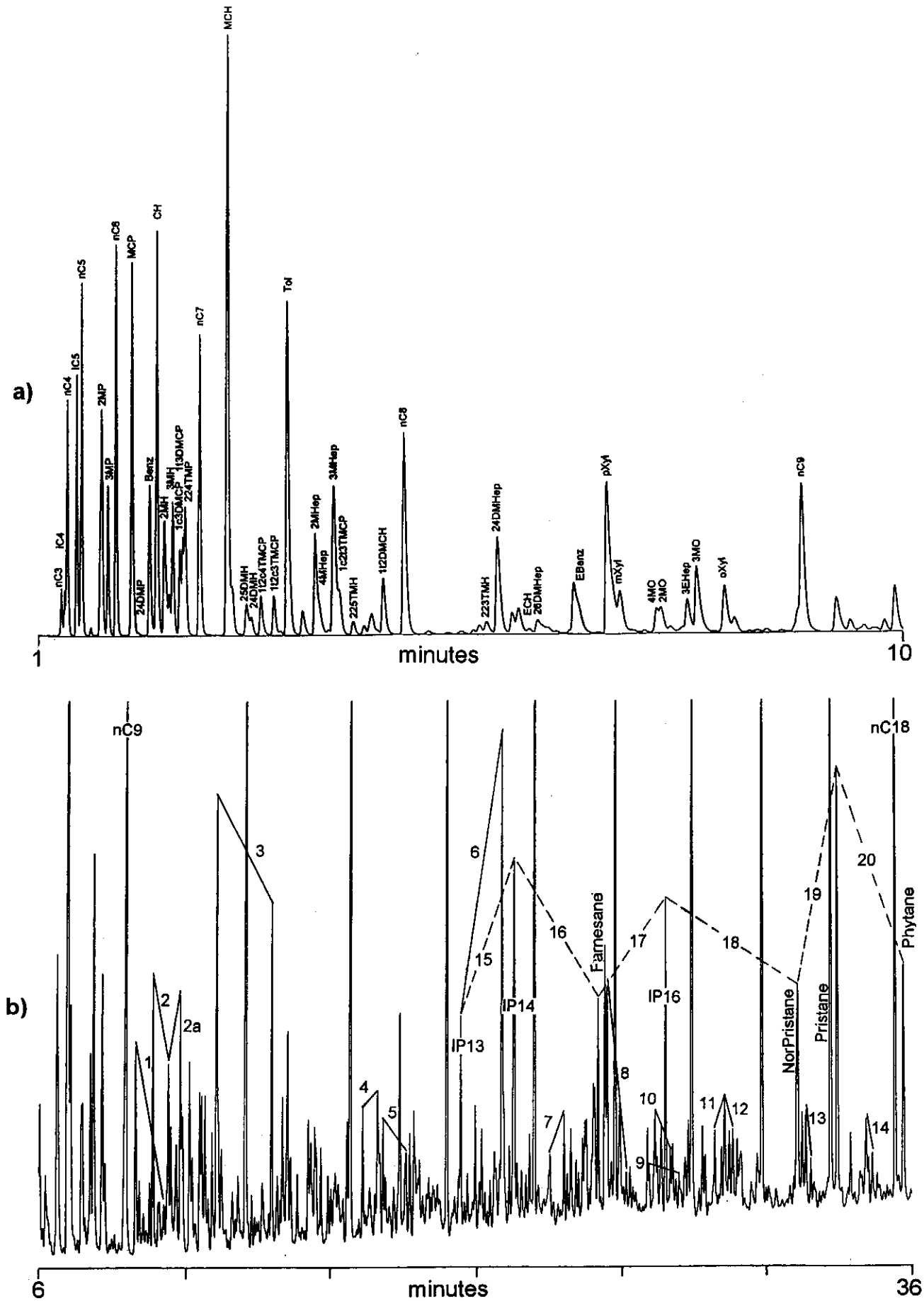

Figure 9.02: Examples of (a) C4-9 and (b) C9-20 annotated gas chromatograms (Well 109, DST1, Column3)

maturity hydrocarbon (e.g. wet gas-condensate), the normal alkane envelope describes an exponentially-declining curve (Fig. 9.01a). Such a fill is likely to have entered the reservoir as a single phase flow, because two phase flow is unlikely to result in such a constant relationship between carbon chain-length and mass proportions. Such an alkane envelope is characteristically generated by thermal cracking which affects all molecules randomly and results in progressively shorter chain lengths and opened aromatic and naphthenic rings. So the products of thermal cracking have similar compound skeletons with only slight variations between individual components from different source rocks. Alkane products of cracking reactions generally show an inverse relationship between mass and proportion (except where large proportions of biologic structures are inherited).

By contrast, where the reservoir fill represents a mixture of hydrocarbons from two different sources, the envelope describes a deeply-divided double-humped shape (Fig. 9.01b). In some cases, the hydrocarbon represents filling from a single source but the chromatogram appears to have two humps, a gas hump and a heavier oil hump. This may be because hydrocarbons entered the reservoir as two separate phases and were not in equilibrium with each other (Fig. 9.01c). A fourth variant is where the analysed liquid contains little gas, perhaps resulting from evaporation, and the envelope describes a single hump offset from the start of the chromatogram (Fig. 9.01d).

Some oil samples have a unimodal envelope (e.g. well 109, Appendix C, Figs. C.25-26) indicating derivation from a single source. Some are bimodal, occasionally possessing a steep concave envelope between nC9 and nC15, representing residual oil dissolved in wet gas-condensate (well 59, Appendix C, Fig. C.64). These interpretive guidelines are used for each sample (Table 9.01).

9.2. CONDENSATE FRACTION (nC4-nC9)

This fraction includes components tested by PVT analyses, but since those analyses do not describe each component in the range, preferring to sum groups with similar molecular weights, the condensate fraction data provide a more complete view of the light oil fraction (Fig. 9.02a).

9.2.1. Peak quantification

Fully quantitative analyses have not been carried out, instead peak heights are measured above a baseline drawn between major valleys. These heights are normalised so that comparison between matching analyses provides a semi-quantitative correlation. Blank analyses were carried out at regular intervals and showed essentially flat baselines corresponding well with the valley-valley baseline.

9.2.2. General similarities between hydrocarbons

The C4-9 data are shown graphically in Appendix C and peak heights are given in Appendix F, Tables F.3 and F.4. Although the general pattern of data from each sample is similar (except where evaporation during storage or sampling reduced the light fraction proportions (e.g. well 11, DST2, Appendix C, Fig. C.47), four aspects help to characterise the samples:

1. similar distributions of aromatic and normal alkanes,
2. small proportions of aromatics (exceptions do occur e.g. in wells 65 and 128),
3. higher ratios of normal:branched/cyclic alkanes in the oil-associated fractions.

The first indicates derivation from broadly similar source rock types, i.e. no dominances of aromatic-rich kerogen indicating dominantly coaly organic matter or alkane-rich kerogen indicative of algal organic matter (Tissot and Welte, 1984, p. 159). The second is used to determine the degree of water-washing which can deplete the more soluble aromatic molecules (Tissot and Welte, 1984, p.312-318; Section 9.2.4.3), but more likely indicates high maturity as single-ring aromatics commonly form during high temperature cracking of polycyclic compounds (Tissot and Welte, 1984, p.187). The third characteristic may indicate differences in either the source organic matter or increased maturity (Tissot and Welte, 1984, p.384-393).

9.2.3. Genesis of hydrocarbons

Very few of the hydrocarbons found in oils and condensates occur naturally in living organisms. Most are generated from precursor molecules by thermal cracking, condensation, hydrogenation and other reactions during burial. For example, Thompson (1983) showed that ratios of C7 components could be used to describe the general nature of oils. The ratios he devised:

$$\text{Heptane Value (HV)} = 100*nC7/(CH+\Sigma MH+\Sigma DMCP+nC7)$$

$$\text{Iso-heptane value (IHV)} = \Sigma MH/\Sigma DMCP$$

matched reservoir temperature and broadly correlated with vitrinite reflectance of adjacent sediments. He also showed that hydrocarbons generated from aliphatic and aromatic source kerogen could be distinguished using these ratios. A matching plot of the HV and IHV of the 85 Bredasdorp Basin samples shows Family 1 oils and Family 5 condensates to locate close to the 'aliphatic' trend whereas Family 2, 3 and 4 condensates locate closer to the 'aromatic' trend (Fig. 9.03). The four labelled samples all have high MH:DMCP ratios, relatively high toluene proportions and elevated formation pressures. Mango (1994) shows that samples with unusually high MH:DMCP ratios are of high maturity. These samples also have reduced formation water salinities (~25000 ppm NaCl). Relative aqueous solubility of the various components shows that water-washing would reduce the ratio IHV faster than ratio HV (Tissot and Welte, 1984,

p. 314; McAuliffe, 1966; Fig. 9.03) so there appears to have been no water-washing, which is confirmed by the high toluene proportions. This suggests a very recent hydrocarbon charge which has had little time to be washed or dissipate, hence the high formation pressures.

Further, Mango (1990; 1991) showed that many C6-9 compounds could not result from thermal cracking as they are remarkably stable under oil generation time and temperature conditions. He showed that catalysis was a prerequisite for formation of these components in large proportions and that there was a consistent reaction sequence which could be followed through the higher maturity oils and condensates (Mango, 1987 and 1994). He pointed out that many of the metals necessary for these catalytic reactions (such as nickel, vanadium etc.) were commonly present in argillaceous sediments and more specifically, associated with deep marine claystones with low oxygen contents such as source rocks (Alexander et al., 1983b). Hence it is likely that little cracking took place in reservoir rocks (Mango, 1992). The implication of this is that condensate compositions (and probably light oils as well) are representative of degradation of the original kerogen and should be source indicators. Although Mango's work did not address the higher homologues (>C8) it is likely that thermocatalysis also affects these, at least up to molecular weights and temperatures at which thermal cracking dominates (>200 mass units, ~>150°C).

Mango (1987) showed the results of 2000 analyses of oils and condensates in which there was an invariance in the ratios of branched C7 compounds, which could not have arisen from thermal cracking alone. This invariance is matched by data from Bredasdorp Basin samples (Fig. 9.04) although the lacustrine oil from the west coast fits less well. Apart from confirming the regional nature of cracking processes, this match with Mango's data also provides some quality control of the analyses and of the peak size measurement procedures used. In a later schematic representation of the breakdown of precursor nC7, Mango (1994) showed that catalytic cracking proceeded in two stages:

(i) nC7 → toluene+methylcyclohexane+methyl hexanes+1,2 dimethyl cyclopentane

(ii) methyl hexanes → 1,1+1,3 dimethyl cyclopentanes+dimethyl pentanes+trimethyl butane.

Ternary plots of the major components participating in these thermo-catalytic routes record only slight differences between the different families (Figs. 9.05 and 9.06) in spite of evident differences between hydrocarbon families. The data lie on subparallel trends which result from differing proportions of catalysts in each source rock.

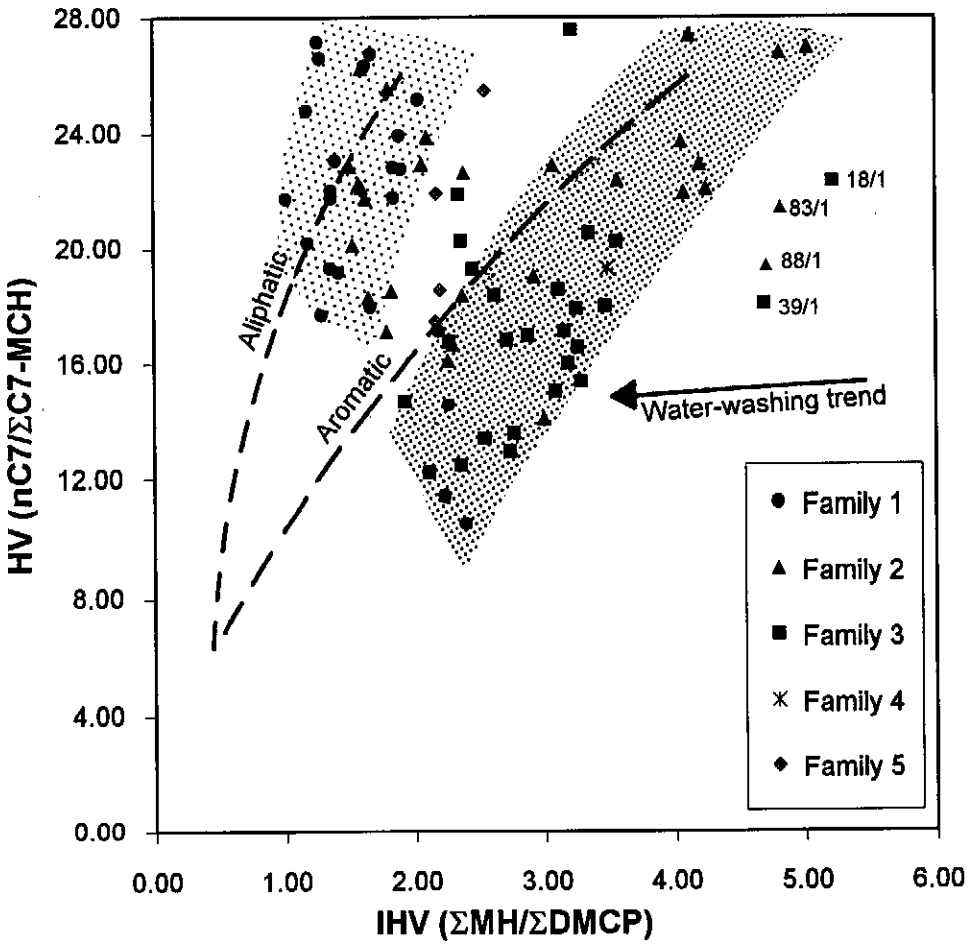

Figure 9.03: Plot of Heptane and Iso-Heptane values showing the aromatic and aliphatic source trends of Thompson (1983). Trends of Bredasdorp Basin data subparallel those of Thompson. The four labelled outlying samples have unusually high ratios methyl hexanes: dimethyl cyclopentanes indicative of high maturity (Mango, 1994) and recent charge.

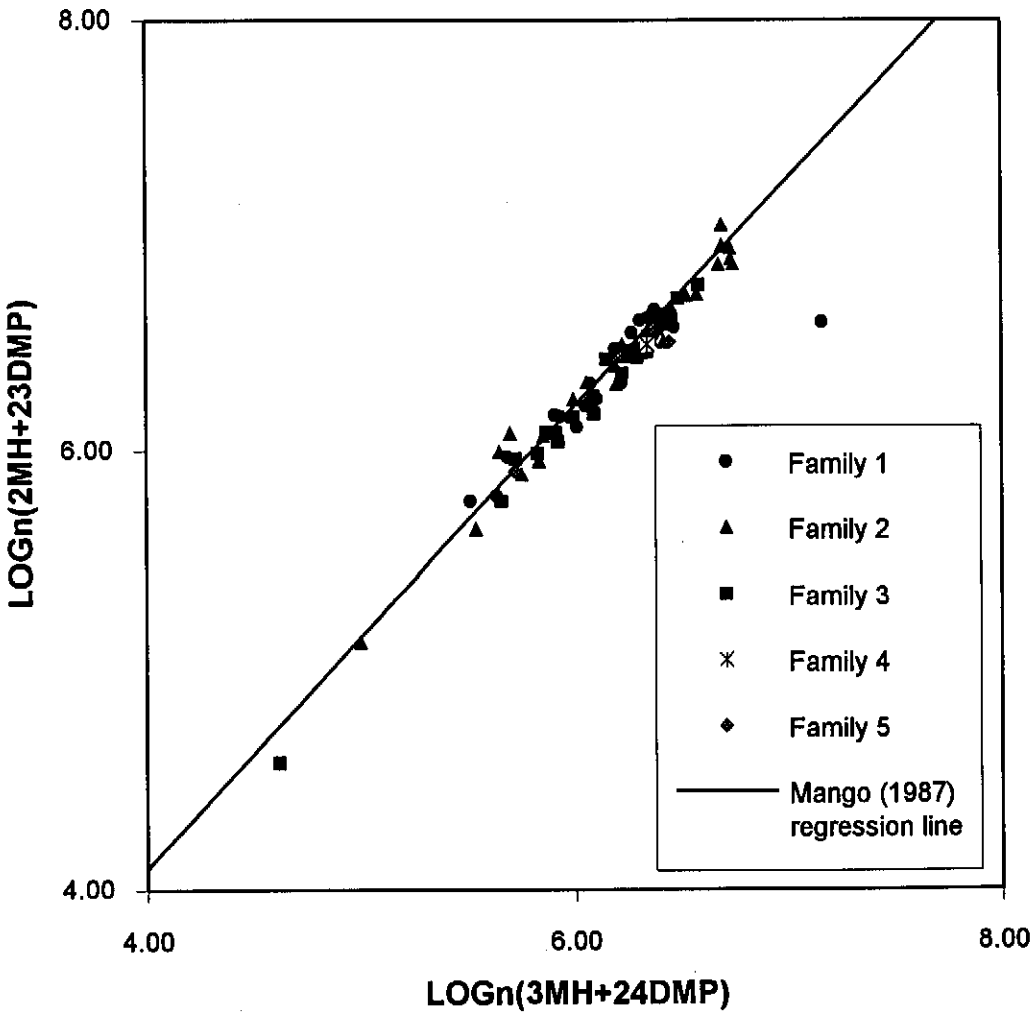

Figure 9.04: Plot of iso-heptane ratios used (Mango, 1987) in interpreting thermo-catalytic activity from the invariance of the C7 hydrocarbon proportionation

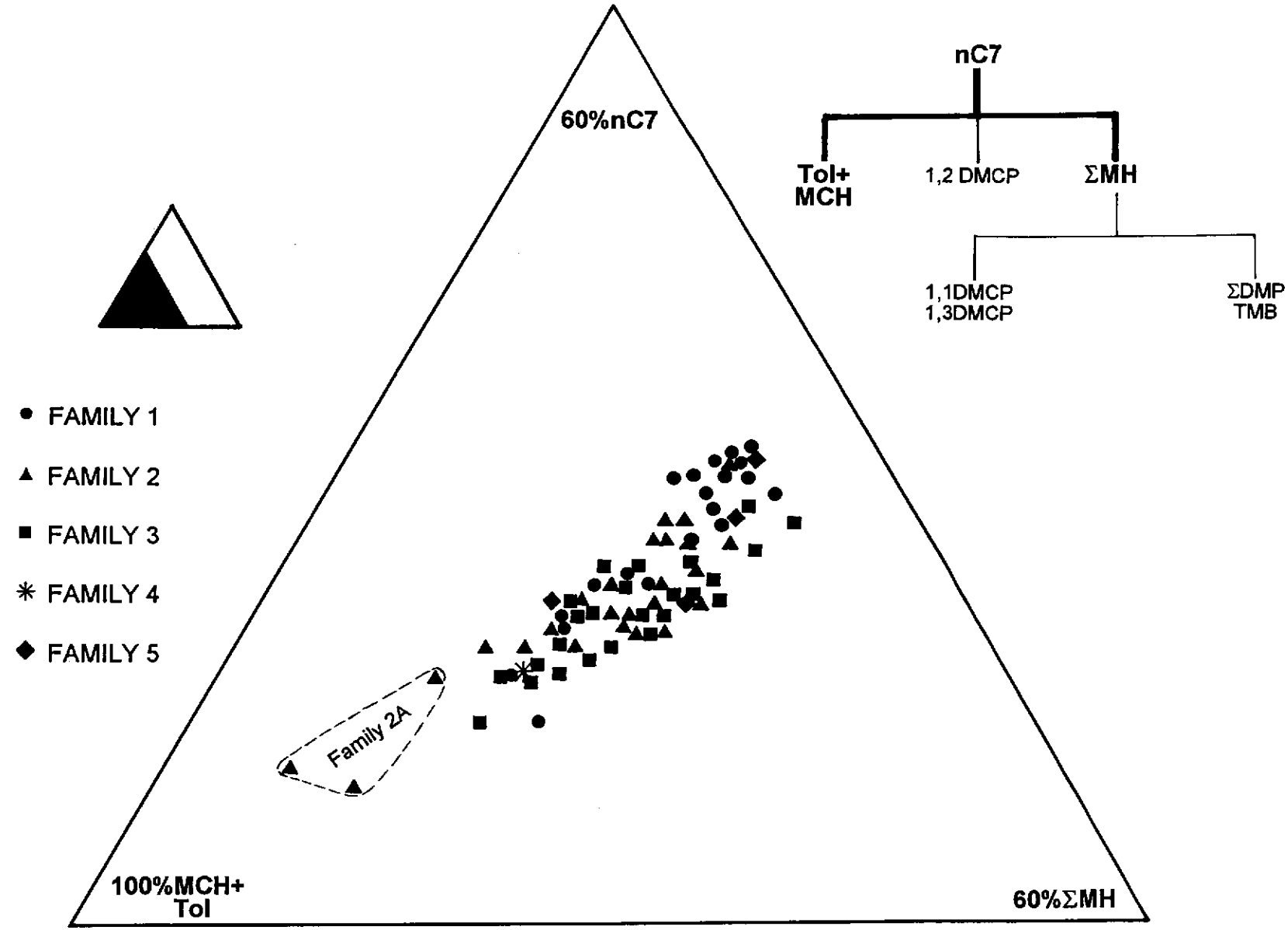

Figure 9.05: Ternary plot of the first stage thermo-catalytic break-down of parent nC7 (after Mango, 1994).

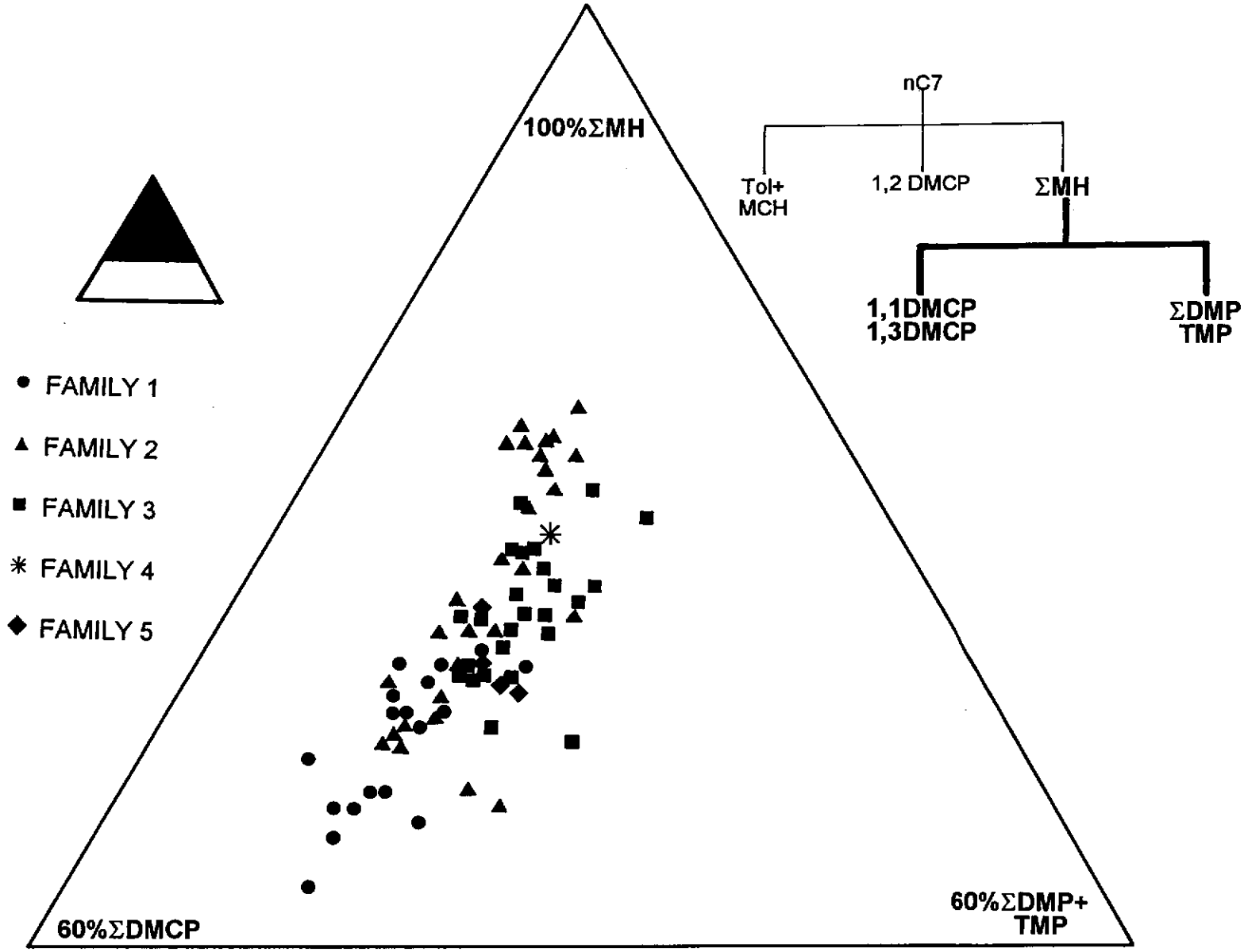

Figure 9.06: Ternary plot of the second stage thermo-catalytic break-down of parent nC7 (after Mango, 1994).

9.2.4. Alteration of hydrocarbon proportions

Major alteration routes which can influence proportions of reservoired hydrocarbons include biodegradation, late-stage thermo-catalytic cracking, evaporative fractionation and water-washing. Evidence for only the last two is available from this data-set.

9.2.4.1. Biodegradation

Aerobic and anaerobic biodegradation of oil affects simple hydrocarbon structures more readily than complex ones, and where of matching complexity, saturates before aromatics. The importance of detecting such degradation is that commercially negative aspects of bacterial growth need to be assessed. Connan (1984) shows that aerobic bacterial degradation more commonly occurs in subsurface environments, under the following conditions:

(i) meteoric water flush
(ii) at the oil-water contact
(iii) where nutrient and oxygen supplies are high
(iv) where microbes are present
(v) at temperatures at which bacteria can thrive.

In the Bredasdorp Basin, many reservoirs have low salinity formation water (Davies, 1995a; Chapter 4), believed to be a residue of a meteoric flush. Such water would contain oxygen, nutrients, bacteria and little salt where it entered the rock. However, all reservoirs encountered to date are presently at temperatures far in excess of the range at which bacteria thrive (40-80°C, esp. <60°C) and have not been at those temperatures since the Early Tertiary. Connan (1984) showed that bacterial alteration starts with loss of C6-15 alkanes (and C2-5 alkane gases) closely followed by loss of heavier and more complex hydrocarbon structures. Peters and Moldowan, (1993, p. 254) describe a similar biodegradation sequence which affects first alkanes then (sequentially) isoalkanes, cyclo-alkanes and aromatics. Some of the samples have reduced proportions of gases but since these are methane and ethane, this probably reflects evaporation rather than biodegradation. Those samples with reduced proportions of C6-15 alkanes, e.g. residual oils, all retain their full complement of heavier alkanes and isoprenoids suggesting in-reservoir evaporation rather than biodegradation. Indeed, none of the samples are thought to have been bacterially altered. Had there been any biodegradation, which was masked by further hydrocarbon migration into the reservoir, increased proportions of certain biomarkers would have been evident (Goodwin et al., 1983; Chapter 12).

9.2.4.2. Evaporative fractionation

A number of the oils and condensates appear to have suffered the effects of in-reservoir evaporative fractionation (Thompson, 1988). When this happens, escaping

gas entrains some of the oil in solution and consequently the most volatile material can become removed. Under these circumstances, the residual oil becomes enriched in aromatics, and cycloalkanes to a lesser extent, whilst the escaping gas condensate is depleted in those components. Thompson (op cit.) also considers that heavier components, possibly as large as naphthalenes, could also be affected by this process. Heums et al. (1986) also showed a variation of this process when they discussed the effects of sequential gas leakage from an oil reservoir forming new condensate-rich reservoir fills. Thompson (op cit.) plotted C7 ratios which included the most and the least volatile components (toluene/nC7 vs nC7/MCH).

The evaporative fractionation trend shown by Thompson (op cit.) does not completely match the majority of the Bredasdorp Basin samples (Fig. 9.07). This is thought to be largely an effect of the different peak size measuring method and partly of the analytical column. Thompson (1983) measured peak areas from data generated using a 100ft SCOT stainless steel squalane column whereas in this study, peak heights were measured from analyses using a 75ft glass WCOT OV101 column. Peak height measurements are not quantitative whereas peak area measurements are. The separation phases have similarly low response (squalane is fractionally lower than OV101) but the different column type and length meant that small differences in response factor result in systematically different peak height:area ratios. Even greater differences are likely due to programming and oven conditions. Thompson (1983) employed cold on-column trapping with a nitrogen-filled Dewar flask to focus the peaks whilst the data in this report were generated from a constant temperature oven using an open split injection method.

Aromatics in general have a greater propensity for donor electrons than alkanes, more than squalane or OV101 phases can supply. Therefore aromatic peaks tend to tail throughout the analysis. Thompson's cold focusing technique results in a narrower peak compared to the results from this study.

The net result of this is that aromatic peaks from these analyses are slightly broader than the alkanes. For a given pair of peaks, the aromatic/alkane ratio is lower. Although there are differences between Thompsons's data and these, the bulk of the difference between most Family 2 condensates and Family 1 and 3 condensates/oils is due to the former having a higher proportion of aromatic (terrigenous) kerogen.

Mango (1990) reviewed Thompson's work and suggested that the evaporative fractionation effect is more likely due to differences in the structure of the kerogen or the thermocatalytic generation rate than to late stage in-reservoir effects, although he did concede the latter to be possible.

The plot of the Bredasdorp Basin samples shows that most data cluster in one corner of the plot but there are two values which plot far away (Fig. 9.07). These two, from the same well (no. 65) indicate an evaporative fractionation effect.

9.2.4.3. Water-washing

Certain hydrocarbons in the C4-9 fraction are highly soluble in fresh water, in particular aromatic hydrocarbons such as benzene and toluene which have aqueous solubilities in excess of 1000 ppm. Normal alkanes of matching carbon number are orders of magnitude less soluble (McAuliffe, 1966; Price, 1976). Osadetz et al. (1992) demonstrated the effect of water-washing on C6 hydrocarbons which have different solubilities (viz. benzene>>cyclohexane>3-methyl pentane). They showed that heavily water-washed samples have CH/benzene and 3MP/benzene ratios of several hundred. A plot of these ratios for the Bredasdorp Basin data shows that 14A oils and Family 5 condensates seem to have suffered some water-washing (Fig. 9.08). Samples which appear to have been more severely water-washed (e.g. well 69 DST1) do not have high values because most of the C6 fraction is missing (Appendix C, Fig. C.54).

Similarly in the C7 hydrocarbons, toluene is much more water-soluble than methylcyclohexane and the plot of the ratio between them against formation water salinity will also show where water-washing has been effective. The Bredasdorp Basin data shows a broad correlation between high salinity and low ratio and vice versa (Fig. 9.09). But within individual hydrocarbon families there is a poorer correlation and some samples, notably from Family 5, have unusually high salinities relative to the ratio. This surprising lack of direct one-to-one correlation between salinity and aromatic proportion may be (i) a function of different source rocks which generate larger or smaller amounts of aromatics, differentiating between terrigenous and marine-dominated source rocks or (ii) lack of contact time between the fresh water and the reservoir fill due to recent flushing by fresh water or hydrocarbons or (iii) due to lack of migration of hydrocarbons through fresh water or (iv) recent changes in formation water salinity. Larter and Aplin (1995) indicate that hydrocarbon losses due to water-washing are likely to be more severe during migration than in the reservoir. This is because of the more intimate contact of the oil with water in the migration route than the limited contact between the water and the base of the reservoir.

Whilst these possibilities cannot be resolved at present, there is at least local evidence that, except where meteoric flushing has occurred, formation water salinities increase downdip (Davies, 1995a), hence water-washing during migration from depth is unlikely. It is also possible that much of the hydrocarbon has been in the reservoir for a relatively short time (Chapter 7), possibly less than 10 Ma so reducing the contact time. In

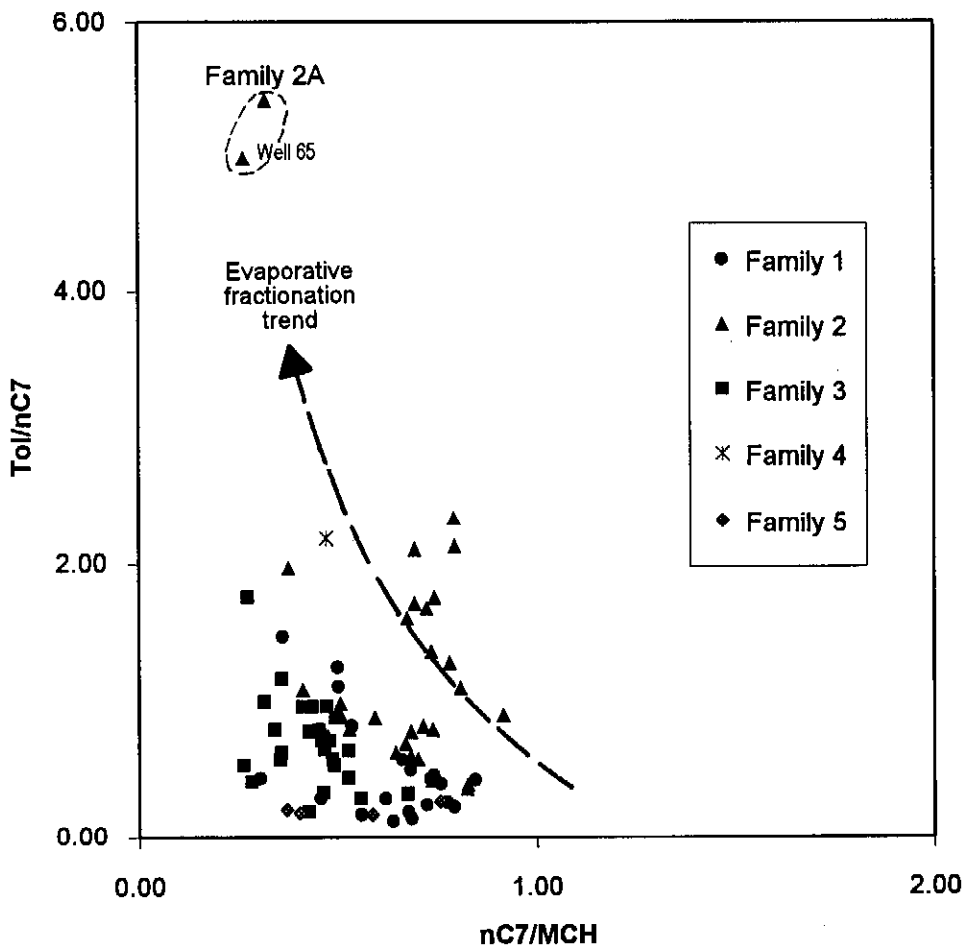

Figure 9.07: Plot of C7 ratios with the evaporative fractionation trend of Thompson (1988) superimposed. Most of these samples locate below the trend, in the area Thompson indicated to contain biodegraded oils. In this case though, this probably a result of the different peak size measuring method. Two samples (both condensates from well 65) locate so far along the trend that they are thought to represent in-reservoir evaporation.

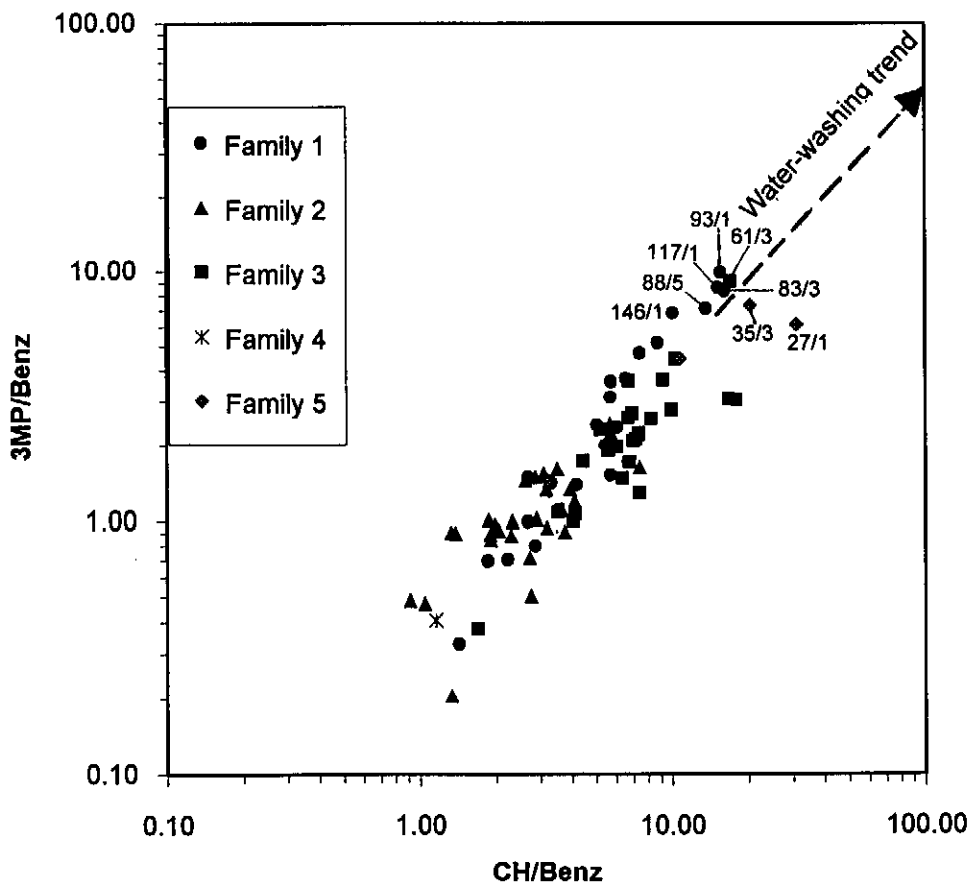

Figure 9.08: Crossplot of C6 ratios used by Osadetz et al. (1992) to test for water-washing.

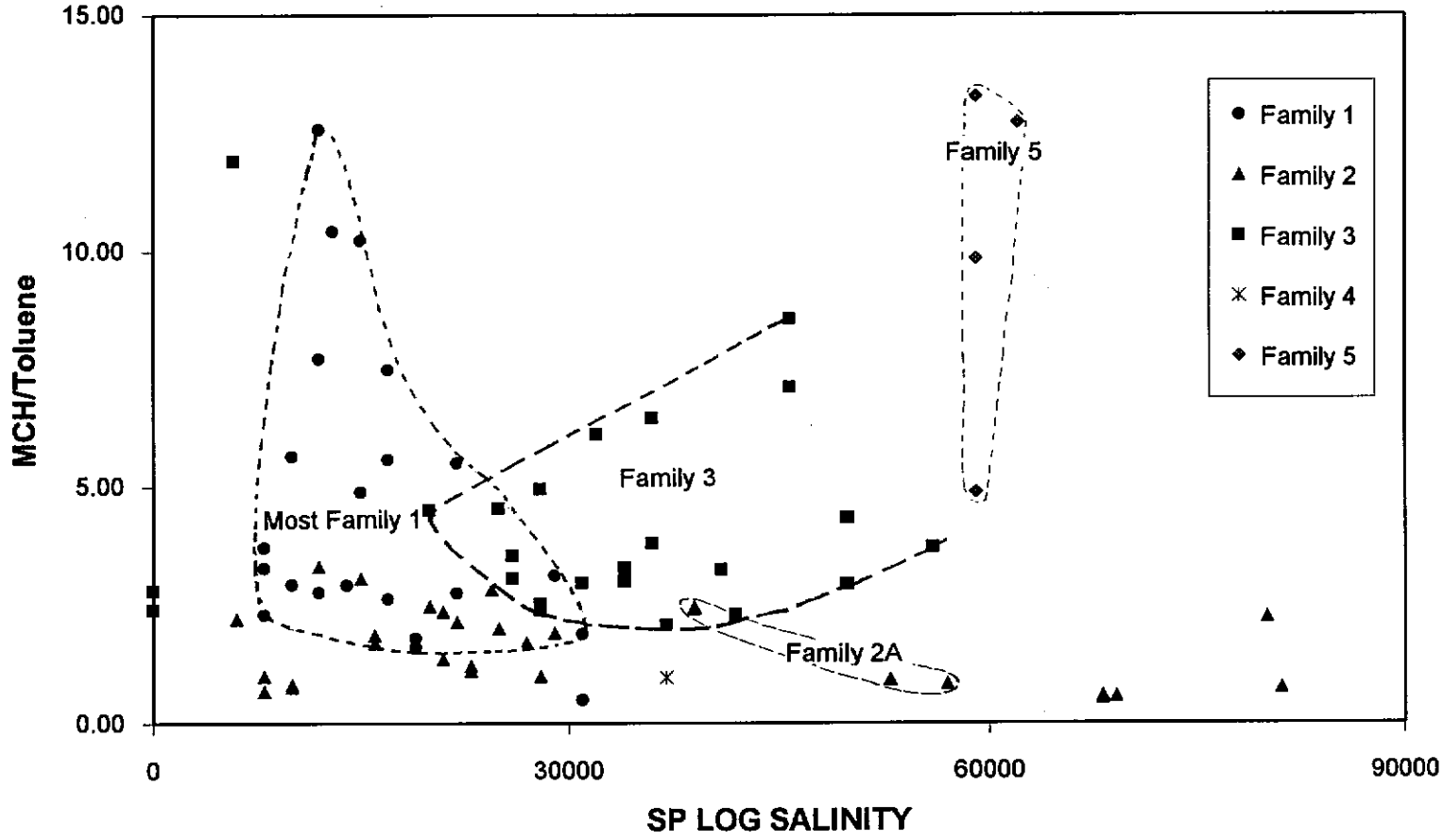

Figure 9.09: Plot of ratio between high and low solubility C7 hydrocarbons vs formation water salinity. Of the four hydrocarbon families with more than one data point, only that of Family 1 displays the expected trend of decreasing MCH/Toluene with increasing formation water salinity and even there the samples with low ratios are mostly the mixed samples.

addition (Appendix C and Fig. 9.09) aromatic proportions can vary dramatically through each family where there is little change in salinity (Family 1) and hardly vary even though salinity does (Family 2). These results may reflect other alteration processes such as evaporative fractionation or maturity differences (Thompson, 1988 and Mango, 1990).

A ternary plot of C7 representatives of the three main hydrocarbon groups (nC7, MCH and toluene) show that despite slight differences caused by subtle column variations (Figs. 9.10a) resulting in overlaps of each family (Fig. 9.10b; C.C. Magnier, 1995, pers. comm.). Since the proportions of these representative compounds are mainly a function of source rock characteristics (i.e. kerogen and catalysts, Mango 1990 and 1992) it is not surprising that they should be able to separate the families.

9.3. FINGERPRINT DATA (C9+)

Throughout this report, this fraction will be referred to as the C9-20 fraction, because that is the range of hydrocarbons used in correlations, although most are <C16 (Fig. 9.02b). Recently published results show that most of the peaks between the normal alkanes and regular isoprenoids, comprising up to 25% of most crudes, are monomethyl and dimethyl iso- and anteiso-alkanes with few monocyclic alkanes (Fowler et al., 1986; Fowler and Douglas, 1987; Kaufman et al., 1987; Kissin, 1987; Kaufman et al., 1990; Hwang et al., 1994). Kissin (op cit.) also showed that the distribution of many isoalkanes could result from acid catalysis of normal alkanes. Since most acid catalysts are found in claystones, this implies that fingerprint GC traces reflect conditions of formation in source rocks rather than reservoirs. Hence matching GC fingerprints could indicate matching source type and, possibly, migration episodes.

Kaufman et al. (1987) show that the proportions of many hydrocarbons are characteristic of its reservoir. Based on proportions of C9-16 iso- and cycloalkane components, Kaufman et al. (1990) show convincing evidence for very detailed correlations down to individual flow units and have used the technique to apportion commingled flow from different reservoirs. The rationale for this is based on empirical observations that "oils from a continuous reservoir display uniform chromatographic fingerprints whereas oils from separate reservoirs exhibit significantly different chromatographic fingerprints" (Hwang et al., 1994).

Based on published data, vertical (and some horizontal) homogenisation occurs at a rate fast enough that through geologic time, liquid hydrocarbons in the same or connected reservoirs will have similar chemical signatures. Generally the closer the reservoirs and the more permeable the connection, the closer the match. In the case of

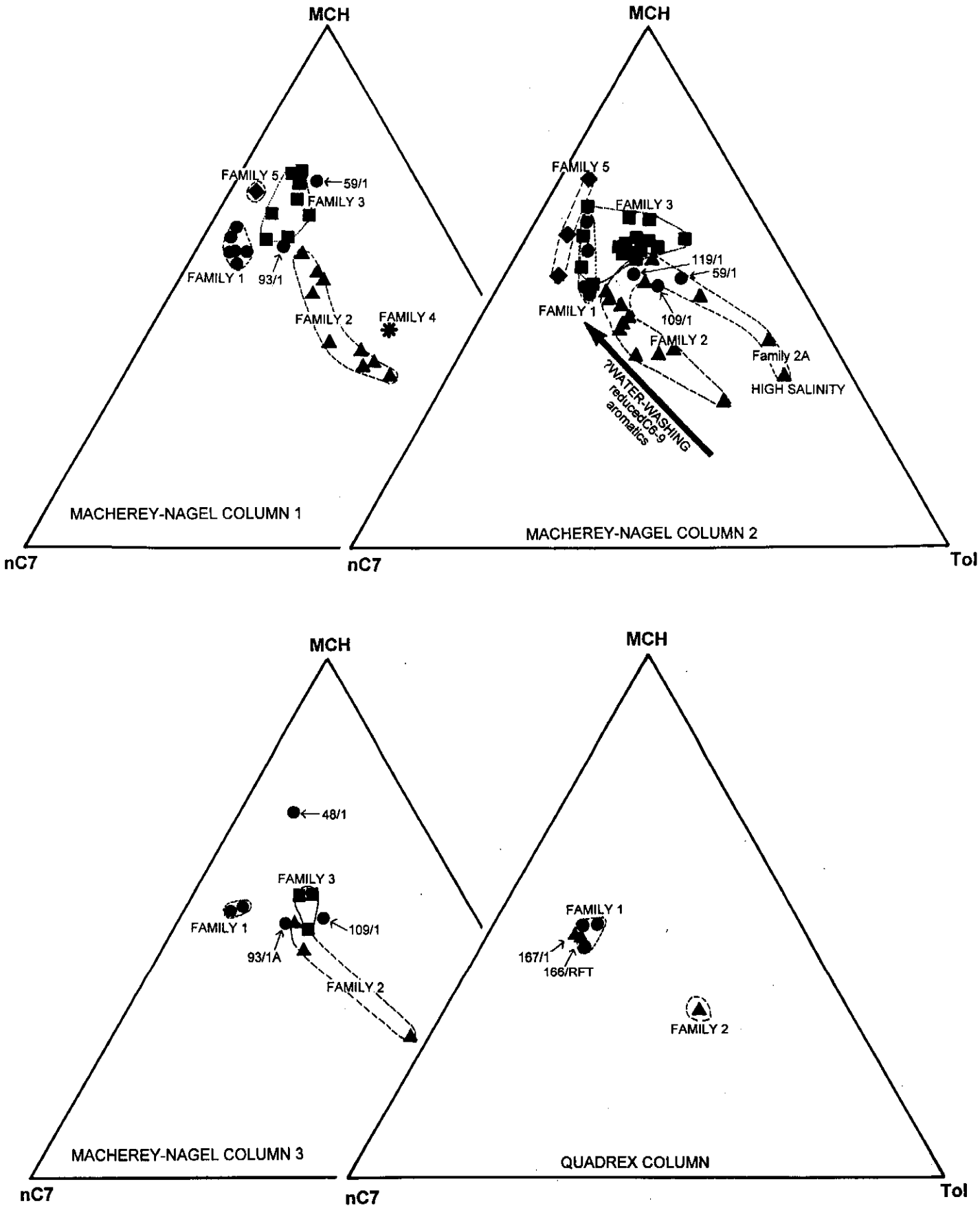

Figure 9.10a: Ternary plots of major C7 hydrocarbon proportions for each column type showing separation into the main hydrocarbon Families. Selected DST and RFT samples are located where outside their group.

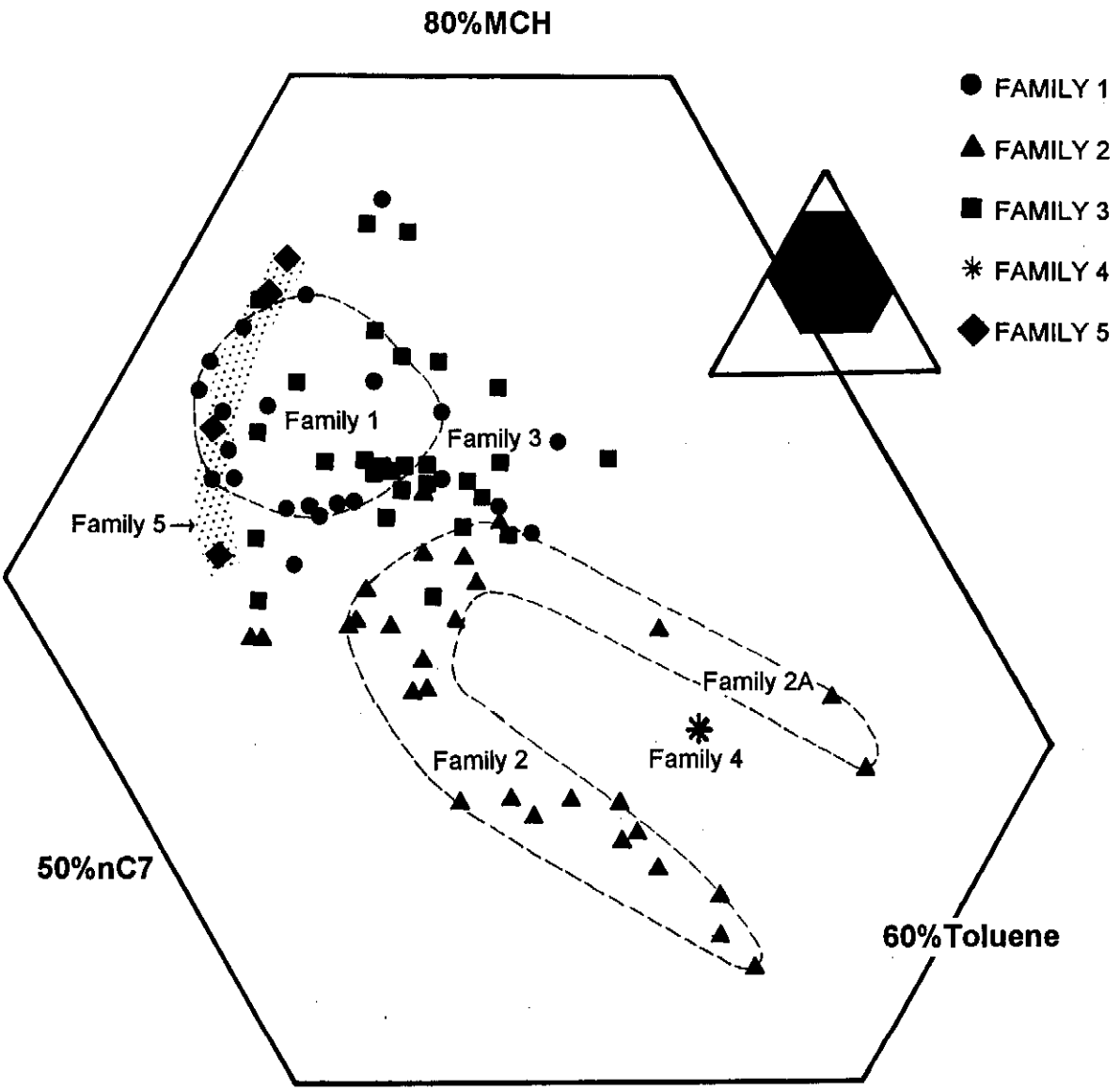

Figure 9.10b: Partial ternary plot of the major C7 hydrocarbons summarised from Figure 9.10a showing separation into the main hydrocarbon families. Mango (1988) shows the proportions of these components to be largely a function of source type and thermo-catalysis.

gaseous hydrocarbons, the rates of diffusion are much faster and horizontal homogenisation proceeds much more rapidly. Hence, similar chemical signatures of gas-phase hydrocarbons in reservoirs, up to 5-10 kilometres apart, may imply connectivity.

Where geochemical signatures match (i.e. where differences between individual peak ratios are no greater than a few percent) the hydrocarbons are considered to be in communication, probably through a part of the hydrocarbon column, i.e. that part of the reservoir where hydrocarbons occupy a substantial proportion of the pore space and the pore fills interconnect (Kaufman et al., 1990). Where the signatures differ by ~5-10%, they are considered to indicate hydraulic communication and where differences are >~10% it indicates lack of communication. Where low molecular weight hydrocarbons do not match, but medium and high molecular weight hydrocarbons do, it is thought to indicate a previous communication, from which the more mobile gas-rich phases have been lost and into which later and different gas-rich phases have been injected. Thus a lack of similarity in only the gas-rich phases suggests recent isolation. Schematic diagrams illustrating communication, non-communication and flow zones are shown in Fig. 9.11a-e.

Previous studies show that peaks in the range C9-20 can be repeatedly analysed with enough precision to allow the establishment of a correlation (Kaufman et al., 1987; 1990). Peaks up to C25 too can be useful in demonstrating a 'heavy ends' correlation, but they suffer from multiple compound overlaps, peak broadening becomes significant and heavy ends are often masked by solubilized residual oil.

9.3.1. Correlation technique

The technique used by the Chevron group (Kaufman et al., 1987; 1990; Hwang et al., 1994) has been to select adjacent and near-adjacent peaks in the range C9-33 which show the largest difference between two oils and to construct ratios of the differences (Fig. 9.12).

In this study, the peaks selected were in the C9-20 range only and did not include either normal alkanes or known aromatics. The reasons for this were:

(i) minimal evaporation discrimination between adjacent peaks
(ii) chromatographic separation and peak definition was excellent up to C20
(iii) no (or few) biological markers were included
(iv) all components were light enough to be mobile whether in the gas or liquid phases
(v) components were essentially non-polar hence there were minimal effects of adsorption onto minerals

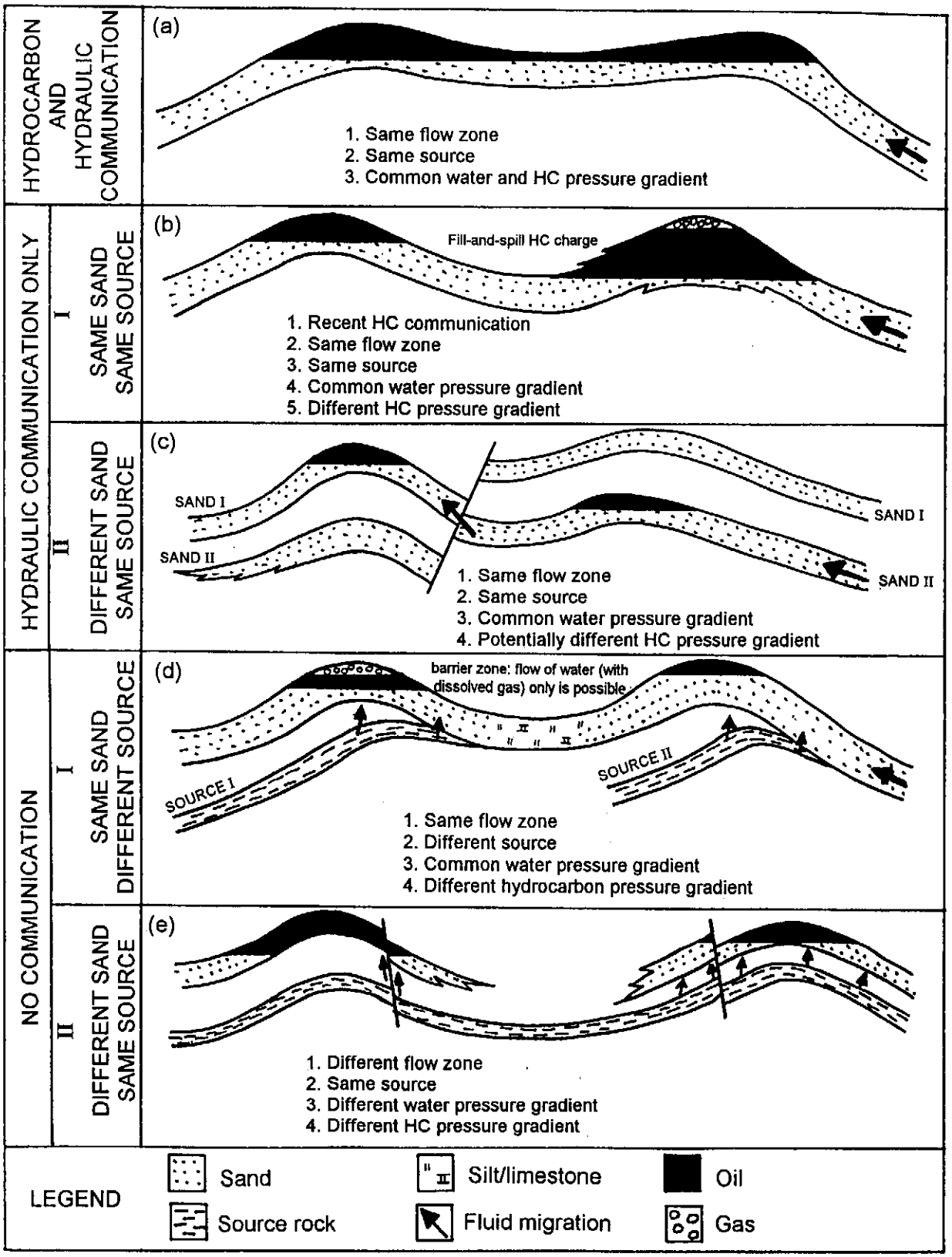

Figure 9.11: Cartoon of definitions of fluid communication used with interpreted C9-20 GC data (from Davies, 1995d).

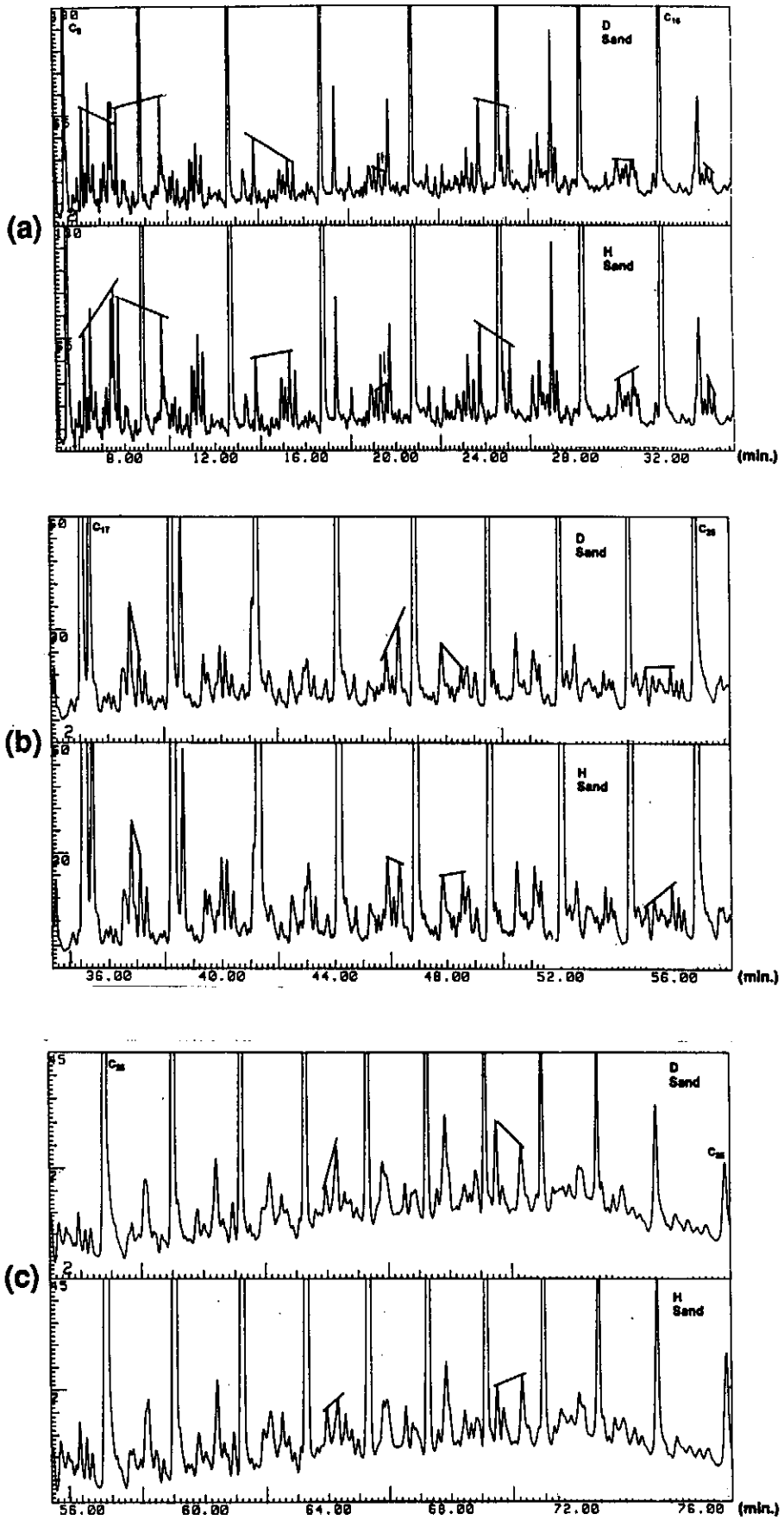

Figure 9.12: Chromatographic plots (a) nC9-16, (b) nC17-25 (c) nC26-36 of oils from separate flow zones but the same structure illustrating peak-pair differences (Hwang et al., 1994).

(vi) the solubility of iso- and cyclo-alkanes of similar mass are similar, whereas aromatics with the same carbon number have much higher aqueous solubilities.

9.3.2. Peak selection

In this study, the peak selection is based on that of Kaufman et al. (1990) and characteristic peak ratios representing different levels of communication between reservoired hydrocarbons largely match theirs. Ratios are plotted on polar plots and grouped to show different levels of reservoir communication. Average differences between peak-pair correlations shown in Kaufman et al. (1990) are as follows:

(i) same structure, same flow zone	<±5%
(ii) same structure and flow zone, gravity segregation (>1000' column)	±8.3%
(iii) same structure, different flow zone	±12.3%
(iv) different structure, same sandstone	±18.7%
(v) same structure, same sandstone, different fault block	±24.4%

For instance, where the differences are close to experimental (shown to be as low as ~2%, Kaufman et al., 1990), these reservoirs are considered to be in hydrocarbon communication. Where differences are small, but larger than experimental, it is taken to indicate communication between adjacent structures through the water leg, and where differences are markedly higher than ±10%, it is taken to show lack of communication.

Fingerprint GC analyses have also been locally used to demonstrate communication between hydrocarbons from the same reservoir flow zone and from different reservoirs (e.g. Davies, 1994a; 1995d; 1995e; 1995f). One proviso has been that the method requires such high resolution analysis that only those results from analyses on the same equipment carried out using the same programme, within a short time of each other and with few intervening analyses, can be utilised.

The results (Table 9.02) show that:

(i) where oil samples were from the same flow zone in hydrocarbon communication, average differences between the most different 10 peak-pairs were <5%

(ii) where samples were from the same flow zone but in hydraulic communication (described in Fig. 9.11, from Davies, 1995c), average differences were 5-10%

(iii) where samples were from different flow zones (but still from the same source rock) and not in hydraulic or hydrocarbon communication, average differences were >10%.

(iv) in samples from different flow zones, different source rocks and different structures, average peak-pair ratio differences were >20%.

9.3.3. Effect of separator conditions on hydrocarbon composition

Separator conditions are optimised to maximise gas yield to better assess possible commercial flow rates and to safely handle the flow. This is done by adjusting the flowing pressure and temperature throughout the test period. Since the gas/liquid ratio is partly a function of the separator conditions, and only partly a function of the reservoir fill, it is possible to significantly alter the volumes of each fraction. The compositions of the whole oil fractions, in particular those near the separation molecular weight, are potentially affected. The phase separation is usually taken to be within the range C4-6, but may occasionally be at a higher carbon-number. Effects resulting from the phase separation might therefore be evident not only in fractions closest to the separation point (~C4-6) but also in adjacent fractions (~C3-7). Consequently tests have been carried out to determine if different separator conditions caused the characteristic differences between each family.

Flowing conditions are routinely recorded during flow periods and the relevant values prevailing at the collection time of each of the sampled fluids are given in Table 9.02. If there was an influence of higher or lower separator temperatures or pressures on peak-pair ratios, they would change in step, most markedly in those ratios closest to the phase change carbon-number. Consequently, cross-plots of two of the ratios used to characterise different hydrocarbon families, one at low molecular weight (Toluene/(nC7+nC8)) and one from higher molecular weight (Ratio6/Ratio15) are plotted against separator temperature and pressure (Figs. 9.13-9.14).

The data within each family form essentially horizontal regions indicating no relationship with either separator pressure or temperature. Family 1 samples (Fig. 9.13b) do record a slight decrease with increasing pressure. This is considered to be a function of the unusually high toluene proportions in samples from well 109, which may be sourced by a facies variant of Family 1 (Davies, 1997c) and well 59 where Family 2 gas has mixed with the oil. Alternatively, these differences could be due to sample evaporation between collection and analysis since toluene is more volatile than the average of the adjacent normal alkanes. It is evident that there is no consistent effect on the peak-pair ratios as a result of different separator conditions.

9.3.4. Graphical analysis

Commonly, graphical comparison of individual whole oil GC peak-pair ratios is used to differentiate between hydrocarbons in different reservoirs (Kaufman et al., 1987; 1990) and samples from different sources (Hwang et al., 1994). In this study, plots of peak-pair ratios largely differentiate between hydrocarbons from different families (Figs. 9.15-9.19). Some ratios are more successful at differentiating some families, other ratios separate other families and there are zones in which mixtures of hydrocarbon families

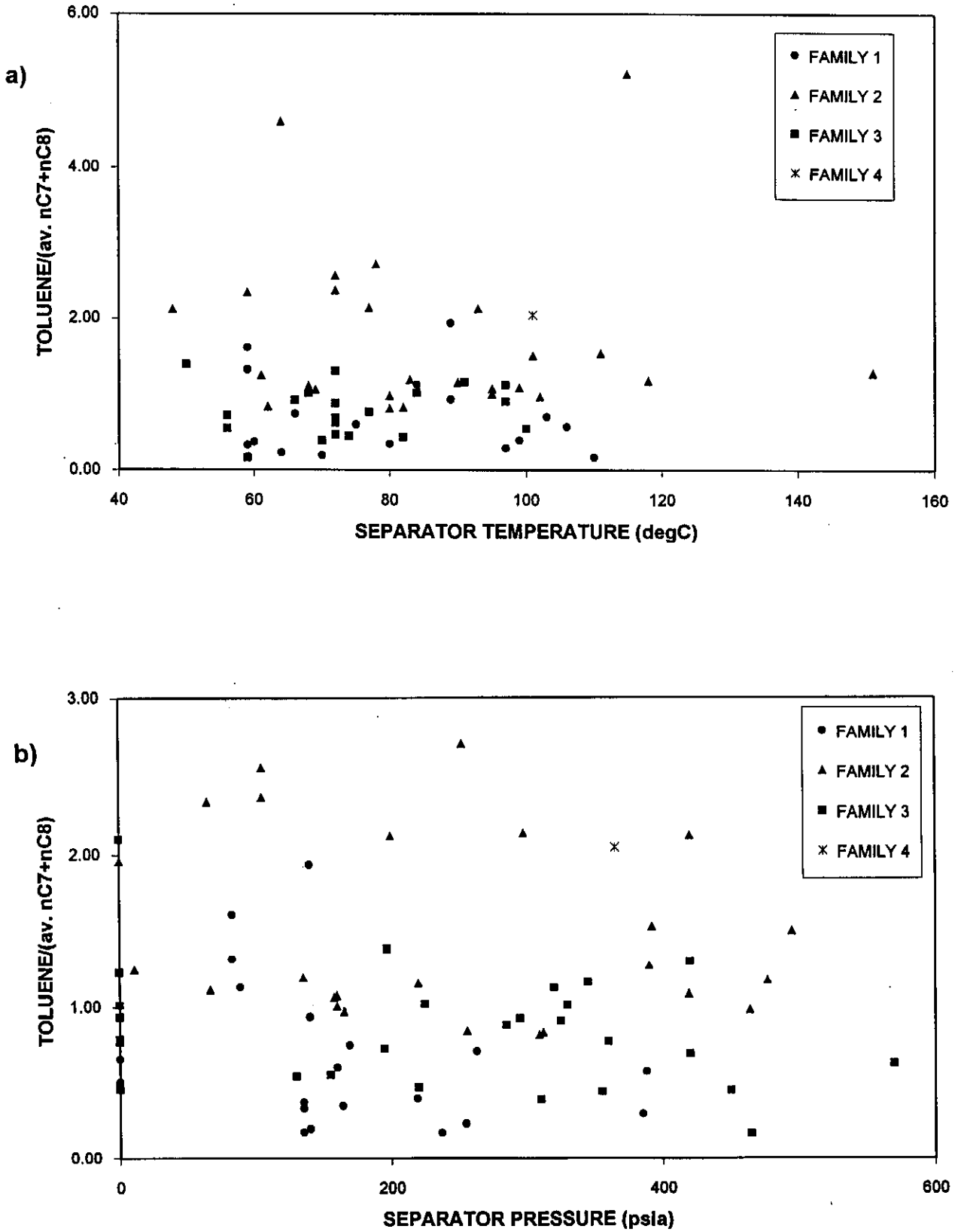

Figure 9.13: Plots of a low carbon number ratio [Toluene/(nC7+nC8)] vs (a) separator temperature and (b) separator pressure showing no temperature or pressure correlation. Family 5 data plot offscale because of their high proportions of Toluene.

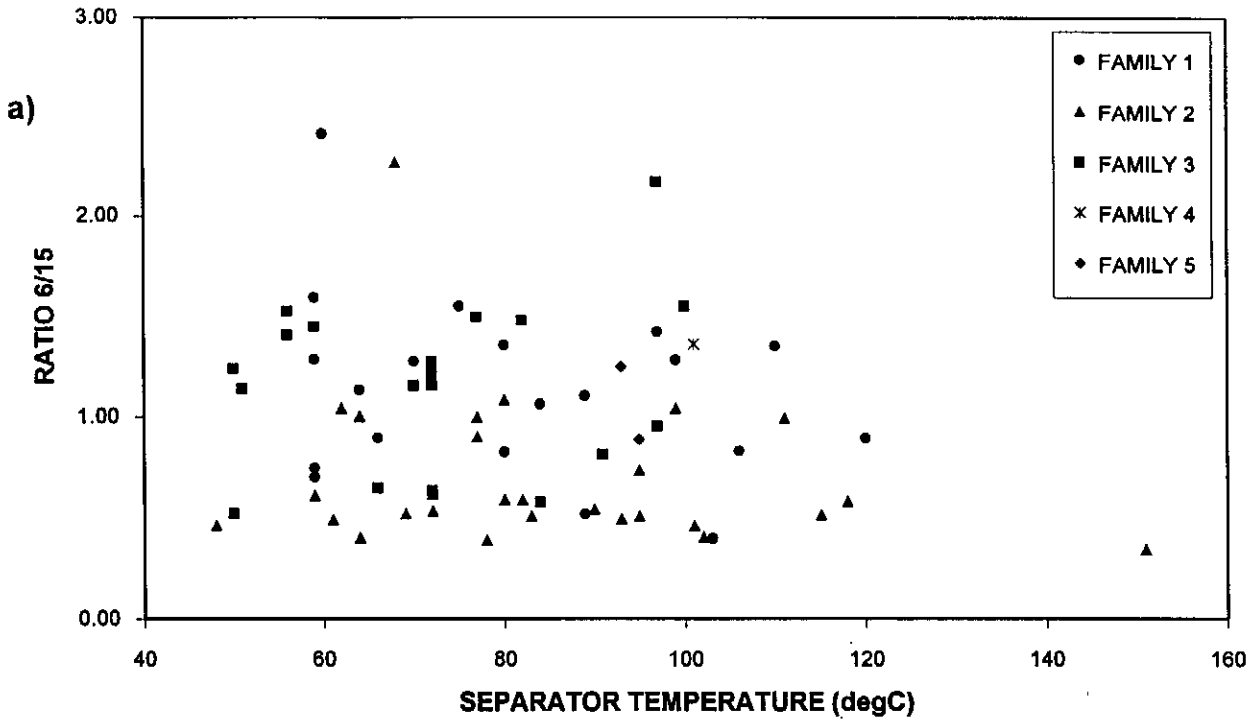

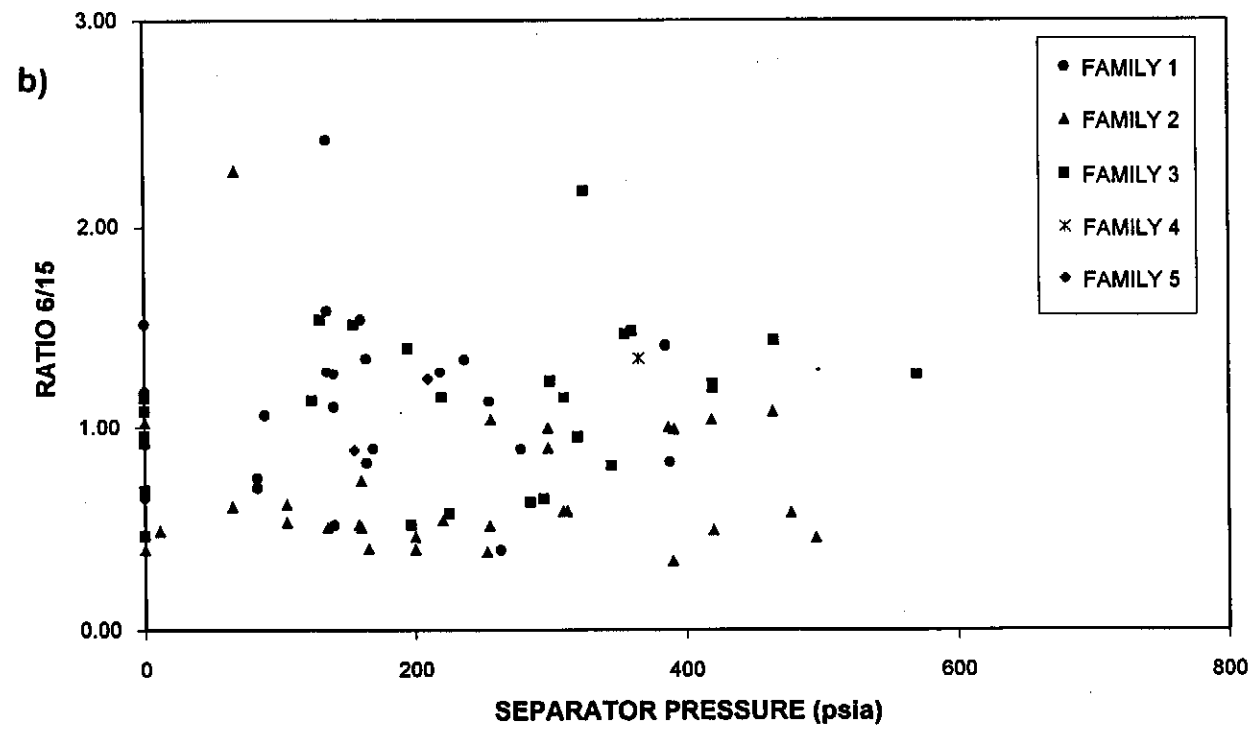

Figure 9.14: Plots of a high carbon number ratio [6/15] vs (a) separator temperature and (b) separator pressure showing no temperature or pressure correlation.

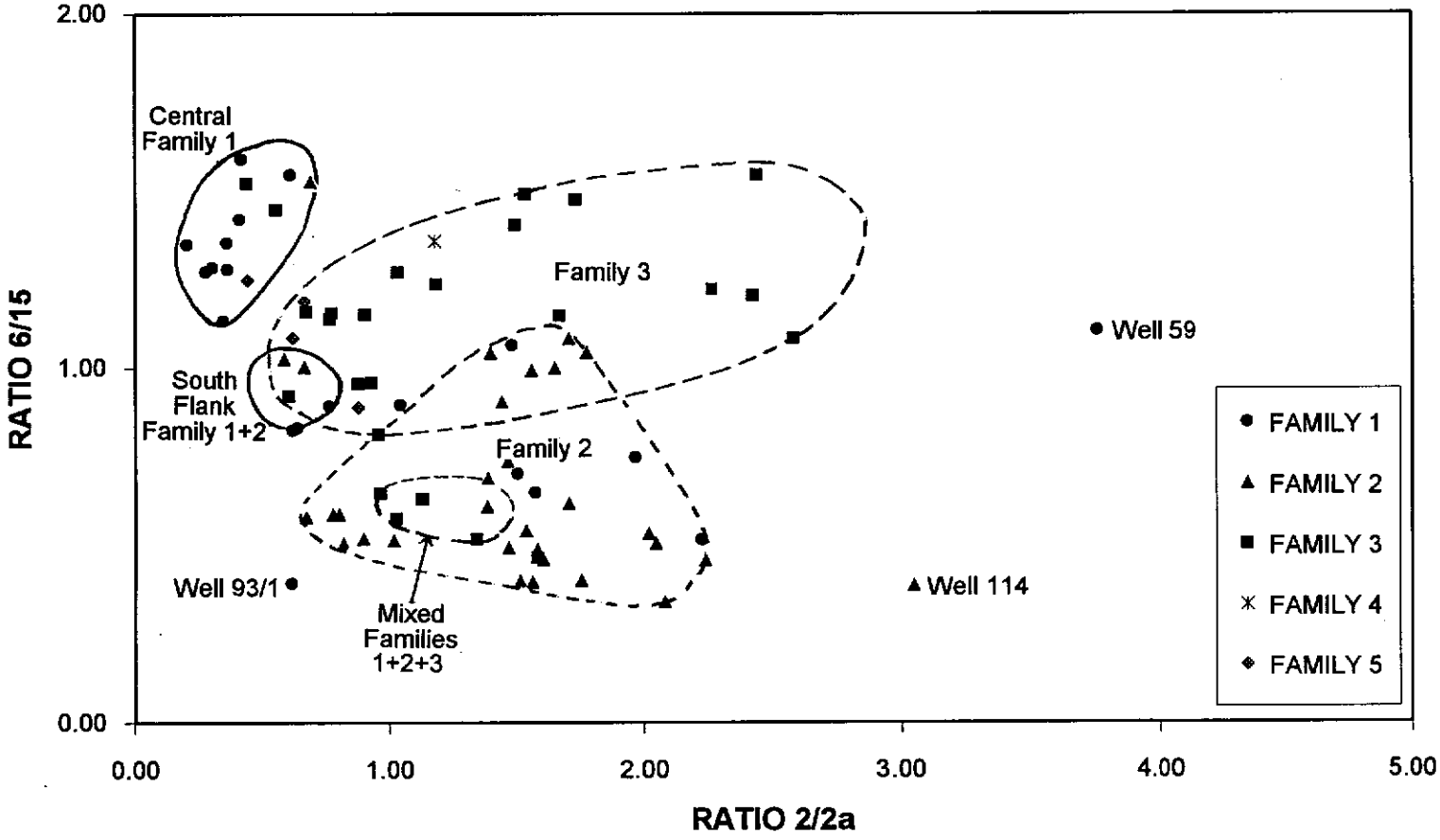

Figure 9.15: Crossplot of ratios 6/15 and 2/2a showing partial separation between the different hydrocarbon families

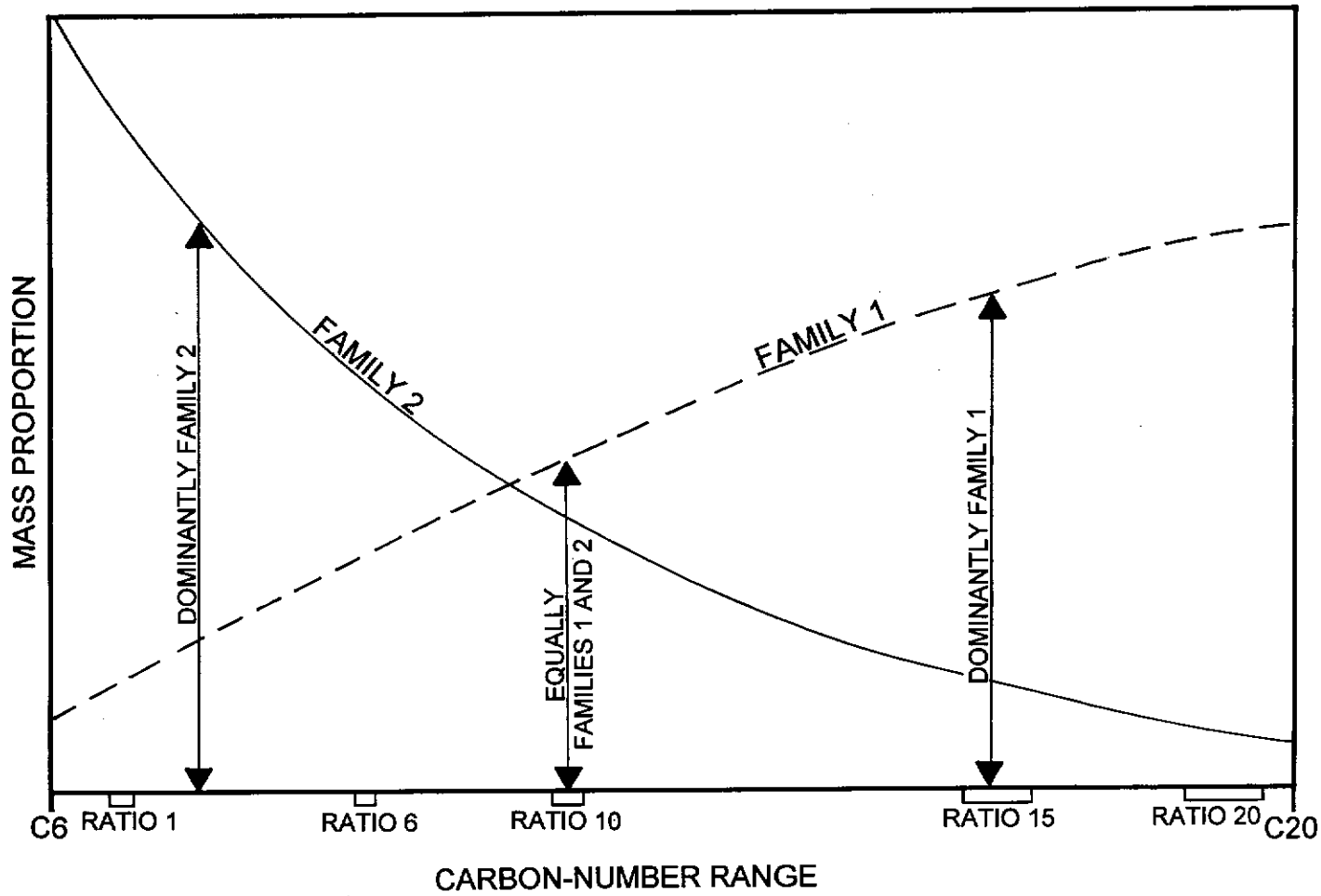

Figure 9.16: Schematic diagram comparing hypothetical mixing proportions of Family 1 and 2 liquid phases with carbon-number range and selected peak-pair ratios.

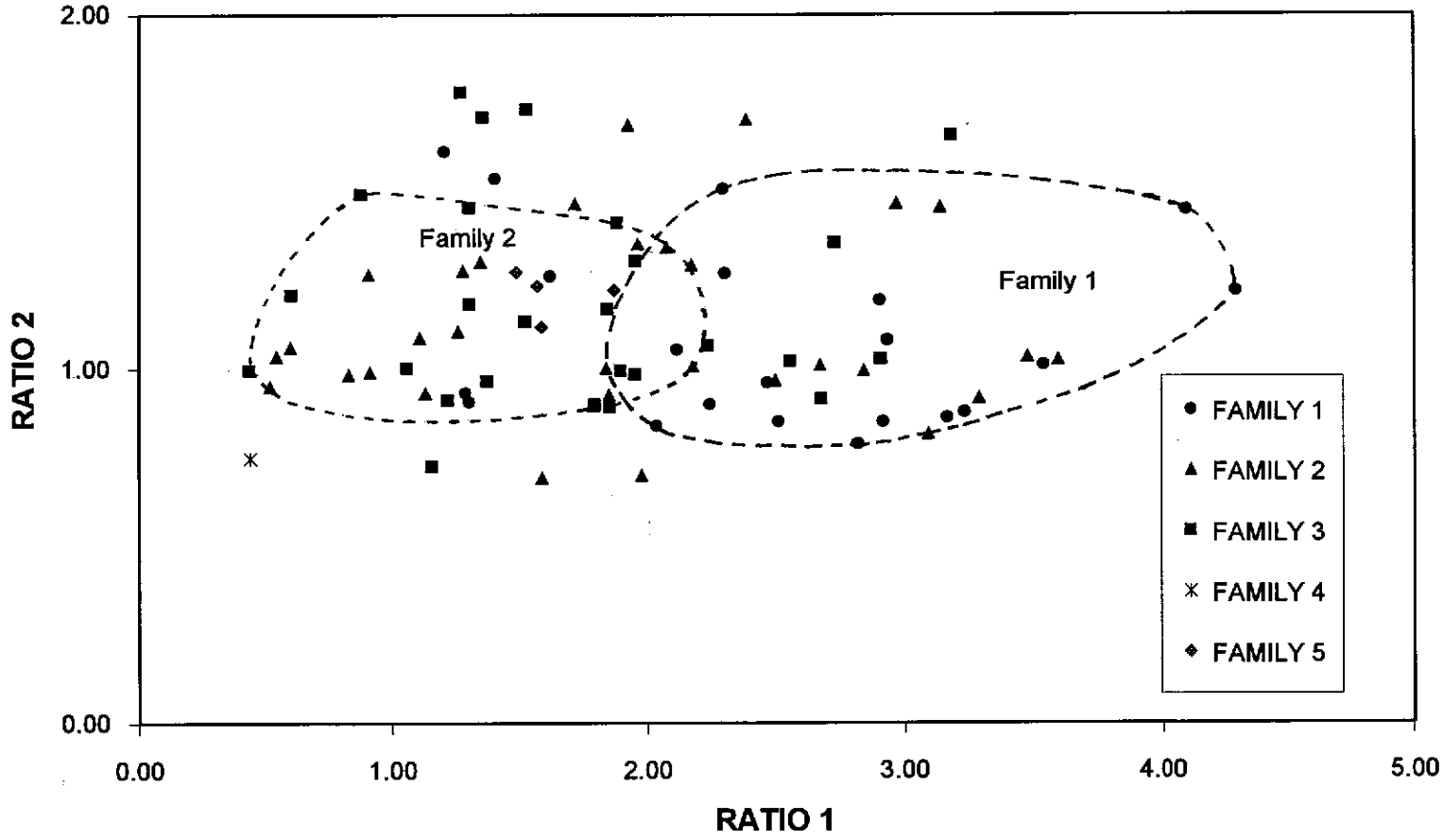

Figure 9.17: Crossplot of ratios 1 vs 2 showing the partial separation between data points of Families 1 and 2.

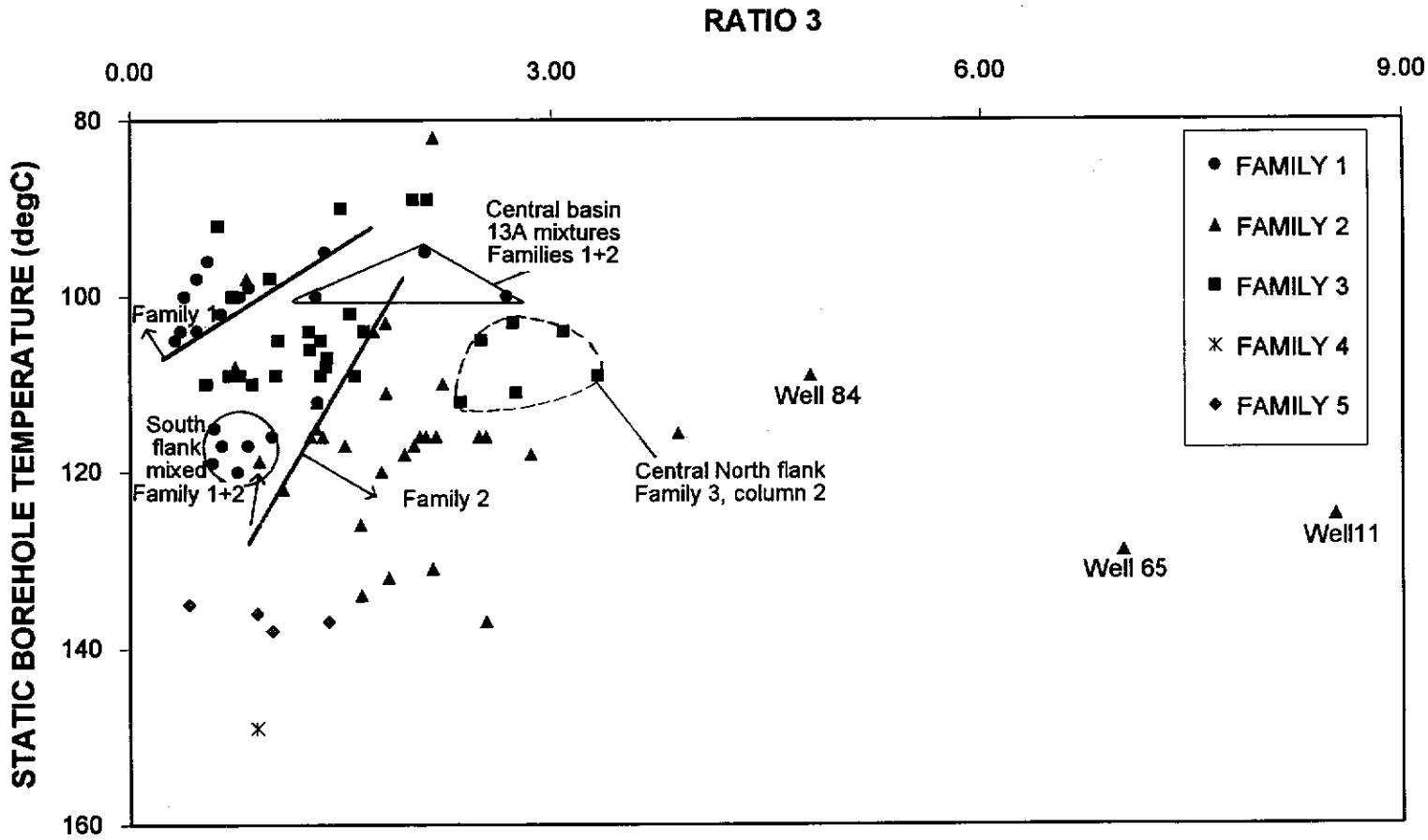

Figure 9.18: Plot of ratio 3 vs static borehole temperature showing the temperature dependant separation of Families 1, 2 and 3 and the Family 1+2 mixed hydrocarbons.

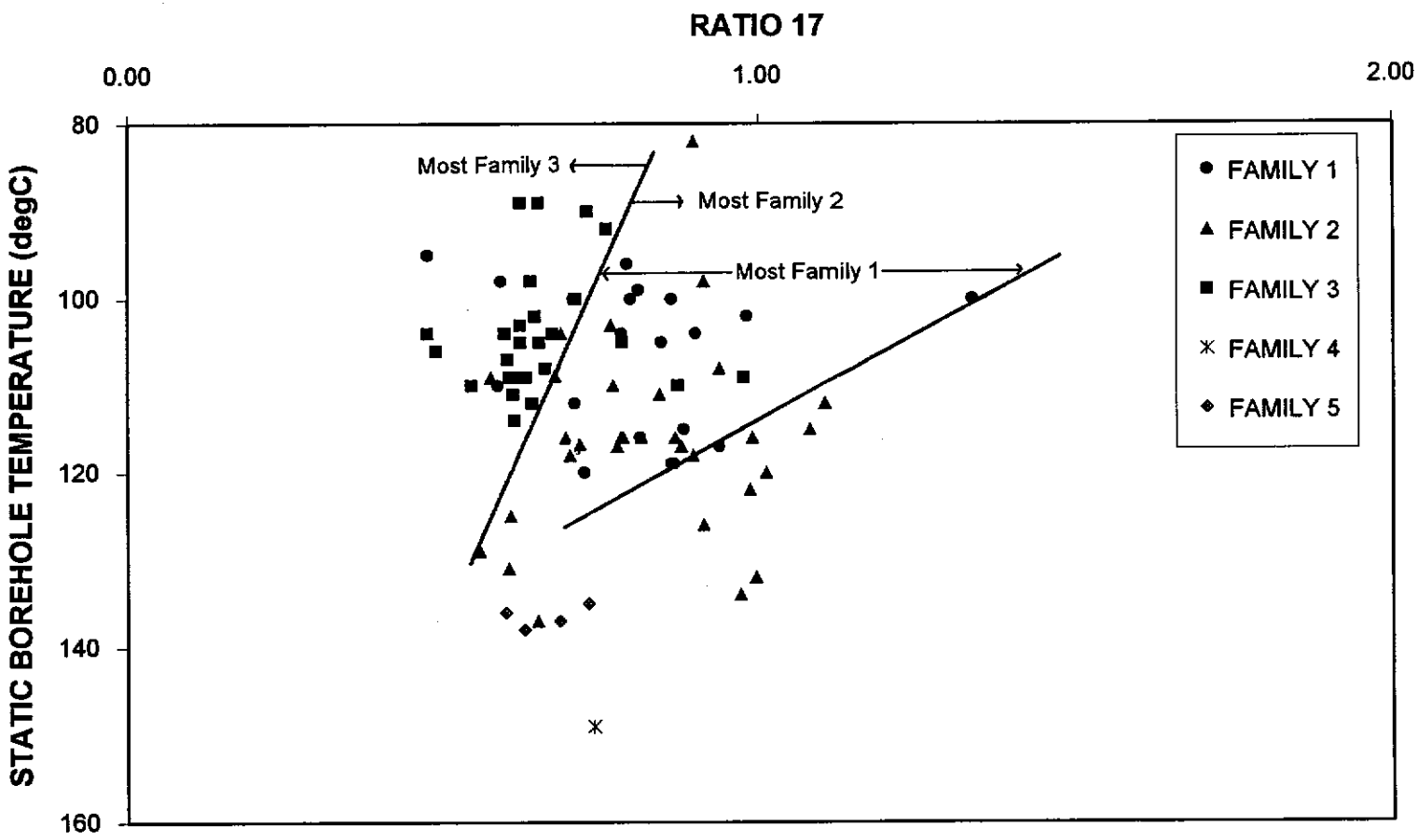

Figure 9.19: Plot of ratio 17 (between C15 and C16 isoprenoids) vs static borehole temperature showing the largely complete temperature dependant separation of Family 3 from the other Families.

are found. Envelopes enclosing a number of samples show where samples of a particular family locate separate from other families .

Samples assigned solely to Families 1, 2 and 3 form largely separate groups, circled on Fig. 9.15. Family 1 samples have high values of ratio 6/15 and low values of ratio 2/2a, whilst samples assigned solely to Family 2 have lower values of ratio 6/15 and higher values of ratio 2/2a (Fig. 9.15). Where Family 1 oils mix with Family 2 condensate, as in some flank wells and 13A reservoirs, they plot midway between the groups, or even within the other group if the second family dominates at that molecular weight as shown schematically in Fig. 9.16. This is also the case with other families in Fig. 9.15 although Families 4 and 5 are not discriminated from Families 2 and 3 by this plot. A cross-plot of ratios 1 vs 2 (Fig. 9.17) largely separates samples assigned solely to Family 1 from those assigned solely to Family 2, although there is a small region of overlap.

In the case of ratio 3, distinction of two or more families is affected by the formation temperature of the samples (Fig. 9.18) and the boundaries between families vary at different temperature rates. For example, the sloping Family 1 and Family 2 boundaries largely separate the two families although there are samples which from their gas, light oil, isotopic and biomarker signatures appear to be mixtures of the two. Family 3 samples are only poorly separated from Family 2 by this ratio, probably because these two gas-rich families are only well separated by non-hydrocarbon gases and some heavier components (Chapters 10-12). The Family 3 samples display no obvious temperature effect although central north flank Family 3 samples analysed on GC column no. 2 locate separate from the rest, suggesting a slight analytical effect.

Comparison of the ratio 17 (between C15 and C16 isoprenoids) with static borehole temperature shows that Family 1 and 2 data overlap but have mostly higher ratios than Family 3 except where samples represent mixtures (Fig. 9.19). Families 4 and 5 plot outside the Family 3 zone suggesting that they do not match.

The plot of ratio 8 with SBHT data shows that Families 2, 4 and 5 are largely distinct from Family 3 data and to some extent Family 1 (Fig. 9.20). The plot also shows that the slight temperature dependency of Families 2, 4 and 5 is in a different direction to the Families 1 and 3 data. This plot shown in Figs. 9.15-9.20, indicate that the fingerprint ratios are affected by formation temperature. It is also known from comparison of source rock maturity and depth maps (Figs. 4.07-4.17 and 4.24-29) that thermal maturity closely parallels present day depths and temperatures. Hence the apparent temperature-dependency may instead reflect source rock maturity.

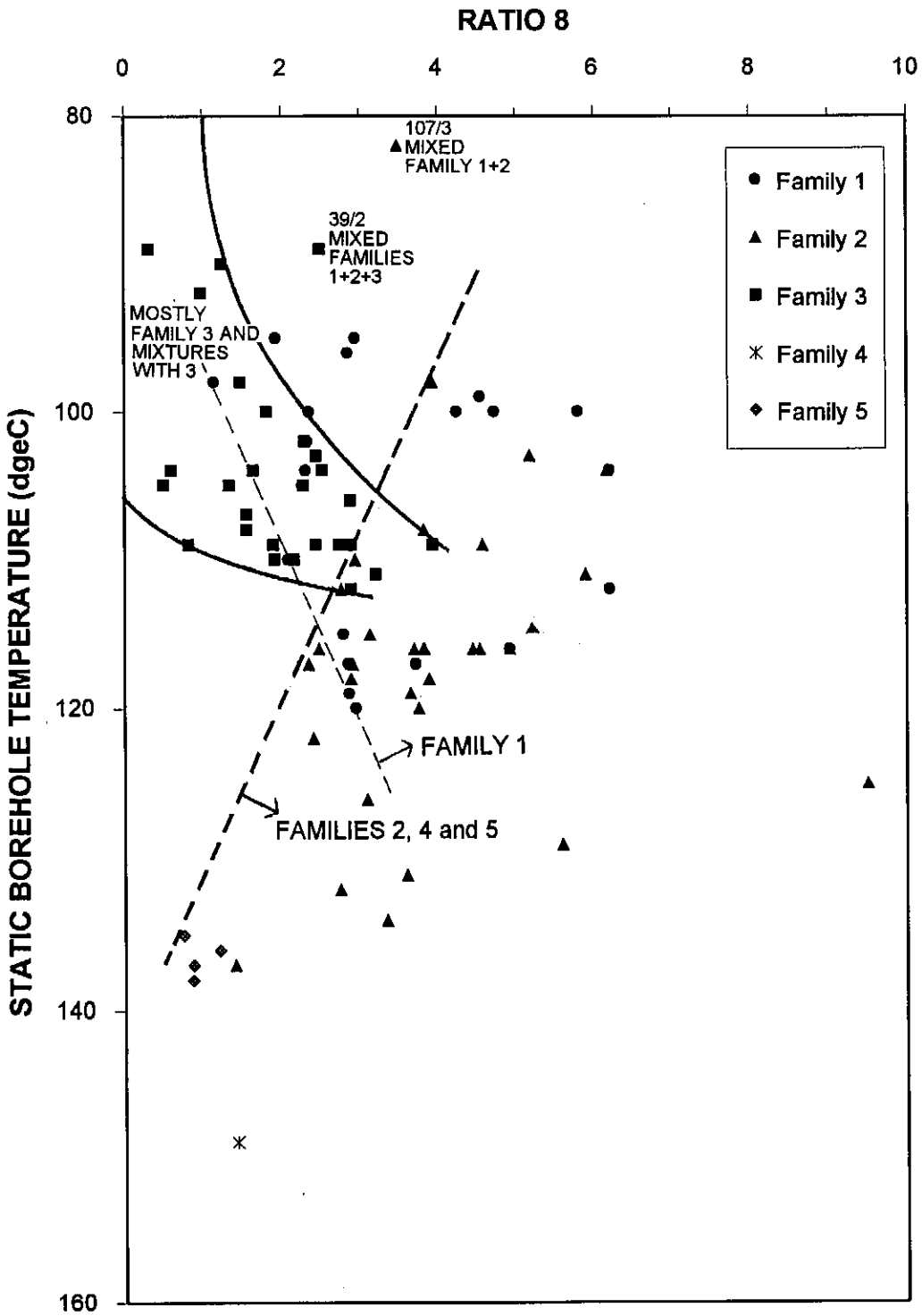

Figure 9.20: Plot of ratio 8 vs static borehole temperature showing the temperature-dependant distinction of Family 1 from Families 2, 4 and 5.

9.3.5. Statistical analysis

Individual ratio plots are able to distinguish one or more hydrocarbon family from the rest but none of the plots is able to completely separate all families. A number of the samples which cause these overlaps are samples which are considered from these data, the gas data and the biomarker and isotopic data (Chapters 11-12) to represent mixtures of hydrocarbon families. Consequently a multivariate statistical method (stepwise discriminant function analysis) was employed with the aim of establishing the best correlation between each hydrocarbon family and those representing mixed families. The analysis was carried out in the Department of Geology, University of Stellenbosch using the VAX programme BMDP (1993).

All hydrocarbons were included in this analysis except condensate from well 128. That sample was excluded from the data-set because it is the only representative of its group (Family 4) and discriminant function analysis requires a minimum of two samples/family. The samples of mixed families were placed in separate groups representing the most common mixtures namely Families 1+2, 1+3, 2+3.

The analysis compared each ratio of each sample and indicated which ones were mathematically closer and which ones would better fit in to a specific group. In cases where there was some doubt about the precise sample assignment, a fresh analysis was made with the sample temporarily assigned to another group. The analysis needed three iterations to establish the best geologically acceptable fit of the data. Final results show that the sample families are clearly separated by the smallest Mahalanobis' D^2 distance and the largest probability coefficients (Table 9.03) whilst the two groups of mixed samples locate intermediately. Canonical variables were constructed from the ratios which gave the greatest distinction between families and the mixed families (ratios 2a, 5, 8, 12 and 6/15; Table 9.04). These variables are plotted in Fig. 9.21 and show the location of Families 1, 2, 3 and 5 which plot separate from each other and the intermediate locations of the mixtures of the families, which plot between the 'pure' end members. The discriminating functions of these variables are given below:

Variable 1 = [(0.360 * ratio 1)+(1.685 * ratio 2a)+(0.948 * ratio 8)+(6.054 * ratio 17)]

Variable 2 = [0.468 * ratio 1)+(1.830 * ratio 2a)+(-0.0323 * ratio 8)+(-5.339 * ratio 17)]

9.3.6. Interpretation of discriminant function analysis results

Discriminant function analysis largely confirms the separation of the flowed samples into 5 distinct families and several mixtures based on the whole oil analyses. The *a posteriori* probabilities (Table 9.03) show that a number of samples may be better located in other families. No further data (such as isotopic or biomarker data) are available for many of these samples so the discrepancies cannot be resolved. Those

TABLE OF 'a posteriori probabilities' FOR LACK OF MATCH														
FAMILY 1	SAMPLE	COLUMN	FAMILY 1		FAMILY 1+2		FAMILY 2		FAMILY 3		FAMILY 1+2+3		FAMILY 5	
1	146/1	3	3.5	0.862	8.4	0.074	14.0	0.005	12.3	0.011	20.8	0.000	9.3	0.049
2	166/1	Q	6.2	0.059	0.7	0.940	13.4	0.002	20.2	0.000	26.1	0.000	23.0	0.000
3	88/5	1	1.2	0.997	14.1	0.002	25.0	0.000	22.7	0.000	33.3	0.000	14.7	0.001
4	156/1	Q	6.0	0.154	2.6	0.846	22.2	0.000	27.6	0.000	32.6	0.000	28.0	0.000
5	93/2	1	22.0	1.000	60.6	0.000	94.7	0.000	92.6	0.000	110.2	0.000	68.6	0.000
6	117/1	1	1.5	0.999	16.6	0.001	34.8	0.000	32.4	0.000	42.3	0.000	21.9	0.000
7	117/1	3	7.2	0.950	13.1	0.050	38.4	0.000	49.7	0.000	60.8	0.000	46.8	0.000
8	83/3	1	2.4	1.000	22.5	0.000	39.2	0.000	34.5	0.000	46.3	0.000	21.7	0.000
9	103/2	1	2.0	1.000	18.1	0.000	28.6	0.000	29.9	0.000	43.8	0.000	21.5	0.000
10	126/1	1	1.9	1.000	20.5	0.000	34.9	0.000	35.1	0.000	49.0	0.000	24.7	0.000
11	126/1	Q	5.4	0.145	1.9	0.835	9.5	0.019	15.2	0.001	22.5	0.000	17.4	0.000
FAMILY 1+2														
12	107/3	2	10.2	0.017	2.0	0.981	14.1	0.002	19.7	0.000	23.5	0.000	22.9	0.000
13	166/RFT	Q	4.1	0.303	2.4	0.696	15.4	0.001	23.8	0.000	31.8	0.000	24.7	0.000
14	109/1	2	42.1	0.000	23.0	0.982	31.0	0.018	63.9	0.000	74.2	0.000	78.1	0.000
15	109/1	3	21.0	0.000	4.2	1.000	23.9	0.000	30.6	0.000	30.2	0.000	37.8	0.000
16	132/2	2	14.8	0.001	0.4	0.996	11.7	0.004	20.3	0.000	23.4	0.000	28.0	0.000
17	132/1	2	15.2	0.001	1.9	0.997	14.4	0.002	24.0	0.000	28.3	0.000	31.9	0.000
18	167/1	Q	7.2	0.108	3.0	0.844	8.8	0.048	20.0	0.000	29.6	0.000	23.9	0.000
19	84/1	2	33.5	0.000	14.2	0.883	30.8	0.000	24.7	0.005	18.3	0.112	30.5	0.000
20	148/1	3	15.8	0.004	4.8	0.954	11.0	0.042	28.6	0.000	38.3	0.000	37.8	0.000
21	119/1	2	15.6	0.002	3.7	0.977	11.4	0.021	23.6	0.000	30.6	0.000	32.2	0.000
22	208/1	2	9.4	0.017	1.3	0.983	17.1	0.000	21.4	0.000	24.5	0.000	24.3	0.000
23	108/2	2	9.7	0.019	1.8	0.981	18.6	0.000	22.2	0.000	24.8	0.000	24.5	0.000
24	110/1A	2	11.5	0.005	1.2	0.940	7.1	0.049	11.6	0.005	15.6	0.001	17.0	0.000
25	110/1B	3	11.1	0.009	1.9	0.873	6.3	0.095	9.4	0.020	13.8	0.002	14.3	0.002
26	110/1B	2	17.0	0.000	2.9	0.473	2.7	0.521	11.8	0.005	17.2	0.000	20.9	0.000
27	93/1A	3	16.1	0.004	4.9	0.996	27.6	0.000	33.8	0.000	34.7	0.000	37.3	0.000
28	93/1	1	12.7	0.008	3.2	0.937	9.0	0.051	14.8	0.003	19.2	0.000	19.4	0.000
29	94/1	2	11.4	0.079	10.1	0.148	7.7	0.482	9.3	0.222	18.5	0.002	11.7	0.066
30	11/2	2	35.3	0.000	19.5	1.000	40.4	0.000	62.4	0.000	70.0	0.000	74.0	0.000
FAMILY 2														
31	63/1	1	35.7	0.000	15.9	0.001	1.7	0.994	12.4	0.005	18.2	0.000	26.1	0.000
32	102/2	2	25.5	0.000	12.3	0.003	1.5	0.698	3.4	0.275	8.5	0.021	12.3	0.003
33	88/4	1	31.3	0.000	12.9	0.020	5.1	0.980	22.6	0.000	30.2	0.000	35.9	0.000
34	120/1	1	34.4	0.000	17.9	0.000	1.3	0.943	7.0	0.054	13.0	0.003	18.8	0.000
35	61/2	2	22.6	0.000	8.0	0.220	5.9	0.638	9.1	0.125	13.2	0.016	18.6	0.001
36	88/3	1	27.4	0.000	12.3	0.014	3.8	0.985	22.1	0.000	32.0	0.000	34.4	0.000
37	88/2	2	25.1	0.000	11.5	0.023	4.0	0.959	12.0	0.017	19.5	0.000	22.9	0.000
38	129/2	1	24.9	0.000	8.0	0.207	5.3	0.779	13.7	0.012	17.3	0.002	23.5	0.000
39	120/1	Q	35.4	0.000	18.5	0.000	1.9	0.857	5.6	0.134	11.0	0.009	17.6	0.000
40	96/1	2	39.9	0.000	21.2	0.000	1.8	0.995	12.3	0.005	20.1	0.000	26.9	0.000
41	96/1	3	31.0	0.000	14.0	0.002	2.2	0.860	6.0	0.126	10.8	0.011	17.8	0.000
42	95/2	2	17.0	0.001	11.2	0.011	4.4	0.333	3.3	0.570	9.9	0.022	7.7	0.064
43	129/1	1	31.2	0.000	12.4	0.008	2.6	0.992	21.1	0.000	30.0	0.000	35.8	0.000
44	83/2	1	22.4	0.000	8.3	0.060	2.8	0.928	11.6	0.012	17.3	0.001	20.7	0.000
45	88/1	1	32.9	0.000	17.6	0.000	1.3	0.996	12.6	0.003	21.7	0.000	25.4	0.000
46	65/2	2	26.8	0.000	9.2	0.330	8.2	0.540	11.5	0.102	14.2	0.027	22.4	0.000
47	114/1	1	41.1	0.000	19.7	0.000	2.4	0.999	16.7	0.001	23.9	0.000	32.6	0.000
48	83/1	1	37.2	0.000	19.7	0.000	2.6	0.999	18.7	0.000	28.9	0.000	33.6	0.000

Table 9.03: 'A posteriori' probabilities of incorrect classification assignments to Families.

FAMILY 1	SAMPLE	COLUMN	FAMILY 1		FAMILY 1+2		FAMILY 2		FAMILY 3		FAMILY 1+2+3		FAMILY 5	
FAMILY 3														
49	61/3	2	29.0	0.000	20.9	0.000	10.2	0.005	0.5	0.665	2.8	0.213	4.0	0.117
50	69/1	2	18.7	0.000	18.3	0.000	14.8	0.001	3.3	0.272	6.7	0.051	1.5	0.677
51	20/4	1	29.6	0.000	18.6	0.000	7.8	0.016	0.2	0.688	2.2	0.253	5.8	0.043
52	20/3	1	37.8	0.000	22.1	0.000	8.2	0.017	1.1	0.596	2.0	0.378	9.7	0.008
53	39/1	1	50.9	0.000	43.2	0.000	21.9	0.000	4.7	0.637	6.5	0.263	8.4	0.100
54	107/2	2	23.2	0.000	14.7	0.003	13.5	0.006	4.8	0.441	5.1	0.391	6.9	0.159
55	18/4	2	31.5	0.000	19.1	0.000	11.0	0.003	0.7	0.471	0.6	0.495	6.2	0.031
56	31/1	1	54.0	0.000	39.5	0.000	20.8	0.000	4.9	0.292	3.1	0.695	11.2	0.012
57	18/3	2	36.0	0.000	28.2	0.000	14.9	0.001	0.9	0.606	2.5	0.277	4.2	0.116
58	21/1	2	32.6	0.000	24.7	0.000	11.2	0.003	0.4	0.718	3.1	0.180	4.3	0.099
59	18/1	2	25.3	0.000	35.1	0.000	27.9	0.000	8.9	0.028	15.2	0.001	1.8	0.971
60	21/2	3	29.7	0.000	16.1	0.000	4.9	0.107	1.1	0.706	3.9	0.174	9.1	0.013
61	19/2	2	32.3	0.000	18.8	0.000	7.0	0.038	1.1	0.713	3.4	0.235	9.0	0.014
62	62/1	2	24.9	0.000	10.6	0.017	5.9	0.177	3.5	0.587	5.6	0.209	11.6	0.010
63	20/2	1	23.3	0.000	20.2	0.000	5.4	0.750	7.8	0.227	18.4	0.001	12.5	0.022
64	55/2	2	26.4	0.000	13.8	0.001	7.5	0.030	1.4	0.635	2.9	0.308	7.9	0.025
65	44/1	2	25.1	0.000	13.3	0.001	7.4	0.026	1.0	0.636	2.5	0.301	6.8	0.035
FAMILY 1+2+3														
66	39/2	1	64.7	0.000	47.7	0.000	23.3	0.000	7.8	0.314	6.3	0.681	16.3	0.004
67	39/2	2	39.2	0.000	21.1	0.000	10.8	0.004	2.3	0.313	0.7	0.679	11.1	0.004
68	59/1	1	52.9	0.000	37.7	0.000	22.4	0.000	4.8	0.209	2.2	0.783	11.4	0.008
69	59/1	2	51.1	0.000	32.6	0.000	16.5	0.001	4.8	0.343	3.5	0.653	14.7	0.002
70	102/4	2	43.9	0.000	32.5	0.000	19.6	0.000	2.7	0.297	1.1	0.663	6.7	0.040
71	46/2	2	40.3	0.000	25.9	0.000	15.5	0.000	2.4	0.260	0.3	0.725	8.1	0.015
72	70/2	2	31.2	0.000	18.0	0.000	10.3	0.004	0.9	0.467	0.7	0.505	6.8	0.024
73	70/1	2	42.3	0.000	27.5	0.000	21.3	0.000	4.8	0.121	0.8	0.869	9.9	0.009
74	54/1	2	32.6	0.000	20.0	0.000	17.8	0.000	5.0	0.184	2.1	0.783	8.4	0.033
75	107/1	2	31.1	0.000	20.8	0.000	24.0	0.000	7.4	0.124	3.7	0.818	8.9	0.058
76	76/1	3	36.5	0.000	21.6	0.000	19.1	0.000	5.6	0.118	1.6	0.870	10.2	0.012
77	48/2	3	47.4	0.000	28.6	0.000	28.0	0.000	11.4	0.024	4.0	0.974	17.0	0.002
78	48/1	1	33.9	0.000	21.4	0.000	16.5	0.000	2.7	0.230	0.4	0.740	6.8	0.030
79	65/1	2	29.2	0.000	14.1	0.002	5.8	0.121	2.5	0.633	4.5	0.236	11.3	0.008
80	37/1	2	40.5	0.000	26.0	0.000	15.5	0.000	2.5	0.259	0.5	0.727	8.3	0.014
FAMILY 5														
81	35/3	1	13.2	0.016	30.0	0.000	31.7	0.000	16.2	0.003	25.0	0.000	4.9	0.981
82	27/1	2	24.3	0.000	28.0	0.000	22.2	0.000	4.5	0.110	8.1	0.018	0.4	0.872
83	35/2B	2	30.7	0.000	24.4	0.000	16.4	0.000	1.9	0.419	2.3	0.333	2.9	0.248
84	35/1	2	27.0	0.000	28.2	0.000	21.4	0.000	3.5	0.166	6.0	0.047	0.4	0.787

Table 9.03 (cont.)

DISCRIMINANT FUNCTION ANALYSIS						
No	WELL/DST	COLUMN	SBHT	FAMILY	X-coord	Y-coord
1	146/1	3	96	1	1.49	1.42
2	166/1	Q	99	1	2.49	0.06
3	88/5	1	100	1	2.44	2.32
4	156/1	Q	100	1	3.11	0.64
5	93/2	1	102	1	6.34	5.24
6	117/1	1	104	1	3.24	2.82
7	117/1	3	104	1	5.03	0.94
8	83/3	1	105	1	3.17	3.37
9	103/2	1	115	1	3.08	2.16
10	126/1	1	119	1	3.48	2.63
11	126/1	Q	119	1	2.02	0.12
12	107/3	2	82	1+2	2.08	-0.01
13	166/RFT	Q	98	1+2	2.97	0.21
14	109/1	2	100	1+2	4.31	-3.77
15	109/1	3	100	1+2	2.37	-0.50
16	132/2	2	103	1+2	1.99	-0.86
17	132/1	2	104	1+2	2.34	-0.87
18	167/1	Q	108	1+2	2.49	-0.57
19	84/1	2	109	1+2	0.32	0.51
20	148/1	3	111	1+2	2.89	-1.76
21	119/1	2	112	1+2	2.31	-1.24
22	108	2	116	1+2	2.30	0.25
23	108/2	2	116	1+2	2.30	0.39
24	110/1A	2	116	1+2	1.25	-0.34
25	110/1B	3	116	1+2	1.03	-0.18
26	110/1B	2	116	1+2	1.00	-1.35
27	93/1A	3	116	1+2	2.94	0.13
28	93/1	1	117	1+2	1.42	-0.38
29	94/1	2	117	1+2	0.77	0.26
30	11/2	2	125	1+2	4.54	-2.03
31	63/1	1	109	2	-0.52	-2.50
32	102/2	2	110	2	-0.80	-1.00
33	88/4	1	112	2	1.00	-2.82
34	120/1	1	113	2	-1.11	-1.87
35	61/2	2	114	2	0.12	-0.93
36	88/3	1	115	2	1.27	-2.69
37	88/2	2	116	2	0.28	-1.58
38	129/2	1	116	2	0.45	-1.55
39	120/1	Q	117	2	-1.36	-1.72
40	96/1	2	118	2	-0.91	-2.65
41	96/1	3	118	2	-0.89	-1.56
42	95/2	2	120	2	-0.29	0.01
43	129/1	1	120	2	0.95	-3.07
44	83/2	1	122	2	0.43	-1.51
45	88/1	1	126	2	-0.29	-2.36
46	65/2	2	129	2	0.03	-1.13
47	114/1	1	132	2	-0.46	-3.13
48	83/1	1	134	2	0.08	-3.04

Table 9.04: Mahalanobis' D^2 canonical variables for the four main discriminant data for Families 1, 2, 3, 5 and mixtures.

No	WELL/DST	COLUMN	SBHT	FAMILY	X-coord	Y-coord
49	61/3	2	90	3	-1.91	0.60
50	69/1	2	92	3	-0.95	1.68
51	20/4	1	100	3	-1.84	0.14
52	20/3	1	102	3	-2.37	-0.40
53	39/1	1	104	3	-3.77	0.92
54	107/2	2	105	3	-0.95	0.88
55	18/4	2	105	3	-2.01	0.42
56	31/1	1	105	3	-3.86	0.42
57	18/3	2	107	3	-2.62	0.92
59	21/1	2	109	?5	-2.27	0.59
58	18/1	2	108	3	-1.49	3.03
60	21/2	3	109	3	-1.56	-0.48
61	19/2	2	109	3	-1.86	-0.29
62	62/1	2	109	3	-0.82	-0.42
63	20/2	1	110	3	-0.42	-0.45
64	55/2	2	111	3	-1.32	0.04
65	44/1	2	112	3	-1.27	0.15
66	39/2	1	89	3+1+2	-4.50	-0.05
67	39/2	2	89	3+1+2	-2.39	-0.27
68	59/1	1	95	3+1+2	-3.75	0.63
69	59/1	2	95	3+1+2	-3.30	-0.26
70	102/4	2	98	3+1+2	-3.22	0.99
71	46/2	2	98	3+1+2	-2.73	0.49
72	70/2	2	103	3+1+2	-1.91	0.29
73	70/1	2	104	3+1+2	-2.76	0.96
74	54/1	2	104	3+1+2	-1.82	0.95
75	107/1	2	106	3+1+2	-1.59	1.69
76	76/1	3	109	3+1+2	-2.08	0.82
77	48/2	3	110	3+1+2	-2.55	0.92
78	48/1	1	110	3+1+2	-2.16	0.91
79	65/1	2	131	3+1+2	-1.32	-0.54
80	37/1	2	137	3+1+2	-2.73	0.46
81	35/3	1	135	5	0.23	3.58
82	27/1	2	136	5	-1.62	2.50
83	35/2B	2	137	5	-2.14	1.35
84	35/1	2	138	5	-1.92	2.30

Table 9.04 (cont.)

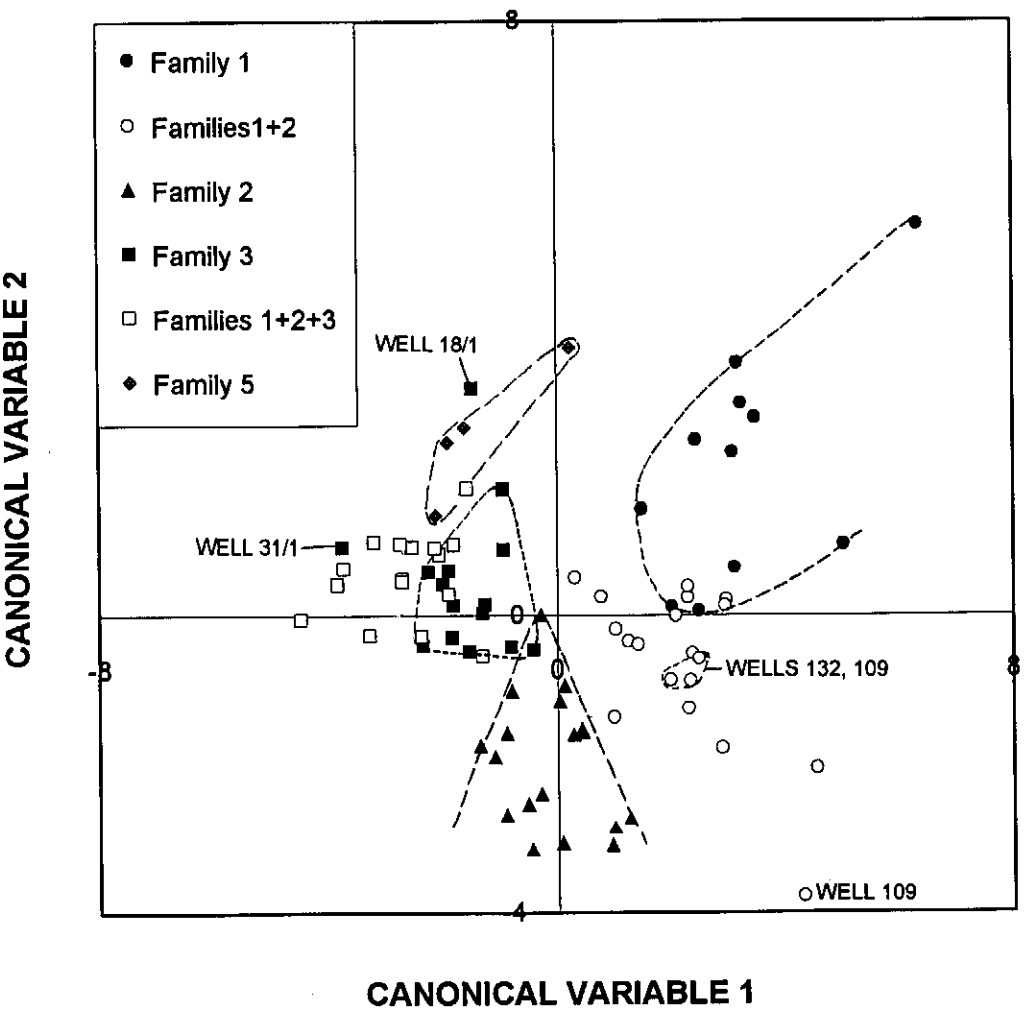

Figure 9.21: Crossplot of the first and second canonical variables showing the separation of the 'pure' Families and the intermediate locations of the hydrocarbon mixtures.

samples are left in the family which better suits them geologically. For example, the DST 1 sample from well 65 is left in the mixed Family 1+2+3 rather than placing it in Family 3 because it has many affinities with Family 2 (high aromatic contents, gas data).

The gas-condensate produced during DST 1, well 18, is shown to more likely belong to the Family 5 group of syn-rift condensates from wells 27 and 35 (with a 97.1% probability of a match with Family 5 and a 2.8% probability of a match with Family 3, Table 9.03). Whilst this appears unlikely in view of their spatial separation (~100 km apart) there are certain geological similarities. The condensates in wells 27 and 35 are associated with a syn-rift graben which is known (from well 16) to contain red beds and evaporites. The DST1 condensate in well 18 is the only one from that structure reservoired in non-marine sandstones and whilst present formation water salinities are relatively fresh (in contrast with those in wells 27 and 35), this could be a late stage alteration. Indeed, maximum formation water salinities in sandstones in adjacent wells (no's. 20, 44 and 58) are very high (50000-80000 ppm). Furthermore, the formation pressure recorded from RFT measurements in the sandstone in well 18, shows the sandstone to lie off the trend of the upper low-salinity (~20000 ppm) sandstones suggesting a separate trap (Fig. 9.22). This and the different chemistry could indicate migration from a different source and hence a different trapping time. Nevertheless there are other parameters which indicate that the sample should not belong with Family 5 (e.g. C7 ternary plot, gas data) hence the sample is left with Family 3.

Gas-condensate produced from well 31 DST1 appears from the gas, C4-9 and low carbon-number fingerprint data to match Family 3. However, the higher carbon number fingerprint data suggest an affiliation which places the sample in the Family 1+3 mixture in the results of the discriminant function analysis (Table 9.03; Fig. 9.21). The whole oil GC shows the sample to have an unusually large oil 'hump' compared to the results from nearby wells (e.g. wells 18, 20 and 44). This suggests that the condensate has dissolved some residual oil influencing the higher molecular weight fingerprint data. The sample is temporarily retained in Family 3 because the bulk of the data indicate that family. Biomarker and isotopic analyses may help to resolve this discrepancy.

Condensate from DST1 in well 69 is also better matched to the syn-rift condensates of wells 27 and 35 than to the next most likely group, with a 67.7% probability of a match with Family 5 and only a 28.3% probability of a match with Family 1+2+3 (Table 9.03). This well too has relatively high salinity formation water (58000 ppm, Davies, 1995a) although it is normally pressured. This well is directly updip of a major syn-rift sediment thickness where gas-prone source rocks could exist (Fig. 4.03 and Burden, 1993).

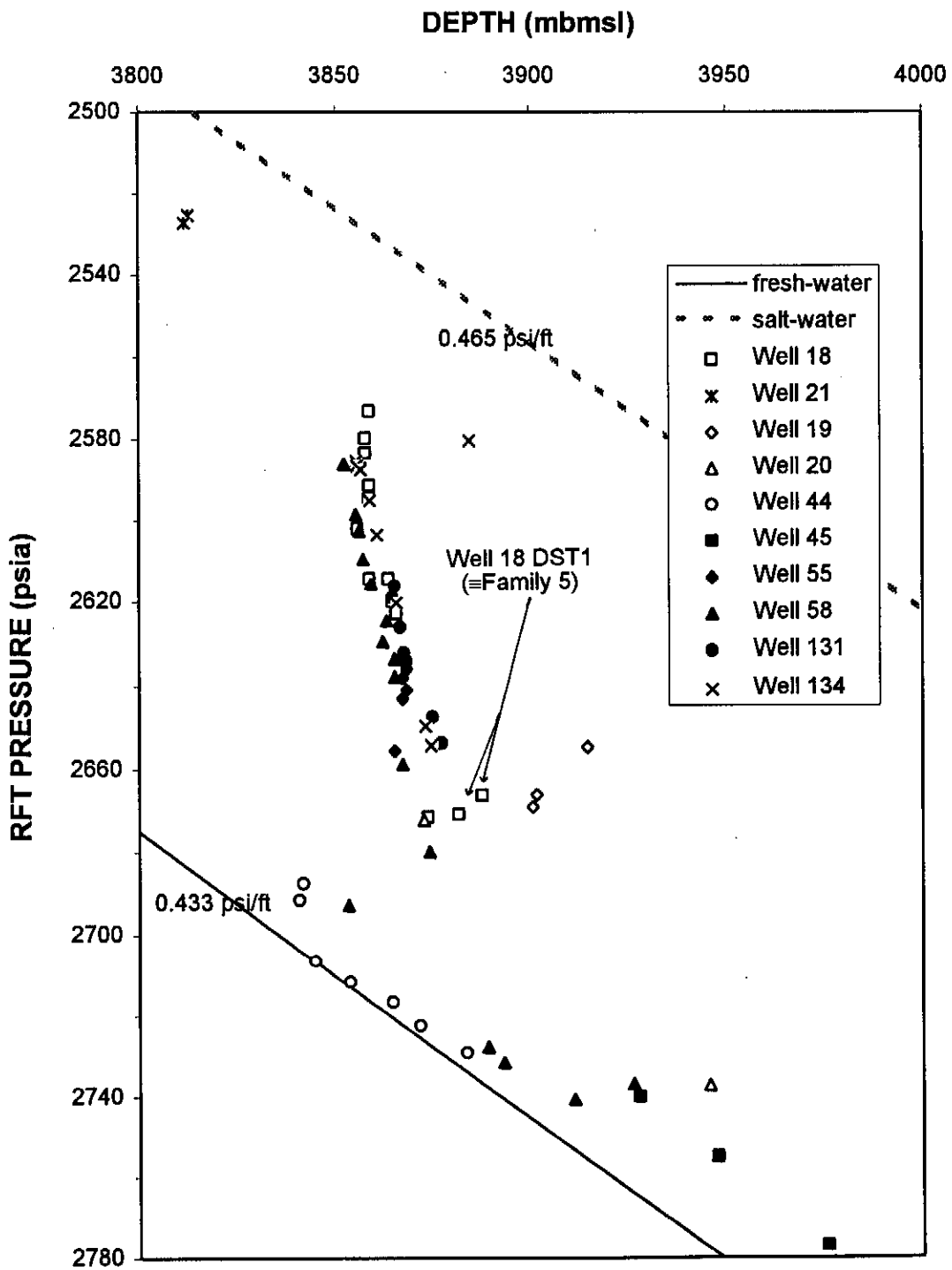

Figure 9.22: Crossplot of RFT pressures for the sands in the eastern part of the north flank showing the isolation of the DST1 sandstone in well 18 from the other wells as suggested by the discriminant function analysis.

Largely because of the great distance between this sample and the Family 5 wells, and the unlikelihood of a migration route between them, this sample too is left in Family 3.

These two unusual correlations suggest the possibility that gas-condensate sourced in syn-rift sediments, either the same source in a single depocentre or similar source rocks in different depocentres, charged sandstones throughout the basin. Evidence of this charge is found in over-pressured sandstones only because they have not been breached and displaced by later migration. If so, there may be other gas reservoirs in traps which have remained sealed since that early charge. Should this apparent similarity be substantiated by further analyses, a whole new trend of gas migration, updip of the present finds, may be suggested.

Three of the Family 1 oils would, on the strength of the *a posteriori* probability coefficients (Table 9.03) be slightly better located in a mixed Family (1+2). These three (plus 3 others) were analysed on the Quadrex column which is known to have introduced a slightly greater measure of misfit than between the other GC separation columns. Repeat analyses of hydrocarbons from wells 156 and 120 on Macherey-Nagel columns (the former not reported here as the data are incomplete and the latter are reported in Tables 9.01; 9.03) confirm their correct assignment to Families 1 and 2 respectively, hence the 'out-of-place' oils are not reassigned. Nevertheless, the 5 Quadrex analyses compare well amongst themselves and are employed in this report, but mainly for correlation using only the whole envelope, the C4-9 fraction and individual ratios.

The western part of the north flank of the basin is the only area of this basin where fingerprint GC data record mixtures of all three major hydrocarbon families. This is the same area as that indicated in Davies (1995c) and Jungslager (1996) as being a possible meeting place for all hydrocarbon streams.

Jungslager (1996) shows that the basin is bounded by master faults which govern its shape and have been active for a long time. He shows that wells in the structure on the north-east flank where Family 3 gas dominates, are bounded by the north flank master fault which downthrows to the north. In addition, he comments on the master fault to the south as another major flow boundary. It is likely that the three different families of hydrocarbons which are found reservoired in north flank structures (Families 1, 2 and 3) migrated towards the north-west as a result of this fault control (Davies, 1996c).

The southern of these two master faults is indicated by Davies (1996c) and Larsen (1995) as a major pressure boundary below horizon 9At1. It is considered that it is only through this fault that oil from the 13A sequence might migrate stratigraphically

downward (but structurally updip) through pre-13A sandstones into pre-1A sandstones and thence to the north flank reservoirs. The available seismic line across the fault (Figs. 9.23a and 9.23b) shows rocks below 13At1 in contact with rocks below 1At1. In all intersections of below horizon 1At1, and in most intersections of horizon 13At1, the subjacent rocks are sandstones. Seismic mapping in the area shows approximately 4 km of overlap between the two horizons (J. Roux, 1995, pers. comm.). Since hydrocarbons migrating through the fault eventually accumulate in the north-west structures (as do any hydrocarbons migrating westwards immediately south of the fault), the area at the western end of this fault is a mixing locus for hydrocarbons of Families 1, 2 and 3. The fingerprint analysis and the results of the discriminant function analyses to support this model as hydrocarbons in that area display characteristics of all three families (Table 9.03). In addition, if the familial assignment predicted for condensates from wells 69 and 18 (DST1) by the discriminant function analysis is correct, then Family 5 gas has also migrated there.

Three of the samples (wells 132 DST's 1 and 2 and well 109) test hydrocarbons which were generated from a sub-group of the Family 1 source rock (Davies, 1997c; Chapter 12). These oils differ only in the proportions of some of their biomarkers and not in proportions of their C9-20 fraction - therefore they have not been reassigned to a separate subset of Family 1. The three samples plot closely together on Fig. 9.21, confirming this similarity. However, the repeat analysis of the sample from well 109 locates far out-of-place. This is due to the presence of abnormally small peaks in the column 2 analysis which affect ratios 3, 4, 10, 16 and 17 (cf. Appendix C, Figs. C.25 and C.26). It may indicate a problem, possibly an intermittent electrical noise, during the analysis of this sample. Since the rest of the analysis gives results which match the repeat analysis, and also the results from adjacent wells, and as the gas data (Chapter 8) and biomarker data (Chapter 12) show that the rest of the data match well, the results of this analysis are retained.

Interpretation of the whole oil GC data (including C4-9 and fingerprint) have shown familial correlations which largely match those determined from the gas data (Chapter 8). Apart from this familial correlation, the results have also pointed the way to a previously unrecognised, possibly basin-wide, gas flux. It is unfortunate that none of these unusual gas-condensates have been further analysed (for biomarkers, stable carbon isotopes), as a result it is not possible to determine the origin of this gas flux.

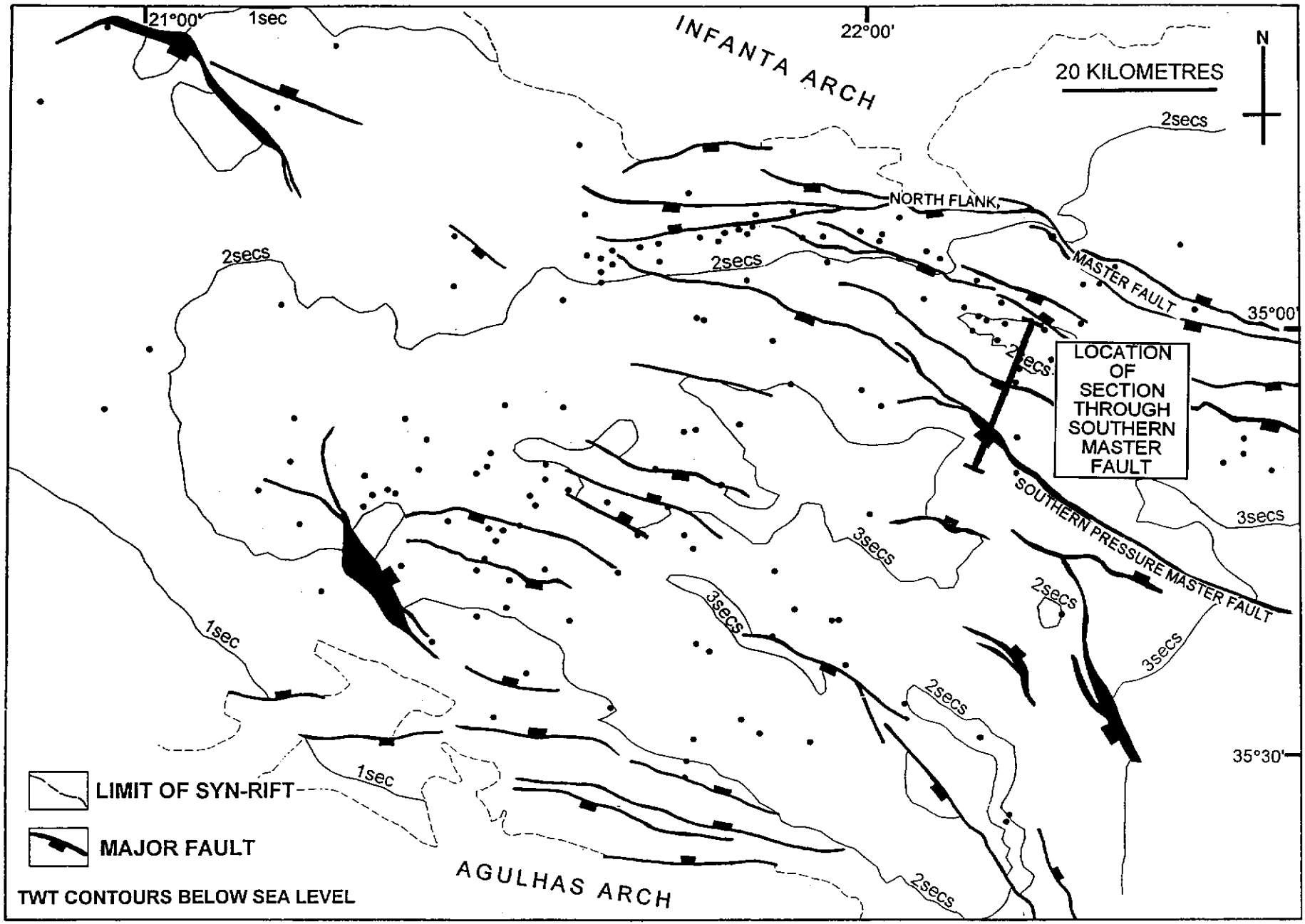

Figure 9.23a: Location map of the section line across the southern master fault (after Figure 3.04).

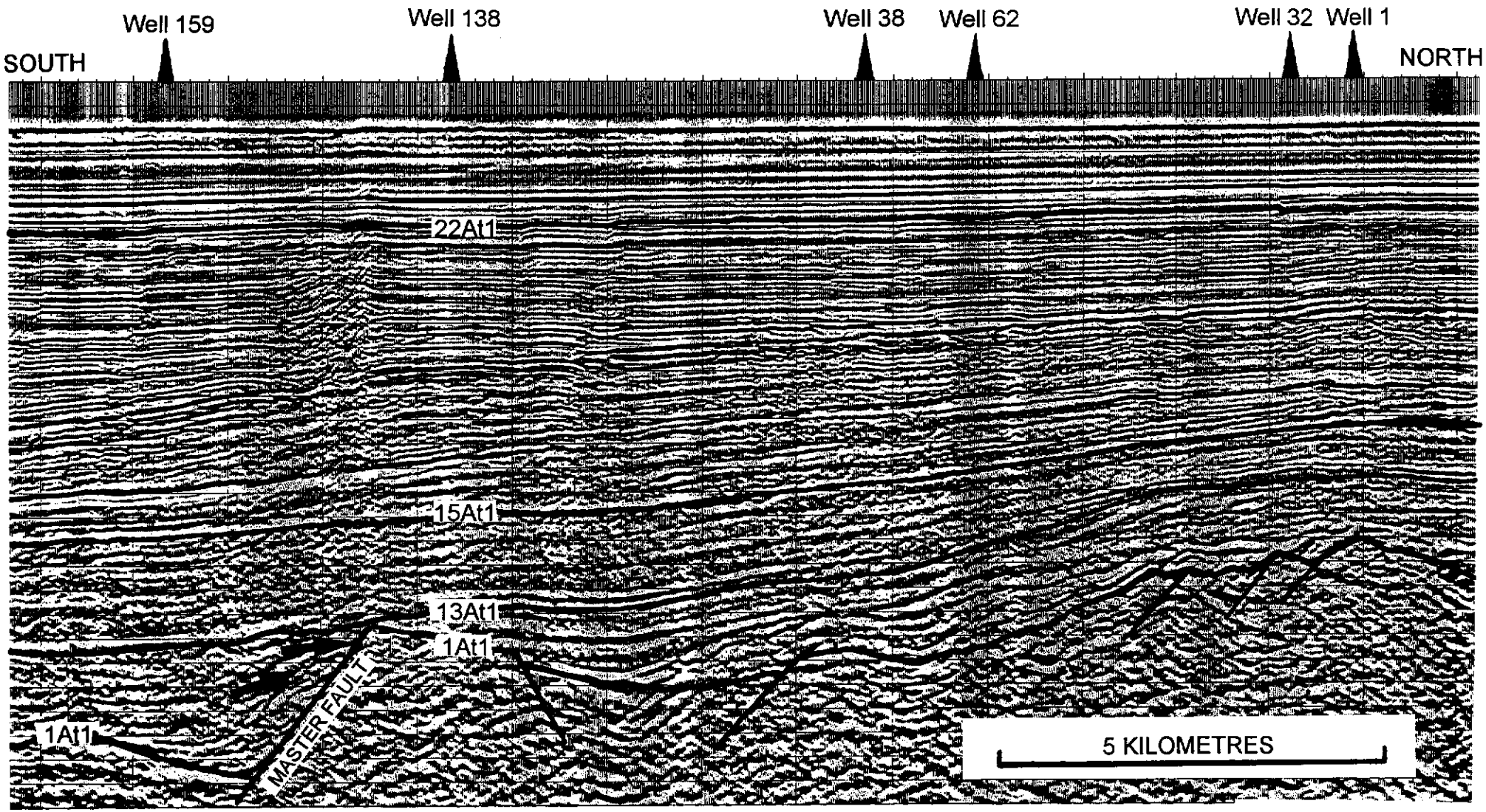

Figure 9.23b: Part of seismic line across the southern master fault through which hydrocarbons could migrate from pre13A sediments into pre1A sandstones on the uptilted fault blocks and thence to the north flank.

CHAPTER 10: HYDROCARBON FRACTIONS AND BULK PROPERTIES

Bulk quantities of solvent extractable bitumen and oils have been determined on several hundred samples throughout the basin. This organic matter is subdivided into two major groups: non-hydrocarbons (resins and asphaltenes) and hydrocarbons (saturates and aromatics). Since the beginnings of petroleum geochemical studies (Bray and Evans, 1965; Martin et al., 1963; Philippi, 1956; 1965), solvent extracts and fractionation analyses have become routine and the proportions of these components have been related to thermal maturity, migration effects or to the organic matter type. Indeed, many of the early interpretation methods based on these bulk data such as total extracted organic matter/TOC, saturates/aromatics (Hunt, 1979a, p.136-142) are still routinely used.

The saturated and aromatic fractions are routinely analysed by high resolution GC. This is done to provide a first view of the composition of the oil or bitumen and to determine if any group of those components amenable to interpretation are present. These data are routinely interpreted in terms of their maturity and organic matter type. For source rock samples, they are used to seek signs of hydrocarbon expulsion whilst evidence for in-reservoir evaporation can be seen in oil gas chromatograms. Saturates GC data are available for 297 shales and 237 oils and aromatic GC data for 160 shales and 142 oils. Of these, 64 samples have been selected from source rock and reservoired hydrocarbons in the Bredasdorp Basin for detailed study of GC and GC-MS data. Analyses of several samples were repeated. These samples include examples of each source rock and a range of reservoired hydrocarbons.

10.1. RESULTS

Data acquired from liquid column and gas chromatography are tabulated in Appendix F, Tables F.02, F.05 and F.14) and plotted in Appendix D, Figs. D.01-D.68.

10.2. INTERPRETATION

Data acquired from these analyses can be subdivided into three groups depending on which fraction they represent, bulk parameters, saturated hydrocarbons, aromatic hydrocarbons, and saturated and aromatic biomarkers which are found in the highest molecular weight fraction investigated.

10.2.1. Bulk parameters

Ratios of bulk and GC parameters determined during hydrocarbon fractionation procedures are plotted against vitrinite reflectance for the samples studied in detail for

this report (Appendix F, Table F.01), and against palaeotemperature for the common Bredasdorp Basin dataset (3315 values). Vitrinite reflectance data are not available for all Bredasdorp Basin samples, but the palaeotemperature value is calculated from other chemical and optical maturity parameters (Table 4.05) and closely approximates vitrinite reflectances (Fig. 10.01).

Total solvent-extracted organic material (EOM) is likely to be present in very small quantities in immature samples because there are few detrital hydrocarbons, but it increases rapidly as generation from kerogen starts in the early oil window. Some low maturity samples are characterised by large amounts of EOM, due to contributions by plant waxes and non-hydrocarbon material (e.g. samples from well 25 in Fig. 10.02a), so high EOM values are not exclusively found in high maturity samples.

Most source rock intersections in the basin have been sampled only once for this analysis. However, the 13A source rock, because of its thickness, richness and great areal extent, was sampled in considerably more detail. Many of these samples are located at either the edge or the centre of thick (>30m) oil-prone source shales. The kerogen in the samples is of comparable WG-OIL and OIL prone quality, as determined from chemical and optical data and from environmental assessments of micropalaeontological and palynological interpretations. Their total EOM values are reported here (Fig. 10.02a). The figure shows that samples from the upper and lower edges of source rocks record significantly less extractable organic matter than equivalent samples from the centre, indicating that material is missing from the edge samples. A few samples have unusually low proportions of EOM which are believed to result from the dilution effects of mud contaminating the samples.

Expulsion is thought to follow the route shown by Pepper (1991), namely build-up of generated products in droplets until they coalesce and form stringers, eventually reaching the edge of the shale and initiating primary migration. This continues until most of the free oil has escaped and the oil stringers break up into droplets again. Where in the oil window, the 'edge' samples contain minimum amounts of EOM (1500~2000 ppm) whilst the centre samples range from 3000-5000 ppm (Fig. 10.02a). Regression lines through the data from samples in the oil window show the likely trends for centre and edge samples. The trend lines have been drawn through the very sparse data above R_o~0.8% towards the top of the oil window. It is possible that the higher amount is the minimum amount needed to initiate expulsion (i.e. droplet coalescence) whilst the lower amount is the amount remaining when the oil droplets are no longer in contact and flow stops. The amount of 4000 ppm represents a pore oil saturation of 30-40% at mid-oil window with a probable porosity 10% and bound water occlusion of 20%, at the lower end of the range suggested by Ejedawe (1986). This is

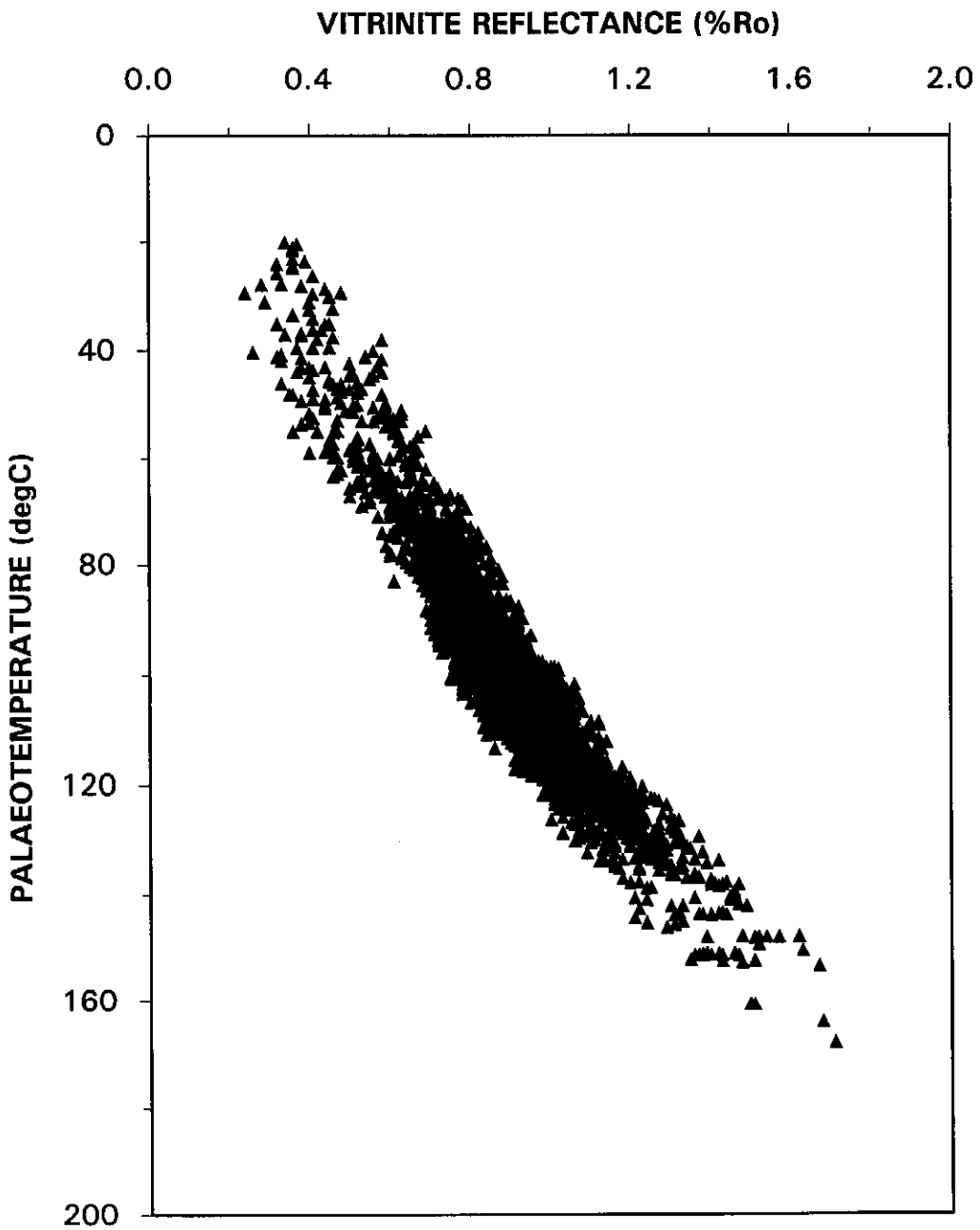

Figure 10.01: Plot of vitrinite reflectance vs calculated palaeotemperature from all shale samples in Bredasdorp Basin wells.

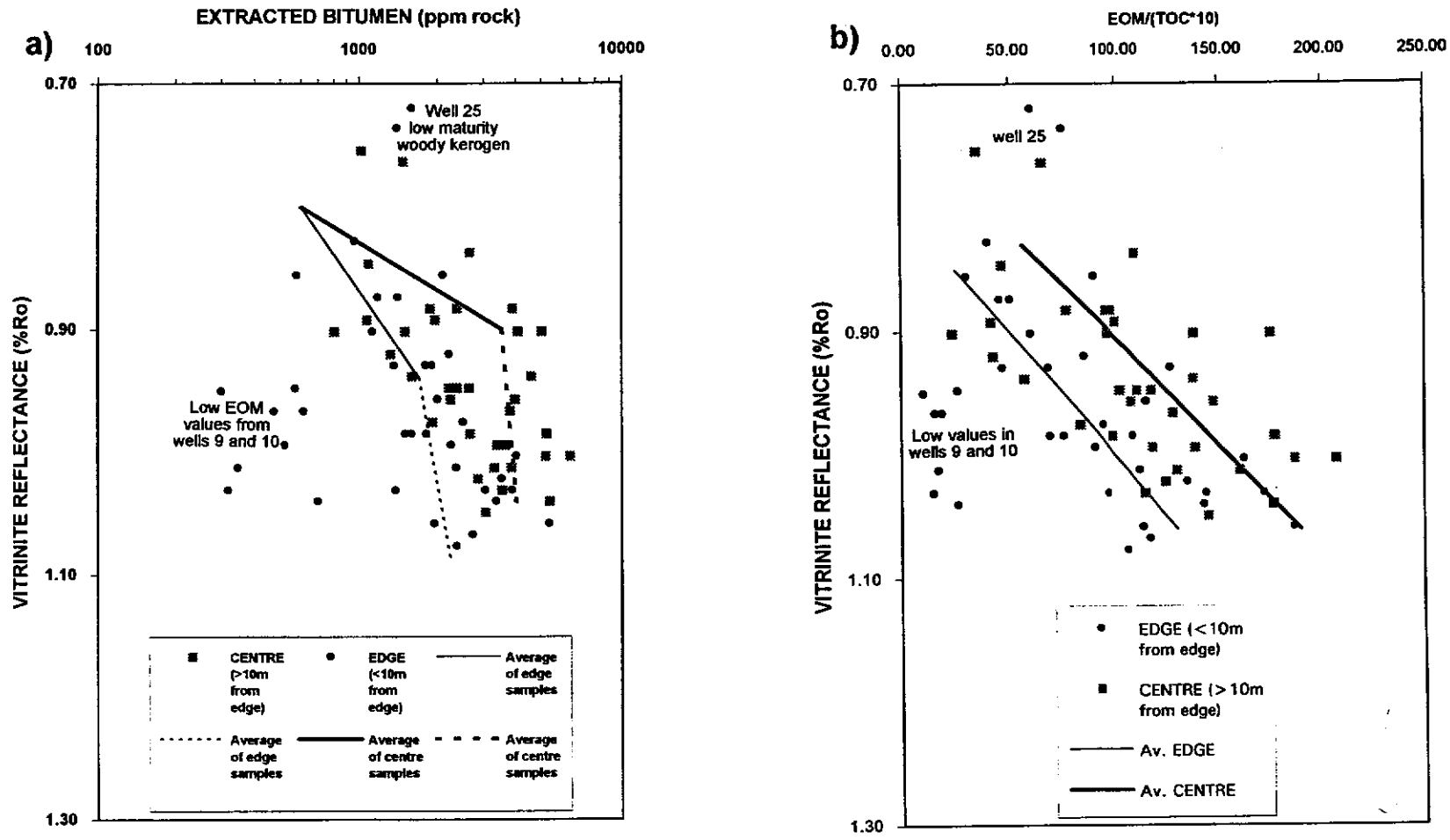

Figures 10.02a and b: Plots of (a) extracted organic matter (EOM) and (b) EOM/TOC vs. vitrinite reflectance for 'centre and edge' samples of 13A source rock showing differences between expelled and unexpelled amounts of oil.

probably an acceptable limit as the source rocks he considered were coaly and highly adsorbant, whilst those in the Bredasdorp Basin are amorphous with a lower adsorbancy. The implication is that expulsion could occur in pulses of ~2000 ppm of oil at a time. The total potential of these shales is up to 12 kg oil/tonne rock (Davies, 1988b), so this implies that several expulsion pulses are needed to deplete the source rock (Welte, 1987).

Although total EOM is a measure of the quantity of oil generated and preserved in the sample it is not a particularly useful assessment of the richness of the source unless normalised to the TOC. This is done in Fig. 10.02b for the same sample population. The regression lines show the likely trends of the centre and edge samples. EOM/TOC values worldwide (Tissot and Welte, 1984, p.176-183) increase rapidly after entry into the oil window, reaching a peak at a few hundred mg/gm TOC, thereafter decreasing rapidly. Data from the centre and edge 13A samples (Fig. 10.02a and b) and from the samples studied by GC-MS in this report (Fig. 10.02c) do not show this decrease but rather remain high. This continued increase may be a function of a lack of expulsion from the more deeply buried samples, which are from lower permeability rocks. EOM/TOC ratios are plotted for all shale samples investigated in the Bredasdorp Basin (Fig. 10.02d) and the envelope describes a sharp decrease below ~120°C ($\equiv R_o$~1.15%) in the same way as the envelopes do in Tissot and Welte (1984, p.180-183). This indicates that the main oil generation window was reached at ~115°C and little oil was generated at palaeotemperatures in excess of 140°C.

The one data point in Fig. 10.02a which does not locate in the envelope is from sample 49 (low maturity Turonian WG prone). The unusually high EOM/TOC ratio relative to its low maturity (R_o=0.58%) is probably not due to impregnation, as the carbon preference index (CPI) at 1.48 is still considerably higher than the other samples. An impregnation would have a lower, more mature CPI and would reduce the total CPI so that it did not match the reflectance (section 10.1.2.2.). The more likely alternative is that the high EOM/TOC ratio is due to quantities of detrital waxes, probably from terrigenous components. The sample is indeed dominated by structured and exinitic organic matter (Appendix F, Table F.01), which is often enriched in waxes.

Other ratios which can provide useful data for estimation of maturity and potentially for correlation of oils with source rocks are the ratios of saturates/aromatics and hydrocarbons/nonhydrocarbons respectively. Plots of the saturates/aromatics ratios are shown in Fig. 10.03. It includes all Bredasdorp Basin shale samples (10.03a), all GC-MS sample shales (10.03b), all Bredasdorp Basin oil/condensate samples (10.03c) and for the centre:edge group of samples (10.03d). The ratios gradually increase through the oil window and into the gas window (Figs. 10.03a and 10.03b) as kerogen

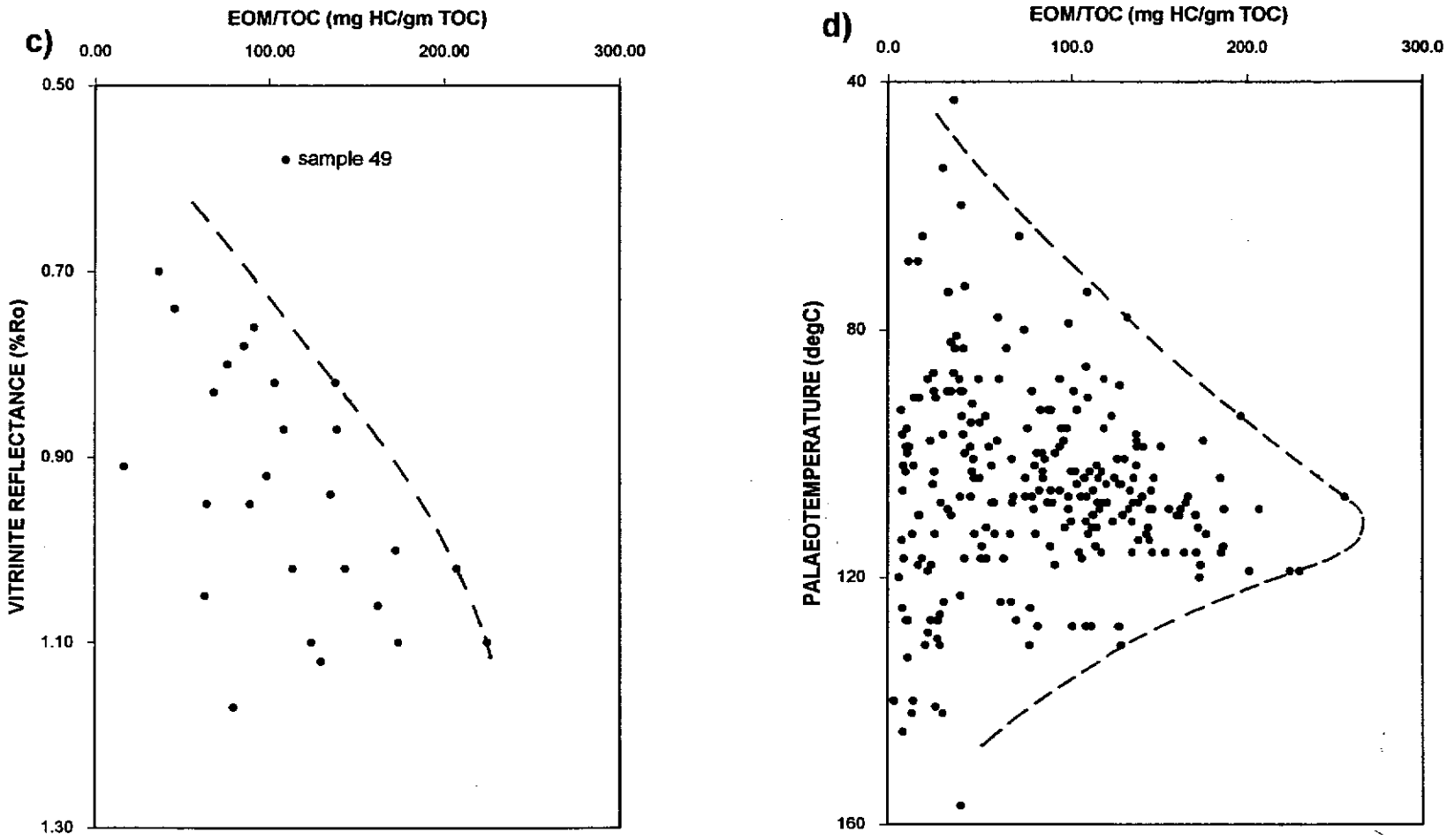

Figures 10.02c and d: Plots of EOM/TOC vs. (c) vitrinite reflectance for GC-MS studied shale samples and (d) palaeotemperature for all Bredasdorp Basin shale samples.

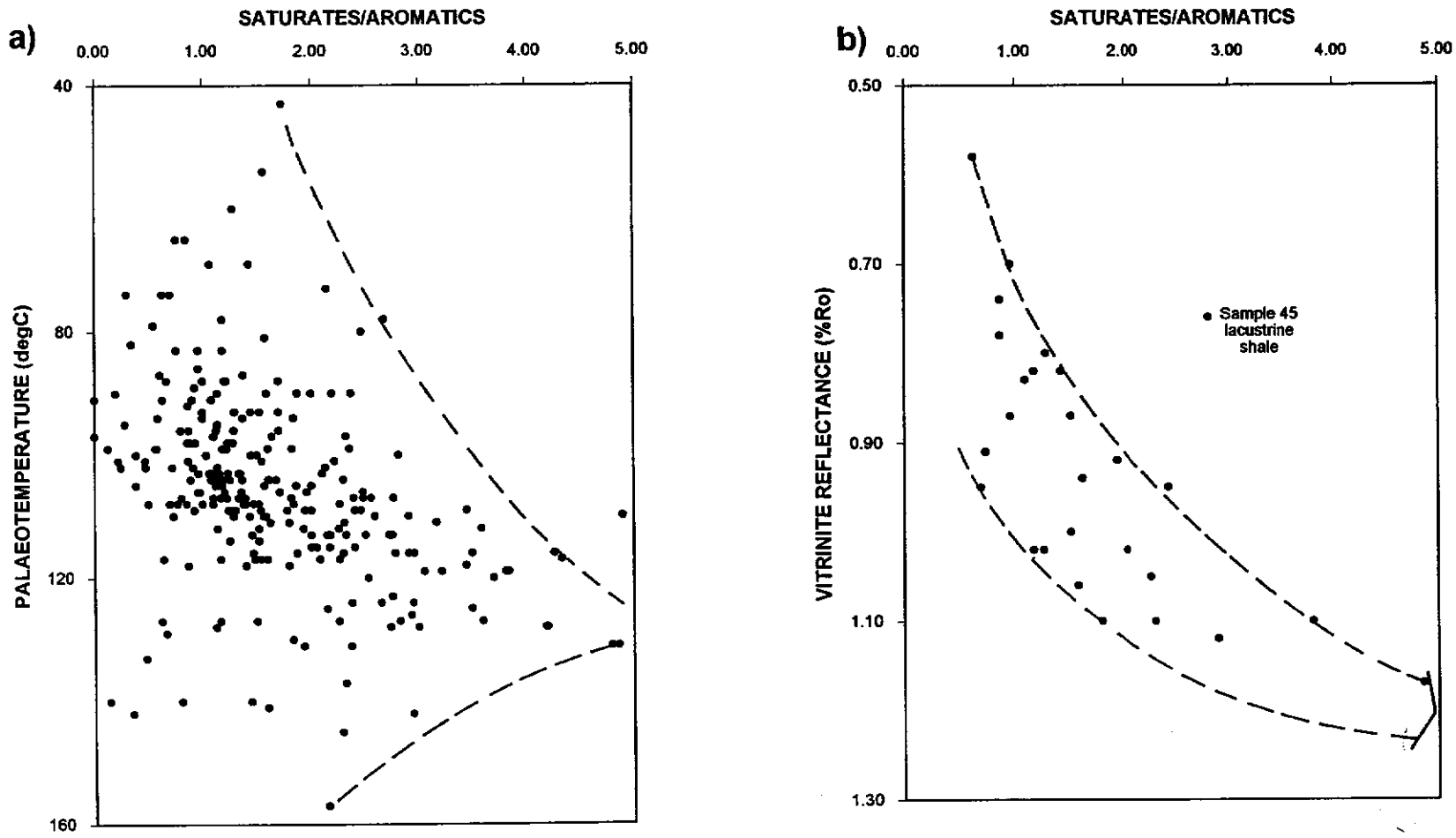

Figures 10.03a and b: Plots of the saturates/aromatics ratios vs. (a) palaeotemperature for all Bredasdorp Basin shale samples, (b) vitrinite reflectance for the GC-MS studied shale samples.

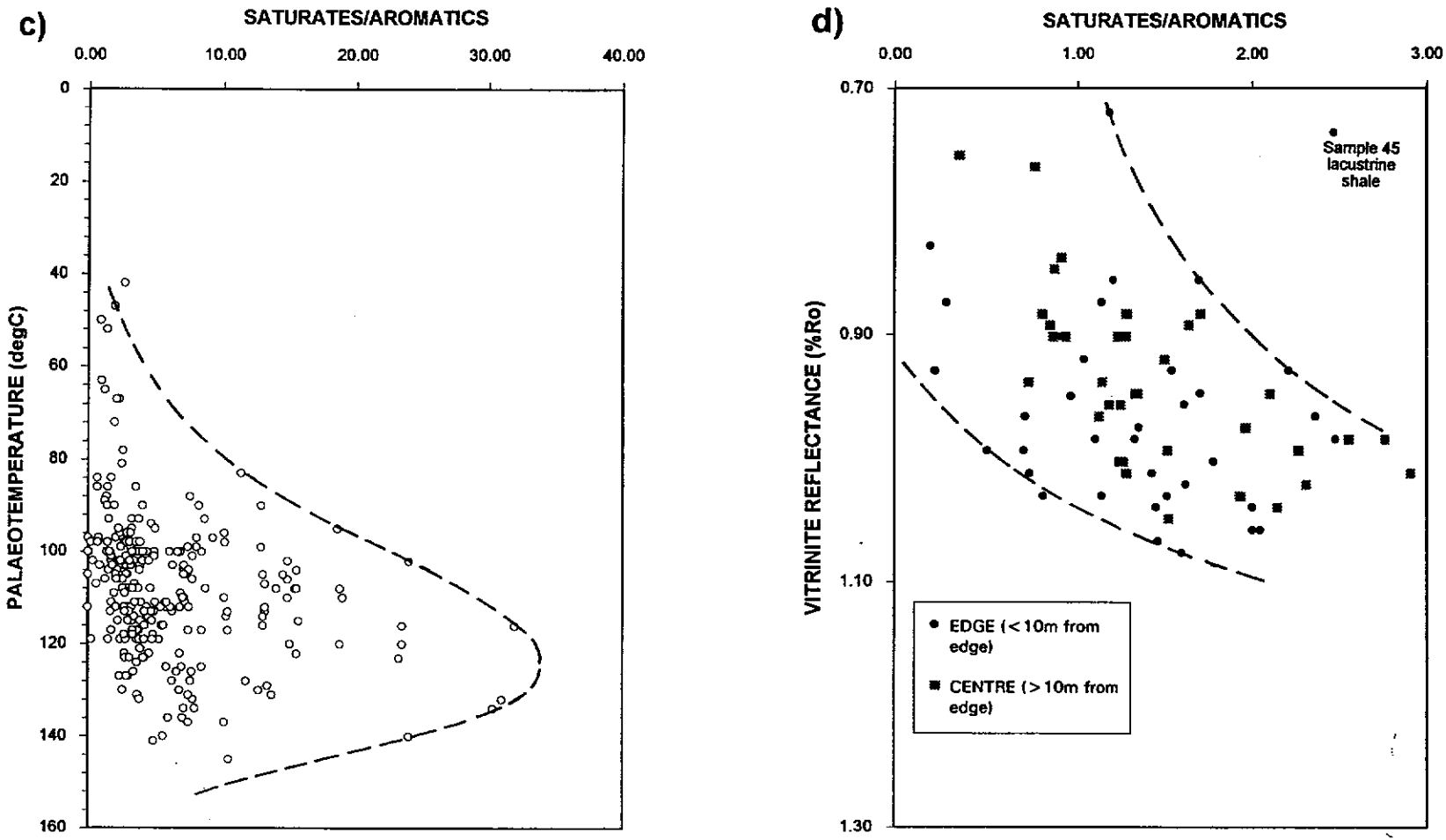

Figures 10.03c and d: Plots of saturates/aromatics ratio vs (c) formation palaeotemperature for all Bredasdorp Basin oil samples and (d) vitrinite reflectance for all 'centre and edge' shale samples.

breaks down. Beyond ~120°C, condensed saturated molecules are cracked to smaller components, some of which are lost during the extraction processing technique. The extract becomes dominated by aromatic molecules as resins and asphaltenes start to be cracked generating soluble residual bitumen with a more aromatic structure (Figs. 10.03a and 10.03c). Eventually cracking affects even those molecules resulting in the sharp cut-off at ~140°C in Figs. 10.03a and 10.03c.

As expected, there is a slight saturates depletion relative to aromatics in the edge samples (Fig. 10.03d) due to the latter's easier mobility, molecular shape and different polarity. Hunt (1979a, p.502) shows that the saturates/aromatics ratio can be used to assess geochromatography during migration from source into reservoir rock.

The proportions of hydrocarbons relative to non-hydrocarbons (Figs. 10.04a-d) mimic the saturates/aromatics ratios by increasing into and through the oil window due to the progressive and continued conversion of kerogen and the heavy fraction of oil and bitumen into light non-polar components (Tissot and Welte, 1984, p.187). Scattered outliers in Figs. 10.04a and 10.04b may indicate impregnation by migrating oil. The envelope shapes match those of the saturates/aromatics ratio suggesting a common origin. In the plot of the centre:edge samples (Fig. 10.04d) the centre samples have, on average, higher proportions of hydrocarbons than the edge samples although the difference is slight. This indicates that expulsion was by bulk movement rather than diffusion or capillary attraction which favours hydrocarbons over non-hydrocarbons.

10.2.1.1. Stable ^{13}carbon isotopes

The distribution of carbon isotopes in organic material and in maturation products depends on the original isotopic composition of the material, isotopic fractionation resulting from thermal stress and fractionation during migration. The last of these is of little importance for this study since migration fractionation has been shown not to significantly alter the isotopic ratios of affected hydrocarbon gases (Fuex, 1980; Schoell, 1983a and b). Diffusion, however, is thought to result in small changes in the isotopic ratio of at least methane and ethane (Prinzhoffer and Huc, 1995). No isotopic analyses have been carried out on gas samples from this basin.

It has been shown that the isotopic signature of terrigenous organic material is generally depleted in ^{13}C compared to that from marine organisms (Stahl, 1974). This difference ranges from 5-10‰ (i.e. 5-10 parts per thousand more ^{13}C isotope than the PDB standard - hence called isotopically heavy) and reflects the different source of carbon in photosynthesis, as terrigenous plants use atmospheric carbon dioxide whilst marine plants use carbonate complexes (Tissot and Welte, 1984, p.89). Since plants are food sources for organisms in both environments, the isotopic proportions in much

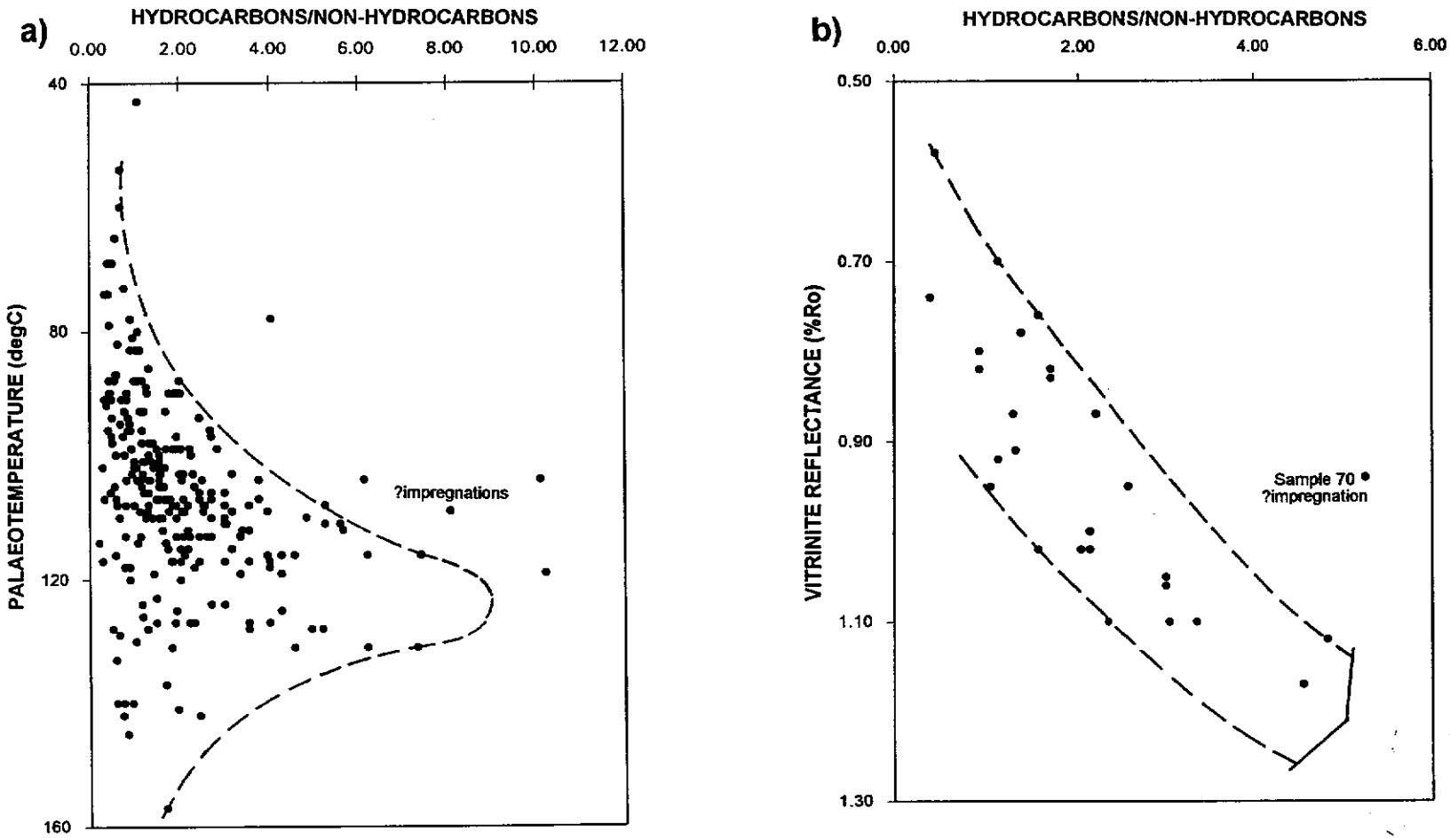

Figures 10.04a and b: Plots of the hydrocarbon/non-hydrocarbon ratios vs. (a) all Bredasdorp Basin shale samples, (b) vitrinite reflectance for the GC-MS studied shale samples.

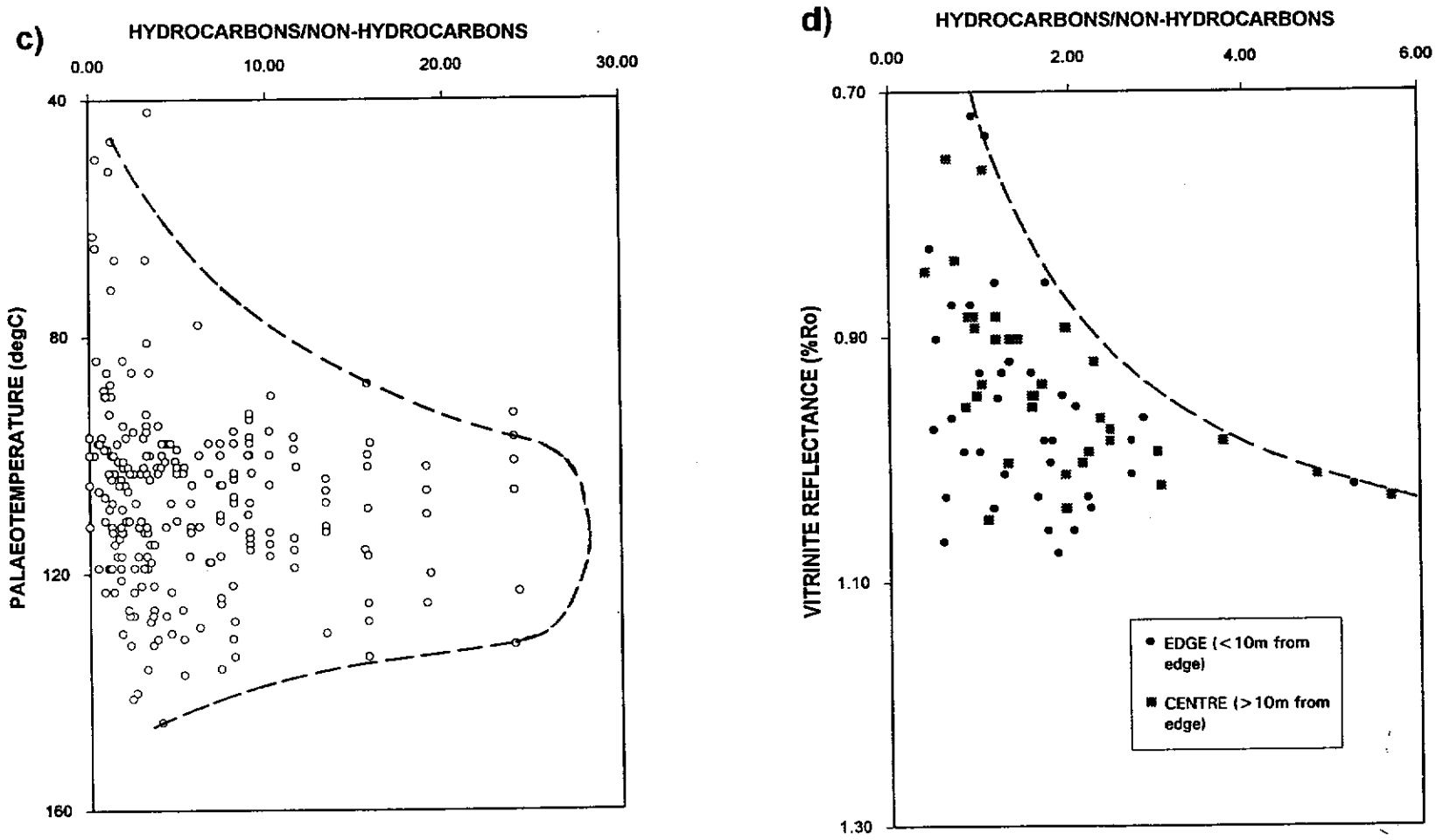

Figures 10.04c and d: Plots of hydrocarbon/non0-hydrocarbon ratios vs (c) formation palaeotemperature for all Bredasdorp Basin oil samples and (d) vitrinite reflectance for the 'centre and edge' shale samples.

of the food chain will reflect this difference. The overall range of ^{13}carbon isotopic proportions in living organisms ranges from ~-30 to -5‰. During diagenesis and maturation, the isotopic composition of bitumen is generally slightly depleted in ^{13}carbon compared to the original kerogen, although the isotopically heavier bonds are barely affected. Hence in petroleums the ^{13}carbon proportion is not only slightly isotopically lighter but the range is significantly narrower (~-38 to -22‰, Fuex, 1977). During maturation, methane generation results in a progressive enrichment of the ^{13}carbon proportion of kerogen and oil and the resulting bitumen is isotopically heavier. In general, maturation through the oil window could be expected to result in a shift of the ^{13}carbon signature by 1-2‰. A number of oil and condensate samples have been analysed for their isotopic composition although in many cases this amounts to determination of the whole oil signature only. Results of the analyses are shown in Appendix F, Table F.25 and plotted in Figs. 10.05a and 10.05b.

For some of the samples that were analysed, only the urea non-adduct fraction was available, hence the results are not directly comparable. However, analyses of n-alkanes and branched alkanes show consistent trends, but are offset by 1-2‰ heavier isotope fractions (Stahl, 1980; Bjorøy et al., 1991). Urea non-adduct fractions (i.e. the cyclo/branched alkane fraction from which the n-alkanes have been removed by trapping in the interstices of the freshly grown urea crystals) were used for the analyses of Family 1 samples (Fig. 10.05b) and if they are relocated by 1-2‰ lighter, they reinforce the maturation trend evident from the Family 1 south samples. GC analysis of the isotopically lightest Family 3 sample, well 62 DST1, shows a high molecular weight 'hump' which could signify the presence of residual oil. This reservoir is upflank of the north flank migration route through which Family 1 oil could migrate into the north flank wells (Fig. 9.20b), so the unusually light signature of the produced oil may reflect admixture of some Family 1 oil.

It is evident that there are too few data to provide any substantive interpretation. The small differences between the hydrocarbons of Families 1, 2 and 3 are barely more than 0.5‰ (Fig. 10.05a). There is a much larger, and more significant difference (>1‰) between the Family 4 signature compared to that of Families 1-3 (Fig. 10.05b).

10.2.2. Normal alkanes

Odd-numbered long-chain paraffin waxes and fatty acids enter the source as part of the detrital organic material (Bray and Evans, 1961; Martin et al., 1963; Hunt, 1979a, Tissot and Welte, 1984, p. 100-109) but are later diagenetically altered by defunctionalisation to long-chain alkanes. Shimoyama and Johns (1972) suggest that this could involve loss of 2 carbon atoms by either reduction in a strongly reducing environment or beta

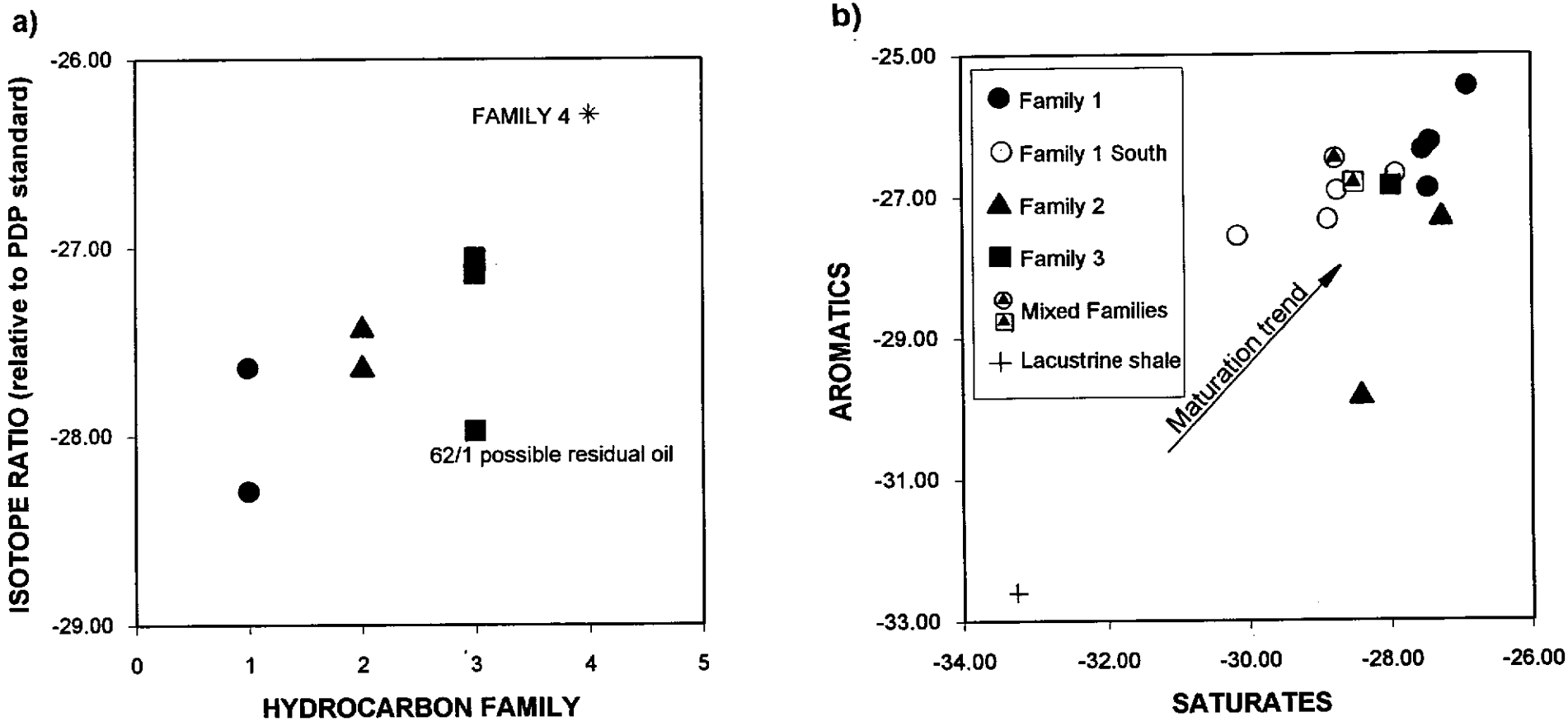

Figures 10.05a and b: Plots of stable ^{13}carbon isotope ratios for samples in the Bredasdorp Basin.

cleavage in a strongly calcareous environment resulting in dominance of even-numbered alkanes and dominance of phytane over pristane (section 10.2.3). Alternatively, loss of one carbon atom could be caused by decarboxylation of fatty acids in the presence of montmorillonite in dysoxic environments resulting in dominance of odd-numbered alkanes and of pristane over phytane.

The implication is that an even-numbered carbon dominance could indicate either calcareous or evaporitic conditions as well as strongly reducing environments, whilst an odd-numbered dominance indicates mildly reducing or dysoxic conditions (Hunt, 1979a, p.90-98; Tissot and Welte, 1984, p.100-110).

10.2.2.1 Environmental indicators

An early summary of alkane chain lengths characteristic of certain types of organic matter by Hunt (1979a) showed carbon number dominances as follows:

(i) C27-44 in animal tissue

(ii) C25-33 in terrigenous plants (lowest in aqueous plants)

(iii) C17-27 in grasses

(iv) C17-21 in bacteria

(v) C15-21 in marine plants.

More recent summaries (Tissot and Welte, 1984; Peters and Moldowan, 1993) both confirm the carbon number dominances and extend it to include biological marker compounds. Few of the Bredasdorp Basin samples show dominance of a particular group of alkane chain lengths other than where maturity is low (e.g. samples 49, 50, 52 and 59, Fig. 10.06a) and where mainly marine material is present. This is partly because the chain length ranges have been influenced by advanced maturity effects (e.g. sample 54, Fig. 10.06b) but mostly because the depositional environment of all drift sequence sources are so similar that differences could not be expected. The major exception to this is the lacustrine sample, no. 45.

The n-alkane envelope of the lacustrine sample is unusual in that the n-alkanes heavier than C25 are present in sharply reduced proportions (Fig. 10.06c). In addition, there is a strongly developed odd-predominance in the C21-25 range but none in the >C25 range. One possible explanation for this is that the bitumen contains some high maturity light oil impregnation (although the reservoir is now water-wet and there are no hydrocarbon shows). If this were so, then the formation of the unusual n-alkane envelope still requires mixture with a bitumen in which the envelope rapidly tails off after ~C20. It has been suggested that some lacustrine sourced oils, in particular those

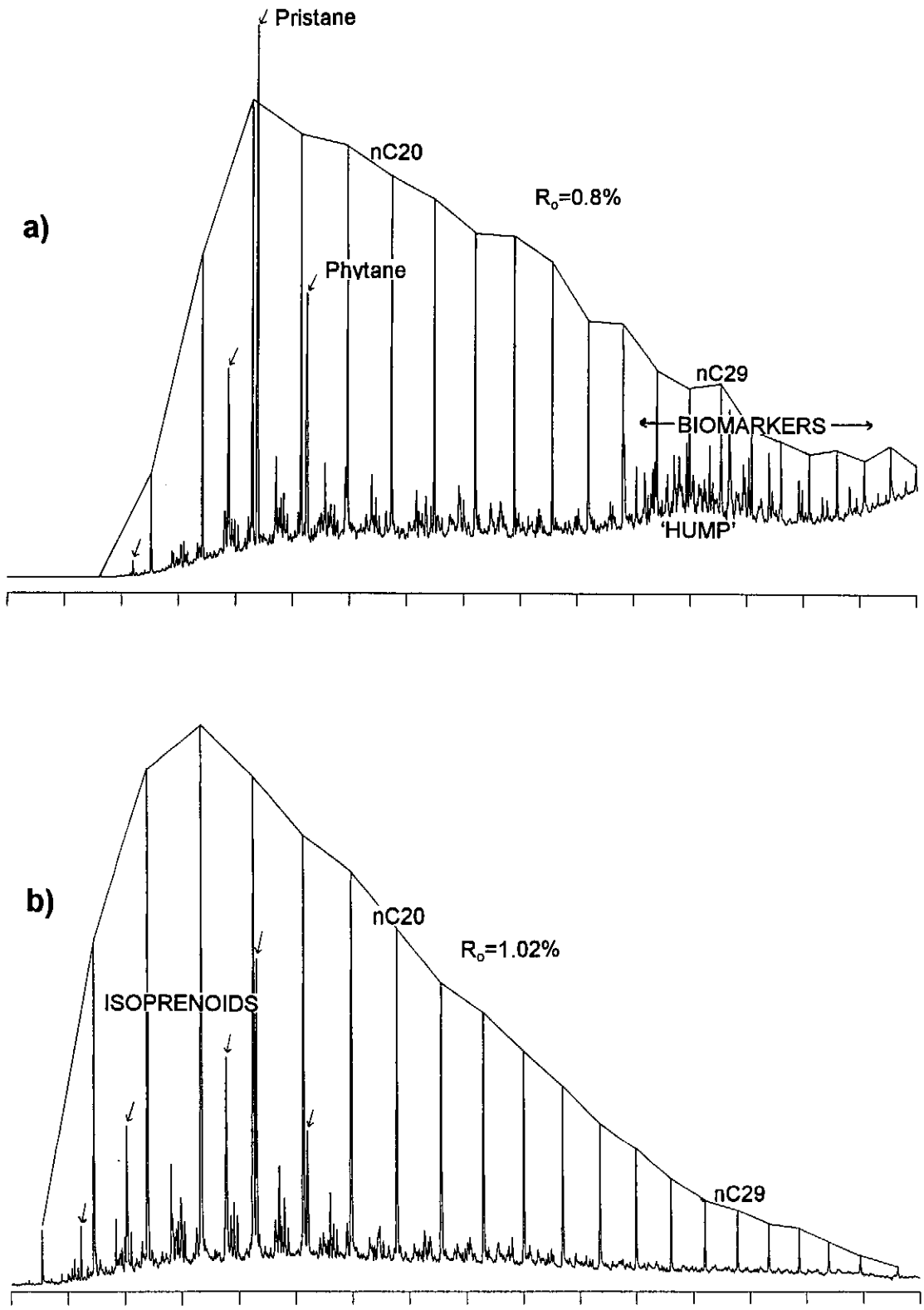

Figures 10.06a and b: Gas chromatograms of (a) low maturity GC-MS shale sample no. 50 and (b) high maturity GC-MS shale sample no. 54.

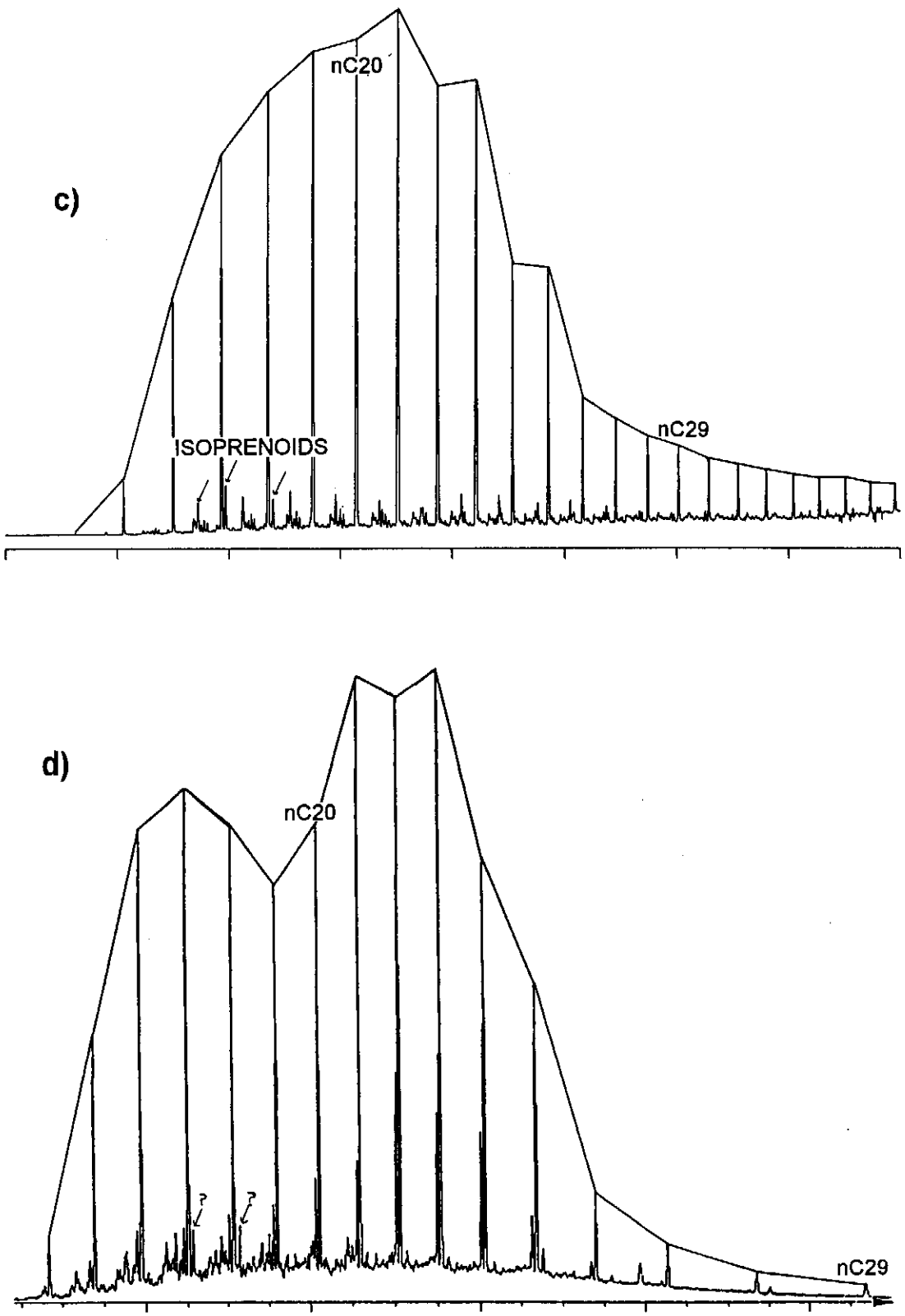

Figures 10.06c and d: Gas chromatograms of (c) moderate maturity GC-MS shale sample no. 45 and (d) pyrolysed immature *Chlorella marina* alga from Derenne et al., 1996.

sourced from *Gloecapsomorpha prisca* (Derenne et al., 1991), have a similar unusual envelope, implying that this lacustrine source might contain some of that organic material. However, they also showed that *G. prisca* sourced saturates were rich in cycloalkanes which this bitumen is not, only small amounts of naphthenic biomarkers having been recorded.

Alternatively, the unusual n-alkane envelope and near absence of regular isoprenoids may be a result of algal sourcing. A GC of laboratory-pyrolysed marine green algae, *Chlorella*, (Fig. 10.06d) bears some similarity (Derenne, et al., 1996). A palynological study of shales in well 89 (sample 45) showed a dominance of lacustrine fauna including botryococcus and near-amorphous organic matter, i.e. an amorphous groundmass but with sharp-edged structured fragments of ?woody material (J.M. Benson, 1993, pers. comm.). The texture of this near-amorphous material is similar to that found in the estuarine Portlandian Colchester member intersected in wells in the onshore Algoa Basin (Davies et al., 1991). In further support of the locally marine nature of the organic matter, there are occasional grains of glauconite in intercalated sandstones. Few of the claystones and siltstones show evidence of the red or green coloration characteristic of sediment deposition under aerobic conditions. Hence the input of the marine alga *Chlorella* into a dominantly lacustrine environment is possible. *Botryococcus* algae can also live in saline water - possibly even in hypersaline conditions (Derenne et al., 1991) so its presence in sediments with marine algae is possible.

10.2.2.2 Maturity

One of the first uses of GC data was in the assessment of thermal maturity of organic matter. Saturated hydrocarbons in bitumens extracted from shales and oils, show smooth normal alkane profiles where thermal maturity is high, but uneven profiles where maturity is low (Figs. 10.06a and 10.06b). This unevenness is a result of dominance of (mainly) odd-numbered normal (and occasionally even-numbered) alkanes (Hunt, 1979a, p.493).

Hunt (1979a, p.302-307) points out that as thermal maturity increases through the early oil window (R_o 0.5-0.7%≡palaeotemperatures 60-80°C), random cracking of kerogen forms large quantities of evenly distributed amounts of odd and even-numbered alkanes. These progressively mask any odd or even predominance in source rocks (cf. Figs. 10.06a and 10.06b). In oil samples, this change is also evident, although less so because many samples represent flowed oils reservoired at shallower levels than prevailed during generation (cf. Figs. 10.07a and 10.07b). Additionally, there are some moderately mature oil samples (cf. Fig. 10.07b, 80-100°C) in which strong carbon-number preference may result from solubilization of low maturity residual oils. Odd-

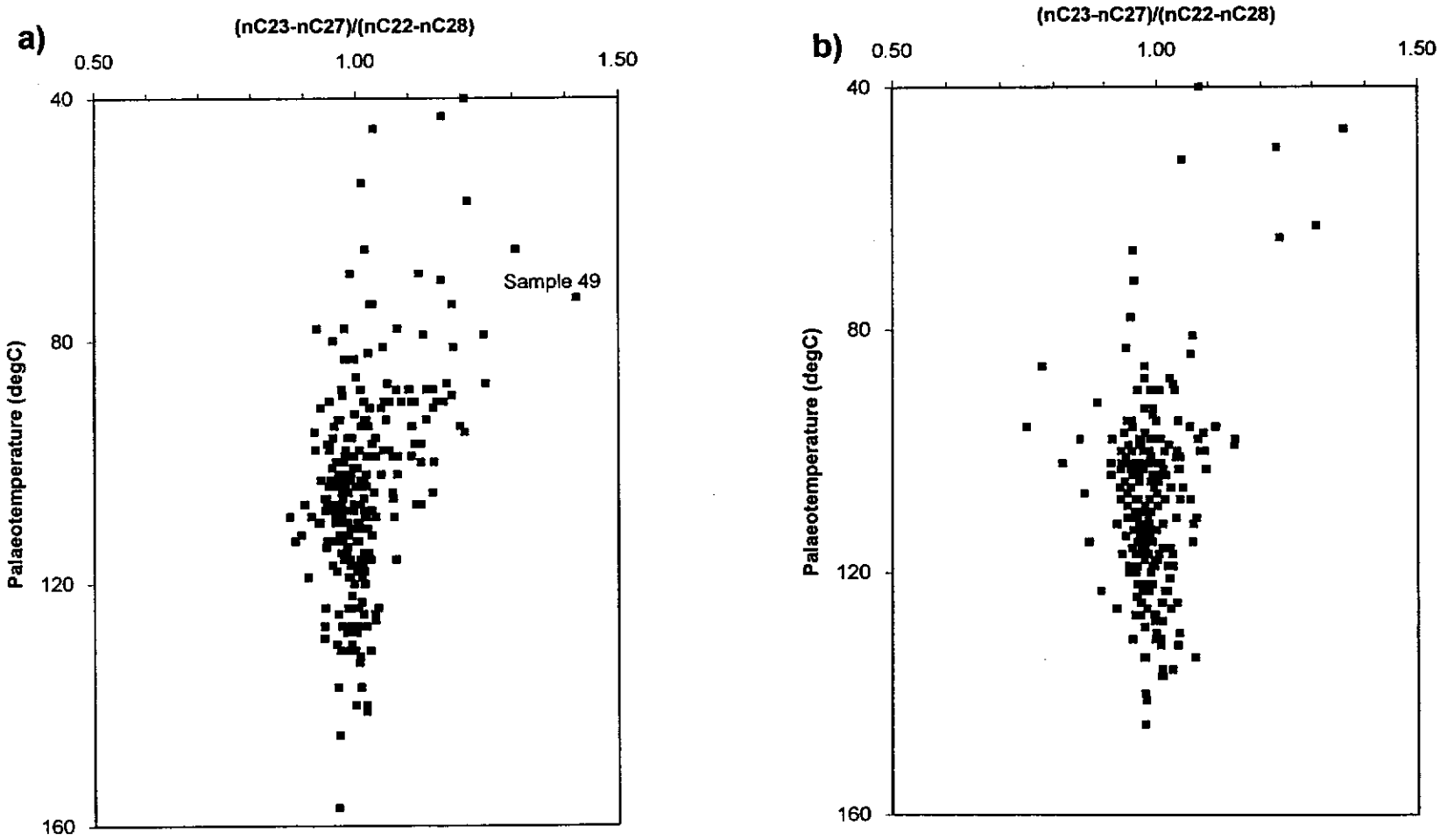

Figures 10.07a and b: Plots of nC23-27 carbon preference index vs. palaeotemperature for all Bredasdorp Basin (a) shale samples and (b) oil samples.

numbered alkanes dominate low maturity Bredasdorp Basin shale samples (Fig. 10.07a), whereas some of the oils (Fig. 10.07b) display an even predominance. This might indicate that the source rocks for these oils have not been sampled so far. In addition to this maturation effect, the generation of more and more low molecular weight alkanes results in the normal alkane envelope of the bitumen becoming skewed towards the lower molecular weight end (Figs. 10.06a and 10.06b).

The effect of different organic matter types is strongly marked by the dominance of particular ranges of alkane carbon number preferences in low maturity kerogen. As maturity increases, these differences are lost by continued generation of progressively lighter compounds so that eventually all oils have the same carbon number distribution as marine plants, i.e. dominated by C15-21 alkanes.

10.2.2.3 In-reservoir evaporation

Losses of low molecular weight hydrocarbons from oils as they evaporate in-reservoir (losing hydrocarbons at rates proportional to their volatility), form residual oils. The effects of these losses are evident on chromatograms and this information is used to help understand migration. For example, the chromatogram of sample 24 from well 75 (Appendix D, Fig. D.24) shows an n-alkane envelope typical of a residual oil peaking at ~C20 and with very small amounts of lighter hydrocarbons. Hence residual oil traces can be recognised by light-end depletion of the normal alkane profile, although not always as the lighter molecules can be replaced through later migration. All oil samples in the detailed dataset with evidence of oil escape are listed in Table 10.01a.

10.2.2.4. Expulsion

Losses of low molecular weight hydrocarbons from mature source rock samples can result from faulty processing. In these samples, the processing has been shown to adequately sample the lighter hydrocarbons. Where it is certain that the processing was carried out properly, alkane depletion is explained as expulsion. Such interpretations have been made of all source rocks studied in depth (Table 10.01b). Leythauser et al. (1983) show that effects attributable to expulsion are most evident in samples from the edges of thick shales and the centres of thin shales, whilst samples from the centre of the thick shales barely record the effect. Studies of bitumen extracts from oil-mature, oil-prone 13A source rock samples (Fig. 4.39) show that n-alkane maxima differ by 3-5 carbon numbers between those samples which have expelled and those which have not and the quantities of extractable bitumen differ by ~2.0 kg/tonne rock (Davies, 1988b; 1997a).

a)

OILS APPEARING TO BE RESIDUAL

SAMPLE	WELL	DEPTH	R_o	n-alkane peak
7	92	2949m	0.99%	nC19-20
8	118	2563.1m	0.85%	nC19
11	91	3220.05m	1.15%	nC20-21
12	104	3017.46m	1.08%	nC20
18	122	2517m	0.93%	nC19
22	16	2614m	0.95%	nC18-21
27	13	2518.86m	0.88%	nC21-22
33	166	2510.43m	0.85%	nC20
38	167	2681.65m	1.00%	nC20
SAMPLES WHICH CONTAIN RESIDUAL OIL				
17	126	2643m	1.04%	cond.
21	48	2620m	1.02%	nC20
24	75	2830.5m	1.05%	nC20
28	103	2718m	1.23%	cond.
	31	2753m	0.97%	cond.
	95	2703m	1.17%	cond.

b)

SHALE SAMPLES WITH EVIDENCE OF EXPULSION

SAMPLE	WELL	DEPTH	R_o	n-alkane peak	EOM
43	83	2792m	0.91%	nC20	345 ppm
61	11	2682m	1.12%	nC19-20	3280 ppm
63	42	3021m	1.10%	nC19	4200 pm
66	65	3160m	1.17%	nC20-21	930 ppm
68	67	2651m	0.95%	nC21-23	1300 ppm
SAMPLES WITH POSSIBLE OIL EXPULSION					
45	89	2660m	0.76%	nC21	1032 ppm
49	99	1820m	0.58%	nC22	1500 ppm
52	130	2331m	0.74%	nC19-21	1086 ppm
69	12	2057m	0.70%	nC22-23	851 ppm

Table 10.01a and b: Bredasdorp Basin samples of (a) oil samples which appear residual and (b) shale showing signs of oil expulsion.

10.2.2.5 Degradation

Another route by which n-alkanes can be lost from oils is through bacterial degradation. This process was described in detail in Chapter 9. None of the samples from the Bredasdorp Basin shows the characteristic results of loss of low-medium molecular weight alkanes relative to isoprenoids or of paraffins relative to aromatics. Connan (1984) showed that even where bacteria had passed through a reservoir, their activity was severely reduced where temperatures exceeded 60°C and especially where it was >80°C. Thus the lack of evidence for bacterial degradation in sandstones which have demonstrably suffered meteoric flushing during recent burial, may be because all the hydrocarbons found to date are reservoired at temperatures in excess of 80°C. Alternatively some of the oils could have been degraded when shallowly buried, but received a later input of non-degraded hydrocarbons which masks the effect of the bacteria. This can be confirmed by increased proportions of demethylated hopanes.

10.2.3. Isoprenoids

The second commonly studied group of alkanes are the regular isoprenoids, in particular phytane and pristane (arrowed on Fig. 10.06). These are derived from the phytol sidechain of chlorophyll either by hydrogenation in reducing environments, resulting in the formation of phytane, or oxidation in dysoxic/oxic environments, forming pristane and lower molecular weight equivalents (Brooks et al., 1969; Maxwell et al., 1973). Ratios of certain isoprenoids relative to adjacent normal alkanes can be related to thermal maturity. Early dominance of pristane and phytane is attributed to (a) common preservation of detrital pristane and (b) early defunctionalisation of phytanic acids and alcohols prior to generation of most n-alkanes (Brooks et al., 1969; Powell and McKirdy, 1973a; 1973b). This early low maturity dominance of isoprenoids quickly decreases as continuously increasing proportions of normal alkanes are formed, probably by random thermal cracking (Fig. 10.08). This results in chromatograms with increasingly small isoprenoid proportions (Figs. 10.06a and 10.06b).

Frequency histograms of pristane and phytane proportions relative to the adjacent normal alkane in shales and oils match closely, which can be interpreted to show that the oil source type and maturity were similar to that of the shales (Fig. 10.09a-d). The major difference lies in the small proportion of shales with very low nC17/pristane ratios (cf. Figs. 10.09a and 10.09b), which is probably due to an abundance of low maturity samples in which isoprenoids dominate (cf. Figs. 10.06a and 10.06b) and from which little oil is expelled. A similar explanation is invoked for the low nC18/phytane ratios in Fig. 10.09c and 10.09d, although there the differences are limited.

Powell and McKirdy (1973b) show the pristane/phytane ratio in coals to be >>2-3 but it is significantly lower in marine shales, hence the proportions can indicate the

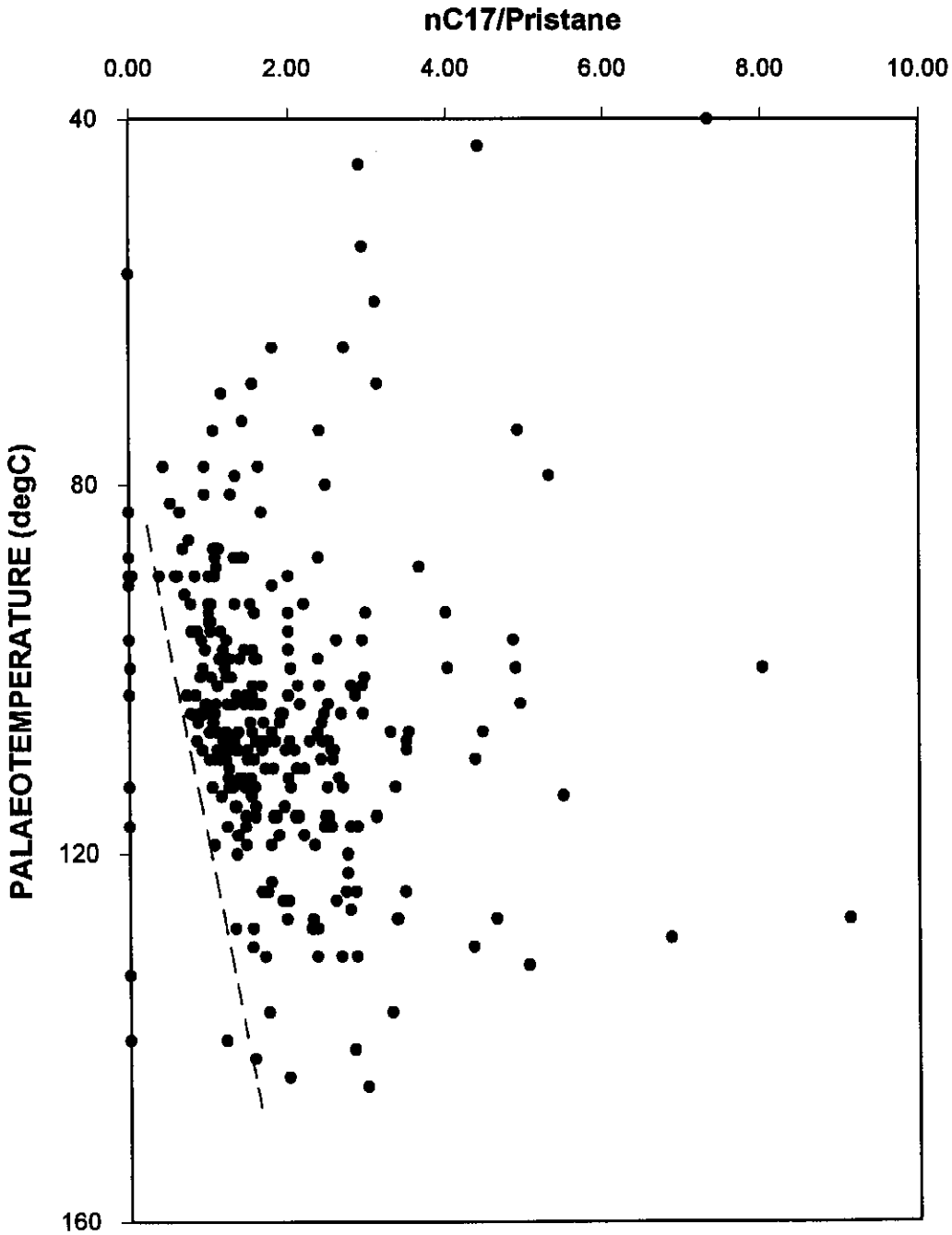

Figure 10.08: Plot of pristane/nC17 vs. palaeotemperature for all Bredasdorp Basin shale samples.

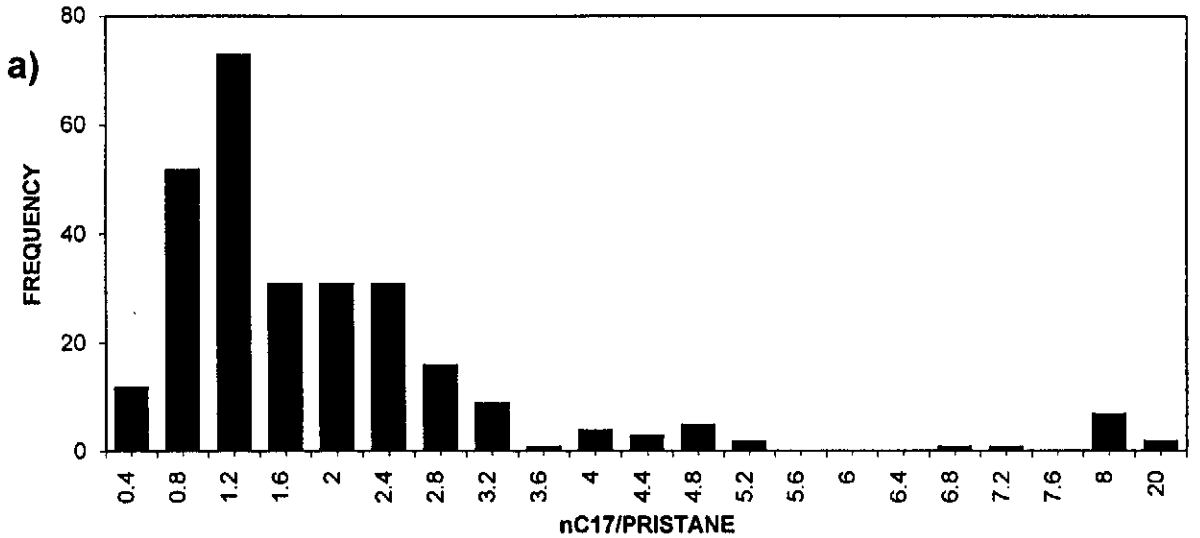

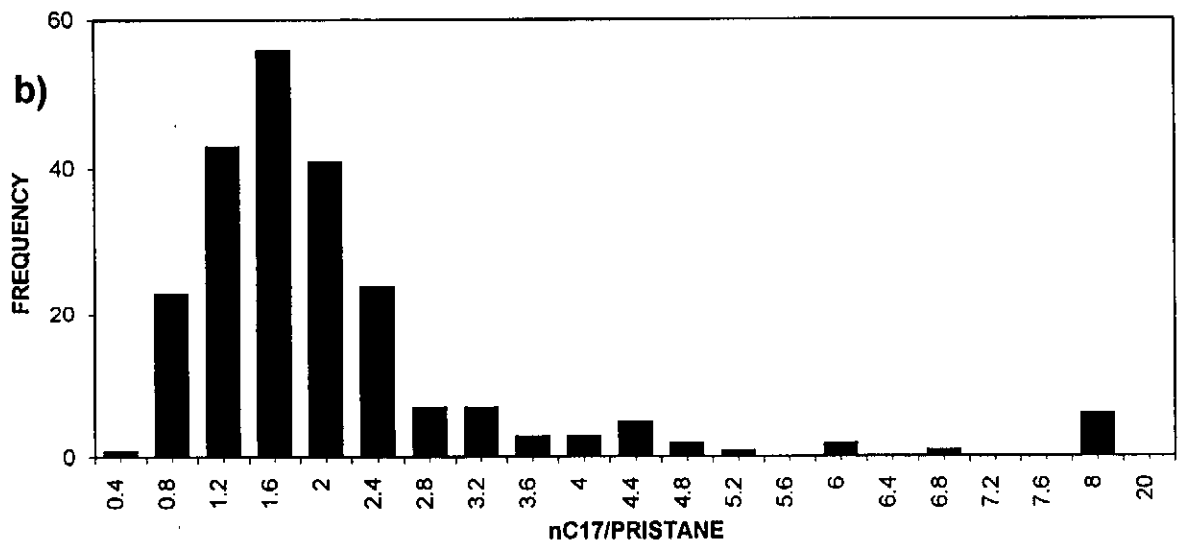

Figures 10.09a and b: Frequency histograms of nC17/pristane for all Bredasdorp basin (a) shale samples and (b) oil samples.

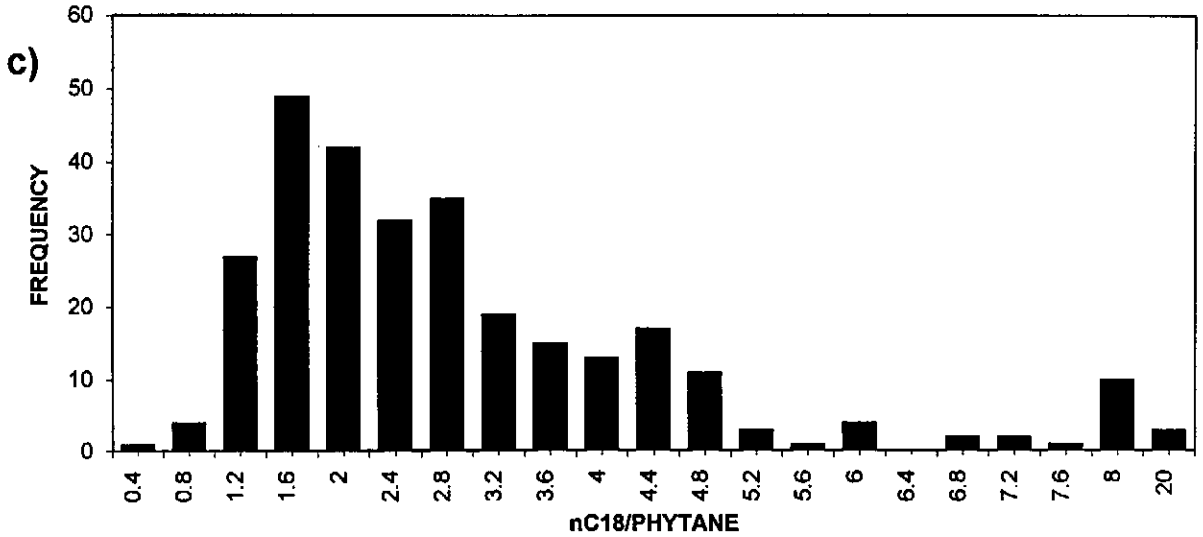

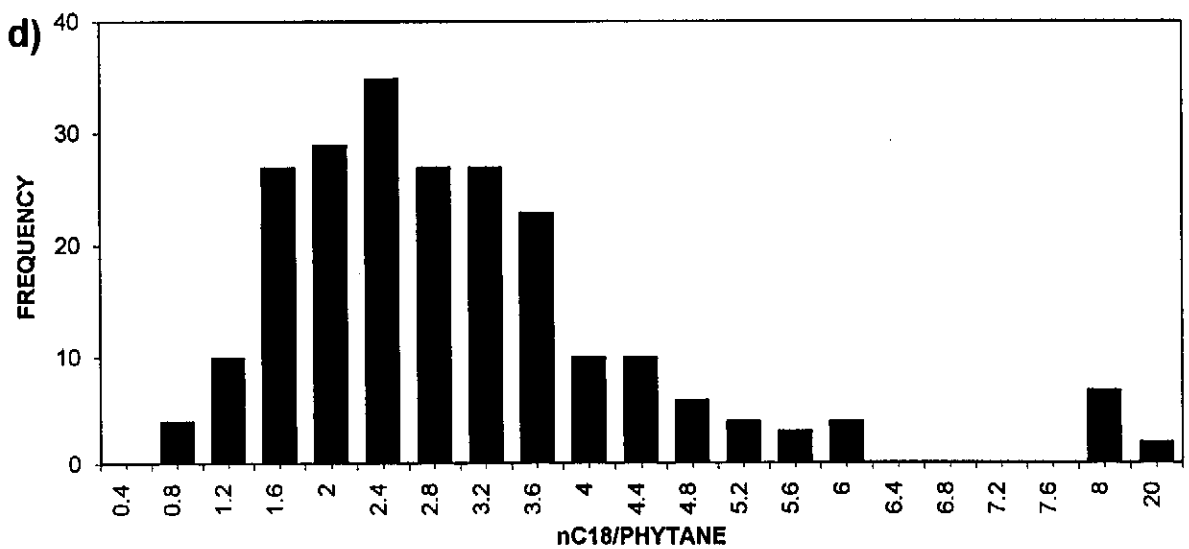

Figures 10.09c and d: Frequency histograms for nC18/phytane for all Bredasdorp Basin (c) shale samples and (d) oil samples.

depositional environment. The plot of the shale samples (Fig. 10.10a) shows a significant proportion of samples with very low Pr/Ph ratios whereas the oils do not (Fig. 10.10b). This difference between the proportions of components with slightly different mass may result from preferential expulsion of the lighter material and retention of the heavier material (Leythauser et al., 1983).

Plots comparing the two main isoprenoid/alkane ratios (Saban et al., 1988; Osadetz et al., 1992) for all oil and shale samples from the Bredasdorp Basin are shown in Figs. 10.11a and 10.11b. They show that there are no samples displaying biodegradational traits, in which n-alkanes are present in smaller amounts than adjacent isoprenoids leading to ratios <1. However, there are a few samples where evaporation has resulted in almost complete loss of nC17 and pristane, leading to spuriously low ratios suggestive of biodegradation (Fig. 10.11a). In those cases, the more normal nC18/phytane ratios show that it results from evaporation, not degradation.

10.2.4. Undifferentiated complex mixture (UCM)

Another maturity indicator which can be derived from the total saturates GC is the presence of a UCM ('baseline hump') as seen on Fig. 10.06a. In early maturation, kerogen often contains large proportions of many complex molecules. These do not separate readily, especially on non-polar columns, but instead form a high temperature 'hump' of overlapping peaks. This 'hump' decreases in size as thermal and diagenetic processes reduce the proportions of these compounds and promote the formation of more readily separated components. In the more mature source rock samples (e.g. Fig. 10.06b) there is no evidence of a UCM.

10.2.5. Aromatic hydrocarbons

The origins of polyaromatic hydrocarbons (PAH) have been summarised by Radke et al. (1982a;1982b) and Radke (1987). They reported that biosynthesis of large proportions is unlikely and that most PAH are derived from non-aromatic biogenic precursors, probably by catalysis on active surfaces of minerals. Since most active catalysts are found in shales, this implies that many of the aromatics are formed in source rocks and their distribution and proportion may therefore be a function of source distribution and maturation. It has also been shown (Tissot et al., 1973; Radke, 1987) that some PAH are derived from biogenic precursors with minimal alteration. The implication is that, although the biological origin of aromatics is less evident than for saturates, some do retain their precursors' characteristics. For example, phenanthrenes have carbon skeletons which closely match the cholesterol skeleton (Radke, 1987). Aromaticity increases with depth as aromatic rings gradually condense to 3 or more rings (Radke et al., 1982b). These gradual changes can be attributed to increased maturity. Hence the ratios of some of the components can be useful maturity

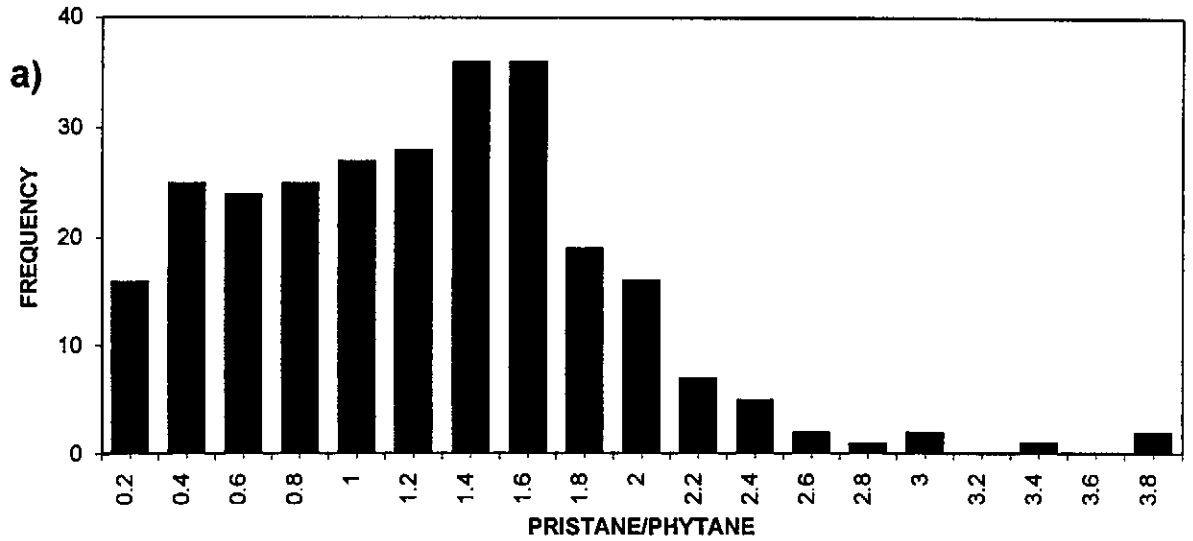

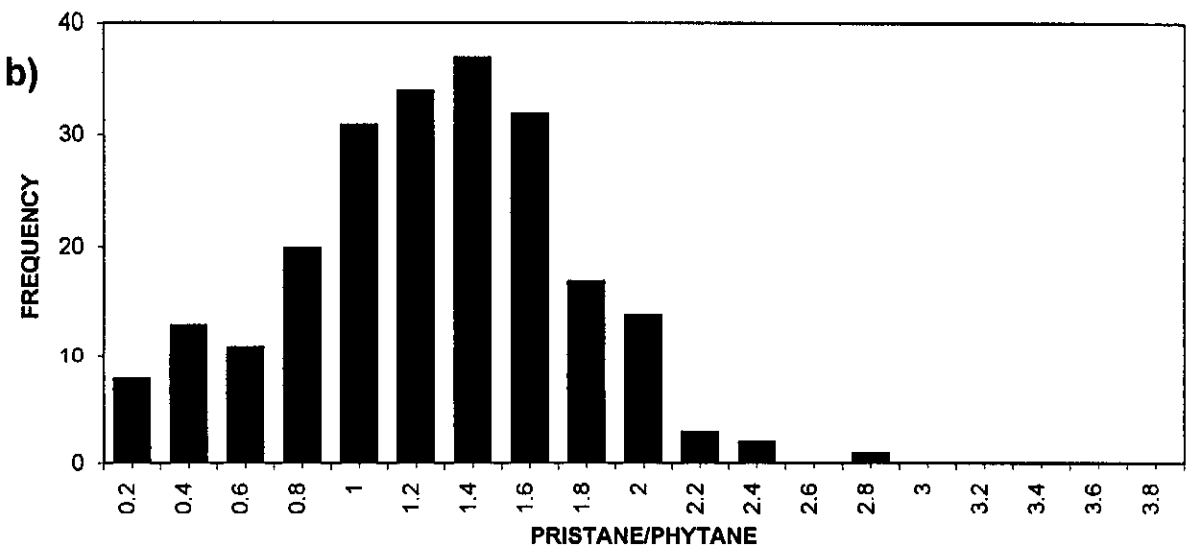

Figures 10.10a and b: Frequency histograms of pristane/phytane for all Bredasdorp Basin (a) shale samples and (b) oil samples.

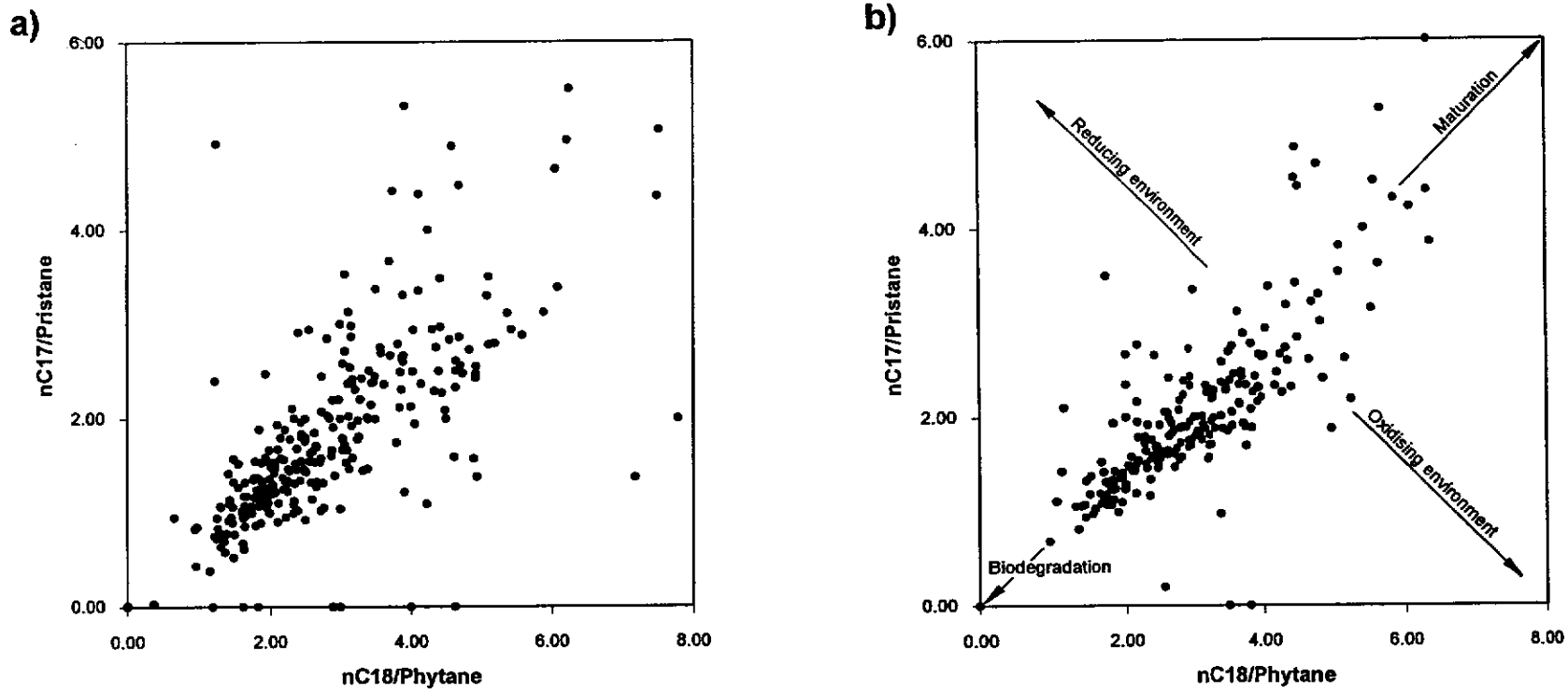

Figures 10.11a and b: Cross-plots of nC17/pristane vs nC18/phytane for all Bredasdorp Basin (a) shale samples and (b) oil samples.

parameters. Aromatic hydrocarbon distributions have been commonly used over the past 10-15 years to evaluate effects of thermal maturity. However, Radke et al. (1982b) show that hydrocarbons typical of different source facies have different PAH distributions and hence the assessment of maturity from these compounds is less than perfect.

Two groups of compounds are used to assess maturity namely phenanthrenes and chrysenes. These have condensed structures with 3 and 4 rings respectively and both structures can have a variety of side groups. The most common of these are the methyl and dimethyl forms. A third common PAH species, naphthalenes, have also been used in maturity investigations (e.g. Radke, 1987). Because they are often overlapped by other compounds on the largely non-polar columns used here, they are best studied from GC-MS data (Chapters 11-12).

10.2.5.1. Phenanthrenes

Radke (1987; 1988) showed that changes in the proportions of methyl and dimethyl phenanthrenes are largely comparable with other measurements of thermal maturity effects such as vitrinite reflectance, at least for type 3 organic matter. These changes largely involve the thermally-controlled shift of methyl groups from the sterically crowded α position to the less crowded β position. Calibration of changes with maturity from the proportions of these methyl homologues with other types of organic matter are less successful, largely because of the scarcity of autochthonous vitrinite and phenanthrenes in those kerogens. Hence any methyl- or dimethyl-phenanthrene parameters determined on samples with wholly amorphous or algal organic matter may not reflect the *in situ* maturity, instead they reflect admixtures of second-cycle vitrinite. Fortunately many of the oil-prone source rocks in the Bredasdorp Basin, as well as the gas-prone source rocks, contain at least small amounts of *in situ* vitrinite so their phenanthrene ratios largely reflect source rock maturity levels. Phenanthrene peaks are located on aromatic GC's in Fig. 10.12.

Three ratios are commonly determined from phenanthrene data:
(i) DPR=(2,6DMP+2,7DMP)/(2,10DMP+1,6DMP), R_{calc}=1.5+1.34log$_{10}$DPR,
(ii) MPI1=1.5(3MP+2MP/(P+9/4MP+1MP), R_{calc}=0.6MPI1+0.4%,
(iii) MPR=3MP/4+9MP, R_{calc}=0.95+1.1log$_{10}$MPR%.

These values have been calculated for all source rock and oil samples from Bredasdorp Basin wells and plotted in Figs. 10.13a-f. In contrast to earlier studies (Radke, 1987) only weakly defined trends are evident for the phenanthrene ratios. Perhaps this poorer correlation reflects the variable organic matter type. This is not surprising, as

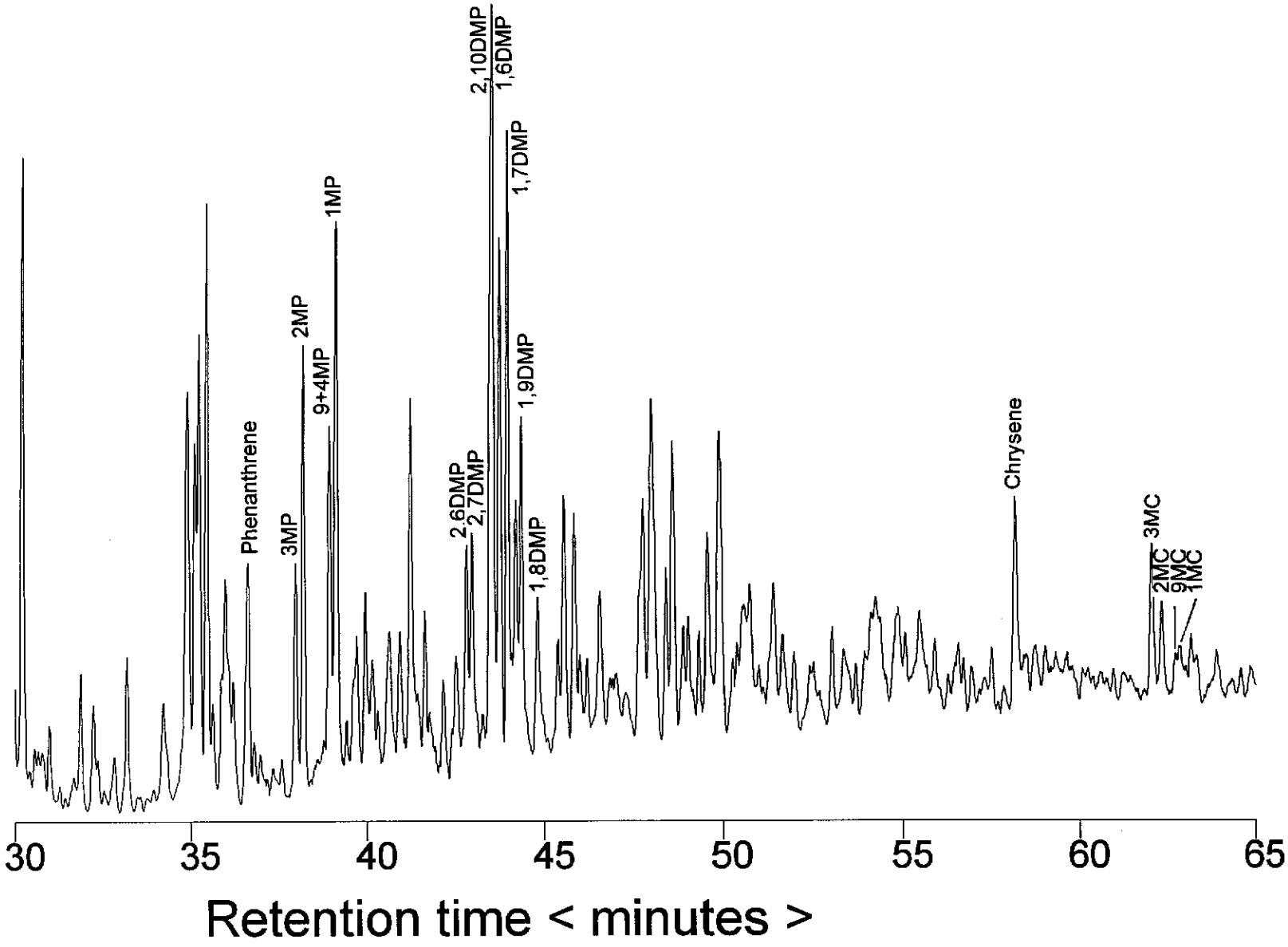

Figure 10.12: Gas chromatogram of aromatic hydrocarbons from sample 6, well 88 DST4 showing the peaks assigned to phenanthrenes and chrysenes

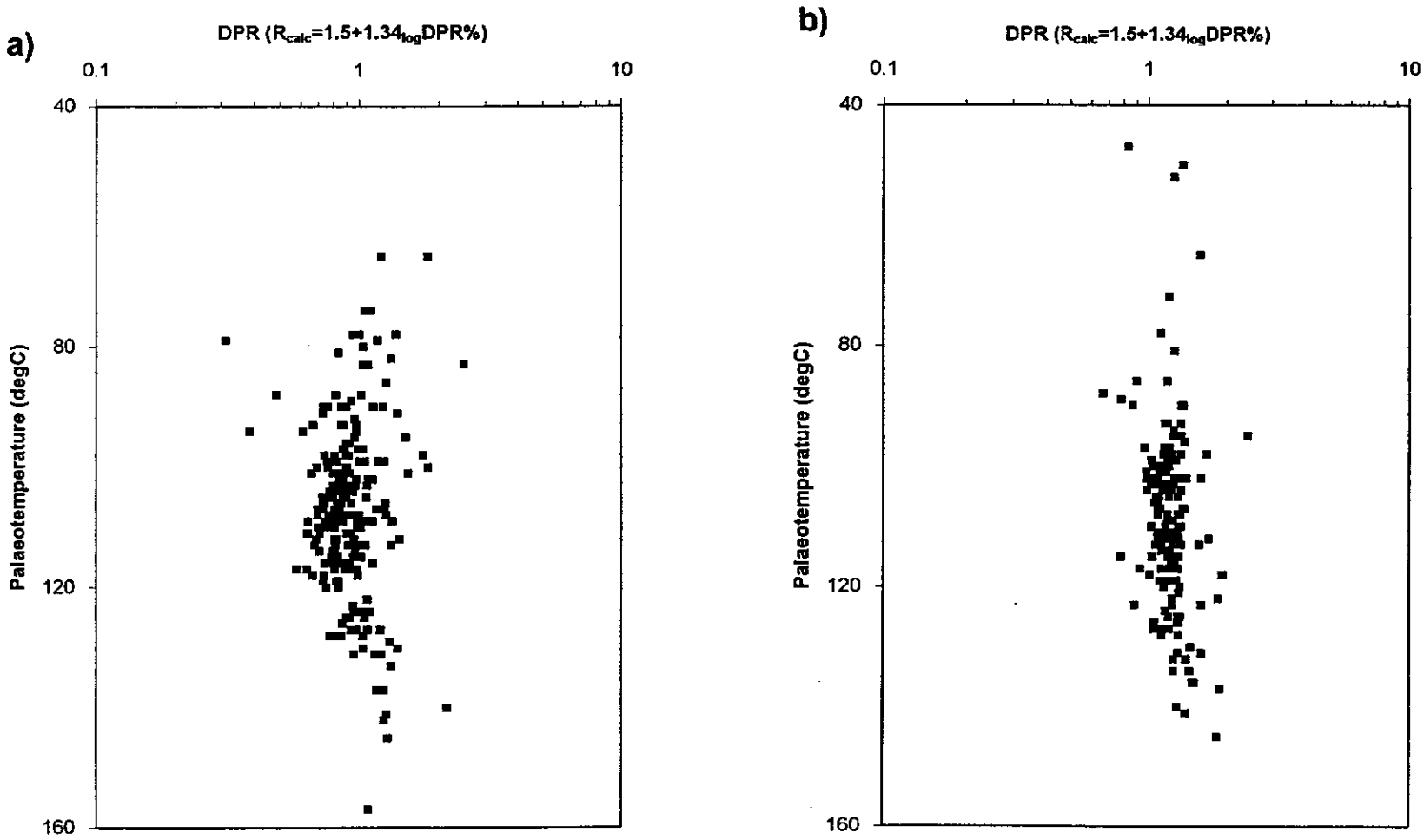

Figures 10.13a and b: Plots of vitrinite reflectances calculated from dimethyl phenanthrene ratio (DPR) (from GC data after Radke, 1987) for all Bredasdorp Basin (a) shale samples and (b) oil samples.

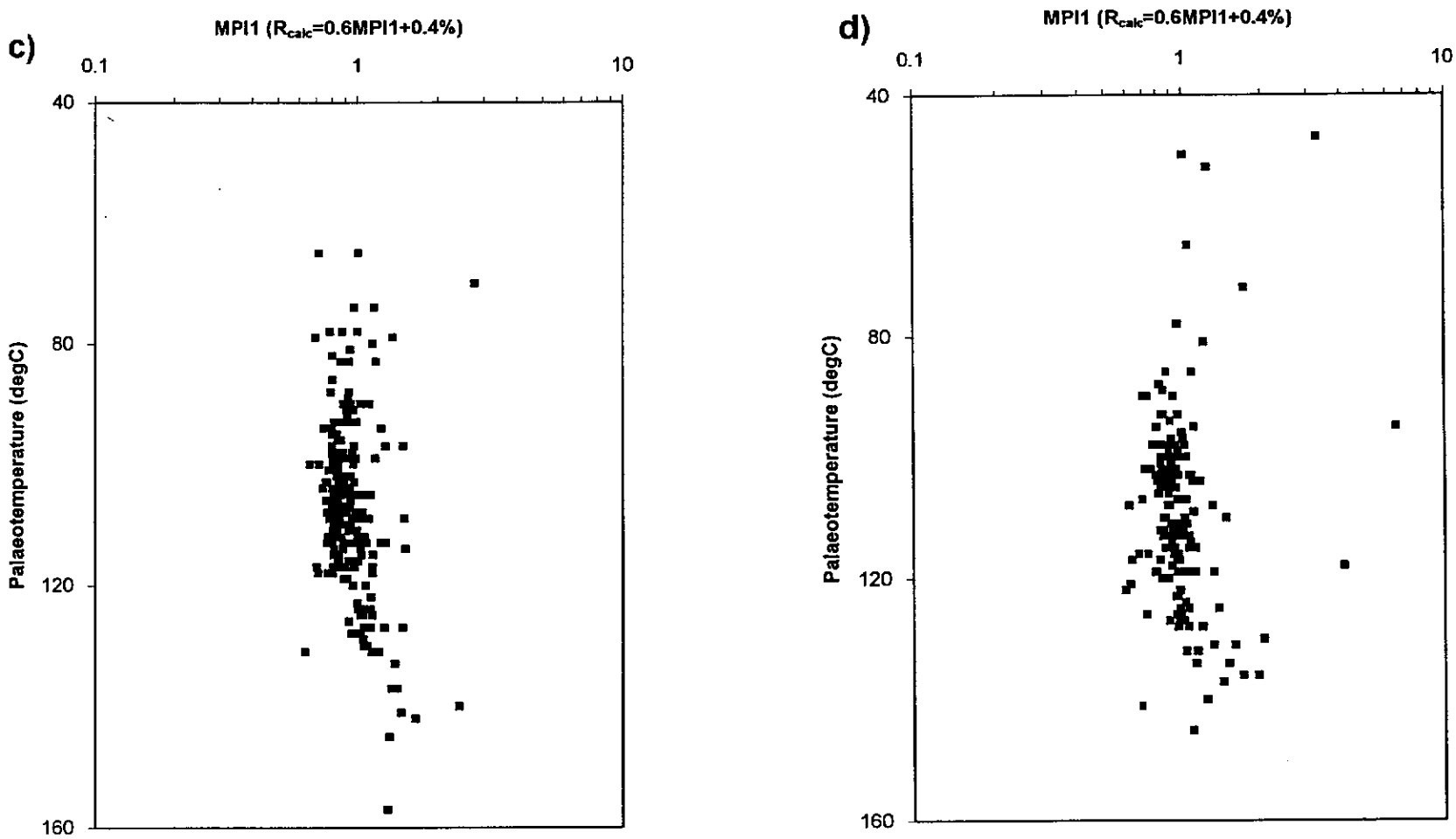

Figures 10.13c and d: Plots of vitrinite reflectances calculated from methyl phenanthrene ratio (MPI1) (from GC data after Radke, 1987) for all Bredasdorp Basin (c) shale samples and (d) oil samples.

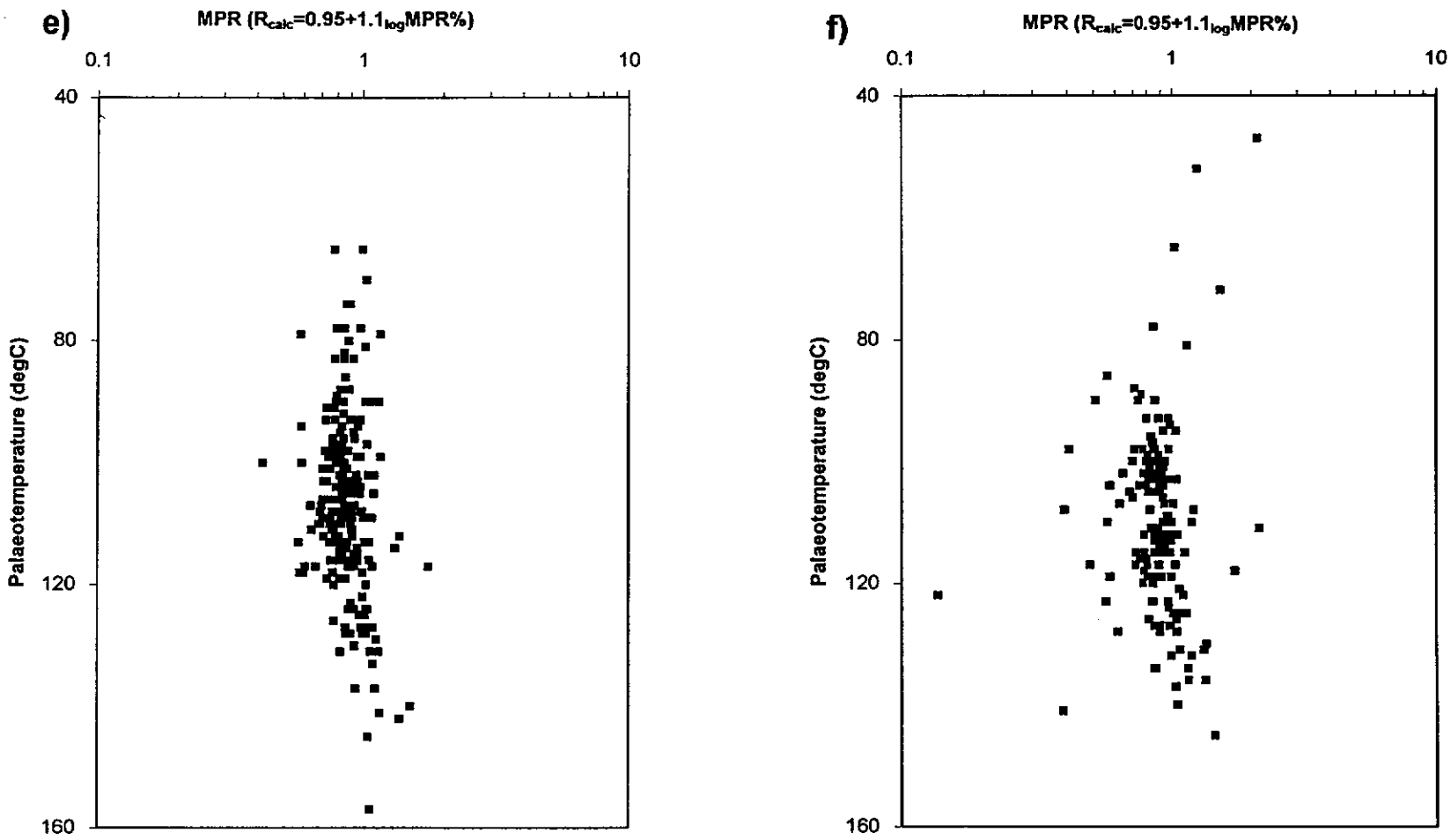

Figures 10.13e and f: Plots of vitrinite reflectances calculated from dimethyl phenanthrene ratio (MPR) (from GC data after Radke, 1987) for all Bredasdorp Basin (e) shale samples and (f) oil samples.

the samples were chosen to maximise hydrocarbon generation potential rather than to sample kerogen monotypes.

The MPI1 ratio has also been calculated from GC-MS data from the oil and shale samples used for the detailed study (Figs. 10.14a and 10.14b). The envelopes of Radke (1988) and Boreham et al. (1988) are constructed therein. All data locate within the extremes of the envelopes indicating that by and large the phenanthrenes are present in maturity-related proportions. However, the envelopes themselves are really too wide to be of any predictive use. Evidence to support the source-related effects is found in these plots. For example the dominantly amorphous samples all plot within Radke's trend whilst the gassier samples mainly plot outside that trend, but still within the outer trend of Boreham et al. (1988).

10.2.5.2. Chrysenes

Chrysenes are benzo-phenanthrenes and as such the methyl homologues are thought to have similar reactivity relationships to the methyl phenanthrenes. It is therefore possible that maturity differences between steric methyl locations in chrysenes are similar to those of phenanthrenes. The four major methyl chrysene isomers matching those of the methyl phenanthrenes are located on each chromatogram using retention indices (Lee et al., 1979) and the two ratios which match those calculated from methyl phenanthrene data are determined.

Such ratios have been commented on previously (Radke, 1987; Benson et al., 1990; Davies and Van der Spuy, 1990). However, there are no standard calibrations to vitrinite reflectance or other maturity parameters so the ratios are plotted against palaeotemperature:

(i) MCI1=(3MC+2MC)/(C+9/4MC+1MC) (Fig. 10.15a and b),

(ii) MCR=(3MC/1MC) (Fig. 10.15c and d).

Weakly defined trends with maturity are present and that of the MCI1 ratio (especially from the shale samples, Fig. 10.13a) appears better defined than the MPI1 ratio. This is perhaps due to variable evaporation of low molecular weight components which has influenced the phenanthrene ratios. Nevertheless the trends are still too poorly defined to allow construction of a usable regression line.

10.2.6. Biomarkers

In the higher molecular weight range of moderately mature bitumens and oils, biomarkers are commonly present, but they are seldom seen in total saturates chromatograms as they generally constitute <<1% of the total extract. However, low maturity source rock and oil samples contain larger proportions of detrital and early

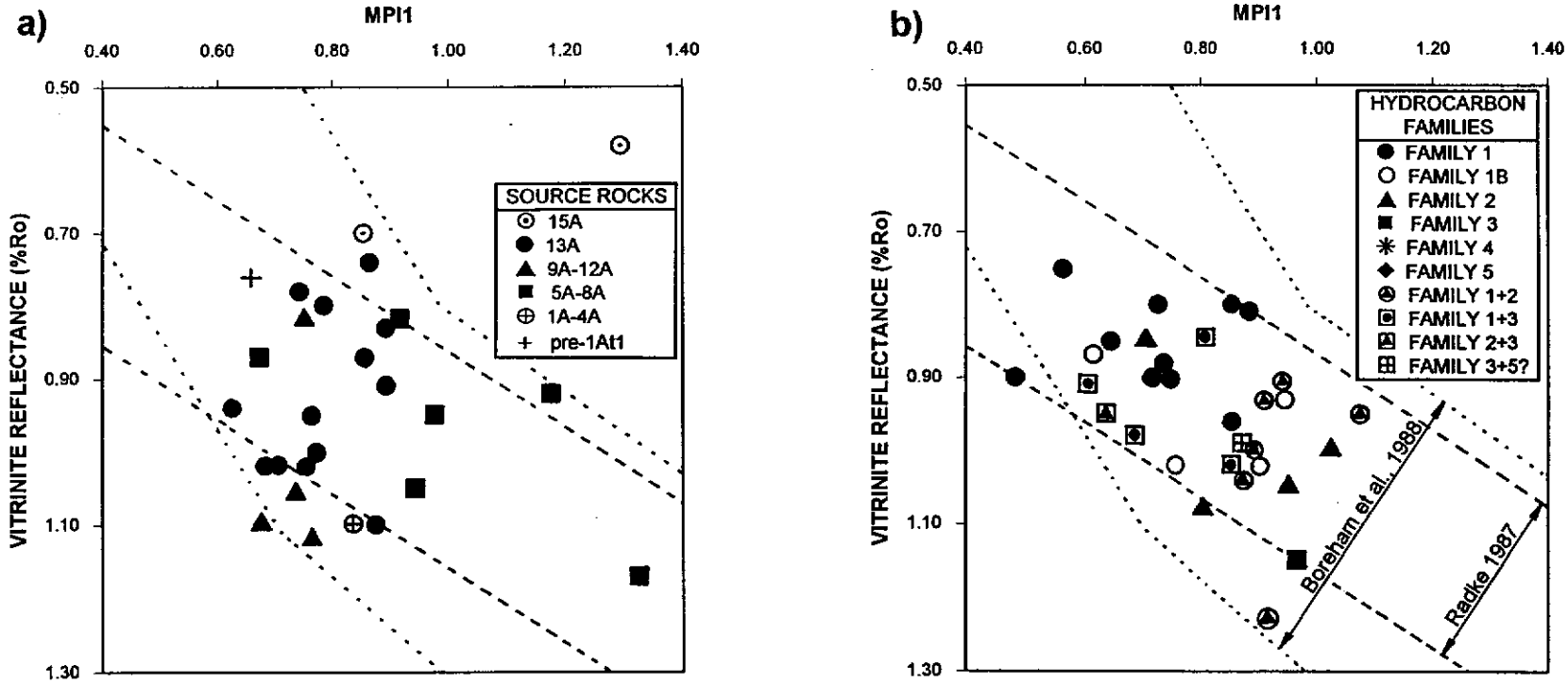

Figures 10.14a and b: Plots of MPI1 calculated from all GC-MS fragmentograms (after Radke, 1987) for (a) shale and (b) oil samples. Envelopes of data from Radke, 1987 and Boreham et al., 1998 are shown.

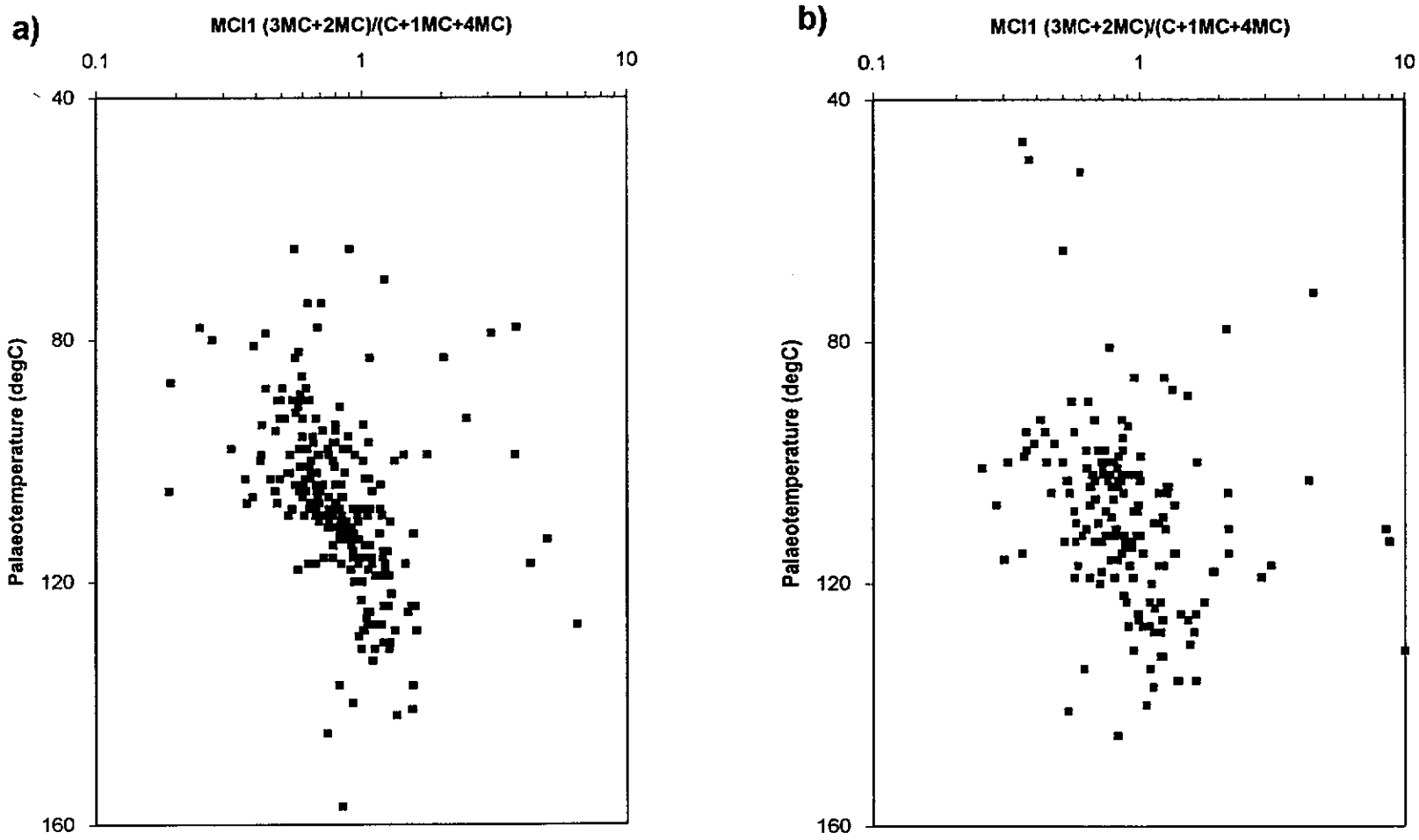

Figures 10.15a and b: Plots of MCI1 calculated from GC data (after the MPI1 formula of Radke, 1987) vs. palaeotemperature for all Bredasdorp Basin (a) shale and (b) oil samples.

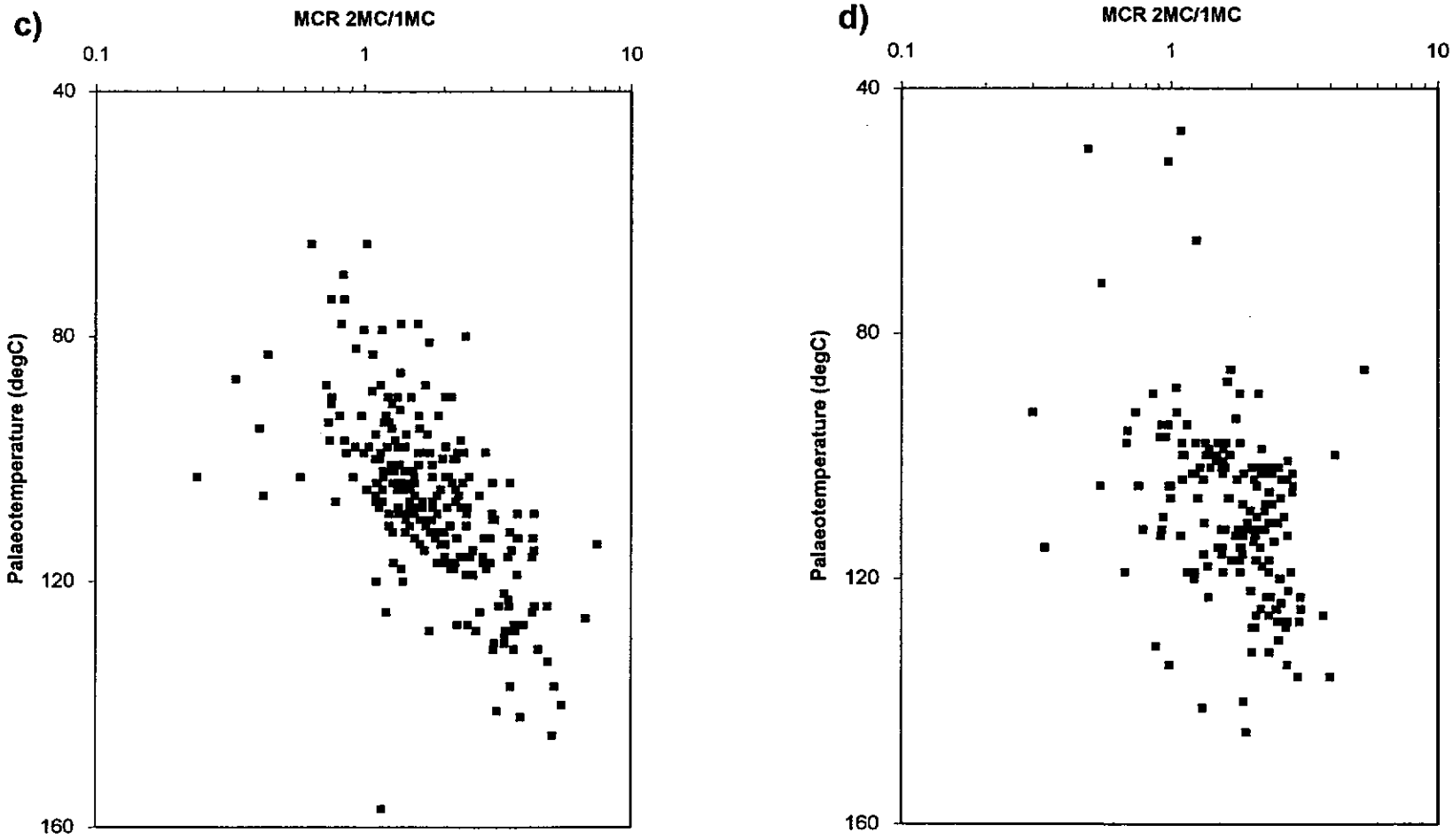

Figures 10.15c and d: Plots of MCR calculated from GC data (after the MPR formula of Radke, 1987) vs. palaeotemperature for all Bredasdorp Basin (c) shale and (d) oil samples.

generated biomarkers which are visible on some chromatograms (e.g. Fig. 10.06a). Indeed in many low maturity shale samples, a full spectrum of biomarkers from C27 steranes to C35 terpanes can be seen (cf. biomarker and GC plots for samples 49 and 50 in Appendix D, Figs. D.36 and D.38).

At the high temperature end of chromatograms, branched and cyclo-alkanes are generally found in very small proportions. However, source rock samples from the Bredasdorp Basin occasionally have peak(s) in that range at retention indices similar to those of carotanes (near nC36-37). Carotanes are commonly found in vegetation (Tissot and Welte, 1984, p. 41) and in lacustrine algal mats (Peters and Moldowan, 1993, p. 164), but rarely in large quantities in marine organisms. Hence they are indicators of terrigenous input. One such peak is seen on the saturated hydrocarbon chromatogram of sample 7, an oil show in well 92 (Appendix D, Fig. D.88). This well is located close to the graben where anoxic lacustrine source rocks are known to exist (cf. Figs. 2.10 and 4.03) and these possible carotane traces may indicate migration of some oil from that source.

10.3. CONCLUSIONS

Not only have the bulk and fractional GC data been widely used to determine environmental and in-reservoir effects and to characterise source rocks, but they have also been extensively used to correlate oils to their source rocks. For example, Deroo et al. (1977) in their regional study of hydrocarbons in W. Canada, established such correlations. Later source rock:oil biological marker correlation studies of similar samples supported the original correlation (Leenheer, 1984). Deroo et al. (1977) studied several different types of source rocks and showed that the oils had been generated at widely different maturity levels. In the Bredasdorp Basin, oils and condensates are all relatively mature and the source rocks are all (except for the lone lacustrine source rock sample) of similar age and from similar deep marine depositional environments. Hence the n-alkane envelope or the proportions of phenanthrenes or other source indicators, rarely provide evidence of different depositional environment conditions for any source rock or oil. Whilst such environmental character does agree closely with the known depositional environment (from palaeontological and sequence stratigraphic evidence (McMillan et al., 1997; Brown et al., 1995) it does not help to establish correlations between individual oils and specific source intervals. Therefore the comparison of different source rocks, and of the hydrocarbons expelled therefrom, will largely depend on characteristics derived from more detailed analytical data, e.g. the biomarker data discussed in Chapters 11 and 12. Stable ^{13}carbon isotopic data show that Family 4 condensates are significantly different from hydrocarbon Families 1-3 but do not so readily differentiate between samples of Families 1-3.

CHAPTER 11. BIOMARKER COMPOUNDS: INTERPRETATION THEORY

A large data-set of biomarker compounds has been generated from Bredasdorp Basin source rock and hydrocarbon samples. The interpretation of this data-set requires constant reference to interpretation theory and practice established from many published studies. To avoid reiteration each time biomarkers are referred to, and for ease of reference, the interpretation theory is compiled in this Chapter and data interpretations are discussed in Chapter 12. Continuing the interpretation styles used in Chapters 8-10, the data is addressed from several different aspects (overview, detailed X:Y plots, statistical analysis) to correlate between the source rocks and hydrocarbons.

11.1. BIOLOGICAL MARKER HISTORY

Biological marker compounds (biomarkers) are "compounds which have chemical structures which can be unequivocally linked to the structures of precursor compounds occurring in original organic matter" (Eglinton and Calvin, 1967) or "any organic compound detected in the geosphere whose basic chemical skeleton suggests an unambiguous link with a known contemporary natural product" (Mackenzie, 1984).
The study of biological marker compounds started some 20-30 years ago (Eglinton and Calvin, 1967; Pym et al., 1974). However it is only since the early 1980's, with the more ready accessibility of GC-MS equipment, that enough studies have been done world-wide to allow clarity in detailing those which are characteristic of specific depositional environments and establishing maturity trends (Moldowan et al., 1985; 1986).

In general, biomarkers have multi-ring condensed saturated and aromatic skeletons with numerous short side-chains. They are usually present in small proportions and are therefore usually barely evident on gas chromatograms of saturated or aromatic hydrocarbons (Fig. 11.01a). In some cases, they can be present in moderate proportions (Fig. 11.01b). They mostly elute in the highly crowded nC25-35 region of saturated hydrocarbon GC's and in the latter parts of aromatic chromatograms near and beyond the elution time of many of the phenanthrenes (Fig. 11.02). In some of the earliest studies, some biomarkers were shown to be highly specific for certain source environments, for example the prevalence of carotanes in lacustrine sediments, gammacerane in highly anoxic or hypersaline sediments and oleananes in deltaic or shelf sediments. Other studies have established maturity trends of characteristic biomarkers and shown that certain biomarkers are particularly useful in determining differences between oils of marine or non-marine sources. In addition, there are a

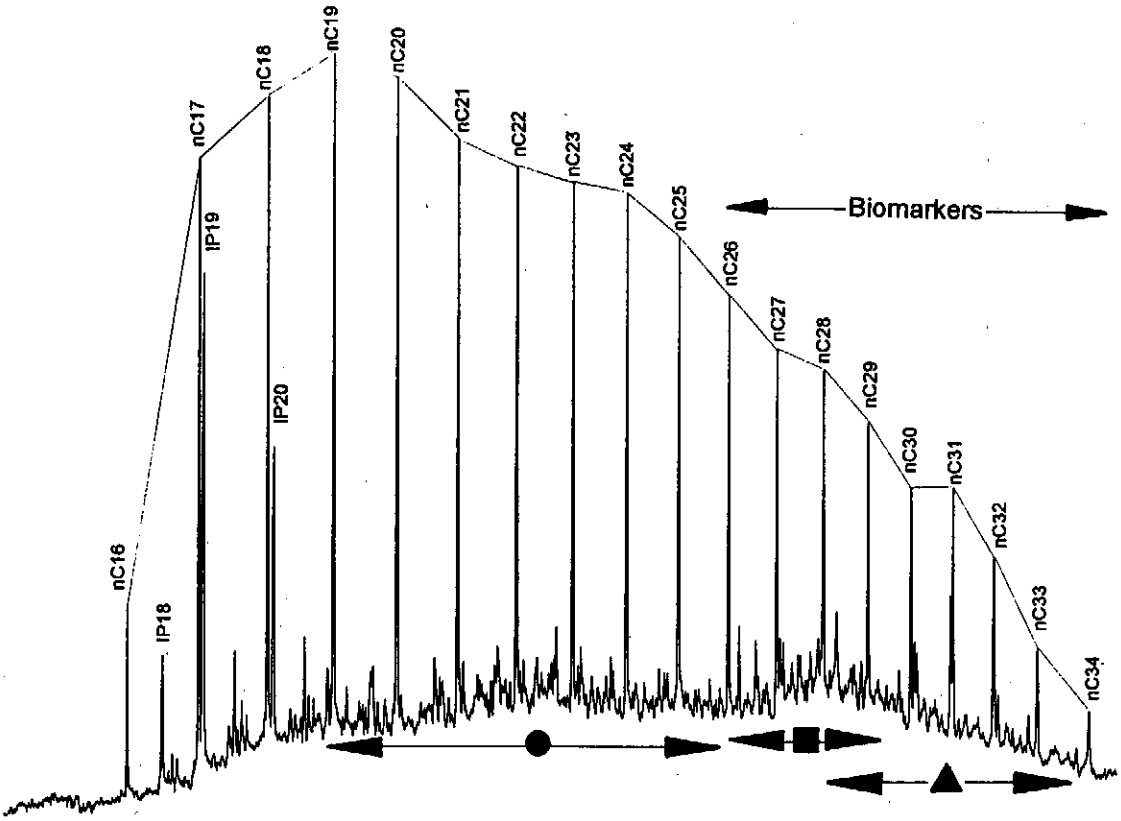

Figure 11.01a: Gas chromatogram of the total saturates fraction of sample 51 (a) with the iso- and monocyclic- alkanes (●), steranes (■) and pentacyclic terpanes (▲) located.

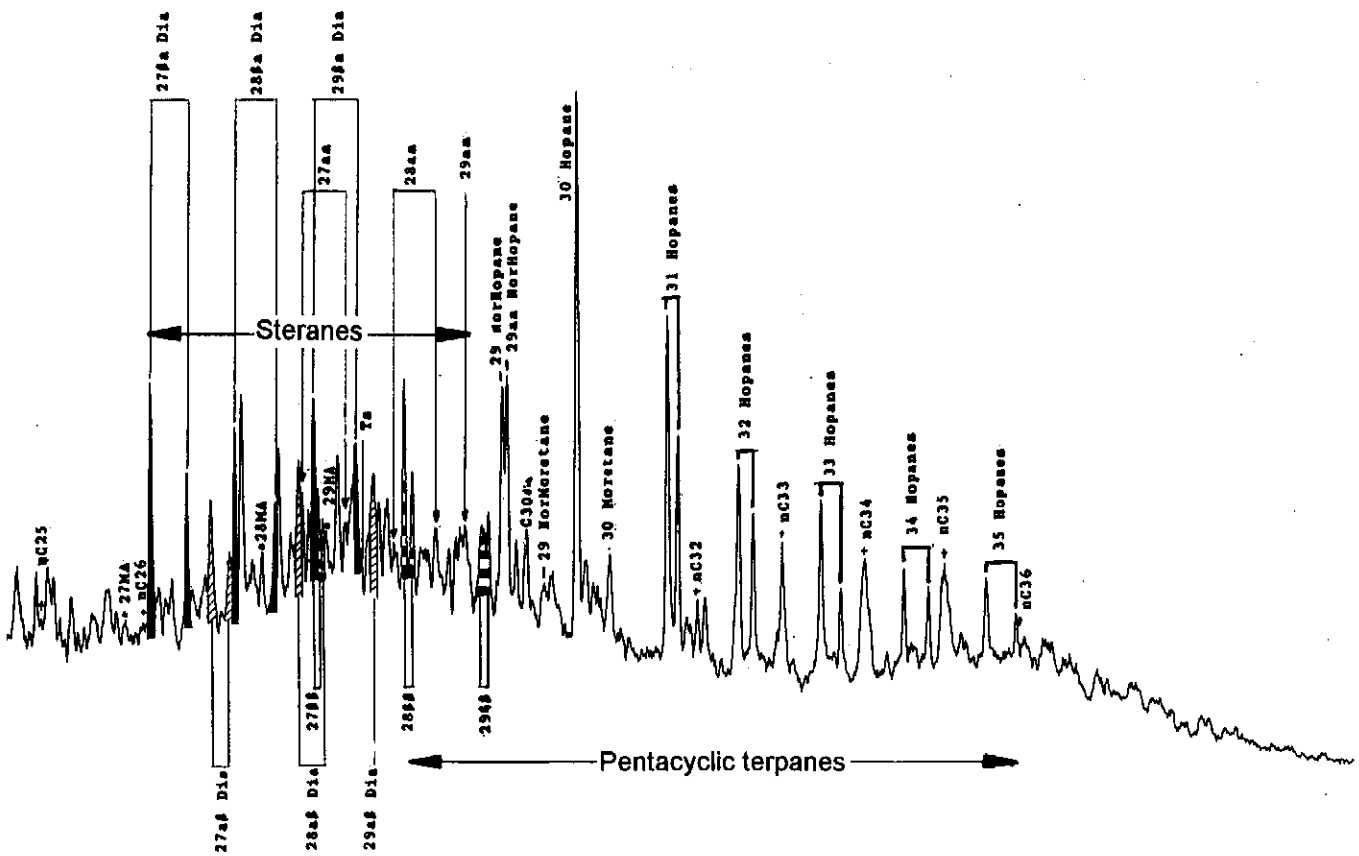

Figure 11.01b: Gas chromatogram of part of the urea non-adduct fraction of sample 51 showing the steranes and pentacyclic terpanes in more detail. Compare this chromatogram to the GC-MS fragmentograms of the m/z 191 and m/z 217 ions for this sample in Appendix E, Figure E.50.

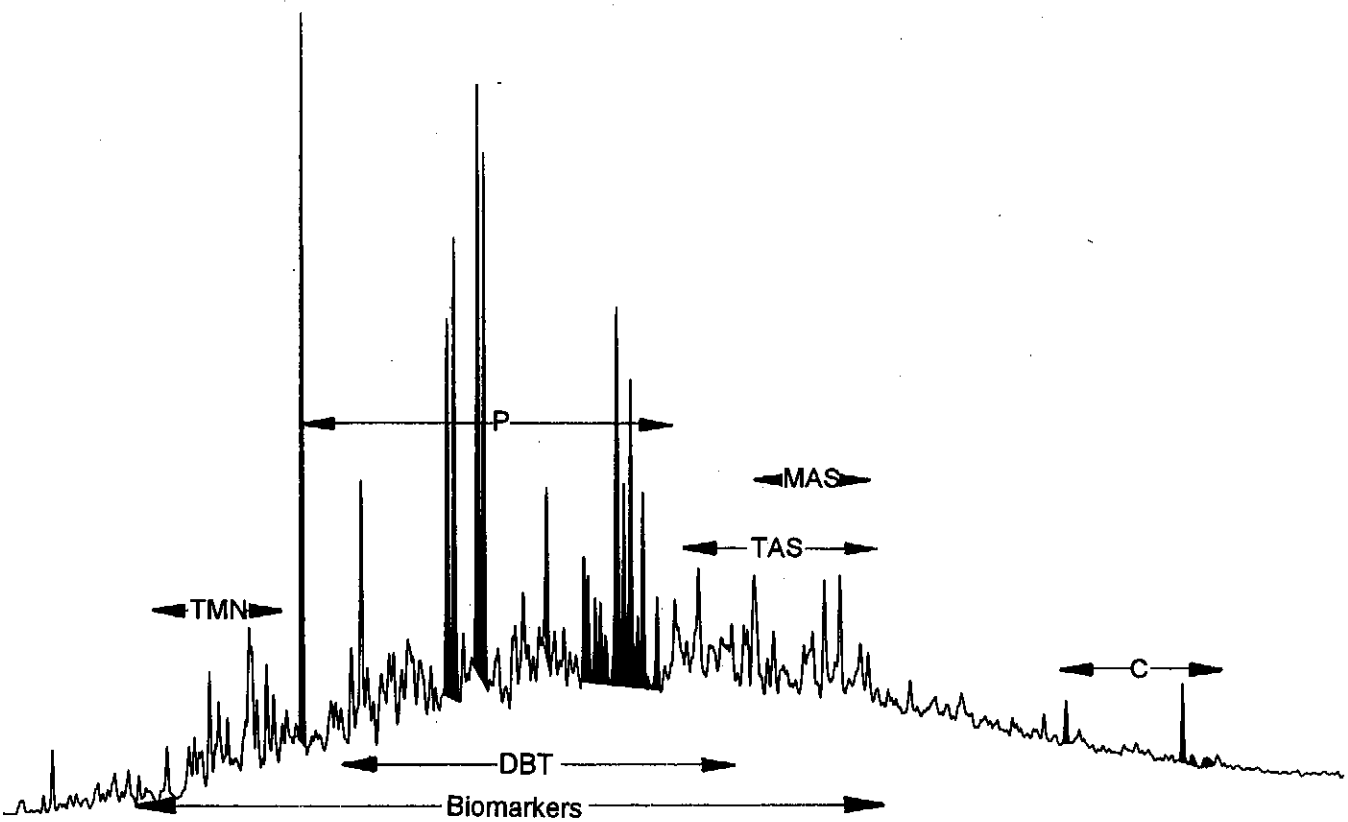

Figure 11.02: Gas chromatogram of the aromatic fraction of sample 51 showing the location of the trimethyl naphthalenes (TMN), dibenzo thiophenes (DBT), mono-aromatic and tri- aromatic steroids (MAS and TAS), phenanthrenes (P) and chrysenes (C) in detail.

number of biomarkers which are present in characteristic concentrations in altered oils, such as large proportions of demethylated hopanes in biodegraded oils.

Some biomarker compounds which were shown to be either maturity- or source-specific (e.g. Tm and Ts compounds, Seifert and Moldowan, 1978) have more recently been shown to have both maturity- and source-specificity. Indeed it is now thought that the concentration of most biomarkers can be affected by both changes in maturity and source environment. In this study, therefore, interpretations of both source and maturity aspects are discussed together and biomarker ratios are plotted as published elsewhere. Where necessary, different ratios are constructed (based on known compound relationships) to better characterise particular source:oil correlations.

11.1.1. Comparison with non-biomarker compounds

Biomarkers differ from compounds investigated in previous chapters (Chapters 9-10), which are generally accepted to derive from biological material but are not usually considered as biological markers, because some are only distantly related to their biological precursors. Some too, such as iso-and anteiso-alkanes, normal alkanes, and single-ring aromatics, have been derived from biological compounds by one of several different routes and hence may not be unique to a contemporary product (Hwang et al., 1994). Many of those compounds are products of thermal and catalytic cracking. Those compounds include those thought particularly useful in distinguishing the effects of biological degradation (Connan, 1984; Williams, et al., 1986), thermal alteration (Simoneit et al., 1981), water-washing (Lafargue and Barker, 1988) or evaporative fractionation (Thompson, 1983; 1988). Their proportions give guidance on the habitat of the source organic material when at low maturity, but are less useful at higher thermal maturation levels. Proportions of long-chain alkanes and 2-3 ring aromatics in mature samples, which appear to have fingerprint correlation potential, often match those from similarly mature oils elsewhere. For example, Bredasdorp Basin alkane envelopes match those from the North Sea (Thomas et al., 1985). Indeed whole oil chromatograms used in fingerprint GC studies elsewhere match those used in the Bredasdorp Basin very closely. In some cases, neoformed compounds can completely mask the range of deposited and preserved biologic compounds (Kissin, 1987). Hence those compounds were considered less useful in matching oils to their source rocks. However, recent work at IFP suggests the 'fingerprint' components are also present in source rocks and useful for oil:source correlations (C.C. Magnier, 1995, pers. comm.).

11.2. USE OF BIOMARKERS FOR CORRELATION.

In order to demonstrate which areas of the basin are likely to contain reserves of hydrocarbons, it is necessary to know where and when hydrocarbons were generated

and in what quantities and in which direction they migrated after expulsion from the source. Previous studies (Davies, 1988b; Davies, 1996a; Davies, 1996c; Davies, 1997a; 1997e) have shown which source rocks generated large amounts of hydrocarbon and how much. The modelling study in this report indicates when those hydrocarbons became available for expulsion and in what proportions. However, the earlier data are not adequate to demonstrate in which direction hydrocarbons migrated or indeed from which source rock each originated. These aspects can only be evaluated once it is possible to correlate each hydrocarbon with its source rock. Once such matches have been demonstrated, it is possible to evaluate the likely fetch area and therefore the migration direction. From knowledge of the expulsion potential of that source rock, the quantities migrating (and their time of migration) can be calculated and hence the amount available for reservoiring in each updip trap can be estimated. Such biomarker correlations are therefore routinely used elsewhere to establish or characterise five aspects of petroleum geochemistry:
(i) correlation between source rocks and hydrocarbons
(ii) characterisation of the origin of the preserved organic material in source rocks and the source for expelled hydrocarbons
(iii) evaluation of the maturation level of the source rock and expelled hydrocarbons and establishing the migration direction and timing
(iv) characterising post-depositional and reservoiring processes affecting hydrocarbons
(v) indicating an approximate age of the source rock.

11.2.1. Oil:source correlation

Correlation between hydrocarbons and their source needs compounds which are:
(i) present in both hydrocarbons and source rocks
(ii) predictably apportioned between hydrocarbons and their source
(iii) present in characteristic proportions for each source rock
(iv) present in large enough quantities for detailed study
(v) in unalterable proportions during migration, or if they do alter, predictably so.

The process of extracting source rock bitumens and oil traces from ground rock with solvent followed by evaporation of the solvent, leads to the loss of all gases and most light oils. This loss extends up to ~C12 but occasionally as far as ~C17, hence compounds lighter than this, such as 'fingerprint' GC data, have less commonly been used for correlation between oils and source rocks. Furthermore, saturates and aromatics in the ~C15-25 range are reportedly largely generated by thermal cracking of larger molecules, and their variability is more a function of the local thermal regime than of the source (Hunt, 1979a). Recent studies (Chapters 8-9) have shown this viewpoint to be limiting.

Only those compounds with biologically-formed skeletons, present in oils and source rocks, are reportedly specific enough to use for correlations and present in enough variety to allow for multiple correlations, although they occur in very small proportions in light condensates. They are assumed to apportion equally between oils and source rocks, although occasionally quantitative differences between the two are reported (Peters and Moldowan, 1993, p. 268). In this semi-quantitative study, biomarkers are assumed to apportion in constant ratios between oils and source rocks. There is also evidence that biomarker ratios can vary during long distance migration, in particular proportions of tricyclics vs pentacyclics (Seifert and Moldowan, 1986). Here again in this study that aspect was investigated but no such evidence could be found. This is largely because there are not enough oil or source rock samples to characterise the two to the accuracy needed to establish that fact. In all samples, enough biomarkers are available to allow for detailed study of their proportions. In some samples, however, the proportions of some biomarkers are too small to be useful.

In highly mature samples, correlations of oils and source rocks using fragmentograms as fingerprints, are more fruitful than pursuing the published biomarker ratios because:
(i) biomarkers characterising certain types of organic matter (gammacerane, oleanane) are depleted by thermal cracking and mass fragmentograms are not source-specific
(ii) many of the reactions which led to concentrations of biomarker isomers at lower maturities, such as back-bone rearrangement of steranes to diasteranes or conversion of regular 14α17α to 14β17β steranes reached completion (or equilibrium) earlier.

Indeed, many biomarker reaction rates are not fully understood in high maturity regimes and studies have recently addressed aspects of this problem (Van Graas, 1990; Raymond and Murchison, 1992; Farrimond et al., 1996). This incomplete understanding is largely a result of most studies concentrating on low to moderate maturity samples (ranging from R_o~0.4-0.8%). This range has been more commonly studied because the samples contain large proportions of biomarkers and because low maturity samples are more characteristic of oil. Many compounds are present in high maturity samples (R_o>~1.0%), but their derivation becomes less certain as thermal cracking reactions progressively alter their skeletons beyond those of their precursors. Nevertheless, detailed fragmentograms of high molecular weight samples can still provide enough biomarker ratios to compare oils with their source rocks and in some circumstances can still record maturity and source-related trends.

11.2.2. Depositional environment parameters

Biomarker parameters which allow evaluation of the depositional environment need to be characteristic of a particular environmentally characteristic organic matter type. Some biomarkers are extremely useful in characterising the input of organic matter from

specific environments and sometimes even of specific types. For example, gammacerane and certain homohopanes are shown to be characteristic of high salinity and high anoxicity environments. Carotanes are also characteristic of anoxic lacustrine environments but can also be found with terrigenous inputs into anoxic environments (Mello et al., 1988; Trindade et al., 1992). However, carotanes rarely survive transport in an oxic environment so these latter examples are rare.

Many of these biomarkers survive migration and can provide information on the origin of the parent organic material of reservoired hydrocarbons (except where severely matured). This facility is most useful where there is more than one potential source rock in the fetch area or where predictions need to be made regarding the presence or absence of source rocks in an untested area. The proportions of characteristic biomarkers in some oils allow establishment of correlations between samples which are far apart and where there is no obvious geologic connection. Oils in the Prudhoe Bay area, Alaskan North Slope, have been correlated with each other and to their source rocks over distances in excess of hundreds of kilometres (Mackenzie et al., 1985; Magoon and Claypool, 1985).

More specifically, trimethyl naphthalenes have been used to characterise source organic matter types (Alexander et al., 1988; Strachan et al., 1988), whilst ratios between certain dibenzothiophenes have found use in distinguishing lacustrine from marine sediments (Hughes, 1984; Davies, 1994b; Chakhmakhchev and Suzuki, 1995). These are based largely on their ability to detect the presence of terrigenous organic material. Other examples are found in the ratios of diasterane isomers which are characteristically developed in rocks deposited in clay-rich environments (Rubinstein et al., 1975). They can also be generated from regular steranes at maturation levels near the base of the oil window (Peters et al., 1990). Since this maturity level is commonly attained in samples from the Bredasdorp Basin, especially in the more deeply buried source rocks, this environmental interpretation tool is less definitive although subtle distinctions between some source rocks are found.

In basins where there are large differences between the source rock types, discrimination between different source rocks and organic matter environments using only sterane and pentacyclic terpane ratios, has proved very successful. However, in the Bredasdorp Basin, where organic material in most source rocks is largely similar, composed mainly of marine organic matter with modest proportions of terrigenous organic matter, and is of similar age (~115-108 Ma), the differences are much more subtle. Hence more subtle measures are needed to establish correlations, and a wider range of biomarkers are routinely studied.

11.2.3. Maturity parameters

Certain biomarker isomers are present in proportions which are characteristic of the maturation level achieved. During burial through the oil window, at least until the maximum or equilibrium ratio is attained, ratios between certain isomers characterise the maturity. Furthermore, even where absolute component proportions decrease through thermal cracking, many of these ratios are unchanged after expulsion. Hence where recorded in oils they indicate the source rock maturation level at the time of expulsion (Waples and Machihara, 1991; Mackenzie, 1984; Jovanicevic et al., 1993).

Biomarker ratios can be modified by addition of more or less mature hydrocarbons from another source. In shales this is not common as there is opportunity only for edge contact between oil in a migration conduit and the adjacent source. This is because source rocks form capillary and even pressure seals to migration (Mackenzie, 1984). Even in the cap rock of a reservoir, where long term diffusion may prevail, only the lightest gases (lighter than ~C8) impregnate the source rock in quantity and even these heavier components may penetrate no more than a few centimetres (Krooss et al., 1988 and 1991). Where the source rock is fractured, hydrocarbon impregnation can occur - but this process usually results in some fluorescent traces or even bitumen veinlets as indicators (Du Rouchet, 1981). Samples must therefore be chosen from locations away from these two characteristic features as well as from the extreme edge of the source rock. In this study, source rock samples were chosen from at least 10 metres away from known hydrocarbon accumulations.

In oils, however, modification of biomarker ratios is more common due to continued displacement by freshly migrating hydrocarbons during multiple phases of migration, as are interpreted to have occurred in the Bredasdorp Basin (Banks et al., 1993; Davies, 1997a and b). A second possibility for alteration of biomarker ratios in migrated hydrocarbons is by solubilization of *in situ* immature biomarkers from source rocks during migration of (generally) gas-condensates. These light oils are often rich in compounds commonly used as solvents, e.g. single-ring aromatics. As discussed above, it is unlikely that large volumes of biomarkers could be dissolved out of source rocks because of the limited contact with migrating hydrocarbons. The exception to this is in the case of largely dry gases, but these are not good solvents of high molecular weight biomarkers. It is likely that wet gas-condensate readily migrates through coaly rocks, because coals have more vertical joint migration pathways, and dissolve biomarkers from the rocks. Hughes and Dzou (1995) discussed one such example from Alaska, where gas-condensate was reservoired in intimate association with aliphatic-rich coals and biomarker ratios were affected. In the Bredasdorp Basin, no coals have been found in rocks older than Latest Cretaceous and the later examples

are not on the migration routes to known structures, so the known gas-condensate biomarker ratios are unlikely to have been affected by solubilization.

Other solubilization examples listed by Hughes and Dzou (op cit.) record small biomarker ratio changes due to solution from biomarker-rich shales in the reservoir. In the Bredasdorp Basin, despite intensive studies of core samples from many reservoirs in Cretaceous and Jurassic sediments, no such juxtaposition of source rocks proximal to or within reservoirs has been found

A third possibility is that of alteration of maturity ratios in-reservoir by either biodegradation or catalytic cracking (the former being briefly discussed later). Catalytic reactions are considered to have occurred in many source rocks, especially argillaceous-rich rocks, and to have resulted in generation of high maturity material at unusually low maturities (Hughes, 1984). They require the presence of large numbers of catalytic sources commonly not found in reservoirs. Most catalysts are either complexed transition metals (Mango, 1992) or high valence cations in clays (Hunt, 1979a, p. 128). In addition, it is known that clays have the ability to acid catalyse isomerisation reactions because of the high concentration of hydrogen ions released by dissociation of water at ionically active interlayer sites (Larcher et al., 1986). These sites are found primarily in montmorillonite clays but montmorillonite is deposited only in low energy environments and uncommon in sandstones, hence the likelihood of this effect occurring in a reservoir is small.

Indeed, catalytic cracking may be even less effective in the generation of hydrocarbons in source rocks because the process requires intimate contact between the organic matter and the catalyst. Kerogen and catalyst-bearing clay minerals can only contact at grain boundaries (Tissot and Welte, 1984) whereas generated oil is in more intimate contact with the clay particles. The opportunities for catalysis are therefore limited to the contact of already generated hydrocarbons with clays before expulsion occurs, hence this effect may be indistinguishable from the normal generation process. This was confirmed by the results of experiments carried out on bituminous coal (Saxby et al., 1992). The results showed that even where a high proportion of clay minerals was present, the maturation level evaluated from terpane compound ratios reflected the original maturity and not any excess effects of catalysis. Therefore, unless unusual circumstances arise, biomarkers in oils have the potential to give information about the maturity level of the source rock at the time of their generation and expulsion.

Indeed, where source rocks are rich, hydrocarbons can be expelled almost immediately and time for catalytic reactions to proceed may be restricted, yet where source rocks are less rich, generation rates are slower and it takes longer to build up enough oil to

saturate pores prior to expulsion so that catalysis can proceed further. Therefore, lower quality source rocks could suffer more from the effects of *in situ* catalysis than rich source rocks, which may be evident in differences between maturation ratios in oils from source rocks of different qualities. This is an area of study which has yet to be addressed and where there exists great potential for further advances.

Some maturation ratios do indeed show unusual reversals and examples of these are found in aromatics, steroids and homohopanes. These reversals may be due to a number of causes:
(i) there may be two processes operating on one of the compounds, but at different maturity levels, one process being in-source catalysis
(ii) a compound can be preserved or left unchanged because of unusual stability giving rise to an increased ratio, but is later thermally cracked and lost leading to a decreased ratio. Such is part of the explanation for the reversal of the methyl phenanthrene ratio MPI1 (Radke, 1988)
(iii) another possibility is that of an overlapping compound with a different maturity relationship. Spectral analysis of the relevant peaks can be used to confirm whether this happens by showing fragments which are unexpected from the known component. This possibility has been addressed for many samples in this study.

Recent studies (Van Graas, 1990, Raymond and Murchison, 1992; Farrimond et al., 1996) show that high rates of maturation, such as thermal increases accompanying igneous intrusive events, can significantly modify biomarker ratios. In extreme cases, some ratios (e.g. Ts/Tm) which normally reached equilibrium values at R_O~0.8% (Peters and Moldowan, 1993) only attained equilibrium after R_O~1.0%. This may be an effect where different proportions of catalysts in source rocks heated at matching rates will affect different hydrocarbons at different rates, and may help to explain the differences observed by Raymond and Murchison (1992) in source rocks containing different organic matter types. Indeed in some experiments with different source rocks heated at high equivalent maturation rates (Peters et al., 1990 and Van Graas, 1990), reversals occurred in samples of one type of organic material and not in others, nor were they recorded in naturally heated sample sets (e.g. regular C-29 sterane isomerization ratios). In some experiments the diasterane/sterane ratio reversed at high experimental maturities (Peters et al., 1990) whereas this did not happen in samples affected by different rates of experimental heating (Van Graas, 1990).

11.2.4. Post-generation alteration

The ubiquity of post-depositional or post-reservoiring alteration processes requires compounds which are only weakly affected by the process, otherwise their absence may be mistaken for different sourcing. Many studies have been carried out on aspects

of the more common alteration processes (i.e. water-washing, biodegradation, evaporative fractionation). The effects of these have been shown to be best characterised by proportions of low molecular weight compounds:
(i) the aqueous solubility of single-ring aromatics is much higher than the equivalent carbon number saturate and ratios of these relative to chain and cyclo alkanes effectively characterises water-washing
(ii) biodegradation readily removes small to medium molecular weight normal alkanes before isoprenoids and isoprenoids before heavy normal alkanes along a well-defined route
(iii) evaporative fractionation removes the most volatile light components such as normal, branched and cycloalkanes from light oils enriching the aromatics.

These processes are well defined, but the situation can arise where altered oils are recharged by input of fresh unaltered oils. The proportions of characteristic compounds can be masked, so other compounds are sought to characterise the alteration. For example, the loss of light alkanes which characterises early biodegradation can be masked by input of later oil which, if from the same source, is probably more mature and richer in alkanes than the preceding charge. Where such input is suspected, changes in proportions of heavier biomarkers typical of biodegradation may be sought, but they may be dominant only at higher levels of degradation.

One such characteristic is the increased proportion of 25-nor demethylated hopanes which have a base peak at m/z 177. Philp (1985, p. 164-174) and Farrimond et al. (1996) show that demethylated hopanes have a m/z 177 fragment which is ~50-70% of the size of the m/z 191 fragment, whereas in other norhopanes the ratio is ~10%. Many norhopanes co-elute with R-isomers of hopanes one carbon number smaller (Chosson et al., 1992; Farrimond et al., 1996). Comparison of the ratios between the S- and R-isomers of extended hopanes in both fragments would indicate any increased R-isomer in the m/z 177 fragment compared to that in the m/z 191 fragment.

Another way biodegradation affects source and maturity ratios is by preferential removal of the biologically-formed R-isomer in hopanes and steranes giving rise to false maturity indications where S/R ratios are employed (Chosson et al., 1992; Peters and Moldowan, 1993, p. 252-265; Peters et al., 1996).

11.2.5. Age determination

Many biomarkers are environment-specific fossils but some have age-specificity too. Oleananes are considered to have derived from angiosperm debris (Ekweozor and Telnaes, 1990, Moldowan et al., 1994). Angiosperms mostly developed during the Mid-Cretaceous although precursors which may have generated oleanane existed in Late

Jurassic (Moldowan et al., op cit.). Nevertheless, the presence of large quantities of these compounds in Early Jurassic and older rocks has been used to confirm the presence of contaminants (Davies, 1994b). A study of the age significance of the C28/C29 ($\beta\alpha$+$\beta\beta$+$\alpha\alpha$ S+R) steranes in oils showed that oils from Cambrian source rocks had the lowest ratios and oils from Tertiary source rocks the highest ratios, although the standard deviations were quite large (Grantham and Wakefield, 1988). A number of other parameters with age connotations have also been recorded, and are listed in Peters and Moldowan (1993, p. 273-274), but they have rather broad age-limits and are not suitable for differentiating the limited age range of Bredasdorp Basin source rocks.

11.3. BIOMARKERS STUDIED

Biomarkers commonly studied, such as C27-30 steranes and rearranged steranes (diasteranes) and C29-35 pentacyclic terpanes, are part of the medium to high molecular weight fractions of oils and source rock extracts. Lower molecular weight biomarkers do exist, notably C19-26 tricyclic terpanes, C20-22 mono- and triaromatic steroids and C20-21 steranes. They are not commonly studied in as great detail as the heavier biomarkers partly because their concentrations can be severely depleted by evaporation both in-reservoir and in-lab. They are often less structurally-specific since their skeletons are further removed from their precursor organisms and are therefore less useful in characterising hydrocarbons and source rocks. However, they can be used in high maturity samples where the higher molecular weight biomarkers are present in much reduced proportions. Some of the diterpanes and diterpenoids are characteristic of certain types of terrigenous organic material found in specific depositional environments (Alexander et al., 1988). In addition, members of the naphthalene and phenanthrene groups are studied, because they too are sensitive to changes in maturity, whilst the benzothiophenes are studied for their environmental and maturity information.

11.3.1. Biomarkers recorded

Biomarkers are generally better known in the saturated than the aromatic fraction because saturated compounds and precursor compounds are more common in living organisms than are aromatic compounds. Hence deposited and preserved organic matter contains a greater variety of saturated compounds from which comparisons can be established. The proportions of these biomarkers in samples are evaluated using specific ion mass fragmentograms. The ion monitored is usually the base peak for that group; for aromatic compounds this is usually the molecular ion. Example plots of each ion annotated with the peaks routinely used are shown in Figs. 11.03-11.09, 11.11 (saturated hydrocarbons) and Figs. 11.10, 11.12-11.19 (aromatic hydrocarbons).

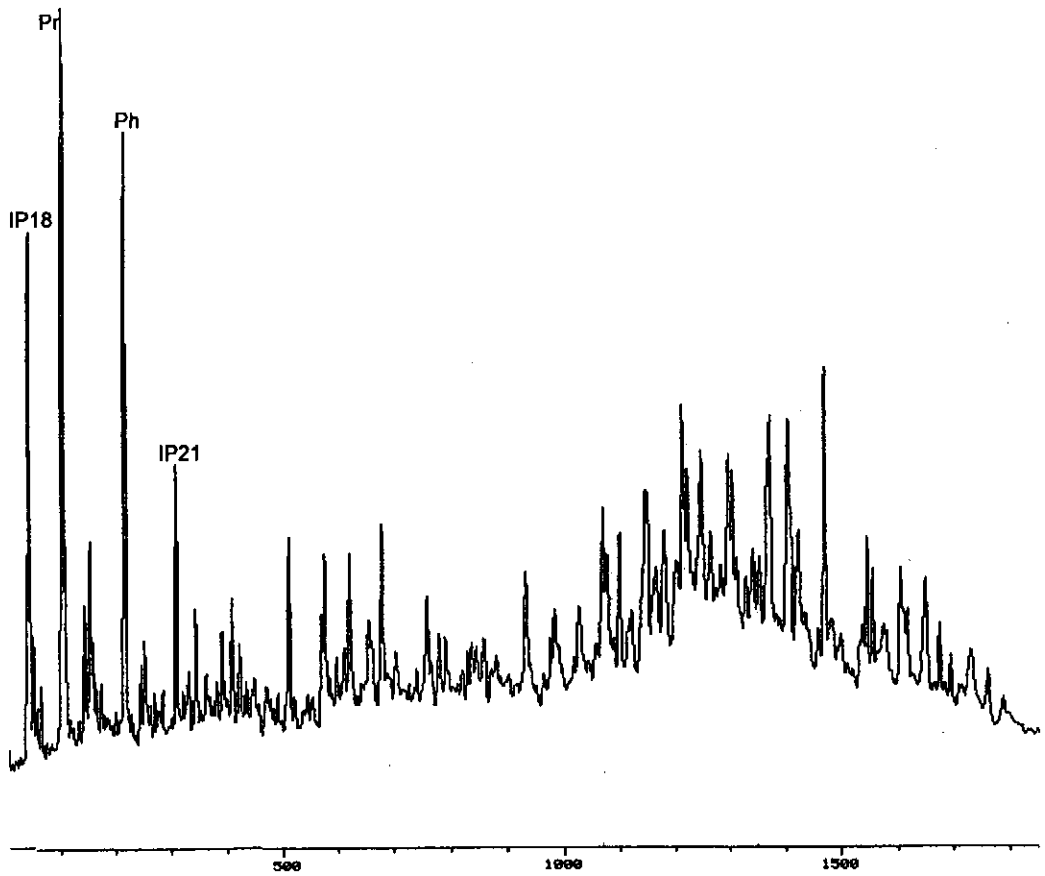

Figure 11.03: Partial fragmentogram of the total ion current (TIC) of an Aptian (13A) oil prone source rock (sample 59) with the regular C18-21 isoprenoids indicated. Labelling as detailed in Appendix G.

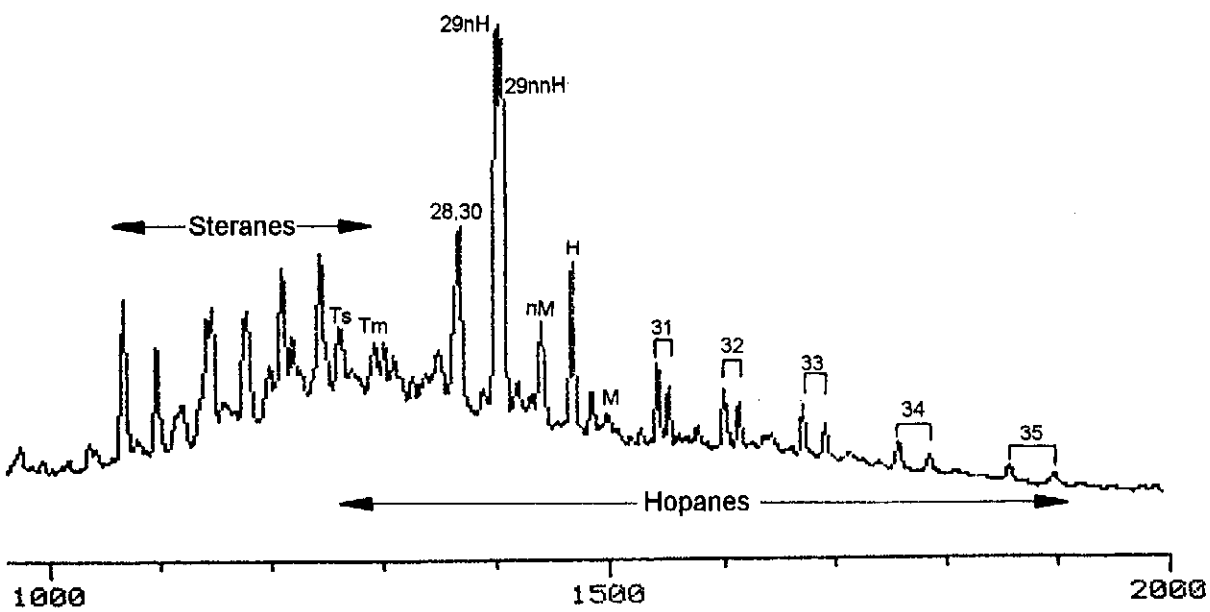

Figure 11.04: Partial fragmentogram of the m/z 177 ion of sample 59, characteristic of demethylated hopanes showing the steranes and pentacyclic terpanes. Labelling as detailed in Appendix G.

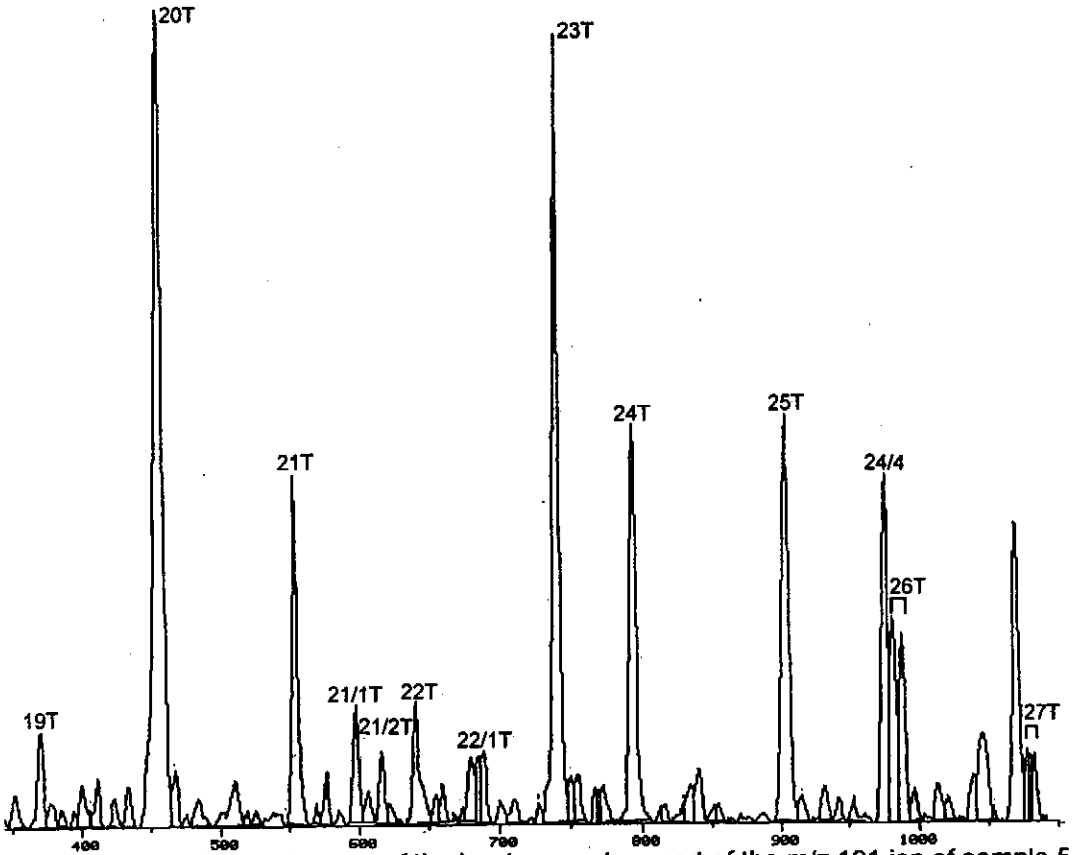

Figure 11.05: Partial fragmentogram of the low temperature part of the m/z 191 ion of sample 59, characteristic of the tricyclic terpanes (labelled T) and the C24 tetracyclic terpane (24/4). The doublets evident for the C26 and C27 homologues record the development of isomerisation at C-22. Labelling as detailed in Appendix G.

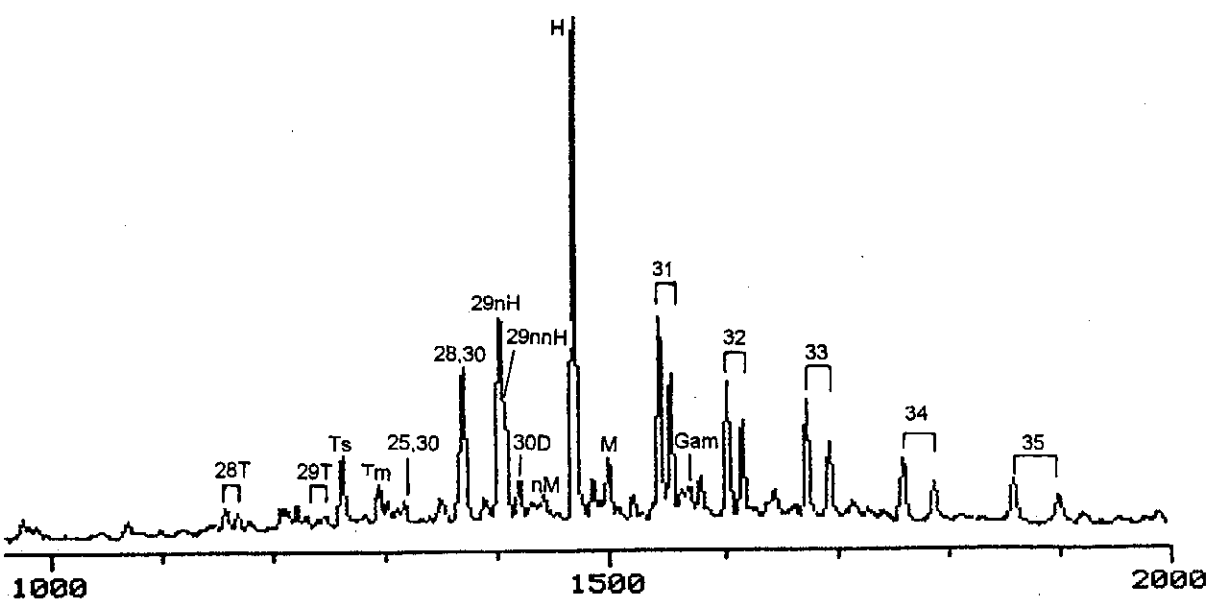

Figure 11.06: Partial fragmentogram of the high temperature part of the m/z 191 ion of sample 59, characteristic of the high molecular weight tricyclic terpanes, pentacyclic terpanes and gammacerane (Gam). Labelling as detailed in Appendix G.

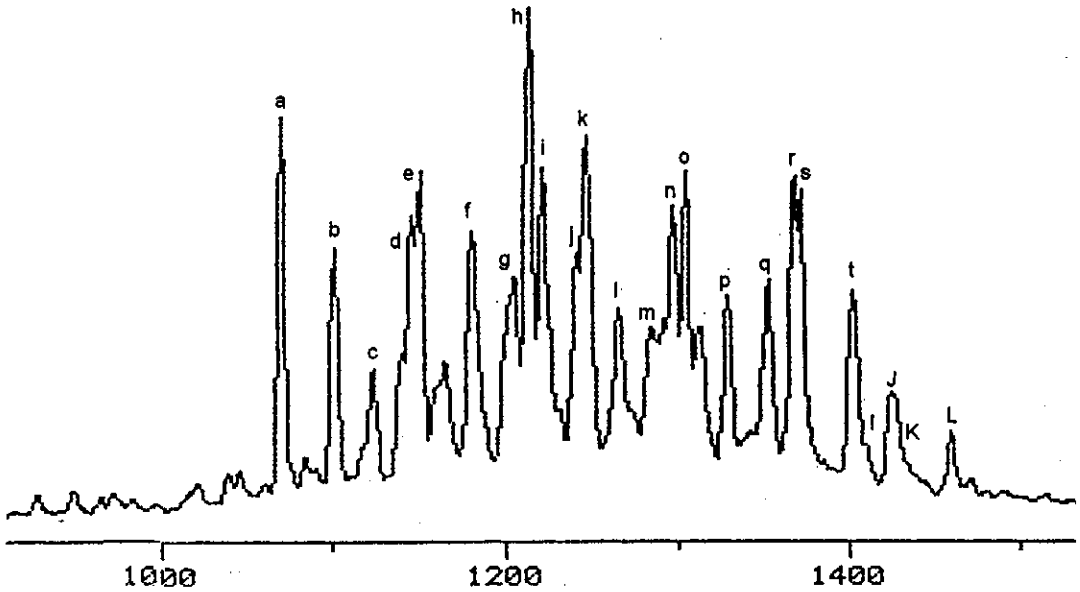

Figure 11.07: Partial fragmentogram of the m/z 217 ion of sample 59 showing the C27-30 steranes and C27-29 diasteranes. Labelling as detailed in Appendix G.

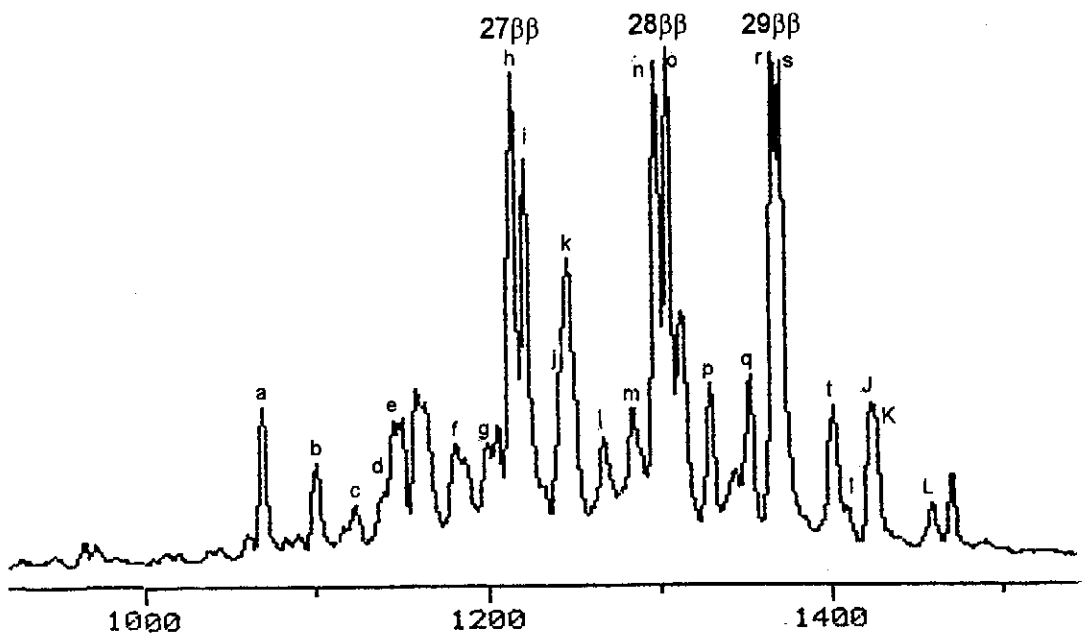

Figure 11.08: Partial fragmentogram of the m/z 218 ion characteristic of the C27-29 ββ steranes of sample 59. Labelling as detailed in Appendix G.

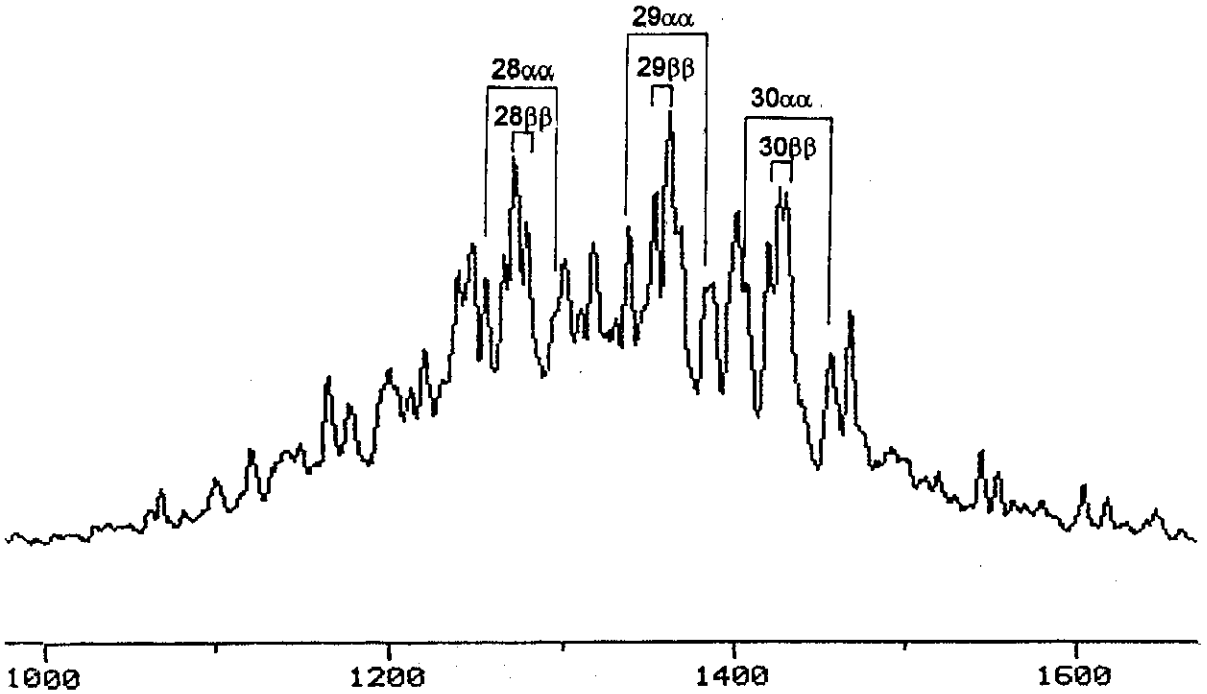

Figure 11.09: Partial fragmentogram of the m/z 231 ion characteristic of the C28-30 4-methyl steranes of sample 59. Labelling as detailed in Appendix G.

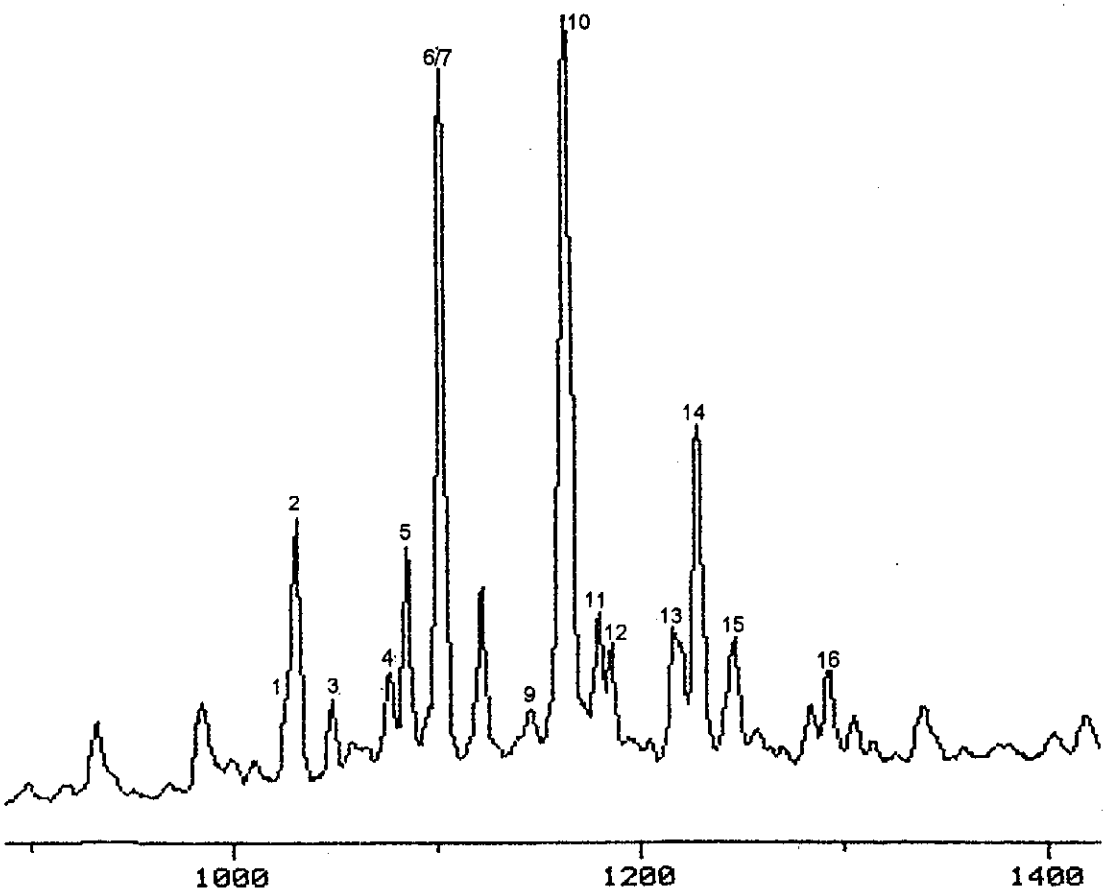

Figure 11.10: Partial fragmentogram of the m/z 253 ion of sample 59 characteristic of the monoaromatic steroids (MAS). This fragmentogram shows the MAS which eluted with the saturated hydrocarbon fraction. Labelling as detailed in Appendix G.

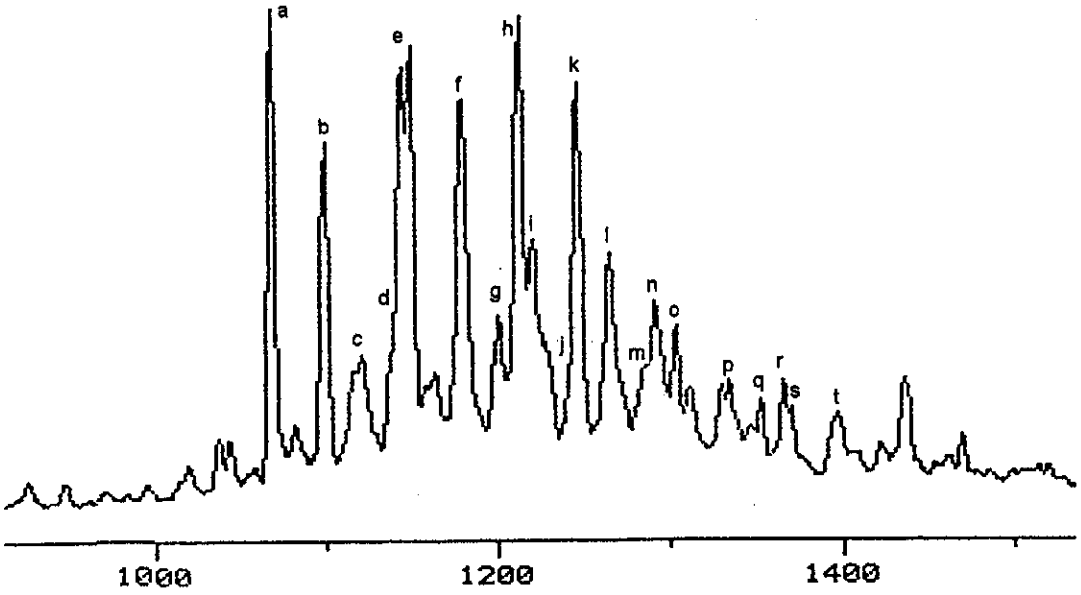

Figure 11.11: Partial fragmentogram of the m/z 259 ion of sample 59 characteristic of the βα diasteranes and showing the C27-29 homologues. Labelling as detailed in Appendix G.

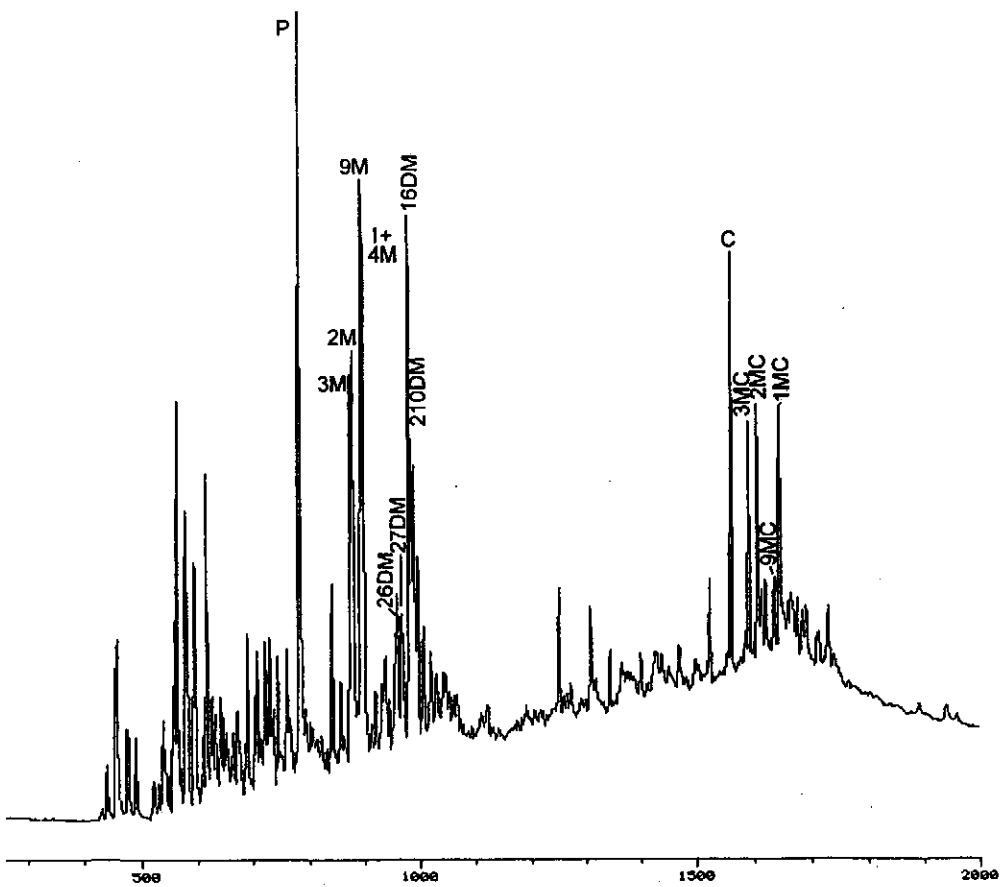

Figure 11.12: Partial fragmentogram of the total ion current from GC-MS analysis of the aromatic fraction of sample 59 with the phenanthrenes and chrysenes located. Labelling as detailed in Appendix G.

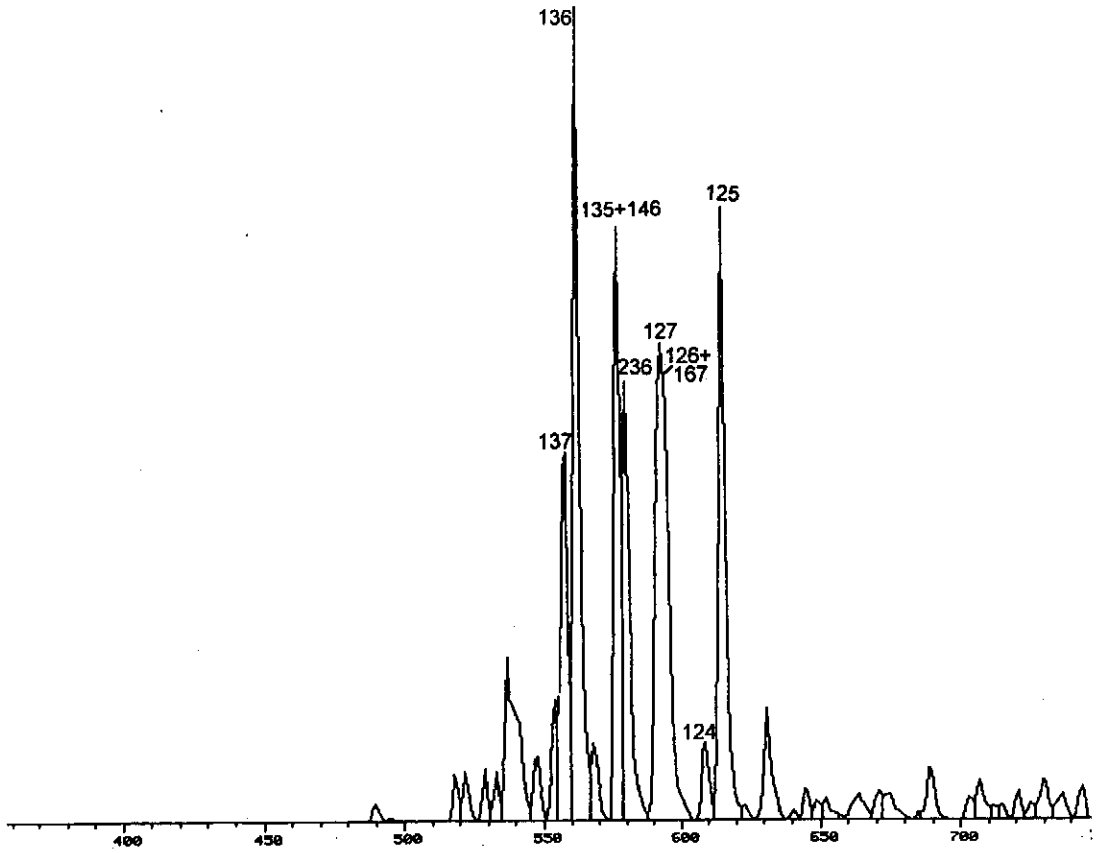

Figure 11.13: Partial fragmentogram of the m/z 170 ion of sample 59 characteristic of the trimethyl naphthalenes. Labelling as detailed in Appendix G.

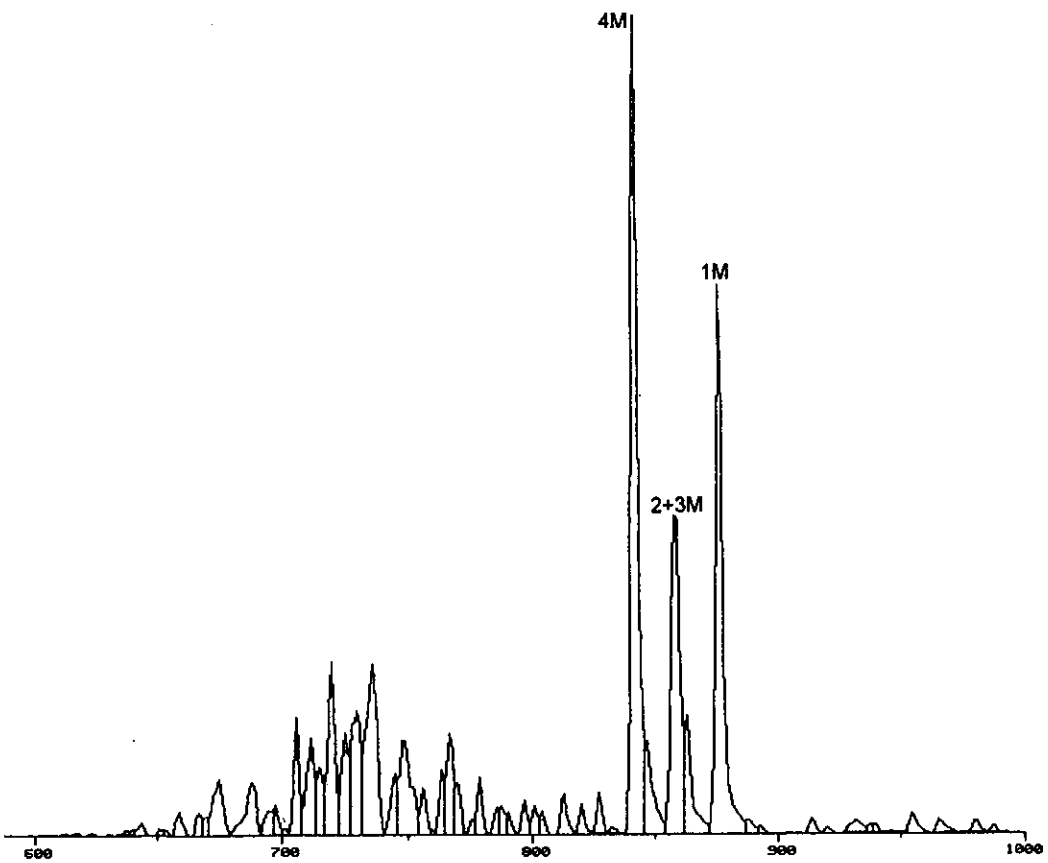

Figure 11.14: Partial fragmentogram of the m/z 198 ion of sample 59 characteristic of the methyl dibenzothiophenes. Labelling as detailed in Appendix G.

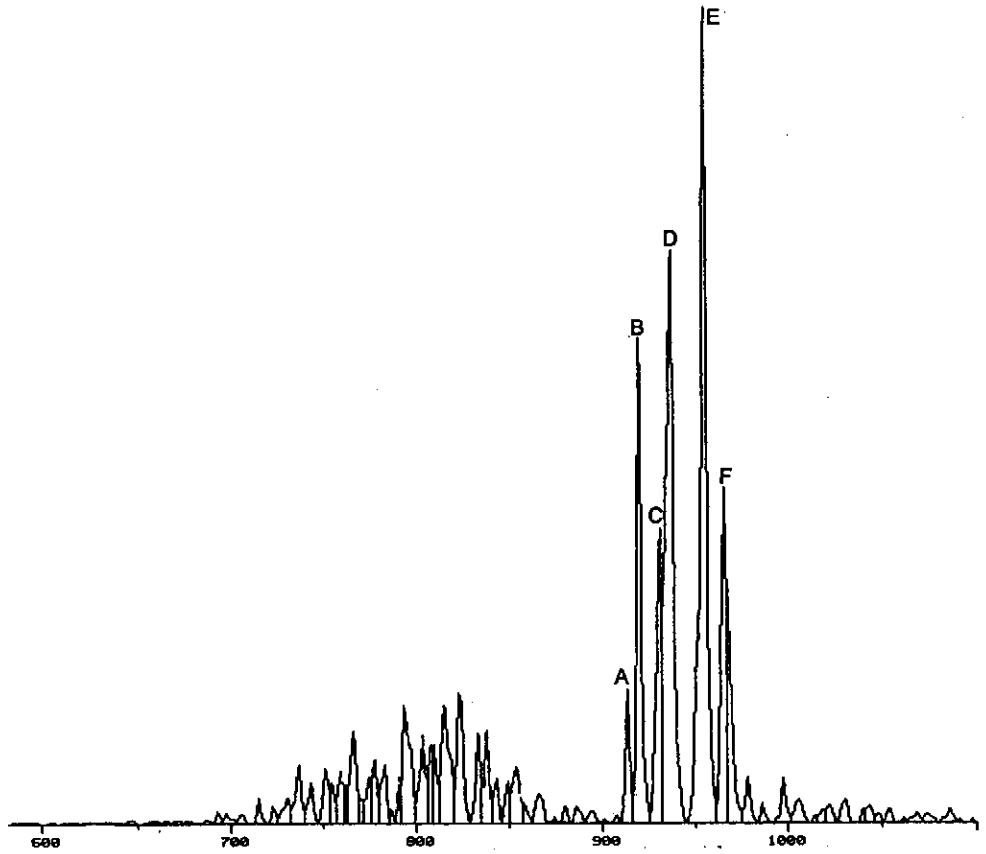

Figure 11.15: Partial fragmentogram of the m/z 212 ion of sample 59 characteristic of the dimethyl dibenzothiophenes. Labelling as detailed in Appendix G.

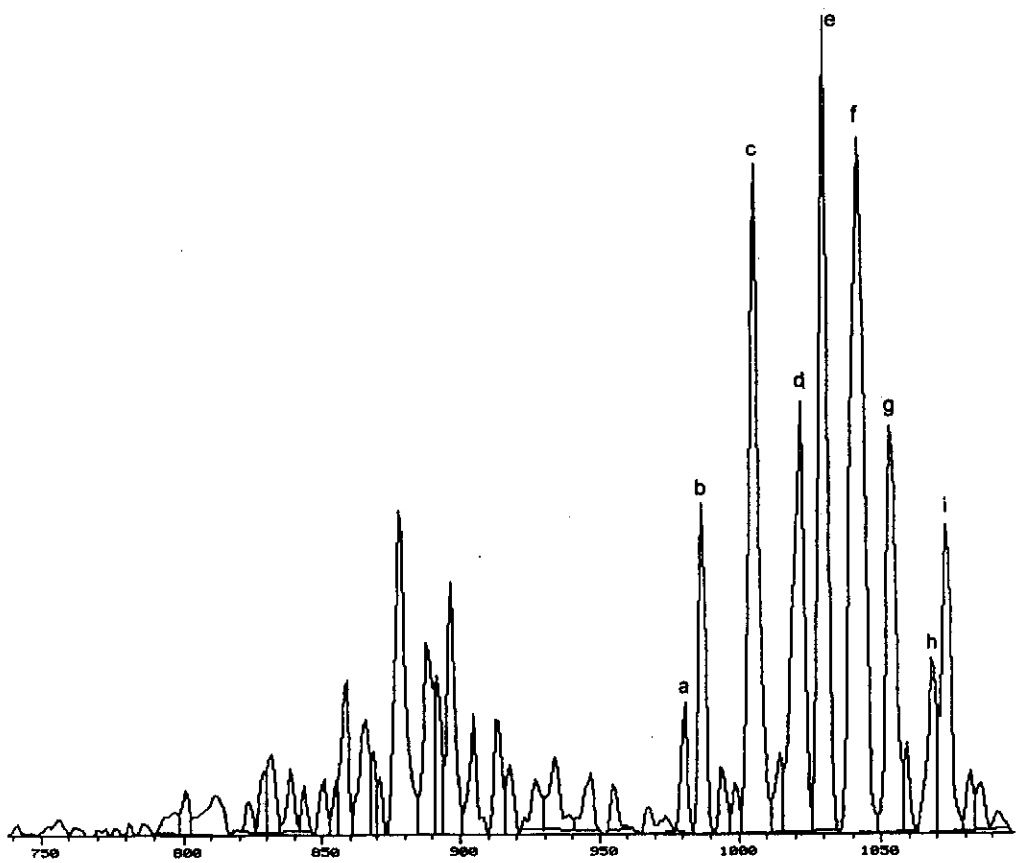

Figure 11.16: Partial fragmentogram of the m/z 226 ion of sample 59 characteristic of the trimethyl dibenzothiophenes. Labelling as detailed in Appendix G.

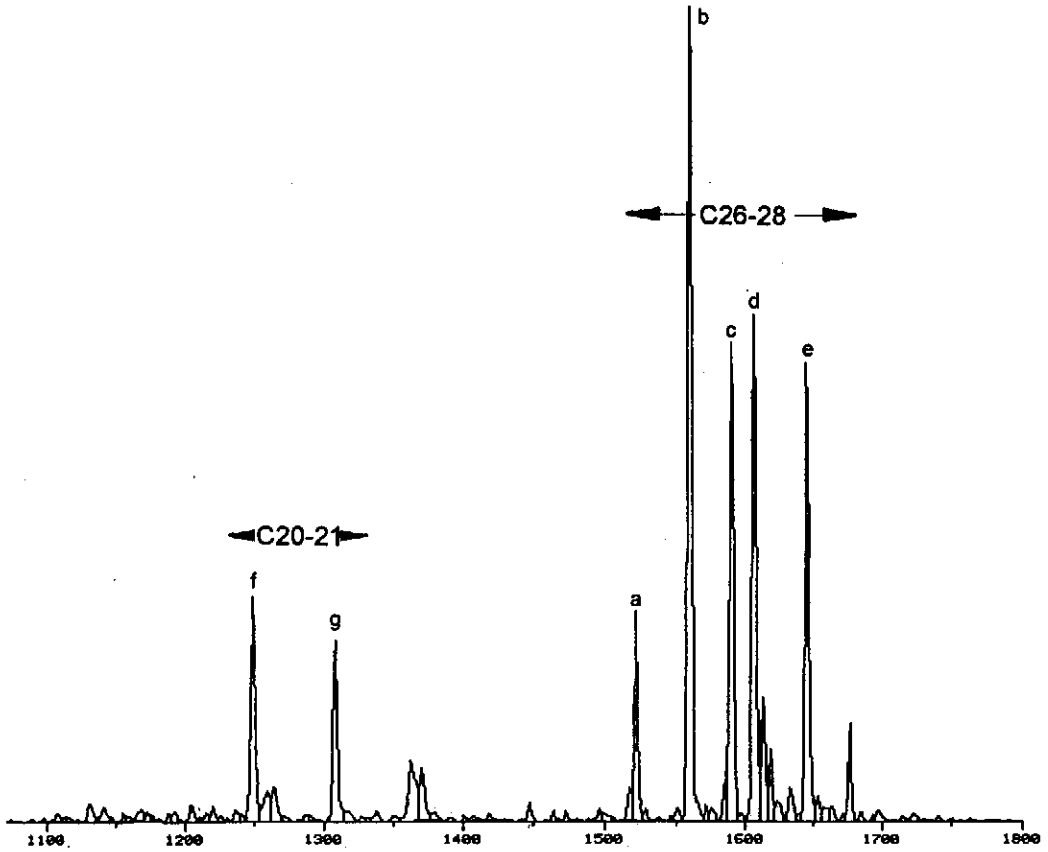

Figure 11.17: Partial fragmentogram of the m/z 231 ion of sample 59 characteristic of the C20-28 triaromatic steroids. Labelling as detailed in Appendix G.

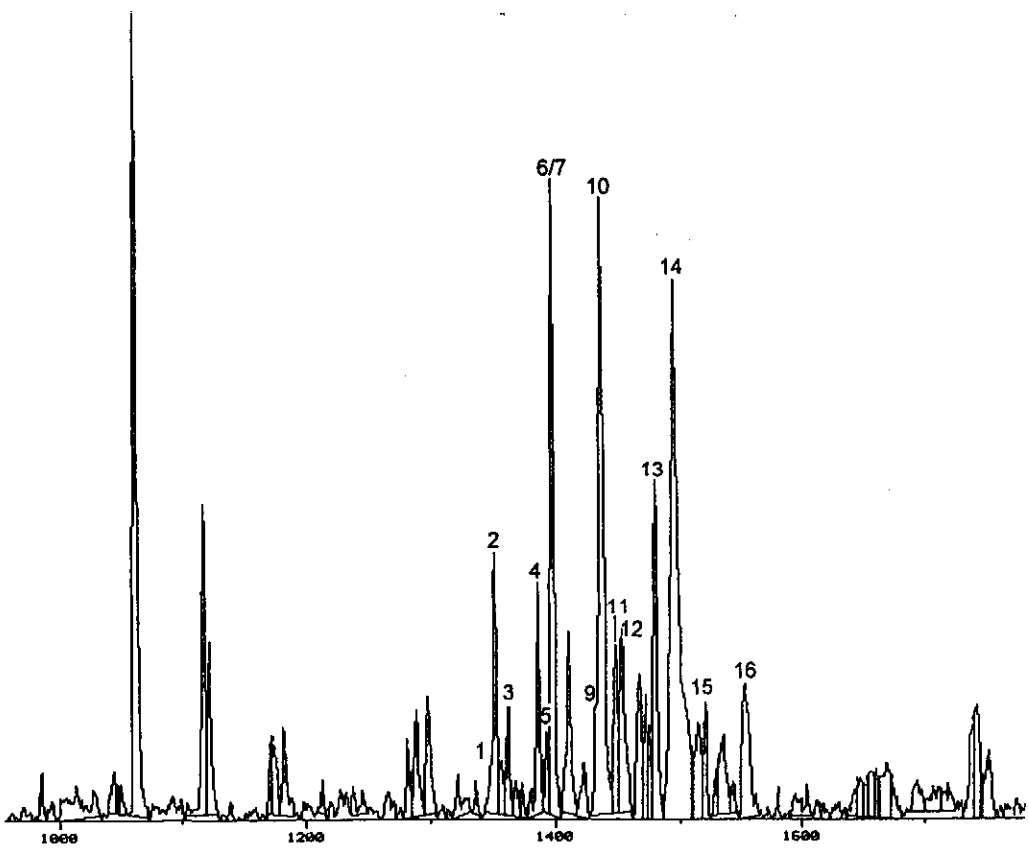

Figure 11.18: Partial fragmentogram of the m/z 253 ion characteristic of the C27-29 monoaromatic steroids (MAS). This fragmentogram shows the MAS eluting with the aromatic fraction. Labelling as detailed in Appendix G. Compare this plot with that in Figure 11.17.

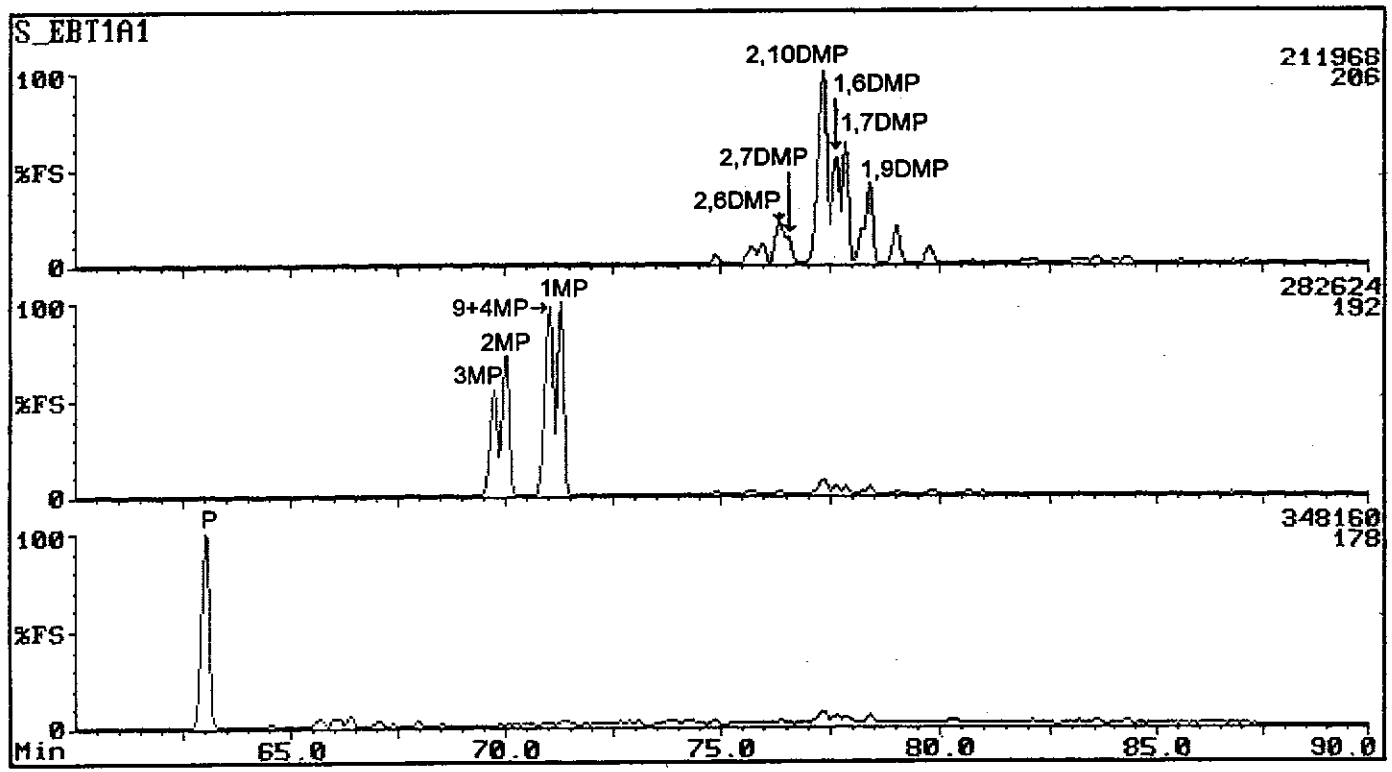

Figure 11.19: Partial fragmentograms of the m/z 178, m/z 192 and m/z 206 ions of sample 58 characteristic of phenanthrene, methyl phenanthrenes and dimethyl phenanthrenes. Labelling as detailed in Appendix G.

11.3.2. Saturated hydrocarbon fraction

The ions used to study the saturated hydrocarbons are:

(i) TIC (total ion current ≡ gas chromatogram): mostly for C18-21 isoprenoid proportions (Fig. 11.03)

(ii) m/z 177: for 25-norhopanes and relative proportions of steranes and hopanes (Fig. 11.04)

(iii) m/z 191: for tri- and tetracyclic terpanes (Fig. 11.05)

(iv) m/z 191: for pentacyclic terpanes (Fig. 11.06)

(v) m/z 217: for C27-30 regular and rearranged steranes (Fig. 11.07)

(vi) m/z 218: for C27-29 14β(H) 17β(H) steranes (Fig. 11.08)

(vii) m/z 231: for C28-30 4-methyl steranes (Fig. 11.09)

(viii) m/z 253: for characterisation of the C27-29 monoaromatic steroids (which mostly elute with the saturated biomarkers) (Fig. 11.10)

(ix) m/z 259: for accentuation of the C27-29 13β(H) 17α(H) diasteranes (Fig. 11.11).

Assignment proofs for at least one peak from each mass fragment are given in Appendix G. In addition, a number of other diagnostic ions are monitored:

(i) m/z 125: for carotanes

(ii) m/z 113 and 448: for botryococcanes

(iii) m/z 183: for isoprenoids

(iv) m/z 205: for diahopanes

(v) m/z 369: for hopanes (in order to differentiate gammacerane from coeluting norhopanes because gammacerane has no m/z 369 fragment)

(vi) m/z 412: for detection of oleananes (hopanes do not fragment to form this ion).

In some cases, biomarkers can be readily identified from gas chromatograms (cf. Fig. 11.01b with 11.06 and 11.07).

11.3.3. Aromatic hydrocarbon fraction

Mass fragmentograms obtained from the GC-MS analysis of the aromatic fractions of each sample are used to identify the following groups of components:

(i) TIC: for proportions of phenanthrenes, chrysenes and contaminants (Fig. 11.12)

(ii) m/z 170: for trimethyl naphthalenes (lighter naphthalenes are occasionally present but are usually lost in evaporation procedures) (Fig. 11.13)

(iii) m/z 198: for methyl dibenzothiophenes (Fig. 11.14)

(iv) m/z 212: for dimethyl dibenzothiophenes (Fig. 11.15)

(v) m/z 226: for trimethyl dibenzothiophenes (Fig. 11.16)

(vi) m/z 231: for triaromatic steroids (Fig. 11.17)

(vii) m/z 253: for monoaromatic steroids apportioned into the aromatic fraction (Figs. 11.10 and 11.18).

One other aromatic fraction mass fragmentogram, which is used (but not plotted in Appendix E) is the summed mass fragmentogram (m/z 178+192+206) (Fig. 11.19). This is used to identify phenanthrenes and to determine the methyl and dimethyl phenanthrene indices after Radke (1987). The groups of phenanthrenes used to calculate those ratios are annotated on the TIC fragmentogram.

Other than samples 1 and 2, which were analysed at the Kernforschungszentrum in Jülich, Germany (KFA) using tandem GC-MS-MS, and samples 28 and 29 analysed on a magnetic sector double-focussing MS by GH Geochemical Services (section 6.3.6), all samples were analysed by low resolution single quadrupole GC-MS (GC-LRMS). The paucity of high resolution analyses meant that identities of some compounds assigned solely from relative retention indices, have not been confirmed. This is especially true for the monoaromatic steroids (MAS). These are not only often present in very small proportions (<1% of TIC), but some also elute with the saturated fraction during the liquid chromatography stage, because the cut point between saturates and aromatics (determined by colour change) is not precise enough. This tends to reduce the concentration of MAS in the aromatic fraction even further. In general, a higher proportion of the MAS are found in the saturated hydrocarbon fraction. This situation could have been avoided if high pressure liquid chromatography (HPLC) had been used for the separation of the hydrocarbon fractions as described in Radke et al. (1980).

Some of the samples were too small (<1 mg) to submit to removal of the normal alkanes, because branched and cyclic material can also be lost in the process, and consequently their analyses show some normal alkanes overlapping some steranes and terpanes (Samples 6 and 33, Appendix E, Figs. E.06 and E.33).

11.4. SOURCE AND DERIVATION OF BIOMARKERS

A brief summary of the mode(s) of formation of each of the most commonly utilised biomarkers or groups of biomarkers and a listing of those discussed is given below where relevant for this study. The concentration of individual biomarkers or groups of biomarkers is a function partly of the amounts incorporated into the sediment and surviving diagenetic alteration, and partly of the changes caused by further burial and maturation. The resultant biomarker proportions are therefore indicators of:
(i) the history of the source rock and the hydrocarbons generated therein
(ii) the maturation level attained and in some cases, the maturation rates
(iii) the alteration processes which have affected the organic matter and hydrocarbons
(iv) the migration history of the expelled hydrocarbons.

11.4.1. Saturated hydrocarbon fraction

Saturated hydrocarbon biomarkers comprise the following:

(i) steranes subdivided into regular, rearranged and 4-methyl

(ii) hopanes subdivided into tri-, tetra- and pentacyclic, norhopanes, diahopanes, gammacerane, carotanes, (which have 191 fragments even though they are not hopanes), oleananes.

11.4.1.1. Steranes

Sterols are sterane precursors and are considered to act as cell wall 'stiffeners' in eukaryote organisms, e.g. higher plants and animals (Nes, 1974). Steranes derived from diagenesis and catagenesis of these sterols are common constituents of virtually all source rocks. They are shown in Figs. 11.07, 11.08 and 11.11.

The derivation of this group of compounds is well-understood in terms of their origin, their diagenesis and maturation in source rocks and their alteration in migrated hydrocarbons. Discussions regarding their formation and alteration are summarised for the compounds used in this study (Mackenzie, 1984; Volkman, 1988; Peters and Moldowan, 1993). Cholesterol and other sterols are 3-ring condensed naphthenic compounds amenable to diagenetic modification by dehydration and microbial reduction before thermal effects become prevalent. These processes can result in the formation of alkanes (Mackenzie, 1984). Alternatively, further clay-catalysed reactions may result in rearrangement of the steroid skeleton to form diasterenes in which the double bond is at C-13 and C-17 (Rubinstein et al., 1975). Aromatization of the A-ring can also occur during diagenesis leading to the formation of aromatic steroids (Hussler et al., 1981). During further burial, steroid hydrocarbons can be significantly affected by maturity related processes giving rise to preference for (i) lower molecular weight compounds, (ii) further aromatization and (iii) isomerization.

Isomerization affects five chiral centres, at C-5, C-14, C-17, C-20 and C-24. The centre at C-5 is in the β configuration in biological components but readily converts to the α configuration during early burial. This conversion is an indicator of very low maturity (or diagenesis, Mackenzie, 1984) but owing to the relatively high maturities found in Bredasdorp Basin samples, has not been recorded in these samples. The centres at C-14 and C-17 are both in the α configuration in deposited organic material, as this is favoured for sterols utilised in cell walls where the molecularly 'flat' configuration provides a greater degree of strengthening (Nes, 1974). With increased maturity, both centres convert to the thermodynamically more stable β form and the ratio $\beta\beta/(\alpha\alpha+\beta\beta)$ is a commonly utilised maturity parameter (Cornford, et al., 1983). This conversion can also occur during diagenesis (Peakman et al., 1989) affecting the maturity ratio, but examples of immature sediments in which this has been found are all from hypersaline

environments. Since none of the samples in this study are known to have been deposited under such conditions, this effect is not expected and the ratio is considered to be a function largely of maturity. Examples of the 14β17α and 14α17β ratios have been found but are rare since they are even less thermodynamically stable than the 14 α17α form (Peakman et al., 1989).

The chiral centre at C-20 also converts with increased maturity from the biological R isomers to approximately equal proportions of the R and S isomers. The apparent proportion of the C29 homologue can be influenced by coelution with an unknown compound (possibly a terpane) and Mackenzie (1984, p. 170) recommends using the m/z 218 fragment to confirm the ratio. However, the C29 αα regular compounds are barely visible in that fragment, because fragmentation generally results in minimal amounts of the m/z 218 fragment and the isomer ratio is poorly visualised. Isomerisation at the C-24 centre is largely a function of the type of organic material incorporated into the sediment. Dominance of higher plant material results in higher proportions of the R isomer and dominance of algae results in higher proportions of the S isomer. Since these overlap on non-polar columns, the distinction is not possible. The absolute amounts of the C27-29 αα steranes decrease significantly with increasing maturation. However their proportions, which are source-specific, remain nearly constant. In addition, the conversion of the αα form to the ββ form tends to preserve the relative proportions so that even at high maturities, the ββ steranes retain the original source-specificity (Peters and Moldowan, 1993, p.223).

C27-29 rearranged steranes, also called diasteranes, form from previously formed diasterenes or in mature samples either by hydrogen exchange reactions (Rullkötter et al., 1984) or by virtue of a greater stability than regular steranes. Carbon-number specificity matches that of regular steranes and the S/R ratio can be used to characterise maturity relationships as in the regular steranes (Mackenzie et al., 1980).

Regular C30 steranes (propyl cholestanes) occur in non-marine sediments (Cornford, 1986). They are evident on m/z 217 fragmentograms but elute close to the times of C30 4-methyl steranes. They can strictly only be distinguished from the 4-methyl steranes by parent-daughter (m/z 412→217 or m/z 414→98) ion relationships in GC-MS-MS analyses, but such analyses are only available for two samples in this study.

11.4.1.2. 4-methyl steranes

The 4-methyl steranes are thought to have been derived from dinoflagellates (Wolff et al., 1986) or if alkylated at C-24, possibly from algae (Volkman, 1988), They can be found in both marine and non-marine petroleum showing that they may not be effective source environment parameters, but almost all samples in which they are found in high

concentrations are from lacustrine sources (Wolff et al., 1986; Brassell et al., 1986). These compounds are best determined from GC-MS-MS analyses but can also be characterised using the m/z 231 ion (Fig. 11.09).

11.4.1.3. Hopanoids

Hopanoids have been shown to be strongly linked to bacterial source, probably bacteriohopanetetrol, which is a 'flat' molecule found as a strengthener in cell walls in prokaryotic organisms such as bacteria and some algae (Ourisson et al., 1984). In this regard they occupy the same ecological niche that steroids occupy in eukaryotic organisms. These hopanoids are comprised of five condensed naphthenic rings with a dominant alkyl chain located at C-24. Hopanoids are generally found in two isomeric series in sediments in the lower diagenetic zone; 17α(H),21β(H) and 17β(H),21α(H). There is also a third series with the form 17β(H),21β(H) but it is thermally unstable and readily breaks down to form the other two series in early diagenesis. Those with the 17 β(H), 21α(H) configuration are called moretanes. They range from C27-C35 but generally only the C29-31 forms are found. They are thermally unstable, breaking down during early oil window maturity, although the commonest two (moretane and normoretane) do survive into late oil window maturity. Those hopanoids with the 17α (H), 21β(H) form are called hopanes. These pentacyclic terpane-based compounds have a wide size range (C27-C35) and comprise several homologous series (Figs. 11.05 and 11.06). In many of these compounds, as in the steranes, the R isomer is readily attacked during bacterial degradation and either removed or converted to the S isomer so that anomalously high S/R ratios are found. However, as with the steranes this only happens at level 6 biodegradation (Peters and Moldowan, 1993, p. 254) or higher.

11.4.1.4. Demethylated hopanes

This series is one in which the usual hopane skeleton has been demethylated at certain carbon atoms. Methyl groups are preferentially absent from carbon atoms in one of two series namely C25-, C28-, C30- and C22-, C29-, C30. Removal of a methyl group is often an indication of thermal or bacterial alteration, the latter taking place either during diagenesis of the kerogen (Subroto et al., 1991; Schoell et al., 1992) or in-reservoir (Peters et al., 1996). One of the commonest norhopanes is C-28,30 bisnorhopane which has been identified in oils from highly anoxic environments (Seifert and Moldowan, 1978; Mackenzie et al., 1988). This compound is thermally unstable and largely absent from samples at maturity levels of R_o>~0.8%. It is sourced from detrital bitumen rather than kerogen, hence its near disappearance above R_o~0.8% may be a function of reduced proportions rather than destruction (Tannenbaum et al., 1986).

Other common norhopanes, the C27 and C29, 17α(H)nor- and 18α(H) norneohopanes (Figs. 11.04 and 11.06), belong to the same series, demethylated at C30-, C29- and C22-. The C27 pair was identified early on as being able to characterise maturity (Seifert and Moldowan, 1978) and were named Tm and Ts to indicate 'stable' and 'maturable' respectively. Indeed, the 18α(H) isomer is shown (Moldowan et al., 1991) to be thermally more stable than the 17α(H) isomer in the C29 and C27 forms, confirming earlier studies (Seifert and Moldowan, 1978). More recently, the C29 analog of Ts has been determined as the peak immediately adjacent to C29 norhopane (Hughes et al., 1985; Sofer, 1988; Moldowan et al., 1991). The ratio between these two C29 terpanes is also shown to have maturity connotations. The maturity connotation of the C27 pair is reduced in carbonate-rich rocks (Mackenzie et al., 1983) whilst Moldowan et al. (1986) show high Tm/(Tm+Ts) (i.e. lower Ts/Tm) ratios where sediments are marls and the organic material is dominantly Type 3.

Hopanes of the 25-nor type are common in biodegraded samples. They are considered to be present in immature oils only and concentrated in biodegraded samples (Armanios et al., 1992; Chosson et al., 1992) but other studies show that they are generated during biodegradation (Seifert and Moldowan, 1979; Goodwin et al., 1983).

11.4.1.5. Diahopanes

C30 diahopane (compound 'X' of Philp and Gilbert, 1986a; 1986b), eluting just after the C29 norhopanes (30D, Fig. 11.06), shows a maturity-related increase relative to the C29 norneohopane (Horstad et al., 1990). Subsequent work has identified this compound as a C30 diahopane (Moldowan et al., 1991) thought, on the basis of ^{13}carbon isotopic data, to be derived from the same precursor as the C27-30 hopanes (Moldowan et al., 1991; Peters and Moldowan, 1993, p. 162). The compound also has a source-specific aspect in its abundance in oxic-suboxic environments (Philp and Gilbert, 1986a) and in clay-rich depositional environments (Peters and Moldowan, 1993, p. 162). The C30 diahopane is now considered to be part of the homologous series of diahopanes extending from C27-C34 (Summons et al., 1988) and showing the same isomer doublets as the homohopanes. The C30 diahopane differs from C29 and C30 hopanes in the rearrangement of alkyl groups on ring-D. Perhaps because of this it is generally more thermally stable than the hopanes and therefore the increase with depth relative to the C29 norhopane is maturity-related. Where diahopanes are abundant in Bredasdorp Basin samples, some of the doublets can be seen eluting just before each homohopane doublet (Appendix F, Figs. F.24, 54, 59 and 61).

11.4.1.6. Gammacerane

This C30 triterpane, which elutes immediately after the C31R homohopane isomer on non-polar columns, is a marker for highly saline, commonly lacustrine, anoxic

depositional environments (Moldowan et al., 1985; Jiang and Fowler, 1986; Mello et al., 1988). It is best visualised using the m/z 191 fragment (Gam, Fig. 11.06), but is most readily distinguished from the hopanes in the m/z 412 fragment where the effects of the near co-elution of the C31 hopane are minimised.

11.4.1.7. Oleananes

A strong correlation exists between the proportions of oleananes and higher plant lipid macerals of angiosperm origin (Ekweozor et al., 1981; Ekweozor and Telnaes, 1990). The two isomers, 18α(H) and 18β(H), elute from non-polar columns immediately before the C30 hopane. They have a larger m/z 412 fragment than the adjacent C30 hopane but are more commonly distinguished by their presence in the m/z 191 fragment and absence from the m/z 369 fragment (Peters and Moldowan, 1993, p. 156).

Oleananes are not likely to be found in source rocks or oils in the Bredasdorp Basin as angiosperm plants reportedly become dominant only during the Latest Cretaceous and continue so through the Tertiary (Peters and Moldowan, 1993, p. 155). However, primitive angiosperm pollen were found in Mid-Cretaceous and younger rocks in wells on the west coast of South Africa (Zavada and Benson, 1987). Their samples ranged in age from Early Turonian to Mid-Campanian, which extends the age-range further than that shown from Nigerian samples (Ekweozor and Udo, 1988) but still within the range shown by Moldowan et al., 1994). The only source rocks in the Bredasdorp Basin which fall within this time range and might contain oleananes are those in the 15A sequence (Turonian). Angiosperm lipid debris is best preserved in shallow marine, deltaic environments close to the material source. Both these samples are from deep marine environments, in which angiosperm material is unlikely to be found in quantity. However, since angiosperm pollen have been found in the region, and the sample from well 99 at least is known to contain terrigenous material, the possible presence of oleanane in Turonian source rock samples was investigated. These compounds would be an invaluable marker for hydrocarbons expelled from these Turonian source rocks. However, fragmentograms of the m/z 191 ion for those two samples do not show the presence of peaks in the expected location (i.e. eluting just before hopane) with the characteristically absent m/z 369 ion. Hence it appears that either angiosperm material did not form part of the deposited organic matter or the environment was not conducive to their preservation.

11.4.1.8. Carotanes

Carotanes are derived from carotenoid pigments which have two dominant sources, namely higher plants and some algae. These pigments are known from both marine and non-marine anoxic depositional environments (Tissot and Welte, 1984, p. 126). Carotenoids undergo reduction in low sulphur environments to form carotanes, but in

high sulfur environments, carotenoids become part of the non-hydrocarbon fraction through reactions with sulphur (Peters and Moldowan, 1993, p. 164). Hence most occurrences of carotanes are in anoxic saline, low sulphur, lacustrine deposits (Hall and Douglas, 1983; Jiang and Fowler, 1986; Peters et al., 1989) although they have more recently been noted in Cretaceous largely calcareous, evaporitic, marine rocks dominated by input of terrigenous material (Mello et al., 1988).

11.4.1.9. Tetracyclic terpanes

Although this group of 4-ring 17,21 secohopanes can extend through C24 to C35 (Aquino Neto et al., 1983), the only one commonly developed is the C24 species (Fig. 11.05). The characteristic ion is m/z 191 although the m/z 329 fragment is also useful for detection of the extended tetracyclic terpanes. Where this latter ion was monitored, there was no evidence in any sample for significant amounts of other species of this series. The compound elutes equidistant between the C25 and C26 tricyclic terpanes on non-polar columns (e.g. OV101) but closer to the C26 S+R doublet on slightly polar columns (e.g. DB5). Tetracyclic terpanes have been shown to be largely absent from low maturity samples (Aquino Neto et al., 1983) suggesting that thermocatalytic degradation of a hopanoid precursor (Philp, 1988) may be the source. Alternatively they could have formed by microbial degradation of hopanoids (Philp, 1988). Certainly the latter route may not always be necessary as tetracyclic terpanes have been generated from non-biodegraded crude oil resin and asphaltene fractions (Aquino Neto et al., 1983). Abundant proportions of the C24 member are an indicator of carbonate (Palacas et al., 1984) or evaporitic environments (Connan and Dessort, 1987; Clark and Philp, 1989). Both the source and maturity connotations of the abundance of the C24 species relative to the adjacent tricyclic terpanes are used in unravelling the hydrocarbon generation history of the Bredasdorp Basin.

11.4.1.10. Tricyclic terpanes

This series of 3-ring naphthenes is considered to be derived from bacterial or algal lipids. Aquino Neto et al. (1983) proposed a source in a hexaprenol, a cell wall constituent. Some authors have shown that their source is largely non-marine organic matter (Volkman, 1988) but they are also known from marine oils (Aquino Neto et al., 1983 and Zumberge, 1983). Their characteristic ion is the m/z 191 fragment, the same as the hopanes, and because their range extends beyond C26, they locally overlap some of the hopanes. For example, C30 tricyclics frequently overlap Ts.

As with the tetracyclic terpanes, the tricyclics can also be generated from resin or asphaltene fractions of oil suggesting a non-kerogenous source such as detrital bitumens (Aquino Neto, et al., 1983; Ekweozor and Strausz, 1983). The variability of the proportions of the different members of the commonly found tricyclics (mainly C19-

26) in different source rocks relative to hopanes indicates that they are a useful source correlation parameter (Seifert et al., 1980; Figs. 11.05; 11.06). They are also found in some reservoirs in ratios, especially that of C23/C21, which are entirely predictable from maturity data. This suggests they too have a maturity connotation (Ekweozor and Strausz, 1983) and it appears that maturity increases affect the secondary tricyclics (e.g. C19-22) rather than the primary tricyclics (e.g. C23-26). They have been found to be largely unaffected by biodegradation, even at level 10 (Peters and Moldowan, 1993, p. 254) and can still provide correlative data where all other hopanes have been removed. Seifert et al. (1980) contend that tricyclic terpanes migrate faster than pentacyclic terpanes (hopanes) and use the ratio between them as a migration distance parameter.

11.4.2. Aromatic hydrocarbons

Aromatic hydrocarbon biomarkers comprise the following:

(i) Trimethyl naphthalenes (Fig. 11.13)

(ii) Phenanthrenes (Figs. 11.02 and 11.19)

(iii) Aromatic steroids, mono- and tri- (Figs. 11.10; 11.17; 11.18)

(iv) Thiophenes, methyl- , dimethyl- and trimethyl- (Figs. 11.14-11.16).

Aromatic hydrocarbons used in biomarker correlation and maturity studies are polycyclic. Usually all rings are aromatic as in the phenanthrenes, but tricyclic mono-aromatic hydrocarbons, in which two of the rings are naphthenic, are also studied. Their origin, where known, is summarised by Radke et al. (1982b) and Radke, (1987) who indicate that the origin of the aromatic hydrocarbons is less well known than the saturates and is somewhat more complicated. They report that biosynthesis in large quantities is unlikely and that polycyclic aromatic hydrocarbons (PAH) are largely derived from non-aromatic precursors, possibly by catalysis on surface-active minerals such as clays. Very few aromatics, other than some 1 or 2-ring naphthalenes and benzenoid moities of, *inter alia*, proteins and lignins, are found in nature. Some increase with depth whilst others increase towards the surface showing their anthropological input (Wakeham et al., 1980). One major natural source for PAH is in soot formed from natural combustion, e.g. forest fires. PAH are therefore known to form from a wide variety of heavily altered biogenic precursors so it is difficult to establish the precursor with certainty (Tissot and Welte, 1984, p.126-127; Radke, 1987, p. 143).

Cholesterol is thought to be a phenanthrene precursor because of their similar molecular shapes (Radke, 1987, p. 143-166). The 2-to-5-ring PAH are formed by clay-catalysed dehydrogenation or hydrogen disproportionation reactions from steroids, suggesting that steroids undergo a complicated transformation process to form mono-

and triaromatic steroids (Mackenzie, 1984, p. 137-144). No matter how far the PAH are removed from their precursor material, in some circumstances, different source organic facies have different concentrations of each PAH and can be distinguished by GC and GC-MS data (Radke et al., 1986). In general, aromaticity increases with depth linked to maturity increases (Radke et al., 1982b) and the effect is clearly evident in phenanthrenes.

11.4.2.1. Trimethyl naphthalenes

At least one of these compounds (1,2,5) originated in natural resin precursors indicative of Araucariaceae conifers (Alexander et al., 1988; 1992), which are relatively common in the Late Jurassic. Unusual proportions of that compound, and possibly others, may be evidence for a strongly terrigenous syn-rift source for the kerogen. Alternatively, they may form by thermal degradation of pentacyclic terpanes and PAH (Peters and Moldowan, 1993, p. 205). Their proportions reflect both the original hydrocarbons from which they were derived and the thermal alteration state achieved. In view of the near ubiquitous presence of these compounds, except where depleted by evaporation, they are more useful for thermal alteration studies (Fig. 11.13).

11.4.2.2. Phenanthrenes

These 3-ring aromatic hydrocarbons are commonly developed in the aromatic fraction, often in larger proportions than any other group. They can comprise up to 20% of the total fraction. In many samples, phenanthrene is usually accompanied by four methyl phenanthrene isomers and a spectrum of 6-10 dimethyl isomers (Figs. 11.02 and 11.19). Their characteristic ions are usually summed (m/z 178+192+206) although they can be readily seen on the TIC fragmentogram. The different positions of the characteristic methyl groups vary as a result of maturity-mediated methyl transfer reactions between sterically crowded (α) and less crowded (β) positions.

The proportions of various methyl and dimethyl phenanthrenes relative to phenanthrene were first utilised routinely for maturity studies by Radke et al. (1982a; 1982b). This long-term usage of the data has lead to acceptance of the rates of change of the isomers with maturity. When plotted to a larger scale (which allows for interpretation of the passage through the oil window) the data given in Radke (1987; 1988) are found to have very large variability. For example, those plots of the ratio MPI1 against vitrinite reflectance show ranges of R_{calc}~±0.25% for a specific measured reflectance which is far too large to be useful. However, Radke (1988) pointed out that the phenanthrene ratios should only be used for these plots where the organic material was coaly, as problems had been found with the ratios where the organic material was amorphous. It is thought that these anomalous values are largely due to either the absence of

phenanthrene precursors and the solution of phenanthrenes from the host rock, or the lack of the necessary reactivity to generate the full suite of phenanthrenes during burial.

Alternatively the formation of phenanthrenes by a different process where amorphous material dominates, has been invoked (Radke, 1987, p. 185). In early maturation, the phenanthrene alkylation ratios are significantly affected by changes in source organic material, but this reduces with increasing maturity (Radke, 1987; 1988). In the Bredasdorp Basin, even where samples have large proportions of amorphous organic material, there are reportedly always small proportions of woody material which should be able to generate phenanthrenes *in situ*.

11.4.2.3. Aromatic steroids

Aromatic steroids are derived from detrital steroids after processes which parallel those which form steranes during diagenesis (Mackenzie, 1984, p. 143-145). Aromatic steroids form two similar series, the mono-aromatic and the tri-aromatic steroids. Mackenzie (op cit.) also showed that the lower molecular weight homologues are enriched (relative to the heavier homologues) through the oil window and into the gas window. Whether this reflects increased stability of the lower molecular weight material relative to the heavier components or direct conversion from heavy to light is not known. However, in Bredasdorp Basin examples, the proportions of mono-aromatic and tri-aromatic steroids tends to increase with increasing burial depth suggesting that the process does indeed involve continued creation rather than solely conversion.

Mono-aromatic steroids (MAS) are those in which ring-C has been aromatised (Mackenzie, 1984, p. 144). They form structural isomers and there are regular and rearranged species, as in the steranes. The MAS range comprises C26-28 forms and a total of 16 components have been identified. These are best visualised using the m/z 253 fragment but there are still a number of overlapping forms (Figs. 11.10; 11.18). Detailed descriptions of the assignments of the relevant peaks to each isomer and of their derivation are shown in Seifert et al. (1983) and Riolo et al. (1986). These reports also indicate that different distributions of MAS are found in rocks from different depositional environments. However, it is very difficult to deconvolve the environmental, diagenetic and maturity aspects of these biomarkers. Hence they are generally used in a 'fingerprint' mode.

Tri-aromatic steroids (TAS) are considered to be generated largely by aromatization of first the B-ring then the C-ring of MAS (Mackenzie, 1984, p. 143-145). This process results in formation of two chiral centres (at C-5 and C-20) although only the latter is considered here as the 5α to 5β conversion happens at very low maturity. Due to overlap, not all the isomers are recorded on GC-MS as generally only 5 peaks in the

C26-28 range are evident (Fig. 11.17; Appendix G). Increased proportions of the C20 and C21 homologues during maturation have been reported to be more a function of their resistance to thermal degradation than to their neoformation from the C26-28 homologues (Mackenzie, 1984, p. 145; Beach et al., 1989). Ratios of C26, C27 and C28 have some source specificity. Riolo et al. (1986) show examples from different environments which record different C28 and C29 proportions. For example, in siliceous environments, the C27 homologue dominates, in marls C27 and C28 form about equal proportions whilst in evaporitic material the C28 dominates. Triaromatic steroids, like the monoaromatic steroids, are essentially unaffected by biodegradation (Seifert and Moldowan, 1979).

11.4.2.4. Benzothiophenes

The origin of the sulphur in organic matter is considered as secondary after microbial activity by reaction with elemental sulphur, produced by chemical reaction with sulphate-bearing sea water, or reaction with H_2S generated by bacterial activity in a sulphur-rich environment, e.g. where evaporites such as anhydrite occur. These reactions generally happen during deposition and early burial mainly in anaerobic environments. Under those conditions, sulphate-reducing bacteria utilise oxygen from sulphate and reduce the sulphur to S^{--}. If there are sulphate-oxidising bacteria in the overlying water column, large quantities of H_2S are produced (Tissot and Welte, 1984, p. 77-79). The sulphur released combines with iron in clay-rich sediments to eventually form pyrite or in iron-poor (e.g. calcareous) muds with organic material. Where large amounts of pyrite are incorporated with the organic matter, the intimate link between the two can later lead to the incorporation of some sulphur into the organic matter. Optical analyses of Bredasdorp Basin source rocks from anoxic environments, reveal the ubiquitous presence of pyrite grains in organic matter.

Sulphur can also become part of the crude oils either as a result of maturation of sulphur-containing organic matter or by bacterial activity (Jobson et al., 1979; Ho et al., 1974). Sulphur-bearing hydrocarbons are commonly represented by the dibenzothiophenes of which there are three series, methyl-, dimethyl- and trimethyl-substituted. The base peaks of these compounds are m/z 198, m/z 212 and m/z 226 (Figs. 11.14-11.16). The base compound, dibenzo thiophene, is less well represented in its base fragmentogram (m/z 184) because it is often depleted in processing by excessive evaporation. Dibenzothiophene elutes slightly earlier than phenanthrene on polar columns (e.g. on SE54, Hughes, 1984) which is itself often depleted by sample evaporation. Hughes et al. (1995) show that the ratio of dibenzothiophene to phenanthrene can, with the pristane/phytane ratio, be used to infer the depositional environment of the source both from oil and rock extract samples.

Methyl dibenzothiophenes (MDBT)

There are four isomers of this compound, 1-, 2-, 3-, and 4- all of which are found naturally, although the 2- and 3- isomers generally co-elute. All these isomers have a base peak at m/z 198 (Fig. 11.14). 1-MDBT appears to have the lowest thermal stability (Radke et al., 1982a; 1982b) whilst 4-MDBT is more stable. The ratio between the two shows an exponential increase with increasing maturity (Dzou et al., 1995; Chakhmakhchev and Suzuki, 1995) although the ratio can reflect some minor organic facies variations (Radke et al., 1982b). Samples of coals and coaly organic matter plot in a much narrower trend typical of monomaceralic material but show minimal variation below R_o~1.10% (Dzou et al., 1995). The 2- and 3- isomers show intermediate thermal stability and have use in confirmation of the thermal response of the other species.

Dimethyl dibenzothiophenes (DMDBT)

Trends for several of the isomer ratios have been shown to be effective indicators of maturity (Radke and Willsch, 1994; Chakhmakhchev and Suzuki, 1995). Only a few of the DMDBT isomers have been assigned, notably peaks D, E, and F are 2,5, 2,4 and 2,3 dimethyl isomers respectively (Tomic et al., 1995; Fig. 11.15). Differences in their relative thermal stability are well known from studies of their variation with maturity increases (Radke et al., 1982a; 1982b; Chakhmakhchev and Suzuki, 1995). Plots of one of the more commonly used ratios, peaks C/E show straight-line increases relative to the more common MDBT maturity ratio (4-MDBT/1-MDBT; Chakhmakhchev and Suzuki, 1995). However, the MDBT ratio does provide an exponential indication of maturity (Dzou et al., 1995) and the DMDBT ratio probably does too. As with the MDBT ratios, samples do locate off the trends and are also assumed to represent different source facies. Indeed, Hughes (1984) shows the relative proportions of the MDBT and DMDBT isomers to be strongly influenced by different source environments.

Trimethyl dibenzothiophenes (TMDBT)

The assignments of the individual isomers are not known, hence all peaks are labelled alphabetically. The thermal stabilities of some peaks are assessed by Chakhmakhchev and Suzuki (1995) who found that peaks 'c' and 'e' (their peaks '3' and '5' respectively) comprised a maturity ratio which matched that of the MDBT and DMDBT ratios (Fig. 11.16). Plots of the ratio between these two compounds show an exponential rate of change. This is believed to be due to maturation rate differences rather than differences in depositional facies, as variations in the latter are as wide for the least mature samples as for the most mature samples.

CHAPTER 12. BIOMARKER INTERPRETATIONS

Representative samples were chosen for biomarker interpretations from 38 of the 167 wells in the Bredasdorp Basin (Fig. 12.01). These samples represent all source rock intervals which are known to have wet gas to oil potential and many of the hydrocarbon families. Source rock samples are listed in Table 12.01 and the hydrocarbon samples in Table 12.02. Sampled wells are highlighted on the relevant horizon and source rock distribution maps (Figs. 12.02-12.08). Not all hydrocarbons separated using the gas, condensate or light oil analyses have been analysed for their biomarker content because of availability of suitable extracted fractions, but at least one sample from each family and each mixture of families has been chosen. These samples form the 'bridge' between the biomarker characterisation of hydrocarbon families, the source rock intervals and the gas-light oil correlations of Chapters 8-9 (Table 12.03).

Biomarker data have not been acquired from the sample of Family 4. The condensate sample was analysed by GC-MS, but without removing the normal alkanes or concentrating the heavy ends by evaporation (IGI, 1994). The resulting fragmentograms show very few peaks at higher retention times than dimethyl phenanthrenes, yet the GC data show a range of compounds up to and beyond the chrysenes. This suggests that sample concentration procedures should succeed in isolating enough biomarkers for an analysis. Bearing in mind the possibility that the source for this gas condensate lies in the Southern Outeniqua Basin, where water depths can be up to 1800 metres deeper than at well 128, hydrocarbon migration could have been from structurally deeper, but stratigraphically younger and less mature intervals. It is therefore possible that some biomarkers may still be found but only after analysis of a concentrated sample is carried out. Biomarker analyses have not yet been attempted on samples of Family 5. The high reservoir maturity (R_o>1.3%) and the dry nature of the gases suggests that most of the indigenous biomarkers have been cracked.

Interpretation of the biomarker data is carried out in three different ways, 'fingerprint' correlation using raw data plots (after Comet et al., 1993), data cross-plots as used in Chapter 11 and statistical assessment of 51 biomarker ratios calculated from the 94 saturated and 70 aromatic compounds using published methods (ratios listed in Appendix F, Tables F18-22).

12.1. FINGERPRINT CORRELATION

The 'fingerprint' interpretation route was chosen in order to study familial characteristics because this can quickly highlight differences between each family. The technique is

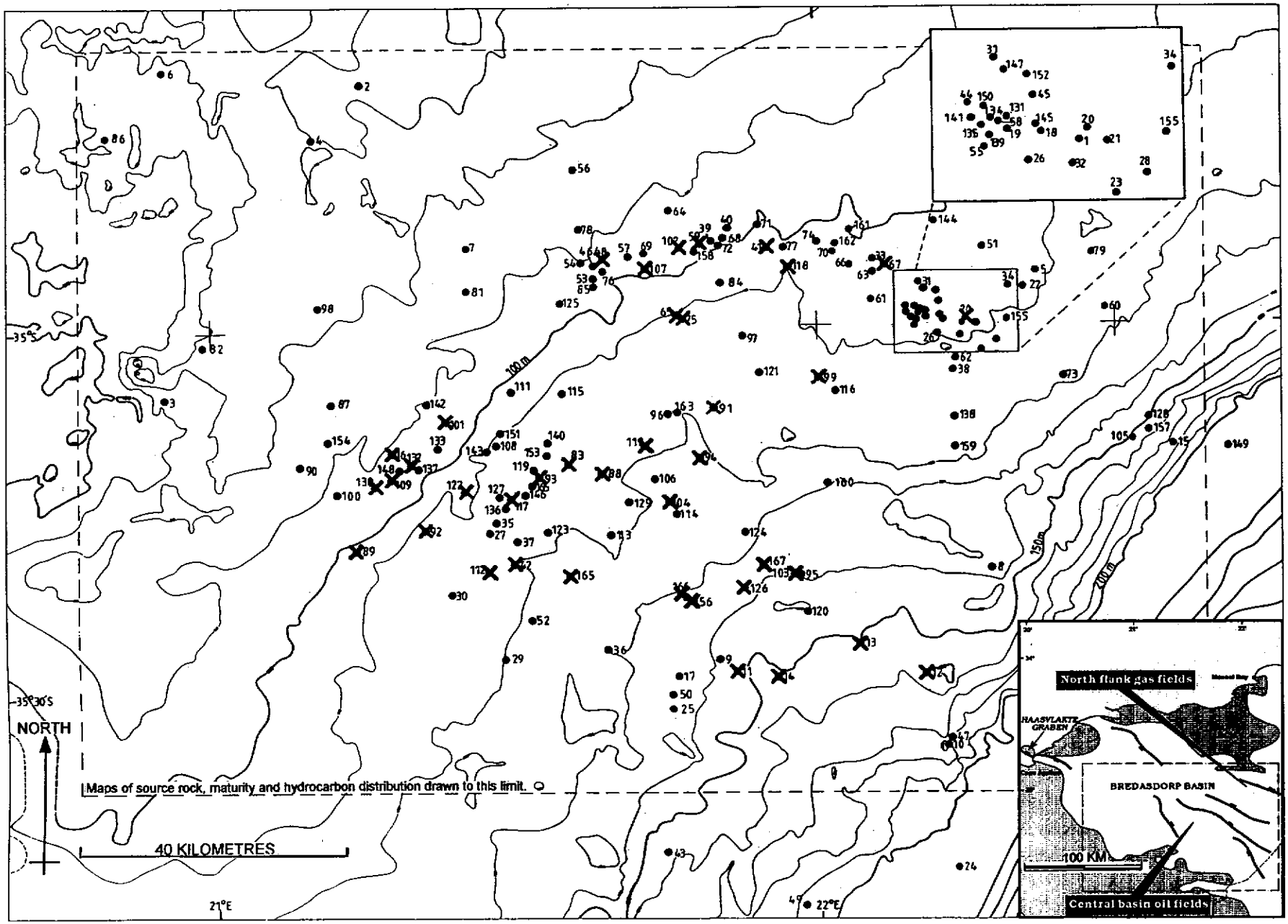

Figure 12.01: Map showing the wells in the Bredasdorp Basin in which GC-MS (biomarker) analyses were carried out (✖) (this map copied from Figure 2.10).

HYDROCARBON SAMPLES						
SAMPLE	WELL	SAMPLE TYPE	DEPTH	SEQUENCE	ANALYST	REMARKS
1	83	DST3	2470m	14A	KFA	few fragmentograms brown oil
2	83.	DST2	2889m	10A	KFA	few fragmentograms light condensate
3	83	"	"	"	US (CE)	heavy brown condensate
4	88	DST5	2507m	14A	US (CE)	sample not adducted
5	88	"	"	"	"	urea adducted sample
6	88	DST4	2827m	10A	US (CE)	heavy brown condensate
7	92	Core1	2949.0m	5A	US (CE)	live oil trace
8	118	Core1	2563.1m	8A	US (F)	residual oil trace
9	102	DST4	2241m	pre1At1	US (CE)	brown oil/condensate
10	102	DST2	2556m	pre1At1	US (CE)	condensate
11	91	Core1	3220.05m	6A	US (F)	residual oil trace
12	104	Core2	3017.46m	10A	US (F)	live oil trace
13	93	Core4	3212.4m	5A	S-R	residual oil trace
14	109	DST1	2630m	13A	S-R	brown oil
15	107	DST2	2565m	pre1At1	US (F)	light condensate
16	110	DST1	3051m	9A	US (F)	condensate
17	126	DST1	2643m	14A	US (F)	light condensate
18	122	SWC	2517m	13B	S-R	live oil trace
19	132	DST2	2662m	13A	S-R	brown condensate
20	132	Core1	2702.43m	13A	S-R	oil trace below OWC
21	48	DST2	2620m	pre1At1	US (F)	brown condensate
22	16	RC	2614m	13A	US (F)	live oil trace
23	59	DST1	2212m	pre1At1	US (CE)	brown oil
24	75	Core1	2830.5m	8A	US (F)	residual oil trace
25	101	Core1	2987.5m	7A	S-R	residual oil trace
26	20	DST2	2699m	pre1At1	US (CE)	light condensate
27	13	Core1	2518.86m	pre1At1	US (F)	live oil show
28	103	DST2	2718m	14A	GHG	light condensate (?oil)
29	94	DST1	2799m	13B	GHG	brown oil
30	156	DST1	2522m	14A	US (CE)	brown oil
31	156	Core1	2525m	14A	US (CE)	residual oil trace
32	166	RFT	2508m	14A	US (CE)	light condensate
33	166	Core1	2510.43m	14A	US (CE)	asphalt layer ('mini-tarmat')
34	166	DST	2520m	14A	US (CE)	brown oil
35	166	Core1	2522.5m	14A	US (CE)	residual oil trace
36	165	RC	2256m	14A	US (CE)	residual heavy oil trace
37	167	DST1	2679m	14A	US (CE)	light condensate
38	167	Core1	2681.65m	14A	US (CE)	residual oil

Biomarker analysts:

KFA=Institute of Petroleum and Organic Geochemistry (ICH-5) at the Research Centre (KFA), Julich, Germany.
S-R=Simon-Robertson Laboratories, Simon Petroleum Technology, Llandudno, N.Wales, UK.
US=University of Stellenbosch, Laboratory for Ecological Chemistry. Sats:(F)=Fisons 8000 GC-MS, (CE)=Carlo-Erba MD1000 GC-MS
GHG=GH Geochemical services, Bebington, Wirral, Cheshire, UK.

Table 12.01: List of hydrocarbon samples used for GC-MS (biomarker) analyses together with annotations regarding the sample type and physical appearance (similar to Table 6.07a).

SOURCE ROCK SAMPLES						
SAMPLE	WELL	SAMPLE TYPE	DEPTH	SEQUENCE	ANALYST	REMARKS
41	83	RC	2702m	13A	US (CE)	WG-OIL prone
42	83	RC	2741m	13A	US (CE)	OIL prone
43	83	RC	2792m	13A	US (CE)	WG-OIL prone
44	92	RC	2610m	?13A	US (CE)	WG-OIL prone
45	89	RC	2660m	pre1At1	US (CE)	WG prone
46	93	RC	2720m	13A	S-R	OIL prone
47	93	RC	2761m	13A	US (CE)	OIL prone
48	93	"	"	"	"	SE52 column
49	99	RC	1820m	15A	US (CE)	WG prone
50	109	RC	2461m	13A	US (CE)	OIL prone
51	109	Core3	2654.15m	13A	S-R	OIL prone
52	130	RC	2331m	13A	US (CE)	OIL prone
53	110	RC	2830m	13A	US (F)	WG prone
54	110	RC	2902m	13A	US (F)	WG prone
55	112	RC	2392m	6A	US (F)	WG prone
56	117	SWC	2918.5m	9-12A	S-R	WG prone
57	117	"	"	"	US (CE)	WG prone
58	117	"	"	"	US (F)	WG prone
59	122	RC	2682m	13A	S-R	OIL prone
60	122	RC	2832m	9-12A	S-R	WG prone
61	11	RC	2682m	9-12A	US (F)	WG-OIL prone
62	14	RC	2721m	13A	US (F)	WG-OIL prone
63	42	RC	3021m	1A-4A	US (F)	WG-OIL prone
64	48	RC	2490m	6A	US (F)	WG prone
65	41	RC	2320m	5A	US (F)	OIL prone
66	65	RC	3160m	5A	US (F)	WG prone
67	75	Core1	2829.0m	8A	US (F)	WG-OIL prone
68	67	RC	2651m	5A	US (F)	WG prone
69	12	RC	2057m	15A	US (F)	OIL prone
70	156	RC	2835m	13A	US (CE)	OIL prone

Table 12.02: List of source rock samples used for GC-MS (biomarker) analyses together with annotations about sample type and source potential evaluated from optical and chemical data (similar to Table 6.07a).

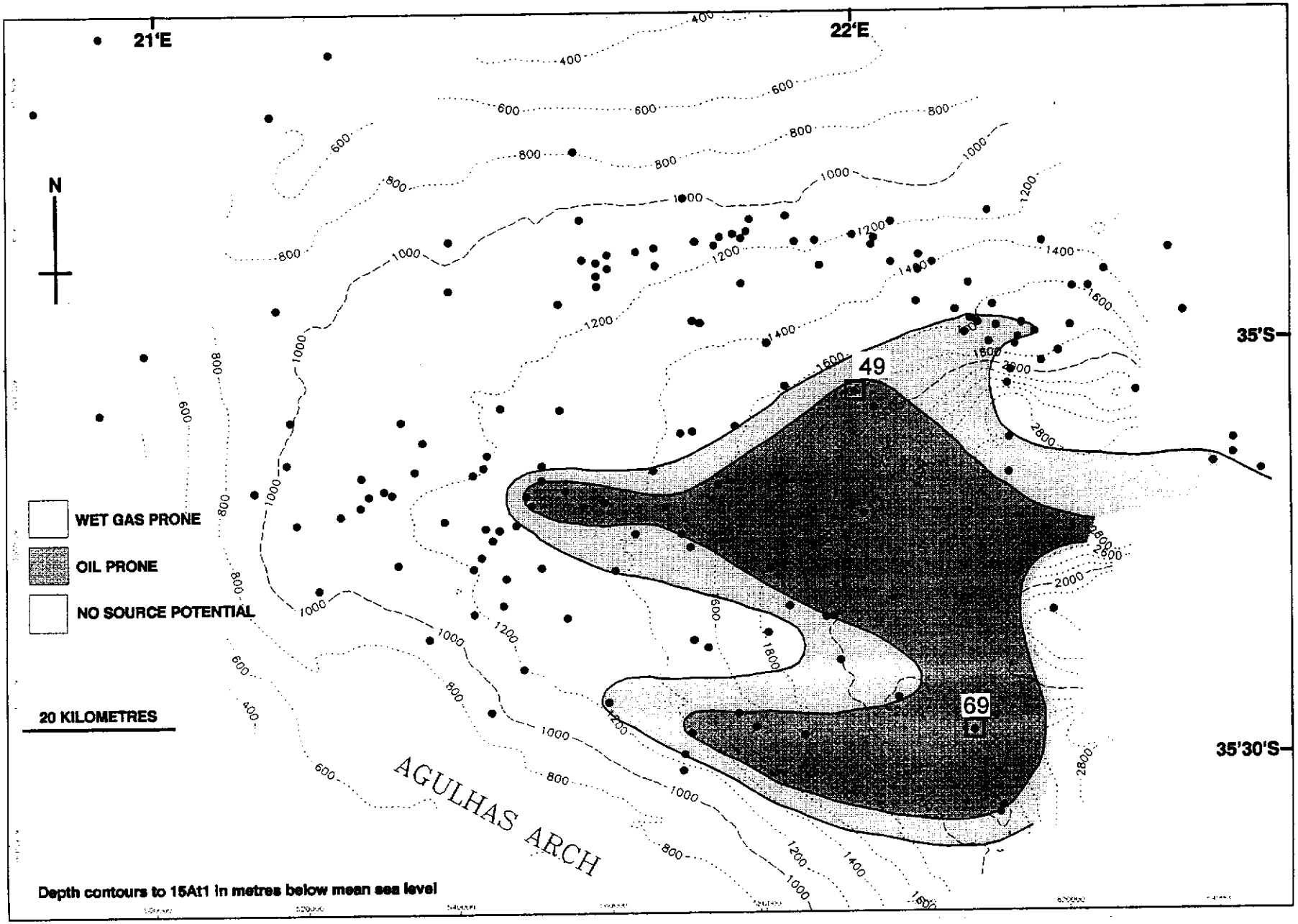

Figure 12.02: Depth map showing the distribution of source rocks in the 15A sequence and the wells from which samples were taken from the source rock for GC-MS (biomarker) analyses (□). Sample codes indicated. Map after Fig. 4.17.

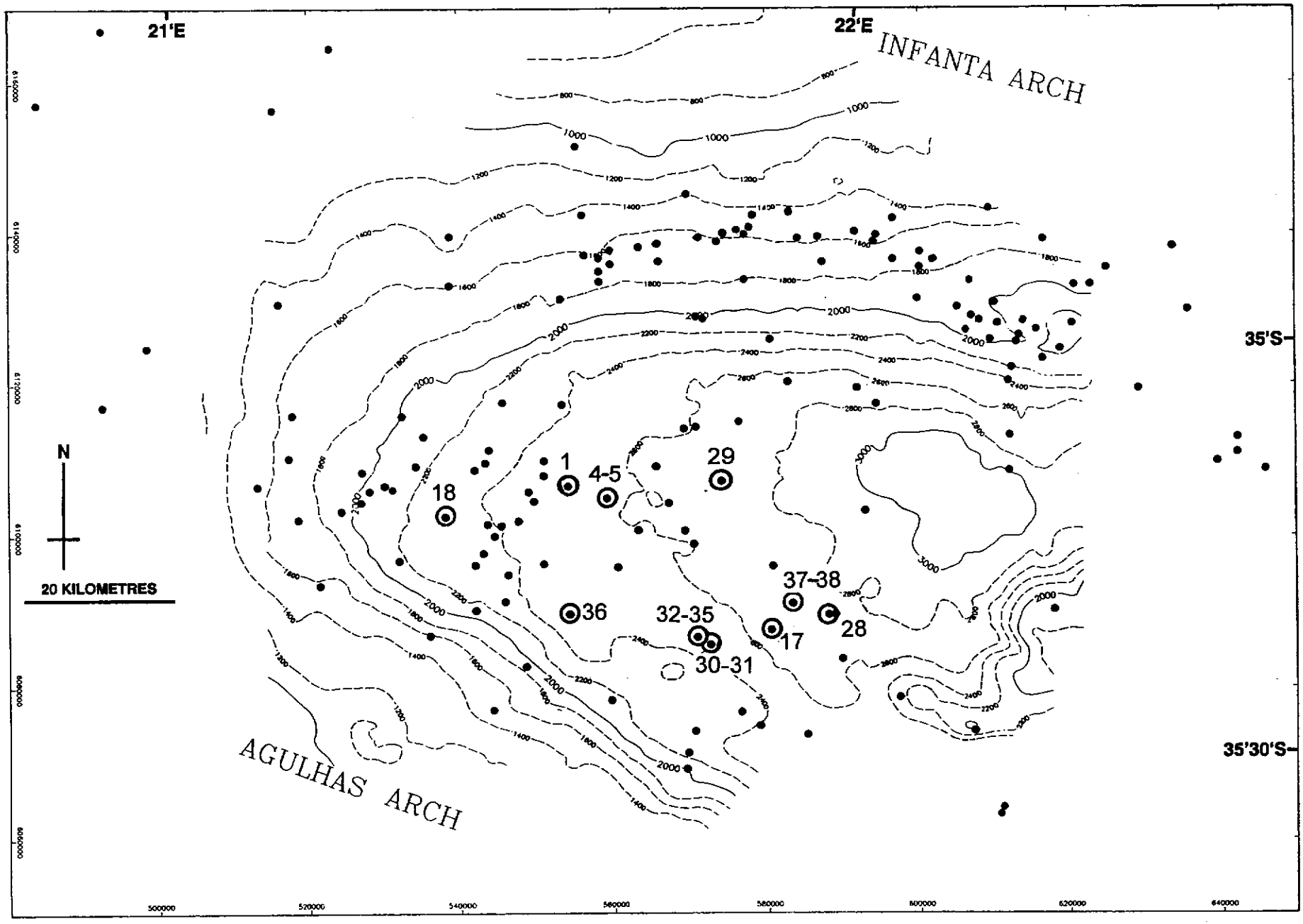

Figure 12.03: Depth map to 14At1 showing the wells from which samples of reservoired fluids were taken for GC-MS (biomarker) analyses (O). Sample codes indicated.

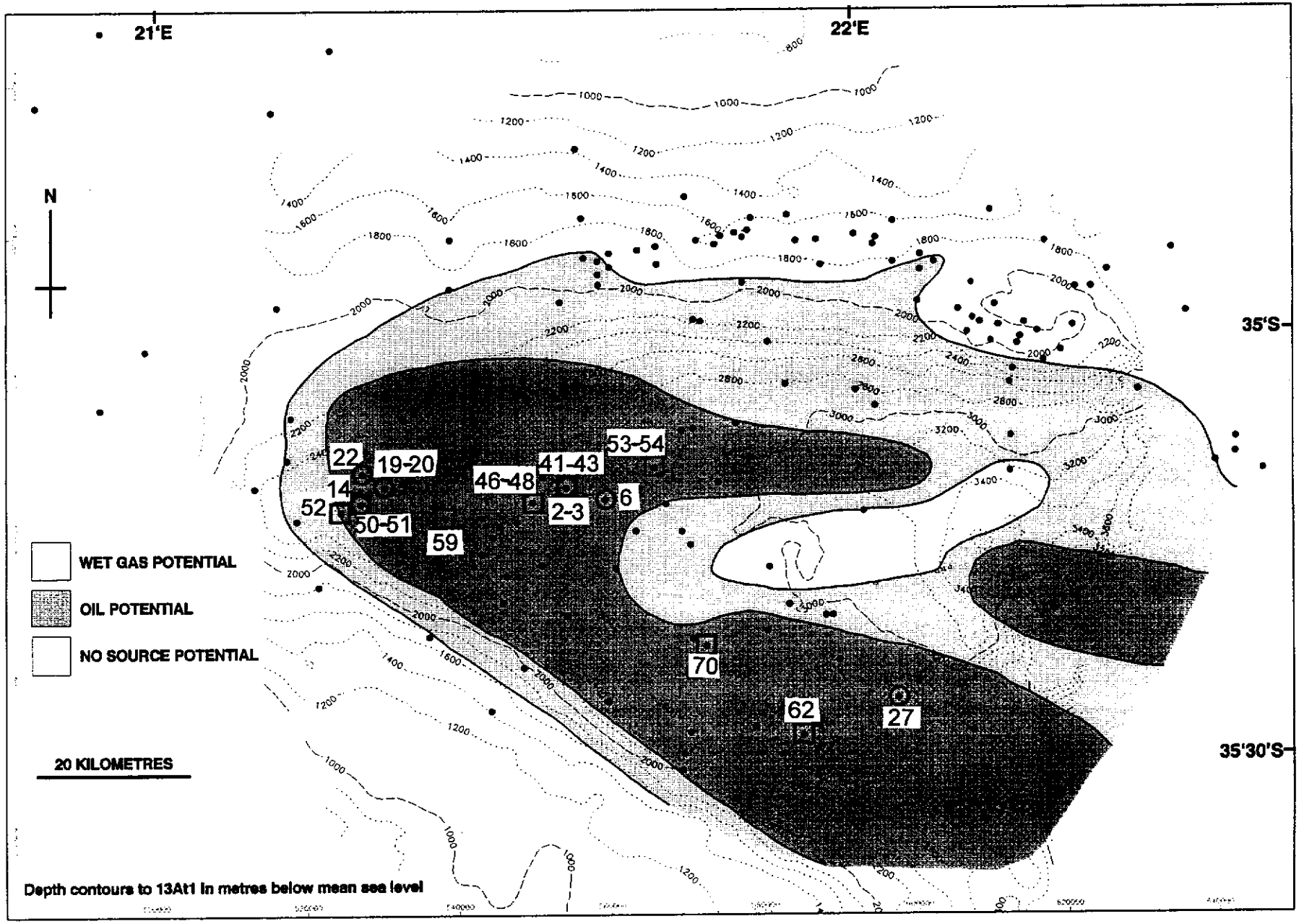

Figure 12.04: Depth map to 13At1 showing the distribution of source rocks and the wells from which samples of source rocks (□) and reservoired hydrocarbons (O) were taken for GC-MS (biomarker) analyses. Sample codes indicated. Map after Fig. 4.15.

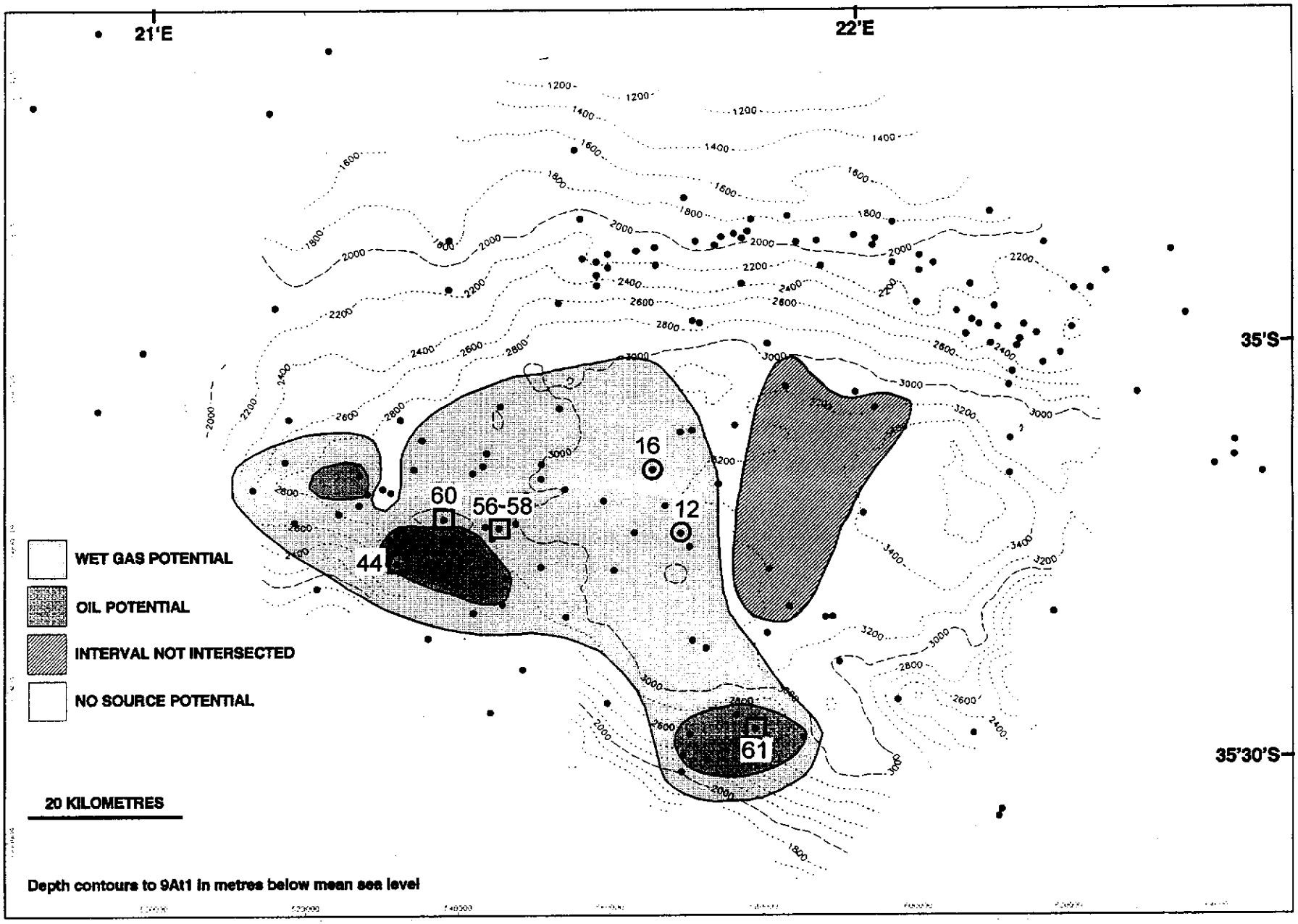

Figure 12.05: Depth map to 9At1 showing the distribution of source rocks and the wells from which samples of source rocks (□) and reservoired hydrocarbons (O) were taken for GC-MS (biomarker) analyses. Sample codes indicated. Map after Fig. 4.13.

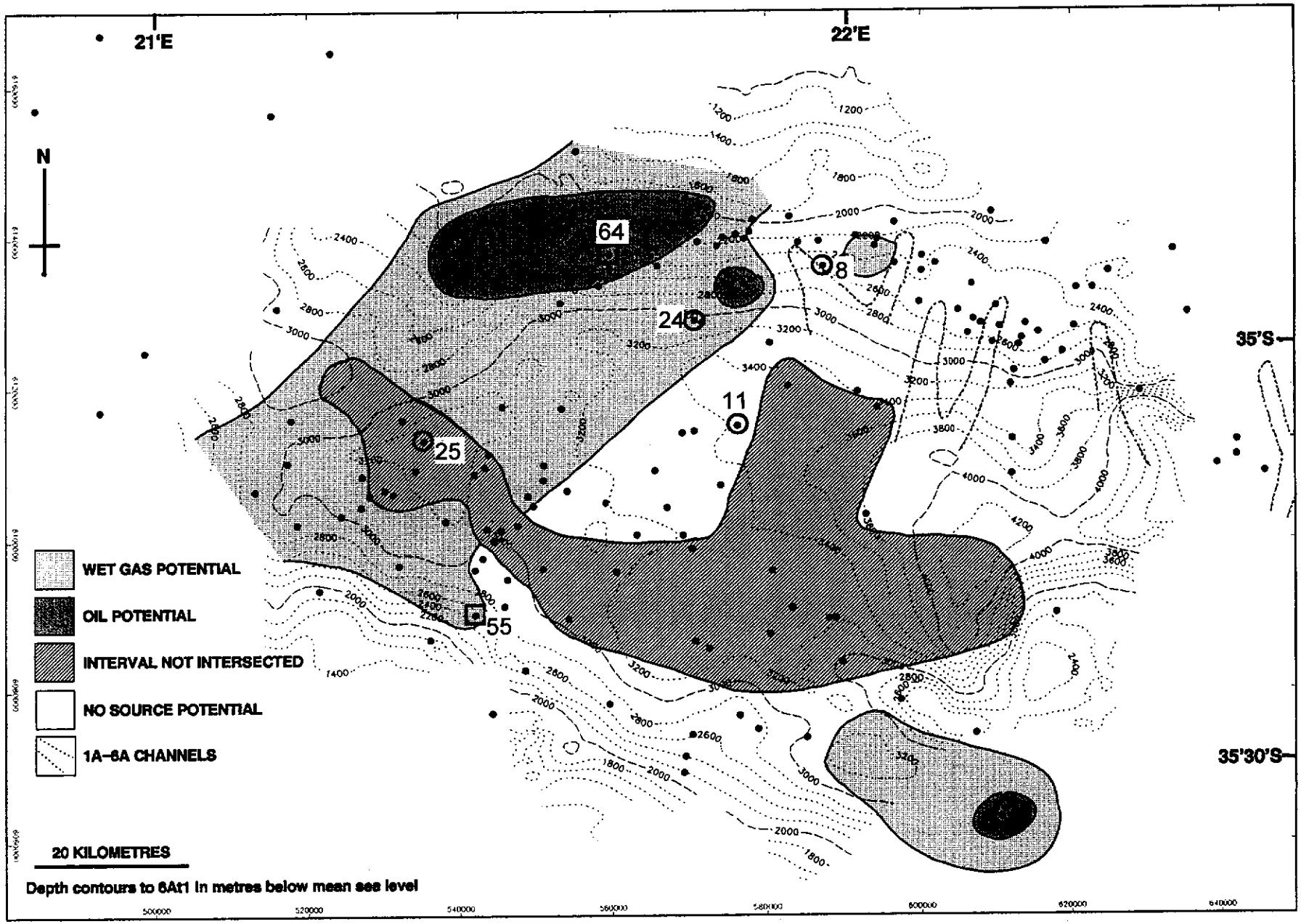

Figure 12.06: Depth map to 6At1 showing the distribution of source rocks and the wells from which samples of source rocks (□) and reservoired hydrocarbons (○) were taken for GC-MS (biomarker) analyses. Sample codes indicated. Map after Fig. 4.11.

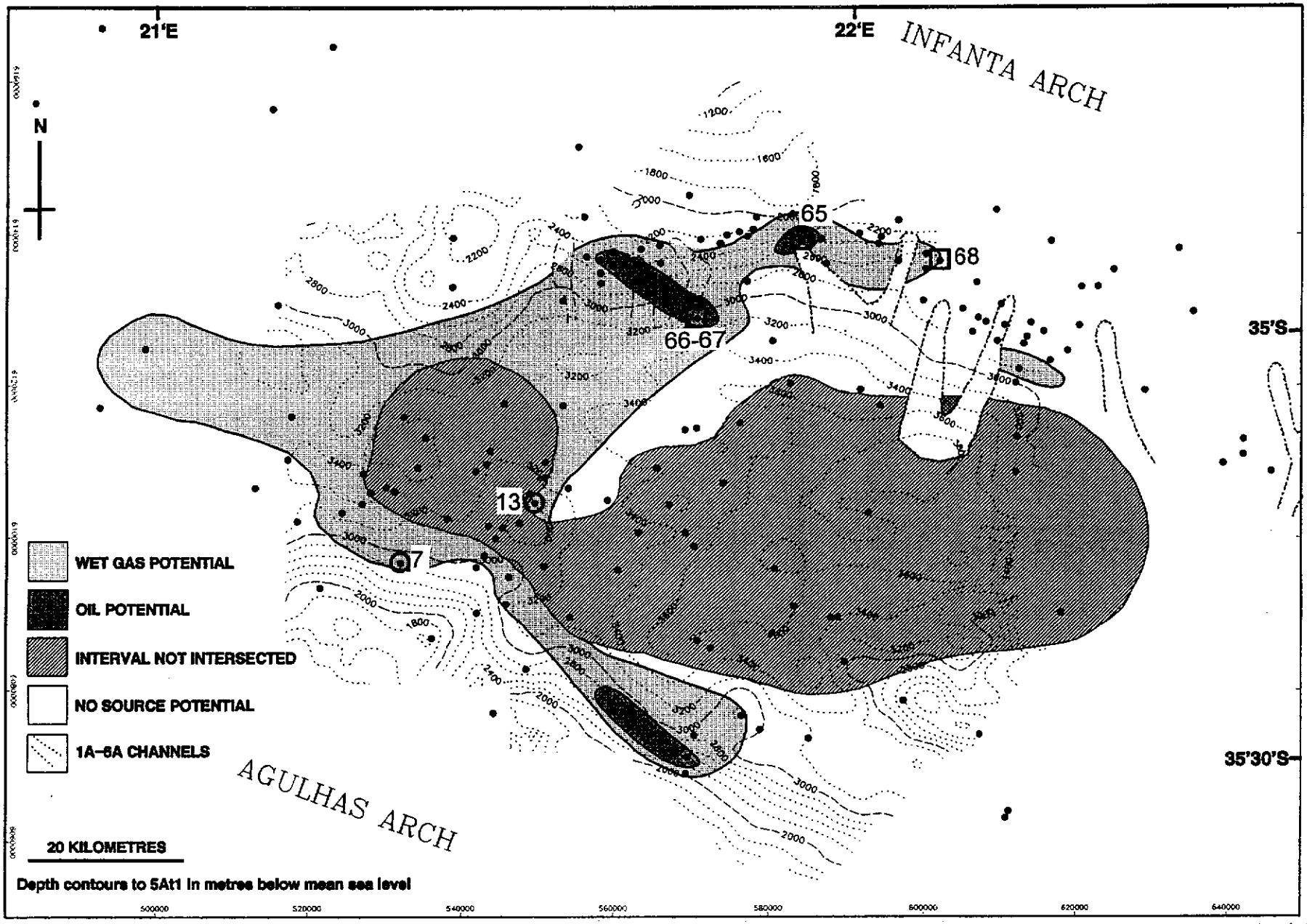

Figure 12.07: Depth map to 5At1 showing the distribution of source rocks and the wells from which samples of source rocks (□) and reservoired hydrocarbons (○) were taken for GC-MS (biomarker) analyses. Sample codes indicated. Map after Fig. 4.09.

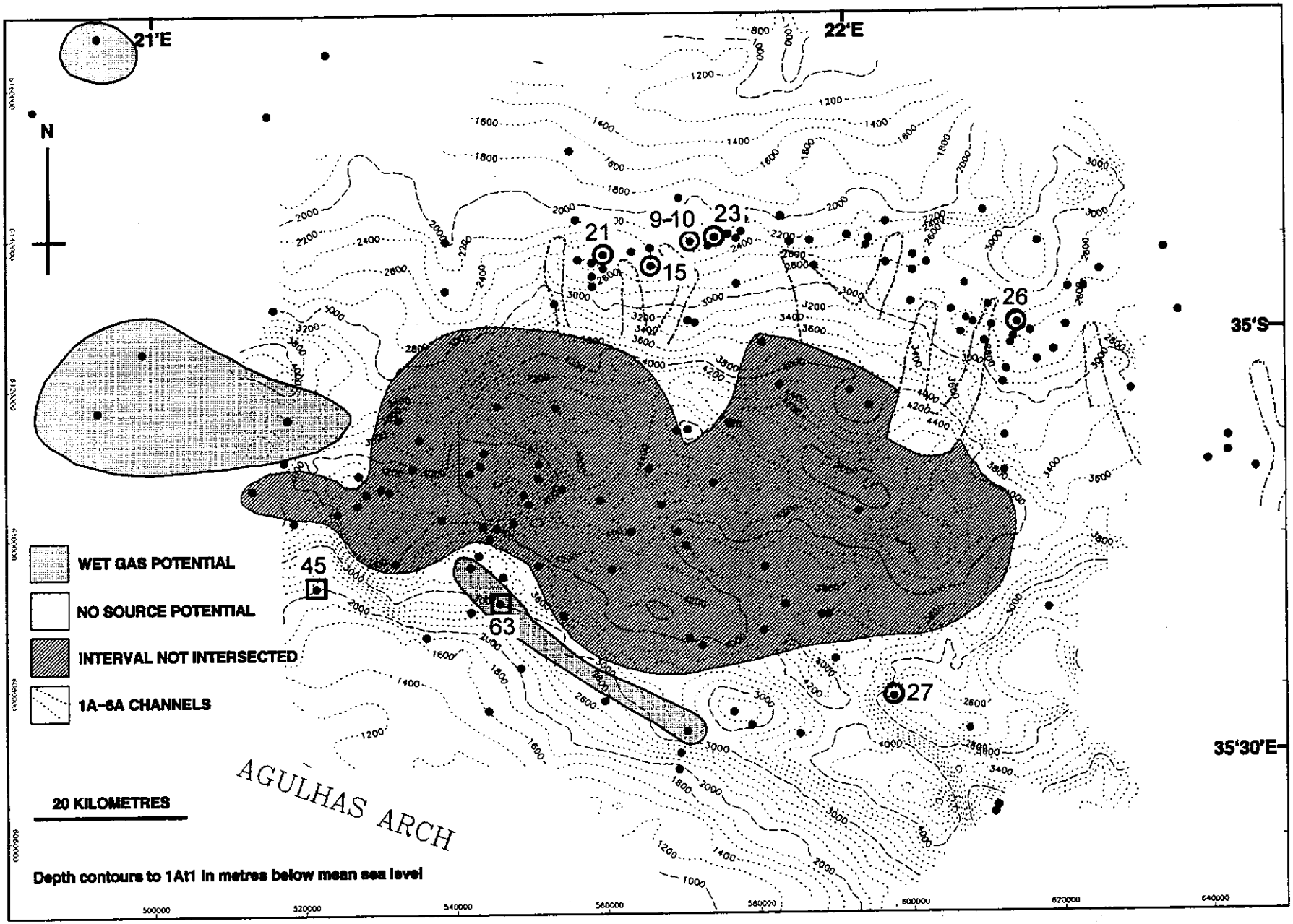

Figure 12.08: Depth map to 1At1 showing the distribution of source rocks and the wells from which samples of source rocks (□) and reservoired hydrocarbons (O) were taken for GC-MS (biomarker) analyses. Sample codes indicated. Map after Fig. 4.07. All hydrocarbon samples shown are from below horizon 1At1.

WELL	TYPE	DEPTH	CODE	FAMILY 1	FAMILY 1B	FAMILY 2	FAMILY 3	FAMILY 1+2	FAMILY 1+3	FAMILY 2+3
59	DST1	2212m	23	Y						
83	DST3	2470m	1	Y						
88	DST5	2507m	4-5	Y						
94	DST1	2799m	29	Y						
102	DST4	2241m	9	Y						
156	DST1	2522m	30	Y						
166	DST1	2520m	34	Y						
109	DST1	2630m	14		Y					
132	DST2	2662m	19		Y(OIL)....	.....Y(GAS)				
132	Core1	2702.43m ≡DST1	20		Y					
110	DST1	3051m	16			Y				
167	DST1	2679m	37			Y				
20	DST2	2699m	26				Y			
83	DST2	2889m	2-3					Y		
88	DST4	2827m	6					Y		
102	DST2	2632m	10					Y		
126	DST1	2643m	17						Y	
48	DST1	2634m	21						Y	
102	DST2	2632m	10							Y
107	DST2	2565m	15							Y

Table 12.03: Samples analysed for biomarkers from the DST intervals used to characterise the hydrocarbon Families.

particularly useful where differences are subtle and do not always conform to standard correlation parameters. Where biomarker proportions reflect generation from higher or lower maturity source rocks, correlations can be ascertained although they are best described graphically. A similar style of assessment was used by Comet et al. (1993) in classifying a large number of oils from the Gulf Coast into a multitude of different classes. That study is discussed in some detail because it is the only published example of such usage of biomarker data.

12.1.1. Previous studies

Comet et al. (1993) show that potential source rocks in the Gulf Coast range in age from Kimmeridgian to Pliocene, some being representative of clastic environments and some of carbonate environments. The oils are reservoired throughout the succession and in deposits in both environments. This wide variability in both source and reservoir rock depositional environments ensure that there are significant chemical differences between the samples. This makes them easy to separate using only the common sterane and terpane ion fragmentograms. From these data, Comet et al. (1993) derived primary sorting parameters to broadly group the oils, e.g. large differences in the relative proportions of diasteranes and steranes or in the proportions of even-numbered extended hopanes. They also further separated the oils using secondary parameters such as the presence of oleanane or 4-methyl steranes, absence of tricyclic terpanes and unusual dominances of 22R extended hopanes. Based on 35 sterane classes and 20 terpane classes, they could potentially characterise 700 subtle differences amongst the oils and broadly indicated which oils represented mixtures from which source rocks.

In this study, there is far less variability amongst both the active source rocks and the reservoir sediments. All source rocks studied, except the lacustrine source rock, are deep marine clastic sediments deposited in largely cold-water environments. The preserved organic matter comprises mixtures of subordinate terrigenous and dominant marine organic matter, locally altered bacterially to a greater or lesser extent. There are no known source rocks or reservoired hydrocarbons in either carbonate or evaporitic rocks and both sources and reservoir rocks are Early Cretaceous in age (Valanginian-Albian, ~126-103 Ma).

As a result of this lack of variability, a far more elaborate separation system was needed and the present one was devised which used 7 major groups of saturated and aromatic hydrocarbon compounds. A total of 9 families of reservoired hydrocarbons and 8 families of source rocks are inferred from this separation (Tables 12.04a and b). Of this large number of hydrocarbon families, 2 (numbers 4 and 5) are determined solely from gas and fingerprint GC data and there are no biomarker data to back up this

SOURCE ROCK FAMILIES

	ACTIVE				From fingerprint GC only		ESSENTIALLY INACTIVE	
Sequence (hydrocarbon family)	13A (≡1)	upper 9A-12A (≡1B)	lower 9A-12A (≡2)	5A-8A (≡3)	4	5	pre1A (≡6)	15A (≡7)
Symbols	●	○ △	▲	■	✳	◆	+	○
Samples	41-43	44	56-58	(55)	nil	nil	45	49
"	46-48	51	61	64-66				69
"	50	60		(67)				
"	52-54			68				
"	59							
"	62							
"	70							

() parentheses represent some uncertainty in the assignment because some of the characteristic hydrocarbons are present in unusual proportions. In particular the following qualifications apply:

(i) Shale sample 63 is unassigned. This sample has some features matching Family 2 but has very low proportions of C28 ββ steranes and C28 and C29 diasteranes are present in equal proportions.
(ii) Samples 43 and 46 are unusual in that proportions of C28 ββ steranes are lower than the adjacent C27 and C29 homologues (≡Family 3), C24 tetracyclic terpane is present in high proportions (≡Family 1B) and C29 diasteranes are high (≡Family 3).
(iii) Sample 45, the sole representative of the lacustrine source rocks in well 89, has affinities with a mixture of Families 1 and 3 except for the absence of C30 steranes and the unusual dominance of C21 tricyclic terpanes.
(iv) Sample 67 may be an impregnation of Family 2 condensate in Family 3 source rock. This is the only sample taken from close to a known reservoired hydrocarbon (residual condensate sample 24).

Table 12.04a: Distribution of source rock Families based on sampled intervals and hydrocarbon types with samples located in relevant groups.

HYDROCARBON FAMILIES

Families	Families from single source				Families from mixed sources			Families from undefined sources	
Family code	1	1B	2	3	1+2	1+3	2+3	4	5
Family symbol	●	○	▲	■	◔	◘	◭	✳	◆
Samples	1	14	12	13	2-3	8	10	Well 27	Well 128
"	4-5	18	16	25	6	21-23	11	Well 35	
"	9	19	24	26	17		(15)		
"	27	20	(37)		28				
"	(29)	(33)			32				
"	30-31				38				
"	34-36								

() parentheses represent some uncertainty in the assignment to a particular family perhaps indicating more than one phase of mixing. In addition, there are several samples in which unusual proportions of characteristic compounds are found:

(i) Sample 7 is unassigned. It may represent a mixture of three Families i.e. 2, 3 and an unknown but possibly non-marine source (because of the possible presence of a carotane).
(ii) Sample 29 is characterised by a restricted range of ion fragmentograms - and those available do not allow for certainty in assignment but it is likely that the sample represents a single Family.
(iii) Sample 36 has unusually large proportions of C29 diasteranes (≡Family 3).
(iv) Sample 9 has lower proportions of the triaromatic steroid compound, C28 20S ('c') (≡Family 3).
(v) Sample 37 has very weak aromatic and m/z 177 ion fragmentograms but is likely to be a mixture of Families 1 and 2.
(vi) Family 2 condensates largely match 9A-12A source rocks. However, the condensates are found locally up to 500 metres below this source and there is no geologically supportable migration route between the two - hence there must be a deeper source rock responsible for many of the Family 2 condensates.

Table 12.04b: Distribution of samples into 'pure' and mixed hydrocarbon Families together with annotations dealing with unusual samples and groups.

characterisation. Three (numbers 1+2, 1+3 and 2+3) are mixtures of Families 1-3. Two different source rock families are thought to have sourced the Family 4 and 5 condensates, although there are no data to support this. A further two source rock families (numbers 6 and 7) are essentially inactive as they appear not to have expelled significant volumes of hydrocarbons. Hence the total number of source rock and hydrocarbon families which are discussed in detail, and which comprise essentially all the hydrocarbons in the basin, are 4 source rocks and 4 hydrocarbons, i.e. 8 in total. These are represented by 24 source rock samples and 36 hydrocarbon samples. The assignments of source rock and hydrocarbon samples to particular families are shown in Tables 12.04a and 12.04b.

Assignment to a particular hydrocarbon family depends on matching the majority of sterane, aromatic steroid and terpane parameters. In a number of cases, the results indicate that the hydrocarbons are a mixture of 2 (or more) families. In each case, this is found where a heavy oil is apparently dissolved in a lighter gas condensate and it is likely that these represent solution of residual oil by later gas influx. Examples of these are found in sample 17 from well 126 in the southern 14A trend and where several streams of hydrocarbons meet at the confluence of migration routes on the north flank of the basin (e.g. sample 21 from well 48). In each case, the early oil either escaped or was displaced from the reservoir and later wet gas-condensate dissolved portions of the remaining residual oil traces. Hence, in spite of this apparent proliferation of source rocks, there are really only 4 demonstrably effective intervals in the basin. There is an additional source for the Family 4 hydrocarbons which is almost certainly located in the Southern Outeniqua Basin. This may be an extension of intervals already studied in the Bredasdorp Basin. There is another source for the Family 5 gas-condensates. This, too, may have been intersected as it may be the syn-rift lacustrine source.

The characteristic low maturity sterane patterns in Family 7 (Turonian, 15A) samples, i.e. dominant 14α,17α 20R steranes, with large amounts of diasteranes denoting a clastic source, and an almost complete absence of C30 diahopane, have not been seen in any oils. In three wells (numbers 21, 32 and 47) there are oil shows near this source rock. In each case, the data show that the source was not close by and it is evident the oil has migrated from much deeper in the succession (Davies, 1997b).

The pre-1At1 source rock sample (no. 45) is significantly different from all oils because of (i) the absence of C30 steranes from the m/z 217 ion fragmentogram and (ii) the unusual dominance of C21 tricyclic terpane. No oil was found associated with this apparently isolated development of lacustrine source rock. The possible influence of syn-rift source rocks in sample 7, assumed from the unusual presence of (?) carotanes, does not extend to sample 45 as this has no signs of carotanes. Indeed studies by

Mello et al. (1988) show that carotanes are not exclusively found in non-marine sediments as was originally thought and can occur in terrigenous kerogen deposited in shallow marine environments (Hall and Douglas, 1983; Peters et al., 1989).

12.1.2. Correlation method

Of the hydrocarbon samples, most are ascribed to the four 'active' source rock families or to one of the mixtures thereof (Table 12.04a and b). Where there are mixtures, the resultant hydrocarbon is not assigned to a new family but is identified as a mixture of two or more families. The distinction of the mixed samples compares well with the mixtures assessed from gas data and light oil data. There are, however, too few data to allow for calculation of the proportions of the mixes. In some samples, perhaps as a result of facies variations amongst source rocks, the local input of different types of organic material or because of maturity effects, some familial recognition patterns are less well developed than others. In those instances, the remaining familial characteristics, however few they may be, are used to decide on the probable source.

A further difference from the methods used by Comet et al. (1993) is the assumption that there are no primary and secondary sorting parameters - all are assumed equal. One source rock sample (no. 67) does appear to contain a mixture of compounds. This sample is the only one taken from very close to a known hydrocarbon impregnation (<1m away) and almost certainly contains some impregnation.

The term 'Family 1B' is used in this study to denote source rocks which are similar in most respects to the Family 1 source rocks but differ in a few respects, notably in the characteristically high proportions of C24 tetracyclic terpane, low proportions of C27 trisnorhopane and the dominance of C28 20S monoaromatic steroids. Two of the three Family 1B source rock samples are presently located within the uppermost 9A-12A sequence shales whilst the third sample (no. 51) is assigned to the basal 13A sequence some 200 metres below the main 13A source rocks in well 109 (cf. samples 41-43). There is some doubt as to whether this is truly a 13A or 9A-12A source (Davies, 1997e).

It may be that these biomarker characteristics represent a purely local influence, perhaps from a particular organic input from the sediment fetch area, which only influenced sediments in a periodically dysoxic region on the shelf. Indeed, Family 1B source rock samples were all deposited near the palaeo-shelf break in one small region of the basin which is at the furthest southerly updip extent of the main 13A and 9A-12A source rocks (Brink et al., 1991; Smit, 1992). Three of the four Family 1B hydrocarbons (no's. 14, 18, 19, 20) are all located very close at the western end of the source trend. The fifth sample, no. 33, has been shown to be part of the earliest phase

of migration of Aptian (13A) oil, at ~60 Ma, along the southern 14A trend (Davies, 1997a). However, its affinity with Family 1B hydrocarbons may reflect one of three possibilities:
(i) early expulsion from local 9A-12A source rocks, when the 13A source rocks were not mature enough to expel oil, followed by vertical migration into the 14A sandstones
(ii) expulsion from a proximal facies variant of the 13A source which included the characteristic 1B precursor organisms.

Although the heavily faulted nature of the area is apparent and would tend to support the first option (Strauss et al., 1996) there are no known oil-prone 9A-12A source rocks in the area. Analyses of further source rock samples from the area should resolve the problem.

A total of 7 ions are used to distinguish between the different source rocks and their related hydrocarbons. Partial fragmentograms of these ions chosen from samples representative of active source rocks, inactive source rocks and reservoired hydrocarbons respectively, are shown in Figs. 12.09-12.11. For each sample, original fragmentograms are available in Appendix E. All the hydrocarbon samples are shown to have affinities either to a single source rock family or to a mixture of source rocks. The absence of samples with unusual characteristics may indicate either that the fetch area contains no other source rocks, or that the characteristic hydrocarbons used are not selective enough to differentiate another effective source rock in the basin. Until more source rock and hydrocarbon analyses are carried out, this aspect will remain uncertain.

12.1.2.1. Steranes and hopanes

The m/z 177 fragment is generally used to assess the contribution of demethylated hopanes which are often present in large proportions in biodegraded oils (section 11.2.4.). However, in this study, where none of the oils display signs of biodegradation, the fragmentogram is used to assess the relative proportions of norhopanes, hopanes and steranes. In his compilation of biomarker spectra, Philp (1985) shows that most steranes and hopanes have m/z 177 fragments which are of similar size (ranging from 9-12%) of the base peak. Hence this ion provides an approximation of the relative proportions of these compounds, mostly C27-29 diasteranes and C27-32 hopanes. Indeed the proportions estimated from the m/z 177 fragmentogram largely match the relative proportions recorded from m/z 217 and m/z 191 fragments.

Family 1 source rocks and hydrocarbons have diasterane proportions which are similar to, or greater than, those of C29 norhopane (Figs. 12.09 and 12.11). Family 2

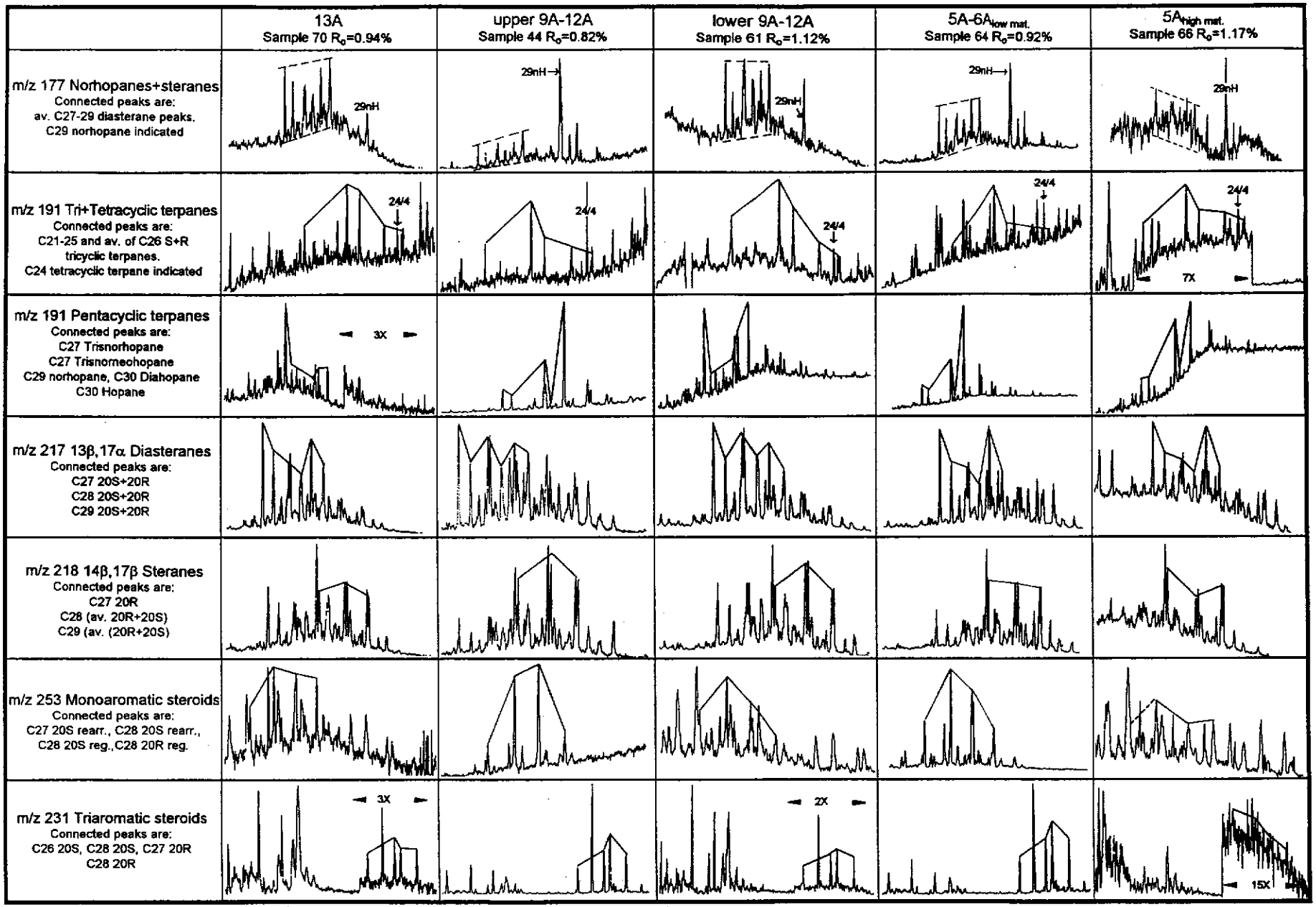

Figure 12.09: Partial mass fragmentograms of examples of characteristic ions from each of the main source rocks. Relevant peaks are highlighted and connected to indicate the differences between each unit of source rock.

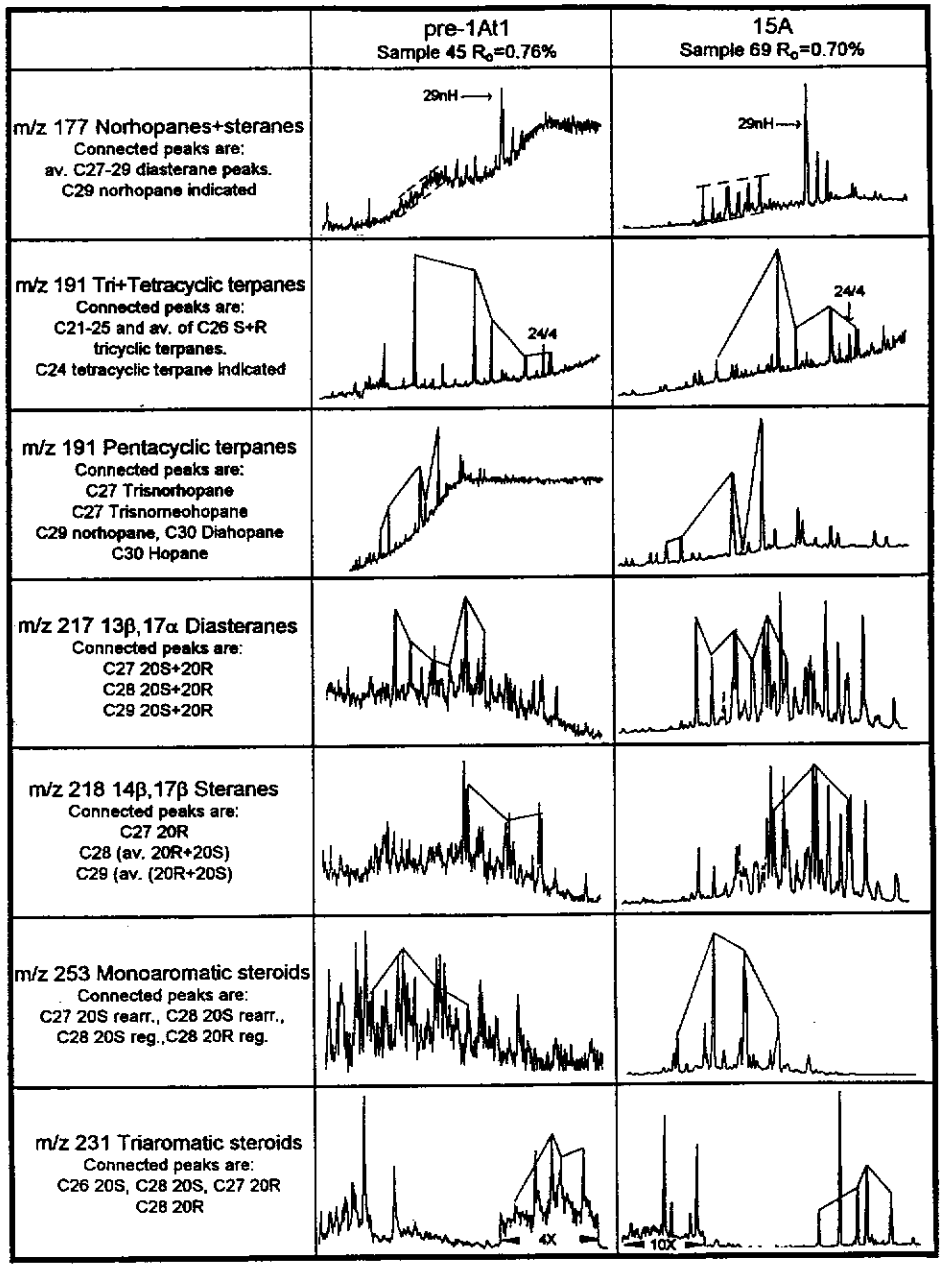

Figure 12.10: Partial mass fragmentograms of examples of characteristic ions from each of the two inactive source rocks. Relevant peaks are highlighted and connected to indicate the differences between each unit of source rock.

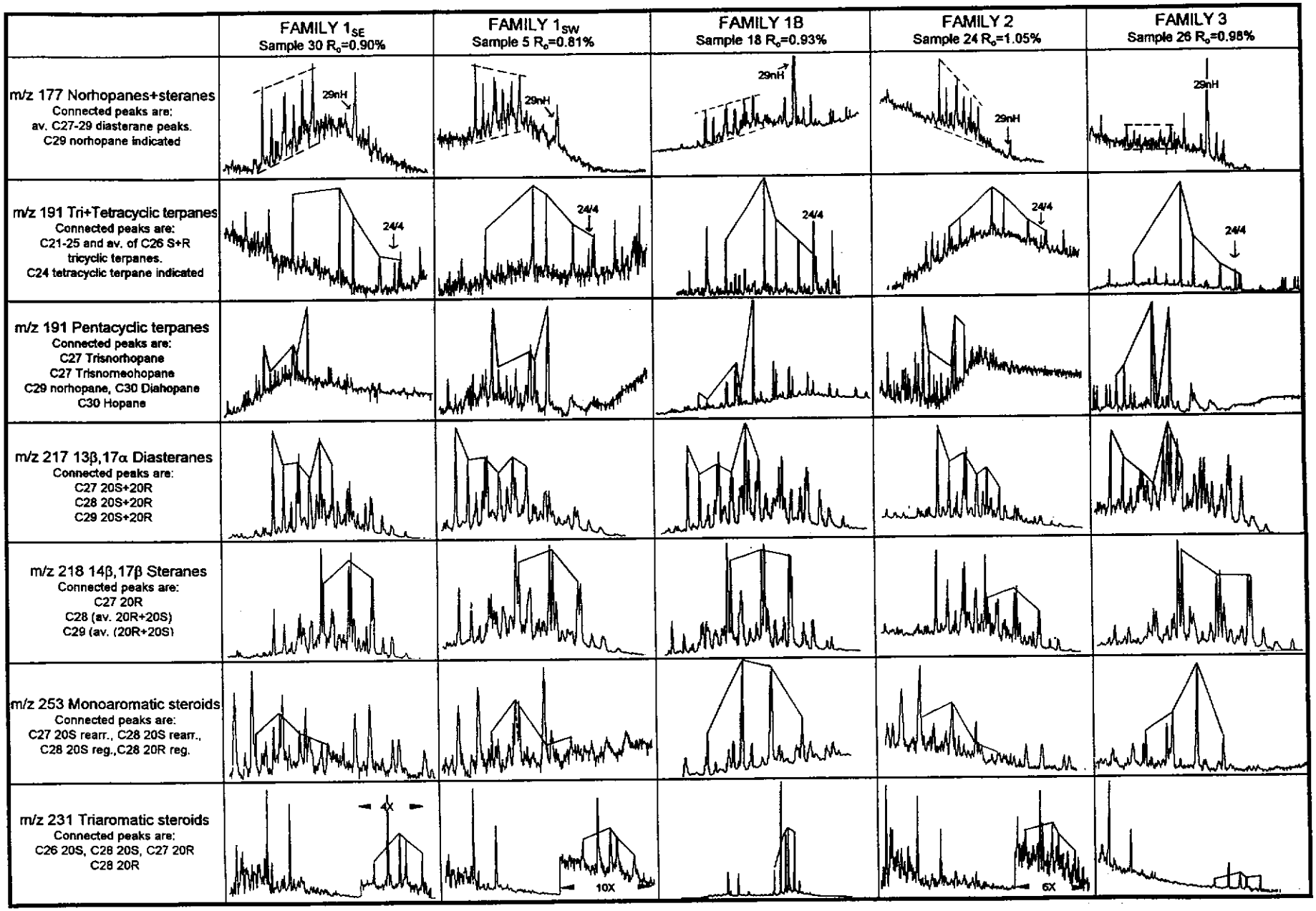

Figure 12.11: Partial mass fragmentograms of examples of characteristic ions from representative samples of each hydrocarbon family. Relevant peaks are highlighted and connected as in Figures 12.09 and 12.10 to indicate the differences which distinguish each hydrocarbon family.

condensates generally have distinctly higher diasterane proportions whilst the opposite is true of samples of Families 1B and 3.

The proportion of diasteranes relative to ββ steranes was shown to increase as maturity increases and in this example reached maximum values after R_o~0.9% (Van Graas, 1990). Most of the samples in this dataset, and in Figs. 12.09 and 12.11 are at maturity levels higher than R_o~0.9%. Connan and Dessort (1987) show the ratio of triterpanes/steranes to be a source parameter and Moldowan et al. (1985) interpret higher sterane proportions as indicative of marine organic matter with algal contributions whilst lower ratios are more typical of terrigenous input. Certainly the Bredasdorp Basin data seem to confirm this as those source rock samples with higher hopane proportions tend to be more gas-prone.

12.1.2.2. Tri- and tetracyclic terpanes (m/z 191)
Three different patterns are evident in the m/z 191 fragmentograms namely:
(i) one with a strong dominance of the C24 tetracyclic terpane over the adjacent tricyclic terpanes in Family 1B samples
(ii) one with a reduced C24 tricyclic terpane relative to the adjacent C25 and C23 homologues
(iii) one with a dominance of C21 tricyclic terpane over the other tricyclic terpanes.

(i) Dominance of C24 tetracyclic terpane, a characteristic of Family 1B material, has been shown to be typical of either evaporitic and carbonate-rich sequences, bacterial or algal near-shore source, or dominance of terrigenous-sourced material (section 11.4.1.9). Family 1B source rocks do not have high carbonate proportions nor are they evaporitic. They were deposited in shelfal not near-shore environments and do not appear to contain large proportions of bacterial or algal organic material. Hence it is likely that the high C24 tetracyclic proportions result from increased terrigenous proportions. Indeed, Family 1B source rocks are located closer to the palaeo-basin edge than Family 1 source rocks where input of land-plant debris is likely to have been higher. Hence the high C24 tetracyclic proportions in Family 1B source rocks, which indicate a significant source-specificity and that the Family 1 and 1B source intervals are not the same. Indeed, other samples from the near-shore region, e.g. samples 55 and 66 from 5A-6A source rocks (in wells 112 and 65 respectively), also contain high C24 tetracyclic proportions. This suggests that generally, there is a depositional or diagenetic reason why source rocks near basin margins should have higher C24 proportions (Sofer, 1988).

(ii) The C25-26 tricyclic terpanes are primary and formed either by thermo-catalytic degradation of a hopanoid precursor or side-chain cleavage of pentacyclic terpanes

rather than by cracking of pentacyclic terpanes. Hence increased proportions of the C25-26 tricyclic terpanes, relative to C24 tetracyclic terpane, probably reflect both the composition of the original starting material as well as the maturity.

(iii) The C21 tricyclic terpane precursor has been suggested as either a tricyclic sesterpenoid (Ekweozor and Strausz, 1983) or a polyprenol (Aquino Neto et al., 1983; Moldowan et al., 1983). Its derivation is therefore not significantly different from the precursors of the rest of the C19-25 tricyclic terpanes. Since they are not present in elevated proportions it would suggest there is no general depositional, diagenetic or maturation reason for the uncommon C21 dominance. Unusually large proportions of the C21 homologue have been recorded in lacustrine samples, but not in sediments deposited in marine-dominated environments (Mello et al., 1988; De Grande et al., 1993). Therefore dominance of this C21 compound in the lacustrine sample (number 45) does help to confirm its depositional environment.

12.1.2.3. Pentacyclic terpanes

The proportions of six compounds are considered to summarise the familial correlation namely C27 18α(H)norneohopane (Ts), C27 17α(H)norhopane (Tm), C29 norhopane (29nH), C29 18α(H)norneohopane (≡C29Ts) (29nnH), C30 diahopane (30D) and C30 hopane (H). The relative proportions of these six compounds (Figs. 12.09-12.11) allow for differentiation between source rock and hydrocarbon families. Family 1 samples generally have more of compound Ts than the C29 norhopane (29nH), which is itself present in much greater proportions than the C29 norneohopane. However, C30 hopane (H) is dominant over these last two compounds. Family 1B samples have similarly small Ts and 29nnH peaks, but somewhat smaller 30D peaks and substantially larger C30 hopane peaks. Family 2 samples also have larger proportions of Ts than 29nH but diahopanes are dominant, mostly over all other peaks. Although the proportions of all of these have been used elsewhere in maturation studies (Seifert and Moldowan, 1978; Hughes et al., 1985; Philp and Gilbert, 1986a and b; Farrimond and Telnaes, 1996) reports also show them to have source facies connotations (Moldowan et al., 1986; Blanc and Connan, 1992; Moldowan et al., 1991; Peters and Moldowan, 1993, p.143-164).

Compound Ts was very early shown to be a thermally generated hopane, the proportions of which increased with thermal stress relative to the proportions of compound Tm (Seifert and Moldowan, 1978). However the relative proportions of Ts and Tm can only be used as a maturation parameter where there is a common source, which implies a source-specificity (Peters and Moldowan, 1993, p. 234). Both the C29 and C30 hopanes (17α(H) configuration) are relatively stable under thermal stress so that non-maturation changes are measured against their proportions.

In this dataset, although the Ts/Tm ratio varies somewhat with maturity, there are major changes which are unrelated to maturity and more likely related to source-specificity. For example, Family 1 and 3 source rocks have matching reflectances but very different Ts/Tm proportions (Fig. 12.09). Other authors have also commented on the source-specificity of these terpanes. McKirdy et al. (1983) record unusually low proportions of Ts in mature carbonate-rich source rocks. This explanation cannot be the answer here as Family 1B source rocks have the lowest Ts proportions relative to their maturity, yet they also have the lowest carbonate contents (Appendix F, Table F1). Moldowan et al. (1986) report increased proportions of Tm in oxidised shales relative to anoxic shales. Peters and Moldowan (1993, p.233) suggested increased Tm proportions are due to different proportions of a coeluting tricyclic or tetracyclic terpane. There are evidently several possible effects which could modify the Ts or Tm proportions; in this case the most important appears to be that of oxicity of the depositional environment.

Moretanes are an epimeric form of pentacyclic terpanes which decrease in proportion relative to the hopanes as maturity increases. The ratio is used as a maturity parameter for low maturity samples, but not here because of the relatively high maturity of most samples. Nevertheless, there is a difference in the moretane abundances between the highest and lowest maturity samples (Figs. 12.12a; 12.12b).

The C30 diahopane (30D≡Compound X) was originally considered to be an indicator of terrigenous origin (Philp and Gilbert, 1986a and b). It has recently been shown to derive from a bacterial precursor (Moldowan et al. 1991). The compound is the dominant homologue of a series of diahopanes, which in these samples ranges up to C33 (Fig. 12.12). A bacterial origin is more likely than a terrigenous source as their presence in Precambrian oils, possibly from a Precambrian or Early Phanerozoic source, implies an aquatic origin (Summons et al., 1988).

It has also recently been shown (Peters and Moldowan, 1993, p 160.; Farrimond and Telnaes, 1996) that these rearranged hopanes may be indicators of oxic environments. In this dataset, there is no strong evidence for a global maturity effect. This is because of the source rock samples with reflectances in excess of R_o 0.9%, only a little over half have dominant diahopanes. However, the sample shown in Fig. 12.12a is from an outer shelf dysoxic environment and lies on the same trend as the Family 2 condensates which all have high diahopane proportions (section 12.2.2.5). There the diahopane proportions record a maturity-dependency and confirm the indication of an oxic depositional environment from the high aromatic proportions.

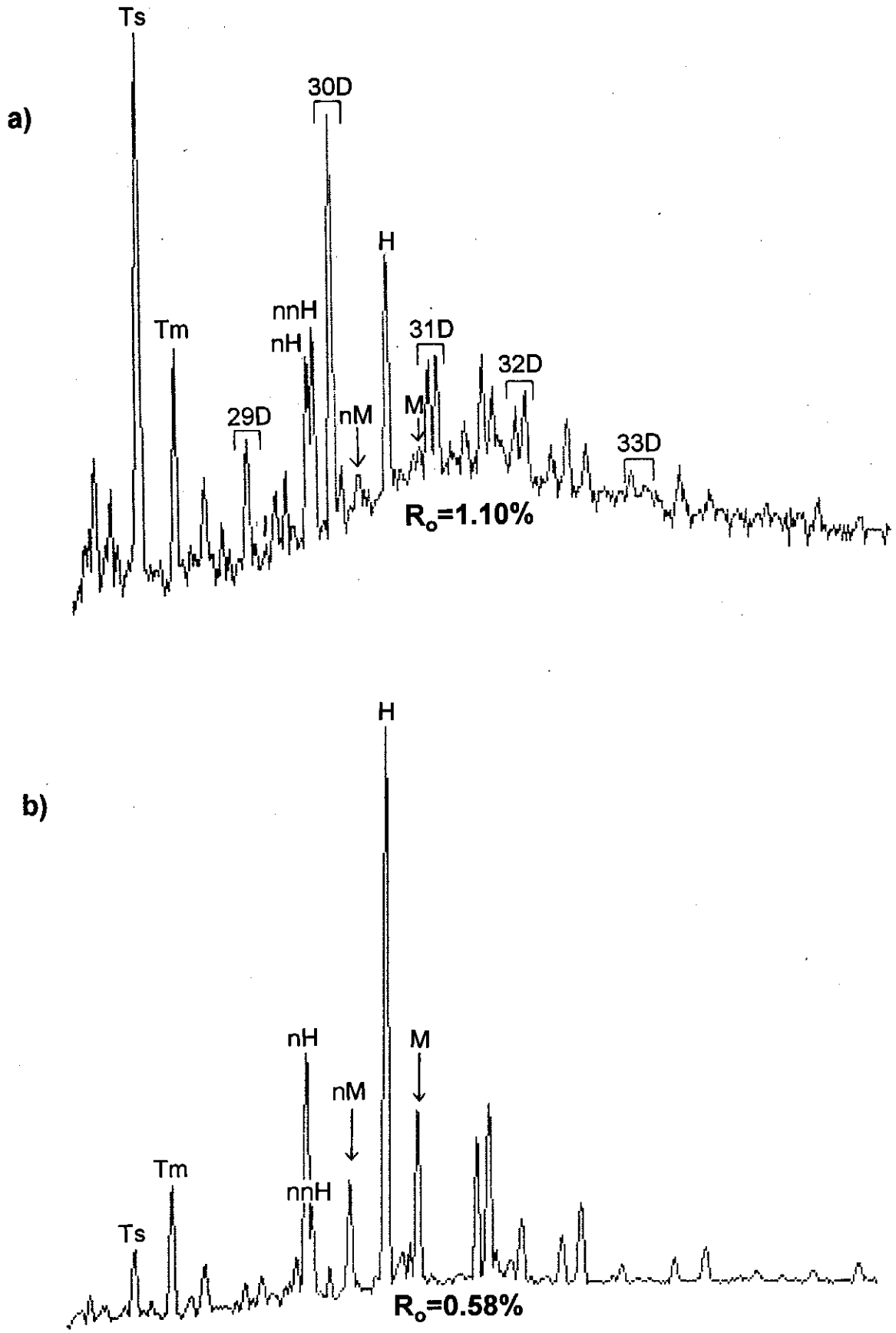

Figure 12.12: Partial m/z 191 mass fragmentograms of (a) a high maturity source rock sample (no. 63) and (b) a low maturity source rock sample (no. 49) showing the development of the C29-33 homologous series of diahopanes in the high maturity and the C29-30 moretane series in the low maturity samples.

12.1.2.4. Steranes and diasteranes

Two groups of compounds are considered for familial characterisation - (i) 14α,17α steranes and (ii) 13β,17α diasteranes.

The 14α,17α steranes dominate in only 2 samples i.e. the Family 7 Turonian (15A) source rocks. No reservoired hydrocarbons of this type have been found, but these source rocks have not expelled quantities of hydrocarbons because their original potential is not so high that they could generate enough oil at their presently low maturity level ($R_o \leq 0.7\%$) There are apparently no other features which could characterise oils from more mature versions of this source and while it is not impossible that more deeply buried equivalents of the 15A source shales in the Bredasdorp Basin have expelled hydrocarbons, geological constraints suggest this to be unlikely (see sections 12.1.1. and 13.3.2.1). Family 7 source rocks are therefore considered essentially inactive.

Most source rock bitumen samples have large proportions of diasteranes and in most cases they dominate over the regular steranes. Apart from increased proportions where the maturity is high, they are still surprisingly dominant which suggests a source-specific influence such as from specific algae or from higher plants in a clay-rich environment (Rubinstein et al., 1975). The distribution of these compounds in each sample have elsewhere proved to be indicators of the type of organic material (Mello et al., 1988; Comet et al., 1993). Diasteranes are found in these samples with three major distribution patterns:

(i) samples with C28 βα approximately midway in height between the C27 and C29 homologues (characteristic of Families 1B and 2)

(ii) samples where C28βα homologues are significantly lower (Families 1 and 3)

(iii) samples where the C29 βα homologues are relatively higher than those of the C27 homologues (Family 3).

The proportions of C27-29 homologous steranes have been used for some time to distinguish between source rock ecosystems (Haung and Meinschein, 1979; Mackenzie et al., 1983), although some later studies show that this environmental interpretation can be inconclusive (Moldowan et al., 1985). For example, Moldowan et al. (1992) showed reduced C28 proportions to be characteristic of Triassic lagoonal source rocks whilst very low C28 proportions were reported by Peters et al. (1989) and Magoon and Anders (1992) from Jurassic marine source rocks. Peters and Moldowan (1993, p. 190) show that the proportions of C27-29 homologues are unaffected by maturation hence they should largely match those of the detrital sterols. However, they point out that use of GC-MSMS is necessary for complete characterisation of diasteranes to avoid co-

elution problems such as elution of C27 14β,17β 20R cholestane with C29 20S 13β,17α diasterane.

12.1.2.5. Regular ββ steranes

Discriminating patterns in this ion fragment rely largely on the relative proportions of C28 20S+20R. In Family 3 samples, C28 components are generally present in smaller proportions than the average of the C27 and C29 homologues whilst in all other families they are present in greater proportions reaching a maximum in Family 1B samples where they are >1.5X larger than the C27 and C29 homologues. The 14β,17β steranes are characteristic of higher maturity samples, and are considered to have been generated either from the matching 14α,17α sterane by a diagenetic methyl-shifting reaction or from a precursor (Mackenzie, 1984, p. 138-143, Rullkötter and Marzi, 1988; Waples and Machihara, 1991, p. 25). Those formation routes result in proportions of the C27-30 homologues which partly reflect the original detrital organic matter and partly the subsequent diagenesis. There are suggestions of ββ sterane formation by sulphur catalysis in source rocks of hypersaline environments (Peters and Moldowan, 1993, p. 241-242). However, that generation route is unlikely in the Bredasdorp Basin where hypersaline sediments are known to be present only in one well. In that interval there are no known source rocks.

Haung and Meinschein (1979) show lacustrine organic material to be dominated by the C28 sterol homologue and Waples and Machihara (1991, p. 42) show the C28 sterane homologue to dominate in mature lacustrine source rocks. However, other authors (Mpanju and Philp, 1993; Comet et al., 1993) show high proportions of C28 steranes to reflect both marine and non-marine hydrocarbons. Grantham and Wakefield (1988) show the ratio of C28/C29 steranes to broadly reflect the age of the source rock, but the spread of values in their plots is so large that they could accommodate most ratios in most age groups. Indeed the sterane proportions in these samples reflect that wide variation. The lacustrine source rock in this dataset (sample 45) is the only source rock to match the low C28 proportions common to Family 3 source rock bitumens and hydrocarbons. It is not impossible that some syn-rift sourced hydrocarbons have mixed with Family 3 condensates. The unusual character of the condensate from fluvial sandstones in well 18 (DST1) (Chapter 9) which partly matches the condensates in wells 27 and 35, may support this interpretation although there are no biomarker data to confirm this.

12.1.2.6. Monoaromatic steroids

The main distinguishing features of monoaromatic steroids (MAS) are the proportions of the C27, C28 and C29 homologues. These are represented by the relative heights of peaks 2, 6, 10 and 14 as shown on Figs. 12.09-12.11.

Family 1 source rocks and hydrocarbons are characterised by a predominance of C27 and C28 rearranged components, based on dominances of peaks 2 and 6. Elsewhere this is considered characteristic of a dominantly clastic terrigenous input (Riolo et al., 1986) but here that is not the case. The explanation may lie in the relatively low maturity of the samples they investigated compared to those from the Bredasdorp Basin. Riolo et al. (1986) do show the proportions of peak 6 to decrease at higher maturation levels. Certainly the modestly mature western Family 1B samples have characteristically strongly developed MAS in which there is a clear dominance of peaks 6 and 10 (C28 20S regular and rearranged). In the eastern Family 1B sample 33, peak 6 is masked by n-alkanes, because the sample was too small to subject to urea adduction. Proportions of peak 2 are also lower in samples at reflectances R_o~0.9-1.0% (samples 46-48, Appendix E, Figs. E.112-114) than in samples from the same source interval with reflectances R_o~0.8-0.9% (samples 41-43, Appendix E, Figs. E.107-109). confirming the results of Riolo et al. (1986). However, samples from the 15A source rock, both at significantly lower maturities, have smaller proportions of peak 2 than almost any other sample. This suggests that either the proportions increase and decrease through the oil window or they demonstrate a strong source-specificity.

Riolo et al. (1986) indicate that peaks 11 and 12 are present in low proportions at high maturity, but show only one sample with a high proportion of peak 12 which was from a low maturity anhydrite-rich source rock. In the Bredasdorp Basin, reduced proportions of these two steroids confirm the elevated maturity level compared to many literature examples.

Seifert et al. (1983) and Mackenzie (1984, p. 143-145) show MAS to be formed by aromatisation of sterenes from detrital sterols during diagenesis. Hence the proportions of different homologues, as with the steranes, probably reflect the proportions of detrital organic matter. Seifert et al. (1983) also comment that the formation of steroids is linked to catalytic conversion. Hence the different proportions could also reflect different proportions of catalysts. Indeed, they employed the C27/C29 ratio as a source parameter and commented that it is especially useful as it is barely affected by modification during migration.

In none of the source rock samples from this area are the C29 homologues (peaks 15 and 16) dominant. Family 3 samples, which are generally the more mature, tend to have higher proportions than most and also have relatively high proportions of the C28 20R regular compound (peak 14). This may indicate kerogen of a very different type in Family 3 source rocks compared to the other source rock intervals.

12.1.2.7. Triaromatic steroids

As with the MAS, the most effective discriminatory parameters are those defining different carbon-number homologues. This includes the proportions of C26 and C28 20S and C27 and C28 20R components (peaks a, c, d, e respectively) in the present study. Family 2 samples have these peaks in roughly equal proportions. In moderately mature Family 1 samples (R_o>0.85%), peak 'c' dominates over peak 'd' (Fig. 12.13a), but in Family 1B samples this ratio is reversed. In Family 3 samples, peak 'c' is significantly subordinate to peak 'd' matching a mature source rock of clastic, mud-rich origin (Riolo et al., 1986). In a few of the shale samples, there is evidence of small amounts of the C29 20R homologue (peak eluting just after peak 'e', e.g. in sample 55, Appendix E, Fig. E.121). Riolo et al. (1986) show that this peak characterises dominantly terrigenous organic matter.

Riolo et al. (op cit.) also show that proportions of the C28 20S homologue (peak c) increase and C27 20R (peak d) decrease during a maturation increase across a depth increment of ~500 metres. The ratio of these peaks in their data change from 0.75-1.46. This depth increment is less than that between the shallowest and deepest Bredasdorp Basin samples (1820-3220m) so that a change in the proportions of peaks 'c' and 'd' would be expected to be at least as large here. Indeed, source rocks of Families 1, 1B and 3 do show similarly increased c/d ratios with increasing maturation (Fig. 12.13a). However, the matching plot for the hydrocarbon samples shows minimal increase with maturity (Fig. 12.13b). This may result from too few samples in each family to derive trends, but more likely because the reservoir maturities do not match the maturities at expulsion. In addition, other than a few from Family 1B, there are no hydrocarbon samples with c/d ratios <0.8. This ratio is indicative of a source rock maturation level of R_o<0.8% for Family 1 and R_o~0.9% for Family 3, suggesting that these reflectance values mark the threshold of first liquids expulsion.

12.2. MATURATION AND SOURCE CORRELATION

Cross-plots of biomarker ratios are commonly used to establish maturation trends and to determine if offsets from these trends characterise bitumen from specific source intervals. A number of the more commonly used biomarker plots are shown with ratios plotted against, mostly, vitrinite reflectance data following conventional formats.

Fragments used throughout are the ones most commonly employed in the literature for the determination of proportions of characteristic compounds. Most have been analysed by low resolution-MS hence some compounds are partly masked by co-elution.

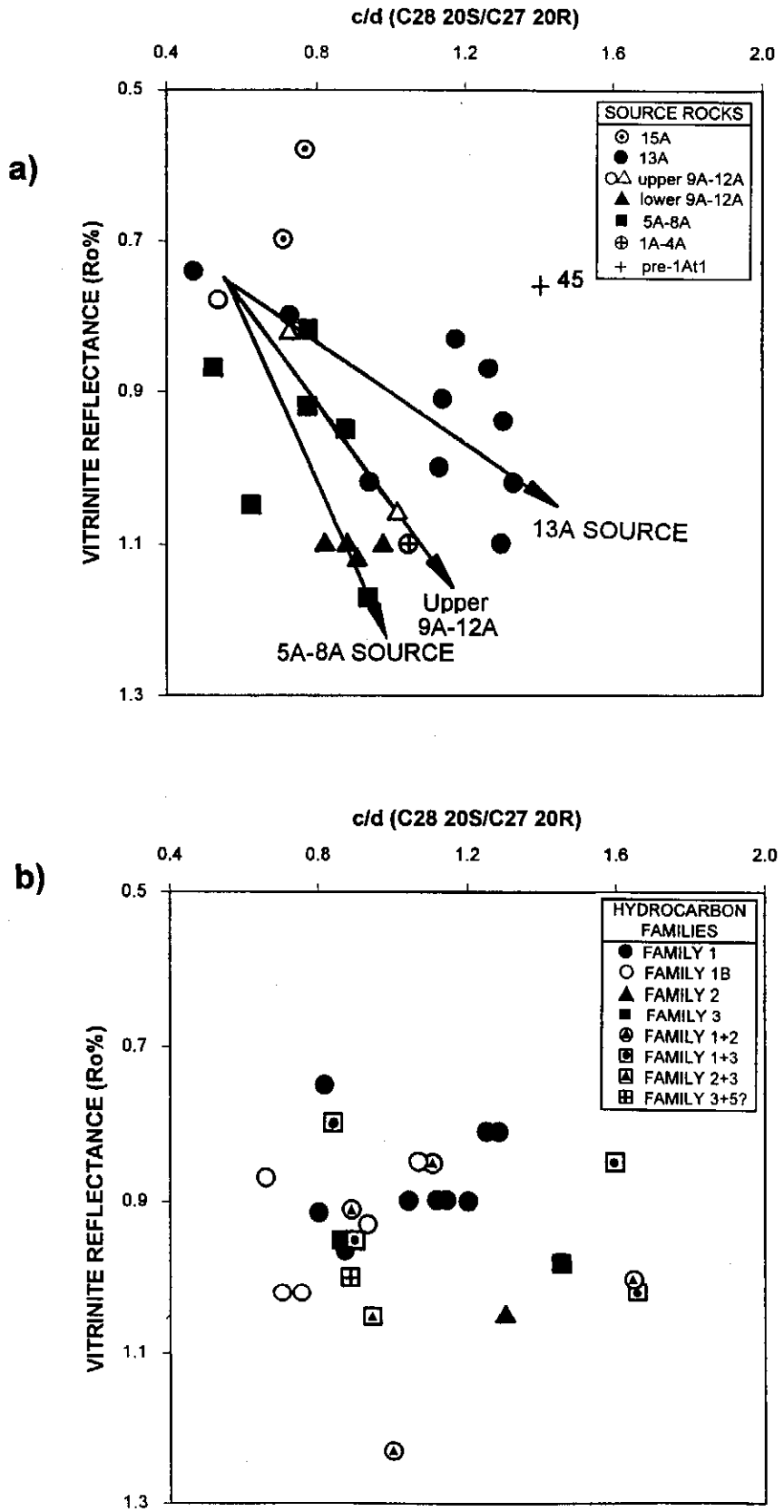

Figure 12.13: Plots of ratio between two triaromatic steroid peaks i.e. c/d (C28 20S/C27 20R) vs vitrinite reflectance data calculated for (a) each source rock and (b) each hydrocarbon sample. Each data point is coded to indicate (a) the source rock intervals sampled and (b) the hydrocarbon families. Regression lines for source rock intervals are drawn through the majority of the data which display a maturity-dependency. These figures are discussed in section 12.1.2.7.

12.2.1. Sterane plots

Most of these data are determined from m/z 217, 218 and 259 ion fragmentograms.

12.2.1.1. C29 14α,17α 20S/(20S+20R) isomerisation of regular steranes

This ratio is probably the one most commonly used in other studies (Waples and Machihara, 1991, p.25; Peters and Moldowan, 1993, p.237-239), because it is relatively easy to determine. Most authors consider it to be uncompromised by co-elution although there is some evidence that co-elution with a number of lesser known compounds can influence the apparent proportions of the C29αα 20S isomer (Gallegos and Moldowan, 1992). As previously discussed (11.4.1.1.), the change from the biologically-derived 20R isomers to the thermally more stable 20S isomers, tracks maturation increases at least until the equilibrium value (~0.55-0.6) is reached (Fig. 12.14). The trend lines are after Waples and Machihara (1991) and not only record the increased maturation, but also differences between samples from different families. For instance, Family 1 hydrocarbons locate at the upper side of the envelope, similar to some of the Family 1 bitumen samples (Figs. 12.14a and b). A few 13A source rock bitumens locate separately from these at the lower side of the envelope. However, these samples have expelled little oil because of low maturity and few of the residual oils contain components from these shales.

Sample 26 however, would only fit within the envelope if the reflectance were R_o~0.7% instead of R_o~1.0%. The reflectance data are considered accurate as there are many similar reflectance values in adjacent wells. The unusually low ratio could reflect one of several possible effects:

(i) it may be derived from solution of low maturity biomarkers from a source during migration. This is unlikely in view of the high formation maturity, and the small amounts of Tertiary sedimentation which would push the age of the backstripped formation at R_o~0.7% to Early Tertiary. The gases are unlikely to have been reservoired that long as surface seepage was continuing (Davies, 1988a)

(ii) the 20R peak may be overprinted by another compound although the mass spectrum does not confirm that. This is similar to the evidence for co-elution with the 20S isomer (Gallegos and Moldowan, 1992)

(iii) the sterane data may be in error, but this is unlikely as no contamination has been found and the peak assignments are clear (Appendix E, Fig. E.26)

(iv) the steranes in the sample could be inherited from a low maturity oil generated from resins although this is unlikely in view of other data (Snowdon, 1979)

(v) the steranes could be derived from the residue of an early low maturity oil charge.

The last option is considered to be the most plausible as there are traces of residual oil in other wells nearby, such as the high molecular weight 'hump' in the sample from well

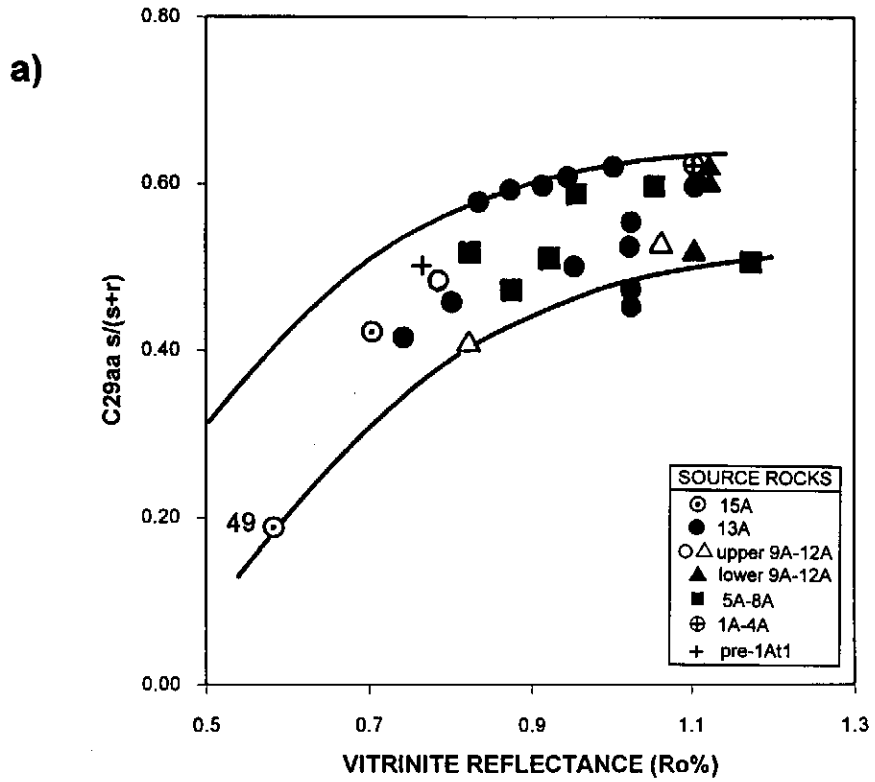

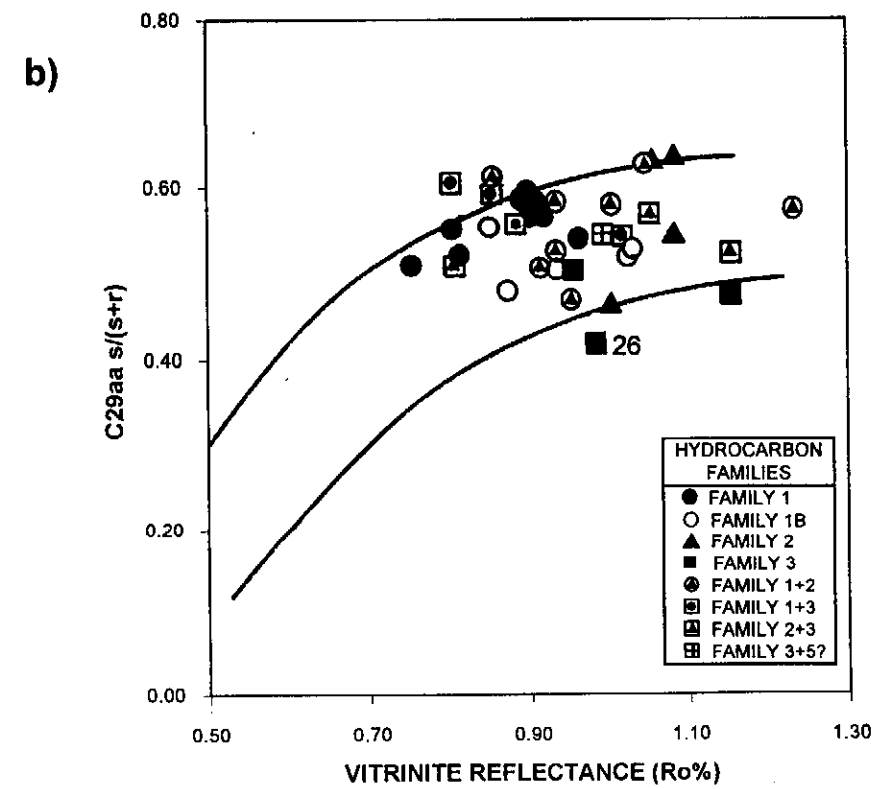

Figure 12.14: Plots of the C29 $\alpha\alpha$ 20S/(20S+20R) sterane isomer ratios vs vitrinite reflectance data for all (a) source rock and (b) hydrocarbon samples. Data zone after Waples and Machihara (1991, p. 25).

31 (Chapter 9). If this anomalous nature is confirmed by other data, then there is support for the presence of an early phase of oil migration through the structure (Banks et al., 1993).

12.2.1.2. C29 14β,17β/(14α,17α+14β,17β) epimerisation of regular steranes

This ratio too is often used in other studies and is also unaffected by co-elution of other steranes (Waples and Machihara, 1991, p.26). This ratio increases with maturity but not at the same rate as the S/(S+R) isomerisation (12.2.1.1.; Figs. 12.15a and b). Peters et al. (1989) do indeed show the ratio to reach its equilibrium value at R_o~0.7%, after the C29 (S/S+R) isomerisation ratio reaches its equilibrium. The trend lines used in Fig. 12.15 are after Cornford et al. (1983); Goodarzi et al. (1989) and Burwood et al. (1990). Most Family 1 and 1B oils locate at the right side of the envelope as do most Family 1 and 1B source rock bitumens. Although this ratio is not recommended as a maturity parameter (Waples and Machihara, 1991, p. 25), largely because ββ proportions can be high in low maturity samples under certain (mainly hyper-saline) diagenetic conditions (Rullkötter and Marzi, 1988; Peakman et al., 1989), it nevertheless does appear that the maturity trends do match for the higher maturity samples. In addition the source-specific distinction between hydrocarbons of different families adds further value to the usefulness of the ratio. The value for condensate sample no. 26 is close to the equilibrium value. As shown in the previous section, if the reflectance value was closer to R_o~0.7% as suggested by the αα 20S/(S+R) ratio (section 12.2.1.1), the sample would locate close to samples 36 and 23, the latter being representative of an early oil migration into the north flank of the basin.

The ratio for sample 22 at R_o=0.95% by contrast, is anomalously low, indicating a somewhat lower maturity (R_o~0.8%). This sample is from a sandstone largely enclosed by shale which would likely contain a mixture of oils expelled during different phases from the surrounding shale.

12.2.1.3. C27-29 αα regular steranes

Proportions of these homologues were amongst the first used to evaluate relative inputs of organic matter typical of different depositional environments (Palmer, 1984; Moldowan et al., 1985; Shanmugam, 1985). In a few cases the proportions have been shown useful in establishing maturation trends (Mackenzie, 1984, p. 191; Curiale, 1986 and 1992; Dzou et al., 1995).

In shale samples, the proportions of the C27 homologue increase largely with increasing maturity (Fig. 12.16a). The trend characterises the maturation level of each data point with a precision of R_o~0.1%, except for sample 66. That sample locates almost R_o~0.25% lower than expected and closest to the C29 apex. Published

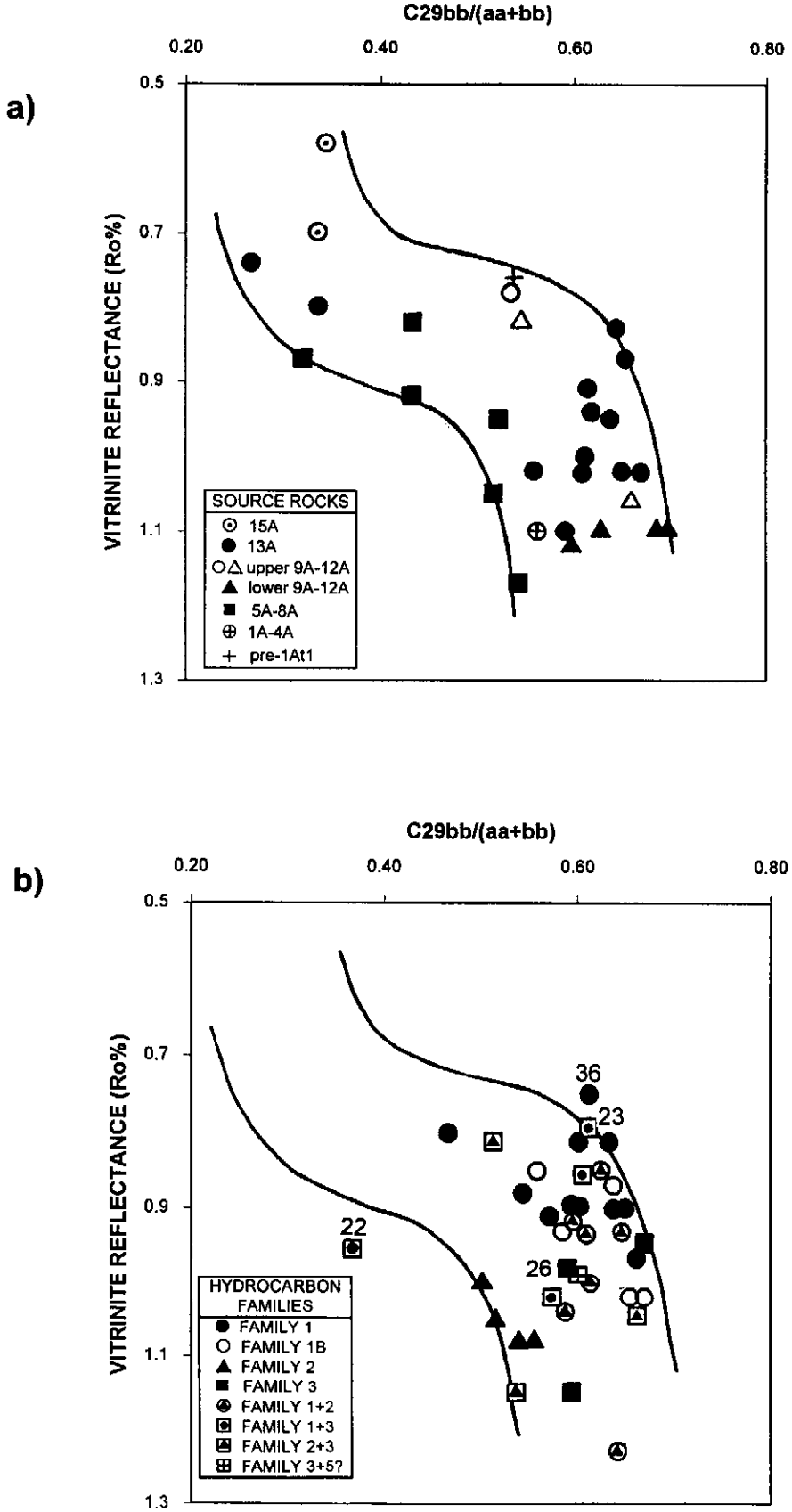

Figure 12.15: Plots of the C29 ββ/(αα+ββ) 20S+R epimer ratio vs vitrinite reflectance data for (a) all source rocks and (b) all hydrocarbon samples. Trend zone after Cornford et al. (1983), Goodarzi et al. (1989) and Burwood et al. (1990). Samples from northern source rocks plot within the low side of the trend.

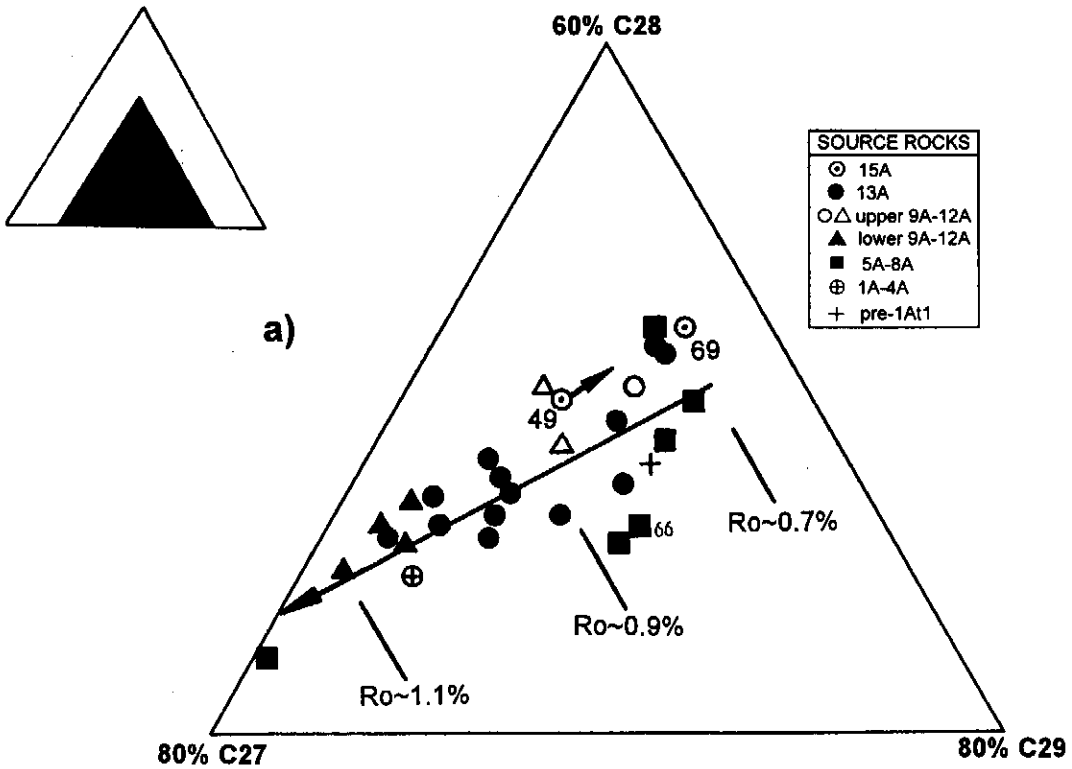

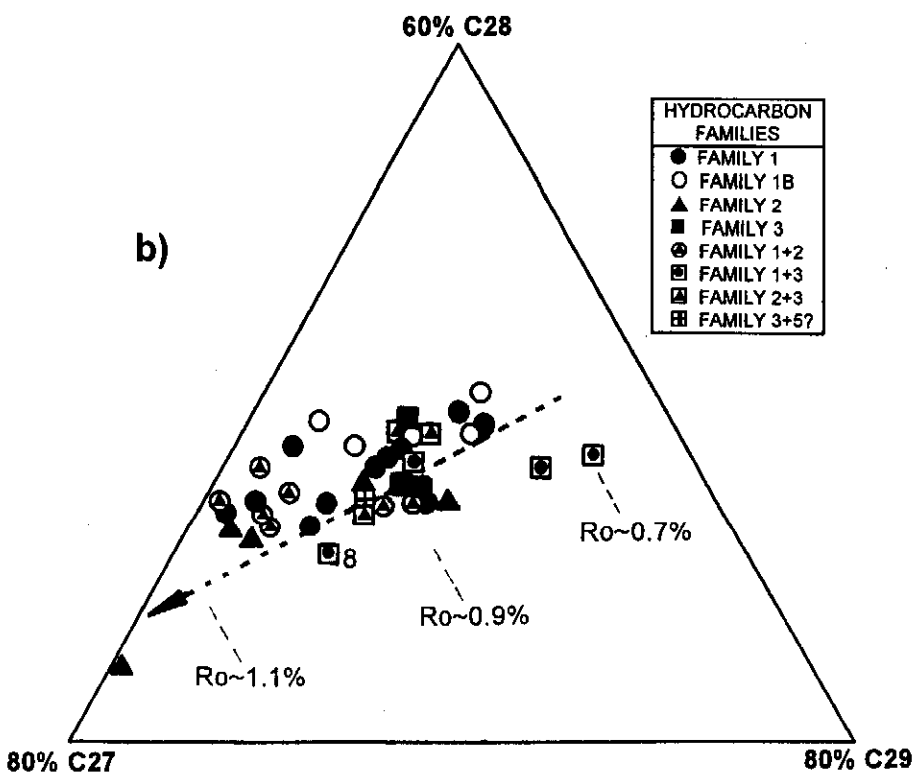

Figure 12.16: Ternary plots of the total 20S+R C27-29 14α,17α steranes for (a) source rock and (b) hydrocarbon samples. Maturation envelope after Mackenzie et al. (1984), Brassell et al. (1986) and Peters et al. (1989).

interpretations show that samples close to this apex are generally comprised of large proportions of higher plant material. It may be that source dependency has an over-riding effect on the carbon-number dominance because this sample, and all other 5A-8A source rocks, generally locate closer to the C29 apex than samples of other source rocks (Fig. 12.16a). This is also generally true of the Family 3 hydrocarbons, and those comprising mixtures with Family 3 (Fig. 12.16b).

Sample 8 locates closer to the R_o~1.1% region than its reservoir reflectance would suggest, by R_o~0.2%. This probably reflects the high maturity at generation of the material compared to its present reservoir maturity. Curiale (1992) shows a maturation trend towards the C28 apex in low maturity samples (R_o<~0.7%). Only one of the samples in this dataset is at a similarly low maturity (sample 49, R_o=0.58%). The trend from that sample to the next most mature sample (also from the Turonian source rock, sample 69) matches Curiale's trend (arrowed on Fig. 12.16a). Haung and Meinschein (1979) show samples close to the C27 apex as dominantly from an open marine environment and containing planktonic debris. Family 1 source rocks and hydrocarbons tend to cluster close to this apex. Palaeontology studies indeed confirm that the source rocks contain significant amounts of radiolaria and dinoflagellates and were deposited in open marine environments. This provides support for that environmental interpretation. Family 1B source rock and hydrocarbon samples tend to locate closer to the C28 apex than most other samples. This apex has been shown to characterise material from near-shore environments (Shanmugam, 1985). Source rocks for Family 1B hydrocarbons are found in a slope marine environment but very close to an advancing shelf. Organic matter is a mixture of near-shore, dominantly Type 3 material, deposited during each shelf advance and Type 2 amorphous material deposited during each quiescent phase (Smit, 1992; Barton and Grobbler, 1997).

12.2.1.4. C27-29 βα diasteranes

The proportions of C27-29 diasteranes (C-20 S and R) are used here to characterise different source rocks (Figs. 12.17a and b; Peters and Moldowan, 1993, p. 190). Skeleton rearrangement of sterenes to form diasteranes does not alter the proportions of the C27-29 homologues, so their proportions are a function of the detrital organic matter (Rubinstein et al., 1975). Grantham (1986) commented that oil samples from Oman had been sourced by a pre-Devonian source rock, yet they had high C29 diasterane proportions. Since land-plants had not developed then, a higher plant origin for the C29 diasteranes was clearly untenable. One possible origin was in marine brown algae (e.g. kelp) in which C29 sterols dominated. Therefore the proportions of C27-29 diasteranes are utilised as indicators of different source organic material even though there is some ambivalence regarding the type of organic material their dominance indicates. Cognisance has also been taken of the possible effects of co-

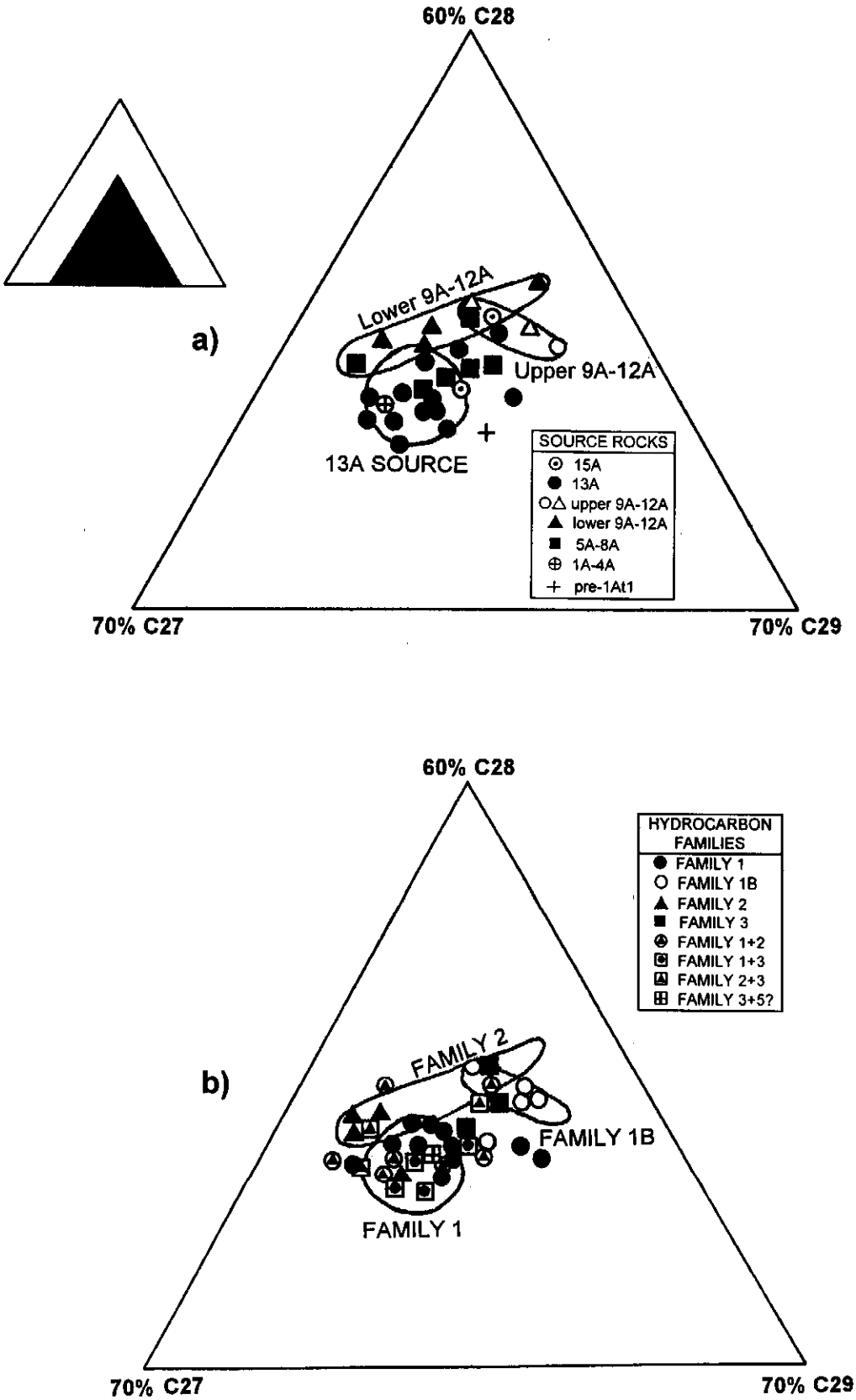

Figure 12.17: Ternary plots of the total 20S+R C27-29 13β,17α diasteranes for (a) each source rock and (b) each hydrocarbon sample. Although the points appear to form an unstructured group, there is a general structure. All Family 1B (and upper 9A-12A source rocks) locate furthest from the C27 apex, all Family 2 samples (and lower 9A-12A and possibly basal 13A source rocks) locate furthest from the C29 apex and all Family 1 samples locate centrally.

elution of C27 ββ 20R sterane with C29 20S diasterane. The former largely influences the mature samples where it dominates the regular steranes, especially where there are high C27 proportions. Family 1 oils and 13A source rocks generally have the lowest C28 proportions and a slight preference for C27 over C29 homologues (Figs. 12.17a and b). Family 1B has significantly lower C27 proportions than Family 1, even though they are similar in other ratios, whilst Family 2 condensates have higher C28 proportions (and lower C29) than most other samples. Family 3 condensates, and 5A-8A source rocks, locate between Families 1, 1B and 2.

12.2.1.5. C29 diasterane/sterane vs C30 diahopane/hopane

This plot compares the rearranged/regular ratios for the two main types of biomarkers. Plots comparing the C29 diasterane proportion against the C30 diahopane/hopane ratio describes an S-shaped curve suggestive of two reactions operating sequentially (Figs. 12.18a and b). The two reactions are those in which rearranged forms of both groups are generated, albeit at different rates. Farrimond and Telnaes (1996) use this plot to differentiate between two series of rearranged hopanes. Their data describe an S-curve indicating that hopane and sterane rearrangement reactions do not happen in parallel. If they did, the plot would describe a straight line. In general upper 9A-12A source rocks and Family 1B hydrocarbon samples lie at the lower end of the plot, whereas Family 1 oils and 13A shales locate just above them closely associated with Family 3 condensates and 5A-8A source rocks. Family 2 condensates mostly plot at the upper end of the figure, in contrast to their possible source rocks in lower 9A-12A shales. These locate higher up the trend perhaps implying that these are the source rocks but only where buried somewhat deeper.

The Family 1 oil from well 94 (sample no. 29) matches Family 2 condensate almost as closely as Family 1, suggesting it may represent a mixture of oil from a Family 1 source and a lighter condensate from Family 2. Indeed this agrees well with the evidence from the statistical analysis of C9-16 hydrocarbons (Fig. 9.18), which clearly locates this oil between Families 1 and 2. This plot is generally of limited value in characterising source-specificity or maturity-dependency, other than for Family 2 hydrocarbons.

12.2.2. Terpane plots

Terpanes are separated into tricyclic and pentacyclic compounds. Most pentacyclic compounds are hopanes. The precursors for the two groups are different, polyprenols and bacteriohopantetrol respectively, which are found in co-existing bacteria. They generally have characteristic fragmentation ions at m/z 191.

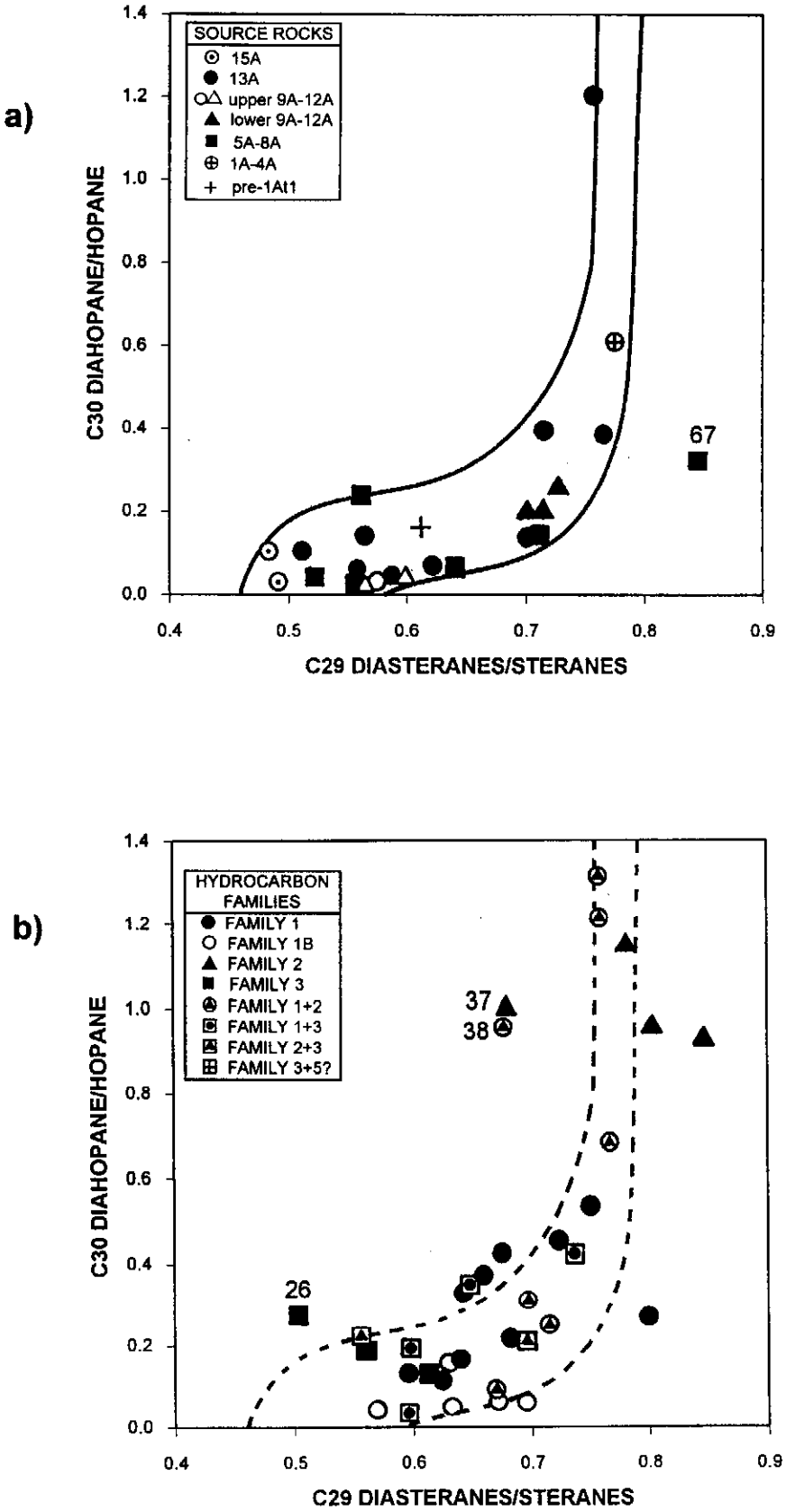

Figure 12.18: Cross-plots of rearranged/regular hopanes vs steranes for (a) source rock and (b) hydrocarbon samples. The envelope was constructed to encompass all matching data from Farrimond and Telnaes (1996). Sample 67 does not fit, perhaps because it contains impregnating condensate.

12.2.2.1. Total steranes/total hopanes vs vitrinite reflectance

Since steranes and hopanes largely represent different types of organic matter (algal/higher plant and bacterial respectively) their proportions are expected to show source-specificity. Indeed, Moldowan et al. (1985) show that high sterane/hopane ratios do typify marine organic matter, especially where dominated by algal or planktonic organisms. A further example is given in data comparing Kimmeridge (siliciclastic) and Hanifa (carbonate) source rocks and oils (Van Graas, 1990). Very large differences between the two groups of hydrocarbons are apparent (Fig. 12.19).

Data from the Bredasdorp Basin generally show a very broad scatter (Fig. 12.20a). Bitumens from 5A-8A source rocks, except for sample 66, show a maturity-related trend. Less evident is a weak maturity trend amongst upper 9A-12A samples. The corresponding Family 1B hydrocarbons do not plot in precisely the same area although they do plot to the left side of the data (Fig. 12.20b). This indicates that if the source rocks are representative of the source of the oils, then geochromatographic effects may alter the proportions of steranes and hopanes. The lacustrine source rock (sample 45, ✚) has the lowest sterane/hopane ratio (Fig. 12.20a), suggesting dominance of bacterial organic material, which is at odds with the known occurrence of Botryococcus masses in the kerogen (Davies et al., 1991). In all though, as with the preceding plot of rearranged/regular steranes and hopanes, these offer little convincing evidence for either source-specificity or maturity-dependency.

12.2.2.2. C24 tetracyclic/C25+C26 tricyclic terpanes

As shown in Figs. 12.09-12.11, Family 1B is characterised by high proportions of C24 tetracyclic terpanes relative to the adjacent C25 and C26 tricyclic terpanes. Such a relationship is detailed in Figs. 12.21a and 12.21b. However, there is no support for a maturity relationship of the ratio similar to that suggested by Aquino Neto et al. (1983). They showed that C24 tetracyclic terpane was thermally more stable (or neoformed at a faster rate) than the tricyclics. Indeed, quite the opposite seems true as the source rock samples with the lowest ratios tend to be the most mature. It may be that there is a slight maturity effect which is mostly overprinted by a larger source effect. There is however, no such maturity effect in the plot of the hydrocarbon samples (Fig. 12.21b). In this regard, Family 2 hydrocarbons and lower 9A-12A wet gas-prone source rocks all have low proportions of the tetracyclic component, confirming the dominantly terrigenous input, whilst Family 1B generally have the highest (Aquino Neto et al., 1983; Philp, 1988).

12.2.2.3. C24 tetracyclic/total terpanes vs C23/C21 tricyclic terpanes.

Ekweozor and Strausz (1983) suggest that the C21/C23 ratio is a measure of thermal maturity, based on pyrolysis data which showed the ratio to consistently decrease with

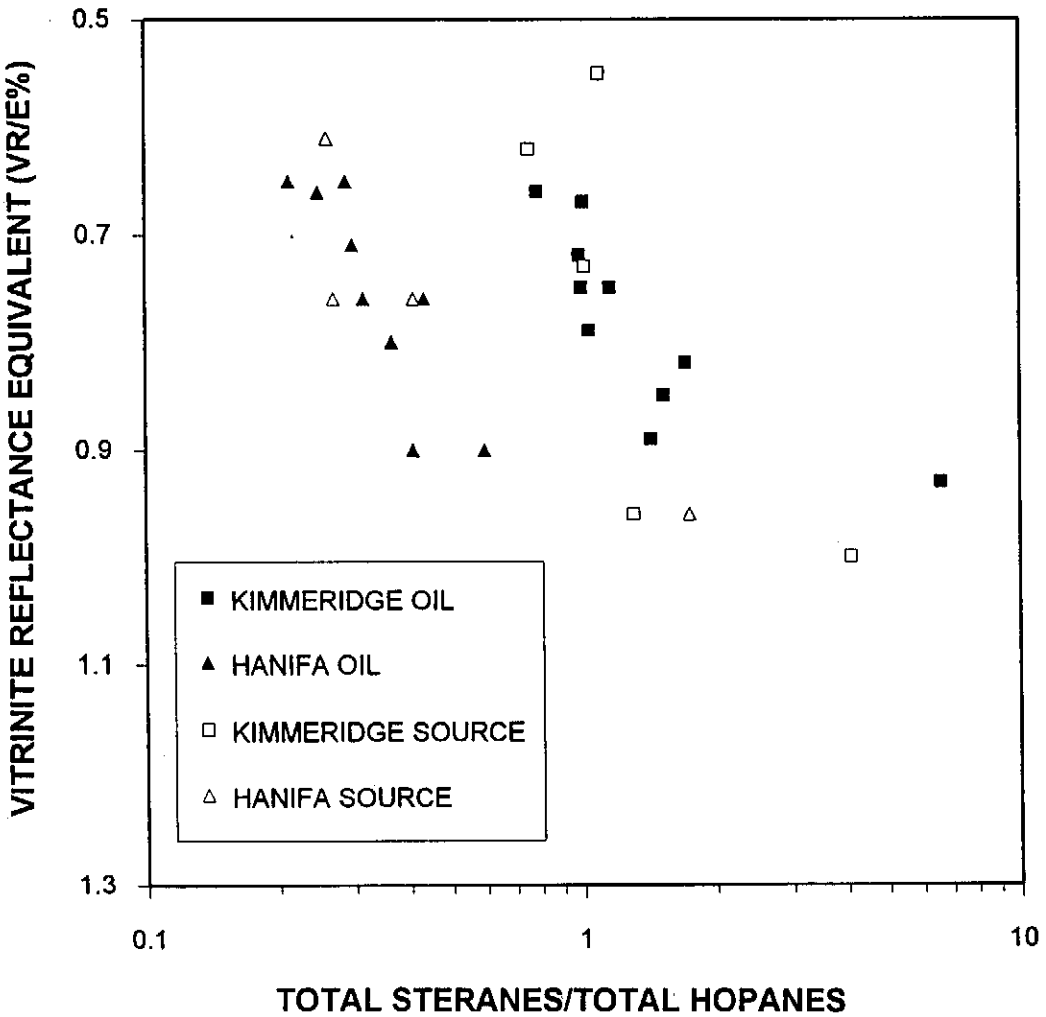

Figure 12.19: Plot of total sterane/hopane ratios vs equivalent vitrinite reflectance data for samples from Van Graas (1990) showing the distinction between two different source rocks.

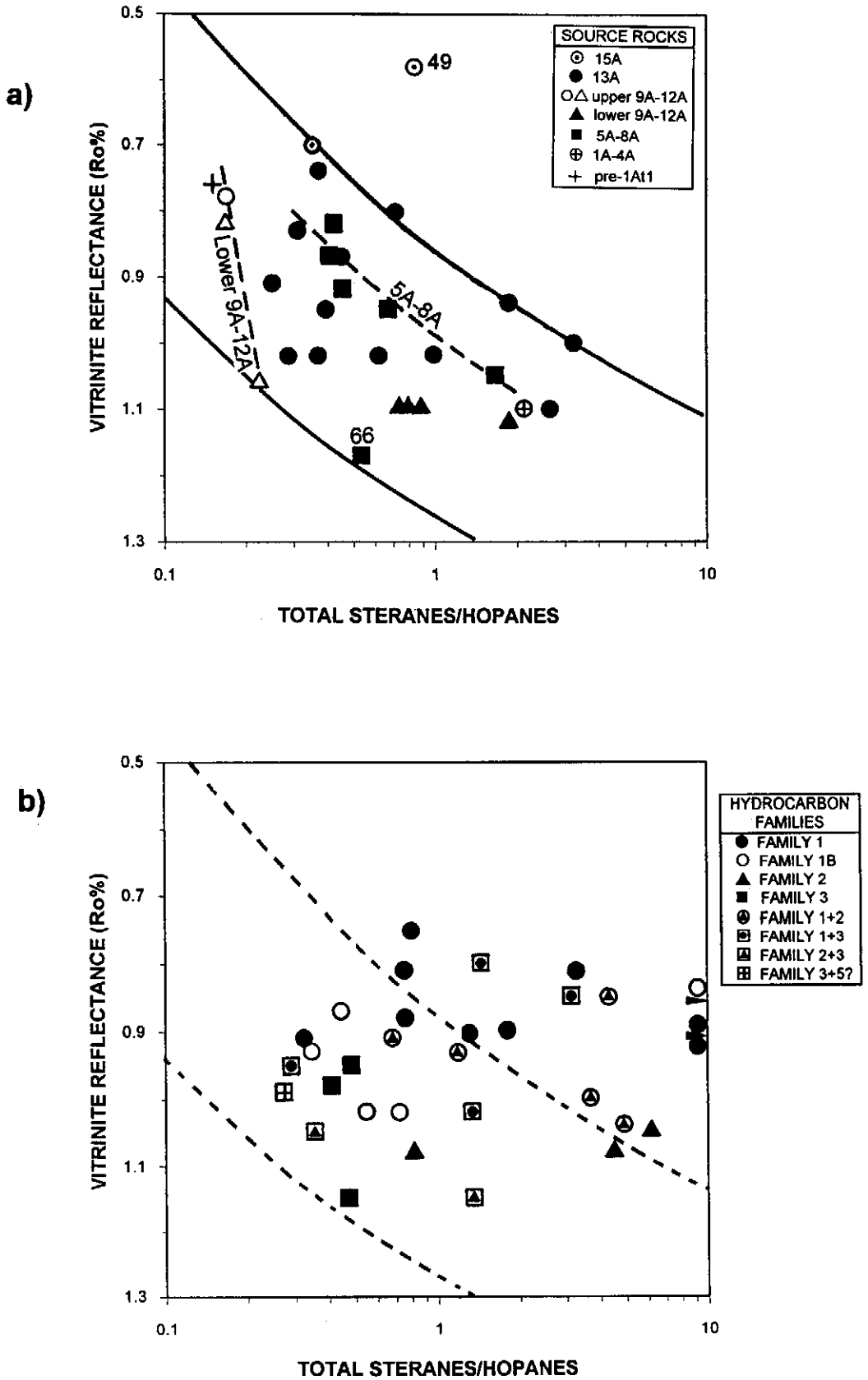

Figure 12.20: Plots of total sterane/hopane ratios vs vitrinite reflectance data for all Bredasdorp Basin samples of (a) source rock and (b) hydrocarbons to scales matching those used in Figure 12.19.

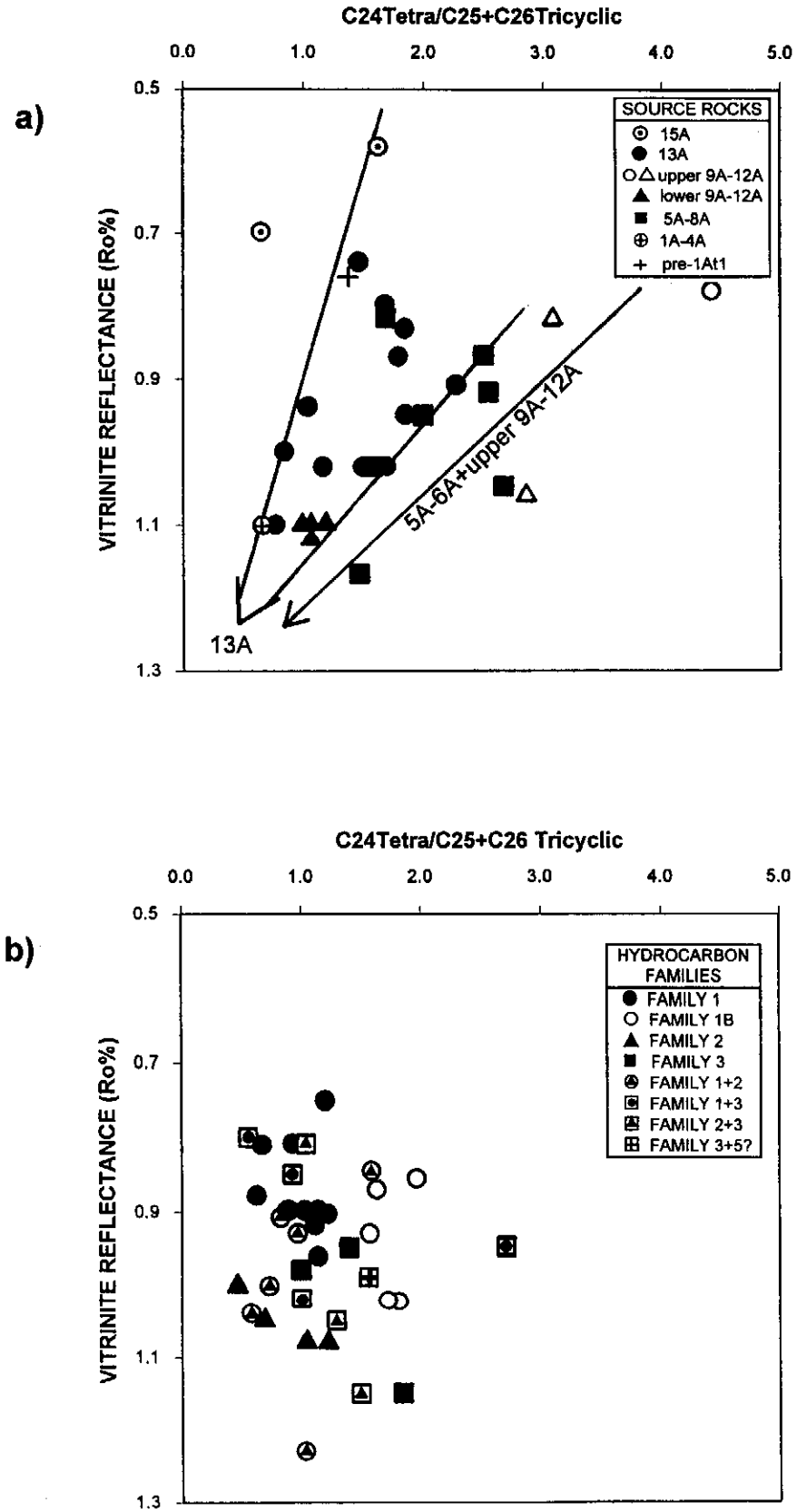

Figure 12.21: Plots of C24 tetracyclic/average C25+26 tricyclic terpane ratios vs vitrinite reflectance data for (a) all source rock and (b) all hydrocarbon samples. The possible maturity trend(s) differ from that expected from increased C24 tetracyclic terpane contents predicted by Aquino Neto et al. (1983). Supporting this unusual trend(s), all Family 1B hydrocarbons and upper 9A-12A (possibly basal 13A) source rocks locate with high values whilst all Family 2 hydrocarbons, and lower 9A-12A source rock samples, locate with very low ratios.

increasing heat. Generally, the data in Figs. 12.22a and 12.22b do support this maturity effect, showing that samples with the highest ratios are those with the lowest reflectances (Turonian samples, no's. 49 and 69). The sample with the lowest ratio is one of the least mature, sample 45 (lacustrine source rock at R_o=0.76%). This sample has an unusually high C21 tricyclic terpane proportion, causing the C23/21 ratio to be so high (Fig. 12.10). This result is similar to that from a freshwater lacustrine deposit in north-eastern Brazil (De Grande et al., 1993) providing further support for the source-specificity of C21 tricyclic terpane. Further published support for a partial source-specificity of this ratio is shown for oils sourced in Late Cretaceous calcareous clays which have high C23/21 ratios in spite of their elevated maturity (evaluated from sterane and hopane parameters) compared to other source rocks with lower ratios (Palacas et al., 1984). The ratio is able to distinguish lower 9A-12A source rocks and Family 2 hydrocarbons by their low ratios. Samples of unmixed Family 3 hydrocarbons have high C23/21 ratios but the equivalent 5A-8A source rocks (■) have ratios which range from ~1.5-3.5 indicating a range of maturities and confirming their known depth-range (~1000 metres). This suggests that only portions of this source in specific maturity windows are responsible for Family 3 gases in mixed samples (e.g. samples 8, 21, 23).

The pair of ratios have only slight maturity-dependency and no source-specificity despite their both being widely used in the industry. This may reflect different types of organic material or an unusual maturation history.

12.2.2.4. Total tricyclics/(tricyclics+pentacyclics)

Van Graas (1990) shows the proportions of tricyclics relative to the total terpane contents to be maturity-dependent, but they do not demonstrate any source-specificity. Peters and Moldowan (1993, p. 174-175), however, show the ratio to largely record source differences. Perhaps the source-specificity is more a function of input of terrigenous organic material, because all of Van Graas's examples were dominated by bacterially reworked algal material.

In the Bredasdorp Basin dataset, the source rock samples (Fig. 12.23a) largely track maturity, but within that overall trend, there are source-specific differences. For example, source rocks considered responsible for Family 1B oils have very low ratios (<0.1 at R_o<0.8%) which show little increase through the oil window. Ratios of Aptian (13A) source rocks believed responsible for Family 1 oils have similar low ratios at low maturity but these increase faster, so that a ratio of ~0.5 is reached at R_o~1.1%. Source rocks in the 5A and 6A sequences, considered possible sources for Family 3 wet gas-condensates, show an even more rapid increase between <0.1 at R_o~0.8% and ~0.6 at R_o>1.1%. However, the lacustrine source rock sample (no. 45, ✚) has a

a)

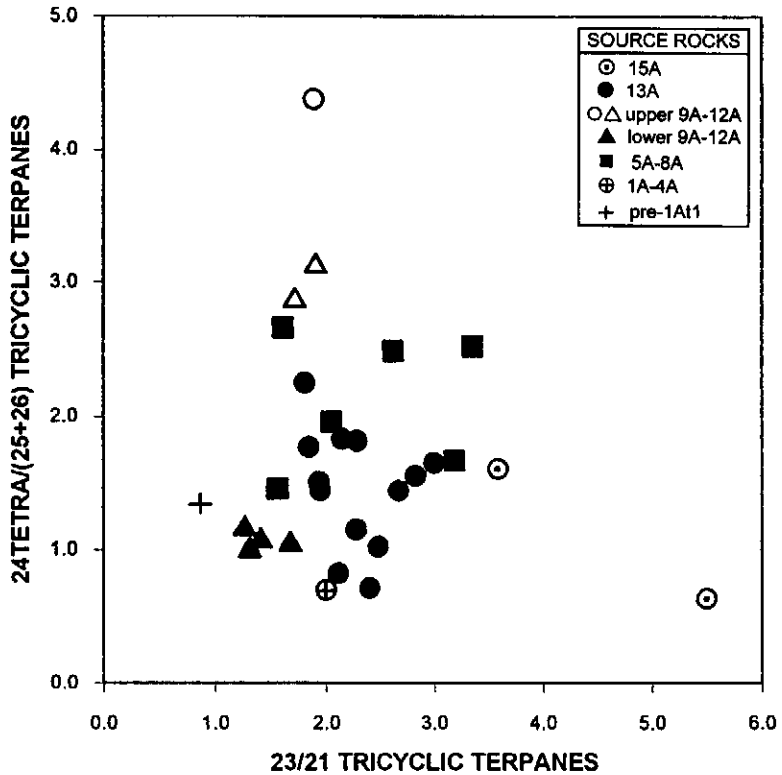

b)

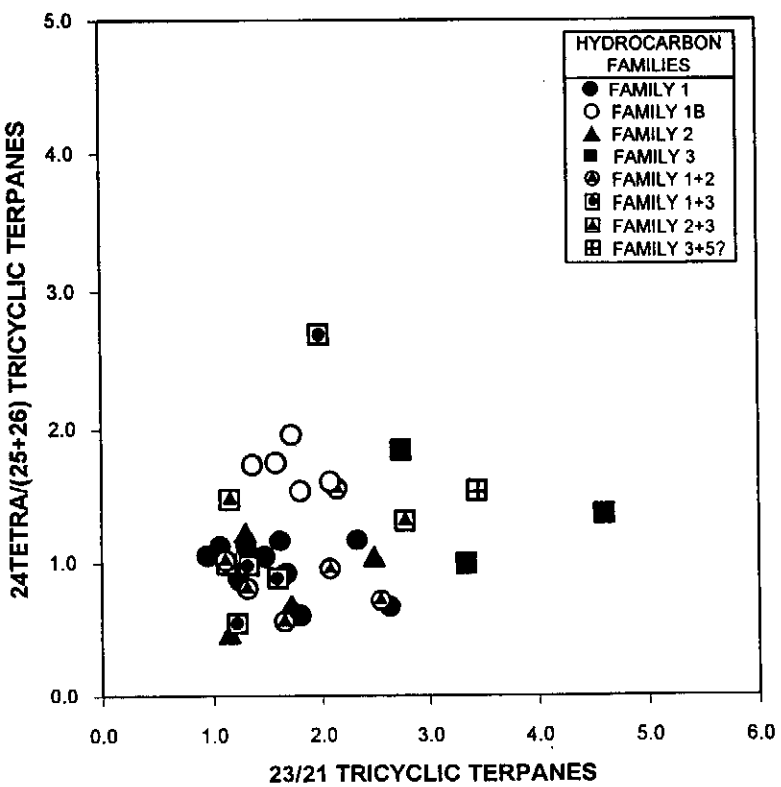

Figure 12.22: Cross-plots of C24 tetracyclic/average C25+26 tricyclic terpane ratios vs C23/C21 tricyclic terpane ratios for (a) all source rock samples and (b) all hydrocarbon samples. The predicted maturity-dependency for the C23/21 ratio is not evident in either data set.

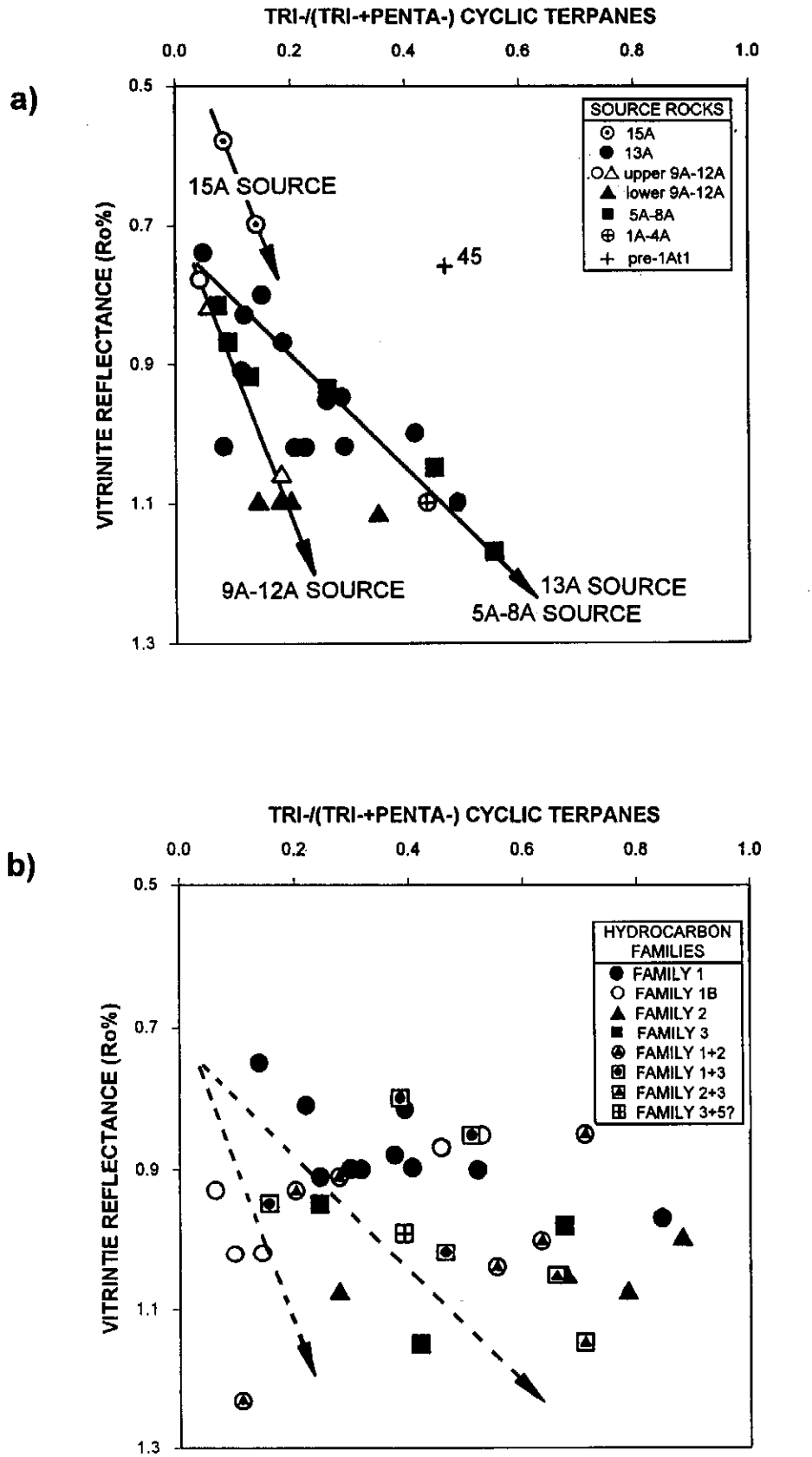

Figure 12.23: Plots of total tricyclic terpanes/total terpanes vs vitrinite reflectance data for (a) all source rock and (b) all hydrocarbon samples. Most sub-parallel trends of source rock data are not matched by the hydrocarbon data.

high ratio at R_o<0.8% which is probably indicative of unusual diagenetic effects converting such a high proportion of hopanoid precursors to tricyclic terpanes. By contrast, the hydrocarbon samples show essentially no source-specificity and appear to be randomly scattered. This probably results from migration from different depths. The ratio is therefore an effective indicator of maturity and a good discriminator of source rocks.

12.2.2.5. C30 diahopane/hopane vs vitrinite reflectance

Initially thought to be a marker for terrigenous input (Sheng et al., 1992; Philp and Gilbert, 1986a and b) C30 17α(H) diahopane is now thought to have bacterial precursors like most other hopanes (Moldowan et al., 1991) and to be derived like hopanes during diagenesis (Farrimond and Telnaes, 1996). Since the diahopanes share a common heritage with hopanes, it is expected that they too retain their source-specificity. The C30 diahopane/hopane ratio has been used to characterise different hydrocarbon types (Cornford et al., 1986; Horstad et al., 1990). In addition, diahopanes are more thermally stable than hopanes and the ratio between them has use as a maturity indicator (Moldowan et al., 1991; Horstad et al., 1990). Indeed, B. Michaelson (1996, pers. comm.) suggests that the C30 diahopane and the C31+ diahopane doublets become dominant only after R_o~1.0%, highlighting their usefulness as high maturity parameters.

In this data-set, diahopane/hopane ratios from hydrocarbons do have mostly well-defined maturity trends separated by family (Fig. 12.24b). These trends are superimposed on the source rock data in Fig. 12.24a. The Family 3 and 1B trends seem to agree quite well with 5A-8A and upper 9A-12A source rock respectively, only sample 67 plots out-of-place on the Family 2 trend. That sample has been shown previously to probably indicate some impregnation by Family 2 hydrocarbons from the reservoir immediately above. Family 2 samples, including hydrocarbon mixtures with Family 2 material, show a strong maturity-dependency with ratios up to 10X higher than those of samples from other families at equivalent maturity. This ratio, therefore, is an effective maturity-dependent and source-specific indicator.

12.2.2.6. C32 Homohopane 22S/22R vs vitrinite reflectance

Isomerisation at the C-22 chiral centre of the C31-35 extended hopanes converts the solely 22R biologic form to a dominance of the 22S thermally more stable form (Mackenzie, 1984). The ratio 22S/22R has been used extensively as a maturity parameter in comparison to depth or vitrinite reflectance (Seifert et al., 1980; Larcher et al., 1986; Peters and Moldowan, 1991). The C32 homologue is preferred, because the C31 species can be partly overlapped by gammacerane, or where biodegradation has occurred, by a C-25 norhopane (Subroto et al., 1991). The C33+ homologues are often

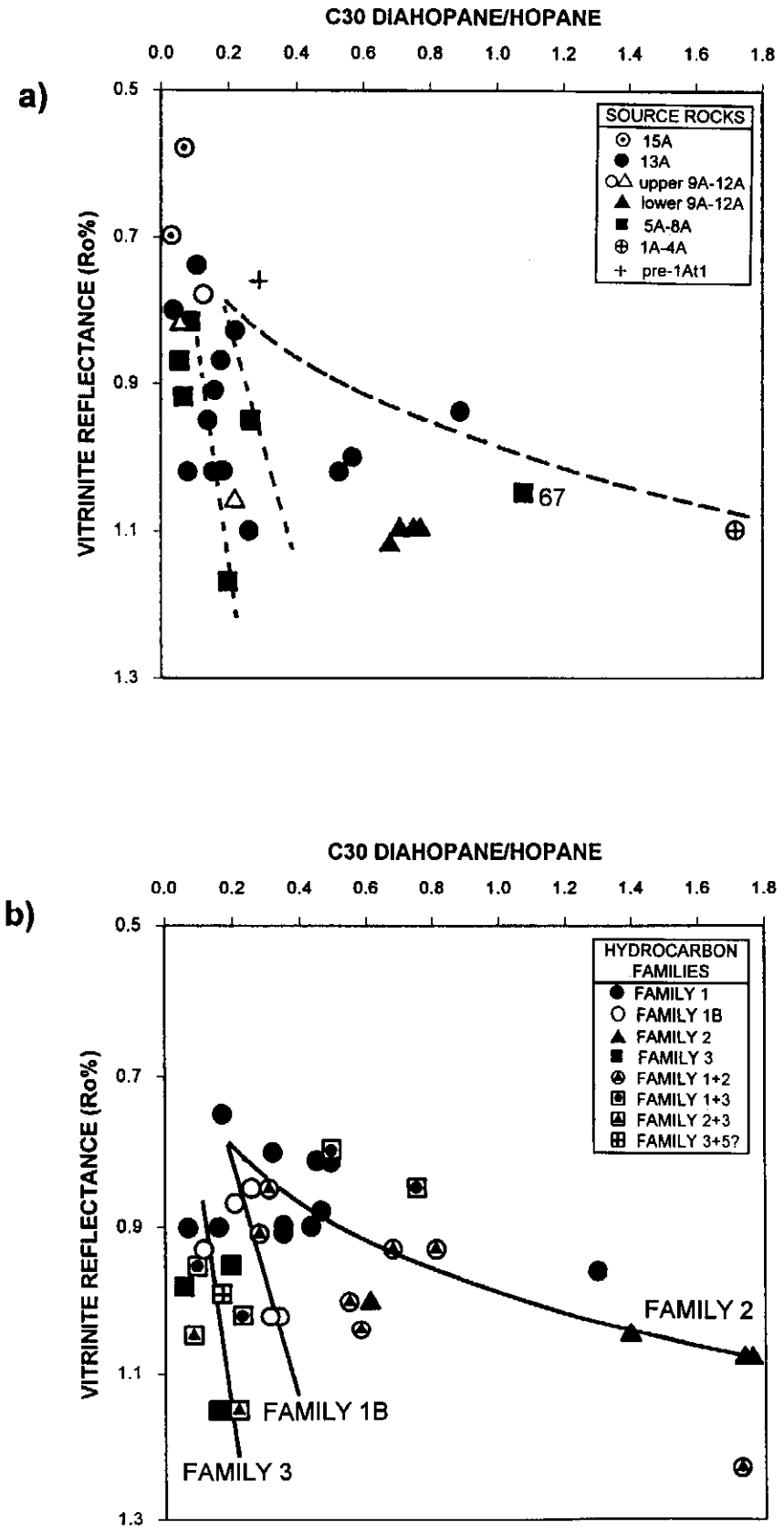

Figure 12.24: Plots of C30 diahopane/hopane vs vitrinite reflectance data for (a) all source rock and (b) all hydrocarbon samples. Maturation-dependent trends are weakly developed for upper 9A-12A source rock and Family 1B hydrocarbon samples and for 5A-8A source rocks and Family 3 hydrocarbons.

present in only small proportions in condensates. In addition, the proportions of the extended hopanes are commonly used as source indicators. For example, samples with high C35 proportions are considered to indicate sediment deposition in highly anoxic environments (Mello et al., 1988).

Available maturity calibrations show the ratio to reach the equilibrium position of ~60% 22S by R_o~0.6% (Mackenzie, 1984, p. 169; Peters and Moldowan, 1993, p. 226-228). However, studies by Van Graas (1990), Raymond and Murchison (1992), Bishop and Abbott (1995) and Farrimond et al. (1996) all show that where heating rates are high, the ratio reaches a similar equilibrium value but at higher maturity levels of up to R_o~1.0%. Indeed, where heating rates are very high, such as where shales are exposed to igneous intrusions, the ratio has been shown to apparently reverse (Bishop and Abbott, 1995; Farrimond et al., 1996). In the Bredasdorp Basin, the 13A source rock samples (Fig. 12.25a) follow a track which reaches a maximum value at R_o~0.9% and subsequently decreases. The same may be said for the 5A-8A samples but there are too few samples from the other Lower Cretaceous source rocks to define their tracks. The decrease matches that shown for a high maturity Aptian oil-prone source rock in a Namibian well, which has also apparently been affected by a hotspot track (Davies and Van der Spuy, 1992/93).

By contrast, the Turonian (15A) source rock samples appear to follow the track of samples heated at low rates reaching the equilibrium position at R_o~0.7%. These maturation rate differences between older and younger source rock samples are considered to be geologically significant and are discussed further in the next chapter (section 13.1.4.). The oil samples (Fig. 12.25b) do not follow any track which indicates that isomerisation is not a function of reservoir maturity but rather of source rock maturity at the time of generation.

12.2.2.7. C29nH/C28 bisnH vs C29nH/C30Diahopane

This plot compares the thermal stability of 3 hopanes, the C28 C-28,30 bisnorhopane, the C29 C-30 norhopane and the C30 rearranged diahopane. Each of these hopanes has been shown to have increasing thermal stabilities (Moldowan et al., 1991). C28 bisnorhopane has been shown to be an indicator of highly anoxic marine source rocks, but dominates only where sediment maturities are low R_o~<0.6% (Cornford et al., 1986; Peters et al. 1989; Waples and Machihara, 1991). Many of the Bredasdorp Basin samples display a peak at the retention location of this compound, but it is generally very small probably because of the high maturity levels (Figs. 12.09-12.11). Samples with significant bisnorhopane peaks are the Family 1B oils (Fig. 12.11) and the low maturity southern trend 14A residual oils (samples 31 and 35). Of the source rocks, only the low maturity Aptian source rocks (samples 46-48, 50, 52 and 53) and the 5A-

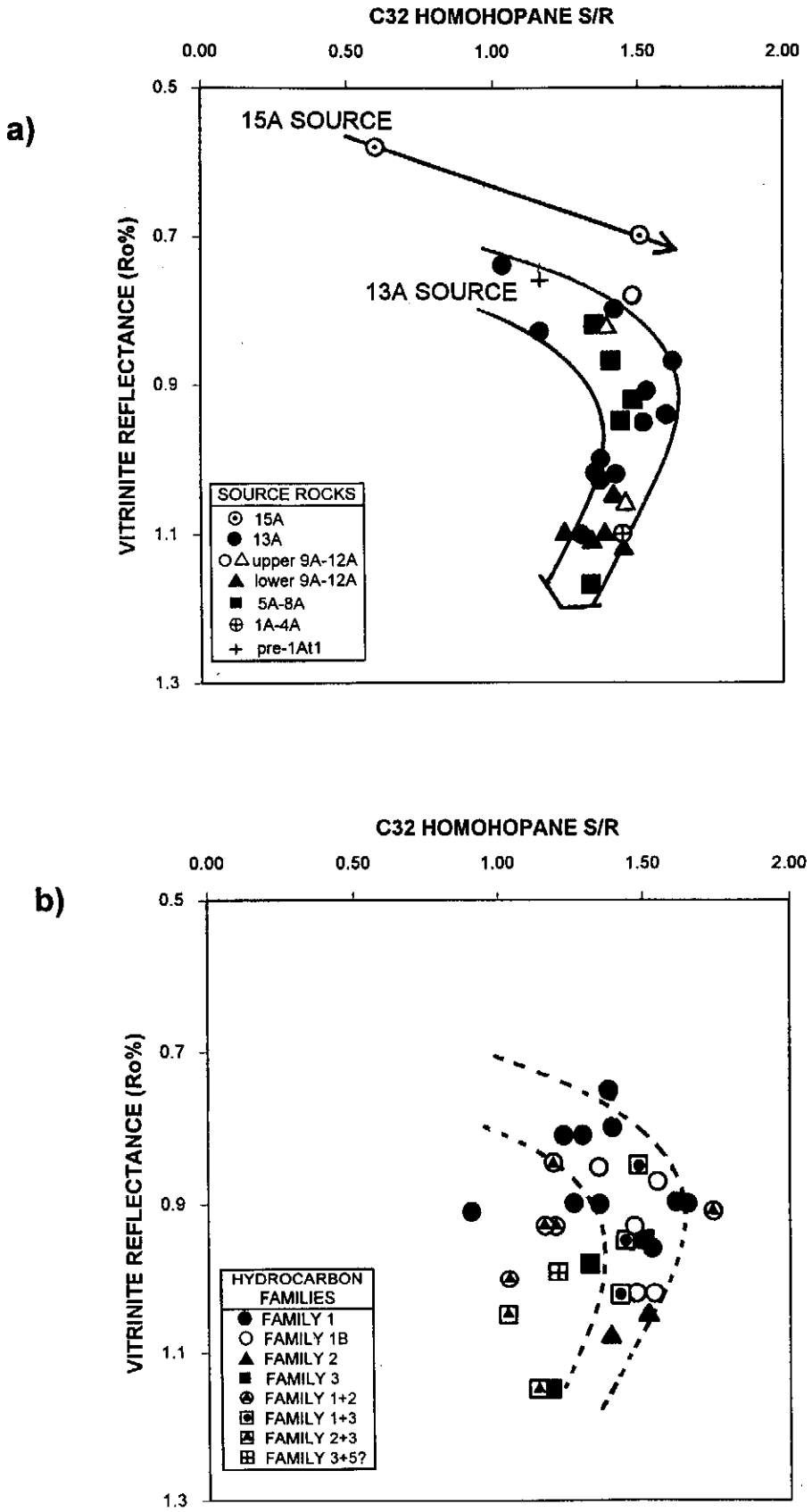

Figure 12.25: Plots of C32 homohopane 22S/R epimerisation ratio vs vitrinite reflectance data for (a) all source rock and (b) all hydrocarbon samples. Two trends are shown, for the 13A and 15A source rocks.

8A source in well 112 (sample 55) have large peaks and these are mostly at maturity levels higher than R_o~0.8%. Hence either the published reflectance value at which the minimum is achieved is not valid for these source rocks or the peaks identified as C28 bisnorhopane is another compound. This can only be resolved from GC-MS-MS analyses which are presently unavailable.

Nevertheless, the bisnorhopane minimum is generally achieved close to R_o~0.8-0.9%. Therefore, when in combination with the adjacent peak of C29 norhopane, the ratio should decrease with increasing maturity above R_o~0.8-0.9% (Fig. 12.26a). C29 norhopane/C30 diahopane too has been shown to be an effective maturation parameter, decreasing with increasing maturity (Philp and Gilbert, 1986b). However, they showed diahopanes to also be source-specific as they commonly occur in large proportions in oxic and sub-oxic depositional environments, i.e. conditions conducive to the preservation of more gas-prone material. The norhopane proportions too show source-related effects hence the plot of these ratios can demonstrate both source-specificity and maturity-dependency. In these samples, the 5A, 6A and lower 9A-12A source rocks ranging from R_o~0.8-1.2% have low ratios (<~5, Fig. 12.26a), whilst moderate ratios (~1-8) are found in 13A and upper 9A-12A source rocks in the same maturity range, i.e. R_o~0.9-1.1%. Matching this, the Family 2 and 3 hydrocarbons all locate with low values whilst Family 1 and 1B hydrocarbons have higher values (Fig. 12.26b), broadly confirming the maturity-dependency.

12.2.2.8. Ts/Tm vs vitrinite reflectance

The Ts/Tm ratio compares the proportions of C27 17α(H) C22, 29, 30 trisnorhopane (Tm) with that of the neoformed C27 18α(H) trisnorneohopane (Ts). The Ts molecule is thought to form during diagenesis by acid-catalysed methyl-shifting reaction of hydroxyhopane (Seifert and Moldowan, 1981) although there is some doubt about the exact derivation of Ts (Rullkötter and Marzi, 1988). It is more resistant to maturation than the companion Tm compound, hence the ratio between them is maturation-related. Published results show the ratio to increase exponentially through the oil window due to interconversion (Tm-to-Ts), fresh generation of Ts and/or destruction of the Tm species (Seifert and Moldowan, 1978; Moldowan et al., 1986; Van Graas, 1990; Raymond and Murchison, 1992). The ratio is most effective when comparing samples from the same organic facies, indicating a source-specificity (McKirdy et al., 1983; Rullkötter and Marzi, 1988). This effect is most apparent where highly calcareous rocks are concerned as the ratio is higher than in adjacent mudstones.

In the Bredasdorp Basin source rocks there is a broadly defined trend of increasing Ts/Tm ratio with increasing vitrinite reflectance (Fig. 12.27a). Within this trend, there are separate groups for different source rock intervals, each with slightly differing

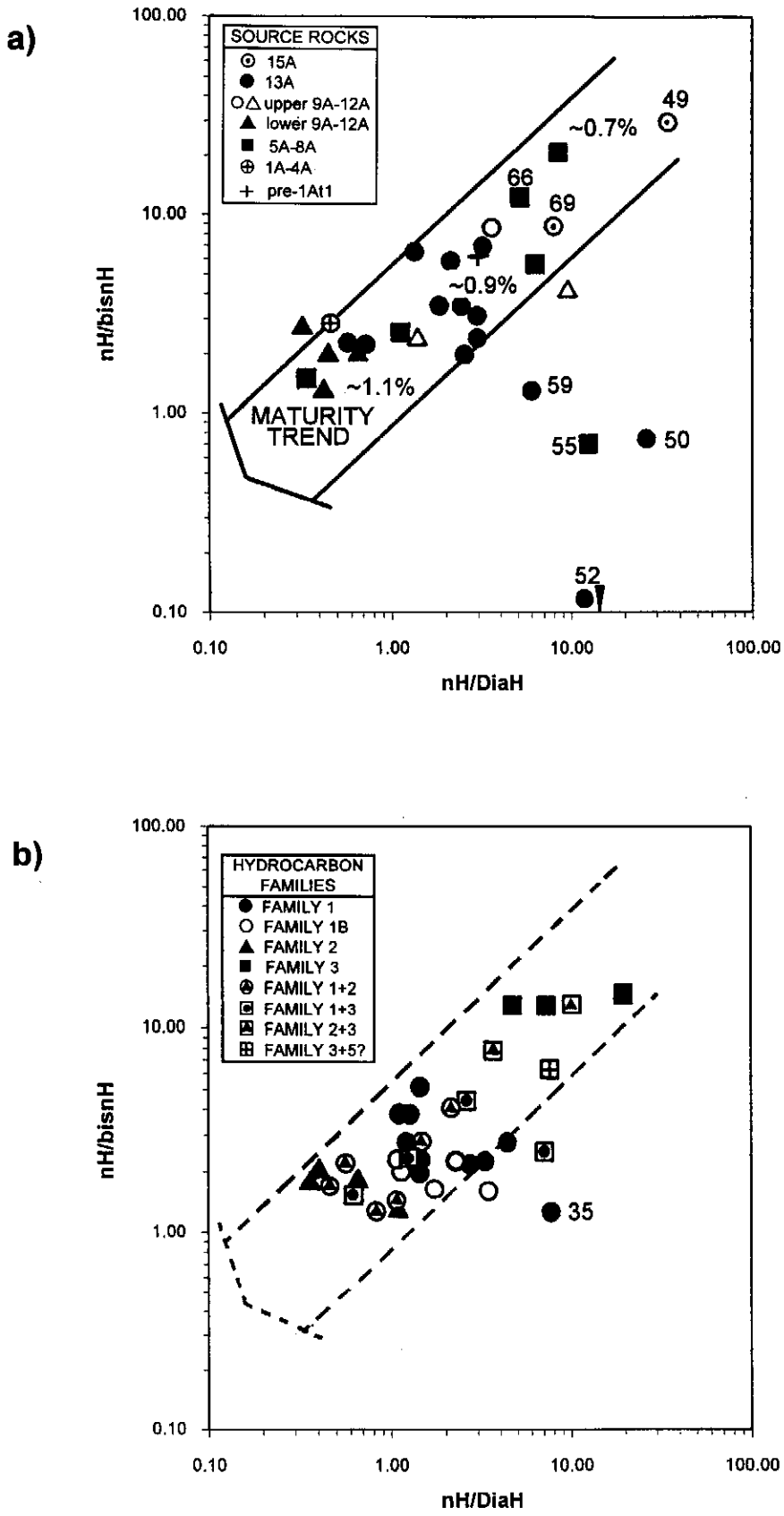

Figure 12.26: Cross-plots of C29 norhopane/C28 bisnorhopane vs C29 norhopane/C30 diahopane for (a) all source rock and (b) all hydrocarbon samples. The group of source rocks with unusually high bisnorhopane proportions are all from relatively low maturity shales deposited in highly anoxic environments.

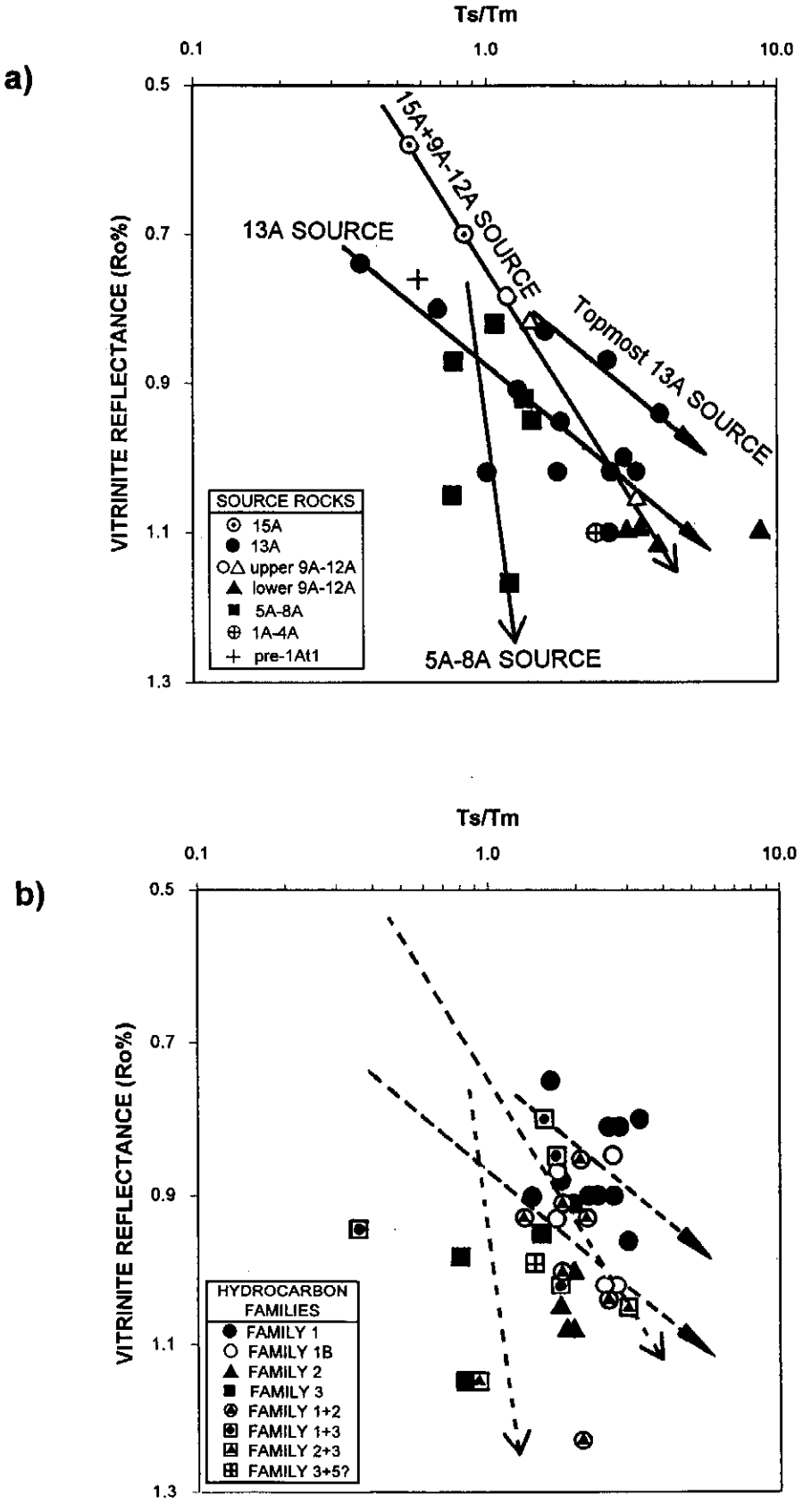

Figure 12.27: Plots of C27 18α(H) norneohopane/17α(H) norhopane vs vitrinite reflectance data for (a) all source rock and (b) all hydrocarbon samples. Several sub-parallel trends are evident in the source rock data. In the hydrocarbon data, the Family 2 (and Family 2 mixture) data locate close to their possible source, the lower 9A-12A interval.

trends. For example, the 5A-8A source rock samples mainly locate to one side of the trend with a minimal maturity-dependency, whilst the 13A samples locate at the other side with a stronger maturity-dependency. Within the hydrocarbon samples, only in Family 1 and Family 1B samples are there signs of maturation trends, indicative of relatively local sourcing, and a slight source-specificity. In other hydrocarbon families, no trends are evident probably because the ratio is determined by maturation in-source not in-reservoir, and those maturation trends are masked by migration over-printing.

12.2.2.9. C29nH/nnH vs vitrinite reflectance

The ratio between C29 17α(H) norhopane and the adjacent C29 18α(H) norneohopane ($\equiv$29Ts) is considered to be an effective maturation parameter (Fowler and Brooks, 1990; Moldowan et al., 1991). These two compounds are thought to form from precursor molecules such as bacteriohopantetrol, but following different routes the former by diagenetic reduction and the latter by a structural rearrangement in which a methyl group is shifted, probably by clay-mediated catalysis (Peters and Moldowan, 1993, p. 162). Moldowan et al. (1991) comment that molecular mechanics show the neo-formed compound should be thermally more stable than the equivalent 17α(H) epimer. Fowler and Brooks (1990) demonstrate the ratio in oils, derived from the same source, to decrease from ~2.5 -~0.9 over a ~2000 metre interval, equivalent to the whole of the oil window.

In the samples from this study, the ratios in source rocks do show a slight maturity-dependency, but vary through lower values than Fowler and Brooks (op cit.) show and apparently following two separate trends (Fig. 12.28a). One of these trends contains the examples of lower 9A-12A source rocks which tend to match Family 2 hydrocarbons (samples 56-58 and 61) whilst the other trend includes all Family 1B, most Family 1 and both Family 7 samples. By contrast, the hydrocarbon samples do not demonstrate either source-related or maturity-dependent trends (Fig. 12.28b). Yet the Family 1B samples all have proportionally higher ratios for their maturity than most Family 2 samples, which largely matches the source rock data proportions. Unusually, one of the 5A-8A source rock samples, which largely match Family 3 condensates (sample 66) and several of the Family 3 hydrocarbons and mixtures, locate with unusually high ratios indicating minimal amounts of the neoformed compound.

Such high ratios are more typical of low maturity biomarkers, similar to those in the Turonian (15A) source rocks, yet none of the other maturity parameters indicate such low maturity. It is unlikely that sample 66 contains impregnating compounds as *inter alia* no fluorescence was recorded and the sample was taken from at least 15-20 metres above the nearest reservoired hydrocarbon. Indeed, the fact that such high ratios are found scattered throughout the basin (hydrocarbon samples 25, 26, 13),

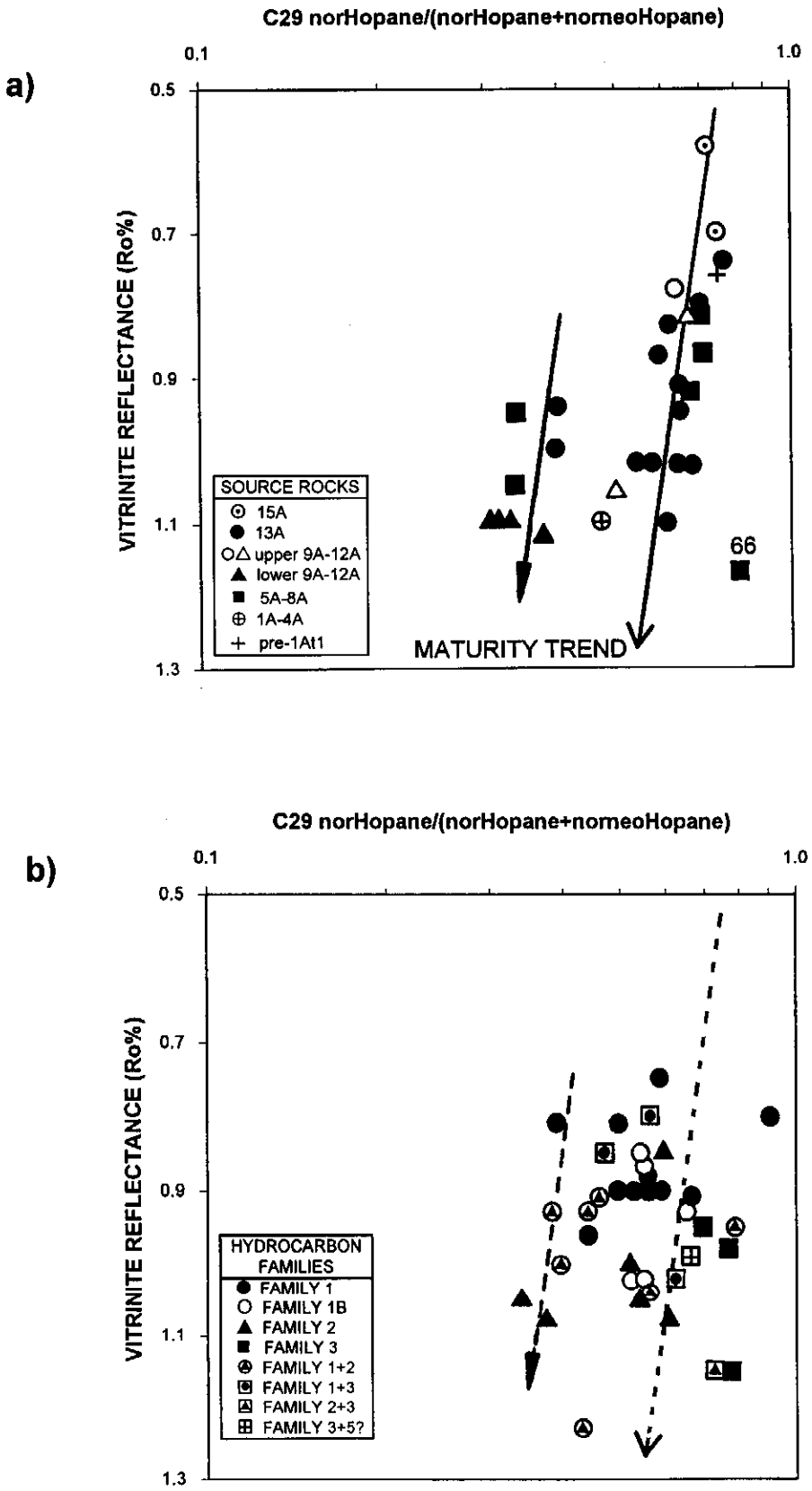

Figure 12.28: Plots of the C29 norhopane/(nor- and norneo-) hopane ratio vs vitrinite reflectance data for (a) all source rock and (b) all hydrocarbon samples. Two maturity-dependent trends are seen in the source rock samples (except sample 66) but are not evident in the hydrocarbon samples.

suggests that this does represent a source-specificity rather than a local sample impregnation. By contrast, other source rock samples from the 5A sequence have very low Ts/Tm ratios, suggesting that they either sample different parts of the sequence, or that the source-specificity is less clear than the maturity-dependency.

12.2.2.10. C27-29/C30/C31+ hopanes

Fan Pu et al. (1991) discuss the differences between proportions of C27-31+ hopanes and show that their carbon-number proportions distinguish families of hydrocarbons from freshwater lacustrine, hypersaline lacustrine and marine facies. A similar approach was attempted for the Bredasdorp Basin samples, with some success.

All samples generally locate in the lower part of the plot, within the area of Fan Pu's zones I-III, but very few lie in their zone III (marine source). In general none correlated well with their groups of hydrocarbons (Figs. 12.29a and b), but a more detailed inspection revealed several discriminatory differences. For example the location of samples 51 and 60 furthest from the C27-29 apex matches the location of most of the Family 1B oils. Samples from the lower 9A-12A source rock, and Family 2 hydrocarbons (and Family 2 mixtures), all locate with low proportions of C30 hopane (Fig. 12.29a). The hydrocarbons, however, all have reduced proportions of C30+hopanes resulting from inefficient expulsion (Fig. 12.29b). However, other than the slightly increased proportions of C30 hopane in the Family 1 source rocks and hydrocarbons, there is no consistency in the location of Family 1 and 3 hydrocarbons or 13A and 5A-8A source rocks. Sample 45, representative of lacustrine source rock, has hopane proportions no different from many marine source rocks - in which regard it differs from the environmental characterisation shown by Fan Pu et al. (1991). This lack of agreement may result from the possibly mixed nature of this source organic material.

12.2.3. Aromatic biomarkers

12.2.3.1. Trimethyl naphthalene ratios (TMN)

Naphthenes, like most condensed multi-ring aromatics, are not found in nature (Radke, 1987, p. 155-162). Conversion of possible algal, bacterial, higher plant and combustion material from sources rich in multi-ring aromatic acids and alcohols was discussed by Laflamme and Hites (1978). They showed that the combustion source may be over-rated in terms of geologic sources for aromatic hydrocarbons. Although bacterial and algal sources are possible, higher plant material is a more significant source of aromatic precursors. Alexander et al. (1992) showed that derivation of specific trimethyl naphthalenes by degradation of aromatic diterpanes, seemingly sourced by resinous plant material, was a likely source. However, this route results in preferential formation

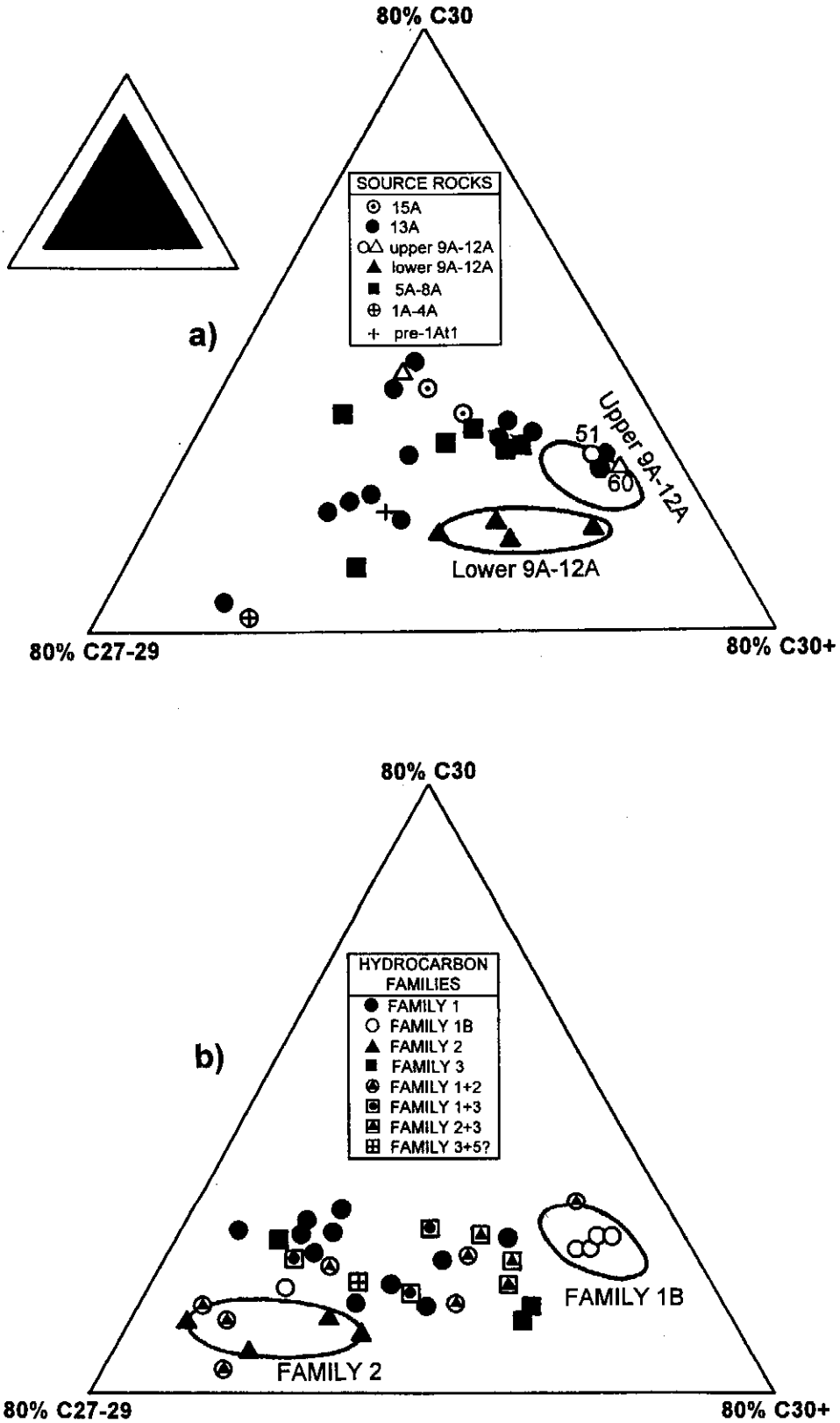

Figure 12.29: Ternary plots of C27-31+ hopanes. All Family 2 and 1B hydrocarbons and source rocks (9A-12A) locate in distinct regions but not matching the depositional environments of Fan Pu et al. (1991).

of only 2 TMN isomers (1,2,5 and 1,3,6) which are not the most common in source rocks or hydrocarbons.

Other isomers from the commonly identified suite of 8-9 TMN isomers can seemingly be formed by isomerisation reactions involving methyl-shifting to more stable configurations (Strachan et al., 1988). Alexander et al. (1992) also showed that the ratio 1,2,5/1,3,6 is potentially a maturity parameter although, like most other biomarkers, with a significant source-specificity. Strachan et al. (1988) used this pair of TMN isomers, and that of another pair (1,2,7/1,3,7), to characterise differences between examples of several different oils and source rocks ranging in age from Ordovician to Late Tertiary. They showed that the proportions of the 1,2,7 and 1,2,5 isomers are characteristic of resin-rich organic matter. They also showed that the 1,2,7 isomer could be formed by a parallel isomerisation reaction from the precursor terpenoid which formed the 1,2,5 isomer during diagenesis, and that a second ratio (1,2,7/1,3,7) also showed a strong maturity relationship as well as some source-specificity. Since both ratios display exponential relationships with maturity, they used log scales to demonstrate the maturation trend and source-specific clustering.

Plots of Bredasdorp Basin data on a similar format (Figs. 12.30a and b) show two parallel trends, offset slightly from each other. Most of the Family 1B hydrocarbons and their putative source (samples 51 and 60) also locate in the same region i.e. with high 1,2,7 isomer proportions. Sample 44 does not locate near this trend, but that portion of the upper 9A-12A source is geographically unlikely to source the Family 1B oils as it lies updip. This dominance of the 1,2,7 isomer may be characteristic of high proportions of resins in the preserved detrital organic matter (Alexander et al., 1992).

Family 2 hydrocarbons, and most Family 2 mixtures, all locate in the trend with lower proportions of the 1,2,7 isomer. The lower 9A-12A source rock samples (no's. 57-58, 61), which have strong affinities with Family 2 hydrocarbons, also plot there. Most Family 3 condensate can be distinguished from Family 1 oils by high 1,2,5/1,3,6 ratios. Interestingly, the Upper Jurassic lacustrine sample (no. 45) locates with all the marine samples of Family 1-3 instead of the high 1,2,5/1,3,6 ratio characteristic of Mid-Mesozoic higher plant material (Alexander et al., 1988). This material would concentrate in nearshore lacustrine rocks such as deltaic coals. Perhaps this difference results from the ecologically-different mix of plants due to the different location of southern Africa during the period of Jurassic source rock deposition.

12.2.3.2. Methyl and dimethyl phenanthrenes

As with the naphthalenes, the phenanthrenes are probably formed from diterpenoid acids, commonly found in higher plant debris such as resins, by clay catalytic

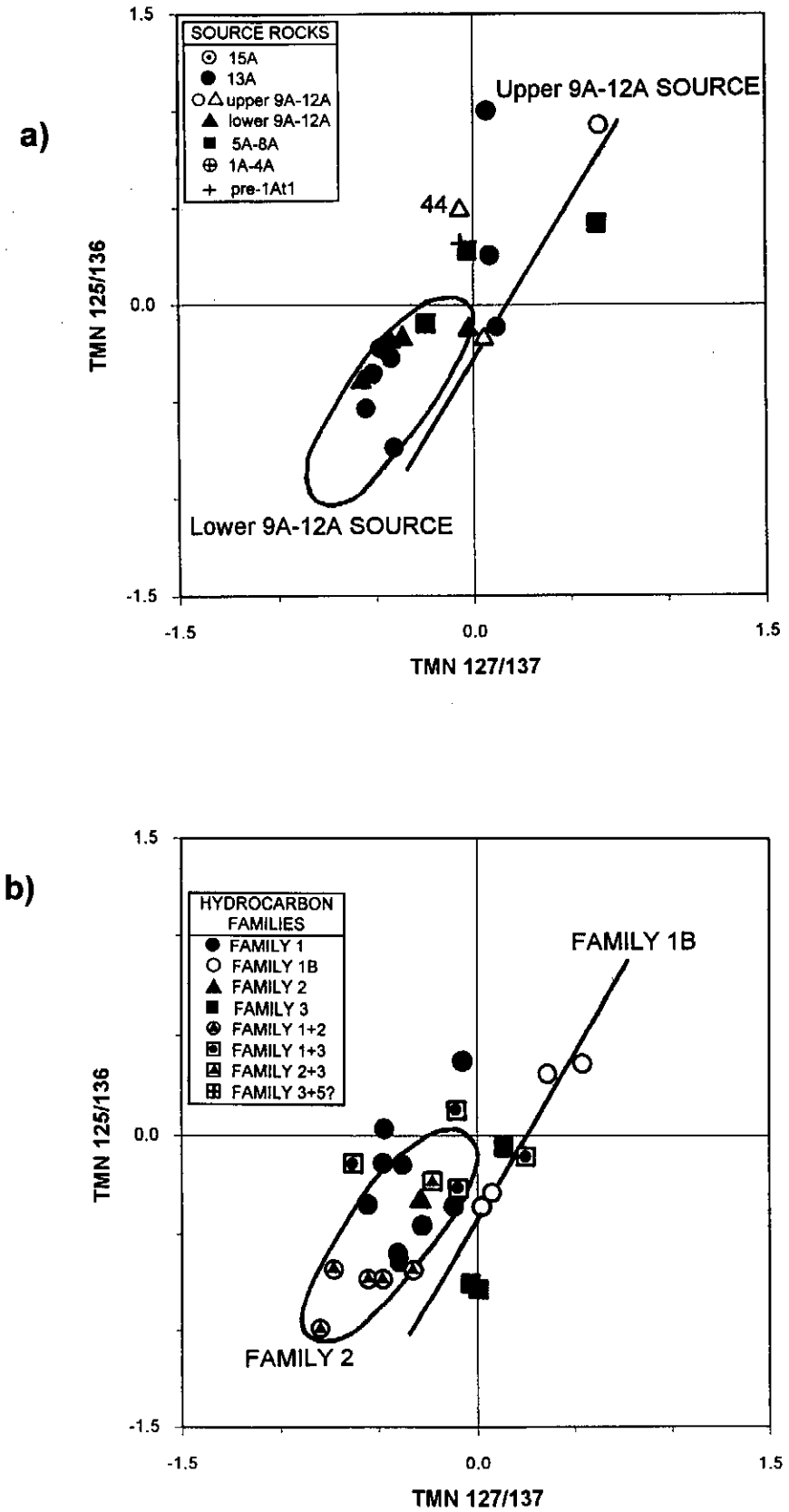

Figure 12.30: Cross-plots of trimethyl naphthalene ratios for (a) all source rock and (b) all hydrocarbon samples. All Family 1B and 2 hydrocarbons and source rock samples (9A-12A) locate in two distinct trends with most Family 3 hydrocarbon/5A-8A source rock samples located between.

conversion (Radke, 1987, p. 166). A number of methyl and dimethyl phenanthrene isomers are more common in rocks of low maturity, but undergo degradation or methyl-shifting reactions which result in dominance of different isomers. For example, 3- and 2-methyl phenanthrene (3MP and 2MP) commonly attain dominance in samples from highly mature source rocks. Indeed, Radke et al., (1982a and b) and Radke (1987, p. 174-179) showed that the MPI1 ratio from coaly organic matter could be linked to increasing vitrinite reflectance by the following formulae:

$$MPI1 = 1.5(3MP+2MP)/(P+9/4MP+1MP)$$

$$R_{calc} = 0.6MPI1 + 0.4.$$

A more recent re-assessment of the ratio by Boreham et al. (1988) from oils and terrigenous rocks of various ages was somewhat different, but confirmed the slight source-specificity for the ratio. However, they did point out that hydrogen-rich organic matter, representative of most of the Bredasdorp Basin samples, showed a poor correlation at low maturities. Radke et al. (1982a and b); Radke (1987) and Boreham et al. (1988) show only small standard errors, the last named authors quoting an accuracy of R_{calc} ~0.06-0.1% through the oil window. Plots of the MPI1 ratio for the Bredasdorp Basin source rock and hydrocarbon samples, together with the envelopes from these published works are plotted in Figs. 12.31a and b. Almost all the source rock data locate within the envelope of Boreham et al. (1988) but describe no apparent useful trend. It is evident that the envelopes of the published datasets are too broad for any practical use. By contrast, the hydrocarbon data not only plot within the envelopes, but also describe a broadly increasing ratio with increasing maturity.

The situation is even less precise for the dimethyl phenanthrene ratio (Figs. 12.32a and b). There the envelope of the dataset of Radke (1988) has been superimposed on the source rock and hydrocarbon data from the Bredasdorp Basin. No evidence of either maturity or source-specific trends is displayed. The lack of trends in these data is unexpected as other data presented here show good correlation with both maturity-dependent and source-specific trends. It may be because the methyl and dimethyl components are often depleted in residual oils, and occasionally lost during processing too, hence these ratios would be affected. However, this does not explain the lack of trends in the DPR ratios which are not affected by evaporation. It may be that the aromatic maturity ratios are simply not useful for correlation at practical or large scales.

12.2.3.3. Tri-/(tri-+mono-) aromatic steroids

Mono- and triaromatic steroids (MAS and TAS) are considered to form from precursor detrital steroids, such as cholesterol, by aromatisation reactions during diagenesis, possibly following some microbial activity. Indeed, TAS have not been found in immature sediments and it is believed they are formed from monoaromatic steroids

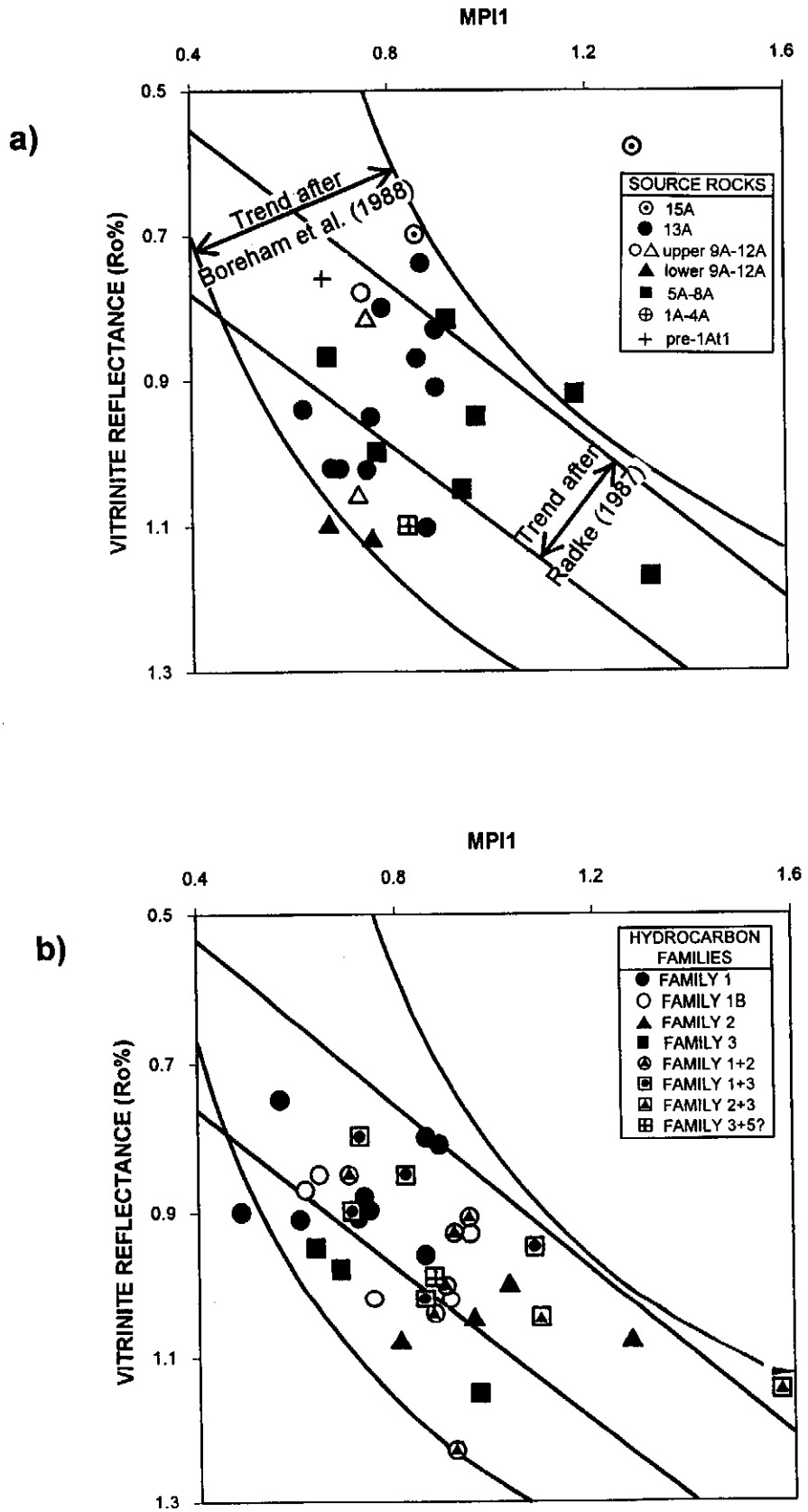

Figure 12.31: Plots of MPI1 (methyl phenanthrene index) for (a) all source rock and (b) all hydrocarbon samples. Data envelope trends of Radke (1987) and Boreham et al. (1988) are shown.

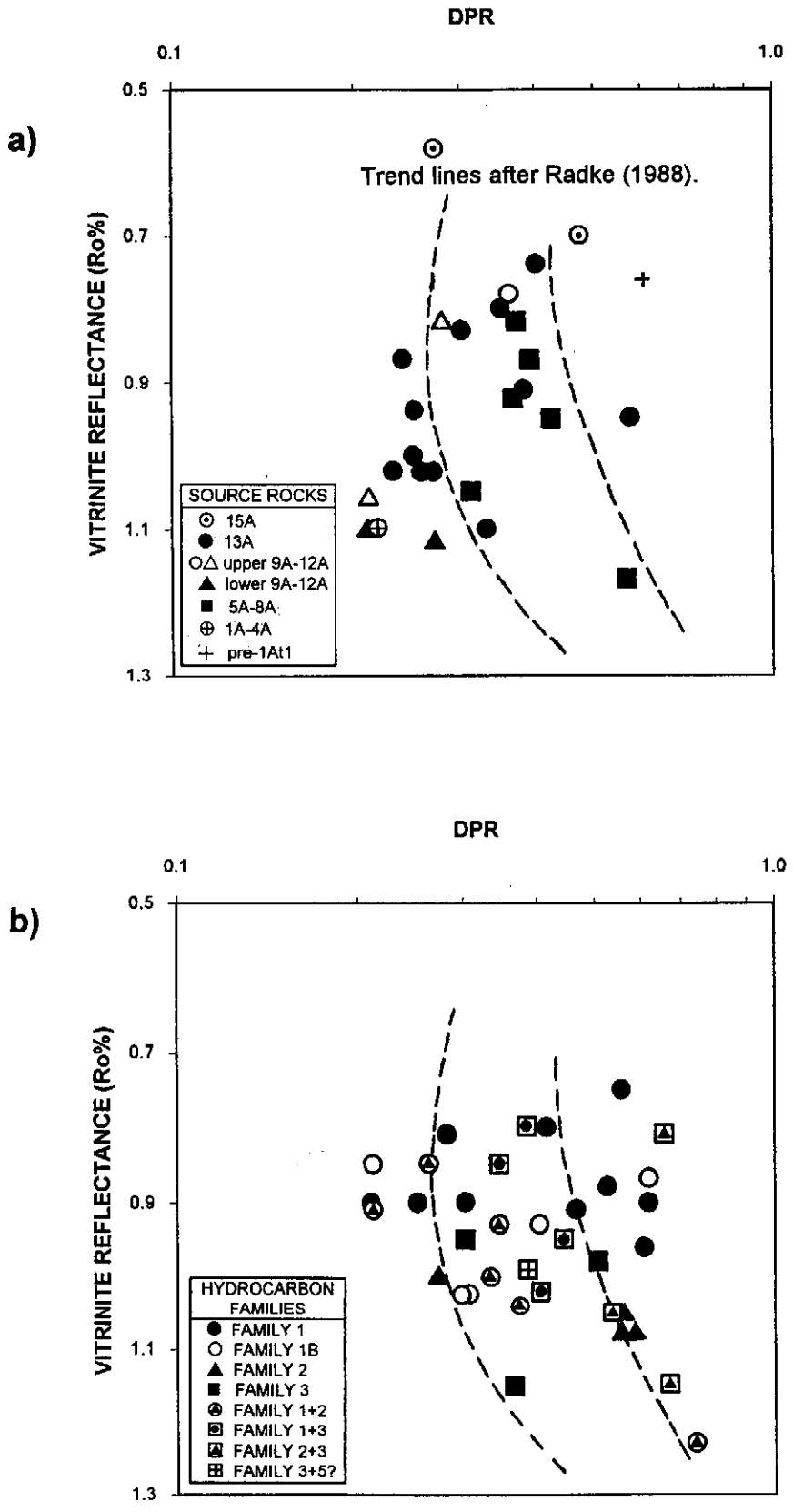

Figure 12.32: Plots of DPR (dimethyl phenanthrene ratio) after Radke (1987) for (a) all source rock and (b) all hydrocarbon samples.

through a thermally driven reaction, increasing their concentrations significantly between 80°C and 110°C (Mackenzie, 1984, p. 136-146). The proportions of TAS increase significantly into the oil window (to R_o~0.9%). With further maturation, the C26-28 TAS dominance is replaced by a C20-22 dominance due to differences in their thermal stability. Hence the ratio C26-28 TAS/(TAS+MAS) increases up to R_o~0.9%, after which it decreases (Mackenzie, 1984, p. 171; Thomas et al., 1985). Similar maturity effects are seen in the Bredasdorp Basin source rock data where the envelope increases to a maximum at R_o~0.85% then decreases, at least as far as R_o~>1.1%, (Fig. 12.33a). Two data values do not fit the envelope. The lacustrine sample plots slightly off the low maturity trend which may result from source-specificity. Contaminant peaks in the m/z 253 fragmentogram of the 6A shale sample (no. 68) have affected the measured peak heights. Correction for these co-eluting contaminants would increase the TAS/(TAS+MAS) ratio and locate it well within the envelope.

A possible alternate cause of the reversal may be the co-elution of some TAS compounds with another compound which is only present at high maturity. Mass spectral analysis has shown no sign of this as the spectra obtained for compounds assigned as TAS match published ones. However, it is not impossible as there are other TAS compounds which might co-elute with these five on certain columns (Peters and Moldowan, 1993, p. 80).

In the hydrocarbon plot the fit within the envelope is less good, as expected since the updip migration of mature hydrocarbons, or the burial of reservoired low maturity hydrocarbons, would result in 'out-of-place' maturity data (Fig. 12.33b). For example the oil traces in sample 22 may have been expelled from the surrounding WG-OIL prone source rock when it was some R_o~0.2% less mature (≡~300 metres less burial), whereas sample 33 contains oil which was expelled at a source maturity level of R_o~0.1% less than the presently attained reservoir maturity. Again, as with the MAS data, there is no strong evidence for source-specificity except possibly for the lacustrine source rock sample (✚).

12.2.3.4. Monoaromatic steroids (MAS)

The ratio compares the proportions of the C27 MAS rearranged/non-rearranged compounds, peaks 1/(2+3), which has been shown to be a source-specific indicator (Moldowan and Fago, 1986; Riolo et al., 1986). However, Moldowan et al. (1986) show that the rearranged/non-rearranged ratio may have some maturity-dependency. The matching ratio from Bredasdorp Basin data shows no corresponding correlation between source rock type and ratio but does show an apparent trend reversal at R_o~0.9% with the source rock data (Fig. 12.34a). This trend is not matched by the hydrocarbon data which largely plot randomly (Fig. 12.34b).

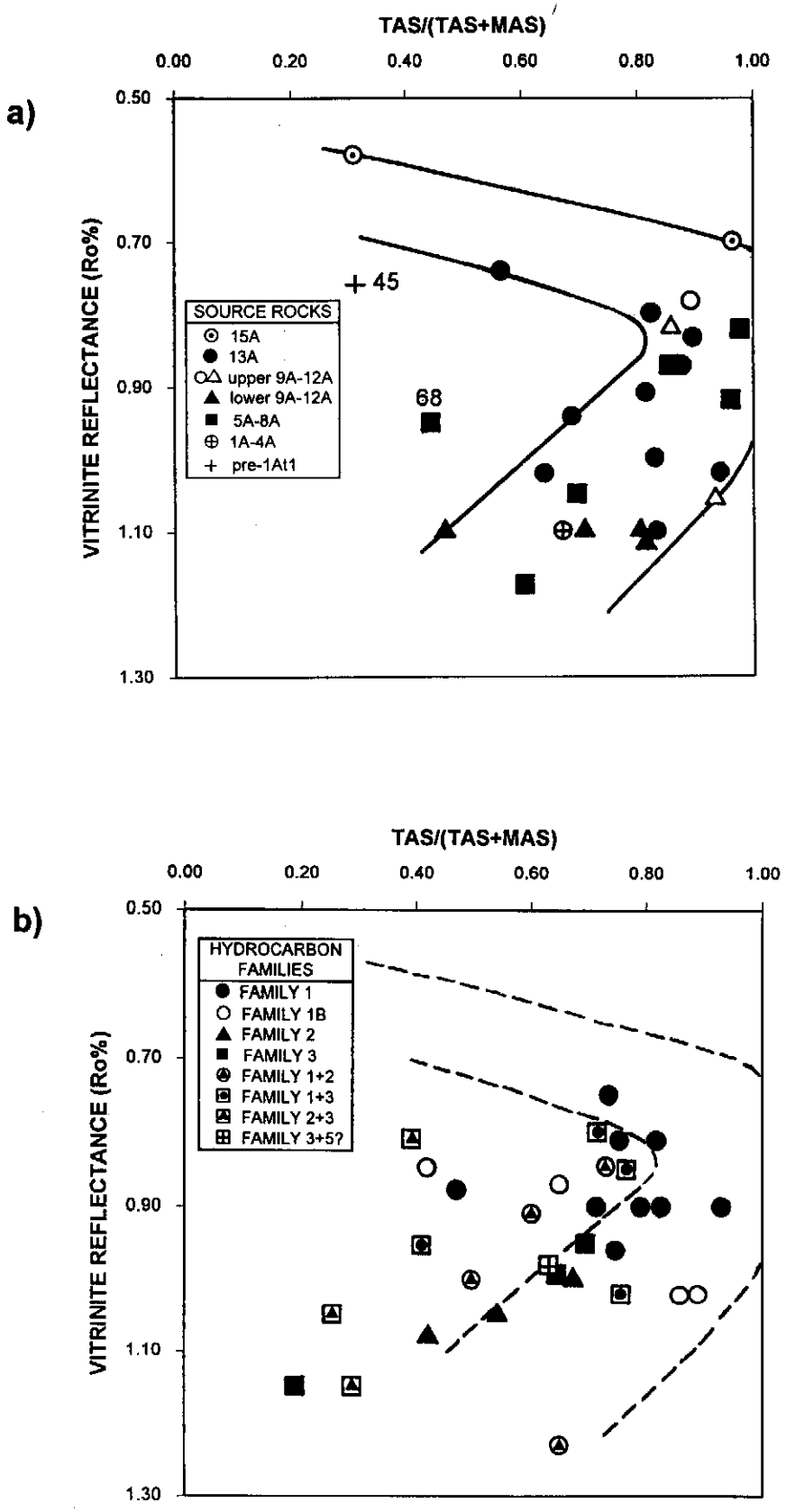

Figure 12.33: Plots of total C26-28 triaromatic /(triaromatic and C27-29 monoaromatic) steroids for (a) all source rock and (b) all hydrocarbon samples. Trend up to R_o~0.9% after Mackenzie (1987) and after R_o~0.9% after Davies (1997, in press). Out of place data due to, in source rock figure (i) peak overlap by contaminating normal alkane (sample 68) and (ii) different source rock type in the lacustrine sample (45) and in the hydrocarbon figure (iii) hydrocarbon migration.

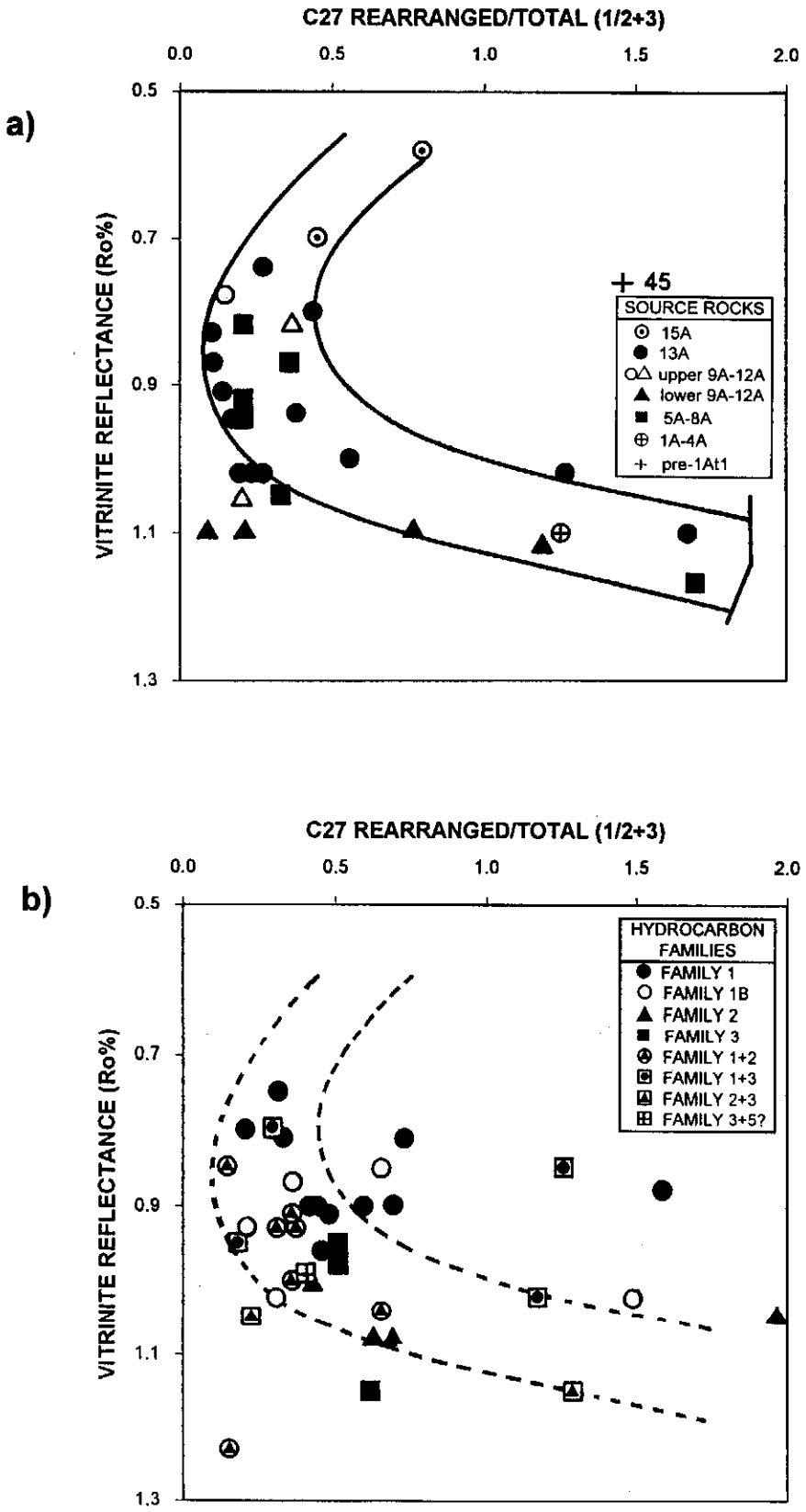

Figure 12.34: Plots of the C27 rearranged/total monoaromatic steroids vs vitrinite reflectance data for (a) all source rock and (b) all hydrocarbon samples. The apparent reversal in the source rock data is not matched by the hydrocarbon data but that may be because there are too few hydrocarbon data above the inflection point (R_o 0.8-0.9%).

12.2.3.5. Triaromatic steroids (TAS)

Proportions of individual TAS isomers can also be used to characterise inputs of different source material and the effects of changing maturation. A plot of the ratios of peaks c/d vs peaks d/e (C28 20S/C27 20R vs C27R/C28R) is used to investigate the TAS group of compounds. The first of these two ratios was shown in Fig. 12.13. These peaks were selected for comparison as (i) they are apparently not overlapped by other isomers (Gallegos and Moldowan, 1992) (ii) they are adjacent so that there could be minimal influence of peak width variations, for example from gas chromatographic temperature programming, and (iii) they represent different homologues and epimers.

The plot shows a gradual increase in preference for the C28 20S+20R epimers relative to the C27 20R epimer with increasing maturity (Figs. 12.35a and b). Part of this increase is probably due to preference for the 20S epimer over the 20R epimer, similar to that found in steranes and terpanes. However, there should also be a preference of C27 20R over C28 20R homologues due to the higher thermal stability of the former, but the opposite seems true (Mackenzie, 1984, p. 145). A possible cause is that of a source-specificity. The gradual increase in C28 proportions of less oil-rich source shales from R_o~0.7 to R_o~1.2% is well defined (5A-8A trend, Fig. 12.35a). A second trend, that of the upper 9A-12A, 13A, 15A and pre1At1 source rocks, lies sub-parallel to this, but does not have the same maturation correlation (lower trend, Fig. 12.35a). The more highly mature 13A samples tend to cluster together even though they show wide maturity variations, whilst the 13A samples which extend along the trend are the low maturity, largely non-expelling, samples 50, 52 and 59. Hence this trend may be reflecting expulsion of higher proportions of the C27 than C28 compounds.

The data from hydrocarbon samples generally matches the source rock trends, but the trend is offset and somewhat steeper (Fig. 12.35b). Family 1B hydrocarbons all lie on a separate trend, outside the Family 3 trend, whilst inside, and with lower C28 proportions, lies the Family 1 and 2 trend. All these trends start at maturation levels (from Fig. 12.35a) of R_o~0.8% for Family 1 and 1B and R_o~1.0% for Family 3 - which largely match the start of expulsion from these source rocks.

To match 5A-8A and lower 9A-12A source rock trends with Family 2 and 3 trends, and the 13A source rock trend with the Family 1 trend, requires accentuated proportions of C28 components in the expelled hydrocarbons. This is not the case for Family 1B hydrocarbons. These mismatches of seemingly well-supported trends are not fully understood. They cannot be due to bacterial degradation as there would be other evidence such as 'missing' alkane components and increased norhopane proportions (Seifert and Moldowan, 1979; Peters and Moldowan, 1993, p. 254). It is extremely

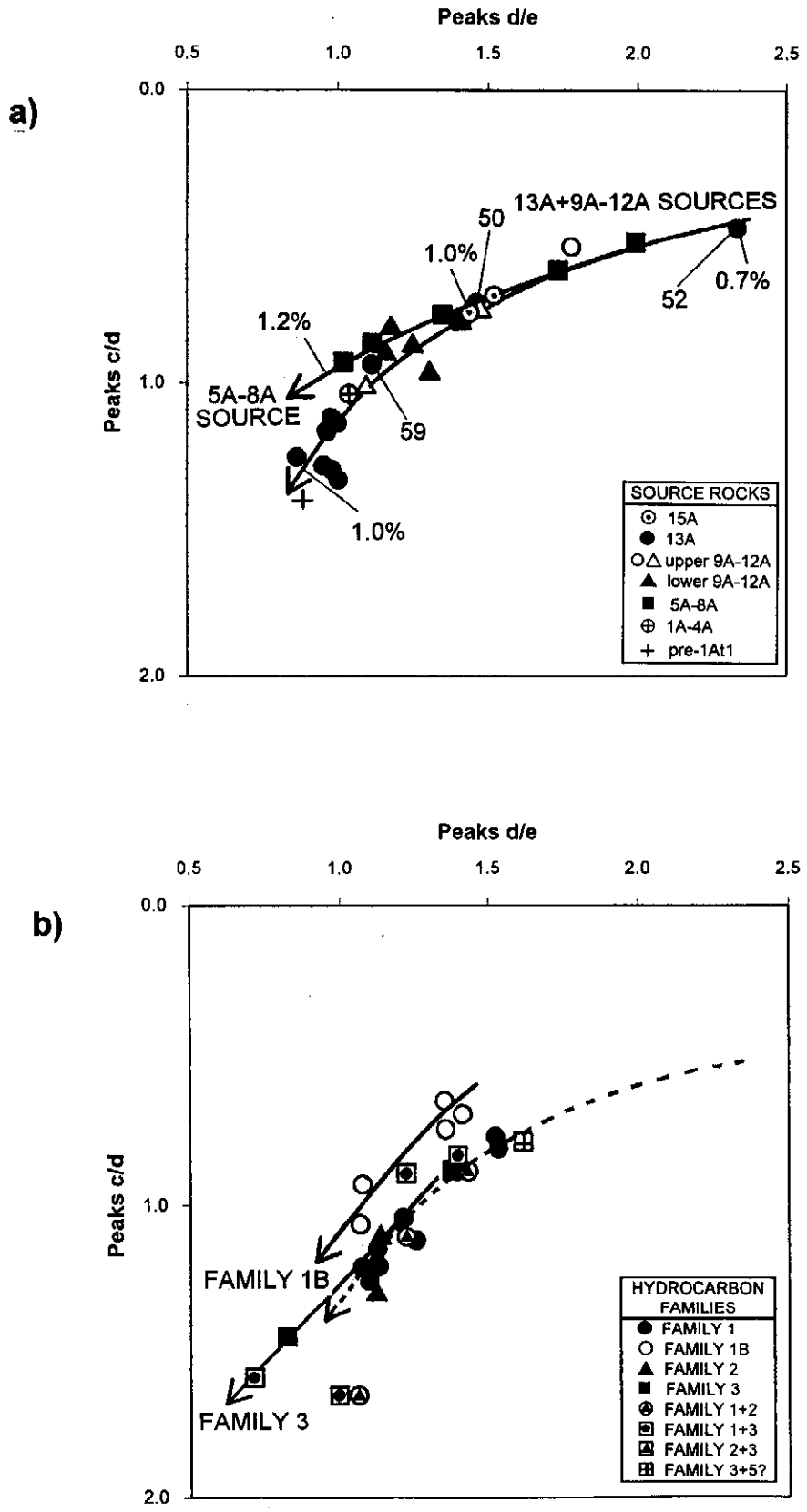

Figure 12.35: Cross-plots of triaromatic steroid ratios (peaks c/d and d/e) for (a) all source rock and (b) all hydrocarbon samples. Equivalent reflectances given for the two trends are based on the available measured data. The slopes of the sub-parallel trends of the Family 1, 1B and 3 data in the hydrocarbon plot match the source rock trends, but are slightly offset.

unlikely that the mismatch is a result of incorrectly assigned peaks, as they clearly match published data (Mackenzie et al., 1983; Gallegos and Moldowan, 1992). It is possible that the mismatch results from geochromatographic effects. Geochromatography refers to compositional changes in the oil occurring during migration. These changes include differential adsorption of polar compounds on ionically active minerals, such as clays, and proportionally slower travel through pore throats by the bulkier molecules, such as those with multiple branches. Alternatively, small variations in volatility or vapour pressures of certain compounds can result in phase changes during migration through different temperature regimes (Leythauser et al., 1984; Mackenzie et al., 1988; Peters et al., 1990). Sajgo et al. (1983) concluded that migration redistribution (≡geochromatography) would cause increases in lower molecular weight homologues in the migrating hydrocarbons and the opposite in the non-migrating hydrocarbons - exactly as seen in Figs. 12.35a and b. The offsets between the source rock and hydrocarbon trends are likely to include these effects. Nevertheless, the trends are useful for correlation between source rocks and hydrocarbons and the size of the offset may be related to the distance of migration.

12.2.3.6. Methyl dibenzothiophenes (MDBT)

Dibenzothiophenes originate shortly after sedimentation during microbially-mediated diagenesis of organic matter, particularly where sulphur-rich minerals are in intimate contact. These compounds are common in all the source rocks and hydrocarbons studied here. Plots of the proportions of the three main MDBT isomers (4MDBT/1MDBT vs 4MDBT/2+3MDBT) determined from source rock samples are shown in Fig. 12.36a. The plot shows closely juxtaposed, but distinct, maturation-related trends for the 5A-8A, 9A-12A and 13A source rocks and for the upper (oil prone) 9A-12A source rocks to the right of the main trend. The matching plot of the hydrocarbons records no such distinction between the different hydrocarbon families except for the Family 1B hydrocarbons which locate to the right of the main trend (Fig. 12.36b). This lack of separation may be due to the 'blurring' effect that migration has on familial characteristics, i.e. where maturation of the source rock at generation and expulsion does not match the present reservoir maturity. In this case, the 'blurring' is contrary to that shown by Chakhmakhchev and Suzuki (1995) and Dzou et al., (1995).

12.2.3.7. Dimethyl dibenzothiophenes (DMDBT)

Dibenzothiophenes have been utilised for some time for maturity studies although the chromatographically easy to distinguish ratio of DMDBT to DBT was used (Joly et al., 1974). Unfortunately the relatively volatile nature of DBT accounts for its common absence from oil extract samples, especially in residual oils, hence the value of such a ratio is limited. However, there is evidence that other thiophenic compounds can reliably indicate maturity in oils. Chakhmakhchev and Suzuki (1995) showed the ratio

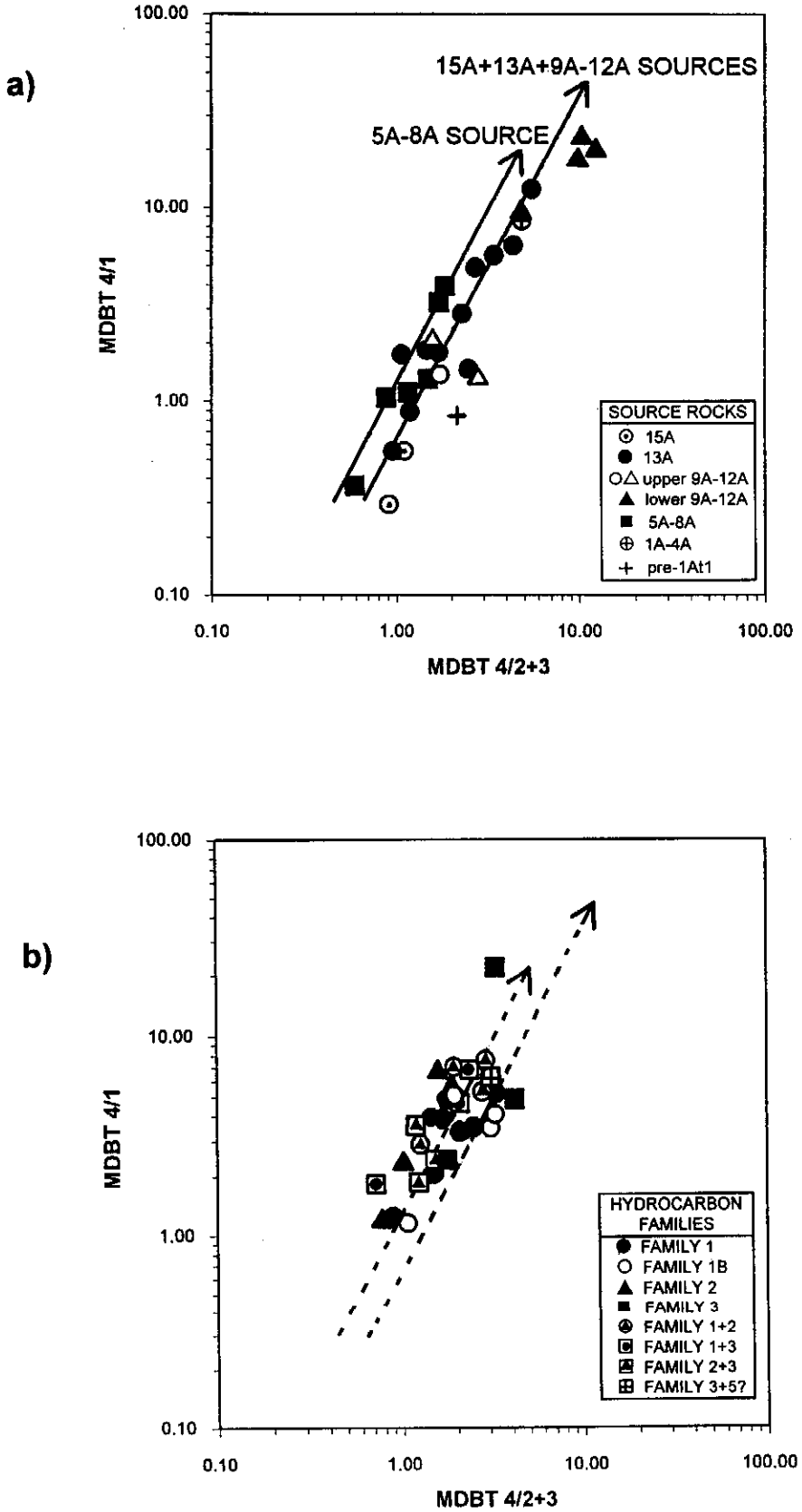

Figure 12.36: Cross-plots of methyl dibenzothiophene ratios (4MDBT/1MDBT vs 4MDBT/2+3MDBT) for (a) all source rock and (b) all hydrocarbon samples. All the source rock and hydrocarbon data locate in the same zone but within that there are subtly different trends for each source rock interval - however only the Family 1B hydrocarbons show any matching trend.

of DMDBT peaks C/E to be an exponential maturation function (Fig. 12.37b). Matching this, the ratio between peaks D/F appears also to be a maturation parameter (Figs. 12.37a). Both plots show the data from well 122 (i.e. samples 59-60) to be anomalous.

The cross-plot of these two ratios for the shale samples does not show the data from well 122 as anomalous, but indicates the north flank 5A-8A source rock bitumens (i.e. excluding sample 55) to follow a different trend from the other data (Fig. 12.38a). From the measured vitrinite reflectance data, it is possible to construct a maturation trend on these data, to which the data agree to within an error of R_o~<0.1%.

Three of these four DMDBT peaks have been assigned to particular isomers and it is possible that the maturation correlation stems from the increasing preference for isomers where methyl groups locate at sterically crowded positions. This is because the higher reactivity isomers are more readily reactive (Radke, 1987, p. 146; Tomic et al., 1995; D=2,5; E=2,4; F=2,3 DMDBT). Using this reasoning, the 4- and 5- methyl positions are likely to be more thermally stable than the 2- and 3- positions. Hence the ratio D/F (2,5-/2,3-) is likely to increase as maturity increases. Although the isomeric assignment for peak C is not known, it would need to be more stable than the E isomer (2,4-) which itself includes a methyl group in a 'crowded' position.

The cross-plot of the two ratios for the hydrocarbon data (Fig. 12.38b), however, does not fit well (Fig. 12.38b). Perhaps this is another 'out-of-place' effect due to migration of mature hydrocarbons into low mature reservoirs. Also, both the main trend and the Family 3 branch are offset by small but consistent amounts. This might indicate some preference during migration for one component over another in each pair. The 2,5-isomer is a more 'bulky' molecule than the 2,3- isomer (annotation on Fig. 12.37a) and likely to be discriminated against during primary migration. Hence the D/F ratio is reduced in the hydrocarbon samples and increased in the shale samples. Whatever the cause of the offset, Family 1B hydrocarbons still locate at maturity levels which are unusually low compared to their other biomarker data. A likely explanation is that these samples represent the least migrated of oils and their ratios are only barely affected by migration-specificity.

There are other anomalous hydrocarbon samples. Sample 12 locates offscale, but there are so few dibenzothiophenes in the sample that it is unlikely that the ratios truly reflect the real proportions of each component (Appendix E, Fig. E.80). Sample 21 from well 48, however, has well defined DMDBT peaks yet it locates at a high equivalent reflectance of R_o~1.1-1.2% (Appendix E. Fig. E.21). This is likely an effect of the mixing of this sample. Whole oil analyses indicate that this sample represents admixtures of two or three different hydrocarbon streams. In addition the sample may

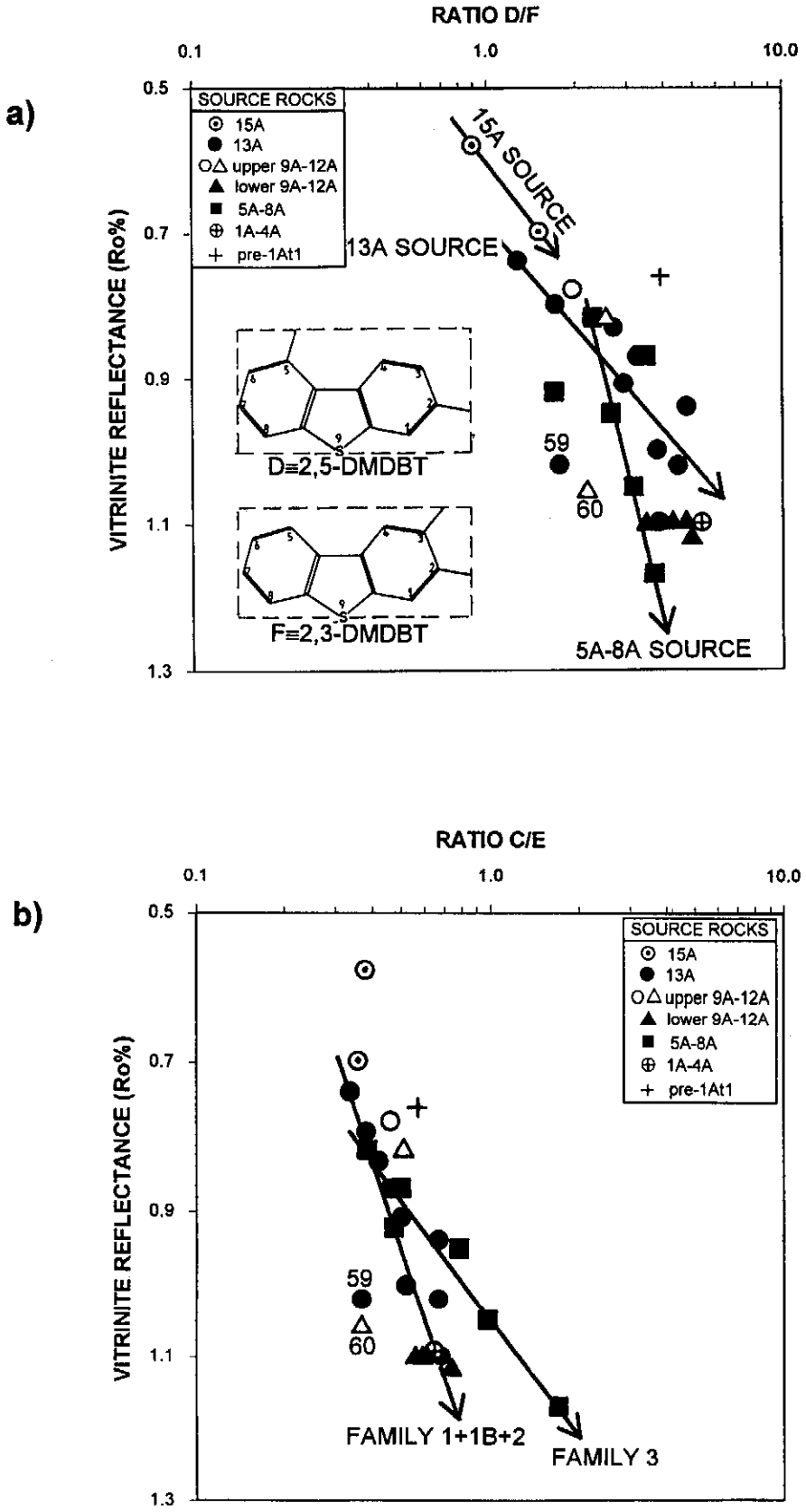

Figure 12.37: Plots of dimethyl dibenzothiophene ratios (C/E) and (D/F) vs vitrinite reflectance data for source rock sample only. Both datasets show differences between the trends of Family 1, 3 and 7 samples. The different molecule shapes, which are thought to affect the relative rates of expulsion, are shown.

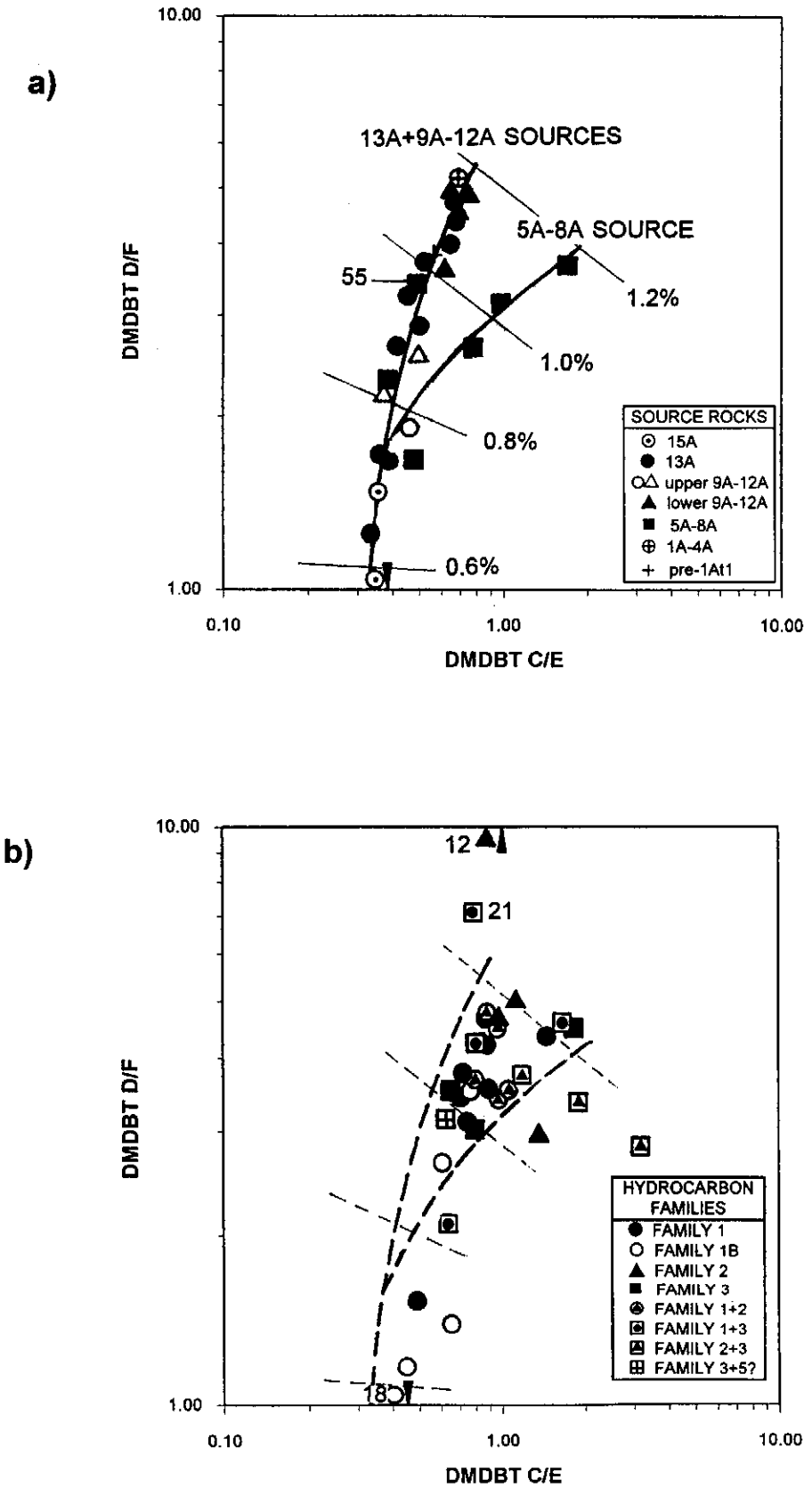

Figure 12.38: Cross-plots of dimethyl dibenzothiophene ratios (C/E vs D/F) for (a) all source rock and (b) all hydrocarbon samples. Well defined trends are apparent in both the plots - although the hydrocarbon trend is offset somewhat. Equivalent vitrinite reflectances have been annotated on the Family 1+1B+2 trends and the Family 3 trend and achieve precisions of R_o~0.1%.

include high maturity residue from yet another source area, such as the nearby syn-rift graben. Certainly the location of well 48, at the end of a major boundary fault where it is known that different hydrocarbon systems meet, would be a favoured location for cross-contamination by oils from varied sources (Davies, 1996c).

In spite of the possible geochromatographically-induced differences between source rock and hydrocarbon trends, the C/E and D/F ratios are useful indicators for source maturity.

12.2.3.8. Trimethyl dibenzothiophenes (TMDBT)

Trimethyl dibenzothiophene peaks are not commonly shown in the literature. Even where fragmentograms of the m/z 226 ion are shown, peaks are rarely labelled and are not assigned to specific isomers, rather they are labelled alphabetically or numerically (e.g. numerically by Chakhmakhchev and Suzuki, 1995). Few ratios are available from published examples other than the thermal stability assessments of Chakhmakhchev and Suzuki (1995). They stated that peaks 'c' and 'e' (their peaks 3 and 5) constituted a maturation parameter. However, they did not plot the data, but merely show ratios. In fact when plotted, the ratio c/e calculated from Bredasdorp Basin source rock samples describes an exponentially increasing maturity trend from which a maturity progression can be evaluated (Fig. 12.39a) as was done for the dimethyl homologues, with a precision of R_o~0.1%.

When the source rock data envelope is compared to that of the hydrocarbon samples, there is an offset of 'source rock value *3.5' (Fig. 12.39b). As in the triaromatic steroids, there are no hydrocarbons at equivalent reflectances R_o<~0.8%, suggesting that this is the beginning of oil expulsion. As in the dimethyl homologues, Family 1B hydrocarbons locate closer to the source rock values than any other family, supporting the hypothesis that the ratio has a migration specificity and that these hydrocarbons have migrated the shortest distance. In this data-set, the hydrocarbon with the lowest calculated maturity (sample 36) is known to represent an early oil migration episode, and other biomarker maturity parameters confirm its maturity at sourcing of R_o~0.7%. The two samples which plot outside the envelope (no's. 9 and 23) are both from wells where input of more mature condensate is suspected and their high ratios match the likely culprit condensate (Family 3) better than do the oil traces (e.g. sample 10). This suggests that the ratio of peaks c/d records the maturity level at the time of sourcing.

12.3. STATISTICAL CORRELATION

Statistical correlations using several different techniques have been attempted on the ratio data-set. Ratio data are used because peak height data are not absolute and as

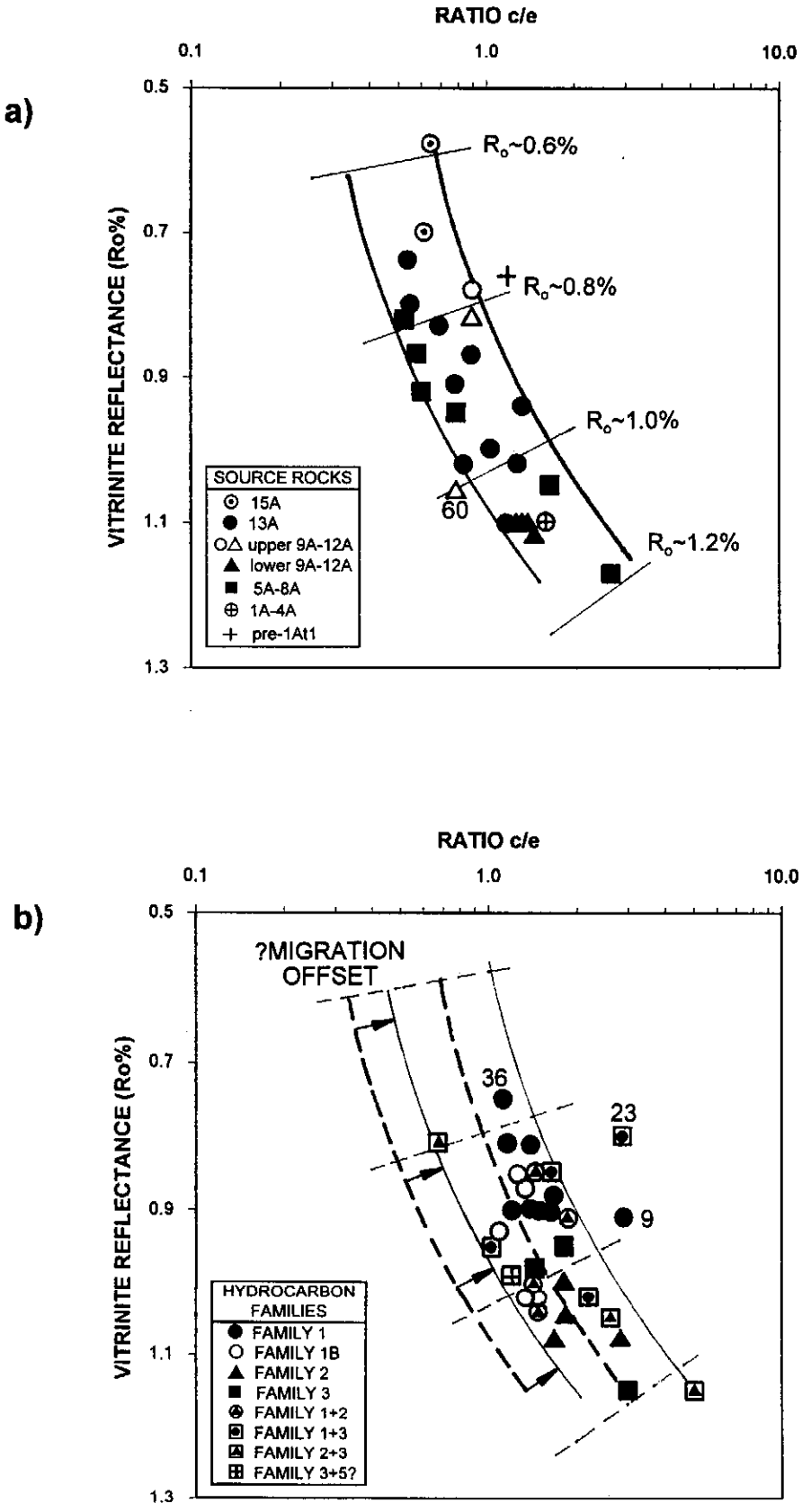

Figure 12.39: Plots of trimethyl dibenzothiophene ratios (c/e) for (a) all source rock and (b) all hydrocarbon samples. All source rock data locate in a maturity-dependent trend - and most hydrocarbon samples also locate in a matching, but offset, trend.

ratios of adjacent peaks remove most bias due to temperature or flow rate changes during analysis.

12.3.1. Cluster analysis

Cluster analysis using squared Euclidean distances and average linking for saturated fraction biomarker ratios was successfully employed (Appendix F, Tables F.18-F.22, R.S. Hatton, 1997, pers. comm.).

The source rock results show that most Family 1 and 3 source rocks locate separate from each other (Fig. 12.40 a). Only one 15A sample (number 49) was included because of the many data missing from the other 15A source sample (no. 69; Table F.18). Nevertheless, sample 49 clearly locates separate from all other samples. Similarly the lacustrine sample (number 45) and the 5A source rock which best matches the pre-1A Family 3 condensates both locate separate from the other samples. The two western basin upper 9A-12A samples which are equivalent to Family 1B oils (i.e. numbers 44 and 51) locate close to each other.

The hydrocarbon results (Fig. 12.40b) show a similarly definite separation. Western basin Family 1B oils all locate at the top of the plot. The Family 1B sample from the eastern part of the basin, sample 33, locates separate from the other samples in a group of quite poorly matched samples. Most Family 1 hydrocarbons locate close by in the top half of the plot although one low maturity Family 1 sample from the south-east corner of the basin, sample 27, locates separate from the rest. This is suggestive of a slightly different source type, not surprising in view of its location in an area where 9A-12A source rocks also have oil potential (Davies, 1997e). Most Family 2 samples locate together in the central region of the plot whilst most Family 3 samples locate at the base.

Bearing in mind that there are quite significant maturity-dependent trends in each family, the close similarities indicated by the cluster analysis confirms the broad distinction of the four main families and the 1B sub-family.

12.3.2. Stepwise discriminant function analysis

Discriminant function analysis was carried out with the source rock data-set with BMDP (1993). The data input for the correlation were saturated hydrocarbon biomarker ratios as listed in Appendix F, Tables F.18-20. The aromatic biomarker ratios were not used because (i) the aromatic fraction of a few samples had not been analysed and (ii) aromatic fractions contained too few biomarkers in other samples. Coefficients of variation and canonical variables were determined for the hydrocarbons using the four main families (1, 1B, 2 and 3) and for the shales using the main families (13A, upper

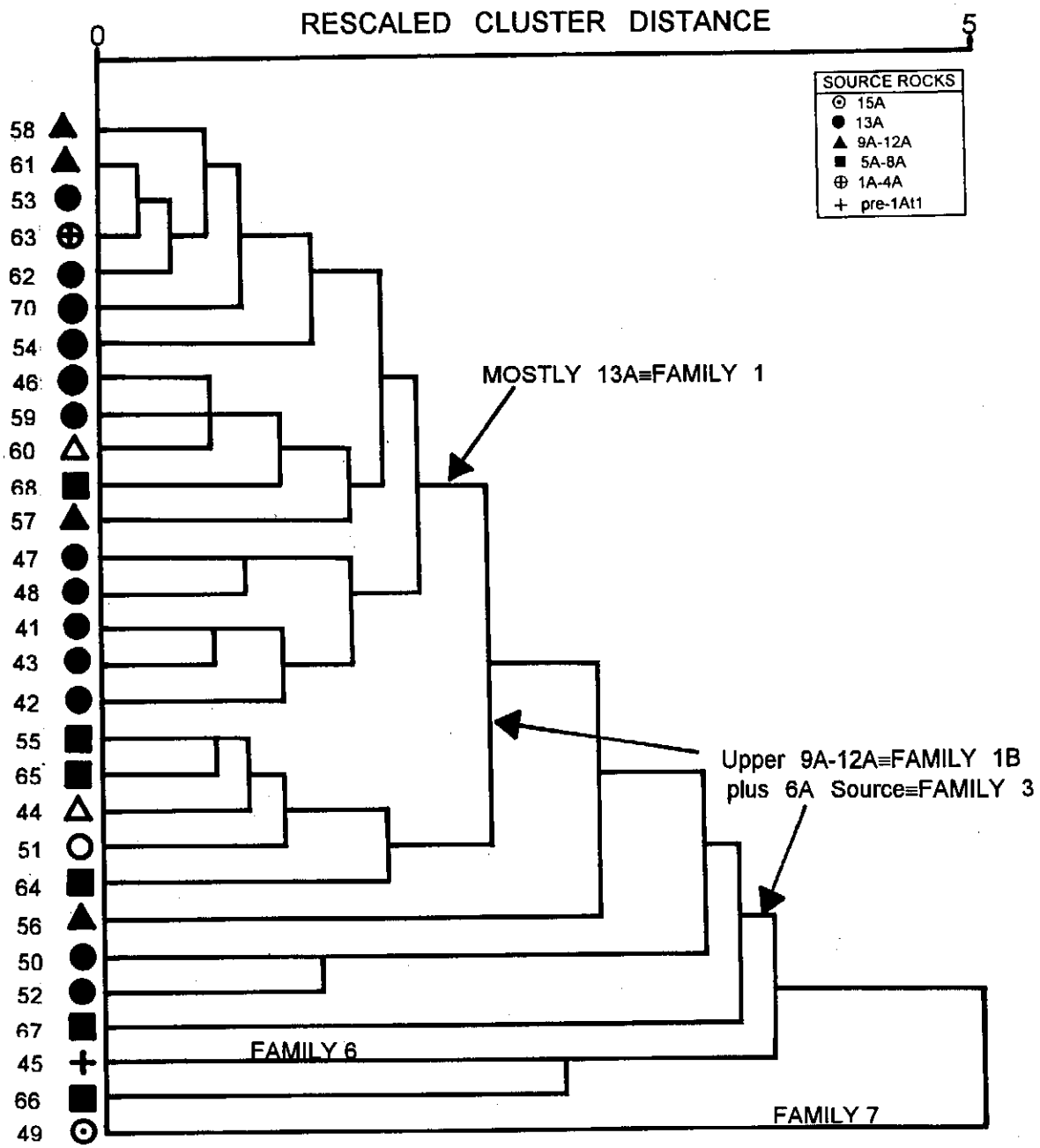

Figure 12.40a: Hierarchical clustering of source rock samples from Euclidean distance analysis of biomarker ratios given in Tables F.18-22.

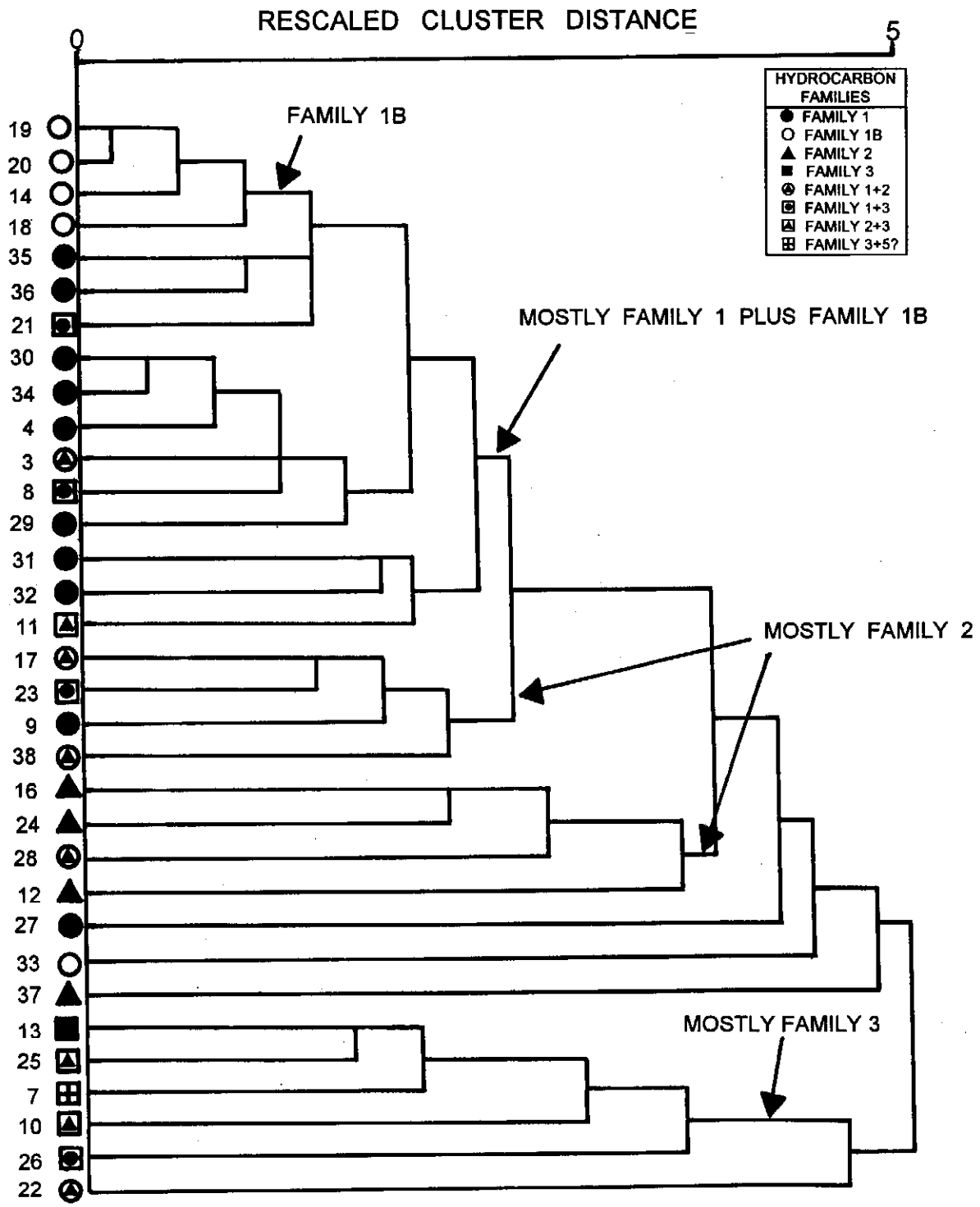

Figure 12.40b: Hierarchical clustering of hydrocarbon samples from Euclidean distance analysis of biomarker ratios given in Tables F18-22.

9A-12A, lower 9A-12A and 5A-8A). The mixed hydrocarbon families and the 15A (Turonian) source rock, Family 7, were excluded from the calculations. This was because the oil families would overlap all family boundaries and because the source rock family was essentially immature and would mask the distinctness of the other families. The mixed families and 15A source Family were re-included in the data sets for the classification procedure (Appendix F, Tables F.26a and 27a). The analyses were successful in that the hydrocarbon families were clearly well separated and the source rock families were largely separated (Figs. 12.41a and b; Appendix F, Tables F.26a and F.26b). These plots are based on the first two canonical variables of each discriminant function. For the source rocks, these are:

Variable 1 = [92.49085*2728bb) + (-1.41135*2456)]

Variable 2 = [(3.76096*2728bb) + (1.14966*2456)]

2728bb=m/z 218 C27ββS+R/C28ββ$+R

2456 = C24 tetracyclic terpane/(C25 + av. C26 tricyclic terpanes)

For the hydrocarbon samples, the variables are:

Variable 1 = [(-4.6841*2928bb) + (-5.9163*32SR) + (-.0089*H24) + (-6.3939*2456) + (-1.8942*nHbis)]

Variable 2 = [(1.8476*2928bb) + (-2.9825*32SR) + (0.0131*H24) + (3.1094*2456) + (-0.3685*nHbis)]

2928bb = m/z 218 C29ββ/C28ββ

32SR = C32 homohopane 24S/24R

H24 = C30 hopane/(hopane+C24 tetracyclic terpane)

2456 = C24 tetracyclic terpane/(C25 + av. C26 tricyclic terpanes)

nH/bis = C29 norhopane/C28 bisnorhopane

In the source rock separation, three samples of Family 3 overlap with some of Family 1. It is known that many of the saturated hydrocarbon fractions were mature enough for their biomarker isomerisation ratios to have attained the equilibrium or maximum value. As shown in Figs. 12.14-39, different source-specific trends reach a similar equilibrium or maximum value at different maturity levels. Hence where they have all reached the same value, there is no difference between them. In addition, most discrimination between the different families at high maturity was done using the aromatic data. This is because those data tend to have a greater effectiveness at higher maturity (Mackenzie, 1984). So the discriminant function analysis is most useful for relatively low maturity samples.

Results of calculation of Mahalanobis' D^2 distances and *a posteriori* probabilities of the correct source rock family assignment recorded a number of mismatched samples apart from the Family 7 samples which are placed in the closest fitting family. Family 1

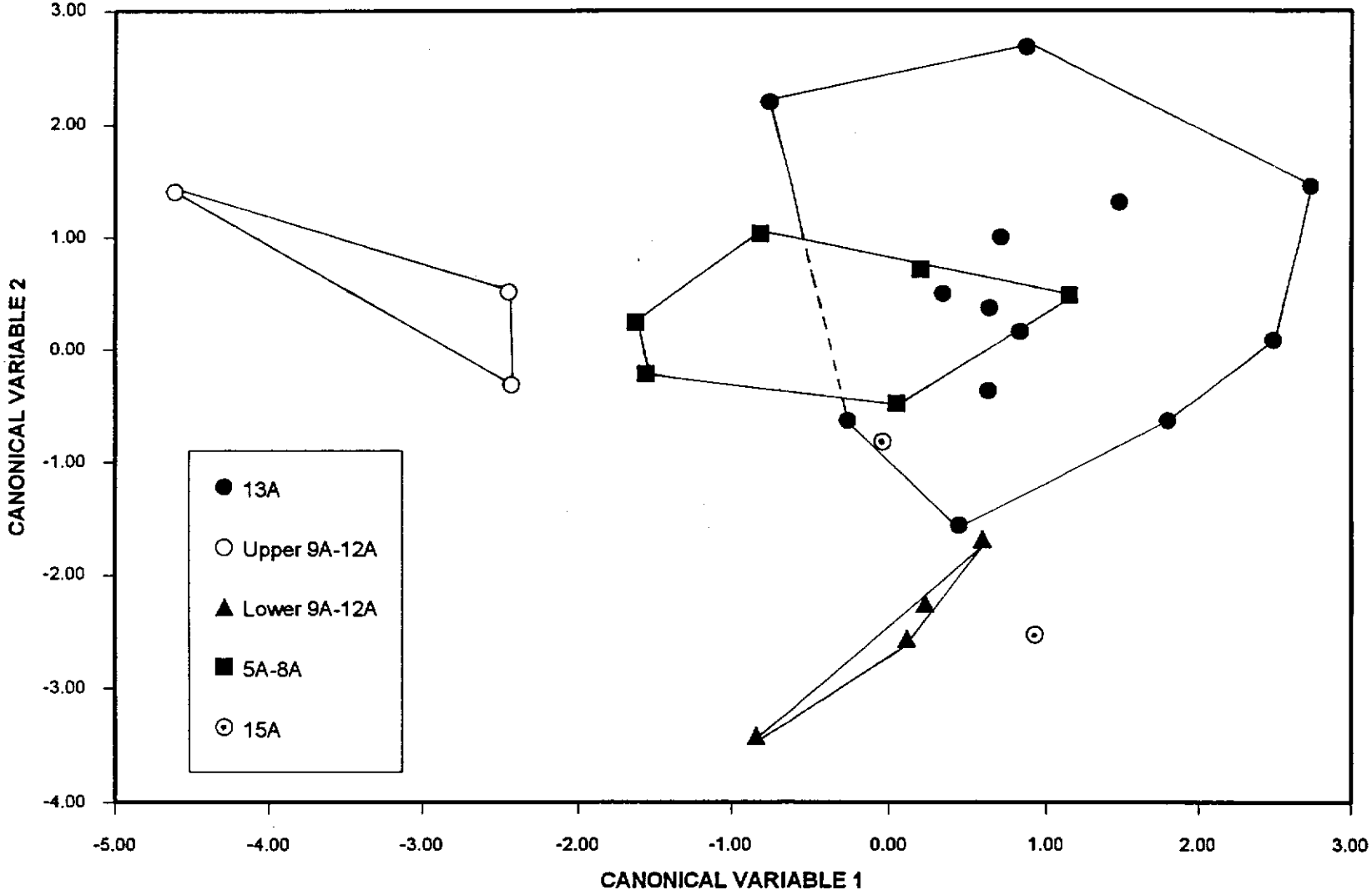

Figure 12.41a: First and second canonical variables of the stepwise discriminant function analysis of the main source rock Families applied to all source rock Families.

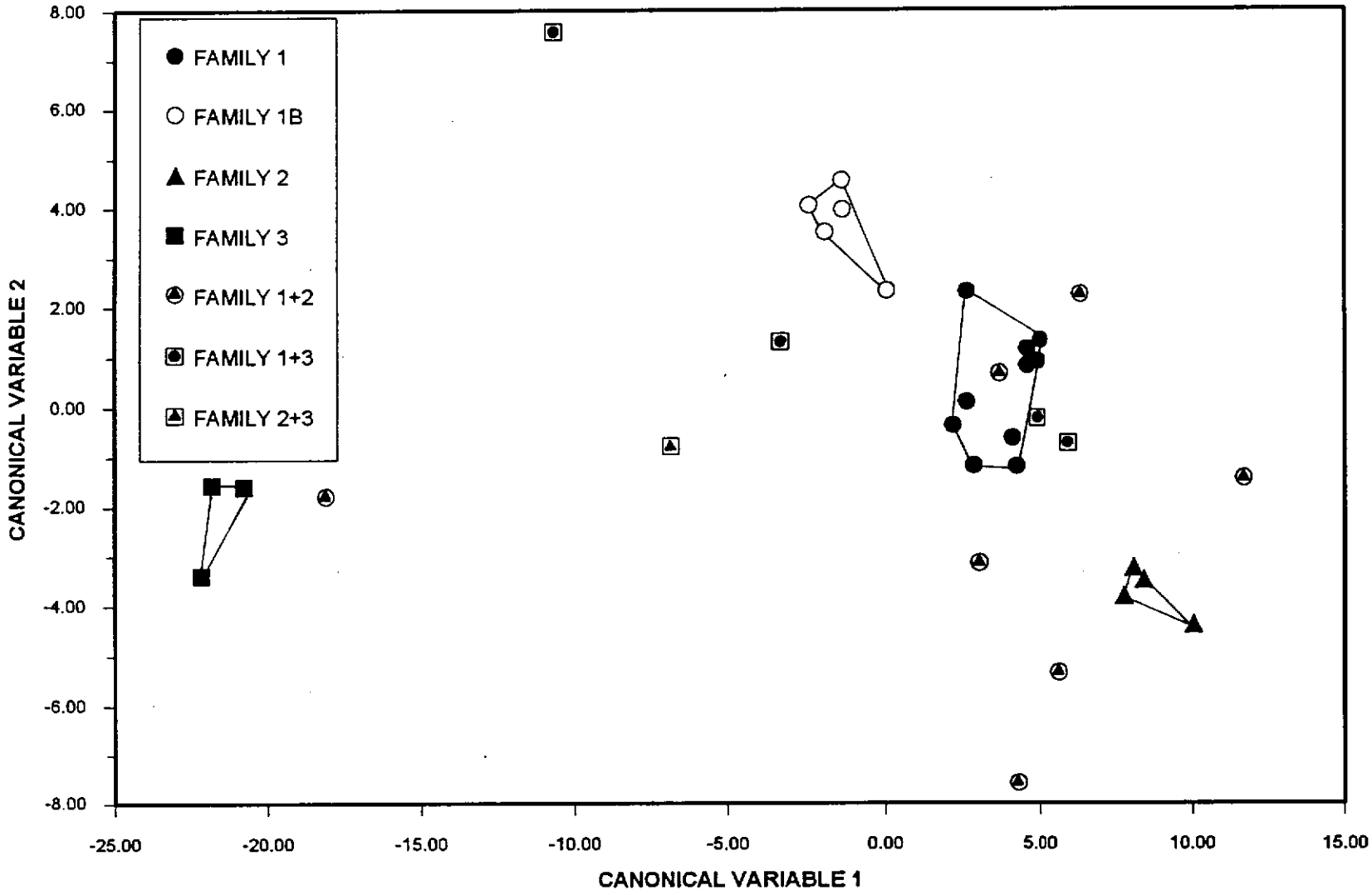

Figure 12.41b: First and second canonical variables of the stepwise discriminant function analysis of the main hydrocarbon Families applied to all hydrocarbons.

samples 42 and 47 are both better assigned to 5A-8A source rocks (Appendix F, Table F.26a). The likelihood of those assignments are 59% and 68% respectively. Both these samples were analysed with normal alkanes included, and it is possible that it has influenced the results. In each case, the samples are part of the 13A source rock and nearby there are samples typical of that sequence. Sample 59 appears better assigned to Family lower 9A-12A on these data although the characteristic dominance of diahopanes is absent (Appendix E, Fig. E.57). Sample 66 is assigned to Family 1 instead of Family 5A-8A. This sample has been most affected by ratio reversals and in some cases has biomarker ratios typical of low maturity samples. By contrast with Family 1 samples it has the characteristically low proportions of C28 β steranes found in Family 3 condensates and Family 5A-8A source rocks (Appendix E, Fig. E.64).

Results of calculation of the Mahalanobis D^2 distance and *a posteriori* probabilities of a correct match for the hydrocarbon samples show complete separation of the main hydrocarbon families (Appendix F, Table F.27b). The mixed hydrocarbons locate scattered throughout the plot as expected.

The hydrocarbon discriminant functions were also used to test the separation of the source rock samples (Fig. 12.42a; Appendix F, Table F.26c). The separation is quite poor with only the upper 9A-12A source rocks well separated, although the lower 9A-12A samples clearly separate from all but a few 13A samples. Complete separation was not expected, partly because the biomarker data most likely to separate the higher maturity samples were not used, and partly because of the maturity-dependency trends described in Chapter 12. Similarly, canonical variables for the hydrocarbon samples were calculated from the source rock discriminant functions. The Family 1B and 3 samples separate whilst the Family 1 and 2 samples do not (Fig. 12.42b). Again this lack of complete separation is considered to be a function of the inability to employ the aromatic data.

There is a second possible explanation for the lack of 1:1 correlation between source rocks and hydrocarbons. Source rock samples represent only a limited area of the basin and it is likely that proportions of kerogen vary somewhat across the basin. Hydrocarbon samples, on the other hand, test the whole of the active fetch area rather than just the basin edges where reservoirs are found, hence they are likely to sample different parts of the source rocks. In addition, source rock samples test the bitumens generated through the whole of the generation period. Hydrocarbons are, however, expelled only periodically through the period of generation and are therefore characteristic of only discrete parts of the generation period. So perfect correlations between hydrocarbon and source rock biomarkers are not to be expected.

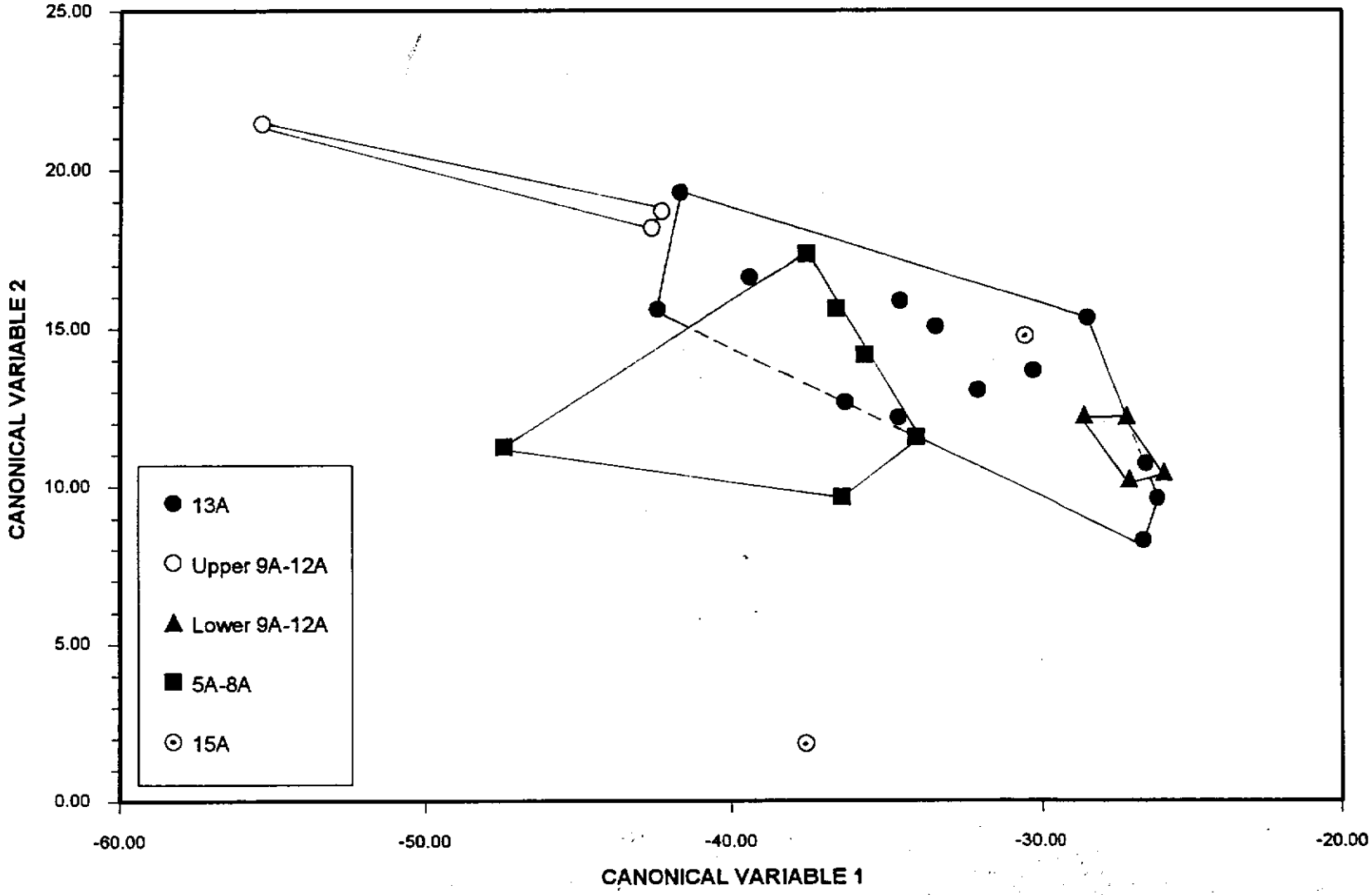

Figure 12.42a: First and second canonical variables of the stepwise discriminant function analysis of the main hydrocarbon Families applied to the source rock Families.

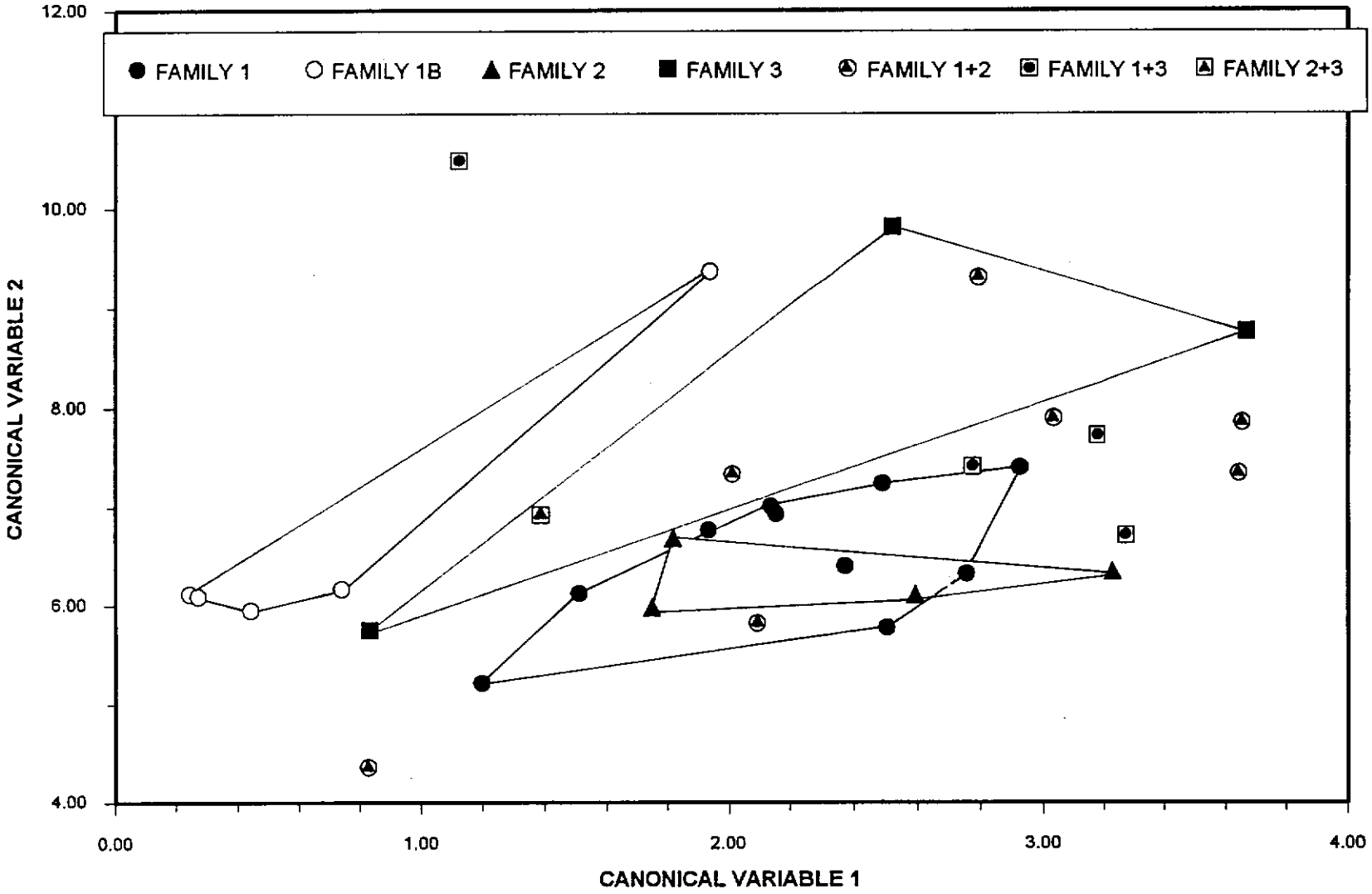

Figure 12.42b: First and second canonical variables of the stepwise discriminant function analysis of the main source rock Families applied to all hydrocarbons.

12.4 CONCLUSIONS

Throughout this chapter, the individual families of hydrocarbons are shown to match specific intervals of source rock with varying degrees of success namely:

13A source rocks	largely match Family 1 oils
upper 9A-12A source rocks	largely match Family 1B oils
lower 9A-12A source rocks	largely match Family 2 gas-condensates
5A-8A source rocks	largely match Family 3 gas-condensates.

These correlations, however, are not absolute and some biomarker ratios are more useful for distinguishing one source-hydrocarbon group from another, whilst another ratio is more specific for a different pair of source rock-hydrocarbon groups. For example, the 15A+9A-12A source trend in Fig. 12.27 matches the trend of the Family 1B oils closely, but the regression line through the 5A-8A source rocks only broadly matches the Family 3 trend. Maturation-dependent trends are commonly found both in source rock and hydrocarbon samples. In a number of cases individual source-hydrocarbon trends are different from each other (e.g. Figs. 12.23, 12.25, 12.27). In some cases there are reversals of the trends which record either development of early dominance of one compound which is later cracked or the later neoformation of a co-eluting compound (Figs. 12.25 and 12.33). Mass spectral analyses have yet to be carried out to confirm this.

In other cases, trends of source rock and hydrocarbon samples do not match perfectly but are evidently related. For example, in Fig. 12.27 and 12.29, the Family 1B trend matches the nearby upper 9A-12A source rock samples very closely indicating minimal migration. The Family 2 samples locate with a similar trend to their probable source rocks, the lower 9A-12A source rocks, but offset perhaps due to a migration effect. Certainly their much higher biomarker maturation level than most Family 1 oils, may indicate longer migration distances from greater depths. In other examples, source rock trends lie near, but sub-parallel to, the trends of matching hydrocarbons (Fig. 12.38). This too is suggestive of a migration fractionation as reported by Larter and Mills (1991) and Peters and Moldowan (1993, p. 112-113). Alternatively, the migration effect may represent the subtle differences between the hydrocarbons generated and expelled from the source rock at earlier times compared to those not expelled from the source. Indeed, the source rock probably retains material generated throughout its history whereas the reservoir may hold hydrocarbons from only one of the expulsion periods (Peters and Moldowan, 1993, p. 113).

Other examples of migration-dependence are seen in Figs. 12.35 and 12.39 where source rock biomarker ratios describe maturation-dependent trends, but most hydrocarbons are found with ratios indicative of only the later part of those trends. This

indicates that few of the early-generated hydrocarbons are available for reservoiring. Migration also results in many hydrocarbon samples having ratios which are out-of-place with the source rock samples. For example, in Fig. 12.33, the well-characterised reversal in the aromatic steroid ratio is not matched by many of the hydrocarbon data, probably because they have formation reflectances lower than those which prevailed in the source rock at expulsion.

The biomarker data also show that there are mixtures of hydrocarbons characteristic of different families. For example in Fig. 12.17, Family 2 hydrocarbons mostly locate in the same region of the plot as the lower 9A-12A source rocks, yet a number of the mixtures of Family 2 condensates with Family 1 and 3 material plot between the relevant families.

The main source rock and hydrocarbon families are therefore matched to each other using more than one biomarker parameter, because no single parameter fully describes their relationships.

CHAPTER 13: DISCUSSION

So far, the study has addressed a number of aspects of the petroleum history of the Bredasdorp Basin in detail, mainly as separate entities. A more co-ordinated assessment of these diverse aspects is discussed here.

The chapter is divided into 3 parts, each using a different method to assess the petroleum potential:
1. the evolutionary approach to hydrocarbon generation, migration and reservoiring, locating each aspect in the relevant time frame,
2. the 'prospect/play' approach viewing the more local communication between source rock and hydrocarbon reservoir,
3. the 'petroleum system approach' viewing the critical aspects of the source-reservoir combination as part of a whole system.

13.1. GENERAL HYDROCARBON EVOLUTION

The six main aspects that impact on the petroleum history of the area are sedimentation, thermal history, tectonism, generation and expulsion, fluid movement and reservoiring.

13.1.1. Depositional history

Mesozoic sedimentation in the region commenced in the Late Jurassic with continental clastics deposited on the Permo-Triassic post-Karoo surface (Gilbert, 1977; Jungslager, 1996; McMillan et al., 1997). These rocks are mainly fluvial but locally lacustrine (wells 10, 47, 65, 89, V.H. Valicenti, 1994, pers. comm.; Jungslager, 1996) and have oil source potential in well 89 offshore and well DWK-1 onshore (Davies et al., 1991).

Gradually overstepping the continental land surface from the east, Late Jurassic deep marine conditions pervaded the region resulting in the deposition of oil-prone source rocks in the eastern part of the Outeniqua Basin (Davies, 1992; Malan, 1993). Encroachment may have extended further west, but no wells have penetrated deep enough to intersect such source intervals. The marine source interval may be present in the deepest part of the early rift in the western part of the Southern Outeniqua Basin. During the Earliest Cretaceous times, the sea retreated again and continental sedimentation again prevailed. With further advances of the sea during Valanginian times, the youngest continental rocks were reworked to form regressive coastal sandstones that are present throughout the four inboard basins and form the main pre-1At1 reservoir sandstone. The rate of advance of these conditions must have been quite steady to result in the matching thicknesses of these sandstones around the basin. One borehole in the centre of the Bredasdorp Basin (well 163) intersected these

sandstones (100-200 m). It is therefore possible that similar thicknesses are developed elsewhere and could contain large volumes of gaseous hydrocarbons (Jungslager, 1996). This proximal marine sandstone was locally uplifted and eroded before being overlapped by deep marine deposits. These formed the seals and sources to the many deep marine turbidite and channel fill sandstone reservoirs in the Bredasdorp and Pletmos Basins.

Soon after rifting at 1At1 times (Early Valanginian), water depths increased quickly as a result of thermal subsidence, resulting in a rapid increase in accommodation space (McMillan et al., 1997). Early sedimentation rates were slow until the Albian so that the marine environment in the basin remained quite deep. Thereafter, the sedimentation rate increased and a rapid influx of sediments during the Albian-Turonian largely filled the basin. Continued thermal subsidence and a much slower rate of sediment fill through to Late Santonian resulted in a further increase in accommodation space. During the Late Cretaceous, this space filled rapidly as two periods of progradation, one from the north and one from the west (sequences 16B and 17A respectively) mostly completed the Mesozoic fill (Fig. 3.07). Hence maximum sedimentation rates do not occur in step with maximum generation rates of accommodation space. This means that estimating changes in heat flow, based on the assumption that relative changes in accommodation space are a function solely of thermal sag, is not correct in this area (White, 1993; K.L. Gallagher, 1996, pers. comm.).

After 5A-6A times, when syn-rift fault blocks were reactivated, pre-1At1 sandstones were eroded from crestal locations. Later doming and steepening of some of these tilted blocks, perhaps during the Late Albian compression, resulted in the crests being displaced to where uneroded sandstones remained. The reactivation of faults also resulted in accentuation of the eastern topographic highs. These acted as barriers to the free interchange of water between the Bredasdorp and Southern Outeniqua Basins, resulting in frequent periods of anoxia. The highs also acted as barriers to transport of sand out of the basin, resulting in their being ponded against some highs generating potential new exploration targets. Large volumes of sand-rich shelf material were reworked into the basin during 6A, 9A-12A, 13B-14A and 14C times (L. Hauterivian, L. Barremian, L. Aptian-Albian and L. Cenomanian) forming further exploration targets.

During early periods, in the organically productive 'greenhouse' Mid-Cretaceous, the hinterland supplied much organic material to the sediments and its bacterial decay occasionally resulted in the development of anoxia. Where these anoxic layers impinged on the coastline, or more probably on shelf edges, source rocks developed. Most of the 5A-12A source rocks were formed in this fashion and hence largely occur around the basin edge and near fluvial debouchments. It is thought that pre-5A source

rocks also formed in the anoxic core of the basin and therefore form a basin-wide layer, although the lack of intersections away from the basin edges renders this an unknown.

During the Aptian and to a lesser extent in the Turonian, anoxic conditions developed regionally. This resulted in the formation of the Aptian and Turonian source rocks in South Africa and adjoining regions, the Falklands Plateau and southern South America. Both these source rocks are probably developed in all the southern offshore basins. The final burial of the eastern basin highs was only achieved during the Aptian and the basin-wide 13A oil-prone source rock overlies many of these highs juxtaposed on pre-1A sandstone (wells 12 and 13, sample 27; Fig. 13.01).

Apart from the regional Turonian source, which is thin throughout the southern African region (Fig. 13.02) and relatively immature, and the apparently locally developed Jurassic lacustrine source, regional source rocks dominate only in a narrow time period (118-111 Ma i.e. 5A-13A). Since these source rocks were all deposited in similar environments and with similar organic matter, in locally different proportions, they can be considered as a single source episode.

13.1.2. Thermal evolution

The Outeniqua Basin in general and the Bredasdorp Basin in particular have been affected by four different heating events: heat associated with rifting during the Late Jurassic, heating due to the Turonian passage of the spreading centre, heat associated with the transit over the Bouvet/Shona hotspot, and heat associated with the African Superswell and ensuing Agulhas Slump (Fig. 13.03). Burial history and thermal modelling studies carried out using drilled data and analysed samples from several widely separated locations throughout the basin, all record similar unusual maturation features confirming that the basin was subjected to a number of unusual events.

Assumptions about the heat input of regional heating events, such as rifting, are based on similar events elsewhere. Maturation effects of the first two heating events on kerogen-rich source rocks cannot be fully evaluated because of the over-printing effect of the later heating periods. However, it is possible that the common bitumen fill in pre-1At1 sandstones in the eastern basin highs, results from early generation from syn-rift lacustrine shales formed during these events. The heat increase associated with the transit of the spreading centre during the Turonian, which altered the heating patterns mainly in the Southern Outeniqua Basin, is derived by analogy with modern rifts (Barnard et al., 1992).

Heat associated with the regional Bouvet/Shona mantle swell and hotspot transit is considered to affect the whole basin and the western part of the Pletmos Basin (Davies,

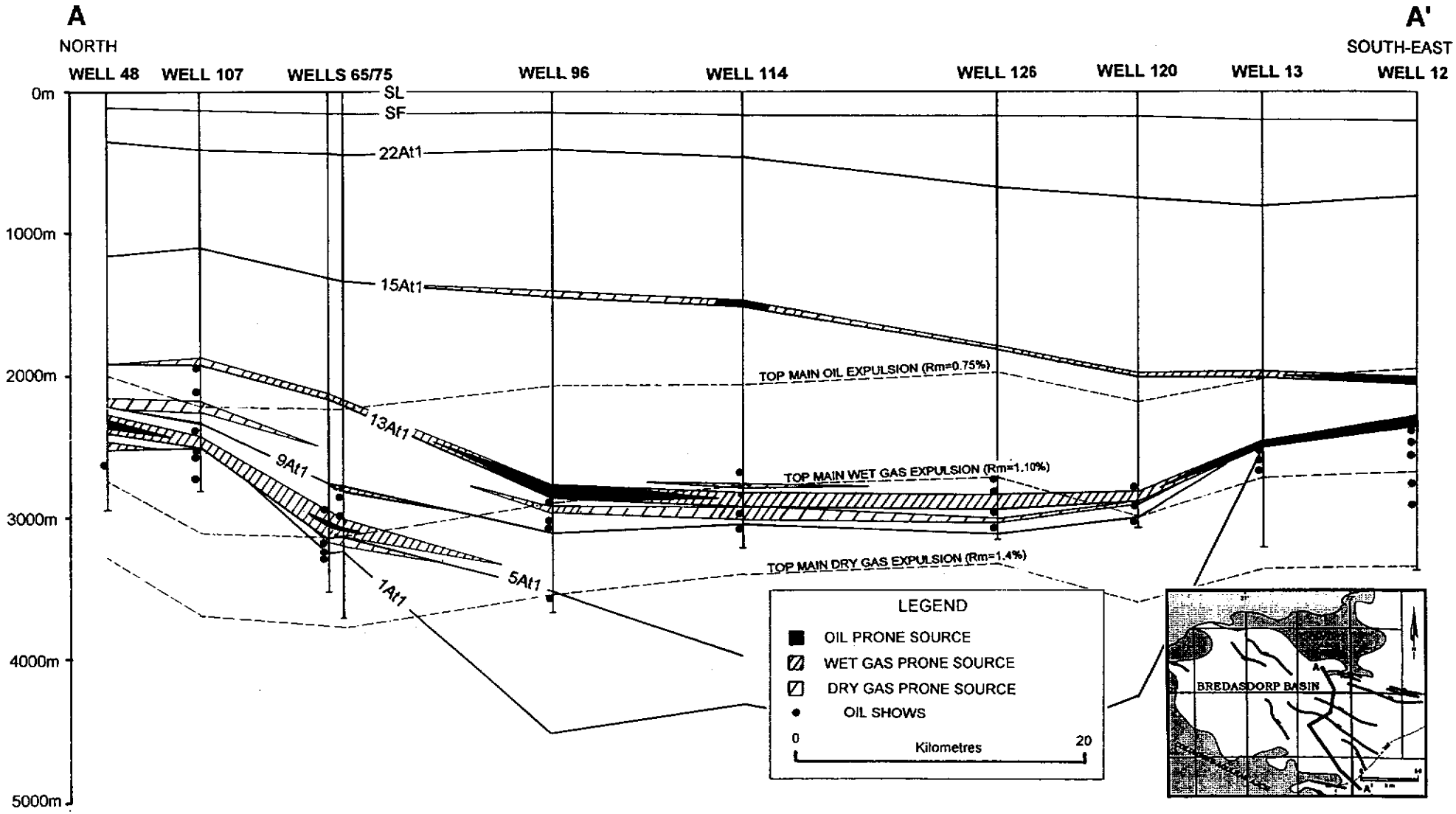

Figure 13.01: Section across the Bredasdorp Basin showing the local extent of pre13A source rocks and the regional extent of 13A and 15A source rock development (after Figure 3.04).

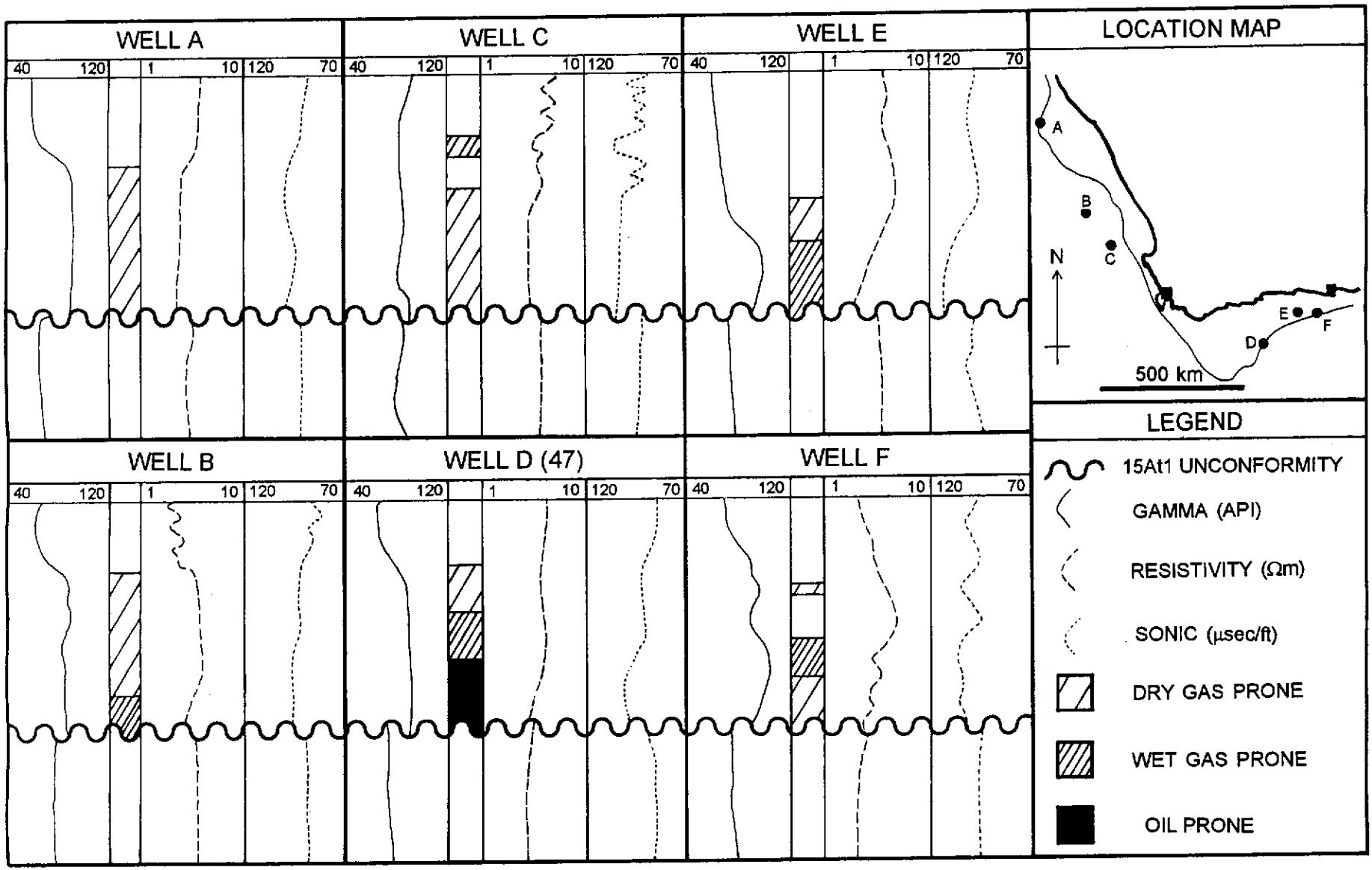

Figure 13.02: Matching thickness, source quality and log character of 15A source rocks from wells around the South African coastline.

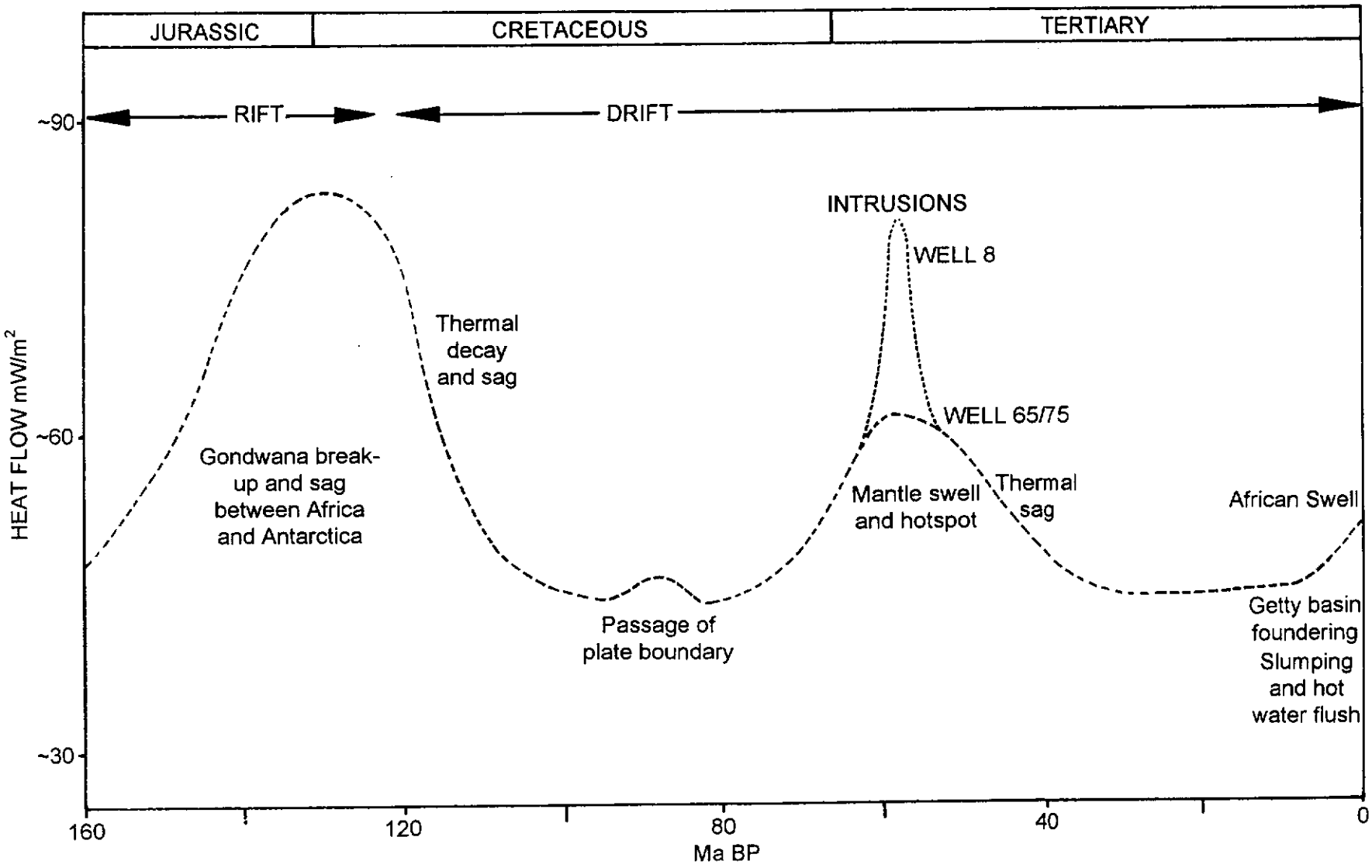

Figure 13.03: Model of heat flows affecting the Bredasdorp Basin since early rifting (after Figure 7.01).

1997c; 1997d). Evidence for the hotspot transit is found *inter alia* in bathymetric and igneous data (Duncan, 1981; Hartnady and Le Roex, 1985) and is indirectly supported by vitrinite reflectance and apatite fission track results (Eurotrack, 1996). The heat needed to cause the near-total annealing of apatite grains just a few hundred metres below the palaeo-surface some 40-50 km away from an intrusive area, could not be due to the intrusions of 'cool' carbonatite magma (Tarling, 1973). It must, therefore, be due to a regionally large heat input.

Even basic intrusive centres often have only local effects on heat flows as shown by an example from New Zealand. In the Banks Peninsula (South Island) heat flows within 20-30 kms of a Late Miocene to Recent volcanic field are at regionally low values (Funnell and Allis, 1996). If the intrusions in the Bredasdorp Basin were responsible for similarly local heat inputs, they could not be responsible for apatite annealing as far away as 40-50 kms.

The hydrothermal episode resulting from the Agulhas Slump is supported also by vitrinite data. Seismic evidence of Late Tertiary cones on the sea floor at the eastern margin of the basin, that are possible mud volcanoes, lend further support (Burden, 1993). Similar maturation effects on shallow sediments are postulated by Gibbons and Herridge (1984), Gibbons and Fry (1986) and Lerche et al. (1997). The probable cause of the slumping, the African Superswell, is characterised by differential uplift from east-to-west across southern Africa, from Late Tertiary biostratigraphic evidence and from results of global tomography (Hartnady and Partridge, 1995). Local tilting associated with this event is interpreted from seismic data across the Agulhas Fracture Ridge (Ben-Avraham et al., 1997). Analysis of temperature, isotopic and water chemistry data from fluid inclusions in quartz or carbonate overgrowths in possible migration conduit or reservoir samples could help to characterise the thermal events and so confirm the postulated hydrothermal charge. A more complete suite of data from apatite fission track analyses would be necessary to confirm the regional heating from the hotspot transit and possibly from the hydrothermal charge.

13.1.3. Tectonic history

Rifting has been effective mainly in three stages namely (i) during the Late Jurassic, when the first evidence for rifting is seen, (ii) during the Valanginian when horizon 1At1 is shown to mark the main period of thermal subsidence and encroachment of marine conditions and (iii) widespread reactivation of basement highs in the Early Hauterivian when latest Valanginian (5A) rocks were stripped off the highs.

In contrast to Du Toit (1976) who suggested that inherited fault directions controlled the formation of the inboard Outeniqua Basins, Jungslager (1996) proposed that the

Bredasdorp Basin is a failed rift, analogous to that of the North Sea. If so, then faulting should essentially cease at the end of rifting, as shown in sections across the North Sea (Park, 1988, p.201-202; Thomas et al., 1985). Yet faulting in the Bredasdorp Basin continued into the Early Barremian (9A) in the north flank of the basin, to Earliest Albian (14A) in the central basin and into the Tertiary in the south flank (Van der Merwe and Fouché, 1992). These renewed faulting episodes lend support to the suggestion that the basin formed during the pull-apart motion along the Agulhas-Falklands Fracture Zone (AFFZ) and continued to develop throughout the period of pull-apart, at least until the plates were no longer in contact.

The importance of this model is that the faulting which appears to have provided the sub-basins for sandstone concentration was also responsible for the development of the 14A structural highs. The inversion results from localised accommodation-space problems caused by intermittent movement along the master wrench faults, evidenced by the positive and negative flower structures that extend into 13B sediments (Holmes, 1994). Local compression and tension effects were caused by drag along the AFFZ, hence the main oil reservoirs result from relative plate motions during drift.

Apart from these effects, the region has suffered from other episodes of significant tectonic change. The two relatively recent periods of mantle heat increase (mantle swell/hotspot transit and African Superswell) are both considered to have dramatically altered the configuration of the basin (Davies, 1997g; Burden, 1997). It is suggested that during the mantle swell/hotspot transit, the whole basin was upwarped then downwarped progressively from north to south. This must have had some effect on the regional reservoiring pattern although this has yet to be confirmed. By analogy with similar events in northern Britain (Cope, 1994) uplifts changed not only the configuration of reservoired traps but also the drainage pattern in the sediment fetch area. Consequences of such effects need to be sought from changes in the sediment types in the basin. For example, the lack of apatite in coarse sediments of the Early and Mid-Cretaceous may indicate a different provenance (Davies, 1997f). Tertiary rocks in the Bredasdorp Basin are indeed quite different from Mesozoic rocks as they record a drastic diminution of clastic debris entering the basin and the dominance of calcareous biogenic deposition. This indicates either a changing climate and the establishment of more temperate vegetation, which stabilised the soil so that erosion was reduced, or elevation of the southern Cape so that drainage directions were away from the basin.

Fault activation in the basin would also be affected through the period of transit. Certainly more faults on the south side of the basin extend into younger rocks than on the north side as expected for the progressive development of tilting across the basin

(Strauss et al., 1996; Fouché et al., 1995; Fouché 1996a and b). The likely changes in basin configuration during the development of the Late Tertiary African Superswell, which tilted the continent by some 1-2° down to the west, must have influenced the faulting (Hartnady and Partridge, 1995). In addition the evidence for Late Tertiary foundering of the Marginal Fracture Ridge, at least in the eastern part of the Outeniqua Basin, also hints at further episodes of deformation (Ben-Avraham et al., 1997).

13.1.4. Generation and expulsion history

Generation and expulsion histories of the Mesozoic source rocks in the basin are a function of thermal, subsidence and depositional histories. Published examples show the beginning of generation near R_o~0.5%, the beginning of expulsion somewhat higher and peak oil generation close to R_o~0.75% (Durand, 1983; Demaison, 1984; Cornford, 1986; Welte, 1987; Demaison et al., 1988). These limits are mainly for (i) rich source rocks, with hydrogen indices (HI) close to 600 and S2>5, and (ii) source rocks heated at rates ranging from 2-5°C/Ma. Burial history modelling using these limits shows that generation starts in the central basin in 13A source rocks during the Mid-Cretaceous and that first expulsion occurred at ~80 Ma (Davies, 1993e).

By contrast, in the Bredasdorp Basin, samples at R_o 0.58% are dominated by saturated hydrocarbons typical of very low maturation levels (sample 49, Appendix E, Fig. E.47). Even at R_o~0.7%, the hydrocarbons in samples still contain early mature material (sample 69, Appendix E, Fig. E.67). Significant generation seems to have started closer to R_o~0.80% and peak generation reached closer to R_o~1.0% (samples 50 and 53, Appendix E. Figs. E.48 and 51). Burial history modelling using these data shows that significant hydrocarbon generation in 13A source rocks only started during the Late Cretaceous. First expulsion probably commenced shortly after that when the necessary proportion of the pore space had been filled, possibly as late as R_o~0.9% (≡ 100°C; Figs. 10.02 and 13.04).

The richest of the source rocks, the oil-prone shales in the 13A, upper 9A-12A and 6A sequences, are as rich as many highly productive source rocks world-wide (Magoon and Dow, 1994) hence their delayed maturation is not a function of lower richness. Furthermore, the apparently delayed maturation cannot be the result of incorrect vitrinite reflectance data, as chemical and other optical maturity data all confirm the maturity estimate. Therefore the reason for the delayed maturation lies elsewhere, possibly a function of the unusual maturation rates that have prevailed. For most of the time since deposition, modelled maturation rates have been very low, <0.3°C/Ma (Davies, 1997d), indeed they are so low that maturation is essentially frozen. However, during the three main heating periods (rapid basin fill, hotspot transit, hydrothermal charge) modelled maturation rates are very high - often in excess of 5-10°C/Ma

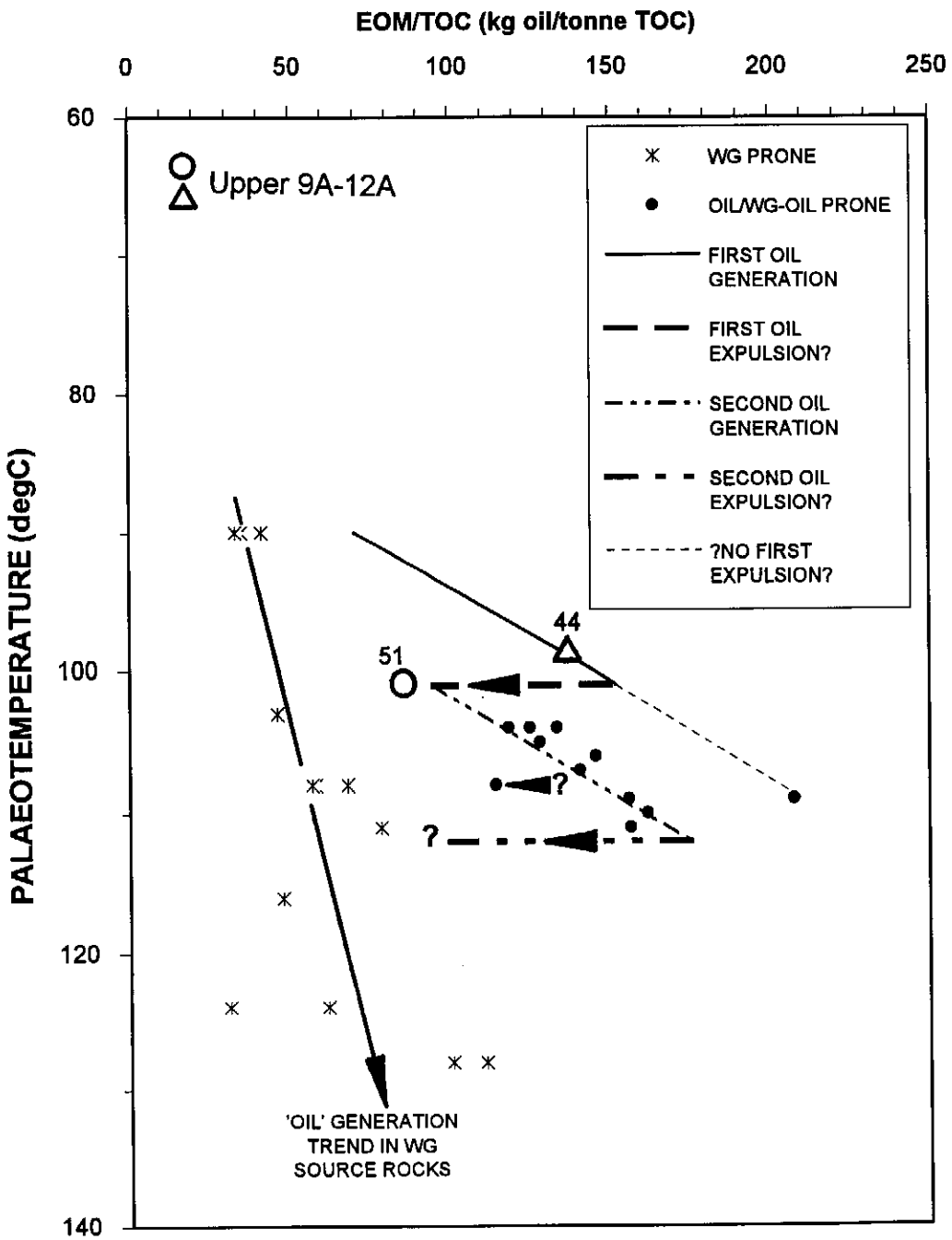

Figure 13.04: Example of extracted organic matter trends for upper and lower 9A-12A source rocks showing the differences in the rates of hydrocarbon generation with maturity and in expulsion thresholds.

(Davies, 1997d). Several studies have shown that high heating rates result in delayed maturity as recorded by higher than normal reflectances for biomarker ratios (Van Graas, 1990; Raymond and Murchison, 1992). Therefore, hydrocarbons expelled at the time of most rapid generation, may also display different biomarker ratios than are usually found at that reflectance level. Reflectance values are largely a function of time and maturity (or temperature). Yukler and Thomsen (1989) show that during periods when there is minimal maturity increase, reflectances might continue to increase, but at best only very slowly. So a comparison of measured reflectances and biomarker maturity ratios from the Bredasdorp Basin could differ significantly from published comparisons.

One complication found throughout the basin is that of reservoired hydrocarbons typical of more than one source rock. Chemical properties of these source rocks are broadly similar because they contain similar kerogen (mixed amorphous and terrigenous), of similar ages (Early Cretaceous), deposited in similar environments (marine dysoxic), and their products differ only slightly. This study, therefore, addressed not only the usual biomarker components to find a match between source rocks and hydrocarbons but also used other less commonly utilised biomarkers as well as a range of lighter compounds in each sample in order to find the best match. In spite of the overall similarities between the sources, there are characteristic biomarker and other differences which distinguish products of adjacent source rocks. Examples of such differences are found in oils reservoired in 13A sandstones in wells 83 and 109 which tap 13A and 9A-12A oil-prone sources respectively (Davies, 1997e).

13.1.5. Fluid migration history

Fluids migrating through this study area are from essentially three different sources:

1. connate water progressively expelled from compacting sediments during burial,
2. fresh meteoric water, introduced from the surface through a permeable, possibly faulted, topographically elevated region. Flow generally occurs where there is recharge at the upper end of the conduit and an outlet at the other end of the conduit,
3. hydrocarbon fluids sourced in several layers in the basin over long time periods.

13.1.5.1. Connate water flow

This fluid is expelled during compaction, mostly from shales, and migrates through porous, permeable layers such as sandstones and along faults. The quantities are large, potentially totalling several pore volumes. Since it is often focused through selected conduits, it can appear to be significantly more. In general, connate water is expelled throughout burial at predictable rates. Indeed, the continuous expulsion of water in a subsiding basin can be likened to an essentially stationary water column, extending to great depths, through which the rocks are buried. However, the amounts

of water expelled can be large during some periods, when shales that have remained uncompacted for some time suddenly compact. An example of this is believed to have occurred during the Agulhas Slump episode when the equivalent of ~60 Ma of sedimentation elsewhere was deposited on the Southern Outeniqua Basin during short episodes each lasting probably no more than ~10^5 years. Pressure and fluid expulsion effects of these events are similar to those reported by Lerche et al. (1997) for periods of ice build-up onshore. The salinity of connate water can vary depending on the original water salinity but in general it is of marine salinity or slightly higher when hosted by marine sediments (Magara, 1978, p.217-242).

There are essentially three separate connate flow regions in the basin:
(i) regions in which salinity is close to marine (25-45000 ppm) and evidently little changed since deposition. These regions tend to show little evidence of hydrocarbon migration probably because the sandstones do not connect to hydrocarbon conduits
(ii) regions in which salinity is high (50-70000 ppm) and generally where formation pressures are also high. These regions clearly do not communicate to either surface or to the surrounding normally pressured regions and represent separate pressure-cells. All sandstones in these cells are gas-saturated throughout (Hodges, 1996)
(iii) regions where salinities are particularly high (>80000 ppm) and possibly indicative of nearby halite deposits. In all cases these are found in pre-1At1 sediments and in most cases, traces of gas and oil are also associated. Examples of these are found near well 16, which did intersect salt at depth, and at wells 7, 14, 27 and 35, although in the last cases there is no evidence that salt deposits exist in the nearby sediments (Davies, 1995a; Grobbler, 1995).

Economically the zone of importance in which formation water may well be connate is in the 9A-12A interval in the central basin where sandstones are gas-saturated. Even in that interval the hydrocarbon charge has varied enormously. There is evidence from oil shows that this interval must have held oil originally. The oil escaped before the regional pressure seal formed by slow exsolution of calcite from saturated formation water as compaction progressed at the cell edges. It is likely that the calcite represents shelly material originally entrained in the sediments and taken into solution as pressure and temperature increased. It is unlikely that large amounts of calcite could be brought into the formation from outside by connate water as this requires a large number of pore water changes, for which there is no evidence (Walderhaug and Bjørkum, 1992).

13.1.5.2. Meteoric water flow.
Quantities can be extremely large as ingress can happen every rainy season throughout the exposure period, potentially up to 10^5 pore volumes each Ma. There are apparently two separate regions where meteoric water has invaded the Bredasdorp

Basin (i) in the central basin 13B-14A sandstone trend which contain relatively fresh water (Fig. 13.05) and (ii) along the north flank margin where marine and fluvial pre-1At1 sandstones in crestal locations have reduced salinity (Fig. 13.06a and b).

Salinities along the 13B-14A trend decrease from ~20000 ppm in the deeper eastern region (near well 94) to ~12000 ppm in the shallower western wells of each trend (wells 164 and 156; Burden and Davies, 1997a).

Pre-1At1 sandstones in the north flank area contain largely matching formation water salinities (<30000 ppm) suggestive of a single filling episode, but probably through several ingress points as they are so widely dispersed around the basin. Gradual replenishment by normal connate water has apparently started as the flanks of the structures have largely marine waters. Alternatively, the flush did not extend so deep as to displace the marine connate water. The ingress points are not known, but in well no. 1 on the far north-west flank of the basin, just north of the main basin-boundary fault, formation water salinity calculated from the SP log in pre-1At1 sandstones reaches ~2000 ppm, suggesting that the ingress point was close to the Arniston Fault (Fig. 2.05). It is likely that the flushing extended progressively further east from the incursion point. The absence of oil traces from the easternmost reservoirs (around wells 20 and 128) compared to the presence of oil traces in all the more westerly highs (e.g. wells 48, 59, 102, 41, 162) may suggest that they were flushed only after the phase of oil migration into the north flank.

In order to initiate the flushing, there must be a topographic high. There are three periods when basin margins were uplifted (or exposed by sea level fall) to allow meteoric water ingress. These are:
(i) Plio-Pleistocene glaciation lowstand
(ii) Mid-Oligocene global sea level lowstand
(iii) Late Maastrichtian-Early Palaeocene regional uplift and erosion.

Of these, it is probable that the last period allowed some ingress of water, but being a short-lived event, the amount of washing and/or bacterial degradation was minimal. The latter effect was also lessened by the high formation temperatures.

The earliest possible flushing episode broadly coincides with the rapid heating due to the mantle swell and hotspot (Eurotrack, 1996; Davies, 1997d; Figure 13.07). There would be minimal bacterial effects as temperatures are shown to exceed 100°C (Connan, 1984). This period may also coincide with the episode of extensive dissolution of calcite from reservoir sands. Volumes of calcite dissolved are unknown, but many sandstones have secondary porosity in excess of 20%, a volumetrically large

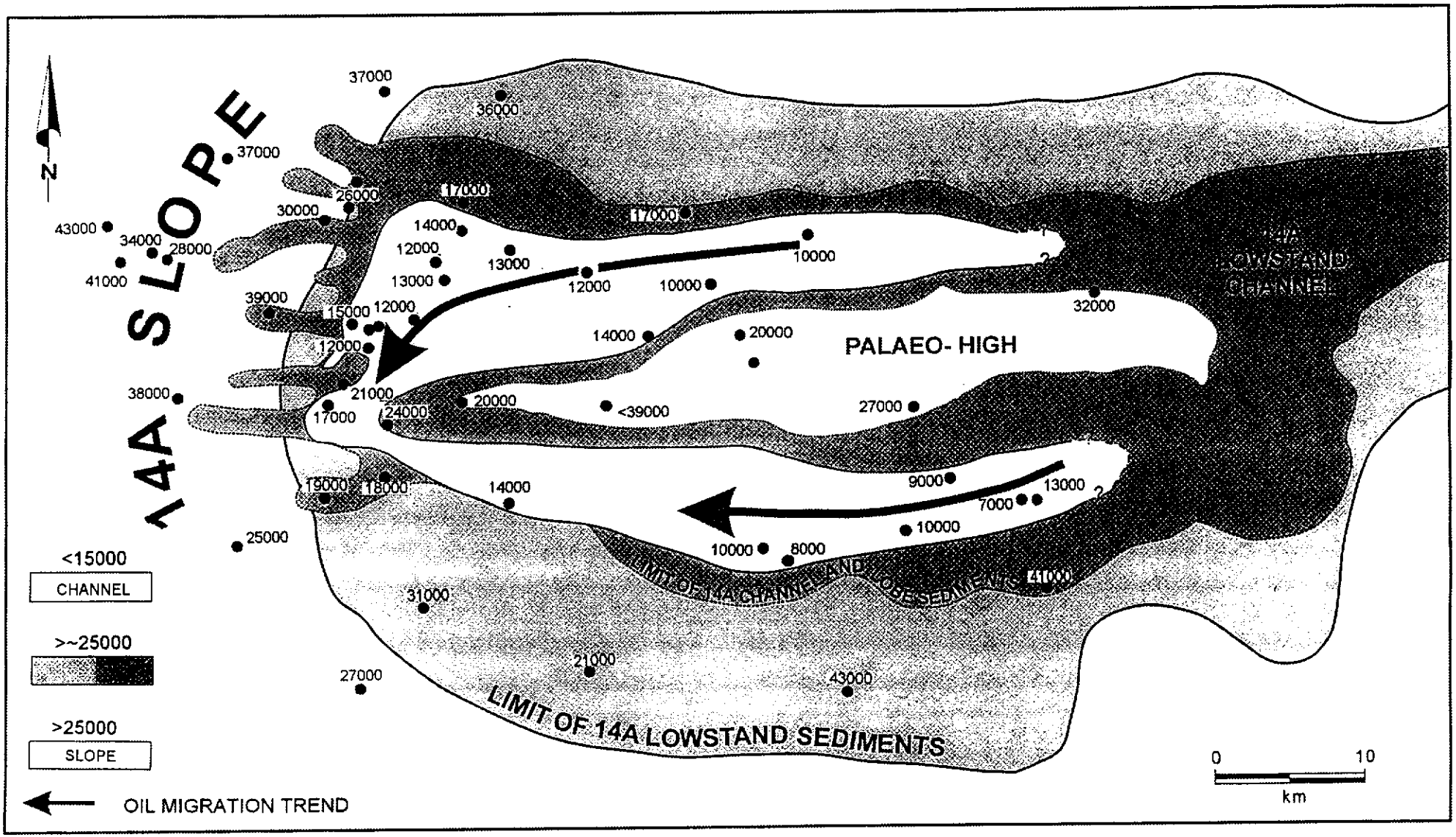

Figure 13.05: Schematic plan of the 14A lowstand channel complex showing salinity variations through the trend (after Davies 1995a; Burden and Davies, 1997a).

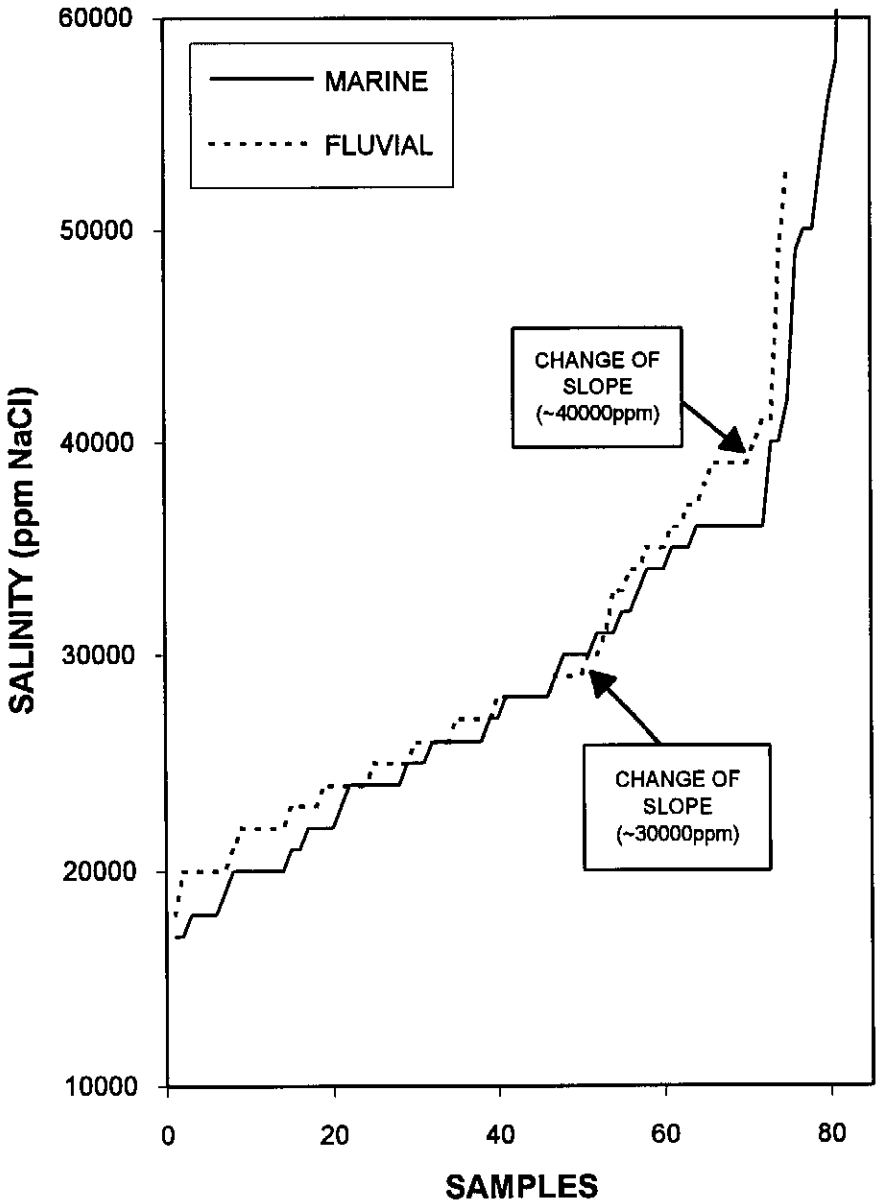

Figure 13.06a: Formation water salinities in the two main types of north flank reservoir sandstones.

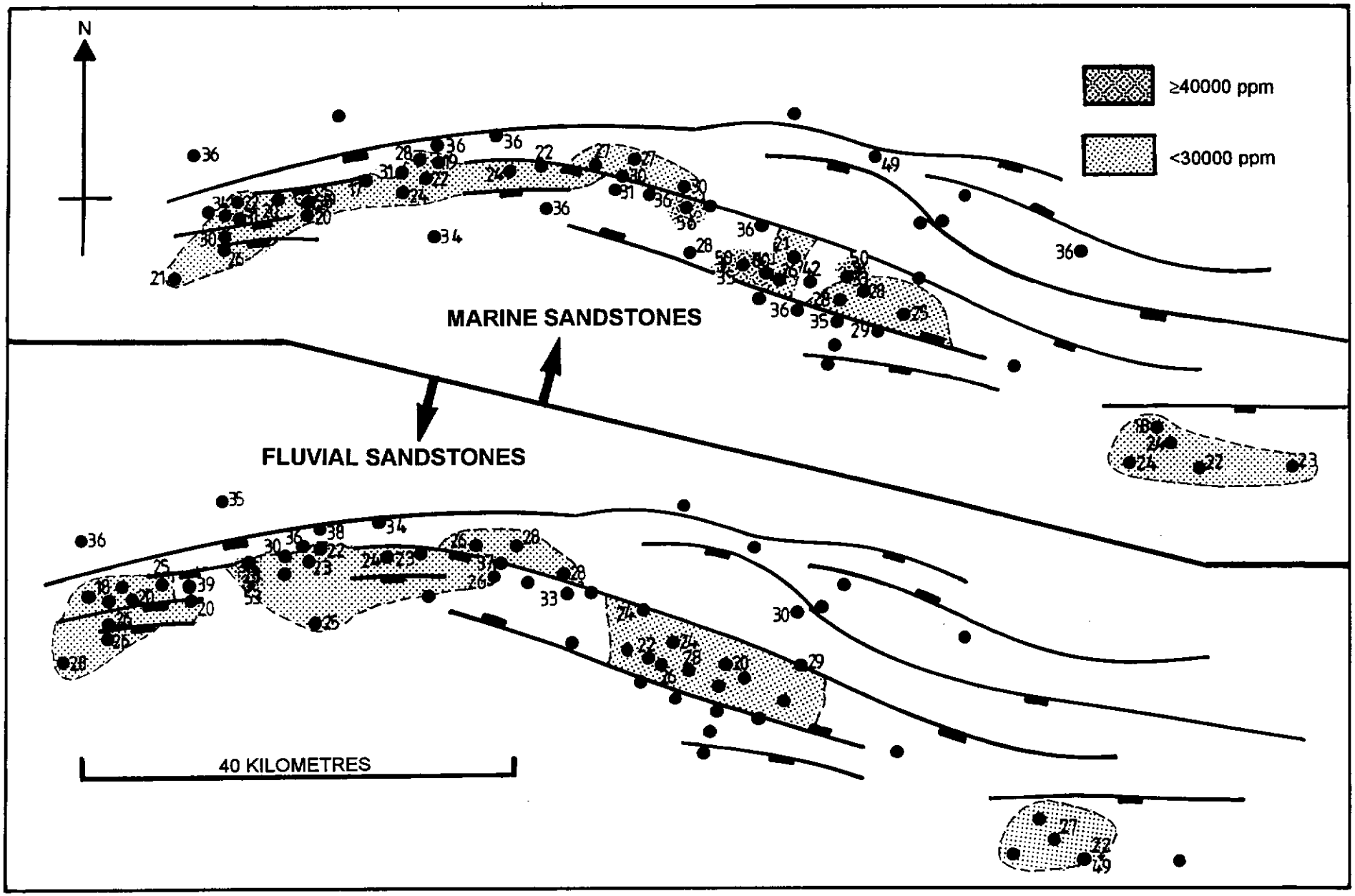

Figure 13.06b: Plans showing the various formation water salinity trends in the marine and fluvial sandstones intersected in north flank wells.

process. Removal of such large amounts of calcite by solution in ascending connate water streams is unlikely and either the constant throughput of calcite-undersaturated surface water or flushing by acidic waters could possibly remove so much calcite. Whilst there is ample opportunity for flushing in all three periods, there are only two possible sources for an acidic meteoric water influx.

Acid rainfall is now considered to have occurred widely at the Cretaceous/Tertiary boundary as a result of the solution of the large amounts of anhydrite ejected into the atmosphere by the bolide impact in the Yucatan peninsula (Retallack, 1996). The north, south and west margins of the Bredasdorp Basin were exposed at that time, probably with an elevation of some 100-200 metres as suggested by the extensive reworking of Latest Maastrichtian fauna into Early Palaeocene sediments (McMillan, 1986; McMillan, 1994, pers. comm.). Meteoric water flow could descend to depths of 10-20 times this distance i.e. to 2000-4000 metres below surface and being relatively acid, could remove significant amounts of calcite from the subsurface.

A second possibility is the input of CO_2-rich fluids accompanying the alkali intrusions in the western and eastern parts of the basin (Dingle and Gentle, 1972 and Rowsell et al., 1979). If there was any extrusive vulcanicity, for which there is minimal evidence although intrusions do reach close to the palaeo-surface in well 8, this would also have added volumes of CO_2-rich corrosive fluid into the subsurface and possibly even into the atmosphere. Certainly the juxtaposition of a Ca-rich lamprophyric intrusion and an unusually permeable sandstone, in which secondary porosity occurs to depths in excess of 3600 metres, seems to point to a direct association. In addition, it is possible that the common presence of sericite in hydrothermally altered argillaceous-rich sandstones in the nearby well 60 is evidence of this. Should this second possibility of late acidic water influx from the intrusions be correct, the area of greatest dissolution should be found surrounding the igneous centres and could constitute a new exploration target.

Surface water invasion during the global Mid-Oligocene lowstand may also have occurred. Dingle et al. (1983, p.304) show that the sea-level was lower by several hundred metres during the mid-Oligocene lowstand. This would result in exposure of the complete surface of the basin, and the margins would have been several hundred metres above sea level. However, based on the fluid flow history discussed here, few reservoirs are thought to have held much hydrocarbon at that time. Recent studies suggest that the Mid-Oligocene sea-level fall may have been far less than originally thought and that the period may have been characterised by minimal sediment transport and minimal accommodation space (I.K. McMillan, 1997, pers. comm.).

During the Late Tertiary, glacial lowstands reached as low as 150-200 metres below present sea level causing rapid but far-reaching regressions (Dingle et al., 1983, p. 304; De Decker and Woodborne, 1996). Meteoric flow through the basin probably occurred during this time, although mostly during the most extensive regressions. It is this influx which is believed to have resulted in the low salinities recorded today, because there have been essentially no bacterial effects recorded (Davies, 1995a).

As in the earlier influx, no bacterial action was likely because of high reservoir temperatures (presently all >80°C), except possibly close to the ingress point where formation temperatures could have been lowered significantly. Perhaps this is the reason why the only evidence for bacterial activity (low n-alkane proportions) in the basin is in some of the shallowest oil-bearing pre-1At1 sandstones (well 78) and in Late Cretaceous rocks in well 47. In addition, water-washing could also occur, which may explain the remarkably low aromatic contents of the condensate in well 69 just a few kilometres downdip of well 78 (Davies, 1997h). Fortunately the effects were not too pervasive as each episode was short-lived, probably lasting <0.1 Ma (De Decker and Woodborne, 1996).

13.1.5.3. Hydrocarbon migration

The total volume of hydrocarbons generated is relatively small, potentially only 1-2 pore volumes. Hydrocarbons are modelled to be generated largely in drift source rocks and expelled during essentially two periods, the Late Cretaceous-Early Tertiary and Late Tertiary (Fig. 13.07). Vitrinite reflectances are higher for oils expelled during the later period than for those expelled in the first period by R_o~0.2-0.3%. This reflects the maturation increase between the end of the first heating episode and the start of the second episode. Flow directions of hydrocarbons through the basin from each source rock during the second episode are constructed using the present day basin configuration (Figs. 13.08a and b). An equivalent figure for the Early Tertiary has not been constructed as the relevant horizon has not been mapped in the basin and back-stripping cannot be done.

Most reservoired hydrocarbons discovered to date are believed to result from the more recent fill episode, most of the earlier fill having been lost during tilting or displacement. It is unlikely that significant amounts of first fill hydrocarbons have been absorbed into the second fill because the first had far higher proportions of biomarkers and their chemical signatures would dominate. Yet a number of remnant oil shows from the first fill have been found.

Evidently this first fill was extensive as there are low maturity traces in 14A sandstones, in central 9A sandstones and in pre-1At1 sandstones (well 93, Davies 1997g; well 165,

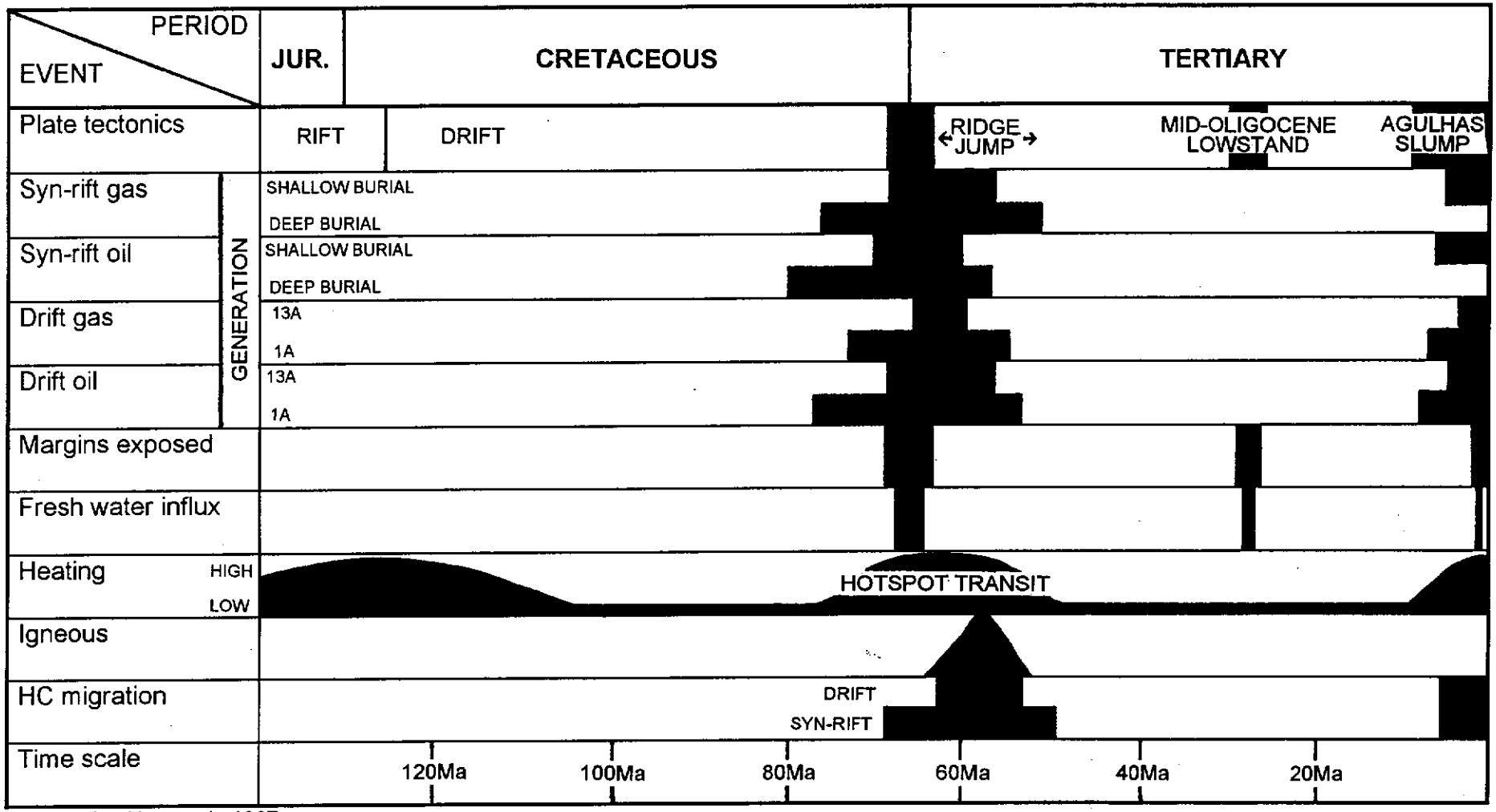

Dates after Haq et al., 1987.

Figure 13.07: Chronographic chart showing the chronology of fluid movements through the Bredasdorp Basin in relation to the heating events.

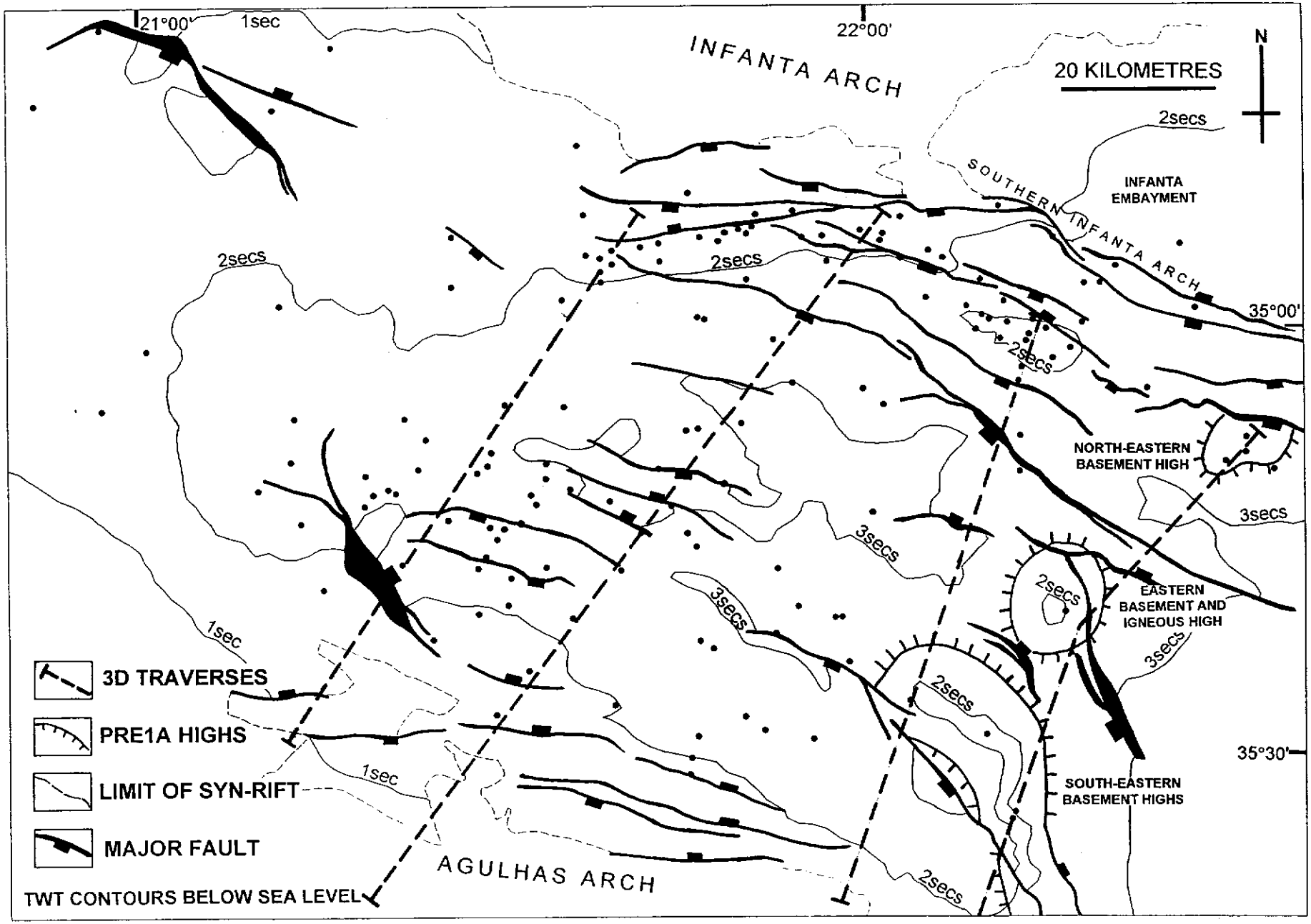

Figure 13.08a: Map showing traverses of the 3D schematic sections across the Bredasdorp Basin shown in Figure 13.08b.

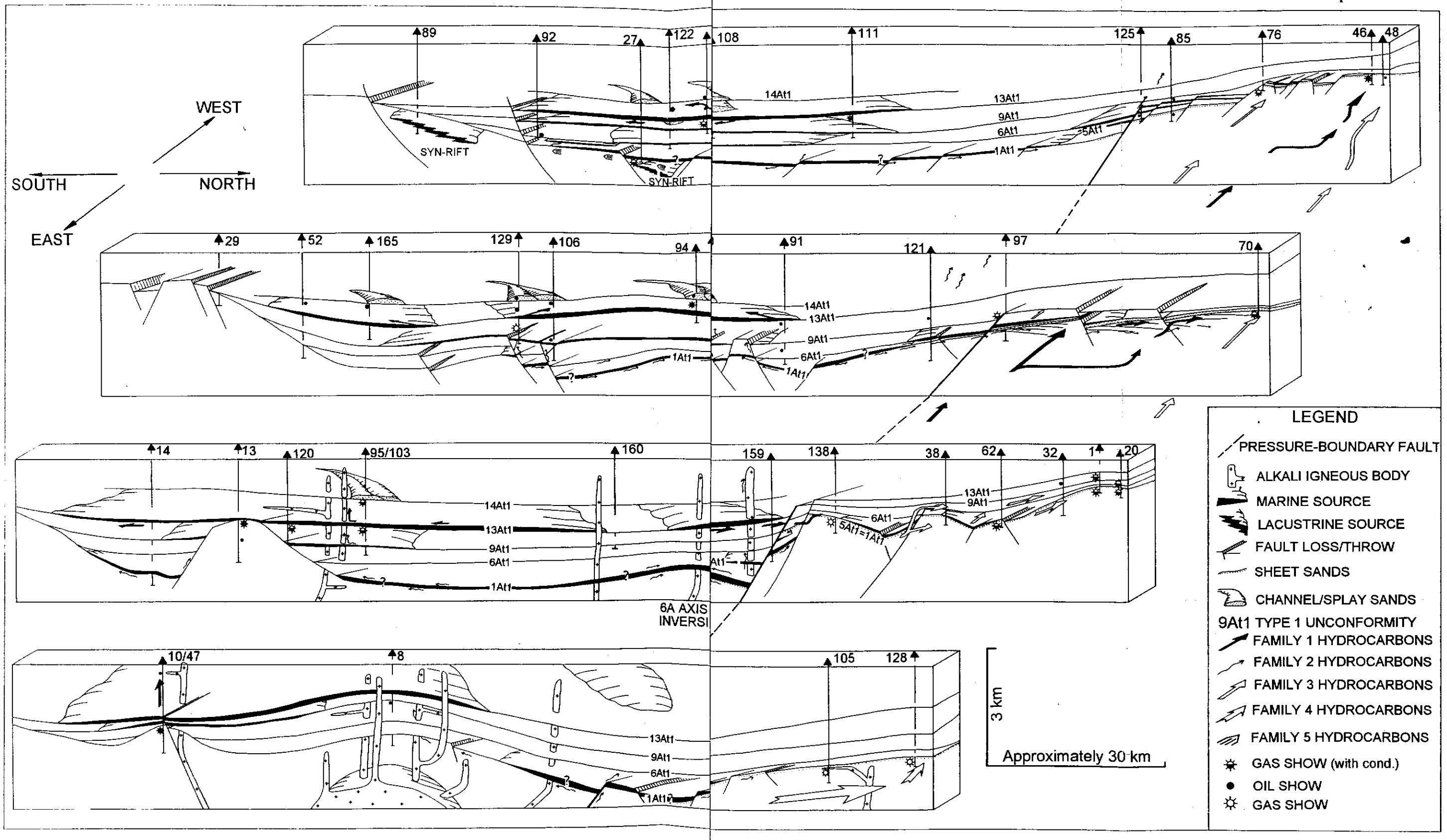

Figure 13.08b: Series of 3-D schematic cross-sections through the Bredasdorp Basin along seismic traverses summarising source rock and reservoir rock development, the igneous bodies and the movement of each hydrocarbon Family.

Davies, 1997a; Davies, 1995e; wells 48, 20, 162, 107). Most of these traces are found in lower permeability sandstones into which they are likely to have migrated if the more permeable sandstones were already oil-filled. This is because hydrocarbons flow by buoyancy and oil droplets and gas bubbles seek the upper surfaces of conduits where significant flow occurs (Thomas and Clouse, 1995). Therefore, flow often results in the establishment of just a few rivulets along the top surface, through which large volumes of oil can migrate essentially unimpeded (Thomas and Clouse, op cit.). Where sandstone is found with oil traces throughout, it is an indication that hydrocarbons originally filled the sandstone at least down to the level of the deepest trace. Hence many of the residual oil shows may well record the composition of previous reservoir fills. In addition, the reservoir volume, shallower than the deepest trace (calculated after back-stripping) may indicate the amount of hydrocarbons that escaped updip.

13.1.6. Reservoir history

It is shown above that two periods of hydrocarbon fill are considered to have prevailed in the basin. There is a possibility of an even earlier period, represented by the 'pyrobitumen' traces found in pre-1At1 sandstones in wells on some of the eastern highs (wells 10, 12-14; Rowsell et al., 1979). However, an alternative explanation for these traces is that the deepest-buried source rocks, which were largely matured during deep burial before the hotspot transit, completed their maturation during the early stages of the transit, whereupon large amounts of oil migrated into the eastern highs. These oils were subsequently coked during the increased heat associated with the nearby igneous intrusions. It is noteworthy that these coked bitumens are only found along the track of the hotspot. So far no biomarkers have been found in these 'pyrobitumens'.

Residual oil traces believed to represent the first demonstrable period of migration have been analysed in this biomarker set. These samples (no's. 31, 33, 35 and 36) are located in the southern 14A trend. Their biomarker ratios show distributions of unusually low (equivalent) maturity relative to the maturation calculated from the present reservoir fill (e.g. samples 30 and 34, section 12.2). The most reasonable explanation for these unusually low biomarker 'maturities' is sequential fill. One example of this is demonstrated from wells 156 and 166.

The 'mini-tarmat' sample (no. 33) has the lowest 'biomarker maturity' by far and is indicative of generation at close to R_o~0.7%, but the latest oil fill samples, no's. 30 and 34, have biomarker maturities $\equiv R_o$~0.9-1.0% indicating a difference of R_o~0.2-0.3% (Figs. 13.09-13.11). This difference matches quite well with the modelled reflectance increase in 13A source rocks at the basin centre during the past ~60 Ma (Fig. 13.12).

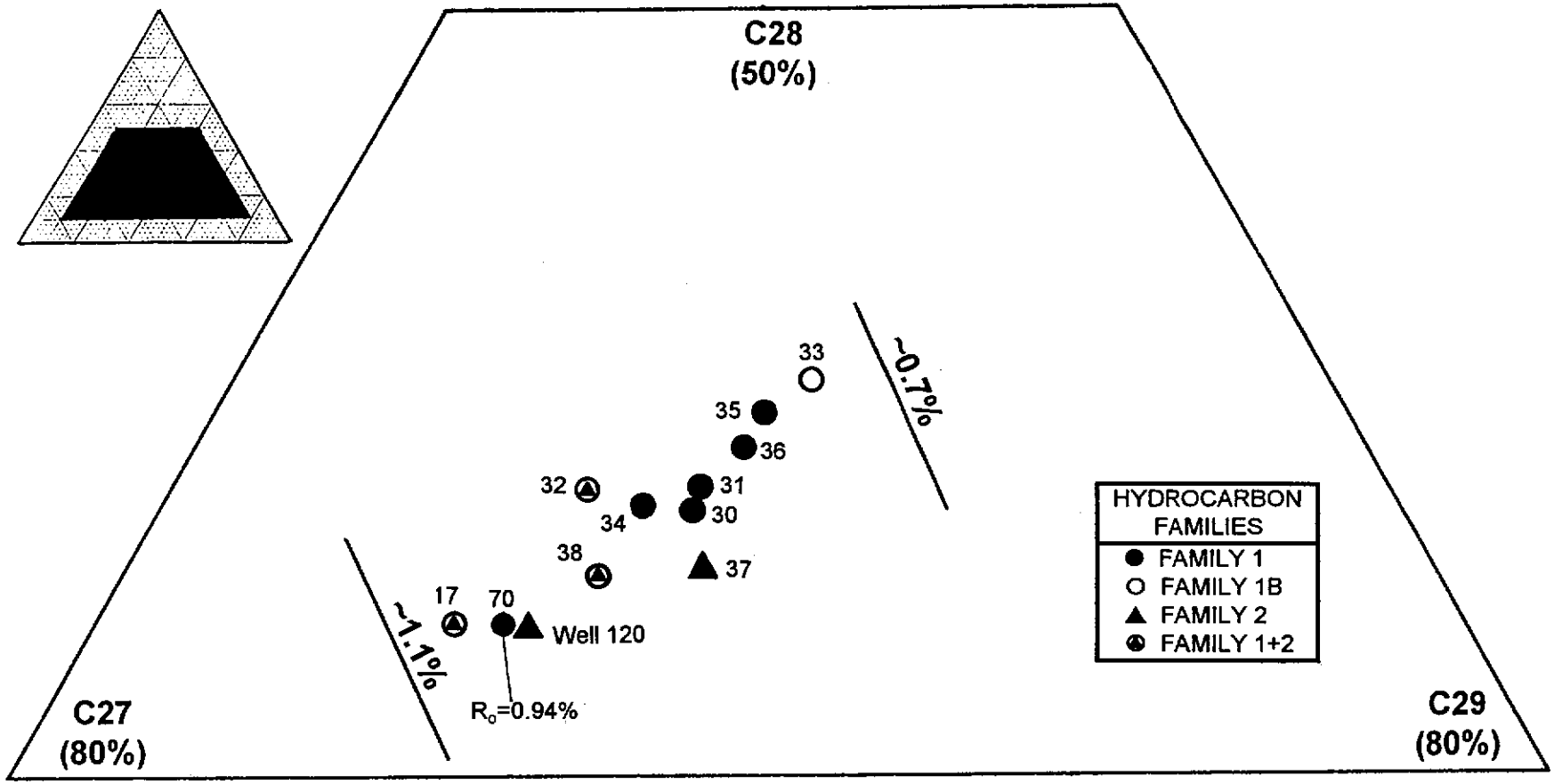

Figure 13.09: Detail of a ternary plot of the C27-29 αα sterane distribution in samples from the southern 14A trend and nearby wells showing the probable maturation spread of the data (after Figure 12.16 and Davies, 1997a).

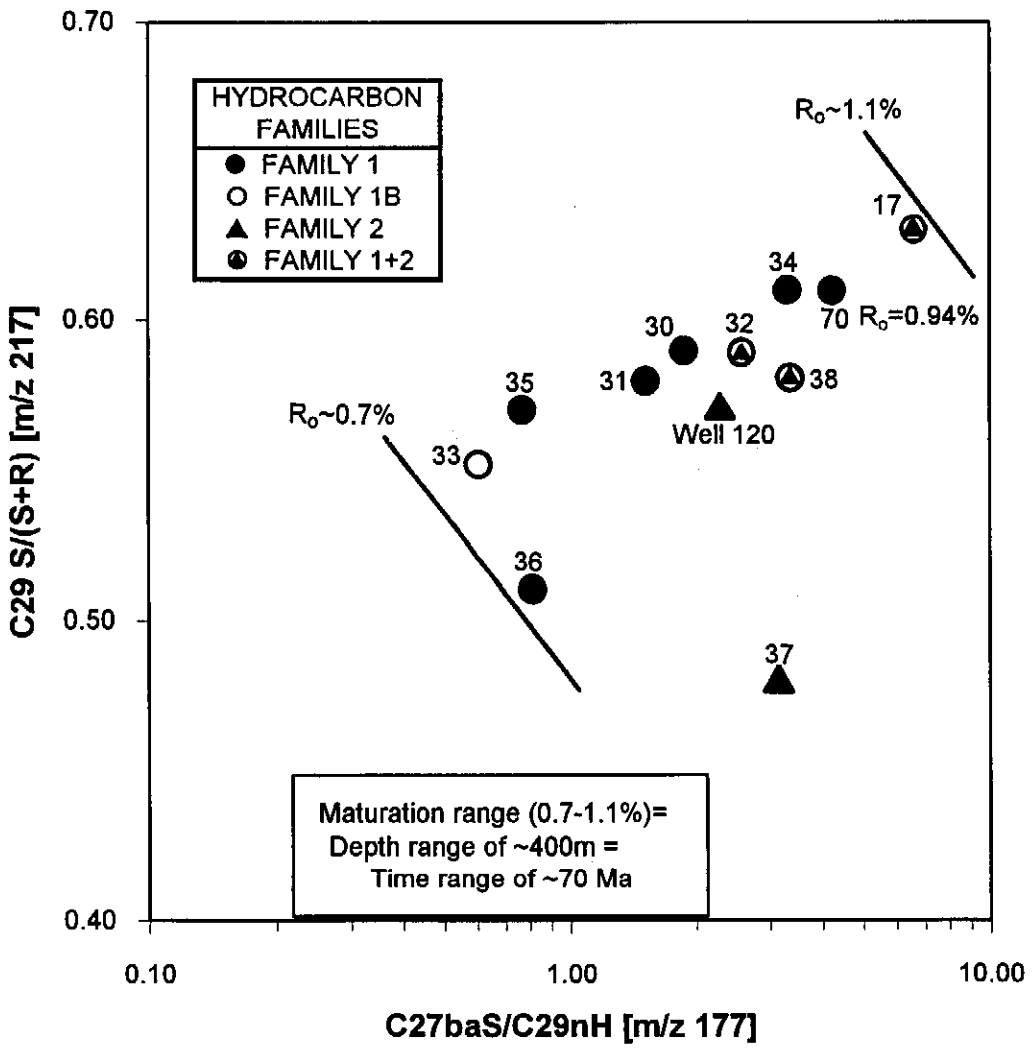

Figure 13.10: Cross-plot of the C29 αα 20S/(20S+20R) sterane ratio vs the ratio of C29 βα20S diasterane/C29 17α norhopane from m/z 177 fragmentogram (after Figure 12.09, section 12.1.2.1) showing the likely maturity-dependency of the ratios. Samples plotted are from the southern 14A trend and relevant adjacent wells (taken from Davies, 1997a)

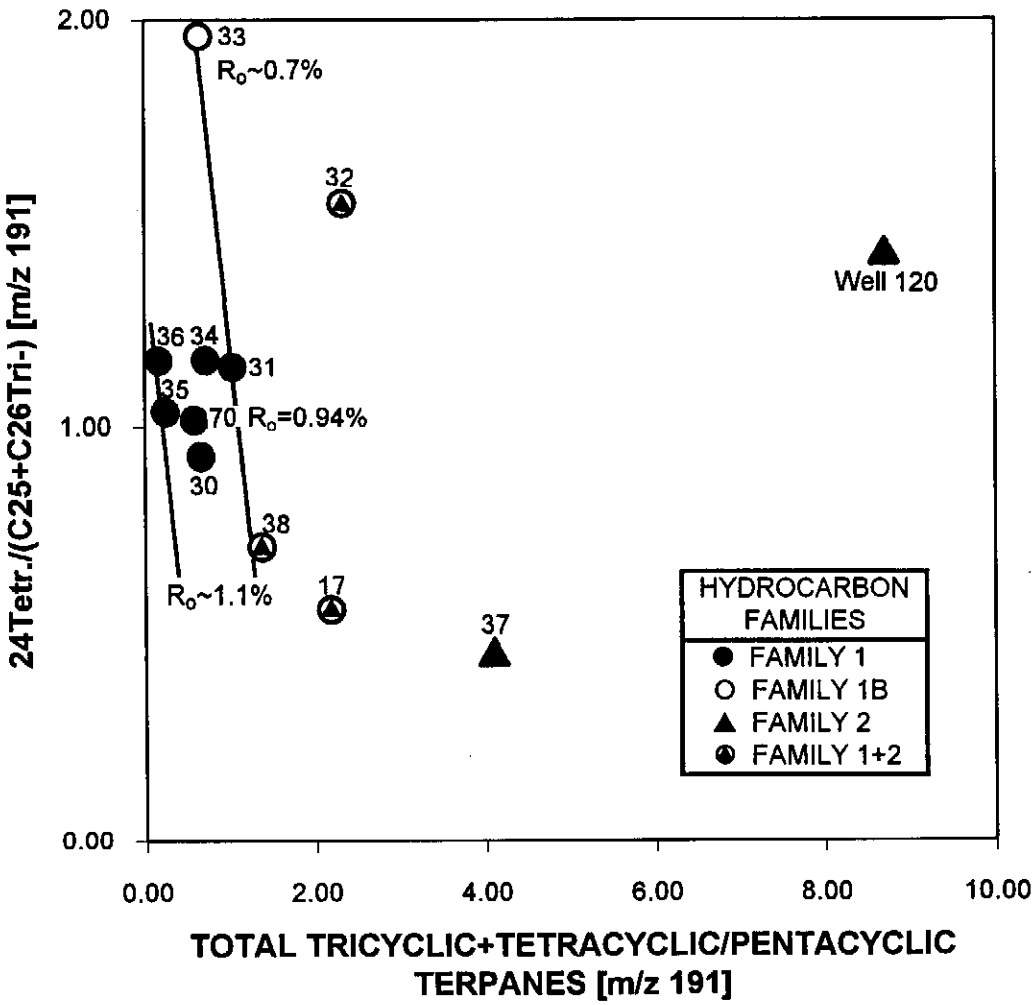

Figure 13.11: Cross-plot of tricyclic and pentacyclic terpane ratios used to characterise the source and maturity characteristics of samples from the southern 14A trend (after Davies, 1997a).

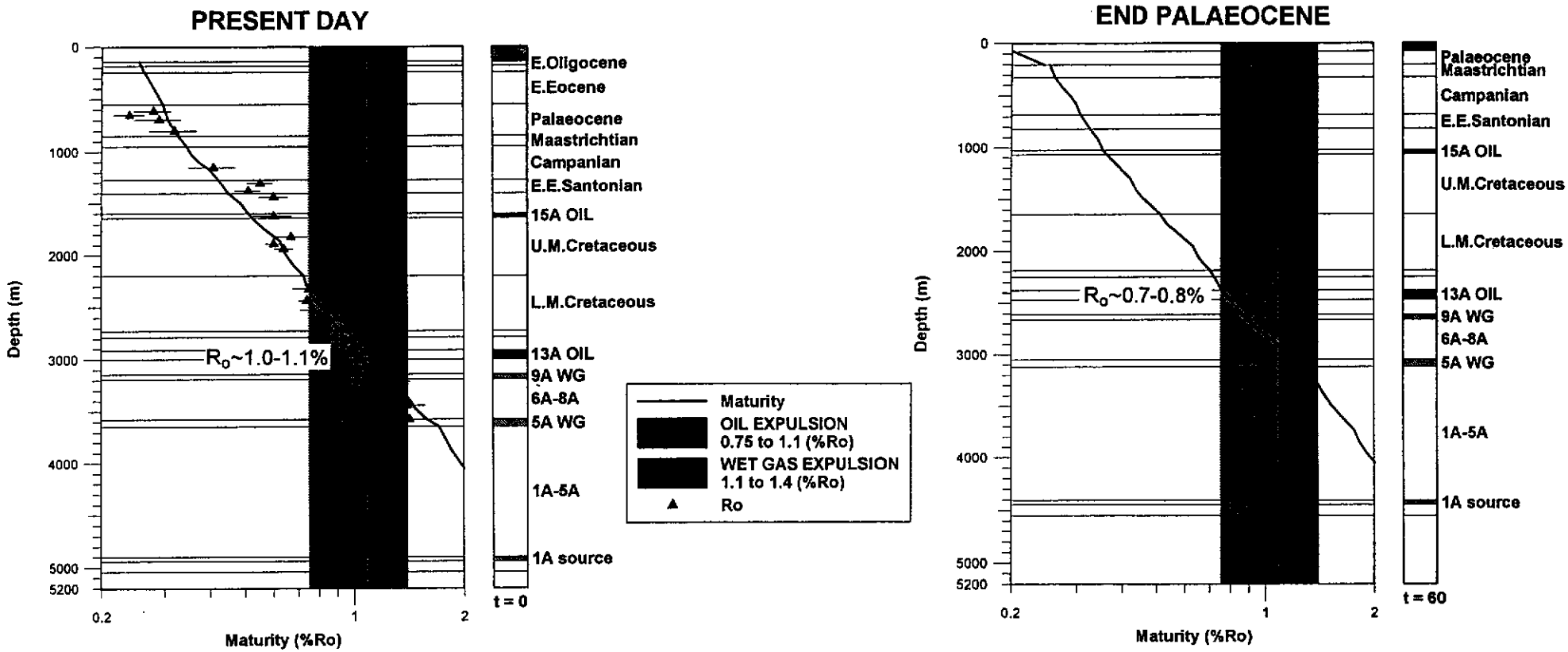

Figure 13.12: Plots of measured and calculated vitrinite reflectance data at the central basin location (see section 7.2.1) comparing the maturity level of the 13A source rock at present and at end of the hotspot transit.

This supports the backstripped estimate of the time of expulsion for the various samples in the southern 14A trend shown in Fig. 13.13.

A paragenesis model of the distinct hydrocarbon fills in this trend, derived essentially from an amalgam of data from wells 156 and 166, has been compiled (Fig. 13.14). These data include the following ratios (a) C27-29 αα steranes, (b) C27/29 βα sterane, (c) total steranes/terpanes, (d) Ts/Tm, (e) C20-21/C27 steranes, (f) C29nH/C30 diaHopane, (g) C23 tricyclic/C30 pentacyclic terpane, (h) tricyclic/pentacyclic terpanes, (i) C/E dimethyl dibenzothiophenes, (j) 125/136 trimethyl naphthalenes, (k) ^{13}C isotopes.

The paragenesis model suggests:
(i) a later gas charge to provide the gas cap at well 166
(ii) renewed oil migration during the Late Pliocene heating
(iii) subsequent loss of gas through diffusion during the intervening ~40 Ma
(iv) loss of most oil either during Palaeocene/Eocene tilting or by gas displacement
(v) an Early Tertiary oil fill from 2-3 expulsion pulses.

Similar sequences of events are likely to have prevailed elsewhere in the basin, such as in wells 109 and 132 where a 'mini-tarmat' was found in the gas zone (Davies, 1997e) and in pre-1At1 sandstones in wells 10 and 47 where low maturity hydrocarbons are found juxtaposed with high maturity oil traces (Davies, 1997b). In addition, there is evidence for possible 'mini-tarmat' formation in other wells in the basin, e.g. well 93 and possibly well 37 (Davies, 1997d).

13.2. SOURCE ROCK: RESERVOIR ASSOCIATIONS (PLAY'S)

Examples of each type of source rock: reservoir association ('play') highlight the variability and complexity of the hydrocarbon charging history and show that certain hydrocarbon types will preferentially be found in characteristic types of plays.

13.2.1. Short distance vertical migration

This is a commonly developed situation in which the reservoir is located only a short distance above the source rock (Fig. 13.15). The sandstone trend was formed along a valley caused by sag over previous lines of weakness, probably during the final separation at 5A-6A times. Reactivation of compression, probably as a result of the wrenching motion along the basin axis (indicated by the presence of flower structures to the south (P.J. Strauss, 1997, pers. comm.) at ~103 Ma, caused the upwarping of these old fault lines and consequent trap formation (Gilbert and Roux, 1992). Some of the faults extend up to, and locally through, the 13A source rocks, but they generally do not extend to the 14A reservoir interval (Van Wyk, 1997; Pferdekämper and Winters, 1997).

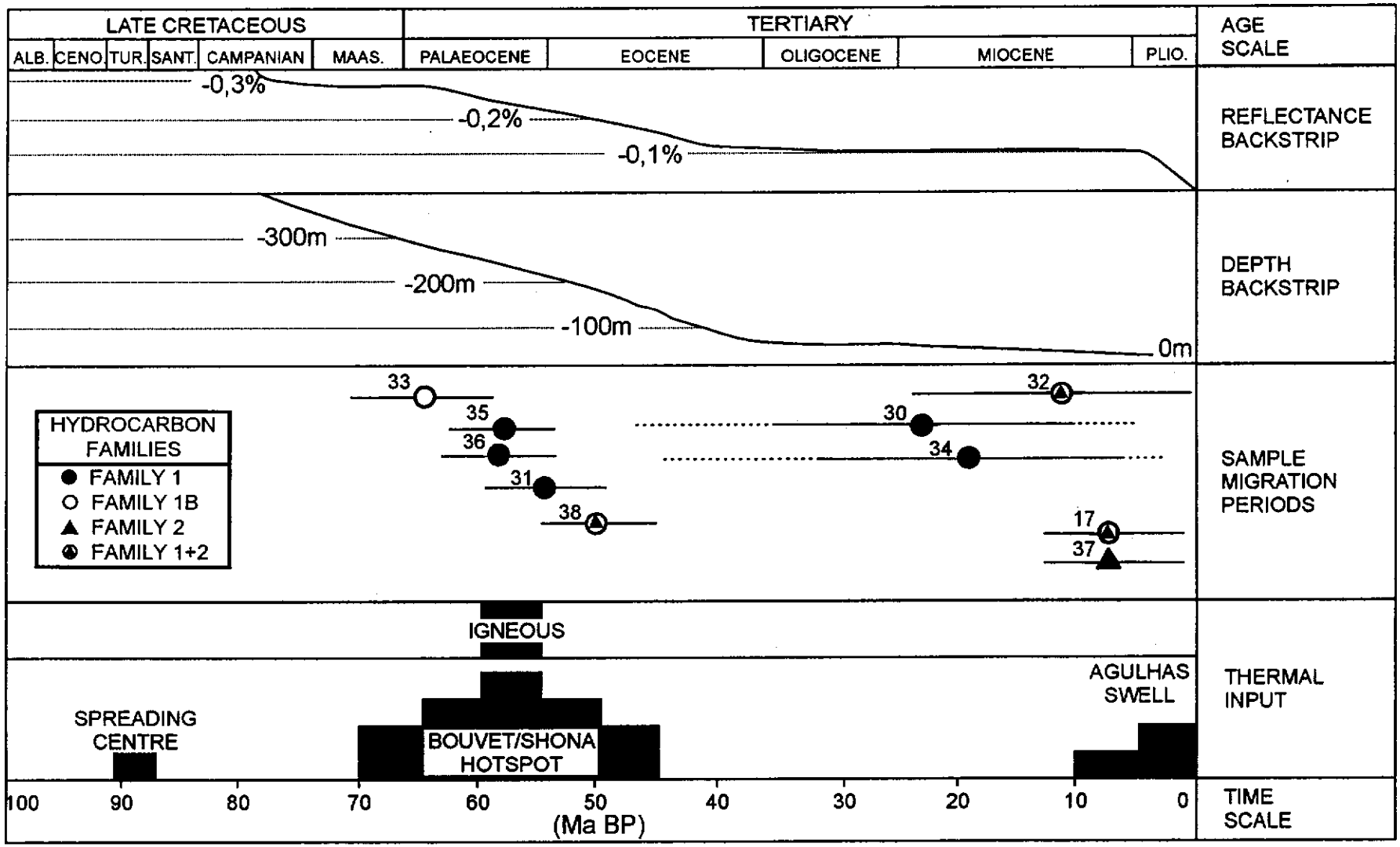

Figure 13.13: Chronographic chart showing the major heating events, the backstripped maturity levels and the biomarker-calculated maturities of oil samples in the southern 14A oil-rich trend (after Davies, 1997a).

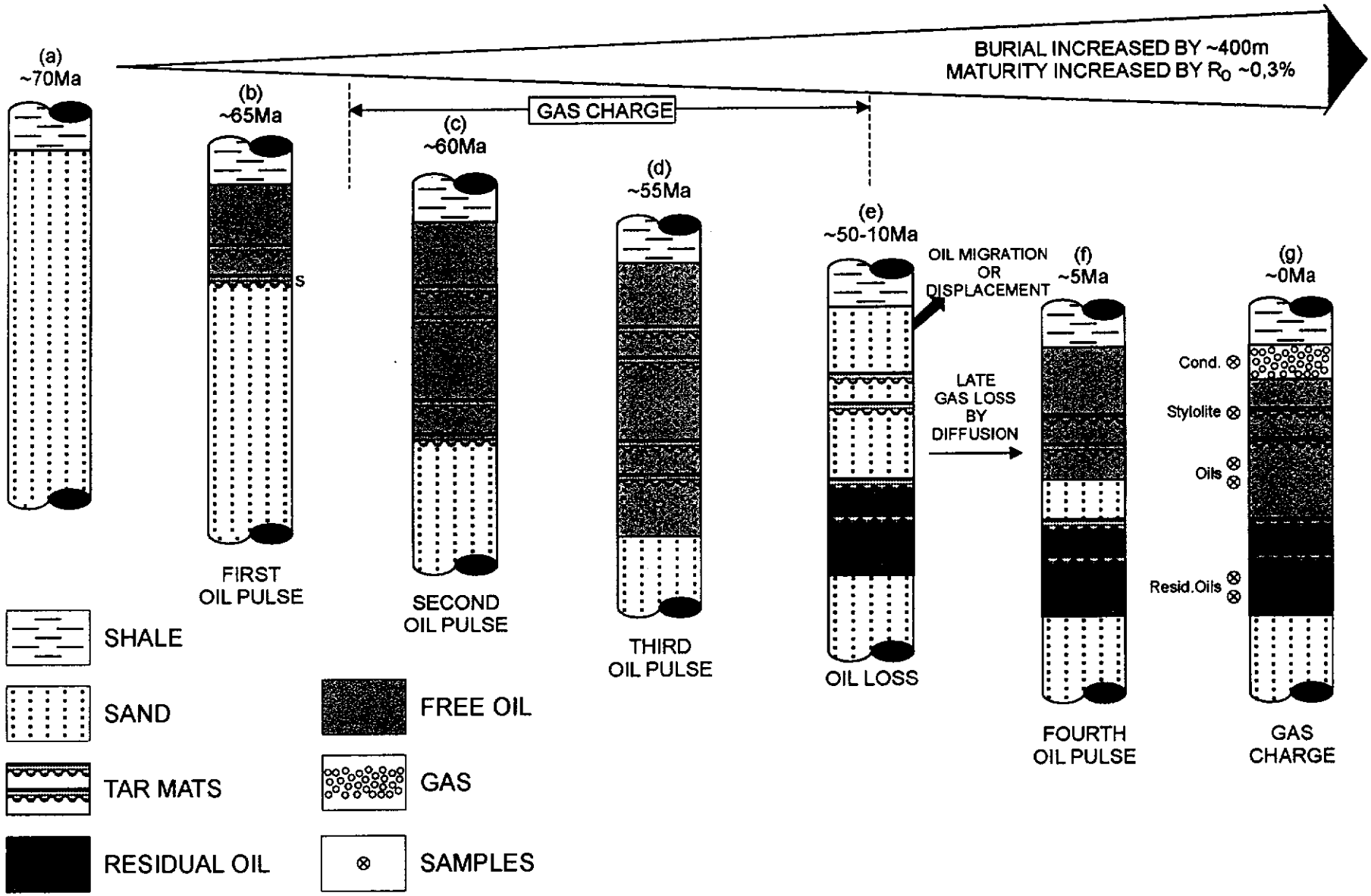

Figure 13.14: Schematic paragenesis of hydrocarbon fills and spills since the start of the hotspot transit to the present, explaining the possible reservoir fills and the biomarker maturity differences between the residual and flowed oils.

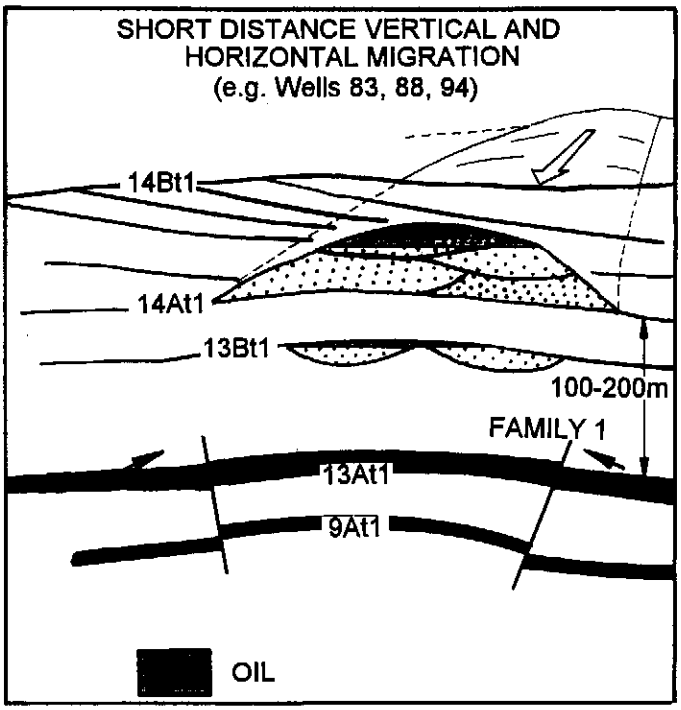

Figure 13.15: Schematic section across the 14A trend sandstones showing the faulting and the hydrocarbon migration routes.

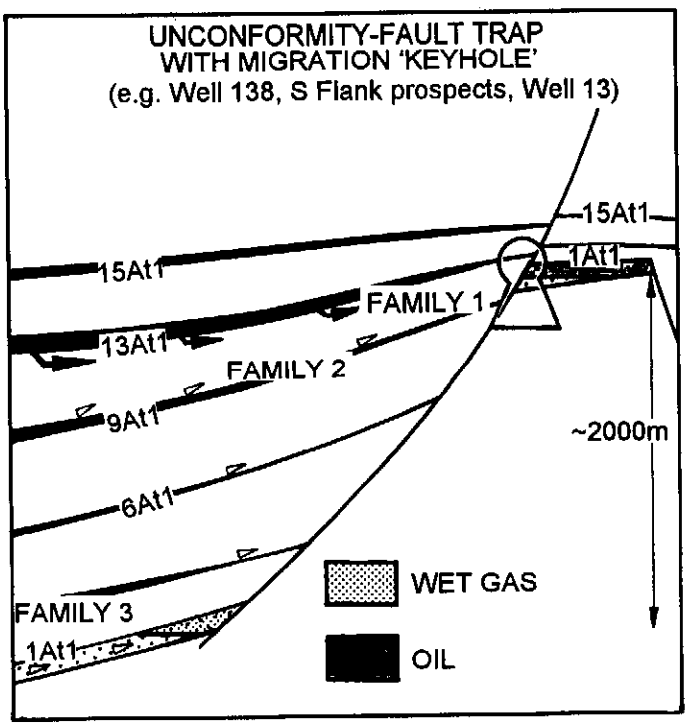

Figure 13.16: Schematic section through the basin margin showing the fault juxtaposition of younger source rock and older reservoir rock which allows stratigraphic down-stepping of migrating oil.

Most of the migration has been updip along the channel axis with only occasional vertical migration through crosscutting faults.

Family 1 oil-bearing sandstones in the 14A and 13B sequences in the central basin show characteristics of short distance migration. There is a misfit between the biomarker 'maturity' levels in reservoirs compared to those in the shales immediately beneath. Indeed the source rock samples from up to 10 km downdip match oils reservoired in wells 83 and 88. A further aspect is that several of these 14A-reservoired oils have matching biomarker maturities, (also well 117 DST1, although not included in this study) indicating they were all sourced from the same location. The main ingress point must have been close to well 110.

In addition, the 13A source rock also acts as a regional seal to hydrocarbons migrating from below so that no Family 2 gas has been detected in any 14A sandstone, although traces were found in 13B sandstones in sample 29 near the eastern end of the trend.
The channelised fill acts as a regional conduit for fill and spill so that the presence of only traces of oil in sandstones in the area does not indicate lack of fill further updip, but merely lack of local reservoiring. As an example, migration of oil along the crest of the trend in narrow rivulets results in only traces of oil in some areas (e.g. in 13B sandstones in wells 106 and 112). Further support for the possibility of 'fill-and-spill' migration having operated here is the presence of a 'mini-tarmat' in oil-bearing sandstones in well 93 (Davies, 1997g).

13.2.2. Fault juxtaposition of source rock and reservoir rock.
In this play, hydrocarbons are able to step stratigraphically downwards through faults, which bring source and reservoir in contact (Fig. 13.16). Here, the distance of migration is less important than the time of conduit opening. Migration through the fault can involve a high proportion of available hydrocarbons, but only where the timing is right. In this regard they are 'keyholes', restricted in both time and space. The area in which there is overlap of the two horizons provides a 2-dimensional view of the conduit. Detailed mapping of the conduit shows the third dimension and indicates a lateral extent of the source: reservoir juxtaposition of ~4 km. Only through back-stripping of decompacted sediments can the fourth dimension, time, be evaluated. In the case of the south flank example, this shows the juxtaposition to have lasted some 30 Ma.

Examples of this type of association are seen in two areas of the basin. In the eastern part of the north flank between wells 159 and 138, oil migration from 13A source rocks into pre-1At1 sandstones (and probably later dry gas migration at a lower level) has occurred (Figs. 9.20b and 13.17). The gas reservoired just above horizon 1At1 in well 138 was extremely dry, unlike either of Family 2 or 3 gases. Only a small amount of

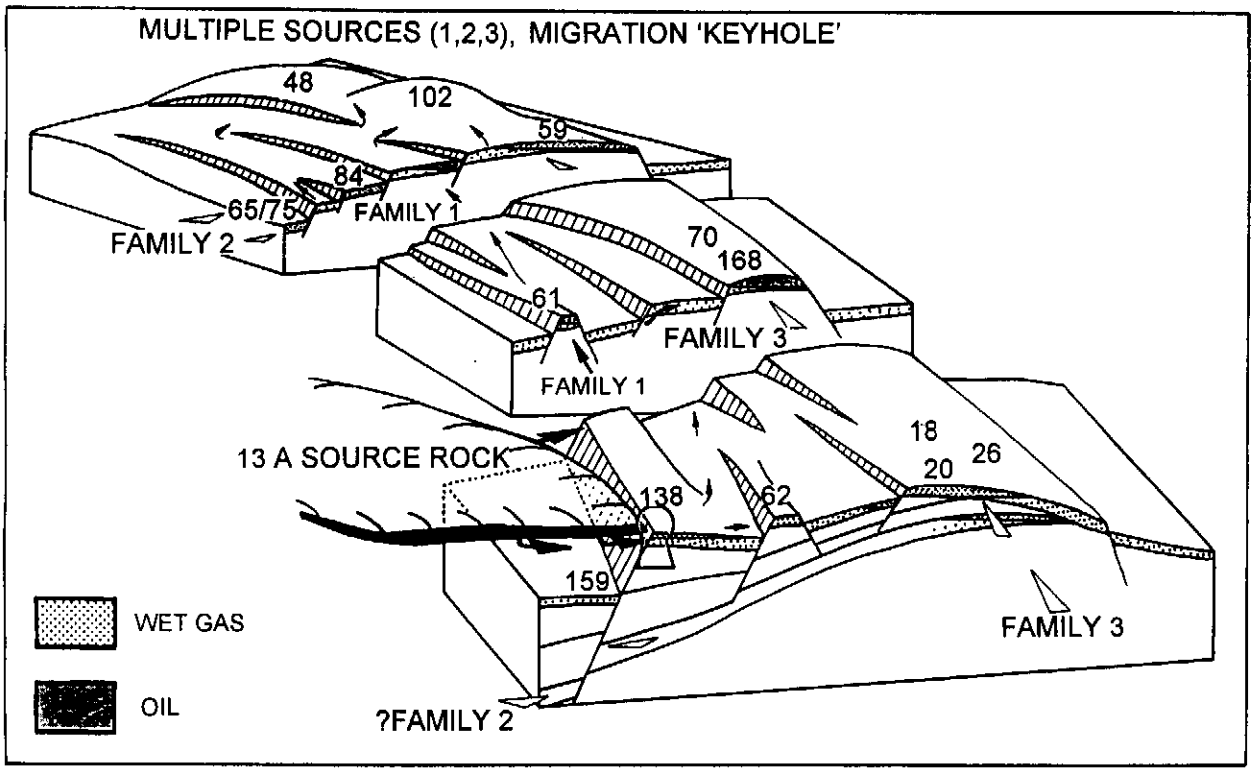

Figure 13.17: Schematic 3-D sections through the north flank of the basin showing the fault juxtaposition of source and reservoir, the migration trends of the different hydrocarbon Families and the probable generally updip migration route by which Family 1 oil reached the northern traps.

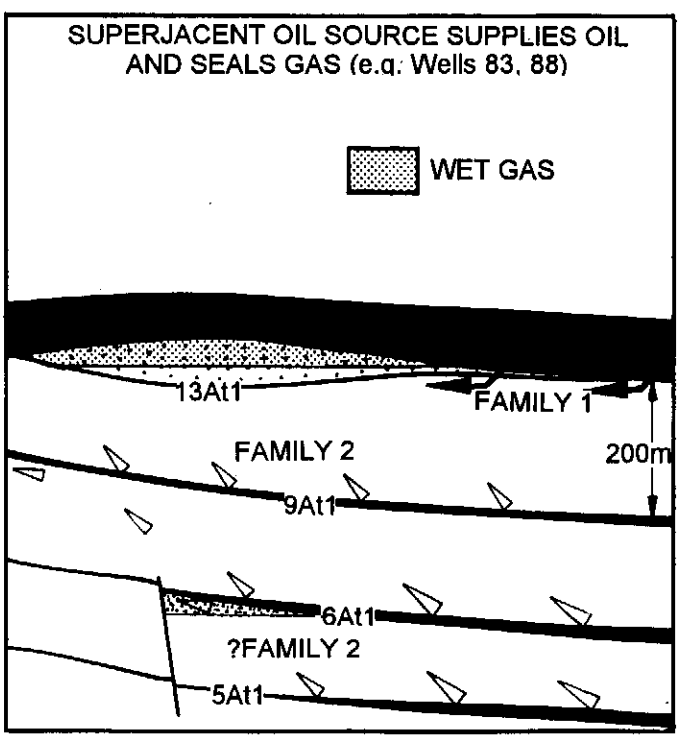

Figure 13.18: Schematic section through sandstone reservoir subjacent to the 13A source rock showing the likely oil and gas migration routes which created the hydrocarbon fills seen today.

condensate was associated with it and it may represent the same source as the gas in well 128, Family 4. Since no analyses have been carried out, and none of the liquid fraction was sampled, it is not possible to precisely characterise its source. Some of the sandstones in the north flank wells also contain hydrocarbons with partial affinities with Family 2 gas-condensates (e.g. wells 61, 63, 70 see section 9.3.6. and a possible Family 5 affinity in DST1 well 18). The 'keyhole' could also allow migration through deeper horizons and it is possible that the early input of Family 2 hydrocarbons to wells 61, 63 and 70 could have been by this route.

The second region is in the south flank of the basin. Two examples are available from the southwest region. Well 13 (sample 27) is located on an early high, which was only overlapped at 13A times. There oil shows have a biomarker maturity matching the superjacent source rock, hence it represents a relatively recent fill. In another example, southwest of well 25, a flat spot suggests the presence of a hydrocarbon column in pre-1At1 sandstones in an upthrown fault block (Strauss et al., 1996; Davies, 1996b). It is likely that several different hydrocarbon types migrated updip towards this fault, but they are unlikely to have crossed the fault where the hanging wall is basement. This could be a multi-level structural trap as well. In this area of the south flank, many of the faults extend into the Tertiary rocks and at seismic resolution appear to intersect basal Eocene rocks. The likelihood of ingress of fresh water and possible bacterial degradation forming a tar layer at the base of the oil column has been assessed as quite high, particularly where these rocks were exposed on palaeo-topographic highs. However, formation water salinities in wells downdip of these faulted regions do not appear unusually fresh so perhaps the faults are locally barriers to migration.

13.2.3. Multiple sources, fault conduits and reservoir levels

Migration through the faulted north flank of the basin has involved at least 3 families of hydrocarbons. The keyhole described in section 13.2.2 allows Family 1 oil, and possibly also deeper gas, to migrate into the 1At1 sandstones. Indeed, it may be that the Family 4 gas that seems to be present in well 18 DST1 as well as wells 27 and 35, has migrated from the nearby deep graben (Fig. 3.04). In addition, the fault allows Family 2 gas-condensate into the north flank through a conduit near well 65. The gas condensate in well 84 is a close match to that in well 65 and the formation pressures and formation water salinities provide a good match (Davies, 1995a). Indeed, this area near the termination of the fault is a likely place for intermixing of Family 1 oil with Family 2 wet gas-condensate and Family 3 wet gas. Hydrocarbons in many wells here do comprise mixtures of all three hydrocarbons (Chapter 9, section 9.3.6.). Input of Family 3 hydrocarbons could have occurred all along the high, although it is only shown from the eastern end, especially since the source sample with the best match for these hydrocarbons is sample 66 in well 65 (Fig. 13.17). However, too few samples have

been studied for their biomarker contents to consider this as the sole source area. It is likely that these hydrocarbons have migrated from other 5A fetch areas as the Family 3 hydrocarbons tend to cluster at the eastern end of the flank and are only rarely found further west.

Oil legs have been found in a number of the north flank sandstones (wells 48, 54, 59, 61, 70, 102, 107, 162). Biomarker analyses of three of these, (48, 59 and 102) show a close, but not perfect match with Family 1 oils. One explanation shows Family 1 oils to migrate into the north flank reservoirs, probably through the 'keyhole' and thence via tortuous routes to the highs. It may be that all north flank structures were originally oil-charged. If so, there should be a progression from east to west in the biomarker maturities of the oil traces. This scenario is planned to be tested later. An alternative explanation shows the oil to migrate from the extension of the 13A source into the western part of the Southern Outeniqua Basin. Later influx of Family 2 and 3 gases, possibly via occasional breaches of the over-pressure bounding fault, may have displaced oil from most reservoir sandstones except the lowest permeability ones. Other reservoir zones are also present above 1At1 in this area. Where the occasional fault extends above horizon 6At1, wetter gas shows are found in 10A sandstones.

13.2.4. Mixing of oil and gas from two sources.

In the 13A sequence in the central basin, lowstand channels and lobe sandstones are developed on the 13At1 surface and they are directly overlapped by the 13A oil-prone shale (Fig. 13.18). These sandstones commonly contain Family 1 oil which migrates down from the source rock, driven by the pressure gradient which developed as a result of undercompaction near the centre of the shale (Brink and Winters, 1989; McAloon et al., 1990). In addition they also contain large amounts of Family 2 wet gas-condensate, probably sourced in the 9A-12A sequences below through faults as shown in Winters and Kuhlmann (1994).

The two hydrocarbons mix and form the characteristic 'heavy condensate' of wells 83 DST2, 88 DST4 and 93 DST1. The hydrocarbons are all of similarly high maturity and their retention in these sands, in spite of their volatility, suggests relatively recent reservoiring with minimal gas loss by diffusion through the overlying 13A shales. Sniffer data do not record seepages above these reservoirs, but the presence of the thick top-seal mitigates against this. It is possible that the oils were also emplaced during the more recent episode of heating, but because the biomarker ratios record only the mixed ratios, they do not reveal different maturities. Since they are only found in the central basin, they do not include Family 1B oils, whose source is very localised in the western end of the region. There is no proof that the reservoirs were originally oil-filled and later suffered gas dilution as *inter alia* no 'mini-tarmats' have been found. Yet, it is possible

that the sandstones have been receiving wet gas charge since the time of the first oil charge, because of the favourable location for migration from the lower 9A-12A wet gas-prone source rocks

13.2.5. Upflank gas-driven oil fill-and-spill migration.

In this source rock-reservoir play, the source rock underlies the 14A reservoir channel trend (Fig. 13.19). However, the greater availability of data in the southern trend allows the recording of several episodes of migration. This extensive potential migration trend allows oil to migrate up the channel axis through fill-and-spill displacement largely as a response to influx of Family 2 wet gas-condensate. The latter hydrocarbons must have entered the trend downdip of the oil-bearing wells, as the 9A-12A source rocks in the vicinity do not have the potential or maturity to generate such large amounts of wet gas-condensate.

Even though the source rock is barely 200 metres below the reservoir trend, the oil is probably sourced much further downdip, some 5-10km away. This is likely because, as with the northern trend, the faults do not extend through the 13A shales into the 14A sandstones (Fig. 3.05, Strauss et al., 1996; Davies, 1996c). In all probability, the gas-condensate entered the system even further downdip near well 160 where the 13A source shales are not developed and hence did not act as a seal (Fig. 4.15). Evidence for fill-and-spill migration is found in the common occurrence of 'mini-tarmats' in gas and oil legs in several wells in this trend (Fig. 13.14). Indeed there are possibly similar 'mini-tarmats' in other wells in this trend (95, 103 and 126) where unexpectedly bright fluorescence was recorded in wet gas-condensate bearing sandstone cores.

Near the probable updip ends of the trend there are heavy tarry hydrocarbons. These may be the furthest migrated along the trend and may represent the earliest fill. In each case and in a similar case at well 123 on the southern part of the northern trend, these oils are associated with deposition of late calcite indicative of relatively late sealing (Brown, 1991; Davies, 1995b). This implies that they lie updip of an over-pressured charge, which is possibly a result of buoyancy effects.

13.2.6. Subjacent oil source, fault-controlled gas influx

A few sandstone reservoirs on the 13A surface tap oil from an interval of wet gas-to-oil prone source rock. This is similar to the Aptian source but located below 13At1 in some wells and only locally developed (Fig. 13.20). There is some uncertainty regarding the exact pick of horizon 13At1 in this area. In some wells this source lies above and in other wells below this horizon, which is why these unusual oils are characterised as a Family 1 variant, i.e. Family 1B rather than as a completely new family. This oil is believed to migrate directly into wells 109 and 132 from the source, but in the latter

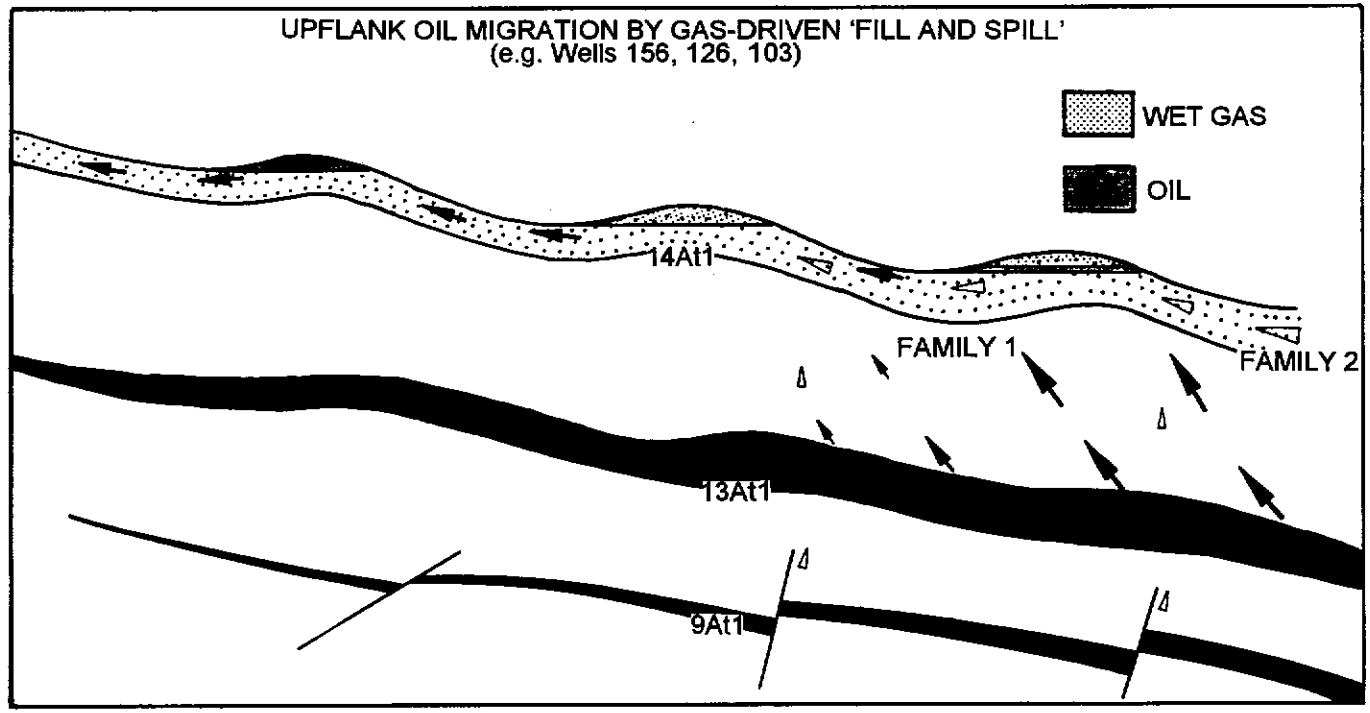

Figure 13.19: Schematic section through the southern 14A trend showing the probable migration routes for the gas and oil known to be in place and the emplaced hydrocarbon (after Davies, 1995c).

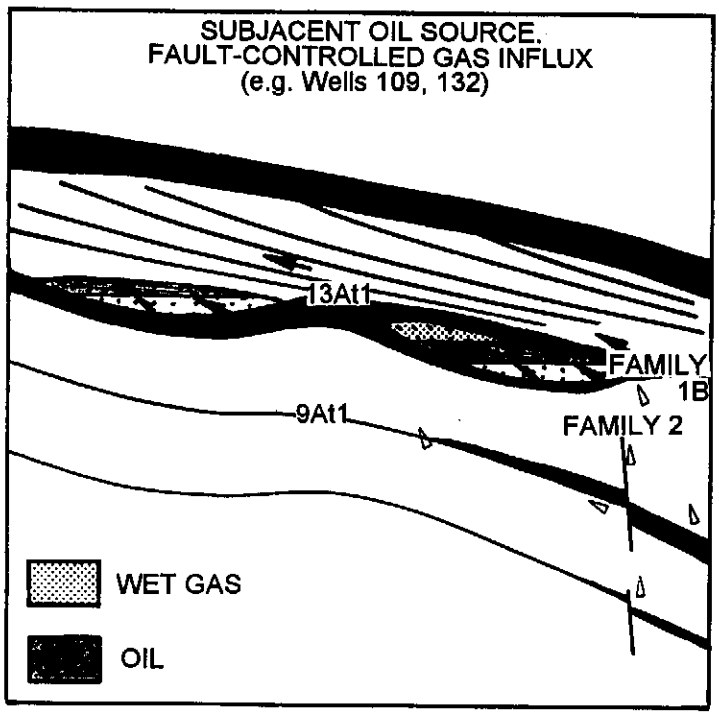

Figure 13.20: Schematic section through the Family 1B reservoirs and their probable source rocks showing the likely migration routes by which the gas and oil migrated into the present structures.

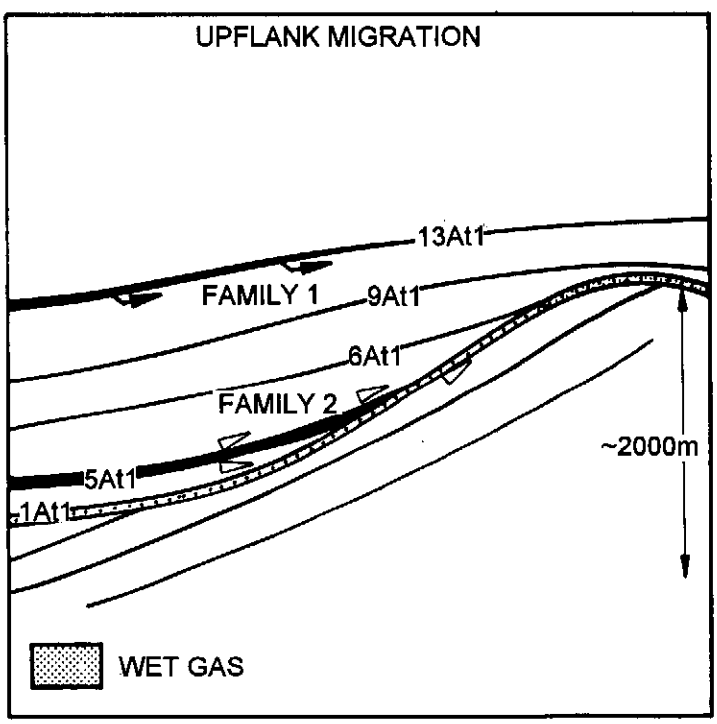

Figure 13.21: Schematic section through the north flank of the basin showing the juxtaposition of the 5A gas prone source rock and the regional pre1At1 regressive coastal sandstone complex through which Family 3 gas probably migrated to the north flank.

case, minor faults deeper down act as conduits allowing Family 2 gas to invade (Winters and Kuhlmann, 1994; Davies, 1997e; Van Wyk, 1997). In well 132, the influx has clearly displaced oil downwards as the asphaltene-rich 'mini-tarmat' in the gas zone is characteristic of gas-deasphalting.

Although no biomarker data are available for this 'mini-tarmat', GC data record unusually low phenanthrene ratios indicative of expulsion from a source at a maturity level some 0.2% lower than the present formation maturity. The cored source rock sample from some 15-20 metres below the oil reservoir matches Family 1B oil quite closely and has reduced proportions of C15-20 saturates, suggestive of at least one episode of expulsion. It appears that oil may have been expelled from this source into the overlying sandstone during the previous heating phase to account for the low maturity. However, gas expulsion is interpreted to be recent as nearby surface gas seeps and gas diffusing through the overlying shales indicate active migration (Davies, 1988a; Brown and Ranoszek, 1990).

It is possible that oil was expelled from the lower sandstone trend in well 132 when gas displacement started, migrating directly into the upper sandstone at well 109. This is an unlikely scenario because the lighter fractions do not match. Perhaps there was some replenishment from the source because the heavier fractions do largely match. Nevertheless there are a few biomarker ratios which do not match between wells 109 and 132. Either the source rock is locally quite variable and the reservoirs were locally filled or one of the three available samples of this source is unrepresentative of the expelled oil because of its lower maturity.

The oil is known to have been generated locally because of several highly characteristic biomarker ratios, *inter alia*, dominance of C24 tetracyclic terpane over the adjacent tricyclic terpanes (Figs. 12.21; 12.22). A sandstone in the 13B sequence above the regional 13A source shale in well 122, contains another example of the same oil. Since this is located some distance above the likely location of this oil family, there may be a conduit from below 13At1. A number of minor faults which could be conduits do cut the 13Bt1 surface and may extend as deep as pre-13At1 (Winters and Kuhlmann, 1994).

Gas migration into the deeper reservoir at well 132 seems to rely on faults that cut the 9A-12A sequences as indicated on Fig. 13.20. These faults do not appear to intersect the reservoir on seismic data. However, seismic detection at this depth is no better than ~10-15 metres and the faulting may be more pervasive than these data show. However, there has been minimal migration of this gas into the shallower sandstone as shown by the presence of some Family 2 characteristics in the oil from well 109 DST (Chapter 9).

13.2.7. Long distance upflank migration

Pre-1At1 sandstones are regionally developed and likely to be present throughout most of the basin (Valicenti, 1995). They can comprise a regional migration conduit which extends to great depth, except where locally eroded. Long distance migration along this conduit is considered to bring Family 3 and 4 hydrocarbons up basin flanks (Fig. 13.21). In this situation, the biomarker maturity of the condensate fraction is likely to be high. Being a relatively light, aromatic-rich fluid, however, it could be easily influenced by the dissolution of residual hydrocarbons in transit.

Family 3 samples match the 5A source in well 65 (sample 66), but these shales cannot be shown to have a widespread distribution because of the limited well cover. In Fig. 13.17, Family 3 gas condensate is shown migrating along the crest because of its buoyancy, but charging may have been through several updip migration conduits from the 5A source in each block. In the vicinity of most crestal wellsites, the 5A-6A shales are not mature enough to expel such large volumes of gas. Further downdip, where buried to higher maturities than even at well 65, and where they may possess a richer potential, they can expel large amounts of gas.

The Family 4 gas reservoir in well 128 is very highly over-pressured (~0.73 psi/ft) and is probably very close to the fracture pressure, indicating that it is well sealed. Yet the seal is only ~28 metres thick and gas is apparently diffusing through in large quantities to an overlying, water-wet sandstone. In addition the formation water salinity is low (~18000 ppm, Davies, 1995a) indicating a recent period of flushing. The probability is that the structure fills only when the rate of gas influx exceeds the rate of leakage. Family 4 gas is suggested to have been expelled from source rocks in the western part of the Southern Outeniqua Basin for a number of reasons. An alternative interpretation of the gas data suggests that Family 4 gas is a high maturity equivalent of Family 3 gas, because they both lie on a trend which parallels that of other trends (Fig. 8.02a). However, the significantly different ^{13}carbon isotope signature (Chapter 12) confirms a different source from the Family 3 gases. Furthermore, Family 4 gas is evidently much more mature than Family 3 gas as biomarkers are almost completely absent (IGI, 1994). This may be partly related to the extremely dry nature of the gas and the fact that heavy fraction concentration was not attempted during the analysis (methane proportion = ~89%, Table 8.02).

13.2.8. Pressurised gas charge from deeper sources

In this play type, central basin 9A sandstones are locally charged by Family 2 wet gas-condensate, migrating from the lower 9A-12A source rocks and probably also from breached deep reservoirs. These were originally charged from similar dominantly

terrigenous source rocks (Fig. 13.22). Two reservoir conditions are encountered (Verfaille, 1993; Hodges; 1996; Davies, 1995a), (i) over-pressured, high salinity, gas-filled and (ii) normally pressured, normal salinity, partly gas-charged.

Pressure gradients in some 9A sandstones, recorded from equivalent mud weights or DST/RFT measurements, reach ~0.5 psi/ft and they have formation water salinities of nearly 50000m ppm (e.g. wells 91, 94, 96, and 163). In deeper sandstones, the over-pressure is greater (up to 0.62 psi/ft) and the salinity is higher (locally up to ~80000 ppm). These sandstones seem to form the top of a regionally large over-pressure cell which extends below horizon 5At1 (Mid-Hauterivian) and possibly even deeper (Verfaille, 1993; Hodges, 1996; Winters, 1996).

Sandstones in 5A and deeper intervals in the west of the basin, the north flank and the south flank are gas-charged. These have locally high formation pressures (up to ~0.7 psi/ft) and very high formation water salinities. Yet other 9A-12A sandstones in the area are normally pressured and have formation water salinities <20000 ppm. Only one well in the area (no. 163) has penetrated far into the over-pressured zone and intersected sandstones below horizon 1At1 that were water-wet. For mechanical reasons few logs were taken across this interval, but it is evident that these sandstones conform to neither group as they are water-wet and appear to have lower formation pressures than the overlying sandstones and have formation water salinities ranging from 38000-49000 ppm (A.V.C. Steyn, 1996, pers. comm.).

In most cases, there are deep-seated faults reaching from near, or even below 1At1, to 9At1 or locally higher. Where these faults die out vertically, the pressures and salinities drop. Where formation pressure gradients and salinities are lower, the reservoirs tend to contain admixtures of hydrocarbons from different families such as sample 29, which is a mixture of mostly Family 1 oil with some Family 2 gas. Traces of brown oil are also associated with some of these central basin pre-13A sandstones, suggestive of an earlier oil fill.

None of the hydrocarbons from the high salinity, high pressure reservoirs have yet been subjected to biomarker analysis. Only whole oil analyses were used in their characterisation. However, fingerprint GC data (Chapter 9) do show distinct similarities with Family 2 hydrocarbons from both lower- and higher-pressured sandstones in wells 110. Biomarker analyses of this sample, one other from the same region (well 104) and one from a sandstone in well 75, match very closely with the lower 9A-12A source rock samples. However, it is also possible that some of the gas and much of the high pressure and highly saline water, could have come from recently breached reservoirs in pre-1At1 sandstones. It is not impossible that these oil traces represent remnants of oil

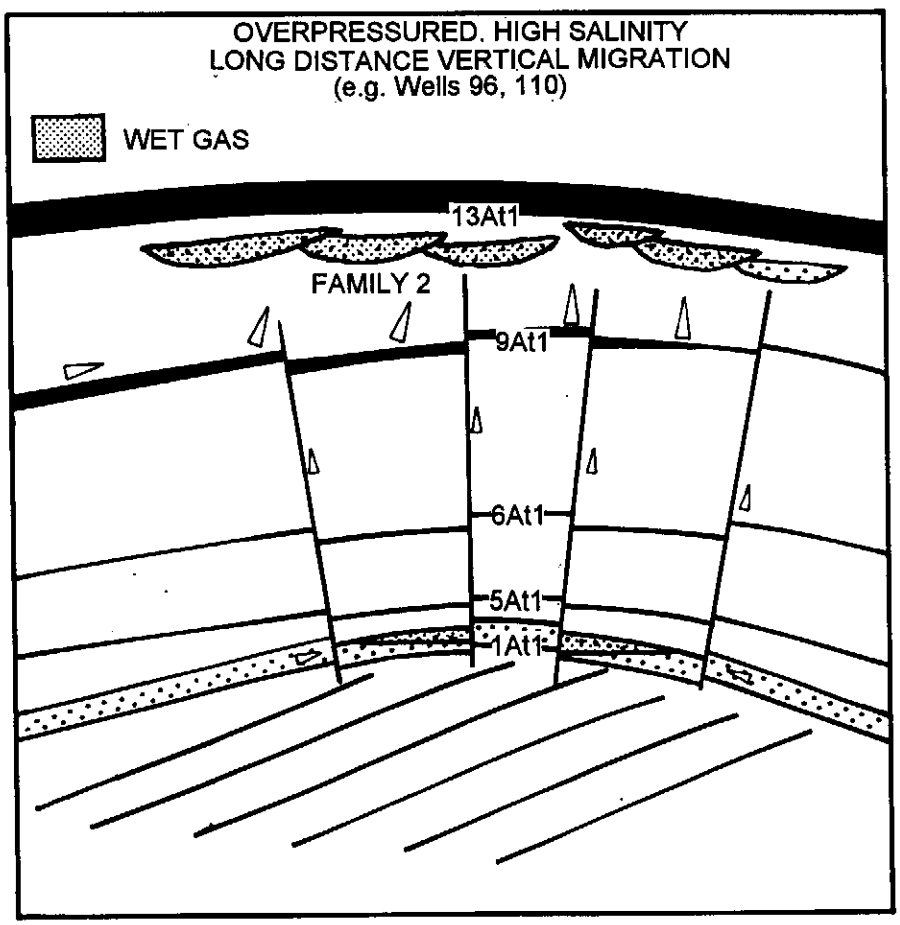

Figure 13.22: Schematic section through the pre13A central basin area where the 13A source acts as a seal as it is mostly gas prone and immature. Sandstones beneath this barrier are gas charged from below, from the lower 9A-12A gas prone source rocks developed immediately below and possibly also from remigrated gas from breached pre1At1 reservoirs up to 2 km below. Graben-bounding tensional faults, rejuvenated during compressional events exist in the area and may be gas conduits.

migrated upwards from these pre-1A sandstones. Perhaps such oil traces were present in all the fully gas-charged sandstones but they have since been dissolved into the present reservoir fill. It is equally possible that the gas associated with deep horizons is largely devoid of biomarkers and comprises mainly C1-6 hydrocarbons. In this case, it would be largely invisible to fingerprint and biomarker correlation, and may even match the Family 4 gases. Hence the assumption that all Family 2 gas is deep-seated may be wrong and further study is required for clarification.

The formation water salinities are unusual as they differ from the more usual case where over-pressured sandstones commonly contain low salinity water (Magara, 1978, p. 228). Perhaps they were originally flushed by low salinity water, which might explain the unexpected lack of apatite in samples throughout well 96 (Eurotrack 1996; Morton, 1986). If this effect is facilitated by faulting, then unfaulted areas may yet retain their gas charge. Alternatively, areas where formation water is heavily charged with dissolved ions, which would otherwise precipitate to occlude pores, may leak from specific points. Near those locations, there would be less effect of destruction of secondary porosity (Wilkinson et al., 1997). Such an area at the edge of the pressure cell, where gas charged, could be a new gas trend.

Miles (1990) shows examples where the fracture leak-off pressure gradient is closer to 0.73 psi/ft than the expected 1.0 psi/ft. If a similar regime operates here, then extrapolating the increasing gradient through the 9A, 6A, 5A and 4A sandstones would reach pre-1At1 sandstones at gradients close to 0.7 psi/ft suggesting imminent leak-off. If the over-pressure were due to hydrocarbon buoyancy effects, the pressure gradient would decrease downhole instead of increasing. It is therefore believed that this reflects intermittent bleed-off, perhaps through microfractured seals, of accumulated pressure from depth. High salinity formation waters do generate higher pressure gradients because of their greater density. In this area, even the highest salinity water (69000 ppm in well 96) has a temperature-corrected density not exceeding ~0.46 psi/ft.

13.2.9. Syn-rift source, syn- and post-rift reservoirs

To date only one well in the Bredasdorp Basin has intersected rocks with source potential in syn-rift sediments (well 89, sample 45) and one well intersected similar source rocks in the onshore Haasvlakte Graben. However, none of the Bredasdorp Basin wells have penetrated deep into any other graben (Fig. 4.03). Most intersect only the top few hundred metres of the syn-rift fill on structural highs and hence the potential is largely unknown. Most of the graben are deeply buried and source rocks within them are presently in the gas window (Fig. 7.09). It is not impossible that the deep central basin gas similar to Family 2, and some of the gas at the northern basin margin, could also result from such a source (Fig. 13.23).

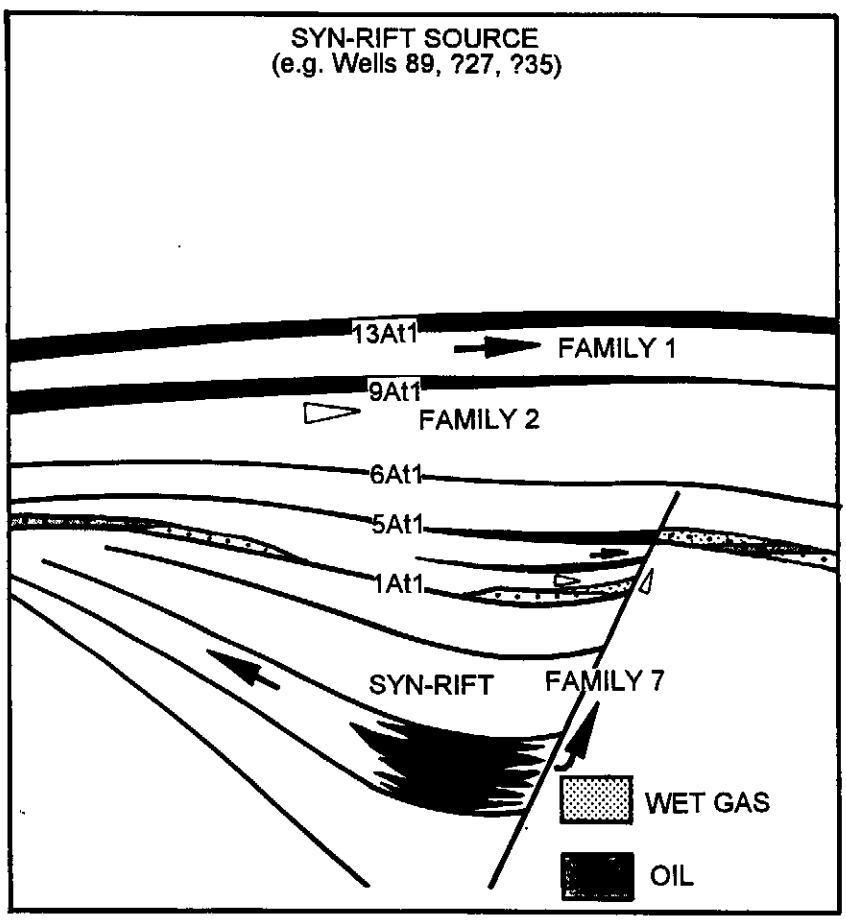

Figure 13.23: Schematic section through the syn-rift fill of a pre-rift graben showing the probable development of lacustrine source rocks (after those found in the A-J1 well on the west coast, Muntingh, 1993) and possible migration routes into adjacent structures.

It is likely that source rocks in these graben are non-marine and that the organic matter is composed dominantly of terrigenous or lacustrine debris, because the Late Jurassic marine incursion is not thought to have extended as far west as this area. If so, then the exclusively marine derivation of the hydrocarbons shows a mismatch with such a source. It is less certain though, that syn-rift source rocks in the western part of the Southern Outeniqua Basin are also non-marine. That region was developed as a structural low very early, hence the Oxfordian beach deposits in borehole DSDP 330 (Gilbert, 1977) on the conjugate margin. Marine source rocks, similar to those in wells in the Algoa and Gamtoos Basins offshore may also be present and they may source, or partly source, Family 4 gas (Malan, 1993).

Assuming that source rocks similar to those in well 89 have developed in some parts of the graben, burial history modelling of earliest syn-rift sediments shows a very early passage through the oil window (~100 Ma or earlier by extrapolation from Fig. 7.17). Hence any oil generated there could have been displaced, remigrated, or dissolved in the later gas generated. One characteristic of such terrigenous-rich organic material is the dominance of waxy saturates. Several examples of waxy oil are known in the basin, mostly in pre-1At1 sediments (e.g. wells 50 and 62) and waxy condensates have been found in wells 27 and 35. Hydrocarbons migrating from syn-rift source rocks could migrate stratigraphically up dip along fault conduits, as may have occurred in wells 27 and 35. They could also migrate structurally updip to post-rift or syn-rift targets as may occur in the central basin (Fig. 13.23). Until these oils and the deep condensates are properly studied, the possibility of syn-rift sourcing cannot be ignored.

Formation water salinities in these non-marine sediments may not necessarily be very low. In borehole A-J1 on the west coast, a fresh-water lacustrine sequence which contained sandstones with formation water salinities close to marine was intersected (Muntingh, 1993). By contrast, formation water salinities in syn-rift sediments intersected in borehole 16 are highly saline because of the nearby halite deposition. Hence low formation water salinities are not exclusively characteristic of syn-rift sediments, but highly saline formation water is often indicative of nearby evaporites (Bjørlykke and Gran, 1994). Individual graben in the basin differ in their sediment contents and where formation water salinities are high it would not be unreasonable to expect other halite developments.

13.3. PETROLEUM SYSTEM APPROACH

The foregoing discussions show the number of possible source-reservoir juxtapositions that characterise the basin. All form part of the same petroleum system.

13.3.1. Introduction

A petroleum system is described as "the genetic relationship between a pod of active source rock and the resulting oil and gas accumulations" and includes all the processes needed for the accumulations to exist. It includes source rock, reservoir rock, seal rock, overburden rock, trap formation, and the generation, migration and accumulation of petroleum, all placed in time and space (Magoon and Dow, 1994, p. 3-15). One requirement in defining a system is that it should include an active source rock and hydrocarbons reservoired from that source.

The compilation by Magoon and Dow (1994) of all the known petroleum systems does not include any system from southern Africa. Within that volume, Klemme (1994) discusses the contribution of Upper Jurassic source rocks to different systems but also shows that many African systems are un-named - in particular those of the southern African region. This study aims to correct those omissions for the south and west coast basins of South Africa. It is proposed herein that the systems for the south coast and west coast basins should be called the Outeniqua(!) and Orange(!) petroleum systems respectively and that where referred to as a whole, the name Outeniqua-Orange(!) should be used.

13.3.2. Attributes of the system

Source and reservoir rocks in the Bredasdorp Basin (Davies, 1996c) were deposited in the initially rifted and later pull-apart basins located south of southern Africa during the Late Mesozoic period. Components of the system range in age from ~140 Ma, probably the maximum age of the oldest source rock, to ~103 Ma, the age of the youngest reservoir. It excludes the youngest source rock (15A, Turonian), which is essentially inactive. This is a fairly wide range for a system and is greater than all those listed in Magoon and Dow (1994) except the Ellesmerian(!) of Alaska which ranges from 220-60 Ma. Many of the source rocks and sand-rich intervals are also common to other basins of the southern offshore area and these areas should be included in the system. In addition, the contribution from the Southern Outeniqua Basin in terms of both its source rocks and the postulated hydrothermal heating should not be ignored. The important facets of the petroleum system are shown in Fig. 13.24.

13.3.2.1. Source rocks

There is no evidence for any hydrocarbon generation in the basin before rifting took place, although the Bokkeveld shales may have done so during the Late Palaeozoic. Mesozoic source rocks are developed through a wide age range, from Late Jurassic lacustrine to Early Turonian marine. Notwithstanding this wide range, all are clastic-dominated, being largely composed of eroded Cape System sediments.

COMPONENTS OF THE OUTENIQUA(!) PETROLEUM SYSTEM

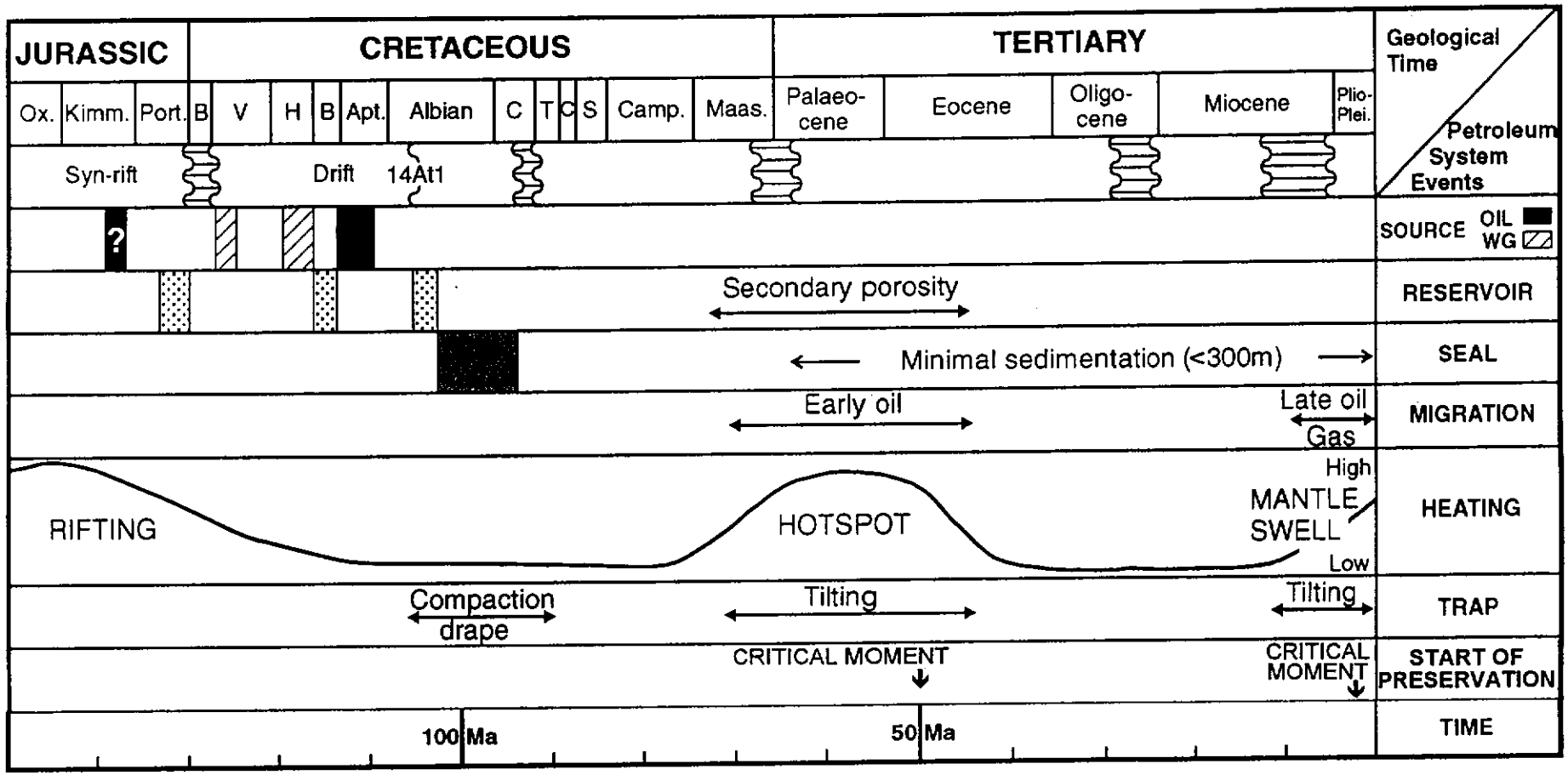

Figure 13.24: Petroleum System Chart showing the development chronology of the various parts of the system (after Davies, 1997i).

High proportions of extractable hydrocarbons show that all source rocks with potential for wet gas and oil generation have generated some oil and gas, although the oldest (pre-1At1, pre-Hauterivian) and youngest (15A, Turonian) source rocks cannot be shown to have expelled hydrocarbons in any quantity in the Bredasdorp Basin. However, the Upper Jurassic source rocks are included in the system because they are known to have generated and expelled hydrocarbons in other south coast basins. These are gas and lacustrine oil in the Pletmos Basin (Davies, 1978; 1996d; 1997c) and oil in the Gamtoos and Algoa Basins (Davies, 1992; Malan, 1993).

By contrast, the Turonian (15A) source shales are not mature enough to have expelled any hydrocarbons in the Bredasdorp Basin (Davies, 1997b), in the central parts of the Southern Outeniqua Basin (Davies, 1996d; 1997b; 1997c) or in the Algoa or Gamtoos Basins. However, modelling shows that those shales could expel oil in a small fetch area in the most westerly part of the Southern Outeniqua Basin (Davies, 1997b). Nevertheless, until such sourcing is demonstrated, the 15A shales are excluded and the proposed system includes Upper Jurassic (140-131 Ma) and Lower Cretaceous (118-111 Ma) source rocks.

13.3.2.2. Reservoir rocks

Three sandstone depositional environments largely characterise the basin, viz. regressive coastal sandstones (pre-1At1), submarine fans (central basin 9A) and channelised lobes and fans in minor inversion graben (e.g. 13A-14A). These reservoir rocks range from Late Jurassic (pre-1At1) to Early Albian (14A; ~140-103 Ma). They are all clastic sandstones, but many were indurated by calcite or silica cement, mostly during early burial or diagenesis. However, later meteoric water flushing removed the occluding cement in areas (Davies, 1995a). In addition to these reservoirs, occasional reservoirs of gas have been found in fractured Table Mountain Sandstone basement (e.g. in the Pletmos Basin, Du Toit, 1972). There are seismic indications of reservoired hydrocarbons at the south flank Bredasdorp Basin locations (e.g. in 15A sandstones, Strauss et al., 1996).

Most hydrocarbon fields are trapped structurally. The structures formed during two major episodes namely (i) early-rifted horst blocks formed during initial stages of rifting in the southeastern basement high (Fig. 3.04) and (ii) Early-Mid Cretaceous tectonism. During the late stages of the Cretaceous tectonism, local compression events resulted from wrench faulting. Some of the earlier minor graben were inverted during these compression events forming structures such as the central basin 14A channel highs (wells 117, 83, 88) and positive flower structures (Holmes, 1994). A few of the

structures also have a stratigraphic component to their trapping mechanisms but these are less common (Burden and Davies, 1997b).

13.3.2.3. Hydrocarbon generation and migration

Burial history modelling using data from wells in the Bredasdorp and Southern Outeniqua Basins (Davies, 1997c), shows generation and migration of hydrocarbons to be concentrated in two intervals. These occur in the Late Cretaceous-Early Tertiary (~75-50 Ma) and Latest Tertiary (~10-0 Ma) resulting from regional heating events driven by global tectonism (Davies, 1997c; 1997f). Evidence supporting these two episodes is found in the biomarker maturities of a number of residual oil traces formed as a result of dysmigration of earlier reservoir fills (Davies, 1997a; 1997b).

Hydrocarbon migration took place along faults, along unconformity surfaces and along sandstone trends. Many of the faults follow trends inherited from the Palaeozoic Cape Fold Belt orogeny, but more recent faults crosscut these, contributing to an intricate network of faults. Where these faults cut over-pressured source shales, they are probably largely sealed, except where throws are very large. Yet where faults cut sandstone-dominated structures, matching oil-water contacts on either side show that the faults leak at least partially (Rathan, 1996).

Hydrocarbon flow along reservoir trends was facilitated by the late injection of large amounts of gas which ultimately resulted in extensive 'fill-and-spill' migration (Davies, 1997a). The presence of both early residual oils and more recently migrated volumes of hydrocarbons from individual source rocks in structures throughout the basin, shows that the recent and palaeo-episodes of migration were pervasive. Indeed, the common occurrence of fluorescence traces in sandstones throughout the basin shows that much of the early fill has migrated away, probably during the tilting phases associated with mantle heating episodes. This remigrated material constitutes a potential future target.

In some parts of the basin, hindrances to migration are found such as the lack of major faults in post-6A formations and the diagenetic plugging of sandstones. Fortunately the former is of reduced importance in the south flank of the basin where some faults extend into the Tertiary and in the central basin where small faults reach to 13At1. The latter too is not a problem where recent meteoric water flushing prevailed, mostly around the basin margins and along the 13B-14A sandstone trend.

13.3.3. Critical moments

Critical moments are defined (Magoon and Dow, 1994, p. 12) as the end of the generation-migration-reservoiring phase and the beginning of the preservation phase.

After this moment, all migrated and reservoired hydrocarbons could be preserved to the present, except where diffusion or leakage processes prevail.

There are two critical moments in the hydrocarbon history of the Bredasdorp Basin. The first critical moment is dated at about 50 Ma and is placed at the time of cessation of tilting associated with the Bouvet/Shona mantle swell-hotspot transit. The second critical moment marks the end of Southern Outeniqua Basin continental shelf slumps. This regionally extensive slumping episode (Dingle, 1977) probably results from regional tilting following initiation of the African Superswell (Hartnady and Partridge, 1995). The episode provided the impetus for further maturation in and hydrocarbon migration through the basin, which continues to the present. Reservoired gas and oil mostly date to the Agulhas Slump so this is the more important event.

13.3.4. Richness of the system

The areal extent of each source interval is well characterised from borehole data and mapped in Davies (1996a). However, because most of the drilling to the deeper horizons has been around the basin margin, there are few intersections of pre-6A source rocks and those maps are necessarily sketchy.

At least 50% of all the hydrocarbons available for migration are from the main oil source rock in the 13A Aptian sequence (Table 13.01). This interval is widely developed and consistently rich, with an original source potential ranging from 8-12 kg HC/tonne rock and maximised above 20 kg/tonne (after Burden, 1992). This is classified as 'good-to-very good source potential' by a number of authors (Clementz et al., 1979; Espitalié et al., 1985; Tissot and Welte, 1984, p. 513). A large input of gases has come from the basin centre. At least some of the associated condensates contain biomarkers characteristic of the 9A-12A source rocks.

The total amounts of hydrocarbons generated and potentially available for migration from each source interval in the Bredasdorp Basin have been calculated (Table 13.01). These quantities take into account the burial depths, maturation levels, richness and potential and the amount which could be absorbed in the source shales. It shows that some ~11B bbls oil and ~9B bbls oil equivalent gas are available for migration, although not all the oil which is available for migration will necessarily be expelled. The total amount of hydrocarbons found to date in reservoirs approximates 3-4 Tcf and 100-200 MM bbls oil. This is some 2-3% of the total available. Examples in Magoon and Dow (1994) show that for well explored basins, the ratio between available and reservoired hydrocarbons can be a lot higher, sometimes reaching 20-30%, but averaging ~8%. The potential for further discoveries in the area is still high.

Source rock interval	Kerogen type and quality	Oil/Gas ratio	Areal extent km^2	Average thickness metres	SG	Proportion of potential realised	Average yield kg/tonne	Proportion expellable oil	Proportion expellable gas	Range of original TOC (%)	Range of original HI	Quantity expellable (MM tonnes) Oil	Quantity expellable (MM tonnes) Gas
15A	II/(III) (WG)-OIL	60/40	3000	10	2.4	0.1	7-10	0.1	0.1	2.0-3.2	230-400	5	5
	III WG	20/80	1070	15	2.4	0.1	3-4	0.1	0.1	1.8-2.5	150-250	2	3
13A	I/II OIL	70/30	3200	100	2.5	0.5	8-12	0.3	0.1	2.6-4.0	310-550	1200	400
	III WG	30/70	2400	75	2.5	0.3	3-5	0.1	0.5	1.7-2.4	220-380	50	270
9A-12A	II OIL	60/40	700	45	2.5	0.6	6-8	0.5	0.1	2.0-2.5	200-400	165	30
	III (DG)-WG	30/70	1900	35	2.5	0.4	2-4	0	0.5	1.8-2.6	180-320	0	100
5A-8A	I/II OIL	70/30	500	50	2.6	0.3	6-8	0.1	0.1	1.4-2.5	220-470	15	15
	III WG	30/70	2600	80	2.6	0.4	3-5	0	0.5	2.0-2.5	180-300	0	430
1A-4A	(II)/III WG-(OIL)	20/80	100	65	2.7	0.3	4-6	0	0.1	1.6-2.6	200-360	0	3
guess	(II)/III WG-(OIL)	40/60	~500	50	2.7	0.5	4-6	0.5	0.5	?	?	80	80
pre1A	I/II WG-OIL	70/30	50	20	2.6	0.2	6-8	0.1	0.1	?	?	1	1
guess	I/II WG-OIL	70/30	500	50	2.7	0.5	6-8	0.6	0.4	2.0-2.3	200-350	150	100
										TOTALS (MM tonnes)		**1787**	**1437**
										TOTAL EXPELLABLE (bbls oil equiv.)		**11B**	**9B**

1 tonne oil = ~6.5 bbls, 1 tonne gas = ~30000 ft^3

2. Expellable quantities = Area x Thickness x SG x Proportion realised x Yield/1000 x Proportion expellable.

Table 13.01: Quantities of oil and gas which could be expelled from each source rock interval in the Bredasdorp Basin, to the present day. These numbers are calculated from measured source rock richness, mapped extent, measured and extrapolated maturity levels and from empirical examples of proportions of expellable hydrocarbons.

13.3.5. System name

In published examples, the formation name(s) of the sediments that characterise the system, in which the source and reservoir rocks are best developed, is used to label the system. In order to best identify the system, the name should be unique, and where source rocks and reservoir rocks are developed in different formations, all formation names are included in the system name to provide specificity. The level of uncertainty is indicated after the system name by (!) for known, (.) for hypothetical or (?) for speculative (Magoon and Dow, 1994, p. 12).

The sediments in which all the source rocks and most of the reservoir rocks are found were first described by Du Toit (1976) as the Sundays River Formation. However, this formation extends from the top of the Late Jurassic through to Mid-Cretaceous and encompasses rocks ranging from fluvial to deep marine. In addition, the type section of this formation is a deltaic sequence only developed onshore and correlation with the largely marine offshore rocks, is tenuous.

Du Toit (1976, his Fig. 11) proposed a four-fold subdivision of the formation and gave depths to the upper and lower horizons for the 17 wells used in that study (Du Toit, 1976, Table II). Results of later biostratigraphic study of these and surrounding wells (I.K. McMillan, 1994, pers. comm. and SOEKOR Biostratigraphic Summaries) show that these formation boundaries are imprecisely picked. For example Du Toit's pick of the top of the Sundays River Formation, Marker 19, ranges from Earliest Aptian in the type well (Ga-B1) to Latest Cenomanian in well E-B1. Since the exact boundaries of the formation cannot be established with any certainty, the formation name cannot be used to properly describe the source and reservoir rock system.

Alternatively, the name(s) of the major sedimentary units could be used for the system name. However, in the Bredasdorp Basin, none of the intervals of rocks are named. All are numbered either with the name of the underlying type 1 unconformity (e.g. 13A source rock) or even less satisfactorily by the name of the overlying unconformity (e.g. pre-1At1 sandstones). Within the interval of interest (i.e. post-14A sandstones-to-pre1At1 sandstones) there are some 20-30 labelled sediment packages, none of which describes the main source or reservoir rocks adequately. Indeed, in some places, the source and reservoir rocks have the same name (such as 13A source and 13A sandstones). The only way to use the currently adopted nomenclature would be to name the system the 'pre-1At1-top 14A sandstone' system - not satisfactory at all and potentially confusing should hydrocarbons be found above the 14A sandstones.

An alternative system name would be that of the major periods which make up the main source/reservoir interval such as Late Jurassic-Early Albian. This too is not satisfactory as such a description could fit many other systems whereas it should be area-specific.

The only name that does lend itself to description of the system is that of the basin itself. There are no precedents for the use of names other than formations in Magoon and Dow (1994), all systems being named after either the main source interval or the main reservoir formation. However, in this case, neither of these options is available. 'Bredasdorp Basin' would be the obvious choice for the name as it best describes the area where the system was first described, but would ignore the matching source and reservoir rock development in the remainder of the Outeniqua Basin. Therefore in adopting a more regional approach, which does allow for inclusion of all the genetically matching parts of this system, it is proposed that the petroleum system for all the south coast basins be named the Outeniqua(!) petroleum system.

13.3.6. Other areas and systems

Other areas of hydrocarbon generation, migration and reservoiring off the west coast of South Africa also contain similar source and reservoir rock components. In that region the main source rocks are the 13A marine source, 6A lacustrine shales and a probable pre-6At1 (syn-rift) gas-prone source. These largely match those of the south coast. In addition, hydrocarbons from all these source rocks have been found reservoired, and the main reservoir rocks are also of similar age, i.e. 14A sandstones, pre-6At1.

It may therefore be acceptable to name that system the same as along the south coast. However, there are characteristic differences in the tectonism, hydrocarbon types and rift times, which indicate a separate, but closely allied, system. It is therefore suggested that the west coast system should be called the Orange(!) system and the combined system should be called the Orange-Outeniqua(!) system.

It is indeed possible that the Upper Jurassic source rocks, which are so far shown to be responsible for few, if any, hydrocarbons in the Bredasdorp Basin, could be considered a separate system, in which case the Sundays River(.) System may be a more appropriate name for those sediments.

Should the Turonian (15A) source rocks be shown to have generated oil, their more regional development and significantly younger age dictates that they should be classed as a separate system. Since these source rocks are found in the Agulhas Formation they could be named the Agulhas(?) system.

CHAPTER 14. CONCLUSIONS

The study addresses aspects of the petroleum geochemistry of the Bredasdorp Basin and its downdip extension, the Southern Outeniqua Basin, from three viewpoints:
(i) sourced hydrocarbons, i.e. the distribution and maturation of source intervals, the types of organic matter they contain, whether they have generated and expelled hydrocarbons, and the chemical character of those hydrocarbons
(ii) migration routes, i.e the relationship between source and reservoir, the migration conduits, the evidence of present and palaeo-migration and barriers
(iii) reservoired hydrocarbons, i.e. their type, distribution, maturation, chemical character and similarity with those bitumens remaining in the source rocks.

No detailed compilation of the geochemistry of the Bredasdorp Basin has previously been carried out although reference to recent geochemical studies is made in a number of geological reviews (Burden, 1993; Winters and Kuhlmann, 1994; Wood, 1995; Davies, 1996c). This study investigates all geochemical aspects, determines the hydrocarbon history of the basin and places it in the overall framework used to assess the exploration potential. In order to establish this framework, a number of facets of the hydrocarbon evolution are addressed, few of which were fully understood or even known before the study started. Some of these have not been previously reported for any other basins worldwide. In particular the following aspects pertinent to petroleum exploration, which have not been previously reported:

1. the thermal effects, in terms of both total heat and rates of heat input, from regional mantle events
2. the significant tilting resulting from these mantle events and which affect hydrocarbon reservoirs
3. the fluid flow and heating effects arising from instantaneous deposition of major thicknesses of slumped sediments
4. the ability to correlate between hydrocarbons from different source rocks using a wide range of whole oil gas chromatography data and the clear characterisation of mixtures of hydrocarbons from different sources
5. the definition of the Outeniqua(!) petroleum system, one of the few reported from Africa.

14.1 SOURCE ROCKS

The source rock distribution is shown to be a function of the basin shape, depositional environment and oxygen levels. Changes in the shape of the basin as sea level rises and falls and as tectonic events unfold, expose different areas to deposition. Within

these areas, reduced oxygen levels lead to localised and regional concentrations of organic matter. As a consequence, basin-wide source rocks (e.g. 13A) developed. During other periods an anoxic layer formed which aided organic matter preservation only where it impinged on the coastline. These conditions promoted the formation of source rocks in swaths paralleling the basin margins (e.g. 6A).

Correlations of maturation-dependent indicators and source-specific indicators in hydrocarbon samples with those of their putative source rocks, confirm the modelled expulsion potential of each source and the times at which hydrocarbons were available for trapping. This occurred mostly in the Palaeocene and the Late Plio-Pleistocene (Fig. 13.07).

Four active source rocks, responsible for the bulk of the hydrocarbons found in the basin, are present within Early Cretaceous sediments. These include oil-prone rocks in the Early Aptian (13A) and Late Barremian (upper 9A-12A), and gas-prone rocks in the Early Barremian (lower 9A-12A) and Late Hauterivian (5A-6A). Since all these source rocks are similar in age, depositional environment and organic matter type, establishing correlations between the source rocks and the hydrocarbons requires much more detailed study than in areas where the source rocks differ significantly as in the Gulf Coast study of Comet et al. (1993).

14.2. THERMAL EFFECTS

Thermal effects relating to mantle-lithosphere boundary conditions are shown to significantly influence the thermal maturity of the basin. In particular, the transit of the African continent over a Late Cretaceous-Early Tertiary mantle swell and its associated hotspot and the recent development of a new mantle swell beneath eastern Africa, both played major roles (Fig. 2.13). Literature on the structural and thermal effects of such events (e.g. Barnard et al., 1992, Underhill and Partington, 1993, Cope 1994) only addresses the possible effects on source rocks in very general terms. None has so far addressed details of the petroleum history nor demonstrated the effects on source:hydrocarbon correlations.

Only by invoking the excess heating associated with these events, can modelled and measured maturation data be shown to coincide. This shows these heating events to be responsible for most of the hydrocarbon generation in the basin. Other effects of these events are the associated thermal uplift and sag, which altered the patterns of fluid flow through the basin and led to remigration of previously reservoired hydrocarbons (Fig. 7.20).

A further effect of the later mantle event was the initiation of the Agulhas Slump (Dingle, 1977; Fig. 3.24). Modelling this event shows that it seriously perturbed the fluid flow regime in the Bredasdorp Basin by injection of large amounts of hot water, thereby increasing the maturity levels of some source rocks (Fig. 3.27). Support for this effect comes from: (i) the presence of mud volcanoes, interpreted from seismic data to be associated with this event. These occur at the easternmost edge of the Bredasdorp Basin, proximal to the source of the hydrothermal charge (Fig. 4.33)
(ii) interpretations of optical vitrinite reflectance data, which record the basin-wide influx of hot water (Fig. 4.34)
(iii) two periods of hydrocarbon generation and expulsion determined from hydrocarbon biomarker maturities (Fig. 7.05).
The migration effect has been determined for three separate source rock-hydrocarbon pairs, one of which is discussed in detail.

A further result of the two short heating events is the unusual situation where wet chemical data record moderately low generation and reduced expulsion whilst optical and pyrolysis maturity parameters show moderately high maturities. This unusual combination is in agreement with published evidence of rapid heating effects (e.g. Van Graas, 1990). In the case of the Bredasdorp Basin, both events resulted in short periods of rapid heating interspersed with long periods of minimal heat increase. This effect is not due to imprecise maturity measurements as both optical and chemical results coincide with published data.

14.3. QUANTITIES OF EXPELLED HYDROCARBONS

The volumes of hydrocarbons generated and expelled during each thermal event are modelled using measured kinetic data. The known reservoired amounts are shown to be commensurate with the proportions available for expulsion times the likely reservoired fraction (Davies, 1997i). Likely available gas and oil total ~20 billion bbls oil equivalent of which less than 5% has been discovered to date.

14.4. FLUID MIGRATION

Evidence of regional migration both past and present is recorded by gas diffusion data (Fig. 4.41). The presence of gas in non-sourcing seals above known reservoirs is probably due to this effect and the proportions of methane and ethane largely match those expected to migrate by diffusion (Krooss et al., 1988). This gas migration effect is interpreted to indicate the type of hydrocarbons originally in the reservoir but subsequently lost.

Evaluation of migration distances has been carried out for oil trapped in the northern 14A reservoir trend. There the source rocks most similar in origin and maturity to the reservoired oils are up to 10 km downdip. Knowledge of this distance helps to define the area of active source and hence refine calculations of the volumes of hydrocarbons available for trapping. The ability to evaluate the amounts of hydrocarbons available is particularly useful in prospect generation where the type and amount of hydrocarbons expected are of critical importance to its value. Use of published guidelines of quantities generated are inappropriate in the Bredasdorp Basin because of the unusual thermal history of the area. A regional model of the migration of each type of hydrocarbon has been derived from the above data and an elaborate 3D model constructed along certain seismic lines (Fig. 13.08).

Formation water salinity data, determined from logs and water samples from sandstones at different levels throughout the basin, record evidence for two periods of fresh water flushing through at least some of the basin. These salinity data also show which regional conduits were open and where fresh water migrated, in contrast to those sandstones where water salinities are high and which are interpreted not to possess open migration conduits. However, in one case, the presence of residual oil stains in a presently high maturity, high salinity, gas-charged sandstone (section 13.1.5.3) bears witness to the previous existence of a fluid escape route. Geological evidence shows that the two periods when flushing was likely were at ~50-60 Ma and 0-10 Ma.

Detailed study of the direction and timing of local flushing conduits could indicate the locations of areas at the opposite end of the open conduits where the dissolved salts precipitate as temperature and pressure decrease and where updip diagenetic seals could be formed. One such region has been predicted along the south flank of the basin in the 14A sequence (Davies, 1995b).

Another outcome of the hydrologic study suggests the lack of ingress of fresh water early into the eastern part of the north flank. This may have resulted in only a very late establishment of the reservoir by porosity-enhancement. If so, this could explain the unexpected lack of evidence of the early oil flux which is now thought to have migrated through most of the north flank.

14.5. SOURCE ROCK-RESERVOIR PLAYS

Individual source rock-reservoir plays have been discussed in detail because they help to characterise the more hydrocarbon-prone areas of the basin. These studies highlight the fact that reservoired hydrocarbons can differ widely, largely as a result of mixing of two or more streams of hydrocarbons. The studies predict where this is likely.

In two places, migration 'keyholes' are described, for example where cross-fault migration could occur due to carrier bed juxtaposition in both time and space (Figs. 13.16 and 13.17). Studies of these regions include the effects due to different hydrocarbons migrating early and late. Indeed, tracking down fugitive hydrocarbons, which remigrated after their early reservoiring at ~50 Ma, could merit investigation.

14.6. CORRELATIONS

Published correlations between hydrocarbons rely on both biomarkers and isotopic data for their distinctiveness. This study shows that gas and light condensate fractions, as well as GC 'fingerprint' data can also be used, and that they are impressively source-specific (Figures 8.02a and 9.18). Indeed these methods are particularly useful in ascertaining source characteristics from mixtures of oils and gases where the biomarkers would not record the gas fraction. Results of analyses have viewed the data graphically (Figs. 12.09-12.11; 12.13-12.39) and statistically (Figs. 12.40-12.41). Each line of study demonstrates matching correlations. One unexpected result of this study was the interpretation that most samples comprise mixtures of two or more hydrocarbon Families. In fact less than one third of all the studied hydrocabon samples represent single hydrocarbon Families. This shows that effective migration routes can be utilised by several different hydrocarbon streams.

One interesting future target would be to follow up the close similarity between the isolated reservoir of wet gas-condensate in well 18 DST1 which matches the material in wells 27 and 35 on the opposite side of the basin. These results point to a syn-rift source for these hydrocarbons. Either this implies a basin-wide flux of this unusual condensate or that a similar syn-rift source potential exists in several separate grabens.

14.7. STRUCTURAL EFFECTS

Structural effects, based on previously published work, have been addressed in some detail because they control the regional migration pathways and the more local reservoiring trends. For instance, the episode of wrench fault inversion, almost certainly related to frictional drag on the Agulhas Fracture Zone, appears responsible for the formation of the oil-productive central basin 14A and 13B traps (section 13.2.1). Superimposed on this motion, there were up- and down-warping thermal effects associated with both the hotspot transit and the initiation of the recent African Swell. A general study of these effects shows that they coincided with the filling of some reservoirs and the emptying of others. More detailed study of these effects could be

useful in characterising other areas where large-scale reservoiring has occurred and where fluid flow directions of both hydrocarbons and water have varied.

14.8. PETROLEUM SYSTEM

Characterisation of the Outeniqua(!) Petroleum System has been carried out as a direct result of these source rock-hydrocarbon correlations following the guidelines of Magoon and Dow (1994, pp10-16). This is the first study to have done so in southern Africa. The elements of the system have been characterised in great detail by comparison with published studies, which tend to ignore differences between hydrocarbons derived from source rocks of slightly different age but similar environments. This study has shown that, despite the overall similarities of the source rocks, the expelled hydrocarbons do differ and have different, but predictable migration and reservoiring histories.

15. REFERENCES

Abreu, V.S. and Savini, R. (1994). Major palaeo-oceanographic events of the Brazilian continental margin: relationships with the giant oil fields of the Oligo-Miocene of Campos Basin, Brazil. 28th Ann. Offshore Tech. Conf., OTC 7411, 335-344.

Alexander, R., Kagi, I.R. and Woodhouse, G.W. (1983a). Variation in the ratio of isomeric butane with sediment temperature in the Carnarvon Basin of Western Australia. in "Advances in Organic Geochemistry 1981". (eds.) Bjorøy, M. et al., John Wiley, Chichester, 76-79.

Alexander, R., Kagi, I.R., Larcher, A.V. and Woodhouse, G.W. (1983b). Aromatic hydrogen exchange in petroleum source rocks. in "Advances in Organic Geochemistry 1981". (eds.) Bjorøy, M. et al., John Wiley, Chichester, 69-71.

Alexander, R., Larcher, A.V., Kagi, R.I. and Price, P.L. (1988). The use of plant-derived biomarkers for correlation of oils with source rocks in the Cooper/Eromanga Basin system, Australia. APEA Jour., 310-324.

Alexander, R., Larcher, A.V., Kagi, R.I. and Price, P.L. (1992). An oil-source correlation study using age-specific plant-derived aromatic biomarkers. in "Biological Markers in Sediments and Petroleum". (eds.) Moldowan, J.M., Albrecht, P. and Philp, R.P., Prentice Hall, New Jersey, 201-221.

Alvarez, L.W., Alvarez, W. Asaro, F and Michel, H.V. (1980). Extraterrestrial cause for the Cretaceous-Tertiary extinction. Science, **208**, 1095-1108.

Aquino Neto, F.R., Trendel, J.M., Restle, A., Connan, J. and Albrecht, P.A. (1983). Occurrence and formation of tricyclic and pentacyclic terpanes in sediments and petroleum. in "Advances in Organic Geochemistry 1981". (eds.) Bjorøy, M. et al., John Wiley, Chichester, 659-667.

Armanios, C., Alexander, R. and Kagi, R.I. (1992). High diahopane and neohopane abundances in biodegraded crude oil from the Barrow Sub-basin of Western Australia. Org. Geochem., **18/5**, 641-645.

Arthur, M.A., Schlanger, S.O. and Jenkyns, H.C. (1987). The Cenomanian-Turonian oceanic anoxic event, 11. Palaeoceanographic controls on organic matter production and preservation. in "Marine Petroleum Source Rocks". (eds.) Brooks, J. and Fleet, A.J., Geol., Soc. Spec. Publ. No. 26, Blackwell, London, 401-420

Bailey, N.J.L., Burwood, R. and Harriman, G.E. (1990). Application of pyrolysate carbon isotope and biomarker technology to organofacies definition and oil correlation problems in the North Sea basins. Org. Geochem., **16/4-6**, 1157-1172.

Baird, S. (1986). "Overpressure". Unpubl. training manual, Gearhart Geodata Services, Aberdeen, pp. var.

Baldwin, B. and Butler, C.O. (1985). Compaction curves. Am. Assoc. Pet. Geol. Bull., **69/4**, 622-626.

Banks, N.L., Light, M.P.R. and Miles, J.A. (1993). Technical audit of the petroleum potential of offshore South Africa and its exploration to date. Unpubl. rept to SOEKOR, 110pp.

Barker, C.E. (1983). Influence of time and metamorphism of sedimentary organic matter in liquid-dominated geothermal systems, western North America. Geology, 11, 384-388.

Barker, C.E. (1990). Calculated volume and pressure changes during the thermal cracking of oil to gas in reservoirs. Am. Assoc. Pet. Geol. Bull., **74/8**, 1254-1261.

Barker, P.F., Dalziel, I.W.D., Dinkelmann, M.G., Elliot, D.H., Gombos Jr, A.M., Harris, W., Lonardi, A., Plafker, G., Sliter, W.V., Tarney, J., Thompson, R.W., Tjalsma, R.C., Von der Borch, C.C. and Wise Jr, S.W. (1977a). 6. Site 330. in "Initial Reports Deep Sea Drilling Project, Vol 36". (eds.) Barker, P.F., Dalziel, I.W.D. et al., Washington (US Govt. Printers Office), 207-257.

Barker, P.F., Dalziel, I.W.D., Dinkelmann, M.G., Elliot, D.H., Gombos Jr, A.M., Harris, W., Lonardi, A., Plafker, G., Sliter, W.V., Tarney, J., Thompson, R.W., Tjalsma, R.C., Von der Borch, C.C. and Wise Jr, S.W,. (1977b). 29. Evolution of the southwestern Atlantic Ocean Basin: results of leg 36, Deep Sea Drilling Project. in "Initial Reports Deep Sea Drilling Project, Vol 36". (eds.) Barker, P.F., Dalziel, I.W.D. et al., Washington (US Govt. Printers Office), 993-1014.

Barnard, P.C. and Thompson, S. (1992). Petroleum source rocks of the Indian Ocean. in "First Indian Ocean Petroleum Seminar". (ed.) Plummer, P.S., U.N. Dept. Tech. Co-op. Dev., Space, Seychelles, 397-414.

Barnard, P.C., Thompson, S., Bastow, M.A., Ducreux, C. and Mathurin, G. (1992). Thermal maturity development and source-rock occurrence in the Red Sea and Gulf of Aden. Jour. Pet. Geol., **15/2**, 173-186.

Barron, E.J. (1983). A warm equable Cretaceous: the nature of the problem. Earth Sci. Rev., **29**, 305-338.

Barron, E.J. and Moore, G.T. (1993). Late Jurassic to mid-Cretaceous source rock, reservoir and evaporitic seal distribution derived from general circulation model simulation. Ann. AAPG-SEPM-EMO-OPA-DEG Conv. Pap. Abstr., 72.

Barton, K.A. (1996). Participation opportunity in Block 9, offshore Republic of South Africa: borehole E-DE1 recommendation. SOEKOR unpubl. rept., SOE-EXP-RPT-370, 17pp.

Barton, K.A. and Grobbler, N.G. (1997). Re-appraisal of the E-CE/E-BD oil and gas fields based on the 1996 reprocessing of the 3-D seismic data. SOEKOR unpubl. rept., SOE-EXP-RPT-430, 36pp.

Barton, R.H., Tomlinson, W.D. and Bartington, G.W. (1988). Use of seabottom magnetic susceptibility measurements in hydrocarbon exploration. in "Remote sensing for geologists proceedings 1". (eds.) 6th Environ. Res. Inst. Mich. et al., Thematic conference, 137-145.

Bathurst, R.G.C. (1976). "Carbonate sediments and their diagenesis". Dev. in Sed. 12, Elsevier, Amsterdam, 658pp.

Beach, F., Peakman, T.M., Abbott, G.D., Sleeman, R. and Maxwell, J.R. (1989). Laboratory thermal alteration of triaromatic steroid hydrocarbons. Org. Geoch., **14/1**, 109-111.

Beamish, G.W.J. (1990). The seismic expression of depositional systems tracts and its application to hydrocarbon exploration in the Bredasdorp Basin, offshore Southern Africa. in "Abstracts Geocongress 90", Geol. Soc. S. Afr., Cape Town, 638-641.

Ben-Avraham, Z., Hartnady, C.J.H. and Malan, J.A. (1993). Early tectonic extension between the Agulhas Bank and the Falklands Plateau due to the rotation of the Lafonia microplate. Earth Planet. Sci. Lett., **117**, 43-58.

Ben-Avraham, Z., Hartnady, C.J.H. and Kitchin, K.A. (1997, in press). Tectonics of the Agulhas-Falklands transform. Tectonophysics, 282, pp. unknown.

Benson, J.M. (1990). Palynofacies characteristics and palynological source rock assessment of the Cretaceous sediments of the northern Orange Basin (Kudu 9A-2 and 9A-3 wells). Communs. Geol. Surv. Namibia, **6**, 31-39.

Benson, J.M., Van der Spuy, D. and Davies, C.P.N. (1990). Correlation between optical and chemical maturation indices and their application to the offshore petroleum geology of southern Africa. "Abstracts Geocongress 90". Geol. Soc. S. Afr., Cape Town, 642-645.

Benson, J.M., Davies, C.P.N., Elliott, S., Hill, S.J., McMillan, I.K., Marot, J.E.B., Petrie, H., Pringle, A., Valicenti, V.H., Van der Spuy, D. and Wickens, H. deV. (1993). The correlation of sandstones within the 14A turbidite system, central Bredasdorp Basin. SOEKOR unpubl. rept., SOE-RPT-GEO-002, 46pp.

Biddle, K.T., Uliana, M.A., Mitchum, R.M., Fitzgerald, M.G. and Wright, R.C. (1986). The stratigraphic and structural evolution of the central and eastern Magellanes Basin, southern South America. in "Foreland Basins", (eds.) Allen, P.A. and Homewood, P., Int. Assoc. Sediment. Spec. Publ. No. 8, 41-61.

Birch, G.F., Rogers, J. and Bremner, J.M. (1986). Texture and composition of surficial sediments of the continental margin of the Republics of South Africa, Transkei and Ciskei. Marine Geoscience Series 3, Geol. Surv. S. Afr., Pretoria, 4 sheets.

Bishop, A.N. and Philp, R.P. (1994). Potential for amorphous kerogen formation via adsorption of organic material at mineral surfaces. Energy and Fuels, **8**, 1494-1497.

Bishop, A.N. and Abbott, G.D. (1995). The interrelationship of biological marker maturity parameters and molecular yields during contact metamorphism. Geochim. et Cosmochim. Acta, **57**, 3661-3668.

Bjørlykke, K. and Gran, K. (1994). Salinity variations in North Sea formation waters: implications for large-scale fluid movements. Mar. Pet. Geol., **11/1**, 5-9.

Bjorøy, M., Hall., K., Gillyon, P. and Jumeau, J. (1991). Carbon isotope variations in n-alkanes and isoprenoids of whole oils. Chem. Geol., **93**, 13-20.

Blackwell, D.D. and Steele, J.L. (1989). Thermal conductivity of sedimentary rocks: measurement and significance. in "Thermal History of Sedimentary Basins". (eds.) Naeser, N.D. and McCulloh, T.H., Springer-Verlag, New York, 13-36.

Blanc, Ph. and Connan, J. (1992). Origin and occurrence of 25 norhopanes: a statistical study. Org. Geochem., **18/6**, 813-828.

BMDP (1993). BMDP Statistical Software Inc., Version 7.1, Los Angeles.

Boreham, C.J, Crick, I.H. and Powell, T.G. (1988). Alternative calibration of the Methylphenanthrene Index against vitrinite reflectance: application to maturity measurements on oils and sediments. Org. Geochem., **12/3**, 289-294.

Bostick, N.H. (1975). Microscopic assessment of the level of catagenesis of solid organic matter in sedimentary rocks to aid exploration for petroleum and to determine former burial temperatures: a review. SEPM Spec. Publ. No. 26, Soc. Econ. Pal. Mineral., 17-43.

Brassell, S.C., Eglinton, G. and Fu Jia Mo. (1986). Biological marker compounds as indicators of the depositional history of the Maoming oil shale. Org. Geochem., **10**, 927-941.

Bray, E.E. and Evans, E.D. (1961). Distribution of n-paraffins as a clue to recognition of source beds. Geochim. et Cosmochim. Acta, **22**, 2-15.

Bray, E.E. and Evans, E.D. (1965). Hydrocarbons in non-reservoir-rock source beds. Am. Assoc. Pet. Geol. Bull., **49/3**, 248-257.

Brink, G.J and Winters, S.J. (1989). Overpressure study of the Bredasdorp Basin. SOEKOR unpubl. rept., 8pp.

Brink, G.J., Kuhlmann, S., Winters, S.J., Fraser, N., Basson, W. and Blagg, J. (1991). Sequence 13A, Bredasdorp Basin: A case study of seismic/sequence stratigraphy integrated with seismic anomaly reservoir and source rock distribution trends. SOEKOR unpubl. rept. SOE-EXP-RPT-004, 33pp.

Broad, D.S. and Mills, S.R. (1993). South Africa offshore exploratory potential in variety of basins. Oil Gas Jour., **91/49**, 38-44.

Broad, D.S. and Turner, J.R. (1982). Stratigraphy, facies and environments of deposition of the C-to-D sequence in the Bredasdorp Basin and Infanta Embayment. SOEKOR unpubl. rept., 58pp.

Brooks, J.D., Gould, K. and Smith, J.W. (1969). Isoprenoid hydrocarbons in coal and petroleum. Nature, **222**, 257-259.

Brooks, J., Cornford, C. and Archer, R. (1987). The role of hydrocarbon source rocks in petroleum exploration. In "Marine Petroleum Source Rocks". (eds.) Brooks, J. and Fleet, A.K., Geol. Soc. Spec. Publ. No. 26, 17-46.

Brown, D.M. (1991). E-AQ1 post-mortem study and implications for overpressure compartments in the Bredasdorp Basin. SOEKOR unpubl. rept., 15pp.

Brown, D.M. and Ranoszek, M.A. (1990). E-BD1: geological well completion report. SOEKOR unpubl. rept., SOE-DRG-WCR-309, 18pp.

Brown, L.F. and Doherty, S. (1992). Drilling success for sequence stratigraphic targets by Soekor (Pty) Ltd., offshore South Africa, 1987-1992. (abs.). Rocky Mountain Assoc. Geol. Appl. Sequ. Strat. Symp.

Brown, L.F., Benson, J.M., Brink, G.J., Doherty, S., Jollands, A., Jungslager, E.H.A., Keenan, J.H.G., Muntingh, A. and Van Wyk, N.J.S. (1995). "Sequence stratigraphy in offshore South African divergent basins". Am. Assoc. Pet. Geol., Stud. Geol. No. 41, 184pp.

Brown, R. W., Rust, D. J., Summerfield, M. A., Gleadow, A. J. and De Wit, M. J. (1990). An early Cretaceous phase of accelerated erosion on the south-western margin of Africa: evidence from apatite fission track analysis and the offshore sedimentary record. Nucl. Tracks Radiat. Meas., **17/3**, 339-350.

Burden, P.L.A. (1991). Re-evaluation of the F-F structure south-eastern Bredasdorp Basin. SOEKOR unpubl. rept., SOE-EXP-RPT-001, 28pp.

Burden, P.L.A. (1992). Soekor, partners explore possibilities in Bredasdorp Basin off South Africa. Oil and Gas Jour., **90/51**, 109-112.

Burden, P.L.A. (1993). Geology and prospectivity of the synrift succession in the Bredasdorp Basin. SOEKOR unpubl. rept., SOE-EXP-RPT-048, 53pp.

Burden, P.L.A. (1997). The geological evolution of the F-S structure in the eastern part of block 9. SOEKOR unpubl. Tech. Note No. 83, 9pp.

Burden, P.L.A. and Gasson, M. (1992). Project: The geology and prospectivity of sequences 1A-to-8A in the Bredasdorp Basin. SOEKOR unpubl. rept., 34pp.

Burden, P.L.A. and Davies, C.P.N. (1997a). Exploration to first production on Block 9 off South Africa. Oil Gas Jour., **95/36**, 92-97.

Burden, P.L.A. and Davies, C.P.N. (1997b). Oribi field is South Africa's first offshore crude oil production. Oil Gas Jour., **95/37**, 63-65.

Burnham, A.K. and Braun. R.L. (1985). General kinetic model of oil shale pyrolysis. In Situ, **9**, 1-23.

Burnham, A.K., Braun, R.L., Gregg, H.R. and Samoun, A.L. (1987). Comparison of methods for measuring kerogen pyrolysis rates and fitting kinetic parameters. Jour. Energy Fuels, **1/6**, 452-458.

Burst, J, F. (1969). Diagenesis of Gulf Coast clayey sediments and its possible relation to petroleum migration. Am. Assoc. Pet. Geol. Bull., **53**, 73-93.

Burwood, R., Cornet, P.J., Jacobs, L. and Paulet, J. (1990). Organofacies variation control on hydrocarbon generation: a Lower Congo coastal basin (Angola) case history. Org. Geochem., **16/1-3**, 325-338.

Burwood, R., Leplat, P., Mycke, B. and Paulet, J. (1992). Rifted margin source rock deposition: a carbon isotope and biomarker study of a West African Lower Cretaceous "lacustrine" section. Org. Geochem., **19/1-3**, 41-52.

Bustin, R.M., Barnes, M.A. and Barnes, W.C. (1990). Determining levels of organic diagenesis in sediments and fossil fuels. in "Diagenesis" (eds.) McIlreath, I.A. and Morrow, D.W., Geoscience Can. Repr. Ser., **4**, 205-226.

Butler, R.W.H., Lickorish, W.H., Grasso, M., Pedley, H.M. and Ramberti, L. (1995). Tectonics and sequence stratigraphy in Messinian basins, Sicily: constraints on the initiation and termination of the Mediterranean salinity crisis. Geol. Soc. Am. Bull., **107/4**, 425-439.

Butzer, K.W., Fock, G.J., Stuckenrath, R. and Zilch, A. (1973). Palaeohydrology of late Pleistocene lake, Alexandersfontein, Kimberley, South Africa. Nature, **243**, 328-330.

Cartwright, J.A. (1989). The structural and stratigraphic development of the Gamtoos and Algoa Basins. SOEKOR unpubl. rept., 26pp.

Cartwright, J.A. (1994). Episodic basin-wide hydrofracturing of over-pressured early Cenozoic mudrock sequences in the North Sea basin. Mar. Pet. Geol., **11/5**, 587-607.

Cassani, F. and Eglinton, G. (1986). 1. Pyrolysis of asphaltenes: a technique for the correlation and maturity evaluation of crude oils. Chem. Geol., **56**. 167-183.

Chakhmakhchev, A. and Suzuki, N. (1995). Aromatic sulphur compounds as maturity indicators for petroleums from the Buzuluk depression, Russia. Org. Geochem., **23/7**, 617-625.

Chosson, P., Connan, J., Dessort, D. and Lanau, C. (1992). In vitro Biodegradation of steranes and terpanes: a clue to understanding geological situations. in "Biological Markers in Sediments and Petroleum". (eds.) Moldowan, J.M., Albrecht, P. and Philp, R.P., Prentice Hall, New Jersey, 320-349.

Christie, A.D.M. (1990). Origin, classification and utilization of oil shales in South Africa. Suid-Afrikaanse Tydskrif vir Wetenskap, **86**, 9-15.

Clark, J.P. and Philp, R.P. (1989). Geochemical characteristics of evaporite and carbonate depositional environments and correlation of associated crude oils in the Black Creek Basin, Alberta. Bull. Can. Pet. Geol., **37**, 401-416.

Claypool, G.E. and Magoon, L.B. (1985). Comparison of oil-source rock correlation data for Alaskan North Slope: techniques, results and conclusions. in "Alaskan North Slope oil/rock correlation study". (eds.) Magoon, L.B. and Claypool, G.E., AAPG Stud. Geol. No. 20, Am. Assoc. Pet. Geol., Tulsa, 49-81.

Clementz, D.M., Demaison, G.J. and Daly, A.R. (1979). Well site geochemistry by programmed pyrolysis. Offshore Tech. Conf. OTC 3410, 465-470.

Cole, D.I. (1992). Evolution and development of the Karoo Basin. in "Inversion tectonics of the Cape Fold Belt, Karoo and Cretaceous basins of Southern Africa." (eds.) De Wit, M.J. and Ransome, I.G.D., A.A. Balkema, Rotterdam, 87-99.

Cole, D.I. and McLachlan, I.R. (1990). Oil potential of the Permian Whitehill Formation in the main Karoo Basin, South Africa. in "Abstracts Geocongress '90". Geol. Soc. S. Afr., Cape Town, 103-105.

Comet, P.A., Rafalska, J.K. and Brooks, J.M. (1993). Sterane and triterpane patterns as diagnostic tools in the mapping of oils, condensates and source rocks of the Gulf of Mexico region. Org. Geochem., **20/8**, 1265-1296.

Condie, K.C. (1989). "Plate Tectonics and Crustal Evolution". Pergamon Press, Oxford, 476pp.

Connan, J. (1984). Biodegradation of crude oils in reservoirs. in "Advances in "Petroleum Geochemistry Vol 1". (eds.) Brooks, J. and Welte, D.H., Academic, London, 299-335.

Connan, J. and Dessort, D. (1987). Novel family of hexacyclic hopanoid alkanes (C32-C35) occurring in sediments and oils from anoxic palaeoenvironments. Org. Geochem., **11**, 103-113.

Cooles, G.P., Mackenzie, A.S. and Quigley, T.M. (1986). Calculation of petroleum masses generated and expelled from source rocks. Org. Geochem., **10**, 235-245.

Cope, J.C.W. (1994). A latest Cretaceous hotspot and the southeasterly tilt of Britain. Jour. Geol. Soc., Lond., **151**, 905-908.

Cornelius, C-D. (1975). Geothermal aspects of hydrocarbon exploration in the North Sea area. Norsk. Geol. Ondersoek, **316**, 26-67.

Cornford, C. (1986). Source rocks and hydrocarbons of the North Sea. in "Introduction to the petroleum geology of the North Sea". (ed.) Glennie, K.W., Oxford Press, London, 197-236.

Cornford, C., Morrow, J.A., Turrington, A., Miles, J.A. and Brooks, J. (1983). Some geological controls on the oil composition in the UK North Sea. in "Petroleum Geochemistry and Exploration of Europe". (ed.) Brooks, J., Geol. Soc. Spec. Publ. No. 12, Blackwell, London, 175-194.

Cornford, C., Needham, C.E.J. and de Walque, L. (1986). Geochemical habitat of North Sea oils and gases. in "Habitat of Hydrocarbons on the Norwegian Continental Shelf". Graham and Trotman, London, 39-54.

Correa da Silva, Z.C. and Cornford, C. (1985). The kerogen type, depositional environment and maturity of the Irati Shale, Upper Permian of Paraña Basin, Southern Brazil. Org. Geochem., **8/6**, 399-411.

Correia, M. and Peniguel, G. (1975). Étude microscopique de la matière organique - ses applications a l'exploration pétrolière. Bull. Centre Rech. Pau - SNPA, **9/2**, 99-127.

Coster, P.W., Lawrence, S.R. and Foster, G. (1989). Mozambique: a new geological framework for hydrocarbon exploration. Jour. Pet. Geol., **12/2**, 205-230.

Creaney, S. and Passey, Q.R. (1993). Recurring patterns of total organic carbon and source rock quality within a sequence stratigraphic framework. Am. Assoc. Pet. Geol. Bull., **77/3**, 386-401.

Curiale, J.A. (1986). Origin of solid bitumens, with emphasis on biological marker results. Org. Geochem., **10**, 559-580.

Curiale, J.A. (1992). Molecular maturity parameters within a single oil family: a case study from the Sverdrup Basin, Arctic Canada. in "Biological Markers in Sediments and Petroleum" (eds.) Moldowan, J.M., Albrecht, P. and Philp, R.P., Prentice Hall, New Jersey, 275-300.

Dahl, B. And Spears, G.C. (1985). Organic geochemistry of the Oseburg field (I). In "Petroleum Geochemistry in Exploration of the Norwegian Shelf". (eds.) Thomas, B.M. et al., Norwegian Petroleum Society, Graham and Trotman, London, 185-195.

Dalziel, I.W.D., Garrett, S.W., Grunow, A.M., Pankhurst, R.J., Storey, B.C. and Vennum, W.R. (1987). The Ellsworth-Whitmore Mountains crustal block: its role in the tectonic evolution of West Antarctica. in "Gondwana Six: structure, tectonics and geophysics". (ed.) McKenzie, G.D., Geophys. Monograph No. 40, Am. Geophys. Union, Washington, 173-182.

Davies, C.P.N. (1978). Geochemical report: borehole Gb-C1. SOEKOR unpubl. rept., 13pp.

Davies, C.P.N. (1979). Geochemical report for the Ga-D1 borehole. SOEKOR unpubl. rept., 10pp.

Davies, C.P.N. (1988a). Offshore hydrocarbon profiling (Sniffer) survey. SOEKOR unpubl. rept., 27pp.

Davies, C.P.N. (1988b). Bredasdorp Basin - south flank hydrocarbon expulsion. SOEKOR unpubl. rept., 17pp.

Davies, C.P.N. (1990). Quantification of oil generation and expulsion from source rocks in the offshore Bredasdorp Basin. Abstracts Geocongress 90, Geol. Soc. S. Afr., Cape Town, 119-122.

Davies, C.P.N. (1991). Geochemistry section: calcimetry analyses - accuracy and repeatability testing. SOEKOR unpubl. rept., 17pp.

Davies, C.P.N. (1992). Gamtoos Basin: geochemical correlation of oils and shales. SOEKOR unpubl. rept., 17pp.

Davies, C.P.N. (1993a). 14 megasequence project: the chemical contribution. SOEKOR unpubl. rept., 37pp.

Davies, C.P.N. (1993b). E-CB1: Modelling of expected hydrocarbons. SOEKOR unpubl. rept., 34pp.

Davies, C.P.N. (1993c). Geochemistry report on features of borehole F-BB1. SOEKOR unpubl. rept., 18pp.

Davies, C.P.N. (1993d). Organic geochemical studies of potential source rocks in the Magellanes Basin, Chile. SOEKOR unpubl. rept., 26pp.

Davies, C.P.N. (1993e). E-S1: source and correlation of oil and condensates with E-CE1 and E-AA1. SOEKOR unpubl. rept., SOE-GCH-RPT-009, 20pp.

Davies, C.P.N. (1994a). Geochemical correlation of oils in 14A reservoirs in wells E-BT1, E-BT01P, E-AR1, E-AA1 and E-AD1. SOEKOR unpubl. rept., SOE-GCH-RPT-131, 41pp.

Davies, C.P.N. (1994b). Kinetic, burial history and biomarker studies of the Neptuno XE-1 and Calafate PK-1 wells in the Magallanes Basin, Chile. SOEKOR unpubl. rept., 27pp.

Davies, C.P.N. (1995a). Log-derived salinity data: an investigation of sands in the Bredasdorp Basin. SOEKOR unpubl. rept., SOE-GCH-RPT-249, 14pp.

Davies, C.P.N. (1995b). Chemical, lithological and pressure evidence of a diagenetic seal trend in proximal 14A sands. SOEKOR unpubl. rept., SOE-GCH-RPT-216, 22pp.

Davies, C.P.N. (1995c). Gas: oil ratios. SOEKOR unpubl. Tech. Note No. 23, 7pp.

Davies, C.P.N. (1995d). Biomarker and fingerprint correlation of hydrocarbons in sands in sequence 14A in wells E-AJ1, E-AJ2, E-AM1, E-BK1 and E-CB1. SOEKOR unpubl. rept., SOE-GCH-RPT-215, 40pp.

Davies, C.P.N. (1995e). Biomarker and fingerprint correlation of oils in wells E-BH1, E-BB1, E-AO2, E-AO1, E-AN1 and E-AD1. SOEKOR unpubl. rept., SOE-GCH-RPT-182, 42pp.

Davies, C.P.N. (1995f). Biomarker and fingerprint correlation of oils and their flow units in E-BD1-2, E-CE1-3 and E-N1. SOEKOR unpubl. rept., SOE-GCH-RPT-153, 43pp.

Davies, C.P.N. (1996a). Source rock summary data: Bredasdorp Basin wells. SOEKOR unpubl. rept., SOE-GCH-RPT-250, 10pp.

Davies, C.P.N. (1996b). Modelling of hydrocarbon generation, migration and reservoiring for the E-DC prospect. SOEKOR unpubl. Tech. Note No. 65, 16pp.

Davies, C.P.N. (1996c). Bredasdorp Basin syn-rift study: a review of hydrocarbons and migration. SOEKOR unpubl. rept., SOE-GCH-RPT-251, 16pp.

Davies, C.P.N. (1996d). Source rocks and hydrocarbons in the Pletmos Basin, offshore South Africa: their tectonic and thermal history. SOEKOR unpubl. rept., SOE-GCH-RPT-253, 17pp.

Davies, C.P.N. (1996e). Gas chromatography fingerprint analyses: test of repeatability. SOEKOR unpubl. rept. Tech Note No. 32, 10pp.

Davies, C.P.N. (1997a). Bredasdorp Basin south-east flank 14A oil trend: hydrocarbon generation and migration. SOEKOR unpubl. rept., SOE-GCH-RPT-254, 40pp.

Davies, C.P.N. (1997b). Oils in F-L wells and their migration implications. SOEKOR Tech. Note No. 79, 15pp

Davies, C.P.N. (1997c in press). Pletmos and Southern Outeniqua Basins, offshore South Africa: hydrocarbon potential reflects multiple heating and sourcing. Accepted for Proceedings of 4th AAAPG Conference, June 2-6 1996, Arusha, Tanzania.

Davies, C.P.N. (1997d in press). Unusual biomarker maturation ratio changes through the oil window, a consequence of varied thermal history. Accepted for Org. Geochem.

Davies, C.P.N. (1997e). Western Bredasdorp Basin: 9A-12A source rocks and associated hydrocarbons. SOEKOR unpubl. Tech. Note No. 85, 16pp.

Davies, C.P.N. (1997f). Results of apatite fission track analyses of samples from borehole E-AN1, Bredasdorp Basin. SOEKOR unpubl. Tech Note No. 84, 6pp.

Davies, C.P.N. (1997g). Earlier oil fill of E-AR structure. SOEKOR unpubl. memo. GCH/1, 23 May 1997, 2pp.

Davies, C.P.N. (1997h). Communication between gas-condensates in the E-M area. SOEKOR unpubl. rept., SOE-GCH-RPT-255, 17pp.

Davies, C.P.N. (1997i). South African Petroleum System(s): their naming and characterisation (with special reference to the Bredasdorp Basin). SOEKOR unpubl. Tech. Note No. 88, 8pp.

Davies, C.P.N. and Ellis, R.B. (1981). Cuttings sample contaminant removal. SOEKOR unpubl. rept., SOE-GCH-RPT-252, 16pp.

Davies, C.P.N. and Van der Spuy, D. (1990). Chemical and optical investigations into the hydrocarbon potential and thermal maturity of the Kudu 9A-2 and 9A-3 boreholes. Communs. Geol. Surv. Namibia, **6**, 49-58.

Davies, C.P.N. and Van der Spuy, D. (1992/93). The Kudu wells: Results of a biomarker study related to burial history modelling. Communs. Geol. Surv. Namibia, **8**, 45-56.

Davies, C.P.N. and Van der Spuy, D. (1997). Basin charge maps: an estimate of volumes of hydrocarbons available for migration. SOEKOR unpubl. Tech. Note No. 80, 6pp.

Davies, C.P.N., Benson, J.M. and Van der Spuy, D. (1991). Geochemical and palaeontological study of AEC DWK-1 borehole, Haasvlakte basin, South Western Cape. SOEKOR unpubl. rept., 38pp.

Davies, C.P.N., Van der Spuy, D. and Venter, H.J. (1994a). A-J1: geochemical data and summary report. SOEKOR unpubl. rept., SOE-GCH-RPT-040, 12pp.

Davies, C.P.N., Van der Spuy, D. and Venter, H.J. (1994b). E-A11: geochemical data and summary report. SOEKOR unpubl. rept., SOE-GCH-RPT-249, 11pp.

Davies, C.P.N., Van der Spuy, D. and Venter, H.J. (1995). E-B1: geochemical data and summary report. SOEKOR unpubl. rept., SOE-GCH-RPT-156, 10pp.

De Decker, R.H. and Woodborne, M.W. (1996). Geological and technical aspects of marine diamond exploration in Southern Africa. OTC 8018, "OTC 96 Proc. Off. Tech. Conf. Vol 1", Houston, 561-572.

De Grande, S.M.B., Aquino Neto, F.R. and Mello, M.R. (1993). Extended tricyclic terpanes in sediments and petroleum. Org. Geochem., **20/7**, 1039-1047

Demaison, G.J. (1984). The generative basin concept. in "Petroleum Geochemistry and Basin Evaluation". (eds.) Demaison, G.J. and Murris, R.J., Am. Assoc. Pet. Geol. Geol. Mem. No. 35, 1-14.

Demaison, G.J. and Moore, G.T. (1980). Anoxic environments and oil source bed genesis. Am. Assoc. Pet. Geol. Bull., **64/8**, 1179-1209.

Demaison, G.J., Holck, A.J.J., Jones, R.W. and Moore, G.T. (1988). Predictive source bed stratigraphy; A guide to regional petroleum occurrence. in "Geochemistry". (comps.) Beaumont, E.A. and Foster, N.H., AAPG Treatise Pet. Geol. Repr. Ser. No. 8, 323-333.

Deming, D. (1994). Factors necessary to define a pressure seal. Am. Assoc. Pet. Geol. Bull., **78/6**, 1005-1009.

DePaolo, D., Stolper, E. and Thomas, D. (1996). Hawaii scientific drilling project: summary of preliminary results. GSA Today, **6/8**, 1-8.

Derbyshire, J. (1964). A hydrological investigation of the Agulhas Current area. Deep-sea Res., **11**, 781-815.

Derenne, S., Largeau, C. and Berkaloff, C. (1996). First example of an algaenan yielding on aromatic-rich pyrolysate. Possible geochemical implications on marine kerogen formation. Org. Geochem., **24/6-7**, 617-627.

Derenne, S., Metzger, P., Largeau, C., Van Bergen, P.F., Gatellier, J.P., Sinninghe Damsté, J.S., De Leeuw, J.W. and Berkaloff, C. (1991). Similar morphological and chemical variation *of Gloecapsomorpha prisca* in Ordovician sediments and cultured *Botryococcus braunii* as a response to changes in salinity. Org. Geochem., **19/4-6**, 299-313.

Deroo, G., Powell, T.G., Tissot, B.P. and McCrossan, R.G. (1977). The origin and migration of petroleum in the Western Canada sedimentary basin, Alberta. Geol. Surv. Can. Bull., **262**, 136pp.

Deroo, G., Herbin, J.P. and Roucaché, J. (1983). Organic geochemistry of Upper Jurassic - Cretaceous sediments from site 511, Leg 71, Western South Atlantic. in "Initial reports of Deep Sea Drilling Project". (eds.) Blakeslee, J.H. and Lee, M., Univ. Calif., Scripps Inst. Ocean., US Govt. Printers Office, Washington DC, 1001-1013.

De Swardt, A.M.J. and McLachlan, I.R. (1982). Petroleum exploration in the South African offshore: the geological framework and hydrocarbon potential. Proc. 12th CMMI Congress. (ed.) Glen, H.W., S. Afr. Inst. Min. Metall., Johannesburg, 147-161.

De Wit, M., Jeffery, M. Bergh, H. and Nicolaysen, L. (1988). Geological map of sectors of Gondwana: reconstruction to their disposition ~150 Ma. Am. Assoc. Pet. Geol. and Univ. Wits., AAPG, Tulsa.

Dingle, R.V. (1971). Tertiary sedimentary history of the continental shelf off Southern Cape Province, South Africa. Trans. Geol. Soc. S. Afr., **74**, 173-185.

Dingle, R.V. (1977). The anatomy of a large submarine slump on a sheared continental margin (SE Africa). Jour. Geol. Soc. Lond., **134**, 293-310.

Dingle, R.V. and Gentle, R.I. (1972). Early Tertiary volcanic rocks on the Agulhas bank, South African continental shelf. Geol. Mag., **109**, 127-136.

Dingle, R.V., Siesser, W.G. and Newton, A.R. (1983). "Mesozoic and Tertiary Geology of Southern Africa". A.A. Balkema, Rotterdam, 375pp.

Dingle, R.V., Birch, G.F., Bremner, J.M., DeDecker, R.H., Du Plessis, A., Engelbrecht, J.C., Fincham, M.J., Fitton, T., Flemming, B.W., Gentle, R.I., Goodlad, S.W., Martin, A.K., Mills, E.G., Moir, G.J., Parker, R.J., Robson, S.H., Rogers, J., Salmon, D.A., Siesser, W.G., Simpson, E.S.W., Summerhayes, C.P., Westall. F., Winter, A. and Woodborne, M.W. (1987). Deep-sea sedimentary environments around Southern Africa (SE Atlantic and SW Indian Oceans). Annals S. Afr. Museum, **98/1**, 1-27.

Dow, W.G. (1974). Application of oil-correlation and source-rock data to exploration in Williston Basin. Am. Assoc. Pet. Geol. Bull., 58/7, 1253-1262.

Dow, W.G. (1977). Kerogen studies and geological interpretation. Jour. Geoch. Expl., **7**, 79-99.

Dow, W.G. and O'Connor, D.J. (1982). Kerogen maturity and type by reflected light microscopy applied to petroleum exploration. in "How to assess Maturation and Palaeotemperatures". (eds.) Staplin, F.L. et al., Soc. Econ. Palaeontol. Mineral. Short Course No. 7, 133-157.

Dowdle, W.L. and Cobb, W.M. (1975). Estimation of static formation temperatures from well logs; an empirical method. Jour. Pet. Tech., **29**, 1326-1330.

Downey, M.W. (1984). Evaluating seals for hydrocarbon accumulation. Am. Assoc. Pet. Geol. Bull., **68/11**, 1752-1763.

Duane, M.J. and Brown, R.W. (1991). Tectonic brines in sedimentary basins: further applications of fission track analysis in understanding Karoo Basin evolution (South Africa). Basin Res., **3**, 187-195.

Duncan, R.A. (1981). Hotspots in the Southern Ocean - an absolute frame of reference for motion of the Gondwana continent. Tectonophys., **74**, 29-42.

Duncan, R.A., Hargraves, R.B. and Brey, G.P. (1978). Age, palaeomagnetism and chemistry of melilite basalts in the Southern Cape, South Africa. Geol. Mag., **115/5**, 317-327.

Durand, B. (1983). Present trends in organic geochemistry in research on migration of hydrocarbons. in "Advances in Organic Geochemistry 1981" (eds.) Bjorøy, M et al., John Wiley, Chichester, 117-128.

Durand, B. (1988). Understanding of hydrocarbon migration in sedimentary basins (present state of knowledge). Org. Geochem., **13/1-3**, 445-459.

Durand, B., Huc, A.Y. and Oudin, J.L. (1987). Oil saturation and primary migration: observations in shales and coals from the Kerbau wells, Mahakam Delta, Indonesia. in "Migration of hydrocarbons in sedimentary basins". (ed.) Doligez, B., Proc. 2nd IFP Expl. Res. Conf., Editions Technip, Paris, 173-196.

Du Rouchet, J. (1981). Stress fields, a key to oil migration. Am. Assoc. Pet. Geol. Bull., **65/1**, 74-85.

Du Toit, A.L. (1954). "Geology of South Africa". Oliver and Boyd, Edinburgh, 611pp.

Du Toit, J.J.L. (1972). Recoverable gas reserves in the Superior A structure. SOEKOR unpubl. rept., 18pp.

Du Toit, S.R. (1976). The Mesozoic geology of the Agulhas Bank, South Africa. Ph.D thesis, Univ. Cape Town, 150pp.

Dzou, L.I.P., Noble, R.A. and Senftle, J.T. (1995). Maturation effects on absolute biomarker concentration in a suite of coals and associated vitrinite concentrates. Org. Geochem., **23/7**, 681-697.

Eglington, B.M., Auret, J.M. and Retief, E.A. (1990). Results of a Rb-Sr isotopic study of biotites from boreholes F-F2 and F-O1. EMATEK (CSIR) unpubl. rept. to SOEKOR, EMA-C 90119, 4pp.

Eglinton, G. and Calvin, M. (1967). Chemical fossils. Sci. Amer., **216**, 32-43.

Ejedawe, J.E. (1986). The expulsion criterion in the evaluation of the petroleum source beds of the Tertiary Niger delta. Jour. Pet. Geol., **9/4**, 439-450.

Ekweozor, C.M., Okogun, J.I., Ekong, D.E.V. and Maxwell, J.R. (1981). C24-27 Degraded triterpanes in Nigerian petroleum: novel molecular markers of source/input or organic maturation. Jour. Geoch. Expl., **15**, 653-662.

Ekweozor, C.M. and Strausz, O.P. (1983). Tricyclic terpanes in the Athabasca oil sands: their geochemistry. in "Advances in Organic Geochemistry 1981". (eds.) Bjorøy, M. et al., John Wiley, Chichester, 746-766.

Ekweozor, C.M. and Udo, O.T. (1988). The oleananes: origin, maturation and limits of occurrence in Southern Nigeria sedimentary basins. Org. Geochem., **13/1-3**, 131-140.

Ekweozor, C.M. and Telnaes, N. (1990). Oleanane parameter: verification by quantitative study of the biomarker occurrence in sediments of the Niger delta. Org. Geochem., **16/1-3**, 401-413.

Erdman, G.J. (1975). Relations controlling oil and gas generation in sedimentary basins. 9th Wor. Pet. Cong., 139-148.

Erlank, A.J., le Roex, A.P., Harris, C., Miller, R.McG. and McLachlan, I.R. (1990). Preliminary note on the geochemistry of basalt samples from the Kudu boreholes. Communs. Geol. Surv. Namibia, **6**, 59-61.

Ernst, R.E., Head, J.W., Parfitt, E., Grosfils, E. and Wilson, L. (1995). Giant radiating dyke swarms on Earth and Venus. Earth Sci. Rev., **39.**, 1-58.

Espitalié, J., Laporte, J.L., Madec, M., Marquis, F., Leplat, P., Paulet, J. and Boutefou, A. (1977). Méthode rapide de caractérisation des roches mères, de leur potential pétrolier et de leur degré d'évolution. Rev. Inst. Fr. Petr., **32**, 23-42.

Espitalié, J., Deroo, G. and Marquis, F. (1985). La pyrolyse Rock-Eval et ses applications, Deuxiéme partie. Rev. Inst. Fr. du Petrole, **40/6**, 755-784.

Espitalié, J. and Joubert, L. (1987). Use of Tmax as a maturation index in petroleum exploration. in "Petroleum Geochemistry and Exploration in the Afro-Asian Region". (eds.) Kumar, R.K. et al., A.A. Balkema, Rotterdam, 67-73.

Espitalié, J., Ungerer, P., Irwin, I. and Marquis, F. (1988). Primary cracking of kerogen. Experimenting and modelling C1, C2-5, C6-15 and C15+ classes of hydrocarbons formed. Org. Geochem., **13/4-6**, 893-899.

Eurotrack (1996). Fission track analyses of apatite from two samples. Unpubl. rept. to SOEKOR, Eurotrack, London, 17pp.

Evans, R.J. and Felbeck, G.J. Jr. (1983). High temperature simulation of petroleum formation - 111. Effect of organic starting structure on hydrocarbon formation. Org. Geochem., **4/3-4**, 153-160.

Falcon, R.M.S. and Snyman, C.P. (1986). An introduction to coal petrography: atlas of petrographic constituents in bituminous coals of Southern Africa. Rev. Pap. Geol. Surv. S. Afr., **2**, 28pp.

Fan Pu, Philp, R.P., Li Zhenxi, Yu Xinki and Ying Guangguo (1991). Biomarker distributions in crude oils and source rocks from different sedimentary environments. Chem. Geol., **93**, 61-78.

Farrimond, P. and Telnaes, N. (1996). Three series of rearranged hopanes in Toarcian sediments (northern Italy). Org. Geochem., **25/3-4**, 165-177.

Farrimond, P., Bevan, J.C. and Bishop, A.N. (1996). Hopanoid hydrocarbon maturation by an igneous intrusion. Org. Geoch., **25/3-4**, 149-164.

Field, J.D. (1985). Organic geochemistry in exploration of the northern North Sea. in "Petroleum Geochemistry in Exploration of the Norwegian Shelf". (ed.) Thomas, B.M. et al., Graham and Trotman, London, 39-57.

Fitzgerald, M.G., Mitchum, R.M.Jr., Uliana, M.A. and Biddle, K.T. (1990). Evolution of the San Jorge Basin, Argentina. Am. Assoc. Pet. Geol. Bull., **74/6**, 879-920.

Fleet, A.J. and Scott, A.C. (1994). Coal and coal-bearing strata as oil-prone source rocks: an overview. in "Coal and coal-bearing strata as oil-prone source rocks?". (eds.) Scott, A.J. and Fleet, A.C., Geol Soc. Lond. Spec. Publ. No. 77, Geol. Soc., London, 1-8.

Flores, G. (1986). The petroleum geology and hydrocarbon prospectivity of Mozambique Vol 1". ENH, Maputo, 134pp.

FM Consultants (1972). Geochronological report on an aegirine-trachyte sample. Unpubl. rept. to SOEKOR, No. FMK/1105, 5pp.

FM Consultants (1973). Geochronological report on syenite cuttings D-A1. Unpubl. rept. to SOEKOR, No. FMK/1138, 4pp.

FM Consultants (1974). Geochronological report on sample No. FM 7396, Kudu 9A-1. Unpubl. rept to SOEKOR No. FMK/1178, 3pp.

FM Consultants (1976). Geochronological report: age determinations on Ba-A1 samples. Unpubl. rept. to Soekor No. FMK/1271, 3pp.

Fouché, J. (1996a). E-DB prospect lead. SOEKOR unpubl. Tech. Note No. 64, 6pp.

Fouché, J. (1996b). A re-evaluation of the structural evolution, depth conversion and volumetrics of the E-M field. SOEKOR unpubl. Tech. Note No. 75, 8pp.

Fouché, J., Bate, K.J. and Van der Merwe, R. (1992). Plate tectonic setting of the Mesozoic basins, southern offshore, South Africa: a review. in "Inversion tectonics of the Cape Fold Belt, Karoo and Cretaceous Basins of Southern Africa". (eds.) De Wit, M.J. and Ransome, I.G.D., A.A. Balkema, Rotterdam, 33-59.

Fouché, J., Brown D.M. and Wood, E.M. (1995). Reservoir reappraisal of the F-AH field incorporating the results of the 3-D seismic survey. SOEKOR unpubl. rept. SOE-EXP-RPT-311, 44pp.

Foresman, J.B. (1978). 11. Organic geochemistry DSDP leg 40, continental rise of southwest Africa. in "Initial reports of the Deep Sea Drilling Project Volume 40". (eds.) Bolli, H.M., Ryan, W.B.F. et al., Washington (US Government Printing Office), 557-567.

Fowler, M.G., Abolins, P. and Douglas, A.G. (1986). Monocyclic alkanes in Ordovician organic matter. Org. Geochem., **10**, 815-823.

Fowler, M.G. and Douglas, A.G. (1987). Saturated hydrocarbon biomarkers in oils of Late Precambrian age from Eastern Siberia. Org. Geochem., **11**, 201-213.

Fowler, M.G. and Brooks, P.W. (1990). Organic geochemistry as an aid in the interpretation of the history of oil migration into different reservoirs at the Hibernia K-18 and Ben Nevis I-45 wells, Jeanne d'Arc Basin, offshore eastern Canada. Org. Geochem., **16/1-3**, 461-475.

Frakes, L.A. and Kemp, E.M. (1972). Influence of continental positions on early Tertiary climates. Nature, **240**, 97-100.

Friedinger, P.J.J. (1988). The hydrocarbon potential of the F-F structure (south eastern Bredasdorp basin). SOEKOR unpubl. rept., 11pp.

Fuex, A.N. (1977). The use of stable carbon isotopes in hydrocarbon exploration. Jour. Geochem. Expl., **7**, 155-188.

Fuex, A.N. (1980). Experimental evidence against an appreciable isotopic fractionation of methane during migration. in "Advances in Organic Geochemistry 1979". (eds.) Douglas, A.G. and Maxwell, J.R., Pergamon Press, Oxford, 725-732.

Funnell, R.H. and Allis, R.G. (1996). Hydrocarbon maturation potential of offshore Canterbury and Great South Basins. in "1996 New Zealand Pet. Conf. Proc. Vol. 1", New Zealand Crown Minerals, Wellington, 22-30.

Gallegos, E.J. and Moldowan, J.M. (1992). The effect of injection hold time on GC resolution and the effect of collision gas on mass spectra in geochemical "biomarker" research. in "Biological markers in sediments and petroleum". (eds.) Moldowan, J.M., Albrecht, P. and Philp, R.P., Prentice-Hall, New Jersey, 157-181.

Gay, S.P.C. (1992). Epigenetic versus syngenetic magnetite as a cause of magnetic anomalies. Geophys., **57/1**, 60-68.

Gerrard. I. and Smith, G.C. (1983). Post-Palaeozoic succession and structure of the south-western African continental margin. in "Studies in Continental Margin Geology" (eds.) Watkins, J.S. and Drake, C.L., Am. Assoc. Pet. Geol. Mem. No. 34, 49-74.

GETECH (1992). African magnetic mapping project - total magnetic field anomaly map. ULIS Ltd., England.

Gibbons, M.J. and Herridge, K.J. (1984). Maturity and source potential of Clipper-1, Canterbury Basin, offshore New Zealand. BP unpubl. rept., GCB/162/84, 7pp.

Gibbons M.J. and Fry, S. (1986). A geochemical study of the Galleon-1 well, Canterbury Basin, offshore New Zealand. BP unpubl. rept., GCB/13/86, 5pp.

Gilbert, D. (1977). Organic facies variation in the Mesozoic South Atlantic. in "Initial Reports Deep Sea Drilling Project Leg 75". (eds.) Hay, W.W., Sibuet, J-C. et al., Washington (US Govt. Printers Office), 1035-1049.

Gilbert, C.E. (1990). Sandstone distribution in the 14At1 level in the E-G area, south-central Bredasdorp Basin: implication for a predictive depositional model. in "Abstracts Geocongress 90". Geol. Soc. S. Afr., Cape Town, 177-180.

Gilbert, C.E. and Roux, J. (1992). Evaluation of the 13A reservoirs at E-AR. SOEKOR unpubl. rept., SOE-PEN-RPT-051, 29pp.

Goodarzi, F., Brooks, P.W. and Embry, A.F. (1989). Regional maturity as determined by organic petrography and geochemistry of the Schei Point Group (Triassic) in the Western Sverdrup Basin, Canadian Arctic archipelago. Mar. Pet. Geol., **6**, 290-302.

Goodwin, N.S., Park, P.J.D. and Rawlinson, A.P. (1983). Crude oil biodegradation under simulated and natural conditions. in "Advances in Organic Geochemistry 1981". (eds.) Bjorøy, M. et al., John Wiley, Chichester, 650-658.

Goodwin, N.S., Mann, A.L. and Patience, R.L. (1988). Structure and significance of the C30 4 methyl steranes in lacustrine shales and oils. Org. Geochem., **12/5**, 495-506.

Grantham, P.J. (1986). The occurrence of unusual C27 and C29 sterane predominances in two types of Oman crude oils. Org. Geochem., **9/1**, 1-10.

Grantham, P.J. and Wakefield, L.L. (1988). Variation in the sterane carbon number distribution of marine source rock derived crude oils through geologic time. Org. Geochem., **12/1**, 61-73.

Green, P.F., Duddy, I.R. and Bray, R.J. (1993). Early Tertiary heating in Northwest England: fluids or burial or (both?). in "Geofluids, '93". (eds.) Parnell, J., Ruffell, A.H. and Moles, N.R., British Gas, UK, 119-123.

Grigo, D., Maragna, B., Arienti, M.T., Fiorani, M., Parisi, A., Marrone, M., Squazzero, P. and Uberg, A.S. (1993). Issues in 3D sedimentary basin modelling and application to Haltenbanken, offshore Norway. In "Basin Modelling: Advances and Applications". (eds.) Doré, A.G. et al., Norwegian Petroleum Society Spec. Publ. 3, Elsevier, Amsterdam, 455-468.

Grobbler, N. (1995). Formation water salinities in the Bredasdorp Basin. SOEKOR unpubl. rept. SOE-GEO-RPT-313, 14pp.

Grunau, H.R. (1987). A worldwide look at the cap-rock problem. Jour. Pet. Geol., **10/3**, 245-266.

Gründlingh, M. (1984). Environmental observations: Sedco K - ocean current and temperature observations. CSIR-NRIO unpubl. rept. to SOEKOR No. C/SEA 7913 (rev.), 4pp.

Gussow, W.C. (1954). Differential entrapment of oil and gas: a fundamental principle. Am. Assoc. Pet. Geol. Bull., **38/5**, 816-853.

Gutjahr, C.C.M. (1966). Carbonization measurements of pollen-grains and spores and their application. Leidse Geologische Mededelingen, **38**, 1-29.

Hälbich, I.W. (1983). The Cape Fold Belt - Agulhas transect across the Gondwana suture, Southern Africa. Global Geosci. Trans., **9**, Geophys. Union, Washington, 18pp.

Hälbich, I.W., Fitch, F.J. and Miller, J.A. (1983). Dating the Cape orogeny. Spec. Publ. Geol. Soc. S. Afr., **12**, 149-164.

Hall, P.B. and Douglas, A.G. (1983). The distribution of cyclic alkanes in two lacustrine deposits. in "Advances in Organic Geochemistry 1981". (eds.) Bjorøy, M. et al., John Wiley, New York, 576-587.

Hall, P.B., Schou, L. and Bjorøy, M. (1985). NPRA Alaska - North Slope oil-source rock correlation study. in "Alaska North Slope Oil/Rock Correlation Study". (eds.) Magoon, L.B. and Claypool, G.E., AAPG Stud. Geol., No. 20, 509-556.

Haq, B.U. and Van Eysinga, F.W.B. (1987). "Geological Time Table", 4th ed., Elsevier, Amsterdam.

Haq, B.U., Hardenbohl, J. and Vail, P.R. (1987). The new chronostratigraphic basis of Cenozoic and Mesozoic sea level cycles. Cushman Foundation Foram. Res. Spec. Publ. No. 24.

Hartnady, C.J.H. and Le Roex, A.P. (1985). Southern Ocean hotspot tracks and the Cenozoic absolute motion of the African, Antarctic and South American plates. Earth Planet. Sci. Let., **75**, 245-257.

Hartnady, C.J.H. and Partridge, T.C. (1995). Neotectonic uplift in Southern Africa: a brief review and geodynamic conjecture. in "Centennial Geocongress (1995): extended abstracts vol 11"., Geol. Soc. S. Afr., 456-459.

Hatch, F.H., Wells, A.K. and Wells, M.K. (1961). "Petrology of the Igneous Rocks". Thomas Murby, London, 515pp.

Haung, W.Y. and Meinschein, W.G. (1979). Sterols as ecological indicators. Geochim. et Cosmochim. Acta, **43**, 739-745.

Hays, J.D., Imbrie, J. and Shackleton, N.J. (1976). Variations in the earth's orbit: pacemaker of the ice ages. Science, **194**, 1121-1132.

Heckel, P.H. (1986). Sea-level curve for Pennsylvanian eustatic marine transgressive-regressive cycles along midcontinent outcrop belt, North America. Geology, **14**, 330-334.

Herbin, J.P., Magniez-Jannin, F. and Muller, C. (1986). Mesozoic organic rich sediments in the South Atlantic: distribution in time and space. SCOPE/UNEP Sonderbund, **60**, 71-97.

Hermanrud, C. (1986). On the importance to the petroleum generation of heating effects from compaction-derived water: an example from the North Sea. in "Thermal modelling in sedimentary basins". (ed.) Burrus, J., Éditions Technip, Paris, 247-269.

Heroux, Y., Chagnon, A. and Bertrand, R. (1979). Compilation and correlation of major thermal maturation indicators. Am. Assoc. Pet. Geol. Bull., **63/12**, 2128-2144.

Heums, O.R., Dalland, A. and Meisingset, K.K. (1986). Habitat of hydrocarbons at Haltenbanken (PVT-modelling as a predictive tool in hydrocarbon exploration). in "Habitat of hydrocarbons on the Norwegian Continental Shelf", Graham and Trotman, London, 259-274.

Hildebrand, A.R., Penfield, G.T., Kring, D.A., Pilkington, M. Camargo, A., Jacobsen, S.B. and Boynton, W.V. (1991). Chicxulub crater: a possible Cretaceous-Tertiary boundary impact crater on the Yucatán Peninsula, Mexico. Geology, **19**, 867-871.

Hill, S.J. (1991). Petrographic subdivison and correlation of the 14A sandstones in the central Bredasdorp Basin. SOEKOR unpubl. rept., 10pp.

Hill, S.J. (1995a). F-A gas field: petrographic appraisal. Halliburton unpubl. rept. to SOEKOR, HALPET R007/95, 22pp.

Hill, S.J. (1995b). Petrographic appraisal of pre1At1 sandstones from the northern flank of the Bredasdorp Basin. Halliburton unpubl. rept. to SOEKOR, HALPET R019/95, 21pp.

Hill, S.J. (1996). Carbonate cementation of 14A sandstones in the southern part of the central Bredasdorp Basin. Halliburton unpubl. rept. to SOEKOR, HALPET R004/96, 11pp.

Hiller, K. and Shoko, U. (1996). Hydrocarbon source potential of the Karoo in Zimbabwe. Jour. Afr. Earth Sci., **23/1**, 31-43.

Ho, T.Y., Rogers, M.A., Drushel, H.V. and Koens, C.B. (1974). Evolution of sulphur compounds in crude oils. Am. Assoc. Pet. Geol. Bull., **38/11**, 2338-2348.

Hodges, K. (1996). The geology of the deep marine sandstones of the 9At1-to-13At1 interval in the central Bredasdorp Basin. SOEKOR unpubl. rept., SOE-EXP-RPT-342, 16pp.

Holmes, A. (1965). "Principles of physical geology", Nelson, London, 482-489.

Holmes, L. (1994). Geological re-evaluation of the F-A gas field, incorporating development data. SOEKOR unpubl. rept. SOE-EXP-RPT-319, 48pp.

Honiball, A. (1995). Palaeogeographic maps of offshore South Africa. SOEKOR unpubl. rept., Tech. Note No. 56, 11pp.

Hood, H., Gutjahr, C.C.M. and Peacock, R.L. (1975). Organic metamorphism and the generation of petroleum. Am. Assoc. Pet. Geol. Bull., **59/6**, 986-996.

Horstad, I., Larter, S.R., Dypvik, H., Aagard, P., Bjornvik, A.M., Johansen, P.E. and Eriksen, S. (1990). Degradation and maturity controls on oil field petroleum column heterogeneity in the Gullfaks field, Norwegian North Sea,. Org. Geochem., **16/1-3**, 497-510.

Hovland, M., Croker, P.F. and Martin, M. (1994). Fault-associated seabed mounds (carbonate knolls?) off western Ireland and north-west Australia. Mar. Pet. Geol., 11/2, 232-246.

Huber, B.T. and Watkins, D.K. (1992). Biogeography of Campanian-Maastrichtian calcareous plankton in the region of the Southern Ocean. in "The Antarctic palaeoenvironment: a perspective on global change-1". (eds.) Kennet, J.P. and Warnke, D.A., Antarctic research series No. 56, Am. Geophys. Union, 31-60.

Hughes, W.B. (1984). Use of thiophenic organosulphur compounds in characterising crude oils derived from Carbonate versus siliciclastic sources. in "Petroleum Geochemistry and Source Rock Potential of Carbonate Rocks". (ed.) Palacas, J.G., AAPG Stud. Geol. No. 18, Tulsa, 181-196.

Hughes, W.B. and Dzou, L.I.P. (1995). Reservoir overprinting of crude oils. Org. Geochem., **23/10**, 905-914.

Hughes, W.B., Holba, A.G., Miller, D.E. and Richardson, J.S. (1985). Geochemistry of greater Ekofisk crude oils. in "Petroleum Geochemistry in Exploration of the Norwegian Shelf". (ed.) Thomas, B.D. et al., Graham and Trotman, London, 75-92.

Hughes, W.B., Holba, A.G. and Dzou, L.I.P. (1995). The ratios of dibenzothiophene to phenanthrene and pristane to phytane as indicators of depositional environment and lithology of petroleum source rocks. Geochim. et Cosmochim. Acta, **59/17**, 3581-3598.

Hunt, A. (1996). Uncertainties remain in predicting paraffin deposition. Oil Gas Jour., **94/3**, 96-103.

Hunt, J.M. (1979a). "Petroleum Geochemistry and Geology". Freeman, San Francisco, 617pp.

Hunt, J.M. (1979b). E-D1 oil. Unpubl. rept. to SOEKOR, JMH.PAC, 6pp.

Hunt, J.M. (1990). Generation and migration of petroleum from abnormally pressured fluid compartments. Am. Assoc. Pet. Geol. Bull., 74/1, 1-12.

Hussler, G., Chappe, B., Wehrung, B. and Albrecht, P. (1981). C27-29 ring-A monoaromatic steroids in Cretaceous black shales. Nature, **294**, 556-558.

Hutton, A.C. and Cook, A.C. (1980). Influence of alginite on the reflectance of vitrinite from Joadja, NSW, and some other coals and oil shales containing alginite. Fuel, **59/10**, 711-714.

Hwang, R.J., Ahmed, A.S. and Moldowan, J.M. (1994). Oil composition variation and reservoir continuity: Unity field, Sudan. Org. Geochem., **21/2**, 171-188.

IGI (1994). Hydrocarbon correlation in the offshore Mossel Bay area, RSA. Unpubl. rept to Soekor, Integrated Geochem. Interpret., Bideford, Devon, 51pp.

Jacobson, S.R. (1991). Petroleum source rocks and organic facies. in "Source and migration processes and evaluation techniques". (ed.) Merrill, R.K., Am. Assoc. Pet. Geol. Treatise Pet. Geol., 3-11.

Jensen, R.P. and Doré, A.G. (1993). A recent Norwegian shelf heating event - fact or fantasy? in "Basin modelling: advances and applications". (eds.) Doré, A.G. et al., NPF Spec. Publ. 3, Elsevier, Amsterdam, 85-106.

Jessop, A.M. and Majorowicz, J.A. (1994). Fluid flow and heat transfer in sedimentary basins. in "Geofluids: origin, migration and evolution of fluids in sedimentary basins". (ed.) Parnell, J., Geol. Soc. Spec. Publ. No. 78, London, 43-54.

Jarvie, D.M. (1991). Total organic carbon (TOC) analysis. in "Source and Migration Processes and Evaluation Techniques". (ed.) Merrill, R.K., AAPG Treatise Pet. Geol., 113-118.

Jiang, Z.S. and Fowler, M.G. (1986). Carotenoid-derived alkanes in oils from northwestern China. Org. Geochem., **10**, 831-839.

Jobson, A.M., Cook, F.D. and Westlake, D.M.S. (1979). Interaction of aerobic and anaerobic bacteria in petroleum degradation. Chem. Geol., **24**, 355-365.

Johnson, M.R. (1990). Provenance and tectonic setting of the Cape-Karoo basin in the eastern Cape Province. in "Abstracts Geocongress 90". Geol. Soc. S. Afr., Cape Town, 690-693.

Joly, D., Vasse, L. and Bordenave, M.L. (1974). Application de méthodes d'analyse physique à la recherche de parenté entre différents pétroles du Moyen-Orient.. in "Advances in Organic Geochemistry 1973". (eds.) Tissot, B.P. and Bienner, F., Éditions Technip, Paris, 531-547.

Jovancicevic, B., Vucelic, D., Saban, M., Wehner, H. and Vitorovic, D. (1993). Investigation of the catalytic effect of indigenous minerals in the pyrolysis of Aleksinac oil shale substrates: steranes, terpanes and triaromatic steroids in the pyrolysates. Org. Geochem., **20/1**, 69-76.

Jungslager, E.H.A. (1996). The syn-rift of the Bredasdorp Basin. SOEKOR unpubl. rept., SOE-GEO-RPT-380, 61pp.

Kajato, H.K. (1982). Gas strike spurs search for oil in Tanzania. Oil Gas Jour., **80/11**, 123-131.

Karweil, J. (1956). Die Metamorphose der Kohlen vom Standpunkt der physikalischen Chemie. Zeit. Deutsch Geol. Ges., **107**, 132-138.

Katz, B.J., Pheifer, R.N. and Schunk, D.J. (1988). Interpretations of discontinuous vitrinite reflectance profiles. Am. Assoc. Pet. Geol. Bull., **72/8**, 926-931.

Kaufman, R.L., Ahmed, A.S. and Hempkins, W.B. (1987). A new technique for the analysis of commingled oils and its application to production allocation calculations. Indon. Pet. Assoc. Proc. 16th Ann. Conv., 247-266.

Kaufman, R.L., Ahmed, A.S. and Elsinger, R.J. (1990). Gas chromatography as a development and production tool for fingerprinting oils from individual reservoirs: applications in the Gulf of Mexico. Gulf Coast Soc. Expl. Prod. Am. Conf., Austin, Texas, 263-282.

Keeley, M.L. and Light, M.P.R. (1993). Basin evolution and prospectivity of the Argentine continental margin. Jour. Pet. Geol., **16/4**, 451-464.

Khanna, S.N. and Pillay, G. (1986). Seychelles: petroleum potential of this Indian Ocean paradise. Oil and Gas Jour., **84/12**, 136-139.

Kissin, Y.V. (1987). Catagenesis and composition of petroleum: Origin of n-alkanes and isoalkanes in petroleum crudes. Geochim. et Cosmochim. Acta, **51**, 2445-2457.

Klemme, H.D. (1994). Petroleum systems of the world involving Upper Jurassic source rock. in "The Petroleum System - from source to trap". (eds.) Magoon, L.B. and Dow, W.G., Am. Assoc. Pet. Geol. Mem. No. 60, AAPG, Tulsa, Oklahoma, 51-72.

Kreuger (1974). Potassium-argon age determination sample U-1. Krueger Enterprises Inc., Geochron laboratories, Cambridge Mass, 1pp.

Kroner, A. (1973). Comment on "Is the African plate stationary". Nature, **243**, 29-30.

Krooss, B.M. (1987). Experimental investigation of the diffusion of low-molecular weight hydrocarbons in sedimentary rocks. in "Migration of hydrocarbons in sedimentary basins". (ed.) Doligez, B., 2nd IFP Expl. Res. Conf., Éditions Technip, Paris, 329-351.

Krooss, B.M., Leythauser, D. and Schaefer, R.G. (1988). Light hydrocarbon diffusion in a caprock. Chem. Geol., **71**, 65-76.

Krooss, B.M., Brothers, L. and Engel, M.H. (1991). Geochromatography in petroleum migration: a review. in "Petroleum Migration" (eds.) England, W.A. and Fleet, A.J., Geol. Soc. Spec. Publ. No. 59, 149-163.

Kvenvolden, K.A., Rapp, J.B. and Bowrell, J.H. (1985). Comparison of molecular markers in crude oils and rocks from the North Slope of Alaska. in 'Alaska North Slope oil/rock correlation study". (eds.) Magoon, L.B. and Claypool, G.E., AAPG Stud. Geol. No. 20, Tulsa, 593-617.

Labuschagne, H. (1993). Geological well completion report of borehole E-BK1. SOEKOR unpubl. rept., SOE-DRG-WCR-278, 24pp.

Lafargue, E. and Barker, C. (1988). Effect of water-washing on crude oil composition. Am. Assoc. Pet. Geol. Bull., **72/3**, 263-276.

Laflamme, R.E. and Hites, R.A. (1978). The global distribution of polycyclic aromatic hydrocarbons in recent sediments. Geochim. et Cosmochim. Acta, **42**, 289-303.

Larcher, A.V., Alexander, R., Rowlands, S.J. and Kagi, R.I. (1986). Acid catalysis of alkyl hydrogen exchange and configurational isomerisation reactions: acyclic isoprenoid acids. Org. Geochem., **10**, 1015-1021.

Larsen, M. (1995). Overpressure study. SOEKOR unpubl. Tech. Note No. 29, 12pp.

Larsen, R.L. (1991). Geological consequences of superplumes. Geology, **19/10**, 963-966.

Larter, S.R. and Aplin, A.C. (1995). Reservoir geochemistry: methods, applications and opportunities. in "The Geochemistry of Reservoirs". (eds.) Cubitt, J.M. and England, W.A., Geol. Soc. Spec. Publ. No. 86, Geological Society, London, 5-32.

Larter, S. and Mills, N. (1991). Phase-controlled molecular fractionation in migrating petroleum charges. in "Petroleum Migration". (eds.) England, W.A. and Fleet, A.J., Geol. Soc. Spec. Publ. No. 59, 137-147.

Lawrence, S.R. and Johnson, M. (1995). Shelf north of Falklands may be new S. Atlantic petroleum province. Oil Gas Jour., **93/9**, 52-55.

Lawver, L.A., Gahagan, L.M. and Coffin, M.F. (1992). The development of palaeoseaways around Antarctica. in "The Antarctic palaeoenvironment: a perspective on global change". (eds.) Kennett, J.P. and Warnke, D.D., Antarctic Res. Ser. **56**, 7-36.

Lee, M.L., Vassilaros, D.L., White, C.M. and Novotny, M. (1979). Retention indices for programmed temperature capillary-column gas chromatography of polycyclic hydrocarbons. Analyt. Chem., **51/6,** 766-774.

Leenheer, M.J. (1984). Mississippi Bakken and equivalent formations as source rocks in the Western Canadian basin. Org. Geochem., **6**, 521-532.

Leith, M.L. and Rowsell, D.M. (1978). Burial history and temperature-depth conditions for hydrocarbon generation and migration in the Agulhas Bank, RSA. SOEKOR unpubl. rept., 18pp.

Leith, T.L., Kaarsted, I., Connan, J., Pierron, J. and Caillet, G. (1993). Recognition of caprock leakage in the Snorre field, Norwegian North Sea. Mar. Pet. Geol., **10**, 29-41.

Lerche, I. (1990). "Basin analysis - quantitative methods, Volume 1". Academic Press, San Diego, 562pp.

Lerche, I., Yu, Z., Tørudbakken, B. and Thomsen, R.O. (1997). Ice loading effects in sedimentary basins with reference to the Barents Sea. Mar. Pet. Geol., **14/3**, 277-338.

Le Roux, D.M., (1983). 7. Geological structure in the Little Karoo about 21°E longitude. Spec. Publ. Geol. Soc. S. Afr., **12**, 65-74.

Le Tran, K. (1975). Analyse et étude des hydrocarbures gazeux occlus dans les sediments. Exemple d'application a l'exploration pétrolière. Bull. Centre Rech. Pau - SNPA, **9**, 223-243.

Lewan, M.D. (1985). Evaluation of petroleum generation by hydrous pyrolysis experimentation. Phil. Trans. R. Soc. Lond., **A315**, 123-134.

Leythauser, D., Mackenzie, A.S., Schaefer, R.G., Altebäumer, F.J. and Bjorøy, M. (1983). Recognition of migration and its effects within two coreholes in shale/sandstone sequences from Svalbard, Norway. in "Advances in Organic Geochemistry 1981". (eds.) Bjorøy, M. et al., John Wiley, Chichester, 136-146.

Leythauser, D., Mackenzie, A.S., Schaeffer, R.G. and Bjorøy, M. (1984). A novel approach for recognition and quantification of hydrocarbon migration effects in shale-sandstone sequences. Am. Assoc. Pet. Geol. Bull., **68/2**, 196-219.

Leythauser, D., Schaefer, R.G. and Radke, M. (1988). Geochemical effects of primary migration of petroleum in Kimmeridge source rocks from Brae field area, North Sea. 1: gross composition of C^{15+}-soluble organic matter and molecular composition of C^{15+}-saturated hydrocarbons. Geochim. et Cosmochim. Acta, **52**, 701-713.

Leythauser, D. and Poelchau, H.S. (1991). Expulsion of petroleum from type III kerogen source rocks in gaseous solution: modelling of solubility fractionation. in "Petroleum Migration". (eds.) England, W.A. and Fleet, A.J., Geol. Soc. Lond. Spec. Publ. No. 59, 33-46.

Light, M.P.R. and Shimutwikeni, H. (1991). Namibia, practically unexplored, may have land, offshore potential. Oil Gas Jour., **89/14**, 85-89.

Limonov, A.F., van Weering, Tj.C.E., Kenyon, N.H., Ivanov, M.K. and Meisner, L.B. (1997). Seabed morphology and gas venting in the Black Sea mudvolcano area: Observations with the MAK-1 deep-tow sidescan sonar and bottom profiler. Mar. Geol., **137**, 121-136.

Lin, R. (1994). An interlaboratory comparison of vitrinite reflectance measurement. Org. Geochem., **22/1**, 1-9.

Littke, R., Rullkötter, J. and Schaefer, R.G. (1991). Organic and carbonate carbon accumulation on Broken Ridge and Ninety East Ridge, Central Indian Ocean. Proc. ODP. Sci. Res., **121**, 467-487.

Littke, R., Krooss, B., Idiz, E. and Frielingsdorf, J. (1995). Molecular nitrogen in natural gas accumulations from sedimentary organic matter at high temperatures. Am. Assoc. Pet. Geol. Bull., **79/3**, 410-430.

Loring, D.H. and Rantala, R.T.T. (1992). Manual for the geochemical analysis of marine sediments and suspended particulate matter. Earth Sci. Rev., **32**, 235-283.

Loutit, T.S., Hardenbol, J., Vail, P.R. and Baum, G.R. (1989). Condensed sections: The key to age dating and correlation of continental margin sequences. in "Sea-level changes: an integrated approach". (eds.) Wilgus, C.K., Hastings, B.S., Kendall, C.G.St.C., Posamentier, H.W., Ross, C.A. and Van Wagoner, J.C., Soc. Pal. Mineral. Spec. Publ. No. 42, 1-40.

Lutjeharms, J.R.E., Bang, N.D. and Valentine, H.R. (1981). Die fisiese oseanologie van die Agulhas Bank. WNNR Navorsingsverslag 386, Stellenbosch, 38pp.

Mackenzie, A.S. (1984). Application of biological markers in petroleum geochemistry. in "Advances in Organic Geochemistry Vol 1". (eds.) Brooks, J. and Welte, D.H., Academic, London, 115-214.

Mackenzie, A.S., Patience, R.L., Maxwell, J.R., Vandenbroucke, M. and Durand, B. (1980). Molecular parameters of maturation in the Toarcian shales, Paris Basin, France-1. Changes in the configurations of acyclic isoprenoid alkanes, steranes and triterpanes. Geochim. et Cosmochim. Acta, **44**, 1709-1721.

Mackenzie, A.S., Li Ren-Wei, Maxwell, J.R., Moldowan, J.M. and Seifert, W.K. (1983). Molecular measurements of thermal maturation of Cretaceous shale from the Overthrust Belt, Wyoming, USA. in "Advances in Organic Geochemistry 1981". (eds.) Bjorøy, M. et al., John Wiley and Sons, Chichester, 496-503.

Mackenzie, A.S., Rullkötter, J., Welte, D.H. and Mankiewicz, P. (1985). Reconstruction of oil formation and accumulation in North Slope, Alaska, using quantitative GC-MS. in "Alaska North Slope Oil/Shale Correlation Study". (eds.) Magoon, L.B. and Claypool, G.E., AAPG Stud. Geol. No. 20, 319-377.

Mackenzie, A.S., Leythauser, D., Muller, P., Quigley, T.M. and Radke, M. (1988). The movement of hydrocarbons in shales. Nature, **331**, 63-65.

Macquaker, J.H.S., Farrimond, P. and Brassell, S.C. (1986). Biological markers in the Rhaetian black shales of South West Britain. Org. Geochem., **10**, 93-100.

Magara, K. (1977). Petroleum migration and accumulation. in "Developments in Petroleum Geology 1". (ed.) Hobson, G.D., Applied Science, London, 83-125.

Magara, K. (1978). "Compaction and Fluid Migration". Developments in Petroleum Science, 9, Elsevier, Amsterdam, 319pp.

Magara, K. (1986). "Geological Models of Petroleum Entrapment", Elsevier, London, 328pp.

Magoon, L.B. and Claypool, G.E. (1985). "Alaska North Slope oil-source rock correlation study". AAPG Stud. Geol. No. 20, Tulsa, 682pp.

Magoon, L.B. and Anders, D.E. (1992). Oil-to-source rock correlation using carbon-isotopic data and biological marker compounds, Cook Inlet - Alaska Peninsula, Alaska. in "Biological Markers in Sediments and Petroleum". (eds.) Moldowan, J.M., Albrecht, P. and Philp, R.P., Preston Hall, New Jersey, 241-274.

Magoon, L.B. and Dow, W.G. (1994). "The Petroleum System - from source to trap". Am. Assoc. Pet. Geol. Mem. No. 60, 655.

Malan, J.A. (1990). The stratigraphy and sedimentology of the Bredasdorp Group, Southern Cape Province. Unpubl. M.Sc. thesis, Univ. Cape Town, 197pp.

Malan, J.A. (1993). Geology, potential of Algoa, Gamtoos basins of South Africa. Oil Gas Jour., **91/46**, 74-77.

Malan, J.A., Martin, A.K. and Cartwright, J.A. (1990). The structural and stratigraphic development of the Gamtoos and Algoa Basins, offshore South Africa. In "Abstracts Geocongress 90", Geol. Soc. S. Afr., Cape Town, 328-331.

Mango, F.D. (1987). An invariance in the iso-heptanes of petroleum. Science, **237**, 514-517.

Mango, F.D. (1990). The origin of light cycloalkanes in petroleum. Geochim. et Cosmochim. Acta, **54**, 23-27.

Mango, F.D. (1991). The stability of hydrocarbons under the time-temperature conditions of petroleum genesis. Nature, **352**, 146-148.

Mango, F.D. (1992). Transition metal catalysis in the generation of petroleum and natural gas. Geochim. et Cosmochim. Acta, **56**, 895-901.

Mango, F.D. (1994). The origin of light hydrocarbons in petroleum: ring preference in the closure of carbocyclic rings. Geochim. et Cosmochim. Acta, **58/2**, 553-555.

Marshall, J.E.A. (1994). Plate tectonics and hydrocarbon generation in the Falklands Islands. Mar. Pet. Geol., **11/5**, 631-636.

Martin, A.K., Hartnady, C.J.H. and Goodlad, S.W. (1981). A revised fit of South America and South Central Africa. Earth Planet. Sci. Lett., **54**, 293-305.

Martin, R.L., Winters, J.C. and Williams, J.A. (1963). Distributions of n-paraffins in crude oils and their implications to origin of petroleum. Nature, **199/4889**, 110-113.

Maslanyi, M., Light, M., Horn, I., Greenwood, J. and Davidson, K. (1992). How similar geology of West Africa and eastern South America evolved. Offshore, **52/2**, 25-27.

Maxwell, J.R., Cox, R.E., Eglinton, G., Pillinger, C.T., Ackman, R.G. and Hooper, S.N. (1973). Stereochemical studies of acyclic isoprenoid compounds - 11. The rôle of chlorophyll in the derivation of isoprenoid-type acids in a lacustrine sediment. Geochim. et Cosmochim. Acta, **37**, 297-313.

McAloon, W., Webster, M. and Elliott, S. (1990). The occurrence of overpressure in the South African continental shelf. Abstracts Geocongress 90, Geol. Soc. S. Afr., 349-352.

McAuliffe, C. (1966). Solubility in water of paraffin, cycloparaffin, olefin, acetylene, cyclo-olefin and aromatic hydrocarbons. Jour. Phys. Chem., **70**, 1267-1275.

McCarthy, T.S. (1978). Report on analytical services. Unpubl. report to Soekor, Wits. Univ., 2pp.

McIver, J.R. and Ferguson, J. (1978). Kimberlitic, melilitic, trachytic and carbonatitic eruptives at Saltpetre Kop, Sutherland, South Africa. In "Extended Abstracts to Second International Kimberlite Conference", October 3-7, 1977, Santa Fe, New Mexico, 3pp.

McKirdy, D.M., Aldridge, A.K. and Ypma, P.J.M .(1983). A geochemical comparison of some crude oils from pre Ordovician carbonate rocks. in "Advances in Organic Geochemistry 1981". (eds.) Bjorøy, M. et al., John Wiley, Chichester, 99-107.

McLachlan, I R. and Fülop, R. (1975). Description of standard palynological processing techniques used at Soekor. Soekor unpubl. rept., PALR3/III-42, 6pp.

McLachlan, I.R. and McMillan, I.K. (1979). Microfaunal biostratigraphy, chronostratigraphy and history of Mesozoic and Cenozoic deposits on the coastal margin of South Africa. Geol. Soc. S. Afr. Spec. Publ. No. 6, 161-181.

McLachlan, I.R., Du Toit, J.J.L., Davies, C.P.N., Wood, E.M. and Marot, J.E.B. (1979). Initial report on alteration and flushing of petroleum reservoirs in the distal Bredasdorp Basin. SOEKOR unpubl. rept., 21pp.

McMillan, I.K. (1986). Cainozoic planktonic and larger foraminifera distribution around Southern Africa and their implication for past changes of oceanic water temperature. S. Afr. Jour. Sci., **82**, 66-69.

McMillan, I.K. (1989). Victoriella conoidea (Rutten, 1914): A guide foraminifera for the late Aquitanian (Early Miocene) marine rocks of Southern Africa. S. Afr. Jour. Geol., **92/2**, 95-101.

McMillan, I.K. (1990). Foraminiferal definition and possible implications of the major mid Cretaceous (Albian to Coniacian) hiatuses of southernmost Africa. in "Abstracts Geocongress 90". Geol. Soc. S. Afr., Cape Town, 363-366.

McMillan, I.K. and Valicenti, V.H. (1986). Palaeontology summary borehole F-R1. SOEKOR unpubl. rept., 1pp.

McMillan, I.K., Broad, D.S. and Brink, G.J. (1992). Late Mesozoic basins off the south coast of South Africa. SOEKOR unpubl. rept., SOE-EXP-RPT-034, 35pp.

McMillan, I.K., Brink, G.J., Broad, D.S. and Maier, J.J. (1997 in press). Late Mesozoic sedimentary basins off the south coast of South Africa. in "Sedimentary Basins of the World: The African Basins", (ed.) Selley, R.C, Elsevier, Amsterdam.

Mello, M.R., Mohriak, W.U., Koutsoukos, A.M. and Figueira, J.C.A. (1991). Brazilian and West African oils: generation, migration, accumulation and correlation. 13th Wor. Pet. Cong., Topic 3 preprints, John Wiley, Chichester, 1-12.

Mello, M.R., Telnaes, N., Gaglianone, P.C., Chicarelli, M.I., Brassell, S.C. and Maxwell, J.R. (1988). Organic geochemical characterisation of depositional palaeoenviroments of source rocks and oils in Brazilian marginal basins. Org. Geochem., **13/1-3**, 31-45.

Miles, J.A. (1989). "Illustrated Glossary of Petroleum Geochemistry". Oxford Univ. Press, Oxford, 137pp.

Miles, J.A. (1990). Secondary migration routes in the Brent sandstones of the Viking Graben and East Shetland Basin: evidence from oil residues and subsurface pressures. Am Assoc. Pet. Geol. Bull., **74/11**, 1718-1735.

Milner, S.C. (1992). The age and emplacement of the Etendeka Formation volcanic rocks and the Damaraland igneous complexes relative to the opening of the South Atlantic: a review. "Abstracts South Western African continental margin conference: evolution and physical characteristics". Geol. Soc. Namibia, April 1992, 44-47.

Mitchell, C., Taylor, G.K. Cox, K.G. and Shaw, J. (1986). Are the Falklands a rotated microplate? Nature, **319**, 131-134.

Mlaba, B.M. (1996). Evaluation of magnetic and seismic anomalies surrounding the F-F high. SOEKOR unpubl. rept., Tech. Note No. 76, 5pp.

Mohriak, W.U., Mello, M.R., Karner, G.D., Dewey, J.F. and Maxwell, J.R. (1989). Structural and stratigraphic evolution of the Campos Basin, offshore Brazil. in "Extensional tectonics and stratigraphy of the North Atlantic margins". (eds.) Tankard, A.J. and Balkwill, H.R., AAPG Mem. No. 46, 599-614.

Moldowan, J.M. and Fago, F.J. (1986). Structure and significance of a novel rearranged monoaromatic steroid hydrocarbon in petroleum. Geochim. et Cosmochim. Acta, **50**, 343-351.

Moldowan, J.M., Sundararaman, P. and Schoell, M. (1986). Sensitivity of biomarker properties to depositional environment and/or source input in the Lower Toarcian of SW Germany. Org. Geochem., **10**, 915-926.

Moldowan, J.M., Seifert, W.K. and Gallegos, E.J. (1983). Identification of an extended series of tricyclic terpanes in petroleum. Geochim. et Cosmochim. Acta, **47**, 1531-1534.

Moldowan, J.M., Seifert, W.K. and Gallegos, E.J. (1985). Relationship between petroleum composition and depositional environments of petroleum source rocks. Am. Assoc. Pet. Geol. Bull., **69/8**, 1255-1268.

Moldowan, J.M., Fago, F.J., Carlson, R.M.K., Young, D.C., Van Duyne, G., Clardy, J., Schoell, M., Pillinger, C.T. and Watt, D.S. (1991). Rearranged hopanes in sediments and petroleum. Geochim. et Cosmochim. Acta, **55**, 3333-3353.

Moldowan, J.M., Lee, C.Y., Sundararaman, P., Salvatori, T., Alajbeg, A., Gjukic, B., Demaison, G.J., Slougui, N-E. and Watt, D.S. (1992). Source correlation and maturity assessment of select oils and rocks from the Central Adriatic Basin (Italy and Yugoslavia). in "Biological Markers in Sediments and petroleum". (eds.) Moldowan, J.M., Albrecht, P. and Philp, R.P., Prentice Hall, New Jersey, 370-401.

Moldowan, J.M., Dahl, J., Huizinga, B.J., Fago, F.J., Hickey, L.J., Peakman, T.M. and Taylor, D.W. (1994). The molecular fossil record of oleanane and its relation to angiosperms. Science, **265**, 768-771.

Momper, J.A. (1982). The Etosha basin re-examined. Oil Gas Jour., **80/40**, 262-287.

Morgan, W.J. (1983). Hotspot tracks and the early rifting of the Atlantic. Tectonophysics, **94**, 123-139.

Morris, R.J. and Calvert, S.E. (1975). Fatty acid uptake by marine sediment particles. Geochim. et Cosmochim. Acta, **39**, 377-381.

Morrow, D.H. and Issler, D.R. (1993). Calculation of vitrinite reflectance from thermal histories: a comparison of some methods. Am. Assoc. Pet. Geol. Bull., **77/4**, 610-624.

Morton, A.C. (1986). Dissolution of apatite in North Sea Jurassic sandstones: implications for the generation of secondary porosity. Clay Mins., **21**, 711-733.

Mpanju, F. and Philp, R.P. (1993). Organic geochemical characterisation of bitumens, seeps, rock extracts and condensates from Tanzania. Org. Geochem., **21/3-4**, 259-371.

Muntingh, A. (1993) Geology, prospects in Orange basin offshore western South Africa. Oil Gas Jour., **91/4**, 106-109.

NASOU, (1973). "Standard encyclopaedia of Southern Africa", **8**, p284.

Natland, M.L., González, E., Cañon, A. and Ernst, M.C. (1974). A system of stages for correlation of Magallanes Basin sediments. Mem. Geol. Soc. Am., **139**, 126pp.

Nes, W.R. (1974). Role of sterols in membranes. Lipids, **9/8**, 596-612.

Noble R.D.P. (1996). Hydrocarbon shows database project. SOEKOR unpubl. Tech. Note No. 55, 3pp.

Noble, R.D.P. and Davies, C.P.N. (1996). Diagenetic seal trend in the proximal 14A sandstones. SOE-EXP-RPT-377, 31pp.

North, F.K. (1985). "Petroleum Geology". Allen and Unwin, Winchester, 607pp.

Nybakken, S. (1991). Sealing fault trap - an exploration concept in a mature petroleum province: Tampen Spur, northern North Sea. First Break, **9/5**, 209-222.

Nyblade, A.A. and Robinson, S.W. (1994). The African superswell. Geophys. Res. Lett., **21/9**, 765-768.

O'Brien, G. and Woods, P. (1995). Hydrocarbon-related diagenetic zones (HRDZs) in the Vulcan sub-basin, Timor Sea: recognition and exploration implications. APEA Jour., **35/1**, 220-252.

O'Connell, S.A., Chandler, M.A. and Ruedy, R. (1996). Implications for the creation of warm saline deep water: late Palaeocene reconstructions and global climate model simulations. Geol. Soc. Am. Bull., **108/3**, 270-284.

Osadetz, K.G., Brooks, P.W. and Snowdon, L.R. (1992). Oil families and their sources in Canadian Williston Basin, (southeastern Saskatchewan and southwestern Manitoba). Bull. Can. Pet. Geol., **40/3**, 254-273.

Ourisson, G., Albrecht, P.A. and Rohmer, M. (1984). The microbial origin of fossil fuels. Sci. Am., **251/2**, 44-51.

Ozkaya, I. and Akbar, A. (1991). An iterative procedure to determine depth and time of primary oil migration and expulsion efficiency of source rocks. Jour. Pet. Sci. Engin., **5**, 371-378.

Palacas, J.G., Anders, D.E. and King, J.D. (1984). South Florida Basin - a prime example of carbonate source rocks of petroleum. in "Petroleum Geochemistry and Source Rock Potential of Carbonate Rocks" (ed.) Palacas, J.G., AAPG Stud. Geol. No. 18, Am. Assoc. pet. Geol., Tulsa, 71-96.

Palmer, S.E. (1984). Hydrocarbon source potential of organic facies of the lacustrine Elko Formation (Eocene/Oligocene), northeast Nevada. in "Hydrocarbon source rocks of the Greater Rocky Mountain Region". (eds.) Woodward, J.E., Meissner, F.F. and Clayton, J.L., Rocky Mtn. Assoc. Geol., Denver, 491-511.

Park, R.G. (1988). "Geological Structures and Moving Plates". Blackie, New York, 337pp.

Partridge, T.C. and Maud, R.R. (1987). Geomorphic evolution of Southern Africa since the Mesozoic. S. Afr. Jour. Geol., **90/2**, 179-208.

Paull, C.K., Buelow, W.J., Ussler III, W. and Borowski, W.S. (1996). Increased continental-margin slumping frequency during sea level lowstands above gas hydrate-bearing sediments. Geology, **24/2**, 143-146.

Peakman, T.M., Ten Haven, H.L., Rechka, J.R., De Leeuw, J.W. and Maxwell, J.R. (1989). Occurrence of (20R)- and (20S)-$\Delta^{8(14)}$ and Δ^{14} 5α(H)-steranes and the origin of 5α(H),14β(H),17β(H)-steranes in immature sediment. Geochim. et Cosmochim. Acta, **53**, 2001-2009.

Pederson, T.F. and Calvert, S.E. (1990). Anoxia vs productivity: what controls the formation of organic carbon-rich sediments and source rocks. Am. Assoc. Pet. Geol. Bull., **74/4**, 454-466.

Pepper, A.S. (1991). Estimating the petroleum expulsion behaviour of source rocks: a novel quantitative approach. in "Petroleum Migration". (eds.) England, W.A. and Fleet, A.J., Geol. Soc. Lond. Spec. Publ. No. 59, London, 9-31.

Peters, K.E. (1986). Guidelines for evaluating petroleum source rocks using programmed pyrolysis. Am. Assoc. Pet. Geol. Bull., **70/3**, 318-329.

Peters, K.E., Ishiwatari, R. and Kaplan, I.R. (1977). Colour of kerogen as index of organic maturity. Am. Assoc. Pet. Geol. Bull., **61/4**, 504-510.

Peters, K.E., Moldowan, J.M., Driscoll, A.R. and Demaison, G.J. (1989). Origin of Beatrice oil by co-sourcing from Devonian and Middle Jurassic source rocks, Inner Moray Firth, United Kingdom. Am. Assoc. Pet. Geol. Bull., **73/4,** 454-471.

Peters, K.E., Moldowan, J.M. and Sundararaman, P. (1990). Effects of hydrous pyrolysis on biomarker thermal maturity parameters: Monterey Phosphatic and Siliceous Members. Org. Geochem., **15/3**, 249-265.

Peters, K.E. and Moldowan, J.M. (1991). Effects of source, thermal history, and biodegradation on the distribution and isomerization of homohopanes in petroleum. Org. Geochem., **17/1**, 47-61.

Peters, K.E. and Moldowan, J.M. (1993). "The Biomarker Guide". Prentice Hall, New Jersey, 363pp.

Peters , K.E., Moldowan, J.M., McCaffrey, M.A. and Fago, F.J. (1996). Selective biodegradation of extended hopanes to 25-norhopanes in petroleum reservoirs. Insights from molecular mechanics. Org. Geochem., **24/8-9**, 765-783.

Petrie, H.S. (1996). F-F2, F-BC1 and F-S1 Tertiary biostratigraphic report. Unpubl. rept. to SOEKOR, Halliburton Services, HAL BIO R05/96, 7pp.

Pferdekämper, H. and Winters, S.J. (1997). Evaluation of the 9At1-13At1 interval in boreholes E-BB/E-AA/E-AD/E-BB/E-CA. SOEKOR unpubl. Tech. Note No. 61, 10pp.

Philippi, G.T. (1956). Identification of oil source beds by chemical means. in Proc. 20th Int. Geol. Cong. (Mexico City) Sect.III Petr. Geol., 25-38.

Philippi, G.T. (1965). On the depth, time and mechanism of petroleum generation. Geochim. et Cosmochim. Acta, **29**, 1021-1049.

Philp, R.P. (1985). "Fossil Fuel Biomarkers". Elsevier, New York, 294pp.

Philp, R.P. (1988). Biological markers in fossil fuel production. in "Geochemistry". (comps.) Beaumont, E.A. and Foster, N.H., AAPG Treatise Pet. Geol. Reprint Ser. No. 8, 337-390.

Philp, R.P. and Engel, M.H. (1987). The effects of migration on the distribution of biomarkers and stable carbon isotopic composition of crude oil. in "Migration of Hydrocarbons in Sedimentary Basins". (ed.) Doligez, B. Éditions Technip, Paris, 615-632.

Philp, R.P. and Gilbert, T.D. (1986a). Biomarker distributions in Australian oils predominantly derived from terrestrial material. Org. Geochem., **10**, 73-84.

Philp, R.P. and Gilbert, T.D. (1986b). A geochemical investigation of oils and source rocks from the Surat basin. APEA Jour., **26**, 172-186.

Philp, R.P. and Oung, J.N. (1988). Biomarkers occurrence, utility and detection. Analyt. Chem., **60/15**, 887-896.

Piper, D.J.W., Shor, A.N., Farre, J.A., O'Connell, S. and Jacobi, R. (1985). Sediment slides and turbidity currents on the Laurentian Fan: sidescan sonar investigations near the epicenter of the 1929 Grand Banks earthquake. Geology, **13**, 538-541.

Pittion, J-L. and Goudain, J. (1991). Source-rocks and oil generation in the Austral Basin. 13th Wor. Pet. Cong., Pre-print, John Wiley, Chichester.

Platte River Associates (1995). "Basinmod 1-D - version 5.00". Platte River Associates, Denver, Colorado, pp. var.

Platt, N.H. and Philip, P.R. (1995). Structure of the southern Falkland Islands continental shelf: initial results from new seismic data. Mar. Pet. Geol., **12/7**, 759-771.

Pocock, S.A.J. (1982). Identification and recording of particulate sedimentary organic matter. in "How to assess maturation and palaeotemperature". (ed.) Staplin, F.L. et al., Soc. Econ. Pal. Mineral., Short Course No. 7, 13-131.

Potter, P.E., Maynard, J.B. and Pryor, W.A. (1980). "Sedimentology of shale". Springer-Verlag, New York, 306pp.

Powell, T.G. (1978). An assessment of the hydrocarbon source rock potential of the Canadian Arctic Islands. Geol. Surv. Can. Pap. 78-12, 82pp.

Powell, T.G. and McKirdy, D.M. (1973a). The effect of source material, rock type and diagenesis on the n-alkane content of sediments. Geochim. et Cosmochim. Acta, **37**, 623-633.

Powell, T.G. and McKirdy, D.M. (1973b). Relationship between ratio of pristane to phytane, crude oil composition and geological environment. Nature Phys. Sci., **243**, 37-39.

Price, L.C. (1976). Aqueous solubility of petroleum as applied to its origin and primary migration. Am. Assoc. Pet. Geol. Bull., **60/2**, 213-244.

Price, L.C. (1982). Organic geochemistry of core samples from an ultra-deep hot well (300°C, 7 km). Chem Geol., **37**, 215-228.

Price, L.C. and Barker, C.F. (1984). Suppression of vitrinite reflectance in amorphous rich kerogen - a major unrecognised problem. Jour. Pet. Geol., **8/1**, 59-84.

Price, L.C., Ging, T., Love, A. and Anders, D. (1986) Organic metamorphism in the Lower Mississippian - Upper Devonian Bakken shales - II: Soxhlet extraction. Jour. Pet. Geol., **9/3**, 313-342.

Prinzhoffer, A.A. and Huc, A-Y. (1995). Genetic and post-genetic molecular and isotopic fractionations in natural gases. Chem Geol., **126/3-4**, 281-290.

Prior, E.M. (1984). ERC course in "Gas Condensates". Energy Resources Consultants Project 83.0639, ERC, London, pp. var.

Pym, J.G., Ray, J.E., Smith, G.W. and Whitehead, E.V. (1974). Petroleum triterpane fingerprints of crude oils. Analyt. Chem., **47/9**, 1617-1622.

Quigley, T.M., Mackenzie, A.S. and Gray, J.R. (1988). Kinetic theory of petroleum generation. in "Migration of Hydrocarbons in Sedimentary Basins". (ed.) Doligez, B., Éditions Technip, Paris, 649-665.

Radke, M. (1987). Organic geochemistry of aromatic hydrocarbons. in "Advances in Petroleum Geochemistry Vol 2". (eds.) Brooks, J. and Welte, D.H., Academic Press, London, 141-207.

Radke, M. (1988). Application of aromatic compounds as maturity indicators in source rocks and crude oils. Mar. Pet. Geol., **5/8**, 224-236.

Radke, M., Willsch, H. and Welte, D.H. (1980). Preparative hydrocarbon group type determination by automated medium pressure liquid chromatography. Anal. Chem., **50**, 663-665.

Radke, M., Welte, D.H. and Willsch, H. (1982). Geochemical study on a well in the western Canada basin: relation of the aromatic distribution pattern to maturity of organic matter. Geochim. et Cosmochim. Acta, **46**, 1-10.

Radke, M., Welte, D. and Willsch, H. (1986). Maturity parameters based on aromatic hydrocarbons: Influence of the organic matter type. Org. Geochem., **10**, 51-63.

Radke, M. and Willsch, H. (1994). Extractable alkyl dibenzothiophenes in Posidonia shale (Toarcian) source rocks: relationship of yields to petroleum formation and expulsion. Geochim. et Cosmochim. Acta, **58**, 5223-5244.

Radke, M., Willsch, H., Leythauser, D. and Teichmüller, M. (1982b). Aromatic components of coal: relation of distribution pattern to rank. Geoch. et Cosmochim. Acta, **46**, 1831-1848.

Rathan, D.G.L. (1996). Update on reservoir model at F-A and impact on production strategy. SOEKOR unpubl. rept., 4pp.

Ravelson, E., Ranasy, J., Sparihariјaona and Ramanampisoa, L. (1991). Bemolanga and Tsimiroro source rocks and hydrocarbon generation. in "Proc. 5th Unitar et al. Heavy Crude and Tar Sands Int. Conf.", **1**, 357-367.

Raymond, A.C. and Murchison, D.G. (1992). Effect of igneous activity on molecular-maturation indices in different types of organic material. Org. Geochem., **18/5**, 725-735.

Reimann, K-U. (1988). Prospects for oil and gas in Zimbabwe, Zambia and Botswana. Episodes, **9/2**, 95-101.

Retallack, G.J. (1996). Acid trauma at the Cretaceous-Tertiary boundary in eastern Montana. GSA Today, **6/5**, 1-7.

Riediger, C.L. (1993). Solid bitumen reflectance and Rock Eval Tmax as maturation indices: An example from the "Nordegg Member", West Canada sedimentary basin. Int. Jour. Coal Geol., **22/3-4**, 295-315.

Riccardi, A.C. (1988). "The Cretaceous System of Southern South America". Mem. Geol. Soc. Am. No. 168, Colorado, 161pp.

Richards, P.C. and Fannin, N. (1994). Falkland Islands offshore offers high risks-costs, good potential. Oil Gas Jour., **92/3**, 67-70.

Rigassi, D.A. and Dixon, G.E. (1970). Cretaceous of the Cape Province, Republic of South Africa. Ibadan Univ. Conf. on African Geol., Dec. 1970, 513-527.

Riolo, J., Hussler, G., Albrecht, P.A. and Connan, J. (1986). Distribution of aromatic steroids in geological samples: their evaluation as geochemical parameters. Org. Geochem., **10**, 981-990.

Robert, P. (1988). "Organic metamorphism and geothermal history: microscopic study of organic matter and thermal evolution of sedimentary basins". Reidel, Dordrecht, 311pp.

Rogers, M.A., McAlary, J.D. and Bailey, N.J.L. (1974). Significance of reservoir bitumens to thermal-maturation studies, Western Canada Basin. Am. Assoc. Pet. Geol. Bull., **58/9**, 1806-1824.

Ronov, A.B. (1958). Organic carbon in sedimentary rocks (in relation to presence of petroleum). Translations in Geochemistry No. 5, 510-536.

Roux, J. (1995). Structural evolution and prospectivity of the F-F/F-P prospect areas. SOEKOR unpubl. Tech. Note No. 34, 5pp.

Roux, J. (1996). Oil finds within the pre1At1 succession of the Bredasdorp Basin (Block 9). SOEKOR unpubl. Tech. Note No. 45, 4pp.

Rowsell, D.M. (1974). The geochemistry, petrography and hydrocarbon source potential of well-sections in the Agulhas Bank area - summary to July 1974. SOEKOR unpubl. rept., 71pp.

Rowsell, D.M. and De Swardt, A.M.J. (1976). Diagenesis in Cape and Karroo sediments, South Africa, and its bearing on their hydrocarbon potential. Trans. Geol. Soc. S. Afr., **79/1**, 81-145.

Rowsell, D.M., Winter, H.de la R. and Davies, C.P.N. (1979). Geochemical report borehole F-F2. SOEKOR unpubl. rept., 8pp.

Rubinstein, I., Sieskind, O. and Albrecht, P. (1975). Rearranged sterenes in a shale: occurrence and simulated formation. Jour. Chem Soc. Perkin Trans., **1**., 1833-1836.

Rullkötter, J., Aizenshtat, Z. and Spiro, B. (1984). Biological markers in bitumens and bituminous pyrolyzates of Upper Cretaceous chalks from the Ghareb Formation (Israel). Geochim. et Cosmochim. Acta, **48**, 151-157.

Rullkötter, J. and Marzi, R. (1988). Natural and artificial maturation of biological markers in a Toarcian shale from northern Germany. Org. Geochem., **13/4-6**, 639-645.

Rullkötter, J., Radke, M. and Schaefer, R.G. (1991). Correlation of two crude oil samples from well E-AA1, South Africa. Unpubl. rept. to SOEKOR, KFA/ICH-5, No. 501491, 10pp.

Saban, M., Jovancicevic, B.S., Saracevic, S. Hollerbach, A. and Vitorovic, D. (1988). Correlative geochemical study of crude oils from southeastern and southern parts of the Pannonian Basin. Org. Geochem., **13/1-3**, 325-333.

SABS (1983). Analysis of E-G1 oil. Unpubl. rept. to SOEKOR no. 321/81264/W22, 4pp.

SADCC (1992). "Oil and Gas Exploration in the SADCC Region". SADCC Energy Sector Seminar, 26-29, Nov. 1986, Arusha, Tanzania, PUBL?, PP??

Sajgo, Cs., Maxwell, J.R. and Mackenzie, A.S. (1983). Evaluation of fractionation effects during the early stages of primary migration. Org. Geochem., **5/2**, 65-73.

Sales, J.K. (1994). Closure vs. seal capacity - fundamental control on the distribution of oil and gas. in "Basin modelling: advances and applications". (eds.) Doré, A.G. et al., NPF Spec. Publ. No. 3, Elsevier, Amsterdam, 399-414.

Saxby, J.D., Chatfield, P., Taylor, G.H., FitzGerald, J.D., Kaplan, I.R. and Lu, S-T. (1992). Effect of clay minerals on products from coal maturation. Org. Geochem., **18/3**, 373-383.

Schlanger, S.O., Arthur, M.A., Jenkyns, H.C. and Scholle, P.A. (1987). The Cenomanian-Turonian oceanic anoxic Event, 1. Stratigraphy and distribution of organic carbon-rich beds and the marine δC^{13} excursion. in "Marine Petroleum Source Rocks" (eds.) Brooks, J. and Fleet, A.J., Geol. Soc. Spec. Publ. No. 26, Blackwell, London, 371-399.

Schlumberger (1989). Log interpretation principles/applications. Schlumberger educ. services, Houston, Texas, pp var.

Schlumberger (1991a). Petroleum Geology. in "Well evaluation conference - Angola", (ed.) Stark, D.M., Éditions Galilée, Paris, 1-11-95.

Schlumberger (1991b). Log interpretation charts. Schlumberger educ. services, Houston, Texas, 171pp.

Schoell, M. (1983a). Genetic characterisation of natural gases. Am. Assoc. Pet. Geol. Bull., **67/12**, 2225-2238.

Schoell, M. (1983b). Isotope techniques for tracing migration of gases in sedimentary basins. Jour. Geol. Soc. Lond., **140**, 415-422.

Schoell, M., McCaffrey, M.A., Fago, F.J. and Moldowan, J.M. (1992). Carbon isotopic compositions of 28,30-bisnorhopanes and other biological markers in a Monterey crude oil. Geochim. et Cosmochim. Acta, **56**, 1391-1399.

Schmoker, J.W. and Hester, T.C. (1990). Formation resistivity as an indicator of oil generation – Bakken Formation of North Dakota and Woodford Shale of Oklahoma. The Log Analyst, **38/1**, 1-9.

Scrutton, R.A. and Du Plessis, A. (1973). Possible marginal fracture ridge south of South Africa. Nature, **242**, 180-182.

Seifert, W.K. and Moldowan, J.M. (1978). Applications of steranes, terpanes and monoaromatics to the maturation, migration and source of crude oils. Geochim. et Cosmochim. Acta, **42/1**, 77-95.

Seifert, W.K. and Moldowan, J.M. (1979). The effect of biodegradation on steranes and terpanes in crude oils. Geochem. et Cosmochim. Acta., **43**, 111-126.

Seifert, W.K. and Moldowan, J.M. (1981). Palaeoreconstruction by biological markers. Geochim. et Cosmochim. Acta, **45**, 783-794.

Seifert, W.K. and Moldowan, J.M. (1986). Use of biological markers in petroleum exploration. in "Methods in Geochemistry and Geophysics". (ed.) Johns, R.B., Elsevier Science, Amsterdam, 261-290.

Seifert, W.K., Moldowan, J.M. and Jones, R.W. (1980). Applications of biological marker chemistry to petroleum exploration. in "10th World Pet. Cong. Vol. 2"., Heyden and Sons, London, 425-438.

Seifert, W.K., Carlson, R.M.K. and Moldowan, J.M. (1983). Geomimetic synthesis, structure assignment, and geochemical correlation application of monoaromatized petroleum steroids. in "Advances in Organic Geochemistry 1981". John Wiley, Chichester, 710-724.

Senftle, J.T. and Landis, C.R. (1991). Vitrinite reflectance as a tool to assess thermal maturity. in "Source and migration processes and evaluation techniques" (ed.) Merrill, R.K., Am. Assoc. Pet. Geol. Treatise Pet. Geol., 119-125.

Shanmugam, G. (1985). Significance of coniferous rain forests and related organic matter in generating commercial quantities of oil, Gippsland Basin, Australia. Am. Assoc. Pet. Geol. Bull., 69/8, 1241-1254.

Sheng, G., Simoneit, B.R.T., Leif, R.N., Chen, X. and Fu, J. (1992). Tetracyclic terpanes enriched in Devonian cuticle humic coals. Fuel, **71/5**, 523-532.

Shimoyama, A. and Johns, J.D. (1972). Formation of alkanes from fatty acids in the presence of Ca CO_3. Geochim. et Cosmochim. Acta, **36**, 87-91.

Simoneit, B.R.T., Brenner, S., Peters, K.E. and Kaplan, I.R. (1981). Thermal alteration of Cretaceous black shale by diabase intrusions in the eastern Atlantic - II. Effects on bitumens and kerogen. Geochim. et Cosmochim. Acta, **45**, 1581-1602.

Smit, G.J. (1992). Geology and prospectivity of the 9A-to-12A sequences, Bredasdorp Basin. SOEKOR unpubl. rept., SOE-EXP-RPT-046, 33pp.

Smith, D.G. (1990). Milankovitch cyclicity and the stratigraphic record - a review. Terra Nova, **1**, 402-404.

Smith, J.T. and Ehrenberg, S.N. (1989). Correlation of carbon dioxide abundance with temperature in clastic hydrocarbon reservoirs: relationship to inorganic chemical equilibrium. Mar. Pet. Geol., **6**, 129-135.

Snowdon, L.R. (1979). Resinite - a potential petroleum source in the Upper Cretaceous/Tertiary of the Beaufort-Mackenzie Basin. Can. Soc. Petrol. Geol. Mem. No. 6, 509-521.

Sofer, Z. (1988). Biomarkers and carbon isotopes of oils in the Jurassic Smackover trend of the Gulf Coast States, USA. Org. Geochem., **12/5**, 421-432.

Stahl, W.J. (1974). Carbon isotope fractionations in natural gases. Nature, **251**, 134-135.

Stahl, W.J. (1980). Compositional changes and $^{13}C/^{12}C$ fractionation during degradation of hydrocarbons by bacteria. Geochim. et Cosmochim. Acta, **44**, 1903-1907.

Staplin, F.L. (1982a). Determination of thermal alteration index from colour of exinite (pollen, spores). In "How to assess maturity and palaeotemperatures". (eds.) Staplin, F.L., Dow, W.G., Milner, C.W.D., O'Connor, D.I., Pocock, S.A.J., van Gijzel, P., Welte, D.H. and Yükler, M.A., Soc. Econ. Pal. Min. Short Course No. 7, SEPM, Tulsa, 7-10.

Staplin, F.L. (1982b). Sedimentary organic matter, organic metamorphism and oil and gas occurrences. Bull. Can. Pet. Geol., **17**, 47-66.

Stear, D.A., Bell, C.P.T., Holmes, L.C., Roux, J. and Van Heerden, M. (1985). Geological well completion report of borehole E-S4. SOEKOR unpubl. rept., 18pp.

Stenhager, E., Abrahamsson, S and McLafferty, F.W. (1974). "Registry of Mass Spectral Data", John Wiley, New York, 3835pp.

Strauss, P., Noble, R.D.P. and Davies, C.P.N. (1996). Recommendation to drill borehole E-DC1. SOEKOR unpubl. rept., SOE-EXP-RPT-0360, 16pp.

Strachan, M.G., Alexander, R. and Kagi, I.R. (1988). Trimethyl naphthalenes in crude oils and sediments: effects of source and maturity. Geochim. et Cosmochim. Acta, **52**, 1255-1264.

Subroto, E., Alexander, R. and Kagi, R. (1991). 30-norhopanes: their occurrence in sediments and crude oils. Chem. Geol., **93**, 179-192.

Summons, R.E., Powell, T.G. and Boreham, C.J. (1988). Petroleum geology and geochemistry of the Middle Proterozoic McArthur Basin, Northern Australia: III composition of extractable hydrocarbons. Geochim. et Cosmochim. Acta, **52**, 1747-1763.

Talukdar, S., Gallango, O. and Chin-A-Lien, M. (1986). Generation and migration of hydrocarbons in the Maracaibo Basin, Venezuela: an integrated basin study. Org. Geochem., **10**, 261-279.

Talwani, M. and Eldholm, O. (1973). Boundary between continental and oceanic crust at the margin of rifted continents. Nature, **241**, 325-330.

Tannenbaum, E., Ruth, E. and Kaplan, I.R. (1986). Steranes and triterpanes generated from kerogen in the absence and presence of minerals. Geochim. et Cosmochim. Acta, **50**, 805-812.

Tarling, D.H. (1973). Metallic deposits and continental drift. Nature, **243**, 193-196.

Teichmüller, M. and Teichmüller, R. (1981). The significance of coalification studies to geology - a review. Bull. Centres Rech. Explor-Prod. Elf-Aquitaine, **5/2**, 491-534.

Teuteberg, B.H., (1995). Agreement for release of hydrographic information. SA Navy Hydrographic Office, 1pp.

Theron, J.A. (1970). A stratigraphical study of the Bokkeveld Group (Series). in "Second Gondwana symposium - proceedings and papers". Int. Union Geol. Sci. Comm. Strat., CSIR, Pretoria, 197-204.

Thomas, B.M., Møller-Pedersen, P., Whitaker, M.F. and Shaw, N.D. (1985). Organic facies and hydrocarbon distribution in the Norwegian North Sea. in (eds.) Thomas, B.M. et al. "Petroleum Geochemistry in Exploration of the Norwegian Shelf". Graham and Trotman, London, 3-26.

Thomas, M.M. and Clouse, J. (1995). Scaled physical model of secondary migration. Am. Assoc. Pet. Geol. Bull., **79/1**, 19-29.

Thompson, K.F.M. (1979). Light hydrocarbons in subsurface sediments. Geochim. et Cosmochim. Acta, **43**, 657-672.

Thompson, K.F.M. (1983). Classification and thermal history of petroleum based on light hydrocarbons. Geochim. et Cosmochim. Acta, **47**, 303-316.

Thompson, K.F.M. (1987). Fractionated aromatic petroleums and the generation of gas-condensates. Org. Geochem., **11/6**, 573-590.

Thompson, K.F.M. (1988). Gas-condensate migration and oil fractionation in deltaic systems. Mar. Pet. Geol., **5/8**, 237-246.

Tissot, B.P. (1969). Premières données sur les mécanismes et la cinétique de la formation du pétrole dans les sédiments. Simulation d'un schéma réactionnel sur ordinateur. Rev. Inst. Fr. Pétr., **24**, 470-501.

Tissot, B.P., Oudin, J.C. and Pelet, R. (1973). Critères d'origine et d'evolution des petroles. Application a l'étude geochimique des bassins sedimentaires. in "Advances in Organic Geochemistry 1971". (eds.) Von Gaertner, H.R. and Wehner, H., Pergamon, Oxford, 113-134.

Tissot, B.P. and Espitalié, J. (1975). L'evolution thermique de la matiére organique des sediments: application d'une simulation mathematique. Rev. Inst. Fr. Pétr., **30**, 743-777.

Tissot, B.P., Pelet, R. and Ungerer, Ph. (1982). Thermal history of sedimentary basins, maturation indices and kinetics of oil and gas generation. Am. Assoc. Pet. Geol. Bull., **71/12**, 1445-1466.

Tissot, B.P. and Welte, D.H. (1984). "Petroleum Formation and Occurrence"., Springer-Verlag, Berlin, 699pp.

Tomic, J., Behar, F., Vandenbroucke, M. and Tang, Y. (1995). Artificial maturation of Monterey kerogen (Type II-S) in a closed system and comparison with Type II kerogen: implications on the fate of sulfur. Org. Geochem., **23/7**, 647-660.

TPDC (1992). Tanzania petroleum exploration potential. Tanzan. Pet. Dev. Corp., unpubl. rept., pp var.

Trindade, L.A.F., Brassell, S.C. and Santos Neto, E.V. (1992). Petroleum migration and mixing in the Potiguar Basin, Brazil. Am. Assoc. Pet. Geol. Bull., **76/12**, 1903-1924.

Underhill, J.R. and Partington, M.A. (1993). Jurassic thermal doming and deflation in the North Sea: implications of the sequence stratigraphic evidence. in "Petroleum Geology of Northwest Europe" (ed.) Parker, J.R., Geol. Soc. Lond., 337-345.

Ungerer, P., Espitalié, J., Marquis, F. and Durand, B. (1986). Use of kinetic models of organic matter evolution for the reconstruction of palaeotemperatures. in "Thermal modelling in sedimentary basins". (ed.) Burrus, J., Éditions Technip, Paris, 531-546.

Ungerer, P., Behar, F., Villalba, M., Heum, O.R. and Audibert, A. (1988). Kinetic modelling of oil cracking. Org. Geochem., **13/4-6**, 857-868.

Ungerer, P., Burrus, J., Doligez, B., Chénet, P.Y. and Bessis, F. (1990). Basin evaluation by integrated two-dimensional modeling of heat transfer, fluid flow, hydrocarbon generation and migration. Am. Assoc. Pet. Geol. Bull., **74/3**, 309-335.

Vail, P.R., Bubb, J.N., Hatelid, W.G., Mitchum, R.M., Sangree, J.B., Thompson, J.B. 111., Todd, R.G. and Widmier, J.M. (1977). Seismic stratigraphy and global changes of sea level, Parts I to II. in "Seismic Stratigraphy - application to hydrocarbon exploration". AAPG Mem. No. 26, 49-212.

Vail, P.R. (1987). Seismic stratigraphy interpretation procedure. In "Atlas of Seismic Stratigraphy". (ed.) Bally, A.W., Am. Assoc. Pet. Geol. Studies Geol. No. 27, AAPG, Tulsa, 1-10.

Valicenti, V.H. (1995). Biostratigraphy, sequence stratigraphy and a depositional model for the Bredasdorp Basin synrift sediments. SOEKOR unpubl. Tech. Note No. 19, 6pp.

Valicenti, V.H. and Broad, D.S. (1994). Dating of the drift onset unconformity in South Africa. SOEKOR unpubl. rept., SOE-PAL-RPT-015, 6pp.

Valicenti, V.H. and Stephens, J.M. (1984). Ostracods from the Upper Valanginian and Upper Hauterivian of the Sundays River Formation, Algoa basin, South Africa. Revista Española de Micropal., **16**, 171-239.

Van der Merwe, R. and Fouché, J. (1992). Inversion tectonics in the Bredasdorp Basin, offshore South Africa. in "Inversion Tectonics of the Cape Fold Belt, Karoo and Cretaceous Basins of Southern Africa". (eds.) De Wit, M.J. and Ransome, I.G.D., A.A. Balkema, Rotterdam, 49-59.

Van der Spuy, D. (1991). Application of the delta logR method of source rock identification. SOEKOR unpubl. rept., SOE-GCH-RPT-003, 12pp.

Van der Spuy, D. (1994a). Geochemistry section: Leco total organic carbon determination procedures. SOEKOR unpubl. rept., SOE-GCH-PM-001, 5pp.

Van der Spuy, D. (1994b). Geochemistry section: reflectance slide preparation procedures. SOEKOR unpubl. rept., SOE-GCH-PM-006, 7pp.

Van der Spuy, D. (1994c). Geochemistry section: reflectance microscopy procedures. SOEKOR unpubl. rept., SOE-GCH-PM-004, 9pp.

Van der Spuy, D. (1995). The vitrinite reflectance validation exercise: results and discussion. Halliburton unpubl. rept. to SOEKOR, HALGEO R003/95, 10pp.

Van der Spuy, D. (1996). E-N1: reappraisal of vitrinite reflectance data. Halliburton unpubl. rept. to SOEKOR, HALGEOR 0028/96, 8pp.

Van der Weide, B.M. (1969). Organic geochemical analysis. SNPA unpubl. rept. to SOEKOR, R/GEO 675/69, 29pp.

Van Graas, G.W. (1990). Biomarker maturity parameters for high maturation: calibration of the working range up to the oil/condensate threshold. Org. Geochem., **16/4-6**, 1025-1032.

Van Heerden, I. Ll. (1984). Report on Agulhas Current measurements - F-Q1 site. Specialist Offshore Surveys unpubl. rept. to SOEKOR, 25pp.

Van Krevelen, D.W. (1984). Organic geochemistry - old and new. Org. Geochem., **6**, 1-10.

Van Wyk, A. and Guest, M. (1992). Depth conversion: Southern Outeniqua Basin. SOEKOR unpubl. rept., SOE-EXP-RPT-004, 23 pp.

Van Wyk, N.J.S. (1990). Application of sequence stratigraphy to oil and gas exploration in the Bredasdorp Basin, offshore South Africa. Abstracts Geocongress 90, Geol. Soc. S. Afr., 566-569.

Van Wyk, N.J.S. (1995). Recommendation to drill borehole E-CB2. SOEKOR unpubl. rept., SOE-EXP-RPT-287, 14pp.

Van Wyk, N.J.S. (1997). Re-appraisal of the E-AR 13A reservoir. SOEKOR unpubl. rept., SOE-EXP-RPT-415, 14pp.

Van Wyk, N.J.S., Roux, J., Broad, D.S., Valicenti, V.H. and Brink, G.J. (1994). Correlation of old and new horizons, South Coast Blocks 7 to 12. SOEKOR unpubl. rept., SOE-EXP-RPT-240, 7pp.

Veevers, J.J. (1990). Tectonic-climate supercycle in the billion-year plate-tectonic eon: Permian Pangean icehouse alternates with Cretaceous dispersed-continents greenhouse. Sed. Geol., **68**, 1-16.

Venter, H.J. (1992). Geochemistry section: calcimeter operation manual. SOEKOR unpubl. rept., 14pp.

Venter, H.J., Davies, C.P.N. and Van der Spuy, D. (1994a). Geochemistry section: calcimetry procedures. SOEKOR unpubl. rept., SOE-GCH-PM-003, 7pp.

Venter, H.J., Davies, C.P.N. and Van der Spuy, D. (1994b). Geochemistry section: dry chemistry sample preparation procedures. SOEKOR unpubl. rept., SOE-GCH-PM-002, 5pp.

Venter, H.J., Meintjes, M. and Van der Spuy, D. (1994c). Geochemistry section: oil extraction and liquid chromatography procedures. SOEKOR unpubl. rept., SOE-GCH-PM-007, 24pp.

Verfaille, E.J.J. (1993). A synopsis of RFT data acquired in wells in the Bredasdorp Basin, including regional plots. SOEKOR unpubl. rept., SOE-PET-RPT-107, 6pp.

Vogt, P.R. (1972). Evidence for global synchronism in mantle plume convection, and possible significance for geology. Nature, **240**, 338-342.

Volkman, J.K. (1988). Biological marker compounds as indicators of the depositional environments of petroleum source rocks. in "Lacustrine Petroleum Source Rocks". (eds.) Fleet, A.J., Kelts, K. and Talbot, M.R., Geol. Soc. Spec. Publ. No. 40, 103-122.

Wakeham, S.G., Schaffner, C. and Giger, W. (1980). Polycyclic aromatic hydrocarbons in recent lake sediments - 11. Compounds derived from biogenic precursors during early diagenesis. Geochim. et Cosmochim. Acta, **44**, 415-429.

Walderhaug, O. and Bjørkum, P.A. (1992). Effect of meteoric flow on calcite cementation in the Middle Jurassic Oseburg Formation, well 30/3-2, Veslefrikk field, Norwegian North Sea. Mar. Pet. Geol., **9/6**, 308-318.

Waples, D.W. (1980). Time and temperature in petroleum formation: application of Lopatin's method to petroleum exploration. Am. Assoc. Pet. Geol. Bull., **64/6**, 916-926.

Waples, D.W. (1984). Thermal models for oil generation. in "Advances in Petroleum Geochemistry Volume 1". (eds.) Brooks, J. and Welte, D., Academic Press, London, 7-67.

Waples, D.W. and Machihara, T. (1991). "Biomarkers for Geologists". AAPG Methods in Expl. Ser. No. 9, Am. Assoc. Pet. Geol., Tulsa, 91pp.

Weber, K.J. (1994). "Reservoir characterisation and management". Unpubl. course notes to SOEKOR, 93pp.

Wenham, M.A., Van Wyk A. and Guest, M. (1991). Re-evaluation of the Southern Outeniqua Basin. SOEKOR unpubl. rept., SOE-EXP-RPT-001, 25pp.

Welte, D.H. (1987). Migration of hydrocarbons: facts and theory. in "Migration of hydrocarbons in sedimentary basins". (ed.) Doligez, B., Éditions Technip, Paris, 393-413.

White, N. (1993). Recovery of strain rate variation from inversion of subsidence data. Nature, **366**, 449-452.

White, R. and McKenzie, D. (1989). Magmatism at rift zones: the generation of volcanic continental margins and flood basalts. Jour. Geophys. Res., **94/B6**, 7685-7729.

Wickens, H. de V. (1993). Sedimentology of the 14A reservoir sandstones, central Bredasdorp Basin, southern offshore South Africa. SOEKOR unpubl. rept., SOE-SED-RPT-001, 80pp.

Wickens, H. de V. and McLachlan, I.R. (1990). The stratigraphy and sedimentology of the reservoir interval of the Kudu 9A-2 and 9A-3 boreholes. Communs. Geol. Surv. Namibia, **6**, 9-22.

Wickens, H. de V., Brink, G.J. and McLachlan, I.R. (1995). Review of the hydrocarbon potential of the Karoo basin and the development of new concepts for exploration. SOEKOR unpubl. rept., SOE-EXP-RPT-101, 52pp.

Wilkinson, M., Darby, D., Haszeldine, R.S. and Couples, G.D. (1997). Secondary porosity generation during deep burial associated with overpressure leak-off: Fulmar Formation, United Kingdom Central Graben. Am. Assoc. Pet. Geol. Bull., **81/5**, 803-813.

Williams, J.A. (1974). Characterization of oil types in Williston Basin. Am. Assoc. Pet. Geol. Bull., 58/7, 1243-1252.

Williams, J.A., Bjorøy, M., Dolcater, D.L. and Winters, J.C. (1986). Biodegradation in South Texas Eocene oils - effects on aromatics and biomarkers. Org. Geochem., **10**, 451-461.

Williamson, M.A. (1992). The subsidence, compaction thermal and maturation history of the Egret Member, source rock, Jeanne D'Arc Basin, offshore Newfoundland. Bull. Can. Pet. Geol., **40/2**, 136-150.

Winter, A. and Martin, A.K. (1990). Late Quaternary history of the Agulhas Current. Palaeoceanography, **5/4**, 479-486.

Winter, H. de la R. (1981). Progress report on geopressure interpretation: volumes 1 and 2. SOEKOR unpubl. rept., 57pp.

Winters, S.J., Unstead, P.J., Petersen, N.D., Brink, G.J. and Erasmus, J.F. (1984). Geological well completion report of borehole E-M2. SOEKOR unpubl. rept., 15pp.

Winters, S.J. (1996). Evaluation of the 4A-5A sandstones in boreholes E-AN1, E-CN1, E-AL1 and E-AM1. SOEKOR unpubl. Tech. Note No. 57, 4pp.

Winters, S.J. and Kuhlmann, S. (1994). Delineation of an oil and gas field within a turbidite system: Bredasdorp Basin, South Africa. GCS SEPM Proc. 15th Ann. Conf.

Wolff, G.A., Lamb, N.A. and Maxwell, J.R. (1986). The origin and fate of 4-methyl steroids-II. Dehydration of sterols and occurrence of C30 4-methyl steranes. Org. Geochem., **10**, 965-974.

Wood, E.M. (1995). Development potential seen in Bredasdorp basin off South Africa. Oil Gas Jour., **93/22**, 54-58.

Wright, J.B. (1973). Continental drift, magmatic provinces and mantle plumes. Nature, **244**, 565-567.

Yukler, M.A. and Thomsen, E. (1989). Effects of heating rates on hydrocarbon generation and occurrence. Am. Assoc. Pet. Geol. Bull., **73/3**, 428-429.

Zavada, M.S. and Benson, J.M. (1987). First fossil evidence for the primitive angiosperm family Lactoridaceae. Amer. Jour. Bot., **74/10**, 1590-1594.

Zhusheng, J., Philp, R.P. and Lewis, C.A. (1988). Fractionation of biological markers in crude oils during migration and the effects on correlation and maturation parameters. Org. Geochem., **13/1-3**, 561-571.

Zielinski, G.W. and Bruchhausen, P.M. (1983). Shallow temperatures and thermal regime in the hydrocarbon province of Tierra del Fuego. Am. Assoc. Pet. Geol. Bull., **67/1**, 166-177.

Zimmerman, H.B., Boersma, A. and McCoy, F.W. (1987). Carbonaceous sediments and palaeoenvironment of the Cretaceous South Atlantic Ocean. in "Marine petroleum source rocks" (eds.) Brooks, J. and Fleet, A.J., Geol. Soc. Spec. Publ. No. 26, London, 271-286.

Zumberge, J.E. (1983). Tricyclic diterpane distribution in the correlation of Palaeozoic crude oils from the Williston Basin. in (eds.) Bjorøy, M et al., "Advances in Organic Geochemistry 1981", John Wiley, Chichester, 738-745.

ACKNOWLEDGEMENTS

I wish to express my gratitude to many people who helped me along the way through this study and gave technical support, and who spurred me on to better understand the geochemistry of the basin. In particular I would like to mention the following:

Drs. I.K. McMillan and J.A. Miles for their initial drive to carry out this study and for their continuing support and assistance, and for the time Dr. Miles painstakingly devoted to an early draft,

SOEKOR management, in particular Messrs A.W. Davies and G.C. Smith, for the support and guidance they gave me and for the free access to data, interpretations and ideas. I also thank my colleagues at SOEKOR, past and present, for their assistance and advice and willingness to answer what may have seemed purposeless questions quite outside the normal realms of a petroleum geochemist. In particular the following experts who bore the brunt of the questions:
for geology; Dr. D.S. Broad and Mr. W. McAloon,
for geophysics; Messrs. E.M. Wood and P.J. Strauss,
for petrography; Mr. S.J. Hill,
for biostratigraphy and palaeo-environments; Dr. I.K. McMillan and Messrs. I.R. McLachlan and V.H. Valicenti,
for petroleum engineering; Messrs. A.V.C. Steyn, J.P. Strauss and J. Egan and Ms. H. Delaporte,
for computing; Messrs. C. Van den Berg and again J. Egan and Ms. H. Delaporte,
for administration; Ms. M. Grandia,
and draughting and technical drawing guidance, Mr. H. Coetzee.
I thank the geochemistry laboratory staff who produced such good datasets, especially Ms. H.J. Venter for pyrolysis data, Ms. M-A. Meintjes for oil extracts and GC data and Mr. D. Van der Spuy for optical studies and vitrinite data.

Mr. R.S. Hatton for guidance and assistance with the statistical calculations

My co-promoter Professor B.V. Burger for the countless hours he spent running my samples through the GC-MS to acquire the best possible results and the efforts he and his laboratory staff made to teach me some chemistry

My promoter, Professor A. Rozendaal who kept me on the right track, gave freely of his expertise and time and helped me produce a much more effective thesis

I also wish to thank the internal examiner, Professor J.P. Le Roux and the two external examiners, Professor D.H. Welte and Dr. A-Y. Huc, who all soldiered through my lengthy work giving useful advice throughout

Lastly, but not least, my wife, Heidi and my children, Anneliese and Alexander, without whose continuing support this part-time study would not have been possible.

HYDROCARBON EVOLUTION OF THE BREDASDORP BASIN, OFFSHORE SOUTH AFRICA: FROM SOURCE TO RESERVOIR

C.P.N. DAVIES

VOLUME 3: APPENDICES

APPENDIX A: MODELLING DATA

BREDOIL REACTION CONSTANTS				
REACTANT	PRODUCT	FRACTION	ACTIVATION ENERGY	FREQUENCY
			kJ/mole	1/Ma
kerogen	C15+	10%	48	1.10E+27
kerogen	C15+	25%	50	1.10E+27
kerogen	C15+	35%	52	1.10E+27
kerogen	C15+	25%	54	1.10E+27
kerogen	C15+	5%	56	1.10E+27
kerogen	C5-14	5%	48	1.10E+27
kerogen	C5-14	25%	50	1.10E+27
kerogen	C5-14	30%	52	1.10E+27
kerogen	C5-14	30%	54	1.10E+27
kerogen	C5-14	10%	56	1.10E+27
kerogen	C2-4	10%	50	1.10E+27
kerogen	C2-4	25%	52	1.10E+27
kerogen	C2-4	25%	54	1.10E+27
kerogen	C2-4	25%	56	1.10E+27
kerogen	C2-4	15%	58	1.10E+27
kerogen	C1	10%	50	1.10E+27
kerogen	C1	20%	52	1.10E+27
kerogen	C1	25%	54	1.10E+27
kerogen	C1	30%	56	1.10E+27
kerogen	C1	15%	58	1.10E+27
kerogen	semi-residue	10%	50	1.10E+27
kerogen	semi-residue	20%	52	1.10E+27
kerogen	semi-residue	30%	54	1.10E+27
kerogen	semi-residue	20%	56	1.10E+27
kerogen	semi-residue	20%	58	1.10E+27
C15+	C5-14	100%	56	3.16E+26
C15+	C2-4	100%	56	3.16E+26
C15+	C1	100%	56	3.16E+26
C15+	semi-residue	100%	56	3.16E+26
C5-14	C2-4	100%	56	1.58E+25
C5-14	C1	100%	56	1.58E+25
C5-14	semi-residue	100%	56	1.58E+25
C2-4	C1	100%	56	3.79E+25
C2-4	semi-residue	100%	56	3.79E+25
semi-residue	C1	100%	56	3.16E+26
semi-residue	residue	100%	56	3.16E+26

Table A.01: Reaction constants for BREDOIL kerogen (LLNL style) based on data from Bredasdorp Basin (page 1 of 4).

BREDWGOIL REACTION CONSTANTS				
REACTANT	PRODUCT	FRACTION	ACTIVATION ENERGY	FREQUENCY
			kJ/mole	1/Ma
kerogen	C15+	5%	48	1.50E+27
kerogen	C15+	11%	50	1.50E+27
kerogen	C15+	20%	52	1.50E+27
kerogen	C15+	50%	54	1.50E+27
kerogen	C15+	10%	56	1.50E+27
kerogen	C15+	4%	58	1.50E+27
kerogen	C5-14	10%	50	1.50E+27
kerogen	C5-14	20%	52	1.50E+27
kerogen	C5-14	50%	54	1.50E+27
kerogen	C5-14	15%	56	1.50E+27
kerogen	C5-14	5%	58	1.50E+27
kerogen	C2-4	10%	50	1.50E+27
kerogen	C2-4	20%	52	1.50E+27
kerogen	C2-4	50%	54	1.50E+27
kerogen	C2-4	15%	56	1.50E+27
kerogen	C2-4	5%	58	1.50E+27
kerogen	C1	10%	50	1.50E+27
kerogen	C1	20%	52	1.50E+27
kerogen	C1	50%	54	1.50E+27
kerogen	C1	15%	56	1.50E+27
kerogen	C1	5%	58	1.50E+27
kerogen	semi-residue	10%	50	1.50E+27
kerogen	semi-residue	20%	52	1.50E+27
kerogen	semi-residue	50%	54	1.50E+27
kerogen	semi-residue	15%	56	1.50E+27
kerogen	semi-residue	5%	58	1.50E+27
C15+	C5-14	100%	56	3.16E+26
C15+	C2-4	100%	56	3.16E+26
C15+	C1	100%	56	3.16E+26
C15+	semi-residue	100%	56	3.16E+26
C5-14	C2-4	100%	56	1.58E+25
C5-14	C1	100%	56	1.58E+25
C5-14	semi-residue	100%	56	1.58E+25
C2-4	C1	100%	56	3.79E+25
C2-4	semi-residue	100%	56	3.79E+25
semi-residue	methane	100%	56	3.16E+26
semi-residue	residue	100%	56	3.16E+26

Table A.01: Reaction constants for BREDWGOIL wet gas-oil prone kerogen (LLNL style) based on data from Bredasdorp Basin (page 2 of 4).

BREDWG REACTION CONSTANTS				
REACTANT	PRODUCT	FRACTION	ACTIVATION ENERGY	FREQUENCY
			kJ/mole	1/Ma
kerogen	C15+	5%	46	3.70E+27
kerogen	C15+	11%	48	3.70E+27
kerogen	C15+	15%	50	3.70E+27
kerogen	C15+	26%	52	3.70E+27
kerogen	C15+	20%	54	3.70E+27
kerogen	C15+	15%	56	3.70E+27
kerogen	C15+	8%	58	3.70E+27
kerogen	C5-14	8%	48	3.70E+27
kerogen	C5-14	12%	50	3.70E+27
kerogen	C5-14	21%	52	3.70E+27
kerogen	C5-14	25%	54	3.70E+27
kerogen	C5-14	22%	56	3.70E+27
kerogen	C5-14	12%	58	3.70E+27
kerogen	C2-4	8%	48	3.70E+27
kerogen	C2-4	15%	50	3.70E+27
kerogen	C2-4	22%	52	3.70E+27
kerogen	C2-4	25%	54	3.70E+27
kerogen	C2-4	18%	56	3.70E+27
kerogen	C2-4	12%	58	3.70E+27
kerogen	C1	9%	48	3.70E+27
kerogen	C1	17%	50	3.70E+27
kerogen	C1	21%	52	3.70E+27
kerogen	C1	25%	54	3.70E+27
kerogen	C1	17%	56	3.70E+27
kerogen	C1	11%	58	3.70E+27
kerogen	semi-residue	10%	48	3.70E+27
kerogen	semi-residue	15%	50	3.70E+27
kerogen	semi-residue	17%	52	3.70E+27
kerogen	semi-residue	21%	54	3.70E+27
kerogen	semi-residue	25%	56	3.70E+27
kerogen	semi-residue	12%	58	3.70E+27
C15+	C5-14	100%	56	3.16E+26
C15+	C2-4	100%	56	3.16E+26
C15+	C1	100%	56	3.16E+26
C15+	semi-residue	100%	56	3.16E+26
C5-14	C2-4	100%	56	1.58E+25
C5-14	C1	100%	56	1.58E+25
C5-14	semi-residue	100%	56	1.58E+25
C2-4	C1	100%	56	3.79E+25
C2-4	semi-residue	100%	56	3.79E+25
semi-residue	methane	100%	56	3.16E+26
semi-residue	residue	100%	56	3.16E+26

Table A.01: Reaction constants for BREDWG wet gas prone kerogen (LLNL style) based on data from Bredasdorp Basin (page 3 of 4).

BREDDG REACTION CONSTANTS				
REACTANT	PRODUCT	FRACTION	ACTIVATION ENERGY	FREQUENCY
			kJ/mole	1/Ma
kerogen	C15+	8%	50	3.70E+27
kerogen	C15+	15%	52	3.70E+27
kerogen	C15+	17%	54	3.70E+27
kerogen	C15+	20%	56	3.70E+27
kerogen	C15+	17%	58	3.70E+27
kerogen	C15+	13%	60	3.70E+27
kerogen	C15+	10%	62	3.70E+27
kerogen	C5-14	8%	50	3.70E+27
kerogen	C5-14	15%	52	3.70E+27
kerogen	C5-14	17%	54	3.70E+27
kerogen	C5-14	20%	56	3.70E+27
kerogen	C5-14	17%	58	3.70E+27
kerogen	C5-14	13%	60	3.70E+27
kerogen	C5-14	10%	62	3.70E+27
kerogen	C2-4	8%	50	3.70E+27
kerogen	C2-4	15%	52	3.70E+27
kerogen	C2-4	17%	54	3.70E+27
kerogen	C2-4	20%	56	3.70E+27
kerogen	C2-4	17%	58	3.70E+27
kerogen	C2-4	13%	60	3.70E+27
kerogen	C2-4	10%	62	3.70E+27
kerogen	C1	8%	50	3.70E+27
kerogen	C1	15%	52	3.70E+27
kerogen	C1	17%	54	3.70E+27
kerogen	C1	20%	56	3.70E+27
kerogen	C1	17%	58	3.70E+27
kerogen	C1	13%	60	3.70E+27
kerogen	C1	10%	62	3.70E+27
C15+	C5-14	1	56	3.70E+27
C15+	C2-4	1	56	3.70E+27
C15+	methane	1	56	3.70E+27
C15+	residue	1	60	3.70E+27
C5-14	C2-4	1	58	3.70E+27
C5-14	methane	1	58	3.70E+27
C5-14	residue	1	60	3.70E+27
C2-4	methane	1	58	3.70E+27
C2-4	residue	1	60	3.70E+27
methane	residue	1	60	3.70E+27

Table A.01: Reaction constants for BREDDG dry gas prone kerogen (LLNL style) based on data from Bredasdorp Basin (page 4 of 4).

BREDOIL													
Reactant	Start	Product 1				Product 2		Product 3		Product 4		Product 5	
	Fraction	Name	Density	Expels	Fraction	Name	Fraction	Name	Fraction	Name	Fraction	Name	Fraction
Kerogen	1	C15+	0.9	Y	0.30	C5-14	0.20	C2-4	0.15	C1	0.10	semi-residue	0.25
C15+	0	C5-14	0.55	Y	0.40	C2-4	0.30	C1	0.20	semi-residue	0.10		
C5-14	0	C2-4	0.1	Y	0.55	C1	0.30	semi-residue	0.15				
C2-4	0	C1	0.007	Y	0.80	semi-residue	0.20						
semi-residue	0	C2-4	1.1	N	0.20	C1	0.20	residue	0.60				

BREDWGOIL													
Reactant	Start	Product 1				Product 2		Product 3		Product 4		Product 5	
	Fraction	Name	Density	Expels	Fraction	Name	Fraction	Name	Fraction	Name	Fraction	Name	Fraction
Kerogen	1	C15+	0.9	Y	0.15	C5-14	0.20	C2-4	0.20	C1	0.00	semi-residue	0.25
C15+	0	C5-14	0.55	Y	0.50	C2-4	0.20	C1	0.10	semi-residue	0.20		
C5-14	0	C2-4	0.1	Y	0.60	C1	0.30	semi-residue	0.10				
C2-4	0	C1	0.007	Y	0.70	semi-residue	0.30						
semi-residue	0	C2-4	1.1	N	0.03	C1	0.03	residue	0.94				

BREDWG													
Reactant	Start	Product 1				Product 2		Product 3		Product 4		Product 5	
	Fraction	Name	Density	Expels	Fraction	Name	Fraction	Name	Fraction	Name	Fraction	Name	Fraction
Kerogen	1	C15+	0.9	Y	0.30	C5-14	0.25	C2-4	0.20	C1	0.15	semi-residue	0.10
C15+	0	C5-14	0.55	Y	0.25	C2-4	0.30	C1	0.30	semi-residue	0.15		
C5-14	0	C2-4	0.1	Y	0.60	C1	0.10	semi-residue	0.30				
C2-4	0	C1	0.007	Y	0.70	residue	0.30						
semi-residue	0	C2-4	1.1	N	0.03	C1	0.03	residue	0.94				

BREDDG													
Reactant	Start	Product 1				Product 2		Product 3		Product 4		Product 5	
	Fraction	Name	Density	Expels	Fraction	Name	Fraction	Name	Fraction	Name	Fraction	Name	Fraction
Kerogen	1	C15+	0.9	Y	0.15	C5-14	0.10	C2-4	0.30	C1	0.35	semi-residue	0.10
C15+	0	C5-14	0.55	Y	0.30	C2-4	0.30	C1	0.30	semi-residue	0.10		
C5-14	0	C2-4	0.1	Y	0.50	C1	0.40	semi-residue	0.10				
C2-4	0	C1	0.007	Y	0.80	residue	0.20						
semi-residue	0	C2-4	1.1	N	0.20	C1	0.10	residue	0.70				

Table A.02a: LLNL reaction products for all four kerogens used (BREDOIL, BREDWGOIL, BREDWG, BREDDG).

BREDOIL CRACKING								
PRIMARY			SECONDARY			CONSTANTS		
Initial HC potential	Activation energy (kcal/mole	Arrhenius constant (1/Ma)	Initial HC potential	Activation energy (kcal/mole	Arrhenius constant (1/Ma)	Primary oil (mg/gm)	Primary gas (mg/gm)	Secondary gas (mg/gm)
0.05	46	1.10E+27	1	54	3.20E+27	400	40	60
0.10	48	1.10E+27						
0.10	50	1.10E+27						
0.40	52	1.10E+27						
0.20	54	1.10E+27						
0.10	56	1.10E+27						
0.05	58	1.10E+27						
BREGWGOIL CRACKING								
PRIMARY			SECONDARY			CONSTANTS		
Initial HC potential	Activation energy (kcal/mole	Arrhenius constant (1/Ma)	Initial HC potential	Activation energy (kcal/mole	Arrhenius constant (1/Ma)	Primary oil (mg/gm)	Primary gas (mg/gm)	Secondary gas (mg/gm)
0.05	48	1.50E+27	1	54	3.20E+27	300	50	60
0.11	50	1.50E+27						
0.20	52	1.50E+27						
0.50	54	1.50E+27						
0.10	56	1.50E+27						
0.04	58	1.50E+27						

Table A.02b: Primary and secondary cracking reaction rates and generation quantities for two kerogens used (BREDOIL and BREDWGOIL) (page 1 of 2).

BREDWG CRACKING								
PRIMARY			SECONDARY			CONSTANTS		
Initial HC potential	Activation energy (kcal/mole	Arrhenius constant (1/Ma)	Initial HC potential	Activation energy (kcal/mole	Arrhenius constant (1/Ma)	Primary oil (mg/gm)	Primary gas (mg/gm)	Secondary gas (mg/gm)
0.05	46	3.70E+27	1	54	3.20E+27	80	150	60
0.11	48	3.70E+27						
0.15	50	3.70E+27						
0.26	52	3.70E+27						
0.20	54	3.70E+27						
0.15	56	3.70E+27						
0.08	58	3.70E+27						

BREDDG CRACKING								
PRIMARY			SECONDARY			CONSTANTS		
Initial HC potential	Activation energy (kcal/mole	Arrhenius constant (1/Ma)	Initial HC potential	Activation energy (kcal/mole	Arrhenius constant (1/Ma)	Primary oil (mg/gm)	Primary gas (mg/gm)	Secondary gas (mg/gm)
0.05	46	2.50E+27	1	54	3.20E+27	50	170	100
0.08	48	2.50E+27						
0.15	50	2.50E+27						
0.23	52	2.50E+27						
0.25	54	2.50E+27						
0.15	56	2.50E+27						
0.09	58	2.50E+27						

Table A.02b: Primary and secondary cracking reaction rates and generation quantities for two kerogens used (BREDWG and BREDDG) (page 2 of 2).

GENERAL DATA	
Model name	Well 14
Model description	South Bredasdorp
Surface temperature	10 degC
Corrected maximum log temperature	150 degC at 3823m
Elevation (m bKb)	-186
Heat flow	52.5 mW/m2
Compaction	Fluid Flow (B-B in source rocks)
Porosity-depth method	Linear
Permeability calculation	Power function
Geothermal calculation	Transient heat flow
Maturation calculation	Lawrence Livermore National Laboratory
Expulsion calculation	Saturation (% pores)
Time interval	5 Ma
Depth interval	200 m
Conductivity calculation	Deming/Chapman

Table A.03: General data for South Bredasdorp Basin model (located at well 14) (page 1 of 7).

GENERAL DATA	
Model name	Well 16
Model description	West Bredasdorp
Surface temperature	10 degC
Corrected maximum log temperature	189 degC at 4862m
Elevation (m bKb)	-127
Heat flow	53.0 mW/m2
Compaction	Fluid Flow (B-B in source rocks)
Porosity-depth method	Linear
Permeability calculation	Power function
Geothermal calculation	Transient heat flow
Maturation calculation	Lawrence Livermore National Laboratory
Expulsion calculation	Saturation (% pores)
Time interval	5 Ma
Depth interval	200 m
Conductivity calculation	Deming/Chapman

Table A.03: General data for West Bredasdorp Basin model (located at well 16) (page 2 of 7).

GENERAL DATA	
Model name	Wells 65/75
Model description	North Bredasdorp
Surface temperature	10 degC
Corrected maximum log temperature	143 degC at 3526m
Elevation (m bKb)	-142
Heat flow	52 mW/m2
Compaction	Fluid Flow (B-B in source rocks)
Porosity-depth method	Linear
Permeability calculation	Power function
Geothermal calculation	Transient heat flow
Maturation calculation	Lawrence Livermore National Laboratory
Expulsion calculation	Saturation (% pores)
Time interval	5 Ma
Depth interval	200 m
Conductivity calculation	Deming/Chapman

Table A.03: General data for North Bredasdorp Basin model (located at wells 65/75) (page 3 of 7).

GENERAL DATA	
Model name	Well 8
Model description	East Bredasdorp
Surface temperature	10 degC
Corrected maximum log temperature	51 degC at 1250m
Corrected maximum log temperature	129 degC at 3143m
Elevation (m bKb)	-168
Heat flow	57 mW/m2
Compaction	Fluid Flow (B-B in source rocks)
Porosity-depth method	Linear
Permeability calculation	Power function
Geothermal calculation	Transient heat flow
Maturation calculation	Lawrence Livermore National Laboratory
Expulsion calculation	Saturation (% pores)
Time interval	5 Ma
Depth interval	200 m
Conductivity calculation	Deming/Chapman

Table A.03: General data for East Bredasdorp Basin model (located at well 8) (page 4 of 7).

GENERAL DATA	
Model name	Wells 91/94
Model description	Central Bredasdorp
Surface temperature	10 degC
Corrected maximum log temperature	157 degC at 3581m
Elevation (m bKb)	-129
Heat flow	57 mW/m2
Compaction	Fluid Flow (B-B in source rocks)
Porosity-depth method	Linear
Permeability calculation	Power function
Geothermal calculation	Transient heat flow
Maturation calculation	Lawrence Livermore National Laboratory
Expulsion calculation	Saturation (% pores)
Time interval	5 Ma
Depth interval	200 m
Conductivity calculation	Deming/Chapman

Table A.03: General data for central Bredasdorp Basin model (located between wells 91 and 94) (page 5 of 7).

GENERAL DATA	
Model name	western Southern Outeniqua
Model description	Line L72-020 SP800
Surface temperature	5degC
Elevation (m bKb)	-1740
Heat flow	60 mW/m2
Compaction	Fluid Flow (B-B in source rocks)
Porosity-depth method	Linear
Permeability calculation	Power function
Geothermal calculation	Transient heat flow
Maturation calculation	Lawrence Livermore National Laboratory
Expulsion calculation	Saturation (% pores)
Time interval	5 Ma
Depth interval	200 m
Conductivity calculation	Deming/Chapman
Time variant	14-4 Ma: 1Ma

Table A.03: General data for western Southern Outeniqua Basin model (located at crossing of 1972 seismic lines 15 and 20) (page 6 of 7).

GENERAL DATA	
Model name	eastern Southern Outeniqua
Model description	Line L72-020 SP400
Surface temperature	5degC
Elevation (m bKb)	-1846
Heat flow	65 mW/m2
Compaction	Fluid Flow (B-B in source rocks)
Porosity-depth method	Linear
Permeability calculation	Power function
Geothermal calculation	Transient heat flow
Maturation calculation	Lawrence Livermore National Laboratory
Expulsion calculation	Saturation (% pores)
Time interval	5 Ma
Depth interval	200 m
Conductivity calculation	Deming/Chapman
Time variant	14-4 Ma: 1Ma

Table A.03: General data for eastern Southern Outeniqua Basin model (located at junction of 1972 seismic lines 19 and 20) (page 7 of 7).

STRATIGRAPHY TABLE: WELL 14													
Formation	Type	Begin	Well top	Present	Missing	Lithology	Kerogen	TOC	Compaction	Permeability	Saturation	Reaction	Potential
Event name		Age (Ma)	(m bKb)	thick (m)	thick (m)			(%)	method	method	threshold	network	mg/g TOC
sea	H	5											
erosion1	E	10			-100								
L.Miocene	D	18			100	2			FF	PR			
E.Miocene	F	25	186	94		2			FF	PR			
L.Oligocene	F	28	280	80		2			FF	PR			
erosion2	E	30			-150								
L.E.Oligocene	D	32			150	2			FF	PR			
E.Oligocene	F	36	360	30		3			FF	PR			
L.Eocene	F	40	390	80		3			FF	PR			
M.Eocene	F	46	470	40		3			FF	PR			
E.Eocene	F	54	510	70		3			FF	PR			
Palaeocene	F	64	580	220		2			FF	PR			
erosion3	E	66			-200								
L.Maastrichtian	D	68			200	4			FF	PR			
Maastrichtian	F	74	800	200		4			FF	PR			
Campanian	F	84	1000	150		4			FF	PR			
Santonian	F	88	1150	300		5			FF	PR			
Coniacian	F	89	1450	310		5			FF	PR			
15A WG-OIL	F	92	1760	50		1	BREDWGOIL	2.2	BB	PR	0.30	BREDWGOIL	350
erosion4	E	92.5			-150								
L.Cenomanian	D	93			150	4			FF	PR			
M.Cenomanian	F	95	1810	140		4			FF	PR			
E.Cenomanian	F	96	1950	129		6			FF	PR			
L.Albian	F	98	2079	330		6			FF	PR			
E.-M.Albian	H	103											
L.Aptian	F	108	2409	300		3			FF	PR			
hiatus1	H	109											
13A OIL	F	111	2709	85		1	BREDOIL	2.5	BB	PR	0.25	BREDOIL	440
9A-12A WG-OIL	F	115	2794	261		1	BREDWGOIL	2.1	BB	PR	0.20	BREDWGOIL	350
hiatus2	H	117											
6A	F	118	3055	120		4			FF				
6A WG-OIL	F	119	3175	50		1	BREDWGOIL	1.9	BB	PR	0.20	BREDWGOIL	350
Top 1A-4A	F	121	3225	190		8			FF	PR			
1A-4A DG	F	122	3415	40		1	BREDWG	1.5	BB	PR	0.20	BREDWG	230
1A-4A	F	124	3455	112		8			FF	PR			
hiatus3	H	126											
Pre 1A	F	130	3567	400		7			FF	PR			
BB = Baldwin and Butler, 1985, FF = fluid flow.													
PR = permeability power function													

Table A.04: Stratigraphy table for South Bredasdorp Basin model (located at well 14) (page 1 of 7).

STRATIGRAPHY TABLE: WELL 16													
Formation	Type	Begin	Well top	Present	Missing	Lithology	Kerogen	TOC	Compaction	Permeability	Saturation	Reaction	Potential
Event name		Age (Ma)	(m bKb)	thick (m)	thick (m)			(%)	method	method	threshold	network	mg/g TOC
sea	H	5											
erosion1	E	10			-200								
L.Miocene	D	18			200	2			FF	PR			
E.Miocene	F	25	127	47		Limestone			FF	PR			
L.Oligocene	F	28	174	74		1			FF	PR			
erosion2	E	34			-200								
L.Eocene	D	40			200	2			FF	PR			
M.Eocene	F	46	248	62		1			FF	PR			
erosion3	E	49			-200								
E-Eocene	D	54			200	2			FF	PR			
Palaeocene	F	64	310	110		1			FF	PR			
erosion4	E	66			-400								
L.Maastrichtian	D	69			400	1			FF	PR			
Maastrichtian	F	74	420	140		2			FF	PR			
Campanian	F	84	560	60		Siltstone			FF	PR			
Santonian	F	88	620	210		3			FF	PR			
Coniacian	F	89	830	230		4			FF	PR			
hiatus	H	90											
E.Turonian	F	92	1060	90		5			FF	PR			
Cenomanian	F	96	1150	330		3			FF	PR			
M-L.Albian	F	102	1480	300		3			FF	PR			
14A	F	103	1780	217		4			FF	PR			
13B	F	110	1997	416		5			FF	PR			
13A OIL	F	111	2413	233		6	BREDOIL	3.0	BB	PR	0.15	BREDOIL	350
9A-12A WG	F	114	2646	190		6	BREDWG	2.2	BB	PR	0.15	BREDWG	250
6A-8A WG	F	117	2836	191		6	BREDWG	2.0	BB	PR	0.10	BREDWG	200
6A	F	118	3027	94		5			FF	PR			
5A	F	120	3121	316		4			FF	PR			
L.1A-4A	F	122	3437	263		7			FF	PR			
M.1A-4A	F	124	3700	350		6			FF	PR			
E.1A-4A	F	126	4050	347		5			FF	PR			
Pre 1A salt	F	128	4397	428		8			FF	PR			
Pre 1A DG	F	130	4825	175		3	BREDDG	1.0	BB	PR	0.10	BREDDG	200
BB = Baldwin and Butler, 1985, FF = fluid flow.													
PR = permeability power function													

Table A.04: Stratigraphy table for West Bredasdorp Basin model (located at well 16) (page 2 of 7).

STRATIGRAPHY TABLE: WELLS 65/75													
Formation	Type	Begin	Well top	Present	Missing	Lithology	Kerogen	TOC	Compaction	Permeability	Saturation	Reaction	Potential
Event name		Age (Ma)	(m bKb)	thick (m)	thick (m)			(%)	method	method	threshold	network	mg/g TOC
sea	H	5											
erosion1	E	10			-200								
L.Miocene	D	16			200	4			FF	PR			
erosion2	E	20			-200								
L.Oligocene	D	28			200	5			FF	PR			
E.Oligocene	F	36	142	48		5			FF	PR			
L.Eocene	F	40	190	110		5			FF	PR			
erosion4	E	49			-100								
E.Eocene	D	50			100	4			FF	PR			
E.E.Eocene	F	54	300	70		4			FF	PR			
erosion4	E	56			-150								
L.Palaeocene	D	58			150	3			FF	PR			
Palaeocene	F	64	370	60		3			FF	PR			
erosion5	E	66			-100								
L.Maastrichtian	D	69			100	3			FF	PR			
Maastrichtian	F	74	430	310		6			FF	PR			
L.Campanian	F	76	740	40		3			FF	PR			
hiatus1	H	84											
Santonian	F	88	780	100		6			FF	PR			
Coniacian	F	89	880	250		3			FF	PR			
hiatus2	H	90											
E.Turonian	F	92	1130	140		3			FF	PR			
M-L.Cenomanian	F	95	1270	140		4			FF	PR			
E.Cenomanian	F	96	1410	110		6			FF	PR			
14A	F	103	1520	535		6			FF	PR			
13B	F	110.5	2055	115		3			FF	PR			
13A DG	F	111	2170	21		1	BREDDG	1.4	BB	PR	0.05	BREDDG	150
9A-13A	F	115	2191	559		3			FF	PR			
8A	F	117	2750	210		6			FF	PR			
6A WG	F	118	2960	97		1	BREDWG	1.8	BB	PR	0.15	BREDWG	220
5A WG	F	120	3057	98		1	BREDWG	2.4	BB	PR	0.15	BREDWG	300
1A-4A	F	126	3155	12		4			FF	PR			
Pre 1A	F	130	3167	333		Sandstone			FF	PR			
B-B = Baldwin and Butler, 1985.													
PR = Permeability Power Function													

Table A.04: Stratigraphy table for North Bredasdorp Basin model (located at wells 65/75) (page 3 of 7).

STRATIGRAPHY TABLE: WELL 8													
Formation	Type	Begin	Well top	Present	Missing	Lithology	Kerogen	TOC	Compaction	Permeability	Saturation	Reaction	Potential
Event name		Age (Ma)	(m bKb)	thick (m)	thick (m)			(%)	method	method	threshold	network	mg/g TOC
sea	H	5											
erosion1	E	10			-100								
L.Miocene	D	18			100	1			FF	PR			
E.Miocene	F	25	168	57		Limestone			FF	PR			
L.Oligocene	F	28	225	25		Limestone			FF	PR			
erosion2	E	30			-50								
E.Oligocene	D	36			50	1			FF	PR			
L.Eocene	F	40	250	200		2			FF	PR			
M.Eocene	F	46	450	70		3			FF	PR			
erosion3	E	49			-150								
E.Eocene	D	54			100	2			FF	PR			
L.Palaeocene	D	58			50	3			FF	PR			
Palaeocene	F	64	520	80		3			FF	PR			
erosion4	E	66			-200								
L.Maastrichtian	D	69			100	8			FF	PR			
M.Maastrichtian	D	70			100	8			FF	PR			
E.Maastrichtian	F	74	600	170		4			FF	PR			
Campanian	F	84	770	70		5			FF	PR			
Santonian	F	88	840	500		4			FF	PR			
L.Coniacian	F	88.2	1340	150		3			FF	PR			
M.Coniacian	F	88.4	1490	90		3			FF	PR			
erosion5	E	88.5			-50								
E.Coniacian	D	89			50	8			FF	PR			
Turonian	F	92	1580	80		4			FF	PR			
L.Cenomanian	F	93	1660	70		3			FF	PR			
erosion6	E	94			-100								
M.Cenomanian	D	95			100	5			FF	PR			
E.Cenomanian	F	96	1730	160		5			FF	PR			
14A	F	103	1890	120		6			FF	PR			
E.Albian	F	108	2010	80		6			FF	PR			
13B	F	110	2090	168		6			FF	PR			
13A WG-OIL	F	111	2258	81		7	BREDWGOIL	3.0	BB	PR	0.10	BREDWGOIL	350
E.Aptian	F	115	2339	261		6			FF	PR			
Barremian	F	124	2600	540		6			FF	PR			
1A-Barremian	F	125	3140	160		6			FF	PR			
1A WG-OIL	F	126	3300	50		7	BREDWGOIL	2.0	BB	PR	0.20	BREDWGOIL	300
Pre 1A	F	130	3350	600		3			FF	PR			
B-B = Baldwin and Butler, 1985.													
PR = Permeability Power Function													

Table A.04: Stratigraphy table for East Bredasdorp Basin model (located at well 8) (page 4 of 7).

STRATIGRAPHY TABLE: WELLS 91/94													
Formation	Type	Begin	Well top	Present	Missing	Lithology	Kerogen	TOC	Compaction	Permeability	Saturation	Reaction	Potential
Event name		Age (Ma)	(m bKb)	thick (m)	thick (m)			(%)	method	method	threshold	network	mg/g TOC
sea	H	5											
erosion1	E	10			-200								
L.Olig.-E.Miocene	D	28			200	4			FF	PR			
E.Oligocene	F	36	129	40		4			FF	PR			
M-L.Eocene	F	42	169	60		3			FF	PR			
erosion2	E	49			-100								
E-M.Eocene	D	50			100	3			FF	PR			
E.Eocene	F	54	229	311		3			FF	PR			
Palaeocene	F	64	540	300		2			FF	PR			
erosion3	E	66			-200								
L.Maastrichtian	D	69			200	5			FF	PR			
Maastrichtian	F	74	840	100		5			FF	PR			
Campanian	F	84	940	330		7			FF	PR			
erosion4	E	85			-200								
E.Santonian	D	86			200	8			FF	PR			
E.E.Santonian	F	88	1270	130		5			FF	PR			
L.Cretaceous	F	89	1400	200		5			FF	PR			
15A OIL	F	92	1600	44		1	BREDOIL	2.5	BB	PR	0.35	BREDOIL	400
U-M.Cretaceous	F	97	1644	556		6			FF	PR			
L-M.Cretaceous	F	101	2200	530		6			FF	PR			
Target sand	F	103	2730	60		Sandstone			FF	PR			
13B	F	110	2790	125		7			FF	PR			
13A WG-OIL	F	111	2915	90		1	BREDOIL	3.0	BB	PR	0.35	BREDOIL	500
9A-12A	F	115	3005	140		4			FF	PR			
9A WG	F	116	3145	50		1	BREDWG	1.9	BB	PR	0.55	BREDWG	250
6A-8A	F	118	3195	385		7			FF	PR			
5A WG	F	120	3580	70		1	BREDWG	2.5	BB	PR	0.40	BREDWG	280
1A-4A	F	126	3650	1250		3			FF	PR			
Pre 1A WG	F	128	4900	40		1	BREDWGOIL	2.5	BB	PR	0.50	BREDWGOIL	455
Pre 1A	F	130	4940	100		Sandstone			FF	PR			
B-B = Baldwin and Butler, 1985.													
PR = Permeability Power Function													

Table A.04: Stratigraphy table for Central Bredasdorp Basin model (located between wells 91 and 94) (page 5 of 7).

STRATIGRAPHY TABLE: WESTERN SOUTHERN OUTENIQUA													
Formation	Type	Begin	Well top	Present	Missing	Lithology	Kerogen	TOC	Compaction	Permeability	Saturation	Reaction	Potential
Event name		Age (Ma)	(m bKb)	thick (m)	thick (m)			(%)	method	method	threshold	network	mg/g TOC
sea	H	5											
slump	F	10	1740	350		1			FF	PR			
founder	H	14											
slump+erosion 1	F	15			-200				FF	PR			
E.Miocene	D	25			50	1			FF	PR			
hiatus	H	32											
E.Oligocene	D	36			20	1			FF	PR			
Eocene	D	54			30	2			FF	PR			
Palaeocene	D	64			50	3			FF	PR			
erosion 2	E	66			-100								
L.L Maastrichtian	D	70			50	3			FF	PR			
Maastrichtian	D	74			100	2			FF	PR			
17At1-22At1	F	80	2090	540		1			FF	PR			
16Bt1-17At1	F	89	2630	530		1			FF	PR			
15At1-16Bt1	F	92	3160	270		1			FF	PR			
13Amfs-15At1	F	110	3430	320		1			FF	PR			
13A WG/OIL	F	111	3750	80		5	Type 2	3.0	B-B	PR	0.15	BREDASDORP	400
6At1-13At1	F	118	3830	390		1			FF	PR			
1At1-6At1	F	124	4220	350		2			FF	PR			
1A WG-OIL	F	126	4570	70		5	Type 2	2.5	B-B	PR	0.15	BREDASDORP	350
L. pre1At1	F	140	4640	360		4			FF	PR			
pre1A OIL	F	145	5000	100		5	Type1	3.5	B-B	PR	0.20	BREDASDORP	500
E. pre1A	F	150	5100	600		4			FF	PR			
B-B = Baldwin and Butler, 1985.													
PR = Permeability Power Function													

Table A.04: Stratigraphy table for western Southern Outeniqua Basin model (located at junction of 1972 seismic lines 15 and 20) (page 6 of 7).

STRATIGRAPHY TABLE: EASTERN SOUTHERN OUTENIQUA													
Formation	Type	Begin	Well top	Present	Missing	Lithology	Kerogen	TOC	Compaction	Permeability	Saturation	Reaction	Potential
Event name		Age (Ma)	(m bKb)	thick (m)	thick (m)			(%)	method	method	threshold	network	mg/g TOC
sea	H	5											
slump	F	10	1846	600		1			FF	PR			
founder	H	14											
slump+erosion 1	F	15			-60				FF	PR			
E.Miocene	D	25			10	1			FF	PR			
hiatus	H	32											
E.Oligocene	D	36			10	1			FF	PR			
Eocene	D	54			20	2			FF	PR			
Palaeocene	D	64			10	3			FF	PR			
erosion 2	E	66			-30								
L.L Maastrichtian	D	70			20	3			FF	PR			
Maastrichtian	D	74			20	2			FF	PR			
17At1-22At1	F	80	2446	400		1			FF	PR			
16Bt1-17At1	F	89	2846	400		1			FF	PR			
15At1-16Bt1	F	92	3246	250		1			FF	PR			
13Amfs-15At1	F	110	3496	460		1			FF	PR			
13A WG/OIL	F	111	3956	60		5	Type 2	3.0	BB	PR	0.15	BREDASDORP	400
6At1-13At1	F	118	4016	570		1			FF	PR			
erosion 3	E	119			-250								
1At1-6At1	D	124			250	2			FF	PR			
1A WG-OIL	F	126	4586	60		5	Type 2	2.5	B-B	PR	0.15	BREDASDORP	350
L. pre1At1	F	140	4646	1254		4			FF	PR			
pre1A OIL	F	145	5900	100		5	Type1	3.5	B-B	PR	0.20	BREDASDORP	500
E. pre1A	F	150	6000	700		4			FF	PR			
B-B = Baldwin and Butler, 1985.													
PR = Permeability Power Function													

Table A.04: Stratigraphy table for eastern Southern Outeniqua Basin model (located at junction of 1972 seismic lines 19 and 20) (page 7 of 7).

LITHOLOGY DEFAULTS, MIXTURES AND PROPERTIES: Southern Bredasdorp																
Name	Pattern	SST%	SLT%	SH%	LST%	DOL%	EVAP%	KER%	IGN%	TOTAL%	Initial porosity	Compaction factor (FM) (1/km)	Exp. factor (SC) (1/km)	SG (gm/cc)	Grain size (mm)	Matrix conductivity (W/m.degC)	Heat capacity (kJ/m3.degC)
Sandstone		100								100	45%	1.75	0.27	2.64	0.5	4.4	2800
Siltstone			100							100	55%	2.2	0.41	2.64	0.0156	2	2650
Shale				100						100	60%	2.4	0.51	2.6	0.0004	1.5	2100
Limestone					100					100	60%	1.5	0.22	2.72	0.5	2.9	2600
Dolomite						100				100	60%	1.5	0.22	2.85	0.5	4.8	2600
Evaporite							100			100	0%	0	0	2.15	0.0004	5.4	1750
Kerogen								100		100	90%	3.5	0.7	1.8	0.0004	0.3	950
Igneous									100	100	0%	0	0	2.65	0.0001	2.9	2500
1	7			90				10		100	63%	2.51	0.52	2.52	0.0004	1.38	1985
2		40	20	20	20					100	53%	1.92	0.33	2.648	0.6	3.04	2590
3		20	10	60	10					100	56%	2.16	0.42	2.624	0.0049	2.27	2345
4			10	80	10					100	59%	2.29	0.47	2.616	0.0011	1.69	2205
5			10	70	20					100	59%	2.2	0.44	2.628	0.0024	1.83	2255
6			10	90						100	59%	2.38	0.5	2.604	0.0005	1.55	2155
7		60	40							100	49%	1.93	0.32	2.64	0.1249	3.44	2740
8		40	20	40						100	53%	2.1	0.39	2.624	0.0144	2.76	2490

Table A.05: Lithology table for South Bredasdorp Basin model (located at well 14) (page 1 of 7).

LITHOLOGY DEFAULTS, MIXTURES AND PROPERTIES: Western Bredasdorp																	
Name	Pattern	SST%	SLT%	SH%	LST%	DOL%	EVAP%	KER%	IGN%	TOTAL%	Initial porosity	Compaction factor (FM) (1/km)	Exp. factor (SC) (1/km)	SG (gm/cc)	Grain size (mm)	Matrix conductivity (W/m.degC)	Heat capacity kJ/m3.degC)
Sandstone		100								100	45%	1.75	0.27	2.64	0.5	4.4	2800
Siltstone			100							100	55%	2.2	0.41	2.64	0.0156	2	2650
Shale				100						100	60%	2.4	0.51	2.6	0.0004	1.5	2100
Limestone					100					100	60%	1.5	0.22	2.72	0.5	2.9	2600
Dolomite						100				100	60%	1.5	0.22	2.85	0.5	4.8	2600
Evaporite							100			100	0%	0	0	2.15	0.0004	5.4	1750
Kerogen								100		100	90%	3.5	0.7	1.8	0.0004	0.3	950
Igneous									100	100	0%	0	0	2.65	0.0001	2.9	2500
1		50			50					100	52%	1.62	0.24	2.68	0.5	3.65	2700
2		30	60		10					100	52%	1.99	0.34	2.648	0.0624	2.81	2690
3		10	50	30	10					100	56%	2.14	0.4	2.636	0.0103	2.18	2495
4		10	10	60	20					100	58%	2.13	0.41	2.632	0.0049	2.12	2325
5			30	70						100	58%	2.34	0.48	2.612	0.0012	1.65	2265
6	7			90				10		100	63%	2.51	0.52	2.52	0.0004	1.38	1985
7		50		50						100	52%	2.07	0.39	2.62	0.0141	2.95	2450
8		10	30	20			40			100	33%	1.31	0.25	2.436	0.0024	3.5	2195

Table A.05: Lithology table for West Bredasdorp Basin model (located at well 16) (page 2 of 7).

LITHOLOGY DEFAULTS, MIXTURES AND PROPERTIES: Northern Bredasdorp																	
Name	Pattern	SST%	SLT%	SH%	LST%	DOL%	EVAP%	KER%	IGN%	TOTAL%	Initial porosity	Compaction factor (FM) (1/km)	Exp. factor (SC) (1/km)	SG (gm/cc)	Grain size (mm)	Matrix conductivity (W/m.degC)	Heat capacity (kJ/m3.degC)
Sandstone		100								100	45%	1.75	0.27	2.64	0.5	4.4	2800
Siltstone			100							100	55%	2.2	0.41	2.64	0.0156	2	2650
Shale				100						100	60%	2.4	0.51	2.6	0.0004	1.5	2100
Limestone					100					100	60%	1.5	0.22	2.72	0.5	2.9	2600
Dolomite						100				100	60%	1.5	0.22	2.85	0.5	4.8	2600
Evaporite							100			100	0%	0	0	2.15	0.0004	5.4	1750
Kerogen								100		100	90%	3.5	0.7	1.8	0.0004	0.3	950
Igneous									100	100	0%	0	0	2.65	0.0001	2.9	2500
1	7			90				10		100	63%	2.51	0.52	2.52	0.0004	1.38	1985
2		30	20		50					100	54%	1.71	0.27	2.68	0.2499	3.17	2670
3		10	10	70	10					100	58%	2.22	0.44	2.62	0.0024	1.98	2275
4		10	20	40	30					100	57%	2.02	0.37	2.648	0.0144	2.31	2430
5		50	20		30					100	51%	1.76	0.28	2.664	0.2499	3.47	2710
6			10	80	10					100	59%	2.29	0.47	2.616	0.0011	1.69	2205

Table A.05: Lithology table for North Bredasdorp Basin model (located at wells 65/75) (page 3 of 7).

LITHOLOGY DEFAULTS, MIXTURES AND PROPERTIES: Eastern Bredasdorp																	
Name	Pattern	SST%	SLT%	SH%	LST%	DOL%	EVAP%	KER%	IGN%	TOTAL%	Initial porosity	Compaction factor (FM) (1/km)	Exp. factor (SC) (1/km)	SG (gm/cc)	Grain size (mm)	Matrix conductivity (W/m.degC)	Heat capacity (KJ/m3.degC)
Sandstone		100								100	45%	1.75	0.27	2.64	0.5	4.4	2800
Siltstone			100							100	55%	2.2	0.41	2.64	0.0156	2	2650
Shale				100						100	60%	2.4	0.51	2.6	0.0004	1.5	2100
Limestone					100					100	60%	1.5	0.22	2.72	0.5	2.9	2600
Dolomite						100				100	60%	1.5	0.22	2.85	0.5	4.8	2600
Evaporite							100			100	0%	0	0	2.15	0.0004	5.4	1750
Kerogen								100		100	90%	3.5	0.7	1.8	0.0004	0.3	950
Igneous									100	100	0%	0	0	2.65	0.0001	2.9	2500
1		20	30		50					100	55%	1.76	0.28	2.68	0.1766	2.93	2655
2				50	50					100	60%	1.95	0.36	2.66	0.0141	2.2	2350
3		30	10	30	30					100	55%	1.91	0.34	2.652	0.0416	2.84	2515
4		20	20	40	20					100	56%	2.05	0.38	2.64	0.0144	2.46	2450
5				70	30					100	60%	2.13	0.42	2.636	0.0033	1.92	2250
6		10	30	60						100	58%	2.32	0.47	2.616	0.0017	1.7	2320
7	7			90				10		100	63%	2.51	0.52	2.52	0.0004	1.38	1985
8		10	20	70						100	57%	2.29	0.46	2.612	0.0016	1.89	2280

Table A.05: Lithology table for East Bredasdorp Basin model (located at well 8) (page 4 of 7).

LITHOLOGY DEFAULTS, MIXTURES AND PROPERTIES (Central Bredasdorp)																
Name	Pattern	SST%	SLT%	SH%	LST%	DOL%	EVAP%	KER%	IGN%	TOTAL%	Initial porosity	Compaction factor (FM) (1/km)	Exp. factor (SC) (1/km)	SG (gm/cc)	Grain size (mm)	Matrix conductivity (W/m.degC)	Heat capacity (kJ/m3.degC)
Sandstone		100								100	45%	1.75	0.27	2.64	0.5	4.4	2800
Siltstone			100							100	55%	2.2	0.41	2.64	0.0156	2	2650
Shale				100						100	60%	2.4	0.51	2.6	0.0004	1.5	2100
Limestone					100					100	60%	1.5	0.22	2.72	0.5	2.9	2600
Dolomite						100				100	60%	1.5	0.22	2.85	0.5	4.8	2600
Evaporite							100			100	0%	0	0	2.15	0.0004	5.4	1750
Kerogen								100		100	90%	3.5	0.7	1.8	0.0004	0.3	950
Igneous									100	100	0%	0	0	2.65	0.0001	2.9	2500
1	7			90				10		100	63%	2.51	0.52	2.52	0.0004	1.38	1985
2		60		10	30					100	51%	1.74	0.27	2.66	0.245	3.66	2670
3		60	20	20						100	50%	1.97	0.34	2.632	0.06	3.34	2630
4		30	10	40	20					100	55%	2	0.37	2.64	0.0204	2.7	2465
5		10	20	60	10					100	57%	2.2	0.43	2.624	0.0034	2.03	2330
6			40	60						100	58%	2.32	0.47	2.616	0.0017	1.7	2320
7		10	10	80						100	58%	2.31	0.47	2.608	0.0011	1.84	2225
8		20	10	10	60					100	56%	1.71	0.27	2.684	0.1732	2.97	2595

Table A.05: Lithology table for Central Bredasdorp Basin model (located between wells 91 and 94) (page 5 of 7).

LITHOLOGY DEFAULTS, MIXTURES AND PROPERTIES (Southern Outeniqua 1)																	
Name	Pattern	SST%	SLT%	SH%	LST%	DOL%	EVAP%	KER%	IGN%	TOTAL%	Initial porosity	Compaction factor (FM) (1/km)	Exp. factor (SC) (1/km)	SG (gm/cc)	Grain size (mm)	Matrix conductivity (W/m.degC)	Heat capacity (KJ/m3.degC)
Sandstone		100								100	45%	1.75	0.27	2.64	0.5	4.4	2800
Siltstone			100							100	55%	2.2	0.41	2.64	0.0156	2	2650
Shale				100						100	60%	2.4	0.51	2.6	0.0004	1.5	2100
Limestone					100					100	60%	1.5	0.22	2.72	0.5	2.9	2600
Dolomite						100				100	60%	1.5	0.22	2.85	0.5	4.8	2600
Evaporite							100			100	0%	0	0	2.15	0.0004	5.4	1750
Kerogen								100		100	90%	3.5	0.7	1.8	0.0004	0.3	950
Igneous									100	100	0%	0	0	2.65	0.0001	2.9	2500
1		30	20	20	30					100	54%	1.89	0.33	2.656	0.06	2.89	2570
2		10	10	60	20					100	56%	2.16	0.42	2.624	0.0049	2.27	2345
3		10	20	70						100	57%	2.29	0.46	2.612	0.0016	1.89	2280
4		30		70						100	58%	2.31	0.47	2.608	0.0011	1.84	2225
5	7			90				10		100	63%	2.51	0.52	2.52	0.0004	1.38	1985

Table A.05: Lithology table for western Southern Outeniqua Basin model (located at junction of 1972 seismic lines 19 and 20) (page 6 of 7).

LITHOLOGY DEFAULTS, MIXTURES AND PROPERTIES (Southern Outeniqua 2)																	
Name	Pattern	SST%	SLT%	SH%	LST%	DOL%	EVAP%	KER%	IGN%	TOTAL%	Initial porosity	Compaction factor (FM) (1/km)	Exp. factor (SC) (1/km)	SG (gm/cc)	Grain size (mm)	Matrix conductivity (W/m.degC)	Heat capacity (kJ/m3.degC)
Sandstone		100								100	45%	1.75	0.27	2.64	0.5	4.4	2800
Siltstone			100							100	55%	2.2	0.41	2.64	0.0156	2	2100
Shale				100						100	60%	2.4	0.51	2.6	0.0004	1.5	2100
Limestone					100					100	60%	1.5	0.22	2.72	0.5	2.9	2600
Dolomite						100				100	60%	1.5	0.22	2.85	0.5	4.8	2600
Evaporite							100			100	0%	0	0	2.15	0.0004	5.4	1750
Kerogen								100		100	90%	3.5	0.7	1.8	0.0004	0.3	950
Igneous									100	100	0%	0	0	2.65	0.0001	2.9	2500
1		30	20	20	30					100	54%	1.89	0.33	2.656	0.06	2.89	2570
2		10	10	60	20					100	56%	2.16	0.42	2.624	0.0049	2.27	2345
3		10	20	70						100	57%	2.29	0.46	2.612	0.0016	1.89	2280
4		30		70						100	58%	2.31	0.47	2.608	0.0011	1.84	2225
5	7			90				10		100	63%	2.51	0.52	2.52	0.0004	1.38	1985

Table A.05: Lithology table for eastern Southern Outeniqua Basin model (located at junction of 1972 seismic lines 15 and 20) (page 7 of 7).
MODELS: APATABL.DOC

FLUID FLOW FACTORS: Southern Bredasdorp								
Name	Initial porosity		Compaction factor		Fraction	Porosity	Initial	Permeability
	Fraction A	Fraction B	A	B	A	reduction	permeability	power
	(%shale)	(%sand)	(expon.)	(linear) 1/Pa	(%)	factor	(mD)	function
Sandstone	0	45%	0	1.35	0	0.000120	2.786221	5.5
Siltstone	55.00%	0	-0.8	0	100%	0.000230	1.013171	5.5
Shale	60.00%	0	-0.8	0	100%	0.000300	1.013171	5.5
Limestone	60.00%	0	-0.8	0	100%	0.000190	2.786221	5.5
Dolomite	60.00%	0	-0.8	0	100%	0.000200	2.786221	5.5
Evaporite	0	0	-0.8	1.35	0	0.050000	1.013171	5.5
Kerogen	90.00%	0	-0.8	0	100%	0.000300	1.013171	5.5
Igneous	0	0	-0.8	1.35	0	0.050000	1.013171	5.5
1	63.00%	0	-0.8	0	100%	0.000300	1.013171	5.5
2	58.33%	45%	-0.8	1.35	60%	0.000180	1.859013	5.5
3	59.37%	45%	-0.8	1.35	80%	0.000232	4.33993	5.5
4	59.50%	0	-0.8	0	100%	0.000279	3.544999	5.5
5	59.50%	0	-0.8	0	100%	0.000267	1.240365	5.5
6	59.50%	0	-0.8	0	100%	0.000292	1.013171	5.5
7	55.00%	45%	-0.8	1.35	40%	0.000156	1.859013	5.5
8	58.33%	45%	-0.8	1.35	60%	0.000197	1.518504	5.5

Table A.06: Fluid flow factors (porosity, compaction, permeability) used in the South Bredasdorp Basin model (at well 14) (page 1 of 7)

FLUID FLOW FACTORS: Western Bredasdorp								
Name	Initial porosity		Compaction factor		Fraction	Porosity	Initial	Permeability
	Fraction A	Fraction B	A	B	A	reduction	permeability	power
	(%shale)	(%sand)	(expon.)	(linear) 1/Pa	(%)	factor	(mD)	function
Sandstone	0	45%	0	1.35E-08	0	0.000120	2.79E+04	5.5
Siltstone	55.00%	0	-0.8	0	100%	0.000230	1.01E-01	5.5
Shale	60.00%	0	-0.8	0	100%	0.000300	1.01E-01	5.5
Limestone	60.00%	0	-0.8	0	100%	0.000190	2.79E+04	5.5
Dolomite	60.00%	0	-0.8	0	100%	0.000200	2.79E+04	5.5
Evaporite	0	0	-0.8	1.35E-08	0	0.050000	1.01E-08	5.5
Kerogen	90.00%	0	-0.8	0	100%	0.000300	1.01E-01	5.5
Igneous	0	0	-0.8	1.35E-08	0	0.050000	1.01E-08	5.5
1	60.00%	45%	-0.8	1.35E-08	50%	0.000151	2.79E+04	5.5
2	55.71%	45%	-0.8	1.35E-08	70%	0.000186	1.52E+01	5.5
3	57.22%	45%	-0.8	1.35E-08	90%	0.000229	1.240365	5.5
4	59.44%	45%	-0.8	1.35E-08	90%	0.000243	4.33993	5.5
5	58.50%	0	-0.8	0	100%	0.000277	1.01E-01	5.5
6	63.00%	0	-0.8	0	100%	0.000300	1.01E-01	5.5
7	60.00%	45%	-0.8	1.35E-08	50%	0.000190	5.31E+01	5.5
8	57.00%	45%	-0.8	1.35E-08	50%	0.001956	5.618444	5.5

Table A.06: Fluid flow factors (porosity, compaction, permeability) used in the West Bredasdorp Basin model (located at well 16) (page 2 of 7)

FLUID FLOW FACTORS: Northern Bredasdorp								
Name	Initial porosity		Compaction factor		Fraction	Porosity	Initial	Permeability
	Fraction A	Fraction B	A	B	A	reduction	permeability	power
	(%shale)	(%sand)	(expon.)	(linear) 1/Pa	(%)	factor	(mD)	function
Sandstone	0	45%	0	1.35E-08	0	0.000120	2.79E+04	5.5
Siltstone	55.00%	0	-0.8	0	100%	0.000230	1.01E-01	5.5
Shale	60.00%	0	-0.8	0	100%	0.000300	1.01E-01	5.5
Limestone	60.00%	0	-0.8	0	100%	0.000190	2.79E+04	5.5
Dolomite	60.00%	0	-0.8	0	100%	0.000200	2.79E+04	5.5
Evaporite	0	0	-0.8	1.35E-08	0	0.050000	1.01E-08	5.5
Kerogen	90.00%	0	-0.8	0	100%	0.000300	1.01E-01	5.5
Igneous	0	0	-0.8	1.35E-08	0	0.050000	1.01E-08	5.5
1	63.00%	0	-0.8	0	100%	0.000300	1.01E-01	5.5
2	58.57%	45%	-0.8	1.35E-08	70%	0.000172	2.28E+03	5.5
3	59.44%	45%	-0.8	1.35E-08	90%	0.000255	1.240365	5.5
4	58.88%	45%	-0.8	1.35E-08	90%	0.000226	1.52E+01	5.5
5	58.00%	45%	-0.8	1.35E-08	50%	0.000157	2.28E+03	5.5
6	59.50%	0	-0.8	0	100%	0.000279	3.55E-01	5.5

Table A.06: Fluid flow factors (porosity, compaction, permeability) used in the North Bredasdorp Basin model (located at wells 65 and 75) (page 3 of 7)

FLUID FLOW FACTORS: Eastern Bredasdorp								
Name	Initial porosity		Compaction factor		Fraction	Porosity	Initial	Permeability
	Fraction A	Fraction B	A	B	A	reduction	permeability	power
	(%shale)	(%sand)	(expon.)	(linear) 1/Pa	(%)	factor	(mD)	function
Sandstone	0	45%	0	1.35E-08	0	0.000120	2.79E+04	5.5
Siltstone	55.00%	0	-0.8	0	100%	0.000230	1.01E-01	5.5
Shale	60.00%	0	-0.8	0	100%	0.000300	1.01E-01	5.5
Limestone	60.00%	0	-0.8	0	100%	0.000190	2.79E+04	5.5
Dolomite	60.00%	0	-0.8	0	100%	0.000200	2.79E+04	5.5
Evaporite	0	0	-0.8	1.35E-08	0	0.050000	1.01E-08	5.5
Kerogen	90.00%	0	-0.8	0	100%	0.000300	1.01E-01	5.5
Igneous	0	0	-0.8	1.35E-08	0	0.050000	1.01E-08	5.5
1	58.12%	45%	-0.8	1.35E-08	80%	0.000184	6.50E+02	5.5
2	60.00%	0%	-0.8	0	100%	0.000239	5.31E+01	5.5
3	59.28%	45%	-0.8	1.35E-08	70%	0.000194	1.86E+02	5.5
4	58.75%	45%	-0.8	1.35E-08	80%	0.000216	1.52E+01	5.5
5	60.00%	0	-0.8	0	100%	0.000262	4.33993	5.5
6	58.00%	0	-0.8	0	100%	0.000253	1.01E-01	5.5
7	63.00%	0%	-0.8	0	100%	0.000300	1.01E-01	5.5
8	58.88%	45%	-0.8	1.35E-08	90%	0.000260	3.54E-01	5.5

Table A.06: Fluid flow factors (porosity, compaction, permeability) used in the East Bredasdorp Basin model (located at well 8) (page 4 of 7)

FLUID FLOW FACTORS: Central Bredasdorp								
Name	Initial porosity		Compaction factor		Fraction	Porosity	Initial	Permeability
	Fraction A	Fraction B	A	B	A	reduction	permeability	power
	(%shale)	(%sand)	(expon.)	(linear) 1/Pa	(%)	factor	(mD)	function
Sandstone	0	45%	0	1.35E-08	0	0.000120	2.79E+04	5.5
Siltstone	55.00%	0	-0.8	0	100%	0.000230	1.01E-01	5.5
Shale	60.00%	0	-0.8	0	100%	0.000300	1.01E-01	5.5
Limestone	60.00%	0	-0.8	0	100%	0.000190	2.79E+04	5.5
Dolomite	60.00%	0	-0.8	0	100%	0.000200	2.79E+04	5.5
Evaporite	0	0	-0.8	1.35E-08	0	0.050000	1.01E-08	5.5
Kerogen	90.00%	0	-0.8	0	100%	0.000300	1.01E-01	5.5
Igneous	0	0	-0.8	1.35E-08	0	0.050000	1.01E-08	5.5
1	63.00%	0	-0.8	0.00E+00	100%	0.000300	1.01E-01	5.5
2	60.00%	45%	-0.8	1.35E-08	40%	0.000151	7.96E+03	5.5
3	57.50%	45%	-0.8	1.35E-08	40%	0.000164	1.86E+02	5.5
4	59.28%	45%	-0.8	1.35E-08	70%	0.000203	5.31E+01	5.5
5	58.88%	45%	-0.8	1.35E-08	90%	0.000248	1.24	5.5
6	58.00%	0	-0.8	0.00E+00	100%	0.000270	1.01E-01	5.5
7	59.44%	45%	-0.8	1.35E-08	90%	0.000267	3.55E-01	5.5
8	59.37%	45%	-0.8	1.35E-08	80%	0.000185	2.28E+03	5.5

Table A.06: Fluid flow factors (porosity, compaction, permeability) used in the Central Bredasdorp Basin model (located between wells 91 and 94) (page 5 of 7)

FLUID FLOW FACTORS: Southern Outeniqua 1								
Name	Initial porosity		Compaction factor		Fraction	Porosity	Initial	Permeability
	Fraction A	Fraction B	A	B	A	reduction	permeability	power
	(%shale)	(%sand)	(expon.)	(linear) 1/Pa	(%)	factor	(mD)	function
Sandstone	0	45%	0	1.35E-08	0	0.000120	2.79E+04	5.5
Siltstone	55.00%	0	-0.8	0	100%	0.000230	1.01E-01	5.5
Shale	60.00%	0	-0.8	0	100%	0.000300	1.01E-01	5.5
Limestone	60.00%	0	-0.8	0	100%	0.000190	2.79E+04	5.5
Dolomite	60.00%	0	-0.8	0	100%	0.000200	2.79E+04	5.5
Evaporite	0	0	-0.8	1.35E-08	0	0.050000	1.01E-08	5.5
Kerogen	90.00%	0	-0.8	0	100%	0.000300	1.01E-01	5.5
Igneous	0	0	-0.8	1.35E-08	0	0.050000	1.01E-08	5.5
1	58.57%	45%	-0.8	1.35	70%	0.000188	1.859013	5.5
2	59.37%	45%	-0.8	1.35	80%	0.000232	4.33993	5.5
3	58.88%	45%	-0.8	1.35	90%	0.000260	3.544999	5.5
4	59.44%	45%	-0.8	1.35	90%	0.000228	3.544999	5.5
5	63.00%	0	-0.8	0	100%	0.000300	1.013171	5.5

Table A.06: Fluid flow factors (porosity, compaction, permeability) used in the western Southern Outeniqua Basin model (located at junction of 1972 lines 15 and 20) (page 6 of 7)

FLUID FLOW FACTORS: Southern Outeniqua 2								
Name	Initial porosity		Compaction factor		Fraction	Porosity	Initial	Permeability
	Fraction A	Fraction B	A	B	A	reduction	permeability	power
	(%shale)	(%sand)	(expon.)	(linear) 1/Pa	(%)	factor	(mD)	function
Sandstone	0	45%	0	1.35E-08	0	0.000120	2.79E+04	5.5
Siltstone	55.00%	0	-0.8	0	100%	0.000230	1.01E-01	5.5
Shale	60.00%	0	-0.8	0	100%	0.000300	1.01E-01	5.5
Limestone	60.00%	0	-0.8	0	100%	0.000190	2.79E+04	5.5
Dolomite	60.00%	0	-0.8	0	100%	0.000200	2.79E+04	5.5
Evaporite	0	0	-0.8	1.35E-08	0	0.050000	1.01E-08	5.5
Kerogen	90.00%	0	-0.8	0	100%	0.000300	1.01E-01	5.5
Igneous	0	0	-0.8	1.35E-08	0	0.050000	1.01E-08	5.5
1	58.57%	45%	-0.8	1.35E-08	70%	0.000188	1.86E+02	5.5
2	59.44%	45%	-0.8	1.35E-08	90%	0.000243	4.34	5.5
3	58.88%	45%	-0.8	1.35E-08	90%	0.000260	3.55E-01	5.5
4	60.00%	45%	-0.8	1.35E-08	70%	0.000228	4.34	5.5
5	63.00%	0	-0.8	0	100%	0.000300	1.01E-01	5.5

Table A.06: Fluid flow factors (porosity, compaction, permeability) used in the eastern Southern Outeniqua Basin model (located at junction of 1972 seismic lines 19 and 20) (page 7 of 7)

TIME VALUES TABLE			
SOUTH BREDASDORP: WELL 14			
Time	Heat flow (mW/m2)	Surface temperature	Sea depth (m)
2	50		
5	45	10	186
6		15	0
10		15	0
11		15	50
12		15	80
28		15	80
29		15	20
30		15	20
31		15	50
48	45		
51	51		
53	54		
60	54		
63		12	100
64	51	12	100
64.1		15	20
66	48	15	20
67		10	80
70	44		
89		8	200
89.1		5	300
92		5	300
92.1		15	50
109		8	200
110	44	5	300
111		5	300
114	50		
117	55	10	200
120	59		
126	75	15	100
130	75	20	40

DELTA HEAT TABLE			
Formation Name	Time (Ma) Start	Time (Ma) End	Generated Heat (muW/m3)
E. Eocene	10	0	60
Palaeocene	10	0	60
Maastrichtian	10	0	70
Campanian	10	0	60
Santonian	10	0	35
Coniacian	10	0	35

VITRINITE REFLECTANCE			
SOUTH BREDASDORP: WELL 14			
Depth (mbKb)	Sample type	Reflectance	Error
730	R	0.38	15%
1380	R	0.55	9%
1443	R	0.56	10%
1525	R	0.65	10%
1613	S	0.59	8%
1983	R	0.81	9%
2121	R	0.81	7%
2361	R	0.90	8%
2511	R	0.96	9%
2742	R	1.02	6%
2781	R	1.04	8%
2834	S	1.02	9%
2871	R	1.08	9%
2922	R	1.14	10%
3021	R	1.18	12%
3120	R	1.18	15%
3260	Core	1.24	8%
3262.5	Core	1.26	5%
3263.1	Core	1.24	8%
3264.6	Core	1.24	10%
3528.3	Core	1.45	8%
3528.4	Core	1.7	12%
3529	Core	1.49	10%
3740	Core	1.80	7%
3740.6	Core	1.51	6%
3742	Core	1.73	6%
3752	R	1.57	4%

Table A.07: Time-heat, delta heat and vitrinite reflectance values for South Bredasdorp Basin model (located at well 14) (page 1 of 7).

TIME VALUES TABLE			
WEST BREDASDORP: WELL 16			
Time	Heat flow	Surface	Sea depth
	(mW/m2)	temperature	(m)
1	50	15	120
2	45		
5	40		
18		15	100
25		20	50
45	40		
56	48	20	50
58	58	20	50
60	50	20	50
64	43	20	50
72	40		
88		10	150
89		15	50
107	40	10	100
108		10	200
111	45		
117	50	10	200
118		15	150
125.5	70	15	100
126		20	10
128.5		20	0
130	75	20	0

DELTA HEAT TABLE			
Formation	Time (Ma)	Time (Ma)	Generated
Name	Start	End	Heat (muW/m3)
Maastrichtian	10	0	50
Campanian	10	0	50
Santonian	10	0	50
Coniacian	10	0	50
E.Turonian	10	0	50
Cenomanian	10	0	50
M-L.Albian	10	0	50

VITRINITE REFLECTANCE			
WEST BREDASDORP: WELL 16			
Depth	Sample	Reflectance	Error
(mbKb)	type		
625	S	0.43	10%
1260	R	0.58	8%
1310	R	0.57	9%
1390	R	0.60	8%
1462	S	0.63	6%
2710	R	1.03	8%
2800	R	1.06	10%
2926	R	1.01	10%
2929	R	1.02	12%
3010	R	1.06	11%
3031	R	1.06	14%
3052	R	1.08	9%
3094	R	1.13	8%
3157	R	1.17	12%
3166	R	1.12	6%
3217	R	1.14	8%
3238	R	1.12	8%
3250	R	1.25	12%
3302	R	1.18	10%
3513.1	Core	1.24	10%
3553	R	1.21	6%
3595	R	1.22	8%
3637	R	1.31	10%
3798	S	1.33	8%
4201.5	S	1.63	9%
4501	R	2.16	10%

Table A.07: Time-heat, delta heat and vitrinite reflectance values for West Bredasdorp Basin model (located at well 16) (page 2 of 7).

TIME VALUES TABLE			
NORTH BREDASDORP: WELLS 65/75			
Time	Heat flow (mW/m2)	Surface temperature	Sea depth (m)
1	52		
2		10	140
8	49		
30		15	80
49	50		
53	55		
58	60		
64	60	10	100
67	56	20	50
71	53		
76	50		
89		10	150
91		20	50
110	52	15	100
110.1		10	200
111		10	200
111.1		15	100
114	55		
117	60	15	100
118.5		10	200
119		10	200
119.1	62	15	100
126	75	15	100
126.1		20	50
130	80	20	50

DELTA HEAT TABLE			
Formation Name	Time (Ma) Start	Time (Ma) End	Generated Heat (muW/m3)
Maas.	10	0	50
L. Camp.	10	0	60
Santonian	10	0	70
Coniacian	10	0	65
E.Turonian	10	0	60
M-L. Ceno.	10	0	55
E. Ceno.	10	0	50

VITRINITE REFLECTANCE			
NORTH BREDASDORP WELLS 65/75			
Depth (mbKb)		Reflectance	Error
1310	R	0.59	10%
1410	R	0.63	9%
1510	R	0.67	10%
1660	R	0.72	8%
1710	R	0.75	9%
1760	R	0.69	10%
1860	R	0.73	8%
1960	R	0.76	7%
2060	R	0.80	10%
2110	R	0.83	11%
2212	R	0.81	11%
2260	R	0.86	8%
2311	R	0.85	9%
2362	R	0.87	6%
2410	R	0.88	10%
2461	R	0.90	7%
2512	R	0.90	8%
2560	R	0.94	9%
2611	R	0.9	10%
2761	R	1.04	8%
2820	R	1.03	10%
2824	Core	0.99	11%
2932.1	Core	0.99	11%
2837.9	Core	1.04	14%
2860	R	1.03	9%
3112	R	1.16	8%
3200	R	1.19	8%
3270.5	Core	1.24	11%
3295.9	Core	1.22	7%
3326.5	Core	1.50	9%

Table A.07: Time-heat, delta heat and vitrinite reflectance values for North Bredasdorp Basin model (located at wells 65/75) (page 3 of 7).

TIME VALUES TABLE

EAST BREDASDORP: WELL 8

Time	Heat flow (mW/m2)	Surface temperature	Sea depth (m)
2	53	10	168
5	50	15	80
24		15	80
30		20	20
31	50	15	80
39	56		
45	63	12	100
50	75	10	120
54	86		
56		15	60
58	92	15	50
59	86		
63	70	15	80
64		15	50
68	60	15	50
69	65	15	80
70	59		
73	52		
75			
83		10	150
88		10	100
88.5		20	30
89		15	100
109		15	100
110	48	10	200
111		10	200
112	50	15	100
124	76	15	100
125		10	200
126	95	10	200
127		20	50
130	99	20	40

DELTA HEAT TABLE

Formation Name	Time (Ma) Start	Time (Ma) End	Generated Heat (muW/m3)
Palaeocene	10	0	45
E.Maas.	10	0	50
Campanian	10	0	55
Santonian	10	0	60
L.Coniacian	10	0	65
M.Coniacian	10	0	60
Turonian	10	0	55
L.Ceno.	10	0	50
E.Ceno.	10	0	45

VITRINITE REFLECTANCE

EAST BREDASDORP: WELL 8

Depth (mbKb)		Reflectance	Error
2117	R	0.99	10%
2216	R	0.93	10%
2249	R	1.02	10%
2267	R	0.99	15%
2273	R	1.10	8%
2279	R	1.04	10%
2288	R	1.06	11%
2306	R	1.08	9%
2312	R	1.17	20%
2663	R	1.32	15%
2663.1	Core	1.28	10%
2696	R	1.25	10%
2894	R	1.36	10%
2897	R	1.45	14%

DELTA THICKNESS

Period	Start	End	Thickness
E. Maas.	58 Ma	56 Ma	50m
Santonain	58 Ma	56 Ma	50m
L. Coniacian	58 Ma	56 Ma	10m
M. Coniacian	58 Ma	56 Ma	10m
Turonian	58 Ma	56 Ma	20m
L. Ceno.	58 Ma	56 Ma	50m
E. Ceno.	58 Ma	56 Ma	50m
14A	58 Ma	56 Ma	10m
E. Albian	58 Ma	56 Ma	20m
13A WG-OIL	58 Ma	56 Ma	10m
E. Aptian	58 Ma	56 Ma	10m
Barremian	58 Ma	56 Ma	40m
1A-Barr.	58 Ma	56 Ma	50m

Table A.07: Time-heat, delta heat, vitrinite reflectance and delta thickness values for East Bredasdorp Basin model (located at well 8) (page 4 of 7).

TIME VALUES TABLE			
CENTRAL BREDASDORP WELLS 91/94			
Time	Heat flow (mW/m2)	Surface temperature	Sea depth (m)
2	50	10	130
5	48	10	80
10		10	80
12		10	80
20		10	80
24		10	115
30			
36	48	15	100
47	55		
54	60		
56		12	150
58		15	80
59	66		
60		15	80
62	63		
66	60	12	150
72	55	10	150
83	50	10	200
88.5		10	200
89		5	300
91		5	300
92	50	10	150
109	55	10	250
110		5	300
111		5	300
112	60	10	200
125	70	15	100
126		20	40
128	75	10	100
130	90	10	50

DELTA HEAT TABLE			
Formation Name	Time (Ma) Start	Time (Ma) End	Generated Heat (muW/m3)
Campanian	10	0	30
E. Sant.	10	0	30
L. Cret.	10	0	30
15A OIL	10	0	30
U.M.Cret.	10	0	30

VITRINITE REFLECTANCE			
CENTRAL BREDASDORP WELLS 91/94			
Depth (mbKb)		Reflectance	Error
600	S	0.28	12%
639	S	0.24	10%
682	S	0.29	15%
786	S	0.32	15%
1140	S	0.41	15%
1295	S	0.55	8%
1368	S	0.51	8%
1426	S	0.60	9%
1612	S	0.60	12%
1812	S	0.67	11%
1877	S	0.6	5%
1924	S	0.64	6%
2310	S	0.75	10%
2421	S	0.74	5%
2515	S	0.77	8%
2547	S	0.83	8%
2590	S	0.89	10%
2701	S	0.92	10%
2706.5	S	0.95	9%
2774.5	S	0.93	7%
2780	S	0.85	6%
2800.6	Core	0.98	10%
2802.6	Core	0.95	8%
2806.3	Core	0.95	10%
2830	S	0.93	9%
2870	S	0.99	5%
2919.5	S	1.01	6%
2935	S	0.99	10%
2985.9	S	1.02	10%
2997.5	S	1.05	9%
3050.9	Core	1.07	8%
3052	Core	1.17	10%
3188.2	Core	1.02	7%
3191.7	Core	1.08	8%
3200	S	1.37	4%
3221.7	Core	1.15	8%
3229	Core	1.16	8%
3300	S	1.33	5%
3431.5	Core	1.40	12%
3567.4	Core	1.42	10%
3737	S	1.63	5%
3810	S	1.67	6%

Table A.07: Time-heat, delta heat and vitrinite reflectance values for Central Bredasdorp Basin model (located between wells 91 and 94) (page 5 of 7).

TIME VALUES TABLE			
western SOUTHERN OUTENIQUA 1			
Time	Heat flow (mW/m2)	Surface temperature	Sea depth (m)
5	60	5	1070
12	55	10	200
15	50	10	180
18		10	150
40	50		
45	50	10	100
50	55	10	80
55	60	10	50
58	65		40
60	60		50
65	55		100
70	50		150
80			200
100	50		
109		5	150
110		5	300
111		5	300
112	55	5	150
122	70	10	100
126	90	15	50
130	100	15	50
140	110	15	100
DELTA HEAT TABLE			
Formation Name	Time (Ma) Start	Time (Ma) End	Generated Heat (muW/m3)
17At1-22At1	10	0	50
16Bt1-17At1	10	0	50
15At1-16Bt1	10	0	50

Table A.07: Time-heat and delta heat values for western Southern Outeniqua Basin model (located at junction of 1972 seismic lines 15 and 20) (page 6 of 7).

TIME VALUES TABLE			
eastern SOUTHERN OUTENIQUA 2			
Time	Heat flow (mW/m2)	Surface temperature	Sea depth (m)
5	65	5	1846
12	55	10	200
15	50	10	180
18		10	150
40	50		
45	50	10	100
50	55	10	80
55	60	10	50
58	65		40
60	60		50
65	55		100
70	50		150
80			200
100	50		
109		5	150
110		5	300
111		5	300
112	55	5	150
122	70	10	100
126	90	15	50
130	100	15	50
140	110	15	100

DELTA HEAT TABLE			
Formation Name	Time (Ma) Start	Time (Ma) End	Generated Heat (muW/m3)
17At1-22At1	10	0	50
16Bt1-17At1	10	0	50
15At1-16Bt1	10	0	50

Table A.07: Time-heat and delta heat values for eastern Southern Outeniqua Basin model (located at junction of 1972 seismic lines 19 and 20) (page 7 of 7).

APPENDIX B: GAS DATA

WELL	Hor.	TEMPS.		DEPTH (TV)		Recombined Formation Fluid (mole percent)															Reservoir	Analyst		%Ro	iC4
and DST		SBHT	DST	top	base	N2	CO2	C1	C2	C3	iC4	nC4	iC5	nC5	C6	C7	C8	C9	C10	C11+	pressure		GLR		nC4
																						S=Schlumberger			
FAMILY 1																						E=Expro			
83 DST3	14A	101.0	98.9	2461	2470	0.16	1.65	37.94	6.48	6.03	1.21	3.39	1.36	1.94	3.06	5.56	6.62	4.42	3.59	16.60	3580	S	454	0.8	0.36
88 DST5	14A	100.0	112.0	2495	2507	0.40	1.70	37.52	6.99	7.30	1.44	3.97	1.53	2.18	3.12	5.31	6.13	4.05	3.32	15.05	3535	S	503	0.81	0.36
102 DST4	pre1A	95.0	106.7	2237	2241	1.01	0.82	39.07	4.11	3.92	1.40	2.54	1.61	1.68	2.91	5.34	6.25	4.36	4.46	20.50	3207	S	576	0.91	0.55
93 DST1	13A	112.0	112.8	2805	2817	0.39	2.02	45.69	9.54	8.57	0.99	3.93	1.17	1.67	1.96	3.73	4.08	2.92	2.28	11.07	3966	S	6256	0.99	0.25
119 DST2	13A	112.0	114.4	2804	2810	0.21	2.06	47.73	9.25	8.24	0.96	3.83	1.20	1.72	2.08	3.71	3.62	2.30	1.78	11.31	3961	S	1203	0.98	0.25
109 DST1	13A	100.0	109.4	2620	2630	0.08	2.11	38.52	7.98	7.12	0.91	3.04	1.20	1.21	1.84	4.28	5.49	4.31	3.72	18.18	3792	S	660	0.87	0.30
126 DST1	14A	119.0	116.7	2624	2643	0.73	3.37	63.62	9.73	6.81	1.15	3.02	1.04	1.41	1.58	2.13	2.03	1.13	0.75	1.49	3803	S	6134	1.04	0.38
117 DST1	14A	104.0	106.7	2382	2399	0.35	1.16	30.32	5.89	7.61	1.48	4.60	1.73	2.60	3.82	6.79	7.57	4.88	4.16	17.05	3465	S	411	0.93	0.32
146 DST1	14A	96.0	101.7	2371	2400	0.33	1.17	31.99	6.09	6.70	1.49	5.21	2.20	3.46	4.04	6.41	6.88	4.13	3.27	16.62	3460	S	376	0.93	0.29
156 DST1	14A	107.0	111.0	2512	2522	0.86	1.81	42.35	8.05	6.12	1.04	3.56	1.46	2.63	3.63	5.79	6.42	3.76	2.49	10.02	3643	S	1581	0.9	0.29
166 DST1	14A	99.0	113.8	2510	2519	0.51	2.09	49.42	9.07	7.25	1.25	3.23	1.19	1.65	2.22	3.52	3.97	2.43	1.99	10.21	3642	S	1360	0.9	0.39
152 DST1	13A	104.0	110.0	2696	2706	0.14	2.33	49.51	8.95	6.72	0.91	3.36	1.20	1.85	2.50	4.51	4.55	2.92	2.17	8.39	3873	S	980	1.02	0.27
48 DST1	pre1A	110.0	104.4	2625	2634	1.70	0.54	44.90	3.34	2.26	0.53	1.17	0.62	0.79	1.49	42.66					3755	S	580	1.02	0.45
59 DST1	pre1A	93.0	99.2	2195	2212	0.33	0.72	36.47	4.94	2.90	0.58	1.20	0.45	0.44	1.19	50.78					3120	S	368	0.8	0.48
FAMILY 2																									
83 DST2	10A	112.0	113.0	2864	2894	0.12	3.67	70.07	8.31	4.36	0.59	1.53	0.51	0.65	0.95	1.70	1.86	1.20	0.85	3.64	4169	S	5464	0.93	0.39
88 DST4	12A	112.0	117.0	2827	2839	0.28	3.63	75.59	7.42	3.48	0.54	1.19	0.43	0.49	0.66	1.09	1.18	0.79	0.56	2.68	3990	S	8750	0.91	0.45
88 DST3	10A	115.0	119.4	2909	2916	0.27	3.80	79.93	7.53	3.23	0.51	1.09	0.39	0.41	0.49	0.68	0.66	0.35	0.25	0.41	4127	S	26873	1.01	0.47
88 DST2	10A	116.0	120.0	2924	2929	0.23	3.82	79.60	7.53	3.26	0.52	1.12	0.41	0.44	0.55	0.75	0.71	0.38	0.24	0.44	4133	S	24393	1.02	0.46
88 DST1	5A	126.0	131.7	3213	3243	0.00	4.08	81.15	7.06	2.83	0.50	0.88	0.36	0.32	0.45	0.64	0.68	0.38	0.22	0.45	7620	S	24667	1.08	0.57
96 DST1	8A	126.0	126.1	3117	3131	0.09	4.85	84.60	5.97	2.13	0.34	0.57	0.22	0.19	0.22	0.26	0.22	0.11	0.07	0.16	5139	S	130300	1.32	0.60
114 DST1	9A	132.0	135.0	3068	3085	0.14	5.13	78.54	8.22	3.53	0.54	1.07	0.39	0.35	0.42	0.51	0.53	0.26	0.14	0.24	4682	S	33694	1.15	0.50
108 DST1	10A	117.0	116.7	2820	2829	0.44	2.98	63.50	10.21	7.55	0.94	3.28	0.99	1.39	1.46	2.16	1.94	1.05	0.72	1.38	4047	S	6211	0.94	0.29
151 DST1	10A	113.0	118.3	2915	2927	0.00	3.26	75.50	8.66	3.79	0.53	1.50	0.54	0.73	0.89	1.40	1.35	0.67	0.35	0.81	4437	S	12500	0.91	0.35
129 DST2	12A	116.0	118.3	2845	2865	0.29	3.31	72.87	10.00	5.23	0.61	1.78	0.50	0.66	0.72	1.16	1.12	0.63	0.38	0.74	4038	S	17726	1	0.34
110 DST1B	10A	120.0	121.1	3037	3050	0.24	3.75	69.82	9.51	5.33	0.64	1.98	0.60	0.85	1.00	1.58	1.57	0.93	0.65	1.55	4280	S	8429	1.08	0.32
132 DST2	13A	103.0	104.4	2654	2662	0.38	2.82	67.53	9.44	6.42	0.81	3.03	0.94	1.34	1.35	1.94	1.70	0.83	0.47	0.99	3873	S	6497	1.02	0.27
148 DST1	13A	104.0	110.6	2674	2684	0.33	2.87	66.75	9.36	5.76	0.82	3.27	1.11	1.60	1.60	2.19	1.70	0.87	0.56	1.19	3870	S	6309	0.95	0.25

Table B.01: Gas data from PVT analyses carried out on DST samples (page 1 of 2).

WELL	Hor.	TEMPS.		DEPTH (TV)		Recombined Formation Fluid (mole percent)															Reservoir	Analyst		%Ro	iC4
and DST		SBHT	DST	top	base	N2	CO2	C1	C2	C3	iC4	nC4	iC5	nC5	C6	C7	C8	C9	C10	C11+	pressure		GLR		nC4
FAMILY 3																									
107 DST2	pre1A	104.0	106.7	2522	2565	4.61	1.39	81.02	5.40	3.13	0.59	1.12	0.39	0.40	0.42	0.52	0.40	0.19	0.14	0.28	3647	S	45482	0.85	0.53
69 DST1	pre1A	102.8	107.2	2388	2435	4.78	1.22	80.25	5.11	3.19	0.71	1.26	0.46	0.45	0.53	0.67	0.56	0.26	0.19	0.36	3463	S	31348	0	0.56
46 DST2	pre1A	98.0	109.4	2540	2560	3.15	1.34	85.05	5.14	2.19	0.35	0.70	0.24	0.24	0.29	0.44	0.42	0.20	0.12	0.23	3715	S	53448	0.97	0.50
54 DST1	pre1A	104.0	112.8	2558	2617	3.29	1.43	85.80	4.96	2.04	0.31	0.62	0.19	0.20	0.22	0.31	0.27	0.13	0.08	0.15	3715	S	89235	0	0.50
76 DST1	pre1A	109.0	107.8	2556	2610	3.26	1.41	84.64	5.34	2.11	0.35	0.68	0.23	0.24	0.29	0.41	0.40	0.21	0.14	0.29	3695	S	46129	0	0.51
39 DST2	9A	89.0	100.6	2209	2229	1.32	1.31	85.86	6.03	2.64	0.51	0.71	0.25	0.20	0.31	0.30	0.27	0.12	0.07	0.10	3229	S	78486	0	0.72
39 DST1	pre1A	99.0	110.6	2451	2576	0.92	0.90	84.35	7.12	3.08	0.61	0.85	0.34	0.27	0.36	0.41	0.38	0.17	0.10	0.14	3675	S	61820	0	0.72
18 DST4	pre1A	105.0	124.4	2602	2635	1.69	1.96	82.66	6.32	3.06	0.62	0.91	0.35	0.28	0.48	0.53	0.42	0.25	0.14	0.33		S	40220	1.12	0.68
18 DST3	pre1A	107.0	121.1	2641	2673	1.83	2.11	81.54	7.00	3.18	0.67	0.93	0.37	0.32	0.39	0.51	0.44	0.19	0.12	0.40	3939	S	42789	1.14	0.72
18 DST1	pre1A	109.0	120.0	2696	2702	1.46	1.30	83.40	7.10	3.00	0.67	0.85	0.30	0.28	0.32	0.36	0.31	0.16	0.11	0.38	3955	S	46584	1.15	0.79
21 DST2	pre1A	108.0	112.8	2552	2559	2.35	1.85	85.72	5.77	2.13	0.46	0.46	0.19	0.13	0.24	0.30	0.23	0.05	0.09		3827	S	47684	0	1.00
19 DST2	pre1A	109.0	118.3	2680	2709	1.69	2.28	80.77	7.22	3.26	0.64	0.97	0.35	0.31	0.41	0.61	0.62	0.31	0.20	0.36	3900	S	31665	0	0.66
44 DST1	pre1A	112.0	128.7	2715	2750	1.43	2.31	78.79	7.38	3.78	0.76	1.20	0.50	0.45	0.63	0.88	0.82	0.38	0.23	0.33	3911	S	19368	0	0.63
55 DST2	pre1A	111.0	118.3	2659	2682	1.29	2.73	80.15	7.59	3.55	0.67	1.06	0.41	0.36	0.45	0.60	0.55	0.23	0.13	0.23	3865	S	38766	0	0.63
61 DST3	9A	90.0	99.3	2113	2130	1.29	1.69	75.70	7.32	5.46	1.09	1.92	0.74	0.67	0.84	1.02	0.94	0.46	0.32	0.54	3095	S	12443	0	0.57
61 DST2	pre1A	114.0	121.7	2718	2770	0.70	2.62	84.67	6.34	2.25	0.37	0.67	0.26	0.23	0.45	0.47	0.45	0.21	0.12	0.19	3940	S	44919	0	0.55
70 DST2	pre1A	103.0	107.2	2411	2428	2.12	1.82	80.14	7.14	3.47	0.63	1.13	0.43	0.40	0.54	0.74	0.67	0.29	0.18	0.30	3475	S	28897	0.85	0.56
162 DST2	pre1A	99.0	107.0	2349	2355	2.23	1.71	81.33	6.57	3.44	0.63	1.14	0.44	0.46	0.83	0.49	0.29	0.20	0.07	0.16	3355	S	29899	0	0.55
31 DST1	pre1A	105.0	117.8	2691	2753	1.83	1.80	78.90	7.22	4.07	0.86	1.35	0.52	0.46	0.57	0.75	0.66	0.31	0.21	0.49	3898	S	21227	0.95	0.64
63 DST1	pre1A	109.0	107.2	2659	2691	0.97	1.87	83.86	6.58	2.81	0.48	0.84	0.31	0.29	0.36	0.51	0.50	0.23	0.14	0.25	3820	S	36478	0.91	0.57
131 DST1	pre1A	107.0	120.0	2669	2752	1.47	2.26	81.64	7.15	2.68	0.54	0.86	0.38	0.35	0.50	0.71	0.67	0.29	0.17	0.34	0	S	17207	0	0.63
135 DST1	pre1A	107.0	126.3	2629	2734	1.54	2.35	81.09	7.20	3.04	0.60	0.95	0.40	0.36	0.47	0.68	0.67	0.25	0.13	0.27	0	S	19821	0	0.63
141 DST1	pre1A	107.0	125.1	2624	2734	1.26	2.45	80.10	7.77	3.17	0.65	1.08	0.47	0.44	0.55	0.74	0.63	0.25	0.14	0.29	0	S	24477	0	0.60
145 DST1	pre1A	107.0	126.3	2626	2678	1.60	2.17	81.58	7.30	2.79	0.59	0.87	0.33	0.38	0.48	0.62	0.58	0.24	0.14	0.32	0	S	21998	0	0.68
147 DST1	pre1A	107.0	121.7	2728	2765	1.97	1.86	80.02	7.40	3.16	0.66	1.08	0.46	0.43	0.53	0.72	0.67	0.31	0.21	0.52	0	S	14624	0	0.61
FAMILY 4																									
128 DST1	pre1A	149.0	154.3	3627	3661	1.35	3.79	89.10	3.84	0.86	0.25	0.14	0.12	0.05	0.11	0.14	0.12	0.04	0.03	0.06	7721	S	376271	1.66	1.79
FAMILY 5																									
35 DST3	pre1A	130.0	134.4	3309	3417	1.90	2.11	58.44	8.09	4.52	1.48	2.82	1.49	1.81	2.54	3.56	3.65	2.12	1.48	3.99	6580	S	2851	1.18	0.52
35 DST3	pre1A	130.0	134.4	3309	3417	2.23	2.25	60.22	8.22	4.75	1.22	2.63	1.16	1.42	1.93	2.77	2.73	1.52	7.15		6580	E	2851	1.2	0.46
35 DST2B	pre1A	132.0	134.4	3354	3417	1.66	2.15	62.66	7.33	4.69	1.38	2.59	1.29	1.53	2.04	2.51	2.58	1.46	6.13		6565	E	4300	1.22	0.53

Table B.01: Gas data from PVT analyses carried out on DST samples (page 2 of 2).

ENVIRONMENTAL DATA							GAS DATA (v/v%) (incl. molecular masses)											
WELL	DST	HOR.	DEPTH	DEPTH	PSIA	SBHT	N2	CO2	He	H2	O2	C1	C2	C3	C4	C5	C6+	REMARKS
			top mbkb	bot.mbkb		degC	28	60	2	2	32	16	30	44	58	72	86	
FAMILY 1																		
83	3	14A	2461	2470	3580	105.0	1.4	3.3	0.003	0.00	0.00	77.10	9.60	6.70	1.30	0.400	0.10	Final flow
88	5	14A	2495	2507	3535	100.0	1.3	3.0	0.010	0.00	0.00	80.60	8.50	5.00	1.05	0.420	0.12	Final flow
93	2	14A	2454	2463	3549	102.0	1.5	2.0	0.000	0.00	0.00	74.50	10.00	6.60	3.60	1.400	0.30	Flow 6
93	1A	13A	2805	2808	3966	117.0	1.3	2.1	0.012	0.00	0.00	75.10	10.60	6.30	3.00	1.200	0.30	Flow 4
93	1	13A	2805	2817	3966	117.0	1.3	2.2	0.008	0.00	0.00	74.00	10.60	6.80	3.30	1.200	0.50	Final flow
59	1	pre1A	2195	2212	3120	95.0	1.4	1.3	0.008	0.00	0.10	82.50	8.80	3.30	2.00	0.400	0.10	Final flow
FAMILY 2																		
83	2	10A	2864	2894	4169	112.0	1.0	4.4	0.011	0.00	0.00	79.00	8.80	4.60	1.20	0.600	0.20	Final flow
83	1	5A	3160	3254	7546	132.0	0.7	4.3	0.002	0.00	0.00	83.90	6.80	2.80	1.00	0.300	0.10	Choke 0.75"
88	4	12A	2827	2839	3990	112.0	0.7	3.8	0.020	0.00	0.00	84.20	6.90	3.00	0.86	0.380	0.13	Flow 3
88	3	10A	2909	2916	4127	115.0	1.0	3.8	0.010	0.00	0.00	83.90	6.80	2.90	0.95	0.460	0.18	Final flow
88	2	10A	2924	2929	4133	116.0	0.6	4.1	0.020	0.00	0.00	83.70	7.00	3.30	0.81	0.330	0.13	Final flow
88	1	5A	3213	3243	7620	126.0	0.6	4.4	0.000	0.00	0.00	85.20	6.20	2.30	0.79	0.310	0.12	Flow 3
84	1	pre1A	2753	2771	3951	110.8	3.0	2.1	0.050	0.00	0.00	87.10	4.90	1.70	0.62	0.240	0.15	Final flow
65	2	pre1A	3167	3189	6409	131.0	1.5	2.2	0.020	0.00	0.00	86.10	6.50	2.00	1.08	0.340	0.11	Final flow
65	1	pre1A	3213	3267	5605	132.8	2.0	2.4	0.020	0.00	0.00	88.30	5.20	1.20	0.57	0.190	0.06	Final flow
FAMILY 3																		
69	1	pre1A	2388	2435	3463	92.0	4.7	1.0	0.030	0.00	0.00	81.30	6.00	3.80	2.33	0.710	0.12	Flow 2
46	2	pre1A	2540	2560	0	98.0	4.5	1.6	0.040	0.00	0.00	85.00	5.90	2.00	0.55	0.160	0.09	Flow 2
54	1	pre1A	2558	2617	3715	104.0	4.1	1.4	0.000	0.00	0.04	85.60	5.00	2.10	0.80	0.900	0.20	Flow 2
39	1	pre1A	2451	2576	3675	105.0	0.0	1.2	0.000	0.00	0.00	83.40	9.70	4.00	1.20	0.300	0.10	Flow 4. Air con?
18	1	pre1A	2696	2702	3955	109.0	2.2	0.0	0.030	0.09	0.70	79.50	7.30	4.50	2.70	1.200	0.90	Flow 4
23	2	pre1A	2365	2380	0	104.6	4.5	0.1	0.050	1.30	0.40	86.90	4.10	2.00	0.50	0.130	0.05	APR
21	2	pre1A	2552	2559	3827	107.0	6.4	1.9	0.050	0.00	1.00	82.60	5.40	1.80	0.60	0.170	0.07	Flow 4
19	2	pre1A	2680	2709	3900	109.0	5.7	2.4	0.040	0.30	3.60	74.80	7.30	3.50	1.00	0.600	0.70	APR-M lower.
20	3	1A-6A	2569	2578	0	96.7	4.3	2.2	0.040	0.00	1.30	81.00	6.30	3.50	0.80	0.300	0.20	Flow 2
20	2	pre1A	2692	2699	0	101.1	4.5	2.0	0.050	0.00	1.30	82.80	6.00	2.30	0.70	0.170	0.10	Flow 2
44	1B	pre1A	2715	2750	3911	112.0	2.7	2.9	0.000	0.00	0.30	77.80	9.40	4.20	1.60	0.700	0.30	Flow 2
55	2	pre1A	2659	2682	3865	109.0	2.3	3.2	0.040	0.00	0.03	78.90	9.00	3.80	1.50	0.700	0.30	Final flow
61	3	9A	2113	2130	3095	90.0	0.1	1.5	0.050	0.00	0.00	78.80	7.50	4.60	5.30	1.500	0.50	Choke 0.625"
61	2	pre1A	2718	2770	3940	114.0	0.2	2.3	0.050	0.00	0.00	84.90	6.50	2.30	2.60	0.800	0.30	Choke 0.50"
70	2	pre1A	2411	2428	3475	103.0	2.8	1.6	0.040	0.00	0.00	80.20	8.10	3.80	1.28	0.900	0.20	Flow 2
63	1	pre1A	2659	2691	3820	109.0	1.8	1.7	0.030	0.00	0.05	85.10	7.00	2.80	0.97	0.350	0.17	Final flow
FAMILY 5																		
35	3	pre1A	3309	3417	6580	135.0	3.2	2.8	0.000	0.00	0.10	72.60	10.50	6.10	3.20	1.000	0.40	Servipetrol cylinder.
35	2B	pre1A	3354	3417	6565	137.0	2.7	2.5	0.000	0.00	0.10	70.80	10.20	6.00	4.10	1.800	1.60	Servipetrol cylinder.

Table B.02: Gas data from SABS analyses carried out on DST samples (page 1 of 2).

CALCULATED DATA								
C2/C3	pCO2	M.Mass total	Mol.% CO2	C1/C1-5 %	C2/C1-5 %	C3/C1-5 %	C4/C1-5 %	C3+/C1-5 %
1.43	3.75	21.66	9.14	81.07	10.09	7.05	1.37	8.83
1.70	3.59	20.82	8.64	84.34	8.89	5.23	1.10	6.77
1.52	2.18	22.80	5.26	77.52	10.41	6.87	3.75	12.07
1.68	2.08	22.45	5.61	78.07	11.02	6.55	3.12	10.91
1.56	2.14	22.90	5.76	77.16	11.05	7.09	3.44	11.78
2.67	1.83	20.03	3.89	85.05	9.07	3.40	2.06	5.88
1.91	4.32	21.52	12.27	83.86	9.34	4.88	1.27	6.79
2.43	2.47	20.35	12.68	88.50	7.17	2.95	1.05	4.32
2.30	4.15	20.22	11.27	88.32	7.24	3.15	0.90	4.45
2.34	3.99	20.34	11.21	88.31	7.16	3.05	1.00	4.54
2.12	4.29	20.39	12.06	87.98	7.36	3.47	0.85	4.67
2.70	2.53	20.10	13.14	89.87	6.54	2.43	0.83	3.59
2.88	2.48	18.92	6.66	92.11	5.18	1.80	0.66	2.71
3.25	1.57	19.31	6.84	89.67	6.77	2.08	1.12	3.56
4.33	2.02	18.74	7.69	92.50	5.45	1.26	0.60	2.05
1.58	1.25	20.36	2.95	86.36	6.37	4.04	2.48	7.27
2.95	0.00	18.98	5.06	90.80	6.30	2.14	0.59	2.89
2.38	1.71	19.40	4.33	90.68	5.30	2.22	0.85	4.03
2.43	1.46	19.73	3.65	84.58	9.84	4.06	1.22	5.58
1.62	0.00	20.94	0.00	83.51	7.67	4.73	2.84	8.82
2.05	0.00	17.90	0.23	92.81	4.38	2.14	0.53	2.81
3.00	2.26	19.41	5.87	91.20	5.96	1.99	0.66	2.84
2.09	2.52	21.51	6.70	85.78	8.37	4.01	1.15	5.85
1.80	0.00	20.18	6.54	88.14	6.86	3.81	0.87	5.01
2.61	0.00	19.55	6.14	90.03	6.52	2.50	0.76	3.45
2.24	3.06	21.40	8.13	83.03	10.03	4.48	1.71	6.94
2.37	3.44	21.20	9.06	84.03	9.58	4.05	1.60	6.39
1.63	1.91	22.41	4.02	80.66	7.68	4.71	5.42	11.67
2.83	2.53	20.31	6.79	87.44	6.69	2.37	2.68	5.87
2.13	2.01	20.24	4.74	85.07	8.59	4.03	1.36	6.34
2.50	2.02	19.45	5.24	88.44	7.27	2.91	1.01	4.28
1.72	1.63	22.98	7.31	77.73	11.24	6.53	3.43	11.03
1.70	1.38	24.37	6.16	76.21	10.98	6.46	4.41	12.81

Table B.02: Gas data from SABS analyses carried out on DST samples (page 2 of 2).

APPENDIX C: WHOLE OIL PLOTS

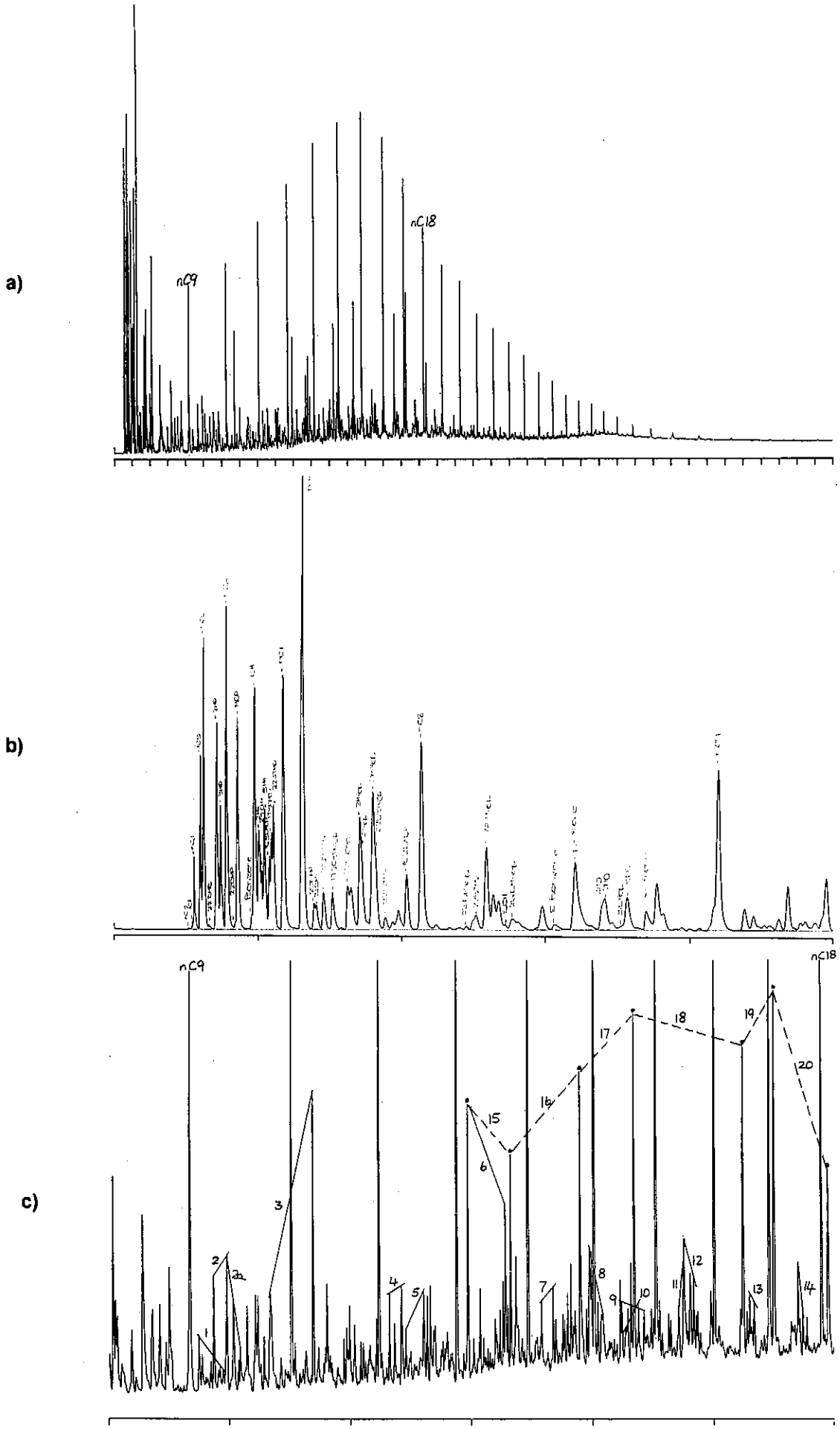

Figure C.01: Whole oil gas chromatograms of oil from well 83 DST3 (a) 0-80 minutes, (b) 0-10 minutes and (c) 6-36 minutes analysed using column 1.

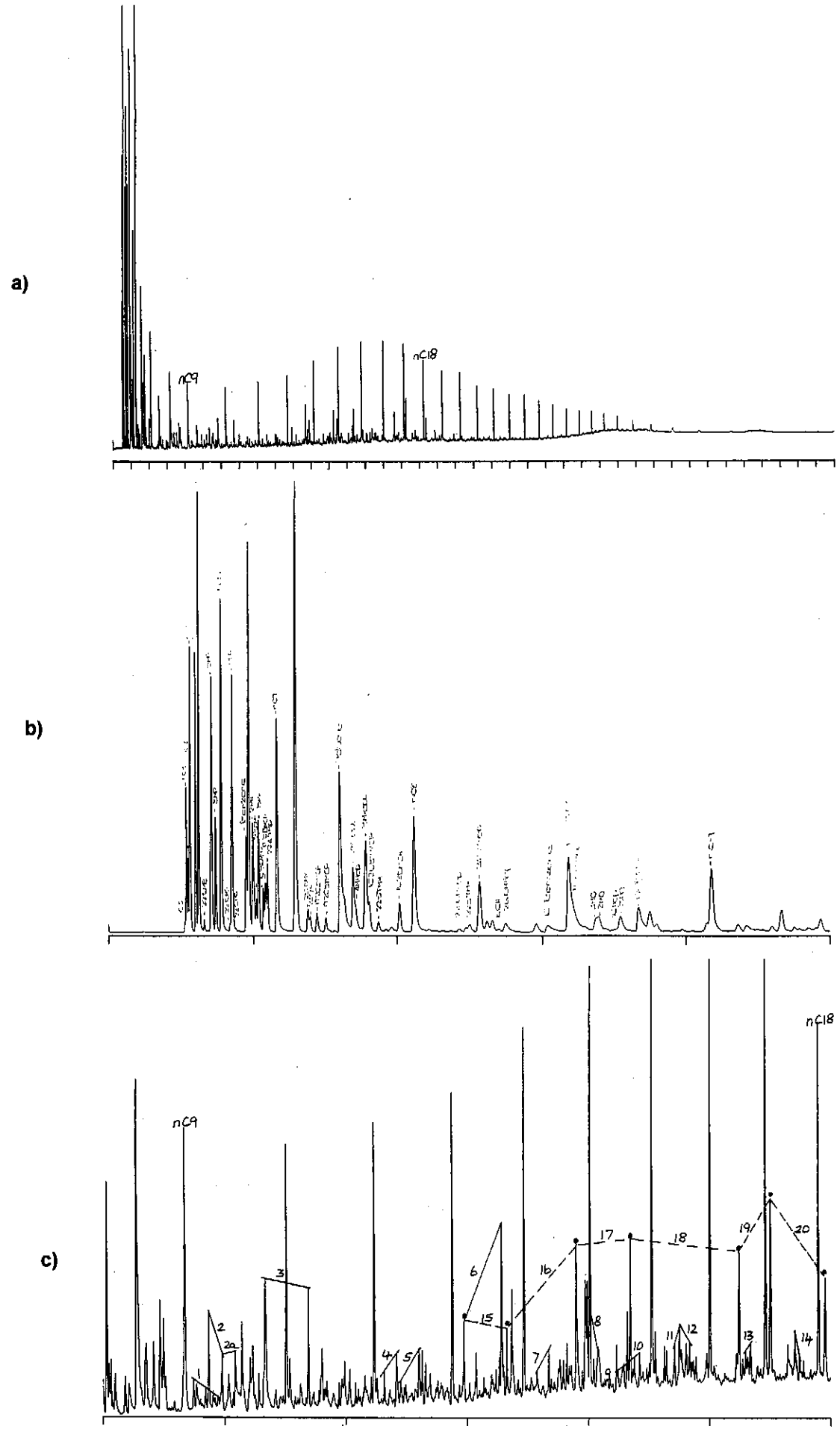

Figure C.02: Whole oil gas chromatograms of condensate from well 83 DST2 (a) 0-80 minutes, (b) 0-10 minutes and (c) 6-36 minutes analysed using column 1.

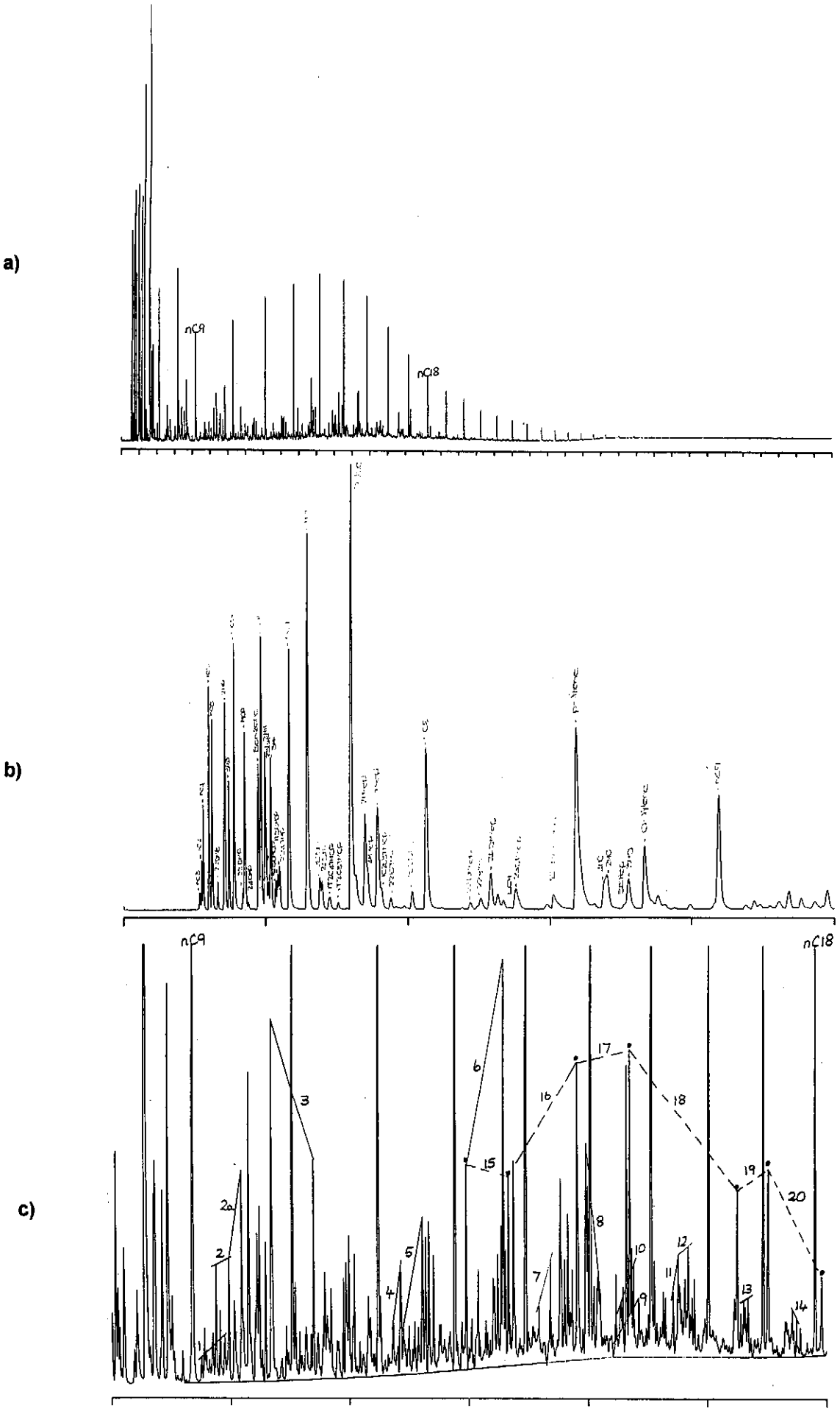

Figure C.03: Whole oil gas chromatograms of condensate from well 83 DST1 (a) 0-80 minutes, (b) 0-10 minutes and (c) 6-36 minutes analysed using column 1.

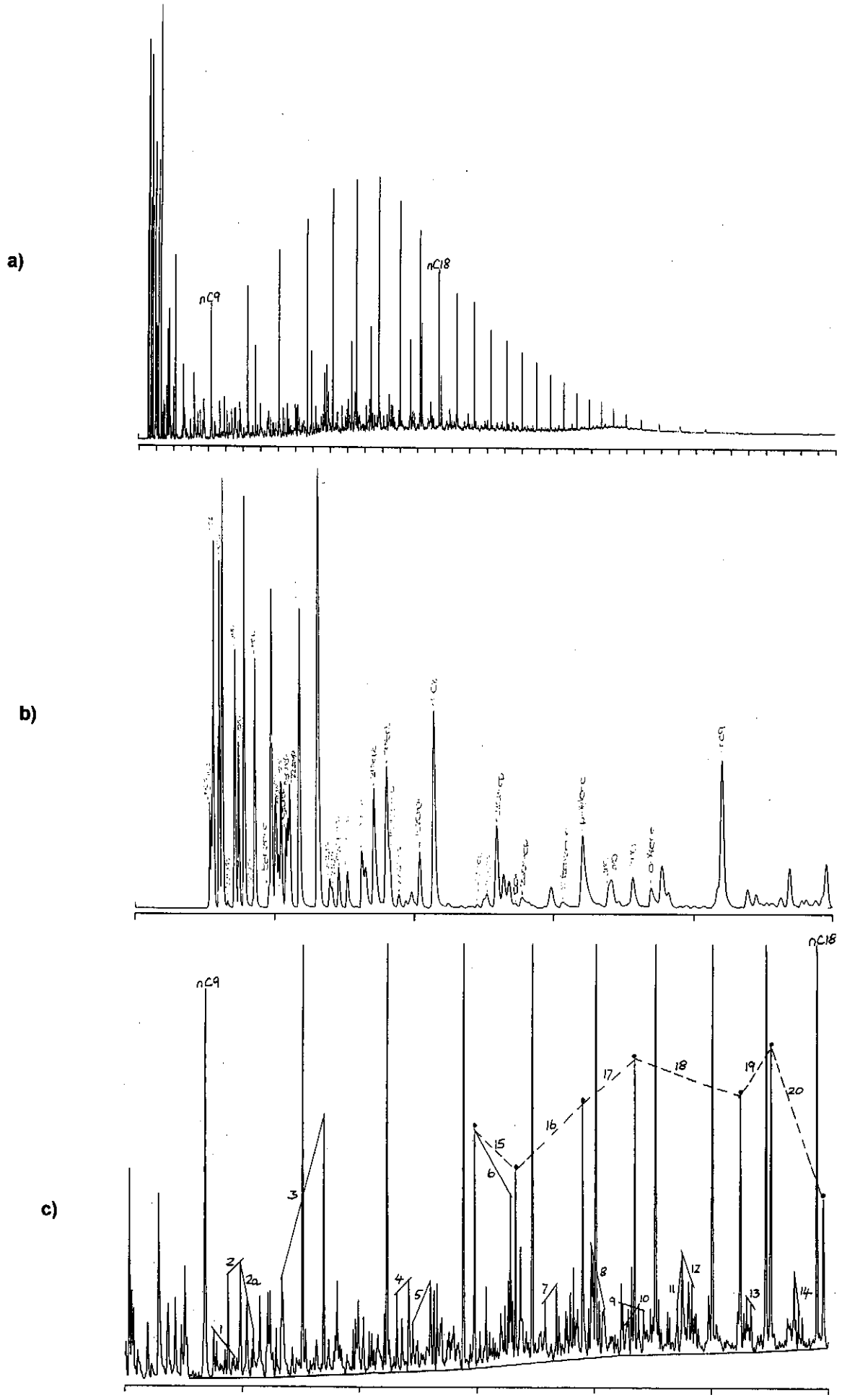

Figure C.04: Whole oil gas chromatograms of oil from well 88 DST5 (a) 0-80 minutes, (b) 0-10 minutes and (c) 6-36 minutes analysed using column 1.

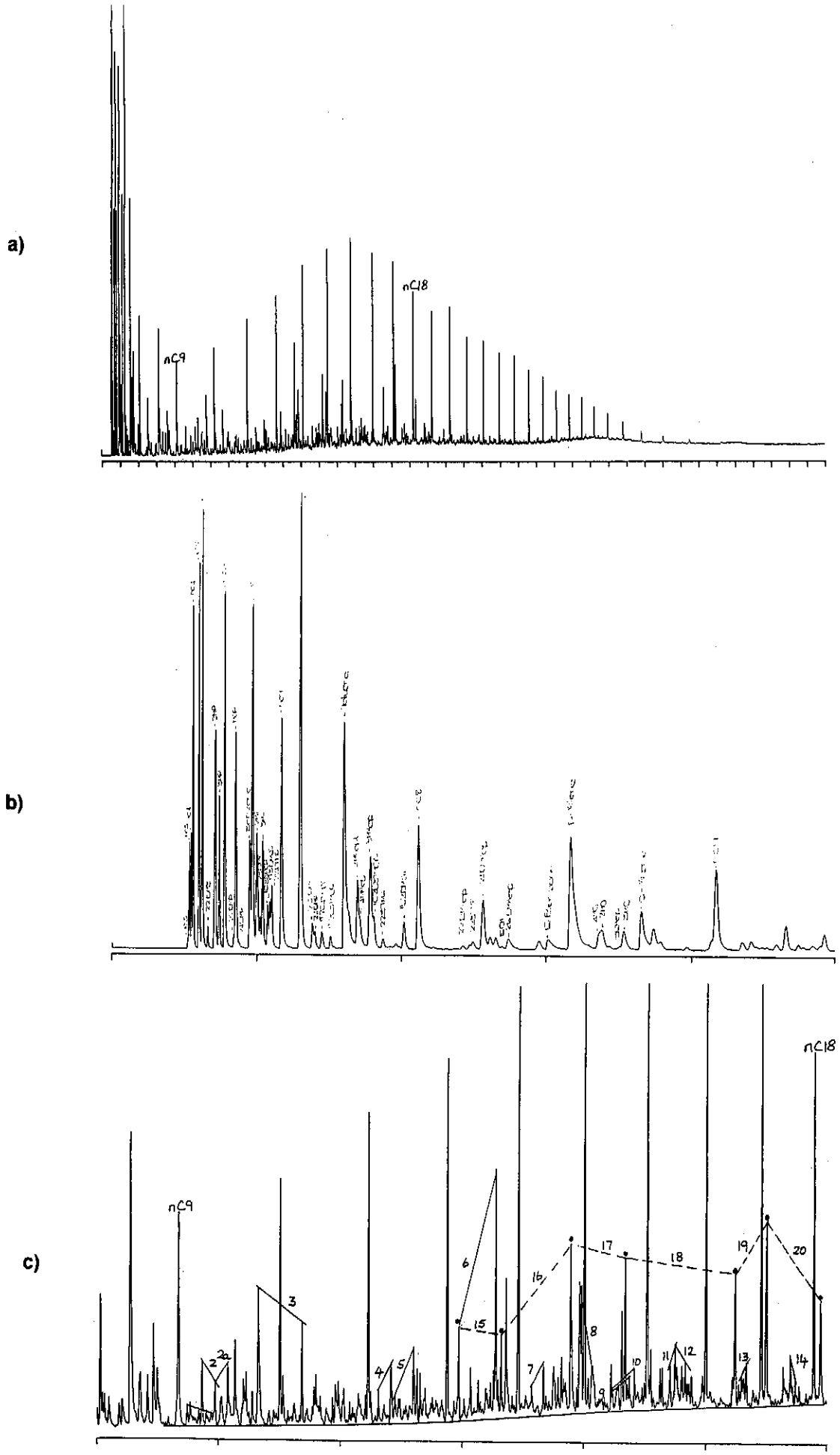

Figure C.05: Whole oil gas chromatograms of condensate from well 88 DST4 (a) 0-80 minutes, (b) 0-10 minutes and (c) 6-36 minutes analysed using column 1.

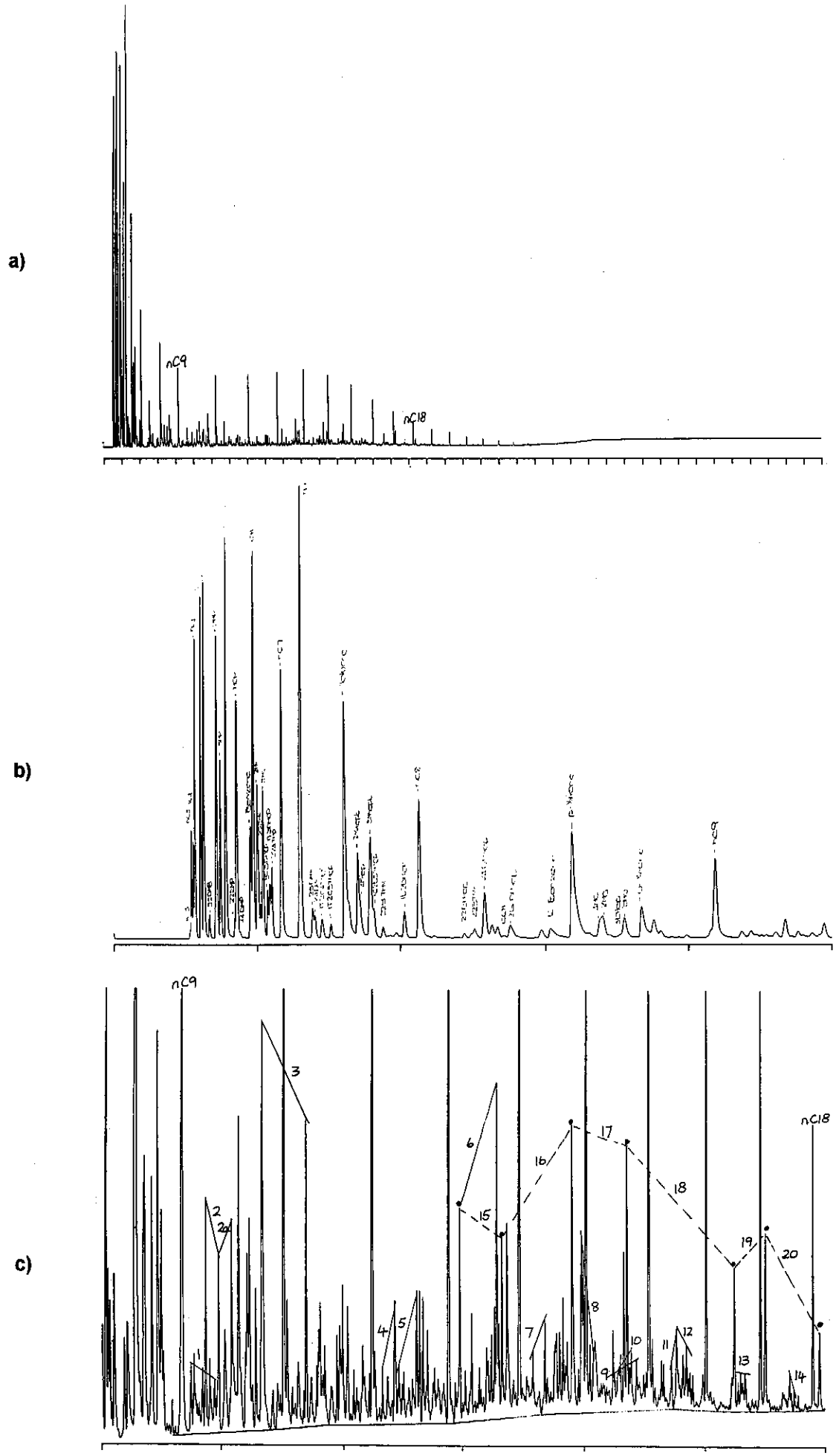

Figure C.06: Whole oil gas chromatograms of condensate from well 88 DST3 (a) 0-80 minutes, (b) 0-10 minutes and (c) 6-36 minutes analysed using column 1.

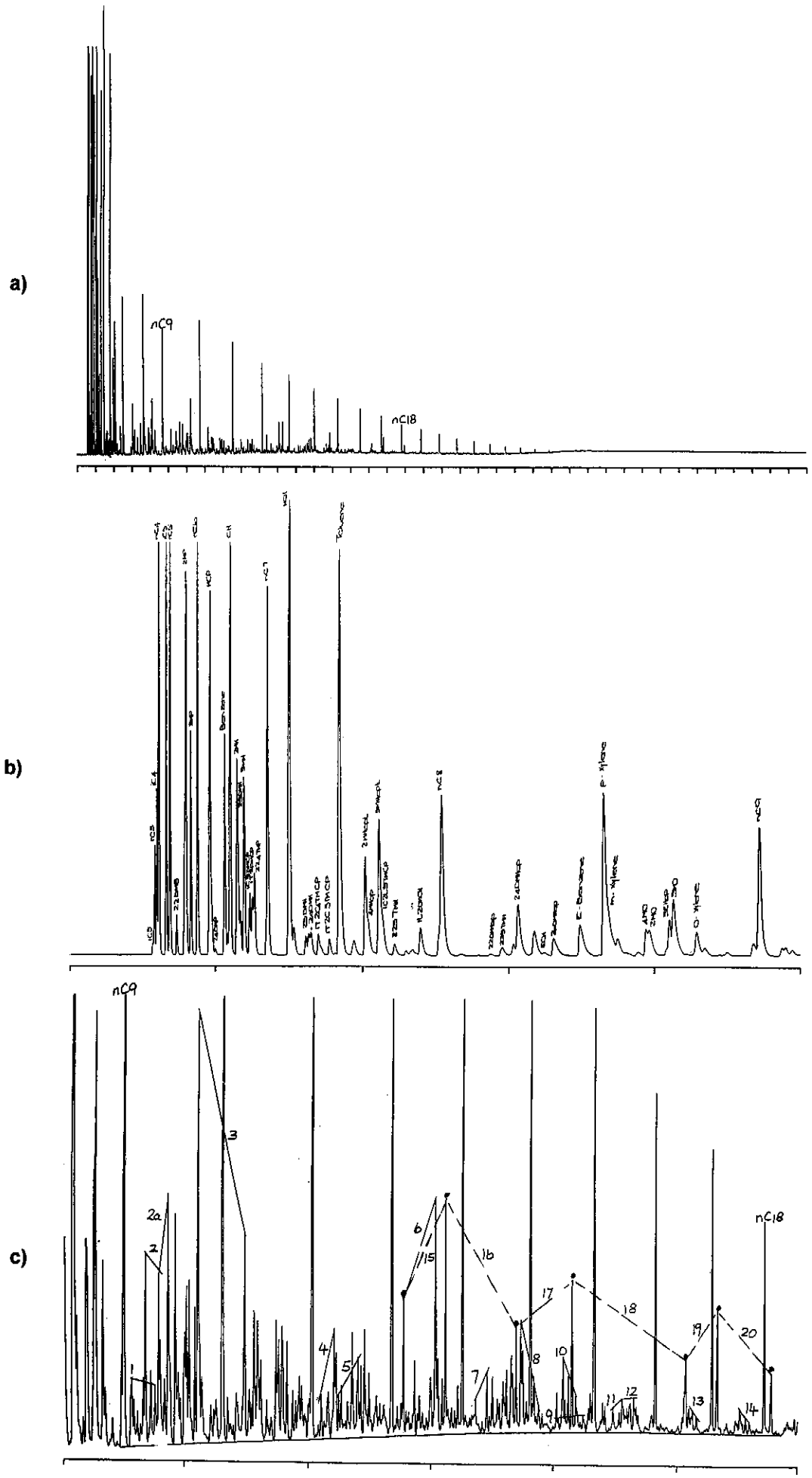

Figure C.07: Whole oil gas chromatograms of condensate from well 88 DST2 (a) 0-80 minutes, (b) 0-10 minutes and (c) 6-36 minutes analysed using column 2.

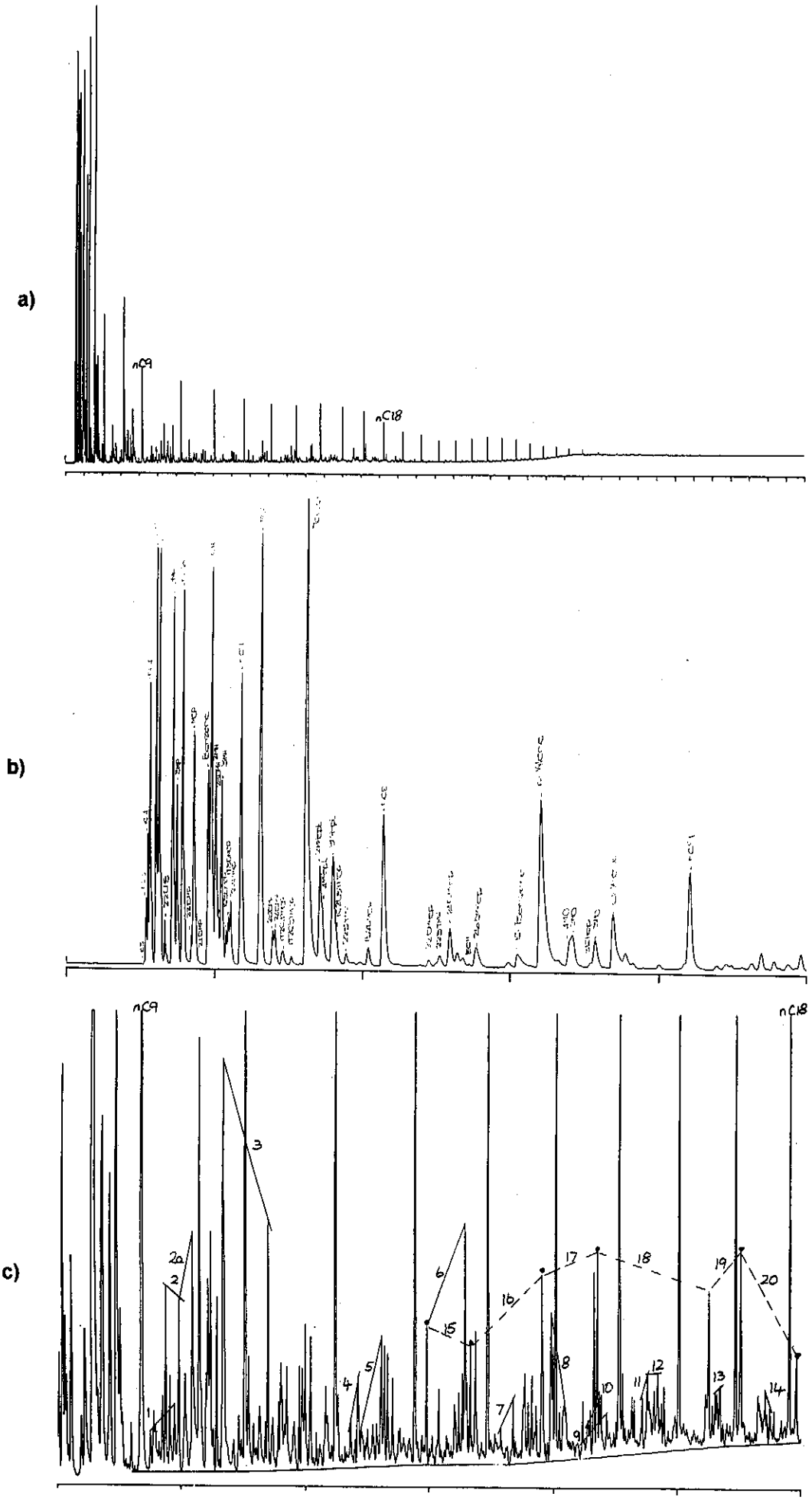

Figure C.08: Whole oil gas chromatograms of condensate from well 88 DST1 (a) 0-80 minutes, (b) 0-10 minutes and (c) 6-36 minutes analysed using column 1.

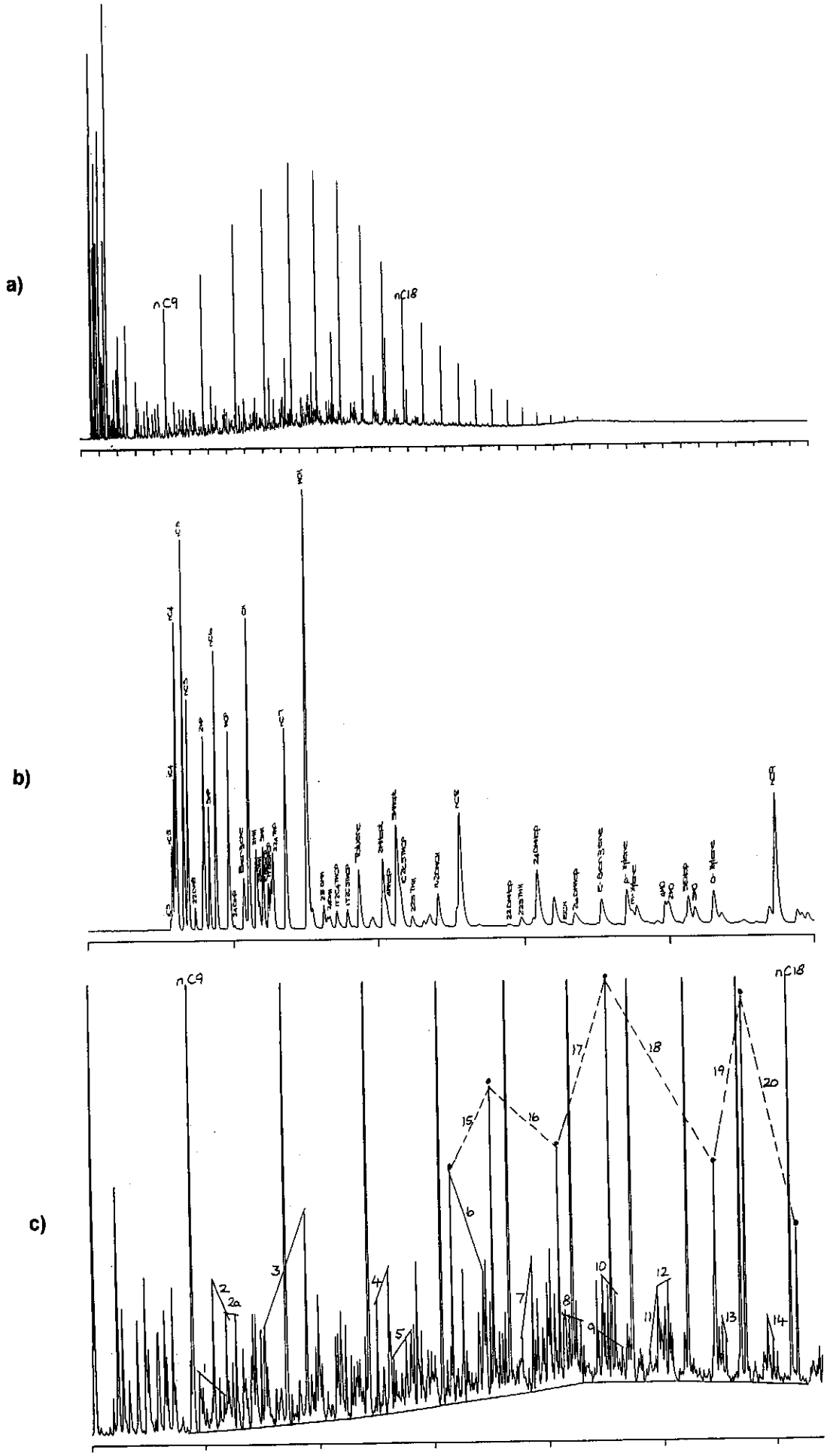

Figure C.09: Whole oil gas chromatograms of oil from well 102 DST4 (a) 0-80 minutes, (b) 0-10 minutes and (c) 6-36 minutes analysed using column 2.

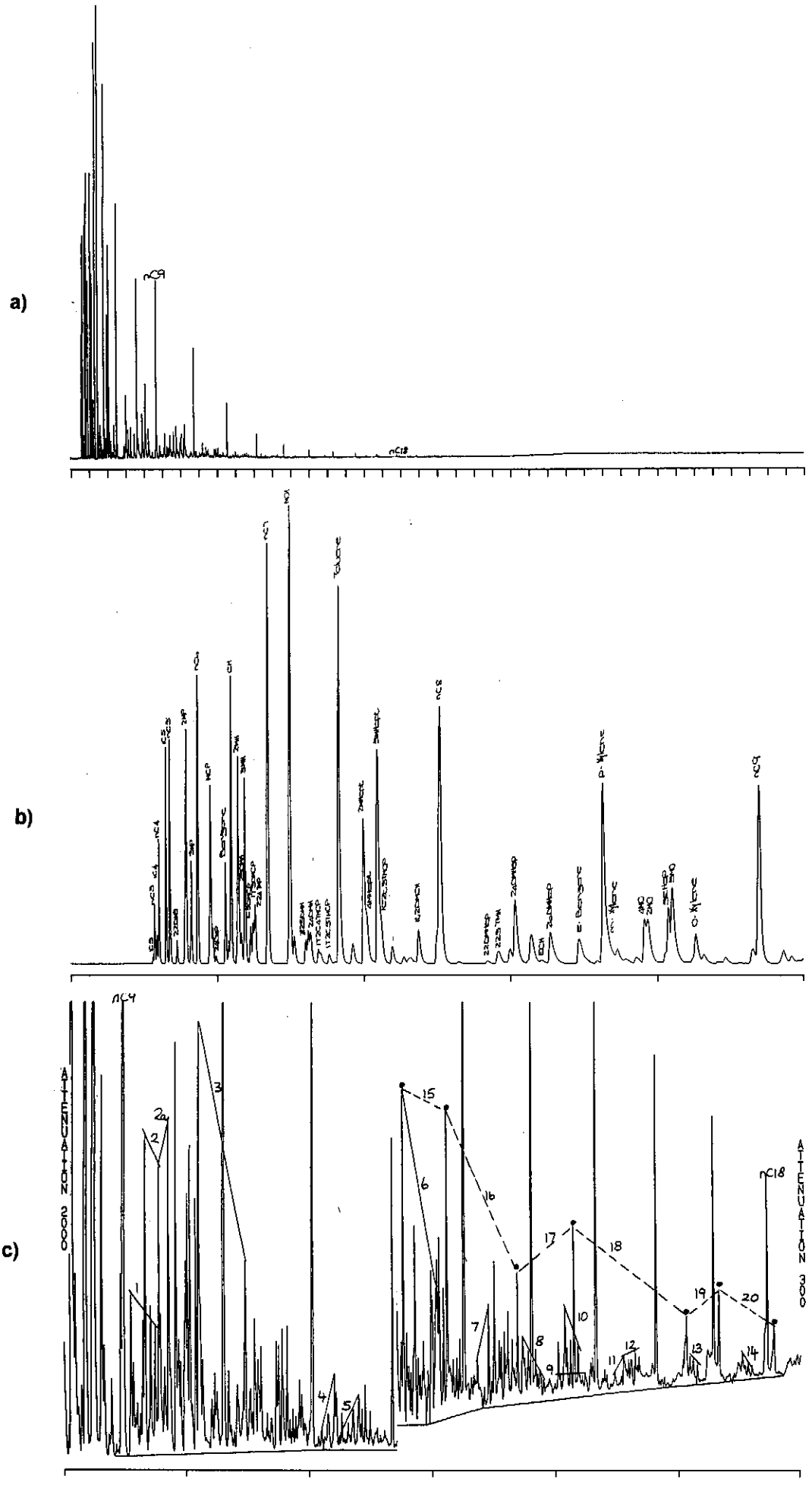

Figure C.10: Whole oil gas chromatograms of condensate from well 102 DST2 (a) 0-80 minutes, (b) 0-10 minutes and (c) 6-36 minutes analysed using column 2.

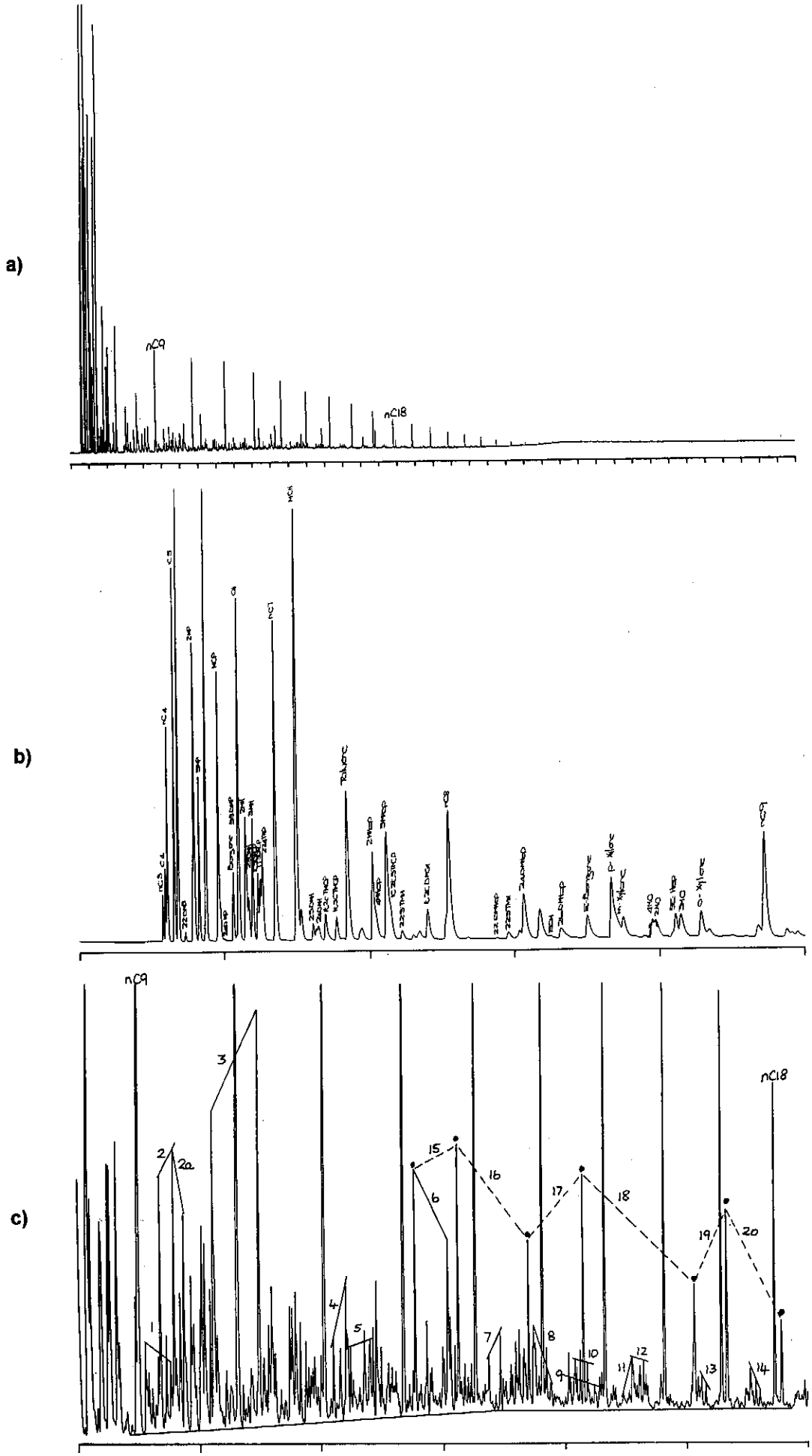

Figure C.11: Whole oil gas chromatograms of condensate from well 95 DST2 (a) 0-80 minutes, (b) 0-10 minutes and (c) 6-36 minutes analysed using column 2.

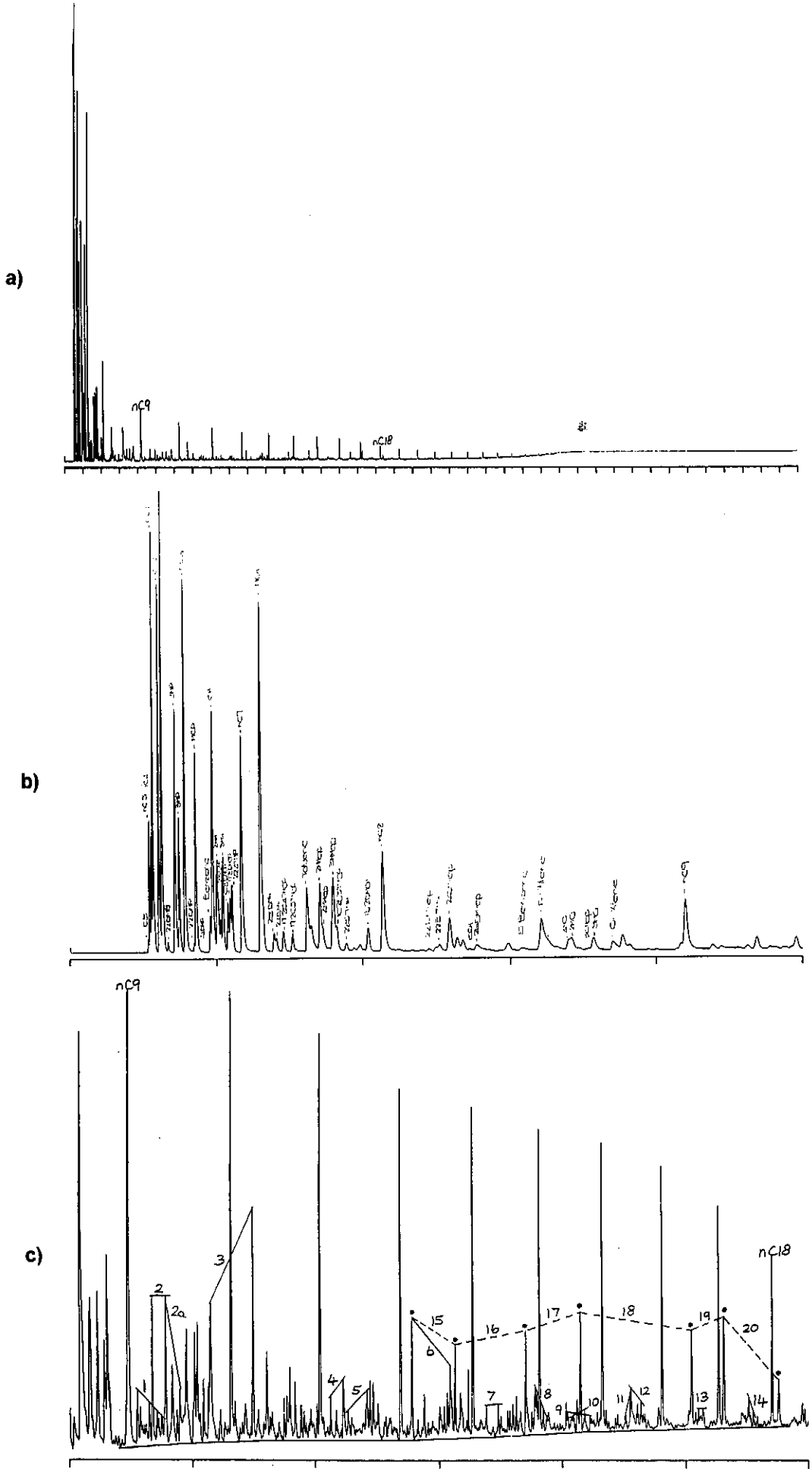

Figure C.12: Whole oil gas chromatograms of condensate from well 103 DST2 (a) 0-80 minutes, (b) 0-10 minutes and (c) 6-36 minutes analysed using column 1.

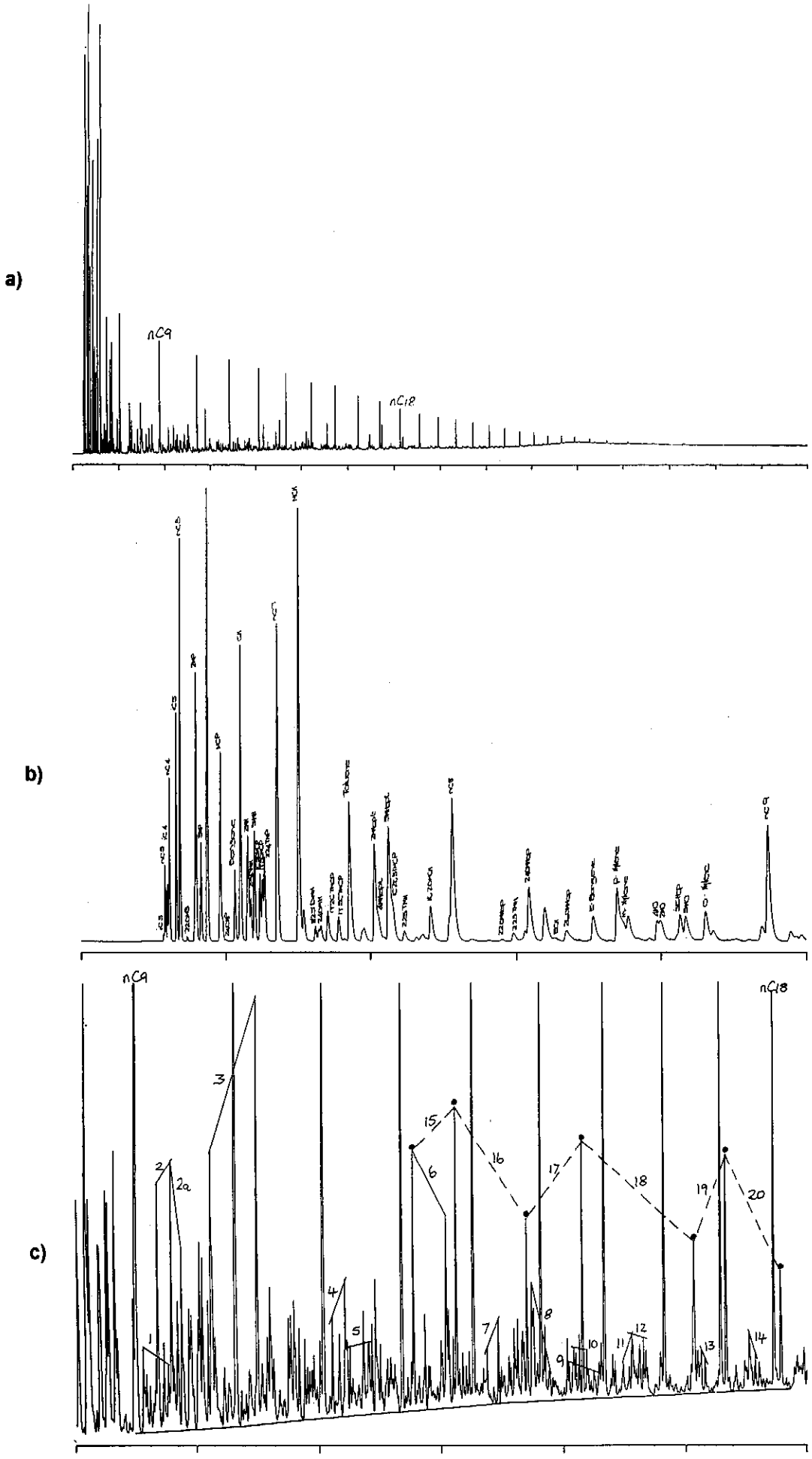

Figure C.13: Whole oil gas chromatograms of oil from well 94 DST1 (a) 0-80 minutes, (b) 0-10 minutes and (c) 6-36 minutes analysed using column 2.

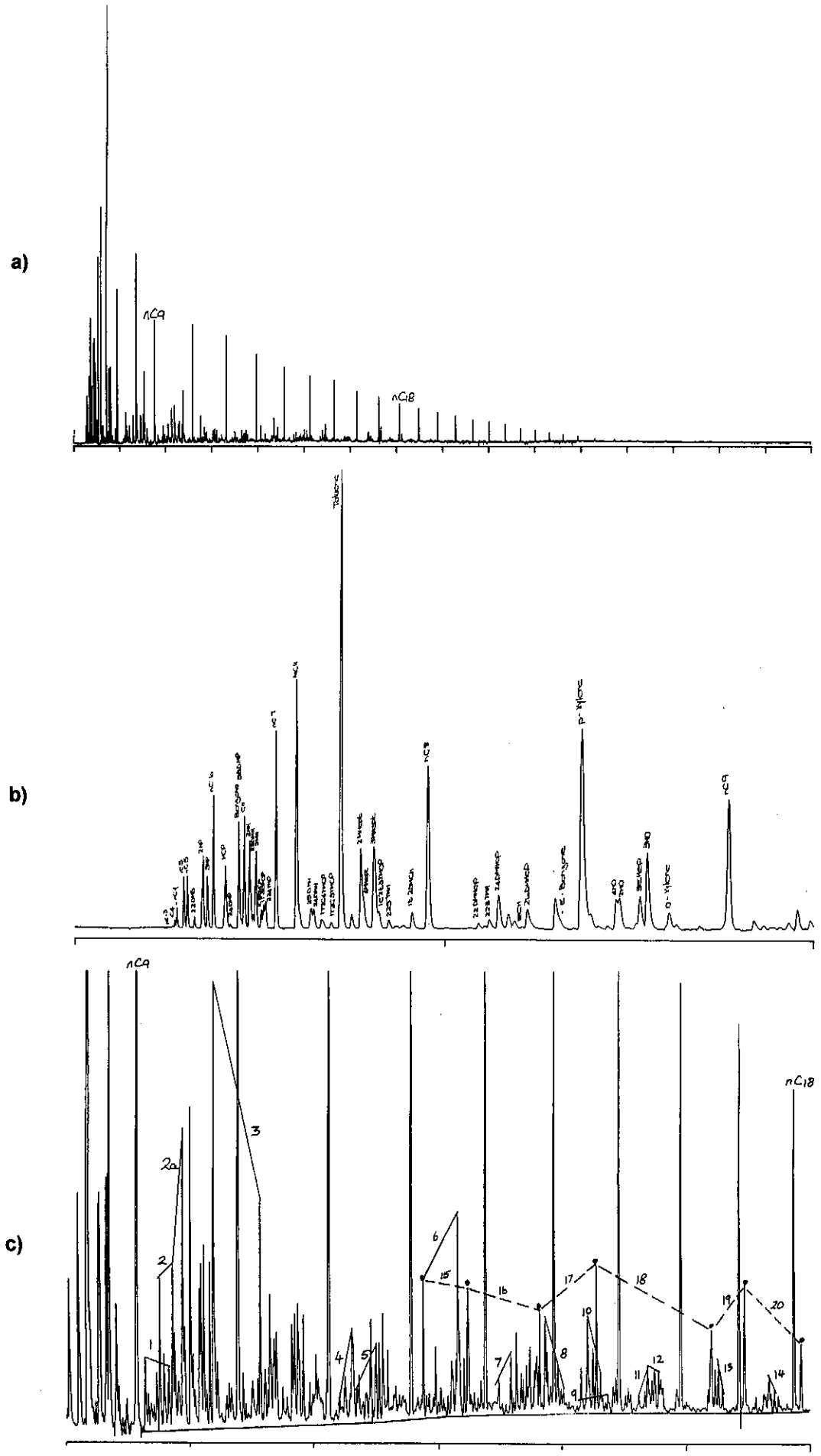

Figure C.14: Whole oil gas chromatograms of condensate from well 96 DST1 (a) 0-80 minutes, (b) 0-10 minutes and (c) 6-36 minutes analysed using column 3.

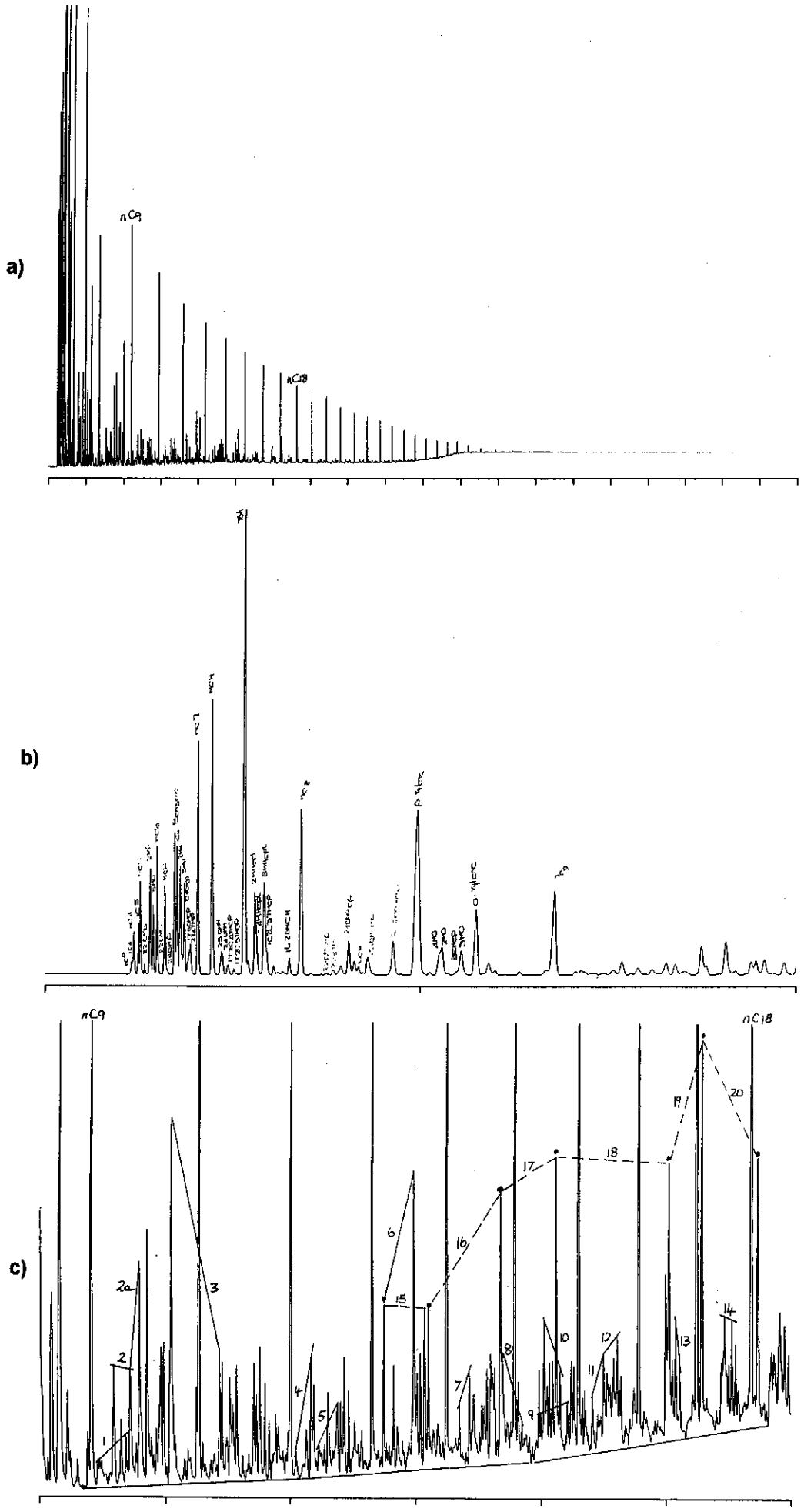

Figure C.15: Whole oil gas chromatograms of condensate from well 96 DST1 (a) 0-80 minutes, (b) 0-10 minutes and (c) 6-36 minutes analysed using column 2.

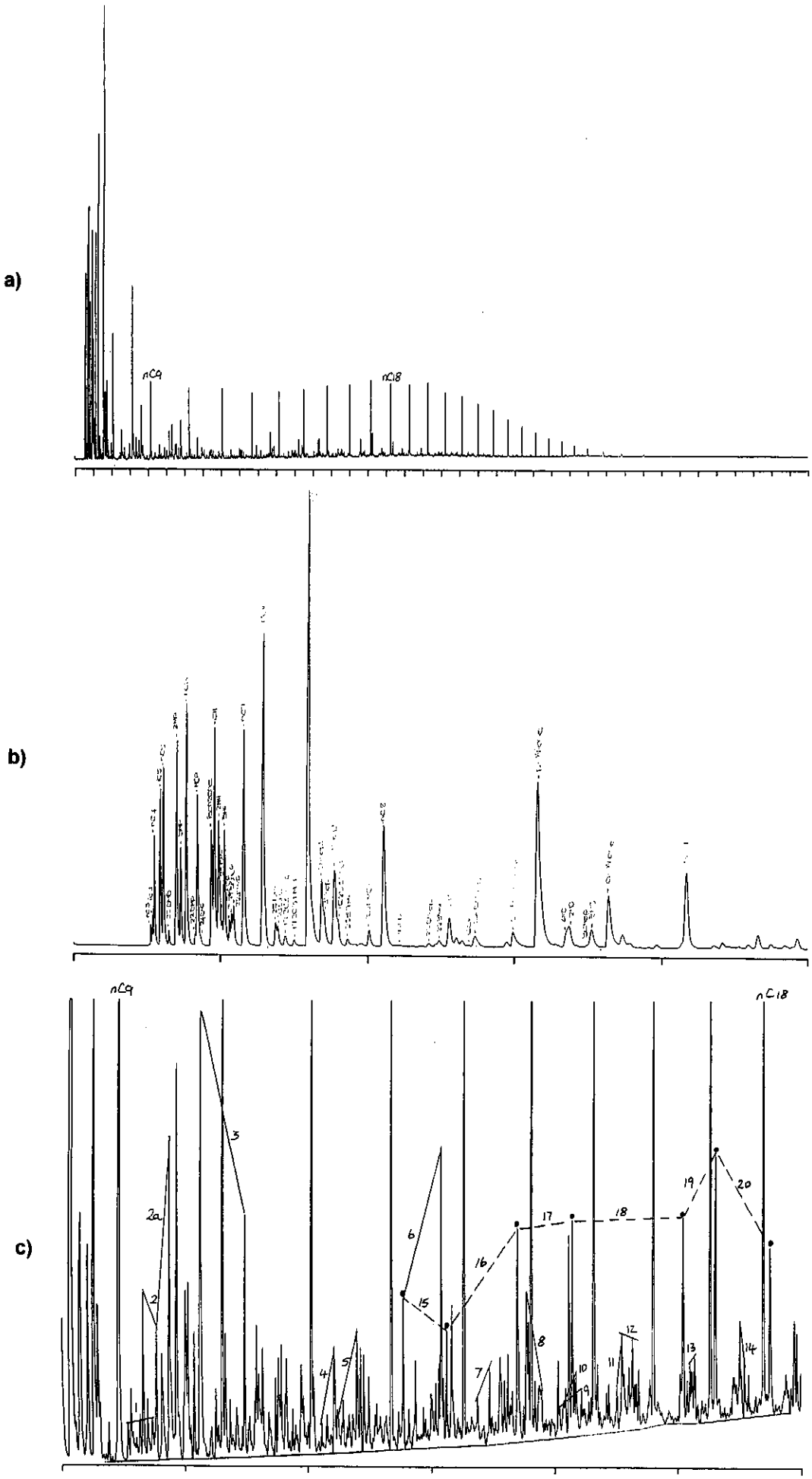

Figure C.16: Whole oil gas chromatograms of condensate from well 114 DST1 (a) 0-80 minutes, (b) 0-10 minutes and (c) 6-36 minutes analysed using column 1.

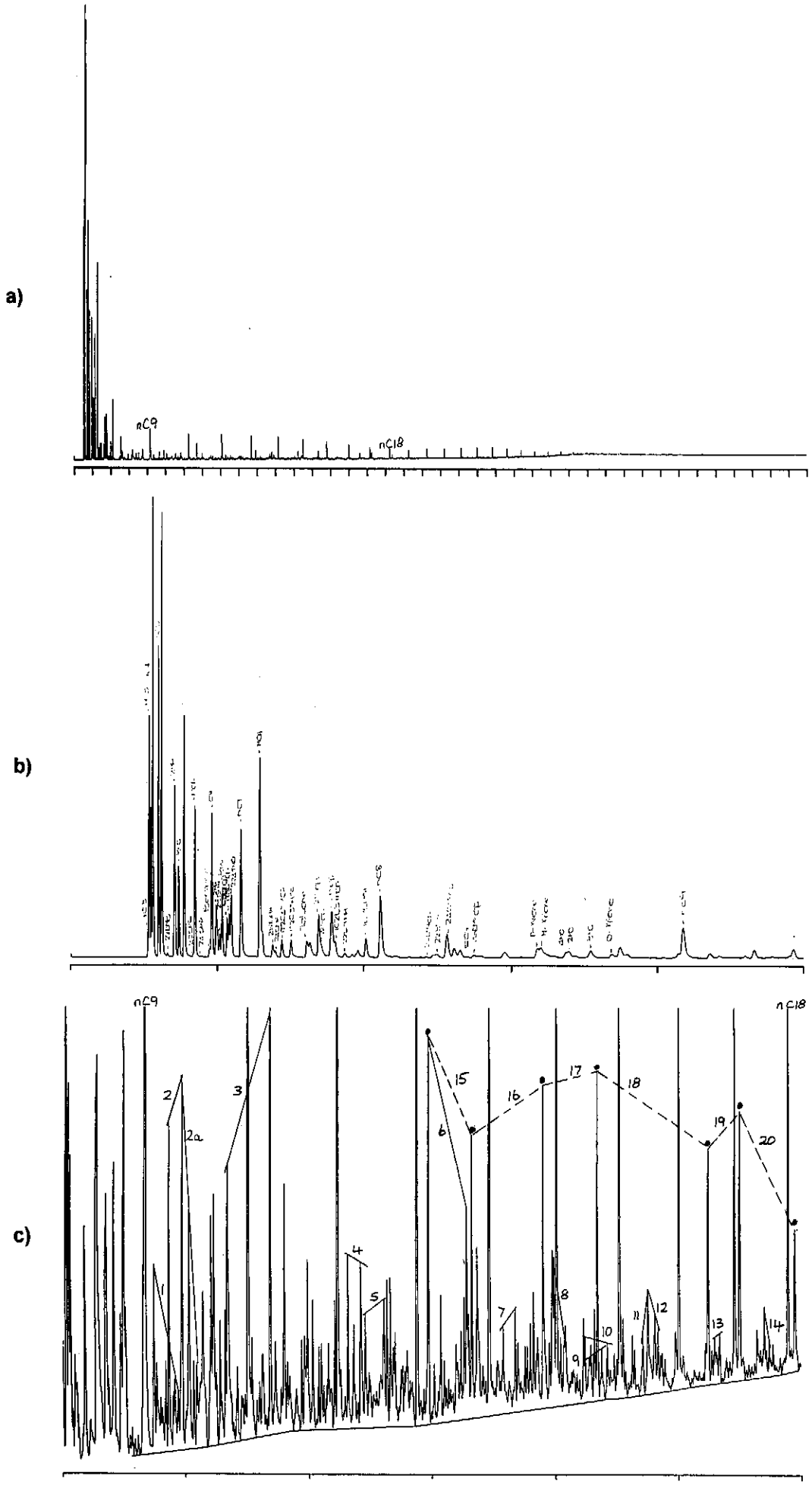

Figure C.17: Whole oil gas chromatograms of oil from well 93 DST2 (a) 0-80 minutes, (b) 0-10 minutes and (c) 6-36 minutes analysed using column 1.

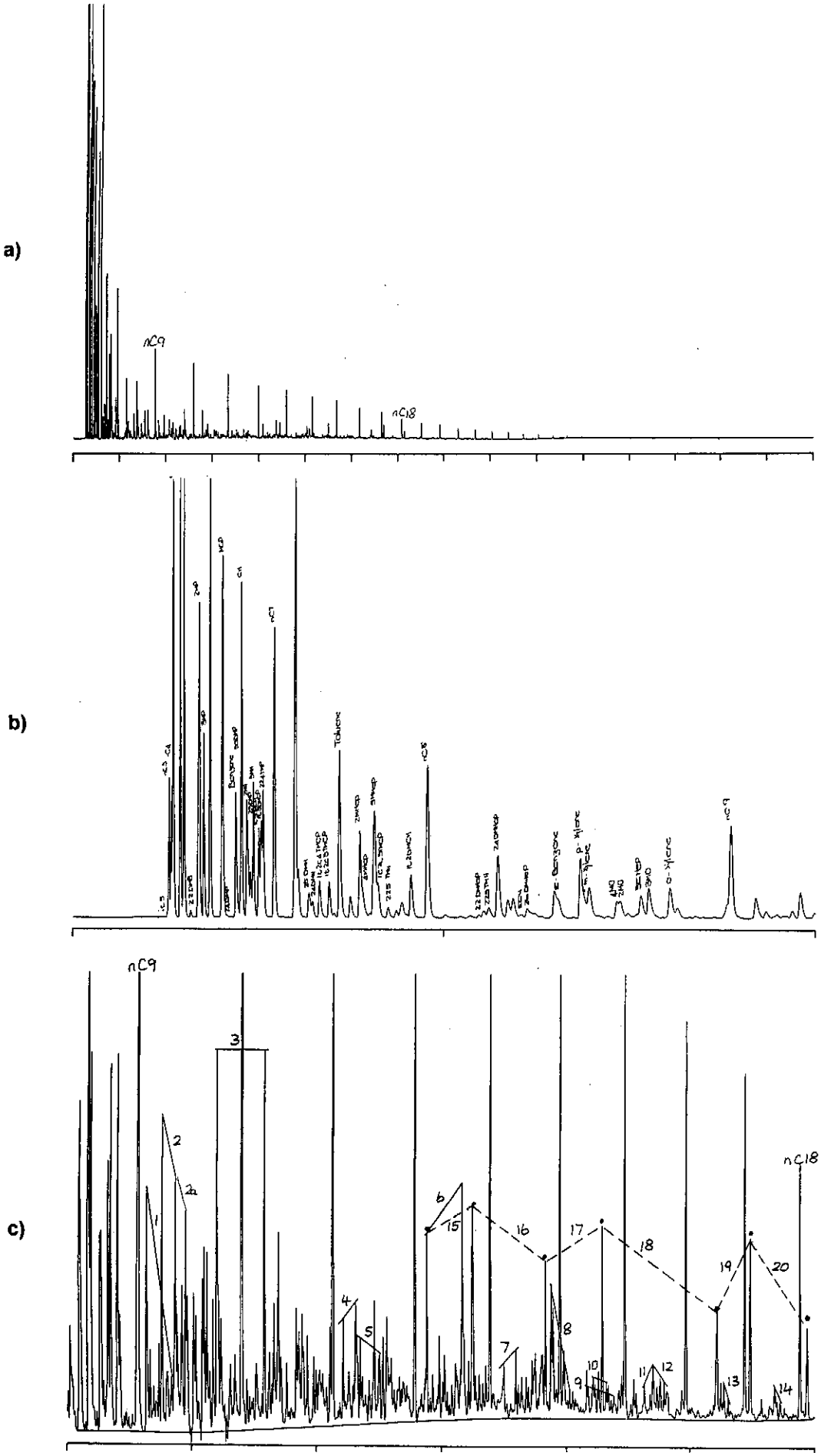

Figure C.18: Whole oil gas chromatograms of condensate from well 93 DST1A (a) 0-80 minutes, (b) 0-10 minutes and (c) 6-36 minutes analysed using column 3.

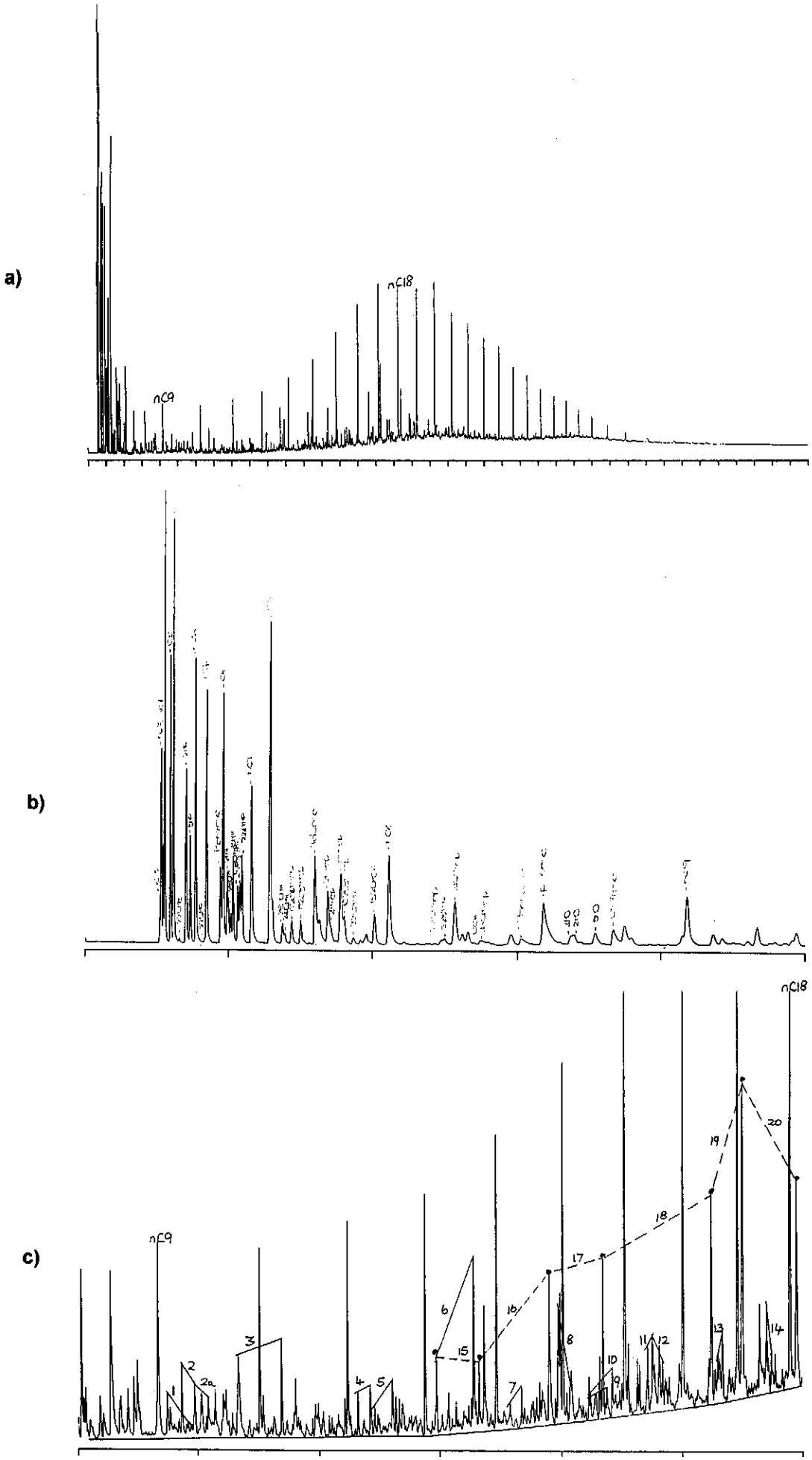

Figure C.19: Whole oil gas chromatograms of condensate from well 93 DST1 (a) 0-80 minutes, (b) 0-10 minutes and (c) 6-36 minutes analysed using column 1.

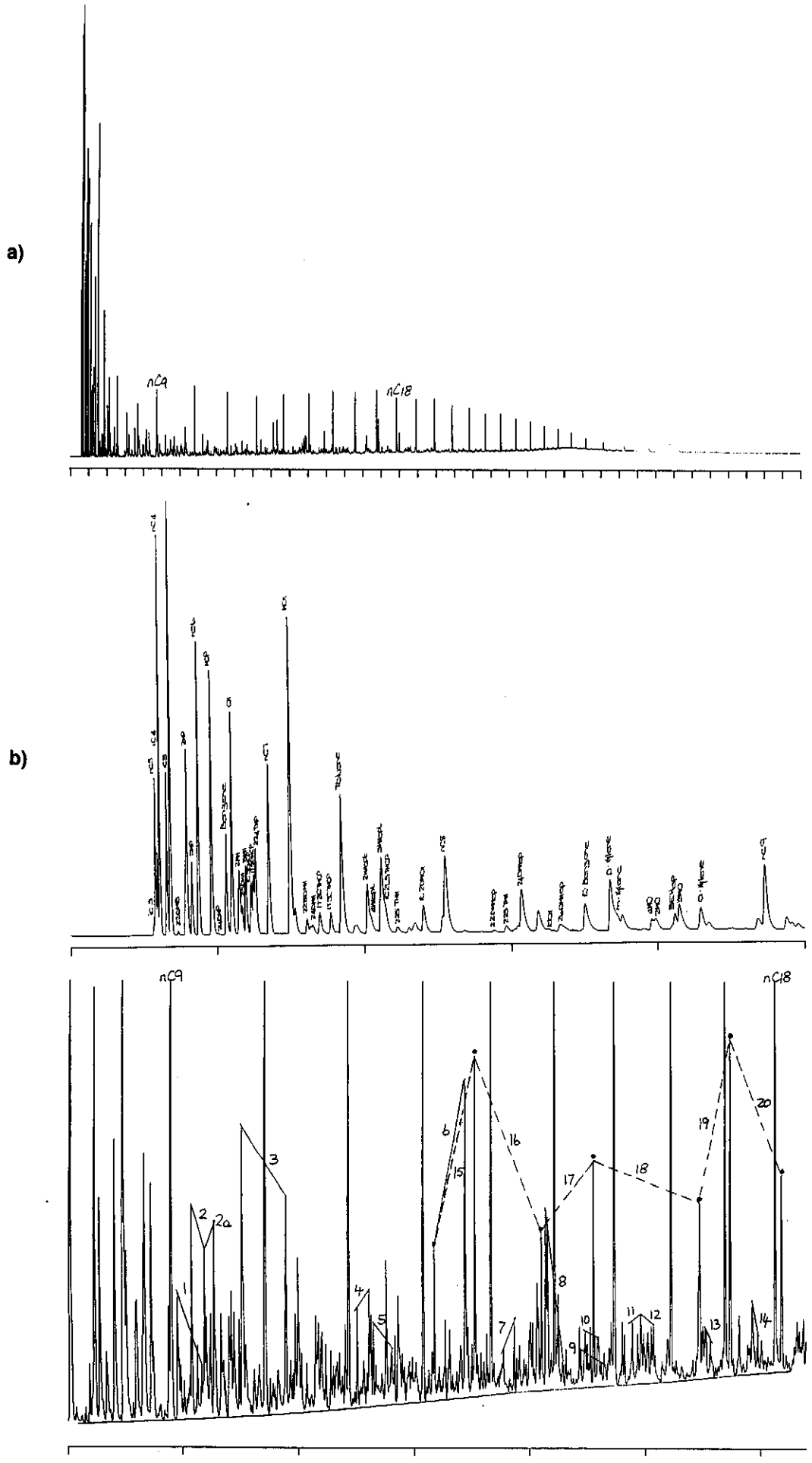

Figure C.20: Whole oil gas chromatograms of condensate from well 119 DST1 (a) 0-80 minutes, (b) 0-10 minutes and (c) 6-36 minutes analysed using column 2.

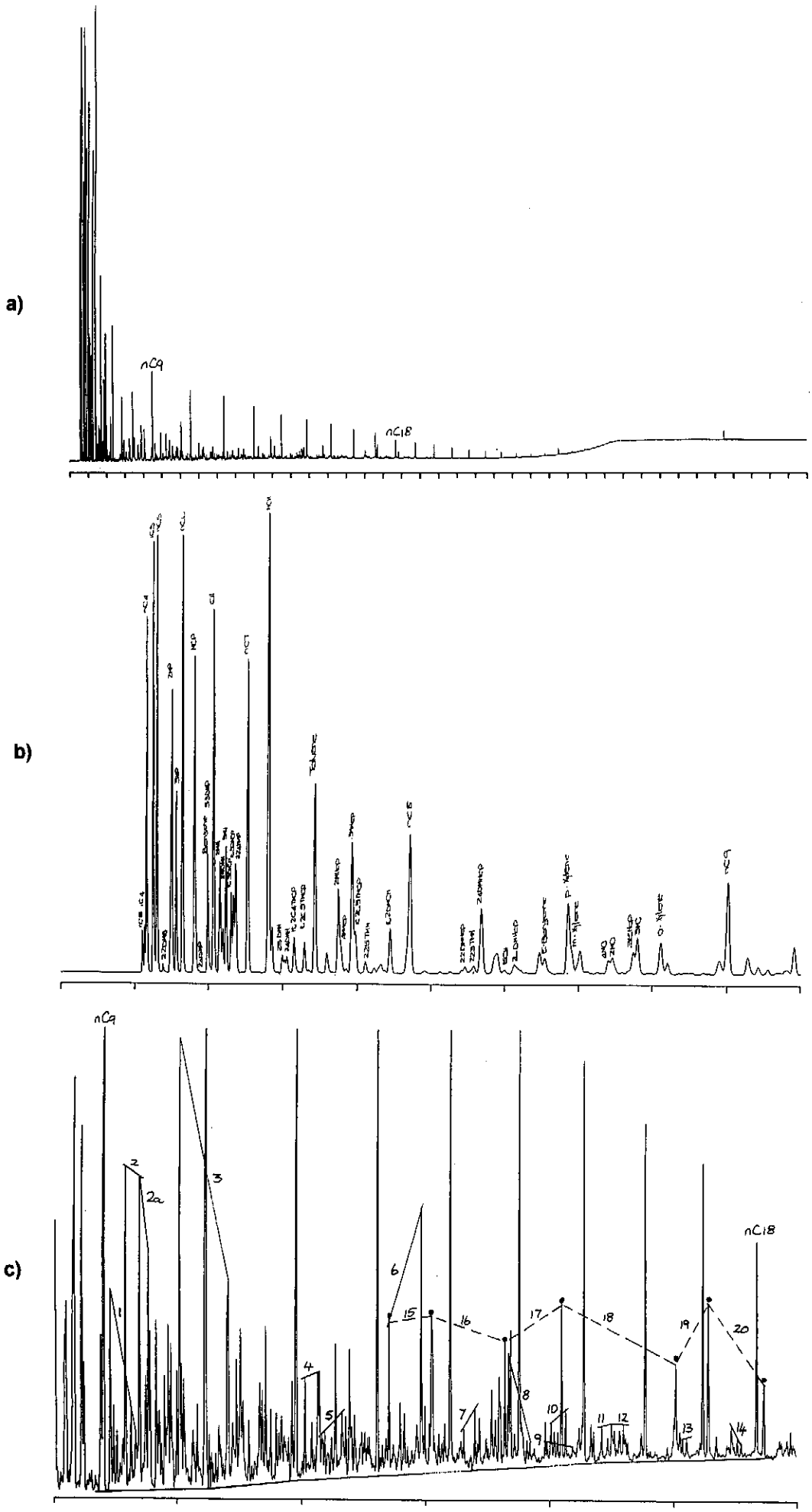

Figure C.21: Whole oil gas chromatograms of condensate from well 108 DST2 (a) 0-80 minutes, (b) 0-10 minutes and (c) 6-36 minutes analysed using column 2.

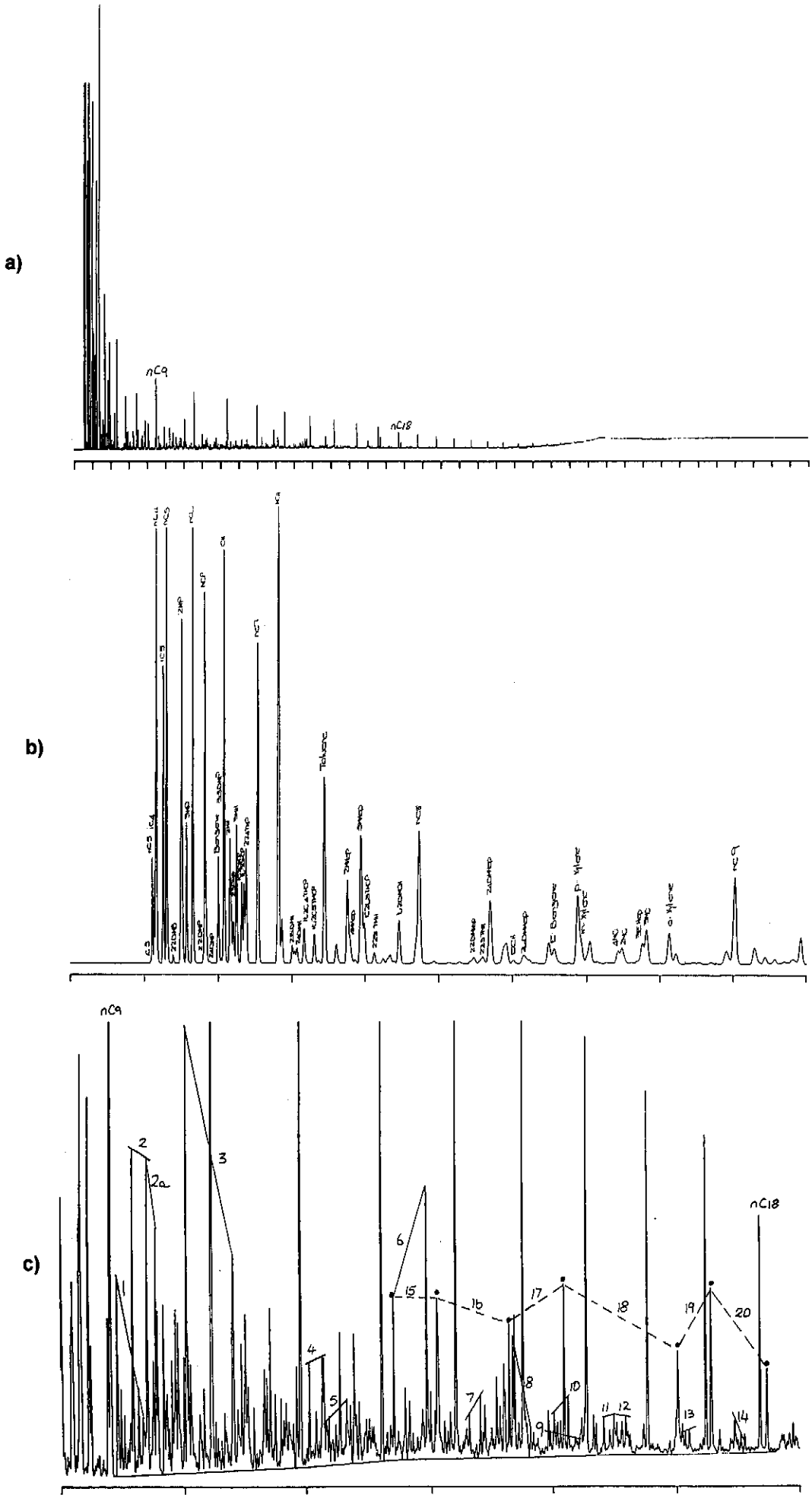

Figure C.22: Whole oil gas chromatograms of condensate from well 108 DST1 (a) 0-80 minutes, (b) 0-10 minutes and (c) 6-36 minutes analysed using column 2.

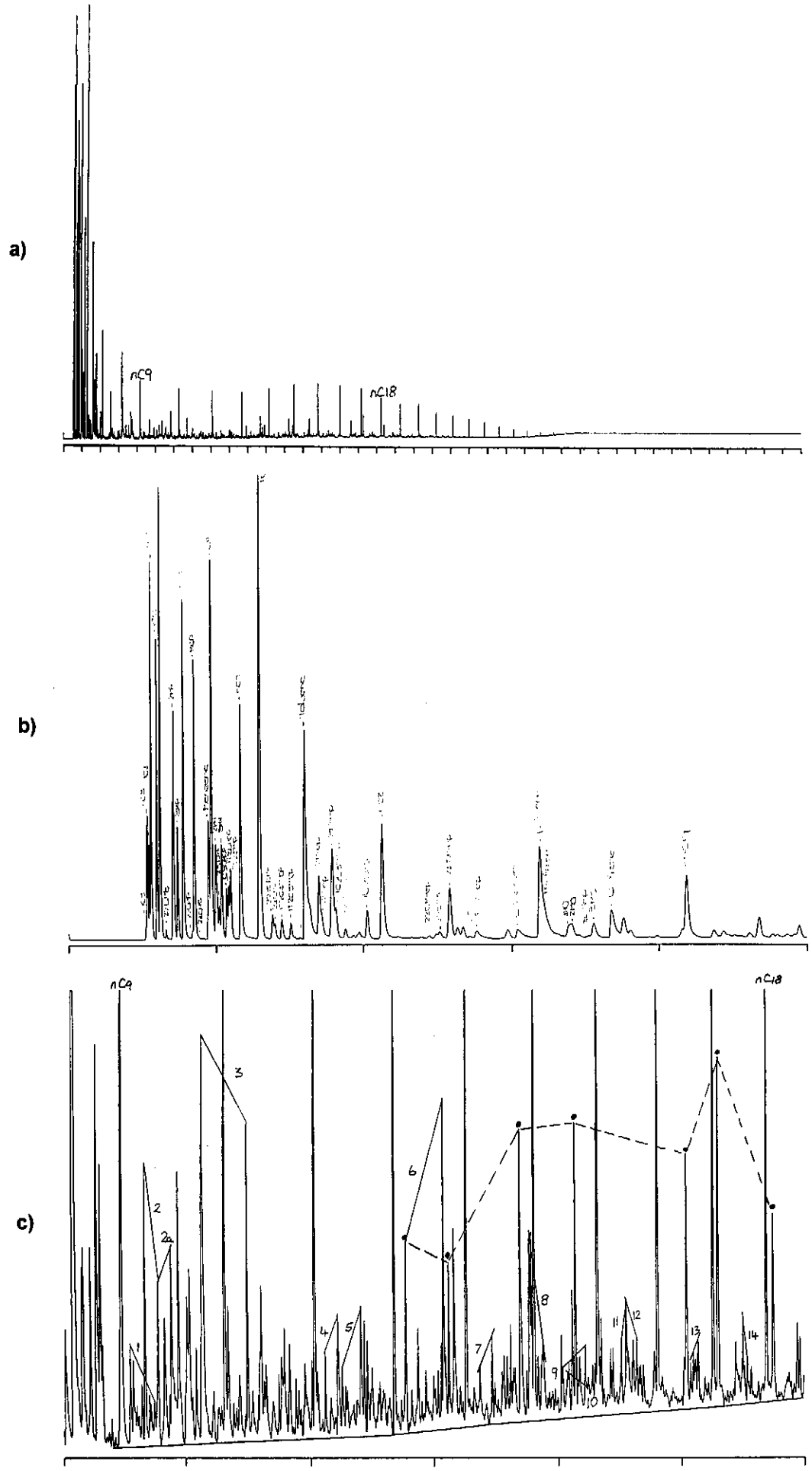

Figure C.23: Whole oil gas chromatograms of condensate from well 129 DST2 (a) 0-80 minutes, (b) 0-10 minutes and (c) 6-36 minutes analysed using column 1.

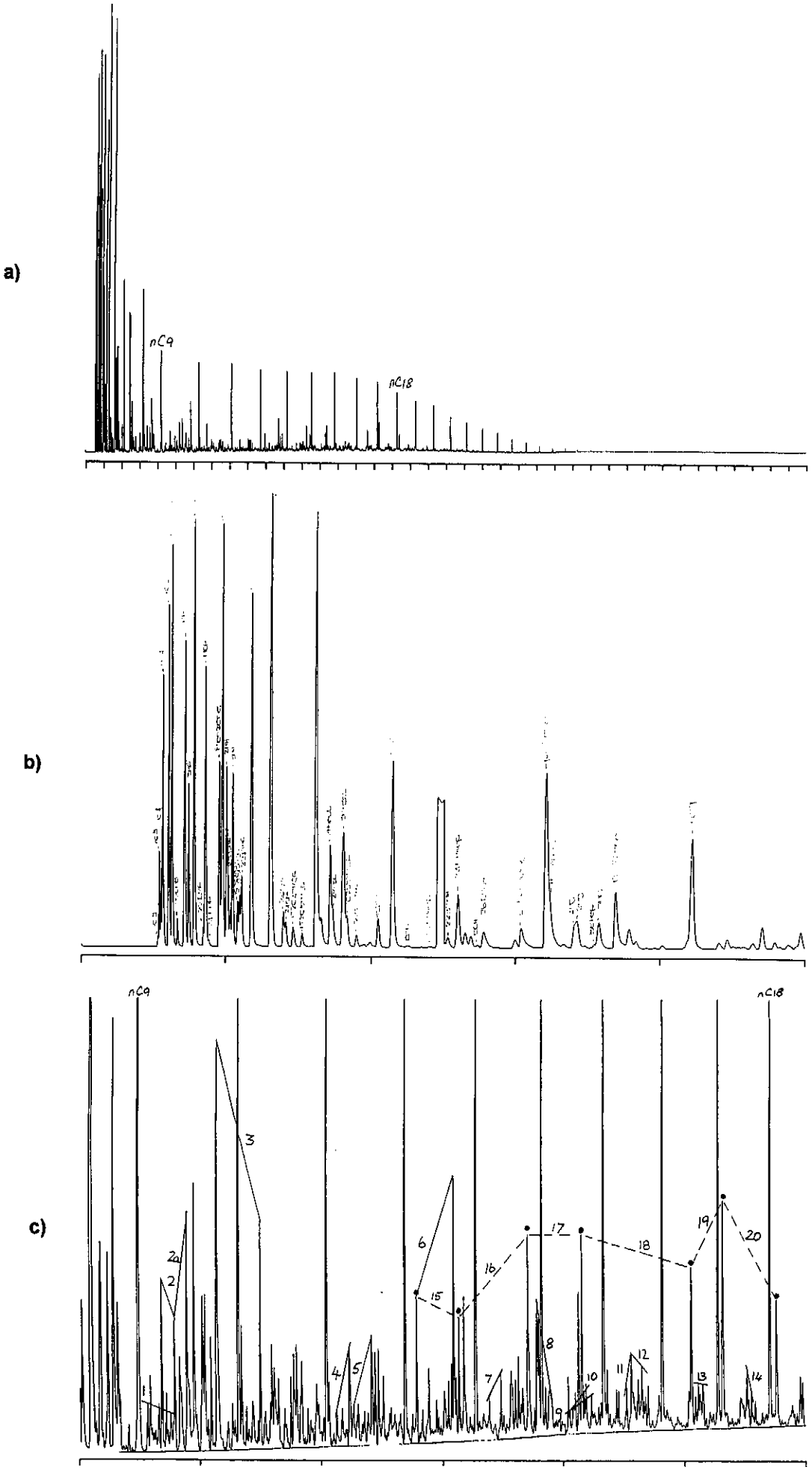

Figure C.24: Whole oil gas chromatograms of condensate from well 129 DST1 (a) 0-80 minutes, (b) 0-10 minutes and (c) 6-36 minutes analysed using column 1.

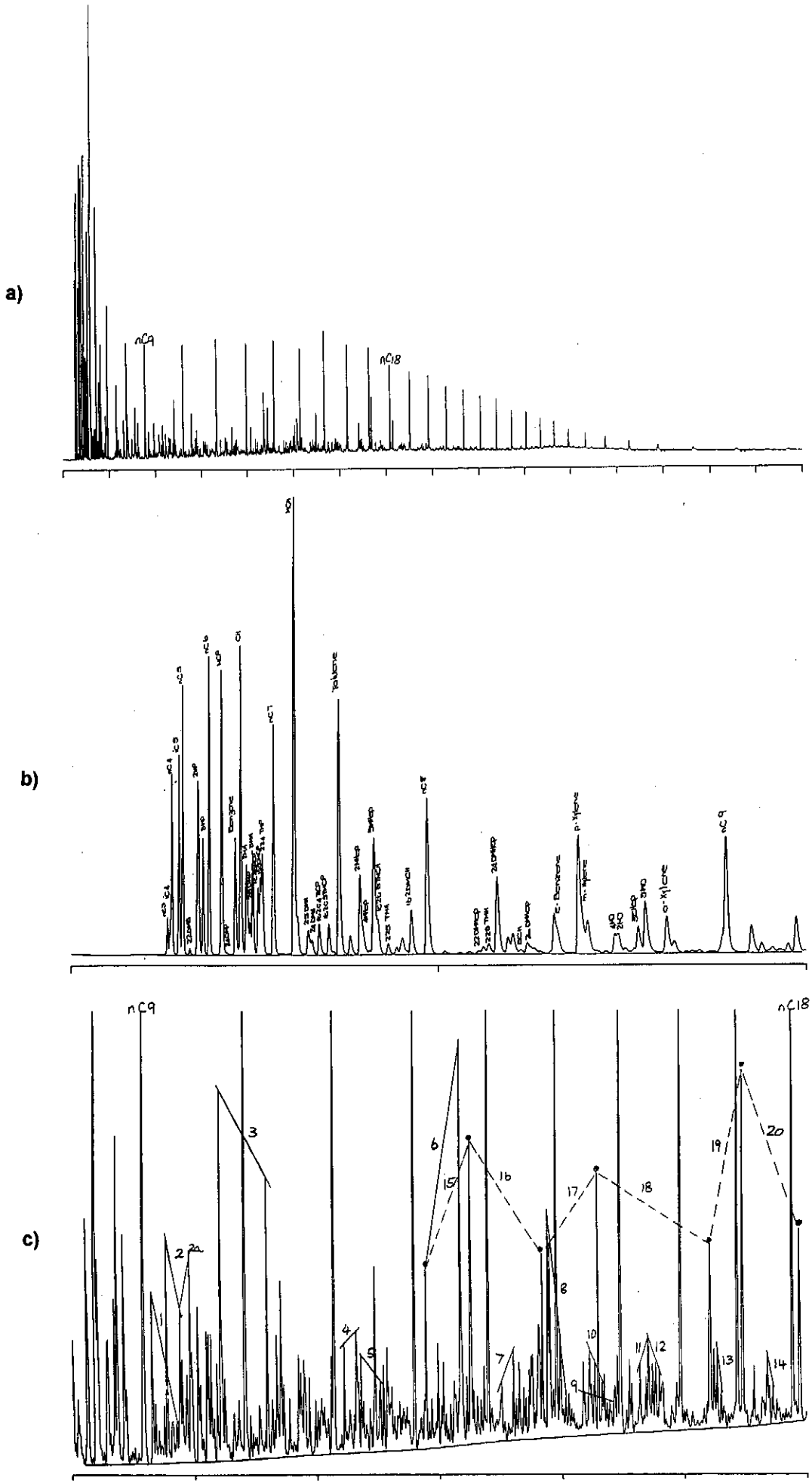

Figure C.25: Whole oil gas chromatograms of oil from well 109 DST1 (a) 0-80 minutes, (b) 0-10 minutes and (c) 6-36 minutes analysed using column 3.

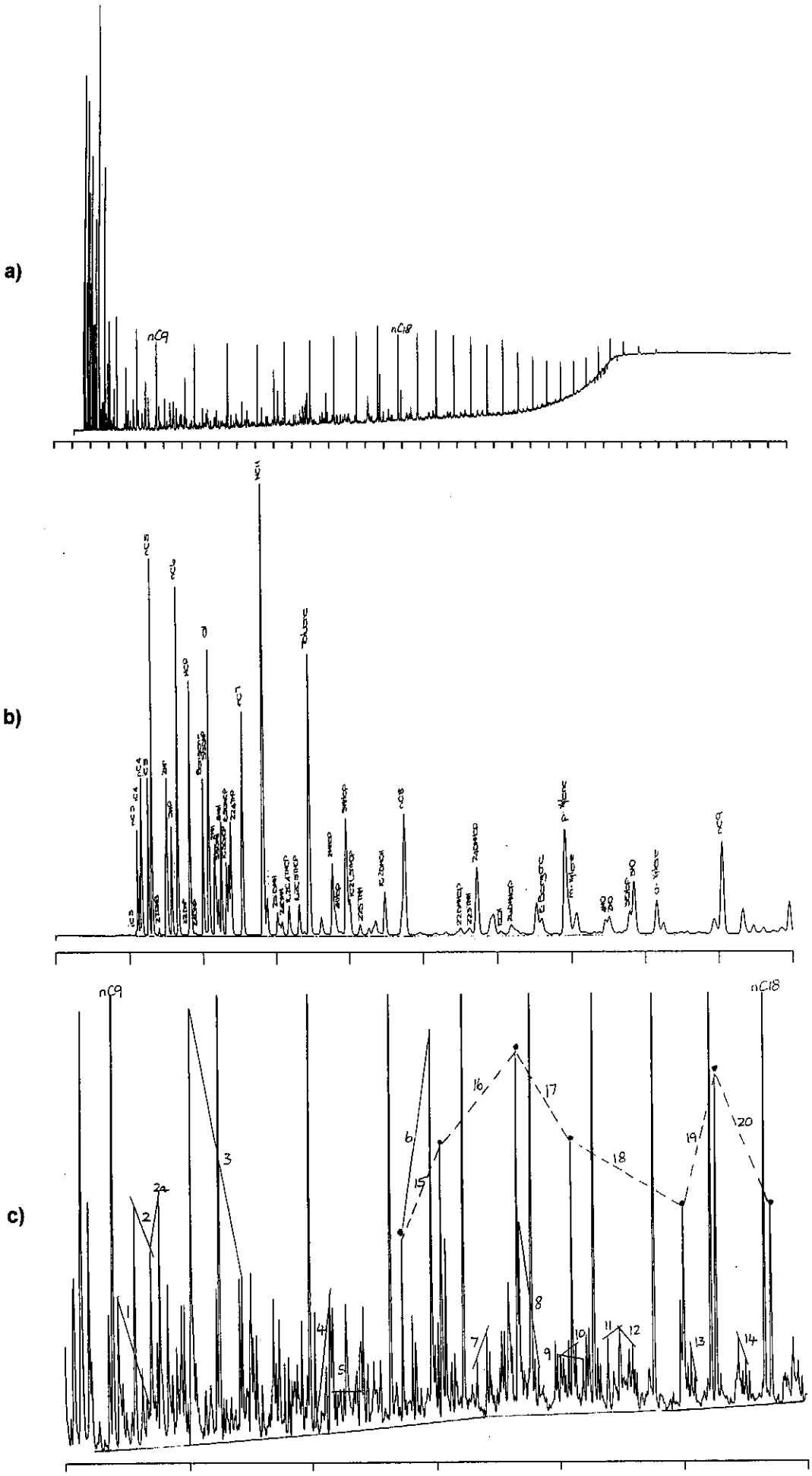

Figure C.26: Whole oil gas chromatograms of oil from well 109 DST1 (a) 0-80 minutes, (b) 0-10 minutes and (c) 6-36 minutes analysed using column 2.

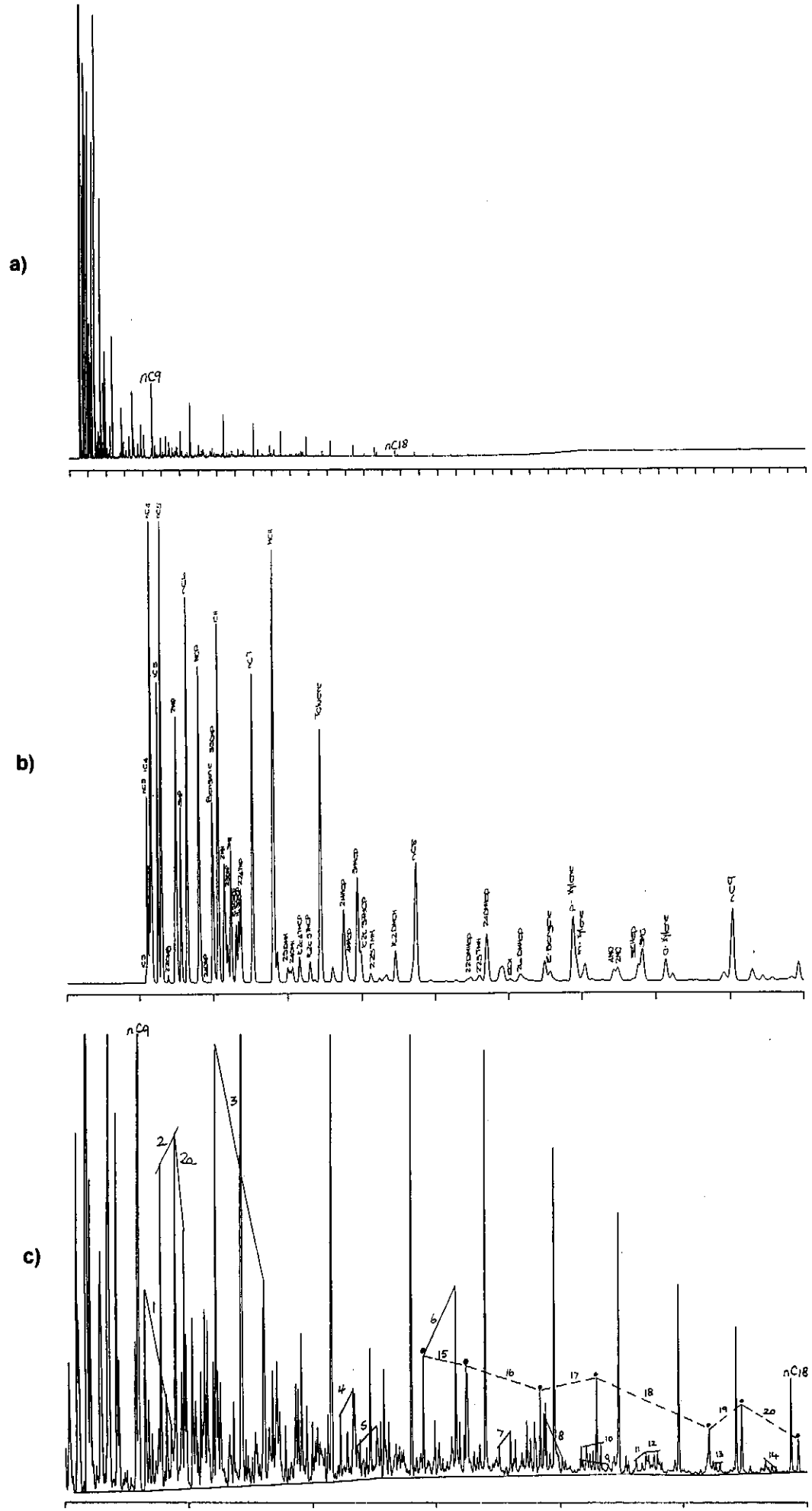

Figure C.27: Whole oil gas chromatograms of condensate from well 107 DST3 (a) 0-80 minutes, (b) 0-10 minutes and (c) 6-36 minutes analysed using column 2.

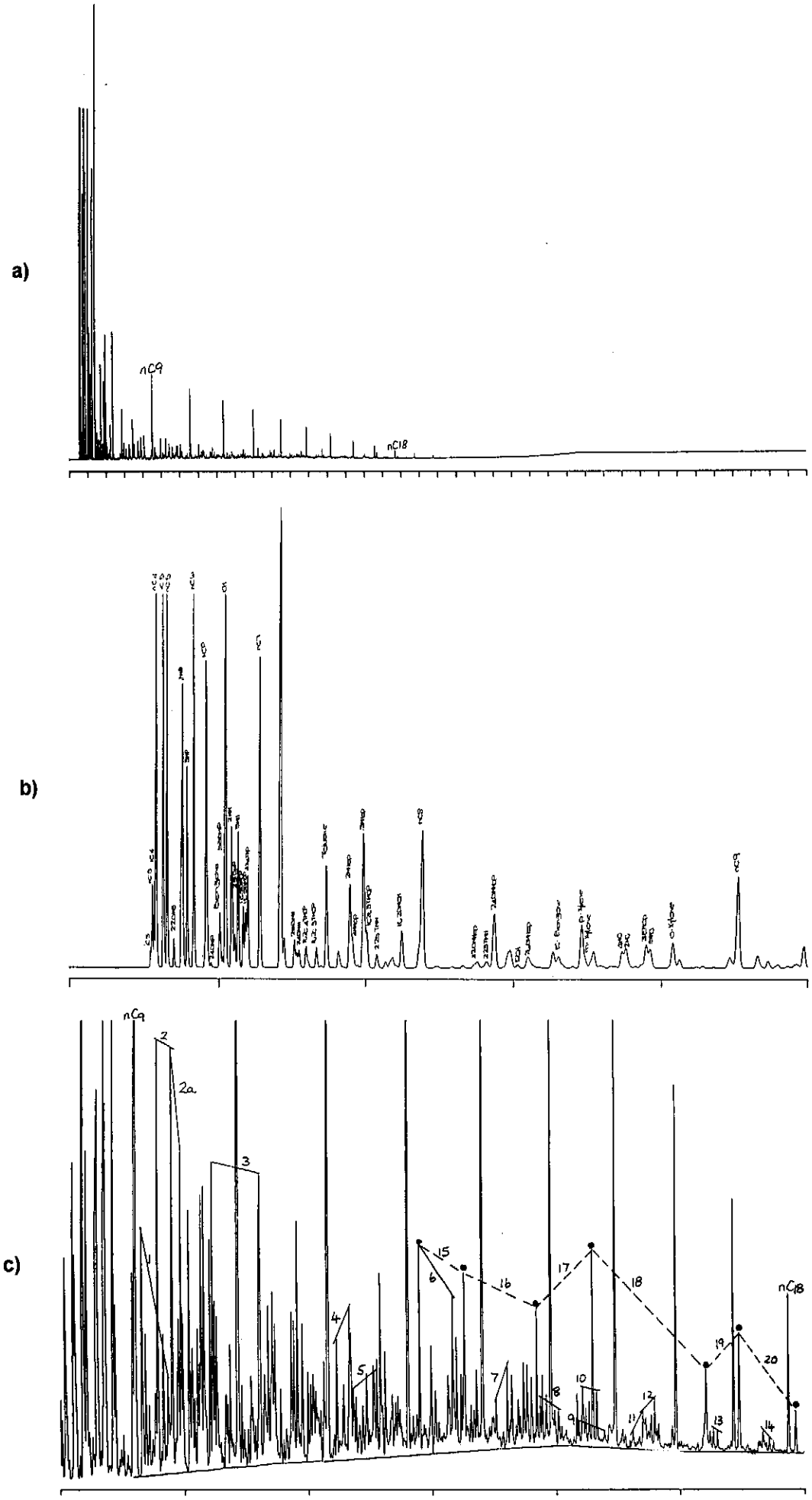

Figure C.28: Whole oil gas chromatograms of condensate from well 107 DST2 (a) 0-80 minutes, (b) 0-10 minutes and (c) 6-36 minutes analysed using column 2.

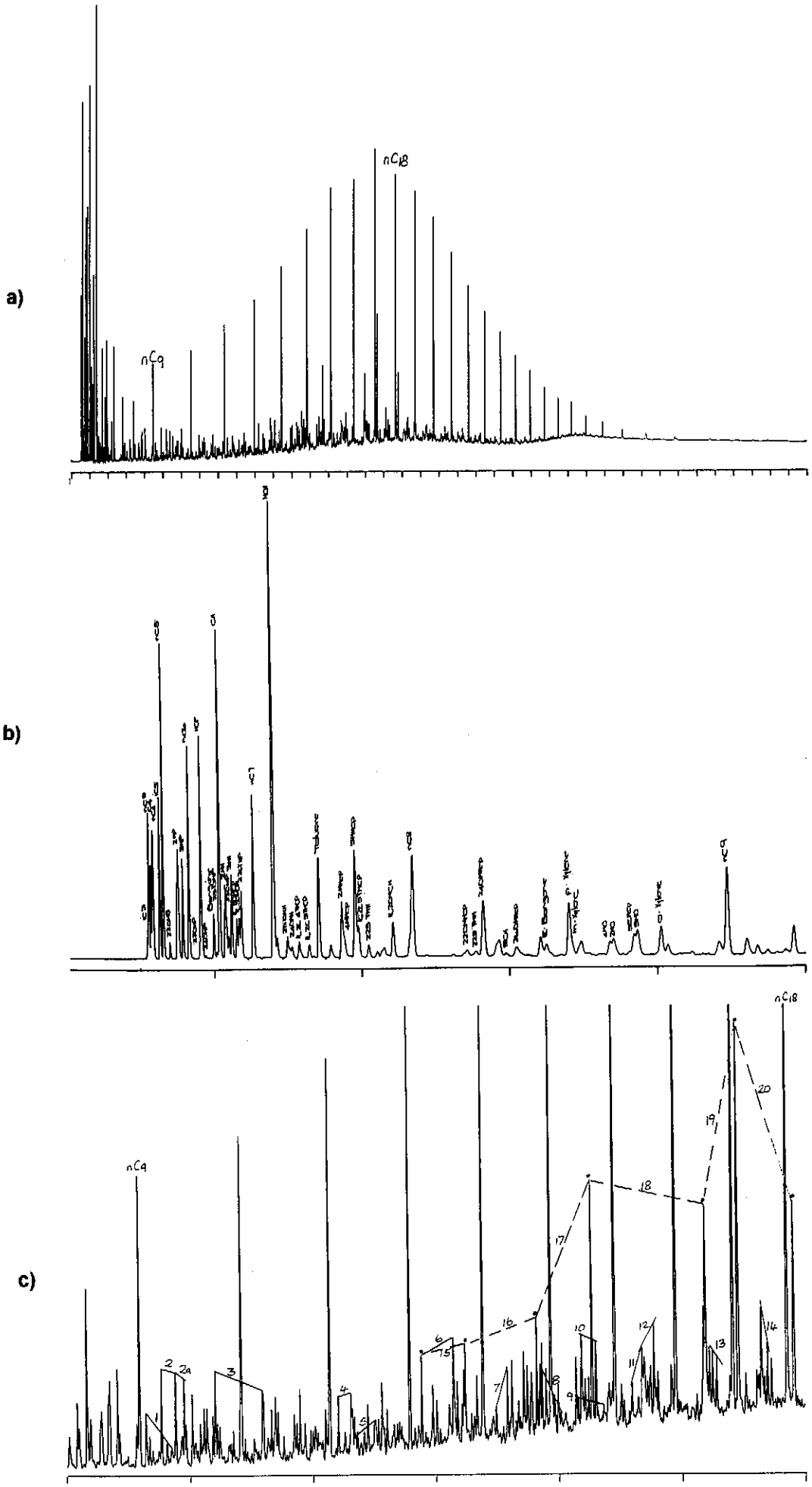

Figure C.29: Whole oil gas chromatograms of oil from well 107 DST1 (a) 0-80 minutes, (b) 0-10 minutes and (c) 6-36 minutes analysed using column 2.

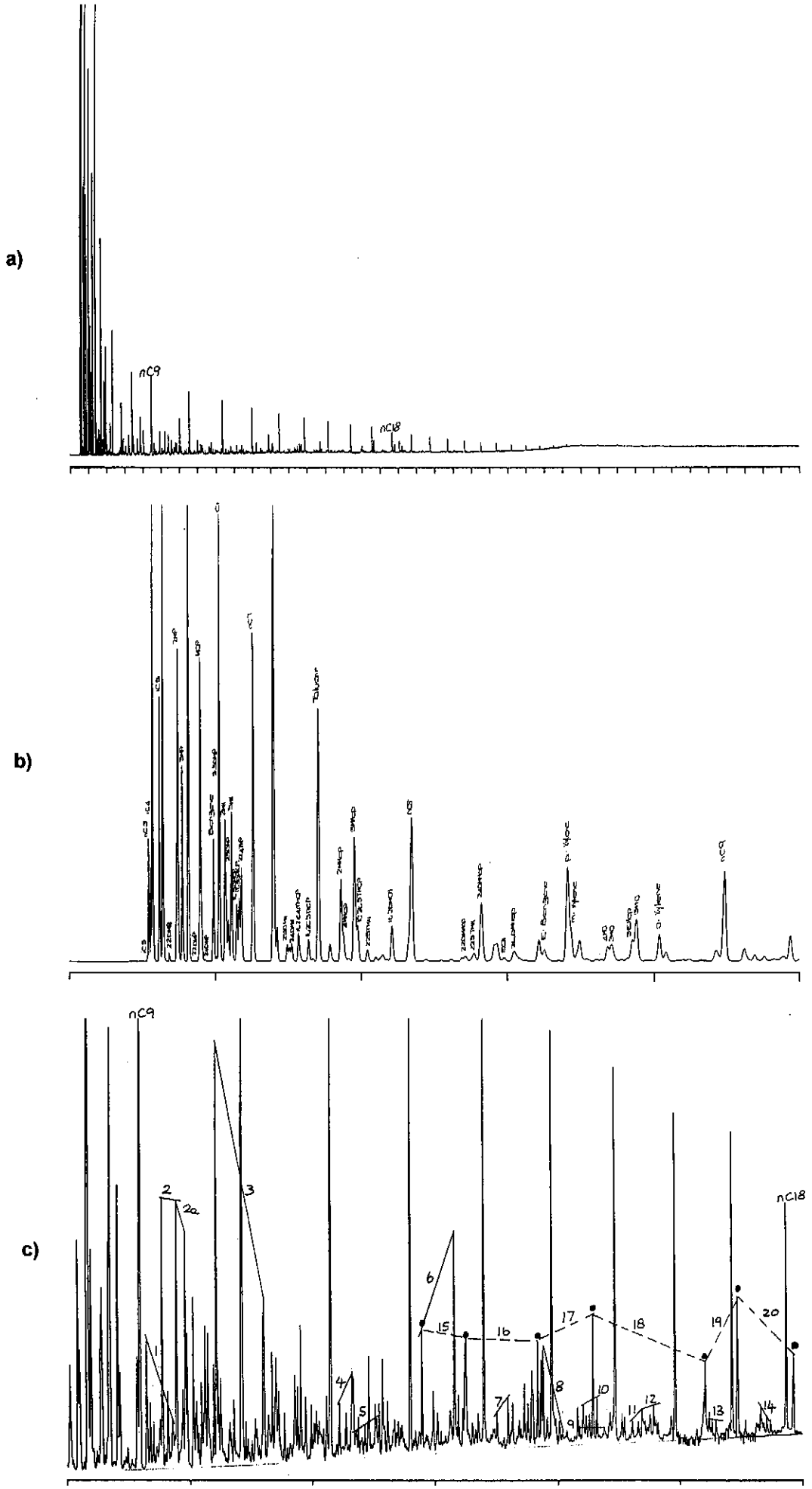

Figure C.30: Whole oil gas chromatograms of condensate from well 110 DST1A (a) 0-80 minutes, (b) 0-10 minutes and (c) 6-36 minutes analysed using column 2.

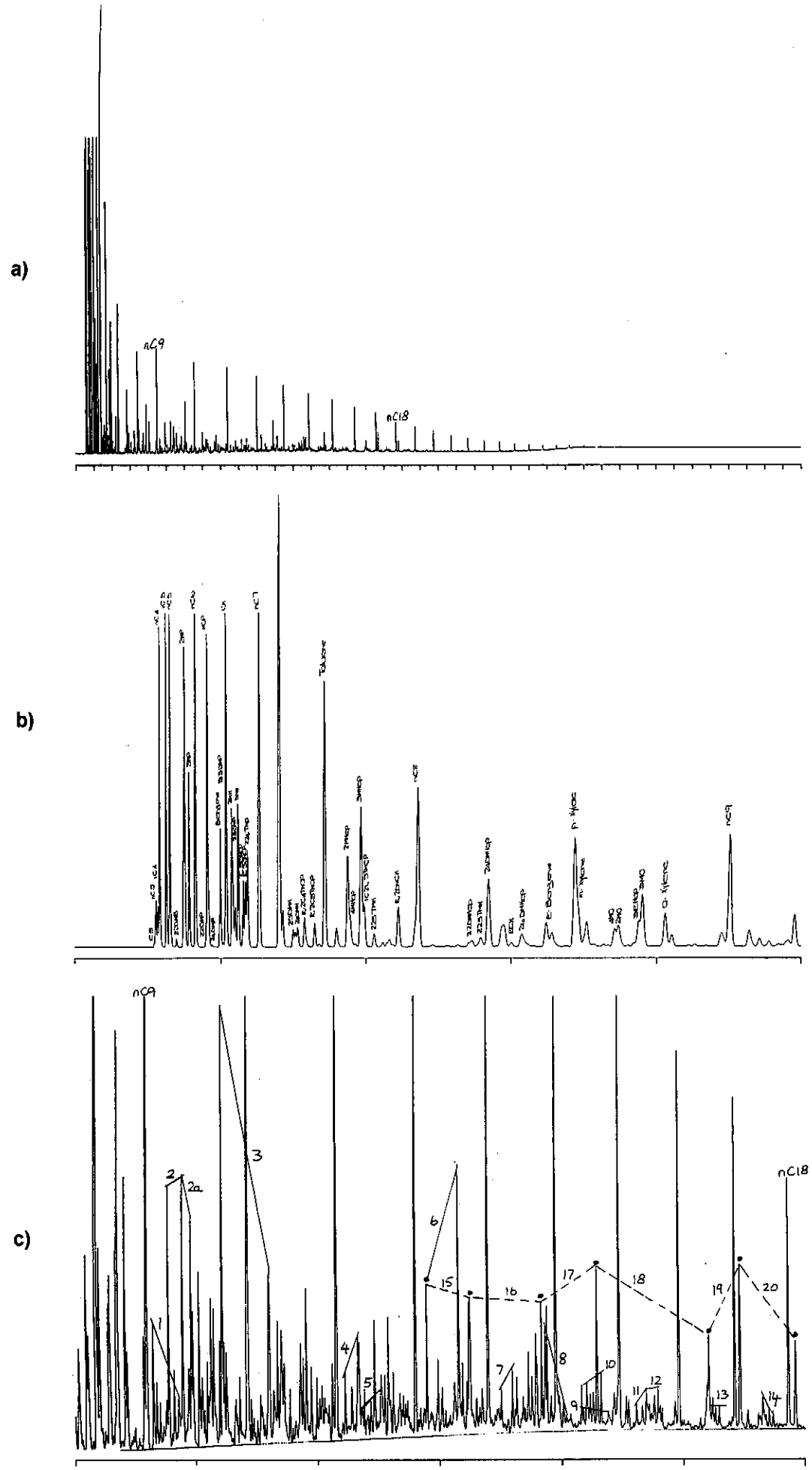

Figure C.31: Whole oil gas chromatograms of condensate from well 110 DST1B (a) 0-80 minutes, (b) 0-10 minutes and (c) 6-36 minutes analysed using column 2.

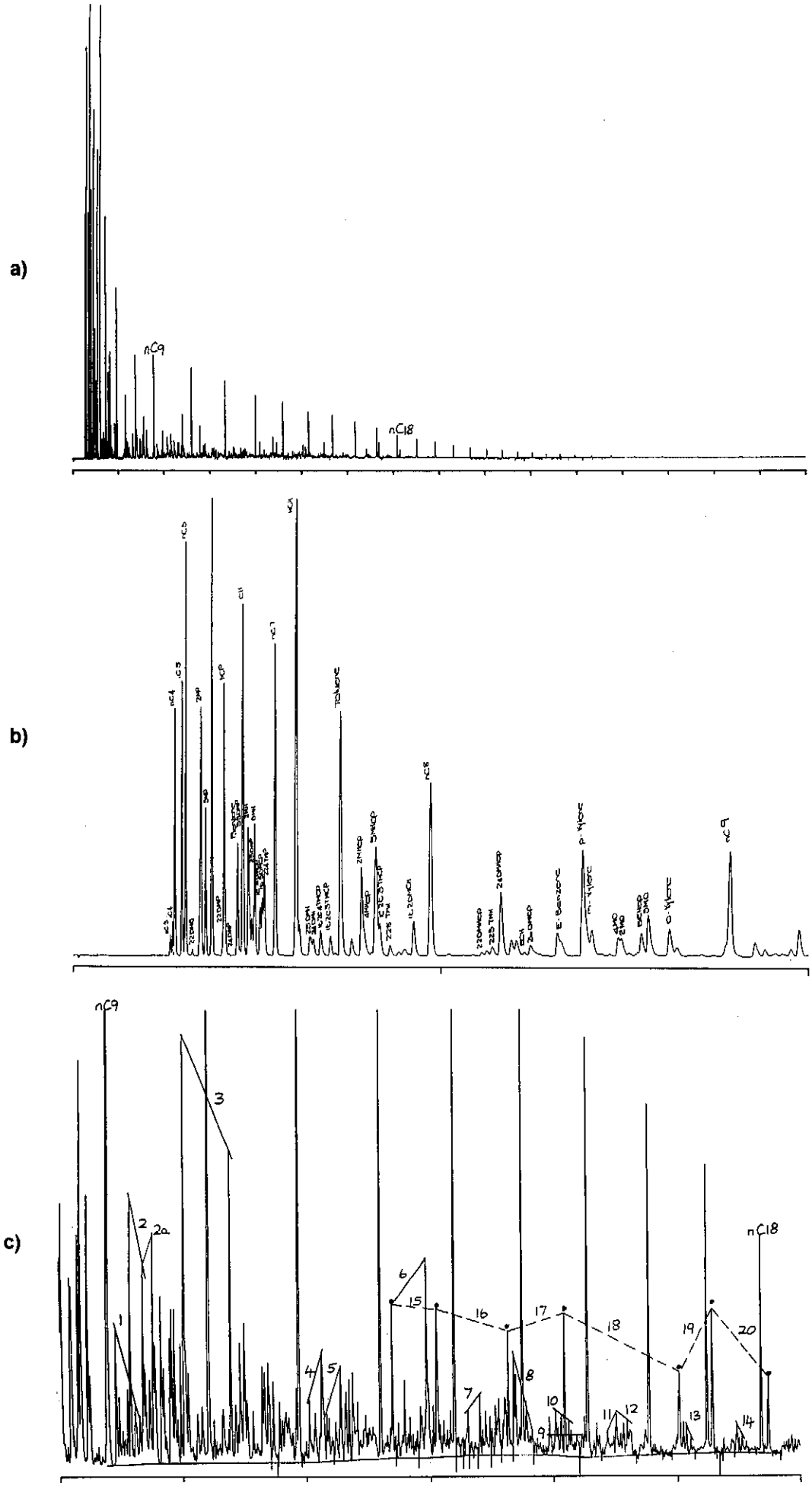

Figure C.32: Whole oil gas chromatograms of condensate from well 110 DST1B (a) 0-80 minutes, (b) 0-10 minutes and (c) 6-36 minutes analysed using column 3.

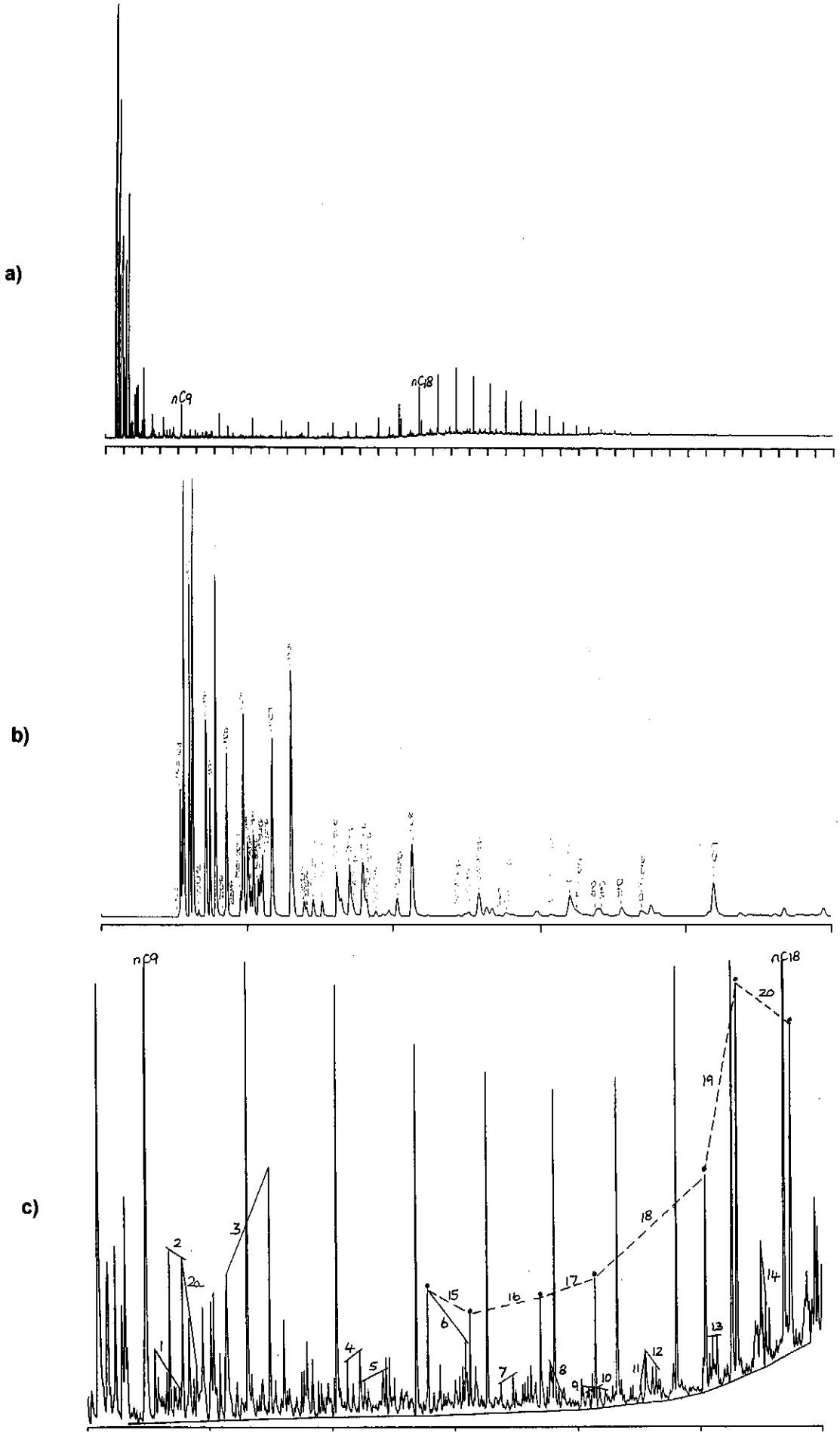

Figure C.33: Whole oil gas chromatograms of condensate from well 126 DST1 (a) 0-80 minutes, (b) 0-10 minutes and (c) 6-36 minutes analysed using column 1.

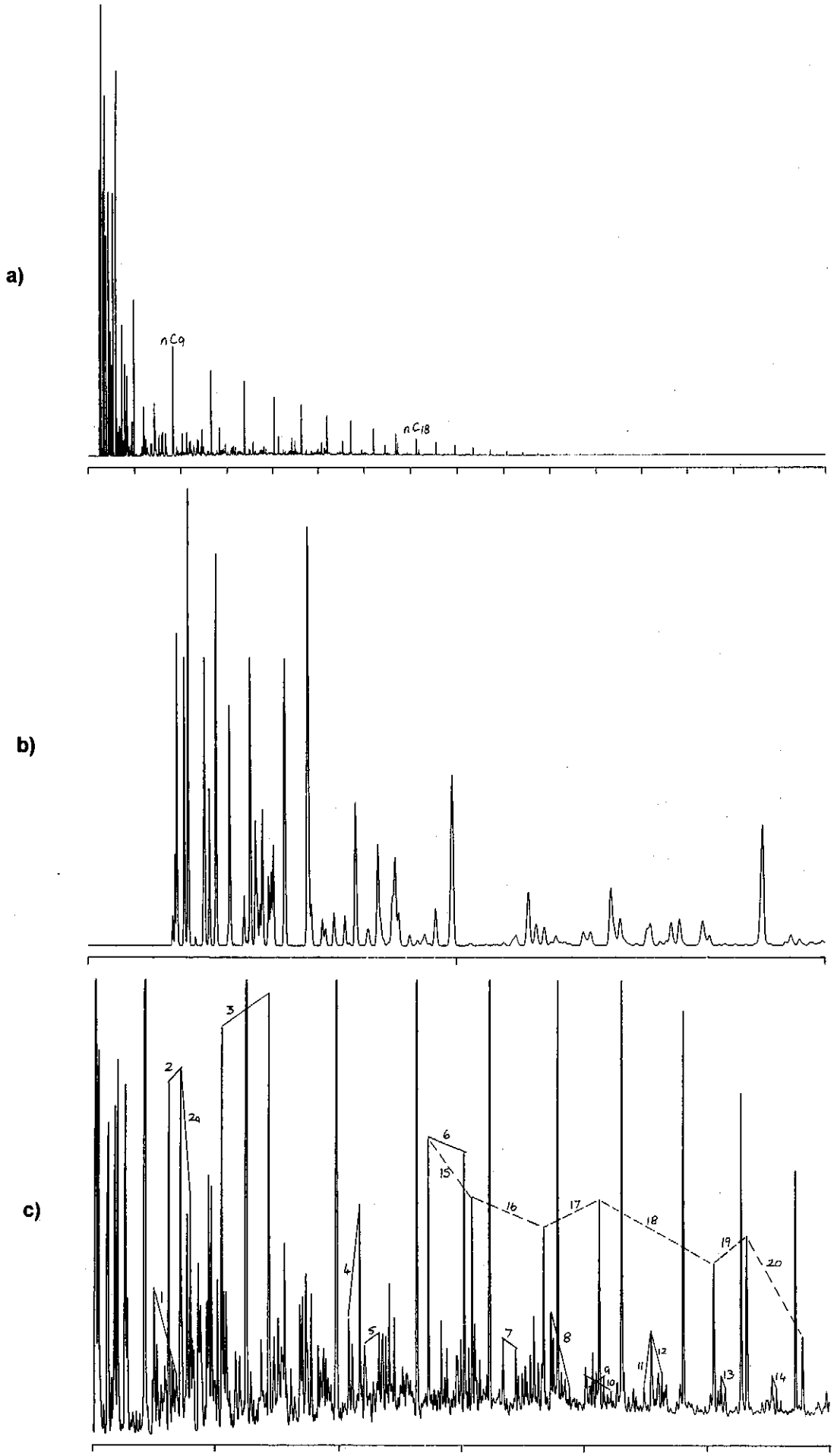

Figure C.34: Whole oil gas chromatograms of condensate from well 126 DST1 (a) 0-80 minutes, (b) 0-10 minutes and (c) 6-36 minutes analysed using column Q.

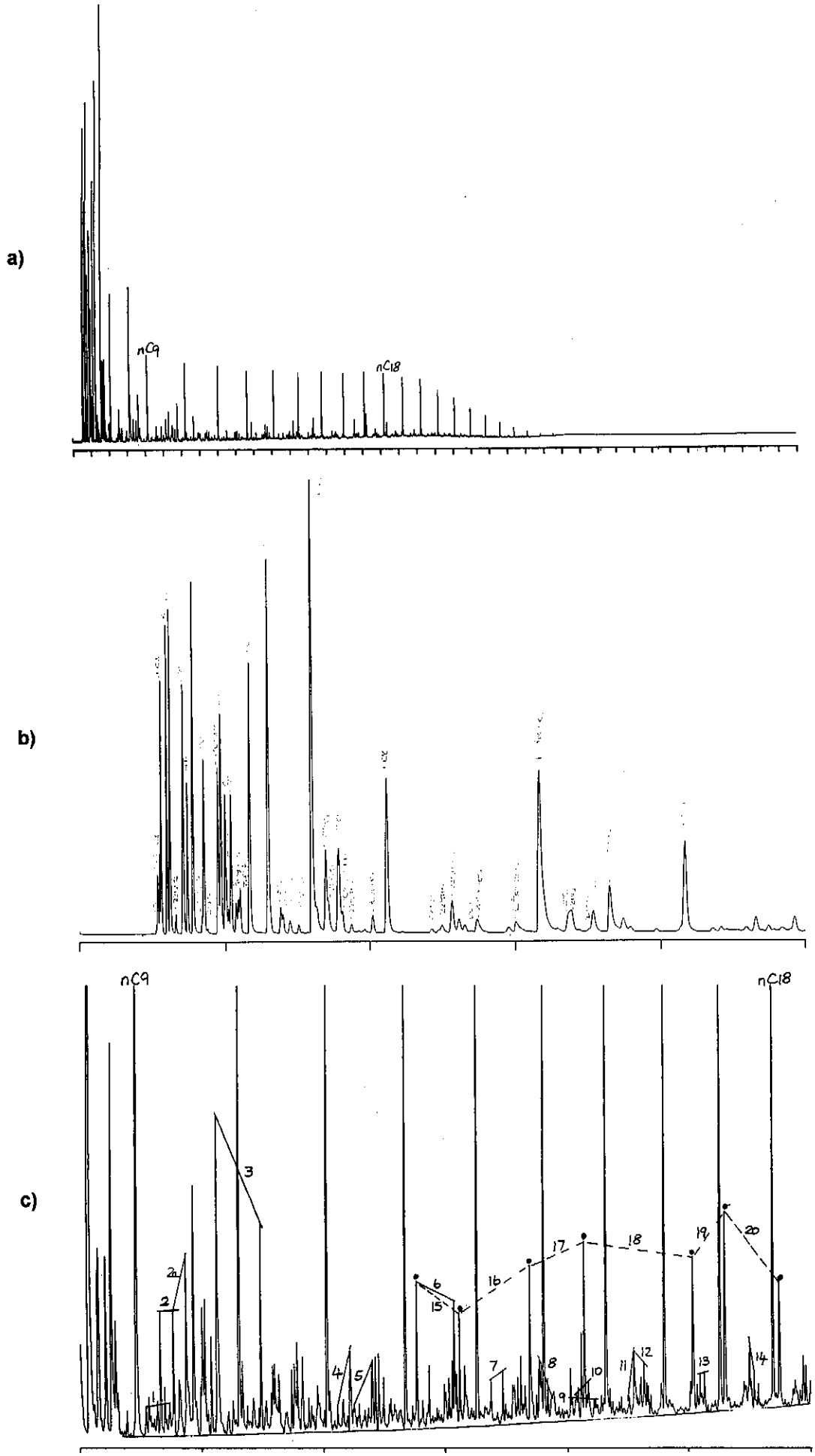

Figure C.35: Whole oil gas chromatograms of condensate from well 120 DST1 (a) 0-80 minutes, (b) 0-10 minutes and (c) 6-36 minutes analysed using column 1.

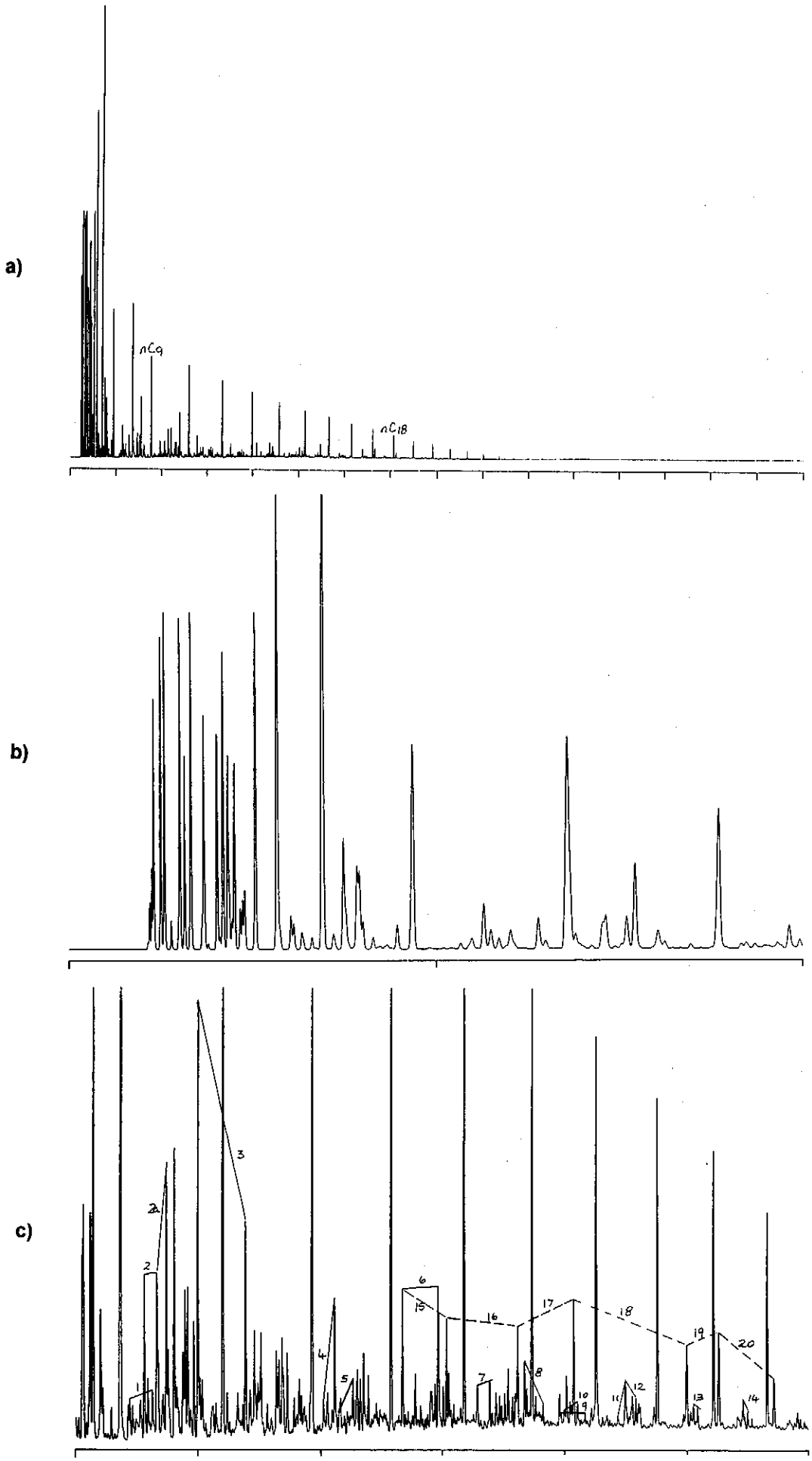

Figure C.36: Whole oil gas chromatograms of condensate from well 120 DST1 (a) 0-80 minutes, (b) 0-10 minutes and (c) 6-36 minutes analysed using column Q.

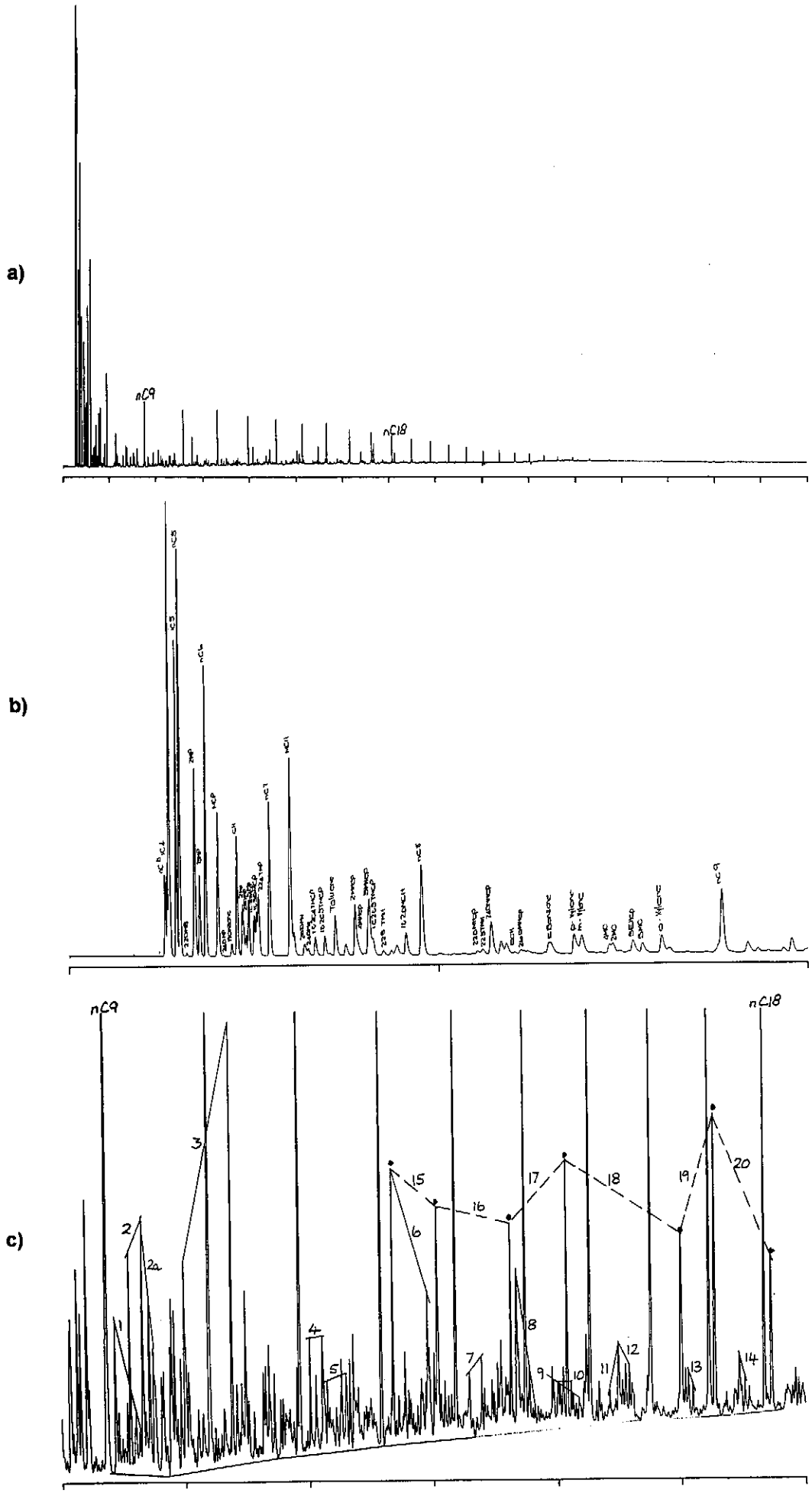

Figure C.37: Whole oil gas chromatograms of oil from well 117 DST1 (a) 0-80 minutes, (b) 0-10 minutes and (c) 6-36 minutes analysed using column 3.

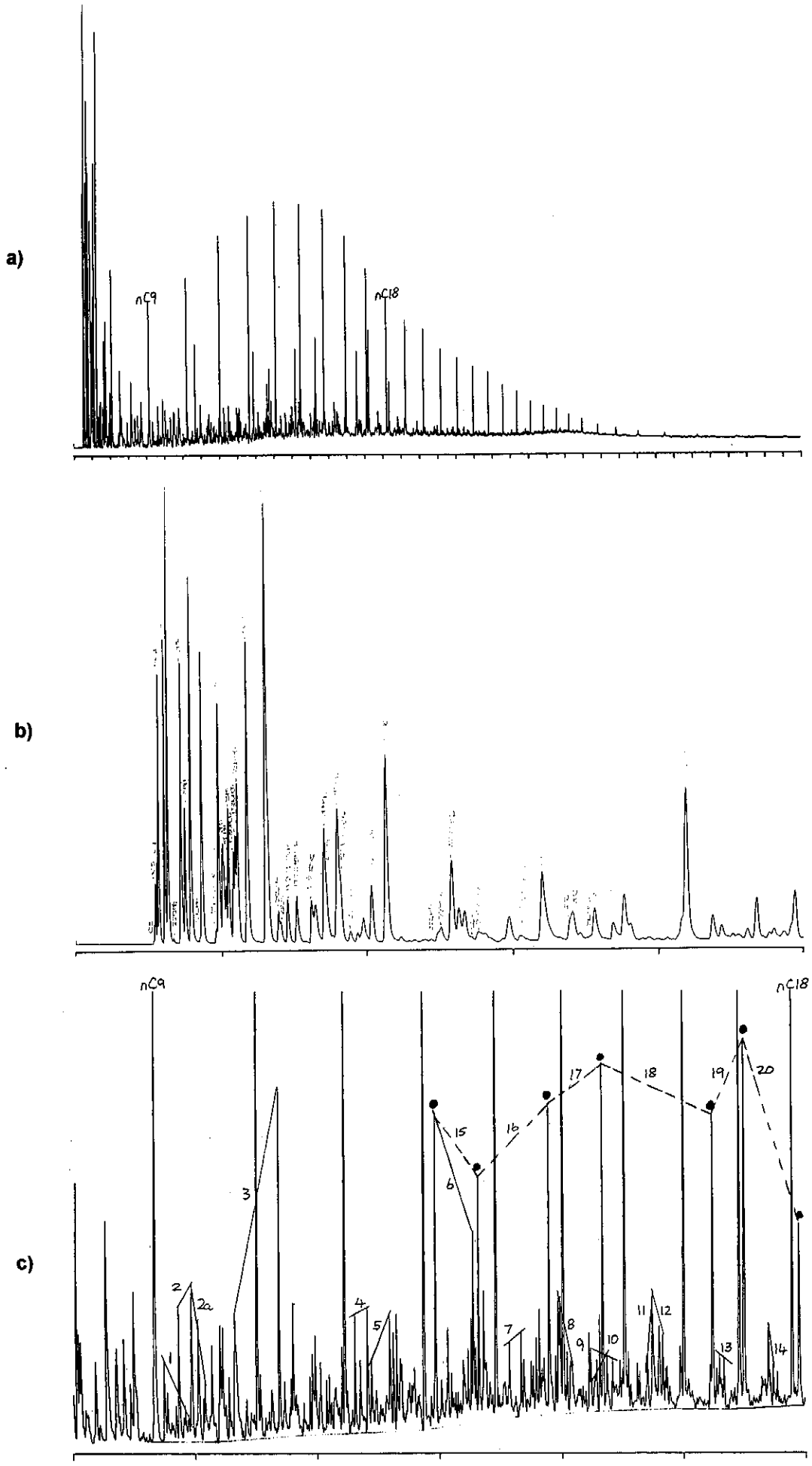

Figure C.38: Whole oil gas chromatograms of oil from well 117 DST1 (a) 0-80 minutes, (b) 0-10 minutes and (c) 6-36 minutes analysed using column 1.

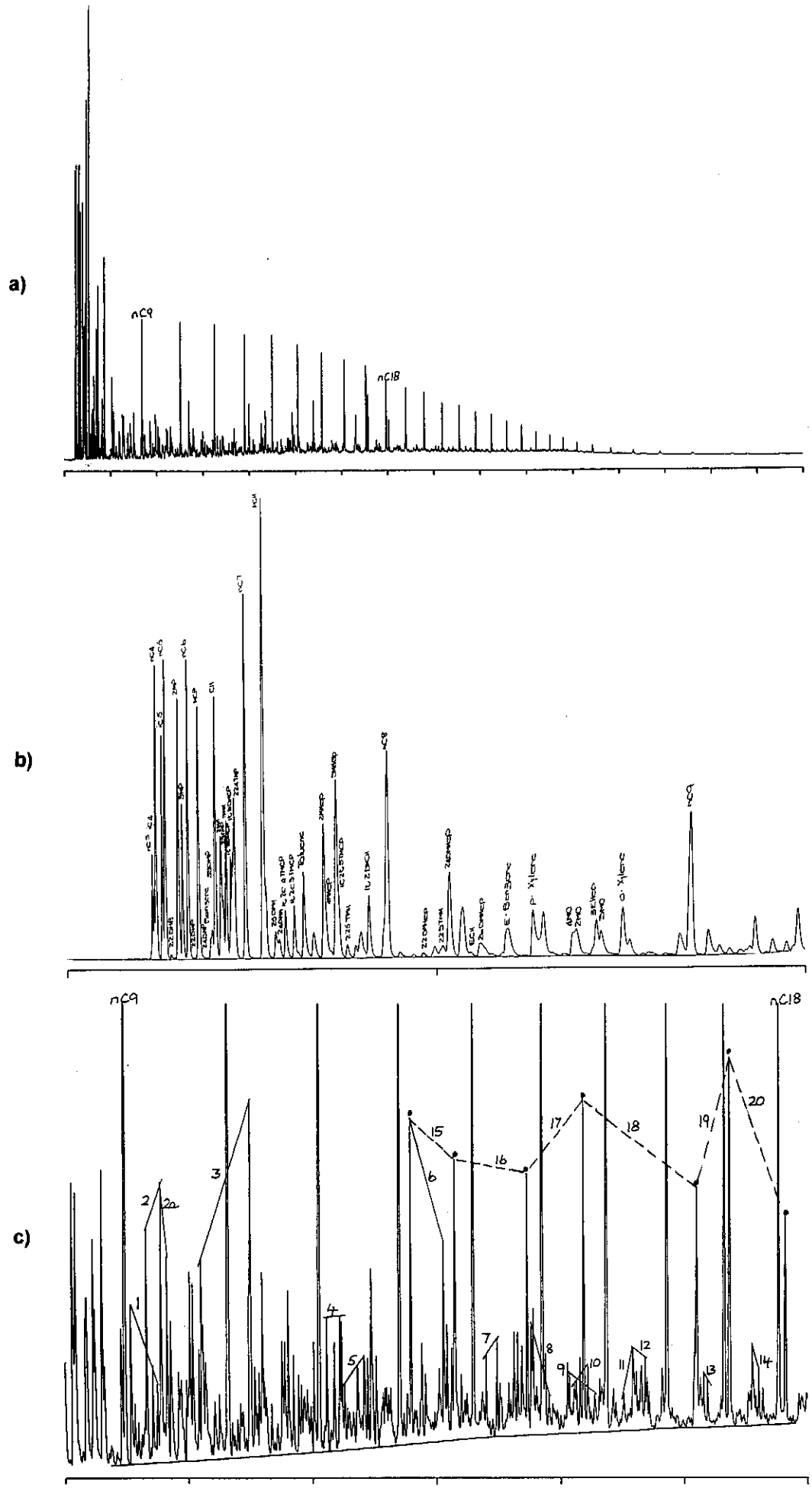

Figure C.39: Whole oil gas chromatograms of oil from well 146 DST1 (a) 0-80 minutes, (b) 0-10 minutes and (c) 6-36 minutes analysed using column 3.

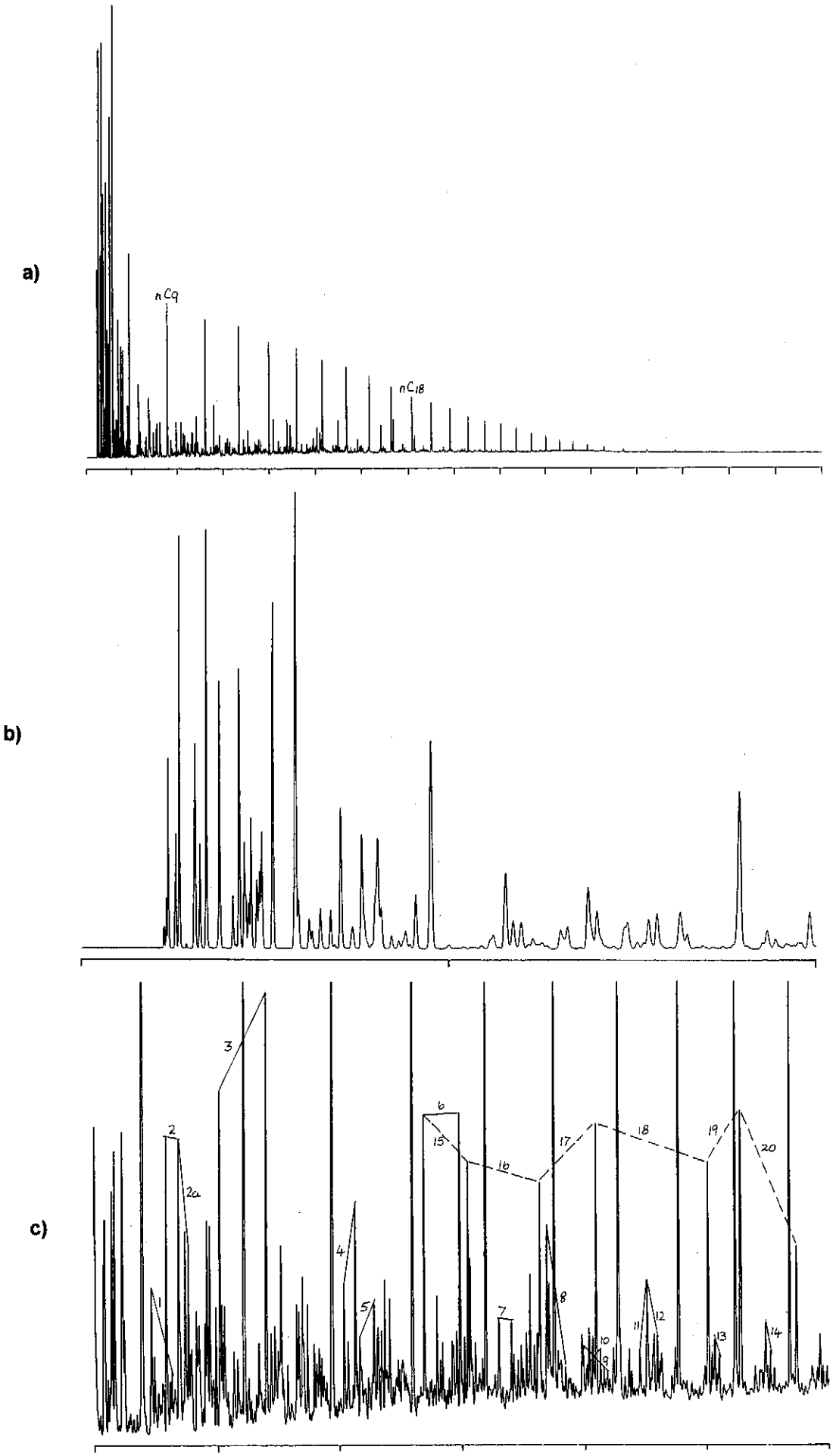

Figure C.40: Whole oil gas chromatograms of oil from well 156 DST1 (a) 0-80 minutes, (b) 0-10 minutes and (c) 6-36 minutes analysed using column Q.

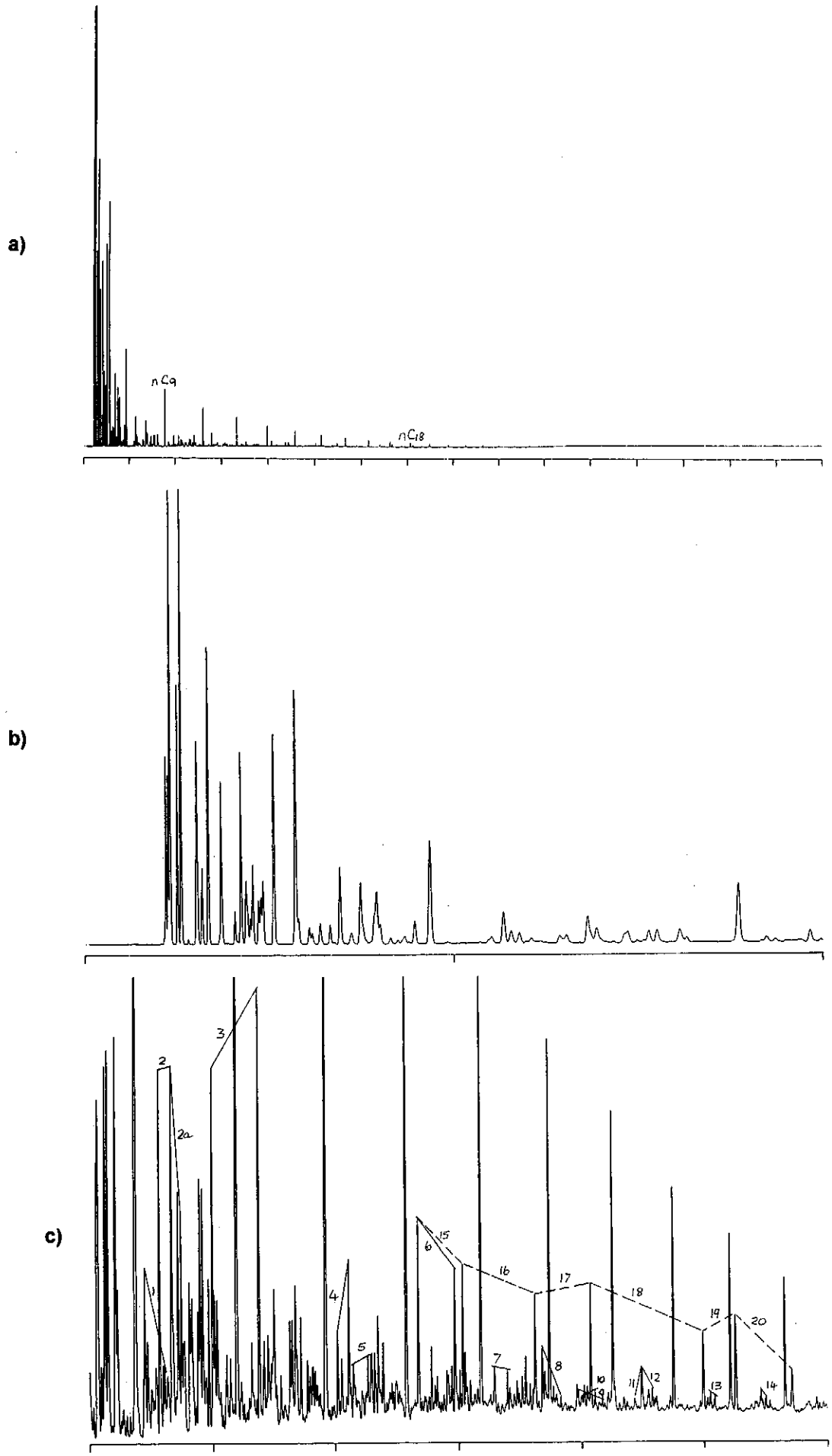

Figure C.41: Whole oil gas chromatograms of condensate from well 166 RFT (a) 0-80 minutes, (b) 0-10 minutes and (c) 6-36 minutes analysed using column Q.

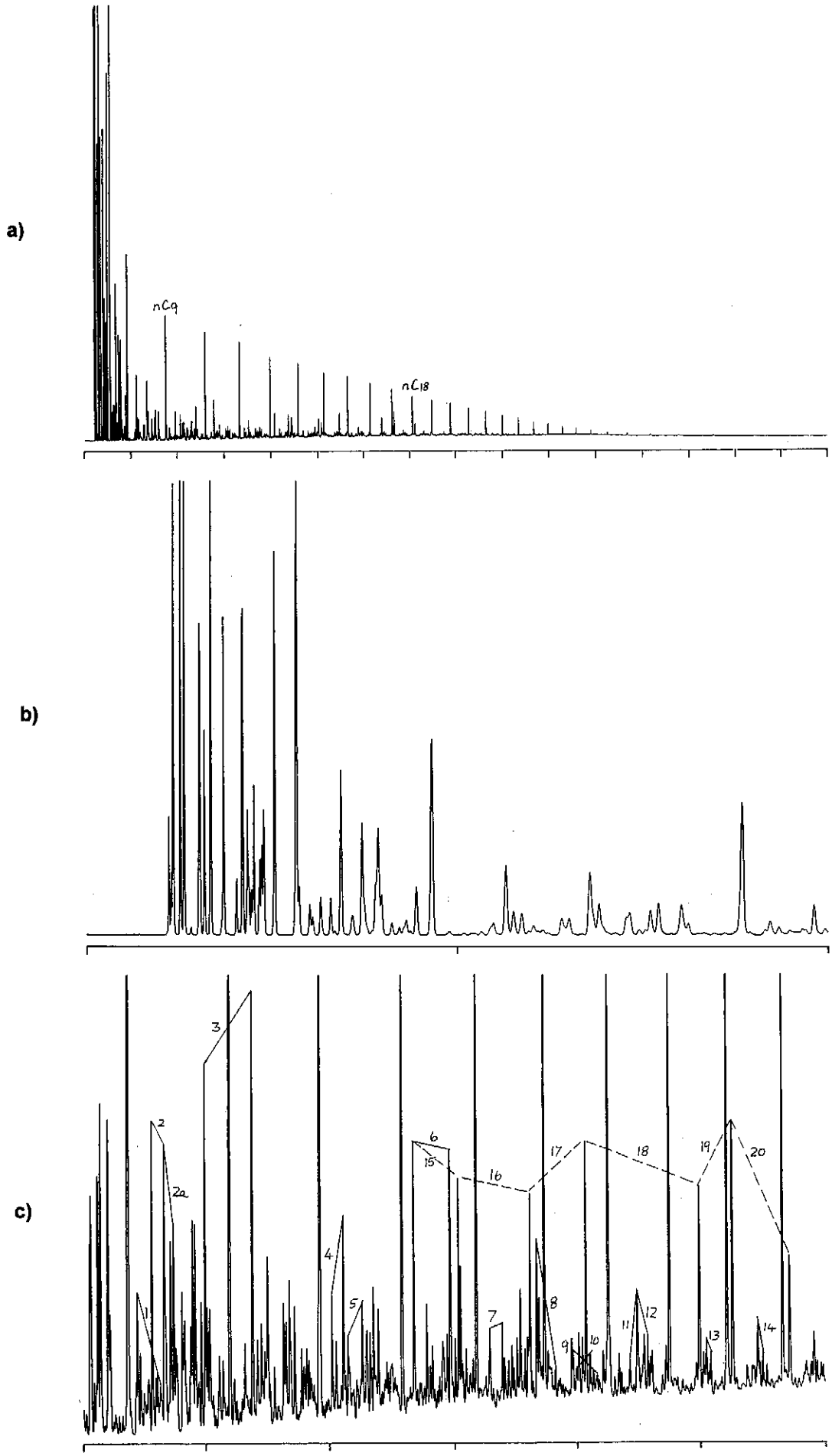

Figure C.42: Whole oil gas chromatograms of oil from well 166 DST1 (a) 0-80 minutes, (b) 0-10 minutes and (c) 6-36 minutes analysed using column Q.

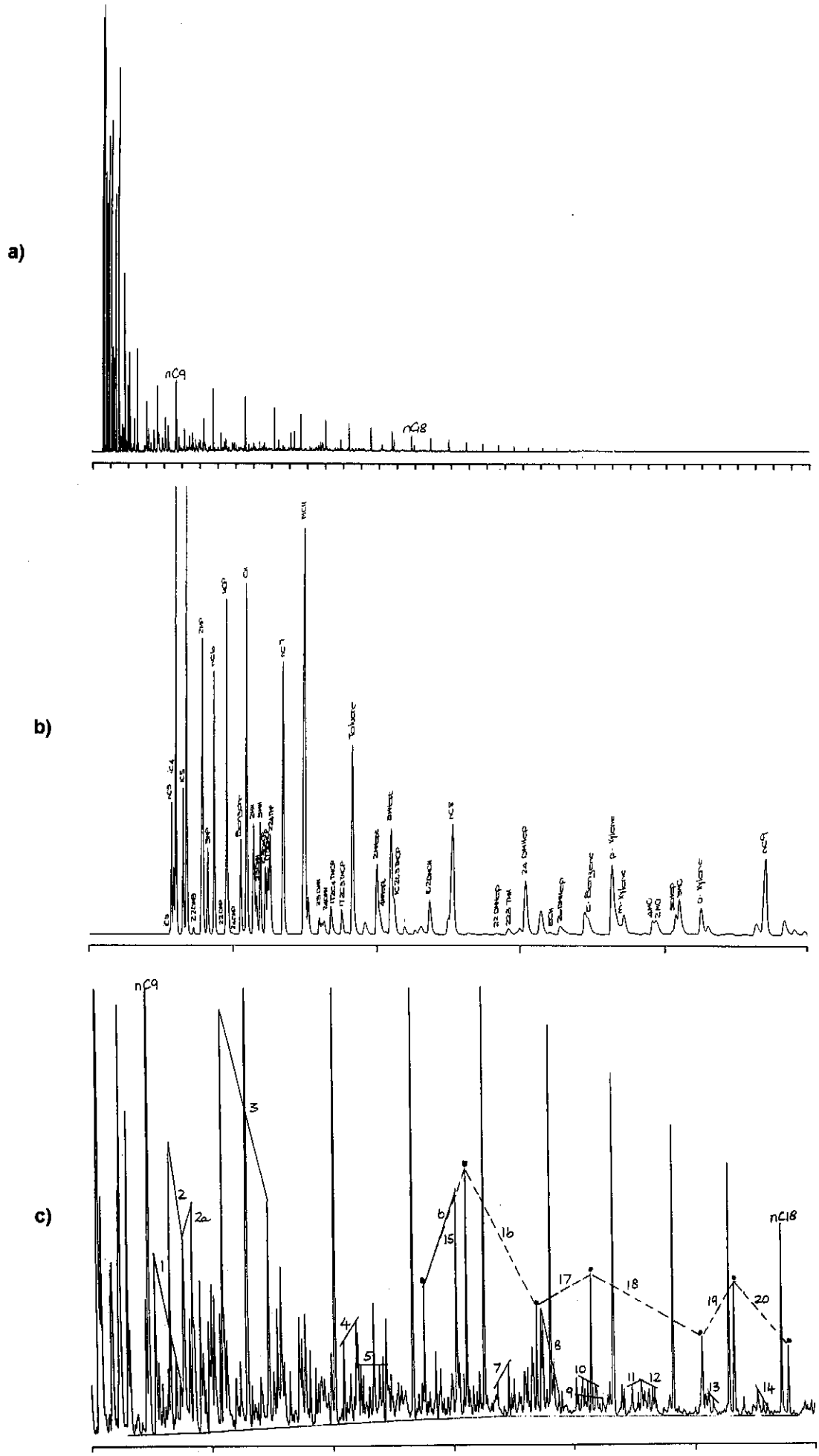

Figure C.43: Whole oil gas chromatograms of condensate from well 132 DST2 (a) 0-80 minutes, (b) 0-10 minutes and (c) 6-36 minutes analysed using column 2.

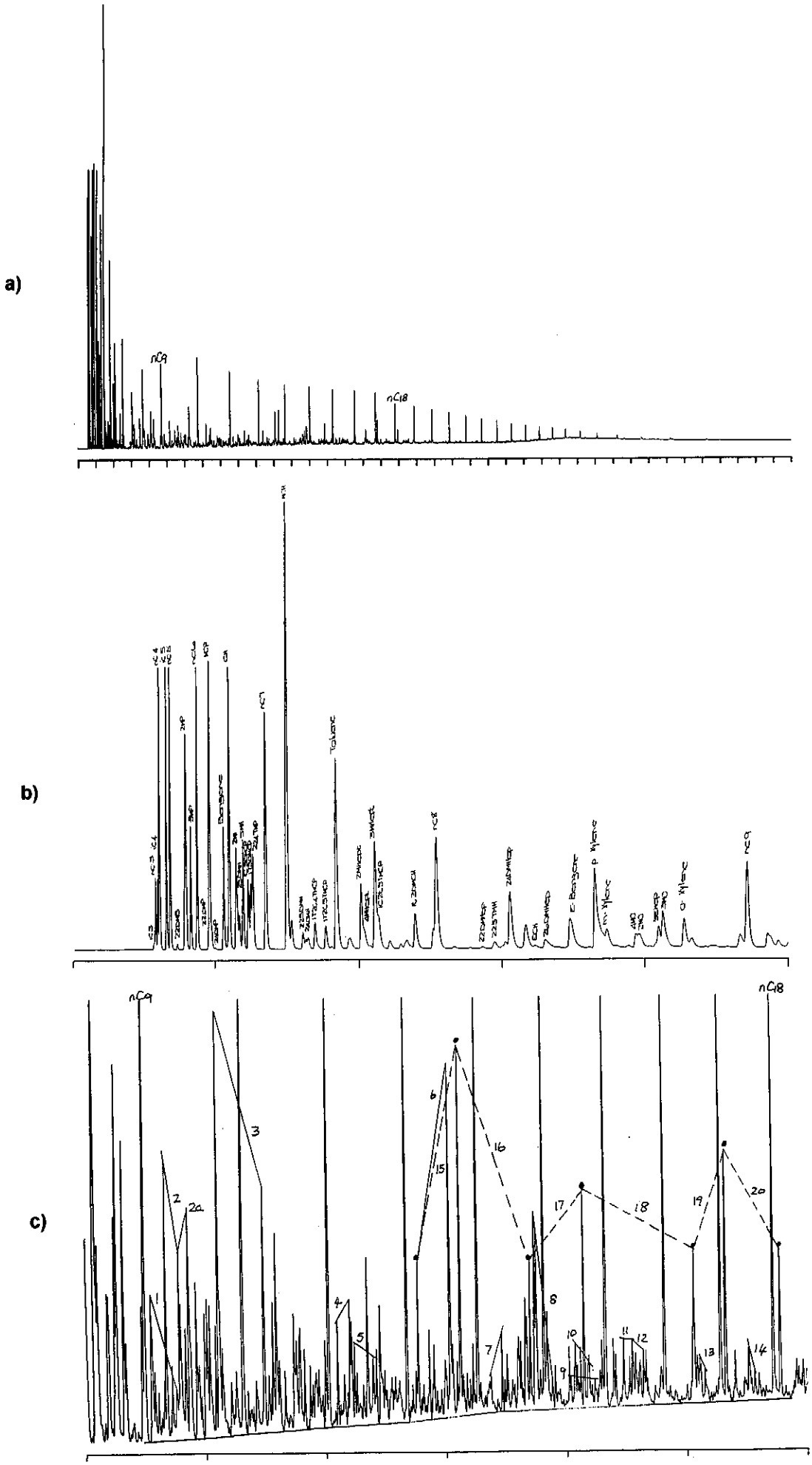

Figure C.44: Whole oil gas chromatograms of oil from well 132 DST1 (a) 0-80 minutes, (b) 0-10 minutes and (c) 6-36 minutes analysed using column 2.

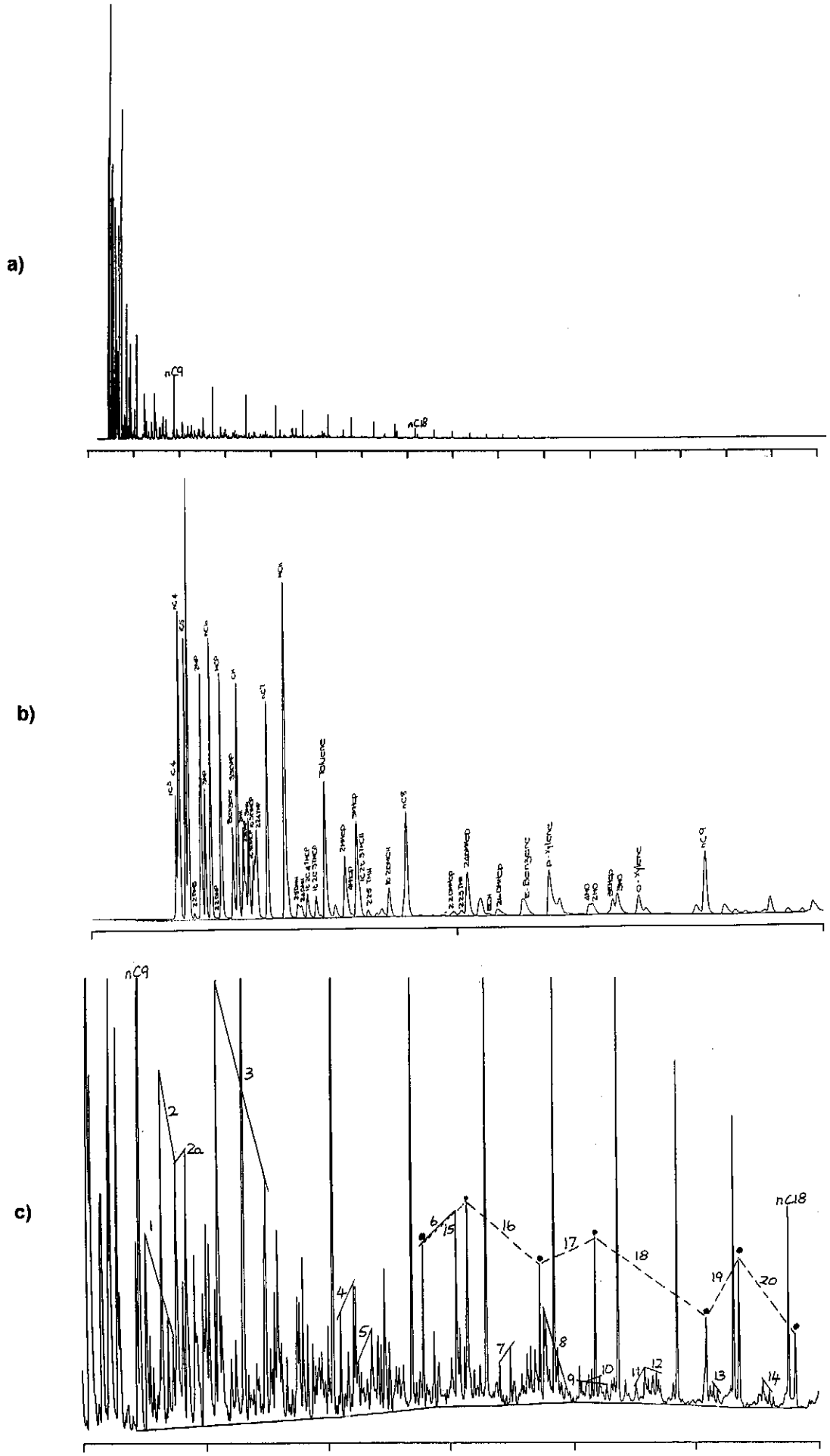

Figure C.45: Whole oil gas chromatograms of condensate from well 148 DST1 (a) 0-80 minutes, (b) 0-10 minutes and (c) 6-36 minutes analysed using column 3.

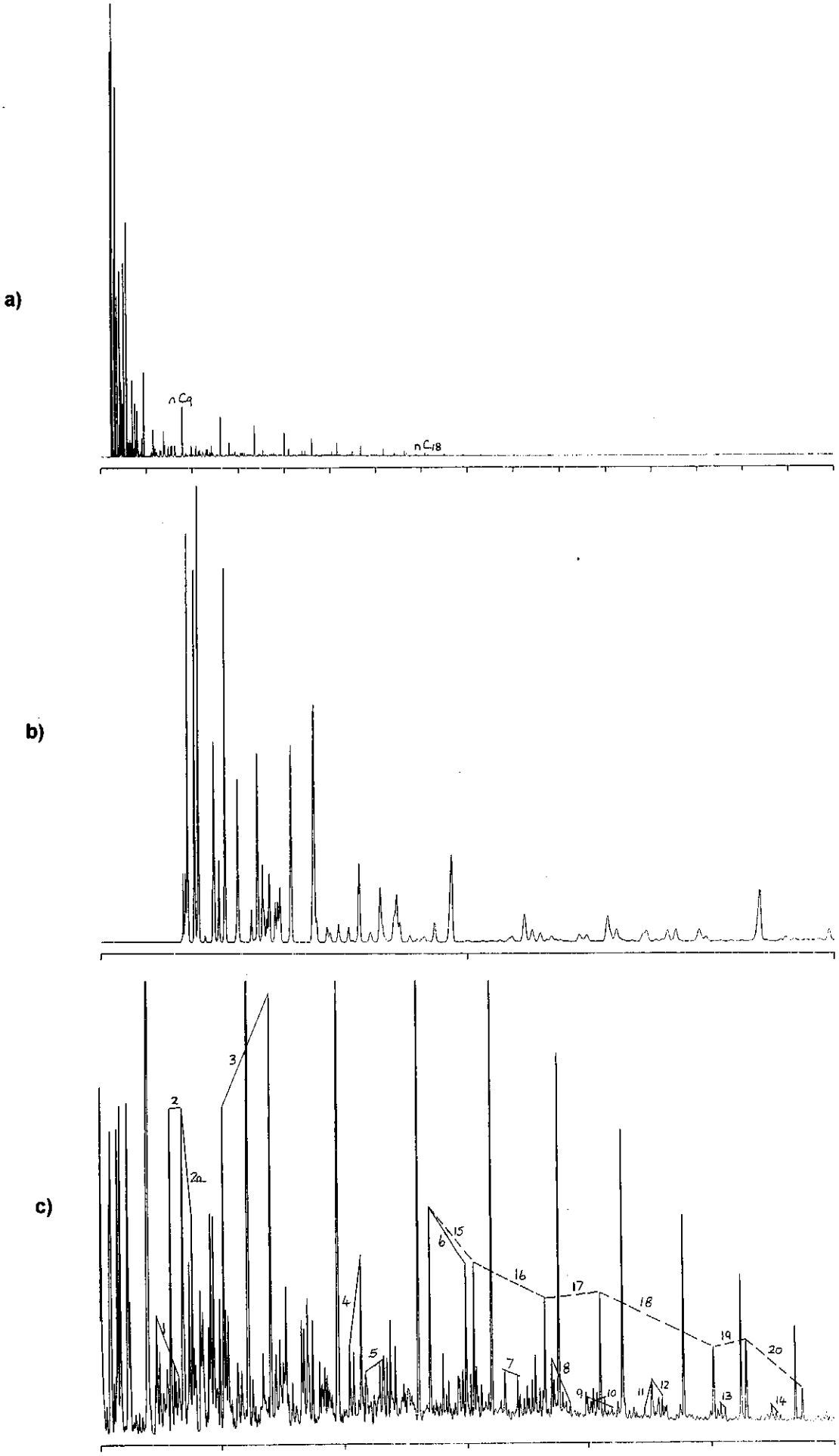

Figure C.46: Whole oil gas chromatograms of condensate from well 167 DST1 (a) 0-80 minutes, (b) 0-10 minutes and (c) 6-36 minutes analysed using column Q.

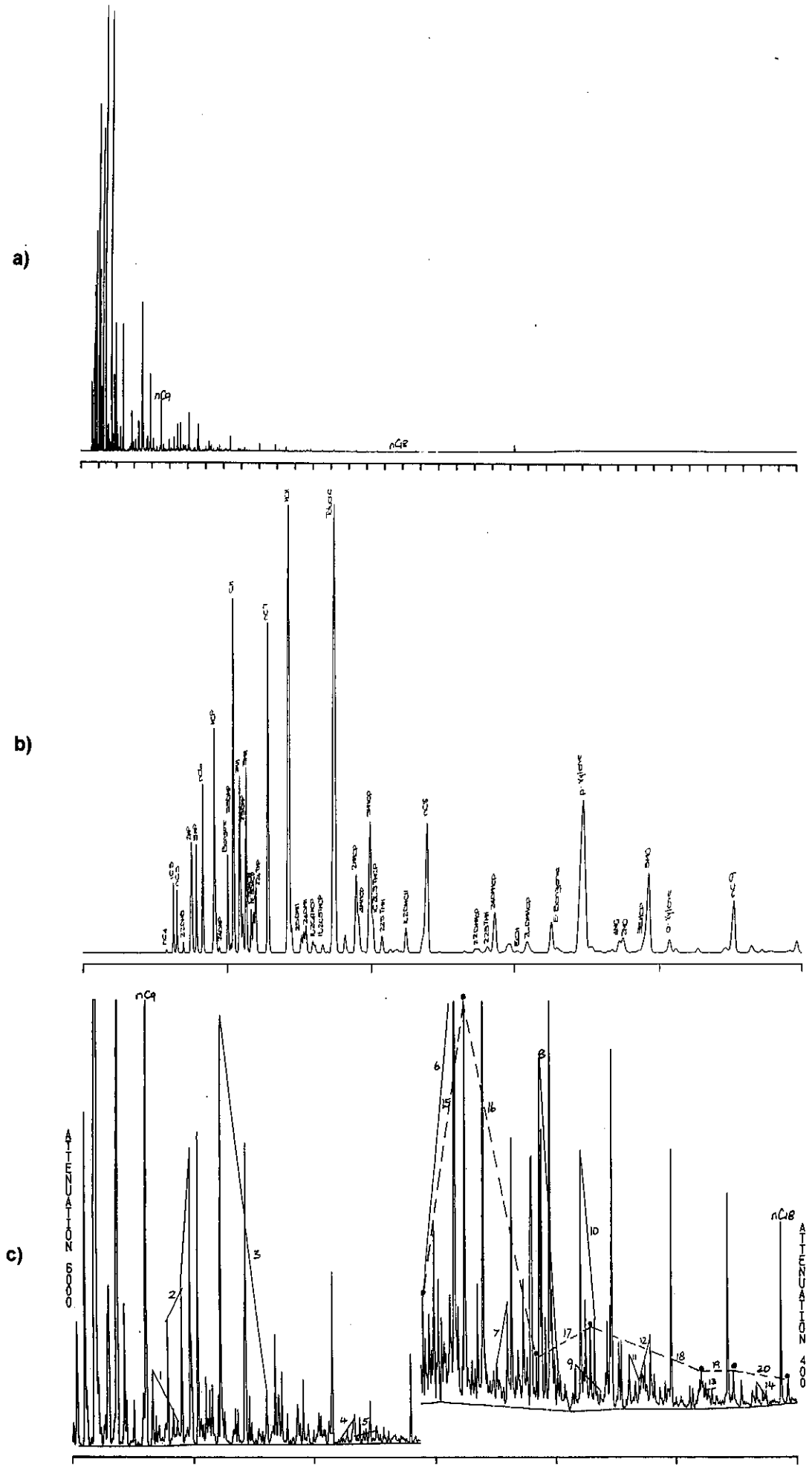

Figure C.47: Whole oil gas chromatograms of condensate from well 11 DST2 (a) 0-80 minutes, (b) 0-10 minutes and (c) 6-36 minutes analysed using column 2.

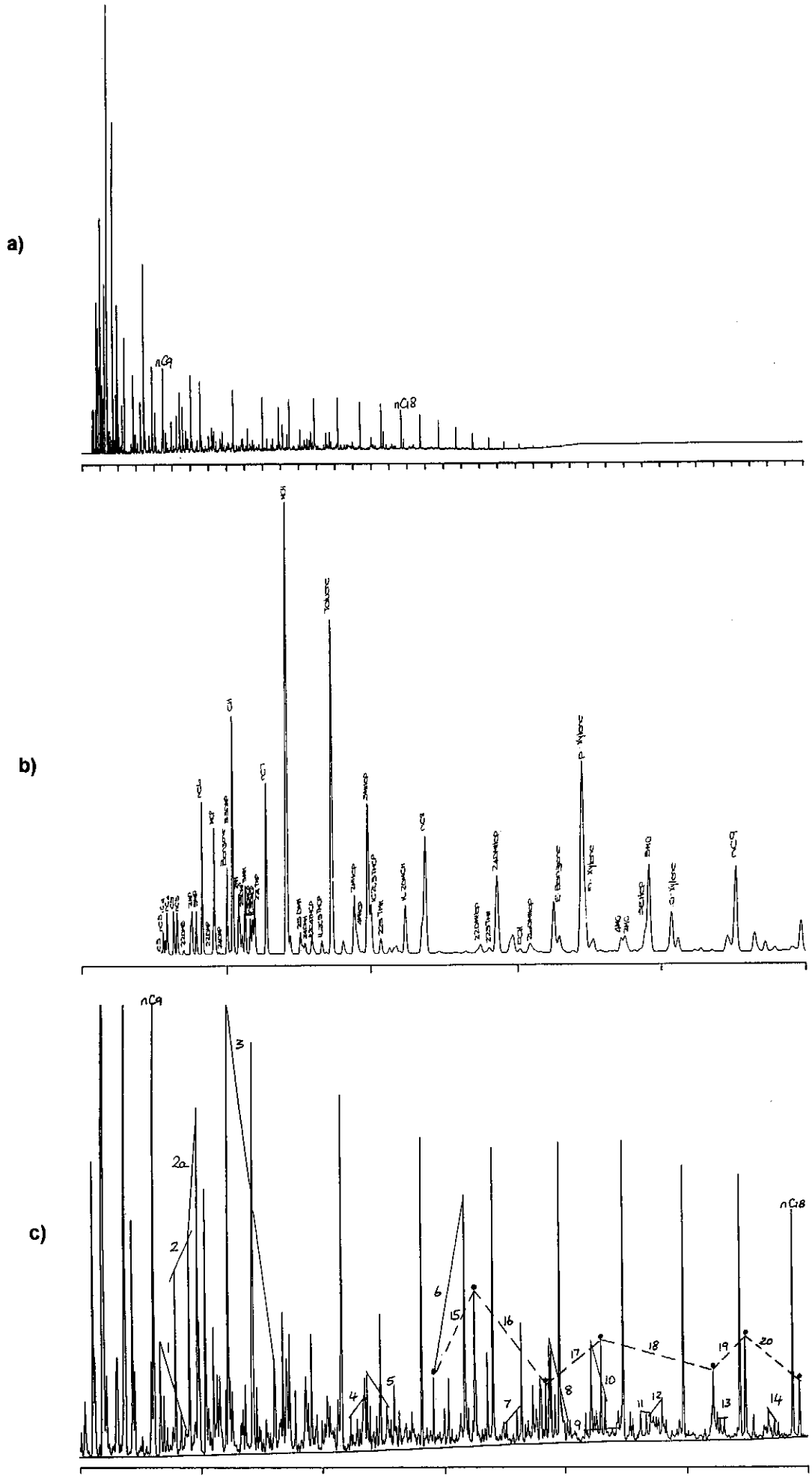

Figure C.48: Whole oil gas chromatograms of condensate from well 84 DST1 (a) 0-80 minutes, (b) 0-10 minutes and (c) 6-36 minutes analysed using column 2.

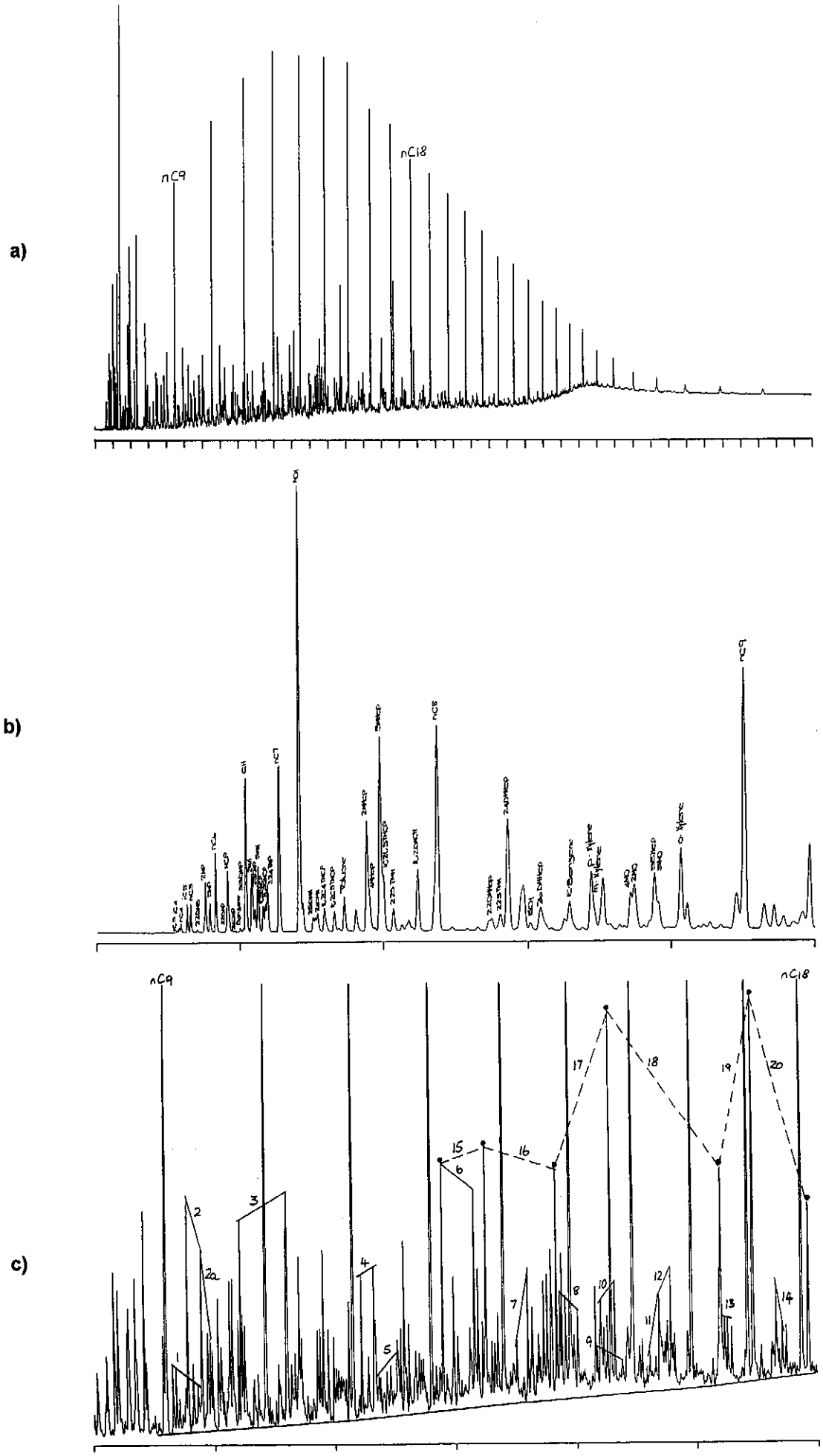

Figure C.49: Whole oil gas chromatograms of condensate from well 27 DST1 (a) 0-80 minutes, (b) 0-10 minutes and (c) 6-36 minutes analysed using column 2.

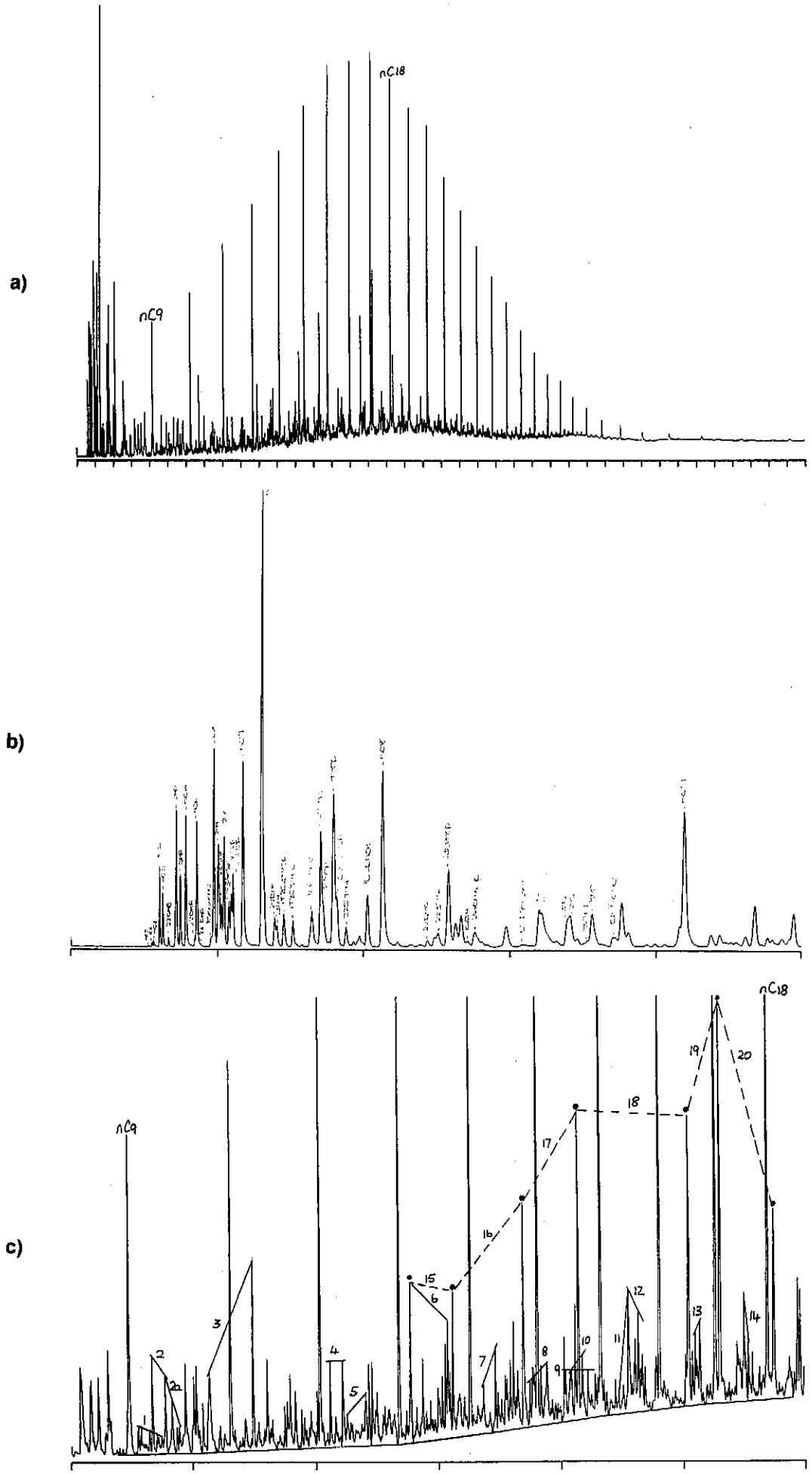

Figure C.50: Whole oil gas chromatograms of condensate from well 35 DST3 (a) 0-80 minutes, (b) 0-10 minutes and (c) 6-36 minutes analysed using column 1.

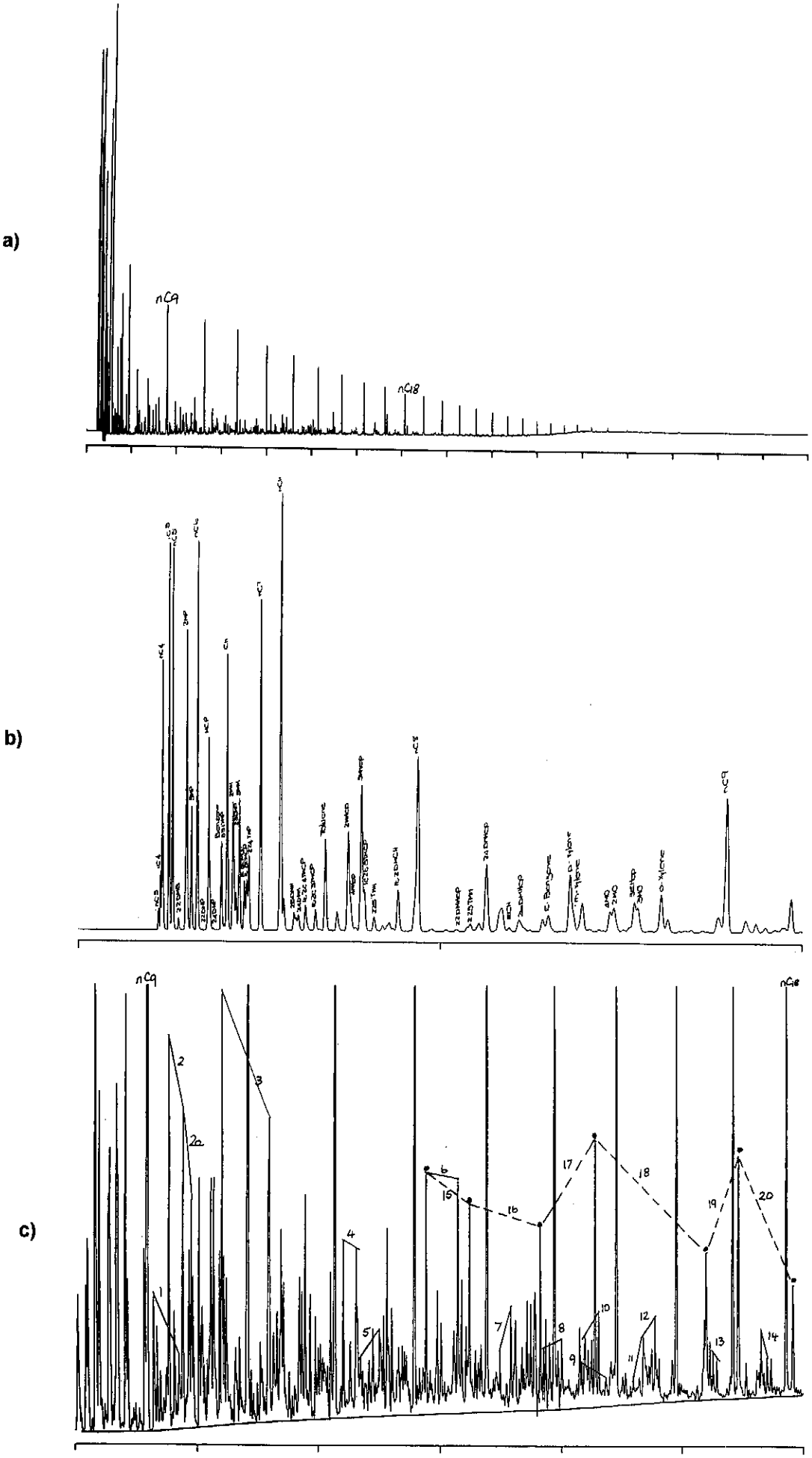

Figure C.51: Whole oil gas chromatograms of condensate from well 35 DST2B (a) 0-80 minutes, (b) 0-10 minutes and (c) 6-36 minutes analysed using column 2.

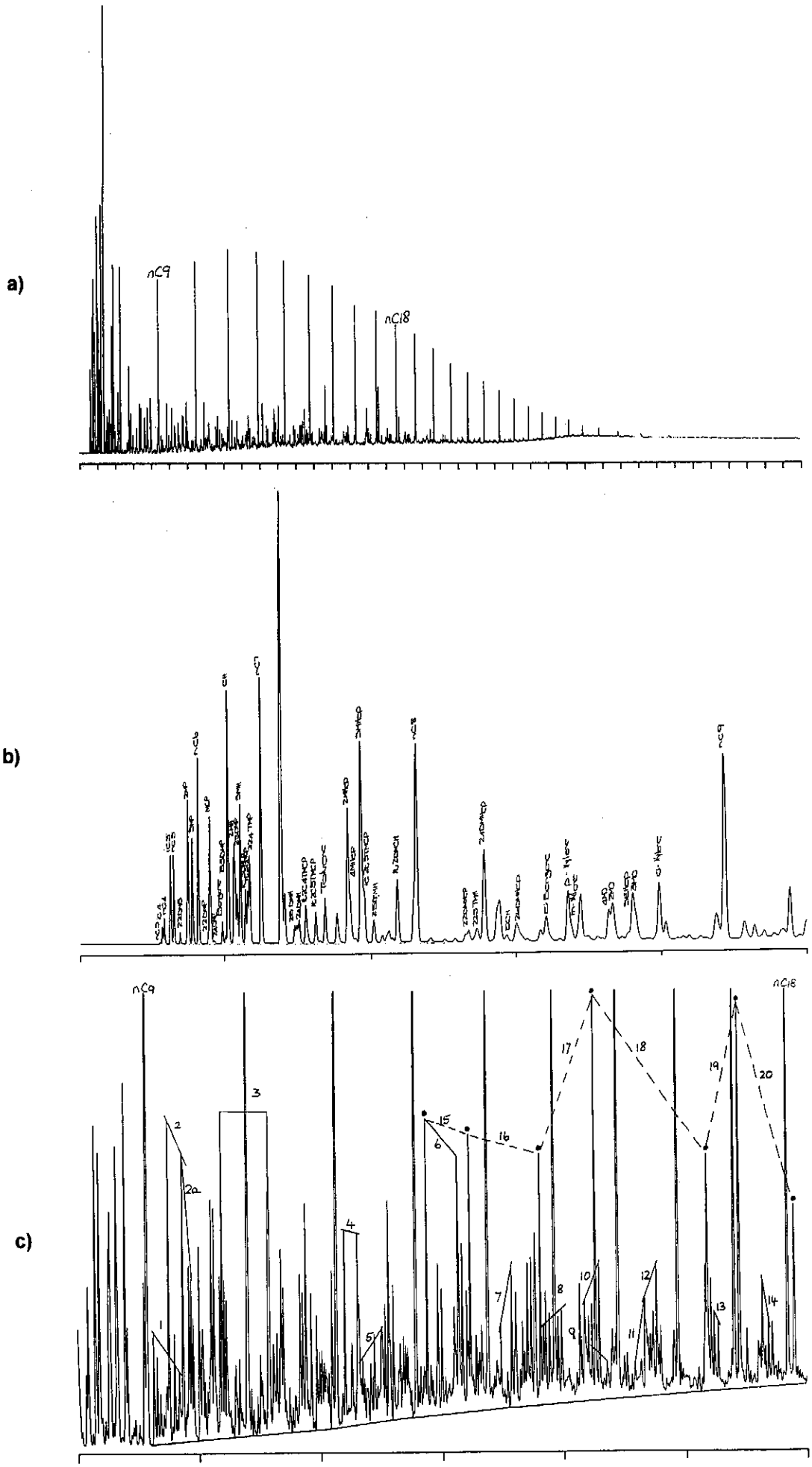

Figure C.52: Whole oil gas chromatograms of condensate from well 35 DST1 (a) 0-80 minutes, (b) 0-10 minutes and (c) 6-36 minutes analysed using column 2.

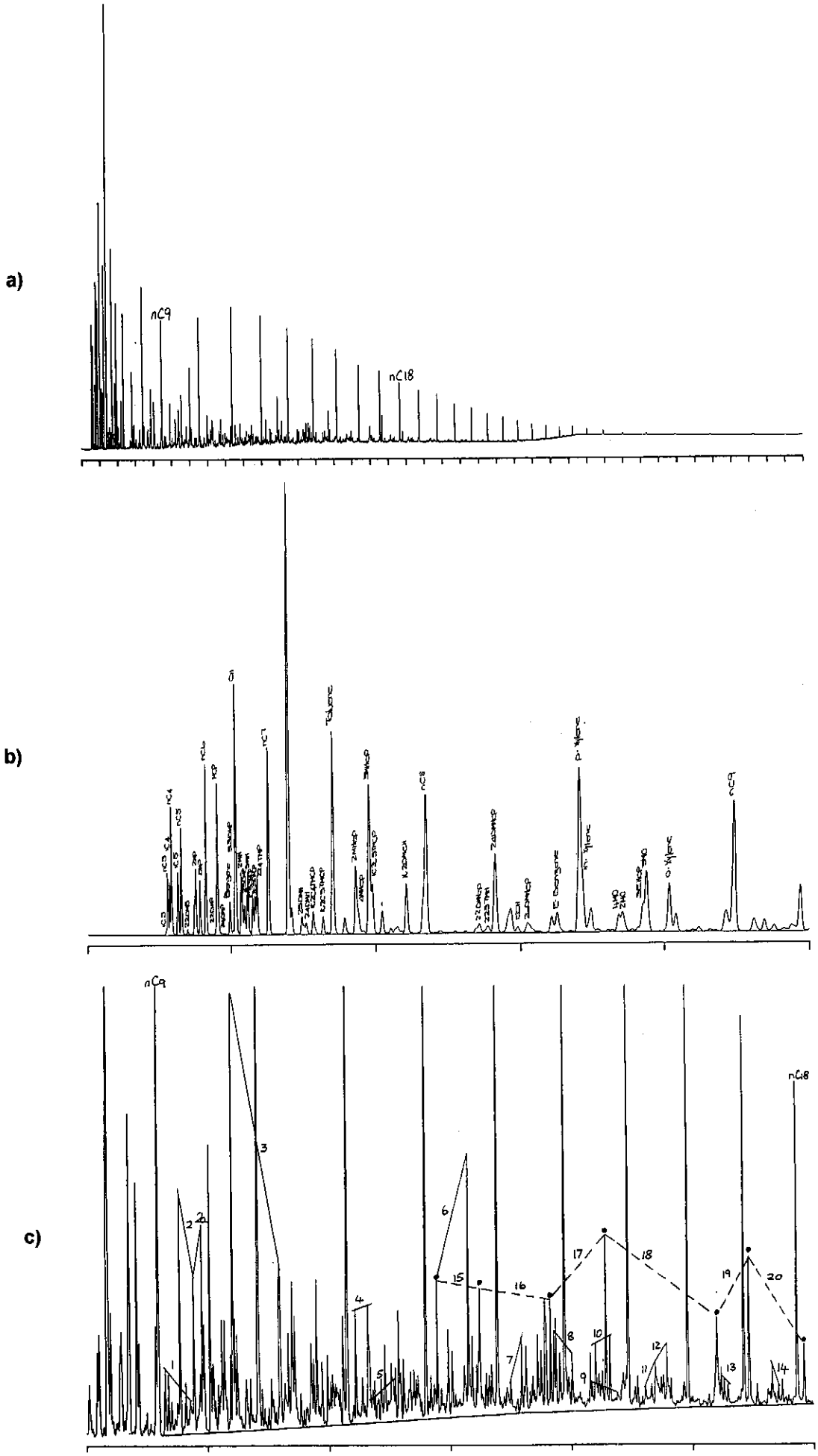

Figure C.53: Whole oil gas chromatograms of condensate from well 37 DST1 (a) 0-80 minutes, (b) 0-10 minutes and (c) 6-36 minutes analysed using column 2.

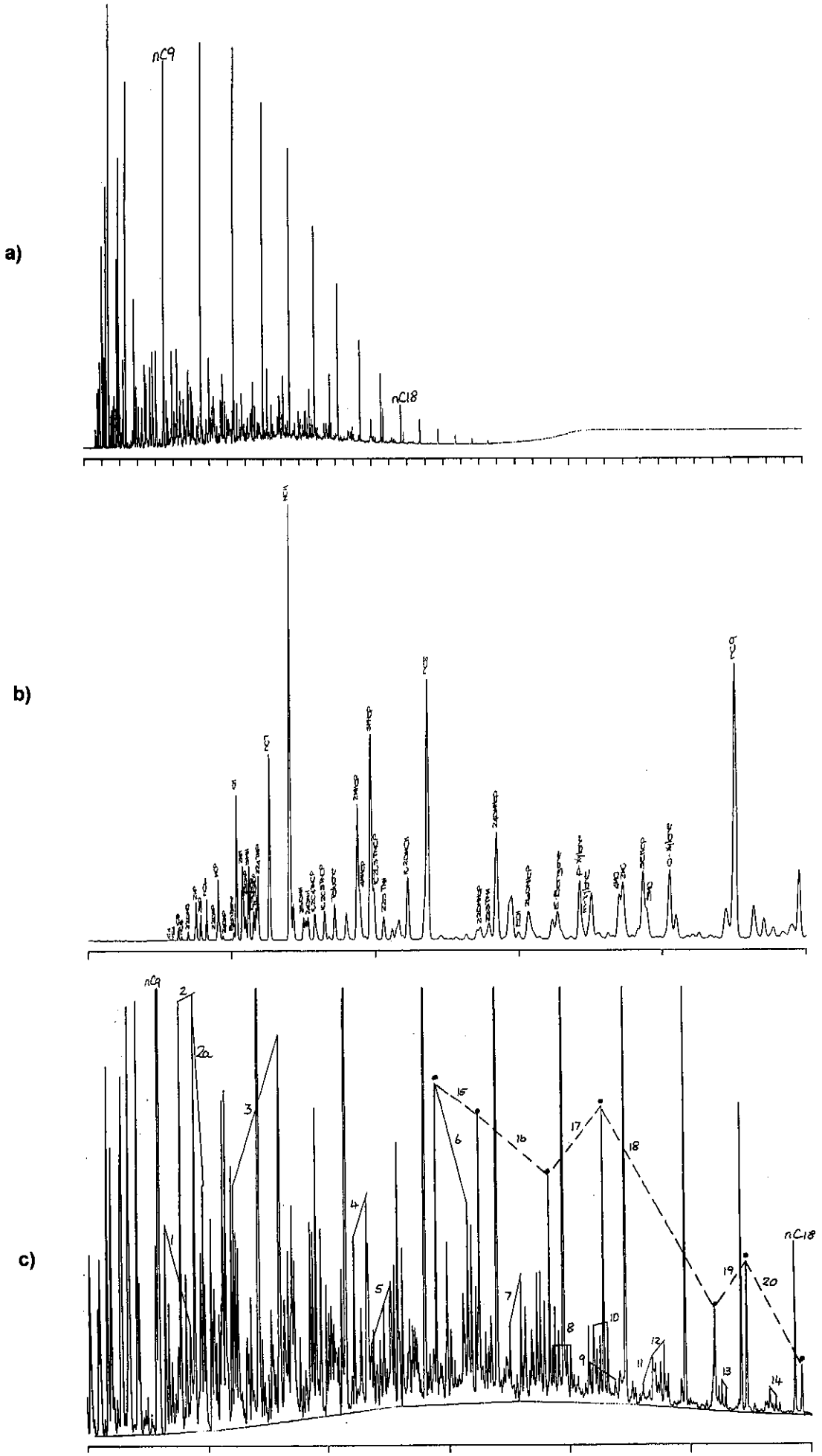

Figure C.54: Whole oil gas chromatograms of condensate from well 69 DST1 (a) 0-80 minutes, (b) 0-10 minutes and (c) 6-36 minutes analysed using column 2.

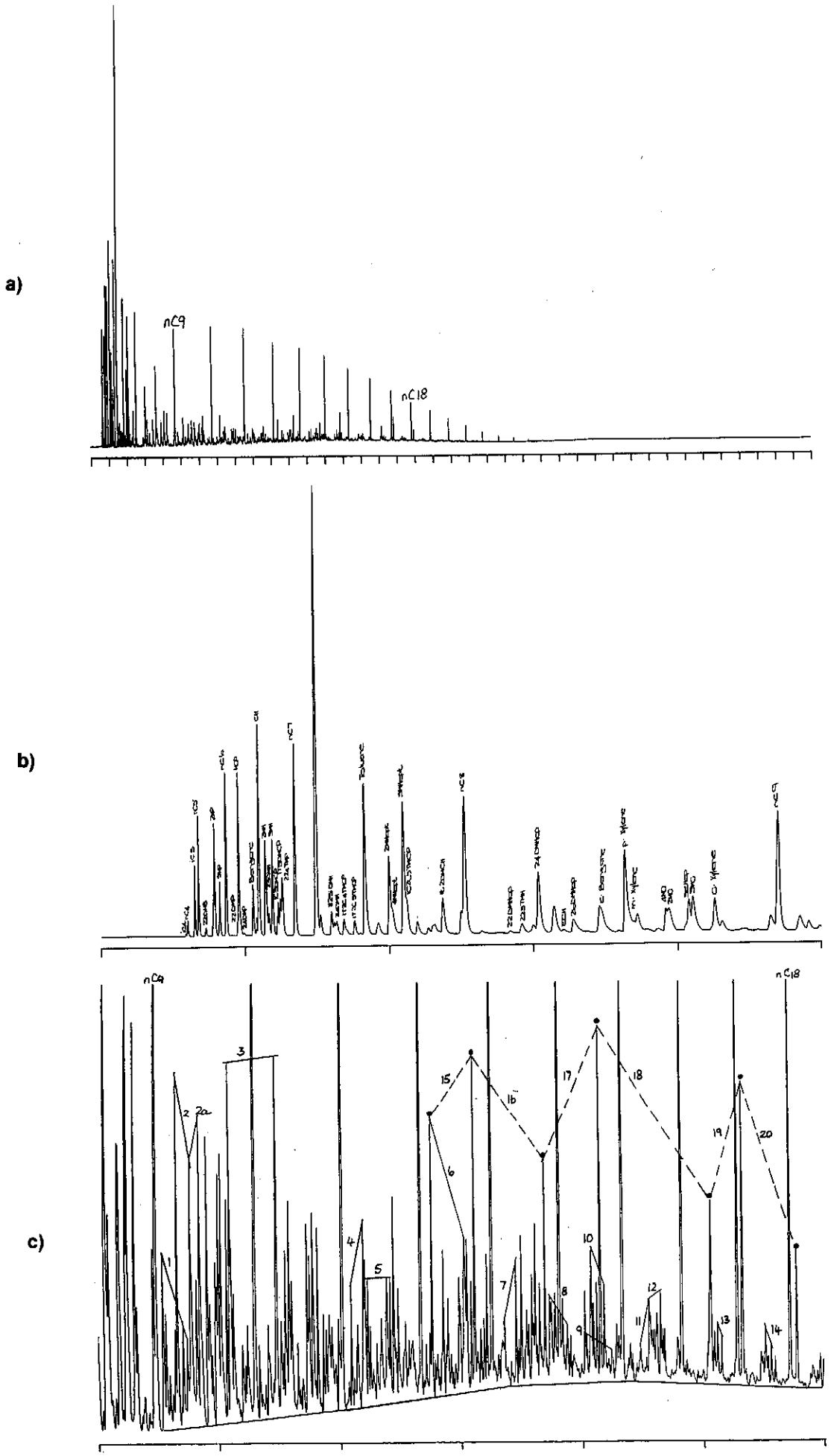

Figure C.55: Whole oil gas chromatograms of condensate (+?oil) from well 46 DST2 (a) 0-80 minutes, (b) 0-10 minutes and (c) 6-36 minutes analysed using column 2.

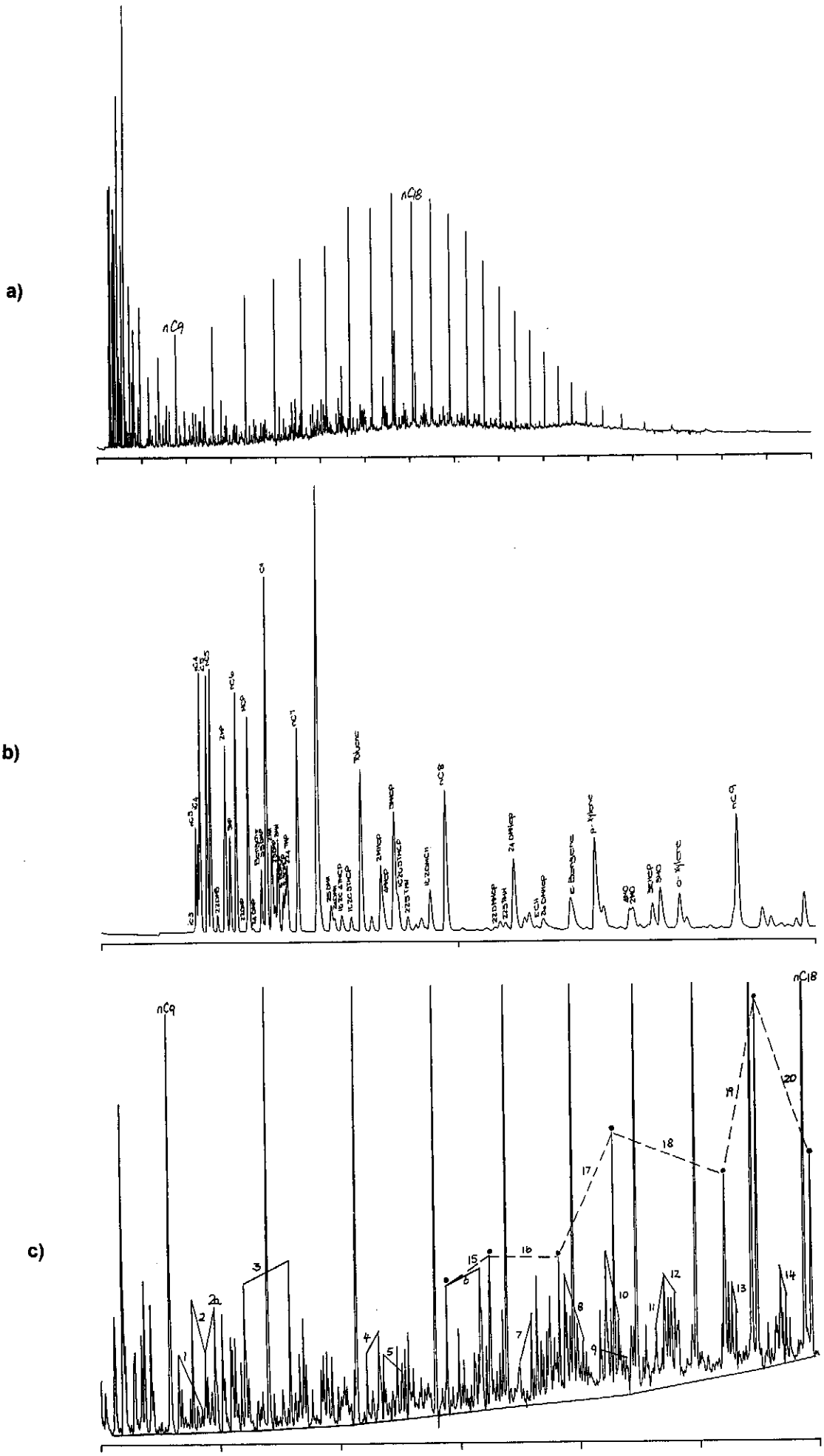

Figure C.56: Whole oil gas chromatograms of condensate from well 48 DST2 (a) 0-80 minutes, (b) 0-10 minutes and (c) 6-36 minutes analysed using column 3.

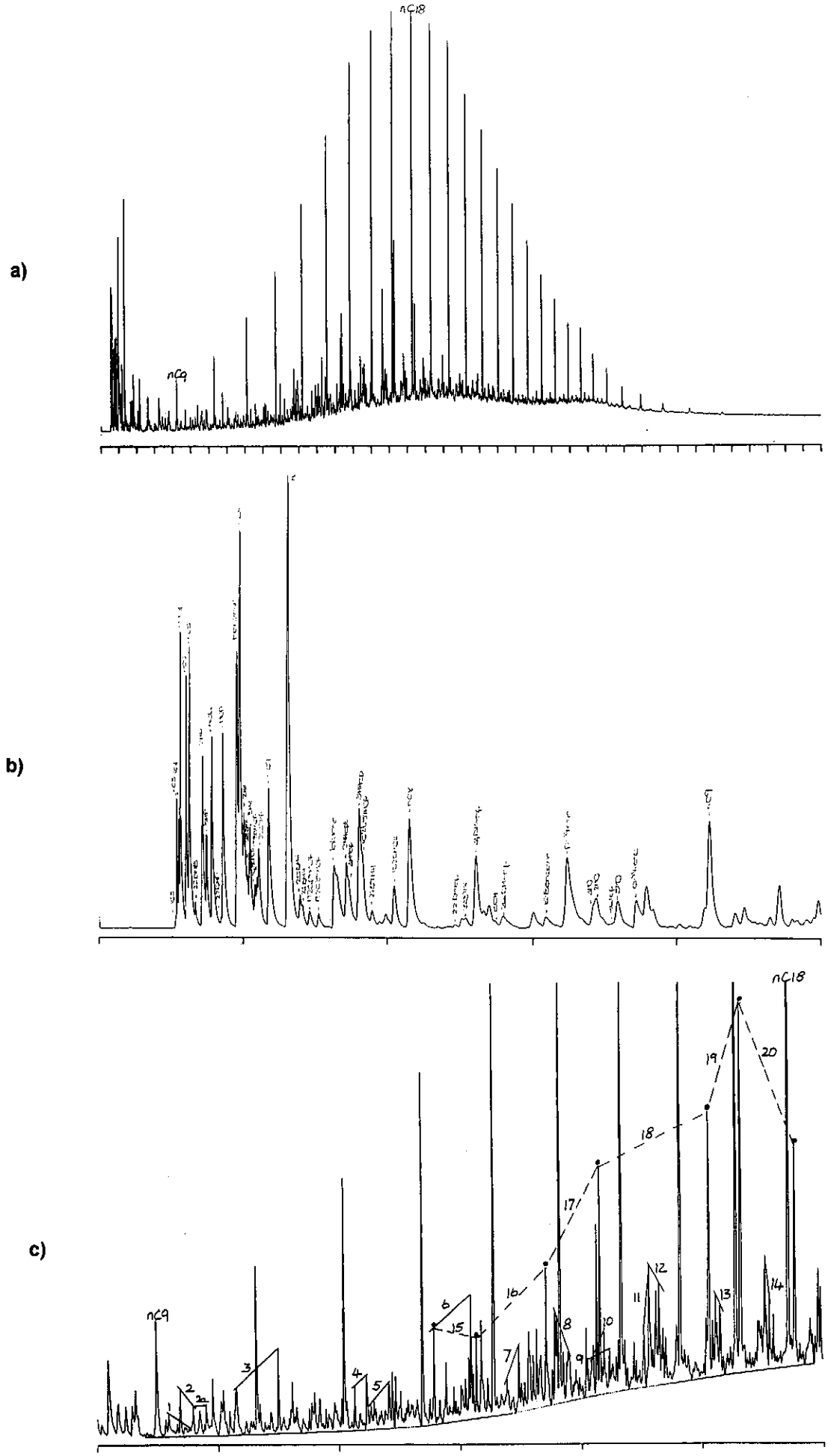

Figure C.57: Whole oil gas chromatograms of ?oil from well 48 DST1 (a) 0-80 minutes, (b) 0-10 minutes and (c) 6-36 minutes analysed using column 1.

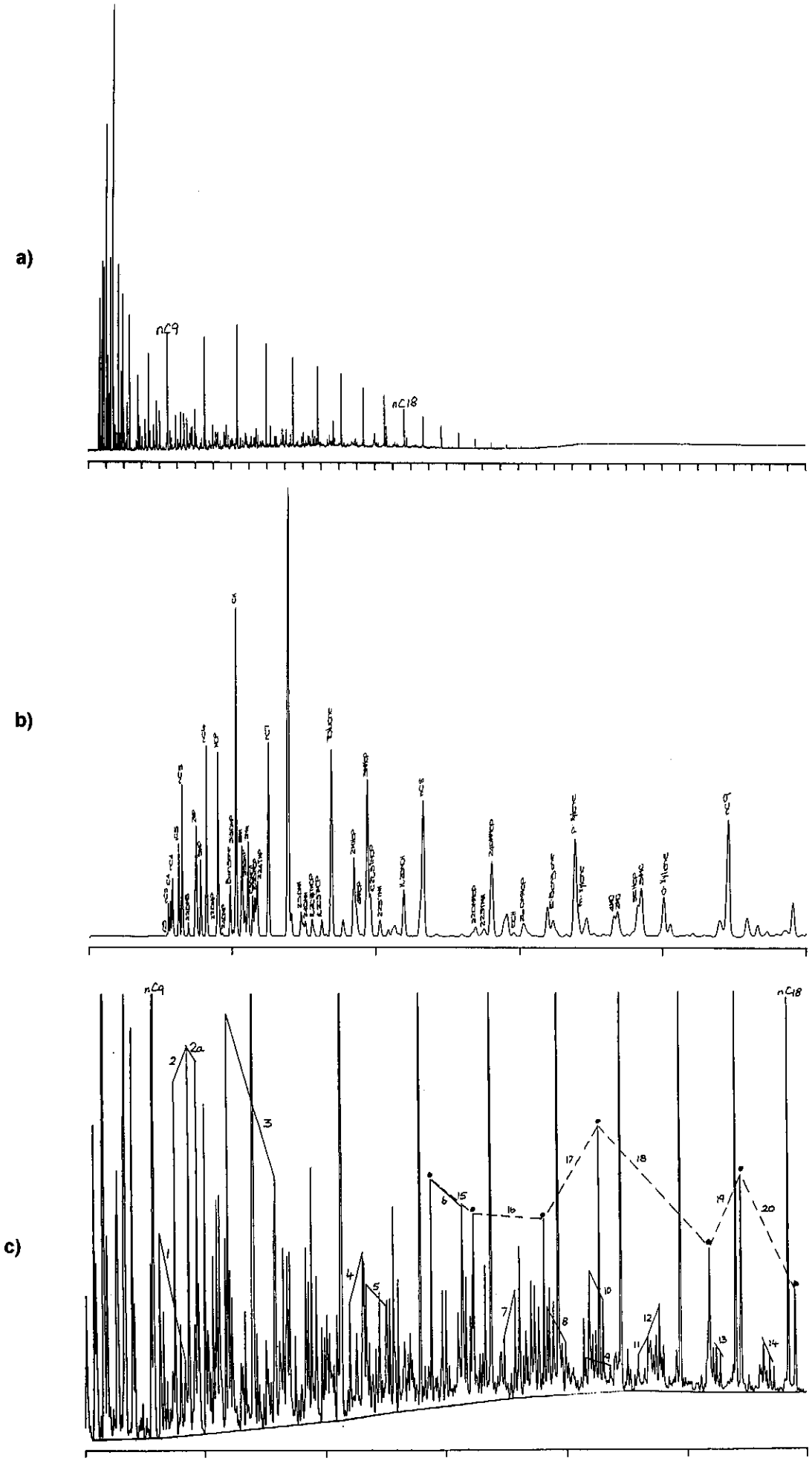

Figure C.58: Whole oil gas chromatograms of condensate from well 54 DST1 (a) 0-80 minutes, (b) 0-10 minutes and (c) 6-36 minutes analysed using column 2.

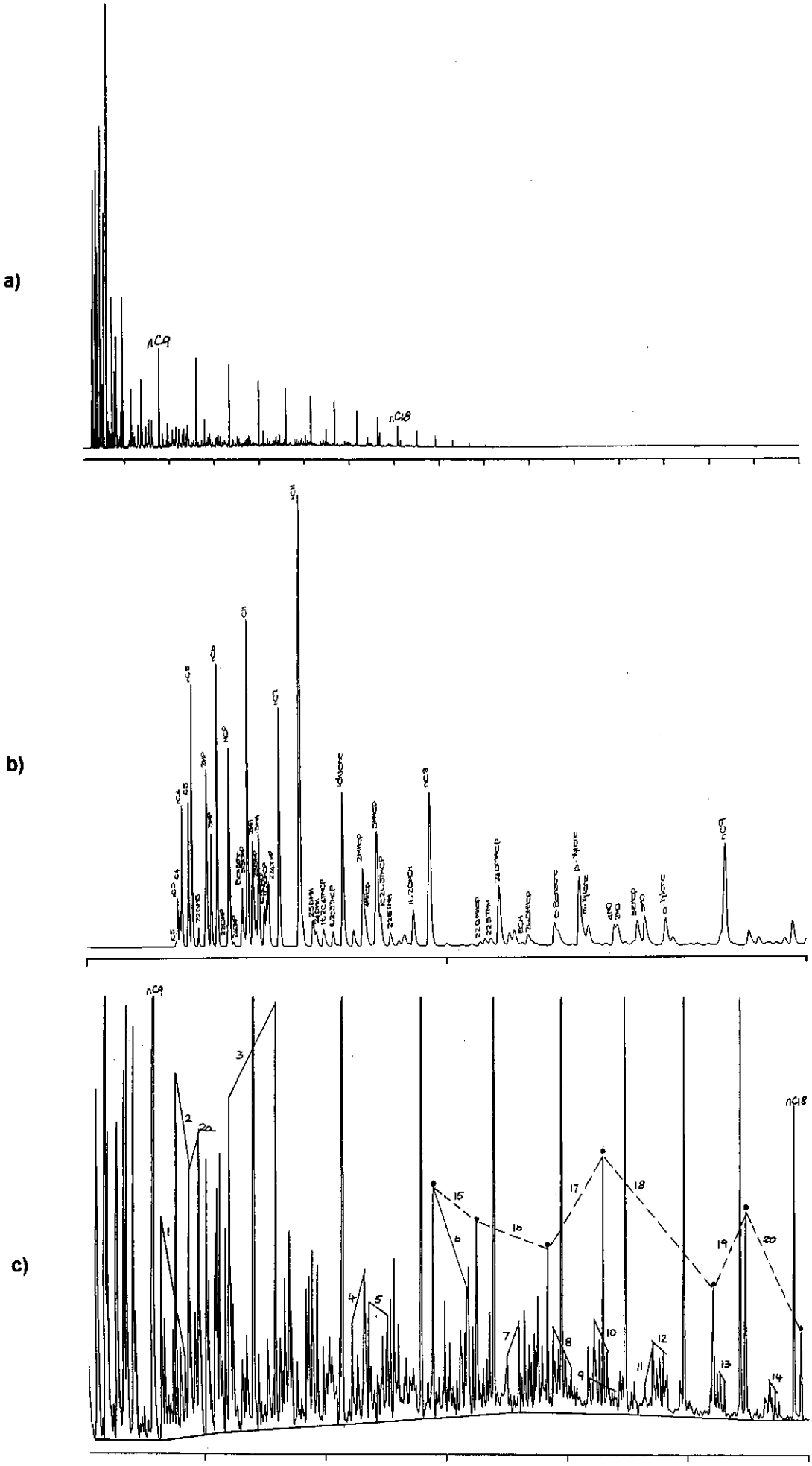

Figure C.59: Whole oil gas chromatograms of condensate from well 76 DST1 (a) 0-80 minutes, (b) 0-10 minutes and (c) 6-36 minutes analysed using column 2.

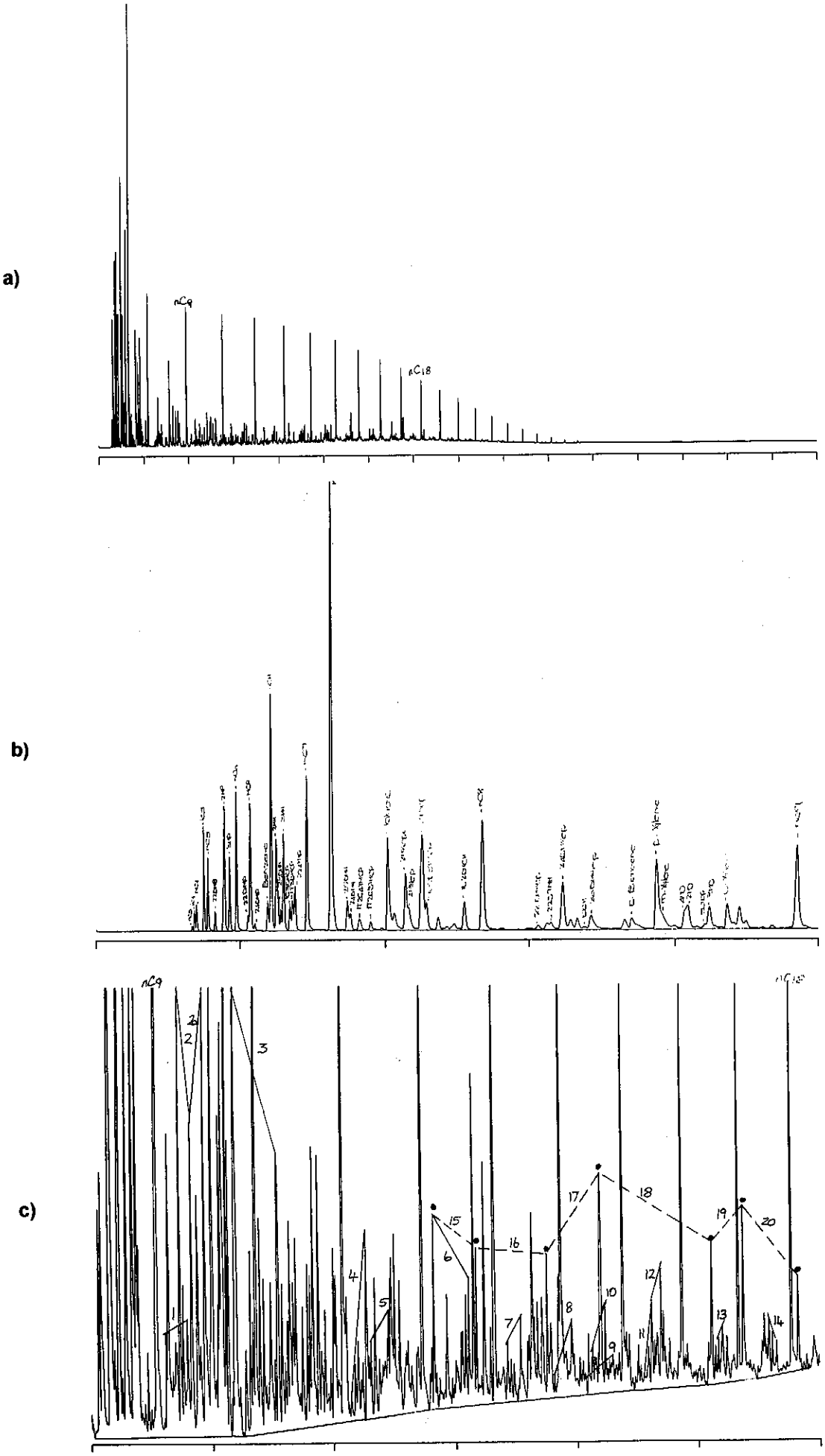

Figure C.60: Whole oil gas chromatograms of condensate from well 39 DST2 (a) 0-80 minutes, (b) 0-10 minutes and (c) 6-36 minutes analysed using column 1.

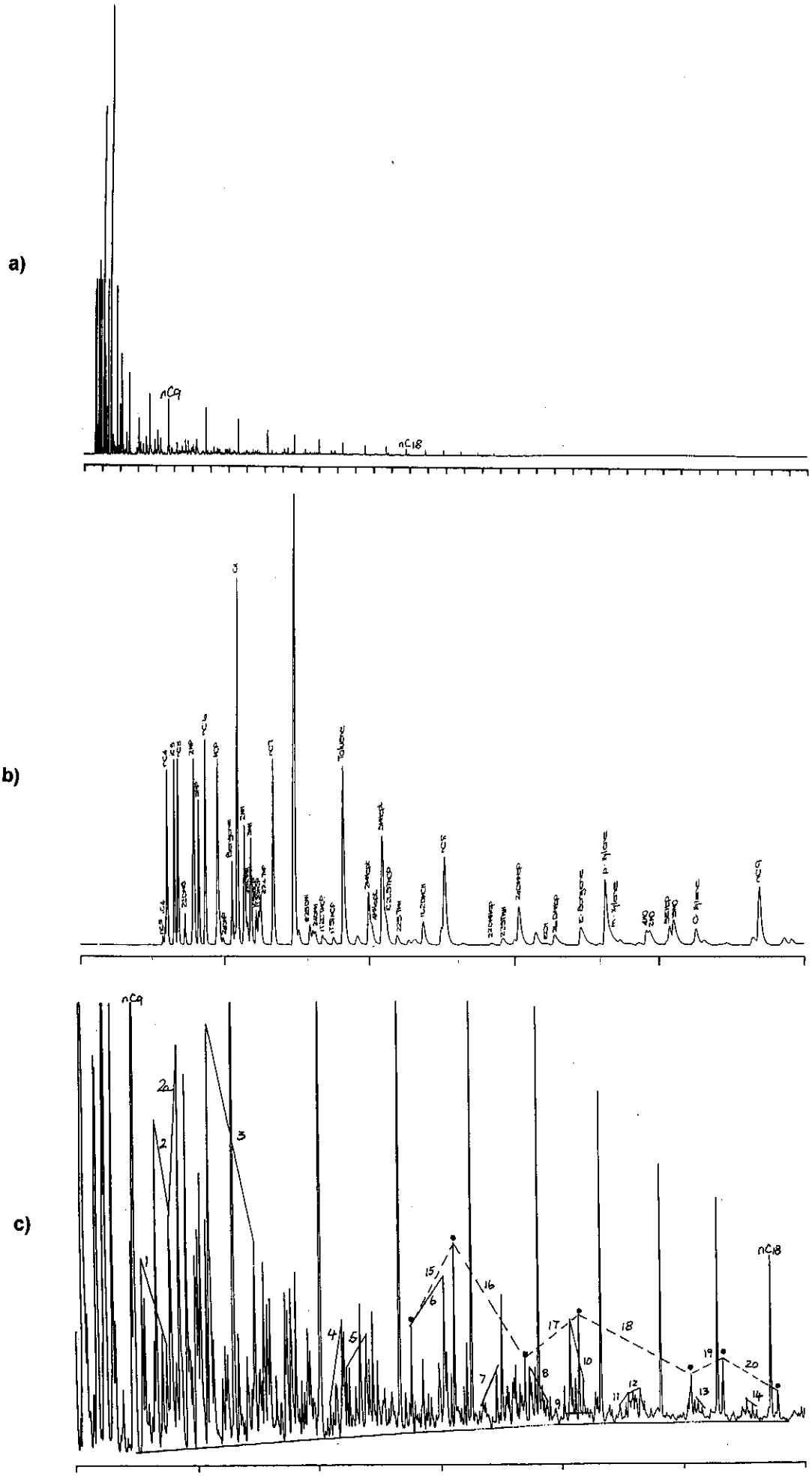

Figure C.61: Whole oil gas chromatograms of condensate from well 39 DST2 (a) 0-80 minutes, (b) 0-10 minutes and (c) 6-36 minutes analysed using column 2.

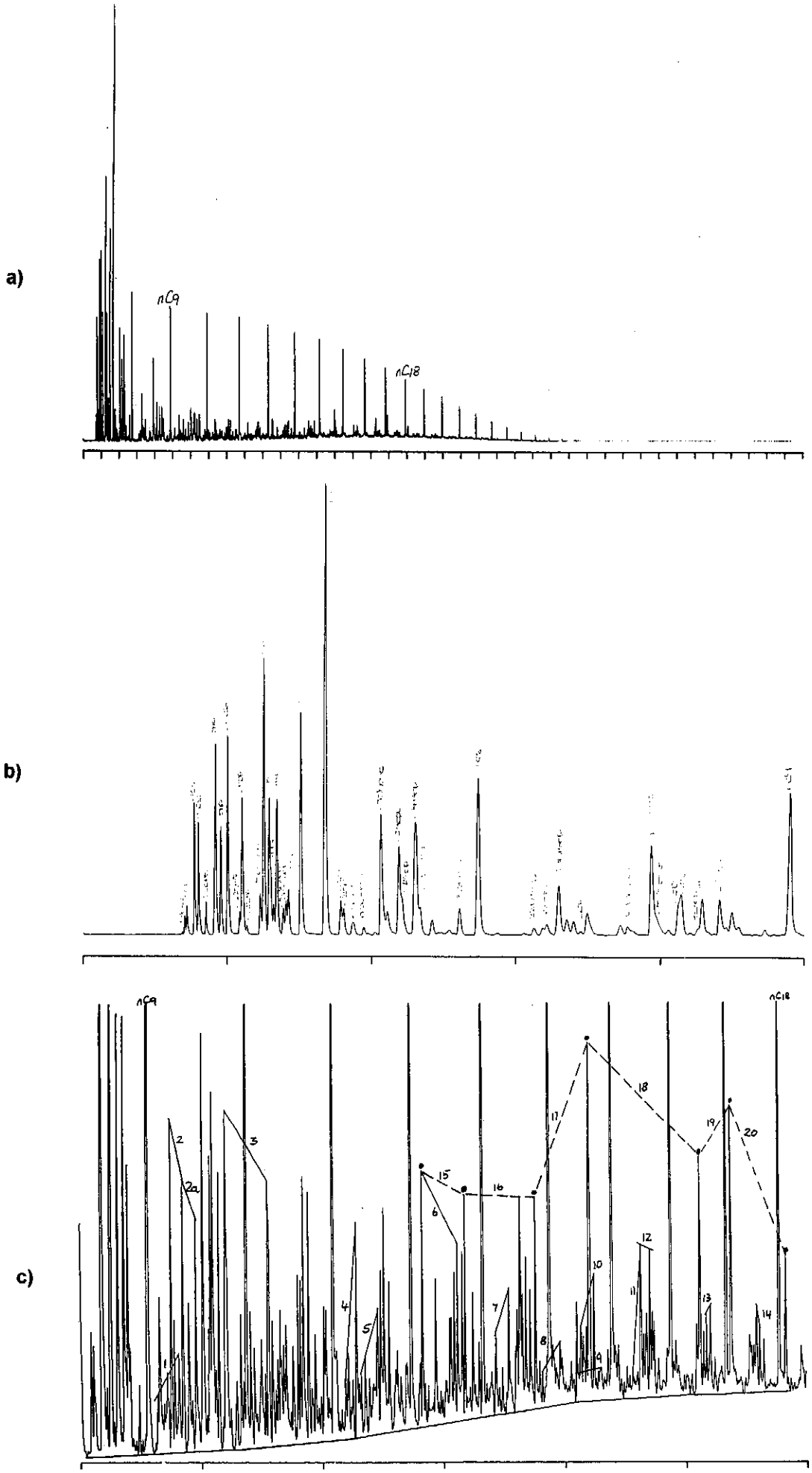

Figure C.62: Whole oil gas chromatograms of condensate from well 39 DST1 (a) 0-80 minutes, (b) 0-10 minutes and (c) 6-36 minutes analysed using column 1.

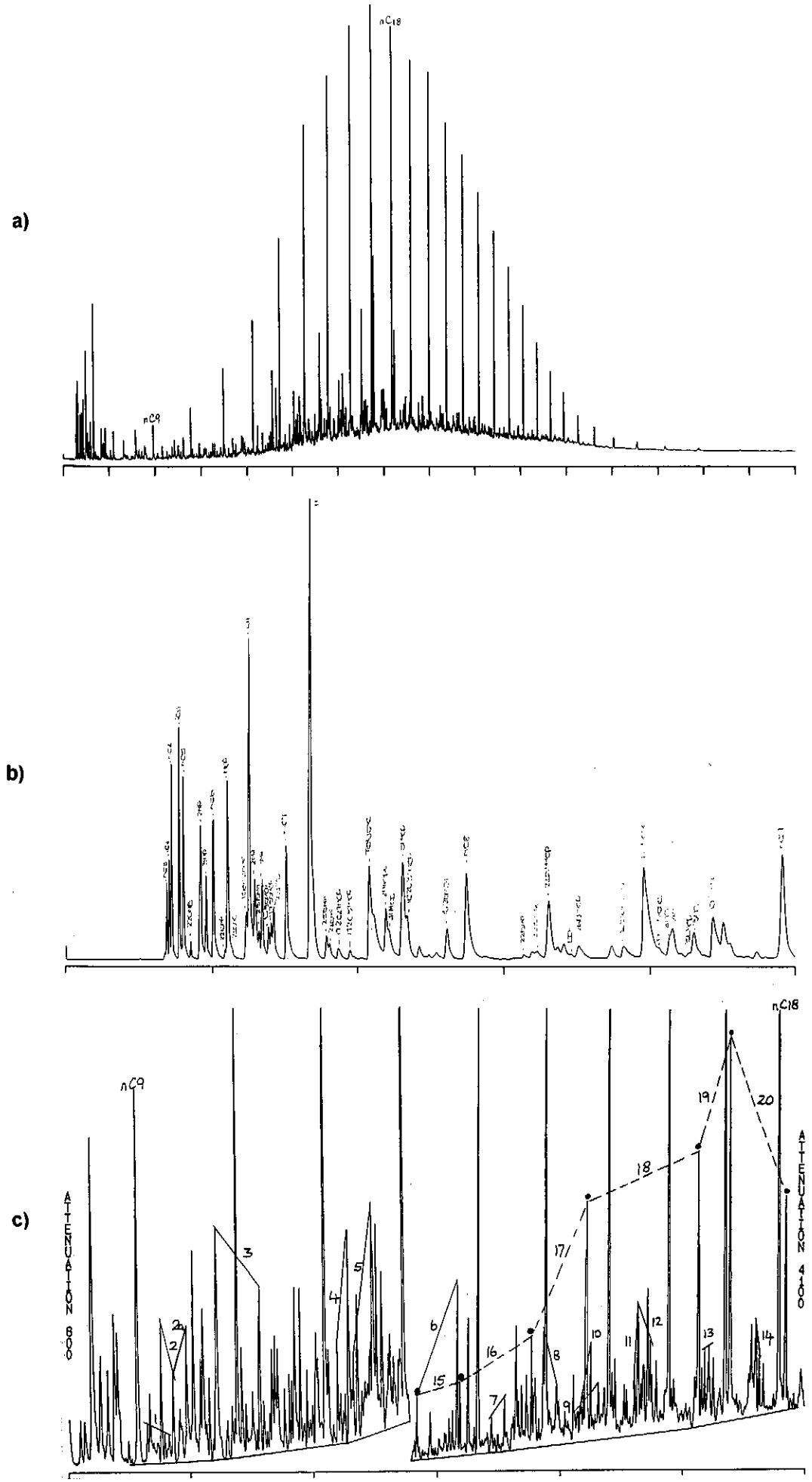

Figure C.63: Whole oil gas chromatograms of oil from well 59 DST1 (a) 0-80 minutes, (b) 0-10 minutes and (c) 6-36 minutes analysed using column 1.

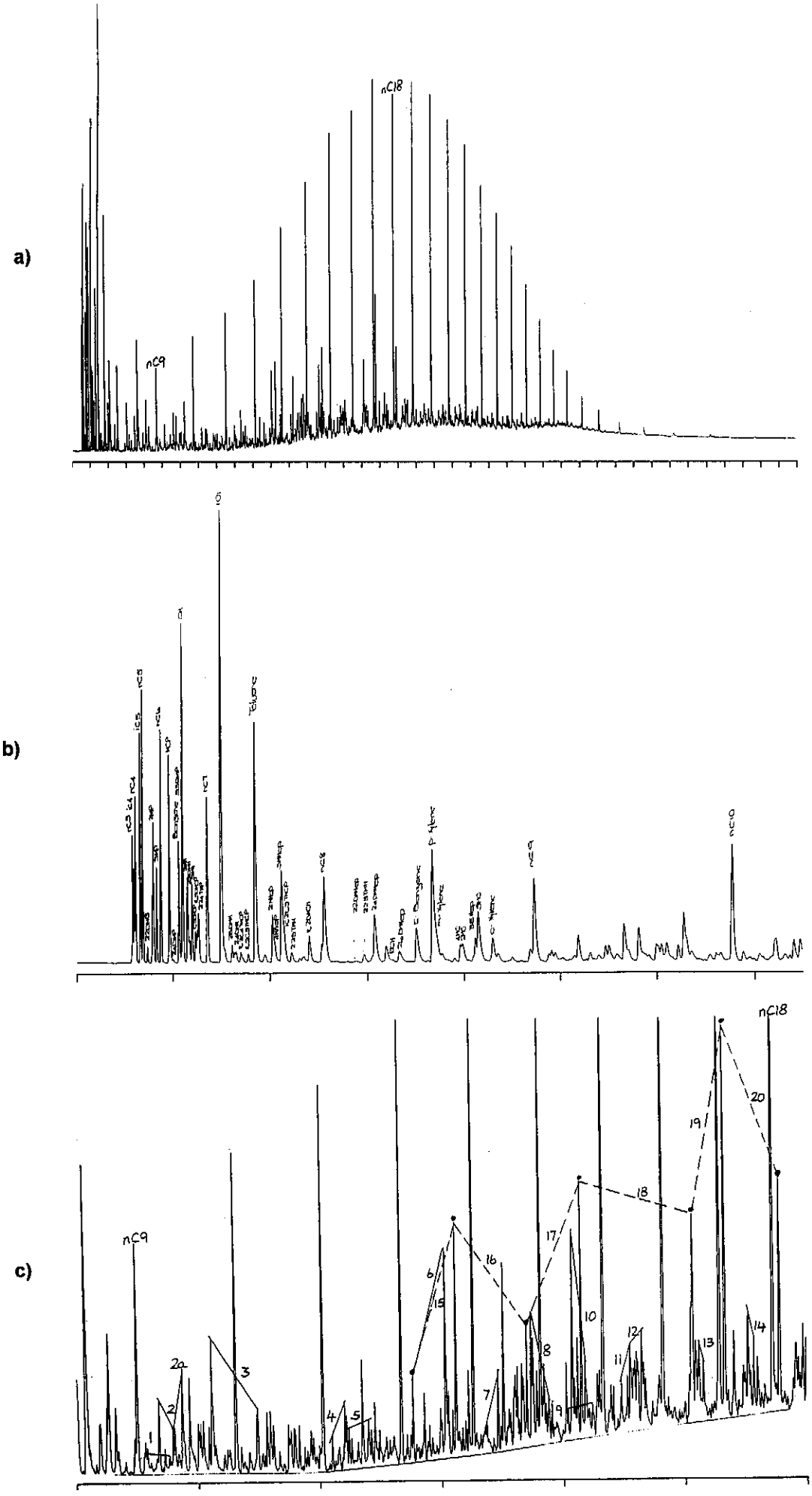

Figure C.64: Whole oil gas chromatograms of oil from well 59 DST1 (a) 0-80 minutes, (b) 0-10 minutes and (c) 6-36 minutes analysed using column 2.

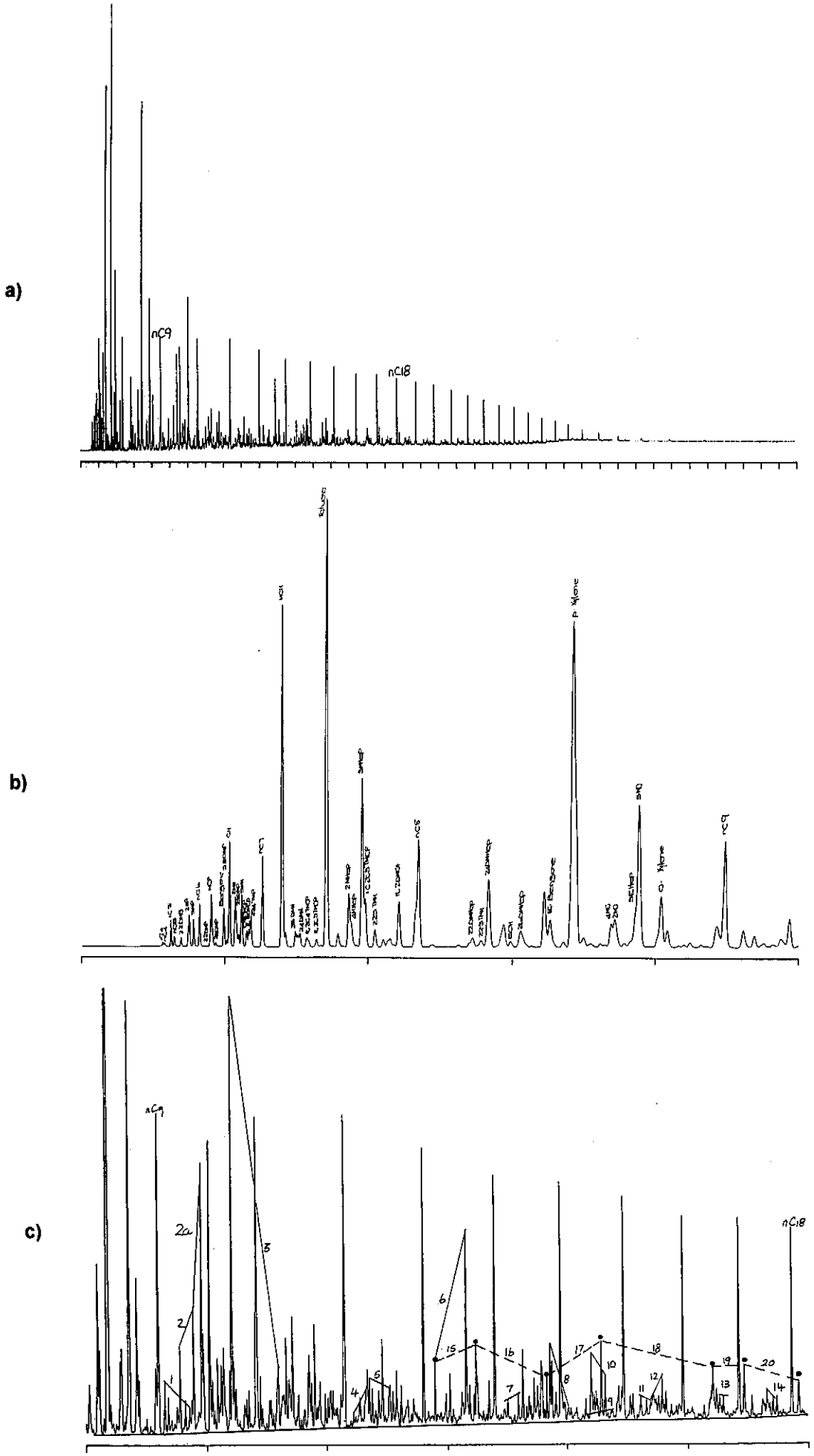

Figure C.65: Whole oil gas chromatograms of condensate from well 65 DST2 (a) 0-80 minutes, (b) 0-10 minutes and (c) 6-36 minutes analysed using column 2.

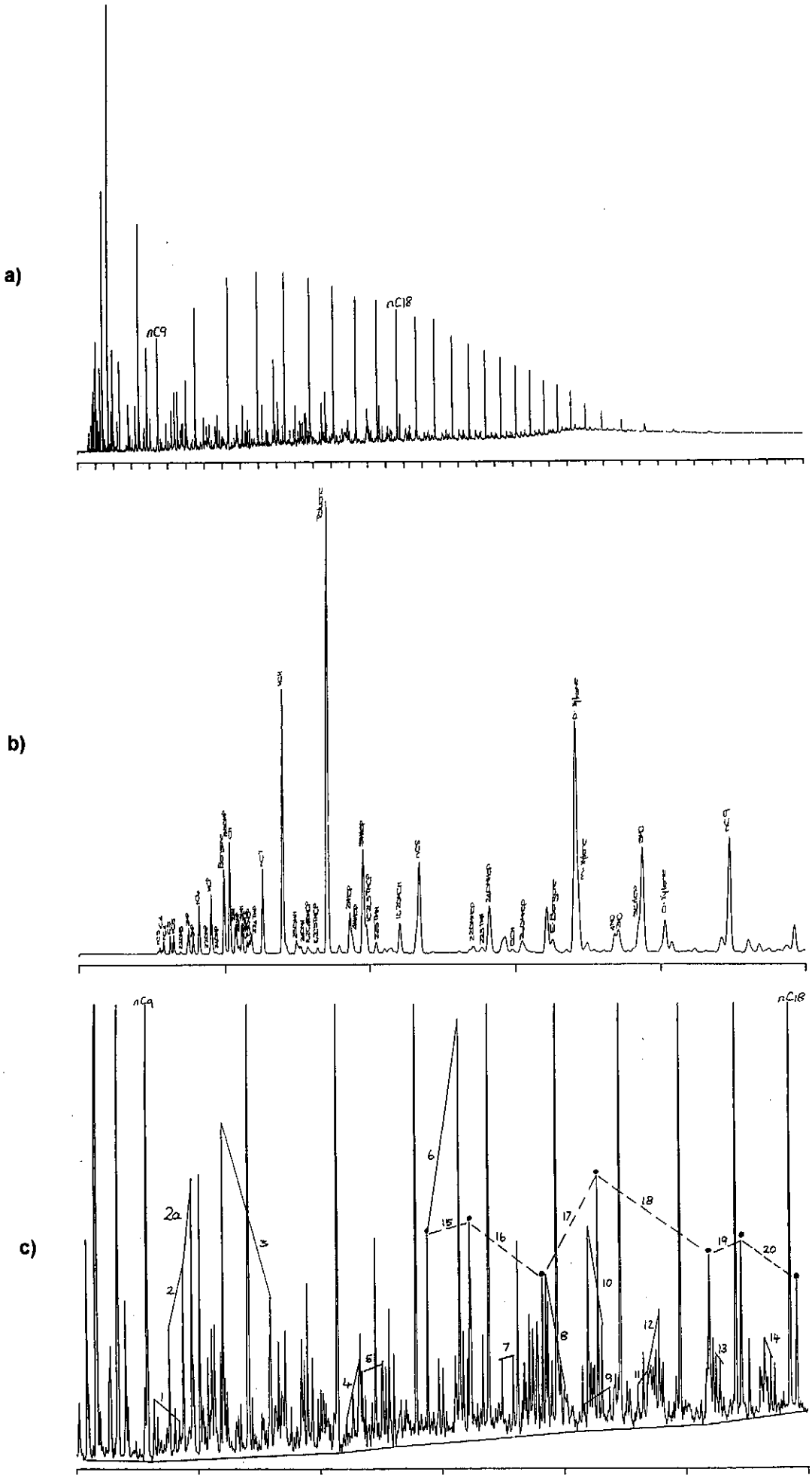

Figure C.66: Whole oil gas chromatograms of condensate from well 65 DST1 (a) 0-80 minutes, (b) 0-10 minutes and (c) 6-36 minutes analysed using column 2.

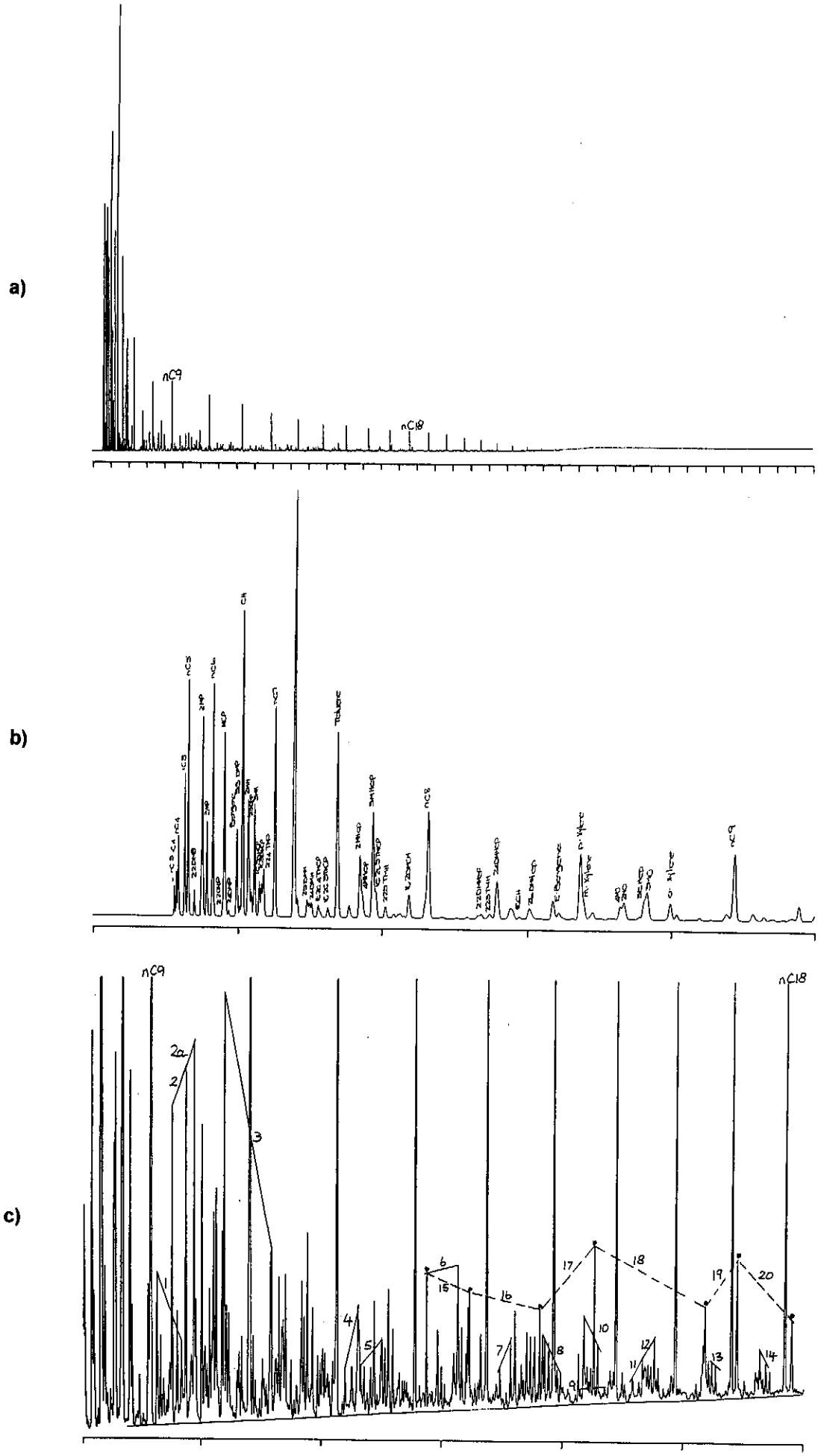

Figure C.67: Whole oil gas chromatograms of condensate from well 18 DST4 (a) 0-80 minutes, (b) 0-10 minutes and (c) 6-36 minutes analysed using column 2.

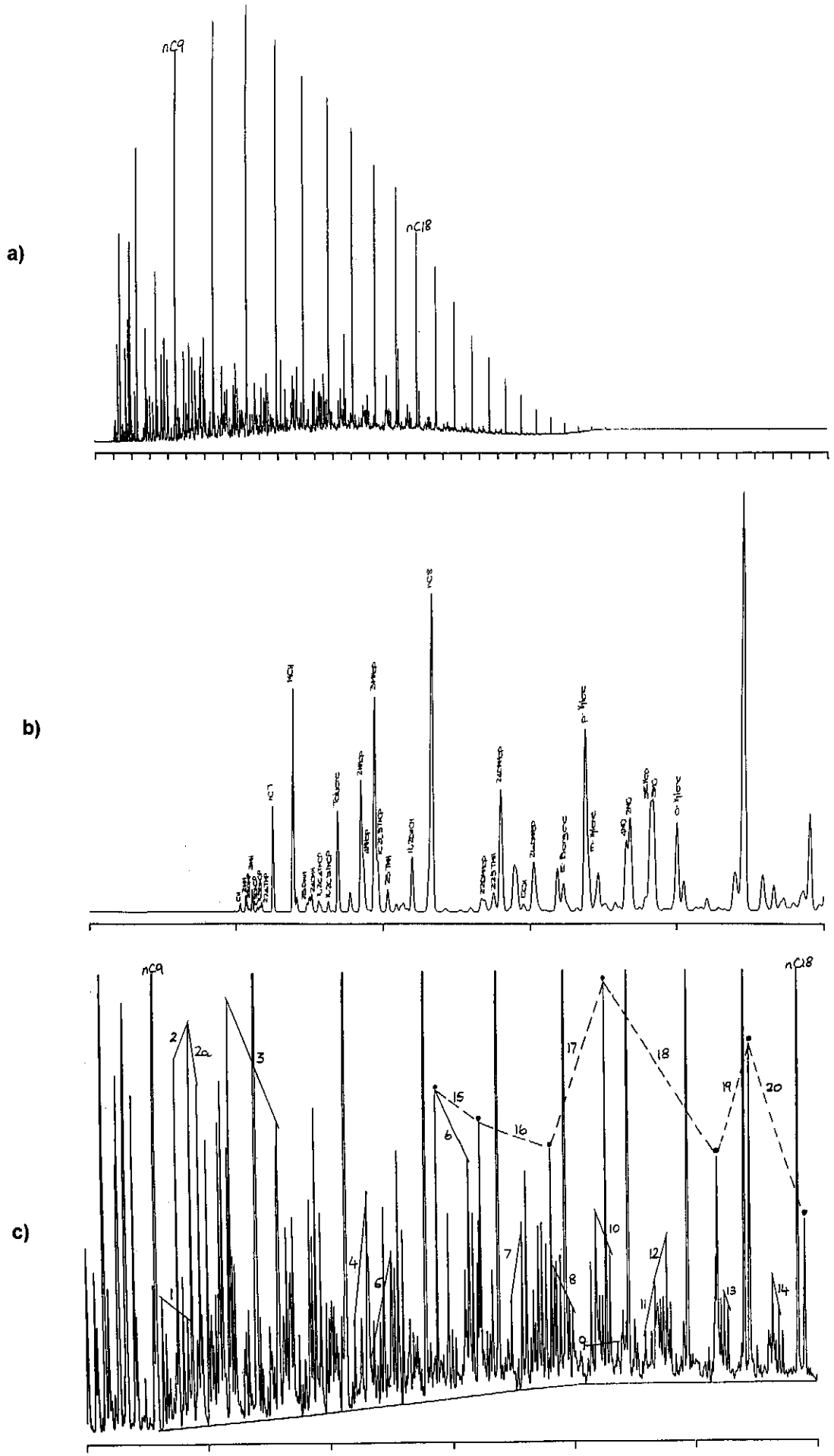

Figure C.68: Whole oil gas chromatograms of condensate from well 18 DST3 (a) 0-80 minutes, (b) 0-10 minutes and (c) 6-36 minutes analysed using column 2.

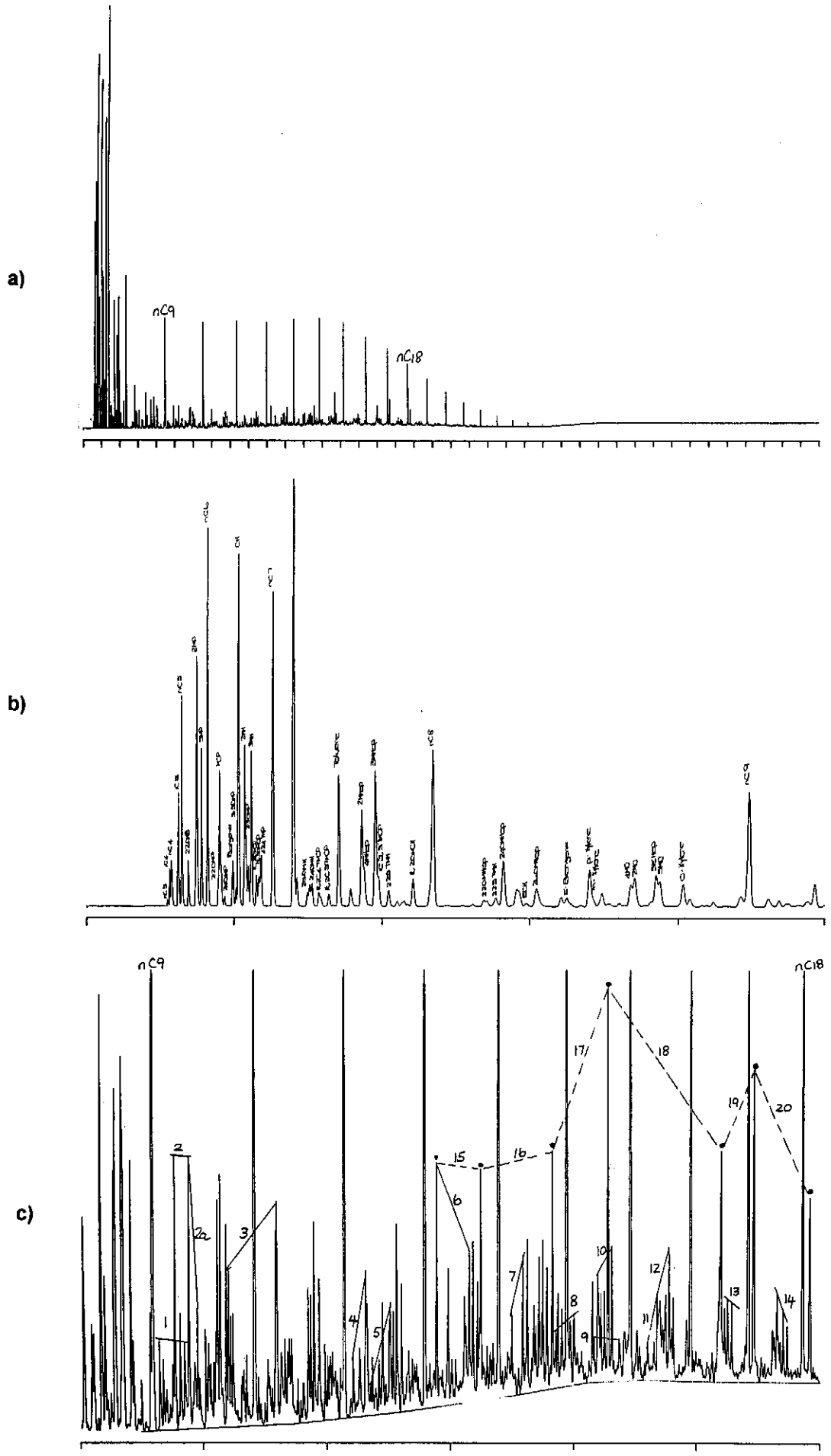

Figure C.69: Whole oil gas chromatograms of condensate from well 18 DST1 (a) 0-80 minutes, (b) 0-10 minutes and (c) 6-36 minutes analysed using column 2.

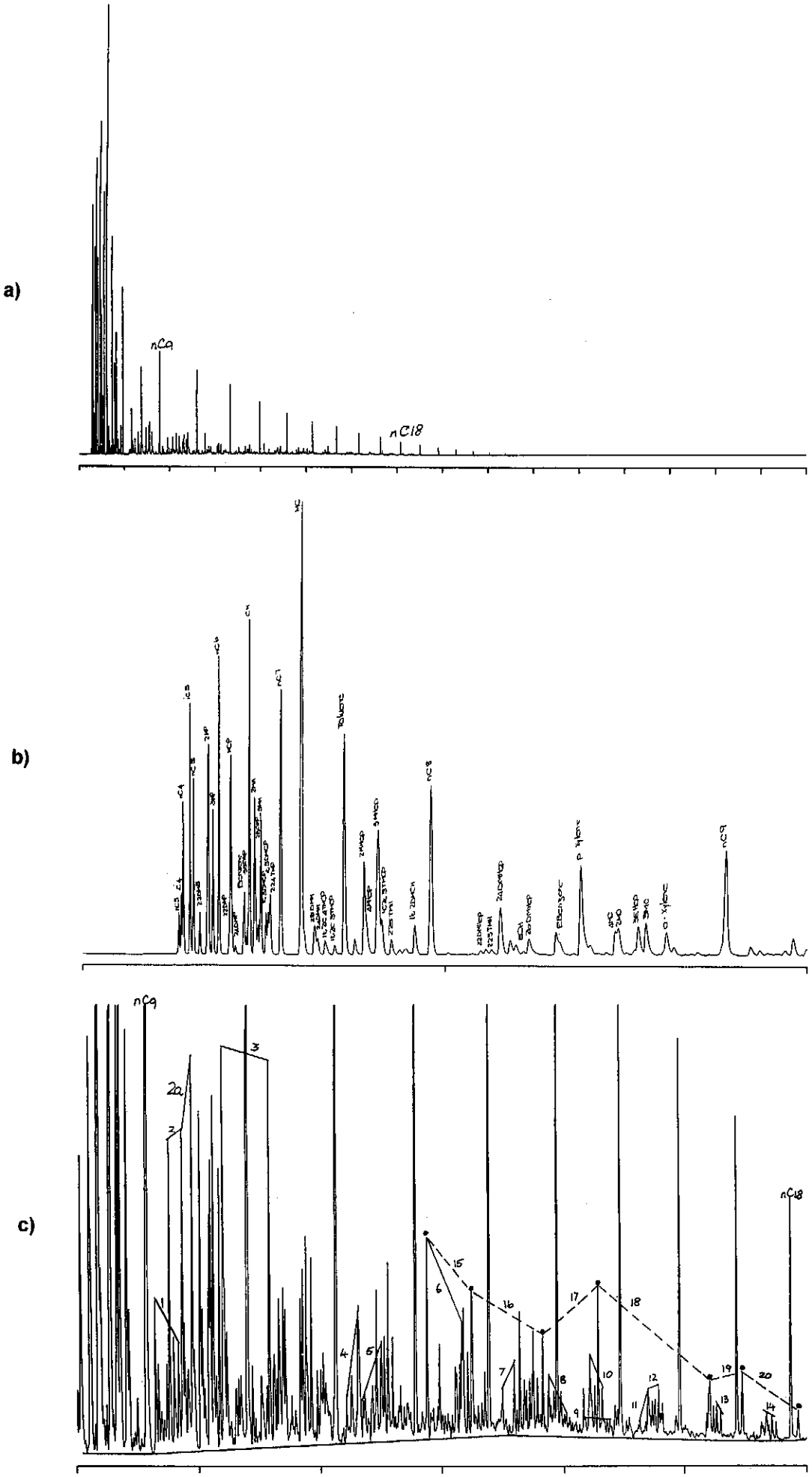

Figure C.70: Whole oil gas chromatograms of condensate from well 21 DST2 (a) 0-80 minutes, (b) 0-10 minutes and (c) 6-36 minutes analysed using column 3.

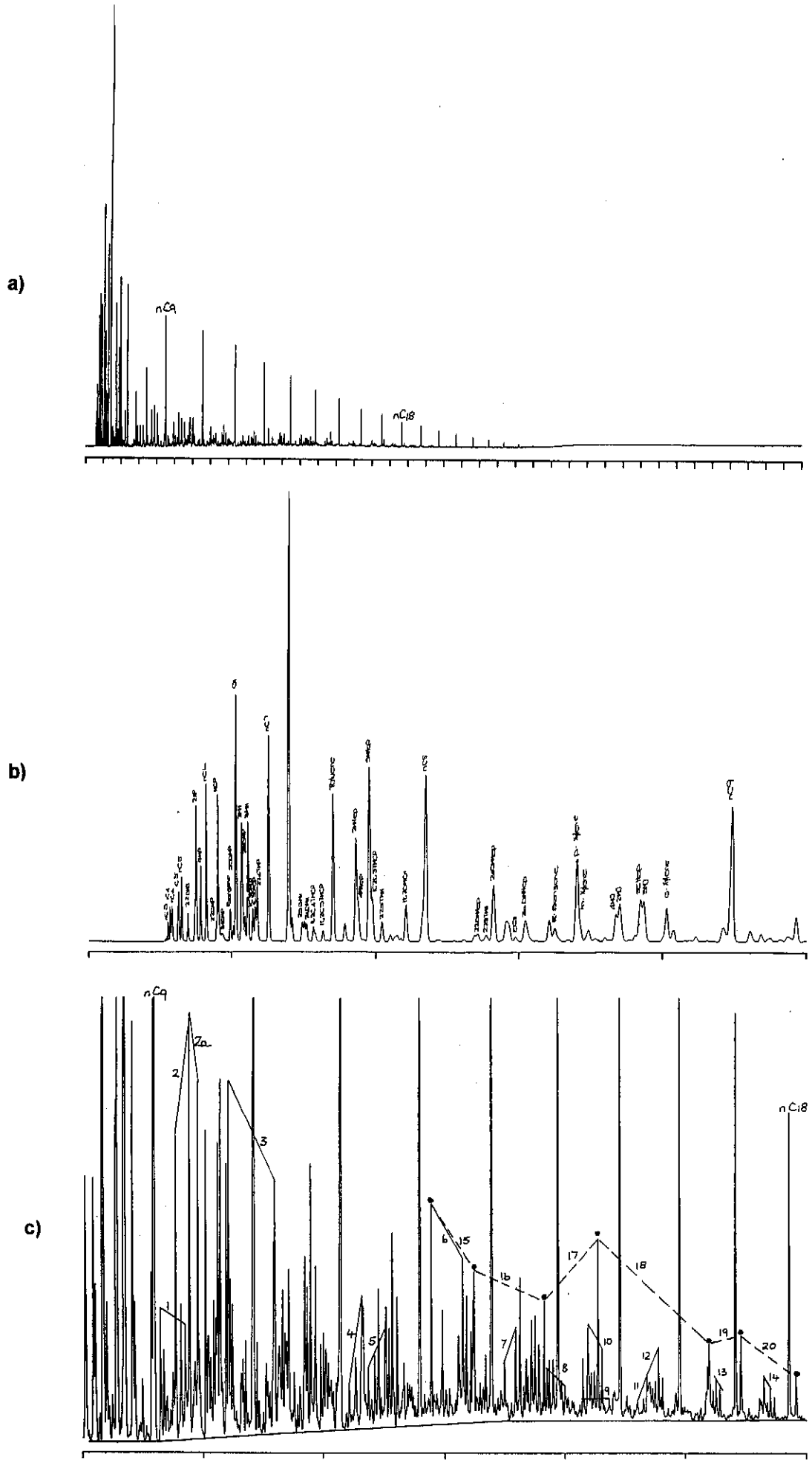

Figure C.71: Whole oil gas chromatograms of condensate from well 21 DST1 (a) 0-80 minutes, (b) 0-10 minutes and (c) 6-36 minutes analysed using column 2.

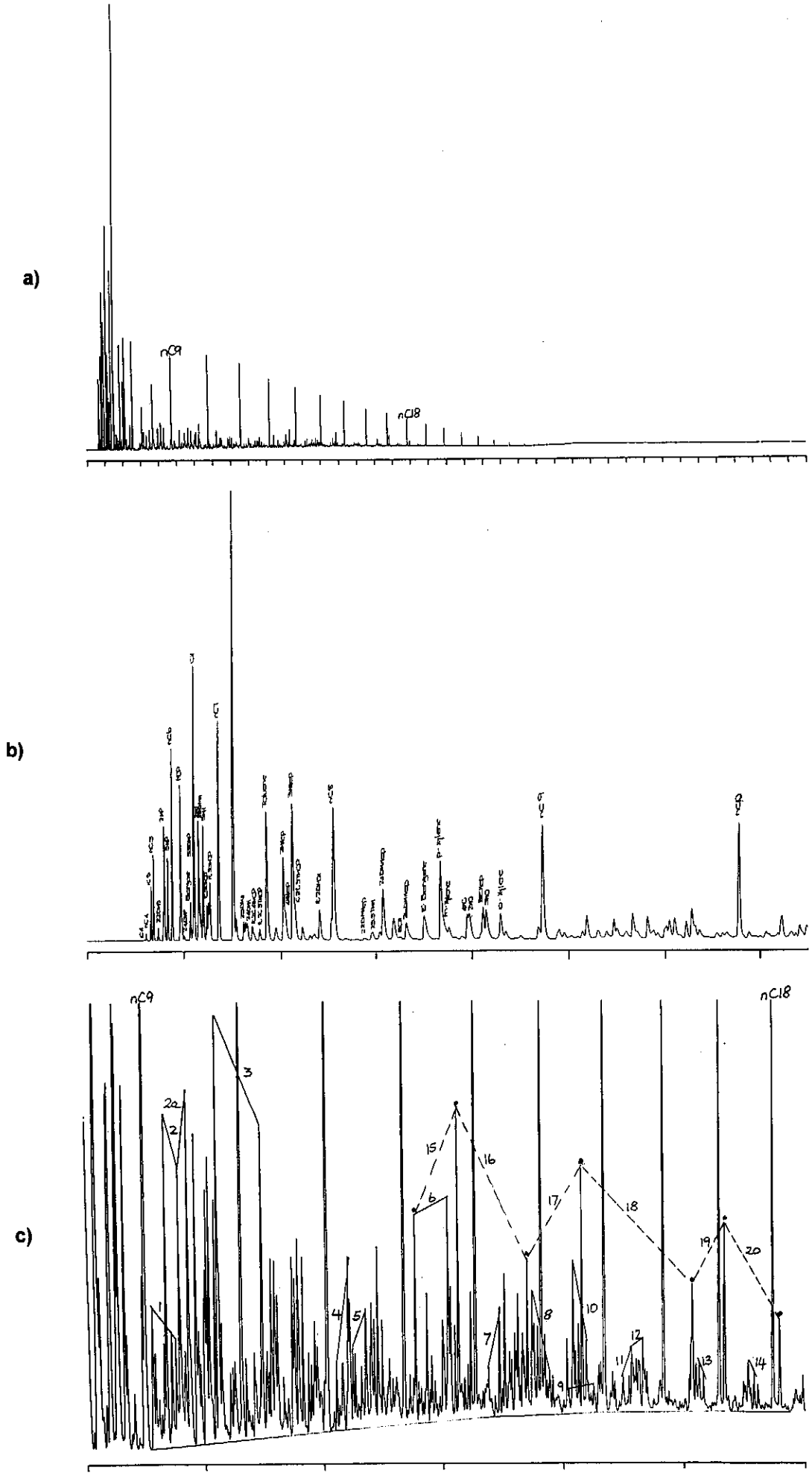

Figure C.72: Whole oil gas chromatograms of condensate from well 19 DST2 (a) 0-80 minutes, (b) 0-10 minutes and (c) 6-36 minutes analysed using column 2.

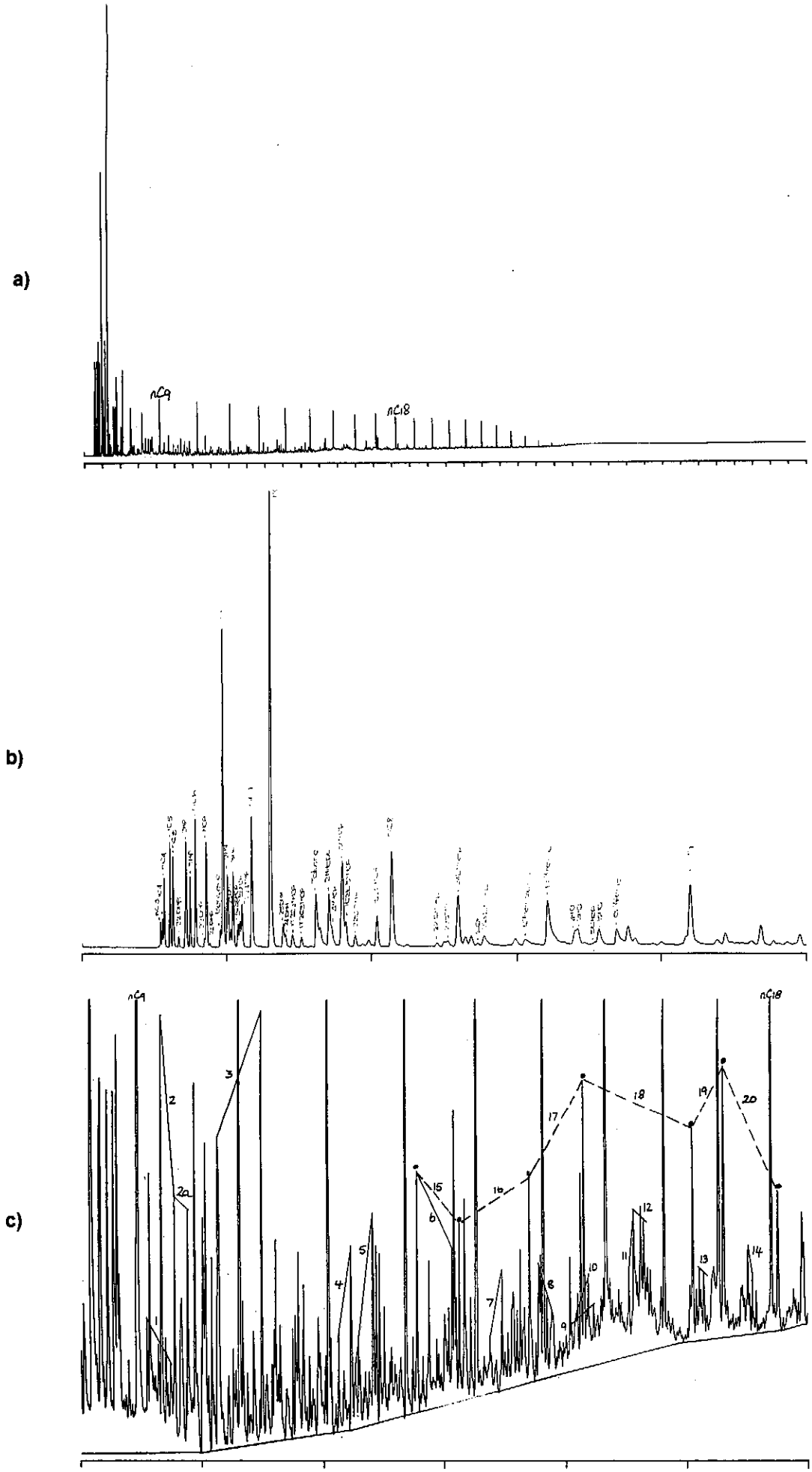

Figure C.73: Whole oil gas chromatograms of condensate from well 20 DST4 (a) 0-80 minutes, (b) 0-10 minutes and (c) 6-36 minutes analysed using column 1.

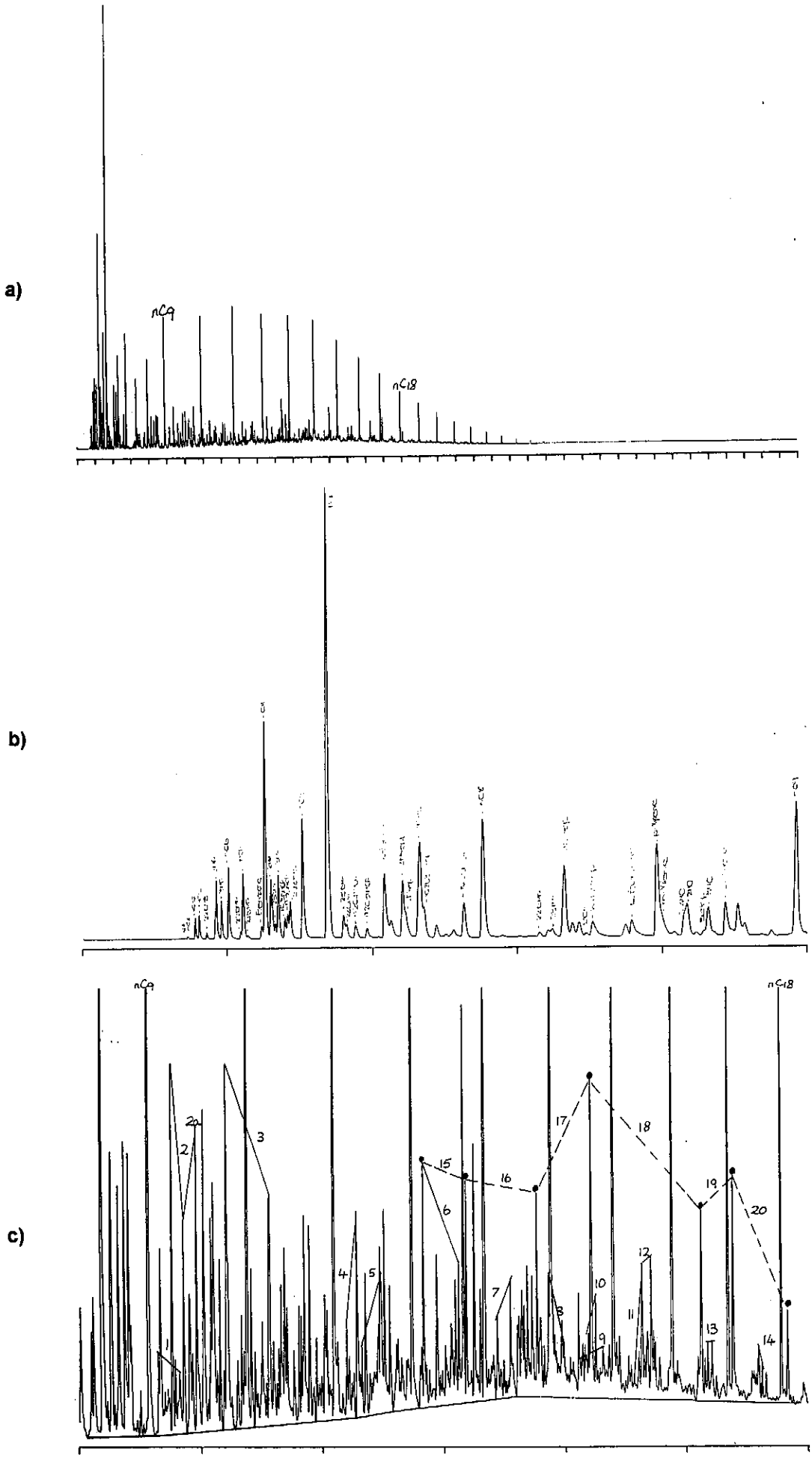

Figure C.74: Whole oil gas chromatograms of condensate from well 20 DST3 (a) 0-80 minutes, (b) 0-10 minutes and (c) 6-36 minutes analysed using column 1.

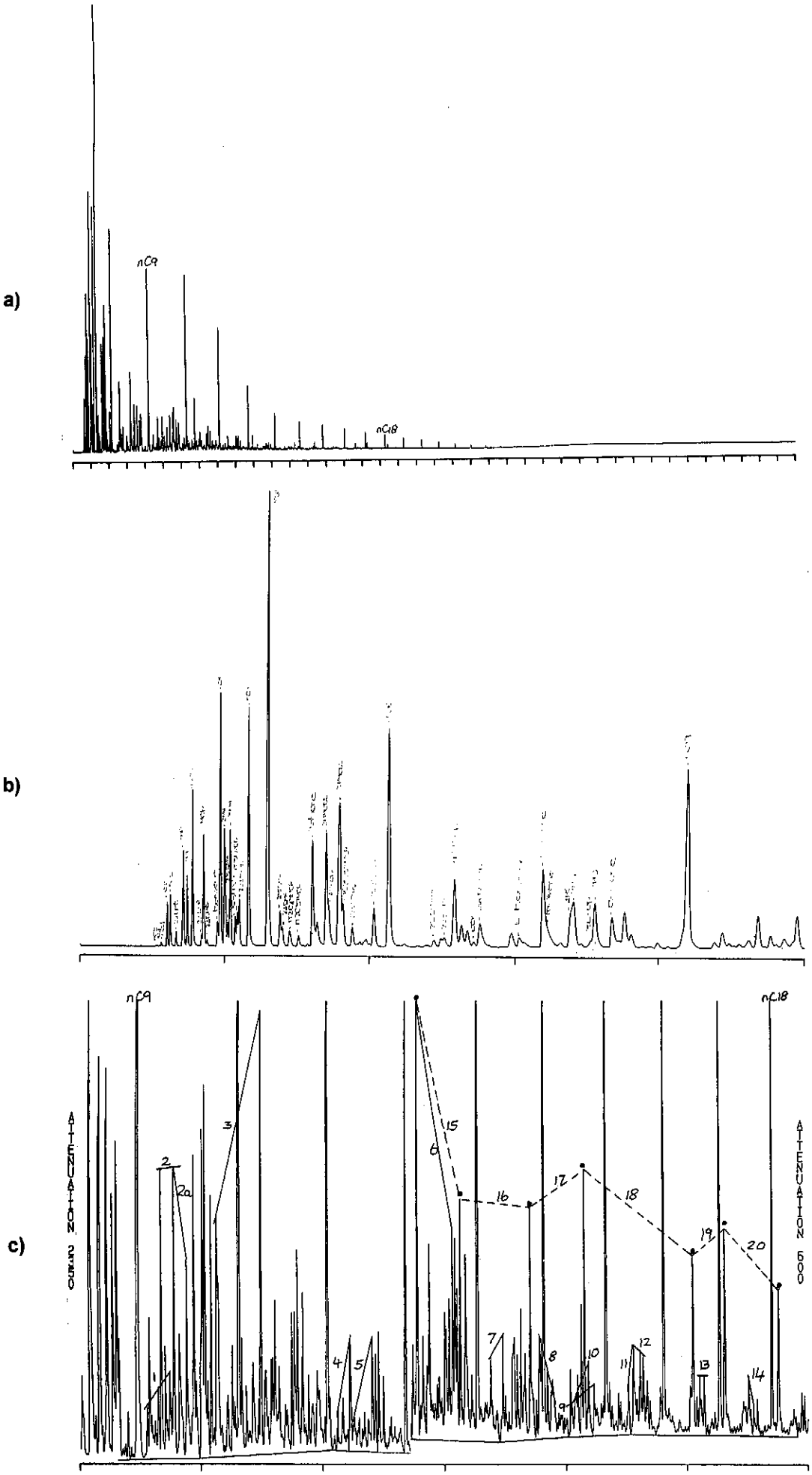

Figure C.75: Whole oil gas chromatograms of condensate from well 20 DST2 (a) 0-80 minutes, (b) 0-10 minutes and (c) 6-36 minutes analysed using column 1.

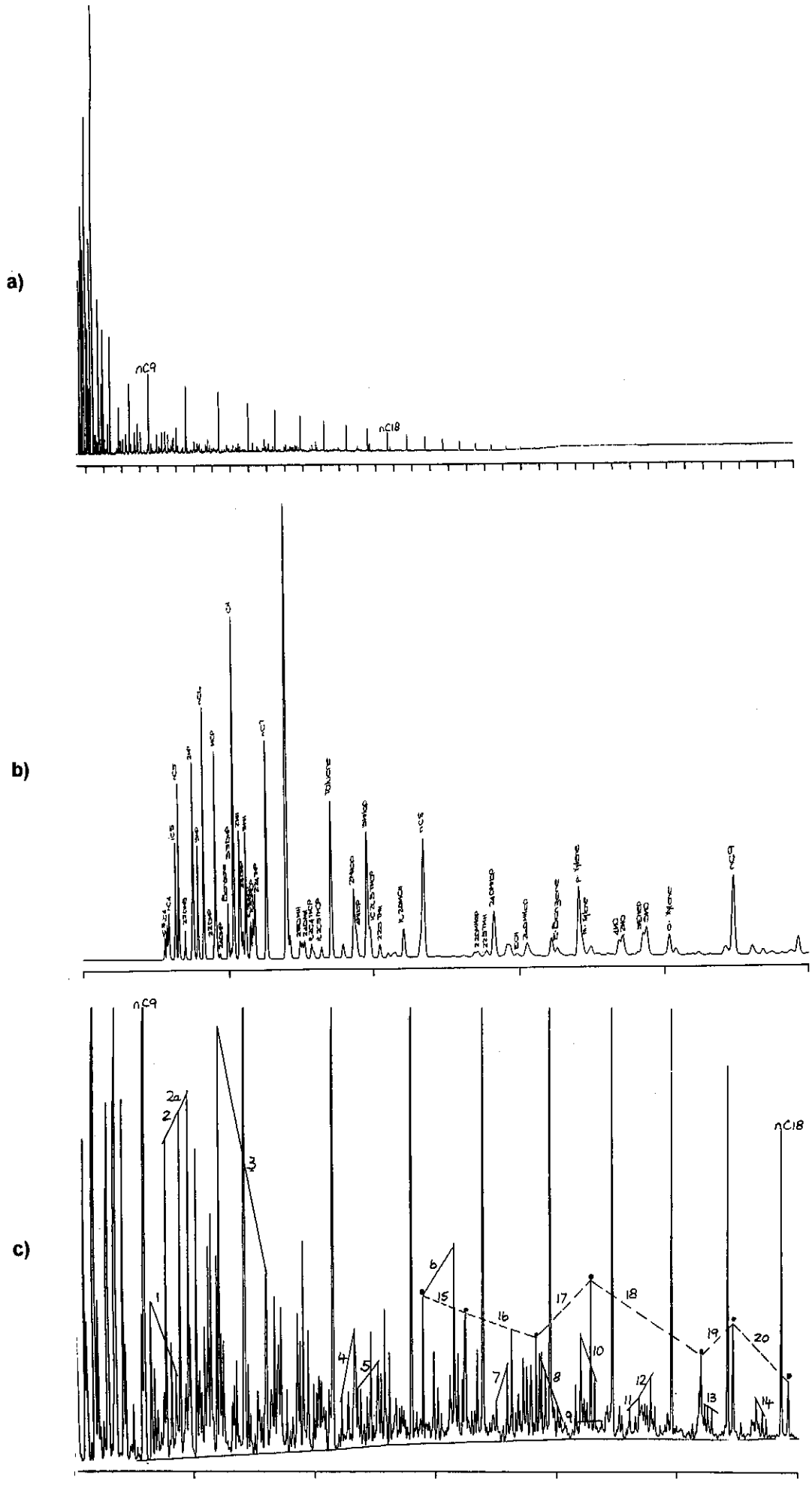

Figure C.76: Whole oil gas chromatograms of condensate from well 44 DST1 (a) 0-80 minutes, (b) 0-10 minutes and (c) 6-36 minutes analysed using column 2.

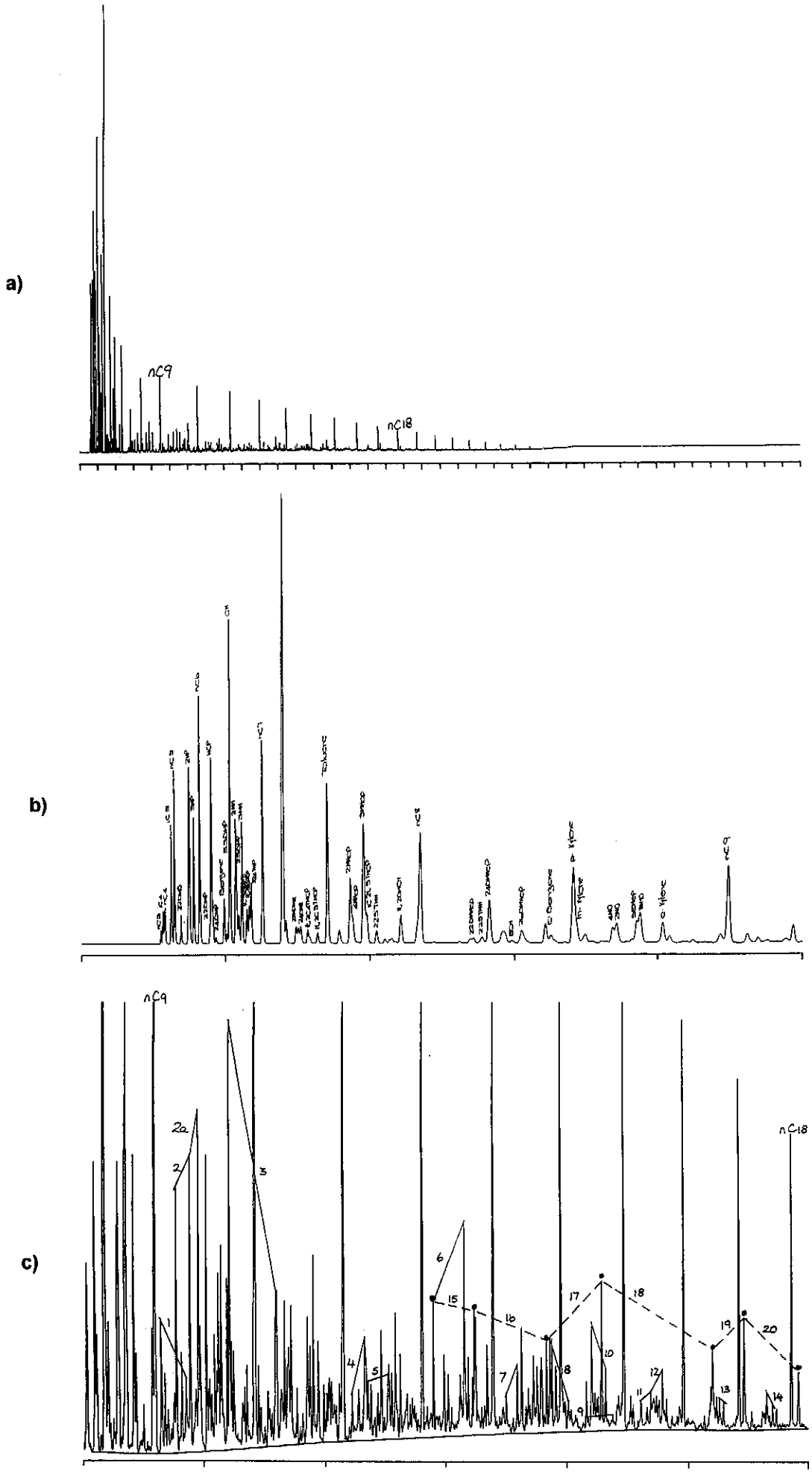

Figure C.77: Whole oil gas chromatograms of condensate from well 55 DST2 (a) 0-80 minutes, (b) 0-10 minutes and (c) 6-36 minutes analysed using column 2.

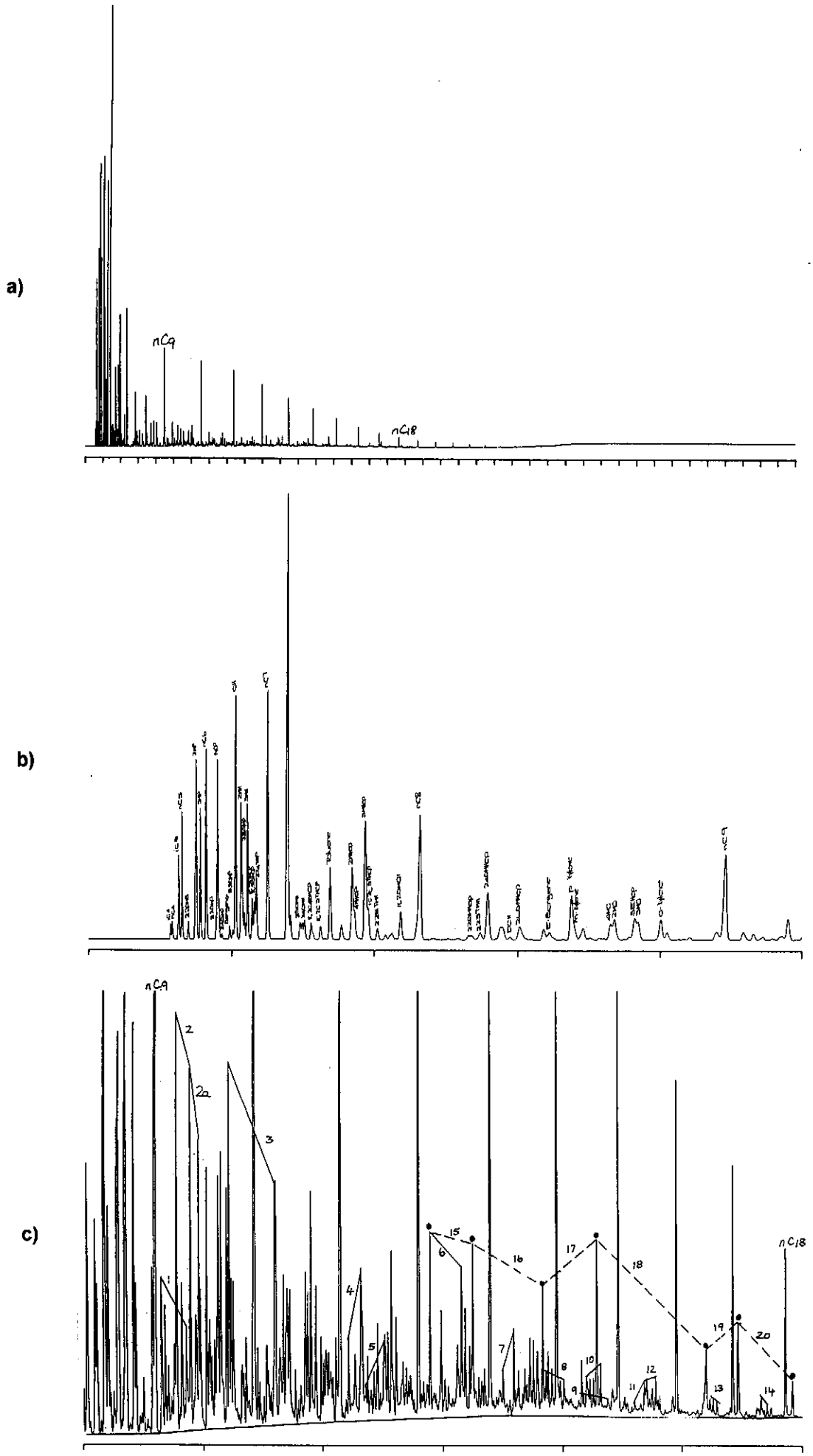

Figure C.78: Whole oil gas chromatograms of condensate from well 61 DST3 (a) 0-80 minutes, (b) 0-10 minutes and (c) 6-36 minutes analysed using column 2.

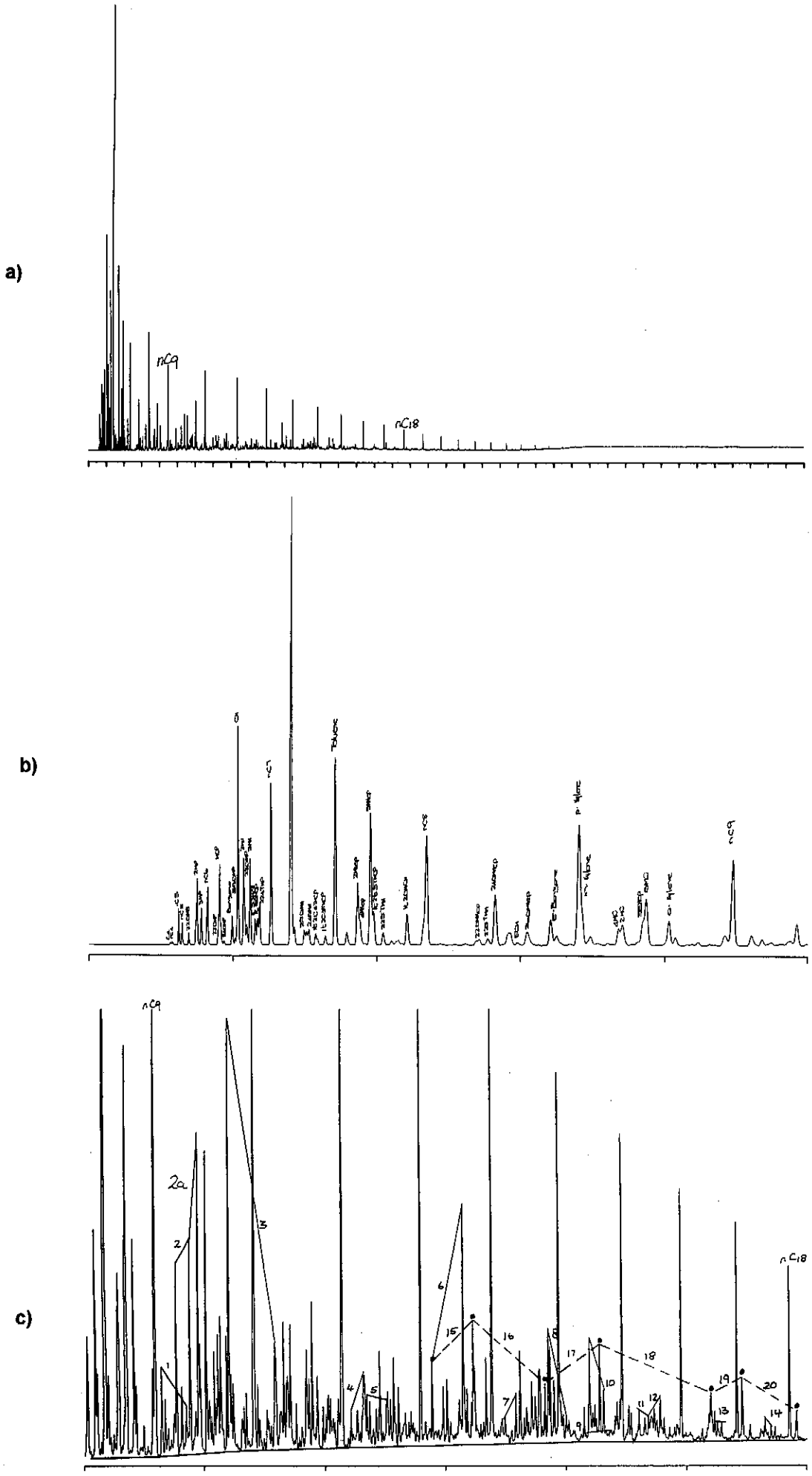

Figure C.79: Whole oil gas chromatograms of condensate from well 61 DST2 (a) 0-80 minutes, (b) 0-10 minutes and (c) 6-36 minutes analysed using column 2.

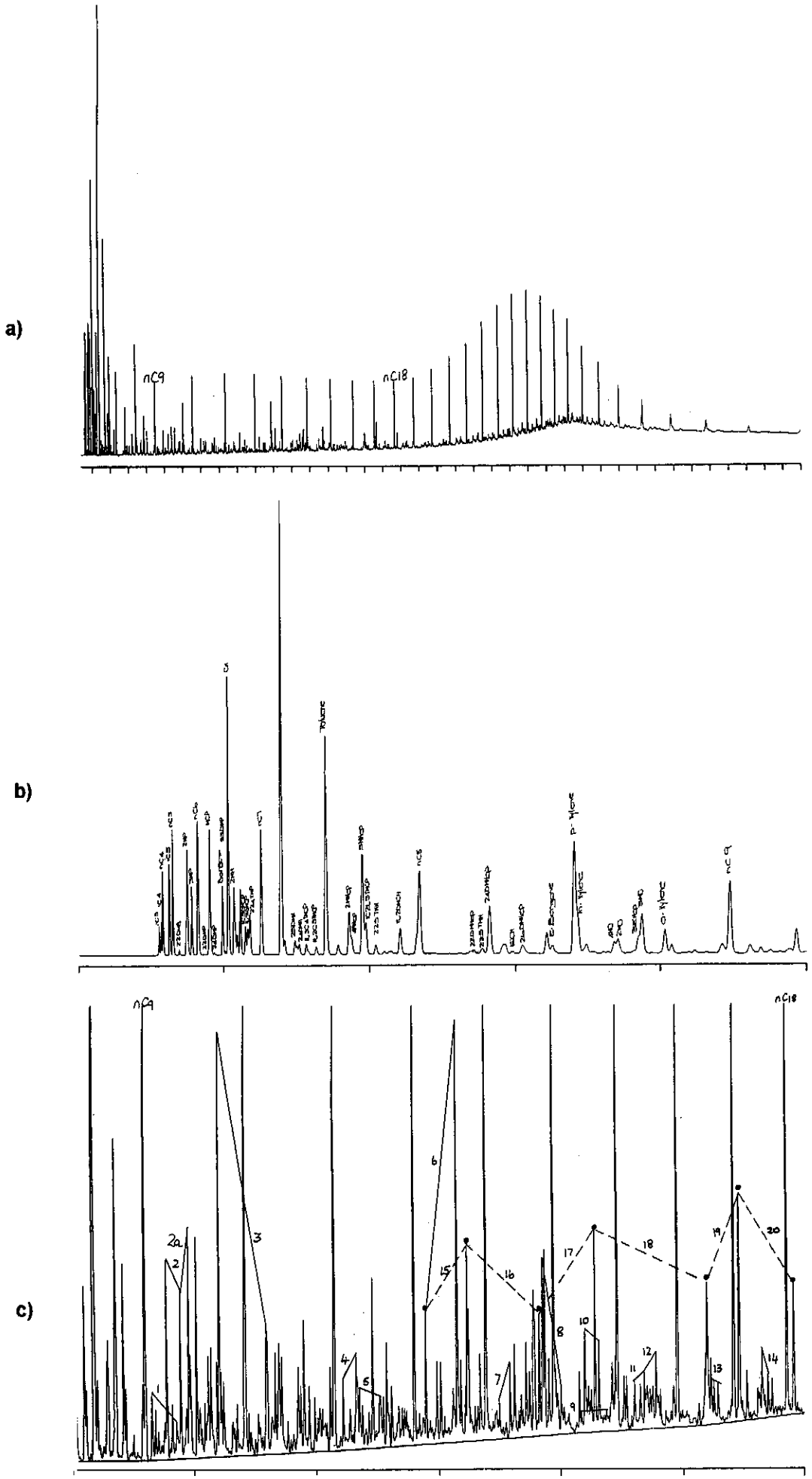

Figure C.80: Whole oil gas chromatograms of oil from well 62 DST1 (a) 0-80 minutes, (b) 0-10 minutes and (c) 6-36 minutes analysed using column 2.

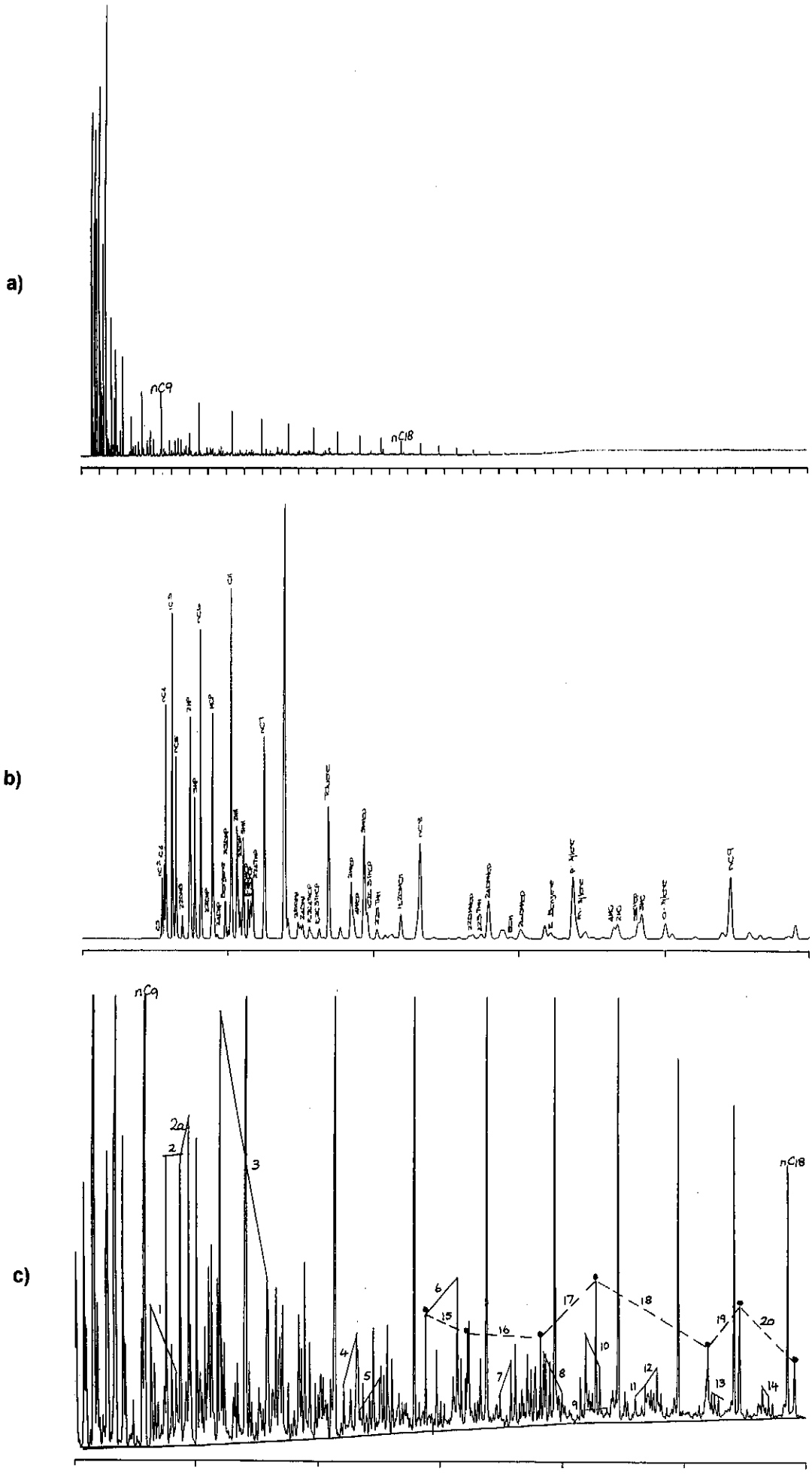

Figure C.81: Whole oil gas chromatograms of condensate from well 70 DST2 (a) 0-80 minutes, (b) 0-10 minutes and (c) 6-36 minutes analysed using column 2.

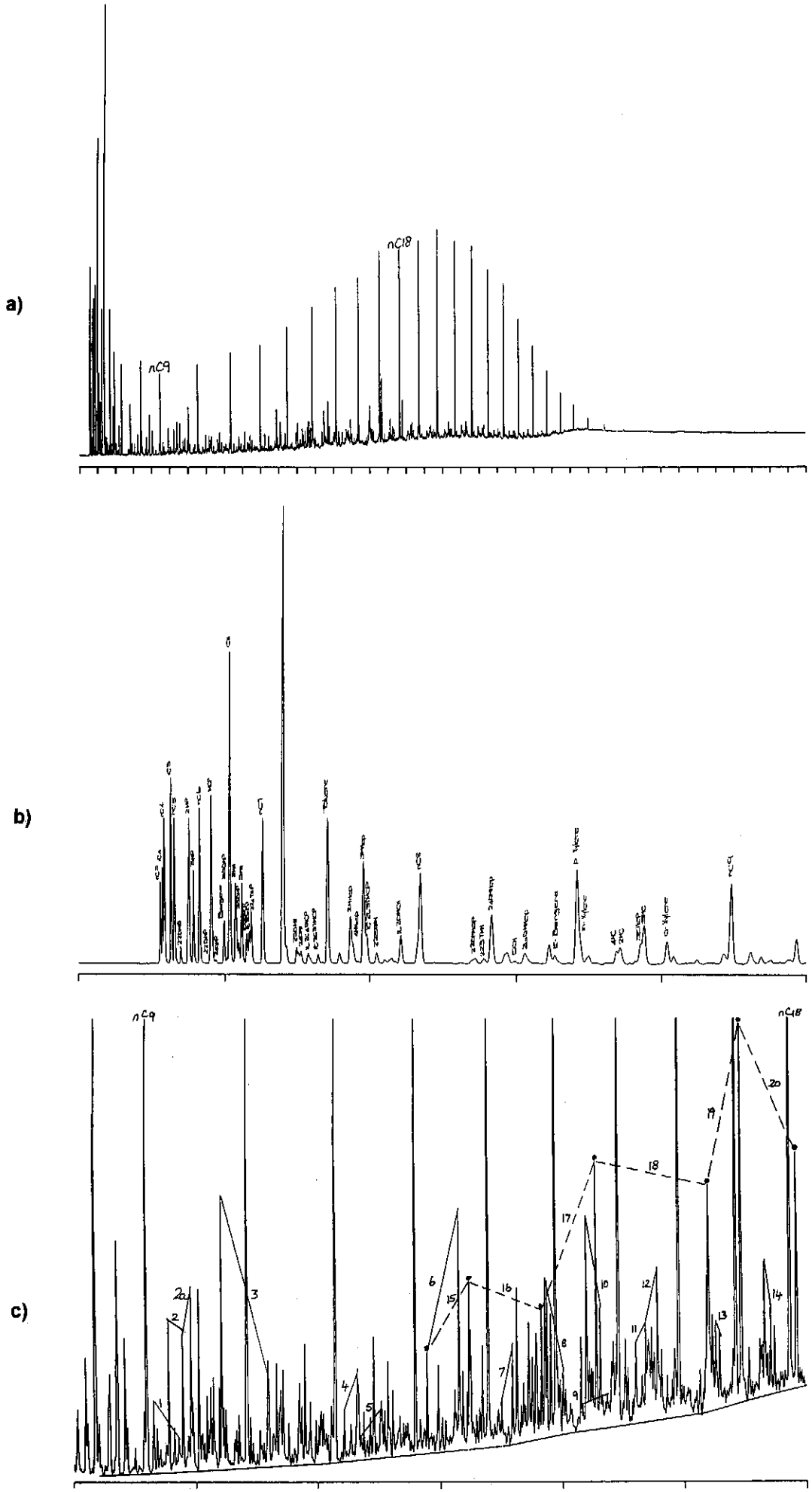

Figure C.82: Whole oil gas chromatograms of oil from well 70 DST1 (a) 0-80 minutes, (b) 0-10 minutes and (c) 6-36 minutes analysed using column 2.

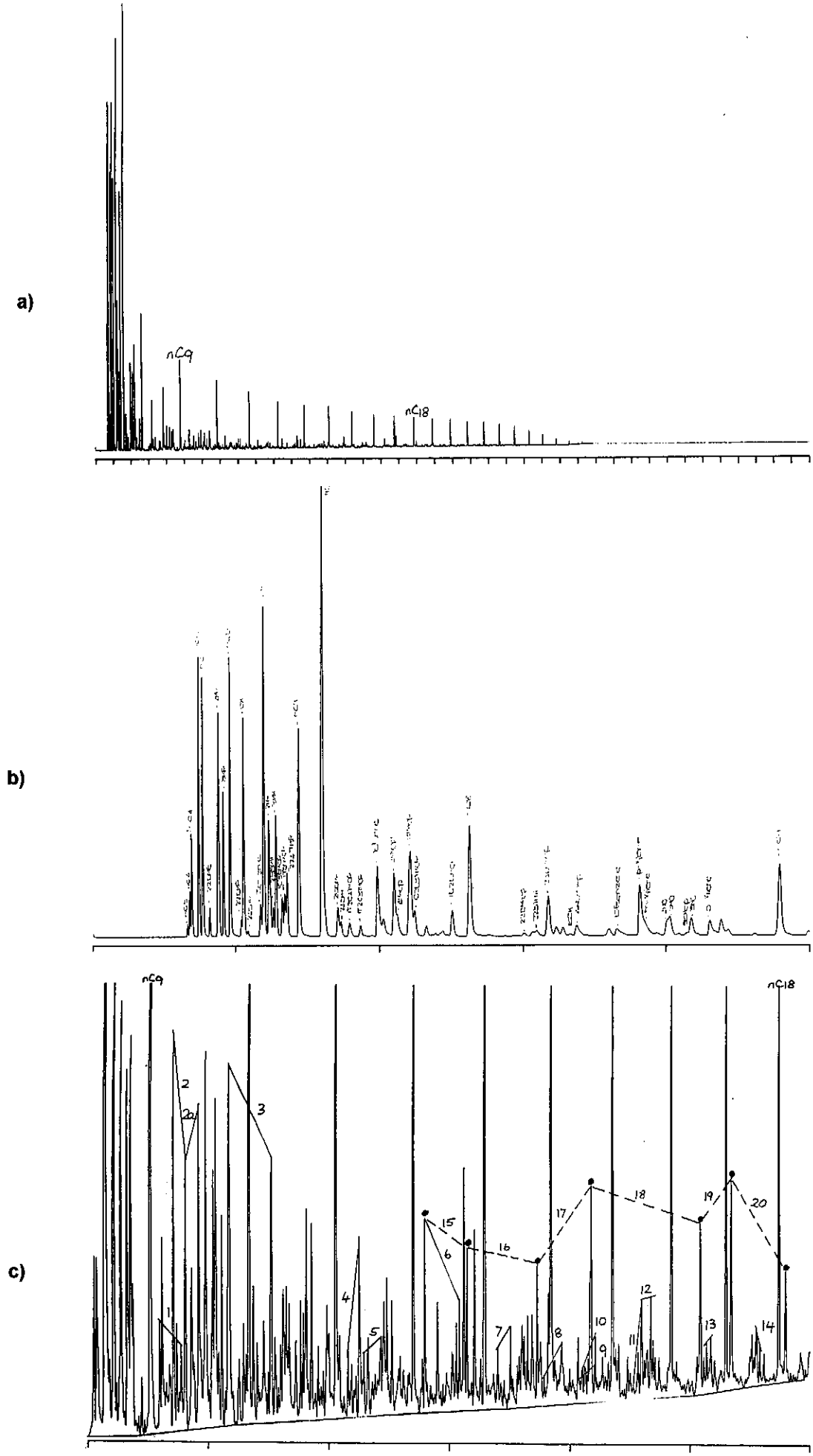

Figure C.83: Whole oil gas chromatograms of condensate from well 31 DST1 (a) 0-80 minutes, (b) 0-10 minutes and (c) 6-36 minutes analysed using column 1.

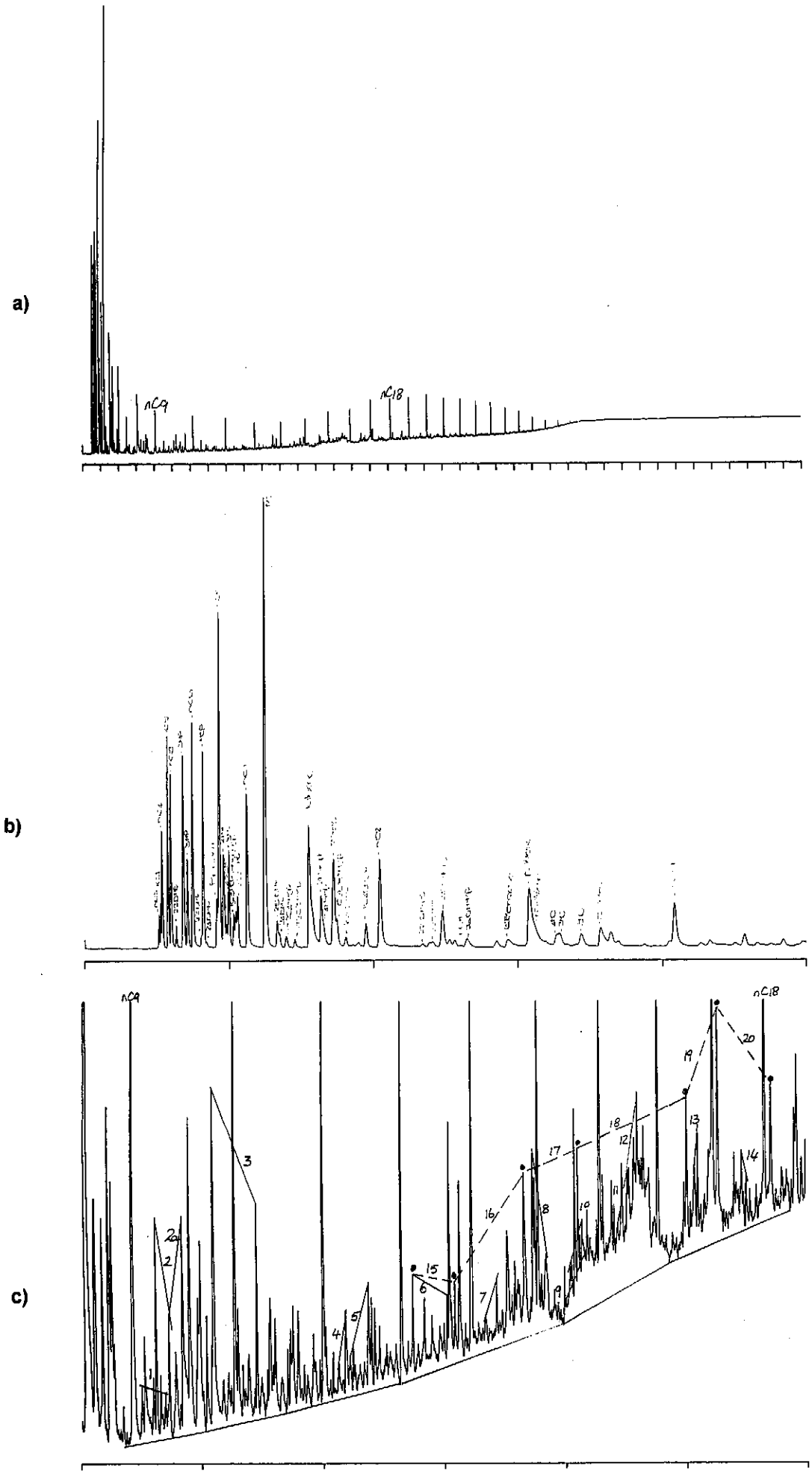

Figure C.84: Whole oil gas chromatograms of condensate from well 63 DST1 (a) 0-80 minutes, (b) 0-10 minutes and (c) 6-36 minutes analysed using column 1.

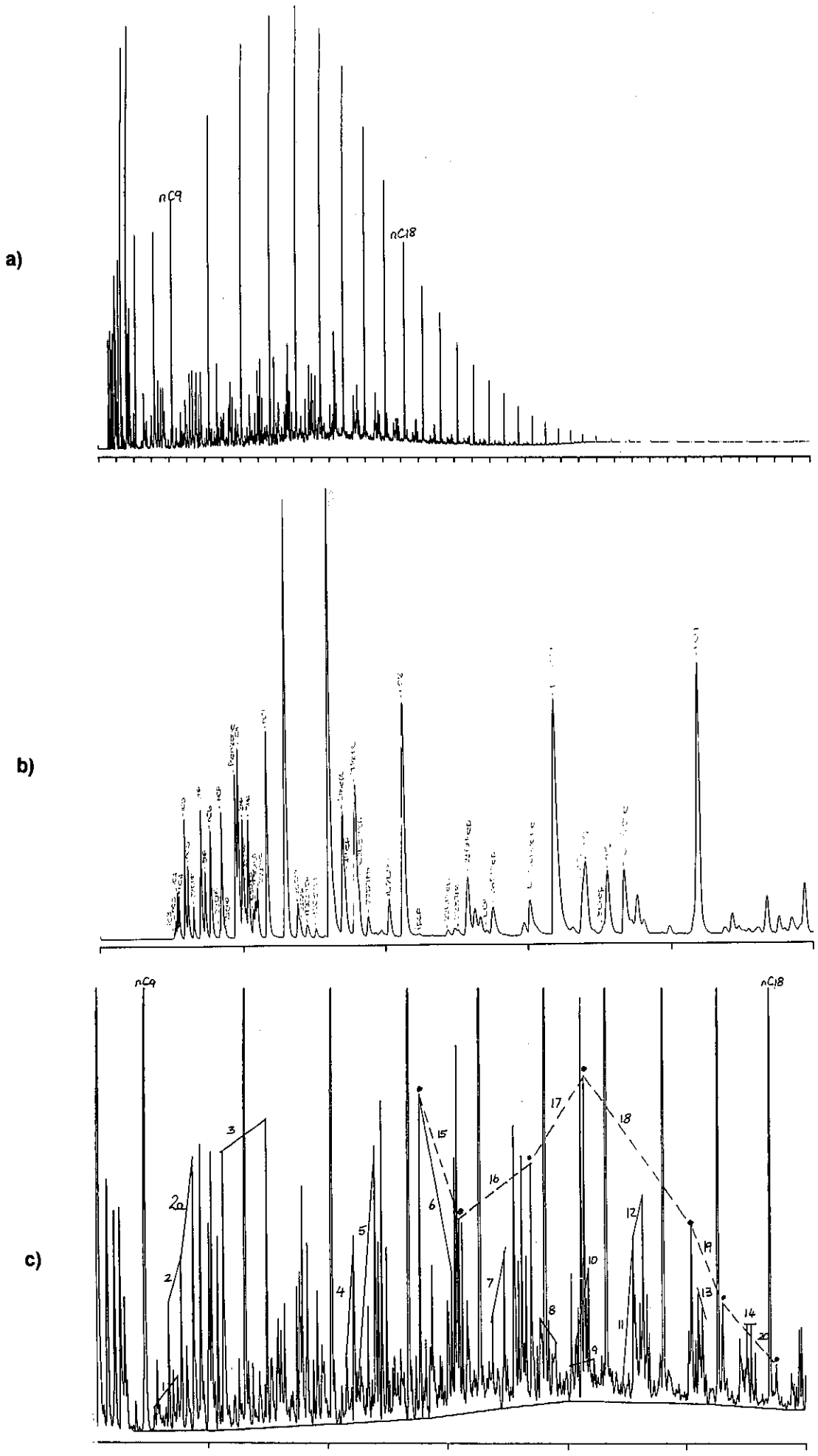

Figure C.85: Whole oil gas chromatograms of condensate from well 128 DST1 (a) 0-80 minutes, (b) 0-10 minutes and (c) 6-36 minutes analysed using column 1.

APPENDIX D: SATURATED AND AROMATIC FRACTION PLOTS

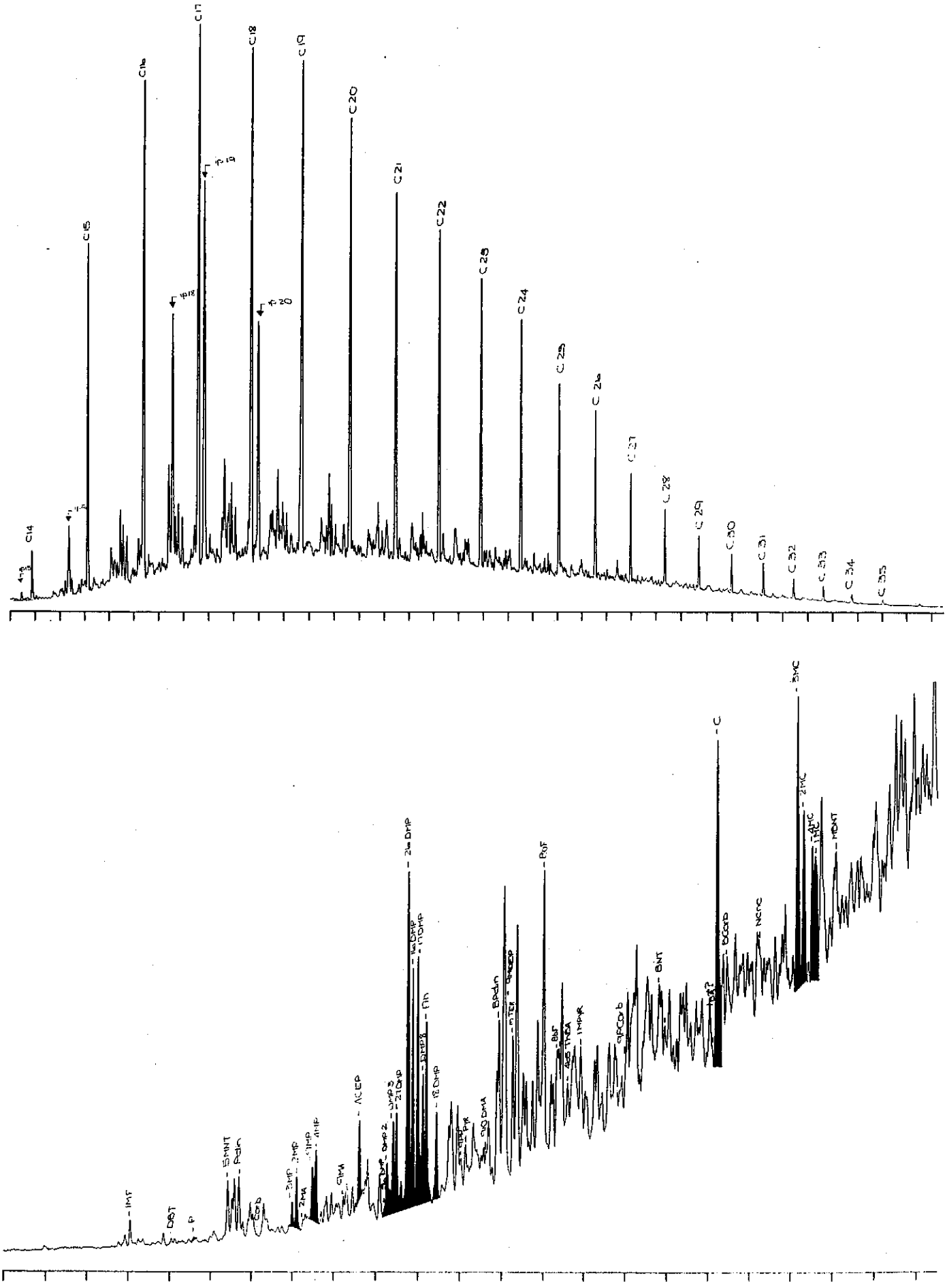

Figure D.01: Gas chromatograms of the total saturated and aromatic fractions of sample 1, well 83 DST 3, 2470m.

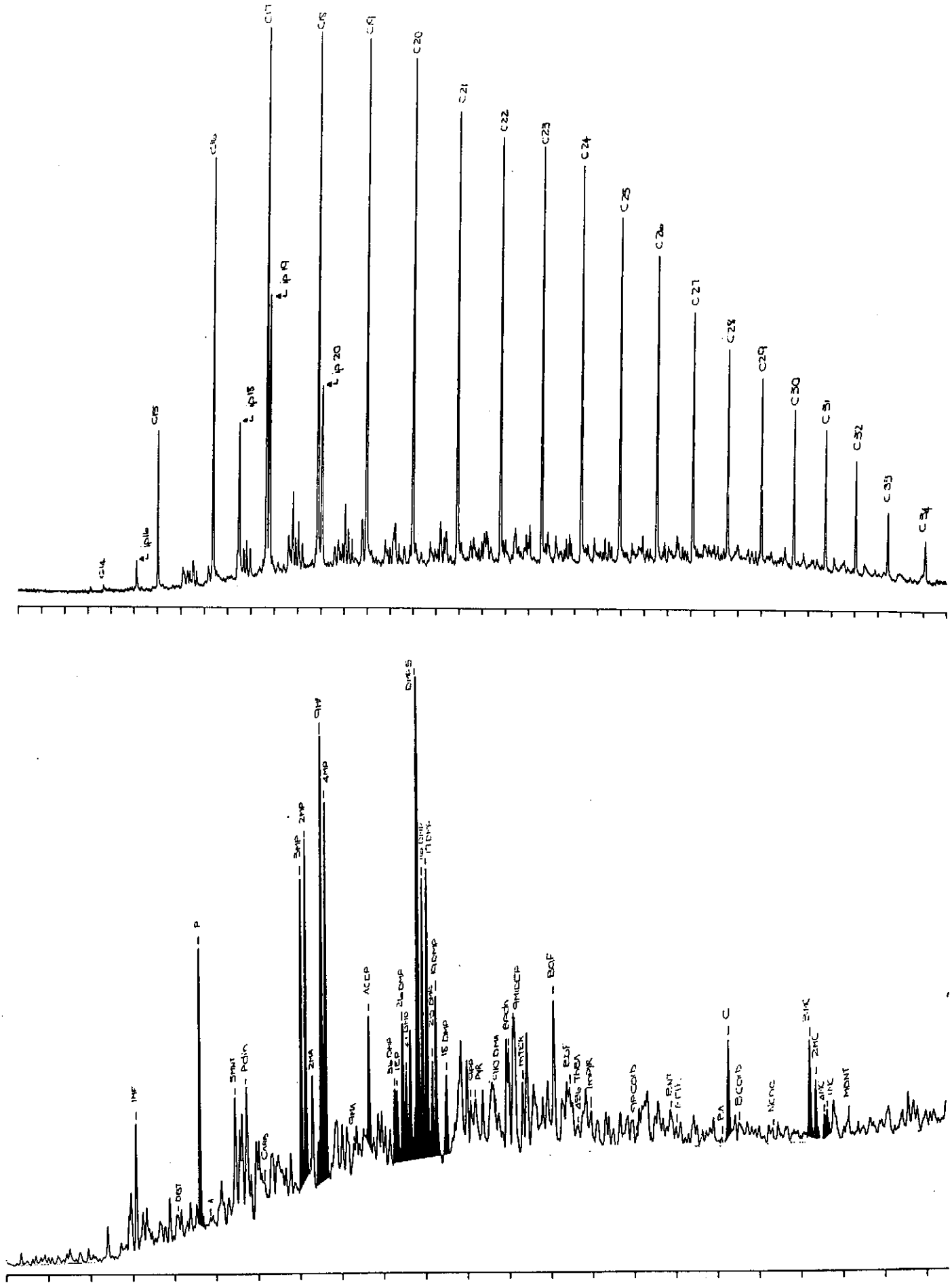

Figure D.02: Gas chromatograms of the total saturated and aromatic fractions of sample 2, well 83 DST 2, 2889m.

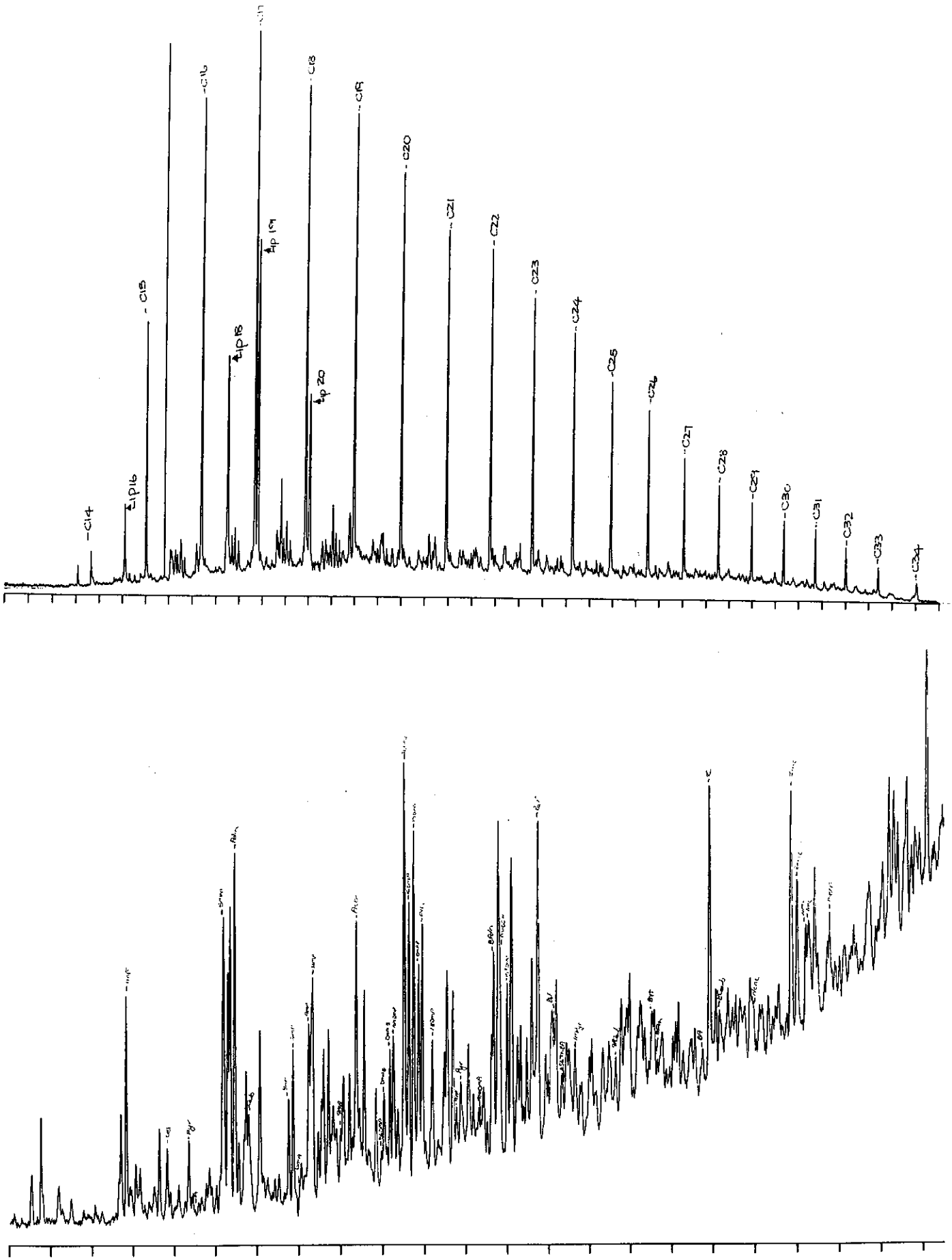

Figure D.03: Gas chromatograms of the total saturated and aromatic fractions of sample 4, well 88 DST 5, 2507m.

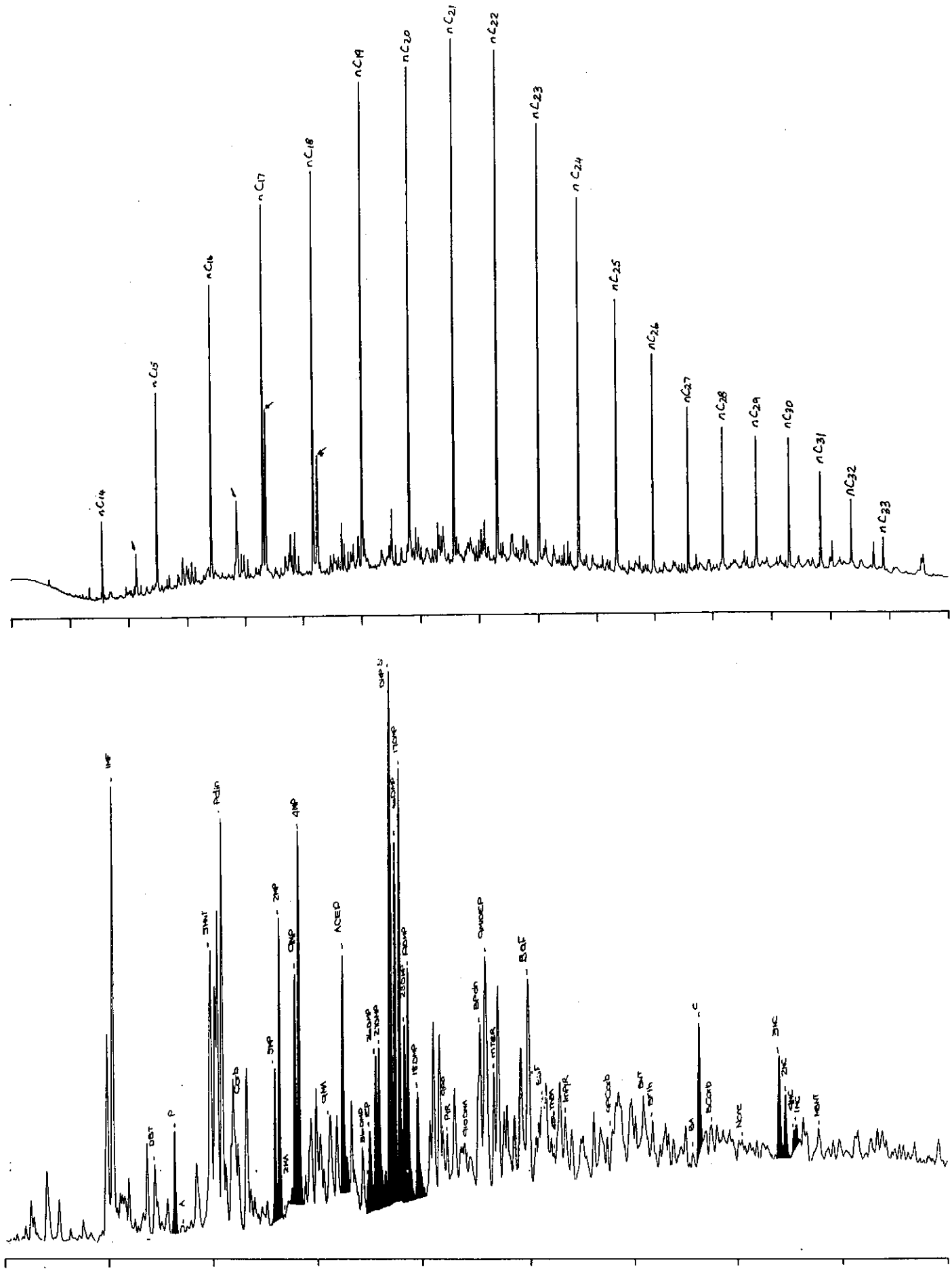

Figure D.04: Gas chromatograms of the total saturated and aromatic fractions of sample 6, well 88 DST 4, 2827m.

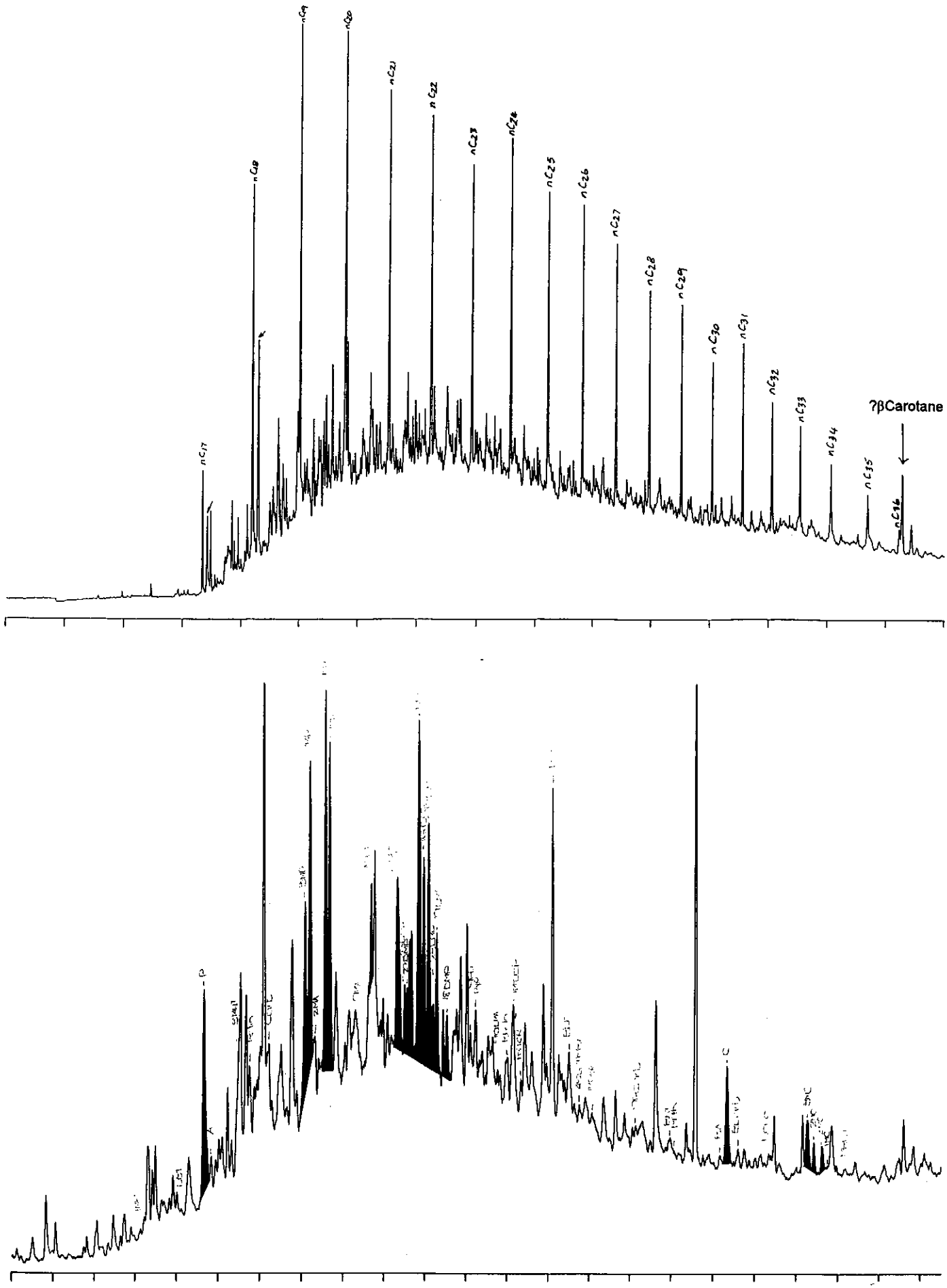

Figure D.05: Gas chromatograms of the total saturated and aromatic fractions of sample 7, well 92 core 1, 2949.0m.

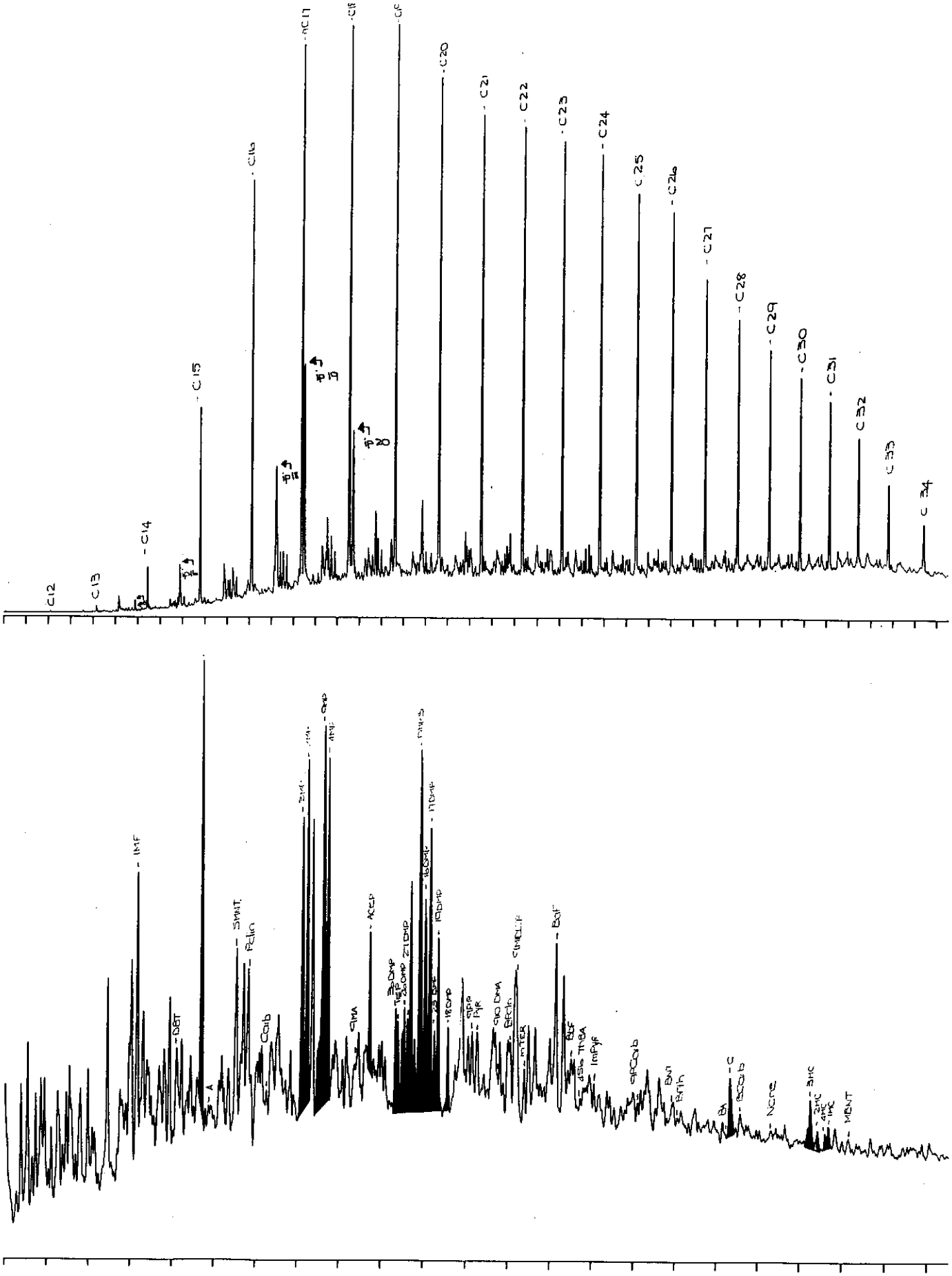

Figure D.06: Gas chromatograms of the total saturated and aromatic fractions of sample 8, well 118 core 1, 2563.1m.

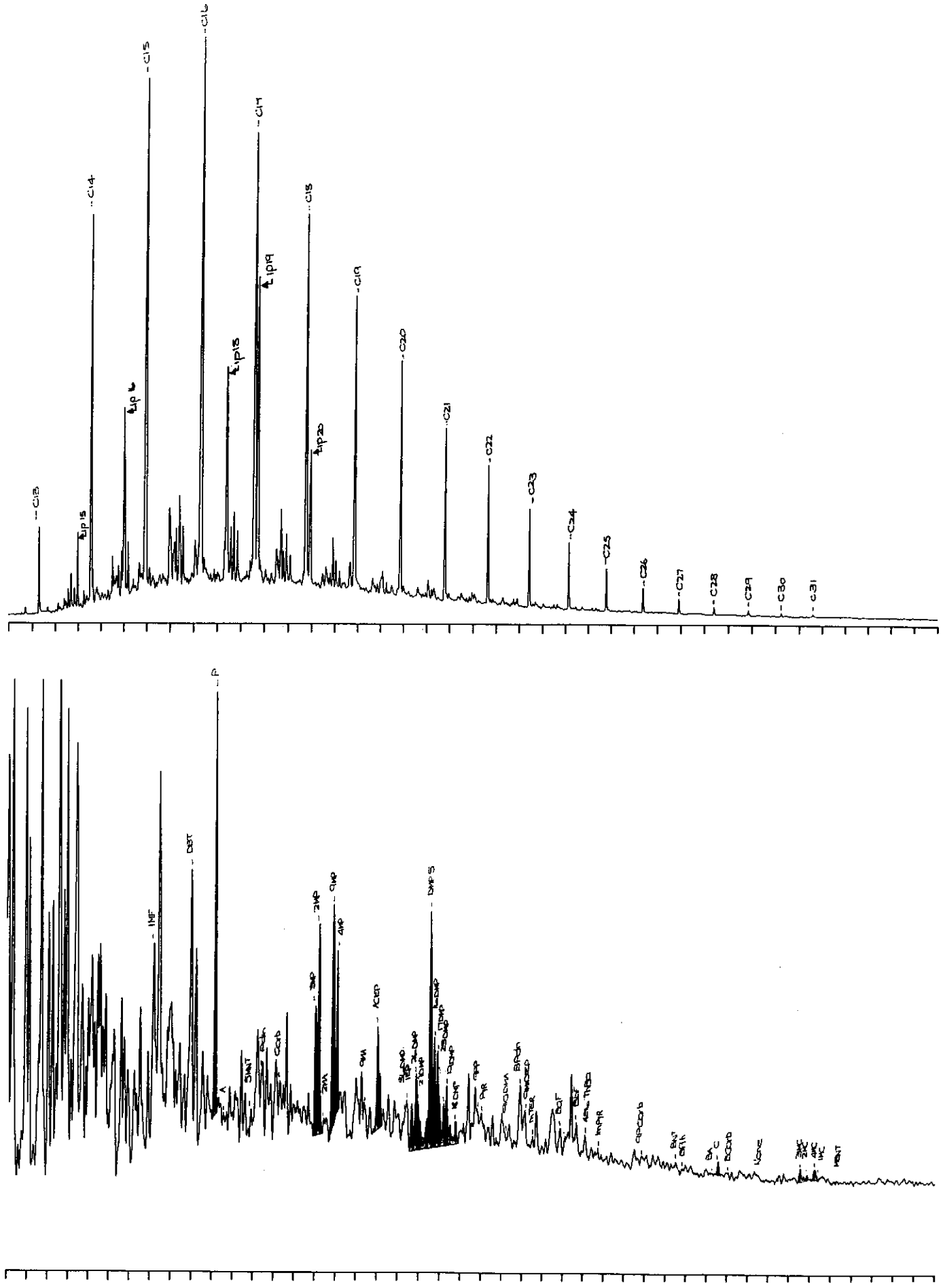

Figure D.07: Gas chromatograms of the total saturated and aromatic fractions of sample 9, well 102 DST 2, 2241m.

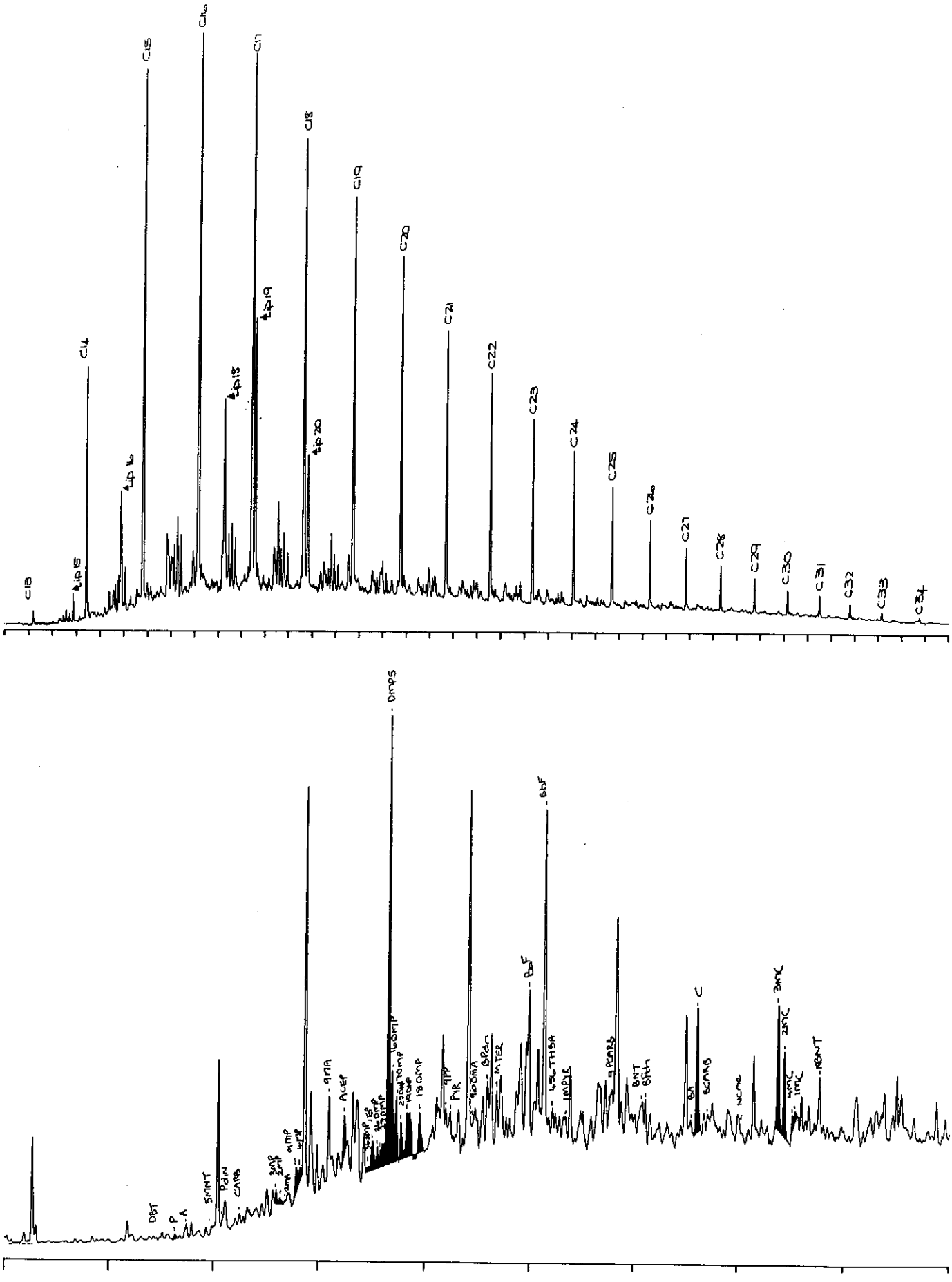

Figure D.08: Gas chromatograms of the total saturated and aromatic fractions of sample 10, well 102 DST 4, 2556m.

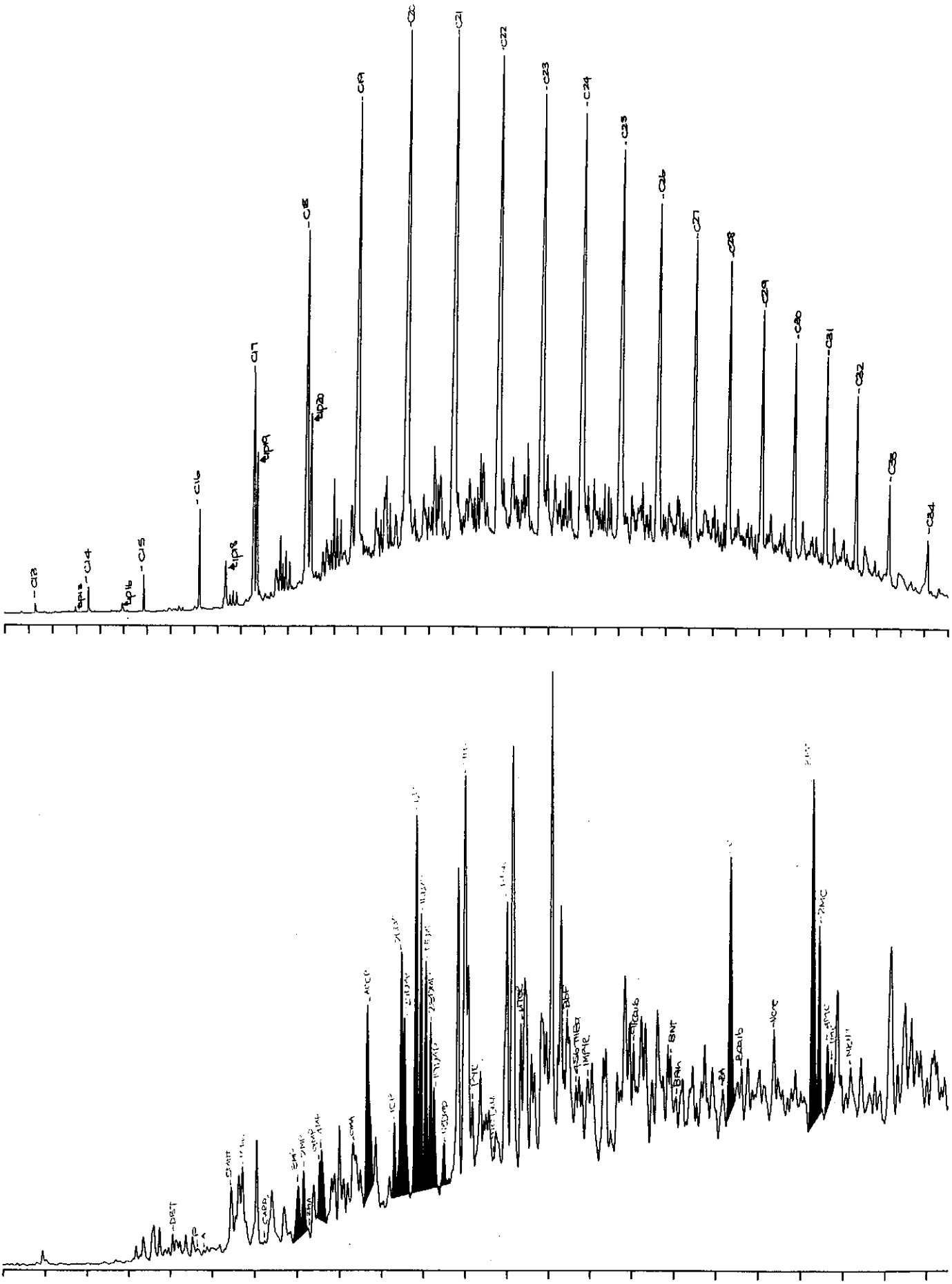

Figure D.09: Gas chromatograms of the total saturated and aromatic fractions of sample 11, well 91 core 1, 3220.05m.

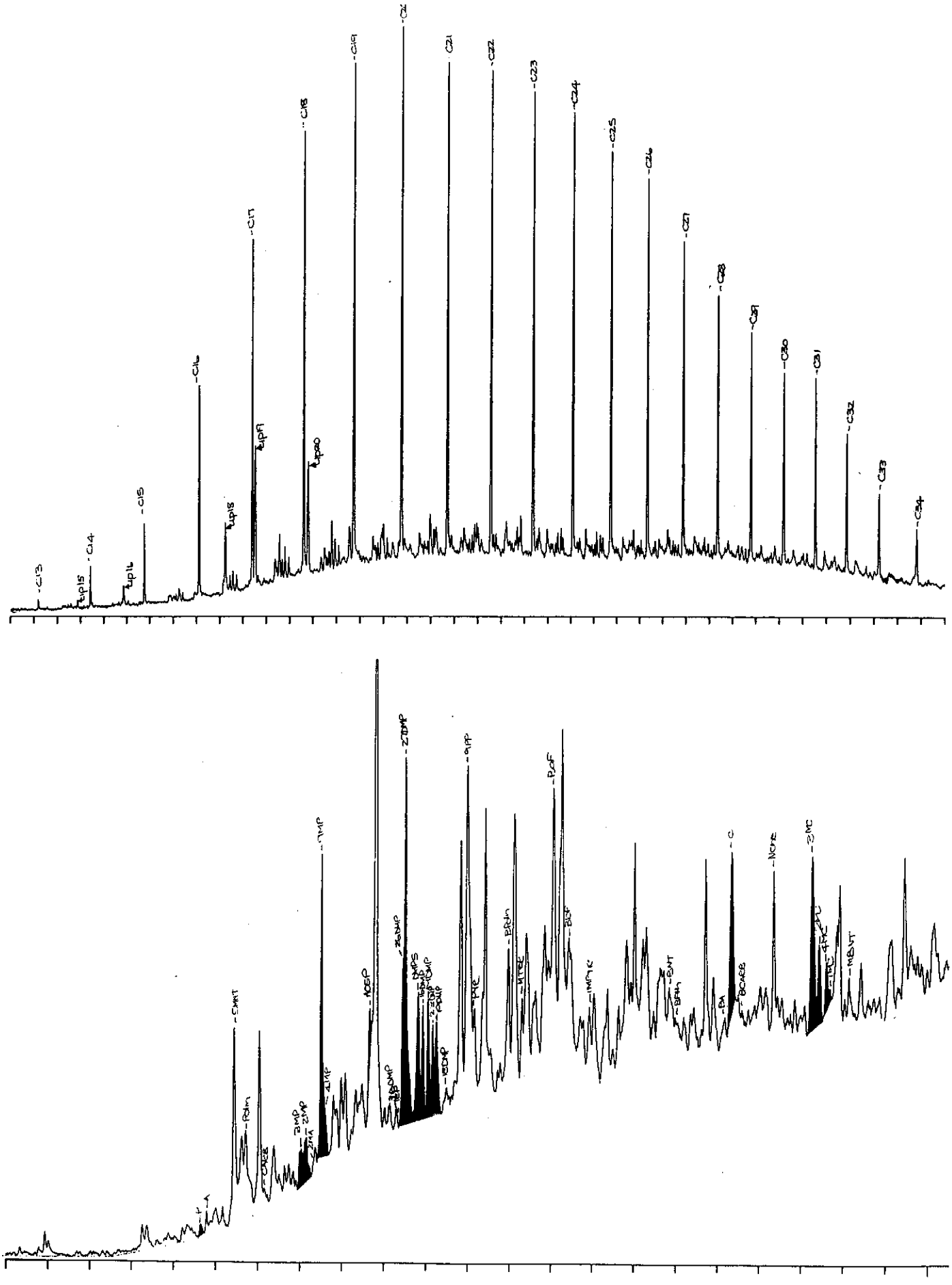

Figure D.10: Gas chromatograms of the total saturated and aromatic fractions of sample 12, well 104 core 2, 3017.46m.

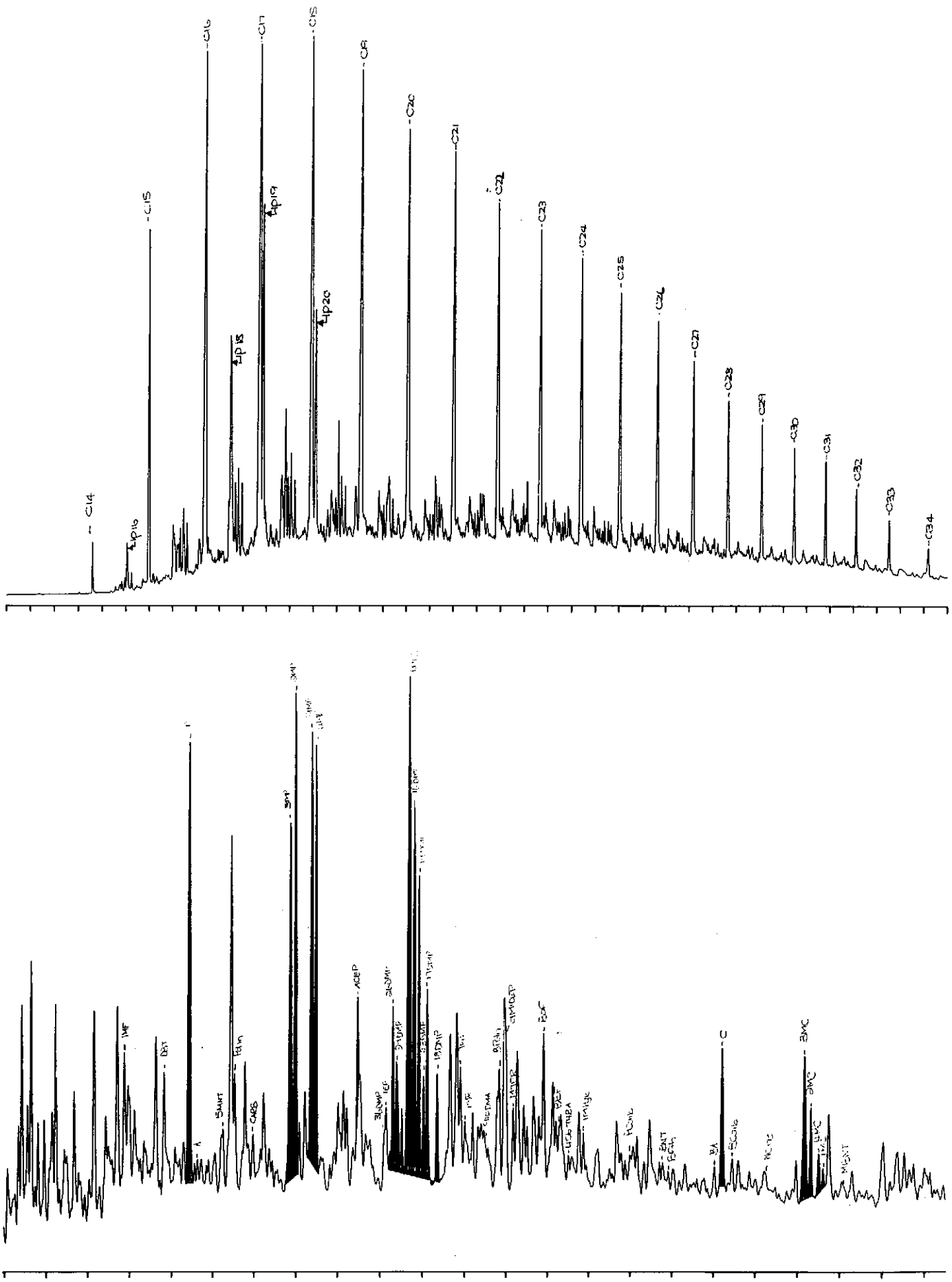

Figure D.11: Gas chromatograms of the total saturated and aromatic fractions of sample 13, well 93 core 4, 3212.4m.

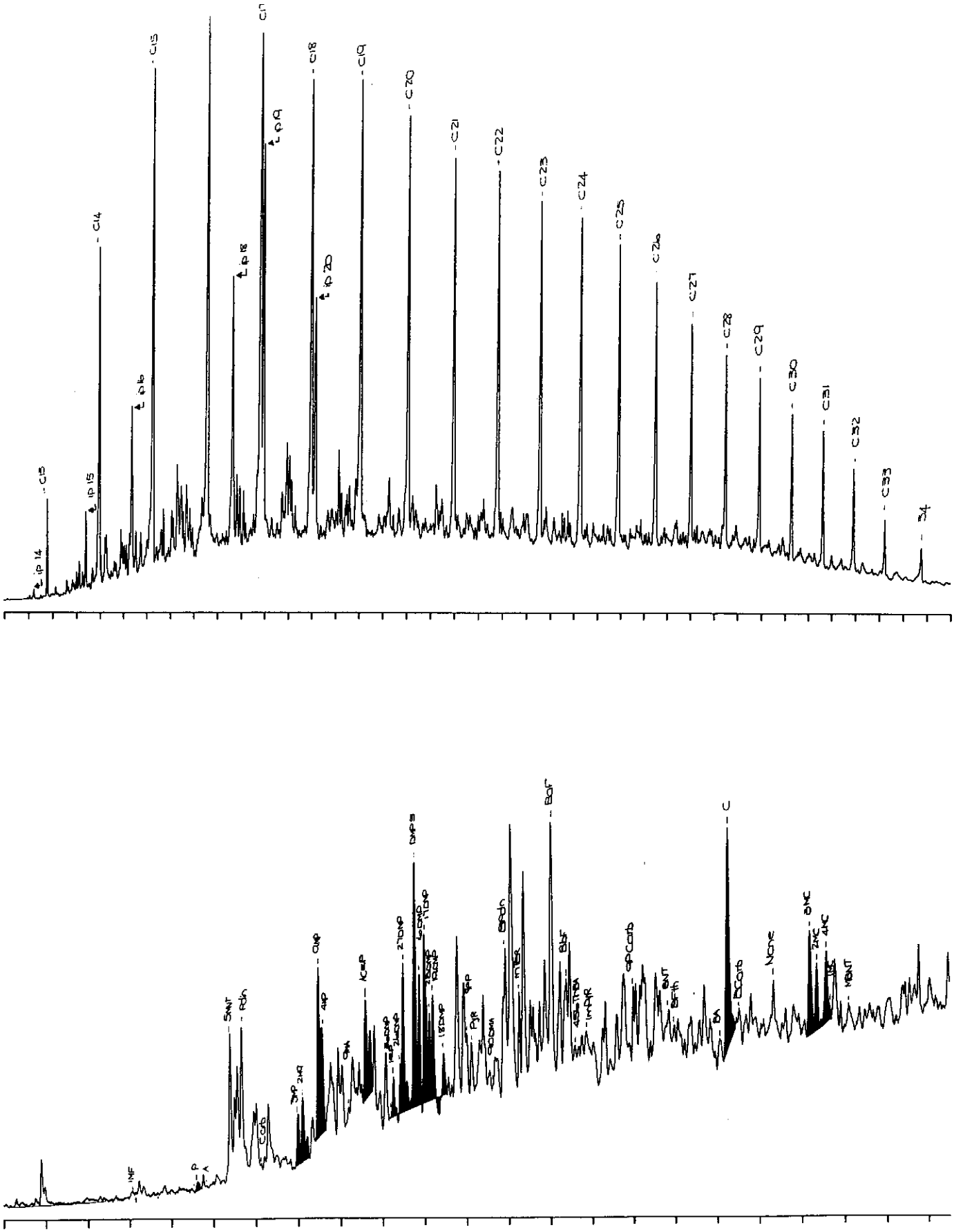

Figure D.12: Gas chromatograms of the total saturated and aromatic fractions of sample 14, well 109 DST 1, 2630m.

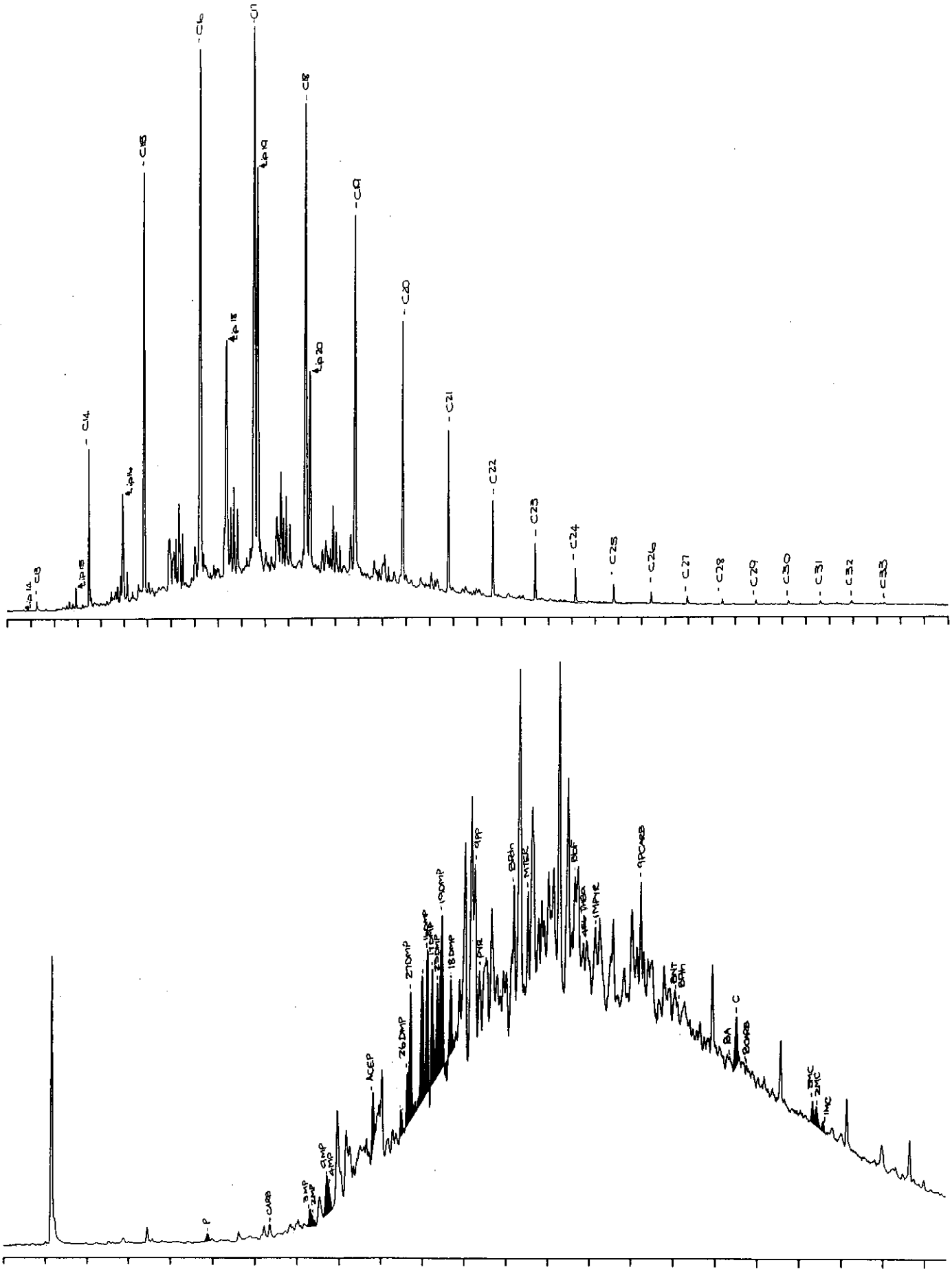

Figure D.13: Gas chromatograms of the total saturated and aromatic fractions of sample 15, well 107 DST 2, 2565m.

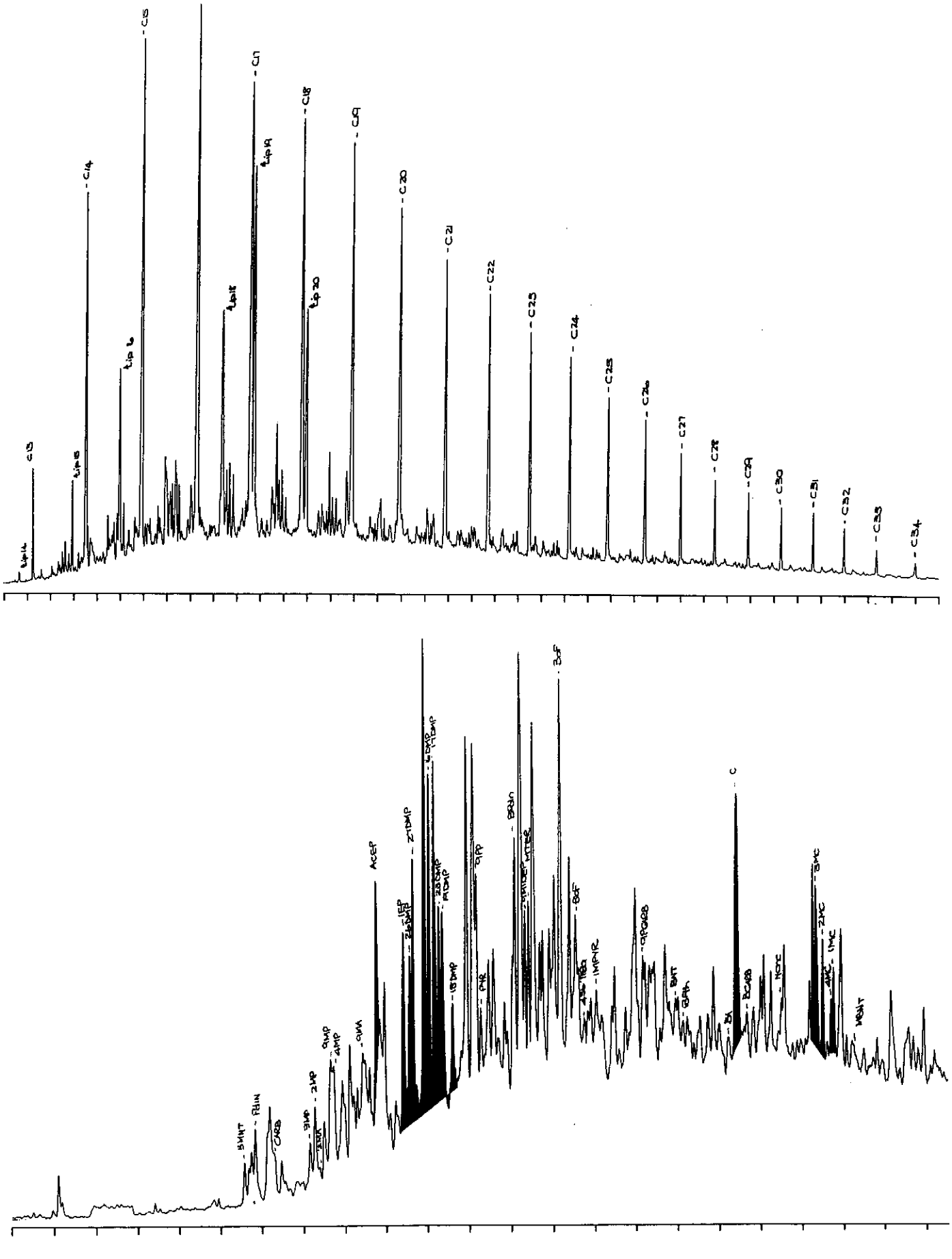

Figure D.14: Gas chromatograms of the total saturated and aromatic fractions of sample 16, well 110 DST 1, 3051m.

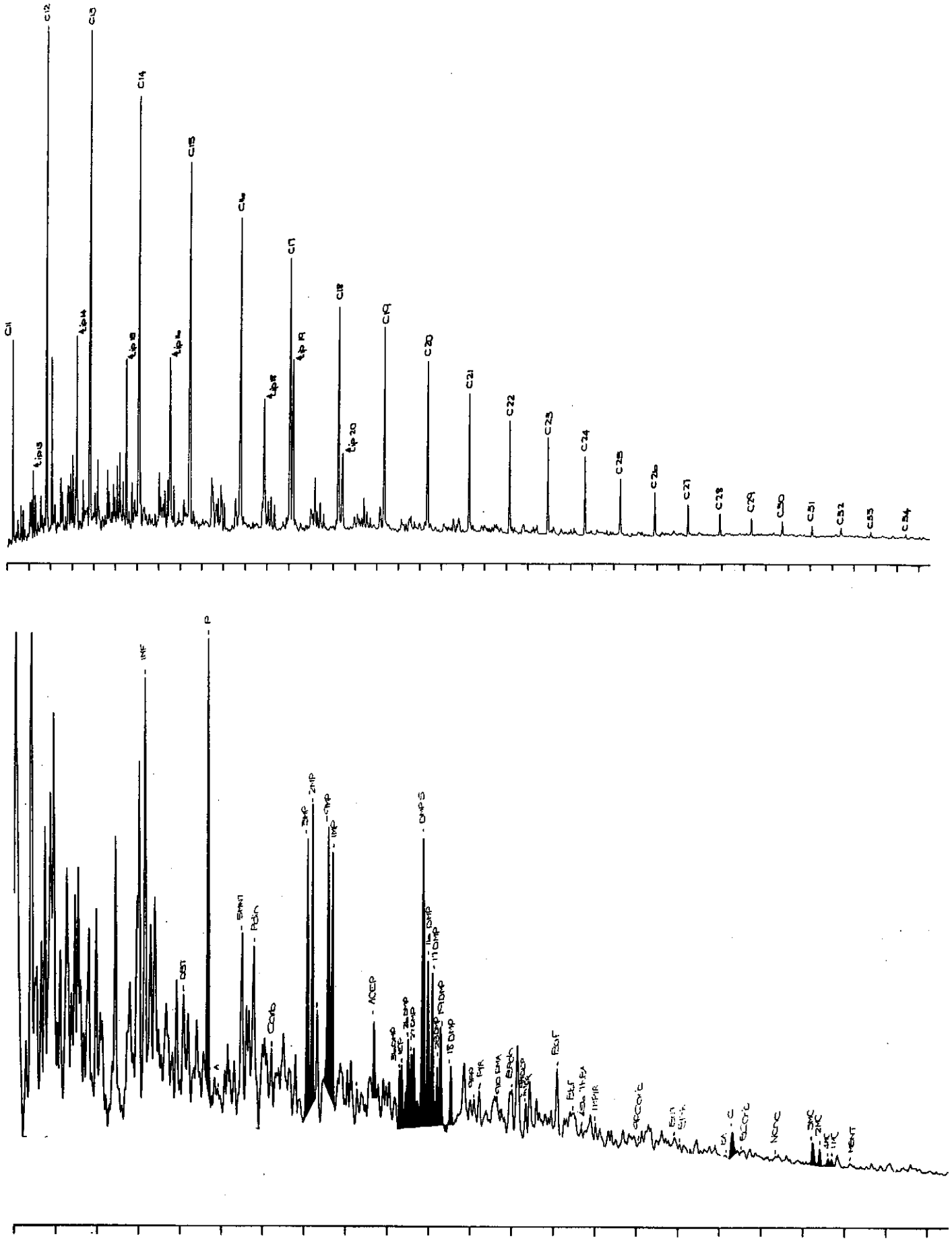

Figure D.15: Gas chromatograms of the total saturated and aromatic fractions of sample 17, well 126 DST 1, 2643m.

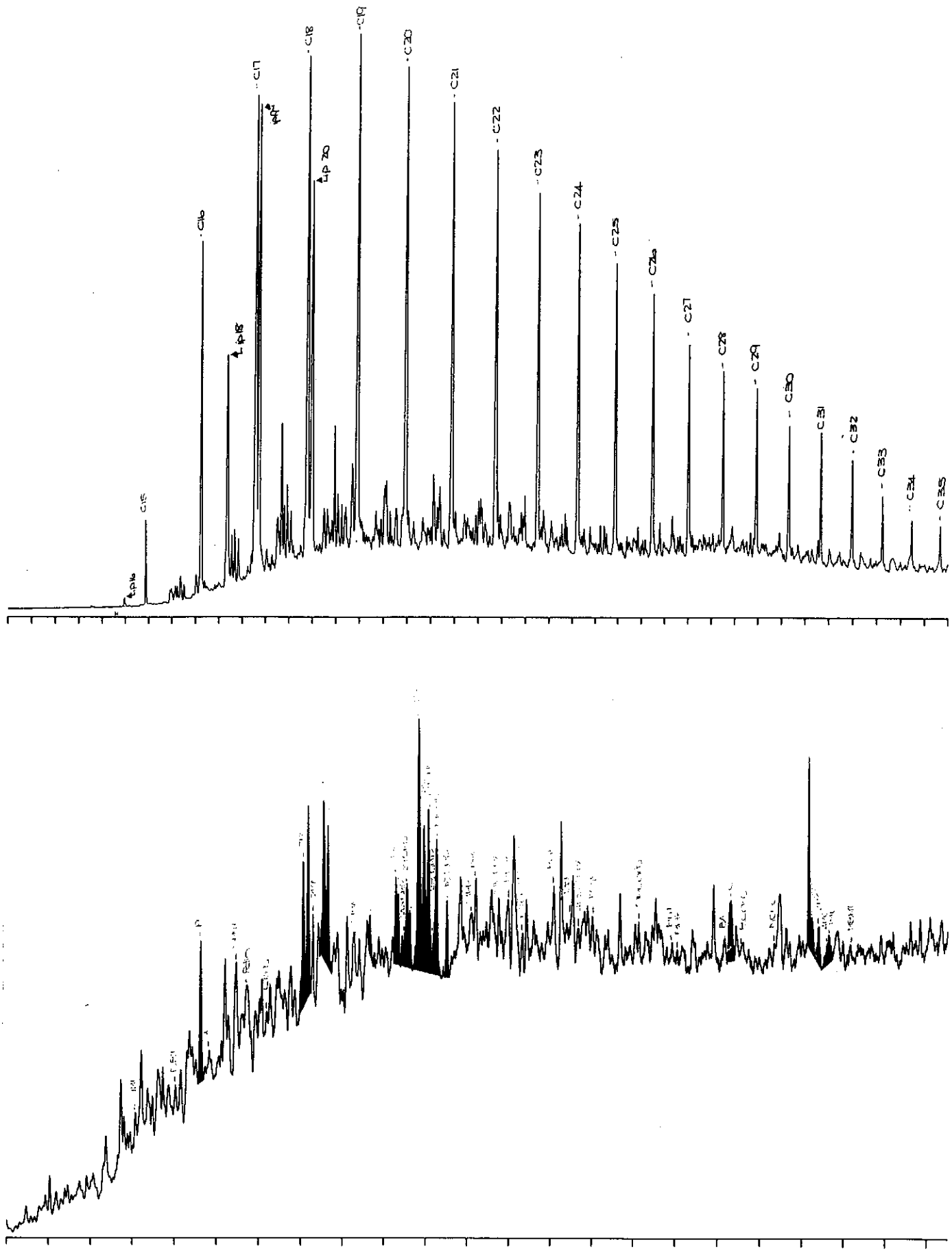

Figure D.16: Gas chromatograms of the total saturated and aromatic fractions of sample 18, well 122 SWC, 2517m.

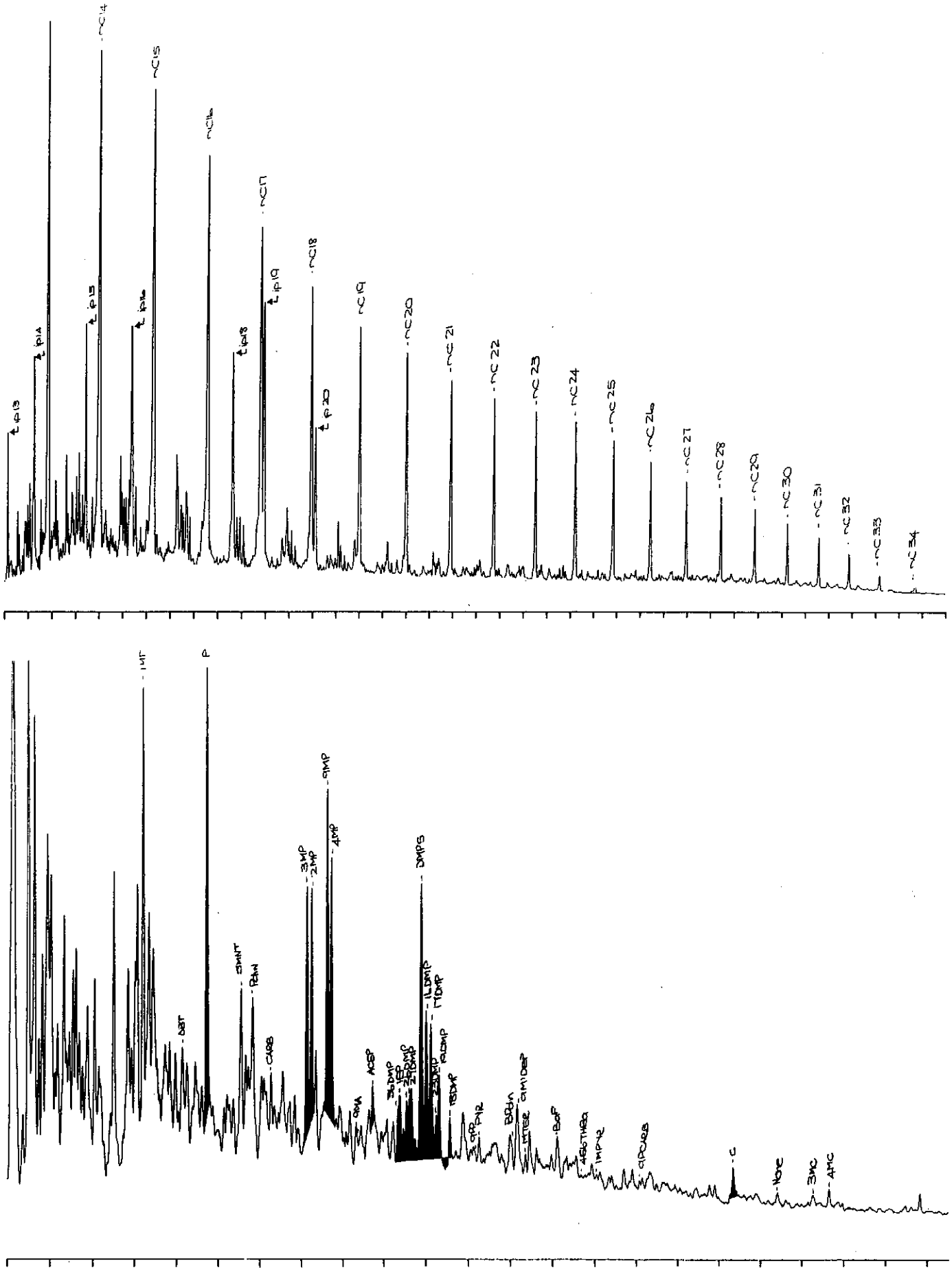

Figure D.17: Gas chromatograms of the total saturated and aromatic fractions of sample 19, well 132 DST 2, 2662m.

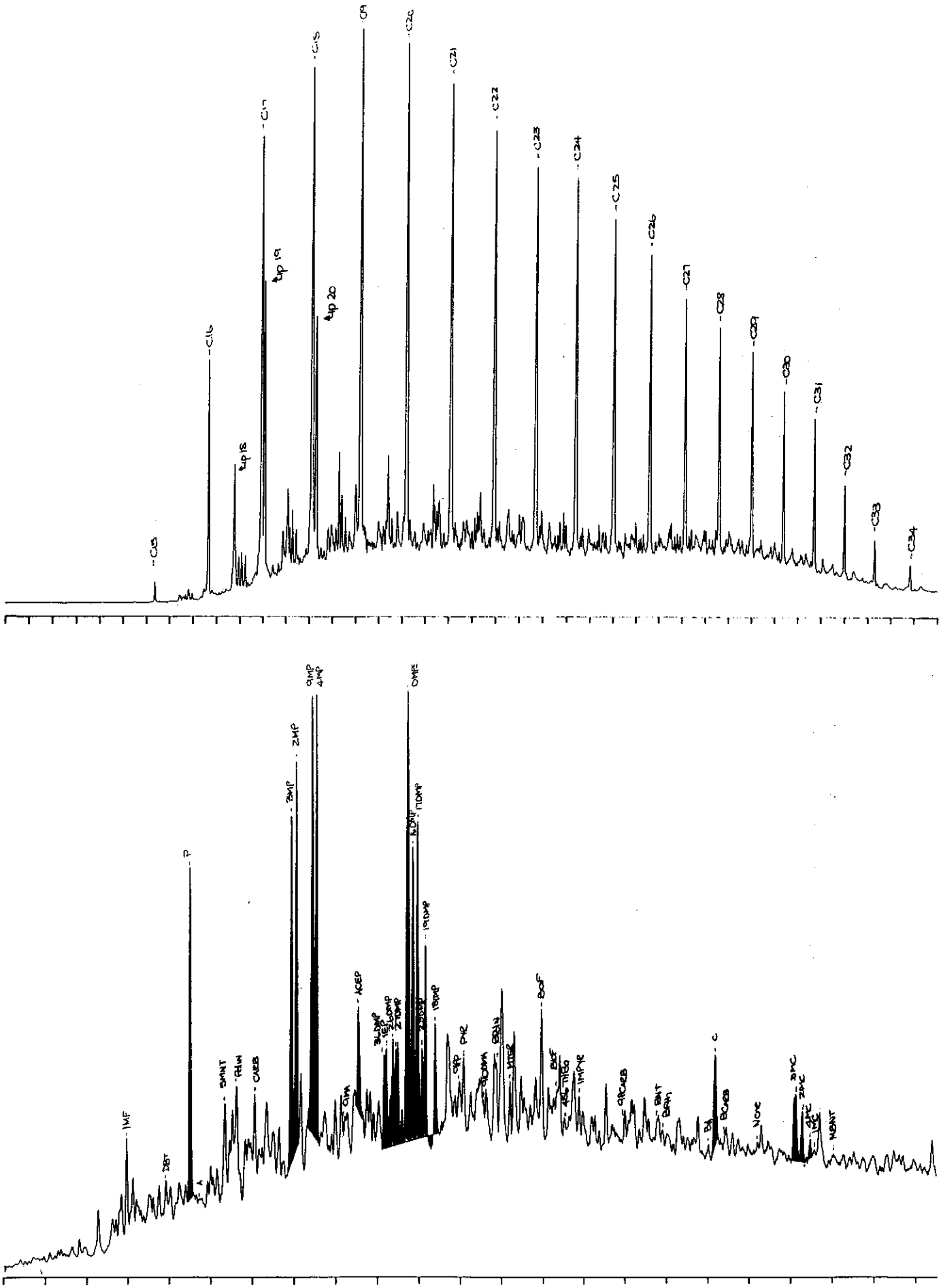

Figure D.18: Gas chromatograms of the total saturated and aromatic fractions of sample 20, well 132 core 1, 2702.43m.

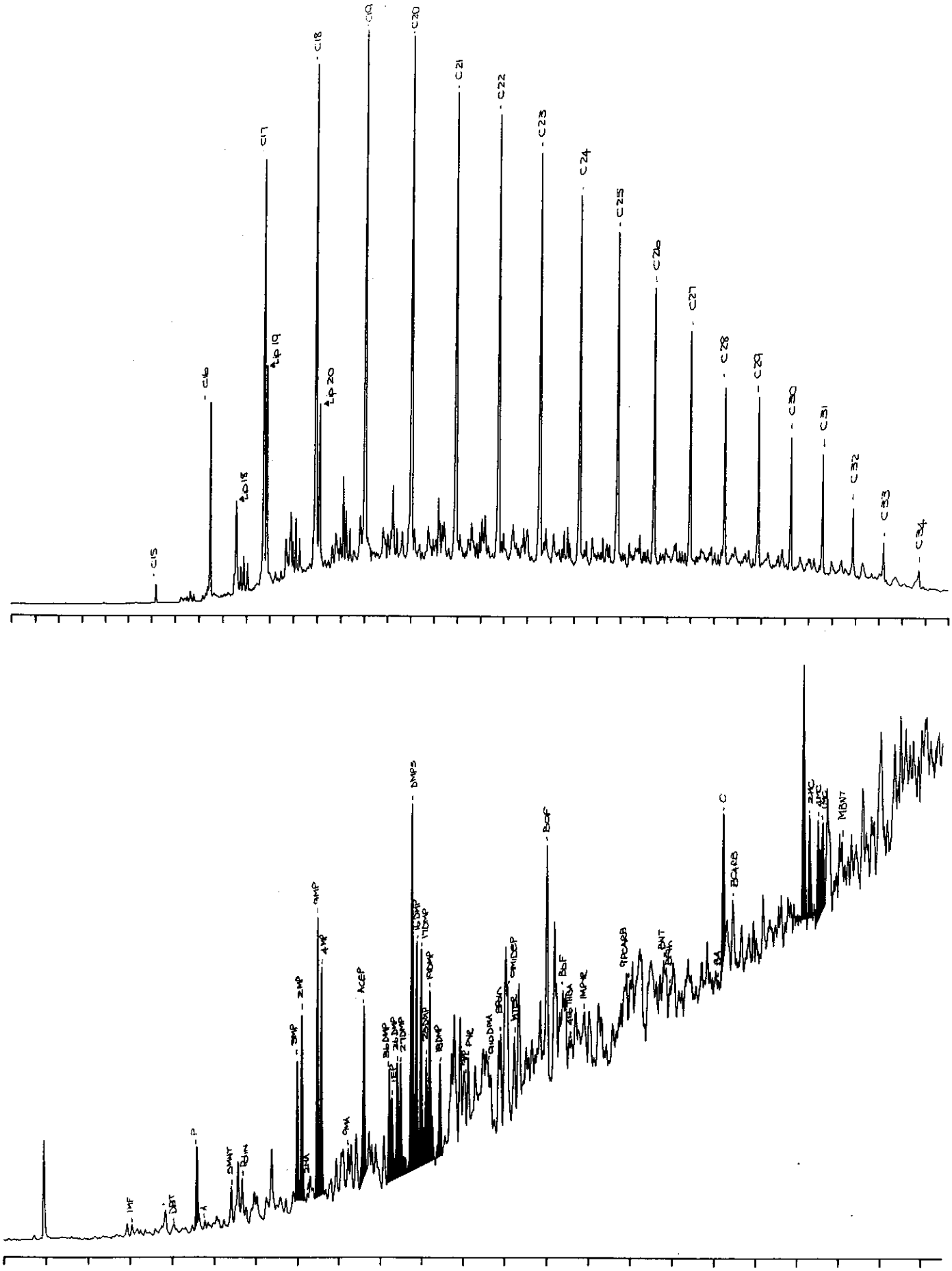

Figure D. 19: Gas chromatograms of the total saturated and aromatic fractions of sample 21, well 48 DST 2, 2620m.

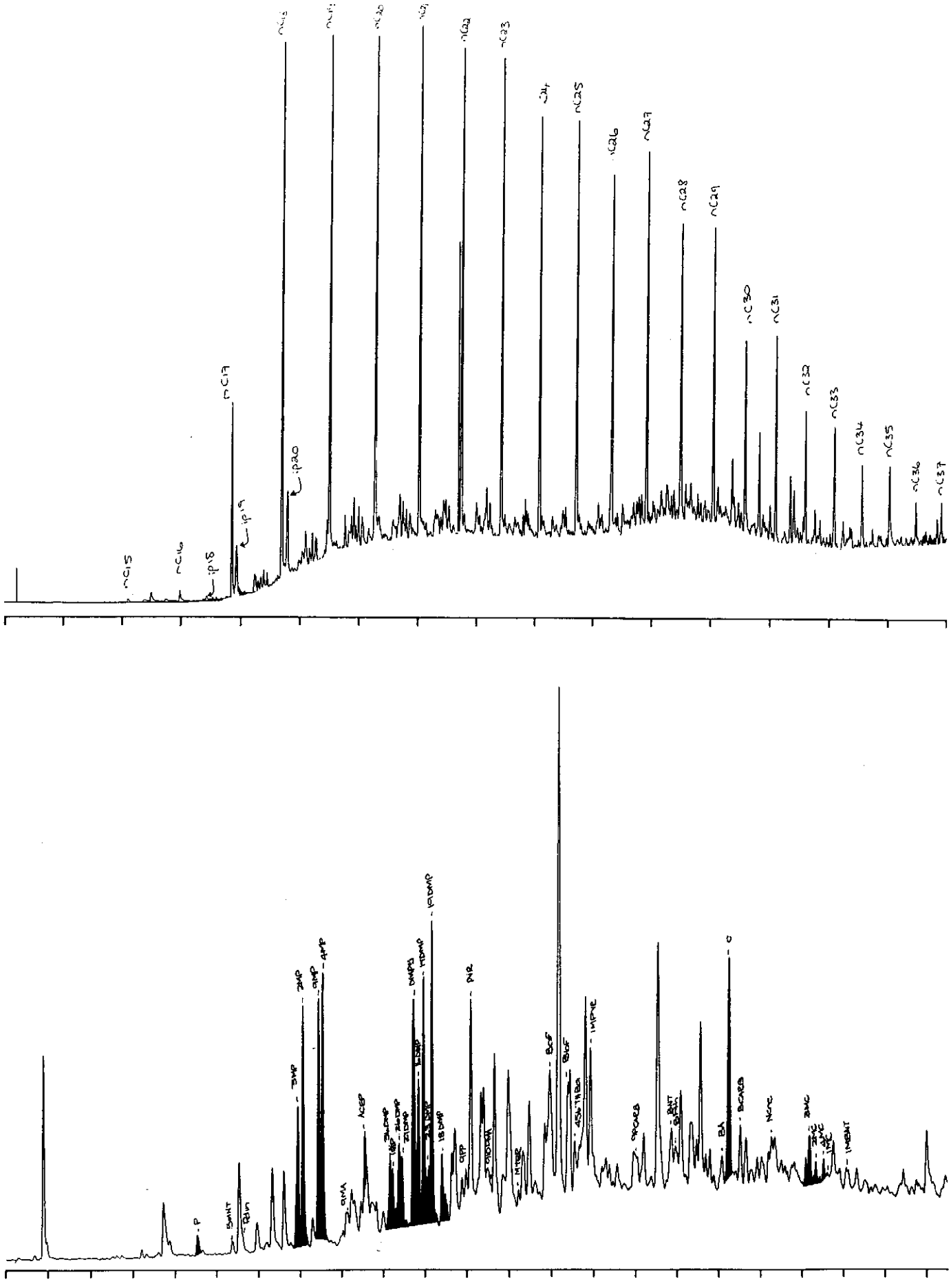

Figure D.20: Gas chromatograms of the total saturated and aromatic fractions of sample 22, well 16 RC, 2614m.

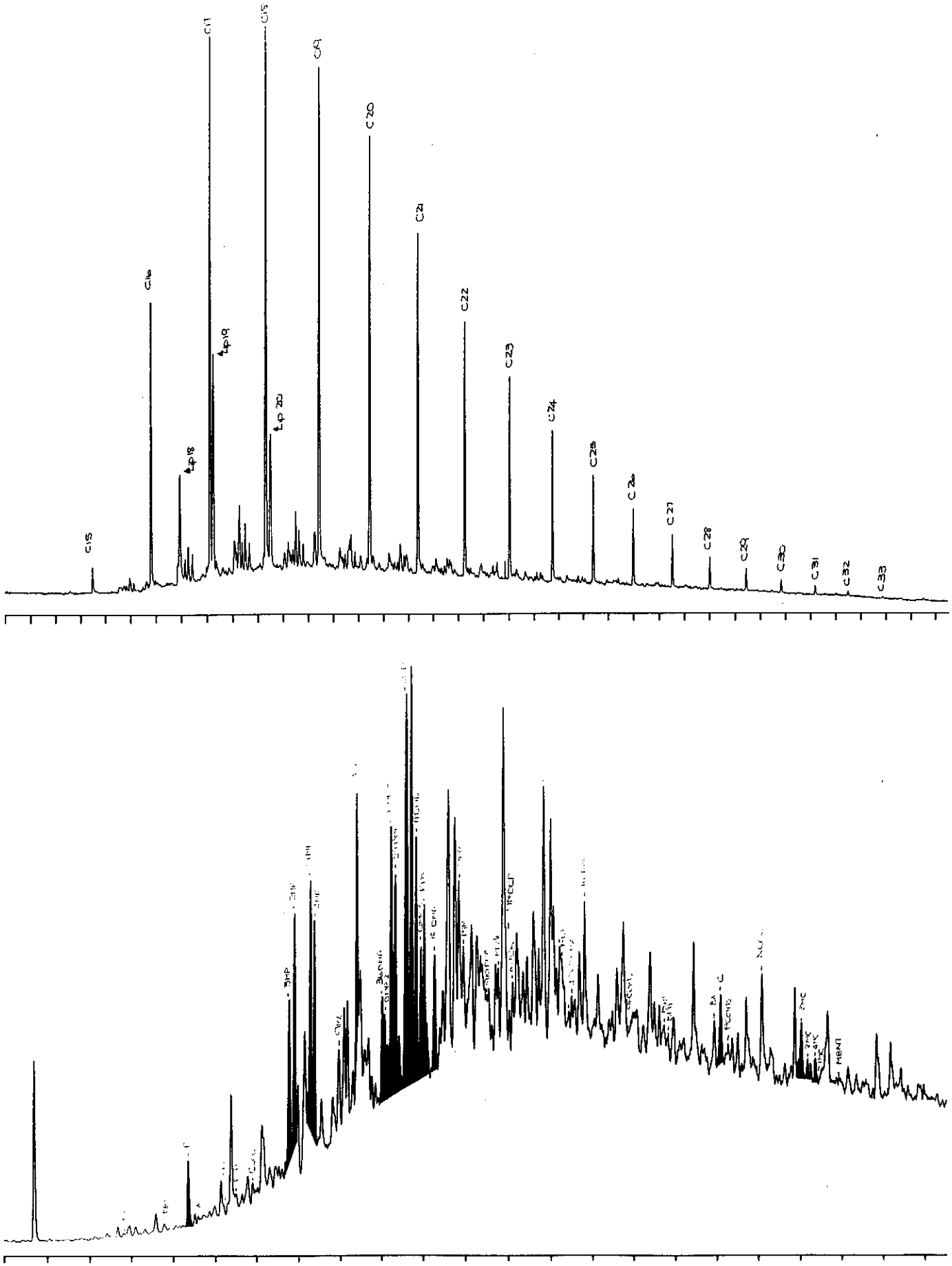

Figure D.21: Gas chromatograms of the total saturated and aromatic fractions of sample 23, well 59 DST 1, 2122m.

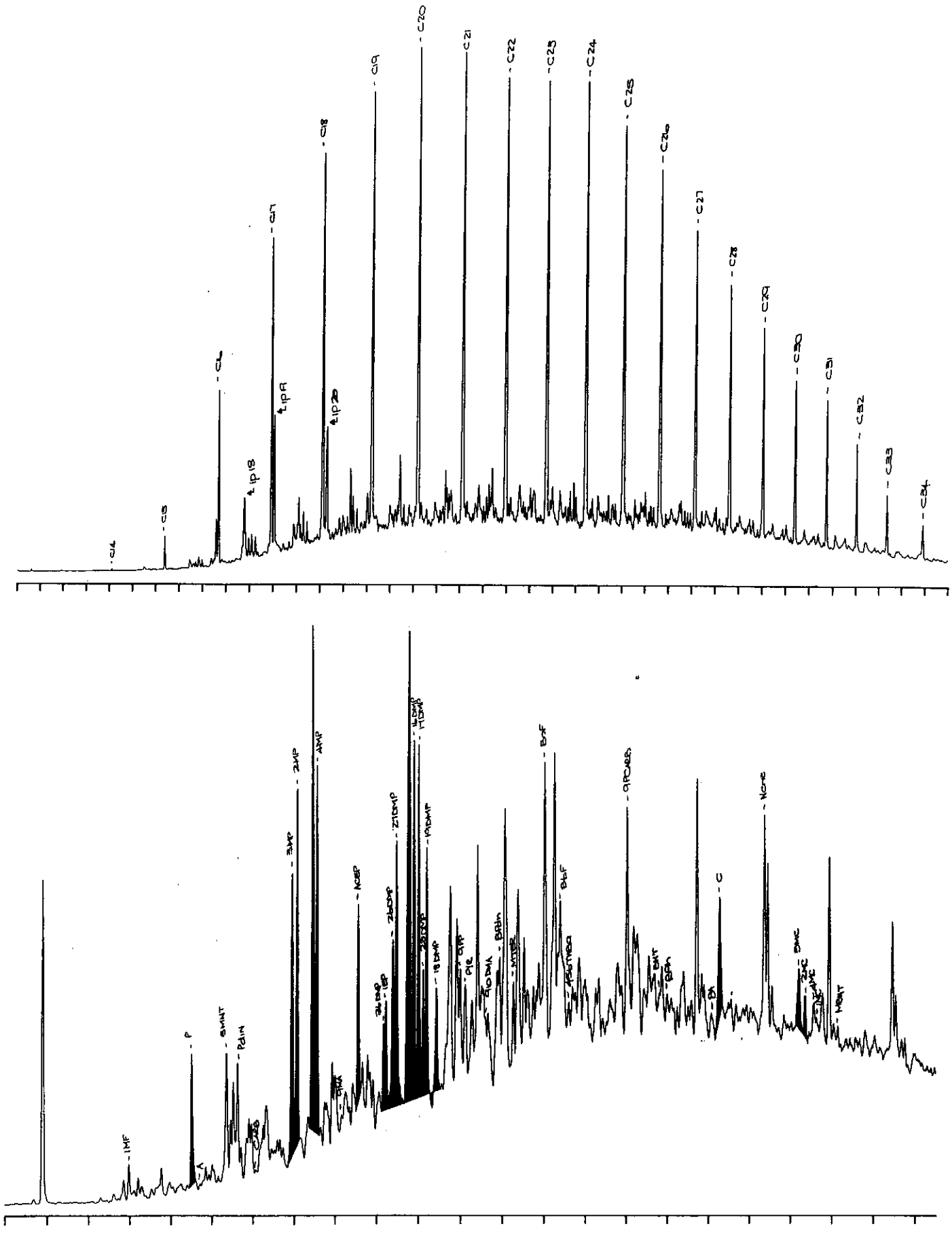

Figure D.22: Gas chromatograms of the total saturated and aromatic fractions of sample 24, well 75 core 1, 2830.5m.

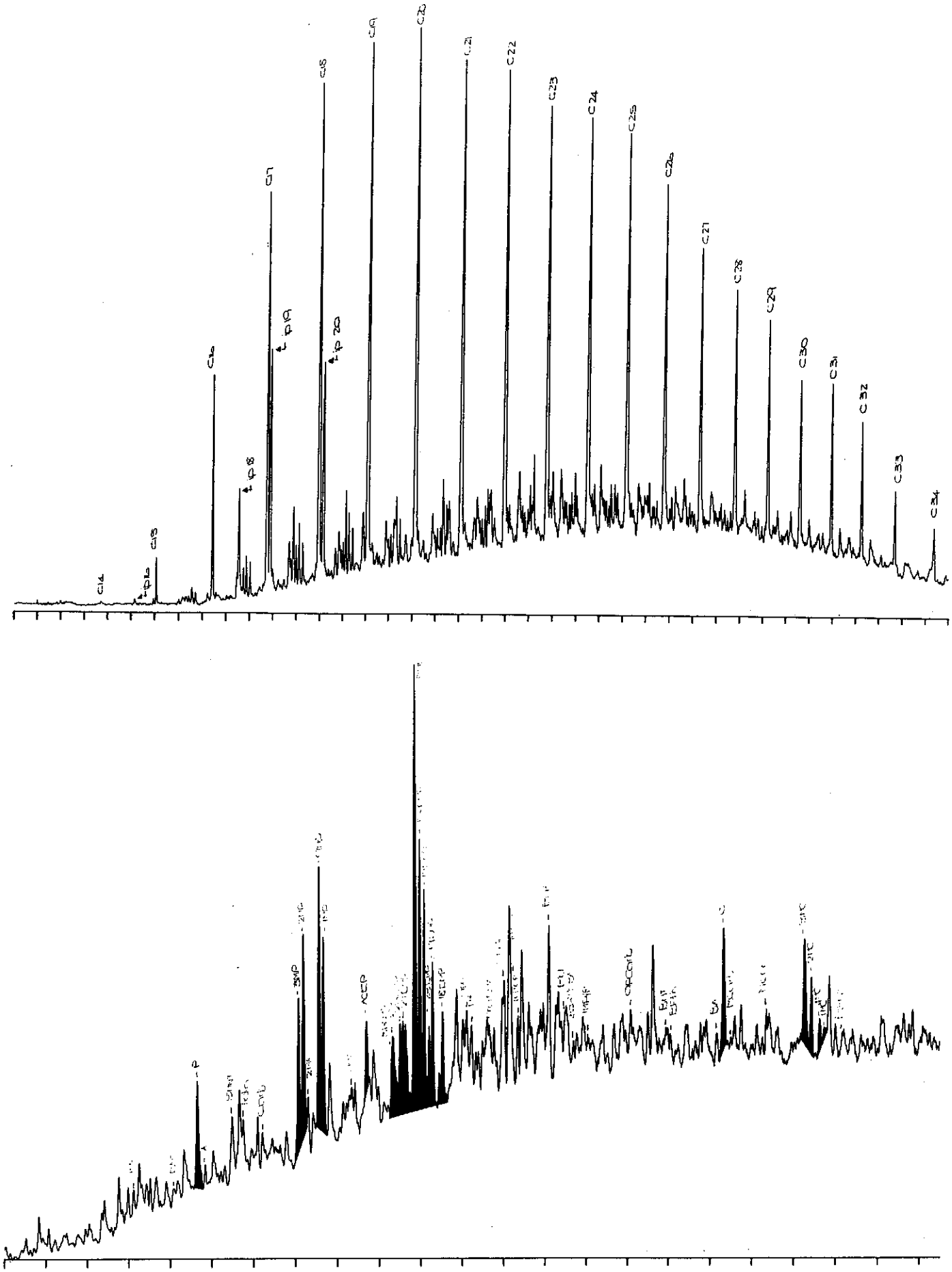

Figure D.23: Gas chromatograms of the total saturated and aromatic fractions of sample 25, well 101 core 1, 2987.5m.

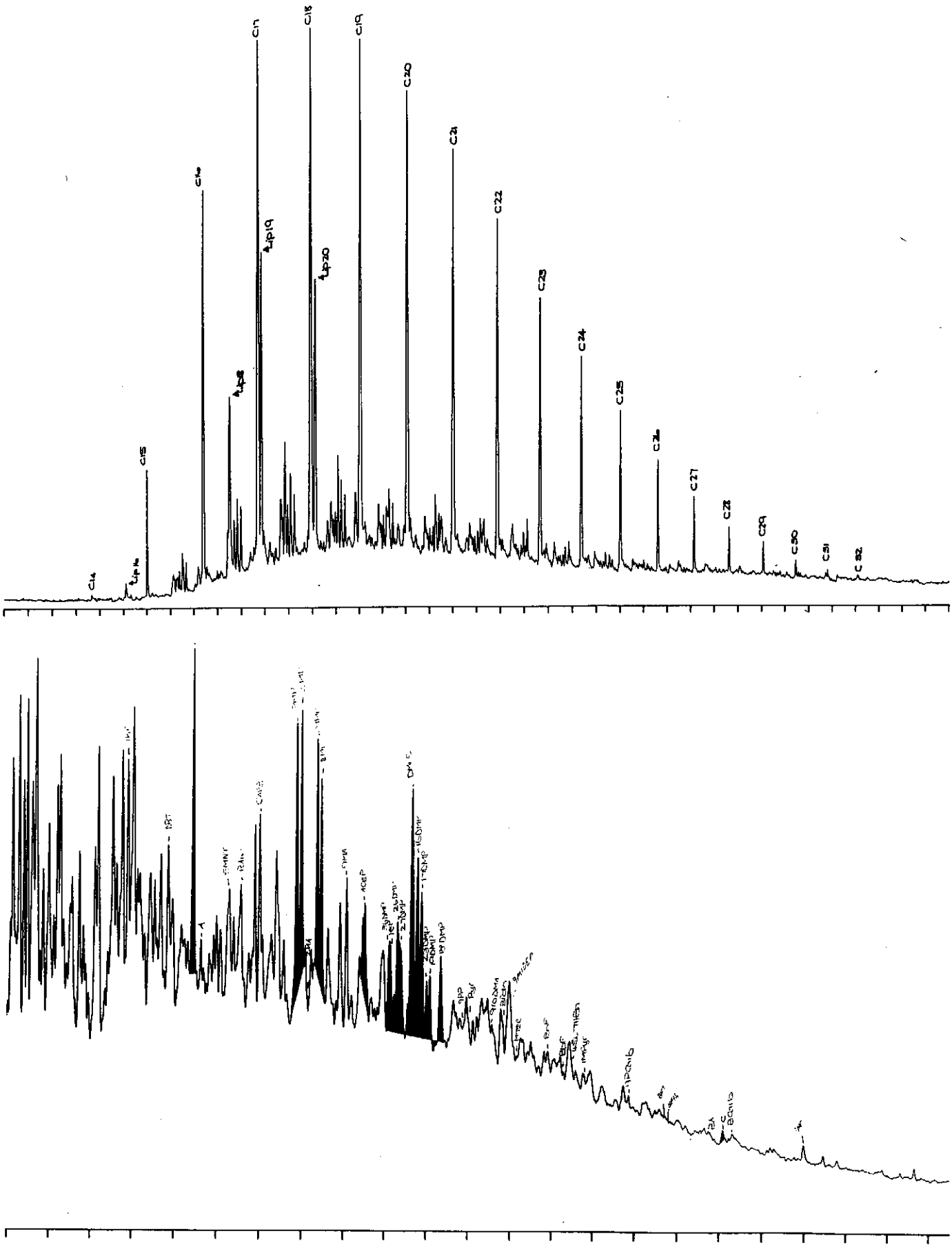

Figure D.24: Gas chromatograms of the total saturated and aromatic fractions of sample 26, well 20 DST2, 2699m.

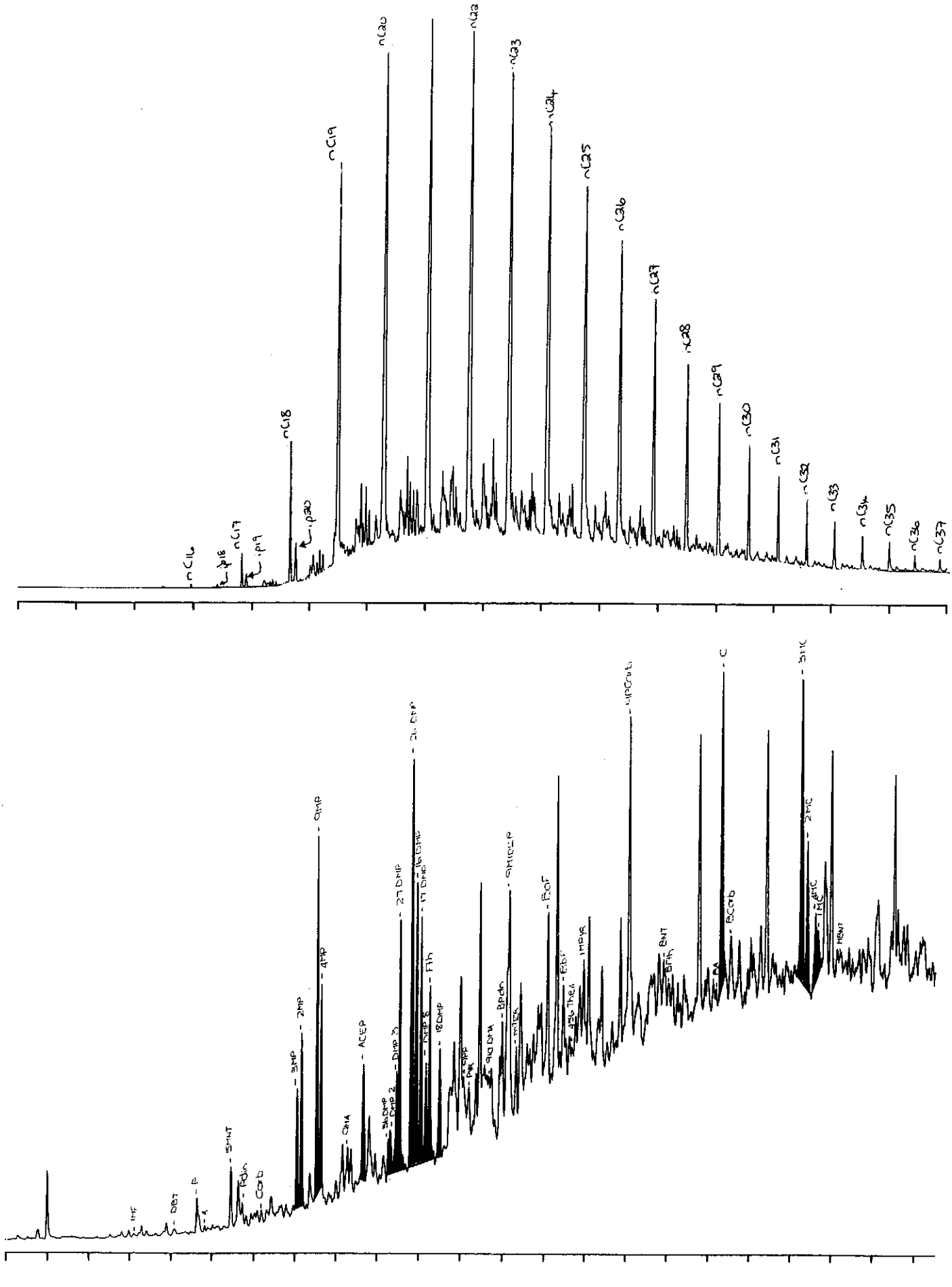

Figure D.25: Gas chromatograms of the total saturated and aromatic fractions of sample 27, well 13 core 1, 2518.86m.

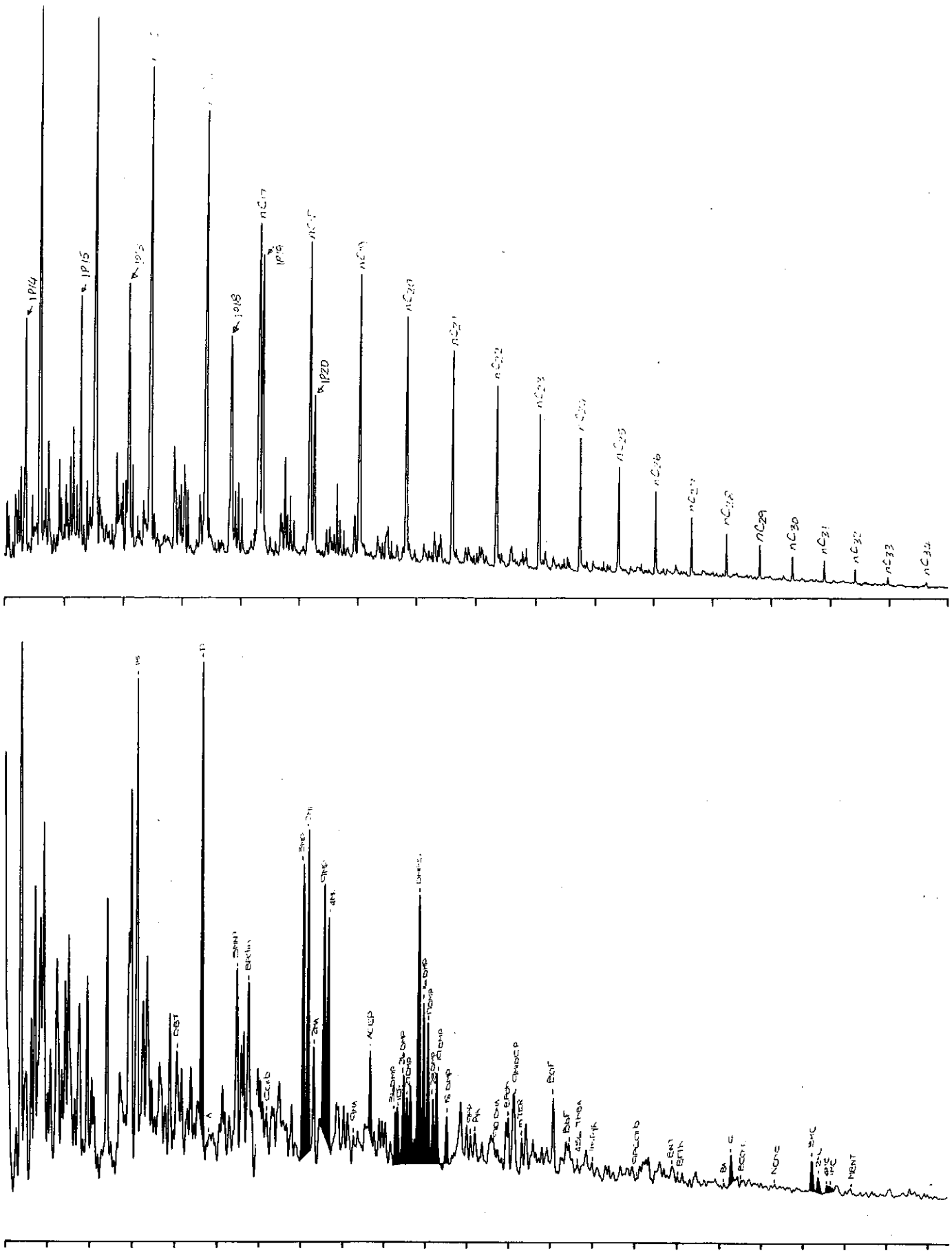

Figure D.26: Gas chromatograms of the total saturated and aromatic fractions of sample 28, well 103 DST 1, 2718m.

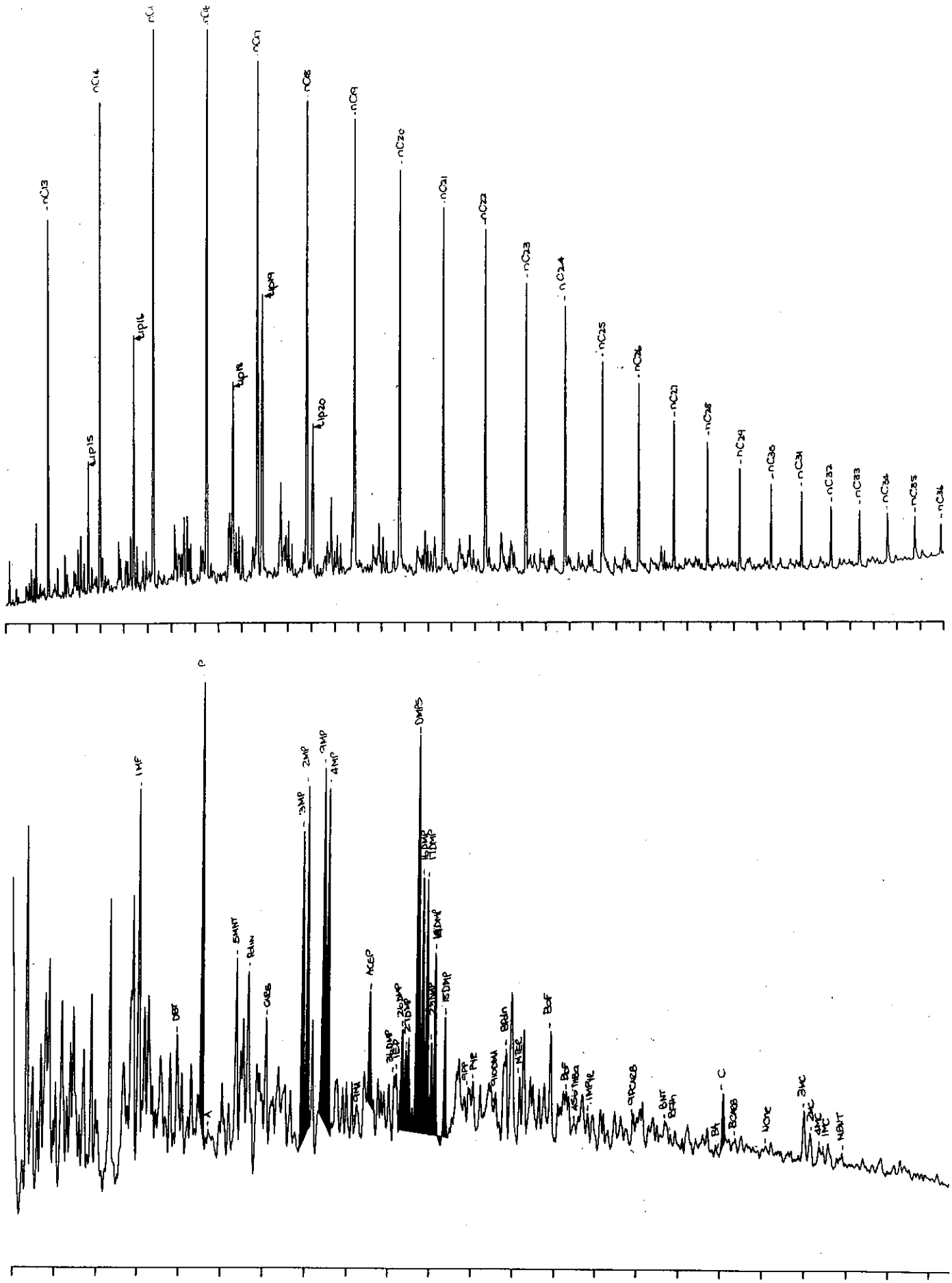

Figure D.27: Gas chromatograms of the total saturated and aromatic fractions of sample 29, well 94 DST 1, 2799m.

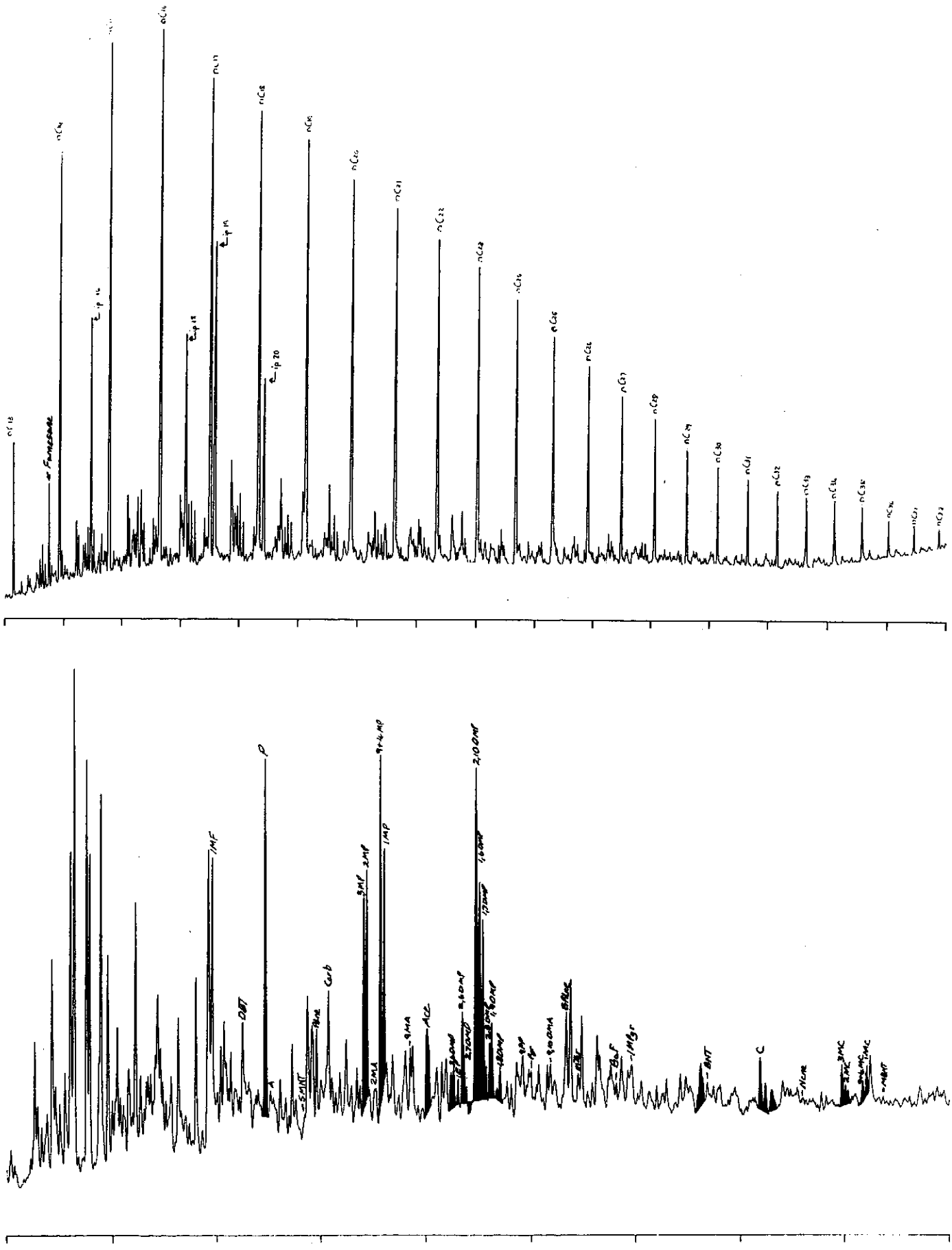

Figure D.28: Gas chromatograms of the total saturated and aromatic fractions of sample 30, well 156 DST 1, 2522m.

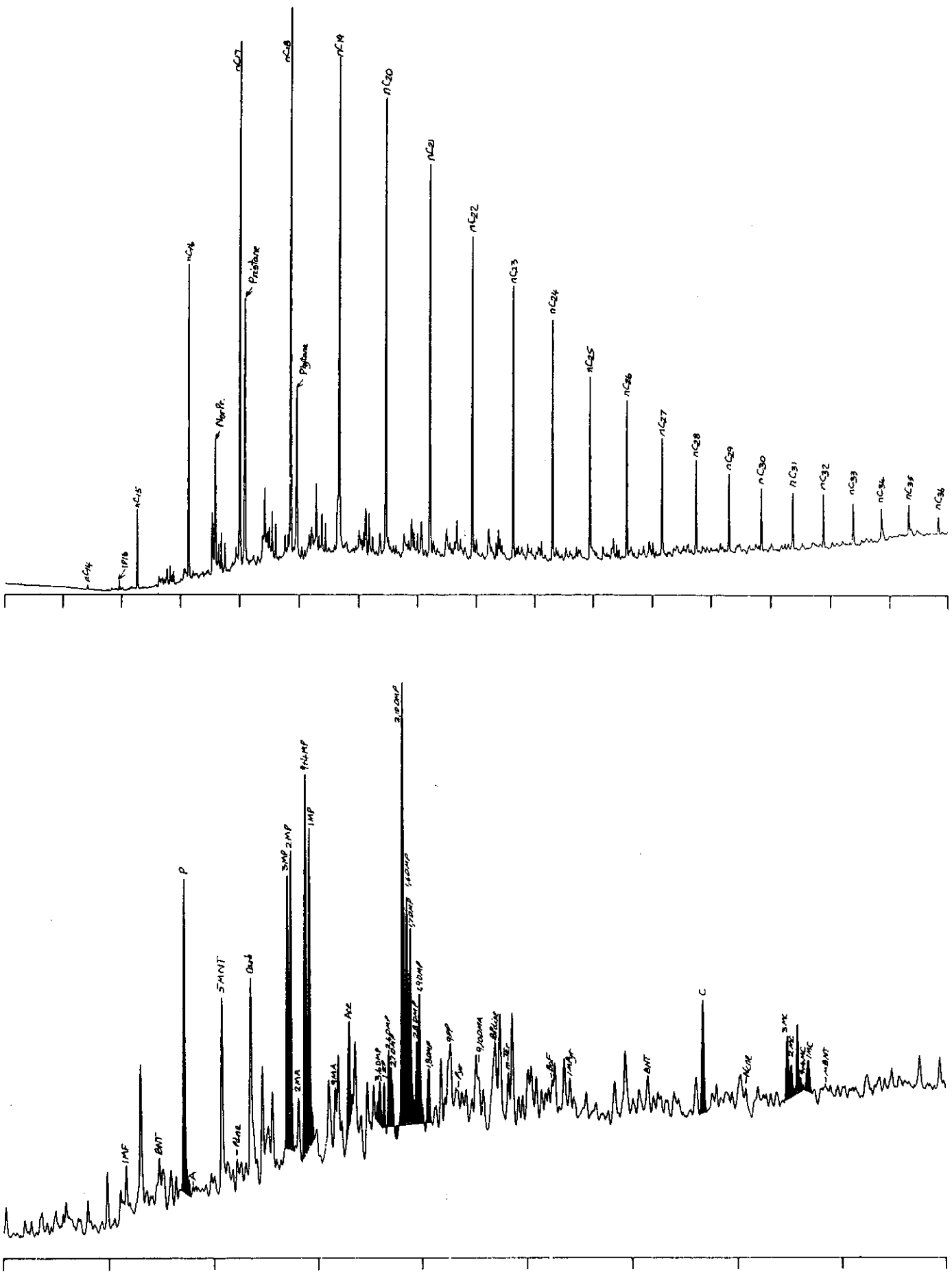

Figure D.29: Gas chromatograms of the total saturated and aromatic fractions of sample 31, well 156 core 1, 2525m.

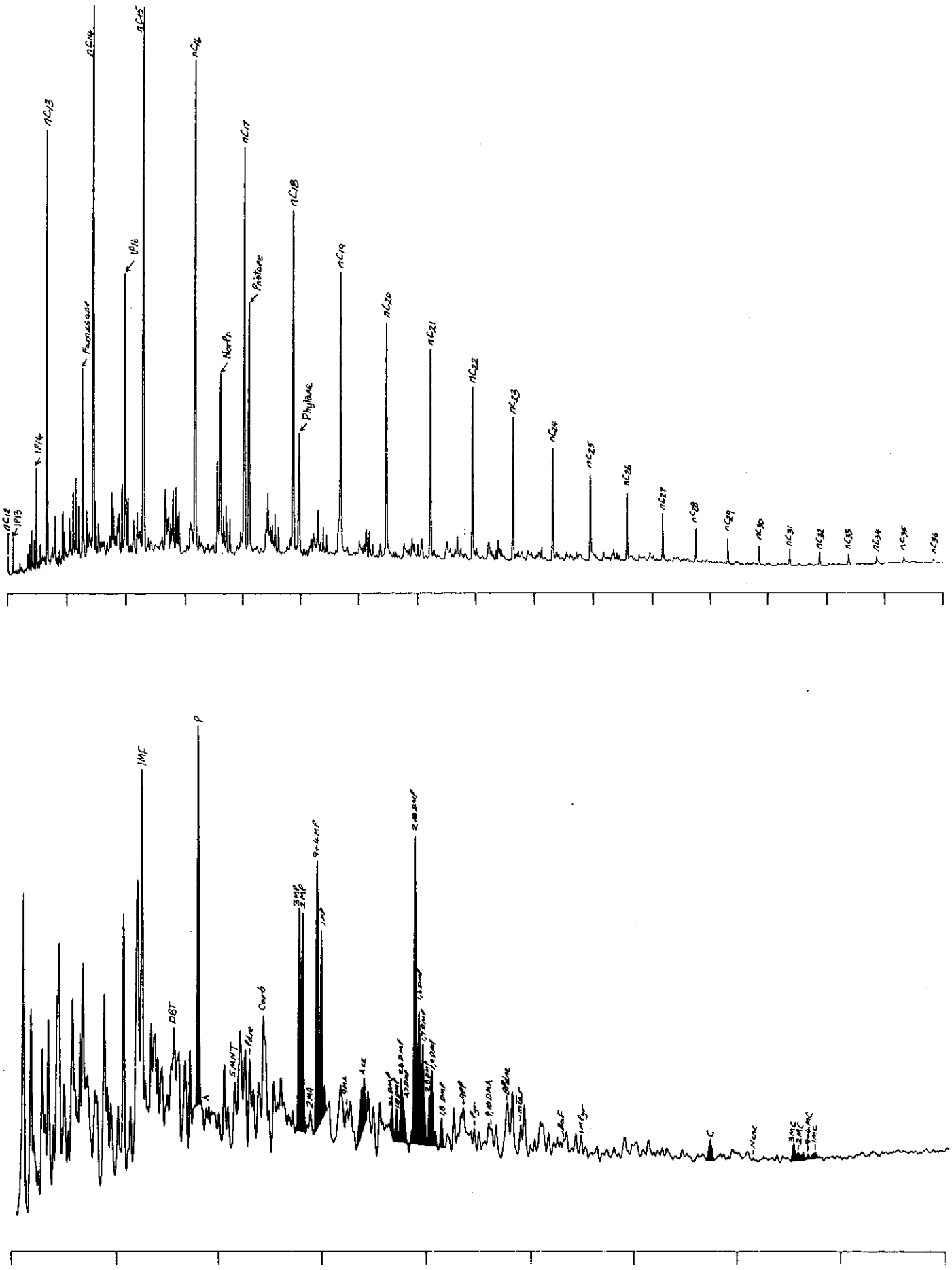

Figure D.30: Gas chromatograms of the total saturated and aromatic fractions of sample 32, well 166 RFT, 2508m.

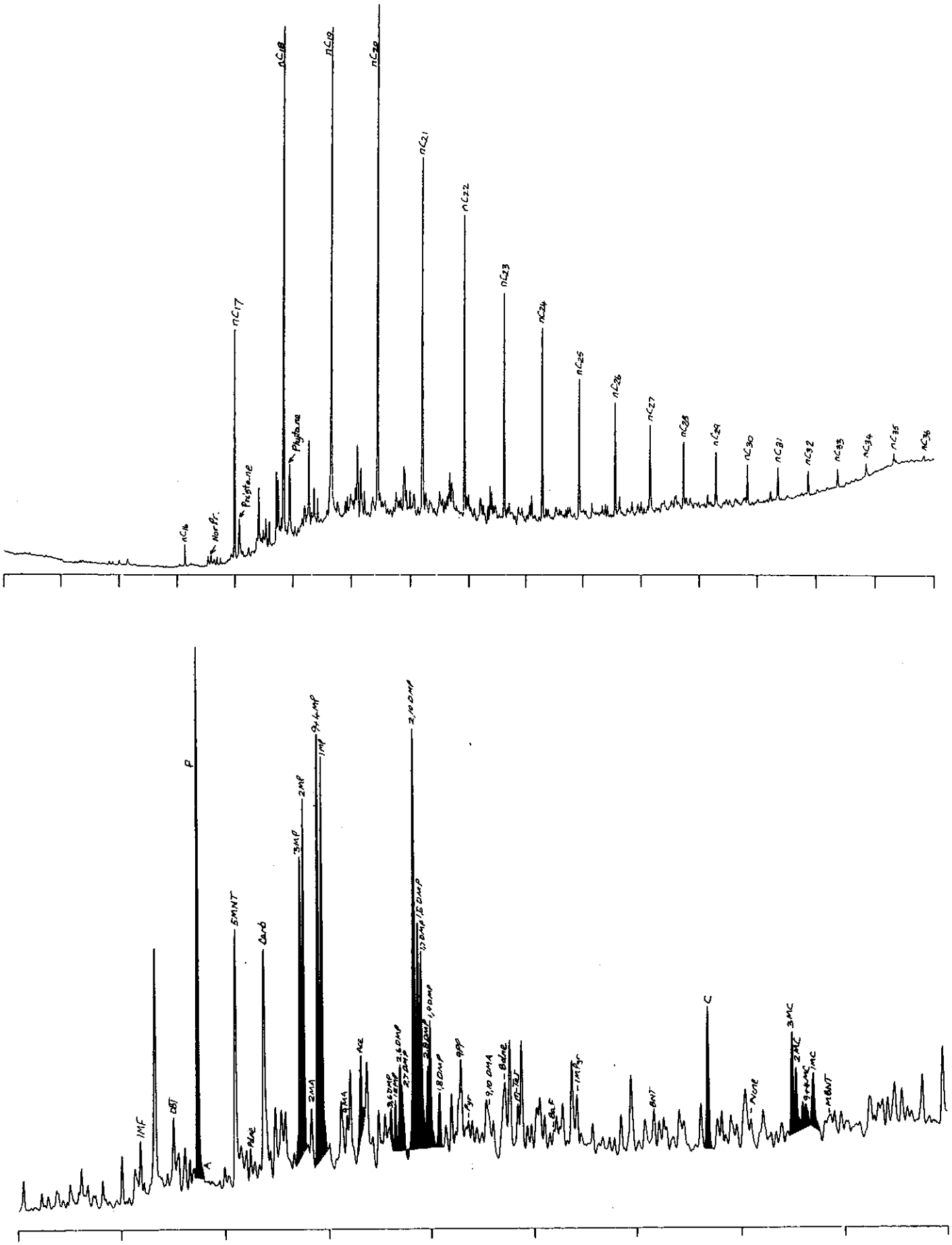

Figure D.31: Gas chromatograms of the total saturated and aromatic fractions of sample 33, well 166 core 1, 2510.43m.

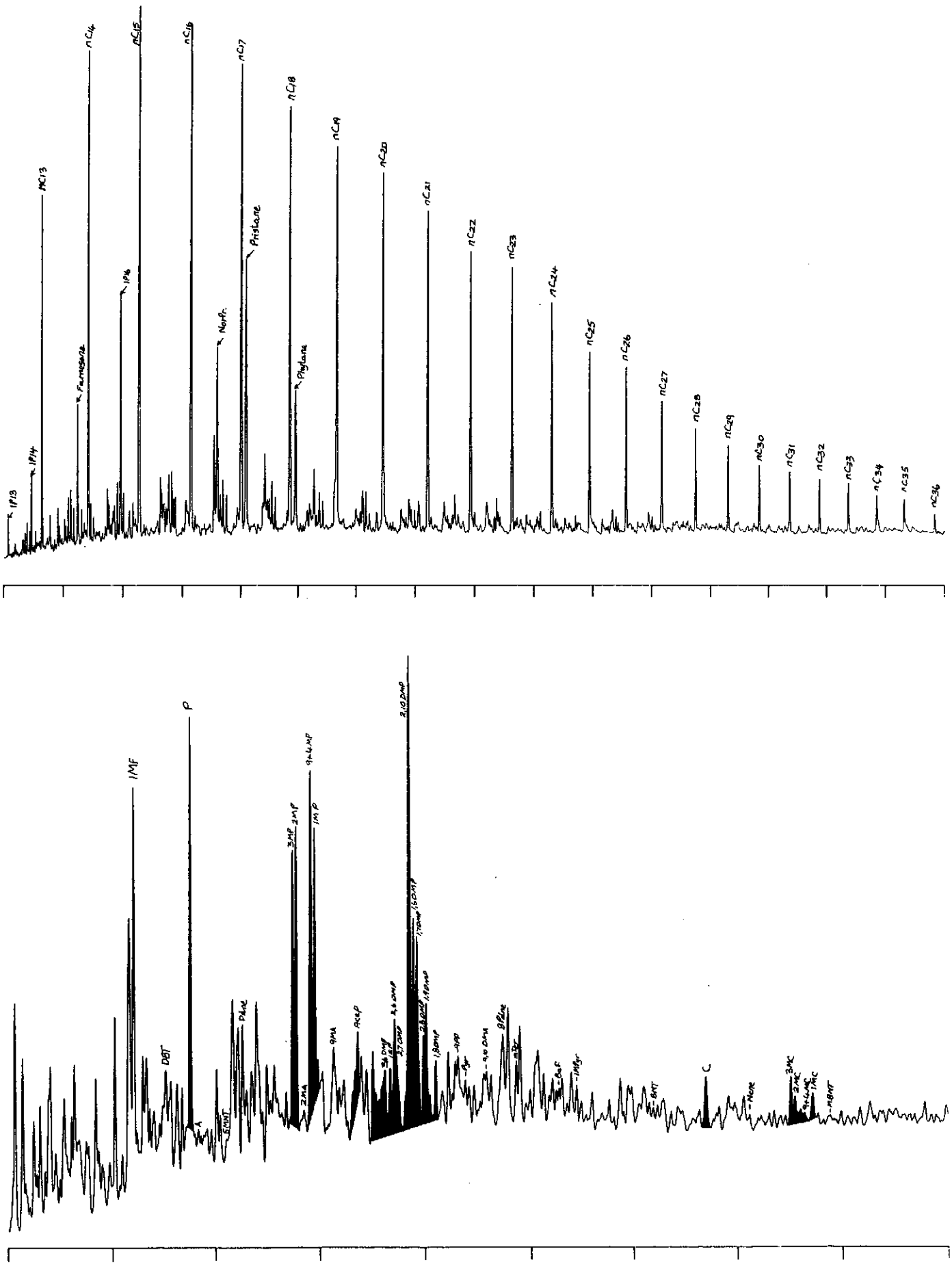

Figure D.32: Gas chromatograms of the total saturated and aromatic fractions of sample 34, well 166 DST 1, 2520m.

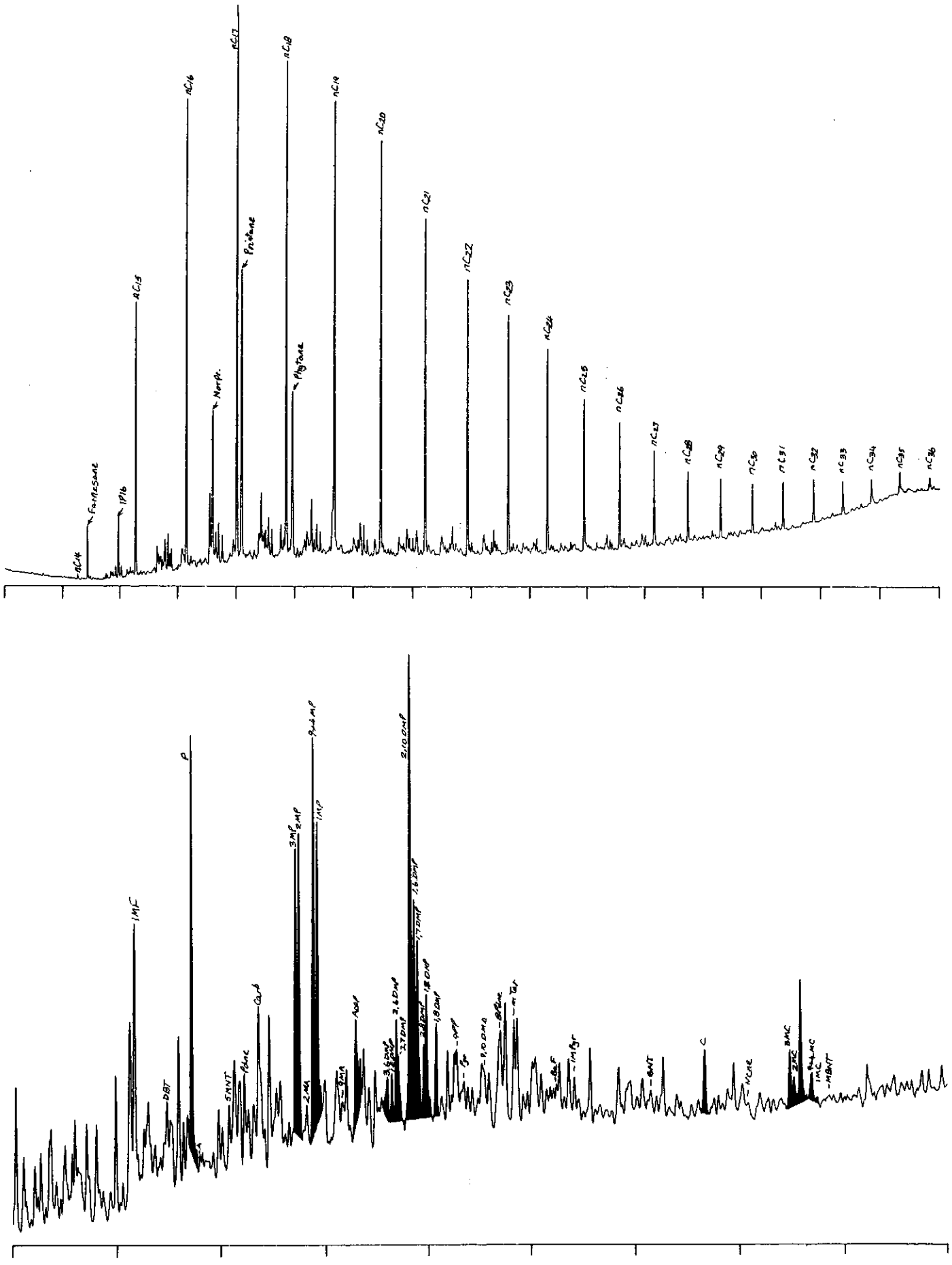

Figure D.33: Gas chromatograms of the total saturated and aromatic fractions of sample 35, well 166 core 1, 2522.5m.

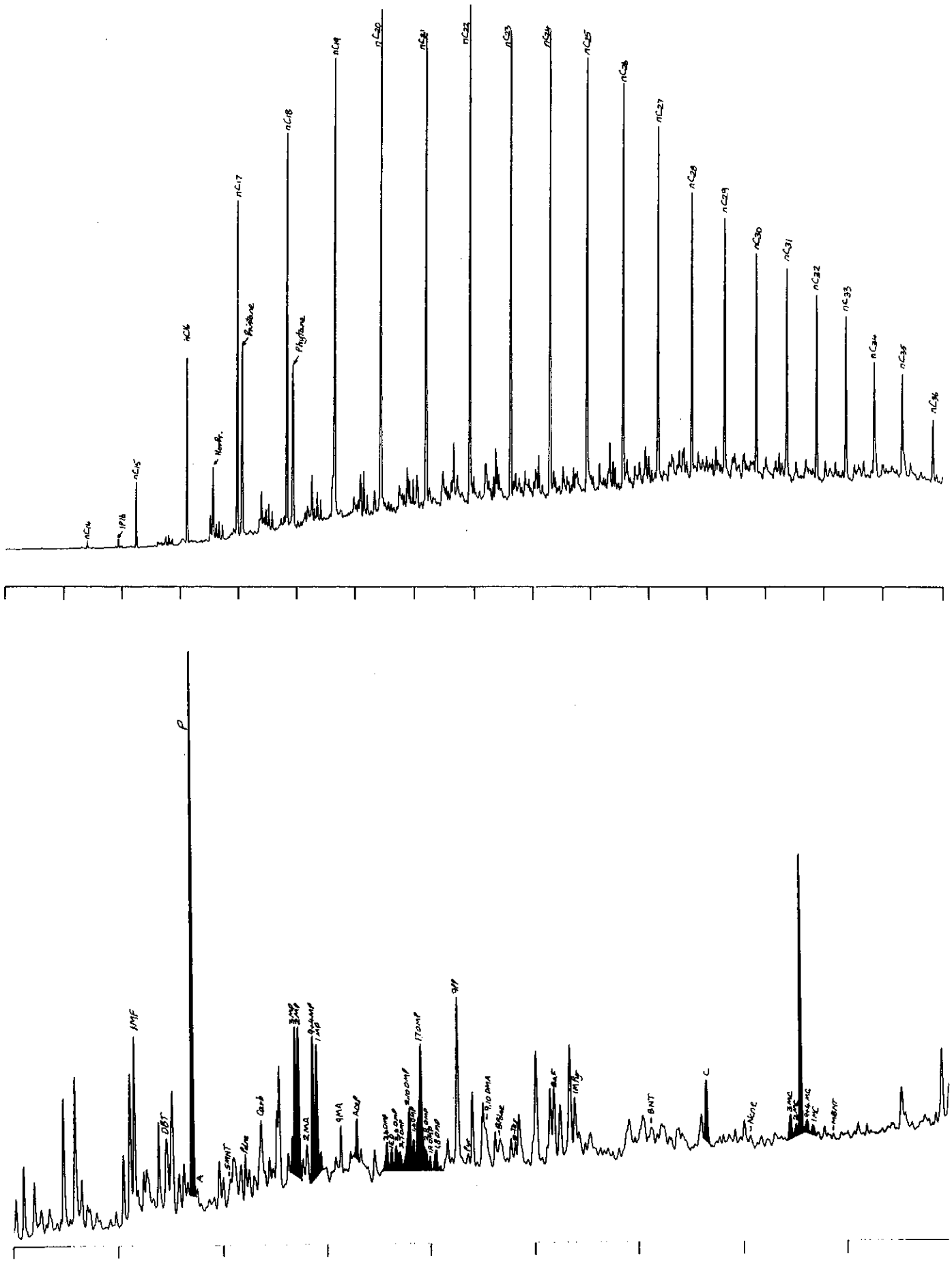

Figure D.34: Gas chromatograms of the total saturated and aromatic fractions of sample 36, well 165 RC, 2256m.

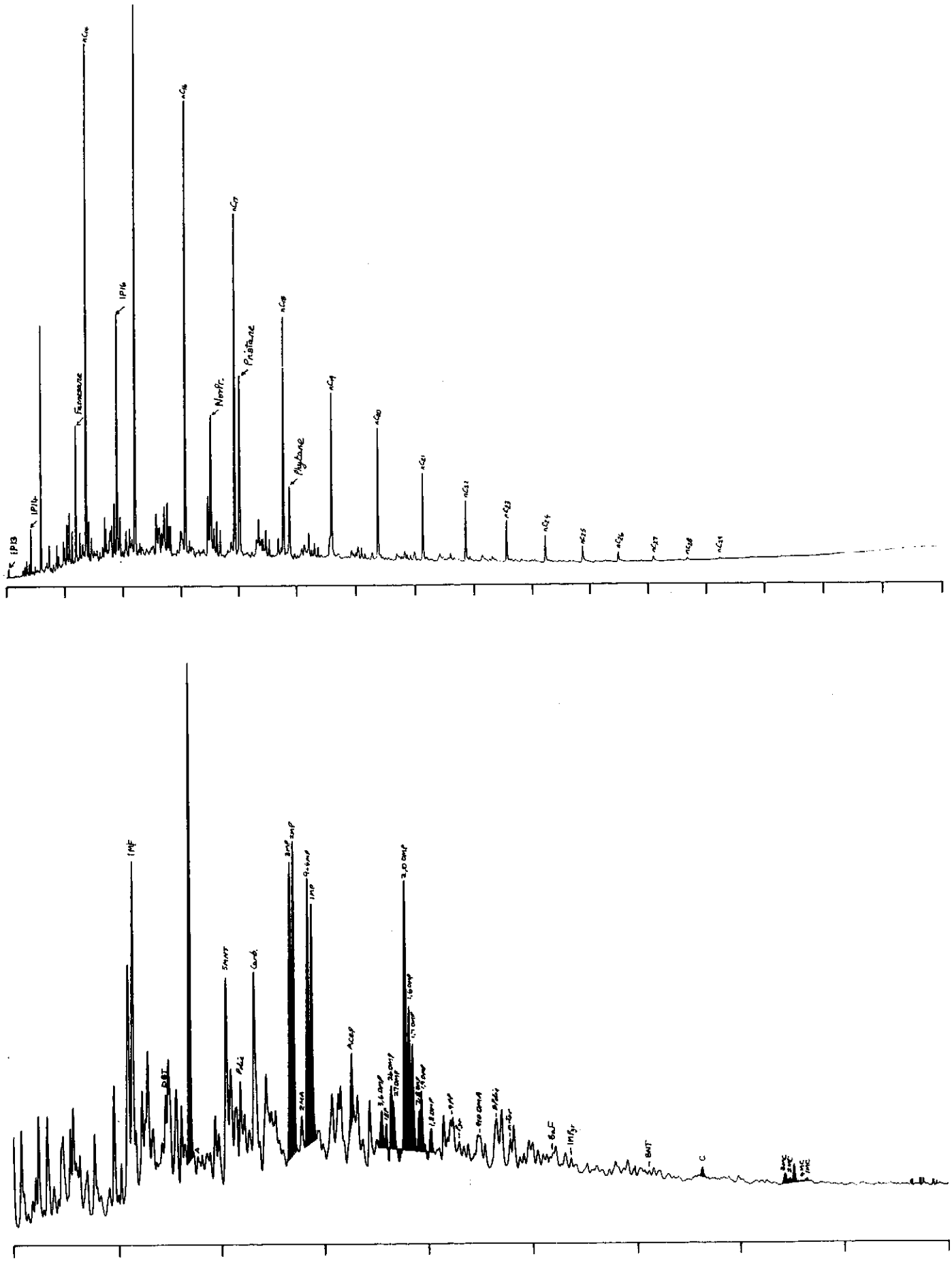

Figure D.35: Gas chromatograms of the total saturated and aromatic fractions of sample 37, well 167 DST 1, 2679m.

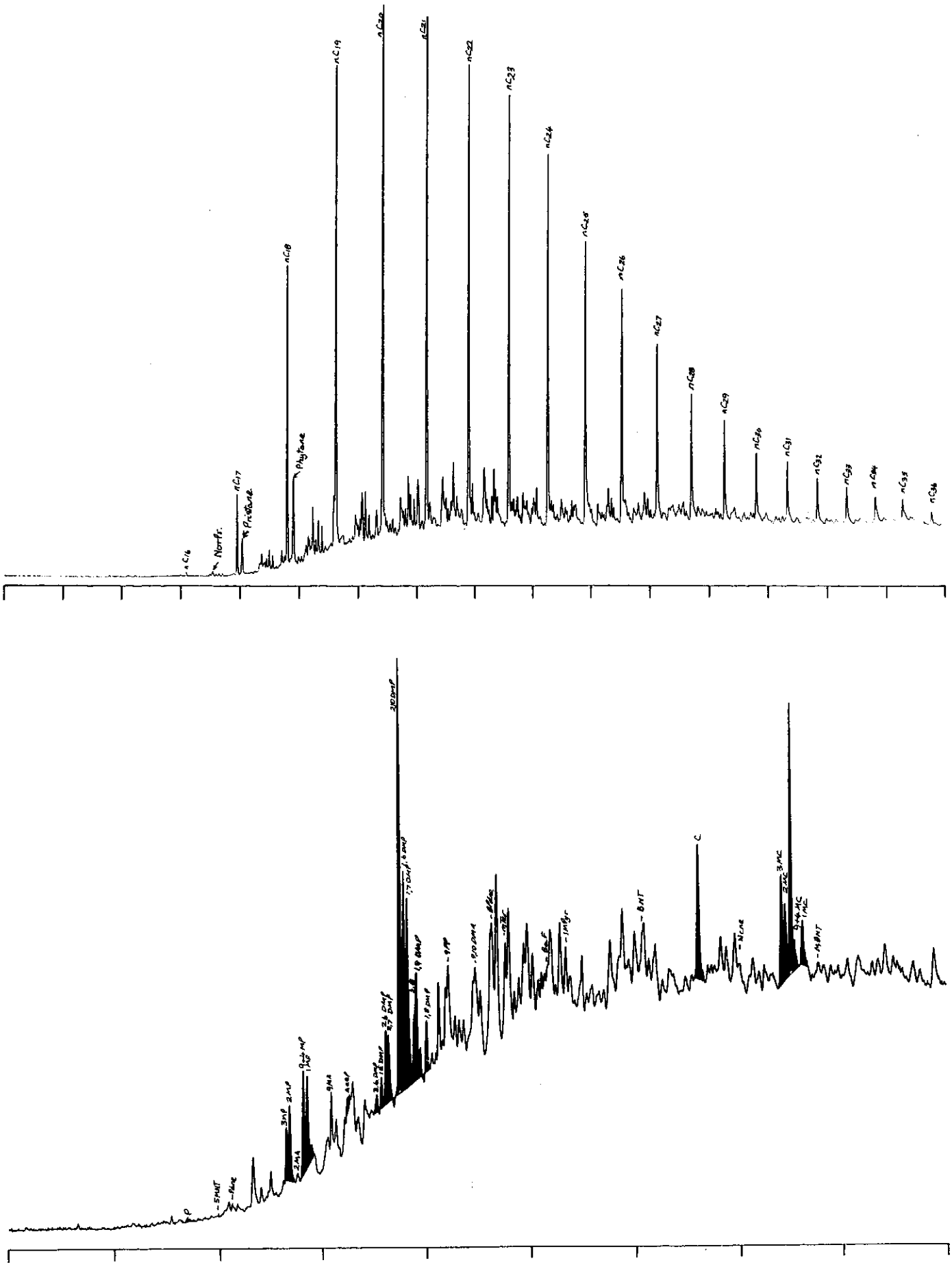

Figure D.36: Gas chromatograms of the total saturated and aromatic fractions of sample 38, well 167 core 1, 2681.65m.

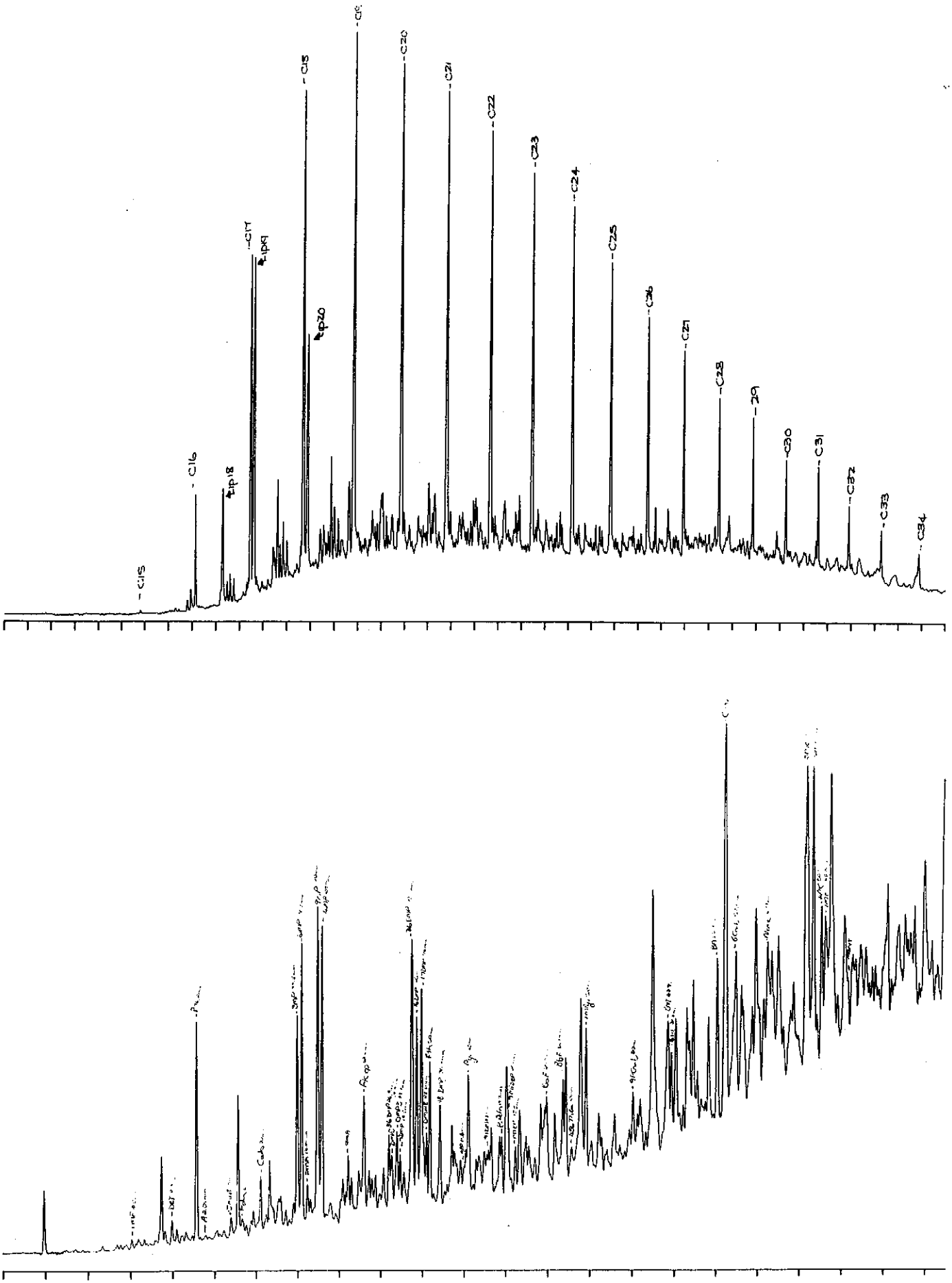

Figure D.37: Gas chromatograms of the total saturated and aromatic fractions of sample 41, well 83 RC, 2702m.

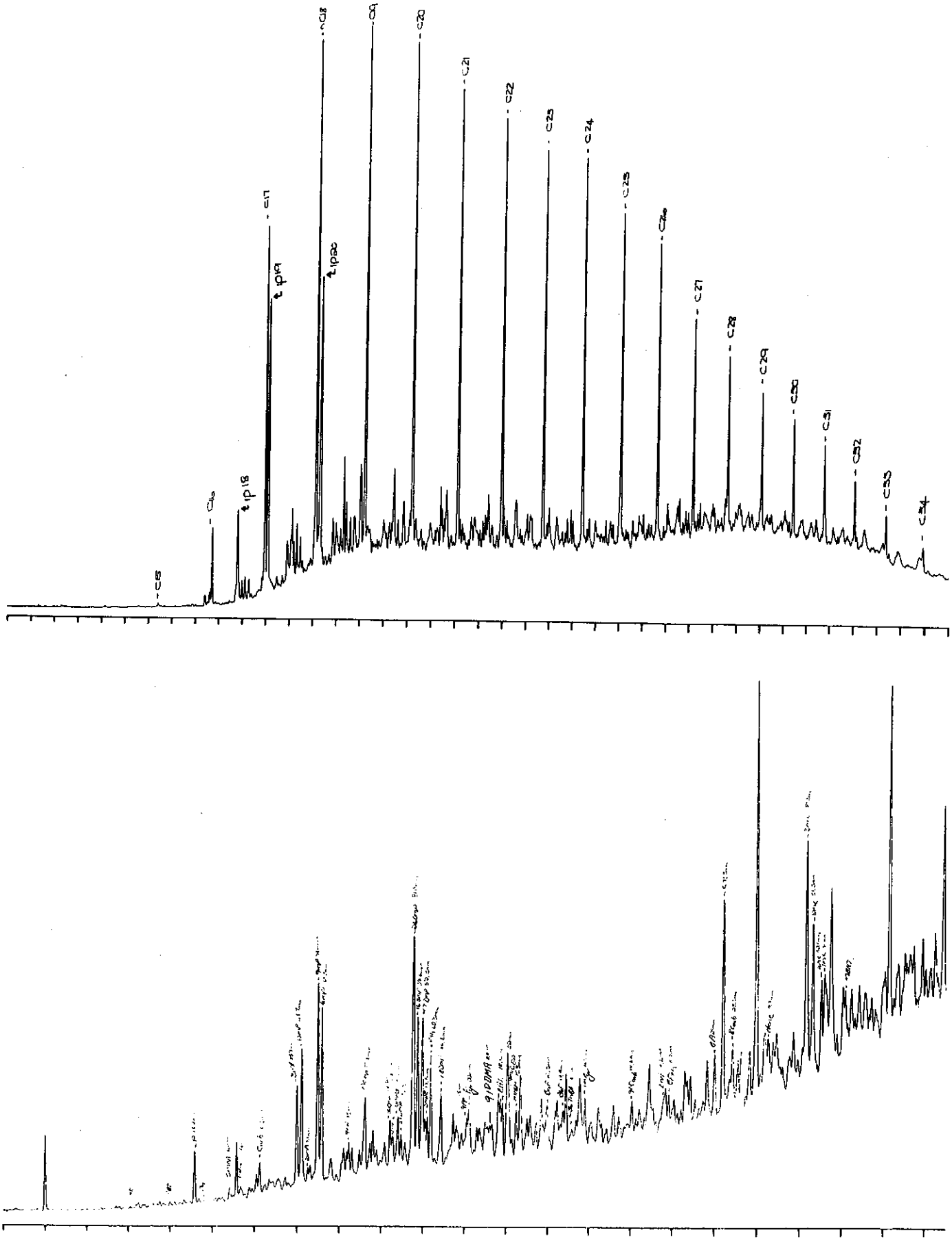

Figure D.38: Gas chromatograms of the total saturated and aromatic fractions of sample 42, well 83 RC, 2741m.

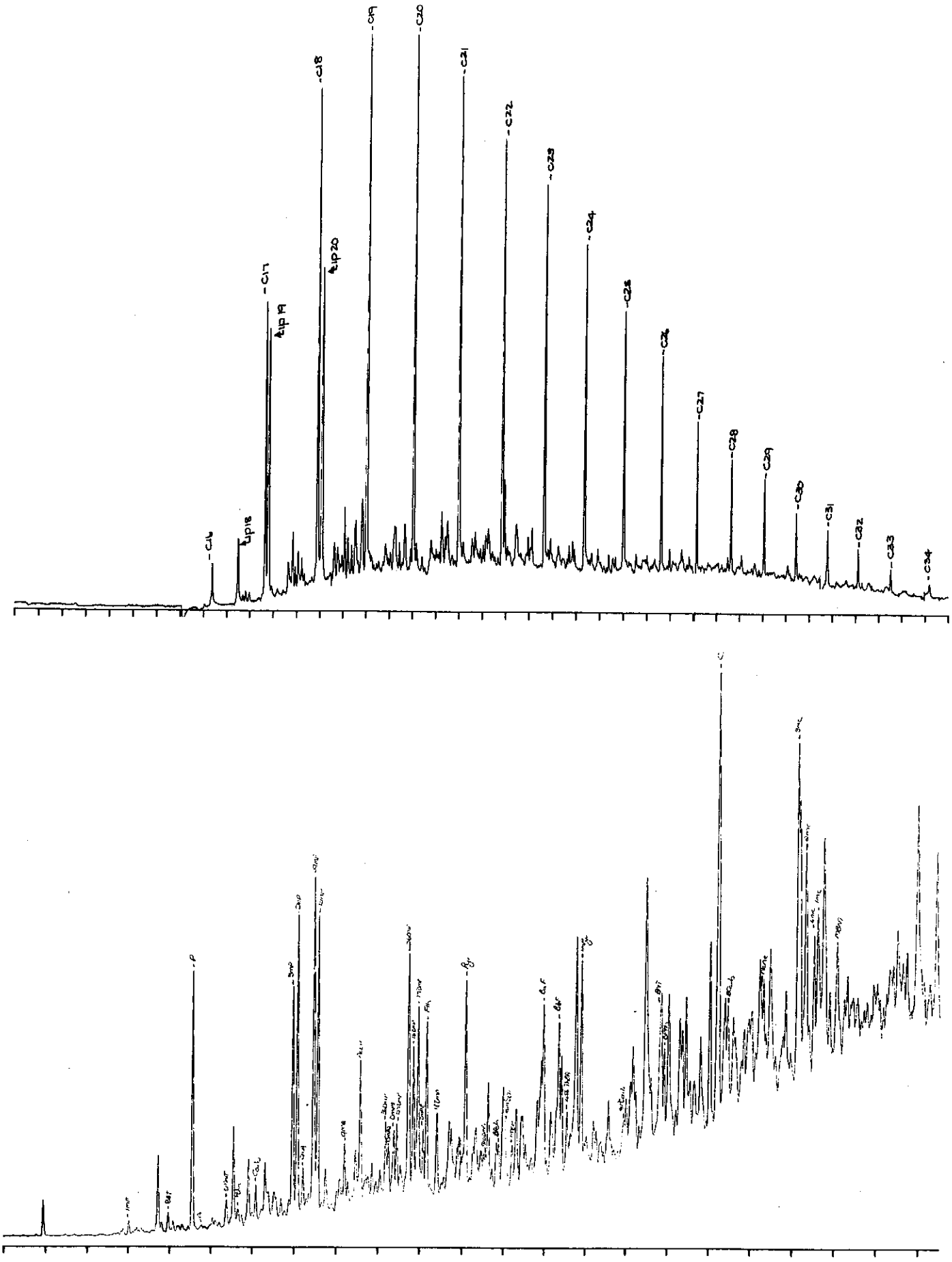

Figure D.39: Gas chromatograms of the total saturated and aromatic fractions of sample 43, well 83 RC, 2792m.

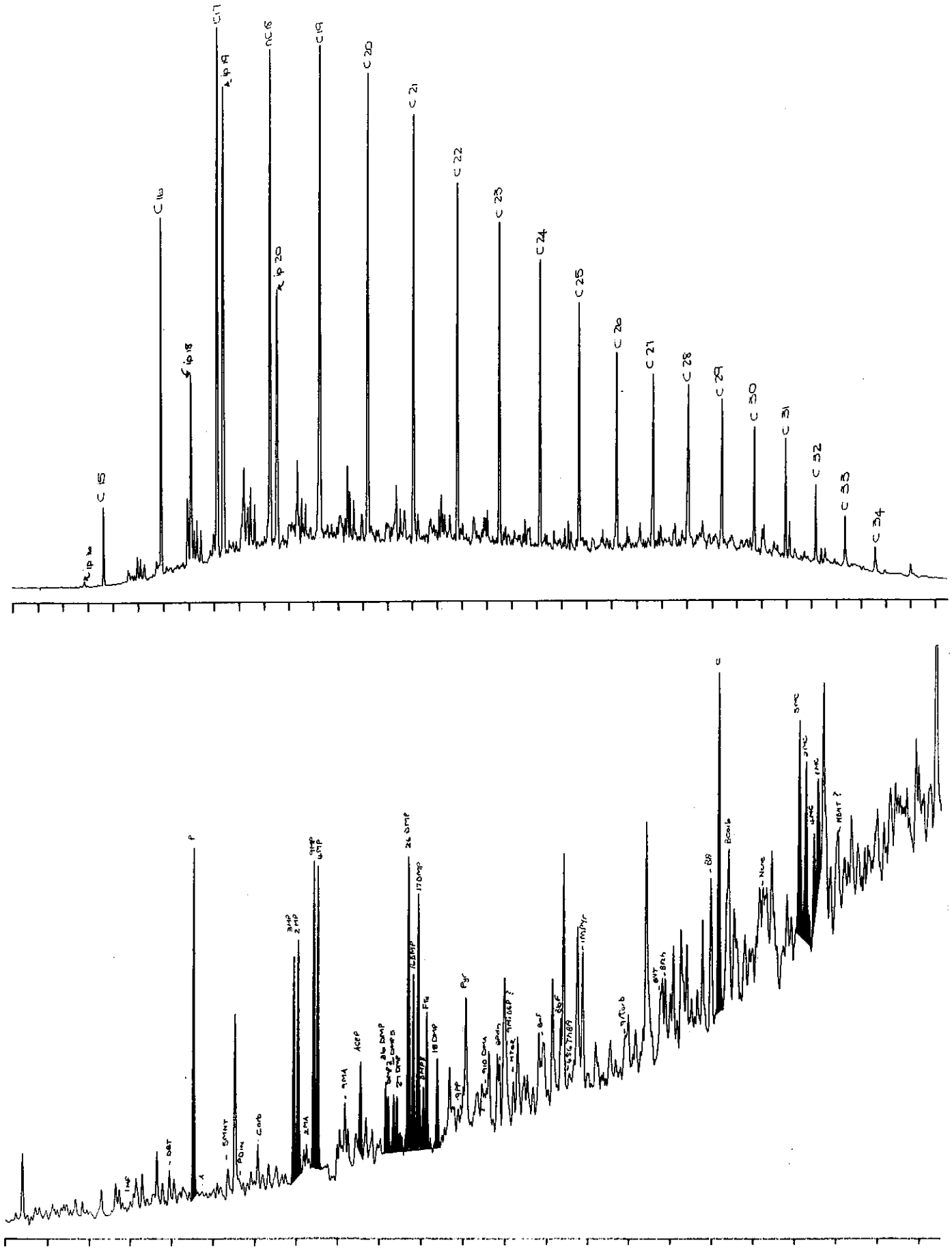

Figure D.40: Gas chromatograms of the total saturated and aromatic fractions of sample 44, well 92 RC, 2610m.

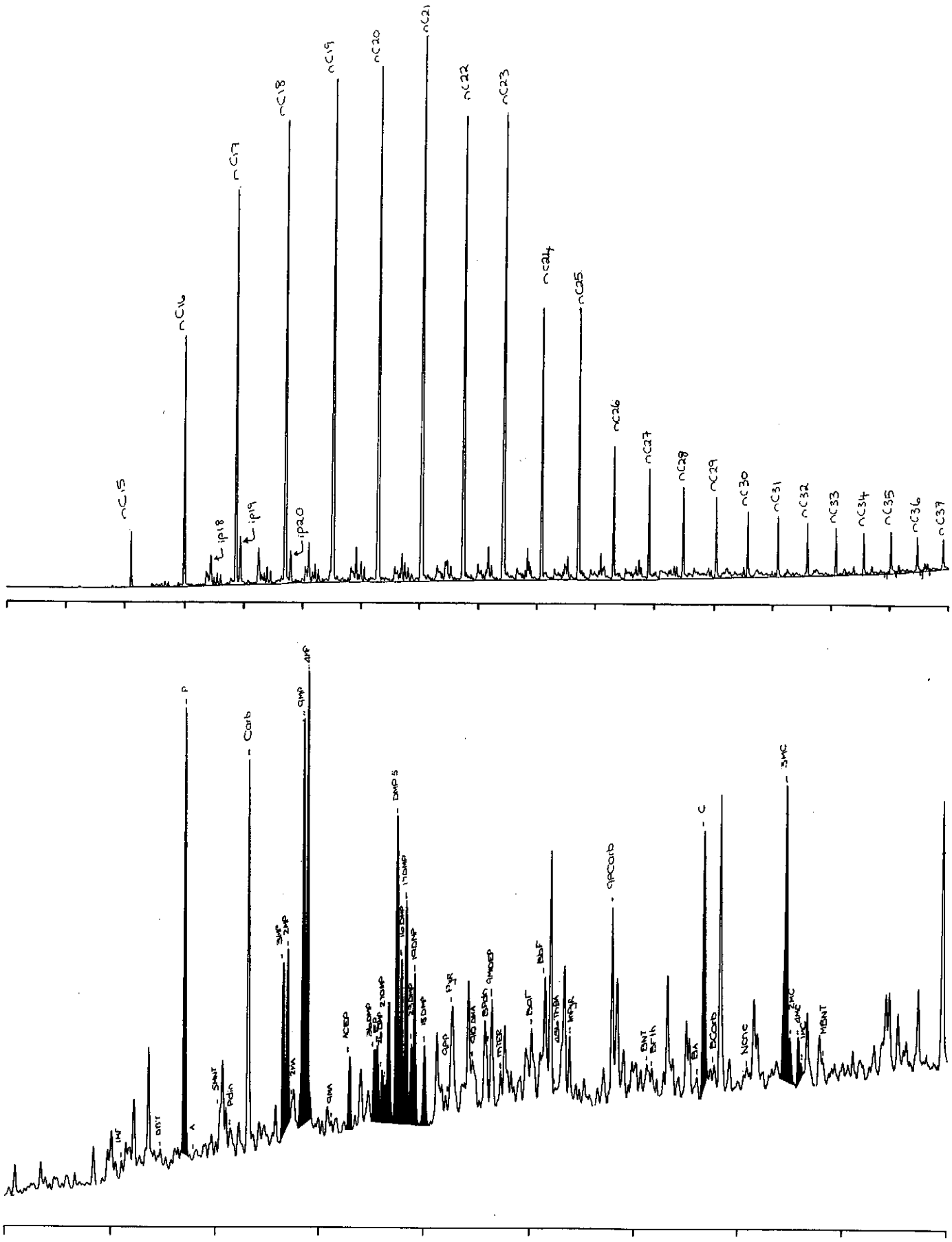

Figure D.41: Gas chromatograms of the total saturated and aromatic fractions of sample 45, well 89 RC, 2660m.

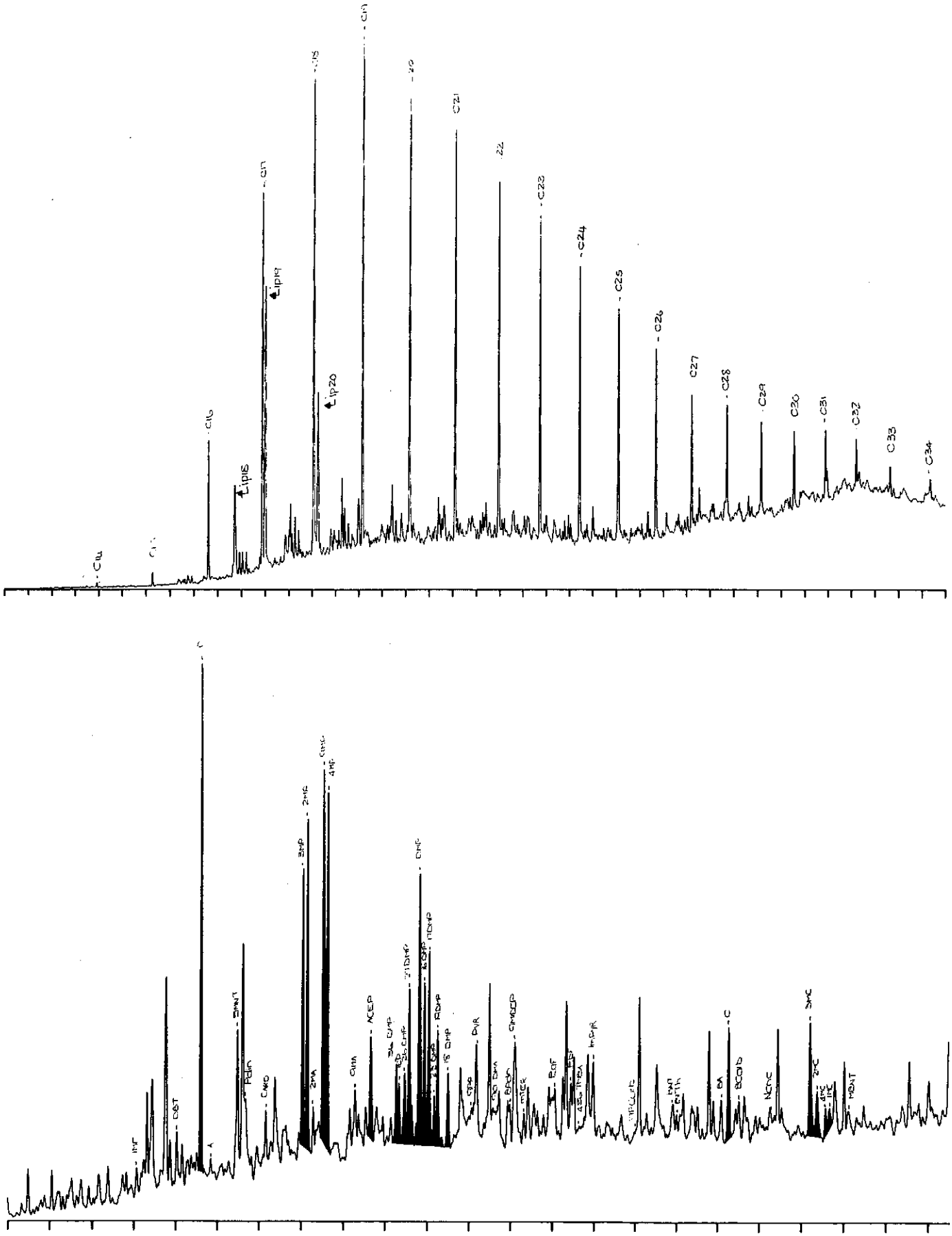

Figure D.42: Gas chromatograms of the total saturated and aromatic fractions of sample 46, well 93 RC, 2720m.

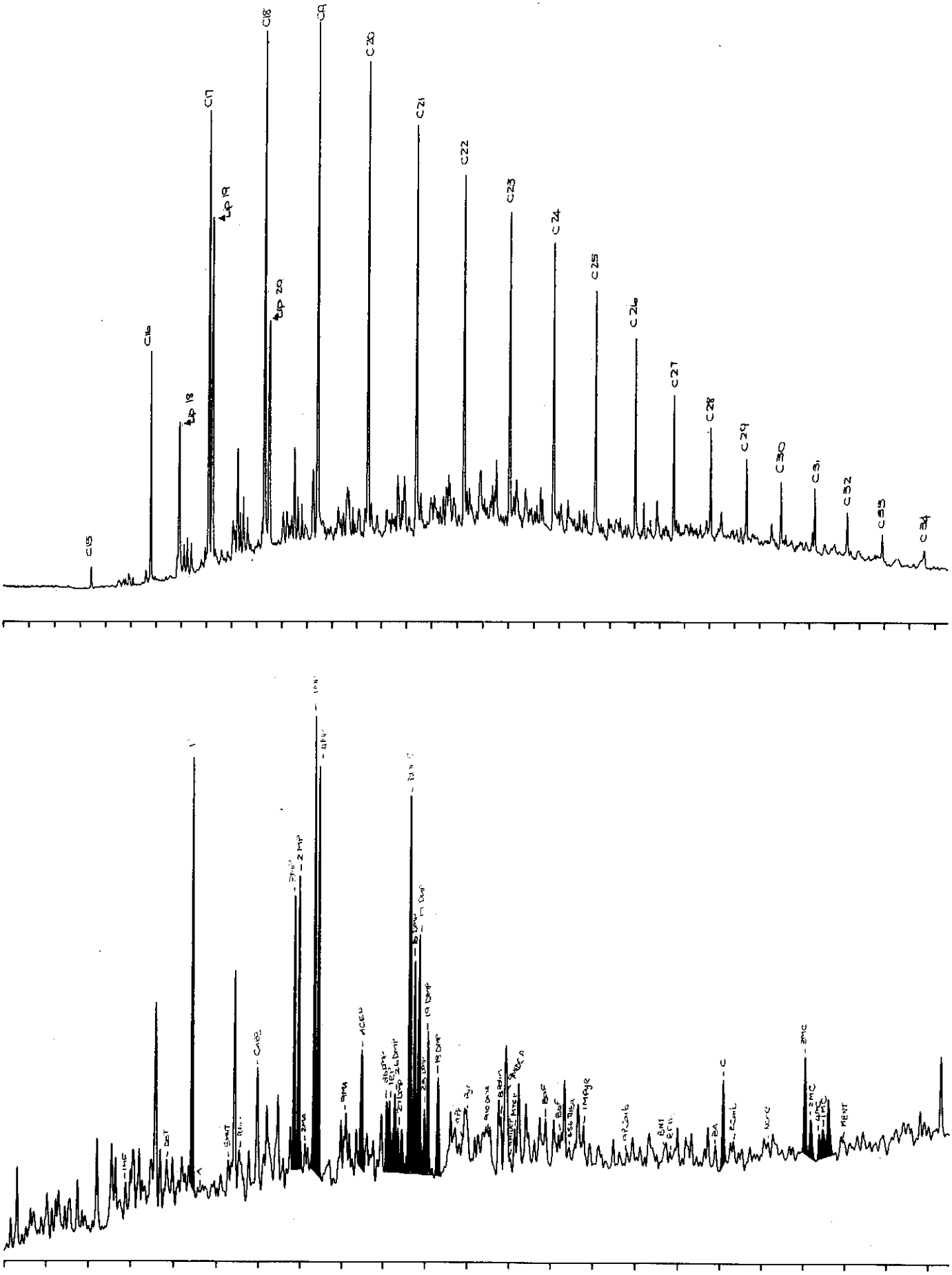

Figure D.43: Gas chromatograms of the total saturated and aromatic fractions of sample 47, well 93 RC, 2761m.

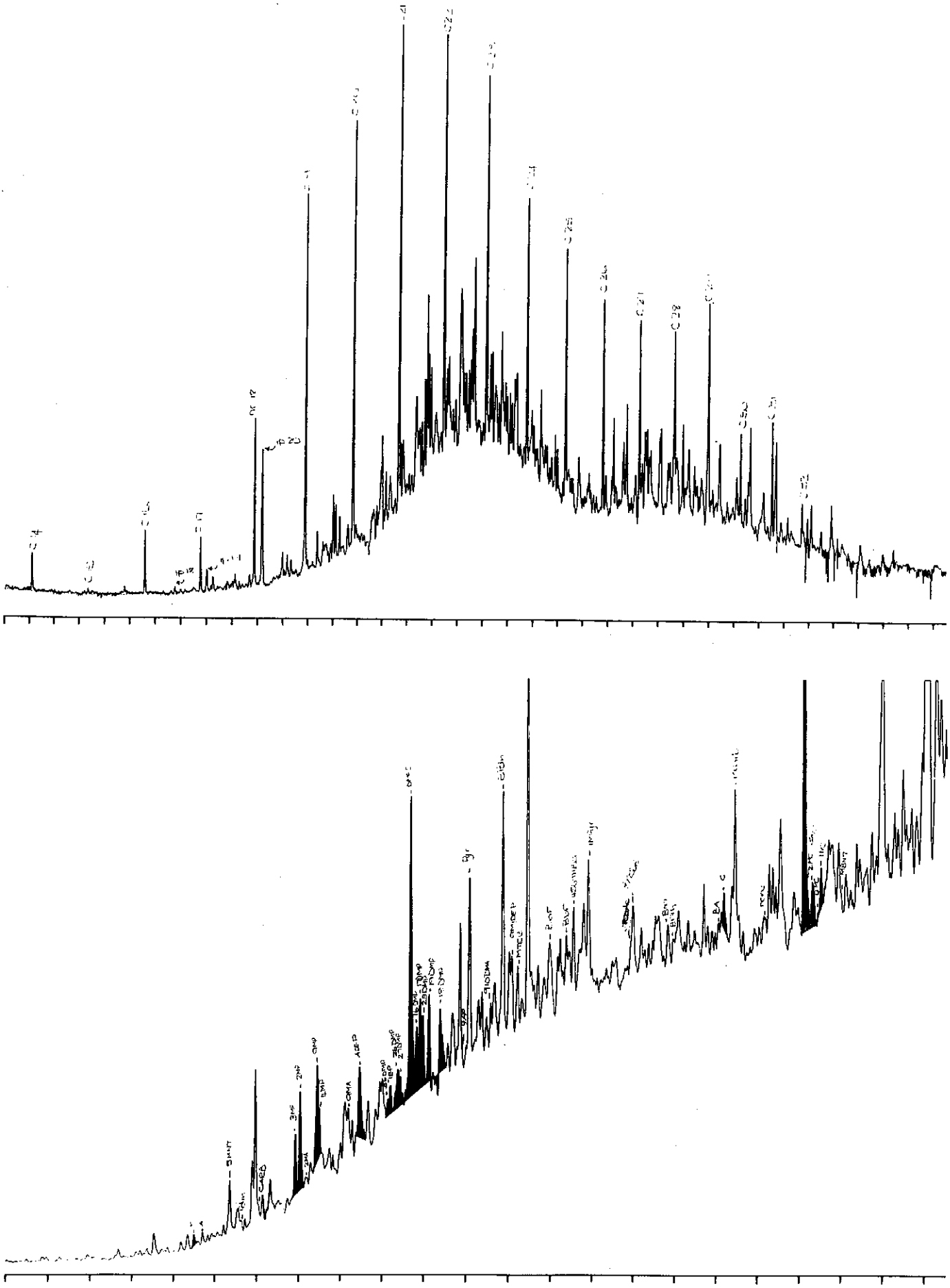

Figure D.44: Gas chromatograms of the total saturated and aromatic fractions of sample 49, well 99 RC, 1820m.

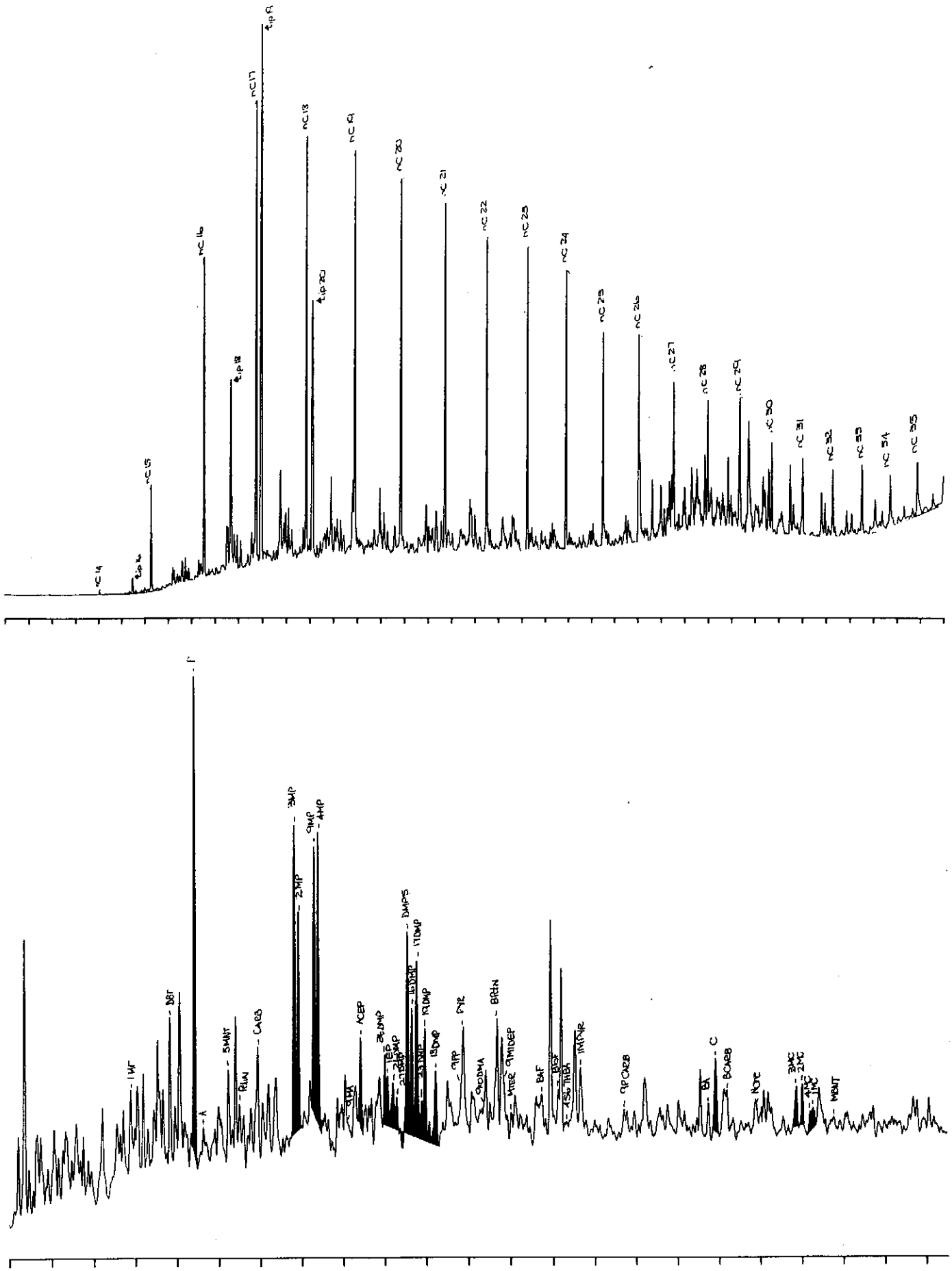

Figure D.45: Gas chromatograms of the total saturated and aromatic fractions of sample 50, well 109 RC, 2461m.

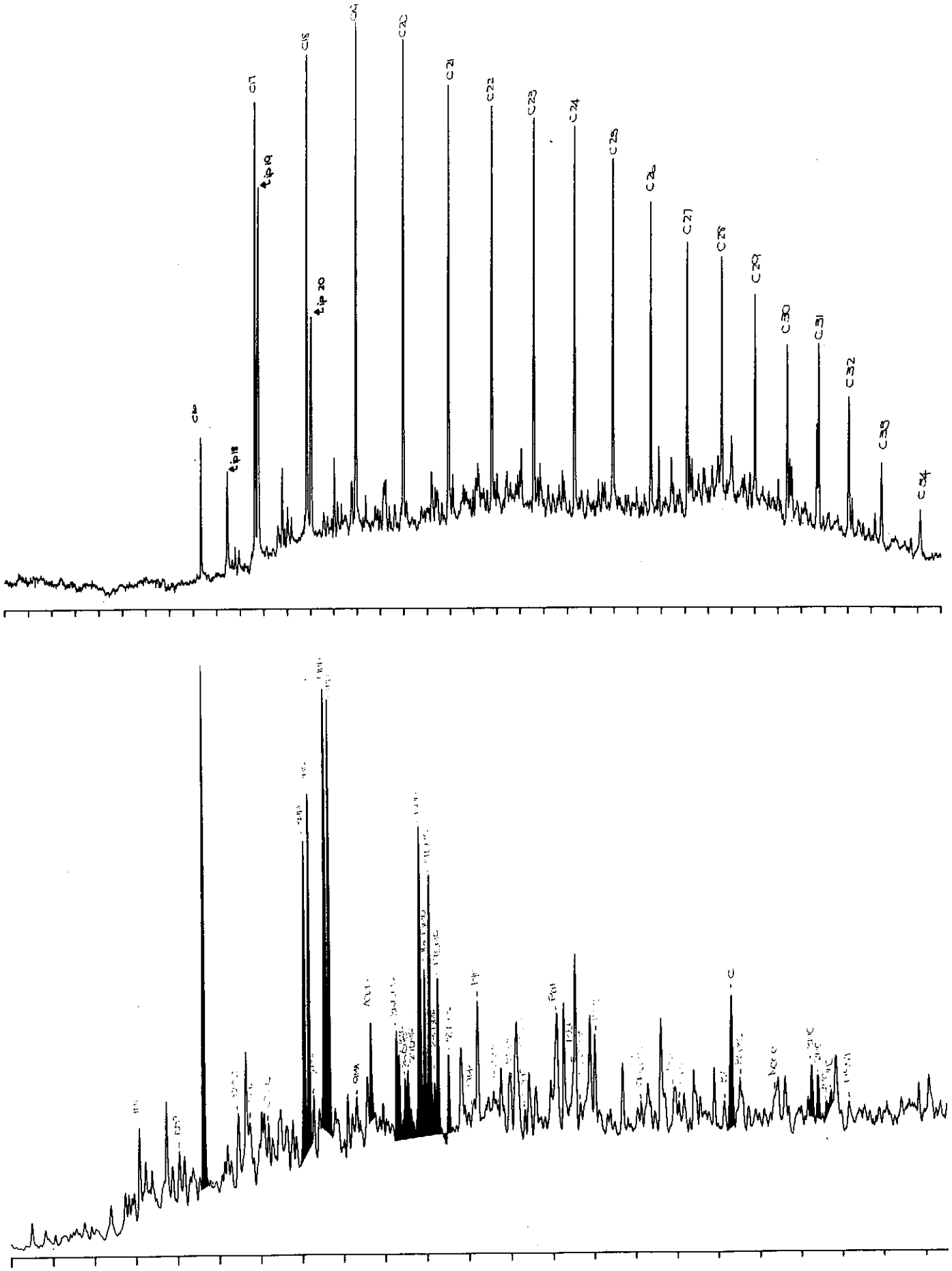

Figure D.46: Gas chromatograms of the total saturated and aromatic fractions of sample 51, well 109 core 3, 2654.15m.

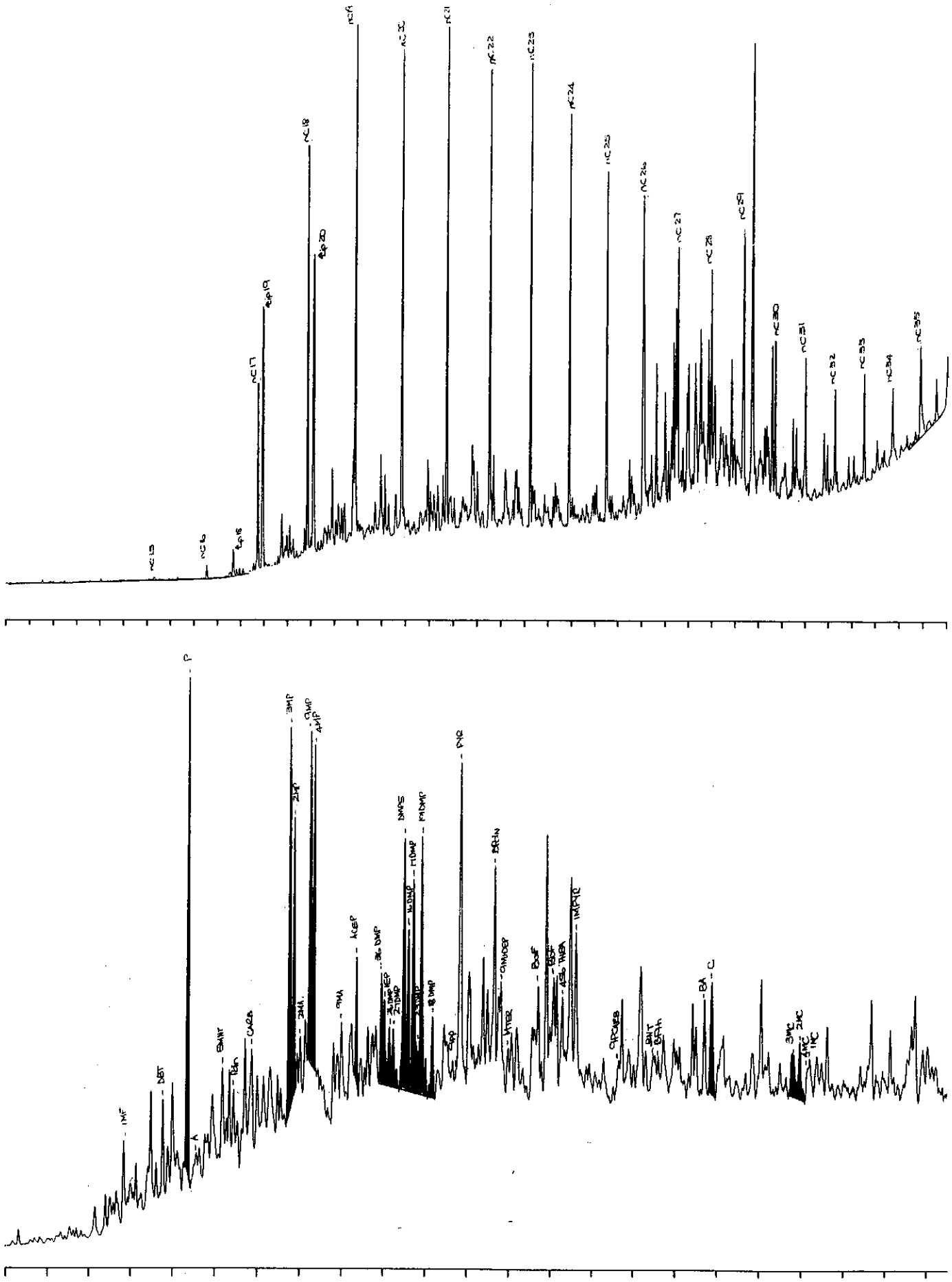

Figure D.47: Gas chromatograms of the total saturated and aromatic fractions of sample 52, well 130 RC, 2331m.

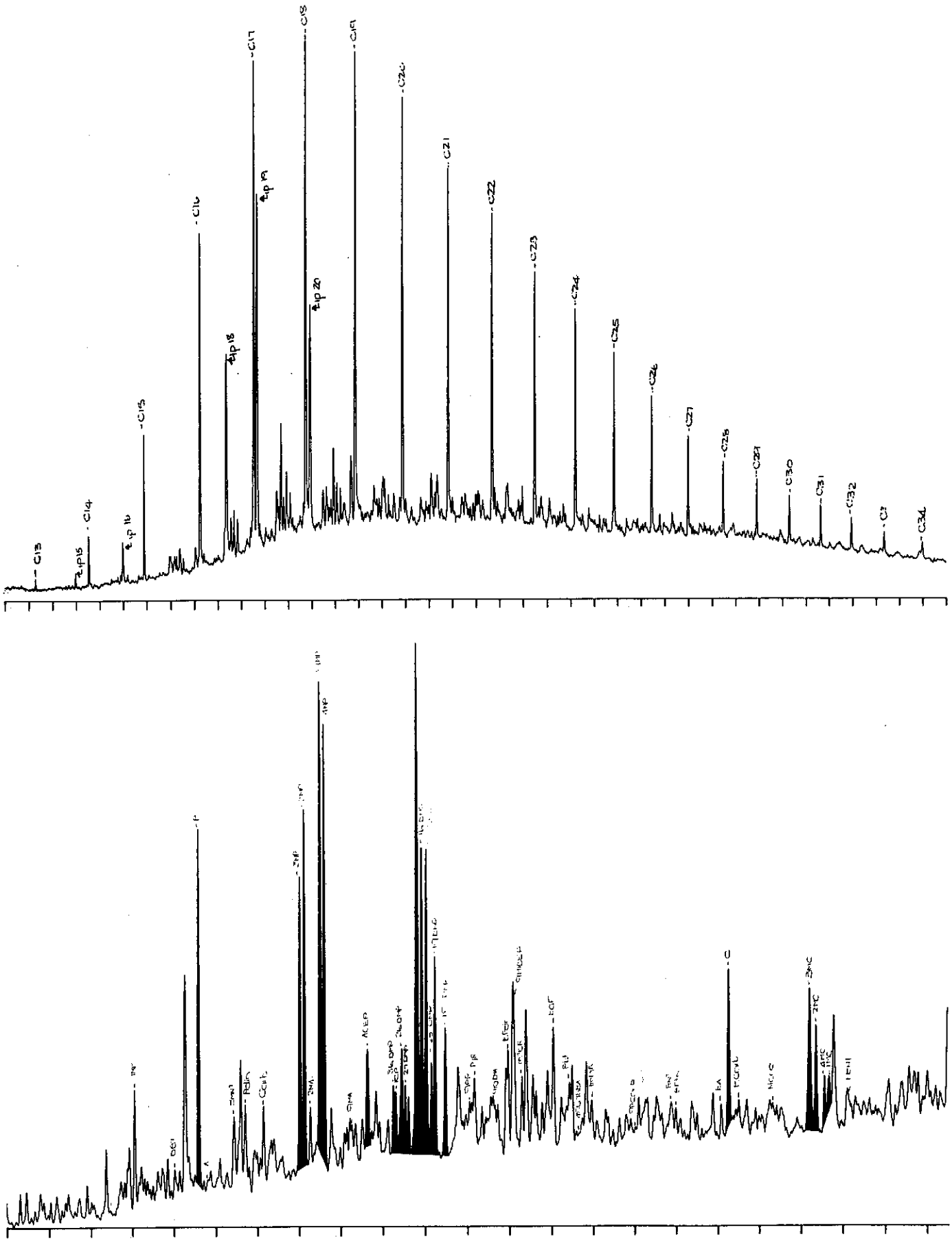

Figure D.48: Gas chromatograms of the total saturated and aromatic fractions of sample 53, well 110 RC, 2830m.

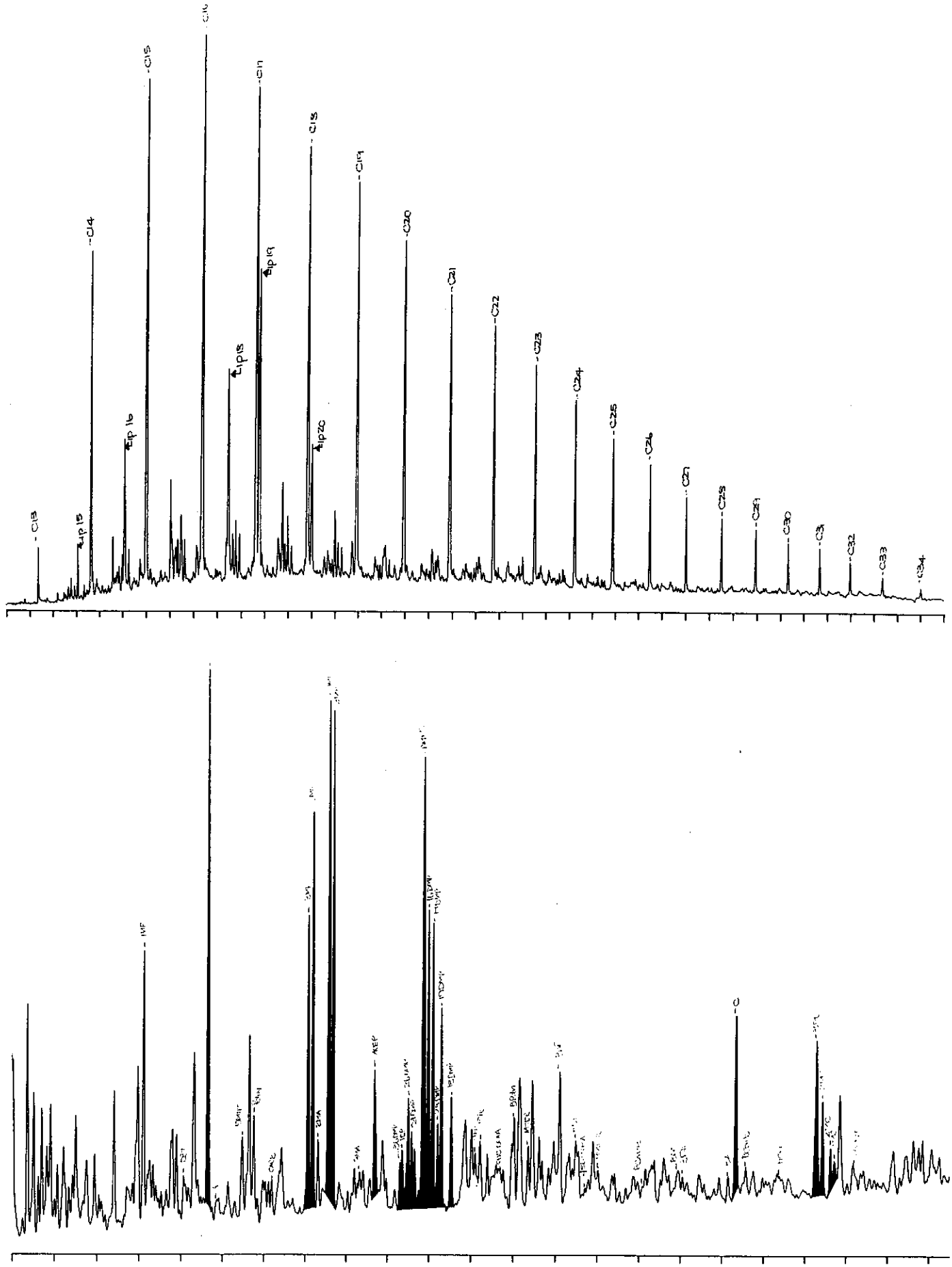

Figure D.49: Gas chromatograms of the total saturated and aromatic fractions of sample 54, well 110 RC, 2902m.

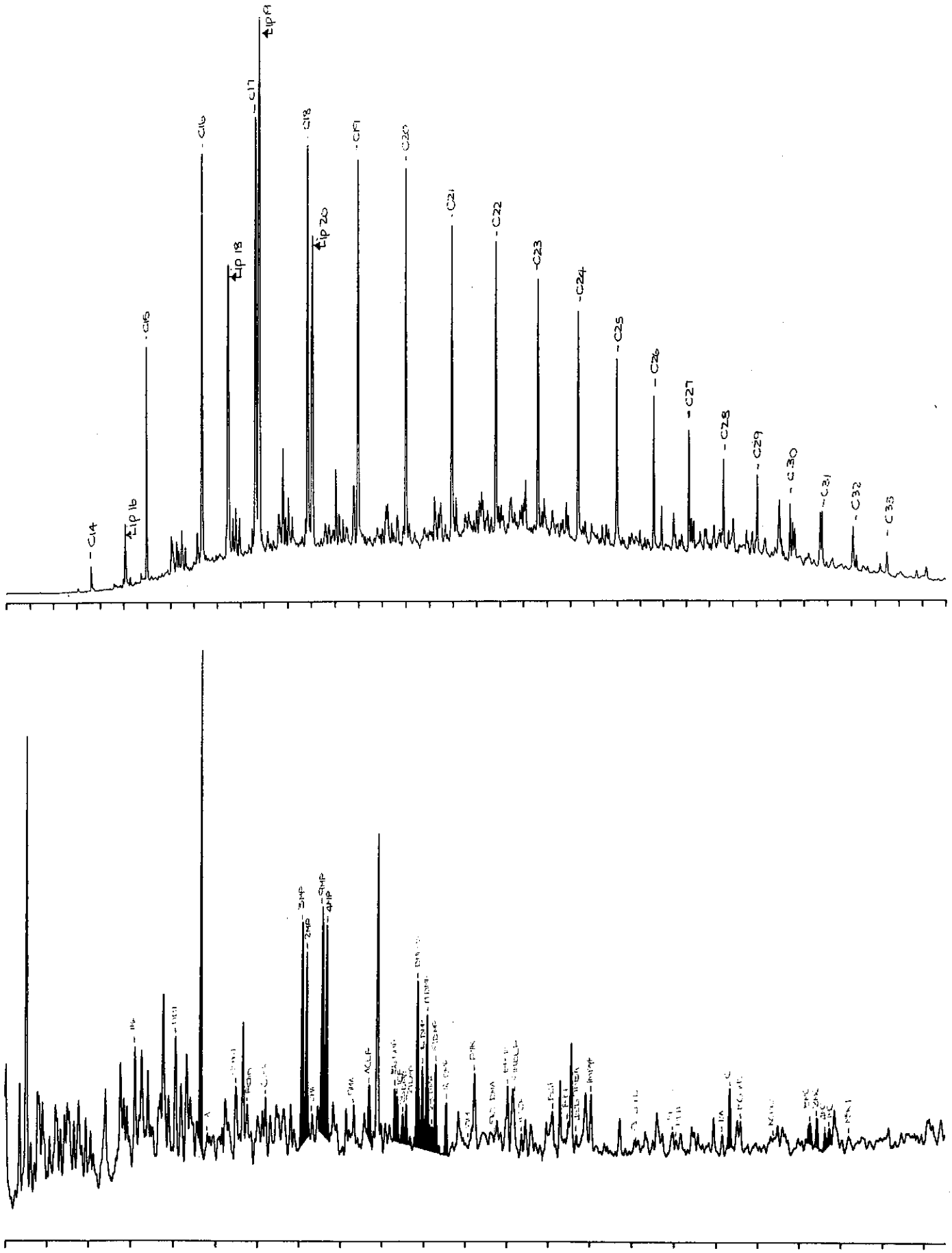

Figure D.50: Gas chromatograms of the total saturated and aromatic fractions of sample 55, well 112 RC, 2392m.

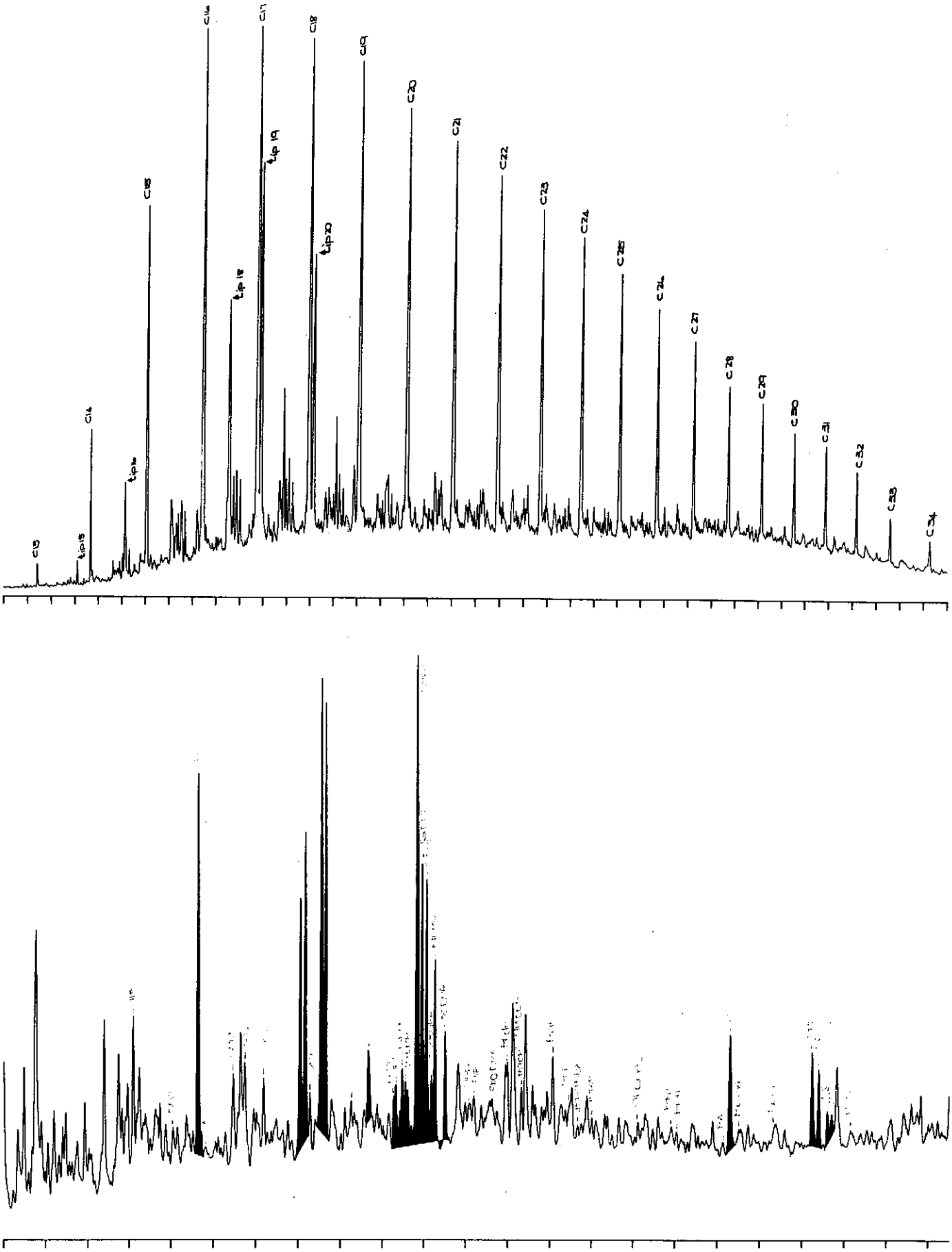

Figure D.51: Gas chromatograms of the total saturated and aromatic fractions of sample 56, well 117 SWC, 2918.5m.

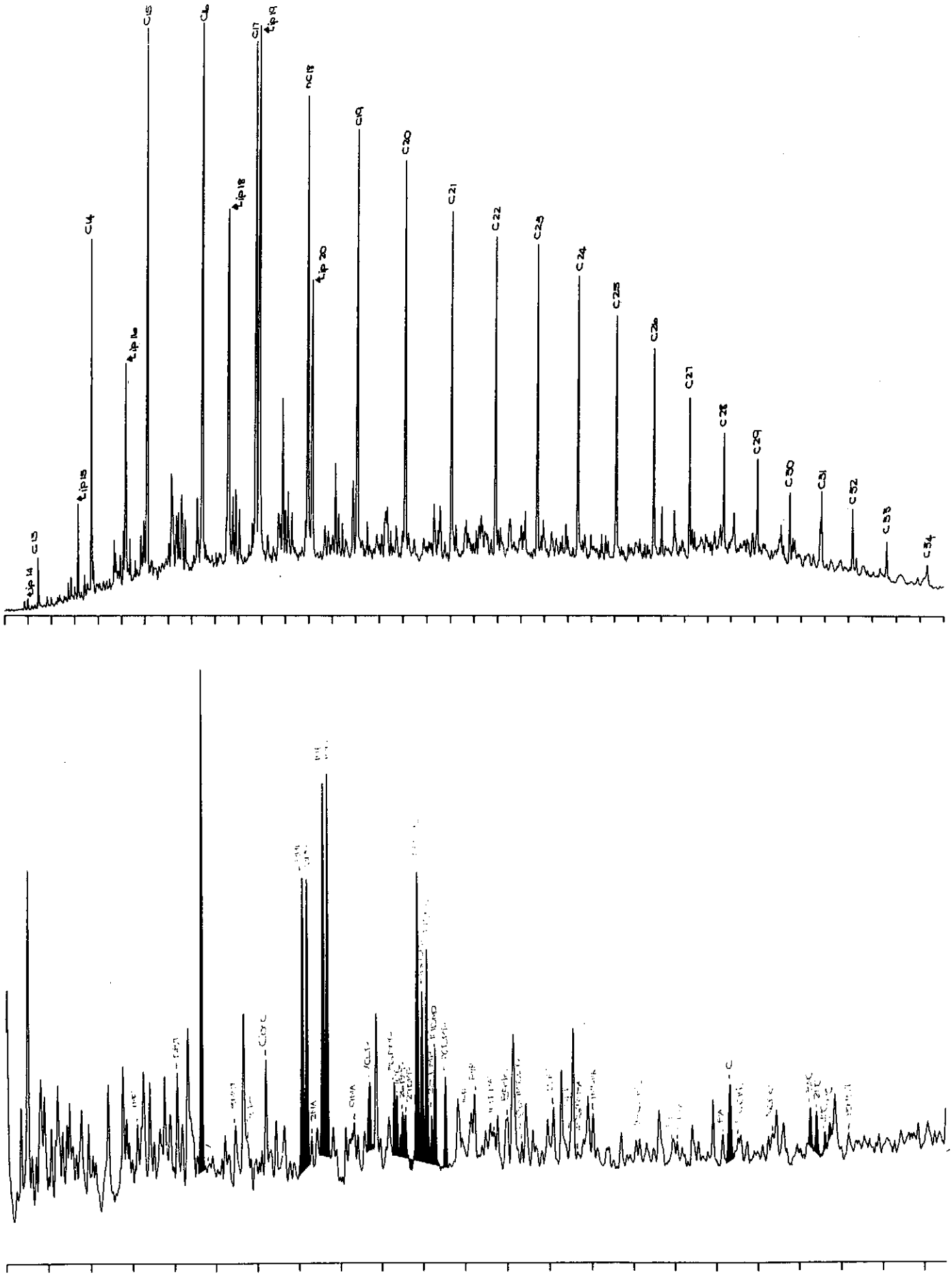

Figure D.52: Gas chromatograms of the total saturated and aromatic fractions of sample 59, well 122 RC, 2682m.

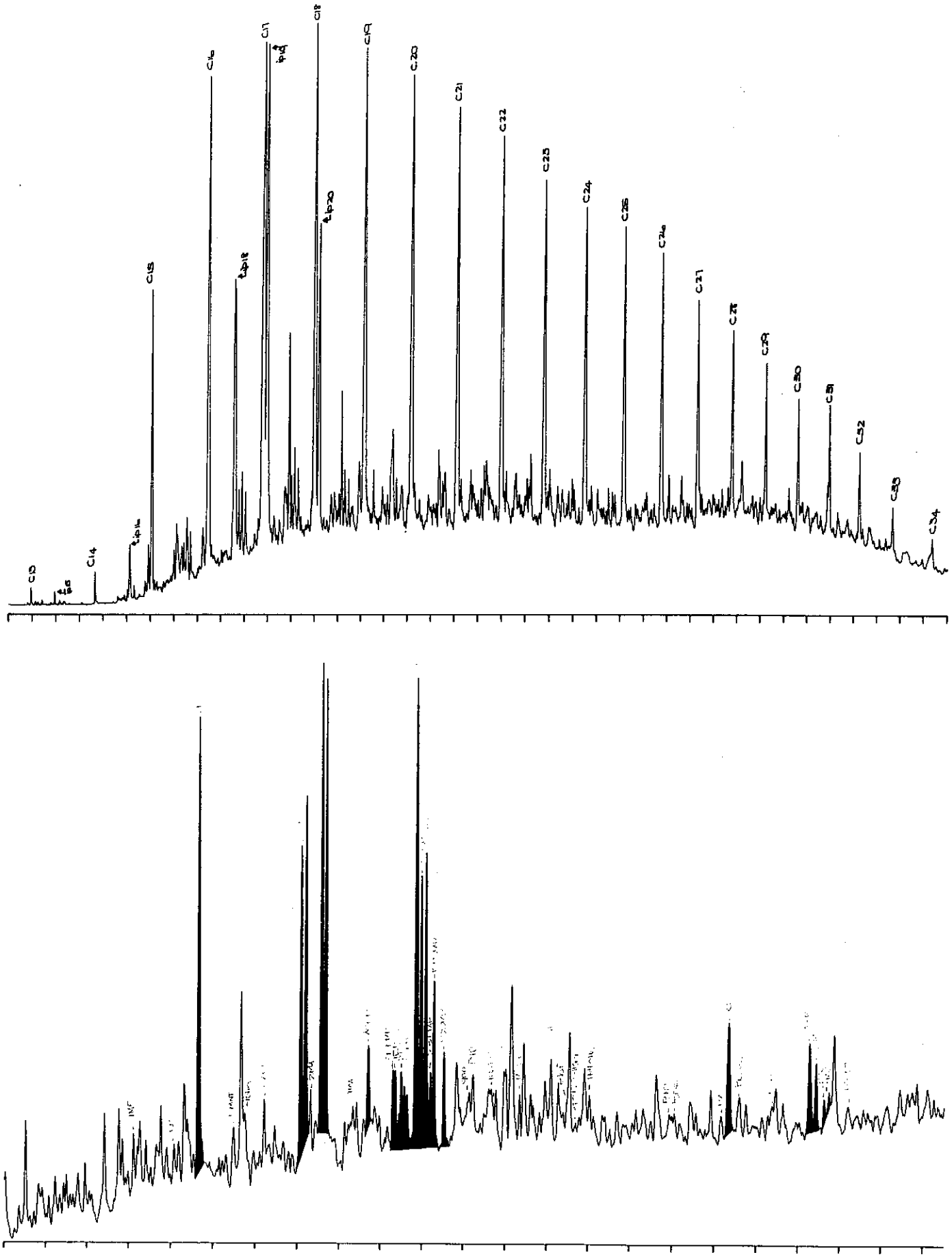

Figure D.53: Gas chromatograms of the total saturated and aromatic fractions of sample 60, well 122 RC, 2832m.

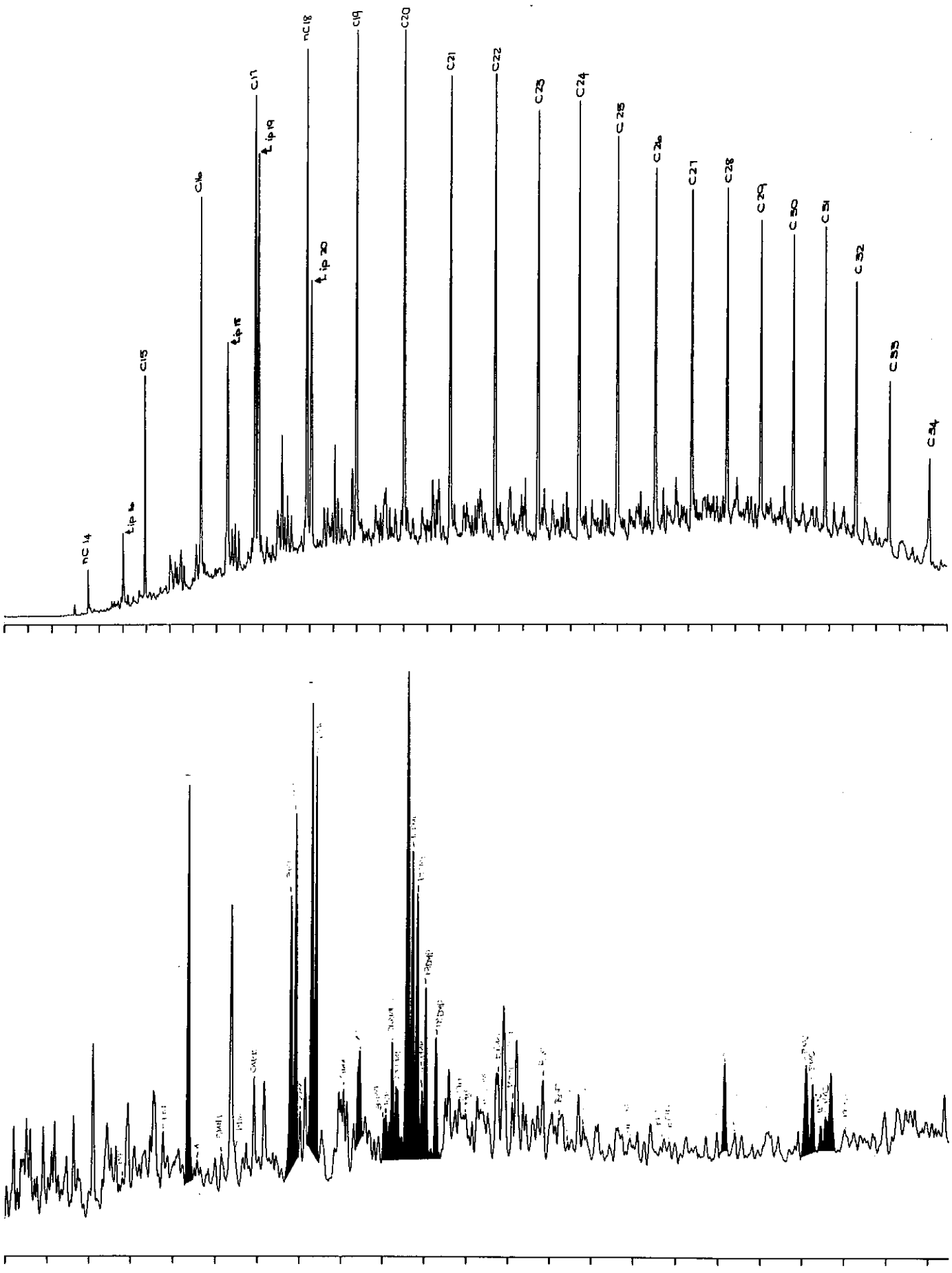

Figure D.54: Gas chromatograms of the total saturated and aromatic fractions of sample 61, well 11 RC, 2682m.

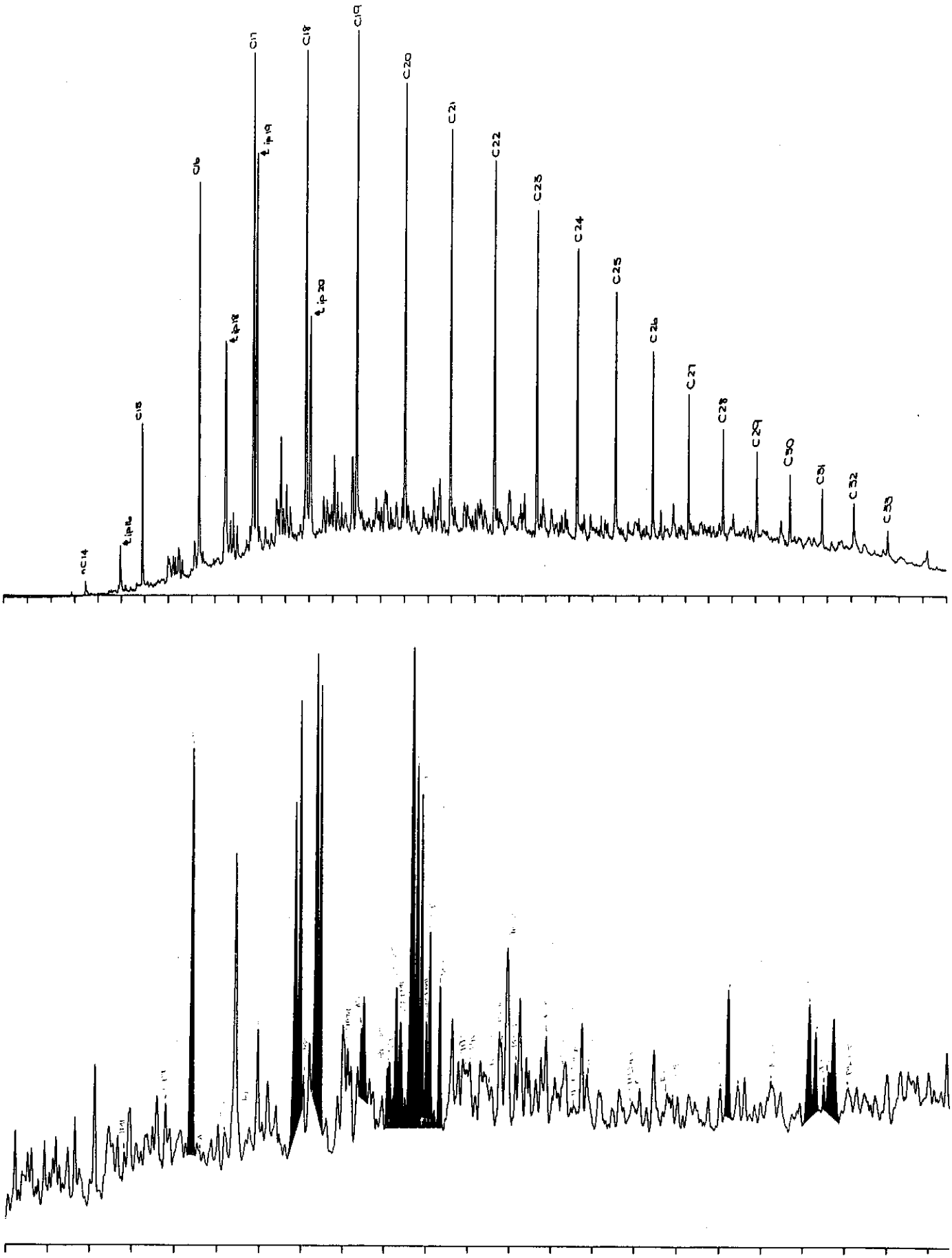

Figure D.55: Gas chromatograms of the total saturated and aromatic fractions of sample 62, well 14 RC, 2721m.

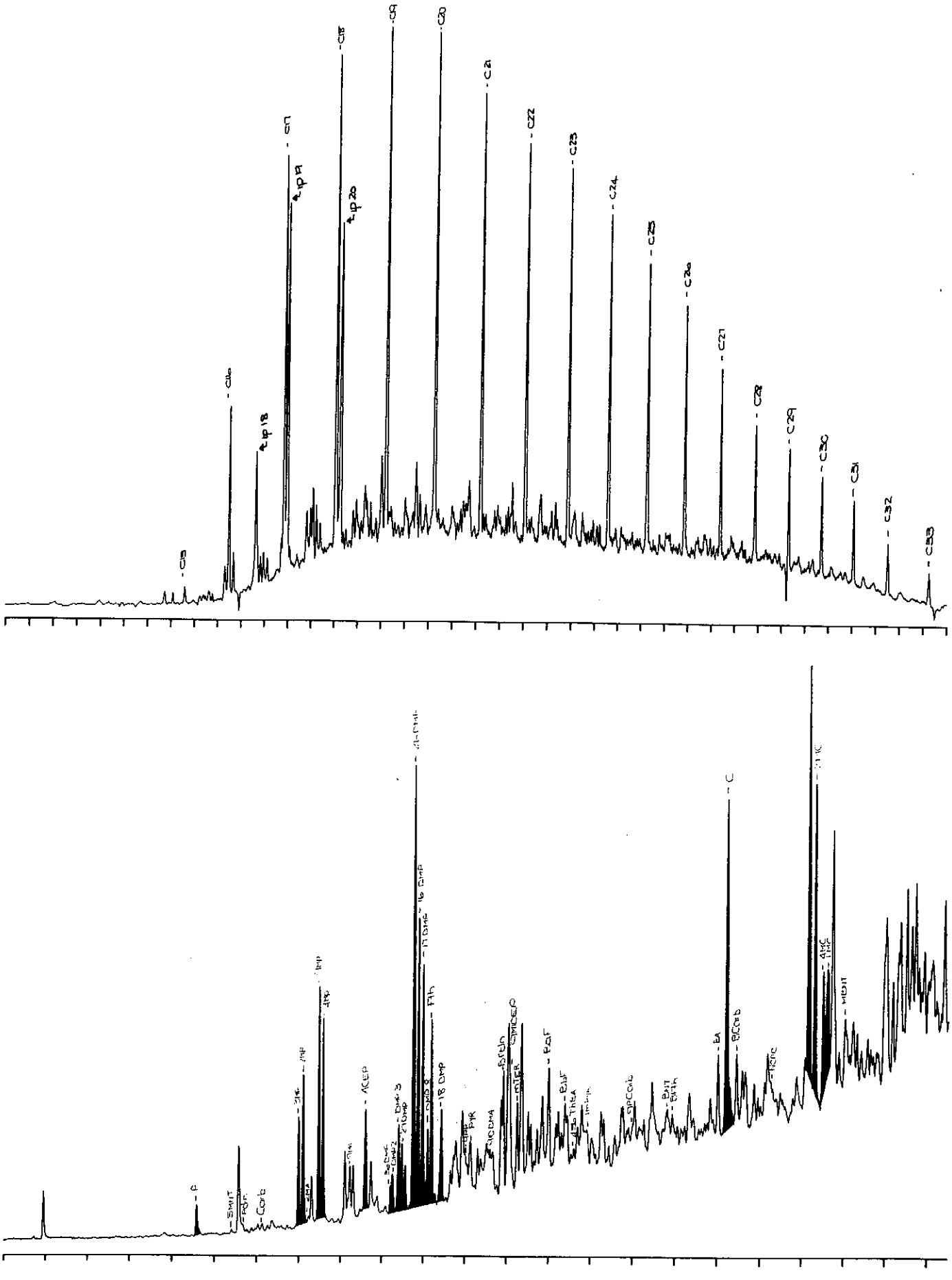

Figure D.56: Gas chromatograms of the total saturated and aromatic fractions of sample 63, well 42 RC, 3021m.

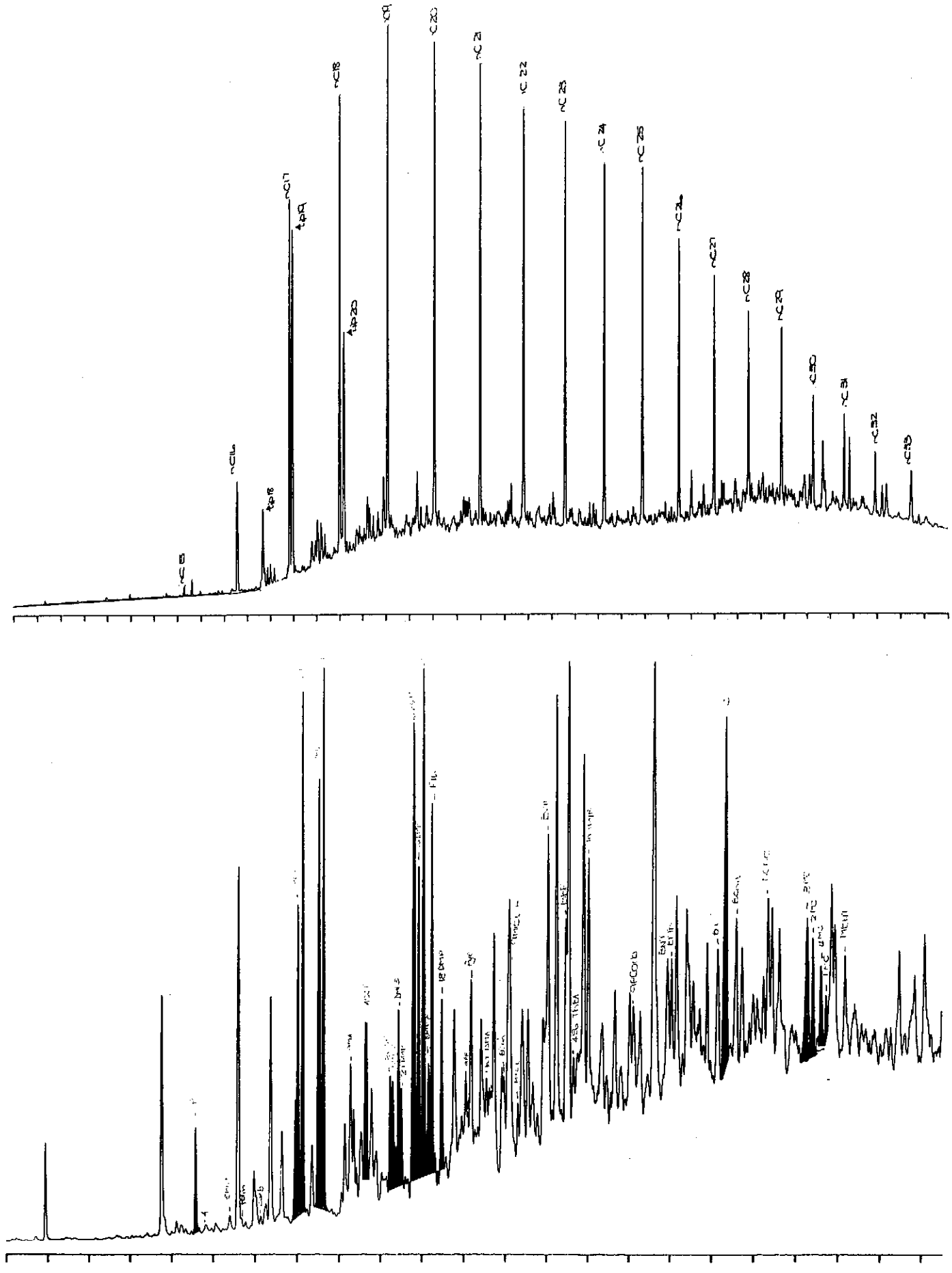

Figure D.57: Gas chromatograms of the total saturated and aromatic fractions of sample 64, well 48 RC, 2490m.

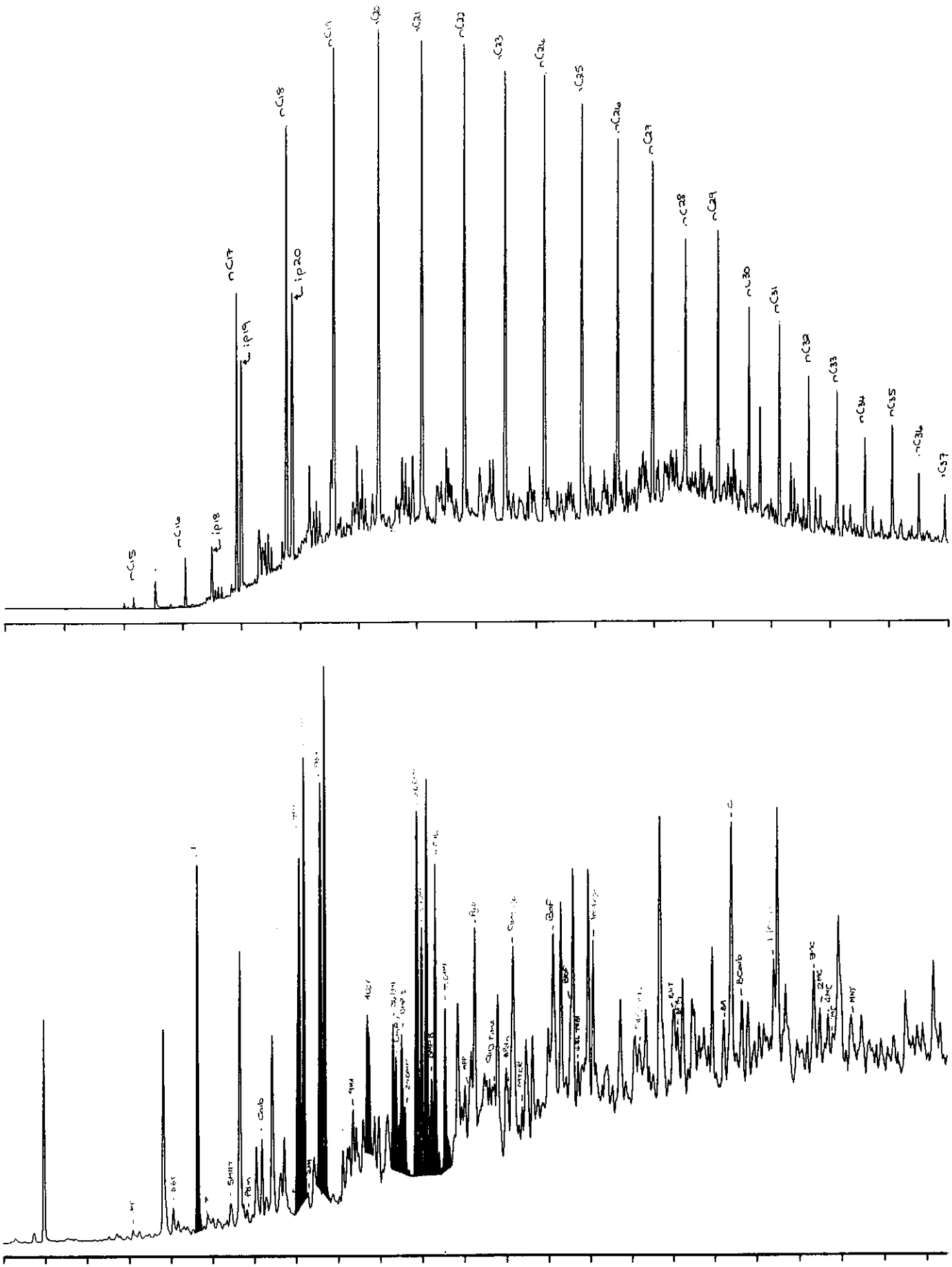

Figure D.58: Gas chromatograms of the total saturated and aromatic fractions of sample 65, well 41 RC, 2320m.

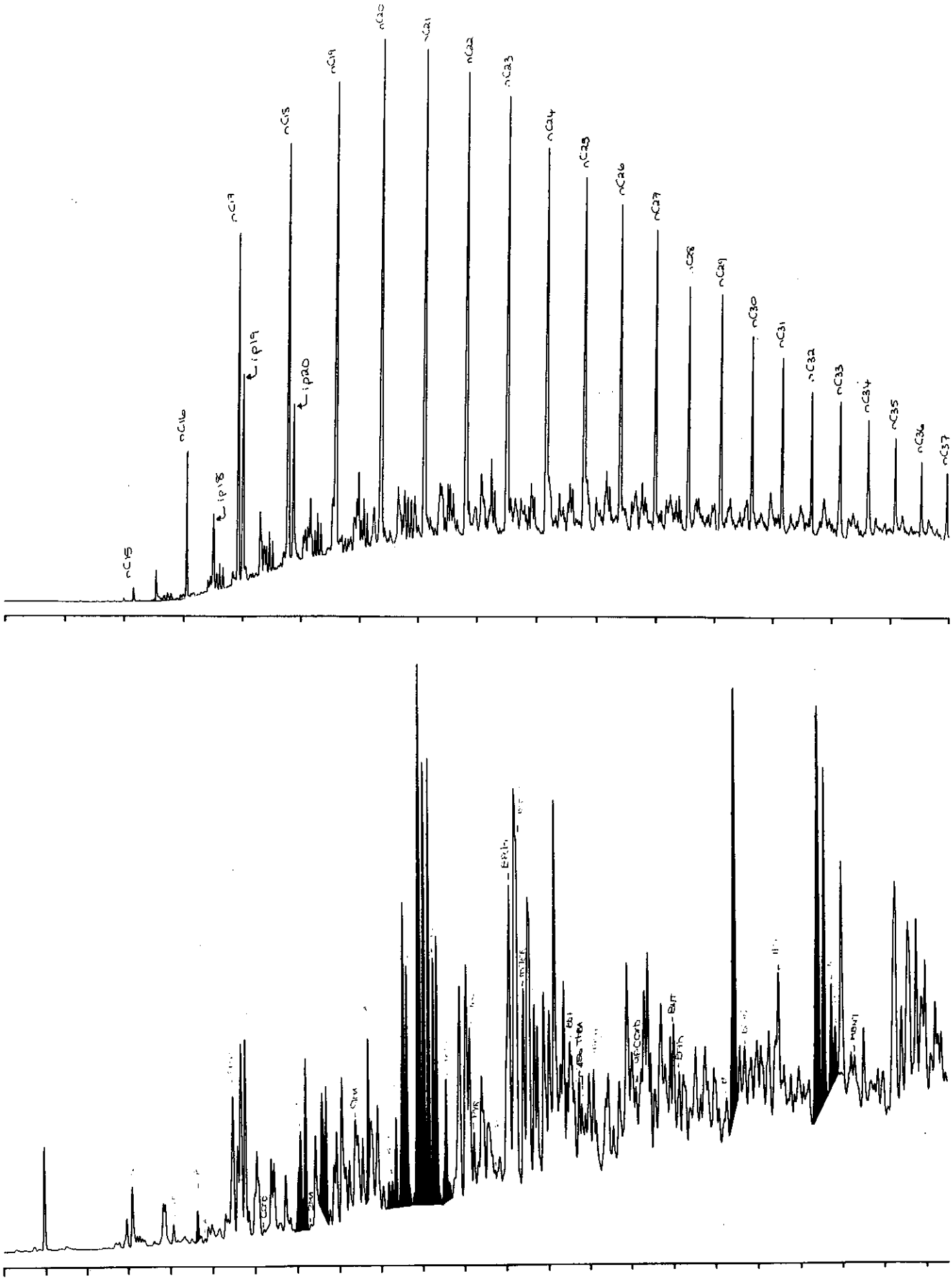

Figure D.59: Gas chromatograms of the total saturated and aromatic fractions of sample 66, well 65 RC, 3160m.

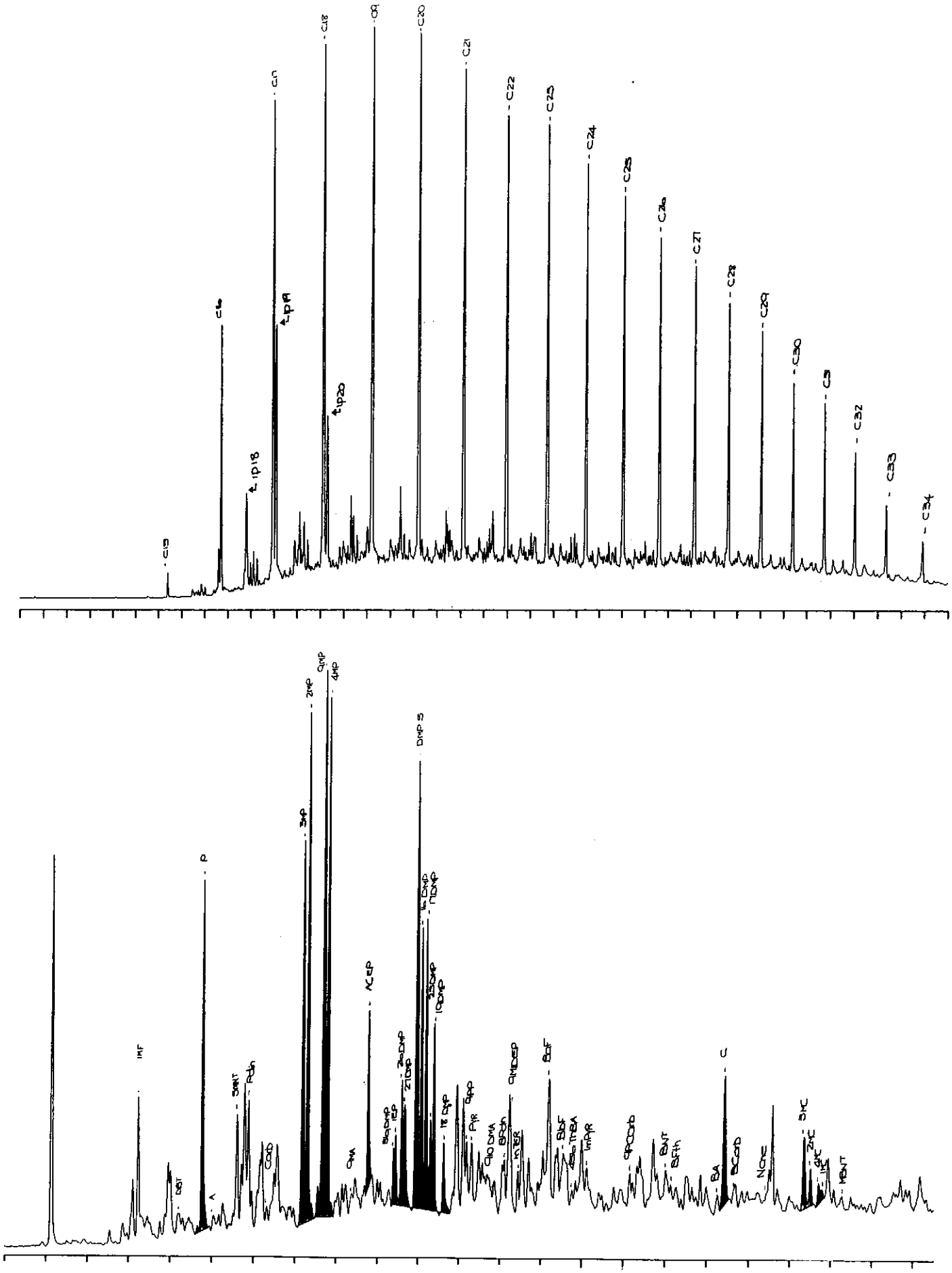

Figure D.60: Gas chromatograms of the total saturated and aromatic fractions of sample 67, well 75 core 1, 2829.0m.

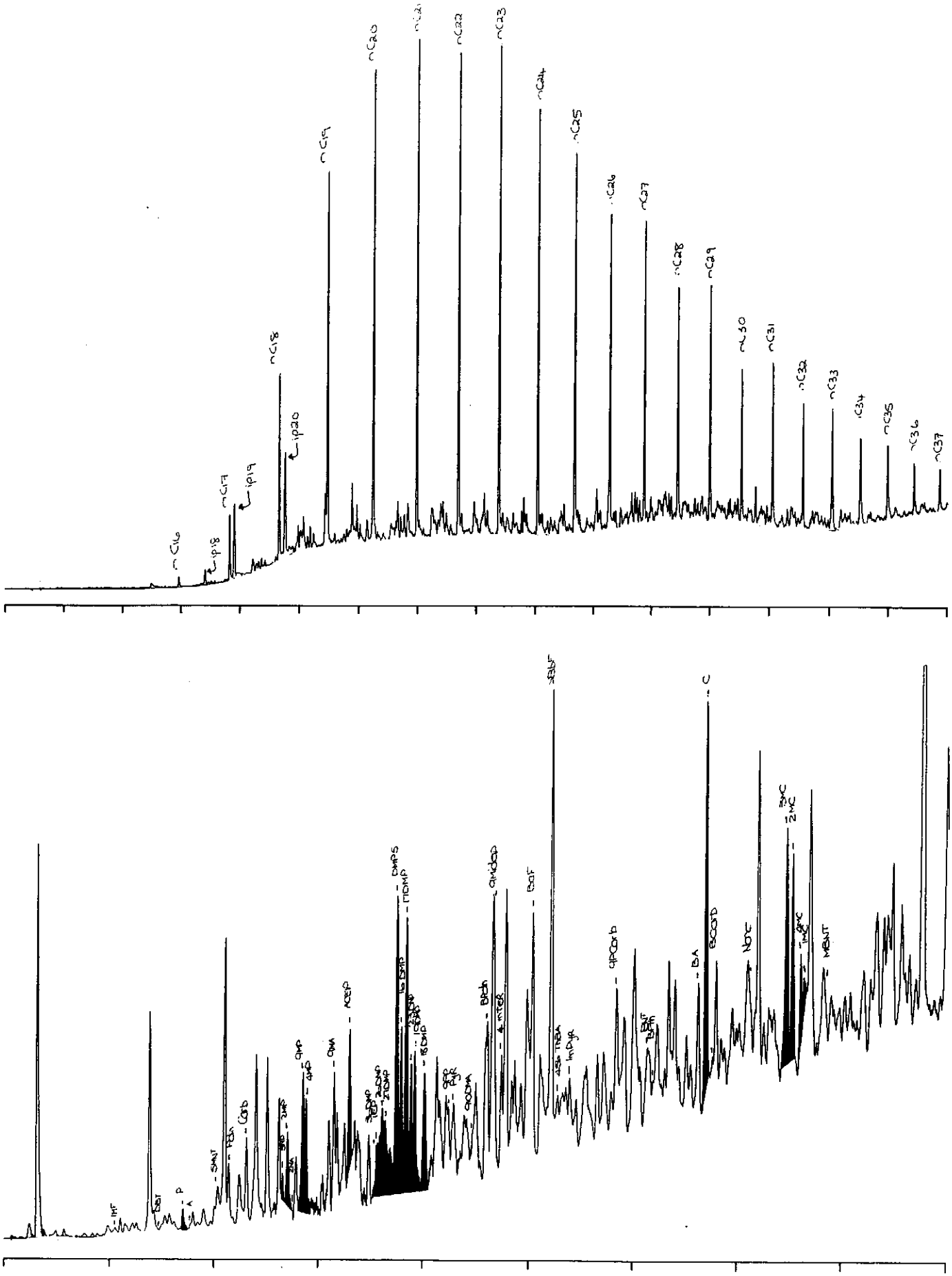

Figure D.61: Gas chromatograms of the total saturated and aromatic fractions of sample 68, well 67 RC, 2651m.

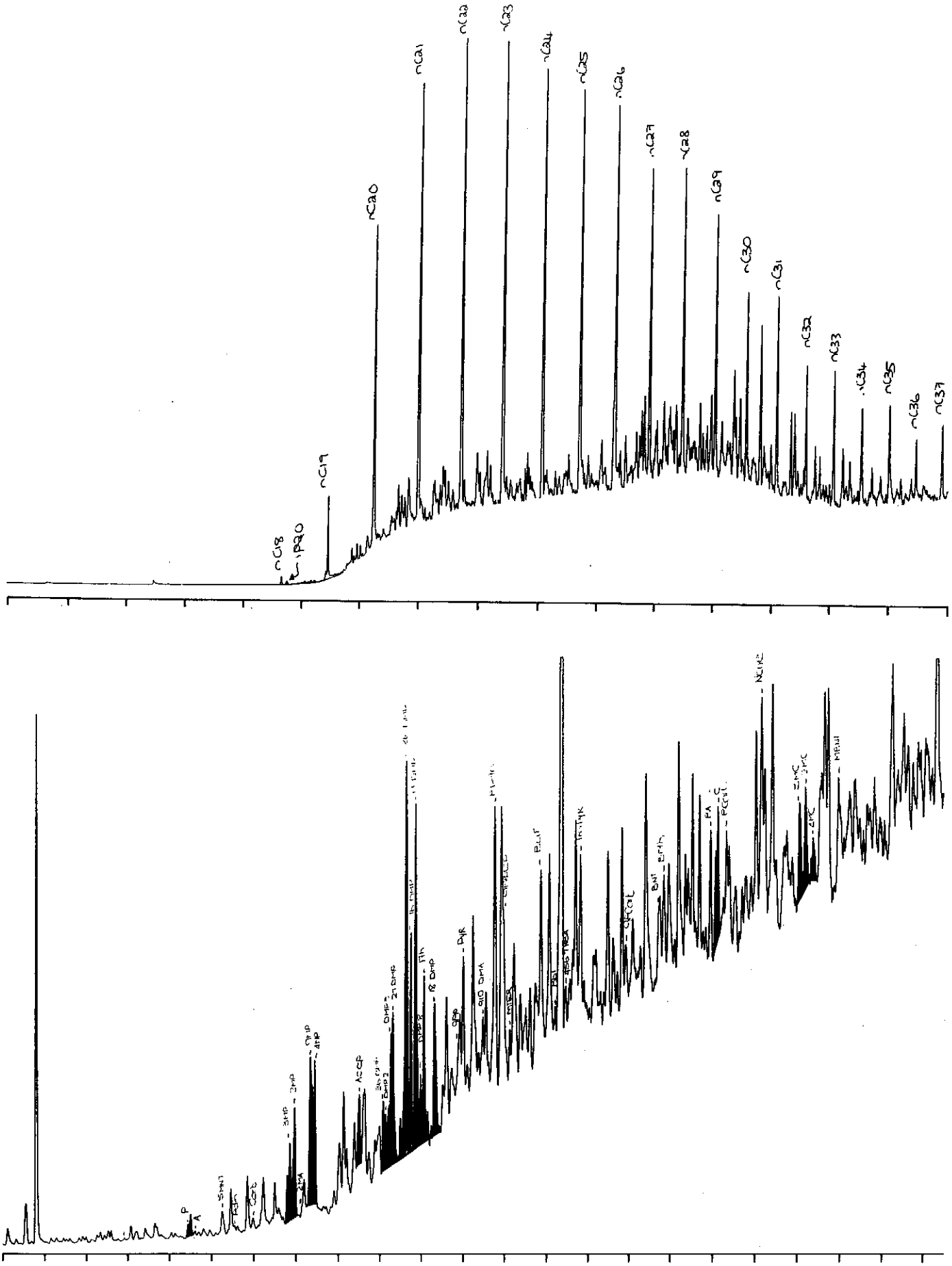

Figure D.62: Gas chromatograms of the total saturated and aromatic fractions of sample 69, well 12 RC, 2057m.

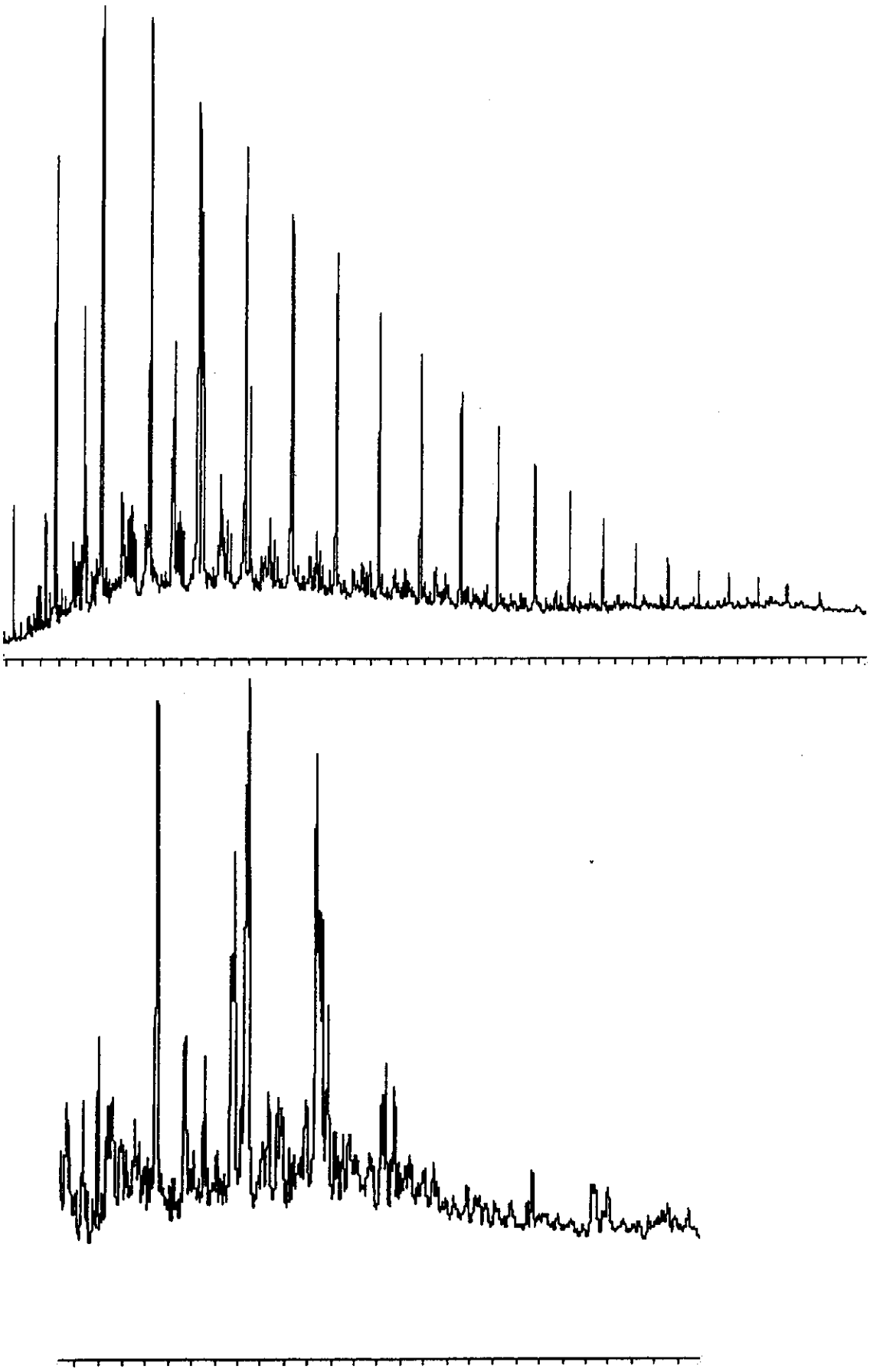

Figure D.63: Gas chromatograms of the total saturated and aromatic fractions of sample 70, well 156 RC, 2805m.

APPENDIX E: SATURATED AND AROMATIC BIOMARKER PLOTS

not analysed

not analysed

a) TIC: Total Ion Count

b) m/z 177: Demethylated Hopanes

not analysed

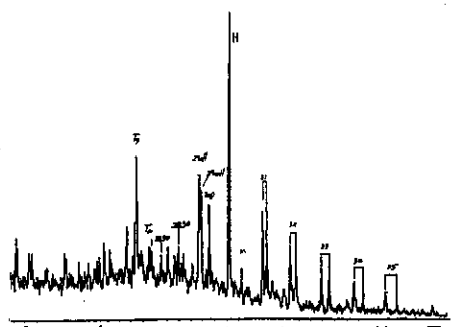

c) m/z 191: Tri and Tetra–cyclic Terpanes

d) m/z 191: Penta–cyclic Terpanes

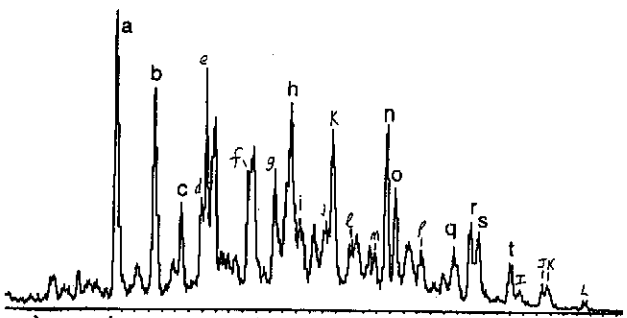

e) m/z 217: Steranes

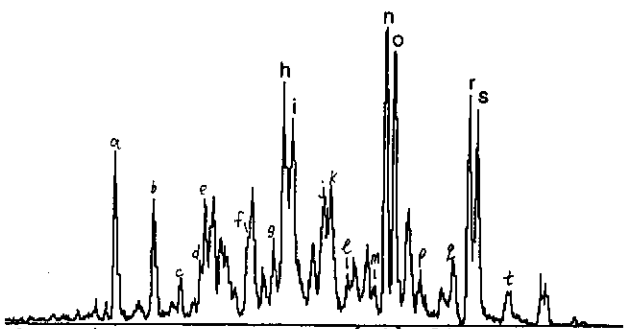

f) m/z 218: Regular (ßß) Steranes

not analysed

not analysed

g) m/z 231: Methyl Steranes

h) m/z 259: Rearranged (ßa) Steranes

Figure E.01: Annotated TIC and single ion fragmentograms of saturated hydrocarbons from sample 1, well 83 DST 1, 2470m.

not analysed

not analysed

a) TIC: Total Ion Count

b) m/z 177: Demethylated Hopanes

not analysed

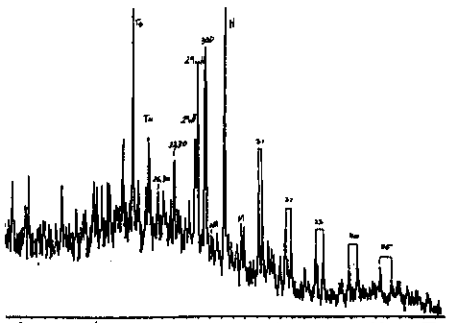

c) m/z 191: Tri and Tetra-cyclic Terpanes

d) m/z 191: Penta-cyclic Terpanes

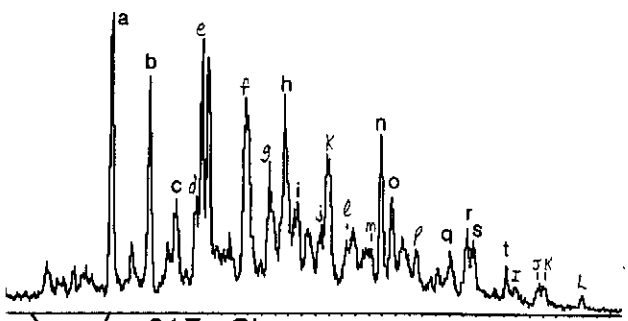

e) m/z 217: Steranes

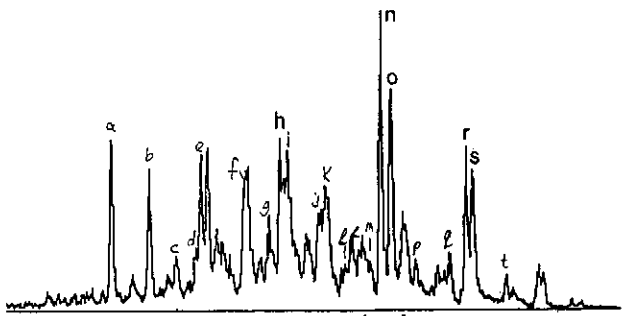

f) m/z 218: Regular (ßß) Steranes

not analysed

not analysed

g) m/z 231: Methyl Steranes

h) m/z 259: Rearranged (ßa) Steranes

Figure E.02: Annotated TIC and single ion fragmentograms of saturated hydrocarbons from sample 2, well 83 DST 2, 2889m.

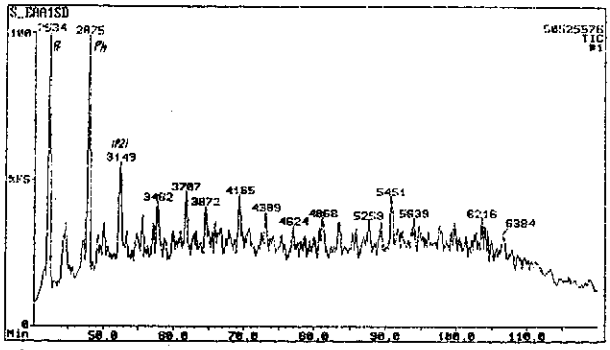

a) TIC: Total Ion Count

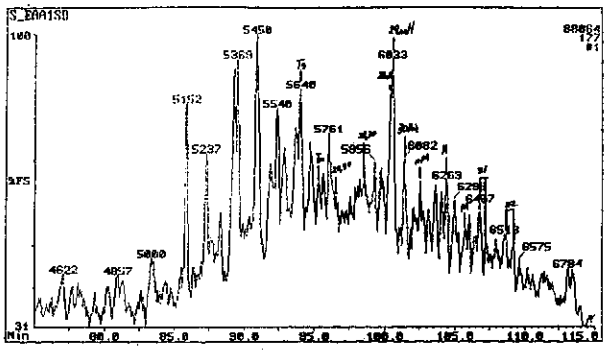

b) m/z 177: Demethylated Hopanes

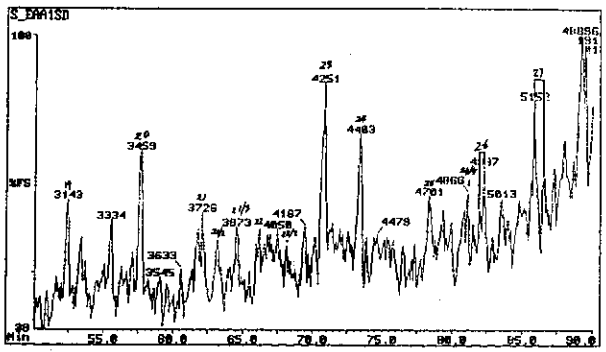

c) m/z 191: Tri and Tetra-cyclic Terpanes

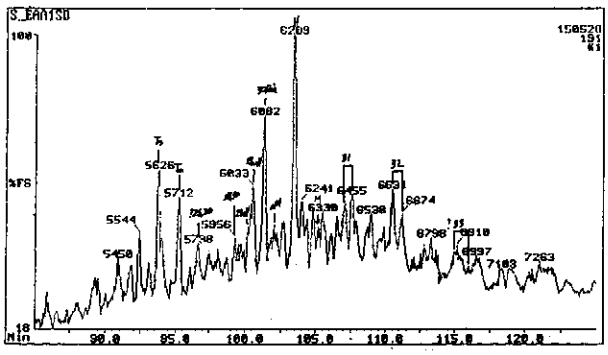

d) m/z 191: Penta-cyclic Terpanes

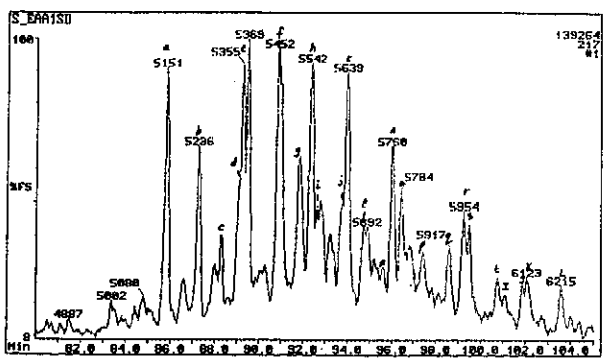

e) m/z 217: Steranes

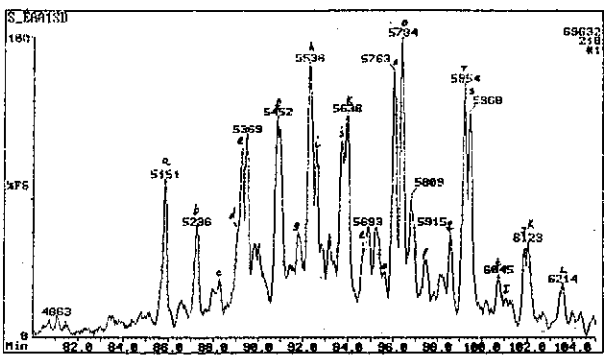

f) m/z 218: Regular (ßß) Steranes

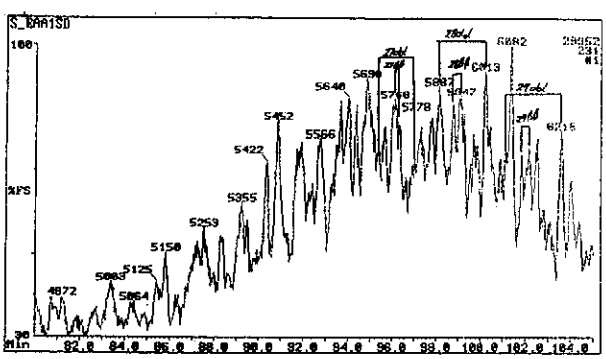

g) m/z 231: Methyl Steranes

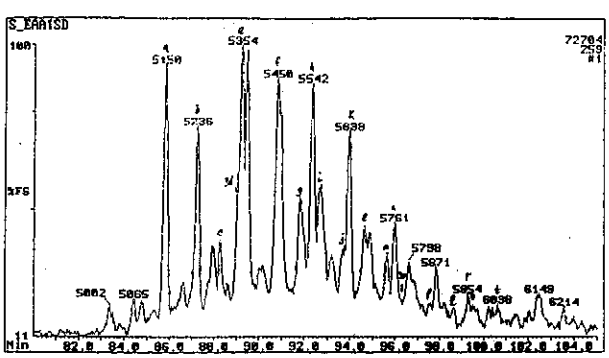

h) m/z 259: Rearranged (ßa) Steranes

Figure E.03: Annotated TIC and single ion fragmentograms of saturated hydrocarbons from sample 3, well 83 DST 2, 2889m.

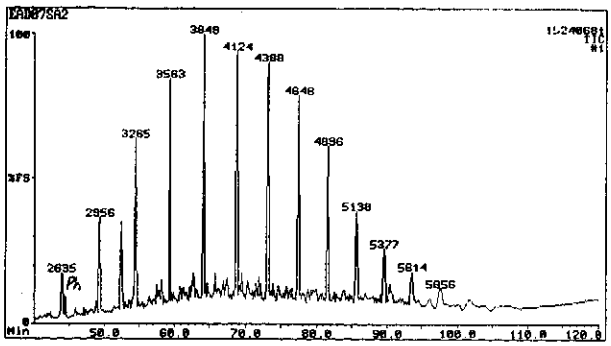

a) TIC: Total Ion Count

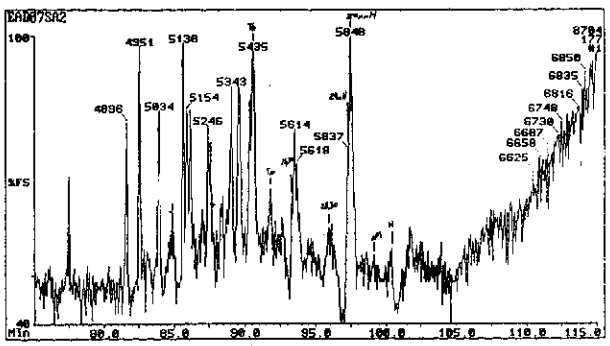

b) m/z 177: Demethylated Hopanes

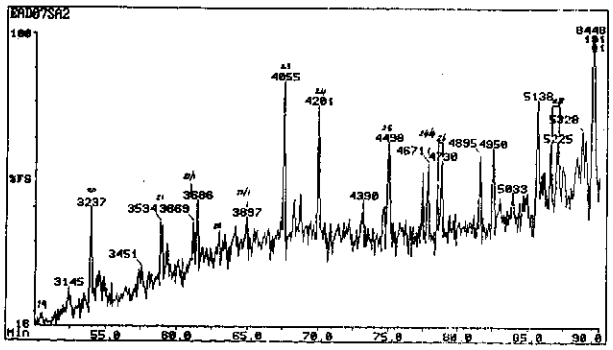

c) m/z 191: Tri and Tetra-cyclic Terpanes

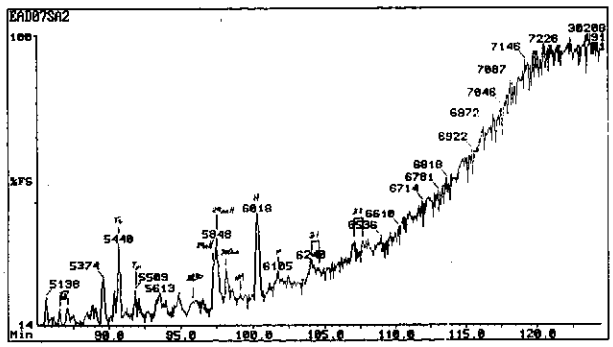

d) m/z 191: Penta-cyclic Terpanes

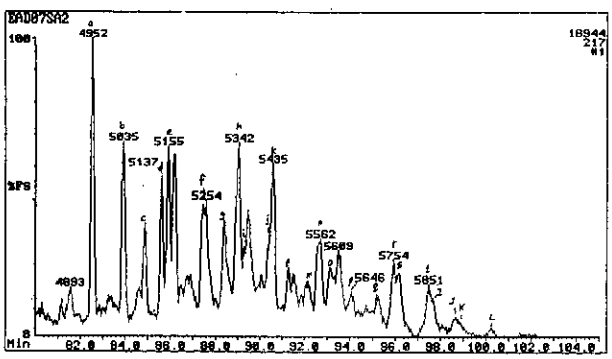

e) m/z 217: Steranes

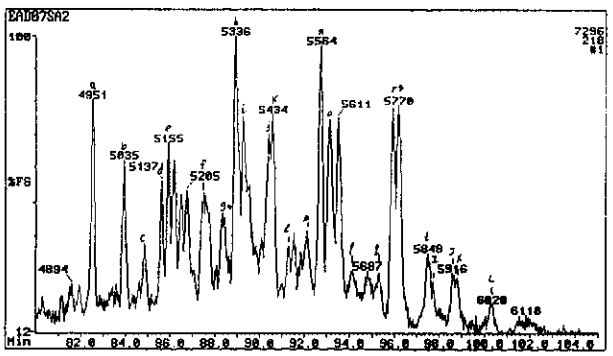

f) m/z 218: Regular (ßß) Steranes

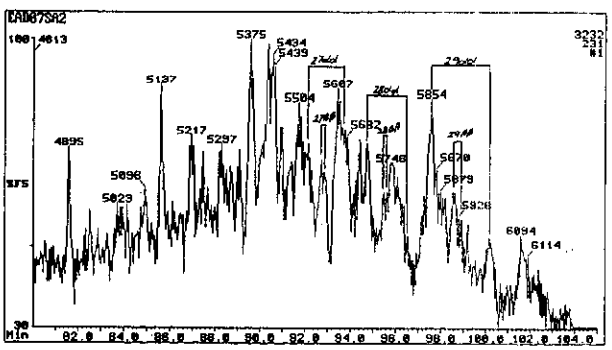

g) m/z 231: Methyl Steranes

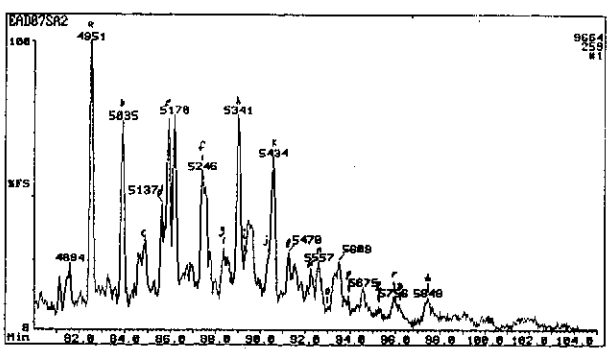

h) m/z 259: Rearranged (ßa) Steranes

Figure E.04: Annotated TIC and single ion fragmentograms of saturated hydrocarbons from sample 4, well 88 DST 5, 2507m.

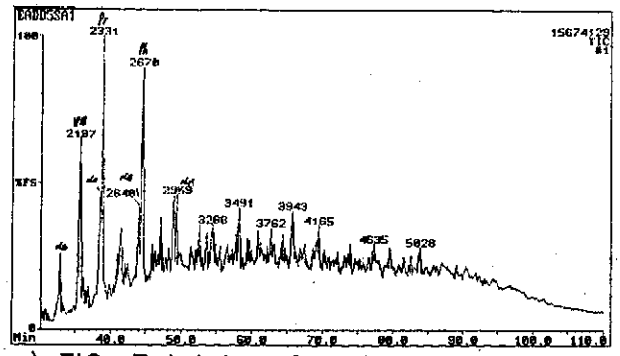

a) TIC: Total Ion Count

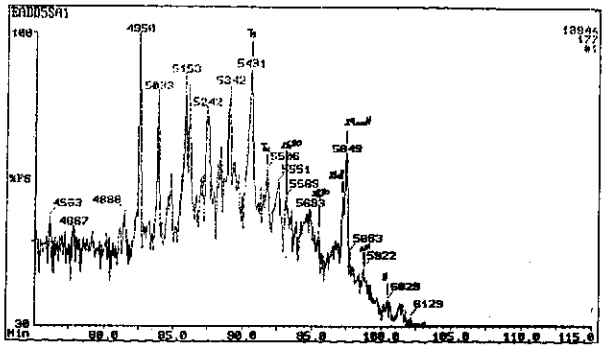

b) m/z 177: Demethylated Hopanes

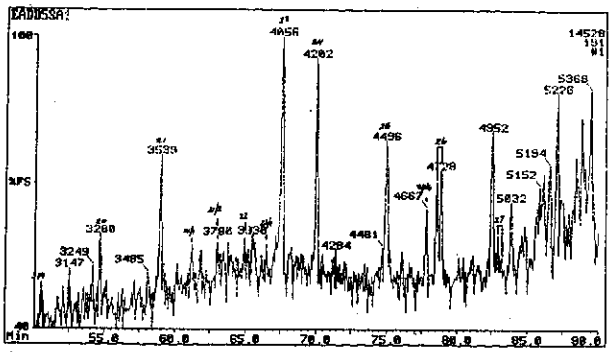

c) m/z 191: Tri and Tetra-cyclic Terpanes

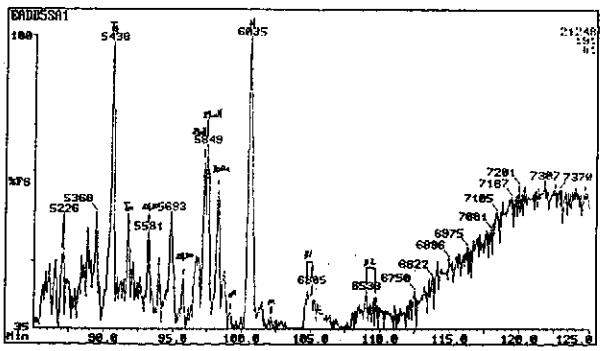

d) m/z 191: Penta-cyclic Terpanes

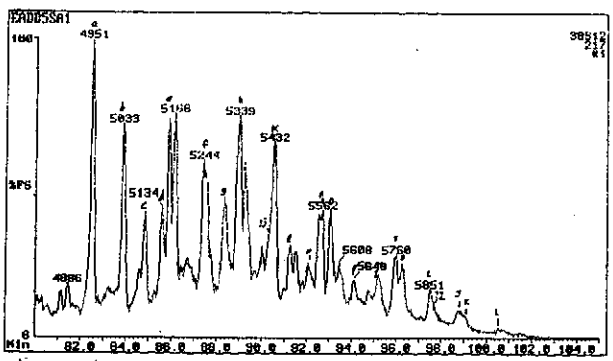

e) m/z 217: Steranes

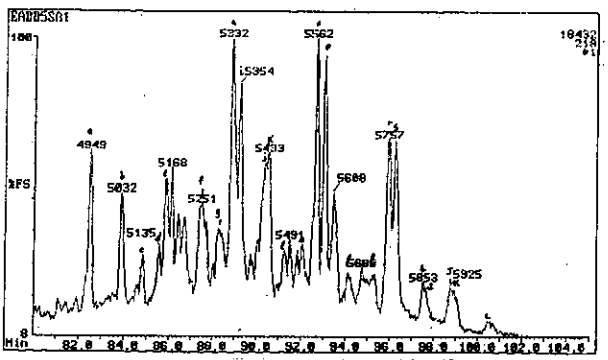

f) m/z 218: Regular (ßß) Steranes

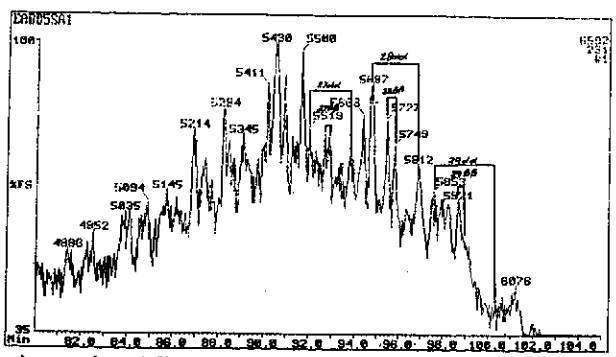

g) m/z 231: Methyl Steranes

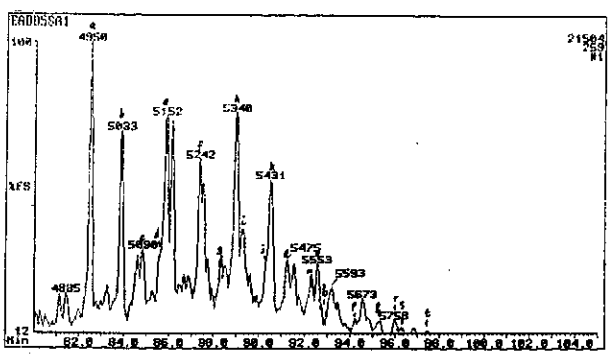

h) m/z 259: Rearranged (ßa) Steranes

Figure E.05: Annotated TIC and single ion fragmentograms of saturated hydrocarbons from sample 5, well 88 DST 5, 2507m.

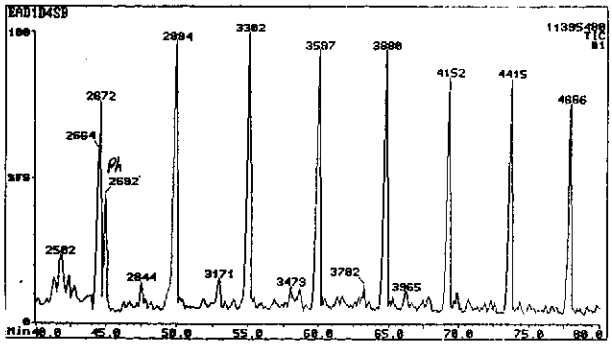

a) TIC: Total Ion Count

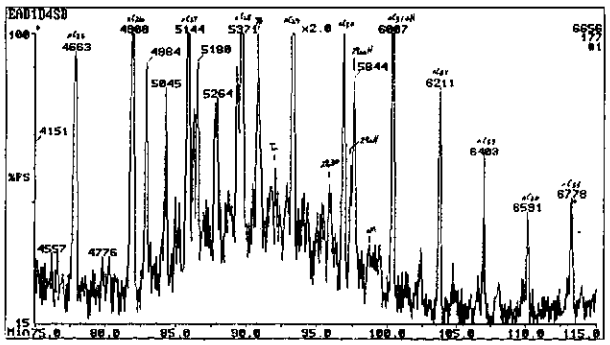

b) m/z 177: Demethylated Hopanes

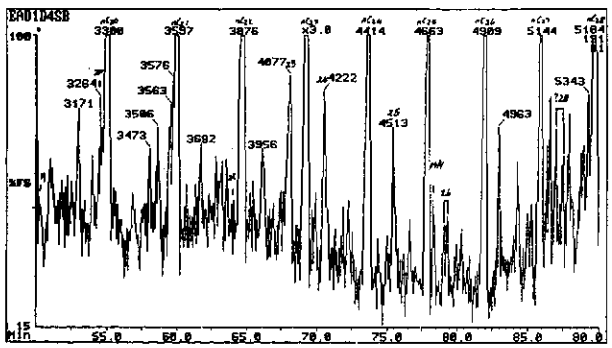

c) m/z 191: Tri and Tetra-cyclic Terpanes

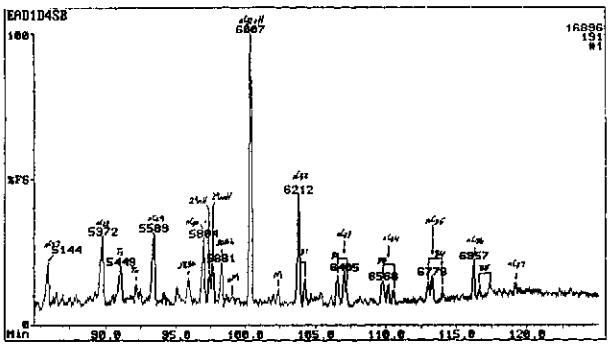

d) m/z 191: Penta-cyclic Terpanes

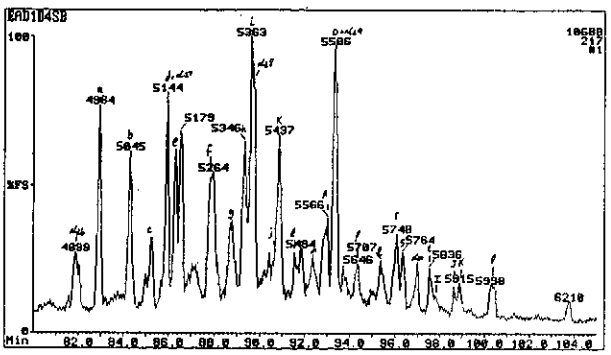

e) m/z 217: Steranes

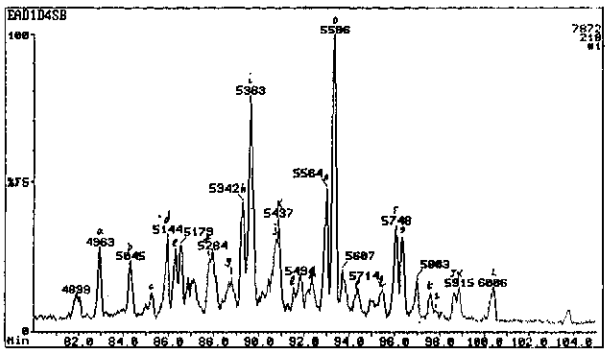

f) m/z 218: Regular (ßß) Steranes

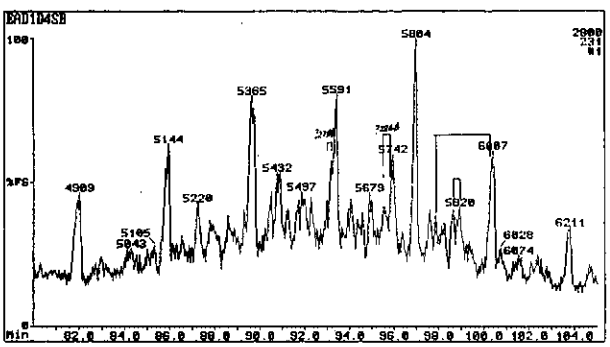

g) m/z 231: Methyl Steranes

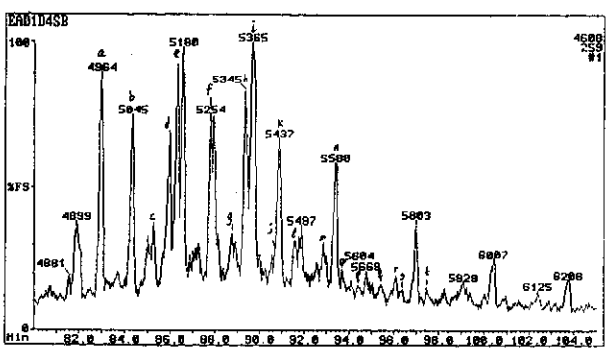

h) m/z 259: Rearranged (ßa) Steranes

Figure E.06: Annotated TIC and single ion fragmentograms of saturated hydrocarbons from sample 6, well 88 DST 4, 2827m.

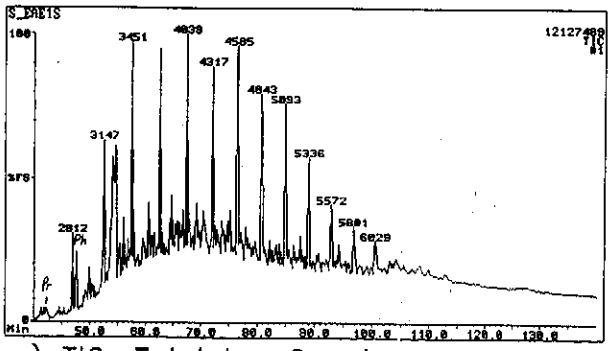

a) TIC: Total Ion Count

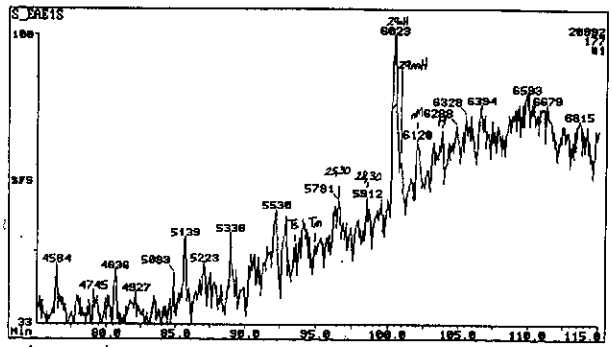

b) m/z 177: Demethylated Hopanes

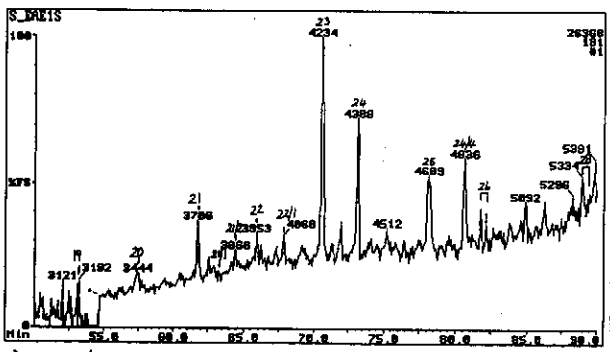

c) m/z 191: Tri and Tetra-cyclic Terpanes

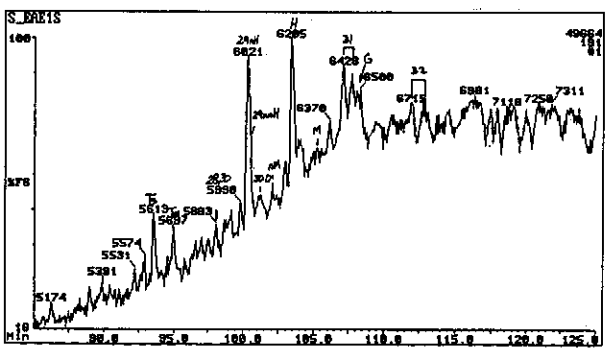

d) m/z 191: Penta-cyclic Terpanes

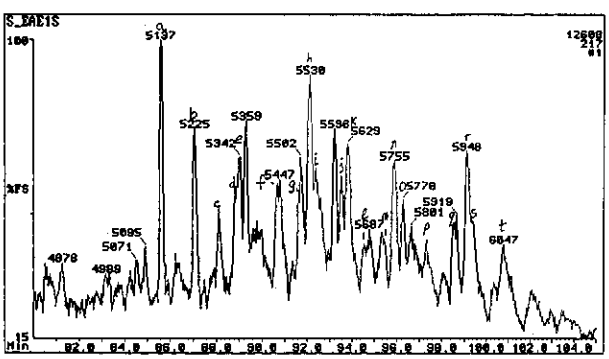

e) m/z 217: Steranes

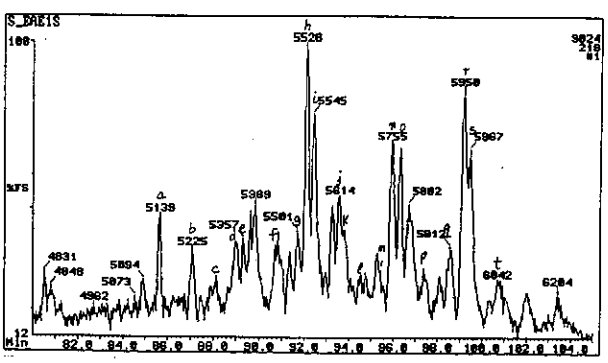

f) m/z 218: Regular (ßß) Steranes

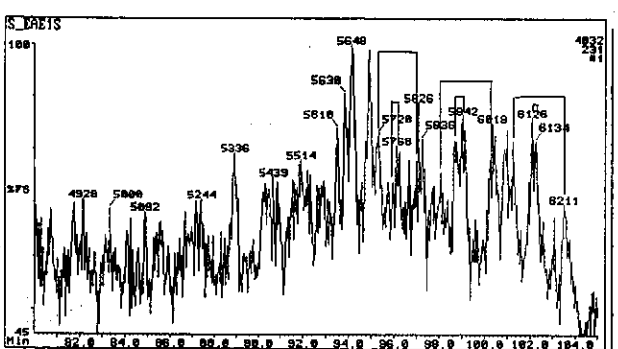

g) m/z 231: Methyl Steranes

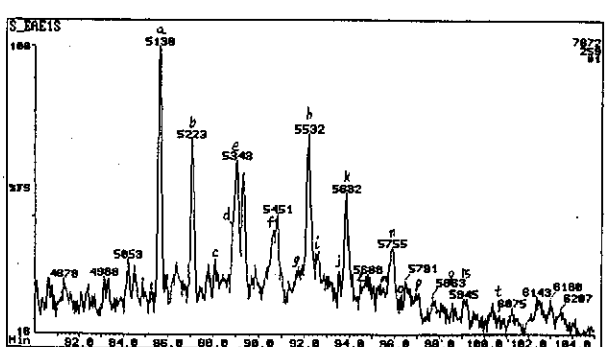

h) m/z 259: Rearranged (ßa) Steranes

Figure E.07: Annotated TIC and single ion fragmentograms of saturated hydrocarbons from sample 7, well 92 core 1, 2949.0m.

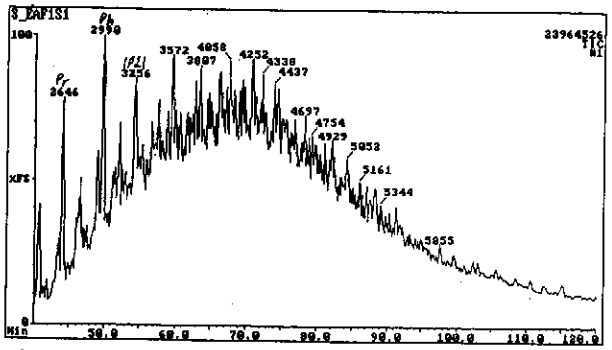

a) TIC: Total Ion Count

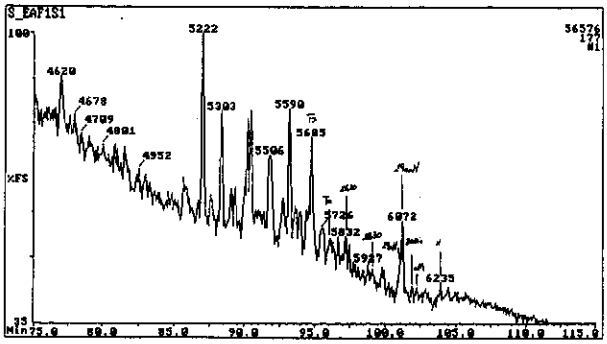

b) m/z 177: Demethylated Hopanes

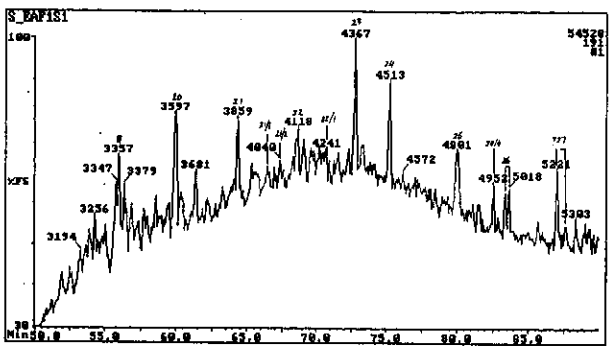

c) m/z 191: Tri and Tetra-cyclic Terpanes

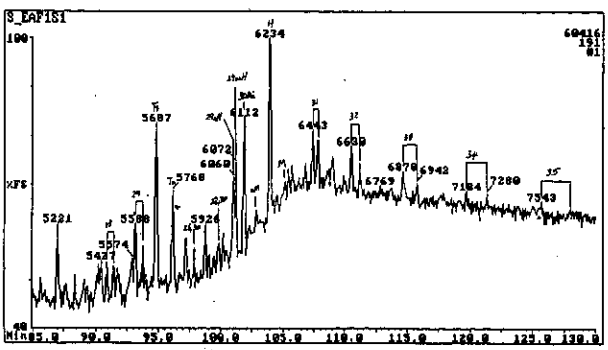

d) m/z 191: Penta-cyclic Terpanes

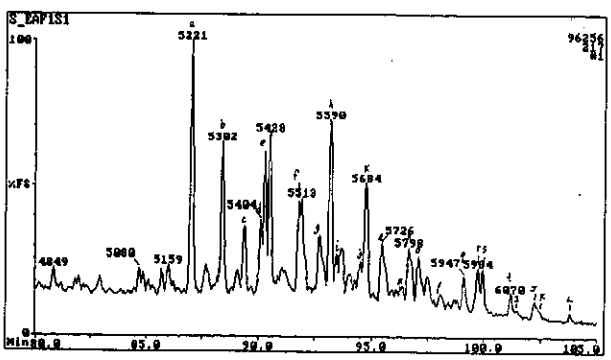

e) m/z 217: Steranes

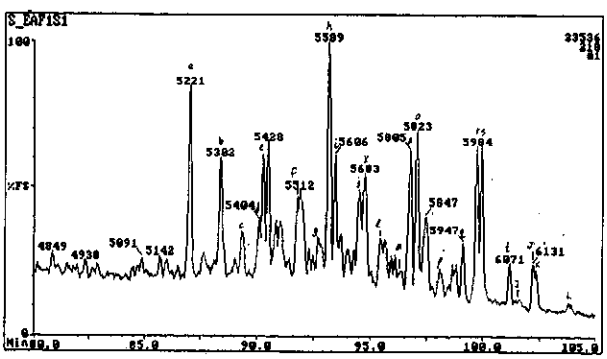

f) m/z 218: Regular (ßß) Steranes

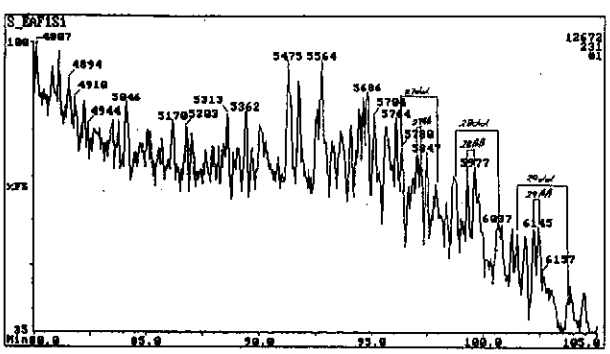

g) m/z 231: Methyl Steranes

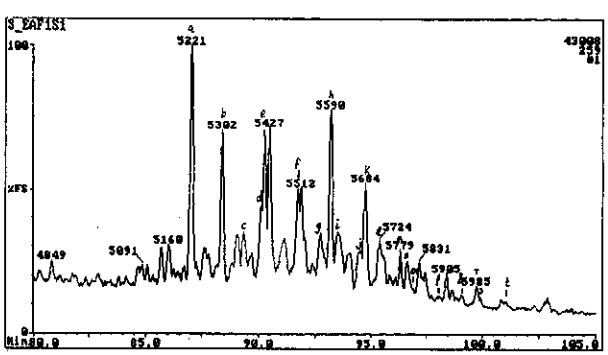

h) m/z 259: Rearranged (ßa) Steranes

Figure E.08: Annotated TIC and single ion fragmentograms of saturated hydrocarbons from sample 8, well 118 core 1, 2563.1m.

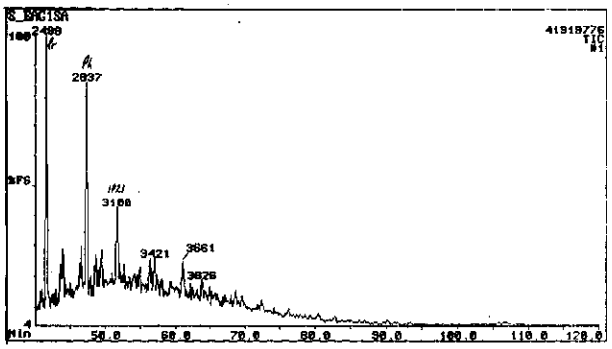

a) TIC: Total Ion Count

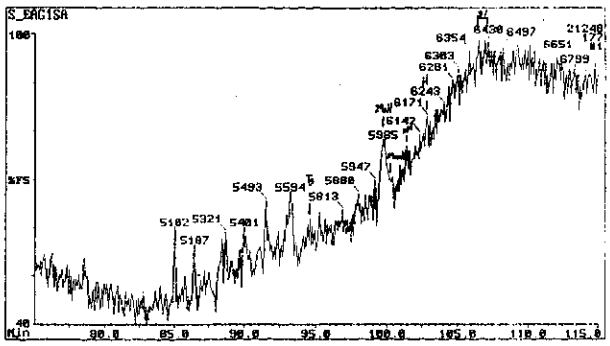

b) m/z 177: Demethylated Hopanes

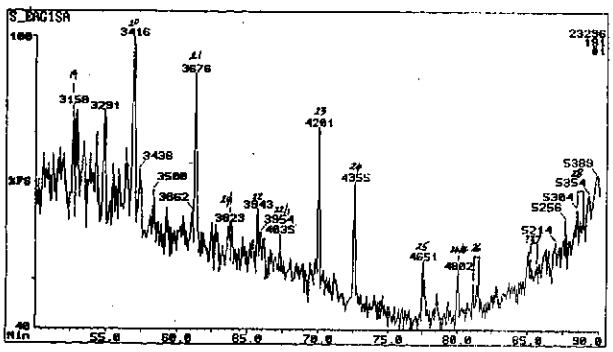

c) m/z 191: Tri and Tetra-cyclic Terpanes

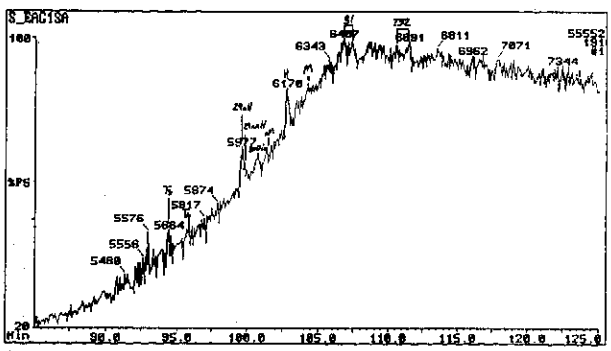

d) m/z 191: Penta-cyclic Terpanes

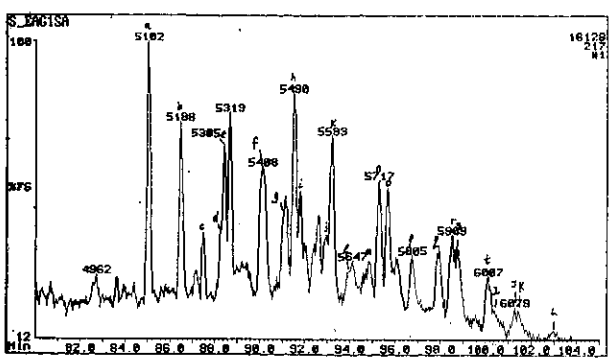

e) m/z 217: Steranes

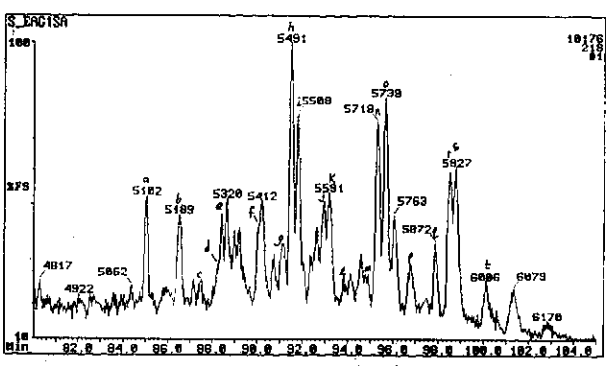

f) m/z 218: Regular (ßß) Steranes

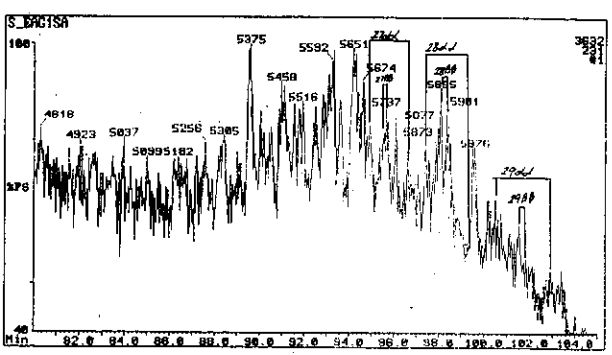

g) m/z 231: Methyl Steranes

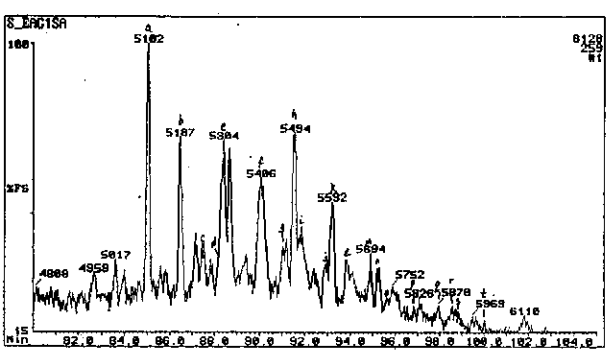

h) m/z 259: Rearranged (ßa) Steranes

Figure E.09: Annotated TIC and single ion fragmentograms of saturated hydrocarbons from sample 9, well 102 DST 4, 2241m.

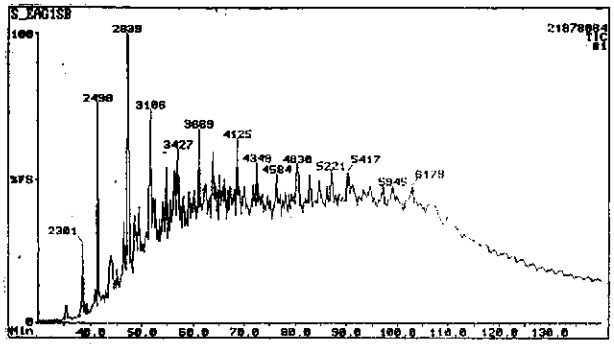

a) TIC: Total Ion Count

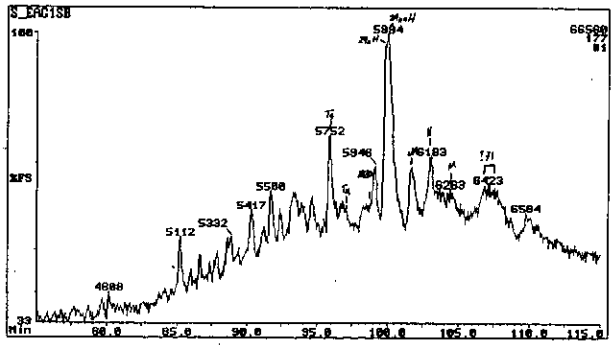

b) m/z 177: Demethylated Hopanes

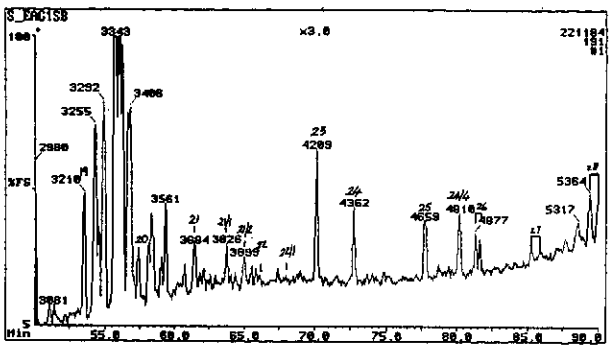

c) m/z 191: Tri and Tetra-cyclic Terpanes

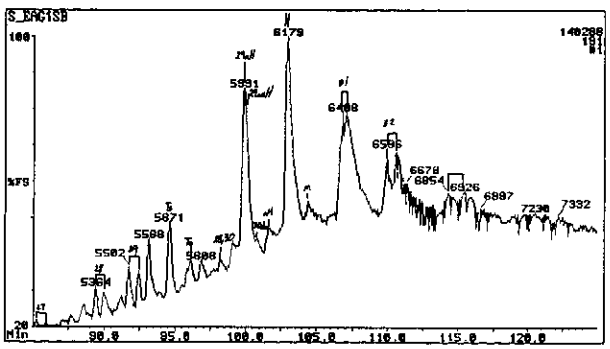

d) m/z 191: Penta-cyclic Terpanes

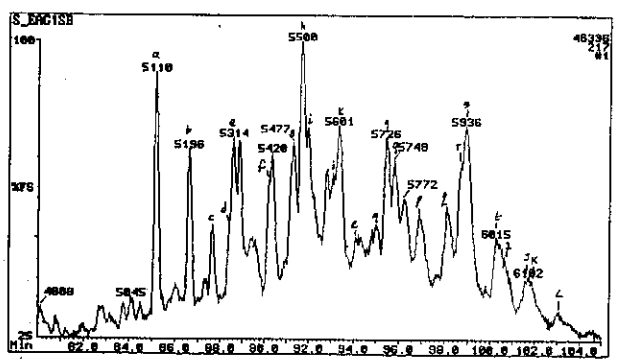

e) m/z 217: Steranes

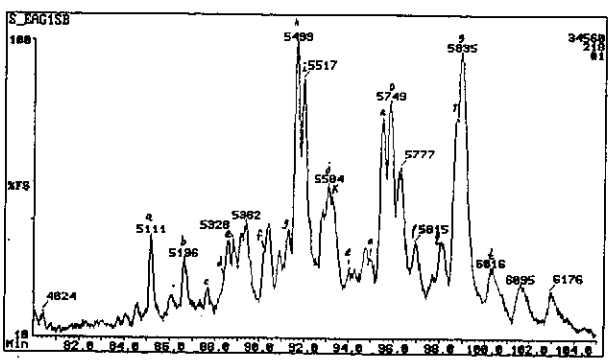

f) m/z 218: Regular (ßß) Steranes

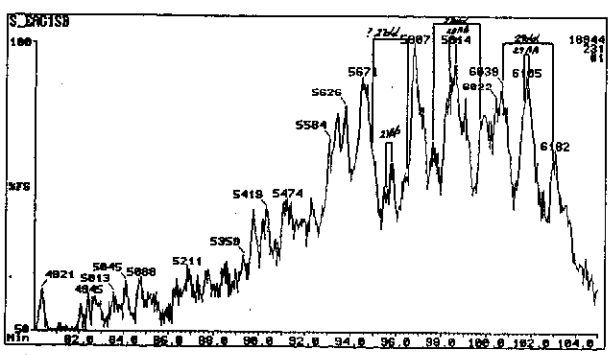

g) m/z 231: Methyl Steranes

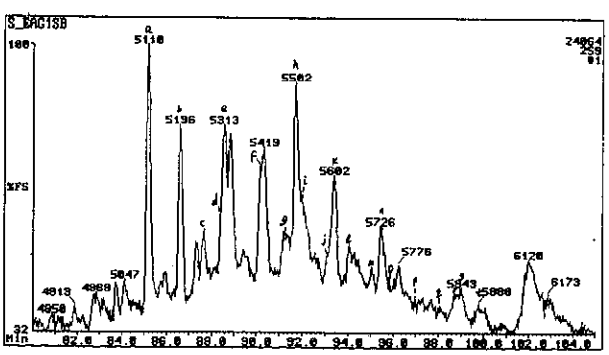

h) m/z 259: Rearranged (ßa) Steranes

Figure E.10: Annotated TIC and single ion fragmentograms of saturated hydrocarbons from sample 10, well 102 DST 2, 2556m.

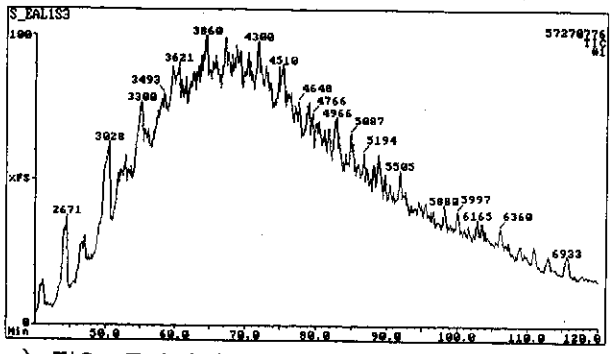

a) TIC: Total Ion Count

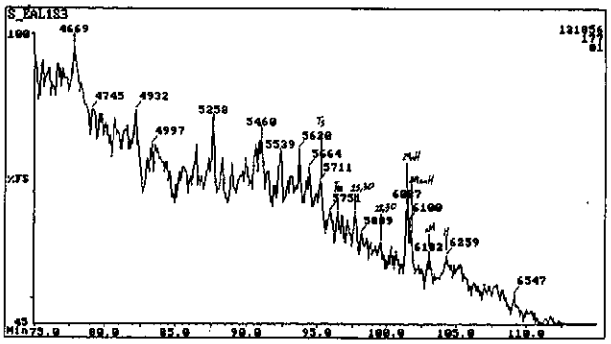

b) m/z 177: Demethylated Hopanes

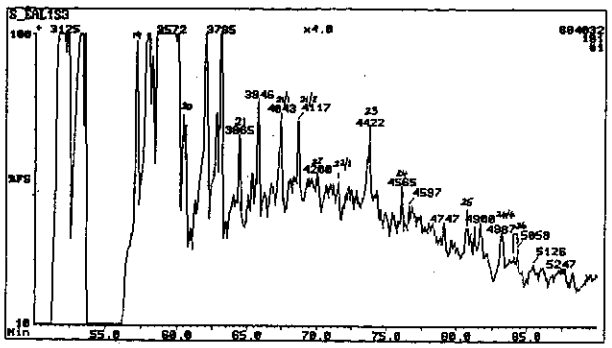

c) m/z 191: Tri and Tetra-cyclic Terpanes

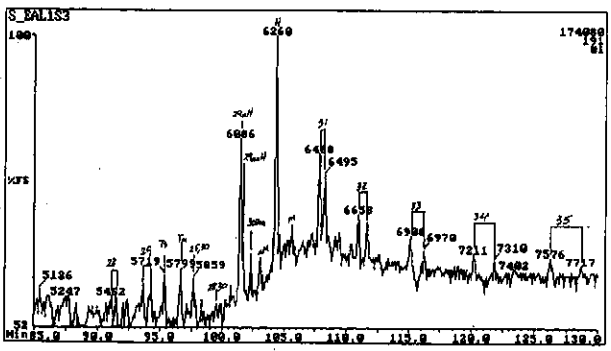

d) m/z 191: Penta-cyclic Terpanes

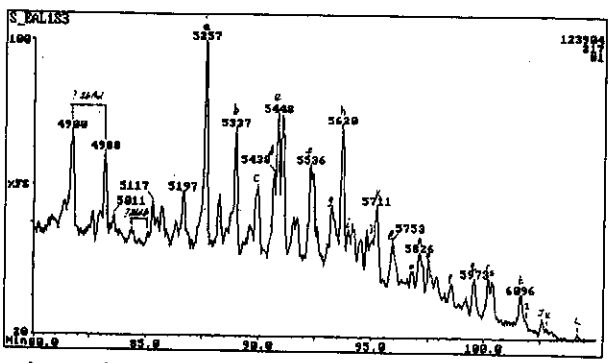

e) m/z 217: Steranes

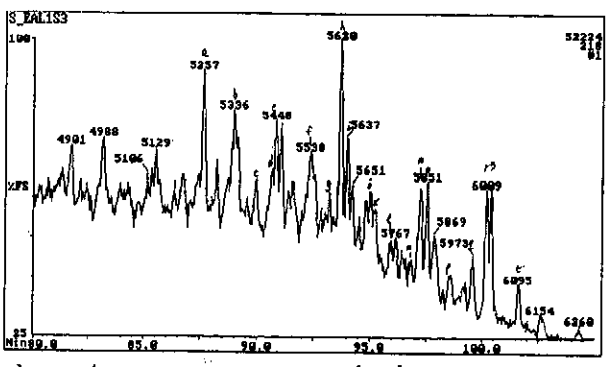

f) m/z 218: Regular (ßß) Steranes

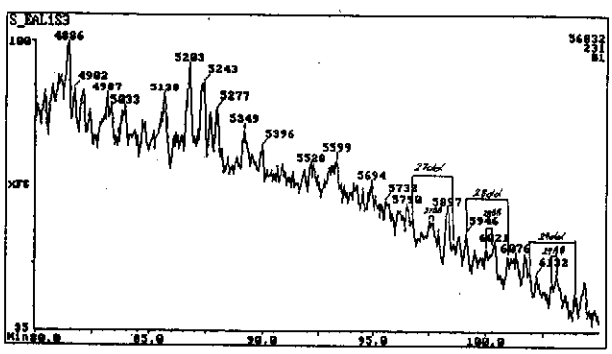

g) m/z 231: Methyl Steranes

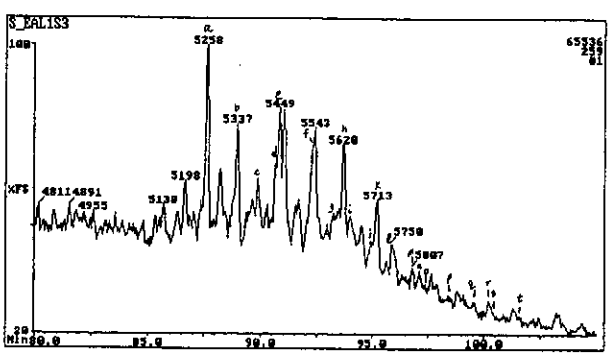

h) m/z 259: Rearranged (ßa) Steranes

Figure E.11: Annotated TIC and single ion fragmentograms of saturated hydrocarbons from sample 11, well 91 core 1, 3220.05m.

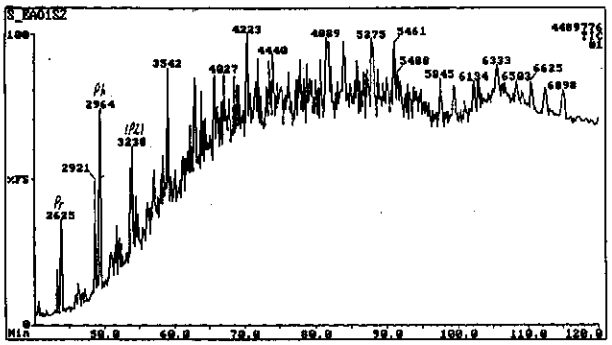

a) TIC: Total Ion Count

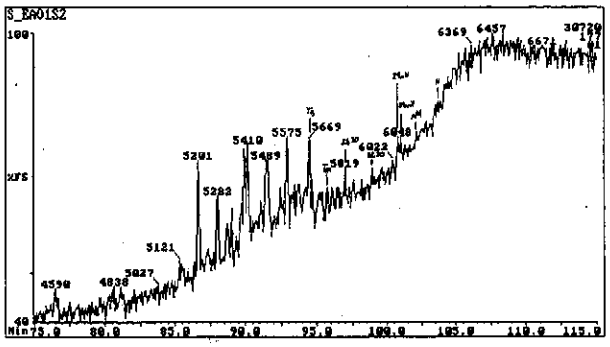

b) m/z 177: Demethylated Hopanes

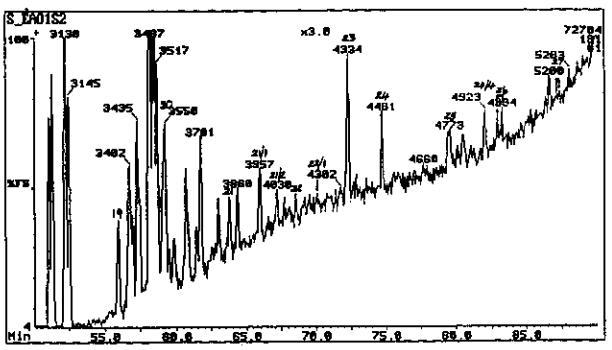

c) m/z 191: Tri and Tetra-cyclic Terpanes

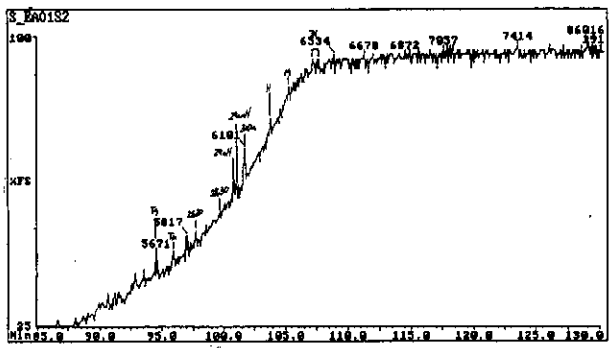

d) m/z 191: Penta-cyclic Terpanes

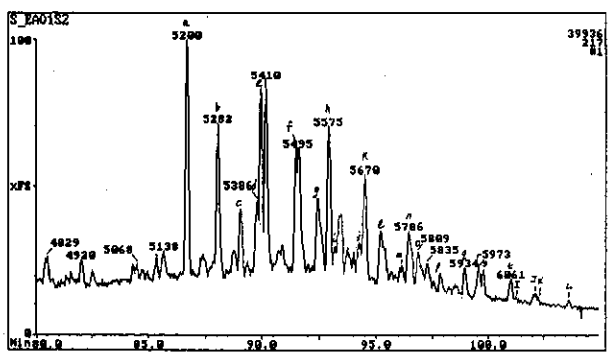

e) m/z 217: Steranes

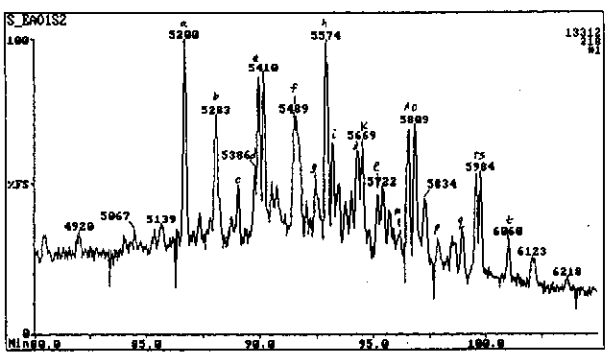

f) m/z 218: Regular (ßß) Steranes

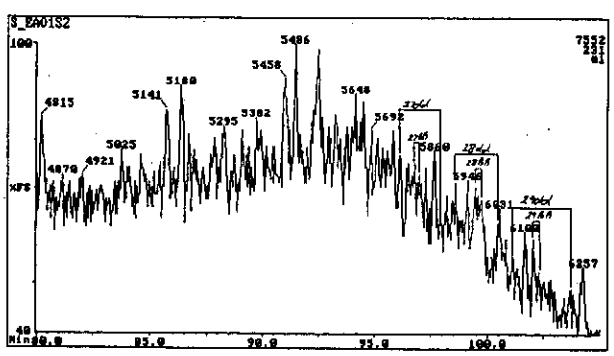

g) m/z 231: Methyl Steranes

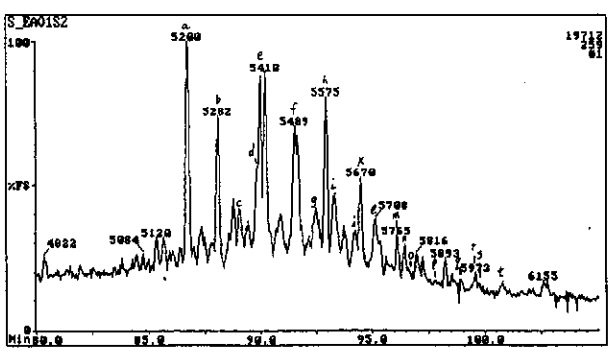

h) m/z 259: Rearranged (ßa) Steranes

Figure E.12: Annotated TIC and single ion fragmentograms of saturated hydrocarbons from sample 12, well 104 core 2, 3017.46m.

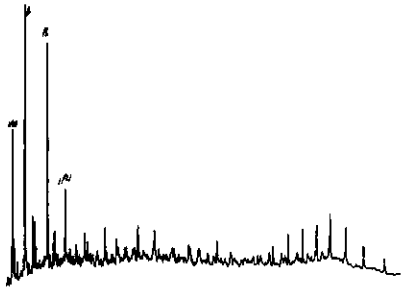

a) TIC: Total Ion Count

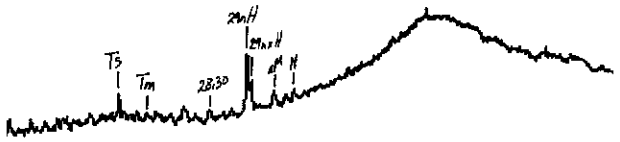

b) m/z 177: Demethylated Hopanes

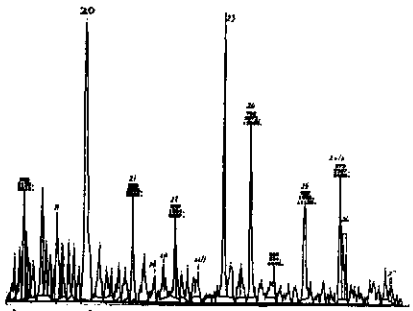

c) m/z 191: Tri and Tetra-cyclic Terpanes

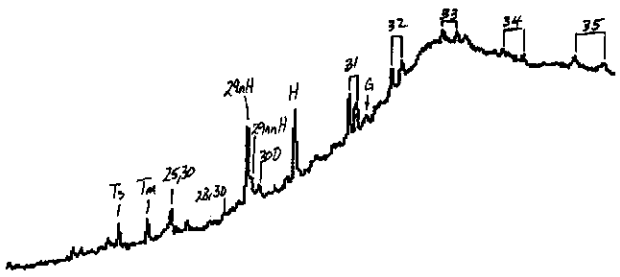

d) m/z 191: Penta-cyclic Terpanes

e) m/z 217: Steranes

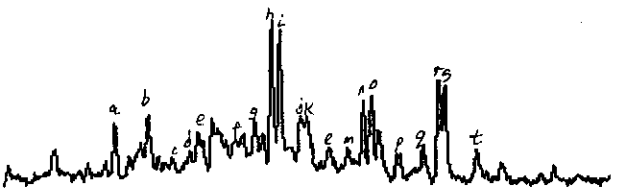

f) m/z 218: Regular (ßß) Steranes

g) m/z 231: Methyl Steranes

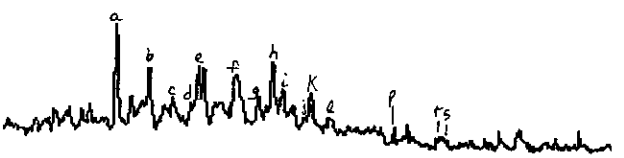

h) m/z 259: Rearranged (ßa) Steranes

Figure E.13: Annotated TIC and single ion fragmentograms of saturated hydrocarbons from sample 13, well 93 core 4, 3212.4m.

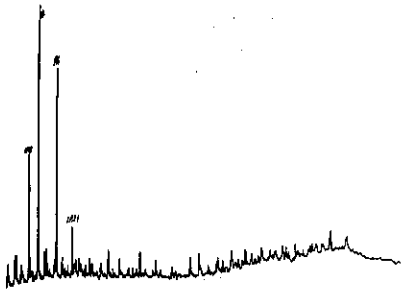

a) TIC: Total Ion Count

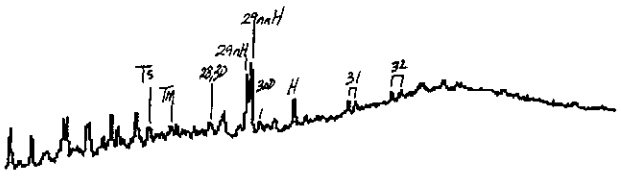

b) m/z 177: Demethylated Hopanes

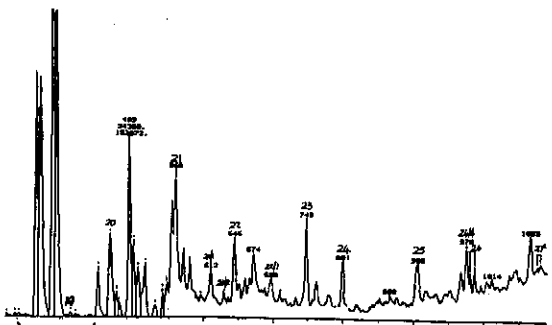

c) m/z 191: Tri and Tetra-cyclic Terpanes

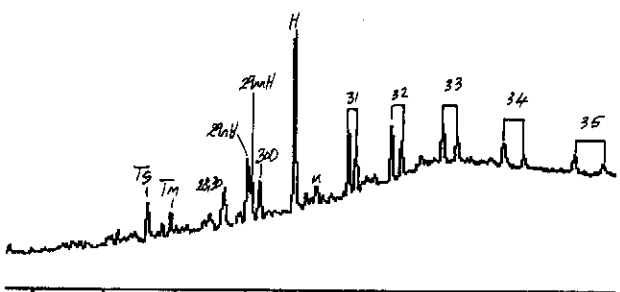

d) m/z 191: Penta-cyclic Terpanes

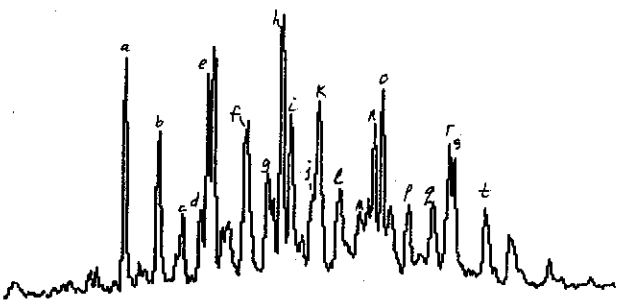

e) m/z 217: Steranes

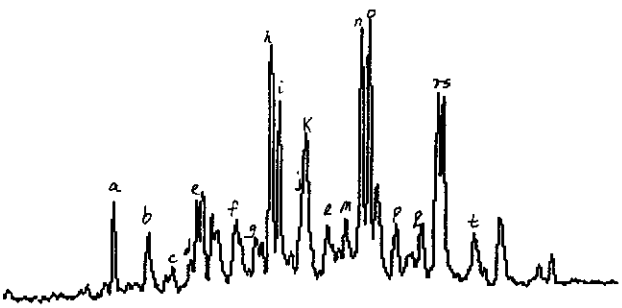

f) m/z 218: Regular (ßß) Steranes

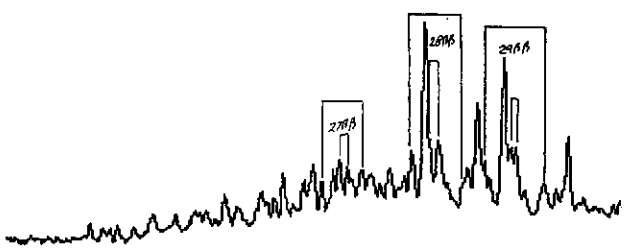

g) m/z 231: Methyl Steranes

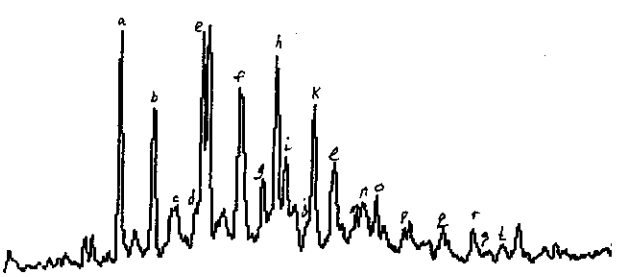

h) m/z 259: Rearranged (ßa) Steranes

Figure E.14: Annotated TIC and single ion fragmentograms of saturated hydrocarbons from sample 14, well 109 DST 1, 2630m.

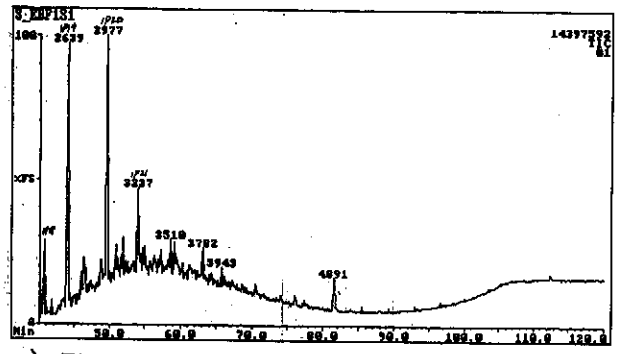

a) TIC: Total Ion Count

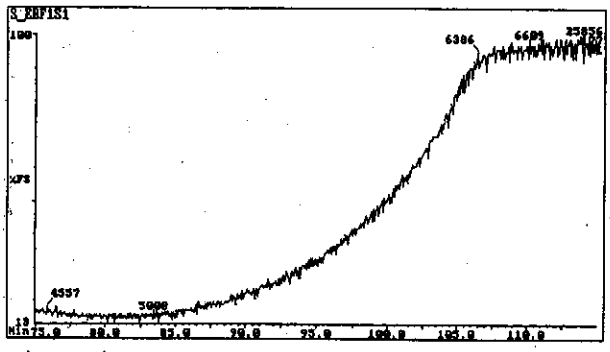

b) m/z 177: Demethylated Hopanes

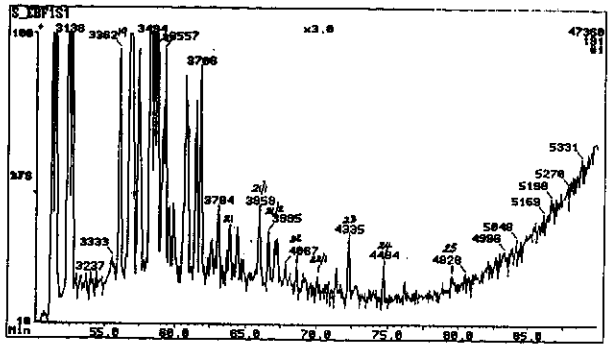

c) m/z 191: Tri and Tetra-cyclic Terpanes

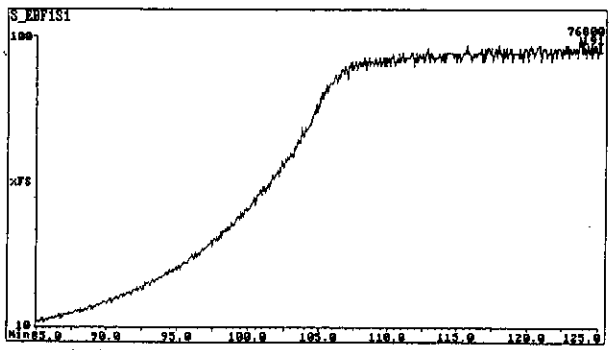

d) m/z 191: Penta-cyclic Terpanes

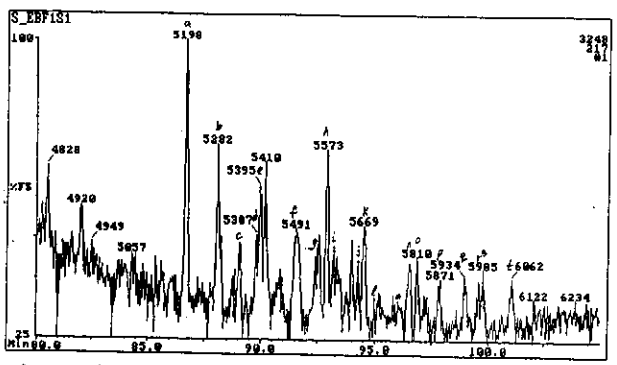

e) m/z 217: Steranes

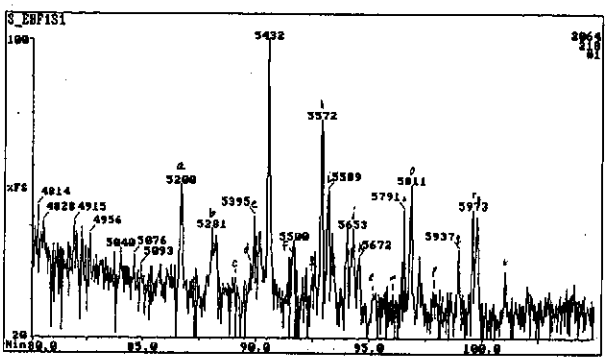

f) m/z 218: Regular (ßß) Steranes

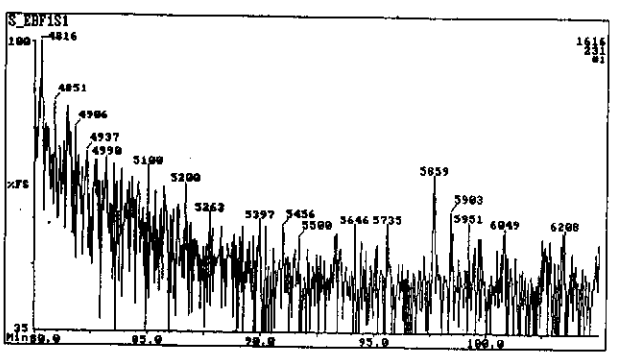

g) m/z 231: Methyl Steranes

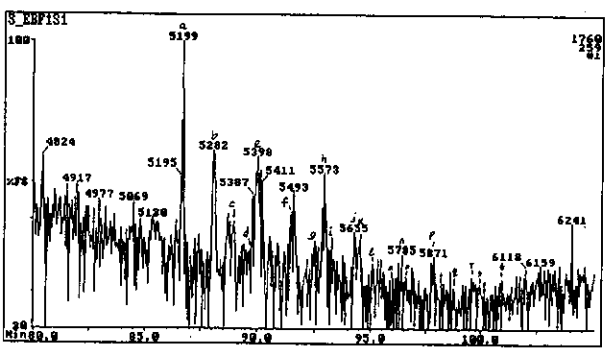

h) m/z 259: Rearranged (ßa) Steranes

Figure E.15: Annotated TIC and single ion fragmentograms of saturated hydrocarbons from sample 15, well 107 DST 2, 2565m.

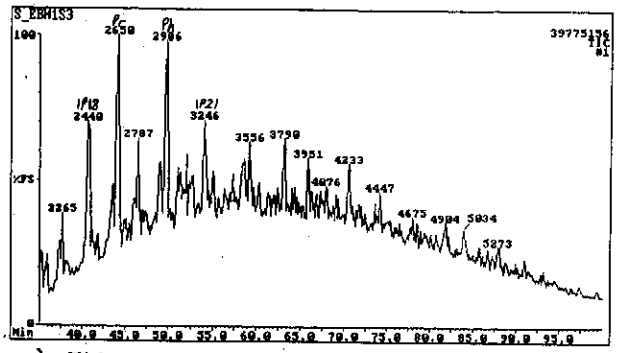

a) TIC: Total Ion Count

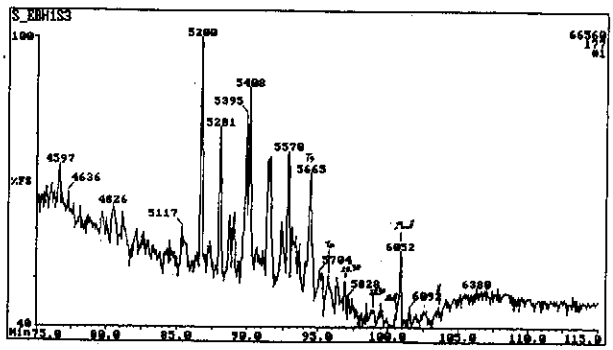

b) m/z 177: Demethylated Hopanes

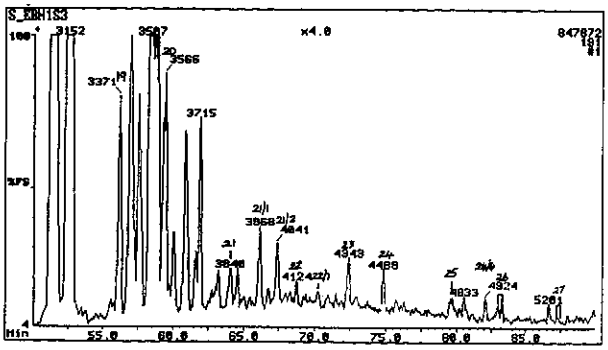

c) m/z 191: Tri and Tetra-cyclic Terpanes

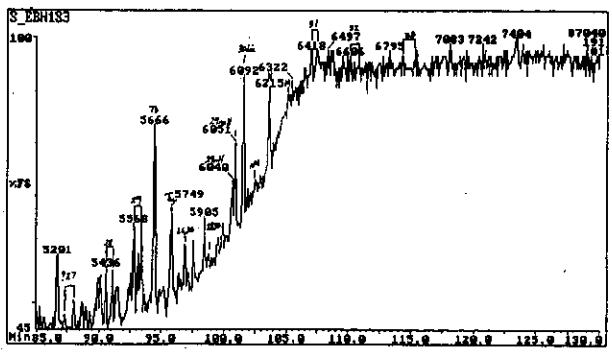

d) m/z 191: Penta-cyclic Terpanes

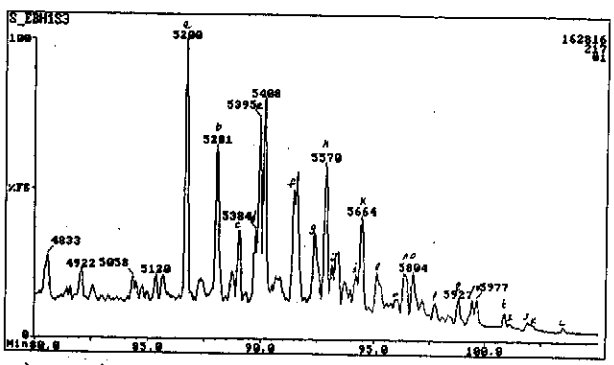

e) m/z 217: Steranes

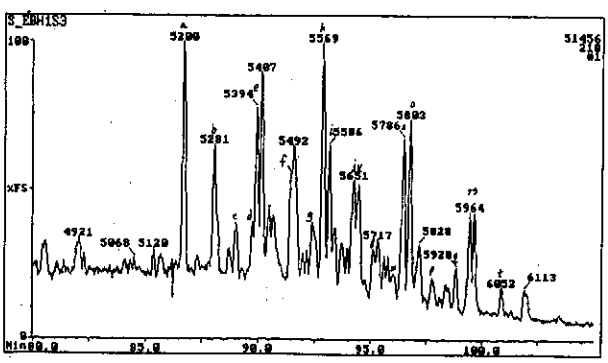

f) m/z 218: Regular (ßß) Steranes

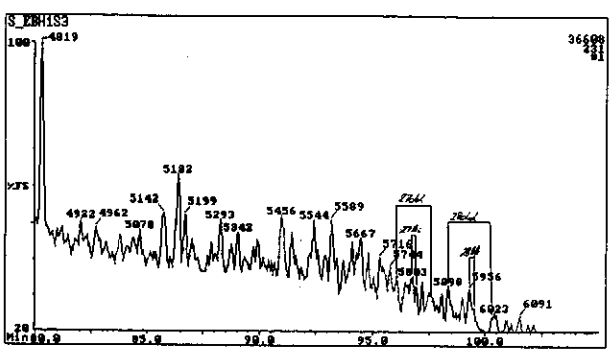

g) m/z 231: Methyl Steranes

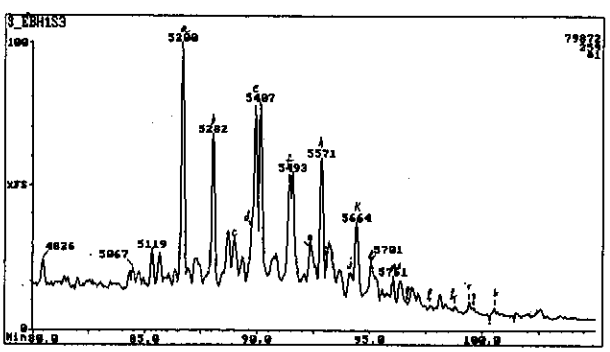

h) m/z 259: Rearranged (ßa) Steranes

Figure E.16: Annotated TIC and single ion fragmentograms of saturated hydrocarbons from sample 16, well 110 DST 1, 3051m.

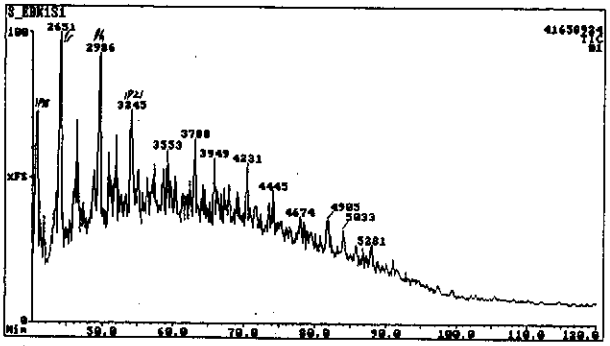

a) TIC: Total Ion Count

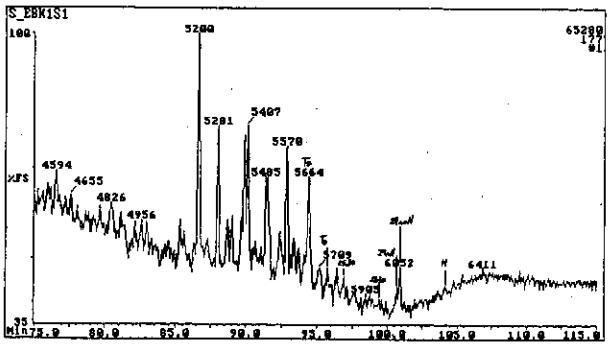

b) m/z 177: Demethylated Hopanes

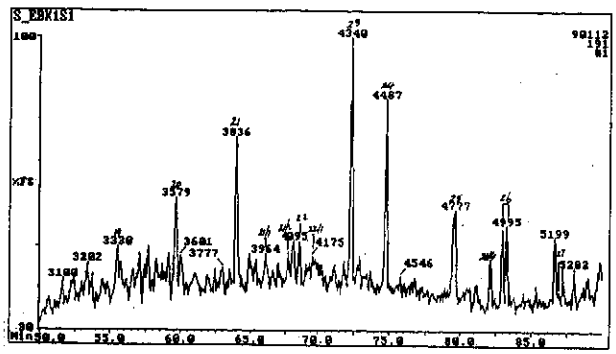

c) m/z 191: Tri and Tetra-cyclic Terpanes

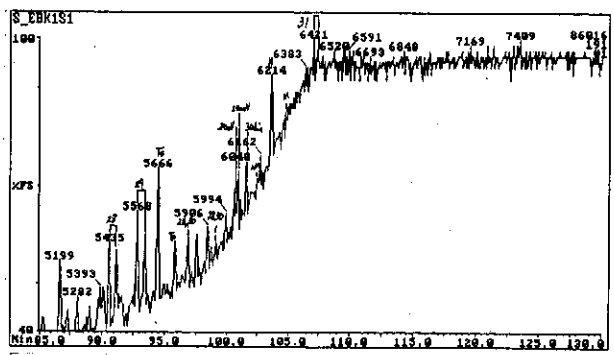

d) m/z 191: Penta-cyclic Terpanes

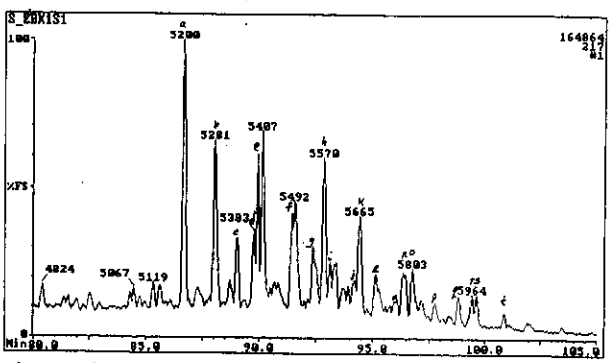

e) m/z 217: Steranes

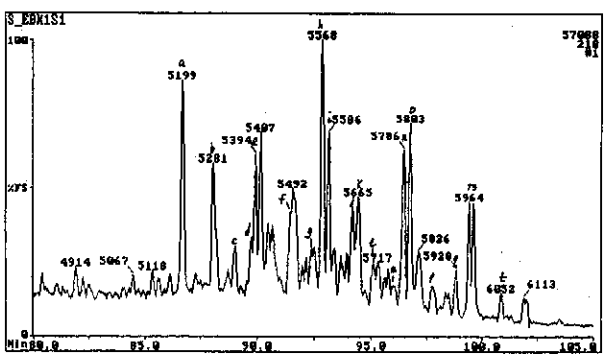

f) m/z 218: Regular (ßß) Steranes

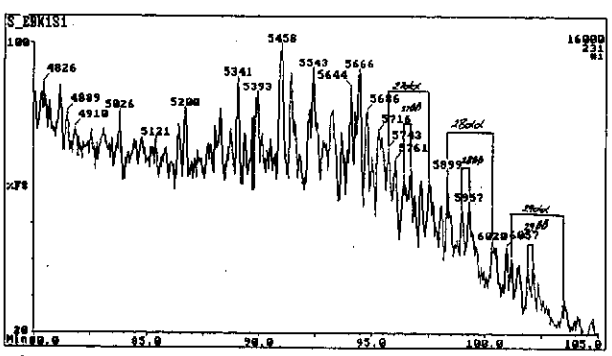

g) m/z 231: Methyl Steranes

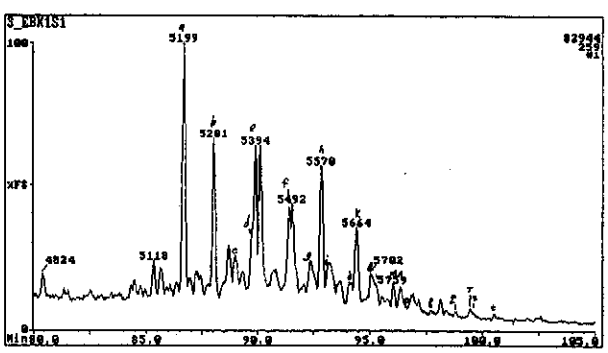

h) m/z 259: Rearranged (ßa) Steranes

Figure E.17: Annotated TIC and single ion fragmentograms of saturated hydrocarbons from sample 17, well 126 DST 1, 2643m.

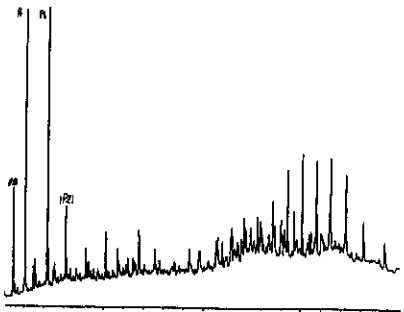

a) TIC: Total Ion Count

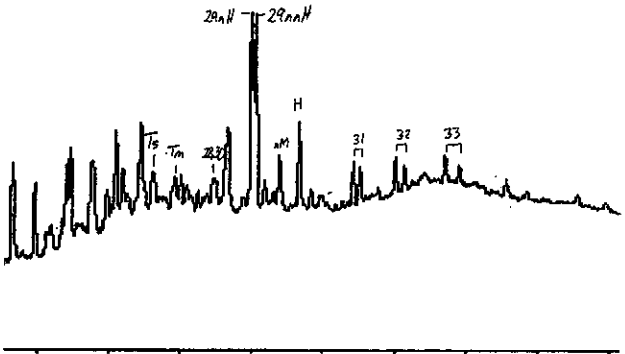

b) m/z 177: Demethylated Hopanes

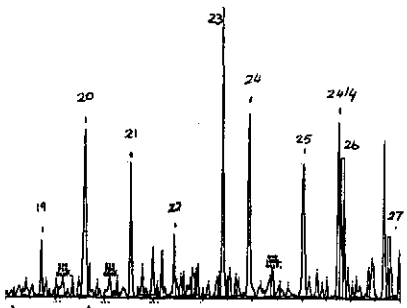

c) m/z 191: Tri and Tetra-cyclic Terpanes

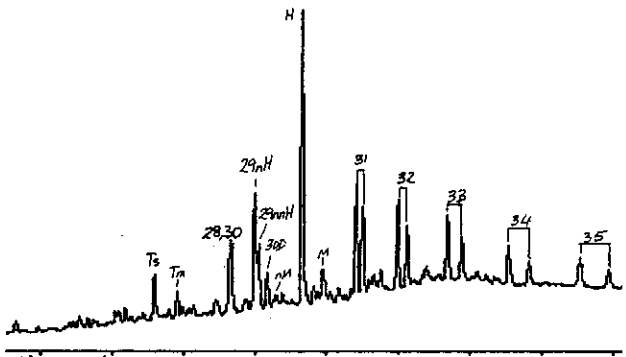

d) m/z 191: Penta-cyclic Terpanes

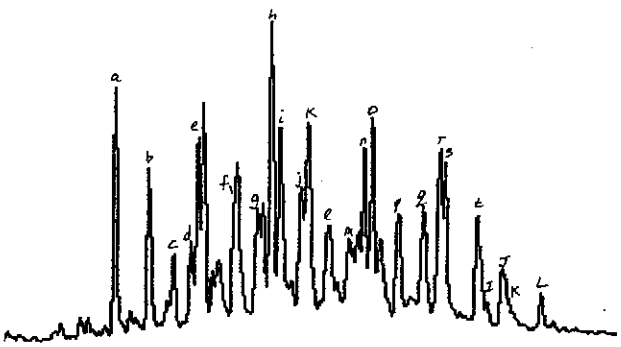

e) m/z 217: Steranes

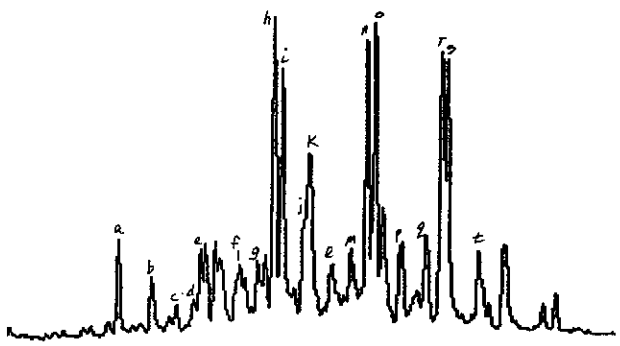

f) m/z 218: Regular (ßß) Steranes

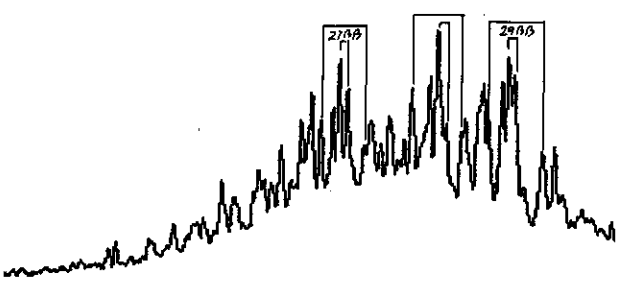

g) m/z 231: Methyl Steranes

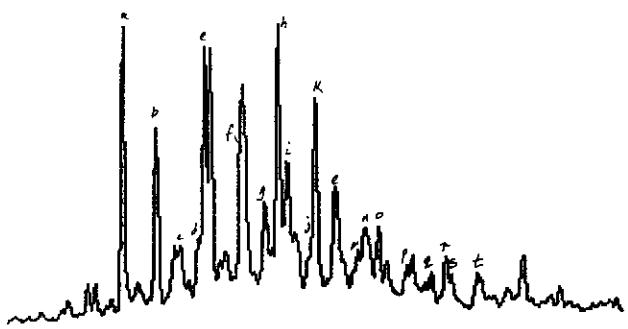

h) m/z 259: Rearranged (ßa) Steranes

Figure E.18: Annotated TIC and single ion fragmentograms of saturated hydrocarbons from sample 18, well 122 SWC, 2517m.

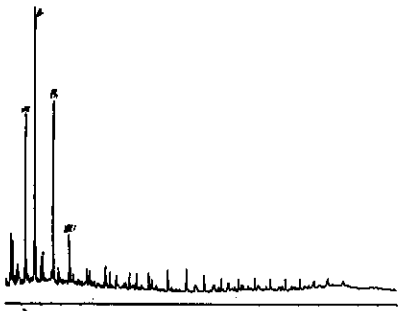

a) TIC: Total Ion Count

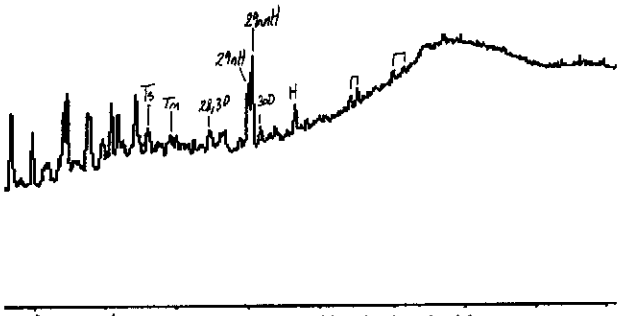

b) m/z 177: Demethylated Hopanes

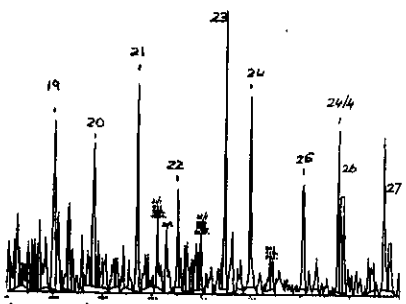

c) m/z 191: Tri and Tetra-cyclic Terpanes

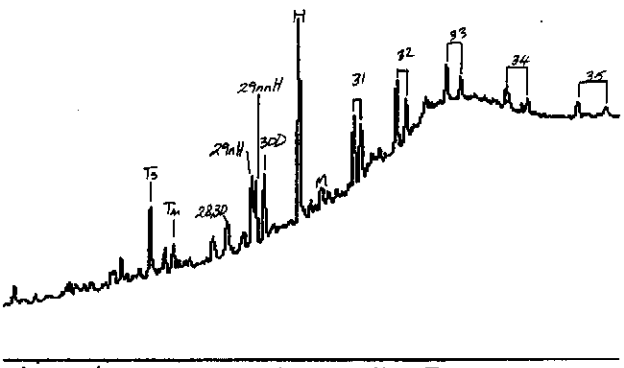

d) m/z 191: Penta-cyclic Terpanes

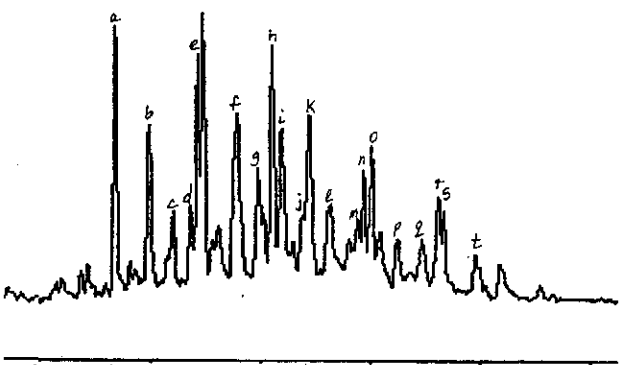

e) m/z 217: Steranes

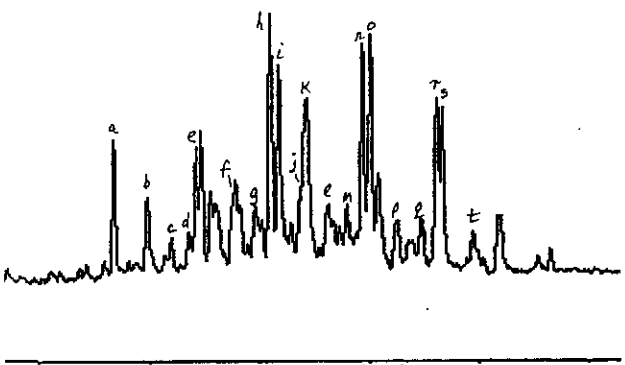

f) m/z 218: Regular (ßß) Steranes

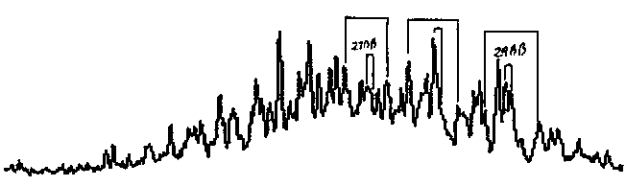

g) m/z 231: Methyl Steranes

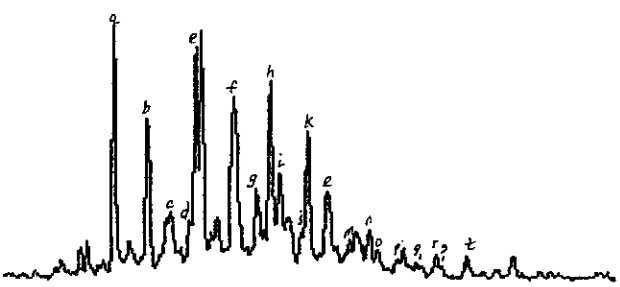

h) m/z 259: Rearranged (ßa) Steranes

Figure E.19: Annotated TIC and single ion fragmentograms of saturated hydrocarbons from sample 19, well 132 DST 2, 2662m.

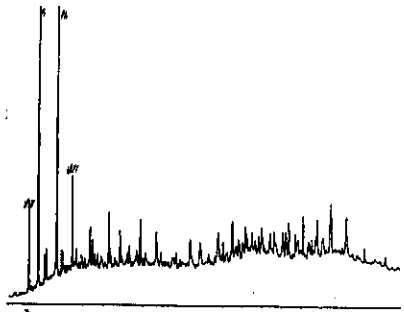

a) TIC: Total Ion Count

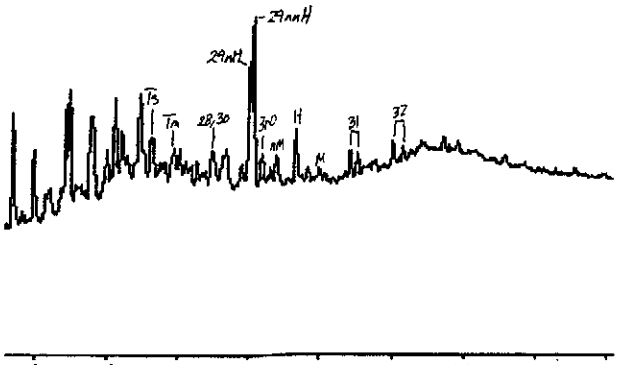

b) m/z 177: Demethylated Hopanes

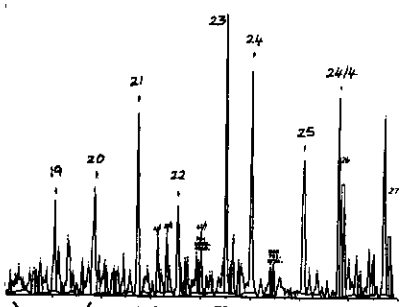

c) m/z 191: Tri and Tetra-cyclic Terpanes

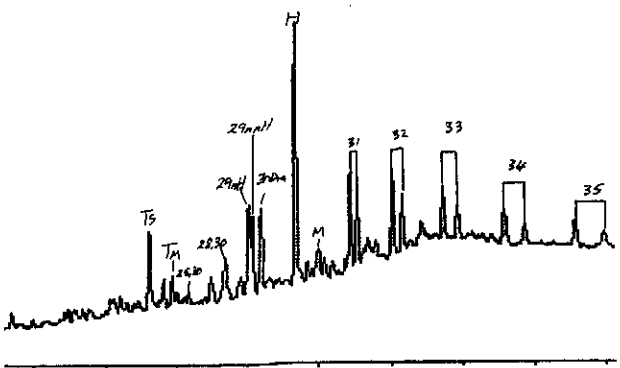

d) m/z 191: Penta-cyclic Terpanes

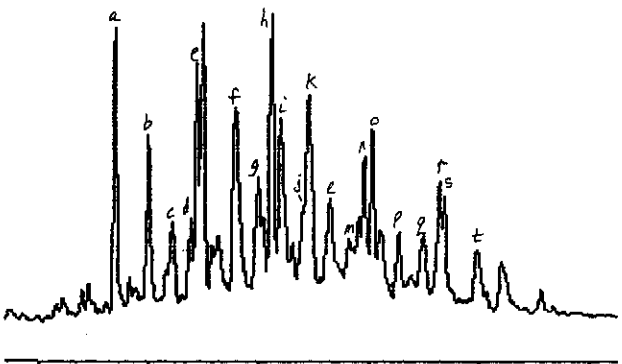

e) m/z 217: Steranes

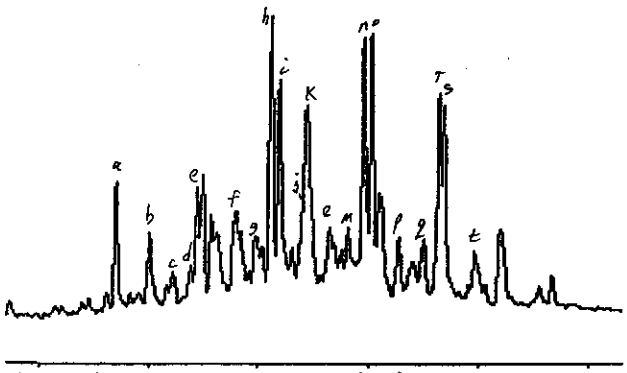

f) m/z 218: Regular (ßß) Steranes

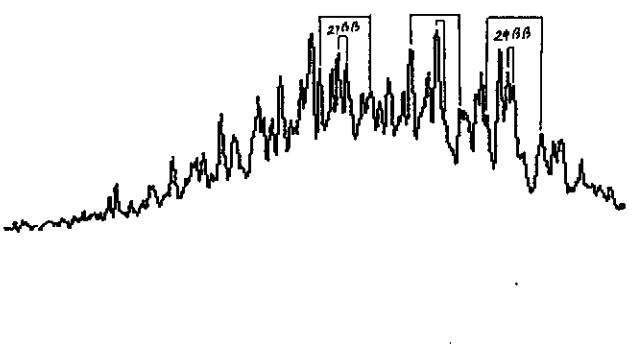

g) m/z 231: Methyl Steranes

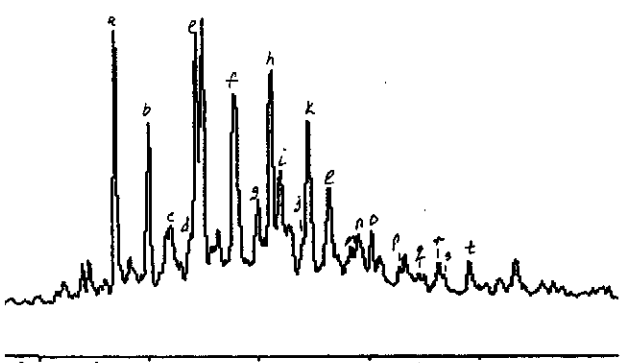

h) m/z 259: Rearranged (ßa) Steranes

Figure E.20: Annotated TIC and single ion fragmentograms of saturated hydrocarbons from sample 20, well 132 core 1, 2702.43m.

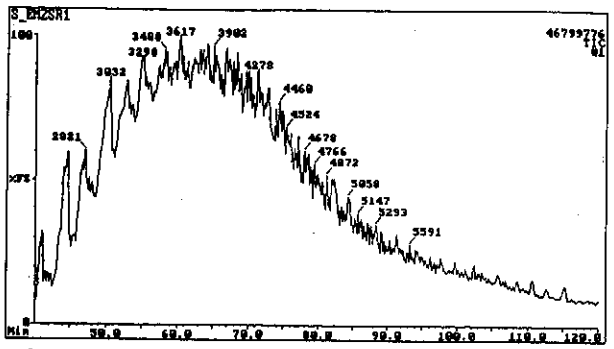

a) TIC: Total Ion Count

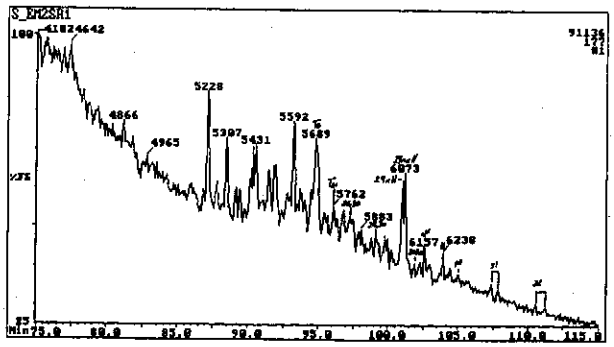

b) m/z 177: Demethylated Hopanes

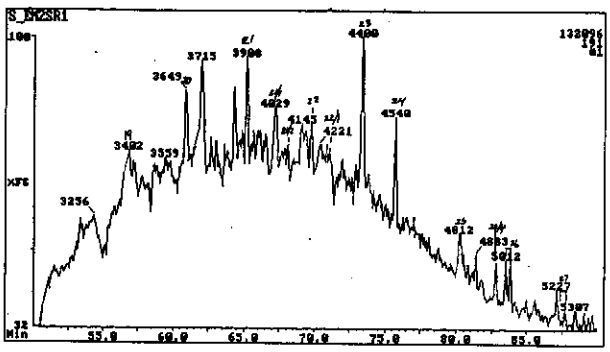

c) m/z 191: Tri and Tetra-cyclic Terpanes

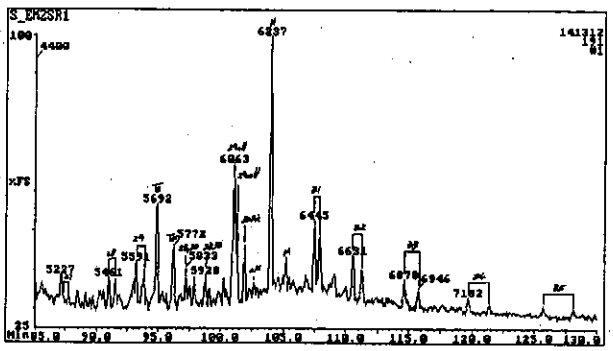

d) m/z 191: Penta-cyclic Terpanes

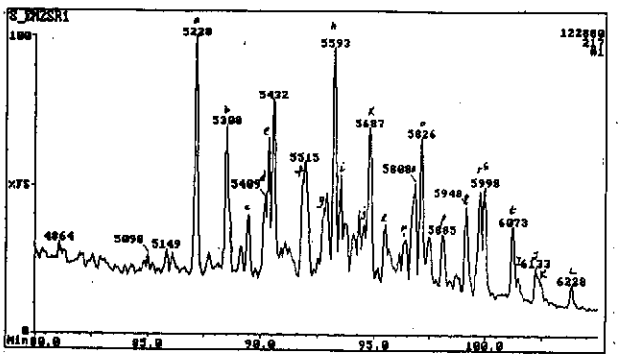

e) m/z 217: Steranes

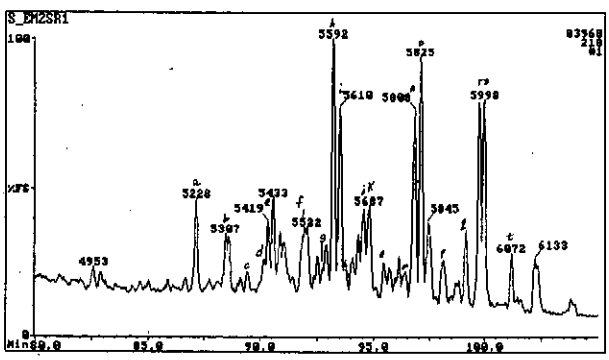

f) m/z 218: Regular (ßß) Steranes

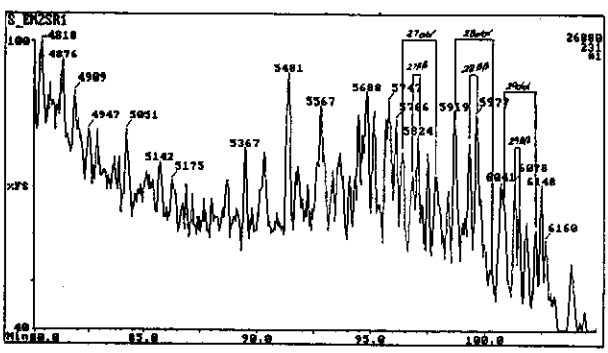

g) m/z 231: Methyl Steranes

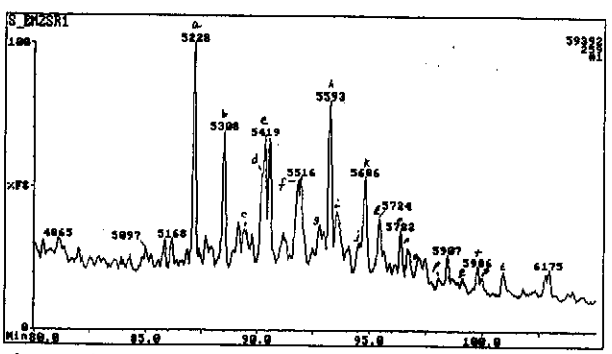

h) m/z 259: Rearranged (ßa) Steranes

Figure E.21: Annotated TIC and single ion fragmentograms of saturated hydrocarbons from sample 21, well 48 DST 2, 2634m.

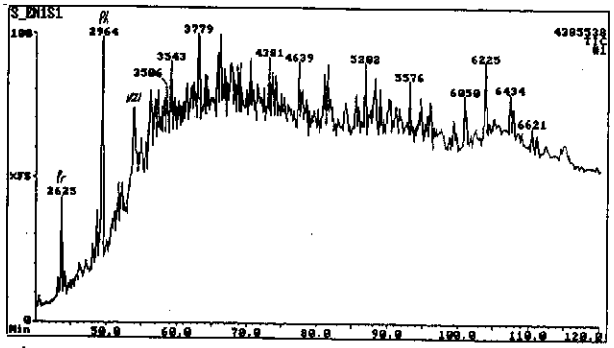

a) TIC: Total Ion Count

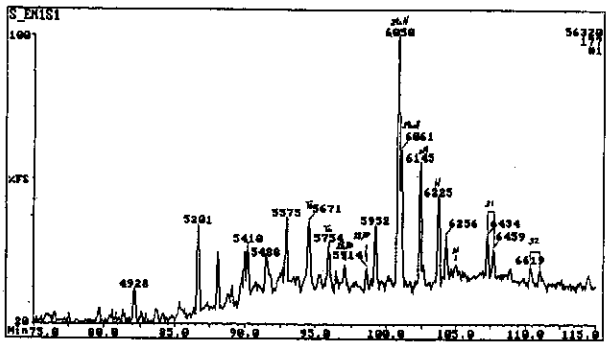

b) m/z 177: Demethylated Hopanes

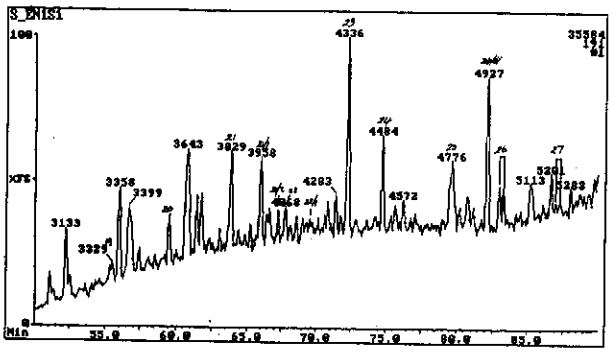

c) m/z 191: Tri and Tetra-cyclic Terpanes

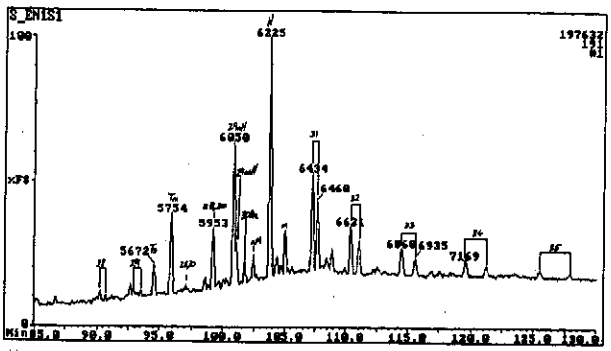

d) m/z 191: Penta-cyclic Terpanes

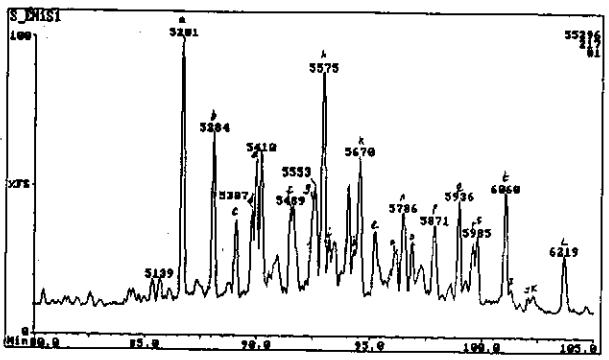

e) m/z 217: Steranes

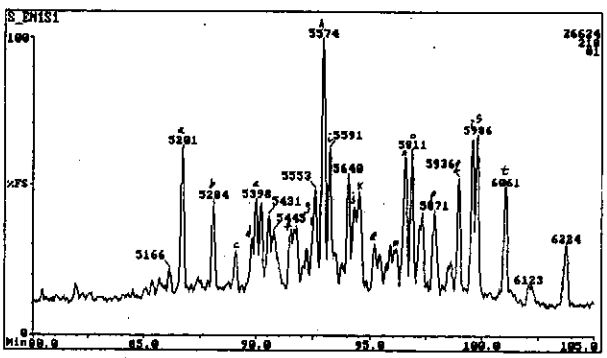

f) m/z 218: Regular (ßß) Steranes

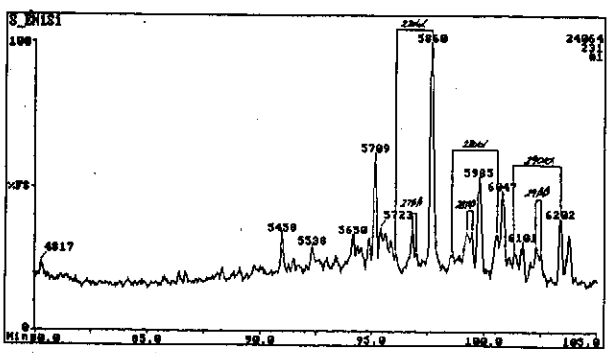

g) m/z 231: Methyl Steranes

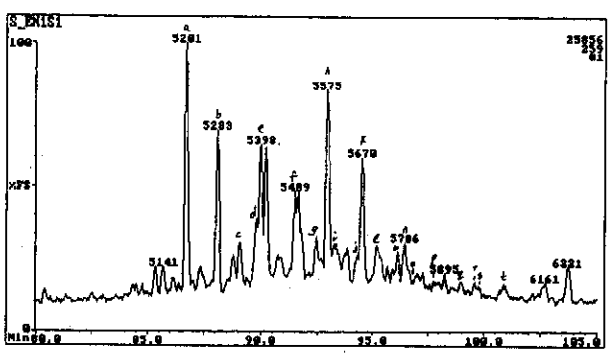

h) m/z 259: Rearranged (ßa) Steranes

Figure E.22: Annotated TIC and single ion fragmentograms of saturated hydrocarbons from sample 22, well 16 RC, 2614m.

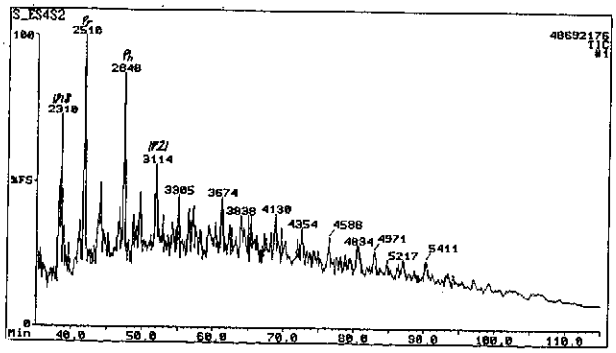

a) TIC: Total Ion Count

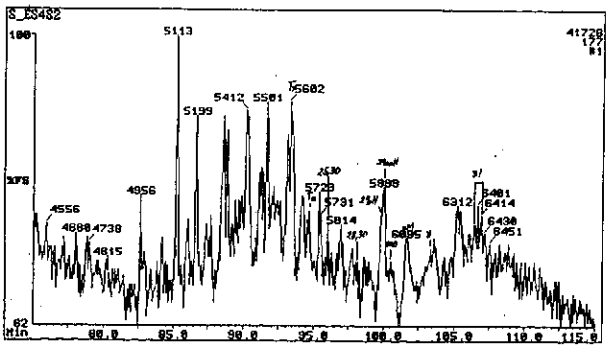

b) m/z 177: Demethylated Hopanes

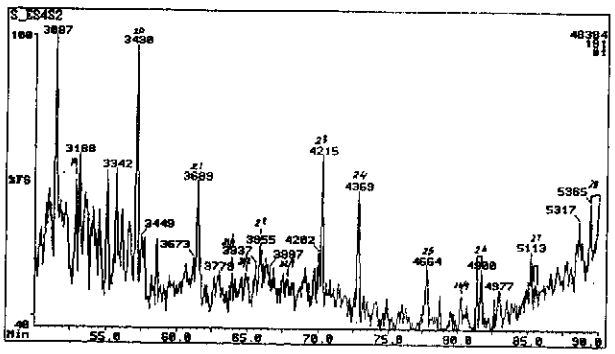

c) m/z 191: Tri and Tetra-cyclic Terpanes

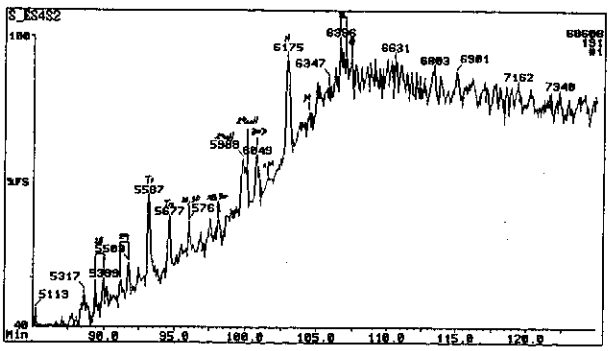

d) m/z 191: Penta-cyclic Terpanes

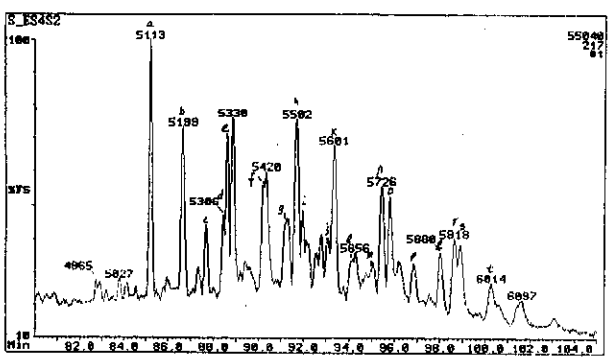

e) m/z 217: Steranes

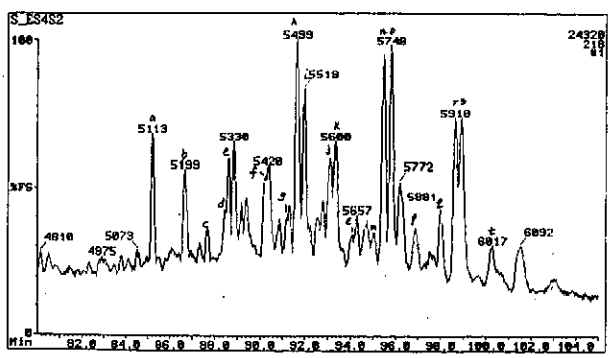

f) m/z 218: Regular (ßß) Steranes

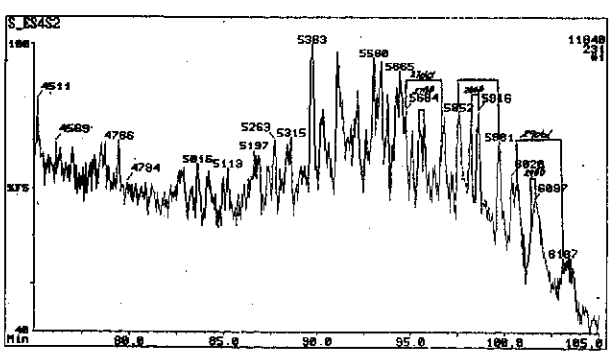

g) m/z 231: Methyl Steranes

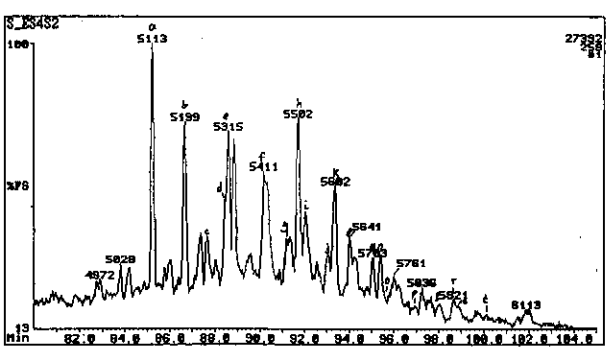

h) m/z 259: Rearranged (ßa) Steranes

Figure E.23: Annotated TIC and single ion fragmentograms of saturated hydrocarbons from sample 23, well 59 DST 1, 2212m.

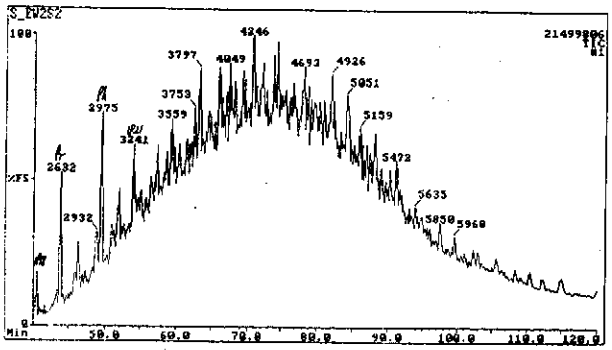

a) TIC: Total Ion Count

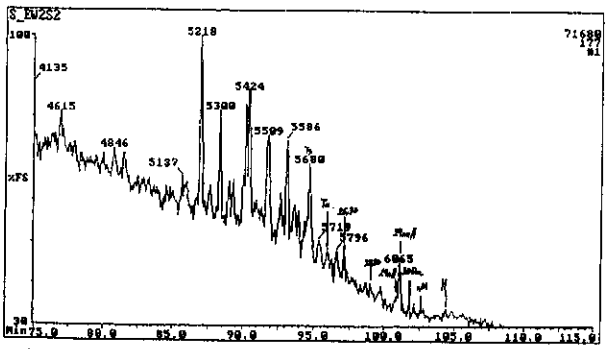

b) m/z 177: Demethylated Hopanes

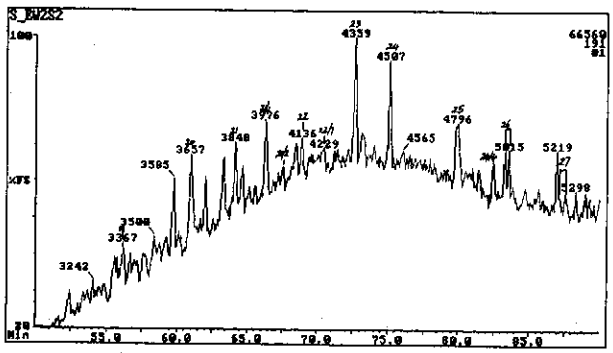

c) m/z 191: Tri and Tetra-cyclic Terpanes

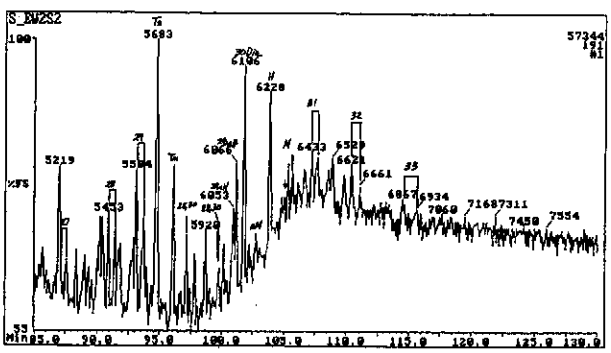

d) m/z 191: Penta-cyclic Terpanes

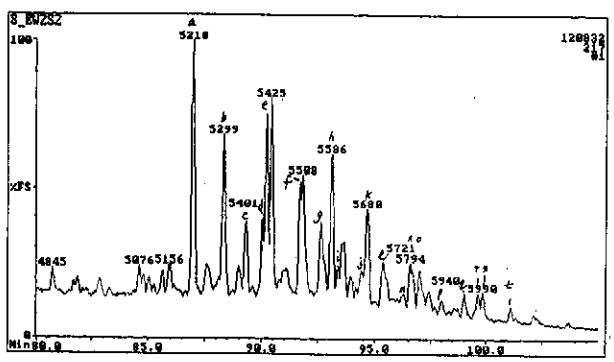

e) m/z 217: Steranes

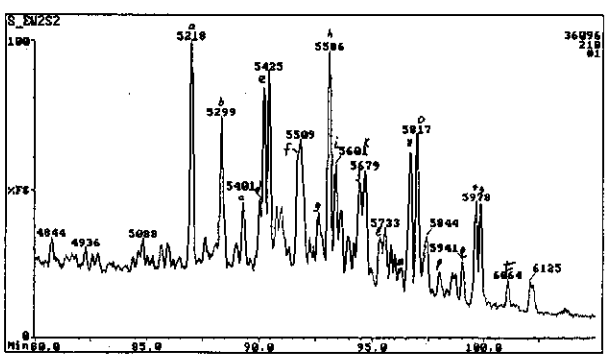

f) m/z 218: Regular (ßß) Steranes

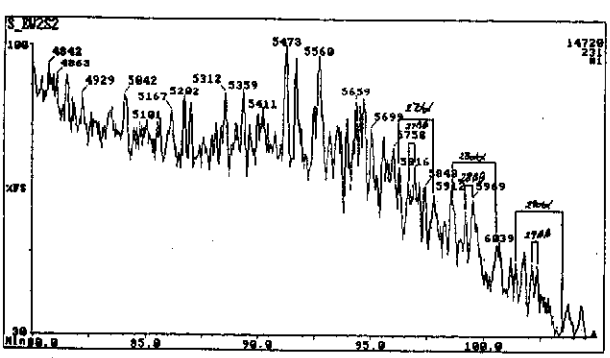

g) m/z 231: Methyl Steranes

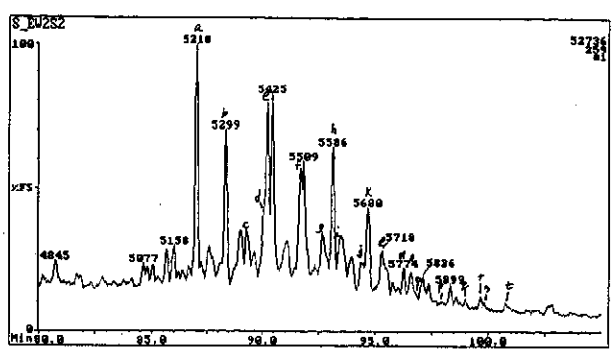

h) m/z 259: Rearranged (ßa) Steranes

Figure E.24: Annotated TIC and single ion fragmentograms of saturated hydrocarbons from sample 24, well 75 core 1, 2830.5m.

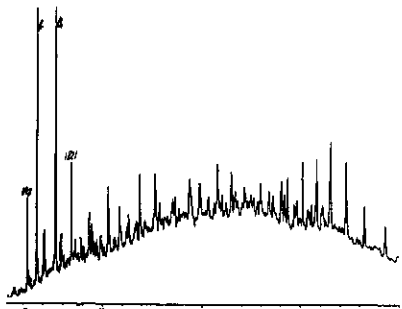

a) TIC: Total Ion Count

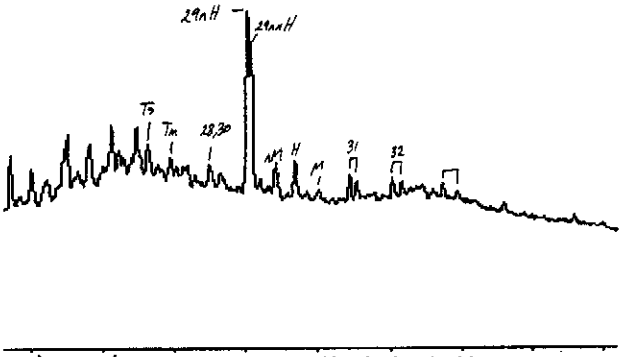

b) m/z 177: Demethylated Hopanes

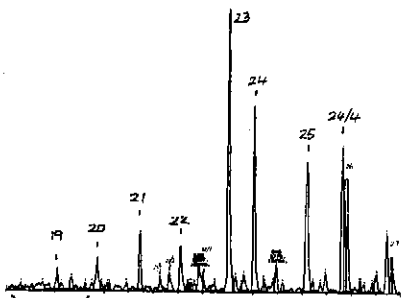

c) m/z 191: Tri and Tetra-cyclic Terpanes

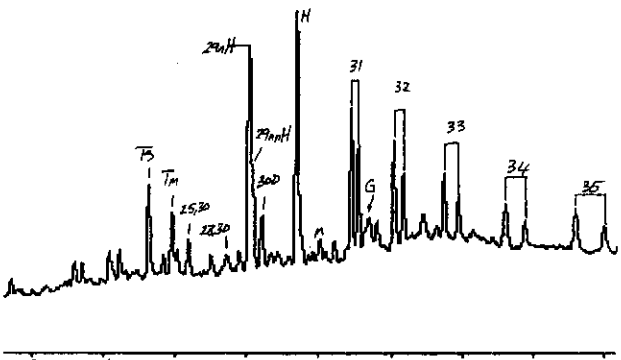

d) m/z 191: Penta-cyclic Terpanes

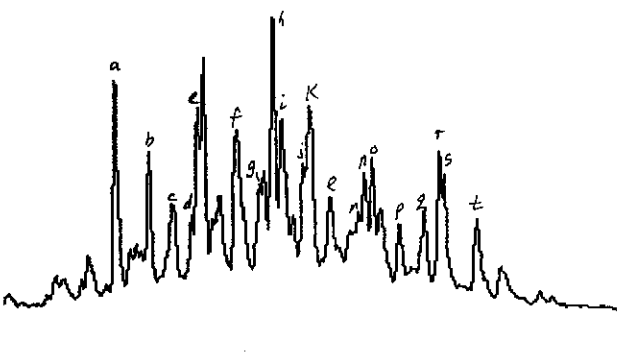

e) m/z 217: Steranes

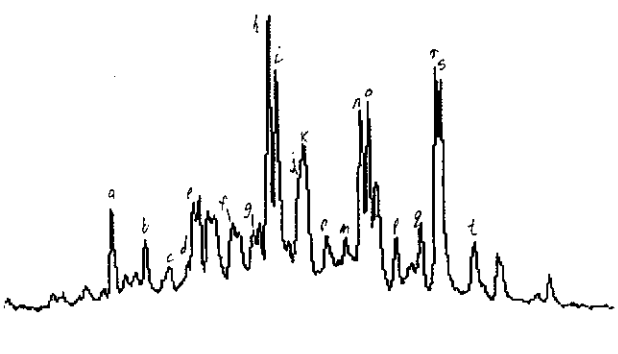

f) m/z 218: Regular (ßß) Steranes

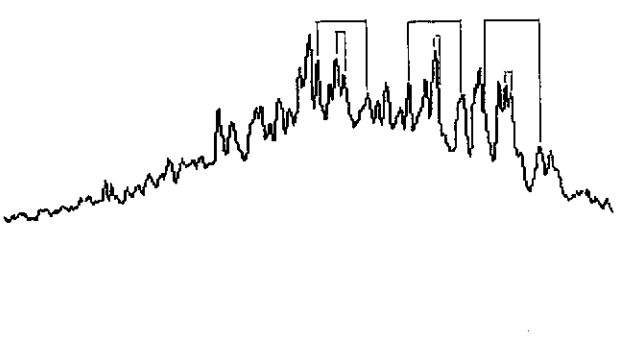

g) m/z 231: Methyl Steranes

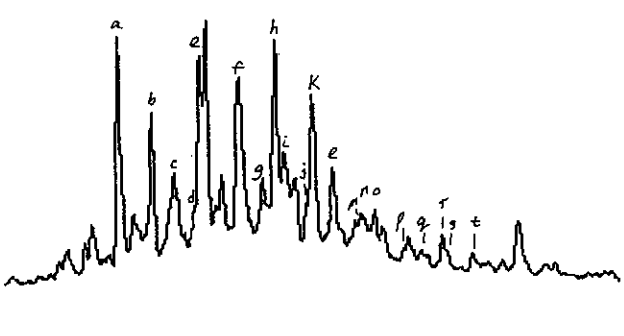

h) m/z 259: Rearranged (ßa) Steranes

Figure E.25: Annotated TIC and single ion fragmentograms of saturated hydrocarbons from sample 25, well 101 core 1, 2987.5m.

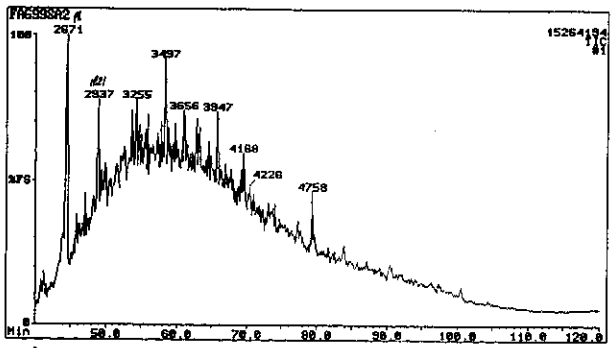

a) TIC: Total Ion Count

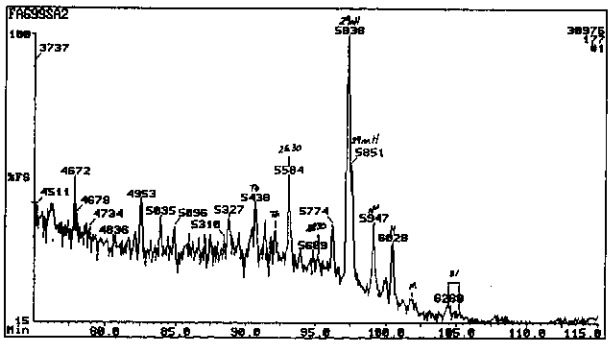

b) m/z 177: Demethylated Hopanes

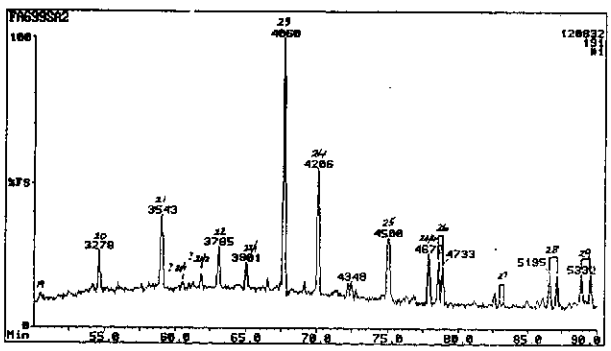

c) m/z 191: Tri and Tetra-cyclic Terpanes

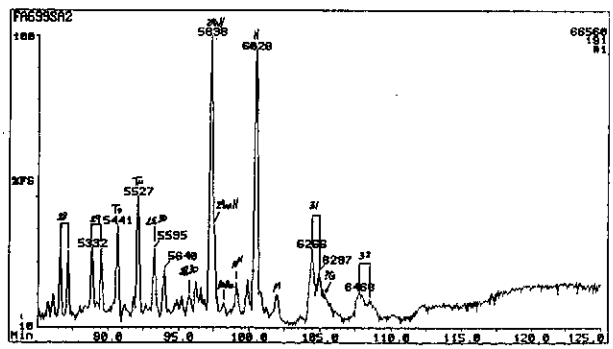

d) m/z 191: Penta-cyclic Terpanes

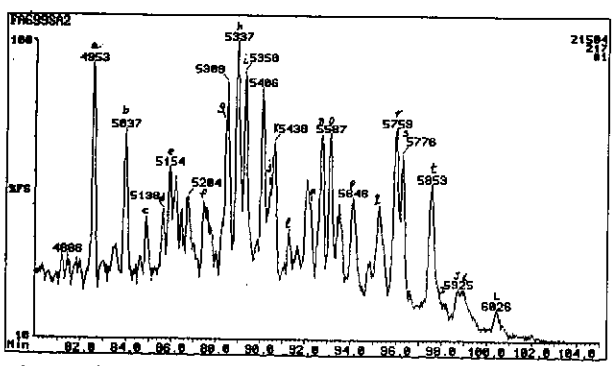

e) m/z 217: Steranes

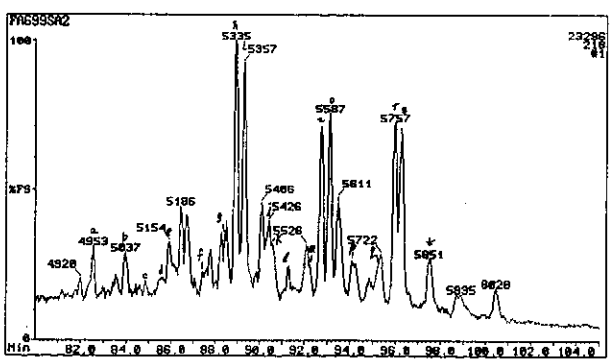

f) m/z 218: Regular (ßß) Steranes

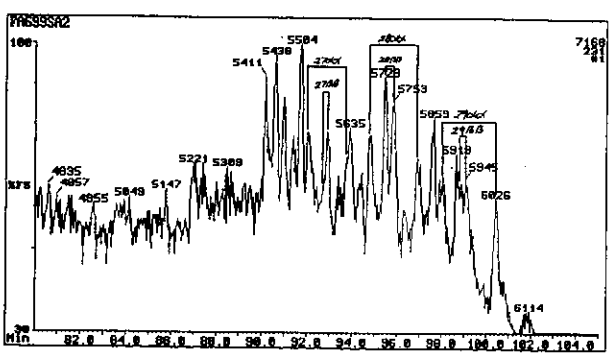

g) m/z 231: Methyl Steranes

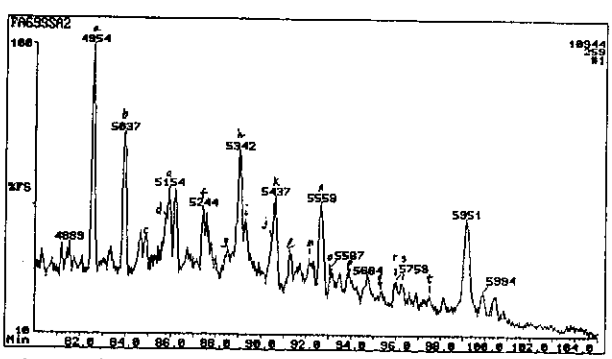

h) m/z 259: Rearranged (ßa) Steranes

Figure E.26: Annotated TIC and single ion fragmentograms of saturated hydrocarbons from sample 26, well 20 DST 2, 2699m.

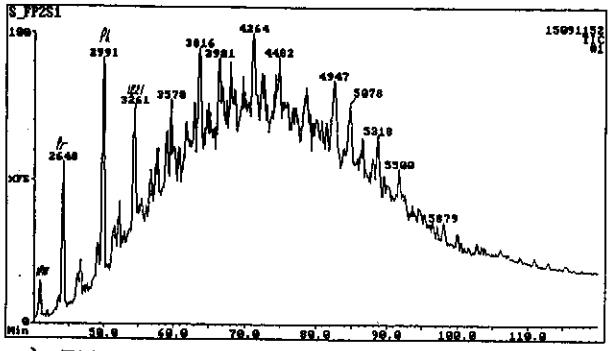

a) TIC: Total Ion Count

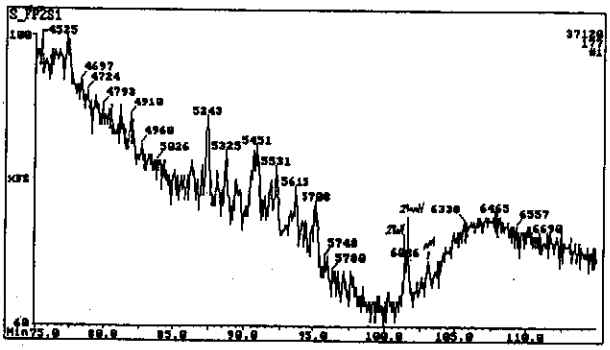

b) m/z 177: Demethylated Hopanes

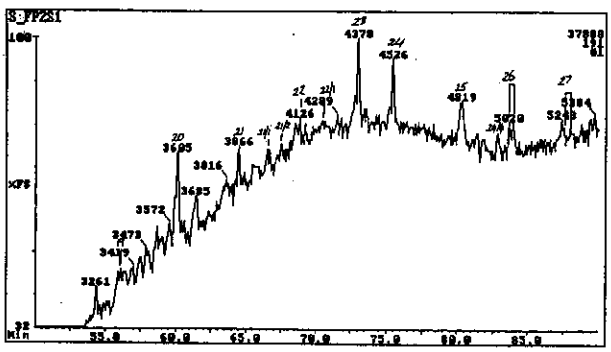

c) m/z 191: Tri and Tetra-cyclic Terpanes

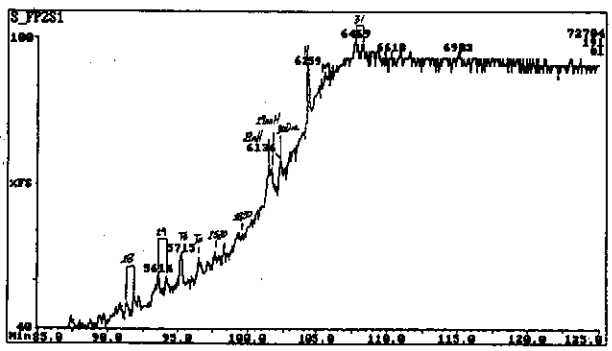

d) m/z 191: Penta-cyclic Terpanes

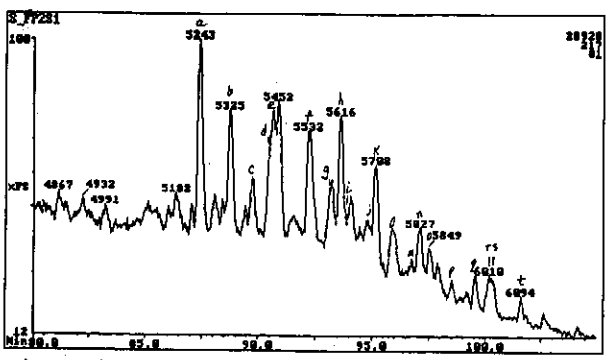

e) m/z 217: Steranes

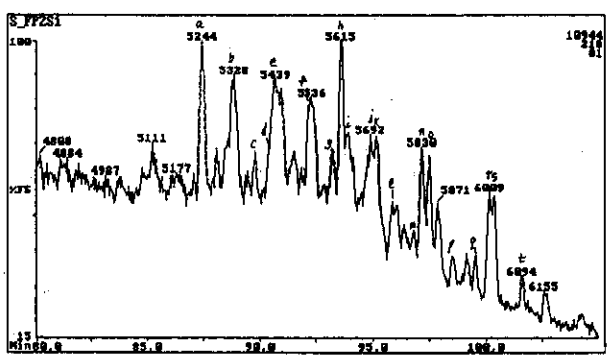

f) m/z 218: Regular (ßß) Steranes

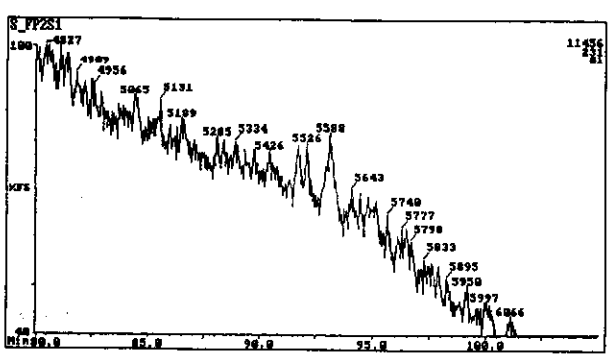

g) m/z 231: Methyl Steranes

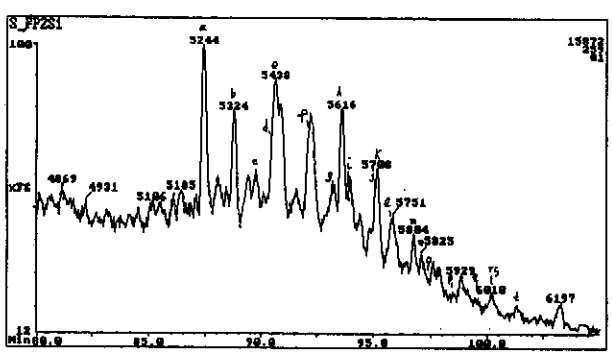

h) m/z 259: Rearranged (ßa) Steranes

Figure E.27: Annotated TIC and single ion fragmentograms of saturated hydrocarbons from sample 27, well 13 core 1, 2518.86m.

not analysed

a) TIC: Total Ion Count

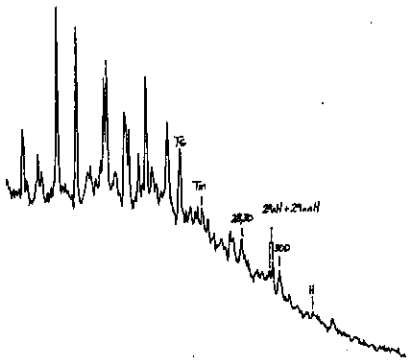

b) m/z 177: Demethylated Hopanes

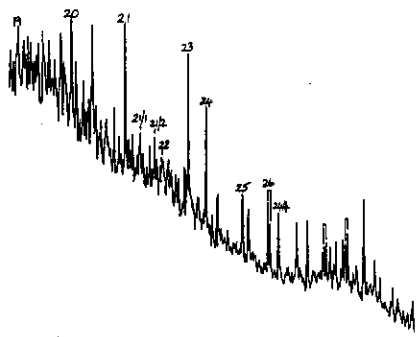

c) m/z 191: Tri and Tetra-cyclic Terpanes

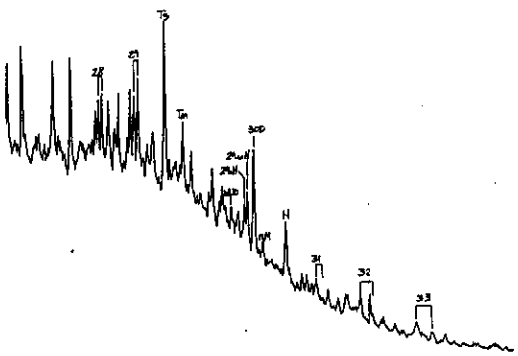

d) m/z 191: Penta-cyclic Terpanes

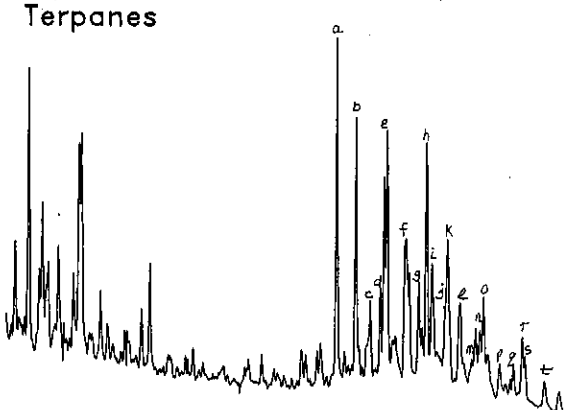

e) m/z 217: Steranes

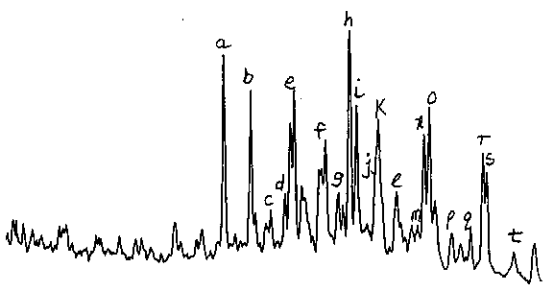

f) m/z 218: Regular (ββ) Steranes

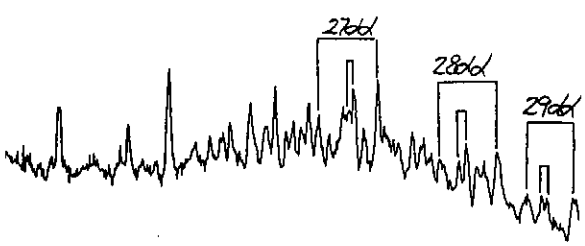

g) m/z 231: Methyl Steranes

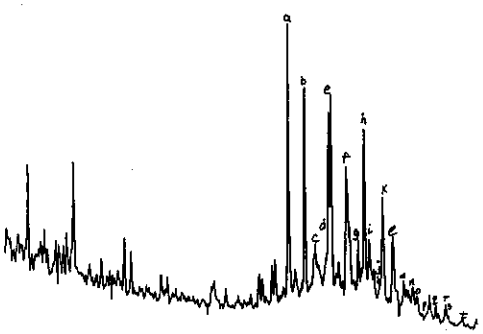

h) m/z 259: Rearranged (βa) Steranes

Figure E.28: Annotated TIC and single ion fragmentograms of saturated hydrocarbons from sample 28, well 103 DST 2, 2718m.

not analysed

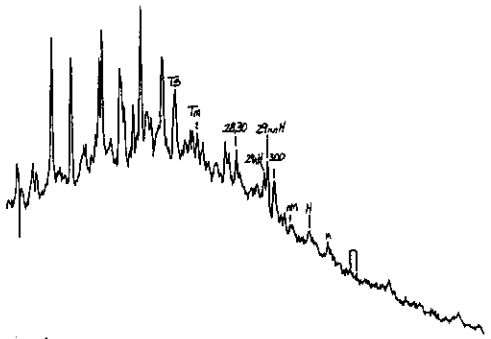

a) TIC: Total Ion Count

b) m/z 177: Demethylated Hopanes

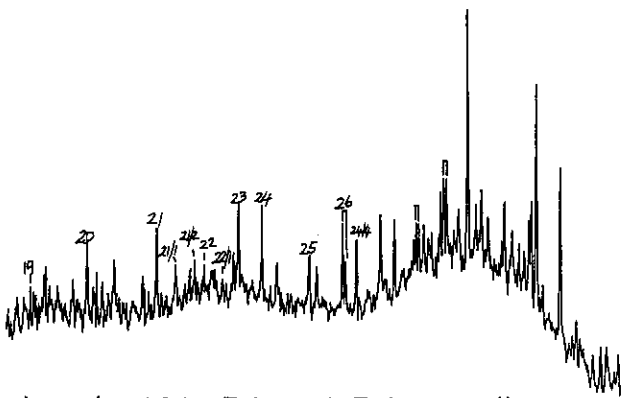

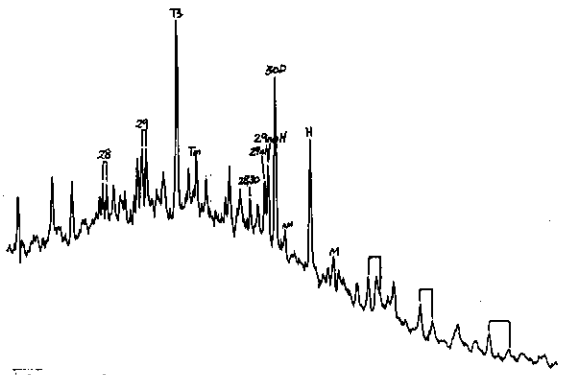

c) m/z 191: Tri and Tetra-cyclic Terpanes

d) m/z 191: Penta-cyclic Terpanes

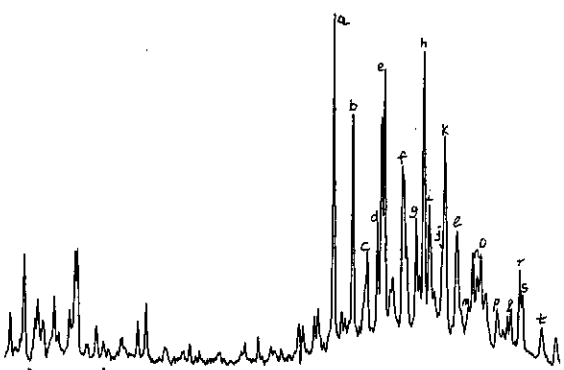

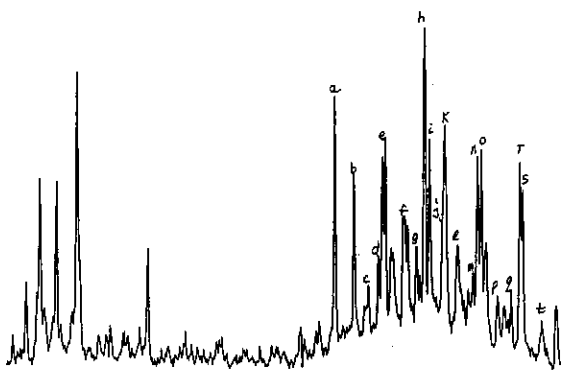

e) m/z 217: Steranes

f) m/z 218: Regular (ßß) Steranes

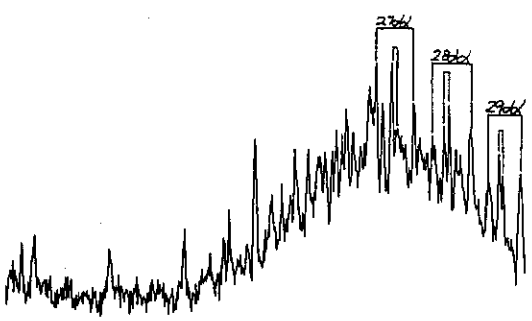

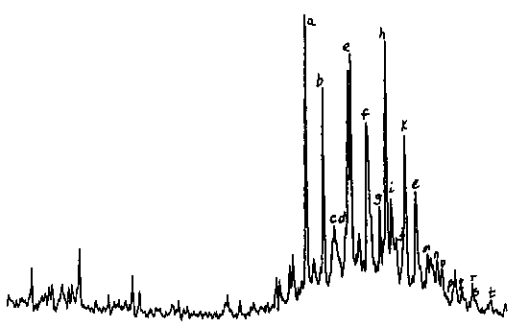

g) m/z 231: Methyl Steranes

h) m/z 259: Rearranged (ßa) Steranes

Figure E.29: Annotated TIC and single ion fragmentograms of saturated hydrocarbons from sample 29, well 94 DST 1, 2799m.

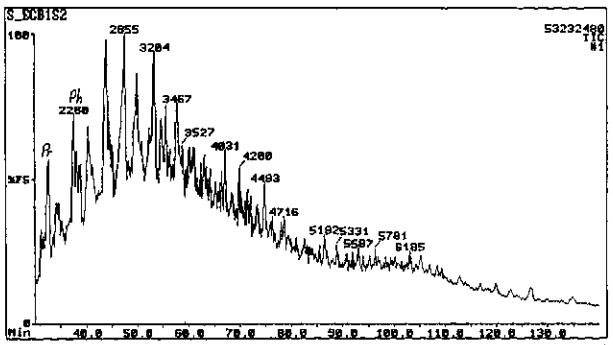

a) TIC: Total Ion Count

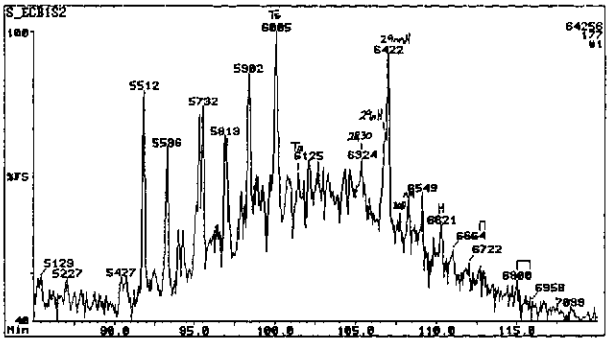

b) m/z 177: Demethylated Hopanes

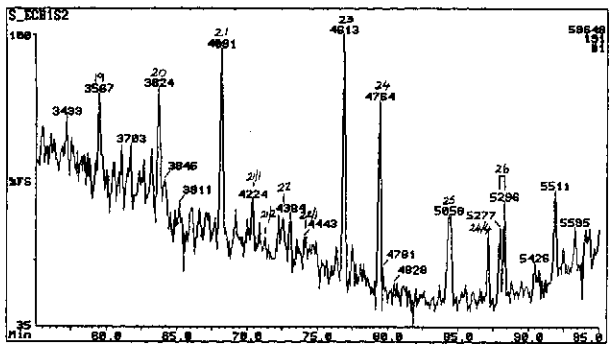

c) m/z 191: Tri and Tetra-cyclic Terpanes

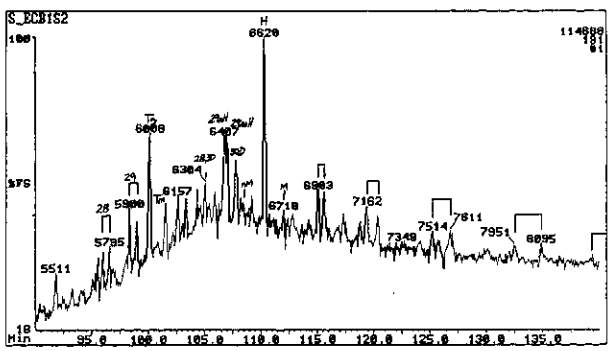

d) m/z 191: Penta-cyclic Terpanes

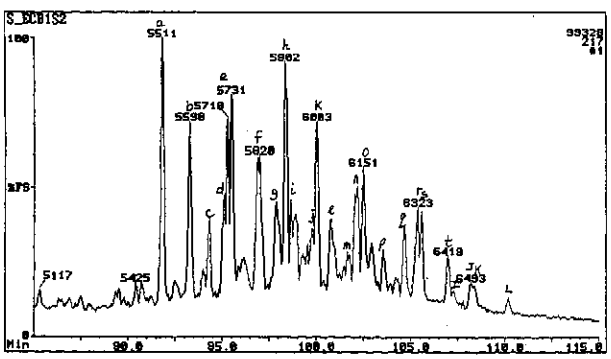

e) m/z 217: Steranes

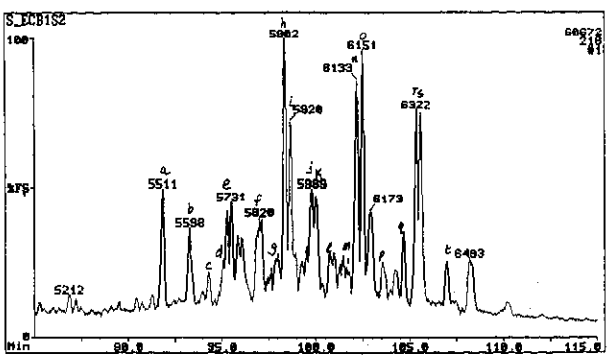

f) m/z 218: Regular (ßß) Steranes

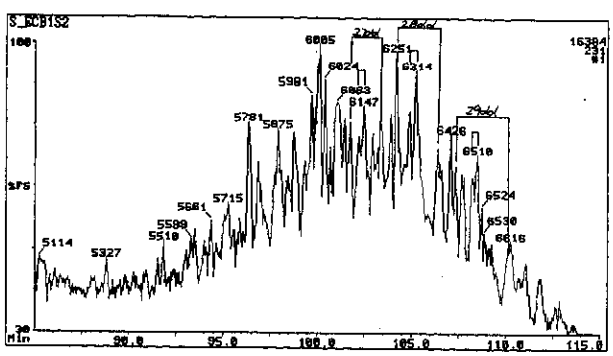

g) m/z 231: Methyl Steranes

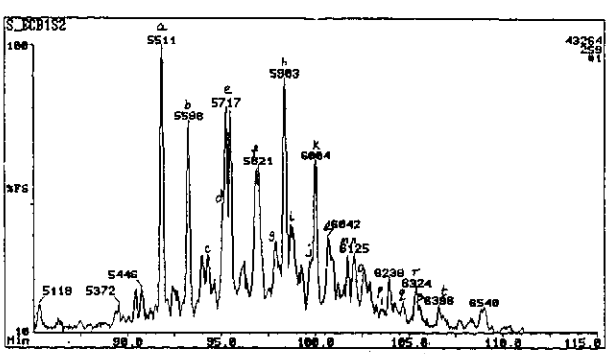

h) m/z 259: Rearranged (ßa) Steranes

Figure E.30: Annotated TIC and single ion fragmentograms of saturated hydrocarbons from sample 30, well 156 DST 1, 2522m.

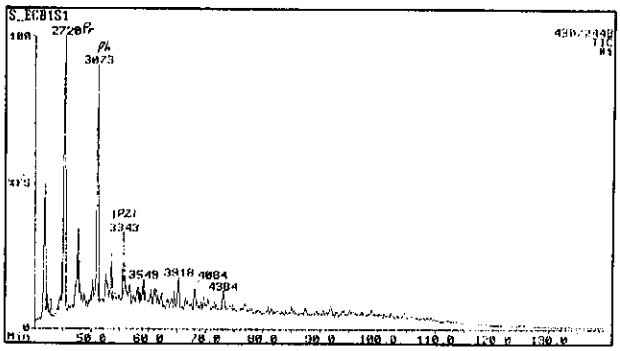

a) TIC: Total Ion Count

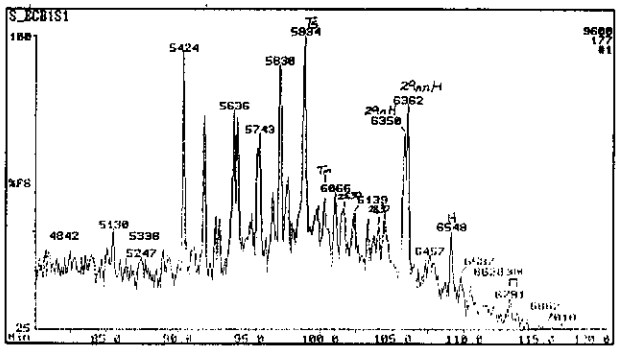

b) m/z 177: Demethylated Hopanes

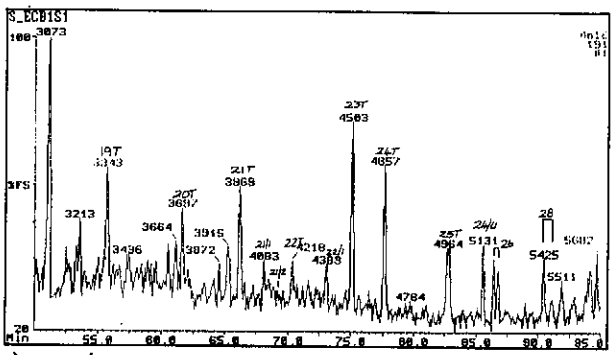

c) m/z 191: Tri and Tetra-cyclic Terpanes

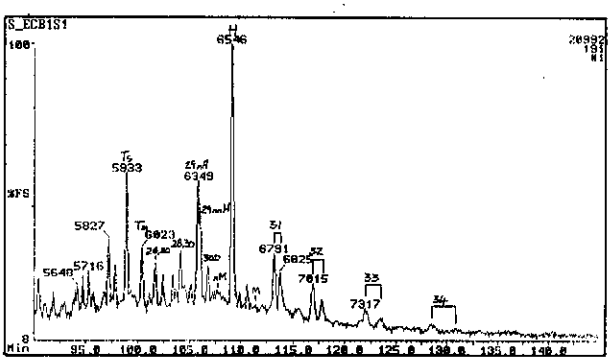

d) m/z 191: Penta-cyclic Terpanes

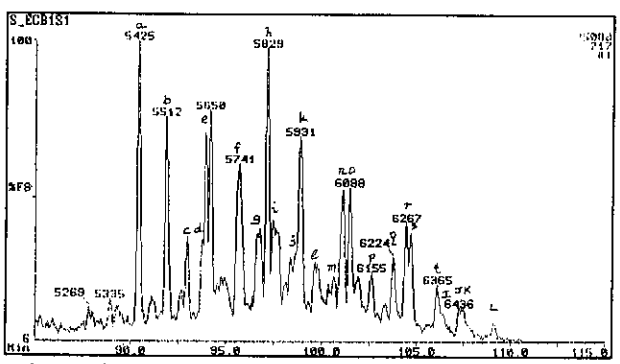

e) m/z 217: Steranes

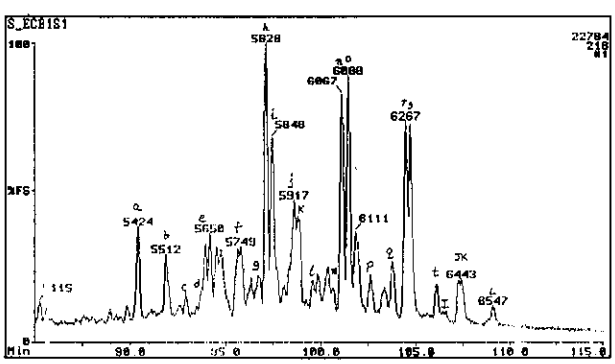

f) m/z 218: Regular (ßß) Steranes

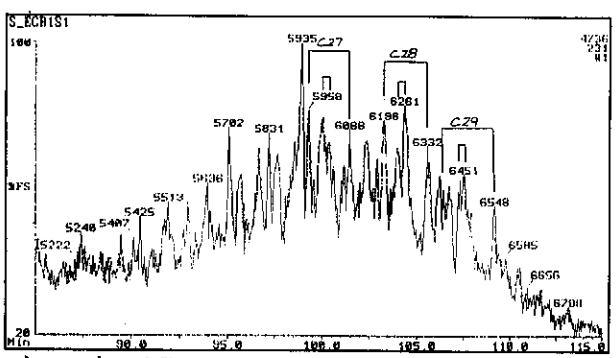

g) m/z 231: Methyl Steranes

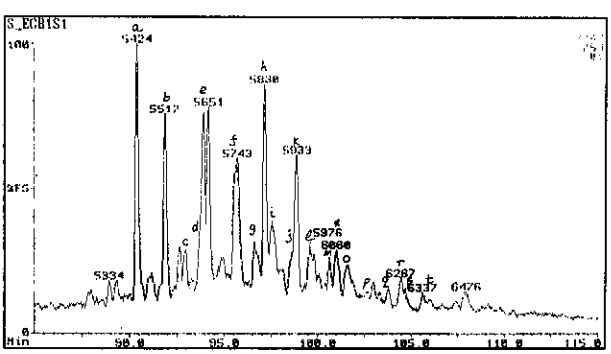

h) m/z 259: Rearranged (ßa) Steranes

Figure E.31: Annotated TIC and single ion fragmentograms of saturated hydrocarbons from sample 31, well 156 core 1, 2525m.

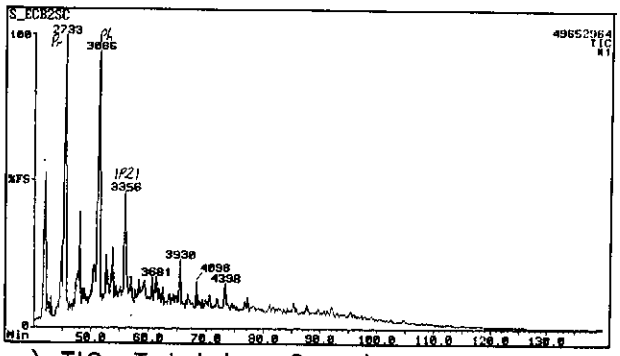

a) TIC: Total Ion Count

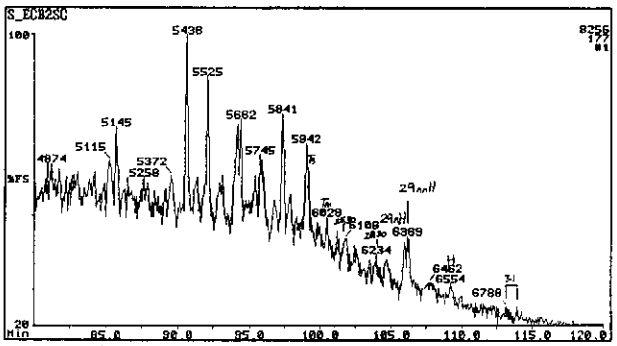

b) m/z 177: Demethylated Hopanes

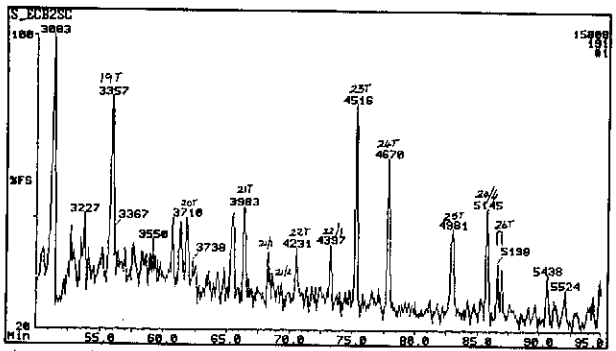

c) m/z 191: Tri and Tetra-cyclic Terpanes

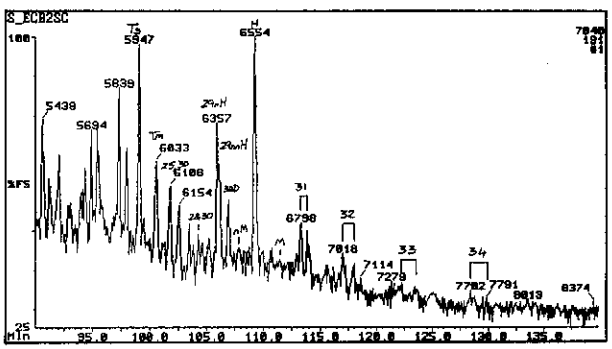

d) m/z 191: Penta-cyclic Terpanes

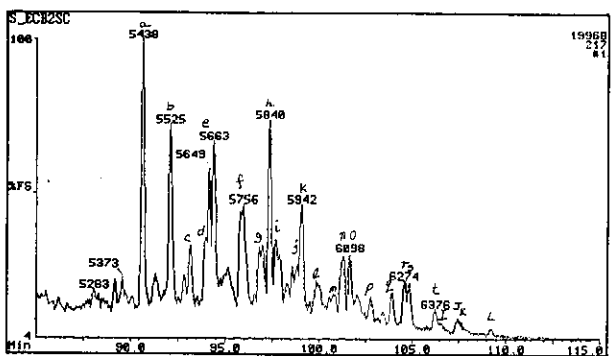

e) m/z 217: Steranes

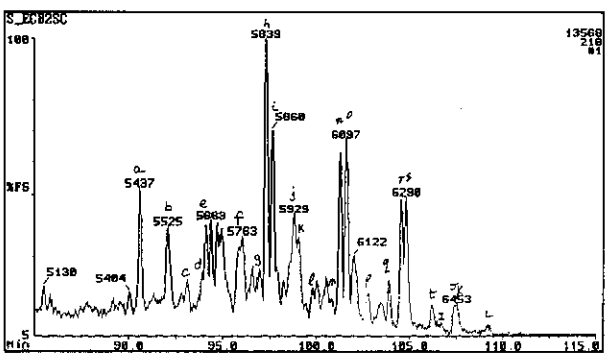

f) m/z 218: Regular (ßß) Steranes

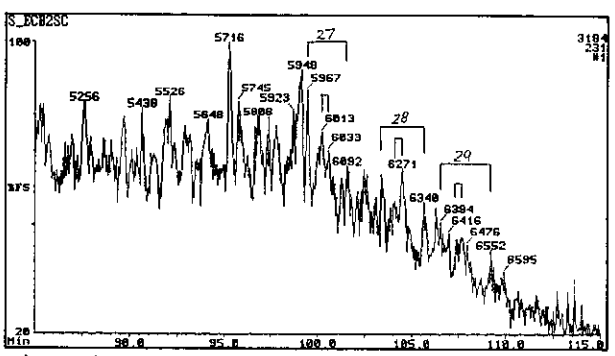

g) m/z 231: Methyl Steranes

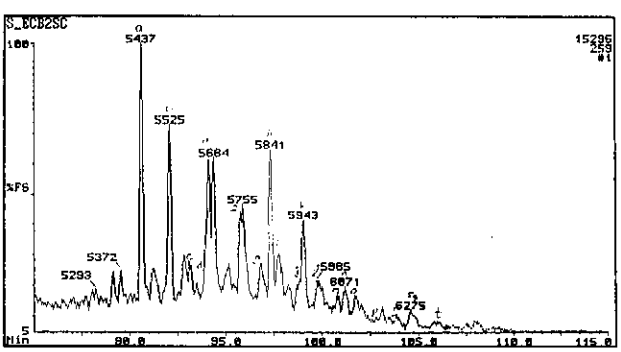

h) m/z 259: Rearranged (ßa) Steranes

Figure E.32: Annotated TIC and single ion fragmentograms of saturated hydrocarbons from sample 32, well 166 RFT, 2508m.

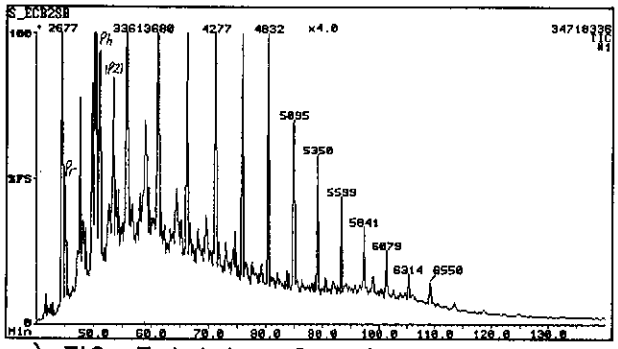

a) TIC: Total Ion Count

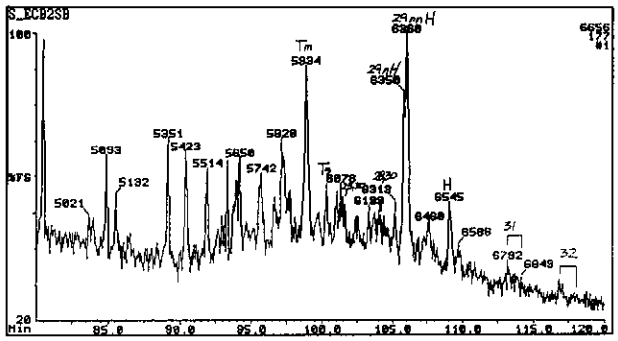

b) m/z 177: Demethylated Hopanes

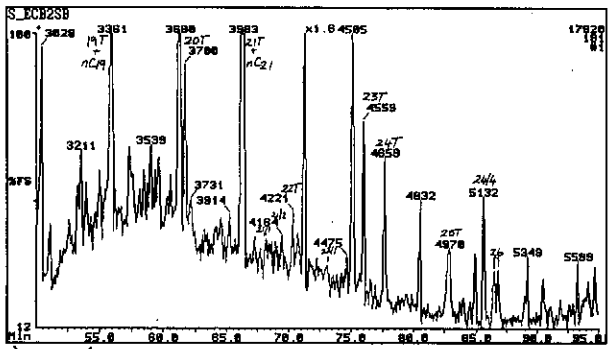

c) m/z 191: Tri and Tetra-cyclic Terpanes

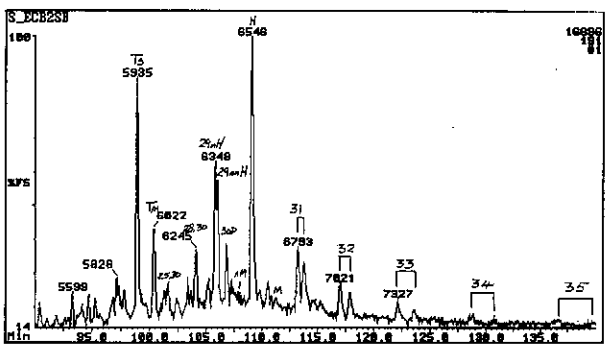

d) m/z 191: Penta-cyclic Terpanes

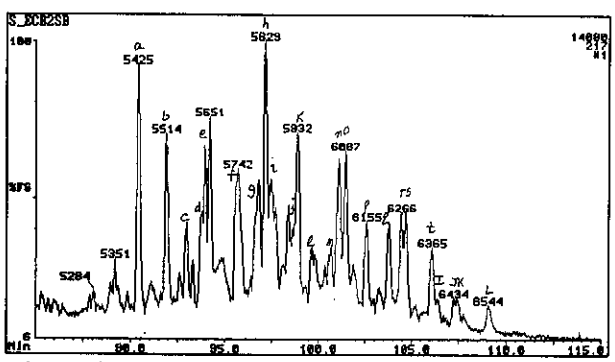

e) m/z 217: Steranes

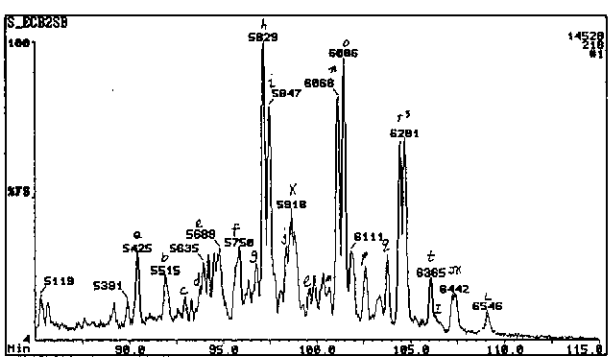

f) m/z 218: Regular (ββ) Steranes

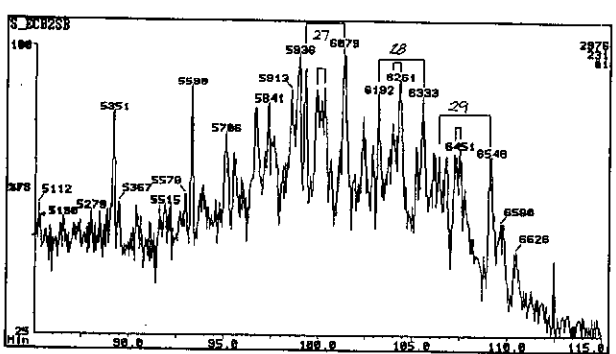

g) m/z 231: Methyl Steranes

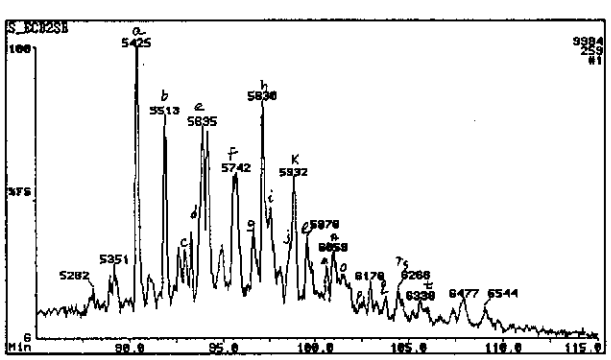

h) m/z 259: Rearranged (βa) Steranes

Figure E.33: Annotated TIC and single ion fragmentograms of saturated hydrocarbons from sample 33, well 166 core 1, 2510.43m.

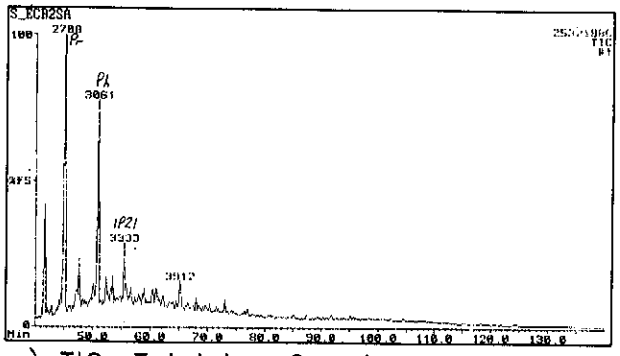

a) TIC: Total Ion Count

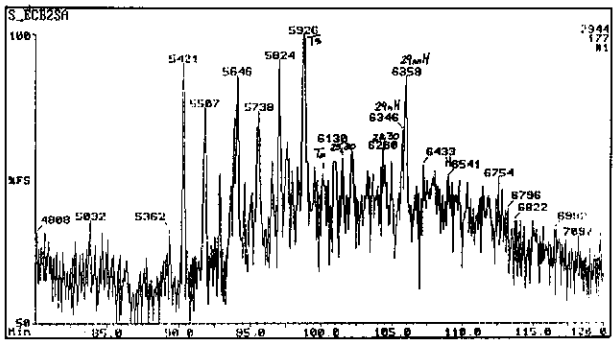

b) m/z 177: Demethylated Hopanes

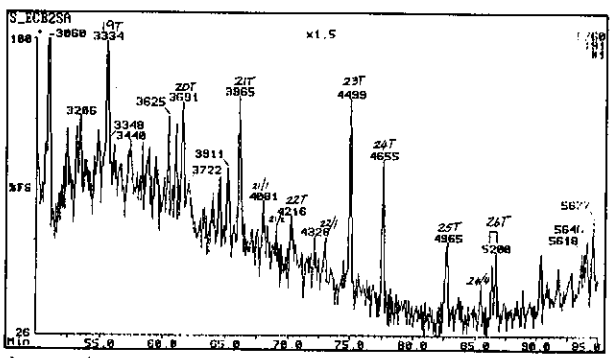

c) m/z 191: Tri and Tetra-cyclic Terpanes

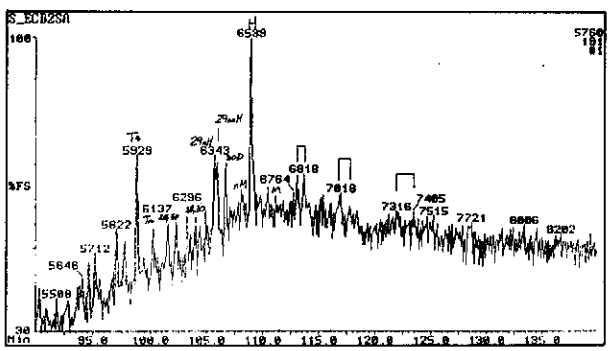

d) m/z 191: Penta-cyclic Terpanes

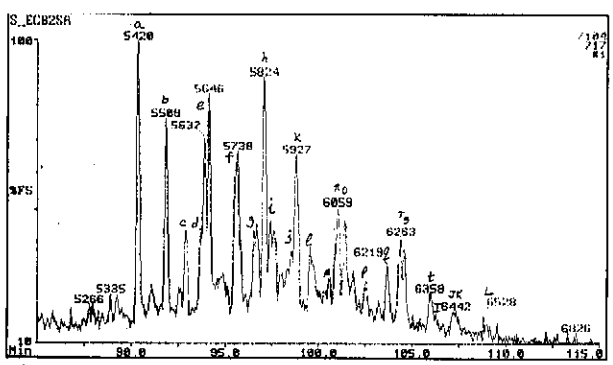

e) m/z 217: Steranes

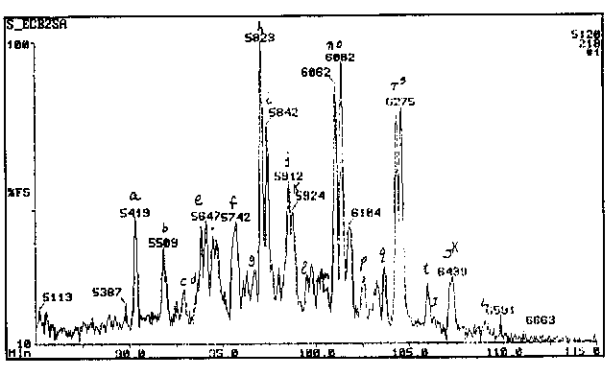

f) m/z 218: Regular (ßß) Steranes

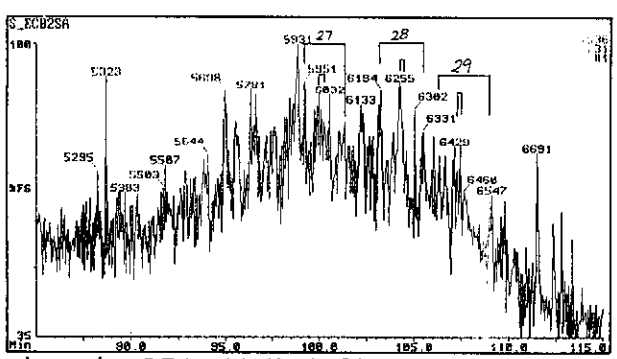

g) m/z 231: Methyl Steranes

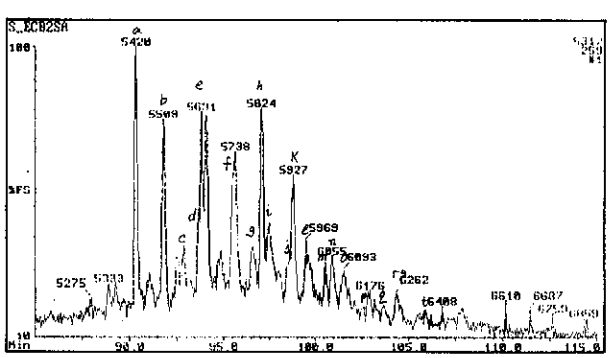

h) m/z 259: Rearranged (ßa) Steranes

Figure E.34: Annotated TIC and single ion fragmentograms of saturated hydrocarbons from sample 34, well 166 DST 1, 2520m.

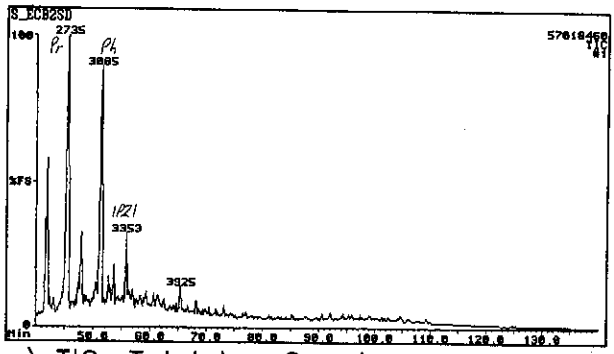

a) TIC: Total Ion Count

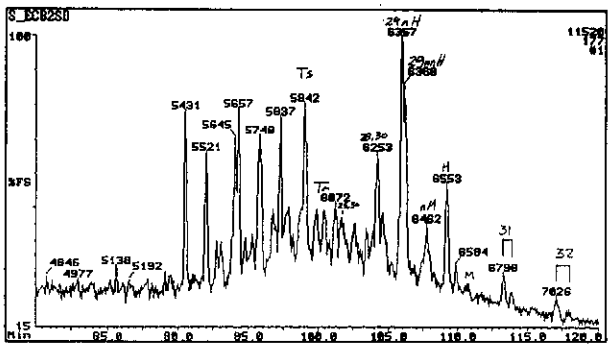

b) m/z 177: Demethylated Hopanes

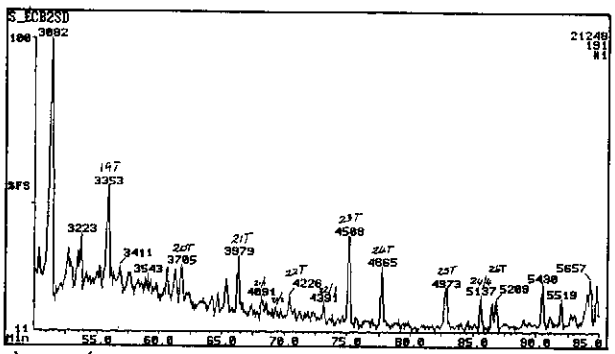

c) m/z 191: Tri and Tetra-cyclic Terpanes

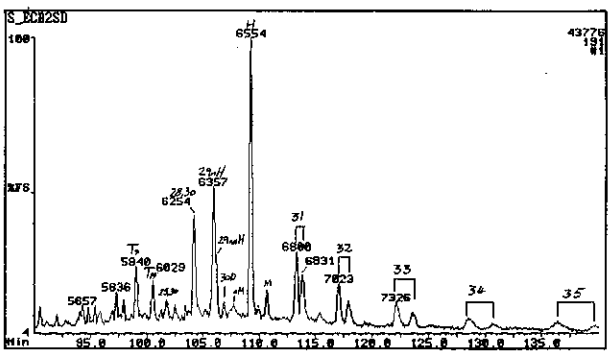

d) m/z 191: Penta-cyclic Terpanes

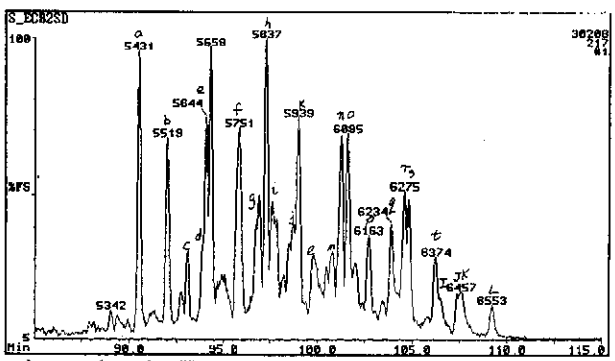

e) m/z 217: Steranes

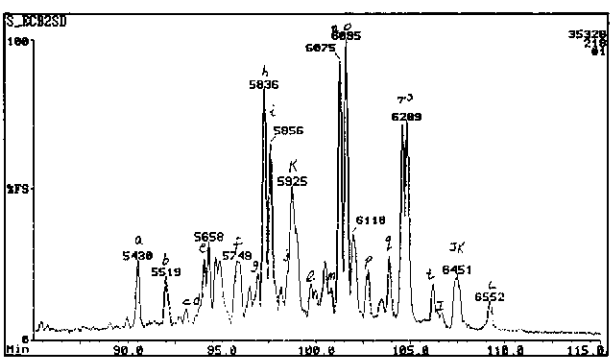

f) m/z 218: Regular (ßß) Steranes

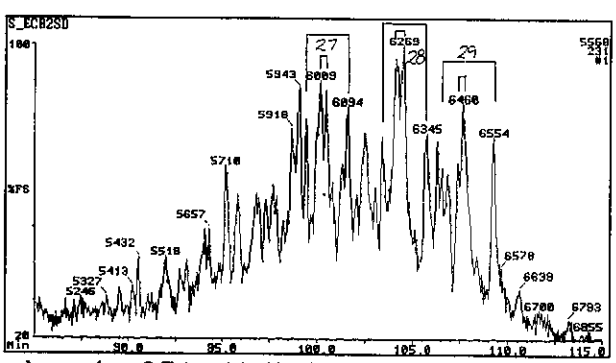

g) m/z 231: Methyl Steranes

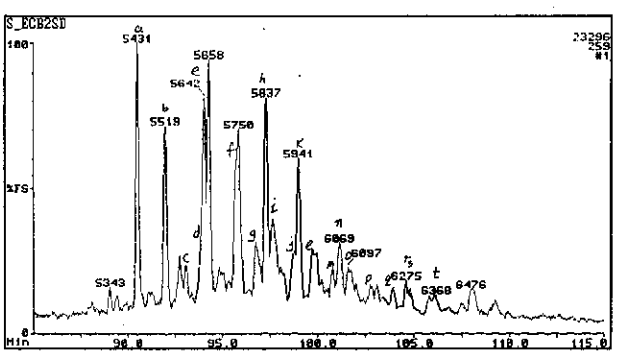

h) m/z 259: Rearranged (ßa) Steranes

Figure E.35: Annotated TIC and single ion fragmentograms of saturated hydrocarbons from sample 35, well 166 core 1, 2522.5m.

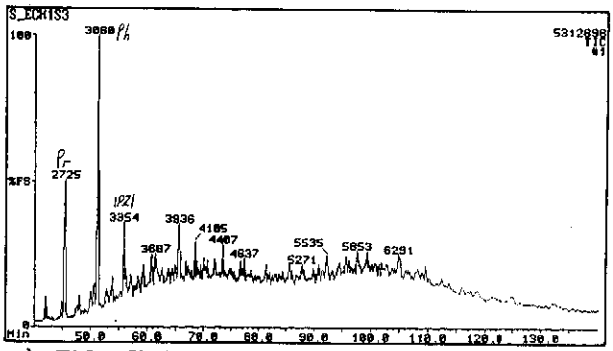

a) TIC: Total Ion Count

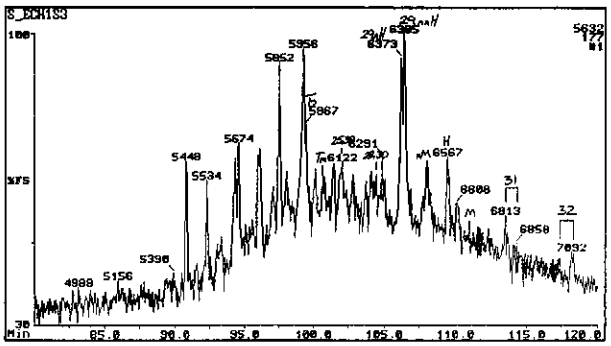

b) m/z 177: Demethylated Hopanes

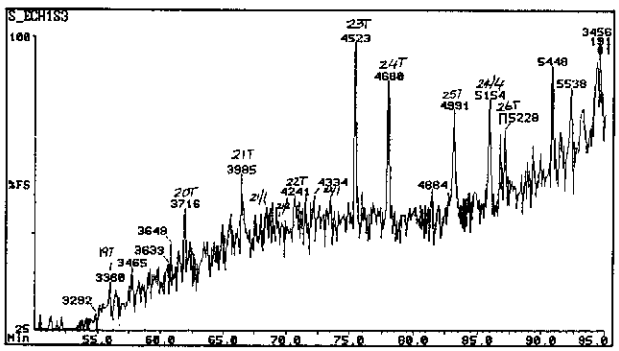

c) m/z 191: Tri and Tetra-cyclic Terpanes

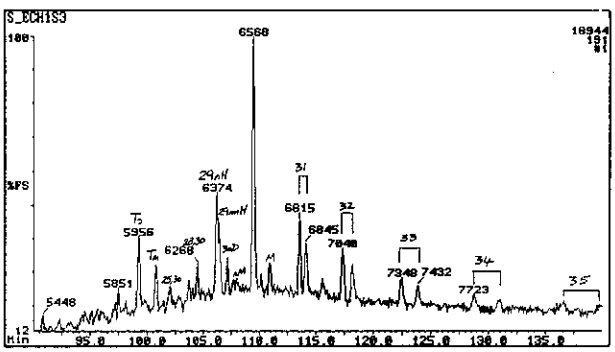

d) m/z 191: Penta-cyclic Terpanes

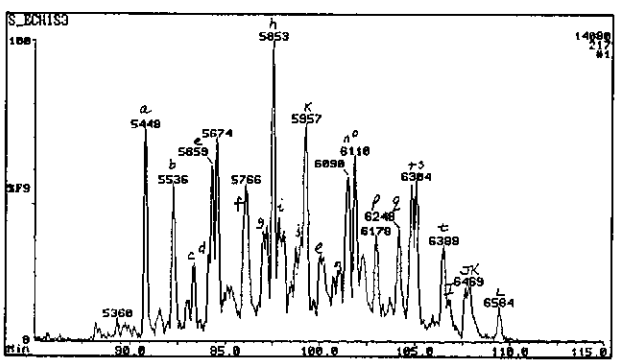

e) m/z 217: Steranes

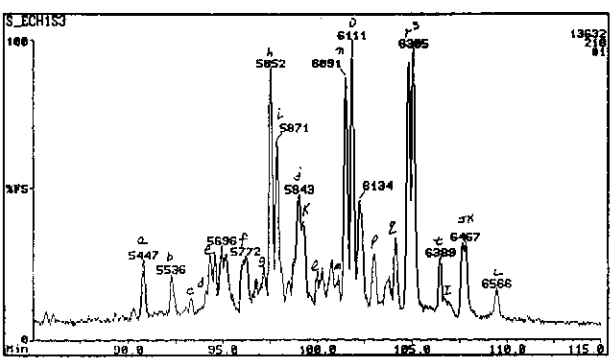

f) m/z 218: Regular (ßß) Steranes

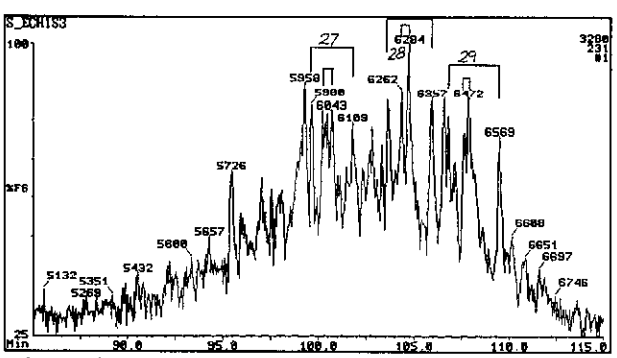

g) m/z 231: Methyl Steranes

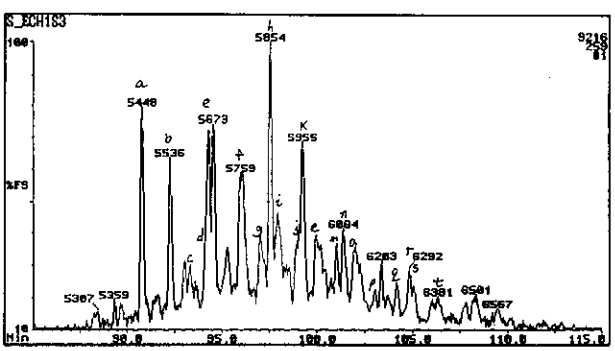

h) m/z 259: Rearranged (ßa) Steranes

Figure E.36: Annotated TIC and single ion fragmentograms of saturated hydrocarbons from sample 36, well 165 RC, 2256m.

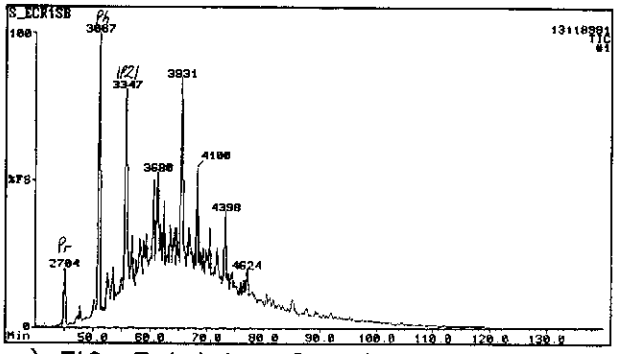

a) TIC: Total Ion Count

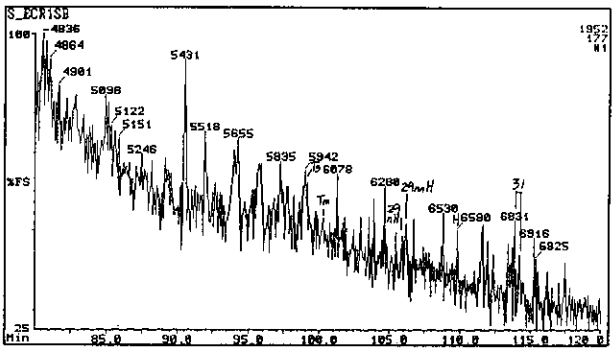

b) m/z 177: Demethylated Hopanes

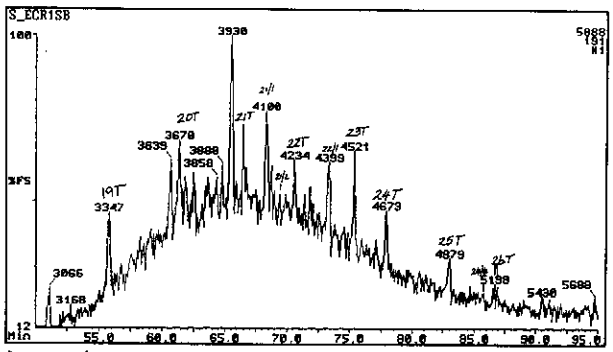

c) m/z 191: Tri and Tetra-cyclic Terpanes

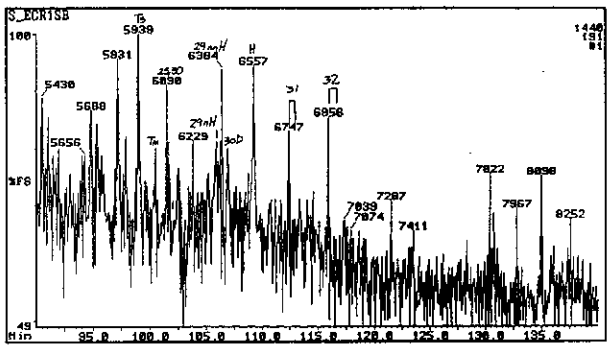

d) m/z 191: Penta-cyclic Terpanes

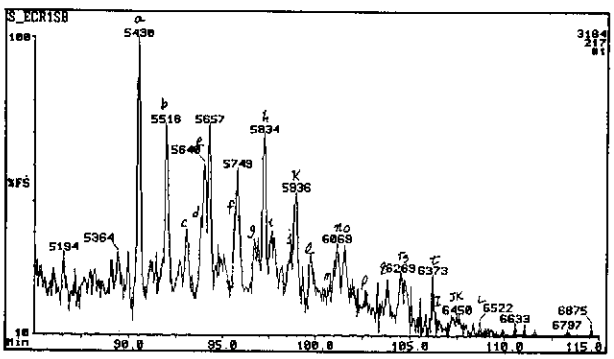

e) m/z 217: Steranes

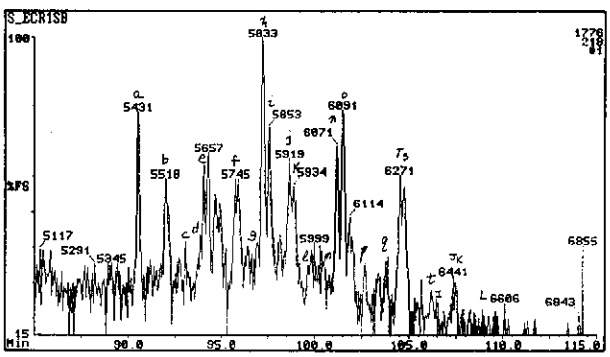

f) m/z 218: Regular (ßß) Steranes

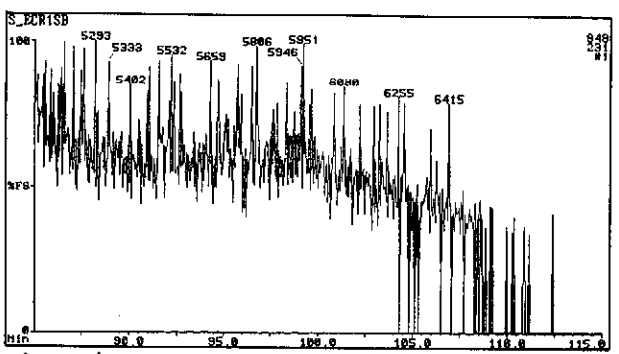

g) m/z 231: Methyl Steranes

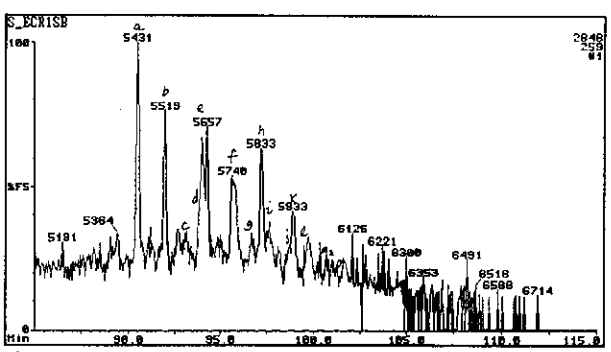

h) m/z 259: Rearranged (ßa) Steranes

Figure E.37: Annotated TIC and single ion fragmentograms of saturated hydrocarbons from sample 37, well 167 DST 1, 2679m.

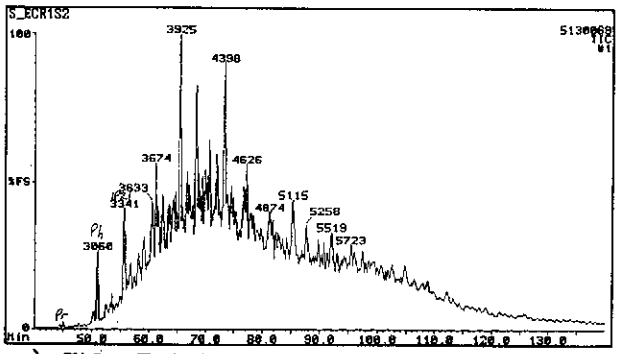

a) TIC: Total Ion Count

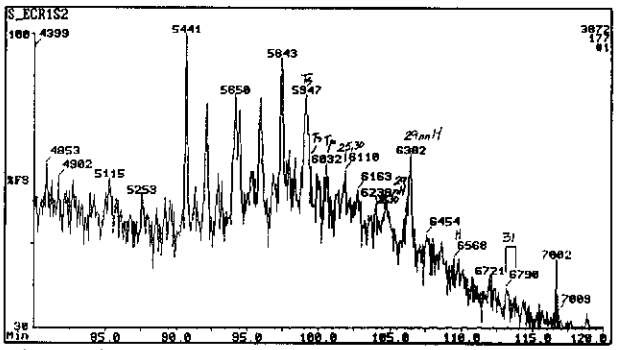

b) m/z 177: Demethylated Hopanes

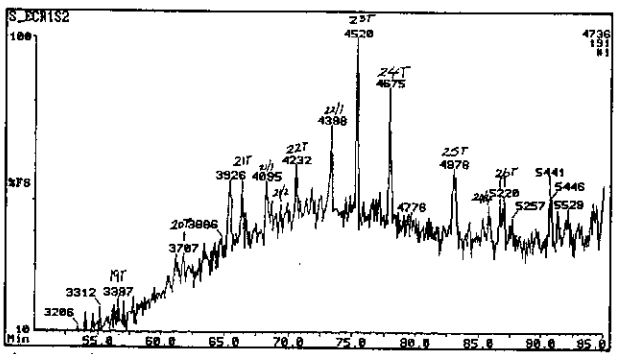

c) m/z 191: Tri and Tetra-cyclic Terpanes

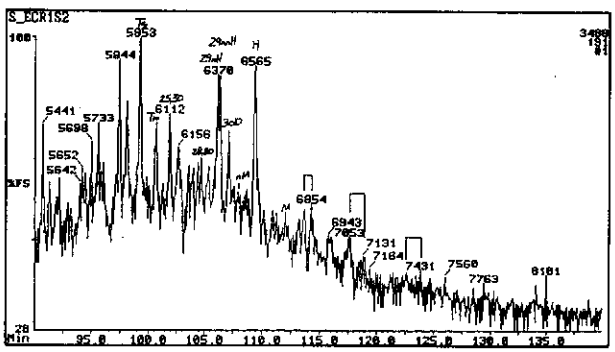

d) m/z 191: Penta-cyclic Terpanes

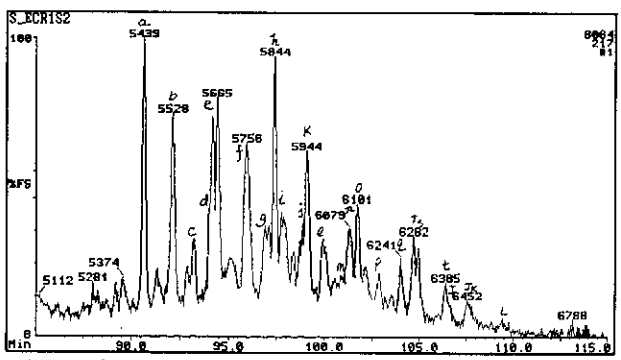

e) m/z 217: Steranes

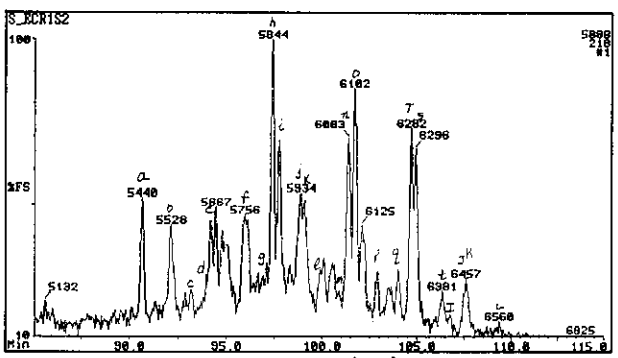

f) m/z 218: Regular (ßß) Steranes

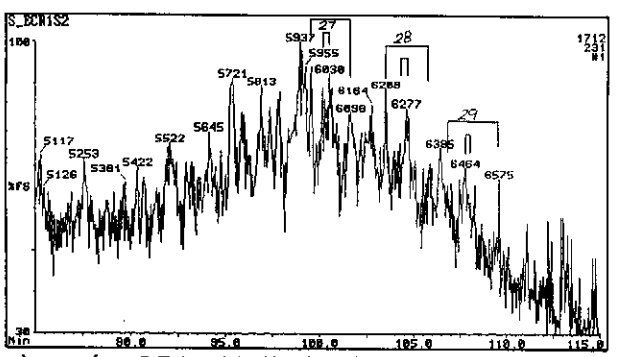

g) m/z 231: Methyl Steranes

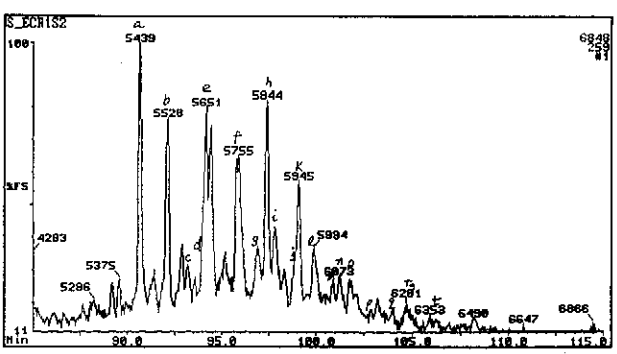

h) m/z 259: Rearranged (ßa) Steranes

Figure E.38: Annotated TIC and single ion fragmentograms of saturated hydrocarbons from sample 38, well 167 core 1, 2681.65m.

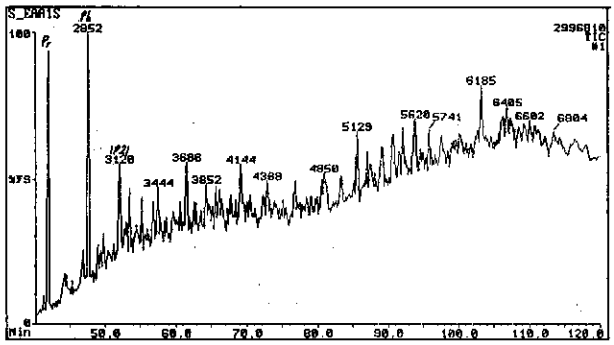

a) TIC: Total Ion Count

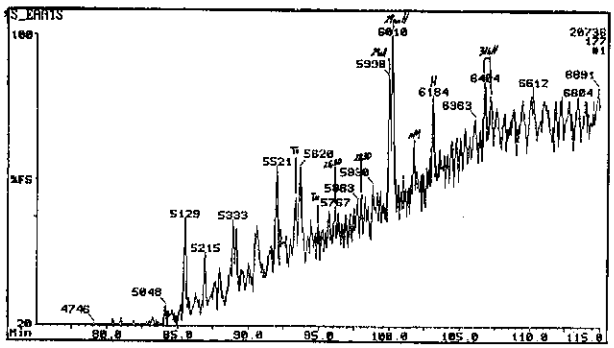

b) m/z 177: Demethylated Hopanes

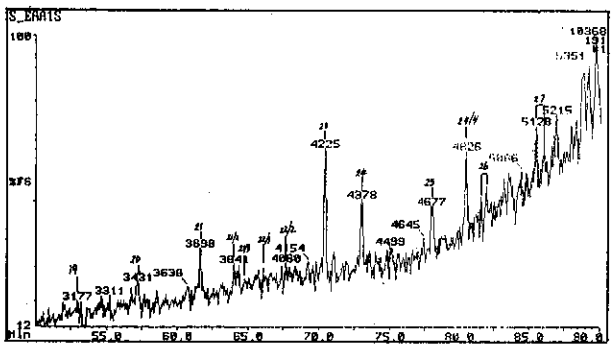

c) m/z 191: Tri and Tetra-cyclic Terpanes

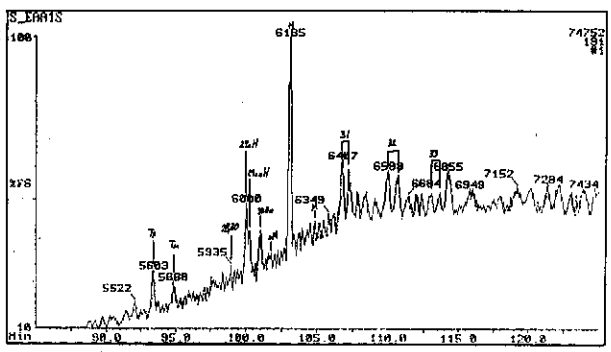

d) m/z 191: Penta-cyclic Terpanes

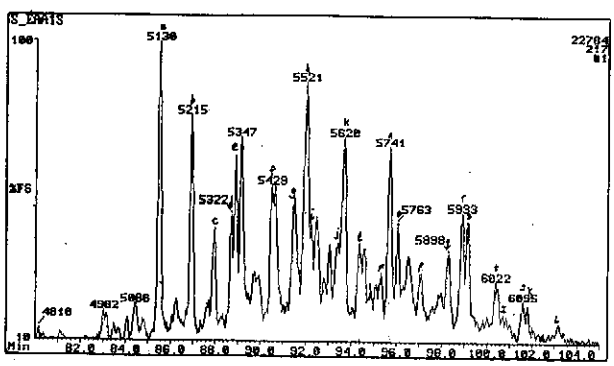

e) m/z 217: Steranes

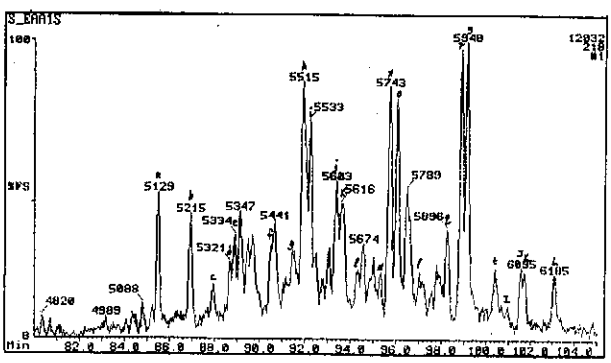

f) m/z 218: Regular (ßß) Steranes

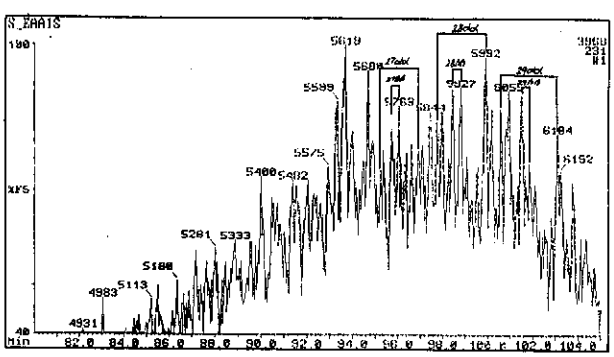

g) m/z 231: Methyl Steranes

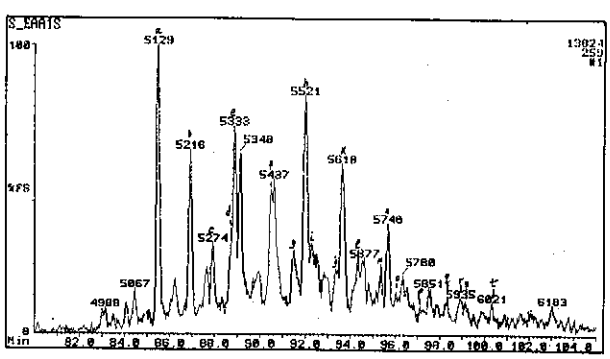

h) m/z 259: Rearranged (ßa) Steranes

Figure E.39: Annotated TIC and single ion fragmentograms of saturated hydrocarbons from sample 41, well 83 RC, 2702m.

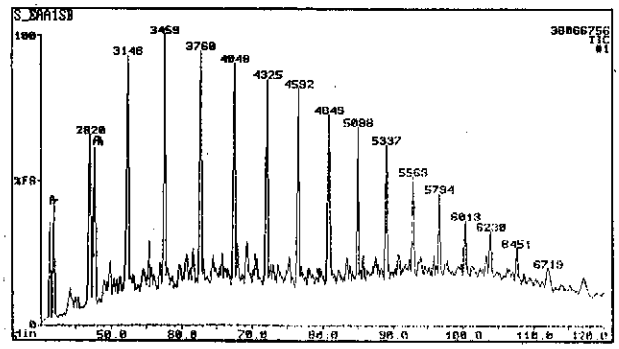

a) TIC: Total Ion Count

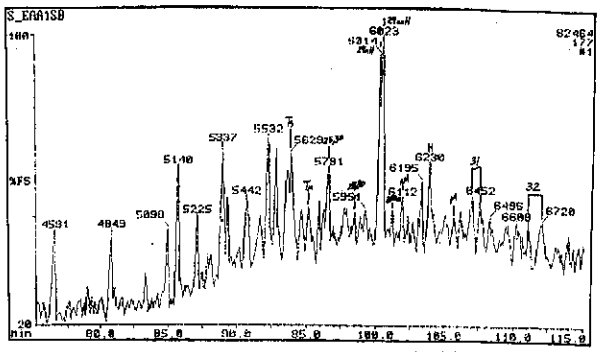

b) m/z 177: Demethylated Hopanes

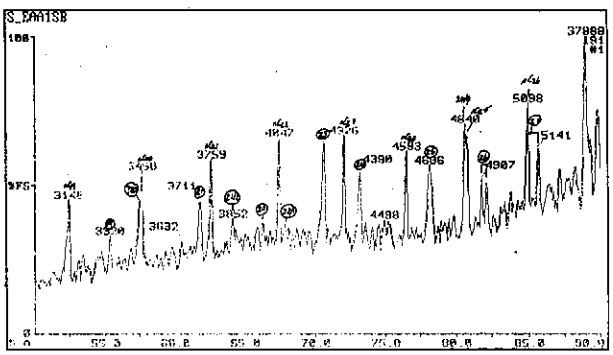

c) m/z 191: Tri and Tetra-cyclic Terpanes

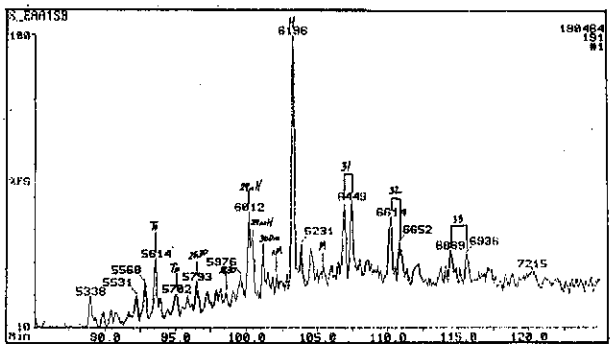

d) m/z 191: Penta-cyclic Terpanes

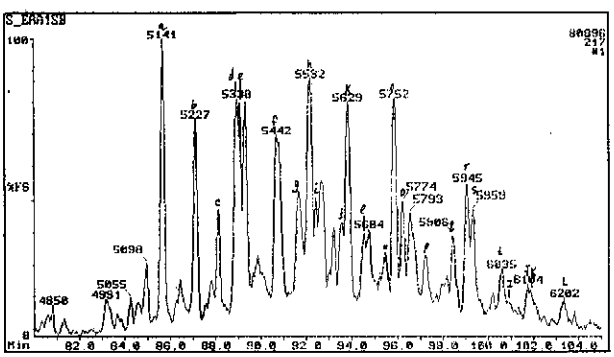

e) m/z 217: Steranes

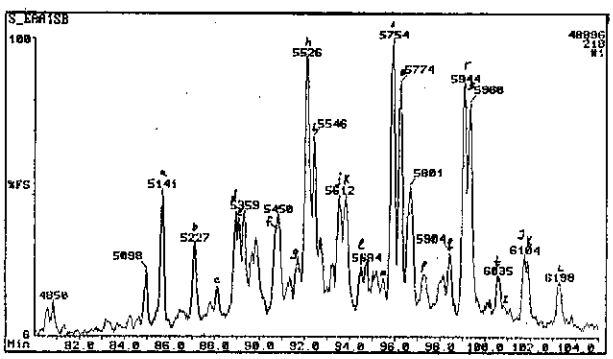

f) m/z 218: Regular (ßß) Steranes

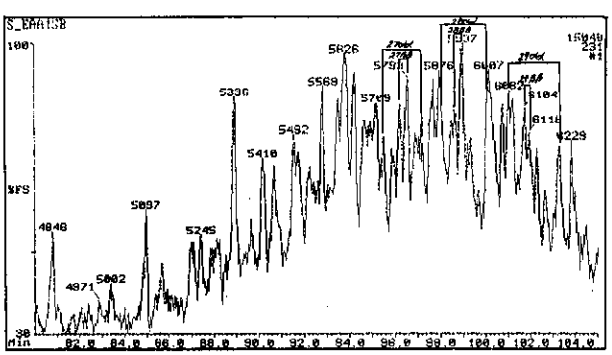

g) m/z 231: Methyl Steranes

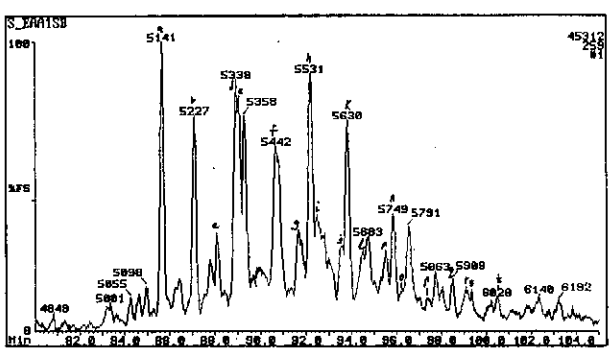

h) m/z 259: Rearranged (ßa) Steranes

Figure E.40: Annotated TIC and single ion fragmentograms of saturated hydrocarbons from sample 42, well 83 RC, 2741m.

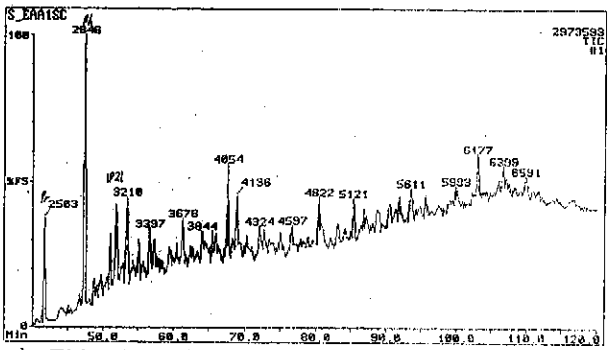

a) TIC: Total Ion Count

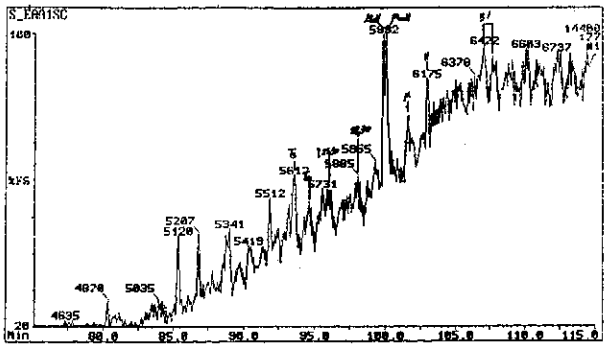

b) m/z 177: Demethylated Hopanes

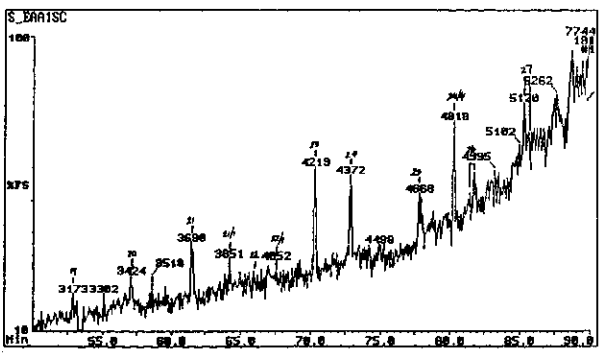

c) m/z 191: Tri and Tetra-cyclic Terpanes

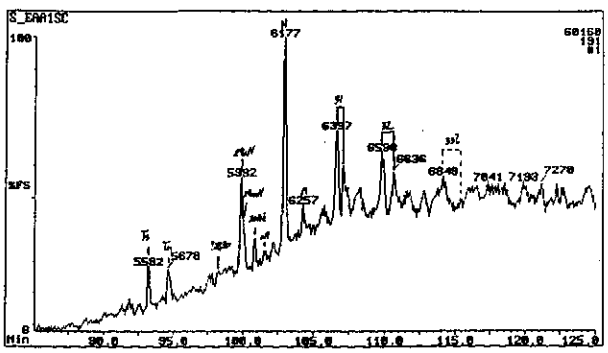

d) m/z 191: Penta-cyclic Terpanes

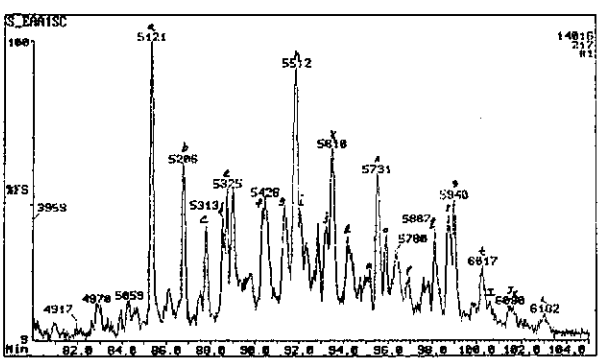

e) m/z 217: Steranes

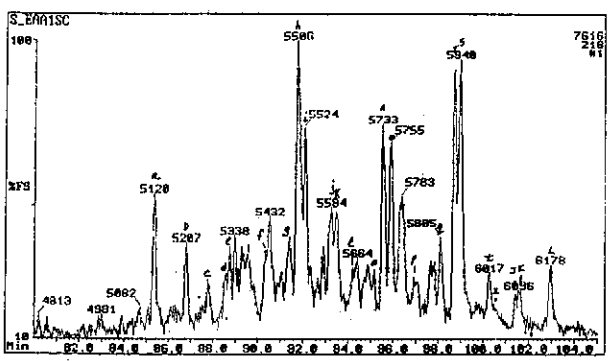

f) m/z 218: Regular (ßß) Steranes

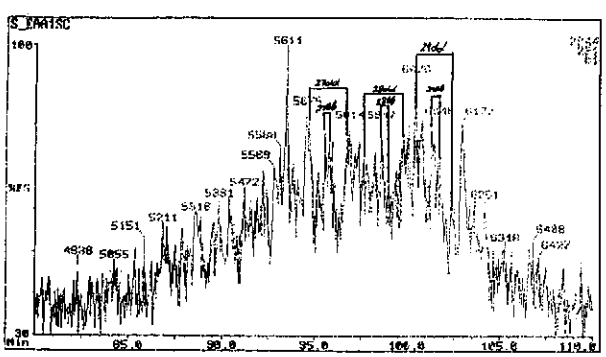

g) m/z 231: Methyl Steranes

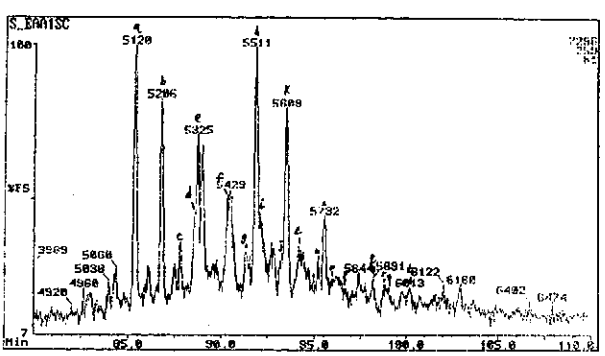

h) m/z 259: Rearranged (ßa) Steranes

Figure E.41: Annotated TIC and single ion fragmentograms of saturated hydrocarbons from sample 43, well 83 RC, 2792m.

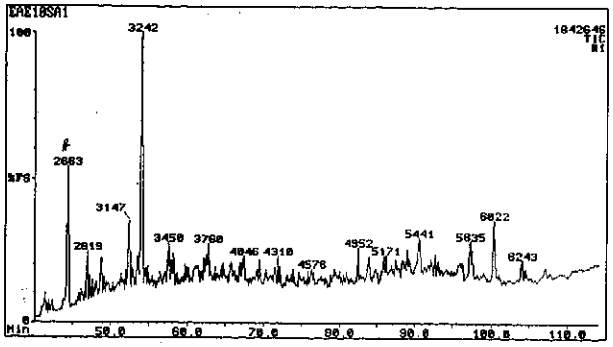

a) TIC: Total Ion Count

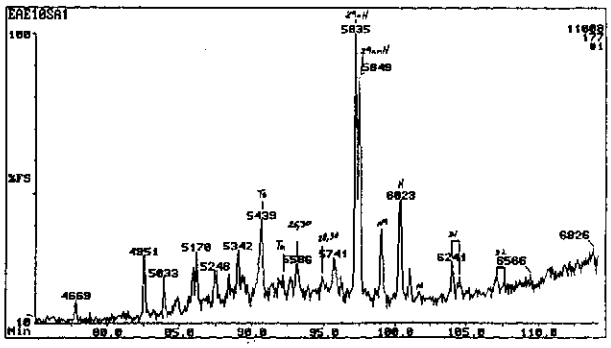

b) m/z 177: Demethylated Hopanes

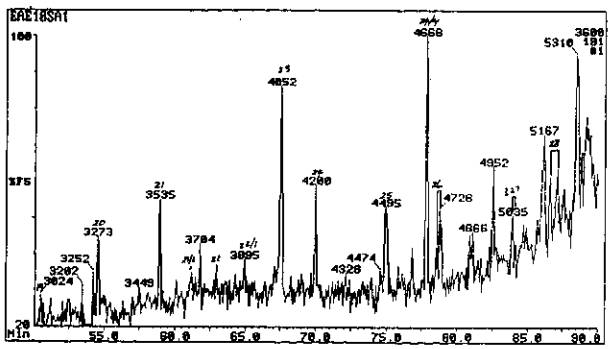

c) m/z 191: Tri and Tetra-cyclic Terpanes

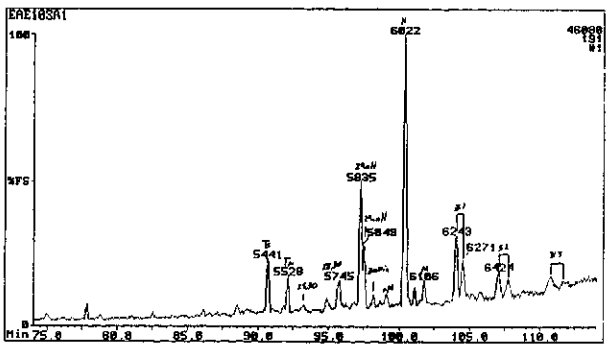

d) m/z 191: Penta-cyclic Terpanes

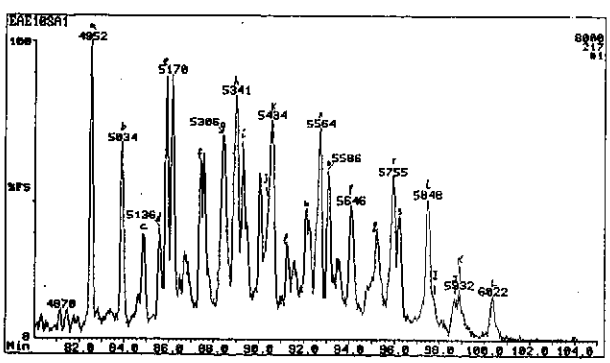

e) m/z 217: Steranes

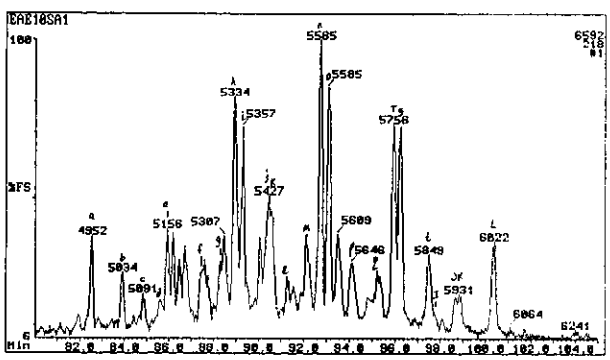

f) m/z 218: Regular (ßß) Steranes

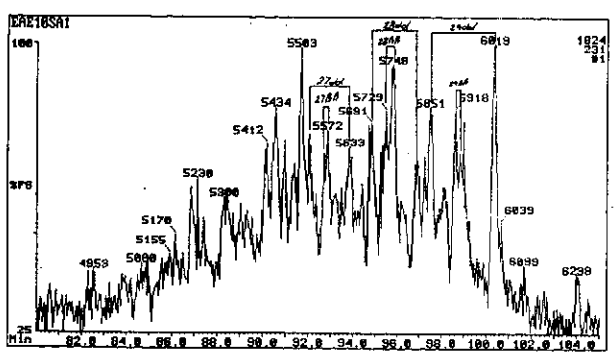

g) m/z 231: Methyl Steranes

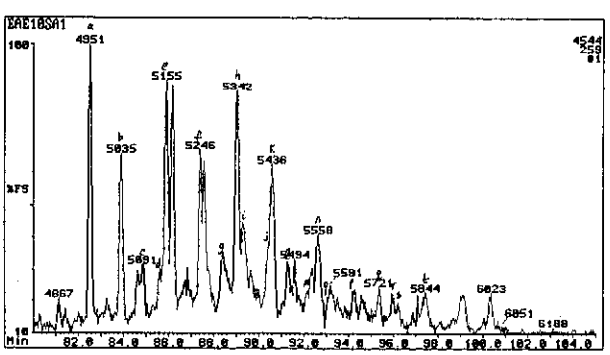

h) m/z 259: Rearranged (ßa) Steranes

Figure E.42: Annotated TIC and single ion fragmentograms of saturated hydrocarbons from sample 44, well 92 RC, 2610m.

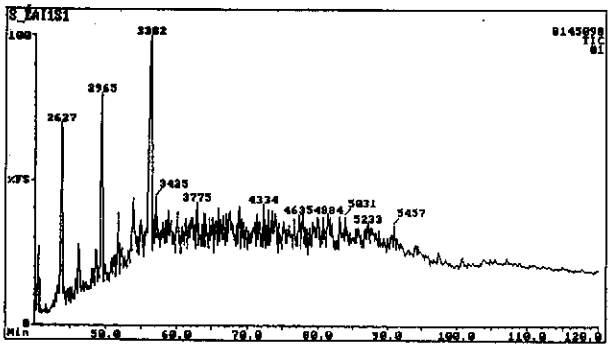

a) TIC: Total Ion Count

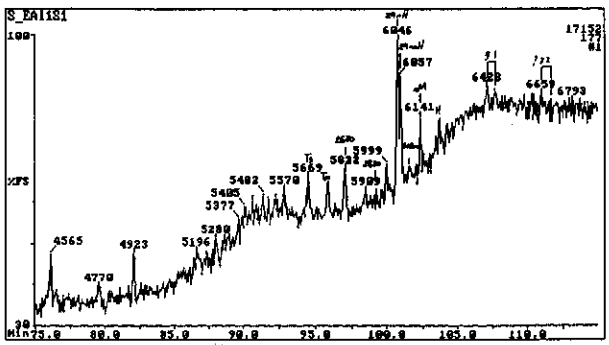

b) m/z 177: Demethylated Hopanes

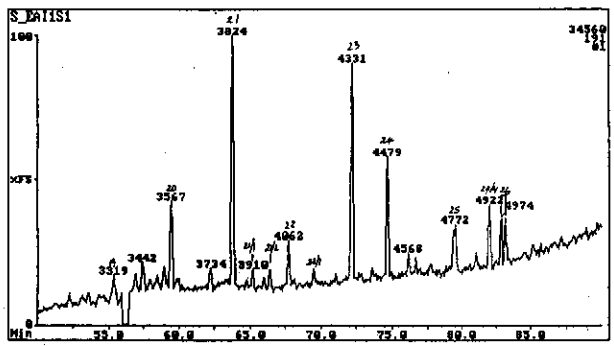

c) m/z 191: Tri and Tetra-cyclic Terpanes

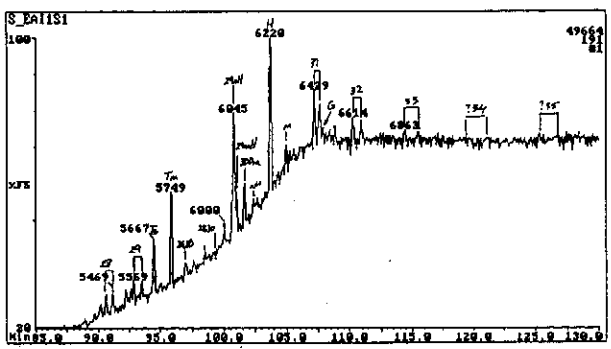

d) m/z 191: Penta-cyclic Terpanes

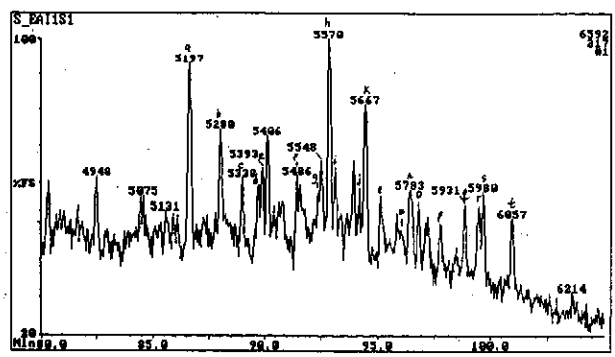

e) m/z 217: Steranes

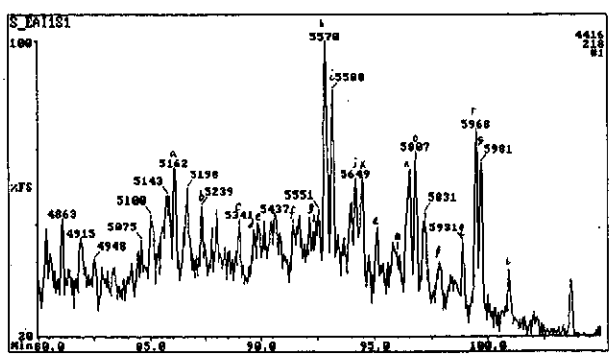

f) m/z 218: Regular (ßß) Steranes

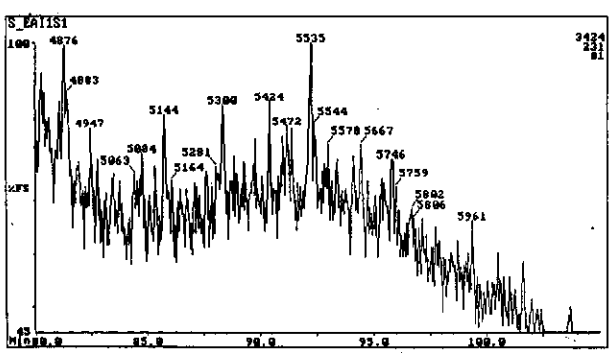

g) m/z 231: Methyl Steranes

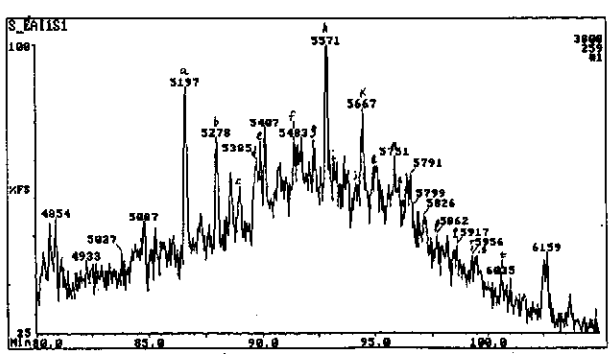

h) m/z 259: Rearranged (ßa) Steranes

Figure E.43: Annotated TIC and single ion fragmentograms of saturated hydrocarbons from sample 45, well 89 RC, 2660m.

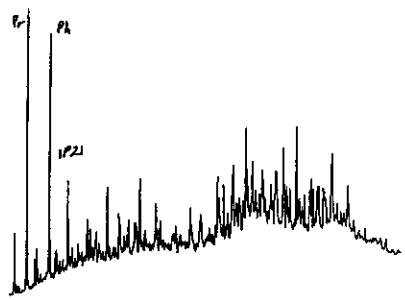

a) TIC: Total Ion Count

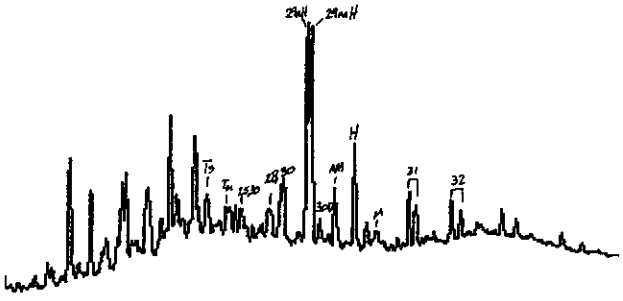

b) m/z 177: Demethylated Hopanes

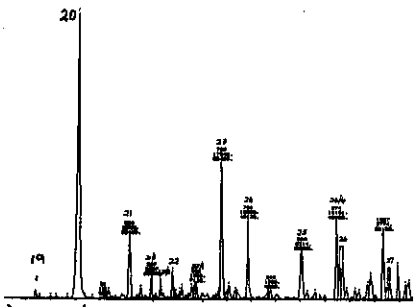

c) m/z 191: Tri and Tetra-cyclic Terpanes

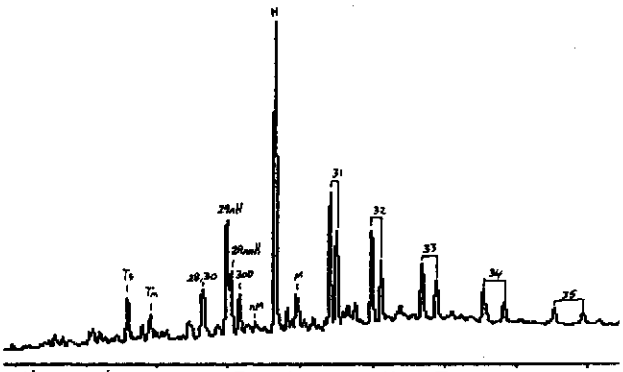

d) m/z 191: Penta-cyclic Terpanes

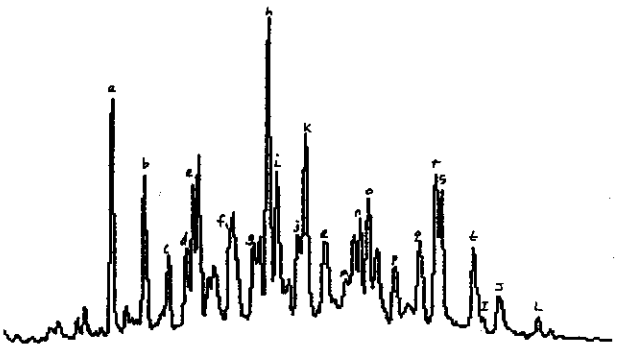

e) m/z 217: Steranes

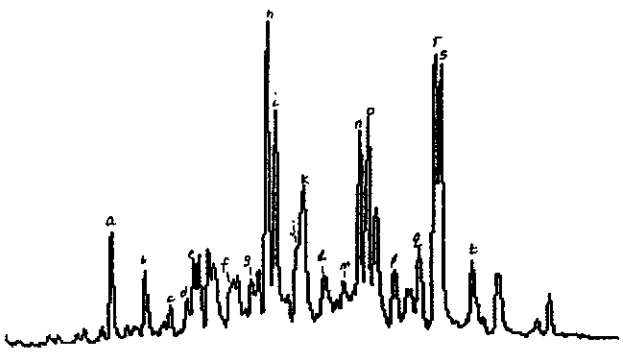

f) m/z 218: Regular (ßß) Steranes

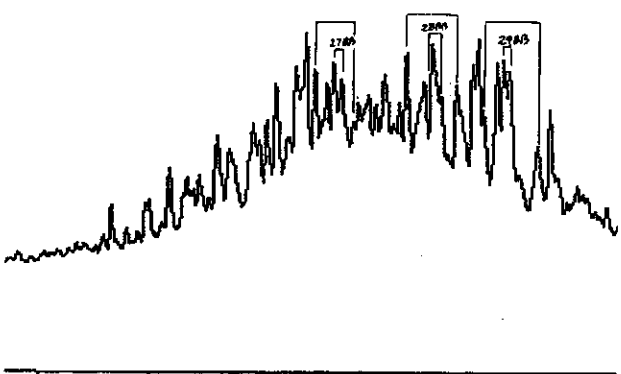

g) m/z 231: Methyl Steranes

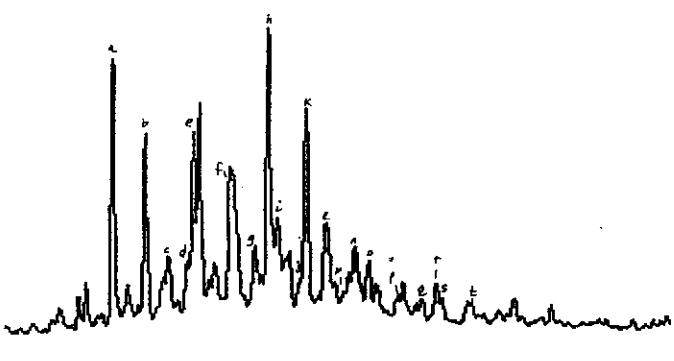

h) m/z 259: Rearranged (ßa) Steranes

Figure E.44: Annotated TIC and single ion fragmentograms of saturated hydrocarbons from sample 46, well 93 RC, 2720m.

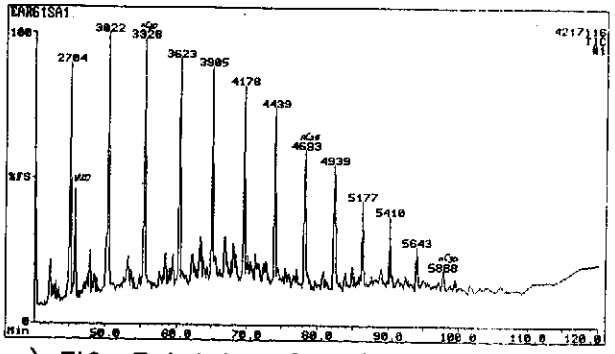

a) TIC: Total Ion Count

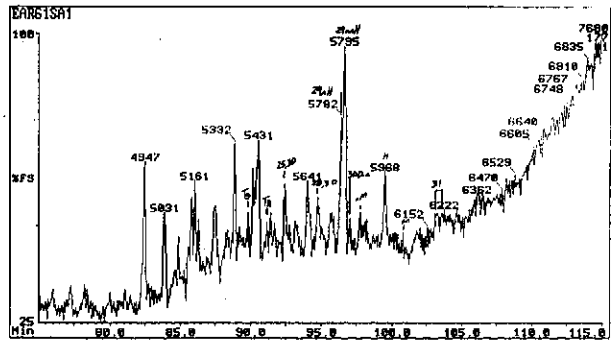

b) m/z 177: Demethylated Hopanes

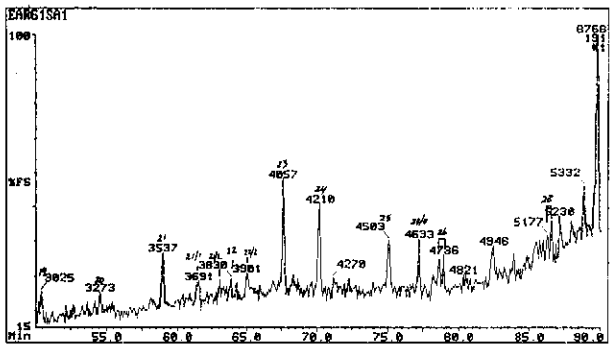

c) m/z 191: Tri and Tetra-cyclic Terpanes

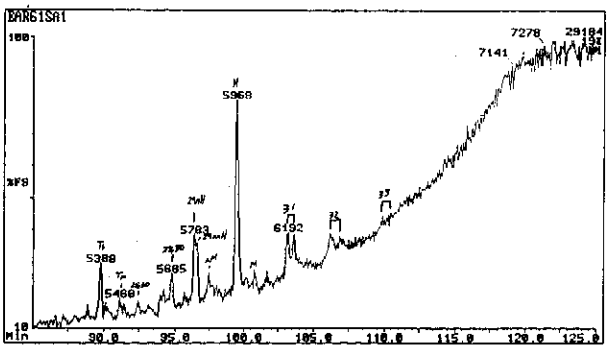

d) m/z 191: Penta-cyclic Terpanes

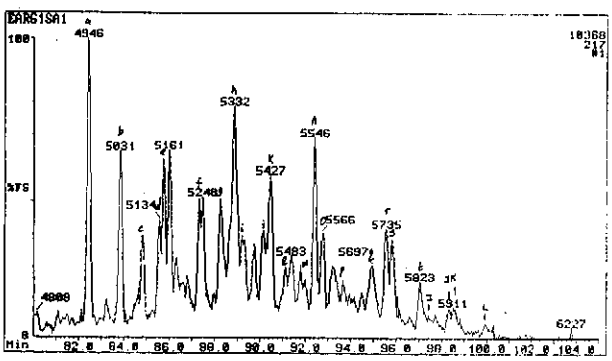

e) m/z 217: Steranes

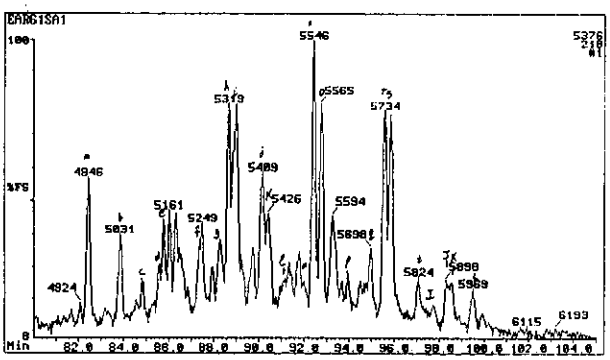

f) m/z 218: Regular (ßß) Steranes

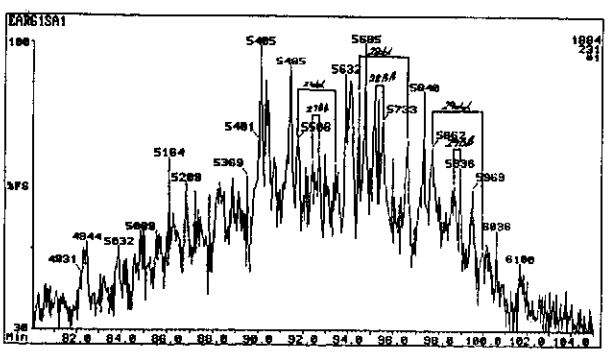

g) m/z 231: Methyl Steranes

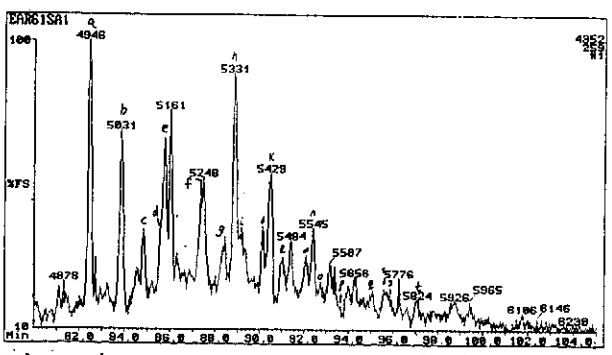

h) m/z 259: Rearranged (ßa) Steranes

Figure E.45: Annotated TIC and single ion fragmentograms of saturated hydrocarbons from sample 47, well 93 RC, 2761m.

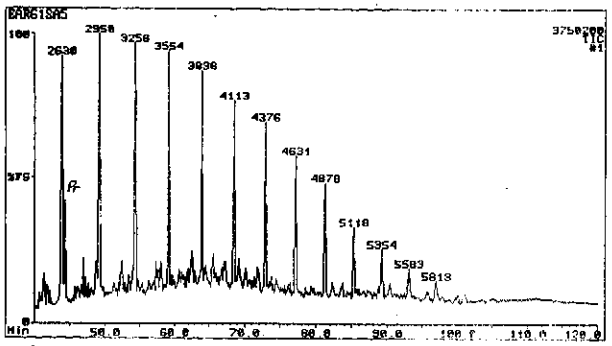

a) TIC: Total Ion Count

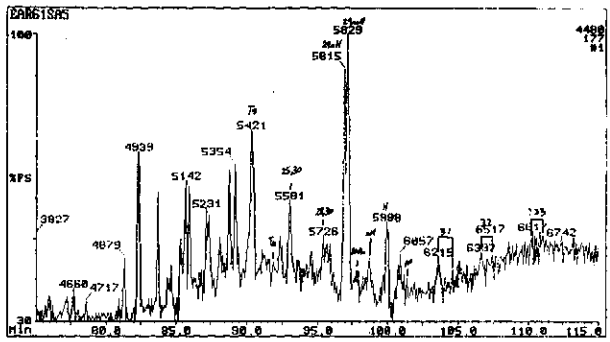

b) m/z 177: Demethylated Hopanes

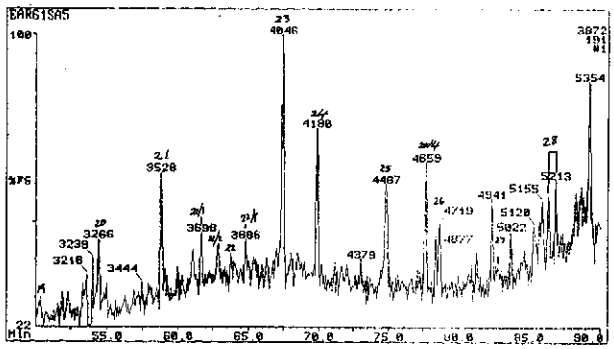

c) m/z 191: Tri and Tetra-cyclic Terpanes

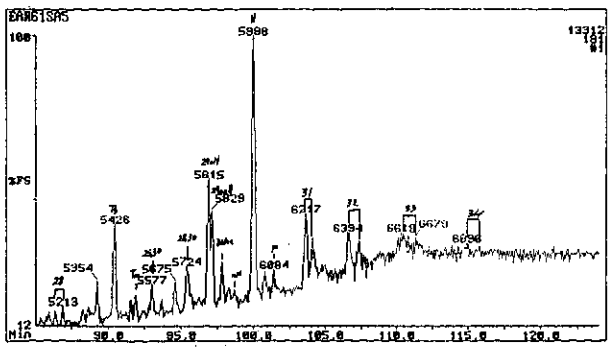

d) m/z 191: Penta-cyclic Terpanes

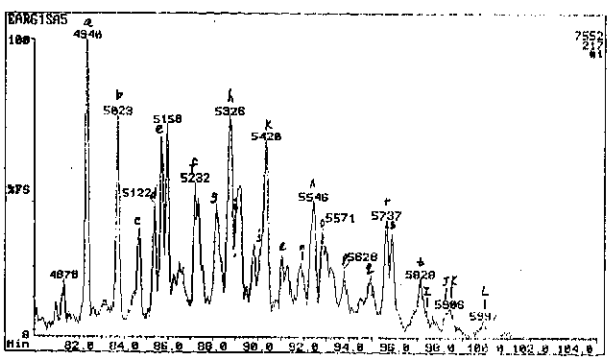

e) m/z 217: Steranes

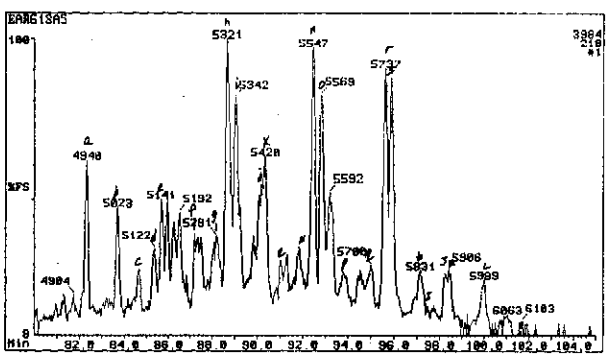

f) m/z 218: Regular (ββ) Steranes

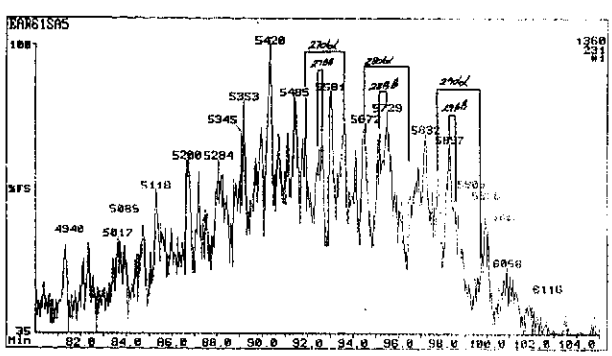

g) m/z 231: Methyl Steranes

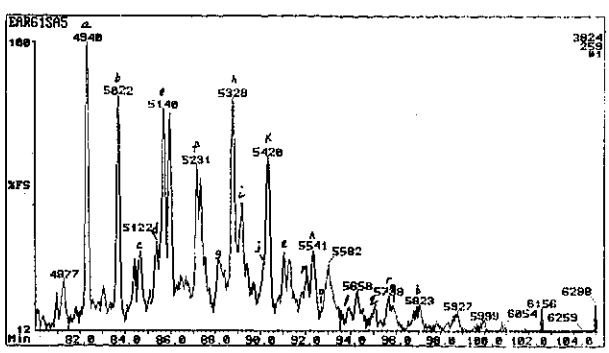

h) m/z 259: Rearranged (βa) Steranes

Figure E.46: Annotated TIC and single ion fragmentograms of saturated hydrocarbons from sample 48, well 93 RC, 2761m.

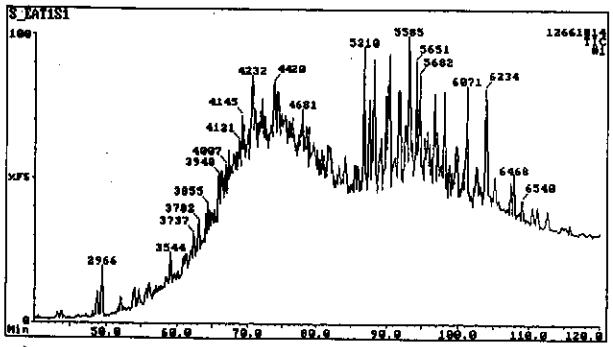

a) TIC: Total Ion Count

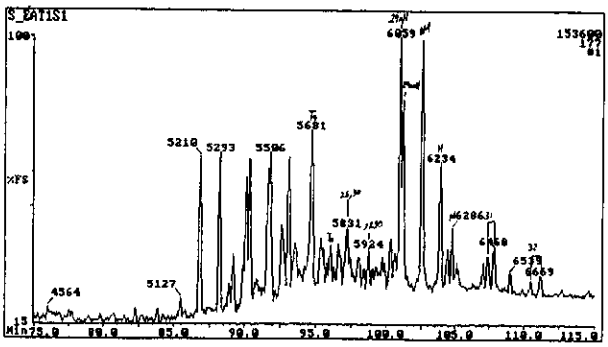

b) m/z 177: Demethylated Hopanes

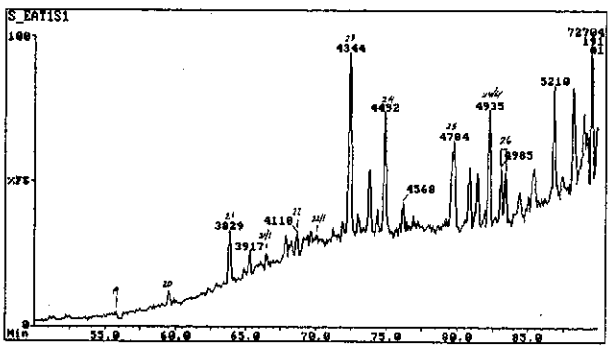

c) m/z 191: Tri and Tetra-cyclic Terpanes

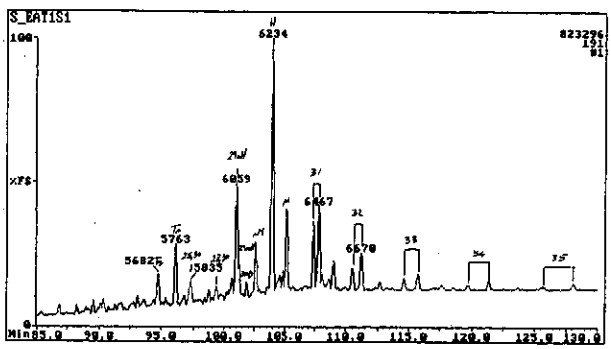

d) m/z 191: Penta-cyclic Terpanes

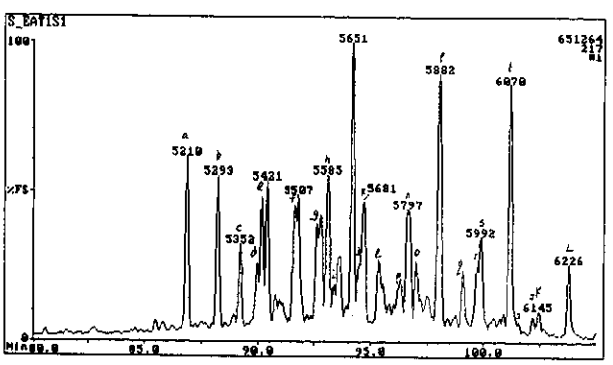

e) m/z 217: Steranes

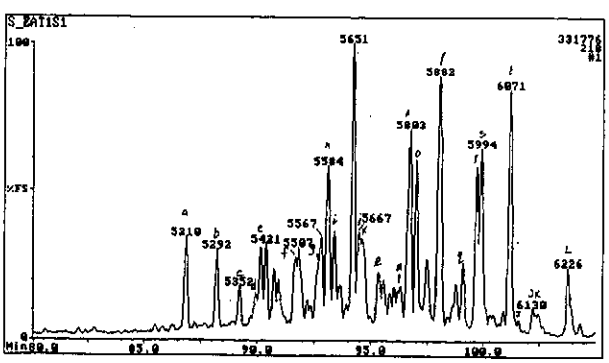

f) m/z 218: Regular (ßß) Steranes

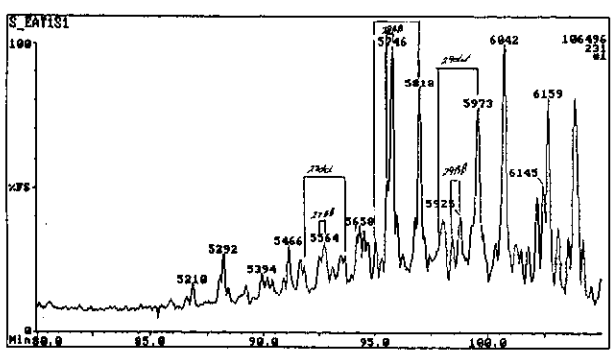

g) m/z 231: Methyl Steranes

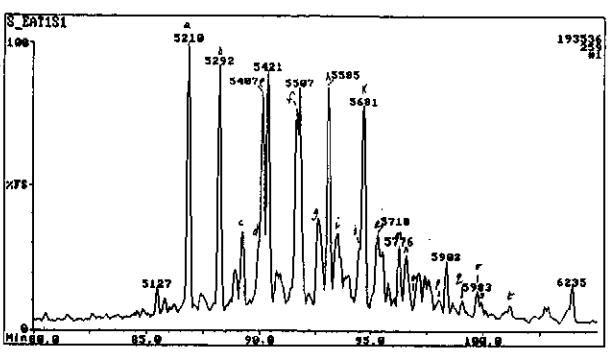

h) m/z 259: Rearranged (ßa) Steranes

Figure E.47: Annotated TIC and single ion fragmentograms of saturated hydrocarbons from sample 49, well 99 RC, 1820m.

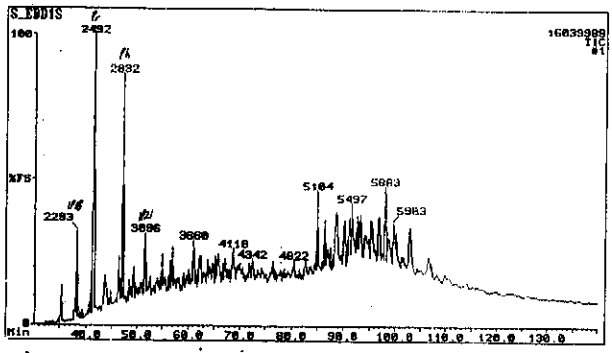

a) TIC: Total Ion Count

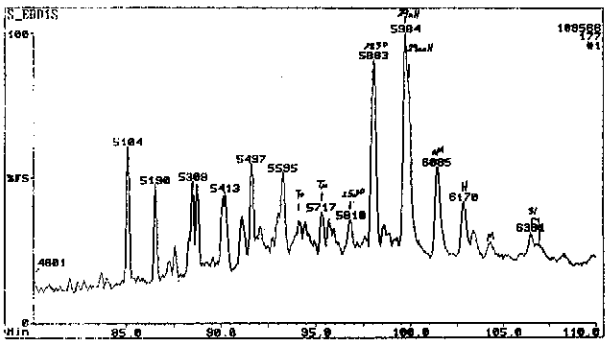

b) m/z 177: Demethylated Hopanes

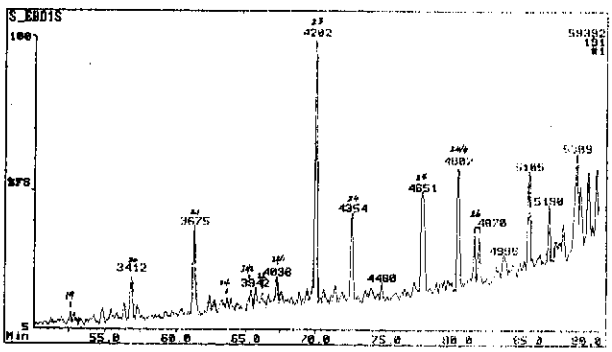

c) m/z 191: Tri and Tetra-cyclic Terpanes

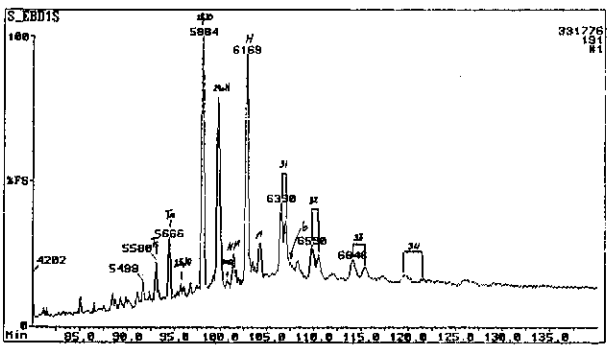

d) m/z 191: Penta-cyclic Terpanes

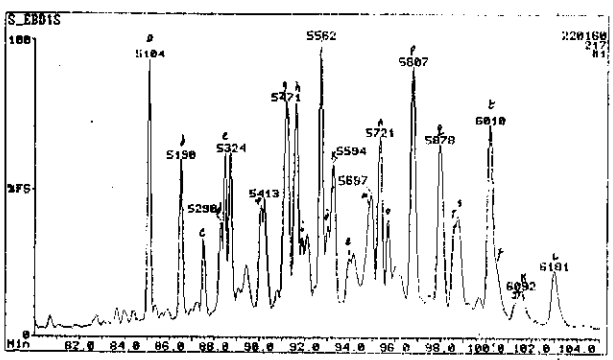

e) m/z 217: Steranes

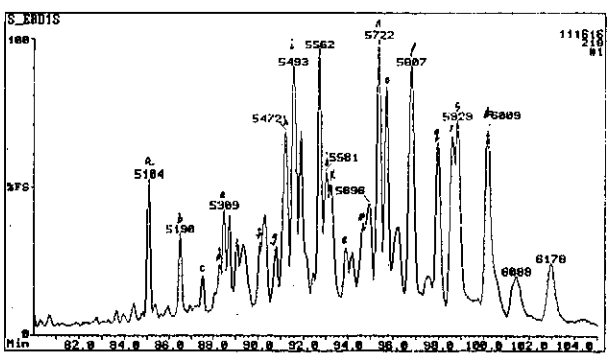

f) m/z 218: Regular (ßß) Steranes

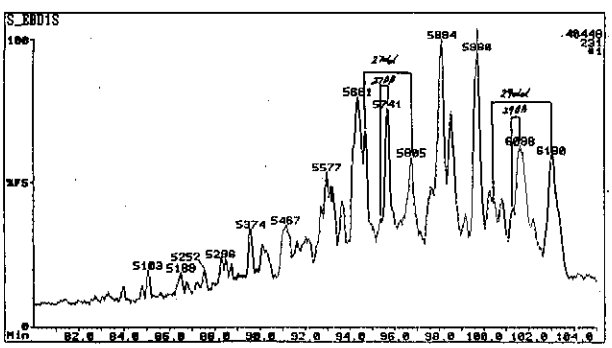

g) m/z 231: Methyl Steranes

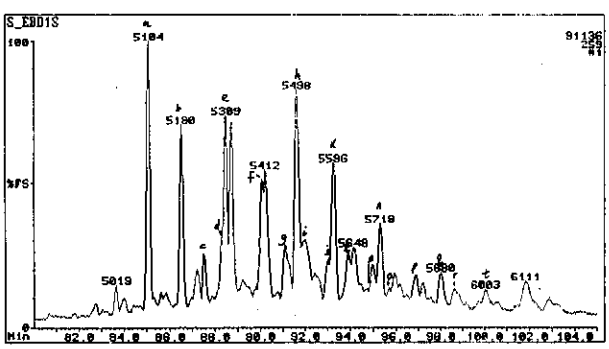

h) m/z 259: Rearranged (ßa) Steranes

Figure E.48: Annotated TIC and single ion fragmentograms of saturated hydrocarbons from sample 50, well 109 RC, 2461m.

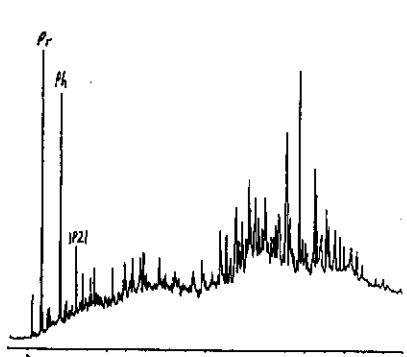

a) TIC: Total Ion Count

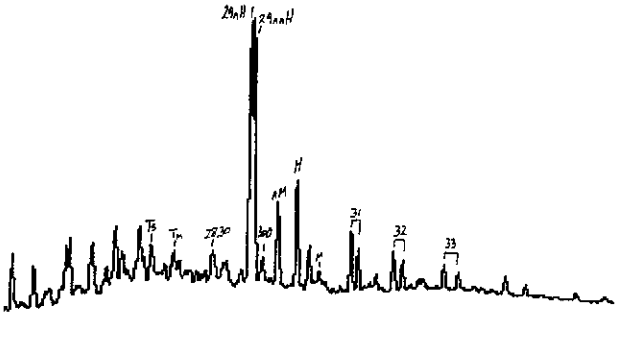

b) m/z 177: Demethylated Hopanes

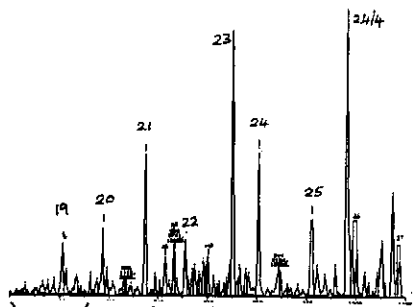

c) m/z 191: Tri and Tetra-cyclic Terpanes

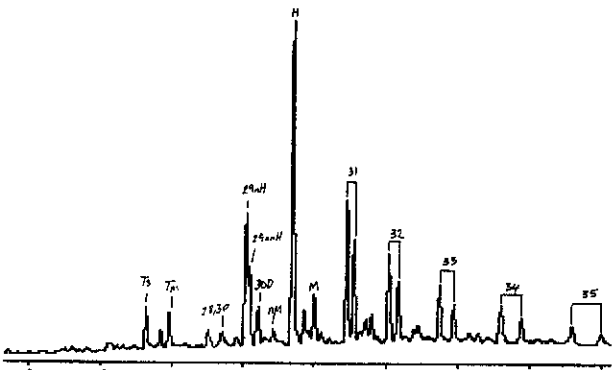

d) m/z 191: Penta-cyclic Terpanes

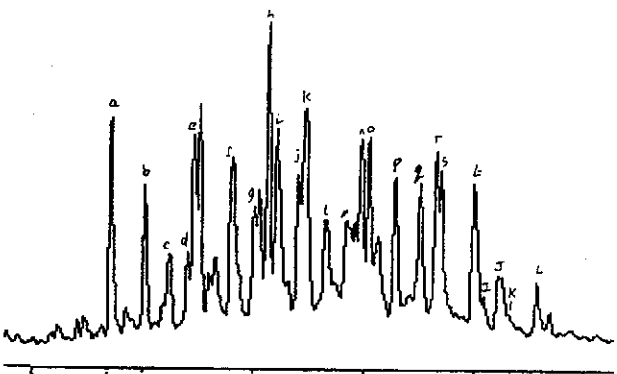

e) m/z 217: Steranes

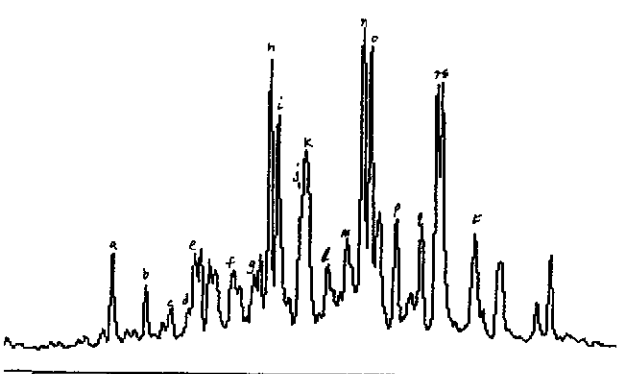

f) m/z 218: Regular (ßß) Steranes

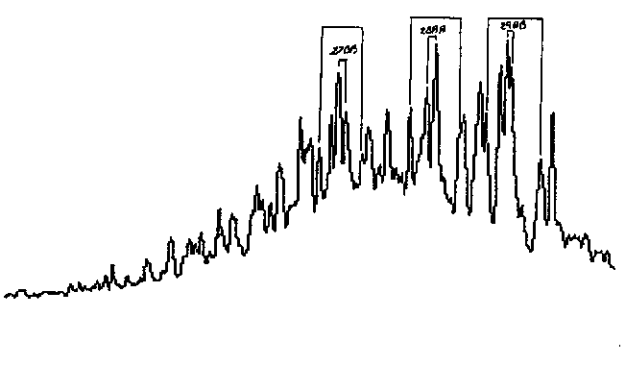

g) m/z 231: Methyl Steranes

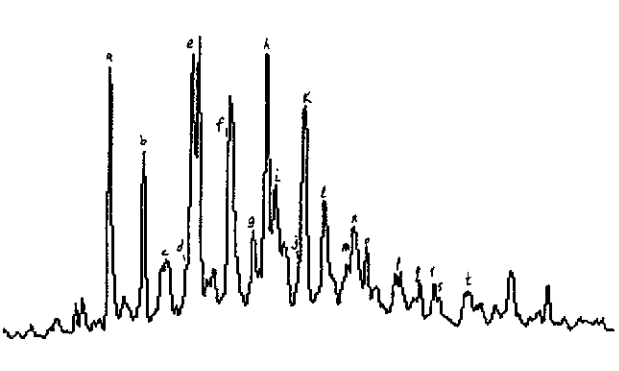

h) m/z 259: Rearranged (ßa) Steranes

Figure E.49: Annotated TIC and single ion fragmentograms of saturated hydrocarbons from sample 51, well 109 core 3, 2654.15m.

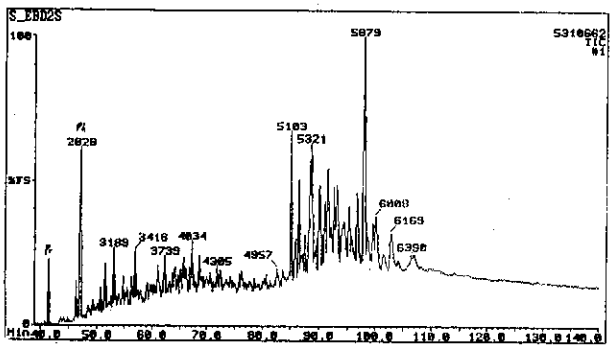

a) TIC: Total Ion Count

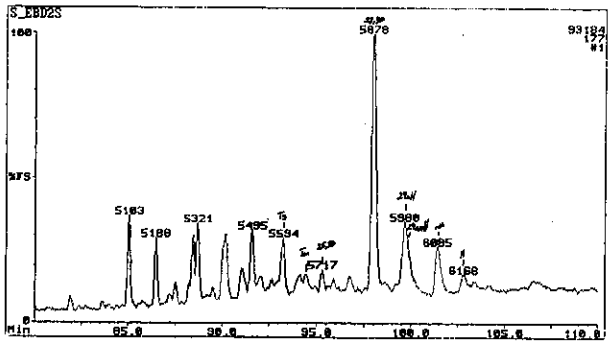

b) m/z 177: Demethylated Hopanes

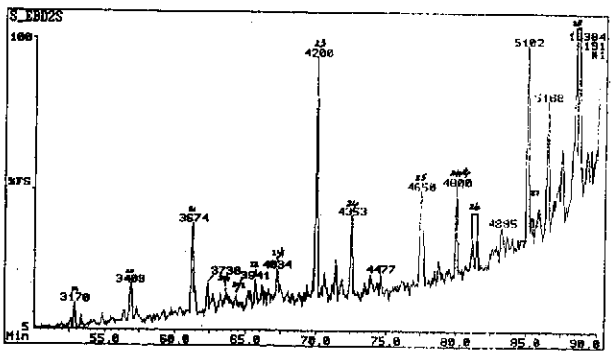

c) m/z 191: Tri and Tetra-cyclic Terpanes

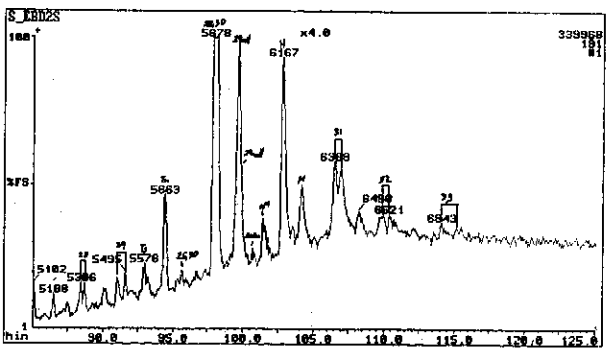

d) m/z 191: Penta-cyclic Terpanes

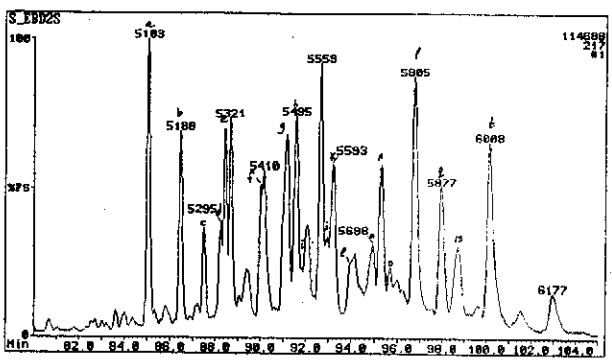

e) m/z 217: Steranes

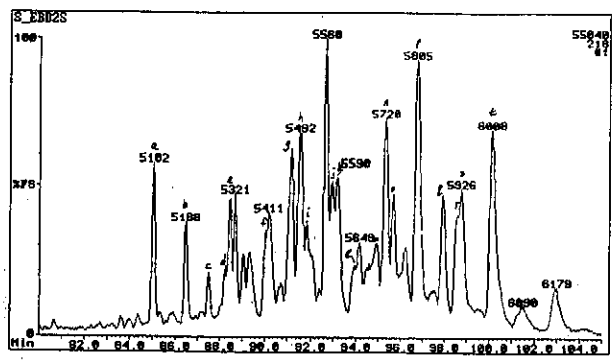

f) m/z 218: Regular (ßß) Steranes

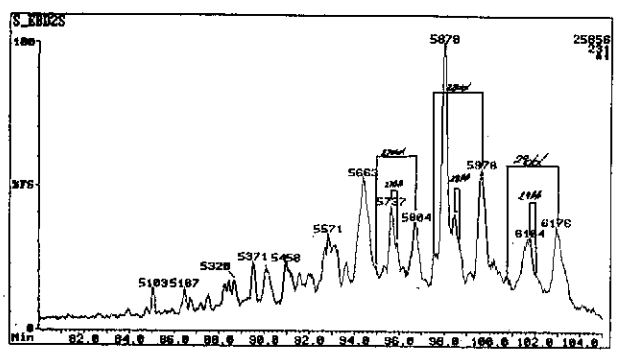

g) m/z 231: Methyl Steranes

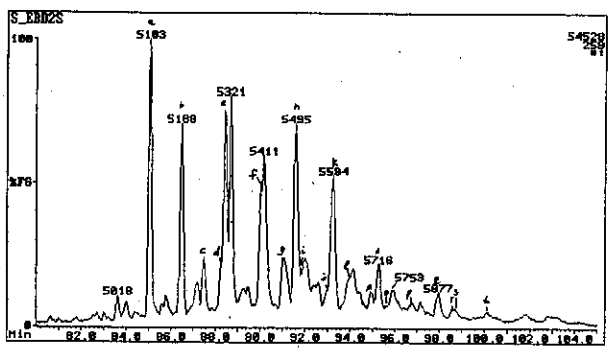

h) m/z 259: Rearranged (ßa) Steranes

Figure E.50: Annotated TIC and single ion fragmentograms of saturated hydrocarbons from sample 52, well 130 RC, 2331m.

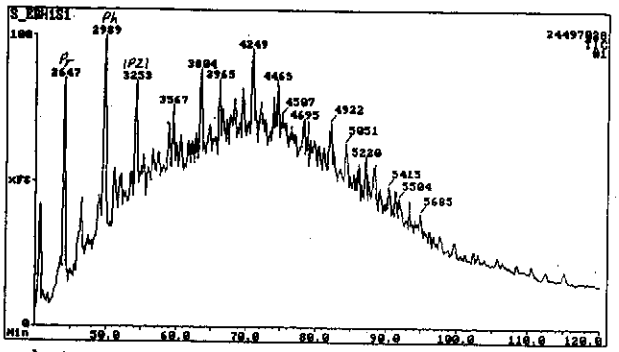

a) TIC: Total Ion Count

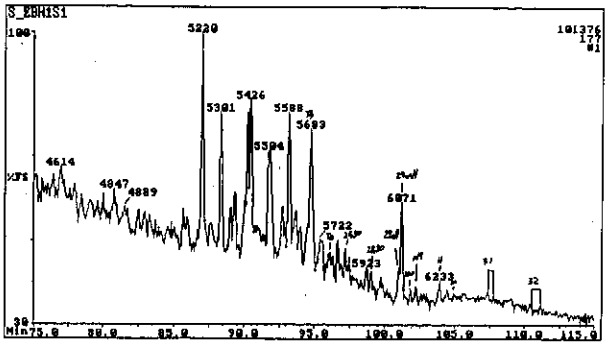

b) m/z 177: Demethylated Hopanes

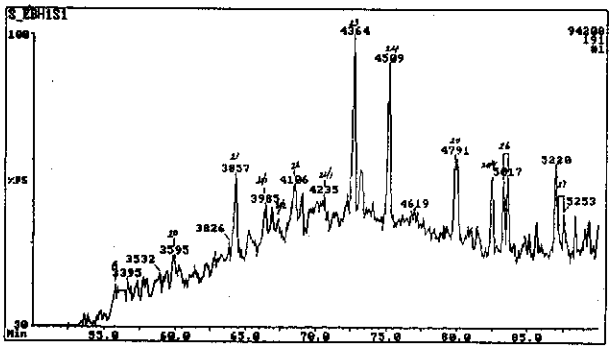

c) m/z 191: Tri and Tetra-cyclic Terpanes

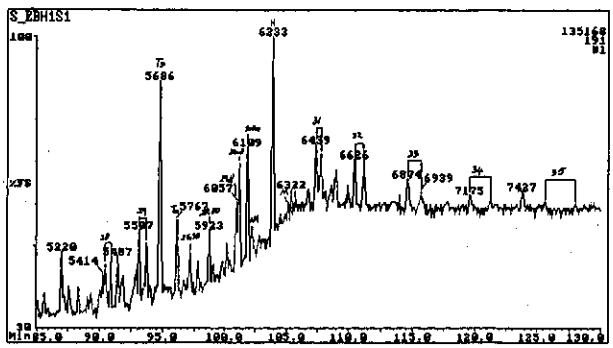

d) m/z 191: Penta-cyclic Terpanes

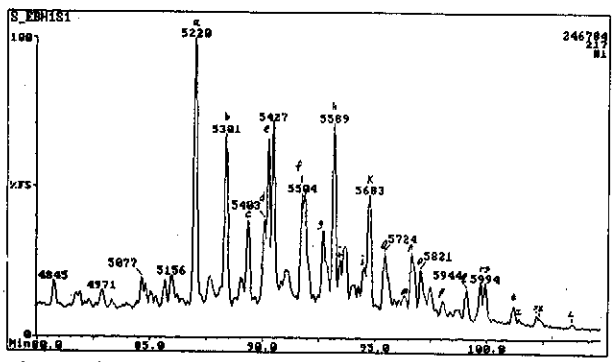

e) m/z 217: Steranes

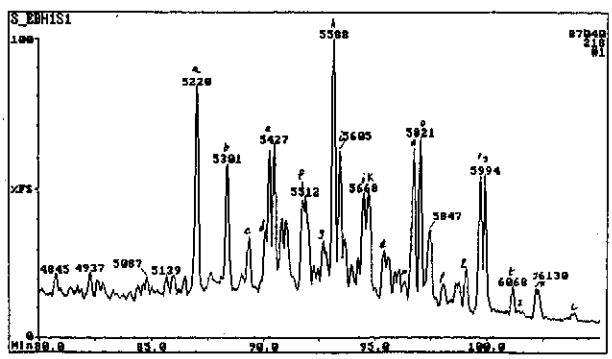

f) m/z 218: Regular (ßß) Steranes

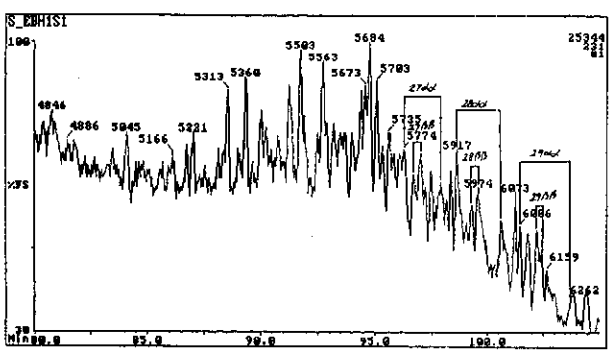

g) m/z 231: Methyl Steranes

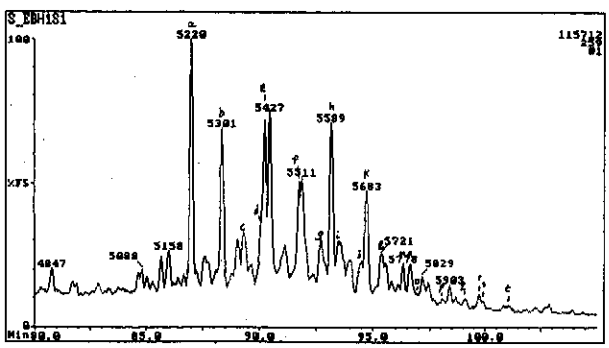

h) m/z 259: Rearranged (ßa) Steranes

Figure E.51: Annotated TIC and single ion fragmentograms of saturated hydrocarbons from sample 53, well 110 RC, 2830m.

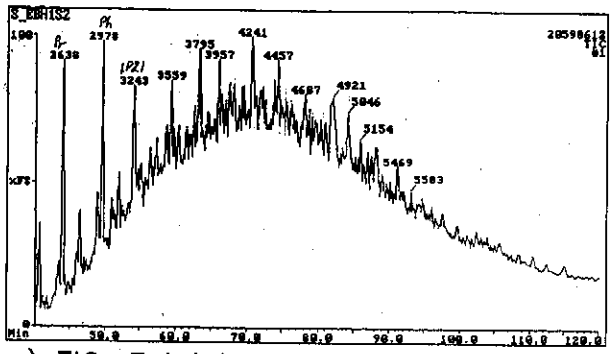

a) TIC: Total Ion Count

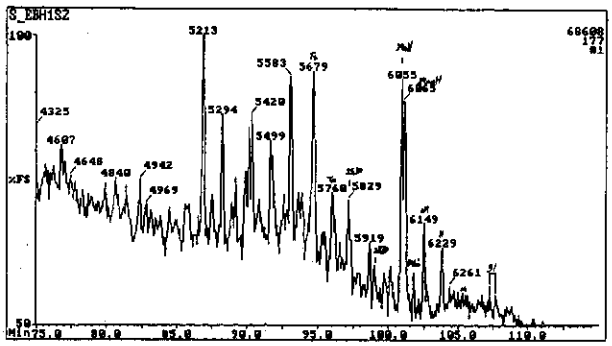

b) m/z 177: Demethylated Hopanes

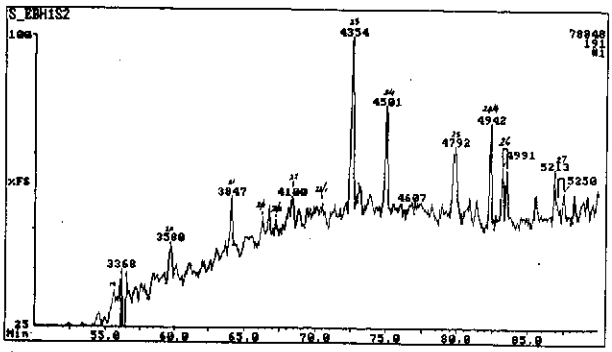

c) m/z 191: Tri and Tetra-cyclic Terpanes

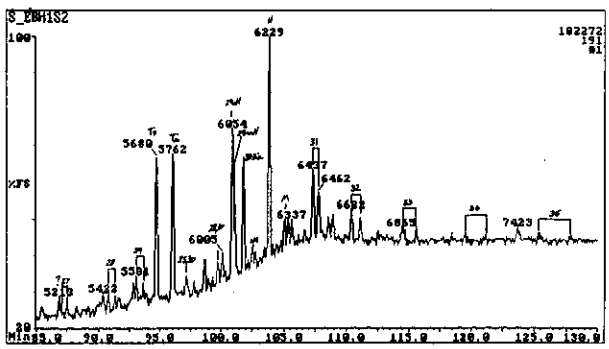

d) m/z 191: Penta-cyclic Terpanes

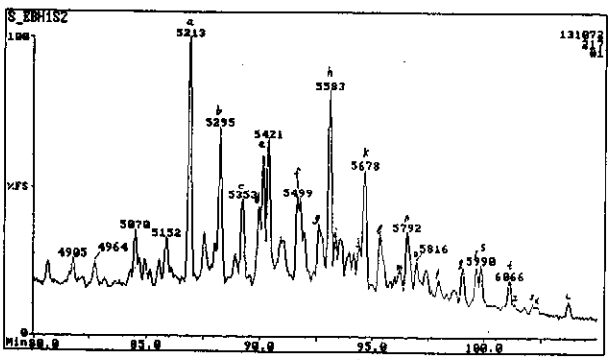

e) m/z 217: Steranes

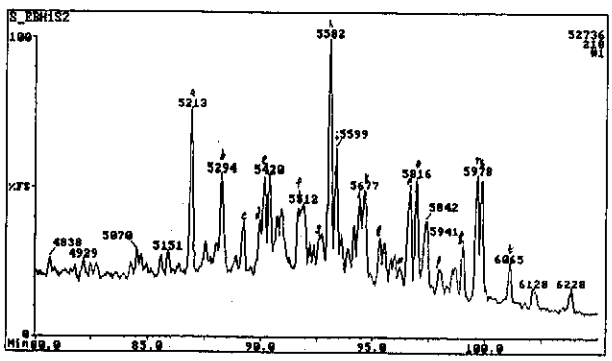

f) m/z 218: Regular (ßß) Steranes

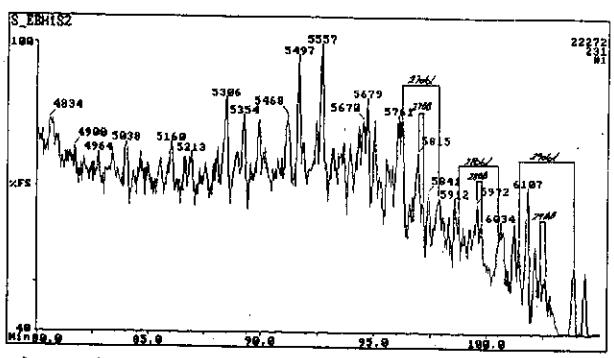

g) m/z 231: Methyl Steranes

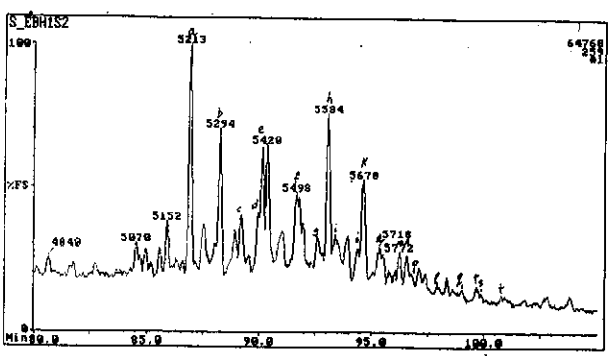

h) m/z 259: Rearranged (ßa) Steranes

Figure E.52: Annotated TIC and single ion fragmentograms of saturated hydrocarbons from sample 54, well 110 RC, 2902m.

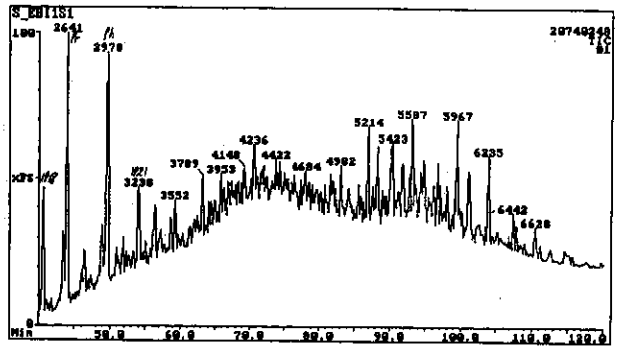

a) TIC: Total Ion Count

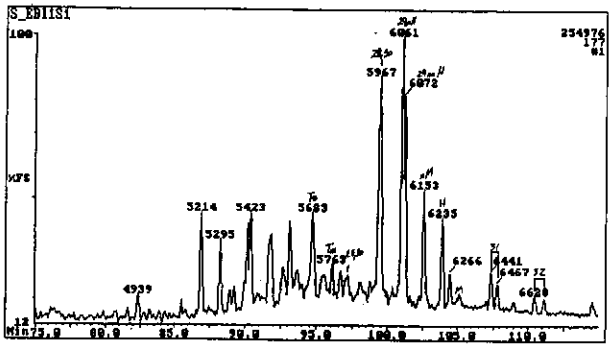

b) m/z 177: Demethylated Hopanes

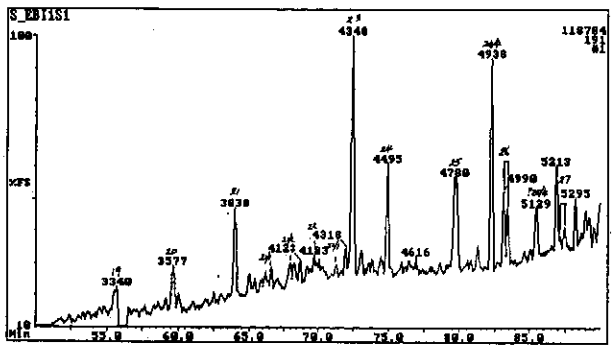

c) m/z 191: Tri and Tetra-cyclic Terpanes

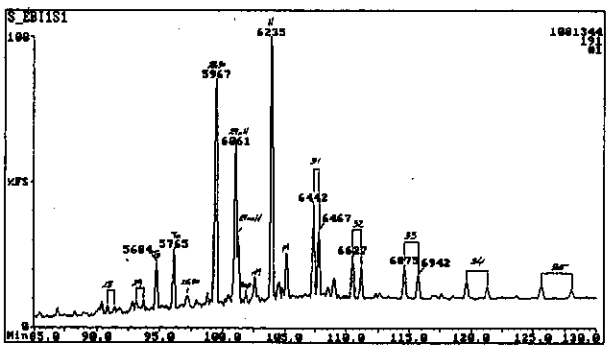

d) m/z 191: Penta-cyclic Terpanes

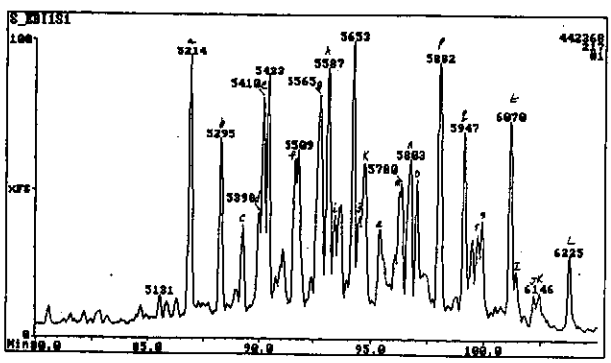

e) m/z 217: Steranes

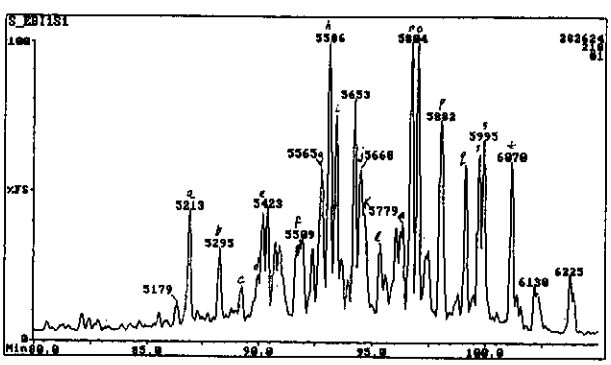

f) m/z 218: Regular (ßß) Steranes

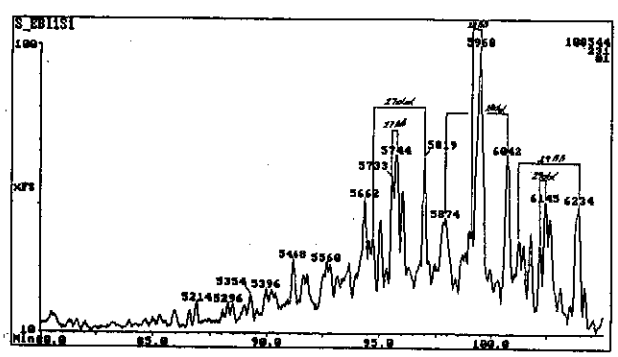

g) m/z 231: Methyl Steranes

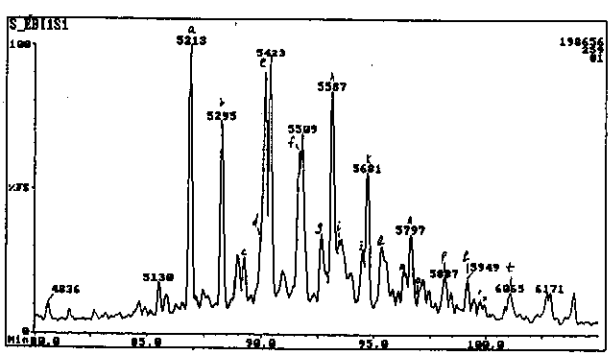

h) m/z 259: Rearranged (ßa) Steranes

Figure E.53: Annotated TIC and single ion fragmentograms of saturated hydrocarbons from sample 55, well 112 RC, 2392m.

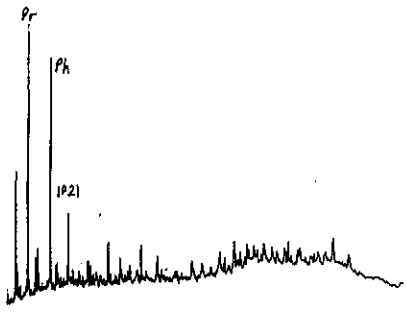

a) TIC: Total Ion Count

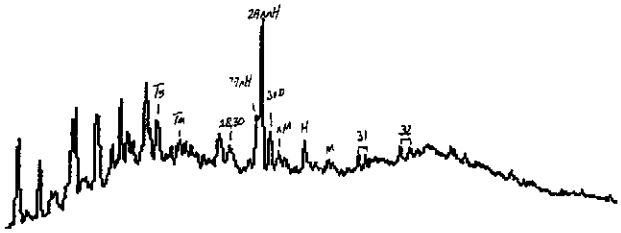

b) m/z 177: Demethylated Hopanes

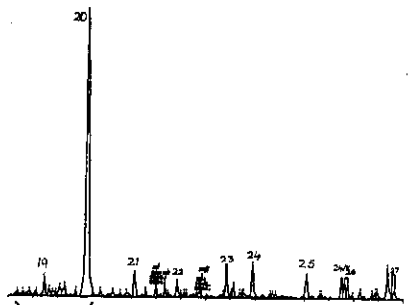

c) m/z 191: Tri and Tetra-cyclic Terpanes

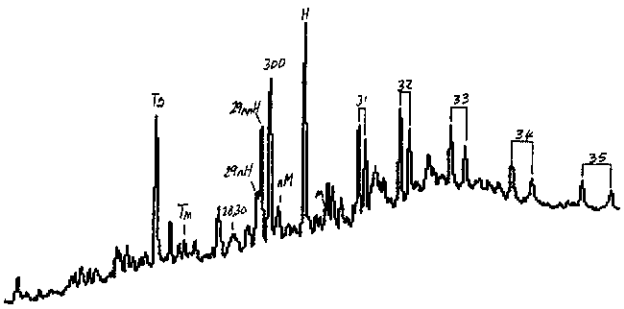

d) m/z 191: Penta-cyclic Terpanes

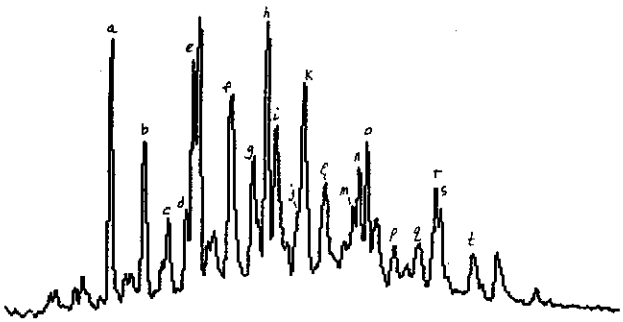

e) m/z 217: Steranes

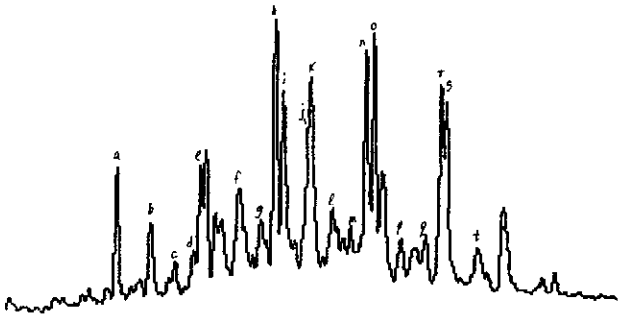

f) m/z 218: Regular (ββ) Steranes

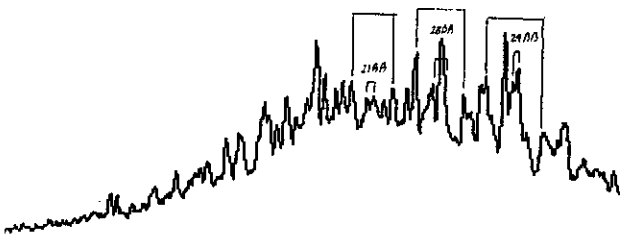

g) m/z 231: Methyl Steranes

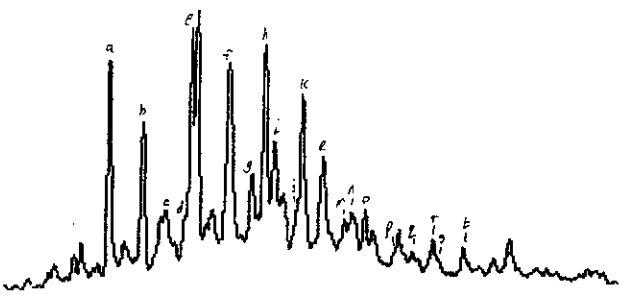

h) m/z 259: Rearranged (βα) Steranes

Figure E.54: Annotated TIC and single ion fragmentograms of saturated hydrocarbons from sample 56, well 117 SWC, 2918.5m.

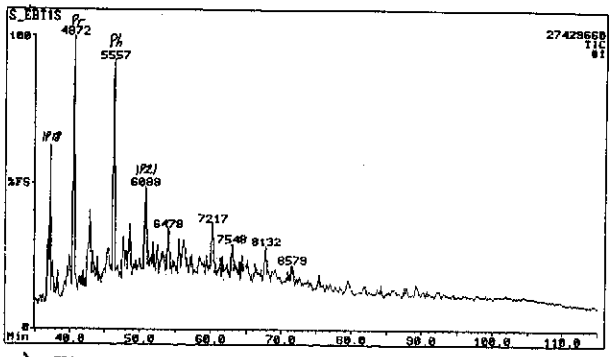

a) TIC: Total Ion Count

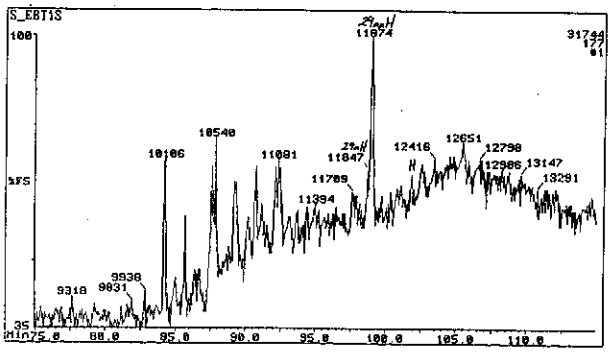

b) m/z 177: Demethylated Hopanes

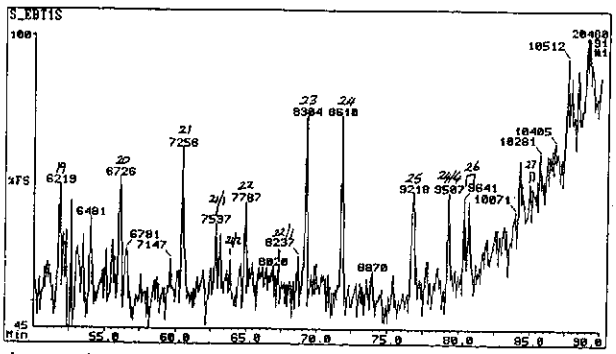

c) m/z 191: Tri and Tetra-cyclic Terpanes

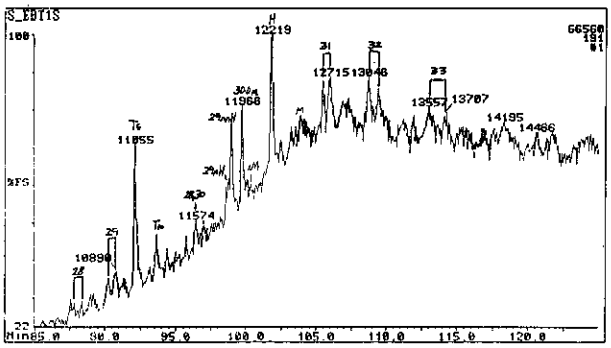

d) m/z 191: Penta-cyclic Terpanes

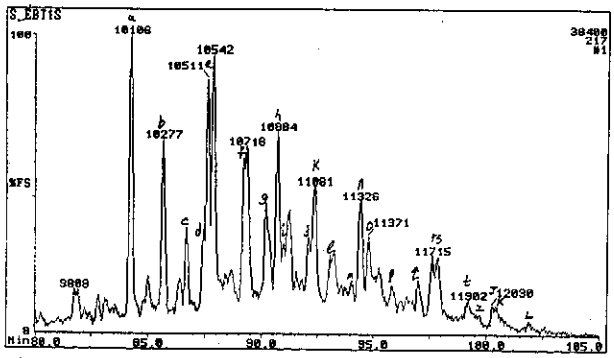

e) m/z 217: Steranes

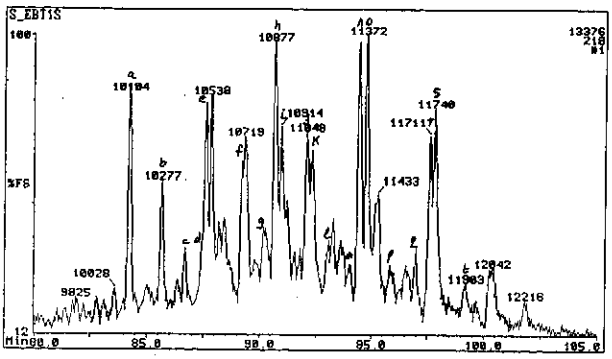

f) m/z 218: Regular (ßß) Steranes

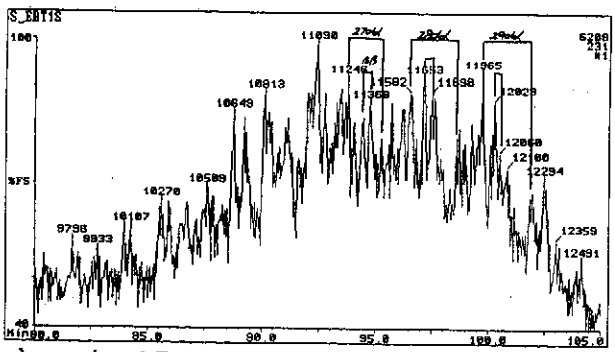

g) m/z 231: Methyl Steranes

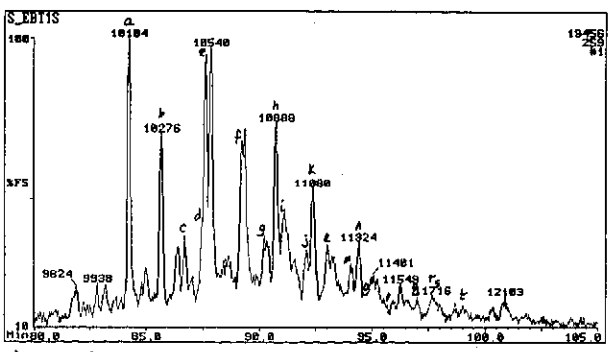

h) m/z 259: Rearranged (ßa) Steranes

Figure E.55: Annotated TIC and single ion fragmentograms of saturated hydrocarbons from sample 57, well 117 SWC, 2918.5m.

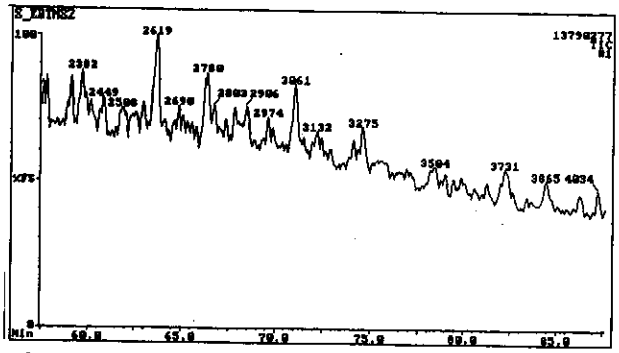

a) TIC: Total Ion Count

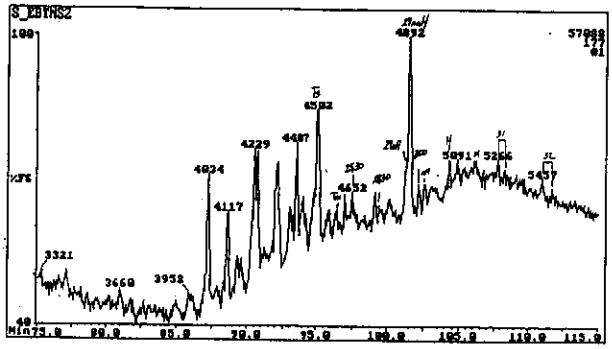

b) m/z 177: Demethylated Hopanes

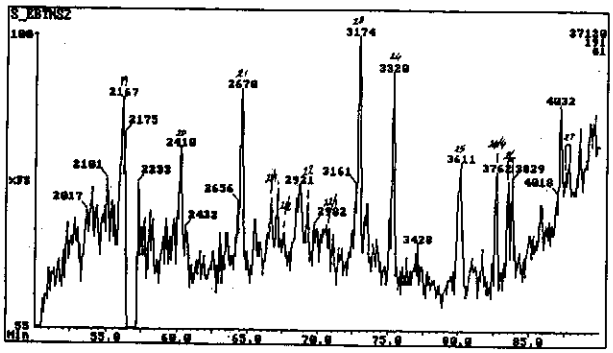

c) m/z 191: Tri and Tetra-cyclic Terpanes

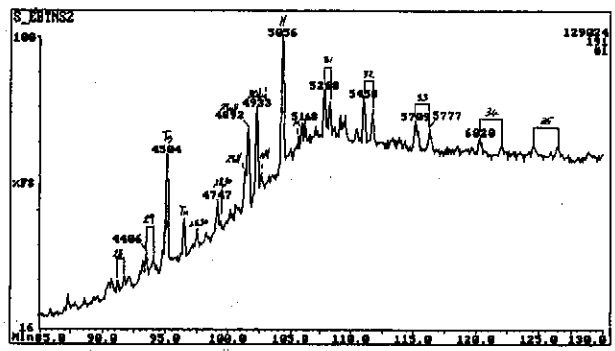

d) m/z 191: Penta-cyclic Terpanes

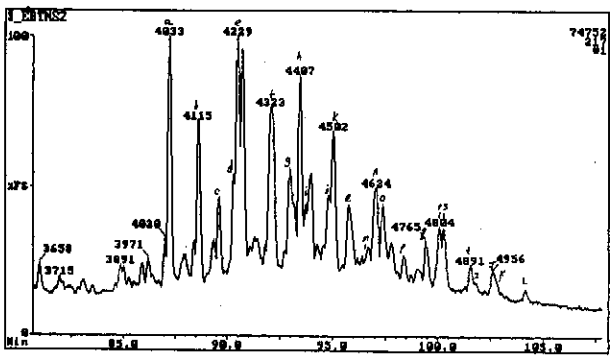

e) m/z 217: Steranes

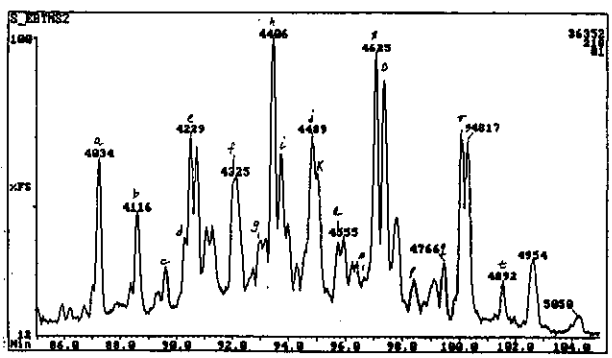

f) m/z 218: Regular (ßß) Steranes

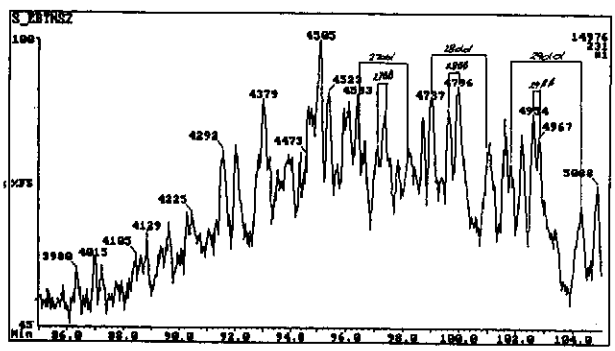

g) m/z 231: Methyl Steranes

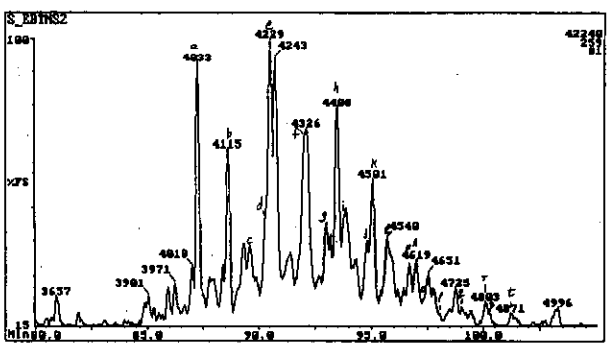

h) m/z 259: Rearranged (ßa) Steranes

Figure E.56: Annotated TIC and single ion fragmentograms of saturated hydrocarbons from sample 58, well 117 SWC, 2918.5m.

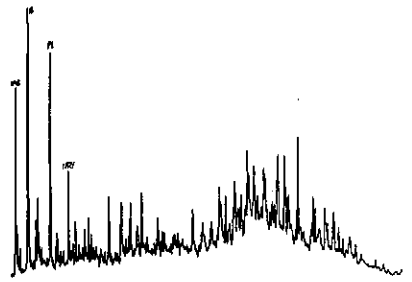

a) TIC: Total Ion Count

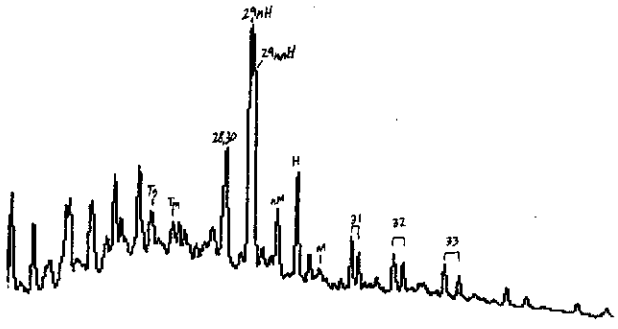

b) m/z 177: Demethylated Hopanes

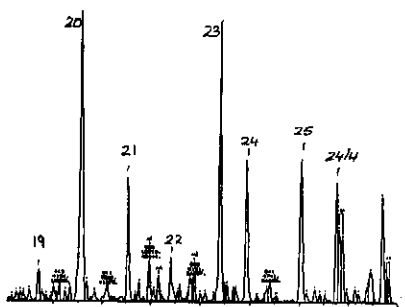

c) m/z 191: Tri and Tetra-cyclic Terpanes

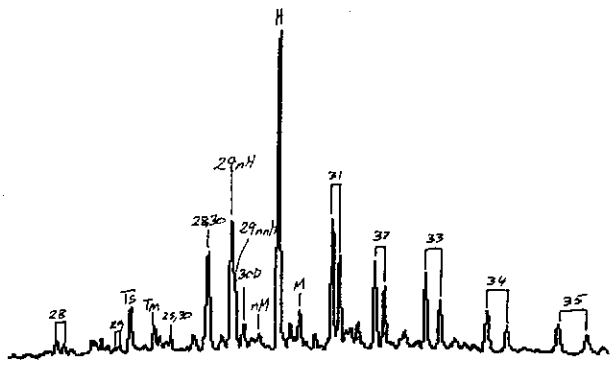

d) m/z 191: Penta-cyclic Terpanes

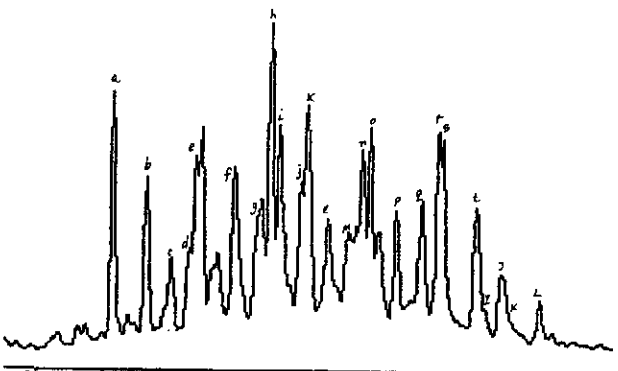

e) m/z 217: Steranes

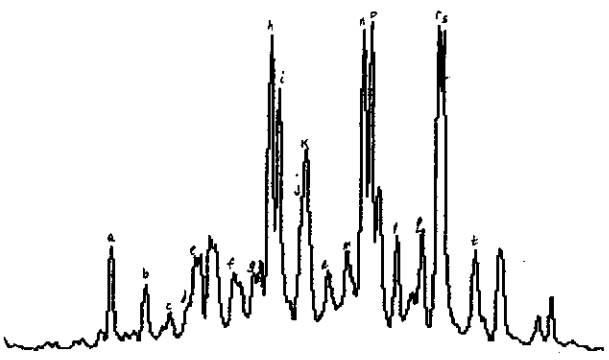

f) m/z 218: Regular (ßß) Steranes

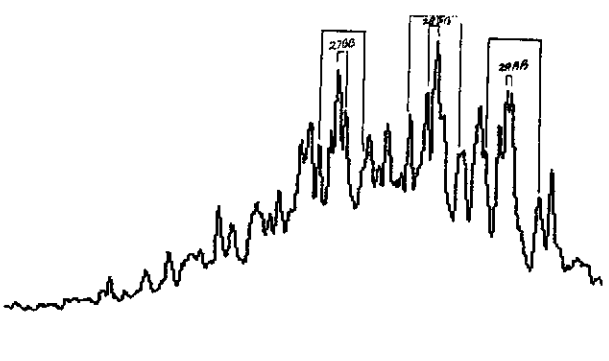

g) m/z 231: Methyl Steranes

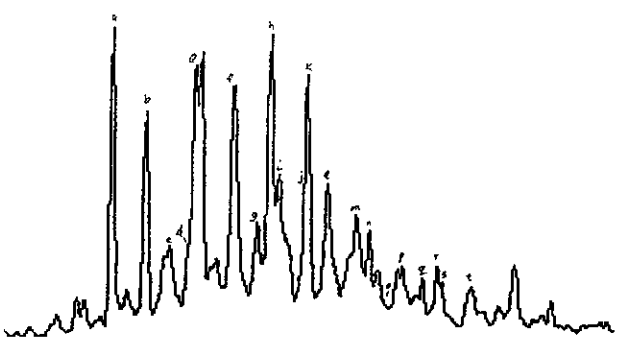

h) m/z 259: Rearranged (ßa) Steranes

Figure E.57: Annotated TIC and single ion fragmentograms of saturated hydrocarbons from sample 59, well 122 RC, 2682m.

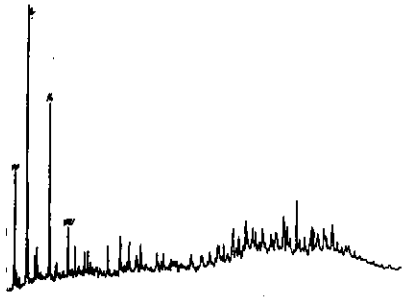

a) TIC: Total Ion Count

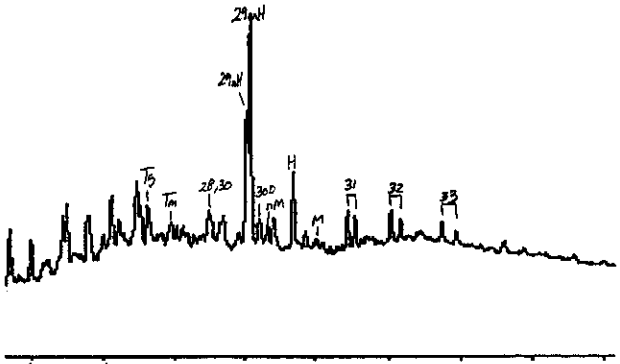

b) m/z 177: Demethylated Hopanes

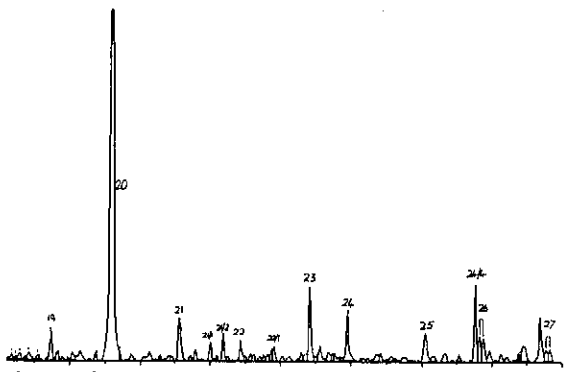

c) m/z 191: Tri and Tetra-cyclic Terpanes

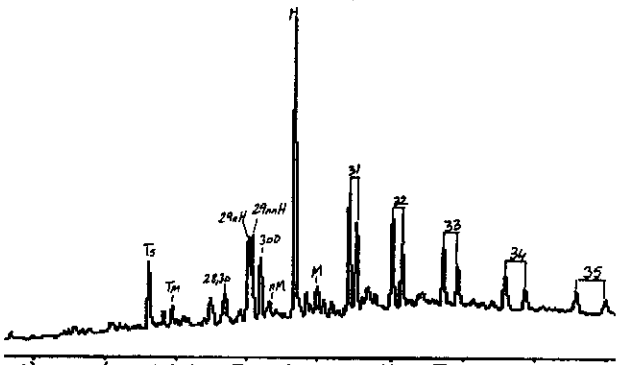

d) m/z 191: Penta-cyclic Terpanes

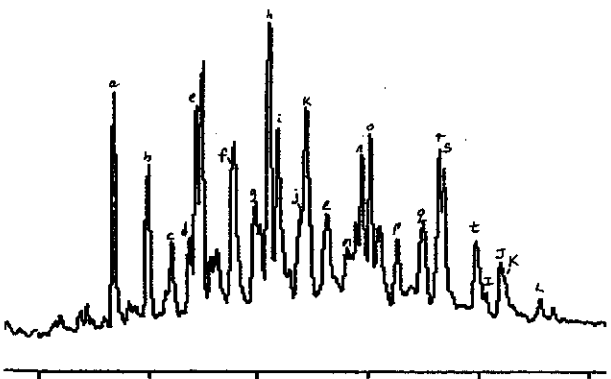

e) m/z 217: Steranes

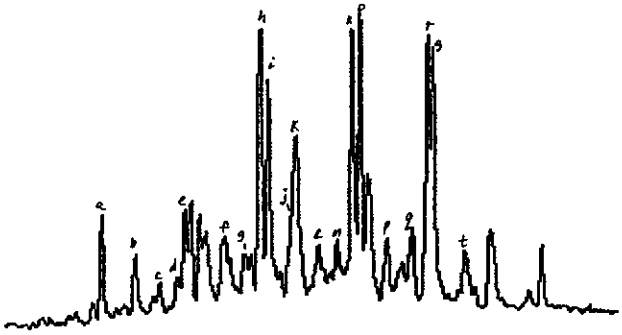

f) m/z 218: Regular (ßß) Steranes

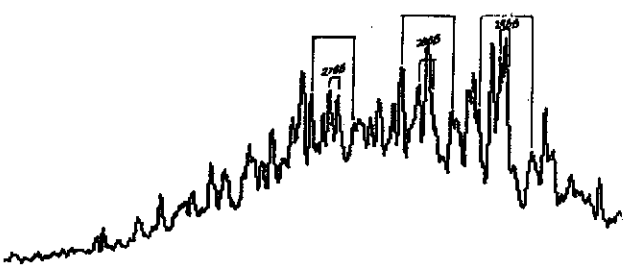

g) m/z 231: Methyl Steranes

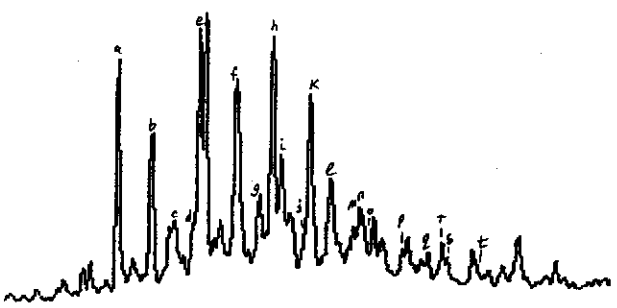

h) m/z 259: Rearranged (ßa) Steranes

Figure E.58: Annotated TIC and single ion fragmentograms of saturated hydrocarbons from sample 60, well 122 RC, 2832m.

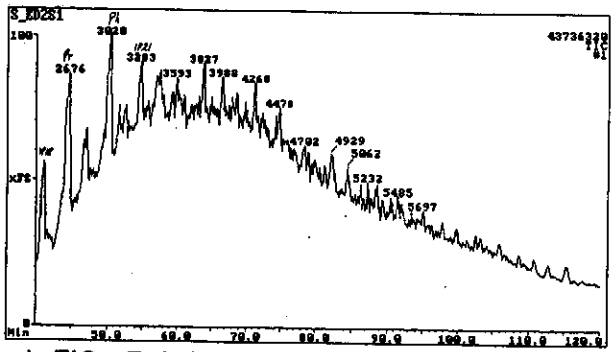

a) TIC: Total Ion Count

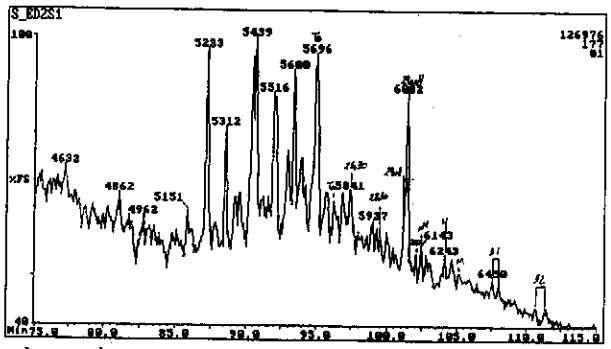

b) m/z 177: Demethylated Hopanes

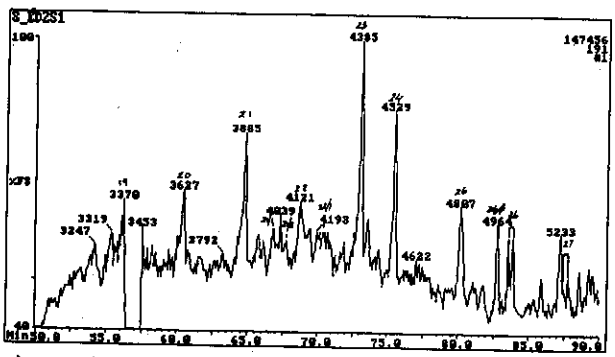

c) m/z 191: Tri and Tetra-cyclic Terpanes

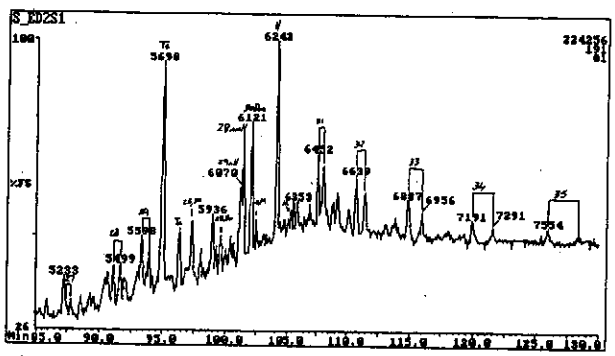

d) m/z 191: Penta-cyclic Terpanes

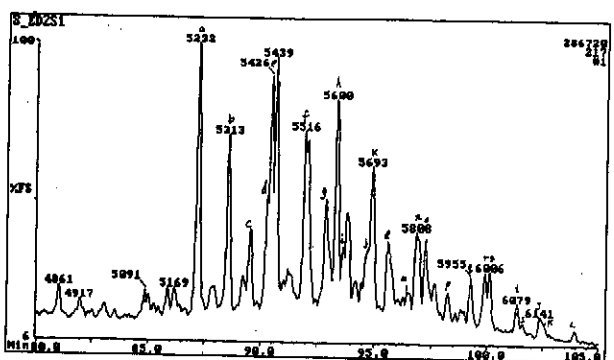

e) m/z 217: Steranes

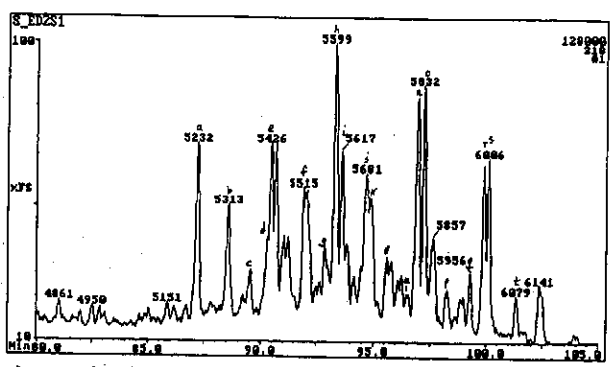

f) m/z 218: Regular (ßß) Steranes

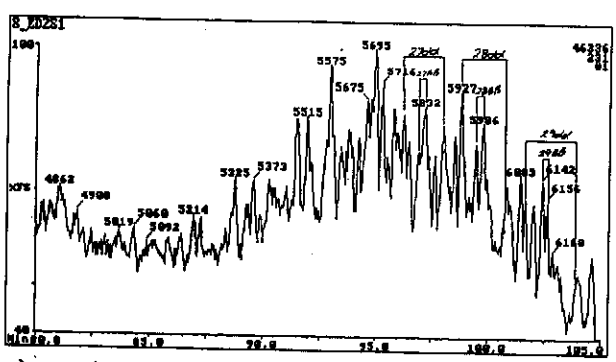

g) m/z 231: Methyl Steranes

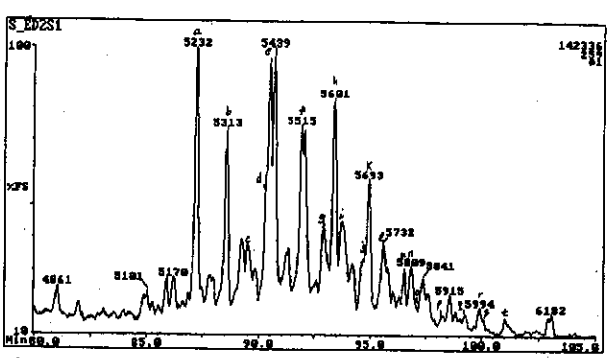

h) m/z 259: Rearranged (ßa) Steranes

Figure E.59: Annotated TIC and single ion fragmentograms of saturated hydrocarbons from sample 61, well 11 RC, 2682m.

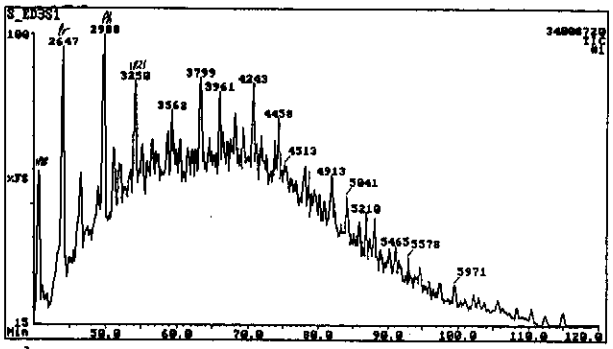

a) TIC: Total Ion Count

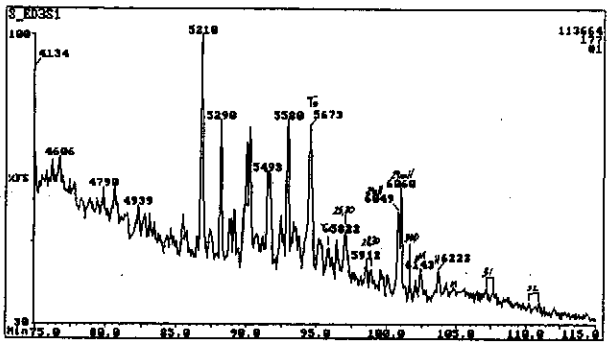

b) m/z 177: Demethylated Hopanes

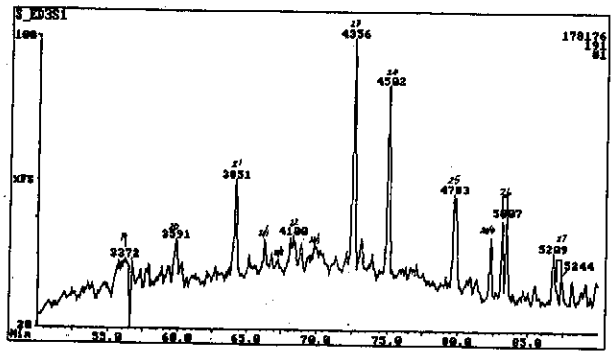

c) m/z 191: Tri and Tetra-cyclic Terpanes

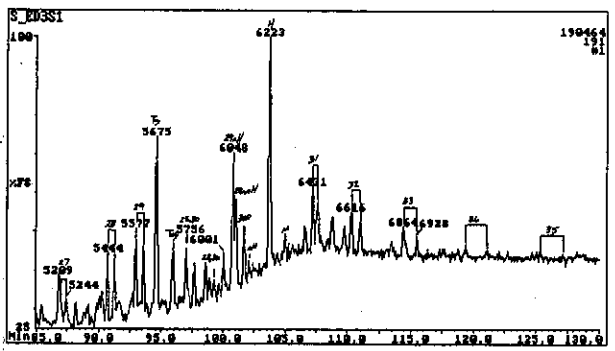

d) m/z 191: Penta-cyclic Terpanes

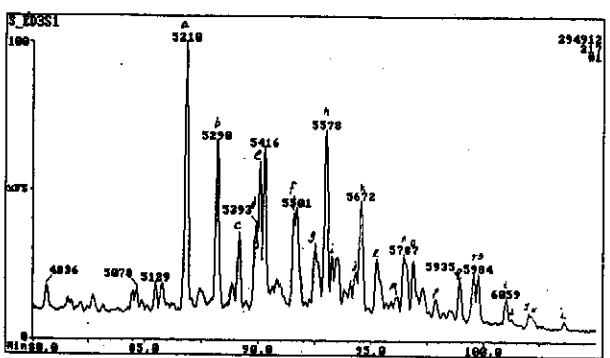

e) m/z 217: Steranes

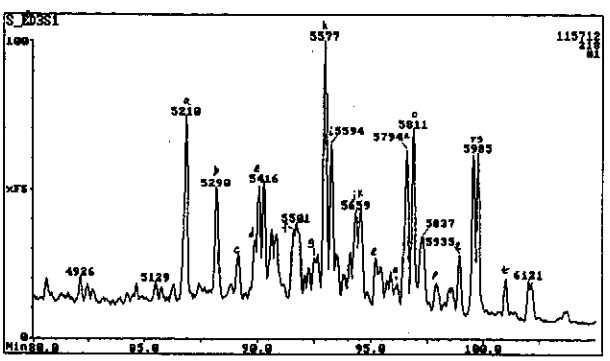

f) m/z 218: Regular (ßß) Steranes

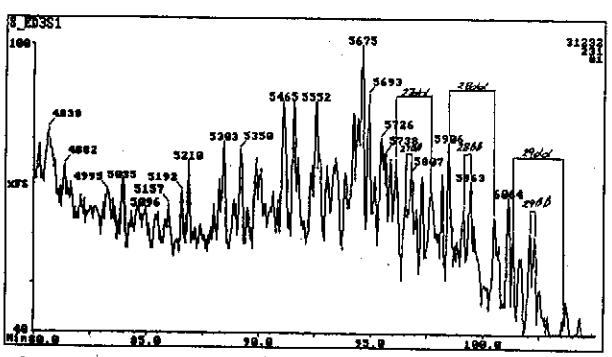

g) m/z 231: Methyl Steranes

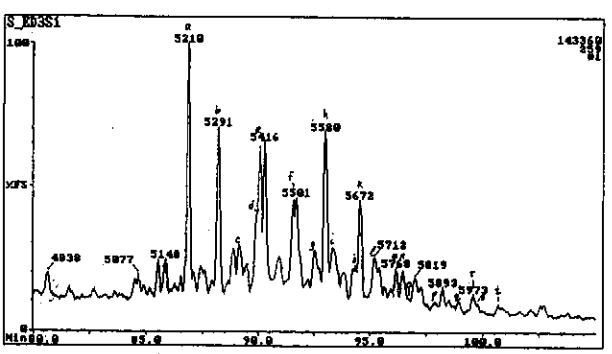

h) m/z 259: Rearranged (ßa) Steranes

Figure E.60: Annotated TIC and single ion fragmentograms of saturated hydrocarbons from sample 62, well 14 RC, 2721m.

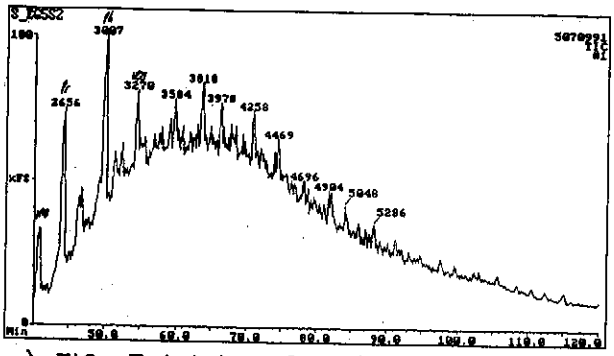

a) TIC: Total Ion Count

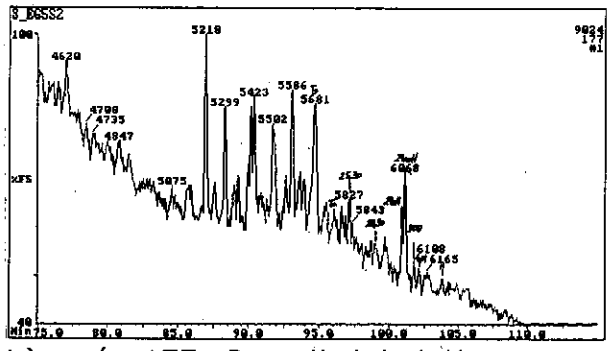

b) m/z 177: Demethylated Hopanes

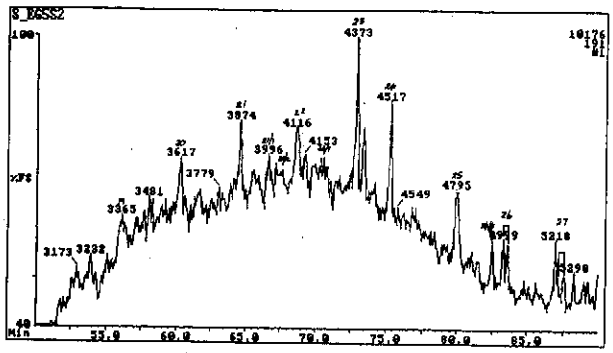

c) m/z 191: Tri and Tetra-cyclic Terpanes

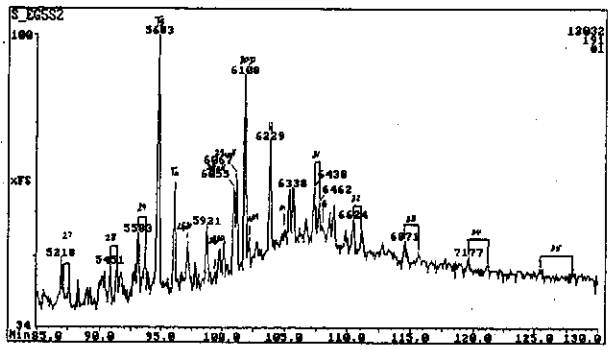

d) m/z 191: Penta-cyclic Terpanes

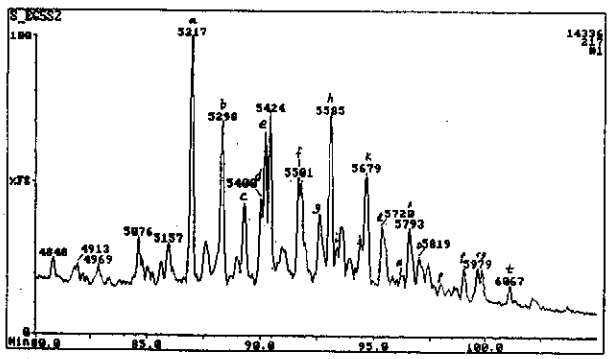

e) m/z 217: Steranes

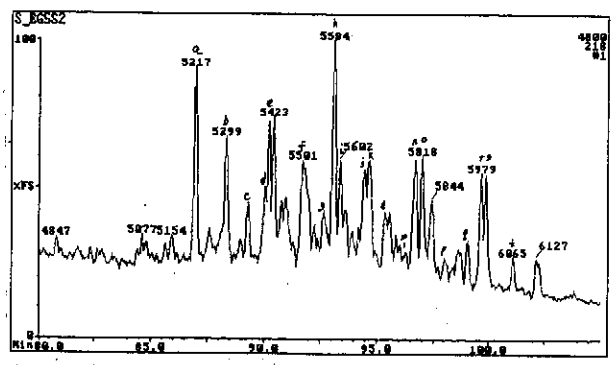

f) m/z 218: Regular (ßß) Steranes

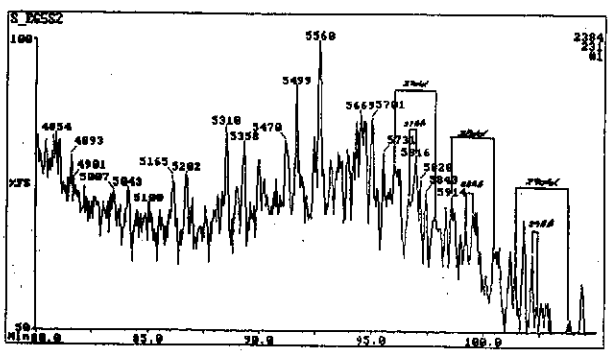

g) m/z 231: Methyl Steranes

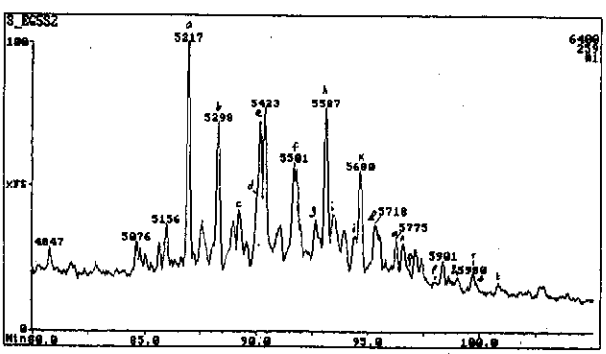

h) m/z 259: Rearranged (ßa) Steranes

Figure E.61: Annotated TIC and single ion fragmentograms of saturated hydrocarbons from sample 63, well 42 RC, 3021m.

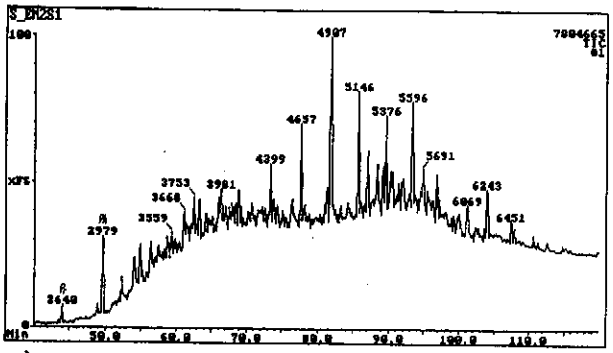

a) TIC: Total Ion Count

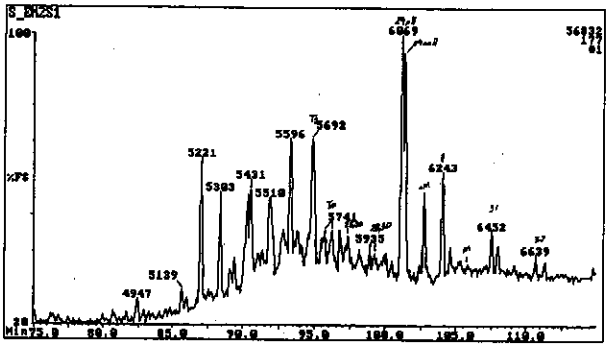

b) m/z 177: Demethylated Hopanes

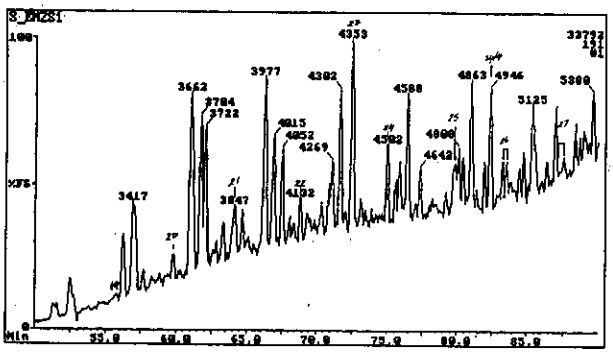

c) m/z 191: Tri and Tetra-cyclic Terpanes

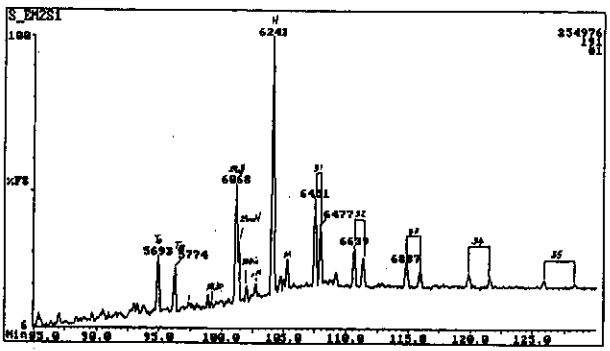

d) m/z 191: Penta-cyclic Terpanes

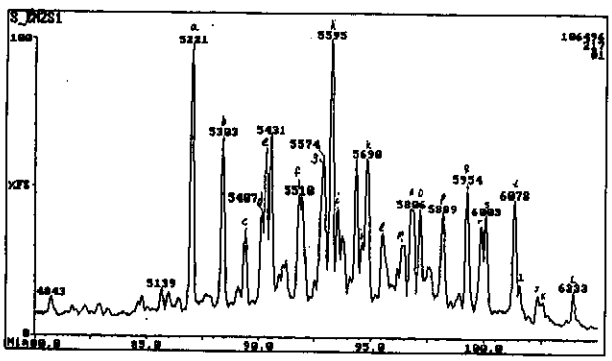

e) m/z 217: Steranes

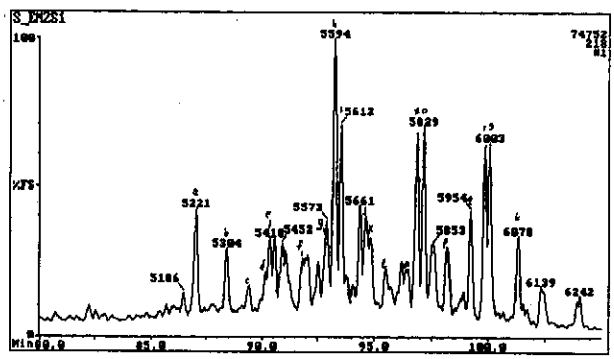

f) m/z 218: Regular (ßß) Steranes

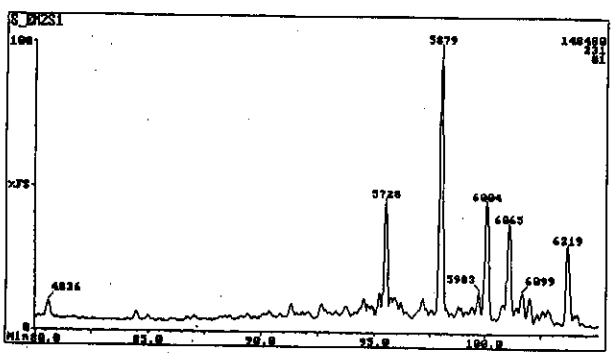

g) m/z 231: Methyl Steranes

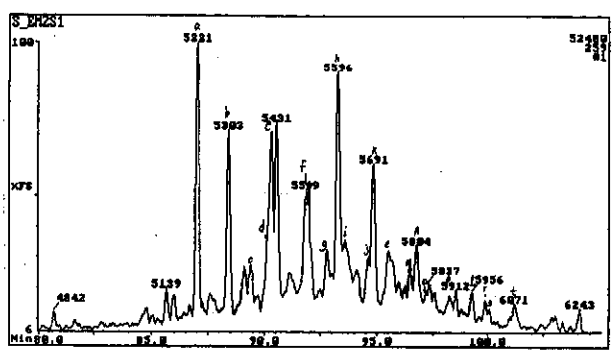

h) m/z 259: Rearranged (ßa) Steranes

Figure E.62: Annotated TIC and single ion fragmentograms of saturated hydrocarbons from sample 64, well 48 RC, 2490m.

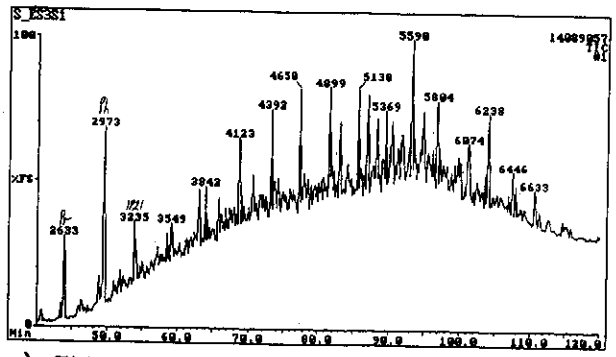

a) TIC: Total Ion Count

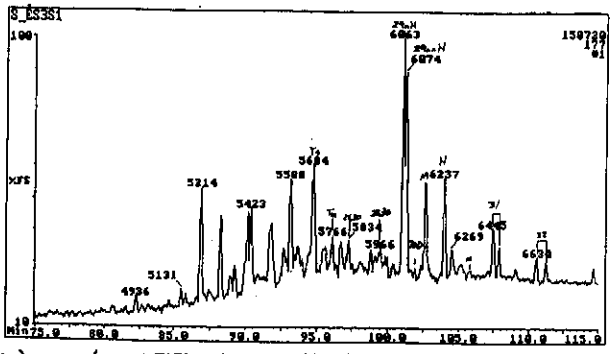

b) m/z 177: Demethylated Hopanes

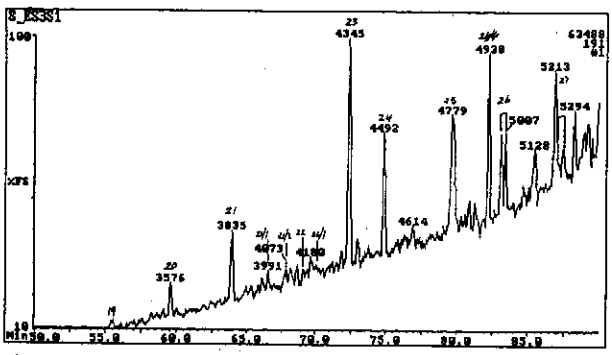

c) m/z 191: Tri and Tetra-cyclic Terpanes

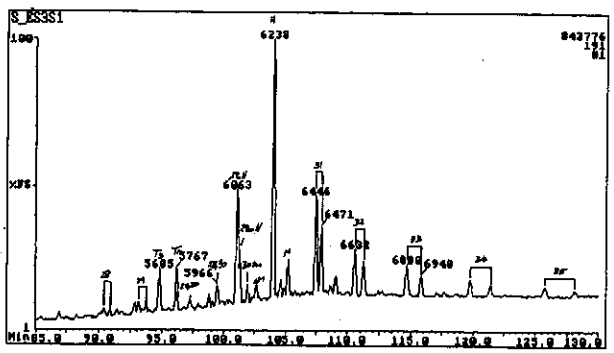

d) m/z 191: Penta-cyclic Terpanes

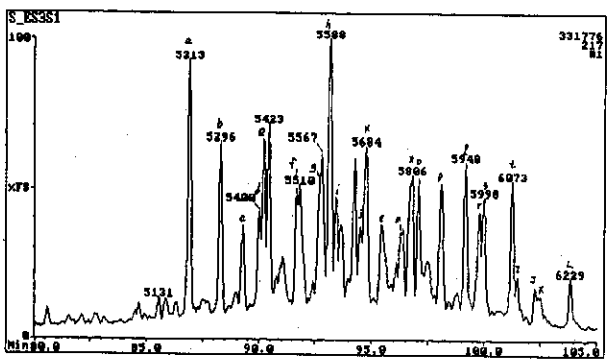

e) m/z 217: Steranes

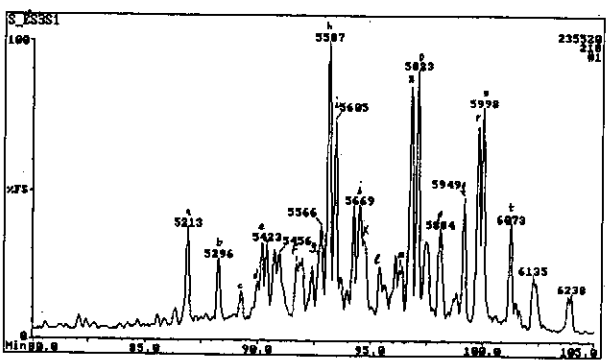

f) m/z 218: Regular (ßß) Steranes

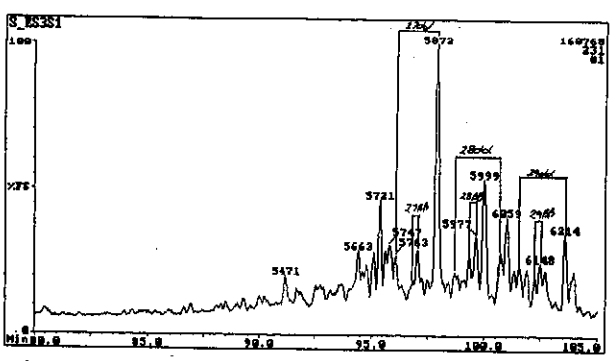

g) m/z 231: Methyl Steranes

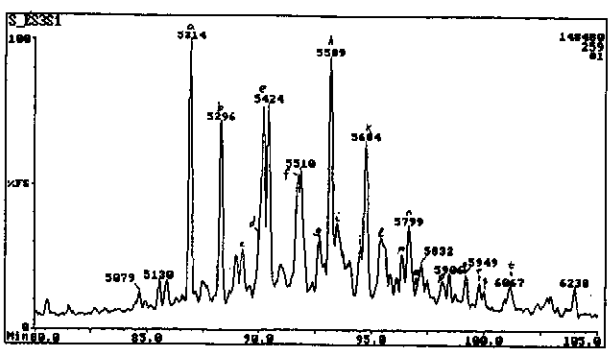

h) m/z 259: Rearranged (ßa) Steranes

Figure E.63: Annotated TIC and single ion fragmentograms of saturated hydrocarbons from sample 65, well 41 RC, 2320m.

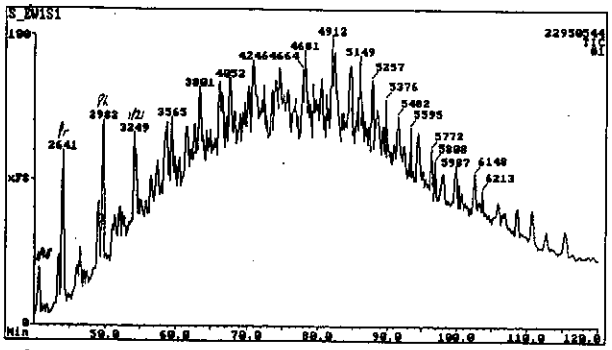

a) TIC: Total Ion Count

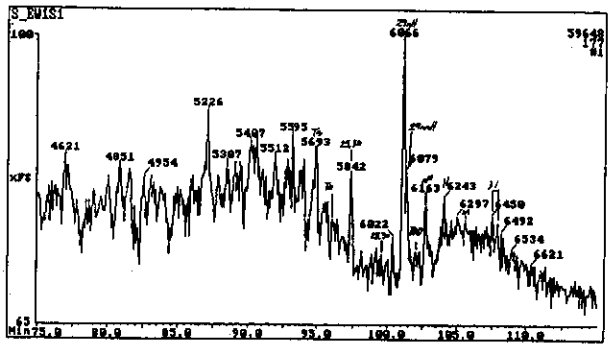

b) m/z 177: Demethylated Hopanes

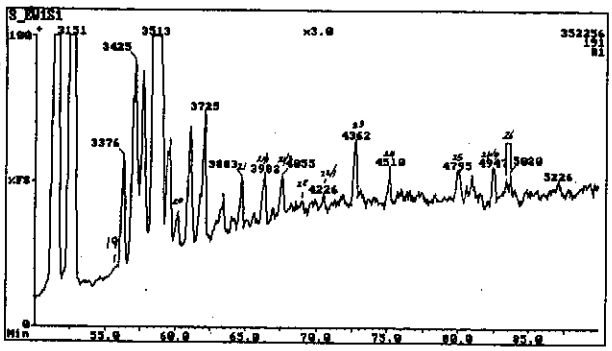

c) m/z 191: Tri and Tetra-cyclic Terpanes

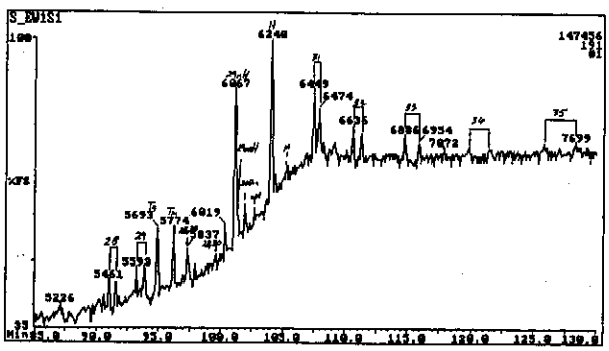

d) m/z 191: Penta-cyclic Terpanes

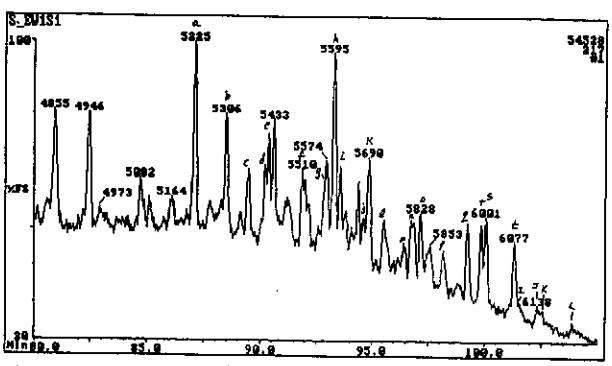

e) m/z 217: Steranes

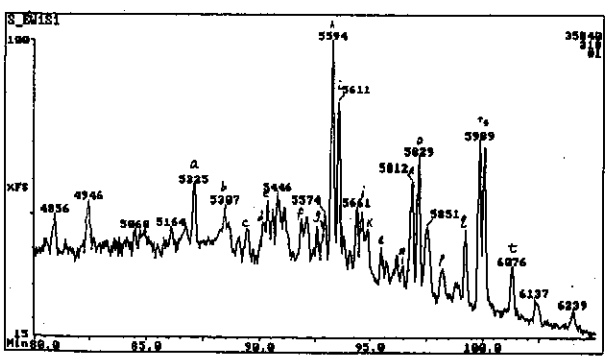

f) m/z 218: Regular (ßß) Steranes

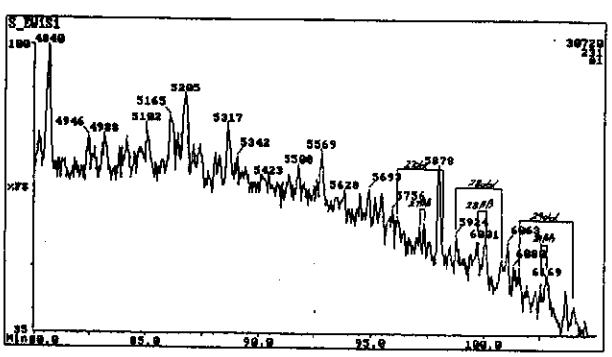

g) m/z 231: Methyl Steranes

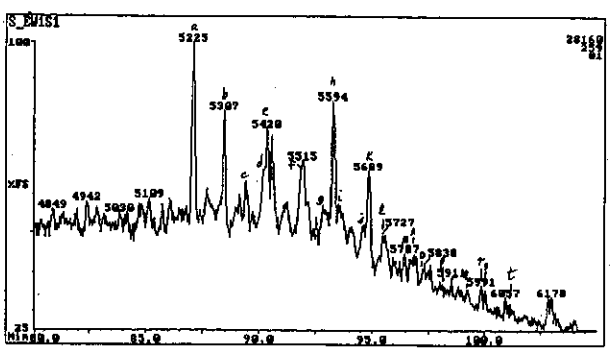

h) m/z 259: Rearranged (ßa) Steranes

Figure E.64: Annotated TIC and single ion fragmentograms of saturated hydrocarbons from sample 66, well 65 RC, 3160m.

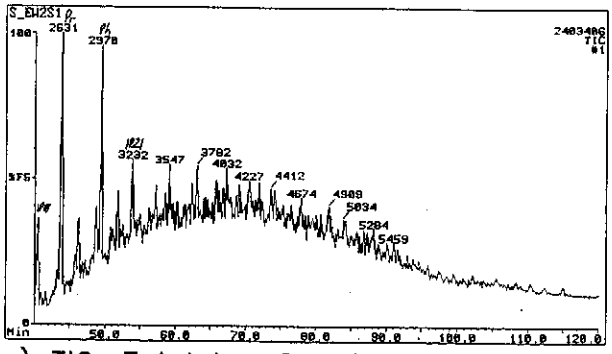

a) TIC: Total Ion Count

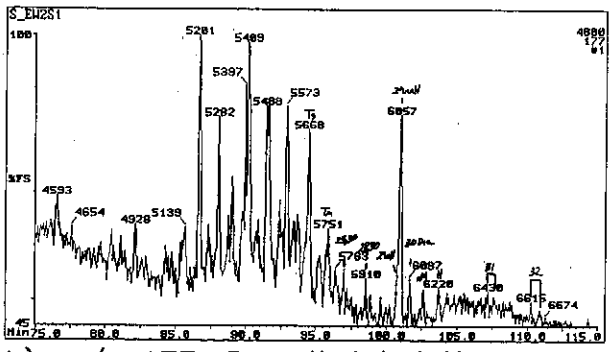

b) m/z 177: Demethylated Hopanes

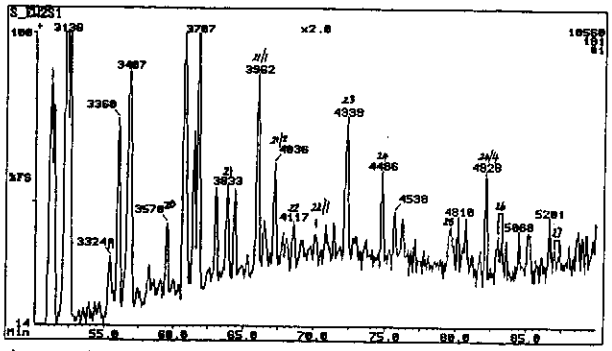

c) m/z 191: Tri and Tetra-cyclic Terpanes

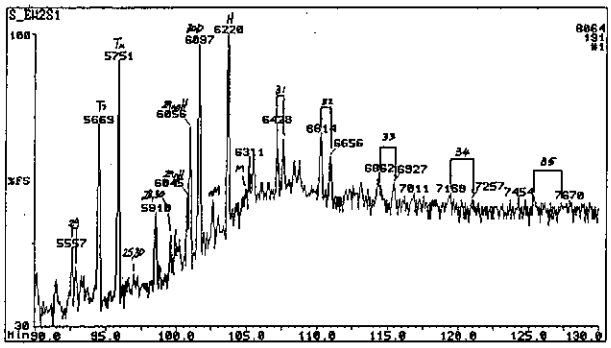

d) m/z 191: Penta-cyclic Terpanes

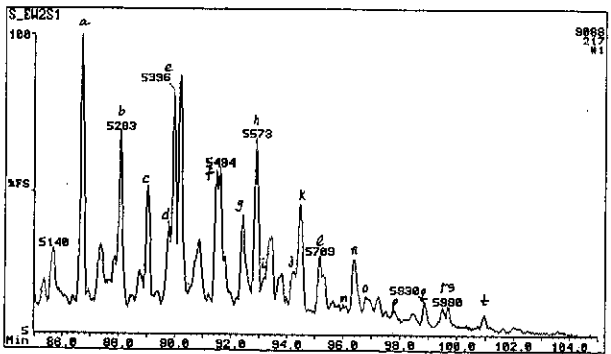

e) m/z 217: Steranes

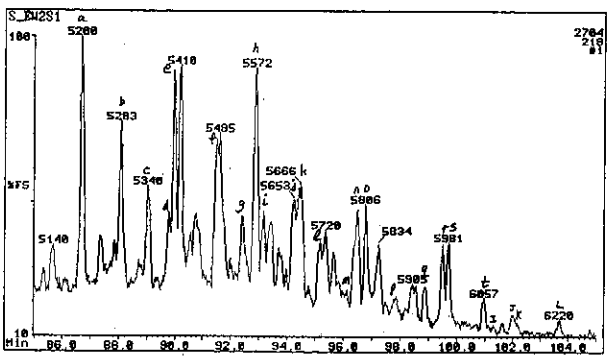

f) m/z 218: Regular (ßß) Steranes

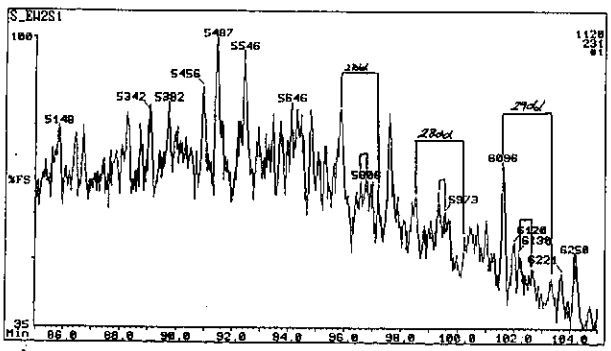

g) m/z 231: Methyl Steranes

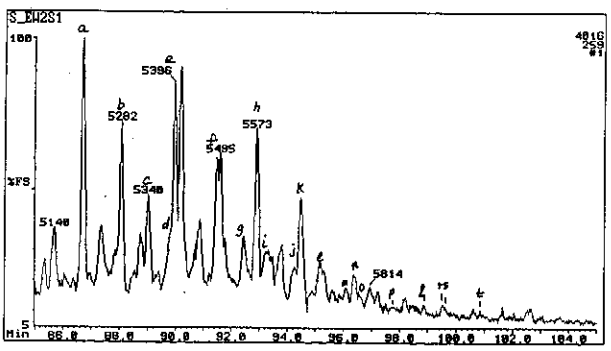

h) m/z 259: Rearranged (ßa) Steranes

Figure E.65: Annotated TIC and single ion fragmentograms of saturated hydrocarbons from sample 67, well 75 core 1, 2829.0m.

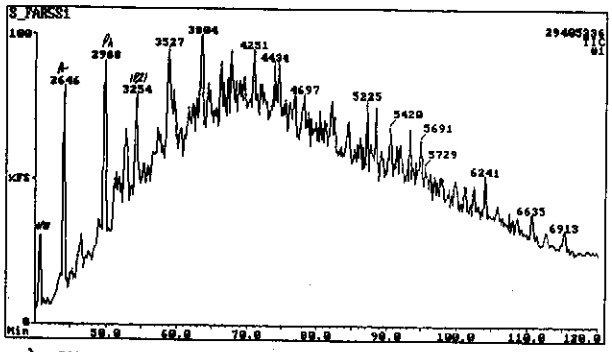

a) TIC: Total Ion Count

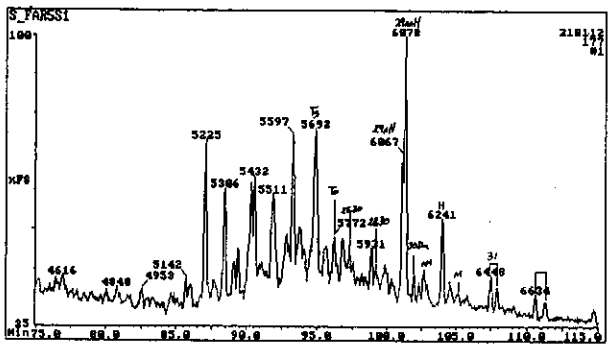

b) m/z 177: Demethylated Hopanes

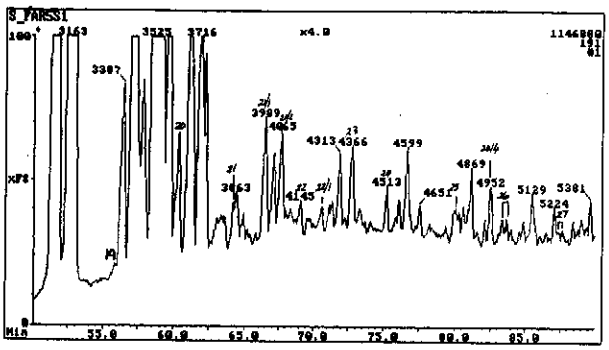

c) m/z 191: Tri and Tetra-cyclic Terpanes

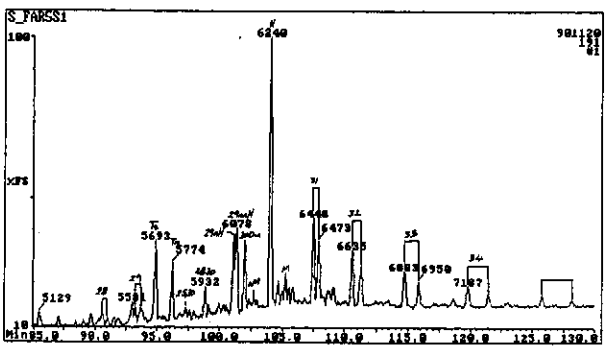

d) m/z 191: Penta-cyclic Terpanes

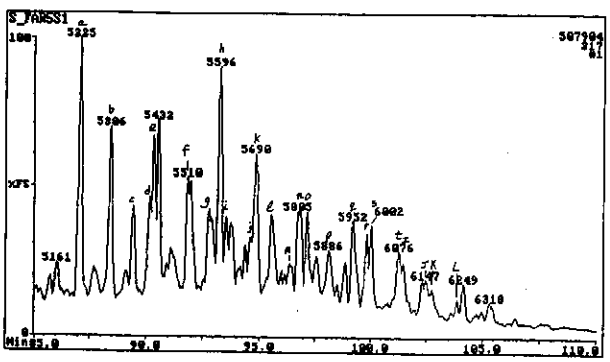

e) m/z 217: Steranes

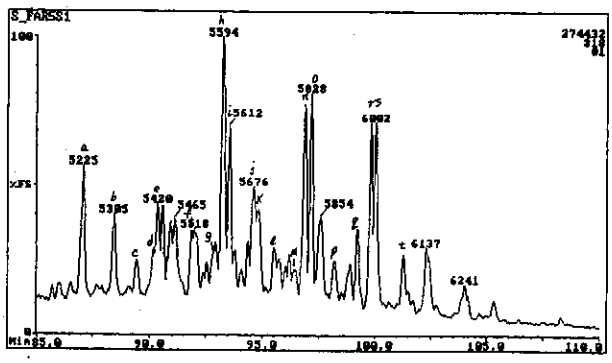

f) m/z 218: Regular (ßß) Steranes

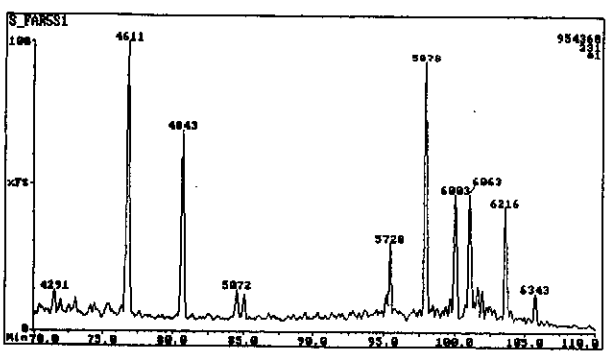

g) m/z 231: Methyl Steranes

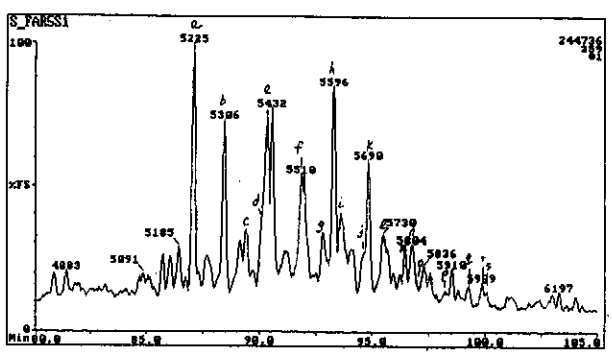

h) m/z 259: Rearranged (ßa) Steranes

Figure E.66: Annotated TIC and single ion fragmentograms of saturated hydrocarbons from sample 68, well 67 RC, 2651m.

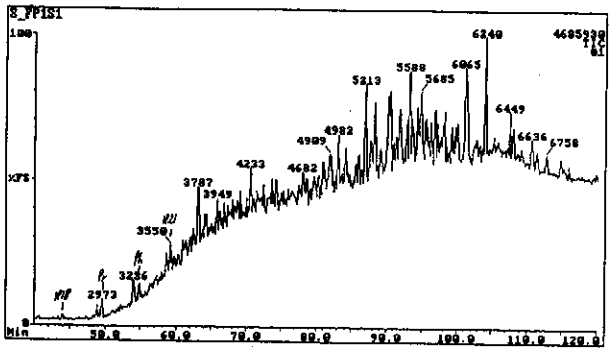

a) TIC: Total Ion Count

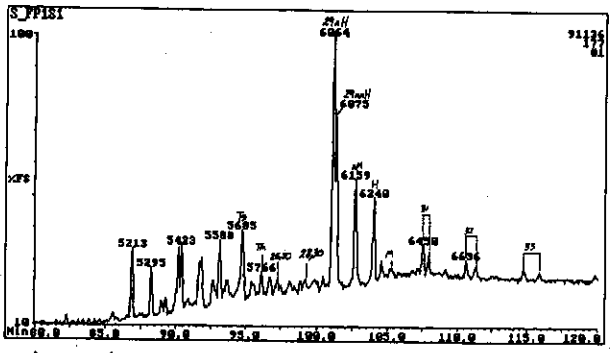

b) m/z 177: Demethylated Hopanes

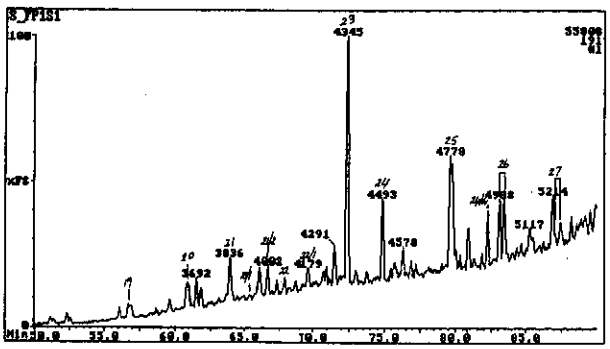

c) m/z 191: Tri and Tetra-cyclic Terpanes

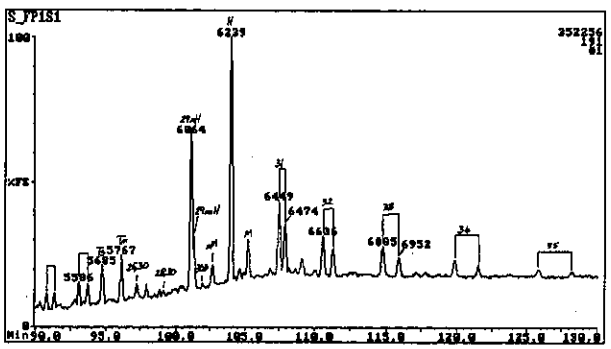

d) m/z 191: Penta-cyclic Terpanes

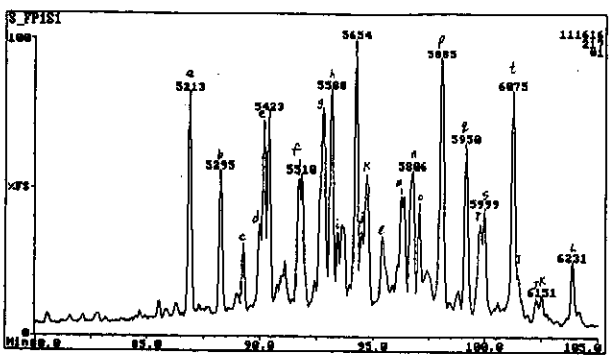

e) m/z 217: Steranes

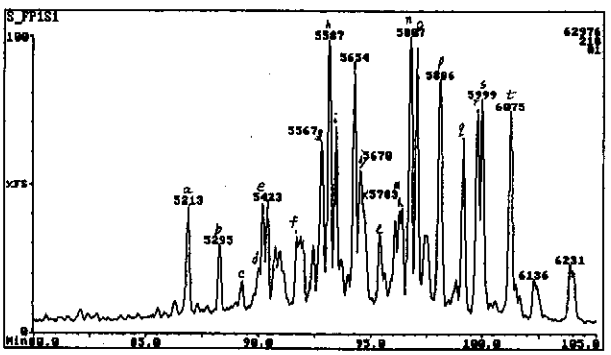

f) m/z 218: Regular (ßß) Steranes

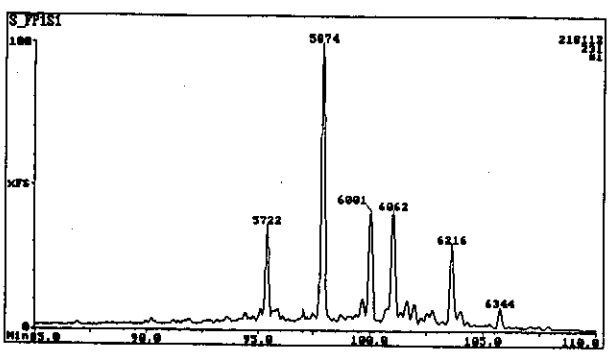

g) m/z 231: Methyl Steranes

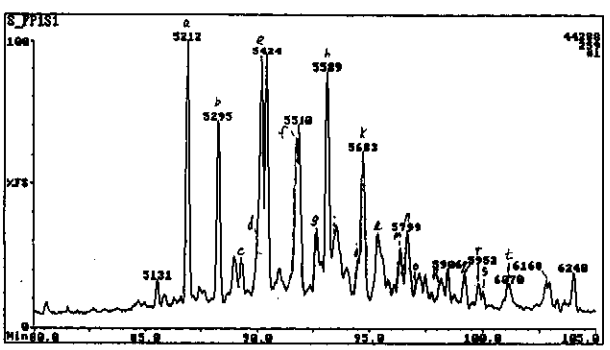

h) m/z 259: Rearranged (ßa) Steranes

Figure E.67: Annotated TIC and single ion fragmentograms of saturated hydrocarbons from sample 69, well 12 RC, 2057m.

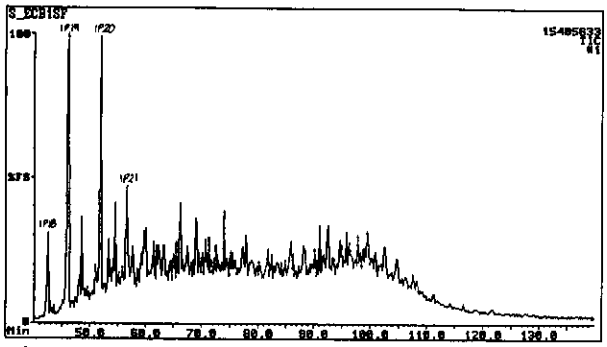

a) TIC: Total Ion Count

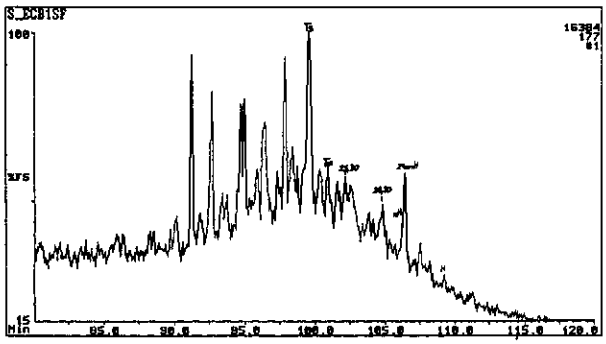

b) m/z 177: Demethylated Hopanes

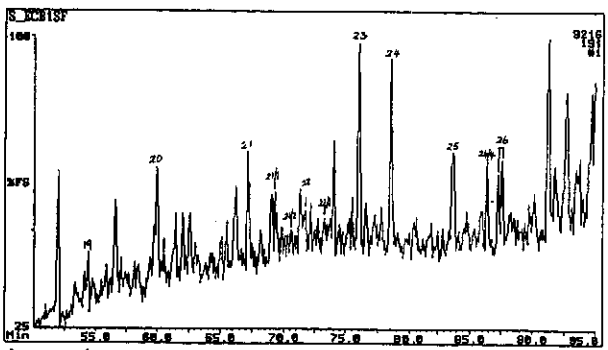

c) m/z 191: Tri and Tetra-cyclic Terpanes

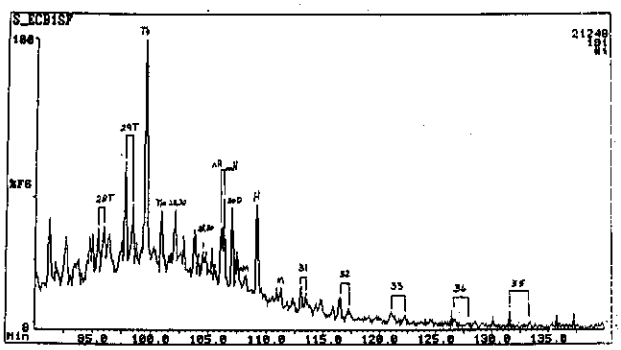

d) m/z 191: Penta-cyclic Terpanes

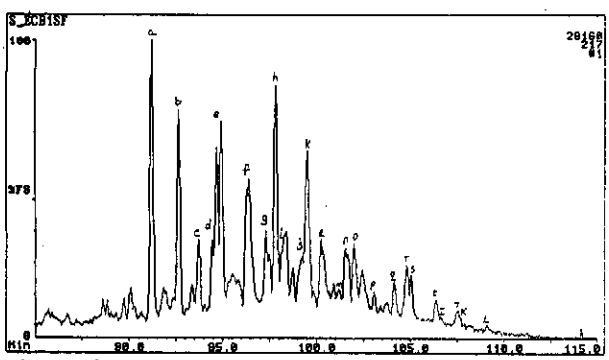

e) m/z 217: Steranes

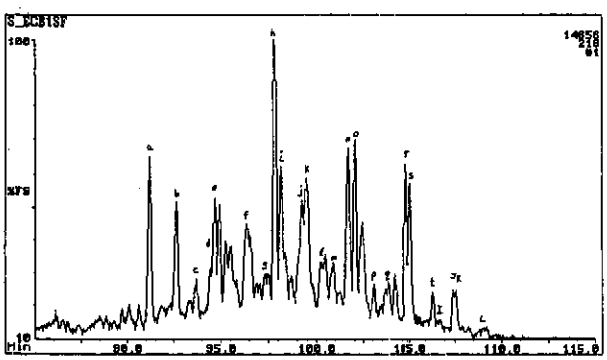

f) m/z 218: Regular (ßß) Steranes

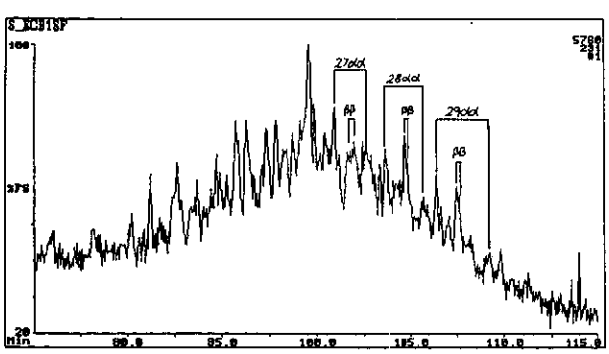

g) m/z 231: Methyl Steranes

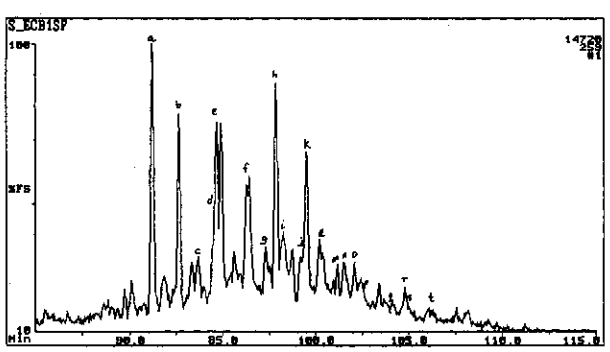

h) m/z 259: Rearranged (ßa) Steranes

Figure E.68: Annotated TIC and single ion fragmentograms of saturated hydrocarbons from sample 70, well 156 RC, 2805m.

not analysed

a) TIC: Total Ion Count

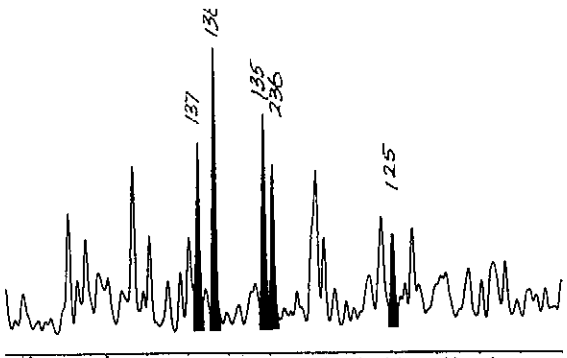

b) m/z 170: Trimethyl Napthalenes
annotated gas chromatogram

not analysed

not analysed

c) m/z 198: Methyl DibenzoThiophenes

d) m/z 212: Dimethyl DibenzoThiophenes

not analysed

e) m/z 226: Trimethyl DibenzoThiophenes

f) m/z 231: Triaromatic Steroids

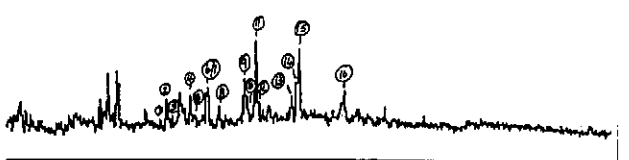

g) m/z 253: Monoaromatic Steroids
(from aromatic fraction)

not analysed

h) m/z 253: Monoaromatic Steroids
(from saturates fraction)

Figure E.69: Annotated TIC and single ion fragmentograms of aromatic hydrocarbons from sample 1, well 83 DST 1, 2470m.

not analysed

a) TIC: Total Ion Count

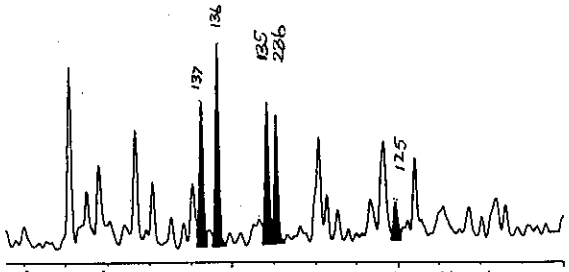

b) m/z 170: Trimethyl Napthalenes
annotated gas chromatogram

not analysed

not analysed

c) m/z 198: Methyl DibenzoThiophenes

d) m/z 212: Dimethyl DibenzoThiophenes

not analysed

e) m/z 226: Trimethyl DibenzoThiophenes

f) m/z 231: Triaromatic Steroids

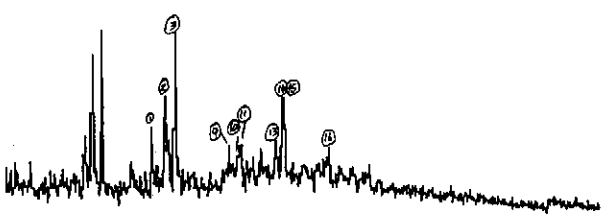

g) m/z 253: Monoaromatic Steroids
(from aromatic fraction)

not analysed

h) m/z 253: Monoaromatic Steroids
(from saturates fraction)

Figure E.70: Annotated TIC and single ion fragmentograms of aromatic hydrocarbons from sample 2, well 83 DST 2, 2889m.

not analysed

not analysed

a) TIC: Total Ion Count

b) m/z 170: Trimethyl Napthalenes

not analysed

not analysed

c) m/z 198: Methyl DibenzoThiophenes

d) m/z 212: Dimethyl DibenzoThiophenes

not analysed

not analysed

e) m/z 226: Trimethyl DibenzoThiophenes

f) m/z 231: Triaromatic Steroids

not analysed

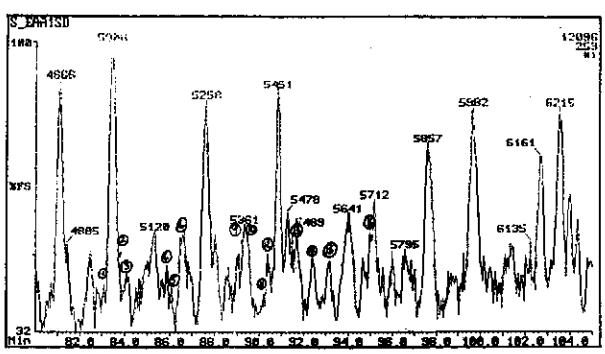

g) m/z 253: Monoaromatic Steroids (from aromatic fraction)

h) m/z 253: Monoaromatic Steroids (from saturates fraction)

Figure E.71: Annotated TIC and single ion fragmentograms of aromatic hydrocarbons from sample 3, well 83 DST 2, 2889m.

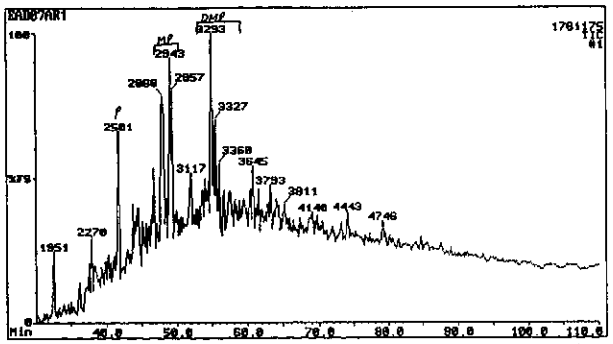

a) TIC: Total Ion Count

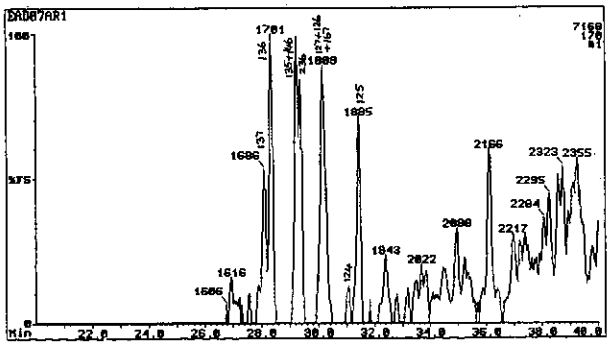

b) m/z 170: Trimethyl Napthalenes

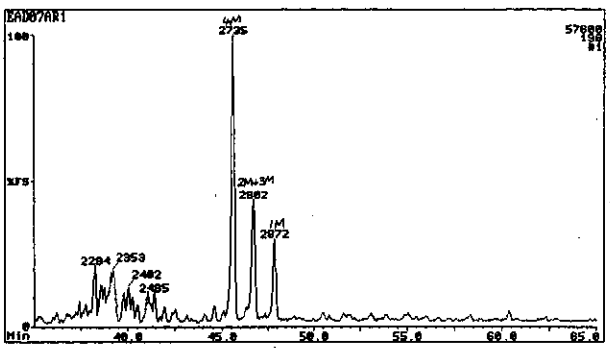

c) m/z 198: Methyl DibenzoThiophenes

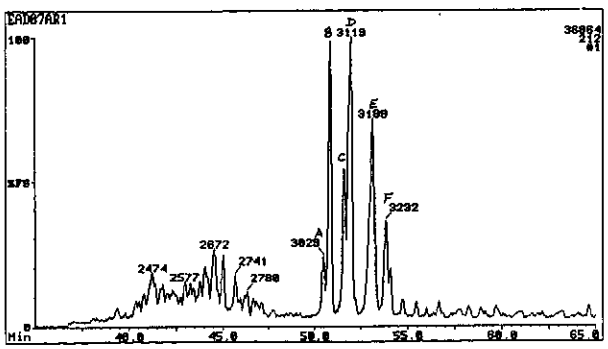

d) m/z 212: Dimethyl DibenzoThiophenes

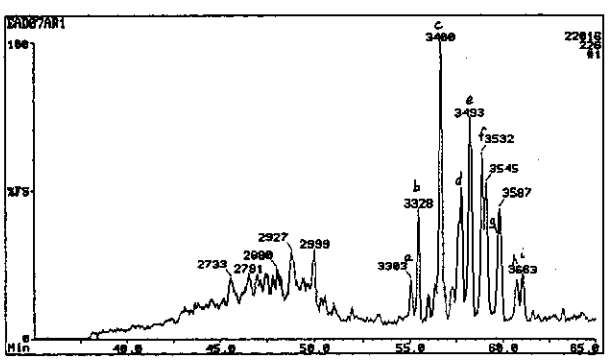

e) m/z 226: Trimethyl DibenzoThiophenes

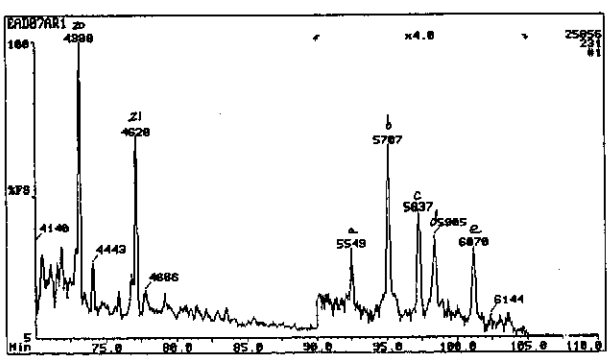

f) m/z 231: Triaromatic Steroids

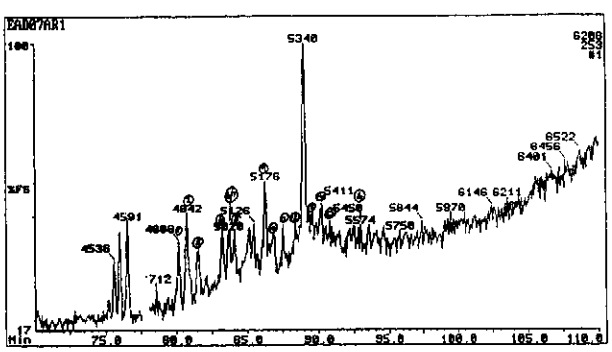

g) m/z 253: Monoaromatic Steroids (from aromatic fraction)

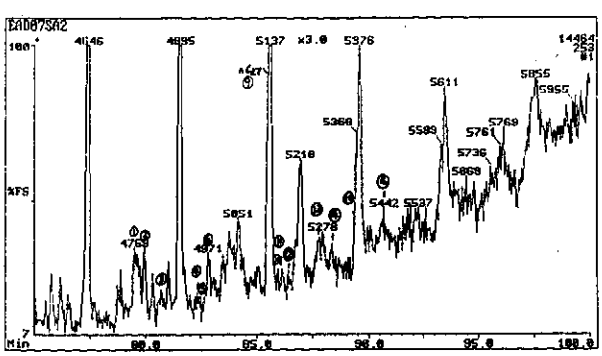

h) m/z 253: Monoaromatic Steroids (from saturates fraction)

Figure E.72: Annotated TIC and single ion fragmentograms of aromatic hydrocarbons from sample 4, well 88 DST 5, 2507m.

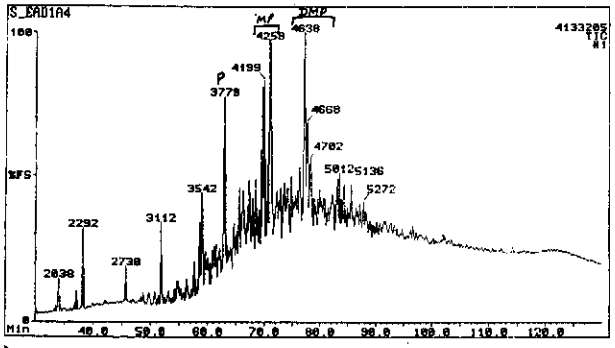

a) TIC: Total Ion Count

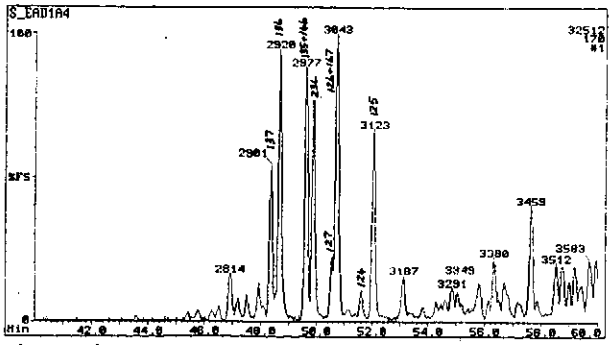

b) m/z 170: Trimethyl Napthalenes

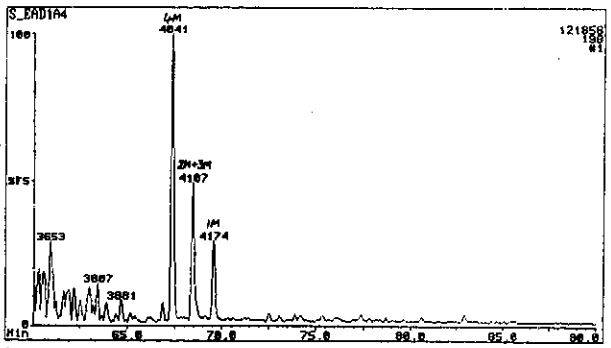

c) m/z 198: Methyl DibenzoThiophenes

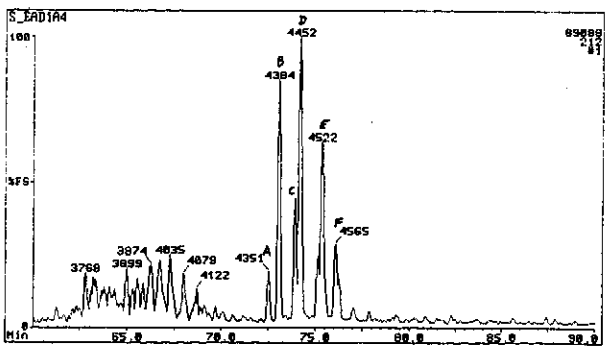

d) m/z 212: Dimethyl DibenzoThiophenes

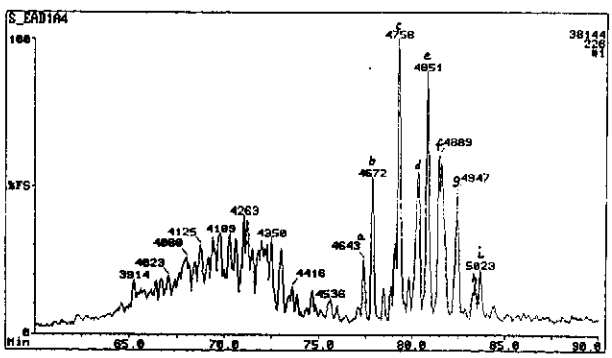

e) m/z 226: Trimethyl DibenzoThiophenes

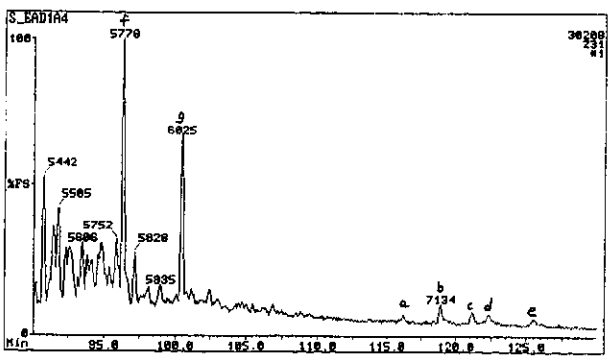

f) m/z 231: Triaromatic Steroids

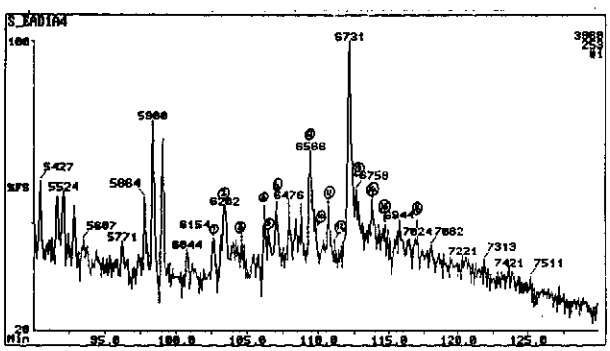

g) m/z 253: Monoaromatic Steroids (from aromatic fraction)

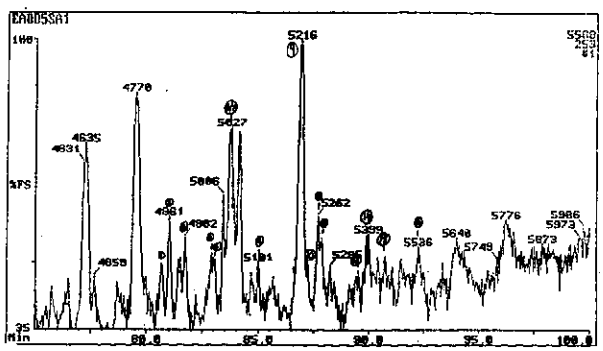

h) m/z 253: Monoaromatic Steroids (from saturates fraction)

Figure E.73: Annotated TIC and single ion fragmentograms of aromatic hydrocarbons from sample 5, well 88 DST 5, 2507m.

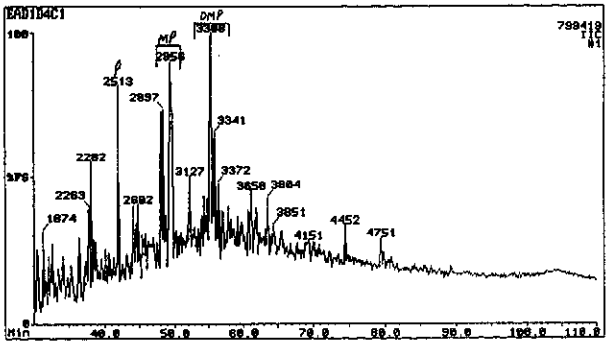

a) TIC: Total Ion Count

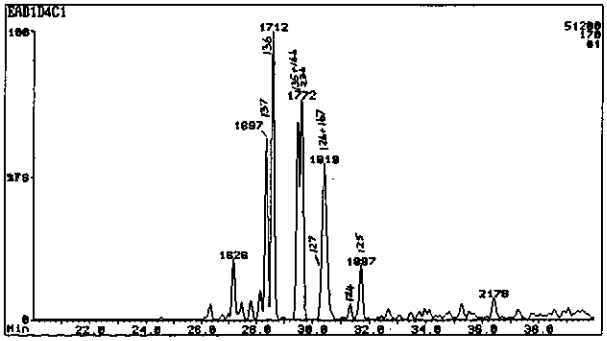

b) m/z 170: Trimethyl Napthalenes

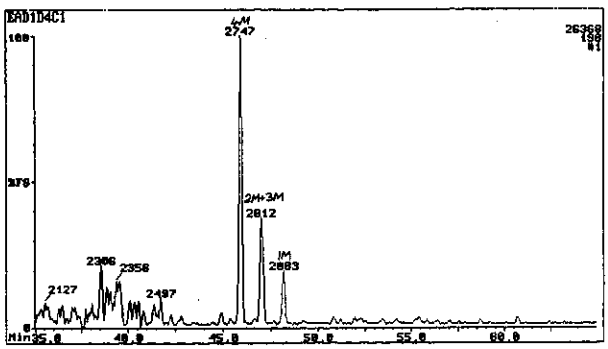

c) m/z 198: Methyl DibenzoThiophenes

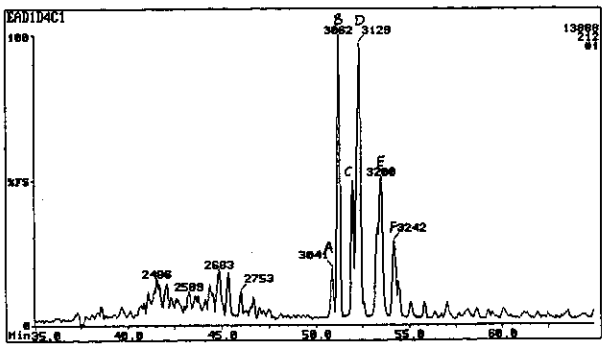

d) m/z 212: Dimethyl DibenzoThiophenes

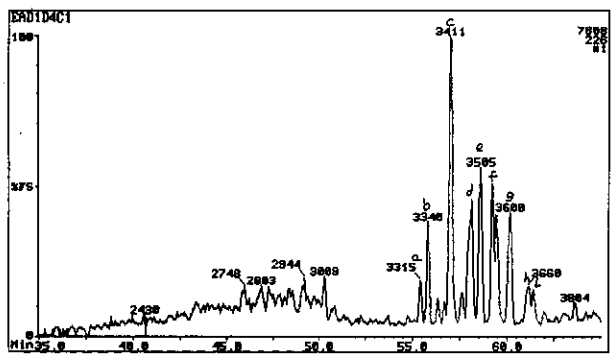

e) m/z 226: Trimethyl DibenzoThiophenes

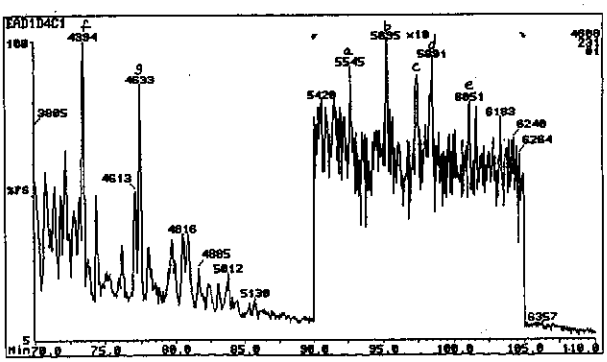

f) m/z 231: Triaromatic Steroids

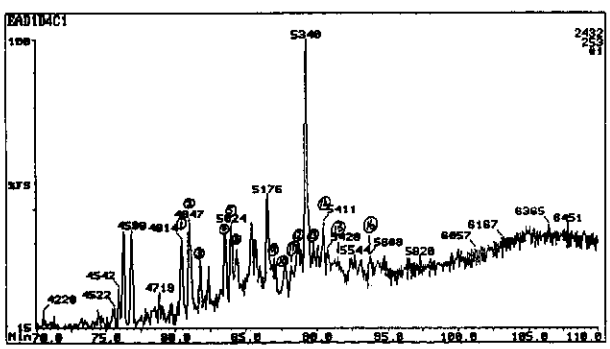

g) m/z 253: Monoaromatic Steroids (from aromatic fraction)

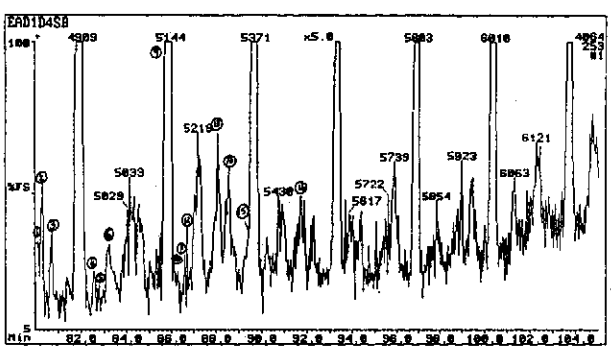

h) m/z 253: Monoaromatic Steroids (from saturates fraction)

Figure E.74: Annotated TIC and single ion fragmentograms of aromatic hydrocarbons from sample 6, well 88 DST 4, 2827m.

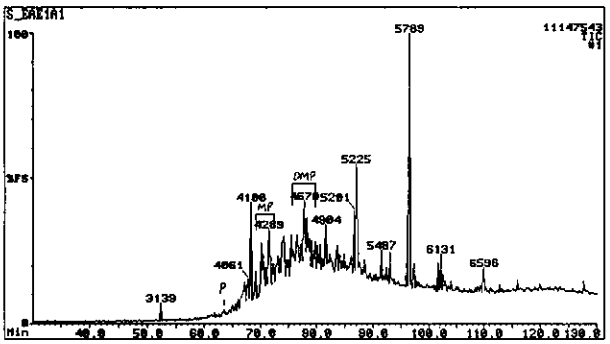

a) TIC: Total Ion Count

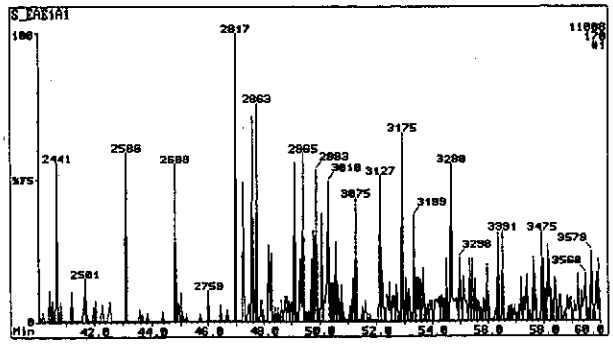

b) m/z 170: Trimethyl Napthalenes

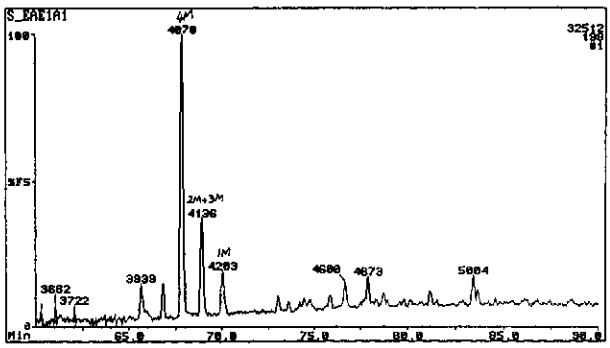

c) m/z 198: Methyl DibenzoThiophenes

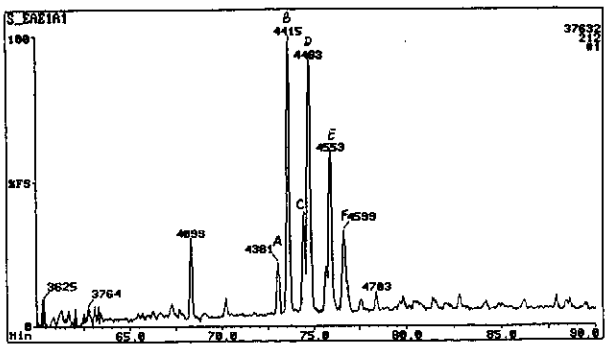

d) m/z 212: Dimethyl DibenzoThiophenes

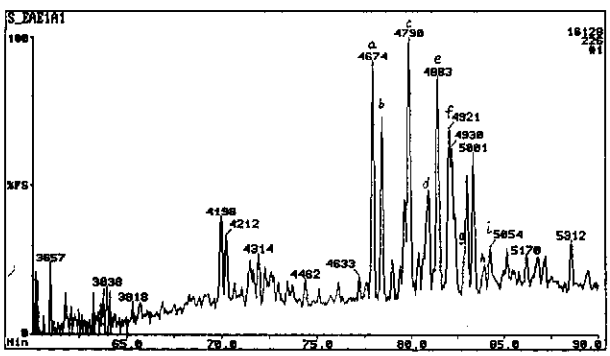

e) m/z 226: Trimethyl DibenzoThiophenes

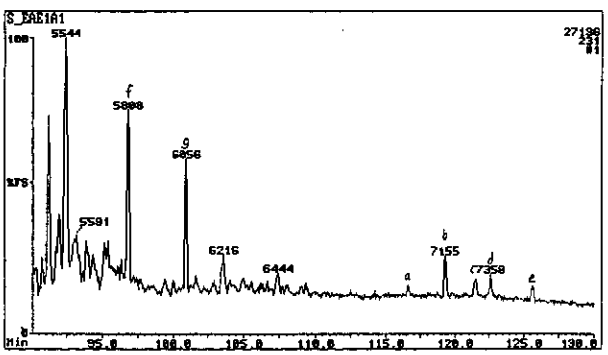

f) m/z 231: Triaromatic Steroids

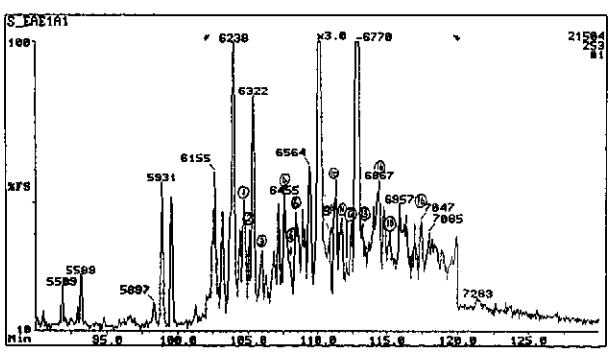

g) m/z 253: Monoaromatic Steroids (from aromatic fraction)

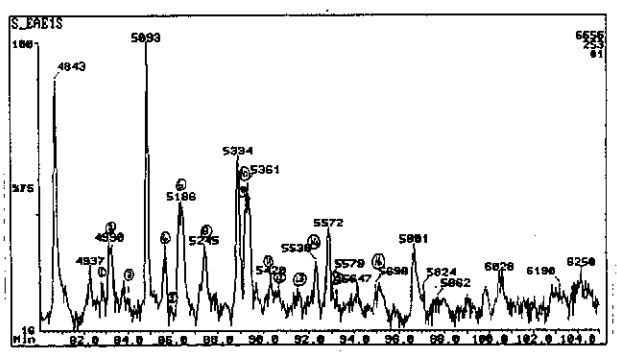

h) m/z 253: Monoaromatic Steroids (from saturates fraction)

Figure E.75: Annotated TIC and single ion fragmentograms of aromatic hydrocarbons from sample 7, well 92 core 1, 2949.0m.

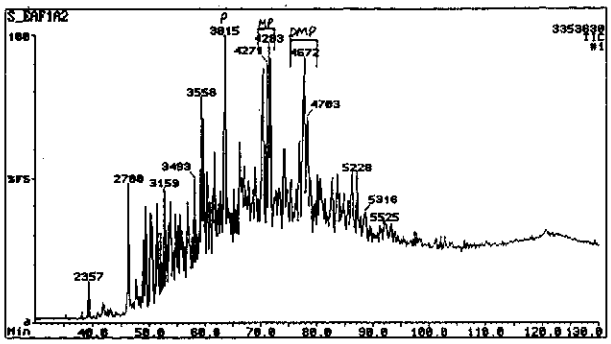

a) TIC: Total Ion Count

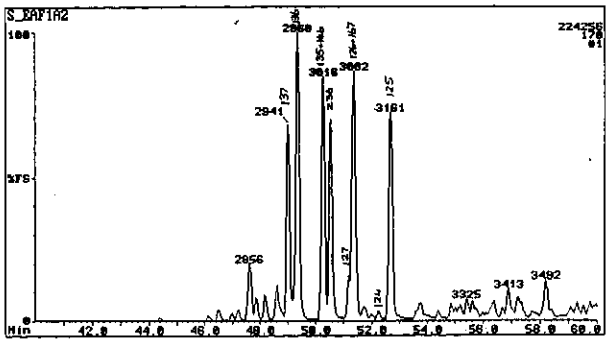

b) m/z 170: Trimethyl Napthalenes

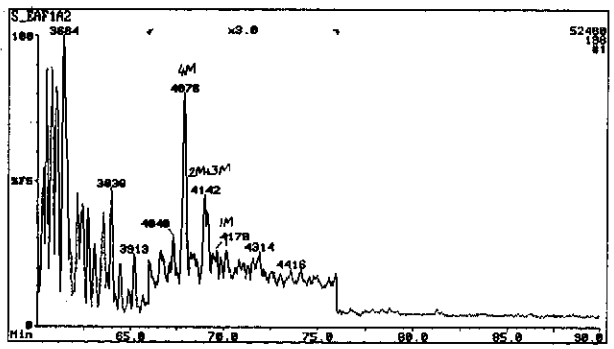

c) m/z 198: Methyl DibenzoThiophenes

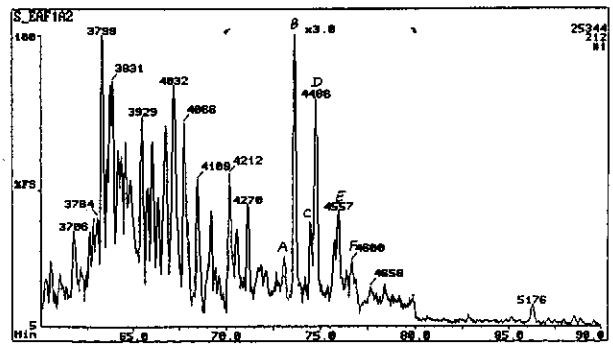

d) m/z 212: Dimethyl DibenzoThiophenes

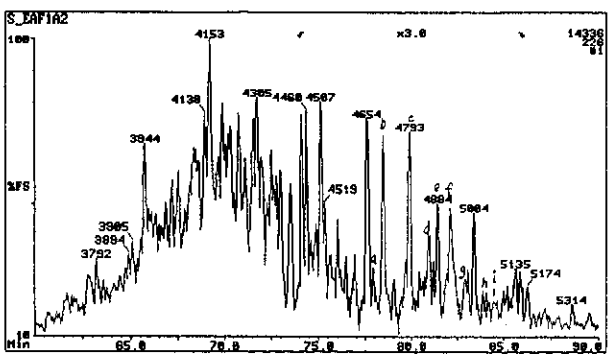

e) m/z 226: Trimethyl DibenzoThiophenes

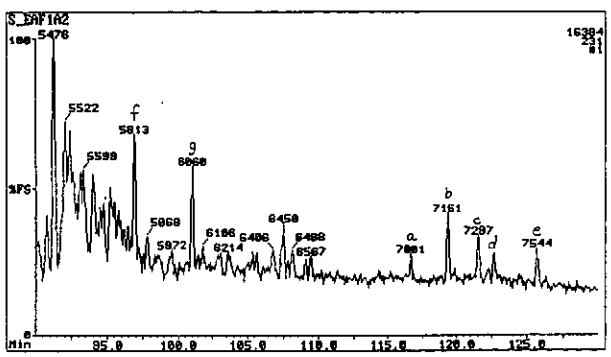

f) m/z 231: Triaromatic Steroids

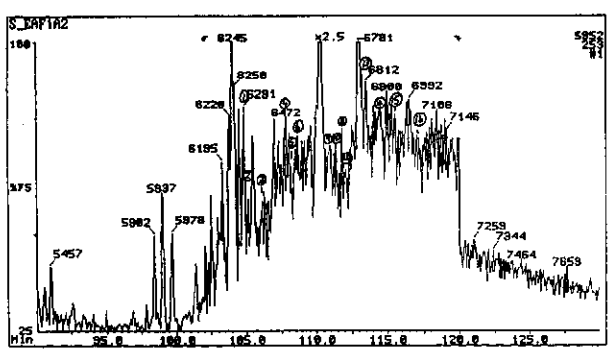

g) m/z 253: Monoaromatic Steroids (from aromatic fraction)

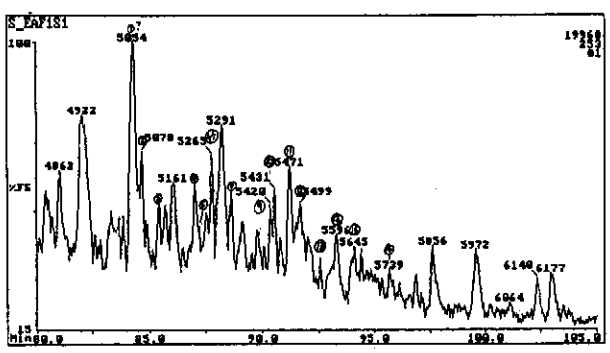

h) m/z 253: Monoaromatic Steroids (from saturates fraction)

Figure E.76: Annotated TIC and single ion fragmentograms of aromatic hydrocarbons from sample 8, well 118 core 1, 2563.1m.

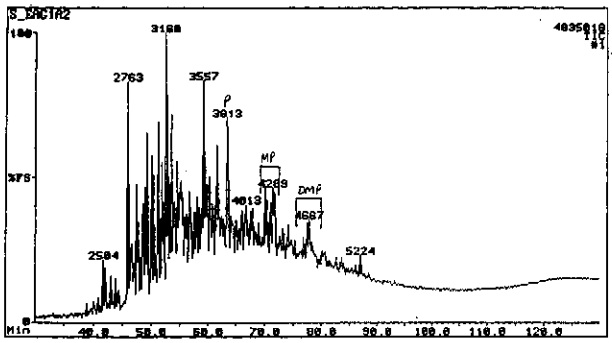

a) TIC: Total Ion Count

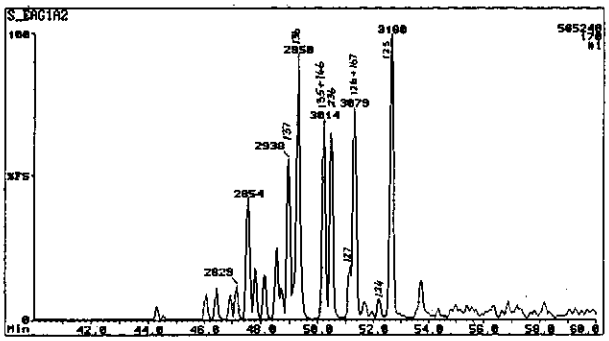

b) m/z 170: Trimethyl Napthalenes

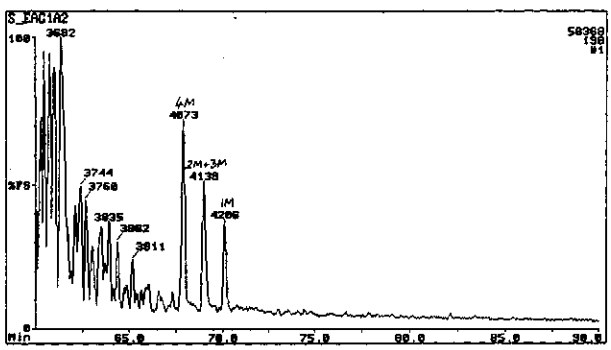

c) m/z 198: Methyl DibenzoThiophenes

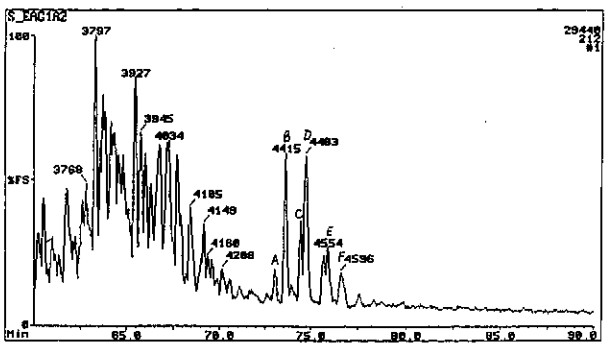

d) m/z 212: Dimethyl DibenzoThiophenes

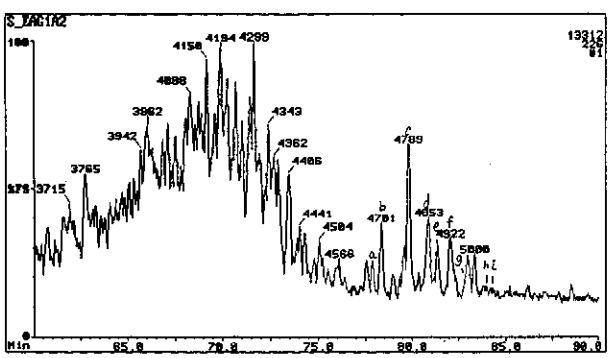

e) m/z 226: Trimethyl DibenzoThiophenes

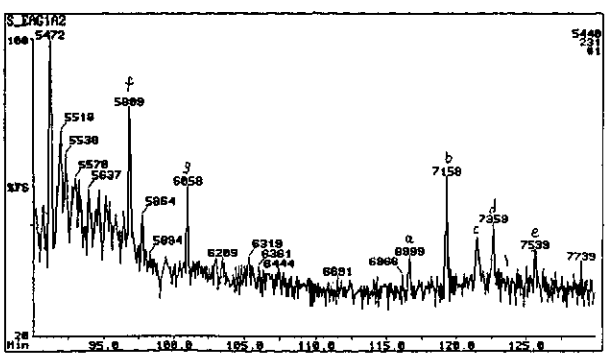

f) m/z 231: Triaromatic Steroids

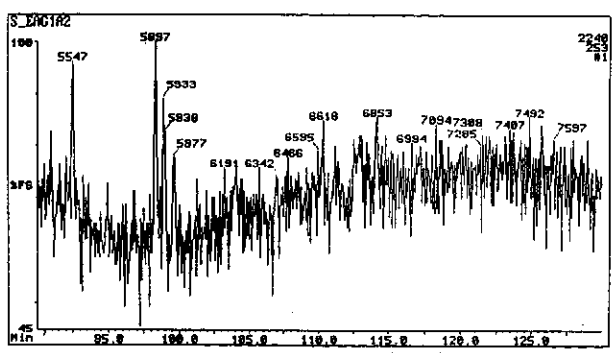

g) m/z 253: Monoaromatic Steroids (from aromatic fraction)

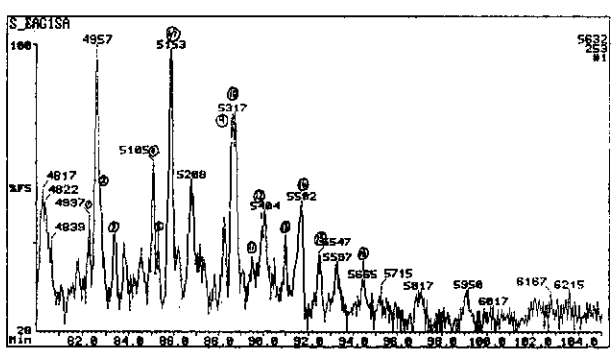

h) m/z 253: Monoaromatic Steroids (from saturates fraction)

Figure E.77: Annotated TIC and single ion fragmentograms of aromatic hydrocarbons from sample 9, well 102 DST 4, 2241m.

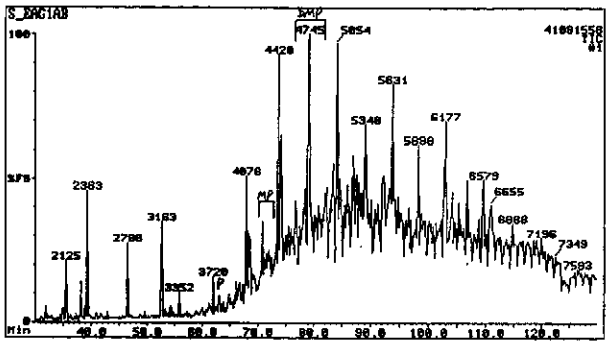

a) TIC: Total Ion Count

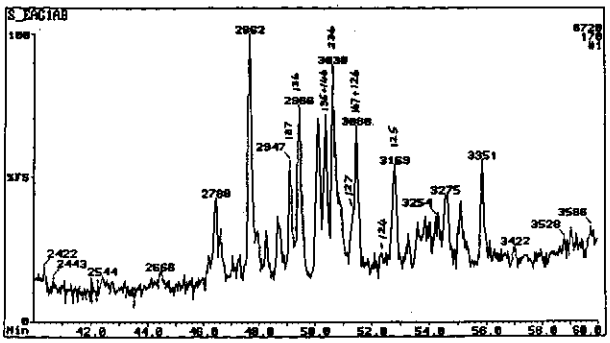

b) m/z 170: Trimethyl Napthalenes

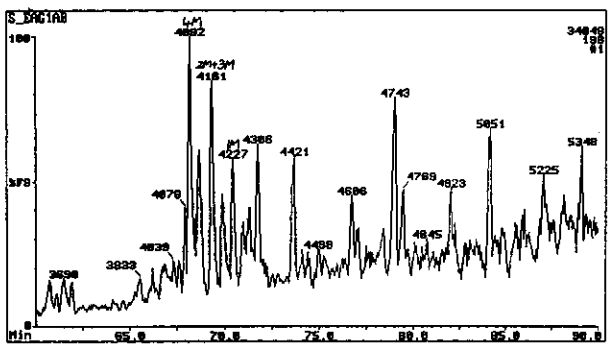

c) m/z 198: Methyl DibenzoThiophenes

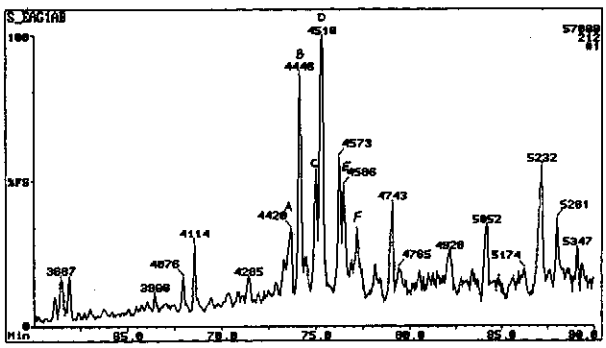

d) m/z 212: Dimethyl DibenzoThiophenes

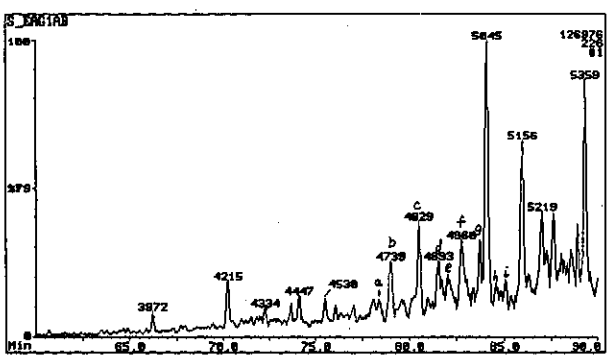

e) m/z 226: Trimethyl DibenzoThiophenes

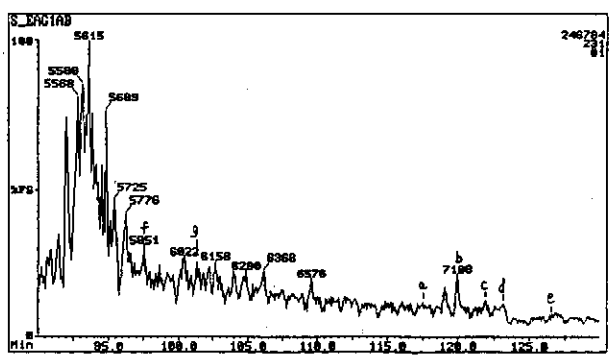

f) m/z 231: Triaromatic Steroids

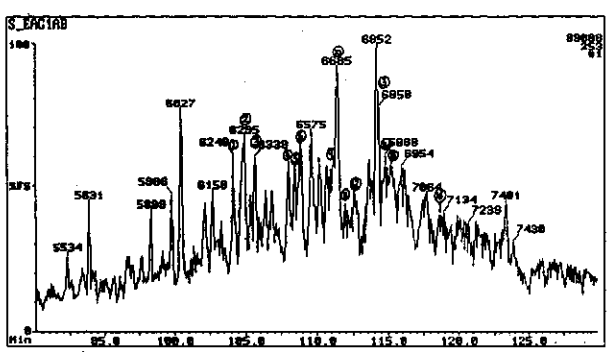

g) m/z 253: Monoaromatic Steroids (from aromatic fraction)

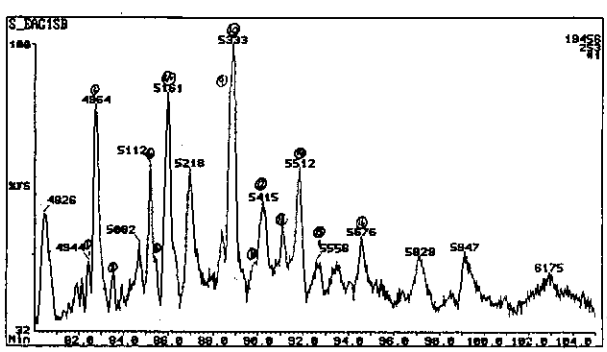

h) m/z 253: Monoaromatic Steroids (from saturates fraction)

Figure E.78: Annotated TIC and single ion fragmentograms of aromatic hydrocarbons from sample 10, well 102 DST 2, 2556m.

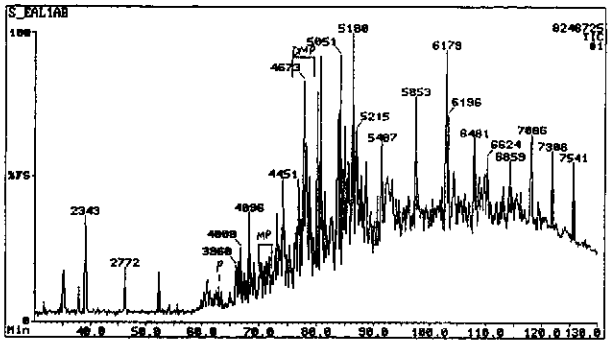

a) TIC: Total Ion Count

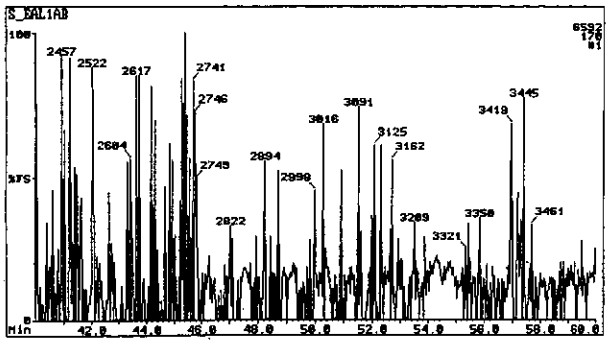

b) m/z 170: Trimethyl Napthalenes

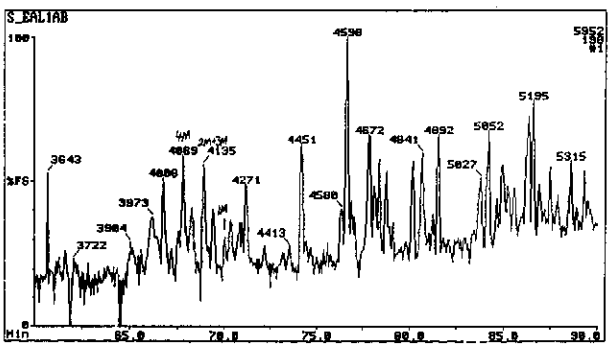

c) m/z 198: Methyl DibenzoThiophenes

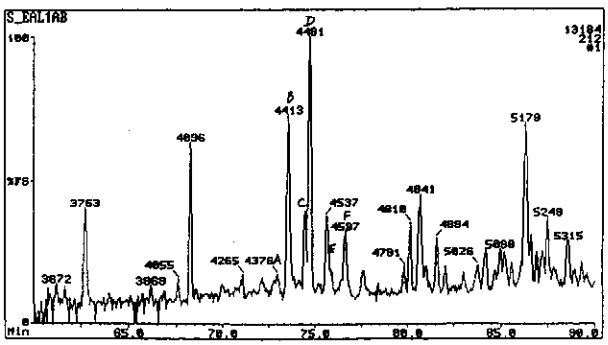

d) m/z 212: Dimethyl DibenzoThiophenes

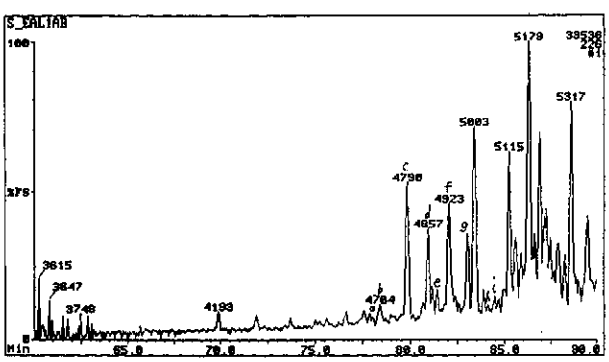

e) m/z 226: Trimethyl DibenzoThiophenes

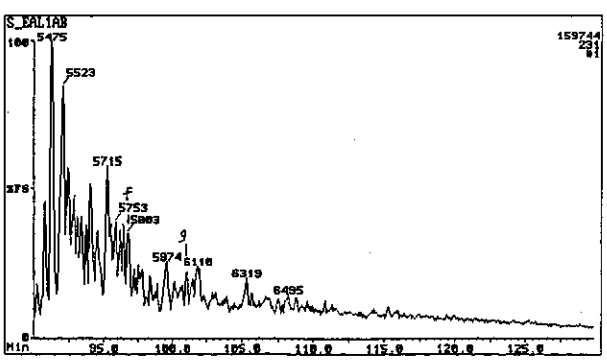

f) m/z 231: Triaromatic Steroids

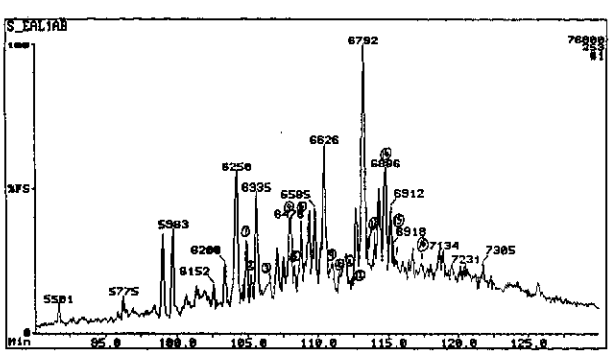

g) m/z 253: Monoaromatic Steroids (from aromatic fraction)

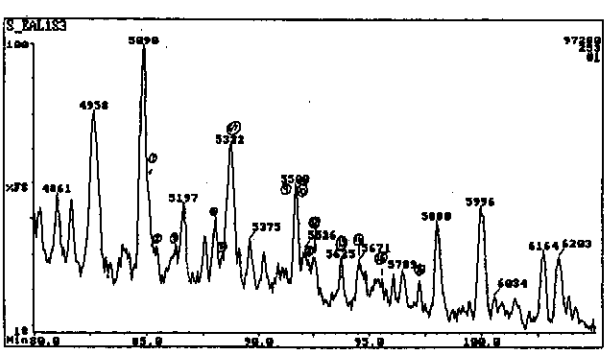

h) m/z 253: Monoaromatic Steroids (from saturates fraction)

Figure E.79: Annotated TIC and single ion fragmentograms of aromatic hydrocarbons from sample 11, well 91 core 1, 3220.05m.

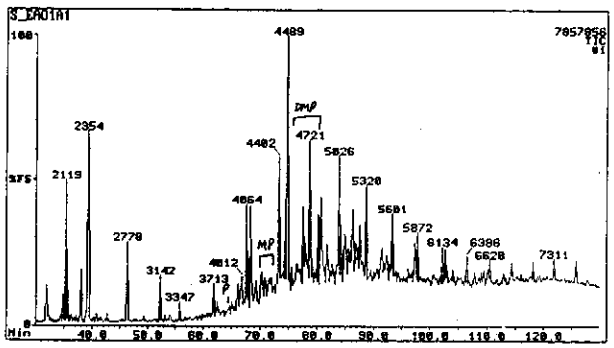

a) TIC: Total Ion Count

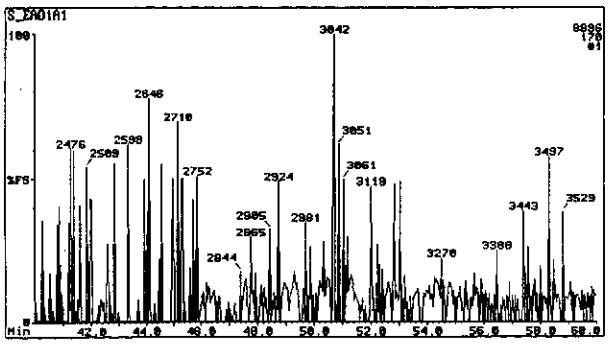

b) m/z 170: Trimethyl Napthalenes

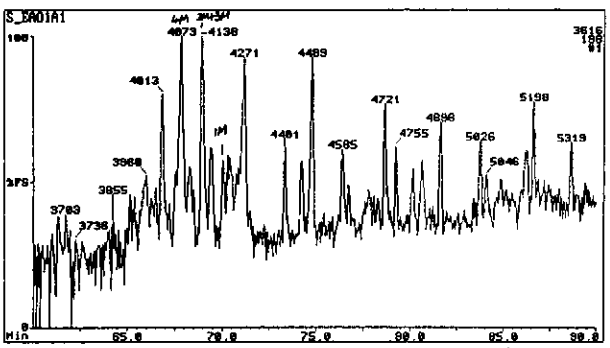

c) m/z 198: Methyl DibenzoThiophenes

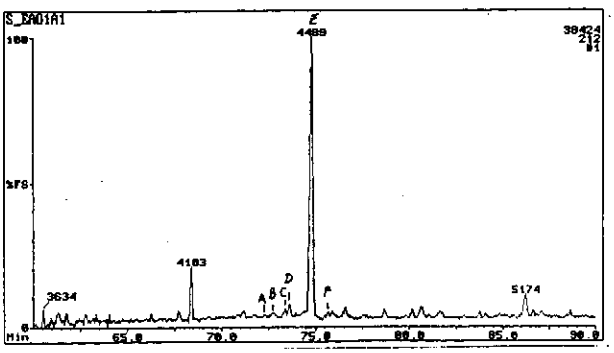

d) m/z 212: Dimethyl DibenzoThiophenes

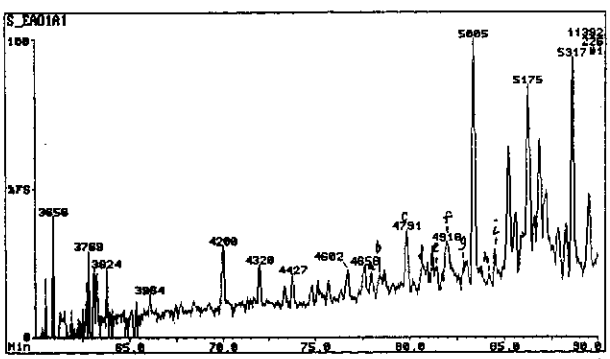

e) m/z 226: Trimethyl DibenzoThiophenes

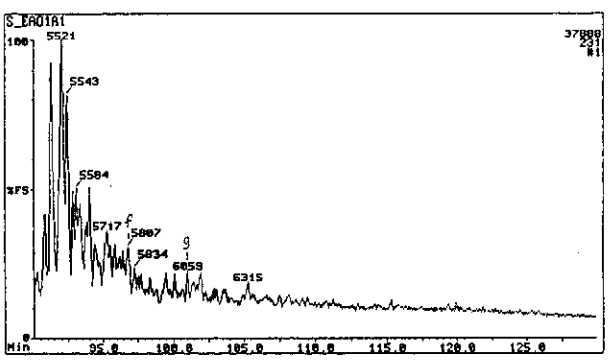

f) m/z 231: Triaromatic Steroids

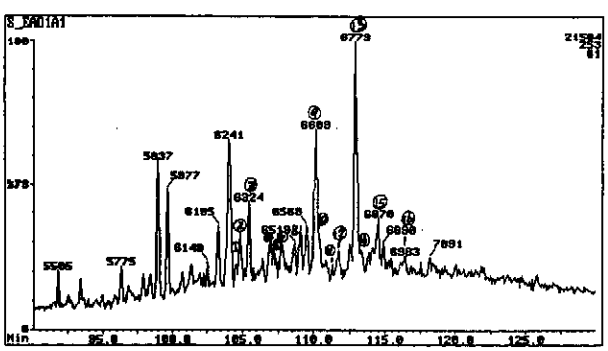

g) m/z 253: Monoaromatic Steroids (from aromatic fraction)

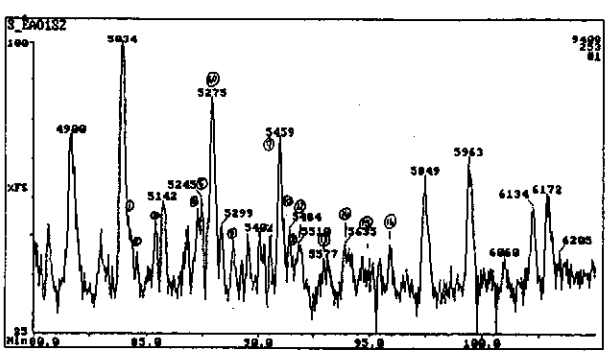

h) m/z 253: Monoaromatic Steroids (from saturates fraction)

Figure E.80: Annotated TIC and single ion fragmentograms of aromatic hydrocarbons from sample 12, well 104 core 2, 3017.46m.

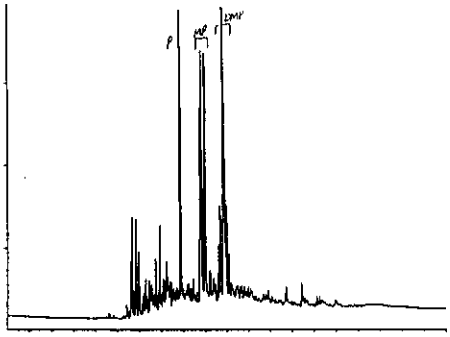

a) TIC: Total Ion Count

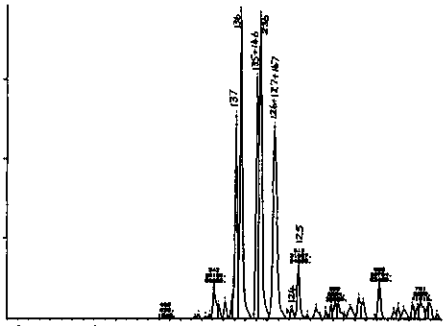

b) m/z 170: Trimethyl Napthalenes

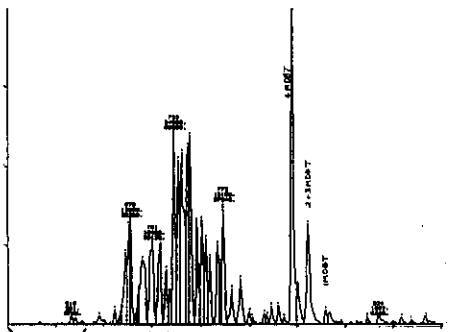

c) m/z 198: Methyl DibenzoThiophenes

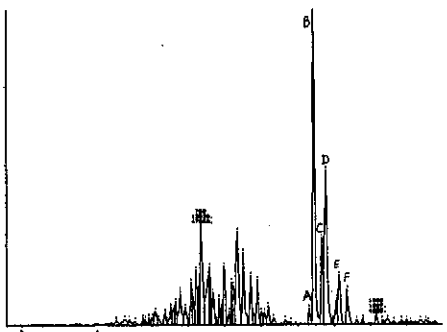

d) m/z 212: Dimethyl DibenzoThiophenes

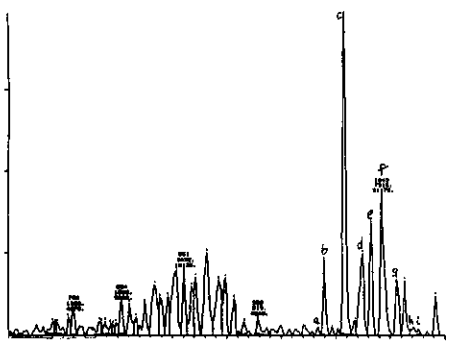

e) m/z 226: Trimethyl DibenzoThiophenes

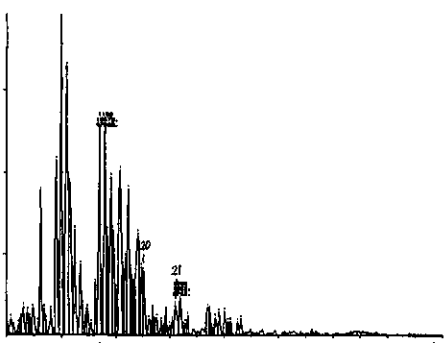

f) m/z 231: Triaromatic Steroids

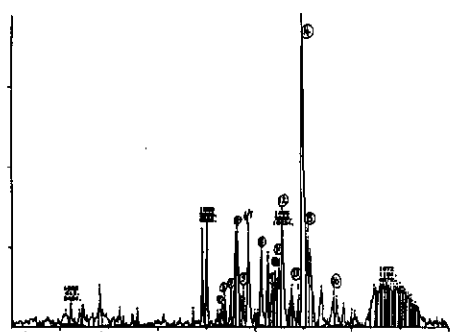

g) m/z 253: Monoaromatic Steroids (from aromatic fraction)

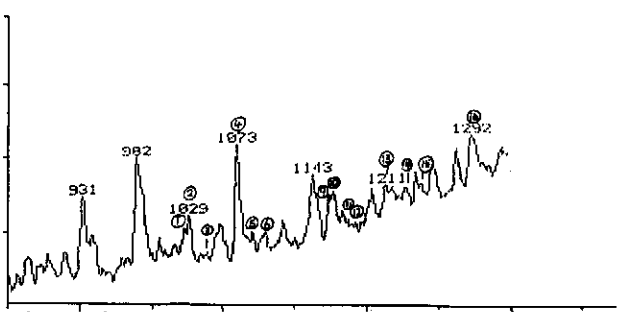

h) m/z 253: Monoaromatic Steroids (from saturates fraction)

Figure E.81: Annotated TIC and single ion fragmentograms of aromatic hydrocarbons from sample 13, well 93 core 4, 3212.4m.

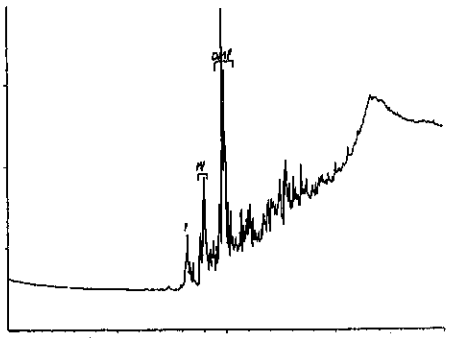

a) TIC: Total Ion Count

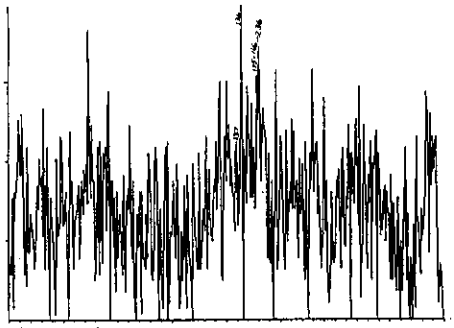

b) m/z 170: Trimethyl Napthalenes

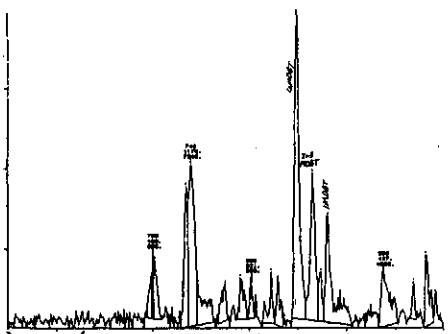

c) m/z 198: Methyl DibenzoThiophenes

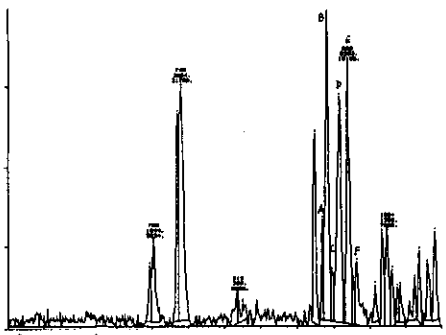

d) m/z 212: Dimethyl DibenzoThiophenes

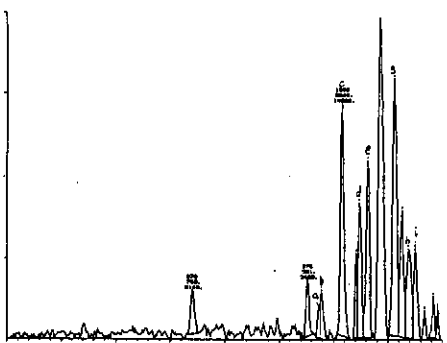

e) m/z 226: Trimethyl DibenzoThiophenes

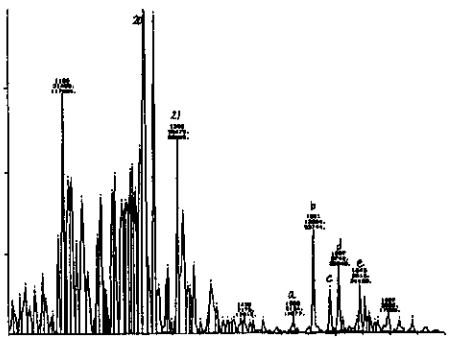

f) m/z 231: Triaromatic Steroids

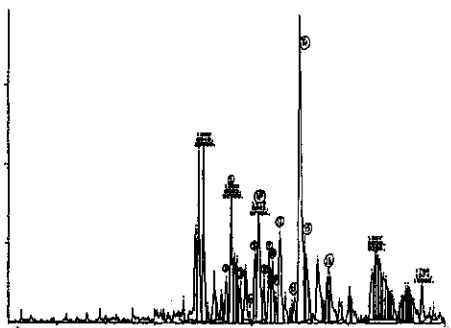

g) m/z 253: Monoaromatic Steroids (from aromatic fraction)

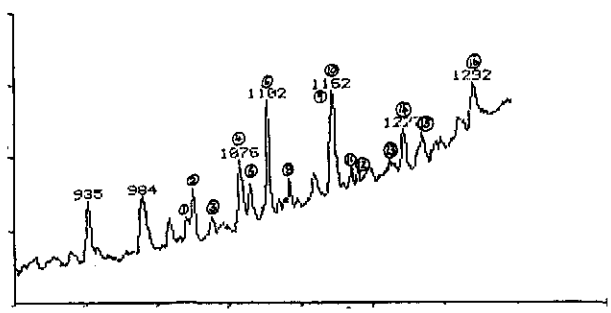

h) m/z 253: Monoaromatic Steroids (from saturates fraction)

Figure E.82: Annotated TIC and single ion fragmentograms of aromatic hydrocarbons from sample 14, well 109 DST 1, 2630m.

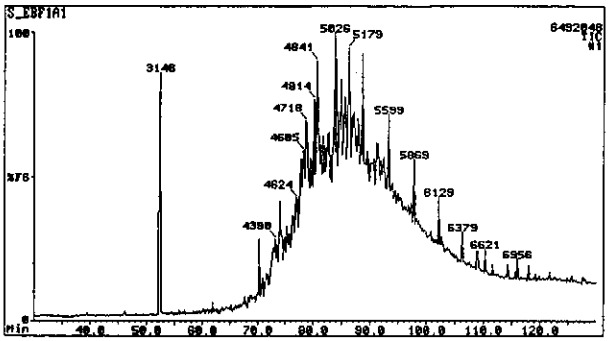

a) TIC: Total Ion Count

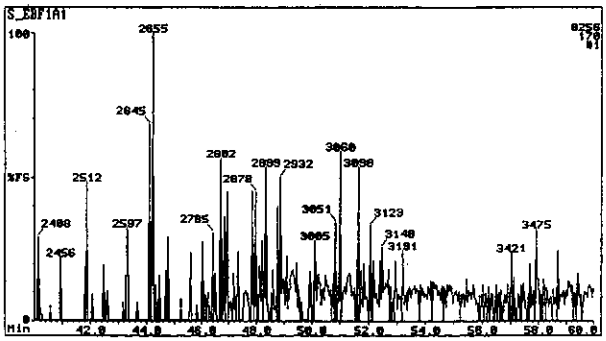

b) m/z 170: Trimethyl Napthalenes

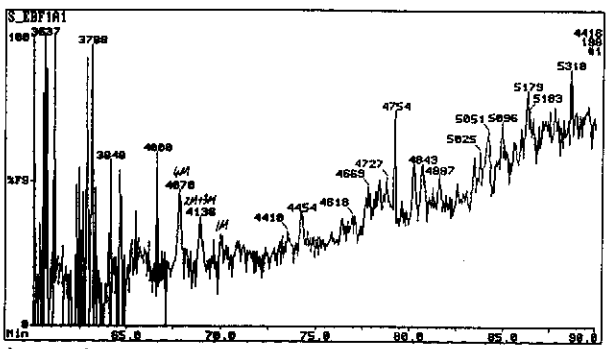

c) m/z 198: Methyl DibenzoThiophenes

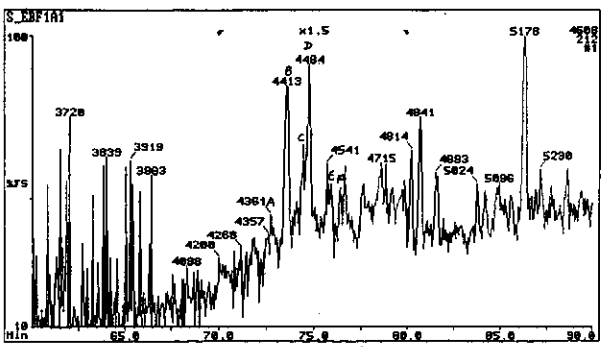

d) m/z 212: Dimethyl DibenzoThiophenes

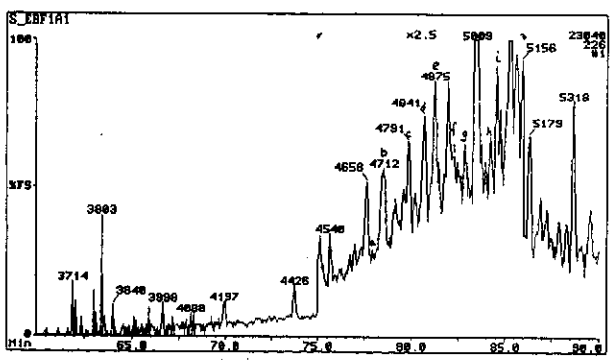

e) m/z 226: Trimethyl DibenzoThiophenes

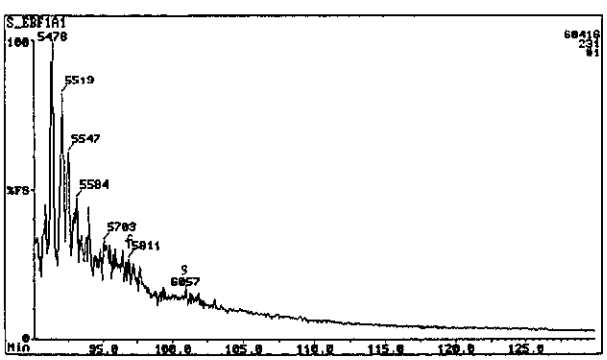

f) m/z 231: Triaromatic Steroids

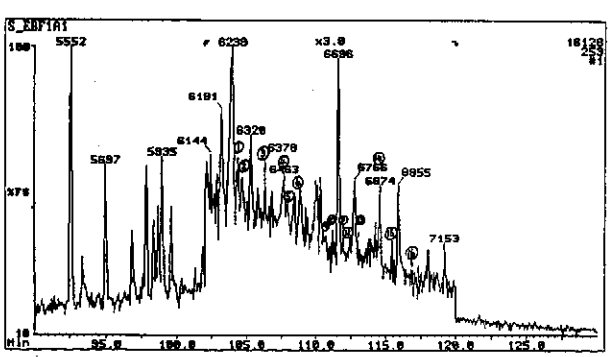

g) m/z 253: Monoaromatic Steroids (from aromatic fraction)

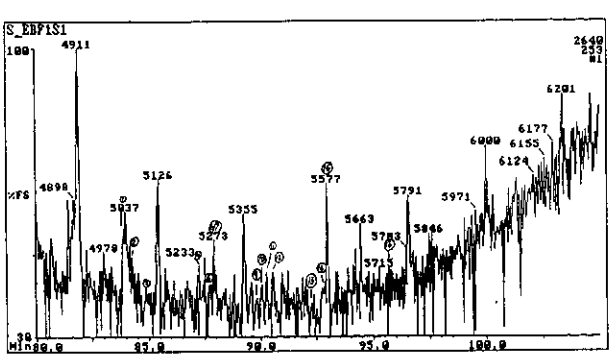

h) m/z 253: Monoaromatic Steroids (from saturates fraction)

Figure E.83: Annotated TIC and single ion fragmentograms of aromatic hydrocarbons from sample 15, well 107 DST 2, 2565m.

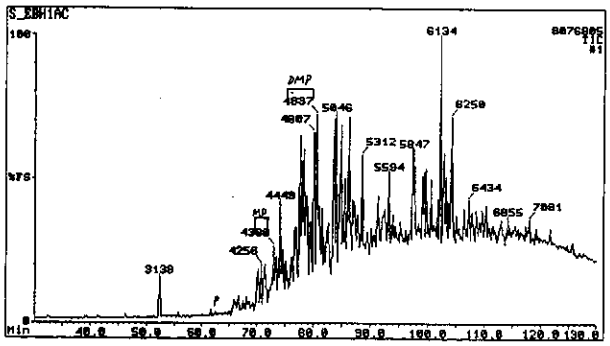

a) TIC: Total Ion Count

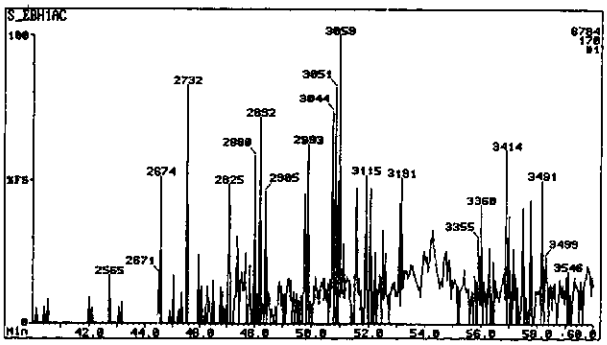

b) m/z 170: Trimethyl Napthalenes

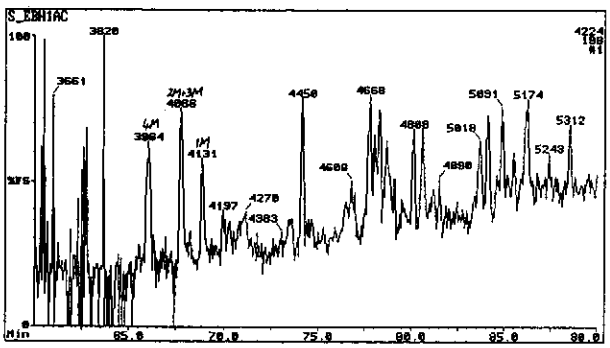

c) m/z 198: Methyl DibenzoThiophenes

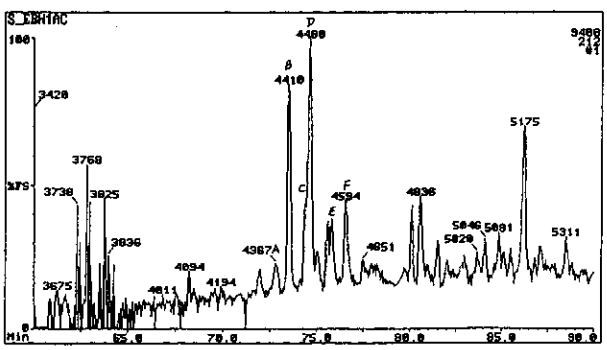

d) m/z 212: Dimethyl DibenzoThiophenes

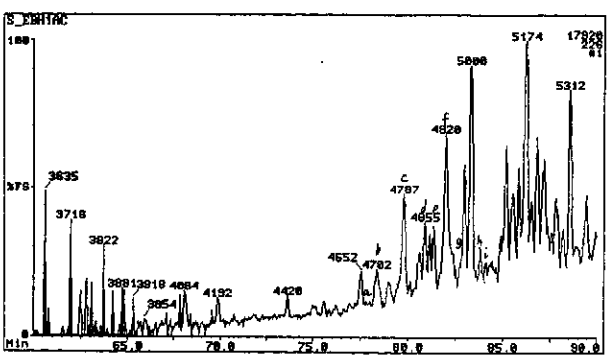

e) m/z 226: Trimethyl DibenzoThiophenes

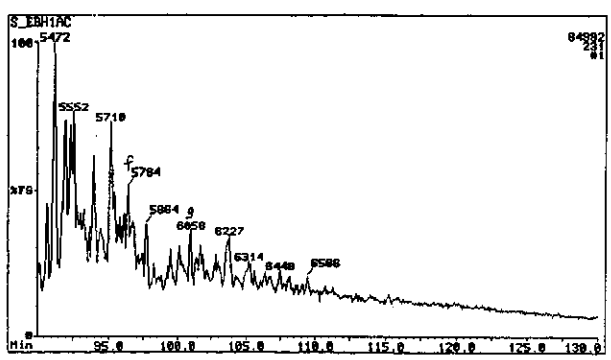

f) m/z 231: Triaromatic Steroids

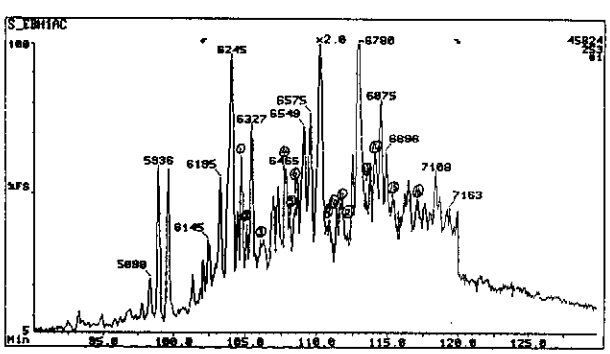

g) m/z 253: Monoaromatic Steroids (from aromatic fraction)

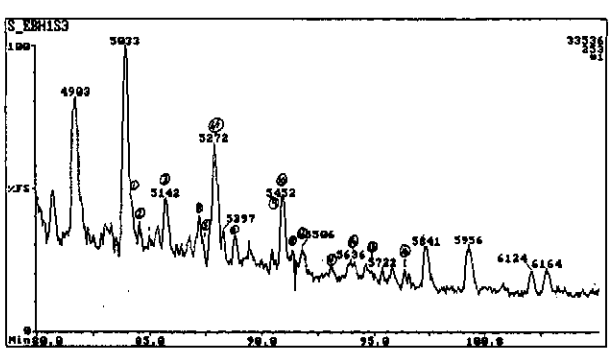

h) m/z 253: Monoaromatic Steroids (from saturates fraction)

Figure E.84: Annotated TIC and single ion fragmentograms of aromatic hydrocarbons from sample 16, well 110 DST 1, 3051m.

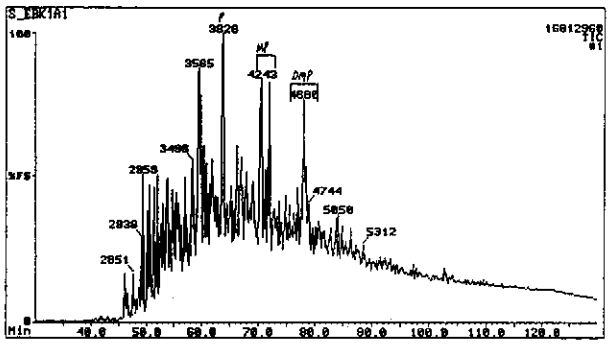

a) TIC: Total Ion Count

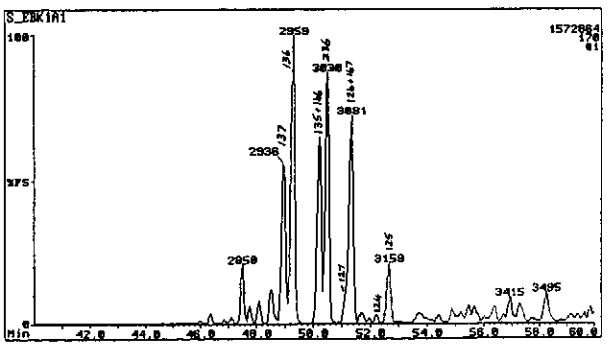

b) m/z 170: Trimethyl Napthalenes

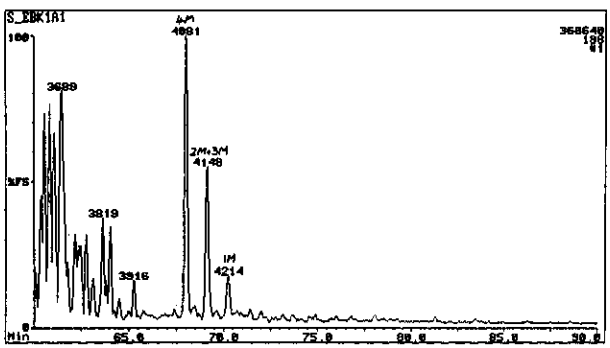

c) m/z 198: Methyl DibenzoThiophenes

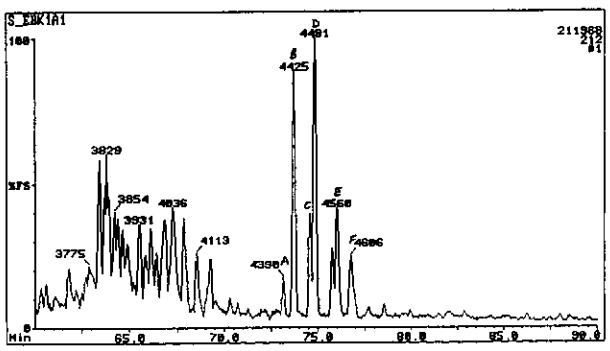

d) m/z 212: Dimethyl DibenzoThiophenes

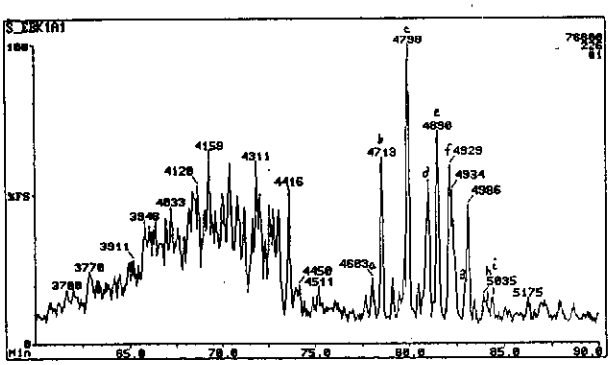

e) m/z 226: Trimethyl DibenzoThiophenes

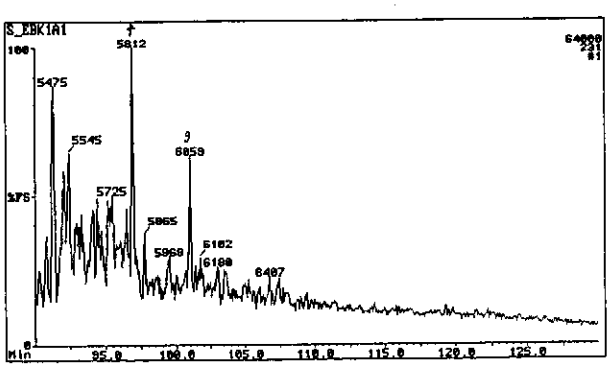

f) m/z 231: Triaromatic Steroids

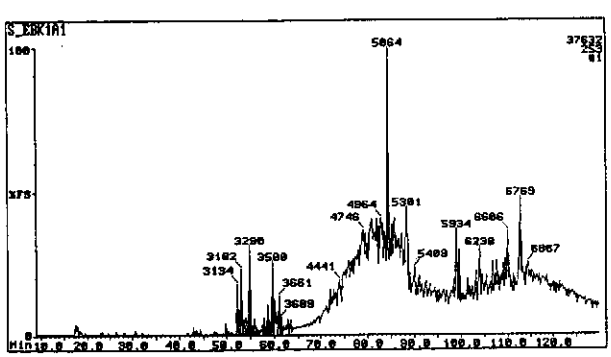

g) m/z 253: Monoaromatic Steroids (from aromatic fraction)

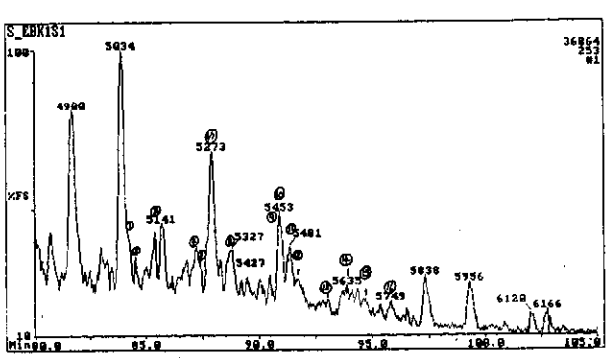

h) m/z 253: Monoaromatic Steroids (from saturates fraction)

Figure E.85: Annotated TIC and single ion fragmentograms of aromatic hydrocarbons from sample 17, well 126 DST 1, 2643m.

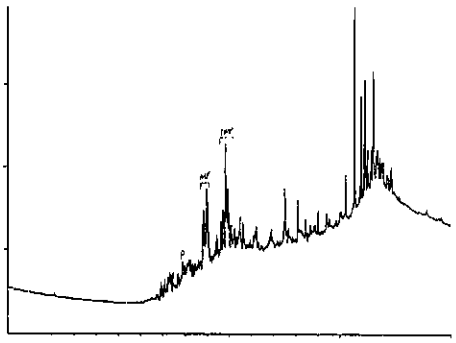

a) TIC: Total Ion Count

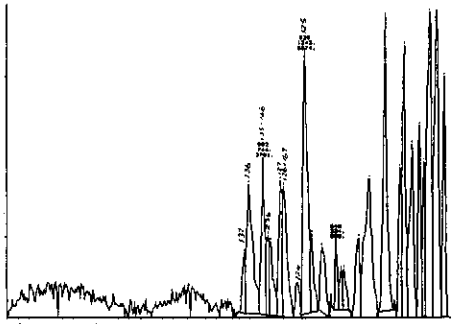

b) m/z 170: Trimethyl Napthalenes

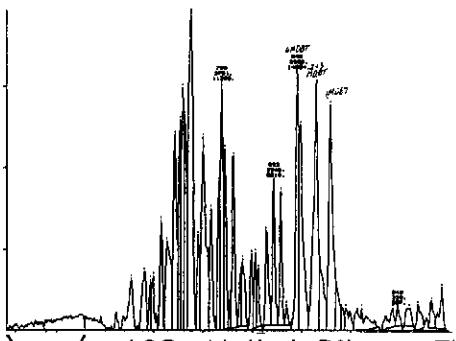

c) m/z 198: Methyl DibenzoThiophenes

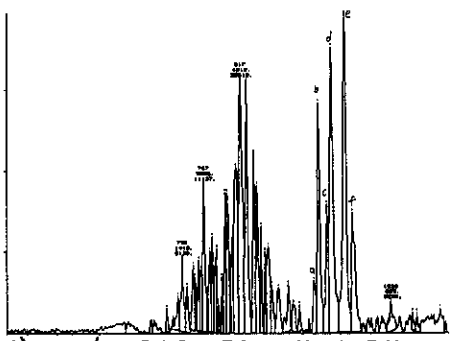

d) m/z 212: Dimethyl DibenzoThiophenes

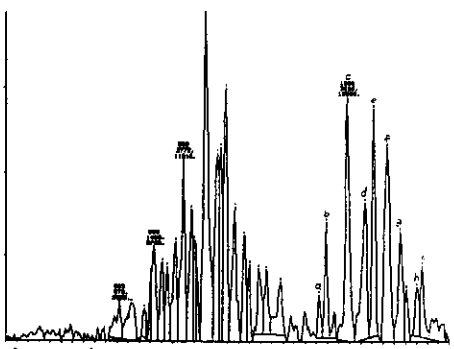

e) m/z 226: Trimethyl DibenzoThiophenes

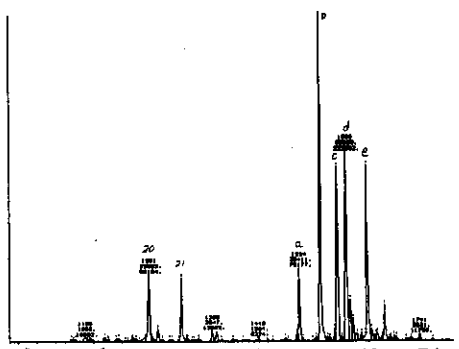

f) m/z 231: Triaromatic Steroids

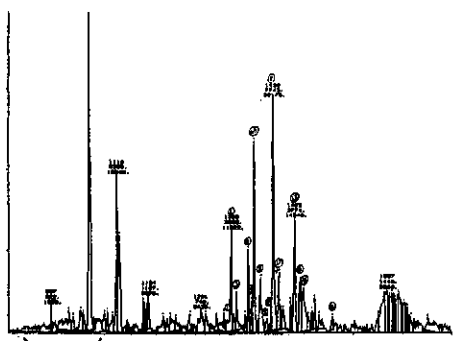

g) m/z 253: Monoaromatic Steroids
(from aromatic fraction)

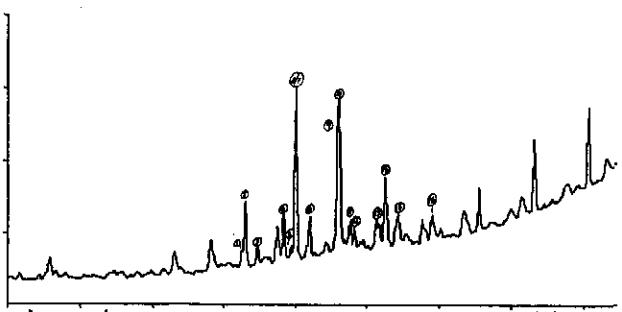

h) m/z 253: Monoaromatic Steroids
(from saturates fraction)

Figure E.86: Annotated TIC and single ion fragmentograms of aromatic hydrocarbons from sample 18, well 122 SWC, 2517m.

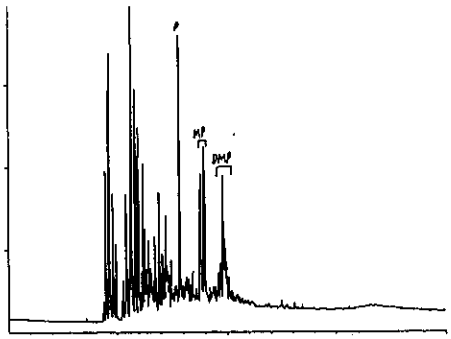

a) TIC: Total Ion Count

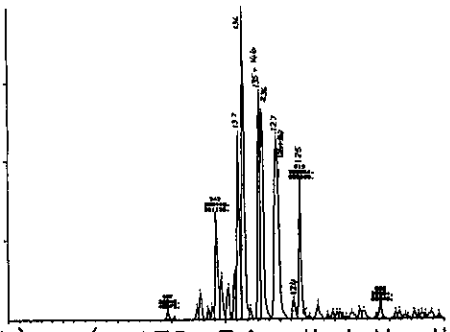

b) m/z 170: Trimethyl Napthalenes

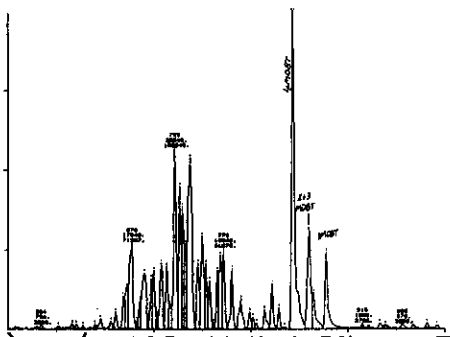

c) m/z 198: Methyl DibenzoThiophenes

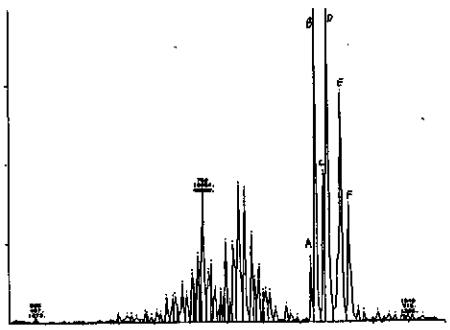

d) m/z 212: Dimethyl DibenzoThiophenes

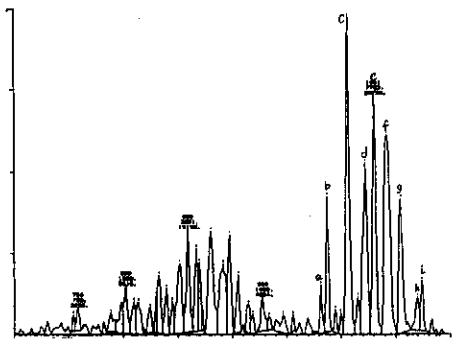

e) m/z 226: Trimethyl DibenzoThiophenes

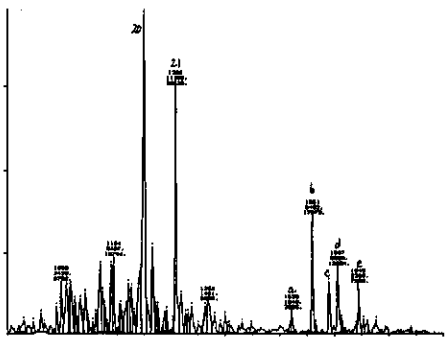

f) m/z 231: Triaromatic Steroids

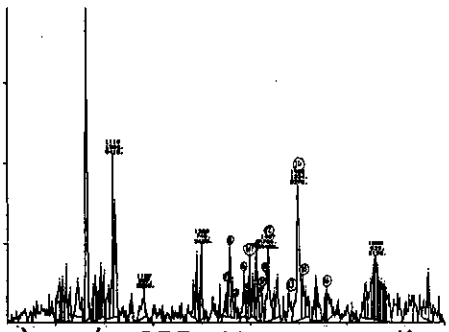

g) m/z 253: Monoaromatic Steroids
(from aromatic fraction)

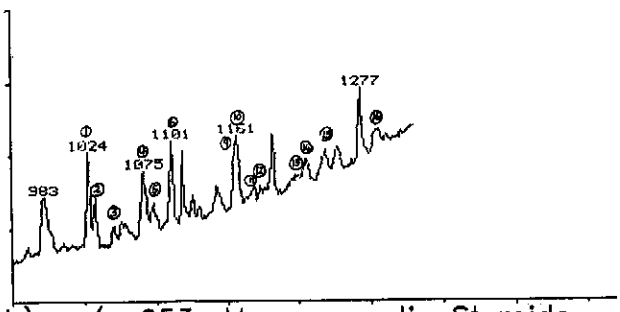

h) m/z 253: Monoaromatic Steroids
(from saturates fraction)

Figure E.87: Annotated TIC and single ion fragmentograms of aromatic hydrocarbons from sample 19, well 132 DST 2, 2662m.

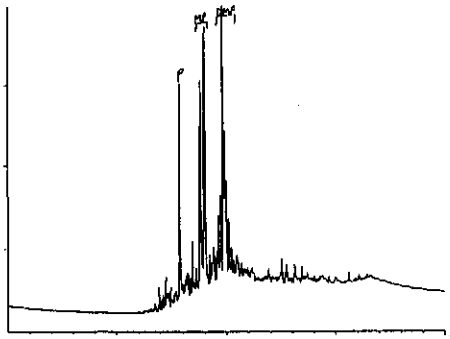

a) TIC: Total Ion Count

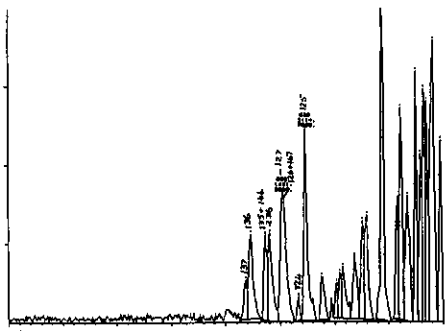

b) m/z 170: Trimethyl Napthalenes

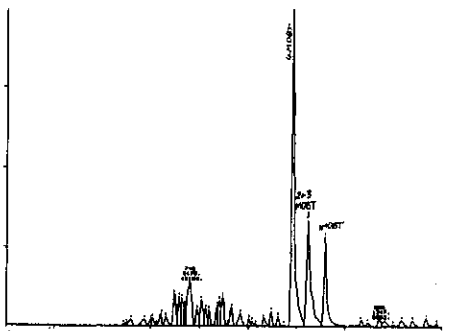

c) m/z 198: Methyl DibenzoThiophenes

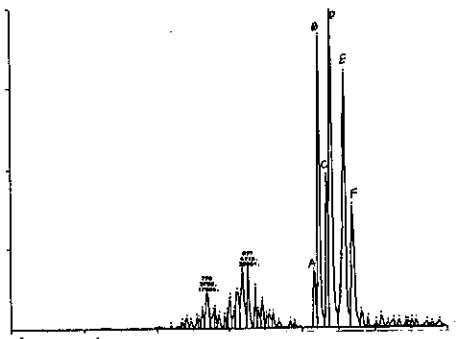

d) m/z 212: Dimethyl DibenzoThiophenes

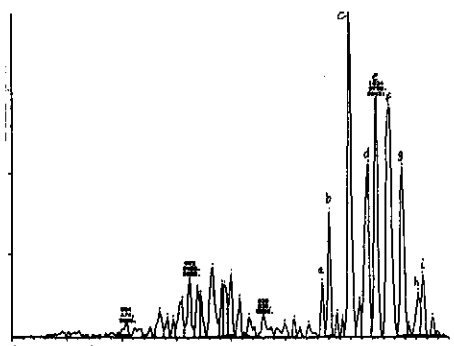

e) m/z 226: Trimethyl DibenzoThiophenes

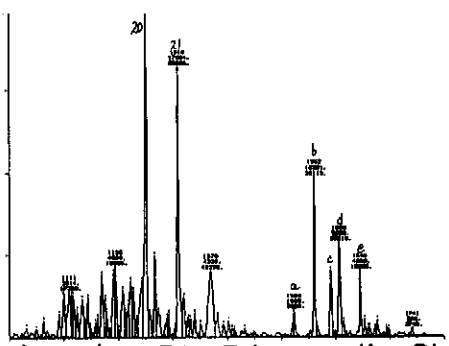

f) m/z 231: Triaromatic Steroids

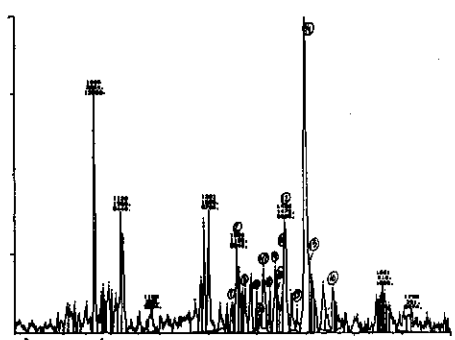

g) m/z 253: Monoaromatic Steroids
(from aromatic fraction)

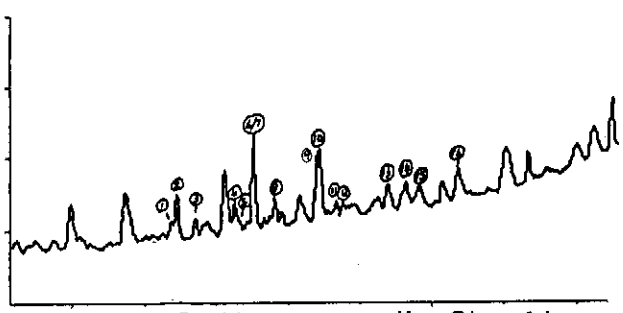

h) m/z 253: Monoaromatic Steroids
(from saturates fraction)

Figure E.88: Annotated TIC and single ion fragmentograms of aromatic hydrocarbons from sample 20, well 132 core 1, 2702.43m.

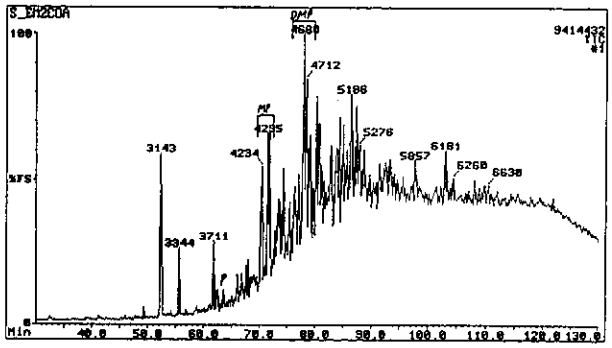

a) TIC: Total Ion Count

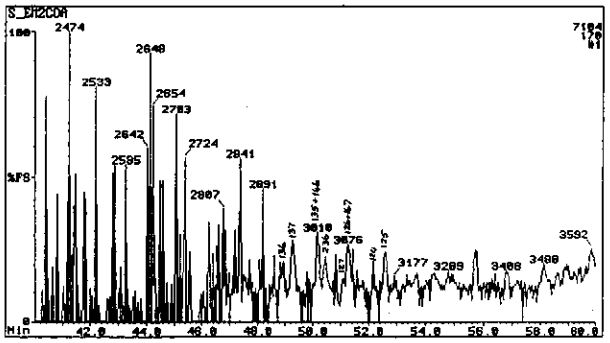

b) m/z 170: Trimethyl Napthalenes

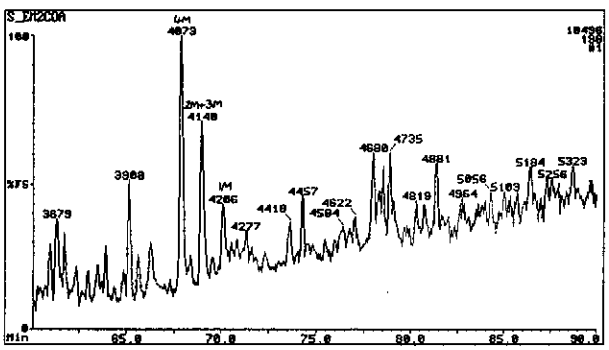

c) m/z 198: Methyl DibenzoThiophenes

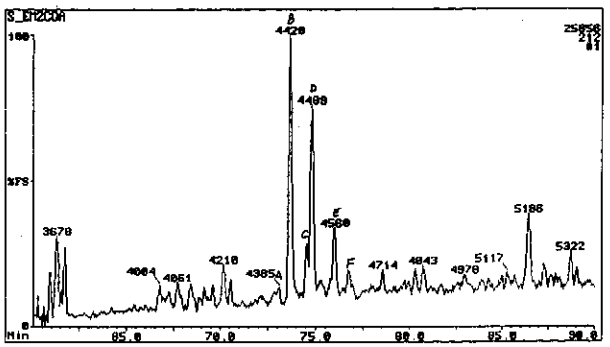

d) m/z 212: Dimethyl DibenzoThiophenes

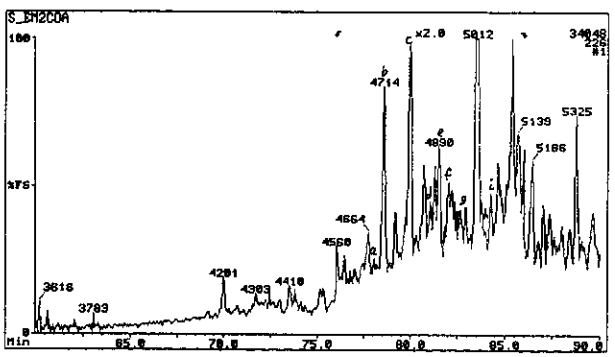

e) m/z 226: Trimethyl DibenzoThiophenes

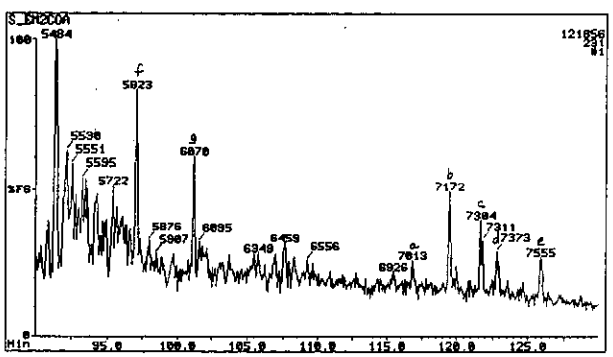

f) m/z 231: Triaromatic Steroids

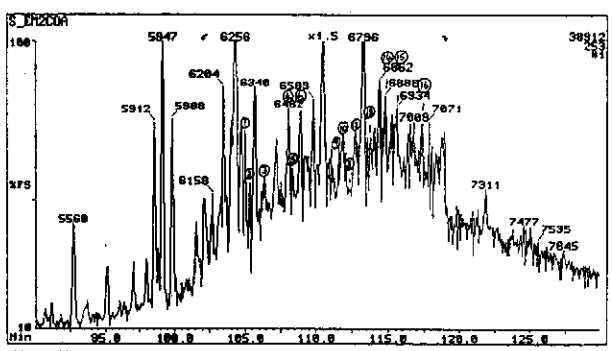

g) m/z 253: Monoaromatic Steroids (from aromatic fraction)

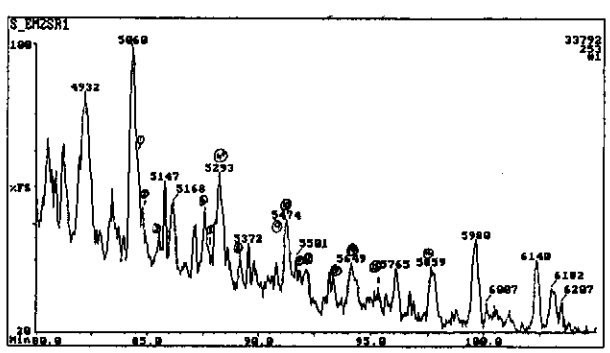

h) m/z 253: Monoaromatic Steroids (from saturates fraction)

Figure E.89: Annotated TIC and single ion fragmentograms of aromatic hydrocarbons from sample 21, well 48 DST 2, 2634m.

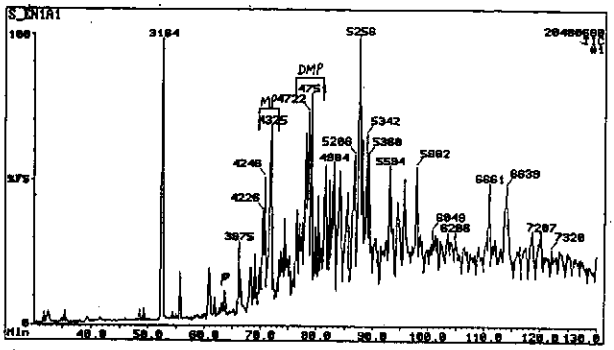

a) TIC: Total Ion Count

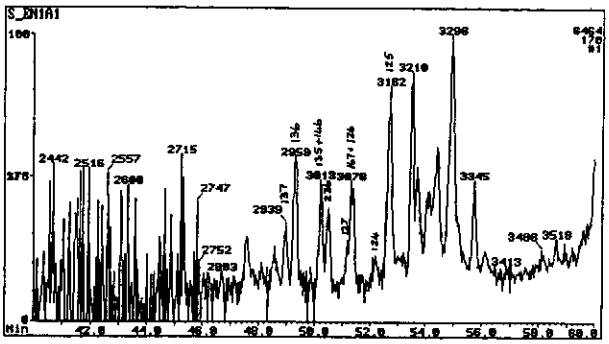

b) m/z 170: Trimethyl Napthalenes

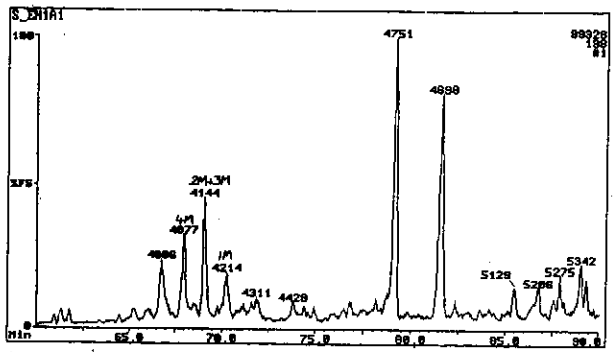

c) m/z 198: Methyl DibenzoThiophenes

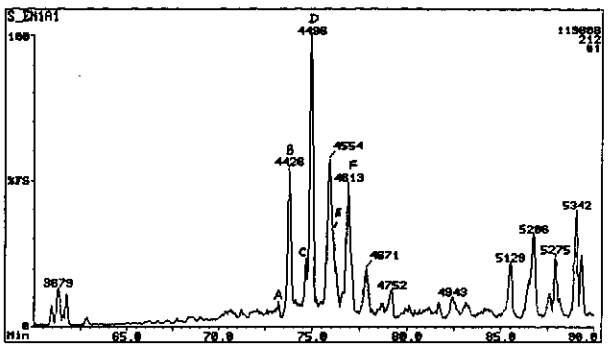

d) m/z 212: Dimethyl DibenzoThiophenes

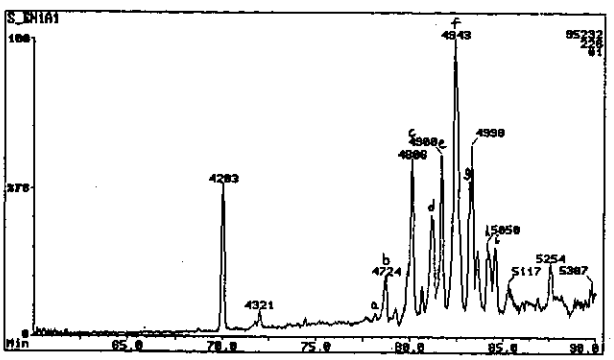

e) m/z 226: Trimethyl DibenzoThiophenes

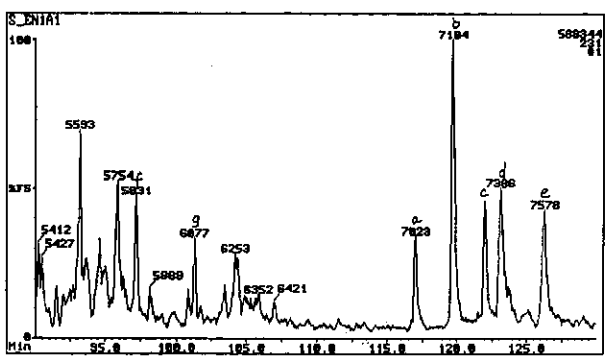

f) m/z 231: Triaromatic Steroids

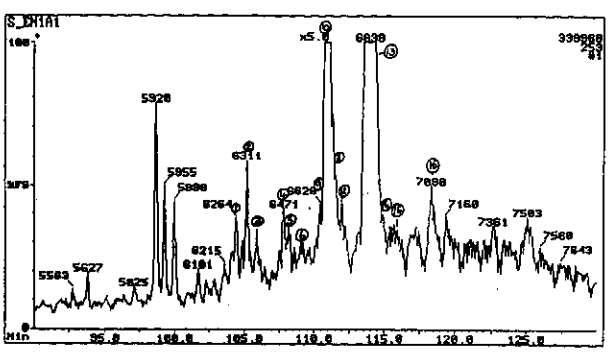

g) m/z 253: Monoaromatic Steroids (from aromatic fraction)

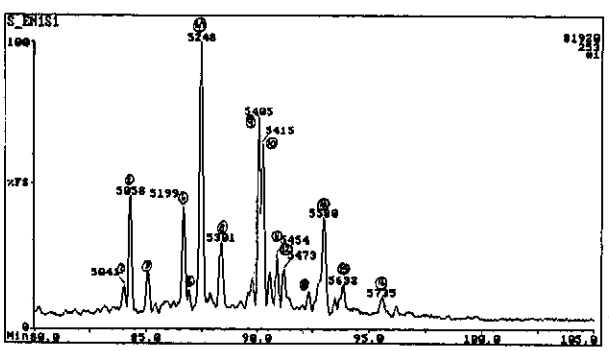

h) m/z 253: Monoaromatic Steroids (from saturates fraction)

Figure E.90: Annotated TIC and single ion fragmentograms of aromatic hydrocarbons from sample 22, well 16 RC, 2614m.

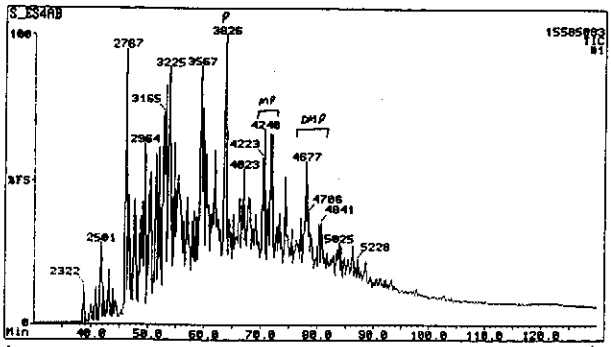

a) TIC: Total Ion Count

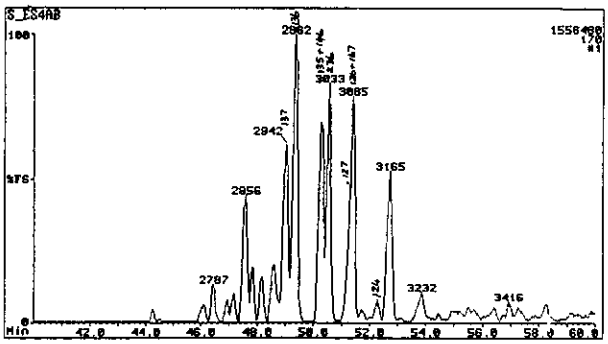

b) m/z 170: Trimethyl Napthalenes

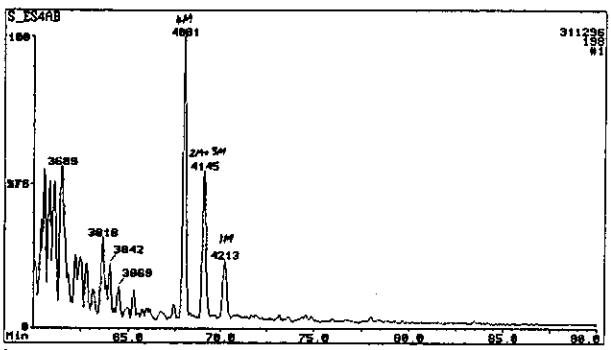

c) m/z 198: Methyl DibenzoThiophenes

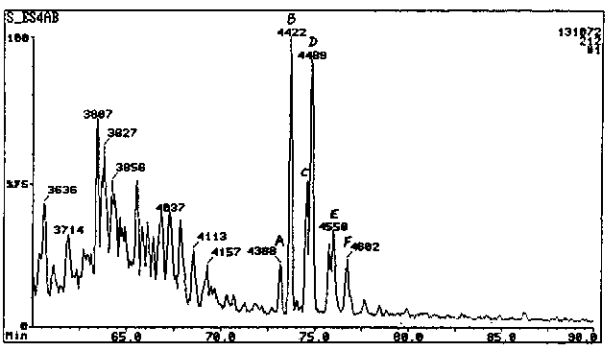

d) m/z 212: Dimethyl DibenzoThiophenes

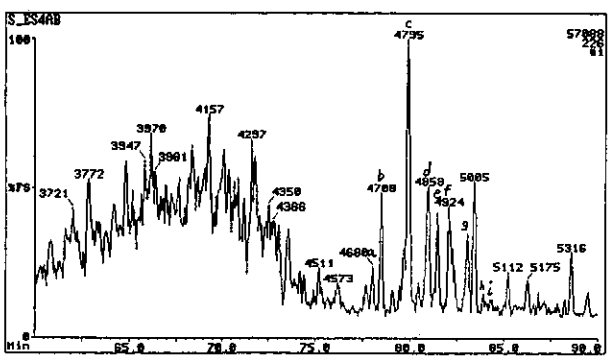

e) m/z 226: Trimethyl DibenzoThiophenes

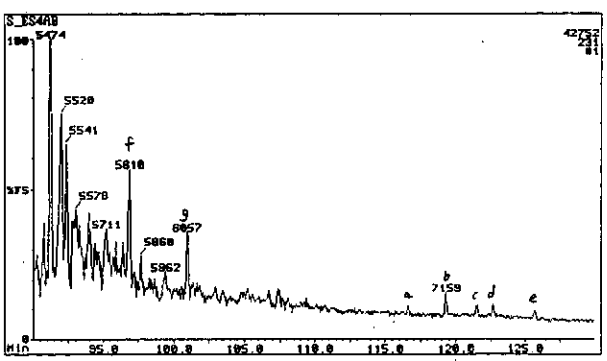

f) m/z 231: Triaromatic Steroids

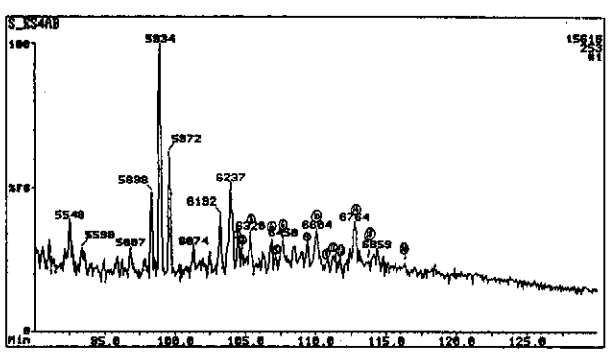

g) m/z 253: Monoaromatic Steroids (from aromatic fraction)

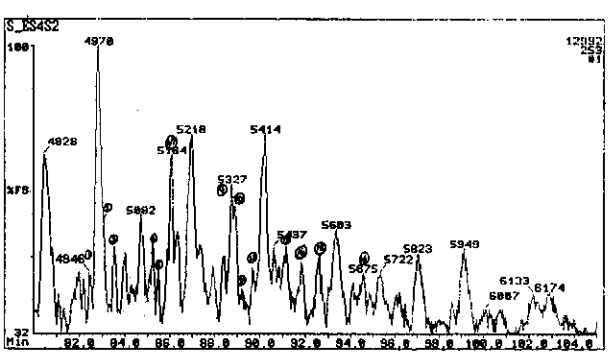

h) m/z 253: Monoaromatic Steroids (from saturates fraction)

Figure E.91: Annotated TIC and single ion fragmentograms of aromatic hydrocarbons from sample 23, well 59 DST 1, 2212m.

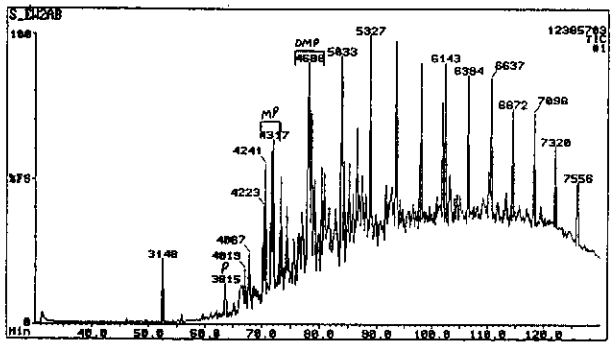

a) TIC: Total Ion Count

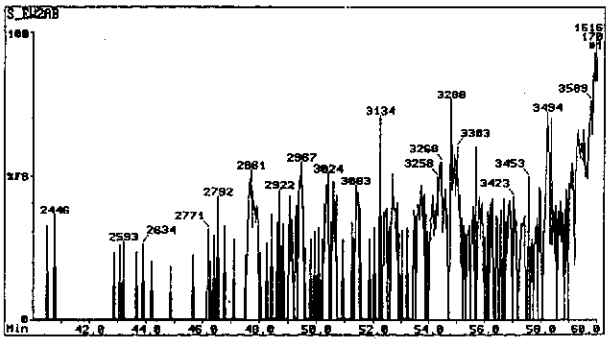

b) m/z 170: Trimethyl Napthalenes

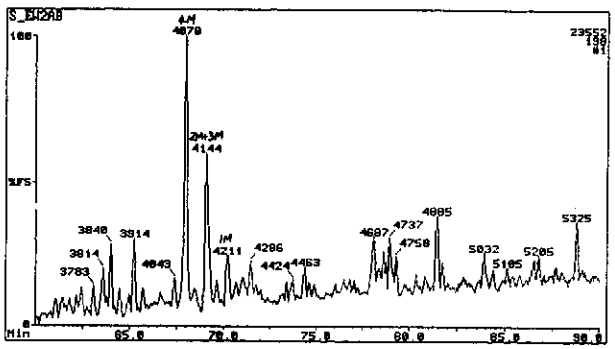

c) m/z 198: Methyl DibenzoThiophenes

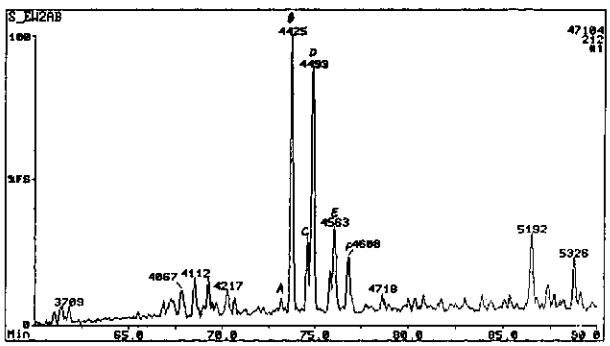

d) m/z 212: Dimethyl DibenzoThiophenes

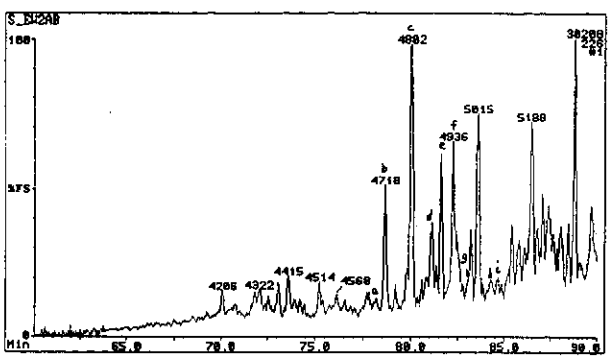

e) m/z 226: Trimethyl DibenzoThiophenes

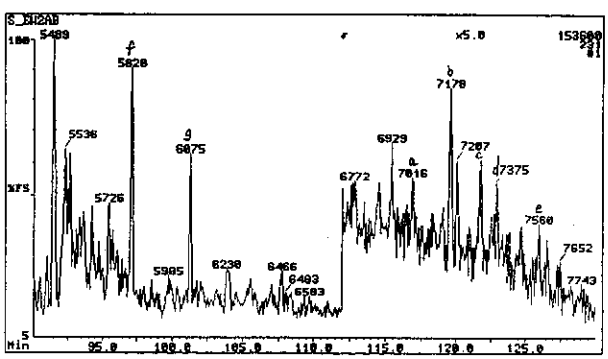

f) m/z 231: Triaromatic Steroids

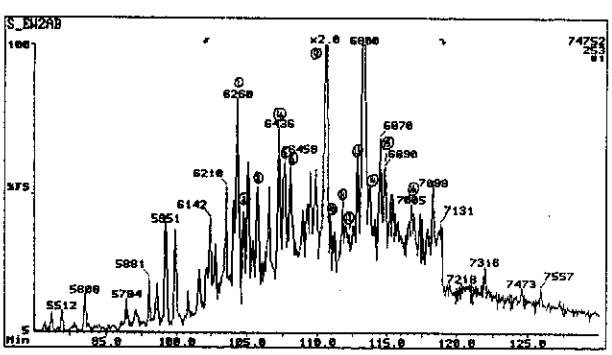

g) m/z 253: Monoaromatic Steroids (from aromatic fraction)

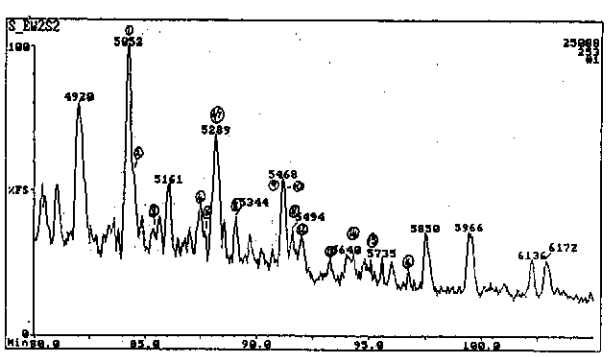

h) m/z 253: Monoaromatic Steroids (from saturates fraction)

Figure E.92: Annotated TIC and single ion fragmentograms of aromatic hydrocarbons from sample 24, well 75 core 1, 2830.5m.

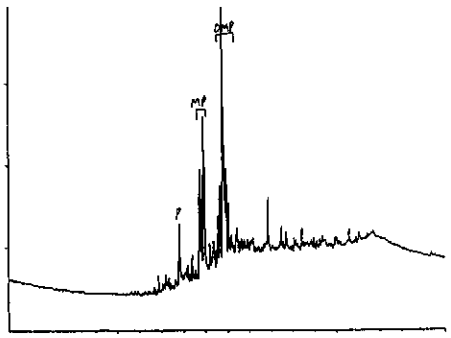

a) TIC: Total Ion Count

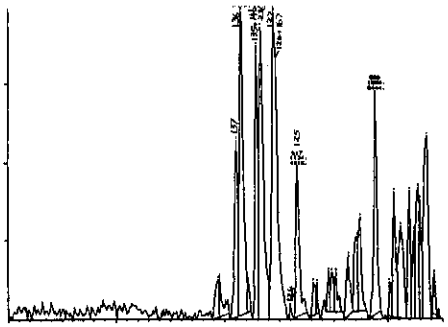

b) m/z 170: Trimethyl Napthalenes

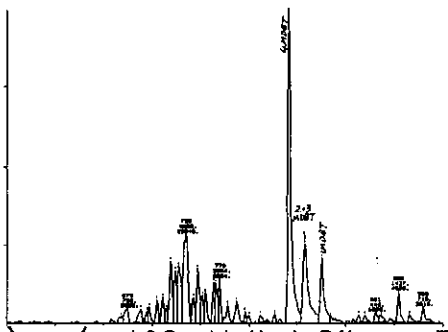

c) m/z 198: Methyl DibenzoThiophenes

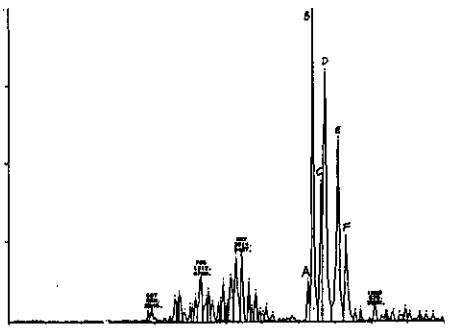

d) m/z 212: Dimethyl DibenzoThiophenes

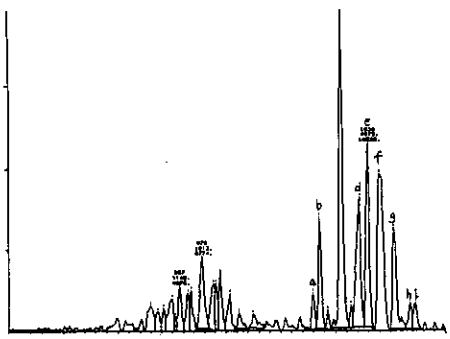

e) m/z 226: Trimethyl DibenzoThiophenes

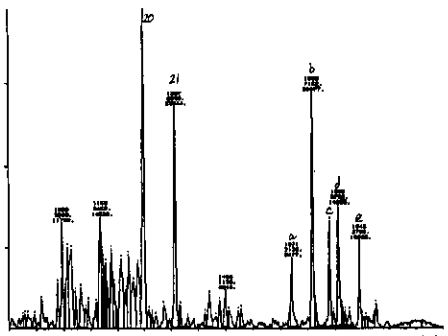

f) m/z 231: Triaromatic Steroids

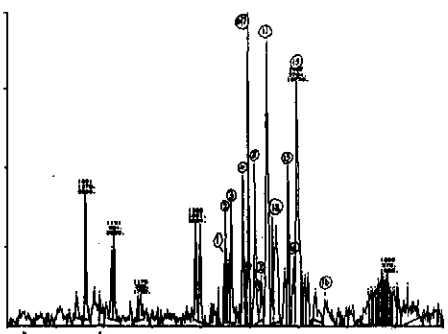

g) m/z 253: Monoaromatic Steroids (from aromatic fraction)

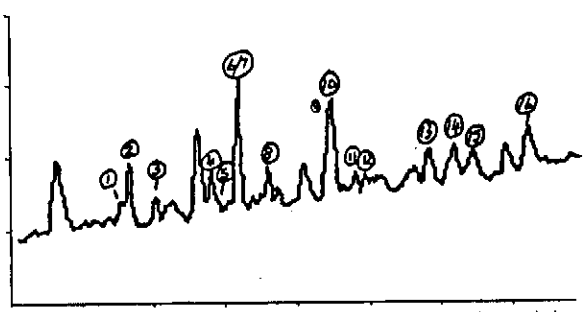

h) m/z 253: Monoaromatic Steroids (from saturates fraction)

Figure E.93: Annotated TIC and single ion fragmentograms of aromatic hydrocarbons from sample 25, well 101 core 1, 2987.5m.

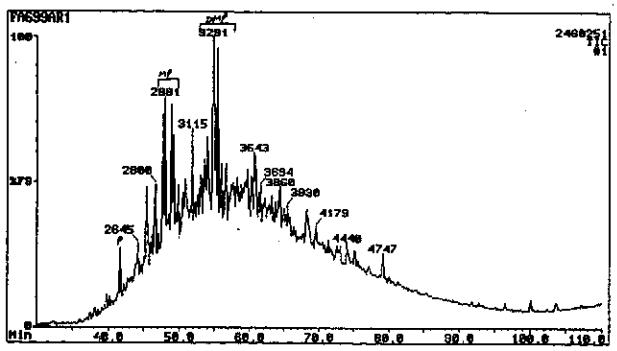

a) TIC: Total Ion Count

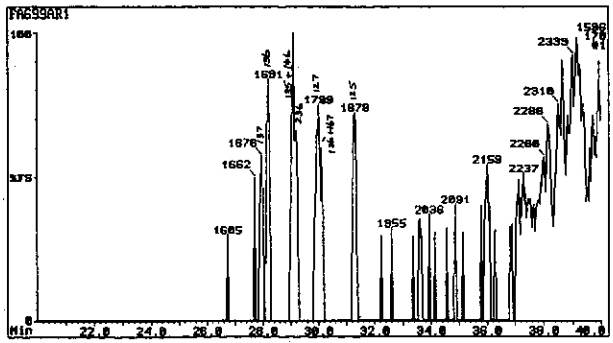

b) m/z 170: Trimethyl Napthalenes

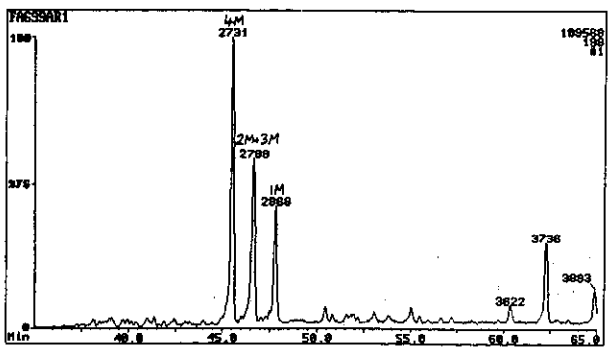

c) m/z 198: Methyl DibenzoThiophenes

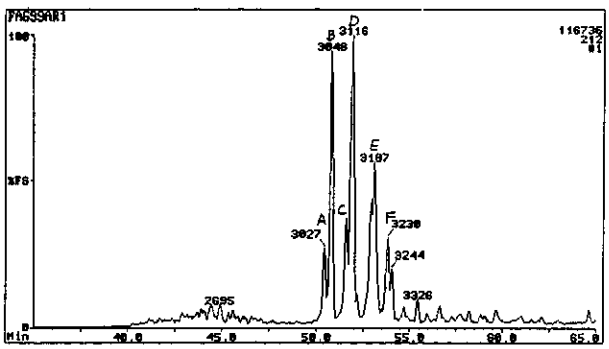

d) m/z 212: Dimethyl DibenzoThiophenes

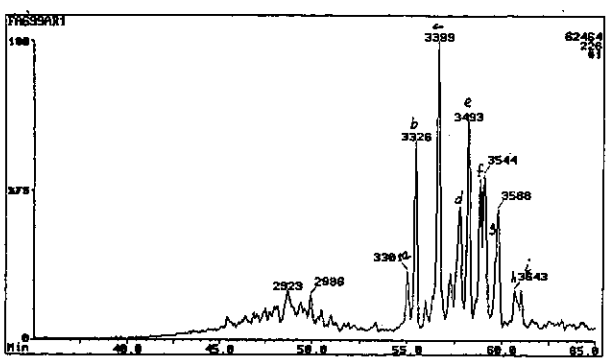

e) m/z 226: Trimethyl DibenzoThiophenes

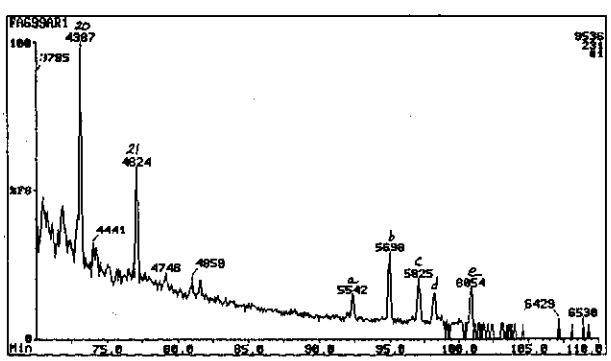

f) m/z 231: Triaromatic Steroids

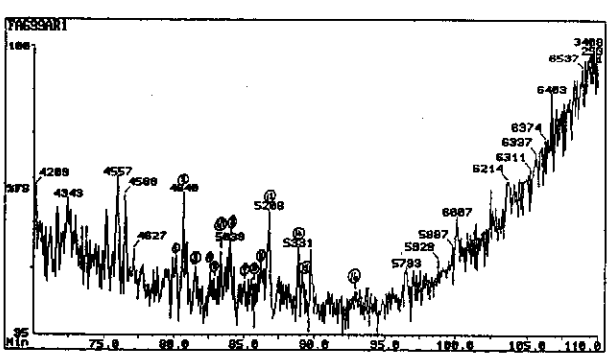

g) m/z 253: Monoaromatic Steroids (from aromatic fraction)

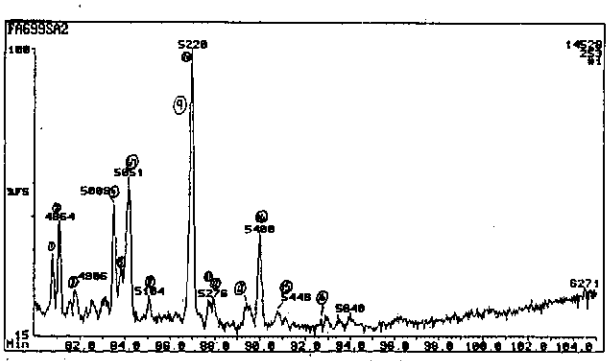

h) m/z 253: Monoaromatic Steroids (from saturates fraction)

Figure E.94: Annotated TIC and single ion fragmentograms of aromatic hydrocarbons from sample 26, well 20 DST 2, 2699m.

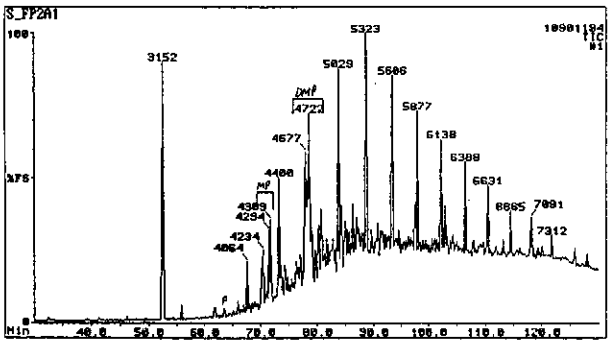

a) TIC: Total Ion Count

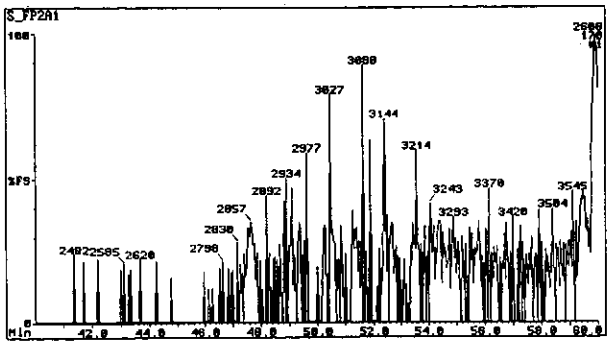

b) m/z 170: Trimethyl Napthalenes

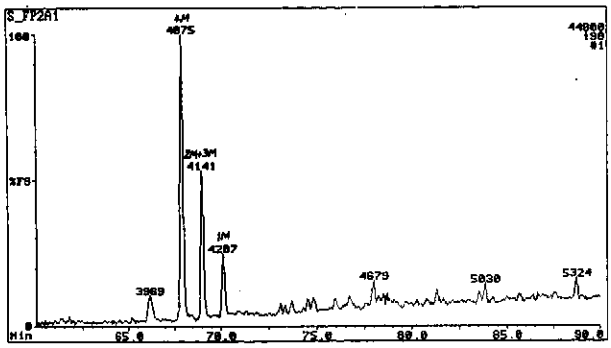

c) m/z 198: Methyl DibenzoThiophenes

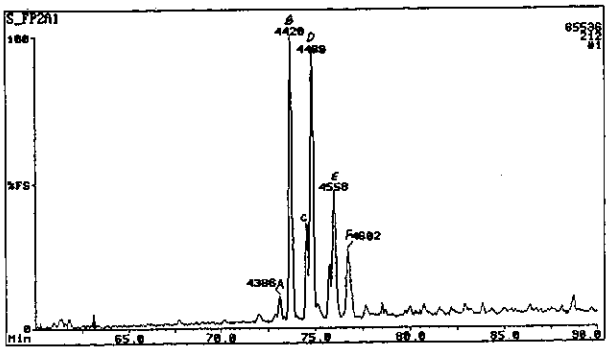

d) m/z 212: Dimethyl DibenzoThiophenes

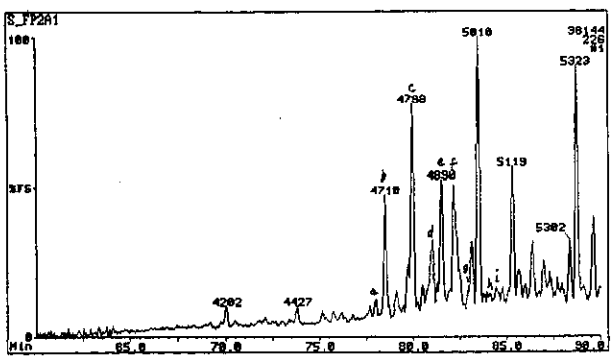

e) m/z 226: Trimethyl DibenzoThiophenes

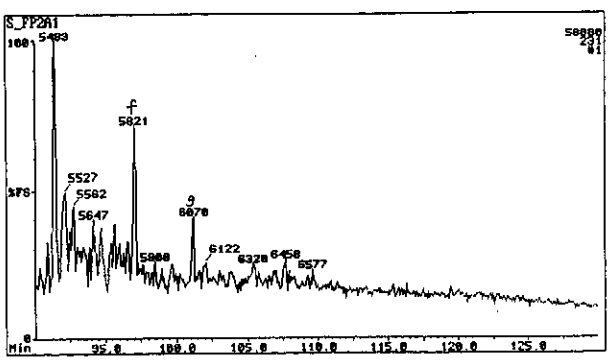

f) m/z 231: Triaromatic Steroids

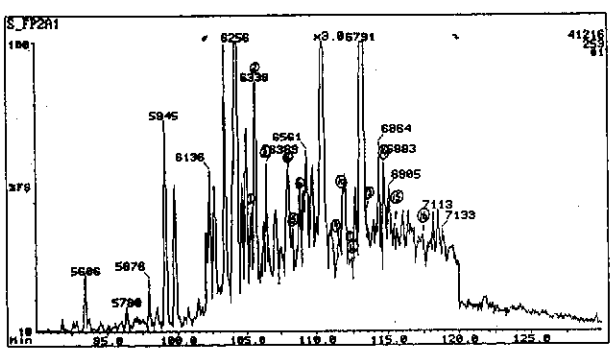

g) m/z 253: Monoaromatic Steroids (from aromatic fraction)

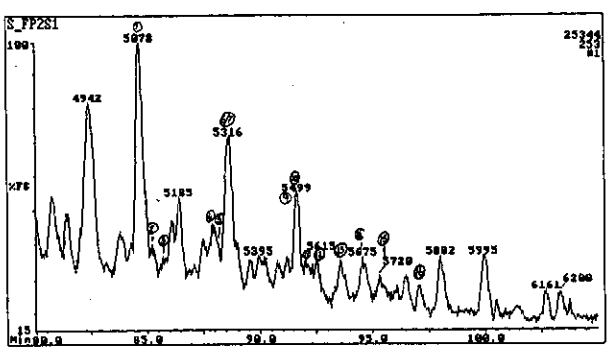

h) m/z 253: Monoaromatic Steroids (from saturates fraction)

Figure E.95: Annotated TIC and single ion fragmentograms of aromatic hydrocarbons from sample 27, well 13 core 1, 2518.86m.

not analysed

not analysed

a) TIC: Total Ion Count

b) m/z 170: Trimethyl Napthalenes

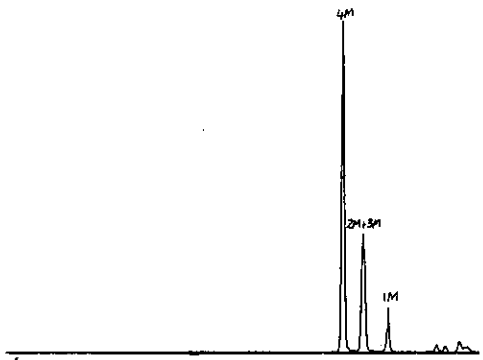

not analysed

c) m/z 198: Methyl DibenzoThiophenes

d) m/z 212: Dimethyl DibenzoThiophenes

not analysed

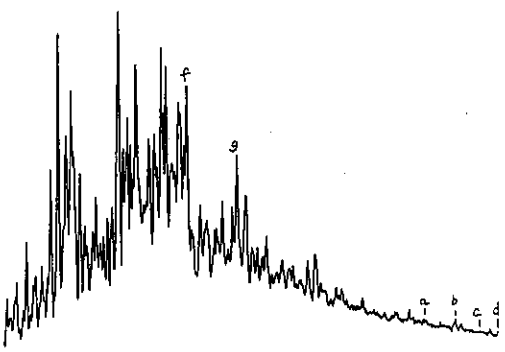

e) m/z 226: Trimethyl DibenzoThiophenes

f) m/z 231: Triaromatic Steroids

not analysed

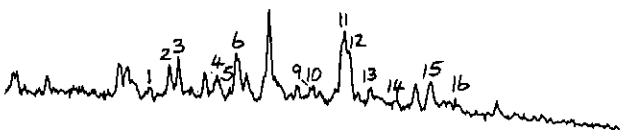

g) m/z 253: Monoaromatic Steroids (from aromatic fraction)

h) m/z 253: Monoaromatic Steroids (from saturates fraction)

Figure E.96: Annotated TIC and single ion fragmentograms of aromatic hydrocarbons from sample 28, well 103 DST 2, 2718m.

not analysed

not analysed

a) TIC: Total Ion Count

b) m/z 170: Trimethyl Napthalenes

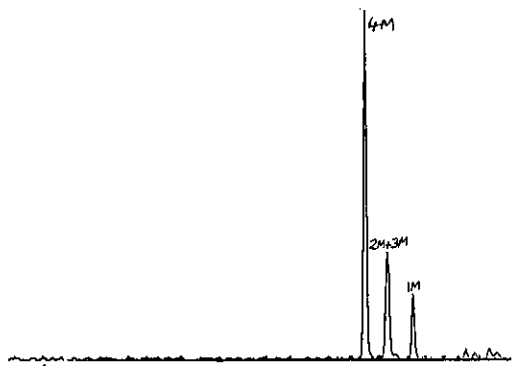

c) m/z 198: Methyl DibenzoThiophenes

not analysed

d) m/z 212: Dimethyl DibenzoThiophenes

not analysed

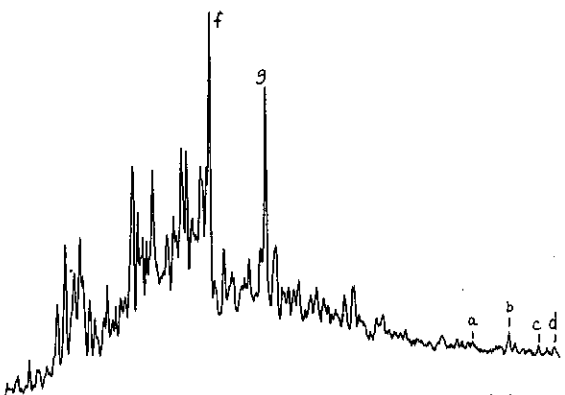

e) m/z 226: Trimethyl DibenzoThiophenes

f) m/z 231: Triaromatic Steroids

not analysed

g) m/z 253: Monóaromatic Steroids (from aromatic fraction)

h) m/z 253: Monoaromatic Steroids (from saturates fraction)

Figure E.97: Annotated TIC and single ion fragmentograms of aromatic hydrocarbons from sample 29, well 94 DST 1, 2799m.

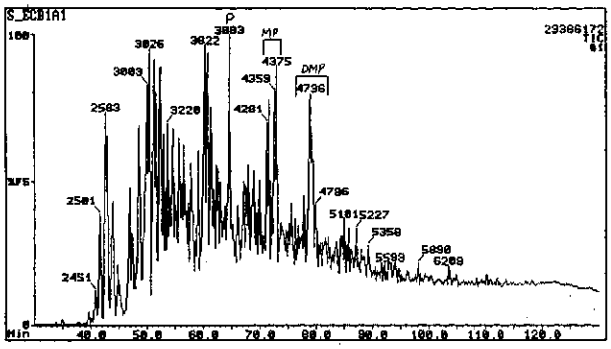

a) TIC: Total Ion Count

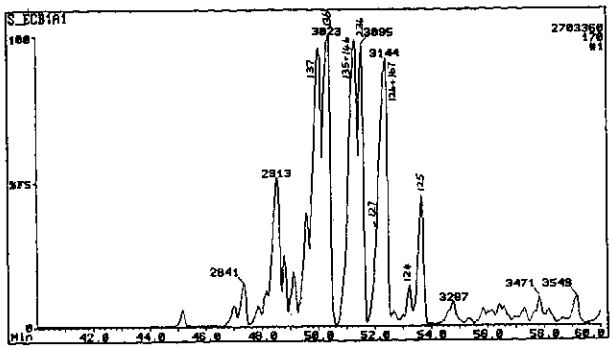

b) m/z 170: Trimethyl Napthalenes

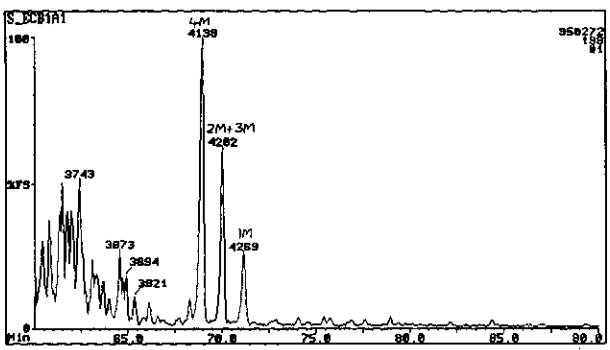

c) m/z 198: Methyl DibenzoThiophenes

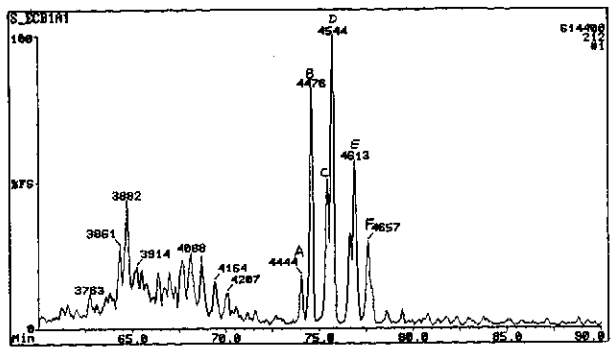

d) m/z 212: Dimethyl DibenzoThiophenes

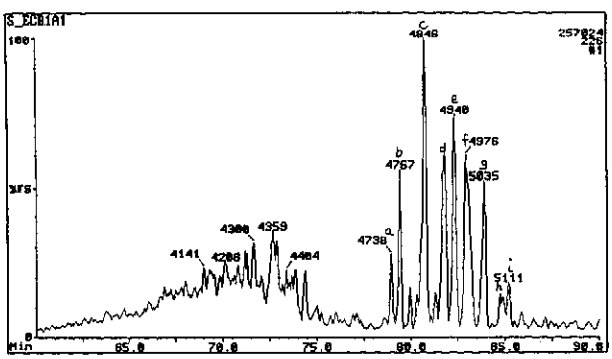

e) m/z 226: Trimethyl DibenzoThiophenes

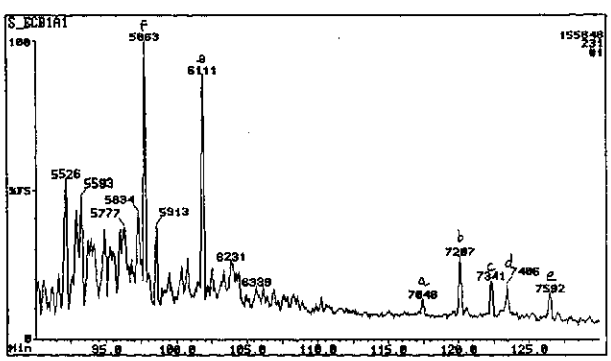

f) m/z 231: Triaromatic Steroids

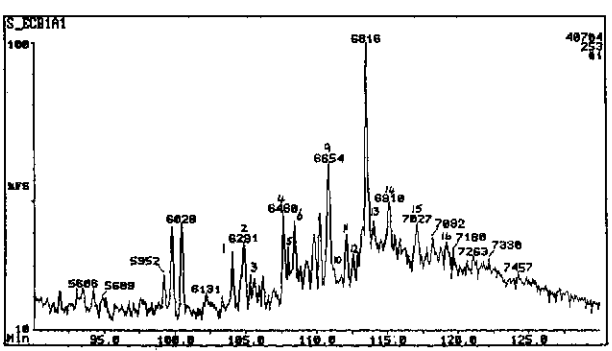

g) m/z 253: Monoaromatic Steroids (from aromatic fraction)

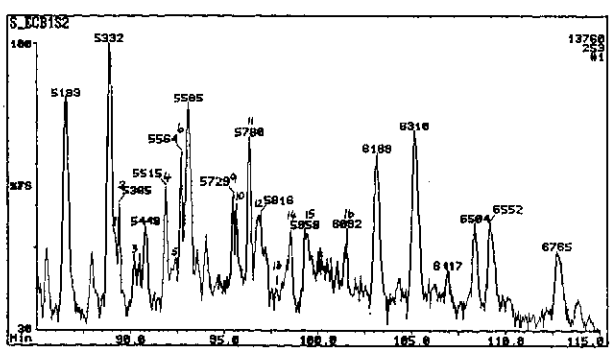

h) m/z 253: Monoaromatic Steroids (from saturates fraction)

Figure E.98: Annotated TIC and single ion fragmentograms of aromatic hydrocarbons from sample 30, well 156 DST 1, 2522m.

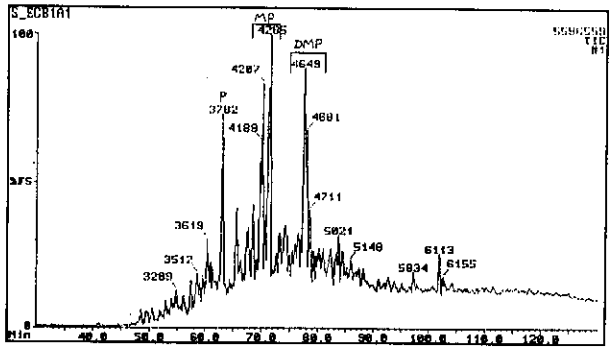

a) TIC: Total Ion Count

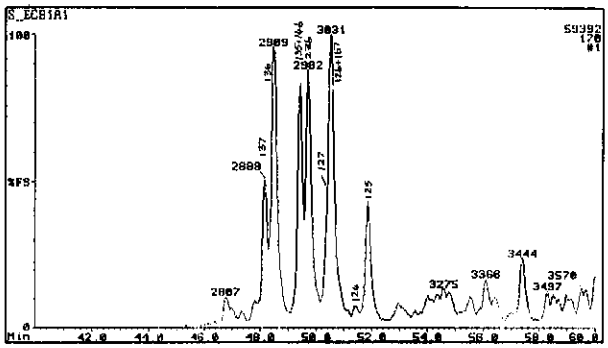

b) m/z 170: Trimethyl Napthalenes

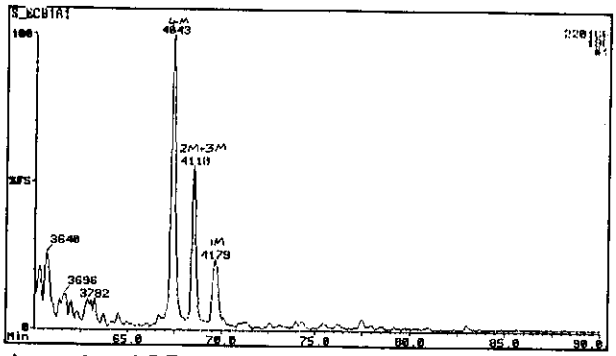

c) m/z 198: Methyl DibenzoThiophenes

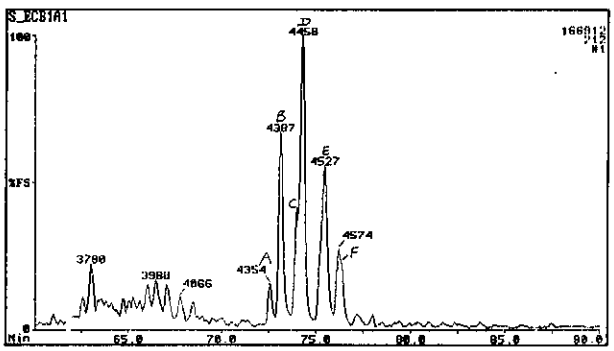

d) m/z 212: Dimethyl DibenzoThiophenes

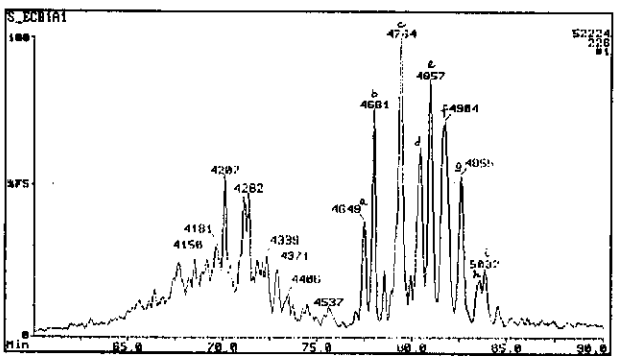

e) m/z 226: Trimethyl DibenzoThiophenes

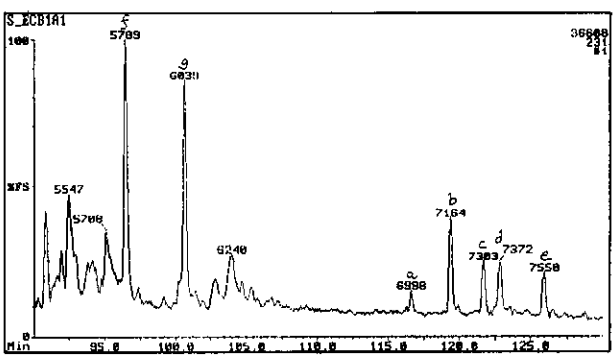

f) m/z 231: Triaromatic Steroids

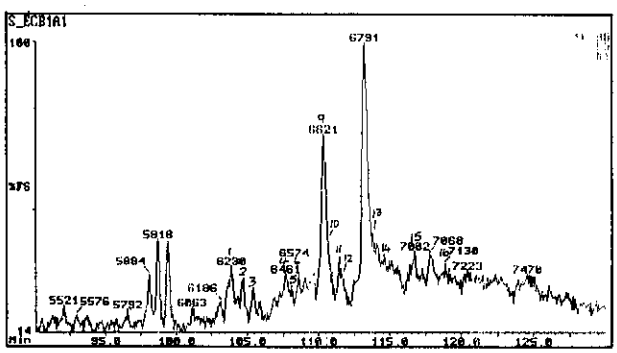

g) m/z 253: Monoaromatic Steroids (from aromatic fraction)

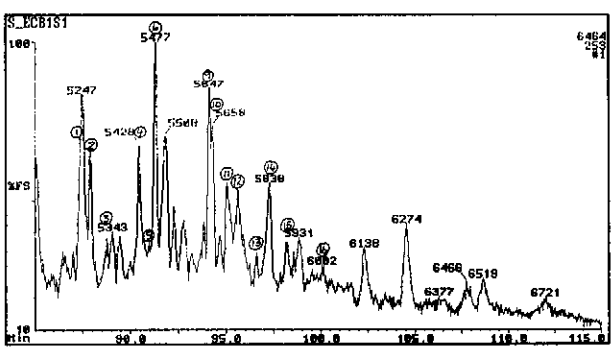

h) m/z 253: Monoaromatic Steroids (from saturates fraction)

Figure E.99: Annotated TIC and single ion fragmentograms of aromatic hydrocarbons from sample 31, well 156 core 1, 2525m.

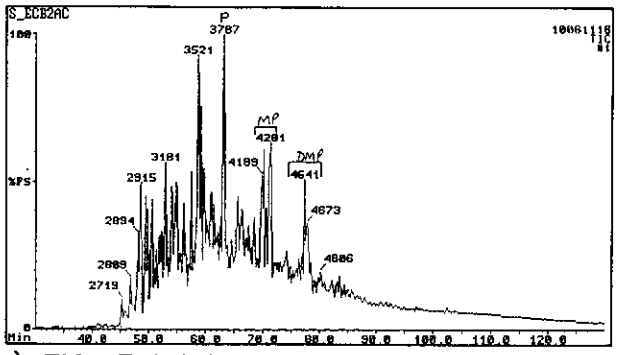

a) TIC: Total Ion Count

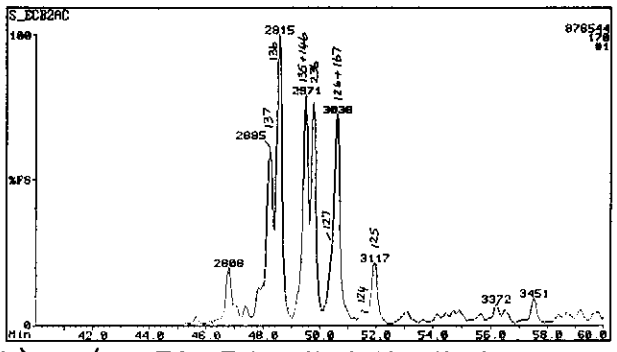

b) m/z 170: Trimethyl Napthalenes

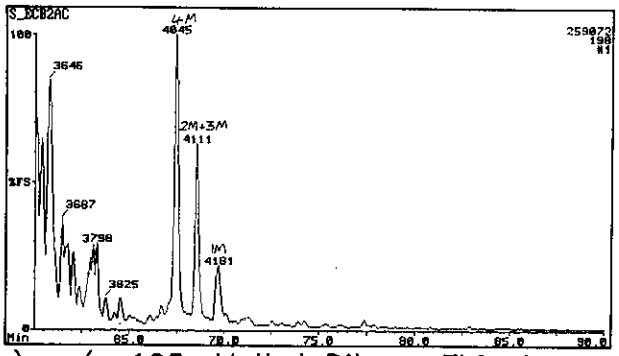

c) m/z 198: Methyl DibenzoThiophenes

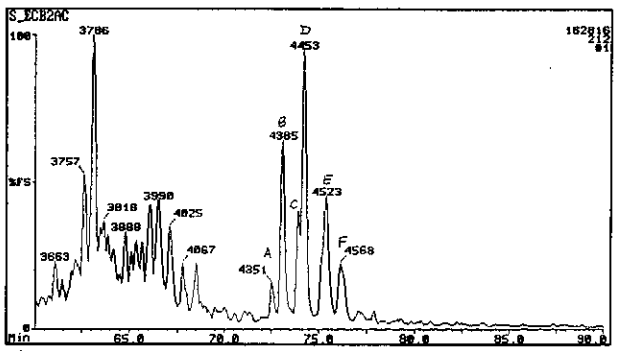

d) m/z 212: Dimethyl DibenzoThiophenes

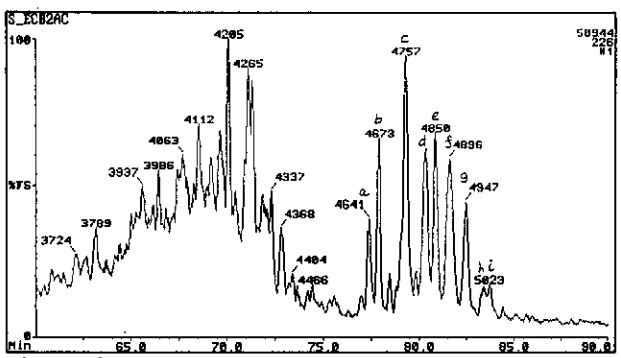

e) m/z 226: Trimethyl DibenzoThiophenes

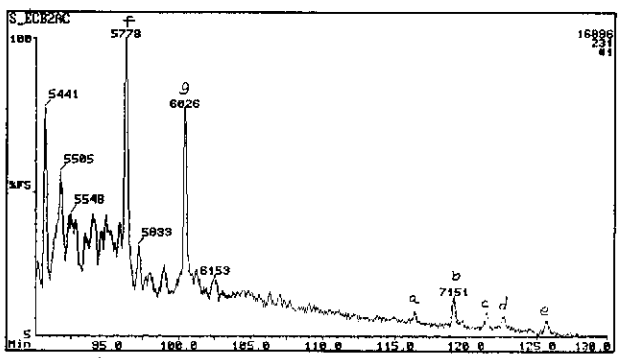

f) m/z 231: Triaromatic Steroids

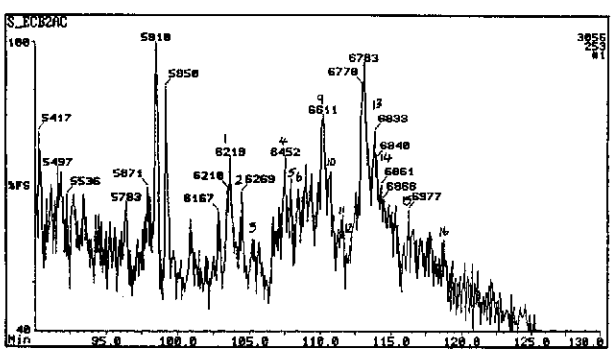

g) m/z 253: Monoaromatic Steroids (from aromatic fraction)

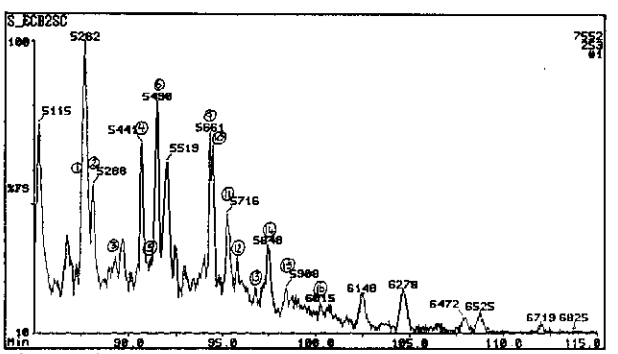

h) m/z 253: Monoaromatic Steroids (from saturates fraction)

Figure E.100: Annotated TIC and single ion fragmentograms of aromatic hydrocarbons from sample 32, well 166 RFT, 2508m.

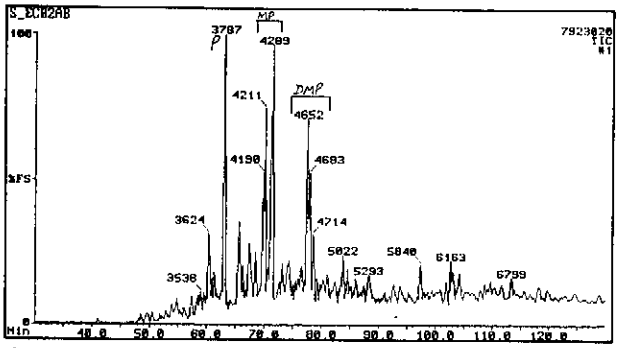

a) TIC: Total Ion Count

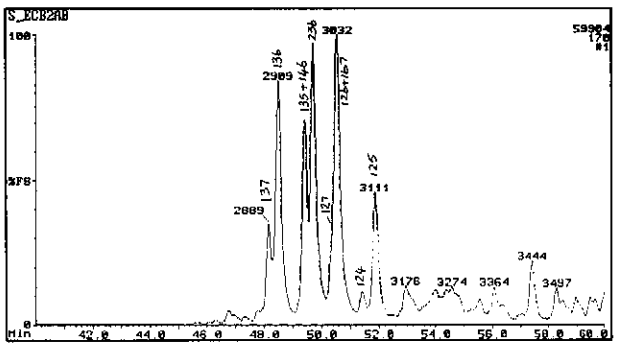

b) m/z 170: Trimethyl Napthalenes

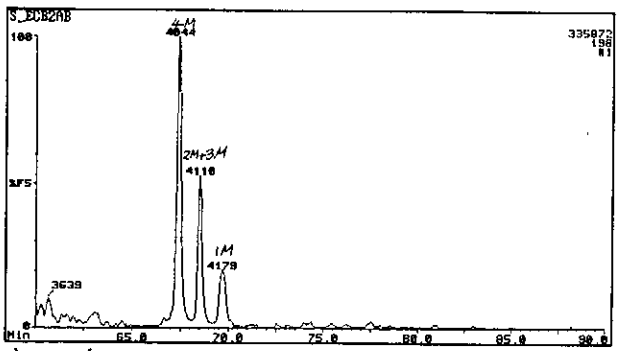

c) m/z 198: Methyl DibenzoThiophenes

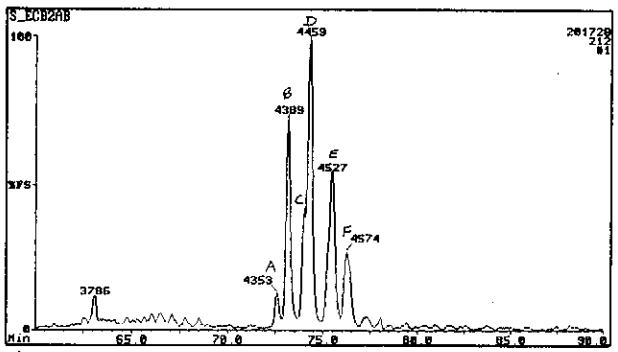

d) m/z 212: Dimethyl DibenzoThiophenes

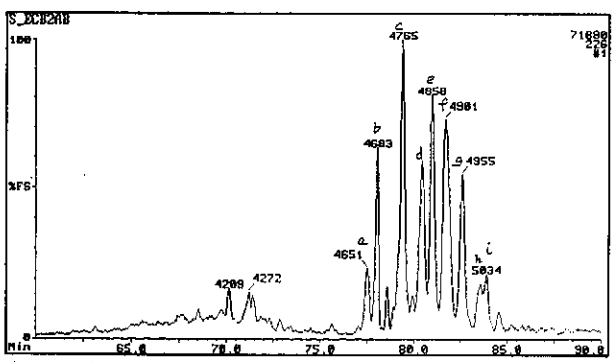

e) m/z 226: Trimethyl DibenzoThiophenes

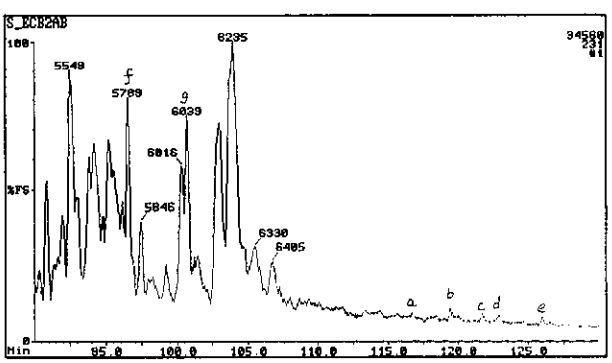

f) m/z 231: Triaromatic Steroids

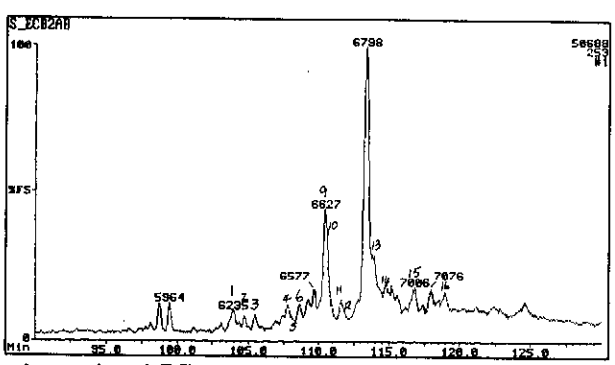

g) m/z 253: Monoaromatic Steroids (from aromatic fraction)

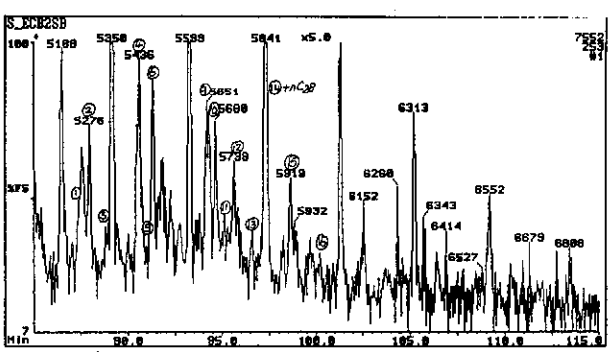

h) m/z 253: Monoaromatic Steroids (from saturates fraction)

Figure E.101: Annotated TIC and single ion fragmentograms of aromatic hydrocarbons from sample 33, well 166 core 1, 2510.43m.

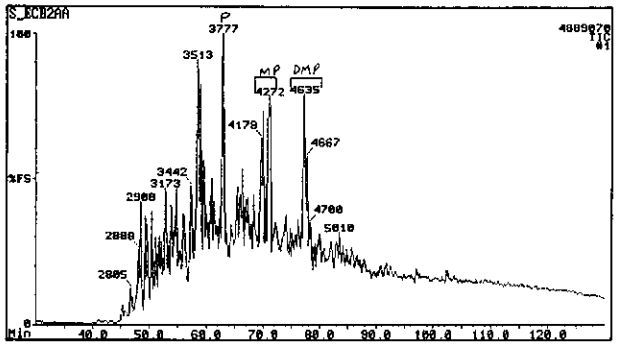

a) TIC: Total Ion Count

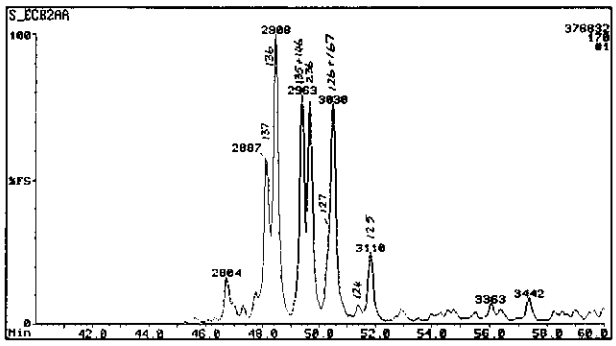

b) m/z 170: Trimethyl Napthalenes

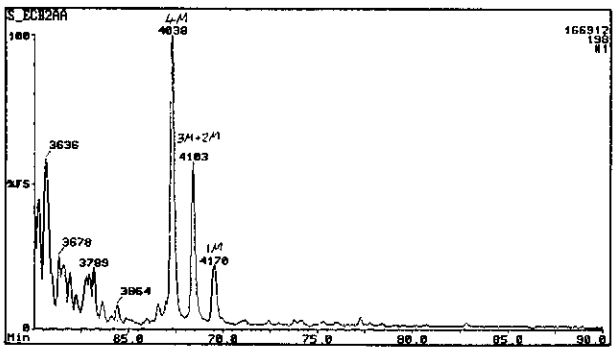

c) m/z 198: Methyl DibenzoThiophenes

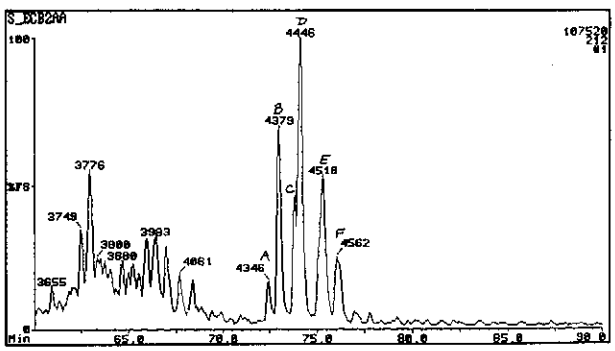

d) m/z 212: Dimethyl DibenzoThiophenes

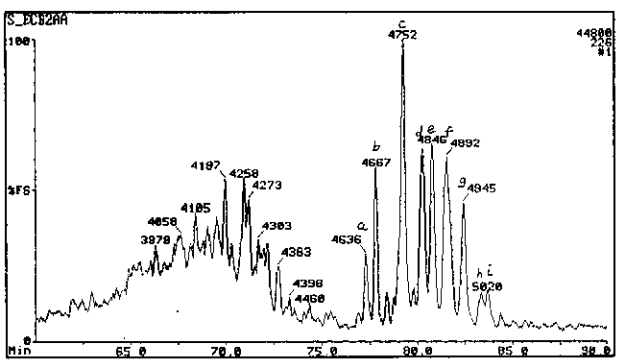

e) m/z 226: Trimethyl DibenzoThiophenes

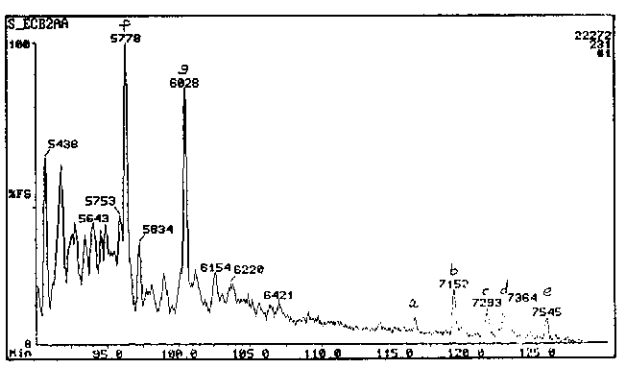

f) m/z 231: Triaromatic Steroids

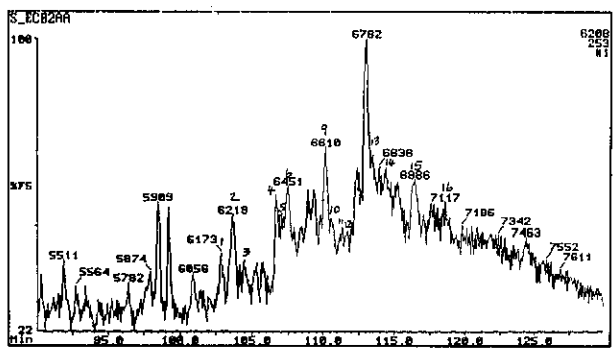

g) m/z 253: Monoaromatic Steroids (from aromatic fraction)

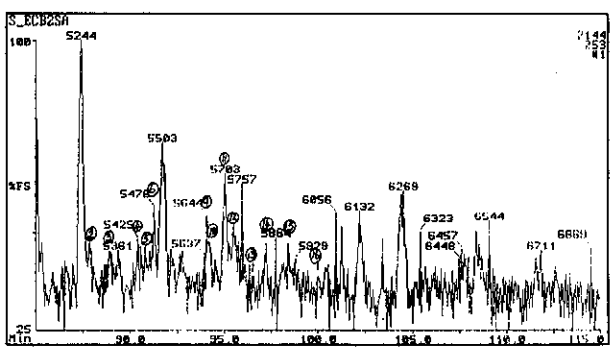

h) m/z 253: Monoaromatic Steroids (from saturates fraction)

Figure E.102: Annotated TIC and single ion fragmentograms of aromatic hydrocarbons from sample 34, well 166 DST 1, 2520m.

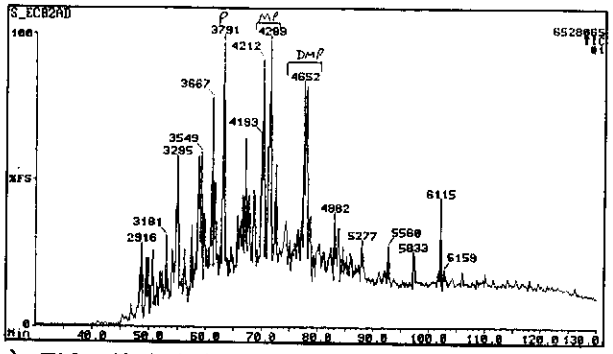

a) TIC: Total Ion Count

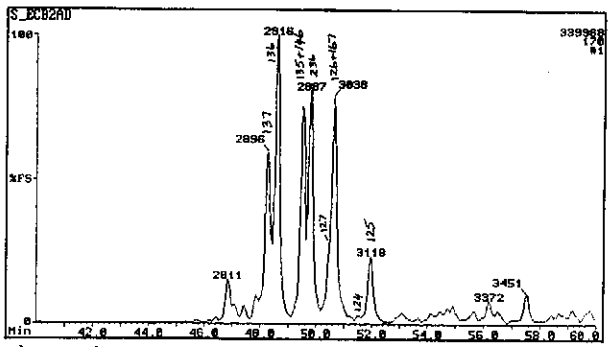

b) m/z 170: Trimethyl Napthalenes

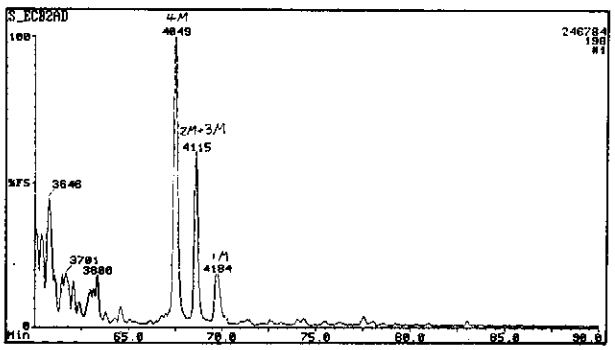

c) m/z 198: Methyl DibenzoThiophenes

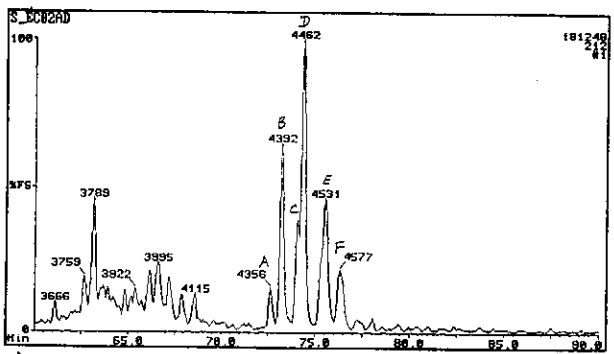

d) m/z 212: Dimethyl DibenzoThiophenes

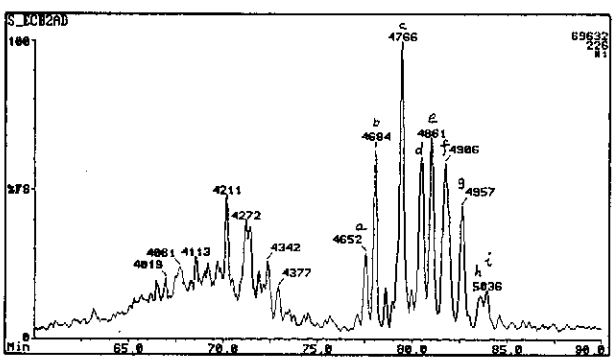

e) m/z 226: Trimethyl DibenzoThiophenes

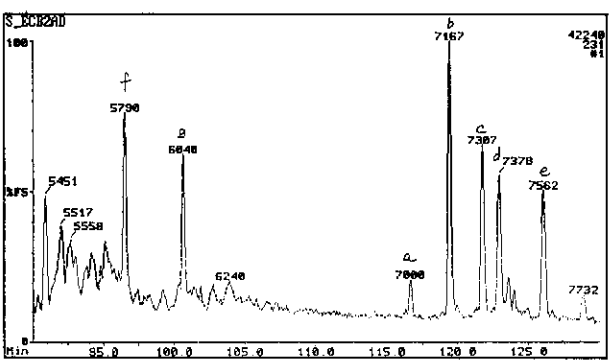

f) m/z 231: Triaromatic Steroids

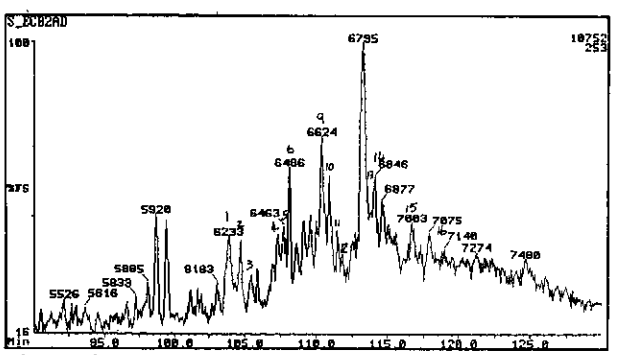

g) m/z 253: Monoaromatic Steroids (from aromatic fraction)

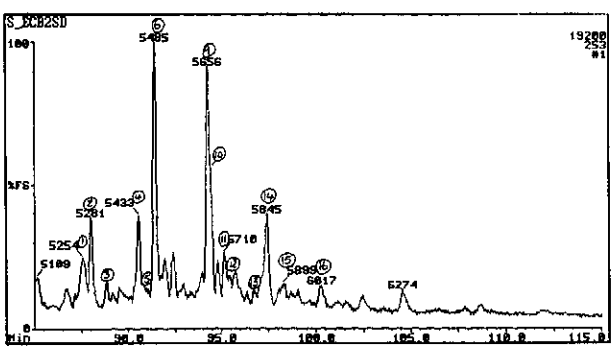

h) m/z 253: Monoaromatic Steroids (from saturates fraction)

Figure E.103: Annotated TIC and single ion fragmentograms of aromatic hydrocarbons from sample 35, well 166 core 1, 2522.5m.

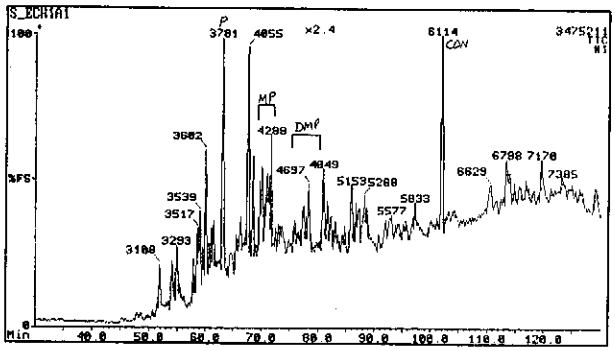

a) TIC: Total Ion Count

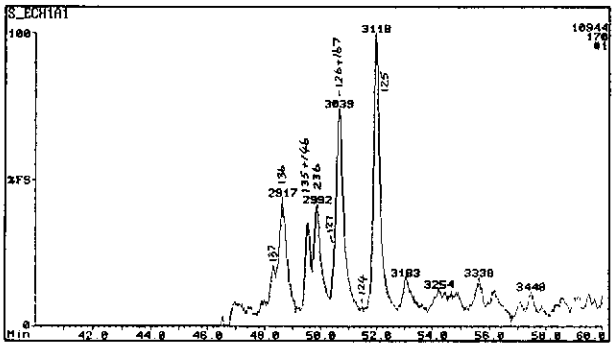

b) m/z 170: Trimethyl Napthalenes

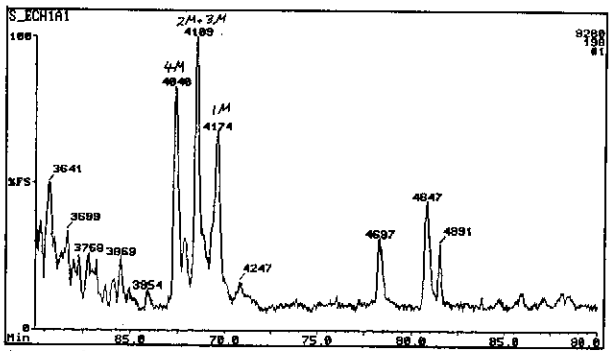

c) m/z 198: Methyl DibenzoThiophenes

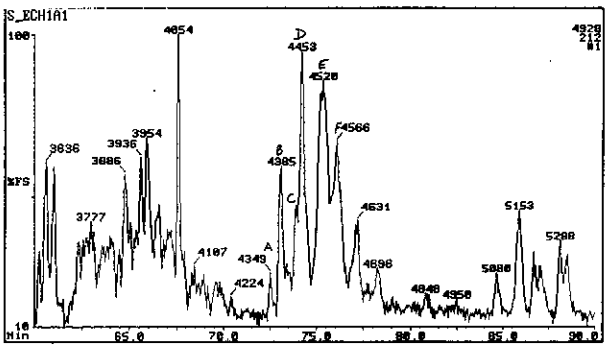

d) m/z 212: Dimethyl DibenzoThiophenes

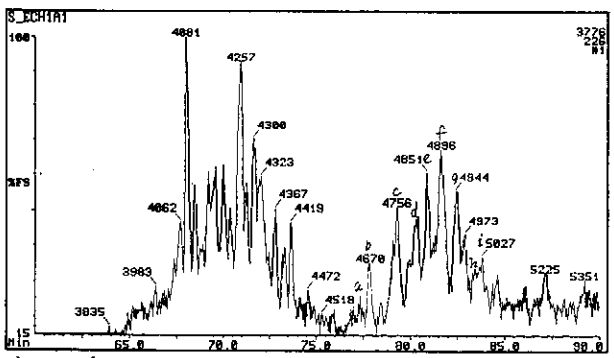

e) m/z 226: Trimethyl DibenzoThiophenes

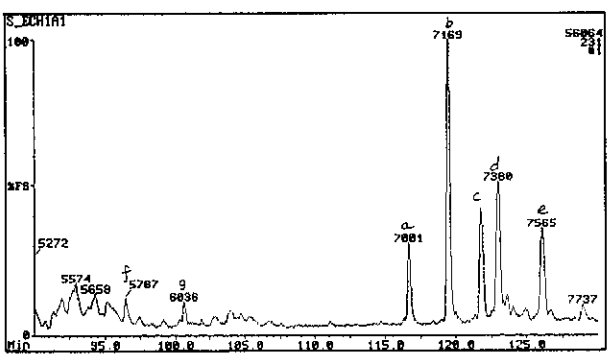

f) m/z 231: Triaromatic Steroids

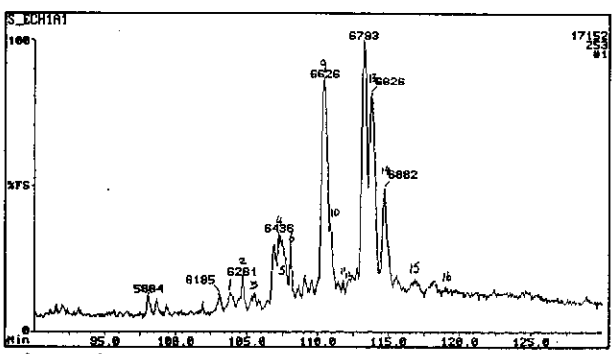

g) m/z 253: Monoaromatic Steroids (from aromatic fraction)

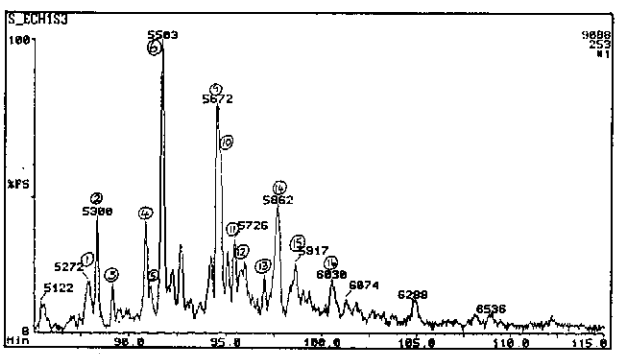

h) m/z 253: Monoaromatic Steroids (from saturates fraction)

Figure E.104: Annotated TIC and single ion fragmentograms of aromatic hydrocarbons from sample 36, well 165 RC, 2256m.

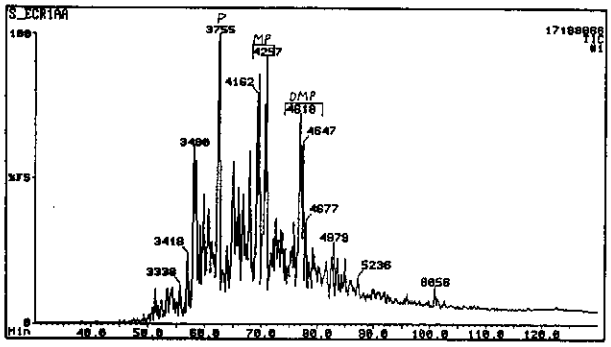

a) TIC: Total Ion Count

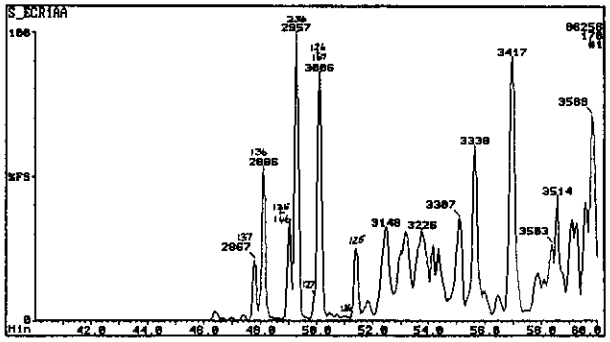

b) m/z 170: Trimethyl Napthalenes

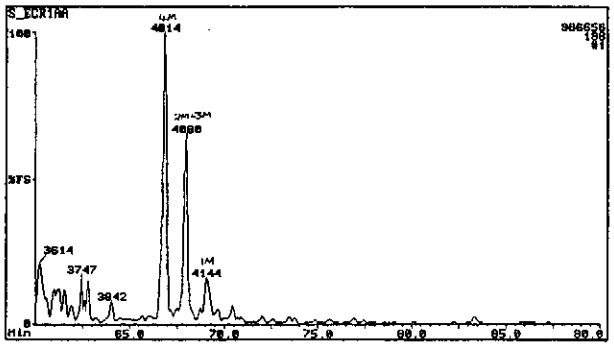

c) m/z 198: Methyl DibenzoThiophenes

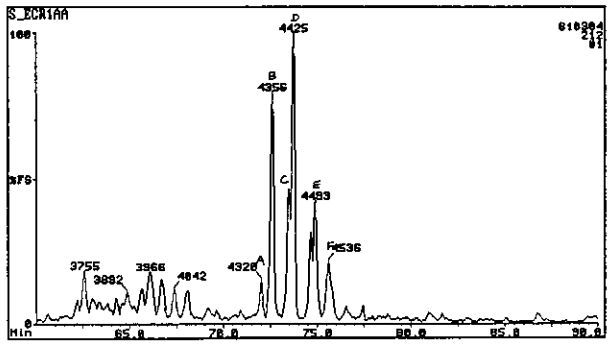

d) m/z 212: Dimethyl DibenzoThiophenes

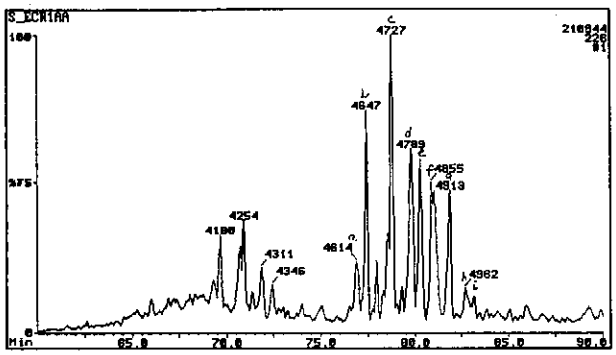

e) m/z 226: Trimethyl DibenzoThiophenes

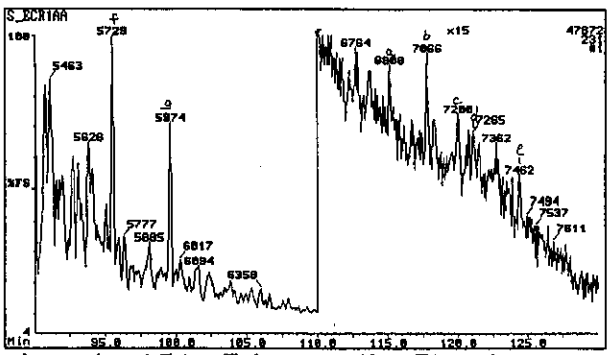

f) m/z 231: Triaromatic Steroids

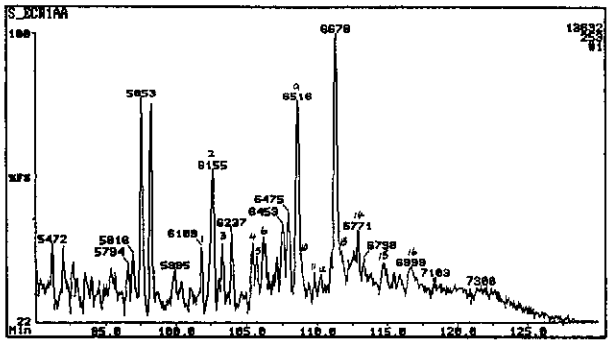

g) m/z 253: Monoaromatic Steroids (from aromatic fraction)

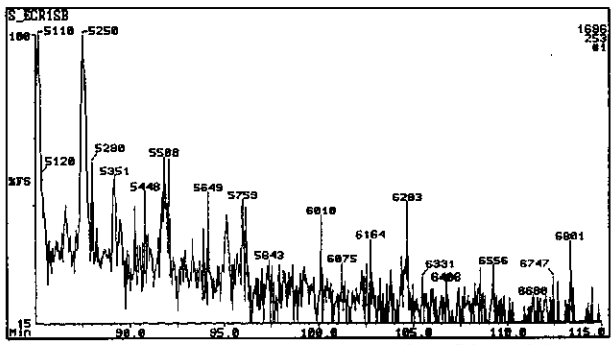

h) m/z 253: Monoaromatic Steroids (from saturates fraction)

Figure E.105: Annotated TIC and single ion fragmentograms of aromatic hydrocarbons from sample 37, well 167 DST 1, 2679m.

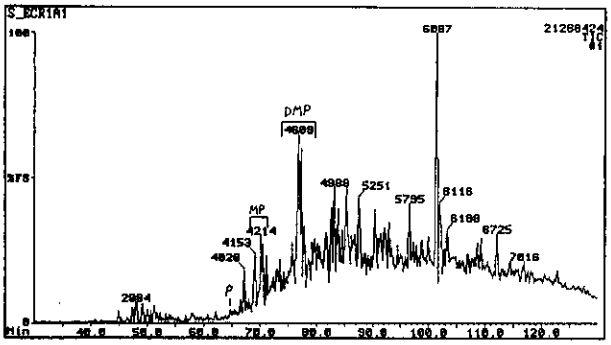

a) TIC: Total Ion Count

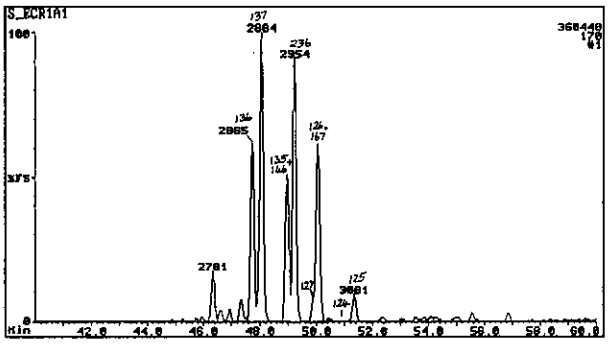

b) m/z 170: Trimethyl Napthalenes

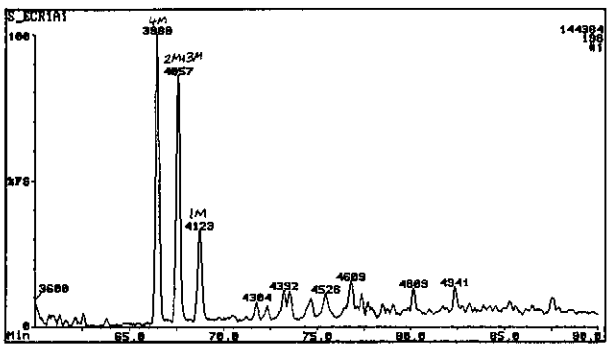

c) m/z 198: Methyl DibenzoThiophenes

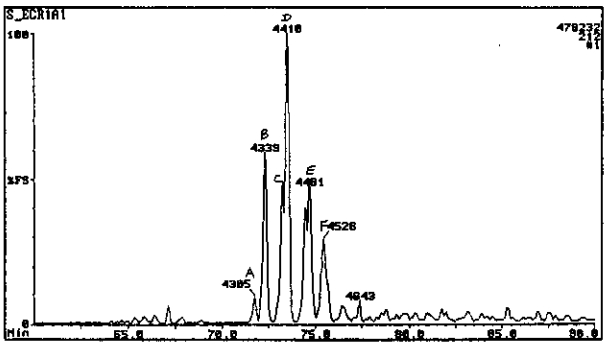

d) m/z 212: Dimethyl DibenzoThiophenes

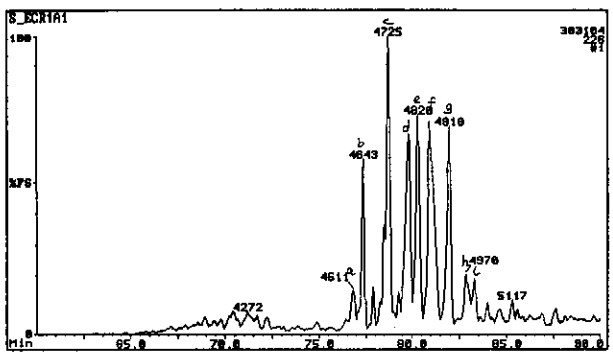

e) m/z 226: Trimethyl DibenzoThiophenes

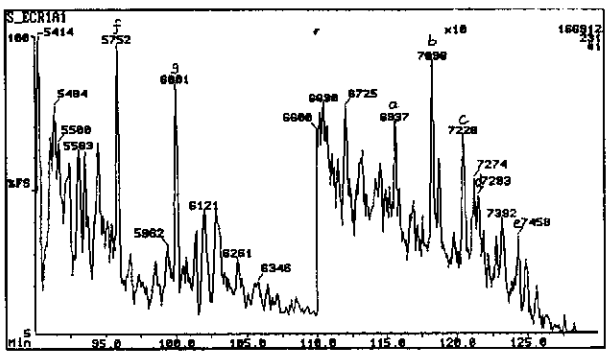

f) m/z 231: Triaromatic Steroids

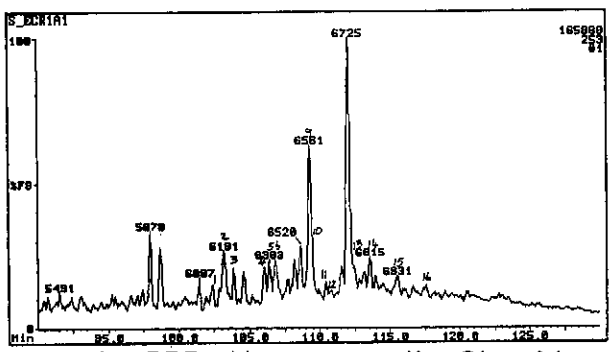

g) m/z 253: Monoaromatic Steroids (from aromatic fraction)

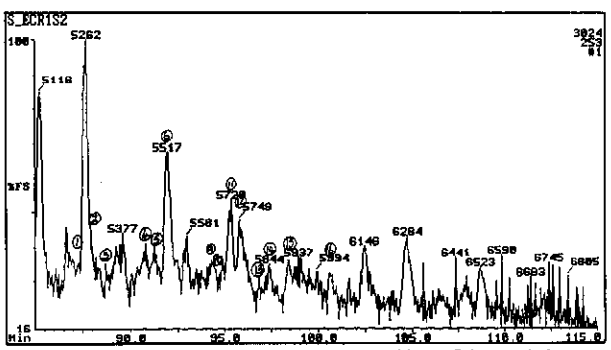

h) m/z 253: Monoaromatic Steroids (from saturates fraction)

Figure E.106: Annotated TIC and single ion fragmentograms of aromatic hydrocarbons from sample 38, well 167 core 1, 2681.65m.

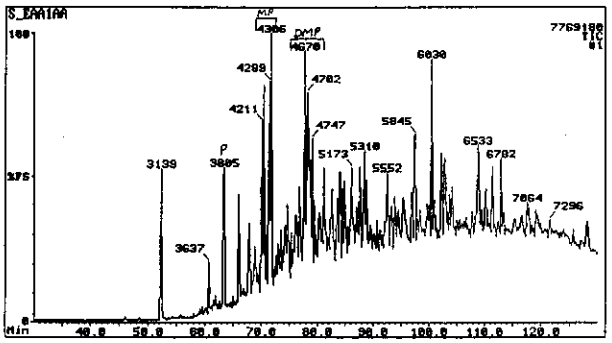

a) TIC: Total Ion Count

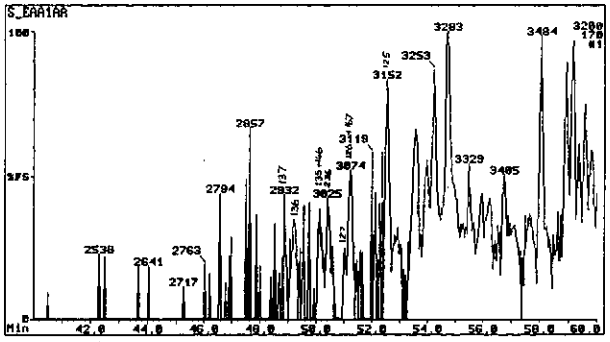

b) m/z 170: Trimethyl Napthalenes

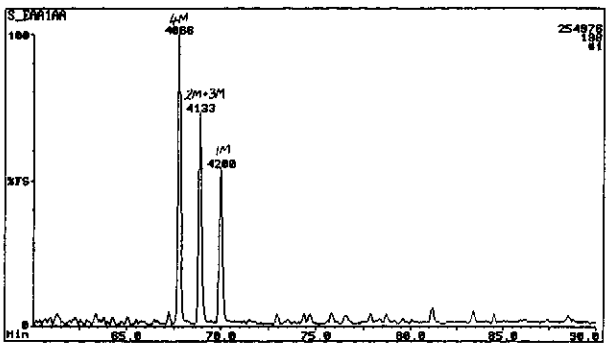

c) m/z 198: Methyl DibenzoThiophenes

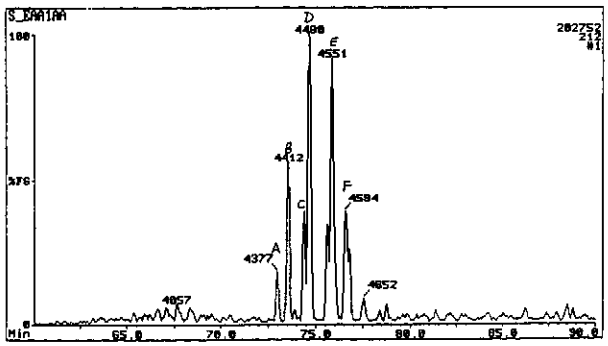

d) m/z 212: Dimethyl DibenzoThiophenes

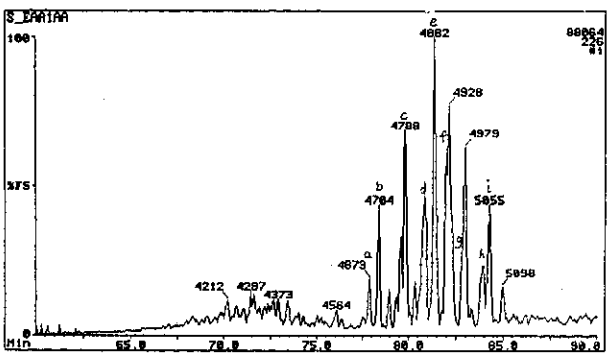

e) m/z 226: Trimethyl DibenzoThiophenes

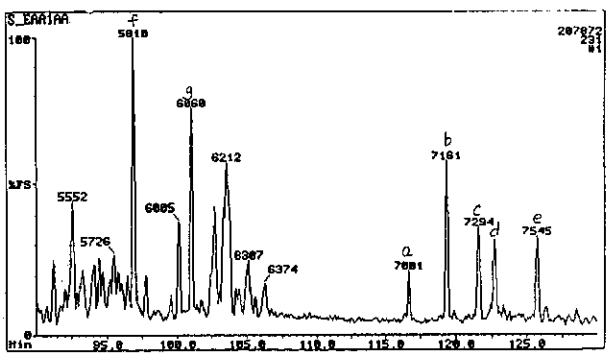

f) m/z 231: Triaromatic Steroids

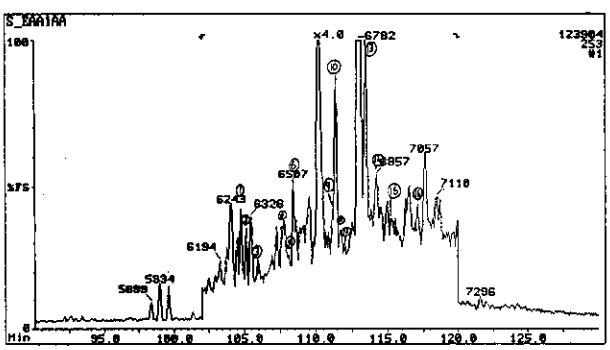

g) m/z 253: Monoaromatic Steroids (from aromatic fraction)

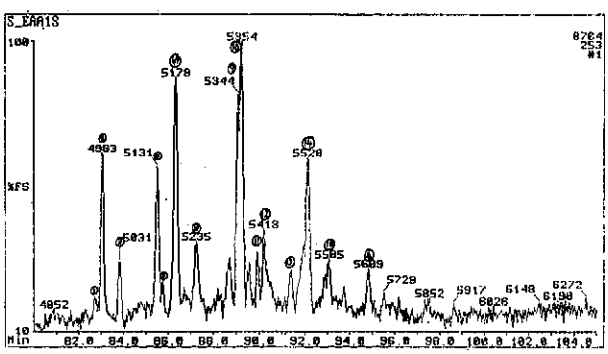

h) m/z 253: Monoaromatic Steroids (from saturates fraction)

Figure E.107: Annotated TIC and single ion fragmentograms of aromatic hydrocarbons from sample 41, well 83 RC, 2702m.

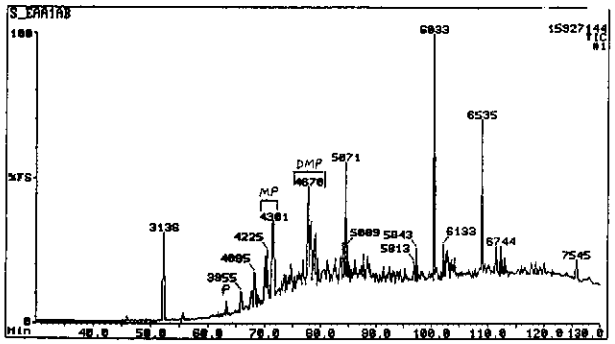

a) TIC: Total Ion Count

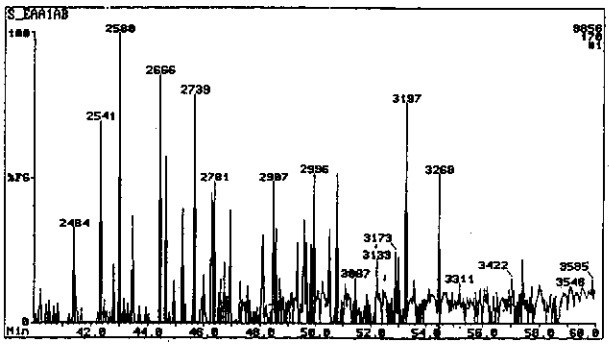

b) m/z 170: Trimethyl Napthalenes

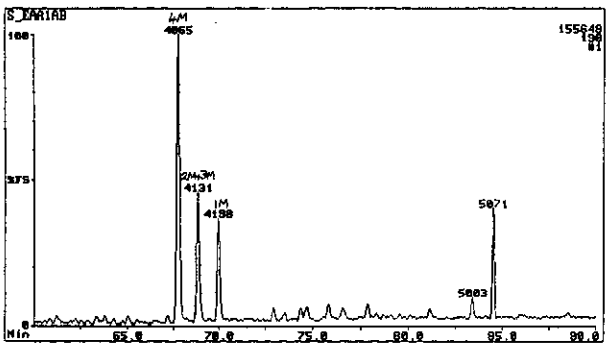

c) m/z 198: Methyl DibenzoThiophenes

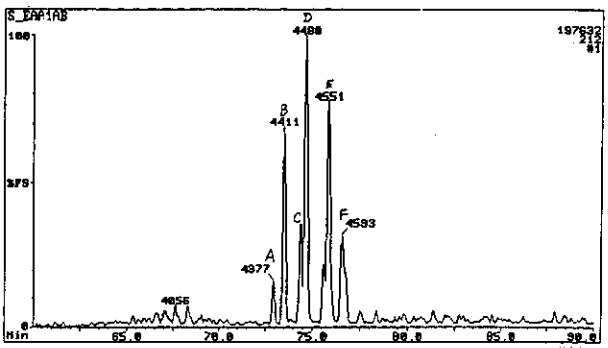

d) m/z 212: Dimethyl DibenzoThiophenes

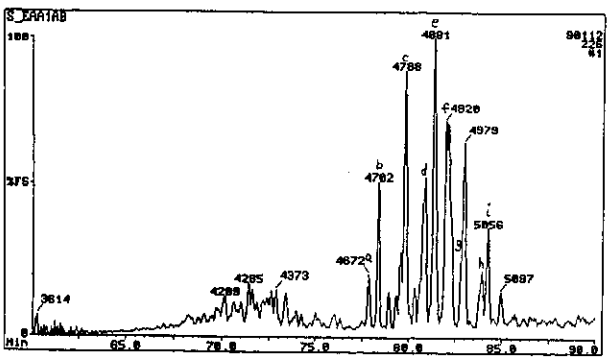

e) m/z 226: Trimethyl DibenzoThiophenes

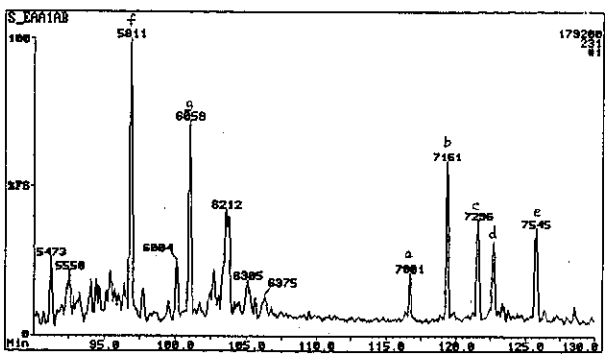

f) m/z 231: Triaromatic Steroids

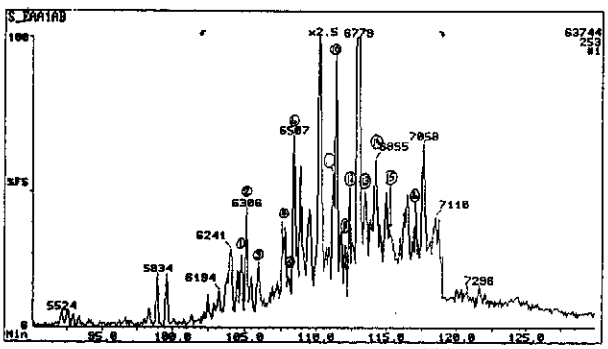

g) m/z 253: Monoaromatic Steroids (from aromatic fraction)

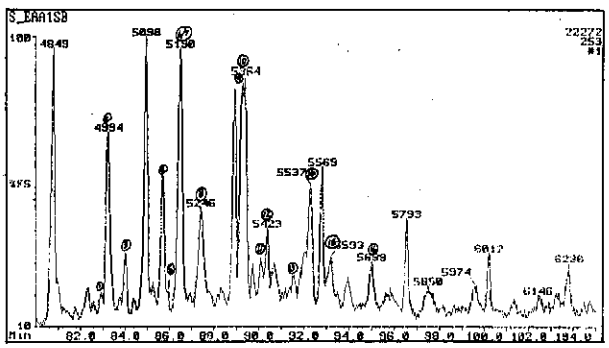

h) m/z 253: Monoaromatic Steroids (from saturates fraction)

Figure E.108: Annotated TIC and single ion fragmentograms of aromatic hydrocarbons from sample 42, well 83 RC, 2741m.

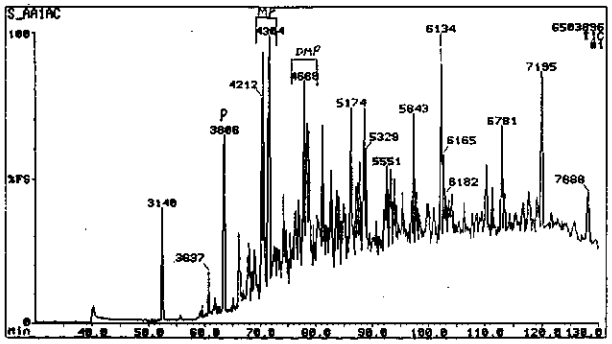

a) TIC: Total Ion Count

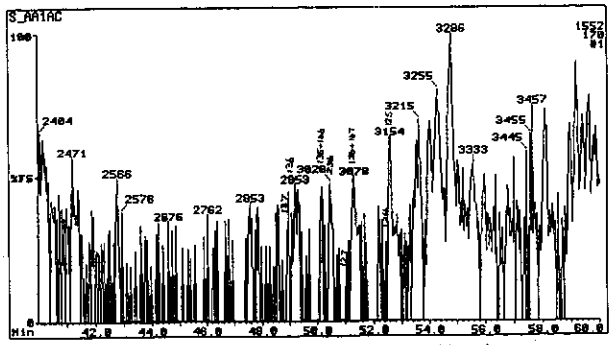

b) m/z 170: Trimethyl Napthalenes

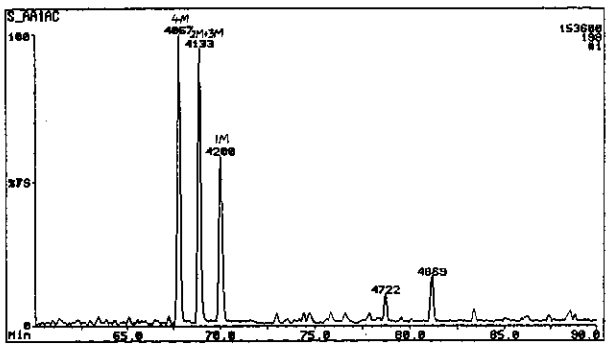

c) m/z 198: Methyl DibenzoThiophenes

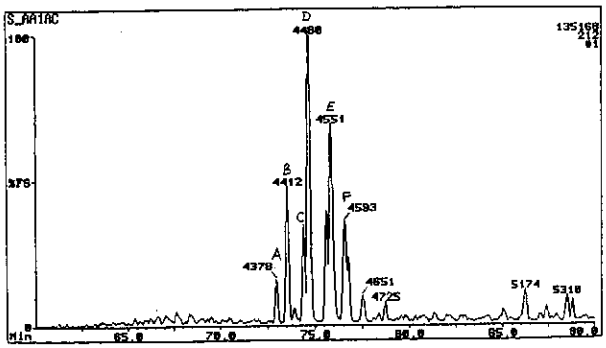

d) m/z 212: Dimethyl DibenzoThiophenes

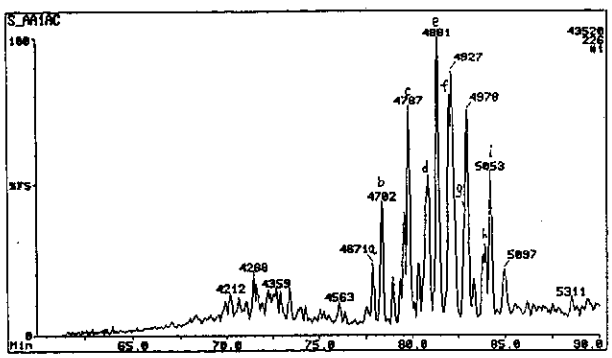

e) m/z 226: Trimethyl DibenzoThiophenes

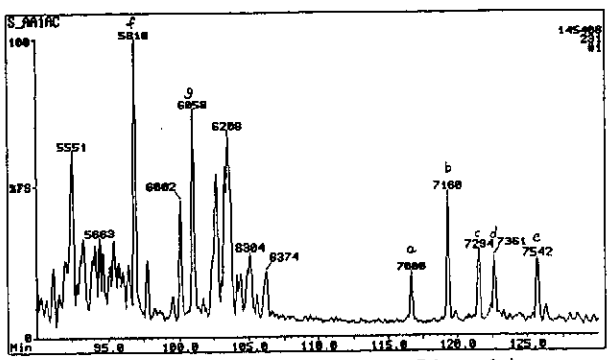

f) m/z 231: Triaromatic Steroids

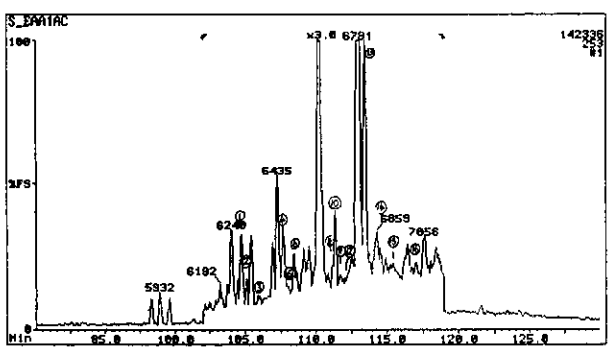

g) m/z 253: Monoaromatic Steroids (from aromatic fraction)

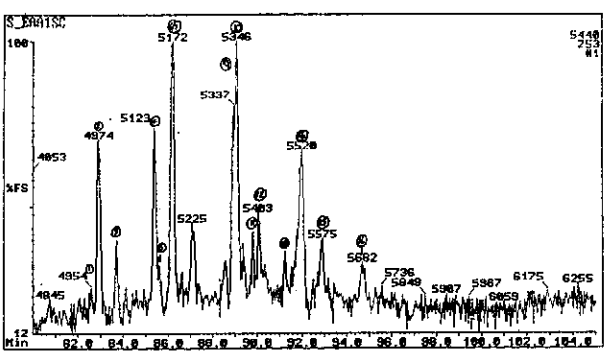

h) m/z 253: Monoaromatic Steroids (from saturates fraction)

Figure E.109: Annotated TIC and single ion fragmentograms of aromatic hydrocarbons from sample 43, well 83 RC, 2792m.

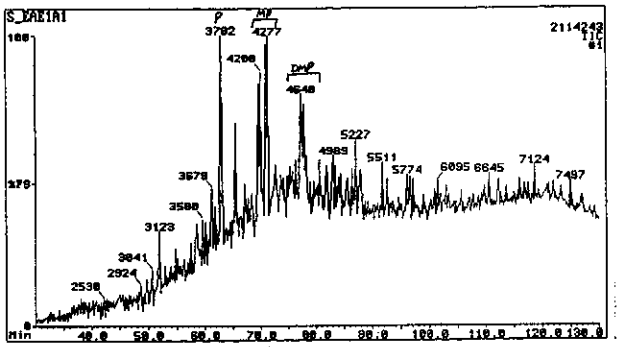

a) TIC: Total Ion Count

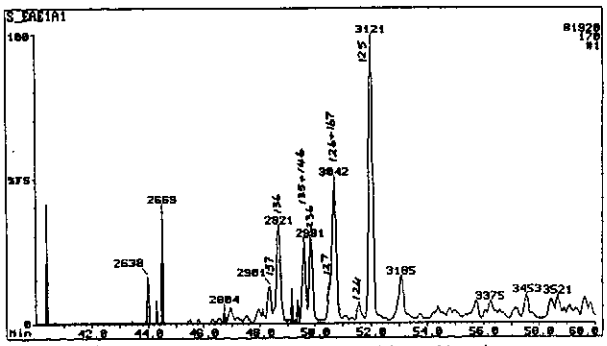

b) m/z 170: Trimethyl Napthalenes

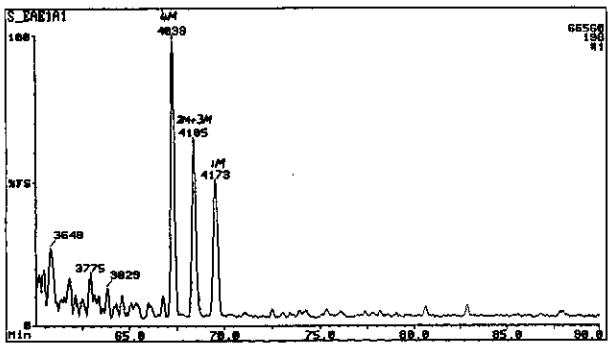

c) m/z 198: Methyl DibenzoThiophenes

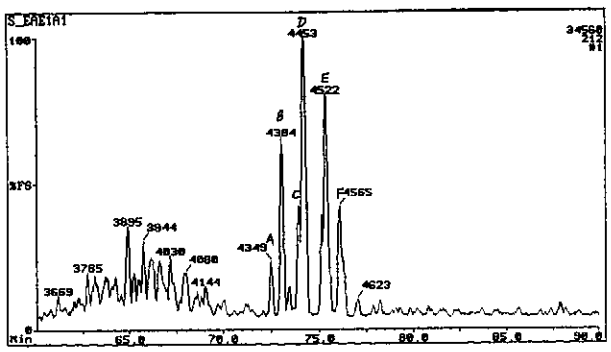

d) m/z 212: Dimethyl DibenzoThiophenes

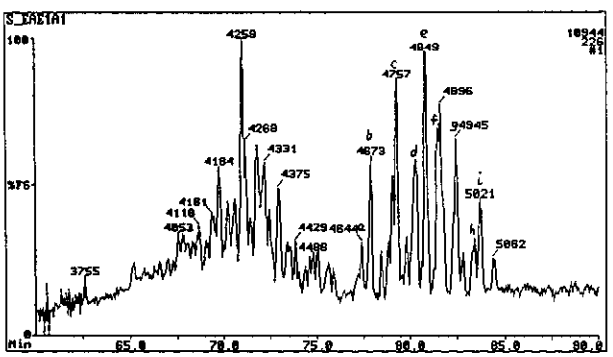

e) m/z 226: Trimethyl DibenzoThiophenes

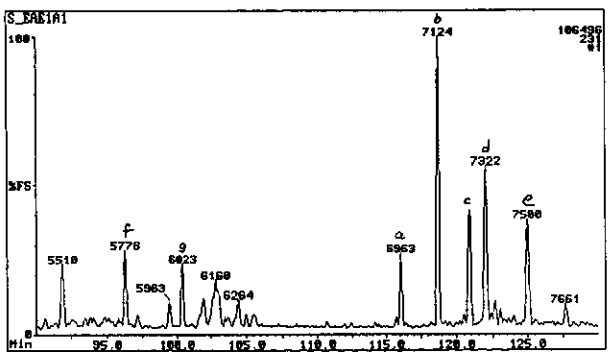

f) m/z 231: Triaromatic Steroids

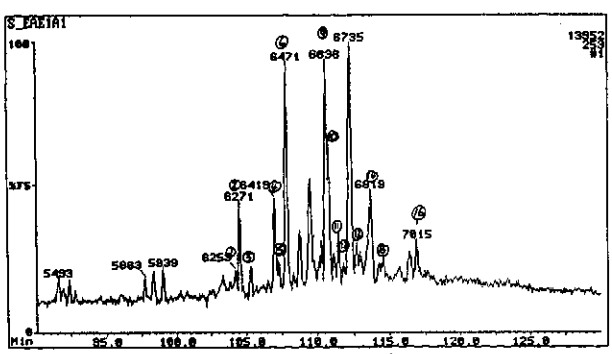

g) m/z 253: Monoaromatic Steroids (from aromatic fraction)

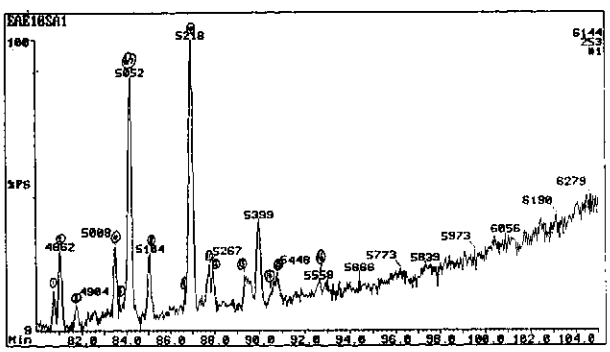

h) m/z 253: Monoaromatic Steroids (from saturates fraction)

Figure E.110: Annotated TIC and single ion fragmentograms of aromatic hydrocarbons from sample 44, well 92 RC, 2610m.

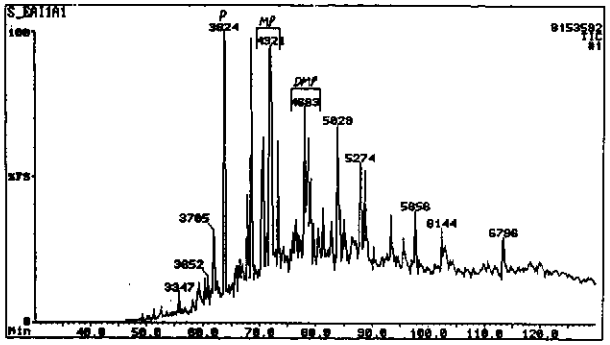

a) TIC: Total Ion Count

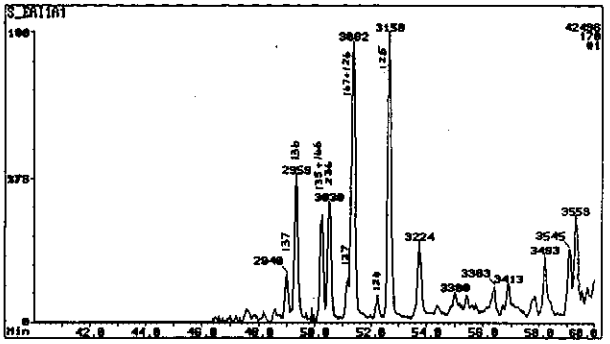

b) m/z 170: Trimethyl Napthalenes

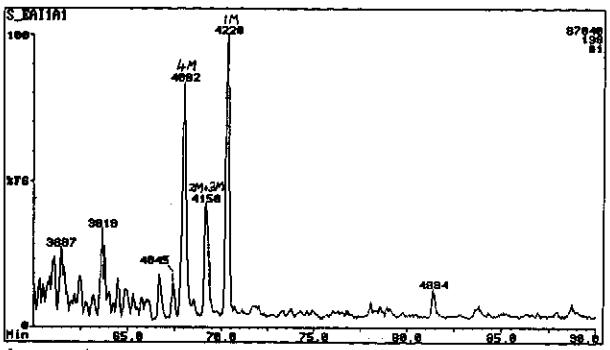

c) m/z 198: Methyl DibenzoThiophenes

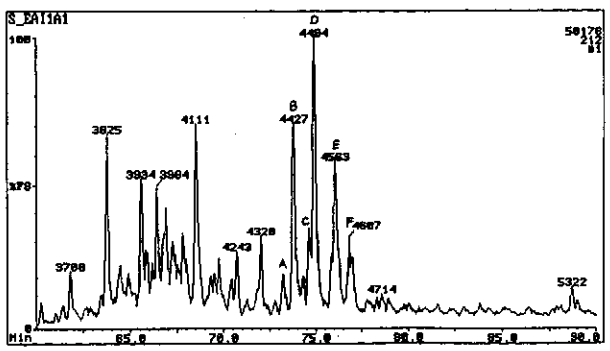

d) m/z 212: Dimethyl DibenzoThiophenes

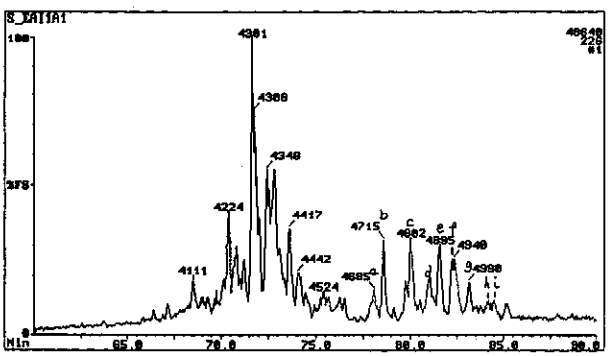

e) m/z 226: Trimethyl DibenzoThiophenes

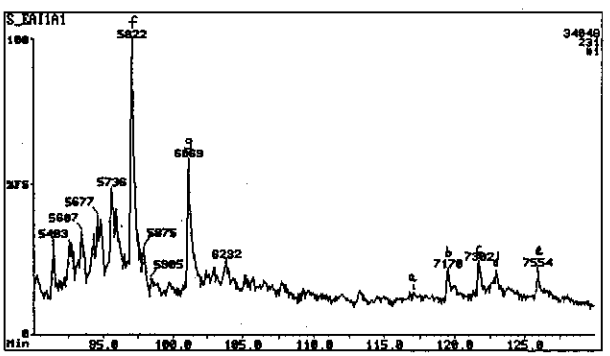

f) m/z 231: Triaromatic Steroids

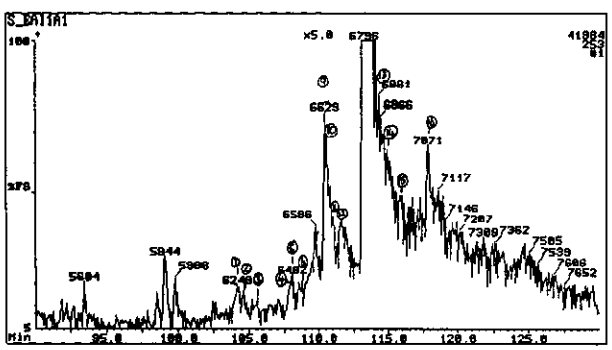

g) m/z 253: Monoaromatic Steroids (from aromatic fraction)

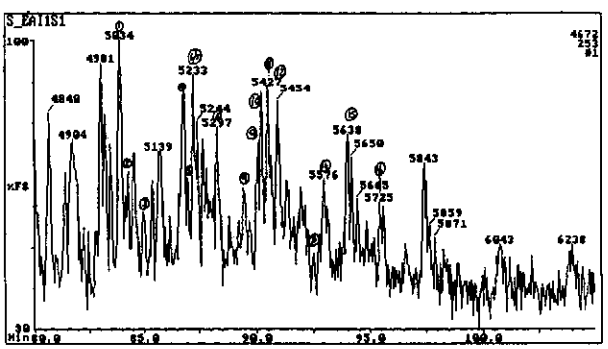

h) m/z 253: Monoaromatic Steroids (from saturates fraction)

Figure E.111: Annotated TIC and single ion fragmentograms of aromatic hydrocarbons from sample 45, well 89 RC, 2660m.

not analysed

not analysed

a) TIC: Total Ion Count

b) m/z 170: Trimethyl Napthalenes

not analysed

not analysed

c) m/z 198: Methyl DibenzoThiophenes

d) m/z 212: Dimethyl DibenzoThiophenes

not analysed

not analysed

e) m/z 226: Trimethyl DibenzoThiophenes

f) m/z 231: Triaromatic Steroids

not analysed

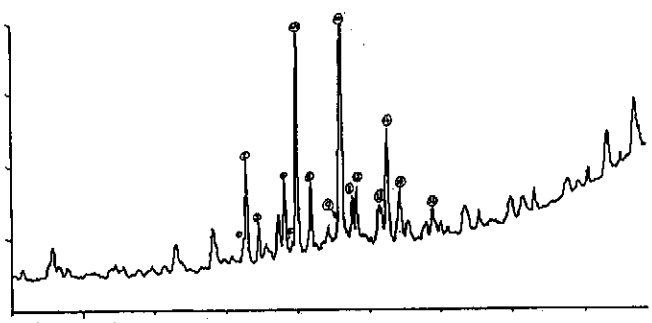

g) m/z 253: Monoaromatic Steroids (from aromatic fraction)

h) m/z 253: Monoaromatic Steroids (from saturates fraction)

Figure E.112: Annotated TIC and single ion fragmentograms of aromatic hydrocarbons from sample 46, well 93 RC, 2720m.

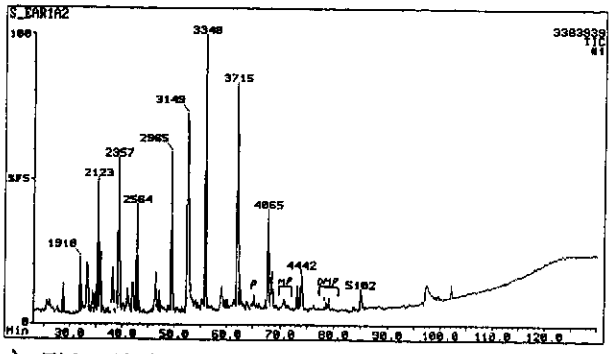

a) TIC: Total Ion Count

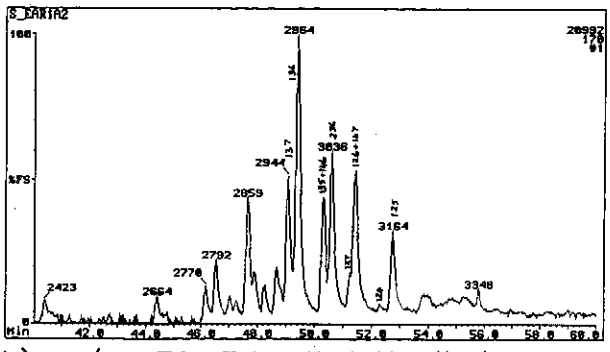

b) m/z 170: Trimethyl Napthalenes

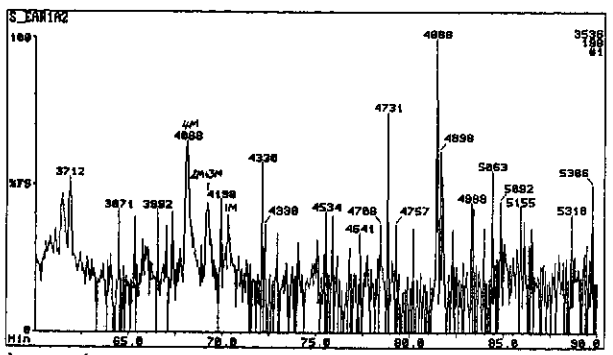

c) m/z 198: Methyl DibenzoThiophenes

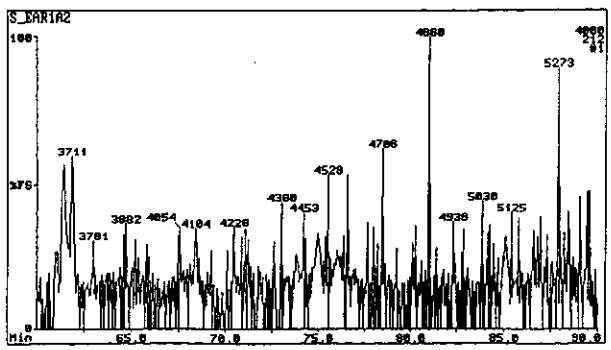

d) m/z 212: Dimethyl DibenzoThiophenes

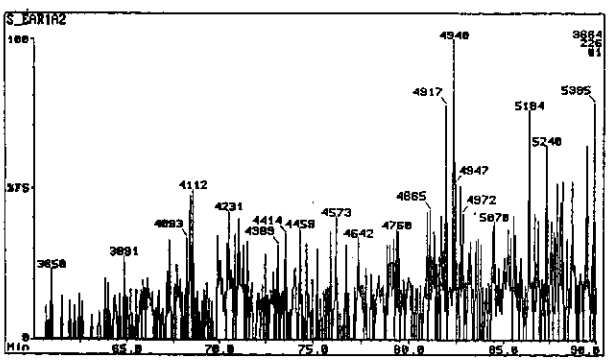

e) m/z 226: Trimethyl DibenzoThiophenes

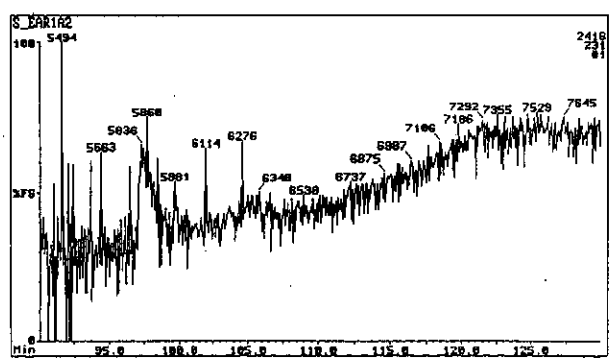

f) m/z 231: Triaromatic Steroids

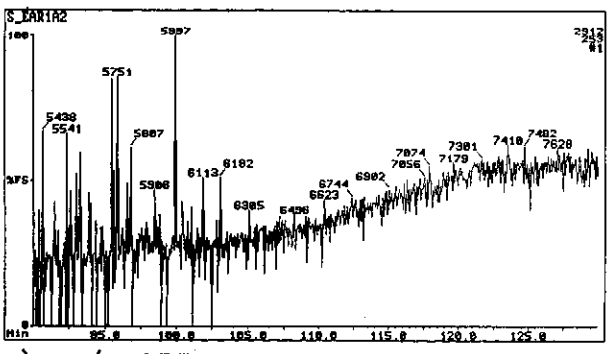

g) m/z 253: Monoaromatic Steroids (from aromatic fraction)

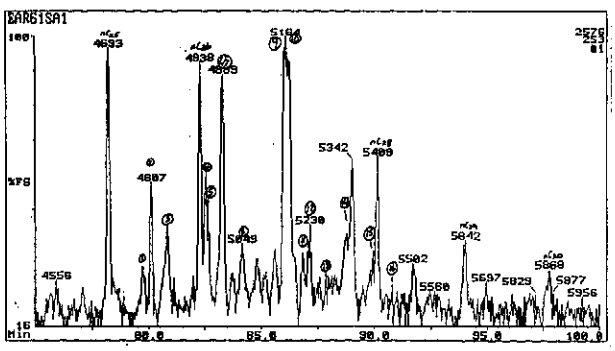

h) m/z 253: Monoaromatic Steroids (from saturates fraction)

Figure E.113: Annotated TIC and single ion fragmentograms of aromatic hydrocarbons from sample 47, well 93 RC, 2761m.

not analysed

not analysed

a) TIC: Total Ion Count

b) m/z 170: Trimethyl Napthalenes

not analysed

not analysed

c) m/z 198: Methyl DibenzoThiophenes

d) m/z 212: Dimethyl DibenzoThiophenes

not analysed

not analysed

e) m/z 226: Trimethyl DibenzoThiophenes

f) m/z 231: Triaromatic Steroids

not analysed

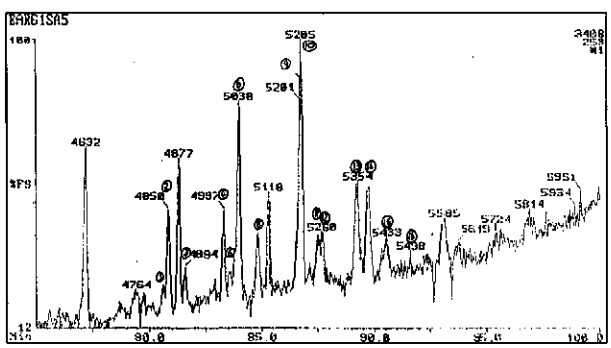

g) m/z 253: Monoaromatic Steroids (from aromatic fraction)

h) m/z 253: Monoaromatic Steroids (from saturates fraction)

Figure E.114: Annotated TIC and single ion fragmentograms of aromatic hydrocarbons from sample 48, well 93 RC, 2761m.

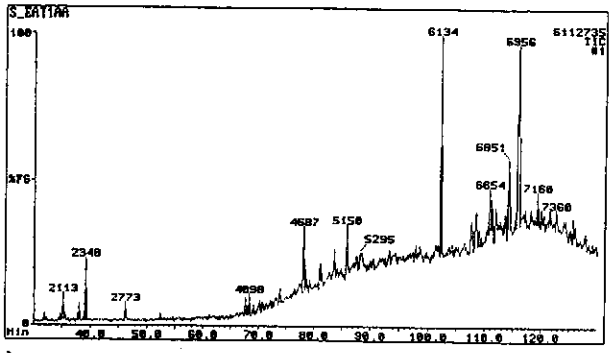

a) TIC: Total Ion Count

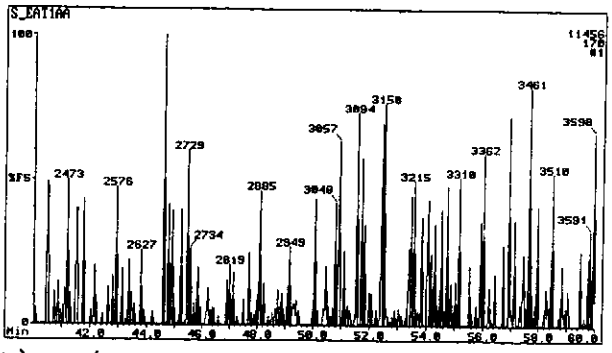

b) m/z 170: Trimethyl Napthalenes

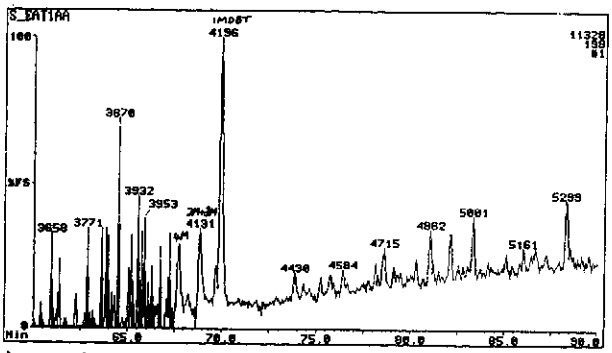

c) m/z 198: Methyl DibenzoThiophenes

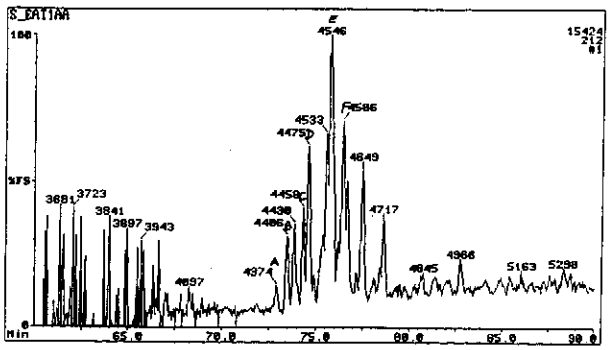

d) m/z 212: Dimethyl DibenzoThiophenes

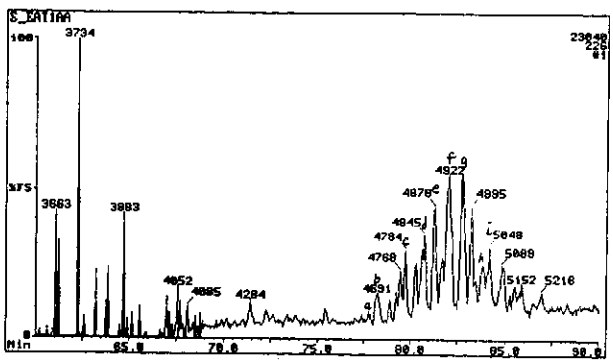

e) m/z 226: Trimethyl DibenzoThiophenes

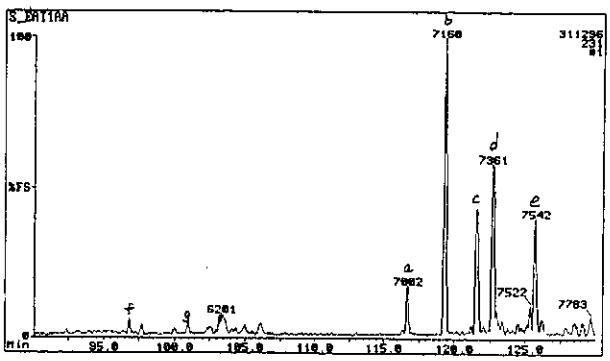

f) m/z 231: Triaromatic Steroids

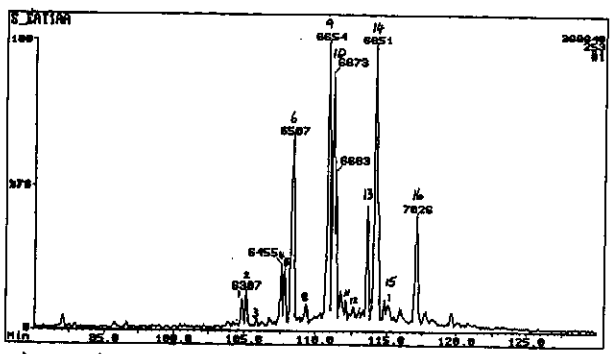

g) m/z 253: Monoaromatic Steroids (from aromatic fraction)

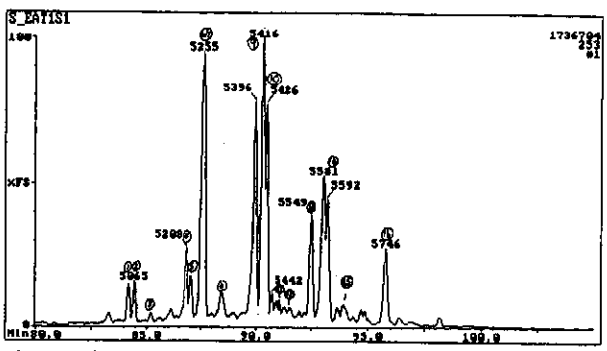

h) m/z 253: Monoaromatic Steroids (from saturates fraction)

Figure E.115: Annotated TIC and single ion fragmentograms of aromatic hydrocarbons from sample 49, well 99 RC, 1820m.

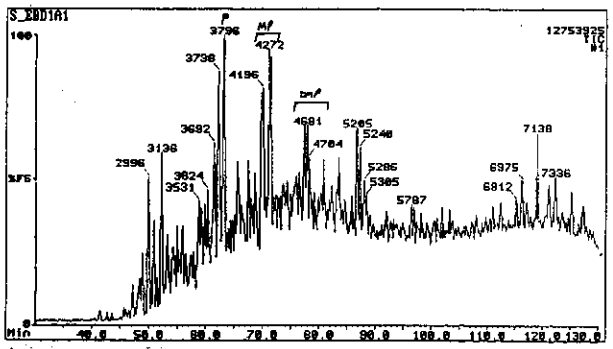

a) TIC: Total Ion Count

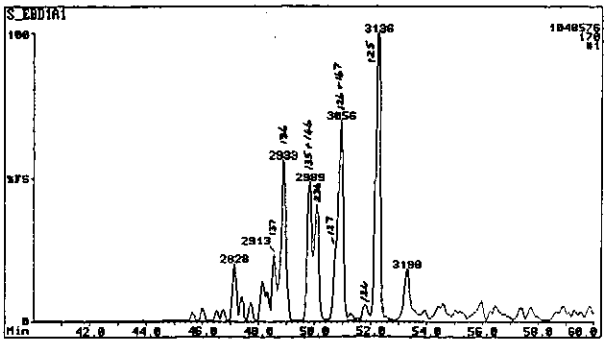

b) m/z 170: Trimethyl Napthalenes

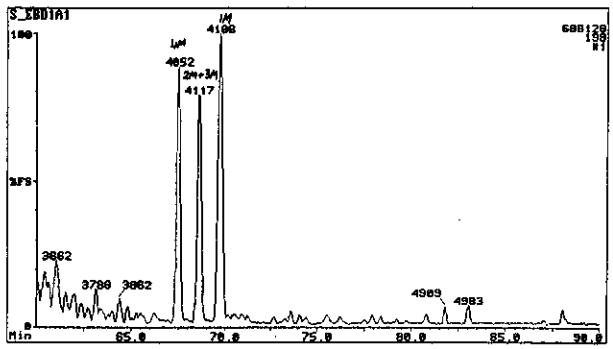

c) m/z 198: Methyl DibenzoThiophenes

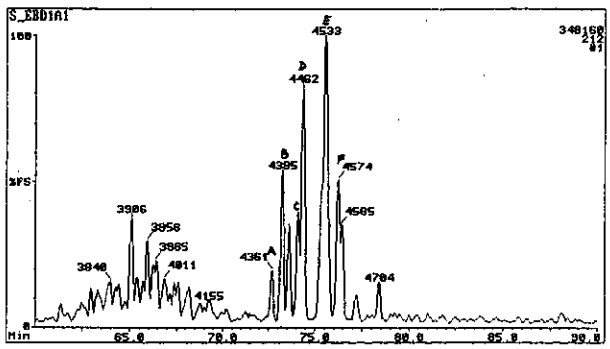

d) m/z 212: Dimethyl DibenzoThiophenes

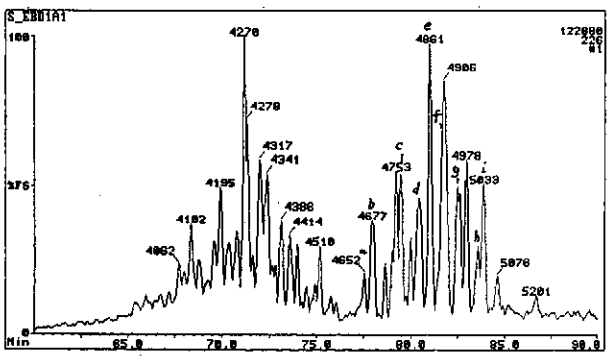

e) m/z 226: Trimethyl DibenzoThiophenes

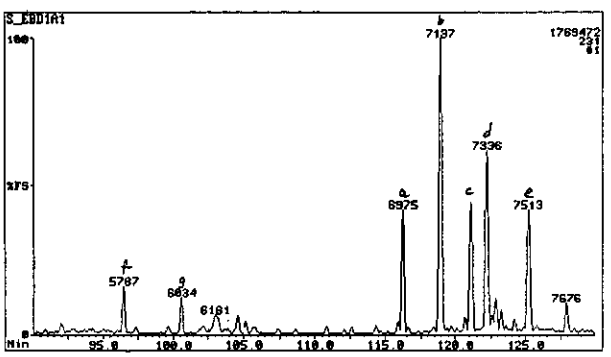

f) m/z 231: Triaromatic Steroids

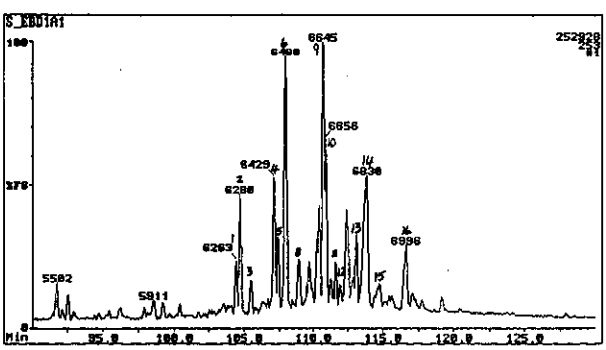

g) m/z 253: Monoaromatic Steroids (from aromatic fraction)

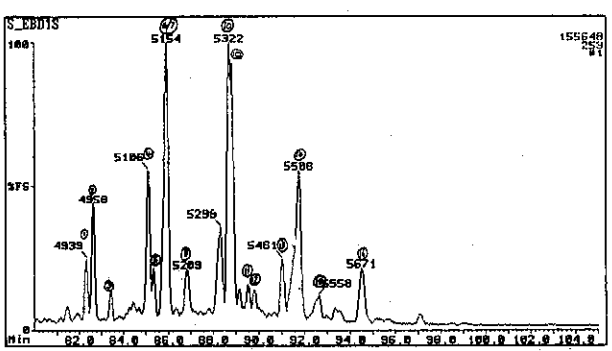

h) m/z 253: Monoaromatic Steroids (from saturates fraction)

Figure E.116: Annotated TIC and single ion fragmentograms of aromatic hydrocarbons from sample 50, well 109 RC, 2461m.

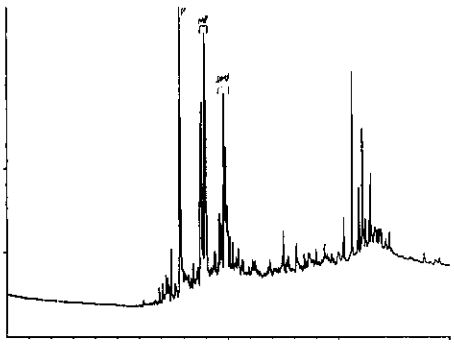

a) TIC: Total Ion Count

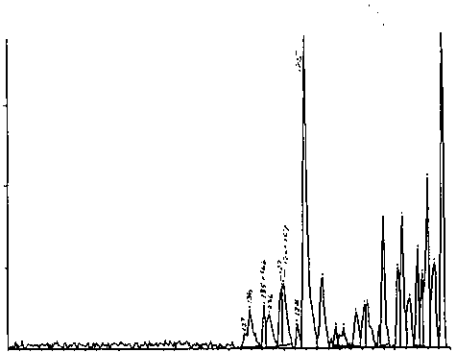

b) m/z 170: Trimethyl Napthalenes

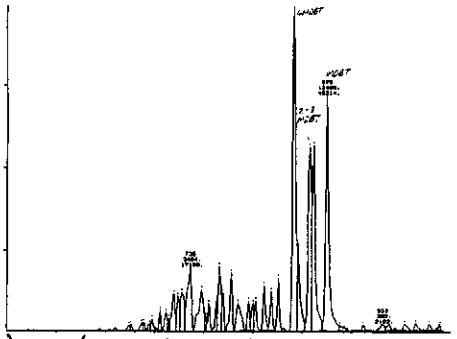

c) m/z 198: Methyl DibenzoThiophenes

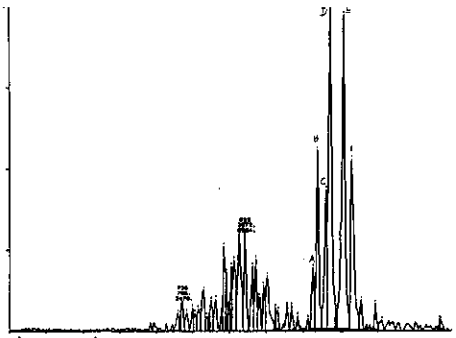

d) m/z 212: Dimethyl DibenzoThiophenes

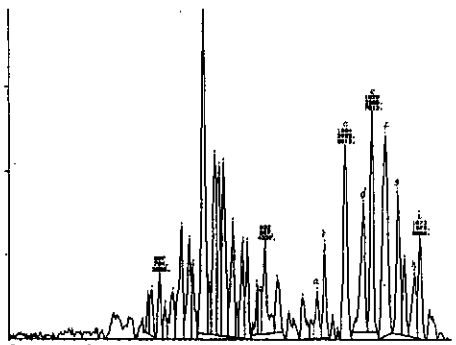

e) m/z 226: Trimethyl DibenzoThiophenes

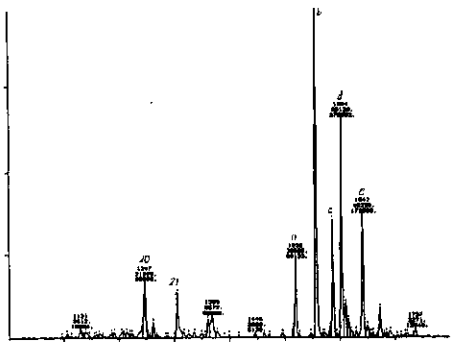

f) m/z 231: Triaromatic Steroids

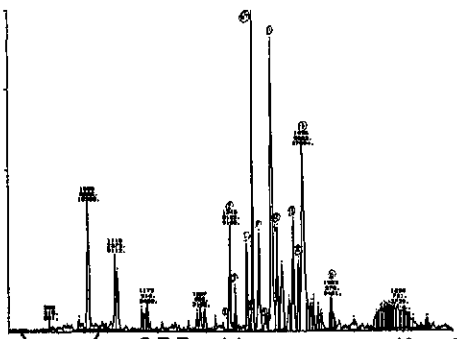

g) m/z 253: Monoaromatic Steroids
(from aromatic fraction)

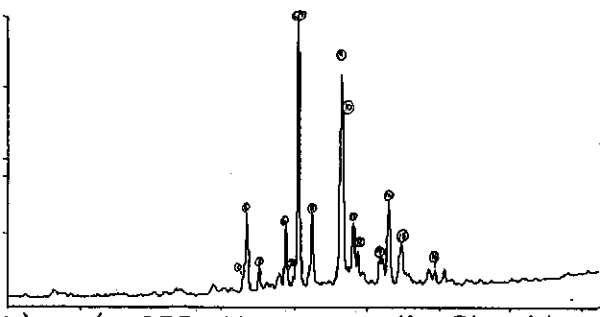

h) m/z 253: Monoaromatic Steroids
(from saturates fraction)

Figure E.117: Annotated TIC and single ion fragmentograms of aromatic hydrocarbons from sample 51, well 109 core 3, 2654.15m.

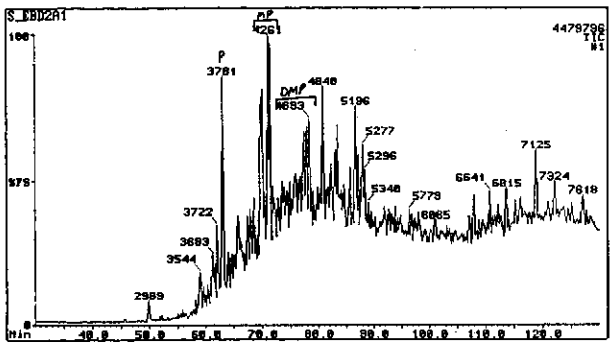

a) TIC: Total Ion Count

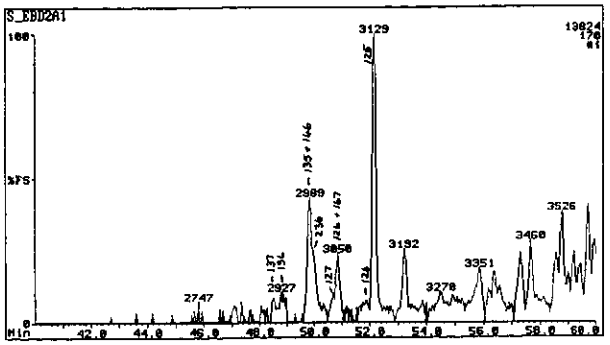

b) m/z 170: Trimethyl Napthalenes

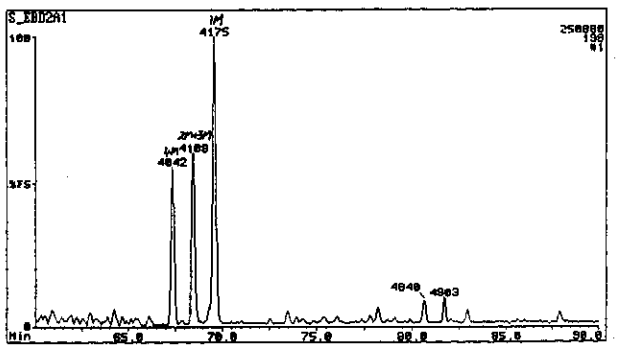

c) m/z 198: Methyl DibenzoThiophenes

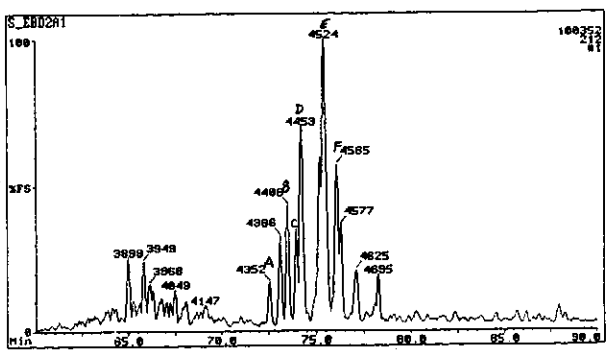

d) m/z 212: Dimethyl DibenzoThiophenes

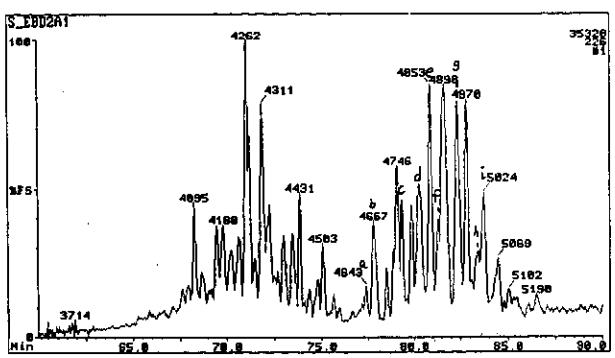

e) m/z 226: Trimethyl DibenzoThiophenes

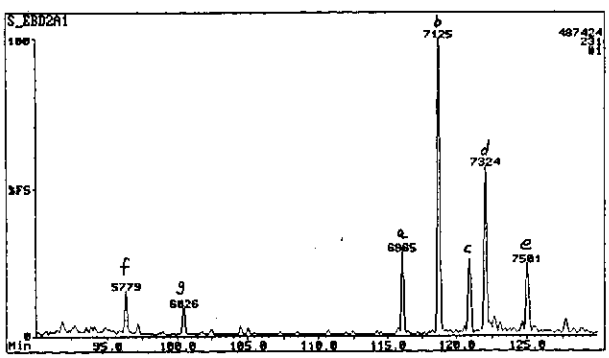

f) m/z 231: Triaromatic Steroids

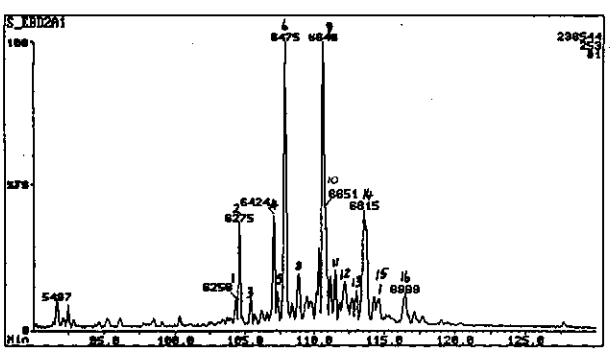

g) m/z 253: Monoaromatic Steroids (from aromatic fraction)

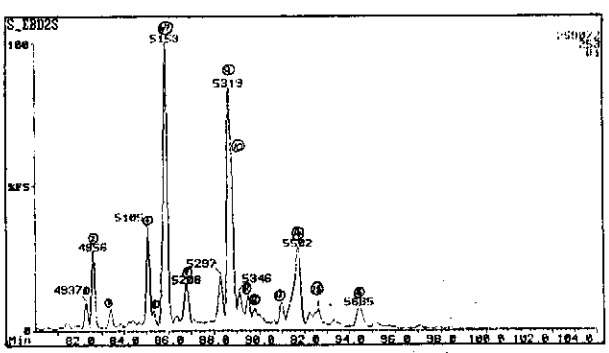

h) m/z 253: Monoaromatic Steroids (from saturates fraction)

Figure E.118: Annotated TIC and single ion fragmentograms of aromatic hydrocarbons from sample 52, well 130 RC, 2331m.

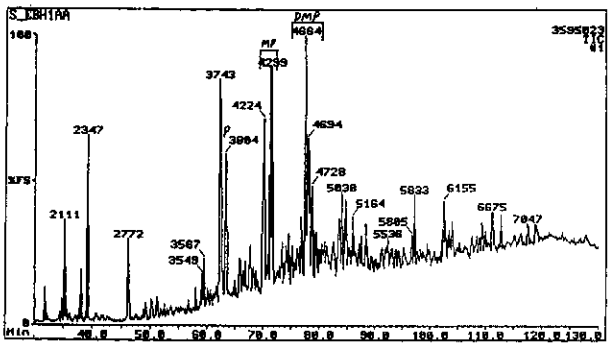

a) TIC: Total Ion Count

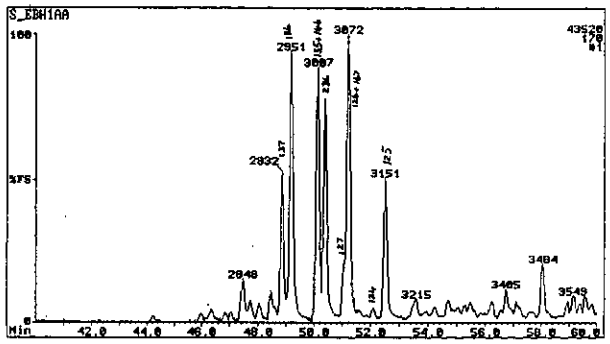

b) m/z 170: Trimethyl Napthalenes

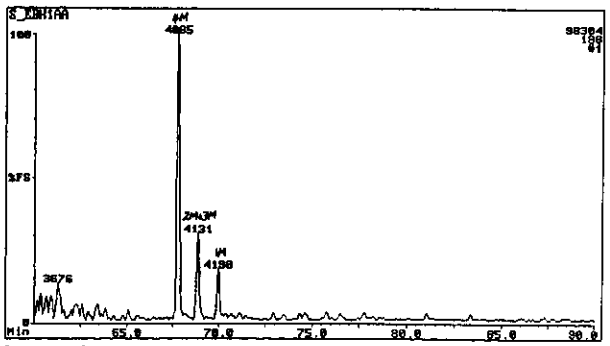

c) m/z 198: Methyl DibenzoThiophenes

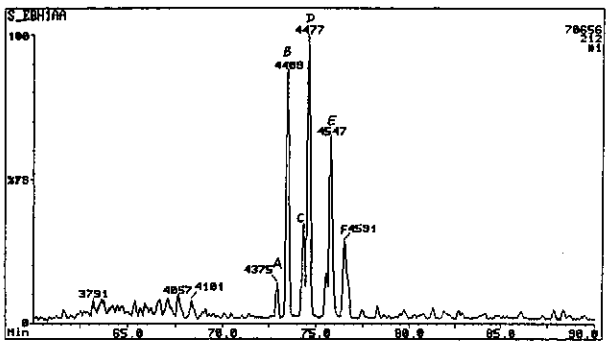

d) m/z 212: Dimethyl DibenzoThiophenes

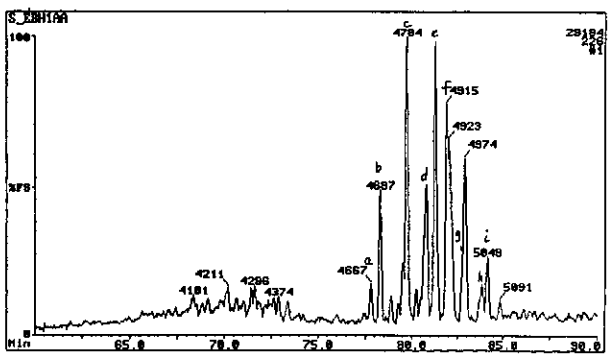

e) m/z 226: Trimethyl DibenzoThiophenes

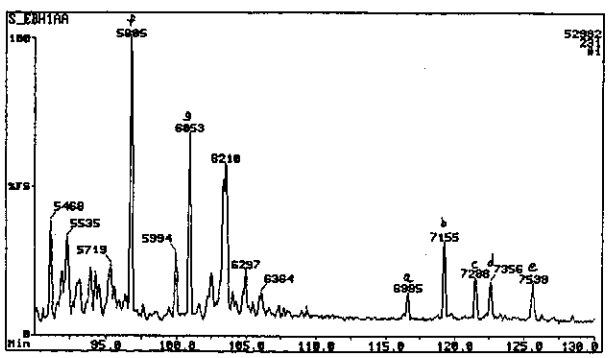

f) m/z 231: Triaromatic Steroids

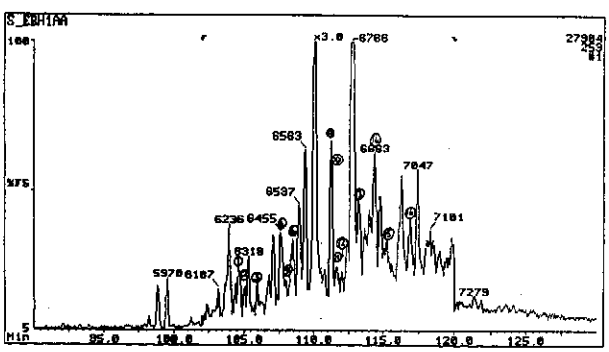

g) m/z 253: Monoaromatic Steroids (from aromatic fraction)

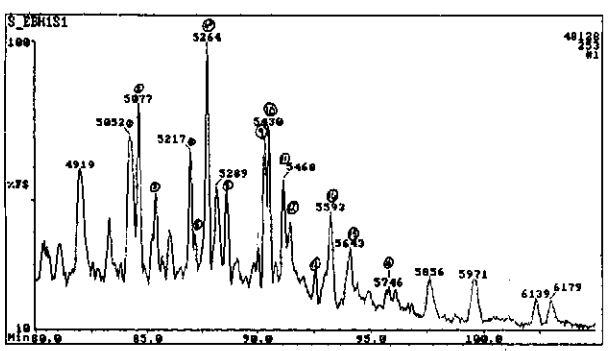

h) m/z 253: Monoaromatic Steroids (from saturates fraction)

Figure E.119: Annotated TIC and single ion fragmentograms of aromatic hydrocarbons from sample 53, well 110 RC, 2830m.

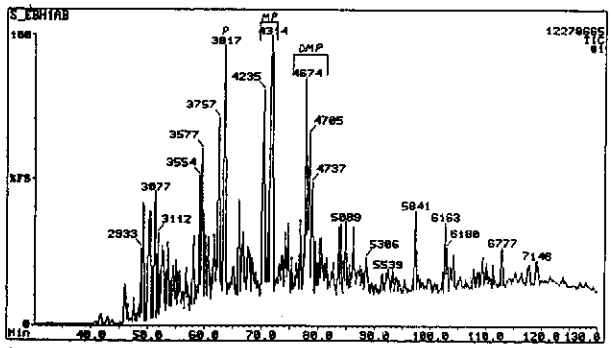

a) TIC: Total Ion Count

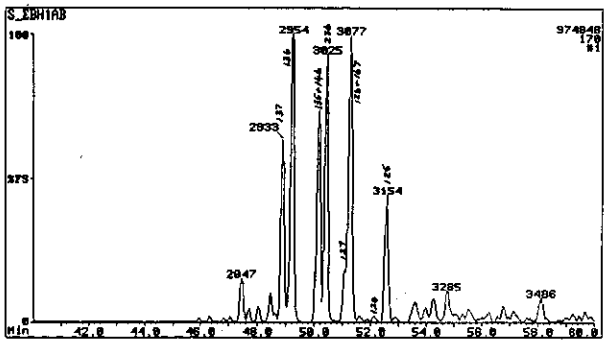

b) m/z 170: Trimethyl Napthalenes

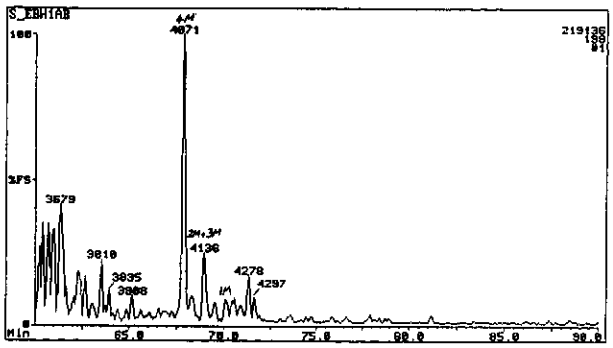

c) m/z 198: Methyl DibenzoThiophenes

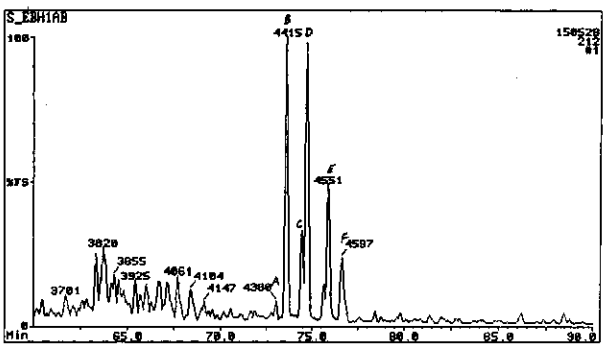

d) m/z 212: Dimethyl DibenzoThiophenes

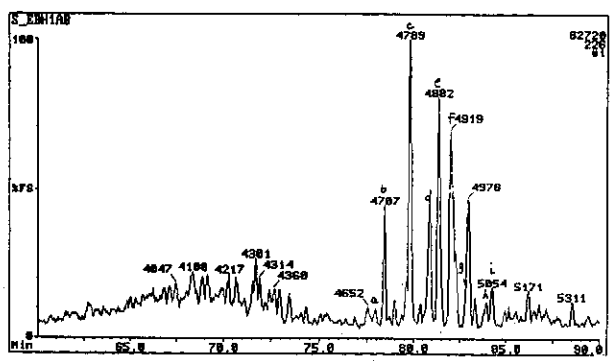

e) m/z 226: Trimethyl DibenzoThiophenes

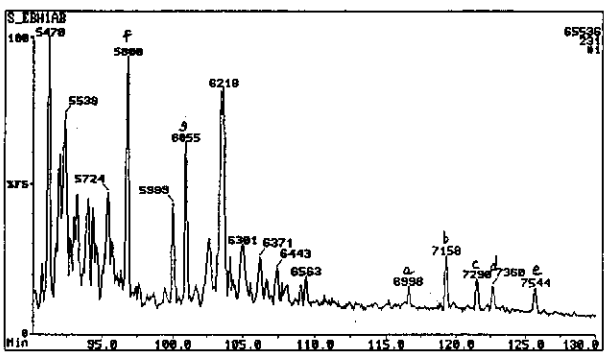

f) m/z 231: Triaromatic Steroids

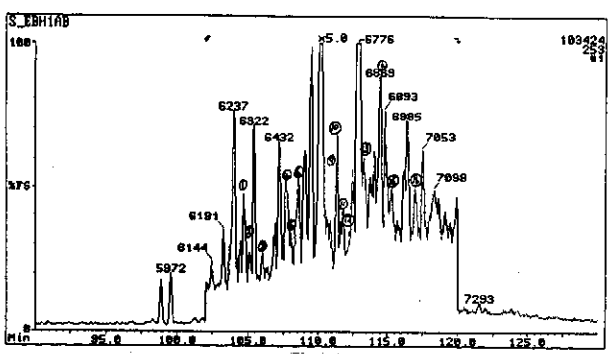

g) m/z 253: Monoaromatic Steroids (from aromatic fraction)

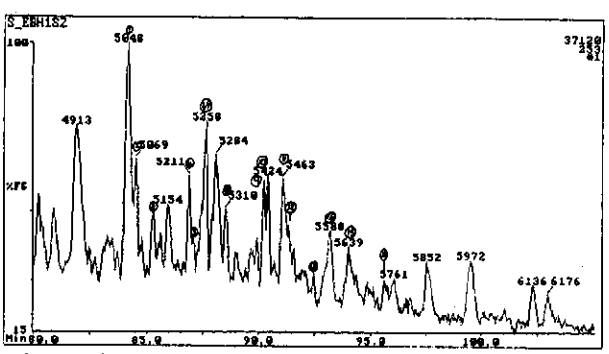

h) m/z 253: Monoaromatic Steroids (from saturates fraction)

Figure E.120: Annotated TIC and single ion fragmentograms of aromatic hydrocarbons from sample 54, well 110 RC, 2902m.

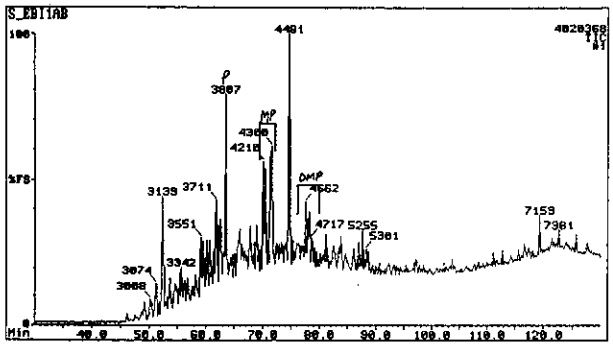

a) TIC: Total Ion Count

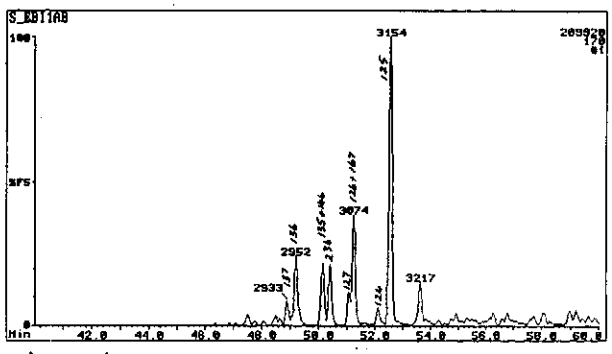

b) m/z 170: Trimethyl Napthalenes

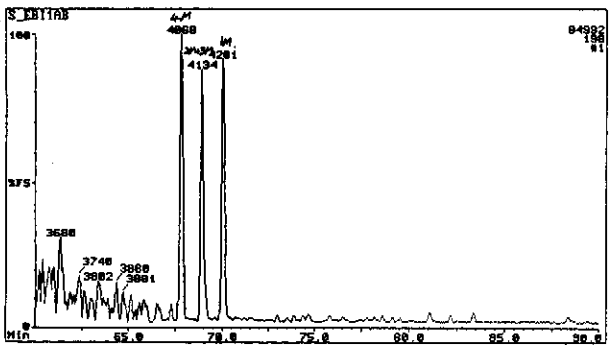

c) m/z 198: Methyl DibenzoThiophenes

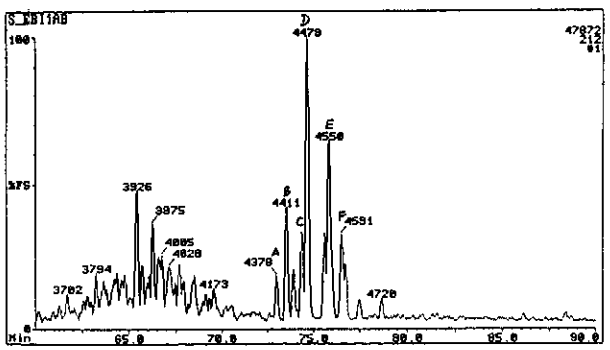

d) m/z 212: Dimethyl DibenzoThiophenes

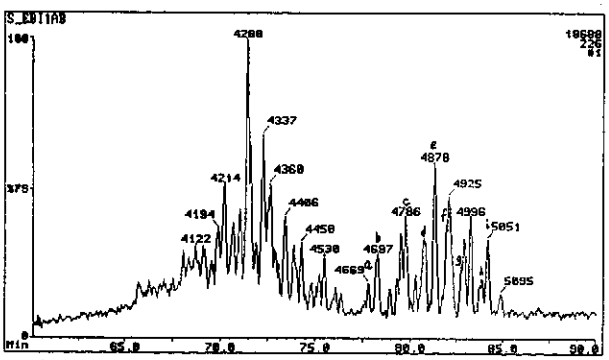

e) m/z 226: Trimethyl DibenzoThiophenes

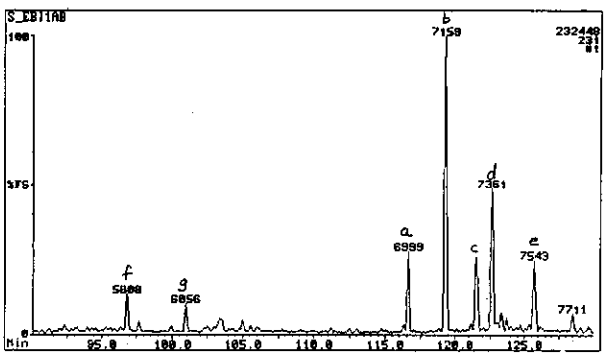

f) m/z 231: Triaromatic Steroids

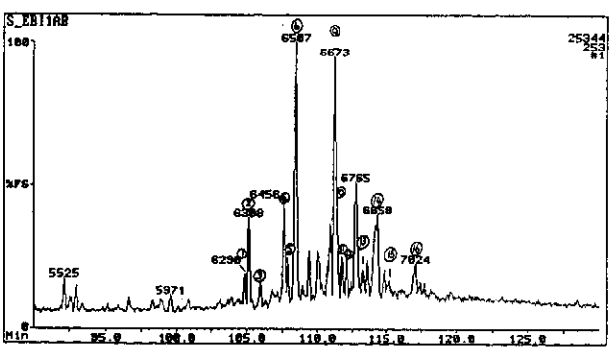

g) m/z 253: Monoaromatic Steroids (from aromatic fraction)

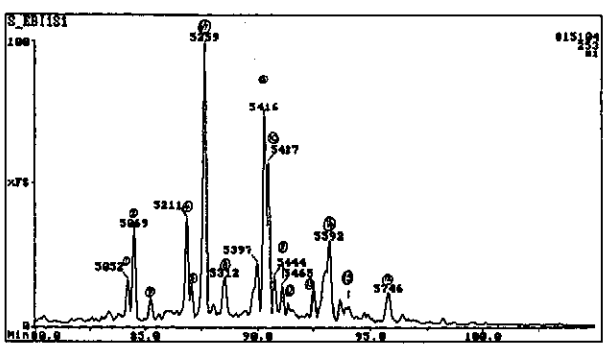

h) m/z 253: Monoaromatic Steroids (from saturates fraction)

Figure E.121: Annotated TIC and single ion fragmentograms of aromatic hydrocarbons from sample 55, well 112 RC, 2392m.

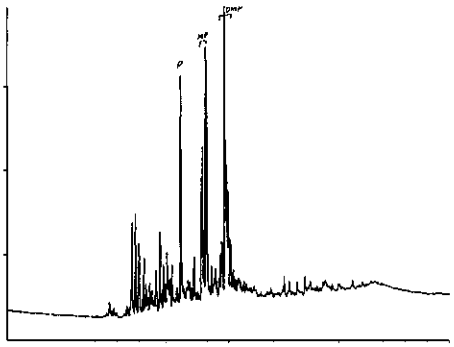

a) TIC: Total Ion Count

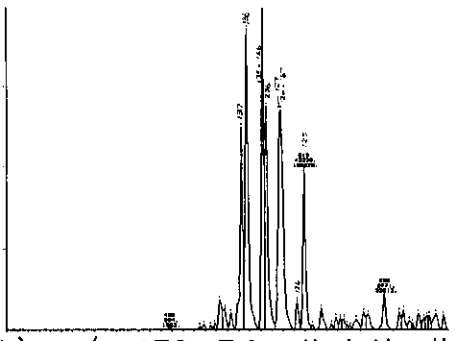

b) m/z 170: Trimethyl Napthalenes

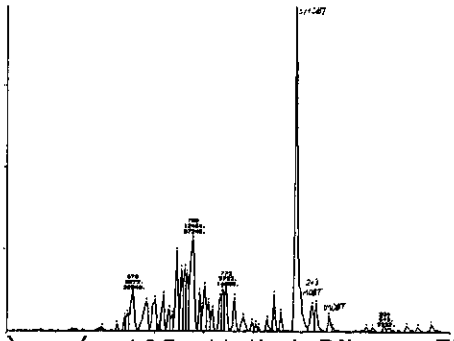

c) m/z 198: Methyl DibenzoThiophenes

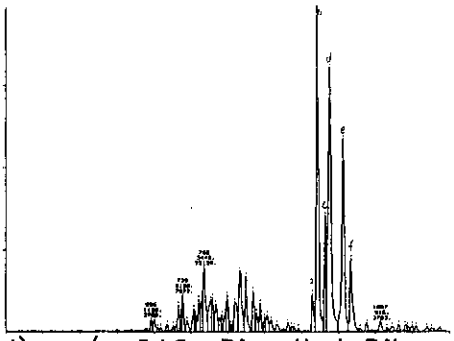

d) m/z 212: Dimethyl DibenzoThiophenes

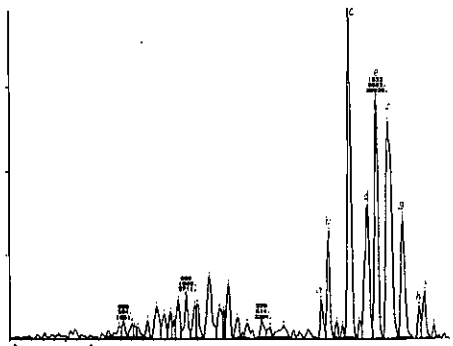

e) m/z 226: Trimethyl DibenzoThiophenes

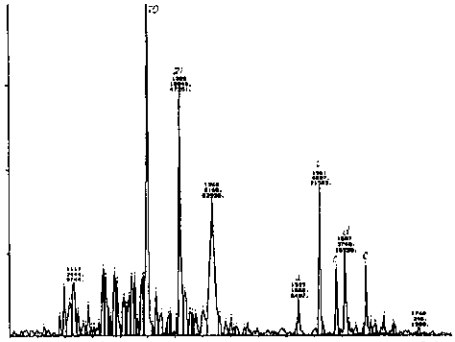

f) m/z 231: Triaromatic Steroids

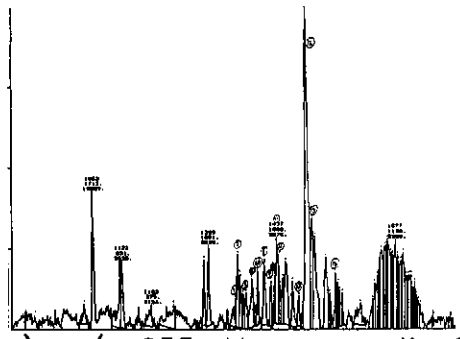

g) m/z 253: Monoaromatic Steroids
(from aromatic fraction)

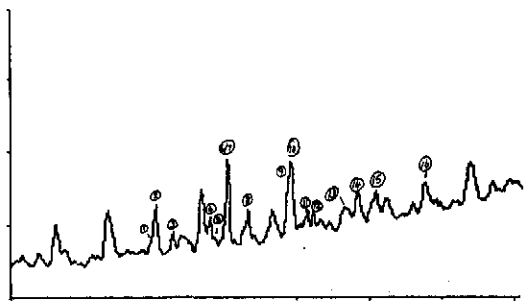

h) m/z 253: Monoaromatic Steroids
(from saturates fraction)

Figure E.122: Annotated TIC and single ion fragmentograms of aromatic hydrocarbons from sample 56, well 117 SWC, 2918.5m.

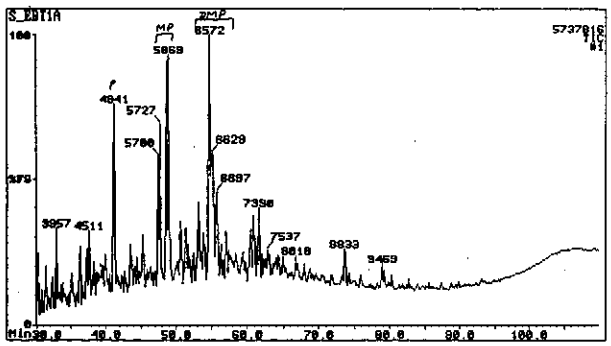

a) TIC: Total Ion Count

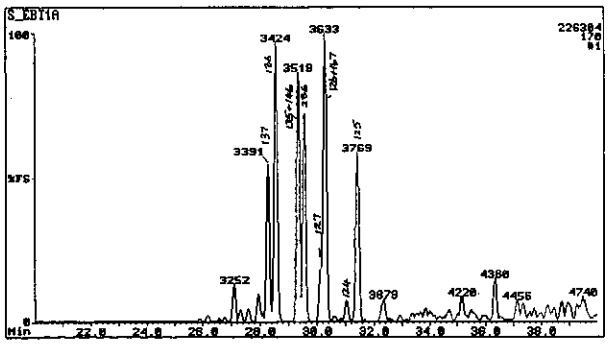

b) m/z 170: Trimethyl Napthalenes

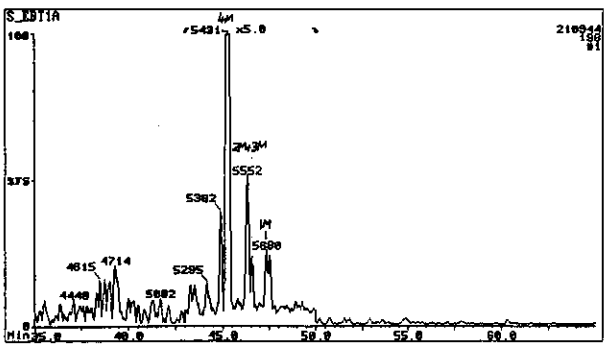

c) m/z 198: Methyl DibenzoThiophenes

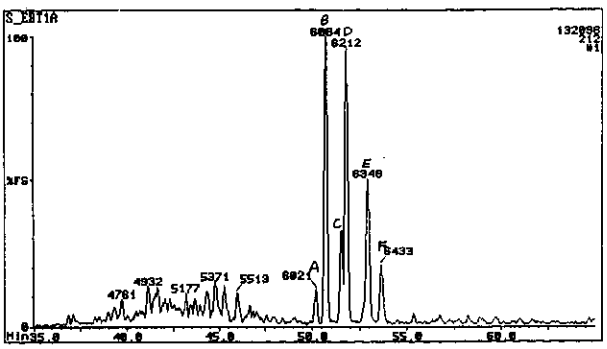

d) m/z 212: Dimethyl DibenzoThiophenes

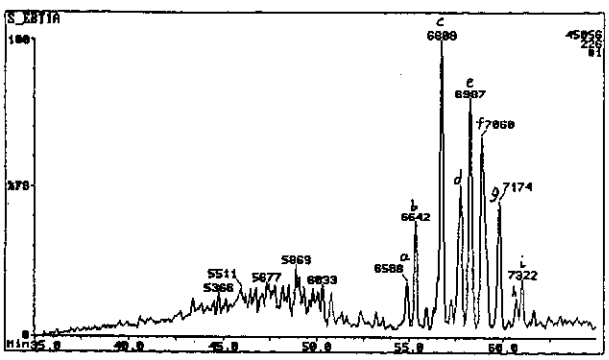

e) m/z 226: Trimethyl DibenzoThiophenes

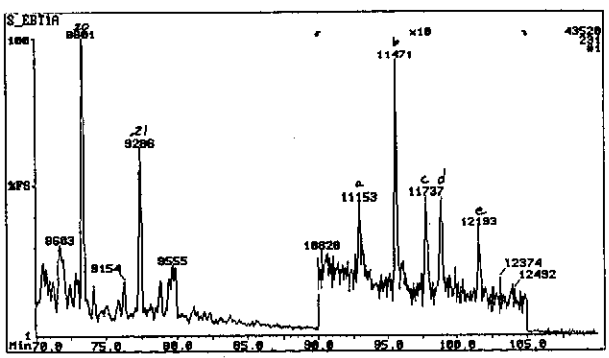

f) m/z 231: Triaromatic Steroids

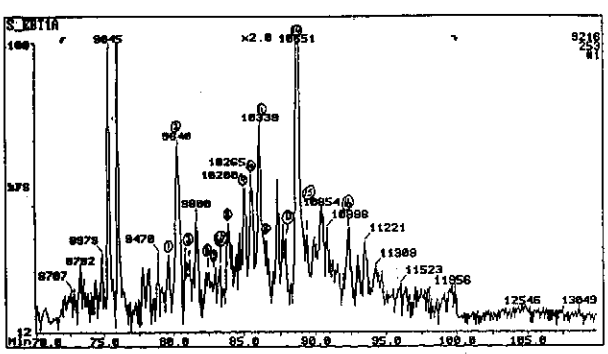

g) m/z 253: Monoaromatic Steroids (from aromatic fraction)

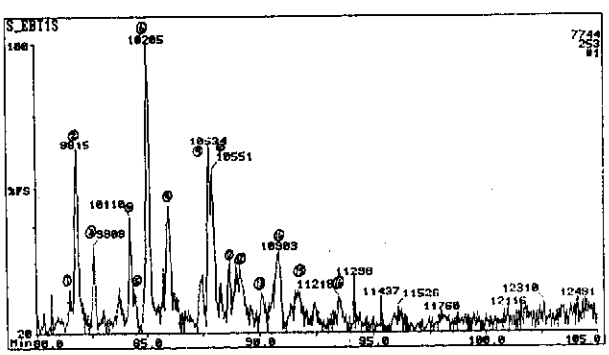

h) m/z 253: Monoaromatic Steroids (from saturates fraction)

Figure E.123: Annotated TIC and single ion fragmentograms of aromatic hydrocarbons from sample 57, well 117 SWC, 2918.5m.

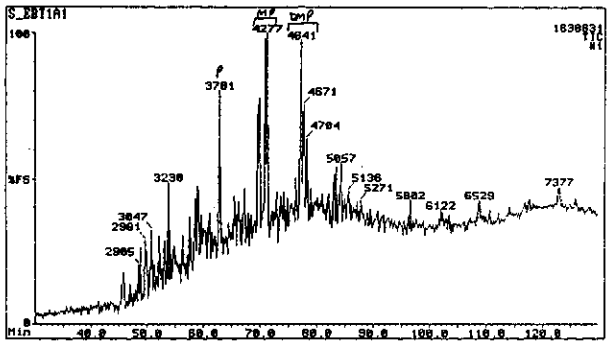

a) TIC: Total Ion Count

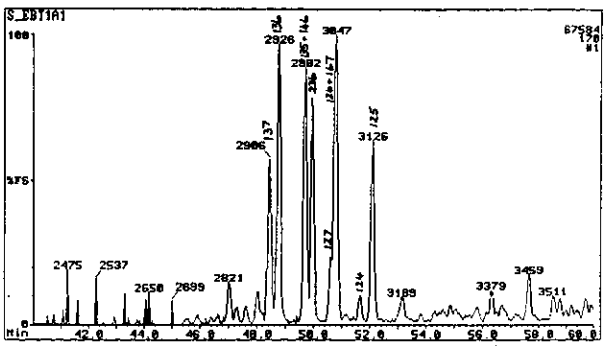

b) m/z 170: Trimethyl Napthalenes

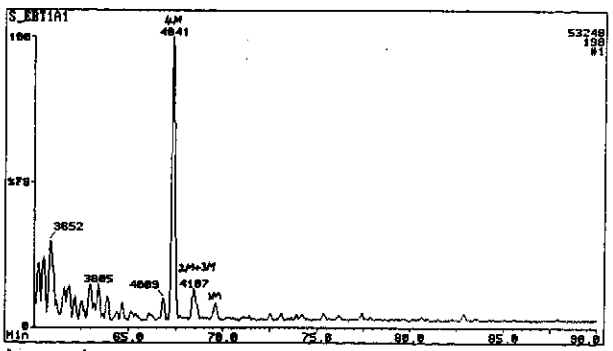

c) m/z 198: Methyl DibenzoThiophenes

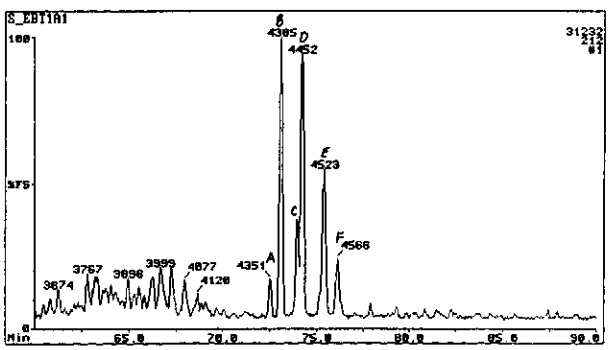

d) m/z 212: Dimethyl DibenzoThiophenes

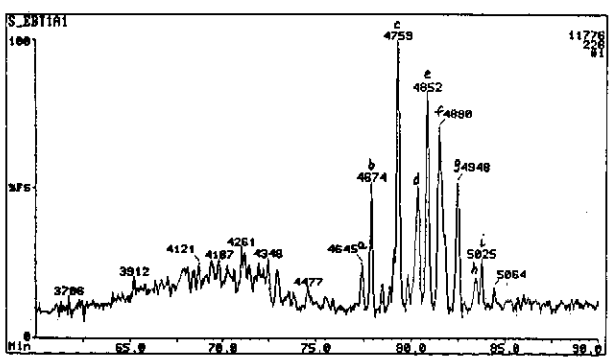

e) m/z 226: Trimethyl DibenzoThiophenes

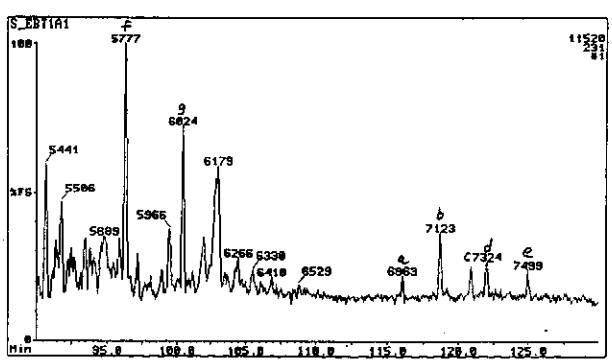

f) m/z 231: Triaromatic Steroids

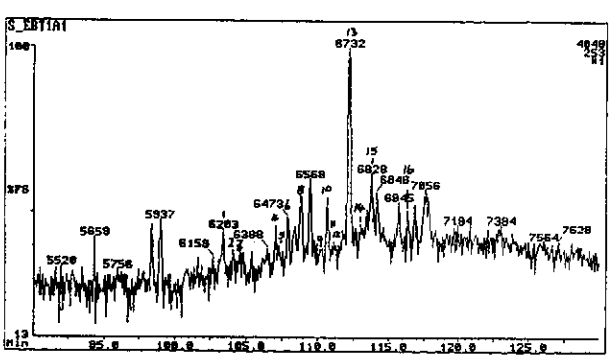

g) m/z 253: Monoaromatic Steroids (from aromatic fraction)

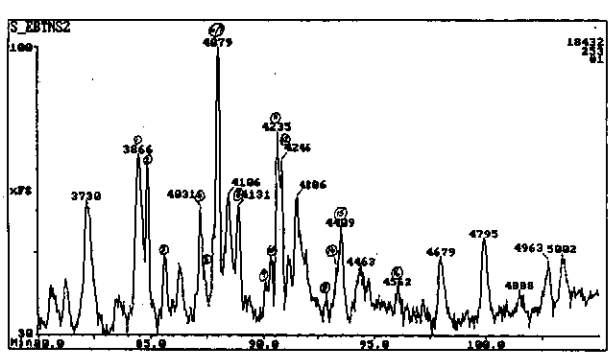

h) m/z 253: Monoaromatic Steroids (from saturates fraction)

Figure E.124: Annotated TIC and single ion fragmentograms of aromatic hydrocarbons from sample 58, well 117 SWC, 2918.5m.

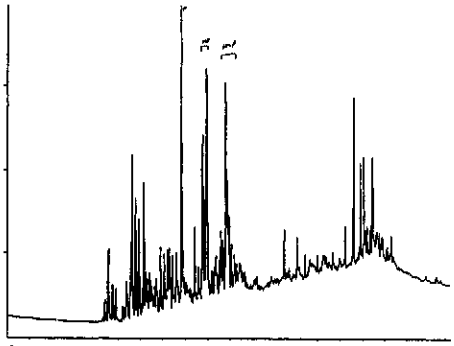

a) TIC: Total Ion Count

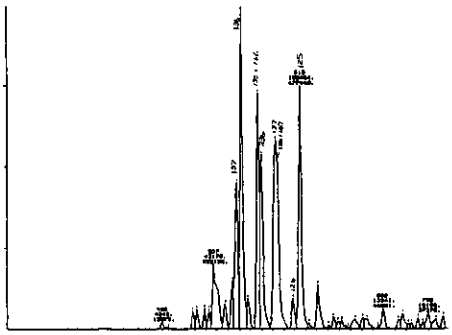

b) m/z 170: Trimethyl Napthalenes

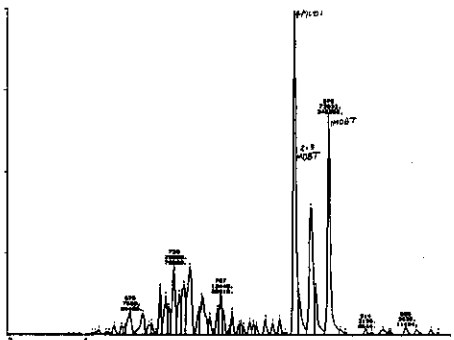

c) m/z 198: Methyl DibenzoThiophenes

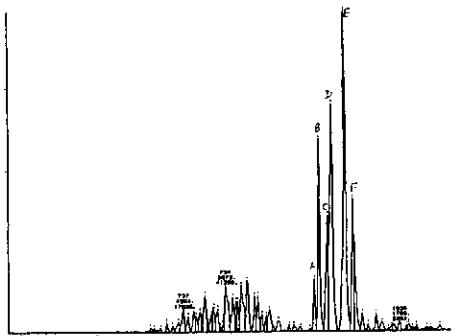

d) m/z 212: Dimethyl DibenzoThiophenes

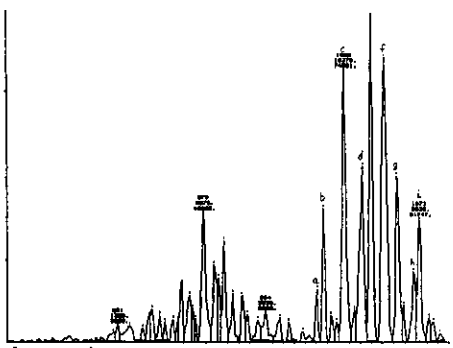

e) m/z 226: Trimethyl DibenzoThiophenes

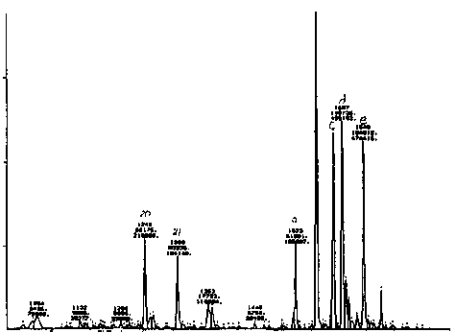

f) m/z 231: Triaromatic Steroids

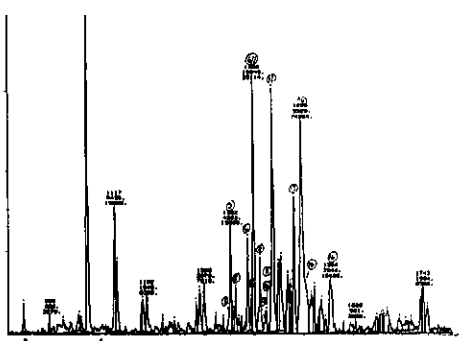

g) m/z 253: Monoaromatic Steroids
(from aromatic fraction)

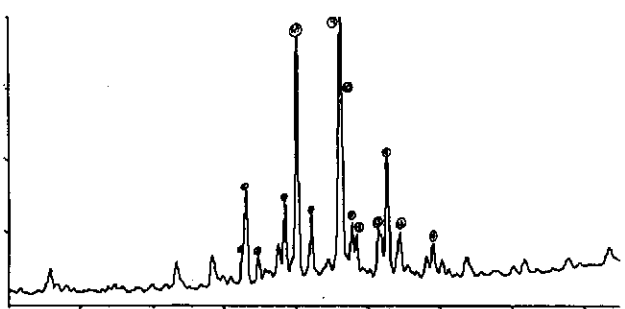

h) m/z 253: Monoaromatic Steroids
(from saturates fraction)

Figure E.125: Annotated TIC and single ion fragmentograms of aromatic hydrocarbons from sample 59, well 122 RC, 2682m.

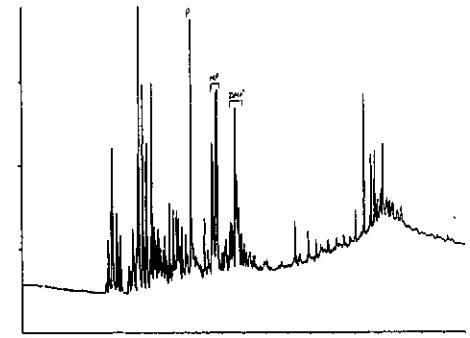

a) TIC: Total Ion Count

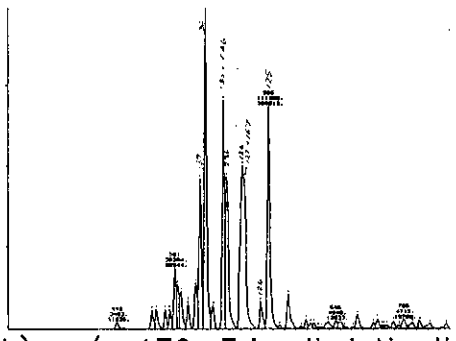

b) m/z 170: Trimethyl Napthalenes

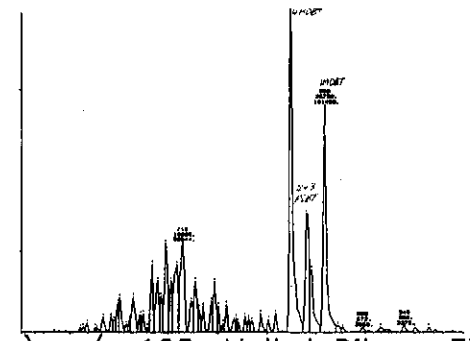

c) m/z 198: Methyl DibenzoThiophenes

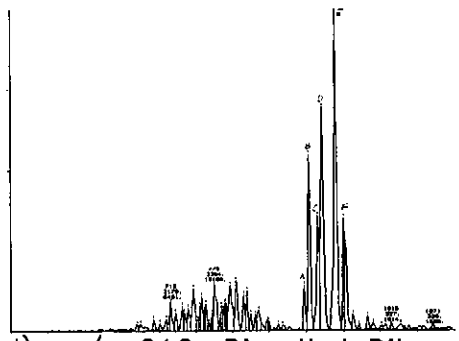

d) m/z 212: Dimethyl DibenzoThiophenes

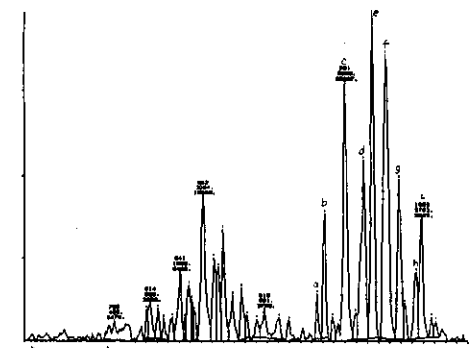

e) m/z 226: Trimethyl DibenzoThiophenes

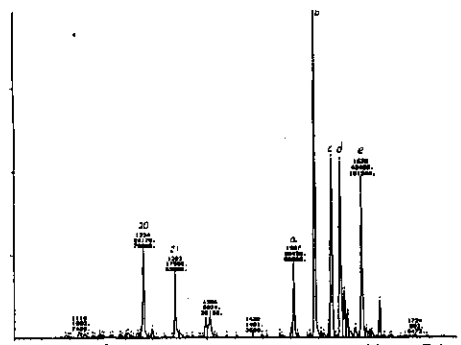

f) m/z 231: Triaromatic Steroids

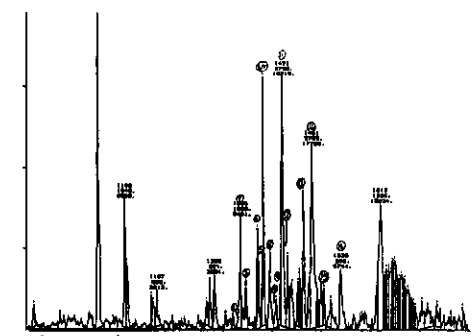

g) m/z 253: Monoaromatic Steroids (from aromatic fraction)

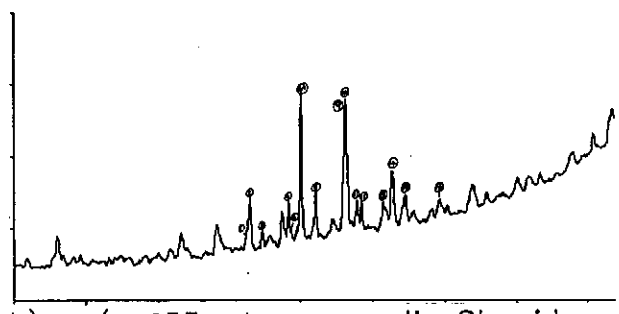

h) m/z 253: Monoaromatic Steroids (from saturates fraction)

Figure E.126: Annotated TIC and single ion fragmentograms of aromatic hydrocarbons from sample 60, well 122 RC, 2832m.

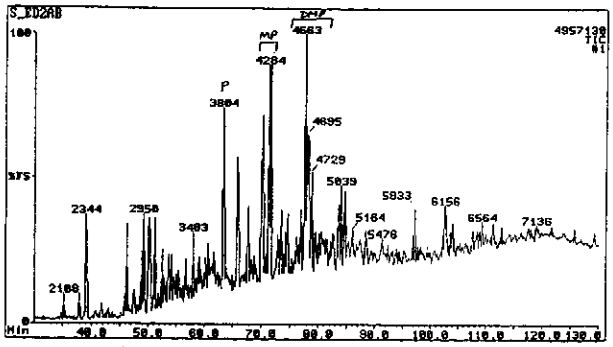

a) TIC: Total Ion Count

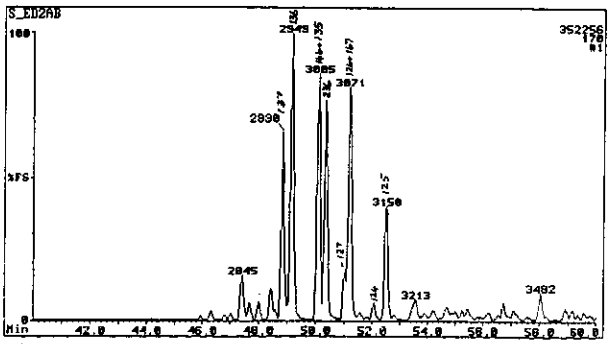

b) m/z 170: Trimethyl Napthalenes

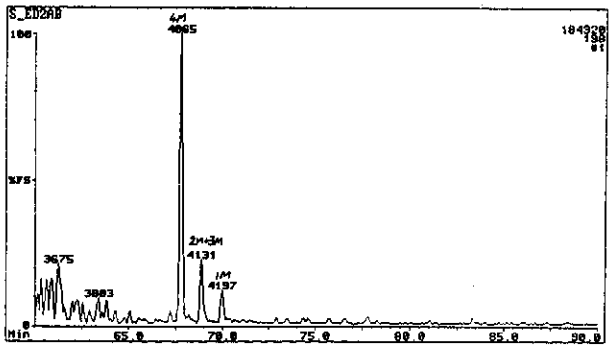

c) m/z 198: Methyl DibenzoThiophenes

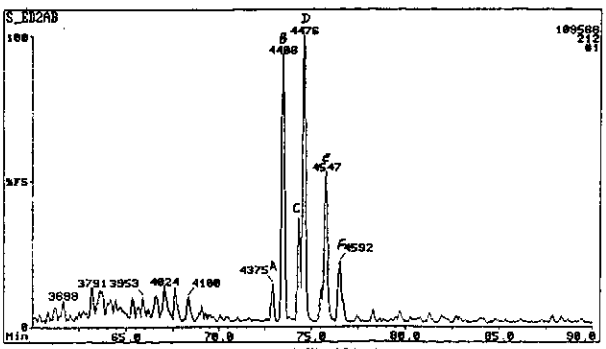

d) m/z 212: Dimethyl DibenzoThiophenes

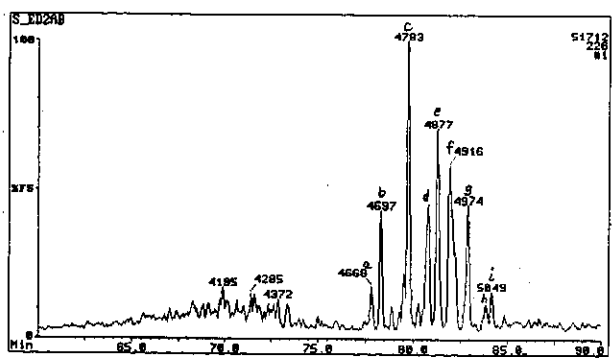

e) m/z 226: Trimethyl DibenzoThiophenes

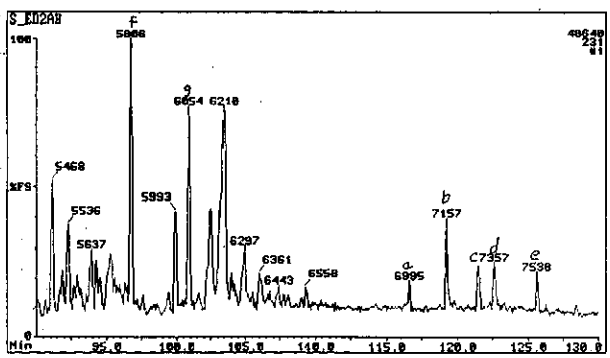

f) m/z 231: Triaromatic Steroids

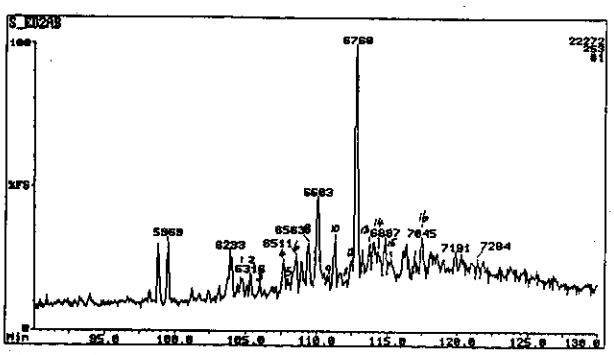

g) m/z 253: Monoaromatic Steroids (from aromatic fraction)

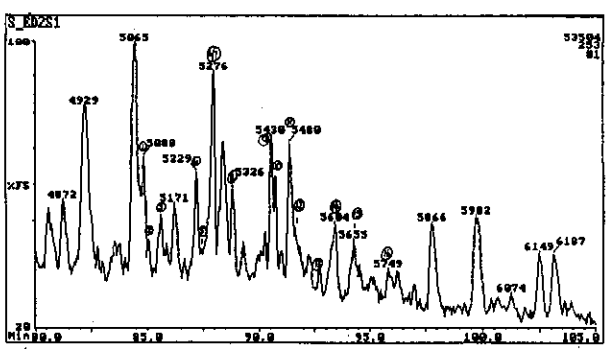

h) m/z 253: Monoaromatic Steroids (from saturates fraction)

Figure E.127: Annotated TIC and single ion fragmentograms of aromatic hydrocarbons from sample 61, well 11 RC, 2682m.

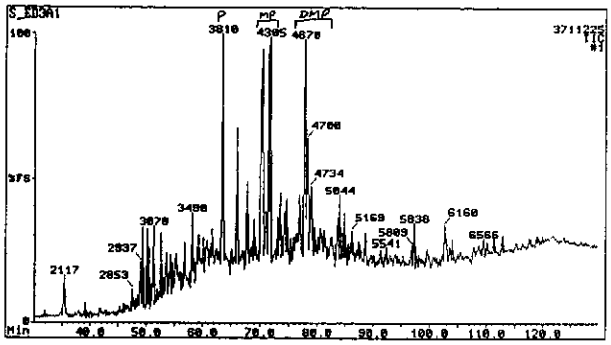

a) TIC: Total Ion Count

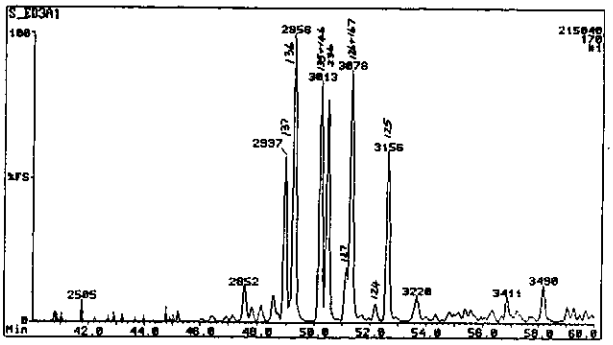

b) m/z 170: Trimethyl Napthalenes

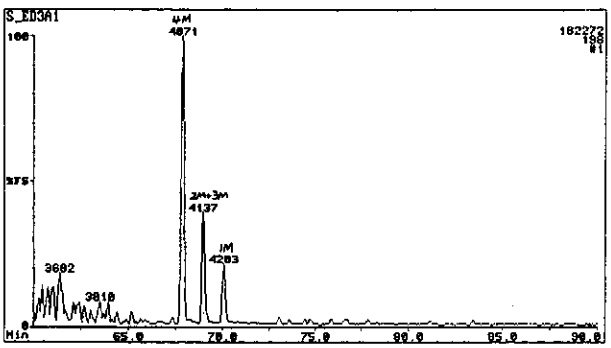

c) m/z 198: Methyl DibenzoThiophenes

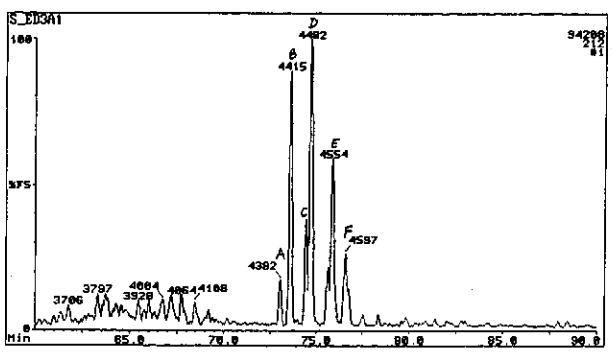

d) m/z 212: Dimethyl DibenzoThiophenes

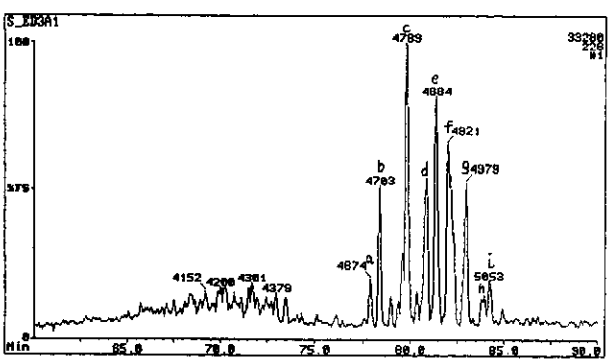

e) m/z 226: Trimethyl DibenzoThiophenes

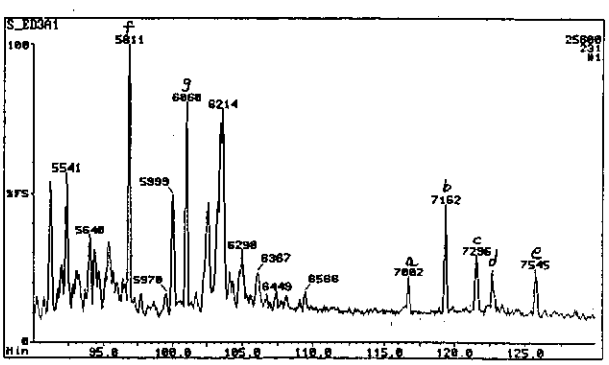

f) m/z 231: Triaromatic Steroids

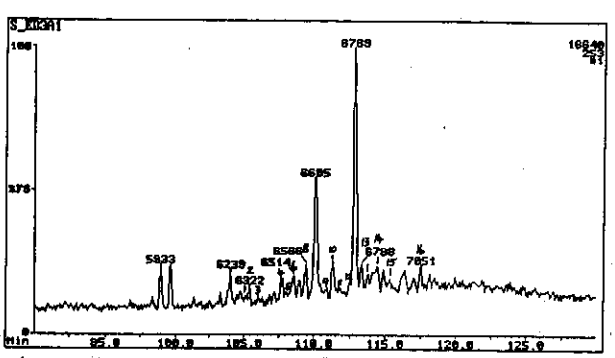

g) m/z 253: Monoaromatic Steroids (from aromatic fraction)

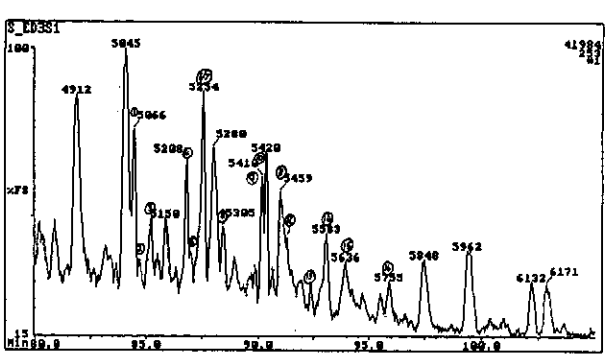

h) m/z 253: Monoaromatic Steroids (from saturates fraction)

Figure E.128: Annotated TIC and single ion fragmentograms of aromatic hydrocarbons from sample 62, well 14 RC, 2721m.

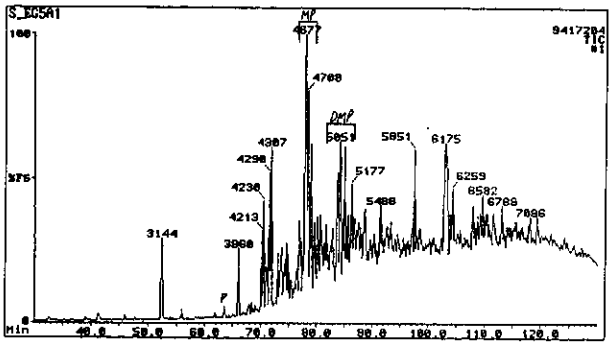

a) TIC: Total Ion Count

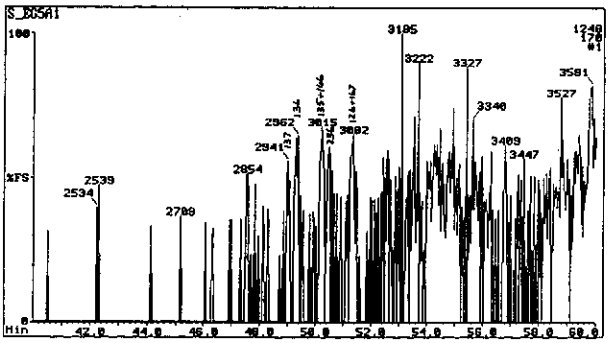

b) m/z 170: Trimethyl Napthalenes

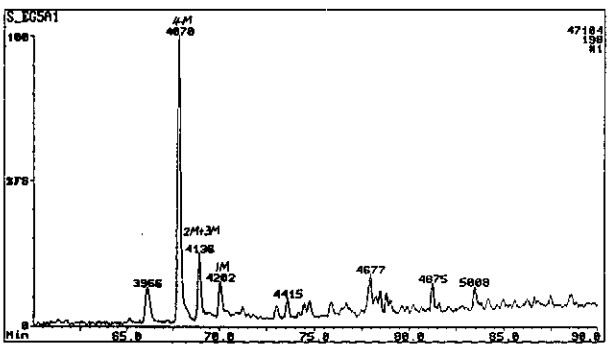

c) m/z 198: Methyl DibenzoThiophenes

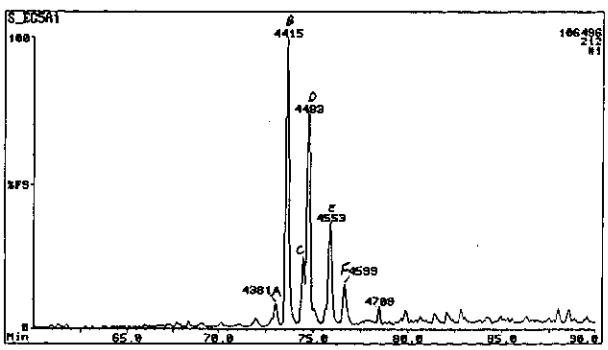

d) m/z 212: Dimethyl DibenzoThiophenes

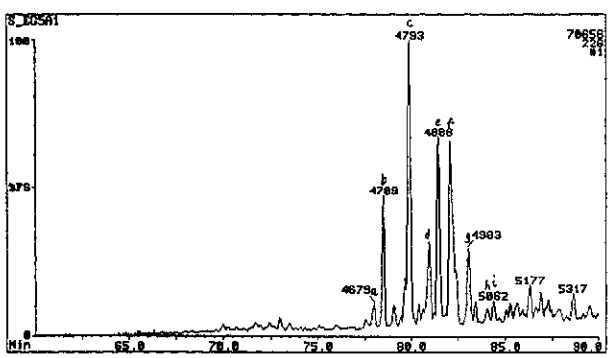

e) m/z 226: Trimethyl DibenzoThiophenes

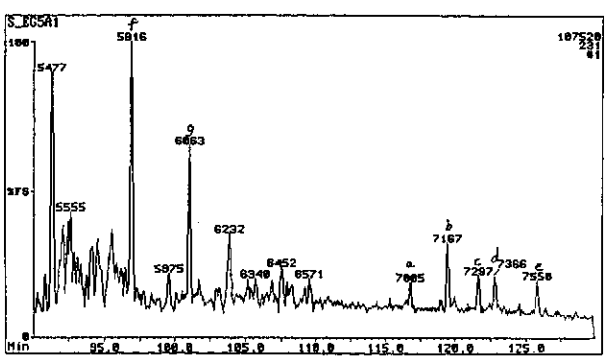

f) m/z 231: Triaromatic Steroids

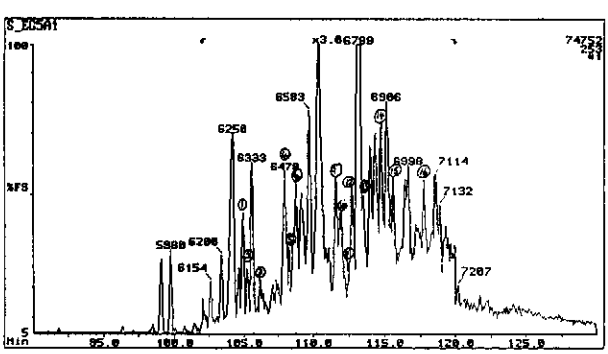

g) m/z 253: Monoaromatic Steroids (from aromatic fraction)

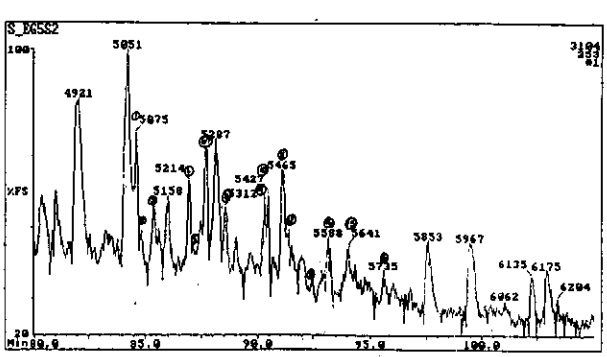

h) m/z 253: Monoaromatic Steroids (from saturates fraction)

Figure E.129: Annotated TIC and single ion fragmentograms of aromatic hydrocarbons from sample 63, well 42 RC, 3021m.

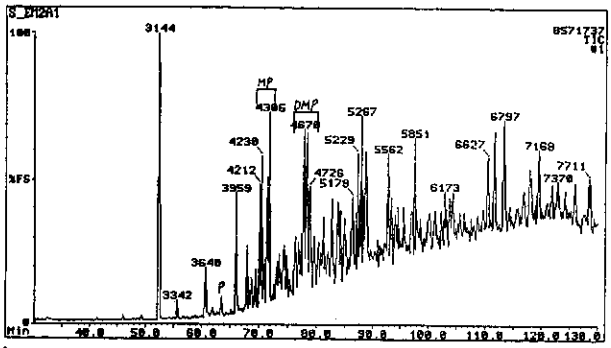

a) TIC: Total Ion Count

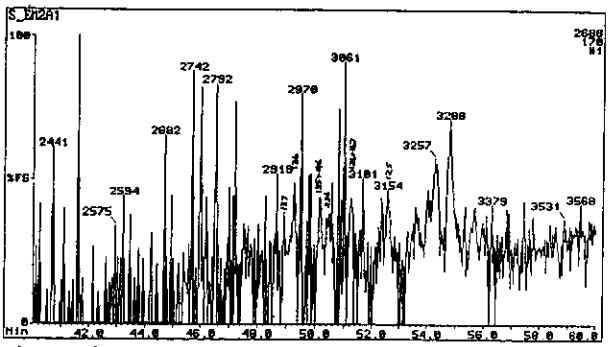

b) m/z 170: Trimethyl Napthalenes

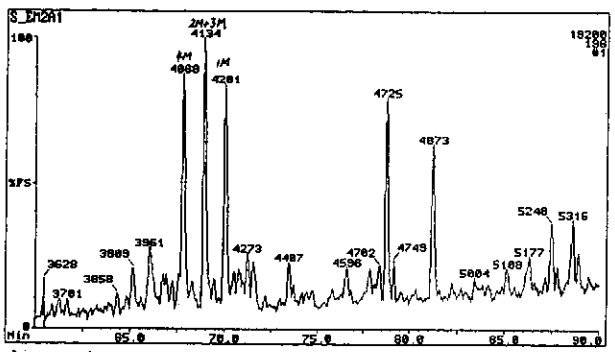

c) m/z 198: Methyl DibenzoThiophenes

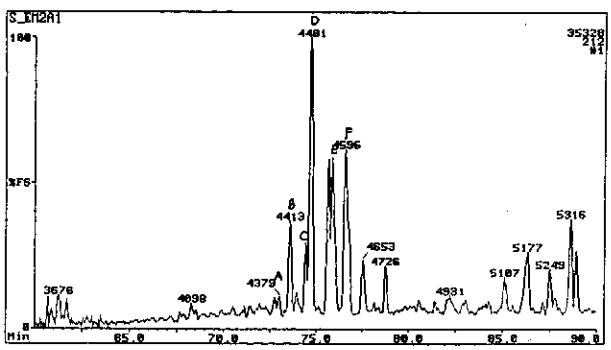

d) m/z 212: Dimethyl DibenzoThiophenes

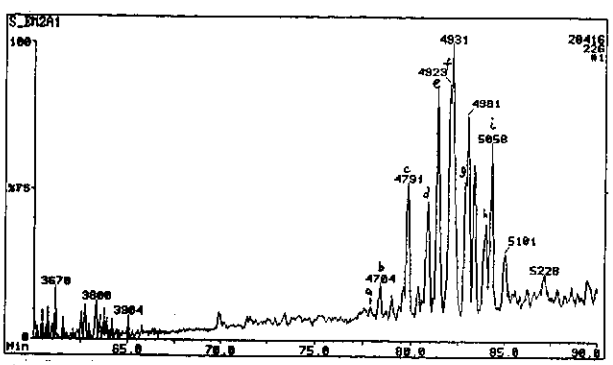

e) m/z 226: Trimethyl DibenzoThiophenes

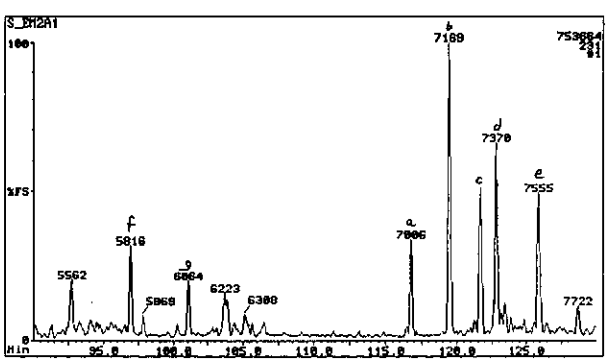

f) m/z 231: Triaromatic Steroids

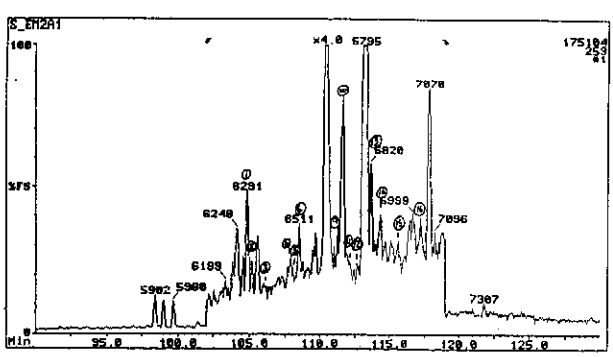

g) m/z 253: Monoaromatic Steroids (from aromatic fraction)

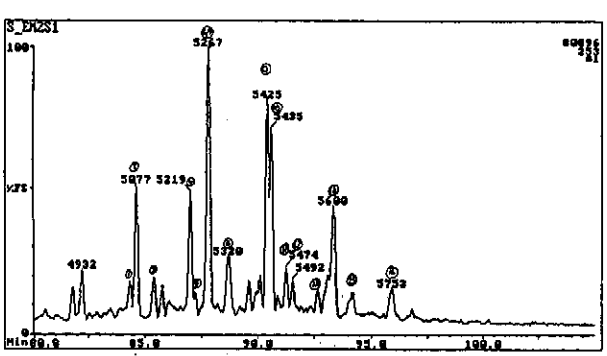

h) m/z 253: Monoaromatic Steroids (from saturates fraction)

Figure E.130: Annotated TIC and single ion fragmentograms of aromatic hydrocarbons from sample 64, well 48 RC, 2490m.

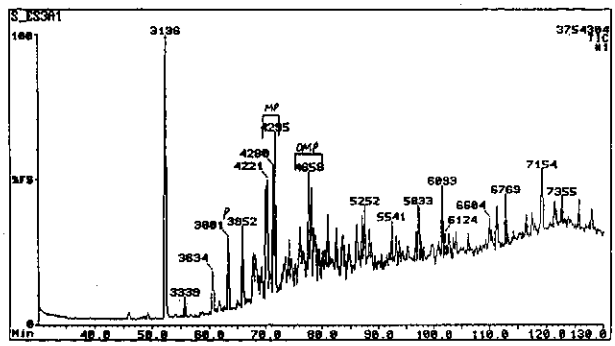

a) TIC: Total Ion Count

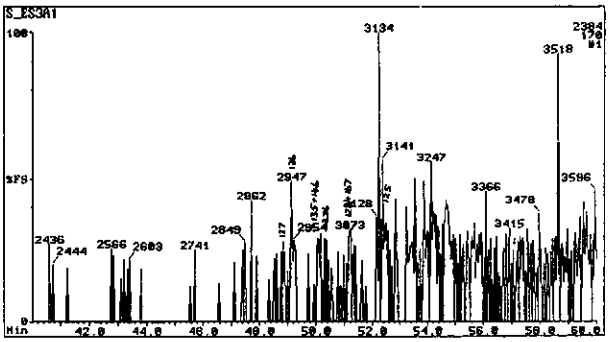

b) m/z 170: Trimethyl Napthalenes

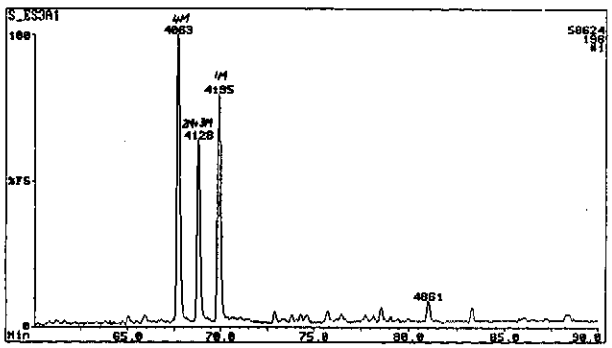

c) m/z 198: Methyl DibenzoThiophenes

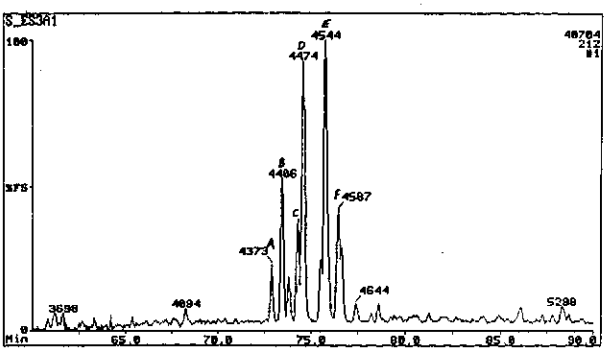

d) m/z 212: Dimethyl DibenzoThiophenes

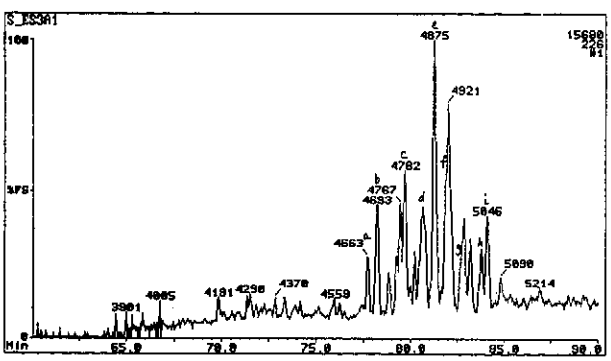

e) m/z 226: Trimethyl DibenzoThiophenes

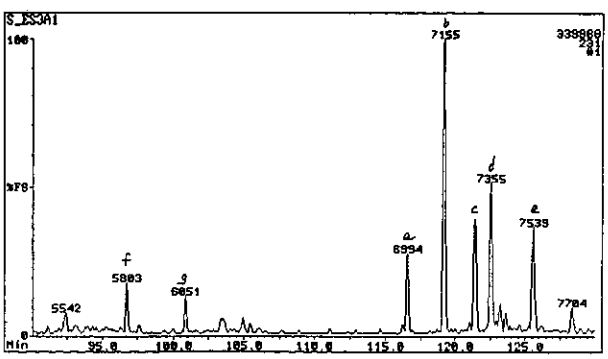

f) m/z 231: Triaromatic Steroids

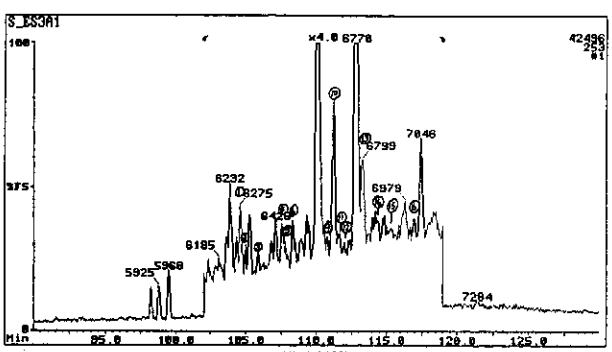

g) m/z 253: Monoaromatic Steroids (from aromatic fraction)

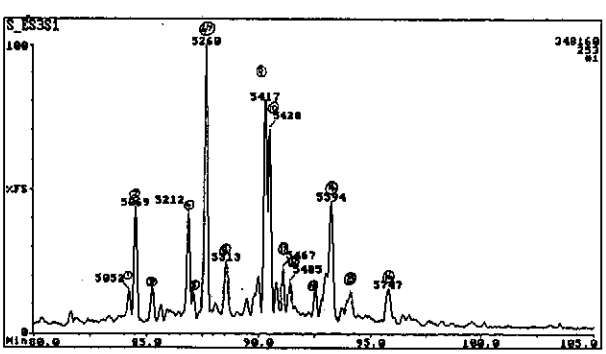

h) m/z 253: Monoaromatic Steroids (from saturates fraction)

Figure E.131: Annotated TIC and single ion fragmentograms of aromatic hydrocarbons from sample 65, well 41 RC, 2320m.

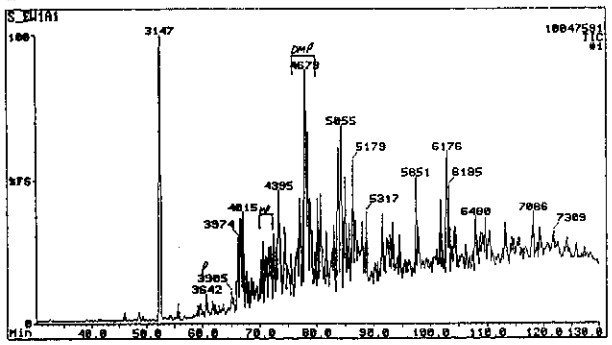

a) TIC: Total Ion Count

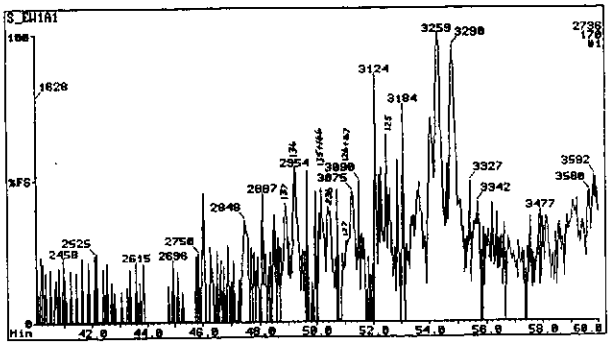

b) m/z 170: Trimethyl Napthalenes

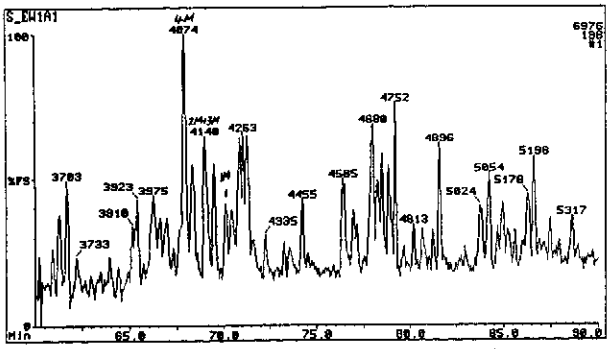

c) m/z 198: Methyl DibenzoThiophenes

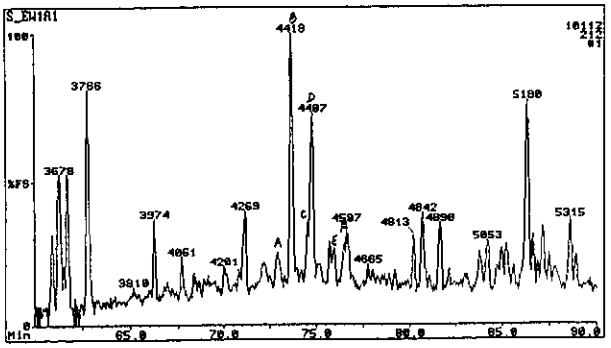

d) m/z 212: Dimethyl DibenzoThiophenes

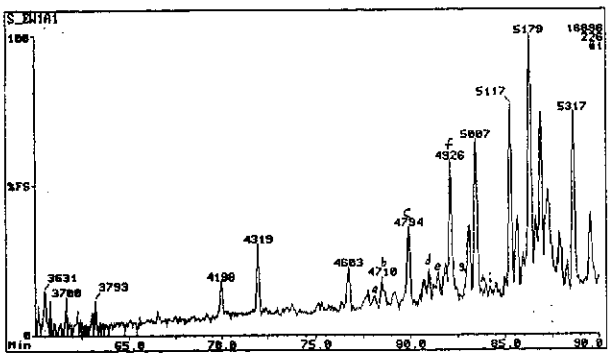

e) m/z 226: Trimethyl DibenzoThiophenes

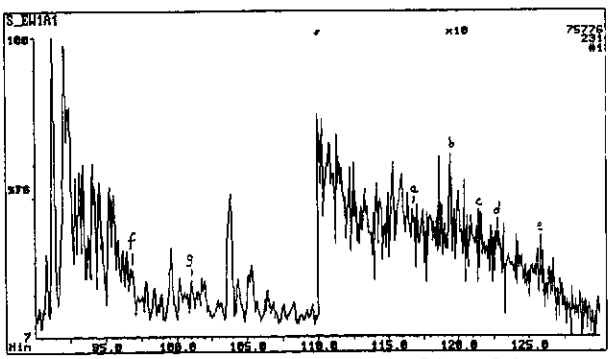

f) m/z 231: Triaromatic Steroids

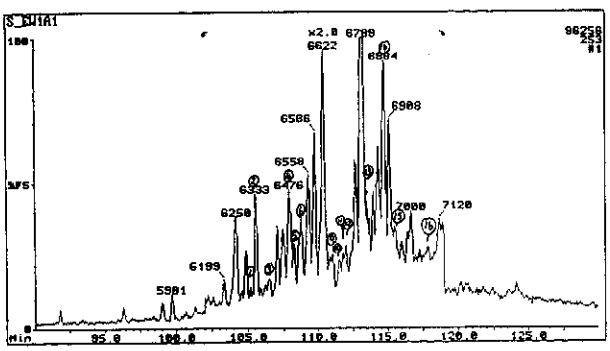

g) m/z 253: Monoaromatic Steroids (from aromatic fraction)

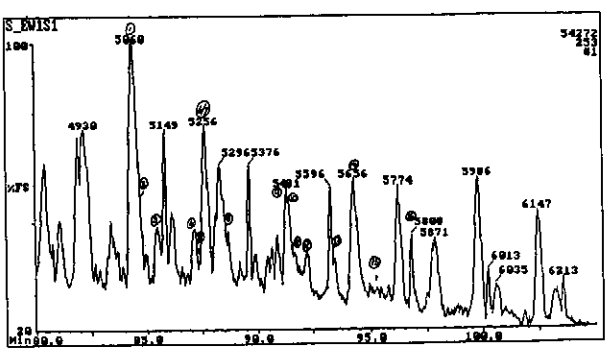

h) m/z 253: Monoaromatic Steroids (from saturates fraction)

Figure E.132: Annotated TIC and single ion fragmentograms of aromatic hydrocarbons from sample 66, well 65 RC, 3160m.

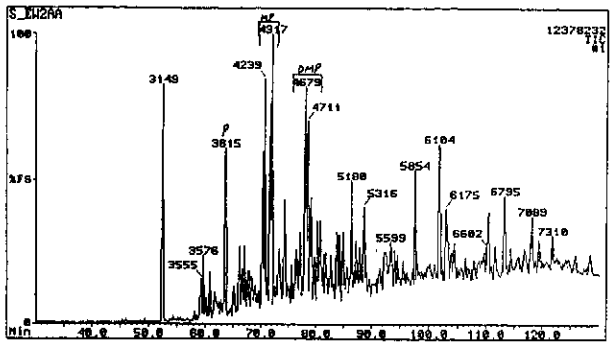

a) TIC: Total Ion Count

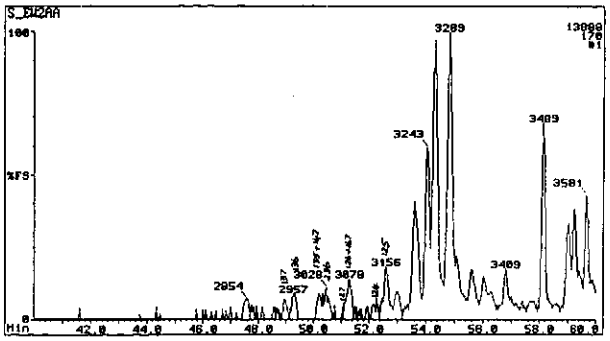

b) m/z 170: Trimethyl Napthalenes

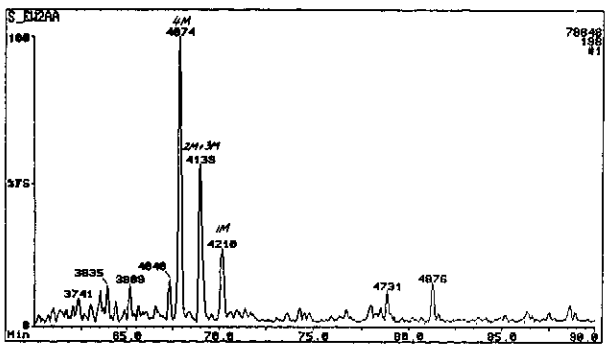

c) m/z 198: Methyl DibenzoThiophenes

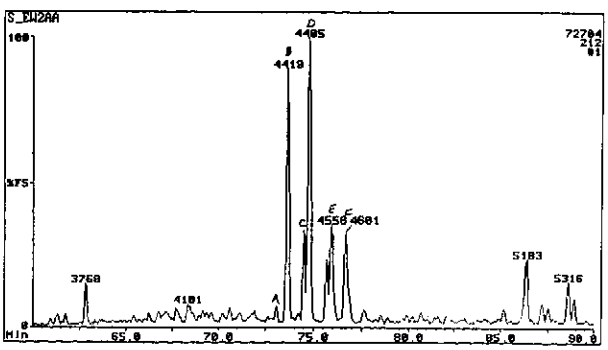

d) m/z 212: Dimethyl DibenzoThiophenes

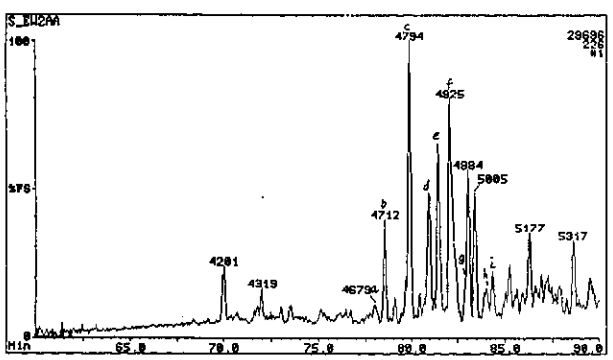

e) m/z 226: Trimethyl DibenzoThiophenes

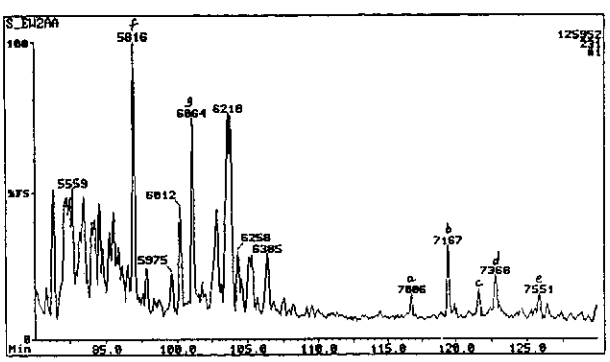

f) m/z 231: Triaromatic Steroids

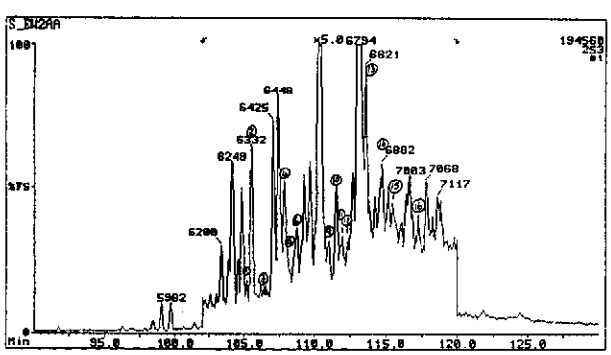

g) m/z 253: Monoaromatic Steroids (from aromatic fraction)

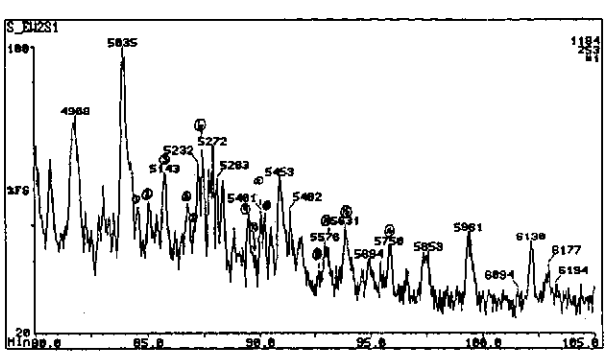

h) m/z 253: Monoaromatic Steroids (from saturates fraction)

Figure E.133: Annotated TIC and single ion fragmentograms of aromatic hydrocarbons from sample 67, well 75 core 1, 2829.0m.

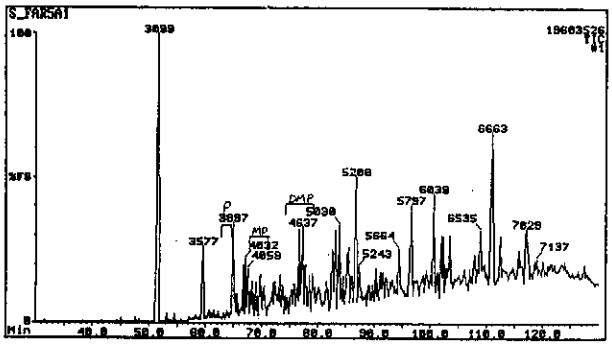

a) TIC: Total Ion Count

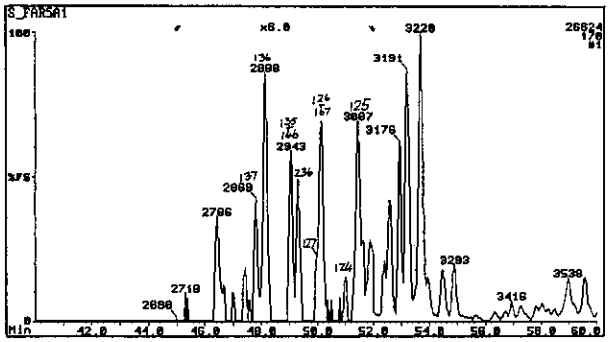

b) m/z 170: Trimethyl Napthalenes

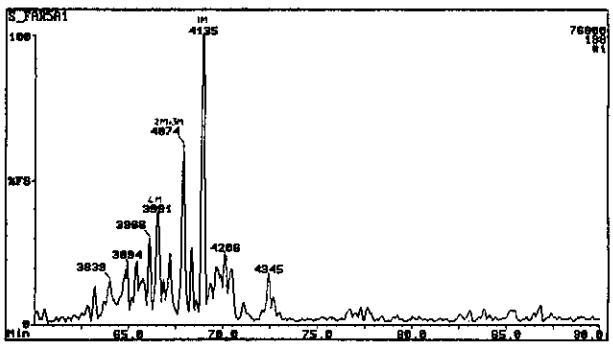

c) m/z 198: Methyl DibenzoThiophenes

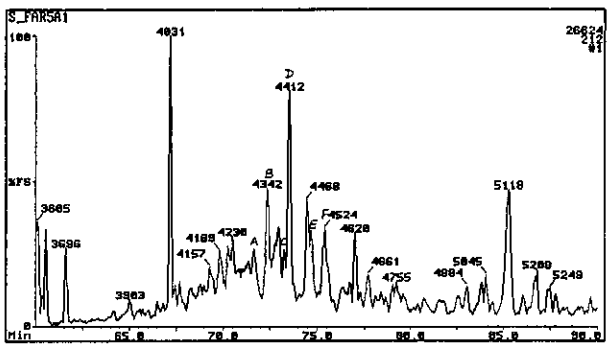

d) m/z 212: Dimethyl DibenzoThiophenes

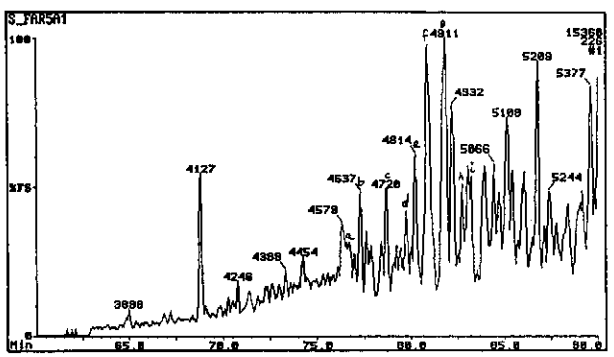

e) m/z 226: Trimethyl DibenzoThiophenes

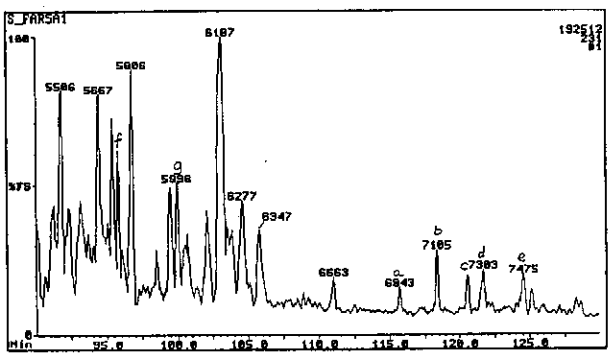

f) m/z 231: Triaromatic Steroids

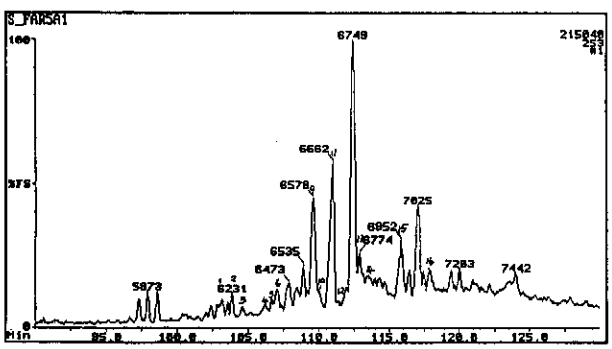

g) m/z 253: Monoaromatic Steroids (from aromatic fraction)

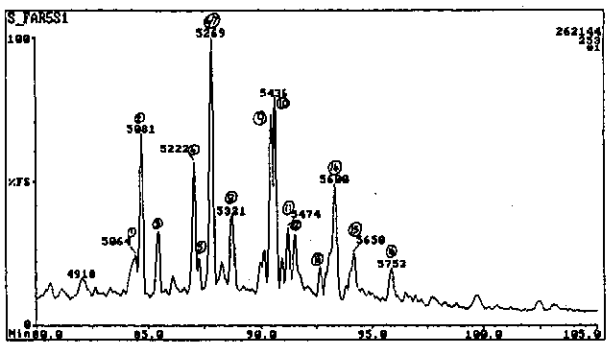

h) m/z 253: Monoaromatic Steroids (from saturates fraction)

Figure E.134: Annotated TIC and single ion fragmentograms of aromatic hydrocarbons from sample 68, well 67 RC, 2651m.

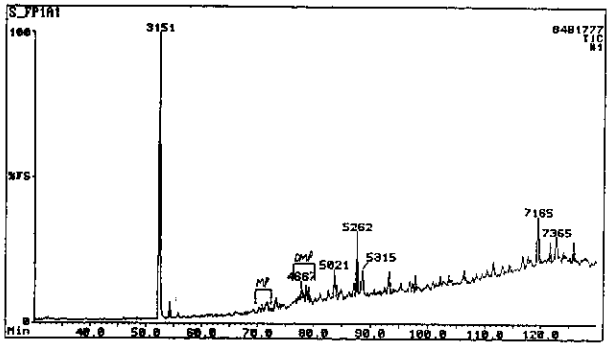

a) TIC: Total Ion Count

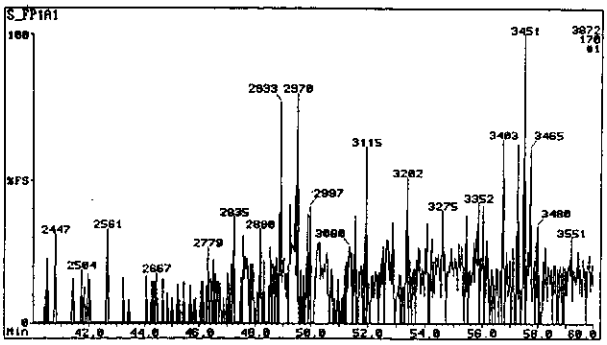

b) m/z 170: Trimethyl Napthalenes

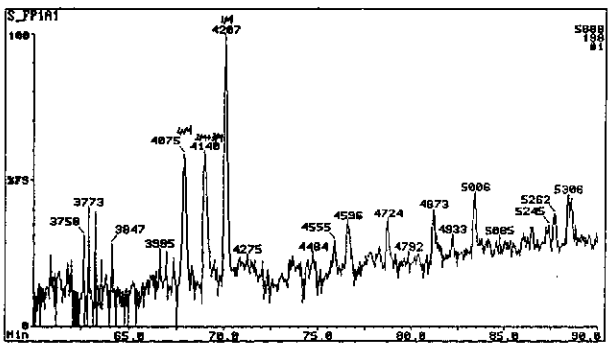

c) m/z 198: Methyl DibenzoThiophenes

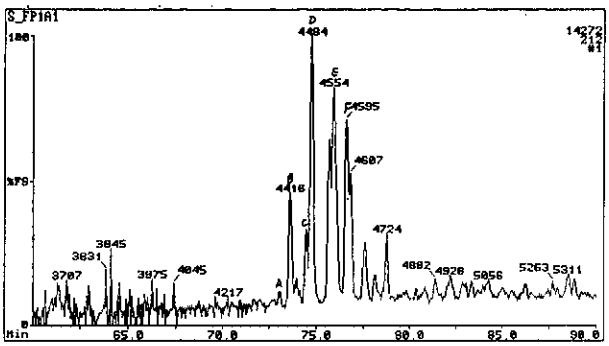

d) m/z 212: Dimethyl DibenzoThiophenes

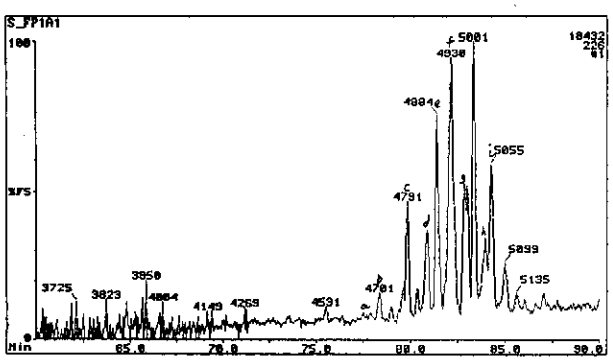

e) m/z 226: Trimethyl DibenzoThiophenes

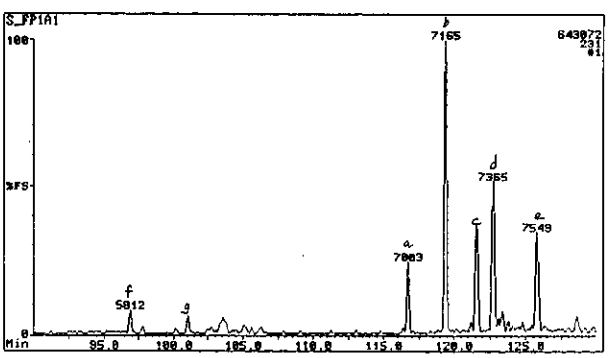

f) m/z 231: Triaromatic Steroids

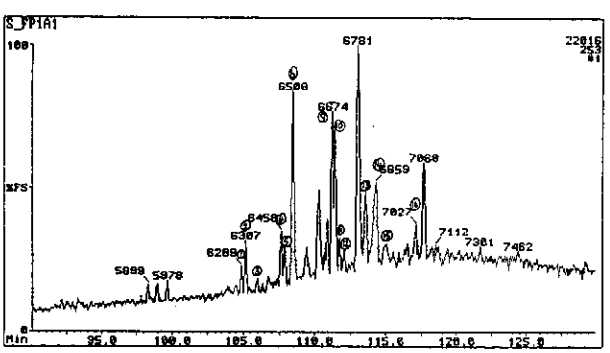

g) m/z 253: Monoaromatic Steroids (from aromatic fraction)

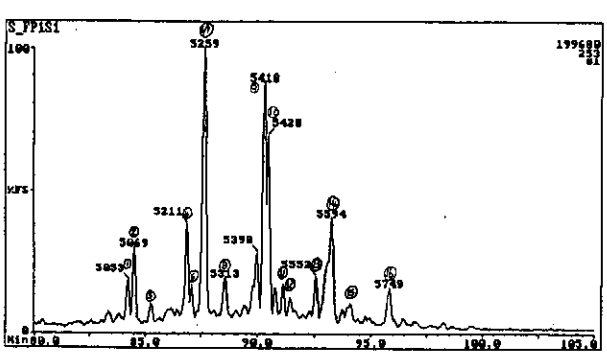

h) m/z 253: Monoaromatic Steroids (from saturates fraction)

Figure E.135: Annotated TIC and single ion fragmentograms of aromatic hydrocarbons from sample 69, well 12 RC, 2057m.

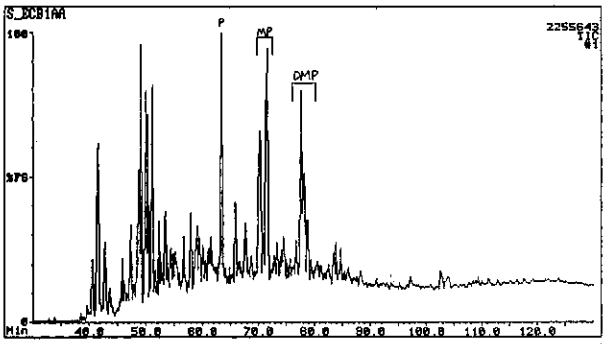

a) TIC: Total Ion Count

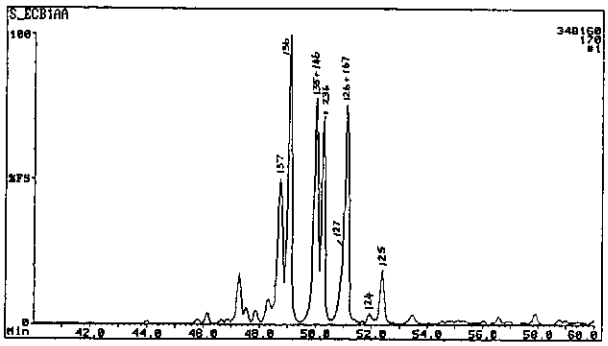

b) m/z 170: Trimethyl Napthalenes

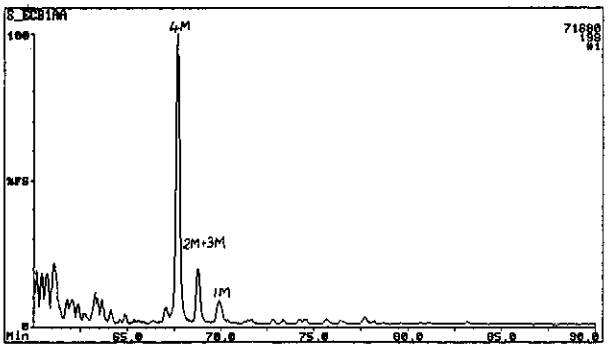

c) m/z 198: Methyl DibenzoThiophenes

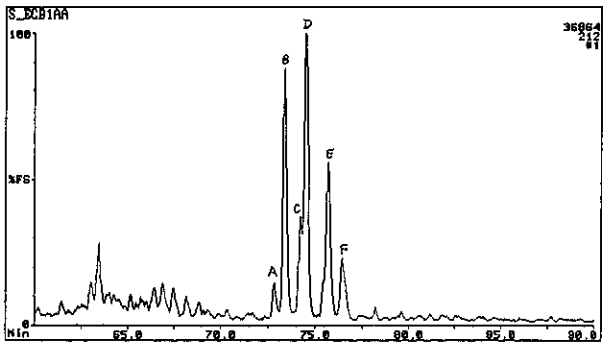

d) m/z 212: Dimethyl DibenzoThiophenes

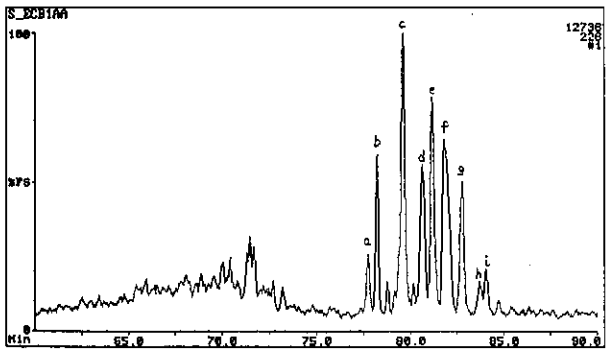

e) m/z 226: Trimethyl DibenzoThiophenes

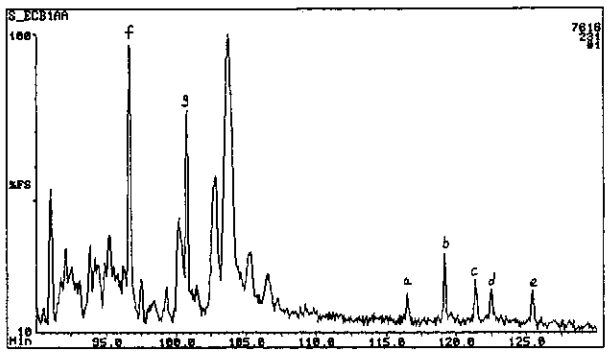

f) m/z 231: Triaromatic Steroids

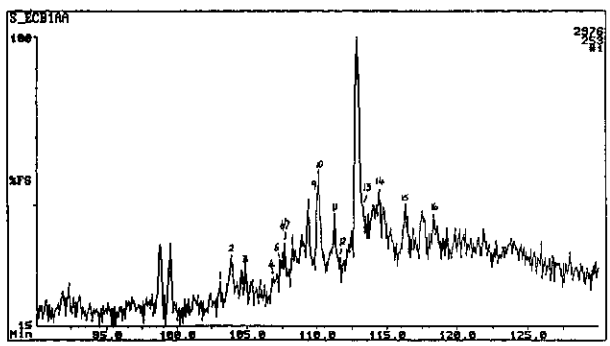

g) m/z 253: Monoaromatic Steroids (from aromatic fraction)

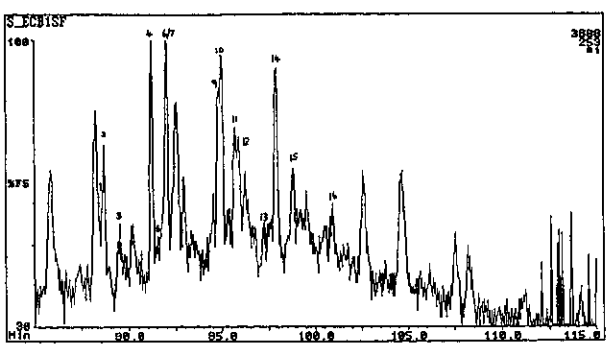

h) m/z 253: Monoaromatic Steroids (from saturates fraction)

Figure E.136: Annotated TIC and single ion fragmentograms of aromatic hydrocarbons from sample 70, well 156 RC, 2805m.

APPENDIX F: WHOLE OIL, FRACTIONAL AND BIOMARKER TABLES

BASIC PYROLYSIS, CALCIMETRY AND OPTICAL DATA.																			
No.	WELL	DEPTH(mbkb)	TOC%	S2	HI	OI	Tmax	PI	Cal	Dol	Ro%	Am	Sp	Ex	Vr	In	S%	Rock T	Sequ
OIL SAMPLES																			
1	83	2470							11	2	0.80						<0.03	101	14A
2	83	2889							1	6	0.93						<0.03	112	10A
3	83	2889							1	6	0.93						<0.03	112	10A
4	88	2507							0	0	0.81						0.13	100	14A
5	88	2507							0	0	0.81						0.13	100	14A
6	88	2827							3	2	0.91							112	10A
7	92	2949							16	1	0.99							111	5A
8	118	2563.1							1	1	0.85							100	8A
9	102	2241							1	1	0.91						0.10	95	pre1At1
10	102	2632									1.05							110	pre1At1
11	91	3220.05									1.15							130	6A
12	104	3017.46									1.08							122	10A
13	93	3212.4									1.15							127	5A
14	109	2630							1	1	0.87							100	13A
15	107	2565							0	3	0.81							98	pre1At1
16	110	3051							1	0	1.08							120	9A
17	126	2643							1	3	1.04							112	14A
18	122	2517									0.93							98	13B
19	132	2662							1	2	1.02							103	13A
20	132	2702.4							1	2	1.02							103	13A
21	48	2620									1.02						0.72	115	pre1At1
22	16	2614							0	3	0.95							97	13A
23	59	2212									0.80						0.27	93	pre1At1
24	75	2830.5							1	0	1.05							117	8A
25	101	2987.5							1	1	0.95							119	7A
26	20	2699									0.98						0.05	110	pre1At1
27	13	2518.86									0.88							107	pre1At1
28	103	2718							1	0	1.23							117	14A
29	94	2799									0.96							113	13B
30	156	2522							1	2	0.90							100	14A
31	156	2525							1	2	0.90							100	14A
32	166	2508									0.85							98	14A
33	166	2510.43									0.85							98	14A
34	166	2520									0.90							99	14A
35	166	2522.5									0.90							99	14A
36	165	2256									0.75							84	14A
37	167	2679									1.00							108	14A
38	167	2681.65							1	4	1.00							108	14A

Table F.01: Basic pyrolysis, calcimetry and optical data from all hydrocarbon samples (page 1 of 2).

No.	WELL	DEPTH(mbkb)	TOC%	S2	HI	OI	Tmax	PI	Cal	Dol	Ro%	Am	Sp	Ex	Vr	In	S%	Rock T	Sequ
SHALE SAMPLES																			
41	83	2702	2.32	3.04	131	41	441	0.14	1	4	0.83	A			S	S		107	13A
42	83	2741	2.61	4.65	178	40	441	0.18	1	6	0.87	A	T	T	S	S		108	13A
43	83	2792	2.03	2.93	144	47	439	0.19	0	5	0.91	A	T	S	S	S		110	13A
44	92	2610	1.64	4.13	252	36	441	0.09	1	1	0.82							99	9A
45	89	2660	1.13	4.25	376	97	449	0.01	2	2	0.76	A	T		S	S		83	pre1At1
46	93	2720	3.50	10.06	287	4	439	0.13	1	4	0.95	A			S	S		108	13A
47	93	2761	2.50	6.46	258	41	439	0.16	8	2	1.02	A			C	C		109	13A
48	93	2761	2.50	6.46	258	41	439	0.16	8	2	1.02	A			C	C		109	13A
49	99	1820	1.37	2.25	164	101	434	0.07	7	3	0.58	T		T	S	C		74	15A
50	109	2461	2.45	8.65	353	36	435	0.05	1	4	0.80	A			C	C		96	12A
51	109	2654.15	1.46	5.05	346	5	440	0.08	1	0	0.78	A			C	C		101	13A
52	130	2331	2.35	6.40	272	23	431	0.04	1	4	0.74	A	T	T		C		92	13A
53	110	2830	2.24	3.18	142	75	449	0.21	9	3	1.00	A		S	S	C		112	13A
54	110	2902	1.71	1.85	108	56	457	0.22	5	1	1.02		T	S	A	C		115	13A
55	112	2392	1.56	3.69	237	54	435	0.08	1	2	0.87	A	S	S	C	S		89	6A
56	117	2918.5	1.97	3.07	156	27	441	0.33	1	2	1.10	A		T	C	S		118	9A
57	117	2918.5	1.97	3.07	156	27	441	0.33	1	2	1.10	A		T	C	S		118	9A
58	117	2918.5	1.97	3.07	156	27	441	0.33	1	2	1.10	A		T	C	S		118	9A
59	122	2682	2.75	8.54	311	44	436	0.12	4	3	1.02	A			C	C		104	13A
60	122	2832	1.58	3.67	232	63	441	0.18	1	3	1.06	A	S		S	S		110	9A
61	11	2682	2.53	3.18	126	65	445	0.39	3	5	1.12	S	T	C	C	C		110	9A
62	14	2721	2.28	2.90	127	35	442	0.29	6	2	1.10	A			C	C		111	13A
63	42	3021	1.87	2.48	133	37	441	0.32	26	1	1.10							119	1A
64	48	2490	1.32	2.52	191	61	434	0.13	6	2	0.92	S	T	A	S	A		109	5A
65	41	2320	1.55	3.08	189	53	437	0.10	2	6	0.82	A	S		C	C		93	5A
66	65	3160	0.69	0.45	65	141	439	0.31	9	2	1.17	C		S	S	S		131	1A-4A
67	75	2829	1.47	2.80	190	10	443	0.10	1	0	1.05	A		A	T	S		117	8A
68	67	2651	1.46	3.18	218	46	438	0.12	2	4	0.95	C	T	S	S	S		106	5A
69	12	2057	2.30	8.21	357	22	428	0.07	20	2	0.70							83	15A
70	156	2805	2.60	4.03	155	41	444	0.22	14	3	0.94	S	T	S	A	S		110	13A
S2 in mgHC/gmROCK. HI=hydrogen index (mgHC/gmTOC). OI=oxygen index (mgCO2/gmTOC). Tmax=pyrolysis maximum temperature.																			
Cal=calcite content m/m. Dol=dolomite content m/m. Ro%=mean random vitrinite reflectance measured in oil%.																			
S%=total sulphur content m/m. Am=amorphous maceral. Sp=sporinite maceral. Ex=exinite maceral. Vr=vitrinite maceral. In=Inertinite maceral.																			
A=abundant. C=common. S=some. T=trace. PI=production index = S1/(S1+S2).																			
RockT=rock temperature from corrected logs. Sequ=chronostratigraphic sequence from which sample taken.																			

Table F.01: Basic pyrolysis, calcimetry and optical data from all source rock samples (plus description of sample annotation codes) (page 2 of 2).

EXTRACT AND GC DATA														ANALYSIS CODES	
No.	EOM	Sats	Aroms	NSO	Asph	Adduct	Rock T	IP14	IP15	IP16	IP18	IP19 (Pr)	IP20 (Ph)	MS Sat	MS Arom
OIL SAMPLES															
1		85	11	4	0	mol.	101	0	228	646	857	1094	568	F32623/1	32623A/1
2		69	16	15	0	mol.	112	0	0	110	551	984	642	F32624/1	32624A/1
3		69	16	15	0	urea	112	0	0	110	551	984	642	S_EAA1SD	na
4		84	10	6	0	nil	100	0	0	281	780	1174	631	EAD07SA2	EAD07AR1
5		84	10	6	0	urea	100	0	0	281	780	1174	631	EADD5SA1	S_EAD1A4
6		69	24	6	1	nil	112	0	48	208	423	838	562	EAD1D4SB	EAD1D4C1
7	110	29	17	47	7	nil	111	0	0	0	12	170	497	S_EAE1S	S_EAE1A1
8	5240	73	17	9	1	urea	100	0	52	150	438	773	522	S_EAF1S1	S_EAF1A2
9		93	5	2	0	urea	95	0	267	666	760	1071	483	S_EAG1SA	S_EAG1A2
10		89	6	5	0	urea	110	0	103	417	670	943	479	S_EAG1SB	S_EAG1AB
11	1000	76	6	14	4	urea	130	0	23	39	161	518	590	S_EAL1S3	S_EAL1AB
12	500	68	10	18	4	urea	122	0	39	77	251	499	400	S_EAO1S2	S_EAO1A1
13	470	49	21	18	12	urea	127	0	0	170	820	1260	869	92c5bc	92c5ar
14		90	7	3	0	urea	100	40	196	450	345	718	386	92c10bc	92c10ar
15		96	2	2	0	urea	98	7	75	372	844	1423	692	S_EBF1S1	S_EBF1A1
16		94	5	1	0	urea	120	35	325	679	812	1290	801	S_EBH1S3	S_EBH1AC
17		75	11	14	0	urea	112	722	629	622	468	609	283	S_EBK1S1	S_EBK1A1
18	9570	60	21	18	1	urea	98	0	0	0	514	1108	877	92c1bc	92c1ar
19		56	20	24	0	urea	103	0	579	798	910	1211	699	92c7bc	92c7ar
20	985	59	24	12	5	urea	103	0	0	0	432	1040	852	92c8bc	92c8ar
21		59	20	20	1	urea	115	0	50	210	410	770	490	S_EM2SR1	S_EM2COA
22	1070	41	25	29	5	urea	97	0	0	0	155	669	461	S_EN1S1	S_EN1A1
23		86	10	4	0	urea	93	0	14	41	38	65	40	S_ES4S2	S_ES4AB
24	3300	84	10	6	0	urea	117	0	0	80	218	315	248	S_EW2S2	S_EW2AB
25	552	63	12	21	4	urea	119	0	0	28	382	849	764	92c9bc	92c9ar
26		95	5	0	0	urea	110	0	21	50	31	37	19	FA699SA2	FA699AR1
27	2460	71	23	5	1	urea	107	0	0	0	5	32	98	S_FP2S1	S_FP2A1
28		83	8	9	0	nil	117	830	888	929	756	1038	557	GHG 131001	whole oil
29		75	17	8	0	nil	113	0	469	882	690	985	537	GHG 131003	whole oil
30		71	19	10	0	urea	100	0	0	889	802	1117	641	S_ECB1SF	S_ECB1AA
31	2774	67	19	13	1	urea	100	0	33	270	464	922	586	S_ECB1S1	S_ECB1A1
32		66	11	22	1	urea	98	353	654	967	624	871	423	S_ECB2SC	S_ECB2AC
33	26343	1	18	6	75	nil	98	0	0	0	35	139	257	S_ECB2SB	S_ECB2AB
34		73	15	11	1	urea	99	271	490	840	647	943	488	S_ECB2SA	S_ECB2AA
35	2815	73	18	8	1	urea	99	0	14	213	537	1010	578	S_ECB2SD	S_ECB2AD
36	1235	60	18	15	7	urea	84	0	0	32	253	656	565	S_ECH1S3	S_ECH1A1

Table F.02: Extract and isoprenoid GC data and GC-MS analysis codes for all hydrocarbon samples (page 1 of 2).

No.	EOM	Sats	Aroms	NSO	Asph	Adduct	Rock T	IP14	IP15	IP16	IP18	IP19 (Pr)	IP20 (Ph)	MS Sat	MS Arom
37		76	5	18	0	urea	108	352	526	761	372	508	188	S_ECR1SB	nil
38	328	67	19	10	4	urea	108	0	0	0	17	121	294	S_ECR1S2	nil
SHALE SAMPLES															
41	1590	33	30	20	17	urea	107	0	0	0	409	1177	860	S_EAA1S	S_EAA1AA
42	3620	41	27	23	8	nil	108	0	0	0	319	1013	1020	S_EAA1SB	S_EAA1AB
43	345	23	31	25	16	urea	110	0	0	0	308	999	1090	S_EAA1SC	S_EAA1AC
44	2260	26	22	27	25	mol.	99	0	0	24	662	1633	899	EAE10SA1	S_EAE1A1
45	1032	45	16	34	5	urea	83	0	0	0	70	115	77	S_EAI1S1	S_EAI1A1
46	2250	21	30	34	15	urea	108	0	0	0	322	999	316	92c4bc	na
47	5180	38	30	25	7	nil	109	0	0	95	339	1500	859	EAR61SA1	S_EAR1A2
48	5180	38	30	25	7	nil	109	0	0	95	339	1500	859	EAR61SA5	na
49	1500	12	19	47	22	urea	74	0	0	0	28	80	472	S_EAT1S1	S_EAT1AA
50	1865	27	21	45	7	urea	96	0	0	58	669	18778	888	S_EBD1S	S_EBD1A1
51	1250	27	31	19	23	urea	101	0	0	0	377	1332	842	92c11bc	92c11ar
52	1086	13	15	67	5	urea	92	0	0	0	93	901	1030	S_EBD2S	S_EBD2A1
53	3860	41	27	21	11	urea	112	0	59	149	717	1233	792	S_EBH1S1	S_EBH1AA
54	1940	45	22	24	9	urea	115	0	198	538	739	1081	475	S_EBH1S2	S_EBH1AB
55	1690	28	29	37	7	urea	86	0	0	218	1042	1897	1113	S_EBI1S1	S_EBI1AB
56	3420	45	25	20	10	urea	118	0	89	333	882	1333	978	92c6bc	92c6ar
57	3420	45	25	20	10	urea	118	0	89	333	882	1333	978	S_EBT1S	S_EBT1A
58	3420	45	25	20	10	urea	118	0	89	333	882	1333	978	S_EBTNS2	S_EBT1A1
59	3940	33	28	31	8	urea	104	42	339	800	1269	1894	967	92c2bc	92c2ar
60	2560	46	29	18	7	urea	110	0	49	196	1004	1785	1112	92c3bc	92c3ar
61	3280	61	21	15	2	urea	110	0	0	253	810	1422	951	S_ED2S1	S_ED2AB
62	2830	53	23	22	3	urea	111	0	0	162	773	1383	773	S_ED3S1	S_ED3A1
63	4200	61	16	23	0	urea	119	0	17	45	51	94	63	S_EG5S2	S_EG5A1
64	1300	35	18	32	15	urea	109	0	0	0	119	548	519	S_EM2S1	S_EM2A1
65	1600	37	26	31	6	urea	93	0	0	0	180	792	920	S_ES3S1	S_ES3A1
66	550	68	14	15	3	urea	131	0	0	0	269	713	552	S_EW1S1	S_EW1A1
67	930	52	23	19	6	urea	117	0	36	202	513	818	382	S_EW2S1	S_EW2AA
68	1300	51	21	23	5	urea	106	0	0	0	53	258	360	S_FAR5S1	na
69	851	26	27	38	9	urea	83	0	0	0	0	11	0	S_FP1S1	S_FP1A1
70	3509	52	32	13	3	urea	111	0	217	581	478	721	383	S_ECB1SF	S_ECB1AA
EOM=extracted organic material (ppm). Sats=saturated fraction%. Arom=aromatic fraction%. NSO=resin fraction%. Asph=asphaltene fraction%.															
IP=regular isoprenoid. MSSat and MSArom are sample analysis codes for GC-MS analyses.															

Table F.02: Extract and isoprenoid GC data and GC-MS analysis codes for all source rock samples (plus description of sample annotation codes).

WELL	DEPTH	TYPE	Col.	Fam.	Att.	SBHT	DSTT	Salinity	psia grad	nC3	iC4	nC4	iC5	nC5	22DMB	2MP	3MP	nC6	22DMP	MCP	24DMP	Benz	33DMP	CH	2MH
Family 1: Aptian oils																									
83	2470	DST3	1	1	8000	105	98.9	13000	0.448	7	36	319	770	1297	22	918	547	1439	38	940	0	66	0	1072	438
88	2507	DST5	1	1	8000	100	112.0	12000	0.426	479	518	1694	1599	1989	37	1187	756	1897	40	1147	0	107	0	1465	500
102	2241	DST4	2	1	10000	98	106.7	17000	0.441	361	657	1349	1710	1004	100	843	533	1220	0	866	21	226	0	1365	346
95	2703	DST2	2	1	14000	120	120.0	14000	0.443	211	320	944	1650	2000	49	1318	722	2003	0	1191	14	300	32	1515	540
103	2718	DST2	1	1	9000	115	93.3	17000	0.441	574	509	1842	1613	2022	46	1065	592	1635	47	872	20	160	0	1053	403
94	2799	DST1	2	1	10000	117	126.0	29000	0.481	329	249	715	1000	1773	23	1181	428	1987	0	827	9	310	15	1300	458
93	2463	DST2	1	1	12000	102	102.8	12000	0.445	1054	651	2017	1360	1949	19	749	392	1057	16	659	11	40	0	627	227
93	2808	DST1A	3	1	17000	116	111.1	17000	0.433	603	499	1904	1908	1906	36	1368	800	1907	0	1570	12	540	168	1457	509
93	2817	DST1	1	1	10000	117	112.8	8000	0.433	863	421	2019	1280	1891	26	769	471	1267	21	1127	29	334	0	1111	312
119	2816	DST1	2	1	16000	112	114.4	8000	0.434	678	352	1747	1353	1882	12	802	303	1271	20	1151	6	431	11	965	270
109	2630	DST1	2	1	4800	100	109.4	19000	0.445	453	259	678	677	1623	39	680	471	1510	40	1095	18	677	22	1264	390
109	2630	DST1	3	1	6500	100	109.4	19000	0.445	152	144	770	852	1161	27	738	489	1285	0	1227	10	493	0	1328	377
126	2643	DST1	1	1	14000	119	116.7	10000	0.444	556	471	1914	1460	1927	36	864	559	1498	30	719	12	119	0	889	322
126	2643	DST1	Q	1	26000	119	116.7	10000	0.444	129	389	1348	1243	1989	42	1247	678	1699	0	1037	9	218	18	1245	538
146	2398	DST1	3	1	25000	96	101.7	22000	0.446	442	308	1262	961	1298	15	1121	662	1287	20	1086	0	128	0	1128	522
117	2399	DST1	3	1	9000	104	106.7	15000	0.445	353	411	1986	1429	1842	14	842	359	1302	22	841	5	53	0	537	228
117	2399	DST1A	1	1	11000	104	106.7	15000	0.445	268	355	1184	1335	2018	29	1233	590	1614	32	1279	0	69	0	1053	434
156	2522	DST1	Q	1	11000	100	111	8000	0.446	93	213	823	487	1802	21	886	444	1826	0	1158	7	223	18	1212	455
166	2520	DST1	Q	1	16500	99	113.8	12000	0	103	269	1951	1962	1961	34	1342	876	1957	0	1368	6	245	17	1406	529
48	2620	DST2	3	3	28000	109	109.4	22000	0.441	462	379	1150	1138	1171	73	830	419	1066	35	958	18	278	37	1585	378
48	2634	DST1	1	1	3800	110	104.4			470	558	1300	1107	1236	112	750	401	837	46	837	854	1220	0	1748	500
59	2212	DST1	1	1	3000	95	99.2	31000	0.438	326	422	839	999	782	79	568	357	603	38	772	47	208	0	1394	349
59	2212	DST1	2	1	5500	95	99.2	31000	0.438	547	403	719	999	1191	73	605	411	1018	0	892	21	515	41	1479	361
Family 2: Barremian wet gas																									
83	2889	DST2	1	2	5500	122	113.0	24500	0.443	636	330	1266	1242	1956	59	1130	504	1483	46	1138	19	423	0	1736	478
83	3254	DST1	1	2	12000	134	128.5	57000	0.728	79	225	467	1004	859	129	934	577	1203	99	799	37	650	0	1232	707
88	2839	DST4	1	2	8000	112	117.0	25000	0.432	463	509	1518	1710	1946	99	967	670	1582	69	957	29	472	0	1527	505
88	2916	DST3	1	2	9000	115	119.4	29000	0.436	474	423	1333	1526	1587	108	1349	790	1788	91	1056	32	492	0	1722	678
88	2929	DST2	2	2	18000	116	120.0	23000	0.435	473	722	1809	1810	1808	178	1682	980	1809	0	1595	31	965	67	1809	857
88	3243	DST1	1	2	6000	126	131.7	53000	0.728	283	560	1210	1802	1798	185	1620	771	1618	121	1001	10	835	0	1717	841
102	2625	DST2	2	2	26000	110	106.0	23000	0.444	257	127	539	937	968	104	1016	440	1253	0	772	35	431	80	1251	899
96	3131	DST1	3	2	15000	118	126.1	68000	0.507	10	32	81	217	219	48	307	217	571	0	264	19	457	40	480	374
96	3131	DST1	2	2	60000	118	126.1	68000	0.507	57	58	183	222	389	48	445	289	528	61	367	23	592	0	542	445

Table F.03: Peak heights of all C3-9 compounds identified from whole oil analyses of all flowed samples from the Bredasdorp Basin (plus totals and ratios used in Chapter 8 and others) (page 1 of 12).

WELL	DEPTH	TYPE	Col.	Fam.	Att.	SBHT	DSTT	Salinity	psia grad	nC3	iC4	nC4	iC5	nC5	22DMB	2MP	3MP	nC6	22DMP	MCP	24DMP	Benz	33DMP	CH	2MH
114	3085	DST1	1	2	19000	132	135.0	8000	0.475	87	132	472	677	774	69	894	420	1054	63	657	41	499	0	952	543
108	2820	DST2	2	2	17000	116	112.2	39000	0.441	186	209	1541	1872	1900	42	1227	783	1902	0	1372	15	509	28	1574	477
108	2829	DST1	2	2	17000	116	116.7	39000	0.441	451	398	1896	1297	1901	42	1502	608	1903	44	1619	14	459	21	1806	488
129	2855	DST2	1	2	8000	116	118.3	6000	0.434	537	409	1645	1310	1972	44	994	489	1481	40	1217	18	517	0	1652	407
129	2945	DST1	1	2	20000	120	123.9	8000	0.436	414	344	1199	1513	1778	126	1352	713	1892	101	1238	29	812	0	1872	789
107	2388	DST3	2	2	25000	82	97.8	27000	0.463	799	501	1999	1298	2000	38	1149	752	1668	37	1367	10	778	39	1550	508
110	3051	DST1A	2	2	14000	116	121.1	16000	0.438	408	310	1789	892	1795	29	1053	609	1795	50	1021	6	409	22	1515	475
110	3051	DST1B	3	2	22000	116	121.1	16000	0.438	92	147	1075	1184	1802	27	1081	639	1988	33	1177	8	482	22	1524	551
110	3051	DST1B	2	2	14000	116	121.1	16000	0.438	209	183	1418	1475	1469	43	1322	763	1473	26	1380	13	513	27	1475	604
120	2931	DST1	1	2	15000	113	121.1	10000	0	265	360	1117	1366	1437	89	1104	663	1558	82	770	21	732	0	972	613
120	2931	DST1	Q	2	30000	113	121.1	10000	0	203	348	1093	1368	1477	128	1448	849	1474	0	1023	27	942	52	1303	848
166	2508	RFT	Q	2	12300	98	113	12000	0.443	809	726	1968	1122	1972	24	873	325	1282	0	697	7	145	14	828	272
132	2662	DST2	2	2	110000	103	104.4	22000	0.448	581	300	1994	647	1995	34	1316	379	1169	27	1490	11	417	24	1562	485
132	2706	DST1	2	2	26000	104	110.0	21000	0.445	319	311	1250	1251	1250	30	957	539	1252	24	1280	11	538	20	1252	442
148	2684	DST1	3	2	26500	111	110.6	20000	0.443	532	435	1341	1220	1928	28	1069	562	1219	31	1068	60	390	101	1021	390
167	2679	DST1	Q	2	110000	108	115	15000	0.444	296	297	1789	1630	2003	32	872	352	1636	0	703	5	145	15	823	333
11	2950	DST2	2	2	67000	125	127.2	28000	0.581	0	0	20	312	279	52	487	474	748	0	995	32	431	49	1575	781
84	2771	DST1	2	2	17500	109	108.9	21000	0.442	104	69	189	196	187	23	197	193	669	21	553	11	380	21	1049	268
37	3495	DST1	2	2	12000	137	136.7	80000	0.552	273	231	567	275	463	28	291	240	744	41	660	10	148	26	1101	273
65	3189	DST2	2	2	14000	129	126.1	81000	0.622	0	21	18	117	48	41	140	122	190	29	232	20	170	30	462	224
65	3267	DST1	2	2	9000	131	127.8	69000	0.537	32	21	58	81	87	17	117	75	210	21	262	9	364	18	486	130
Family 3: Hauterivian wet-dry gas																									
107	2565	DST2	2	3	20000	87	106.7	25000	0.446	358	371	1620	1620	1619	131	1228	870	1621	33	1330	28	240	51	1618	608
107	2590	DST1	2	3	7000	106	106.7	20000	0.433	622	400	546	690	1356	77	468	425	914	78	957	20	193	33	1415	317
69	2435	DST1	2	3	10000	92	107.2	5800	0.439	0	11	9	59	25	43	174	116	187	47	270	24	38	38	638	330
46	2560	DST2	2	3	45000	98	109.4	34000	0.451	0	16	72	317	528	40	497	242	726	70	722	18	227	32	935	418
54	2588	DST1	2	3	15000	104	112.8	1	0.442	151	160	261	410	678	69	491	339	849	74	820	21	231	36	1464	399
76	2610	DST1	3	3	18600	109	107.8	31000	0.445	211	172	618	623	1150	82	768	488	1245	0	872	16	258	62	1438	457
39	2229	DST2	2	3	40000	89	100.6	28000	0.451	47	129	770	813	815	140	817	635	903	0	814	38	368	67	1624	525
39	2229	DST2	1	3	25000	89	100.6	28000	0.451	17	89	111	451	320	83	537	320	594	65	548	29	125	0	1030	387
39	2556	DST1	1	3	25000	104	110.6	36000	0.462	14	83	125	573	486	145	835	469	876	100	598	40	182	0	1219	600
18	2635	DST4	2	3	17000	105	124.4	42000	0.45	141	198	350	630	1046	122	880	418	1030	40	813	31	385	50	1353	518
18	2673	DST3	2	3	7000	107	121.1	42000	0.46	0	0	0	0	0	0	0	0	0	0	0	0	0	0	44	79
18	2703	DST1	2	3	17000	109	120.0	41000	0.452	31	163	197	494	915	196	1088	680	1643	109	588	49	294	82	1530	699
21	2559	DST2	3	3	26000	107	112.8	26000	0.466	179	266	665	1104	768	180	922	630	1313	5	875	38	272	74	1478	685

Table F.03: Whole oil GC peak heights (page 2 of 12).

WELL	DEPTH	TYPE	Col.	Fam.	Att.	SBHT	DSTT	Salinity	psia grad	nC3	iC4	nC4	iC5	nC5	22DMB	2MP	3MP	nC6	22DMP	MCP	24DMP	Benz	33DMP	CH	2MH
21	2585	DST1	3	3	26000	108	117.2	26000	0.461	90	152	159	220	286	128	595	333	690	76	644	39	149	72	1092	522
19	2700	DST2	2	3	29000	109	118.3	26000	0.449	0	6	32	241	375	58	498	361	844	20	682	25	173	54	1211	522
20	2515	DST4	1	3	9000	100	101.1	46000		111	127	305	452	396	46	453	309	553	36	452	10	822	50	1392	320
20	2579	DST3	1	3	28000	102	100.6	46000		0	5	10	91	100	26	251	161	306	29	281	8	53	25	948	255
20	2699	DST2	1	3	21000	110	99.4	50000	0.442	5	2	19	198	227	69	417	311	684	57	489	32	112	0	1114	513
44	2750	DST1	2	3	21000	112	128.7	50000	0.438	100	158	201	502	760	130	852	490	1099	97	902	29	249	53	1501	553
55	2681	DST2	2	3	22500	111	118.3		0.447	64	149	163	522	767	130	784	558	1099	120	820	35	208	50	1440	551
61	2128	DST3	2	3	40500	90	99.3	32000	0.452	4	75	83	378	561	82	799	583	846	79	799	29	64	45	1086	610
61	2770	DST2	2	3	20000	114	121.7	28000	0.438	0	13	16	160	100	57	292	167	256	49	357	21	131	28	969	380
62	2549	DST1	2	3	6000	109	110.6	37000		130	149	370	398	542	28	453	302	580	33	542	17	302	19	1222	298
70	2428	DST2	2	3	18000	103	107.2	34000	0.444	263	318	1029	1434	798	103	974	619	1361	95	992	28	169	42	1544	494
70	2452	DST1	2	3	5200	104	108.3	34000	0.442	350	410	624	805	624	76	626	400	670	51	728	20	190	31	1361	344
31	2753	DST1	1	3	17000	105	117.8	36000	0.446	55	200	443	1235	1246	130	1987	633	1233	73	963	24	142	50	1460	507
63	2690	DST1	1	3	4000	109	107.2	56000	0.437	151	194	513	930	762	101	843	372	992	52	864	21	218	0	1478	400
Family 4: ?Southern Outeniqua dry gas																									
128	3640	DST1	1	4	12000	149	154.3	18000	0.65	86	207	192	528	325	143	569	298	477	53	556	49	727	0	842	522
Family 5: ?Valanginian wet gas																									
27	3164	DST1	2	5	3800	136	136.1	62000	0.545	12	25	45	130	130	13	228	134	353	21	276	13	22	20	685	260
35	3309	DST3	1	5	5000	135	134.4	59000	0.612	10	21	26	341	236	41	591	306	564	49	532	18	42	0	861	445
35	3354	DST2B	2	5	11500	137	134.4	59000	0.602	95	251	1185	1704	1682	55	1316	539	1711	38	842	12	375	22	1209	552
35	3397	DST1	2	5	8500	138	135.6	59000	0.554	10	70	117	384	383	59	632	460	816	58	559	20	103	40	1112	440

Table F.03: Whole oil GC peak heights (page 3 of 12).

23DMP	3MH	13DMCP	1t3DMCP	224TMP	nC7	MCH	25DMH	24DMH	124TMCP	12c3TMCP	Tol	2MH7	4MH7	3MH7	1c23TMCP	14DMCH	225TMH	12DMCH	nC8	22DMH7
259	529	528	423	547	1129	2025	1119	107	168	167	194	494	368	608	357	0	59	243	830	18
246	572	362	405	559	1369	2024	137	99	188	169	262	542	0	640	267	0	64	257	900	18
127	357	202	221	330	878	1933	107	60	71	89	258	300	123	447	191	0	57	149	498	16
198	536	298	272	378	1415	1911	80	71	117	106	651	385	133	470	170	0	48	136	567	10
147	415	212	231	290	948	1532	84	60	92	80	274	291	117	319	115	0	37	104	432	11
189	480	291	169	365	1395	1909	68	69	138	109	609	421	129	491	179	0	48	156	622	11
100	269	175	189	267	554	869	58	29	65	77	69	187	66	199	70	0	18	80	261	1
198	587	386	416	551	1260	1909	101	70	168	154	724	373	122	460	150	0	44	182	672	14
138	380	259	279	387	695	1431	90	49	107	101	384	236	92	310	129	0	31	135	390	10
122	289	221	252	363	735	1380	643	32	93	889	600	203	82	323	131	0	24	121	329	10
162	486	314	304	489	971	1951	102	66	132	137	1211	310	109	503	163	0	56	195	528	37
135	438	281	320	417	988	1978	99	58	128	130	1095	932	113	492	151	43	58	183	662	0
118	354	169	186	269	780	1079	67	44	79	70	191	222	187	230	79	0	27	80	310	6
182	587	297	313	432	1241	1823	118	78	146	132	620	432	128	377	146	0	48	162	737	33
252	589	429	453	684	1579	1996	118	78	200	221	362	569	208	760	278	52	57	263	885	0
92	243	176	191	264	687	887	53	37	85	91	181	231	79	247	80	20	45	103	397	18
260	588	400	468	699	1322	1935	144	98	193	207	189	499	269	586	303	0	57	254	825	14
197	561	297	329	498	1506	1987	127	74	169	167	603	484	228	468	177	0	53	228	898	42
188	638	317	379	530	1654	1960	132	78	159	155	707	472	226	452	167	0	53	206	838	34
118	408	171	188	291	903	1991	116	59	72	65	719	293	140	525	162	20	68	173	622	20
231	437	193	226	342	606	1997	143	99	74	63	266	279	214	512	321	0	76	181	473	14
121	350	137	155	223	483	2004	101	67	49	42	3984	218	123	412	186	55	30	133	365	0
114	347	151	162	232	711	1981	79	49	44	39	1047	211	94	390	157	50	30	121	369	0
149	492	198	224	304	945	2005	106	77	91	69	706	289	128	403	139	0	49	128	506	15
127	680	130	158	198	1176	1699	140	127	57	31	2017	427	193	455	99	0	56	83	725	32
144	470	196	215	279	1020	2022	114	80	80	61	1004	307	149	405	147	0	50	122	544	18
152	650	213	242	311	1193	2019	135	102	85	61	1050	376	171	446	134	0	49	122	616	22
293	775	274	258	356	1615	1999	89	107	97	75	1780	427	168	589	187	0	52	128	697	12
202	797	146	202	269	1255	1864	148	152	58	35	2018	423	269	466	161	38	53	81	651	0
135	804	161	178	257	1831	1999	108	140	68	49	1650	626	237	929	220	0	81	150	1118	17
58	330	74	97	110	855	1080	72	80	39	27	1996	342	136	350	70	0	40	68	703	27
67	378	62	109	128	929	1172	100	92	43	27	1975	348	191	387	102	0	40	73	695	0

Table F.03: Whole oil GC peak heights (page 4 of 12).

23DMP	3MH	13DMCP	1t3DMCP	224TMP	nC7	MCH	25DMH	24DMH	124TMCP	12c3TMCP	Tol	2MH7	4MH7	3MH7	1c23TMCP	14DMCH	225TMH	12DMCH	nC8	22DMH7
108	500	114	142	176	946	1367	100	86	57	32	1997	286	154	327	120	0	38	75	526	18
194	544	345	332	469	1362	2000	84	77	161	139	821	363	135	568	188	0	57	198	602	38
183	600	348	342	493	1401	2001	83	72	158	131	811	360	127	557	178	0	54	192	572	34
146	409	219	228	305	1022	2022	109	68	79	70	911	271	119	389	140	0	45	123	497	12
168	765	206	230	318	1569	2011	162	113	89	65	2011	443	180	499	144	0	58	127	817	7
168	562	251	268	400	1337	1873	70	73	112	99	1093	313	118	449	140	0	46	140	510	27
138	499	191	212	311	1109	1789	59	63	93	77	851	278	99	414	124	0	38	119	481	19
161	565	211	257	336	1355	1985	83	74	111	88	1060	379	116	468	141	40	50	150	747	16
179	623	294	290	419	1475	2002	84	90	134	109	1173	396	149	611	188	0	61	178	696	32
114	612	143	159	209	1199	1660	1023	90	62	43	2015	373	149	378	103	0	46	84	683	20
136	814	178	218	258	1477	1993	145	109	76	54	2590	478	353	334	121	0	55	105	893	30
112	335	183	198	273	898	1089	72	43	86	80	328	263	126	221	81	0	26	98	435	19
176	494	304	298	440	1210	1810	80	62	130	115	839	315	112	470	168	0	45	160	487	16
156	478	311	291	419	1051	1997	80	56	121	110	841	290	92	470	151	0	43	158	489	11
159	431	244	270	380	941	1463	65	57	103	94	590	266	122	416	152		33	127	452	10
104	294	173	175	238	853	1034	64	42	76	64	336	234	116	205	83	0	30	87	373	13
178	820	194	183	294	1468	2000	82	123	57	44	2001	349	170	580	160	0	78	113	572	22
93	304	160	160	247	749	1999	100	51	78	62	1475	260	103	658	220	0	72	218	511	43
128	274	162	170	257	819	2000	80	51	100	78	890	298	129	651	219	0	100	216	600	41
57	234	73	80	132	401	1520	71	60	44	37	2000	240	120	741	219	0	79	207	470	46
39	139	59	60	91	368	1159	58	37	33	28	1995	180	87	449	130	0	50	134	397	33
150	583	268	241	397	1348	2002	127	81	99	93	439	361	146	579	168	0	64	167	591	34
102	354	172	177	292	699	1975	100	57	76	64	437	242	100	457	140	0	57	156	432	33
109	329	130	149	287	823	1942	106	107	120	134	163	597	220	914	232	0	109	280	1158	59
101	422	152	169	260	850	1998	109	65	74	69	665	347	120	588	163	0	61	168	605	18
120	420	183	178	253	864	2003	117	74	85	80	832	349	150	699	193	0	81	214	607	49
118	488	177	209	284	1048	2000	113	70	79	70	671	339	138	496	142	0	58	159	671	18
110	465	157	164	227	817	2001	94	67	48	41	787	240	101	477	141	0	48	109	383	11
91	413	113	131	195	688	1957	129	72	48	39	394	345	99	406	120	55	32	122	467	0
131	596	114	141	195	975	1995	151	114	56	36	523	379	168	491	123	50	69	116	685	11
115	498	161	152	210	931	1895	80	69	57	48	820	271	126	463	126	0	52	109	471	22
19	101	26	30	50	458	978	46	84	57	52	440	573	241	938	220	0	100	234	1388	62
171	672	133	130	219	1370	1861	62	101	61	57	570	414	169	588	130	0	73	124	680	31
132	618	181	182	263	1169	2000	128	68	62	43	969	400	153	542	152	0	67	130	745	21

Table F.03: Whole oil GC peak heights (page 5 of 12).

23DMP	3MH	13DMCP	1t3DMCP	224TMP	nC7	MCH	25DMH	24DMH	124TMCP	12c3TMCP	Tol	2MH7	4MH7	3MH7	1c23TMCP	14DMCH	225TMH	12DMCH	nC8	22DMH7
118	529	148	155	241	911	2001	90	88	70	51	651	458	190	770	199	0	92	164	735	41
120	503	159	171	207	967	1998	87	80	66	55	562	366	132	602	169	0	62	137	581	12
78	330	191	117	184	564	2008	104	56	55	42	234	232	97	373	111	361	51	137	412	22
65	278	91	104	161	514	1973	98	57	52	42	277	248	113	409	131	50	53	151	510	30
109	510	136	152	209	1052	2009	159	88	69	49	462	492	184	627	192	0	88	172	957	32
122	547	169	180	283	952	2003	82	84	65	57	680	306	130	546	141	0	61	130	511	28
136	536	159	175	276	900	2002	84	84	70	57	712	294	123	530	142	0	64	132	493	30
128	600	188	174	277	1113	2003	84	91	82	67	327	329	137	527	152	0	58	130	554	28
92	380	119	120	192	712	2002	71	78	57	45	830	279	119	579	152	0	60	144	479	33
90	289	129	120	184	543	2000	68	49	51	41	957	188	82	436	140	0	48	119	368	23
122	441	175	170	268	891	1919	80	73	58	50	580	249	110	449	120	0	51	113	421	28
93	349	131	142	224	627	2002	75	58	49	48	627	209	99	440	130	0	52	127	388	29
128	529	170	191	278	918	1992	128	66	61	49	308	274	96	368	112	20	47	112	478	20
102	416	142	153	218	672	1989	121	64	50	37	533	230	112	382	128	60	47	105	382	42
139	520	130	169	226	923	1968	154	81	61	40	2017	555	299	675	243	0	91	168	1047	27
107	292	120	131	218	739	2001	69	87	109	91	157	490	200	870	259	0	104	277	919	57
182	479	195	232	308	801	1994	135	91	141	112	150	482	178	655	204	0	81	221	762	30
162	568	217	223	318	1453	1921	83	68	110	93	392	429	152	632	179	20	61	178	759	20
228	610	243	240	386	1171	2002	84	107	170	141	203	591	228	885	244	0	108	282	872	58

Table F.03: Whole oil GC peak heights (page 6 of 12).

223TMH	24DMH7	ECH	26DMH7	EBen	pXyl	mXyl	4MO	2MO	3EH	3MO	oXyl	nC9		MCH/	MANGO RATIOS (% of total peak height)							
													Tol C3-9	TOL	P2	P3	N2	P2+N2	nC7/MH	T+M%	DMP%	DMCP%
															MH	DMP	DMCP					
66	365	25	51	25	299	0	112	139	21	148	84	708	20124	10.44	4.81	1.48	7.44	12.25	1.17	11.03	1.48	4.73
64	370	21	49	28	337	0	112	130	0	140	92	674	24512	7.73	4.37	1.17	5.41	9.78	1.05	9.33	1.17	3.13
44	247	22	61	117	159	70	104	106	127	80	149	563	18864	7.49	3.73	0.78	3.99	7.72	1.61	11.61	0.78	2.24
36	202	16	49	102	261	111	84	81	105	106	116	455	22485	2.94	4.79	1.09	4.22	9.00	1.05	11.39	1.09	2.54
27	149	10	28	11	142	49	46	52	8	55	39	218	19078	5.59	4.29	1.12	3.84	8.13	1.38	9.47	1.12	2.32
38	230	19	49	112	229	91	88	90	114	110	131	503	20256	3.13	4.63	1.05	4.07	8.70	1.20	12.43	1.05	2.27
17	103	6	13	0	45	47	25	31	0	32	18	137	14905	12.59	3.33	0.85	4.23	7.56	2.28	6.29	0.85	2.44
41	265	16	37	80	257	104	71	70	86	125	128	398	25406	2.64	4.31	1.49	5.33	9.64	1.03	10.36	1.49	3.16
29	188	11	22	29	184	0	40	46	0	51	68	211	18453	3.73	3.75	1.02	5.01	8.76	1.63	9.84	1.02	2.92
24	179	12	33	117	216	50	52	52	73	109	100	275	19388	2.30	2.88	0.82	4.31	7.20	2.02	10.21	0.82	2.44
38	290	23	48	75	470	157	70	81	106	228	151	409	20268	1.61	4.32	1.19	5.46	9.78	1.29	15.60	1.19	3.05
41	318	15	46	108	498	143	137	82	83	219	153	489	20086	1.81	4.06	0.72	5.07	9.13	1.39	15.30	0.72	2.99
20	104	9	17	9	95	36	30	35	7	40	29	149	16503	5.65	4.10	0.97	3.78	7.88	1.67	7.70	0.97	2.15
48	235	83	45	61	251	91	77	97	103	117	108	512	21689	2.94	5.19	0.96	4.80	9.99	1.00	11.26	0.96	2.81
46	360	18	60	121	192	100	100	114	153	109	203	611	22460	5.51	4.95	1.21	6.97	11.92	1.02	10.50	1.21	3.93
27	147	11	20	53	87	83	39	45	60	42	79	278	15402	4.90	3.06	0.77	4.10	7.15	2.40	6.93	0.77	2.38
69	353	26	48	27	303	0	103	129	20	141	80	669	22771	10.24	4.49	1.28	6.88	11.37	1.10	9.33	1.28	3.81
62	322	112	46	77	253	108	88	113	124	146	155	668	21035	3.30	4.83	1.06	5.34	10.17	1.11	12.31	1.06	2.98
53	294	97	42	73	267	104	79	96	104	132	128	559	25399	2.77	4.59	0.83	4.83	9.42	0.97	10.50	0.83	2.74
29	309	12	51	141	403	50	96	98	119	186	157	501	19253	2.77	4.08	1.08	3.38	7.46	1.44	14.08	1.08	1.86
43	309	29	52	48	297	46	102	129	20	115	119	458	20490	7.51	4.57	5.52	3.71	8.29	1.20	11.04	5.52	2.04
34	245	21	58	52	385	50	98	132	20	113	178	444	18851	0.50	3.71	1.09	2.73	6.44	1.62	31.76	1.09	1.55
33	209	11	47	148	480	142	77	80	104	219	108	357	17668	1.89	4.01	1.00	3.08	7.09	1.59	17.14	1.00	1.77
33	25	14	41	30	330	140	65	71	15	69	109	280	20691	2.84	4.69	1.03	3.51	8.20	1.16	13.10	1.03	2.04
53	163	12	96	67	816	0	130	154	20	131	277	507	20037	0.84	6.92	1.31	2.43	9.35	0.81	18.55	1.31	1.44
34	221	11	48	43	489	0	79	90	17	85	169	357	22093	2.01	4.41	1.10	3.12	7.54	1.16	13.70	1.10	1.86
42	200	12	58	43	468	0	87	101	17	90	144	349	23209	1.92	5.72	1.18	3.30	9.02	0.85	13.22	1.18	1.96
39	226	18	81	139	708	207	122	120	162	249	111	556	29311	1.12	5.57	1.33	3.03	8.60	0.69	12.89	1.33	1.82
50	161	16	89	58	718	48	119	140	18	112	227	405	25821	0.92	6.34	1.29	2.39	8.73	0.69	15.03	1.29	1.35
58	280	20	139	110	780	151	194	192	249	326	129	771	23266	1.21	7.32	1.07	2.56	9.88	0.66	15.68	1.07	1.46
40	140	13	80	51	866	0	122	130	139	330	70	565	12436	0.54	5.66	0.94	2.26	7.92	1.60	24.73	0.94	1.38
20	141	32	75	142	695	50	96	115	16	100	273	350	13272	0.59	6.20	1.14	2.25	8.45	1.37	23.71	1.14	1.29

Table F.03: Whole oil GC peak heights (page 7 of 12).

223TMH	24DMH7	ECH	26DMH7	EBen	pXyl	mXyl	4MO	2MO	3EH	3MO	oXyl	nC9		MCH/	MANGO RATIOS (% of total peak height)							
31	125	11	49	68	719	0	76	91	13	80	224	323	16313	0.68	6.39	1.30	2.65	9.04	1.08	20.62	1.30	1.57
42	288	26	48	70	317	122	71	85	109	167	148	399	24206	2.44	4.22	0.98	4.73	8.95	1.11	11.65	0.98	2.80
37	276	21	44	72	297	119	62	76	96	153	139	371	24909	2.47	4.37	1.05	4.75	9.12	1.04	11.29	1.05	2.77
30	219	11	36	39	397	156	57	62	11	61	120	264	21379	2.22	3.82	0.95	3.52	7.33	1.38	13.72	0.95	2.09
46	237	14	71	89	769	247	109	123	19	117	253	478	26726	1.00	5.81	1.12	2.82	8.64	0.73	15.05	1.12	1.63
36	211	18	39	49	281	110	60	69	80	144	99	318	24056	1.71	4.45	1.06	3.82	8.27	1.06	12.33	1.06	2.16
26	198	12	33	37	311	111	49	58	72	138	88	298	20573	2.10	4.73	1.05	3.47	8.20	1.16	12.83	1.05	1.96
42	272	12	50	103	453	118	83	81	103	177	122	452	22293	1.87	5.01	1.00	3.61	8.61	1.01	13.66	1.00	2.10
44	299	21	59	66	471	195	81	98	118	229	150	484	23891	1.71	5.14	1.03	4.20	9.33	0.92	13.29	1.03	2.44
38	149	10	61	50	710	0	90	102	18	98	210	399	22249	0.82	5.51	0.98	2.30	7.80	0.92	16.52	0.98	1.36
48	195	52	73	136	928	70	115	145	141	364	80	607	25954	0.77	6.40	0.83	2.52	8.92	0.68	17.66	0.83	1.53
32	137	47	25	33	118	58	43	48	54	57	59	257	16998	3.32	3.57	0.78	3.85	7.42	1.86	8.34	0.78	2.24
35	240	19	48	107	313	116	64	68	94	159	122	337	21884	2.16	4.47	1.09	4.76	9.24	1.15	12.10	1.09	2.75
33	252	18	41	133	350	74	65	64	100	164	130	377	20142	2.37	4.57	1.05	5.07	9.64	1.23	14.09	1.05	2.99
29	197	16	32	70	199		49	50	69	94	83	270	18928	2.48	4.34	1.85	4.72	9.06	1.38	10.85	1.85	2.72
24	120	38	24	32	112	51	39	49	52	56	55	222	16399	3.08	3.82	0.76	3.57	7.40	1.80	8.35	0.76	2.12
30	181	14	54	27	675	0	56	69	66	349	62	229	17535	1.00	9.13	1.48	3.83	12.96	0.71	22.82	1.48	2.15
27	344	20	43	78	839	262	67	78	106	386	182	378	14503	1.36	3.94	1.01	3.91	7.85	1.97	23.95	1.01	2.21
31	344	27	44	87	720	278	78	88	124	265	209	569	15498	2.25	3.53	1.32	3.80	7.33	2.06	18.65	1.32	2.14
35	302	30	74	125	1456	680	110	128	190	630	232	470	13157	0.76	3.48	1.03	2.17	5.65	2.47	26.75	1.03	1.16
27	208	20	54	61	1010	357	85	104	139	457	144	500	10680	0.58	2.52	0.81	1.97	4.49	4.20	29.53	0.81	1.11
36	237	19	52	53	188	51	76	89	108	87	116	394	22790	4.56	5.23	1.15	3.98	9.20	0.95	10.71	1.15	2.23
30	245	20	48	59	232	78	70	80	101	120	131	370	16217	4.52	4.14	1.44	3.95	8.09	1.68	14.87	1.44	2.15
78	470	39	133	130	263	109	202	256	304	140	308	1222	13631	11.91	4.83	1.60	4.15	8.99	1.71	15.44	1.60	2.05
46	272	20	61	120	361	50	108	106	144	160	149	520	13981	3.00	6.01	1.58	4.16	10.16	1.34	19.05	1.58	2.30
40	331	23	68	79	431	140	99	115	144	220	128	519	16341	2.41	5.01	1.54	3.76	8.77	1.38	17.35	1.54	2.21
33	259	12	52	71	304	80	92	92	108	124	120	441	17596	2.98	5.37	1.11	3.81	9.18	1.19	15.18	1.11	2.19
34	173	16	50	85	286	70	71	69	88	115	80	259	16389	2.54	6.04	1.31	3.34	9.38	1.14	17.01	1.31	1.96
23	205	9	61	49	298	68	82	101	22	92	109	349	12090	4.97	6.62	1.53	3.63	10.25	1.41	19.45	1.53	2.02
49	222	18	101	41	383	57	140	178	33	158	159	627	15630	3.81	7.65	1.73	2.88	10.53	0.94	16.11	1.73	1.63
27	170	15	51	36	289	95	64	80	90	130	77	291	16096	2.31	6.31	1.47	3.25	9.56	1.11	16.87	1.47	1.94
84	529	38	209	120	790	206	300	400	471	480	380	1834	12061	2.22	1.49	0.16	0.88	2.37	6.27	11.76	0.16	0.46
40	192	19	80	39	158	43	97	125	136	110	99	492	18004	3.26	7.61	2.28	2.68	10.29	0.82	13.50	2.28	1.46
22	205	47	69	100	384	55	104	117	129	143	104	453	19411	2.06	6.71	1.28	3.22	9.94	0.87	15.30	1.28	1.87

Table F.03: Whole oil GC peak heights (page 8 of 12).

223TMH	24DMH7	ECH	26DMH7	EBen	pXyl	mXyl	4MO	2MO	3EH	3MO	oXyl	nC9		MCH/	MANGO RATIOS (% of total peak height)							
36	254	28	101	65	364	105	128	171	191	185	158	599	15334	3.07	6.85	1.99	3.55	10.40	1.07	17.29	1.99	1.98
40	229	19	80	110	348	98	117	119	147	138	118	503	14204	3.56	7.22	1.54	3.78	11.00	1.10	18.02	1.54	2.32
22	222	10	42	23	194	90	63	701	10	69	70	259	13368	8.58	4.86	1.30	3.68	8.54	1.74	16.77	1.30	2.30
36	310	12	65	70	392	250	105	142	28	125	143	580	10214	7.12	5.22	1.24	3.49	8.70	2.12	22.03	1.24	1.91
42	300	22	105	42	339	109	162	198	29	192	130	782	14449	4.35	7.08	1.37	3.44	10.52	1.10	17.10	1.37	1.99
30	203	17	63	40	304	99	73	95	104	130	98	346	16355	2.95	6.73	1.84	3.86	10.59	1.03	16.40	1.84	2.13
33	198	20	67	43	342	127	78	97	107	141	98	342	16152	2.81	6.73	2.11	3.78	10.51	1.04	16.80	2.11	2.07
40	221	20	68	43	207	78	80	103	107	91	101	388	14719	6.13	8.22	1.91	4.34	12.56	0.93	15.83	1.91	2.46
37	230	19	68	49	530	180	83	99	117	214	117	382	11664	2.41	6.52	1.63	3.70	10.21	1.49	24.28	1.63	2.05
29	213	14	45	41	497	202	59	69	80	177	109	320	13165	2.09	4.46	1.21	3.29	7.75	1.92	22.46	1.21	1.89
31	172	18	49	37	276	95	61	78	84	112	78	274	17996	3.31	5.20	1.59	3.41	8.60	1.21	13.89	1.59	1.92
26	217	17	50	40	399	136	60	77	90	171	100	346	14938	3.19	4.64	1.31	3.33	7.97	1.63	17.60	1.31	1.83
23	172	8	48	30	221	50	70	83	15	78	67	314	17905	6.47	5.79	1.54	3.57	9.35	1.09	12.85	1.54	2.02
28	161	8	39	33	260	47	56	63	10	58	85	183	14907	3.73	5.47	1.17	3.44	8.92	1.38	16.92	1.17	1.98
25	263	20	124	152	1052	0	238	322	42	282	286	1211	19124	0.98	5.45	1.26	2.75	8.19	1.08	20.84	1.26	1.56
68	496	36	105	130	260	100	168	206	252	126	359	1169	13139	12.75	4.20	1.23	3.57	7.77	2.05	16.42	1.23	1.91
56	330	18	63	10	156	50	115	131	23	137	38	580	13223	13.29	6.99	1.88	5.56	12.55	1.22	16.21	1.88	3.23
29	291	17	51	71	247	50	88	102	129	104	159	581	21545	4.90	5.20	1.00	3.52	8.72	1.01	10.74	1.09	2.04
67	400	37	88	117	229	90	142	169	211	139	254	812	16871	9.86	6.22	2.05	5.15	11.37	1.08	13.07	2.05	2.86

Table F.03: Whole oil GC peak heights (page 9 of 12).

		nC7 Ternary				MANGO (Science, 1987)		C7-9 A vs N		CHAPTER 9 RATIOS					
tot.MH%	MH/DMCP	SigmaC7	(T+M)/C7%	MH/C7%	nC7/SigmaC7	2MH+23DMP	3MH+24DMP	Arom	Norm	3MP/B	CH/B	Tol/nC7	nC7/MCH	HV	IHV
										Family 1					
22.41	1.02	4315	51.4	22.4	26.2	6.55	6.27	2.99	13.25	8.29	16.24	0.17	0.56	21.74	1.02
22.68	1.40	4727	48.4	22.7	29.0	6.61	6.35	2.93	12.01	7.07	13.69	0.19	0.68	23.09	1.40
18.64	1.66	3772	58.1	18.6	23.3	6.16	5.93	3.99	10.28	2.36	6.04	0.29	0.45	18.00	1.66
21.29	1.89	5053	50.7	21.3	28.0	6.60	6.31	5.52	10.84	2.41	5.05	0.46	0.74	23.91	1.89
22.90	1.85	3572	50.6	22.9	26.5	6.31	6.08	2.70	8.38	3.70	6.58	0.29	0.62	21.79	1.85
19.34	2.04	4851	51.9	19.3	28.8	6.47	6.19	5.79	12.44	1.38	4.19	0.44	0.73	25.17	2.04
24.95	1.36	1988	47.2	24.9	27.9	5.79	5.63	1.20	6.39	9.80	15.68	0.12	0.64	21.76	1.36
21.97	1.37	4989	52.8	22.0	25.3	6.56	6.40	5.09	9.17	1.48	2.70	0.57	0.66	22.02	1.37
21.61	1.29	3202	56.7	21.6	21.7	6.11	6.01	3.60	7.02	1.41	3.33	0.55	0.49	17.69	1.29
17.07	1.18	3274	60.5	17.1	22.4	5.97	5.69	5.59	6.91	0.70	2.24	0.82	0.53	20.20	1.18
17.49	1.42	5009	63.1	17.5	19.4	6.31	6.22	10.18	9.41	0.70	1.87	1.25	0.50	19.18	1.42
16.71	1.36	4876	63.0	16.7	20.3	6.24	6.10	9.94	10.65	0.99	2.69	1.11	0.50	19.34	1.36
24.80	1.90	2726	46.6	24.8	28.6	6.09	5.90	2.18	7.51	4.70	7.47	0.24	0.72	22.78	1.90
23.39	1.84	4809	50.8	23.4	25.8	6.58	6.39	5.21	11.48	3.11	5.71	0.50	0.68	22.84	1.84
22.01	1.26	5048	46.7	22.0	31.3	6.65	6.38	4.35	13.69	5.17	8.81	0.23	0.79	27.16	1.26
21.16	1.28	2226	48.0	21.2	30.9	5.77	5.51	3.14	8.84	6.77	10.13	0.26	0.77	26.61	1.28
22.87	1.18	4468	47.5	22.9	29.6	6.54	6.38	2.63	12.37	8.55	15.26	0.14	0.68	24.79	1.18
19.87	1.62	5112	50.7	19.9	29.5	6.48	6.34	5.69	14.60	1.99	5.43	0.40	0.76	26.32	1.62
21.26	1.68	5488	48.6	21.3	30.1	6.58	6.47	5.04	12.01	3.58	5.74	0.43	0.84	26.73	1.68
17.87	2.19	4399	61.6	17.9	20.5	6.21	6.05	7.64	10.52	1.51	5.70	0.80	0.45	17.15	2.19
24.62	2.24	3806	59.5	24.6	15.9	6.59	7.16	3.79	7.50	0.33	1.43	0.44	0.30	11.46	2.24
9.75	2.39	7170	83.5	9.7	6.7	6.15	5.98	24.66	6.85	1.72	6.70	8.25	0.24	10.55	2.39
15.92	2.26	4447	68.1	15.9	16.0	6.16	5.91	10.90	8.13	0.80	2.87	1.47	0.36	14.57	2.26
						Mango (1987) regression line		-7.20	7.70						
								-8.00	8.00	Family 2					
20.97	2.30	4626	58.6	21.0	20.4	6.44	6.24	6.36	8.37	1.19	4.10	0.75	0.47	16.71	2.30
22.09	4.82	6279	59.2	22.1	18.7	6.73	6.58	15.86	12.02	0.89	1.90	1.72	0.69	21.41	4.82
19.42	2.37	5021	60.3	19.4	20.3	6.48	6.21	7.72	8.70	1.42	3.24	0.98	0.50	18.40	2.37
23.76	2.92	5590	54.9	23.8	21.3	6.72	6.53	7.35	9.30	1.61	3.50	0.88	0.59	19.05	2.92
23.23	3.07	7026	53.8	23.2	23.0	7.05	6.69	10.05	9.78	1.02	1.87	1.10	0.81	22.89	3.07
24.18	4.71	6775	57.3	24.2	18.5	6.95	6.69	11.89	8.95	0.92	2.06	1.61	0.67	19.39	4.71
23.71	5.02	7183	50.8	23.7	25.5	6.94	6.73	12.12	15.99	1.02	2.90	0.90	0.92	26.99	5.02
15.19	4.12	4635	66.4	15.2	18.4	6.07	5.86	23.99	17.07	0.47	1.05	2.33	0.79	27.41	4.12
16.80	4.81	4899	64.2	16.8	19.0	6.24	5.99	23.62	14.87	0.49	0.92	2.13	0.79	26.80	4.81

Table F.03: Whole oil GC peak heights (page 10 of 12).

		nC7 Ternary				MANGO (Science, 1987)		C7-9 A vs N		CHAPTER 9 RATIOS					
19.48	4.07	5353	62.8	19.5	17.7	6.48	6.29	18.44	11.00	0.84	1.91	2.11	0.69	21.96	4.07
19.62	1.51	5204	54.2	19.6	26.2	6.51	6.33	6.11	9.76	1.54	3.09	0.60	0.68	22.86	1.51
20.52	1.58	5301	53.0	20.5	26.4	6.51	6.42	5.77	9.41	1.32	3.93	0.58	0.70	22.25	1.58
17.10	1.83	4771	61.5	17.1	21.4	6.32	6.06	7.59	8.34	0.95	3.20	0.89	0.51	18.54	1.83
21.75	3.56	7145	56.3	21.7	22.0	6.86	6.68	12.61	10.72	0.88	2.31	1.28	0.78	22.40	3.56
19.91	2.06	5373	55.2	19.9	24.9	6.52	6.35	6.78	9.00	0.97	1.99	0.82	0.71	22.93	2.06
20.62	2.42	4723	55.9	20.6	23.5	6.42	6.22	6.80	9.18	1.49	3.70	0.77	0.62	20.59	2.42
20.23	2.38	5516	55.2	20.2	24.6	6.57	6.35	8.33	11.46	1.33	3.16	0.78	0.68	22.66	2.38
20.88	2.10	5877	54.0	20.9	25.1	6.66	6.46	8.60	11.11	1.49	2.88	0.80	0.74	23.87	2.10
20.09	4.06	6099	60.3	20.1	19.7	6.59	6.45	13.42	10.25	0.91	1.33	1.68	0.72	23.71	4.06
21.52	4.20	7722	59.3	21.5	19.1	6.89	6.73	14.66	11.47	0.90	1.38	1.75	0.74	22.95	4.20
20.77	1.59	2922	48.5	20.8	30.7	5.95	5.83	3.51	9.35	2.24	5.71	0.37	0.82	26.24	1.59
20.24	1.63	4838	54.8	20.2	25.0	6.49	6.22	6.84	9.29	0.91	3.75	0.69	0.67	21.76	1.63
19.13	1.53	4809	59.0	19.1	21.9	6.39	6.19	7.59	9.52	1.00	2.33	0.80	0.53	20.13	1.53
21.52	1.60	3815	53.8	21.5	24.7	6.31	6.20	4.98	8.79	1.44	2.62	0.63	0.64	22.16	1.60
22.00	1.80	2850	48.1	22.0	29.9	6.08	5.70	3.57	8.83	2.43	5.68	0.39	0.82	25.56	1.80
22.64	4.25	7070	56.6	22.6	20.8	6.87	6.75	15.77	12.94	1.10	3.65	1.36	0.73	22.10	4.25
11.93	1.79	4795	72.5	11.9	15.6	5.89	5.75	19.55	11.29	0.51	2.76	1.97	0.37	17.14	1.79
12.85	1.65	4256	67.9	12.9	19.2	5.99	5.65	14.09	12.83	1.62	7.44	1.09	0.41	18.33	1.65
10.46	2.99	4379	80.4	10.5	9.2	5.64	5.54	34.15	10.19	0.72	2.72	4.99	0.26	14.11	2.99
7.10	2.26	3791	83.2	7.1	9.7	5.13	5.00	33.40	11.84	0.21	1.34	5.42	0.32	16.13	2.26
										Family 3					
23.92	2.34	4980	49.0	23.9	27.1	6.63	6.42	3.72	10.24	3.63	6.74	0.33	0.67	21.89	2.34
17.74	1.92	3782	63.8	17.7	18.5	6.04	5.92	5.78	9.26	2.20	7.33	0.63	0.35	14.68	1.92
18.37	2.36	3587	58.7	18.4	22.9	6.08	5.87	7.14	23.50	3.05	16.79	0.20	0.42	20.26	2.36
19.30	2.62	4353	61.2	19.3	19.5	6.25	6.09	9.62	14.13	1.07	4.12	0.78	0.43	18.39	2.62
18.13	2.27	4518	62.7	18.1	19.1	6.25	6.09	9.85	12.18	1.47	6.34	0.96	0.43	16.78	2.27
20.26	2.45	4664	57.3	20.3	22.5	6.35	6.22	7.08	12.28	1.89	5.57	0.64	0.52	19.30	2.45
21.55	3.08	4595	60.7	21.5	17.8	6.45	6.22	7.98	8.90	1.73	4.41	0.96	0.41	15.04	3.08
20.84	3.28	3839	61.2	20.8	17.9	6.17	6.09	7.59	12.44	2.56	8.24	0.57	0.35	15.37	3.28
25.51	4.69	4689	53.7	25.5	20.8	6.59	6.46	7.44	14.63	2.58	6.70	0.54	0.49	18.11	4.69
21.79	3.25	4662	58.2	21.8	20.0	6.45	6.27	8.18	10.52	1.09	3.51	0.88	0.49	17.92	3.25
8.75	3.21	2056	69.0	8.8	22.3	4.58	4.62	16.05	30.51	0.01	0.01	0.96	0.47	27.59	3.21
26.51	5.21	5172	47.0	26.5	26.5	6.77	6.58	5.05	14.12	2.31	5.20	0.42	0.74	22.34	5.21
23.95	3.59	5441	54.6	23.9	21.5	6.71	6.49	8.30	12.19	2.32	5.43	0.83	0.58	19.65	3.59

Table F.03: Whole oil GC peak heights (page 11 of 12).

		nC7 Ternary				MANGO (Science, 1987)		C7-9 A vs N		CHAPTER 9 RATIOS					
22.78	3.47	4614	57.5	22.8	19.7	6.46	6.34	8.76	14.64	2.23	7.33	0.71	0.46	18.02	3.47
22.52	3.11	4552	56.2	22.5	21.2	6.46	6.27	8.70	14.44	2.09	7.00	0.58	0.48	18.59	3.11
18.81	2.11	3456	64.9	18.8	16.3	5.99	5.83	4.57	9.24	0.38	1.69	0.41	0.28	12.22	2.11
16.17	2.73	3297	68.2	16.2	15.6	5.77	5.66	11.08	15.70	3.04	17.89	0.54	0.26	12.95	2.73
22.50	3.55	4546	54.4	22.5	23.1	6.43	6.30	7.49	19.32	2.78	9.95	0.44	0.52	20.24	3.55
23.23	3.15	4735	56.7	23.2	20.1	6.51	6.36	7.47	11.06	1.97	6.03	0.71	0.48	17.13	3.15
23.12	3.25	4701	57.7	23.1	19.1	6.53	6.35	8.18	10.74	2.68	6.92	0.79	0.45	16.58	3.25
26.00	3.34	4653	50.1	26.0	23.9	6.60	6.44	5.14	13.96	9.11	16.97	0.29	0.56	20.57	3.34
17.66	3.18	4304	65.8	17.7	16.5	6.16	5.99	14.63	13.49	1.27	7.40	1.17	0.36	16.03	3.18
14.36	2.36	4087	72.4	14.4	13.3	5.96	5.72	13.72	9.35	1.00	4.05	1.76	0.27	12.48	2.36
21.62	2.71	4325	57.8	21.6	20.6	6.42	6.15	5.92	8.81	3.66	9.14	0.65	0.46	16.85	2.71
17.55	2.54	3949	66.6	17.5	15.9	6.08	5.91	8.72	9.11	2.11	7.16	1.00	0.31	13.39	2.54
24.35	2.87	4254	54.1	24.4	21.6	6.45	6.32	3.78	9.55	4.46	10.28	0.34	0.46	16.98	2.87
20.35	2.77	4010	62.9	20.3	16.8	6.22	6.08	6.43	8.30	1.71	6.78	0.79	0.34	13.56	2.77
										Family 4					
17.51	3.48	5950	67.0	17.5	15.5	6.49	6.34	18.34	16.63	0.41	1.16	2.19	0.47	19.33	3.48
										Family 5					
16.00	2.20	3449	62.6	16.0	21.4	5.91	5.72	7.66	21.52	6.09	31.14	0.21	0.37	18.58	2.20
23.88	2.16	3869	55.4	23.9	20.7	6.44	6.21	3.06	16.21	7.29	20.50	0.19	0.40	17.49	2.16
22.92	2.55	4886	47.3	22.9	29.7	6.57	6.36	4.27	12.96	1.44	3.22	0.27	0.76	25.48	2.55
23.72	2.17	4426	49.8	23.7	26.5	6.50	6.45	5.29	16.92	4.47	10.80	0.17	0.58	21.95	2.17

Table F.03: Whole oil GC peak heights (page 12 of 12).

MSCHEV PEAKS				PEAK HEIGHT RATIOS																					
RATIOS			Analysis	1	2	2a	3	4	5	6	7	8	9	10	11	12	13	14	15	16	17	18	19	20	Separator	
SAMPLE	Col.	SBHT	Date	Branched and cyclo-alkanes															Isoprenoids						psi	TF
FAMILY 1: APTIAN (13A)																									
Well 83 DST3 2470m	1	105	20-08-91	2.51	0.85	3.04	0.33	0.94	0.59	1.59	0.83	2.27	1.22	0.64	0.42	1.47	1.16	2.23	1.25	0.74	0.85	1.12	0.86	1.99	140	70
Well 88 DST5 2507m	1	100	21-08-91	2.25	0.90	2.58	0.39	1.17	0.54	1.37	0.81	2.35	1.13	0.63	0.47	1.40	1.13	1.92	1.21	0.77	0.86	1.15	0.85	2.02	255	64
Well 102 DST4 2241m	2	98	1-04-92	1.62	1.26	1.01	0.48	0.80	0.70	1.80	0.47	1.14	1.44	1.18	0.33	0.94	1.38	1.45	0.74	1.31	0.59	1.85	0.56	2.49	135	60
Well 95 DST2 2703m	2	120	2-04-92	1.30	0.91	1.29	0.77	0.59	0.89	1.41	0.70	2.96	1.34	1.09	0.34	1.10	1.33	1.46	0.92	1.56	0.73	1.88	0.63	2.21	0	0
Well 103 DST2 2718m	1	115	26-08-91	1.85	1.00	2.73	0.60	0.73	0.59	1.68	0.98	2.79	1.36	0.74	0.37	1.56	1.00	1.84	1.31	0.89	0.88	1.20	0.89	2.31	219	99
Well 94 DST1 2799m	2	117	2-04-92	1.29	0.93	1.53	0.65	0.74	0.95	1.35	0.66	3.72	1.38	1.06	0.57	1.08	1.35	1.54	0.87	1.62	0.72	1.71	0.64	1.99	160	75
Well 93 DST1 2817m	1	117	26-08-91	2.82	0.79	1.28	0.84	0.87	0.54	0.44	0.60	2.86	0.57	0.82	0.88	1.53	0.68	2.15	1.11	0.46	0.94	0.76	0.67	1.51	263	103
Well 93 DST1A 2808m	3	116	16-02-93	4.29	1.22	1.17	1.01	0.87	1.24	0.79	0.79	4.93	1.44	1.12	0.63	1.41	1.74	1.65	0.88	1.35	0.81	1.79	0.60	1.95	169	66
Well 93 DST2 2463m	1	102	27-08-91	3.23	0.88	4.27	0.65	1.05	0.90	1.83	0.83	2.33	1.16	0.85	0.59	1.64	0.94	2.06	1.36	0.88	0.98	1.38	0.89	1.89	237	110
Well 119 DST1 2816m	2	112	2-04-92	2.31	1.27	0.86	1.34	0.85	1.46	0.48	0.60	6.21	1.72	0.51	0.90	1.21	1.39	1.73	0.45	2.12	0.71	1.28	0.52	1.71	89	84
Well 109 DST1 2630m	2	100	23-12-92	2.91	1.20	0.79	2.68	0.13	1.06	0.47	0.82	4.25	1.11	0.86	0.91	1.23	1.79	1.48	0.67	0.76	1.33	1.34	0.61	1.68	83	59
Well 109 DST1 2630m	3	100	18-02-93	4.09	1.45	0.74	1.32	0.89	1.39	0.45	0.65	5.81	1.29	1.59	0.73	1.55	1.85	1.72	0.60	1.63	0.71	1.41	0.52	1.84	83	59
Well 126 DST1 2643m	1	119	27-08-91	2.12	1.06	2.90	0.58	0.85	0.80	1.68	0.80	2.87	1.32	0.82	0.39	1.39	1.03	1.68	1.24	0.90	0.87	0.61	0.55	1.20	164	80
Well 126 DST1 2643m	Q	119	07-11-95	2.47	0.96	1.55	0.93	0.49	0.87	1.07	1.14	3.66	1.56	0.79	0.31	1.87	1.35	1.54	1.29	1.18	0.86	1.42	0.85	2.25	164	80
Well 146 DST1 2564m	3	96	18-05-93	2.03	0.84	2.03	0.56	1.00	0.71	1.65	0.84	2.86	1.53	0.77	0.45	1.14	1.15	1.13	1.16	1.07	0.79	1.38	0.65	1.77	385	97
Well 117 DST1 2399m	1	104	28-08-91	2.92	0.85	2.79	0.37	0.96	0.61	1.63	0.90	2.31	1.19	0.61	0.45	1.53	1.09	1.86	1.27	0.80	0.90	1.16	0.81	1.99	135	59
Well 117 DST1 2399m	3	104	22-02-93	3.16	0.86	2.04	0.48	0.99	0.93	1.88	0.80	6.21	1.72	0.99	0.43	1.41	1.46	1.63	1.18	1.11	0.78	1.44	0.62	1.96	135	59
Well 156 DST1 2522m	Q	100	07-11-95	3.53	1.01	1.58	0.79	0.64	0.69	1.00	1.02	4.73	1.87	0.66	0.40	1.81	1.33	1.62	1.21	1.11	0.80	1.17	0.82	1.91	388	106
Well 166 DST1 2520m	Q	99	09-11-95	2.93	1.08	1.41	0.85	0.61	0.71	1.04	0.94	4.55	1.95	0.75	0.37	1.73	1.24	1.65	1.17	1.10	0.81	1.24	0.77	2.05	278	120
Well 48 DST1 2634m	1	110	4-09-91	2.30	1.51	0.96	0.55	0.82	0.54	0.77	0.51	2.08	0.88	0.58	0.48	1.20	1.16	1.57	1.18	0.60	0.59	0.86	0.72	1.67	0	0
Well 59 DST1 2212m	1	95	29-08-91*	1.41	1.54	0.69	1.39	0.48	0.37	0.45	0.65	1.93	0.56	0.30	0.44	1.42	0.97	1.43	0.86	0.78	0.48	0.87	0.72	1.79	140	89
Well 59 DST1 2212m	2	95	3-04-92	1.21	1.62	0.43	2.10	0.50	0.86	0.40	0.30	2.94	0.94	2.73	0.63	0.87	1.28	1.34	0.36	1.91	0.48	1.23	0.54	1.67	140	89
FAMILY 2: pre-BARREMIAN (deep central)																									
Well 83 DST1C 3254m	1	134	21-08-91	0.52	0.95	0.59	1.65	0.49	0.31	0.50	0.58	3.35	0.30	0.58	0.64	0.93	0.95	1.24	1.09	0.63	0.97	1.85	0.89	2.34	200	48
Well 83 DST2 2889m	1	122	21-08-91	1.92	1.69	0.96	1.09	0.66	0.47	0.46	0.57	2.41	0.56	0.74	0.69	1.42	0.81	2.12	1.15	0.48	0.99	1.15	0.72	1.80	165	102
Well 88 DST1 3243m	1	126	22-08-91	0.60	1.06	0.72	1.64	0.53	0.29	0.57	0.55	3.09	0.40	0.60	0.74	1.00	0.91	1.38	1.16	0.64	0.91	1.29	0.82	2.28	420	93
Well 88 DST2 2929m	2	116	1-04-92	1.11	1.09	0.70	2.06	0.41	0.55	0.58	0.55	4.93	0.86	2.03	0.71	0.94	1.32	1.41	0.58	2.23	0.69	2.07	0.60	2.05	391	111
Well 88 DST3 2916m	1	115	22-08-91	1.35	1.30	0.85	1.32	0.46	0.43	0.64	0.68	3.13	0.73	0.70	0.61	1.30	1.02	1.95	1.17	0.64	1.08	1.82	0.81	2.27	220	90
Well 88 DST4 2839m	1	112	22-08-91	1.72	1.47	0.71	1.33	0.59	0.37	0.38	0.59	2.76	0.55	0.67	0.71	1.34	0.72	1.81	1.10	0.49	1.11	1.17	0.72	1.78	390	151
Well 102 DST2 2632m	2	110	2-04-92*	1.26	1.11	0.86	2.23	0.46	0.22	0.57	0.48	2.94	1.03	1.12	0.55	0.93	1.19	1.93	0.25	2.31	0.77	2.48	0.75	1.84	67	68
Well 96 DST1 3131m	2	118	30-11-92	0.54	1.04	0.51	2.85	0.25	0.45	0.55	0.66	2.89	0.93	1.59	0.60	0.87	1.48	1.04	1.04	0.59	0.90	1.09	0.71	1.46	105	72
Well 96 DST1 3131m	3	118	16-02-93	1.13	0.93	0.55	1.95	0.27	0.46	0.67	0.60	3.89	0.74	2.40	0.39	1.17	1.88	1.54	1.08	1.22	0.70	1.80	0.66	1.84	105	72

Table F.04A: Peak height ratios of 'fingerprint' peaks measured from all whole oil GC plots, listed in their major Families (these include known regular isoprenoids and separator conditions) (page 1 of 3).

RATIOS			Analysis	1	2	2a	3	4	5	6	7	8	9	10	11	12	13	14	15	16	17	18	19	20	Separator	
Well 114 DST1 3085m	1	132	2-08-91	0.91	1.27	0.42	1.84	0.34	0.35	0.50	0.63	2.75	0.64	0.57	0.49	1.06	0.89	1.83	1.30	0.54	1.00	1.05	0.77	1.61	253	78
Well 108 DST1 2829m	2	116	28-04-92	3.47	1.04	1.29	2.11	0.94	0.68	0.59	0.69	4.54	1.37	0.75	0.94	1.05	0.92	1.83	1.00	1.20	0.78	1.67	0.63	1.96	309	80
Well 108 DST2 2820m	2	116	28-04-92	3.59	1.03	1.32	2.18	0.95	0.69	0.58	0.70	4.45	1.44	0.77	0.91	1.04	0.96	1.71	0.98	1.24	0.78	1.65	0.62	2.14	312	82
Well 129 DST1 2946m	1	120	19-08-91	1.28	1.28	0.57	1.79	0.38	0.35	0.55	0.64	3.76	0.61	0.62	0.58	1.23	1.04	1.71	1.19	0.61	1.01	1.24	0.71	1.82	495	101
Well 129 DST2 2865m	1	116	27-08-91	2.39	1.71	0.83	1.28	0.70	0.54	0.58	0.64	2.48	0.71	1.25	0.63	1.52	0.81	2.23	1.14	0.57	0.99	1.16	0.73	1.87	135	83
Well 107 DST3 2388m	2	82	28-04-92	3.28	0.92	1.36	2.16	0.74	0.66	0.63	0.65	3.49	1.42	0.91	0.65	0.92	0.97	1.54	1.09	1.28	0.90	2.04	0.67	2.13	477	118
Well 110 DST1A 3051m	2	116	29-04-92	2.68	1.01	1.13	2.53	0.66	0.71	0.57	0.71	3.83	1.16	0.85	0.66	0.96	1.03	1.53	1.09	1.07	0.81	1.59	0.59	1.70	158	69
Well 110 DST1B 3051m	2	116	29-04-92	2.50	0.97	1.18	2.48	0.66	0.65	0.56	0.70	3.70	1.18	0.83	0.63	0.95	1.00	1.59	1.11	1.07	0.79	1.73	0.58	1.88	160	95
Well 110 DST1B 3051m	3	116	19-02-93	2.17	1.30	0.88	1.37	0.60	0.52	0.77	0.75	3.82	0.87	0.83	0.55	1.29	1.73	1.61	1.04	1.20	0.87	1.73	0.57	1.91	160	95
Well 120 DST1 2931m	1	113	28-08-91	0.91	0.99	0.69	1.53	0.32	0.37	1.16	0.88	2.35	1.09	0.71	0.32	1.28	0.97	1.96	1.28	0.74	0.88	1.14	0.79	1.60	298	77
Well 120 DST1 2931m	Q	113	08-11-95	0.83	0.99	0.60	2.02	0.22	0.38	1.28	0.93	2.91	0.86	0.67	0.24	1.58	1.13	1.61	1.28	1.10	0.78	1.53	0.87	1.93	298	77
Well 166 RFT 2508m	Q	98	09-11-95	2.84	1.00	1.70	0.83	0.56	0.88	1.37	1.06	3.93	1.82	0.73	0.32	1.83	1.18	1.48	1.33	1.28	0.91	1.61	0.84	2.28	0	0
Well 132 DST1 2706m	2	104	30-03-92	2.97	1.47	0.83	1.73	0.84	1.20	0.45	0.52	6.17	1.17	1.42	1.02	1.22	1.36	2.01	0.43	2.47	0.69	1.42	0.62	1.67	419	99
Well 132 DST2 2662m	2	103	30-03-92	3.14	1.46	0.85	1.82	0.82	1.02	0.58	0.62	5.19	1.27	1.20	0.91	1.22	1.19	1.73	0.54	2.27	0.77	1.79	0.60	1.87	464	80
Well 148 DST1 2684m	3	111	19-05-93	2.08	1.34	0.96	1.82	0.78	0.61	0.84	0.76	5.90	1.18	0.81	0.57	1.12	1.37	1.50	0.80	1.46	0.84	1.84	0.60	2.01	256	62
Well 167 DST1 2679m	Q	108	07-12-95	2.18	1.01	1.51	0.75	0.45	0.79	1.36	1.12	3.82	1.72	0.72	0.30	1.74	1.40	1.44	1.35	1.31	0.94	1.72	0.90	2.49	387	64
Well 11 DST2 2950m	2	125	29-04-92*	3.09	0.82	0.52	8.52	0.24	0.70	0.11	0.41	9.50	2.60	2.84	1.77	0.40	0.94	1.67	0.27	7.76	0.61	2.23	1.01	1.54	0	0
Well 84 DST1 2771m	2	109	29-04-92	4.38	0.85	0.62	4.83	0.65	1.74	0.28	0.69	4.58	0.95	2.10	1.12	0.62	0.97	1.71	0.46	2.66	0.58	1.44	0.69	1.83	65	59
Well 37 DST1 3495m	2	137	30-04-92	1.96	1.35	0.86	2.53	1.00	0.59	0.53	0.43	1.41	1.64	0.89	0.50	0.72	1.15	1.79	1.08	1.12	0.65	1.94	0.60	2.48	11	61
Well 65 DST1 3267m	2	131	4-05-92	1.59	0.69	0.68	2.15	0.35	0.95	0.49	0.98	3.61	0.65	1.93	6.32	0.50	1.11	1.28	0.96	1.41	0.61	1.51	0.95	1.38	255	115
Well 65 DST2 3189m	2	129	4-05-92	1.98	0.70	0.46	6.99	0.36	1.28	0.32	0.81	5.60	0.44	1.57	1.09	0.47	1.03	1.39	0.79	1.77	0.56	1.55	0.96	1.54	200	64
FAMILY 3: HAUTERIVIAN (5A)																										
Well 107 DST2 2565m	2	105	28-04-92	2.56	1.02	1.33	1.06	0.79	0.82	1.33	0.58	1.33	1.48	1.05	0.46	0.75	1.09	1.21	1.17	1.16	0.79	2.40	0.70	2.77	124	51
Well 69 DST1 2436m	2	92	30-04-92	1.95	0.98	1.77	0.63	0.81	0.52	1.62	0.60	0.97	1.68	0.96	0.42	0.76	1.29	1.45	1.12	1.28	0.76	2.93	0.67	3.01	465	59
Well 46 DST2 2560m	2	98	31-03-92	1.95	1.31	0.86	1.00	0.66	1.05	1.79	0.55	1.48	1.52	1.39	0.45	0.91	1.22	1.40	0.82	1.49	0.64	1.93	0.60	2.21	325	97
Well 48 DST2 2620m	3	110	19-02-93	3.18	1.66	0.64	0.88	0.76	1.43	0.90	0.49	2.16	1.18	1.94	0.54	1.22	1.38	1.34	0.83	1.07	0.55	1.30	0.55	1.80	0	0
Well 54 DST1 2617m	2	104	5-05-92	2.69	0.92	1.04	1.67	0.70	1.24	1.15	0.57	1.64	1.37	1.33	0.65	0.64	1.12	1.41	1.21	1.06	0.67	1.85	0.66	2.10	320	97
Well 76 DST1 2610m	3	109	19-02-93	2.74	1.36	0.88	0.79	0.66	1.14	1.78	0.65	1.89	1.55	1.53	0.40	1.14	1.18	1.27	1.19	1.19	0.63	1.98	0.62	2.36	360	77
Well 39 DST1 2567m	1	104	29-08-91	0.60	1.21	1.17	1.28	0.26	0.51	1.43	0.67	0.60	0.90	0.60	0.17	1.04	0.91	1.27	1.13	1.06	0.60	1.49	0.84	2.07	570	72
Well 39 DST2 2229m	1	89	29-08-91*	0.88	1.49	0.66	2.02	0.16	0.73	1.51	0.72	0.31	0.56	0.55	0.18	0.76	0.83	1.29	1.24	1.10	0.65	1.56	0.81	1.84	420	72
Well 39 DST2 2229m	2	89	3-04-92	1.88	1.41	0.58	2.12	0.29	0.68	0.69	0.46	2.49	1.06	2.51	0.65	0.87	1.33	1.26	0.57	2.77	0.62	2.26	0.77	2.06	420	72
Well 44 DST1 2750m	2	112	5-05-92	1.85	0.92	0.95	2.35	0.45	1.12	0.74	0.52	2.89	0.95	1.70	1.15	0.42	1.10	1.49	1.15	1.26	0.64	1.90	0.73	2.02	295	66
Well 55 DST2 2680m	2	111	5-05-92	1.79	0.90	0.87	2.75	0.48	0.91	0.63	0.98	3.20	0.86	1.74	0.77	0.62	1.11	1.49	1.09	1.35	0.61	1.88	0.71	1.99	225	84
Well 18 DST1 2703m	2	109	4-05-92	1.06	1.00	2.27	0.71	0.42	0.30	1.62	0.61	0.81	1.09	0.80	0.42	0.63	1.04	1.22	1.06	0.97	0.61	1.69	0.75	1.68	155	56
Well 18 DST3 2673m	2	107	18-05-92	1.22	0.91	1.18	1.41	0.41	0.33	1.31	0.55	1.55	0.92	1.28	0.50	0.71	1.15	1.41	1.13	1.14	0.60	1.75	0.67	2.07	220	72
Well 18 DST4 2635m	2	105	18-05-92	1.85	0.89	0.93	2.50	0.43	0.64	0.95	0.59	2.28	0.94	1.46	0.57	0.68	1.09	1.32	1.17	1.21	0.62	1.67	0.68	1.01	345	91

Table F.04A: Peak height ratios of 'fingerprint' peaks measured from all whole oil GC plots (page 2 of 3).

RATIOS			Analysis	1	2	2a	3	4	5	6	7	8	9	10	11	12	13	14	15	16	17	18	19	20	Separator	
Well 21 DST1 2585m	2	108	5-05-92	1.15	0.72	1.19	1.40	0.35	0.60	1.33	0.65	1.55	0.97	1.35	0.43	0.61	1.18	1.29	1.44	1.26	0.66	2.35	0.91	2.00	0	0
Well 21 DST2 2559m	3	109	16-02-93	1.37	0.97	0.82	1.04	0.33	0.45	1.72	0.63	2.74	1.17	1.68	0.37	0.92	1.31	1.13	1.39	1.42	0.68	2.49	0.86	2.31	300	50
Well 19 DST2 2709m	2	109	30-03-92	1.31	1.19	0.79	1.36	0.38	0.69	0.93	0.46	2.89	0.89	2.13	0.60	0.86	1.27	1.33	0.66	2.04	0.62	1.98	0.67	2.08	195	56
Well 20 DST2 2699m	1	110	20-08-91*	0.44	1.00	1.48	0.54	0.36	0.24	2.25	0.80	1.91	0.68	0.53	0.58	1.11	1.00	1.54	1.94	1.04	0.87	1.50	0.87	1.40	0	0
Well 20 DST3 2579m	1	102	29-08-91	1.36	1.71	0.70	1.57	0.48	0.50	1.71	0.69	2.30	0.77	0.51	0.17	0.94	0.98	1.41	1.10	1.08	0.65	1.64	0.85	2.43	130	100
Well 20 DST4 2515m	1	100	4-09-91	1.53	1.74	1.04	0.73	0.54	0.30	1.57	0.48	1.81	0.78	0.61	0.56	1.10	1.07	1.54	1.37	0.86	0.71	1.35	0.79	1.93	0	0
Well 61 DST2 2770m	2	114	6-05-92	1.79	0.90	0.67	3.95	0.46	1.13	0.22	0.53	5.07	0.81	2.04	1.20	0.88	1.03	1.53	0.43	2.07	0.61	2.05	0.75	2.24	197	50
Well 61 DST3 2128m	2	90	6-05-92	1.52	1.14	1.25	1.50	0.54	0.44	1.24	0.52	1.24	1.20	0.74	0.40	0.94	1.20	1.50	1.07	1.35	0.73	2.62	0.71	2.59	310	70
Well 62 DST1 2549m	2	109	6-05-92	1.84	1.17	0.74	3.32	0.75	1.16	0.31	0.53	3.94	1.00	1.14	0.89	0.73	1.10	1.58	0.67	1.60	0.61	1.42	0.62	1.75	0	0
Well 70 DST1 2452m	2	104	6-05-92	2.24	1.07	0.76	3.08	0.57	0.48	0.42	0.44	2.53	0.83	1.78	0.83	0.65	1.17	1.51	0.61	1.31	0.48	1.18	0.60	1.60	0	0
Well 70 DST2 2428m	2	103	7-05-92	1.89	1.00	0.88	2.72	0.50	0.45	0.76	0.49	2.45	0.91	1.60	0.70	0.67	1.11	1.40	1.20	1.10	0.62	1.92	0.66	2.07	285	72
Well 31 DST1 2753m	1	105	30-08-91	1.31	1.46	0.84	1.36	0.37	0.82	1.77	0.74	0.50	0.56	0.51	0.13	0.98	0.90	1.49	1.20	1.15	0.65	1.26	0.81	1.92	355	82
Well 63 DST1 2691m	1	109	30-08-91	1.27	1.78	0.56	1.60	0.41	0.36	1.45	0.55	2.43	0.33	0.57	0.53	0.61	0.67	1.49	1.26	0.49	0.98	1.05	0.69	1.70	330	68
FAMILY 4: F-O																										
Well 128 DST1 3661m	1	149	20-08-91	0.44	0.75	0.63	0.91	0.35	0.13	2.28	0.59	1.43	0.84	0.46	0.13	0.78	1.14	1.00	1.68	0.80	0.74	1.86	1.71	2.30	365	101
FAMILY 5: E-G																										
Well 27 DST1 3161m	2	136	29-04-92	1.49	1.28	1.91	0.90	0.96	0.67	1.13	0.50	1.21	1.45	0.85	0.44	0.79	1.02	1.68	0.95	1.12	0.60	1.77	0.57	2.26	0	0
Well 35 DST3 3309-3416m	1	135	28-08-91	1.57	1.24	2.78	0.42	0.99	0.61	1.35	0.59	0.75	1.05	0.79	0.11	1.23	0.87	1.68	1.08	0.65	0.73	1.06	0.73	2.08	210	93
Well 35 DST2B 3354-3416m	2	137	7-05-92	1.87	1.22	1.39	1.41	1.06	0.67	1.03	0.58	0.87	1.65	0.76	0.37	0.77	1.15	1.64	1.16	1.14	0.69	1.82	0.61	1.70	155	95
Well 35 DST1 3397-3416m	2	138	18-05-92	1.59	1.12	1.80	1.01	1.03	0.70	1.16	0.60	0.86	1.69	0.73	0.30	0.73	1.15	1.65	1.07	1.10	0.63	1.69	0.62	2.13	0	0

Table F.04A: Peak height ratios of 'fingerprint' peaks measured from all whole oil GC plots (page 3 of 3).

MSCHEV PEAKS				PEAK HEIGHT RATIOS																					
RATIOS				1	2	2a	3	4	5	6	7	8	9	10	11	12	13	14	15	16	17	18	19	20	6(15)	2(2a)
SAMPLE	Col.	SBHT	Date	Branched and cyclo-alkanes															Isoprenoids						
FAMILY 1																									
Well 146 DST1 2564m	3	96	18-05-93	2.03	0.84	2.03	0.56	1.00	0.71	1.65	0.84	2.86	1.53	0.77	0.45	1.14	1.15	1.13	1.16	1.07	0.79	1.38	0.65	1.77	1.42	0.41
Well 166 DST1 2520m	Q	99	09-11-95	2.93	1.08	1.41	0.85	0.61	0.71	1.04	0.94	4.55	1.95	0.75	0.37	1.73	1.24	1.65	1.17	1.10	0.81	1.24	0.77	2.05	0.89	0.77
Well 88 DST5 2507m	1	100	21-08-91	2.25	0.90	2.58	0.39	1.17	0.54	1.37	0.81	2.35	1.13	0.63	0.47	1.40	1.13	1.92	1.21	0.77	0.86	1.15	0.85	2.02	1.13	0.35
Well 109 DST1 2630m	2	100	23-12-92	2.91	1.20	0.79	2.68	0.13	1.06	0.47	0.82	4.25	1.11	0.86	0.91	1.23	1.79	1.48	0.67	0.76	1.33	1.34	0.61	1.68	0.70	1.51
Well 109 DST1 2630m	3	100	18-02-93	4.09	1.45	0.74	1.32	0.89	1.39	0.45	0.65	5.81	1.29	1.59	0.73	1.55	1.85	1.72	0.60	1.63	0.71	1.41	0.52	1.84	0.75	1.97
Well 156 DST1 2522m	Q	100	07-11-95	3.53	1.01	1.58	0.79	0.64	0.69	1.00	1.02	4.73	1.87	0.66	0.40	1.81	1.33	1.62	1.21	1.11	0.80	1.17	0.82	1.91	0.83	0.64
Well 93 DST2 2463m	1	102	27-08-91	3.23	0.88	4.27	0.65	1.05	0.90	1.83	0.83	2.33	1.16	0.85	0.59	1.64	0.94	2.06	1.36	0.88	0.98	1.38	0.89	1.89	1.35	0.21
Well 117 DST1 2399m	1	104	28-08-91	2.92	0.85	2.79	0.37	0.96	0.61	1.63	0.90	2.31	1.19	0.61	0.45	1.53	1.09	1.86	1.27	0.80	0.90	1.16	0.81	1.99	1.28	0.30
Well 117 DST1 2399m	3	104	22-02-93	3.16	0.86	2.04	0.48	0.99	0.93	1.88	0.80	6.21	1.72	0.99	0.43	1.41	1.46	1.63	1.18	1.11	0.78	1.44	0.62	1.96	1.59	0.42
Well 83 DST3 2470m	1	105	20-08-91	2.51	0.85	3.04	0.33	0.94	0.59	1.59	0.83	2.27	1.22	0.64	0.42	1.47	1.16	2.23	1.25	0.74	0.85	1.12	0.86	1.99	1.27	0.28
FAMILY1(2M)																									
Well 59 DST1 2212m	1	95	29-08-91	1.41	1.54	0.69	1.39	0.48	0.37	0.45	0.65	1.93	0.56	0.30	0.44	1.42	0.97	1.43	0.86	0.78	0.48	0.87	0.72	1.79	0.52	2.23
Well 59 DST1 2212m	2	95	3-04-92	1.21	1.62	0.43	2.10	0.50	0.86	0.40	0.30	2.94	0.94	2.73	0.63	0.87	1.28	1.34	0.36	1.91	0.48	1.23	0.54	1.67	1.11	3.75
Well 102 DST4 2241m	2	98	1-04-92	1.62	1.26	1.01	0.48	0.80	0.70	1.80	0.47	1.14	1.44	1.18	0.33	0.94	1.38	1.45	0.74	1.31	0.59	1.85	0.56	2.49	2.42	1.25
Well 119 DST1 2816m	2	112	2-04-92	2.31	1.27	0.86	1.34	0.85	1.46	0.48	0.60	6.21	1.72	0.51	0.90	1.21	1.39	1.73	0.45	2.12	0.71	1.28	0.52	1.71	1.06	1.48
Well 103 DST2 2718m	1	115	26-08-91	1.85	1.00	2.73	0.60	0.73	0.59	1.68	0.98	2.79	1.36	0.74	0.37	1.56	1.00	1.84	1.31	0.89	0.88	1.20	0.89	2.31	1.28	0.37
Well 93 DST1A 2808m	3	116	16-02-93	4.29	1.22	1.17	1.01	0.87	1.24	0.79	0.79	4.93	1.44	1.12	0.63	1.41	1.74	1.65	0.88	1.35	0.81	1.79	0.60	1.95	0.90	1.05
Well 94 DST1 2799m	2	117	2-04-92	1.29	0.93	1.53	0.65	0.74	0.95	1.35	0.66	3.72	1.38	1.06	0.57	1.08	1.35	1.54	0.87	1.62	0.72	1.71	0.64	1.99	1.55	0.61
Well 93 DST1 2817m	1	117	26-08-91	2.82	0.79	1.28	0.84	0.87	0.54	0.44	0.60	2.86	0.57	0.82	0.88	1.53	0.68	2.15	1.11	0.46	0.94	0.76	0.67	1.51	0.39	0.62
Well 126 DST1 2643m	1	119	27-08-91	2.12	1.06	2.90	0.58	0.85	0.80	1.68	0.80	2.87	1.32	0.82	0.39	1.39	1.03	1.68	1.24	0.90	0.87	0.61	0.55	1.20	1.36	0.36
Well 126 DST1 2643m	Q	119	07-11-95	2.47	0.96	1.55	0.93	0.49	0.87	1.07	1.14	3.66	1.56	0.79	0.31	1.87	1.35	1.54	1.29	1.18	0.86	1.42	0.85	2.25	0.83	0.62
Well 95 DST2 2703m	2	120	2-04-92	1.30	0.91	1.29	0.77	0.59	0.89	1.41	0.70	2.96	1.34	1.09	0.34	1.10	1.33	1.46	0.92	1.56	0.73	1.88	0.63	2.21	1.52	0.70
FAMILY 2																									
Well 132 DST1 2684m	3	111	19-05-93	2.08	1.34	0.96	1.82	0.78	0.61	0.84	0.76	5.90	1.18	0.81	0.57	1.12	1.37	1.50	0.80	1.46	0.84	1.84	0.60	2.01	1.04	1.40
Well 88 DST4 2839m	1	112	22-08-91	1.72	1.47	0.71	1.33	0.59	0.37	0.38	0.59	2.76	0.55	0.67	0.71	1.34	0.72	1.81	1.10	0.49	1.11	1.17	0.72	1.78	0.34	2.08
Well 120 DST1 2931m	1	113	28-08-91	0.91	0.99	0.69	1.53	0.32	0.37	1.16	0.88	2.35	1.09	0.71	0.32	1.28	0.97	1.96	1.28	0.74	0.88	1.14	0.79	1.60	0.90	1.45
Well 120 DST1 2931m	Q	113	08-11-95	0.83	0.99	0.60	2.02	0.22	0.38	1.28	0.93	2.91	0.86	0.67	0.24	1.58	1.13	1.61	1.28	1.10	0.78	1.53	0.87	1.93	1.00	1.65
Well 88 DST3 2916m	1	115	22-08-91	1.35	1.30	0.85	1.32	0.46	0.43	0.64	0.68	3.13	0.73	0.70	0.61	1.30	1.02	1.95	1.17	0.64	1.08	1.82	0.81	2.27	0.54	1.54
Well 88 DST2 2929m	2	116	1-04-92	1.11	1.09	0.70	2.06	0.41	0.55	0.58	0.55	4.93	0.86	2.03	0.71	0.94	1.32	1.41	0.58	2.23	0.69	2.07	0.60	2.05	0.99	1.56
Well 129 DST2 2865m	1	116	27-08-91	2.39	1.71	0.83	1.28	0.70	0.54	0.58	0.64	2.48	0.71	1.25	0.63	1.52	0.81	2.23	1.14	0.57	0.99	1.16	0.73	1.87	0.51	2.05
Well 110 DST1A 3051m	2	116	29-04-92	2.68	1.01	1.13	2.53	0.66	0.71	0.57	0.71	3.83	1.16	0.85	0.66	0.96	1.03	1.53	1.09	1.07	0.81	1.59	0.59	1.70	0.52	0.90

Table F.04B: Peak height ratios of 'fingerprint' peaks measured from all whole oil GC plots, listed in their minor families (page 1 of 3).

RATIOS				1	2	2a	3	4	5	6	7	8	9	10	11	12	13	14	15	16	17	18	19	20	6(15)	2(2a)
Well 110 DST1B 3051m	2	116	29-04-92	2.50	0.97	1.18	2.48	0.66	0.65	0.56	0.70	3.70	1.18	0.83	0.63	0.95	1.00	1.59	1.11	1.07	0.79	1.73	0.58	1.88	0.51	0.82
Well 110 DST1B 3051m	3	116	19-02-93	2.17	1.30	0.88	1.37	0.60	0.52	0.77	0.75	3.82	0.87	0.83	0.55	1.29	1.73	1.61	1.04	1.20	0.87	1.73	0.57	1.91	0.74	1.47
Well 96 DST1 3131m	2	118	30-11-92	0.54	1.04	0.51	2.85	0.25	0.45	0.55	0.66	2.89	0.93	1.59	0.60	0.87	1.48	1.04	1.04	0.59	0.90	1.09	0.71	1.46	0.53	2.02
Well 96 DST1 3131m	3	118	16-02-93	1.13	0.93	0.55	1.95	0.27	0.46	0.67	0.60	3.89	0.74	2.40	0.39	1.17	1.88	1.54	1.08	1.22	0.70	1.80	0.66	1.84	0.62	1.71
Well 129 DST1 2946m	1	120	19-08-91	1.28	1.28	0.57	1.79	0.38	0.35	0.55	0.64	3.76	0.61	0.62	0.58	1.23	1.04	1.71	1.19	0.61	1.01	1.24	0.71	1.82	0.46	2.24
Well 83 DST2 2889m	1	122	21-08-91	1.92	1.69	0.96	1.09	0.66	0.47	0.46	0.57	2.41	0.56	0.74	0.69	1.42	0.81	2.12	1.15	0.48	0.99	1.15	0.72	1.80	0.40	1.75
Well 11 DST2 2950m	2	125	29-04-92	3.09	0.82	0.52	8.52	0.24	0.70	0.11	0.41	9.50	2.60	2.84	1.77	0.40	0.94	1.67	0.27	7.76	0.61	2.23	1.01	1.54	0.40	1.56
Well 88 DST1 3243m	1	126	22-08-91	0.60	1.06	0.72	1.64	0.53	0.29	0.57	0.55	3.09	0.40	0.60	0.74	1.00	0.91	1.38	1.16	0.64	0.91	1.29	0.82	2.28	0.49	1.47
Well 65 DST2 3189m	2	129	4-05-92	1.98	0.70	0.46	6.99	0.36	1.28	0.32	0.81	5.60	0.44	1.57	1.09	0.47	1.03	1.39	0.79	1.77	0.56	1.55	0.96	1.54	0.40	1.52
Well 65 DST1 3267m	2	131	4-05-92	1.59	0.69	0.68	2.15	0.35	0.95	0.49	0.98	3.61	0.65	1.93	6.32	0.50	1.11	1.28	0.96	1.41	0.61	1.51	0.95	1.38	0.52	1.02
Well 114 DST1 3085m	1	132	2-08-91	0.91	1.27	0.42	1.84	0.34	0.35	0.50	0.63	2.75	0.64	0.57	0.49	1.06	0.89	1.83	1.30	0.54	1.00	1.05	0.77	1.61	0.39	3.05
Well 83 DST1C 3254m	1	134	21-08-91	0.52	0.95	0.59	1.65	0.49	0.31	0.50	0.58	3.35	0.30	0.58	0.64	0.93	0.95	1.24	1.09	0.63	0.97	1.85	0.89	2.34	0.46	1.61
Well 37 DST1 3495m	2	137	30-04-92	1.96	1.35	0.86	2.53	1.00	0.59	0.53	0.43	1.41	1.64	0.89	0.50	0.72	1.15	1.79	1.08	1.12	0.65	1.94	0.60	2.48	0.49	1.58
FAMILY 2(1M)																										
Well 107 DST3 2388m	2	82	28-04-92	3.28	0.92	1.36	2.16	0.74	0.66	0.63	0.65	3.49	1.42	0.91	0.65	0.92	0.97	1.54	1.09	1.28	0.90	2.04	0.67	2.13	0.58	0.67
Well 166 RFT 2508m	Q	98	09-11-95	2.84	1.00	1.70	0.83	0.56	0.88	1.37	1.06	3.93	1.82	0.73	0.32	1.83	1.18	1.48	1.33	1.28	0.91	1.61	0.84	2.28	1.03	0.59
Well 132 DST2 2662m	2	103	30-03-92	3.14	1.46	0.85	1.82	0.82	1.02	0.58	0.62	5.19	1.27	1.20	0.91	1.22	1.19	1.73	0.54	2.27	0.77	1.79	0.60	1.87	1.08	1.71
Well 132 DST1 2706m	2	104	30-03-92	2.97	1.47	0.83	1.73	0.84	1.20	0.45	0.52	6.17	1.17	1.42	1.02	1.22	1.36	2.01	0.43	2.47	0.69	1.42	0.62	1.67	1.05	1.78
Well 167 DST1 2679m	Q	108	07-12-95	2.18	1.01	1.51	0.75	0.45	0.79	1.36	1.12	3.82	1.72	0.72	0.30	1.74	1.40	1.44	1.35	1.31	0.94	1.72	0.90	2.49	1.00	0.67
Well 84 DST1 2771m	2	109	29-04-92	4.38	0.85	0.62	4.83	0.65	1.74	0.28	0.69	4.58	0.95	2.10	1.12	0.62	0.97	1.71	0.46	2.66	0.58	1.44	0.69	1.83	0.61	1.39
Well 102 DST2 2632m	2	110	2-04-92	1.26	1.11	0.86	2.23	0.46	0.22	0.57	0.48	2.94	1.03	1.12	0.55	0.93	1.19	1.93	0.25	2.31	0.77	2.48	0.75	1.84	2.27	1.28
Well 108 DST1 2829m	2	116	28-04-92	3.47	1.04	1.29	2.11	0.94	0.68	0.59	0.69	4.54	1.37	0.75	0.94	1.05	0.92	1.83	1.00	1.20	0.78	1.67	0.63	1.96	0.59	0.80
Well 108 DST2 2820m	2	116	28-04-92	3.59	1.03	1.32	2.18	0.95	0.69	0.58	0.70	4.45	1.44	0.77	0.91	1.04	0.96	1.71	0.98	1.24	0.78	1.65	0.62	2.14	0.59	0.78
FAMILY 3																										
Well 61 DST3 2128m	2	90	6-05-92	1.52	1.14	1.25	1.50	0.54	0.44	1.24	0.52	1.24	1.20	0.74	0.40	0.94	1.20	1.50	1.07	1.35	0.73	2.62	0.71	2.59	1.15	0.91
Well 69 DST1 2436m	2	92	30-04-92	1.95	0.98	1.77	0.63	0.81	0.52	1.62	0.60	0.97	1.68	0.96	0.42	0.76	1.29	1.45	1.12	1.28	0.76	2.93	0.67	3.01	1.45	0.56
Well 20 DST4 2515m	1	100	4-09-91	1.53	1.74	1.04	0.73	0.54	0.30	1.57	0.48	1.81	0.78	0.61	0.56	1.10	1.07	1.54	1.37	0.86	0.71	1.35	0.79	1.93	1.15	1.67
Well 20 DST3 2579m	1	102	29-08-91	1.36	1.71	0.70	1.57	0.48	0.50	1.71	0.69	2.30	0.77	0.51	0.17	0.94	0.98	1.41	1.10	1.08	0.65	1.64	0.85	2.43	1.55	2.44
Well 54 DST1 2617m	2	104	5-05-92	2.69	0.92	1.04	1.67	0.70	1.24	1.15	0.57	1.64	1.37	1.33	0.65	0.64	1.12	1.41	1.21	1.06	0.67	1.85	0.66	2.10	0.96	0.88
Well 39 DST1 2567m	1	104	29-08-91	0.60	1.21	1.17	1.28	0.26	0.51	1.43	0.67	0.60	0.90	0.60	0.17	1.04	0.91	1.27	1.13	1.06	0.60	1.49	0.84	2.07	1.27	1.03
Well 107 DST2 2565m	2	105	28-04-92	2.56	1.02	1.33	1.06	0.79	0.82	1.33	0.58	1.33	1.48	1.05	0.46	0.75	1.09	1.21	1.17	1.16	0.79	2.40	0.70	2.77	1.14	0.77
Well 18 DST4 2635m	2	105	18-05-92	1.85	0.89	0.93	2.50	0.43	0.64	0.95	0.59	2.28	0.94	1.46	0.57	0.68	1.09	1.32	1.17	1.21	0.62	1.67	0.68	1.01	0.81	0.96
Well 31 DST1 2753m	1	105	30-08-91	1.31	1.46	0.84	1.36	0.37	0.82	1.77	0.74	0.50	0.56	0.51	0.13	0.98	0.90	1.49	1.20	1.15	0.65	1.26	0.81	1.92	1.48	1.74
Well 18 DST3 2673m	2	107	18-05-92	1.22	0.91	1.18	1.41	0.41	0.33	1.31	0.55	1.55	0.92	1.28	0.50	0.71	1.15	1.41	1.13	1.14	0.60	1.75	0.67	2.07	1.16	0.77
Well 21 DST1 2585m	2	108	5-05-92	1.15	0.72	1.19	1.40	0.35	0.60	1.33	0.65	1.55	0.97	1.35	0.43	0.61	1.18	1.29	1.44	1.26	0.66	2.35	0.91	2.00	0.92	0.61

Table F.04B: Peak height ratios of 'fingerprint' peaks measured from all whole oil GC plots (page 2 of 3).

RATIOS				1	2	2a	3	4	5	6	7	8	9	10	11	12	13	14	15	16	17	18	19	20	6(15)	2(2a)
Well 76 DST1 2610m	3	109	19-02-93	2.74	1.36	0.88	0.79	0.66	1.14	1.78	0.65	1.89	1.55	1.53	0.40	1.14	1.18	1.27	1.19	1.19	0.63	1.98	0.62	2.36	1.49	1.54
Well 18 DST1 2703m	2	109	4-05-92	1.06	1.00	2.27	0.71	0.42	0.30	1.62	0.61	0.81	1.09	0.80	0.42	0.63	1.04	1.22	1.06	0.97	0.61	1.69	0.75	1.68	1.52	0.44
Well 21 DST2 2559m	3	109	16-02-93	1.37	0.97	0.82	1.04	0.33	0.45	1.72	0.63	2.74	1.17	1.68	0.37	0.92	1.31	1.13	1.39	1.42	0.68	2.49	0.86	2.31	1.24	1.19
Well 19 DST2 2709m	2	109	30-03-92	1.31	1.19	0.79	1.36	0.38	0.69	0.93	0.46	2.89	0.89	2.13	0.60	0.86	1.27	1.33	0.66	2.04	0.62	1.98	0.67	2.08	1.41	1.50
Well 62 DST1 2549m	2	109	6-05-92	1.84	1.17	0.74	3.32	0.75	1.16	0.31	0.53	3.94	1.00	1.14	0.89	0.73	1.10	1.58	0.67	1.60	0.61	1.42	0.62	1.75	0.47	1.58
Well 20 DST2 2699m	1	110	33470.00	0.44	1.00	1.48	0.54	0.36	0.24	2.25	0.80	1.91	0.68	0.53	0.58	1.11	1.00	1.54	1.94	1.04	0.87	1.50	0.87	1.40	1.16	0.68
Well 55 DST2 2680m	2	111	5-05-92	1.79	0.90	0.87	2.75	0.48	0.91	0.63	0.98	3.20	0.86	1.74	0.77	0.62	1.11	1.49	1.09	1.35	0.61	1.88	0.71	1.99	0.58	1.03
Well 44 DST1 2750m	2	112	5-05-92	1.85	0.92	0.95	2.35	0.45	1.12	0.74	0.52	2.89	0.95	1.70	1.15	0.42	1.10	1.49	1.15	1.26	0.64	1.90	0.73	2.02	0.65	0.97
Well 61 DST2 2770m	2	114	6-05-92	1.79	0.90	0.67	3.95	0.46	1.13	0.22	0.53	5.07	0.81	2.04	1.20	0.88	1.03	1.53	0.43	2.07	0.61	2.05	0.75	2.24	0.52	1.35
FAMILY 3(1M)																										
Well 39 DST2 2229m	1	89	29-08-91	0.88	1.49	0.66	2.02	0.16	0.73	1.51	0.72	0.31	0.56	0.55	0.18	0.76	0.83	1.29	1.24	1.10	0.65	1.56	0.81	1.84	1.22	2.27
Well 39 DST2 2229m	2	89	3-04-92	1.88	1.41	0.58	2.12	0.29	0.68	0.69	0.46	2.49	1.06	2.51	0.65	0.87	1.33	1.26	0.57	2.77	0.62	2.26	0.77	2.06	1.20	2.43
Well 46 DST2 2560m	2	98	31-03-92	1.95	1.31	0.86	1.00	0.66	1.05	1.79	0.55	1.48	1.52	1.39	0.45	0.91	1.22	1.40	0.82	1.49	0.64	1.93	0.60	2.21	2.18	1.52
Well 70 DST2 2428m	2	103	7-05-92	1.89	1.00	0.88	2.72	0.50	0.45	0.76	0.49	2.45	0.91	1.60	0.70	0.67	1.11	1.40	1.20	1.10	0.62	1.92	0.66	2.07	0.63	1.13
Well 70 DST1 2452m	2	104	6-05-92	2.24	1.07	0.76	3.08	0.57	0.48	0.42	0.44	2.53	0.83	1.78	0.83	0.65	1.17	1.51	0.61	1.31	0.48	1.18	0.60	1.60	0.69	1.40
Well 63 DST1 2691m	1	109	30-08-91	1.27	1.78	0.56	1.60	0.41	0.36	1.45	0.55	2.43	0.33	0.57	0.53	0.61	0.67	1.49	1.26	0.49	0.98	1.05	0.69	1.70	1.15	3.18
Well 48 DST2 2620m	3	110	19-02-93	3.18	1.66	0.64	0.88	0.76	1.43	0.90	0.49	2.16	1.18	1.94	0.54	1.22	1.38	1.34	0.83	1.07	0.55	1.30	0.55	1.80	1.08	2.59
Well 48 DST1 2634m	1	110	4-09-91	2.30	1.51	0.96	0.55	0.82	0.54	0.77	0.51	2.08	0.88	0.58	0.48	1.20	1.16	1.57	1.18	0.60	0.59	0.86	0.72	1.67	0.65	1.57
FAMILY 4																										
Well 128 DST1 3661m	1	149	20-08-91	0.44	0.75	0.63	0.91	0.35	0.13	2.28	0.59	1.43	0.84	0.46	0.13	0.78	1.14	1.00	1.68	0.80	0.74	1.86	1.71	2.30	1.36	1.18
FAMILY 5																										
Well 35 DST3 3309-3416m	1	135	28-08-91	1.57	1.24	2.78	0.42	0.99	0.61	1.35	0.59	0.75	1.05	0.79	0.11	1.23	0.87	1.68	1.08	0.65	0.73	1.06	0.73	2.08	1.25	0.44
Well 27 DST1 3161m	2	136	29-04-92	1.49	1.28	1.91	0.90	0.96	0.67	1.13	0.50	1.21	1.45	0.85	0.44	0.79	1.02	1.68	0.95	1.12	0.60	1.77	0.57	2.26	1.19	0.67
Well 35 DST2B 3354-3416m	2	137	7-05-92	1.87	1.22	1.39	1.41	1.06	0.67	1.03	0.58	0.87	1.65	0.76	0.37	0.77	1.15	1.64	1.16	1.14	0.69	1.82	0.61	1.70	0.89	0.88
Well 35 DST1 3397-3416m	2	138	18-05-92	1.59	1.12	1.80	1.01	1.03	0.70	1.16	0.60	0.86	1.69	0.73	0.30	0.73	1.15	1.65	1.07	1.10	0.63	1.69	0.62	2.13	1.09	0.62

Table F.04B: Peak height ratios of 'fingerprint' peaks measured from all whole oil GC plots (page 3 of 3).

NORMAL ALKANE PEAK HEIGHTS (FROM GAS CHROMATOGRAMS).																					
No.	nC13	nC14	nC15	nC16	nC17	nC18	nC19	nC20	nC21	nC22	nC23	nC24	nC25	nC26	nC27	nC28	nC29	nC30	nC31	nC32	nC33
OIL SAMPLES																					
1	260	1131	1870	1948	1792	1428	1210	1048	833	751	611	555	415	340	250	171	111	78	52	28	0
2	0	29	557	1483	1921	1884	1848	1774	1587	1495	1456	1388	1207	1074	873	752	658	557	502	403	0
3	0	29	557	1483	1921	1884	1848	1774	1587	1495	1456	1388	1207	1074	873	752	658	557	502	403	237
4	0	129	913	1677	1900	1700	1599	1382	1184	1122	961	849	680	590	426	339	284	230	213	161	0
5	0	129	913	1677	1900	1700	1599	1382	1184	1122	961	849	680	590	426	339	284	230	213	161	0
6	19	338	1062	1383	1592	1623	1599	1485	1286	1201	1044	1021	891	764	638	539	430	382	340	278	0
7	0	0	10	26	282	868	1150	1047	882	813	700	780	681	673	600	506	481	370	420	295	255
8	23	152	679	1433	1877	1924	1920	1726	1593	1550	1502	1461	1322	1270	1019	873	774	661	582	459	0
9	302	1362	1801	1916	1580	1362	1037	824	602	484	349	238	151	89	51	30	21	15	11	0	0
10	49	862	1842	1930	1849	1556	1362	1164	918	780	639	535	408	309	217	159	124	89	77	53	0
11	39	91	130	349	799	1225	1604	1798	1734	1648	1521	1470	1359	1184	1072	1012	858	770	747	632	0
12	40	149	281	740	1212	1551	1750	1860	1730	1691	1622	1551	1418	1328	1110	928	804	674	667	490	0
13	0	182	1233	1812	1813	1813	1878	1448	1342	1180	1096	1007	893	805	673	548	473	408	371	289	0
14	342	814	1135	1165	1242	1076	1030	1020	800	790	830	708	586	521	417	296	240	170	140	95	0
15	36	543	1469	1867	1915	1621	1249	913	559	336	195	120	70	47	29	20	15	12	11	10	0
16	390	1313	1809	1899	1589	1462	1390	1179	1009	899	771	701	571	501	392	269	221	211	161	105	0
17	1796	1554	1307	1106	965	796	725	610	495	405	346	283	206	158	114	85	67	54	38	36	0
18	0	12	180	869	1461	1512	1576	1605	1530	1708	1713	1744	1668	1671	1432	1409	1356	1222	1260	1079	950
19	1245	1721	1870	1891	1740	1481	1289	1202	1021	1017	952	963	860	816	699	590	521	429	345	210	0
20	0	0	71	819	1550	1734	1849	1782	1630	1469	1340	1311	1171	1047	890	791	721	598	533	330	0
21	15	206	620	1000	1426	1498	1655	1753	1663	1472	1410	1089	977	768	646	487	422	271	231	138	0
22	0	0	11	556	1963	1862	1262	1045	987	890	841	699	560	504	508	401	291	239	181	129	0
23	20	80	115	126	139	147	145	132	118	110	104	98	73	67	48	32	24	12	8	4	0
24	50	135	291	546	781	914	1058	1202	1201	1239	1202	1209	1082	973	696	471	320	226	148	91	0
25	0	18	167	791	1396	1739	1847	1867	1736	1672	1522	1460	1400	1221	992	870	781	589	609	507	0
26	51	137	167	152	134	107	92	74	60	48	36	24	15	8	4	0	0	0	0	0	0
27	0	0	0	5	82	351	997	1225	1281	1239	1150	1014	978	753	612	469	384	289	231	165	129
28	1891	1840	1672	1525	1144	1082	983	844	740	624	535	462	368	291	211	158	124	90	78	55	0
29	1311	1698	1933	1920	1792	1650	1586	1401	1269	1190	1003	928	736	660	530	451	359	300	271	215	0
30	546	1521	1848	1868	1692	1571	1470	1334	1229	1121	1025	925	780	694	588	512	409	351	313	279	0
31	0	10	270	1081	1805	1893	1711	1570	1348	1105	934	825	626	542	405	320	267	222	196	183	141
32	1515	1905	1892	1707	1410	1195	982	813	724	596	492	386	300	234	165	119	95	68	61	50	37
33	0	0	10	78	802	1788	1718	1780	1246	1064	800	678	492	398	308	243	195	142	116	86	64
34	1229	1697	1828	1768	1620	1466	1328	1236	1106	968	916	799	631	577	456	357	300	231	212	186	172
35	5	183	944	1620	1920	1720	1578	1440	1168	959	830	708	528	443	332	248	211	177	170	152	117
36	0	21	222	640	1163	1368	1604	1750	1637	1720	1618	1615	1505	1404	1235	981	897	773	730	641	568
37	1550	1885	1700	1323	957	678	459	350	242	178	127	88	50	38	22	12	7	5			
38	0	0	2	10	276	1027	1658	1826	1759	1582	1479	1274	976	803	608	436	346	237	210	151	122

Table F.05: Normal alkane peak heights measured from GC plots of saturated hydrocarbons from all hydrocarbon samples (page 1 of 2).

SHALE SAMPLES																					
41	0	0	20	399	1190	1711	1862	1713	1603	1470	1327	1210	1018	835	724	570	512	370	362	246	0
42	0	0	11	271	1269	1850	1829	1767	1601	1496	1387	1353	1159	1050	779	640	508	415	353	256	0
43	0	0	19	289	1071	1425	1479	1560	1472	1289	1248	1100	950	876	755	622	579	348	277	169	125
44	0	0	272	1235	1848	1736	1734	1633	1487	1254	1125	1003	862	689	611	571	523	442	418	274	0
45	0	5	123	595	955	1120	1220	1250	1320	1125	1140	665	660	320	270	220	195	155	140	128	112
46	0	20	49	487	1320	1698	1826	1599	1480	1285	1154	968	810	656	480	419	339	292	290	252	140
47	0	41	760	1598	1821	1769	1670	1549	1281	1131	869	734	530	438	291	220	179	122	104	77	20
48	0	41	760	1598	1821	1769	1670	1549	1281	1131	869	734	530	438	291	220	179	122	104	77	20
49	0	129	24	222	192	580	1307	1480	1668	1476	1329	989	878	750	698	677	786	354	407	159	0
50	0	10	358	1099	1612	1463	1410	1300	1212	1087	1073	980	753	730	542	445	472	329	297	250	190
51	0	0	0	520	1633	1752	1829	1725	1533	1459	1410	1358	1262	1105	963	921	799	644	672	517	480
52	0	0	22	51	630	1403	1808	1686	1758	1601	1622	1436	1222	1108	869	749	943	529	503	358	0
53	43	181	508	1160	1699	1729	1650	1485	1239	1081	889	770	632	491	359	277	220	170	150	120	0
54	199	1201	1779	1908	1716	1507	1382	1185	1000	899	763	650	527	440	333	260	229	181	170	124	0
55	88	810	1432	1541	1430	1361	1320	1116	1061	933	829	662	535	420	335	297	208	199	156	88	0
56	86	535	1266	1840	1807	1735	1625	1469	1357	1243	1127	1037	914	794	689	548	498	410	374	303	280
57	86	535	1266	1840	1807	1735	1625	1469	1357	1243	1127	1037	914	794	689	548	498	410	374	303	280
58	86	535	1266	1840	1807	1735	1625	1469	1357	1243	1127	1037	914	794	689	548	498	410	374	303	280
59	182	1244	1942	1930	1837	1618	1496	1387	1216	1128	1102	991	858	749	589	479	399	292	310	257	0
60	65	116	1057	1733	1798	1809	1678	1586	1474	1374	1219	1126	1060	969	806	700	589	466	478	449	0
61	0	152	778	1335	1629	1753	1799	1784	1619	1622	1493	1522	1393	1270	1182	1187	1077	1032	1083	917	700
62	0	49	570	1346	1738	1697	1759	1565	1407	1303	1135	1007	860	656	508	387	322	260	222	191	0
63	4	34	69	96	100	93	91	85	75	67	65	62	54	45	33	26	23	17	13	7	0
64	0	0	21	119	607	1103	1437	1549	1539	1518	1430	1279	1302	1100	1049	768	680	459	470	320	0
65	0	0	38	168	1052	1517	1698	1732	1675	1652	1558	1549	1440	1297	1200	883	970	728	720	542	0
66	0	0	48	520	1216	1474	1630	1767	1690	1600	1520	1336	1231	1132	1049	854	828	678	618	501	0
67	54	240	998	1680	2024	1810	1652	1510	1288	1136	933	850	790	665	530	360	272	172	122	68	0
68	0	0	0	34	223	648	1313	1629	1722	1668	1688	1473	1321	1087	1061	808	818	529	582	438	0
69	0	0	0	0	0	32	302	1122	1541	1633	1612	1493	1409	1348	1083	1068	922	668	692	478	0
70	259	894	1138	1101	929	838	721	651	545	475	406	348	279	228	173	123	95	67	61	58	42

Table F.05: Normal alkane peak heights measured from GC plots of saturated hydrocarbons from all source rock samples (page 2 of 2).

STERANE PEAK HEIGHTS (FROM m/z 217 FRAGMENTOGRAM).																					
code:	27baS	27baR	27abS	27abR	27aaS	27aaR	27bbR	27bbS	28baS	28baR	28abS	28abR	28aaS	28aaR	28bbR	28bbS	29baS	29baR	29abS	29abR	29aaS
OIL SAMPLES																					
1	750	530	235	240	295	162	467	168	570	300	295	168	111	112	427	265	467	405	120	427	131
2	735	660	240	238	313	155	485	210	645	470	313	210	100	104	400	234	385	335	116	400	111
3	935	620	285	455	510	352	860	335	880	910	510	335	122	190	560	400	860	820	270	560	230
4	1005	675	340	340	345	230	645	435	655	480	345	435	135	90	335	335	645	565	200	335	130
5	1050	655	345	510	320	215	610	225	620	390	320	225	105	95	265	165	610	535	150	265	100
6	755	580	265	0	285	135	580	0	575	455	285	0	165	150	310	0	580	600	170	310	170
7	1090	650	345	420	500	420	805	460	525	410	500	460	192	230	495	360	805	535	165	495	350
8	940	550	250	270	210	130	635	145	510	325	210	145	55	47	205	180	635	420	205	205	125
9	978	665	250	250	370	235	750	390	555	475	370	390	155	200	455	425	750	600	105	455	265
10	895	580	280	280	490	355	865	540	575	380	490	540	0	250	505	425	865	530	115	505	310
11	780	460	255	305	230	140	535	155	530	360	230	155	80	80	155	145	535	285	165	155	132
12	887	570	255	280	285	135	545	110	690	450	285	110	66	68	205	135	545	385	185	205	101
13	2070	1280	570	480	610	1020	2170	1495	915	720	610	1495	395	460	680	535	2170	890	380	680	630
14	1990	1310	595	585	810	610	2170	1290	1740	1300	810	1290	395	575	1190	1500	2170	1430	640	1190	555
15	1010	640	300	328	250	250	640	290	505	305	250	290	130	218	270	290	640	380	150	270	220
16	950	570	265	265	260	125	520	155	665	410	260	155	60	65	165	170	520	350	150	165	95
17	980	605	255	275	230	115	545	170	550	340	230	170	53	68	162	180	545	355	145	162	101
18	1860	1200	545	615	770	860	2170	1345	1390	1225	770	1345	480	760	1180	1420	2170	1385	580	1180	795
19	2160	1280	595	620	845	435	1840	1150	1840	1315	845	1150	420	370	830	1050	1840	1270	550	830	350
20	2170	1285	620	615	850	525	2095	1250	1800	1380	850	1250	305	490	965	1200	2095	1435	1635	965	460
21	870	540	220	285	235	190	840	370	500	345	235	370	140	180	360	520	840	545	200	360	305
22	955	590	272	305	300	150	795	190	475	310	300	190	145	260	295	190	795	485	220	295	360
23	950	620	260	290	240	195	615	285	580	390	240	285	124	140	405	375	615	530	120	405	215
24	940	590	270	288	272	120	520	125	660	415	272	125	43	50	170	148	520	347	162	170	88
25	1830	1120	640	515	715	815	2170	1220	1455	1205	715	1220	305	500	840	985	2170	1360	585	840	630
26	835	575	245	265	705	325	865	750	415	280	705	750	375	350	555	560	865	490	190	555	340
27	715	465	220	315	225	160	495	175	470	405	225	175	90	75	220	155	495	380	180	220	125
28	1277	968	296	342	369	272	878	441	742	511	369	441	118	120	232	357	878	542	318	232	132
29	1228	818	300	398	401	295	1014	455	778	587	401	455	111	134	233	321	1014	715	376	233	144
30	973	647	289	360	318	319	825	220	632	475	318	319	137	149	373	437	825	601	251	373	257
31	1048	757	305	284	292	217	979	337	673	546	292	337	142	168	454	461	979	635	183	454	240
32	978	661	224	251	229	165	684	254	494	343	229	254	79	92	223	240	684	390	120	223	121
33	858	601	279	316	303	250	897	419	542	435	303	419	196	302	500	523	897	573	182	500	317
34	1013	718	312	285	282	202	834	322	629	568	282	322	133	133	383	382	834	550	229	383	205
35	1016	627	265	270	324	328	995	402	726	533	324	402	239	278	652	659	995	708	216	652	358
36	748	532	254	278	312	286	1004	367	574	376	312	367	178	294	498	578	1004	694	230	498	330
37	968	640	248	291	222	217	598	250	477	379	222	250	103	130	277	272	598	412	203	277	189

Table F.06: Peak heights of steranes measured from GC-MS plots for all hydrocarbon samples (page 1 of 8).

			total peak	NORMALISED PEAKS																
29aaR	29bbR	29bbS	height	27baS	27baR	27abS	27abR	27aaS	27aaR	27bbR	27bbS	28baS	28baR	28abS	28abR	28aaS	28aaR	28bbR	28bbS	29baS	29baR
106	202	178	7131	10.52	7.43	3.30	3.37	4.14	2.27	6.55	2.36	7.99	4.21	4.14	2.36	1.56	1.57	5.99	3.72	6.55	5.68
100	177	150	7286	10.09	9.06	3.29	3.27	4.30	2.13	6.66	2.88	8.85	6.45	4.30	2.88	1.37	1.43	5.49	3.21	5.28	4.60
165	380	335	11879	7.87	5.22	2.40	3.83	4.29	2.96	7.24	2.82	7.41	7.66	4.29	2.82	1.03	1.60	4.71	3.37	7.24	6.90
120	230	195	9245	10.87	7.30	3.68	3.68	3.73	2.49	6.98	4.71	7.08	5.19	3.73	4.71	1.46	0.97	3.62	3.62	6.98	6.11
195	245	195	8410	12.49	7.79	4.10	6.06	3.80	2.56	7.25	2.68	7.37	4.64	3.80	2.68	1.25	1.13	3.15	1.96	7.25	6.36
165	280	210	7025	10.75	8.26	3.77	0.00	4.06	1.92	8.26	0.00	8.19	6.48	4.06	0.00	2.35	2.14	4.41	0.00	8.26	8.54
290	595	350	11447	9.52	5.68	3.01	3.67	4.37	3.67	7.03	4.02	4.59	3.58	4.37	4.02	1.68	2.01	4.32	3.14	7.03	4.67
82	163	160	6802	13.82	8.09	3.68	3.97	3.09	1.91	9.34	2.13	7.50	4.78	3.09	2.13	0.81	0.69	3.01	2.65	9.34	6.17
200	315	300	9903	9.88	6.72	2.52	2.52	3.74	2.37	7.57	3.94	5.60	4.80	3.74	3.94	1.57	2.02	4.59	4.29	7.57	6.06
240	470	610	11095	8.07	5.23	2.52	2.52	4.42	3.20	7.80	4.87	5.18	3.42	4.42	4.87	0.00	2.25	4.55	3.83	7.80	4.78
121	150	140	6278	12.42	7.33	4.06	4.86	3.66	2.23	8.52	2.47	8.44	5.73	3.66	2.47	1.27	1.27	2.47	2.31	8.52	4.54
85	111	105	6798	13.05	8.38	3.75	4.12	4.19	1.99	8.02	1.62	10.15	6.62	4.19	1.62	0.97	1.00	3.02	1.99	8.02	5.66
700	1040	885	22880	9.05	5.59	2.49	2.10	2.67	4.46	9.48	6.53	4.00	3.15	2.67	6.53	1.73	2.01	2.97	2.34	9.48	3.89
605	1060	960	26770	7.43	4.89	2.22	2.19	3.03	2.28	8.11	4.82	6.50	4.86	3.03	4.82	1.48	2.15	4.45	5.60	8.11	5.34
210	205	245	8286	12.19	7.72	3.62	3.96	3.02	3.02	7.72	3.50	6.09	3.68	3.02	3.50	1.57	2.63	3.26	3.50	7.72	4.59
55	90	95	6580	14.44	8.66	4.03	4.03	3.95	1.90	7.90	2.36	10.11	6.23	3.95	2.36	0.91	0.99	2.51	2.58	7.90	5.32
60	115	112	6523	15.02	9.27	3.91	4.22	3.53	1.76	8.36	2.61	8.43	5.21	3.53	2.61	0.81	1.04	2.48	2.76	8.36	5.44
790	1220	1130	27185	6.84	4.41	2.00	2.26	2.83	3.16	7.98	4.95	5.11	4.51	2.83	4.95	1.77	2.80	4.34	5.22	7.98	5.09
320	710	615	23230	9.30	5.51	2.56	2.67	3.64	1.87	7.92	4.95	7.92	5.66	3.64	4.95	1.81	1.59	3.57	4.52	7.92	5.47
415	885	770	26310	8.25	4.88	2.36	2.34	3.23	2.00	7.96	4.75	6.84	5.25	3.23	4.75	1.16	1.86	3.67	4.56	7.96	5.45
260	370	385	9465	9.19	5.71	2.32	3.01	2.48	2.01	8.87	3.91	5.28	3.65	2.48	3.91	1.48	1.90	3.80	5.49	8.87	5.76
410	205	240	8732	10.94	6.76	3.11	3.49	3.44	1.72	9.10	2.18	5.44	3.55	3.44	2.18	1.66	2.98	3.38	2.18	9.10	5.55
140	280	260	8559	11.10	7.24	3.04	3.39	2.80	2.28	7.19	3.33	6.78	4.56	2.80	3.33	1.45	1.64	4.73	4.38	7.19	6.19
52	90	100	6537	14.38	9.03	4.13	4.41	4.16	1.84	7.95	1.91	10.10	6.35	4.16	1.91	0.66	0.76	2.60	2.26	7.95	5.31
620	1140	950	24545	7.46	4.56	2.61	2.10	2.91	3.32	8.84	4.97	5.93	4.91	2.91	4.97	1.24	2.04	3.42	4.01	8.84	5.54
475	630	540	12640	6.61	4.55	1.94	2.10	5.58	2.57	6.84	5.93	3.28	2.22	5.58	5.93	2.97	2.77	4.39	4.43	6.84	3.88
100	140	125	6350	11.26	7.32	3.46	4.96	3.54	2.52	7.80	2.76	7.40	6.38	3.54	2.76	1.42	1.18	3.46	2.44	7.80	5.98
98	241	168	10342	12.35	9.36	2.86	3.31	3.57	2.63	8.49	4.26	7.17	4.94	3.57	4.26	1.14	1.16	2.24	3.45	8.49	5.24
122	305	215	11053	11.11	7.40	2.71	3.60	3.63	2.67	9.17	4.12	7.04	5.31	3.63	4.12	1.00	1.21	2.11	2.90	9.17	6.47
175	328	317	9918	9.81	6.52	2.91	3.63	3.21	3.22	8.32	2.22	6.37	4.79	3.21	3.22	1.38	1.50	3.76	4.41	8.32	6.06
173	378	339	10673	9.82	7.09	2.86	2.66	2.74	2.03	9.17	3.16	6.31	5.12	2.74	3.16	1.33	1.57	4.25	4.32	9.17	5.95
78	168	161	7345	13.32	9.00	3.05	3.42	3.12	2.25	9.31	3.46	6.73	4.67	3.12	3.46	1.08	1.25	3.04	3.27	9.31	5.31
256	356	358	10582	8.11	5.68	2.64	2.99	2.86	2.36	8.48	3.96	5.12	4.11	2.86	3.96	1.85	2.85	4.73	4.94	8.48	5.41
145	329	289	9764	10.37	7.35	3.20	2.92	2.89	2.07	8.54	3.30	6.44	5.82	2.89	3.30	1.36	1.36	3.92	3.91	8.54	5.63
273	478	456	12176	8.34	5.15	2.18	2.22	2.66	2.69	8.17	3.30	5.96	4.38	2.66	3.30	1.96	2.28	5.35	5.41	8.17	5.81
314	498	515	11041	6.77	4.82	2.30	2.52	2.83	2.59	9.09	3.32	5.20	3.41	2.83	3.32	1.61	2.66	4.51	5.24	9.09	6.29
231	223	193	7870	12.30	8.13	3.15	3.70	2.82	2.76	7.60	3.18	6.06	4.82	2.82	3.18	1.31	1.65	3.52	3.46	7.60	5.24

Table F.06: Peak heights of steranes for all hydrocarbon samples (page 2 of 8) and annotation description.

									m/z217	STERANE PEAK HEI										
29abS	29abR	29aaS	29aaR	29bbR	29bbS	TIC	217	%	% of TIC	code:	27baS	27baR	27abS	27abR	27aaS	27aaR	27bbR	27bbS	28baS	28baR
1.68	5.99	1.84	1.49	2.83	2.50	not given	14140	100	0.0000	1	0.00	0.00	0.00	0.00	0.00	0.00	0.00	0.00	0.00	0.00
1.59	5.49	1.52	1.37	2.43	2.06	not given	17792	100	0.0000	2	0.00	0.00	0.00	0.00	0.00	0.00	0.00	0.00	0.00	0.00
2.27	4.71	1.94	1.39	3.20	2.82	50525576	139386	91	0.2510	3	1.98	1.31	0.60	0.96	1.08	0.74	1.82	0.71	1.86	1.92
2.16	3.62	1.41	1.30	2.49	2.11	15240681	18944	92	0.1144	4	1.24	0.83	0.42	0.42	0.43	0.28	0.80	0.54	0.81	0.59
1.78	3.15	1.19	2.32	2.91	2.32	15674129	38912	94	0.2334	5	2.91	1.82	0.96	1.42	0.89	0.60	1.69	0.62	1.72	1.08
2.42	4.41	2.42	2.35	3.99	2.99	11395480	10688	100	0.0938	6	1.01	0.77	0.35	0.00	0.38	0.18	0.77	0.00	0.77	0.61
1.44	4.32	3.06	2.53	5.20	3.06	12127489	12608	85	0.0884	7	0.84	0.50	0.27	0.32	0.39	0.32	0.62	0.36	0.41	0.32
3.01	3.01	1.84	1.21	2.40	2.35	23964526	96256	100	0.4017	8	5.55	3.25	1.48	1.59	1.24	0.77	3.75	0.86	3.01	1.92
1.06	4.59	2.68	2.02	3.18	3.03	41919776	16128	88	0.0339	9	0.33	0.23	0.09	0.09	0.13	0.08	0.26	0.13	0.19	0.16
1.04	4.55	2.79	2.16	4.24	5.50	21878084	46336	75	0.1588	10	1.28	0.83	0.40	0.40	0.70	0.51	1.24	0.77	0.82	0.54
2.63	2.47	2.10	1.93	2.39	2.23	57270776	123904	80	0.1731	11	2.15	1.27	0.70	0.84	0.63	0.39	1.47	0.43	1.46	0.99
2.72	3.02	1.49	1.25	1.63	1.54	4489776	39936	100	0.8895	12	11.61	7.46	3.34	3.66	3.73	1.77	7.13	1.44	9.03	5.89
1.66	2.97	2.75	3.06	4.55	3.87	2797560	3280	100	0.1172	13	1.06	0.66	0.29	0.25	0.31	0.52	1.11	0.77	0.47	0.37
2.39	4.45	2.07	2.26	3.96	3.59	1650680	19584	100	1.1864	14	8.82	5.81	2.64	2.59	3.59	2.70	9.62	5.72	7.71	5.76
1.81	3.26	2.66	2.53	2.47	2.96	14397592	3248	75	0.0169	15	0.21	0.13	0.06	0.07	0.05	0.05	0.13	0.06	0.10	0.06
2.28	2.51	1.44	0.84	1.37	1.44	39775156	162816	100	0.4093	16	5.91	3.55	1.65	1.65	1.62	0.78	3.23	0.96	4.14	2.55
2.22	2.48	1.55	0.92	1.76	1.72	41658924	164864	100	0.3957	17	5.95	3.67	1.55	1.67	1.40	0.70	3.31	1.03	3.34	2.06
2.13	4.34	2.92	2.91	4.49	4.16	2060280	53376	100	2.5907	18	17.73	11.44	5.19	5.86	7.34	8.20	20.68	12.82	13.25	11.67
2.37	3.57	1.51	1.38	3.06	2.65	3481590	15744	100	0.4522	19	4.20	2.49	1.16	1.21	1.64	0.85	3.58	2.24	3.58	2.56
6.21	3.67	1.75	1.58	3.36	2.93	1816570	35520	100	1.9553	20	16.13	9.55	4.61	4.57	6.32	3.90	15.57	9.29	13.38	10.26
2.11	3.80	3.22	2.75	3.91	4.07	46799776	122880	100	0.2626	21	2.41	1.50	0.61	0.79	0.65	0.53	2.33	1.03	1.39	0.96
2.52	3.38	4.12	4.70	2.35	2.75	4385538	55296	100	1.2609	22	13.79	8.52	3.93	4.40	4.33	2.17	11.48	2.74	6.86	4.48
1.40	4.73	2.51	1.64	3.27	3.04	48692176	55040	90	0.1017	23	1.13	0.74	0.31	0.34	0.29	0.23	0.73	0.34	0.69	0.46
2.48	2.60	1.35	0.80	1.38	1.53	21499806	120832	100	0.5620	24	8.08	5.07	2.32	2.48	2.34	1.03	4.47	1.07	5.67	3.57
2.38	3.42	2.57	2.53	4.64	3.87	2564090	39040	100	1.5226	25	11.35	6.95	3.97	3.19	4.44	5.06	13.46	7.57	9.03	7.47
1.50	4.39	2.69	3.76	4.98	4.27	15264194	21504	90	0.1268	26	0.84	0.58	0.25	0.27	0.71	0.33	0.87	0.75	0.42	0.28
2.83	3.46	1.97	1.57	2.20	1.97	15091152	28928	88	0.1687	27	1.90	1.24	0.58	0.84	0.60	0.43	1.31	0.46	1.25	1.08
3.07	2.24	1.28	0.95	2.33	1.62	not given	3.00E+07	100	0.0000	28	0.00	0.00	0.00	0.00	0.00	0.00	0.00	0.00	0.00	0.00
3.40	2.11	1.30	1.10	2.76	1.95	not given	3.60E+06	100	0.0000	29	0.00	0.00	0.00	0.00	0.00	0.00	0.00	0.00	0.00	0.00
2.53	3.76	2.59	1.76	3.31	3.20	53232480	99328	100	0.1866	30	1.83	1.22	0.54	0.68	0.60	0.60	1.55	0.41	1.19	0.89
1.71	4.25	2.25	1.62	3.54	3.18	43072448	25088	94	1.0000	31	9.82	7.09	2.86	2.66	2.74	2.03	9.17	3.16	6.31	5.12
1.63	3.04	1.65	1.06	2.29	2.19	49652964	19968	96	0.0386	32	0.51	0.35	0.12	0.13	0.12	0.09	0.36	0.13	0.26	0.18
1.72	4.73	3.00	2.42	3.36	3.38	34718336	14080	100	2.0000	33	16.22	11.36	5.27	5.97	5.73	4.73	16.95	7.92	10.24	8.22
2.35	3.92	2.10	1.49	3.37	2.96	25321986	7104	90	0.0252	34	0.26	0.19	0.08	0.07	0.07	0.05	0.22	0.08	0.16	0.15
1.77	5.35	2.94	2.24	3.93	3.75	57018460	30208	95	3.0000	35	25.03	15.45	6.53	6.65	7.98	8.08	24.52	9.90	17.89	13.13
2.08	4.51	2.99	2.84	4.51	4.66	5312698	14080	91	0.2412	36	1.63	1.16	0.55	0.61	0.68	0.62	2.19	0.80	1.25	0.82
2.58	3.52	2.40	2.94	2.83	2.45	13118981	3184	90	4.0000	37	49.20	32.53	12.60	14.79	11.28	11.03	30.39	12.71	24.24	19.26

Table F.06: Peak heights of steranes for all hydrocarbon samples (page 3 of 8).

HTS (from m/z 217 fragmentogram) (ppm of TIC)														ppm
28abS	28abR	28aaS	28aaR	28bbR	28bbS	29baS	29baR	29abS	29abR	29aaS	29aaR	29bbR	29bbS	total
OIL SAMPLES														
0.00	0.00	0.00	0.00	0.00	0.00	0.00	0.00	0.00	0.00	0.00	0.00	0.00	0.00	0.00
0.00	0.00	0.00	0.00	0.00	0.00	0.00	0.00	0.00	0.00	0.00	0.00	0.00	0.00	0.00
1.08	0.71	0.26	0.40	1.18	0.85	1.82	1.73	0.57	1.18	0.49	0.35	0.80	0.71	25.10
0.43	0.54	0.17	0.11	0.41	0.41	0.80	0.70	0.25	0.41	0.16	0.15	0.28	0.24	11.44
0.89	0.62	0.29	0.26	0.74	0.46	1.69	1.48	0.42	0.74	0.28	0.54	0.68	0.54	23.34
0.38	0.00	0.22	0.20	0.41	0.00	0.77	0.80	0.23	0.41	0.23	0.22	0.37	0.28	9.38
0.39	0.36	0.15	0.18	0.38	0.28	0.62	0.41	0.13	0.38	0.27	0.22	0.46	0.27	8.84
1.24	0.86	0.32	0.28	1.21	1.06	3.75	2.48	1.21	1.21	0.74	0.48	0.96	0.94	40.17
0.13	0.13	0.05	0.07	0.16	0.15	0.26	0.21	0.04	0.16	0.09	0.07	0.11	0.10	3.39
0.70	0.77	0.00	0.36	0.72	0.61	1.24	0.76	0.16	0.72	0.44	0.34	0.67	0.87	15.88
0.63	0.43	0.22	0.22	0.43	0.40	1.47	0.79	0.45	0.43	0.36	0.33	0.41	0.39	17.31
3.73	1.44	0.86	0.89	2.68	1.77	7.13	5.04	2.42	2.68	1.32	1.11	1.45	1.37	88.95
0.31	0.77	0.20	0.24	0.35	0.27	1.11	0.46	0.19	0.35	0.32	0.36	0.53	0.45	11.72
3.59	5.72	1.75	2.55	5.27	6.65	9.62	6.34	2.84	5.27	2.46	2.68	4.70	4.25	118.64
0.05	0.06	0.03	0.04	0.06	0.06	0.13	0.08	0.03	0.06	0.04	0.04	0.04	0.05	1.69
1.62	0.96	0.37	0.40	1.03	1.06	3.23	2.18	0.93	1.03	0.59	0.34	0.56	0.59	40.93
1.40	1.03	0.32	0.41	0.98	1.09	3.31	2.15	0.88	0.98	0.61	0.36	0.70	0.68	39.57
7.34	12.82	4.57	7.24	11.25	13.53	20.68	13.20	5.53	11.25	7.58	7.53	11.63	10.77	259.07
1.64	2.24	0.82	0.72	1.62	2.04	3.58	2.47	1.07	1.62	0.68	0.62	1.38	1.20	45.22
6.32	9.29	2.27	3.64	7.17	8.92	15.57	10.66	12.15	7.17	3.42	3.08	6.58	5.72	195.53
0.65	1.03	0.39	0.50	1.00	1.44	2.33	1.51	0.55	1.00	0.85	0.72	1.03	1.07	26.26
4.33	2.74	2.09	3.75	4.26	2.74	11.48	7.00	3.18	4.26	5.20	5.92	2.96	3.47	126.09
0.29	0.34	0.15	0.17	0.48	0.45	0.73	0.63	0.14	0.48	0.26	0.17	0.33	0.31	10.17
2.34	1.07	0.37	0.43	1.46	1.27	4.47	2.98	1.39	1.46	0.76	0.45	0.77	0.86	56.20
4.44	7.57	1.89	3.10	5.21	6.11	13.46	8.44	3.63	5.21	3.91	3.85	7.07	5.89	152.26
0.71	0.75	0.38	0.35	0.56	0.56	0.87	0.49	0.19	0.56	0.34	0.48	0.63	0.54	12.68
0.60	0.46	0.24	0.20	0.58	0.41	1.31	1.01	0.48	0.58	0.33	0.27	0.37	0.33	16.87
0.00	0.00	0.00	0.00	0.00	0.00	0.00	0.00	0.00	0.00	0.00	0.00	0.00	0.00	0.00
0.00	0.00	0.00	0.00	0.00	0.00	0.00	0.00	0.00	0.00	0.00	0.00	0.00	0.00	0.00
0.60	0.60	0.26	0.28	0.70	0.82	1.55	1.13	0.47	0.70	0.48	0.33	0.62	0.60	18.66
2.74	3.16	1.33	1.57	4.25	4.32	9.17	5.95	1.71	4.25	2.25	1.62	3.54	3.18	100.00
0.12	0.13	0.04	0.05	0.12	0.13	0.36	0.20	0.06	0.12	0.06	0.04	0.09	0.00	3.78
5.73	7.92	3.70	5.71	9.45	9.88	16.95	10.83	3.44	9.45	5.99	4.84	6.73	0.00	193.23
0.07	0.08	0.03	0.03	0.10	0.10	0.22	0.14	0.06	0.10	0.05	0.04	0.09	0.07	2.52
7.98	9.90	5.89	6.85	16.06	16.24	24.52	17.44	5.32	16.06	8.82	6.73	11.78	11.24	300.00
0.68	0.80	0.39	0.64	1.09	1.26	2.19	1.52	0.50	1.09	0.72	0.69	1.09	0.00	22.99
11.28	12.71	5.24	6.61	14.08	13.82	30.39	20.94	10.32	14.08	9.61	11.74	11.33	0.00	390.19

Table F.06: Peak heights of steranes for all hydrocarbon samples (page 4 of 8).

code:	27baS	27baR	27abS	27abR	27aaS	27aaR	27bbR	27bbS	28baS	28baR	28abS	28abR	28aaS	28aaR	28bbR	28bbS	29baS	29baR	29abS	29abR	29aaS
38	996	698	228	327	255	261	880	306	665	537	255	306	97	138	268	368	880	531	227	268	208
SHALE SAMPLES																					
41	1085	800	370	400	420	260	845	340	610	475	420	340	0	165	610	340	845	640	260	610	260
42	1050	730	390	770	385	280	800	365	750	600	385	365	105	185	750	380	800	720	248	750	272
43	960	530	305	315	315	245	775	280	415	312	315	280	0	120	445	255	775	500	225	445	275
44	1060	670	320	328	630	400	780	600	885	550	630	600	375	385	670	510	780	690	235	670	315
45	715	470	290	265	238	245	818	330	330	305	238	330	130	200	290	260	818	565	237	290	292
46	1690	1100	530	560	525	570	2170	1010	990	750	525	1010	215	405	680	850	2170	1295	505	680	580
47	1055	630	305	355	405	290	740	270	565	405	405	270	160	110	620	280	740	495	100	620	180
48	1039	741	338	400	369	221	691	270	646	462	369	270	164	151	289	398	691	601	189	398	163
49	630	550	300	225	360	1025	530	135	470	425	360	135	125	920	420	230	530	440	230	420	210
50	965	575	280	330	750	280	735	250	575	375	750	250	310	865	600	300	735	500	160	600	585
51	1600	1060	545	515	770	970	2170	1340	1365	1160	770	1340	590	1005	1220	1240	2170	1480	630	1220	960
52	1050	695	340	350	650	275	715	160	685	485	650	160	195	855	535	160	715	540	175	535	465
53	975	611	305	310	265	150	650	165	590	395	265	165	60	60	215	160	650	410	205	215	111
54	900	570	310	280	210	140	695	165	465	310	210	165	75	62	220	115	695	430	200	220	130
55	955	635	320	360	765	325	865	335	775	540	765	335	420	900	540	470	865	515	280	540	655
56	2150	1245	600	640	930	540	2060	1180	1830	1460	930	1180	230	305	850	1080	2060	1530	685	850	340
57	1032	635	308	308	338	232	603	200	824	503	338	200	50	80	371	242	603	417	172	371	123
58	910	580	290	355	365	270	700	235	855	580	365	235	100	91	320	260	700	500	245	320	162
59	1840	1150	545	580	795	925	2170	1360	1255	1120	795	1360	535	770	1180	1365	1270	1510	660	1180	830
60	1810	1180	580	575	775	600	2170	1305	1570	1220	775	1305	335	500	1070	1260	2170	1450	615	1070	615
61	995	630	290	405	390	210	745	210	840	625	390	210	77	100	300	280	745	510	250	300	170
62	980	615	280	310	230	140	650	190	530	340	230	190	61	65	220	195	650	400	192	220	145
63	900	590	290	305	240	140	595	125	540	365	240	125	45	45	225	125	595	395	215	225	115
64	970	620	275	330	510	210	950	340	555	485	510	340	210	345	350	350	950	515	245	350	455
65	930	620	310	355	545	275	960	385	695	420	545	385	260	455	475	465	960	565	285	475	540
66	705	450	255	280	330	170	740	330	400	280	330	330	80	155	225	265	740	400	195	225	285
67	989	636	435	295	331	135	611	103	770	496	331	103	22	32	193	67	611	385	201	193	74
68	960	615	315	345	295	190	825	265	560	410	295	265	112	180	308	305	825	500	280	308	305
69	815	520	245	310	720	270	785	270	680	468	720	270	402	910	492	378	785	475	255	492	605
70	1038	752	273	265	271	175	787	190	591	428	271	190	73	78	228	249	787	552	253	228	138
No.	a	b	c	d	g+	j	h+	i+	e	f	g+	i+	m	p	n+	o	h+	k	l	n+	q
code= carbon number, C-13,17 (H) or C-14,17 (H) isomer, stereoisomerism at C-20 (S or R).																					
ba=13b(H), 17a(H). ab=13a(H), 17b(H). aa=14a(H), 17a(H). bb=14b(H), 17b(H).																					
Peak 'l' for sample 5: peak overlapped or obscured. '+' means peak represents 2 compounds.																					

Table F.06: Peak heights of steranes for all source rock samples (including annotation descriptions) (page 5 of 8).

29aaR	29bbR	29bbS	height	27baS	27baR	27abS	27abR	27aaS	27aaR	27bbR	27bbS	28baS	28baR	28abS	28abR	28aaS	28aaR	28bbR	28bbS	29baS	29baR
152	298	258	9407	10.59	7.42	2.42	3.48	2.71	2.77	9.35	3.25	7.07	5.71	2.71	3.25	1.03	1.47	2.85	3.91	9.35	5.64
190	420	390	11095	9.78	7.21	3.33	3.61	3.79	2.34	7.62	3.06	5.50	4.28	3.79	3.06	0.00	1.49	5.50	3.06	7.62	5.77
185	465	385	12115	8.67	6.03	3.22	6.36	3.18	2.31	6.60	3.01	6.19	4.95	3.18	3.01	0.87	1.53	6.19	3.14	6.60	5.94
185	335	395	9002	10.66	5.89	3.39	3.50	3.50	2.72	8.61	3.11	4.61	3.47	3.50	3.11	0.00	1.33	4.94	2.83	8.61	5.55
465	525	385	13458	7.88	4.98	2.38	2.44	4.68	2.97	5.80	4.46	6.58	4.09	4.68	4.46	2.79	2.86	4.98	3.79	5.80	5.13
291	298	350	8595	8.32	5.47	3.37	3.08	2.77	2.85	9.52	3.84	3.84	3.55	2.77	3.84	1.51	2.33	3.37	3.03	9.52	6.57
580	1060	960	21410	7.89	5.14	2.48	2.62	2.45	2.66	10.14	4.72	4.62	3.50	2.45	4.72	1.00	1.89	3.18	3.97	10.14	6.05
165	335	295	9795	10.77	6.43	3.11	3.62	4.13	2.96	7.55	2.76	5.77	4.13	4.13	2.76	1.63	1.12	6.33	2.86	7.55	5.05
202	385	342	9789	10.61	7.57	3.45	4.09	3.77	2.26	7.06	2.76	6.60	4.72	3.77	2.76	1.68	1.54	2.95	4.07	7.06	6.14
905	230	350	10155	6.20	5.42	2.95	2.22	3.55	10.09	5.22	1.33	4.63	4.19	3.55	1.33	1.23	9.06	4.14	2.26	5.22	4.33
695	305	345	12115	7.97	4.75	2.31	2.72	6.19	2.31	6.07	2.06	4.75	3.10	6.19	2.06	2.56	7.14	4.95	2.48	6.07	4.13
1020	1195	1055	27390	5.84	3.87	1.99	1.88	2.81	3.54	7.92	4.89	4.98	4.24	2.81	4.89	2.15	3.67	4.45	4.53	7.92	5.40
655	255	150	11450	9.17	6.07	2.97	3.06	5.68	2.40	6.24	1.40	5.98	4.24	5.68	1.40	1.70	7.47	4.67	1.40	6.24	4.72
68	140	140	7280	13.39	8.39	4.19	4.26	3.64	2.06	8.93	2.27	8.10	5.43	3.64	2.27	0.82	0.82	2.95	2.20	8.93	5.63
105	140	155	6967	12.92	8.18	4.45	4.02	3.01	2.01	9.98	2.37	6.67	4.45	3.01	2.37	1.08	0.89	3.16	1.65	9.98	6.17
730	295	355	13540	7.05	4.69	2.36	2.66	5.65	2.40	6.39	2.47	5.72	3.99	5.65	2.47	3.10	6.65	3.99	3.47	6.39	3.80
320	800	640	24435	8.80	5.10	2.46	2.62	3.81	2.21	8.43	4.83	7.49	5.98	3.81	4.83	0.94	1.25	3.48	4.42	8.43	6.26
83	225	221	8479	12.17	7.49	3.63	3.63	3.99	2.74	7.11	2.36	9.72	5.93	3.99	2.36	0.59	0.94	4.38	2.85	7.11	4.92
105	225	220	8988	10.12	6.45	3.23	3.95	4.06	3.00	7.79	2.61	9.51	6.45	4.06	2.61	1.11	1.01	3.56	2.89	7.79	5.56
920	1375	1320	26810	6.86	4.29	2.03	2.16	2.97	3.45	8.09	5.07	4.68	4.18	2.97	5.07	2.00	2.87	4.40	5.09	4.74	5.63
555	1190	1055	25750	7.03	4.58	2.25	2.23	3.01	2.33	8.43	5.07	6.10	4.74	3.01	5.07	1.30	1.94	4.16	4.89	8.43	5.63
105	200	205	9182	10.84	6.86	3.16	4.41	4.25	2.29	8.11	2.29	9.15	6.81	4.25	2.29	0.84	1.09	3.27	3.05	8.11	5.55
97	171	176	7277	13.47	8.45	3.85	4.26	3.16	1.92	8.93	2.61	7.28	4.67	3.16	2.61	0.84	0.89	3.02	2.68	8.93	5.50
70	120	115	6745	13.34	8.75	4.30	4.52	3.56	2.08	8.82	1.85	8.01	5.41	3.56	1.85	0.67	0.67	3.34	1.85	8.82	5.86
435	310	360	10970	8.84	5.65	2.51	3.01	4.65	1.91	8.66	3.10	5.06	4.42	4.65	3.10	1.91	3.14	3.19	3.19	8.66	4.69
505	362	425	12197	7.62	5.08	2.54	2.91	4.47	2.25	7.87	3.16	5.70	3.44	4.47	3.16	2.13	3.73	3.89	3.81	7.87	4.63
280	300	330	8080	8.73	5.57	3.16	3.47	4.08	2.10	9.16	4.08	4.95	3.47	4.08	4.08	0.99	1.92	2.78	3.28	9.16	4.95
50	665	66	7794	12.69	8.16	5.58	3.78	4.25	1.73	7.84	1.32	9.88	6.36	4.25	1.32	0.28	0.41	2.48	0.86	7.84	4.94
215	260	300	9238	10.39	6.66	3.41	3.73	3.19	2.06	8.93	2.87	6.06	4.44	3.19	2.87	1.21	1.95	3.33	3.30	8.93	5.41
831	328	391	12417	6.56	4.19	1.97	2.50	5.80	2.17	6.32	2.17	5.48	3.77	5.80	2.17	3.24	7.33	3.96	3.04	6.32	3.83
89	196	167	8269	12.55	9.09	3.30	3.20	3.28	2.12	9.52	2.30	7.15	5.18	3.28	2.30	0.88	0.94	2.76	3.01	9.52	6.68
t	r	s																			

Table F.06: Peak heights of steranes for all source rock samples (page 6 of 8).

29abS	29abR	29aaS	29aaR	29bbR	29bbS	TIC	217	%	% of TIC	code:	27baS	27baR	27abS	27abR	27aaS	27aaR	27bbR	27bbS	28baS	28baR
2.41	2.85	2.21	1.62	3.17	2.74	5130069	8064	92	0.1446	38	1.53	1.07	0.35	0.50	0.39	0.40	1.35	0.47	1.02	0.83
									0.0000											
2.34	5.50	2.34	1.71	3.79	3.52	2996810	22784	90	0.6842	31	6.69	4.93	2.28	2.47	2.59	1.60	5.21	2.10	3.76	2.93
2.05	6.19	2.25	1.53	3.84	3.18	38066756	80896	92	0.1955	32	1.69	1.18	0.63	1.24	0.62	0.45	1.29	0.59	1.21	0.97
2.50	4.94	3.05	2.06	3.72	4.39	2973593	14016	91	0.4289	33	4.57	2.53	1.45	1.50	1.50	1.17	3.69	1.33	1.98	1.49
1.75	4.98	2.34	3.46	3.90	2.86	1842646	8000	92	0.3994	34	3.15	1.99	0.95	0.97	1.87	1.19	2.31	1.78	2.63	1.63
2.76	3.37	3.40	3.39	3.47	4.07	8145098	6592	80	0.0647	35	0.54	0.35	0.22	0.20	0.18	0.18	0.62	0.25	0.25	0.23
2.36	3.18	2.71	2.71	4.95	4.48	1466360	96512	100	6.5817	36	51.95	33.82	16.29	17.22	16.14	17.52	66.71	31.05	30.43	23.06
1.02	6.33	1.84	1.68	3.42	3.01	4217116	10368	92	0.2262	37	2.44	1.45	0.70	0.82	0.94	0.67	1.71	0.62	1.30	0.94
1.93	4.07	1.67	2.06	3.93	3.49	3750200	7552	92	0.1853	38	1.97	1.40	0.64	0.76	0.70	0.42	1.31	0.51	1.22	0.87
2.26	4.14	2.07	8.91	2.26	3.45	12661814	651264	100	5.1435	39	31.91	27.86	15.20	11.40	18.23	51.92	26.84	6.84	23.81	21.53
1.32	4.95	4.83	5.74	2.52	2.85	16039989	220160	100	1.3726	40	10.93	6.51	3.17	3.74	8.50	3.17	8.33	2.83	6.51	4.25
2.30	4.45	3.50	3.72	4.36	3.85	1478650	87680	100	5.9297	41	34.64	22.95	11.80	11.15	16.67	21.00	46.98	29.01	29.55	25.11
1.53	4.67	4.06	5.72	2.23	1.31	5310662	114688	100	2.1596	42	19.80	13.11	6.41	6.60	12.26	5.19	13.49	3.02	12.92	9.15
2.82	2.95	1.52	0.93	1.92	1.92	24497028	246784	100	1.0074	43	13.49	8.45	4.22	4.29	3.67	2.08	8.99	2.28	8.16	5.47
2.87	3.16	1.87	1.51	2.01	2.22	20598612	131072	100	0.6363	44	8.22	5.21	2.83	2.56	1.92	1.28	6.35	1.51	4.25	2.83
2.07	3.99	4.84	5.39	2.18	2.62	20740248	442368	100	2.1329	45	15.04	10.00	5.04	5.67	12.05	5.12	13.63	5.28	12.21	8.51
2.80	3.48	1.39	1.31	3.27	2.62	2625530	37952	100	1.4455	46	12.72	7.37	3.55	3.79	5.50	3.19	12.19	6.98	10.83	8.64
2.03	4.38	1.45	0.98	2.65	2.61	27429660	38400	92	0.1288	47	1.57	0.96	0.47	0.47	0.51	0.35	0.92	0.30	1.25	0.76
2.73	3.56	1.80	1.17	2.50	2.45	13790277	74752	100	0.5421	48	5.49	3.50	1.75	2.14	2.20	1.63	4.22	1.42	5.16	3.50
2.46	4.40	3.10	3.43	5.13	4.92	4440060	226048	100	5.0911	49	34.94	21.84	10.35	11.01	15.10	17.57	41.21	25.83	23.83	21.27
2.39	4.16	2.39	2.16	4.62	4.10	2494460	48576	100	1.9474	50	13.69	8.92	4.39	4.35	5.86	4.54	16.41	9.87	11.87	9.23
2.72	3.27	1.85	1.14	2.18	2.23	43736320	286720	94	0.6162	51	6.68	4.23	1.95	2.72	2.62	1.41	5.00	1.41	5.64	4.19
2.64	3.02	1.99	1.33	2.35	2.42	34008720	294912	100	0.8672	52	11.68	7.33	3.34	3.69	2.74	1.67	7.75	2.26	6.32	4.05
3.19	3.34	1.70	1.04	1.78	1.70	5070991	14336	100	0.2827	53	3.77	2.47	1.22	1.28	1.01	0.59	2.49	0.52	2.26	1.53
2.23	3.19	4.15	3.97	2.83	3.28	7804665	106496	100	1.3645	54	12.07	7.71	3.42	4.10	6.34	2.61	11.82	4.23	6.90	6.03
2.34	3.89	4.43	4.14	2.97	3.48	14089057	331776	100	2.3548	55	17.96	11.97	5.99	6.85	10.52	5.31	18.53	7.43	13.42	8.11
2.41	2.78	3.53	3.47	3.71	4.08	22950544	54528	80	0.1901	56	1.66	1.06	0.60	0.66	0.78	0.40	1.74	0.78	0.94	0.66
2.58	2.48	0.95	0.64	8.53	0.85	2403406	9088	95	0.3592	57	4.56	2.93	2.00	1.36	1.53	0.62	2.82	0.47	3.55	2.29
3.03	3.33	3.30	2.33	2.81	3.25	29405236	507904	100	1.7273	58	17.95	11.50	5.89	6.45	5.52	3.55	15.43	4.95	10.47	7.67
2.05	3.96	4.87	6.69	2.64	3.15	4685930	111616	100	2.3819	59	15.63	9.98	4.70	5.95	13.81	5.18	15.06	5.18	13.04	8.98
3.06	2.76	1.67	1.08	2.37	2.02	15405633	28160	94	0.1718	60	2.16	1.56	0.57	0.55	0.56	0.36	1.64	0.39	1.23	0.89

Table F.06: Peak heights of steranes for all source rock samples (page 7 of 8).

28abS	28abR	28aaS	28aaR	28bbR	28bbS	29baS	29baR	29abS	29abR	29aaS	29aaR	29bbR	29bbS	total
0.39	0.47	0.15	0.21	0.41	0.57	1.35	0.82	0.35	0.41	0.32	0.23	0.46	0.40	14.46
	SHALE SAMPLES													
2.59	2.10	0.00	1.02	3.76	2.10	5.21	3.95	1.60	3.76	1.60	1.17	2.59	2.41	68.42
0.62	0.59	0.17	0.30	1.21	0.61	1.29	1.16	0.40	1.21	0.44	0.30	0.75	0.62	19.55
1.50	1.33	0.00	0.57	2.12	1.22	3.69	2.38	1.07	2.12	1.31	0.88	1.60	1.88	42.89
1.87	1.78	1.11	1.14	1.99	1.51	2.31	2.05	0.70	1.99	0.93	1.38	1.56	1.14	39.94
0.18	0.25	0.10	0.15	0.22	0.20	0.62	0.43	0.18	0.22	0.22	0.22	0.22	0.26	6.47
16.14	31.05	6.61	12.45	20.90	26.13	66.71	39.81	15.52	20.90	17.83	17.83	32.59	29.51	658.17
0.94	0.62	0.37	0.25	1.43	0.65	1.71	1.14	0.23	1.43	0.42	0.38	0.77	0.68	22.62
0.70	0.51	0.31	0.29	0.55	0.75	1.31	1.14	0.36	0.75	0.31	0.38	0.73	0.65	18.53
18.23	6.84	6.33	46.60	21.27	11.65	26.84	22.29	11.65	21.27	10.64	45.84	11.65	17.73	514.35
8.50	2.83	3.51	9.80	6.80	3.40	8.33	5.66	1.81	6.80	6.63	7.87	3.46	3.91	137.26
16.67	29.01	12.77	21.76	26.41	26.85	46.98	32.04	13.64	26.41	20.78	22.08	25.87	22.84	592.97
12.26	3.02	3.68	16.13	10.09	3.02	13.49	10.18	3.30	10.09	8.77	12.35	4.81	2.83	215.96
3.67	2.28	0.83	0.83	2.98	2.21	8.99	5.67	2.84	2.98	1.54	0.94	1.94	1.94	100.74
1.92	1.51	0.68	0.57	2.01	1.05	6.35	3.93	1.83	2.01	1.19	0.96	1.28	1.42	63.63
12.05	5.28	6.62	14.18	8.51	7.40	13.63	8.11	4.41	8.51	10.32	11.50	4.65	5.59	213.29
5.50	6.98	1.36	1.80	5.03	6.39	12.19	9.05	4.05	5.03	2.01	1.89	4.73	3.79	144.55
0.51	0.30	0.08	0.12	0.56	0.37	0.92	0.63	0.26	0.56	0.19	0.13	0.34	0.34	12.88
2.20	1.42	0.60	0.55	1.93	1.57	4.22	3.02	1.48	1.93	0.98	0.63	1.36	1.33	54.21
15.10	25.83	10.16	14.62	22.41	25.92	24.12	28.67	12.53	22.41	15.76	17.47	26.11	25.07	509.11
5.86	9.87	2.53	3.78	8.09	9.53	16.41	10.97	4.65	8.09	4.65	4.20	9.00	7.98	194.74
2.62	1.41	0.52	0.67	2.01	1.88	5.00	3.42	1.68	2.01	1.14	0.70	1.34	1.38	61.62
2.74	2.26	0.73	0.77	2.62	2.32	7.75	4.77	2.29	2.62	1.73	1.16	2.04	2.10	86.72
1.01	0.52	0.19	0.19	0.94	0.52	2.49	1.66	0.90	0.94	0.48	0.29	0.50	0.48	28.27
6.34	4.23	2.61	4.29	4.35	4.35	11.82	6.41	3.05	4.35	5.66	5.41	3.86	4.48	136.45
10.52	7.43	5.02	8.78	9.17	8.98	18.53	10.91	5.50	9.17	10.43	9.75	6.99	8.21	235.48
0.78	0.78	0.19	0.36	0.53	0.62	1.74	0.94	0.46	0.53	0.67	0.66	0.71	0.78	19.01
1.53	0.47	0.10	0.15	0.89	0.31	2.82	1.77	0.93	0.89	0.34	0.23	3.06	0.30	35.92
5.52	4.95	2.09	3.37	5.76	5.70	15.43	9.35	5.24	5.76	5.70	4.02	4.86	5.61	172.73
13.81	5.18	7.71	17.46	9.44	7.25	15.06	9.11	4.89	9.44	11.61	15.94	6.29	7.50	238.19
0.56	0.39	0.15	0.16	0.47	0.52	1.64	1.15	0.53	0.47	0.29	0.18	0.41	0.35	17.18

Table F.06: Peak heights of steranes for all source rock samples (page 8 of 8).

STERANE PEAK HEIGHT RATIOS m/z 217/218.											bb PEAK HEIGHTS (m/z218)					
No.	27baS+R	27abS+R	27aaR	28baS+R	28aaS+R	28bbS	29baR	29abS	29aaS+R	29bbS+R	27bbR	27bbS	28bbR	28bbS	29bbR	29bbS
OIL SAMPLES																
1	3.40	3.90	1.1	3.40	1.55	0.8	2.6	2.6	2.10	0.65	595	495	745	680	595	555
2	3.25	3.65	1.2	2.75	1.50	0.8	2.1	2.5	1.80	0.80	411	381	740	532	418	358
3	3.55	3.70	1.2	2.85	2.20	0.8	2.4	2.9	1.75	0.90	870	540	820	960	840	735
4	3.60	4.00	1.1	3.30	1.65	0.8	2.4	2.7	2.05	0.75	930	760	950	885	620	615
5	3.45	3.65	1.0	2.85	1.90	0.7	2.2	2.1	1.90	0.80	965	660	960	685	775	790
6	3.85	4.00	1.3	0.00	2.00	0.0	0.0	0.0	0.00	0.00	395	790	445	1015	335	290
7	3.40	2.95	1.4	2.40	1.90	0.8	2.6	1.5	1.90	0.85	982	713	615	600	825	640
8	3.65	3.80	1.1	3.20	2.10	0.9	3.0	3.4	1.60	0.80	870	445	510	590	575	585
9	3.35	3.35	1.0	2.65	1.85	0.8	2.4	1.6	1.70	0.85	950	685	685	780	530	560
10	3.30	3.60	1.1	2.65	1.80	0.7	1.9	1.7	1.70	0.80	942	798	645	720	700	950
11	3.30	3.40	1.3	3.20	1.90	0.9	3.3	3.1	1.70	0.75	760	405	380	415	470	480
12	3.50	3.45	1.2	3.25	1.75	0.8	2.9	2.4	1.60	0.85	740	345	490	520	380	390
13	2.25	2.50	1.6	1.90	1.30	0.5	1.3	1.4	1.55	0.75	2170	2030	1095	1200	1520	1430
14	3.30	3.65	0.9	3.10	1.60	0.9	1.5	2.2	1.80	0.85	2020	1510	2065	2170	1620	1600
15	3.25	2.45	1.1	2.35	2.40	0.9	2.4	2.1	1.40	0.80	715	460	410	500	420	400
16	3.60	4.00	1.0	3.35	1.95	0.8	2.8	2.7	1.75	0.80	895	510	590	670	372	368
17	3.60	4.00	1.0	3.20	1.95	0.8	2.6	2.6	1.70	0.80	950	600	580	680	425	420
18	3.35	3.50	1.5	3.65	1.55	0.8	1.4	2.1	1.65	0.70	2170	1795	1950	2130	2000	1940
19	3.35	3.60	1.3	3.50	1.80	0.9	1.6	2.3	1.60	0.85	2170	1690	1840	1990	1485	1400
20	3.40	3.75	1.2	3.35	1.60	1.0	1.6	2.5	1.70	0.85	2170	1615	1925	1990	1620	1540
21	3.70	4.00	0.9	2.45	2.15	0.9	2.4	2.3	1.70	0.70	925	670	685	885	740	750
22	3.70	3.65	1.1	3.05	2.00	0.8	2.8	2.7	1.95	0.85	915	500	475	505	555	580
23	3.85	3.75	1.1	2.95	1.75	0.9	2.5	2.2	1.75	0.95	815	635	800	840	600	605
24	3.70	3.65	1.1	3.40	1.85	0.9	2.9	3.0	1.75	0.85	810	390	550	575	390	375
25	3.30	3.65	1.3	3.25	1.70	0.9	1.7	2.7	1.70	0.75	2170	1680	1300	1435	1910	1800
26	3.30	3.55	1.0	2.35	1.85	0.7	2.1	1.4	1.80	0.75	930	840	615	660	655	635
27	2.85	3.65	1.1	2.85	1.80	0.9	2.5	2.3	1.90	0.90	640	320	450	435	400	395
28	3.55	3.70	1.5	3.45	1.80	1.1	2.2	2.6	1.80	0.90	584	389	345	411	318	371
29	3.70	4.30	2.4	3.70	2.10	1.3	2.6	3.1	2.00	1.05	1102	696	672	701	704	609
30	3.70	3.80	0.9	3.10	1.85	0.9	2.7	4.4	1.65	0.75	950	629	789	814	707	696
31	3.24	3.12	0.6	2.50	1.58	0.6	2.0	1.8	1.28	0.52	987	628	785	860	713	702
32	3.14	2.71	0.7	2.25	1.35	0.5	2.0	1.6	1.13	0.52	1003	664	606	659	469	480
33	3.27	2.88	0.6	2.27	1.57	0.6	1.9	1.7	1.31	0.53	968	739	779	912	640	660
34	3.47	2.93	0.6	2.63	1.41	0.6	2.1	2.3	1.21	0.56	981	670	829	924	753	786
35	3.01	3.20	0.6	2.18	1.58	0.5	1.8	1.5	1.39	0.53	834	629	922	1000	702	719
36	3.18	3.63	0.7	2.18	1.47	0.6	2.1	1.8	1.31	0.51	868	597	828	964	895	954
37	2.54	21.50	0.8	1.76	1.35	0.7	1.9	2.9	1.80	0.71	946	612	602	738	574	541
38	2.88	2.95	0.9	2.43	1.33	0.6	1.9	2.5	1.45	0.57	978	598	644	824	717	642

Table F.07: Peak heights of ββ steranes (from m/z 218 ion) and m/z 217/218 ratios from all hydrocarbon samples (page 1 of 2).

No.	27baS+R	27abS+R	27aaR	28baS+R	28aaS+R	28bbS	29baR	29abS	29aaS+R	29bbS+R	27bbR	27bbS	28bbR	28bbS	29bbR	29bbS
SHALE SAMPLES																
41	3.75	4.05	1.0	3.50	1.95	0.8	3.0	3.2	1.60	0.75	751	625	763	725	906	938
42	3.65	4.30	1.1	3.30	2.00	0.7	2.8	2.6	1.75	0.85	930	630	990	825	855	780
43	3.75	3.60	1.4	2.95	1.90	0.9	2.9	3.2	2.00	0.85	890	590	600	545	815	855
44	3.70	3.55	1.1	3.35	1.85	0.7	2.2	1.9	2.00	0.80	805	690	1010	840	720	710
45	2.90	2.05	1.0	2.50	1.60	0.7	2.2	1.5	1.90	0.75	850	660	465	540	690	565
46	3.45	3.60	1.6	3.30	1.75	0.9	2.0	2.7	1.70	0.80	2170	1495	1280	1420	2010	1930
47	3.70	3.70	1.1	3.20	1.60	0.7	2.8	2.1	1.65	0.85	745	560	970	735	745	735
48	3.54	3.72	1.6	3.15	1.91	0.8	1.6	1.0	2.22	0.80	969	741	925	744	881	841
49	3.70	3.95	1.3	3.40	2.05	0.8	2.9	2.5	1.90	0.95	565	330	705	590	580	650
50	3.70	4.00	1.2	3.20	2.15	0.8	2.4	1.8	2.00	1.00	870	615	945	765	620	680
51	3.35	3.30	1.6	3.50	1.80	0.9	1.6	2.3	1.80	0.85	2100	1635	2170	2080	1940	1955
52	3.85	4.05	1.2	3.35	2.30	0.9	2.3	2.3	2.15	1.10	645	330	670	390	355	450
53	3.70	4.05	1.1	3.35	2.25	0.8	3.1	3.3	1.80	0.80	925	515	565	595	502	510
54	3.85	3.85	1.2	3.45	2.05	0.7	3.2	2.9	1.70	0.85	855	445	382	410	455	440
55	3.70	3.80	1.0	3.20	2.10	0.7	2.2	1.7	1.85	0.85	990	715	995	995	595	645
56	3.40	3.75	2.6	3.35	1.55	0.9	1.7	2.7	1.60	0.75	2170	1530	1845	2040	1725	1580
57	3.95	4.05	1.2	3.25	1.50	0.7	2.5	2.7	1.60	0.95	930	610	950	980	655	760
58	3.20	3.45	0.9	2.90	1.45	0.6	2.2	2.3	1.55	0.70	930	505	930	825	685	640
59	3.35	3.60	1.4	3.25	1.65	0.8	1.5	2.6	1.70	0.75	2030	1630	1900	2000	2170	2135
60	3.30	3.30	1.1	2.80	1.55	0.8	1.7	2.7	1.90	0.75	2095	1690	2010	2170	2115	2015
61	3.60	3.80	1.0	3.25	1.75	0.7	2.8	2.7	1.70	0.75	990	580	820	875	610	640
62	3.75	3.95	1.1	3.35	2.05	0.8	3.0	2.9	1.75	0.80	950	565	570	650	580	590
63	3.85	3.65	1.2	3.10	2.05	0.9	3.1	3.2	1.85	0.85	820	375	405	430	415	410
64	3.60	3.80	0.9	3.40	1.90	0.8	2.9	2.5	1.75	0.75	980	660	635	660	625	635
65	3.65	3.95	0.9	3.15	2.20	0.7	3.1	2.3	1.80	0.75	980	690	815	885	715	785
66	3.15	3.00	1.1	2.60	1.45	0.7	3.3	2.1	1.75	0.75	835	600	415	510	620	595
67	3.74	3.98	1.4	3.42	1.52	0.6	3.3	3.2	1.66	0.77	789	271	350	378	300	308
68	3.85	4.15	0.9	3.20	1.75	0.7	3.0	3.2	1.95	0.75	940	605	710	755	675	675
69	3.70	4.00	1.0	3.30	2.05	0.7	2.4	1.8	1.85	0.85	965	635	980	940	745	785
70	3.40	3.60	0.9	2.80	1.15	0.8	2.3	2.8	1.55	0.70	971	511	589	624	573	503
Columns headed ..S or ..R are ratios of individual peaks and resultant average is given to 1 decimal place only.																
All other columns are averages using both isomers.																
Data from sample 5: peaks overlapped or obscured.																

Table F.07: Peak heights of ββ steranes (from m/z 218 ion) and m/z 217/218 ratios from all source rock samples (including annotation descriptions) (page 2 of 2).

4-METHYL STERANE PEAK HEIGHTS (MEASURED FROM m/z 231 FRAGMENTOGRAM).																NORMALIZED PEAK HEIGHTS								
	C28				C29				C30							C28				C29				
No.	aaS	bbR	bbS	aaR	aaS	bbR	bbS	aaR	aaS	bbR	bbS	aaR	Height	217 ht	(231/217)%	aaS	bbR	bbS	aaR	aaS	bbR	bbS	aaR	aaS
OIL SAMPLES																								
1																								
2																								
3	170	380	300	160	450	390	430	550	270	280	320	440	4140	126730	16.5	4.11	9.18	7.25	3.86	10.87	9.42	10.39	13.29	6.52
4	140	170	160	135	400	310	270	260	180	300	180	70	2575	36577	11.1	5.44	6.60	6.21	5.24	15.53	12.04	10.49	10.10	6.99
5	395	360	325	495	490	325	320	140	680	420	330	270	4550	17428	13.0	8.68	7.91	7.14	10.88	10.77	7.14	7.03	3.08	14.95
6	0	0	0	0	0	0	0	0	0	0	0	0	0			0.00	0.00	0.00	0.00	0.00	0.00	0.00	0.00	0.00
7	320	180	320	320	250	470	540	430	460	570	540	360	4760	10597	20.9	6.72	3.78	6.72	6.72	5.25	9.87	11.34	9.03	9.66
8	305	305	285	105	280	290	360	220	240	310	320	160	3180	96256	8.6	9.59	9.59	8.96	3.30	8.81	9.12	11.32	6.92	7.55
9	250	240	280	190	190	470	480	90	190	200	100	140	2820	16128	13.5	8.87	8.51	9.93	6.74	6.74	16.67	17.02	3.19	6.74
10	270	140	220	630	240	440	540	270	390	360	470	270	4240	34752	27.3	6.37	3.30	5.19	14.86	5.66	10.38	12.74	6.37	9.20
11	74	60	105	70	110	85	130	90	70	80	115	90	1079	99123	37.3	6.86	5.56	9.73	6.49	10.19	7.88	12.05	8.34	6.49
12	240	200	170	100	110	250	250	100	100	220	130	100	1970	39936	11.3	12.18	10.15	8.63	5.08	5.58	12.69	12.69	5.08	5.08
13	690	680	700	260	450	560	950	600	350	560	480	430	6710	3280	32.0	10.28	10.13	10.43	3.87	6.71	8.35	14.16	8.94	5.22
14	330	520	390	290	540	640	750	310	290	710	710	280	5760	19584	31.9	5.73	9.03	6.77	5.03	9.38	11.11	13.02	5.38	5.03
15	0	0	0	0	0	0	0	0	0	0	0	0	0	2436	43.1	0.00	0.00	0.00	0.00	0.00	0.00	0.00	0.00	0.00
16	100	120	85	80	130	100	135	55	30	25	20	10	890	162816	18.0	11.24	13.48	9.55	8.99	14.61	11.24	15.17	6.18	3.37
17	270	200	250	230	310	225	260	185	155	150	180	95	2510	164864	7.8	10.76	7.97	9.96	9.16	12.35	8.96	10.36	7.37	6.18
18	950	1750	1310	480	1150	1420	2130	920	1070	2150	1960	1020	16310	53376	11.4	5.82	10.73	8.03	2.94	7.05	8.71	13.06	5.64	6.56
19	910	1290	1060	740	1340	1240	2060	870	840	1570	1400	810	14130	15744	9.1	6.44	9.13	7.50	5.24	9.48	8.78	14.58	6.16	5.94
20	1080	1420	1240	720	1550	1260	2130	900	840	1770	1540	870	15320	35520	9.8	7.05	9.27	8.09	4.70	10.12	8.22	13.90	5.87	5.48
21	340	260	300	280	550	460	590	110	375	510	435	327	4537	122880	13.1	7.49	5.73	6.61	6.17	12.12	10.14	13.00	2.42	8.27
22	60	150	65	850	65	150	145	165	85	130	115	240	2220	55296	43.5	2.70	6.76	2.93	38.29	2.93	6.76	6.53	7.43	3.83
23	270	320	310	300	380	425	465	400	300	180	305	175	3830	49536	13.9	7.05	8.36	8.09	7.83	9.92	11.10	12.14	10.44	7.83
24	220	200	270	180	250	195	280	175	145	175	190	70	2350	120832	8.5	9.36	8.51	11.49	7.66	10.64	8.30	11.91	7.45	6.17
25	1400	1470	1190	410	1080	1310	2170	1220	1070	1940	1870	1010	16140	39080	10.5	8.67	9.11	7.37	2.54	6.69	8.12	13.44	7.56	6.63
26	290	140	330	260	350	570	480	300	260	370	340	410	4100	19784	27.2	7.07	3.41	8.05	6.34	8.54	13.90	11.71	7.32	6.34
27	0	0	0	0	0	0	0	0	0	0	0	0	0	25457	27.0	0.00	0.00	0.00	0.00	0.00	0.00	0.00	0.00	0.00
28	92	100	141	170	68	75	113	112	60	66	65	82	1144	3.00E+07	43.3	8.04	8.74	12.33	14.86	5.94	6.56	9.88	9.79	5.24
29	376	377	180	263	183	228	297	277	169	272	221	272	3115	3.60E+06	19.2	12.07	12.10	5.78	8.44	5.87	7.32	9.53	8.89	5.43
30	348	289	400	337	592	400	572	335	316	335	447	232	4603	99328	11.5	7.56	6.28	8.69	7.32	12.86	8.69	12.43	7.28	6.87
31	445	434	317	353	403	319	489	372	253	332	371	313	4401	23583	16.1	10.11	9.86	7.20	8.02	9.16	7.25	11.11	8.45	5.75
32	467	335	277	254	230	207	345	255	180	169	190	200	3109	19169	13.3	15.02	10.78	8.91	8.17	7.40	6.66	11.10	8.20	5.79
33	501	286	661	397	492	388	560	542	372	436	478	521	5634	14080	15.9	8.89	5.08	11.73	7.05	8.73	6.89	9.94	9.62	6.60
34	297	272	310	411	503	369	572	423	400	474	495	392	4918	6394	15.6	6.04	5.53	6.30	8.36	10.23	7.50	11.63	8.60	8.13
35	518	667	620	560	368	776	827	529	392	462	692	621	7032	28698	15.5	7.37	9.49	8.82	7.96	5.23	11.04	11.76	7.52	5.57
36	498	458	463	411	520	564	744	572	360	488	528	567	6173	12813	19.2	8.07	7.42	7.50	6.66	8.42	9.14	12.05	9.27	5.83
37	0	0	0	0	0	0	0	0	0	0	0	0	0	2866	33.1	0.00	0.00	0.00	0.00	0.00	0.00	0.00	0.00	0.00
38	453	365	427	297	425	256	400	260	238	285	374	345	4125	7419	16.2	10.98	8.85	10.35	7.20	10.30	6.21	9.70	6.30	5.77

Table F.08: Peak heights of 4-methyl steranes (from m/z 231 ion) from all hydrocarbon samples (page 1 of 4).

			Total ion counts				4-METHYL STERANE PEAKS (from m/z 231 fragmentogram) (ppm TIC).												
C30								C28				C29				C30			
bbR	bbS	aaR	231	%	TIC	231% of TIC	No.	aaS	bbR	bbS	aaR	aaS	bbR	bbS	aaR	aaS	bbR	bbS	aaR
							OIL SAMPLES												
			628560	100	not given		1	0.00	0.00	0.00	0.00	0.00	0.00	0.00	0.00	0.00	0.00	0.00	0.00
			170480	100	not given		2	0.00	0.00	0.00	0.00	0.00	0.00	0.00	0.00	0.00	0.00	0.00	0.00
6.76	7.73	10.63	29952	70	50525576	0.0415	3	17.04	38.09	30.07	16.04	45.11	39.09	43.10	55.13	27.06	28.07	32.07	44.10
11.65	6.99	2.72	3232	70	15240681	0.0148	4	8.07	9.80	9.22	7.78	23.06	17.87	15.57	14.99	10.38	17.29	10.38	4.04
9.23	7.25	5.93	6592	65	15674129	0.0273	5	23.73	21.63	19.53	29.74	29.44	19.53	19.23	8.41	40.85	25.23	19.83	16.22
0.00	0.00	0.00	2800	100	11395480	0.0246	6	0	0	0	0	0	0	0	0	0	0	0	0
11.97	11.34	7.56	4032	55	12127489	0.0183	7	12.29	6.91	12.29	12.29	9.60	18.06	20.74	16.52	17.67	21.90	20.74	13.83
9.75	10.06	5.03	12672	65	23964526	0.0344	8	32.97	32.97	30.80	11.35	30.26	31.34	38.91	23.78	25.94	33.51	34.59	17.29
7.09	3.55	4.96	3632	60	41919776	0.0052	9	4.61	4.42	5.16	3.50	3.50	8.66	8.85	1.66	3.50	3.69	1.84	2.58
8.49	11.08	6.37	19844	50	21878084	0.0454	10	28.88	14.97	23.53	67.39	25.67	47.06	57.76	28.88	41.71	38.51	50.27	28.88
7.41	10.66	8.34	56832	65	57270776	0.0645	11	44.24	35.87	62.77	41.85	65.76	50.81	77.71	53.80	41.85	47.82	68.75	53.80
11.17	6.60	5.08	7552	60	4489776	0.1009	12	122.95	102.46	87.09	51.23	56.35	128.07	128.07	51.23	51.23	112.71	66.60	51.23
8.35	7.15	6.41	1048	100	2797560	0.0375	13	38.52	37.96	39.08	14.52	25.12	31.26	53.04	33.50	19.54	31.26	26.80	24.01
12.33	12.33	4.86	6248	100	1650680	0.3785	14	216.86	341.71	256.28	190.57	354.85	420.57	492.85	203.71	190.57	466.57	466.57	184.00
0.00	0.00	0.00	1616	65	14397592	0.0073	15	0	0	0	0	0	0	0	0	0	0	0	0
2.81	2.25	1.12	36608	80	39775156	0.0736	16	82.73	99.28	70.32	66.18	107.55	82.73	111.69	45.50	24.82	20.68	16.55	8.27
5.98	7.17	3.78	16000	80	41658924	0.0307	17	33.05	24.48	30.60	28.16	37.95	27.54	31.83	22.65	18.97	18.36	22.03	11.63
13.18	12.02	6.25	6096	100	2060280	0.2959	18	172.34	317.47	237.65	87.08	208.62	257.60	386.41	166.90	194.11	390.03	355.57	185.04
11.11	9.91	5.73	1436	100	3481590	0.0412	19	26.56	37.66	30.94	21.60	39.11	36.20	60.13	25.40	24.52	45.83	40.87	23.64
11.55	10.05	5.68	3480	100	1816570	0.1916	20	135.05	177.56	155.06	90.03	193.82	157.56	266.35	112.54	105.04	221.33	192.57	108.79
11.24	9.59	7.21	26880	60	46799776	0.0345	21	25.83	19.75	22.79	21.27	41.78	34.94	44.81	8.36	28.48	38.74	33.04	24.84
5.86	5.18	10.81	24064	100	4385538	0.5487	22	148.30	370.75	160.66	2100.93	160.66	370.75	358.39	407.83	210.09	321.32	284.24	593.20
4.70	7.96	4.57	11840	60	48692176	0.0146	23	10.29	12.19	11.81	11.43	14.48	16.19	17.71	15.24	11.43	6.86	11.62	6.67
7.45	8.09	2.98	14720	70	21499806	0.0479	24	44.87	40.79	55.06	36.71	50.99	39.77	57.10	35.69	29.57	35.69	38.75	14.28
12.02	11.59	6.26	4096	100	2564090	0.1597	25	138.56	145.49	117.78	40.58	106.89	129.66	214.77	120.75	105.90	192.01	185.08	99.96
9.02	8.29	10.00	7168	70	15264194	0.0329	26	23.25	11.22	26.46	20.85	28.06	45.70	38.48	24.05	20.85	29.66	27.26	32.87
0.00	0.00	0.00	11456	60	15091152	0.0455	27	0	0	0	0	0	0	0	0	0	0	0	0
5.77	5.68	7.17	1.60E+07	100	not given		28	0	0	0	0	0	0	0	0	0	0	0	0
8.73	7.09	8.73	6.90E+05	100	not given		29	0	0	0	0	0	0	0	0	0	0	0	0
7.28	9.71	5.04	16384	70	53232480	0.0215	30	16.29	13.53	18.72	15.77	27.71	18.72	26.77	15.68	14.79	15.68	20.92	10.86
7.54	8.43	7.11	4736	80	43072448	0.0088	31	8.89	8.67	6.34	7.06	8.05	6.38	9.77	7.44	5.06	6.64	7.42	6.26
5.44	6.11	6.43	3184	80	49652964	0.0051	32	7.71	5.53	4.57	4.19	3.80	3.42	5.69	4.21	2.97	2.79	3.14	3.30
7.74	8.48	9.25	2976	75	34718336	0.0064	33	5.72	3.26	7.54	4.53	5.61	4.43	6.39	6.18	4.24	4.98	5.45	5.95
9.64	10.07	7.97	1536	65	25321986	0.0039	34	2.38	2.18	2.49	3.30	4.03	2.96	4.59	3.39	3.21	3.80	3.97	3.14
6.57	9.84	8.83	5568	80	57018460	0.0078	35	5.75	7.41	6.89	6.22	4.09	8.62	9.19	5.88	4.35	5.13	7.69	6.90
7.91	8.55	9.19	3280	75	5312698	0.0463	36	37.36	34.35	34.73	30.83	39.01	42.31	55.81	42.91	27.00	36.61	39.61	42.53
0.00	0.00	0.00	948	100	13118981	0.0072	37	0.00	0.00	0.00	0.00	0.00	0.00	0.00	0.00	0.00	0.00	0.00	0.00
6.91	9.07	8.36	1712	70	5130069	0.0234	38	25.65	20.67	24.18	16.82	24.07	14.50	22.65	14.72	13.48	16.14	21.18	19.54

Table F.08: Peak heights of 4-methyl steranes (from m/z 231 ion) from all hydrocarbon samples (page 2 of 4).

	C28				C29				C30							C28				C29				
No.	aaS	bbR	bbS	aaR	aaS	bbR	bbS	aaR	aaS	bbR	bbS	aaR	Height	217 ht	(231/217)%	aaS	bbR	bbS	aaR	aaS	bbR	bbS	aaR	aaS
SHALE SAMPLES																								
41	200	320	400	210	320	390	400	160	370	440	280	440	3930	22784	13.1	5.09	8.14	10.18	5.34	8.14	9.92	10.18	4.07	9.41
42	270	370	470	210	310	340	600	500	505	440	370	380	4765	74424	14.2	5.67	7.76	9.86	4.41	6.51	7.14	12.59	10.49	10.60
43	340	300	310	340	240	240	320	270	510	360	290	160	3680	12755	15.7	9.24	8.15	8.42	9.24	6.52	6.52	8.70	7.34	13.86
44	400	340	400	330	450	450	700	340	530	570	480	950	5940	7360	18.6	6.73	5.72	6.73	5.56	7.58	7.58	11.78	5.72	8.92
45	0	0	0	0	0	0	0	0	0	0	0	0	0	5273	38.9	0.00	0.00	0.00	0.00	0.00	0.00	0.00	0.00	0.00
46	1229	1290	1040	680	1500	1140	1790	1230	1060	2070	1940	960	15929	96512	6.3	7.72	8.10	6.53	4.27	9.42	7.16	11.24	7.72	6.65
47	290	230	280	170	420	470	400	380	400	270	350	160	3820	9539	13.8	7.59	6.02	7.33	4.45	10.99	12.30	10.47	9.95	10.47
48	440	370	560	435	430	420	480	320	500	570	380	430	5335	6948	12.7	8.25	6.94	10.50	8.15	8.06	7.87	9.00	6.00	9.37
49	410	570	650	810	105	310	655	790	165	460	540	700	6165	331776	19.8	6.65	9.25	10.54	13.14	1.70	5.03	10.62	12.81	2.68
50	440	90	520	290	100	810	500	170	150	130	400	410	4010	220160	16.9	10.97	2.24	12.97	7.23	2.49	20.20	12.47	4.24	3.74
51	600	1360	880	350	970	1250	1770	880	1210	2150	1900	1010	14330	87680	14.2	4.19	9.49	6.14	2.44	6.77	8.72	12.35	6.14	8.44
52	50	290	150	240	120	270	150	440	50	210	90	280	2340	114688	22.6	2.14	12.39	6.41	10.26	5.13	11.54	6.41	18.80	2.14
53	245	180	270	180	360	200	270	220	260	290	210	120	2805	246784	7.2	8.73	6.42	9.63	6.42	12.83	7.13	9.63	7.84	9.27
54	420	320	150	190	150	260	180	160	200	260	220	260	2770	131072	10.2	15.16	11.55	5.42	6.86	5.42	9.39	6.50	5.78	7.22
55	80	100	500	265	60	230	940	570	230	240	430	420	4065	442368	22.1	1.97	2.46	12.30	6.52	1.48	5.66	23.12	14.02	5.66
56	920	810	830	470	1390	920	1700	870	640	1410	1700	700	12360	37952	12.5	7.44	6.55	6.72	3.80	11.25	7.44	13.75	7.04	5.18
57	275	305	355	180	390	460	420	290	305	430	295	240	3945	35712	10.4	6.97	7.73	9.00	4.56	9.89	11.66	10.65	7.35	7.73
58	280	270	390	220	410	410	530	190	310	520	460	210	4200	74752	11.1	6.67	6.43	9.29	5.24	9.76	9.76	12.62	4.52	7.38
59	810	1800	1250	480	970	1390	2170	880	1050	2020	1990	950	15760	226048	11.6	5.14	11.42	7.93	3.05	6.15	8.82	13.77	5.58	6.66
60	950	970	900	450	1230	1080	1670	840	970	1840	2170	740	13810	48576	13.5	6.88	7.02	6.52	3.26	8.91	7.82	12.09	6.08	7.02
61	220	390	230	140	450	330	340	125	390	260	280	280	3435	269517	13.9	6.40	11.35	6.70	4.08	13.10	9.61	9.90	3.64	11.35
62	370	225	345	275	490	300	410	200	345	350	330	120	3760	294912	6.4	9.84	5.98	9.18	7.31	13.03	7.98	10.90	5.32	9.18
63	310	210	355	170	255	180	265	195	210	265	105	85	2605	14336	11.8	11.90	8.06	13.63	6.53	9.79	6.91	10.17	7.49	8.06
64	0	0	0	0	0	0	0	0	0	0	0	0	0	106496	139.4	0.00	0.00	0.00	0.00	0.00	0.00	0.00	0.00	0.00
65	155	65	180	950	90	165	230	185	130	105	160	280	2695	331776	48.5	5.75	2.41	6.68	35.25	3.34	6.12	8.53	6.86	4.82
66	80	110	130	95	140	145	175	130	140	100	130	95	1470	43622	45.8	5.44	7.48	8.84	6.46	9.52	9.86	11.90	8.84	9.52
67	427	181	189	174	202	250	186	189	502	165	120	120	2705	9088	8.0	15.79	6.69	6.99	6.43	7.47	9.24	6.88	6.99	18.56
68	0	0	0	0	0	0	0	0	0	0	0	0	0	507904	187.9	0.00	0.00	0.00	0.00	0.00	0.00	0.00	0.00	0.00
69	0	0	0	0	0	0	0	0	0	0	0	0	0	218112	51.2	0.00	0.00	0.00	0.00	0.00	0.00	0.00	0.00	0.00
70	346	175	215	200	222	305	226	127	253	257	229	103	2658	26752	17.2	13.02	6.58	8.09	7.52	8.35	11.47	8.50	4.78	9.52
Height=total of peak heights. 217 ht=maximum ion height of m/z 217 fragmentogram x baseline factor.																								
231/217%=ratio of the two fragmentogram ion heights.																								
Sample 5: peak C29aaR overlapped by nC30.																								

Table F.08:-Peak heights of 4-methyl steranes (from m/z 231 ion) from all source rock samples (including annotation descriptions) (page 3 of 4).

C30								C28				C29				C30			
bbR	bbS	aaR	231	%	TIC	231% of TIC	No.	aaS	bbR	bbS	aaR	aaS	bbR	bbS	aaR	aaS	bbR	bbS	aaR
								SHALE SAMPLES											
11.20	7.12	11.20	3968	60	2996810	0.0794	41	40.43	64.69	80.86	42.45	64.69	78.84	80.86	32.34	74.80	88.95	56.60	88.95
9.23	7.76	7.97	15040	70	38066756	0.0277	42	15.67	21.48	27.28	12.19	17.99	19.73	34.82	29.02	29.31	25.54	21.48	22.06
9.78	7.88	4.35	2944	70	2973593	0.0693	43	64.03	56.50	58.38	64.03	45.20	45.20	60.26	50.85	96.05	67.80	54.61	30.13
9.60	8.08	15.99	1824	75	1842646	0.0742	44	49.99	42.49	49.99	41.25	56.24	56.24	87.49	42.49	66.24	71.24	59.99	118.74
0.00	0.00	0.00	3424	55	8145098	0.0231	45	0	0	0	0	0	0	0	0	0	0	0	0
13.00	12.18	6.03	6096	100	1466360	0.4157	46	320.75	336.67	271.42	177.47	391.48	297.52	467.16	321.01	276.64	540.24	506.31	250.55
7.07	9.16	4.19	1884	70	4217116	0.0313	47	23.74	18.83	22.92	13.92	34.38	38.48	32.75	31.11	32.75	22.10	28.65	13.10
10.68	7.12	8.06	1360	65	3750200	0.0236	48	19.44	16.35	24.74	19.22	19.00	18.56	21.21	14.14	22.09	25.18	16.79	19.00
7.46	8.76	11.35	106496	100	12661814	0.8411	49	559.36	777.64	886.78	1105.07	143.25	422.93	893.60	1077.78	225.11	627.57	736.71	955.00
3.24	9.98	10.22	40448	100	16039989	0.2522	50	276.69	56.60	327.00	182.37	62.89	509.37	314.43	106.90	94.33	81.75	251.54	257.83
15.00	13.26	7.05	12432	100	1478650	0.8408	51	352.03	797.94	516.31	205.35	569.12	733.40	1038.49	516.31	709.93	1261.44	1114.76	592.59
8.97	3.85	11.97	25856	100	5310662	0.4869	52	104.03	603.39	312.10	499.35	249.68	561.77	312.10	915.48	104.03	436.93	187.26	582.58
10.34	7.49	4.28	25344	70	24497028	0.0724	53	63.25	46.47	69.71	46.47	92.95	51.64	69.71	56.80	67.13	74.87	54.22	30.98
9.39	7.94	9.39	22272	60	20598612	0.0649	54	98.37	74.95	35.13	44.50	35.13	60.89	42.16	37.47	46.84	60.89	51.52	60.89
5.90	10.58	10.33	108544	90	20740248	0.4710	55	92.70	115.87	579.35	307.06	69.52	266.50	1089.19	660.46	266.50	278.09	498.24	486.66
11.41	13.75	5.66	4728	100	2625530	0.1801	56	134.04	118.01	120.93	68.48	202.51	134.04	247.68	126.75	93.24	205.43	247.68	101.99
10.90	7.48	6.08	6208	60	27429660	0.0136	57	9.47	10.50	12.22	6.20	13.42	15.83	14.46	9.98	10.50	14.80	10.15	8.26
12.38	10.95	5.00	14976	55	13790277	0.0597	58	39.82	38.40	55.46	31.29	58.31	58.31	75.37	27.02	44.09	73.95	65.42	29.86
12.82	12.63	6.03	26208	100	4440060	0.5903	59	303.37	674.16	468.16	179.78	363.30	520.60	812.73	329.59	393.26	756.55	745.32	355.81
13.32	15.71	5.36	6544	100	2494460	0.2623	60	180.47	184.27	170.97	85.48	233.66	205.16	317.24	159.57	184.27	349.54	412.22	140.57
7.57	8.15	8.15	46336	60	43736320	0.0636	61	40.71	72.17	42.56	25.91	83.27	61.07	62.92	23.13	72.17	48.11	51.82	51.82
9.31	8.78	3.19	31232	60	34008720	0.0551	62	54.22	32.97	50.56	40.30	71.81	43.96	60.08	29.31	50.56	51.29	48.36	17.59
10.17	4.03	3.26	2384	50	5070991	0.0235	63	27.97	18.95	32.03	15.34	23.01	16.24	23.91	17.60	18.95	23.91	9.47	7.67
0.00	0.00	0.00	148480	100	7804665	1.9025	64	0	0	0	0	0	0	0	0	0	0	0	0
3.90	5.94	10.39	160768	100	14089057	1.1411	65	656.28	275.22	762.13	4022.37	381.07	698.62	973.84	783.30	550.43	444.58	677.45	1185.54
6.80	8.84	6.46	30720	65	22950544	0.0870	66	47.35	65.11	76.94	56.23	82.86	85.82	103.58	76.94	82.86	59.19	76.94	56.23
6.10	4.44	4.44	1120	65	2403406	0.0303	67	47.82	20.27	21.16	19.48	22.62	27.99	20.83	21.16	56.21	18.48	13.44	13.44
0.00	0.00	0.00	954368	100	29405236	3.2456	68	0	0	0	0	0	0	0	0	0	0	0	0
0.00	0.00	0.00	218112	100	4685930	4.6546	69	0	0	0	0	0	0	0	0	0	0	0	0
9.67	8.62	3.88	5760	80	15405633	0.0299	70	38.94	19.69	24.19	22.51	24.98	34.32	25.43	14.29	28.47	28.92	25.77	11.59

Table F.08: Peak heights of 4-methyl steranes (from m/z 231 ion) from all source rock samples (page 4 of 4).

STERANE PEAK HEIGHT RATIOS m/z 217/259.													
No.	27baS+R	27abS+R	27aaR	28baS+R	28aaS	28aaR	28bbS	29baS+R	29abS+R	29aaS	29aaR	29bbR	29bbS
OIL SAMPLES													
1													
2													
3	1.85	2.15	3.8	1.95	0.0	1.9	39.2	2.6	1.9	6.9	3.6	6.2	7.7
4	1.80	2.70	2.2	1.70	1.5	1.6	9.9	2.2	1.9	5.7	11.6	8.9	12.5
5	1.90	2.90	2.5	1.70	2.7	4.6	16.2	2.0	1.5	4.4	3.8	5.1	5.1
6													
7	1.70	2.55	5.4	2.00	0.0	3.6	8.9	2.0	2.8	8.6	9.3	9.5	10.4
8	2.25	2.65	2.7	2.05	0.8	7.0	10.1	2.3	2.4	7.4	6.6	4.5	9.0
9	2.15	2.95	3.0	2.10	1.4	8.2	15.8	3.1	1.2	6.8	9.1	7.6	8.2
10	1.85	2.15	3.8	1.95	3.9	11.7	12.9	2.7	1.5	16.4	6.0	9.2	9.6
11	2.00	1.90	2.6	1.85	1.9	5.0	9.1	2.0	2.3	6.2	11.4	4.7	8.8
12	2.05	2.05	2.0	1.90	0.8	6.9	9.1	2.2	1.8	4.1	5.8	2.8	5.2
13	2.15	2.10	9.9	1.55	4.7	3.7	7.2	2.6	2.6	13.6	8.9	8.3	10.6
14	2.15	3.55	5.3	2.05	3.1	6.2	7.1	2.5	1.9	8.2	4.8	8.4	11.7
15	1.95	1.80	1.6	1.65	2.0	1.9	3.6	2.4	1.7	5.1	3.7	2.6	3.9
16	2.25	2.65	2.8	2.00	2.2	13.3	17.3	2.5	2.2	8.1	9.4	3.9	8.8
17	2.00	4.00	3.1	2.00	1.1	11.3	17.9	2.4	2.4	11.2	6.0	7.4	11.1
18	2.15	3.50	8.7	1.90	4.0	7.7	7.0	2.3	1.9	8.2	8.5	8.1	11.2
19	2.05	3.20	3.4	2.00	3.0	6.4	6.4	2.3	1.9	8.6	6.7	8.0	15.0
20	2.05	3.30	4.5	1.70	2.7	6.8	6.3	2.5	2.0	7.6	3.4	8.2	12.2
21	1.95	2.70	3.6	2.60	1.6	8.9	15.4	3.1	1.9	12.6	6.3	7.7	13.3
22	2.15	3.00	3.4	2.00	5.2	18.5	7.4	2.3	3.5	16.4	17.5	8.8	16.1
23	2.00	2.35	4.3	2.00	0.0	11.6	15.6	2.7	1.1	8.1	8.8	6.7	8.7
24	2.35	2.80	2.6	2.30	0.9	7.6	11.3	2.5	2.3	6.1	11.9	4.3	8.2
25	2.00	2.95	5.4	2.00	2.2	9.6	9.1	2.3	2.0	11.2	9.3	8.9	13.1
26	2.00	2.75	3.4	2.30	5.4	9.1	10.4	2.7	2.3	13.3	15.5	13.0	11.8
27	1.95	3.30	2.6	1.75	0.9	3.9	4.6	2.0	0.9	5.7	3.6	3.5	3.5
28	1.80	2.85	6.8	1.60	1.7	6.6	7.6	2.1	1.9	3.5	5.4	5.2	6.7
29	1.80	2.70	3.3	1.60	1.2	4.4	4.4	2.3	1.5	4.6	4.9	11.4	21.7
30	2.30	2.85	3.2	2.20	1.6	8.8	6.5	2.7	2.3	8.8	14.4	6.1	11.7
31	1.36	2.26	1.8	1.39	1.1	4.3	5.3	1.3	1.3	3.9	4.9	3.9	5.4
32	1.16	2.53	2.1	1.19	1.3	5.8	3.7	1.5	1.4	3.5	3.7	3.3	4.6
33	1.26	1.85	1.8	1.36	1.8	7.9	5.7	1.8	1.1	5.7	6.3	4.4	6.2
34	1.34	1.46	1.5	1.42	1.0	4.1	3.2	1.5	1.3	3.6	2.7	3.6	4.3
35	1.19	2.16	2.2	1.17	2.1	8.0	5.4	1.6	1.3	4.6	4.3	4.7	5.6
36	1.40	2.71	1.5	1.26	1.2	5.5	4.1	1.8	1.4	4.2	4.7	4.2	6.3
37	1.08	2.57	1.7	0.98	0.9	0.0	3.6	1.6	1.2	0.0	0.0	2.3	2.9
38	1.18	2.54	1.8	1.06	0.9	3.6	3.2	1.4	1.2	3.6	3.6	3.7	5.1

Table F.09: Regular and rearranged sterane ratios of m/z 217/259 for all hydrocarbon samples (page 1 of 2).

No.	27baS+R	27abS+R	27aaR	28baS+R	28aaS	28aaR	28bbS	29baS+R	29abS+R	29aaS	29aaR	29bbR	29bbS
SHALE SAMPLES													
41	1.85	2.40	2.8	1.55	0.0	5.2	5.9	1.9	2.3	4.4	8.7	6.8	7.2
42	1.75	2.00	2.4	1.75	1.8	6.5	19.0	1.9	2.3	3.0	3.5	6.8	5.9
43	1.70	2.50	3.4	1.55	1.5	3.9	6.1	1.5	1.6	7.9	4.2	6.3	8.2
44	1.85	3.00	2.6	1.70	7.1	6.6	15.3	2.2	2.0	3.9	6.7	7.6	7.3
45	1.95	2.15	2.6	1.90	0.9	3.4	6.9	2.8	2.1	4.5	4.7	4.6	5.1
46	2.20	3.70	7.2	2.00	2.3	7.7	11.5	2.4	2.2	10.0	9.7	10.5	14.4
47	2.35	2.60	2.7	2.25	3.5	0.0	6.2	2.6	1.5	4.2	4.5	7.1	7.6
48	1.87	2.95	2.7	1.70	2.4	5.2	3.4	1.9	2.3	4.5	4.8	6.8	9.3
49	2.05	3.35	3.2	1.95	1.8	62.0	15.5	1.9	2.8	1.2	51.7	7.8	18.7
50	2.15	3.30	4.5	2.05	18.8	22.0	1.0	2.4	2.3	11.8	21.0	11.4	15.2
51	2.10	3.50	8.0	1.85	5.5	8.6	23.3	2.6	2.1	9.5	10.5	11.4	15.2
52	2.05	3.85	8.9	2.05	6.8	42.7	16.8	2.3	3.3	10.6	39.3	15.8	0.0
53	2.20	3.00	3.5	2.10	0.9	6.4	11.4	2.2	2.7	6.6	7.2	5.6	10.7
54	2.10	2.65	2.5	2.10	1.1	6.3	15.5	2.3	3.2	7.5	7.6	4.6	8.7
55	2.05	3.60	3.5	2.10	13.0	21.1	19.1	2.3	2.7	10.8	15.5	9.4	15.8
56	2.10	2.95	3.0	1.90	1.6	5.3	5.1	2.3	1.7	7.0	8.8	5.7	9.8
57	2.00	2.30	2.6	1.85	2.6	3.7	10.0	2.0	1.7	3.2	3.4	5.1	7.6
58	1.70	2.15	2.2	1.70	1.0	8.1	9.2	1.9	1.8	4.8	3.7	4.4	7.1
59	2.00	2.65	9.9	1.80	2.2	6.6	26.9	2.3	2.0	7.9	7.8	8.9	12.3
60	2.10	2.65	4.6	1.80	2.5	5.2	6.7	2.3	2.0	6.4	6.7	8.8	12.1
61	2.05	2.30	2.1	1.95	0.9	6.0	9.8	2.2	2.1	6.9	7.1	5.1	10.2
62	2.05	2.80	2.4	2.05	2.5	5.4	20.1	2.2	2.6	7.3	10.0	5.0	10.9
63	2.35	2.85	2.5	2.25	0.7	5.6	8.0	2.4	2.7	5.1	4.5	3.8	6.8
64	1.85	2.65	2.4	2.00	2.6	23.3	11.8	2.0	2.5	8.4	10.4	7.4	12.6
65	2.05	3.50	3.1	2.00	3.3	5.8	17.3	2.1	2.8	9.6	11.9	8.1	13.2
66	2.00	2.45	2.7	2.10	1.7	7.1	7.3	2.3	2.9	9.1	11.6	6.5	8.5
67	2.25	2.88	2.3	2.25	0.7	7.2	4.3	2.2	2.8	4.3	3.5	3.5	4.5
68	2.05	3.20	2.6	1.90	1.3	9.4	12.7	2.1	2.6	8.8	9.9	6.0	10.9
69	2.00	3.80	3.2	1.95	5.2	35.3	11.9	2.2	2.6	12.2	29.1	8.7	15.2
70	2.00	2.60	2.2	1.85	1.1	5.8	3.0	1.9	2.1	6.6	5.6	3.7	3.9
Columns headed ..S or ..R are ratios of individual peaks.													
All other columns are averages calculated using both isomers.													
Sample 5: C29aaR peak overlapped by nC30.													

Table F.09: Regular and rearranged sterane ratios of m/z 217/259 for all source rock samples (including annotation descriptions) (page 2 of 2).

DEMETHYLATED HOPANE PEAKS (FROM m/z 177 FRAGMENTOGRAM).														NORMALIZED PEAK HEIGHTS (%)									
No.	Ts	Tm	28n	25n	bis	nH	nnH	nM	H	M	31S	31R	total	Ts	Tm	28n	25n	bis	nH	nnH	nM	H	M
OIL SAMPLES																							
1																							
2																							
3	510	133	335	92	150	525	670	265	300	140	240	115	3475	14.68	3.83	9.64	2.65	4.32	15.11	19.28	7.63	8.63	4.03
4	590	250	225	180	195	330	510	120	55	0	0	0	2455	24.03	10.18	9.16	7.33	7.94	13.44	20.77	4.89	2.24	0.00
5	910	403	285	381	313	625	1058	215	232	0	0	0	4422	20.58	9.11	6.45	8.62	7.08	14.13	23.93	4.86	5.25	0.00
6	420	165	144	147	184	236	400	101	0	0	0	0	1797	23.37	9.18	8.01	8.18	10.24	13.13	22.26	5.62	0.00	0.00
7	130	89	100	205	145	680	390	210	150	0	0	0	2099	6.19	4.24	4.76	9.77	6.91	32.40	18.58	10.00	7.15	0.00
8	460	100	122	137	64	140	292	61	84	32	0	0	1492	30.83	6.70	8.18	9.18	4.29	9.38	19.57	4.09	5.63	2.14
9	295	135	166	125	145	293	184	110	0	0	0	0	1453	20.30	9.29	11.42	8.60	9.98	20.17	12.66	7.57	0.00	0.00
10	165	130	120	85	95	700	735	220	255	110	0	0	2615	6.31	4.97	4.59	3.25	3.63	26.77	28.11	8.41	9.75	4.21
11	178	110	82	132	55	280	195	115	112	0	0	0	1259	14.14	8.74	6.51	10.48	4.37	22.24	15.49	9.13	8.90	0.00
12	310	102	75	145	40	130	115	55	45	0	0	0	1017	30.48	10.03	7.37	14.26	3.93	12.78	11.31	5.41	4.42	0.00
13	265	342	250	610	190	2170	1080	493	365	48	290	150	6253	4.24	5.47	4.00	9.76	3.04	34.70	17.27	7.88	5.84	0.77
14	535	420	445	270	735	1835	2170	388	888	180	440	345	8651	6.18	4.85	5.14	3.12	8.50	21.21	25.08	4.49	10.26	2.08
15	0	0	0	0	0	0	0	0	0	0	0	0		0.00	0.00	0.00	0.00	0.00	0.00	0.00	0.00	0.00	0.00
16	485	120	128	120	50	75	290	25	0	0	0	0	1293	37.51	9.28	9.90	9.28	3.87	5.80	22.43	1.93	0.00	0.00
17	430	115	127	102	58	113	136	50	35	0	0	0	1166	36.88	9.86	10.89	8.75	4.97	9.69	11.66	4.29	3.00	0.00
18	395	342	374	273	735	2170	2150	590	965	141	460	391	8986	4.40	3.81	4.16	3.04	8.18	24.15	23.93	6.57	10.74	1.57
19	615	485	440	261	510	1530	2170	335	690	160	302	348	7846	7.84	6.18	5.61	3.33	6.50	19.50	27.66	4.27	8.79	2.04
20	538	402	417	290	480	1600	2170	368	691	153	310	278	7697	6.99	5.22	5.42	3.77	6.24	20.79	28.19	4.78	8.98	1.99
21	350	114	117	105	70	330	370	120	108	40	55	42	1821	19.22	6.26	6.43	5.77	3.84	18.12	20.32	6.59	5.93	2.20
22	266	185	70	88	250	950	520	470	330	60	155	110	3454	7.70	5.36	2.03	2.55	7.24	27.50	15.06	13.61	9.55	1.74
23	608	219	304	221	160	372	486	300	142	0	0	0	2812	21.62	7.79	10.81	7.86	5.69	13.23	17.28	10.67	5.05	0.00
24	360	78	91	95	35	70	190	45	30	0	0	0	994	36.22	7.85	9.15	9.56	3.52	7.04	19.11	4.53	3.02	0.00
25	340	275	195	218	120	2170	1825	392	457	122	300	234	6648	5.11	4.14	2.93	3.28	1.81	32.64	27.45	5.90	6.87	1.84
26	230	132	58	350	72	947	455	272	232	47	53	28	2876	8.00	4.59	2.02	12.17	2.50	32.93	15.82	9.46	8.07	1.63
27	0	0	0	145	0	200	210	118	0	0	0	0	673	0.00	0.00	0.00	21.55	0.00	29.72	31.20	17.53	0.00	0.00
28	287	119	94	61	111	67	112	41	51	0	60	30	1033	27.78	11.52	9.10	5.91	10.75	6.49	10.84	3.97	4.94	0.00
29	273	149	118	62	157	157	206	0	65	0	32	31	1250	21.84	11.92	9.44	4.96	12.56	12.56	16.48	0.00	5.20	0.00
30	787	208	226	202	232	375	684	197	200	0	111	65	3287	23.94	6.33	6.88	6.15	7.06	11.41	20.81	5.99	6.08	0.00
31	864	268	270	216	173	553	672	147	273	106	100	57	3699	23.36	7.25	7.30	5.84	4.68	14.95	18.17	3.97	7.38	2.87
32	400	163	134	122	121	215	237	71	87	36	65	75	1726	23.17	9.44	7.76	7.07	7.01	12.46	13.73	4.11	5.04	2.09
33	741	250	220	261	1667	681	929	193	302	84	95	81	5504	13.46	4.54	4.00	4.74	30.29	12.37	16.88	3.51	5.49	1.53
34	757	212	250	253	283	364	564	160	230	0	0	0	3073	24.63	6.90	8.14	8.23	9.21	11.85	18.35	5.21	7.48	0.00
35	660	253	283	224	483	922	744	242	420	60	128	71	4490	14.70	5.63	6.30	4.99	10.76	20.53	16.57	5.39	9.35	1.34
36	709	261	261	268	283	652	735	287	333	92	203	124	4208	16.85	6.20	6.20	6.37	6.73	15.49	17.47	6.82	7.91	2.19
37	288	131	0	0	360	198	245	159	305	0	353	239	2278	12.64	5.75	0.00	0.00	15.80	8.69	10.76	6.98	13.39	0.00
38	467	243	157	237	172	240	400	133	130	90	114	100	2483	18.81	9.79	6.32	9.54	6.93	9.67	16.11	5.36	5.24	3.62

Table F.10: Peak heights of hopanes (from m/z 177 ion) for all hydrocarbon samples (page 1 of 4).

		Fragmentogram heights				Demeth. Hopanes (from m/z 177 fragmentogram) as ppm of TIC.													
31S	31R	177	%	TIC	177% of TIC	No.	Ts	Tm	28n	25n	bis	nH	nnH	nM	H	M	31S	31R	total
						OIL SAMPLES													
				not given		1													
				not given		2													
6.91	3.31	88064	69	50525576	0.12	3	1.77	0.46	1.16	0.32	0.52	1.82	2.32	0.92	1.04	0.48	0.83	0.40	12.03
0.00	0.00	8704	60	15240681	0.03	4	0.82	0.35	0.31	0.25	0.27	0.46	0.71	0.17	0.08	0.00	0.00	0.00	3.43
0.00	0.00	18944	70	15674129	0.08	5	1.74	0.77	0.55	0.73	0.60	1.20	2.02	0.41	0.44	0.00	0.00	0.00	8.46
0.00	0.00	6656	85	11395480	0.05	6	1.16	0.46	0.40	0.41	0.51	0.65	1.11	0.28	0.00	0.00	0.00	0.00	4.96
0.00	0.00	20992	67	12127489	0.12	7	0.72	0.49	0.55	1.13	0.80	3.76	2.15	1.16	0.83	0.00	0.00	0.00	11.60
0.00	0.00	56576	65	23964526	0.15	8	4.73	1.03	1.25	1.41	0.66	1.44	3.00	0.63	0.86	0.33	0.00	0.00	15.35
0.00	0.00	21248	60	41919776	0.03	9	0.62	0.28	0.35	0.26	0.30	0.61	0.39	0.23	0.00	0.00	0.00	0.00	3.04
0.00	0.00	66560	67	21878084	0.20	10	1.29	1.01	0.94	0.66	0.74	5.46	5.73	1.71	1.99	0.86	0.00	0.00	20.38
0.00	0.00	121856	55	57270776	0.12	11	1.65	1.02	0.76	1.23	0.51	2.60	1.81	1.07	1.04	0.00	0.00	0.00	11.70
0.00	0.00	30720	60	4489776	0.41	12	12.51	4.12	3.03	5.85	1.61	5.25	4.64	2.22	1.82	0.00	0.00	0.00	41.05
4.64	2.40	3552	100	2797560	0.13	13	0.54	0.69	0.51	1.24	0.39	4.41	2.19	1.00	0.74	0.10	0.59	0.30	12.70
5.09	3.99	8544	100	1650680	0.52	14	3.20	2.51	2.66	1.62	4.40	10.98	12.98	2.32	5.31	1.08	2.63	2.06	51.76
0.00	0.00	25856	87	14397592	0.16	15	0.00	0.00	0.00	0.00	0.00	0.00	0.00	0.00	0.00	0.00	0.00	0.00	0.00
0.00	0.00	66560	60	39775156	0.10	16	3.77	0.93	0.99	0.93	0.39	0.58	2.25	0.19	0.00	0.00	0.00	0.00	10.04
0.00	0.00	65280	65	41658924	0.10	17	3.76	1.00	1.11	0.89	0.51	0.99	1.19	0.44	0.31	0.00	0.00	0.00	10.19
5.12	4.35	25216	100	2060280	1.22	18	5.38	4.66	5.09	3.72	10.01	29.56	29.28	8.04	13.14	1.92	6.27	5.33	122.39
3.85	4.44	5168	100	3481590	0.15	19	1.16	0.92	0.83	0.49	0.96	2.89	4.11	0.63	1.31	0.30	0.57	0.66	14.84
4.03	3.61	15152	100	1816570	0.83	20	5.83	4.36	4.52	3.14	5.20	17.34	23.52	3.99	7.49	1.66	3.36	3.01	83.41
3.02	2.31	91136	75	46799776	0.15	21	2.81	0.91	0.94	0.84	0.56	2.65	2.97	0.96	0.87	0.32	0.44	0.34	14.61
4.49	3.18	56320	80	4385538	1.03	22	7.91	5.50	2.08	2.62	7.44	28.26	15.47	13.98	9.82	1.78	4.61	3.27	102.74
0.00	0.00	41728	38	48692176	0.03	23	0.70	0.25	0.35	0.26	0.19	0.43	0.56	0.35	0.16	0.00	0.00	0.00	3.26
0.00	0.00	71680	70	21499806	0.23	24	8.45	1.83	2.14	2.23	0.82	1.64	4.46	1.06	0.70	0.00	0.00	0.00	23.34
4.51	3.52	31680	100	2564090	1.24	25	6.32	5.11	3.62	4.05	2.23	40.33	33.92	7.29	8.49	2.27	5.58	4.35	123.55
1.84	0.97	30976	85	15264194	0.17	26	1.38	0.79	0.35	2.10	0.43	5.68	2.73	1.63	1.39	0.28	0.32	0.17	17.25
0.00	0.00	37120	40	15091152	0.10	27	0.00	0.00	0.00	2.12	0.00	2.92	3.07	1.73	0.00	0.00	0.00	0.00	9.84
5.81	2.90	1.60E+07	100	not given	0.00	28	0.00	0.00	0.00	0.00	0.00	0.00	0.00	0.00	0.00	0.00	0.00	0.00	0.00
2.56	2.48	2.00E+06	100	not given	0.00	29	0.00	0.00	0.00	0.00	0.00	0.00	0.00	0.00	0.00	0.00	0.00	0.00	0.00
3.38	1.98	64256	60	53232480	0.07	30	1.73	0.46	0.50	0.45	0.51	0.83	1.51	0.43	0.44	0.00	0.24	0.14	7.24
2.70	1.54	9600	75	43072448	0.02	31	0.39	0.12	0.12	0.10	0.08	0.25	0.30	0.07	0.12	0.05	0.05	0.03	1.67
3.77	4.35	8256	80	49652964	0.01	32	0.31	0.13	0.10	0.09	0.09	0.17	0.18	0.05	0.07	0.03	0.05	0.06	1.33
1.73	1.47	6656	75	34718336	0.01	33	0.19	0.07	0.06	0.07	0.44	0.18	0.24	0.05	0.08	0.02	0.02	0.02	1.44
0.00	0.00	2944	50	25321986	0.01	34	0.14	0.04	0.05	0.05	0.05	0.07	0.11	0.03	0.04	0.00	0.00	0.00	0.58
2.85	1.58	11520	84	57018460	0.02	35	0.25	0.10	0.11	0.08	0.18	0.35	0.28	0.09	0.16	0.02	0.05	0.03	1.70
4.82	2.95	5632	70	5312698	0.07	36	1.25	0.46	0.46	0.47	0.50	1.15	1.30	0.51	0.59	0.16	0.36	0.22	7.42
15.50	10.49	1952	75	13118981	0.01	37	0.14	0.06	0.00	0.00	0.18	0.10	0.12	0.08	0.15	0.00	0.17	0.12	1.12
4.59	4.03	3872	70	5130069	0.05	38	0.99	0.52	0.33	0.50	0.37	0.51	0.85	0.28	0.28	0.19	0.24	0.21	5.28

Table F.10: Peak heights of hopanes (from m/z 177 ion) for all hydrocarbon samples (page 2 of 4).

No.	Ts	Tm	28n	25n	bis	nH	nnH	nM	H	M	31S	31R	total	Ts	Tm	28n	25n	bis	nH	nnH	nM	H	M
SHALE SAMPLES																							
41	280	86	111	110	114	420	535	185	290	110	212	156	2609	10.73	3.30	4.25	4.22	4.37	16.10	20.51	7.09	11.12	4.22
42	395	181	195	310	120	715	787	190	228	135	205	215	3676	10.75	4.92	5.30	8.43	3.26	19.45	21.41	5.17	6.20	3.67
43	270	160	175	155	130	555	570	217	255	115	120	210	2932	9.21	5.46	5.97	5.29	4.43	18.93	19.44	7.40	8.70	3.92
44	305	88	82	135	85	1015	830	280	391	42	41	72	3366	9.06	2.61	2.44	4.01	2.53	30.15	24.66	8.32	11.62	1.25
45	192	138	61	205	100	595	430	235	140	50	110	75	2331	8.24	5.92	2.62	8.79	4.29	25.53	18.45	10.08	6.01	2.15
46	395	285	302	298	642	2170	2150	565	991	162	530	381	8871	4.45	3.21	3.40	3.36	7.24	24.46	24.24	6.37	11.17	1.83
47	600	95	195	340	230	880	1015	180	340	95	145	92	4207	14.26	2.26	4.64	8.08	5.47	20.92	24.13	4.28	8.08	2.26
48	578	77	182	332	216	870	1010	161	305	88	147	79	4045	14.29	1.90	4.50	8.21	5.34	21.51	24.97	3.98	7.54	2.18
49	595	150	158	225	80	955	660	943	480	240	128	170	4784	12.44	3.14	3.30	4.70	1.67	19.96	13.80	19.71	10.03	5.02
50	340	132	173	147	771	926	721	366	230	75	121	84	4086	8.32	3.23	4.23	3.60	18.87	22.66	17.65	8.96	5.63	1.84
51	265	235	150	82	181	2160	2170	668	872	145	490	332	7750	3.42	3.03	1.94	1.06	2.34	27.87	28.00	8.62	11.25	1.87
52	204	69	88	50	960	265	200	175	68	0	0	0	2079	9.81	3.32	4.23	2.41	46.18	12.75	9.62	8.42	3.27	0.00
53	530	122	0	135	83	135	385	78	86	0	43	33	1630	32.52	7.48	0.00	8.28	5.09	8.28	23.62	4.79	5.28	0.00
54	604	256	114	270	80	730	660	290	205	30	90	65	3394	17.80	7.54	3.36	7.96	2.36	21.51	19.45	8.54	6.04	0.88
55	320	130	108	100	860	1020	800	450	345	50	140	100	4423	7.23	2.94	2.44	2.26	19.44	23.06	18.09	10.17	7.80	1.13
56	608	336	337	288	357	780	2170	260	441	185	230	180	6172	9.85	5.44	5.46	4.67	5.78	12.64	35.16	4.21	7.15	3.00
57	335	140	148	150	80	213	692	95	120	0	0	0	1973	16.98	7.10	7.50	7.60	4.05	10.80	35.07	4.82	6.08	0.00
58	490	98	152	153	81	210	667	71	132	89	92	51	2286	21.43	4.29	6.65	6.69	3.54	9.19	29.18	3.11	5.77	3.89
59	365	288	305	240	1015	2170	2115	600	970	163	465	322	9018	4.05	3.19	3.38	2.66	11.26	24.06	23.45	6.65	10.76	1.81
60	356	200	171	170	318	1270	2170	285	730	115	362	292	6439	5.53	3.11	2.66	2.64	4.94	19.72	33.70	4.43	11.34	1.79
61	675	146	193	217	81	208	680	105	120	41	80	58	2604	25.92	5.61	7.41	8.33	3.11	7.99	26.11	4.03	4.61	1.57
62	525	100	135	165	50	215	405	110	98	25	0	0	1828	28.72	5.47	7.39	9.03	2.74	11.76	22.16	6.02	5.36	1.37
63	480	100	150	205	140	200	430	65	62	0	0	0	1832	26.20	5.46	8.19	11.19	7.64	10.92	23.47	3.55	3.38	0.00
64	472	140	146	123	75	910	848	335	397	26	157	103	3732	12.65	3.75	3.91	3.30	2.01	24.38	22.72	8.98	10.64	0.70
65	421	145	122	128	81	897	778	362	380	21	180	113	3628	11.60	4.00	3.36	3.53	2.23	24.72	21.44	9.98	10.47	0.58
66	361	117	93	380	105	950	430	340	230	0	160	140	3306	10.92	3.54	2.81	11.49	3.18	28.74	13.01	10.28	6.96	0.00
67	622	278	141	161	168	178	802	135	132	0	0	0	2617	23.77	10.62	5.39	6.15	6.42	6.80	30.65	5.16	5.04	0.00
68	560	162	151	165	100	540	1000	130	330	55	135	92	3420	16.37	4.74	4.42	4.82	2.92	15.79	29.24	3.80	9.65	1.61
69	270	100	73	68	53	952	644	410	318	38	113	90	3129	8.63	3.20	2.33	2.17	1.69	30.43	20.58	13.10	10.16	1.21
70	698	211	168	204	175	168	357	132	91	66	41	47	2358	29.60	8.95	7.12	8.65	7.42	7.12	15.14	5.60	3.86	2.80
Ts=C27 18a trisnorneohopane. Tm=C27 17a trisnorhopane. 28n=25,28,30 trisnorhopane. 25n=25,30 bisnorhopane. bis=28,30 bisnorhopane.																							
nH=C29 norhopane. nnH=C29 18a norneohopane. nM=normoretane. H=hopane. M=moretane. 31S or R=C31 homohopane 24S or 24R.																							
Height=height of maximum ion in m/z 177 fragmentogram x baseline factor.																							
Total=sum of peak heights. 217height=height of maximum ion in m/z 217 fragmentogram x baseline factor. 217%=ratio of m/z 177/217.																							

Table F.10: Peak heights of hopanes (from m/z 177 ion) for all source rock samples (including annotation descriptions) (page 3 of 4).

31S	31R	177	%	TIC	177% of TIC	No.	Ts	Tm	28n	25n	bis	nH	nnH	nM	H	M	31S	31R	total
												SHALE SAMPLES							
8.13	5.98	20736	80	2996810	0.55	41	5.94	1.82	2.36	2.33	2.42	8.91	11.35	3.93	6.15	2.33	4.50	3.31	55.35
5.58	5.85	62464	80	38066756	0.13	42	1.41	0.65	0.70	1.11	0.43	2.55	2.81	0.68	0.81	0.48	0.73	0.77	13.13
4.09	7.16	14400	80	2973593	0.39	43	3.57	2.11	2.31	2.05	1.72	7.33	7.53	2.87	3.37	1.52	1.59	2.77	38.74
1.22	2.14	11008	90	1842646	0.54	44	4.87	1.41	1.31	2.16	1.36	16.21	13.26	4.47	6.25	0.67	0.65	1.15	53.77
4.72	3.22	17152	70	8145098	0.15	45	1.21	0.87	0.39	1.30	0.63	3.76	2.72	1.49	0.89	0.32	0.70	0.47	14.74
5.97	4.29	38912	100	1466360	2.65	46	11.82	8.53	9.03	8.91	19.20	64.91	64.31	16.90	29.64	4.85	15.85	11.40	265.36
3.45	2.19	7680	75	4217116	0.14	47	1.95	0.31	0.63	1.10	0.75	2.86	3.30	0.58	1.10	0.31	0.47	0.30	13.66
3.63	1.95	4480	70	3750200	0.08	48	1.19	0.16	0.38	0.69	0.45	1.80	2.09	0.33	0.63	0.18	0.30	0.16	8.36
2.68	3.55	153600	85	12661814	1.03	49	12.82	3.23	3.41	4.85	1.72	20.58	14.23	20.33	10.35	5.17	2.76	3.66	103.11
2.96	2.06	109668	100	16039989	0.68	50	5.69	2.21	2.89	2.46	12.90	15.49	12.06	6.12	3.85	1.25	2.02	1.41	68.37
6.32	4.28	90112	100	1478650	6.09	51	20.84	18.48	11.80	6.45	14.23	169.85	170.64	52.53	68.57	11.40	38.53	26.11	609.42
0.00	0.00	93184	100	5310662	1.75	52	17.22	5.82	7.43	4.22	81.02	22.37	16.88	14.77	5.74	0.00	0.00	0.00	175.47
2.64	2.02	101376	70	24497028	0.29	53	9.42	2.17	0.00	2.40	1.48	2.40	6.84	1.39	1.53	0.00	0.76	0.59	28.97
2.65	1.92	68608	50	20598612	0.17	54	2.96	1.26	0.56	1.32	0.39	3.58	3.24	1.42	1.01	0.15	0.44	0.32	16.65
3.17	2.26	254976	88	20740248	1.08	55	7.83	3.18	2.64	2.45	21.04	24.95	19.57	11.01	8.44	1.22	3.42	2.45	108.19
3.73	2.92	18944	100	2625530	0.72	56	7.11	3.93	3.94	3.37	4.17	9.12	25.37	3.04	5.16	2.16	2.69	2.10	72.15
0.00	0.00	31744	65	27429660	0.08	57	1.28	0.53	0.56	0.57	0.31	0.81	2.64	0.36	0.46	0.00	0.00	0.00	7.52
4.02	2.23	57088	60	13790277	0.25	58	5.32	1.06	1.65	1.66	0.88	2.28	7.25	0.77	1.43	0.97	1.00	0.55	24.84
5.16	3.57	135936	100	4440060	3.06	59	12.39	9.78	10.35	8.15	34.46	73.67	71.80	20.37	32.93	5.53	15.79	10.93	306.16
5.62	4.53	46912	100	2494460	1.88	60	10.40	5.84	4.99	4.97	9.29	37.09	63.38	8.32	21.32	3.36	10.57	8.53	188.06
3.07	2.23	126976	60	43736320	0.17	61	4.52	0.98	1.29	1.45	0.54	1.39	4.55	0.70	0.80	0.27	0.54	0.39	17.42
0.00	0.00	113664	70	34008720	0.23	62	6.72	1.28	1.73	2.11	0.64	2.75	5.18	1.41	1.25	0.32	0.00	0.00	23.40
0.00	0.00	9024	60	5070991	0.11	63	2.80	0.58	0.87	1.19	0.82	1.17	2.51	0.38	0.36	0.00	0.00	0.00	10.68
4.21	2.76	56832	80	7804665	0.58	64	7.37	2.19	2.28	1.92	1.17	14.20	13.24	5.23	6.20	0.41	2.45	1.61	58.25
4.96	3.11	158720	90	14089057	1.01	65	11.77	4.05	3.41	3.58	2.26	25.07	21.74	10.12	10.62	0.59	5.03	3.16	101.39
4.84	4.23	59648	35	22950544	0.09	66	0.99	0.32	0.26	1.05	0.29	2.61	1.18	0.94	0.63	0.00	0.44	0.39	9.10
0.00	0.00	4800	55	2403406	0.11	67	2.61	1.17	0.59	0.68	0.71	0.75	3.37	0.57	0.55	0.00	0.00	0.00	10.98
3.95	2.69	218112	75	29405236	0.56	68	9.11	2.64	2.46	2.68	1.63	8.78	16.27	2.11	5.37	0.89	2.20	1.50	55.63
3.61	2.88	91136	90	4685930	1.75	69	15.10	5.59	4.08	3.80	2.96	53.26	36.03	22.94	17.79	2.13	6.32	5.03	175.04
1.74	1.99	16384	85	15405833	0.09	70	2.68	0.81	0.64	0.78	0.67	0.64	1.37	0.51	0.35	0.25	0.16	0.18	9.04

Table F.10: Peak heights of hopanes (from m/z 177 ion) for all source rock samples (page 4 of 4).

TRI- AND TETRACYCLIC TERPANE PEAK HEIGHTS																	NORMALIZED PEAK HEIGHTS									
No.	19T	20T	21T	21/1T	21/2T	22T	22/1T	23T	24T	25T	24Tetr	26TR	26TS	27TR	27TS	Height	19T	20T	21T	21/1T	21/2T	22T	22/1T	23T	24T	25T
OIL SAMPLES																	OIL SAMPLES									
1																										
2																										
3	445	620	370	260	290	265	175	760	565	340	315	240	400	525	205	5775	7.71	10.74	6.41	4.50	5.02	4.59	3.03	13.16	9.78	5.89
4	170	340	595	235	250	215	180	960	895	630	370	465	505	610	220	6640	2.56	5.12	8.96	3.54	3.77	3.24	2.71	14.46	13.48	9.49
5	0	390	255	210	90	135	170	665	560	415	320	245	325	330	135	4245	0.00	9.19	6.01	4.95	2.12	3.18	4.00	15.67	13.19	9.78
6	230	625	585	445	400	235	310	760	750	675	410	320	350	665	360	7120	3.23	8.78	8.22	6.25	5.62	3.30	4.35	10.67	10.53	9.48
7	170	90	250	30	115	160	125	855	540	305	355	160	142	0	0	3297	5.16	2.73	7.58	0.91	3.49	4.85	3.79	25.93	16.38	9.25
8	430	480	355	110	115	230	135	560	415	265	195	165	185	0	0	3640	11.81	13.19	9.75	3.02	3.16	6.32	3.71	15.38	11.40	7.28
9	395	740	690	170	80	250	180	640	495	250	200	130	125	140	70	4555	8.67	16.25	15.15	3.73	1.76	5.49	3.95	14.05	10.87	5.49
10	151	240	60	55	39	24	22	165	97	73	80	54	43	22	15	1140	13.25	21.05	5.26	4.82	3.42	2.11	1.93	14.47	8.51	6.40
11	175	127	82	94	86	34	29	93	49	32	44	23	32	0	0	900	19.44	14.11	9.11	10.44	9.56	3.78	3.22	10.33	5.44	3.56
12	117	190	71	84	50	22	24	175	95	52	57	50	50	0	0	1037	11.28	18.32	6.85	8.10	4.82	2.12	2.31	16.88	9.16	5.01
13	790	2120	780	195	260	590	200	2120	1290	1710	1910	410	340	220	120	13055	6.05	16.24	5.97	1.49	1.99	4.52	1.53	16.24	9.88	13.10
14	27	88	63	51	20	62	31	130	74	58	77	33	42	16	15	787	3.43	11.18	8.01	6.48	2.54	7.88	3.94	16.52	9.40	7.37
15	290	270	380	495	280	170	125	415	275	105	100	100	85	0	0	3090	9.39	8.74	12.30	16.02	9.06	5.50	4.05	13.43	8.90	3.40
16	200	198	36	74	58	22	13	46	38	18	20	15	16	0	0	754	26.53	26.26	4.77	9.81	7.69	2.92	1.72	6.10	5.04	2.39
17	205	355	575	130	87	168	116	940	720	355	185	295	310	0	0	4441	4.62	7.99	12.95	2.93	1.96	3.78	2.61	21.17	16.21	7.99
18	460	1270	1220	390	375	480	270	2170	1390	1010	1335	705	740	230	230	12275	3.75	10.35	9.94	3.18	3.05	3.91	2.20	17.68	11.32	8.23
19	1280	1095	1590	530	460	760	430	2140	1445	800	1240	640	600	200	245	13455	9.51	8.14	11.82	3.94	3.42	5.65	3.20	15.90	10.74	5.95
20	680	810	1370	410	415	690	320	2140	1665	1015	1520	770	710	1310	300	14125	4.81	5.73	9.70	2.90	2.94	4.88	2.27	15.15	11.79	7.19
21	300	375	440	250	115	200	160	600	410	150	160	185	170	0	0	3515	8.53	10.67	12.52	7.11	3.27	5.69	4.55	17.07	11.66	4.27
22	75	190	380	345	130	140	80	745	365	270	570	162	150	0	0	3602	2.08	5.27	10.55	9.58	3.61	3.89	2.22	20.68	10.13	7.50
23	395	975	485	125	120	220	95	575	485	235	120	192	225	230	95	4572	8.64	21.33	10.61	2.73	2.62	4.81	2.08	12.58	10.61	5.14
24	175	355	290	300	80	147	93	500	405	242	150	205	212	0	0	3154	5.55	11.26	9.19	9.51	2.54	4.66	2.95	15.85	12.84	7.67
25	175	260	475	120	145	370	100	2170	1395	990	1120	710	585	460	165	9240	1.89	2.81	5.14	1.30	1.57	4.00	1.08	23.48	15.10	10.71
26	35	165	290	25	60	165	110	960	480	250	200	165	150	55	30	3140	1.11	5.25	9.24	0.80	1.91	5.25	3.50	30.57	15.29	7.96
27	110	360	190	85	70	115	75	340	260	180	95	130	135	92	66	2303	4.78	15.63	8.25	3.69	3.04	4.99	3.26	14.76	11.29	7.82
28	241	412	572	191	208	153	0	631	494	252	243	265	197	0	0	3859	6.25	10.68	14.82	4.95	5.39	3.96	0.00	16.35	12.80	6.53
29	126	234	263	141	135	112	61	275	286	180	228	282	172	72	68	2635	4.78	8.88	9.98	5.35	5.12	4.25	2.31	10.44	10.85	6.83
30	406	550	773	251	115	204	157	971	762	368	310	301	397	82	148	5795	7.01	9.49	13.34	4.33	1.98	3.52	2.71	16.76	13.15	6.35
31	480	359	453	179	74	183	182	721	583	298	310	252	211	0	0	4285	11.20	8.38	10.57	4.18	1.73	4.27	4.25	16.83	13.61	6.95
32	200	287	369	204	99	231	249	778	582	332	419	218	202	0	0	4170	4.80	6.88	8.85	4.89	2.37	5.54	5.97	18.66	13.96	7.96
33	186	361	332	73	89	141	53	564	308	151	261	114	117	0	0	2750	6.76	13.13	12.07	2.65	3.24	5.13	1.93	20.51	11.20	5.49
34	418	329	412	177	132	171	158	527	411	232	128	171	200	0	0	3466	12.06	9.49	11.89	5.11	3.81	4.93	4.56	15.20	11.86	6.69
35	97	156	238	89	56	96	83	345	238	166	187	101	107	0	0	1959	4.95	7.96	12.15	4.54	2.86	4.90	4.24	17.61	12.15	8.47
36	153	289	311	158	92	188	166	716	570	448	438	292	305	0	0	4126	3.71	7.00	7.54	3.83	2.23	4.56	4.02	17.35	13.81	10.86
37	105	228	355	416	115	264	311	406	247	158	55	96	77	0	0	2833	3.71	8.05	12.53	14.68	4.06	9.32	10.98	14.33	8.72	5.58
38	118	136	278	218	104	242	348	698	538	307	189	223	231	0	0	3630	3.25	3.75	7.66	6.01	2.87	6.67	9.59	19.23	14.82	8.46

Table F.11: Peak heights of tri-and tetra-cyclic terpanes (from m/z 191 ion) for all hydrocarbon samples (page 1 of 4).

	NORMALIZED PEAK HEIGHTS								PEAK HEIGHTS AS ppm TIC															total
24Tetr	26TR	26TS	27TR	27TS	191/3	%	TIC	TIC%	19T	20T	21T	21/1T	21/2T	22T	22/1T	23T	24T	25T	24Tetr	26TR	26TS	27TR	27TS	Height
OIL SAMPLES									OIL SAMPLES															
							not given																	
							not given																	
5.45	4.16	6.93	9.09	3.55	48896	62	50525576	0.060	0.46	0.64	0.38	0.27	0.30	0.28	0.18	0.79	0.59	0.35	0.33	0.25	0.42	0.55	0.21	6.00
5.57	7.00	7.61	9.19	3.31	8448	84	15240681	0.047	0.12	0.24	0.42	0.16	0.18	0.15	0.13	0.67	0.63	0.44	0.26	0.33	0.35	0.43	0.15	4.66
7.54	5.77	7.66	7.77	3.18	14528	60	15674129	0.056	0.00	0.51	0.33	0.28	0.12	0.18	0.22	0.87	0.73	0.54	0.42	0.32	0.43	0.43	0.18	5.56
5.76	4.49	4.92	9.34	5.06	7552	85	11395480	0.056	0.18	0.49	0.46	0.35	0.32	0.19	0.25	0.60	0.59	0.53	0.32	0.25	0.28	0.53	0.28	5.63
10.77	4.85	4.31	0.00	0.00	26368	100	12127489	0.217	1.12	0.59	1.65	0.20	0.76	1.06	0.82	5.64	3.56	2.01	2.34	1.06	0.94	0.00	0.00	21.74
5.36	4.53	5.08	0.00	0.00	54528	70	23964526	0.159	1.88	2.10	1.55	0.48	0.50	1.01	0.59	2.45	1.82	1.16	0.85	0.72	0.81	0.00	0.00	15.93
4.39	2.85	2.74	3.07	1.54	23296	60	41919776	0.033	0.29	0.54	0.51	0.12	0.06	0.18	0.13	0.47	0.36	0.18	0.15	0.10	0.09	0.10	0.05	3.33
7.02	4.74	3.77	1.93	1.32	221184	100	21878084	1.011	13.39	21.28	5.32	4.88	3.46	2.13	1.95	14.63	8.60	6.47	7.09	4.79	3.81	1.95	1.33	101.10
4.89	2.56	3.56	0.00	0.00	228010	88	57270776	0.350	6.81	4.94	3.19	3.66	3.35	1.32	1.13	3.62	1.91	1.25	1.71	0.90	1.25	0.00	0.00	35.04
5.50	4.82	4.82	0.00	0.00	24235	100	4489776	0.540	6.09	9.89	3.70	4.37	2.60	1.15	1.25	9.11	4.94	2.71	2.97	2.60	2.60	0.00	0.00	53.98
14.63	3.14	2.60	1.69	0.92	5680	100	2797560	0.203	1.23	3.30	1.21	0.30	0.40	0.92	0.31	3.30	2.01	2.66	2.97	0.64	0.53	0.34	0.19	20.30
9.78	4.19	5.34	2.03	1.91	39104	100	1650680	2.369	8.13	26.49	18.96	15.35	6.02	18.66	9.33	39.13	22.27	17.46	23.18	9.93	12.64	4.82	4.52	236.90
3.24	3.24	2.75	0.00	0.00	9472	90	14397592	0.059	0.56	0.52	0.73	0.95	0.54	0.33	0.24	0.80	0.53	0.20	0.19	0.19	0.16	0.00	0.00	5.92
2.65	1.99	2.12	0.00	0.00	169574	100	39775156	0.426	11.31	11.20	2.04	4.18	3.28	1.24	0.74	2.60	2.15	1.02	1.13	0.85	0.90	0.00	0.00	42.63
4.17	6.64	6.98	0.00	0.00	90112	70	41658924	0.151	0.70	1.21	1.96	0.44	0.30	0.57	0.40	3.20	2.45	1.21	0.63	1.01	1.06	0.00	0.00	15.14
10.88	5.74	6.03	1.87	1.87	10448	100	2060280	0.507	1.90	5.25	5.04	1.61	1.55	1.98	1.12	8.96	5.74	4.17	5.52	2.91	3.06	0.95	0.95	50.71
9.22	4.76	4.46	1.49	1.82	3856	100	3481590	0.111	1.05	0.90	1.31	0.44	0.38	0.63	0.35	1.76	1.19	0.66	1.02	0.53	0.49	0.16	0.20	11.08
10.76	5.45	5.03	9.27	2.12	7040	100	1816570	0.388	1.87	2.22	3.76	1.12	1.14	1.89	0.88	5.87	4.57	2.78	4.17	2.11	1.95	3.59	0.82	38.75
4.55	5.26	4.84	0.00	0.00	132096	68	46799776	0.192	1.64	2.05	2.40	1.37	0.63	1.09	0.87	3.28	2.24	0.82	0.87	1.01	0.93	0.00	0.00	19.19
15.82	4.50	4.16	0.00	0.00	35584	100	4385538	0.811	1.69	4.28	8.56	7.77	2.93	3.15	1.80	16.78	8.22	6.08	12.84	3.65	3.38	0.00	0.00	81.14
2.62	4.20	4.92	5.03	2.08	48384	52	48692176	0.052	0.45	1.10	0.55	0.14	0.14	0.25	0.11	0.65	0.55	0.27	0.14	0.22	0.25	0.26	0.11	5.17
4.76	6.50	6.72	0.00	0.00	66560	80	21499806	0.248	1.37	2.79	2.28	2.36	0.63	1.15	0.73	3.93	3.18	1.90	1.18	1.61	1.66	0.00	0.00	24.77
12.12	7.68	6.33	4.98	1.79	27424	100	2564090	1.070	2.03	3.01	5.50	1.39	1.68	4.28	1.16	25.12	16.15	11.46	12.96	8.22	6.77	5.32	1.91	106.95
6.37	5.25	4.78	1.75	0.96	120832	100	15264194	0.792	0.88	4.16	7.31	0.63	1.51	4.16	2.77	24.20	12.10	6.30	5.04	4.16	3.78	1.39	0.76	79.16
4.13	5.64	5.86	3.99	2.87	37888	68	15091152	0.171	0.82	2.67	1.41	0.63	0.52	0.85	0.56	2.52	1.93	1.33	0.70	0.96	1.00	0.68	0.49	17.07
6.30	6.87	5.10	0.00	0.00	1.80E+07	100	not given																	
8.65	10.70	6.53	2.73	2.58	1.90E+06	100	not given																	
5.35	5.19	6.85	1.42	2.55	59648	65	53232480	0.073	0.073	0.073	0.073	0.073	0.073	0.073	0.073	0.073	0.073	0.073	0.073	0.073	0.073	0.073	0.073	0.073
7.23	5.88	4.92	0.00	0.00	14016	80	43072448	0.026	0.026	0.026	0.026	0.026	0.026	0.026	0.026	0.026	0.026	0.026	0.026	0.026	0.026	0.026	0.026	0.026
10.05	5.23	4.84	0.00	0.00	15808	80	49652964	0.025	0.025	0.025	0.025	0.025	0.025	0.025	0.025	0.025	0.025	0.025	0.025	0.025	0.025	0.025	0.025	0.025
9.49	4.15	4.25	0.00	0.00	17920	90	34718336	0.046	0.046	0.046	0.046	0.046	0.046	0.046	0.046	0.046	0.046	0.046	0.046	0.046	0.046	0.046	0.046	0.046
3.69	4.93	5.77	0.00	0.00	5760	75	25321986	0.017	0.017	0.017	0.017	0.017	0.017	0.017	0.017	0.017	0.017	0.017	0.017	0.017	0.017	0.017	0.017	0.017
9.55	5.16	5.46	0.00	0.00	21248	88	57018460	0.033	0.033	0.033	0.033	0.033	0.033	0.033	0.033	0.033	0.033	0.033	0.033	0.033	0.033	0.033	0.033	0.033
10.62	7.08	7.39	0.00	0.00	3456	75	5312698	0.049	0.049	0.049	0.049	0.049	0.049	0.049	0.049	0.049	0.049	0.049	0.049	0.049	0.049	0.049	0.049	0.049
1.94	3.39	2.72	0.00	0.00	5888	88	13118981	0.039	0.039	0.039	0.039	0.039	0.039	0.039	0.039	0.039	0.039	0.039	0.039	0.039	0.039	0.039	0.039	0.039
5.21	6.14	6.36	0.00	0.00	4736	90	5130069	0.083	0.083	0.083	0.083	0.083	0.083	0.083	0.083	0.083	0.083	0.083	0.083	0.083	0.083	0.083	0.083	0.083

Table F.11: Peak heights of tri-and tetra-cyclic terpanes (from m/z 191 ion) for all hydrocarbon samples (page 2 of 4).

No.	19T	20T	21T	21/1T	21/2T	22T	22/1T	23T	24T	25T	24Tetr	26TR	26TS	27TR	27TS	Height	19T	20T	21T	21/1T	21/2T	22T	22/1T	23T	24T	25T
SHALE SAMPLES																										
41	90	140	225	140	75	100	110	510	305	215	350	165	180	250	130	2985	3.02	4.69	7.54	4.69	2.51	3.35	3.69	17.09	10.22	7.20
42	162	250	225	150	110	115	95	410	285	290	420	205	180	0	0	2897	5.59	8.63	7.77	5.18	3.80	3.97	3.28	14.15	9.84	10.01
43	120	155	250	75	100	90	120	445	395	225	425	120	185	310	180	3195	3.76	4.85	7.82	2.35	3.13	2.82	3.76	13.93	12.36	7.04
44	0	335	440	140	245	155	170	825	465	380	995	190	330	430	110	5210	0.00	6.43	8.45	2.69	4.70	2.98	3.26	15.83	8.93	7.29
45	110	335	960	80	80	180	65	820	455	180	235	172	169	0	0	3841	2.86	8.72	24.99	2.08	2.08	4.69	1.69	21.35	11.85	4.69
46	70	2170	170	60	50	75	40	360	205	130	210	97	100	35	44	3816	1.83	56.87	4.45	1.57	1.31	1.97	1.05	9.43	5.37	3.41
47	130	105	240	100	60	95	105	460	370	220	520	140	150	155	65	2915	4.46	3.60	8.23	3.43	2.06	3.26	3.60	15.78	12.69	7.55
48	150	289	482	218	158	117	168	920	576	421	511	232	289	0	0	4531	3.31	6.38	10.64	4.81	3.49	2.58	3.71	20.30	12.71	9.29
49	0	60	200	0	0	80	0	710	475	345	445	220	205	0	0	2740	0.00	2.19	7.30	0.00	0.00	2.92	0.00	25.91	17.34	12.59
50	46	182	337	55	35	82	115	1000	340	385	470	195	178	375	45	3840	1.20	4.74	8.78	1.43	0.91	2.14	2.99	26.04	8.85	10.03
51	410	510	1070	300	400	400	300	1990	1080	600	2155	435	335	0	280	10265	3.99	4.97	10.42	2.92	3.90	3.90	2.92	19.39	10.52	5.85
52	100	155	350	880	0	102	135	925	310	360	350	125	135	760	0	4687	2.13	3.31	7.47	18.78	0.00	2.18	2.88	19.74	6.61	7.68
53	90	135	340	170	85	200	135	710	605	345	265	293	318	0	0	3691	2.44	3.66	9.21	4.61	2.30	5.42	3.66	19.24	16.39	9.35
54	95	160	230	92	60	128	72	645	395	265	365	210	200	0	0	2917	3.26	5.49	7.88	3.15	2.06	4.39	2.47	22.11	13.54	9.08
55	120	175	345	80	45	95	100	895	430	365	790	292	255	0	0	3987	3.01	4.39	8.65	2.01	1.13	2.38	2.51	22.45	10.79	9.15
56	155	2170	210	95	90	135	40	290	260	180	180	140	110	40	65	4160	3.73	52.16	5.05	2.28	2.16	3.25	0.96	6.97	6.25	4.33
57	535	545	615	320	175	395	170	750	760	470	430	365	340	310	160	6340	8.44	8.60	9.70	5.05	2.76	6.23	2.68	11.83	11.99	7.41
58	615	505	705	325	300	290	200	915	800	510	450	395	385	160	170	6725	9.14	7.51	10.48	4.83	4.46	4.31	2.97	13.61	11.90	7.58
59	250	2170	930	320	190	330	190	2100	1070	1080	925	550	500	190	180	10975	2.28	19.77	8.47	2.92	1.73	3.01	1.73	19.13	9.75	9.84
60	185	2170	240	105	155	115	80	405	285	160	420	140	130	70	75	4735	3.91	45.83	5.07	2.22	3.27	2.43	1.69	8.55	6.02	3.38
61	310	335	535	155	105	250	150	880	660	380	355	300	300	0	0	4715	6.57	7.10	11.35	3.29	2.23	5.30	3.18	18.66	14.00	8.06
62	140	185	375	140	55	145	110	890	725	370	240	300	320	0	0	3995	3.50	4.63	9.39	3.50	1.38	3.63	2.75	22.28	18.15	9.26
63	200	270	330	180	130	290	175	655	460	295	170	205	190	0	0	3550	5.63	7.61	9.30	5.07	3.66	8.17	4.93	18.45	12.96	8.31
64	48	105	216	0	0	168	133	712	303	190	446	165	159	141	82	2868	1.67	3.66	7.53	0.00	0.00	5.86	4.64	24.83	10.56	6.62
65	40	140	275	70	36	105	95	870	475	465	655	325	325	0	0	3876	1.03	3.61	7.09	1.81	0.93	2.71	2.45	22.45	12.25	12.00
66	25	130	200	55	160	50	60	85	49	31	48	33	37	24	13	1000	2.50	13.00	20.00	5.50	16.00	5.00	6.00	8.50	4.90	3.10
67	118	143	164	349	186	74	71	260	165	77	192	75	61	37	28	2000	5.90	7.15	8.20	17.45	9.30	3.70	3.55	13.00	8.25	3.85
68	0	115	41	116	100	31	25	83	48	31	55	25	25	0	0	695	0.00	16.55	5.90	16.69	14.39	4.46	3.60	11.94	6.91	4.46
69	50	105	170	115	120	60	80	930	315	440	215	245	235	90	90	3260	1.53	3.22	5.21	3.53	3.68	1.84	2.45	28.53	9.66	13.50
70	232	475	442	259	121	187	143	787	731	391	362	294	342	0	0	4766	4.87	9.97	9.27	5.43	2.54	3.92	3.00	16.51	15.34	8.20
Height=total height of all peaks.																										
Optical isomers of C26 and C27 labelled S or R.																										
T=tricyclic terpane. 21/1=intermediate peak after Zumberge, 1983. Tetr=tetracyclic terpane.																										

Table F.11: Peak heights of tri-and tetra-cyclic terpanes (from m/z 191 ion) for all source rock samples (including annotations) (page 3 of 4).

24Tetr	26TR	26TS	27TR	27TS	191/3	%	TIC	TIC%	19T	20T	21T	21/1T	21/2T	22T	22/1T	23T	24T	25T	24Tetr	26TR	26TS	27TR	27TS	Height
									SHALE SAMPLES															
11.73	5.53	6.03	8.38	4.36	10368	88	2996810	0.304	0.92	1.43	2.29	1.43	0.76	1.02	1.12	5.20	3.11	2.19	3.57	1.68	1.84	2.55	1.33	30.45
14.50	7.08	6.21	0.00	0.00	37888	100	38066756	0.100	0.56	0.86	0.77	0.52	0.38	0.40	0.33	1.41	0.98	1.00	1.44	0.70	0.62	0.00	0.00	9.95
13.30	3.76	5.79	9.70	5.63	7744	90	2973593	0.234	0.88	1.14	1.83	0.55	0.73	0.66	0.88	3.26	2.90	1.65	3.12	0.88	1.36	2.27	1.32	23.44
19.10	3.65	6.33	8.25	2.11	3600	80	1842646	0.156	0.00	1.00	1.32	0.42	0.73	0.46	0.51	2.47	1.39	1.14	2.98	0.57	0.99	1.29	0.33	15.63
6.12	4.48	4.40	0.00	0.00	34560	100	8145098	0.424	1.22	3.70	10.60	0.88	0.88	1.99	0.72	9.06	5.03	1.99	2.60	1.90	1.87	0.00	0.00	42.43
5.50	2.54	2.62	0.92	1.15	103680	100	1466360	7.071	12.97	402.07	31.50	11.12	9.26	13.90	7.41	66.70	37.98	24.09	38.91	17.97	18.53	6.49	8.15	707.06
17.84	4.80	5.15	5.32	2.23	8786	85	4217116	0.177	0.79	0.64	1.46	0.61	0.36	0.58	0.64	2.79	2.25	1.34	3.16	0.85	0.91	0.94	0.39	17.71
11.28	5.12	6.38	0.00	0.00	3872	78	3750200	0.081	0.27	0.51	0.86	0.39	0.28	0.21	0.30	1.64	1.02	0.75	0.91	0.41	0.51	0.00	0.00	8.05
16.24	8.03	7.48	0.00	0.00	72704	100	12661814	0.574	0.00	1.26	4.19	0.00	0.00	1.68	0.00	14.88	9.95	7.23	9.33	4.61	4.30	0.00	0.00	57.42
12.24	5.08	4.64	9.77	1.17	59392	95	16039989	0.352	0.42	1.67	3.09	0.50	0.32	0.75	1.05	9.16	3.11	3.53	4.31	1.79	1.63	3.44	0.41	35.18
20.99	4.24	3.26	0.00	2.73	21024	100	1478650	1.422	5.68	7.06	14.82	4.16	5.54	5.54	4.16	27.56	14.96	8.31	29.85	6.03	4.64	0.00	3.88	142.18
7.47	2.67	2.88	16.22	0.00	16384	95	5310662	0.293	0.63	0.97	2.19	5.50	0.00	0.64	0.84	5.78	1.94	2.25	2.19	0.78	0.84	4.75	0.00	29.31
7.18	7.94	8.62	0.00	0.00	94208	70	24497028	0.269	0.66	0.98	2.48	1.24	0.62	1.46	0.98	5.18	4.41	2.52	1.93	2.14	2.32	0.00	0.00	26.92
12.51	7.20	6.86	0.00	0.00	78848	75	20598612	0.287	0.93	1.57	2.26	0.91	0.59	1.26	0.71	6.35	3.89	2.61	3.59	2.07	1.97	0.00	0.00	28.71
19.81	7.32	6.40	0.00	0.00	118784	90	20740248	0.515	1.55	2.26	4.46	1.03	0.58	1.23	1.29	11.57	5.56	4.72	10.21	3.78	3.30	0.00	0.00	51.54
4.33	3.37	2.64	0.96	1.56	46720	100	2625530	1.779	6.63	92.82	8.98	4.06	3.85	5.77	1.71	12.40	11.12	7.70	7.70	5.99	4.71	1.71	2.78	177.95
6.78	5.76	5.36	4.89	2.52	20480	55	27429660	0.041	0.35	0.35	0.40	0.21	0.11	0.26	0.11	0.49	0.49	0.30	0.28	0.24	0.22	0.20	0.10	4.11
6.69	5.87	5.72	2.38	2.53	37120	45	13790277	0.121	1.11	0.91	1.27	0.59	0.54	0.52	0.36	1.65	1.44	0.92	0.81	0.71	0.69	0.29	0.31	12.11
8.43	5.01	4.56	1.73	1.64	71296	100	4440060	1.606	3.66	31.75	13.61	4.68	2.78	4.83	2.78	30.72	15.66	15.80	13.53	8.05	7.32	2.78	2.63	160.57
8.87	2.96	2.75	1.48	1.58	49280	100	2494460	1.976	7.72	90.54	10.01	4.38	6.47	4.80	3.34	16.90	11.89	6.68	17.52	5.84	5.42	2.92	3.13	197.56
7.53	6.36	6.36	0.00	0.00	147456	60	43736320	0.202	1.33	1.44	2.30	0.66	0.45	1.07	0.64	3.78	2.83	1.63	1.52	1.29	1.29	0.00	0.00	20.23
6.01	7.51	8.01	0.00	0.00	178176	80	34008720	0.419	1.47	1.94	3.93	1.47	0.58	1.52	1.15	9.34	7.61	3.88	2.52	3.15	3.36	0.00	0.00	41.91
4.79	5.77	5.35	0.00	0.00	10176	60	5070991	0.120	0.68	0.92	1.12	0.61	0.44	0.98	0.59	2.22	1.56	1.00	0.58	0.70	0.64	0.00	0.00	12.04
15.55	5.75	5.54	4.92	2.86	33792	100	7804665	0.433	0.72	1.59	3.26	0.00	0.00	2.54	2.01	10.75	4.57	2.87	6.73	2.49	2.40	2.13	1.24	43.30
16.90	8.38	8.38	0.00	0.00	63488	90	14089057	0.406	0.42	1.46	2.88	0.73	0.38	1.10	0.99	9.10	4.97	4.87	6.85	3.40	3.40	0.00	0.00	40.56
4.80	3.30	3.70	2.40	1.30	117419	100	22950544	0.512	1.28	6.65	10.23	2.81	8.19	2.56	3.07	4.35	2.51	1.59	2.46	1.69	1.89	1.23	0.67	51.16
9.60	3.75	3.05	1.85	1.40	5280	86	2403406	0.189	1.11	1.35	1.55	3.30	1.76	0.70	0.67	2.46	1.56	0.73	1.81	0.71	0.58	0.35	0.26	18.89
7.91	3.60	3.60	0.00	0.00	286720	100	29405236	0.975	0.00	16.13	5.75	16.27	14.03	4.35	3.51	11.64	6.73	4.35	7.72	3.51	3.51	0.00	0.00	97.51
6.60	7.52	7.21	2.76	2.76	55808	100	4685930	1.191	1.83	3.84	6.21	4.20	4.38	2.19	2.92	33.98	11.51	16.07	7.85	8.95	8.59	3.29	3.29	119.10
7.60	6.17	7.18	0.00	0.00	9216	75	15405633	0.045	0.22	0.45	0.42	0.24	0.11	0.18	0.13	0.74	0.69	0.37	0.34	0.28	0.32	0.00	0.00	4.49

Table F.11: Peak heights of tri-and tetra-cyclic terpanes (from m/z 191 ion) for all source rock samples (page 4 of 4).

PENTACYCLIC (AND SOME TRICYCLIC) TERPANE PEAK HEIGHTS.																										
No.	28TR	28TS	29TR	29TS	Ts	Tm	30TS	30TR	bis	29nH	29nnH	30Dia	nM	Hop	Mor	31S	31R	GAM	32S	32R	33S	33R	34S	34R	35S	35R
OIL SAMPLES																										
1	158	103	238	199	661	203	0	0	208	580	503	444	70	1430	182	482	328	125	325	231	222	212	159	100	110	68
2	262	166	330	355	1210	570	0	0	267	586	960	1060	160	1330	310	530	335	250	335	285	290	250	175	182	185	120
3	140	75	270	150	485	370	170	120	155	261	330	580	170	865	100	210	250	0	290	205	140	120	0	0	0	0
4	395	150	0	0	1020	375	0	0	160	605	680	505	55	1085	40	135	165	0	140	115	0	0	0	0	0	0
5	58	62	70	165	290	112	0	0	45	170	270	150	42	330	90	85	40	0	78	61	0	0	0	0	0	0
6	180	145	175	0	465	250	0	0	325	410	490	505	0	1890	215	520	325	20	380	220	290	180	260	195	250	175
7	100	45	0	0	290	205	0	0	105	660	350	90	85	580	50	315	280	210	100	83	0	0	0	0	0	0
8	165	145	285	190	640	380	185	130	200	310	355	505	100	680	80	220	185	45	185	125	120	80	67	59	56	32
9	0	0	0	0	122	66	0	0	40	170	90	62	65	180	80	120	90	0	68	76	0	0	0	0	0	0
10	120	92	166	139	290	95	0	0	50	665	580	65	85	770	40	410	390	0	260	255	120	120	0	0	0	0
11	130	90	185	155	195	220	180	105	82	640	255	180	135	890	140	385	310	60	195	170	170	130	100	75	90	60
12	65	54	77	68	126	67	80	61	51	90	60	142	0	81	56	67	55	0	0	0	0	0	0	0	0	0
13	315	250	380	740	620	740	160	270	170	2170	670	315	190	2030	270	1295	875	220	700	605	470	330	250	230	375	285
14	90	82	100	150	445	260	90	60	460	740	620	440	50	2170	220	780	655	120	640	415	450	305	280	150	210	135
15	0	0	0	0	0	0	0	0	0	0	0	0	0	0	0	0	0	0	0	0	0	0	0	0	0	0
16	215	200	360	285	705	375	190	170	110	200	340	550	70	315	95	117	112	0	76	55	70	60	0	0	0	0
17	322	290	400	295	510	200	215	175	93	260	210	190	130	330	95	140	80	0	0	0	0	0	0	0	0	0
18	82	70	90	105	330	195	87	80	540	860	475	255	88	2170	245	830	635	100	650	445	475	310	285	175	205	125
19	105	87	135	132	740	275	110	104	355	740	675	700	70	2170	210	725	560	165	641	420	550	380	255	110	170	100
20	95	82	135	150	640	260	110	100	340	750	640	680	45	2170	235	810	615	0	715	485	455	285	290	175	230	130
21	125	115	185	150	400	230	150	115	120	520	330	210	60	960	130	275	212	0	170	120	105	65	57	28	42	32
22	22	19	32	24	114	305	33	16	230	540	155	81	104	905	170	365	255	0	175	122	100	63	60	37	25	13
23	130	65	150	52	360	235	0	0	110	245	195	205	50	420	70	230	140	110	0	0	0	0	0	0	0	0
24	355	300	545	430	1040	595	335	260	161	320	480	820	125	590	80	193	180	0	215	145	130	88	0	0	0	0
25	230	195	275	265	800	530	220	300	150	1920	880	420	105	2170	195	1250	830	240	900	600	565	360	370	220	345	225
26	265	255	272	265	355	455	0	0	72	1045	340	55	125	1005	100	280	185	0	105	80	40	25	0	0	0	0
27	60	50	100	70	135	77	0	0	27	140	115	100	0	220	60	95	70	0	0	0	0	0	0	0	0	0
28	300	325	337	418	702	342	0	0	131	185	249	443	100	257	0	96	38	0	111	50	74	46	0	0	0	0
29	187	182	279	277	744	248	0	0	163	253	327	675	117	525	141	132	97	0	126	83	87	41	0	0	0	0
30	161	172	271	197	503	191	0	0	173	347	362	253	118	737	100	196	189	0	166	132	105	111	73	86	53	0
31	0	0	264	173	508	228	168	123	208	461	338	145	48	970	73	235	168	144	89	82	53	31	21	0	0	0
32	0	0	598	382	785	382	317	253	139	560	400	268	92	887	117	232	209	0	161	136	91	78	56	37	0	0
33	0	0	157	114	885	333	141	78	243	545	472	243	105	982	90	248	189	0	138	102	89	62	50	43	0	0
34	0	0	292	234	530	233	227	234	172	361	326	287	72	691	113	213	224	0	178	133	140	145	0	0	0	0
35	64	72	118	81	202	147	78	60	389	488	380	62	52	1030	104	251	171	0	147	93	96	58	40	18	32	20
36	52	56	126	71	302	187	96	54	160	398	291	151	72	952	114	317	202	0	206	151	110	82	65	46	44	31
37	0	0	786	600	886	467	704	401	378	503	710	477	328	790	300	0	0	0	0	0	0	0	0	0	0	0
38	0	0	613	456	682	383	428	307	251	355	551	348	130	643	168	217	237	0	122	118	0	0	0	0	0	0

Table F.12: Peak heights of pentacyclic terpanes (from m/z 191 ion) for all hydrocarbon samples (page 1 of 8).

total	NORMALIZED PEAK HEIGHTS																						
height	28TR	28TS	29TR	29TS	Ts	Tm	30TS	30TR	bis	29nH	29nnH	30Dia	nM	Hop	Mor	31S	31R	GAM	32S	32R	33S	33R	34S	34R
	OIL SAMPLES																							
7341	2.15	1.40	3.24	2.71	9.00	2.77	0.00	0.00	2.83	7.90	6.85	6.05	0.95	19.48	2.48	6.57	4.47	1.70	4.43	3.15	3.02	2.89	2.17	1.36
10503	2.49	1.58	3.14	3.38	11.52	5.43	0.00	0.00	2.54	5.58	9.14	10.09	1.52	12.66	2.95	5.05	3.19	2.38	3.19	2.71	2.76	2.38	1.67	1.73
5456	2.57	1.37	4.95	2.75	8.89	6.78	3.12	2.20	2.84	4.78	6.05	10.63	3.12	15.85	1.83	3.85	4.58	0.00	5.32	3.76	2.57	2.20	0.00	0.00
5625	7.02	2.67	0.00	0.00	18.13	6.67	0.00	0.00	2.84	10.76	12.09	8.98	0.98	19.29	0.71	2.40	2.93	0.00	2.49	2.04	0.00	0.00	0.00	0.00
2118	2.74	2.93	3.31	7.79	13.69	5.29	0.00	0.00	2.12	8.03	12.75	7.08	1.98	15.58	4.25	4.01	1.89	0.00	3.68	2.88	0.00	0.00	0.00	0.00
7865	2.29	1.84	2.23	0.00	5.91	3.18	0.00	0.00	4.13	5.21	6.23	6.42	0.00	24.03	2.73	6.61	4.13	0.25	4.83	2.80	3.69	2.29	3.31	2.48
3548	2.82	1.27	0.00	0.00	8.17	5.78	0.00	0.00	2.96	18.60	9.86	2.54	2.40	16.35	1.41	8.88	7.89	5.92	2.82	2.34	0.00	0.00	0.00	0.00
5524	2.99	2.62	5.16	3.44	11.59	6.88	3.35	2.35	3.62	5.61	6.43	9.14	1.81	12.31	1.45	3.98	3.35	0.81	3.35	2.26	2.17	1.45	1.21	1.07
1229	0.00	0.00	0.00	0.00	9.93	5.37	0.00	0.00	3.25	13.83	7.32	5.04	5.29	14.65	6.51	9.76	7.32	0.00	5.53	6.18	0.00	0.00	0.00	0.00
4712	2.55	1.95	3.52	2.95	6.15	2.02	0.00	0.00	1.06	14.11	12.31	1.38	1.80	16.34	0.85	8.70	8.28	0.00	5.52	5.41	2.55	2.55	0.00	0.00
5327	2.44	1.69	3.47	2.91	3.66	4.13	3.38	1.97	1.54	12.01	4.79	3.38	2.53	16.71	2.63	7.23	5.82	1.13	3.66	3.19	3.19	2.44	1.88	1.41
1200	5.42	4.50	6.42	5.67	10.50	5.58	6.67	5.08	4.25	7.50	5.00	11.83	0.00	6.75	4.67	5.58	4.58	0.00	0.00	0.00	0.00	0.00	0.00	0.00
14925	2.11	1.68	2.55	4.96	4.15	4.96	1.07	1.81	1.14	14.54	4.49	2.11	1.27	13.60	1.81	8.68	5.86	1.47	4.69	4.05	3.15	2.21	1.68	1.54
10117	0.89	0.81	0.99	1.48	4.40	2.57	0.89	0.59	4.55	7.31	6.13	4.35	0.49	21.45	2.17	7.71	6.47	1.19	6.33	4.10	4.45	3.01	2.77	1.48
0	0.00	0.00	0.00	0.00	0.00	0.00	0.00	0.00	0.00	0.00	0.00	0.00	0.00	0.00	0.00	0.00	0.00	0.00	0.00	0.00	0.00	0.00	0.00	0.00
4670	4.60	4.28	7.71	6.10	15.10	8.03	4.07	3.64	2.36	4.28	7.28	11.78	1.50	6.75	2.03	2.51	2.40	0.00	1.63	1.18	1.50	1.28	0.00	0.00
3935	8.18	7.37	10.17	7.50	12.96	5.08	5.46	4.45	2.36	6.61	5.34	4.83	3.30	8.39	2.41	3.56	2.03	0.00	0.00	0.00	0.00	0.00	0.00	0.00
9907	0.83	0.71	0.91	1.06	3.33	1.97	0.88	0.81	5.45	8.68	4.79	2.57	0.89	21.90	2.47	8.38	6.41	1.01	6.56	4.49	4.79	3.13	2.88	1.77
10684	0.98	0.81	1.26	1.24	6.93	2.57	1.03	0.97	3.32	6.93	6.32	6.55	0.66	20.31	1.97	6.79	5.24	1.54	6.00	3.93	5.15	3.56	2.39	1.03
10622	0.89	0.77	1.27	1.41	6.03	2.45	1.04	0.94	3.20	7.06	6.03	6.40	0.42	20.43	2.21	7.63	5.79	0.00	6.73	4.57	4.28	2.68	2.73	1.65
4906	2.55	2.34	3.77	3.06	8.15	4.69	3.06	2.34	2.45	10.60	6.73	4.28	1.22	19.57	2.65	5.61	4.32	0.00	3.47	2.45	2.14	1.32	1.16	0.57
3965	0.55	0.48	0.81	0.61	2.88	7.69	0.83	0.40	5.80	13.62	3.91	2.04	2.62	22.82	4.29	9.21	6.43	0.00	4.41	3.08	2.52	1.59	1.51	0.93
2767	4.70	2.35	5.42	1.88	13.01	8.49	0.00	0.00	3.98	8.85	7.05	7.41	1.81	15.18	2.53	8.31	5.06	3.98	0.00	0.00	0.00	0.00	0.00	0.00
7387	4.81	4.06	7.38	5.82	14.08	8.05	4.53	3.52	2.18	4.33	6.50	11.10	1.69	7.99	1.08	2.61	2.44	0.00	2.91	1.96	1.76	1.19	0.00	0.00
14560	1.58	1.34	1.89	1.82	5.49	3.64	1.51	2.06	1.03	13.19	6.04	2.88	0.72	14.90	1.34	8.59	5.70	1.65	6.18	4.12	3.88	2.47	2.54	1.51
5324	4.98	4.79	5.11	4.98	6.67	8.55	0.00	0.00	1.35	19.63	6.39	1.03	2.35	18.88	1.88	5.26	3.47	0.00	1.97	1.50	0.75	0.47	0.00	0.00
1319	4.55	3.79	7.58	5.31	10.24	5.84	0.00	0.00	2.05	10.61	8.72	7.58	0.00	16.68	4.55	7.20	5.31	0.00	0.00	0.00	0.00	0.00	0.00	0.00
4204	7.14	7.73	8.02	9.94	16.70	8.14	0.00	0.00	3.12	4.40	5.92	10.54	2.38	6.11	0.00	2.28	0.90	0.00	2.64	1.19	1.76	1.09	0.00	0.00
4684	3.99	3.89	5.96	5.91	15.88	5.29	0.00	0.00	3.48	5.40	6.98	14.41	2.50	11.21	3.01	2.82	2.07	0.00	2.69	1.77	1.86	0.88	0.00	0.00
4696	3.43	3.66	5.77	4.20	10.71	4.07	0.00	0.00	3.68	7.39	7.71	5.39	2.51	15.69	2.13	4.17	4.02	0.00	3.53	2.81	2.24	2.36	1.55	1.83
4530	0.00	0.00	5.83	3.82	11.21	5.03	3.71	2.72	4.59	10.18	7.46	3.20	1.06	21.41	1.61	5.19	3.71	3.18	1.96	1.81	1.17	0.68	0.46	0.00
6180	0.00	0.00	9.68	6.18	12.70	6.18	5.13	4.09	2.25	9.06	6.47	4.34	1.49	14.35	1.89	3.75	3.38	0.00	2.61	2.20	1.47	1.26	0.91	0.60
5309	0.00	0.00	2.96	2.15	16.67	6.27	2.66	1.47	4.58	10.27	8.89	4.58	1.98	18.50	1.70	4.67	3.56	0.00	2.60	1.92	1.68	1.17	0.94	0.81
4805	0.00	0.00	6.08	4.87	11.03	4.85	4.72	4.87	3.58	7.51	6.78	5.97	1.50	14.38	2.35	4.43	4.66	0.00	3.70	2.77	2.91	3.02	0.00	0.00
4253	1.50	1.69	2.77	1.90	4.75	3.46	1.83	1.41	9.15	11.47	8.93	1.46	1.22	24.22	2.45	5.90	4.02	0.00	3.46	2.19	2.26	1.36	0.94	0.42
4336	1.20	1.29	2.91	1.64	6.96	4.31	2.21	1.25	3.69	9.18	6.71	3.48	1.66	21.96	2.63	7.31	4.66	0.00	4.75	3.48	2.54	1.89	1.50	1.06
7330	0.00	0.00	10.72	8.19	12.09	6.37	9.60	5.47	5.16	6.86	9.69	6.51	4.47	10.78	4.09	0.00	0.00	0.00	0.00	0.00	0.00	0.00	0.00	0.00
6009	0.00	0.00	10.20	7.59	11.35	6.37	7.12	5.11	4.18	5.91	9.17	5.79	2.16	10.70	2.80	3.61	3.94	0.00	2.03	1.96	0.00	0.00	0.00	0.00

Table F.12: Peak heights of pentacyclic terpanes (from m/z 191 ion) for all hydrocarbon samples (page 2 of 8).

					m/z 191	PEAK HEIGHTS AS ppm TI														
35S	35R	191/5	%	TIC	% of TIC	28TR	28TS	29TR	29TS	Ts	Tm	30TS	30TR	bis	29nH	29nnH	30Dia	nM	Hop	Mor
1.50	0.93	10453	100	not given																
1.76	1.14	6878	100	not given																
0.00	0.00	150604	82	50525576	0.2444	0.62	0.33	1.19	0.66	2.14	1.63	0.75	0.53	0.68	1.15	1.45	2.56	0.75	3.81	0.84
0.00	0.00	30208	86	15240681	0.1705	1.20	0.45	0.00	0.00	3.09	1.14	0.00	0.00	0.48	1.83	2.06	1.53	0.17	3.29	0.12
0.00	0.00	21248	65	15674129	0.0881	0.24	0.26	0.29	0.69	1.21	0.47	0.00	0.00	0.19	0.71	1.12	0.62	0.17	1.37	0.37
3.18	2.23	16896	100	11395480	0.1483	0.34	0.27	0.33	0.00	0.88	0.47	0.00	0.00	0.61	0.77	0.92	0.95	0.00	3.56	0.41
0.00	0.00	49664	84	12127489	0.3440	0.97	0.44	0.00	0.00	2.81	1.99	0.00	0.00	1.02	6.40	3.39	0.87	0.82	5.62	0.48
1.01	0.58	60416	60	23964526	0.1513	0.45	0.39	0.78	0.52	1.74	1.03	0.50	0.35	0.54	0.84	0.97	1.38	0.27	1.85	0.30
0.00	0.00	55552	80	41919776	0.1060	0.00	0.00	0.00	0.00	1.05	0.57	0.00	0.00	0.35	1.47	0.78	0.53	0.56	1.55	0.69
0.00	0.00	140288	80	21878084	0.5130	1.31	1.00	1.81	1.51	3.16	1.03	0.00	0.00	0.54	7.24	6.31	0.71	0.93	8.38	0.44
1.69	1.13	174080	48	57270776	0.1459	0.36	0.25	0.51	0.42	0.53	0.60	0.49	0.29	0.22	1.75	0.70	0.49	0.37	2.44	0.38
0.00	0.00	86016	75	4489776	1.4369	7.78	6.47	9.22	8.14	15.09	8.02	9.58	7.30	6.11	10.78	7.18	17.00	0.00	9.70	6.71
2.51	1.91	8000	100	2797560	0.2860	0.60	0.48	0.73	1.42	1.19	1.42	0.31	0.52	0.33	4.16	1.28	0.60	0.36	3.89	0.52
2.08	1.33	46720	100	1650680	2.8303	2.52	2.29	2.80	4.20	12.45	7.27	2.52	1.68	12.87	20.70	17.35	12.31	1.40	60.71	6.15
0.00	0.00	76800	90	14397592	0.4801	0	0	0	0	0	0	0	0	0	0	0	0	0	0	0
0.00	0.00	87040	55	39775156	0.1204	0.55	0.52	0.93	0.73	1.82	0.97	0.49	0.44	0.28	0.52	0.88	1.42	0.18	0.81	0.24
0.00	0.00	86016	60	41658924	0.1239	1.01	0.91	1.26	0.93	1.61	0.63	0.68	0.55	0.29	0.82	0.66	0.60	0.41	1.04	0.30
2.07	1.26	162560	100	2060280	7.8902	6.53	5.57	7.17	8.36	26.28	15.53	6.93	6.37	43.01	68.49	37.83	20.31	7.01	172.82	19.51
1.59	0.94	23520	100	3481590	0.6756	0.66	0.55	0.85	0.83	4.68	1.74	0.70	0.66	2.24	4.68	4.27	4.43	0.44	13.72	1.33
2.17	1.22	69376	100	1816570	3.8191	3.42	2.95	4.85	5.39	23.01	9.35	3.95	3.60	12.22	26.97	23.01	24.45	1.62	78.02	8.45
0.86	0.65	141312	75	46799776	0.2265	0.58	0.53	0.85	0.69	1.85	1.06	0.69	0.53	0.55	2.40	1.52	0.97	0.28	4.43	0.60
0.63	0.33	197632	100	4385538	4.5064	2.50	2.16	3.64	2.73	12.96	34.66	3.75	1.82	26.14	61.37	17.62	9.21	11.82	102.86	19.32
0.00	0.00	68608	60	48692176	0.0845	0.40	0.20	0.46	0.16	1.10	0.72	0.00	0.00	0.34	0.75	0.60	0.63	0.15	1.28	0.21
0.00	0.00	57344	45	21499806	0.1200	0.57	0.48	0.87	0.69	1.66	0.95	0.54	0.42	0.26	0.51	0.77	1.31	0.20	0.94	0.32
2.37	1.55	87808	100	2564090	3.4245	5.41	4.59	6.47	6.23	18.82	12.47	5.17	7.06	3.53	45.16	20.70	9.88	2.47	51.04	4.59
0.00	0.00	66560	90	15264194	0.3924	1.95	1.88	2.00	1.95	2.62	3.35	0.00	0.00	0.53	7.70	2.51	0.41	0.92	7.41	0.74
0.00	0.00	72704	60	15091152	0.2891	1.31	1.10	2.19	1.53	2.96	1.69	0.00	0.00	0.59	3.07	2.52	2.19	0.00	4.82	1.31
0.00	0.00	9.60E+06	100	not given	0.0000	0.00	0.00	0.00	0.00	0.00	0.00	0.00	0.00	0.00	0.00	0.00	0.00	0.00	0.00	0.00
0.00	0.00	1.90E+06	100	not given	0.0000	0.00	0.00	0.00	0.00	0.00	0.00	0.00	0.00	0.00	0.00	0.00	0.00	0.00	0.00	0.00
1.13	0.00	114688	82	53232480	0.1767	0.61	0.65	1.02	0.74	1.89	0.72	0.00	0.00	0.65	1.31	1.36	0.95	0.44	2.77	0.38
0.00	0.00	20992	80	43072448	0.0390	0.00	0.00	0.23	0.15	0.44	0.20	0.14	0.11	0.18	0.40	0.29	0.12	0.04	0.83	0.06
0.00	0.00	7040	75	49652964	0.0106	0.00	0.00	0.10	0.07	0.14	0.07	0.05	0.04	0.02	0.10	0.07	0.05	0.02	0.15	0.02
0.00	0.00	16896	89	34718336	0.0433	0.00	0.00	0.13	0.09	0.72	0.27	0.12	0.06	0.20	0.44	0.39	0.20	0.09	0.80	0.07
0.00	0.00	5760	70	25321986	0.0159	0.00	0.00	0.10	0.08	0.18	0.08	0.08	0.08	0.06	0.12	0.11	0.10	0.02	0.23	0.04
0.75	0.47	43776	96	57018460	0.0737	0.11	0.12	0.20	0.14	0.35	0.25	0.14	0.10	0.67	0.85	0.66	0.11	0.09	1.78	0.18
1.01	0.71	18944	88	5312698	0.3138	0.38	0.41	0.91	0.51	2.19	1.35	0.69	0.39	1.16	2.88	2.11	1.09	0.52	6.89	0.83
0.00	0.00	1440	51	13118981	0.0056	0.00	0.00	0.06	0.05	0.07	0.04	0.05	0.03	0.03	0.04	0.05	0.04	0.03	0.06	0.02
0.00	0.00	3488	72	5130069	0.0490	0.00	0.00	0.50	0.37	0.56	0.31	0.35	0.25	0.20	0.29	0.45	0.28	0.11	0.52	0.14

Table F.12: Peak heights of pentacyclic terpanes (from m/z 191 ion) for all hydrocarbon samples (page 3 of 8).

											total
31S	31R	GAM	32S	32R	33S	33R	34S	34R	35S	35R	Height
0.93	1.10	0.00	1.28	0.90	0.62	0.53	0.00	0.00	0.00	0.00	24.44
0.41	0.50	0.00	0.42	0.35	0.00	0.00	0.00	0.00	0.00	0.00	17.05
0.35	0.17	0.00	0.32	0.25	0.00	0.00	0.00	0.00	0.00	0.00	8.81
0.98	0.61	0.04	0.72	0.41	0.55	0.34	0.49	0.37	0.47	0.33	14.83
3.05	2.71	2.04	0.97	0.80	0.00	0.00	0.00	0.00	0.00	0.00	34.40
0.60	0.50	0.12	0.50	0.34	0.33	0.22	0.18	0.16	0.15	0.09	15.13
1.04	0.78	0.00	0.59	0.66	0.00	0.00	0.00	0.00	0.00	0.00	10.60
4.46	4.25	0.00	2.83	2.78	1.31	1.31	0.00	0.00	0.00	0.00	51.30
1.05	0.85	0.16	0.53	0.47	0.47	0.36	0.27	0.21	0.25	0.16	14.59
8.02	6.59	0.00	0.00	0.00	0.00	0.00	0.00	0.00	0.00	0.00	143.69
2.48	1.68	0.42	1.34	1.16	0.90	0.63	0.48	0.44	0.72	0.55	28.60
21.82	18.32	3.36	17.90	11.61	12.59	8.53	7.83	4.20	5.87	3.78	283.03
0	0	0	0	0	0	0	0	0	0	0	0
0.30	0.29	0.00	0.20	0.14	0.18	0.15	0.00	0.00	0.00	0.00	12.04
0.44	0.25	0.00	0.00	0.00	0.00	0.00	0.00	0.00	0.00	0.00	12.39
66.10	50.57	7.96	51.77	35.44	37.83	24.69	22.70	13.94	16.33	9.96	789.02
4.58	3.54	1.04	4.05	2.66	3.48	2.40	1.61	0.70	1.07	0.63	67.56
29.12	22.11	0.00	25.71	17.44	16.36	10.25	10.43	6.29	8.27	4.67	381.91
1.27	0.98	0.00	0.78	0.55	0.48	0.30	0.26	0.13	0.19	0.15	22.65
41.48	28.98	0.00	19.89	13.87	11.37	7.16	6.82	4.21	2.84	1.48	450.64
0.70	0.43	0.34	0.00	0.00	0.00	0.00	0.00	0.00	0.00	0.00	8.45
0.31	0.29	0.00	0.34	0.23	0.21	0.14	0.00	0.00	0.00	0.00	12.00
29.40	19.52	5.64	21.17	14.11	13.29	8.47	8.70	5.17	8.11	5.29	342.45
2.06	1.36	0.00	0.77	0.59	0.29	0.18	0.00	0.00	0.00	0.00	39.24
2.08	1.53	0.00	0.00	0.00	0.00	0.00	0.00	0.00	0.00	0.00	28.91
0.00	0.00	0.00	0.00	0.00	0.00	0.00	0.00	0.00	0.00	0.00	0.00
0.00	0.00	0.00	0.00	0.00	0.00	0.00	0.00	0.00	0.00	0.00	0.00
0.74	0.71	0.00	0.62	0.50	0.40	0.42	0.27	0.32	0.20	0.00	17.67
0.20	0.14	0.12	0.08	0.07	0.05	0.03	0.02	0.00	0.00	0.00	3.90
0.04	0.04	0.00	0.03	0.02	0.02	0.01	0.01	0.01	0.00	0.00	1.06
0.20	0.15	0.00	0.11	0.08	0.07	0.05	0.04	0.04	0.00	0.00	4.33
0.07	0.07	0.00	0.06	0.04	0.05	0.05	0.00	0.00	0.00	0.00	1.59
0.43	0.30	0.00	0.25	0.16	0.17	0.10	0.07	0.03	0.06	0.03	7.37
2.29	1.46	0.00	1.49	1.09	0.80	0.59	0.47	0.33	0.32	0.22	31.38
0.00	0.00	0.00	0.00	0.00	0.00	0.00	0.00	0.00	0.00	0.00	0.56
0.18	0.19	0.00	0.10	0.10	0.00	0.00	0.00	0.00	0.00	0.00	4.90

Table F.12: Peak heights of pentacyclic terpanes (from m/z 191 ion) for all hydrocarbon samples (page 4 of 8).

No.	28TR	28TS	29TR	29TS	Ts	Tm	30TS	30TR	bis	29nH	29nnH	30Dia	nM	Hop	Mor	31S	31R	GAM	32S	32R	33S	33R	34S	34R	35S	35R
SHALE SAMPLES																										
41	0	0	0	0	180	115	0	0	90	310	195	175	70	830	95	260	220	120	180	155	85	85	0	0	0	0
42	0	0	0	0	230	90	0	0	58	338	236	165	73	960	150	300	310	92	250	155	141	122	0	0	0	0
43	30	20	50	60	155	122	0	0	50	340	190	110	45	745	125	342	210	0	228	150	0	0	0	0	0	0
44	16	16	45	25	211	148	0	0	118	485	240	52	55	1020	100	260	161	10	105	76	56	28	0	0	0	0
45	86	90	94	82	208	358	60	48	76	474	165	160	70	580	100	220	155	60	106	91	54	46	22	20	40	30
46	72	60	105	81	305	173	62	55	333	795	447	275	68	2170	252	940	660	115	650	430	380	265	225	140	120	80
47	0	0	0	0	215	82	0	0	135	270	230	110	55	750	90	180	155	0	95	70	0	0	0	0	0	0
48	50	62	0	0	345	108	0	0	158	489	363	171	68	1008	104	288	192	0	175	136	96	71	50	41	0	0
49	31	47	25	48	125	232	35	83	50	435	170	56	204	960	310	265	321	0	86	145	45	63	20	31	13	26
50	68	46	96	54	165	242	28	40	1016	760	335	30	130	915	160	315	240	0	135	96	79	55	0	0	0	0
51	32	18	51	29	270	230	25	25	100	875	515	255	100	2170	330	945	670	0	590	400	370	235	240	152	115	71
52	120	110	105	110	140	380	75	50	4065	860	270	70	170	755	240	305	275	0	82	80	70	55	0	0	0	0
53	200	215	300	250	850	295	165	120	123	260	400	440	70	780	60	252	208	65	190	140	128	80	71	53	44	35
54	80	63	120	90	545	550	80	55	87	560	270	430	85	820	80	265	185	35	133	98	60	52	38	29	31	23
55	36	28	41	40	172	226	0	0	855	600	255	50	95	990	172	350	242	0	165	118	125	82	61	42	42	26
56	205	165	300	275	1550	430	210	195	200	530	1185	1640	120	2170	140	945	740	410	960	695	630	430	395	240	290	190
57	85	72	108	70	540	168	0	0	122	155	355	380	70	540	140	220	220	60	210	170	140	110	115	85	0	0
58	0	0	100	75	435	145	80	50	80	155	305	350	50	500	40	180	140	0	165	125	110	82	61	33	37	40
59	93	78	91	42	300	173	95	88	670	865	490	150	87	2170	260	860	590	100	595	420	510	330	275	175	195	120
60	60	45	60	40	490	145	60	55	255	600	610	450	60	2170	220	860	630	160	640	440	410	275	240	150	150	100
61	150	145	190	200	875	230	240	120	135	290	485	505	125	750	80	290	240	0	230	160	155	110	85	56	58	50
62	265	265	340	270	675	265	230	170	150	520	340	220	80	865	100	250	190	0	162	125	115	80	55	28	41	26
63	155	145	255	195	975	415	180	105	115	325	370	720	75	420	45	205	160	65	130	90	92	60	61	37	30	28
64	0	0	0	0	220	170	0	0	22	450	230	55	55	960	115	330	220	0	155	105	95	65	55	35	28	15
65	33	28	48	37	162	155	38	22	78	435	200	70	65	970	142	375	253	0	178	130	122	72	64	41	36	22
66	130	111	148	140	282	242	130	65	50	605	145	120	65	625	70	285	200	75	140	105	110	72	52	38	48	46
67	0	0	239	162	681	913	0	0	177	263	519	796	168	743	79	264	195	45	265	188	137	103	87	64	82	61
68	50	36	63	58	315	220	46	40	118	300	325	270	40	1020	125	330	240	0	215	150	135	95	80	50	43	24
69	65	65	94	85	148	178	64	59	20	595	210	18	77	925	145	279	185	0	155	103	114	74	65	45	27	18
70	175	178	400	246	838	216	0	0	93	200	305	293	63	333	66	89	69	0	82	52	45	37	30	16	62	28
T=tricyclic. 28,30 bis=28,30 bisnorhopane. nH=C29 norhopane. nnh=C29 norneohopane. Dia=C30 diahopane. nM=C30 normoretane. H=hopane. Mor=moretane.																										
GAM=gammacerane. 31S....=C31-35 24S or 24R stereo-isomers. bis=28,30 bisnorhopane.																										
Height=total peak heights.																										

Table F.12: Peak heights of pentacyclic terpanes (from m/z 191 ion) for all source rock samples (including annotation descriptions) (page 5 of 8).

height	28TR	28TS	29TR	29TS	Ts	Tm	30TS	30TR	bis	29nH	29nnH	30Dia	nM	Hop	Mor	31S	31R	GAM	32S	32R	33S	33R	34S	34R
3165	0.00	0.00	0.00	0.00	5.69	3.63	0.00	0.00	2.84	9.79	6.16	5.53	2.21	26.22	3.00	8.21	6.95	3.79	5.69	4.90	2.69	2.69	0.00	0.00
3670	0.00	0.00	0.00	0.00	6.27	2.45	0.00	0.00	1.58	9.21	6.43	4.50	1.99	26.16	4.09	8.17	8.45	2.51	6.81	4.22	3.84	3.32	0.00	0.00
2972	1.01	0.67	1.68	2.02	5.22	4.10	0.00	0.00	1.68	11.44	6.39	3.70	1.51	25.07	4.21	11.51	7.07	0.00	7.67	5.05	0.00	0.00	0.00	0.00
3227	0.50	0.50	1.39	0.77	6.54	4.59	0.00	0.00	3.66	15.03	7.44	1.61	1.70	31.61	3.10	8.06	4.99	0.31	3.25	2.36	1.74	0.87	0.00	0.00
3495	2.46	2.58	2.69	2.35	5.95	10.24	1.72	1.37	2.17	13.56	4.72	4.58	2.00	16.60	2.86	6.29	4.43	1.72	3.03	2.60	1.55	1.32	0.63	0.57
9258	0.78	0.65	1.13	0.87	3.29	1.87	0.67	0.59	3.60	8.59	4.83	2.97	0.73	23.44	2.72	10.15	7.13	1.24	7.02	4.64	4.10	2.86	2.43	1.51
2437	0.00	0.00	0.00	0.00	8.82	3.36	0.00	0.00	5.54	11.08	9.44	4.51	2.26	30.78	3.69	7.39	6.36	0.00	3.90	2.87	0.00	0.00	0.00	0.00
3975	1.26	1.56	0.00	0.00	8.68	2.72	0.00	0.00	3.97	12.30	9.13	4.30	1.71	25.36	2.62	7.25	4.83	0.00	4.40	3.42	2.42	1.79	1.26	1.03
3826	0.81	1.23	0.65	1.25	3.27	6.06	0.91	2.17	1.31	11.37	4.44	1.46	5.33	25.09	8.10	6.93	8.39	0.00	2.25	3.79	1.18	1.65	0.52	0.81
5005	1.36	0.92	1.92	1.08	3.30	4.84	0.56	0.80	20.30	15.18	6.69	0.60	2.60	18.28	3.20	6.29	4.80	0.00	2.70	1.92	1.58	1.10	0.00	0.00
8813	0.36	0.20	0.58	0.33	3.06	2.61	0.28	0.28	1.13	9.93	5.84	2.89	1.13	24.62	3.74	10.72	7.60	0.00	6.69	4.54	4.20	2.67	2.72	1.72
8387	1.43	1.31	1.25	1.31	1.67	4.53	0.89	0.60	48.47	10.25	3.22	0.83	2.03	9.00	2.86	3.64	3.28	0.00	0.98	0.95	0.83	0.66	0.00	0.00
5844	3.42	3.68	5.13	4.28	14.54	5.05	2.82	2.05	2.10	4.45	6.84	7.53	1.20	13.35	1.88	4.31	3.56	1.11	3.25	2.40	2.19	1.37	1.21	0.91
4884	1.64	1.29	2.46	1.84	11.16	11.26	1.64	1.13	1.78	11.47	5.53	8.80	1.74	16.79	2.05	5.43	3.79	0.72	2.72	2.01	1.23	1.06	0.78	0.59
4813	0.75	0.58	0.85	0.83	3.57	4.70	0.00	0.00	17.76	12.47	5.30	1.04	1.97	20.57	3.57	7.27	5.03	0.00	3.43	2.45	2.60	1.70	1.27	0.87
15570	1.32	1.06	1.93	1.77	9.96	2.76	1.35	1.25	1.28	3.40	7.61	10.53	0.77	13.94	3.02	6.07	4.75	2.63	6.17	4.46	4.05	2.76	2.54	1.54
4135	2.06	1.74	2.61	1.69	13.06	4.06	0.00	0.00	2.95	3.75	8.59	9.19	1.69	13.06	3.39	5.32	5.32	1.45	5.08	4.11	3.39	2.66	2.78	2.06
3398	0.00	0.00	2.94	2.21	12.80	4.27	2.35	1.47	2.35	4.56	8.98	10.30	1.47	14.71	2.94	5.30	4.12	0.00	4.86	3.68	3.24	2.41	1.80	0.97
9822	0.95	0.79	0.93	0.43	3.05	1.76	0.97	0.90	6.82	8.81	4.99	1.53	0.89	22.09	2.65	8.76	6.01	1.02	6.06	4.28	5.19	3.36	2.80	1.78
9375	0.64	0.48	0.64	0.43	5.23	1.55	0.64	0.59	2.72	6.40	6.51	4.80	0.64	23.15	2.35	9.17	6.72	1.71	6.83	4.69	4.37	2.93	2.56	1.60
5984	2.51	2.42	3.18	3.34	14.62	3.84	4.01	2.01	2.26	4.85	8.10	8.44	2.09	12.53	1.84	4.85	4.01	0.00	3.84	2.67	2.59	1.84	1.42	0.94
5827	4.55	4.55	5.83	4.63	11.58	4.55	3.95	2.92	2.57	8.92	5.83	3.78	1.37	14.84	1.72	4.29	3.26	0.00	2.78	2.15	1.97	1.37	0.94	0.48
5613	2.76	2.58	4.54	3.47	17.37	7.39	3.21	1.87	2.05	5.79	6.59	12.83	1.34	7.48	3.65	3.65	2.85	1.16	2.32	1.60	1.64	1.07	1.09	0.66
3380	0.00	0.00	0.00	0.00	6.51	5.03	0.00	0.00	0.65	13.31	6.80	1.63	1.63	28.40	3.40	9.76	6.51	0.00	4.59	3.11	2.81	1.92	1.63	1.04
3776	0.87	0.74	1.27	0.98	4.29	4.10	1.01	0.58	2.07	11.52	5.30	1.85	1.72	25.69	3.76	9.93	6.70	0.00	4.71	3.44	3.23	1.91	1.69	1.09
4099	3.17	2.71	3.61	3.42	6.88	5.90	3.17	1.59	1.22	14.76	3.54	2.93	1.59	15.25	1.71	6.95	4.88	1.83	3.42	2.56	2.68	1.76	1.27	0.93
6331	0.00	0.00	3.78	2.56	10.76	14.42	0.00	0.00	2.80	4.15	8.20	12.57	2.65	11.74	2.83	4.17	3.08	0.71	4.19	2.97	2.16	1.63	1.37	1.01
4388	1.14	0.82	1.44	1.32	7.18	5.01	1.05	0.91	2.69	6.84	7.41	6.15	0.91	23.25	2.85	7.52	5.47	0.00	4.90	3.42	3.08	2.16	1.82	1.14
3813	1.70	1.70	2.47	2.23	3.88	4.67	1.68	1.55	0.52	15.60	5.51	0.47	2.02	24.26	3.80	7.32	4.85	0.00	4.07	2.70	2.99	1.94	1.70	1.18
3916	4.47	4.55	10.21	6.28	21.40	5.52	0.00	0.00	2.37	5.11	7.79	7.48	1.61	8.50	1.69	2.27	1.76	0.00	2.09	1.33	1.15	0.94	0.77	0.41

Table F.12: Peak heights of pentacyclic terpanes (from m/z 191 ion) for all source rock samples (page 6 of 8).

35S	35R	191/5	%	TIC	% of TIC	28TR	28TS	29TR	29TS	Ts	Tm	30TS	30TR	bis	29nH	29nnH	30Dia	nM	Hop	Mor
0.00	0.00	74752	90	2996810	2.2449	0.00	0.00	0.00	0.00	12.77	8.16	0.00	0.00	6.38	21.99	13.83	12.41	4.97	58.87	6.74
0.00	0.00	190464	90	38066756	0.4503	0.00	0.00	0.00	0.00	2.82	1.10	0.00	0.00	0.71	4.15	2.90	2.02	0.90	11.78	1.84
0.00	0.00	60160	92	2973593	1.8613	1.88	1.25	3.13	3.76	9.71	7.64	0.00	0.00	3.13	21.29	11.90	6.89	2.82	46.66	7.83
0.00	0.00	46080	100	1842646	2.5008	1.24	1.24	3.49	1.94	16.35	11.47	0.00	0.00	9.14	37.58	18.60	4.03	4.26	79.04	7.75
1.14	0.86	49664	80	8145098	0.4878	1.20	1.26	1.31	1.14	2.90	5.00	0.84	0.67	1.06	6.62	2.30	2.23	0.98	8.09	1.40
1.30	0.86	258560	100	1466360	17.6328	13.71	11.43	20.00	15.43	58.09	32.95	11.81	10.48	63.42	151.42	85.14	52.38	12.95	413.30	48.00
0.00	0.00	29184	90	4217116	0.6228	0.00	0.00	0.00	0.00	5.49	2.10	0.00	0.00	3.45	6.90	5.88	2.81	1.41	19.17	2.30
0.00	0.00	13312	88	3750200	0.3124	0.39	0.49	0.00	0.00	2.71	0.85	0.00	0.00	1.24	3.84	2.85	1.34	0.53	7.92	0.82
0.34	0.68	823296	100	12661814	6.5022	5.27	7.99	4.25	8.16	21.24	39.43	5.95	14.11	8.50	73.93	28.89	9.52	34.67	163.15	52.68
0.00	0.00	331776	100	16039989	2.0684	2.81	1.90	3.97	2.23	6.82	10.00	1.16	1.65	41.99	31.41	13.84	1.24	5.37	37.81	6.61
1.30	0.81	533504	100	1478650	36.0805	13.10	7.37	20.88	11.87	110.54	94.16	10.24	10.24	40.94	358.23	210.84	104.40	40.94	888.40	135.10
0.00	0.00	339968	99	5310662	6.3376	9.07	8.31	7.93	8.31	10.58	28.71	5.67	3.78	307.17	64.99	20.40	5.29	12.85	57.05	18.14
0.75	0.60	135168	70	24497028	0.3862	1.32	1.42	1.98	1.65	5.62	1.95	1.09	0.79	0.81	1.72	2.64	2.91	0.46	5.16	0.73
0.63	0.47	182272	80	20598612	0.7079	1.16	0.91	1.74	1.30	7.90	7.97	1.16	0.80	1.26	8.12	3.91	6.23	1.23	11.89	1.45
0.87	0.54	1081344	100	20740248	5.2137	3.90	3.03	4.44	4.33	18.63	24.48	0.00	0.00	92.62	65.00	27.62	5.42	10.29	107.24	18.63
1.86	1.22	47040	100	2625530	1.7916	2.36	1.90	3.45	3.16	17.84	4.95	2.42	2.24	2.30	6.10	13.64	18.87	1.38	24.97	5.41
0.00	0.00	66560	78	27429660	0.1893	0.39	0.33	0.49	0.32	2.47	0.77	0.00	0.00	0.56	0.71	1.62	1.74	0.32	2.47	0.64
1.09	1.18	129024	80	13790277	0.7485	0.00	0.00	2.20	1.65	9.58	3.19	1.76	1.10	1.76	3.41	6.72	7.71	1.10	11.01	2.20
1.99	1.22	826368	100	4440060	18.6116	17.62	14.78	17.24	7.96	56.85	32.78	18.00	16.68	126.96	163.91	92.85	28.42	16.49	411.19	49.27
1.60	1.07	225536	100	2494460	9.0415	5.79	4.34	5.79	3.86	47.26	13.98	5.79	5.30	24.59	57.87	58.83	43.40	5.79	209.28	21.22
0.97	0.84	224256	74	43736320	0.3794	0.95	0.92	1.20	1.27	5.55	1.46	1.52	0.76	0.86	1.84	3.08	3.20	0.79	4.76	0.70
0.70	0.45	190464	75	34008720	0.4200	1.91	1.91	2.45	1.95	4.87	1.91	1.66	1.23	1.08	3.75	2.45	1.59	0.58	6.24	0.72
0.53	0.50	12032	66	5070991	0.1566	0.43	0.40	0.71	0.54	2.72	1.16	0.50	0.29	0.32	0.91	1.03	2.01	0.21	1.17	0.57
0.83	0.44	254976	94	7804665	3.0710	0.00	0.00	0.00	0.00	19.99	15.45	0.00	0.00	2.00	40.89	20.90	5.00	5.00	87.22	10.45
0.95	0.58	843776	99	14089057	5.9290	5.18	4.40	7.54	5.81	25.44	24.34	5.97	3.45	12.25	68.30	31.40	10.99	10.21	152.31	22.30
1.17	1.12	147456	65	22950544	0.4176	1.32	1.13	1.51	1.43	2.87	2.47	1.32	0.66	0.51	6.16	1.48	1.22	0.66	6.37	0.71
1.30	0.96	8064	70	2403406	0.2349	0.00	0.00	0.89	0.60	2.53	3.39	0.00	0.00	0.66	0.98	1.93	2.95	0.62	2.76	0.66
0.98	0.55	901120	90	29405236	2.7580	3.14	2.26	3.96	3.65	19.80	13.83	2.89	2.51	7.42	18.86	20.43	16.97	2.51	64.11	7.86
0.71	0.47	352256	100	4685930	7.5173	12.81	12.81	18.53	16.76	29.18	35.09	12.62	11.63	3.94	117.30	41.40	3.55	15.18	182.36	28.59
1.58	0.72	21248	92	15405633	0.1269	0.57	0.58	1.30	0.80	2.72	0.70	0.00	0.00	0.30	0.65	0.99	0.95	0.20	1.08	0.21

Table F.12: Peak heights of pentacyclic terpanes (from m/z 191 ion) for all source rock samples (page 7 of 8).

31S	31R	GAM	32S	32R	33S	33R	34S	34R	35S	35R	Height
18.44	15.60	8.51	12.77	10.99	6.03	6.03	0.00	0.00	0.00	0.00	224.49
3.68	3.80	1.13	3.07	1.90	1.73	1.50	0.00	0.00	0.00	0.00	45.03
21.42	13.15	0.00	14.28	9.39	0.00	0.00	0.00	0.00	0.00	0.00	186.13
20.15	12.48	0.77	8.14	5.89	4.34	2.17	0.00	0.00	0.00	0.00	250.08
3.07	2.16	0.84	1.48	1.27	0.75	0.64	0.31	0.28	0.56	0.42	48.78
179.03	125.70	21.90	123.80	81.90	72.37	50.47	42.85	26.66	22.86	15.24	1763.28
4.60	3.96	0.00	2.43	1.79	0.00	0.00	0.00	0.00	0.00	0.00	62.28
2.26	1.51	0.00	1.38	1.07	0.75	0.56	0.39	0.32	0.00	0.00	31.24
45.04	54.55	0.00	14.62	24.64	7.65	10.71	3.40	5.27	2.21	4.42	650.22
13.02	9.92	0.00	5.58	3.97	3.26	2.27	0.00	0.00	0.00	0.00	206.84
386.88	274.30	0.00	241.55	163.76	151.48	96.21	98.26	62.23	47.08	29.07	3608.05
23.05	20.78	0.00	6.20	6.05	5.29	4.16	0.00	0.00	0.00	0.00	633.76
1.67	1.37	0.43	1.26	0.93	0.85	0.53	0.47	0.35	0.29	0.23	38.62
3.84	2.68	0.51	1.93	1.42	0.87	0.75	0.55	0.42	0.45	0.33	70.79
37.91	26.21	0.00	17.87	12.78	13.54	8.88	6.61	4.55	4.55	2.82	521.37
10.87	8.52	4.72	11.05	8.00	7.25	4.95	4.55	2.76	3.34	2.19	179.16
1.01	1.01	0.27	0.96	0.78	0.64	0.50	0.53	0.39	0.00	0.00	18.93
3.96	3.08	0.00	3.63	2.75	2.42	1.81	1.34	0.73	0.82	0.88	74.85
162.96	111.80	18.95	112.75	79.59	96.64	62.53	52.11	33.16	36.95	22.74	1861.16
82.94	60.76	15.43	61.72	42.43	39.54	26.52	23.15	14.47	14.47	9.64	904.15
1.84	1.52	0.00	1.46	1.01	0.98	0.70	0.54	0.36	0.37	0.32	37.94
1.80	1.37	0.00	1.17	0.90	0.83	0.58	0.40	0.20	0.30	0.19	42.00
0.57	0.45	0.18	0.36	0.25	0.26	0.17	0.17	0.10	0.08	0.08	15.66
29.98	19.99	0.00	14.08	9.54	8.63	5.91	5.00	3.18	2.54	1.36	307.10
58.88	39.73	0.00	27.95	20.41	19.16	11.31	10.05	6.44	5.65	3.45	592.90
2.90	2.04	0.76	1.43	1.07	1.12	0.73	0.53	0.39	0.49	0.47	41.76
0.98	0.72	0.17	0.98	0.70	0.51	0.38	0.32	0.24	0.30	0.23	23.49
20.74	15.08	0.00	13.51	9.43	8.49	5.97	5.03	3.14	2.70	1.51	275.80
55.00	36.47	0.00	30.56	20.31	22.48	14.59	12.81	8.87	5.32	3.55	751.73
0.29	0.22	0.00	0.27	0.17	0.15	0.12	0.10	0.05	0.20	0.09	12.69

Table F.12: Peak heights of pentacyclic terpanes (from m/z 191 ion) for all source rock samples (page 8 of 8).

MONOAROMATIC STEROIDS (MEASURED FROM SATURATED FRACTION)																total	NORMALIZED PEAK HEIGHTS								NORMAL	
No.	1	2	3	4	5	6+7	9	10	11	12	13	14	15	16	height	1	2	3	4	5	6+7	9	10	11	12
OIL SAMPLES																Oil samples										
1	32	105	60	127	49	222	34	66	100	190	32	57	91	56	1221	2.62	8.60	4.91	10.40	4.01	18.18	2.78	5.41	8.19	15.56
2	41	63	49	127	75	129	42	127	106	137	59	70	103	70	1198	3.42	5.26	4.09	10.60	6.26	10.77	3.51	10.60	8.85	11.44
3	155	330	180	220	147	340	352	334	83	234	290	223	218	323	3429	4.52	9.62	5.25	6.42	4.29	9.92	10.27	9.74	2.42	6.82
4	245	425	345	510	760	745	1050	472	395	315	170	318	324	200	6274	3.91	6.77	5.50	8.13	12.11	11.87	16.74	7.52	6.30	5.02
5	295	282	127	73	64	222	820	172	90	83	181	150	230	205	2994	9.85	9.42	4.24	2.44	2.14	7.41	27.39	5.74	3.01	2.77
6	287	495	315	152	94	253	1050	189	161	250	592	461	250	355	4904	5.85	10.09	6.42	3.10	1.92	5.16	21.41	3.85	3.28	5.10
7	160	310	95	290	60	460	472	519	161	124	85	206	101	135	3178	5.03	9.75	2.99	9.13	1.89	14.47	14.85	16.33	5.07	3.90
8	850	440	240	318	160	427	281	323	435	310	145	130	240	145	4444	19.13	9.90	5.40	7.16	3.60	9.61	6.32	7.27	9.79	6.98
9	360	487	275	545	280	980	734	735	200	282	305	440	236	155	6014	5.99	8.10	4.57	9.06	4.66	16.30	12.20	12.22	3.33	4.69
10	205	800	150	540	180	800	674	832	127	353	260	483	137	240	5781	3.55	13.84	2.59	9.34	3.11	13.84	11.66	14.39	2.20	6.11
11	340	130	137	252	110	530	423	393	150	161	182	172	120	130	3230	10.53	4.02	4.24	7.80	3.41	16.41	13.10	12.17	4.64	4.98
12	300	162	281	335	375	730	623	249	192	232	194	242	202	240	4357	6.89	3.72	6.45	7.69	8.61	16.75	14.30	5.71	4.41	5.32
13	92	124	28	286	55	50	98	108	47	20	81	56	53	126	1224	7.52	10.13	2.29	23.37	4.49	4.08	8.01	8.82	3.84	1.63
14	68	136	56	175	108	296	225	262	57	43	42	109	80	121	1778	3.82	7.65	3.15	9.84	6.07	16.65	12.65	14.74	3.21	2.42
15	0	0	0	0	0	0	0	0	0	0	0	0	0	0	0	0.00	0.00	0.00	0.00	0.00	0.00	0.00	0.00	0.00	0.00
16	220	127	228	178	85	451	262	298	61	112	50	83	61	78	2294	9.59	5.54	9.94	7.76	3.71	19.66	11.42	12.99	2.66	4.88
17	230	132	227	171	101	532	99	108	230	113	25	110	55	75	2208	10.42	5.98	10.28	7.74	4.57	24.09	4.48	4.89	10.42	5.12
18	66	251	70	182	60	648	508	584	118	97	111	272	122	101	3190	2.07	7.87	2.19	5.71	1.88	20.31	15.92	18.31	3.70	3.04
19	245	122	43	165	75	218	166	180	35	36	31	60	68	51	1495	16.39	8.16	2.88	11.04	5.02	14.58	11.10	12.04	2.34	2.41
20	50	115	48	81	31	240	169	178	39	33	61	70	58	78	1251	4.00	9.19	3.84	6.47	2.48	19.18	13.51	14.23	3.12	2.64
21	410	218	135	202	42	270	293	312	141	143	55	141	199	185	2746	14.93	7.94	4.92	7.36	1.53	9.83	10.67	11.36	5.13	5.21
22	105	435	155	385	75	1015	725	660	211	152	75	350	105	70	4518	2.32	9.63	3.43	8.52	1.66	22.47	16.05	14.61	4.67	3.36
23	200	403	290	290	195	625	500	450	85	198	270	208	237	183	4134	4.84	9.75	7.01	7.01	4.72	15.12	12.09	10.89	2.06	4.79
24	780	300	90	205	100	470	352	331	161	87	91	101	91	78	3237	24.10	9.27	2.78	6.33	3.09	14.52	10.87	10.23	4.97	2.69
25	114	167	62	117	65	253	279	297	58	61	69	132	101	121	1896	6.01	8.81	3.27	6.17	3.43	13.34	14.72	15.66	3.06	3.22
26	235	365	105	440	190	555	697	851	105	110	100	364	75	20	4212	5.58	8.67	2.49	10.45	4.51	13.18	16.55	20.20	2.49	2.61
27	530	121	215	221	161	551	371	387	136	156	165	169	100	141	3424	15.48	3.53	6.28	6.45	4.70	16.09	10.84	11.30	3.97	4.56
28	21	62	81	44	15	9	27	31	141	101	32	21	55	31	671	3.13	9.24	12.07	6.56	2.24	1.34	4.02	4.62	21.01	15.05
29	108	191	49	113	26	225	126	112	169	118	37	68	86	91	1519	7.11	12.57	3.23	7.44	1.71	14.81	8.29	7.37	11.13	7.77
30	241	268	145	347	216	305	478	185	191	110	217	266	173	114	3256	7.40	8.23	4.45	10.66	6.63	9.37	14.68	5.68	5.87	3.38
31	275	502	168	498	137	892	712	568	360	351	119	389	183	112	5266	5.22	9.53	3.19	9.46	2.60	16.94	13.52	10.79	6.84	6.67
32	120	457	403	553	132	714	621	570	322	170	68	248	102	70	4550	2.64	10.04	8.86	12.15	2.90	15.69	13.65	12.53	7.08	3.74
33	556	637	237	851	132	772	664	632	259	464	214	302	229	192	6141	9.05	10.37	3.86	13.86	2.15	12.57	10.81	10.29	4.22	7.56
34	275	248	156	253	204	363	341	236	505	272	123	256	180	187	3599	7.64	6.89	4.33	7.03	5.67	10.09	9.47	6.56	14.03	7.56
35	191	341	100	328	70	988	990	550	186	113	58	342	82	91	4430	4.31	7.70	2.26	7.40	1.58	22.30	22.35	12.42	4.20	2.55
36	173	411	158	369	69	1042	782	594	178	193	142	398	190	149	4848	3.57	8.48	3.26	7.61	1.42	21.49	16.13	12.25	3.67	3.98
37	251	472	152	332	184	400	442	135	365	229	163	235	197	402	3959	6.34	11.92	3.84	8.39	4.65	10.10	11.16	3.41	9.22	5.78

Table F.13: Peak heights of monoaromatic steroids from saturates fraction (m/z 253) for all hydrocarbon samples (page 1 of 4).

ZED PEAK HEIGHTS				Calibration peaks			height%	PEAK HEIGHTS IN ppm TIC													total
13	14	15	16	253	%	TIC	of TIC	1	2	3	4	5	6+7	9	10	11	12	13	14	15	16	height
2.62	4.67	7.45	4.59	151208	100	not given																
4.92	5.84	8.60	5.84	36062	100	not given																
8.46	6.50	6.36	9.42	12096	68	50525576	0.02	0.07	0.16	0.09	0.10	0.07	0.16	0.17	0.16	0.04	0.11	0.14	0.11	0.10	0.15	1.63
2.71	5.07	5.16	3.19	14464	93	15240681	0.09	0.34	0.60	0.49	0.72	1.07	1.05	1.48	0.66	0.56	0.44	0.24	0.45	0.46	0.28	8.83
6.05	5.01	7.68	6.85	5568	65	15674129	0.02	0.23	0.22	0.10	0.06	0.05	0.17	0.63	0.13	0.07	0.06	0.14	0.12	0.18	0.16	2.31
12.07	9.40	5.10	7.24	4064	95	11395480	0.03	0.20	0.34	0.22	0.11	0.06	0.17	0.73	0.13	0.11	0.17	0.41	0.32	0.17	0.25	3.39
2.67	6.48	3.18	4.25	6656	84	12127489	0.05	0.23	0.45	0.14	0.42	0.09	0.67	0.68	0.75	0.23	0.18	0.12	0.30	0.15	0.20	4.61
3.26	2.93	5.40	3.26	19968	85	23964526	0.07	1.35	0.70	0.38	0.51	0.25	0.68	0.45	0.51	0.69	0.49	0.23	0.21	0.38	0.23	7.08
5.07	7.32	3.92	2.58	5632	72	41919776	0.01	0.06	0.08	0.04	0.09	0.05	0.16	0.12	0.12	0.03	0.05	0.05	0.07	0.04	0.02	0.97
4.50	8.35	2.37	4.15	19456	68	21878084	0.06	0.21	0.84	0.16	0.56	0.19	0.84	0.71	0.87	0.13	0.37	0.27	0.51	0.14	0.25	6.05
5.63	5.33	3.72	4.02	97280	82	57270776	0.14	1.47	0.56	0.59	1.09	0.47	2.29	1.82	1.69	0.65	0.69	0.78	0.74	0.52	0.56	13.93
4.45	5.55	4.64	5.51	9408	75	4489776	0.16	1.08	0.58	1.01	1.21	1.35	2.63	2.25	0.90	0.69	0.84	0.70	0.87	0.73	0.87	15.72
6.62	4.58	4.33	10.29	30016	100	2797560	1.07	8.06	10.87	2.45	25.07	4.82	4.38	8.59	9.47	4.12	1.75	7.10	4.91	4.65	11.04	107.29
2.36	6.13	4.50	6.81	22720	100	1650680	1.38	5.26	10.53	4.34	13.55	8.36	22.91	17.42	20.28	4.41	3.33	3.25	8.44	6.19	9.37	137.64
0.00	0.00	0.00	0.00	2640	70	14397592	0.01	0.00	0.00	0.00	0.00	0.00	0.00	0.00	0.00	0.00	0.00	0.00	0.00	0.00	0.00	0.00
2.18	3.62	2.66	3.40	33536	100	39775156	0.08	0.81	0.47	0.84	0.65	0.31	1.66	0.96	1.10	0.22	0.41	0.18	0.31	0.22	0.29	8.43
1.13	4.98	2.49	3.40	36834	90	41658924	0.08	0.83	0.48	0.82	0.62	0.36	1.92	0.36	0.39	0.83	0.41	0.09	0.40	0.20	0.27	7.96
3.48	8.53	3.82	3.17	37120	100	2060280	1.80	3.73	14.18	3.95	10.28	3.39	36.60	28.69	32.98	6.66	5.48	6.27	15.36	6.89	5.70	180.17
2.07	4.01	4.55	3.41	22496	100	3481590	0.65	10.59	5.27	1.86	7.13	3.24	9.42	7.17	7.78	1.51	1.56	1.34	2.59	2.94	2.20	64.61
4.88	5.60	4.64	6.24	26272	100	1816570	1.45	5.78	13.29	5.55	9.36	3.58	27.75	19.54	20.58	4.51	3.82	7.05	8.09	6.71	9.02	144.62
2.00	5.13	7.25	6.74	33792	80	46799776	0.06	0.86	0.46	0.28	0.42	0.09	0.57	0.62	0.66	0.30	0.30	0.12	0.30	0.42	0.39	5.78
1.66	7.75	2.32	1.55	81920	100	4385538	1.87	4.34	17.98	6.41	15.92	3.10	41.96	29.97	27.29	8.72	6.28	3.10	14.47	4.34	2.89	186.80
6.53	5.03	5.73	4.43	12992	68	48692176	0.02	0.09	0.18	0.13	0.13	0.09	0.27	0.22	0.20	0.04	0.09	0.12	0.09	0.10	0.08	1.81
2.81	3.12	2.81	2.41	25088	100	21499806	0.12	2.81	1.08	0.32	0.74	0.36	1.69	1.27	1.19	0.58	0.31	0.33	0.36	0.33	0.28	11.67
3.64	6.96	5.33	6.38	37184	100	2564090	1.45	8.72	12.77	4.74	8.95	4.97	19.35	21.34	22.72	4.44	4.67	5.28	10.10	7.73	9.25	145.02
2.37	8.64	1.78	0.47	14528	85	15264194	0.08	0.45	0.70	0.20	0.85	0.36	1.07	1.34	1.63	0.20	0.21	0.19	0.70	0.14	0.04	8.09
4.82	4.94	2.92	4.12	25344	85	15091152	0.14	2.21	0.50	0.90	0.92	0.67	2.30	1.55	1.61	0.57	0.65	0.69	0.70	0.42	0.59	14.27
4.77	3.13	8.20	4.62	1.80E+07	100	not given																
2.44	4.48	5.66	5.99	1.50E+06	100	not given																
6.66	8.17	5.31	3.50	13760	70	53232480	0.02	0.13	0.15	0.08	0.19	0.12	0.17	0.27	0.10	0.11	0.06	0.12	0.15	0.10	0.06	1.81
2.26	7.39	3.48	2.13	6464	90	43072448	0.01	0.07	0.13	0.04	0.13	0.04	0.23	0.18	0.15	0.09	0.09	0.03	0.10	0.05	0.03	1.35
1.49	5.45	2.24	1.54	7552	90	49652964	0.01	0.04	0.14	0.12	0.17	0.04	0.21	0.19	0.17	0.10	0.05	0.02	0.07	0.03	0.02	1.37
3.48	4.92	3.73	3.13	7552	92	34718336	0.02	0.18	0.21	0.08	0.28	0.04	0.25	0.22	0.21	0.08	0.15	0.07	0.10	0.07	0.06	2.00
3.42	7.11	5.00	5.20	2144	75	25321986	0.01	0.05	0.04	0.03	0.04	0.04	0.06	0.06	0.04	0.09	0.05	0.02	0.05	0.03	0.03	0.64
1.31	7.72	1.85	2.05	19200	100	57018460	0.03	0.15	0.26	0.08	0.25	0.05	0.75	0.75	0.42	0.14	0.09	0.04	0.26	0.06	0.07	3.37
2.93	8.21	3.92	3.07	9088	92	5312698	0.16	0.56	1.33	0.51	1.20	0.22	3.38	2.54	1.93	0.58	0.63	0.46	1.29	0.62	0.48	15.74
4.12	5.94	4.98	10.15	1696	85	13118981	0.01	0.07	0.13	0.04	0.09	0.05	0.11	0.12	0.04	0.10	0.06	0.05	0.07	0.05	0.11	1.10

Table F.13: Peak heights of monoaromatic steroids from saturates fraction (m/z 253) for all hydrocarbon samples (page 2 of 4).

No.	1	2	3	4	5	6+7	9	10	11	12	13	14	15	16	height	1	2	3	4	5	6+7	9	10	11	12
38	185	380	137	227	217	562	173	141	409	333	123	230	195	159	3471	5.33	10.95	3.95	6.54	6.25	16.19	4.98	4.06	11.78	9.59
SHALE SAMPLES																									
41	100	645	375	570	130	900	812	1020	228	310	150	575	200	180	6195	1.61	10.41	6.05	9.20	2.10	14.53	13.11	16.46	3.68	5.00
42	85	630	220	470	65	880	193	761	148	226	85	400	165	280	4608	1.84	13.67	4.77	10.20	1.41	19.10	4.19	16.51	3.21	4.90
43	130	685	305	685	170	110	981	1178	290	350	205	586	258	190	6123	2.12	11.19	4.98	11.19	2.78	1.80	16.02	19.24	4.74	5.72
44	135	285	90	290	100	935	100	1035	172	150	125	270	320	70	4077	3.31	6.99	2.21	7.11	2.45	22.93	2.45	25.39	4.22	3.68
45	980	420	260	745	370	620	498	537	802	747	150	435	612	320	7496	13.07	5.60	3.47	9.94	4.94	8.27	6.64	7.16	10.70	9.97
46	100	400	152	291	50	841	90	853	195	225	152	433	200	121	4103	2.44	9.75	3.70	7.09	1.22	20.50	2.19	20.79	4.75	5.48
47	210	520	340	515	410	880	1080	973	224	323	145	578	184	125	6507	3.23	7.99	5.23	7.91	6.30	13.52	16.60	14.95	3.44	4.96
48	108	389	170	380	140	780	750	840	221	237	385	359	159	100	5018	2.15	7.75	3.39	7.57	2.79	15.54	14.95	16.74	4.40	4.72
49	145	155	30	275	170	1010	1050	882	63	38	65	461	58	290	4692	3.09	3.30	0.64	5.86	3.62	21.53	22.38	18.80	1.34	0.81
50	235	440	110	555	185	1040	1028	935	121	88	220	558	91	200	5806	4.05	7.58	1.89	9.56	3.19	17.91	17.71	16.10	2.08	1.52
51	54	291	96	238	70	1018	798	678	232	124	104	302	152	55	4212	1.28	6.91	2.28	5.65	1.66	24.17	18.95	16.10	5.51	2.94
52	95	290	70	365	50	1075	880	686	101	51	78	290	59	78	4168	2.28	6.96	1.68	8.76	1.20	25.79	21.11	16.46	2.42	1.22
53	491	600	300	440	160	825	511	537	386	250	105	308	195	80	5188	9.46	11.57	5.78	8.48	3.08	15.90	9.85	10.35	7.44	4.82
54	830	420	240	365	145	560	381	419	411	241	102	256	212	100	4682	17.73	8.97	5.13	7.80	3.10	11.96	8.14	8.95	8.78	5.15
55	155	355	85	375	125	1055	777	598	119	56	118	190	56	112	4176	3.71	8.50	2.04	8.98	2.99	25.26	18.61	14.32	2.85	1.34
56	41	139	61	86	30	235	173	204	53	48	61	81	85	80	1377	2.98	10.09	4.43	6.25	2.18	17.07	12.56	14.81	3.85	3.49
57	80	665	280	395	140	990	709	653	269	260	150	306	153	130	5180	1.54	12.84	5.41	7.63	2.70	19.11	13.69	12.61	5.19	5.02
58	660	610	260	430	190	1035	142	238	710	600	95	183	350	135	5638	11.71	10.82	4.61	7.63	3.37	18.36	2.52	4.22	12.59	10.64
59	115	351	105	290	80	910	980	735	200	155	178	450	168	125	4842	2.38	7.25	2.17	5.99	1.65	18.79	20.24	15.18	4.13	3.20
60	55	208	72	171	65	565	501	517	123	104	116	225	117	77	2916	1.89	7.13	2.47	5.86	2.23	19.38	17.18	17.73	4.22	3.57
61	460	140	250	410	115	800	572	475	553	230	94	292	231	102	4724	9.74	2.96	5.29	8.68	2.43	16.93	12.11	10.06	11.71	4.87
62	580	94	255	480	140	745	460	511	421	252	109	302	208	157	4714	12.30	1.99	5.41	10.18	2.97	15.80	9.76	10.84	8.93	5.35
63	520	160	260	370	120	510	369	376	248	414	80	250	222	140	4039	12.87	3.96	6.44	9.16	2.97	12.63	9.14	9.31	6.14	10.25
64	132	500	150	460	84	1020	798	710	158	112	94	413	94	116	4841	2.73	10.33	3.10	9.50	1.74	21.07	16.48	14.67	3.26	2.31
65	115	440	130	405	100	1035	809	736	181	129	105	449	111	125	4870	2.36	9.03	2.67	8.32	2.05	21.25	16.61	15.11	3.72	2.65
66	920	340	205	240	102	507	398	374	113	173	155	472	71	274	4344	21.18	7.83	4.72	5.52	2.35	11.67	9.16	8.61	2.60	3.98
67	175	211	328	223	141	435	255	86	260	255	85	180	261	203	3098	5.65	6.81	10.59	7.20	4.55	14.04	8.23	2.78	8.39	8.23
68	160	615	250	505	140	980	678	698	261	235	120	436	178	130	5386	2.97	11.42	4.64	9.38	2.60	18.20	12.59	12.96	4.85	4.36
69	160	292	70	360	125	1030	884	760	122	71	160	393	66	140	4633	3.45	6.30	1.51	7.77	2.70	22.23	19.08	16.40	2.63	1.53
70	321	589	272	920	168	908	686	911	542	373	170	753	372	271	7256	4.42	8.12	3.75	12.68	2.32	12.51	9.45	12.56	7.47	5.14
Peaks labelled after Riolo et al., 1986, Org. Geochem. 10, 981-990 and Mackenzie et al., 1983, Advances in Org. Geoch., 1981.																									
Height=height of maximum ion in m/z 253 fragmentogram.																									
1=C27 20S Reg5b. 2=C27 20S Dia10b. 3=C27 20S Dia10a. 4=C27 20R Reg5b+10b. 5=C27 20S Reg5a. 6=C28 20S Reg5b.																									
7=C27 20R Dia10a+C28 20S Dia10b. 9=C27 20R Reg5a+C28 20S Reg5a. 10=C28 20R Reg5b+Dia10b+C29 20S Reg5b+Dia10b. 11=C28 20R Dia10a.																									
12=C29 20S Dia10a. 13=C29 20S Reg5a. 14=C28 20R Reg5a+C29 20R Reg5b+Dia10b. 15=C29 20R Dia10a. 16=C29 20R Reg5a.																									

Table F.13: Peak heights of monoaromatic steroids from saturates fraction (m/z 253) for all source rock samples (including annotations) (page 3 of 4).

13	14	15	16	253	%	TIC	of TIC	1	2	3	4	5	6+7	9	10	11	12	13	14	15	16	height
3.54	6.63	5.62	4.58	3024	84	5130069	0.05	0.26	0.54	0.20	0.32	0.31	0.80	0.25	0.20	0.58	0.48	0.18	0.33	0.28	0.23	4.95
2.42	9.28	3.23	2.91	8704	90	2996810	0.26	0.42	2.72	1.58	2.41	0.55	3.80	3.43	4.30	0.96	1.31	0.63	2.43	0.84	0.76	26.14
1.84	8.68	3.58	6.08	22272	90	38066756	0.05	0.10	0.72	0.25	0.54	0.07	1.01	0.22	0.87	0.17	0.26	0.10	0.46	0.19	0.32	5.27
3.35	9.57	4.21	3.10	5440	88	2973593	0.16	0.34	1.80	0.80	1.80	0.45	0.29	2.58	3.10	0.76	0.92	0.54	1.54	0.68	0.50	16.10
3.07	6.62	7.85	1.72	6144	91	1842646	0.30	1.00	2.12	0.67	2.16	0.74	6.96	0.74	7.70	1.28	1.12	0.93	2.01	2.38	0.52	30.34
2.00	5.80	8.16	4.27	4672	70	8145098	0.04	0.52	0.22	0.14	0.40	0.20	0.33	0.27	0.29	0.43	0.40	0.08	0.23	0.33	0.17	4.02
3.70	10.55	4.87	2.95	32128	100	1466360	2.19	5.34	21.36	8.12	15.54	2.67	44.91	4.81	45.55	10.41	12.02	8.12	23.12	10.68	6.46	219.10
2.23	8.88	2.83	1.92	2576	84	4217116	0.05	0.17	0.41	0.27	0.41	0.32	0.69	0.85	0.77	0.18	0.25	0.11	0.46	0.15	0.10	5.13
7.67	7.15	3.17	1.99	3408	88	3750200	0.08	0.17	0.62	0.27	0.61	0.22	1.24	1.20	1.34	0.35	0.38	0.61	0.57	0.25	0.16	8.00
1.39	9.83	1.24	6.18	1736704	100	12661814	13.72	42.39	45.31	8.77	80.39	49.70	295.25	306.95	257.83	18.42	11.11	19.00	134.76	16.96	84.78	1371.61
3.79	9.61	1.57	3.44	155648	100	16039989	0.97	3.93	7.35	1.84	9.28	3.09	17.38	17.18	15.63	2.02	1.47	3.68	9.33	1.52	3.34	97.04
2.47	7.17	3.61	1.31	107136	100	1478650	7.25	9.29	50.06	16.51	40.94	12.04	175.12	137.27	116.63	39.91	21.33	17.89	51.95	26.15	9.46	724.55
1.87	6.96	1.42	1.87	259072	100	5310662	4.88	11.12	33.94	8.19	42.72	5.85	125.82	103.00	80.29	11.82	5.97	9.13	33.94	6.91	9.13	487.83
2.02	5.94	3.76	1.54	48128	90	24497028	0.18	1.67	2.04	1.02	1.50	0.55	2.81	1.74	1.83	1.32	0.85	0.36	1.05	0.66	0.27	17.68
2.18	5.47	4.53	2.14	37120	85	20598612	0.15	2.72	1.37	0.79	1.19	0.47	1.83	1.25	1.37	1.34	0.79	0.33	0.84	0.69	0.33	15.32
2.83	4.55	1.34	2.68	815104	100	20740248	3.93	14.59	33.41	8.00	35.29	11.76	99.29	73.12	56.28	11.20	5.27	11.11	17.88	5.27	10.54	393.01
4.43	5.88	6.17	5.81	29056	100	2625530	1.11	3.30	11.17	4.90	6.91	2.41	18.89	13.90	16.40	4.26	3.86	4.90	6.51	6.83	6.43	110.67
2.90	5.91	2.95	2.51	7744	80	27429660	0.02	0.03	0.29	0.12	0.17	0.06	0.43	0.31	0.28	0.12	0.11	0.07	0.13	0.07	0.06	2.26
1.68	3.25	6.21	2.39	18432	70	13790277	0.09	1.10	1.01	0.43	0.71	0.32	1.72	0.24	0.39	1.18	1.00	0.16	0.30	0.58	0.22	9.36
3.68	9.29	3.47	2.58	104448	100	4440060	2.35	5.59	17.05	5.10	14.09	3.89	44.21	47.61	35.71	9.72	7.53	8.65	21.86	8.16	6.07	235.24
3.98	7.72	4.01	2.64	28064	100	2494460	1.13	2.12	8.03	2.78	6.60	2.51	21.80	19.33	19.95	4.75	4.01	4.48	8.68	4.51	2.97	112.51
1.99	6.18	4.89	2.16	53504	80	43736320	0.10	0.95	0.29	0.52	0.85	0.24	1.66	1.19	0.98	1.15	0.48	0.19	0.60	0.48	0.21	9.79
2.31	6.41	4.41	3.33	41984	85	34008720	0.10	1.29	0.21	0.57	1.07	0.31	1.66	1.02	1.14	0.94	0.56	0.24	0.67	0.46	0.35	10.49
1.98	6.19	5.50	3.47	3104	80	5070991	0.05	0.63	0.19	0.32	0.45	0.15	0.62	0.45	0.46	0.30	0.50	0.10	0.30	0.27	0.17	4.90
1.94	8.53	1.94	2.40	80896	100	7804665	1.04	2.83	10.71	3.21	9.85	1.80	21.84	17.09	15.20	3.38	2.40	2.01	8.84	2.01	2.48	103.65
2.16	9.22	2.28	2.57	348160	100	14089057	2.47	5.84	22.33	6.60	20.55	5.07	52.52	41.05	37.35	9.18	6.55	5.33	22.78	5.63	6.34	247.11
3.57	10.87	1.63	6.31	54272	80	22950544	0.19	4.01	1.48	0.89	1.05	0.44	2.21	1.73	1.63	0.49	0.75	0.68	2.06	0.31	1.19	18.92
2.74	5.81	8.42	6.55	856	65	2403406	0.02	0.13	0.16	0.25	0.17	0.11	0.33	0.19	0.06	0.19	0.19	0.06	0.13	0.20	0.15	2.32
2.23	8.10	3.30	2.41	262144	100	29405236	0.89	2.65	10.18	4.14	8.36	2.32	16.22	11.22	11.55	4.32	3.89	1.99	7.22	2.95	2.15	89.15
3.45	8.48	1.42	3.02	199680	100	4685930	4.26	14.72	26.86	6.44	33.11	11.50	94.74	81.31	69.90	11.22	6.53	14.72	36.15	6.07	12.88	426.13
2.34	10.38	5.13	3.73	3888	70	15405633	0.02	0.08	0.14	0.07	0.22	0.04	0.22	0.17	0.22	0.13	0.09	0.04	0.18	0.09	0.07	1.77

Table F.13: Peak heights of monoaromatic steroids from saturates fraction (m/z 253) for all source rock samples (page 4 of 4).

METHYL AND DIMETHYL PHENANTHRENE AND TRIMETHYL NAPHTHALENE PEAK HEIGHTS																								
Phenanthrenes from GC										Phenanthrenes from GC-MS					Naphthalenes									total	
No.	P	3MP	2MP	9MP	4+1MP	26DMP	27DMP	16DMP	210DMP	P	3MP	2MP	4+9MP	1MP	137	136	134/146	236	127	126/167	124	125	height	137
OIL SAMPLES																								
1	20	75	135	155	195	240	355	845	600	not analysed					353	531	404	309	181	290	90	183	GC only	
2	705	805	900	1130	970	380	270	1200	720	not analysed					275	378	262	244	90	196	70	71	GC only	
3										repeat GC-MS sample														
4	620	695	680	820	895	280	391	1443	911	570	580	518	705	575	589	1032	970	836	240	1092	115	727	5601	10.52
5										repeat GC-MS sample					585	1095	1085	920	190	975	140	785	5775	10.13
6	260	390	760	610	960	190	250	1300	826	735	575	580	730	660	685	1087	749	837	192	591	58	202	4401	15.56
7	540	565	900	1065	925	386	401	1283	815	90	235	317	450	410	0	0	0	0	0	0	0	0	0	0.00
8	1153	725	850	920	845	350	381	1369	812	770	560	580	675	625	730	1082	906	749	168	932	27	778	5372	13.59
9	1110	340	535	585	475	281	376	940	503	470	215	165	220	210	600	1008	755	698	197	799	71	1080	5208	11.52
10	0	0	0	0	0	0	0	0	0	135	265	430	439	387	438	650	605	798	250	558	70	391	3760	11.65
11	0	135	168	176	205	625	450	935	700	48	298	452	284	270	0	0	0	0	0	0	0	0	0	0.00
12	0	0	0	0	0	440	904	340	297	80	353	435	537	528	0	0	0	0	0	0	0	0	0	0.00
13	1130	920	1225	1130	1095	452	643	1701	1320	2573	1737	2170	2155	2020	1390	2170	1665	2090	1300	1320	65	375	10375	13.40
14	40	181	224	565	397	270	480	770	465	81	902	1200	1861	2177	0	0	0	0	0	0	0	0	0	0.00
15	0	0	0	0	0	165	350	370	417	332	78	146	204	224	0	0	0	0	0	0	0	0	0	0.00
16	20	115	197	295	272	458	688	1202	870	21	238	437	402	451	0	0	0	0	0	0	0	0	0	0.00
17	1190	715	795	745	680	230	201	725	430	770	585	610	275	600	605	1095	707	955	112	794	32	231	4531	13.35
18	350	310	340	375	315	120	172	471	255	750	1283	1223	2174	1927	410	870	1060	540	925	880	230	1790	6705	6.11
19	1200	670	760	910	740	161	178	695	385	3847	1641	1695	2172	1927	1265	2165	1550	1420	1260	1200	130	950	9940	12.73
20	870	910	1040	1190	1190	300	270	1135	757	1852	1402	1678	2123	2170	265	575	590	605	895	855	160	1325	5270	5.03
21	212	371	481	709	591	300	292	908	581	85	450	560	460	705	152	247	272	177	89	219	155	191	1502	10.12
22	51	350	600	611	672	225	188	570	372	292	556	628	865	782	281	542	462	345	219	444	126	735	3154	8.91
23	1220	460	670	630	510	222	168	641	365	825	355	465	455	455	673	1090	759	908	523	866	88	579	5486	12.27
24	340	720	930	1300	960	458	698	1185	920	132	371	512	558	589	0	0	0	0	0	0	0	0	0	0.00
25	310	420	570	720	550	268	272	1121	698	887	1252	1353	2165	1720	1390	2170	1656	2085	1322	850	68	371	9912	14.02
26	852	713	743	686	592	291	243	610	452	167	257	317	322	247	620	908	1081	717	816	638		782	5562	11.15
27	91	317	451	917	560	267	638	1011	714	114	340	487	636	640	0	0	0	0	0	0	0	0	0	0.00
28	1769	1080	1199	1012	900	276	355	600	269	2299	747	1306	1451	1037									0	0.00
29	1707	1155	1303	1353	1288	352	429	939	364	2662	672	1135	1450	1113									0	0.00
30	1945	1169	1301	1859	1398	556	328	1710	1195	1070	805	844	896	943	1038	1085	1072	1042	287	1000	142	481	6147	16.89
31	1126	1043	1119	1358	1175	353	290	1578	865	1035	607	921	892	1066	529	1018	887	936	392	1064	60	446	5332	9.92
32	1450	853	838	1016	778	272	201	1107	504	1077	435	557	487	552	649	1077	850	823	297	779	46	223	4744	13.68
33	1885	1113	1308	1520	1438	354	283	1510	850	1090	425	646	623	791	362	901	757	1037	432	1068	102	473	5132	7.05
34	1591	1057	1134	1313	1116	422	293	1641	758	1074	4779	646	609	630	605	1076	853	827	233	816	63	260	4733	12.78
35	1568	1088	1137	1446	1162	433	307	1668	842	1089	508	727	611	809	632	1072	801	863	248	837	19	238	4710	13.42
36	1920	583	581	543	511	114	93	243	129	1082	277	318	256	267	187	437	335	402	155	748	40	1028	3332	5.61
37	1808	1082	1153	1022	936	280	229	992	558	1074	901	938	872	901	229	583	357	1087	115	936	21	272	3600	6.36
38	20	228	296	388	362	332	306	1555	828	107	318	428	495	432	670	1096	553	995	106	668	0	112	4200	15.95

Table F.14: Peak heights of phenanthrenes from GC and GC-MS (m/z 178+192+206) and trimethyl naphthalenes (m/z 170) from all hydrocarbon samples (page 1 of 4).

NORMALIZED PEAK HEIGHTS							CORRELATING PEAKS				PEAK HEIGHTS AS ppm TIC								
										% of									total
136	134/146	236	127	126/167	124	125	TIC	170	%	TIC	137	136	134/146	236	127	126/167	124	125	height
							not anal.												
							not anal.												
							not anal.												
18.43	17.32	14.93	4.28	19.50	2.05	12.98	1761175	7168	100	0.407	4.28	7.50	7.05	6.07	1.74	7.94	0.84	5.28	40.70
18.96	18.79	15.93	3.29	16.88	2.42	13.59	4133205	32512	100	0.787	7.97	14.91	14.78	12.53	2.59	13.28	1.91	10.69	78.66
24.70	17.02	19.02	4.36	13.43	1.32	4.59	7899419	51200	100	0.648	10.09	16.01	11.03	12.33	2.83	8.70	0.85	2.97	64.81
0.00	0.00	0.00	0.00	0.00	0.00	0.00	11147543	11008	100	0.099									
20.14	16.87	13.94	3.13	17.35	0.50	14.48	3353630	224256	100	6.687	90.87	134.69	112.78	93.23	20.91	116.01	3.36	96.84	668.70
19.35	14.50	13.40	3.78	15.34	1.36	20.74	4835016	565248	100	11.691	134.69	226.27	169.48	156.68	44.22	179.36	15.94	242.43	1169.07
17.29	16.09	21.22	6.65	14.84	1.86	10.40	41091556	6720	100	0.016	0.19	0.28	0.26	0.35	0.11	0.24	0.03	0.17	1.64
0.00	0.00	0.00	0.00	0.00	0.00	0.00	8246725	6592	100	0.080									
0.00	0.00	0.00	0.00	0.00	0.00	0.00	7857856	8896	100	0.113									
20.92	16.05	20.14	12.53	12.72	0.63	3.61	673792	180736	100	26.824	359.37	561.04	430.47	540.35	336.10	341.28	16.81	96.95	2682.37
0.00	0.00	0.00	0.00	0.00	0.00	0.00	448000	228	100	0.051									
0.00	0.00	0.00	0.00	0.00	0.00	0.00	6492048	8256	100	0.127									
0.00	0.00	0.00	0.00	0.00	0.00	0.00	8076805	6784	100	0.084									
24.17	15.60	21.08	2.47	17.52	0.71	5.10	16812960	1572760	100	9.354	124.90	226.07	145.96	197.16	23.12	163.92	6.61	47.69	935.45
12.98	15.81	8.05	13.80	13.12	3.43	26.70	189952	1510	100	0.795	4.86	10.31	12.57	6.40	10.97	10.43	2.73	21.22	79.49
21.78	15.59	14.29	12.68	12.07	1.31	9.56	721920	594944	100	82.411	1048.80	1794.98	1285.09	1177.30	1044.65	994.91	107.78	787.63	8241.13
10.91	11.20	11.48	16.98	16.22	3.04	25.14	391680	3460	100	0.883	4.44	9.64	9.89	10.14	15.00	14.33	2.68	22.21	88.34
16.44	18.11	11.78	5.93	14.58	10.32	12.72	9414432	7104	100	0.075	0.76	1.24	1.37	0.89	0.45	1.10	0.78	0.96	7.55
17.18	14.65	10.94	6.94	14.08	3.99	23.30	20480680	6464	100	0.032	0.28	0.54	0.46	0.35	0.22	0.44	0.13	0.74	3.16
19.87	13.84	16.55	9.53	15.79	1.60	10.55	15585093	1556480	100	9.987	122.52	198.43	138.17	165.30	95.21	157.65	16.02	105.40	998.70
0.00	0.00	0.00	0.00	0.00	0.00	0.00	12385703	1616	100	0.013									
21.89	16.71	21.04	13.34	8.58	0.69	3.74	220928	2352	100	1.065	14.93	23.31	17.79	22.39	14.20	9.13	0.73	3.98	106.46
16.33	19.44	12.89	14.67	11.47	0.00	14.06	2460251	1596	100	0.065	0.72	1.06	1.26	0.84	0.95	0.74	0.00	0.91	6.49
0.00	0.00	0.00	0.00	0.00	0.00	0.00	10901194	2608	100	0.024									
0.00	0.00	0.00	0.00	0.00	0.00	0.00	not anal.												
0.00	0.00	0.00	0.00	0.00	0.00	0.00	not anal.												
17.65	17.44	16.95	4.67	16.27	2.31	7.82	23386172	2703360	100	11.560	195.20	204.04	201.59	195.95	53.97	188.05	26.70	90.45	1155.97
19.09	16.64	17.55	7.35	19.95	1.13	8.36	5596559	59392	100	1.061	10.53	20.26	17.65	18.63	7.80	21.18	1.19	8.88	106.12
22.70	17.92	17.35	6.26	16.42	0.97	4.70	10061116	8876544	100	88.226	1206.97	2002.94	1580.78	1530.57	552.34	1448.74	85.55	414.72	8822.62
17.56	14.75	20.21	8.42	20.81	1.99	9.22	7923020	59904	100	0.756	5.33	13.27	11.15	15.28	6.36	15.73	1.50	6.97	75.61
22.73	18.02	17.47	4.92	17.24	1.33	5.49	4889070	376832	100	7.708	98.52	175.23	138.91	134.68	37.94	132.88	10.26	42.34	770.76
22.76	17.01	18.32	5.27	17.77	0.40	5.05	6528065	339968	100	5.208	69.88	118.53	88.57	95.42	27.42	92.55	2.10	26.32	520.78
13.12	10.05	12.06	4.65	22.45	1.20	30.85	3475211	10944	100	0.315	1.77	4.13	3.17	3.80	1.46	7.07	0.38	9.72	31.49
16.19	9.92	30.19	3.19	26.00	0.58	7.56	17189866	96256	100	0.560	3.56	9.07	5.55	16.91	1.79	14.56	0.33	4.23	56.00
26.10	13.17	23.69	2.52	15.90	0.00	2.67	21268424	360448	100	1.695	27.04	44.23	22.31	40.15	4.28	26.95	0.00	4.52	169.48

Table F.14: Peak heights of phenanthrenes from GC and GC-MS (m/z 178+192+206) and trimethyl naphthalenes (m/z 170) from all hydrocarbon samples (page 2 of 4).

Phenanthrenes from GC										Phenanthrenes from GC-MS					Naphthalenes								total	
SHALE SAMPLES																								
41	545	525	705	790	740	195	288	930	660	520	635	765	775	950	0	0	0	0	0	0	0	0	0	0.00
42	130	258	347	500	435	130	191	810	526	55	172	188	255	300	0	0	0	0	0	0	0	0	0	0.00
43	640	560	735	820	720	270	247	852	525	670	720	895	865	955	0	0	0	0	0	0	0	0	0	0.00
44	975	620	710	875	805	231	240	1049	645	975	620	710	845	670	131	375	308	297	148	542	65	1075	2941	4.45
45	1110	452	489	1018	1131	151	118	762	418	1000	390	505	840	850	178	545	398	455	153	1048	87	1077	3941	4.52
46	1270	746	860	971	918	598	307	983	610	not analysed														
47	474	621	653	1075	990	223	378	1638	954	1425	314	410	306	317	520	1065	422	592	140	531	23	302	3595	14.46
48					repeat	sample				not analysed					520	1065	422	592	140	531	23	302	3595	14.46
49	32	178	272	86	303	142	122	775	210	28	164	188	291	318	0	0	0	0	0	0	0	0	0	0.00
50	1215	821	613	758	794	178	138	543	358	825	535	550	700	670	251	605	528	441	300	760	63	1091	4039	6.21
51	1340	860	970	1210	1180	340	317	1163	675	2647	1392	1447	2170	2060	95	260	290	230	410	430	170	2095	3980	2.39
52	1232	1015	797	986	949	221	215	662	440	790	540	581	765	725	89	108	473	272	103	249	72	1080	2446	3.64
53	904	750	907	1208	1104	297	210	1270	778	540	475	630	825	820	551	1022	953	831	200	1072	41	541	5211	10.57
54	1350	735	985	1247	1220	290	197	1102	735	945	555	770	895	970	692	1095	802	1014	201	1085	20	480	5389	12.84
55	1262	591	520	629	584	121	147	450	238	695	400	375	415	445	91	262	237	233	129	423	67	1092	2534	3.59
56	965	642	788	1160	1100	212	182	1200	704	1994	1068	1265	2170	2026	1360	2150	2170	1495	1455	1475	195	1080	11380	11.95
57	965	642	788	1160	1100	212	182	1200	704	337	229	286	398	404	595	1040	946	788	208	1092	78	641	5388	11.04
58	965	642	788	1160	1100	212	182	1200	704	not analysed					610	1046	953	842	247	1030	98	689	5515	11.06
59	1287	762	758	980	1007	168	161	747	461	2922	1278	1378	2170	2098	975	2170	1575	1165	1265	1150	200	1630	10130	9.62
60	1179	820	930	1240	1210	220	185	1165	695	3100	1307	1318	2135	2170	1000	2170	1535	1010	1090	1000	180	1490	9475	10.55
61	1007	709	904	1157	1025	331	218	1218	791	680	450	620	805	810	718	1086	934	831	185	881	65	431	5131	13.99
62	1050	865	1106	1212	1131	400	308	1205	923	900	650	800	810	840	618	1084	907	836	198	946	65	640	5294	11.67
63	78	272	379	590	510	217	168	1081	712	50	295	410	505	600	0	0	0	0	0	0	0	0	0	0.00
64	249	790	1295	1080	1335	462	270	1150	805	85	450	560	460	705	0	0	0	0	0	0	0	0	0	0.00
65	895	868	1096	1034	1302	368	187	892	613	310	415	445	480	610	0	0	0	0	0	0	0	0	0	0.00
66	82	247	423	331	348	740	589	1302	1066	92	253	450	291	351	0	0	0	0	0	0	0	0	0	0.00
67	874	943	1245	1337	1271	308	250	1090	694	635	585	850	750	1000	71	97	95	117	61	152	61	197	851	8.34
68	50	118	219	360	298	236	217	741	423	153	227	285	278	362	75	156	107	89	42	125	28	125	747	
69	58	200	281	399	389	341	372	955	547	42	215	293	437	445	0	0	0	0	0	0	0	0	0	0.00
70	830	406	560	667	832	123	172	714	464	1087	325	514	620	745	532	1078	836	768	200	812	31	195	4452	11.95
Phenanthrenes: M=methyl, DM=dimethyl. measured from aromatic gas chromatograms.																								
HEIGHT=maximum ion height of naphthalenes in m/z 170 fragmentogram x baseline factor.																								
Trimethyl naphthalenes measured from m/z 170 fragmentogram except where noted.																								

Table F.14: Peak heights of phenanthrenes from GC and GC-MS (m/z 178+192+206) and trimethyl naphthalenes (m/z 170) from all source rock samples (including annotation descriptions) (page 3 of 4).

										% of									total
0.00	0.00	0.00	0.00	0.00	0.00	0.00	7769180	3200	100	0.041									
0.00	0.00	0.00	0.00	0.00	0.00	0.00	15927144	9856	100	0.062									
0.00	0.00	0.00	0.00	0.00	0.00	0.00	6503896	1552	100	0.024									
12.75	10.47	10.10	5.03	18.43	2.21	36.55	2114243	81920	100	3.875	17.26	49.41	40.58	39.13	19.50	71.41	8.56	141.63	387.47
13.83	10.10	11.55	3.88	26.59	2.21	27.33	8153592	42496	100	0.521	2.35	7.21	5.26	6.02	2.02	13.86	1.15	14.24	52.12
							not anal.												
29.62	11.74	16.47	3.89	14.77	0.64	8.40	3383939	20992	100	0.620	8.97	18.38	7.28	10.22	2.42	9.16	0.40	5.21	62.03
29.62	11.74	16.47	3.89	14.77	0.64	8.40	not anal.												
0.00	0.00	0.00	0.00	0.00	0.00	0.00	6112735	11456	100	0.187									
14.98	13.07	10.92	7.43	18.82	1.56	27.01	12753925	1048576	100	8.222	51.09	123.15	107.48	89.77	61.07	154.70	12.82	222.08	822.16
6.53	7.29	5.78	10.30	10.80	4.27	52.64	240128	3992	100	1.662	3.97	10.86	12.11	9.61	17.13	17.96	7.10	87.51	166.24
4.42	19.34	11.12	4.21	10.18	2.94	44.15	4479796	13824	100	0.309	1.12	1.36	5.97	3.43	1.30	3.14	0.91	13.63	30.86
19.61	18.29	15.95	3.84	20.57	0.79	10.38	3595023	43520	100	1.211	12.80	23.74	22.14	19.30	4.65	24.90	0.95	12.57	121.06
20.32	14.88	18.82	3.73	20.13	0.37	8.91	12278665	974848	100	7.939	101.95	161.32	118.15	149.39	29.61	159.85	2.95	70.72	793.94
10.34	9.35	9.19	5.09	16.69	2.64	43.09	4020368	209920	100	5.221	18.75	53.99	48.83	48.01	26.58	87.16	13.81	225.01	522.14
18.89	19.07	13.14	12.79	12.96	1.71	9.49	339456	87168	100	25.679	306.88	485.14	489.66	337.34	328.32	332.83	44.00	243.70	2567.87
19.30	17.56	14.63	3.86	20.27	1.45	11.90	5737816	226304	100	3.944	43.55	76.13	69.25	57.68	15.23	79.94	5.71	46.92	394.41
18.97	17.28	15.27	4.48	18.68	1.78	12.49	1638631	67584	100	4.124	45.62	78.23	71.27	62.97	18.47	77.03	7.33	51.53	412.44
21.42	15.55	11.50	12.49	11.35	1.97	16.09	494592	210432	100	42.547	409.51	911.41	661.51	489.31	531.31	483.01	84.00	684.61	4254.66
22.90	16.20	10.66	11.50	10.55	1.90	15.73	214016	161792	100	75.598	797.87	1731.38	1224.73	805.85	869.68	797.87	143.62	1188.82	7559.81
21.17	18.20	16.20	3.61	17.17	1.27	8.40	4957130	352256	100	7.106	99.44	150.40	129.35	115.09	25.62	122.01	9.00	59.69	710.60
20.48	17.13	15.79	3.74	17.87	1.23	12.09	3711225	215040	100	5.794	67.64	118.64	99.27	91.50	21.67	103.54	7.11	70.05	579.43
0.00	0.00	0.00	0.00	0.00	0.00	0.00	9417204	1248	100	0.013									
0.00	0.00	0.00	0.00	0.00	0.00	0.00	8571737	2688	100	0.031									
0.00	0.00	0.00	0.00	0.00	0.00	0.00	3754304	2384	100	0.064									
0.00	0.00	0.00	0.00	0.00	0.00	0.00	10047591	2736	100	0.027									
11.40	11.16	13.75	7.17	17.86	7.17	23.15	12378232	13888	100	0.112	0.94	1.28	1.25	1.54	0.80	2.00	0.80	2.60	11.22
							not anal.												
0.00	0.00	0.00	0.00	0.00	0.00	0.00	8481777	3872	100	0.046									
24.21	18.78	17.25	4.49	18.24	0.70	4.38	2255643	348160	100	15.435	184.44	373.74	289.84	266.27	69.34	281.52	10.75	67.61	1543.51

Table F.14: Peak heights of phenanthrenes from GC and GC-MS (m/z 178+192+206) and trimethyl naphthalenes (m/z 170) from all source rock samples (page 4 of 4).

THIOPHENE PEAK HEIGHTS																						
	Methyl Dibenzothiophenes					Dimethyl Dibenzothiophenes							Trimethyl Dibenzothiophenes									
No.	4	2+3	1	Total ht.	MDBT/TIC%	A	B	C	D	E	F	Total ht.	a	b	c	d	e	f	g	h	i	Total ht.
1																						
2																						
3																						
4	1075	528	317	1920	6.90	185	903	449	1064	663	309	3573	222	520	1035	541	911	600	463	125	175	4592
5	502	210	192	904	1.40	107	493	268	500	353	162	1883	82	205	491	234	358	295	202	77	91	2035
6	1078	397	201	1676	3.30	182	1063	510	1028	527	293	3603	155	372	1041	455	570	511	408	137	126	3775
7	1060	363	172	1595	0.30	201	1050	375	952	602	303	3483	885	681	962	378	813	602	171	102	168	4762
8	235	104	34	373	1.60	56	333	103	257	123	61	933	70	229	232	107	144	136	51	26	27	1022
9	727	500	355	1582	1.20	131	562	304	557	213	128	1895	127	278	571	281	201	211	89	40	34	1832
10	975	800	498	2273	0.08	255	838	472	972	415	268	3220	78	213	343	188	135	258	249	87	93	1644
11	525	448	147	1120	0.07	93	701	330	995	108	354	2581	28	78	517	337	105	415	298	28	61	1867
12	783	798	342	1923	0.05	4	52	30	900	31	45	1062	92	82	232	113	84	175	114	42	128	1062
13	2170	690	95	2955	5.80	105	2170	590	1040	330	240	4475	45	490	2170	540	740	945	370	50	35	5385
14	2109	1000	720	3829	0.50	90	1300	680	2170	1550	1780	7570	180	330	1550	900	1185	2170	1710	600	640	9265
15	360	232	147	739	0.07	140	433	272	467	147	139	1598	17	127	140	166	210	78	87	77	180	1082
16	541	640	428	1609	0.05	121	790	358	950	265	324	2808	10	147	391	266	238	563	131	125	72	1943
17	1060	568	152	1780	0.20	152	934	396	1062	418	235	3197	152	581	1005	508	688	558	161	72	89	3814
18	1740	1670	1510	4920	2.60	360	1570	870	1920	2170	800	7690	280	740	1580	885	1470	1250	710	310	460	7685
19	2115	700	530	3345	8.70	430	2170	1010	2170	1565	790	8135	320	910	2170	1150	1585	1320	920	220	330	8925
20	2170	735	620	3525	14.50	375	1975	1020	2170	1720	820	8080	350	820	2170	1140	1570	1490	1110	275	380	9305
21	962	600	275	1837	0.10	67	995	202	718	263	102	2347	34	342	397	88	185	122	67	24	91	1350
22	313	452	170	935	0.50	55	560	212	1048	328	491	2694	41	172	576	363	572	995	473	256	236	3684
23	1060	562	231	1853	2.00	186	1040	508	959	310	210	3213	165	432	1000	455	354	381	282	70	52	3191
24	1042	581	183	1806	0.20	55	1045	295	927	321	202	2845	51	468	972	305	547	593	78	68	73	3155
25	2170	540	455	3165	6.50	270	2170	940	1710	1245	555	6890	250	760	2170	865	1220	1045	685	170	175	7340
26	505	295	210	1010	4.50	130	480	180	510	280	150	1730	100	320	495	205	350	260	200	62	65	2057
27	1080	552	232	1864	0.40	92	1072	362	1002	481	268	3277	68	457	761	242	465	457	81	34	62	2627
28	1455	517	194	2166	0.00							0										0
29	1451	450	278	2179	0.00							0										0
30	1080	673	282	2035	12.00	181	882	532	1073	605	303	3576	277	573	1067	623	779	623	533	126	167	4768
31	1076	600	247	1923	3.93	159	713	438	1074	598	285	3267	377	783	1051	640	889	733	532	157	202	5364
32	1065	653	222	1940	2.57	141	669	403	1006	463	214	2896	358	647	956	610	670	574	420	113	120	4468
33	1087	576	219	1882	4.24	131	796	449	1080	581	298	3335	238	668	1063	613	856	763	560	166	200	5127
34	1070	612	230	1912	3.41	160	739	477	1067	562	253	3258	276	577	1038	642	659	611	442	126	140	4511
35	1072	647	194	1913	3.78	160	697	408	1076	492	232	3065	284	687	1049	622	692	600	448	121	138	4641
36	825	1011	660	2496	0.03	160	561	414	987	868	644	3634	132	250	439	400	548	629	472	192	236	3298
37	1073	698	164	1935	5.62	150	858	491	1079	448	217	3243	217	771	1047	624	588	502	471	116	87	4423
38	1073	822	341	2236	0.68	95	631	522	1078	507	305	3138	139	606	1067	689	755	728	712	174	155	5025

Table F.15: Peak heights of mono-, di- and tri-methyl dibenzothiophenes (m/z 198+212+226) for all hydrocarbon samples (page 1 of 6).

				Normalized MDBT							Dimethyl Dibenzothiophenes (as ppm of TIC)								
fragmentogram heights											fragmentogram heights								
198	%	TIC	% of TIC	4	2+3	1	4.00	2+3	1.00	tot. ht.	212	%	TIC	%TIC	B	C	D	E	F
OIL SAMPLES																			
		not anal.																	
		not anal.																	
		not anal.																	
57600	100	1761175	3.271	55.99	27.50	16.51	76.56	37.61	22.58	136.75	36864	100	1761175	2.093	20.17	98.44	48.95	116.00	72.28
121856	100	4133205	2.948	55.53	23.23	21.24	72.73	30.42	27.82	130.97	89088	100	4133205	2.155	25.51	117.55	63.90	119.22	84.17
26368	100	7899419	0.334	64.32	23.69	11.99	9.53	3.51	1.78	14.82	13888	100	7899419	0.176	1.91	11.15	5.35	10.78	5.53
32512	100	11147543	0.292	66.46	22.76	10.78	6.49	2.22	1.05	9.77	37632	100	11147543	0.338	4.25	22.22	7.94	20.15	12.74
17493	100	3353630	0.522	63.00	27.88	9.12	11.99	5.31	1.74	19.04	8448	95	3353630	0.239	3.59	21.36	6.61	16.49	7.89
58368	100	4835016	1.207	45.95	31.61	22.44	47.91	32.95	23.39	104.25	29440	100	4835016	0.609	5.04	21.63	11.70	21.44	8.20
34048	100	41091556	0.083	42.89	35.20	21.91	4.91	4.03	2.51	11.46	57088	100	41091556	0.139	1.56	5.12	2.88	5.94	2.54
5952	100	8246725	0.072	46.88	40.00	13.13	2.03	1.73	0.57	4.33	13184	100	8246725	0.160	1.33	10.01	4.71	14.20	1.54
3616	100	7857856	0.046	40.72	41.50	17.78	3.39	3.46	1.48	8.33	39424	100	7857856	0.502	0.10	1.36	0.78	23.48	0.81
39040	100	673792	5.794	73.43	23.35	3.21	233.48	74.24	10.22	317.95	39616	100	673792	5.880	20.89	431.76	117.39	206.93	65.66
2228	100	448000	0.497	55.08	26.12	18.80	11.32	5.37	3.86	20.55	3976	100	448000	0.888	2.09	30.13	15.76	50.30	35.93
4416	100	6492048	0.068	48.71	31.39	19.89	2.26	1.46	0.92	4.65	3072	100	6492048	0.047	0.90	2.77	1.74	2.99	0.94
4224	100	8076805	0.052	33.62	39.78	26.60	1.46	1.72	1.15	4.33	9408	100	8076805	0.116	0.88	5.72	2.59	6.88	1.92
368640	100	16812960	2.193	59.55	31.91	8.54	60.94	32.65	8.74	102.33	211968	100	16812960	1.261	10.77	66.15	28.05	75.22	29.61
4936	100	189952	2.599	35.37	33.94	30.69	58.84	56.47	51.06	166.36	6224	100	189952	3.277	23.98	104.56	57.94	127.87	144.52
62592	100	721920	8.670	63.23	20.93	15.84	205.46	68.00	51.49	324.95	26560	100	721920	3.679	47.29	238.67	111.09	238.67	172.13
56960	100	391680	14.542	61.56	20.85	17.59	339.14	114.87	96.90	550.91	32064	100	391680	8.186	87.09	458.66	236.88	503.95	399.44
10496	100	9414432	0.111	52.37	32.66	14.97	7.94	4.96	2.27	15.17	25856	100	9414432	0.275	1.00	14.88	3.02	10.73	3.93
99328	100	20480680	0.485	33.48	48.34	18.18	4.12	5.95	2.24	12.31	119808	100	20480680	0.585	3.44	35.04	13.26	65.57	20.52
311296	100	15585093	1.997	57.20	30.33	12.47	66.35	35.18	14.46	115.99	131072	100	15585093	0.841	8.44	47.20	23.06	43.53	14.07
23552	100	12385703	0.190	57.70	32.17	10.13	6.28	3.50	1.10	10.88	47104	100	12385703	0.380	1.16	22.01	6.21	19.52	6.76
14272	100	220928	6.460	68.56	17.06	14.38	190.98	47.53	40.05	278.56	12976	100	220928	5.873	50.10	402.69	174.44	317.33	231.04
109568	100	2460251	4.454	50.00	29.21	20.79	109.34	63.87	45.47	218.67	116736	100	2460251	4.745	61.07	225.50	84.56	239.59	131.54
44800	100	10901194	0.411	57.94	29.61	12.45	16.90	8.64	3.63	29.16	65536	100	10901194	0.601	2.97	34.57	11.68	32.32	15.51
120000000	100	not anal.		67.17	23.87	8.96													
11000000	100	not anal.		66.59	20.65	12.76													
950272	100	23386172	4.063	53.07	33.07	13.86	92.04	57.35	24.03	173.43	614400	100	23386172	2.627	23.37	113.87	68.68	138.52	78.11
166912	100	5598559	2.981	55.95	31.20	12.84	59.80	33.35	13.73	106.88	166912	100	5596559	2.982	24.66	110.58	67.93	166.57	92.74
259072	100	10061116	2.575	54.90	33.66	11.44	61.38	37.63	12.79	111.81	162816	100	10061116	1.618	11.76	55.81	33.62	83.92	38.62
335872	100	7923020	4.239	57.76	30.61	11.64	89.88	47.63	18.11	155.61	201728	100	7923020	2.546	17.72	107.69	60.74	146.11	78.60
166912	100	4889070	3.414	55.96	32.01	12.03	80.98	46.32	17.41	144.70	107520	100	4889070	2.199	18.40	85.00	54.86	122.73	64.64
246784	100	6528065	3.780	56.04	33.82	10.14	87.32	52.70	15.80	155.82	181248	100	6528065	2.776	23.22	101.16	59.22	156.17	71.41
9280	100	3475211	0.267	33.05	40.50	26.44	6.68	8.19	5.34	20.21	4928	90	3475211	0.128	0.82	2.87	2.12	5.05	4.44
966656	100	17189866	5.623	55.45	36.07	8.48	136.42	88.74	20.85	246.02	610304	100	17189866	3.550	27.52	157.43	90.09	197.98	82.20
144384	100	21268424	0.679	47.99	36.76	15.25	14.50	11.11	4.61	30.21	479232	100	21268424	2.253	9.57	63.59	52.60	108.63	51.09

Table F.15: Peak heights of mono-, di- and tri-methyl dibenzothiophenes (m/z 198+212+226) for all hydrocarbon samples (page 2 of 6).

	Trimethyl Dibenzothiophenes (as ppm of TIC)															
	fragmentogram heights															
tot. ht.	226	%	TIC	% of TIC	a	b	c	d	e	f	g	h	i	tot. ht.		Ro%
																0.8
																0.93
																0.93
33.69	22016	100	1761175	1.250	6.04	14.16	28.18	14.73	24.80	16.33	12.60	3.40	4.76	125.01		0.81
38.63	38144	100	4133205	0.923	3.72	9.30	22.27	10.61	16.24	13.38	9.16	3.49	4.13	92.29		0.81
3.07	7808	100	7899419	0.099	0.41	0.97	2.73	1.19	1.49	1.34	1.07	0.36	0.33	9.88		0.91
6.41	16128	100	11147543	0.145	2.69	2.07	2.92	1.15	2.47	1.83	0.52	0.31	0.51	14.47		0.99
3.91	4779	90	3353630	0.128	0.88	2.87	2.91	1.34	1.81	1.71	0.64	0.33	0.34	12.83		0.85
4.93	13312	100	4835016	0.275	1.91	4.18	8.58	4.22	3.02	3.17	1.34	0.60	0.51	27.53		0.91
1.64	126976	100	41091556	0.309	1.47	4.00	6.45	3.53	2.54	4.85	4.68	1.64	1.75	30.90		1.05
5.05	33536	100	8246725	0.407	0.61	1.70	11.26	7.34	2.29	9.04	6.49	0.61	1.33	40.67		1.15
1.17	11392	100	7857856	0.145	1.26	1.12	3.17	1.54	1.15	2.39	1.56	0.57	1.75	14.50		1.08
47.75	16640	100	673792	2.470	2.06	22.47	99.52	24.76	33.94	43.34	16.97	2.29	1.61	246.96		1.15
41.26	5576	100	448000	1.245	2.42	4.43	20.82	12.09	15.92	29.15	22.97	8.06	8.60	124.46		0.87
0.89	9216	100	6492048	0.142	0.22	1.67	1.84	2.18	2.76	1.02	1.14	1.01	2.36	14.20		0.81
2.35	17920	100	8076805	0.222	0.11	1.68	4.46	3.04	2.72	6.43	1.50	1.43	0.82	22.19		1.08
16.64	76800	100	16812960	0.457	1.82	6.96	12.04	6.08	8.24	6.68	1.93	0.86	1.07	45.68		1.04
53.28	5104	100	189952	2.687	9.79	25.87	55.24	30.94	51.40	43.71	24.82	10.84	16.08	268.70		0.93
86.89	10592	100	721920	1.467	5.26	14.96	35.67	18.91	26.06	21.70	15.12	3.62	5.42	146.72		1.02
190.43	13376	100	391680	3.415	12.85	30.09	79.64	41.84	57.62	54.68	40.74	10.09	13.95	341.50		1.02
1.52	17024	100	9414432	0.181	0.46	4.58	5.32	1.18	2.48	1.63	0.90	0.32	1.22	18.08		1.02
30.72	95232	100	20480680	0.465	0.52	2.17	7.27	4.58	7.22	12.56	5.97	3.23	2.98	46.50		0.95
9.53	57088	100	15585093	0.366	1.89	4.96	11.48	5.22	4.06	4.37	3.24	0.80	0.60	36.63		0.8
4.25	30208	100	12385703	0.244	0.39	3.62	7.51	2.36	4.23	4.58	0.60	0.53	0.56	24.39		1.05
102.99	8152	100	220928	3.690	12.57	38.21	109.09	43.48	61.33	52.53	34.44	8.55	8.80	368.99		0.95
70.47	62464	100	2460251	2.539	12.34	39.50	61.10	25.30	43.20	32.09	24.69	7.65	8.02	253.89		0.98
8.64	38144	100	10901194	0.350	0.91	6.09	10.14	3.22	6.19	6.09	1.08	0.45	0.83	34.99		0.88
																1.23
																0.96
39.12	257024	100	23386172	1.099	6.38	13.21	24.59	14.36	17.96	14.36	12.29	2.90	3.85	109.90		0.9
44.20	52224	100	5596559	0.933	6.56	13.62	18.28	11.13	15.47	12.75	9.25	2.73	3.51	93.31		0.9
17.85	50944	100	10061116	0.506	4.06	7.33	10.83	6.91	7.59	6.50	4.76	1.28	1.36	50.63		0.85
40.32	71680	100	7923020	0.905	4.20	11.79	18.76	10.82	15.10	13.46	9.88	2.93	3.53	90.47		0.85
29.10	44800	100	4889070	0.916	5.61	11.72	21.09	13.04	13.39	12.41	8.98	2.56	2.84	91.63		0.9
33.67	69632	100	6528065	1.067	6.53	15.79	24.11	14.30	15.90	13.79	10.30	2.78	3.17	106.67		0.9
3.29	3776	85	3475211	0.092	0.37	0.70	1.23	1.12	1.53	1.76	1.32	0.54	0.66	9.24		0.75
39.82	210944	100	17189866	1.227	6.02	21.39	29.05	17.31	16.31	13.93	13.07	3.22	2.41	122.71		1
30.74	303104	100	21268424	1.425	3.94	17.19	30.26	19.54	21.41	20.65	20.19	4.93	4.40	142.51		1

Table F.15: Peak heights of mono-, di- and tri-methyl dibenzothiophenes (m/z 198+212+226) for all hydrocarbon samples (page 3 of 6).

	Methyl Dibenzothiophenes					Dimethyl Dibenzothiophenes							Trimethyl Dibenzothiophenes									
No.	4	2+3	1	Total ht.	MDBT/TIC%	A	B	C	D	E	F	Total ht.	a	b	c	d	e	f	g	h	i	Total ht.
SHALE SAMPLES																						
41	1085	788	578	2451	3.30	183	598	404	1075	983	407	3650	182	460	722	479	1060	635	283	224	448	4493
42	1075	483	382	1940	1.00	160	742	378	1075	831	330	3516	201	523	936	531	1061	738	240	198	353	4781
43	1090	1035	632	2757	2.40	162	502	365	1070	738	371	3208	218	451	802	517	1035	818	395	263	530	5029
44	1055	680	522	2257	3.10	212	669	411	1040	824	412	3568	201	519	795	472	899	604	573	201	353	4617
45	878	429	1048	2355	1.10	147	706	305	1016	552	266	2992	113	295	290	137	255	196	120	59	62	1527
46				0	0.00							0										0
47	561	339	298	1198	0.10	0	0	0	0	0	0	0	0	0	0	0	0	0	0	0	0	0
48				0	0.00							0										0
49	297	332	1033	1662	0.20	102	278	366	588	990	665	2989	42	108	248	293	392	500	496	160	232	2471
50	961	859	1088	2908	5.40	189	563	408	890	1073	529	3652	162	308	522	435	972	670	468	245	473	4255
51	2170	1225	1560	4955	7.20	420	1190	925	2160	2100	1145	7940	310	610	1250	830	1420	1280	920	415	670	7705
52	592	649	1085	2326	5.60	160	444	352	737	1055	591	3339	123	365	428	471	814	325	741	206	431	3904
53	1080	327	190	1597	2.70	125	941	353	1075	691	290	3475	147	500	1046	503	1022	801	256	131	236	4642
54	1075	257	170	1502	1.80	70	1068	341	1057	520	242	3298	66	441	1048	449	832	710	148	81	141	3916
55	1066	935	972	2973	2.10	160	418	320	1060	661	314	2933	115	227	316	285	555	338	192	141	287	2456
56	2150	180	110	2440	12.30	155	2170	775	1750	1270	490	6610	255	695	2175	870	1590	1400	805	220	310	8320
57	1075	108	47	1230	3.60	120	1080	338	1032	531	210	3311	170	392	1063	523	847	691	468	113	182	4449
58	1065	112	61	1238	3.30	148	1053	363	983	552	219	3318	181	475	1000	458	804	667	466	122	189	4362
59	2170	870	1490	4530	21.70	350	1285	780	1520	2170	890	6995	350	885	1780	1165	2175	1855	995	470	830	10505
60	2170	800	1535	4505	17.60	295	1190	775	1510	2170	705	6645	310	835	1690	1180	2170	1870	1065	400	805	10325
61	1078	234	118	1430	3.70	131	990	477	1065	655	220	3538	156	437	1050	458	730	597	456	93	137	4114
62	1088	413	225	1726	4.90	169	950	396	1071	627	269	3482	178	814	1041	537	841	652	513	108	160	4844
63	1072	232	126	1430	0.50	81	1070	252	787	378	151	2719	91	482	1060	295	675	669	271	52	73	3668
64	895	1018	845	2758	0.20	78	351	270	1040	578	620	2937	47	132	490	401	825	848	501	317	601	4162
65	1082	675	847	2604	1.60	220	548	397	985	1058	429	3637	222	416	523	391	1001	523	206	231	348	3861
66	915	542	280	1737	0.07	141	951	251	650	152	178	2323	50	121	291	125	111	501	81	52	39	1371
67	1073	595	274	1942	0.60	62	948	355	1070	368	342	3145	66	375	1035	458	640	818	150	102	171	3815
68	391	642	1059	2092	0.46	247	469	240	834	309	318	2417	208	383	382	298	489	892	913	361	383	4309
69	550	555	981	2086	0.07	69	438	288	1021	817	693	3326	39	118	447	333	741	952	481	278	541	3930
70	1078	204	88	1370	0.50	137	931	381	1067	584	227	3327	228	588	1036	551	797	643	491	120	168	4622
MDBT/TIC%=maximum ion height of MDBT from m/z 198 fragmentogram/TIC maximum height%.																						
tot. height = sum of all peak heights.																						

Table F.15: Peak heights of mono-, di- and tri-methyl dibenzothiophenes (m/z 198+212+226) for all source rock samples (including annotation descriptions) (page 4 of 6).

fragmentogram heights											fragmentogram heights								
198	%	TIC	% of TIC	4	2+3	1	4.00	2+3	1.00	tot. ht.	212	%	TIC	%TIC	B	C	D	E	F
254976	100	7769180	3.282	44.27	32.15	23.58	79.25	57.56	42.22	179.03	202752	100	7769180	2.610	19.48	63.67	43.02	114.46	104.66
155648	100	15927144	0.977	55.41	24.90	19.69	21.97	9.87	7.81	39.65	197632	100	15927144	1.241	10.23	47.46	24.18	68.76	53.15
153600	100	6503896	2.362	39.54	37.54	22.92	51.19	48.60	29.68	129.47	135168	100	6503896	2.078	12.21	37.84	27.51	80.66	55.63
66560	100	2114243	3.148	46.74	30.13	23.13	71.94	46.37	35.59	153.90	34560	100	2114243	1.635	15.35	48.45	29.77	75.32	59.68
87040	100	8153592	1.068	37.28	18.22	44.50	61.38	29.99	73.26	164.63	50176	100	8153592	0.615	3.84	18.45	7.97	26.55	14.42
		not anal.																	
3536	100	3383939	0.104	46.83	28.30	24.87					4000	100	3383939	0.118	0.00	0.00	0.00	0.00	0.00
		not anal.																	
11328	100	6112735	0.185	17.87	19.98	62.15	2.23	2.49	7.75	12.46	15424	100	6112735	0.252	1.55	4.22	5.56	8.93	15.03
688128	100	12753925	5.395	33.05	29.54	37.41	121.86	108.92	137.96	368.74	348160	100	12753925	2.730	17.74	52.85	38.30	83.55	100.73
17248	100	240128	7.183	43.79	24.72	31.48	202.29	114.20	145.43	461.92	8528	100	240128	3.551	30.10	85.29	66.30	154.82	150.52
250880	100	4479796	5.600	25.45	27.90	46.65	84.92	93.10	155.64	333.66	100352	100	4479796	2.240	15.41	42.76	33.90	70.98	101.60
98304	100	3595023	2.734	67.63	20.48	11.90	63.62	19.26	11.19	94.07	70656	100	3595023	1.965	15.38	115.81	43.44	132.30	85.04
219136	100	12278665	1.785	71.57	17.11	11.32	48.99	11.71	7.75	68.45	150528	100	12278665	1.226	5.71	87.17	27.83	86.27	42.44
84992	100	4020368	2.114	35.86	31.45	32.69	91.76	80.48	83.67	255.91	47872	100	4020368	1.191	6.41	16.74	12.82	42.45	26.47
41728	100	339456	12.293	88.11	7.38	4.51	317.66	26.59	16.25	360.50	26688	100	339456	7.862	49.94	699.20	249.71	563.87	409.21
210944	100	5737816	3.676	87.40	8.78	3.82	88.83	8.92	3.88	101.64	132096	100	5737816	2.302	22.46	202.14	63.26	193.16	99.39
53248	100	1638631	3.250	86.03	9.05	4.93	79.34	8.34	4.54	92.23	31232	100	1638631	1.906	22.79	162.12	55.89	151.34	84.98
107136	100	494592	21.661	47.90	19.21	32.89	447.46	179.40	307.24	934.09	59648	100	494592	12.060	93.18	342.10	207.66	404.66	577.71
37760	100	214016	17.644	48.17	17.76	34.07	370.81	136.71	262.30	769.82	22528	100	214016	10.526	68.93	278.05	181.09	352.82	507.04
184320	100	4957130	3.718	75.38	16.36	8.25	97.43	21.15	10.66	129.25	109568	100	4957130	2.210	20.25	153.02	73.73	164.61	101.24
182272	100	3711225	4.911	63.04	23.93	13.04	110.31	41.87	22.81	175.00	94208	100	3711225	2.538	24.86	139.72	58.24	157.51	92.21
47104	100	9417204	0.500	74.97	16.22	8.81	14.62	3.16	1.72	19.50	106496	100	9417204	1.131	6.41	84.62	19.93	62.24	29.89
19200	100	8571737	0.224	32.45	36.91	30.64	4.82	5.48	4.55	14.84	35328	100	8571737	0.412	1.17	5.25	4.03	15.54	8.64
58624	100	3754304	1.562	41.55	25.92	32.53	43.76	27.30	34.26	105.31	40704	100	3754304	1.084	9.16	22.82	16.53	41.01	44.05
6976	100	10047591	0.069	52.68	31.20	16.12	4.63	2.74	1.42	8.80	10112	100	10047591	0.101	0.82	5.51	1.45	3.77	0.88
78848	100	12378232	0.637	55.25	30.64	14.11	17.92	9.93	4.57	32.43	72704	100	12378232	0.587	1.88	28.67	10.74	32.36	11.13
76800	100	19603526	0.392	18.69	30.69	50.62	3.55	5.84	9.63	19.02	26624	100	19603526	0.136	1.60	3.04	1.56	5.41	2.01
5888	100	8481777	0.069	26.37	26.61	47.03	0.97	0.98	1.73	3.68	14272	100	8481777	0.168	0.56	3.53	2.32	8.24	6.59
71680	100	2255643	3.178	78.69	14.89	6.42	74.12	14.03	6.05	94.19	36864	100	2255643	1.634	16.34	111.06	45.45	127.28	69.67

Table F.15: Peak heights of mono-, di- and tri-methyl dibenzothiophenes (m/z 198+212+226) for all source rock samples (including annotation descriptions) (page 5 of 6).

	fragmentogram heights															
tot. ht.	226	%	TIC	% of TIC	a	b	c	d	e	f	g	h	i	tot. ht.		Ro%
43.34	88064	100	7769180	1.134	4.59	11.60	18.21	12.08	26.74	16.02	7.14	5.65	11.30	113.35		0.83
21.11	90112	100	15927144	0.566	2.38	6.19	11.08	6.28	12.56	8.73	2.84	2.34	4.18	56.58		0.87
27.97	43520	100	6503896	0.669	2.90	6.00	10.67	6.88	13.77	10.88	5.26	3.50	7.05	66.91		0.91
29.84	10944	100	2114243	0.518	2.25	5.82	8.91	5.29	10.08	6.77	6.42	2.25	3.96	51.76		0.82
6.95	48640	100	8153592	0.597	4.41	11.52	11.33	5.35	9.96	7.66	4.69	2.30	2.42	59.65		0.76
																0.95
0.00	3664	100	3383939	0.108												1.02
																1.02
10.10	23040	100	6112735	0.377	0.64	1.65	3.78	4.47	5.98	7.63	7.57	2.44	3.54	37.69		0.58
49.66	122880	100	12753925	0.963	3.67	6.97	11.82	9.85	22.01	15.17	10.60	5.55	10.71	96.35		0.8
82.07	3508	100	240128	1.461	5.88	11.57	23.70	15.74	26.92	24.27	17.44	7.87	12.70	146.09		0.78
56.92	35328	100	4479796	0.789	2.48	7.37	8.65	9.51	16.44	6.56	14.97	4.16	8.71	78.86		0.74
35.69	29184	100	3595023	0.812	2.57	8.74	18.29	8.80	17.87	14.01	4.48	2.29	4.13	81.18		1
19.75	62720	100	12278665	0.511	0.86	5.75	13.67	5.86	10.85	9.26	1.93	1.06	1.84	51.08		1.02
12.58	18688	100	4020368	0.465	2.18	4.30	5.98	5.39	10.50	6.40	3.63	2.67	5.43	46.48		0.87
157.88	11600	100	339456	3.417	10.47	28.55	89.33	35.73	65.31	57.50	33.06	9.04	12.73	341.72		1.1
39.31	45056	100	5737816	0.785	3.00	6.92	18.76	9.23	14.95	12.20	8.26	1.99	3.21	78.52		1.1
33.72	11776	100	1638631	0.719	2.98	7.83	16.48	7.55	13.25	10.99	7.68	2.01	3.11	71.86		1.1
236.94	22272	100	494592	4.503	15.00	37.94	76.30	49.94	93.23	79.52	42.65	20.15	35.58	450.31		1.02
164.73	7656	100	214016	3.577	10.74	28.93	58.55	40.88	75.18	64.79	36.90	13.86	27.89	357.73		1.06
34.00	51712	100	4957130	1.043	3.96	11.08	26.62	11.61	18.51	15.14	11.56	2.36	3.47	104.32		1.12
39.56	33280	100	3711225	0.897	3.30	15.07	19.27	9.94	15.57	12.07	9.50	2.00	2.96	89.67		1.1
11.94	70656	100	9417204	0.750	1.86	9.86	21.68	6.03	13.81	13.68	5.54	1.06	1.49	75.03		1.1
9.27	28416	100	8571737	0.332	0.37	1.05	3.90	3.19	6.57	6.75	3.99	2.52	4.79	33.15		0.92
17.86	15680	100	3754304	0.418	2.40	4.50	5.66	4.23	10.83	5.66	2.23	2.50	3.76	41.77		0.82
1.03	16896	100	10047591	0.168	0.61	1.48	3.57	1.53	1.36	6.15	0.99	0.64	0.48	16.82		1.17
10.34	29696	100	12378232	0.240	0.42	2.36	6.51	2.88	4.02	5.14	0.94	0.64	1.08	23.99		1.05
2.06	15360	100	19603526	0.078	0.38	0.70	0.69	0.54	0.89	1.62	1.66	0.66	0.70	7.84		0.95
5.59	18432	100	8481777	0.217	0.22	0.65	2.47	1.84	4.10	5.26	2.66	1.54	2.99	21.73		0.7
27.08	12736	100	2255643	0.565	2.79	7.18	12.66	6.73	9.74	7.85	6.00	1.47	2.05	56.46		0.94

Table F.15: Peak heights of mono-, di- and tri-methyl dibenzothiophenes (m/z 198+212+226) for all source rock samples (including annotation descriptions) (page 6 of 6).

MONOAROMATIC STEROIDS (MEASURED FROM AROMATIC FRACTION)																NORMALIZED PEAK HEIGHTS									
No.	1	2	3	4	5	6+7	9	10	11	12	13	14	15	16	Height	1	2	3	4	5	6+7	9	10	11	12	13
OIL SAMPLES																										
1																										
2																										
3																										
4	201	308	197	278	178	283	435	136	242	68	232	253	150	131	3092	6.50	9.96	6.37	8.99	5.76	9.15	14.07	4.40	7.83	2.20	7.50
5	270	360	195	220	215	200	351	152	168	162	187	211	139	128	2958	9.13	12.17	6.59	7.44	7.27	6.76	11.87	5.14	5.68	5.48	6.32
6	300	376	207	275	306	197	132	104	102	188	180	248	117	102	2834	10.59	13.27	7.30	9.70	10.80	6.95	4.66	3.67	3.60	6.63	6.35
7	127	90	64	126	42	104	94	122	79	23	67	121	51	64	1174	10.82	7.67	5.45	10.73	3.58	8.86	8.01	10.39	6.73	1.96	5.71
8	244	109	80	176	97	133	89	87	107	53	164	115	100	62	1616	15.10	6.75	4.95	10.89	6.00	8.23	5.51	5.38	6.62	3.28	10.15
9	0	0	0	0	0	0	0	0	0	0	0	0	0	0	0	0.00	0.00	0.00	0.00	0.00	0.00	0.00	0.00	0.00	0.00	0.00
10	425	500	401	365	354	427	352	713	182	232	538	350	329	147	5315	8.00	9.41	7.54	6.87	6.66	8.03	6.62	13.41	3.42	4.37	10.12
11	241	108	71	292	110	278	108	73	47	53	125	419	71	50	2046	11.78	5.28	3.47	14.27	5.38	13.59	5.28	3.57	2.30	2.59	6.11
12	81	200	310	152	147	152	562	200	42	102	881	91	212	68	3200	2.53	6.25	9.69	4.75	4.59	4.75	17.56	6.25	1.31	3.19	27.53
13	220	55	655	650	290	105	100	496	262	340	195	2170	1060	180	6778	3.25	0.81	9.66	9.59	4.28	1.55	1.48	7.32	3.87	5.02	2.88
14	280	650	440	350	65	470	230	285	490	421	130	1455	2170	310	7746	3.61	8.39	5.68	4.52	0.84	6.07	2.97	3.68	6.33	5.44	1.68
15	78	58	82	76	43	69	24	253	17	33	34	114	47	19	945	8.25	5.93	8.68	8.04	4.55	7.30	2.54	26.77	1.80	3.49	3.60
16	235	101	57	188	81	97	65	84	92	30	97	168	82	68	1445	16.26	6.99	3.94	13.01	5.61	6.71	4.50	5.81	6.37	2.08	6.71
17	0	0	0	0	0	0	0	0	0	0	0	0	0	0	0	0.00	0.00	0.00	0.00	0.00	0.00	0.00	0.00	0.00	0.00	0.00
18	120	670	260	550	220	1280	62	91	202	1558	760	348	297	90	6508	1.84	10.30	4.00	8.45	3.38	19.67	0.95	1.40	3.10	23.94	11.68
19	145	210	255	290	20	410	40	195	180	495	210	147	920	220	3737	3.88	5.62	6.82	7.76	0.54	10.97	1.07	5.22	4.82	13.25	5.62
20	190	580	290	392	47	295	121	297	250	465	160	400	2170	300	5957	3.19	9.74	4.87	6.58	0.79	4.95	2.03	4.99	4.20	7.81	2.69
21	287	146	141	278	117	254	121	155	10	155	130	230	195	187	2406	11.93	6.07	5.86	11.55	4.86	10.56	5.03	6.44	0.42	6.44	5.40
22	275	488	212	271	195	126	263	4250	600	278	828	203	167	311	8467	3.25	5.76	2.50	3.20	2.30	1.49	3.11	50.19	7.09	3.28	9.78
23	63	161	79	133	61	101	55	70	68	51	41	82	41	33	1039	6.06	15.50	7.60	12.80	5.87	9.72	5.29	6.74	6.54	4.91	3.95
24	372	150	187	285	215	210	850	98	120	54	201	143	181	107	3173	11.72	4.73	5.89	8.98	6.78	6.62	26.79	3.09	3.76	1.70	6.33
25	470	750	820	1030	290	2170	67	296	846	1965	1100	448	1675	170	12097	3.89	6.20	6.78	8.51	2.40	17.94	0.55	2.45	6.99	16.24	9.09
26	210	460	190	240	180	285	200	167	262	395	260	265	165	105	3384	6.21	13.59	5.61	7.09	5.32	8.42	5.91	4.93	7.74	11.67	7.68
27	97	257	149	139	54	102	50	104	20	14	63	122	44	31	1246	7.78	20.63	11.96	11.16	4.33	8.19	4.01	8.35	1.61	1.12	5.06
28																										
29																										
30	241	268	145	347	216	305	478	185	191	110	217	266	173	114	3256	7.40	8.23	4.45	10.66	6.63	9.37	14.68	5.68	5.87	3.38	6.66
31	227	173	138	86	103	165	663	561	171	71	250	166	159	108	3041	7.46	5.69	4.54	2.83	3.39	5.43	21.80	18.45	5.62	2.33	8.22
32	345	550	408	301	331	520	647	406	253	113	533	571	305	243	5526	6.24	9.95	7.38	5.45	5.99	9.41	11.71	7.35	4.58	2.04	9.65
33	36	82	63	44	62	98	406	162	72	20	222	114	96	76	1553	2.32	5.28	4.06	2.83	3.99	6.31	26.14	10.43	4.64	1.29	14.29
34	217	346	162	317	261	343	421	306	147	86	321	372	216	157	3672	5.91	9.42	4.41	8.63	7.11	9.34	11.47	8.33	4.00	2.34	8.74
35	141	300	268	255	274	491	564	302	189	106	365	263	192	104	3814	3.70	7.87	7.03	6.69	7.18	12.87	14.79	7.92	4.96	2.78	9.57
36	78	128	63	220	150	268	820	271	58	55	736	388	61	32	3328	2.34	3.85	1.89	6.61	4.51	8.05	24.64	8.14	1.74	1.65	22.12
37	246	532	253	237	195	263	758	183	104	88	169	238	109	100	3475	7.08	15.31	7.28	6.82	5.61	7.57	21.81	5.27	2.99	2.53	4.86
38	87	213	138	132	158	153	570	65	57	29	113	150	79	47	1991	4.37	10.70	6.93	6.63	7.94	7.68	28.63	3.26	2.86	1.46	5.68

Table F.16: Peak heights of monoaromatic steroids from aromatic fraction (m/z 253) for all hydrocarbon samples (page 1 of 4).

NORMALIZED PEAK HEIGHTS							PEAK HEIGHTS AS ppm OF TIC														
14	15	16	253	%	TIC	% of TIC	1	2	3	4	5	6+7	9	10	11	12	13	14	15	16	Height
								OIL SAMPLES													
					not anal.																
					not anal.																
					not anal.																
8.18	4.85	4.24	6208	100	1761175	0.352	2.29	3.51	2.25	3.17	2.03	3.23	4.96	1.55	2.76	0.78	2.64	2.88	1.71	1.49	35.25
7.13	4.70	4.33	3968	80	4133205	0.077	0.70	0.93	0.51	0.57	0.56	0.52	0.91	0.39	0.44	0.42	0.49	0.55	0.36	0.33	7.68
8.75	4.13	3.60	2432	85	7899419	0.026	0.28	0.35	0.19	0.25	0.28	0.18	0.12	0.10	0.09	0.17	0.17	0.23	0.11	0.09	2.62
10.31	4.34	5.45	7168	90	11147543	0.058	0.63	0.44	0.32	0.62	0.21	0.51	0.46	0.60	0.39	0.11	0.33	0.60	0.25	0.32	5.79
7.12	6.19	3.84	2381	75	3353630	0.053	0.80	0.36	0.26	0.58	0.32	0.44	0.29	0.29	0.35	0.17	0.54	0.38	0.33	0.20	5.32
0.00	0.00	0.00	2240	55	4835016	0.025	0.00	0.00	0.00	0.00	0.00	0.00	0.00	0.00	0.00	0.00	0.00	0.00	0.00	0.00	0.00
6.59	6.19	2.77	89088	100	41091556	0.217	1.73	2.04	1.64	1.49	1.44	1.74	1.44	2.91	0.74	0.95	2.19	1.43	1.34	0.60	21.68
20.48	3.47	2.44	76800	100	8246725	0.931	10.97	4.92	3.23	13.29	5.01	12.65	4.92	3.32	2.14	2.41	5.69	19.07	3.23	2.28	93.13
2.84	6.63	2.13	21504	100	7857856	0.274	0.69	1.71	2.65	1.30	1.26	1.30	4.81	1.71	0.36	0.87	7.53	0.78	1.81	0.58	27.37
32.02	15.64	2.66	8152	100	673792	1.210	3.93	0.98	11.69	11.60	5.18	1.87	1.78	8.85	4.68	6.07	3.48	38.73	18.92	3.21	120.99
18.78	28.01	4.00	16224	100	448000	3.621	13.09	30.39	20.57	16.36	3.04	21.97	10.75	13.32	22.91	19.68	6.08	68.02	101.45	14.49	362.14
12.06	4.97	2.01	5376	90	6492048	0.075	0.62	0.44	0.65	0.60	0.34	0.54	0.19	2.00	0.13	0.26	0.27	0.90	0.37	0.15	7.45
11.63	5.67	4.71	22912	95	8076805	0.269	4.38	1.88	1.06	3.51	1.51	1.81	1.21	1.57	1.72	0.56	1.81	3.13	1.53	1.27	26.95
0.00	0.00	0.00	37632	100	16812960	0.224	0.00	0.00	0.00	0.00	0.00	0.00	0.00	0.00	0.00	0.00	0.00	0.00	0.00	0.00	0.00
5.35	4.56	1.38	10752	100	189952	5.660	10.44	58.27	22.61	47.84	19.13	111.33	5.39	7.91	17.57	135.51	66.10	30.27	25.83	7.83	566.04
3.93	24.62	5.89	3088	100	721920	0.428	1.66	2.40	2.92	3.32	0.23	4.69	0.46	2.23	2.06	5.67	2.40	1.68	10.53	2.52	42.77
6.71	36.43	5.04	4088	100	391680	1.044	3.33	10.16	5.08	6.87	0.82	5.17	2.12	5.20	4.38	8.15	2.80	7.01	38.02	5.26	104.37
9.56	8.10	7.77	25941	90	9414432	0.248	2.96	1.50	1.45	2.87	1.21	2.62	1.25	1.60	0.10	1.60	1.34	2.37	2.01	1.93	24.80
2.40	1.97	3.67	67994	100	20480680	0.332	1.08	1.91	0.83	1.06	0.76	0.49	1.03	16.66	2.35	1.09	3.25	0.80	0.65	1.22	33.20
7.89	3.95	3.18	15616	100	15585093	0.100	0.61	1.55	0.76	1.28	0.59	0.97	0.53	0.68	0.66	0.49	0.40	0.79	0.40	0.32	10.02
4.51	5.70	3.37	37376	100	12385703	0.302	3.54	1.43	1.78	2.71	2.04	2.00	8.08	0.93	1.14	0.51	1.91	1.36	1.72	1.02	30.18
3.70	13.85	1.41	3496	100	220928	1.582	6.15	9.81	10.73	13.47	3.79	28.39	0.88	3.87	11.07	25.70	14.39	5.86	21.91	2.22	158.24
7.83	4.88	3.10	3408	65	2460251	0.090	0.56	1.22	0.51	0.64	0.48	0.76	0.53	0.44	0.70	1.05	0.69	0.71	0.44	0.28	9.00
9.79	3.53	2.49	13739	90	10901194	0.113	0.88	2.34	1.36	1.27	0.49	0.93	0.46	0.95	0.18	0.13	0.57	1.11	0.40	0.28	11.34
					not anal.																
					not anal.																
8.17	5.31	3.50	40704	90	23386172	0.157	1.16	1.29	0.70	1.67	1.04	1.47	2.30	0.89	0.92	0.53	1.04	1.28	0.83	0.55	15.66
5.46	5.23	3.55	10688	86	5596559	0.164	1.23	0.93	0.75	0.46	0.56	0.89	3.58	3.03	0.92	0.38	1.35	0.90	0.86	0.58	16.42
10.33	5.52	4.40	3056	60	10061116	0.018	0.11	0.18	0.13	0.10	0.11	0.17	0.21	0.13	0.08	0.04	0.18	0.19	0.10	0.08	1.82
7.34	6.18	4.89	50688	100	7923020	0.640	1.48	3.38	2.60	1.81	2.55	4.04	16.73	6.67	2.97	0.82	9.15	4.70	3.95	3.13	63.98
10.13	5.88	4.28	6208	78	4889070	0.099	0.59	0.93	0.44	0.86	0.70	0.93	1.14	0.83	0.40	0.23	0.87	1.00	0.58	0.42	9.90
6.90	5.03	2.73	10752	84	6528065	0.138	0.51	1.09	0.97	0.93	0.99	1.78	2.05	1.10	0.69	0.38	1.32	0.95	0.70	0.38	13.84
11.66	1.83	0.96	17152	100	3475211	0.494	1.16	1.90	0.93	3.26	2.22	3.97	12.16	4.02	0.86	0.82	10.92	5.75	0.90	0.47	49.36
6.85	3.14	2.88	13632	78	17189866	0.062	0.44	0.95	0.45	0.42	0.35	0.47	1.35	0.33	0.19	0.16	0.30	0.42	0.19	0.18	6.19
7.53	3.97	2.36	165888	100	21268424	0.780	3.41	8.34	5.41	5.17	6.19	5.99	22.33	2.55	2.23	1.14	4.43	5.88	3.09	1.84	78.00

Table F.16: Peak heights of monoaromatic steroids from aromatic fraction (m/z 253) for all hydrocarbon samples (page 2 of 4).

No.	1	2	3	4	5	6+7	9	10	11	12	13	14	15	16	Height	1	2	3	4	5	6+7	9	10	11	12	13
SHALE SAMPLES																										
41	74	54	23	50	16	85	47	118	24	16	200	71	27	41	846	8.75	6.38	2.72	5.91	1.89	10.05	5.56	13.95	2.84	1.89	23.64
42	89	158	71	121	34	246	174	365	64	146	132	172	58	88	1918	4.64	8.24	3.70	6.31	1.77	12.83	9.07	19.03	3.34	7.61	6.88
43	90	34	12	89	16	52	31	65	12	5	307	64	22	21	820	10.98	4.15	1.46	10.85	1.95	6.34	3.78	7.93	1.46	0.61	37.44
44	95	353	105	342	108	861	840	546	180	69	141	336	94	166	4236	2.24	8.33	2.48	8.07	2.55	20.33	19.83	12.89	4.25	1.63	3.33
45	139	119	83	88	126	77	665	565	259	233	620	372	182	393	3921	3.55	3.03	2.12	2.24	3.21	1.96	16.96	14.41	6.61	5.94	15.81
46																										
47	0	0	0	0	0	0	0	0	0	0	0	0	0	0	0	0.00	0.00	0.00	0.00	0.00	0.00	0.00	0.00	0.00	0.00	0.00
48																										
49	100	136	26	222	215	708	1055	919	79	47	437	1030	62	415	5451	1.83	2.49	0.48	4.07	3.94	12.99	19.35	16.86	1.45	0.86	8.02
50	201	461	122	510	268	963	1009	555	160	72	263	501	89	342	5516	3.64	8.36	2.21	9.25	4.86	17.46	18.29	10.06	2.90	1.31	4.77
51	130	700	290	585	135	2170	50	72	1240	1960	740	470	1240	220	10002	1.30	7.00	2.90	5.85	1.35	21.70	0.50	0.72	12.40	19.60	7.40
52	94	385	100	398	115	1055	1052	410	185	137	112	413	82	113	4651	2.02	8.28	2.15	8.56	2.47	22.68	22.62	8.82	3.98	2.95	2.41
53	56	31	32	91	28	80	193	174	35	26	110	168	53	73	1150	4.87	2.70	2.78	7.91	2.43	6.96	16.78	15.13	3.04	2.26	9.57
54	70	24	20	72	30	71	76	98	38	13	72	131	44	42	801	8.74	3.00	2.50	8.99	3.75	8.86	9.49	12.23	4.74	1.62	8.99
55	131	341	100	361	172	987	918	367	155	147	102	323	60	128	4292	3.05	7.95	2.33	8.41	4.01	23.00	21.39	8.55	3.61	3.42	2.38
56	150	205	375	345	180	400	42	310	322	581	225	200	2170	380	5885	2.55	3.48	6.37	5.86	3.06	6.80	0.71	5.27	5.47	9.87	3.82
57	111	328	209	75	29	143	158	147	280	107	103	158	168	150	2166	5.12	15.14	9.65	3.46	1.34	6.60	7.29	6.79	12.93	4.94	4.76
58	95	125	88	185	86	210	71	260	92	78	810	137	317	162	2716	3.50	4.60	3.24	6.81	3.17	7.73	2.61	9.57	3.39	2.87	29.82
59	200	715	300	630	175	1700	78	142	297	1640	905	185	1435	365	8767	2.28	8.16	3.42	7.19	2.00	19.39	0.89	1.62	3.39	18.71	10.32
60	200	760	330	680	120	1700	104	192	360	1670	935	355	1235	410	9051	2.21	8.40	3.65	7.51	1.33	18.78	1.15	2.12	3.98	18.45	10.33
61	57	98	67	132	58	137	53	198	26	50	141	111	72	141	1341	4.25	7.31	5.00	9.84	4.33	10.22	3.95	14.77	1.94	3.73	10.51
62	41	79	31	91	33	93	32	153	30	15	72	96	47	92	905	4.53	8.73	3.43	10.06	3.65	10.28	3.54	16.91	3.31	1.66	7.96
63	132	59	44	170	74	153	143	98	100	20	313	197	126	112	1741	7.58	3.39	2.53	9.76	4.25	8.79	8.21	5.63	5.74	1.15	17.98
64	101	34	11	30	16	58	49	174	16	13	105	54	28	42	731	13.82	4.65	1.50	4.10	2.19	7.93	6.70	23.80	2.19	1.78	14.36
65	68	31	20	41	26	42	19	147	20	11	83	21	11	20	560	12.14	5.54	3.57	7.32	4.64	7.50	3.39	26.25	3.57	1.96	14.82
66	21	197	34	197	92	139	60	42	52	63	141	375	77	25	1515	1.39	13.00	2.24	13.00	6.07	9.17	3.96	2.77	3.43	4.16	9.31
67	16	118	12	82	14	42	27	67	24	19	145	68	36	27	697	2.30	16.93	1.72	11.76	2.01	6.03	3.87	9.61	3.44	2.73	20.80
68	77	97	41	38	54	91	416	68	541	48	181	97	213	102	2064	3.73	4.70	1.99	1.84	2.62	4.41	20.16	3.29	26.21	2.33	8.77
69	113	209	50	214	145	735	628	590	139	88	290	324	82	145	3752	3.01	5.57	1.33	5.70	3.86	19.59	16.74	15.72	3.70	2.35	7.73
70	106	198	147	86	136	194	357	417	231	75	231	277	200	135	2790	3.80	7.10	5.27	3.08	4.87	6.95	12.80	14.95	8.28	2.69	8.28
Peaks labelled after Riolo et al., 1986, Org. Geochem. 10, 981-990 and Mackenzie et a., 1983, Advances in Organic Geochemistry 1981.																										
1=C27 20S Reg5b. 2=C27 20S Dia10b. 3=C27 20S Dia10a. 4=C27 20R Reg5b+10b. 5=C27 20S Reg5a. 6=C28 20S Reg5b.																										
7=C27 20R Dia10a+C28 20S Dia10b. 9=C27 20R Reg5a+C28 20S Reg5a. 10=C28 20R Reg5b+Dia10b+C29 20S Reg5b+Dia10b. 11=C28 20R Dia10a.																										
12=C29 20S Dia10a. 13=C29 20S Reg5a. 14=C28 20R Reg5a+C29 20R Reg5b+Dia10b. 15=C29 20R Dia10a. 16=C29 20R Reg5a.																										
Height=height of maximum ion in m/z 253 fragmentogram x baseline factor.																										
%TIC=Height as % of TIC height.																										

Table F.16: Peak heights of monoaromatic steroids from aromatic fraction (m/z 253) for all source rock samples (including annotation descriptions) (page 3 of 4).

14	15	16	253	%	TIC	% of TIC	1	2	3	4	5	6+7	9	10	11	12	13	14	15	16	Height
										SHALE SAMPLES											
8.39	3.19	4.85	30976	100	7769180	0.399	3.49	2.54	1.08	2.36	0.75	4.01	2.22	5.56	1.13	0.75	9.43	3.35	1.27	1.93	39.87
8.97	3.02	4.59	25498	94	15927144	0.150	0.70	1.24	0.56	0.95	0.27	1.93	1.37	2.86	0.50	1.15	1.04	1.35	0.46	0.69	15.05
7.80	2.68	2.56	47445	100	6503896	0.729	8.01	3.02	1.07	7.92	1.42	4.63	2.76	5.78	1.07	0.44	27.31	5.69	1.96	1.87	72.95
7.93	2.22	3.92	13952	100	2114243	0.660	1.48	5.50	1.64	5.33	1.68	13.41	13.09	8.51	2.80	1.07	2.20	5.23	1.46	2.59	65.99
9.49	4.64	10.02	8397	95	8153592	0.098	0.35	0.30	0.21	0.22	0.31	0.19	1.66	1.41	0.65	0.58	1.55	0.93	0.45	0.98	9.78
					not anal.																
0.00	0.00	0.00	2912	100	3383939	0.086															
					not anal.																
18.90	1.14	7.61	368640	100	6112735	6.031	11.06	15.05	2.88	24.56	23.79	78.33	116.72	101.67	8.74	5.20	48.35	113.95	6.86	45.91	603.07
9.08	1.61	6.20	252928	100	12753925	1.983	7.23	16.57	4.39	18.34	9.64	34.62	36.28	19.95	5.75	2.59	9.46	18.01	3.20	12.30	198.31
4.70	12.40	2.20	9744	100	240128	4.058	5.27	28.40	11.77	23.73	5.48	88.04	2.03	2.92	50.31	79.52	30.02	19.07	50.31	8.93	405.78
8.88	1.76	2.43	236544	100	4479796	5.280	10.67	43.71	11.35	45.18	13.06	119.77	119.43	46.55	21.00	15.55	12.72	46.89	9.31	12.83	528.02
14.61	4.61	6.35	9301	95	3595023	0.246	1.20	0.66	0.68	1.94	0.60	1.71	4.12	3.72	0.75	0.56	2.35	3.59	1.13	1.56	24.58
16.35	5.49	5.24	20684	100	12278665	0.168	1.47	0.50	0.42	1.51	0.63	1.49	1.60	2.06	0.80	0.27	1.51	2.76	0.93	0.88	16.85
7.53	1.40	2.98	25344	100	4020368	0.630	1.92	5.01	1.47	5.30	2.53	14.50	13.48	5.39	2.28	2.16	1.50	4.74	0.88	1.88	63.04
3.40	36.87	6.46	4008	100	339456	1.181	3.01	4.11	7.52	6.92	3.61	8.03	0.84	6.22	6.46	11.66	4.51	4.01	43.54	7.62	118.07
7.29	7.76	6.93	9536	100	5737816	0.166	0.85	2.52	1.60	0.58	0.22	1.10	1.21	1.13	2.15	0.82	0.79	1.21	1.29	1.15	16.62
5.04	11.67	5.96	4048	87	1638631	0.215	0.75	0.99	0.70	1.46	0.68	1.66	0.56	2.06	0.73	0.62	6.41	1.08	2.51	1.28	21.49
2.11	16.37	4.16	14064	100	494592	2.844	6.49	23.19	9.73	20.43	5.68	55.14	2.53	4.61	9.63	53.19	29.35	6.00	46.54	11.84	284.36
3.92	13.64	4.53	4904	100	214016	2.291	5.06	19.24	8.35	17.22	3.04	43.04	2.63	4.86	9.11	42.28	23.67	8.99	31.27	10.38	229.14
8.28	5.37	10.51	22272	100	4957130	0.449	1.91	3.28	2.24	4.42	1.94	4.59	1.78	6.63	0.87	1.68	4.72	3.72	2.41	4.72	44.93
10.61	5.19	10.17	16640	100	3711225	0.448	2.03	3.91	1.54	4.51	1.63	4.61	1.59	7.58	1.49	0.74	3.57	4.76	2.33	4.56	44.84
11.32	7.24	6.43	24917	95	9417204	0.251	1.91	0.85	0.64	2.45	1.07	2.21	2.06	1.41	1.44	0.29	4.52	2.84	1.82	1.62	25.14
7.39	3.83	5.75	43776	100	8571737	0.511	7.06	2.38	0.77	2.10	1.12	4.05	3.42	12.16	1.12	0.91	7.34	3.77	1.96	2.93	51.07
3.75	1.96	3.57	10624	100	3754304	0.283	3.44	1.57	1.01	2.07	1.31	2.12	0.96	7.43	1.01	0.56	4.19	1.06	0.56	1.01	28.30
24.75	5.08	1.65	48128	100	10047591	0.479	0.66	6.23	1.07	6.23	2.91	4.39	1.90	1.33	1.64	1.99	4.46	11.86	2.43	0.79	47.90
9.76	5.16	3.87	38912	100	12378232	0.314	0.72	5.32	0.54	3.70	0.63	1.89	1.22	3.02	1.08	0.86	6.54	3.07	1.62	1.22	31.44
4.70	10.32	4.94	215040	100	19603526	1.097	4.09	5.16	2.18	2.02	2.87	4.84	22.11	3.61	28.75	2.55	9.62	5.16	11.32	5.42	109.69
8.64	2.19	3.86	22016	100	8481777	0.260	0.78	1.45	0.35	1.48	1.00	5.08	4.34	4.08	0.96	0.61	2.01	2.24	0.57	1.00	25.96
9.93	7.17	4.84	2976	85	2255643	0.112	0.43	0.80	0.59	0.35	0.55	0.78	1.43	1.68	0.93	0.30	0.93	1.11	0.80	0.54	11.21

Table F.16: Peak heights of monoaromatic steroids from aromatic fraction (m/z 253) for all source rock samples (page 4 of 4).

TRIAROMATIC STEROIDS											NORMALIZED PEAK HEIGHTS						
No.	f	g	a	b	c	d	e	Height	AROM TIC	TAS/TOT%	f	g	a	b	c	d	e
OIL SAMPLES																	
1																	
2																	
3																	
4	981	660	58	161	99	75	73	2107	1761175	1.70	46.56	31.32	2.75	7.64	4.70	3.56	3.46
5	990	670	65	163	106	85	78	2157	4133205	0.60	45.90	31.06	3.01	7.56	4.91	3.94	3.62
6	922	800	45	59	48	54	38	1966	799419	0.50	46.90	40.69	2.29	3.00	2.44	2.75	1.93
7	652	498	42	147	65	82	51	1537	11147543	0.20	42.42	32.40	2.73	9.56	4.23	5.34	3.32
8	471	402	111	273	182	114	162	1715	3353630	0.50	27.46	23.44	6.47	15.92	10.61	6.65	9.45
9	561	362	172	438	200	251	176	2160	4835016	0.10	25.97	16.76	7.96	20.28	9.26	11.62	8.15
10	164	130	38	152	68	72	18	642	41091556	0.60	25.55	20.25	5.92	23.68	10.59	11.21	2.80
11	252	143	0	0	0	0	0	395	8246725	1.90	63.80	36.20	0.00	0.00	0.00	0.00	0.00
12	0	0	0	0	0	0	0		7857856	0.10	0.00	0.00	0.00	0.00	0.00	0.00	0.00
13	425	200	0	0	0	0	0	625	673792	2.50	68.00	32.00	0.00	0.00	0.00	0.00	0.00
14	2170	1290	100	700	290	445	330	5325	448000	9.60	40.75	24.23	1.88	13.15	5.45	8.36	6.20
15	92	68	0	0	0	0	0	160	6492048	0.90	57.50	42.50	0.00	0.00	0.00	0.00	0.00
16	341	208	0	0	0	0	0	549	8076805	1.10	62.11	37.89	0.00	0.00	0.00	0.00	0.00
17	916	502	0	0	0	0	0	1418	16812960	0.40	64.60	35.40	0.00	0.00	0.00	0.00	0.00
18	430	410	470	2170	1140	1230	1150	7000	189952	61.30	6.14	5.86	6.71	31.00	16.29	17.57	16.43
19	2170	1640	150	780	340	455	340	5875	721920	2.10	36.94	27.91	2.55	13.28	5.79	7.74	5.79
20	2170	1800	180	1060	430	620	440	6700	391680	5.40	32.39	26.87	2.69	15.82	6.42	9.25	6.57
21	690	475	133	391	295	178	180	2342	9414432	1.30	29.46	20.28	5.68	16.70	12.60	7.60	7.69
22	468	325	341	1050	456	508	418	3566	20480680	2.80	13.12	9.11	9.56	29.44	12.79	14.25	11.72
23	442	246	37	88	42	50	36	941	15505093	0.30	46.97	26.14	3.93	9.35	4.46	5.31	3.83
24	875	561	52	132	78	60	54	1812	12385703	1.20	48.29	30.96	2.87	7.28	4.30	3.31	2.98
25	2170	1465	460	1580	710	810	590	7785	220928	4.50	27.87	18.82	5.91	20.30	9.12	10.40	7.58
26	835	430	91	252	160	110	135	2013	2460251	0.40	41.48	21.36	4.52	12.52	7.95	5.46	6.71
27	487	275	0	0	0	0	0	762	10901194	0.50	63.91	36.09	0.00	0.00	0.00	0.00	0.00
28	765	495	20	50	15	15	0	1360			56.25	36.40	1.47	3.68	1.10	1.10	0.00
29	1102	846	33	74	34	39	0	2128			51.79	39.76	1.55	3.48	1.60	1.83	0.00
30	968	841	66	225	141	126	101	2468	23386172	0.70	39.22	34.08	2.67	9.12	5.71	5.11	4.09
31	982	829	91	350	200	192	160	2804	5596559	0.65	35.02	29.56	3.25	12.48	7.13	6.85	5.71
32	918	687	45	112	63	57	47	1929	10061116	0.17	47.59	35.61	2.33	5.81	3.27	2.95	2.44
33	733	672	29	57	35	33	31	1590	7923020	0.44	46.10	42.26	1.82	3.58	2.20	2.08	1.95
34	965	805	61	168	112	98	88	2297	4889070	0.46	42.01	35.05	2.66	7.31	4.88	4.27	3.83
35	705	563	145	1005	629	523	468	4038	6528065	0.64	17.46	13.94	3.59	24.89	15.58	12.95	11.59
36	109	95	296	1067	429	526	345	2867	3475211	0.16	3.80	3.31	10.32	37.22	14.96	18.35	12.03
37	917	627	21	30	20	18	16	1649	17189866	0.28	55.61	38.02	1.27	1.82	1.21	1.09	0.97
38	940	821	44	73	48	29	27	1982	21268424	0.78	47.43	41.42	2.22	3.68	2.42	1.46	1.36

Table F.17: Peak heights of triaromatic steroids from aromatic fraction (m/z 231) for all hydrocarbon samples (page 1 of 4).

fragmentogram heights (ppm TIC)												
231	%	TIC	% of TIC	f	g	a	b	c	d	e	Height	
		not anal.										
		not anal.										
		not anal.										
25856	100	1761175	1.468	68.35	45.99	4.04	11.22	6.90	5.23	5.09	146.81	
30208	100	4133205	0.731	33.54	22.70	2.20	5.52	3.59	2.88	2.64	73.09	
4608	95	7899419	0.055	2.60	2.26	0.13	0.17	0.14	0.15	0.11	5.54	
27136	100	11147543	0.243	10.33	7.89	0.67	2.33	1.03	1.30	0.81	24.34	
16384	100	3353630	0.489	13.42	11.45	3.16	7.78	5.18	3.25	4.61	48.85	
5440	80	4835016	0.090	2.34	1.51	0.72	1.83	0.83	1.05	0.73	9.00	
246784	100	41091556	0.601	15.34	12.16	3.55	14.22	6.36	6.74	1.68	60.06	
159744	100	8246725	1.937	123.58	70.13	0.00	0.00	0.00	0.00	0.00	193.71	
37888	100	7857856	0.482	0	0	0	0	0	0	0	0	
16864	100	673792	2.503	170.19	80.09	0.00	0.00	0.00	0.00	0.00	250.28	
43008	100	448000	9.600	391.21	232.56	18.03	126.20	52.28	80.23	59.49	960.00	
60416	100	6492048	0.931	53.51	39.55	0.00	0.00	0.00	0.00	0.00	93.06	
84992	100	8076805	1.052	65.36	39.87	0.00	0.00	0.00	0.00	0.00	105.23	
64000	100	16812960	0.381	24.59	13.48	0.00	0.00	0.00	0.00	0.00	38.07	
116352	100	189952	61.253	376.27	358.77	411.27	1898.85	997.55	1076.31	1006.31	6125.34	
14896	100	721920	2.063	76.21	57.60	5.27	27.39	11.94	15.98	11.94	206.34	
21152	100	391680	5.400	174.91	145.08	14.51	85.44	34.66	49.97	35.46	540.03	
121856	100	9414432	1.294	38.13	26.25	7.35	21.61	16.30	9.84	9.95	129.44	
569344	100	20480680	2.780	36.48	25.34	26.58	81.85	35.55	39.60	32.59	277.99	
42752	100	15585093	0.274	12.88	7.17	1.08	2.57	1.22	1.46	1.05	27.43	
153600	95	12385703	1.178	56.89	36.48	3.38	8.58	5.07	3.90	3.51	117.81	
9952	100	220928	4.505	125.56	84.77	26.62	91.42	41.08	46.87	34.14	450.46	
9536	100	2460251	0.388	16.08	8.28	1.75	4.85	3.08	2.12	2.60	38.76	
58880	100	10901194	0.540	34.52	19.49	0.00	0.00	0.00	0.00	0.00	54.01	
16000000	100	not anal.										
3.00E+06	100	not anal.										
155648	100	23386172	0.666	26.10	22.68	1.78	6.07	3.80	3.40	2.72	66.56	
36608	100	5596559	0.654	22.91	19.34	2.12	8.16	4.67	4.48	3.73	65.41	
16896	95	10061116	0.160	7.59	5.68	0.37	0.93	0.52	0.47	0.39	15.95	
34560	100	7923020	0.436	20.11	18.44	0.80	1.56	0.96	0.91	0.85	43.62	
22272	92	4889070	0.419	17.61	14.69	1.11	3.07	2.04	1.79	1.61	41.91	
42240	100	6528065	0.647	11.30	9.02	2.32	16.10	10.08	8.38	7.50	64.71	
56064	98	3475211	1.581	6.01	5.24	16.32	58.84	23.66	29.01	19.02	158.10	
47872	96	17189866	0.267	14.87	10.17	0.34	0.49	0.32	0.29	0.26	26.74	
166912	95	21268424	0.746	35.36	30.88	1.66	2.75	1.81	1.09	1.02	74.55	

Table F.17: Peak heights of triaromatic steroids from aromatic fraction (m/z 231) for all hydrocarbon samples (page 2 of 4).

No.	f	g	a	b	c	d	e	Height	AROM TIC	TAS/TOT%	f	g	a	b	c	d	e
SHALE SAMPLES																	
41	1035	770	200	582	352	300	312	3551	7769180	2.70	29.15	21.68	5.63	16.39	9.91	8.45	8.79
42	1040	725	176	584	372	295	345	3537	15927144	1.10	29.40	20.50	4.98	16.51	10.52	8.34	9.75
43	1035	761	200	480	271	238	241	3226	6503896	2.20	32.08	23.59	6.20	14.88	8.40	7.38	7.47
44	285	237	272	1064	423	572	391	3244	2114243	2.00	8.79	7.31	8.38	32.80	13.04	17.63	12.05
45	935	492	38	116	129	92	105	1907	8153592	0.40	49.03	25.80	1.99	6.08	6.76	4.82	5.51
46																	
47	0	0	0	0	0	0	0		3383939	0.10	0.00	0.00	0.00	0.00	0.00	0.00	0.00
48																	
49	58	34	177	1073	460	604	421	2827	6112735	5.10	2.05	1.20	6.26	37.96	16.27	21.37	14.89
50	178	137	459	1088	482	661	455	3460	12753925	13.90	5.14	3.96	13.27	31.45	13.93	19.10	13.15
51	365	295	510	2170	770	1425	805	6340	240128	53.90	5.76	4.65	8.04	34.23	12.15	22.48	12.70
52	162	98	300	1085	285	600	258	2788	4479796	10.90	5.81	3.52	10.76	38.92	10.22	21.52	9.25
53	1035	672	101	281	152	135	138	2514	3595023	1.50	41.17	26.73	4.02	11.18	6.05	5.37	5.49
54	917	582	82	194	121	91	91	2078	12278665	0.50	44.13	28.01	3.95	9.34	5.82	4.38	4.38
55	131	100	292	1073	272	518	261	2647	4020360	5.80	4.95	3.78	11.03	40.54	10.28	19.57	9.86
56	2170	1585	245	980	450	550	470	6450	339456	4.40	33.64	24.57	3.80	15.19	6.98	8.53	7.29
57	982	606	33	87	38	39	30	1815	5737816	0.80	54.10	33.39	1.82	4.79	2.09	2.15	1.65
58	935	608	95	252	121	138	111	2260	1630631	0.70	41.37	26.90	4.20	11.15	5.35	6.11	4.91
59	595	475	550	2170	1265	1345	1215	7615	494592	48.50	7.81	6.24	7.22	28.50	16.61	17.66	15.96
60	580	430	490	2170	1155	1140	1050	7015	214016	41.70	8.27	6.13	6.99	30.93	16.46	16.25	14.97
61	1000	743	110	329	158	174	151	2665	4957130	1.00	37.52	27.88	4.13	12.35	5.93	6.53	5.67
62	975	765	134	395	212	164	173	2818	3711225	0.70	34.60	27.15	4.76	14.02	7.52	5.82	6.14
63	982	595	106	253	137	132	128	2333	9417204	1.10	42.09	25.50	4.54	10.84	5.87	5.66	5.49
64	331	205	356	1070	538	696	518	3714	8571737	8.80	8.91	5.52	9.59	28.81	14.49	18.74	13.95
65	186	137	294	1075	418	539	381	3030	3754304	9.10	6.14	4.52	9.70	35.48	13.80	17.79	12.57
66	162	117	17	36	18	19	21	390	10047591	0.75	41.54	30.00	4.36	9.23	4.62	4.87	5.38
67	975	698	95	272	103	165	95	2403	12370232	1.00	40.57	29.05	3.95	11.32	4.29	6.87	3.95
68	556	447	109	239	144	165	148	1808	192512	0.98	30.75	24.72	6.03	13.22	7.96	9.13	8.19
69	82	64	261	1062	393	557	368	2807	8481777	7.60	2.92	2.28	9.30	38.55	14.00	19.84	13.11
70	1010	748	112	257	160	123	126	2536	15405633	0.50	39.83	29.50	4.42	10.13	6.31	4.85	4.97
f=C21TAS. g=C22TAS. a=C26 20S TAS. b=C27(S+R) TAS. c=C28 20S TAS. d=C27 20R TAS. e=C28 20R TAS. (from m/z231 fragmentogram).																	
Height=total of all peak heights. AROM TIC=total ion height of aromatic TIC.																	
TAS/TOT=Height as percentage of TIC height.																	

Table F.17: Peak heights of triaromatic steroids from aromatic fraction (m/z 231) for all source rock samples (including annotation descriptions) (page 3 of 4).

231	%	TIC	% of TIC	f	g	a	b	c	d	e	Height	
207872	100	7769180	2.676	77.98	58.02	15.07	43.85	26.52	22.60	23.51	267.56	
179200	100	15927144	1.125	33.08	23.06	5.60	18.58	11.83	9.38	10.97	112.51	
145408	100	6503896	2.236	71.73	52.74	13.86	33.27	18.78	16.49	16.70	223.57	
106496	100	2114243	5.037	44.25	36.80	42.23	165.21	65.68	88.82	60.71	503.71	
34048	100	8153592	0.418	20.47	10.77	0.83	2.54	2.82	2.01	2.30	41.76	
		not anal.										
2416	100	3383939	0.071									
		not anal.										
311296	100	6112735	5.093	10.45	6.12	31.88	193.29	82.86	108.81	75.84	509.26	
1769472	100	12753925	13.874	71.37	54.93	184.05	436.27	193.27	265.05	182.45	1387.39	
129536	100	240128	53.945	310.56	251.00	433.94	1846.37	655.16	1212.48	684.94	5394.46	
487424	100	4479796	10.880	63.22	38.25	117.08	423.43	111.22	234.16	100.69	1088.05	
52992	100	3595023	1.474	60.69	39.40	5.92	16.48	8.91	7.92	8.09	147.40	
65536	100	12278665	0.534	23.55	14.95	2.11	4.98	3.11	2.34	2.34	53.37	
232448	100	4020368	5.782	28.61	21.84	63.78	234.37	59.41	113.15	57.01	578.18	
14896	100	339456	4.388	147.63	107.83	16.67	66.67	30.62	37.42	31.98	438.82	
43520	100	5737816	0.758	41.04	25.32	1.38	3.64	1.59	1.63	1.25	75.85	
11520	100	1638631	0.703	29.09	18.91	2.96	7.84	3.76	4.29	3.45	70.30	
239872	100	494592	48.499	378.95	302.52	350.29	1382.05	805.66	856.61	773.82	4849.90	
89344	100	214016	41.746	345.16	255.89	291.60	1291.37	687.34	678.42	624.86	4174.64	
48640	100	4957130	0.981	36.82	27.36	4.05	12.11	5.82	6.41	5.56	98.12	
25600	100	3711225	0.690	23.87	18.73	3.28	9.67	5.19	4.01	4.23	68.98	
107520	100	9417204	1.142	48.06	29.12	5.19	12.38	6.70	6.46	6.26	114.17	
753664	100	8571737	8.792	78.36	48.53	84.28	253.31	127.36	164.77	122.63	879.24	
339968	100	3754304	9.055	55.59	40.94	87.86	321.27	124.92	161.08	113.87	905.54	
75776	100	10047591	0.754	31.33	22.63	3.29	6.96	3.48	3.67	4.06	75.42	
125952	100	12378232	1.018	41.29	29.56	4.02	11.52	4.36	6.99	4.02	101.75	
192512	100	19603526	0.982	30.20	24.28	5.92	12.98	7.82	8.96	8.04	98.20	
643072	100	8481777	7.582	22.15	17.29	70.50	292.25	106.15	150.45	99.40	758.18	
7616	90	2255643	0.304	12.10	8.96	1.34	3.08	1.92	1.47	1.51	30.39	

Table F.17: Peak heights of triaromatic steroids from aromatic fraction (m/z 231) for all source rock samples (page 4 of 4).

HOPANES AND NORHOPANES AND SATURATED HYDROCARBON RATIOS										
	Hopanes and norhopanes					Normal alkanes and isoprenoids				
No.	1n/nn	2n/nn	nn/bis	1T/T	2T/T	CPI	nC17/Pr	nC18/Ph	Pr/Ph	17/27
OIL SAMPLES										
1		0.892	2.42		3.26	0.94	1.64	2.51	1.52	7.17
2		0.380	3.60		2.12	0.99	1.95	2.93	1.67	2.20
3	0.439	0.436	2.13	3.83	1.31	0.99	1.95	2.93	1.67	2.20
4	0.393	0.491	4.25	2.36	2.72	0.96	1.62	2.69	1.54	4.46
5		0.386	6.00		2.57	0.96	1.62	2.69	1.54	4.46
6		0.456	1.57		1.86	0.97	1.90	2.89	1.64	2.50
7	0.636	0.653	3.33	1.46	1.42	0.97	1.66	1.75	4.00	0.47
8	0.324	0.466	1.78	4.60	1.68	0.98	2.43	3.69	1.67	1.84
9	0.614	0.654	2.25	2.19	1.85	0.95	1.48	2.82	1.45	31.00
10	0.488	0.534	11.60	1.27	3.05	0.97	1.96	3.25	1.52	8.52
11	0.589	0.715	3.11	1.62	0.89	0.99	1.54	2.08	2.13	0.75
12	0.531	0.600	1.18	3.04	1.88	0.99	2.43	3.88	1.79	1.09
13	0.668	0.764	3.94	0.82	0.84	0.99	1.44	2.12	1.59	2.49
14	0.458	0.544	1.35	1.27	1.71	1.03	1.73	2.79	1.54	2.98
15			0.00			0.86	1.35	2.34	1.49	66.00
16	0.205	0.370	3.09	4.04	1.88	0.97	1.23	1.83	1.61	4.05
17	0.454	0.553	2.26	3.74	2.55	0.97	1.58	2.81	1.47	8.46
18	0.502	0.644	0.88	1.16	1.69	0.98	1.32	1.72	1.79	1.02
19	0.414	0.523	1.90	1.27	2.69	0.98	1.44	2.12	1.59	2.49
20	0.424	0.540	1.88	1.34	2.46	0.99	1.49	2.04	1.82	1.74
21	0.471	0.612	2.75	3.07	1.74	1.07	1.85	3.06	1.64	2.21
22	0.646	0.777	0.67	1.44	0.37	1.01	2.93	4.04	1.69	3.86
23	0.435	0.557	1.77	2.78	1.53	0.97	2.14	3.68	1.61	2.90
24	0.182	0.336	2.98	2.24	0.75	0.97	2.48	3.69	1.67	1.84
25	0.543	0.686	5.87	1.24	1.51	1.00	1.64	2.28	1.89	1.41
26	0.675	0.755	4.72	1.74	0.78	0.98	3.62	5.63	1.52	33.50
27	0.488	0.549	4.26	0.00	1.75	1.01	2.46	3.58	3.85	0.14
28	0.374	0.426	1.90	2.41	2.05	0.98	1.10	1.94	1.86	5.42
29	0.433	0.436	2.01	1.83	3.00	0.94	1.82	3.07	1.83	3.38
30	0.354	0.489	2.09	3.78	2.63	0.98	1.51	2.45	1.74	2.88
31	0.760	0.577	1.63	3.22	2.23	0.95	1.96	3.23	1.57	4.46
32	0.476	0.583	2.88	2.45	2.05	0.98	1.62	2.83	2.06	8.55
33	0.424	0.536	1.94	2.96	2.66	0.93	5.77	6.96	0.54	2.60
34	0.392	0.525	2.10	3.57	2.27	0.99	1.72	3.00	1.93	3.55
35	0.553	0.562	0.98	2.61	1.42	0.97	1.90	2.98	1.75	5.78
36	0.470	0.578	1.82	2.72	1.61	1.00	1.77	2.42	1.16	0.94
37	0.447	0.513	1.26	2.20	1.90	0.90	1.88	3.61	2.70	43.50
38	0.375	0.392	2.19	1.92	1.78	1.00	2.28	3.49	0.41	0.45

Table F.18: Norhopane ratios (m/z 177 and m/z 191) and normal alkane and isoprenoid ratios for all hydrocarbon samples (page 1 of 2).

	Hopanes and norhopanes					Normal alkanes and isoprenoids				
SHALE SAMPLES										
41	0.44	0.61	2.17	3.26	1.57	1.01	1.01	1.99	1.72	1.64
42	0.48	0.59	4.07	2.18	2.56	0.96	1.25	1.81	2.00	1.63
43	0.49	0.64	3.80	1.69	1.27	1.03	1.07	1.31	2.08	1.42
44	0.55	0.67	2.03	3.46	1.43	1.00	1.13	1.93	1.54	3.02
45	0.58	0.74	2.17	1.39	0.58	1.23	8.30	14.51	1.67	3.54
46	0.50	0.64	1.34	1.39	1.76	0.98	1.32	5.37	1.32	3.15
47	0.46	0.54	1.70	6.32	2.62	0.93	1.21	2.06	1.56	6.26
48	0.46	0.57	2.30	7.51	3.19	0.93	1.21	2.06	1.56	6.26
49	0.59	0.71	3.40	3.97	0.54	1.11	2.40	1.23	6.67	0.28
50	0.56	0.69	0.33	2.58	0.68	0.99	0.86	1.65	1.47	2.97
51	0.50	0.63	5.15	1.13	1.17	1.00	1.23	2.08	1.64	1.70
52	0.57	0.76	0.07	2.96	0.37	1.07	0.70	1.36	2.13	0.72
53	0.26	0.39	3.25	4.34	2.88	0.97	1.38	2.18	1.64	4.73
54	0.53	0.68	3.10	2.36	0.99	0.98	1.59	3.17	1.43	5.15
55	0.56	0.70	0.30	2.46	0.76	0.98	0.75	1.22	1.59	4.27
56	0.26	0.30	5.93	1.81	8.55	1.01	1.36	1.77	1.72	2.62
57	0.24	0.31	2.91	2.39	3.21	1.01	1.36	1.77	1.72	2.62
58	0.24	0.33	3.81	4.90	3.00	1.01	1.36	1.77	1.72	2.62
59	0.51	0.64	0.73	1.27	1.73	1.01	0.97	1.66	1.52	3.12
60	0.37	0.50	2.39	1.78	3.38	0.99	1.01	1.63	1.61	2.23
61	0.23	0.37	3.59	4.62	3.80	0.97	1.15	1.84	1.67	1.38
62	0.35	0.61	2.27	5.25	2.55	1.00	1.26	2.20	1.56	3.42
63	0.32	0.47	3.22	4.80	2.35	1.00	1.06	1.48	1.67	3.03
64	0.52	0.66	10.50	3.37	1.29	1.08	1.11	2.13	1.92	0.58
65	0.54	0.69	2.56	2.90	1.05	1.05	1.33	1.65	2.17	0.88
66	0.69	0.81	2.90	3.09	1.17	1.04	1.71	2.67	1.79	1.16
67	0.18	0.34	2.93	2.24	0.75	1.00	2.47	4.74	1.47	3.82
68	0.35	0.34	2.75	3.46	1.43	1.09	0.86	1.80	2.38	0.21
69	0.60	0.74	10.50	2.70	0.83	0.99				
70	0.32	0.40	3.28	3.31	3.88	0.98	1.29	2.19	1.88	5.37
1n/nn=m/z177 C29nH/(C29nh+C29nnH). 2n/nn= m/z191 C29nH/(C29nH+C29nnH)										
nn/bis=C29nnH/C28,30 bisnorhopane, 1T/T=m/z 177 Ts/Tm, 2T/T=m/z 191 Ts/Tm.										
CPI=Carbon preference index nC23-29/nC22-30.										
nC17/Pr=nC17/Pristane, nC18/Ph=nC18/Phytane, Pr/Ph=Pristane/Phytane										

Table F.18: Norhopane ratios (m/z 177 and m/z 191) and normal alkane and isoprenoid ratios for all source rock samples (including annotation descriptions) (page 2 of 2).

Sterane ratios m/z 217															m/z 218	
No.	Dia%	Dia/bb	S/S+R	bb/Reg	bb/aa	29/tot	ab/Dia	27/28bb	29/28bb	28/279	27/29bb	27/28ba	27-29ba%	29/28ba	28/279	279/27
OIL SAMPLES																
1	0.64	3.73	0.55	0.47	1.60	0.313	0.271	1.47	1.01	1.36	1.67	1.47	5.72	1.00	1.27	-0.06
2	0.71	4.09	0.53	0.61	1.55	0.254	0.256	1.25	0.65	1.24	2.12	1.25	9.26	0.65	1.62	0.02
3	0.70	3.51	0.58	0.65	1.81	0.316	0.258	0.87	0.94	1.00	1.67	0.87	-1.05	0.94	1.19	-0.12
4	0.72	4.11	0.52	0.63	1.70	0.262	0.288	1.48	1.07	0.89	2.55	1.48	5.08	1.07	1.26	0.27
5	0.68	3.55	0.00	0.60	1.49	0.273	0.333	1.69	1.13	0.67	1.90	1.69	6.66	1.13	1.03	0.04
6	0.67	3.39	0.51	0.59	1.46	0.295	0.364	1.30	1.15	1.43	1.59	1.30	2.21	1.15	1.61	0.47
7	0.56	2.12	0.55	0.60	1.48	0.313	0.305	1.86	1.43	0.77	1.34	1.86	3.49	1.43	0.77	0.14
8	0.73	4.54	0.60	0.61	1.56	0.294	0.259	1.78	1.26	0.70	2.41	1.78	6.40	1.26	0.89	0.12
9	0.64	3.11	0.57	0.57	1.33	0.315	0.233	1.60	1.31	0.55	1.85	1.60	2.96	1.31	1.08	0.33
10	0.55	1.87	0.56	0.66	1.96	0.323	0.246	1.55	1.46	0.75	1.30	1.54	0.72	1.46	0.81	0.05
11	0.70	4.28	0.52	0.53	1.15	0.280	0.311	1.39	0.92	0.61	2.37	1.39	6.69	0.92	0.75	0.19
12	0.80	10.52	0.54	0.54	1.16	0.231	0.269	1.28	0.82	0.88	5.67	1.28	7.75	0.82	1.09	0.29
13	0.56	2.14	0.47	0.59	1.45	0.322	0.239	2.05	1.87	0.44	1.91	2.05	1.27	1.87	0.64	0.30
14	0.63	2.69	0.48	0.64	1.74	0.278	0.263	1.09	1.18	0.98	1.72	1.09	-1.12	1.18	1.26	0.09
15	0.62	3.20	0.51	0.51	1.05	0.280	0.276	2.04	1.26	0.81	2.06	2.04	7.60	1.26	0.91	0.30
16	0.78	6.41	0.63	0.55	1.23	0.228	0.259	1.41	0.81	0.78	3.65	1.41	9.88	0.81	1.18	0.47
17	0.76	5.32	0.63	0.59	1.41	0.242	0.254	1.78	1.01	0.72	3.15	1.78	10.50	1.01	1.05	0.46
18	0.57	2.26	0.50	0.58	1.39	0.426	0.275	1.17	1.36	0.89	1.49	1.17	-1.82	1.36	1.03	0.01
19	0.69	3.39	0.52	0.66	1.98	0.279	0.262	1.09	0.99	0.87	2.26	1.09	1.42	0.99	1.14	0.25
20	0.67	3.10	0.53	0.65	1.89	0.303	0.263	1.09	1.11	0.80	1.38	1.09	-0.29	1.11	1.13	0.17
21	0.60	2.58	0.54	0.57	1.34	0.345	0.264	1.67	1.64	0.89	1.60	1.67	0.26	1.64	1.02	0.07
22	0.60	4.03	0.47	0.37	0.58	0.357	0.272	1.97	1.63	0.82	2.21	1.97	3.03	1.63	0.77	0.20
23	0.65	3.09	0.61	0.60	1.52	0.300	0.259	1.62	1.18	1.08	1.66	1.62	4.97	1.18	1.24	0.17
24	0.85	10.61	0.63	0.51	1.06	0.229	0.310	1.42	0.81	0.51	3.84	1.42	10.14	0.81	1.15	0.36
25	0.61	2.37	0.50	0.67	1.67	0.332	0.281	1.11	1.33	0.67	1.62	1.11	-2.36	1.33	0.72	0.04
26	0.50	1.71	0.42	0.59	1.44	0.318	0.266	2.03	1.95	0.80	1.38	2.03	0.44	1.95	0.83	0.27
27	0.72	4.81	0.56	0.54	1.18	0.278	0.590	1.35	1.00	0.80	2.53	1.35	4.80	1.00	1.01	0.17
28	0.76	4.82	0.57	0.64	1.78	0.252	0.221	1.79	1.13	0.68	3.22	1.79	7.98	1.13	0.91	0.29
29	0.75	4.50	0.54	0.66	1.95	0.283	0.254	1.50	1.27	0.56	2.83	1.50	2.87	1.27	0.88	0.27
30	0.66	3.18	0.60	0.60	1.49	0.316	0.290	1.44	1.29	0.91	1.77	1.46	1.96	1.29	1.08	0.11
31	0.80	2.26	0.58	0.64	1.74	0.341	0.325	1.44	0.79	0.45	1.84	1.48	1.79	1.32	0.54	0.12
32	0.77	4.33	0.61	0.62	1.65	0.183	0.225	2.00	0.71	0.73	2.85	1.96	7.69	1.28	0.48	0.43
33	0.63	3.01	0.55	0.55	1.26	0.468	0.290	1.89	0.70	1.09	1.85	1.49	-0.10	1.50	1.12	0.24
34	0.67	3.23	0.59	0.64	1.77	0.189	0.345	1.51	0.81	0.86	1.87	1.45	3.55	1.16	1.10	0.07
35	0.62	2.76	0.57	0.60	1.48	0.424	0.246	1.07	0.71	1.13	1.50	1.31	-0.49	1.35	1.33	0.03
36	0.59	2.40	0.51	0.61	1.57	0.335	0.305	1.27	0.94	0.90	1.35	1.35	-3.79	1.79	1.08	-0.26
37	0.68	2.43	0.46	0.50	1.20	0.210	0.252	1.55	0.76	0.87	1.04	1.88	7.60	1.18	1.00	0.28
38	0.68	3.42	0.58	0.61	1.54	0.359	0.247	1.87	0.87	0.73	2.13	1.41	3.01	1.17	1.00	0.14

Table F.19: Sterane ratios (m/z 217 and 218) for all hydrocarbon samples (page 1 of 2).

No.	Dia%	Dia/bb	S/S+R	bb/Reg	bb/aa	29/tot	ab/Dia	27/28bb	29/28bb	28/279	27/29bb	27/28ba	27-29ba%	29/28ba	28/279	279/27
SHALE SAMPLES																
41	0.65	2.91	0.58	0.64	1.80	0.321	0.290	1.74	1.37	0.95	1.46	1.74	3.61	1.37	0.92	-0.34
42	0.66	2.96	0.60	0.65	1.86	0.348	0.395	1.32	1.13	1.12	1.37	1.32	2.15	1.13	1.14	-0.05
43	0.62	2.66	0.60	0.61	1.59	0.340	0.326	2.05	1.75	0.79	1.45	2.05	2.39	1.75	0.73	-0.13
44	0.59	2.61	0.41	0.54	1.17	0.302	0.272	1.21	1.02	1.03	1.52	1.21	1.93	1.02	1.27	0.04
45	0.61	2.95	0.50	0.54	1.11	0.361	0.319	1.87	2.18	0.61	1.77	1.87	-2.30	2.18	0.73	0.17
46	0.59	2.30	0.50	0.64	1.74	0.366	0.281	1.60	1.99	0.59	1.58	1.60	-3.15	1.99	0.71	-0.08
47	0.67	3.10	0.52	0.65	1.83	0.299	0.281	1.74	1.27	1.10	1.60	1.74	4.59	1.27	1.22	-0.13
48	0.63	2.59	0.45	0.67	1.99	0.304	0.293	1.61	1.17	0.81	1.32	1.61	4.99	1.17	0.97	-0.01
49	0.49	2.79	0.19	0.34	0.52	0.355	0.367	1.32	1.08	1.04	1.15	1.32	2.07	1.08	1.22	-0.37
50	0.51	3.09	0.46	0.34	0.50	0.324	0.284	1.62	1.30	1.11	1.53	1.62	2.52	1.30	1.23	0.13
51	0.57	2.44	0.48	0.53	1.14	0.355	0.285	1.06	1.45	0.85	1.56	1.05	-3.61	1.45	1.11	-0.04
52	0.56	4.85	0.42	0.27	0.36	0.397	0.296	1.49	1.07	1.09	2.16	1.49	4.28	1.07	1.19	0.17
53	0.76	5.28	0.62	0.61	1.56	0.267	0.280	1.61	1.08	0.68	2.90	1.61	7.23	1.08	0.94	0.30
54	0.70	2.35	0.55	0.56	1.26	0.287	0.286	1.90	1.45	0.58	2.91	1.90	4.95	1.45	0.72	0.31
55	0.52	1.08	0.47	0.32	0.47	0.313	0.300	1.21	1.05	1.09	1.85	1.21	1.55	1.05	1.35	0.27
56	0.71	3.51	0.52	0.69	2.21	0.297	0.285	0.76	1.09	0.82	2.22	1.03	-0.80	1.09	1.11	0.11
57	0.70	3.35	0.60	0.69	2.26	0.263	0.270	1.26	0.77	0.97	1.73	1.26	7.63	0.77	1.31	0.08
58	0.71	3.97	0.61	0.63	1.67	0.273	0.302	1.04	0.84	0.58	2.10	1.04	3.23	0.84	1.27	0.08
59	0.55	2.05	0.47	0.61	1.54	0.337	0.273	1.26	1.17	0.71	1.64	1.26	0.78	1.17	0.98	-0.18
60	0.56	1.92	0.53	0.66	1.92	0.312	0.279	1.07	1.30	0.81	1.55	1.07	-2.45	1.30	1.06	-0.09
61	0.73	4.46	0.62	0.60	1.47	0.271	0.299	1.11	0.86	0.85	2.35	1.11	4.03	0.86	1.20	0.20
62	0.71	4.21	0.60	0.59	1.43	0.282	0.270	1.83	1.21	0.70	2.41	1.83	7.49	1.21	0.91	0.23
63	0.77	6.09	0.62	0.56	1.27	0.274	0.285	1.65	1.09	0.52	3.07	1.65	7.41	1.09	0.83	0.31
64	0.57	3.07	0.51	0.43	0.75	0.330	0.276	1.53	1.41	0.71	1.91	1.53	1.14	1.41	0.89	0.23
65	0.56	2.90	0.52	0.43	0.75	0.343	0.300	1.39	1.37	0.89	1.71	1.39	0.20	1.37	1.07	0.10
66	0.56	2.36	0.50	0.54	1.17	0.343	0.317	1.71	1.68	0.57	1.62	1.70	0.19	1.68	0.70	0.15
67	0.84	10.61	0.60	0.51	1.06	0.229	0.210	1.28	0.79	0.51	3.84	1.28	8.07	0.79	0.87	0.43
68	0.64	3.42	0.59	0.52	1.08	0.328	0.295	1.62	1.37	0.74	1.94	1.62	2.71	1.37	1.01	0.13
69	0.48	2.79	0.42	0.33	0.50	0.333	0.294	1.16	1.10	0.98	1.47	1.16	0.60	1.10	1.23	0.04
70	0.76	5.01	0.61	0.62	1.60	0.291	0.234	2.10	0.78	0.69	2.69	1.76	5.45	1.31	0.93	0.30
DIA%=C29Dia/(C29Dia+C29Reg). Dia/bb=C29(ab+ba)/bb. S/S+R=C29aa 20S/(20S+20R). bb/Reg=C29bb/(bb+aa). bb/aa=C29bb/C29aa.																
29/tot=C29Dia+Reg/(C27-C29 Dia+Reg). ab/Dia=C27ab/C27Dia. 28/279=m/z218 2*(C28bbS+R)/((C27bbS+R)+(C29bbS+R)).																
27/28ba=(C27baS+baR)/(C28baS+baR), 29/28ba = (C29baS+baR)/(C28baS+baR), 279/27=m/z218 ((C27bbS+R)-(C29bbS+R))/(C27bbS+R).																
27-29ba%=(C27baS+R)-(C29baS+R) as %total steranes. Sample 5: overlap of C29aaR with nC30.																

Table F.19: Sterane ratios (m/z 217 and 218) for all source rock samples (including annotation descriptions) (page 2 of 2).

Tricyclic, tetracyclic and pentacyclic terpane ratios.																							
No.	C31S/R	C32S/R	C33S/R	C34S/R	C35S/R	H/24%	Tr/H	20/T	23T/H	nH/H	S/H	d/(d+nH)	bis/H	30D/H	T/P	24T/Tot	24Tet/tot	n/(n+nn)	23/21	24/(25+26)	nH/Dia	Ts/Tm	nH/bis
OIL SAMPLES																							
1	1.47	1.39	1.05	1.59	1.62	0.00	0.00	0	0.00	406	0.001	43.4	0.15	0.31	0.00	0.00	0.00	892	0.00	0.00	1.31	3.26	2.79
2	1.58	1.18	1.16	0.96	1.54	0.00	0.00	0	0.00	441	0.001	64.4	0.20	0.80	0.00	0.00	0.00	380	0.00	0.00	0.55	2.12	2.17
3	0.84	1.16	1.17	0.00	0.00	91.80	1.64	107	4.83	450	1.16	69.0	0.18	0.67	0.32	9.78	5.45	442	2.05	0.95	0.45	1.31	1.68
4	0.82	1.22	0.00	0.00	0.00	82.30	4.39	45	4.88	558	0.743	45.5	0.15	0.47	0.93	13.48	5.57	471	2.61	0.66	1.19	2.72	3.78
5	2.13	1.28	0.00	0.00	0.00	78.80	0.69	92	1.58	515	3.182	35.7	0.14	0.45	0.69	13.19	7.54	386	1.61	0.91	1.13	2.59	3.78
6	1.60	1.73	1.61	1.33	1.43	92.00	0.32	84	5.93	217	0.676	55.2	0.17	0.27	0.32	10.53	5.76	456	1.30	0.81	0.81	1.86	1.26
7	1.13	1.20	0.00	0.00	0.00	72.10	3.59	27	1.00	1140	0.268	12.0	0.18	0.16	0.59	16.38	10.77	653	3.42	1.54	7.33	1.42	6.29
8	1.19	1.48	1.50	1.14	1.75	76.80	6.24	119	0.76	456	3.092	62.0	0.29	0.74	0.95	11.40	5.36	466	1.58	0.89	0.61	1.68	1.55
9	1.33	0.90	0.00	0.00	0.00	74.10	8.36	155	3.31	944	0.319	26.7	0.22	0.34	1.27	10.87	4.39	654	0.93	1.06	4.25	1.85	2.74
10	1.05	1.02	1.00	0.00	0.00	74.70	2.31	213	0.57	864	0.348	8.9	0.06	0.08	0.42	8.51	7.02	534	2.75	1.31	10.20	3.05	13.30
11	1.24	1.15	1.31	1.33	1.50	73.70	8.68	118	0.67	719	1.326	22.0	0.09	0.21	1.76	5.44	4.89	715	1.13	1.47	3.56	0.89	7.80
12	1.22	0.00	0.00	0.00	0.00	55.90	13.04	203	1.06	110	0.794	61.2	0.63	1.75	1.33	9.16	5.50	600	2.46	1.02	0.63	1.88	1.76
13	1.48	1.16	1.42	1.09	1.32	60.00	4.48	144	1.18	1069	0.462	12.7	0.08	0.15	0.71	9.88	14.63	764	2.72	1.83	6.89	0.84	12.76
14	1.19	1.54	1.48	1.87	1.56	94.40	0.59	114	1.55	341	0.437	37.3	0.21	0.20	0.13	9.40	9.78	544	2.06	1.61	1.68	1.71	1.61
15	0.00	0.00	0.00	0.00	0.00	0.00	0.00	0	0.00	0	1692	0.0	0.00	0.00	0.00	8.90	3.24	0	1.09	0.99	0.00	0.01	0.00
16	1.04	1.38	1.17	0.00	0.00	47.10	42.39	305	0.31	635	4.4	73.3	0.35	1.75	3.43	5.04	2.65	370	1.28	1.20	0.36	1.88	1.82
17	1.75	0.00	0.00	0.00	0.00	59.40	17.72	74	0.32	788	4.783	42.2	0.28	0.57	2.54	16.21	4.17	553	1.63	0.56	1.37	2.55	2.80
18	1.31	1.46	1.53	1.63	1.64	96.20	0.42	89	19.28	396	0.34	22.9	0.25	0.11	0.10	11.32	10.88	644	1.78	1.54	3.30	1.69	1.59
19	1.29	1.53	1.45	2.32	1.70	91.40	1.02	81	7.79	341	0.699	48.6	0.16	0.32	0.22	10.74	9.22	523	1.56	1.75	1.06	2.69	2.08
20	1.32	1.47	1.60	1.66	1.77	93.40	0.66	57	13.29	346	0.535	47.6	0.16	0.31	0.14	11.79	10.76	540	1.35	1.73	1.10	2.46	2.21
21	1.30	1.42	1.62	2.04	1.31	87.60	3.19	104	1.35	542	1.313	28.8	0.13	0.22	0.75	11.66	4.55	612	1.36	0.98	2.48	1.74	4.33
22	1.43	1.43	1.59	1.62	1.92	89.80	0.72	53	6.13	597	0.287	13.0	0.25	0.09	0.17	10.13	15.82	777	1.96	2.68	6.67	0.36	2.35
23	1.64	0.00	0.00	0.00	0.00	83.20	8.18	200	1.97	583	1.405	45.6	0.26	0.48	1.45	10.61	2.62	557	1.19	0.54	1.20	1.53	2.23
24	1.07	1.51	1.48	0.00	0.00	65.60	13.13	95	0.24	542	5.981	71.9	0.27	1.39	1.49	12.84	4.76	400	1.72	0.67	0.39	1.75	1.99
25	1.51	1.50	1.57	1.68	1.53	86.10	1.35	28	2.03	885	0.476	17.9	0.07	0.19	0.23	15.10	12.12	686	4.57	1.37	4.57	1.51	12.80
26	1.51	1.31	1.60	0.00	0.00	73.50	6.46	46	0.31	1040	0.403	5.0	0.07	0.05	1.55	15.29	6.37	755	3.31	0.98	19.00	0.78	14.51
27	1.36	0.00	0.00	0.00	0.00	81.50	5.46	156	1.91	636	0.741	41.7	0.12	0.45	1.18	11.29	4.13	549	1.78	0.61	1.40	1.75	5.19
28	2.52	2.22	1.61	0.00	0.00	36.10	2.78	98	0.00	720	0.001	70.5	0.51	1.72	2.78	12.80	6.30	426	1.10	1.01	0.42	2.05	1.41
29	0.69	1.52	2.12	0.00	0.00	64.70	5.68	79	0.00	482	0.001	72.7	0.31	1.29	0.79	10.85	8.65	436	1.05	1.12	0.37	3.00	1.55
30	1.04	1.26	0.95	0.85	0.00	82.10	4.09	95	2.27	491	1.273	42.2	0.23	0.34	0.77	13.15	5.35	489	1.26	0.86	1.37	2.63	2.01
31	1.40	1.61	1.55	1.48	0.00	84.30	2.57	84	1.91	475	28.39	23.9	0.21	0.15	0.69	13.61	7.23	577	1.59	1.17	3.18	2.23	2.22
32	1.11	1.18	1.15	1.51	0.00	46.90	12.60	62	0.32	631	4.22	32.4	0.16	0.30	2.30	13.96	10.05	583	2.11	1.55	2.09	2.05	4.03
33	1.31	1.35	1.44	1.19	0.00	77.80	3.00	131	0.84	1150	47.01	30.8	0.25	0.25	0.65	11.20	9.49	535	1.70	1.96	2.24	2.66	2.24
34	0.95	1.34	0.97	0.00	0.00	83.40	5.37	95	0.88	522	1.781	44.3	0.25	0.42	1.02	11.86	3.69	525	1.28	1.15	1.26	2.27	2.10
35	1.48	1.64	1.71	1.76	1.76	94.40	0.82	82	3.09	474	44.18	11.8	0.38	0.06	0.23	12.15	9.55	670	1.45	1.04	7.46	1.39	1.26
36	1.53	1.37	1.28	1.32	1.35	93.30	0.67	70	8.14	418	0.788	27.5	0.17	0.16	0.16	13.81	10.62	578	2.30	1.17	2.63	1.61	2.16
37	0.00	0.00	0.00	0.00	0.00	67.10	25.30	80	0.11	637	0.001	48.7	0.48	0.60	4.07	8.72	1.94	415	1.14	0.45	1.05	1.90	1.33
38	0.92	1.03	0.00	0.00	0.00	66.70	9.58	375	0.33	552	3.593	49.5	0.39	0.54	1.38	14.82	5.21	392	2.51	0.71	1.02	1.78	1.41

Table F.20: Tri-, tetra- and penta-cyclic terpane ratios for all hydrocarbon samples (page 1 of 2).

No.	C31S/R	C32S/R	C33S/R	C34S/R	C35S/R	H/24%	Tr/H	20/T	23T/H	nH/H	S/H	d/(d+nH)	bis/H	30D/H	T/P	24T/Tot	24Tet/tot	n/(n+nn)	23/21	24/(25+26)	nH/Dia	Ts/Tm	nH/bis
SHALE SAMPLES						0.00	0.00					0.0			0.00								
41	1.18	1.16	1.00	0.00	0.00	94.60	0.56	42	11.32	373	0.305	36.1	0.11	0.21	0.15	10.22	11.73	613	2.27	1.81	1.77	1.57	3.44
42	0.97	1.61	1.16	0.00	0.00	91.20	0.67	86	8.36	353	0.434	32.8	0.06	0.17	0.17	9.84	14.50	589	1.82	1.76	2.05	2.56	5.83
43	1.63	1.52	0.00	0.00	0.00	93.70	0.59	41	14.29	456	0.244	24.4	0.07	0.15	0.17	12.36	13.30	642	1.78	2.25	3.09	1.27	6.80
44	1.61	1.38	2.00	0.00	0.00	92.90	0.40	63	31.94	475	0.165	9.7	0.12	0.05	0.14	8.93	19.10	669	1.88	3.11	9.33	1.43	4.11
45	1.42	1.16	1.17	1.10	1.33	73.90	5.76	87	0.89	817	0.148	25.2	0.13	0.28	0.88	11.85	6.12	742	0.85	1.34	2.96	0.58	6.24
46	1.42	1.51	1.43	1.61	1.50	96.30	0.71	569	6.20	366	0.387	25.2	0.15	0.13	0.17	5.37	5.50	640	2.12	1.83	2.89	1.76	2.39
47	1.16	1.36	0.00	0.00	0.00	98.00	1.00	42	6.86	360	0.363	28.9	0.18	0.15	0.33	12.69	17.84	540	1.92	1.43	2.45	2.62	2.00
48	1.55	1.37	1.17	1.72	0.00	86.90	1.35	63	4.84	475	0.61	25.4	0.16	0.17	0.32	12.71	11.28	573	1.91	1.50	2.86	3.19	3.09
49	0.82	0.59	0.71	0.65	0.50	96.10	0.25	22	10.97	453	0.824	11.4	0.05	0.06	0.07	17.34	16.24	711	3.55	1.60	7.77	0.54	8.70
50	1.31	1.41	1.44	0.00	0.00	91.60	0.87	41	4.13	831	0.701	3.4	1.11	0.03	0.17	8.85	12.24	694	2.97	1.65	25.33	0.68	0.75
51	1.41	1.48	1.57	1.58	1.62	96.20	0.19	49	32.23	403	0.167	22.6	0.05	0.12	0.05	10.52	20.99	629	1.86	4.38	3.43	1.17	8.75
52	1.11	1.03	1.27	0.00	0.00	91.80	1.01	39	9.86	1139	0.36	7.5	5.38	0.10	0.10	6.61	7.47	0	2.64	1.43	12.29	0.37	0.10
53	1.21	1.36	1.60	1.34	1.26	84.00	3.95	32	1.00	333	3.124	62.9	0.16	0.56	0.66	16.39	7.18	394	2.09	0.81	0.59	2.88	2.11
54	1.43	1.36	1.15	1.31	1.35	83.90	1.70	50	1.87	683	0.969	43.4	0.11	0.52	0.31	13.54	12.51	675	2.80	1.55	1.30	0.99	6.44
55	1.45	1.40	1.52	1.45	1.62	92.70	0.41	43	9.27	606	0.422	7.7	0.86	0.05	0.09	10.79	19.81	702	2.59	2.48	12.00	0.76	0.70
56	1.00	1.24	1.27	1.35	0.00	85.60	2.53	84	2.01	287	0.859	71.0	0.09	0.76	0.37	6.25	4.33	303	1.22	1.18	0.32	8.55	2.65
57	1.28	1.38	1.47	1.65	1.53	92.40	1.90	522	5.09	244	0.74	75.6	0.23	0.70	0.29	11.99	6.78	309	1.38	1.05	0.41	3.21	1.27
58	1.29	1.32	1.34	1.85	0.00	79.50	3.81	76	6.68	310	0.764	69.3	0.16	0.70	0.62	11.90	6.69	337	1.30	1.00	0.44	3.00	1.94
59	1.46	1.42	1.55	1.57	1.63	96.40	0.44	198	13.38	399	0.282	14.8	0.31	0.07	0.10	9.75	8.43	638	2.26	1.15	5.77	1.73	1.29
60	1.37	1.45	1.49	1.60	1.50	95.90	0.48	458	12.39	276	0.22	42.9	0.12	0.21	0.12	6.02	8.87	496	1.69	2.85	1.33	3.38	2.35
61	1.21	1.44	1.41	1.52	1.16	79.90	3.35	71	1.26	387	1.834	63.5	0.18	0.67	0.52	14.00	7.53	374	1.64	1.04	0.57	3.80	2.15
62	1.32	1.30	1.44	1.96	1.58	78.30	4.95	43	0.67	601	2.567	29.7	0.17	0.25	1.00	18.15	6.01	605	2.37	0.71	2.36	2.55	3.47
63	1.28	1.44	1.53	1.65	0.00	76.20	7.58	65	0.53	774	2.084	68.9	0.27	1.71	0.68	12.96	4.79	468	1.98	0.69	0.45	2.35	2.83
64	1.50	1.48	1.46	1.57	1.87	94.20	0.57	26	8.11	469	0.444	11.1	0.02	0.06	0.16	10.56	15.55	662	3.30	2.52	8.18	1.29	20.50
65	1.48	1.37	1.69	1.56	1.64	95.60	0.27	36	16.73	448	0.413	13.9	0.08	0.07	0.08	12.25	16.90	685	3.16	1.66	6.21	1.05	5.58
66	1.43	1.33	1.53	1.37	1.04	78.00	8.44	91	1.46	968	0.523	16.6	0.08	0.19	1.62	4.90	4.80	807	1.55	1.45	5.04	1.17	12.10
67	1.35	1.41	1.33	1.36	1.34	50.30	4.38	74	1.12	353	1.633	60.5	0.24	1.07	0.51	8.25	9.60	336	1.59	2.65	0.33	0.75	1.49
68	1.38	1.43	1.42	1.60	1.79	92.90	1.11	144	5.51	227	0.657	47.4	0.12	0.26	0.28	6.91	7.91	480	2.02	1.96	1.11	1.43	2.54
69	1.51	1.50	1.54	1.45	1.50	96.50	0.56	32	5.37	643	0.345	2.9	0.02	0.02	0.15	9.66	6.60	739	5.47	0.63	33.06	0.83	29.75
70	1.29	1.59	1.22	1.89	2.21	70.10	2.52	105	1.46	601	1.818	31.9	0.28	0.88	0.50	15.34	7.60	396	2.45	1.02	0.68	3.88	2.15

C31-35=C31-C35 homohopane 24S/24R. H/24=10*Hopane/(Hopane+C24tetracyclic). Tr/H=1000*total tricyclics/Hopane. 20/T=*C20tricyclic/total tricyclic terpanes. nH/H=1000*C29 norhopane/Hopane.

S/H=total steranes/total pentacyclic terpanes. d/(d+nH)=1000*C30 diahopane/(C30Dia+C29norhopane). b/h=28,30 bisnorhopane/Hopane. 30D/H=C30 diahopane/Hopane.

T/P=total tricyclic terpanes/pentacyclic terpanes. 24T/Tot=1000*C24 tricyclic terpane/total tri- and tetracyclic terpanes. 24Tet./tot=ditto but tetracyclic. n/(n+nn)=1000*C29 norhopane/(C29 norh-+norneohopane).

23/21=C23/C21 tricyclic terpanes. 24/(25+26)=C24 tetracyclic/av.C25+(C26(S+R) tricyclic terpanes)/2. nH/Dia=C29 norhopane/C30 diahopane. nH/bis=C29 norhopane/28,30 bisnorhopane.

23T/H=23Tricyclic terpaqne/C30 Hopane, Ts/Tm = 18a trisnorneohopane/17a trisnorhopane.

Table F.20: Tri-, tetra- and penta-cyclic terpane ratios for all source rock samples (including annotation descriptions) (page 2 of 2).

PHENANTHRENE, MAS, TAS, THIOPHENE AND NAPHTHALENE RATIOS.																		
	PHENANTHRENES				MAS		TAS			MDBT							TMN	
No.	MPI1MS	MPRGC	MPRMS	DPRMS	MAS D/R	27 D/R	20-28	g/(g+e)	T/T+M	4/2+3	4/1.	C/E	D/F	c/e	d/e	e/f	125/136	127/137
OIL SAMPLES																		
1	0.85	0.69	0.96	0.41	1.39	0.442	0.01	0.00	0.01	0.01	0.01	0.01	0.01	0.01	0.01	0.01	-0.46	-0.29
2	0.91	0.93	1.11	0.34	1.29	0.315	0.01	0.00	0.01	0.01	0.01	0.01	0.01	0.01	0.01	0.01	-0.73	-0.49
3	0.91	0.93	0.01	0.34	0.78	0.494	0.01	0.00	0.01	0.01	0.01	0.01	0.01	0.01	0.01	0.01	0.01	0.01
4	0.88	0.76	0.90	0.28	0.84	0.337	3.52	0.97	0.81	2.04	3.39	0.68	3.44	1.14	0.59	1.52	-0.15	-0.39
5	0.88	0.76	0.81	0.28	0.89	0.486	3.34	0.90	0.75	2.39	3.54	0.74	3.10	1.37	0.65	1.22	-0.14	-0.49
6	0.94	0.79	0.88	0.21	1.17	0.603	7.06	0.95	0.60	2.72	5.36	0.97	3.51	1.83	0.80	1.12	-0.73	-0.55
7	0.87	0.97	0.63	0.38	0.56	0.443	2.97	0.91	0.64	2.92	6.16	0.62	3.14	1.18	0.46	1.35	0.01	0.01
8	0.81	1.01	0.93	0.34	0.98	0.339	1.04	0.71	0.76	2.26	6.91	0.84	4.21	1.61	0.74	1.06	-0.14	-0.64
9	0.60	1.13	0.79	0.46	0.70	0.391	0.50	0.67	0.01	1.45	2.05	1.43	4.35	2.84	1.40	0.95	0.03	-0.48
10	1.08	0.01	1.08	0.53	0.93	0.507	0.84	0.88	0.25	1.22	1.96	1.14	3.63	2.54	1.39	0.52	-0.22	-0.24
11	1.88	0.82	1.04	0.66	0.58	0.276	0.01	0.00	0.29	1.17	3.57	3.06	2.81	4.92	3.21	0.25	0.01	0.01
12	1.33	0.01	1.21	0.58	0.56	0.305	0.01	0.00	0.01	0.98	2.29	0.97	20.00	2.76	1.35	0.48	0.01	0.01
13	0.96	1.12	1.07	0.36	0.56	0.260	5.12	0.90	0.19	3.15	21.70	1.75	4.47	2.93	1.24	0.79	-0.76	-0.03
14	0.61	0.56	0.44	0.61	0.56	0.354	1.86	0.80	0.65	2.11	2.92	0.44	1.17	1.31	0.76	0.54	0.01	0.01
15	0.01	0.01	0.64	0.65	1.38	0.389	0.01	0.00	0.39	1.55	2.45	1.85	3.36	0.67	0.79	2.69	0.01	0.01
16	0.80	0.72	0.77	0.55	0.64	0.424	0.01	0.00	0.42	0.85	1.26	1.35	2.93	1.64	1.12	0.42	0.01	0.01
17	0.87	1.17	1.12	0.37	0.76	0.417	0.01	0.00	0.01	1.87	6.97	0.95	4.52	1.46	0.74	1.23	-0.68	-0.73
18	0.94	1.08	0.63	0.40	0.71	0.510	0.14	0.26	0.01	1.03	1.15	0.40	0.88	1.07	0.60	1.18	0.31	0.35
19	0.75	1.03	0.88	0.31	0.46	0.254	1.85	0.83	0.88	3.14	4.09	0.64	1.39	1.37	0.73	1.17	-0.36	0.01
20	0.90	0.87	0.77	0.30	0.62	0.279	1.45	0.80	0.85	2.95	3.50	0.60	2.65	1.38	0.72	1.06	0.36	0.53
21	0.85	0.81	0.85	0.40	0.81	0.351	0.99	0.73	0.75	1.60	3.50	0.77	7.04	2.15	0.48	1.52	-0.11	0.23
22	1.07	0.89	0.80	0.44	0.77	0.511	0.29	0.44	0.41	0.69	1.84	0.65	2.13	1.01	0.63	0.57	0.13	-0.11
23	0.72	1.24	1.02	0.38	0.84	0.503	2.72	0.87	0.71	1.89	4.59	1.64	4.57	2.82	1.29	0.93	-0.27	-0.11
24	0.95	0.97	0.87	0.55	0.48	0.264	3.77	0.91	0.54	1.79	5.69	0.92	4.59	1.78	0.56	0.92	0.01	0.01
25	0.63	1.04	0.79	0.30	0.65	0.436	0.88	0.71	0.69	3.98	4.82	0.76	3.03	1.78	0.71	1.16	-0.77	-0.02
26	0.68	1.26	1.28	0.50	0.73	0.352	1.69	0.76	0.63	1.73	2.44	0.64	3.52	1.41	0.58	1.36	-0.06	0.12
27	0.73	0.81	0.72	0.52	0.48	0.269	0.01	0.00	0.47	1.96	4.66	0.75	3.74	1.64	0.52	1.02	0.01	0.01
28	0.91	1.33	1.25	0.73	4.27	0.641	12.60	0.00	0.64	2.81	7.50	0.01	0.01	0.01	0.01	0.01	0.01	0.01
29	0.85	1.01	1.04	0.60	1.22	0.493	10.82	0.00	0.75	3.22	5.22	0.01	0.01	0.01	0.01	0.01	0.01	0.01
30	0.71	0.93	0.93	0.30	0.66	0.339	2.76	0.89	0.93	1.60	3.83	0.88	3.54	1.37	0.80	1.25	-0.35	-0.56
31	0.71	0.95	0.88	0.61	0.73	0.424	1.82	0.84	0.79	1.79	4.36	0.73	3.77	1.18	0.72	1.21	-0.36	-0.13
32	0.70	1.08	1.01	0.26	0.55	0.302	4.94	0.94	0.73	1.63	4.80	0.87	4.71	1.43	0.91	1.17	-0.68	-0.34
33	0.64	0.91	0.82	0.21	0.79	0.362	7.59	0.96	0.41	1.89	4.96	0.77	3.62	1.24	0.72	1.12	-0.28	0.08
34	0.48	1.02	1.03	0.21	0.99	0.356	3.36	0.90	0.71	1.75	4.65	0.85	4.22	1.58	0.97	1.08	-0.62	-0.41
35	0.74	0.98	0.90	0.25	0.35	0.428	0.46	0.55	0.82	1.66	5.53	0.83	4.64	1.52	0.90	1.15	-0.65	-0.41
36	0.56	0.59	1.19	0.55	0.51	0.482	0.08	0.22	0.73	0.82	1.25	0.48	1.53	1.10	0.73	0.87	0.37	-0.08
37	1.02	0.89	0.82	0.27	0.96	0.449	14.86	0.98	0.67	1.54	6.54	1.10	4.97	1.78	1.06	1.17	-0.33	-0.30
38	0.89	0.83	1.23	0.33	1.12	0.452	7.97	0.97	0.49	1.31	3.15	1.03	3.53	1.41	0.91	1.04	-0.99	-0.80

Table F.21: Phenanthrene, mono and tri-aromatic steroid, dibenzothiophene and trimethyl naphthalene ratios for all hydrocarbon samples (page 1 of 2).

	PHENANTHRENES				MAS		TAS			MDBT							TMN	
SHALE SAMPLES																		
41	0.89	0.95	0.87	0.30	1.15	0.560	1.03	0.71	0.89	1.38	1.88	0.41	2.64	0.68	0.45	1.67	0.01	0.01
42	0.85	0.80	0.76	0.24	0.92	0.578	1.00	0.68	0.87	2.23	2.81	0.45	3.26	0.88	0.50	1.44	0.01	0.01
43	0.89	1.02	0.93	0.38	1.13	0.501	1.26	0.76	0.81	1.05	1.72	0.49	2.88	0.77	0.50	1.27	0.01	0.01
44	0.75	0.88	0.88	0.28	0.76	0.417	0.19	0.38	0.87	1.55	2.02	0.50	2.52	0.88	0.53	1.49	0.46	-0.05
45	0.66	0.23	0.75	0.60	1.08	0.245	2.97	0.82	0.31	2.05	0.84	0.55	3.82	1.14	0.54	1.30	0.30	-0.07
46	0.76	0.94	0.00	0.57	0.98	0.556	0.01	0.00	0.01	0.01	0.01	0.01	0.01	0.01	0.01	0.01	0.01	0.01
47	0.75	0.66	0.74	0.23	0.86	0.431	0.01	0.00	0.01	1.65	1.88	0.01	0.01	0.01	0.01	0.01	-0.54	-0.57
48	0.75	0.66	0.00	0.23	0.87	0.471	0.01	0.00	0.01	0.01	0.01	0.01	0.01	0.01	0.01	0.01	0.01	0.01
49	1.29	1.43	0.57	0.27	0.14	0.239	0.03	0.07	0.31	0.89	0.29	0.37	0.88	0.63	0.74	0.78	0.01	0.01
50	0.78	0.77	0.85	0.35	0.43	0.361	0.10	0.23	0.82	1.12	0.88	0.38	1.68	0.54	0.45	1.45	0.25	0.08
51	0.74	0.82	0.90	0.36	0.74	0.517	0.12	0.27	0.89	1.76	1.38	0.45	1.92	0.88	0.58	1.12	0.91	0.64
52	0.86	0.84	0.88	0.40	0.39	0.414	0.10	0.28	0.56	0.91	0.55	0.33	1.25	0.53	0.58	2.50	1.00	0.06
53	0.77	0.82	0.79	0.25	1.02	0.452	2.17	0.83	0.83	3.30	5.68	0.51	3.71	1.01	0.49	1.28	-0.28	-0.44
54	0.68	0.81	0.88	0.26	0.85	0.330	2.59	0.86	0.64	4.18	6.32	0.66	4.37	1.26	0.54	1.17	-0.36	-0.54
55	0.67	0.89	0.87	0.39	0.41	0.402	0.10	0.28	0.85	1.14	1.10	0.48	3.38	0.57	0.51	1.64	0.41	0.62
56	0.67	0.72	0.78	0.21	0.84	0.560	1.39	0.77	0.80	11.94	19.40	0.60	3.59	1.37	0.55	1.14	-0.13	-0.03
57	0.67	0.72	0.70	0.21	1.04	0.606	2.00	0.95	0.46	9.95	22.87	0.64	4.91	1.26	0.38	1.22	-0.21	-0.45
58	0.67	0.72	0.79	0.21	1.17	0.405	2.12	0.85	0.70	9.51	17.46	0.66	4.49	1.24	0.57	1.21	-0.18	-0.39
59	0.70	0.75	0.76	0.27	0.75	0.292	0.16	0.28	0.94	2.49	1.46	0.36	1.71	0.82	0.53	1.18	-0.12	0.11
60	0.73	0.77	0.71	0.21	0.75	0.490	0.17	0.29	0.93	2.71	1.41	0.36	2.14	0.78	0.54	1.16	-0.16	0.04
61	0.76	0.88	0.88	0.27	0.84	0.284	1.89	0.83	0.81	4.61	9.14	0.73	4.84	1.44	0.63	1.22	-0.40	-0.59
62	0.87	0.98	0.95	0.33	0.68	0.225	1.61	0.82	0.83	2.63	4.83	0.63	3.98	1.24	0.64	1.29	-0.23	-0.49
63	0.83	0.74	0.81	0.21	0.98	0.294	2.09	0.82	0.67	4.62	8.51	0.67	5.21	1.57	0.44	1.01	0.01	0.01
64	1.17	0.97	0.84	0.37	0.69	0.490	0.17	0.28	0.96	0.88	1.06	0.47	1.68	0.59	0.49	0.97	0.01	0.01
65	0.91	0.84	0.81	0.37	0.65	0.479	0.12	0.26	0.98	1.60	1.28	0.38	2.30	0.52	0.39	1.91	0.01	0.01
66	1.32	1.22	1.07	0.56	0.45	0.302	2.51	0.85	0.61	1.69	3.27	1.65	3.65	2.62	1.13	0.22	0.01	0.01
67	0.94	0.98	0.94	0.31	1.23	0.500	2.29	0.88	0.69	1.80	3.92	0.96	3.13	1.62	0.72	0.78	0.31	-0.07
68	0.97	0.73	0.79	0.42	0.98	0.518	1.25	0.75	0.44	0.61	0.37	0.78	2.62	0.78	0.61	0.55	-0.10	-0.25
69	0.85	0.72	0.73	0.47	0.37	0.359	0.05	0.15	0.96	0.99	0.56	0.35	1.47	0.60	0.45	0.78	0.01	0.01
70	0.62	0.67	0.69	0.25	0.91	0.379	2.26	0.86	0.68	5.28	12.25	0.65	4.70	1.30	0.69	1.24	-0.74	-0.42
MPI1=1.5(3MP+2MP)/(P+9MP+1MP+4MP). MPR=2MP/(1MP+4MP). DPR=(2,6-DMP+2,7-DMP)/(1,6-DMP+2.10-DMP). TAS=Triaromatic steroids.																		
To optimize plotting, nul or zero values are given as 0.01.																		
Samples 14 and 15 have low GC-MS MPR and MPI1 due to evaporation of light phenanthrenes.																		
MAS D/R=Monoaromatic steroids from saturated fraction Dia(2+3+11+12+15)/Reg(1+5+6+9+16). 27 D/R=C27 saturated MAS Dia/Dia+Reg (2+3)/(1+2+3+4+5).																		
T/T+M=TAS/(TAS+MAS)(aromatic fraction). 4/2+3 and 4/1=methyl dibenzo thiophene ratios. C/E and D/F=dimethyl dibenzo thiophene ratios. c/e, d/e and e/f=trimethyl dibenzo thiophene ratios.																		
g/(g+e)=C21/(C21+C28R) TAS, 20-28=(C20+C21)/(C26-C28) TAS ratios. 125/136 and 127/137=log(10) trimethyl naphthalene ratios.																		

Table F.21: Phenanthrene, mono and tri-aromatic steroid, dibenzothiophene and trimethyl naphthalene ratios for all source rock samples (including annotation descriptions) (page 2 of 2).

No.	27Dia	28Dia	29Dia	27Reg	28Reg	29Reg	27aa	28aa	29aa	27bb	28bb	29bb	27-29Hop	30Hop	30+Hop	27MAS	28MAS	29MAS	26-28DH	29DH	30+DH
SHALE SAMPLES																					
41	387	269	344	419	285	296	469	221	310	402	323	275	250	343	407	364	486	150	175	368	457
42	389	278	333	402	312	286	470	206	324	371	359	270	227	332	441	361	475	164	201	274	525
43	392	246	362	431	251	318	444	192	364	425	282	293	269	325	406	357	476	167	191	310	499
44	321	359	320	400	321	279	402	296	302	398	340	262	331	400	269	245	592	163	141	196	663
45	358	248	394	436	235	329	346	236	418	489	234	277	433	241	326	424	326	250	191	217	592
46	329	277	394	445	224	331	381	216	403	473	227	300	174	296	530	264	566	170	96	292	612
47	395	276	329	443	304	253	531	206	263	398	354	248	312	413	275	386	479	135	213	206	581
48	410	284	306	426	275	300	465	248	287	405	289	306	347	378	365	320	480	200	208	196	596
49	362	294	344	268	366	366	391	295	314	351	343	306	286	347	367	343	559	98	221	301	478
50	353	320	327	335	345	320	296	337	367	389	356	255	389	304	306	357	528	115	180	194	626
51	268	335	397	388	300	312	327	300	373	427	299	274	188	295	517	215	662	123	75	276	649
52	382	310	308	355	344	301	298	339	363	443	352	205	460	251	289	285	642	73	339	84	577
53	431	278	291	563	227	210	581	168	251	554	255	191	415	230	355	444	424	132	489	121	390
54	433	242	325	547	214	239	485	189	326	577	225	198	488	242	270	489	363	148	326	148	526
55	330	351	319	344	350	306	287	348	365	420	353	227	318	315	367	343	567	90	155	218	627
56	262	379	359	507	265	228	552	201	247	489	291	220	234	216	550	338	448	214	191	211	598
57	400	327	273	492	266	241	629	143	228	427	326	247	322	202	476	375	479	146	317	80	603
58	360	343	297	514	253	233	581	175	244	477	296	227	332	226	441	355	418	227	322	199	479
59	310	342	348	426	267	307	360	273	367	458	263	279	177	286	537	242	608	150	95	280	625
60	290	340	370	425	276	299	407	247	346	432	289	279	169	297	534	256	577	167	101	273	626
61	375	334	291	520	253	227	570	168	262	492	299	209	390	210	400	353	499	148	409	149	442
62	443	261	296	517	231	252	501	171	328	524	259	217	430	255	315	386	446	168	457	90	453
63	436	265	299	612	173	214	580	137	282	598	207	195	638	116	246	400	420	180	456	49	495
64	357	308	335	417	260	323	333	256	411	484	263	253	289	331	380	340	562	98	200	224	576
65	339	312	349	372	299	329	290	288	422	437	307	256	249	322	429	312	578	110	193	236	571
66	368	292	340	446	206	348	385	181	434	482	221	297	404	228	368	488	360	152	200	222	578
67	432	312	256	690	160	150	735	70	195	664	215	173	491	173	336	380	369	251	447	66	487
68	394	269	337	455	233	312	405	160	435	482	271	248	260	317	423	378	485	137	251	213	536
69	313	354	333	331	337	332	265	351	384	399	329	272	306	307	387	304	590	106	147	221	632
70	415	264	321	539	238	223	541	183	275	542	257	201	645	138	217	407	429	164	541	146	313
All data recorded as ppt of the summed mass ranges.																					
Dia=total of ba+ab rearranged steranes. Reg=total of bb+aa regular steranes. aa=total of aa steranes. bb=total of bb steranes. Hop=total identified hopane peaks.																					
MAS=Monoaromatic steroid peaks (saturated fraction) C27=1+2+3+4+5+9, C28=6+10+11+14, C29=12+13+15+16. DH=Identified demethylated hopane peaks.																					
Sample 5: C29aaR peak overlapped by nC30.																					

Table F.22: Sterane, terpane, norhopane and monoaromatic steroid ternary plot ratios for all source rock samples (including annotation descriptions) (page 2 of 2).

Sterane, terpane, demethylated terpane and monoaromatic sterane data for ternary plots.																					
No.	27Dia	28Dia	29Dia	27Reg	28Reg	29Reg	27aa	28aa	29aa	27bb	28bb	29bb	27-29Hop	30Hop	30+Hop	27MAS	28MAS	29MAS	26-28DH	29DH	30+DH
OIL SAMPLES																					
1	389	297	314	416	272	312	498	243	259	372	405	223	282	280	438	333	364	303			
2	395	345	260	458	212	330	530	231	239	420	382	198	370	209	421	331	361	308			
3	308	354	338	463	286	251	549	199	252	416	334	250	348	271	381	349	289	362	244	302	454
4	392	318	290	513	278	209	548	214	238	497	308	195	549	298	153	414	418	168	484	32	484
5	452	273	275	501	230	269	519	194	287	490	252	258	491	283	226	312	448	240	407	72	521
6	350	287	363	381	357	262	432	222	346	358	417	225	194	325	481	324	386	290	479	0	521
7	391	296	313	432	254	314	464	213	323	413	279	308	460	231	309	465	398	137	152	104	744
8	431	255	314	523	228	249	524	157	319	523	260	217	418	214	368	501	301	198	505	105	390
9	367	306	327	477	228	295	425	249	326	510	215	275	401	202	397	407	419	174	474	0	526
10	337	329	334	430	259	311	464	234	302	411	272	317	311	228	461	405	413	182	141	174	685
11	427	302	271	514	223	263	473	204	323	539	234	227	291	245	464	364	434	202	329	128	543
12	411	317	272	581	256	163	568	181	251	590	306	104	511	186	303	391	410	199	587	64	349
13	359	305	336	498	195	306	427	225	348	539	179	282	315	187	498	582	202	216	129	181	690
14	298	341	361	416	312	272	400	273	327	424	329	247	189	284	526	380	444	176	140	272	588
15	449	266	285	444	282	274	391	272	336	479	289	232				398	259	343			
16	434	315	251	542	286	172	584	189	227	566	280	155	614	151	235	437	421	142	624	0	376
17	460	279	261	555	242	203	550	193	257	557	266	177	638	217	145	425	451	124	657	42	301
18	296	332	372	395	295	310	358	272	370	415	307	278	180	282	537	250	592	158	105	279	616
19	325	361	314	477	299	224	465	289	245	483	303	214	221	274	505	514	353	133	175	238	587
20	291	329	380	462	290	248	452	261	287	414	286	300	206	271	523	343	457	200	153	233	614
21	361	273	366	394	289	317	324	244	432	425	309	266	358	299	343	441	334	225	329	174	497
22	409	246	345	377	280	343	277	249	474	489	290	221	311	294	395	320	579	101	175	254	571
23	401	283	316	408	319	273	412	251	337	405	351	244	515	258	227	412	361	227	452	78	470
24	439	309	252	690	160	150	735	70	195	664	215	173	491	173	336	520	363	117	602	41	357
25	301	337	362	460	246	294	427	225	348	464	250	286	301	201	498	379	421	200	107	195	698
26	311	348	341	409	284	307	401	282	317	414	286	300	519	281	200	387	527	86	170	169	661
27	402	299	299	506	259	235	497	213	290	512	286	202	478	299	223	457	409	134			
28	417	298	285	572	241	187	578	215	207	569	254	177	647	135	218	373	301	327	559	194	247
29	376	304	320	577	213	210	577	203	220	578	218	204	534	226	240	369	403	228	462	140	398
30	371	289	340	436	284	280	428	228	344	440	312	248	360	255	385	521	291	188	409	155	436
31	369	284	347	337	345	318	413	252	335	294	395	311	493	274	233	463	399	138	821	88	91
32	436	272	292	516	224	260	516	224	260	543	267	190	462	253	285	499	410	91	502	331	167
33	348	288	364	400	325	275	340	307	353	321	400	279	540	237	223	501	320	179	358	494	148
34	399	259	342	453	283	264	445	240	315	318	377	305	484	207	309	410	377	213	487	361	152
35	323	295	382	377	336	287	362	287	351	384	360	256	457	294	249	456	466	78	360	430	210
36	309	278	413	381	299	320	349	275	376	396	311	293	440	313	247	405	456	139	380	420	200
37	432	268	300	445	270	285	406	216	378	468	303	229	659	194	147	463	287	350	367	210	423
38	381	297	322	488	250	262	464	212	324	499	267	234	624	181	195	379	387	233	451	327	222

Table F.22: Sterane, terpane, norhopane and monoaromatic steroid ternary plot ratios for all hydrocarbon samples (page 1 of 2).

SATURATES FRAGMENTOGRAM HEIGHT AND BASELINE FACTOR																				
No.	WELL	DEPTH	TIC	177	%	191/3	%	191/5	%	217/T	217	%	218	%	231	%	253	%	259	%
OIL SAMPLES																				
1	83	2470						10453	100		14140	100	6973	100	628560	100	151208	100		
2	83	2889						7073	100		17792	100	9815	100	170480	100	36062	100		
3	83	2889	50525576	88064	69	48896	62	150528	82	139264	139264	91	69632	92	29952	70	12096	68	72704	89
4	88	2507	15240681	8704	60	8448	84	30208	86	18944	18944	92	7296	88	3232	70	14464	93	9664	92
5	88	2507	15674129	18944	70	14528	60	21248	65	38912	38912	94	18432	92	6592	65	5568	65	21504	88
6	88	2827	11395480	6656	85	7552	85	16896	100	10688	10688	100	7872	100	2800	100	4064	95	4608	100
7	92	2949	12127489	20992	67	26368	100	49664	84	12608	12608	85	9024	88	4032	55	6656	84	7872	84
8	118	2563.1	23964526	56576	65	54528	70	60416	60	96256	96256	100	33536	100	12672	65	19968	85	43008	100
9	102	2241	41919776	21248	60	23296	60	55552	80	16128	16128	88	10176	90	3632	60	5632	72	8128	85
10	102	2632	21878084	66560	67	221184	100	140288	80	46336	46336	75	34560	82	19844	50	19456	68	24064	68
11	91	3220.05	57270776	121856	55	228010	88	174080	48	154624	123904	80	52224	75	56832	65	97280	82	65536	80
12	104	3017.46	4489776	30720	60	24235	100	86016	75	39936	39936	100	13312	100	7552	60	9408	75	19712	100
13	93	3212.4	2797560	3552	100	5680	100	8000	100	9488	3280	100	2984	100	1048	100	30016	100	1520	100
14	109	2630	1650680	8544	100	39104	100	46720	100	19584	19584	100	14720	100	6248	100	22720	100	8464	100
15	107	2565	14397592	25856	87	9472	90	76800	90	3248	3248	75	2064	80	1616	65	2640	70	1760	80
16	110	3051	39775156	66560	60	169574	100	87040	55	162816	162816	100	51456	100	36608	80	33536	100	79872	100
17	126	2643	41658924	65280	65	90112	70	86016	60	164864	164864	100	57088	100	16000	80	36834	90	82944	100
18	122	2517	2060280	25216	100	10448	100	162560	100	64576	53376	100	43584	100	6096	100	37120	100	21984	100
19	132	2662	3481590	5168	100	3856	100	23520	100	15744	15744	100	8816	100	1436	100	22496	100	7552	100
20	132	2702.4	1816570	15152	100	7040	100	69376	100	43904	35520	100	22336	100	3480	100	26272	100	16608	100
21	48	2620	46799776	91136	75	132096	68	141312	75	151552	122880	100	83968	100	26880	60	33792	80	59392	100
22	16	2614	4385538	56320	80	35584	100	197632	100	55296	55296	100	26624	100	24064	100	81920	100	25856	100
23	59	2212	48692176	41728	38	48384	52	68608	60	55040	55040	90	24320	100	11840	60	12992	68	27392	87
24	75	2830.5	21499806	71680	70	66560	80	57344	45	120832	120832	100	36096	100	14720	70	25088	100	52736	100
25	101	2987.5	2564090	31680	100	27424	100	87808	100	55104	39040	100	29216	100	4096	100	37184	100	16176	100
26	20	2699	15264194	30976	85	120832	100	66560	90	41472	21504	90	23296	100	7168	70	14528	85	10944	90
27	13	2518.86	15091152	37120	40	37888	68	72704	60	28928	28928	88	10944	85	11456	60	25344	85	15872	88
28	103	2718		1.60E+07	100	1.80E+07	100	9.60E+06	100	3.00E+07	3.00E+07	100	2.00E+07	100	1.60E+07	100	1.80E+07	100	1.70E+07	100
29	94	2799		2.00E+06	100	1.90E+06	100	1.90E+06	100	3.60E+06	3.60E+06	100	1.30E+06	100	6.90E+05	100	1.50E+06	100	1.90E+06	100
30	156	2522	53232480	64256	60	59648	65	114688	82	99328	99328	100	60672	100	16384	70	13760	70	43264	90
31	156	2525	43072448	9600	75	14016	80	20992	92	25088	25088	94	22784	100	4736	80	6464	90	18944	100
32	166	2508	49652964	82565	80	15808	80	7040	75	19968	19968	96	13568	95	3184	80	7552	90	15296	95
33	166	2510.43	34718336	6656	75	17920	90	16896	89	33536	14080	100	14528	100	2976	75	7552	92	9984	100
34	166	2520	25321986	2944	50	5760	75	5760	70	7104	7104	90	5120	90	1536	65	2144	75	5312	90
35	166	2522.5	57018460	11520	84	21248	88	43776	96	30208	30208	95	35328	100	5568	80	19200	100	23296	100
36	165	2256	5312698	5632	70	3456	75	18944	88	14080	14080	91	13632	100	3280	75	9088	92	9216	90
37	167	2679	13118981	1952	75	5888	88	1440	51	5376	3184	90	1776	85	948	100	1696	85	2848	100
38	167	2681.65	5130069	3872	70	4736	90	3488	72	8064	8064	92	5888	90	1712	70	3024	84	6848	89

Table F.23: Saturated fraction TIC and fragmentogram heights and baseline factors for all hydrocarbon samples (page 1 of 2).

No.	WELL	DEPTH	TIC	177	%	191/3	%	191/5	%	217/T	217	%	218	%	231	%	253	%	259	%
SHALE SAMPLES																				
41	83	2702	2996810	20736	80	10368	88	74752	90	22784	22784	90	12032	92	3968	60	8704	90	13824	92
42	83	2741	38066756	62464	80	37888	100	190464	90	80896	80896	92	48896	94	15040	70	22272	90	45312	92
43	83	2792	2973593	14400	80	7744	90	60160	92	14016	14016	91	7616	90	2944	70	5440	88	7296	93
44	91	2610	1842646	11008	90	3600	80	46080	100	8000	8000	92	6592	94	1824	75	6144	91	4544	90
45	89	2660	8145098	17152	70	34560	100	49664	80	7488	6592	80	4416	80	3424	55	4672	70	3808	75
46	93	2720	1466360	38912	100	103680	100	258560	100	112256	96512	100	62080	100	6096	100	32128	100	34880	100
47	93	2761	4217116	7680	75	8786	85	29184	90	10368	10368	92	5376	92	1884	70	2576	84	4352	90
48	93	2761	3750200	4480	70	3872	78	13312	88	7552	7552	92	3984	92	1360	65	3408	88	3824	88
49	99	1820	12661814	153600	85	72704	100	823296	100	651264	651264	100	331776	100	106496	100	1736704	100	193536	100
50	109	2461	16039989	109668	100	59392	95	331776	100	220160	220160	100	111616	100	40448	100	155648	100	91136	100
51	109	2654.15	1478650	90112	100	21024	100	533504	100	104832	87680	100	61120	100	12432	100	107136	100	32096	100
52	130	2331	5310662	93184	100	16384	95	339968	99	114688	114688	100	55040	100	25856	100	259072	100	54528	100
53	110	2830	24497028	101376	70	94208	70	135168	70	246784	246784	100	87040	100	25344	70	48128	90	115712	100
54	110	2902	20598612	68608	50	78848	75	182272	80	131072	131072	100	52736	100	22272	60	37120	85	64786	100
55	112	2392	20740248	254976	88	118784	90	1081344	100	442368	442368	100	282624	100	108544	90	815104	100	198656	100
56	117	2918.5	2625530	18944	100	46720	100	47040	100	49344	37952	100	21344	100	4728	100	29056	100	18368	100
57	117	2918.5	27429660	31744	65	20480	55	66560	78	38400	38400	92	13376	88	6208	60	7744	80	19456	90
58	117	2918.5	13790277	57088	60	37120	45	129024	80	74752	74752	100	36352	88	14976	55	18432	70	42240	85
59	122	2682	4440060	135936	100	71296	100	826368	100	272896	226048	100	188928	100	26208	100	104448	100	91520	100
60	122	2832	2494460	46912	100	49280	100	225536	100	61248	48576	100	33792	100	6544	100	28064	100	21152	100
61	11	2682	43736320	126976	60	147456	60	224256	74	286720	286720	94	128000	90	46336	60	53504	80	142336	90
62	14	2721	34008720	113664	70	178176	80	190464	75	294912	294912	100	115712	100	31232	60	41984	85	143360	100
63	42	3021	5070991	9024	60	10176	60	12032	66	14336	14336	100	4800	100	2384	50	3104	80	6400	100
64	48	2490	7804665	56832	80	33792	100	254976	94	106496	106496	100	74752	100	148480	100	80896	100	52480	94
65	41	2320	14089057	158720	90	63488	90	843776	99	331776	331776	100	235520	100	160768	100	348160	100	148480	100
66	65	3160	22950544	59648	35	117419	100	147456	65	74752	54528	80	35840	85	30720	65	54272	80	28160	75
67	75	2829	2403406	4800	55	5280	86	8064	70	9088	9088	95	2704	90	1120	65	856	65	4016	95
68	67	2651	29405236	218112	75	286720	100	901120	90	507904	507904	100	274432	100	954368	100	262144	100	244736	100
69	12	2057	4685930	91136	90	55808	100	352256	100	111616	111616	100	62976	100	218112	100	199680	100	44288	100
70	156	2805	15405633	16384	85	9216	75	21248	92	28160	28160	94	14656	90	5760	80	3888	70	14720	90
Baseline factor given as percentage multiplication.																				
Some samples have the maximum ion heights recorded in exponential notation. The full number of significant figures have been reported.																				

Table F.23: Saturated fraction TIC and fragmentogram heights and baseline factors for all source rock samples (including annotation descriptions) (page 2 of 2).

AROMATIC FRAGMENTOGRAM HEIGHT AND BASELINE FACTOR																	
No.	WELL	DEPTH	TIC	170	%	198	%	212	%	226	%	Phen	%	231	%	253	%
OIL SAMPLES																	
1	83	2470															
2	83	2889															
3	83	2889															
4	88	2507	1761175	7168	100	57600	100	36864	100	22016	100	51968	100	25856	100	6208	100
5	88	2507	4133205	32512	100	121856	100	89088	100	38144	100	729088	100	30208	100	3968	80
6	88	2827	7899419	51200	100	26368	100	13888	100	7808	100	799419	100	4608	95	2432	85
7	92	2949	11147543	11008	100	32512	100	37632	100	16128	100	425984	100	27136	100	7168	90
8	118	2563.1	3353630	224256	100	17493	100	8448	95	4779	90	745472	100	16384	100	2381	75
9	102	2241	4835016	565248	100	58368	100	29440	100	13312	100	688128	100	5440	80	2240	55
10	102	2632	41091556	6720	100	34048	100	57088	100	126976	100	843776	100	246784	100	89088	100
11	91	3220.05	8246725	6592	100	5952	100	13184	100	33536	100	991232	100	159744	100	76800	100
12	104	3017.46	7857856	8896	100	3616	100	39424	100	11392	100	196608	100	37888	100	21504	100
13	93	3212.4	673792	180736	100	39040	100	39616	100	16640	100	503808	100	16864	100	8152	100
14	109	2630	448000	228	100	2228	100	3976	100	5576	100	116096	100	43008	100	16224	100
15	107	2565	6492048	8256	100	4416	100	3072	100	9216	100	111616	100	60416	100	5376	90
16	110	3051	8076805	6784	100	4224	100	9408	100	17920	100	786432	100	84992	100	22912	95
17	126	2643	16812960	1572760	100	368640	100	211968	100	76800	100	3014656	100	64000	100	37632	100
18	122	2517	189952	1510	100	4936	100	6224	100	5104	100	38656	100	116352	100	10752	100
19	132	2662	721920	594944	100	62592	100	26560	100	10592	100	329216	100	14896	100	3088	100
20	132	2702.4	391680	3460	100	56960	100	32064	100	13376	100	300544	100	21152	100	4088	100
21	48	2620	9414432	7104	100	10496	100	25856	100	17024	100	1228800	100	121856	100	25941	90
22	16	2614	20480680	6464	100	99328	100	119808	100	95232	100	2228224	100	569344	100	67994	100
23	59	2212	15585093	1556480	100	311296	100	131072	100	57088	100	2998272	100	42752	100	15616	100
24	75	2830.5	12385703	1616	100	23552	100	47104	100	30208	100	1572864	100	153600	95	37376	100
25	101	2987.5	220928	2352	100	14272	100	12976	100	8152	100	99840	100	9952	100	3496	100
26	20	2699	2460251	1596	100	109568	100	116736	100	62464	100	339968	100	9536	100	3408	65
27	13	2518.86	10901194	2608	100	44800	100	65536	100	38144	100	856064	100	58880	100	13739	90
28	103	2718				120000000	100					620000000	100	16000000	100		
29	94	2799				11000000	100					58000000	100	3.00E+06	100		
30	156	2522	23386172	2703360	100	950272	100	614400	100	257024	100	2795008	100	155648	100	40704	90
31	156	2525	5596559	59392	100	220160	100	166912	100	52224	100	996944	100	36608	100	10688	86
32	166	2508	10061116	876544	100	259072	100	162816	100	50944	100	1643592	100	16896	95	3056	60
33	166	2510.43	7923020	59904	100	335872	100	201728	100	71680	100	2066508	100	34560	100	50688	100
34	166	2520	4889070	376832	100	166912	100	107520	100	44800	100	932136	100	22272	92	6208	78
35	166	2522.5	6528065	339968	100	246784	100	181248	100	69632	100	1346888	100	42240	100	10752	84
36	165	2256	3475211	10944	100	9280	100	4928	90	3776	85	385476	99	56064	98	17152	100
37	167	2679															
38	167	2681.65															

Table F.24: Aromatic fraction TIC and fragmentogram heights and baseline factors for all hydrocarbon samples (page 1 of 2).

No.	WELL	DEPTH	TIC	170	%	198	%	212	%	226	%	Phen	%	231	%	253	%
SHALE SAMPLES																	
41	83	2702	7769180	3200	100	254976	100	202752	100	88064	100	1409024	100	207872	100	30976	100
42	83	2741	15927144	9856	100	155648	100	197632	100	90112	100	1015808	100	179200	100	25498	94
43	83	2792	6503896	1552	100	153600	100	135168	100	43520	100	1261568	100	145408	100	47445	100
44	92	2610	2114243	81920	100	66560	100	34560	100	10944	100	589824	100	106496	100	13952	100
45	89	2660	8153592	42496	100	87040	100	50176	100	48640	100	1835008	100	34048	100	8397	95
46	93	2720															
47	93	2761	3383939	20992	100	3536	100	4000	100	3664	100	13888	100	2416	100	2912	100
48	93	2761	1638631	67584	100	53248	100	31232	100	11776	100	348160	100	11520	100	4048	87
49	99	1820	6112735	11456	100	11328	100	15424	100	23040	100	24320	100	311296	100	368640	100
50	109	2461	12753925	1048576	100	688128	100	348160	100	122880	100	2916352	100	1769472	100	252928	100
51	109	2654.15	240128	3992	100	17248	100	8528	100	3508	100	170752	100	129536	100	9744	100
52	130	2331	4479796	13824	100	250880	100	100352	100	35328	100	1130496	100	487424	100	236544	100
53	110	2830	3595023	43520	100	98304	100	70656	100	29184	100	614400	100	52992	100	9301	95
54	110	2902	12278665	974848	100	219136	100	150528	100	62720	100	2981888	100	65536	100	20684	100
55	112	2392	4020368	209920	100	84992	100	47872	100	18688	100	815104	100	232448	100	25344	100
56	117	2918.5	339456	87168	100	41728	100	26688	100	11600	100	248832	100	14896	100	4008	100
57	117	2918.5	5737816	226304	100	210944	100	132096	100	45056	100			43520	100	9536	100
58	117	2918.5	1638631	67584	100	53248	100	31232	100	11776	100	348160	100	11520	100	4048	87
59	122	2682	494592	210432	100	107136	100	59648	100	22272	100	325120	100	239872	100	14064	100
60	122	2832	214016	161792	100	37760	100	22528	100	7656	100	112896	100	89344	100	4904	100
61	11	2682	4957130	352256	100	184320	100	109568	100	51712	100	1028096	100	48640	100	22272	100
62	14	2721	3711225	215040	100	182272	100	94208	100	33280	100	987136	100	25600	100	16640	100
63	42	3021	9417204	1248	100	47104	100	106496	100	70656	100	1490944	100	107520	100	24917	95
64	48	2490	8571737	2688	100	19200	100	35328	100	28416	100	1228800	100	753664	100	43776	100
65	41	2320	3754304	2384	100	58624	100	40704	100	15680	100	462848	100	339968	100	10624	100
66	65	3160	10047591	2736	100	6976	100	10112	100	16896	100	1343488	100	75776	100	48128	100
67	75	2829	12378232	13888	100	78848	100	72704	100	29696	100	2195456	100	125952	100	38912	100
68	67	2651															
69	12	2057	8481777	3872	100	5888	100	14272	100	18432	100	130048	100	643072	100	22016	100
70	156	2875	2255643	348160	100	71680	100	36864	100	12736	100	492020	100	7616	90	2976	85
Sample 47: data are from analysis S_EBT1A.																	
Sample 48: data are from analysis S_EBT1A1.																	

Table F.24: Aromatic fraction TIC and fragmentogram heights and baseline factors for all source rock samples (including annotation descriptions) (page 2 of 2).

STABLE CARBON 13 ISOTOPE DATA										
WELL	DEPTH	SAMPLE	SATURATES	AROMATICS	RESINS	ASPHALTENES	WHOLE OIL	DATE	SOURCE	REMARKS
83	2470m	DST 3	-27.44	-26.26	-25.74	-26.40		Oct. 1989	CSIR	NBS 22 = -29.91 (international standard = -29.86).
83	"	DST 3	-27.50	-26.33				"	"	"
88	2839m	DST4	-28.74	-26.51				"	"	"
88	"	DST4	-28.79					"	"	"
83	3254m	DST 1					-27.64	Feb. 1994	IGI	oil topped at 35degC.
103	2718m	DST 2					-28.30	"	"	"
94	2799m	DST 1					-27.22	"	"	"
46	2620m	DST 1					-27.14	"	"	"
65	3267m	DST 2					-27.43	"	"	"
20	2515m	DST 4					-27.08	"	"	"
62	2549m	DST 1					-27.98	"	"	"
70	2452m	DST 1					-27.08	"	"	"
128	3661m	DST 1					-26.29	"	"	"
92	2949m	core 1	-28.55	-26.89				Mar. 1995	GHG	urea non-adduct. NBS 22 = -29.75
89	2660m	RC shale	-33.25	-32.56				"	"	"
20	2699m	DST 2	-27.96	-26.84				"	"	"
109	2630m	DST 1	-27.45	-26.89				"	"	"
109	"	"	-27.49					"	"	"
102	2241m	DST 4	-26.87	-25.45				"	"	"
102	2632m	DST 2	-27.26	-27.29				"	"	"
Depths given to bottom of tested/sampled interval in metres bKb.										
CSIR, (Oct. 16, 1989). "13C in oil". EMA/3590, Earth, Marine and Atmospheric Science and Technology, CSIR, PO Box 395, Pretoria, 0001, 2pp. (A.S.Talma).										
IGI, (Feb. 1994). "Hydrocarbon correlations in the offshore Mossel Bay area, RSA". IGI, Hallsannery, Bideford, Devon, UK, 51pp. (Cornford, C.).										
GHG, (March, 1995). Carbon Isotope Data, GHG, 24 Higher Bebington Road, Bebington, Wirral, UK, 9pp. (Harriman, G.H.).										

Table F.25: Stable ^{13}carbon isotopic ratio data.

CANONICAL CORRELATIONS			
CANONICAL MEAN		0.81002	0.7547
VARIABLE		CV1	CV2
13M	2728bb	2.49085	3.76096
32AF	2456	-1.41135	1.14966
2728bb = m/z 218 bb steranes C27/C28			
C24 tetracyclic terpane/(av. C25+C26 tricyclic terpanes)			
PLOTTING COORDINATES			
SAMPLE	SOURCE	XCOORD	YCOORD
41	13A	0.71	1.00
42	13A	-0.26	-0.63
43	13A	0.87	2.68
46	13A	0.34	0.50
47	13A	-0.75	2.20
48	13A	0.83	0.16
50	13A	0.64	0.37
52	13A	0.63	-0.37
53	13A	1.80	-0.63
54	13A	1.48	1.31
59	13A	0.45	-1.56
62	13A	2.49	0.08
70	13A	2.73	1.45
44	Upper 9A-12A	-2.44	0.51
51	Upper 9A-12A	-4.61	1.40
60	Upper 9A-12A	-2.42	-0.32
56	Lower 9A-12A	-0.84	-3.41
57	Lower 9A-12A	0.59	-1.68
58	Lower 9A-12A	0.11	-2.56
61	Lower 9A-12A	0.23	-2.25
55	5A-8A	-1.55	-0.22
64	5A-8A	-0.81	1.03
65	5A-8A	0.05	-0.48
66	5A-8A	1.15	0.48
67	5A-8A	-1.62	0.24
68	5A-8A	0.20	0.72
49	15A	-0.04	-0.82
69	15A	0.93	-2.53

Table F.26a: Canonical variables 1 and 2 for shale samples calculated from discriminant functions and raw data.

STEPWISE DISCRIMINANT FUNCTION ANALYSIS USING MAIN SOURCE FAMILIES ONLY										
			13A		Upper 9A-12A		Lower 9A-12A		5A-8A	
SAMPLE	FAMILY	CORRECT	D2	PP	D2	PP	D2	PP	D2	PP
41	13A		0.3	0.680	15.2	0.000	12.6	0.001	1.8	0.318
42	13A	5A-8A	2.7	0.240	9.7	0.007	3.5	0.163	0.9	0.590
43	13A		4.7	0.787	20.8	0.000	27.2	0.000	7.3	0.212
46	13A		0.3	0.532	12.2	0.001	8.9	0.007	0.6	0.460
47	13A	5A-8A	5.7	0.258	8.6	0.061	22.4	0.000	3.7	0.681
48	13A		0.1	0.665	16.0	0.000	7.6	0.016	1.6	0.319
50	13A		0.1	0.623	14.4	0.000	8.5	0.010	1.2	0.367
52	13A		0.9	0.543	15.1	0.000	4.8	0.076	1.6	0.380
53	13A		2.1	0.794	25.9	0.000	6.5	0.085	5.8	0.121
54	13A		1.0	0.864	22.1	0.000	16.4	0.000	4.7	0.135
59	13A	Lower 9A-12A	4.5	0.128	17.4	0.000	1.0	0.725	4.2	0.146
62	13A		2.7	0.945	32.1	0.000	12.6	0.007	8.6	0.049
70	13A		4.2	0.972	35.5	0.000	22.7	0.000	11.3	0.028
44	Upper 9A-12A		11.3	0.004	0.5	0.853	14.9	0.001	4.1	0.143
51	Upper 9A-12A		31.3	0.000	2.9	1.000	36.5	0.000	18.7	0.000
60	Upper 9A-12A		11.8	0.004	1.3	0.815	10.6	0.008	4.4	0.174
56	Lower 9A-12A		18.4	0.000	20.9	0.000	1.6	0.998	13.9	0.002
57	Lower 9A-12A		4.9	0.111	18.9	0.000	1.0	0.781	4.9	0.108
58	Lower 9A-12A		10.0	0.007	20.2	0.000	0.0	0.979	8.4	0.014
61	Lower 9A-12A		8.1	0.018	19.2	0.000	0.1	0.951	6.9	0.031
55	5A-8A		6.6	0.050	3.1	0.284	7.6	0.031	1.5	0.635
64	5A-8A		3.3	0.203	5.8	0.059	13.0	0.002	0.7	0.737
65	5A-8A		1.7	0.346	11.3	0.003	4.0	0.113	0.8	0.583
66	5A-8A	13A	0.1	0.770	18.5	0.000	10.0	0.005	2.5	0.224
67	5A-8A		6.5	0.047	2.5	0.353	10.1	0.008	1.4	0.593
68	5A-8A		0.6	0.500	11.3	0.002	10.3	0.004	0.6	0.494
49	15A	5A-8A	2.7	0.260	11.6	0.003	2.7	0.248	1.4	0.489
69	15A	Lower 9A-12A	9.2	0.015	26.1	0.000	0.8	0.975	9.9	0.011

Table F.26b: Stepwise discriminant functions of shale samples showing Mahalanobis' D^2 value and *a posteriori* probabilities of incorrect match.

SHALE SAMPLES X OIL CANONICAL VARIABLES																		
		VARIABLE 1			VARIABLE 2			VARIABLE 3			VARIABLE 4			VARIABLE 5				
			CV1	CV2		CV1	CV2		CV1	CV2		CV1	CV2		CV1	CV2	TOTAL	
SAMPLE	FAMILY	2928bb	-4.68408	1.84761	32SR	-5.91634	-2.98247	H24	-0.00891	0.01308	2456	-6.39393	3.10941	-1.89	-0.36852	-0.34669	CV1	CV2
41	13A	1.37	-6.41719	2.53123	1.16	-6.86295	-3.45967	946	-8.42886	12.37368	1.81	-11.57301	5.62803	3.44	-1.26771	-1.19261	-34.55	15.88
42	13A	1.13	-5.29301	2.08780	1.61	-9.52531	-4.80178	912	-8.12592	11.92896	1.76	-11.25332	5.47256	5.83	-2.14847	-2.02120	-36.35	12.67
43	13A	1.75	-8.19714	3.23332	1.52	-8.99284	-4.53335	937	-8.34867	12.25596	2.25	-14.38634	6.99617	6.80	-2.50594	-2.35749	-42.43	15.59
46	13A	1.99	-9.32132	3.67674	1.51	-8.93367	-4.50353	963	-8.58033	12.59604	1.83	-11.70089	5.69022	2.39	-0.88076	-0.82859	-39.42	16.63
47	13A	1.27	-5.94878	2.34646	1.36	-8.04622	-4.05616	980	-8.7318	12.8184	2.85	-18.22270	8.86182	2.00	-0.73704	-0.69338	-41.69	19.28
48	13A	1.17	-5.48037	2.16170	1.37	-8.10539	-4.08598	869	-7.74279	11.36652	1.50	-9.59090	4.66412	3.09	-1.13873	-1.07127	-32.06	13.04
50	13A	1.30	-6.08930	2.40189	1.41	-8.34204	-4.20528	916	-8.16156	11.98128	1.65	-10.54998	5.13053	0.75	-0.27639	-0.26002	-33.42	15.05
52	13A	1.07	-5.01197	1.97694	1.03	-6.09383	-3.07194	918	-8.17938	12.00744	1.43	-9.14332	4.44646	0.10	-0.03685	-0.03467	-28.47	15.32
53	13A	1.08	-5.05881	1.99542	1.36	-8.04622	-4.05616	840	-7.4844	10.9872	0.81	-5.17908	2.51862	2.11	-0.77758	-0.73152	-26.55	10.71
54	13A	1.45	-6.79192	2.67903	1.36	-8.04622	-4.05616	839	-7.47549	10.97412	1.55	-9.91059	4.81959	6.44	-2.37327	-2.23268	-34.60	12.18
59	13A	1.17	-5.48037	2.16170	1.42	-8.40120	-4.23511	964	-8.58924	12.60912	1.15	-7.35302	3.57582	1.29	-0.47539	-0.44723	-30.30	13.66
62	13A	1.21	-5.66774	2.23561	1.30	-7.69124	-3.87721	783	-6.97653	10.24164	0.71	-4.53969	2.20768	3.47	-1.27876	-1.20301	-26.15	9.60
70	13A	0.78	-3.65358	1.44114	1.59	-9.40698	-4.74213	701	-6.24591	9.16908	1.02	-6.52181	3.17160	2.15	-0.79232	-0.74538	-26.62	8.29
44	Upper 9A-12A	1.02	-4.77776	1.88456	1.38	-8.16455	-4.11581	929	-8.27739	12.15132	3.11	-19.88512	9.67027	4.11	-1.51462	-1.42490	-42.62	18.17
51	Upper 9A-12A	1.45	-6.79192	2.67903	1.48	-8.75618	-4.41406	962	-8.57142	12.58296	4.38	-28.00541	13.61922	8.75	-3.22455	-3.03354	-55.35	21.43
60	Upper 9A-12A	1.30	-6.08930	2.40189	1.45	-8.57869	-4.32458	959	-8.54469	12.54372	2.85	-18.22270	8.86182	2.35	-0.86602	-0.81472	-42.30	18.67
56	Lower 9A-12A	1.09	-5.10565	2.01389	1.24	-7.33626	-3.69826	856	-7.62696	11.19648	1.18	-7.54484	3.66910	2.65	-0.97658	-0.91873	-28.59	12.26
57	Lower 9A-12A	0.77	-3.60674	1.42266	1.38	-8.16455	-4.11581	924	-8.23284	12.08592	1.05	-6.71363	3.26488	1.27	-0.46802	-0.44030	-27.19	12.22
58	Lower 9A-12A	0.84	-3.93463	1.55199	1.32	-7.80957	-3.93686	795	-7.08345	10.3986	1.00	-6.39393	3.10941	1.94	-0.71493	-0.67258	-25.94	10.45
61	Lower 9A-12A	0.86	-4.02831	1.58894	1.44	-8.51953	-4.29476	799	-7.11909	10.45092	1.04	-6.64969	3.23379	2.15	-0.79232	-0.74538	-27.11	10.23
55	5A-8A	1.05	-4.91828	1.93999	1.40	-8.28288	-4.17546	927	-8.25957	12.12516	2.48	-15.85695	7.71134	0.70	-0.25796	-0.24268	-37.58	17.36
64	5A-8A	1.41	-6.60455	2.60513	1.48	-8.75618	-4.41406	942	-8.39322	12.32136	2.52	-16.11270	7.83571	20.50	-7.55466	-7.10715	-47.42	11.24
65	5A-8A	1.37	-6.41719	2.53123	1.37	-8.10539	-4.08598	956	-8.51796	12.50448	1.66	-10.61392	5.16162	5.58	-2.05634	-1.93453	-35.71	14.18
66	5A-8A	1.68	-7.86925	3.10398	1.33	-7.86873	-3.96669	780	-6.9498	10.2024	1.45	-9.27120	4.50864	12.10	-4.45909	-4.19495	-36.42	9.65
67	5A-8A	0.79	-3.70042	1.45961	1.41	-8.34204	-4.20528	503	-4.48173	6.57924	2.65	-16.94391	8.23994	1.49	-0.54909	-0.51657	-34.02	11.56
68	5A-8A	1.37	-6.41719	2.53123	1.43	-8.46037	-4.26493	929	-8.27739	12.15132	1.96	-12.53210	6.09444	2.54	-0.93604	-0.88059	-36.62	15.63
49	15A	1.08	-5.05881	1.99542	0.59	-3.49064	-1.75966	961	-8.56251	12.56988	1.60	-10.23029	4.97506	8.70	-3.20612	-3.01620	-30.55	14.76
69	15A	1.10	-5.15249	2.03237	1.50	-8.87451	-4.47371	965	-8.59815	12.6222	0.63	-4.02818	1.95893	29.75	-10.96347	-10.31403	-37.62	1.83

Table F.26c: Canonical variables 1 and 2 for shale samples using hydrocarbon discriminant functions and shale raw data.

CANONICAL CORRELATIONS				
CANONICAL MEAN		0.9952	0.9406	0.6600
VARIABLE		CV1	CV2	CV3
18 R	2928bb	-4.6841	1.8476	-0.1250
24 X	32SR	-5.9163	-2.9825	-4.1200
25 Y	H24	-0.0089	0.0131	0.0050
36 AJ	2456	-6.3939	3.1094	-2.0450
39 AM	nHbis	-1.8942	-0.3685	0.0642
2928bb = m/z 218 bb steranes total C29/C28				
32SR = C32 homohopane 24S/24R				
H24 = hopane/(C24 tetracyclic terpane + hopane)				
2456 = C24 tetracyclic terpane/(C25 and av.C26 tricyclic terpanes)				
nHbis = C29 norhopane/C28 bisnorhopane				

PLOTTING COORDINATES			
SAMPLE	FAMILY	XCOORD	YCOORD
4	FAMILY 1	4.08	-0.64
5	1	2.16	-0.39
9	1	5.00	1.31
27	1	2.84	-1.19
29	1	4.22	-1.21
30	1	4.91	0.90
31	1	2.63	0.09
34	1	4.54	0.81
35	1	4.55	1.14
36	1	2.63	2.30
14	FAMILY 1B	-1.37	3.95
18	1B	-1.41	4.54
19	1B	-1.94	3.50
20	1B	-2.44	4.05
33	1B	0.05	2.31
12	FAMILY 2	8.07	-3.23
16	2	7.75	-3.80
24	2	8.40	-3.48
37	2	10.03	-4.38
13	FAMILY 3	-21.81	-1.57
25	3	-20.75	-1.61
26	3	-22.16	-3.39
3	FAMILY 1+2	6.32	2.22
6	1+2	3.64	0.65
10	1+2	-18.07	-1.80
17	1+2	5.65	-5.34
28	1+2	4.26	-7.59
32	1+2	3.00	-3.14
38	1+2	11.70	-1.45
8	FAMILY 1+3	4.90	-0.25
21	1+3	-3.33	1.30
22	1+3	-10.66	7.56
23	1+3	5.95	-0.75
11	FAMILY 2+3	-6.83	-0.79

Table F.27a: Canonical variables 1 and 2 for hydrocarbon samples calculated from discriminant functions and raw data.

STEPWISE DISCRIMINANT FUNCTION USING MAIN FAMILIES ONLY										
			F1		F1B		F2		F3	
SAMPLE	FAMILY	CORRECT	D2	PP	D2	PP	D2	PP	D2	PP
4	FAMILY 1		2.4	1.000	57.0	0.000	38.1	0.000	664.4	0.000
5	1		3.1	1.000	32.9	0.000	55.9	0.000	567.6	0.000
9	1		8.1	1.000	58.8	0.000	50.6	0.000	726.0	0.000
27	1		7.5	1.000	55.1	0.000	52.9	0.000	604.7	0.000
29	1		10.8	1.000	59.5	0.000	28.9	0.000	672.1	0.000
30	1		3.5	1.000	53.9	0.000	41.1	0.000	713.9	0.000
31	1		4.7	1.000	30.5	0.000	51.2	0.000	592.7	0.000
34	1		1.9	1.000	46.4	0.000	39.6	0.000	692.2	0.000
35	1		4.6	1.000	45.5	0.000	43.3	0.000	696.3	0.000
36	1		5.5	1.000	21.6	0.000	74.9	0.000	607.0	0.000
14	FAMILY 1B		42.8	0.000	0.9	1.000	158.3	0.000	447.5	0.000
18	1B		47.8	0.000	3.3	1.000	170.5	0.000	454.0	0.000
19	1B		46.4	0.000	0.5	1.000	162.5	0.000	419.6	0.000
20	1B		54.7	0.000	1.2	1.000	181.5	0.000	405.7	0.000
33	1B		28.2	0.000	9.5	1.000	114.2	0.000	495.6	0.000
12	FAMILY 2		35.2	0.000	138.1	0.000	1.0	1.000	881.6	0.000
16	2		41.7	0.000	142.6	0.000	3.2	1.000	868.1	0.000
24	2		37.3	0.000	148.1	0.000	0.8	1.000	900.5	0.000
37	2		65.7	0.000	198.5	0.000	5.2	1.000	1006.7	0.000
13	FAMILY 3		663.1	0.000	446.0	0.000	930.1	0.000	4.3	1.000
25	3		608.2	0.000	405.9	0.000	868.4	0.000	4.2	1.000
26	3		686.5	0.000	484.7	0.000	949.0	0.000	3.9	1.000
3	FAMILY 1+2	FAMILY 1	12.2	1.000	71.0	0.000	49.6	0.000	802.1	0.000
6	1+2	FAMILY 1	7.8	1.000	42.3	0.000	51.1	0.000	650.8	0.000
10	1+2	FAMILY 3	485.5	0.000	317.3	0.000	723.5	0.000	18.7	1.000
17	1+2	FAMILY 2	44.5	0.000	135.4	0.000	15.4	1.000	757.2	0.000
32	1+2	FAMILY 2	117.5	0.000	195.1	0.000	68.9	1.000	742.2	0.000
38	1+2	FAMILY 1	27.4	0.999	75.5	0.000	40.9	0.001	616.6	0.000
8	1+2	FAMILY 2	69.5	0.000	207.4	0.000	24.2	1.000	1113.0	0.000
21	FAMILY 1+3	FAMILY 1	5.6	1.000	59.2	0.000	29.6	0.000	707.9	0.000
22	1+3	FAMILY 1B	57.2	0.000	17.9	1.000	175.6	0.000	351.5	0.000
23	1+3	FAMILY 1B	277.3	0.000	108.2	1.000	504.3	0.000	226.5	0.000
11	1+3	FAMILY 1	8.6	0.999	80.9	0.000	23.1	0.001	763.6	0.000
	FAMILY 2+3	FAMILY 1B	120.6	0.000	58.0	1.000	254.5	0.000	226.8	0.000

Table F.27b: Stepwise discriminant functions of hydrocarbon samples showing Mahalanobis' D^2 value and *a posteriori* probabilities of incorrect match.

OIL SAMPLES X SHALE CANONICAL VARIABLES									
		VARIABLE	CV1	CV2	VARIABLE	CV1	CV2	TOTAL	
SAMPLE	FAMILY	2728bb	2.49085	3.76096	2456	-1.41135	1.14966	CV1	CV2
4	FAMILY 1	1.48	3.69	5.57	0.66	-0.93	0.76	2.75	6.32
5	1	1.69	4.21	6.36	0.91	-1.28	1.05	2.93	7.40
9	1	1.60	3.99	6.02	1.06	-1.50	1.22	2.49	7.24
27	1	1.35	3.36	5.08	0.61	-0.86	0.70	2.50	5.78
29	1	1.50	3.74	5.64	1.12	-1.58	1.29	2.16	6.93
30	1	1.44	3.59	5.42	0.86	-1.21	0.99	2.37	6.40
31	1	1.44	3.59	5.42	1.17	-1.65	1.35	1.94	6.76
34	1	1.51	3.76	5.68	1.15	-1.62	1.32	2.14	7.00
35	1	1.07	2.67	4.02	1.04	-1.47	1.20	1.20	5.22
36	1	1.27	3.16	4.78	1.17	-1.65	1.35	1.51	6.12
14	FAMILY 1B	1.09	2.72	4.10	1.61	-2.27	1.85	0.44	5.95
18	1B	1.17	2.91	4.40	1.54	-2.17	1.77	0.74	6.17
19	1B	1.09	2.72	4.10	1.75	-2.47	2.01	0.25	6.11
20	1B	1.09	2.72	4.10	1.73	-2.44	1.99	0.27	6.09
33	1B	1.89	4.71	7.11	1.96	-2.77	2.25	1.94	9.36
12	FAMILY 2	1.28	3.19	4.81	1.02	-1.44	1.17	1.75	5.99
16	2	1.41	3.51	5.30	1.20	-1.69	1.38	1.82	6.68
24	2	1.42	3.54	5.34	0.67	-0.95	0.77	2.59	6.11
37	2	1.55	3.86	5.83	0.45	-0.64	0.52	3.23	6.35
13	FAMILY 3	2.05	5.11	7.71	1.83	-2.58	2.10	2.52	9.81
25	3	1.11	2.76	4.17	1.37	-1.93	1.58	0.83	5.75
26	3	2.03	5.06	7.63	0.98	-1.38	1.13	3.67	8.76
3	FAMILY 1+2	0.87	2.17	3.27	0.95	-1.34	1.09	0.83	4.36
6	1+2	1.30	3.24	4.89	0.81	-1.14	0.93	2.09	5.82
10	1+2	1.55	3.86	5.83	1.31	-1.85	1.51	2.01	7.34
17	1+2	1.78	4.43	6.69	0.56	-0.79	0.64	3.64	7.34
28	1+2	1.79	4.46	6.73	1.01	-1.43	1.16	3.03	7.89
32	1+2	2.00	4.98	7.52	1.55	-2.19	1.78	2.79	9.30
38	1+2	1.87	4.66	7.03	0.71	-1.00	0.82	3.66	7.85
8	FAMILY 1+3	1.78	4.43	6.69	0.89	-1.26	1.02	3.18	7.72
21	1+3	1.67	4.16	6.28	0.98	-1.38	1.13	2.78	7.41
22	1+3	1.97	4.91	7.41	2.68	-3.78	3.08	1.12	10.49
23	1+3	1.62	4.04	6.09	0.54	-0.76	0.62	3.27	6.71
11	FAMILY 2+3	1.39	3.46	5.23	1.47	-2.07	1.69	1.39	6.92

Table F.27c: Canonical variables 1 and 2 for hydrocarbon samples using shale discriminant functions and hydrocarbon raw data.

APPENDIX G: BIOMARKER COMPOUND ASSIGNMENT EXAMPLES

APPENDIX G - MASS SPECTRA AND MOLECULAR STRUCTURES

Spectral analysis of at least one sample of each species of homologous compounds is detailed below. For each compound a spectrum from the literature and from one of the samples in this study are compared, the fragmentogram of the base peak is provided as is a fragmentation structure of the molecule. In each case, examples of fragmentograms given in the literature have been used to determine the relative retention indices from which the other peak assignments in the base peak fragmentograms have been made.

The groups of compounds detailed here are:
(i) Dibenzothiophenes
(ii) Isoprenoids
(iii) Methyl steranes
(iv) Monoaromatic steroids
(v) Pentacyclic terpanes
(vi) Steranes
(vii) Triaromatic steroids
(viii) Tricyclic terpanes
(ix) Trimethyl naphthalenes.

G. 1. DIBENZOTHIOPHENES

The compound used as an example is 4 methyl dibenzothiophene which is assigned to the peak '4M' (S.R. Thompson, 1992, pers. comm.). The spectrum available for this compound is from the NBS library no. 18331 (Fig. G.01) and is equivalent to the spectrum from Stenhager et al. (1974, p958). The comparison spectrum from sample 57 is shown and the m/z 198 fragmentogram locating on which the compound is located are also shown.

The spectrum from sample 57 has nearly equally dominant base peaks at mass 197 and 198 characteristic of an aromatic hydrocarbon. It also has a well developed ion at m/z 165 which is 32 mass units lower than the molecular ion signifying the presence of a sulphur atom in the molecule. This is confirmed by the presence of a fragment at m/z 200, approximately 5% of the height of the m/z 198 ion, indicating the presence of the ^{34}S isotope which occurs naturally at ~4% of the molecular ion. The extremely weakly developed ion at m/z 183 indicates the presence of a methyl group attached adjacent to a carbon-sulphur bonding location such as is found in the C-4 position.

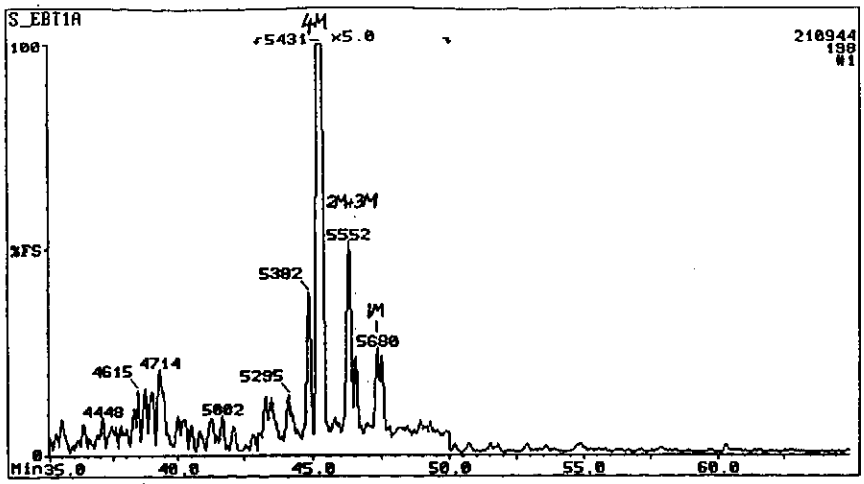

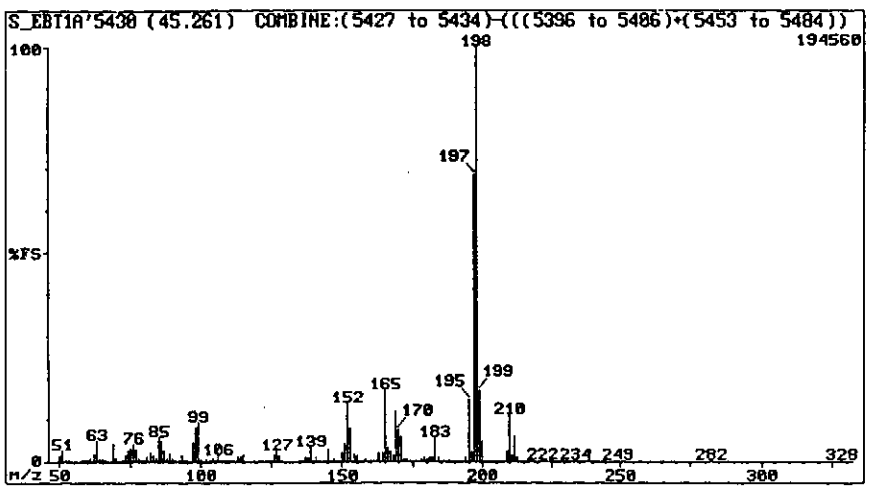

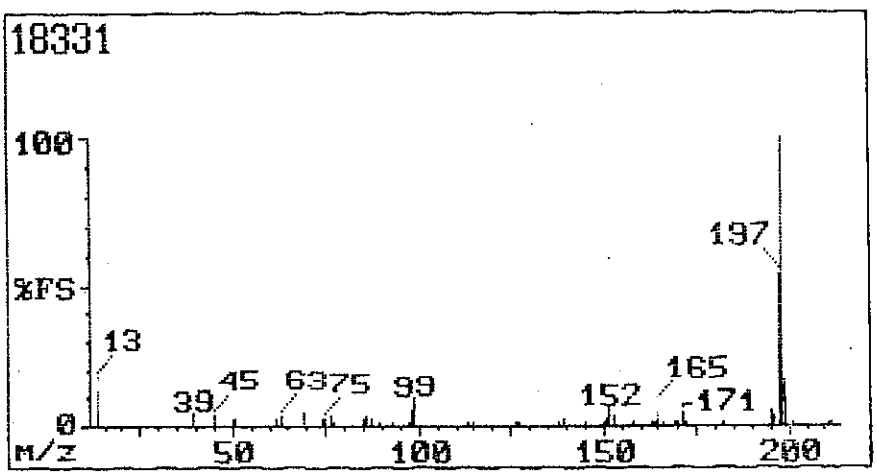

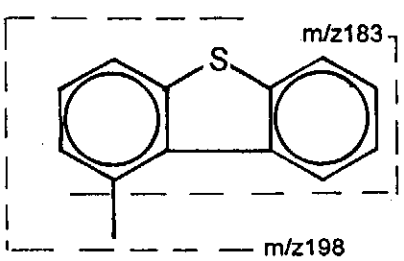

Figure G.01: m/z 198 fragmentogram of aromatic fraction of sample 57 and the mass spectrum of compound '4MDBT' (4--methyl dibenzothiophene) compared to the equivalent mass spectrum from the NBS library and its molecular structure (showing the major fragment ions)

G. 2. ISOPRENOID

Pristane is one of the most important and easily recognised of the regular acyclic isoprenoids. It has a distinctive spectrum due to the characteristic fragmentation of the regular isoprene unit. The spectrum provided by Philp (1985, p.71) matches that obtained from the peak 'Pr' in sample 48 which elutes from the GC column immediately after nC17 (Fig. G.02). The isoprene building block, which has 5 carbon atoms, has a base peak at m/z 57 and a strongly developed ion at 71 mass units corresponding to the C5H11+. The strong ions at m/z 85 and m/z 183 are due to bond rupture between the C-6 and C-7 carbons forming C6 and C13 fragments. The characteristically weak ions at m/z 99 and m/z 169 can only be formed by the breaking of two carbon-carbon bonds because of the regularity of the side-chain at C-5. The molecular ion at m/z 268 is very poorly developed, though, because of the difficulty of breaking the carbon-carbon bonds adjacent to the branch points.

G. 3. METHYL STERANES

The 4-methyl steranes were earlier thought to represent dominantly lacustrine algae but are now considered to have formed from methyl sterols found in both brown and red algae. They are therefore not as environment-specific as the dinosteranes (Goodwin et al., 1988). They are useful, though, for confirmation of the maturity of the oil because the standard sterane ratios are seen to respond similarly to maturation increases in this group (C29$\alpha\alpha$ S/(S+R) and C29 $\beta\beta/(\alpha\alpha+\beta\beta)$; Wolff et al., 1986). However, as shown in Appendix E and Fig. G.03, they are usually present in small quantities and the ratios may therefore be unreliable.

Goodwin et al. (1988) provide spectra of various 4-methyl steranes but, because they used low maturity samples, there were few 14β(H),17β(H) isomers and their spectra are therefore derived only from the isomers of the biologically formed, low maturity 14α(H),17α(H) species.

The spectrum obtained from sample 21 was of the $\beta\beta$ isomers because the $\alpha\alpha$ isomers were interpreted to be present in very small amounts (because of the high maturity) and are partly overlapped by other components. The spectrum, therefore, only partly matches that from Goodwin et al. (op cit.). The mismatch is primarily related to the presence of the extra mass commonly found in $\beta\beta$ isomers (cf. the m/z 218 fragment). Nevertheless the major fragments (m/z 97/98, m/z 150/151, m/z 163, m/z 217, m/z 231/232, m/z 290, m/z 399 and m/z 414) are clearly present and confirm the pick of the

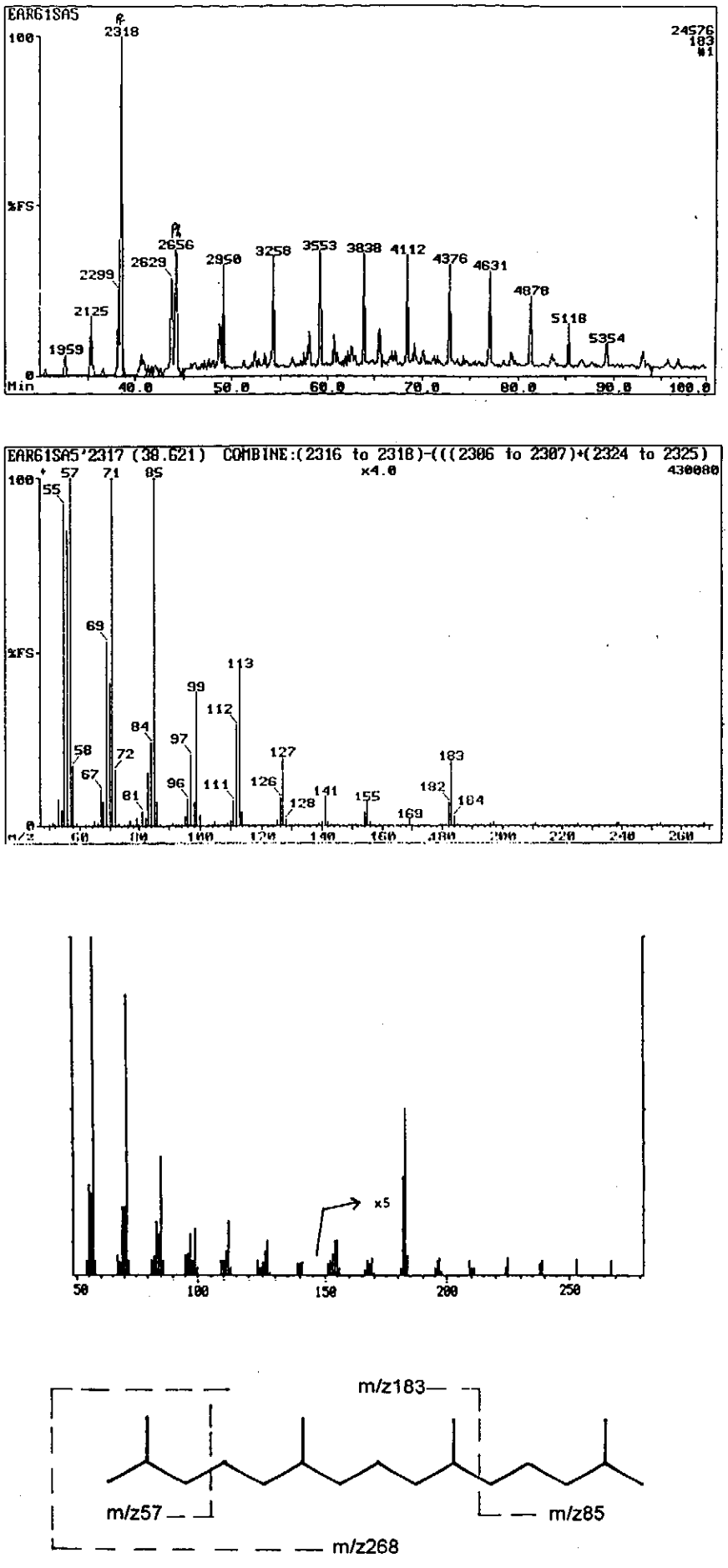

Figure G.02: m/z 183 fragmentogram of the saturated fraction of sample 48 and the mass spectrum of compound 'Pr' (Pristane) compared to the equivalent mass spectrum from Philp (1985) and its molecular structure (showing the major fragment ions).

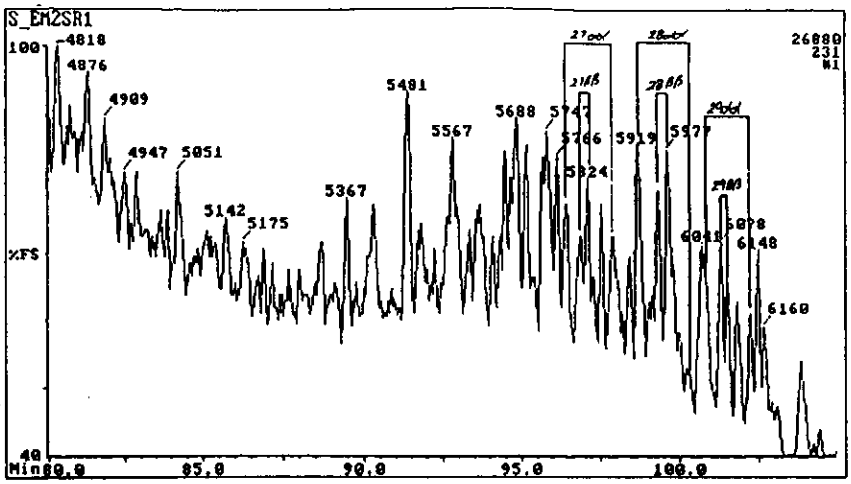

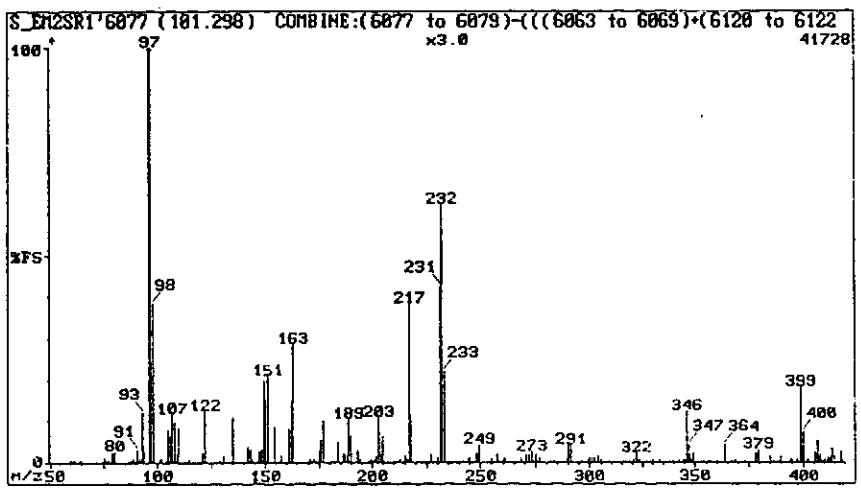

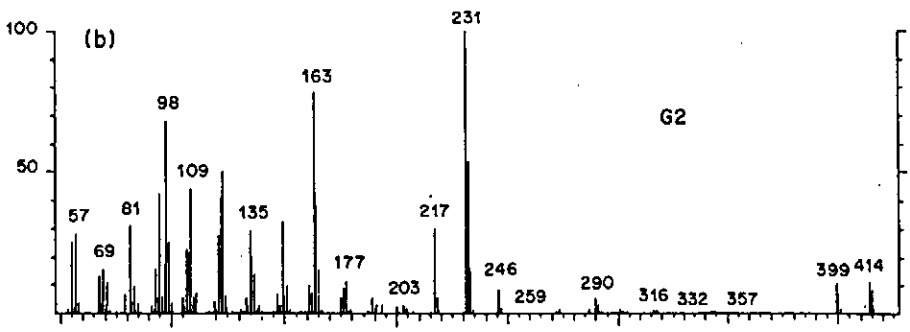

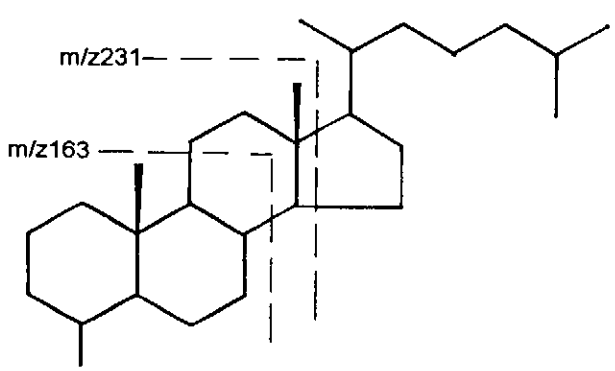

Figure G.03: m/z 231 fragmentogram of the saturated fraction of sample 21 and the mass spectrum of compound '28ββ' (C29 4-methyl 14β,17β sterane) compared to the equivalent mass spectrum from the NBS library and its molecular structure (showing the major fragment ions).

peak in this sample as being one of the C30 14β(H),17β(H) 4-methyl steranes. Each of these is labelled in Appendix F by reference to the equivalent sterane peak i.e. the C30 methyl sterane is labelled as for the C29 sterane.

G. 4. MONOAROMATIC STEROIDS

These compounds are formed from detrital sterols by early defunctionalization followed by dehydrogenation and found in varying amounts in all oil and shale extract samples (Mackenzie et al., 1982). Seifert et al. (1983) provide a spectrum of the C27 homologue which is similar to the spectrum taken from sample 50 (Fig. G.04; equivalent to peak number 1 of Riolo et al., 1986). Distinctive features are the major ion at m/z 253 (with its adjacent ion, one mass unit higher, generated by rearrangement of one of the carbon-carbon bonds in ring C) and the secondary ion at m/z 143.

At greater detail, there are similarities in the relative proportions of the ions at m/z 195 and m/z 322. Seifert et al.(op cit.) used the m/z 351 and m/z 366 ions, visible in the greatly expanded portion of their spectrum, to distinguish between different families of these components. Such differences are not evident in the spectrum from the sample.

This is not due to a mass spectrometer calibration error as it was tested using the internal standard, perfluorokerosene. The difference may be a reflection of the very small peak size containing noise which affects the reliability of the data.

G. 5. PENTACYCLIC TERPANES

Compounds in this class are valuable to the geochemist because of they use in determination of the source rock or oil maturation level and the evaluation of the depositional environment and post-generation diagenesis. Examples of spectra are therefore provided for two components namely C27 trisnorhopane (Tm) and C31 22S bishomohopane.

G. 5. 1. C27 17α(H) Trisnorhopane.

The spectrum of Tm from sample 26 compares well with the spectrum given in Philp (1985, p.167). In particular the proportions of the molecular ion at m/z 370, the fragment (one methyl group less) at m/z 355 and the base peak at m/z 191 all match well (Fig. G.05). Many of the other fragments are also present in proportions matching the standard spectrum noteworthy of these being the m/z 149 and m/z 95 ions which have been generated by fragmentation of the B ring.

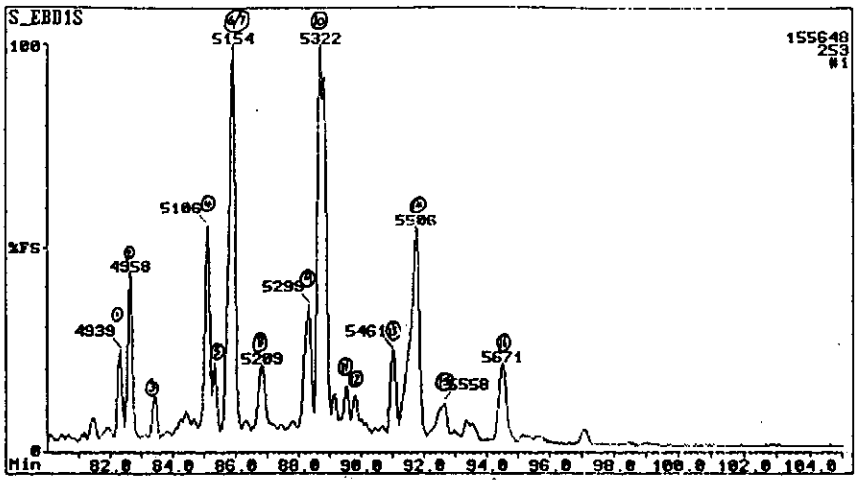

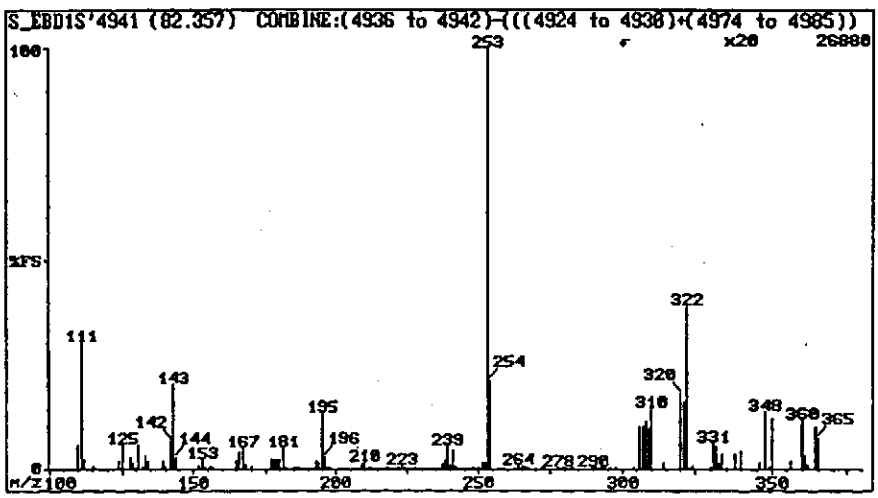

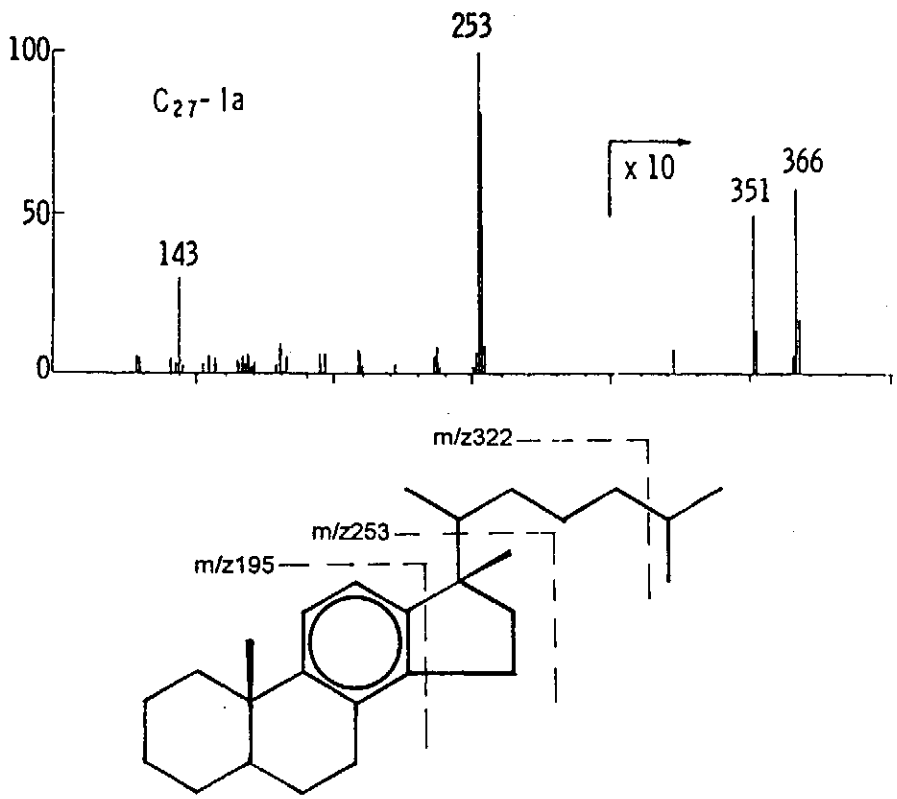

Figure G.04: m/z 253 fragmentogram of the saturated fraction of sample 50 and the mass spectrum of compound '1' (C27 5β monoaromatic steroid) compared to the equivalent mass spectrum from Seifert et al. (1983) and its molecular structure (showing the major fragment ions).

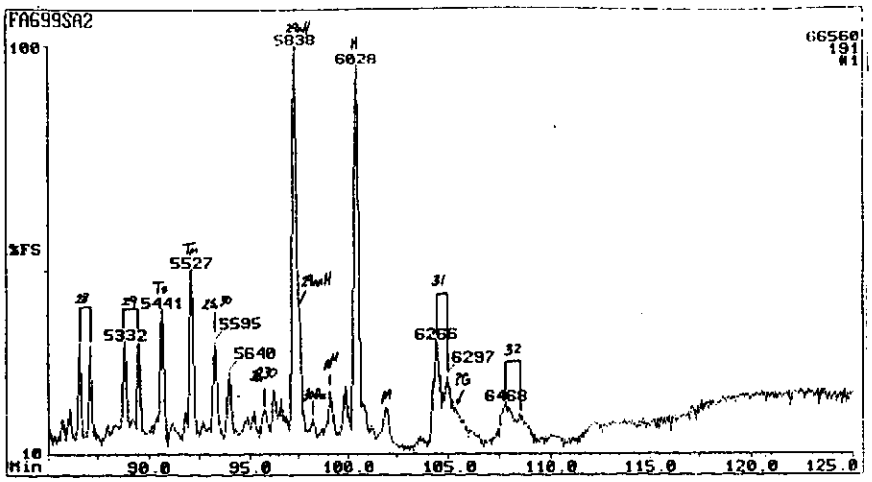

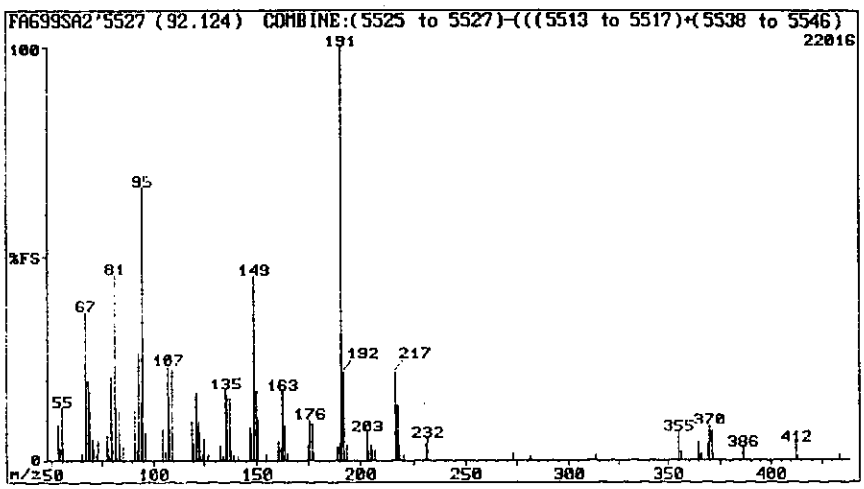

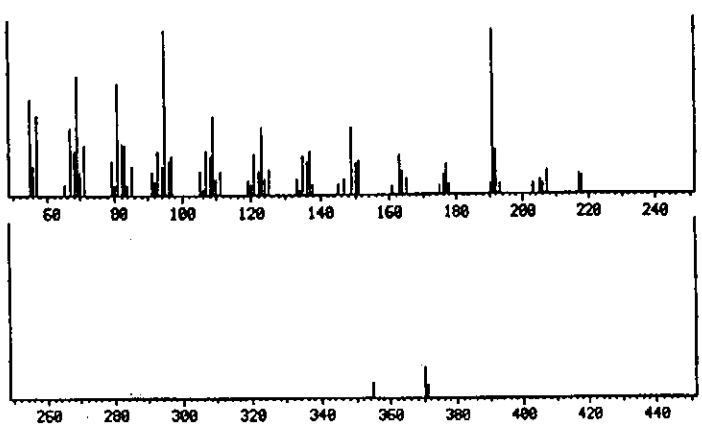

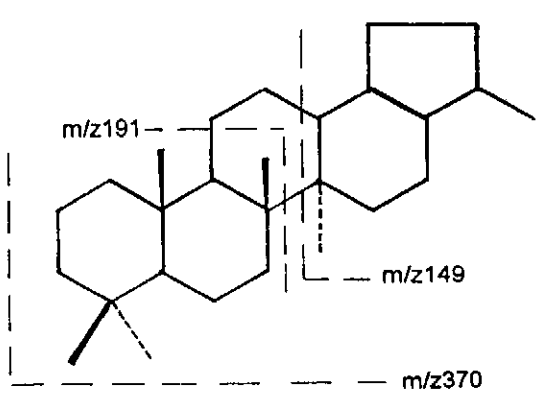

Figure G.05: m/z 191 fragmentogram of the saturated fraction of sample 26 and the mass spectrum of compound 'Tm' (C27 22,29,30 trisnorhopane) compared to the equivalent mass spectrum from Philp (1985) and its molecular structure (showing the major fragment ions).

G. 5. 2. C31 Bishomohopane

The spectrum of C31 22S bishomohopane, taken from sample 44, is compared to the spectrum given in Philp (1985, p.169) and Fig. G.06. The molecular ion (m/z 428) is present in the same proportions in both spectra at approximately 5% of the height of the base peak (m/z 191). The secondary dominance of the m/z 95 fragment is due to the cleavage of rings B and D resulting in the formation of two fragments (from rings A and C) per molecule. The low content of the m/z 149 fragment is a reflection of the difficulty of formation of a double ring fragment from the molecule. This is because several bond cleavages and rearrangements are necessary to create this fragment.

G. 6. STERANES

Important environmental and source correlation interpretations can be made utilising sterane compounds. This dictates the need for rigorous support of the peak assignments. Therefore spectra of five components are provided as follows:

G. 6. 1. C27 13β(H),17α(H) 20S diasterane.

An example of the spectrum of peak 'a' (C27 13β(H),17α(H) 20S diasterane) is given in Seifert and Moldowan (1978). The corresponding spectrum from sample 50 closely matches the example (Fig. G.07). The most significant features are the small m/z 218 fragment (confirming that the compound is not a 14β17β cholestane) and the major m/z 259 fragment present at almost half the height of the m/z 217 base peak which Seifert and Moldowan (op cit.) show to be characteristic of the 13β17α isomer.

G. 6. 2. C27 13α(H),17β(H) 20R diasterane.

The spectrum of peak 'd' (C27 13α(H),17β 20R diasterane), also from sample 50, agrees well with the spectrum given by Philp (1985, p.253; Fig. G.08). In particular, the molecular ion (m/z 372), the extreme dominance of the m/z 217 ion over the m/z 218 ion and the low m/z 259 ion all match the relative ratios for these fragments given by Seifert and Moldowan (op cit.). Other major ions (e.g. m/z 189, m/z 163 and m/z 149) also match closely.

G. 6. 3. C28 13β(H),17α(H) 20S diasterane.

In the same sample, the spectrum of peak 'e' (C28 13β17α diasterane) matches that given by Seifert and Moldowan (1979) for the C27 homologue in all respects (Fig. G.09) except for it having a C28 molecular ion at m/z 386. This peak is also considered to represent the C28 13β(H),17α(H) diasterane by Peters and Moldowan (1993, p.191), Comet et al.(1993), Kvenvolden et al. (1985) and Mackenzie et al. (1985).

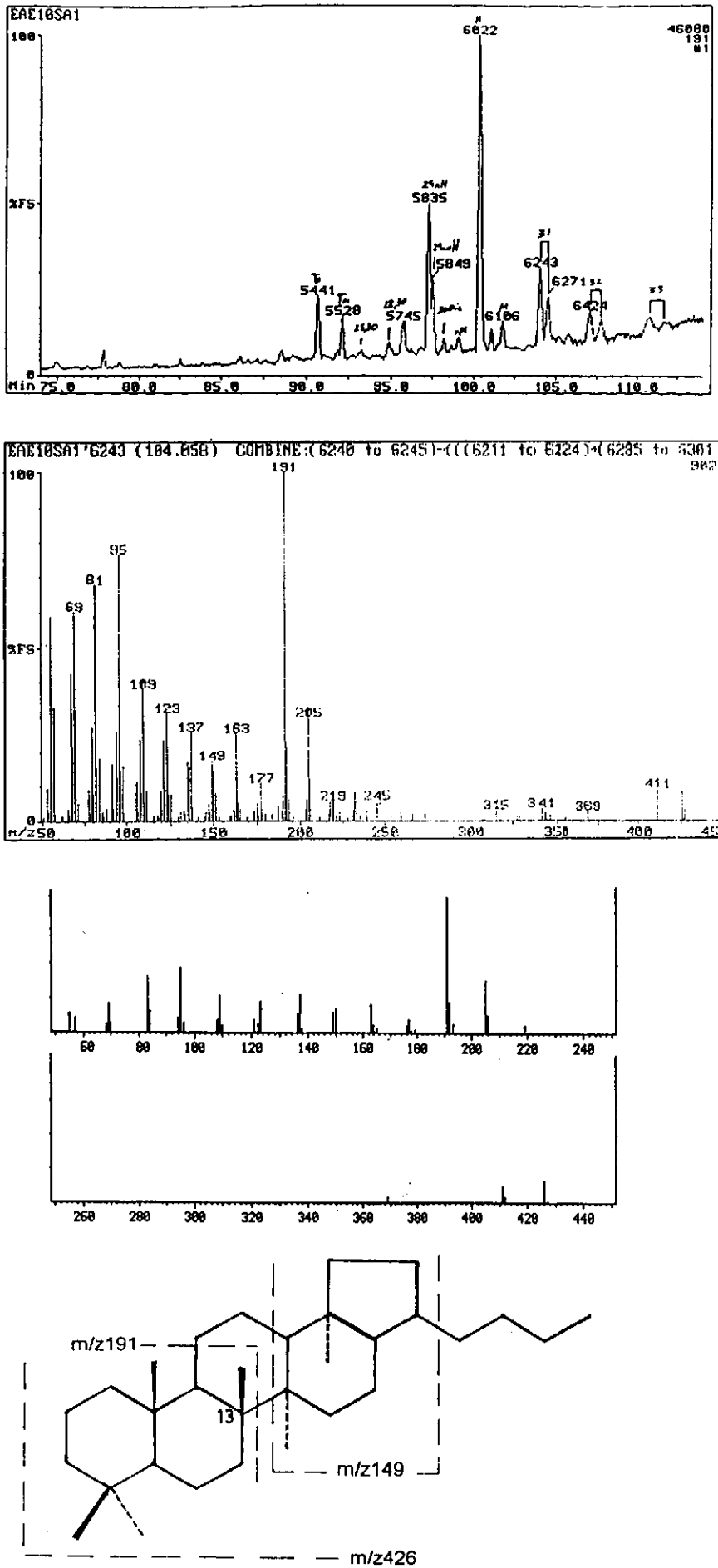

Figure G.06: m/z 191 fragmentogram of the saturated fraction of sample 44, the mass spectrum of compound '31' (C31 22S homohopane) compared to the equivalent mass spectrum from Philp (1985) and its molecular structure (showing the major fragment ions).

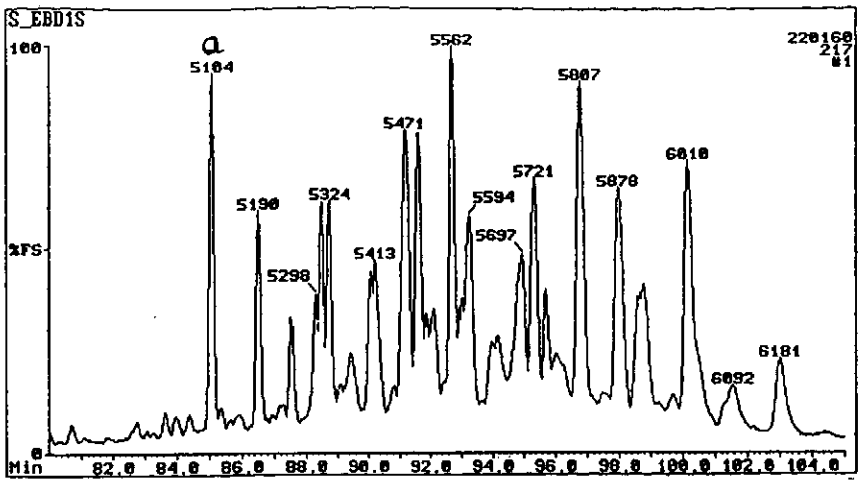

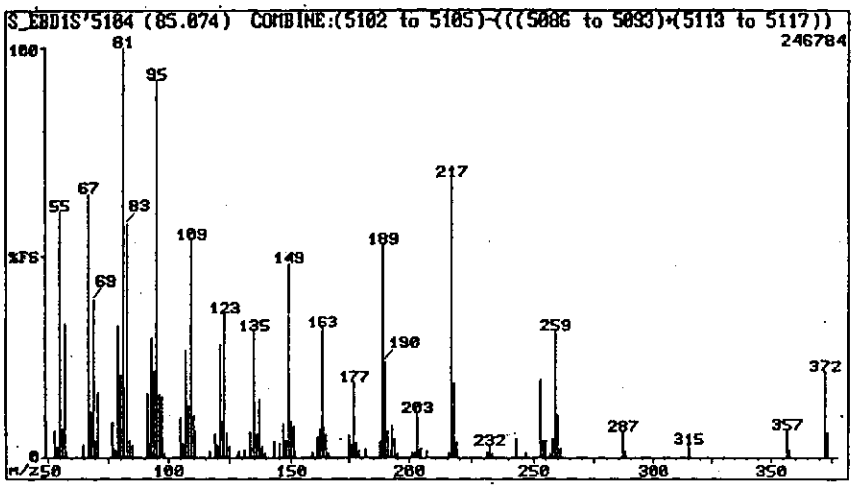

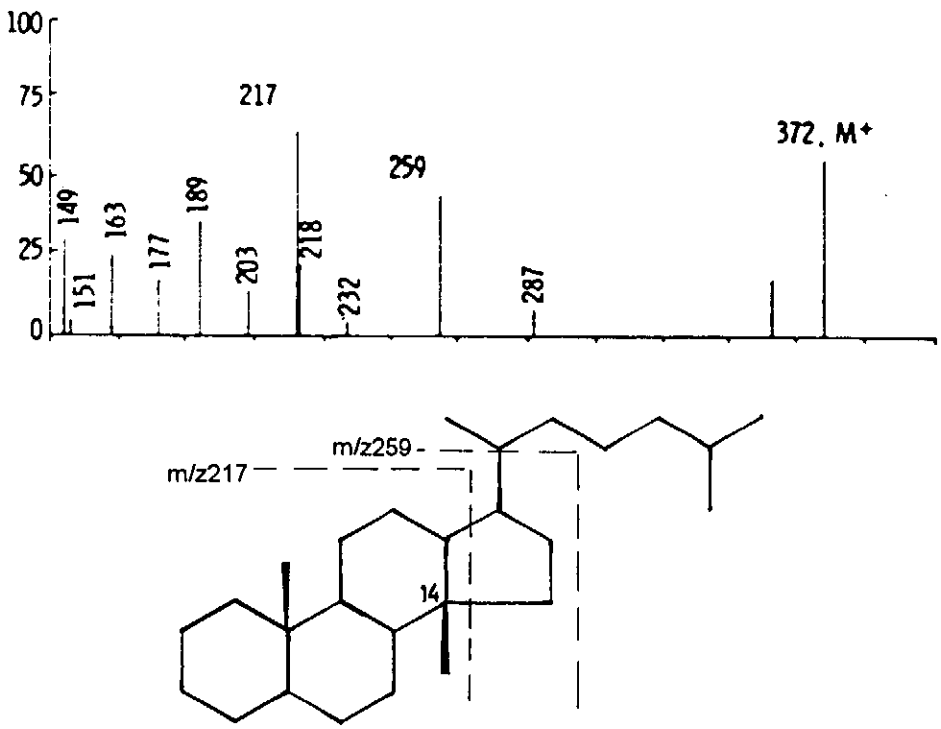

Figure G.07: m/z 217 fragmentogram of saturated fraction of sample 50 and the mass spectrum of compound 'a' (C27 13β,17α diasterane) compared to the equivalent mass spectrum from Seifert and Moldowan (1978) and its molecular structure (showing the major fragment ions).

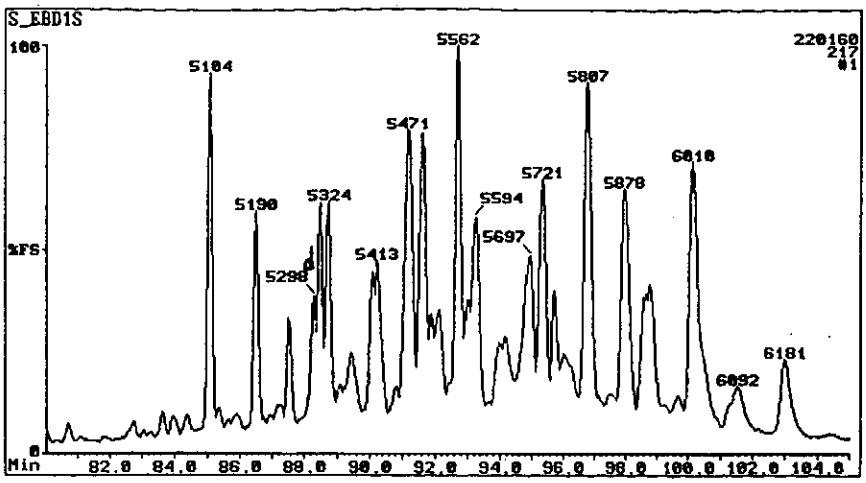

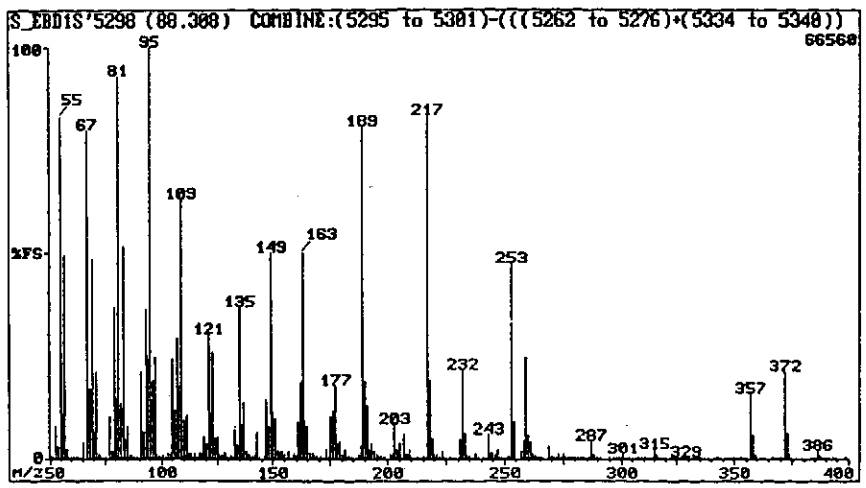

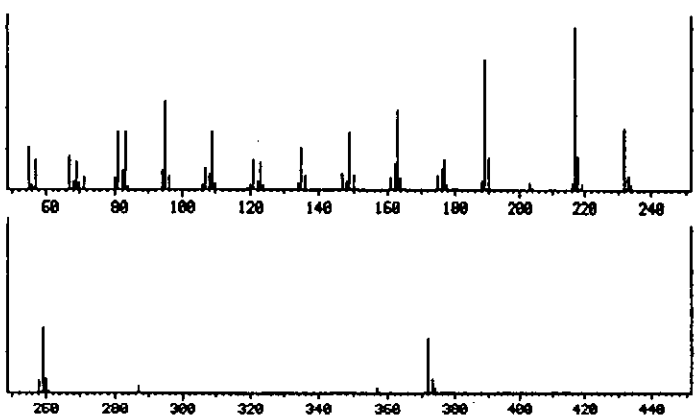

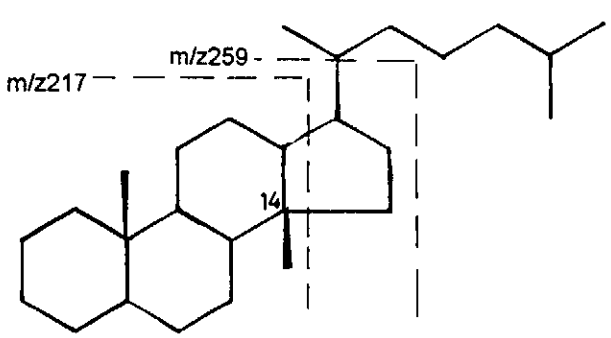

Figure G.08: m/z 217 fragmentogram of the saturated fraction of sample 50 and the mass spectrum of compound 'd' (C27 13α,17β diacholestane) compared to the equivalent mass spectrum from Philp (1985) and its molecular structure (showing the major fragment ions).

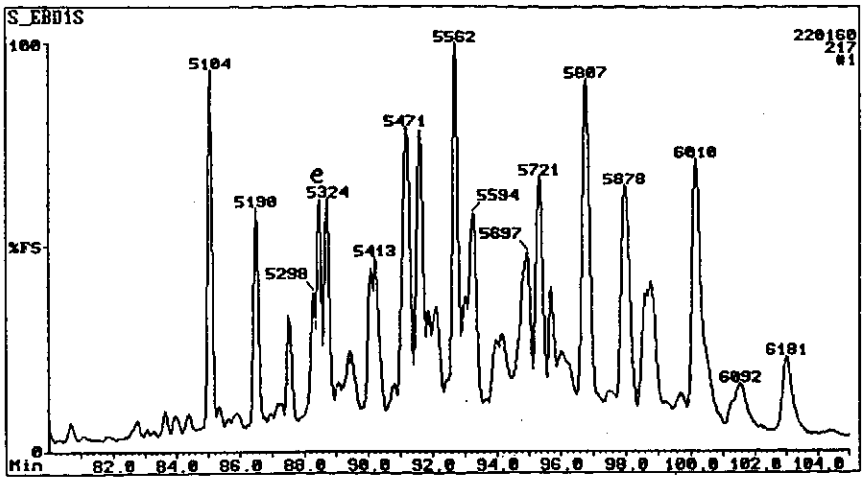

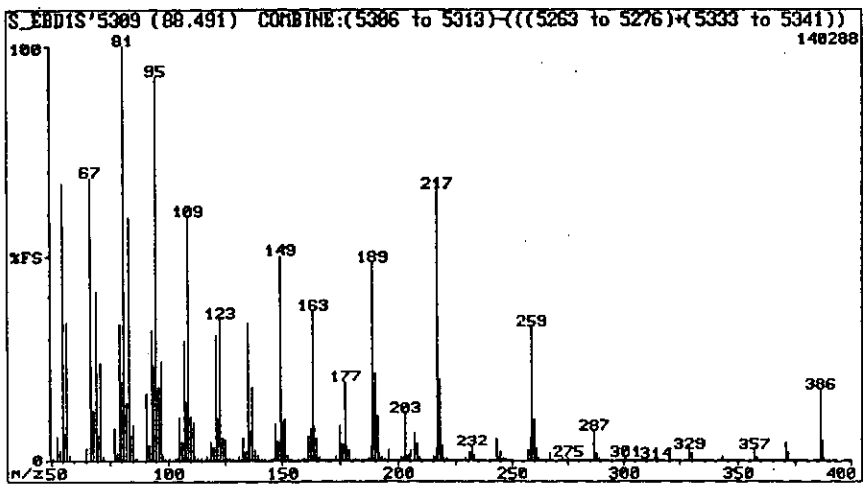

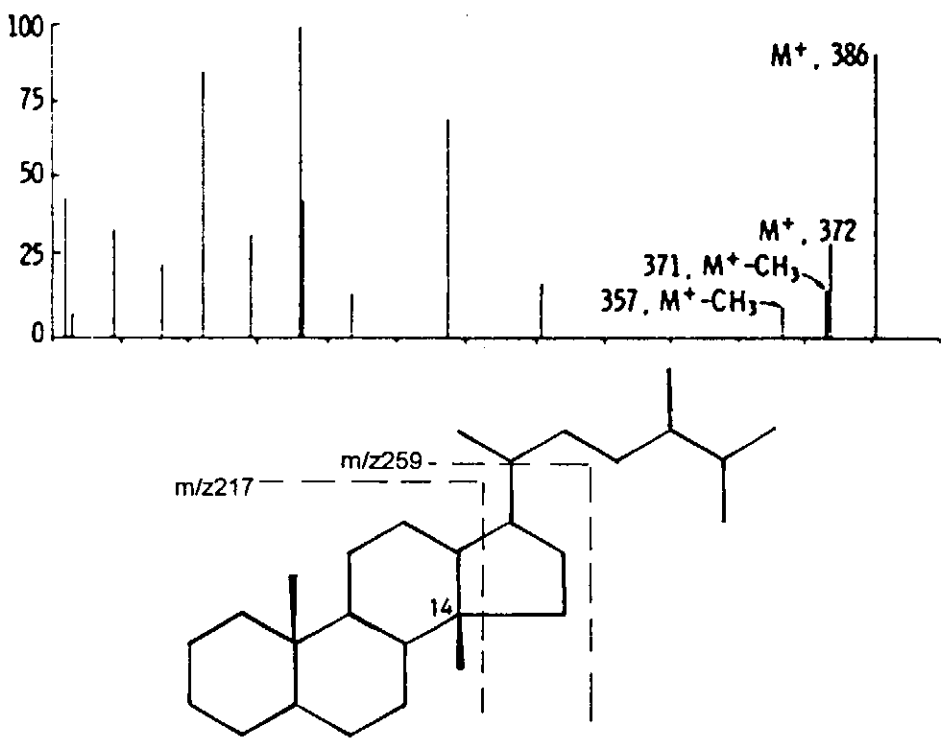

Figure G.09: m/z 217 fragmentogram of the saturated fraction of sample 50 and the mass spectrum of compound 'e' (C28 13β,17α diacholestane) compared to the equivalent mass spectrum from Seifert and Moldowan (1978) and its molecular structure (showing the major fragment ions).

The identification of this peak (and the adjacent peak 'd') is not universally adhered to. An alternative assignment exists which shows peak 'e' to represent the C27 13α(H),17β (H) 20R diasterane and the adjacent peak (scan 5324 of Fig. G.09) to represent the C28 13β(H),17α)H) 20S diasterane. The alternative assignment cannot be tested using the C27 and C29 homologues because they are overlapped by other biomarker compounds.

G. 6. 4. C28 13β(H),17α(H) 20R diasterane.

The spectrum of peak 'f', from sample 50, is shown compared to the spectrum from Seifert and Moldowan (1978; Fig. G.10). It is not possible to distinguish the 20S and 20R isomers using this method, i.e. peaks 'e' and 'f' are quite similar (with only subtle differences in the contents of the fragments with ions at m/z 67 and m/z 71) so these two components cannot be separated by spectrum alone. Nevertheless, it is evident that peak 'f' has the same range of fragments as peak 'e' confirming that it, too, is a 13β 17α diasterane.

G. 6. 5. C30 14β(H),17β(H) 20R sterane.

Probably the most important single family of steranes are the C30 sterane homologues represented by peak 'J' (C30 14β17β 20R). As shown in Chapter 11, if the family is comprised of C30 steranes with a propyl group at the C-24 position, then the series are almost certainly derived from dinoflagellates (Goodwin et al., 1988). These indicate a marine depositional environment. If, on the other hand, they are composed of 4-methyl, 24-ethyl or 4, 23, 24 trimethyl components they could be sourced by organic matter living in both marine and non-marine environments (Volkman, 1988).

The 4-methyl steranes are characterised by the major fragment at m/z 231. This is because the typical sterane fragmentation pattern allows the methyl group at the C-4 position to become part of the major fragment (Fig. G.03). However, the spectrum of this peak from sample 21 shows (Fig. G.11) that the compound is not a 4-methyl sterane because of the very small m/z 231 and m/z 232 ions and the large m/z 217 and m/z 218 ions.

Even so, the evidence is not strongly in favour of propyl ion fragmentation because the peak, expected at m/z 369, is very small. The compound is confirmed as a 14β17β cholestane from the distinctive ratio of the m/z 217 and m/z 218 fragments which is similar to that reported by Seifert and Moldowan (1979), shown by Philp (1985, p.247) and calculated from known homologues in this study (Appendix F, Table F.07).

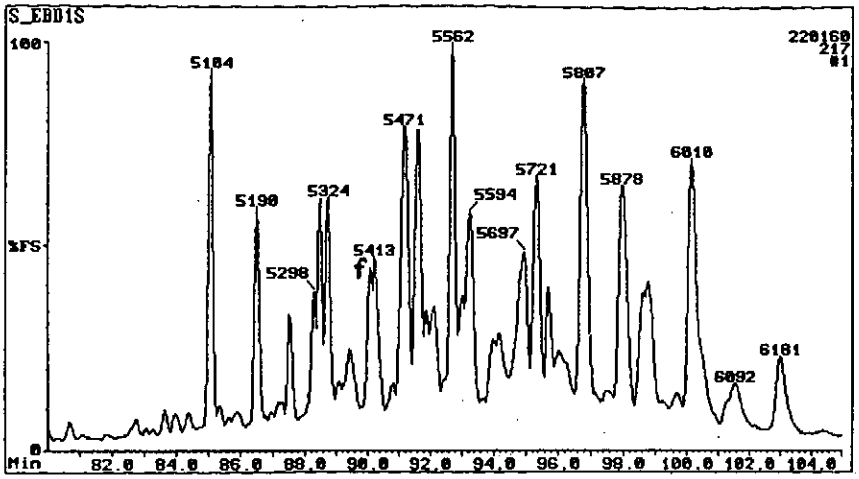

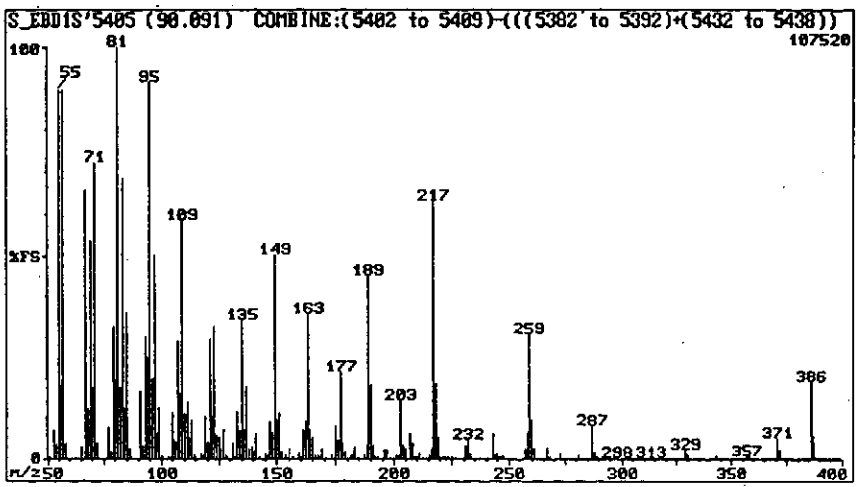

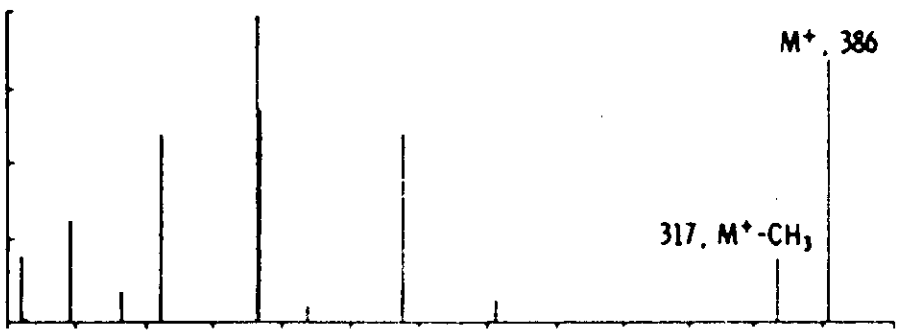

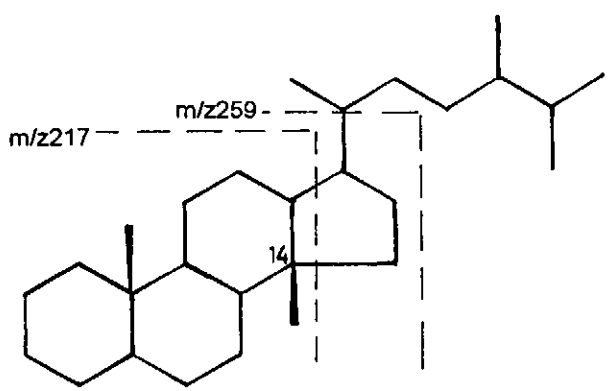

Figure G.10: m/z 217 fragmentogram of the saturated fraction of sample 50 and the mass spectrum of compound 'f' (C28 13β,17α diasterane) compared to the equivalent mass spectrum from Seifert and Moldowan (1978) and its molecular structure (showing the major fragment ions).

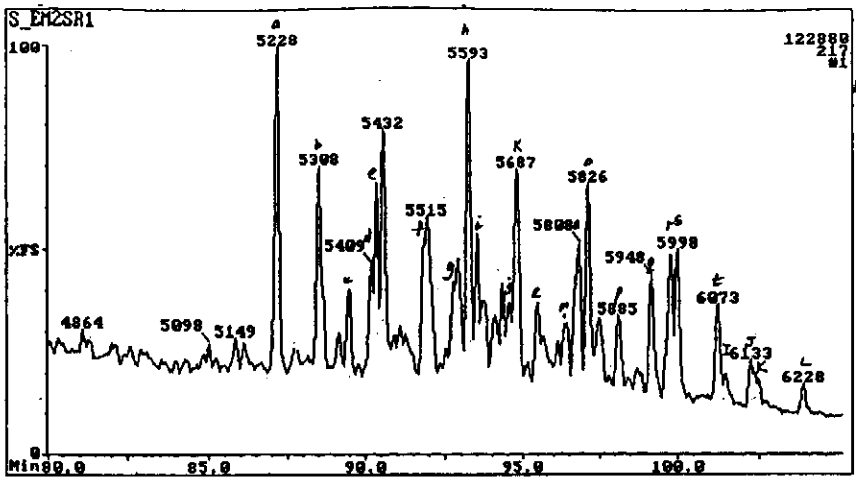

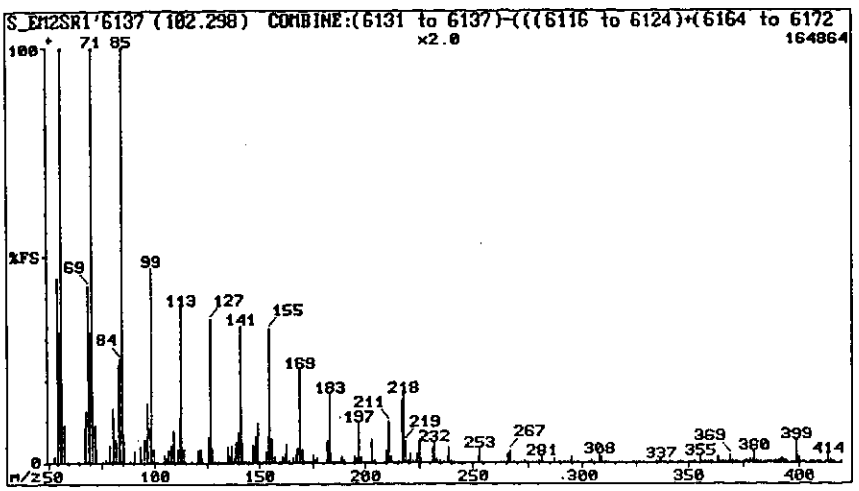

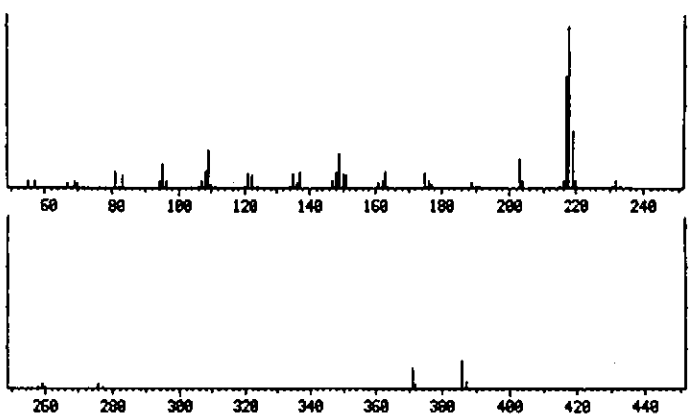

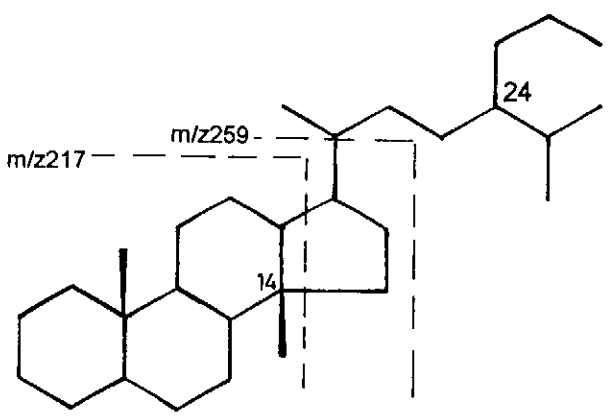

Figure G.11: m/z 217 fragmentogram of saturated fraction of sample 21 and the mass spectrum of compound 'J' (C30 14β,17β 24-propyl sterane) compared to the equivalent mass spectrum from Philp (1985) and its molecular structure (showing the major fragment ions).

Further confirmation that the compounds have the C30, 24-propyl form, is derived from the comparison of relative retention indices with those acquired by GC-MS-MS metastable transition monitoring of two oil samples (no's. 1 and 4; Rullkötter et al., 1991). The peaks labelled I-L are interpreted to be $\alpha\alpha$ and $\beta\beta$steranes having the 24-propyl form because they locate on the same trend of the $\alpha\alpha$ and $\beta\beta$ steranes projected from the C27-C29 homologues (Fig. G.12a). When these traces are time-shifted and centered on the 13β17α 20R diasterane homologue (cf. peaks 'a' and 'b', Fig. G.12b) it becomes evident that the C30 series match their C29 equivalents. Peters and Moldowan (1993, p.187) and MacQuaker et al. (1986) also show that the 4-methyl, 24-ethyl and 4, 23, 24 trimethyl isomers do not elute with the same retention time as the 24-propyl isomers. Hence the position of these peaks is characteristic of the C-24 propyl series.

Fig. G.12b also provides guidance on the problem of the assignment of the peaks 'd', 'e' and 'f' as it shows that the assignment adopted throughout (and in particular in Figs. 11.07, 11.08 and 11.11) are supported by the GC-MS-MS data.

G. 7. TRIAROMATIC STEROIDS

The fragmentogram of the base peak (m/z 231) of the triaromatic steroids is particularly distinctive because the C20-21 homologues elute much earlier than the C26-28 forms. The first group has a methyl or ethyl group (respectively) at the C-22 position (Philp, 1985, p.50). However, the heavier homologues have rather longer chain alkyl fragments and the spectrum given (Fig. G.13) is from the first named of these, i.e. peak 'a' from sample 44. This compound is characterised by the m/z 215 and m/z 270 fragments and by the molecular ion at m/z 344. The fragmentation is essentially the same as that given by Philp (op cit.). The most frequent use of these compounds in biomarker studies is to estimate maturity. Philp (1988) and Mackenzie (1984) both comment on the ratio between the triaromatic and monoaromatic steroids being maturity dependant whilst Mackenzie (op cit.) shows that the C20/C27 monoaromatic steroid ratio can be used as a maturity parameter up to R_o~1.3%.

G. 8. TRICYCLIC TERPANES

This distinctive group of compounds is shown here to extend from C19 to C29, although Moldowan et al. (1983) showed that the series extends up to C45. A spectrum of the C25 compound is used to demonstrate that the peak assignments of this important correlative group are well supported (Fig. G.14). The spectrum, taken from sample 26 is compared with that of an example from Ekweozor and Strausz (1983). The molecular

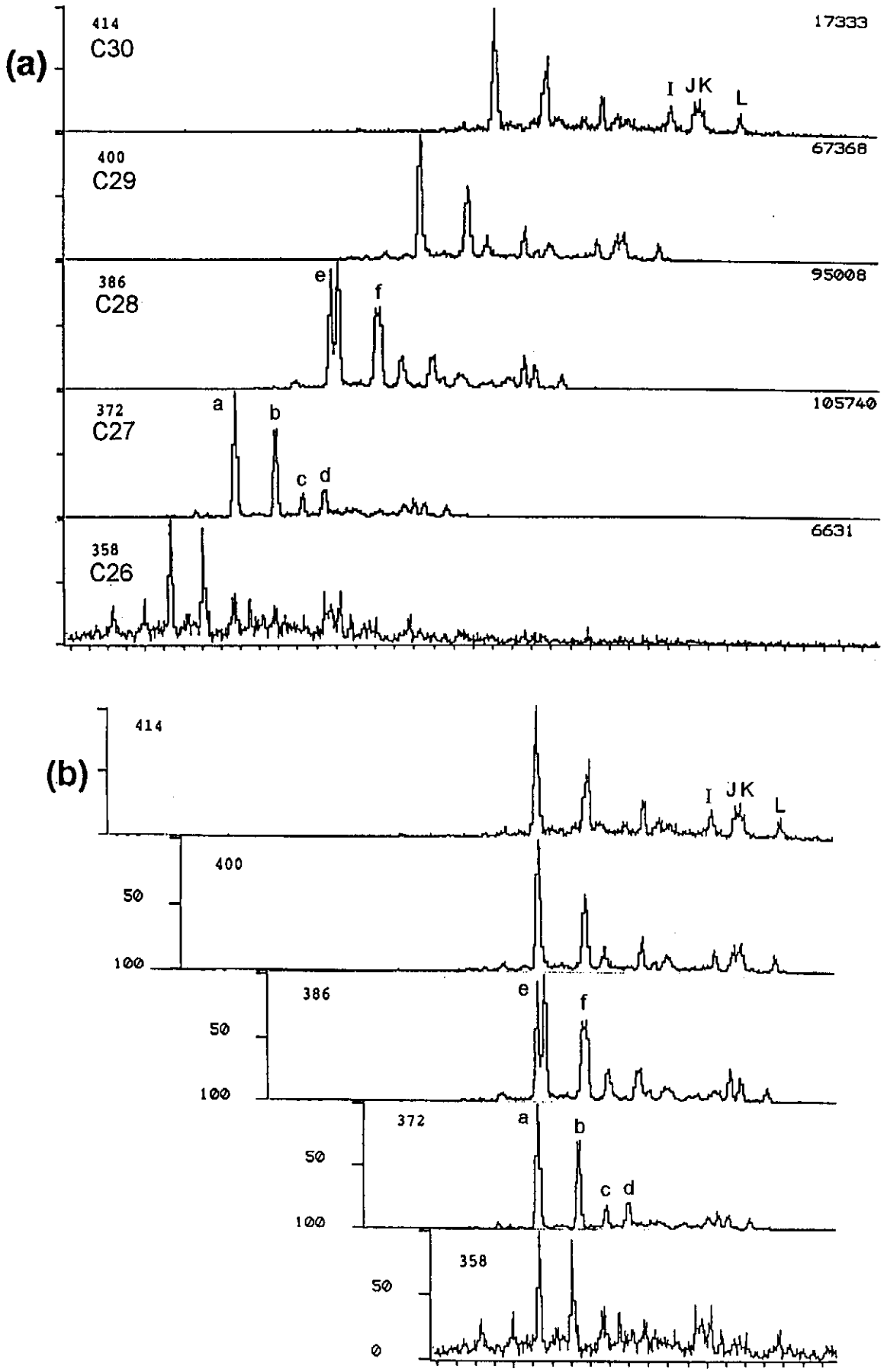

Figure G.12: Raw (a) and time-shifted (b) metastable ion monitoring of sterane daughter fragments (414/400/386/372/358-217) of sample 2 from Rullkötter et al. (1991) Note the maximum peak height of the C26 series (6631 units) is only ~6% of the maximum height of the C27 series (105740 units).

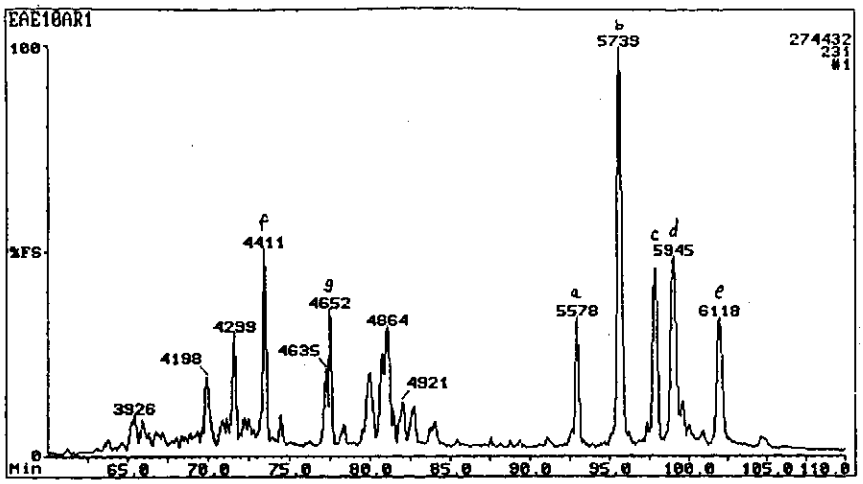

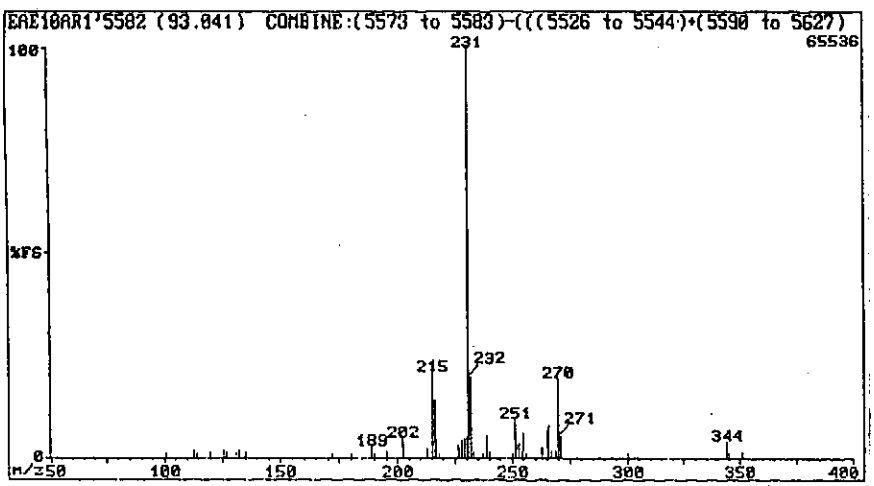

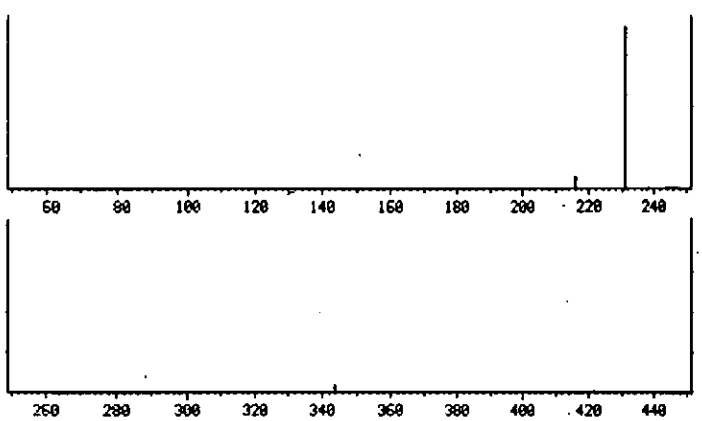

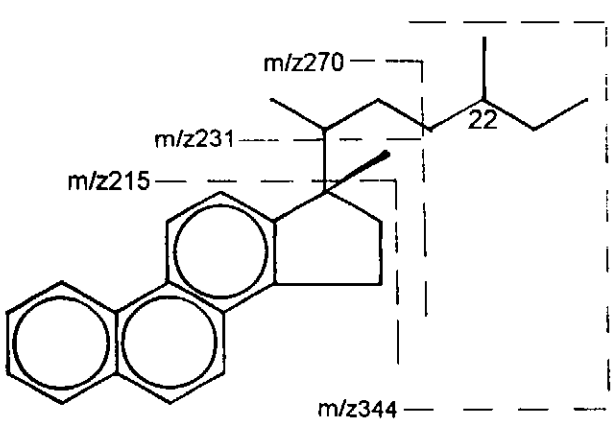

Figure G.13: m/z 231 fragmentogram of the aromatic fraction of sample 44 and the mass spectrum of compound 'a' (C26 triaromatic steroid) compared to the equivalent mass spectrum from Philp (1985) and its molecular structure (showing the major fragment ions).

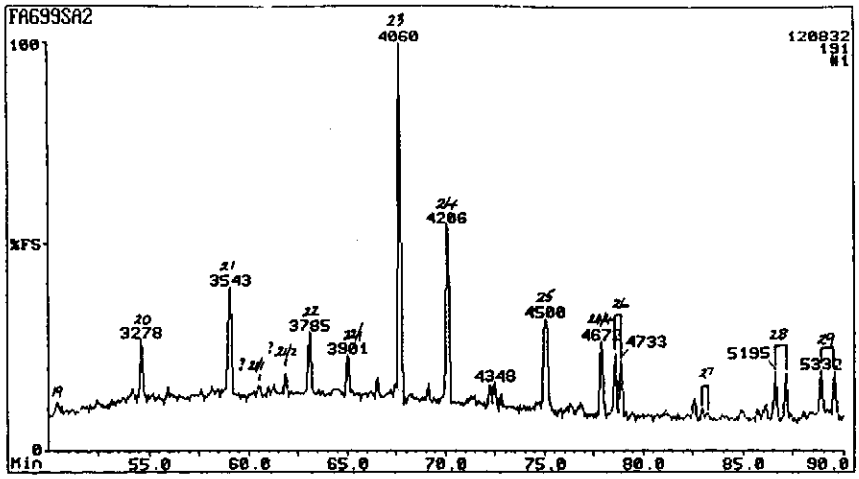

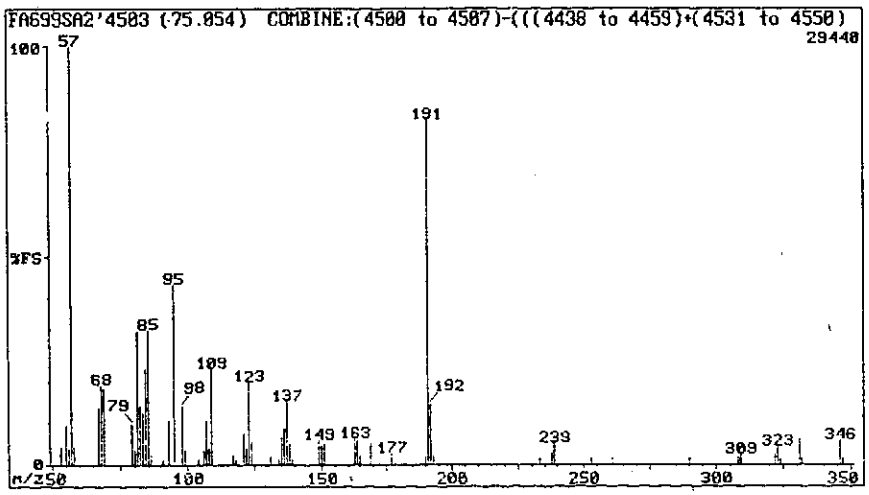

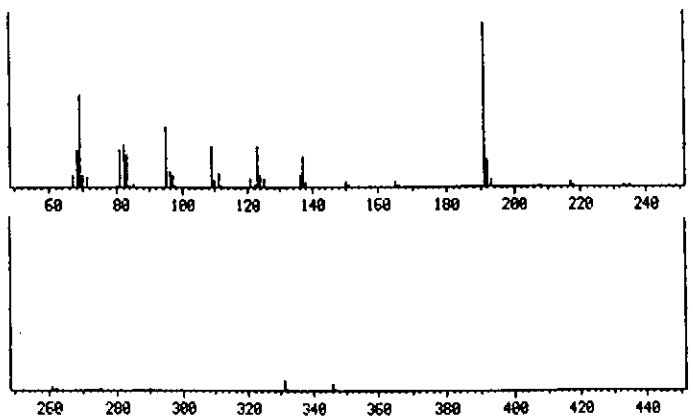

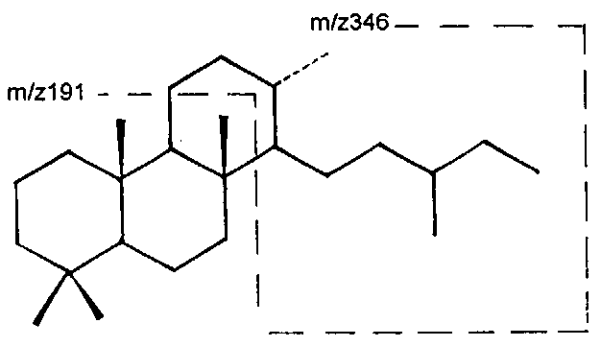

Figure G.14: m/z 191 fragmentogram of the saturated fraction of sample 26 and the mass spectrum of compound '25T' (C25 tricyclic terpane) compared to the equivalent mass spectrum from Ekweozor and Strausz (1983) and its molecular structure (showing the major fragment ions).

ion (m/z 346), the base peak at m/z 191 with its subordinate ion one mass unit higher and the other major fragments at m/z 95, m/z 109, m/z 123 and m/z 137 all match the example spectrum confirming that the assignments are correct.

G. 9. TRIMETHYL NAPHTHALENES

A spectrum of peak '2,3,6' from sample 57 is compared (Fig. G.15) to the spectrum from the Lab-Base programme (no.12802) which is equivalent to that given by Stenhager et al. (1974). Each spectrum has two characteristic ions, the base peak at m/z 155 and the molecular ion at m/z 170. In addition, fragments with ions at m/z 115 and m/z 128 are also developed, but only weakly, because each requires rupture of two bonds in the molecule for its formation.

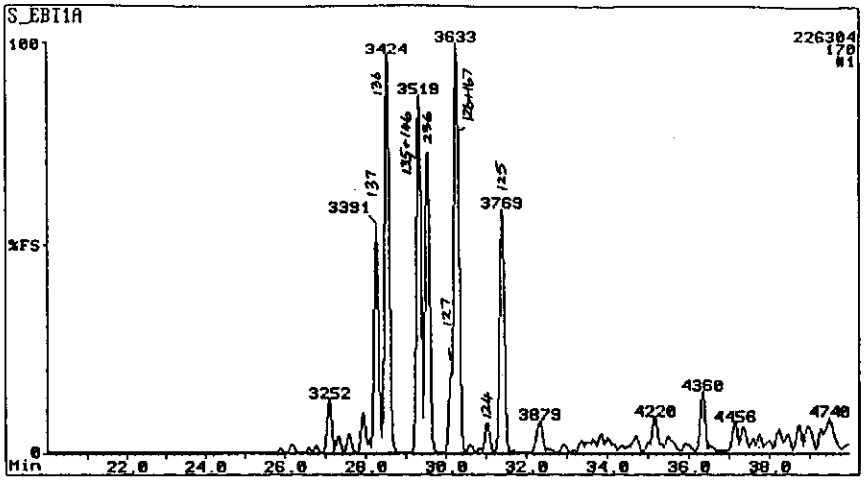

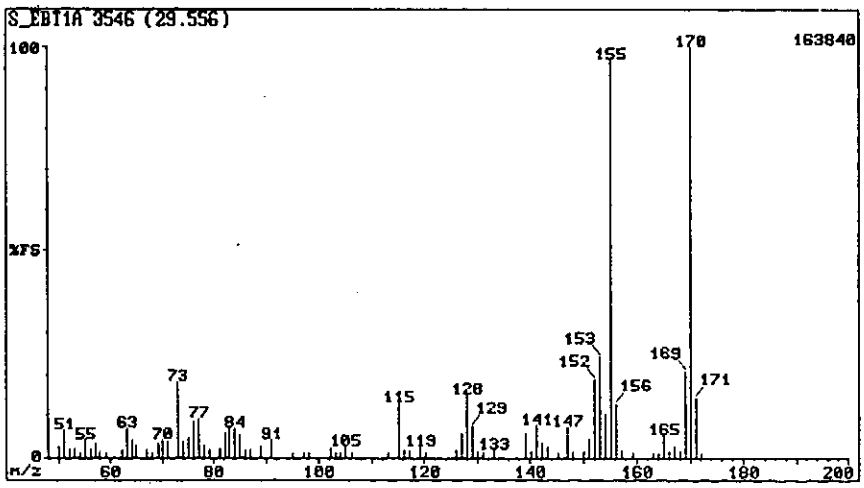

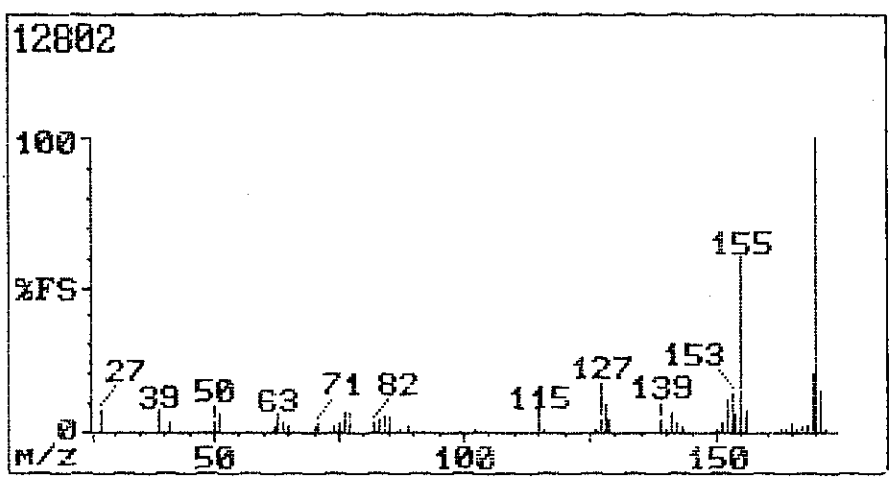

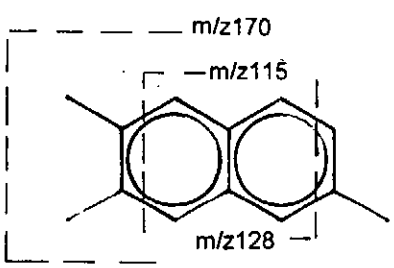

Figure G.15: m/z 170 fragmentogram of aromatic fraction of sample 57 and the mass spectrum of compound '236' (2,3,6-trimethyl naphthalene) compared to the equivalent mass spectrum from NBS library and its molecular structure (showing the major fragment ions).

APPENDIX H: WHOLE OIL, FRACTIONAL AND BIOMARKER COMPOUND CODES

APPENDIX H: COMPOUND DATA

This appendix provides the list of each named component used in this study. The tables give the sample code (used on the gas chromatograms and mass fragmentograms), the molecular formula and mass (in arbitrary mass units) and, in the case of the mass fragmentograms, the base peak.

H. 1. GAS CHROMATOGRAPHY DATA

H. 1.1. Condensate Compounds.

Code	Carbon number	Compound name	Molecular formula	Molecular mass
nC3	C3	normal propane	C3H8	amu 44
iC4	C4	iso-butane	C4H10	amu 58
nC4	C4	normal butane	"	"
iC5	C5	iso-pentane	C5H12	amu 72
nC5	C5	normal pentane	"	"
2MP	C6	2-methyl pentane	C6H14	amu 86
3MP	C6	3-methyl pentane	"	"
nC6	C6	normal hexane	"	"
MCP	C6	methyl cyclopentane	C6H12	amu 84
24DMP	C7	2,4-dimethyl pentane	C7H16	amu 100
Benz	C7	benzene	C6H6	amu 78
CH	C7	cyclohexane	C6H12	amu 84
2MH	C7	2-methyl hexane	C7H16	amu 100
23DMH	C8	2,3,-dimethyl hexane	C8H18	amu 114
3MH	C7	3-methyl hexane	C7H16	amu 100
1c3DMCP	C7	1 cis 3-dimethyl cyclopentane	C7H14	amu 98
1t3DMCP	C7	1 trans 3-dimethyl pentane	"	"
224TMP	C8	2,2,4-trimethyl pentane	C8H18	amu 114
nC7	C7	normal heptane	C7H16	amu 100
MCH	C7	methyl cyclohexane	C7H14	amu 98
25DMH	C8	2,5-dimethyl hexane	C8H18	amu 114
24DMH	C8	2,4-dimethyl hexane	"	"
1t2c4TMCP	C8	1 trans 2 cis 4-trimethyl cyclopentane	C8H16	amu 112
1t2c3TMCP	C8	1 trans 2 cis 3-trimethyl cyclopentane	"	"
Tol	C7	methyl benzene (toluene)	C7H8	amu 92
2MHep	C8	2-methyl heptane	C8H18	amu 114
4MHep	C8	4-methyl heptane	"	"
3MHep	C8	3-methyl heptane	"	"
1c2t3TMCP	C8	1 cis 2 trans 3-trimethyl cyclopentane	C8H16	amu 112
225TMH	C9	2,2,5-trimethyl hexane	C9H20	amu 128
1t2DMCH	C8	1 trans 2-dimethyl cyclohexane	C8H16	amu 112
nC8	C8	normal octane	C8H18	amu 114
223 TMH	C9	2,2,3-trimethyl hexane	C9H20	amu 128
24DMHep	C9	2,4-dimethyl heptane	"	"
ECH	C8	ethyl cyclohexane	C8H16	amu 112
26DMHep	C9	2,6-dimethyl heptane	C9H20	amu 128
EBenz	C8	ethyl benzene	C8H10	amu 106
pXyl	C8	1,4-dimethyl benzene (para-xylene)	"	"
mXyl	C8	1,3-dimethyl benzene (meta-xylene)	"	"
4MO	C9	4-methyl octane	C9H20	amu 128
2MO	C9	2-methyl octane	"	"
3EHep	C9	3-ethyl octane	"	"
3MO	C9	3-methyl octane	"	"
oXyl	C8	1,2-dimethyl benzene (ortho-xylene)	C8H10	amu 106
nC9	C9	normal nonane	C9H20	amu 128

Compound names after Hunt (1979b).

H. 1.2. Saturated compounds.

Code	Compound name/description	Formula	Molecular mass	Fragment base peak
nC12	normal dodecane	C12H26	amu 170	m/z 85
IP13	2,6-dimethyl undecane	C13H28	amu 184	m/z 183
IP14	2,6,10-trimethyl undecane	C14H30	amu 198	"
nC13	normal tridecane	C13H28	amu 184	m/z 85
IP15	2,6,10-trimethyl dodecane (farnesane)	C15H32	amu 212	m/z 183
nC14	normal tetradecane	C14H30	amu 198	m/z 85
IP16	2,6,10-trimethyl tridecane	C16H34	amu 226	m/z 183
nC15	normal pentadecane	C15H32	amu 212	m/z 85
nC16	normal hexadecane	C16H34	amu 226	"
IP18 (NorPr)	2,6,10-trimethyl pentadecane (norpristane)	C18H38	amu 254	m/z 183
nC17	normal heptadecane	C17H36	amu 240	m/z 85
IP19 (Pr)	2,6,10,14-tetramethyl pentadecane (pristane)	C19H40	amu 268	m/z 183
nC18	normal octadecane	C18H38	amu 254	m/z 85
IP20 (Ph)	2,6,10,14-tetramethyl hexadecane (phytane)	C20H42	amu 282	m/z 183
nC19	normal nonadecane	C19H40	amu 268	m/z 85
nC20	normal eicosane	C20H42	amu 282	"
nC21	normal heneicosane	C21H44	amu 296	"
nC22	normal docosane	C22H46	amu 310	"
nC23	normal tricosane	C23H48	amu 324	"
nC24	normal tetracosane	C24H50	amu 338	"
nC25	normal pentacosane	C25H52	amu 352	"
nC26	normal hexacosane	C26H54	amu 366	"
nC27	normal heptacosane	C27H56	amu 380	"
nC28	normal octacosane	C28H58	amu 394	"
nC29	normal nonacosane	C29H60	amu 408	"
nC30	normal triacontane	C30H62	amu 422	"
nC31	normal hentriacontane	C31H64	amu 436	"
nC32	normal dotriacontane	C32H66	amu 450	"
nC33	normal tritriacontane	C33H68	amu 464	"

H. 1.3. Aromatic compounds.

Code	Compound name/description	Formula	Molecular mass	Fragment base peak
P	phenanthrene	C14H10	amu 178	m/z 178
A	anthracene	"	"	TIC
3MP	3-methyl phenanthrene	C15H12	amu 192	m/z 192
2MP	2-methyl phenanthrene	"	"	"
2MA	2-methyl anthracene	"	"	TIC
9MP	9-methyl phenanthrene	"	"	m/z 192
1MP (+4MP)	1 (+4)-methyl phenanthrene	"	"	"
Ace	acephenanthrene	"	"	TIC
26DMP	2,6-dimethyl phenanthrene	C16H14	amu 206	m/z 206
27DMP	2,7-dimethyl phenanthrene	"	"	"
16DMP	1,6-dimethyl phenanthrene	"	"	"
210DMP	2,10-dimethyl phenanthrene	"	"	"
F	fluoranthrene	C16H10	amu 202	TIC
18DMP	1,8-dimethyl phenanthrene	C16H14	amu 206	m/z 206
BA	Benz-anthracene	C18H12	amu 228	m/z 228
C	Chrysene (benzo phenanthrene)	"	"	"
3MC	3-methyl chrysene	C19H14	amu 242	m/z 242
2MC	2-methyl chrysene	"	"	"
9MC	9-methyl chrysene	"	"	"
1MC	1-methyl chrysene	"	"	"

Compound names and identification after Tissot and Welte (1984) and Radke (1987).

H. 2 MASS SPECTROMETRY DATA

H. 2.1. Saturated Hydrocarbon Compounds

H. 2.1.1. Steranes

Code	Compound name and description	Formula	Molecular mass	Fragment base peak
a	C27 13β(H),17α(H) 20S diasterane	C27H48	amu 372	m/z 259
b	C27 13β(H),17α(H) 20R diasterane	"	"	"
c	C27 13α(H),17β(H) 20S diasterane	"	"	m/z 217
d	C27 13α(H),17β(H) 20R diasterane	"	"	"
e	C28 13β(H),17α(H) 20S 24-methyl diasterane	C28H50	amu 386	m/z 259
f	C28 13β(H),17α(H) 20R 24-methyl diasterane	"	"	"
g	C28 13α(H),17β(H) 20S 24-methyl diasterane + C27 14α(H),17α(H) 20S cholestane	" C27H48	" amu 372	m/z 217 "
h	C29 13β(H),17α(H) 20S 24-ethyl diasterane + C27 14β(H),17β(H) 20R cholestane	C29H52 C27H48	amu 400 amu 372	m/z 259 m/z 218
i	C27 14β(H),17β(H) 20S cholestane + C28 13α(H),17β(H) 20R 24-methyl diasterane	" C28H50	" amu 386	" m/z 217
j	C27 14α(H),17α(H) 20R cholestane	C27H48	amu 372	"
k	C29 13β(H),17α(H) 20R 24-ethyl diasterane	C29H52	amu 400	m/z 259
l	C29 13α(H),17β(H) 20S 24-ethyl diasterane	"	"	m/z 217
m	C28 14α(H),17α(H) 20S 24-methyl cholestane	C28H50	amu 386	"
n	C29 13α(H),17β(H) 20R 24-ethyl diasterane + C28 14β(H),17β(H) 20R 24-methyl cholestane	C29H52 C28H50	amu 400 amu 386	" m/z 218
o	C28 14β(H),17β(H) 20S 24-methyl cholestane	"	"	"
p	C28 14α(H),17α(H) 20R 24-methyl cholestane	"	"	m/z 217
q	C29 14α(H),17α(H) 20S 24-ethyl cholestane	C29H52	amu 400	"
r	C29 14β(H),17β(H) 20R 24-ethyl cholestane	"	"	m/z 218
s	C29 14β(H),17β(H) 20S 24-ethyl cholestane	"	"	"
t	C29 14α(H),17α(H) 20R 24-ethyl cholestane	"	"	m/z 217
I	C30 14α(H),17α(H) 20S 24-propyl cholestane	C30H54	amu 414	"
J	C30 14β(H),17β(H) 20R 24-propyl cholestane	"	"	m/z 218
K	C30 14β(H),17β(H) 20S 24-propyl cholestane	"	"	"
L	C30 14α(H),17α(H) 20R 24-propyl cholestane	"	"	m/z 217

Compound names and identification after Mackenzie et al. (1985).

NB: methyl cholestane ≡ ergostane, ethyl cholestane ≡ stigmastane.

H. 2.1.2. Methyl steranes 4β

Equivalents of all diasteranes and the C30 cholestanes have not been recorded in the methyl sterane fragments. Compound codes and descriptions are the same as the steranes except that they have an extra methyl group located at the C-4 position. In these mature samples, this is generally present in the 4β configuration.

Compounds named and identified after S.R. Thompson (1992, pers comm).

H. 2.1.3. Tri and tetracyclic terpanes

Code	Compound name and description	Formula	Molecular mass	Fragment base peak
19T	C19 tricyclic terpane	C19H34	amu 262	m/z 191
20T	C20 tricyclic terpane	C20H36	amu 276	"
21T	C21 tricyclic terpane	C21H38	amu 290	"
21/1T	C21 tricyclic terpane	"	"	"
21/2T	C21 tricyclic terpane	"	"	"
22T	C22 tricyclic terpane	C22H40	amu 304	"
22/1T	C22 tricyclic terpane	"	"	"
23T	C23 tricyclic terpane	C23H42	amu 318	"
24T	C24 tricyclic terpane	C24H44	amu 332	"
25T	C25 tricyclic terpane	C25H46	amu 346	"
24/4	C24 17,21 secohopane (tetracyclic terpane)	C24H42	amu 330	"
26TR	C26 tricyclic terpane 22R	C26H48	amu 360	"
26TS	C26 tricyclic terpane 22S	"	"	"
27TR (?)	C27 tricyclic terpane 22R	C27H50	"	"
27TS (?)	C27 tricyclic terpane 22S	"	"	"

Compound names and identifications after Zumberge (1983) and Ekweozor and Strausz (1983).

H. 2.1.4. Tri and pentacyclic terpanes and non-hopanes

Code	Compound name and description	Formula	Molecular mass	Fragment base peak
28TS	C28 tricyclic terpane 22S	C28H52	amu 388	m/z 191
28TR	C28 tricyclic terpane 22R	"	"	"
29TS	C29 tricyclic terpane 22S	C29H54	amu 402	"
29TR	C29 tricyclic terpane 22R	"	"	"
Ts	C27 18α(H),21β(H) 22,29,30-trisnorneohopane	C27H46	amu 370	"
Tm	C27 17α(H),21β(H) 22,29,30-trisnorhopane	"	"	"
30TS	C30 tricyclic terpane 22S	C30H56	amu 416	"
30TR	C30 tricyclic terpane 22R	"	"	"
25,30	C28 17α(H),21β(H) 25,30-bisnorhopane	C28H48	amu 384	"
28,30	C28 17α(H),21β(H) 28,30-bisnorhopane	"	"	"
29nH	C29 17α(H) 30-norhopane	C29H50	amu 398	"
29nnH	C29 18α(H) 30-norneohopane	"	"	"
30D	C30 14α(H),17α(H),21β(H) diahopane	C30H52	amu 412	"
nM	C29 17β(H),21α(H) 30-normoretane	C29H50	amu 398	"
H	C30 17α(H),21β(H) hopane	C30H52	amu 412	"
M	C30 17β(H),21α(H) moretane	"	"	"
31S	C31 17α(H) homohopane 22S	C31H54	amu 426	"
31R	C31 17α(H) homohopane 22R	"	"	"
G	gammacerane	C30H52	amu 412	"
32S	C32 17α(H) bishomohopane 22S	C32H56	amu 440	"
32R	C32 17α(H) bishomohopane 22R	"	"	"
33R	C33 17α(H) trishomohopane 22S	C33H58	amu 454	"
33S	C33 17α(H) trishomohopane 22R	"	"	"
34S	C34 17α(H) tetrakishomohopane 22S	C34H60	amu 468	"
34R	C34 17α(H) tetrakishomohopane 22R	"	"	"
35S	C35 17α(H) pentakishomohopane 22S	C35H62	amu 484	"
35R	C35 17α(H) pentakishomohopane 22R	"	"	"

Compound names and identifications after Mackenzie et al. (1985) and Aquino Neto et al. (1983).

H. 2.2. AROMATIC COMPOUNDS

H. 2.2.1. Trimethyl naphthalenes

Code	Compound name and description	Formula	Molecular mass	Fragment base peak
137	1,3,7-trimethyl naphthalene	C13H24	amu 170	m/z 170
136	1,3,6-trimethyl naphthalene	"	"	"
135/146	1,3,5 and 1,4,6-trimethyl naphthalene	"	"	"
236	2,3,6-trimethyl naphthalene	"	"	"
127	1,2,7-trimethyl naphthalene	"	"	"
126/167	1,2,6 and 1,6,7-trimethyl naphthalene	"	"	"
124	1,2,4-trimethyl naphthalene	"	"	"
125	1,2,5-trimethyl naphthalene	"	"	"

Compound names and identifications after Rullkötter et al. (1991).

H. 2.2.2. Dibenzothiophenes

Code	Compound name and description	Formula	Molecular mass	Fragment base peak
4M	4-methyl dibenzothiophene	C12H10S	amu 198	m/z 198
2+3M	2 and 3-methyl dibenzothiophene	"	"	"
1M	1-methyl dibenzothiophene	"	"	"

Compound names and identifications after Rullkötter et al. (1991).

H. 2.2.3. Dimethyl dibenzothiophenes

Code	Compound name and description	Formula	Molecular mass	Fragment base peak
A	dimethyl dibenzothiophene (low stability)	C13H12S	amu 212	m/z 212
B	?2,8-dimethyl dibenzothiophene (mod. stability)	"	"	"
C	?1,8-dimethyl dibenzothiophene (high stability)	"	"	"
D	2,5-dimethyl dibenzothiophene (mod. stability)	"	"	"
E	2,4-dimethyl dibenzothiophene (mod. stability)	"	"	"
F	2,3-dimethyl dibenzothiophene (low stability)	"	"	"

NB: stability records the resistance of the compound to the cracking effects of advanced maturation i.e. the peak with the high stability remains high at a higher maturation level. Peaks identified as dimethyl dibenzothiophenes by S.R. Thompson (1992, pers comm.) and Tomic et al. (1995).

H. 2.2.4. Trimethyl dibenzothiophenes

Code	Compound name and description	Formula	Molecular mass	Fragment base peak
a	trimethyl dibenzothiophene (low stability)	C14H14S	amu 226	m/z 226
b	trimethyl dibenzothiophene (low stability)	"	"	"
c	trimethyl dibenzothiophene (mod. stability)	"	"	"
d	trimethyl dibenzothiophene (high stability)	"	"	"
e	trimethyl dibenzothiophene (mod. stability)	"	"	"
f	trimethyl dibenzothiophene (low stability)	"	"	"
g	trimethyl dibenzothiophene (low stability)	"	"	"
h	trimethyl dibenzothiophene (v. low stability)	"	"	"
i	trimethyl dibenzothiophene (v. low stability)	"	"	"

NB: stability as above. Peaks identified as trimethyl dibenzothiophenes by S.R. Thompson (1992, pers comm.) and Chakhmakhchev and Suzuki (1995).

H. 2.2.5. Monoaromatic steroids

Code	Compound name and description	Formula	Molecular mass	Fragment base peak
1	C27 5β(H) cis 20S regular	C27H42	amu 366	m/z 253
2	C27 10β(H) 20S rearranged	"	"	"
3	C27 10α(H) 20S rearranged	"	"	"
4	C27 5β(H) cis 20R regular +C27 10β(H) 20R rearranged	" "	" "	" "
5	C27 5α(H) trans 20S regular	"	"	"
6/7	C28 5β(H) cis 20S regular	C28H44	amu 380	"
9	C27 5α(H) trans 20R regular +C28 5α(H) trans 20S regular	C27H42 C28H44	amu 366 amu 380	" "
10	C28 5β/10β(H) cis 20R regular/rearranged + C29 5β/10β(H) cis 20S regular/rearranged	" C29H46	" amu 394	" "
11	C28 10α(H) 20R rearranged	C28H44	amu 380	"
12	C29 10α(H) 20S rearranged	C29H46	amu 394	"
13	C29 5α(H) trans regular	"	"	"
14	C28 5α(H) trans 20R regular + C29 5β/10β(H) cis 20R regular/rearranged	C28H44 C29H46	amu 380 amu 394	" "
15	C29 10α(H) 20R rearranged	"	"	"
16	C29 5α(H) trans 20R regular	"	"	"

Compounds named and identified after Riolo et al., (1986) and Seifert et al. (1983).

H. 2.2.6. Triaromatic steroids

Code	Compound name and description	Formula	Molecular mass	Fragment base peak
f	C21 11β,11-ethyl triaromatic steroid	C21H22	amu 274	m/z 231
g	C22 11β,11-propyl triaromatic steroid	C22H24	amu 288	"
a	C26 20S 11β,12β triaromatic steroid	C26H32	amu 344	"
b	C26 20R 11β,12α triaromatic steroid + C27 20S 11β,12β,16-methyl triaromatic steroid	" C27H34	" amu 358	" "
c	C28 20S 11β,12β,16-ethyl triaromatic steroid	C28H36	amu 372	"
d	C27 20R 11β,12α,16-methyl triaromatic steroid	C27H34	amu 358	"
e	C28 20R 11β,12α,16-ethyl triaromatic steroid	C28H36	amu 372	"

Compounds named and identified after Rullkötter et al. (1991).